VOL - 1

# HYDRO 2020
# INTERNATIONAL CONFERENCE

(Hydraulics, Water Resources & Coastal Engineering)

Silver Jubilee Year

26-28 March 2021

## Proceedings




1961 - 2021, 60 Glorious Years of Service







*Organized by*
Department of Civil Engineering,
National Institute of Technology Rourkela
Odisha, India

*In Association with*
Indian Society for Hydraulics, Pune

# *Significant Milestones of NIT Rourkela*

**2021** Diamond Jubilee Celebrations

**2020** Inauguration of Golden Jubilee Building,The tallest structure and pride of Rourkela City

**2010** Celebrated Golden Jubilee

**2007** Declared Institute of National Importance via Act of Parliment

**2002** Renamed National Institute of Technology (NIT) Rourkela

**1994** Achieved Academic Autonomy

**1986** Celebrated Silver Jubilee

**1965** Inclusion of Science departments into the REC system

**1961** 15th August — Founded as Regional Engineering College (REC) Rourkela



# XXV HYDRO 2020 INTERNATIONAL CONFERENCE

**(Hydraulics, Water Resources & Coastal Engineering)**
**March, 26-28, 2021**

Silver Jubilee Year


Editors

**Prof. Kanhu Charan Patra**

**Prof. Kishanjit Kumar Khatua**

**Dr. (Mrs) Sanat Nalini Sahoo**

Associate Editors

**Dr. Ratnakar Swain**

**Dr. Anurag Sharma**



***Organized by***

**Department of Civil Engineering,**
**National Institute of Technology Rourkela**
**Odisha, India**

***In Association with***

**Indian Society for Hydraulics, Pune**

All rights are reserved. No part of this publication which is material protected by this copyright notice may not be reproduced or transmitted or utilized or stored in any form or by any means now known or hereinafter invented, electronic, digital or mechanical, including photocopying, scanning, recording or by any information storage or retrieval system, without prior written permission from Paramount Publishing House.

Information contained in this book has been published by Paramount Publishing House, Hyderabad and has been obtained by its Author(s) from sources believed to be reliable and are correct to the best of their knowledge. However, the Publisher and its Author(s) shall in no event be liable for any errors, omissions or damages arising out of use of this information and specifically disclaim any implied warranties or merchantability or fitness for any particular use.

***Disclaimer***
The Publisher and the Organisers of the HYDRO 2020 conference, including the editors have no responsibility, what ever, for the accuracy of the data, statements made, results and opinions expressed by authors of any of the papers in this publication of the conference proceedings. The authors are solely responsible for the contents published in their respective papers.

**HYDRO 2020**

**INTERNATIONAL CONFERENCE**
**(Hydraulics, Water Resources & Coastal Engineering)**

**First Edition - 2021**

Copyright © **Prof. Kishanjit Kumr Khatua, Prof. Kanhu Charan Patra, Dr. (Mrs) Sanat Nalini Sahoo**

ISBN : 978-93-90631-56-8

**Paramount Publishing House**

A-531,H.No.4-32-521,Phase-1,AllwynColony,Kukatpally,
Hyderabad-500072. Ph.:7799000082

***Sales Offices :***

**Hyderabad**
A-531,H.No.4-32-521,Phase-1,AllwynColony,Kukatpally,
Hyderabad-500072. Ph.:7799000082

**New Delhi**

C/14,SDIDCWorkCentreJhilmilColony,NewDelhi-100095.Phone:
011-2162365. paramountpublishers@gmail.com |
alluriasr2005@yahoo.com

Published by Krishna Prasad Alluri for Paramount Publishing House and printed by him at Sai Tirumala Printers.

## *Chief Patron*

**Prof. A. Biswas**

Director, NIT Rourkela

## *Patrons*

**Prof. C. R. Patra**

HOD, CE, NIT Rourkela

**Prof. P. K. Das**

Register, NIT Rourkela

## *Chairman*

**Prof. K. C. Patra**

Professor, CE, NIT Rourkela

**Prof. M. C. Deo**

ISH President

## *Organizing Secretary*

**Prof. Kishanjit Kumar Khatua**

Professor, CE, NIT Rourkela

## *Co-organizing Secretaries*

D**r. (Mrs) Sanat Nalini Sahoo,** Asst. Prof., NIT Rourkela

**Dr. L. R. Rangnath,** Secretary, ISH, Pune

**Dr. R. Swain,** Asst. Prof., NIT Rourkela

## *Organising Committee*

**Prof. T. I. Eldo,** Vice President, ISH, Pune

**Dr. R. G. Patil,** Vice President, ISH, Pune

**Shri Amit Kulkhare,** Treasurer, ISH, Pune

**Dr. Anurag Sharma,** Asst. Prof., NIT Rourkela

# Preface

HYDRO 2020 International Conference on Hydraulics, Water Resources, Coastal & Environmental Engineering, being organized at NIT Rourkela under the aegis of the Indian Society for Hydraulics, is an annual get together of Scientists, Researchers, Academicians, Practicing Engineers, and Consultants all over the world related to Water Engineering that has evolved over the years. The conference earned an international reputation and recognition in this topic. The conference mainly focuses on state-of-the-art technologies and applied research in the field of Hydraulics, Water Resources, Coastal & Environmental Engineering. The present 25th (silver jubilee) episode of the conference is being organized at the National Institute of Technology Rourkela.

NIT Rourkela was established on 15 August 1961. Its foundation stone was laid by the first Prime Minister of India, Pt. Jawaharlal Nehru. NIT Rourkela is a premier institute of national importance funded by the Government of India and is committed to quality technical education in the country. It is a fully residential campus offering accommodation to faculty, staff, and students. The campus of the Institute consisting of the Academic area, halls of residence area, and faculty staff colony located at the eastern end of Rourkela steel city. The green and beautiful campus has all the amenities for developing personal, social, and academic skills of the student, faculty, and staff. HYDRO 2020 International Conference, organized at NIT Rourkela in its silver jubilee year has coincided with the diamond jubilee year of NIT Rourkela online mode. It is our proud privilege to have welcomed you all to this renowned International Conference. Despite the current pandemic situations throughout the globe, more than five hundred abstracts of the papers have been received and after the review, about 292 full papers have been finally accepted. Ten senior scientists of high expertise from abroad and twenty-four senior scientists from reputed Institutes/ Universities of our country have delivered their expertise and knowledge in the emerging field of Water Resources Engineering. Around 60 senior scientists/ Professors from reputed Institutes/ Universities have chaired the sessions covering all the themes of the Conference.

The HYDRO 2020 proceedings volume contains peer-reviewed technical papers under 29 themes and covers a wide spectrum of research studies, experimental outputs, case studies, review papers, and others related to the management of Water Resources and Coastal Engineering. We are indeed happy to bring on this occasion, souvenir containing abstracts of the Keynotes and Invited talks along with the quality technical papers selected for the presentation. Further, proceedings of the conference are also released in electronic forms that are arranged theme-wise.

We take this opportunity to express our sincere thanks and gratitude to all members of the International and National Advisory Committee members, the Technical Committee as well as the Organizing Committee members along with student volunteers, authors, and reviewers. We appreciate the untiring efforts of conference organizers, generous support from sponsors, continuous guidance, support, and encouragement from all academic and research institutions. We strongly hope that the deliberations and discussions at the HYDRO 2020 International Conference shall promoted useful and fruitful interactions among participants and thus help professionals working in the field of Hydraulics, Water Resources, and Coastal Engineering.

-Editors

# VOLUME I

# CONTENTS


| THEME NO. | NAME OF THE THEME |
|---|---|
| Theme I | Coastal and Ocean Engineering |
| Theme II | River and Coastal Engineering |
| Theme III | Impact of Climate Change on Water Resources |
| Theme IV | Hydraulic & Hydrologic Modelling |
| Theme V | RS/GIS Application for Water Resources Management |
| Theme VI | River Hydraulics |
| Theme VII | Coastal and Ocean Engineering |
| Theme VIII | Hydraulic & Hydrologic Modelling |
| Theme IX | Flood Forecasting and Management |
| Theme X | Urban Water Management |
| Theme XI | Watershed Management |
| Theme XII | Hydraulic Structures and Hydropower Engineering |
| Theme XIII | Groundwater Modelling and Management |
| Theme XIV | Computational Fluid Dynamics / Numerical Modelling |
| Theme XV | Sediment Transport |

| Sl.No. | Paper ID No | Title | Page No. |
|---|---|---|---|
| **THEME I** | | | |
| **Theme I<br>Coastal and Ocean Engineering** | | | |
| 1 | **071** | Factors affecting the Vessel Turnaround time in a Seaport<br>*Dayananda Shetty K, Vijayanand.Gurudev, Dwarakish.G.S* | 2 |
| 2 | **077** | Diffraction Studies Pertaining to Functional Design of Breakwaters-A case Study of Gangavaram Port, East Coast of India<br>*G. Lenin Reddy, M. G. Muni Reddy, T. V. Ramana Murthy, M. L. Narasimham* | 22 |
| 3 | **083** | Innovative soft option of coastal protection by floating seaweed farm - a review<br>*Surakshitha, Manu, Subba Rao* | 35 |
| 4 | **112** | Study of sediment behaviour along the Mangalore coast through granulometric studies<br>*Aseem V, Dwarakish G S* | 43 |
| 5 | **114** | Study of shoreline change along Kasaragod district in Kerala, West Coast of India<br>*AnjitaN A, Makhdumi W and Dwarakish G S* | 53 |
| 6 | **129** | Ascertaining the effect of Mesh resolution in MIKE 21 Spectral Wave model results<br>*Ms. Soniya Xaviour, Dr. J.D Agrawal* | 61 |
| 7 | **131** | Mathematical modelling to ascertain the effect of Groyne field on beach fill stability<br>*Mr. Ishfakh M Shafeekh, Mr. M. Phani Kumar* | 68 |
| 8 | **383** | Effect of Porous Baffle on Sloshing Dynamics Placed At *L /2* Location In A Sway Excited Rectangular Tank<br>*Sahaj K V, Pavan Kumar, Nasar T* | 76 |
| 9 | **426** | Forecasting of Natural Disasters, A Case Study on Coastal Part of Odisha<br>*Karanam Raviteja, M Uma Maheswar Rao, K.C. Patra* | 86 |
| 10 | **470** | Mathematical Modelling and Simulation of Ocean Disposal of Harbour Dredged Materials<br>*Anil Bagwan, Jiwcshwar Sinha, Prabhat Chandra* | 96 |
| **Theme II<br>River and Coastal Engineering** | | | |
| 11 | **006** | Flood Estimation Based On Water Surface Velocity using Non-Contact Sensing and Regression Analysis<br>*M. Selva Balan, K.V.Manisa, Yash D, Shraddha Khot & Malathi Khole* | 106 |

| | | | |
|---|---|---|---|
| 12 | **025** | Hydraulic Physical Model Studies For The Development Of Coast Guard Jetty At New Mangalore Port, Panambur, Karnataka – A Case Study<br>*Jagadeesh H.B., Chalawadi A. S. & Prabhat Chandra* | 115 |
| 13 | **167** | Suitability of Regular And Random Sea Wave Generators In Hydraulic Physical Model Studies – Key Factors For Selection<br>*Jagadeesh H B, Kashyape P A, Prabhat Chandra* | 127 |
| 14 | **174** | Assessment of Littoral Drift And Shoreline Changes For A Fishery Harbour on South West Coast of India<br>*N Jha, J Sinha, Prabhat Chandra* | 139 |
| 15 | **175** | Assessment Of Wave Tranquillity And Littoral Drift Studies Using Time Dependent Wave Parameters To Develop Tourist Harbour In Andhra Pradesh<br>*Vighe K S, Barve K H, Ranganath L R, Agrawal J D* | 147 |
| 16 | **176** | Numerical Model Studies For Assessment Of Wave Tranquility And Littoral Drift For Proposed Passenger Jetty In An Inlet Harbour At Kalingapatnam.<br>*Vighe K S, Sawant Rahul, Barve K H, Ranganath L R, Agrawal J D* | 157 |
| 17 | **177** | Wave Hindcasting And Storm Surge Analysis At Porbandar, Gujarat<br>*Santosh Kori, Dr Prabhat Chandra* | 170 |
| 18 | **178** | Importance Of Optimization Of Over Lapping Of Breakwater At Fishing Harbour Entrance<br>*R.K.Chaudhari, S.K. Kori, Dr. Prabhat Chandra* | 175 |
| 19 | **179** | Utilization Of Numerical Model For Shoreline Changes To Evolve The Suitable Coastal Protection Work At Hosabettu, Karnataka<br>*R. K. Chaudhari, S. K. Kori, Dr. Prabhat Chandra* | 184 |
| 20 | **180** | Shoreline Changes Studies For Development Of Passenger Terminal At Kashid, Maharashtra<br>*Dr. Prabhat Chandra, R.K.Chaudhari, S.K. Kori* | 193 |
| **Theme III<br>Impact of Climate Change on Water Resources** | | | |
| 21 | **016** | Effect of Climate Change on Precipitation for Bhopal, India<br>*Priyank Agrawal, H. L. Tiwari and Ankit Balvanshi* | 203 |
| 22 | **048** | A Morphological Comparison of Two Different Climatic Settings And Its Significance on Their Sediment Yield<br>*N. Sahoo, P. K. Das & J. Meher* | 210 |
| 23 | **091** | Sensitivity change of water deficit droughts on evapotranspiration methods in the Indian subcontinent<br>*Femin C Varghese, Subhasis Mitra* | 220 |
| 24 | **132** | Generation of Intensity-Duration-Frequency Curve For A River Basin In South Kerala By Incorporating Climate Changes<br>*Lini R. Chandran, Aiswarya B. Babu, Krishna Priya S. B., Sumina, Sini S. Nair* | 226 |
| 25 | **152** | A Review On Climate Change Impact Analysis Using | 236 |

| | | | |
|---|---|---|---|
| | | Statistical Tools<br>*Parth Sinroza, Mohdzuned Shaikh* | |
| 26 | **370** | Climate Variability Influences on Seasonal Precipitation-Temperature Associations across Florida<br>*Priyank J. Sharma, Ramesh S. V. Teegavarapu* | 240 |
| 27 | **419** | Assessment of Climate Change for Generating Grid Wise Future Scenarios of Precipitation and Temperature Over Lower Godavari Sub Basin Maharashtra State, India<br>*Barokar Y. J., Regulwar D.G* | 249 |
| 28 | **420** | Effect of Climate Change on the Precipitation of Saraikela-Kharsawan District of Jharkhand by Statistical Downscaling Method<br>*Nirup Sundar Mandal, Sanat Nalini Sahoo* | 258 |
| 29 | **421** | Ranking of CMIP6 based Global Climate Models for Prediction of Temperature in Godavari river basin<br>*Narapareddi Manasa, M Uma Maheswar Rao, K.C. Patra* | 267 |
| 30 | **463** | Climate Change or Land-Use Dominated Streamflow Variations: An Empirical Model-Based Contribution Analysis of the Baitarani River Basin, India<br>*Sushree Swagatika Swain, Ashok Mishra, Chandranath Chatterjee, Bhabagrahi Sahoo* | 280 |
| **Theme IV<br>Hydraulic & Hydrologic Modelling** | | | |
| 31 | **120** | Rainfall-Runoff Simulation in Mahi Bajaj Sagar Dam Catchment, India, Using HEC-HMS<br>*Biltu Pal, Prof. Mahender Choudhary, Prof. Y.P. Mathur* | 291 |
| 32 | **209** | Prediction of Water Level/Runoff Using Physics Based Hydrological Model in Lower Tapi Basin, India.<br>*Shubham M. Jibhakate, P. V. Timbadiya, P. L. Patel* | 301 |
| 33 | **212** | Identification of Hydrologically Efficient Regions in Semi-Arid Yerli Sub-Catchment of Upper Tapi Basin, India.<br>*Lalit Kumar Gehlot, P. L. Patel and P. V. Timbadiya* | 311 |
| 34 | **224** | Activation of Central Channel Using Novel Method In River Kosi, Bihar<br>*Arun Kumar, Dr. R. G. Patil* | 321 |
| 35 | **244** | Development of a distributed physics hydrological model for prediction of inflows into Hathnur Reservoir from Main Tapi River in Upper Tapi basin, India.<br>*Nikita Saptarishy, P. L. Patel* | 330 |
| 36 | **258** | A comparison between Flood models developed using topographical details from field survey and SRTM DEM using MIKE HYDRO River<br>*Anju B, Drissia T.K, Nowshaja P.T* | 341 |
| 37 | **269** | A Rainfall- Runoff Simulation Model for Estimation of Floods for Purna River Basin Part of Upper Tapi Basin<br>*Darshan Mehta, Dr. S. M. Yadav, Ankita Patel* | 351 |
| 38 | **270** | Hydrodynamic Challenges And Role Of Physical Model In | 365 |

| | | | |
|---|---|---|---|
| | | Evolving Layout of Boat Landing Facility at Confluence of Elephanta Deep And Nhava Creek<br>*Anil Purohit, Animesh Basu, Kumar Chavan, Jagottam Agrawal* | |
| 39 | **281** | Hydrodynamic Modelling of Upper Tapi River, India<br>*M. Sayan, P.V. Timbadiya* | 375 |
| 40 | **312** | Optimization Of Common Energy Dissipator For The Two-Tier Spillway<br>*R. R. Bhate, Amit Kulhare, Dr. M. R. Bhajantri* | 387 |
| **Theme V<br>RS/GIS Application for Water Resources Management** | | | |
| 41 | **019** | Study on Vegetation, Rainfall pattern and Temperature for the state of Maharashtra<br>*M L Harshavardhan, Anirban Mandal* | 397 |
| 42 | **036** | Estimation of surface heat fluxes using Remote Sensing Method<br>*Ankan Jana, Prof. Mahesh Kumar Jat & Prof. Mahender Choudhary* | 407 |
| 43 | **037** | Assessment of grape crop acreage using geospatial technique for command area of Palkhed Reservoir (Maharashtra)<br>*Shradhha Kuwar, Sunil Gaikwad and Makarand Kulkarni* | 416 |
| 44 | **038** | Hydro-cover Mapping by Remote Sensing and GPS Technology: A case study of Nashik District, Maharashtra, India.<br>*Anita Morkar, Santosh Wagh & Makarand Kulkarni* | 424 |
| 45 | **070** | Impact of land use land cover on the response of the Mahanadi river basin in a sub-basin scale using SWAT<br>*Shasanka Sekhar Barik, Dr. Janhabi Meher, Laxmipriya Mohanty* | 433 |
| 46 | **102** | Comparison of Land Surface Temperature for Bare soil from MODIS and ASTER data<br>*Sreelakshmi C V and Jairaj P G* | 442 |
| 47 | **164** | Hydrological Geophysical and GIS Approach in Delineation of Suitable Artificial Recharge Site<br>*Rolland Andrade* | 452 |
| 48 | **219** | Estimation of Soil Loss from Bagmati River Basin using RUSLE model and GIS Technique<br>*Mani Kumar Singh, Vivekanand Singh* | 462 |
| 49 | **235** | Studies For Proposed Bank Protection Works Along Existing Ghats of Nira And Bhima Rivers At Nira Narsingpur - A Case Study<br>*Jotsana G. Ambekar, B. Raghuram Singh, Dr. R. G. Patil* | 469 |
| 50 | **411** | Assessment of Water Balance Components in the Genale River Basin, Ethiopia Using SWAT Model<br>*Tufa Feyissa Negewo, Arup Kumar Sarma* | 476 |

| | | | |
|---|---|---|---|
| **Theme VI**<br>**River Hydraulics** | | | |
| 51 | **011** | Experimental Investigation of Friction Factor in Alluvial Channel<br>*Anurag Sharma, Nikhitha Elsa Sam, Asmita Tanwani, Hardipsinh Jadeja & Bimlesh Kumar* | 487 |
| 52 | **047** | Effect of Dense Stream bank Vegetation With Steep Sloping Riverbanks on Manning's Roughness Coefficient of 0.11 In Hydraulic Model Studies<br>*Ashish A. Doshi & Pramod B. Deolalikar* | 497 |
| 53 | **087** | Discharge Predictions of Meandering River using Artificial Neural Networks<br>*Tushar Khankhoje, Susmita Ghosh* | 507 |
| 54 | **122** | Investigation of The Issues in The Inter Linking of Rivers: A Case Study for Godavari- Krishna Link Indira Sagar Polavaram Project<br>*Gurusamy B. T, Vasudeo A. D, Gautam N.R, Godbole S. P and Ghare A. D* | 519 |
| 55 | **143** | MEMS Based Remote Operated Bed Profiler For River Model<br>*M. Selva Balan, Pratiksha Mete, Ruchita Pagar, Harshada Shelkande , Dipali Bangar* | 534 |
| 56 | **286** | Hydrodynamic Modelling Of Middle Tapi River Using MIKE 11<br>*K. B. Baladaniya, P. L. Patel* | 543 |
| 57 | **293** | Simulation of Channel Bed Level Variation And Its Experimental Validation<br>*G. Yatirajulu and P. V. Timbadiya* | 553 |
| 58 | **298** | Water Security Assessment of Karuvannur Watershed - Current And Future Scenario<br>*Anjana Ramesh, Reeba Thomas* | 563 |
| 59 | **307** | Evaluating Periodic Changes of River Discharge Carrying Capacity: A Case Study of Lower Tapi River<br>*Vineela Nandam, Patel P. L* | 573 |
| 60 | **339** | Study of unsteady flow parameters and hysteresis effect in a simple channel under unsteady flow condition<br>S.Sahoo, K.Devi, J.R.Khuntia, K.K.Khatua | 581 |
| **Theme VII**<br>**Coastal and Ocean Engineering** | | | |
| 61 | **081** | Numerical Model Studies to Assess the Morphological Changes due to Coastal Front Development- A Case Study<br>*B. Krishna, G. A. Rajkumar, Karthikeyan. M, L.R. Ranganath, J.D Agrawal* | 591 |
| 62 | **184** | Historical and Future Sea Level Rise at Major Indian Ports<br>*Priyen Somaiya, Raghavendra G. Patil and M C Deo* | 602 |

| | | | |
|---|---|---|---|
| 63 | **190** | Stabilization of Inlet And Restoration Of River Mouth In Puthiyangadi<br>*V. B. Sharma, Shivani Sahu, Vaibhav Konde, Prabhat Chandra* | 612 |
| 64 | **194** | Restoration of tidal creek inlet for navigation using pile jetty – a case study<br>*Shivani Sahu, Jiweshwar Sinha, Vaibhawi Roy, Prabhat Chandra* | 622 |
| 65 | **200** | Estimation of Wave Loads on Deck Structures at Indian Ports in a Changing Climate<br>*Akhila Padmajan, Rameeza Moideen, Manasa Ranjan Behera* | 630 |
| 66 | **204** | Effect of wave steepness on wave overtopping discharge of an emerged quarter-circle breakwater<br>*Vishwanatha Mane, Subba Rao, A.Vittal Hegde* | 640 |
| 67 | **222** | Numerical Modelling for Wave Transformation along the Ratnagiri Coast- Case Study<br>*Pranav Vaishampayan, Amol S. Borkar, Varun Khengare, Ketan Jadhav, Abhishek Deshmukh, Prof. Shilpi Bhuinyan, Dr. Prabhat Chandra* | 648 |
| 68 | **243** | Effect of Marine Growth on Wave Loading on Small Diameter Tubular Structural Members<br>*Sarath Suresh, Rameeza Moideen, Manasa Ranjan Behera* | 655 |
| 69 | **261** | Performance Evaluation of Detached Breakwater in Poonthura Coast using Boussinesq Wave Approach<br>*Aleena Elsa Mathew, Ram Kumar J, Satya Kiran Raju, Sridhar Muddada, M V Ramanamurthy* | 666 |
| 70 | **416** | Behaviour of Rubberized Concrete when Subjected to Exposure Along Coastal Zone<br>*Bejay Kumar Yadav, Showmen Saha* | 674 |
| **Theme VIII<br>Hydraulic & Hydrologic Modelling** | | | |
| 71 | **035** | Construction Of Temporary Pile Bridge For Erection Of Fly Over Bridge Across An Estuarine River<br>*Uday B. Patil, Dr. Prabhat Chandra* | 685 |
| 72 | **125** | Evaluation of Run-Off and Its Impact on Confluence of Tributary Due to Rapid Urbanization in Shipra River Basin<br>*Dr. Munendra Kumar and Mr. Jaganniwas* | 695 |
| 73 | **128** | Selection of the Optimal Design Run-off Coefficient for Urban Drainage System<br>*Dr. Munendra Kumar and Mr. Jaganniwas* | 702 |
| 74 | **186** | Mathematical Model Studies for Surge Analysis of Haldi Purani Lift Irrigation Scheme<br>*G. V. R. Murthy, Y. N. Srivastava, V.S. Telgote* | 709 |
| 75 | **205** | Utility Of Physical Wave Model For The Development Of Fishing Harbour On Open Coast<br>*Sudheer S. Chavan, Hradaya Prakash Dr. Prabhat Chandra* | 715 |
| 76 | **208** | Acquisition of Depth Profile Using Bathymetry Survey Near | 722 |

| | | | |
|---|---|---|---|
| | | Left Bank Spillway And Proposed Additional Spillway Of Hirakud Dam, Odisha - A case study<br>*M. S. Bist, Ajay Sonawane, Ajit Singh, J. K. Singh, M. Selva Balan* | |
| 77 | **220** | Morphological Changes Around Sogal Channel of Deendayal Port, Gujarat In the Approaches<br>*Chaudharee B. B, Hradaya Prakash, Dr.Prabhat Chandra* | 729 |
| 78 | **450** | Wave Simulation for Optimization of Breakwater Layout- A Case Study.<br>*A. Pardeshi, A. S. Borkar, B. L. Meena, Dr. Prabhat Chandra* | 736 |
| 79 | **492** | Numerical Simulation of Energy Loss at Drops mechanism by Volume of Fluid Method<br>*Pranaya Keshari Nahak, Adwaith Gupta* | 747 |
| 80 | **507** | Impact of deforestation and urbanization on extreme temperature and humidity over Brahmani River Basin<br>*Ratnakar Swain* | 755 |
| **Theme IX<br>Flood Forecasting and Management** | | | |
| 81 | **014** | Flood Frequency Analysis Using Gumbel's Distribution Method: A Case Study of Sita River, Karnataka, India.<br>*Soumya S Nyamathi & Dwarakish G.S* | 764 |
| 82 | **066** | Investigating the role of streamflow forecasts to mitigate floods in the delta region of Mahanadi River basin<br>*Amina Khatun, Chandranath Chatterjee, Bhabagrahi Sahoo* | 770 |
| 83 | **088** | Flood risk assessment and mapping using AHP: A case study in Thuthapuzha river basin, Kerala<br>*Athira K, Dr. Sarmistha Singh* | 778 |
| 84 | **097** | Application of L-Moment based Regional Flood Frequency Analysis for Krishna River Basin<br>*Amit Kumar Singh, Sagar Rohidas Chavan* | 787 |
| 85 | **202** | Assessment of floodplain mapping of Ulhas River basin usingHEC-RAS1D/2D hydraulic simulation.<br>*Sachin Bhere, M. Janga Reddy* | 798 |
| 86 | **249** | Flood Inundation Mapping of Chalakkudy River using HEC RAS<br>*Jeslin Jose A, Dr. Sumam K S* | 809 |
| 87 | **291** | Non-stationary Flood Frequency Analysis of West flowing Rivers of Kerala using Bayesian Inference Approach<br>*Anjitha U.G., Meera G.Mohan, Adarsh S, Gopakumar R* | 820 |
| 88 | **458** | Web Interface for Random Sea Wave Generation and Data Acquisition System for Hydraulic Physical Model Studies<br>*V. Jagadeesh, R. S. Erande* | 830 |

| | | | |
|---|---|---|---|
| 89 | **462** | 2-D Flash Flood Modelling of Vamasadhara River basin<br>*R. Venkata Raman, V.S. Jeyakanthan, Y.R. Satyaji Rao and T. Vijay* | 842 |
| 90 | **490** | Flood Resistant and Amphibious Houses: An Overview<br>*Dev Vrat Singh, Saurabh Agnihotri, Javed Alam and Mohd. Muzzammil* | 850 |
| **Theme X<br>Urban Water Management** | | | |
| 91 | **008** | Assessing Flow Parameters In Sand Nalla in The Vicinity of Mouda STPP of NTPC, Maharashtra<br>*N. A. Sonawane, Kuldeep Malik, Ku. Madhavi Gajre, M. K. Pawar* | 860 |
| 92 | **073** | Morphometric Analysis of Trident Campus of Budhani in Madhya Pradesh<br>*Jitendra Yadav, Ruchi Khare, Jyoti Sarup* | 871 |
| 93 | **161** | A Study of Greywater Reuse System For An Urban Household<br>*Susen Sinha, Sandeep Kr. Chouksey* | 880 |
| 94 | **239** | Alignment of RRTS Railway Bridge Across River Yamuna for Delhi-Ghaziabad- Meerut Corridor at New Delhi: A Case Study<br>*S. S. Kerimani, S. P. Hedaoo, R. G. Patil* | 892 |
| 95 | **256** | Issues and Challenges of the Urban Water Supply System in Ethiopia: A Case Study of Dire Dawa<br>*Bahar Adem Beker and Mitthan Lal Kansal* | 899 |
| 96 | **275** | Evolutionary Optimization Techniques for Optimal Design of Water Distribution Networks<br>*S N Poojitha, Gagandeep Singh, Vinayakam Jothiprakash* | 911 |
| 97 | **292** | Water Urbanism: Strategies for stormwater management through rainfall-runoff analysis using SCS- CN method and GIS in watersheds of Ajmer, Rajasthan<br>*Aspruha Swain, Prof. Ashwani Kumar* | 920 |
| 98 | **309** | Transient Analysis for Water Supply Pipeline for Pokaran Villages<br>*Jyothi Prakash Arkadu, Seetarami Naidu Malla, Abdul Rahiman P M, Ramappa Govindappa Patil* | 935 |
| 99 | **454** | Traditional stormwater management system in watershed of wetland, a study and overview of “Dong” systems in wetland fringe villages of Assam<br>*Anushri Barman, Dr. Ramakar Jha* | 946 |
| 100 | **477** | An Overview of Dam Failure and It’s Analysis Methods<br>*Umesh Meena, K. K. Khatua* | 953 |

| | | | |
|---|---|---|---|
| | | **Theme XI**<br>**Watershed Management** | |
| 101 | **012** | Variability Analysis of Hydrological Parameters of Faridabad District (Haryana State)<br>*Mridula Sharma & Arun Goel* | 964 |
| 102 | **057** | Comparison of spatial interpolation methods for filling missing observations in daily rainfall data<br>*C. Reshma & R. Arunkumar* | 974 |
| 103 | **133** | An environment concerned risk based approach for evaluating watershed health<br>*Smaranika Mahapatra, Madan K. Jha* | 983 |
| 104 | **169** | Surface Water Balance Study of River Sarada<br>*Jagannath Patro, Vazeer Mahammood* | 992 |
| 105 | **181** | Analysing the Response of Meteorological Droughts on Stream Flow in the Pennar River Basin<br>*Arunav Nanda, Dr. Bhaskar R. Nikam, Dr. Vaibhav Garg, Dr. S.P. Aggarwal* | 1002 |
| 106 | **253** | Estimation of Peak Flood Discharge for Ungauged Catchments By Hydrometeorological Approaches<br>*C. Srishailam, N. Vivekanandan, R.G. Patil* | 1023 |
| 107 | **266** | Flood Routing In A River By Modified Pul's Method<br>*Souvick Kumar Shaw, K. K. Khatua* | 1032 |
| 108 | **276** | Wastewater Management through Water Drainage System: A Case Study<br>*Jagpreet Singh Kamboj, Sahibpreet Singh, Mahesh Patel* | 1041 |
| 109 | **317** | River Discharge Estimation Using SARIMA Model And OLS Regression From Satellite Altimetry Data –A Case Study Of Amazon River<br>*Raviraj Dave, Udit Bhatia* | 1048 |
| 110 | **390** | Distribution, Trend, and Concurrence of Meteorological, Hydrological and Agricultural Droughts over Madhya Pradesh, India<br>*Vikas Poonia, Manish K. Goyal* | 1058 |
| | | **Theme XII**<br>**Hydraulic Structures and Hydropower Engineering** | |
| 111 | **005** | Flow Pattern Around Multiple Vane Arrangement<br>*Karan Solankia & Himanshu Sharmaa* | 1067 |
| 112 | **024** | Study of Energy Dissipator with Different Blocks to Reduce Basin Width and Trajectory : A Review<br>*Shilpi Sippi Bhuinyan& Prof. Dr. Anand Kr. Sinha* | 1077 |
| 113 | **039** | Hydraulic modelling of headpond with lateral spillway weir structure for the Tamskoshi-V hydroelectric project, Nepal<br>*Pradyumna Machhkhand* | 1084 |
| 114 | **076** | Stage discharge relationship by weir theory for channel flow | 1094 |

| | | | |
|---|---|---|---|
| | | measurements using the conical central baffles<br>*Ankur Kapoor, Aniruddha D. Ghare, Avinash M. Badar* | |
| 115 | **082** | Study on Aeration Performance of P.K. weir with its Alternatives: A Review<br>*Deepak Singh and Munendra Kumar* | 1100 |
| 116 | **103** | Study of Flow Characteristic Of Rectangular Labyrinth Weir<br>*Saurabh Sah, Munendra Kumar* | 1108 |
| 117 | **110** | Hydrodynamic Cavitation: A Treatment to Secondary Effluent of STP to Reuse<br>*Neha S. Baghele, Anjali K. Khambete, Robin A. Christian* | 1116 |
| 118 | **148** | New Methodology of Optimisation of Water Conductor System in Hydropower<br>*Satyajeet Sinha* | 1124 |
| 119 | **165** | Numerical Simulation to Study Cavitation Characteristics of Centrifugal Pump<br>*Ruchi Khare, Vishnu Prasad, Chinky Yadav* | 1138 |
| 120 | **321** | Estimation of Reservoir Capacity of Singda Dam, Manipur using Modern Integrated Bathymetry System (IBS) – A case study<br>*Ajit Singh, Mahender Singh Bist, Ajay Sonawane, K Subbarao Murthy, M Selvabalan* | 1148 |
| **Theme XIII<br>Groundwater Modelling and Management** | | | |
| 121 | **027** | Study on Subsurface Hydraulic Conductivity and Soil Moisture using Ground Magnetic Resonance (GMR<br>*Uttam Singh and Pramod K. Sharma* | 1156 |
| 122 | **054** | MODFLOW, MODPATH and MT3DMS based simulation of groundwater flow and leachate transport from landfill<br>*Shikha Kataki, Dr. Triptimoni Borah* | 1165 |
| 123 | **061** | Hydro-Chemical Characterization and Quality Appraisal of Groundwater using Water Quality Index in District Jaipur, Rajasthan<br>*Santosh Ojha, Gunwant Sharma, Deepesh Machiwal* | 1178 |
| 124 | **221** | Assessment of Groundwater Potential Zones Using AHP Technique in Darbhanga District of Bihar<br>*Sumit Kumar, Vivekanand Singh* | 1187 |
| 125 | **241** | Identification and Mapping Potential zones of Submarine Groundwater Discharge (SGD) along Mangalore to Udupi Coast, Karnataka<br>*Sunilkumar P S, Dr. Ramesh H* | 1198 |
| 126 | **242** | Surface Water Groundwater Interactions in Estimating Groundwater Recharge using Genetic Programming<br>*Ajay, Chidara Nagamanikanta Sai & Om Prakash* | 1212 |
| 127 | **315** | A review of evolutionary algorithms in inverse modeling for groundwater flow and transport parameter estimation<br>*Alice Thomas, Eldho T I* | 1223 |
| 128 | **417** | Impact of Climate Change on Groundwater Recharge | 1233 |

| | | | |
|---|---|---|---|
| | | *Puja Tripathy, M. Uma Maheswar Rao, K.C. Patra* | |
| 129 | **425** | Appraising Prolific Zones of Groundwater in hard rock phreatic aquifers from sub-watersheds of Upper Bhima Basin, Western India using Geospatial and MIF technique<br>*Himanshu Gaikwad, Bhavana Umrikar, Mandira Majumdar, C Krishnaiah* | 1246 |
| 130 | **430** | Estimating confined aquifer parameters using Particle Swarm Optimization technique<br>*R. A. Panchal, Dr. H. M. Patel* | 1264 |
| **Theme XIV<br>Computational Fluid Dynamics / Numerical Modelling** | | | |
| 131 | **034** | CFD Analysis of Flow through Concentric, Eccentric and Segmental Orifice Meters<br>*Dr. I. Siva Parvathi & Miss. G. PremaSwathi* | 1273 |
| 132 | **096** | Hydraulic Structure Design with 3-D CFD Model<br>*Prashant Huddar, Vishwanath Bhave* | 1283 |
| 133 | **130** | Performance of MacCormack finite difference scheme with TVD and Artificial Viscosity<br>*Jyotiprakash Tarei, Bandita Barman* | 1291 |
| 134 | **217** | Development of two dimensional 9- noded lagrangian quadratic isoparametric element mesh generation tool for finite element models<br>*Lokesh Mangal, C. Gowri Shankar, Manasa Ranjan Behera* | 1301 |
| 135 | **254** | Application of computational fluid dynamics in investigating orifice spillway flow<br>*M. S. Bhadange, R. R. Bhate, Dr. S. D. Khandekar* | 1310 |
| 136 | **257** | Study On Influence Of Vegetation In Open Channel Using Cfd Model<br>*Anitha Gopinath A., Miji Cherian R.* | 1320 |
| 137 | **277** | Computation of Gradually Varied Flow depths in a Channel System Using Numerical method<br>*Rohini Rani, Kishanjit K Khatua, Pravas Ranjan Pradhan* | 1330 |
| 38 | **283** | Numerical solution of 1D Saint-Venant equation using Numerical method<br>*Pravas Ranjan Pradhan, Kishanjit Kumar Khatua, Rohini Rani* | 1340 |
| 139 | **342** | Numerical Simulation Of Undular Hydraulic Jump Using Ansys Fluent<br>*G Rahul Indivar, Kishanjit Kumar Khatua* | 1349 |
| 140 | **471** | Numerical modelling in shoreline evolution prediction: case study of inlet channel at Kasargod, Kerala.<br>*Jiweshwar Sinha, S.N. Jha, Vaibhawi Roy, Prabhat Chandra* | 1356 |
| **Theme XV<br>Sediment Transport** | | | |
| 141 | **059** | Breakwater Construction Effects on Hydrodynamics And Sedimentation Pattern in Open Coast | 1364 |

| | | | |
|---|---|---|---|
| | | *A K Singh, Naval S Jagatap, L. R. Ranganath & J. D. Agrawal* | |
| 142 | **063** | Interlinking Prospect of Godavari River with Krishna River<br>*Kamalini Devi, Bhabani Shakar Das, Jnana Ranjan Khuntia, Gutha Ruthwikesh Reddy, Annepu Laxmi Prasad* | 1377 |
| 143 | **149** | Estimation of Sediment Production Rate using Josh and Dash model- A Case Study of Rel River, Banaskantha District<br>*Himadri Shah, Sudhanshu S. Dixit, V. M. Patel, Nimrabanu Memon, Dhruvesh P. Patel* | 1388 |
| 144 | **182** | Evaluation of Hydrodynamics and Sedimentation Due To Construction Of Jetty<br>*A. K. Singh, Naval S. Jagatap, L. R. Ranganath, J. D. Agrawal* | 1395 |
| 145 | **188** | Comparison of Sedimentation in Dredged Open Basin And Enclosed Basin– A Case<br>*V. B. Sharma, M D Sawant, Dr. Prabhat Chandra* | 1407 |
| 146 | **197** | Erosion of River Ganga Upstream and Downstream of Farakka Barrage- A Review<br>*Mayuraksha Bardhan* | 1416 |
| 147 | **214** | A Study of Flow and Sediment Transport Analysis using HEC-RAS<br>*Harapriya Panda, Ratnakar Swain, Bibhuti Bhusan Mukharjee* | 1426 |
| 148 | **237** | Flood protection measures and anti- erosion works along Palhori Khala tributary of River Yamuna<br>*B. Raghuram Singh, Jotsana G. Ambekar, Dr. R. G. Patil* | 1436 |
| 149 | **250** | Estimation of Sediment Yield in Chalakudy River<br>*Maneesha K Sankar, Dr. Suman K. S* | 1446 |
| 150 | **300** | 1-D Hydrodynamic Modelling in HEC-RAS for Prediction of Water Levels and Sediment Transport in Narmada River<br>*V. K. Bind, B. K. Samtani* | 1456 |

# THEME I

# COASTAL & OCEAN ENGINEERING

IN PROCEEDINGS OF 25th HYDRO 2020, INTERNATIONAL CONFERENCE,
NATIONAL INSTITUTE OF TECHNOLOGY ROURKELA, ODISHA, INDIA
26-28, March 2021, ISBN 978-93-90631-56-8

Paper ID - 071

# Factors affecting the Vessel Turnaround time in a Seaport

**Dayananda Shetty K[1] Vijayanand.Gurudev[2] Dwarakish.G.S.[3]**

[1]*Assistant Engineer, Civil Engineering Department, New Mangalore Port Trust, Panambur, Mangalore, Karnataka, - P.O.-575010*

[2] *Engineer, No.1248,3rd Cross, Gange Road,Kuvempunagar,Mysuru Karnataka -570023*

*3ProfessorDepartment of Applied Mechanics and Hydraulics, National Institute of Technology Karnataka,Surathkal, Srinivasnagar P.O.-575025(D.K)*

*Email: dpunmaya@yahoo.com, vgurudev@gmail.com, dwaraki.gs@gmail.com*

***Abstract:***

*Turnaround time in a seaport exhibits the capability and ability of a port in providing efficient services. Ship turnaround time is one of the most significant Port performance indicators. This is the total time, spent by the vessel in port, during a given call. It is the sum of waiting time, plus berthing time, plus service time (i.e. ship's time at berth), plus sailing delay. Indian ports play a crucial role in trade and economy, as 95 % of merchandise trade is handled by ports. However, port turnaround time remains key problem. It is significantly slower than across peer ports in other developing countries, being several times higher than for ports in China, Singapore and Malaysia. To reduce the turnaround time of a vessel in a seaport, the port processes are to be streamlined and capacity augmented. This paper is aimed at identifying the factors that are responsible for turnaround time of vessels at the port. This study is motivated by the rapid development in Indian port sector, in providing efficient and effective services and high port productivity, with the aim to achieve optimum port performance. The turnaround time is a function of port operations and port facilities. As currently it is not possible to determine significant factor(s) that influence port performance, in terms of turnaround time. The primary data of vessel arrival/departure in New Mangalore Port trust recorded at VTMS are used. This study is very useful in decision making of port Authorities as well as ship operators in any given budget or resource input, the output results in time minimization and it is possible to tackle all the delay causing factors by the port Management in providing efficient and effective services and high port productivity, with the aim to achieve optimum port performance*

***Key words****: Port, Performance, Indicators, turnaround time, Quality of service, port facilities, optimization, Port management*

## 1. Introduction

The globalization of trade and removal of trade barriers between the various countries have resulted in tremendous growth in maritime transportation. This intern demands stiff competitions among the Port operators. Therefore, port authorities have to consider lower turnaround time for vessel in order to benchmark good productivity and performance for their terminals. Ship turnaround time is one of the most significant indicators of service to ship operators. This is the total time, spent by the vessel in port, during a given call. It is the sum of waiting time, plus berthing time, plus service time (i.e. ship's time at berth), plus sailing delay. Indian ports play a crucial role in trade and economy, as 95 % of merchandise trade is handled by ports. However, port turnaround time remains key problem. It is significantly slower than across peer ports in other developing countries, being several times higher than for ports in China, Singapore and

Malaysia. The port processes are to be streamlined and capacity augmented to reduce the turnaround time. New Mangalore Port trust is the 9th Major Port in India and located in the state of Karnataka. There is a wide range of studies on port efficiency but curiously enough, these studies have never focused on turnaround times in ports, despite this being considered as a key indicator of efficiency. The present research is aimed at optimizing the various port activities to arrive at a reduced turnaround time of vessels at the port. This study is motivated by the rapid development in Indian port sector, in providing efficient and effective services and high port productivity, with the aim to achieve optimum port performance. The turnaround time is a function of port throughputs and port facilities, as currently it is not possible to determine significant factor(s) that influence port performance, in terms of turnaround time. The primary data of vessel arrival/departure in New Mangalore Port trust recorded at VTMS is to be used. The proposed study is very useful in decision making of port Authorities as well as ship operators in any given budget or resource input, the output results in time minimization and it is possible to tackle all the delay causing factors by the port Management in providing efficient and effective services and high port productivity, with the aim to achieve optimum port performance

### 1.1. Literature review

The turnaround time issue, which has been discussed and argued by many scholars since the emergence of containerization for the last three decades have evolved a lot of development. According to (UNCTAD, 1976) under operational indicator, it states clearly turnaround time is crucial to be considered, where it portrays port capability and ability to provide tremendous services with high productivity and performance to port user. The most important objective for a Port is to increase its throughput or in other word is to decrease the turnaround times of vessels. The managers and authorities at ports have increasingly been under pressure to improve port performance by ensuring that the port provides services on an internationally competitive basis (Simoes and Marques, 2010) As a result, the turnaround time of a vessel is depending on the effectiveness of allocating and scheduling key resources such as, quay cranes, yard cranes, berths and trucks. The issue of turnaround time for vessel is related with berthing cost for shippers and increment voyage for vessel itself. Hence objective is to minimize the time vessels spent at berth. Port users are looking into berthing side as it is actually can determine the whole aspects such as cost, voyage, marketing, planning and scheduling. The pivotal key here is turnaround time for vessel, because it is able to solve a lot of things for shipping industry. Consequently, taken into consideration supply chain process, high turnaround time means the process from raw material to user is able to reduce, therefore economic of scale is able to be achieved

The turnaround time is one of the factors that should be included when measuring port performance; the other factors are material handling or labour productivity and berth occupancy (Oram and Baker, 1971). Port performance indicators are useful in getting distinction between port efficiency and effectiveness as well as in measuring port performance(Tongzon, 1995).Port efficiency as a whole may be understood from various perspectives and its influence on trade facilitation (Clark et al. 2004). For this reason, optimization of facilities and operations is the common goal in most current measurement systems. In a supply chain context, measuring performance is managerial tool that assists in planning and organizing activities, motivating workpeople, and controlling events within acceptable parameters (Morgan, 2004). Widely accepted performance measurements are unavailable, although there is a wide range of measures and indicators for port efficiency and performance, as ports are very dissimilar (Bichou and

Gray, 2004). This means ports need to enhance their planning and operation capability by deploying innovative equipment's and state-of-the-art technology in order to optimize terminal logistic process. In order to optimize port terminal resources, it is really vital to ensure that port operational flow is able to operate smoothly. Singapore, ( Gordan et. al.,2005) mention, even a small nation is able to surpass its natural constraint by evidently successfully applying information technology in critical areas with the reason to increase the island's capacity to handle huge throughput in port container terminal. Apart from that, Singapore is also providing supportive government policies to shipping line, ample investment from government and private, as well as operations, location, and deep water draft for vessel, and simultaneously sustains Singapore's port among port users..In fact, empirical estimation of port efficiency differs across many factors, including the method used for measuring efficiency, the type of data and the region or country in which ports are located, (Odeck and Brathen,2012).Based on efficiency scores for ports, previous studies had dissimilar results and conclusions; some shoed high scores and others showed low efficiency scores. This raises the question of whether there is something wrong with the techniques used or simply whether something is not captured by the existing studies (Bichou 2012). The current outlook and increasing globalization of economies call for higher efficiency from all actors in the transport sector, especially ports, where there is massive public input in their production processes (Berqantino, et.al., 2013).Efficiency plays a key role in container port completion, (Yuen et.al., 2013). It is the time to think about long – term plan for boost up by upgrading infrastructure facilities in the major ports (Rajasekar, et. al., 2014). Reforms initiated at major ports have given boost to their performance and enhanced market expectations on their efficiency levels. Therefore, it is important to check the actual efficiency levels at these ports so that appropriate future plans can be envisaged for their sustainable growth. The study found better efficiency levels at a majority of these major ports (BhanuPrakash, et.al, 2016).Modernization of Indian infrastructure and optimum capacity utilization of resources in sea ports are the need of the hour to cope up with the world standards. Hence, the ports and shipping industry is bound to undergo substantial changes in their maritime web. (Padmasani and Tamilselvi,2016)

## 2.0 Objectives and study area

There are a wide range of studies on port efficiency but curiously enough, these studies have never focused on turnaround time in ports, despite this being considered as a key performance indicator. More often we see studies in operation research about queuing models of vessels in relation to port planning and berth allocation and port productivity, but there is a drastic lack of systematic recording and analysis of ship turnaround times.

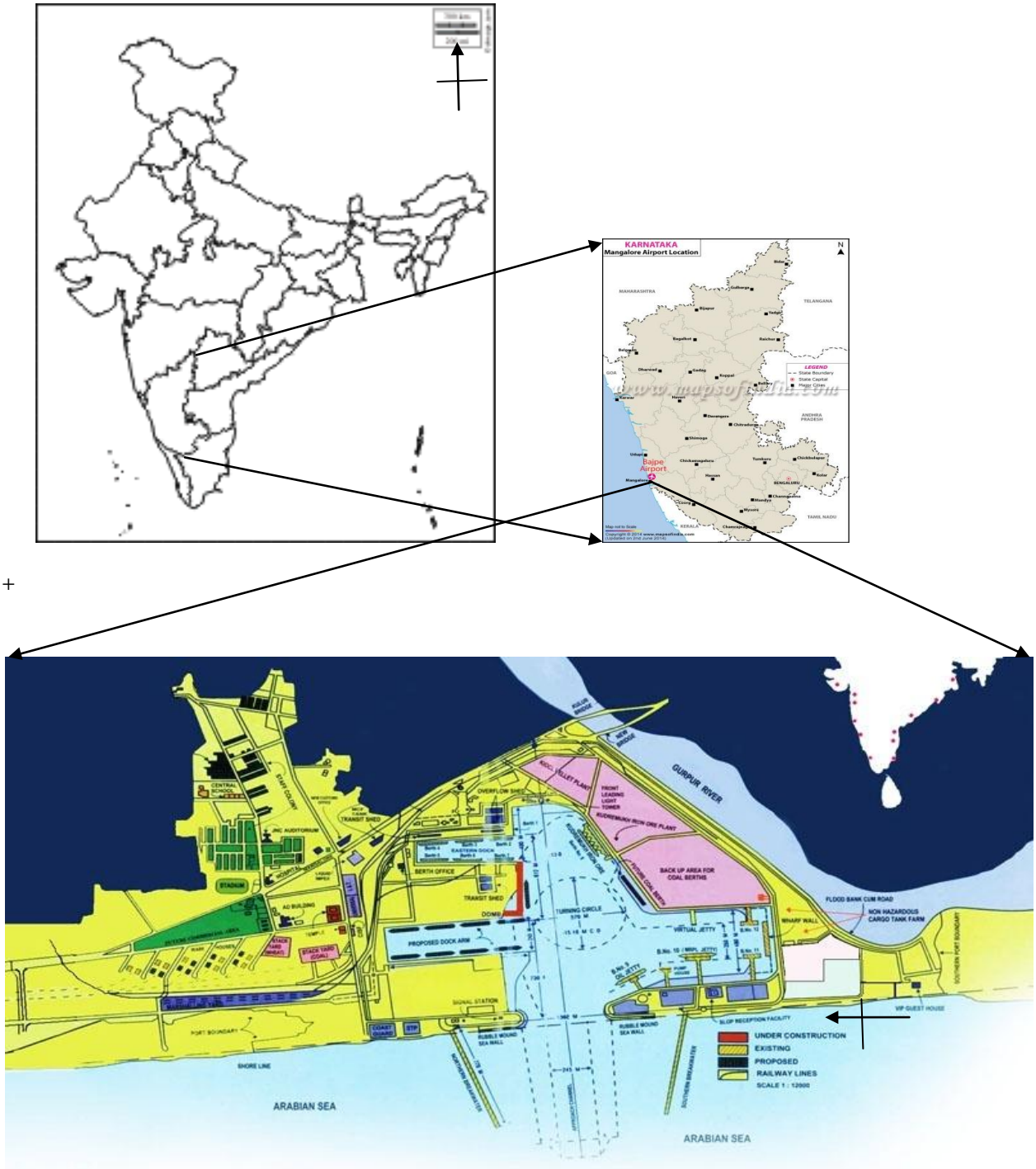
The purpose of the research is identification of factors responsible for delays turnaround time in the New Mangalore Port Trust as well as modeling them. The objective function isto minimize time relative to the identified constraint factors. In pursuant of this goal, the following objectives will be addressed. The main objective is to evaluate the time optimization factors, which causes delay in turnaround time of vessels calling on to the Port.

The specific objectives include.

1. To identify the specific factors influencing the turnaround time of Vesselsto know the port performance.
2. To determine the weightage for each factor this causes the delay in TRT to take corrective measures.

3. To determine the critical factors responsible for higher TRT for optimization of TRT.

The present study is confined to New Mangalore Port trust. It is deep water all weather port located at Panambur, Mangalore on the west coast of India, in Karnataka state.( Latitude : $12^0$55'N ,Longitude :$74^0$ 48' E). The location and layout of New Mangalore Port is shown in Figure.1.




4.

Figure 1. Location of New Mangalore Port Trust, Karnataka, West Coast of India

Table No.1 shows the average vessel turnaround time of New Mangalore Port Trust for a period of 1990-91 to 2017-18

Table.-1. Average turnaround time for New MangalorePort Trust

| Sl.No. | Period | Average Turnaround Time (in Days) | Sl.No. | Period | Average Turnaround Time (in Days) |
|---|---|---|---|---|---|
| 1 | 1990-91 | 4.90 | 15 | 2004-05 | 2.96 |
| 2 | 1991-92 | 5.31 | 16 | 2005-06 | 3.00 |
| 3 | 1992-93 | 6.36 | 17 | 2006-07 | 3.00 |
| 4 | 1993-94 | 5.24 | 18 | 2007-08 | 3.21 |
| 5 | 1994-95 | 5.72 | 19 | 2008-09 | 3.00 |
| 6 | 1995-96 | 5.13 | 20 | 2009-10 | 3.06 |
| 7 | 1996-97 | 4.37 | 21 | 2010-11 | 2.71 |
| 8 | 1997-98 | 4.10 | 22 | 2011-12 | 2.95 |
| 9 | 1998-99 | 3.74 | 23 | 2012-13 | 3.30 |
| 10 | 1999-00 | 3.80 | 24 | 2013-14 | 3.18 |
| 11 | 2000-01 | 2.89 | 25 | 2014-15 | 2.46 |
| 12 | 2001-02 | 2.73 | 26 | 2015-16 | 2.82 |
| 13 | 2002-03 | 2.37 | 27 | 2016-17 | 2.43 |
| 14 | 2003-04 | 2.35 | 28 | 2017-18 | 3.34 |

Source: NMPT Port statistics

***Figure 1:*** **Average turnaround time for New Mangalore Port Trust (in days)**

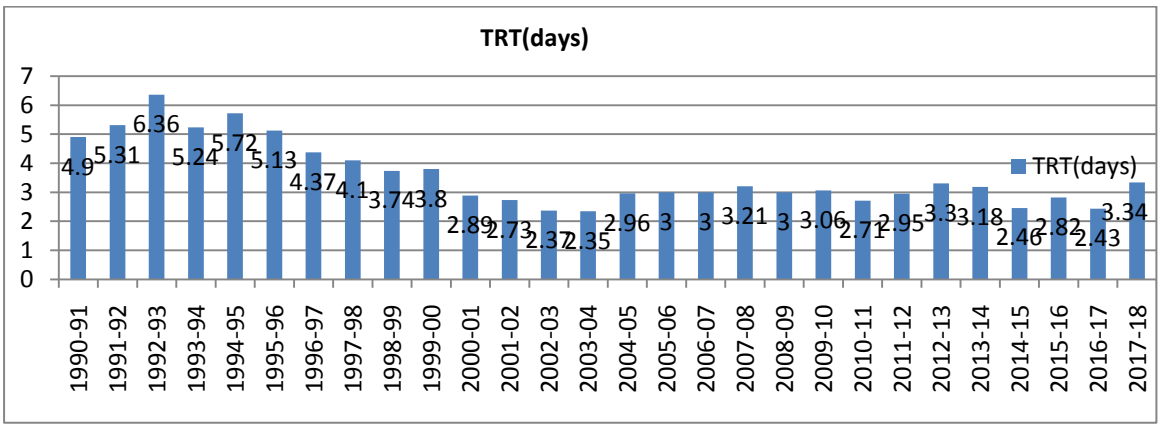
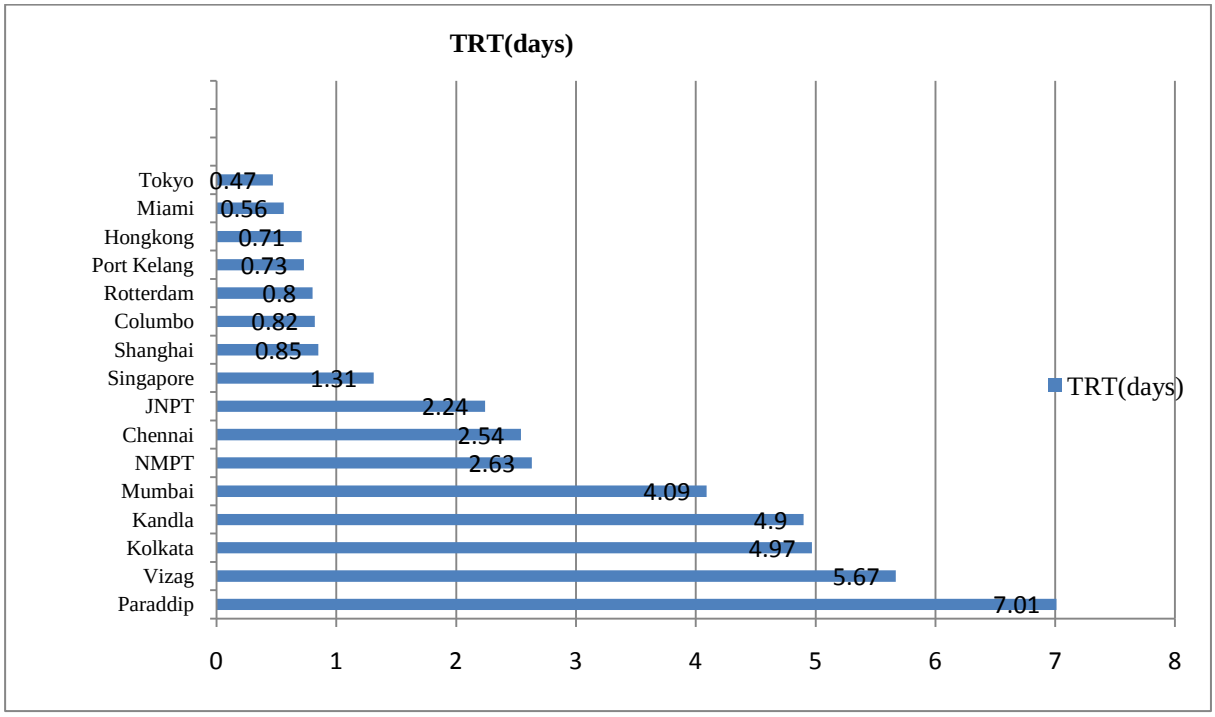


***Figure 3**: Comparison of turnaround time of Indian ports with major international ports*




## 3.0 Data and Methodology

The primary data of vessel arrival/departure in New Mangalore Port trust recorded at VTMS were collected and used to develop optimization model that relates the turnaround time to the port facility and port operations. The data is collected from New Mangalore port trust statistical division. This source is considered to be among the most comprehensive of databases on vessel arrival /departure information related to NMPT. The database records over 1200 movements made by the world's merchant fleet every year to NMPT. The data provides arrival and departure times from terminals for all vessels on most major trade lanes. It is thus possible to determine the amount of time ships spend in port on each port call. The categories and the details of the real time data observed and recorded for each and every vessel calling on to the port are shown in the Table. No. 2.

Table.2. Real time data captured for a vessels calling on to NMPT

| Sl.No. | Major groups of Data | Details of Data |
|---|---|---|
| 1 | Basic Vessel data | Unique vessel identifier<br>Vessel name<br>Category Export/Import Tonnage/ TEU's<br>Commodity 1<br>Commodity 2<br>Commodity 3<br>Total tonnage<br>NRT<br>GRT<br>LOA<br>Nationality<br>Original Port of departure<br>Previous port o<br>Next port of call<br>Draft |
| 2 | Date and Time parameters | Arrive at anchorage date and time<br>Readiness of the vessel date and time<br>Departure for berth (Pilot boarding) Date and time<br>Arrive at berth(Berthing) date and time<br>Cargo operation start date and time<br>Cargo operation completed date and time<br>Departure from the Berth date and time<br>Departure from the port date and time |
| 3 | Pre commencement and post Commencement(Documentation) | Customs Formalities inward<br>Documentation inward<br>Survey inward<br>Customs Formalities outward<br>Documentation outward<br>Survey outward |

## 4.0 VESSEL TRUNAROUND TIME (VTRT) MODEL

### 4.1 General

The Turnaround time of a vessel comprises of waiting time, Inward movement time, berthing time, service time and outward movement time. It is a measure of port capability and ability to provide tremendous services with high productivity and performance to port user. It is also a function of port facilities and the level of service provided at a seaport. The Shorter the turnaround time, it is beneficial to both the ports and port users.

### 4.2Factors affecting the vessel turnaround time

The various factors which are responsible for the vessel turnaround time (V-TRT) are identified from the real time data collected and from the ground truth verification. The identified factors are tabulated are then categorized in to seven categories based on the activities involved in the turnaround process and the constraints faced by a vessel calling on the port. The identified factors responsible for the vessel turnaround time as tabulated in the Table.No.3

Table.3 Identified factors responsible for V-TRT

| Sl.No. | Category | Factors |
|---|---|---|
| 1 | Pre-Berthing Delay factors | Non availability of berth<br>Non availability of tugs/crafts<br>Non availability of mooring gangs<br>Condition and capacity of tugs<br>Non availability of pilots<br>Pilots not ready<br>Delay in pilot boarding<br>Delay in notice to signal station.<br>Bunching of vessels<br>Draft restriction<br>Unidirectional channel<br>Night Navigation<br>Channel Buoys<br>Strike/stoppage<br>Ships account<br>Shippers account<br>Documents not ready<br>Tidal/weather restrictions<br>Want of cargo<br>Others |
| 2 | Pre commencement and post Commencement Factors(Documentation) | Customs Formalities inward<br>Documentation inward<br>Survey inward<br>Immigration documentation<br>Customs Formalities outward<br>Documentation outward<br>Sealing and Inspection<br>Survey outward<br>Departure formalities |

| | | |
|---|---|---|
| 3 | Port Constraints | Holiday Recess<br>Ullage Constrains<br>Pipe line fittings<br>Draft restrictions<br>Shifting Time<br>Non availability of Berths<br>Non availability of Labour gangs<br>Non availability of Ports crafts/Tugs<br>Non availability of cargo handling equipment's<br>Non availability of Pilots<br>Lighting<br>Equipment beak down<br>Non availability of labour gangs<br>Shore tank change over<br>Priority berthing<br>Other vessel movement<br>Strike/stoppage<br>Power failure<br>Shed congestion<br>Breakdown of equipment<br>Lack of storage/silos<br>Any other factors |
| 4 | Non-Port Constraints | Want of Cargo<br>Break down of equipment's<br>Sampling<br>Lab tests<br>PHO's Role<br>Immigration<br>Waiting for shore side readiness<br>Hatch arrangements<br>Hatch opening/closing<br>Nature of cargo.<br>Trimming of cargo post loading<br>Berth cargo evacuation truck turnaround<br>Intermediate stoppage for shifting to other cargo<br>Detained by MMD<br>Bunkering<br>Line changing process<br>Any other factors |
| 5 | Idle Time at Berth | No work<br>Holiday Recess<br>Ports Equipment break down<br>Power problems<br>Labour breakup<br>Stoppage for mock drill<br>Break during shifts<br>Shifting or evacuation of cargo from berth<br>Any other factors |
| | Environmental factors | Weather/rain |

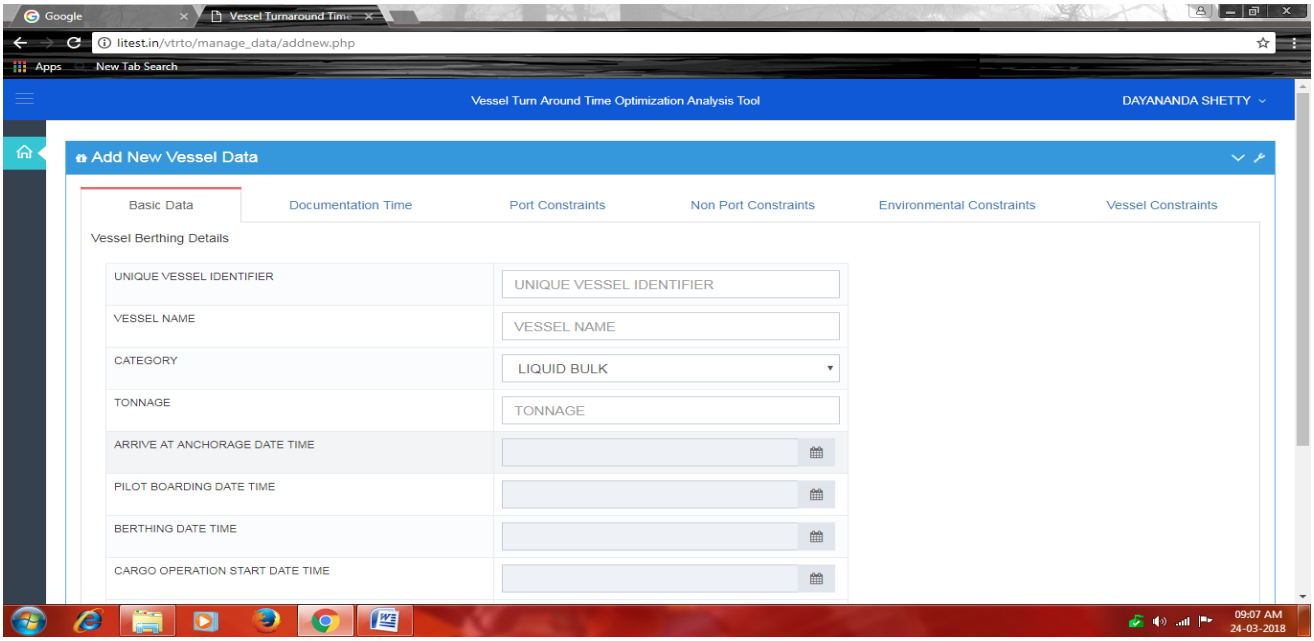
| | | |
|---|---|---|
| 6 | | Tide<br>Cyclone<br>Night Navigation<br>Any other factors |
| 7 | Vessel constraints | Engine failure<br>Lashing/unlashing<br>Vessel advance berthing<br>Vessel ullage constraints<br>Hot water flushing<br>Line flushing<br>Tank value problems<br>Vessel repair or its equipment's<br>Pump capacity<br>Waiting for ship side readiness<br>Slope discharge<br>Delay in sailing<br>Any other factors |

### 4.3 VTRT Model

The real time data of vessel arrival/departure in New Mangalore Port Trust recorded at VTMS were used to develop VTRT model. The various factors that determine optimum turnaround time have been identified and a vessel turnaround time model has been developed.

The model/software being developed by using following programming languages and other available modules

- PHP
- MySQL
- HTML5
- CSS3
- JQuery
- Google Charts
- Apache Tomcat Server
- Ubuntu Operating System




## 5.0 RESULTS AND DISCUSSION

The model relates turnaround time with identified pre-berthing delay factors, Pre commencement and post commencement (Documentation) factors, Port constraints, Non-Port constraints, Vessel constraints, Environmental Constraints and available port facilities.

Using the VTRT model the following analysis and results are generated.

1. Year on year TRT in days, which is the average of monthly TRT of all the vessels sailed from the port.
2. Year wise analysis of TRT
3. Commodity wise TRT analysis
4. Year wise TRT Constraints analysis
5. Commodity wise TRT constraints analysis.

### 5.1 Year on year TRT

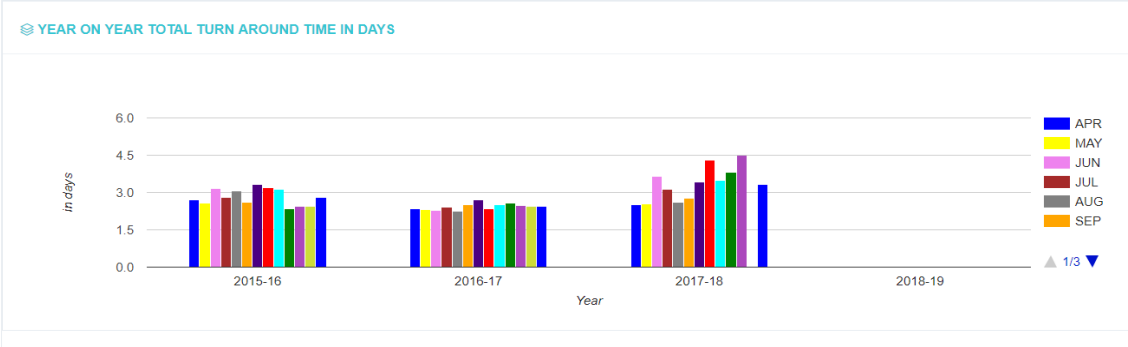



***Figure 4**: year on year TRT of vessels handled in NMPT*

From this module one can generate the port performance indicators such has pre-berthing waiting time (PBWT), vessel turnaround time (TRT), Non-working time at berth(NWTB) Number of vessels handled, output per ship berth day(OSBD) and port productivity.

### 5.2 Year wise analysis of TRT

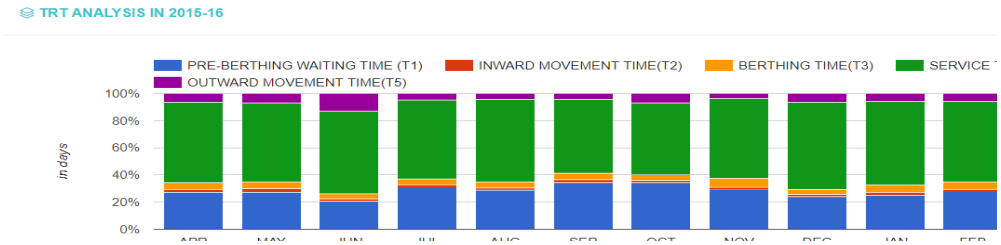



***Figure 5**: Monthly distribution of TRT components for 2015-16*

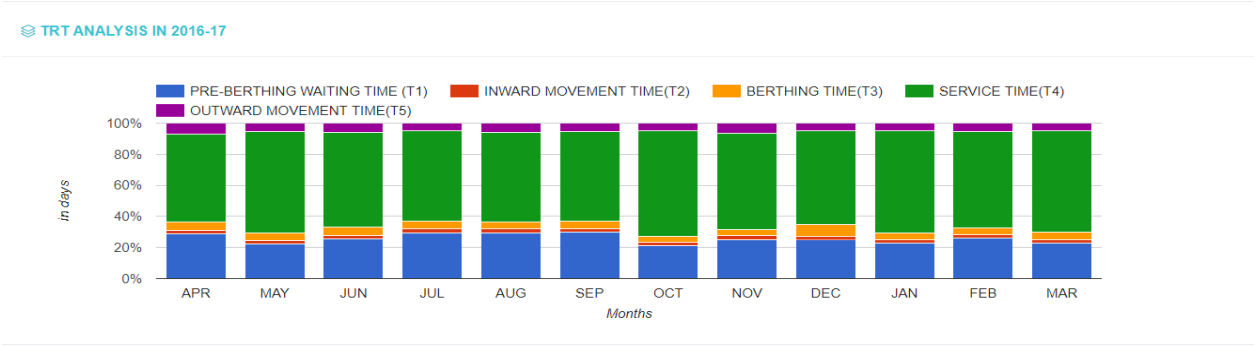



***Figure 6**: Monthly distribution of TRT components for2016-17*

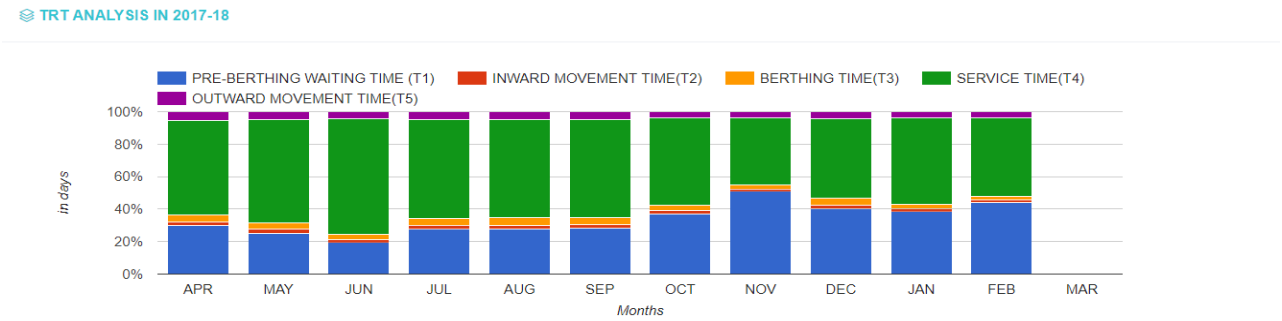



***Figure 7**: Monthly distribution of TRT components for2017-18*

The Turn Round Time shall comprise the following components:

(i) Pre-Berthing Waiting Time,(ii) Inward Movement Time,(iii) Berthing/Shifting Time

(iv) Service Time, (v) Outward Movement Time

**TRT = PBWT (T1) +IM (T2) +BT (T3) +ST (T4) +OM (T5)**

From the results of year wise analysis of TRT it is observed that the pre-berthing time and service time contributes to the maximum percentage of vessel turnaround time. The service time is on higher side during the monsoon months and the pre berthing time is higher side in the non-monsoon months. It is also observed that the outward movement time more compared to inward movement time of vessels calling on to the port.

### 5.3 Commodity wise TRT analysis

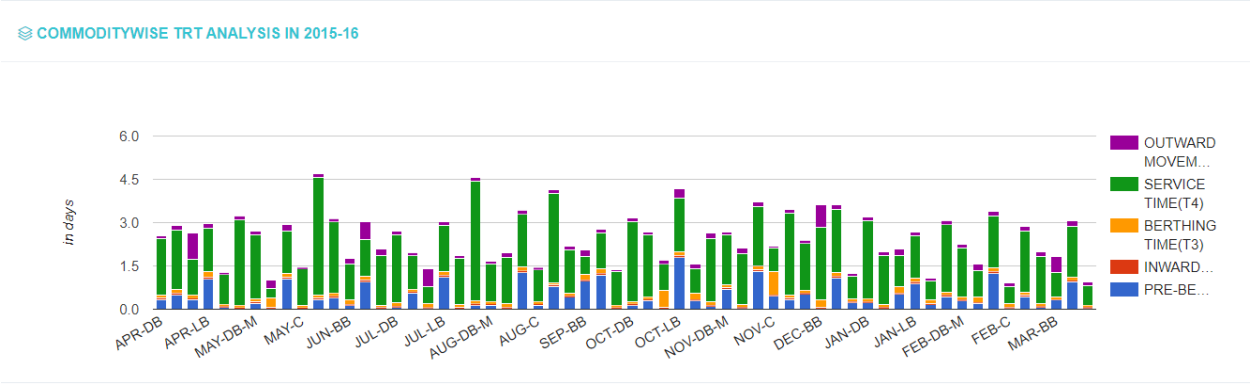



***Figure 8**: Commodity wise distribution of TRT components for2015-16*

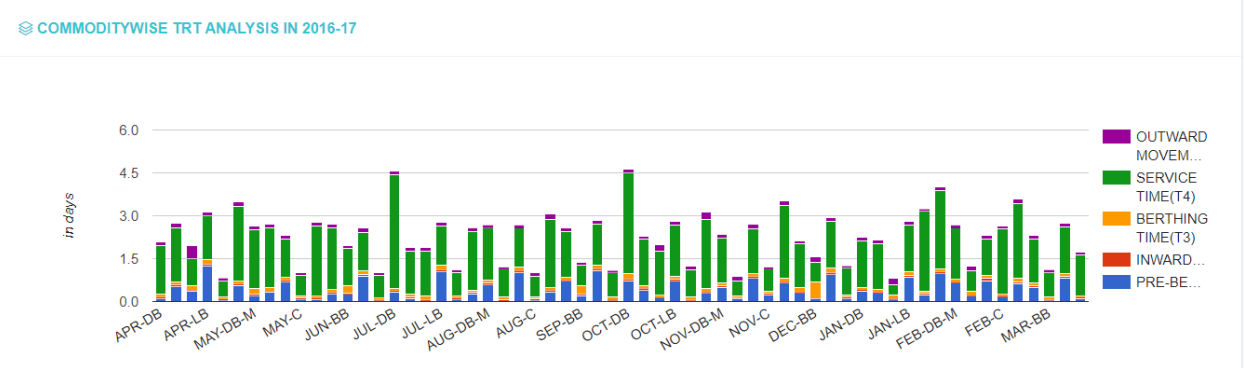



***Figure 9**: Commodity wise distribution of TRT components for2016-17*

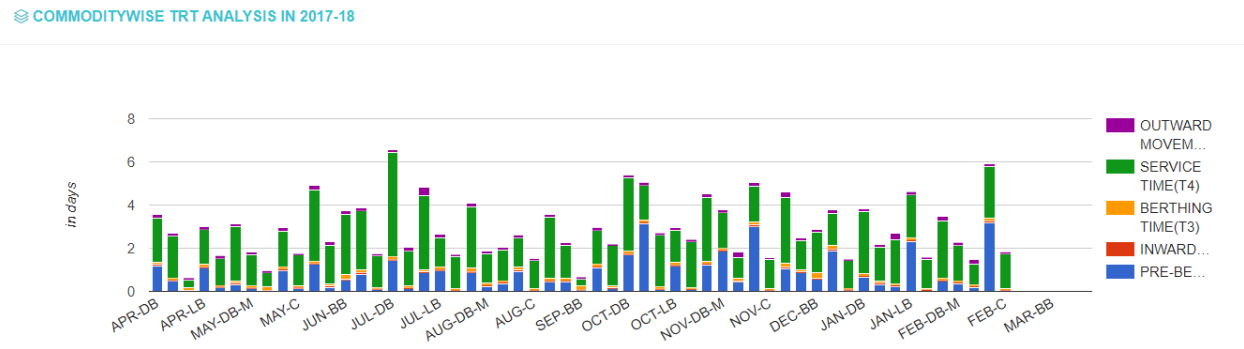



***Figure 10**: Commodity wise distribution of TRT components for2017-18*

The commodity wise analysis of the TRT reflects that the TRT for the dry bulk cargo is highest and whereas TRT for container cargo is least. The service time for Dry bulk is high and service time for liquid bulk is low. The pre berthing weighting time for Liquid bulk is always high compared to all other categories of cargo. From this we can conclude that the number of berths to handle liquid berth at NMPT are not optimal.

### 5.4 Year wise TRT constraints analysis

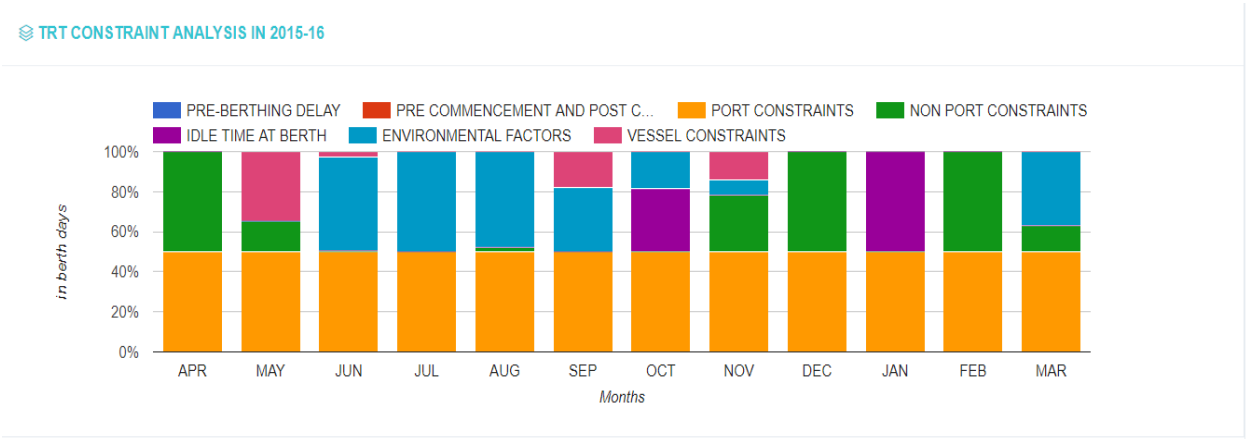



***Figure 11**: Monthly Analysis of TRT constraints for 2015-16*

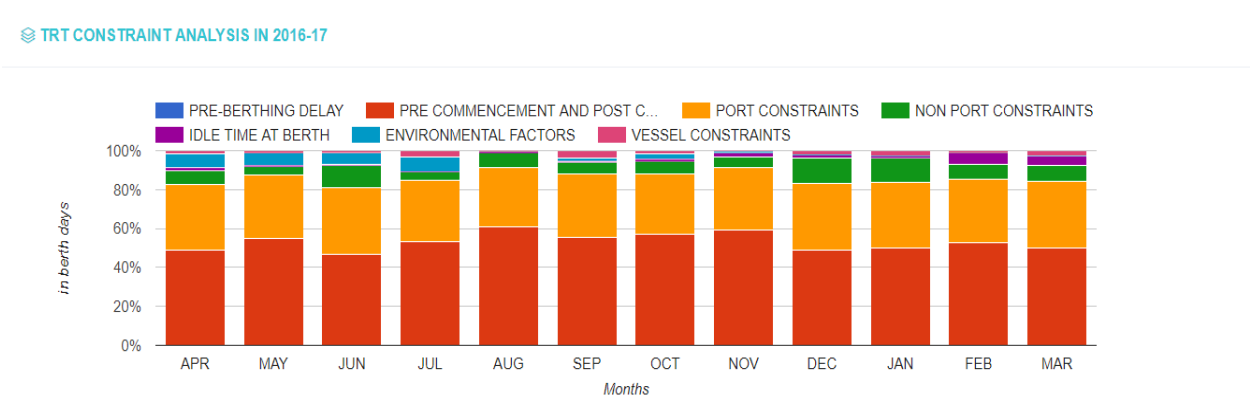



***Figure 12**: Monthly Analysis of TRT constraints for 2016-17*

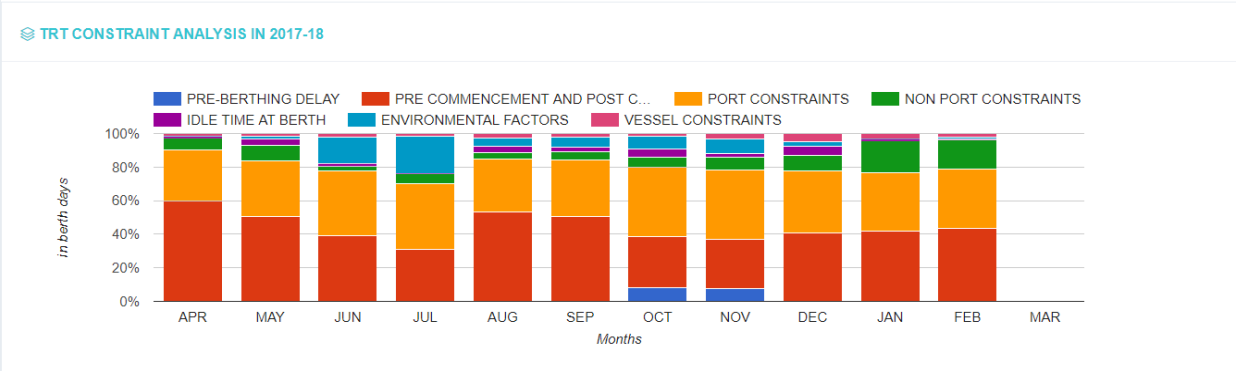



***Figure 13**: Monthly Analysis of TRT constraints for 2017-18*

## 5.5 Commodity wise TRT constraints analysis

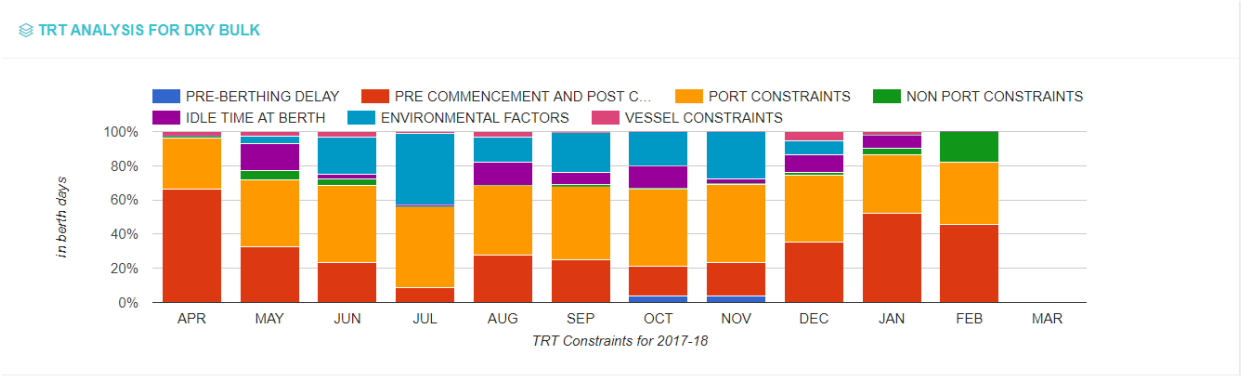



***Figure 14**: Analysis of TRT Constraints for Dry Bulk-Manual handling*

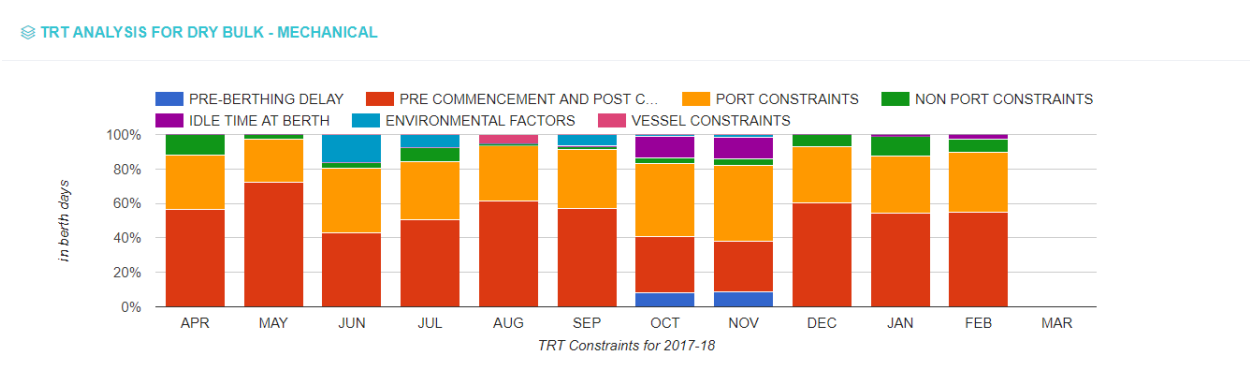



***Figure 15**: Analysis of TRT Constraints for Dry Bulk- Mechanized handling*

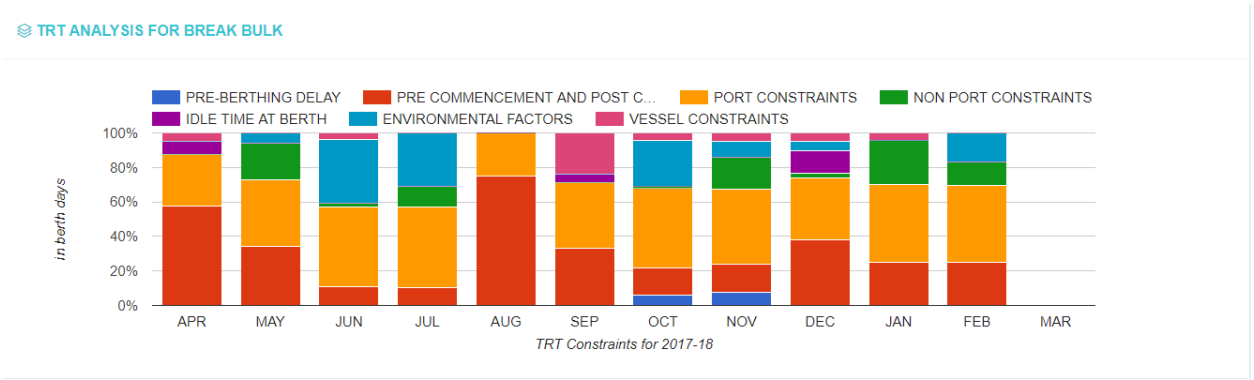



***Figure 16**: Analysis of TRT Constraints for Break Bulk*

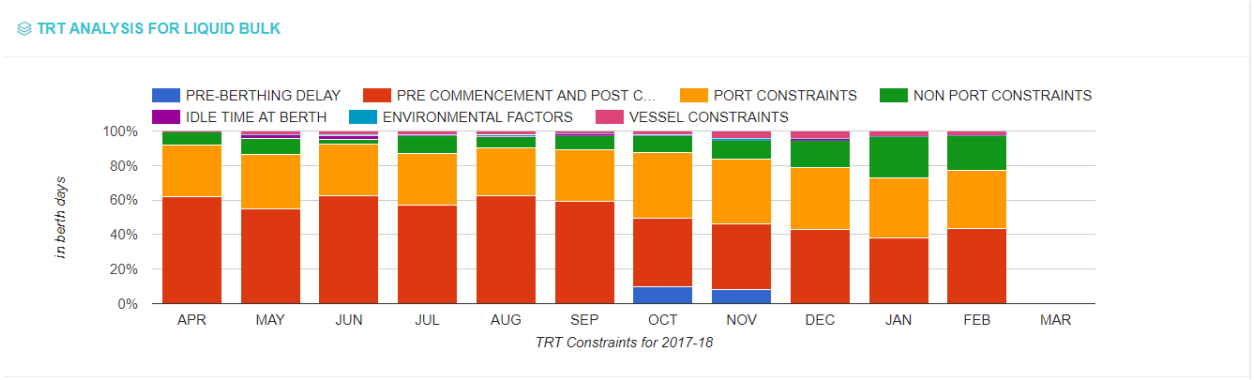



***Figure 17**: Analysis of TRT Constraints for Liquid Bulk*

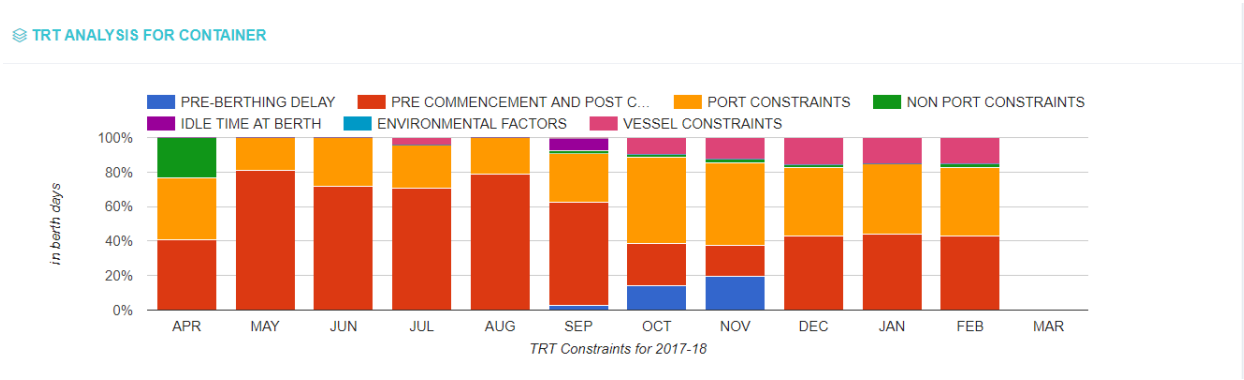



***Figure 18**: Analysis of TRT Constraints for Container*

The year wise TRT constraint analysis reveals that pre commencement and post commencement factors and port constraints are the major contributing the delay in the TRT. In the monsoon months the environmental constrains also having the share on the increased TRT of the vessels. Other than the monsoon months the non-port constraints also affects the TRT

## 6.0 CONCLUSIONS

From the Year on year TRT module one can generate the port performance indicators such has pre-berthing waiting time (PBWT), vessel turnaround time (TRT), Non-working time at berth(NWTB) Number of vessels handled, output per ship berth day(OSBD) and port productivity.

From the year wise analysis of TRT it is observed that the pre-berthing time and service time contributes to the maximum percentage of vessel turnaround time. The service time is on higher side during the monsoon months and the pre berthing time is higher side in the non-monsoon months. It is also observed that the outward movement time more compared to inward movement time of vessels calling on to the port.

From the seasonal TRT analysis, it is observed that service time is on higher side during the monsoon months and the pre berthing time is on higher side in the non-monsoon months. It is also observed that the outward movement time more compared to inward movement time of vessels calling on to the port.

Thus this VTRT model will able to help the port management to verify the problems in an identified area and to come out with better solutions in providing services and improving the port activities to ensure increased port productivity and efficiency. The proposed programming model is also very useful in decision making for port Authorities as well as ship operators in any given budget or resource input, the output results in time and cost minimization. It is also possible to tackle all the delay causing factors by the port management in providing efficient and effective services and increased port productivity, with the aim to achieve optimum port performance. The outcome of the research is to determine the factors which are most significant to determine the turnaround time for vessel. The model can also be useful in generating various MIS outputs, Port performance indicators (PPI) with respect to the category of cargo handled, Berth wise, on daily/monthly/yearly basis.

**References:**


1. Bhanu.Prakash,Tarun.DhingraandBangar.Raju, (2016): "Efficiency assessment at major ports of India for the period 2007-08 to 2013-14 using Data Envelopment Analysis (DEA)". Energy, Infrastructure and Transportation Challenges and Way Forward.Conference Proceedings of International Conference on Management of Infrastructure (ICMI) 2016, 46-61
2. Bergantino.A.S, Musso.E and F.Porcelli,(2013): " Port management performance and contextual variables: Which relationship? Methodological and empiricalissues", Research in Transportation Business and management
3. Bichou and Gray, (2004): "A Logistics and Supply Chain Management Approach to Port Performance Measurement". Maritime Policy and Management. 31(1), 47-67.
4. Bichou, K, (2012): "Linking theory with practice in port performance and benchmarking". International Journal of Ocean Systems Management, 1(3-4),316–338.
5. Bichou, K. (2007): "Review of Port Performance Approaches and A Supply Chain Framework to Port Performance Benchmarking", Transportation Economics. 17, 567-598
6. Clark, X., Dollar, D., and Micco, A. (2004): "Port Efficiency, Maritime transport costs, and bilateral trade". Journal of Development Economics.(6), 1-34.
7. DayanandaShetty K and G.S.Dwarakish (2018) "Measuring port performance and productivity" – ISH Journal of Hydraulic Engineering DOI: https:// doi.org/10.1080/09715010.2018.1473812.
8. DayanandaShetty K and G.S.Dwarakish (2018) "Performance appraisal of Indian major ports", Indian Ports - Journal of Indian Port Association. Volume 48, 29-34.
9. Gordan, J.R.M., Lee, P.M., and Lucas H.C.Jr. (2005): "A resource-based view of competitive advantage at port of Singapore". Strategic Information Systems.(14), 69-86.
10. Indian Shipping Statistics 2015, Transport Research Wing, Ministry of Shipping and Ministry of Road Transport & Highways, Government of India.
11. Marlow, P.B., and Paixao, A.C. (2003). Measuring Lean Ports Performance. International Journal of Transport Management. 189-202.
12. Morgan, C. (2004): "Structure, speed, and salience: performance measurement in the supply chain". Business Process Management Journal. 10 (5), 522-536.
13. Odeck.J and Brathen.A, (2013): "A meta-analysis of DEA and SFA studies of the technical efficiency of seaports: A comparison of fixed and random-effects regression models". Transportationresearch Part A:Policy and Practice.46,1574-1585
14. Oram, R.B, and Baker, C.C.R. (1971): "The Efficient Port. London: The Commonwealth and International Library".
15. Padmasani, and Tamilselvi(2016): "An assessment of Indian major sea ports performance and efficiency" International Journal of Multidisciplinary Research and Development Volume 3;

16. Rajasekar T, Sania Ashraf and P Malabika Deo P(2014): "Measurement of efficiency of major ports in India – a data envelopment analysis approach" International journal of environmental sciences Volume 4, No 5, 2014
17. Simoes, P. and Marques, R. (2010):"Seaport performance analysis using robust nonparametric efficiency estimators", *Transportation Planning and Technology.* 33(5), 435-451.
18. Tongzon, J. (1995) „Determinants of Port Performance and Efficiency Transportation Research Part A. 29 (3) pp. 245-252.
19. UNCTAD (2012), "Review of Maritime Transport" United Nations Conference on Trade and Development.
20. UNCTAD (1976) "Port Performance Indicators". United Nations Conference on Trade and Development.
21. Yuen, A.Zhang, and W.Cheung (2013):, " Foreign participation and competition: A way to improve the container port efficiency in China" Transportation Research Part A: Policy and practice,49,220-231

IN PROCEEDINGS OF 25th HYDRO 2020, INTERNATIONAL CONFERENCE,
NATIONAL INSTITUTE OF TECHNOLOGY ROURKELA, ODISHA, INDIA
26-28, March 2021, ISBN 978-93-90631-56-8

Paper ID - 077

# Diffraction Studies Pertaining To Functional Design of Breakwaters-A case Study of Gangavaram Port, East Coast of India

G. Lenin Reddy[1], M. G. Muni Reddy[2], T. V. Ramana Murthy[3], M. L. Narasimham[4]

[1]*Research scholar, Andhra University College of Engineering, Visakhapatnam, 530003, India*
[2]*Associate Professor, Andhra University College of Engineering, Visakhapatnam, 530003, India*
[3]*Scientist-F (Rtd.), National Institute of Oceanography, Regional center, Visakhapatnam, 530017, India*
[4]*Professor (Rtd.), Andhra University College of Engineering, Visakhapatnam, 530003, India*
*Email: devicharanarya@gmail.com,munireddy9@rediffmail.com, tvrmurty@gmail.com*
*9490660005, 9494572898, 9000744136, 8895860950*

## Abstract

Development of port requires the selection of proper alignment, a significant step in the functional design of breakwater which in turn can be decided through diffraction studies. Towards this objective, a model has been developed for the determination of diffraction coefficients for given environmental settings. The model has been applied for the analysis of the diffraction pattern for coastal waters off Gangavaram located in the East Coast of India ($17^0$ 37' 30'' N latitude, $83^0$ 14' East longitude) using the available data of physical, meteorological and topographical parameters. The outcome of the study enabled us to suggest a suitable layout of breakwater for the selected port location. The simulated diffraction coefficients obtained through model developed with an approach angle $60^0$ with respect to wave direction have been found to be varying between 0.05 and 0.67 covering 20 Sq. km area, which is indicative of relatively stable and calm water in the leeward side of break water independent of seasons, for the data considered.

***Keywords:*** *Breakwater alignment; Functional design; Diffraction coefficient; Approach angle*

## 1. Introduction

### 1.1 *General*

From the time immemorial people started inhabiting the coastal regions. More than 40% of world's population is living close to the coastal areas. As regards the situation in our country, the density of population is more on the east coast compared to west coast. The total length of Indian coast line is approximately 7500 km, out of which the east coast (Digha to Kanniyakumari) measures approximately 2464 km. Increased sea transport ultimately led to the development of ports and harbours. Twelve major ports and several minor ports exist along the coastal regions of India for transshipment of material and men to meet the requirements of various industrial sectors. Visakhapatnam port is one among the major ports established in East coast of India and has lot of shipment potential. Visakhapatnam is among the fastest growing cities on the industrial map of the India. Abundant natural resources in its hinterland, well developed transport facilities, telecommunication, infrastructure, etc., provide Visakhapatnam an unlimited potential for industrial growth. In spite of many developed cargo facilities several ships await at the high seas for berthing. Several industries developed around Visakhapatnam such as the gigantic integrated steel plant, petroleum refinery, and fertilizer factory, zinc plant, thermal power plants and many more came up in recent times. To set up a new port offshore infrastructure facilities such as breakwaters to create a harbour basin, berthing facilities like jetties, berthing structures are required. For planning and design of these structures a detailed back ground information on spatial and time distribution of different parameters on the shoaling, refraction, and diffraction etc is required. Wave refraction and diffraction studies constitute an important part in the sitting and planning of the new port. The diffraction of water waves plays a major part in the functional design of break water provides a relatively calm area. Mathematically diffraction coefficient is a measure of the physical process of diffraction of water. Diffraction coefficient is defined as the ratio of diffracted wave height and incident wave height.

Several investigations in the past have carried out a thorough study on the other aspects and identified the area, near off Gangavaram to be suitable location for a minor port. The information/data collected in the study area by the National Institute of Oceanography (NIO) will be of immense help to go ahead with the studies.

## 1.2 *Identification of the problem*

For planning construction activities such as a minor port, in the near shore regions, the wave refraction, diffraction pattern and the details of wave forces in that coastal and wave environment are a pre-requisite. The collection of field data on wave topography and its interaction is expensive and this problem needs to be studied through the analysis of analysis of wave refraction and diffraction pattern using the available mathematical models and with some modification in some of them to suit topographical and environmental settings, in recent years, with the availability of fast computers, the numerical methods are found to be more convenient for usage and to check wave diffraction studies. With the objective of mapping of diffraction coefficients of waters, off Visakhapatnam, to suggest suitable alignment for a breakwater in coastal waters off Gangavaram site has been taken up, as a case study. In the following section the relevant theory methodology, numerical experiments, software details etc. are described.

### 1.3 *Study area*

The near shore waters off Visakhapatnam, in general, have been taken up for the studies. Visakhapatnam is situated on the East Coast of India, which is engulfed by Bay of Bengal waters. The actual study area is Gangavaram which is located at the co-ordinates of 17° 37’ 30” N latitude and 83° 14’ E longitude and is situated 10 km South of Visakhapatnam. The environmental settings viz. Coastal Geomorphology, Climatology, near shore Oceanography, Environmental parameters are detailed for better understanding of the study area from the published works (P. Chandra Mohan et al. 1981, Chandra Mohan and Narasimha Rao 1984).

#### 1.3.1 *Climatology*

The climate of Visakhapatnam is dominated by the monsoons and cyclonic storms, which divides the year approximately into four seasons. (a) The North East monsoon from end of November to end of January with predominantly north westerly winds. b) The pre-monsoon period from March to May when the winds shift to Southwesterly direction and cyclones are frequent. (c) The South West monsoon from middle of May to middle of October with predominantly south westerly winds. (d) Post-monsoon period from October to end of January with variable weather and occurrence of frequent cyclones (P. Chandra Mohan et al. 1981; Chandra Mohan and Narasimha Rao 1984). The cyclonic storms occurring in Bay of Bengal are generally associated with heavy rains, and considerable rise in sea level due to storm surges.

#### 1.3.2 *Wave Data*

Sub-surface wave sensors or surface buoys or ship borne wave recorder is normally carrying out the measurement of ocean waves. The wave speed and direction for different seasons with wave directions viz. NE, SW, SSW, and S are taken from wave atlas (P. Chandra Mohan et al. 1990). The atlas containing the data based on ship observations provide information on wave direction also, whereas the wave recording system being used in India provides only wave height and wave period statistics.

Wave periods on cyclonic days are varying from 6 sec to 12 sec and on normal days 8 sec to 10 sec. Thus relating to the variation of wave periods has been obtained from the studies arrives at NIO (P. Chandra Mohan et al. 1981; Chandra Mohan and Narasimha Rao 1984). The same is presented in table 1. Without the loss of generality, simulation experiments have been carried out with the model for minimum, maximum, average periods (6 sec, 12 sec and 9 sec respectively) representing all the

seasons to compute the diffraction coefficients for interpretation. The calculated deep water wave length is 56.2m, 126.37m, 224.83m for wave periods of 6 sec, 9 sec and 12 sec respectively. Although the diffraction coefficient does not depend upon the wave height for the purpose of generality and completion of exercise on data collection, the wave height pattern variation pattern was also looked into. This information is also presented here in table 3.

**Table 1** Wave directions Off Gangavaram (17°37' 30" N, 83°14' E)
Source: Wave atlas (P. Chandra Mohan et al. 1990)

| Period of the Year | Wave direction | $\theta_{atlas}$ |
|---|---|---|
| November-February | North East | 45° |
| March | South -South West | 180°-225°(200° assumed) |
| April | South West | 225° |
| May-September | South | 180° |

**Table 2** Wave periods Off Gangavaram during various periods of a year
Source: (P. Chandra Mohan et al. 1981; Chandra Mohan and Narasimha Rao 1984)

| Period of the Year | Wave Period (Sec) |
|---|---|
| Cyclone days | 6-12 |
| Most part of the year | 6-10 |

**Table 3** Wave heights Off Gangavaram during various periods of a year
(P. Chandra Mohan et al. 1981; Chandra Mohan and Narasimha Rao 1984)

| Period of the Year | Wave height(m) |
|---|---|
| May-September (South West Monsoon) | 1-3 |
| October – December (on cyclone days) | >6 |
| (Other than cyclone days) | calm |

1.3.3 *Geomorphology*

The area near the selected site is near hillocks and plains are used for agriculture purpose. Lands are used for salt industries. The alignment of the coast between Gangavaram and Appikonda lies North East and Southwest direction. There is a shallow bay off Gangavaram having a narrow tidal inlet feeding salt water to the salt pans. The continental shelf off Visakhapatnam is narrow extending up to about 45 km from the coast (P. Chandra Mohan et al. 1981; Chandra Mohan and Narasimha Rao 1984).

1.3.4 *Near shore oceanography*

During May to September the sea is rough with wave heights ranging from 1m-3m. During October to December the sea is generally calm except on cyclonic days. For remaining part of the year, the sea is generally calm with light swells. The wave periods generally vary between 8 and 10 seconds during the greater part of the year and on cyclonic days 6 and 12 seconds. During February and April i.e. after the Northeast monsoon season, the surface flow is towards Northeast. The flow is offshore along this region during May and July. In August the flow is variable and inconsistent in direction. With the offset of Southwest monsoon, by September, a Southwesterly flow is established. By December, the flow is shoreward. The coastal waters are highly productive and rich in prawns catfish and trichirus etc. Major part of the beach undergoes erosion during Southwest monsoon. During Northeast monsoon and calm weather period deposition occurs. Waves approaches from South and break at an angle of 5° to the shoreline during Southwest monsoon period during March and September. A reversal of direction of wave approach is observed during Northeast monsoon period (October-February) and wave break at an angle of about 5° to the shore (Chandra Mohan and Narasimha Rao 1984).

### 1.3.5 *Environmental conditions at the site*

For the study area under consideration four predominant wave directions are noted from the wave atlas. They are North East (NE) from November to February, South West (SW) during March, South-South West (SSW) from April to September and South (S) during October. The study area is represented for the convenience in the form of rectangular grid parallel to latitude and longitude axis. For every grid point i.e. for a particular latitude and longitude, water depth contours are obtained from linear interpolation and tabulated as latitude, longitude and depth. For accurate analysis Digital Global Positioning System (DGPS) and Echo sounder are usually used to obtain the field data. DGPS gives the position i.e. latitude and longitude and Echo sounder gives the depth of the seabed at the point of observation. At any point in sea action of various forces can act in eight different directions viz., North, North East, East, South East, South, South West, West, and North West. Owing to the orientation of coast line of about 70° with respect to the North, various forces in the study area is limited to upon South West to North East region in the anti-clockwise direction.

### *1.3.6 Basic equations*

Somerfield in 1896 proposed the theory of light waves at the edge of the semi-infinite screen (Somerfield 1896), and his hypothesis enabled other investigators to take up the study in further detail. Penny and Price (1944) have shown that Somerfield's solution of the optical diffraction problem is also solution for wave diffraction problem. The solution of Penny and Price (1944) is for the diffraction of the ocean waves at the end of semi-infinite barrier, such as a long breakwater. Superimposing two such solutions for semi-infinite breakwater extending in two directions provides a good qualitative picture of the water surface behind a breakwater with a gap, but the solution is not exact. Putnam and Arthur (1948) presented a form of this solution, which is modified form the original, and which appears to be particularly adopted to wave application. Putnam and Arthur, Blur and Johnson (1938) and Johnson have verified the theory by means of models.

The Somerfield's solution of optical diffraction as applied by Penny and Price (1944) results in the following equation.

$$F(r,\theta)=\frac{\partial^2 F}{\partial r^2}+\frac{1}{r}\cdot\frac{\partial F}{\partial r}+\frac{1}{r^2}\frac{\partial F^2}{\partial \theta^2}+\kappa^2 F=0 \qquad (1)$$

Where F = Function in cylindrical co-ordinates, $\kappa = 2\pi/L$ (wave number) L= wave length
Putnam and Arthur (1948) (Arthur T. Ippen, 1965; Richard Silvester et al.) have shown that diffraction coefficient is analogous to F(r, θ) and can be obtained by the equation 1.

$$F(r,\theta)=F(u_1)\exp[i\kappa r\cos(\theta_0-\theta)]+F(u_2)\exp[i\kappa r\cos(\theta_0-\theta)] \qquad (2)$$

Where r = position vector (the distance between break water tip and any point under consideration = $\sqrt{x^2+y^2}$, $\theta_0$ = Approach angle, θ = Angular co-ordinate of any grid point with respect to break water arm, i = $\sqrt{-1}$,

$$F(u_1)=\frac{1+i}{2}\int_{-\infty}^{u_1}\exp(i\kappa u^2)du \qquad (3)$$

$$F(u_2) = \frac{1+i}{2}\int_{-\infty}^{u_2} \exp(i\kappa u^2)du \quad (4)$$

$$\text{where } u_1 = 4\sqrt{\frac{\kappa r}{\pi}}\sin(\frac{\theta_0-\theta}{2}) \quad (5)$$

$$\text{where } u_2 = -4\sqrt{\frac{\kappa r}{\pi}}\sin(\frac{\theta_0-\theta}{2}) \quad (6)$$

In the above equation F ($u_1$) and F ($u_2$) are Fresnel Integrals. It is further observed that the modulus of the equation 1 gives the numerical value of the diffraction coefficient 'K'. Thus from equations 1 to 4

$$K=\left| F(r,\theta) \right| = F(u_1) - \frac{0.225}{u_2} \quad (7)$$

The value of $u_2$ will be less than -2 for the greater part of the region beyond the breakwater (Arthur T. Ippen 1965). From the above equations one can conclude to know that diffraction coefficient 'K' is a function of θ, $\theta_0$, r/L i.e. K= F ($\theta_0$, θ, r/L).

## 2. Methodology Data and Computational Procedure

### 2.1 *General*

The methodology involved in arriving at the evaluation of various parameters required for the computation of the diffraction coefficients viz. angular co-ordinates of grid points (θ), approach angle of the break water ($\theta_0$), the procedure of calculating the angle between breakwater and the straight parallel line parallel to latitude axis ($\theta_{cal}$), used in the determination '$\theta_0$' and the Regula - Falsi iteration method used in the determination of wavelength 'L' are illustrated in section 2.2.5. Section 2.2.6 deals with the computation of diffraction coefficients obtained through the numerical experiments carried out from the software developed.

### 2.2 *Methodology*

The methodology involves the generation of Bathymetry at required points, Determination of angular co-ordinate (θ) of the grid points, Determination of the approach angle of the breakwater ($\theta_0$), Determination of wave Length (L), and Determination of diffraction coefficient (K).

#### 2.2.1 *Generation of grid*

A local system of rectangular Cartesian co-ordinates X, Y, Z is used with origin 'O' located at the tip of breakwater (Fig. 1). The Y-axis is defined along the wave direction in the shadow zone and X-axis is along the wave front. The predominant wave directions prevailing in the study region in general are obtained from the wave atlas (P. Chandra Mohan et al. 1990).

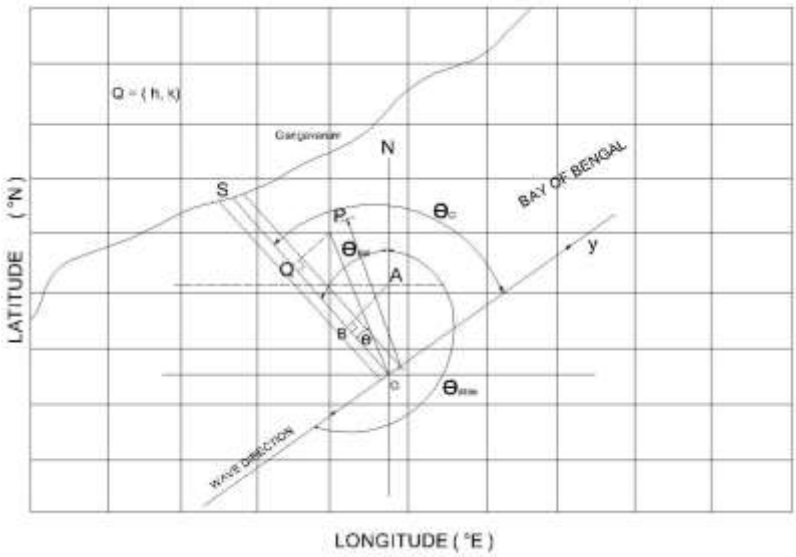



**Figure 1** Co-ordinate system for wave diffraction description

### 2.2.2 *Determination of angular co-ordinate (θ)*

Angle of any point on the grid with respect to breakwater arm is the angular co-ordinate (θ) as shown in Figure1. The two co-ordinates of the break water tip and end are given in the input data. The straight line equation of the breakwater is defined. At any point on the grid, the co-ordinate of the foot of the perpendicular on the equation of the straight line through breakwater is obtained through the formulae

$$h^{*} = \frac{-m(m \cdot lat - long + long_1)}{m^2 + 1} + lat \tag{8}$$

$$k^{*} = \frac{(m \cdot lat - long + long_1)}{m^2 + 1} + long \; ; \; m = \frac{(long_2 - long_1)}{(lat_2 - lat_1)} \tag{9}$$

Where h* = latitude co-ordinate of foot of perpendicular in degrees, k* = longitude co-ordinate of the foot of the perpendicular in degrees, lat1 = latitude co-ordinate of tip of break water in degrees, long1 = longitude co-ordinate of tip of break water in degrees, m = slope of the straight line passing through tip and end co-ordinates of break water, lat = latitude co-ordinate of any other point on the grid in degrees, long = longitude co-ordinate of any other point on grid in degrees, lat2 = latitude co-ordinate of any other point of break water in degrees, long2 = longitude co-ordinate of any point of breakwater water in degrees.

From any grid point co-ordinate (P), co-ordinate of the foot of the perpendicular (Q), co-ordinate of the tip of breakwater (O), the distances PQ, OQ are computed from the general expression (Fig. 1)

$$D = \frac{\pi R}{180 \cdot \sqrt{(\Delta\phi)^2 + \cos\phi_1 \cos\phi_2 + (\Delta\lambda)^2}} \tag{10}$$

Where $\phi_1$ = latitude in degrees at point 1, $\phi_2$ = latitude in degrees at point 2, $\Delta\phi$ = Difference in

latitude between two points in degrees, $\Delta\lambda$ = Difference in longitude between two points in degrees, R = Radius of the earth (≈6371km)

$$\theta = \tan^{-1}\left(\frac{PQ}{OQ}\right) \tag{11}$$

Where PQ = the distance between any point on the grid and its foot of perpendicular,
OQ = the distance between the tipoff breakwater and foot of the perpendicular of any grid point.

### 2.2.3 *Determination of ($\theta_{cal}$)*

$\theta_{cal}$ (θ calculated) is the computed angle between the breakwater and axis parallel to latitude axis passing through tip co-ordinates of breakwater. This quantity $\theta_{cal}$ is needed for the computation of approach angle of breakwater ($\theta_0$). First it is calculated by finding out the mid co-ordinates of the given two co-ordinates of breakwater using the simple co-ordinate geometry formula $\left(\frac{x_1+x_2}{2}, \frac{y_1+y_2}{2}\right)$. The point 'B' (Fig. 1) which is the point of intersection of the lines (a) Parallel to longitude axis and passing through, mid-ordinate of co-ordinates of breakwater at tip O(lat1, long1) and shore S(lat2, long2). (b) Parallel to latitude axis and passing through tip of breakwater. Obviously the point 'B' is $\left(\frac{lat_1+lat_2}{2}, long_1\right)$. With respect to point 'B', foot of the perpendicular on the straight line through breakwater is erected using the formula as discussed in the evaluation of 'θ' in the previous section. Once again the foot of the perpendicular is erected the distances OB, AB are calculated by using similar procedure adopted in evaluation of 'θ' as described in the previous section. Now $\theta_{cal}$ is computed as

$$\theta_{cal} = \tan^{-1}\left(\frac{AB}{BO}\right) \tag{12}$$

### 2.2.4 *Determination of Approach angle '$\theta_0$'*

Approach angle '$\theta_0$' is the angle between the wave direction and breakwater in the diffracted region. It clearly indicates that for a particular configuration of breakwater, approach angle is different for different wave directions. In the study area four predominant wave directions are encountered in different times of the year as inferred from wave rose diagrams of wave atlas (P. Chandra Mohan et al. 1990). The four wave directions are North East, South, South Southwest and Southwest. Wave directions in different times of the year and their respective direction with respect to the North, is described as '$\theta_{atlas}$' (table 1). In each wave direction the approach angle is computed using the following formulae for different cases arises in the environment and also check will be made to know whether each grid point lies in the shadow zone or not for consideration. If it doesn't lie in the shadow zone, the data grid points of the bathymetry are skipped off. The computation of approach angle for case b (South Southwest, Southwest direction) is as shown in figure 2 and 3.

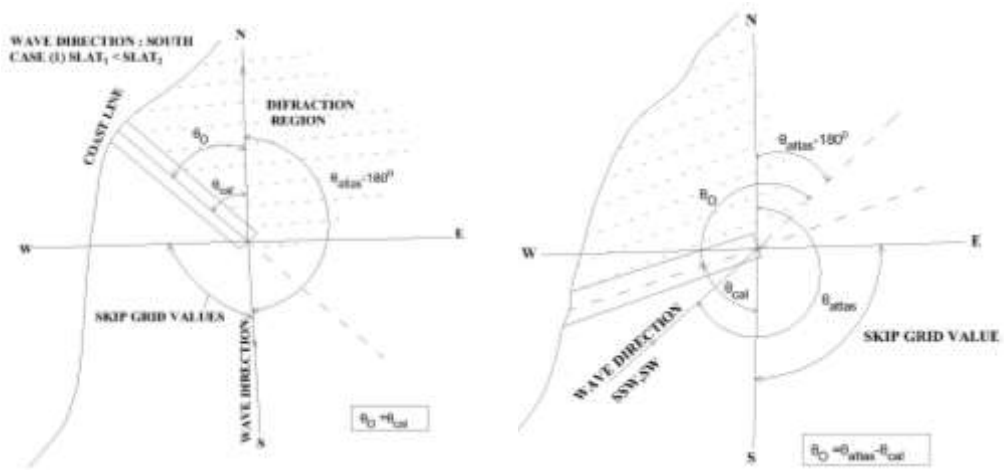



**Figure 2, 3** Calculation of Approach angle for Wave direction South, Southsouth west, Southwest

(a) Wave direction: Northeast.
Case (1) slat1 < slat2;

$$\theta_0 = 360^\circ - (180^\circ + \theta_{atlas} + \theta_{cal}) \quad (13)$$

Case (2) slat1 > slat2;

$$\theta_0 = (\theta_{cal} - \theta_{atlas}) \quad (14)$$

(b) Wave direction: South-Southwest, Southwest.
Case (1) slat1 < slat2;

$$\theta_0 = (\theta_{atlas} + \theta_{cal} - 180^\circ) \quad (15)$$

Case (2) slat1 > slat2;

$$\theta_0 = (\theta_{atlas} - \theta_{cal}) \quad (16)$$

(c) Wave direction: South
Case (1) slat1< slat2;

$$\theta_0 = \theta_{cal} \quad (17)$$

Case (2) slat1> slat2;

$$\theta_0 = 180^\circ - \theta_{cal} \quad (18)$$

2.2.5 *Determination of Wave Length 'L'.*

Wavelength is obtained by solving the dispersion relation i.e.

$$\frac{L}{L_0} = \text{Tanh}\left(\frac{\kappa_0 h}{\frac{L}{L_0}}\right) \quad (19)$$

Where '$L_0$'= Deep water wave length=$\frac{gT^2}{2\pi}$, $\kappa_0$= wave number = $\frac{2\pi}{L_0}$ and using Regula Falsi technique which is a powerful tool for solving the above equation. There are two methods, for solving the above equation i.e. for determining 'L'. They are (1) Graphical, (2) Iteration. Iteration consists of a repeated execution of same process where at each step the result of the preceding step is used.

Newton Rap son method, method of bisection and method of false position or Regula Falsi are some of available techniques, one can adopt, for solving the nature given by equation (20) and (21). In Newton Rap son method, if the slope of the curve tends to zero, the solution doesn't converge. The Bisection method guarantees that the iterative process will converge. It is however slow. But in the third method such a case doesn't arise and also the process is very fast towards convergence. In view of this, the third method i.e. Regula Falsi method has been adopted.

$$L_{21} = L_0 - \frac{(L_1 - L_0^l)}{F(L_1 - L_0^l)} \times F(L_0^l) \tag{20}$$

$$F(L) = L - L_0^l \ \mathrm{Tanh}\left(\frac{2\pi}{L}\right)h = 0 \tag{21}$$

We start this procedure by locating the points $L_1$ and $L_0^l$ where function has opposite signs. We now connect the two points $F(L_0^l)$ and F ($L_1$) by a straight line and find where it connects L axis. Let it cut the L axis at $L_{21}$. If F ($L_{21}$) and $F(L_0^l)$ are of opposite signs then replace $L_{21}$ by $L_{22}$ and draw a straight line connecting F ($L_{22}$) and $F(L_0^l)$ to find the new intersection point. If F ($L_{22}$) and $F(L_0^l)$ are of it signs then $L_0^l$ are replaced by $L_{22}$ and proceed as before. In both the cases the new interval to reach is smaller than the initial interval and ultimately it is guaranteed to converge to the root. Likewise the wavelength for all grid points is evaluated.

### 2.2.6 *Determination of Diffraction coefficient 'K'*

After evaluating the values of $\theta_0, \theta$, r, L the argument $u_1$ in the Fresnel Integral is computed as follows.

$$u_1 = -\sqrt{8 \cdot \left(\frac{r}{L}\right)} \ \mathrm{Sin}\left(\frac{\theta_0 - \theta}{2}\right) \tag{22}$$

From the value of $u_1$, F ($u_1$), which is the length of the first vector (argument is zero) is obtained from the interpolation of spline function of the tabulated values of Fresnel integrals. The length of the second vector is determined using the value of $u_2$ with the following expression.

$$\text{Length of second vector} = \frac{1}{(\pi\sqrt{2}u_2)} \mathrm{Sin}\left(\frac{\theta_0 + \theta}{2}\right) = \frac{0.225}{u_2} \tag{23}$$

$$\text{where } u_2 = -\sqrt{8 \cdot \left(\frac{r}{L}\right)} \ \mathrm{Sin}\left(\frac{\theta_0 + \theta}{2}\right) \tag{24}$$

Finally diffraction coefficient 'K' is computed from the following expression.

$$K = F(u_1) - \text{Length of second vector} \tag{25}$$

The computational procedure from the main program (DC.FOR) of the software developed is presented in next section. From the output of this, bathymetric contours, wavelengths, diffraction coefficient maps are prepared using Surfer for time period of 6, 9, 12 seconds for South, South southwest, Southwest and Northeast wave directions for approach angle of 60°. The diffraction

coefficient maps of all the four wave directions for only a time period of 12 second are only presented (Fig. 4 to Fig. 7).

## 2.3 *Computational Procedure*

The basic data required for computation of diffraction coefficients during various seasons have been taken from naval hydrographic chart no: 308. This data has been manually digitized in the closed interval for the site of Gangavaram located at 17.63° N latitude, 83.63° E longitude, and away 10 km south of Visakhapatnam. The digitized bathymetry data is stored in a file named EX1.dat for computation purpose during the running of main program DC.FOR. The input data for running the main program is bathymetry, tip and end co-ordinates (latitude and longitude) of break water, wave direction and period. Next to the input, is to run the model, season wise wave direction. The output of the program is mainly wavelength and diffraction coefficients at the grid points that fall in the leeward side of the breakwater corresponding to a selected alignment (Fresnel Zone). Using the surfer package, wave length, diffraction coefficient contours have been obtained and only the diffraction coefficient contours are shown in figure4 to figure 7.

## 2.4 *Discussions of Results*

This section contains discussions on results viz., bathymetric contours, wave lengths, diffraction coefficients, for different environmental settings, in the respective Fresnel zones. Diffraction coefficient is a function of $\theta$, $\theta_0$, r/L. Wave length is computed by solving the dispersion relation. The dispersion relation is a function of mean water depth, i.e. bathymetry; therefore diffraction coefficient is a function of bathymetry. Accurate generation of data bank of bathymetry gives the precise results of the output of diffraction coefficients. Initial data bank is prepared by digitization of hydrographic charts. The up-gradation of the data bank of the study area can be done by conducting field investigations.

### 2.4.1 *Bathymetric contours*

3D view of contour map of bathymetry for the region between 83°E longitude to 83° 41’ 41.02” E longitude and 17° 20’ 40.63” N latitude to 17° 45’ N latitude has been obtained using surfer package and already been referred to section 3.3. With the change in wave direction, the Fresnel zone for a given breakwater layout will change. Finally the depths in the grid points that fall in Fresnel zone are only required in the computation of diffraction coefficient. Hence in the present investigation for each of the orientations of the breakwater layouts considered the Fresnel zones has been identified and the depths at the various grid points in that zone are considered for further computation. The depths at grid points falling out side are skipped off.

### 2.4.2 *Wave length*

The isolines along the wave length and mean water depth contours and wavelengths in the Fresnel zones have been contoured using surfer for different wave directions and wave periods, (T = 12, 9, 6sec respectively). The interesting inference is that the gradients of depth contours as well as wavelength for longer periods, for all the seasons from deepwater to the shore is more as compared to the small wave period 6sec. This indicates that the waves with longer wave periods feel the bottom after passing through the tip of the breakwater into the shadow zone and energy gets dissipated as a consequence the wave length decreases. Following the principle of conservation of energy, the wave heights in-turn has to increase. This phenomenon is reflected in the increase of diffraction coefficients.

### 2.4.3 *Diffraction coefficients*

Using the model developed, the values of the diffraction coefficients for different wave conditions are obtained. The results were obtained considering several layouts of the breakwater alignment as already indicated. The diffraction pattern changes with the wave direction and wave periods (Fig. 4 to Fig. 7) indicate the diffraction pattern of the wave direction considered. It is also seen that diffraction coefficients for 12 sec wave period in the shadow zone area near the coast found to be higher as compared to the other wave periods 6sec, 9 sec irrespective of all seasons. It is further seen that minimum value of diffraction coefficient is 0.05 in SW wave direction for wave period 6sec. Figs. 4 to Fig. 7 reveal that overall variation of minimum values of diffraction coefficients irrespective of season and breakwater configuration is between 0.053 and 0.069 near the coast and maximum variation is between 1.12 and 1.17 away from the shadow zone. From table 1 it can be also seen that the wave direction is North East during the months of November to February and for the remaining period it is varying between South to Southwest. Further a period of six months (May to October) corresponds to a wave propagation direction of South. For the balance of the period the waves are limited to only Southwest direction. Thus it can be said that for the study areas, the predominant wave direction are South, South of Southwest. From Fig.5 and Fig.6 it can be seen that diffraction coefficients varied between 1.06 and 0.06 for all the three periods. For this alignment of breakwater the approach angle is seen to be 60°. Considering the approach angle to be 60° breakwater alignments were changed considering the wave direction as Northeast and Southwest. Fig. 4 and Fig.7 show that the changed alignment of breakwater and resulting patterns of diffraction. It can be seen from the figures the diffraction coefficients varied from 0.06 to 1.06 in the Fresnel zones.

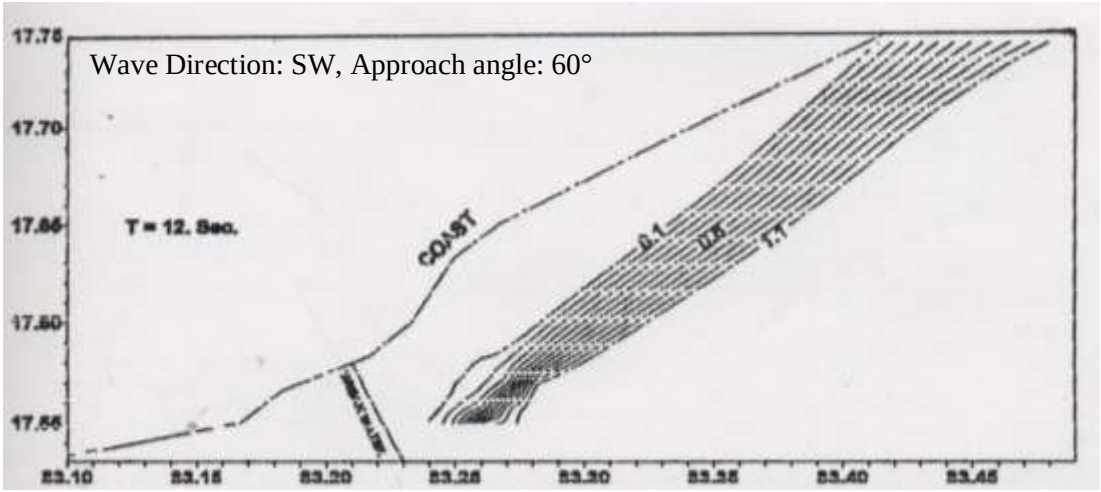



**Figure 4** Diffraction coefficients for Latitude (°N) Versus Longitude (°E)

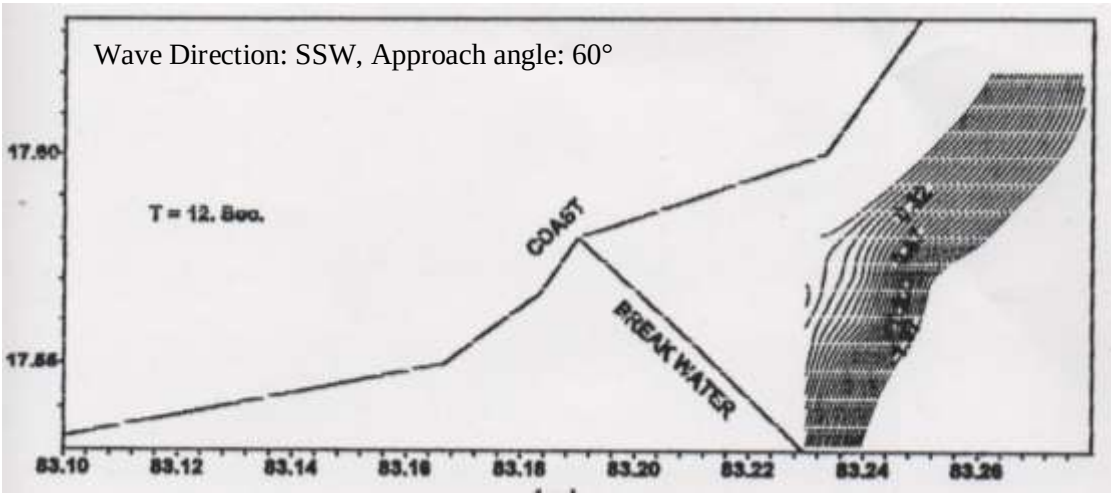



**Figure 5** Diffraction coefficients for Latitude (°N) Versus Longitude (°E)

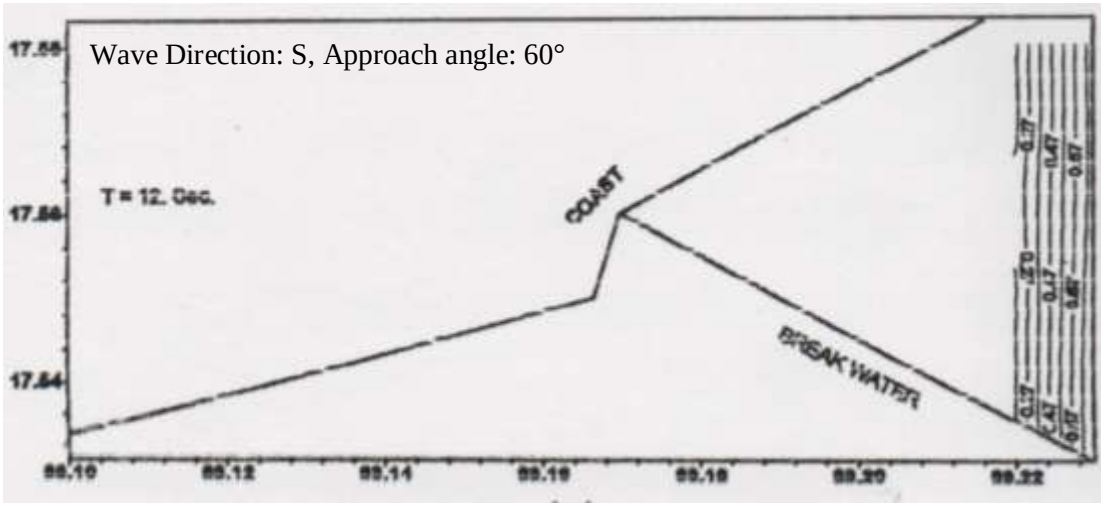



**Figure 6** Diffraction coefficients for Latitude (°N) Versus Longitude (°E)

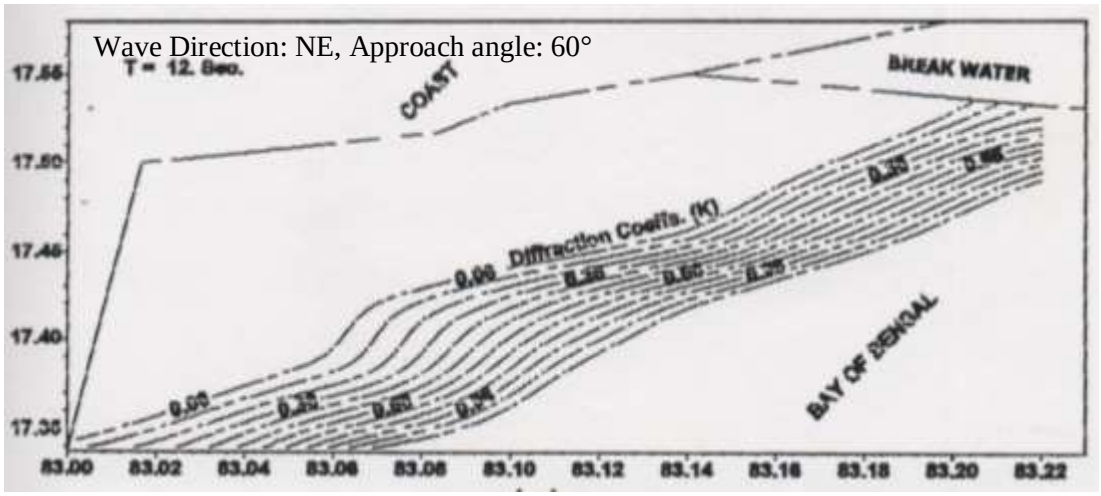



**Figure 7** Diffraction coefficients for Latitude (°N) Versus Longitude (°E)

### 2.4.4 *Functional Design of Breakwater Layout*

The purpose of selecting a particular layout of breakwater is to obtain the relatively calm area in the leeward side i.e. low values of diffraction coefficient. In general diffraction coefficients reduce in shoreward direction. A diffraction coefficient of 0.5 may be preferred at berthing. It has to be decided whether the depth available along the isoline of 0.5 diffraction coefficient is sufficient for allowing vessels of various sizes. In the present study an analysis has been made to evaluate the depth corresponding to the value of K equal to 0.5 for different wave directions. From this table it is observed that about 20m to 22m is available where the diffraction coefficient is equal to 0.5. For all points shoreward of this isoline the diffraction coefficient will be less than 0.5 and hence the zone is a suitable area for berthing. However a decision cannot be obtained as regards to the functional satisfaction of breakwater alignment unless the available depth is compared with the required draft of vessels for vessels of different categories.

**Table 4** Water depth available at 0.5 diffraction coefficient at breakwater tip

| Wave direction | Water depth available(m) |
|---|---|
| South | 20 |
| Southwest | 22 |

Using this criterion the maximum required for berthing the vessels of various categories has been observed to be varying 10m and 12m (Alonzo Def. Quinn 1961). The diffraction coefficient is around 0.3 which shows that the area is calm zone. From table 4 and maximum draft required, it is observed that the water depth available is greater than maximum draft required for all categories of vessels. Thus the suggested layout is functionally satisfactory. The above statement is however subjected to certain limitations that are listed below.

1. The bathymetric data is correct and not varying. The bathymetry in any region will be varying slightly from season to season due to littoral changes. Thus for a precise design of the layout the model has to be run, for different possible bathymetric configurations, which can be taken up for further study.
2. The alignment suggested pertains to predominant wave directions of wave propagation viz. South-Southwest. A detailed study has to be carried out by fixing the alignment and obtaining the wave diffraction pattern for the angle of wave propagation relative to break water subject to in-situ bathymetry site data in closed form, which is not possible from hydrographic charts, for other wave directions also.

## 3. Conclusions

An algorithm for the determination of diffraction coefficient at various grid points in the leeward side of breakwater has been obtained in the present study using Huygens principle. A diffraction model has been developed to arrive at diffraction coefficient for various environmental settings at a site.
(1) For all wave directions at selected location the minimum value of diffraction coefficient encountered during smallest wave period i.e. 6sec and maximum value during highest wave period i.e. 12sec. (2) The simulated diffraction coefficients obtained through model developed through approach angle 60° with respect to breakwater have been found to be varying between 0.05 and 0.67 covering 20 sq. km area which is indicative of relative calm and stable area and also independent of all seasons.
(3) Values of diffraction coefficient 'K' for South and Southwest direction, which are predominant wave directions varied with a minimum of 0.06 and 1.17.

## References

1. Alonzo Def. Quinn, 1961, Design and Construction of Ports and Maritime structures, Mc Graw Hill Company, pp. 610
2. Arthur T. Ippen, 1965, "Estuary and Coast line Hydrodynamics" Mc Graw Hill Company, INC, pp.744.
3. Bascom. W, 1964, "Waves and Beaches: The dynamics of the ocean surface", Garden city, New York, Doubleday and Co., Inc., 1964.
4. Chandra Mohan and T. V. Narasimha Rao, "Study of Long shore Current equations for Currents in Visakhapatnam Beach", Indian Journal of Marine Sciences, March 1984, Vol.13, pp. 27.
5. Eugene Hect, Alfred Zagac, "Optics", Edison-Wesley, Publishing Company, pp. 366.
6. Jerome Williams, "Introduction to Marine Pollution control", John Wiley and Sons, pp. 173.
7. Johnson J. W. 1935, "Engineering Aspects of Diffraction and wave Refraction", Pro. ASCE, pp. 118.
8. Komar. P., 1976, "Beach Processes and Sedimentation", Emgle Woodcliffs, NJ, Prentice Hall, Inc., 1976.
9. N. P. Fofonoff, C. Froese: P. O. G "Manuscipt Report Series No 72", pp. 26.
10. P. Chandra Mohan, 1981, T. V. Narasimha Rao, D. Panakala Rao & B. Prabhakara Rao, "Study of beach changes at Visakhapatnam", Mahasagar Bulletin of NIO, 14(2) pp. 115.
11. Penny W. G. and A. T. Price, "Diffraction of sea waves, by Breakwaters", Directorate of Miscellaneous Weapons development, Technical History No. 26, Artificial Harbours, Sec. 3-4.
12. Putnam J. A. and Arthur R. S. 1948, "Diffraction of water waves by breakwaters", Trans. Amer. Geo Physics Union (AGU), 29(4), pt. 1.
13. Richard Silvester, Needlands W. A, "Developments in Geo-technical Engineering" 4A, Coastal Engineering, Vol.1, pp. 303.
14. Robert L. Wiegel, 1964, Oceanographical Engineering", Prentice Hall International series, in theoretical and applied fluid mechanics, pp. 532.
15. Somerfield, 1896, "Mathematische Theorie Difraktion", Math. Ann., 47:317.

*IN PROCEEDINGS OF 25th HYDRO 2020, INTERNATIONAL CONFERENCE, NATIONAL INSTITUTE OF TECHNOLOGY ROURKELA, ODISHA, INDIA 26-28, March 2021, ISBN 978-93-90631-56-8*

Paper ID - 83

# INNOVATIVE SOFT OPTION OF COASTAL PROTECTION BY FLOATING SEAWEED FARM - A REVIEW

Surakshitha[1], Manu[2], Subba Rao[2]

[1] *Research scholar, Department of Water Resources and Ocean Engineering, National Institute of Technology Karnataka, Surathkal 575025, India*

[2]*Associate Professor, Department **of** Water Resources and Ocean Engineering, National Institute of Technology Karnataka, Surathkal 575025, India, Email: manunitk77@gmail.com*

[2]*Professor, Department **of** Water Resources and Ocean Engineering, National Institute of Technology Karnataka, Surathkal 575025, India, Email: surakrec@gmail.com*

*Email**:**Surakshithaks14@gmail.com*
*Telephone/Mobile No.: +91 9686421564*

## Abstract

Increased human activity along the coastal zone increased the vulnerability and altered the equilibrium of the coast for many years; it also accelerated the innovation in breakwater design for improvised efficiency and less destructive to the environment. Hard solutions to coastal protection are heavy structures, deployed where sensitive areas are to be protected against strong waves. A soft solution includes converting natural features as a buffer zone. It can be used in a mild wave environment or in the area requiring partial tranquility conditions. Once people started realizing the mangrove forest acted as a protective barrier against the destructive 2004 Indian Ocean tsunami and saved several villages, there was more curiosity started to build-up towards natural barriers such as mangrove forest, coral reef, seagrass meadow for coastal protection. Seaweeds are naturally occurring macroalgae living in the surf zone and they are farmed on a large scale throughout the world adopting the off-bottom method, unlike other natural barriers that are bottom fixed. Evaluating their effect on hydrodynamics is essential to understand the consequences of the farm in the coastal protection. In this paper research related to seaweed, their farming and their applicability for coastal erosion mitigation is reviewed. The current status of seaweed farming in India is also addressed.

***Keywords:*** *Coastal protection, coastal vegetation; kelp farm; seaweed farming.*

## 1. INTRODUCTION

The main aim of any coastal defense structure is to offer some resistance to the adverse impact of sea waves, reduce the turbulence, and create the tranquility condition. The hard solution of coastal protection such as breakwater and seawall effectively dissipate the wave energy but their performance needs to be maintained in future to address the current scenario of constant sea-level rise. Whereas the Nature-based infrastructure(Zhu et al. 2020) such as coastal vegetation, coral and oyster reefs, and mangroves which has the potential to dissipate waves, tends to accumulate sediment and grow along, thereby it increases its wave damping ability with rising seawater level.

Seaweeds are macroalgae living in shallow or deep seawater. Unlike land plants, these plants don't have roots but they use holdfast to attach themselves to hard substance(Hoq et al. 2016). Some of the species freely float in the water. They are usually found in the subtidal zone, the region having rocky morphology and experiencing high wave activity(Mach et al. 2007; Mach, 2009). Laminariales are species of large brown algae (Fig.1 (b)) that grow as a forest in cooler region with an individual plant growing up to 45 m long. (Rosman et al. 2007)

Seaweeds are cultivated to extract raw material for medicinal, cosmetic, and food processing applications. It is a rich source of iodine and essential minerals(Kandale et al. 2011). Some species of seaweeds are used directly as food. Because of Excellent water retention capacity, their extraction has been used in viscous component/thickening agent like jelly, agar production. Biodegradable plastics are also can be developed from seaweed (Siah et al. 2015).They have a wide range of applications in the medicinal industry, starting from the preparation of capsule cover to the treatment of

cancer(Laminaria sp., Sargassum, Bryopsis) and extraction of antiviral substances (Kandale et al. 2011). They are called as 'Medical Food of the 21st century (Mohammed, 2015). Now seaweeds are being farmed in 42 countries around the world, China is the highest producer of world seaweed supply.

### 1.1 *Floating Seaweed Farming*

Floating Seaweed farming is less destructive compare to other forms of aquaculture. Because of the floating nature, it neither disturb the seabed nor does it contaminate the water as it requires no fertilizers, making it nearly harmless for the existing aquatic life. Large-scale farming is being practiced in many parts of the world. The coastal belt of Tanzania growing Red species of seaweed Euchema denticulatum and kappaphycus alvarezii in more than 65 hectares.(Hedberg et al. 2018)

#### 1.1.1 *Techniques Adopted To Farming*

In Laminaria farming liquid containing gametophytes are spayed to the strings (Rolin et al. 2014) or algae sheet( 2 x 10 m) and young plants are made to grow with temperature and nutrient controlled environment in the lab. Then the ropes or algae sheet is transferred to the sea and deployed in various configurations as shown in Fig.1 (a).

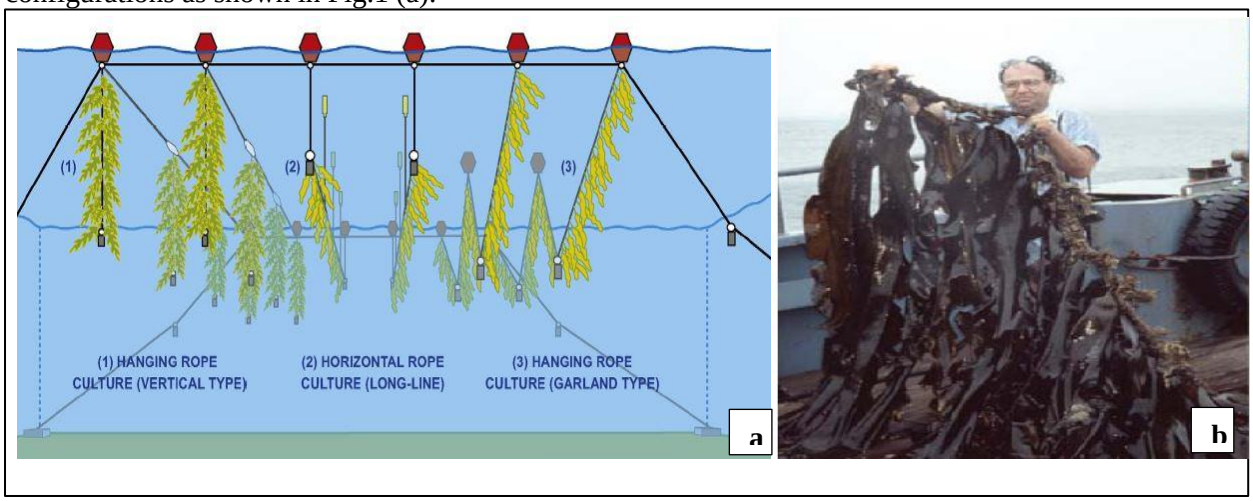



Fig. 1 (a) various methods of kelp farming. source: (Peteiro et al. 2016)
(b) Fully grown Laminaria in long line method.

Source: http://site.iugaza.edu.ps/elnabris/files/2010/02/6_Algae_3__Culturing.pdf

Kappaphycus alvarezii (Selvavinayagam & Dharmar, 2017), Gracilaria edulis, Gracilaria dura, Gracilaria verrucosa and Gelidiella acerosa (Mantri et al. 2017; Ganesan et al. 2017) are some of the species that are being cultivated in the Indian coast.

The floating bamboo raft method (FBR) is one of the methods used for seaweed cultivation in India Fig. 2 (a), where a Raft of 3 m x 3 m size is prepared; the corner of the raft is firmly supported by diagonal bamboos. About 20 Rope with the seedling is tied and placed in the location by using anchors and float. In the Floating Long line method Fig. 2 (b) polypropylene ropes tied horizontally between two sticks which are vertically inserted to the sea bed and the seedling segment is then tied around the rope. (Athithan, 2014; Mohammed, 2015). In net pouch method net bags filled with seedling are hung at regular intervals along the horizontally positioned polypropylene rope. When the seaweeds are fully grown they are taken out from the bags (Veeragurunathan et al. 2018).

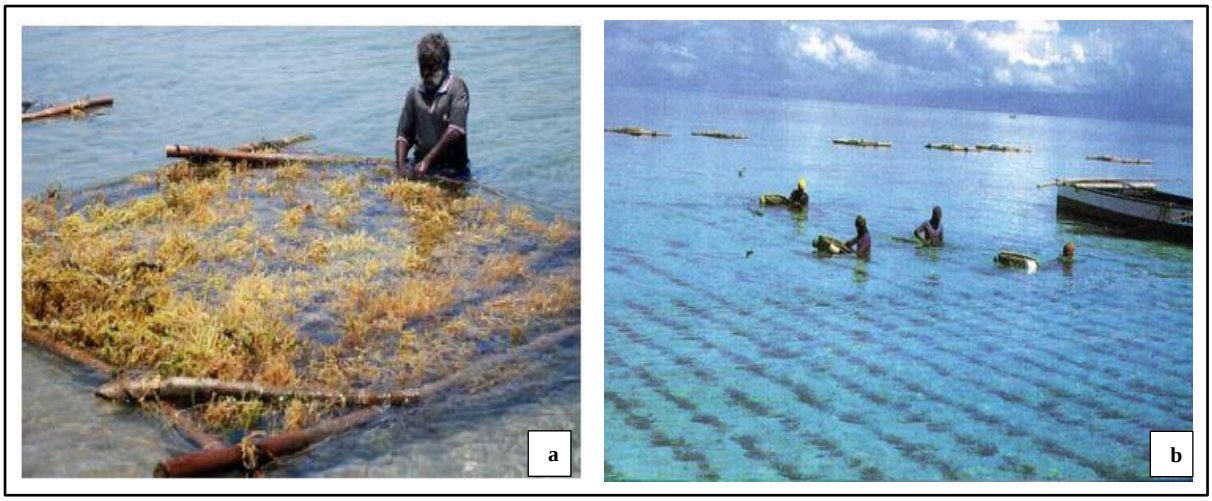



Fig. 2 (a) floating bamboo raft method source:(Johnson et al. 2017) (b) long line method

## 2. FIELD INVESTIGATION

Floating seaweed farming is sustainable farming adopted in many countries throughout the world. Kelp Laminaria japonica Aresch is cultivated in Heini Bay of china since 1980. They are growing on several ropes of 100 m length that suspended at 0.5 m below the sea surface. The site had a water depth of 5 m to 20 m with a maximum wave height ranging from 4-7 m. Field measurements such as flow velocity and direction, temperature, salinity are collected for about 6 months in and around the cultural area which includes both culture and non-culture period. The average flow velocity was found to be reduced for about 49.5% in the presence of a kelp farm. A significant change in seabed siltation was also observed around the site.(Z. Zhang et al. 2016)

It is also noted that the Southwestern part of Norway was experiencing increased wave activity and sand dune erosion along the coast after harvesting the seaweed kelp Laminaria hyperborean which is commercially growing for a decade. Løvås & Tørum, (2001) carried out an experiment to investigate the role of kelp farming along the Norwegian coast in terms of sand dune erosion and wave damping. Experiments were conducted in the wave flume with 5000 artificial kelp plants made from plastic liquid. They were cast in such a way that it represents the shape and stiffness of the real kelp. The sand dune with beach having a proper slope dimensions which are the same as that of scale downed prototype were also constructed in the flume. They found that the presence of the kelp field fastens the equilibrium of sand dune, therefore, end the erosion, however high water level causes significant damage even in the presence of the kelp.

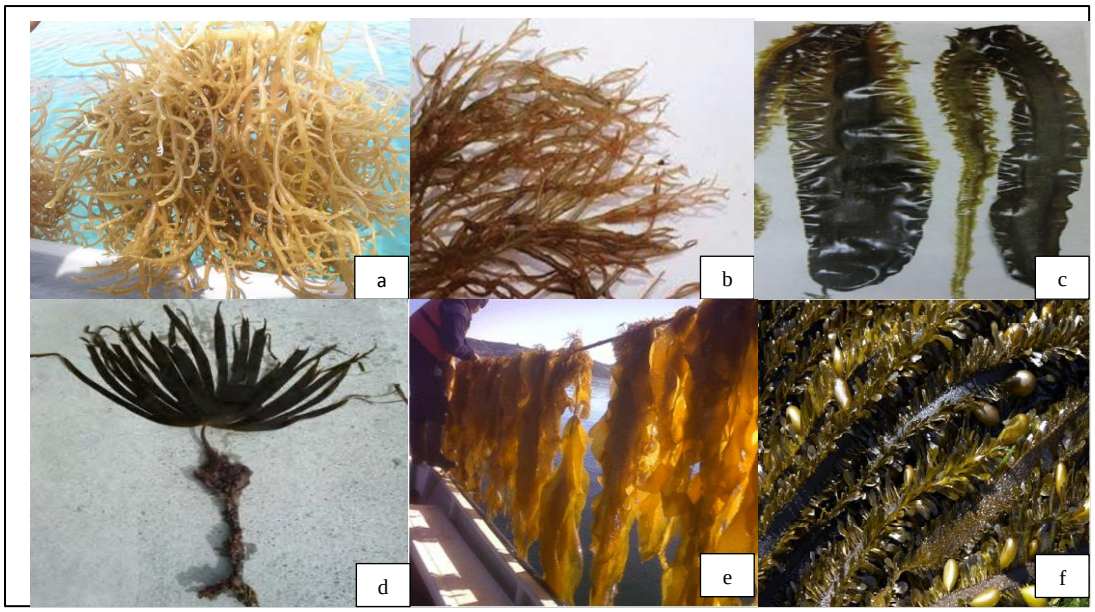



Fig. 3 (a) Kappaphycus Alvarezii (b) Gracilaria edulis (c) Laminaria japonica Aresch (d) Laminaria hyperborean ( e) Macrocystis pyrifera (f) egregia menziesii

Wild kelp forest of Macrocystis pyrifera in Santa Cruz, California is studied for their interaction with surrounding hydrodynamic process. Acoustic Doppler Current Profilers is fixed to the bottom of the seabed in and around the forest to obtain velocity profile. Analysis of data obtained from Field measurement show reduced current speed within the kelp forest (Figure 4), however they were varied with amount of kelp covering surface, kelp density per area (Rosman et al. 2007).

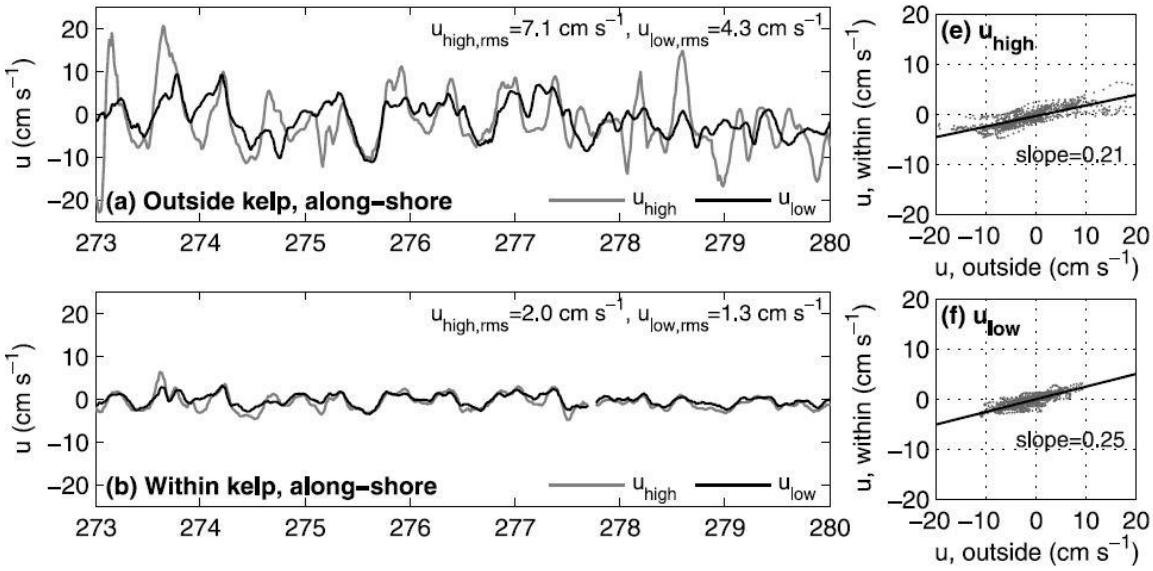



Fig. 4 comparison of velocity (a) outside of the kelp forest and (b) inside the forest, x axis represent days of 2003.

## 3. EFFECT ON COASTAL HAZARD MITIGATION

Bottom fixed Coastal vegetation was extensively used in the beach stabilization purpose in many areas(Anderson & Smith, 2014). Abundance research on rigid and flexible vegetation stem after 2004 Indian Ocean tsunami also supports the observation evidence of wave and flow damping property of mangroves. It was estimated to save 1800 km$^2$ of land from inundation in Gulf Coast of South Florida during hurricane induced storm surge.( Zhang et al. 2012; Gedan et al. 2011) Among bottom fixed

and suspended vegetation, the suspended vegetation was found to be more effective in attenuating the wave and can be used as a living breakwater to enhance coastal resilience (Zhu et al. 2020).
Also, the free-surface vegetated breakwaters which is Deployed in the Mississippi River Delta remain undamaged when it is attacked by 90-MPH category-1 hurricane (Wang et al. 2019). This breakwater visually somewhat resembles the floating vegetation farm; with plate breakwater having vegetation stems covers the water surface and roots floats below the water surface as shown in Figure 5(a). This event shows that there exists a possibility of floating seawater farms in coastal hazard mitigation work.

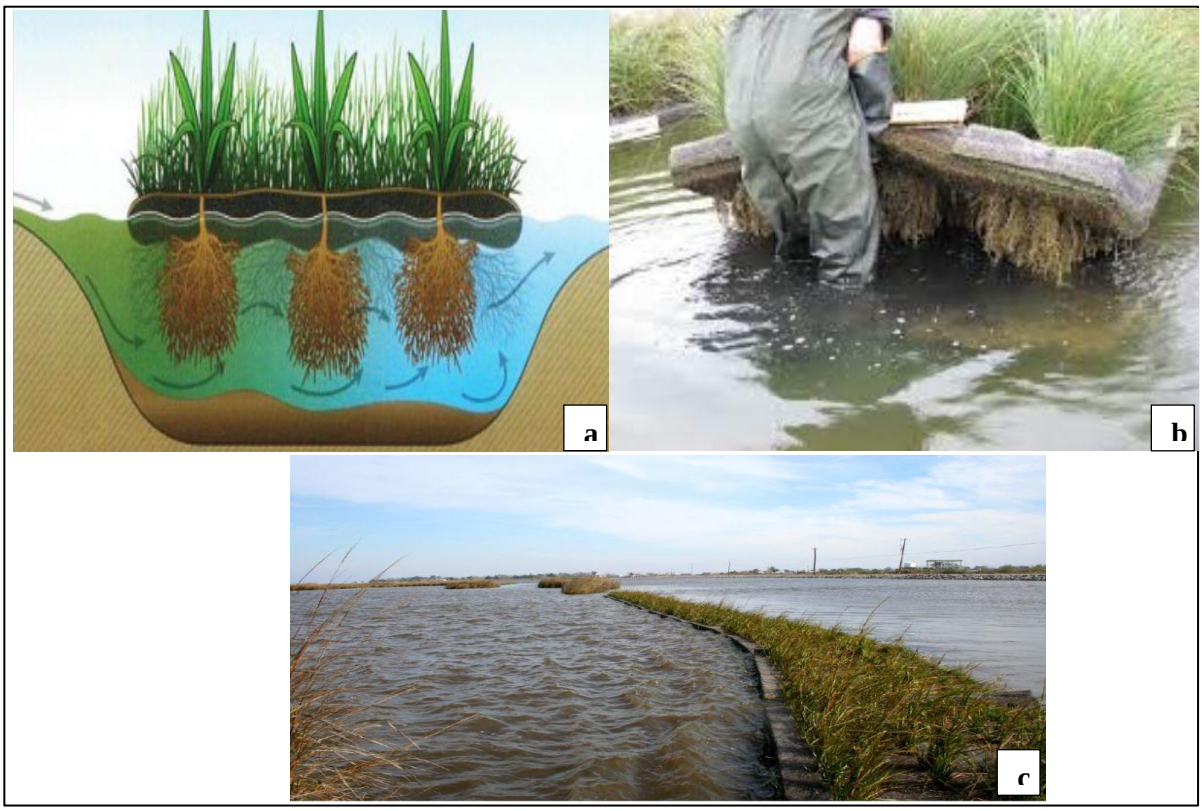



Fig. 5: (a) BIOHAVEN® Floating Breakwater showing vegetation growing in platform made from recycled plastic, injected foams and growing media. (b) Installation procedure (c) after installation. Source: http://martinecosystems.com/wp-content/uploads/2017/07/BioHaven-Floating-Technology-White-Paper-.pdf

Few studies have been recorded on the effect of off bottom vegetation on flow structure. The flume experiment of the suspended canopy is conducted by (Plew, 2011). They used a group of the rigid aluminum cylinder of 9.54 mm dia. This is vertically positioned below the free surface. The velocity profile with respect to depth shows reduced velocity inside the suspended canopy and it started to increase below the canopy layer, reached a maximum at some point between the bottom of the canopy and bed. Thus turbulence is reduced in the water surface. Suspended canopy has a free water surface at top of the canopy and free flow below the canopy hence both the bottom friction and vegetation affect the velocity profile. Once the space between the bottom of the canopy and bed is reduced, the velocity started to increase inside the canopy layer. Along with suspended seaweed farming shellfish culture is also practiced in some of the countries (Fernández et al. 2019). Shellfish suspended farming alone has a significant effect on flow structure (Newell & Richardson, 2014). Numerical investigation of such an integrated farm in Sungo Bay from china revealed a 54% reduction of current speed.(Grant & Bacher, 2001)

## 4. EXPERIMENTAL INVESTIGATION

Seaweed undergoes Reconfiguration in a harsh wave environment to prevent damage. It is the process in which utilizing its flexibility it bends in the direction of flow. Basically changing its shape, size, and orientation, because of which it experiences the least hydrodynamic force and reduces the risk of damage (Miler et al. 2010; Vettori & Nikora 2019; Koehl et al. 2008).

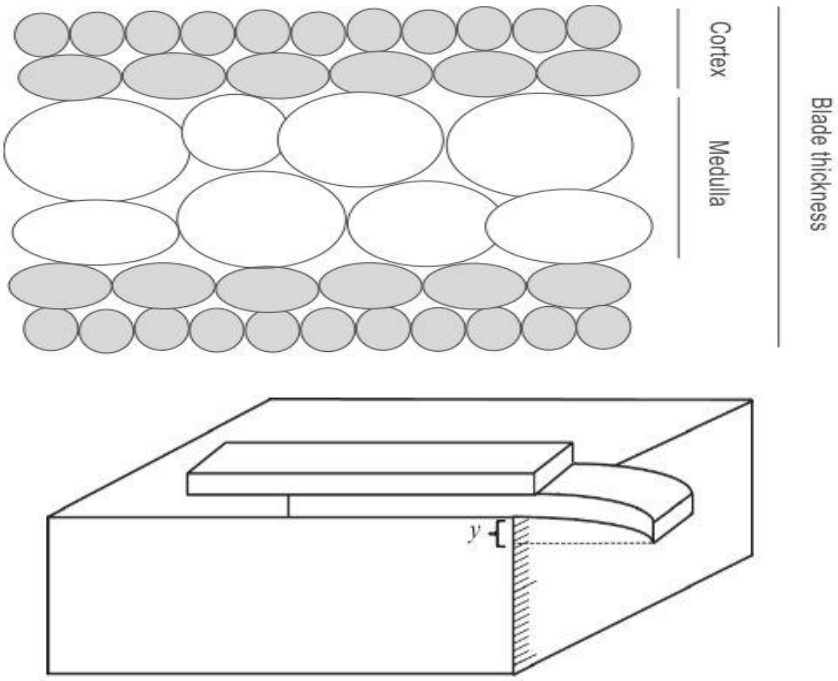



Fig. 6 (a) cross section of the seaweed showing blade thickness. (b) Beam theory deflection method to evaluate flexural rigidity, experiment conducted by standard size cut specimens from the different species.

Demes et al. (2011) conducted an experiment to determine the flexural rigidity of 16 red species of microalgae. Their effect on drag force was determined by keeping constant size and shape. Flexural stiffness ranged from 6 ± 1 ($\mu Nm^2$) for Holmesia to 749 ± 329($\mu Nm^2$) for Neodilsea ($\mu Nm^2$). They found increased blade thickness decrease the reconfiguration but their ability to withstand the drag increased along with stiffness. However, Polyneura latissima displayed high EI than the expected for its thickness, the reason being the thick vein running through its blade. The material and mechanical properties of the seaweeds depend on the physical conditions of the growing habitat. Interestingly seasonal variation in the growth and properties was also observed when the seaweed Egregia menziesii was studied for 2 years. During the winter when the coast was observed to have more wave activity, the growth rate was very low and it remained small throughout the winter so that it experiences less hydrodynamic force thereby increasing the surviving rate. This means that the material properties of different species of seaweed are highly varied for the same location; however, having a wide range of size and shape helps them to survive the same wave force.

## 5. SUMMARY:

The numbers of breakwater seawall groins are increasing as coastal system becomes more vulnerable to hazards such as hurricane, storms, which reduce the interaction of coastal process with natural features and the landscape, consequently changing natural equilibrium. This is one of the reasons for the usage of Natural barrier in coastal protection gaining momentum.

Since the Suspended vegetation induce different flow pattern than the submerged vegetation and few investigations of field measurement also support the wave damping characteristics of large scale seaweed farming, strategically implementing the floating seaweed farm is expected to perform

effectively in achieving stabilizing shoreline. This paper highlights the studies of seaweed on flow structures. Numerous studies are available to determine the biomechanical properties of various seaweeds (Harder et al. 2006; Boller & Carrington, 2007) that can be used as a base to model the farm and to evaluate their interaction with different hydrodynamic conditions. Furthermore, floating vegetation has been used for coastal protection work in few places, where roots also helps to attenuate the flow but the floating seaweed farm has more dense and long formation below the water surface which will offer more resistance to the flow, thus exploring its possibilities in coastal resilience has great scope in the field of innovative design for less environmental impact.

## References

Anderson, M. E., & Smith, J. M. (2014). Wave attenuation by flexible, idealized salt marsh vegetation. *Coastal Engineering*, *83*, 82–92. https://doi.org/10.1016/j.coastaleng.2013.10.004

Athithan, S. (2014). Growth performance of a Seaweed, Kappaphycus alvarezii under lined earthen pond condition in Tharuvaikulam of Thoothukudi coast, South East of India. *Research Journal of Animal Res. J. Animal*, *2*(1), 6–10.

Boller, M. L., & Carrington, E. (2007). Interspecific comparison of hydrodynamic performance and structural properties among intertidal macroalgae. *Journal of Experimental Biology*, *210*(11), 1874–1884. https://doi.org/10.1242/jeb.02775

Demes, K. W., Carrington, E., Gosline, J., & Martone, P. T. (2011). Variation in anatomical and material properties explains differences in hydrodynamic performances of foliose red macroalgae (rhodophyta). *Journal of Phycology*, *47*(6), 1360–1367. https://doi.org/10.1111/j.1529-8817.2011.01066.x

Fernández, P. A., Leal, P. P., & Henríquez, L. A. (2019). Co-culture in marine farms: macroalgae can act as chemical refuge for shell-forming molluscs under an ocean acidification scenario. *Phycologia*, *58*(5), 542–551. https://doi.org/10.1080/00318884.2019.1628576

Ganesan, M., Eswaran, K., & Reddy, C. R. K. (2017). Farming of agarophytes in India—a long-time sustainability for the industry and preserving wild stocks. *Journal of Applied Phycology*, *29*(5), 2239–2248. https://doi.org/10.1007/s10811-017-1128-0

Gedan, K. B., Kirwan, M. L., Wolanski, E., Barbier, E. B., & Silliman, B. R. (2011). The present and future role of coastal wetland vegetation in protecting shorelines: Answering recent challenges to the paradigm. *Climatic Change*, *106*(1), 7–29. https://doi.org/10.1007/s10584-010-0003-7

Grant, J., & Bacher, C. (2001). A numerical model of flow modification induced by suspended aquaculture in a Chinese bay. *Canadian Journal of Fisheries and Aquatic Sciences*, *58*(5), 1003–1011. https://doi.org/10.1139/cjfas-58-5-1003

Harder Deane L. , Hurd Catriona L., & Speck Thomas (2006) Comparison Of Mechanical Properties Of Four Large, Wave-Exposed Seaweeds.

Hedberg, N., von Schreeb, K., Charisiadou, S., Jiddawi, N. S., Tedengren, M., & Nordlund, L. M. (2018). Habitat preference for seaweed farming – A case study from Zanzibar, Tanzania. *Ocean and Coastal Management*, *154*(April 2017), 186–195. https://doi.org/10.1016/j.ocecoaman.2018.01.016

Hoq, M., Haque, M., & Islam, M. (2016). Feasibility of seaweed culture in Inani and Bakkhali coast of Cox's Bazar, Bangladesh. *Pakistan Journal of Marine Sciences*, *25*(1&2), 27–36.

Johnson, B., Narayanakumar, R., Abdul Nazar, A. K., Kaladharan, P., & Gopakumar, G. (2017). Economic analysis of farming and wild collection of seaweeds in Ramanathapuram district, Tamil Nadu. *Indian Journal of Fisheries*, *64*(4), 94–99. https://doi.org/10.21077/ijf.2017.64.4.61828-13

Kandale, A., Meena, a K., Rao, M. M., Panda, P., Mangal, a K., Reddy, G., & Babu, R. (2011). Marine Algae: An Introduction, Food Value and Medicinal Uses. *Journal of Pharmacy Research*, *4*(1), 219–221.

Koehl, M. A. R., Silk, W. K., Liang, H., & Mahadevan, L. (2008). How kelp produce blade shapes suited to different flow regimes: A new wrinkle. *Integrative and Comparative Biology*, *48*(6), 834–851. https://doi.org/10.1093/icb/icn069

Løvås, S. M., & Tørum, A. (2001). Effect of the kelp Laminaria hyperborea upon sand dune erosion and water particle velocities. *Coastal Engineering*, *44*(1), 37–63. https://doi.org/10.1016/S0378-3839(01)00021-7

Mach, K. J. (2009). Mechanical and biological consequences of repetitive loading: Crack initiation and fatigue failure in the red macroalga Mazzaella. *Journal of Experimental Biology*, *212*(7), 961–976. https://doi.org/10.1242/jeb.026989

Mach, K. J., Nelson, D. V., & Denny, M. W. (2007). Techniques for predicting the lifetimes of wave-swept macroalgae: A primer on fracture mechanics and crack growth. *Journal of Experimental Biology*, *210*(13), 2213–2230. https://doi.org/10.1242/jeb.001560

Mantri, V. A., Eswaran, K., Shanmugam, M., Ganesan, M., Veeragurunathan, V., Thiruppathi, S., Reddy, C. R.

K., & Seth, A. (2017). An appraisal on commercial farming of Kappaphycus alvarezii in India: success in diversification of livelihood and prospects. *Journal of Applied Phycology*, *29*(1), 335–357. https://doi.org/10.1007/s10811-016-0948-7

Miler, O., Albayrak, I., Nikora, V., Crane, T., & O'Hare, M. (2010). Biomechanics of aquatic plants and its role in flow-vegetation interactions. *River Flow*, 245–251.

Mohammed, G. (2015). Current trends and Prospects of Seaweed Farming in India. *Winter School on Technological Advances in Mariculture for Production Enhancement and Sustainability Course Manual.*, 78–84.

Newell, C. R., & Richardson, J. (2014). The effects of ambient and aquaculture structure hydrodynamics on the food supply and demand of mussel rafts. *Journal of Shellfish Research*, *33*(1), 257–272. https://doi.org/10.2983/035.033.0125

Peteiro, C., Sánchez, N., & Martínez, B. (2016). Mariculture of the Asian kelp Undaria pinnatifida and the native kelp Saccharina latissima along the Atlantic coast of Southern Europe: An overview. *Algal Research*, *15*, 9–23. https://doi.org/10.1016/j.algal.2016.01.012

Plew, D. R. (2011). Depth-averaged drag coefficient for modeling flow through suspended canopies. *Journal of Hydraulic Engineering*, *137*(2), 234–247. https://doi.org/10.1061/(ASCE)HY.1943-7900.0000300

Rolin, C., Inkster, R., Laing, J., Hedges, J., & Mcevoy, L. (2014). Seaweed cultivation manual Shetland Seaweed Growers Project 2014-16. *Shetland Seaweed Growers Project 2014-16*, 39. https://www.nafc.uhi.ac.uk/t4-media/one-web/nafc/research/document/seaweed-cultivation/Seaweed-Cultivation-Manual.pdf

Rosman, J. H., Koseff, J. R., Monismith, S. G., & Grover, J. (2007). A field investigation into the effects of a kelp forest (Macrocystis pyrifera) on coastal hydrodynamics and transport. *Journal of Geophysical Research: Oceans*, *112*(2). https://doi.org/10.1029/2005JC003430

Seaweeds, W. (2020). *Comparison of Mechanical Properties of Four Large , Wave-Exposed Seaweeds Author ( s ): Deane L . Harder , Catriona L . Hurd and Thomas Speck Published by : Wiley Stable URL : https://www.jstor.org/stable/4123125 REFERENCES Linked references are available*. *93*(10), 1426–1432.

Selvavinayagam, K. T., & Dharmar, K. (2017). Selection of potential method for cultivation and seed stock maintenance of Kappaphycus alvarezii during the northeast monsoon in southeast coast of India. *Journal of Applied Phycology*, *29*(1), 359–370. https://doi.org/10.1007/s10811-016-0967-4

Siah, W. M., Aminah, A., & Ishak, A. (2015). Edible films from seaweed (Kappaphycus alvarezii). *International Food Research Journal*, *22*(6), 2230–2236.

Veeragurunathan, V., Vadodariya, N., Chaudhary, J. P., Gogda, A., Saminathan, K. R., & Meena, R. (2018). Experimental cultivation of Gelidium pusillum in open sea along the south east Indian coast. *Indian Journal of Geo-Marine Sciences*, *47*(2), 336–345.

Vettori, D., & Nikora, V. (2019). Flow-seaweed interactions of Saccharina latissima at a blade scale: turbulence, drag force, and blade dynamics. *Aquatic Sciences*, *81*(4), 1–16. https://doi.org/10.1007/s00027-019-0656-x

Wang, Y., Yin, Z., & Liu, Y. (2019). Numerical study of solitary wave interaction with a vegetated platform. *Ocean Engineering*, *192*(April), 106561. https://doi.org/10.1016/j.oceaneng.2019.106561

Zhang, K., Liu, H., Li, Y., Xu, H., Shen, J., Rhome, J., & Smith, T. J. (2012). The role of mangroves in attenuating storm surges. *Estuarine, Coastal and Shelf Science*, *102–103*, 11–23. https://doi.org/10.1016/j.ecss.2012.02.021

Zhang, Z., Huang, H., Liu, Y., Yan, L., & Bi, H. (2016). Effects of suspended culture of the seaweed Laminaria japonica aresch on the flow structure and sedimentation processes. *Journal of Ocean University of China*, *15*(4), 643–654. https://doi.org/10.1007/s11802-016-2994-9

Zhu, L., Huguenard, K., Zou, Q. P., Fredriksson, D. W., & Xie, D. (2020). Aquaculture farms as nature-based coastal protection: Random wave attenuation by suspended and submerged canopies. *Coastal Engineering*, *160*(June), 103737. https://doi.org/10.1016/j.coastaleng.2020.103737

*IN PROCEEDINGS OF 25th HYDRO 2020, INTERNATIONAL CONFERENCE, NATIONAL INSTITUTE OF TECHNOLOGY ROURKELA, ODISHA, INDIA 26-28, March 2021, ISBN 978-93-90631-56-8*

Paper ID - 112

# Study of sediment behaviour along the Mangalore coast through granulometric studies

Aseem V[1], Dwarakish G S[2]

[1]*Master of Technology, Department of Water Resources and Ocean Engineering, National Institute of Technology Karnataka, Surathkal, 575025, Mangalore, Karnataka, India*
[2]*Professor, Department of Water Resources and Ocean Engineering, National Institute of Technology Karnataka, Surathkal, 575025, Mangalore, Karnataka, India*
*Email: aseemvillan@gmail.com*

## Abstract

Studying sediment behavior and identifying sediment transport pattern is essential in coastal engineering and management projects. In the present study, grain size characteristics of the foreshore beach sand along the Mangalore Coast, West Coast of India, were examined to study the sediment behaviour along the coast. Mode of sediment transportation and deposition of sediments can be inferred from the grain size analysis. Sediment movement trends can be identified from grain size statistical parameters using the technique Sediment Trend Analysis (STA). In STA, the spatial variation of grain size parameters (mean grain size, sorting and skewness) occurring during the sediment transport process from sedimentary source to deposit is analyzed to define the sediment transport path. The grain size statistical parameters show that the foreshore beaches are significantly composed of fine sand (31%) and medium sand (52%). The grains are slightly coarser (0.719 ϕ) on the southern side of the study area and finer (2.185 ϕ) towards the northern side. Sediments are very well sorted (0.312 ϕ) to moderately sorted (0.991 ϕ) along the beach dominated by moderately well sorted (66%) samples. Sand samples were identified as positive (48%) to negative (52%) skewed with platykurtic, mesokurtic and leptokurtic characters. The average skewness of the beach is obtained as symmetrical, indicative of an environment having balanced erosion and deposition. The sediment transport along the coast was studied for the months receiving minimum rainfall, December 2019 and January 2020. Study shows that the net littoral drift along the coast during this period is very less as sediment trends are obtained in both directions.

***Keywords:*** *Sediment transport; Sediment Trend Analysis; Grain size statistical parameters; Littoral drift.*

## 1. Introduction

The coast is one of the most dynamic natural features in the environment. The coast is altered by the action of wind and waves along with the sediments. A considerable amount of sediments is discharged from rivers also. So it is essential to study the sediment behavior and granulometric properties along the coast for any coastal engineering projects. In the present study, the foreshore beach sand's grain size characteristics along the Mangalore Coast, West Coast of India, were examined to study the sediment behavior along the coast. The coastal stretch having two river mouths (Netravati – Gurpur river mouth and Mulki – Pavanje river mouth) and New Mangalore Port is taken as the study area. Sediment movement patterns and hydrodynamic mechanisms can be inferred from the grain size analysis of the sediments. Granulometric properties such as mean grain size, sorting and skewness are used to study sediment behavior. The sediment movement patterns can be identified by analysing the spatial variation in grain size parameters using Sediment Trend Analysis (STA). McLaren (1981) introduced this STA modelling technique initially based on the assumption that the sediment transport mechanism affects the sediment properties at deposits. This paper presents the results of granulometric studies and sediment movement patterns inferred from STA using the McLaren and Bowles (1985) method along the Mangalore Coast.

## 2. Study area

For studying the sediment behavior along the Mangalore Coast, a stretch of coast starting from Ullal Beach (12º 49′ N, 74º 50′ E) in the south and Sasihithlu Beach (13º 04′ N, 74º 46′ E) in the north along the west coast of India is selected as the study area (Figure 1). It is located in Dakshina Kannada District in Karnataka, along the West Coast of India. The coastline selected for the study area has a length of 29 km. The study area consists of Nethravathi – Gurpur river mouth, North and South breakwater, harbor and approach channel of New Mangalore Port and Sasihithlu Estuary (also known as Mulki – Pavanje Rivermouth).

The climate at the Mangalore region is mainly governed by the monsoons. The average annual rainfall is approximately 3,467 mm. The area receives heavy rainfall when the south-west monsoon occurs (June – September). The study area experiences moderate temperatures throughout the year and varies from 22° C to 36° C. The predominant direction of waves at open sea in the vicinity of Mangalore Port during the monsoon months of June, July, and August is west and south-west. Tides in the region are characterized by a mixed type, predominantly semi-diurnal. The average tidal range at Mangalore is 1.50 m during spring tide and 0.30 m during neap tide (Khare et al. 2019).

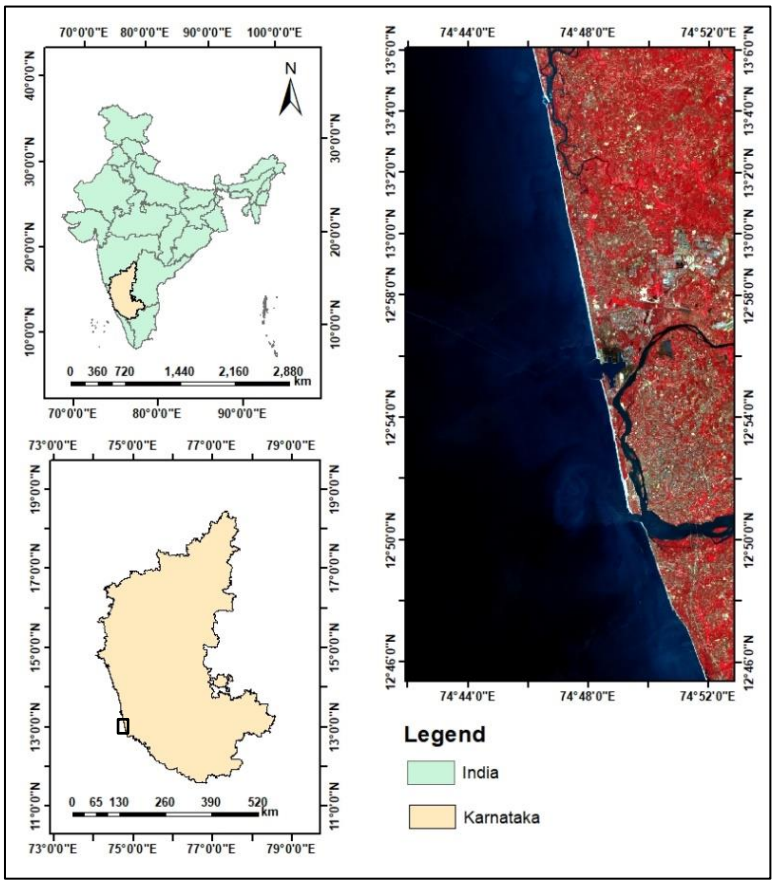



**Figure 1** Study Area

## 3. Materials and methodology

### *3.1 Sediment sampling and analysis*

The beach face sediment samples were collected at 29 different locations at a spacing of nearly 1.0 km. Around 1 kg of the sample was collected at each location by hand grab method at a depth of 4 to 10 cm (Figure 2). Samples were collected on the foreshore zone because this zone is continuously

worked by water forces and thus more affected by the environmental conditions. Sediment sampling was done twice during December 2019 and January 2020 at the same locations with the help of Trimble Handheld GPS. The study area has been divided into four segments for the analysis of sediment movement on each stretch.

After washing and oven drying the collected samples, 200 grams of each sample were taken to perform grain size analysis. Dry sieve analysis using conventional sieves (spaced at half ϕ-interval) has been performed according to IS: 2720 (Part 4) – 1985. Statistical parameters such as mean, sorting and skewness of all the sediment samples were calculated using GRADISTAT (Blott and Pye, 2001).

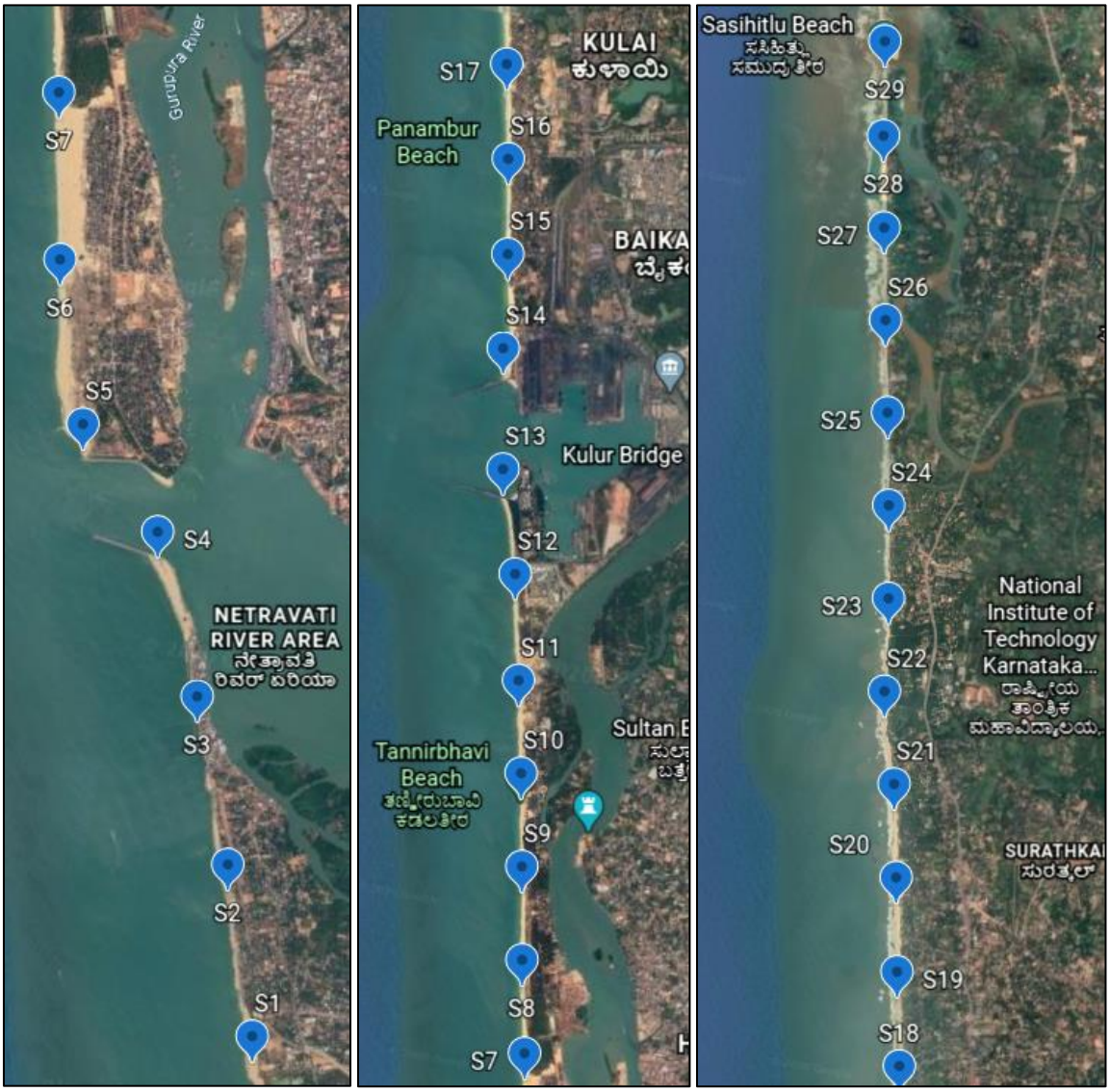



**Figure 2** Sampling Locations

### *3.2 Sediment Trend Analysis (STA)*

In STA, sediment transport paths are identified by comparing the grain size statistical parameters (mean grain size, sorting and skewness) of all sampling stations along the sampling line. In the present study, STA proposed by McLaren and Bowles (1985) has been used.

According to McLaren and Bowles (1985), grain-size distributions will change in response to erosion, transport, and deposition in such a way that a lag will be coarser and more positively skewed than its

source (Case A). In contrast, sequential deposits will become either, finer (F) and more negatively (-) skewed (Case B) or coarser (C) and more positively (+) skewed (Case C). Sediment becomes better (B) sorted in all mentioned cases after deposition. It is noted that Case A and Case C produce similar trends and that Case A by itself does not provide a transport direction. Here, sediment transport patterns are categorized into either Case B (FB-) or Case C (CB+) after comparing the statistical parameters.

Spreadsheets were developed using Excel VBA for the preparation of Sediment Trend Matrix (STM) using grain size parameters (Mean, Sorting and Skewness). Sediment Trend Paths (STP) is drawn from STM in AutoCAD using the developed algorithm. A typical STM is shown in Figure 3.

| | | SEDIMENT SOURCE | | | | | | | | | |
|---|---|---|---|---|---|---|---|---|---|---|---|
| | | S5 | S6 | S7 | S8 | S9 | S10 | S11 | S12 | S13 | |
| SEDIMENT DEPOSIT | S5 | | F | C | F | C | C | C | C | C | Mean |
| | | | P | B | B | B | B | B | B | P | Sorting |
| | | | + | - | + | + | + | + | + | + | Skewness |
| | S6 | C | | C | C | C | C | C | C | C | Mean |
| | | B | | B | B | B | B | B | B | B | Sorting |
| | | - | | - | - | + | - | + | + | + | Skewness |
| | S7 | F | F | | F | C | F | C | C | C | Mean |
| | | P | P | | B | B | B | B | B | P | Sorting |
| | | + | + | | + | + | + | + | + | + | Skewness |
| | S8 | C | F | C | | C | C | C | C | C | Mean |
| | | P | P | P | | B | B | P | P | P | Sorting |
| | | - | + | - | | + | + | + | + | + | Skewness |
| | S9 | F | F | F | F | | F | C | C | C | Mean |
| | | P | P | P | P | | P | P | P | P | Sorting |
| | | - | - | - | - | | - | + | + | - | Skewness |
| | S10 | F | F | C | F | C | | C | C | C | Mean |
| | | P | P | P | P | B | | P | P | P | Sorting |
| | | - | + | - | - | + | | + | + | + | Skewness |
| | S11 | F | F | F | F | F | F | | F | C | Mean |
| | | P | P | P | B | B | B | | P | P | Sorting |
| | | - | - | - | - | - | - | | - | - | Skewness |
| | S12 | F | F | F | F | F | F | C | | C | Mean |
| | | P | P | P | B | B | B | B | | P | Sorting |
| | | - | - | - | - | - | - | + | | - | Skewness |
| | S13 | F | F | F | F | F | F | F | F | | Mean |
| | | B | P | B | B | B | B | B | B | | Sorting |
| | | - | - | - | - | + | - | + | + | | Skewness |

**Figure 3** STM – December 2019

## 4. Results and discussion

### *4.1 Granulometric studies*

Grain size statistical parameters of all the samples were calculated using GRADISTAT. Statistical parameters such as mean grain size (ϕ), sorting (ϕ) and skewness (ϕ) of all the samples for December 2019 are given in Table 1. Grain size statistical parameters show that the beaches are significantly

composed of medium sand and fine sand. Sediments are very well sorted to poorly sorted along the beach dominated by moderately well sorted samples. Sand samples were identified as positively to negatively skewed.

During the period of December 2019, sand samples are coarser on the southern side and finer towards the northern side of the study area (Figure 4 and Table 1). This may be due to winnowing off of finer materials by waves and current at the beach face. The present study showed that 52% of the samples are medium sand, and 31% were fine sand, 17% of total samples were found as coarse sand. Sediment samples were very well sorted (0.312 ϕ) to moderately sorted (0.991 ϕ) along the beach dominated by moderately well sorted (66%) samples. Sorting indicates the fluctuations in the depositing agent's kinetic energy or velocity conditions (Sahu 1964). The sediments are moderately well sorted in most of the stretches, which could be attributed to moderate wave energy activities on the beach (Bramha et al. 2017).

Skewness value indicated that 52% and 48% of the samples were negatively skewed and positively skewed. Positive skewness characterizes a beach with deposition of sand, whereas negative skewness indicates erosion or non-deposition (Duane 1964). On the South of Netravati – Gurupur Rivermouth, all the samples are negatively skewed, which could be due to the sediments' winnowing off (erosion). Average skewness on the coastal stretches along South and North of NMPT Breakwaters is -0.016 and 0.008, which suggests the sediments are generally symmetrically skewed, indicating an environment where the effect of erosion and deposition are almost balanced.

**Table 1** Grain Size Statistical Parameters of the Samples – December 2019

| Station | Mean (ϕ) | Sorting (ϕ) | Skewness (ϕ) | |
|---|---|---|---|---|
| S1 | 0.719 | 0.734 | -0.359 | |
| S2 | 0.857 | 0.409 | -0.253 | South of Netravati – Gurupur Rivermouth |
| S3 | 0.842 | 0.574 | -0.263 | |
| S4 | 0.694 | 0.991 | -0.049 | |
| S5 | 1.450 | 0.583 | 0.323 | |
| S6 | 0.993 | 0.312 | -0.011 | |
| S7 | 1.816 | 0.665 | 0.325 | |
| S8 | 1.428 | 0.709 | 0.196 | South of NMPT Breakwater |
| S9 | 1.830 | 0.930 | -0.214 | |
| S10 | 1.806 | 0.824 | 0.081 | |
| S11 | 2.319 | 0.699 | -0.354 | |
| S12 | 2.198 | 0.698 | -0.342 | |
| S13 | 2.883 | 0.361 | -0.146 | |
| S14 | 2.400 | 0.617 | -0.327 | |
| S15 | 1.817 | 0.704 | 0.287 | |
| S16 | 2.248 | 0.655 | -0.310 | |
| S17 | 1.865 | 0.669 | 0.351 | |
| S18 | 2.153 | 0.668 | -0.280 | North of NMPT Breakwater |
| S19 | 2.174 | 0.674 | -0.230 | |
| S20 | 2.421 | 0.653 | -0.366 | |
| S21 | 1.853 | 0.655 | 0.284 | |
| S22 | 1.636 | 0.650 | 0.321 | |
| S23 | 1.631 | 0.548 | 0.353 | |
| S24 | 1.784 | 0.501 | 0.532 | |
| S25 | 1.719 | 0.659 | 0.269 | |
| S26 | 1.852 | 0.686 | 0.234 | South of Mulki – Pavanje Rivermouth |
| S27 | 1.767 | 0.616 | 0.315 | |
| S28 | 2.185 | 0.643 | -0.390 | |
| S29 | 1.748 | 0.702 | 0.231 | |

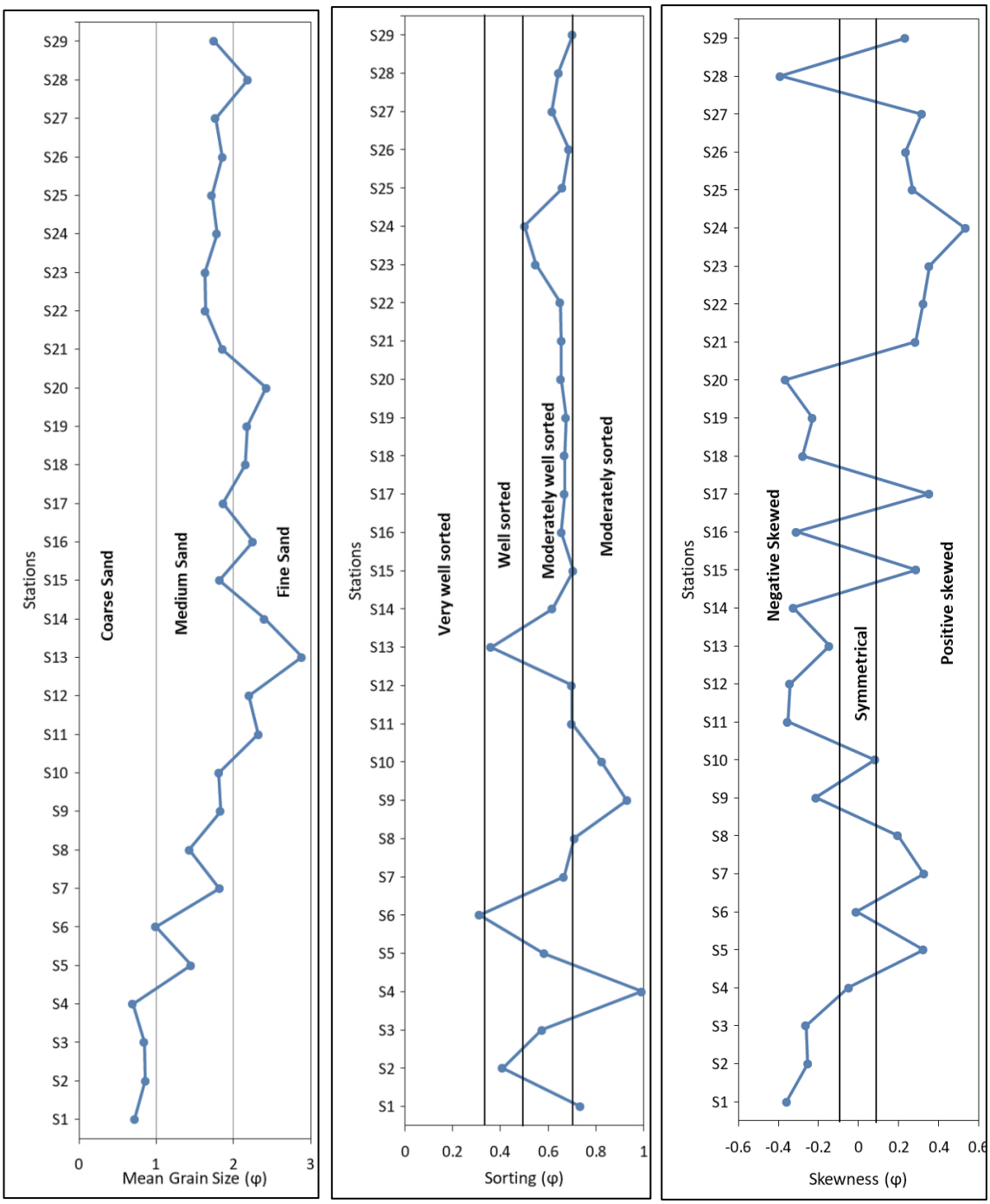



**Figure 4** Variation of Grain Size Statistical Parameters (a) Mean Grain Size (b) Sorting and (d) Skewness – December 2019

Sedimentologists use bivariate plots to discriminate the sedimentary environment and processes. Some of such plots are used in this study. The relationship between mean grain size and sorting are given in Figure 5 (left). It indicated that most of the samples with medium sand and fine sand are moderately well sorted. But the coarse sand sample in the present study showed some covariance between mean grain size and sorting with an obvious general trend of increasing sorting values with an increase in mean grain size. The bivariate plot of mean grain size and skewness are shown in Figure 5 (right). It indicates that most of the fine and coarse sand samples are coarse skewed. But in both cases, medium sand samples are dominated by fine skewed. The sediments of negative skewness ensure in a high energy environment and the positive skewness occurs under the low energy environments.

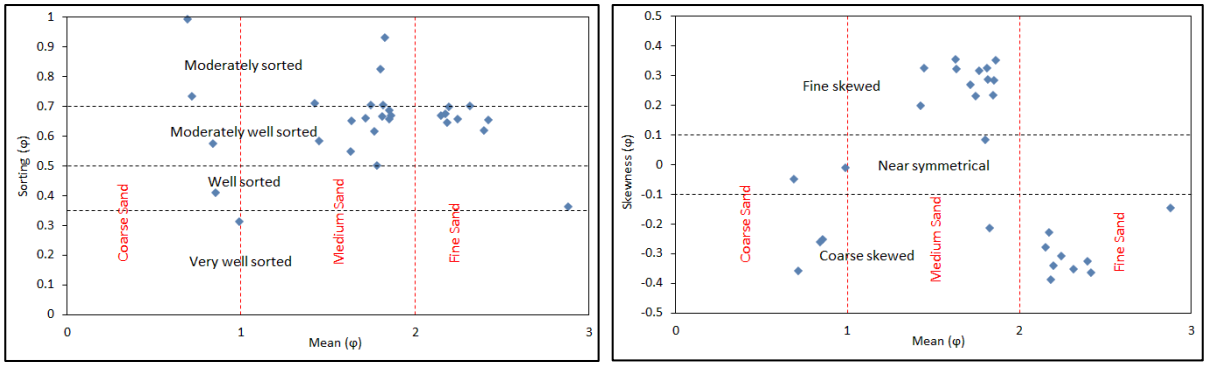



**Figure 5** Bivariate Plot of Sorting (ϕ) vs. Mean (ϕ) and Skewness (ϕ) vs. Mean (ϕ) – December 2019

### *4.2 Sediment movement patterns*

Sediment transport paths between sampling locations are identified using the STA method by McLaren and Bowles (1985). STA has been performed using the calculated statistical parameters for the following four stretches of coasts.

1. South of Netravati – Gurupur Rivermouth
2. North of Netravati – Gurupur Rivermouth to South of NMPT Breakwater
3. North of NMPT Breakwater to NITK Beach
4. South of Mulki – Pavanje Rivermouth to NITK Beach

Sediment Transport Paths (STP) is developed based on the McLaren and Bowles (1985) concept. The STP consists of a straight baseline representing the sampling line along the coast and sampling locations are marked. This line is a virtual line and the distance between the stations is not to scale. The curves (paths) above the baseline represents the sediment movement from South to North and North to South sediment movement is represented by curves below the baseline. Case B and Case C are represented by Red and Blue color curves, respectively.

#### *4.2.1 South of Netravati – Gurupur Rivermouth*

STP developed for South of Netravati – Gurupur Rivermouth for December 2019 and January 2020 are shown in Figure 6. STP shows that net sediment transport is from North to South during these two months along these coastal stretches. Sampling station near to the southern breakwater of Netravati – Gurupur Rivermouth, i.e., station S4 acts as the primary source for sediment transport in both the cases. This may be due to the erosion on these coastal stretches, which is also indicated by negative skewness on these locations.

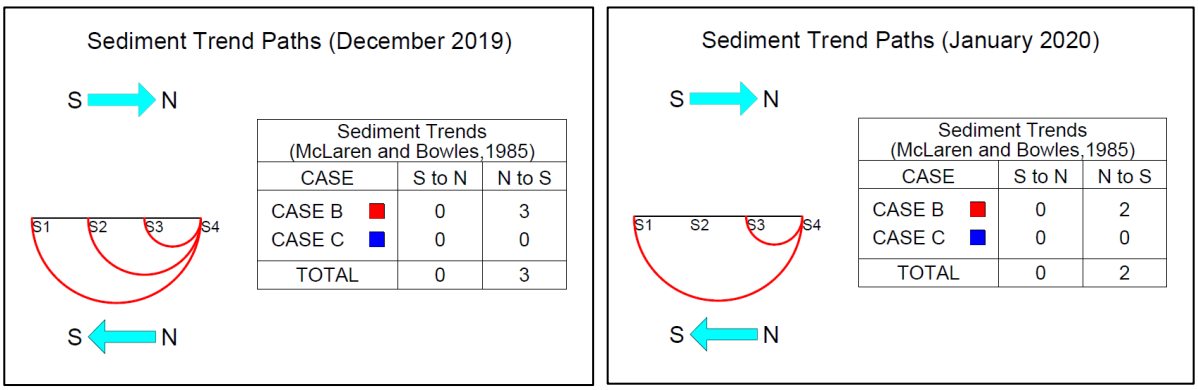



**Figure 6** STP for South of Netravati – Gurupur Rivermouth

### *4.2.2 North of Netravati – Gurupur Rivermouth to South of NMPT Breakwater*

Figures 7 and 8 show the STP for North of Netravati – Gurupur Rivermouth to South of NMPT Breakwater for December 2019 and January 2020. During December 2019, from STP, it is inferred that the littoral drift is negligible as sediment trends are identified in both directions are almost equal. Stations near to breakwater (S13 and S12) are the major sinks for the northern sediment trends. Whereas for southern sediment trends, stations near to river mouth (S5 and S6) are the major sinks. During January 2020, there is a little littoral drift towards the north, as there are eight northern trends compared to three southern trends. Here also, the sampling station near to breakwater (S13) is the major sink for the northern trends.

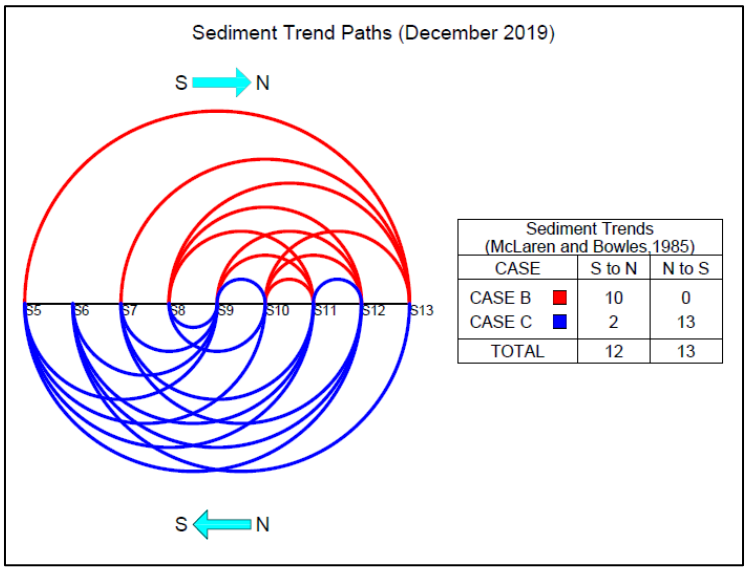



**Figure 7** STP for South of NMPT Breakwater – December 2019

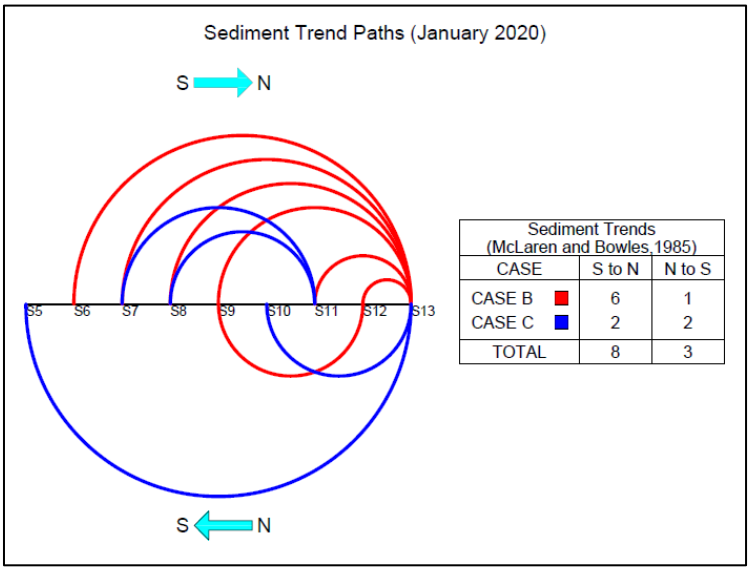



**Figure 8** STP for South of NMPT Breakwater – January 2020

### *4.2.3 North of NMPT Breakwater to NITK Beach*

STP generated for North of NMPT Breakwater to NITK Beach for December 2019 and January 2020 is shown in Figures 9 and 10. In both months, sediment trends are present in both directions. But

during December 2019, northern trends are dominant (27 northern trends and 13 southern trends) as compared to sediment trends of January 2020 (15 northern trends and 14 southern trends). In the southern sediment trends, sampling stations near to breakwater acts as the major sinks, i.e., there is a sediment movement towards the breakwater.

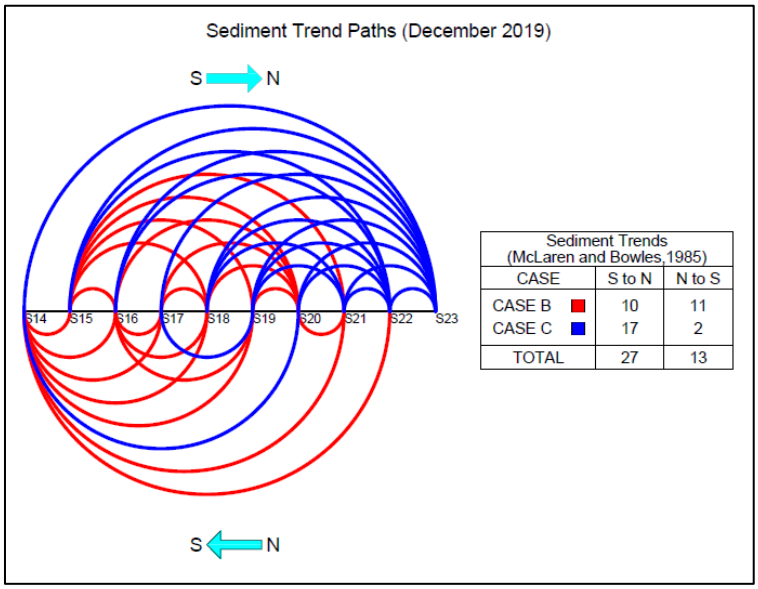



**Figure 9** STP for North of NMPT Breakwater to NITK Beach – December 2019

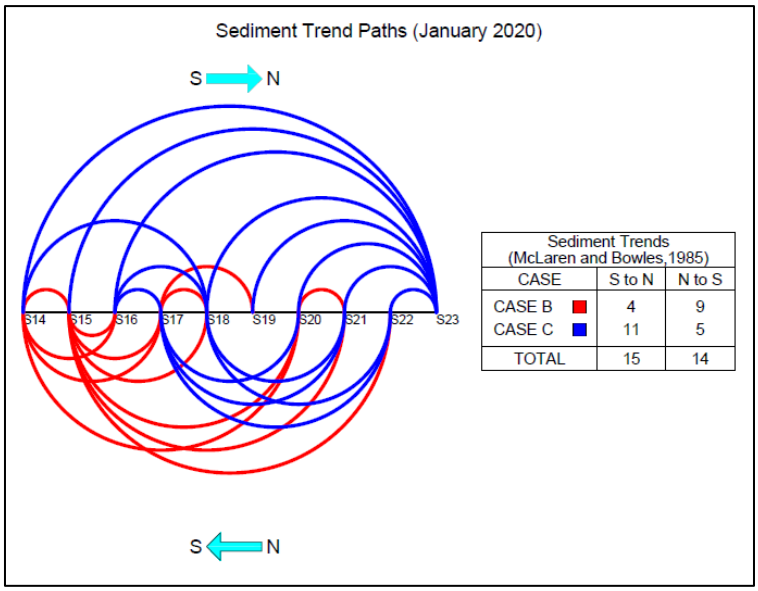



**Figure 10** STP for North of NMPT Breakwater to NITK Beach – January 2020

### *4.2.4 South of Mulki – Pavanje Rivermouth*

Figure 11 shows the STP for South of Mulki – Pavanje Rivermouth for December 2019 and January 2020. In both months, sediment trends are dominated by southern sediment trends. Sampling stations near to the river mouth (S29 and S28) are the major sources for sediment transport in both months. This could be due to the movement of sediments from the river mouth towards the south. During both months, Case C is the predominant type of sediment trends in the southern trends.

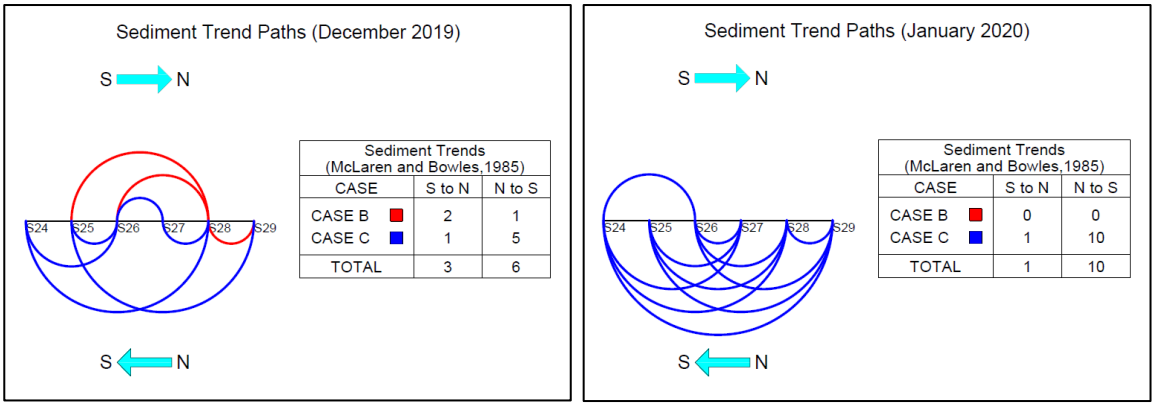



**Figure 11** STP for South of Mulki – Pavanje Rivermouth

## 5. Conclusions

Granulometric properties of the Mangalore Coast extending from Ullal Beach on the south to Sasihithlu river mouth in the north have been studied. The present study was carried out with the samples collected from 29 different locations during the months receiving minimum rainfall (December 2019 and January 2020). From the granulometric study, it can be concluded the foreshore beach is significantly composed of medium sand and fine sand. The sand sample becomes finer towards the north of the study area as compared with the samples in the south. Average skewness is found to be near symmetrical in the coastal stretches, which are almost in dynamic equilibrium. Average skewness is obtained as negatively skewed in the coastal stretches, which are in the state of erosion. Most of the sand samples are found to be moderately well sorted.

Sediment movement patterns along the coast have been studied using the STA method. From the study, it can be concluded that net littoral drift is minimum in the region as there is sediment movement in both directions. Station near to Mulki-Pavanje river mouth acts as a source for the sediment movement towards the south. The coastal stretch on the southern side of the Netravati-Gurpur river mouth is in a state of erosion. A little longshore sediment movement can be observed from south to north during these months. These findings are in agreement with the previous studies done by Rao et al. (2001) and Rajawat et al. (2005).

## References

Bramha, S. N., Mohanty, A. K., Samantara, M. K., Panigrahi, S. N., and Satpathy, K. K. (2017). Textural characteristics of beach sediments along Kalpakkam, south east coast of India. *Indian Journal of Geo Marine Sciences*, *46(8)*, 1562–1574.

Duane, D. B. (1964). Significance Of Skewness In Recent Sediments, Western Pamlico Sound, North Carolina. *Journal of Sedimentary Petrology*, *34(4)*, 864–874.

Khare, V., Khare, C., Nema, S., and Baredar, P. (2019). *Tidal Energy Systems: Design, Optimization and Control*.

Blott, S. J., and Pye, K. (2001). GRADISTAT : A Grain Size Distribution and Statistics Package for the Analysis of Unconsolidated Sediments. *Earth Surface Processes and Landforms*, *26*, 1237–1248.

McLaren, P. (1981). An interpretation of trends in grain size measures. *Journal of Sedimentary Petrology*, *51(2)*, 611–624.

McLaren P, and Bowles D (1985). The effects of sediment transport on grain-size distributions. *Journal of Sedimentary Petrology*, *55(4)*, 457–470.

Sahu, B. K. (1964). Depositional mechanisms from the size analysis of clastic sediments. *Journal of Sedimentary Petrology*, *34(1)*, 73–83.

Rajawat, A. S., Gupta, M., Pradhan, Y., Thomaskutty, A. V., and Nayak, S. (2005). Coastal processes along the Indian coast - Case studies based on synergistic use of IRS-P4 OCM and IRS-1C/1D Data. *Indian Journal of Geo Marine Sciences*, *34(4)*, 459–472.

Rao S, Shirlal KG, Khan PH (2001). An interpretation of sediment trends along D. K. Coast. *ISH Journal of Hydraulic Engineering*, *7(1)*, 33–39.

*IN PROCEEDINGS OF 25th HYDRO 2020, INTERNATIONAL CONFERENCE, NATIONAL INSTITUTE OF TECHNOLOGY ROURKELA, ODISHA, INDIA 26-28, March 2021, ISBN 978-93-90631-56-8*

Paper ID - 114

# Study of shoreline change along the Kasaragod district in Kerala, West Coast of India

Anjita N A[1], Makhdumi W[2] and Dwarakish G S[3]

[1]*Master of Technology, Department of Water Resources and Ocean Engineering, National Institute of Technology Karnataka, Surathkal, 575025, Mangalore, Karnataka, India*
[2]*Ph.D. Research Scholar, Department of Water Resources and Ocean Engineering, National Institute of Technology Karnataka, Surathkal, 575025, Mangalore, Karnataka, India*
[3]*Professor, Department of Water Resources and Ocean Engineering, National Institute of Technology Karnataka, Surathkal, 575025, Mangalore, Karnataka, India*
*Email: anjitaneelatt@gmail.com*
*Telephone/Mobile No.: +91 8139893190*

## Abstract

Study of the effects of oceanographic processes such as erosion and accretion are very important to understand the nature of a coast. Coastlines exhibit a wide range of changes depending on the interactions of tide and wave energy, sediment supply and more importantly human intervention. Generally, the coastline of Kasaragod district (Kerala state) along the west coast of India is dominated by both erosion and a stable condition. In view of this, the present study has been carried out to calculate the long term shoreline change rates along the Kasaragod coast using delineated Landsat images obtained during 1990-2020, at 5-year intervals and to identify the critical erosion zones. Transects were cast at 500-m intervals perpendicular to the coast and long-term shoreline change rates were calculated at each transect based on a linear regression method using Digital Shoreline Analysis System (DSAS), which is an extension of the ArcGIS software. The long-term analysis results indicate an average shoreline change rate of −0.21 m/year along the study area coast. Further, the rates obtained were classified as stable (-1 to +1 m/year), erosion (more than 1 m/year) and accretion (more than 1 m/year). Based on this classification, about 25.43% of the coast is eroding, 66.48% is stable and the remaining 8.09% is accreting in nature.

***Keywords:*** *Shoreline change; DSAS; Stable coast; Erosion; Accretion*

## 1. Introduction

Ideally, a shoreline is defined as the physical interface between land and water (Dolan et al. 1980) and it is highly dynamic in nature. Shoreline change is a consequence of both natural processes and human interventions (Camfield and Morang 1996). Despite the dynamic behavior of the shorelines, coastal zones are focal points of human activities. It has been estimated that 23% of the world population in 1990 lives within 100 km of the coast and less than 100 m above the sea level (Small and Nicholls 2003). The rate of shoreline change is one of the most common measurements used by coastal scientists and engineers to study the coastal dynamics (Dolan et al. 1991). Remote sensing and Geographical Information System (GIS) techniques have been widely used to analyze shoreline changes due to their cost effectiveness, reduced manual error and usefulness in the absence of field surveys (Maiti and Bhattacharya 2009).

Eroding coastlines affect human structures and natural habitats and result in the reduction of beach capacity for recreation or tourism (Dominguez et al., 2005). Coastal erosion has been reported from various parts along the Kasaragod coast in the past years. Several instances have been reported where houses have been destroyed or partially damaged and trees being uprooted along the coast. The situation is grim as the beaches are slowly disappearing due to erosion. The number of turtle nesting sites along the coast has also drastically reduced, reflecting the bad health of the coastal ecosystem.

The present work was carried out using Landsat images obtained from 1990-2020 at 5-year intervals to estimate the long term shoreline change rates along the coastal stretch of Kasaragod district, west coast of India using the Digital Shoreline Analysis System (DSAS) tool which is an extension of the ArcGIS software (Thieler et al. 2017).

## 2. Study Area

The coastal zone of Kasaragod district along the west coast of India in Kerala is the selected study area. The district lies in the northern tip of Kerala between 12º02′20″ - 12º47′38″ north latitudes and 74º51′59″ - 75º25′59″ east longitudes (Figure 1). It has a total population of 1,307,375, of which 38.9% is urban as per the 2011 census (District Census Handbook 2011). The area experiences a tropical to sub-tropical climate and the average maximum and minimum temperatures are 37ºC and 17ºC, respectively. The district also receives an annual average rainfall of 3350 mm, two-thirds of which is received during the period from June to August from the southwest monsoon (Source: https://kasargod.nic.in/climate/). There are 14 rivers flowing through the district, of which the Chandragiri river is the longest.

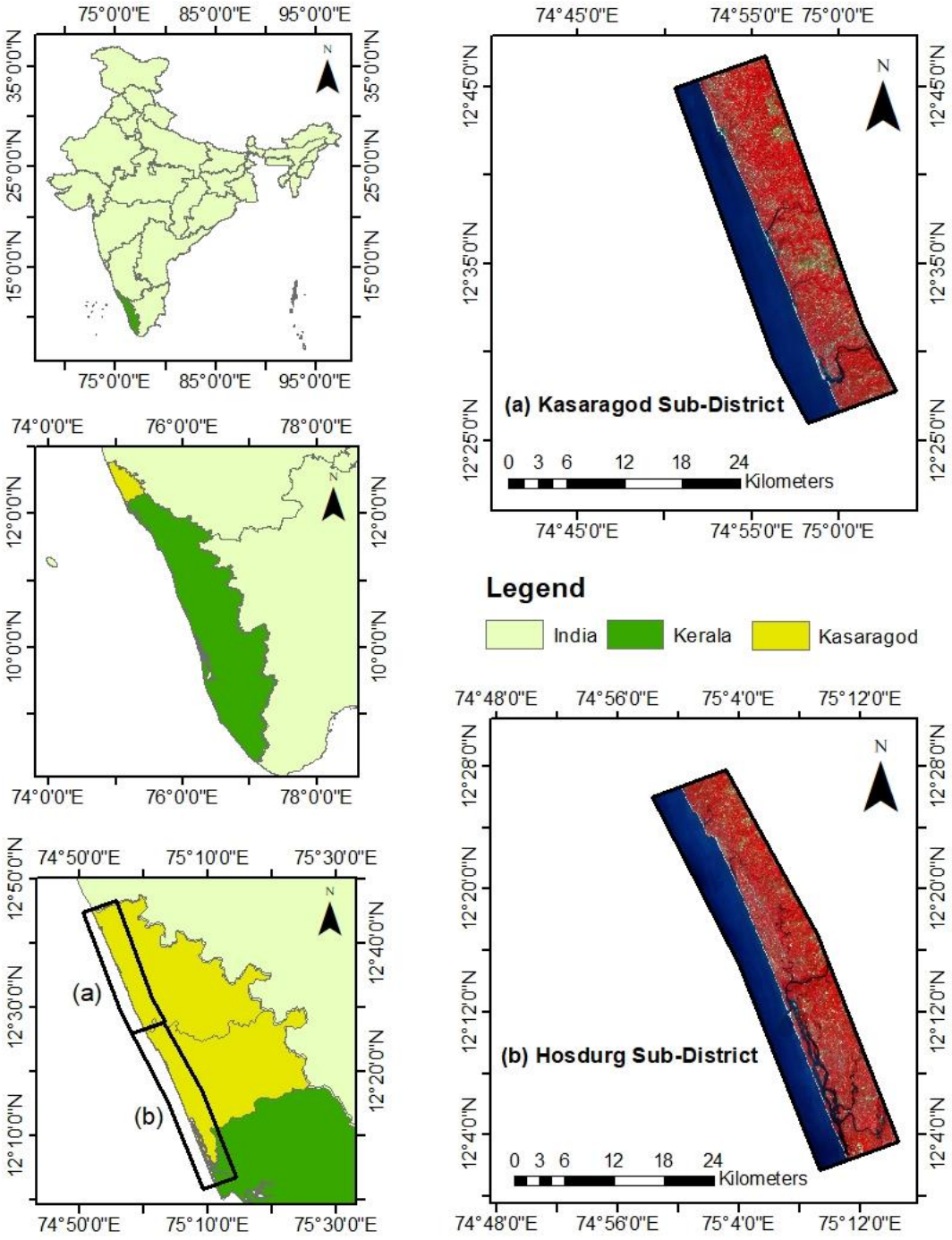



**Figure 1** Study Area

Kasaragod's coastline is approximately 83.6 km long (Kankara et al. 2018) and it is oriented along the NNW–SSE direction. Tides in the region are characterized by a mixed, predominantly semi-diurnal type with two high and two low waters of different amplitudes, occurring in a day. The coast is well known for its sandy beaches, river mouths, sand dunes, mangroves and turtle nesting sites. Main economic activities along the coast include fisheries, agriculture, tourism and industrialization. All these activities are directly or indirectly increasing the vulnerability of the Kasaragod coast.

## 3. Data Sources

In this study, satellite images of the study area from 1990 to 2020 were downloaded from USGS Earth Explorer (http://earthexplorer.usgs.gov/) for the analysis.. The details of the downloaded satellite data are shown in Table 1. The images were obtained for the winter season (December to March) in order to obtain cloud free data.

**Table 1** Satellite data used in the study

| Satellite and Sensor | Acquired date | Resolution |
|---|---|---|
| Landsat-5 TM | 17/12/1990 | 30m |
| Landsat-5 TM | 13/01/1995 | 30m |
| Landsat-7 ETM+ | 23/03/2000 | 30m |
| Landsat-7 ETM+ | 05/03/2005 | 30m |
| Landsat-7 ETM+ | 30/01/2010 | 30m |
| Landsat-8 OLI/TIRS | 05/02/2015 | 30m |
| Landsat-8 OLI/TIRS | 03/02/2020 | 30m |

## 4. Methodology

To perform the shoreline change analysis, shorelines were extracted from the near infrared band of the satellite images through manual digitization. An onshore baseline was created almost parallel to the coast, approximately 500m behind the shorelines and transects were cast at 500m intervals perpendicular to this baseline across the Kasaragod coastline (Figure 3). Erosion/accretion rates were then calculated at each transect based on a linear regression method using the Digital Shoreline Analysis System (DSAS) tool. Flowchart of the shoreline change analysis using DSAS is given in Figure 2.

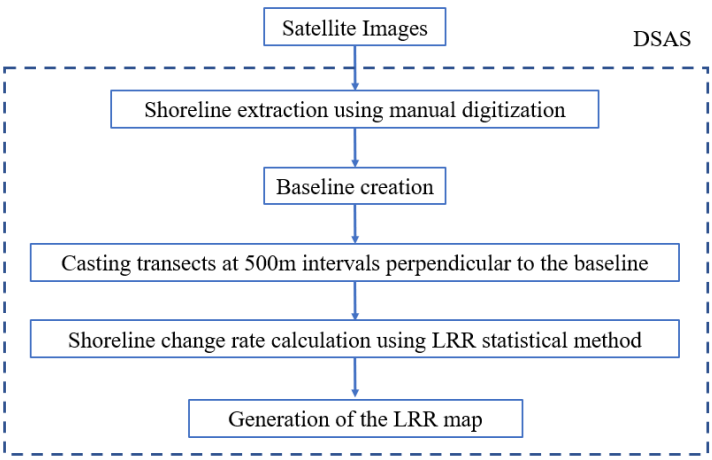



**Figure 2** Flowchart of the shoreline change analysis

The DSAS is a software extension of ArcGIS (Thieler et al. 2017) and it has been widely used in the past to analyze shoreline changes by several authors (Sheik and Chandrasekar 2011; Murali et al. 2015; Hegde and Akshaya 2015; Yadav et al. 2018; Nassar et al. 2018). DSAS has a set of statistical methods to calculate the rate of shoreline change out of which the LRR method is most commonly used for long term shoreline analysis (Nateshan et al. 2015). The LRR method uses all the available shoreline data to find a least-squares regression line so that the sum of the squared residuals (determined by squaring the offset distance of each data point from the regression line and adding the squared residuals together) is minimized (Crowell and Leatherman 1999).

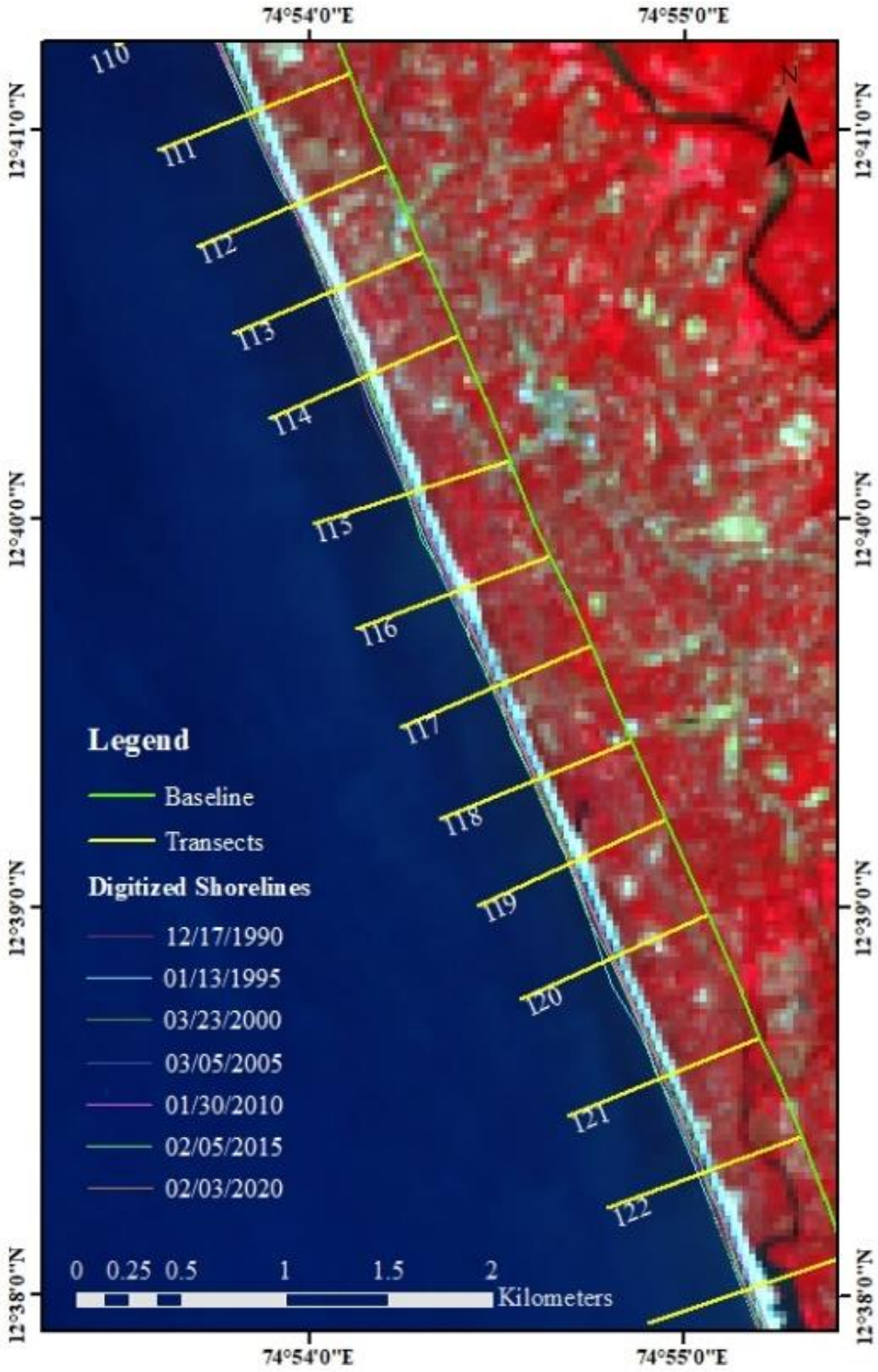



**Figure 3** Digitized shorelines, baseline and the DSAS generated transects

## 5. Results and Discussion

Remote sensing and geospatial techniques coupled with DSAS, an extension of ArcGIS is very useful for the shoreline change analysis. Also, remote sensing techniques can be cost effective, reduce manual error and reduce the subjectivity of conventional field techniques.

Long-term shoreline change analysis results indicate an average shoreline change rate of −0.21 m/year along the Kasaragod coast. Highest accretion and erosion rates were estimated as +10.69 m/year and −3.02 m/year to the north and south of the Chandragiri river, respectively. Figure 4 represents the shoreline change rates obtained at each transect along the coast. Transects 1-75 fall in the Kasaragod sub-district and 76-173 fall in the Hosdurg sub-district.

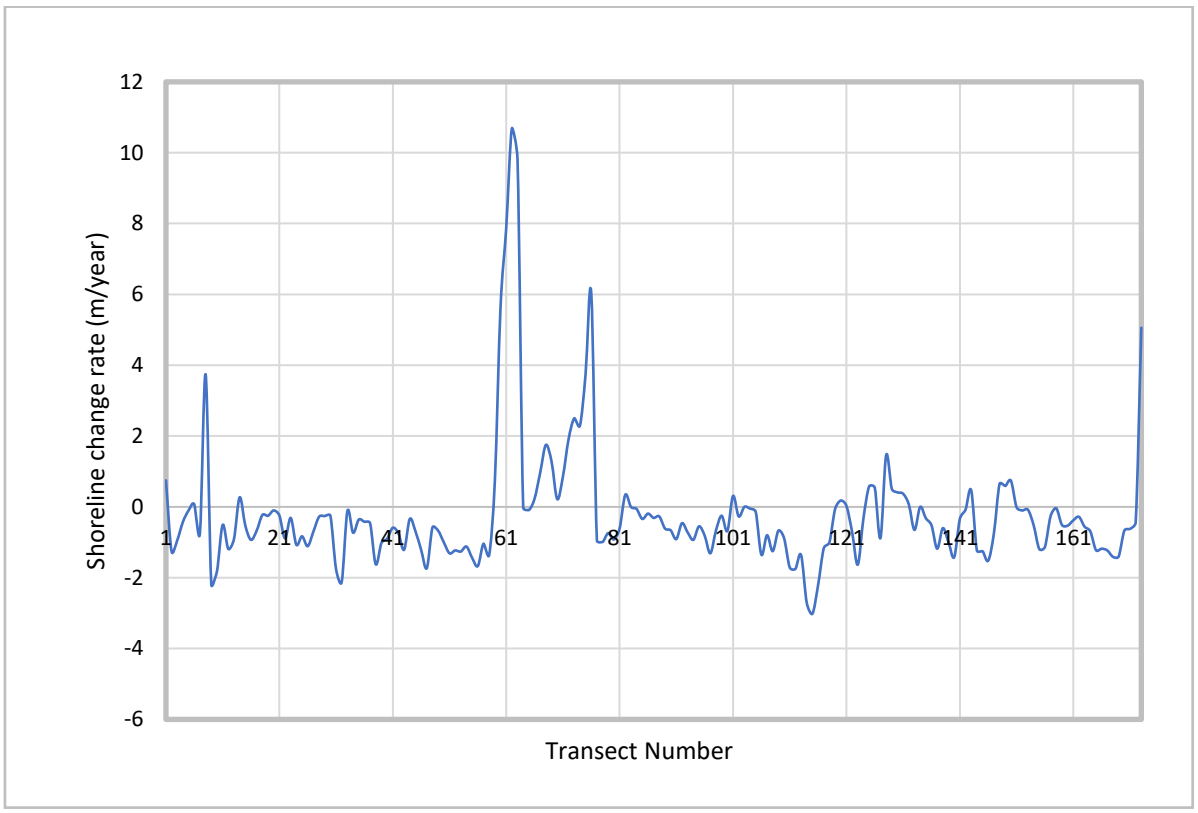



**Figure 4** Shoreline change rate along Kasaragod coast (Transects 1-75 in the Kasaragod sub-district and 76-173 in the Hosdurg sub-district)

The rates obtained were classified as stable (-1 to +1 m/year), eroding (more than 1 m/year) and accreting (more than 1 m/year). Based on this classification, 25.43% of the entire Kasaragod district coast was observed to be eroding, 66.48% - stable and the remaining 8.09% - accreting in nature. Shoreline change analysis carried out by Kankara et al. (2018) also points to the same fact that the Kasaragod coast is dominated by both erosion and stable condition with few pockets of accretion. LRR maps prepared for the sub-districts of Kasaragod and Hosdurg are shown in Figure 5 and 6.

Some of the factors that may be considered responsible for the causes of shoreline changes along the Kasaragod coast are the steepness of the near shore and the critical angle at which the waves strike the coast, deposition of the sediments transported by rivers in the reservoirs, lagoons and estuaries before reaching the Arabian Sea, the presence of mud banks in near-shore/inner-shore regions (Rao et al. 1985).

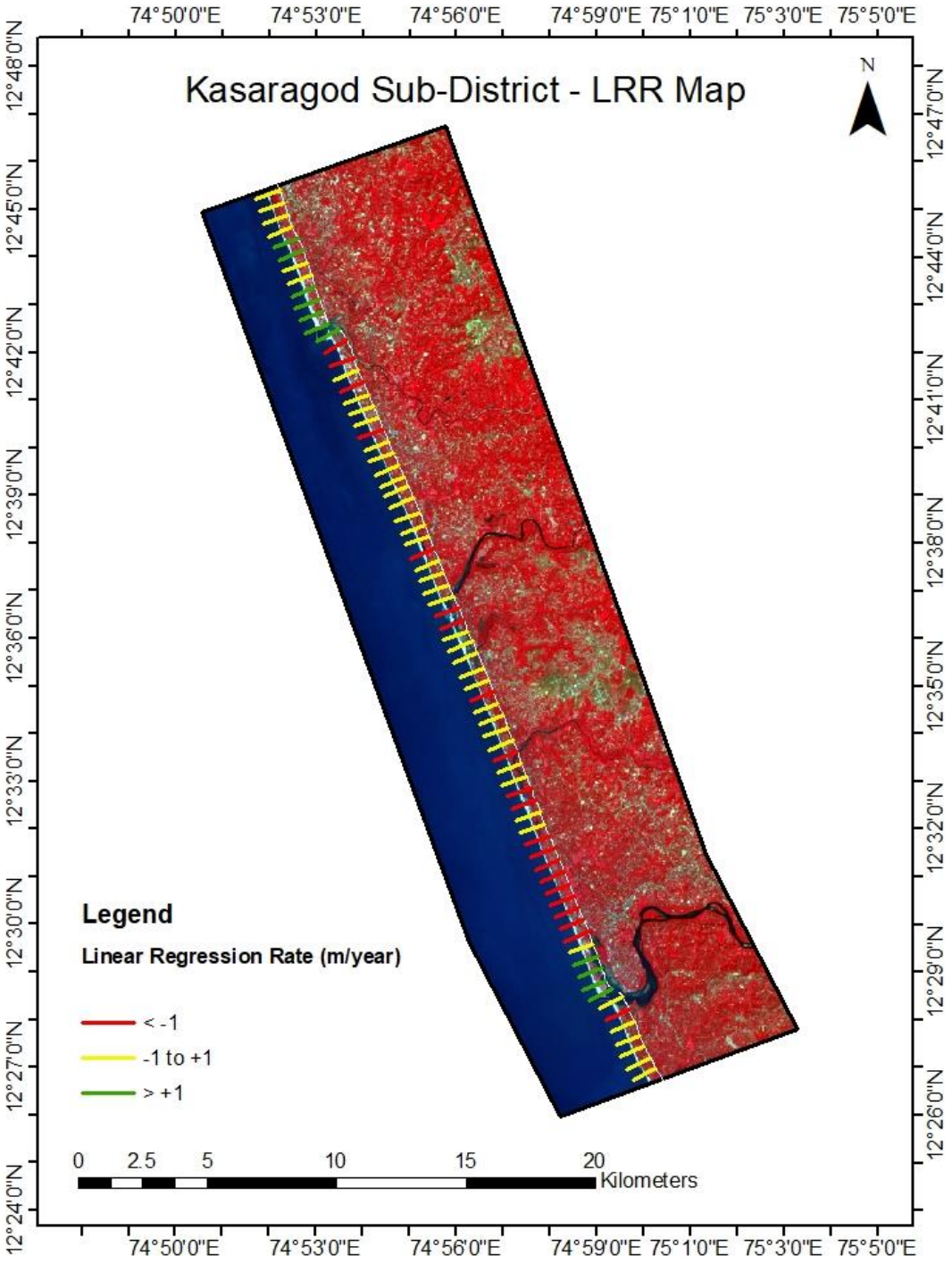



**Figure 5** LRR map of Kasaragod sub-district showing erosion and accretion

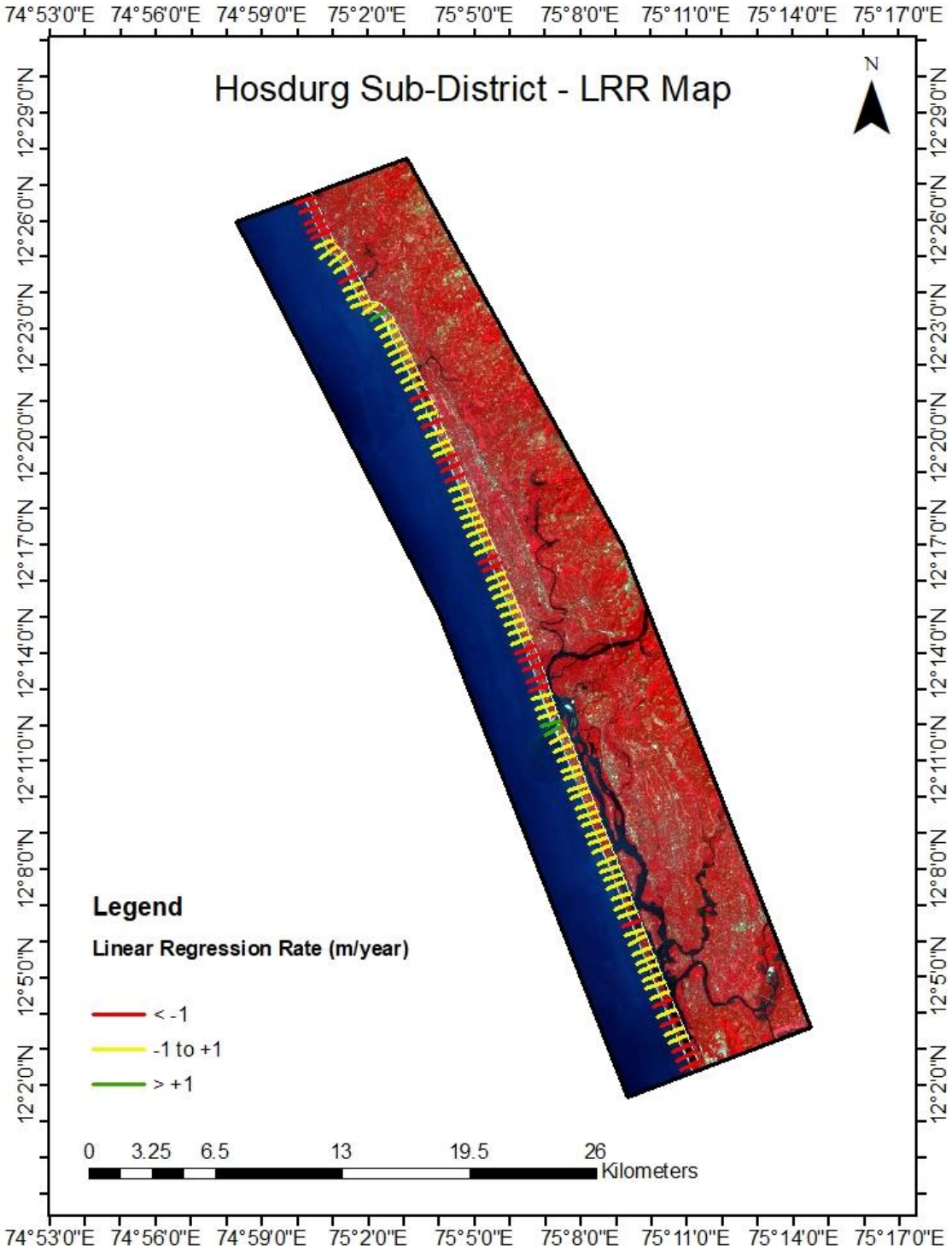



**Figure 6** LRR map of Hosdurg sub-district showing erosion and accretion

## 5. Conclusions

The primary objective of the study was to find the rate of change of shoreline over a period of 30 years from 1990-2020 using Landsat imagery. The LRR method was used to carry out the long-term shoreline change analysis in DSAS and a map showing erosion and accretion was prepared for both the sub-districts, Kasaragod and Hosdurg. Shoreline change rates were classified as stable (-1 to +1 m/year), eroding (more than 1 m/year) and accreting (more than 1 m/year). Based on this classification, 25.43% of the entire Kasaragod district coast was observed to be eroding, 66.48% - stable and the remaining 8.09% - accreting in nature. Based on the present study, it can also be concluded that multi-dated satellite data along with statistical and computational techniques can be used in the analysis of shorelines in the coastal regions.

## References

Camfield, F.E. and Morang, A. (1996). Defining and interpreting shoreline change. Ocean and Coastal Management. 32(3): 129-151.

Crowell, M. and Leatherman, S. P. (1999). Coastal erosion mapping and management. Journal of Coastal Research. Special Issue. 28: 1–196.

District Census Handbook. (2011). *Census of India 2011* (Kerala). Kasaragod: Ministry of Home Affairs, Government of India. https://censusindia.gov.in/ (last access: 16.07.2020).

Dolan, R., Hayden, B.P., May, P. and May, S. (1980). The Reliability of Shoreline Change Measurements from Aerial Photographs. Shore and Beach. Volume 48: 22-29.

Dolan, R., Fenster, M.S. and Holme, S.J. (1991). Temporal analysis of shoreline recession and accretion. Journal of Coastal Research. 7(3):723-744.

Dominguez, L., Anfuso, G., Gracia, F.J. (2005). "Vulnerability assessment of a retreating coast in SW Spain." *Environ. Geol.* 47, 1037-1044.

Hegde, A.V. and Akshaya, B.J. (2015). Shoreline Transformation Study of Karnataka Coast: Geospatial Approach. Aquatic Procedia. 4: 151-156.

Murali, R.M., Dhiman, R., Choudhary, R., Seelam, J.K, Ilangovan, D. and Vethamony, P. (2015). Environmental Earth Sciences. 74(10): 7201-7213.

Kankara, R.S., Murthy, M.V.R., Rajeevan, M., (2018). "National assessment of shoreline changes along Indian Coast: Status report for 26 years (1990-2016)." NCCR Publication, available at NCCR Web site http://www.nccr.gov.in (last access: 16.07.2020).

Maiti, S. and Bhattacharya, A.K. (2009). Shoreline change analysis and its application to prediction: A remote sensing and statistics-based approach. Marine Geology. 257:11–23.

Nassar, K., Mahmod, W.E., Fath, H., Masria, A., Nadaoka, K. and Negm, A. (2018). Shoreline change detection using DSAS technique: Case of North Sinai coast, Egypt. Marine Georesources & Geotechnology: 1-15.

Natesan, U., Parthasarathy, A., Vishnunath, R., Kumar, G.E.K and Ferrer, V.A. (2015). Aquatic Procedia. 4: 325-332.

Rao, P.P., Nair, M.M., and Raju, D.V., (1985). Assessment of the role of remote sensing techniques in monitoring shoreline changes: a case study of the Kerala coast, International Journal of Remote Sensing, 6:3-4, 549-558, DOI: 10.1080/01431168508948477

Sheik, M. and Chandrasekar. (2011). A shoreline change analysis along the coast between Kanyakumari and Tuticorin, India, using digital shoreline analysis system. Geo-spatial Information Science.14: 282–293. DOI: 10.1007/s11806-011-0551-7

Small, C. and Nicholls, R.J. (2003). A global analysis of human settlement in coastal zones. Journal of Coastal Research. 19(3): 584-599.

Thieler, E.R., Himmelstoss, E.A., Zichichi, J.L. and Ergul, A. (2017). The Digital Shoreline Analysis System (DSAS) version 4.0 - an ArcGIS Extension for Calculating Shoreline Change. U.S. Geological Survey Open-File Report: 2008-1278.

Yadav, A., Dodamani, B.M. and Dwarakish, G.S. (2018). Shoreline analysis using Landsat-8 satellite image. ISH Journal of Hydraulic Engineering. DOI: 10.1080/09715010.2018.1556569

*IN PROCEEDINGS OF 25th HYDRO 2020, INTERNATIONAL CONFERENCE, NATIONAL INSTITUTE OF TECHNOLOGY ROURKELA, ODISHA, INDIA 26-28, March 2021, ISBN 978-93-90631-56-8*

Paper ID - 129

# Ascertaining the effect of Mesh resolution in MIKE 21 Spectral Wave model results

Ms. Soniya Xaviour[1], Dr. J.D Agrawal[2]

[1]*MTech student, MTech in Coastal and Harbour Engineering, Kerala University of Fisheries and Ocean Studies, Kochi, Kerala, 682040, India.*

[2]*Scientist E, Central Water and Power Research Station, Khadakwasla, Pune, 411024, India.*
*Email: [1]soniaxavier36@gmail.com, [2]agrawal_jd@cwprs.gov.in*

## Abstract

Mesh resolution is one of the main parameters to be considered while setting up a numerical model as it may influence the model results. A flexible mesh approach is used in numerical modeling using MIKE 21 Spectral Wave (SW) module. The effect of different mesh resolutions in numerical modeling results of MIKE 21 Spectral Wave (SW) module is investigated in this paper. The wave transformation model for deep water to shallow waters was modeled using MIKE 21 SW. The Thrikunnapuzha coastline in Alappuzha district in Kerala was selected for setting up the model. The model simulations were carried out with 10 different mesh resolutions ranging from 50m to 500m to study the effect on output wave parameters like wave height and Time period. The analysis of results reveals that the mesh resolution did not have considerable effect in the output wave parameters. The inference obtained from this study would provide a basic idea regarding choosing an appropriate mesh resolution to setup an optimized MIKE 21 SW model which will take less computational time and memory without compromising the accuracy of the output results.

***Keywords:*** *Numerical model, MIKE 21, Spectral Wave model, Mesh resolution.*

## 1. Introduction

Numerical modeling is one of the most advanced tools employed to study the coastal hydrodynamic problems. Different types of numerical models are available and modelling techniques differ based on the purpose of the models ranging from Wave transformation models, coastal morphology models, models for design of coastal structures etc. The real challenge lies in the adopting the proper numerical models to the coastal problems. Numerical modeling being a predictive tool will involve certain assumptions and limitations, hence it should be applied only by having the comprehensive understanding of the problem domain.

Wave modelling is the most important part of many studies related to coastal environments. Coastal engineering studies such as coastal morphology, hydrodynamics etc. requires wave modeling as the basis. MIKE software by Danish Hydraulic Institute (DHI) is one of the most popular and advanced tools used for numerical modeling for water and coastal related applications. The professional wave modelling modules include basic wave modules; Spectral Wave, MIKE 21 SW and the Boussinesq Wave module, MIKE 21 BW. Using MIKE 21 SW, we can simulate the growth, decay and transformation of wind-generated waves and swells. MIKE 21 BW is used for analyzing the wave disturbances in harbours, ports and coastal areas. Both the modules come with plenty of tools to design models, manage bathymetries, specify boundary conditions and analyze and give results.

MIKE 21 Spectral Wave Model (MIKE-SW) solves the spectral wave action balance equation which is formulated in Cartesian or spherical co-ordinates. The wave field is represented by discrete two-dimensional wave action density spectrum at each element. The model will include wave growth by the action of wind, wave-current interaction, non-linear wave-wave interaction, dissipation by white capping, by wave breaking, due to bottom friction, and refraction due to depth variations. The wave transformation from offshore to near shore can be conveniently modelled using this model. The SW model is a flexible mesh model and works on triangular mesh grid. The grids can be varied based on

the requirement and accuracy of the output needed. A coarser mesh is usually used for offshore area and very fine mesh can be used in areas of interest.

This numerical model study was carried out to ascertain the effect mesh resolution on the MIKE 21 SW results. The MIKE 21 SW results include main wave parameters like Significant Wave height, Maximum Wave height, Mean Wave period, Peak Wave period. Also, the effect of mesh resolution on the computational time and memory used for simulation is also compared in this study. The Thrikunnapuzha coastline of Alappuzha district in Kerala, India is taken to setup the model. Model domain includes 23 km stretch of shoreline and offshore west boundary at 30-40km from shoreline.

## 2. Methodology

The study basically involves setting up of MIKE 21 SW models with various mesh resolutions ranging from coarse mesh to fine mesh. The input files needed to setup the model is the satellite imagery, bathymetry data and Wave data. The bathymetry data of the Thrikunnapuzha coastline was taken from MIKE C-map data and wave data was taken from Indian Meteorological Department (IMD) and Ship observed data. The entire model domain was divided into 3 sub sections from offshore to near shore location. This is done to generate mesh with smooth transition from deep water to shallow waters.

### *2.1.Mesh specifications*

The mesh resolution selected for the study ranges from 50m fine mesh to 500m coarse mesh. A total of 10 mesh resolutions starting from 50m and increasing at 50m increment up to 500m is taken. Near shore area is sub-divided into 2 polygons so as to generate finer mesh compared to offshore areas.

**Table 1** Specification of Types of Mesh used

| Mesh | One side of the Triangle (m) | Area ($m^2$) |
|---|---|---|
| Mesh 1 | 50m | 1083 |
| Mesh 2 | 100m | 4330 |
| Mesh 3 | 150m | 9743 |
| Mesh 4 | 200m | 17321 |
| Mesh 5 | 250m | 27063 |
| Mesh 6 | 300m | 38971 |
| Mesh 7 | 350m | 53044 |
| Mesh 8 | 400m | 69282 |
| Mesh 9 | 450m | 87685 |
| Mesh 10 | 500m | 108253 |

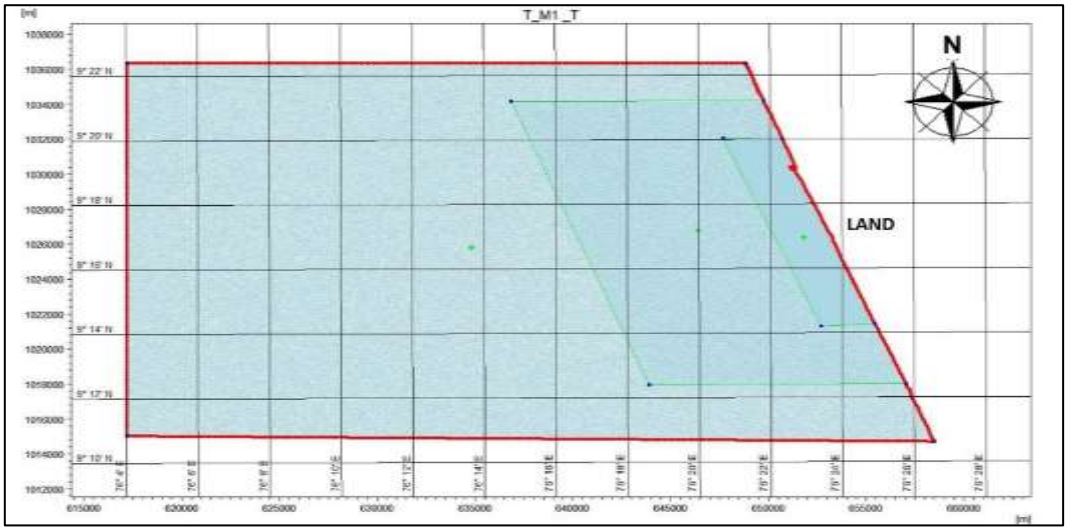



**Figure 1** Model domain with mesh M 1

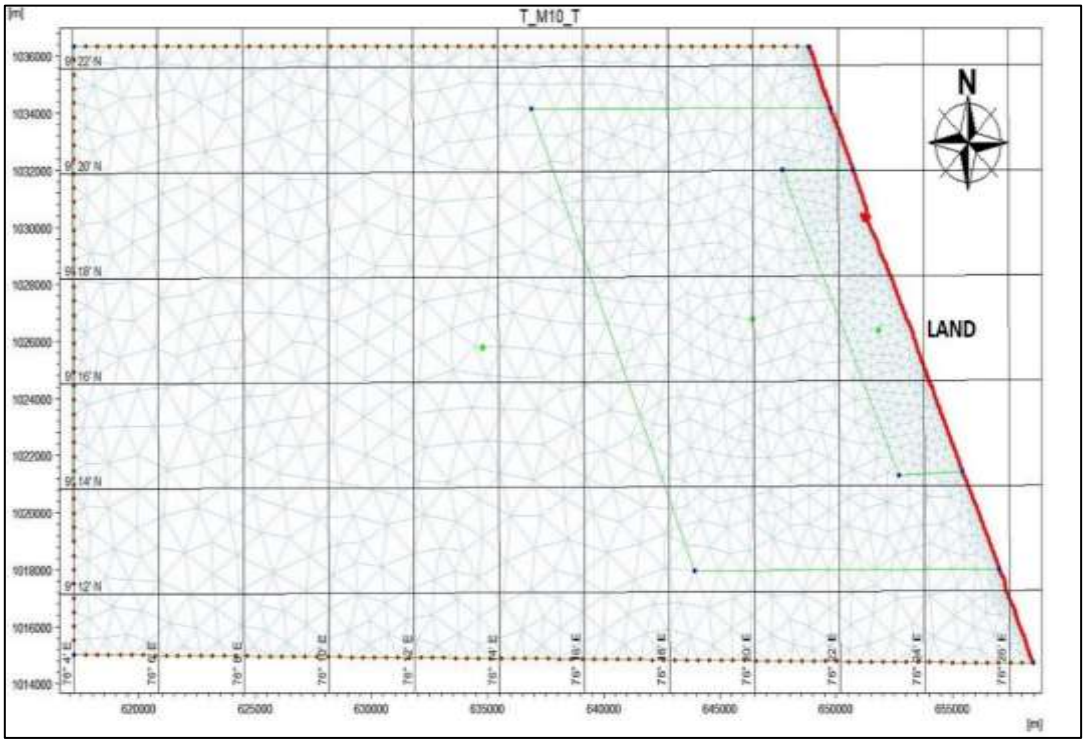



**Figure 2** Model domain with mesh M 10

Ten different bathymetry files were created using the ten different mesh resolutions. These bathymetry files will be used to run separate simulations in MIKE 21 SW and results can be compared.

### *2.2. Model setup*

The spectral wave module in MIKE 21 is setup for the model simulations. The bathymetry file is given as Domain and the North, West and South boundaries are specified. The simulation time parameters are specified; Number of time steps was given as 100, Time step interval was specified as 30 sec. Directionally decoupled parametric formulation is specified as the Spectral formulation. The time formulation is the Quasi stationary formulation. The directional discretization is 360 degree rose and number of directions as 16. The solution technique is Low order, fast algorithm. The method of iteration is Newton-Raphson iteration. The wave breaking is specified by constant Gamma value 0.8. The bottom friction is specified by Nikuradse roughness, $k_n$ 0.04. Zero spectra is chosen for initial conditions. The boundary conditions are to be set for each boundary, South and North boundaries are specified as Lateral boundaries. The wave parameters are specified in West boundary. At the west boundary a wave of 1m significant wave height with 8sec wave period was imposed. The values of Mean wave direction is 270 degrees and Directional spreading index, n is 5. No water level variation and no current variation is specified. The parameters like Ice coverage, wind forcing, Diffraction, white capping are excluded from the model. The output wave parameters like Significant wave height, Maximum wave height, Mean wave period and Peak wave period is specified as point output. The numerical model results were obtained after successful completion of simulation runs.

## 3. Results and Discussions

The model simulations for ten different mesh resolution was carried out successfully and output files were analyzed by plotting graphs of each parameters. The output values were extracted for typical points in offshore and near-shore locations.

### *3.1. Wave height parameters*

The Significant wave height values and Maximum wave height values were plotted for a typical near shore and offshore location for different meshes are as shown below:

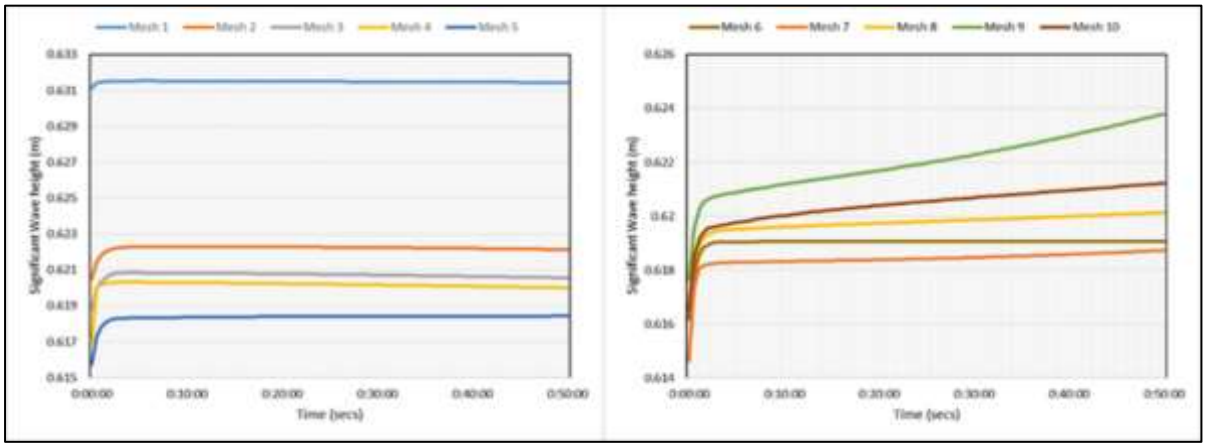



**Figure 3** Significant Wave height at Nearshore for Mesh 1,2,3,4,5,6,7,8,9 and 10

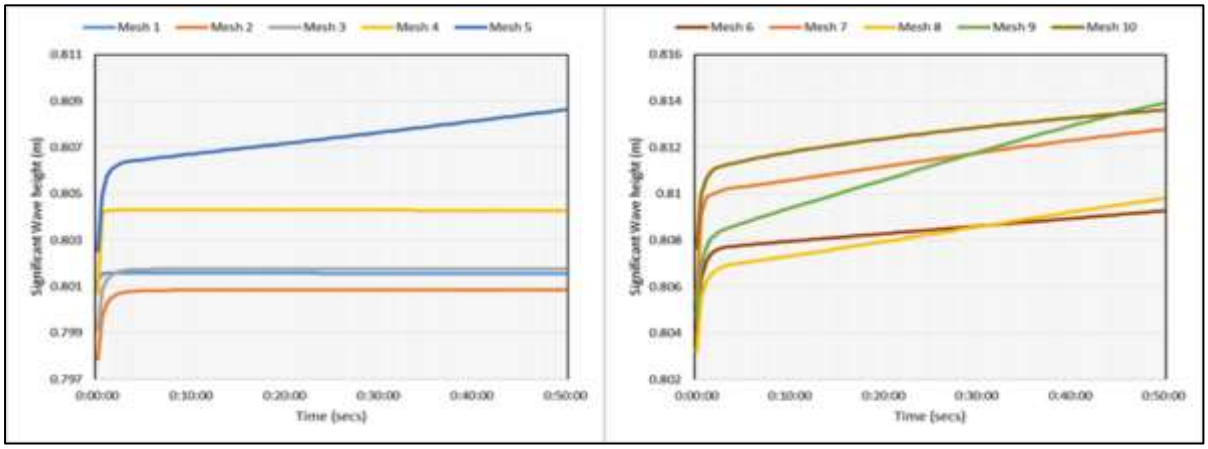



**Figure 4** Significant Wave height at Offshore for Mesh 1,2,3,4,5,6,7,8,9 and 10

From the above graphs, it was observed for Significant wave height at nearshore location a maximum variation of 0.013m and for the offshore location a maximum variation of 0.017m was noticed.

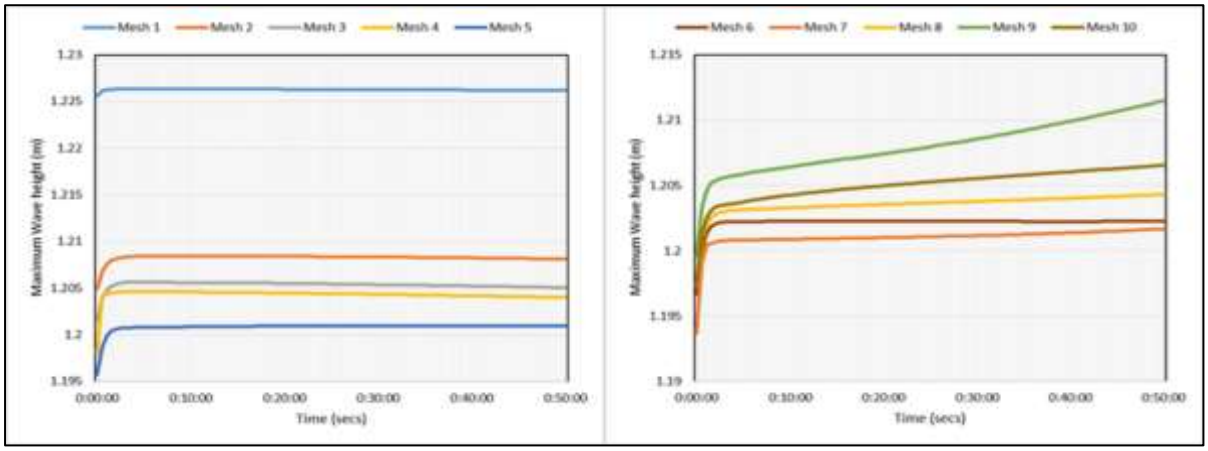



**Figure 5** Maximum Wave height at Nearshore for Mesh 1,2,3,4,5,6,7,8,9 and 10

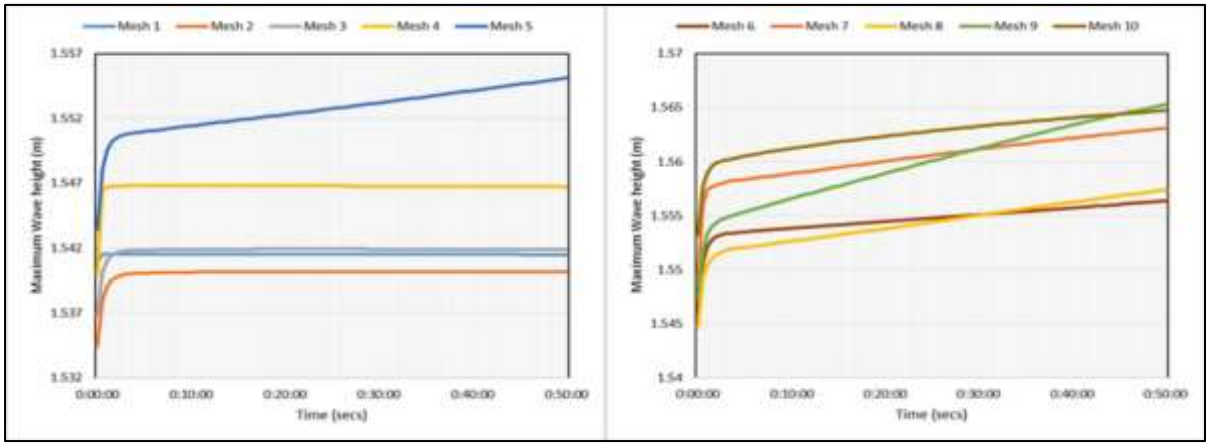



**Figure 6** Maximum Wave height at Offshore for Mesh 1,2,3,4,5,6,7,8,9 and 10

From the above graphs, it was observed that at nearshore location a maximum variation of 0.026 m was observed. For the offshore location a maximum variation of 0.022 m was noticed. As the variations of wave height parameters were found to be within 2%, the effect of mesh resolution on wave heights can be said to be negligible.

### *3.2. Wave period parameters*

The peak wave period and mean wave period values plotted for a typical near shore and offshore location for different meshes are as shown below:

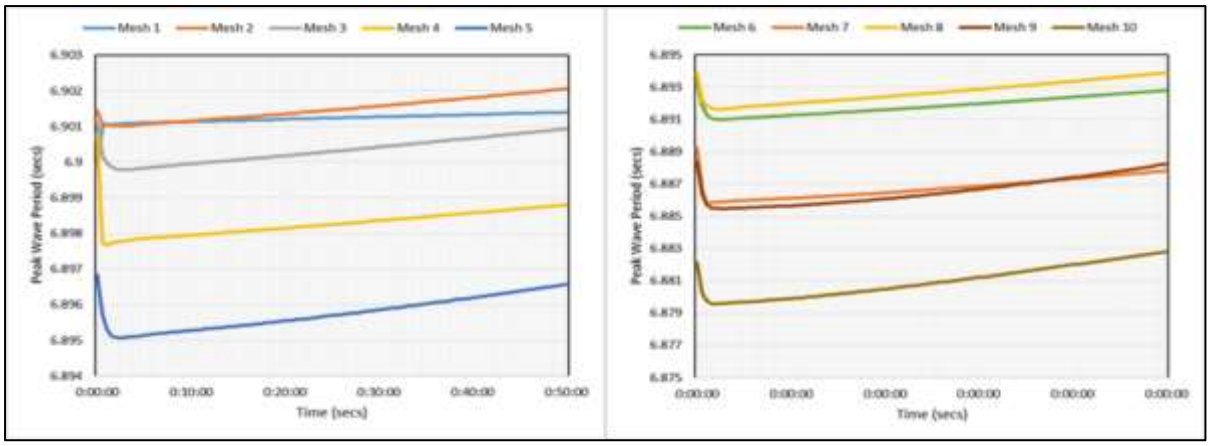



**Figure 7** Peak Wave period at Nearshore for Mesh 1,2,3,4,5,6,7,8,9 and 10

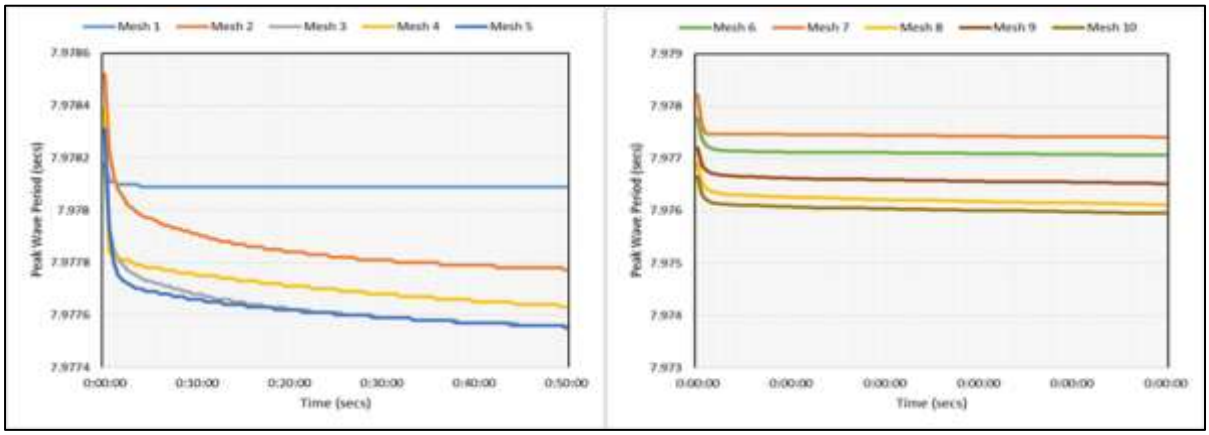



**Figure 8** Peak Wave period at Offshore for Mesh 1,2,3,4,5,6,7,8,9 and 10

From the above graphs, it was observed that at nearshore location and offshore location the values of peak wave period have no significant variations.

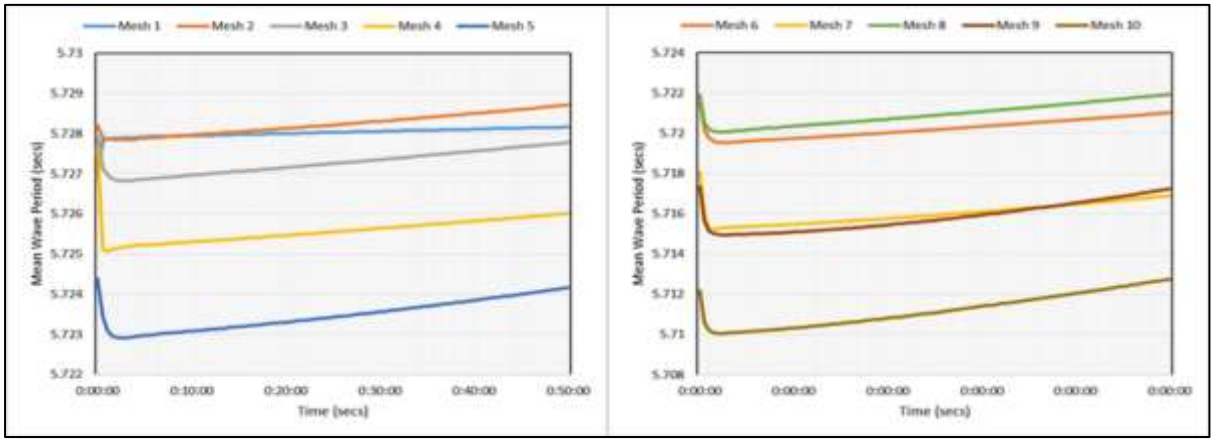



**Figure 9** Mean Wave period at Nearshore for Mesh 1,2,3,4,5,6,7,8,9 and 10

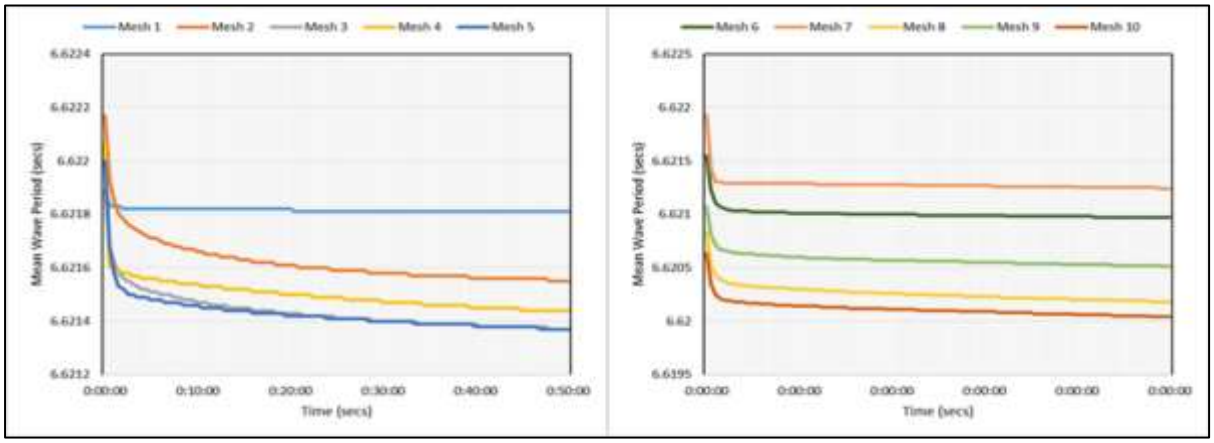



**Figure 10** Mean Wave period at Offshore for Mesh 1,2,3,4,5,6,7,8,9 and 10

From the above graphs, it was observed that at nearshore location and offshore location the values of mean wave period have no significant variations. The variation was observed only for second and third decimal place values, hence it can be concluded that there is no considerable effect of mesh resolution on wave period parameter results.

### *3.3. Computational time and Memory taken*

The computational time taken for the simulation run is a one of the important factors in numerical modeling. As seen from the simulation log file, it was clear that the computational time and memory taken for the model simulations are decreasing from Mesh 1 to Mesh 10. Finer mesh resolutions take more computational time and memory compared to coarser mesh sizes. As seen from earlier observations, since there is no much variations in results of Mesh 1 and Mesh 10, it can be said that coarser mesh resolution can be used to get fairly accurate results with reduced computational time and memory used.

## 4. Conclusions

An attempt to find out the effect of mesh resolution on the MIKE 21 Spectral Wave (SW) model was successfully done in the present research. The model simulation runs which includes 10 simulation runs with different mesh resolution for MIKE 21 SW were completed successfully and outputs were post

processed to arrive at the suitable results and conclusions. On analyzing and comparing the main wave parameters for different mesh resolutions, it was seen that for Significant wave height and Maximum wave height showed very less significant variation (less than 2% variation) in results for finer and coarser meshes. Also, the Peak wave period and Mean wave period did not have any significant changes in values as only second and third decimal value changes were observed which is very insignificant. The computational time and memory taken for simulation runs showed a decreasing trend from finer mesh to coarser meshes with finer mesh taking more computational time and memory compared to coarser meshes. Summing up all the above findings, it can be concluded that MIKE 21 Spectral Wave models can be setup with coarser mesh resolutions so as to get an optimized model which gives fairly accurate results while taking less computational time and memory. The study was helpful in arriving at satisfactory conclusion regarding the effect of mesh resolutions in MIKE 21 SW model results.

## 5. References

A.M Vaidya et al. (2013); *'Influence of Mesh Resolution on Simulation of Wave Propagation in Coastal Area'*; HYDRO 2013 International.

Boris Dibinsky et al. (2017); *'Parameters of Wind Seas and Swells in Black sea based on Numerical modeling'*; Oceanologia 2017.

DHI (2014); MIKE 21 FM SW, *User guide.*

DHI (2014); MIKE 21FM SW, *Step- by -step training guide.*

DHI (2014); MIKE 21 BW, *Step- by -step training guide*.

Joanna Szmelter et al. (2015); *'An Unstructured mesh atmospheric model for Non-Hydrostatic Dynamic: Towards optional mesh resolution'*; Journal of Computational Physics; Vol.294.

Justin Thomas. T (2015*); 'Numerical Wave modelling- a review'*; International Conference on Water Resource, Coastal and Ocean Engineering; 2015.

Parvathy K.G et al. (2014); *'Wave Transformation along Southwest coast of India using MIKE 21'*; International Journal of Ocean and Climate Systems, Vol. 5, Number 1,2014.

Parvathy K.G et al. (2015); *'Wave Transformation along Trivandrum coast of India using MIKE 21'*; Ocean Society of India,2015.

*IN PROCEEDINGS OF 25th HYDRO 2020, INTERNATIONAL CONFERENCE, NATIONAL INSTITUTE OF TECHNOLOGY ROURKELA, ODISHA, INDIA 26-28, March 2021, ISBN 978-93-90631-56-8*

Paper ID - 131

# Mathematical modelling to ascertain the effect of Groyne field on Beach Fill stability

Mr. Ishfakh M Shafeekh[1], Mr. M. Phani Kumar[2]

*[1]MTech student, M.Tech in Coastal and Harbour Engineering, Kerala University of Fisheries and Ocean Studies, Kochi-682506, Kerala, India.*
*[2]Scientist C, Central Water and Power Research Station, Khadakwasla-411024, Pune, India.*
*Email: [1]ishfakh.m.shafeekh@gmail.com, [2]mphanikumar2005@yahoo.com*
*Telephone/Mobile No.: [1]+91 9656325496, [2]+91 9423011618.*

## Abstract

The project work involves setting up of mathematical models using MIKE 21 FM software (Integrated coupled models). The study area taken into consideration is the Visakhapatnam northern coastline adjacent to Visakhapatnam port. The stretch up to Waltair point comprising of Ramakrishna beach on North side of Visakhapatnam Outer harbour is the main study area. In order to study the morphological aspects, coupled model comprising of three modules viz; Hydrodynamic (HD), Spectral Wave (SW) and Sediment transport (ST) was setup. Model simulations were carried out to arrive at appropriate hard measures like groyne field, so as to improve the stability of a conceptual beach fill at the Visakhapatnam coast. The model was setup to represent the South-West monsoon season which is the predominant season for Visakhapatnam coast. A conceptual beach fill was modelled for the study area. The different model simulation runs were carried out for beach fill and beach fill with groynes. The model output parameters like Sediment Transport rate, Wave height parameters and Wave run-up are analyzed. Useful inferences about effect of groynes on the beachfill were derived with systematic post-processing of the model results. This in-turn is useful to evolve suitable coastal protection measures incorporating both soft and hard measures to address the issues like 'coastline stability' which is very essential for 'littoral drift' prone east coast of India.

***Keywords:*** *MIKE 21 FM, Coupled Model, Beach fill, Groyne field, Waves, Sediment Transport.*

## 1. Introduction

Coastal erosion is one of the most challenging problem faced by coastal engineers around the world. The protection of beaches from erosion is the very important aspect of coastal engineering. The beaches naturally remain in equilibrium but this equilibrium maybe disturbed by natural phenomenon or human interventions. The two main types of coastal protection measures are Hard protection measures and Soft protection measures. The hard protection measures are widely used as they are highly capable of resisting extreme wave climate. But however, they sometimes lead to detrimental effects and may accelerate erosion in usually at the downdrift side of the structures. Soft measures are mostly ecofriendly methods but are highly susceptible to damages by extreme wave climate. In order to increase the longevity of soft measures like artificial beach fills, hard measures like groyne field can be incorporated.

In this study we are analyzing the effect of groyne field on stability of an artificial beach fill by numerical modeling using MIKE software. The study area selected is the Visakhapatnam northern coastline adjacent to Visakhapatnam port. The conceptual artificial beachfill is setup for a stretch up to Waltair point comprising of Ramakrishna beach on North side of Visakhapatnam Outer harbor. This stretch is undergoing progressive erosion mainly due to littoral drift and deficit supply of sediments due to Visakhapatnam outer habour breakwaters, although Visakhapatnam Port Trust is doing sand by-passing regularly.

The numerical modeling was carried out using MIKE21/3 Coupled model which allows dynamic coupling of Hydrodynamic (HD), Spectral Wave module (SW) module and Sand Transport (ST) module. The HD and SW modules simulates mutual interaction between waves and currents. The feedback on bed level changes are simulated using ST module. The morphological model was run with

suitable speed-up factor to get fairly accurate results with less computational time. The model was setup and model simulations runs were completed successfully and results were extracted and analyzed to arrive at suitable conclusion regarding the effect of groyne field on artificial beach fill stability.

## 2. Methodology

The study basically involves modeling an artificial beach fill on Ramakrishna beach on the Vishakhapatnam coastline and incorporating the groynes with the beach fill so that the beach fill is stabilized. The study area was digitized using georeferenced images extracted from Google Earth Pro software. The wave data needed to setup the model was taken from Wave data available at CWPRS, Pune. The tide data was extracted from Global tide model in MIKE 21 and sediment transport tables were generated using MIKE 21 Toolbox. The bathymetry data was taken from data available at CWPRS, Pune and Beach profile charts by Visakhapatnam Port Trust. The model runs includes a Baseline model to model the present site conditions and the model was calibrated, and then followed by model with only beach fill, Beach fill with single groyne and then finally beach fill with multiple groynes. The brief description of model setup is discussed in the following sections.

### *2.1. Model description*

The size of the model domain extends from Yarada beach on South to North end of Lawson's Bay. The spatial domain taken is almost 18.6 km from South to North boundaries and almost 6 km from coastline to East boundary as shown in Figure 1. The model simulation is setup so as to represent the South-West monsoon season which is the predominant season for Visakhapatnam coast i.e.; from June to October. The SW monsoon season has the relatively intense wave climate causing northerly drift and hence gives an idea about the significant impact that the waves can cause on the coastline.




**Figure 1** Extend of model boundaries and areas enclosed

### *2.2. Modeling of Beach fill and groynes*

The beach fill extends for 4km stretch from North of catamaran harbour including Ramakrishna beach up to Waltair point. The beach fill consists of two dove tailed tapered portions on two ends and flat fill straight portion with +5m elevation. The frontal slopes were fixed to be 1 in 30 slopes as it was found to be more stable than steeper slopes. The straight beach fill portion extends up to 3km length and 500m length on two tapered ends. The beach fill has a width of 200m on two straight end portions which is

tapered to match the existing bathymetry on both sides. The widest portion of beach fill has a width of 290m. The 1 in 30 frontal slopes has width of 450m and starts from +5m beach fill up to -10m depth where it joins with the existing bathymetry.

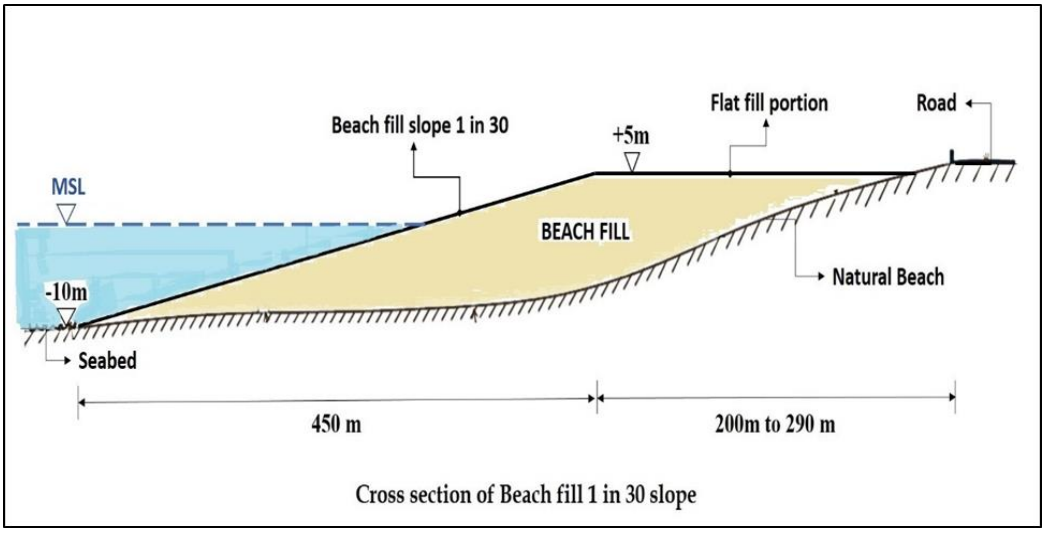



**Figure 2** Cross section of Beach fill with 1 in 30 frontal slopes

In case of the conceptual beach fill, providing a series of groynes would provide sufficient retention for the beach fill from littoral alongshore drift and also may protect the beach fill during extreme wave climates. The length and spacing of groynes were fixed by giving a simulation run with a single groyne of approximately 40m width and 500m length extending from existing coastline boundary to -2m depth on beach fill slope. The results of simulation run with the single groyne on mid portion of beach fill was studied and analysed and was found that only the sloping portion of beach fill was affected by wave attack and +5m flat fill portion was relatively undisturbed. So, the length of groyne was reduced to 210m starting from front end portion +5m fill to -2m depth on sloping portion. The retention effect of groyne was found to be effective for a length of 325m on downdrift side of groyne for SW monsoon. So, a total of eight groynes of approx..40m width were provided in straight fill portion covering 3km beach fill stretch. The first groyne was placed at distance of 400m from South end of flat beach fill portion as the North breakwater of Vizag outer harbour offers protection to some extent in that region. All the remaining groynes were placed at 325 m spacing.

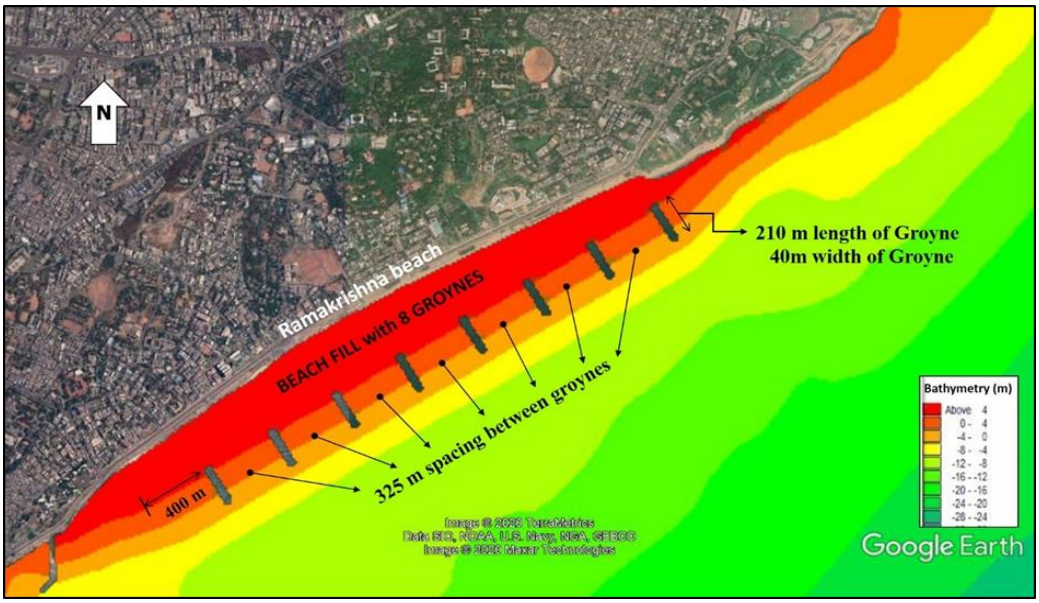



**Figure 3** Beach fill with 8 groynes (Top view)

### *2.3. Model Setup*

The entire model domain was divided into the three subsections to provide different mesh resolutions for offshore regions to beach fill area. For the larger domain in the mesh, a resolution of 400 m was used progressively reducing to 300 m for area between South of Vishakhapatnam port to North of Lawsons Bay and 100m for the coastline of interest i.e.; stretch from Ramakrishna beach to Waltair headland and a resolution of 50 m was applied beach fill portion.
The model setup in MIKE 21/3 coupled model consists of mainly three modules viz; Hydrodynamic module (HD), Spectral Wave module (SW) and Sand Transport module (ST). The simulation period was taken for 3 months of SW monsoon, and a speed-up factor of 2 was taken so that output represents the entire SW monsoon period of 6 months (3months simulation x 2 speed-up factor = 6 months). The Courant–Friedrichs–Lewy (CFL) number was chosen as 0.9 for stability of the model run. The boundary conditions of wave and tide were specified as per the requirement in HD and SW modules. The sediment transport table is given as input in ST module.
The Baseline model representing the present actual site conditions was used as calibration model. The calibration model result was validated using the available field data of current speed value at a known location. The total load magnitude value was taken to compute the quantity of alongshore transport for SW monsoon and was found to be matching with the actual transport quantity estimated for Visakhapatnam coast.

## 3. Results and Discussions

The model simulations for South-West monsoon wave conditions was carried out successfully for different scenarios of beach fill without groyne and beach fill with groynes. The main parameters like Total load-magnitude, Bed Level Change, Rate of Bed Level Change, Significant wave height, Maximum wave height were analysed to arrive at the desired results and conclusions. The observations and analysis of the results were done by plotting graphs of the parameters and the effect of groyne field on beach fill stability was concluded.

### *3.1. Sediment Transport*

The values of total load magnitude obtained by conditional averaging (in order to separate alongshore transport from total load magnitude) was taken for both only beach fill scenario and beach fill with groyne field scenario and was compared to know the effect of groyne field on alongshore transport. The total load magnitude and direction values of both the cases were plotted in rose plot (Figure 4) for better understanding.

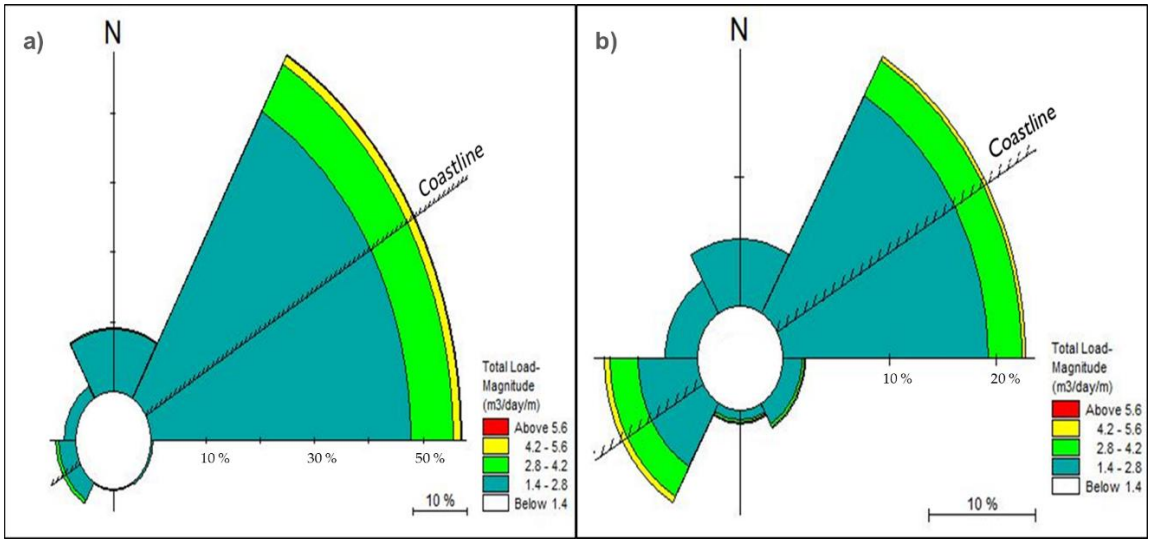



**Figure 4** Total load magnitude for a) Only Beach fill b) Beach fill with groynes

The mean total load magnitude values calculated along different profiles are given below:

**Table 1** Mean Total load magnitude computed at different locations on beach fill

| Location (+3m to -4m depth) | Only Beach fill ($m^3$/day/m) | Beach fill with 8 Groynes ($m^3$/day/m) |
|---|---|---|
| Updrift side of Flat portion | 1.663 | 0.898 |
| Mid portion of Beach fill | 2.635 | 1.503 |
| Downdrift side of Flat portion | 2.732 | 1.08 |
| End portion of Flat fill | 3.464 | 1.78 |

From the above table of Total load magnitude values, it is clear that almost 50% reduction in alongshore sediment transport has happened in case of beach fill with groynes compared to Only beach fill scenario. This shows the reduction in material loss from beach fill due to littoral drift and hence can be attributed as a positive effect of groynes.

### *3.2. Bed Level*

The bed level for typical points between groynes at different depths were extracted for both the cases and the Bed level time series plots were created which shows the variation in bed level for the entire season. The spatial plots of bed levels (Figure 5, 6) were found to be showing siltation trends for beach fill with groynes compared to erosive trend or reduced siltation for only beach fill scenario. This proves the positive effect of using groyne field in the beach fill.
The statistical mean values of Bed level change for area between the groynes was extracted as follows:

**Table 2** Statistical mean values of Bed level parameters

| Parameters | Only Beach fill (m) | Beach fill with 8 Groynes (m) |
|---|---|---|
| Bed level change (m) | 0.32 | 0.53 |
| Rate of bed level change (m/day) | 0.002 | 0.005 |

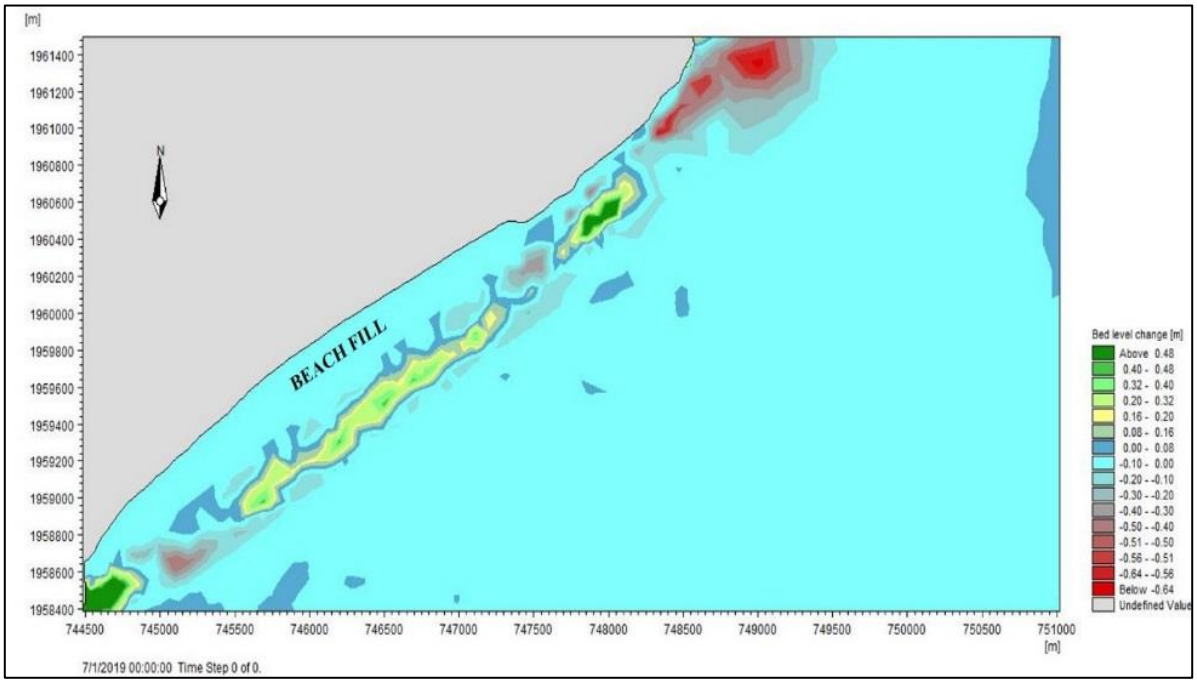



**Figure 5** Statistical mean of Bed Level Change for Beach fill without groynes

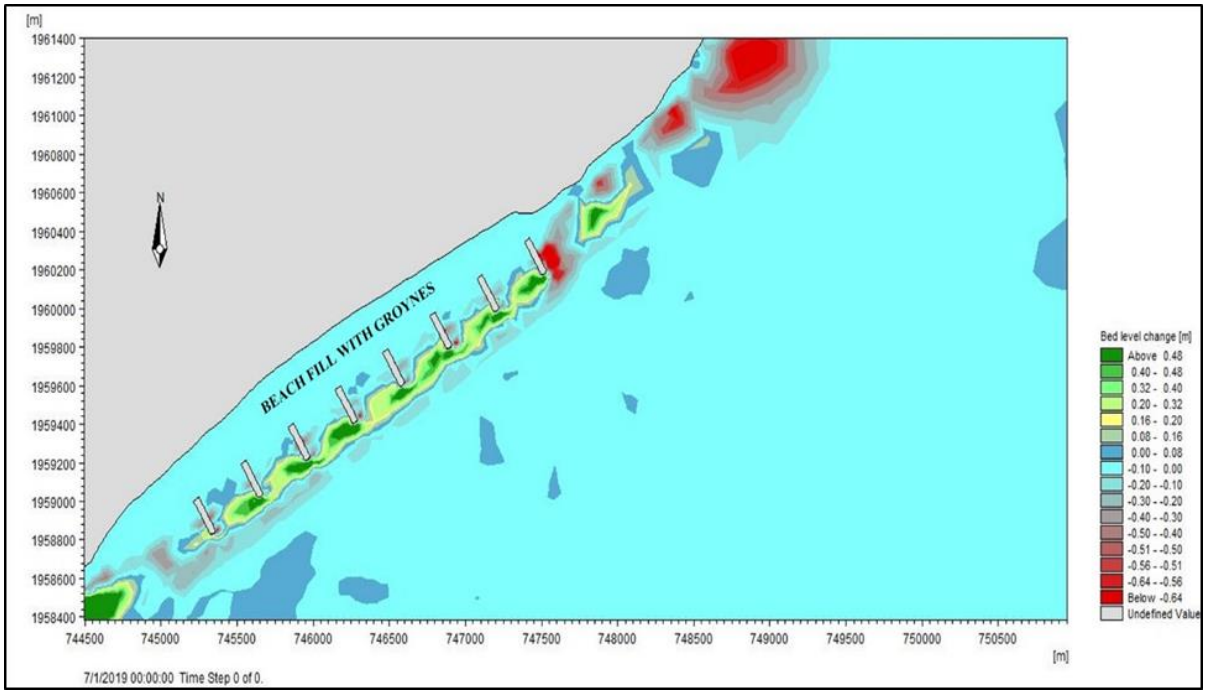



**Figure 6** Statistical mean of Bed Level Change for Beach fill with groynes

### *3.3. Significant Wave Height and Maximum Wave Height*

The wave parameters like Significant wave height ($H_s$), Maximum wave height ($H_{max}$) gives an idea about the intensity of wave action on the face of beach fill. Both these wave height parameters were extracted for typical points on surf zone area on face of beach fill. The mean significant wave height values extracted for typical points on beach fill at +1m contour for both cases were obtained as given below:

**Table 3** Statistical mean values of Significant Wave Height for typical points on Beach fill

| Location | Only Beach fill (m) | Beach fill with 8 Groynes (m) |
|---|---|---|
| Fill portion on updrift side of groynes | 0.62 | 0.33 |
| Mid portion of beach fill between groynes | 0.67 | 0.45 |
| Fill portion on downdrift side of groynes | 0.50 | 0..35 |

The statistical mean maximum wave height values extracted for typical points on beach fill at +1m contour for both cases were obtained as given below:

**Table 4** Statistical mean values of Maximum Wave Height for typical points on Beach fill

| Location | Only Beach fill (m) | Beach fill with 8 Groynes (m) |
|---|---|---|
| Fill portion on updrift side of groynes | 0.62 | 0.33 |
| Mid portion of beach fill between groynes | 0.67 | 0.45 |
| Fill portion on downdrift side of groynes | 0.50 | 0..35 |

The Wave run-up on beach fill slope was another observation made to compare the effect of groynes on beach fill. The wave run-up for both cases can be clearly seen in the figure given below:

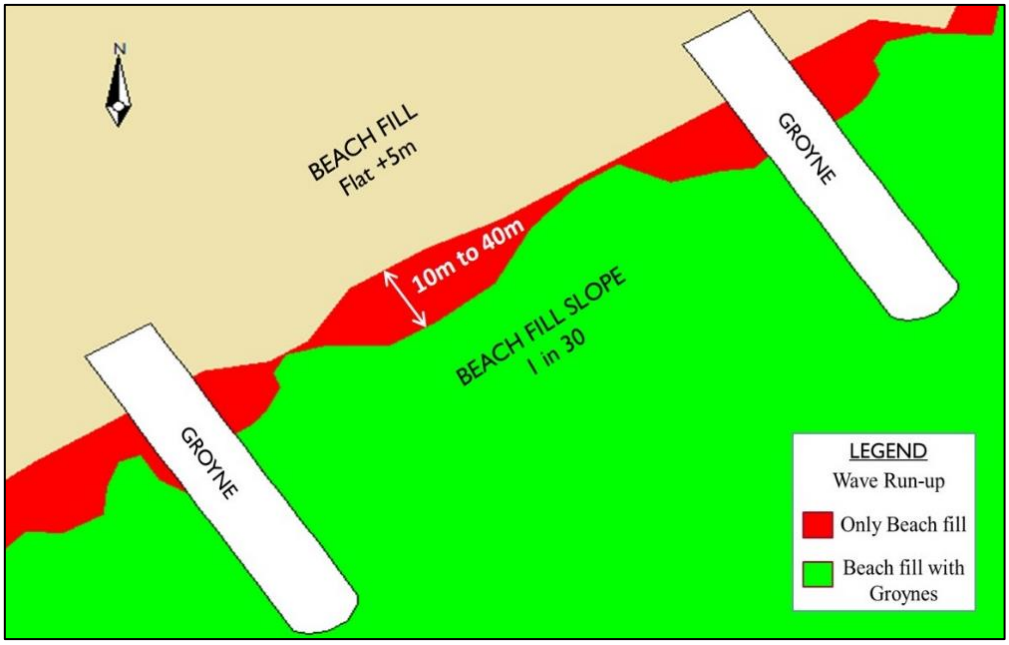



**Figure 7** Extent of wave run-up in beach fill slope portion with and without groynes

From the above figure it is evident that the extend of wave run-up was reduced on beach fill with groynes. The wave run-up distance on beach fill slope was reduced by 10m to 40m with the introduction of groynes on beach fill. This proves that the groyne field helps in reducing wave attack on beach fill slopes and back side flat portions of beach fill is unaffected thus, leaving the beach fill intact without greater damage to the slopes.

## 4. Conclusions

An attempt to find out a solution for coastal erosion along Vishakhapatnam coast by adopting a conceptual artificial beach fill and studying the effect of hard structures such as groynes on the beach fill was successfully done in the present research. A 2D model with flexible mesh was created using MIKE21/3 Coupled model which was calibrated with the current data available for the location. The model simulation runs which includes the baseline model, Beach fill model and beach fill with groyne field model runs were completed successfully and outputs were analysed to arrive at the suitable results and conclusions. The important findings can be summarized as follows:

- The solution of providing an artificial beach fill for the eroding Vishakhapatnam coastline has proven to be successful as it was found to act as a buffer for the existing coastline even during extreme wave climate. Only the beach fill slopes were affected by wave attack and flat fill portion of beach fill was completely undisturbed and hence protecting the existing shoreline areas.
- The beach fill was found to be more stable by the incorporation of groyne field on the beach fill compared to the beach fill without groynes.
- The bed level changes and rate of bed level change has improved significantly by using groyne field on beach fill compared to that without groyne field as less erosion and more accretion took place with use of groyne field.
- The sediment transport rates have been significantly reduced by almost 50% in case of beach fill with groynes compared to Only beach fill scenario, which shows the reduction in beach fill erosion due to littoral drift. The material that is lost from beach fill has reduced hence increasing the longevity of beach fill.
- From the significant wave height and maximum wave height results, almost 30-50 % reduction in wave heights were observed in case of beach fill with groynes, which proves that groynes helped to reduce the effect of wave attack on beach fill.

- The reduction in wave run-up up to 10m to 40m on beach fill slopes was also observed by use of groynes in beach fill.

From the above findings, it is clear that artificial beach fill with groyne field is the best long-term solution that could be adopted for the littoral drift prone coastlines like Vishakhapatnam coastline. The numerical model results were found to be satisfactory in finding the efficacy of use of beach fill for eroding shorelines of Visakhapatnam coast and to prove the positive effect of using groynes on the beach fill. However, before applying these measures to the real-life scenario proper physical model studies are also necessary to arrive at an agreement with the numerical model results obtained.

## 5. References

Coastal Engineering Research Center; Department of the Army, U.S Army Corps of Engineers (1984); *'Shore Protection Manual; Volume 1'*; 1984.

DHI (2014); MIKE 21 FM SW, *User guide*.

DHI (2014); MIKE 21 FM HD, *User guide.*

DHI (2014); MIKE 21 FM ST, *User guide.*

DHI (2014); MIKE 21/3 Coupled Model FM, *Step- by -step training guide*.

Kannan et al. (2016); *'Detection of Shoreline Changes Visakhapatnam Coast, Andhra Pradesh from Multi-Temporal Satellite Images'*; Journal of Remote Sensing & GIS 2016, 5:1.

M. Phani Kumar et al. (2020); *'Application of Principal Component Analysis to Ascertain the Beach Morphological Conditions Adjacent to a Major Port'*; International Journal of Research in Engineering and Science (IJRES), Volume 8 Issue 2 Ser. I ǁ 2020 ǁ PP. 07-15.

M. Phani Kumar et al. (2011);*' Littoral Drift Management – A Success Story of Visakhapatnam Port'*, ISH Journal of Hydraulics Engineering, Vol 17, No.2, 2011.

M Phani Kumar et al. (2005). *'Beach Nourishment on Down-Drift Side of a Major Port in Large Littoral Drift Region'*; Proceedings of HYDRO conference. SIT, Tumkur.

N. Sharmila et al.;(2019). *'Studies on the Morphological Changes by Numerical Modelling Along Kakinada Coasts'*, Proceedings of the Fourth International Conference in Ocean Engineering (ICOE2018).

Parvathy K.G et al. (2014); *'Wave Transformation along Southwest coast of India using MIKE 21'*; International Journal of Ocean and Climate Systems, Vol. 5, Number 1,2014.

Report by Coastal & Environmental Engineering group, National Institute of Ocean Technology, Chennai (2015)*; 'Beach Erosion Studies and Engineering Mitigation Measures for Visakhapatnam'*; July 2015.

Report by DELTARES (2019); *'Coastal Erosion Mitigation and Shoreline Management Plan for Visakhapatnam-Numerical modelling of the reference situation'*; 2019.

V.Sanil Kumar (2004); *'Wave characteristics off Visakhapatnam coast during a cyclone'*; Current Science, Vol. 86, No. 11, 10 June 2004.

*IN PROCEEDINGS OF 25th HYDRO 2020, INTERNATIONAL CONFERENCE, NATIONAL INSTITUTE OF TECHNOLOGY ROURKELA, ODISHA, INDIA 26-28, March 2021, ISBN 978-93-90631-56-8*

Paper ID - 383

# EFFECT OF POROUS BAFFLE ON SLOSHING DYNAMICS PLACED AT *L /2* LOCATION IN A SWAY EXCITED RECTANGULAR TANK

Sahaj K V[1 +], Pavan Kumar[2], Nasar T [3]

*Department of water resources and ocean engineering, National Institute of Technology, Karnataka, Surathkal, Mangalore, 575025, India*

*[1]Research scholar, Email: sahaj30.k.v@gmail.com*

*[2]M.Tech student, Email: pavanpatil415@gmail.com*

*[3]Associate Professor, Email: t.nasar@gmail.com*

## Abstract

The large liquid movement in tanks creates highly localized impact pressure on tank walls and also displays a violent disturbance in the fluid. Hence, this highly nonlinear nature of the problem is the greatest hindrance in solving such a problem analytically and even computationally. Ship structures are likely subjected to impact pressure actions arising from sloshing, slamming, and green seas while in service. The accelerations arising from the motions of a ship in a sea way produce sloshing loads, that is, inertial reactions, on partially filled liquid cargo tank structures of the ship. Motions of liquid cargo vessels such as oil tankers often produce severe sloshing loads. Tanks of moored floating, production, storage, and offloading units are continuously loaded and unloaded, and sloshing in the tanks is unavoidable. In view of this difficulty, an experimental study has been carried out to assess the sloshing oscillation expected on the side walls of the tank. A liquid fill level with an aspect ratio ($h_S$ /*l*, where $h_S$ is static liquid depth, *l* is tank length) of 0.1625 and 0.325 is considered which corresponds to 25% and 50% liquid fill level. In view of suppressing sloshing oscillation and baffle wall configurations with different porosities (4.4%, 6.8% and 9.2%) by placing baffle at a distance of *L/2* in a rectangular tank are studied. The sloshing tank of model scale 1:43 is fitted into the horizontal shake table.

***Keywords:*** *Shake table, Sloshing tank, Porous baffles.*

## 1. Introduction

Sloshing occurs in partially filled tank due to external excitations like Wave motion, earthquake and underwater explosions or with fluid of changing states. This sloshing force depends on the volume of the ship, the larger the volume of a ship, the more possible its exposure to excessive sloshing loads during the ship operation life. This sloshing is important in various engineering disciplines and can occurs in ships carrying oil, trucks, elevated tanks, in a reservoir and space aircraft and rockets, due to the external excitation force. Wave motion, earthquake or underwater explosions may cause, large-amplitude sloshing motions and even structural damage to ships and other oil carrying tanks. In such situation, this influent together with the liquid which is inside the liquid tanks or any other oil carrying tank, which will oscillate along with the tank, may cause additional damages to ship structures, which is a great threat to the structural strength and safety of the ship. Even it will cause a more threat to the structural strength and ship safety, especially when the frequency of liquid sloshing matches the natural frequency of the ship or tank which carries the oil. Therefore, the studies of the sloshing characteristics and mechanisms of liquid tanks have great significances for the ship stability and security. Liquid sloshing in oil carrying ship or tank is a complex nonlinear motion due it involves free surface oscillation, splashing and complex coupling motion of liquid and the hull. Therefore, many scholars have focused on this dynamic problem. As the fluid sloshing in a tank is of a non-linear movement, there is no theoretical solution exists so far. Hence, the experimental is the main methods used in present studies.

To minimize the potential sloshing damage due to sloshing to the structures, the use of Baffle walls has been suggested to control the sloshing behavior and to reduce the effect of sloshing in an oil carrying tank. Even, the damping mechanism of baffle wall is still not fully understood due to the complexity and highly nonlinear nature of the sloshing problems. Hence to reduce the sloshing force, baffle walls are made up with different porosity. Numerous amounts of work on finding of sloshing loads using

vertical baffles with different porosities have been carried out in recent years. Studies have been made on effects of perforated baffle on reducing sloshing in rectangular tank oil carrying tank and found that vertical baffles are effective at external excitation frequencies lower than the natural frequency of the tank and when the excitation frequency exceeds the natural frequency of tank, perforated vertical baffles performed better. In this study an experimental study to investigate the effectiveness of one vertical mounted baffle configurations in suppressing the sloshing force under a wide range of sloshing frequencies has conducted by placing the wall at a distance *L/2*. In this present work, the problem was confined to liquid sloshing in a rectangular tank on shake table experiment under dynamic sway excitations to investigate the variations of the dynamic forces and the effectiveness of vertical baffle on damping liquid sloshing forces. Experiments are carried out for a sloshing tank with and without baffles for different fill levels. For each, water filling ratio, the excitation frequency is chosen close to the fundamental frequency of oscillation of the contained liquid to provide maximum slosh forces. The different design parameters of the baffles and tank have been tested, these include the tank filling ratio, excitation amplitude, excitation frequency and baffle porosity.

Armenio and La Rocca (1996) investigated sloshing oscillation behaviour in a roll excited tank by both experimental and numerical approaches. Cariou and Casella (1999) reviewed the state of the art of the codes available to predict sloshing oscillation and consequent sloshing pressure. Celebi and Akyildiz (2002) solved Navier Stokes equation using finite difference method and investigated the liquid sloshing in a 2D moving tank. Saghi (2016) developed a numerical model using coupled boundary element methods to determine pressure distribution on the rectangular and trapezoidal storage tanks. The above studies are deal either translational or rotational degree of excitation. Studies have also been carried out to estimate liquid sloshing pressure on its containment in the combined mode of excitation. A computational study by Celebi and Akyildiz (2002) traced the pressure time history on a tank wall subjected to combined heave and roll excitation. Nasar et al (2008 and 2012) carried out an experimental work and discussed wave induced sloshing pressure / impact pressure. Xue et al. (2017) investigated liquid sloshing phenomena in cubic tank with horizontal baffle, perforated vertical baffle, and their combinatorial configurations under the harmonic motion excitation. Warnitchai and Pinkaew (1998), observed the performance of various devices and a wire mesh screen device is chosen for further investigation. Akyildiz (2012), investigated the effects of the vertical baffle based on the liquid sloshing in a moving partially filled 2-D-ractangular tank. The objective is to evaluate the sloshing dynamics in a sway excited rectangular tank with 25% and 50% fill levels for three different porosities.

To reduce the negative effects of longitudinal liquid sloshing on tankers, baffle walls are placed at *l/2* distances. The objective of this research is to investigate the influence of the porous baffles on a sway excited rectangular tank and compare the experimental results of with and without porous baffles.

## 2. Methodology

The Figure.1 shows the procedure to be flowed for the experiment and steps followed to arrive at the required results. `

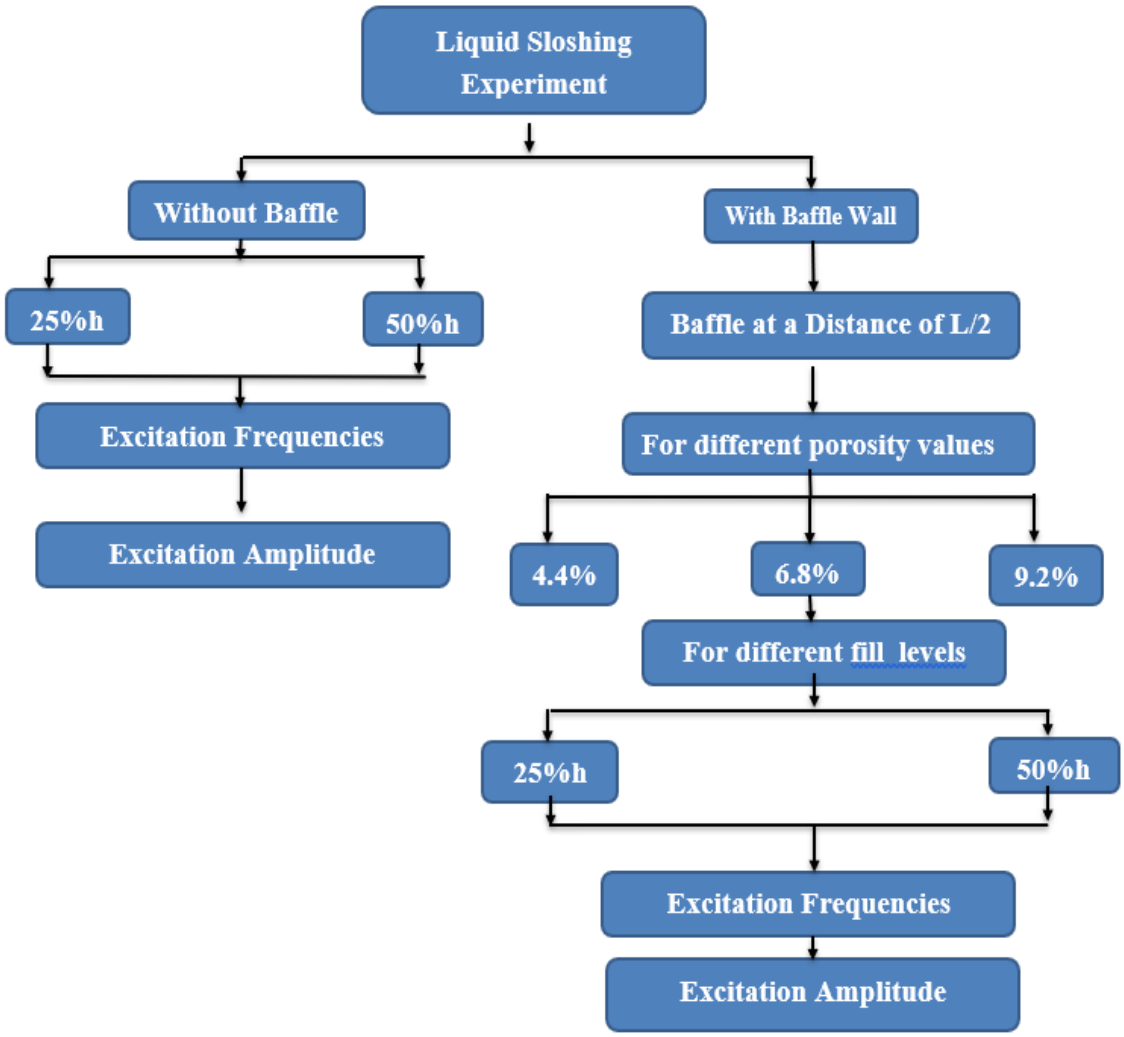



**Figure 1:** Flow Chart of Methodology

## 3. Experimental set-up

A 1:43 scaled liquid sloshing tank was used in this study. A tank was fabricated using acrylic sheets of 12*mm* thickness with inner dimensions of 1.0*m* (*l*) x 0.4*m* (*b*) x 0.65*m* (*h*). A rectangular tank is placed on shake table, the shake table setup consists of two platforms to secure the sloshing tank and dead weight, a driving unit and a Data Acquisition System (DAQ).The Fig.2 shows schematic sketch of experimental setup and Fig. 3. Shows Experimental Setup of Liquid Sloshing Tank. The driving unit encompasses input software to the Shake Table and hydraulic power pack. The liquid tank is positioned on the shake table such that during the sway excitations, the sloshing oscillations occurs along the longitudinal axis. The DAQ consists of 16channel 16*bit* resolution data logger. Capacitance type wave probes were used to measure the free surface response. Two waves probes were used which were placed at the end walls of the tank. The instrumentation is used to capture the free surface response and table motion.

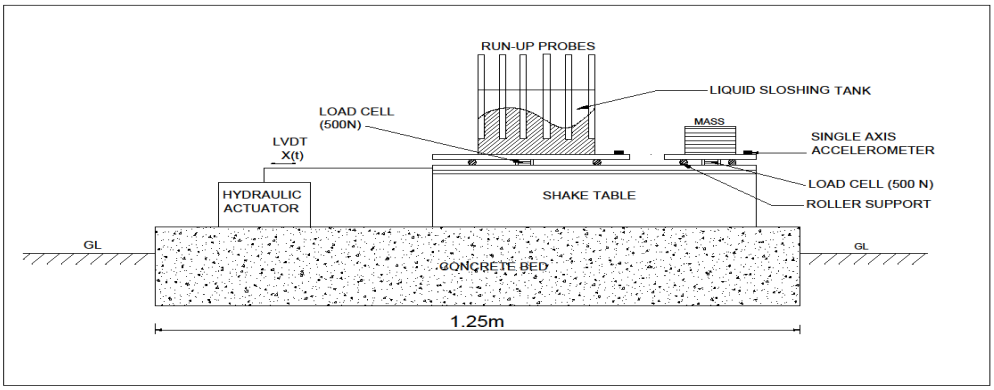



**Figure 2:** Schematic Sketch of Experimental Setup.



**Figure 3:** Experimental Setup of Liquid Sloshing Tank.

## 4. Results and Discussion

In the present study we have conducted the experiment for knowing the dynamic sloshing water surface elevation in a rectangular sloshing tank for without porous baffles and with porous baffle condition. The liquid-sloshing behaviour in the partially filled tank depends on the excitation frequency and amplitude, size of the tank, geometry of the tank, liquid-filled depth and baffle arrangements, if any. Consequently, the sloshing pressure may be of non- impulsive or impulsive type. We considered low frequency modes i.e. 1 to 5 modes and one value of volt peak to peak for the sloshing experiment.

The experiment is conducted for above conditions, giving input data as excitation frequency and excitation amplitude. This inputs given to shake table experiments, the tank which is placed on shake table which start moving forth and back. During this movement, there develops water oscillation due to the water inertial force. To capture wave data four wave probes are used and to capture water inertial force.

### *4.1 Free Surface Response*

The time series of normalized free surface of sloshing oscillation with respect to different time intervals. This graph represents the variations of free surface of water and magnitudes of the free surface of water with and without porous baffles, the baffle wall is placed at a distance at *l/2*. The graph is plotted for the frequencies of $f_1$, $f_2$, $f_3$, $f_4$, and $f_5$ excitation frequencies and considered respective excitation

amplitude and for water fill levels of 25% & 50% of the tank. Fig. 4 and Fig.5 explains the normalised free surface oscillation and demonstrate the comparison between without baffle and with baffle condition for 25% and 50% fill condition. Free surface of the water is normalized with respect to the depth of the water, equation shows below.

$$\eta' = \frac{\eta}{h_s} \tag{1}$$

Where $\eta$ is free surface elevation of the water and $h_s$is the static water depth.

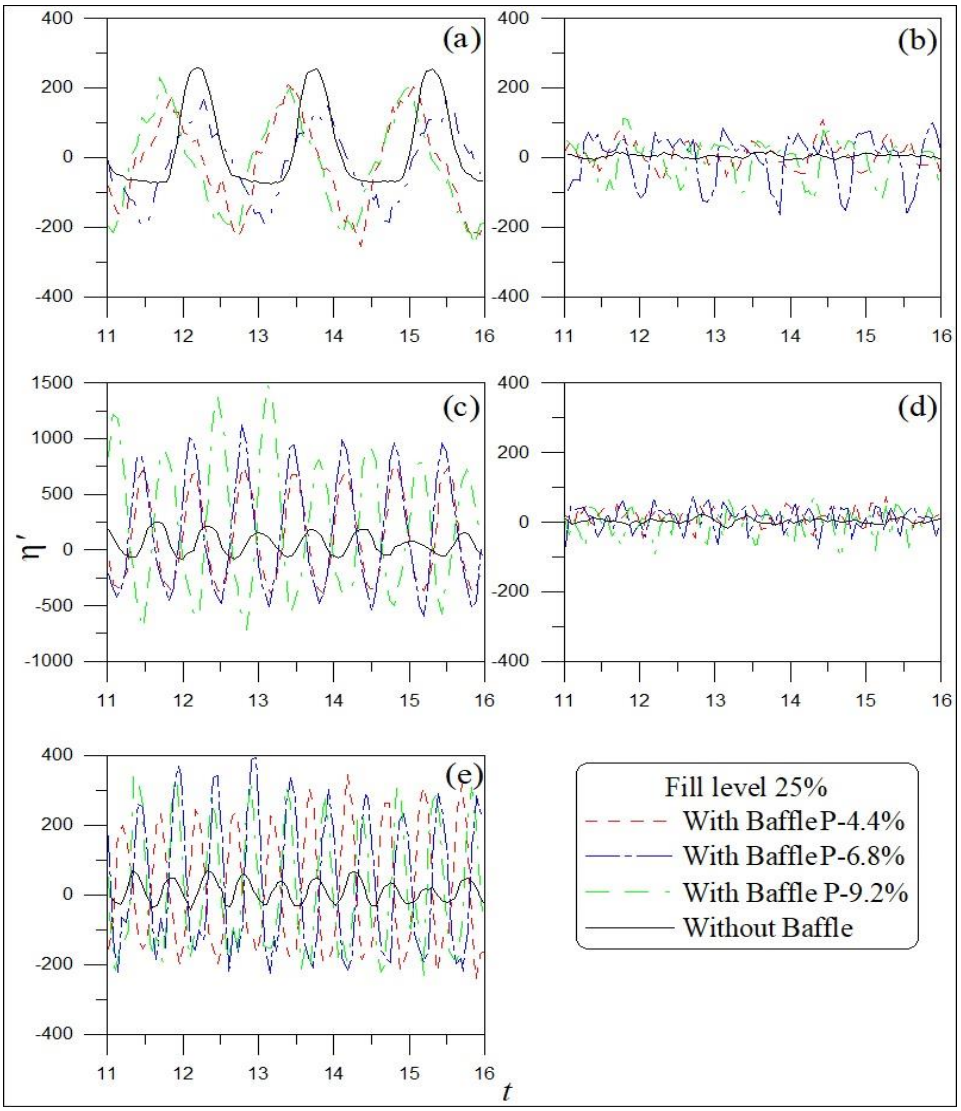



**Figure 4:** Experimental Free Surface Elevation Response for *hs*/*l* = 0.163 and Excitation at Natural Sloshing Frequencies (a) *f* = 0.7755 *Hz* ($f_1$), (b) *f* = 1.2277 *Hz* ($f_2$), (c) *f* = 1.5270 *Hz* ($f_3$), (d) *f* = 1.7666 *Hz* ($f_4$) and, (e) *f* = 1.9756 *Hz* ($f_5$).

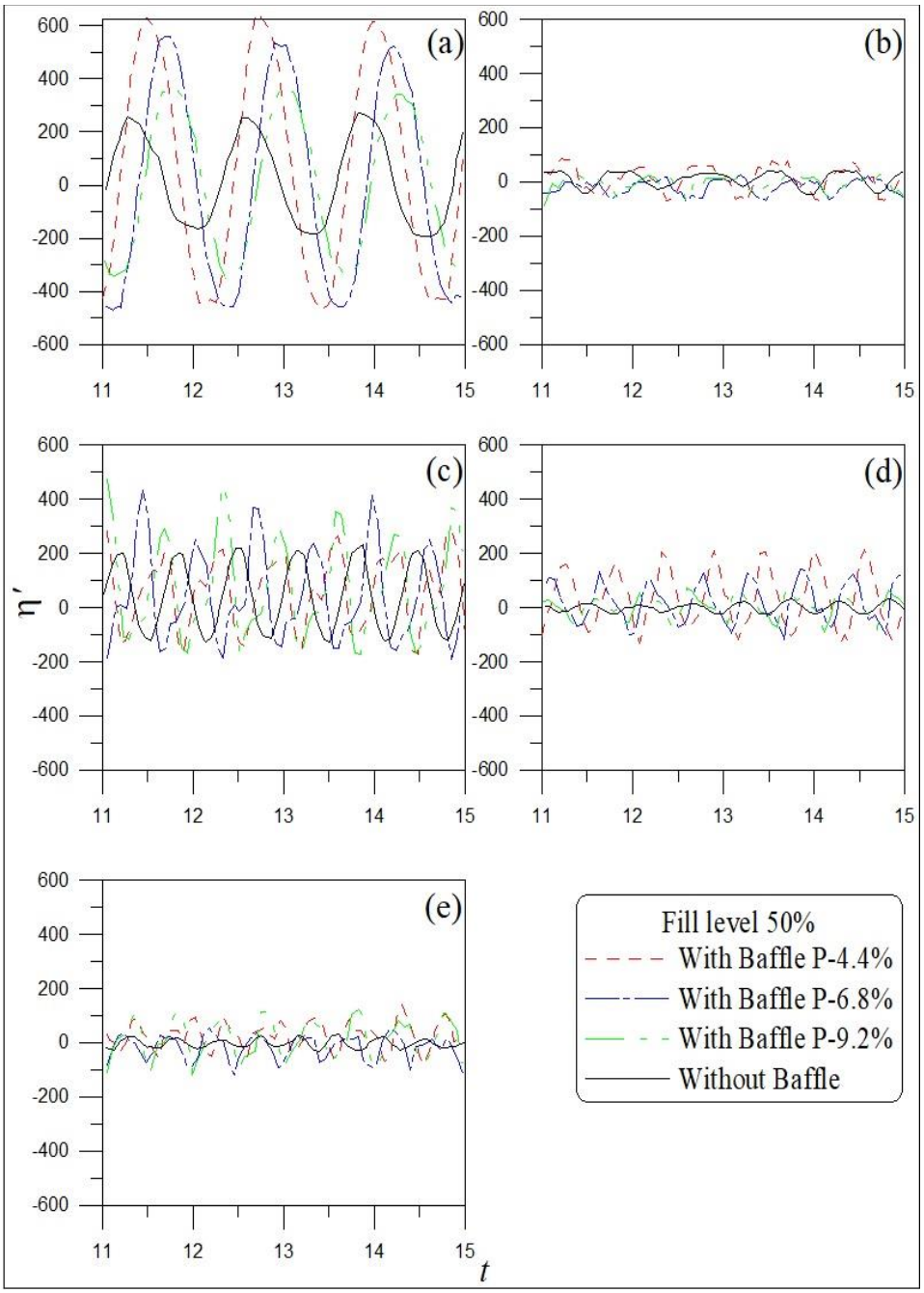



**Figure 5:** Experimental Free Surface Elevation Response for *hs/l* = 0.325: and Excitation at Natural Sloshing Frequencies (a) $f$ = 0.7755 *Hz* ($f_1$), (b) $f$ = 1.2277 *Hz* ($f_2$), (c) $f$ = 1.5270 *Hz* ($f_3$), (d) $f$ = 1.7666 *Hz* ($f_4$) and, (e) $f$ = 1.9756 *Hz* ($f_5$).

Comparition of above free surface elevation response results of with and without porous baffle of different porosities leads to the following oberservations:

- As seen from graphs for both with and without baffle conditions, for the odd mode frequencies i.e, $f_1$, $f_3$, and $f_5$the normalized free surface elevation is more compared to the even mode frequencies i.e, $f_2$ and $f_4$for 25% fill level.
- As in case of 50% of water depth there is slight changes, for the last mode frequency ($f_5$), the normalized free surface elevation is slighlty lower than even mode frequencies.

- In all the cases normalized free surface elevation is more with baffle condition compared to without baffle condition.
- In case of without baffle the normalized free surface elevation mangitude is keep deccreasing with the increases in excitation frequency for both the fill levels. But in case of with baffle the pattern is not same, the normalized free surface elevation for $h_s/l$=0.1625 condition is getting more value for $f_3$ and in case of $h_s/l$=0.325 condition more value getting at $f_1$.
- For third mode frequency ($f_3$) the normalized free surface sloshing amplitude is more compared to all other mode frequencies and it increases with increasing the porosity of the baffle for both 25% fill level and in case of 50% fill level it is occuring at first mode frequency ($f_1$).
- For both with and without baffle cases $h_s/l$=0.1625 tank has high free surface response amplitude than the $h_s/l$=0.325 tank.
- For porous baffle third sloghing mode is the critical mode of sloshing.
- For second and fourth sloshing modes normalized free surface apmplitude increases with increasing the porosity of the baffles.

### *4.2 Spectral Moment ($m_0$)*

The area under the wave spectrum gives the total energy of the irregular wave system per plan area and also the variance value of the water surface fluctuations. $m_0$ is calculated for the different excitation frequencies and excitation amplitude.Below Fig. 6 shows the graph between the $m_0$ verses frequency ratio. The graph of the spectral density function versus wave frequency is called the wave spectrum.Sea surface elevation being considered at a point which is at a horizontal distance '$x$' from any chosen origin and at time instant '$t$' ($\eta$ ($x$, $t$)) is,

$$\eta(x,t) = \sum_{n=1}^{M} a_j \cos(k_j x - \omega_j t + \theta_j) \tag{2}$$

Where,

$M$ Number of linear waves being added together. $A_j$ Amplitude of the $j^{th}$ wave$K_j$ Wave number of the j$^{th}$ wave ((2 π)/Length of the j$^{th}$ wave), $\Omega_j$ Angular wave frequency ((2π) / Period of the $j^{th}$ wave = (2 π) x frequency in cycles per second of the j$^{th}$ wave), $\theta_j$ Phase of the j$^{th}$ wave assumed to be uniformly distributed over the interval (0, 2 π).

The amplitude ($a_j$) of the component wave is related to an important statistical function called the Spectral Density Function by the relationship.

$$a_j = \sqrt{2S_\eta(\omega_j)\Delta\omega} \tag{3}$$

Where,

$S_\eta(\omega_j)$ Spectral density function corresponding to the frequency $\omega_j$ for sea surface ($\eta$), $\Delta\omega$ frequency step or interval used in calculating above mentioned function.

Once a wave spectrum is known, a variety of information can be deduced from it. The significant information obtained is that of the wave frequency composition in a given wave sample. Further the area under the wave spectrum gives the total energy of the irregular wave system per plan area and also the variance value of the water surface fluctuations. Through the MATLAB coding $m_0$ can be found for the different excitation frequencies and same excitation amplitude. The graph is plotted for 25% and 50% fill level and for $f_1$, $f_2$, $f_3$, $f_4$, and $f_5$ excitation frequencies.

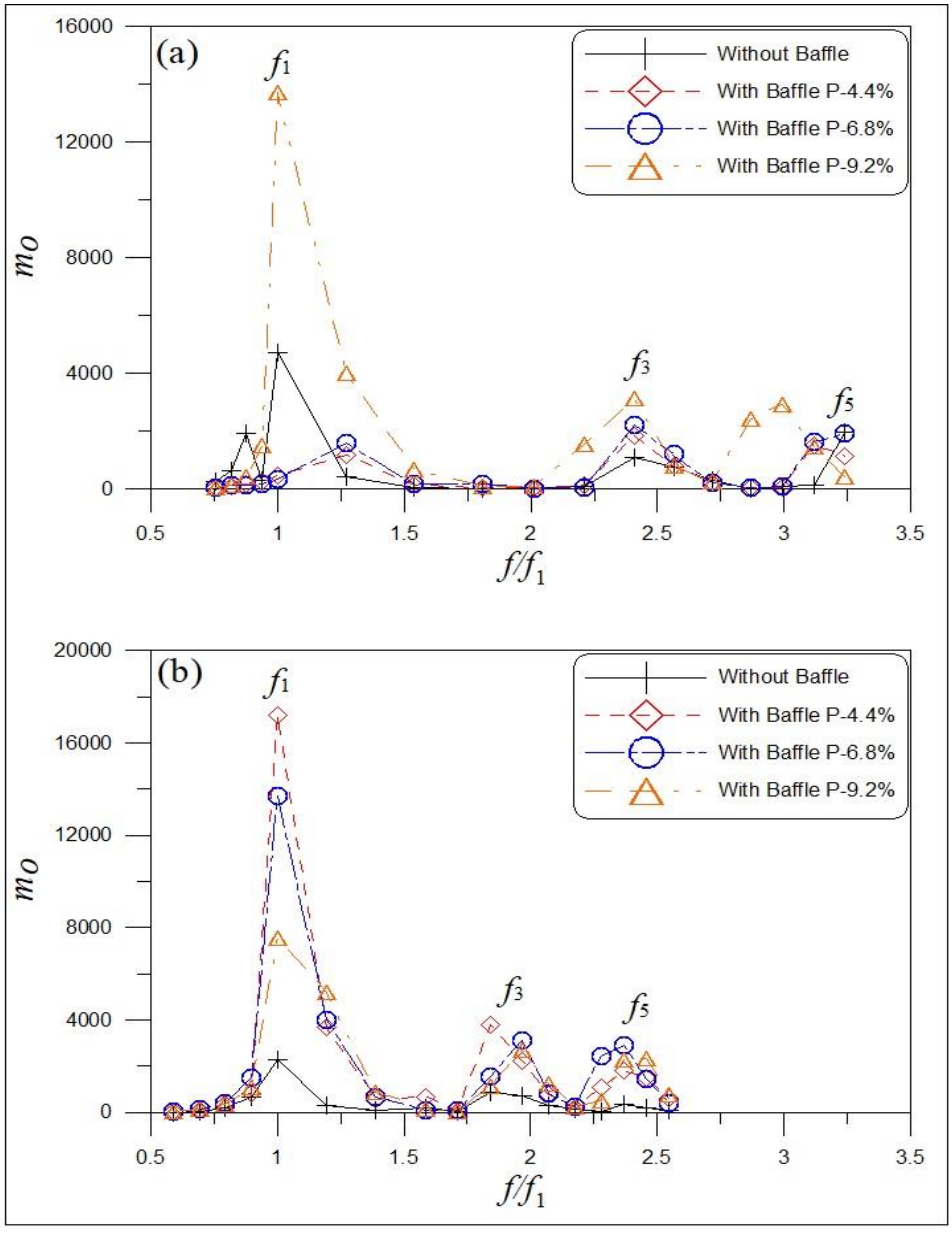



**Figure 6:** Variation of Spectral Energy ($m_o$) with Different Frequencies Ratio ($f/f_1$);

for (a) $hs/l$ = 0.1625 and, (b) $hs/l$ = 0.325

Comparing the below plots of $m_0$ versus frequency ratio of with and without porous baffles of different porosities leads to the following oberservations:

- In below graphs it is observed that the maximun $m_0$ value is getting at odd mode frequency i.e. $f_1$, $f_3$ and $f_5$ respectively.
- $m_0$ value of with baffle is greater than the without baffle condition for both the 25% and 50% of water fill level.
- In 25% fill level for 9.2% porosities $m_0$ value is greater than the 4.4% and 6.8% porosity and without baffle.
- In case of the 50% fill level for $m_0$ value for 4.4% porosities is greater than 6.8% of porosity, and this value greater than 9.2% porosity.
- As comparing two fill levels, 50% fill level $m_0$ magnitude is greater than 25% fill level.

## 5. Conclusions

- Porous baffle walls found to be effective in reducing the sloshing pressure in a rectangular tank.
- Due to the presence of the porous baffles the free surface oscillation is less compared to without baffle.
- For with and without porous baffles conditions $h_s/l$=0.1625 tank has more free surface elevation than the $h_s/l$=0.325 tank.
- For porous baffle third mode sloshing frequency is the critical mode.
- With graphical illustration, it is found that the increasing liquid filling level in the rectangular tank will increase the nonlinearity of the liquid motion during the sloshing.

## References

Akyildiz, H. (2012). A numerical study of the effects of the vertical baffle on liquid sloshing in two-dimensional rectangular tank. *Journal of Sound and Vibration*, *331*(1), 41-52.

Armenio, V., and La Rocca, M. (1996). On the analysis of sloshing of water in rectangular containers: numerical study and experimental validation. *Ocean engineering*, *23*(8), 705-739.

Cariou, A., and Casella, G. (1999). Liquid sloshing in ship tanks: a comparative study of numerical simulation. Marine structures, 12(3), 183-198.

Celebi, M. S., and Akyildiz, H. (2002). Nonlinear modelling of liquid sloshing in a moving rectangular tank. Ocean Engineering, 29(12), 1527-1553.

Kim, Y. (2001). Numerical simulation of sloshing flows with impact load. Applied Ocean Research, 23(1), 53-62.

Nasar, T., Sannasiraj, S. A., and Sundar, V. (2008). Experimental study of liquid sloshing dynamics in a barge carrying tank. *Fluid Dynamics Research*, *40*(6), 427.

Nasar, T., Sannasiraj, S. A., and Sundar, V. (2012). Liquid sloshing dynamics in a barge carrying container subjected to random wave excitation. *J. Naval Architecture and Marine Eng.*, *9(*1), 43-65.

Saghi, H. (2016). The pressure distribution on the rectangular and trapezoidal storage tanks' perimeters due to liquid sloshing phenomenon. *International Journal of Naval Architecture and Ocean Engineering*, *8*(2), 153-168.

Warnitchai, P., and Pinkaew, T. (1998). Modelling of liquid sloshing in rectangular tanks with flow-dampening devices. *Engineering structures*, *20*(7), 593-600.

Xue, M. A., Zheng, J., Lin, P. and Yuan, X. (2017). Experimental study on vertical baffles of different configurations in suppressing sloshing pressure. *Ocean Eng.*, *136*, 178-189.

*IN PROCEEDINGS OF 25th HYDRO 2020, INTERNATIONAL CONFERENCE, NATIONAL INSTITUTE OF TECHNOLOGY ROURKELA, ODISHA, INDIA 26-28, March 2021, ISBN 978-93-90631-56-8*

Paper ID - 426

# FORECASTING OF NATURAL DISASTERS, A CASE STUDY ON COASTAL PART OF ANDHRA PRADESH

Karanam Raviteja[1], Kanhu Charan patra[2], Uma Maheswar rao[3]

[1]*MTech Scholar, Department of Civil Engineering, NIT Rourkela, Odisha 769008, India*
[2]*Professor, Department of Civil Engineering, NIT Rourkela, Odisha 769008, India*
[3]*PhD Scholar, Department of Civil Engineering, NIT Rourkela, Odisha 769008, India*
*Email:* karanamraviteja97@gmail.com

## Abstract

India has been vulnerable to natural disasters particularly floods, cyclones, droughts, extreme heatwaves, landslides, and tsunamis on account of its change in the climate. According to the Global Climate Risk Index report 2019, India is the 14th most vulnerable country in the world due to extreme weather-related events. In India, it is found that these disasters frequently hit the coastal belt, so here an attempt is done to estimate the future magnitude of the disasters at the coastal belt of Odisha and Andhra Pradesh. After the industrial revolution the data indicates that the frequency as well as magnitude of all-natural disasters increased. The damage due to natural disasters affects people and the environment in all directions. It is hard to predict the occurring of natural disasters but with the latest forecasting techniques by machine learning algorithms attempt can be done to forecast the magnitude of the disasters. It is time to forecast the magnitudes of natural hazards to mitigate the damage to infrastructure, economy, and fatalities. Statistical analysis can be done with the historical natural disaster data to find the trend and correlation among the climatic parameters concerning time and changing land use land cover. The result of this study would help the local authorities for better planning and management of disasters and take appropriate emergency action plans to reduce the damage in the particular area.

***Keywords:*** *Natural disasters and management, Machine learning algorithms, Statistical analysis*

## 1. Introduction

A natural disaster is a catastrophe or tragedy that occurs in any place as a consequence of natural causes and causes significant Deaths, property destruction, and environmental destruction are all possible outcomes. Natural calamities include earthquakes, volcanoes, floods, tsunamis, cyclones, heat and cold waves, droughts, wildfires, solar flares, and many others. Geological catastrophes, Hydrologic disasters, Meteorological disasters, and Space disasters are the four types of natural disasters that can occur. Geological disasters cause significant damage, but their frequency and scale in India are minimal when compared to Hydrologic and Meteorological Disasters, according to historical statistics. India is extremely vulnerable to natural calamities, both hydrologic and meteorological. Not only in India, but around the world, the frequency and size of these calamities have been steadily growing. It is apparent that the frequency of catastrophic calamities has begun to rise since the industrial revolution. The industrial revolution and increasing urbanization resulted in significant climate change, as well as changes in land cover/use and vegetation cover. Variations in rainfall intensity and frequency resulted from these changes, as well as an increase in global average temperature. Around 5700 km of India's coastal line, out of a total of 7516 km, is often subjected to tsunamis and cyclones. According to the 2019 Global Climate Risk Index report, India is the world's 14th most susceptible country. Floods are India's most common natural disaster, accounting for 52 percent of all calamities, followed by cyclones (30 per cent).

## 1.1 Climate Change

The burning of fossil fuels, which releases heat-trapping gases into the atmosphere, is a major contributor to global warming. is responsible for a wide range of global occurrences. In addition to the increasing temperature trends indicated by global warming, these phenomenon include sea-level rise, the Arctic, Antarctica, ice mass loss in Greenland, and mountain glaciers all around world, plant blossoming, and weather extremes.

## 1.2 Climate change's impact on Natural Disasters

Natural catastrophes can have devastating effects the environment, on societies and the economic prosperity of the countries affected. Extreme events are putting a strain on industries that are strongly linked to the climate, such as agriculture, tourism, and water(Field et al. 2012). The Intergovernmental Panel on Climate Change assessed the impact of climate change on severe events, and also the societal and environmental consequences of these occurrences, and also the implications for risk management (IPCC). Climate extremes are a normal feature of the climate system, according to the IPCC report, but "extreme weather and climate events alter in frequency, geographic area, severity, length, and timing as a result of climate change, which can lead to unexpected extreme climate and weather occurrences" (IPCC 2012b). Extreme events can thus occur as a result of changes in the variance, mean climate, or probability. A change in the mean temperature distribution, for example, could increase extreme hot weather while decreasing severe cold weather.

Extreme hot and cold weather could become more common as a result of increased variability. The tails of the probability distribution function of climate variables, where the biggest change is reported in percentage terms, document climate extremes(Trenberth 2011).

Hansen et al. (2012)(Hansen, Sato, and Ruedy 2012) represented the movement in the distribution of global temperature anomalies during the last 30 years by examining historic summer temperatures and expressed them in standard deviation units, as part of the analysis of a shifting probability distribution. They show how, in comparison to the 1951–1980 mean, the anomalous distribution has widened over the last three decades, making exceptionally hot summers more common. They also determined that the proportion of global land area experiencing exceptionally warm summer outliers of $+3\sigma$ has increased by nearly an enormous margin.

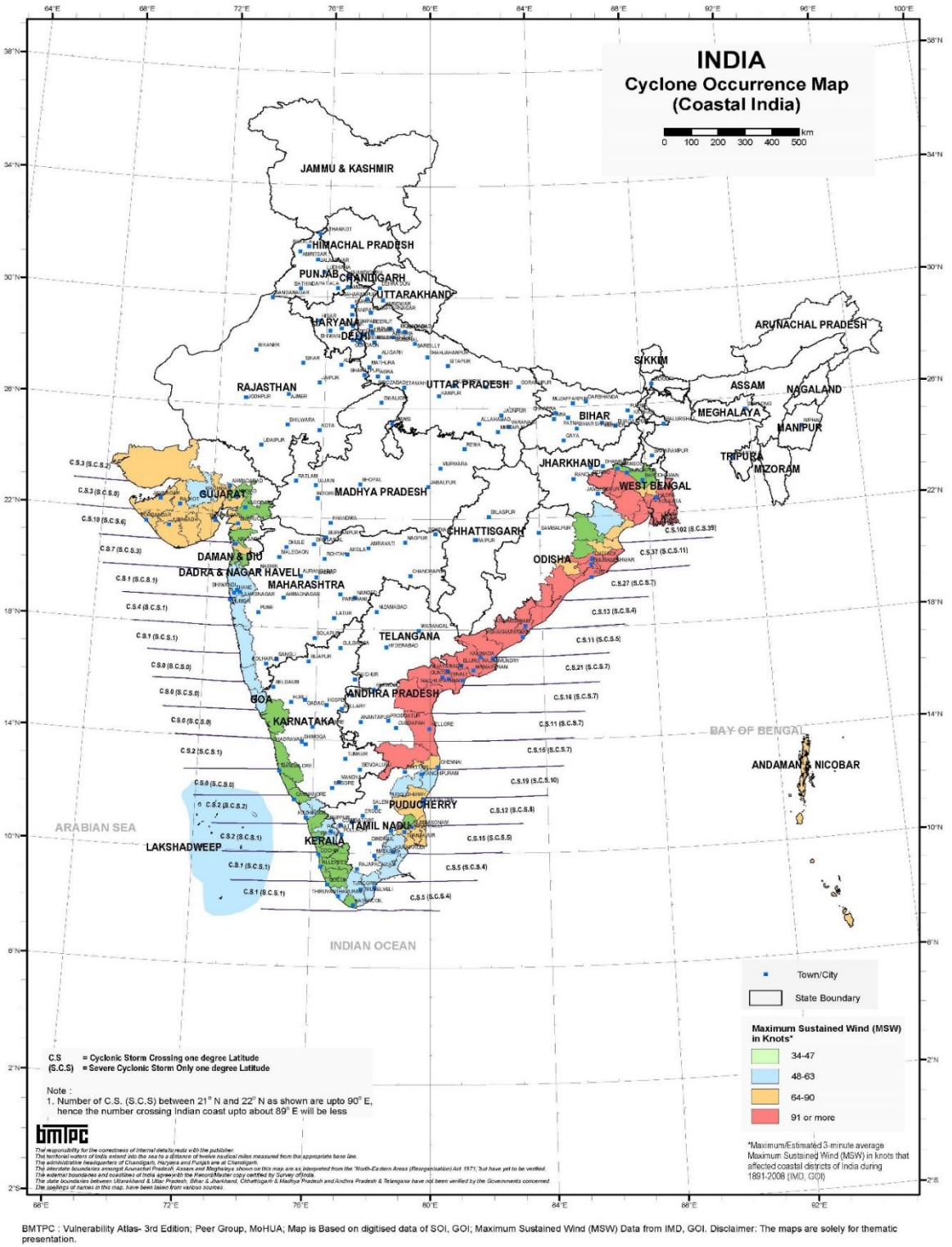
Extreme occurrences are rare by definition, as a result establishing long-term patterns and formulating future estimates is difficult. However, with varying degrees of confidence, some previous trends and future projections can be made.

To differentiate the impact of climate change from observational improvement, non-climate occurrences could be reported. Earthquakes, for example, are not climatic events, but they can be used to assess the effects on information access versus climate change(Peduzzi 2005). Since 1970, both the number of recorded earthquakes and the number of recorded climatic disasters has increased, owing to improved access to information. However, the number of earthquakes has stayed stable since the initial spike, whereas the number of floods, for example, has continued to rise. The fact that tectonic events are stable but climatic events are growing raises concerns about climate change's impact on natural disaster frequency.

Observational data shows that weather and climate extremes have changed since 1950 as a result of human influence on the climate system. The number of cold days and nights has reduced, while the number of warm days and nights has increased. Heatwaves have become more common in most parts of Europe, Asia, and Australia(Stocker et al. 2013).Furthermore, several places have seen a statistically significant rise in heavy precipitation events (e.g., 95th percentile). This is in line with the rising temperature and reported water vapour levels in the atmosphere. Droughts, floods, and cyclone activity have less stable tendencies. Some areas have had more severe and longer droughts, while others have seen a drop.

## 1.3. Analysis of Natural Disasters in India

The natural features of India are extremely diverse. Its peculiar geo-climatic circumstances make it one of the most vulnerable countries in the world to natural disasters. In India, disasters strike frequently, and though society as a whole has adapted to these recurring events, the economic and social consequences continue to rise year after year. It is extremely vulnerable to floods, droughts, cyclones, earthquakes, landslides, and other natural disasters. Almost every portion of India is affected by one or more of these occurrences. Because of their geological features, several parts of India are extremely prone to natural calamities. Seismic damage to buildings affects about 59 percent of the country's total area (BMTPC, 1997 & 2006). According to India's current seismic zone map, the most vulnerable places include the Himalayan and Sub-Himalayan regions, Kutch, and the Andaman & Nicobar Islands, all of which are highly earthquake-prone.




BMTPC : Vulnerability Atlas- 3rd Edition; Peer Group, MoHUA; Map is Based on digitised data of SOI, GOI; Maximum Sustained Wind (MSW) Data from IMD, GOI. Disclaimer: The maps are solely for thematic presentation.

*Figure 1 Cyclone occurrence map of India*

## 2. Study Area

Cyclones, storm surges, floods, and droughts all threaten Andhra Pradesh. Every two to three years, a storm of moderate to severe severity will make landfall. Tropical storms and related dangers threaten about 44% of the state. The bulk of cyclones originate in India during in the pre-monsoon (Apr to May) and post-monsoon (Oct to Dec) seasons. Cyclones mostly on east coast mainly originate in the Bay of Bengal, the Andaman Sea, or even the South China Sea, and then make their way to the shores of states Tamil Nadu, Andhra Pradesh, Orissa, and

West Bengal, are the most vulnerable. In October 1971 and November 1977, respectively, two of the deadliest cyclones of the twentieth century struck Orissa and Andhra Pradesh, killing over 10,000 people in each case. The mega-storm that hit Orissa in 1999 killed several people and destroyed a lot of property.

Cyclones, floods, earthquakes, and drought have all wreaked havoc on Andhra Pradesh. Cyclones and floods hit the coastal region frequently. The central and state governments of India, as well as international donor communities, responded appropriately to the 1977 cyclone and tidal wave, which resulted in a large number of deaths, as did 1979, 1990, and 1996 cyclones and tidal waves. Floods in the Godavari and Krishna Rivers wreaked havoc in the East Godavari, West Godavari and Krishna districts respectively.

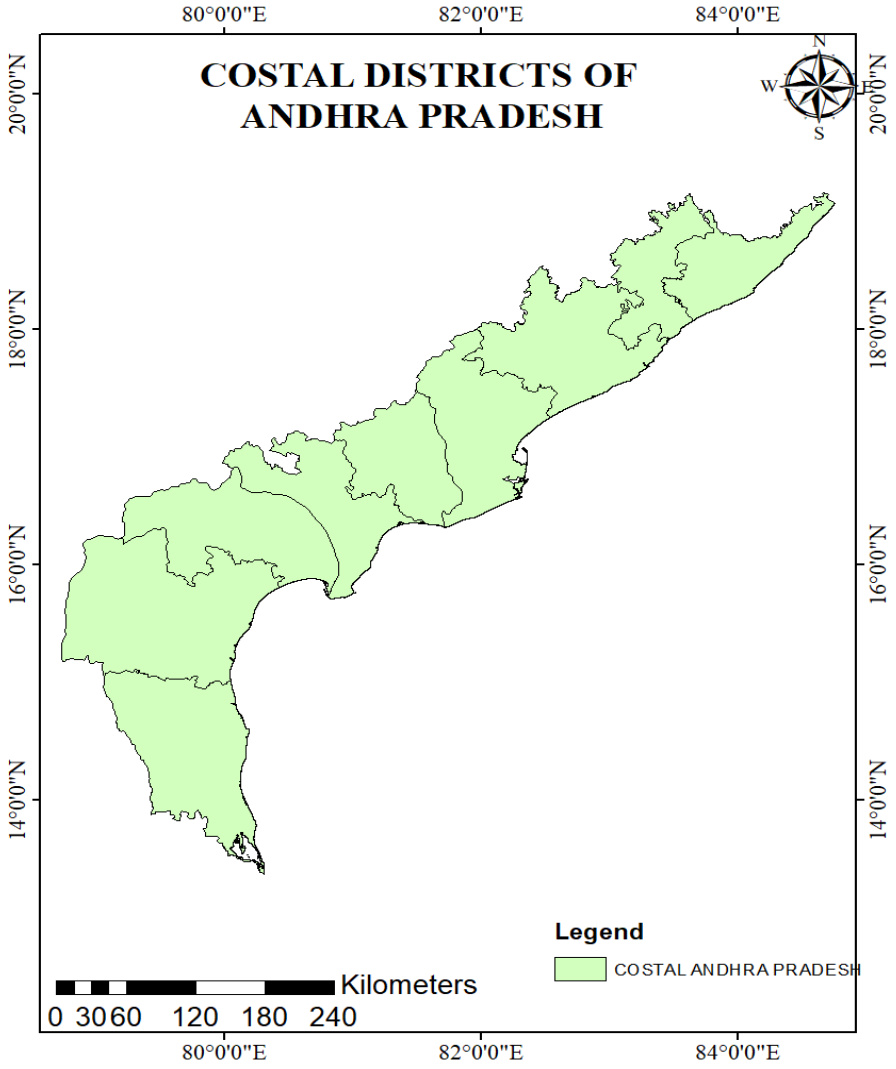



*Figure 2 Coastal Districts of Andhra Pradesh*

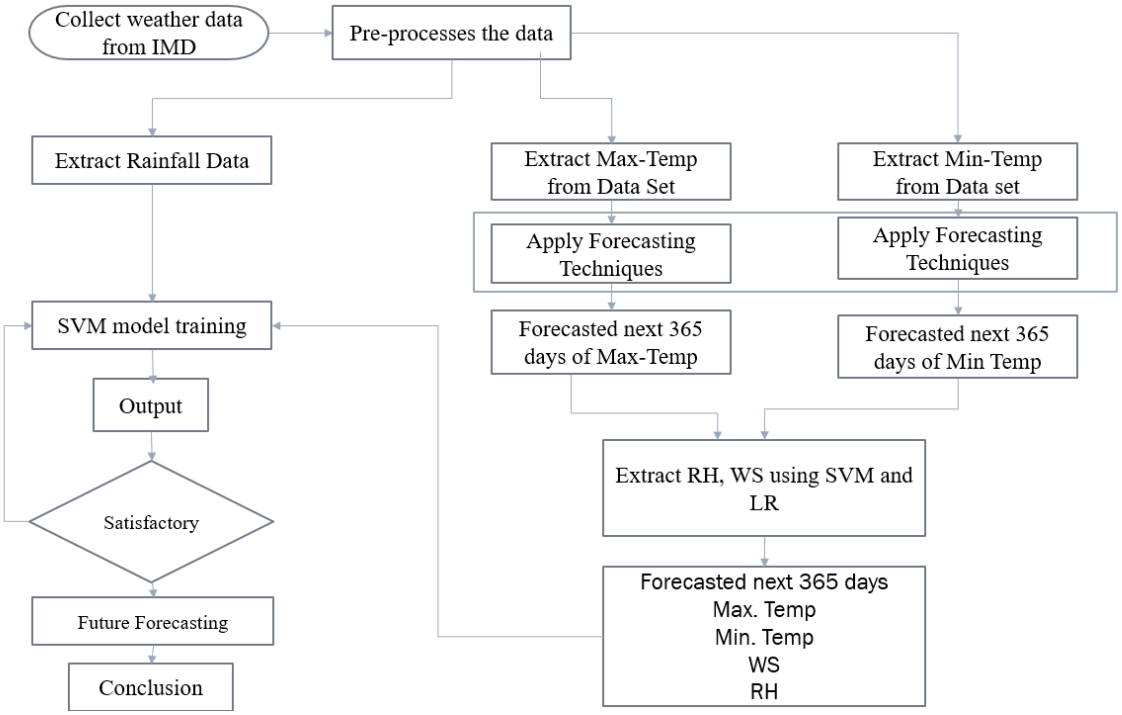
AP has been hit by more than sixty cyclones this century. The frequency of cyclones appears to have increased in recent decades, to the point that severe cyclones have become a typical occurrence every two to three years, wreaking havoc on the state's economy and putting financial and institutional resources to the test. In Coastal AP, about 9 million people are vulnerable to cyclones and their effects, with 3.3 million living within five kilometres of the beach.In November 1977, the deadliest typhoon in the last two decades struck, killing almost 10,000 people. More recently, the May 1990 hurricane, which killed over 1,000 people and damaged ten districts, including the whole coast, caused US$1.25 billion in damage. Cyclones and floods claimed the lives of over 13,000 people and 338,000 cattle between 1977 and 1992, causing damage to roughly 3.3 million homes.

*Table 1 Input data sources of WEKA model*

| DATA TYPE | SOURCE | TIME PERIOD | RESOLUTION |
|---|---|---|---|
| Daily Precipitation | Indian Meteorological Department/ NASA Power | 1983-2017/ 2018-2020 | 0.25*0.25 |
| Maximum Temperature | Indian Meteorological Department/ NASA Power | 1983-2017/ 2018-2020 | 1*1 |
| Minimum Temperature | Indian Meteorological Department/ NASA Power | 1983-2017/ 2018-2020 | 1*1 |
| Wind Speed | NASA Power | 1983-2020 | 05*05 |
| Relative Humidity | NASA Power | 1983-2020 | 0.5*0.5 |

## 3. Methodology

The required data for this study has been collected from Indian Meteorological Department and NASA Power Data. The daily precipitation, max temperature, min temperature, wind speed and relative humidity data has been collected from 1971 to 2020. Observed daily Precipitation is collected from 1971 to 2017 from IMD and from 2018 to 2020, it has been collected from NASA Power Data. Observed Daily Precipitation is in gridded data and the grid size is 0.25*0.25.



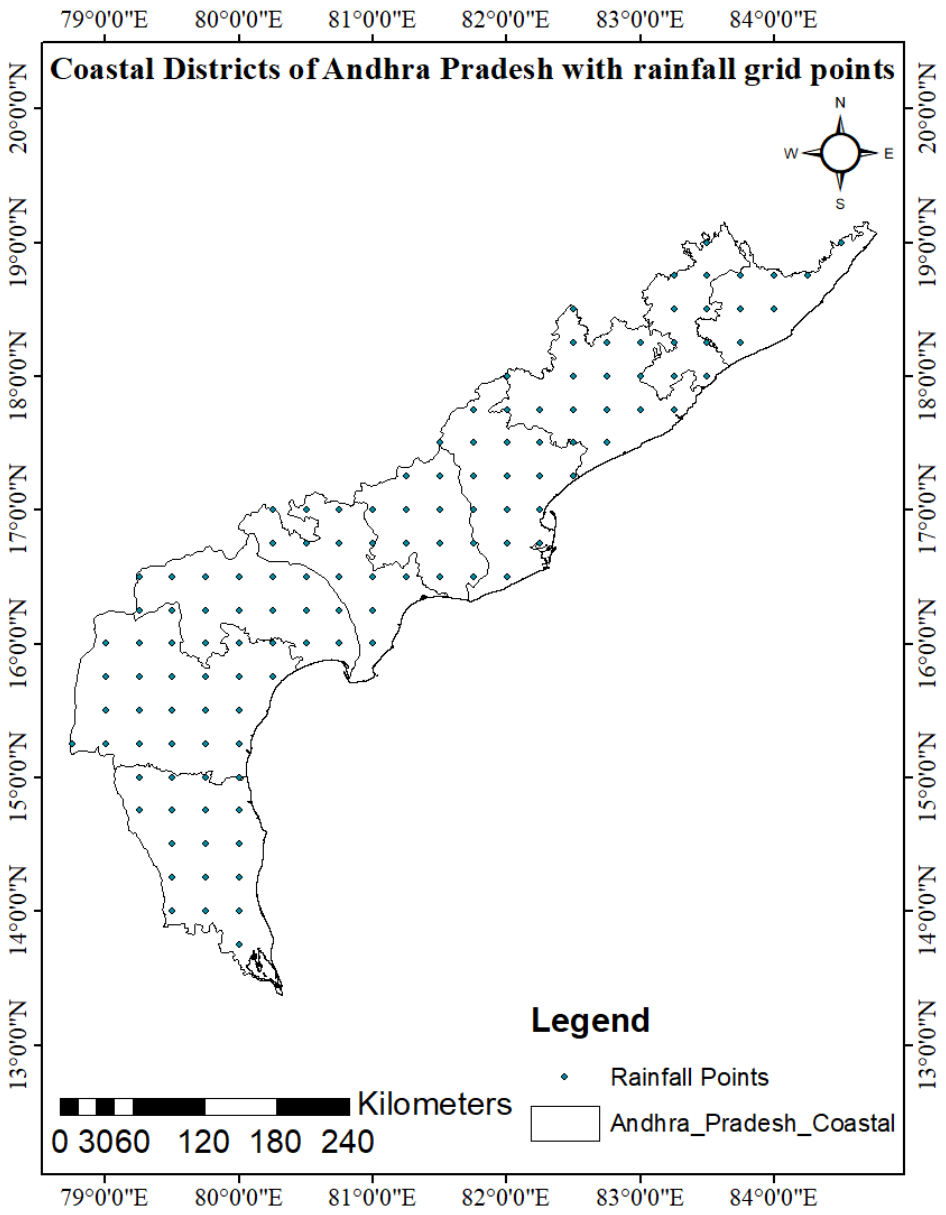



*Figure 3 Coastal districts of Andhra Pradesh with rainfall grid points*

## 3.1. WEKA

WEKA is a computer program created by the University of Waikato in New Zealand. Weka is a software package that provides data analysis and predictive modelling data sets and algorithms, as well as graphical user interfaces for easy access to these capabilities. The graphic below depicts all of the functions that can be used in WEKA.

Begin with the raw data collected in the field. This data may contain a number of null values and worthless fields. WEKA data pre-processing tools are used to clean up the data. Then, depending on the type of ML model you're trying to develop, select one of the options, such as Classify, Cluster, or Associate. The Attributes Selection function allows you to choose features automatically in order to reduce the dataset's size. WEKA makes it possible to use a wide range of algorithms. You'd pick an algorithm, set the parameters, and run it on the data. The model's statistics would be provided by WEKA. It has a data visualization tool.

## 4. Results

The Linear Regression model is applied using WEKA tool to predict the Maximum Temperature, Minimum Temperature and Wind speed in the selected study area.

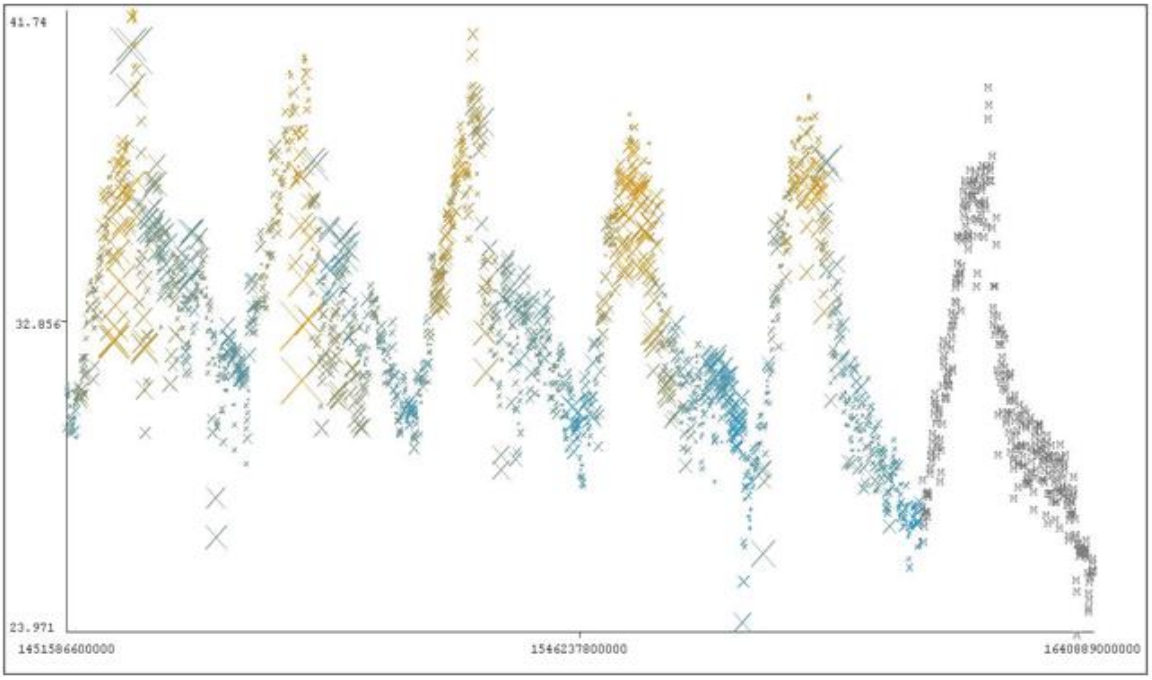



*Figure 4 Graph showing observed and predicted Maximum temperature*

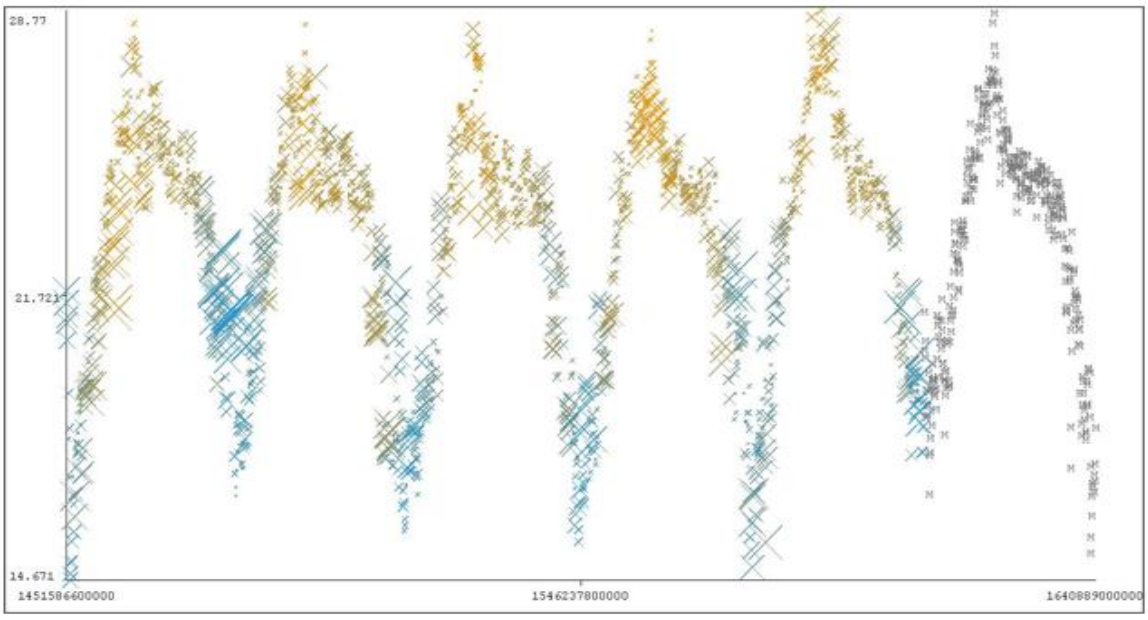



*Figure 5 Graph showing observed and predicted Minimum temperature*

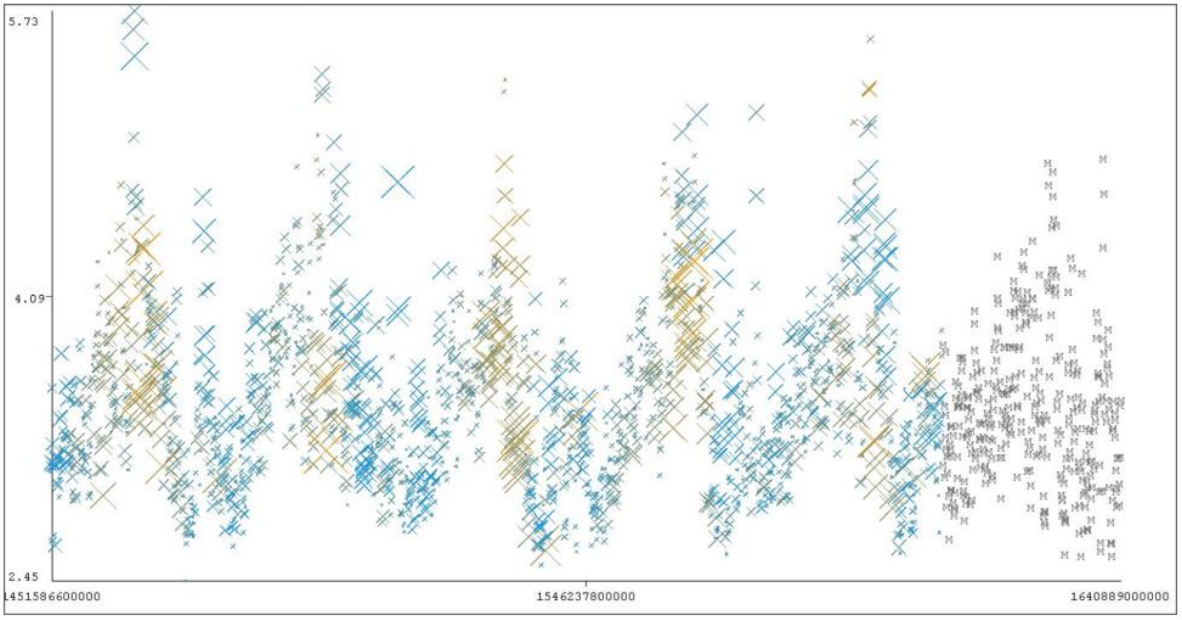



*Figure 6 Graph showing observed and predicted Wind Speed*

The prediction of Relative Humidity has been carried out by creating a Support Vector Machine model and taking Maximum Temperature, Minimum Temperature and Wind Speed as attributes. Along with the observed data of these attributes, the predicted data from linear regression models is used to predict relative humidity in coastal districts of Andhra Pradesh.

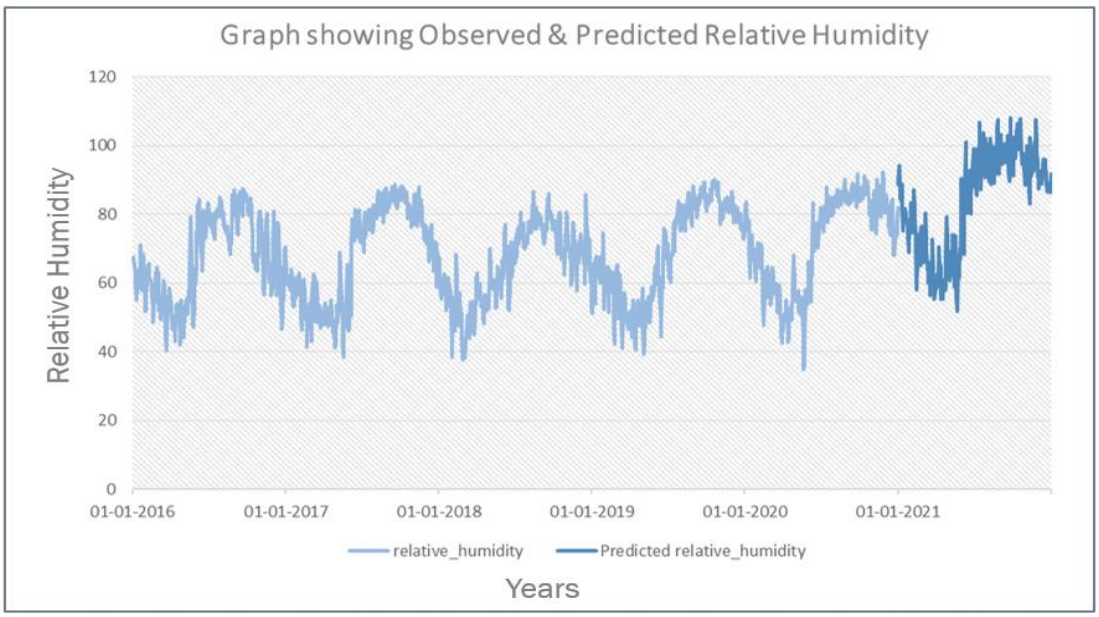



*Figure 7 Graph showing observed and predicted Relative Humidity*

The prediction of precipitation has been carried out by creating a Support Vector Machine model and taking Maximum Temperature, Minimum Temperature, Wind Speed and Relative Humidity as attributes. Along with the observed data of these attributes, the predicted data from linear regression models as well as support vector machine model are used to predict precipitation in coastal districts of Andhra Pradesh.

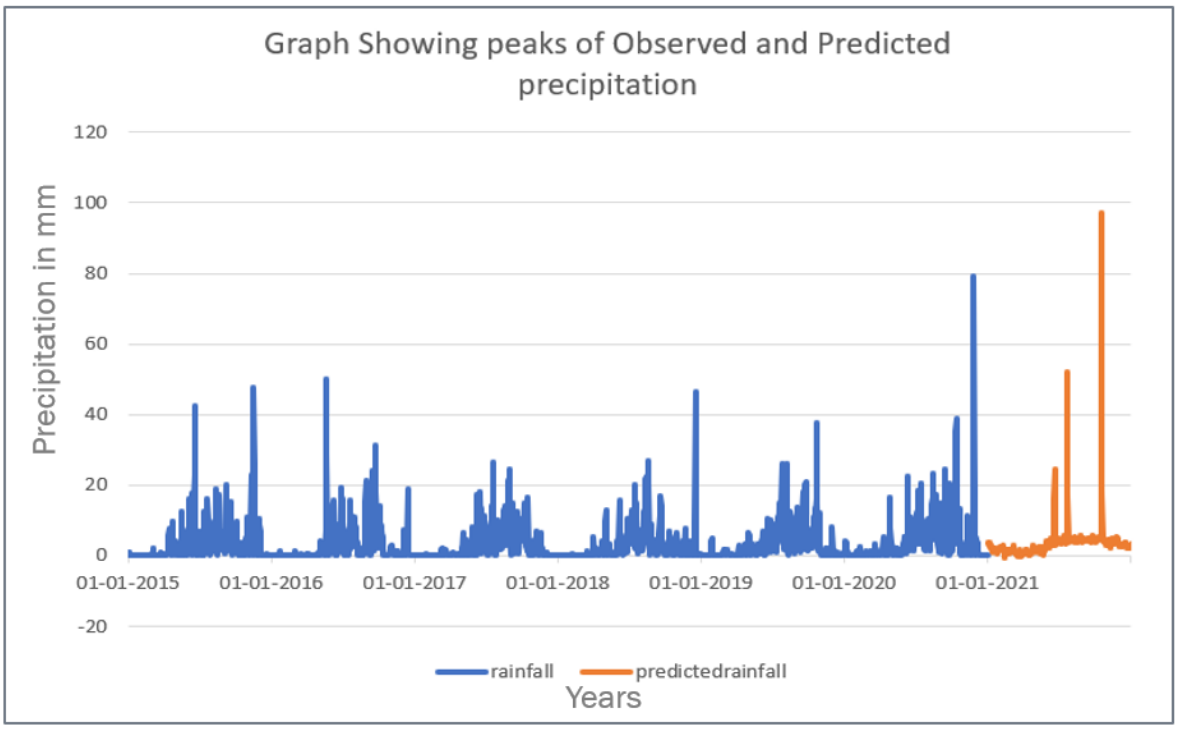



*Figure 8 Graph showing observed and predicted Peaks of Precipitation*

For all these Linear Regression and Support Vector Machine model validation, the entire data set has been divided into 5 sets. During each run, one subset was chosen for validation while all other sets are chosen for training. In this study Correlation and Root mean square error are used as performance indicators.

*Table 2 Performance Indicators*

| Model | RMSE | Co-relation | | |
|---|---|---|---|---|
| | | Training | Validation | Testing |
| Linear Regression | 0.5 | 0.81 | 0.83 | 0.87 |
| Support Vector Machine | 0.7 | 0.83 | 0.87 | 0.89 |

## 3. Conclusion

The precipitation during cyclone events in coastal districts of Andhra Pradesh is predicted using SVM model. The effect of Relative humidity and Temperature is more on precipitation when compared with wind speed. With this rate of change in the variables, the magnitude of precipitation in cyclones is increasing in the nearby future. The developed model applied for precipitation prediction in cyclones and test results indicate that the model can effectively forecast the rainfall.

## References


1. Bromirski, Peter D., and James P. Kossin. 2008. "Increasing Hurricane Wave Power along the U.S. Atlantic and Gulf Coasts." *Journal of Geophysical Research: Oceans* 113 (7): 1–10. https://doi.org/10.1029/2007JC004706.
2. Chen, Rui, Weimin Zhang, and Xiang Wang. 2020. "Machine Learning in Tropical Cyclone Forecast Modeling: A Review." *Atmosphere* 11 (7): 1–29. https://doi.org/10.3390/atmos11070676.
3. Emanuel, Kerry, and Adam Sobel. 2013. "Response of Tropical Sea Surface Temperature, Precipitation, and Tropical Cyclone-Related Variables to Changes in Global and Local Forcing." *Journal of Advances in Modeling Earth Systems* 5 (2): 447–58. https://doi.org/10.1002/jame.20032.
4. Evan, Amato T., Gregory R. Foltz, and Dongxiao Zhang. 2012. "Physical Response of the Tropical-Subtropical North Atlantic Ocean to Decadal-Multidecadal Forcing by African Dust." *Journal of Climate* 25 (17): 5817–29. https://doi.org/10.1175/JCLI-D-11-00438.1.
5. Field, Christopher B., Vicente Barros, Thomas F. Stocker, Qin Dahe, David Jon Dokken, Kristie L. Ebi, Michael D. Mastrandrea, et al. 2012. "Managing the Risks of Extreme Events and Disasters to Advance Climate Change Adaptation: Special Report of the Intergovernmental Panel on Climate Change." *Managing the Risks of Extreme Events and Disasters to Advance Climate Change Adaptation: Special Report of the Intergovernmental Panel on Climate Change* 9781107025: 1–582. https://doi.org/10.1017/CBO9781139177245.
6. Grinsted, Aslak, John C. Moore, and Svetlana Jevrejeva. 2012. "Homogeneous Record of Atlantic Hurricane Surge Threat since 1923." *Proceedings of the National Academy of Sciences of the United States of America* 109 (48): 19601–5. https://doi.org/10.1073/pnas.1209542109.
7. Hansen, James, Makiko Sato, and Reto Ruedy. 2012. "Perception of Climate Change." *Proceedings of the National Academy of Sciences of the United States of America* 109 (37). https://doi.org/10.1073/pnas.1205276109.
8. I. Diaz E. F. Combarro et al, S M Mazza. 2017. "Machine Learning Applied to Go." *Springer* 15 (2).
9. Karl, Thomas R. 2011. "Weather and Climate Extremes in a Changing Climate (Regions of Focus: North America, Hawaii, Caribbean, and U.S. Pacific Islands)." *Impact of Weather and Climate Extremes*, no. June: 1–235.
10. Kaur, Manpreet, R. Phani Murali Krishna, Susmitha Joseph, Avijit Dey, Raju Mandal, Rajib Chattopadhyay, Atul Kumar Sahai, Parthasarathi Mukhopadhyay, and Sukumarapillai Abhilash. 2020. "Dynamical Downscaling of a Multimodel Ensemble Prediction System: Application to Tropical Cyclones." *Atmospheric Science Letters* 21 (8): 1–11. https://doi.org/10.1002/asl.971.
11. Knutson, Thomas R., John L. McBride, Johnny Chan, Kerry Emanuel, Greg Holland, Chris Landsea, Isaac Held, James P. Kossin, A. K. Srivastava, and Masato Sugi. 2010. "Tropical Cyclones and Climate Change." *Nature Geoscience* 3 (3): 157–63. https://doi.org/10.1038/ngeo779.
12. Kossin, James P., and Suzana J. Camargo. 2009. "Hurricane Track Variability and Secular Potential Intensity Trends." *Climatic Change* 97 (1): 329–37. https://doi.org/10.1007/s10584-009-9748-2.

*IN PROCEEDINGS OF 25th HYDRO 2020, INTERNATIONAL CONFERENCE, NATIONAL INSTITUTE OF TECHNOLOGY ROURKELA, ODISHA, INDIA 26-28, March 2021, ISBN 978-93-90631-56-8*

Paper ID - 470

# MATHEMATICAL MODELLING AND SIMULATION OF OCEAN DISPOSAL OF HARBOUR DREDGED MATERIALS

Anil Bagwan[1], Jiweshwar Sinha[2], Prabhat Chandra[3]

*[1]'Asst. Research Officer, Mathematical Modelling in Coastal Engineering, Central Water and Power Research Station, Pune — 411 024, India, anilbagwan@rediffmail.com*
*[2]Scientist D, Mathematical Modelling in Coastal Engineering, Central Water and Power Research Station, Pune - 411 024, India, Email: jsinha_cwprs@yahoo.com [2]Scientist E, Mathematical Modelling in Coastal Engineering, Central Water and Power Research Station, Pune - 411 024, India*

## ABSTRACT

Sedimentation is a major problem for coastal management authorities to maintain the depth for smooth movement of large vessels in and around the ports. Maintenance dredging is required periodically to maintain the desired depths in navigational channel and inside the port. Uncontrolled dumping of the dredged materials might create negative impacts on the living marine resources. Selection of disposal sites in open sea is one of the most important steps of dredge material management process to minimize the possible negative impacts on navigational channels, ports, harbours and other coastal structures.

Two-dimensional mathematical model studies undertaken for identification of disposal grounds of the dredged material due to expansion of captive jetty facilities for an existing port located at about 22 km away from the mouth of Dharamtar creek on the right bank of Amba River at Dolvi in Raigad district of Maharashtra. Hydrodynamic and dispersion model studies using MIKE 21 FM software were carried out to assess the changes likely to occur in flow fields and identification of disposal ground in open sea for disposal of dredged material from capital and maintenance dredging. Two disposal sites with prevailing depth of about -15.0 m CD in open sea near Mumbai harbour were considered. Simulation results using regional model indicated that equilibrium dispersion could be obtained after 3 days of real time. Area of the sustained spread of the material with maximum concentration of about 0.06 kg/m$^3$ was found to be about 15 km$^2$. Simulation results further indicated that the disposed material would not enter into the navigational channel or into the Mumbai port channel or any other area near the shore.

***Keywords**: Dredging; disposal; dispersion; hydrodynamics; creek; river.*

## 1. INTRODUCTION

Disposal of dredged sediment material in open sea is a common practice adopted by the coastal management authorities. Like other anthropogenic activities, it can have a negative impact on the marine environment and due to the dynamic nature of the sea, such impacts may not only be restricted to the immediate area of disposal. In dynamic coastal areas, beforehand assessment is required about spreading of the dredged material and its dispersion mechanism to avoid the return of the sediment in navigational channels and in nearshore regions so that no important life-form can be harmed. Further, any improper selection of disposal location could cause returning back of disposed materials in operational areas resulting into loss of depth. Based on these criteria, investigation for locating a suitable disposal location can be done by using mathematical models. A number of research articles are available dealing with the dispersion of dredged material (Collins, 1990; Truitt, 1988; Van den Eynde, 2004; Van Parijs et al., 2002; Wurpts, 2006) in open water area.

The present paper presents mathematical modelling of disposal and dispersion of the dredged sediment carried out for Dharamtar port using MIKE 21 software. The disposable dredged sediment is likely to be generated due to re-dredging of 26 km long existing navigational channel leading to the port from -3 m CD to -5.5 m CD. Dharamtar Port (Lat. 18$^0$ 42’ 03’’N, Long. 73$^0$ 01’ 46”E) is situated

on the right bank of river Amba at Dolvi in Raigad district, Maharashtra which is about 22 km away from the mouth of Dharamtar creek in the Arabian Sea. Location map of the study area is shown in Figure 1. The port has been planned to enhance its material handling facilities upto 10 MTPA in a phased manner expansion. The area is well protected from the fury of waves by the headlands of Mumbai and Navkhar at the northern and southern ends, respectively.




**Figure 1** Location map of the study area

## 2. MATHEMATICAL MODEL SETUP AND INPUT

2-D mathematical model using MIKE 21 FM (DHI, 2014) software is developed and simulated for the study area as described below.

MIKE 21 is a generalised mathematical modelling system designed for a wide range of marine and estuaries applications and can be applied to oceanographic studies, water pollution and sedimentation studies. The system solves the 2D momentum and continuity equations obtained through vertically integrating the three-dimensional Navier-Stokes equations of motion (Abbott, 1979) under the following assumptions for simulating unsteady flow taking into account bathymetry and external forcing such as meteorology, tidal elevations, currents and other hydrographic conditions.

i) The flow is incompressible,
ii) The flow is well mixed (no variation in density) vertical accelerations are negligible,
iii) Bed shear stress can be modelled.

MIKE 21 is a finite volume model with an unstructured horizontal grid. It can be run on a single grid or with dynamically nested grids. An approximate Riemann solver (Roe's scheme) is used to calculate convective fluxes at the interface of cells. The scheme used is computationally efficient and widely used in solving shallow water flow equations. In this study hydrodynamic module, MIKE 21 HD is applied coupled with dispersion module, MIKE 21 AD.

The basic inputs for the present studies are bathymetry, tidal data, current data, wave data, bed characteristics, suspended sediment load etc. Bathymetry covering an area of about 62 km upto -48 m contour depth in offshore direction using C-MAP software and 15 km in nearshore region covering portions of both the river and the creek is used in simulations. From bathymetric data, it is apparent

that the contours are mostly parallel to the coastline. Bathymetry of the area along with locations of current observation and disposal points is depicted in Figure 2.

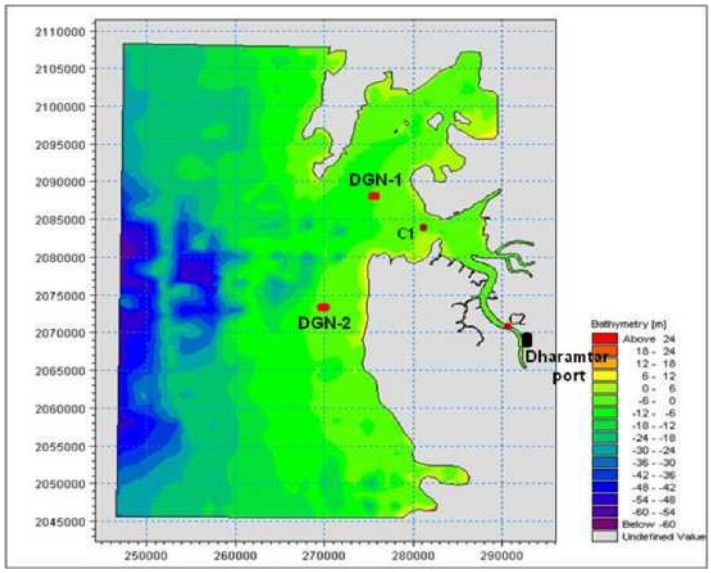



**Figure 2** Bathymetry of model area, locations of current observation (C1 & 2) and disposal point (DGN-1 & 2)

The model area was discretized into a number of triangular grids with flexible mesh. Predicted tide for a period of one year, i.e., 2014 at Bandra and Revdanda sites (Figure 3) extracted from C-MAP software is used as boundary conditions in the model simulations. The tide prevailing at the study area is semi-diurnal in nature. It is also seen that the tidal range during spring and neap tide is about 5.0 m and 1.6 m, respectively. Average daily discharge of river Amba was observed to be about 95 cumec during monsoon period. Bed material of the area is mainly composed of silt and silty-clay with mean grain size $D_{50}$ of 0.05 mm.

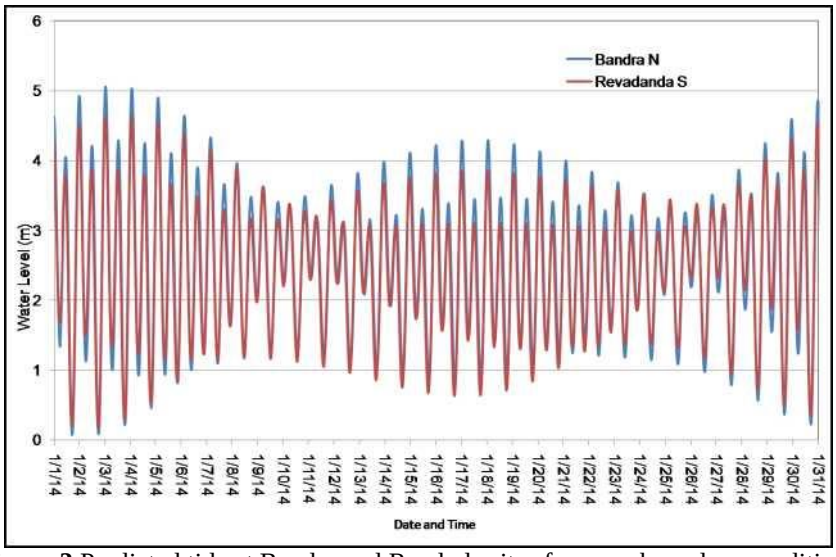



**Figure 3** Predicted tide at Bandra and Revdnda sites for open boundary conditions

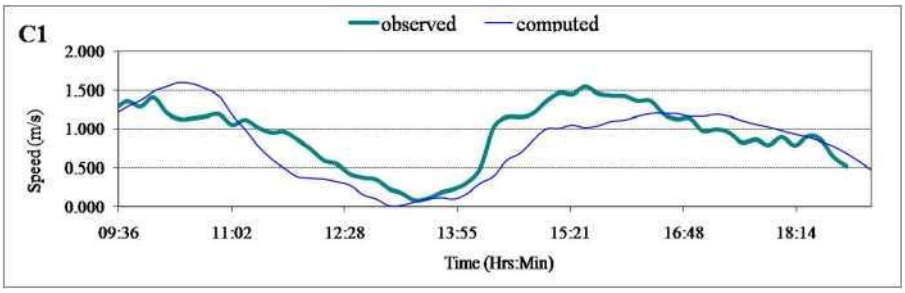
## 3. MODEL CALIBRATION

The study area is influenced by tides and river discharge accordingly the hydrodynamic model is simulated for the prescribed flow conditions at various boundaries. For calibration of the model, various model parameters are adjusted to get the prototype conditions prevailing at the site. The model is simulated under the existing condition for 14-days continuously covering both spring and neap tides. In the present study, the model boundaries and other parameters (eddy viscosity 0.28; bed resistance 40 $m^{1/3}/s$) are adjusted in such a way that the observed and the simulated tidal currents near the port area and

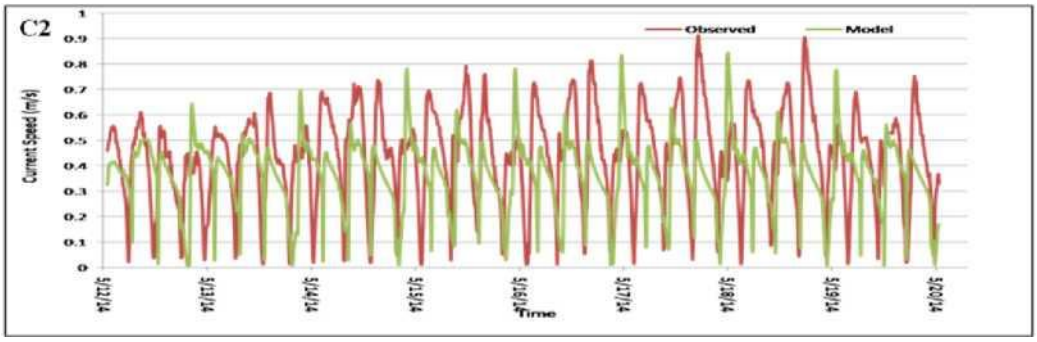
near the disposal location in the open sea would be generated upto their limits. Tidal elevations in terms of time series are applied to the open boundaries with appropriate phase lag and elevation difference. Comparison of the observed and the computed current magnitude at Locations C1 and C2 is shown in Figure 4. From the figure, it can be seen that computational currents follow the trend of observational parameters except at few occasions where it either over-predict or under-predict it. Computed velocity magnitudes correspond well with the measured data during most of the periods. The current peaks are reproduced to a high degree and phase errors are very low. In the neap tide period in bottom plot of location C2, the model slightly under predicts the current peak values, which is not unusual in models of this sort. However, peak current during the model simulation obtained at the location C1 and C2 is of the order of 1.5 m/s and 0.85 m/s respectively.

## 4. MODEL RESULTS AND DISCUSSIONS

Numerical experiment with the calibrated model is carried out for the proposed scenario of the study area under the prescribed boundary conditions. In the proposed condition the 26 km long approach channel with bed width 132 m and depth -5.5 m CD leading to the port is incorporated in the model. The navigational channel is discretized into triangular elements.




(a) At location C1




(b) At location C2

**Figure 4** Comparison of observed and computed current magnitude at different locations

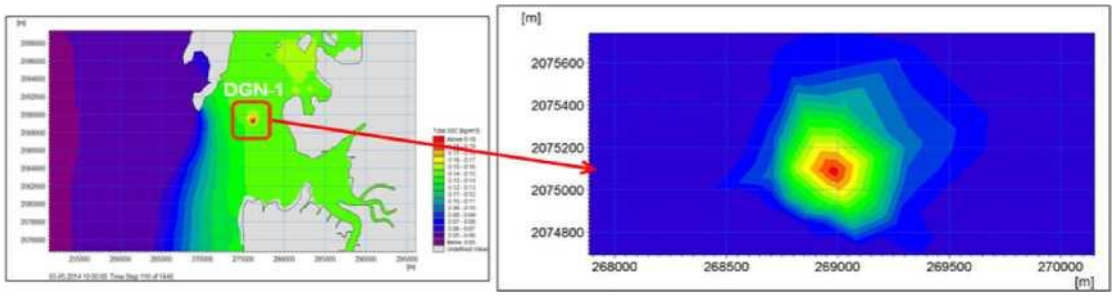
The quantity of dredging is obtained from the simulation of siltation model for the proposed condition. It is estimated that the total quantity of dredged material comprising silt and silty-clay obtained from dredging of the navigational channel would be approximately 8.3 $Mm^3$. Part of the dredged material to be used for reclamation and rest of the dredged material would be disposed off at suitable locations in an economical and environmental friendly manner. Therefore, the studies for ascertaining suitability of disposal ground are carried out using dispersion model under the proposed condition.

While carrying out the studies for identification of disposal sites, two sites viz. Disposal point 1 (DGN-1) and Disposal point 2 (DGN-2) earmarked in Mumbai harbour namely off Karanja were considered (refer Figure 3). These sites with prevailing depth of about -15.0 m CD in open sea are located in the open sea at $18^0$ 52' 29.96" N, $72^0$ 52' 17.98" E and $18^0$ 45' 11.97" N, $72^0$ 48' 24" E. Identification of disposal grounds is carried out through the dispersion of disposed materials using the model simulations. Considering actual rate of disposal and other aspects of dredging, detailed dispersion and suitability of the site for disposal are presented as under. The calibrated model is run for tides of 30 days cycle covering spring, neap and average tides. The hydrodynamic model is coupled with dispersion model for simulating of dispersion of the disposed materials. Disposal of the materials is considered as source discharge at the

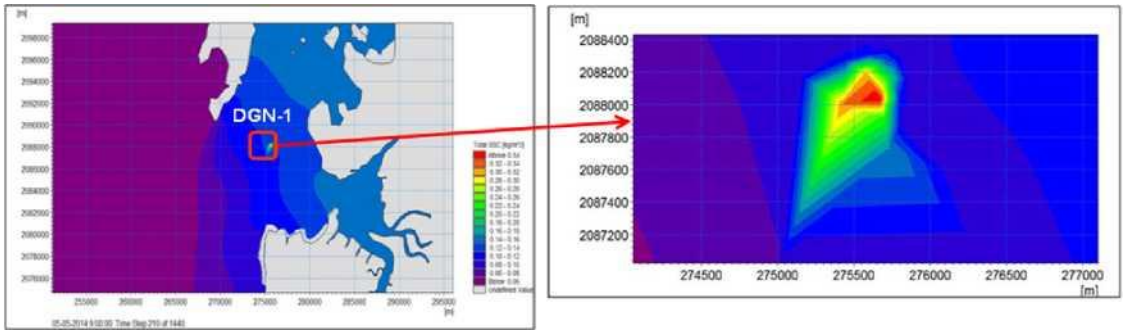
disposal site DGN-1 and the likely dispersion at the site is obtained from the model. The disposal of the material is considered to be continuous. The density of the fluid would be about 1250 kg/m$^3$.

### *4.1 Disposal at Site DGN-1*

Simulation results of the dispersion studies indicated that equilibrium dispersion could be obtained after about 10 to 12 days of real time. The results of the dispersion model are presented in Figures 5(a-d). From these results, it can be seen that the maximum concentration at the disposal location would be about 0.06 kg/m$^3$.



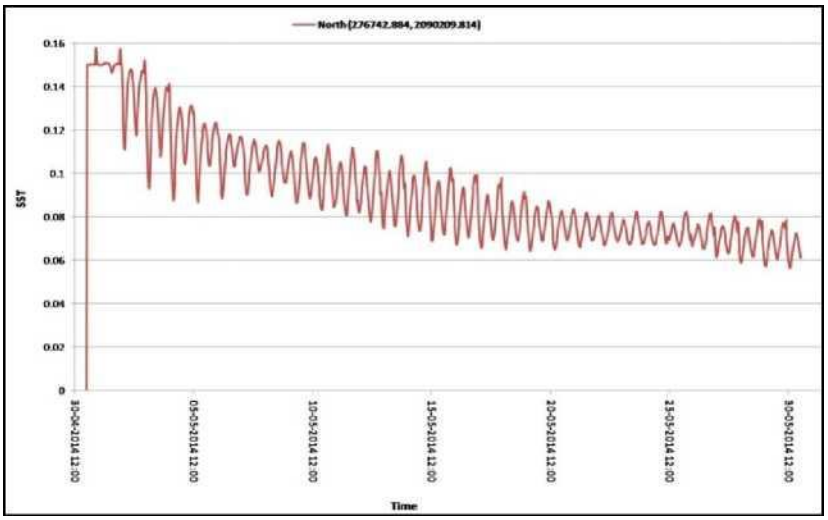

(a) During ebb tide



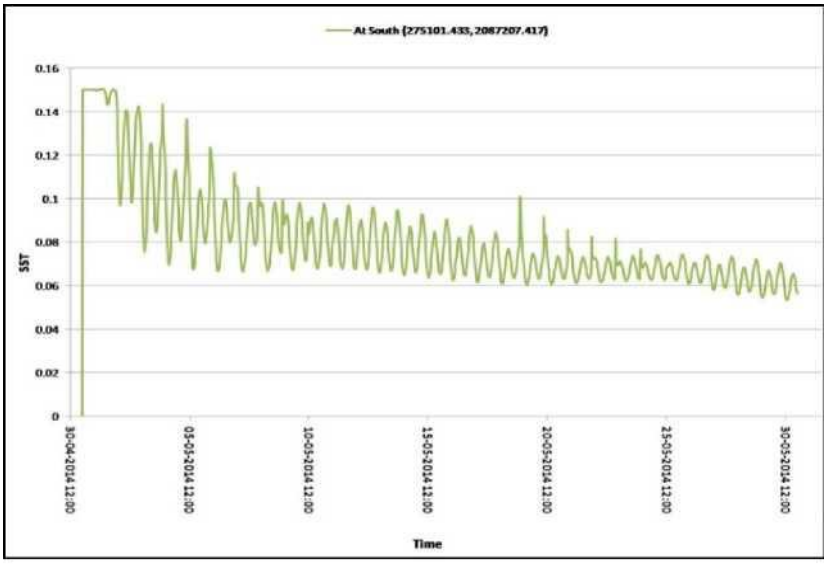

(b) During flood tide

**Figure 5** Dispersion of material at DGN-1

The area of sustained spread of the material as observed on the model is about 15 km$^2$. The area of sustained spread and time series of concentration of dispersed material during flood and ebb tides is shown in Figure 5and Figure 6, respectively. The results clearly indicated that the disposed material would not enter into the navigational channel or into the Mumbai port channel or any other area near the shore.




(a) During ebb tide

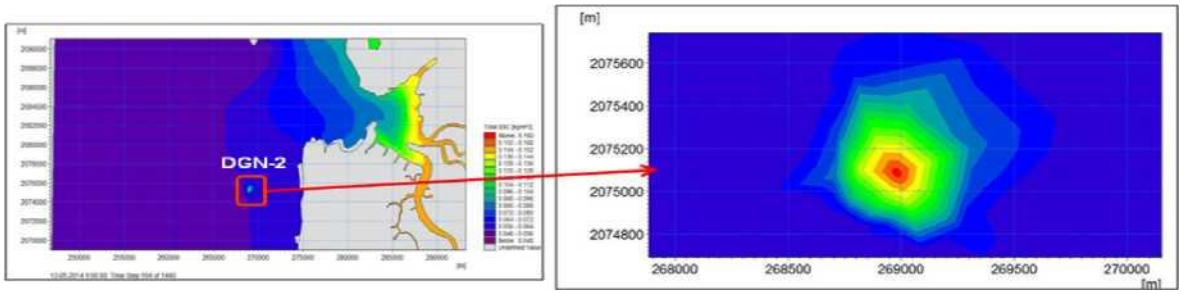



(b) During flood tide

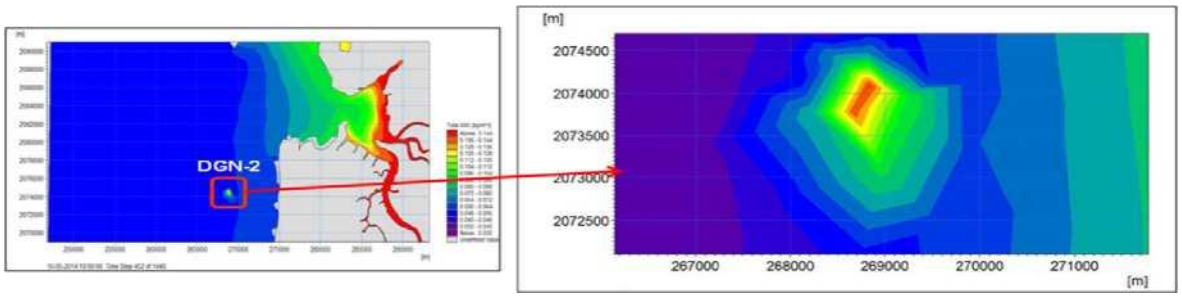
**Figure 6** Extent of material dispersion at DGN-1

## *4.2 Disposal at Site DGN-2*

Simulation results of the dispersion studies disposed at site DGN-2 indicated that equilibrium dispersion could be obtained after about 3 days of real time i.e. for about six tidal cycles. The results obtained from the studies indicated that the maximum concentration at the disposal location would be about 0.06 kg/m$^3$. The area of sustained spread of the material is observed to be about 12.5 km$^2$. The area of sustained spread and time series of concentration of dispersed material during flood and ebb tides is shown in Figure 7 and Figure 8, respectively. The results also indicated that the disposed material would not enter into the navigational channel or any other area near the shore.

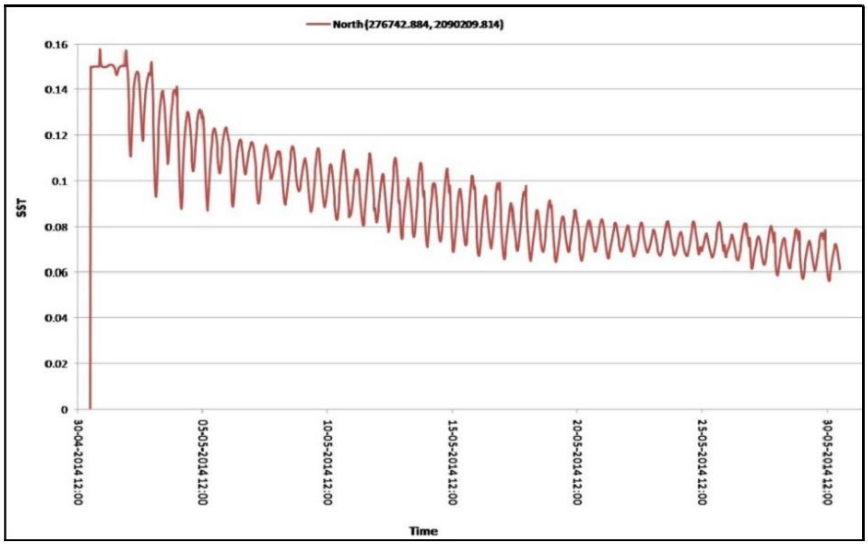



(a) During ebb tide

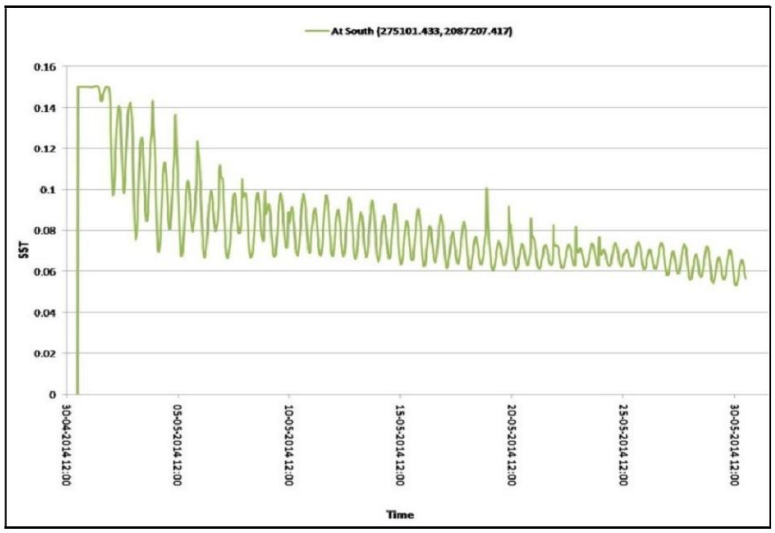



(b) During flood tide

**Figure 7** Dispersion of material at DGN-2




(a) During ebb tide




(b) During flood tide

**Figure 6** Extent of material dispersion at DGN-1

## 5. Conclusions

The following conclusions can be drawn from the study:

1. The hydrodynamics simulations indicate that the peak tidal currents in the vicinity of the Disposal Ground are in the range of 1.5 m/s which may help in the dispersion of the dredged material which comprise of silt and silty-clay with mean grain size $D_{50}$ of 0.05 mm.
2. The disposal of material is to be carried out in both phases of tide.
3. The Suspended sediment concentrations fluctuate with the tide and is likely to attain lowest value of 0.06 kg/m$^3$ at the dumping location.
4. The time required to restore the ambient conditions after the dumping ceases would be about 15 to 17 days at location DGN-1 and 5 to 7 days at location DGN-2.
5. From these studies disposal sites, both DGN-1 and DGN-2 are found suitable for disposing of dredged materials. However, site DGN-1 requires minimum turnaround time for the barge/ dredger. The disposal site, DGN-1 is nearer to the navigational channel for Dharamtar port. Therefore, this site can be conveniently used for the disposal of the dredged materials resulting from dredging of the existing navigational channel.

## ACKNOWLEGDMENT

The authors are grateful to Shri A.K. Agrawal, Director, CWPRS for his guidance. The authors express their deep gratitude for according permission to publish this paper. The authors are thankful to the Project Authority for providing data during the course of the studies.

## References

Abbott,M.B.(1979). "Computational Hydraulics: Elements of the Theory of Free Surface Flows," Pitman, London, 1979.

TR 4089 (2004). Monsoon field investigations for Rewas-Aware port, Mumbai. CWPRS, Pune.

TR 4266 (2005). Mathematical model studies for flow conditions, sedimentation and identification of offshore dumping sites for Rewas-Aware port, Mumbai. CWPRS, Pune.

TR 5444 (2016). Mathematical model studies for tidal hydrodynamics, siltation and identification of dumping locations for the expansion of captive jetty facilities in Dharamtar creek at Raigarh, Maharashtra. Collins,M.,(1990). The behaviour of cohesive and non-cohesive sediments. In Alzieu, C. and Galenne, B. eds. Proceedings of the international seminar on the environmental aspects of dredging activities. Nantes, Port Autonome de Nantes Saint-Nazaire, pp. 15-32.

DHI (2014). MIKE 21 FM, Scientific background, DHI, Denmark.

Truitt,C.L., (1988). Dredged material behaviour during open water disposal. Journal of Coastal Research, 4, 389-397.

Van den Eynde, D. (2004). Interpretation of tracer experiments with fine-grained dredging material at the Belgian Continental Shelf by the use of numerical models. J. of Mar. Systems 48, 171-189.

Van Parijs,M., Dumon,G., Pieters,A., Claeys,S., Lanckneus,J., Van Lancker,V., Vangheluwe, M., Van Sprang,P., Speleers,L., Janssen,C., (2002). Environmental monitoring of dredge operations MOBAG 2000. In: Van Lancker, V. et al. (ED.) Symposium 'Coastal zone management from a geo-ecological and economical perspective', 16-17 May 2002, Oostende. VLIZ Special Publication 10, pp. 1-22.

WURPTS,A. (2006). Morphodynamic-numerical simulations of dredged matter open disposal. Terra et Aqua, 102, 9 p.

# Theme II

# River and Coastal Engineering

Paper ID - 06

*IN PROCEEDINGS OF 25th HYDRO 2020, INTERNATIONAL CONFERENCE, NATIONAL INSTITUTE OF TECHNOLOGY ROURKELA, ODISHA, INDIA 26-28, March 2021, ISBN 978-93-90631-56-8*

# FLOOD ESTIMATION BASED ON WATER SURFACE VELOCITY USING NON-CONTACT SENSING AND REGRESSION ANALYSIS

M. Selva Balan[1], K.V.Manisa[2], Yash D[3], Shraddha Khot[4], Malathi Khole[5]

[1] *Scientist D, Instrumentation and Control Dept., CWPRS, Khadakwasla, Pune-411024, India*
[2]*Final Year Engineering in E&TC, NBNSSOE, Ambegaon, Pune-411044, India*
[3] *Final Year Engineering in E&TC, NBNSSOE, Ambegaon, Pune-411044, India*
[4] *Final Year Engineering in E&TC, NBNSSOE, Ambegaon, Pune-411044, India*
[5]*Final Year Engineering in E&TC, NBNSSOE, Ambegaon, Pune-411044, India*
*Email: instcwprs@gmail.com*

## ABSTRACT

Flood is the flow which is not handled within the river banks. This is normally caused due to excess discharge due to release of water from dam arising due to heavy downpour in upstream catchments within short span of time. These conditions are most destructive and highly complex in nature. The Food estimation models contributed to reduction of risk, minimization of loss of human life, and reduction of the property damage associated with Flood. However, measurement of such events is challenging. In this paper, the flood is estimated by image analysis methods applied to estimate the discharge in river stream with improved accuracy within a fraction of time. The estimation of flood is analysed with 'Logistic Regression' using a machine learning algorithm and compared with existing state-of-art methods. This is then used to train and test the model. The results shown in the paper are calculated on the Khadakwasala canal and Mutha River in Pune region**.** Video Processing is proposed to extract the displacement of the object in water from the frames of the video captured by a camera. Based on the cross-section of the river which is taken in Literature Survey using Distance Sensor the Area of the river is calculated. The discharge is then eventually estimated. A data logger is made to estimate the discharge based on the surface velocity and the cross section profile extracted from literature as well as measured before the flooding instances. For the estimation of flood "Logistic Regression" algorithm is used. This algorithm is one of the most used machine learning (ML) algorithms for Binary classification. The model is first trained and then tested using 3:1 ratio. 75% of the dataset is used for Training the model and 25% of the dataset is used for testing the model. The detailed analysis of the performance of the proposed algorithm is analysed and accuracy is estimated. The trained model is then used to plot a graph to show Flood and non-Flood conditions.

***Keywords****: Flood, Discharge, video Processing, Data Logger, Machine Learning, Logistic Regression, Test-Train model.*

## I. INTRODUCTION

Flood estimation basically needs calculation of Discharge in a river. During monsoon months, large quantities of water flow as runoff. When water fills a river beyond its capacity, water flows out of river to its neighbouring land, causing flood .This paper aims at the proposed system to estimate flood based on non contact image processing method. The output of the study will be more precise than the existing measurement systems which uses contact type sensors to measure velocity and more complex Machine Learning (ML) algorithms. Image based technique is an emerging and new measurement technique that is changing the way of measuring surface water resources. Data-driven methods of prediction assimilate the measured climate indices and hydro-meteorological parameters to provide better insight. This method is fast, automated and computerized.

## II. BASIC PRINCIPLE

A. Velocity calculation:

The cheapest and easiest way to determine water surface velocity is to simply float something down the stream and see how fast it goes. In this study, we used the water surface velocity measured in the middle of the river stream[1]. The video of flow is taken and the movement of flow is estimated from the pair of consecutive frames. The frames are converted into gray scale images using RGB to gray scale conversion. Canny edge detection algorithm is applied to detect object in the frames, and finally Euclidean distance is calculated to calculate velocity. The velocity values are then multiplied with the Area of the canal to obtain Discharge[1]. The obtained Discharge value is then used to estimate Flood.

B. Flood Estimation:

Machine learning (ML) methods provides better performance and cost-effective solutions [6][7]. Due to the better efficiency and potential of ML, its popularity dramatically increased among hydrologists. The Proposed architecture mainly focuses on "Logistic Regression" method which handles a large number of dataset having both flood and non-flood conditions [7]. This method is effectively used when we want output in Binary form, that is, is it a Flood condition or not.

Figure 1 shows the Block diagram of working of the proposed methodology:

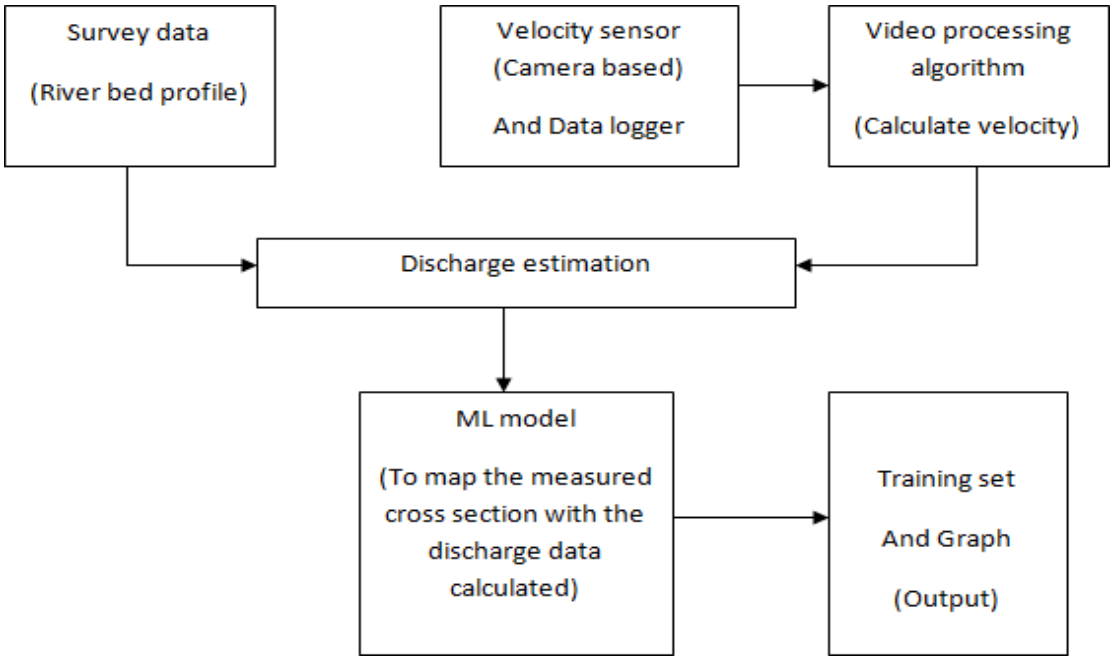



Figure [1]: General block diagram of processing system

## III. DISCHARGE CALCULATION

A. Float

For measurement, object detection is very important. The object should be lighter than the density of water, and should flow with the water. The object needs to be cheap and environmental friendly. Many instances there are floating particles present in the river stream, which is tracked by the algorithm.

B. Video Recorder

The video of the flow of the object in water surface is recorded using a small webcam camera of resolution 2592x1944. It has 30fps (Frames per Second) and 720p. The function, size, price, and power dissipation and also the performance parameters are better than other digital cameras such as Sony, Samsung. This camera is small in size and has better performance.

C. Discharge Calculation

1. The captured video is converted into grey scale using RGB to grey scale converter.

   The conversion formula is as given in equation 1:
   Gray Scale= ((0.3 * R) + (0.59 * G) + (0.11 * B)) (i)

   Red has contributed 30%, Green has contributed 59% which is greater in all three colors and Blue has contributed 11%.

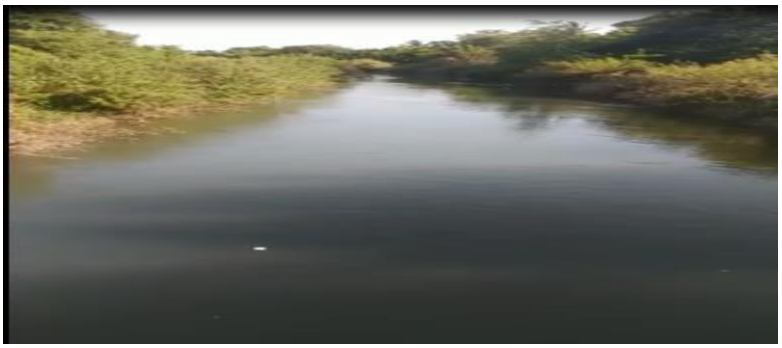


Figure [2]: Original Captured Frame

2. Then Canny edge detector algorithm is applied to remove noise and hence the object is detected [12] preciesly. This algorithm works as follows:
   Noise reduction, Gradient calculation, Non-maximum Suppression, Double threshold, Edge tracking.
   Canny edge detector detects edges in a noisy state by applying the thresholding method. Presence of Gaussian filter allows removing of any noise in an image. It gives good localization response and is immune to a noisy environment.
   The Detected object frame is as shown in figure 3:




Figure [3]: RGB to Grey Converted and Object Detected Frame

The two captured frames are superimposed as shown in figure 4:




Figure [4]: Superimposed Frame

3. Read the two successive frames from captured image. Box point coordinates are taken from the two frames. [Top Right corner, Top Left corner, Bottom Left corner, Bottom Right corner]
   Then using mid-point formula, Midpoint coordinate is obtained from the two images.

4. The distance between any two points on the real line is absolute value of the numerical difference of their coordinates. It is common to identify the name of a point with its Cartesian coordinate.
   In the Euclidean plane, if **p** = ($p_1$, $p_2$) and **q** = ($q_1$, $q_2$) then the distance is given by equation 2:-

$$D(p, q) = \sqrt{(q_1 - p_1)^2 + (q_2 - p_2)^2} \quad \text{(ii)}$$

5. Compute the Euclidean distance between the middle points of the objects.

6. Use formula given in equation 3:

$$\text{Speed} = \frac{Distance}{Time} \quad \text{(iii)}$$

   This gives velocity

7. Calculate Discharge using equation 4 :

$$\text{Discharge} = \text{Area} * \text{Velocity} \quad \text{(iv)}$$

   Print Discharge value in meter per second (m/s).

## IV. DATA LOGGER

A Data Logger is used for collecting data from different sensors like LM35 for temperature, DHT11 for humidity, optical laser sensor for calculating area of cross-section of river[8] and raspberry pi with camera for velocity calculation. This data is then used for storage and processing. Arduino UNO is configured and programmed to function as the Data Logger with SD card interfacing and LCD (Liquid Crystal Display) interfacing[8]. SD card is used for storing purpose and LCD for displaying purpose.

The connection Diagram is as given in figure 5:

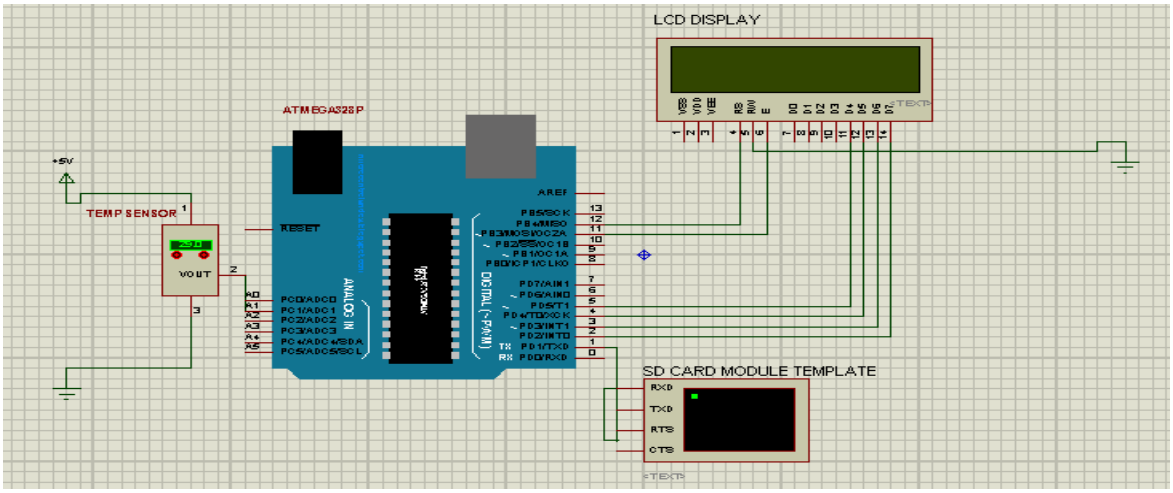



Figure [5]: Connection Diagram

## V. FLOOD ESTIMATION

The Proposed architecture mainly focuses on "Logistic Regression" method which handles a large number of dataset having both flood and non-flood conditions. The velocity of water along with the dataset used contributes to the estimation of the flood. The steps involved in this algorithm are given as below:

### A. Pre-processing

To enhance the features needed for further processing, we employ two steps:

1. Discharge Calculation

The surface water velocity is calculated using image processing algorithms the discharge is calculated using equation 3.

2. Dataset Creation

A dataset is created using past years data using different parameters like temperature, Rainfall, Humidity, Wind speed and the Discharge calculated using image processing algorithm. These values are collected from Indian Metrological Department (IMD) site which provides Day-to-Day weather report. The collected Day-to-Day weather report is then updated in an Excel sheet with required parameters. For the proposed methodology at most 336 days data are collected.

### B. Estimation of Flood

For the estimation of flood "Logistic Regression" algorithm is used. This algorithm is one of the most used machine learning (ML) algorithms for Binary classification.
The model is first Trained and then Tested using 3:1 ratio. 75% of the dataset is used for Training the model and 25% of the dataset is used for Testing the model.
By considering our Literature review, we have obtained the maximum and minimum threshold. By continuous trial and error, we have classified the flood extent as high and low within these threshold values[2].
The detailed analysis of the performance of the proposed algorithm is analysed and accuracy is estimated.
Figure 6 shows the Flowchart of Flood estimation steps and working of algorithm:

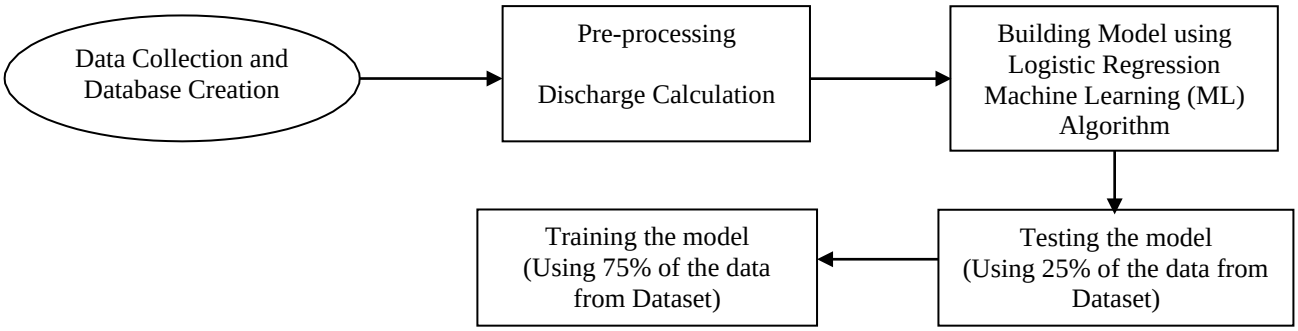



Figure [6]: Flow of Machine Learning (ML) model

## VI. RESULTS

**Profile Extraction:**
Area is calculated by conducting literature survey or directly taken from user.
The experimental setup consists of Optical Laser Distance sensor and traditional method of Levelling the device using thread and stick for calculations.

The device is set to 544m MSL (Mean Sea Level) as a reference point and all readings are taken respectively. The graph in figure 7 denotes the approximation of ground profile and the pictures of the location where the experiment was conducted is shown in figure 8:

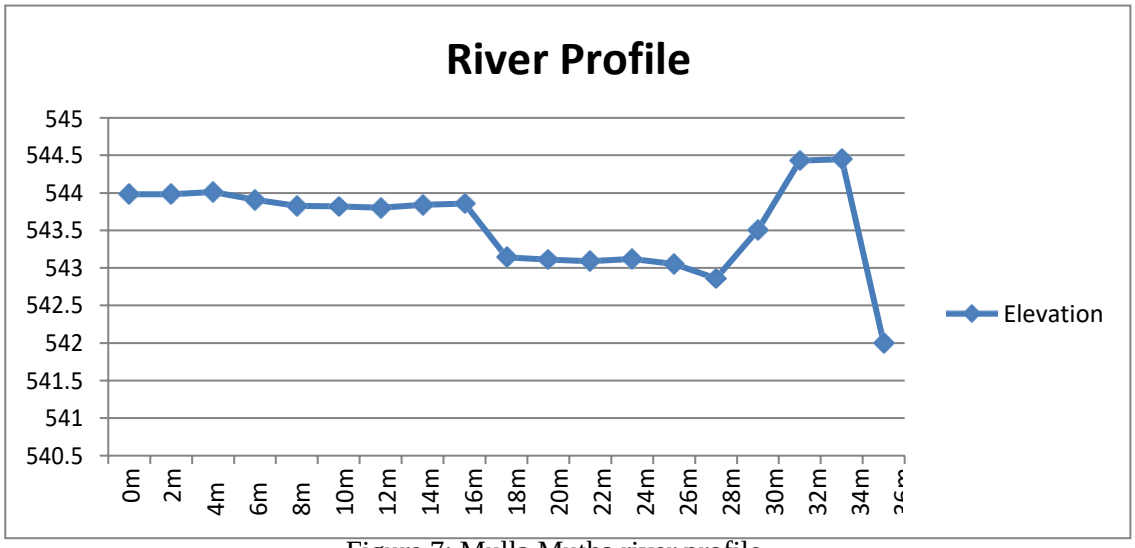



Figure 7: Mulla Mutha river profile

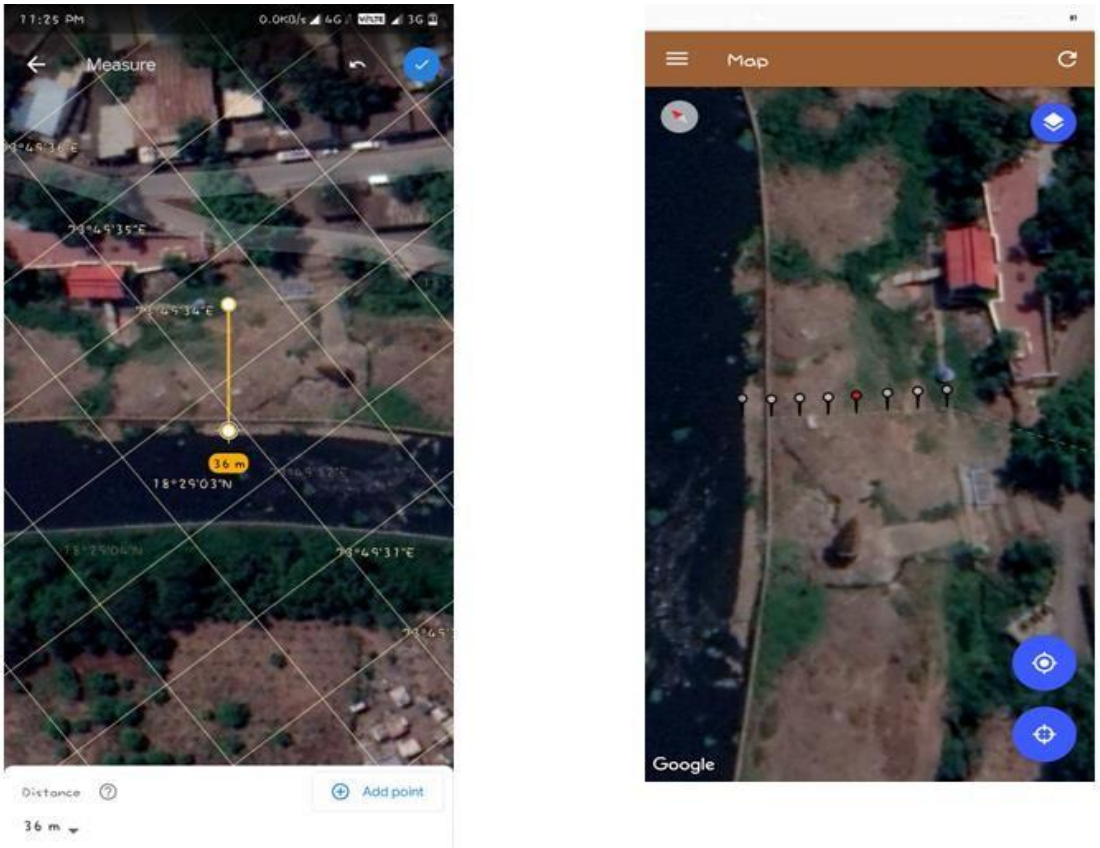



Figure 8: Google earth location of river

The model is tested on the obtained dataset and the results are formulated.
In the proposed algorithm various major computations factors contributing to the final module of estimation of flood like Average rainfall, wind speed and Temperature is used.
Data logger is developed to display and store values in SD card. Some values are taken from IMD site. These are then used to prepare a database in excel of ".csv" file as shown in figure 9:

| | A | B | C | D | E | F | G | H |
|---|---|---|---|---|---|---|---|---|
| 73 | Day | Avg. Temp (.C) | Max. Temp (.C) | Min. Temp (.C) | Atm. Pressure(hPa) | Avg. Humidity(%) | Total Rainfall(mm) | Avg. Wind Speed(Km/h) |
| 74 | Jun-12 | 25.8 | 30.2 | 22.7 | 1001.6 | 76 | 0 | 2 |
| 75 | Jun-13 | 26.3 | 29.8 | 21.9 | 1003.2 | 77 | 4.06 | 4.4 |
| 76 | Jun-14 | 27.9 | 32.4 | 22.8 | 1003.5 | 65 | 1.02 | 5.2 |
| 77 | Jun-15 | 27 | 31.3 | 23.5 | 1005.2 | 72 | 2.03 | 5.4 |
| 78 | Jun-16 | 28.2 | 33.6 | 23.6 | 1006 | 63 | 0 | 6.3 |
| 79 | Jun-17 | 27.8 | 31.8 | 23.9 | 1006.4 | 63 | 0 | 10.9 |
| 80 | Jun-18 | 27.4 | 32.2 | 23.4 | 1004.4 | 68 | 0 | 5.9 |
| 81 | Jun-19 | 26.1 | 28.8 | 23.3 | 1004 | 78 | 0.25 | 3.7 |
| 82 | Jun-20 | 27.9 | 31.7 | 23.1 | 1004.3 | 61 | 0.51 | 6.3 |
| 83 | Jun-21 | 28.2 | 33.6 | 23.3 | 1003.9 | 64 | 0 | 6.7 |
| 84 | Jun-22 | 28.1 | 32.6 | 23.9 | 1003.1 | 65 | 0 | 5 |
| 85 | Jun-23 | 27.6 | 32.2 | 24.5 | 1002.5 | 70 | 0 | 4.4 |
| 86 | Jun-24 | 26.1 | 31.6 | 23.7 | 1004.2 | 80 | 1.02 | 2.8 |
| 87 | Jun-25 | 26.8 | 32.6 | 22.9 | 1005 | 78 | 4.06 | 2 |
| 88 | Jun-26 | 26.8 | 30.8 | 23.2 | 1004.5 | 78 | 12.95 | 1.9 |
| 89 | Jun-27 | 25.2 | 30 | 23.2 | 1003.9 | 86 | 0.76 | 2 |
| 90 | Jun-28 | 23.7 | 25.1 | 22.7 | 1004.2 | 92 | 72.9 | 2.4 |
| 91 | Jun-29 | 23.4 | 24.6 | 21.7 | 1004.5 | 89 | 59.94 | 4.4 |

Table [1]: Database.csv

A flood occurrence graph is obtained using only rainfall values obtained from datasheet. Pune experienced Maximum rainfall and flood conditions on September 24, 25, 26 and 27 on year 2019. The graph obtained clearly depicts these flood conditions as 1 and non flood days as 0. These data is used to train the model. The graph is shown in figure 9:

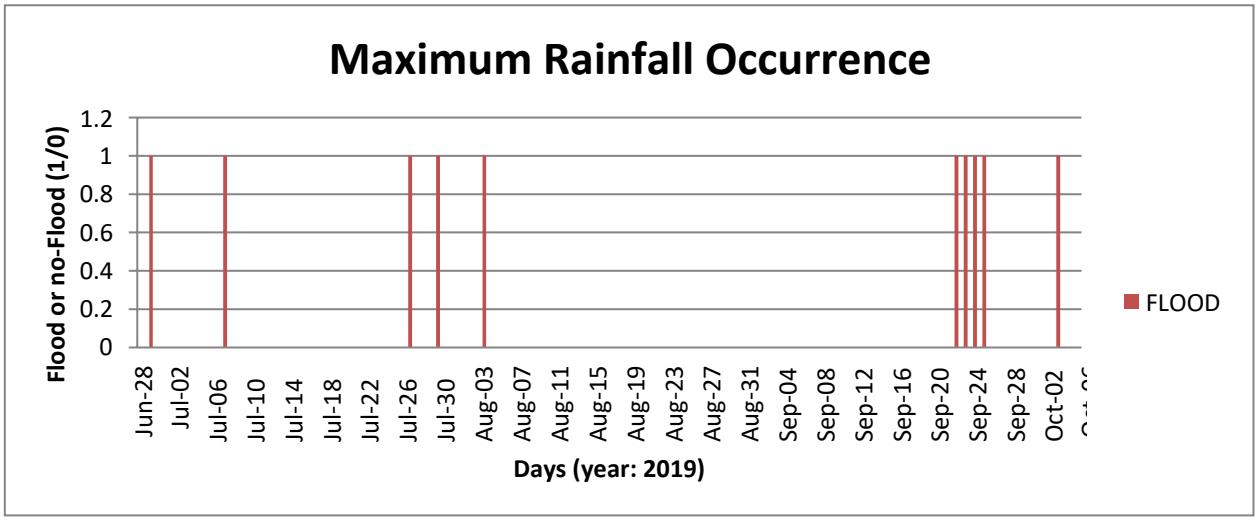



Figure 9: Maximum Rainfall Occurrence graph

A confusion matrix is developed from these classifications which are used to calculate the efficiency and accuracy of the proposed method. There are 68 flood data out of which 65 are correctly classified into flood category and 3 is misclassifies. On the other hand, there are 32 non flood data and 24 of them are correctly classified. Remaining of them is misclassified as flood condition. The obtained Confusion matrix is as shown in table 2:

TABLE 2

CONFUSION MATRIX

| n = 100 | Predicted: Yes | Predicted: No |
|---|---|---|
| Actual: Yes | TP = 65 | FN = 3 |
| Actual: No | FP = 8 | TN = 24 |

Here: TP: True Positive, TN: True Negative, FP: False Positive, FN: False Negative

The accuracy of the proposed algorithm is 0.89. To increase the accuracy more number of parameters can be considered. The more the accuracy the more reliable is the model[11]. With greater accuracy, the estimation is accurate.

The trained model is then used to plot a graph to show Flood and non-Flood conditions as shown in figure 10:

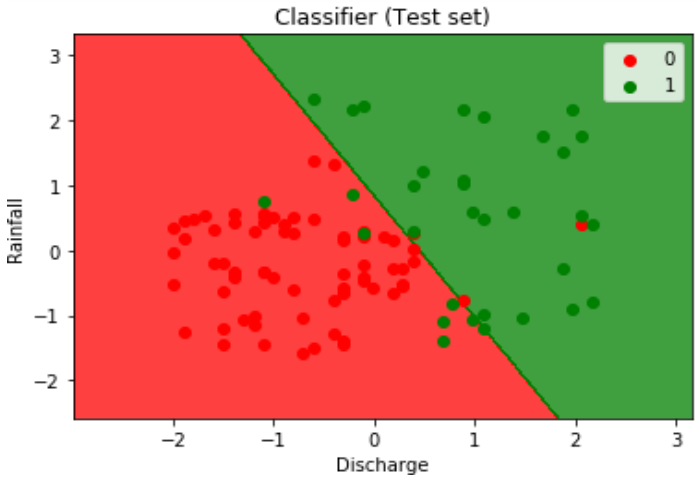



Figure [10]: Graph of Discharge vs. Rainfall

## VII. CONCLUSIONS

The Flood is estimated using the surface velocity and the dataset. The result obtained from this methodology is useful for flood prone areas, downstream of dam or canal and river flow. The surface water velocity measurement using image based technique is a reliable, easy, cheapest measurement approach. The model is trained using previous year's data having both flood and non-flood conditions. The result has been achieved with an accuracy of 89%, which makes the model more reliable. This method aims at flood detection in a very reliable way without harming the environment. We plan to extend our work considering more factors like Wind speed, velocity at different points in a canal relative to area of canal and estimate flood so that the accuracy is increased.

## VIII. ACKNOWLEDGEMENT

The authors thank Shri A K Agrawal, Director, CWPRS for permitting this study to be taken up. We also thank the Khadakwasla Irrigation authorities for sharing the data pertains to the cross section, rainfall, water level, discharge etc., We are also grateful to M/s. Horizon electro solutions, Pune for providing the design of data logger technology.

## REFERENCES

1. G. Farina, M. Bolognesi, S. Alvisi, M. Franchini, A. Pellegrinelli, P. Russo, "Estimating discharge in drainage channels through measurements of surface velocity alone: A case study", Flow Measurement and Instrumentation, Elsevier, Volume 54, April 2017.
2. Onur Genç , Mehmet Ardıçlıoğlu , Necati Ağıralioğlu, "Calculation of mean velocity and discharge using water surface velocity in small streams", Flow Measurement and Instrumentation, Elsevier, Volume 41, March 2015.
3. Christopher Tomaszewski, Paul Scerri, John Dolan, "Augmenting LSPIV Surface Current Measurement with Drifting ASVs", Conference Paper, Proceedings of the 2018 IEEE OCEANS Conference, pp. 1-6, May 2018.
4. Franco Lin, Wen-Yi Chang, Lung-Cheng Lee, and Hung-Ta Hsiao, Whey-fone Tsai, "Applications of Image Recognition for Real-Time Water Level and Surface Velocity", IEEE Volume 1, 2013.
5. Matilde Welber, Jer ome Le Coz, Jonathan B. Laronne, Guido Zolezzi, Daniel Zamler, Guillaume Dramais, Alexandre Hauet, and Martino Salvaro, "Field Assessment of Non-Contact Stream Gauging using portable Surface Velocity Radars (SVR)", Water Resources Research, Volume 52, January 2016.
6. Amitkumar Baburao Ranit, Dr. P. V. Durge, "Flood Forecasting by using Machine Learning", Proceedings of the Fourth International Conference on Communication and Electronics Systems (ICCES 2019) IEEE Conference.
7. Yue Zhou, Jinyao Yan, "A Logistic Regression Based Approach for Software Test Management", 2016 International Conference on Cyber-Enabled Distributed Computing and Knowledge Discovery.
8. C.M. Vancea, L. Viman, "Wireless data logger for thermal validation systems'', 2011 IEEE 17th International Symposium for Design and Technology in Electronic Packaging (SIITME).
9. Vladimir Mitroviü, Milan Mijalkoviü, "Power Quality Data Logger with internet access", 19th International Symposium Power Electronics Ee2017, October 2017.
10. Devi Munandar,Djohr Syamsi, have worked on "Data logger Management Software Design for Maintenance and Utility in Remote'', 2014 1st International Conference on Information Technology, Computer and Electrical Engineering (ICITACEE).
11. Geetha M, Megha Manoj, Sarika A S, Muktha Mohan and Sethuraman N Rao, "Detection and Estimation of the Extent of Flood from Crowd Sourced Images", International Conference on Communication and Signal Processing, IEEE, April 6-8, 2017, India.
12. Qianyu Zhang , Nattha Jindapetch , Rakkrit Duangsoithong and Dujdow Buranapanichkit, "Investigation of Image Processing based Real-time Flood Monitoring", Proc. of the 2018 IEEE 5th International Conference on Smart Instrumentation, Measurement and Applications (ICSIMA 2018).

IN PROCEEDINGS OF 25th HYDRO 2020, INTERNATIONAL CONFERENCE,
NATIONAL INSTITUTE OF TECHNOLOGY ROURKELA, ODISHA, INDIA
26-28, March 2021, ISBN 978-93-90631-56-8

Paper ID - 025

# Hydraulic physical model studies for the development of Coast Guard jetty at New Mangalore port, Panambur, Karnataka - a case study

H. B. Jagadeesh [1], A.S. Chalawadi [2], Prabhat Chandra[3]

[1] Scientist D, Central Water and Power Research Station, Pune - 411024, India.
[2] Assistant Research Officer, Central Water and Power Research Station, Pune - 411024, India.
[3] Scientist E, Central Water and Power Research Station, Pune - 411024, India.
Email: jagadeeshhb@yahoo.co.in[1]

## Abstract

Physical model studies were carried out at CWPRS for the proposed development of Coast Guard jetty at New Mangalore Port. The initial proposed location of the jetty was on the return of berth No. 18 in Western dock arm(Alt - 1). The said location is adjacent to the harbour entrance. The Coast Guard ships which are to be berthed are small draft vessels. As the proposed place is very near to the harbour entrance, the ship generated waves attack on the broader side of the berthed Coast Guard vessel. The waves entering through harbour opening also make disturbance to the berthed Coast Guard vessels. Hydraulic physical model studies were conducted in a 3-D rigid bed, multi-directional random wave model for wave tranquillity and approaching direction of wave. Since the proposed Coast Guard jetty is to be operative for all round the year, model studies were conducted by generating waves from three critical directions viz. West, South-West, and North-West which are prevalent for different seasons for this port. Wave tranquillity studies were conducted by random waves by generating Scott spectra with $H_S$=2.5m, $T_Z$=10sec. Wave approaching direction at the proposed jetty was observed by conducting experiments with regular waves of H=2.5m and T=10 sec. Studies were also conducted for a separate harbour (*Alt - 2*) exclusively for Coast Guard vessels on North of North breakwater. Taking the shelter of existing North breakwater, the Alt-2 harbour comprises of two breakwaters - outer breakwater and inner breakwater with a dredged depth of -8m in harbour area. The wave tranquillity results for both the alternatives and sketches of separate harbour are presented.

***Keywords: -*** *Coast Guard jetty, wave tranquillity, wave direction, jetty alignment, breakwater.*

## 1.0 Introduction

The Indian Coast Guard (ICG) is a multi-mission organization, conducting round the-year real-life operations at sea with a motto of 'we protect'. Along with patrolling the vast Indian coast, it also provides life saving services to the people in emergency cases in the sea, search operations in sea, safety and protection of islands, offshore terminals and other installations, assistance to the Department of Customs and other authorities in anti-smuggling operations, Law enforcement in territorial as well as international waters etc. The Indian Coast Guard has five regions viz. Western Region(W), Eastern Region (E), North-East Region (NE) Andaman and Nicobar Region(A&N) and North-West Region (NW). It's regional, district head quarter and Coast Guard Stations are located at various places along the Indian coast. On western coast, one of its district head quarter (DHQ 3) is located in Panambur, Mangalore in Karnataka state which was commissioned in the year 1991 and located close to the New Mangalore Port.

The New Mangalore Port is one of the major ports of India located on the West coast in Karnataka state and operating since 1974 (Fig. 1). It is an artificially developed lagoon type of port which operates throughout the year. This port has a maximum draft of -15.1m inside the harbour basin and -15.4m in approach channel at present. Predominant waves for this port are from West, South West and North West directions.




**Fig 1.** Location map and satellite image of New Mangalore Port
(Source: Wikimapia)

In the absence of a dedicated berthing facility, at present ICG vessels are usually berthed at berth No.1 or inside the oil dock arm (southern dock) of port. The Fig. 2 shows berthing of ICG boats inside southern dock arm of NMP. Now, there is a proposal to construct a 180 m long dedicated jetty for Indian Coast Guard vessels at suitable location.

It is observed that, at location inside lagoon selected, even though required draft for Coast Guard ships is -8m, there is a need to go beyond -24m since the selected location is in the proximity of port approach channel. This increases the cost of construction of the jetty. Hence alternatively it was explored for a separate harbour on the north side of North breakwater by taking shelter of North breakwater. For our convenience, the proposal on return of berth No. 18 is referred in this paper as Alternative -1 and separate harbour on North side of North breakwater as Alternative – 2.




**Fig. 2:** Satellite image of Southern Dock and berthed CG boats (Image Source: Google)

The locations of Alt – 1 and Alt- 2 are shown in Fig. 3. The proposed location for the jetty in Alt -1 is adjacent to the harbour entrance, wherein all the major port traffic passes along this route.




**Fig. 3 :** Location of proposed Coast Guard Jetty and alternative harbour at NMP.
(Image Source: Google)

The Photos 1 and 2 show actual site view of Alt -1 proposal.




**Photo 1 & 2:** View of the proposed CG Jetty location(Alt-1) from Berth No.18 and from harbour entrance.

## 2.0 Hydraulic model studies

### 2.1 *Description of Physical Model*

It is a rigid bed model simulated with latest bathymetry and other existing features to a scale of 1:120 (G.S.), housed in a hangar of size 72m x 45m (Fig. 4). The model bed is simulated with smooth cement plaster to minimize the effect of the bed friction. Truncated approach channel is reproduced in the model for a distance of about 4000m from port basin entrance up to contour of -11.0 MCD. Two shore connected breakwaters each measuring 770m were also simulated in model. The proposal of development of Coast Guard Jetty was studied in the model by conducting experiments from West, South West, and North-West which are predominant for the proposed development. This model is equipped with hydraulic power system (HPS) for regular and random wave generation facilities from the three critical directions for the harbour entrance.

Wave tranquility and directional propagation were recorded for all salient locations by conducting experiments from three predominant directions mentioned above and these results are presented in this paper.

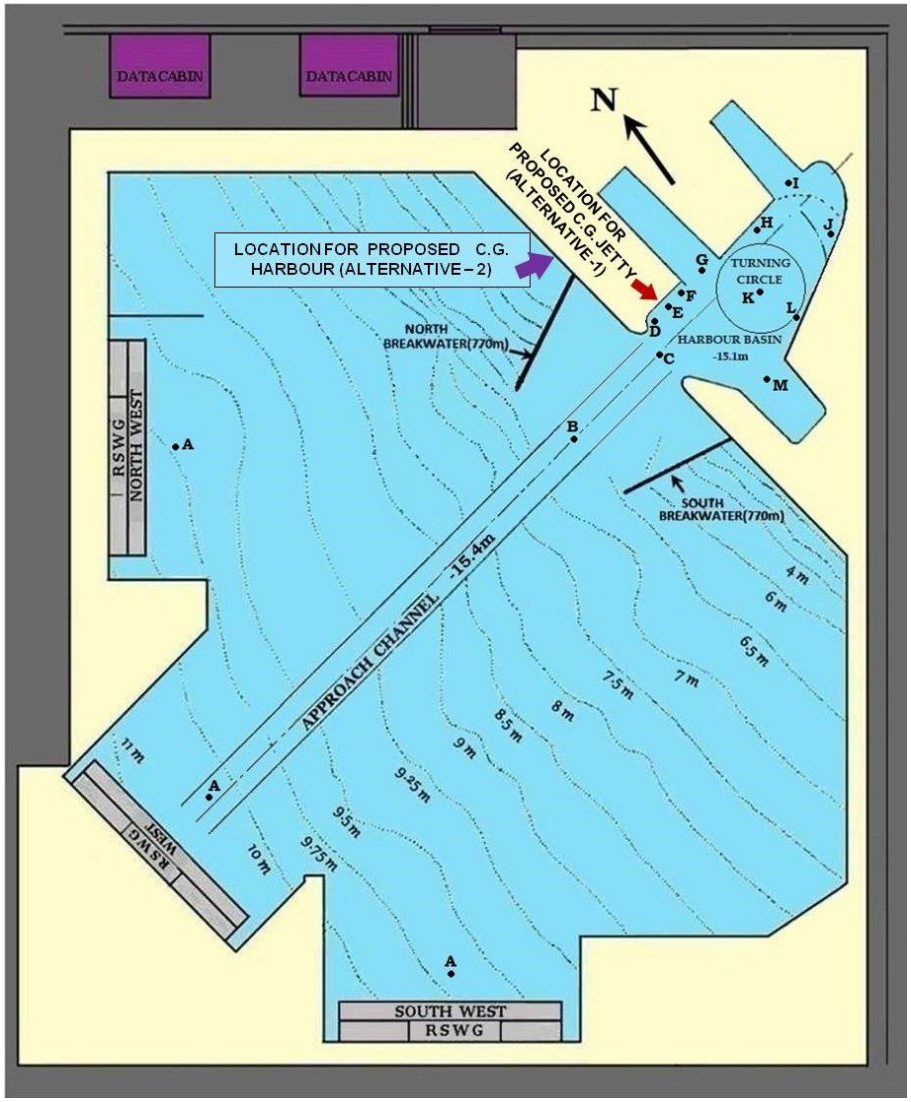



**Fig. 4:** Model Layout of New Mangalore Port with wave probe locations

### *2.2 Testing Conditions*

Random waves with Scott spectra having significant wave height Hs = 2.5m, Time period Tp = 10sec were considered as the boundary condition in the model. The tested conditions are in tune with the prototype observations and for various studies in the model adopted successfully.

### *2.3 Wave Tranquillity Limits*

The wave tranquility limits for proposed Coast Guard vessels were not specified by the project authorities. In the absence of specific wave tranquility limits, a wave height of 0.50m for its 120m long ships and wave height of 0.30m for small size vessels is considered as acceptable wave heights in this study. The allowable Wave Heights near the Berths as per standard wave tranquility limits for vessels of similar sizes.

## 3.0 Model studies

### 3.1 *Wave Tranquillity Studies for Alternative – 1*

A jetty, at location in side lagoon as suggested by port authorities, was simulated in the model on the return of berth No.18. The studies were carried out by generating regular and random waves from West, South-West and North-West directions. The regular wave model studies were done for sketching the wave pattern at the proposed berthing locations. Random wave model studies were useful in the estimation of wave tranquility at the proposed Coast Guard jetty and various other salient locations in the harbor basin with the construction of Coast Guard Jetty. The dredged depth in the approach channel was -15.4 MCD and turning circle was -15.1 MCD as per the conditions prevailing in the prototype. Studies were conducted by simulating a wave absorptive surface on the rear side of the proposed Coast Guard Jetty by suitably placing absorptive surface. This is effective in reducing the reflection effects from the proposed jetty, which in turn helps in reducing wave effects in the harbour basin. Photos 4 and 5 show before and after the simulation of proposed Coast Guard Jetty in the model.




**Photo 4 & 5:** Before and after simulation of proposed C.G. jetty for Alt-1 in model

#### 3.1.1 *Observations for West, North West and South West Direction Waves*

The wave heights at various locations in the port basin were observed for incident waves with Hs = 2.5m / Tp=10 sec at generation point from West, North West and South West direction. The observed wave heights at the Coast Guard jetty are 0.50, 0.45, 0.45m for waves from South West, 0.50, 0.45, 0.40m for waves from West and 0.45, 0.40, 0.35m for waves from North West. The wave heights at

locations near the Coast Guard jetty are within the permissible limit of 0.50m considered for bigger ships but exceeds the limit considered for small size vessels.

A table containing consolidated tranquillity values at salient locations for waves from three directions is given below in Table No.3 (Ref. Fig. 4).

**TABLE 3** Wave heights at various locations for Alternative -1

| Location | Wave height in meters | | |
|---|---|---|---|
| | SW | W | NW |
| A | 2.50 | 2.50 | 2.50 |
| B | 0.75 | 0.70 | 0.70 |
| C | 0.65 | 0.65 | 0.55 |
| D | 0. 50 | 0.50 | 0.45 |
| E | 0.45 | 0.45 | 0.40 |
| F | 0.45 | 0.40 | 0.35 |
| G | 0.35 | 0.30 | 0.30 |
| H | 0.40 | 0.35 | 0.30 |
| I | 0.15 | 0.15 | 0.10 |
| J | 0.40 | 0.35 | 0.35 |
| K | 0.40 | 0.40 | 0.30 |
| L | 0.30 | 0.35 | 0.25 |
| M | 0.30 | 0.25 | 0.25 |

### 3.2 *Wave Tranquillity Studies for Alternative – 2*

The Alt-2 is development of an independent small harbour on the North side of existing North breakwater of New Mangalore port. Here, taking benefit of existing North breakwater, it would consist of two breakwaters - one outer and inner breakwater. Existing North breakwater and proposed location for Alt-2 harbour is shown in Fig.5.




**Fig.5:** Satellite image showing the location of Coast Guard harbour (Alt-2)

The Photos 6 and 7 show the site images which give details of site for the proposed Alt -2. In these photos, proposed location for Alt -2, North breakwater and Coast Guard office can be seen.




**Photo 6 and 7:** Location of alt-2 harbour site on North of North breakwater.

Preliminary wave tranquility studies were conducted by varying the lengths and alignments of inner and outer breakwaters and an optimal length and alignment as shown in layout plan (Fig.6) was arrived. As per this the outer breakwater of length 625m and inner breakwater of length 265m with harbour entrance towards west, an approach channel of 925m length and base width of 50m were finalised. Depth in the harbour basin area was kept at -8.0m and in the approach channel at -9.0m with side slopes of 1:15.

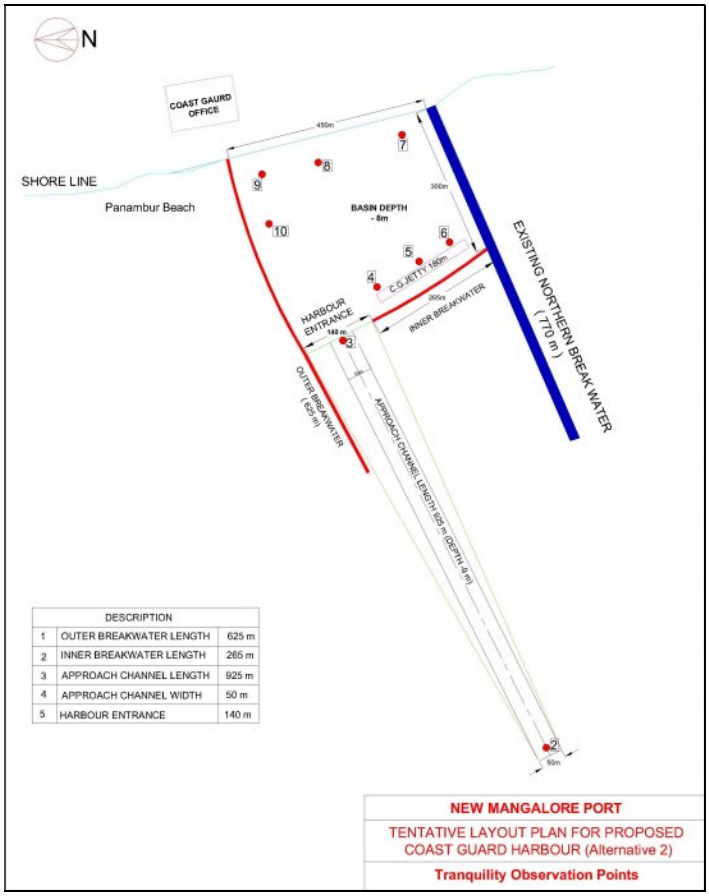



**Fig. 6:** The tentative layout for Alternative-2 and probe positions

All the above important features for development of harbour basin were simulated on the northern side of existing North breakwater of the port model. Wave tranquility studies were conducted for waves from the three directions Viz. South West, West and North West on this layout.

The Photos 8 and 9 were taken while conducting the model studies for the suggested harbour with wave height recording probes at desired locations in the harbour and approach channel.



**Photo 8:** A view of Coast Guard harbour (Alt -2) with Westerly waves



**Photo 9:** Another View of Coast Guard harbour (Alt-2) for North Westerly Waves

The wave heights at the proposed jetty location in the alternative harbour were between 0.15m to 0.30m for waves from all the three directions. The wave heights at the jetty are in acceptable range for lighter vessels. A table containing consolidated tranquillity values of all the above three directions is given below in Table No.4 (for probe locations Ref. Fig. 6).

**TABLE 4** Wave heights at various locations for Alternative -2

| LOCATION | WAVE HEIGHT IN METERS | | |
|---|---|---|---|
| | SW | W | NW |
| 1 | 2.50 | 2.50 | 2.50 |
| 2 | 1.55 | 1.70 | 1.80 |
| 3 | 0.75 | 0.65 | 0.85 |
| 4 | 0.30 | 0.25 | 0.30 |
| 5 | 0.20 | 0.20 | 0.20 |
| 6 | 0.15 | 0.15 | 0.15 |
| 7 | 0.25 | 0.35 | 0.25 |
| 8 | 0.35 | 0.40 | 0.35 |
| 9 | 0.45 | 0.45 | 0.45 |
| 10 | 0.60 | 0.55 | 0.60 |

## 4.0 WAVE PATTERNS AT THE PROPOSED JETTY IN ALT 1 AND 2 LOCATIONS

The model studies with regular waves with incident waves of H=2.5m and T=10 sec were conducted from West, South-West and North-West directions. Wave crest pattern were observed at the proposed Coast Guard jetty locations (Alt 1 and 2) for the three directions. The wave crest patterns for the westerly incident waves which are most critical for the proposed location are as shown in the Fig. 7. In both the alternates, it was observed that the waves were approaching head on for berthed vessels at jetty.

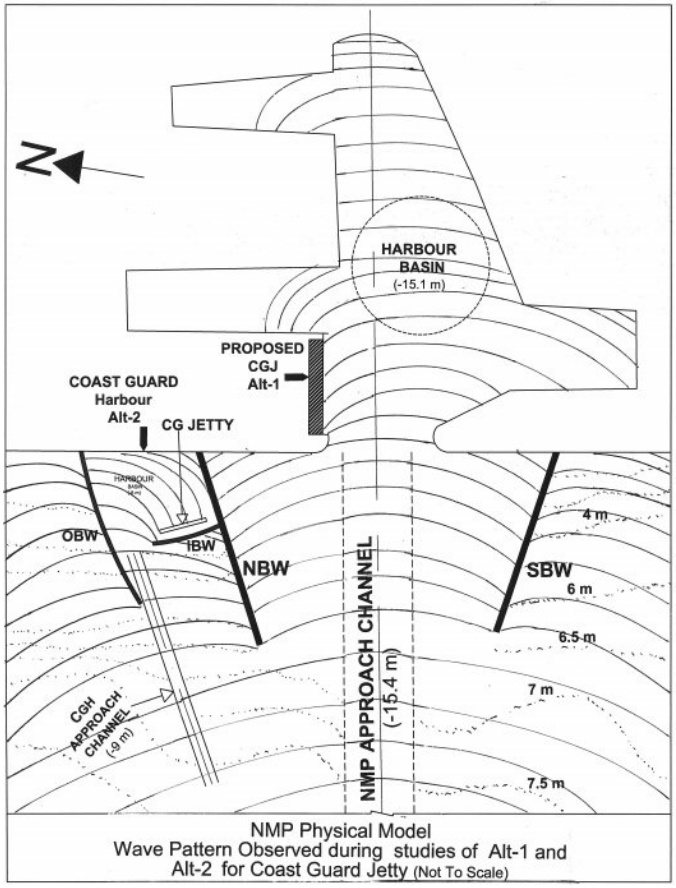



**Fig. 7:** Wave pattern sketch for Coast Guard jetty (waves from West)

## 5.0 Discussion on results

The wave tranquility studies were conducted for Hs=2.5m at generator (which corresponds about 3.66m at deep water) is very rare from North-West direction and from West, South-West direction it may occur for about 10 days in a year.

Alternative – 1 Layout

- The wave heights at the proposed ICG jetty vary from 0.30m to 0.50m for waves from all the three directions tested. These wave heights are just adequate for bigger ships of ICG but exceed the limit for small vessels.

- As the proposed jetty location is near to the harbor entrance, the waves generated by the large ships need to be considered while developing the proposed jetty as these waves may approach on broader side the berthed ship which is not desirable from the safety of the light weight ICG ships.

- Model studies also indicated that there is no adverse effect on wave tranquility due to the development of Coast Guard jetty to other existing berths in the lagoon.

Alternative-2 Layout

- The wave heights for waves from all the three directions at the proposed jetty vary from 0.15m to 0.30m and along the land (beach) facing inside the harbour vary from 0.25m to 0.45m.

- For future development of berthing of ships along land facing area, a small spur of about 50m length may be provided near the proposed Coast Guard harbour entrance. The location and length of the spur may be decided after optimizing the approach channel dimensions through mathematical model studies.

- The existing foundation of North breakwater of New Mangalore Port may interfere with the dredging if Indian Coast Guard harbour basin to -8m CD. Based on the extent of existing North breakwater foundation, a proportional shift of outer breakwater may be decided. This would also increase the length of inner breakwater proportionately. However, such minor shifts in harbour layout will not change the harbour tranquility in general.

- The waves after entering from the harbor entrance will diffract and becomes almost perpendicular to the berthing structure which makes it favorable condition to berthed ships.

- Approach to the jetty may be made by independent trestle bridge with piled structure or by paved road on existing North breakwater.

## 6.0 Conclusion

1. The wave boundary conditions were selected based similar to wave tranquility studies on the same physical model for various berths at New Mangalore port basin.

2. In the absence of any wave tranquility limit specified by the project authorities, a wave disturbance of 0.30m is assumed for small size ICG ships and 0.50m for bigger size ships of 120m long at the proposed jetty.

3. The wave tranquility conditions for the incident waves from the predominant directions for the proposed ICG jetty at Alt-1 will be just adequate for bigger size ICG ships but inadequate for the small size ICG ships.

4. The waves formed by the movement of the large ships may hit the berthed ship on its broader side at proposed jetty in Alt-1 which is not desirable from the safety of the light weight ICG ships. So it is not a very favorable site for the development of C.G. jetty.

5. Even though the draught requirement for the coast guard ships is only about -8m CD, the proposed jetty structures at Alt-1 site is required to be developed to deeper levels of about -24m considering the future deepening of the harbour. This will lead to unnecessary increase in the cost of development.
6. For Alt-2 layout, an independent small harbour development on the North side of existing North breakwater of NMP, the wave tranquility conditions at the jetty proposed on the lee side of the inner breakwater are adequate and are within the considered wave limits and the wave approach directions as well.

7. For the proposed jetty on the lee side of inner breakwater, approach may be provided by constructing road along the top of existing North breakwater or alternatively by constructing a trestle bridge on pilled structure. In either way, the wave tranquility for the proposed jetty will not have any adverse effects.

8. The development of the independent small harbour development on the North side of existing North breakwater will not make any adverse effect on use of the Panambur beach by general public as this location is used by very minimum public. The approach road joins the beach at a distance of about 500m North of North breakwater. After reaching the beach, most of the public prefer to move towards north side as that side beach is much longer in length, many eateries and children attractions like water game equipment vendors available in this side.

9. Having a separate harbor for ICG will be useful in future development works like training academy etc for Coast Guard staff.

10. It is suggested to carryout following additional studies for Alternative-2 before finalizing the proposal.

    i) Mathematical model studies for the littoral drift and hydrodynamic studies for siltation and maintenance dredging.

    ii) Mathematical model studies for Navigation and optimization of harbour approach channel dimensions.

    iii) Desk and Wave flume studies for design of Breakwater.

ACKNOWLEDGEMENT

The authors are thankful to Shri. A. K. Agrawal, Director CWPRS for the encouragement and granting permission to publish the paper. Authors are also thankful to the Indian Coast Guard and New Mangalore Port Trust authorities for sponsoring the model studies.

## Reference

CWPRS Technical report No.4298 (2006) Model studies (1/120 G.S.) for the development of deep draft multipurpose berth at New Mangalore Port, Mangalore, Karnataka.

CWPRS Technical report No. 5159 (2014); Hydraulic Physical model studies for flotilla berths at New Mangalore Port, Mangalore, Karnataka.

CWPRS Technical report No. 5706 (2019) Physical Model studies for Wave Tranquillity for the proposed development of Coast Guard Jetty at New Mangalore Port, Karnataka

H.B. Jagadeesh, A.S. Chalawadi, T. Nagendra and C.N. Kanetkar (2008) ―Development of deep draft multipurpose berth (Berth No 14) at New Mangalore Port – Model studies and prototype behavior - technical paper published in proceedings INCHAE 2008, Pune, India.

IN PROCEEDINGS OF 25th HYDRO 2020, INTERNATIONAL CONFERENCE,
NATIONAL INSTITUTE OF TECHNOLOGY ROURKELA, ODISHA, INDIA
26-28, March 2021, ISBN 978-93-90631-56-8

Paper ID - 167

# SUITABILITY OF REGULAR AND RANDOM SEA WAVE GENERATORS IN HYDRAULIC PHYSICAL MODEL STUDIES - KEY FACTORS FOR SELECTION

Dr. H.B. Jagadeesh[1] Kashyape P A[2] Dr. Prabhat Chandra[3]

[1] *Scientist D, Central Water and Power Research Station, Pune - 411024, India.*
[2] *Scientist B, Central Water and Power Research Station, Pune - 411024, India.*
[3] *Scientist E, Central Water and Power Research Station, Pune - 411024, India*
*Email: jagadeeshhb@yahoo.co.in*[1]
*Telephone/Mobile No.: +919421011813*

## ABSTRACT

Hydraulic models either physical or mathematical are commonly used modeling tools in coastal engineering. Physical models are having advantages such as – they allow complex geometries, bed topography to be modeled and their visual nature draws attention to small scale flow features. These models are very useful to model complex wave hydrodynamics near shallow water regions for the analysis and design of the harbor and other structures near shore.

Hydraulic model studies in basic and applied investigations of wave induced phenomena are conducted on regular wave or random sea wave (wave spectrum) generating physical model. Earlier days physical model studies for coastal engineering investigations are exclusively conducted with regular waves. Where as in actual sea waves are random in nature. With advancement in the hydraulic modeling technique it is possible to simulate the wave spectra with close approximation to natural conditions by advanced instrumentation and automation techniques. Having random wave generating facility on a model, it is also possible to generate regular waves also by giving suitable input data. This paper presents the comparative analysis of the results of regular wave and random sea wave generators and their suitability in hydraulic model studies for coastal engineering project development studies. The results of the Regular and Random waves on various physical model studies conducted at CWPRS are presented in this paper highlighting the pros and cons. The suggestive measures for type of wave generator in physical model studies depending on study needs are presented.

***Key words:*** *Hydraulic physical models, regular wave, random sea wave, wave generation and wave hydrodynamics.*

## 1. Introduction

In design of any coastal structure the study of effects of hydraulic phenomenon like waves, tides, density currents and movement of sediments are important. Hydraulic models either physical or mathematical are commonly used modeling tools for design of coastal development works. Computer based numerical models are widely used for this purpose, however physical models play an important role in proving the numerical models and are having advantages over numerical models such as – they allows complex geometries, bed topography to be modeled without schematic simplification and they have no restriction on grid size so far as data is concerned (Falconer et. al. 1995); their visual nature draws attention to small scale flow features, such as separation which are important in understanding the flow field and improvement of design wherever necessary (Falconer 1982). Physical modeling is often the only technique able to model some more complex physical phenomena properly and very useful tool to study the complex wave hydrodynamic near shallow water regions for the analysis and design of the harbor and other structures near shore (Anoopdas et. al. 2016). Hence, scaled hydraulic physical model studies plays a very important role in the decision making process of

development of any coastal projects as well as helpful in avoiding costly mistakes before making huge investments in coastal development projects.

Since 1930s coastal structure were designed by trial and error method (Bill et. al. 2016) by using physical models studies. In these early years physical model studies for coastal engineering investigations are exclusively conducted by generating regular sinusoidal waves (i.e. regular waves) mechanically by moving the wave board with required amplitude and period. However, in actual sea waves are random in nature. With the advancement in control system theory and computers it is now possible to simulate the wave spectra (i.e. random sea waves) with close approximation to natural conditions in the hydraulic physical models. With the capability of generation of irregular characteristics of sea in the model physical modeling become a more reliable tool for coastal engineers. However in the modeling studies of coastal engineering problems both regular waves and random waves studies have their equal role in obtaining and interpretation of the results for optimum solutions; such as regular waves studies are very good to give the results for directional spread of waves while random waves studies are reliable to obtain the wave tranquility, breaking of waves pattern at the point of interest etc.

The comparative study of results from physical model studies performed with regular wave and random sea wave are seldom studied. This paper focuses on suitability of regular wave and random sea wave generators in hydraulic model studies for coastal engineering projects by discussing the results of model studies performed for various development proposals of New Mangalore Port Trust and Kamrajar Port Ltd. on physical models of these ports at Central Water & Power Research Station (CWPRS) Pune.

## 2. Methodology

### 2.1 *Theory of Wave Generation in Physical Models*

*2.1.1 Regular Wave*

In hydraulic modeling practice regular waves in the model are generated mechanically by moving wave board (flap) with required amplitude and period resulting in unidirectional wave train having specific wave height, time period and wave crests parallel to wave board. These waves are regular sinusoidal waves conform well to linear wave theory. The regular wave with its propagation in a direction is generated by the wave paddle motion described by Biesel and Suquet during 1951 (Hughes 1993 & Nohora 2000) is given below. The wave paddle motion $\eta_i(t)$ of the *i*-th segmented wave paddle at time t is formulated for flap type wave paddle is given as
in the following. Mathematical equation developed

$$\eta_i(t) = \frac{a}{2F} \sin(\sigma t - ikb\cos\theta) \quad (1)$$

where *a, s, b* and *t* denotes amplitude, angular frequency, wave paddle width and time respectively and F denotes transfer function for wave generation i.e. wave height to stroke ratio ($h/S_o$). F is represented by

$$F = \frac{4\sinh(kh)}{kh} \frac{1-\cosh(kh)+(kh)\sinh(kh)}{2kh+\sinh(2kh)} \quad (2)$$

Where *h* means uniform water depth in the basin and *k* is wave number and a solution of the dispersion is as

$s^2 = kg\tanh(kh)$ …… here *g* is acceleration due to gravity. (3)

*2.1.2 Random Wave*

With the advances in digital control system and computer hardware technology of wave generation in hydraulic physical models have been developed rapidly during past few decades. Since the real sea waves are highly irregular and 3-D in nature, coastal engineers generally reproduce these natural waves as a 2-D process (Ketabdari et. al. 2009), since these 2-D irregular waves are more acceptable to theoretical treatment and offers some understanding of 3-D real sea state. Waves in the sea can be expressed by their energy spectrum viz. JONSWAP, ISSC, Bretschneider-Mitsuyasu, SCOTT etc. over a range of frequencies. Hence, random waves in hydraulic physical models are generated by considering them as summation of sinusoidal waves of different frequencies.

$$\eta_i(t) = \sum_{n=1}^{N} \frac{a_n}{F_n} \sin(\sigma_n t - i k_n b \cos\theta + \varepsilon_n) \quad (4)$$

Where $N$, $s_n$, $k_n$, $e_n$ and $F_n$ are the number of component waves in frequency, angular frequency of $n^{th}$ component wave, the wave number of $n^{th}$ component wave, the random phase lag defined from 0 to 2p of $n^{th}$ component wave and transfer function for wave generation of $n^{th}$ component wave respectively. $F_n$ for flap type wave paddle is represented by following equation

$$F_n = \frac{4\sinh(k_n h)}{k_n h} \frac{1 - \cosh(k_n h) + (k_n h)\sinh(k_n h)}{2k_n h + \sinh(2k_n h)} \quad (5)$$

Where $k_n$ is obtained by

$$s^2_n = k_n g \tanh(k_n h) \quad (6)$$

### *2.1.3 Servo-Hydraulic Sea Wave Generation System*

Servo-hydraulic system is used to generate sea waves (either regular or random waves) in physical hydraulic models for studying coastal engineering problems at CWPRS, Pune. This system consist of Hydraulic Power Pack (HPP), SCADA controlled electro-hydraulic servo system, wave board (paddle), data acquisition system. Schematic flow chart of this system is shown in figure 1.

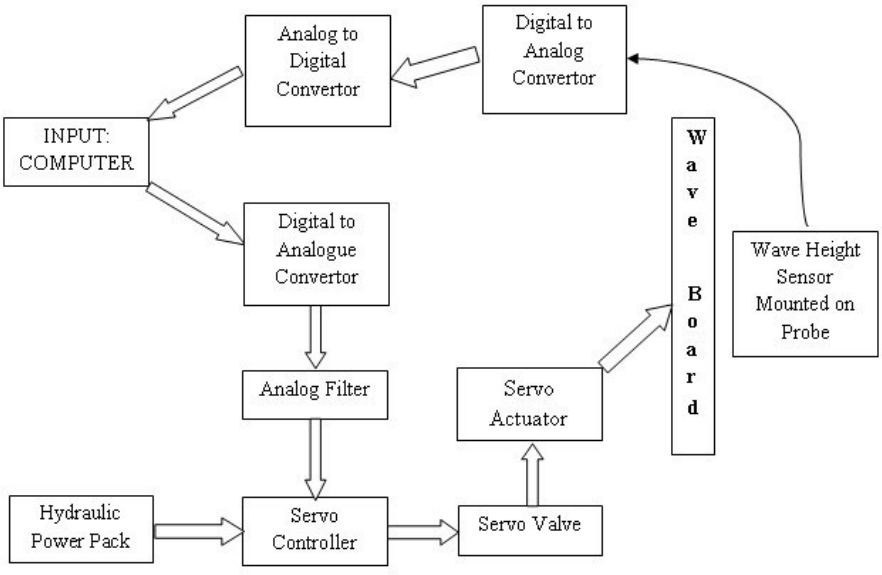



**Figure 1:** Flow Chart of Sea Wave Generation System at CWPRS.

In this wave generation system wave board (paddle) is driven by ram operated by an electro-hydraulic servo system which is controlled by a signal generating unit (Chary et. al. 2016). Pressurized oil is supplied to servo-actuator by a hydraulic power pack. The servo controller receives analogue command signal from micro processor and generates error signal by comparing it with feedback signal obtained from the displacement transducers (Chary et. al. 2016). The error signal from servo amplifier is converted into a current suitable for driving a

servo-valve, which in turn controls oil flow to the actuators causing the displacement of the wave board which results in development of the waves in the basin filled with water as shown in Figure 2.



**Figure 2:** Typical Sea Wave Generation System at CWPRS.



**Figure 3** Photograph of New Manglore Port Model

## 2.2 *Physical Model of New Mangalore Port & Kamrajar Port at CWPRS*

New Mangalore Port (NMP) is one of the major port located on the west coast of India. It is an artificial lagoon type port operating throughout the year and developed in stages during past five decades to suit the traffic requirement. During these development phases (Phase I to Phase IV) physical model studies for the various development proposals by New Mangalore Port Trust had been carried out on physical model of NMP. This physical model of NMP is exists at CWPRS, Pune since late 1950s. This is 3-D geometrically similar hydraulic physical model to the scale of 1:120 and housed in a hanger of size 72m x 45m. Figure 3 shows photograph of the model. This is a rigid bed model with latest bathymetry simulated and is equipped with computarised regular and random wave generation facilities from three directions namely West, South West and North West..Truncated approach channel is simulated in the model for a distance of about 4000m from port basin entrance up to a depth of -11/0 m CD (Chalawadi et. al. 2018). Untill 1995 all studies were conducted with regular wave modeling there after the model was upgraded to random wave and all studies are carried out using this facility.

Kamrajar Port is located at a distance of 24 km north of Chennai Port on east coast of India. Physical model of Kamrajar Port is 3-D rigid bed and geometrical similar having scale of 1:120. This model is having computarised regular and random wave generation facility from $130^0$ N direction, which is the critical direction during SW monsoon season for southerly entrance of the port.



**Figure 4** Photograph of Kamrajar Port Model

These models are also equipped with multichannel data acquisition system for waves and electronic water level indicators to monitor the water level during the course of experiments.

## 3. Case Studies

To understand the suitability of regular and random sea wave generators in the hydraulic physical model studies for coastal engineering projects/problems a discussion on the results of model studies conducted for proposed deep draft multipurpose berth (berth no. 17), coast guard jetty at NMP and development proposals & VLCC vessels related developments at Kamrajar port, Ennore are presented in this paper. These studies are carried out at CWPRS on physical model of NMP and Kamrajar Port, Ennore as mentioned in earlier section.

### 3.1 Testing Conditions for Studies of New Manglore Port

Model studies were performed by simulating Regular and Random waves from three directions viz. West (W), South-West (SW) and North- West (NW) which are the critical directions for harbor entrance. Regular waves are generated in the model during testing with wave height H of 2.5 m with time period T of 10 sec. while random waves are generated with SCOTT spectra having significant wave height $H_s$ of 2.5 m with time period $T_p$ of 10 sec. Studies were conducted by simulating a wave absorptive surface on the rear side of the proposed development.

#### *3.1.1 Physical Model Study for Wave Tranquility and Directional Spread Near Deep Draft Multipurpose Berth (DDMB, Berth No. 17) at New Mangalore Port.*

As mentioned earlier the study with regular and random waves from three directions West, South-West and North-West were performed for the proposed deep draft multipurpose berths. Figure 5 shows the locations of Wave probes to measure the wave height at location of proposed multipurpose berth and other salient locations in the port. Results are presented in Table 1.

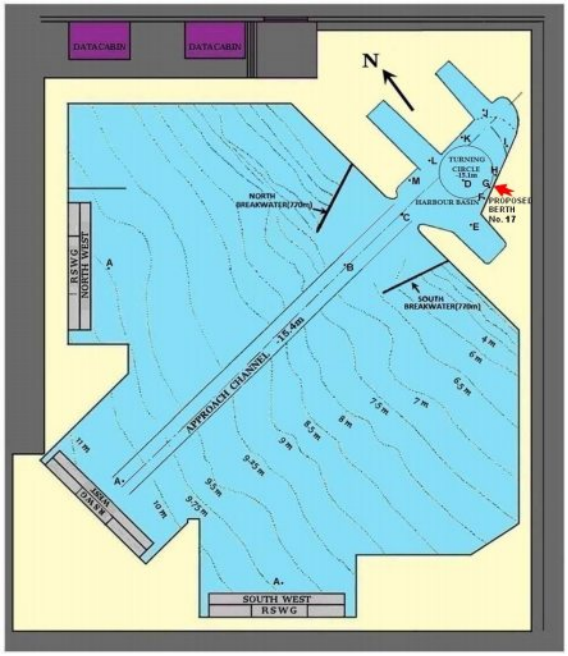



**Figure 5 A:** NMP Model Layout with wave probe locations.

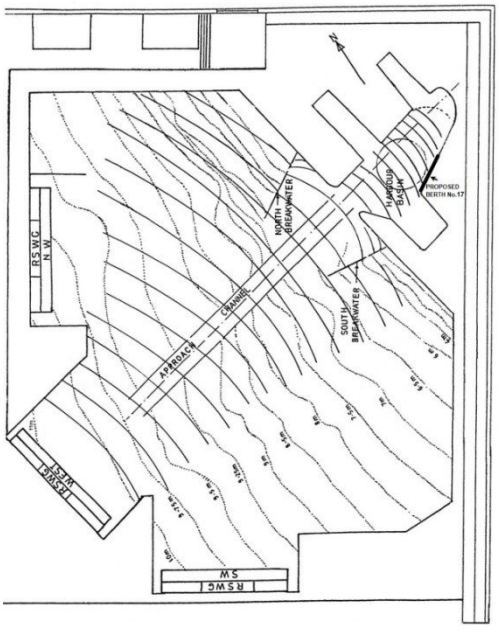



**Figure 5 B:** Wave Pattern in The Harbour Zone

Model studies with regular and random waves indicate that for regular waves, wave disturbances are more at many selected locations. This can be attributed to generation of waves of higher magnitude continuously during regular wave study as compared to random wave wherein waves of different magnitude were generated to simulate the natural phenomenon. Wave tranquility results from 3 critical directions as presented in Table 1.

**Table 1:** Observed Wave Heights in Model Studies for DDMB.

| Location of Probe | | Wave Height in Meters | | | | | |
|---|---|---|---|---|---|---|---|
| | | SW | | W | | NW | |
| | | Regular | Random | Regular | Random | Regular | Random |
| Wave generation point | A | 2.50 | 2.50 | 2.50 | 2.50 | 2.50 | 2.50 |
| In approach channel between the tips of breakwaters | B | 0.85 | 0.75 | 0.85 | 0.80 | 0.80 | 0.70 |
| In the entrance of lagoon area | C | 0.65 | 0.55 | 0.60 | 0.50 | 0.65 | 0.55 |
| In the turning circle | D | 0.35 | 0.30 | 0.40 | 0.30 | 0.35 | 0.30 |
| Entrance of Southern dock arm | E | 0.25 | 0.20 | 0.25 | 0.15 | 0.20 | 0.15 |
| Western end of proposed multipurpose Berth-17 | F | 0.25 | 0.20 | 0.25 | 0.25 | 0.25 | 0.20 |
| Middle of the proposed multipurpose Berth-17 | G | 0.25 | 0.20 | 0.30 | 0.20 | 0.25 | 0.20 |
| Eastern end of proposed multipurpose Berth-17 | H | 0.35 | 0.30 | 0.35 | 0.30 | 0.30 | 0.25 |
| At the Kudremukh iron ore berth | I | 0.40 | 0.35 | 0.45 | 0.35 | 0.30 | 0.25 |
| At the entrance of Eastern dock arm | J | 0.15 | 0.10 | 0.15 | 0.10 | 0.15 | 0.10 |
| At multipurpose berth No 14 | K | 0.40 | 0.35 | 0.40 | 0.35 | 0.25 | 0.20 |
| Entrance of Western dock arm | L | 0.35 | 0.25 | 0.30 | 0.25 | 0.25 | 0.15 |
| Return of West face of Western dock arm | M | 0.35 | 0.30 | 0.30 | 0.25 | 0.30 | 0.25 |

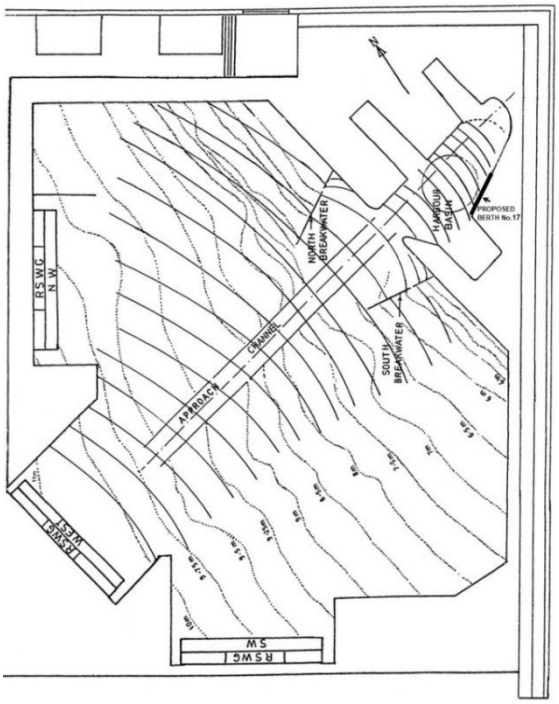



**Figure 6:** Wave pattern near proposed Deep Draft Multipurpose berth No. 17

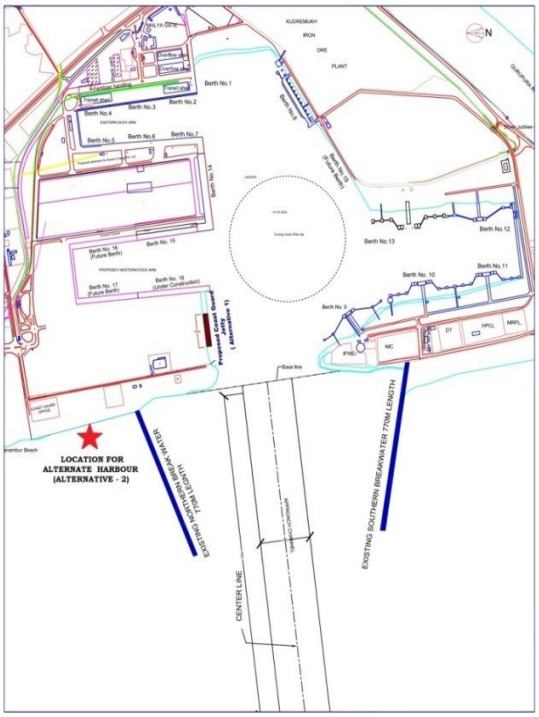



**Figure 7:** NMP Model Layout with proposed Coast Guard Jetty in Alternative 1 & 2

The directional spread of waves study was performed with regular waves for three critical directions. Due to near shore refraction and diffraction along the port structure the direction of wave approach are almost same at the proposed location of DDMB (Berth no.17) Fig 6. Based on such observations the berth alignments can be finalized having best approach angle to minimize the effect on the vessels at berth. While sketching the wave pattern in the running model the regular wave model runs gives good results. Thus for wave tranquility the random waves provides the optimum results whereas for wave directional sketching regular waves are very useful.
This phenomenon prevailed for various other studies conducted in this model and accordingly suggestions were provided to the project authorities for executing the works in field.

### *3.1.2 Physical Model for Wave Tranquility for the Proposed Development of Coast Guard Jetty at New Mangalore Port.*

Indian Coast Guard has proposed to have a dedicated berth for their ships at New Mangalore Port. Two alternatives (Alternative 1 and Alternative 2) have been studied on the model. Figure 7 shows the layout of New Mangalore Port with proposed Coast Guard Jetty in Alternative 1 & 2.

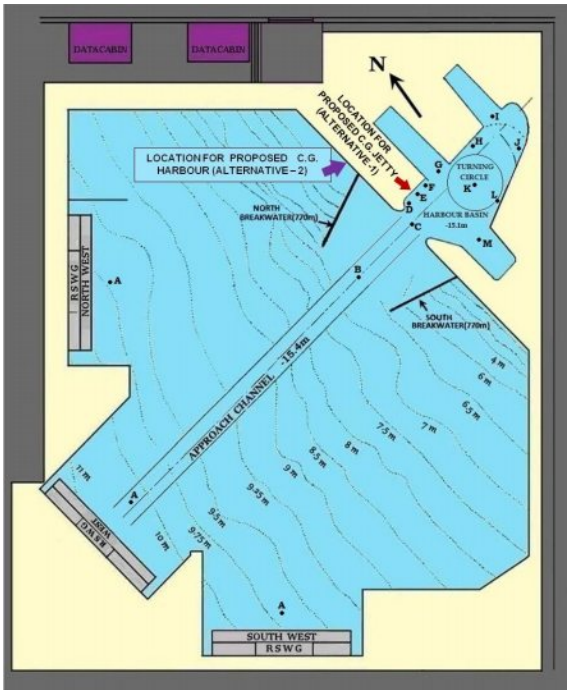



**Figure 8A:** NMP Model Layout with wave probe Locations for Proposed Coast Guard Jetty Alternative -1

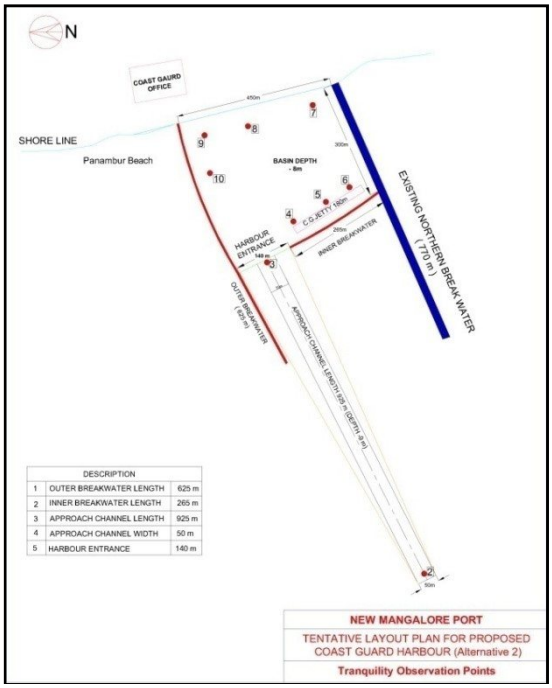



**Figure 8B:** Alternaive 2 for Coast Guard Jetty

Model studies with regular waves from three critical directions as mentioned earlier are performed for proposed coastguard jetty ( alternative 1 & 2) the wave crest pattern for the incident waves for the proposed location are shown in Figure 9.

## 3.2 Testing Conditions for Studies of Kamrajar Port Physical Model.

Model studies were performed by simulating Regular and Random waves from $130^0$ N direction which is the critical directions for the existing harbor entrance. Regular waves are generated in the model during testing with wave height H of 2.5m and 4.0 m with time period T of 11 sec. while random waves are generated with SCOTT spectra having significant wave height, $H_s$ of 2.5 m and 4.0 m having time period $T_p$ of 11 sec. Studies were conducted by simulating a wave absorptive surface on the rear side of the proposed development.

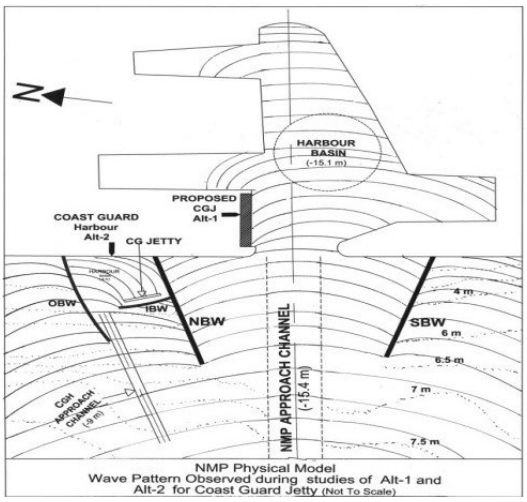



**Figure 9:** Wave pattern sketch for Coast Guard jetty

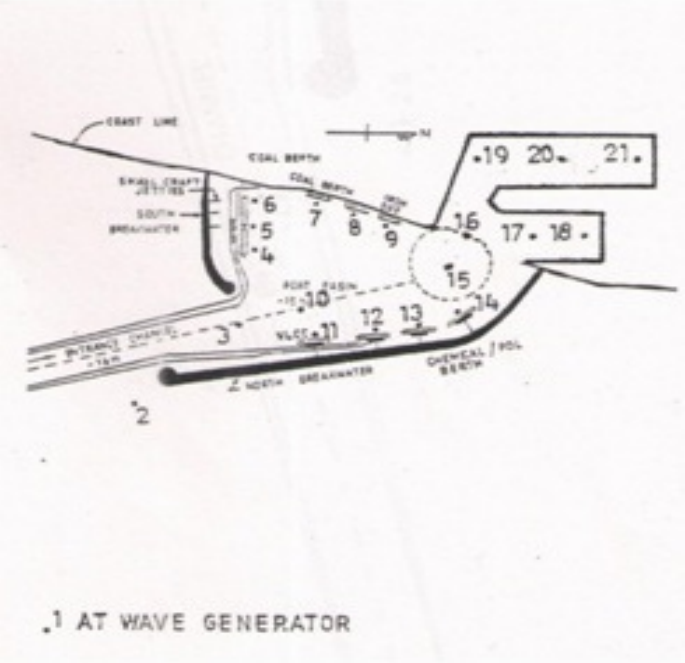



**Figure 10:** Kamrajar Port Model Wave Probe Locations.

### *3.2.1 Physical Model studies for development proposals of Kamrajar Port(Ennore),*

As mentioned above the study with regular and random waves from $130^0$ N direction were performed for the development proposal by Kamrajar Port Ltd. Figure 10 shows the locations of Wave probes to measure the wave height at location of proposed multipurpose berth and other salient locations in the port. Results are presented in Table 2. Two alternatives Alternative-1 and Alternative-2 for the proposed development were tested and the wave tranquility results and the wave flux distribution pattern under the proposed development proposal under Alternative -1 (for outer basin only) under existing condition of breakwater layout and approach channel indicate that the wave tranquility conditions at various locations of berths are achieved under normal design wave condition of $H_s$ of 2.5 m and time period $T_p$ of 11 sec from $130^0$ N direction. However for wave tranquility studies for more severe condition i.e. $H_s$ of 4.0 m and time period $T_p$ of 11 sec from $130^0$ N direction the wave disturbances at all proposed berths in outer basin are well within tranquility limit, though they are higher by 40% to 50% as compared to normal maximum wave climate. The wave disturbances both under normal and severe wave climate for developments uner Alternative – 2 (inner basin) conditions are well within the permissible limits.

The wave tranquility studies for the tested conditions in most of the cases have indicated the wave disturbances are lesser in case of random waves as compared to regular wave for the reasons as explained in the earlier case. Again the directional distribution of waves were sketched by generating regular waves and are as shown in fig11.

**Table 2:** Observed Wave Heights in Model Studies for development proposals by Kamrajar Port

| Location of Probe. | | Alternative 1 | | | | Alternative 2 | | | |
|---|---|---|---|---|---|---|---|---|---|
| | | Regular | | Random | | Regular | | Random | |
| | | 2.5 m | 4.0 m | 2.5 m | 4.0 m | 2.5 m | 4.0 m | 2.5 m | 4.0 m |
| At wave generator | 1 | 2.50 | 4.00 | 2.54 | 4.15 | 2.50 | 4.00 | 2.50 | 4.00 |
| Harbour Entrance | 2 | 2.25 | 3.95 | 2.18 | 3.40 | 2.25 | 3.95 | 2.10 | 3.35 |
| Harbour Entrance | 3 | 0.60 | 1.00 | 0.42 | 0.65 | 0.60 | 1.00 | 0.55 | 0.80 |
| Existing Coal Berth | 4 | 0.25 | 0.35 | 0.25 | 0.30 | 0.25 | 0.35 | 0.20 | 0.35 |
| | 5 | 0.20 | 0.30 | 0.20 | 0.30 | 0.20 | 0.30 | 0.20 | 0.25 |
| | 6 | 0.25 | 0.25 | 0.25 | 0.25 | 0.20 | 0.25 | 0.20 | 0.20 |
| Shore Connected to Wharfs | 7 | 0.30 | 0.40 | 0.18 | 0.30 | 0.30 | 0.40 | 0.25 | 0.40 |
| | 8 | 0.40 | 0.45 | 0.20 | 0.40 | 0.40 | 0.45 | 0.25 | 0.45 |
| | 9 | 0.35 | 0.40 | 0.30 | 0.30 | 0.35 | 0.40 | 0.35 | 0.40 |
| Harbour Entrance | 10 | 0.45 | 0.50 | 0.40 | 0.45 | 0.40 | 0.50 | 0.40 | 0.35 |
| Lee side of north Breakwater | 11 | 0.30 | 0.40 | 0.20 | 0.40 | 0.30 | 0.40 | 0.30 | 0.40 |
| | 12 | 0.30 | 0.45 | 0.25 | 0.25 | 0.30 | 0.45 | 0.30 | 0.25 |
| | 13 | 0.30 | 0.40 | 0.20 | 0.35 | 0.30 | 0.40 | 0.20 | 0.35 |
| | 14 | 0.20 | 0.20 | 0.15 | 0.20 | 0.20 | 0.20 | 0.15 | 0.15 |
| Turning Circle | 15 | 0.30 | 0.45 | 0.25 | 0.30 | 0.20 | 0.30 | 0.30 | 0.30 |
| Inner Harbour Dock No. 1 | 16 | - | - | - | - | 0.15 | 0.20 | 0.21 | 0.15 |
| | 17 | - | - | - | - | 0.10 | 0.20 | 0.18 | 0.15 |
| | 18 | - | - | - | - | 0.10 | 0.15 | 0.14 | 0.15 |
| Inner Harbour Dock No. 2 | 19 | - | - | - | - | 0.10 | 0.15 | - | 0.10 |
| | 20 | - | - | - | - | 0.05 | 0.10 | 0.05 | 0.05 |
| | 21 | - | - | - | - | 0.05 | 0.10 | 0.10 | 0.10 |

Berthing structure orientation were finalized by considering wave angle and wave disturbance in accordance with BIS and PIANC standards as shown in Table-3.

**Table 3:** Allowable Wave Heights As per PIANC and IS 4651 (Part V)

| Wave Height as per PIANC Near Berths | | |
|---|---|---|
| Type of Vessel | Approximate Acceptable Wave Heights - $H_s$ (m) | |
| | Incident Angle $0^0$ (Head on) | Incident Angle ($45^0$ - $90^0$) |
| Conventional general cargo | 1.0 | 0.8 |
| Container Vessels | 0.5 | 0.4 |
| Dry bulk carrier 30 – 100,000 DWT (loading) | 1.5 | 1.0 |
| Dry bulk carrier 30 – 100,000 DWT (unloading) | 1.0 | 0.8 – 1.0 |

| Allowable Wave Height near Berth (IS 4651 Part V) | | |
|---|---|---|
| Type of Vessel | Approximate Acceptable Wave Heights - $H_s$ (m) | |
| | At Berth | At Turning Circle |
| General Cargo | 0.65 | 0.9 |
| Bulk Cargo | 0.90 | 1.20 |
| Container Cargo | 0.65 | 1.20 |
| Dredgers | - | 0.45 – 2.0 |

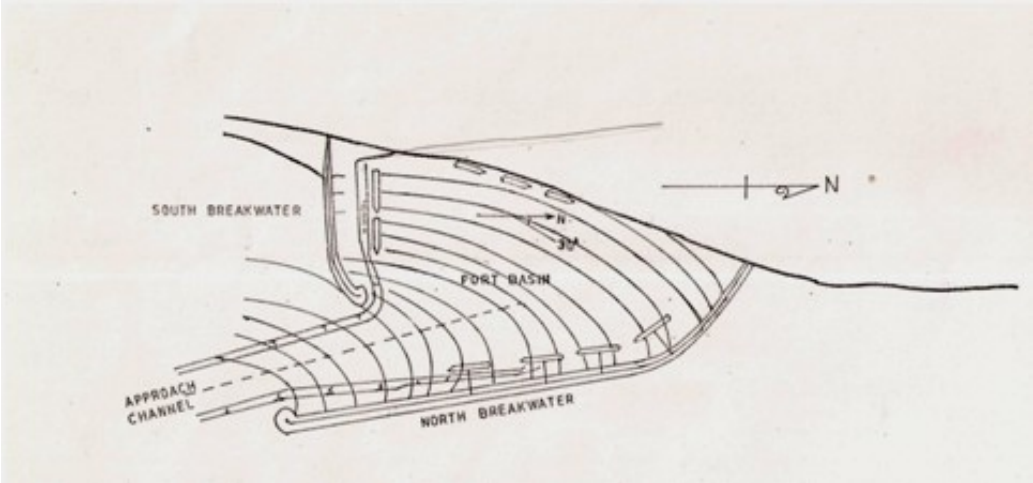



**Figure 11:** Kamrajar Port Model Wave Pattern.

### *3.2.2 Physical Model studies for development proposals of Kamrajar) Port ltd., (Ennore ), Wave pattern sketch.*

In the earlier section the wave tranquility studies for Alternative – 1 and Alternative – 2 along with existing facilities at port were simulated and studied. The proposal for the development of VLCC berth at Kamrajar port, Ennore is simulated and studied as Alternative – 3 and Alternative – 4 and results for wave tranquility are presented in Table 4.

**Table 4:** Observed Wave Heights in Model Studies for VLCC vessels related development proposals by Kamrajar Port

| Location of Probe. | | Alternative 3 | | | | Alternative 4 | | | |
|---|---|---|---|---|---|---|---|---|---|
| | | Regular | | Random | | Regular | | Random | |
| | | 2.5 m | 4.0 m | 2.5 m | 4.0 m | 2.5 m | 4.0 m | 2.5 m | 4.0 m |
| At wave generator | 1 | 2.50 | 4.00 | 2.50 | 4.00 | 2.50 | 4.00 | 2.50 | 4.00 |
| Harbour Entrance | 2 | 2.90 | 4.30 | 2.77 | 4.25 | 3.25 | 4.60 | 3.10 | 4.50 |
| Harbour Entrance | 3 | 1.25 | 3.20 | 1.20 | 2.50 | 1.30 | 2.55 | 1.10 | 2.45 |
| Existing Coal Berth | 4 | 0.55 | 0.80 | 0.45 | 0.70 | 0.50 | 1.20 | 0.45 | 1.00 |
| | 5 | 0.35 | 0.60 | 0.30 | 0.50 | 0.50 | 0.80 | 0.35 | 0.60 |
| | 6 | 0.50 | 0.75 | 0.45 | 0.65 | 0.30 | 0.60 | 0.30 | 0.50 |
| Shore Connected to Wharfs | 7 | 0.75 | 0.90 | 0.70 | 0.80 | 0.50 | 0.70 | 0.45 | 0.65 |
| | 8 | 0.80 | 1.45 | 0.75 | 1.00 | 1.00 | 1.55 | 0.90 | 1.35 |
| | 9 | 1.10 | 1.10 | 0.90 | 1.00 | 0.95 | 1.35 | 0.85 | 1.20 |
| Harbour Entrance | 10 | 0.80 | 1.10 | 0.75 | 1.05 | 1.30 | 1.60 | 1.20 | 1.45 |
| Lee side of north Breakwater | 11 | 0.60 | 0.90 | 0.55 | 0.85 | 0.65 | 1.20 | 0.55 | 1.05 |
| | 12 | 0.45 | 0.85 | 0.45 | 0.70 | 0.70 | 0.95 | 0.60 | 0.75 |
| | 13 | 0.50 | 0.85 | 0.45 | 0.75 | 0.55 | 0.90 | 0.45 | 0.75 |
| | 14 | 0.95 | 1.10 | 0.80 | 1.00 | 0.75 | 1.25 | 0.60 | 1.15 |
| Turning Circle | 15 | 1.05 | 1.50 | 0.85 | 1.30 | 0.85 | 1.45 | 0.70 | 1.20 |
| Inner Harbour Dock No. 1 | 16 | - | - | - | - | 0.60 | 1.30 | 0.50 | 1.05 |
| | 17 | - | - | - | - | 0.40 | 0.50 | 0.30 | 0.40 |
| | 18 | - | - | - | - | 0.20 | 0.40 | 0.20 | 0.30 |
| Inner Harbour Dock No. 2 | 19 | - | - | - | - | 0.20 | 0.25 | 0.15 | 0.20 |
| | 20 | - | - | - | - | 0.10 | 0.15 | 0.10 | 0.10 |
| | 21 | - | - | - | - | 0.05 | 0.20 | 0.05 | 0.10 |

From these selected averaged results also it can be noticed that the wave disturbances are lesser or equal at most of the locations for random waves as compared to regular waves for the same reason as explained above cases. This confirms the reason attributed for the lower wave disturbances at most of the locations in the model studies explained above. The

photographs of the model during regular and random wave model studies have indicated that the sketching pattern is clear and legible for regular waves as compared with random waves.

### 3.3 Breaking of Waves

While performing studies on these models using regular waves it was observed that wave breaking phenomena was observed at same location at depth around -4.5 m CD. However when model studies were performed using random waves breaking of waves phenomena was observed at different locations within the -3.0 m to - 6.5 m CD. Hence random wave modeling is more akin to nature and is appropriate for qualitative injection studies for sediment transport along coastline.

## 4. Discussion & Conclusion

- The wave disturbance results from regular wave generation are more compared to random wave generation.
- While generating the regular waves in the model more amount of energy is driven to the wave paddle as compared to that required to generate random waves in model.
- The regular wave model studies are useful in sketching the wave crest pattern at desired locations and very useful for finalizing the berthing structure alignments.
- The random wave model studies are useful for the wave tranquility assessment at salient locations in the model and optimizing the harbor openings, lengths of breakwater/s, etc.,
- In order to obtain the economical design for port layout, breakwater alignment, orientation and length etc. the random wave studies are more appropriate.
- For understanding the wave breaking effects along the coast line random wave model studies are more appropriate. Thus for qualitative injection studies using tracer material along the coast line random wave generation is more appropriate**.**

## Acknowledgement

The authors are thankful to Shri. A. K. Agrawal, Director, CWPRS for the encouragement and granting permission to publish the paper. Authors are also thankful to the New Manglore Port Trust and Kamarajar Port Ltd., authorities for sponsoring the model studies.

## References

Anoopdas, S., Jagadeesh H. B., Subba Rao. (2016) – "Laboratory wave generation techniques for shallow basin harbor modeling studies". IJRSET, Vol. 5, Issue 9, May 2016, pp. 910 – 916.

Ben T. Nohara (2000) – "A survey of the generation of ocean waves in a test basin", Jour. Of Brazilian Socety of Mechanical Science, Vol. 22,. No. 2, 2000.

Bill Baird, Seth Logan, Wim Van Der Molen, Trevor Elliot, Don Zimmer (2016) – "Thoughts on the future of physical models in coastal engineering". Proc. 6th International Conference on the application of physical modeling in Coastal and Port Engineering & Science, Coastlab – 2016, Ottawa, Canada.

Chalawadi, A. S., Jagadeesh H. B., Nagendra T. (2018) – "Hydraulic physical model studies for wave tranquility and direction spread for deep draft multipurpose berth at New Manglore Port – A case study". Proc. 6th National Conference on Coastal, Harbour and Ocean Engineering, INCHOE – 2018, Pune, India.

Chary, Prabhakar V., Erande, R. S., Ranade, S. D., Kudale, M. D. (2017) – "Design of hydraulic power pack system for servo-hydraulic random sea wave generators for design of port layouts", IJRMET, Vol. 7, Issue 1, Nov. 2016, pp. 80 – 88.

Falconer, R. A. (1982) – "An application of numerical and physical models in harbour design". The Dock & Harbour Authority, Vol. 63, no. 737, pp. 34 – 37.

Falconer, R. A., Chapman, B. C. (1995). ―Design and operation of a laboratory tidal basin for model harbour studies. https://www.researchgate.net/publication/292545728. (accessed on 24, May 2017).

Kashyape, P. A., Jagadeesh, H. B., Nagendra, T. (2017) ― "Design of multipurpose tidal basin model for estuarine port development studies". Proc.22nd HYDRO-2017 International, Ahmedabad, India.

Ketabdari, M. J., Ranginkaman, A. (2009) – "Simulation of random irregular sea waves for numerical and physical models using digital filters", Transaction B: Mechanical Engineering, Vol. 16, No. 3, pp. 240 – 247.

Steven A Hughes (1993) – "Physical models and laboratory techniques in coastal engineering", Advance Series on Ocean Engineering – Volume 7, World Scientific.

Technical report No. 4032 (2003) – Regular wave model studies for the development proposals of Ennore Port Limited, Tamilnadu under existing conditions.

Technical report No. 4095 (2004) – Random wave model studies for the development proposals of Ennore Port Limited, Tamilnadu under existing conditions.

Technical report No. 4097 (2004) – Regular and random wave model studies for the VLCC (300000 DWT) Vessels related developments at Ennore Port Limited, Tamilnadu.

Technical report No. 5159 (2014) – Hydraulic physical model studies for flotilla berths at New Mangalore Port Karnataka.

Technical report No. 5653 (2018) – Hydraulic physical model studies for wave tranquility and directional spread near proposed deep draft multipurpose berth (berth n0. 17) at New Mangalore Port, Karnataka.

Technical report No. 5706 (2019) – Physical model studies for wave tranquility for the proposed development of coast guard jetty at New Mangalore Port, Karnataka.

IN PROCEEDINGS OF 25th HYDRO 2020, INTERNATIONAL CONFERENCE,
NATIONAL INSTITUTE OF TECHNOLOGY ROURKELA, ODISHA, INDIA
26-28, March 2021, ISBN 978-93-90631-56-8

Paper ID - 174

# Assessment of Littoral Drift and Shoreline Changes for a Fishery Harbour on South West Coast of India

S N Jha[1*], J Sinha[1] and Prabhat Chandra[1]
[1]*Central Water and Power Research Station, Khadakwasla, Pune-411024, India*
[*]*E-Mail: snj202003@yahoo.co.in*

## Abstract

Development of marine fisheries infrastructure has gained considerable importance in recent years. To cater the demand of national and international markets, many fishery harbour and fish landing centre are being planned. However, this results in obstruction to natural course of sediment along the shoreline. If due consideration is not given during construction of hydraulic structures, it may cause severe siltation on one side of structure and erosion on the other side resulting in failure to coastal structures and huge economic losses. Thus, it is an essential requirement to carry out scientific studies to assess possible impact of the proposed structures of fishing harbour before undertaking any such project implementation in the field. In the present paper, an assessment of littoral drift distribution and shoreline changes has been made for the proposed open sea fishing harbour located at Thrikkunnapuzha in Kerala on the south west coast of India.

***Keywords:*** *littoral drift; shoreline change; breakwater; fishery harbour; siltation*

## 1. Introduction

Fisheries, and more specifically marine fisheries, are one of the major components of Indian economy. There has been increased focus on the development of marine fisheries infrastructure in recent years in the coastal states of India. Among all the states, Kerala has been in the forefront in the development of marine fisheries infrastructure. The development of infrastructure includes construction of major and minor fisheries harbour associated with the construction of breakwaters to provide tranquil condition in harbour area for their smooth operation. However, construction of breakwaters may cause severe siltation on one side of structure and erosion on the other side resulting in failure to coastal structures and huge economic losses. Thus, it is essential to conduct model studies with site specific data before finalising the location and layout of the harbour to avoid undesirable consequences in future.

An open sea fishing harbour ($9^0$ 15’ 0” N, $76^0$ 24’ 0” E) is proposed to be built at Thrikkunnapuzha of district Allahapuzha, Kerala located at about 61 km north of Kollam and about 25 km south of Alappuzha on the west coast of India for channelizing fishing activities of the area. Location map of the proposed harbour is shown in Fig.1. Proposed fishing harbour consisting of two breakwaters; northern and southern, and an inlet in between were considered for the mathematical model studies of littoral drift distribution and shoreline changes.

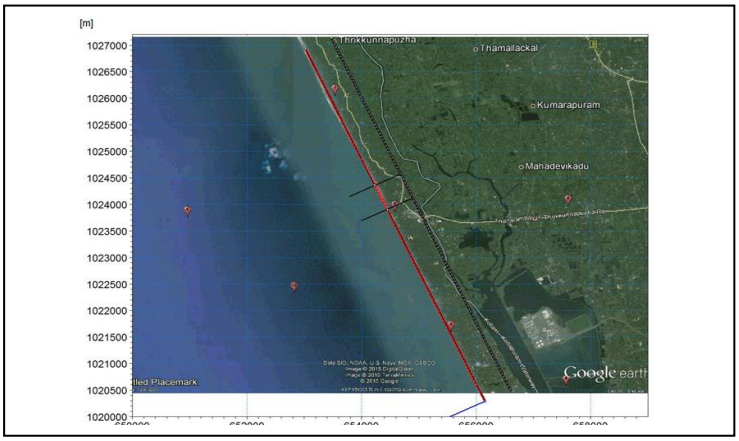



**Fig.1(a)** Location of fishery harbour at Thrikkunnapuzha

## 2. Site Conditions

The important data with respect to model studies for littoral drift studies includes bathymetric data and wave data. Topographic survey of the site was carried out by HED, Kerala during December 2011, This data was used along with depth data available from admiralty charts for preparation of bathymetry. Wave data reported herein was obtained from literature which was recorded at Alappuzha site for two periods in a year. The periods were marked as rough season during the month of May through October and fair season during the month of November through April. The observed wave data has been summarized in Table 1.

**Table 1** Wave characteristics at Alappuzha **site**

| Parameters | Rough season | Fair season |
|---|---|---|
| Significant wave height (Hs) | 3.0 m | 1.4 m |
| Highest wave height (Hmax) | 3.4 m | 2.0 m |
| Predominant wave direction ($^0$N) | 250-265 | 230-240 |
| Time period (s) | 8-10 | 10-11 |

Similarly, wind data for the period of 2005 to 2012 was collected from the metrological station at Asramam, Kollam located at $8^0$ 53' 34" N and $76^0$ 35' 18" E. Based on tidal data of Alappuzha site, it was seen that in the proposed harbour area semi diurnal tides exists with the maximum tidal range of 0.60 m. Table 2 provides important tidal levels at Alappuzha.

**Table2** Important tidal level at Alappuzha

| Levels | Depth wrt to CD |
|---|---|
| MSL | +0.60 m |
| MHHWL | +0.90 m |
| MHLWL | +0.60 m |
| MLHWL | +0.80 m |
| MLLWL | +0.30 m |

The bed material in the vicinity of the proposed site at Thrikkunnapuzha is mainly composed of sand having mean grain size, $D_{50}$ of the order of 0.4 mm. The wave data observed by the ships plying in offshore region of Thrikkunnapuzha reported by India Meteorological Department (IMD) during the past 30 years were considered to arrive at nearshore wave data at a location of -10 m depth contour near the proposed fishery harbour using the SW module of MIKE 21 software.

It was observed that in the offshore region the waves approach predominantly from West, WNW and WSW directions during south-west monsoon with the maximum wave height of the order of 4.5 m. During north-east monsoon period, waves approach predominantly from North and NNW directions with the maximum wave height of the order of 4 m. In non-monsoon period, the predominant directions of waves are NNW, North and NW direction with the maximum wave height of the order of 4 m. The wave climate during the entire year indicates that the predominant wave directions in deep water are West, North, NNW and WNW with the maximum wave height of the order of 4.5 m as shown in Fig. 2.

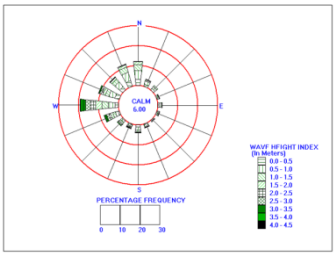



**Fig.2** Offshore Rose Wave Diagram for Annual Period

## 3. Literature Review

Longshore sediment transport rates for Alleppey coastal regions are estimated and reported in literature (Sajeev et al.(1997)) as presented in Table 3. It is reported that the littoral drift of low magnitude exists in southward direction during south-west monsoon. It is further reported that during all other seasons the drift is towards north. However, maximum northerly drift was estimated up to 0.013 MCM during the month of April. Alleppey is located at about 25.0 km north of the proposed site at Thrikkunnapuzha. Thottapally region located at about 6.3 km north of Thrikkunnapuzha shows littoral drift in northern direction. Similarly, Valliyazheekal which is about 15.5 km south of the present site location indicates northward drift. It is also reported by the Project Authority that on either side of the site under study, there exist littoral drift in northward direction.

**Table 3**:Longshore sediment transport at Alleppey region
(Sajeev et al., (1997))

| | | NET | GROSS |
|---|---|---|---|
| At Allepey | Annual | 0.016929 | 0.062519 |
| | NE | 0.00738 | 0.007614 |
| | NM | 0.029765 | 0.033577 |
| | SW | -0.02022 | 0.021328 |

## 4. Modelling Techniques

Bathymetry in the offshore region of Thrikkunnapuzha is fairly simple, consists of almost parallel contours from -10 m depth up to -65 m depth. The bathymetric data in the offshore were taken from CMAP database. It was seen that the bed slope in the vicinity of the proposed harbour at Thrikkunnapuzha is mild (1:500).However, as per data supplied for near shore region the bed slope up to -3 m contour is quite steep.

Wave transformations from deeper water to shallow water region were computed using the MIKE 21 Spectral Wave (SW) model. This model can compute growth, transformation and decay of wind generated waves and swells in both offshore and coastal areas. MIKE 21 SW model is based on unstructured meshes, which can handle non-linear wave- wave interaction and all other important wave phenomena like wave breaking, bottom friction, wave diffraction, refraction and shoaling effects etc. This model will provide the important wave parameter like significant wave height, mean wave direction and radiation stresses at the chosen point or region in the shallower depth. Wave action balance equation is solved using cell centred finite volume method. In horizontal Cartesian co-ordinates wave action balance equation is given as

$$\frac{\partial N}{\partial t} + \nabla.(\vec{\nu} N) = \frac{S}{\sigma} \qquad ..(1)$$

**Nomenclature**

$N(\vec{x}, \sigma, \theta, t)$ = the action density,
t = time (sec),
$\vec{x}$ (x,y) = Cartesian co- ordinates,
$\vec{\nu}$ (Cx, Cy, Cσ, Cθ) = propagation velocity of a wave group in four dimensional phase space $\vec{x}$, $\sigma$ and $\theta$
S = source term for the energy balance equation.
$\nabla$ = the four dimensional differential operator in $\vec{x}$, $\sigma$ and $\theta$

An area of 180 km alongshore and 40 km cross-shore with an unstructured mesh was considered for the simulation of MIKE 21 SW model. In the cross-shore, it extends from high water line near the shore to -65 m depth contour in deep sea. The model was run for incident waves of wave height 4 m for all the predominant wave directions in deep sea viz. SE, SSE, South, SSW, SW, WSW, West, WNW, NW, NNW and North

Wave heights and wave directions, at -10 m depth contour near the location of the proposed fishing harbour were extracted from the model results for all the incident wave directions. The extracted information of wave heights and directions at -10 m depth contour was applied to seasonal and yearly offshore wave climate to obtain frequency distribution of wave heights and wave directions near the location of the proposed harbour site.

It was observed that in the nearshore region, the waves having the maximum wave height of the order of 3.5 m approach predominantly from West and WSW directions with percentage of occurrence 59% and 15%, respectively during south-west monsoon. During the NE monsoon period, waves having the maximum wave height of the order of 3.0 m approach predominantly from WNW, SSW and West directions with the percentage of occurrence of 22%, 13% and 11%, respectively. In the non-monsoon period, the predominant directions of waves having maximum wave height of the order of 3.5 m are from WNW, SSW and West predominant directions with percentage occurrence of 37%, 15% and 12%, respectively. The wave climate during the entire year indicates that the predominant wave directions are from West and WNW with the maximum wave height of the order of 3.5 m and the percentage occurrence of 26% and 21%, respectively as shown in Fig. 3.

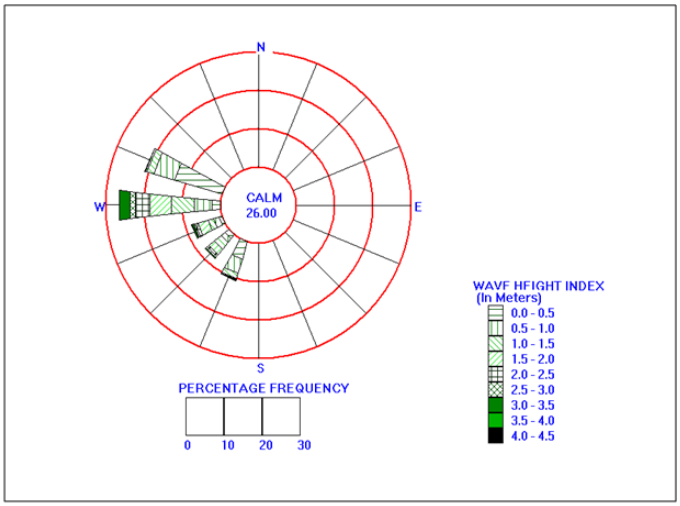



**Fig.3** Nearshore Rose Wave Diagram for Annual Period

## 5. Model Simulations and Results

Some of the most important parameters that needs to be accounted in simulation of littoral drift are waves (both regular and irregular), currents induced by tide, wind effect, type and size of sediments and bottom friction. Further, wave breaking, wave refraction and wave shoaling influence the quantum and distribution of the drift. LITPACK model, which takes into consideration all the above parameters for an arbitrary beach profile, was used for the present study. Details of the method of computation and model capabilities are available in the reference.

In the model, wave condition obtained from the SW model was taken as input for different season. Suspended load and bed load under the influence of wave breaking and current condition were computed for each incident wave. To compute total annual drift, sediment transport obtained from each incident waves was combined. Cross-shore sediment transport was computed using sediment profile and bathymetry of Thrikkunnapuzha.

The model assumes the depth contours parallel to the seashore. Figure 4 shows the beach profile (cross-shore bed profile) near the proposed site which is used for the littoral drift computation. Profile covers a distance of about 4.0 km extending upto about -10 m depth contour. It could be seen from the figure that -5 m depth contour is about 1.0 km from the coastline. Profile is discretised into 400 grid points with uniform grid size of 10 m. Littoral drift was simulated using LITDRIFT module of LITPACK, which takes into account the cross-shore profile, the sediment characteristics and the wave climate as input.

The general orientation of the coastline at the proposed site is NW-SE with normal to shoreline making an angle of about $250^0$ with respect to north. Further, depending on the wave direction with respect to the coastline, the littoral drift will be either directed northward or southward along the shoreline. The model was simulated for the cross-shore profiles for the seasonal and the annual wave climates.

Based on the simulation of littoral drift, the annual net and the gross transports were estimated to be of the order of 0.02 and 0.3 million $m^3$ respectively. The model was also used to compute seasonal transport rates. The distribution of littoral transport rates for the for the annual period is shown in Fig.4. It may be noted that the northward drift is indicated as negative and the southward drift is indicated as positive in the figures. It was seen that during SW monsoon, southward transport is more than the northward transport and the transport occurs within a range of 200 m from the shoreline. It was also seen that main drift moves within a range of 50 m from coastline. It was found that during NE monsoon also, northward transport is more than southward transport and the transport is mainly confined to a range of 150m from the shoreline. During non-monsoon period also, the northward transport is predominant and the major transport occurs within a range of 150 m from the shoreline. The distribution of annual transport (Fig.4), indicates that the sediment drift moves within a range of 200 m from the shoreline as the cross-shore profile has extremely steep slope near the shore. Further, it could be seen that the northward transport is more than the southward transport during all the seasons except SW monsoon. It could also be seen that the peak transport occurs at about 50 m from the shoreline and about 75% transport occurs between 0 m to 100 m from shoreline i.e. between 0.0 m to – 3.0 m depth contours.

Annual and seasonal net and gross littoral drift were estimated using LITDRIFT model. The northward and the southward drift are calculated based on the gross and the net littoral drift. The littoral drifts are reported in the following table:

**Table 4** Transport Rates for IMD Data (million cum)

| Period | Northward | Southward | Net | Gross |
|---|---|---|---|---|
| SW monsoon | 0.043 | 0.057 | -0.015 | 0.1 |
| NE monsoon | 0.034 | 0.01 | 0.025 | 0.043 |
| Non-monsoon | 0.034 | 0.014 | 0.021 | 0.048 |
| Annual | 0.16 | 0.14 | 0.02 | 0.3 |

Field observed near shore wave data was also used to confirm the findings based on IMD data. Wave data for different seasons indicated that the significant wave height during pre-monsoon period was varied from 0.25m to 0.7m whereas during monsoon period, it was in between 0.85m and 2.05m and during post monsoon period, the significant wave height was varied between 0.3m and 0.9m

Based on the simulation of littoral drift using the field observed data, the annual net and the gross transports were estimated to be of the order of 0.006 and 0.18 million $m^3$ respectively as shown in table 5. The model was used to compute seasonal transport rates.Annual and seasonal net and gross littoral drift were estimated for the field observed data. The northward and the southward drift are calculated based on the gross and the net littoral drift as explained earlier.

**Table 5** Transport Rates for Field Data (million cum)

| Period | Northward | Southward | Net | Gross |
|---|---|---|---|---|
| SW monsoon | 0.073 | 0.084 | -0.011 | 0.16 |
| NE monsoon | 0.014 | 0.0 | 0.014 | 0.014 |
| Non-monsoon | 0.005 | 0.002 | 0.003 | 0.007 |
| Annual | 0.092 | 0.086 | 0.006 | 0.18 |

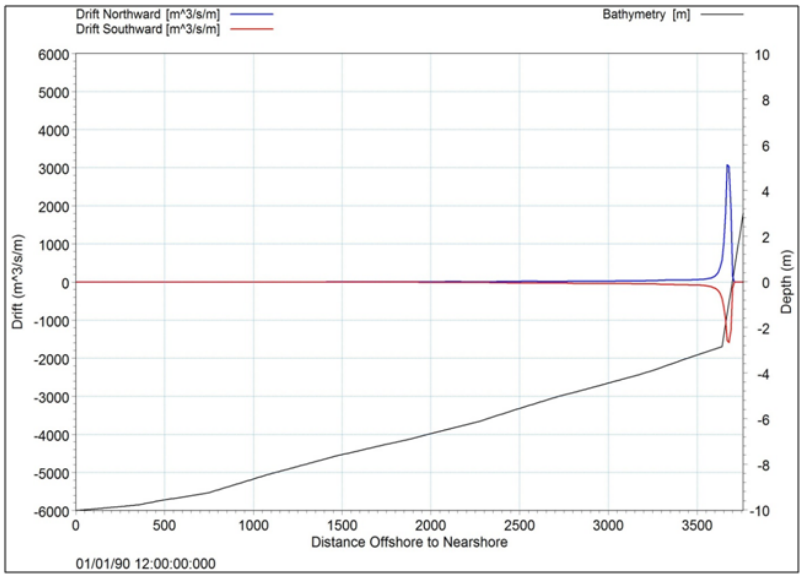



**Fig. 4** Cross-shore Distribution of Littoral Drift for Annual Period

For predicting coastline changes over a period of years, LITLINE module of LITPACK modelling system was used. This model can simulate the effect of various coastal structures on natural sediment transport and predict accretion or erosion in the coastal region. The continuity equation used in the model allows introduction of source or sink in the model as per the site condition. The input parameters consist of depth profile, coastline positions, tide and wave data, size and position of structures on the coastline. The model is divided into definite number of grids and computation is performed for each individual grid. The integration of data over a period of time provides shoreline evolution over a period of time.

For the shoreline evolution model, a shoreline of 7.1 km length was considered. The length was divided into 710 grid points with uniform grid size of 10 m. The proposed location of the breakwaters was schematically located in the middle of the coastline. The transport rates were computed for the above mentioned profile, which was used as input to the shoreline evolution model for LITLINE module of LITPACK software.

Based on field investigation and data available of the site for the proposed fishing harbour, it was found that the area was naturally prone to siltation and erosion due to northward littoral drift persist in the area. The model was simulated for the proposed condition considering the optimised layout suggested based on model studies of wave tranquillity and siltation in which the northern breakwater of length 450 m and southern breakwater of length 400 m was considered. The model was run with the schematic layout of the proposed fishing harbour for a period of 10 years. The predicted shoreline change obtained from the model simulation is shown in Fig. 5. As the net transport was directed towards north, the deposition on the south side of the southern breakwater was noticed while on the north side of the northern breakwater erosion was observed. However, due to the presence of seawall all along the shoreline, erosion would not be felt at the site. Further, based on the field investigation report, some of the accretion occurring due to littoral drift at south side of the southern breakwater would get eroded due to high wave action during monsoon season.

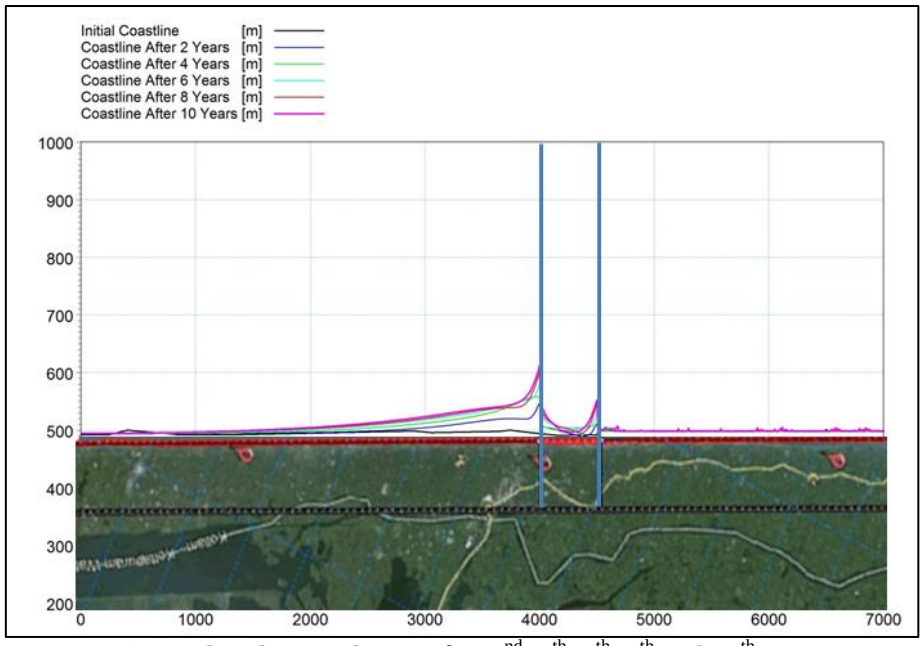



**Fig. 5** Shoreline evolution after 2nd, 4th, 6th, 8th and 10th year

Further, model was simulated subsequently for a period of 2, 4, 6, 8 and 10 years and the maximum cross-shore advancement of south side of the southern breakwater for each period would be as 50 m, 67 m, 78 m, 90 m and 110 m, respectively from the prevailing position of coastline. But due to the presence of seawall along the shore at the proposed location erosion is unlikely to occur beyond the existing shoreline. It may be noted that during the LITPACK model simulation, it has been assumed that the shoreline consisted of erodible material. Further, the corresponding longshore effect of deposition was felt for a length of about 2.0 km and but longshore effect of erosion was not felt due to seawall. The maximum cross-shore advancement of the shoreline in 10 years period would be of the order of 150 m.

However, model simulation was also carried out for the case of without seawall all along the seashore at the site. Based on these results it was found that after 2,4,6,8 and 10 years period, the deposition on south side of southern breakwater would remain similar to that as in earlier case i.e. with seawall, but erosion on north side of the northern breakwater would be of the order of 25 m, 35 m, 40 m, 46 m and 52 m after 2,4,6,8 and 10 years, respectively and extent of erosion would be felt upto 2.5 km in the north side along the shore.

## 6. Conclusions

Mathematical model studies have been carried out to estimate littoral drift at the proposed site of fishing harbour at Thrikkunnapuzha and to examine the likely changes in the coastline due to the construction of open sea fishing harbour having two breakwaters; northern and southern, and an inlet in between. Following are the main conclusions of the model studies:

1. The annual southward and northward transports using IMD wave data were computed to be 0.14 million cum and 0.16 million cum, respectively with the net and the gross transports being 0.02 million cum and 0.3 million cum, respectively. The net longshore transport is towards north and the major northward transport occurs during all the seasons except the SW monsoon.

2. The annual southward and northward transports using field observed wave data were computed to be 0.086 million cum and 0.092 million cum, respectively with the net and the gross transports being 0.006 million cum and 0.18 million cum, respectively. The net longshore

transport is towards north and the major northward transport occurs during all the seasons except the SW monsoon.

3. Drift directions obtained for both these data are same.

4. The difference in nearshore wave data is mainly due to the fact that the observed data corresponds to one year period only.

5. Based on the distribution of annual longshore transport, the transport is confined within a range of 200 m from the shore as extremely steep slope exist near the shore and the northward transport is more than the southward transport. The peak transport occurs at about 50 m from the shoreline and about 75% transport occurs in the range of 0 m to 100 m from shoreline i.e. between +0.0 m to –3.0 m depth contours.

6. As the net transport is directed towards north the deposition is expected on the south side of the proposed southern breakwater. After a period of 2, 4, 6, 8 and 10 years the maximum cross-shore advancement would be about 50 m, 67 m, 78 m, 90 m and 110 m, respectively from the prevailing coastline position. The corresponding longshore effect on southern side of the southern breakwater would be felt upto 2.0 km.

7. The erosion is unlikely to occur beyond the existing shoreline at the proposed site due to presence of seawall along it and so the protected coastline is not likely to suffer erosion.

**Acknowledgements** The authors are grateful to Shri A. K. Agrawal, Director, CWPRS for his guidance and constant encouragement. The authors express their deep gratitude for according permission to publish this paper.

## References

1. C-MAP (2005), Danish Hydraulic Institute (DHI), Denmark.
2. LITPACK (2015), An Integrated Modelling System for Littoral Processes and Coastal Kinetics, Danish Hydraulic Institute.
3. MIKE 21 SW(2013), User manual, Danish Hydraulic Institute (DHI), Denmark.
4. Sajeev R, chandramohan P Josanto V and sankarnarayanan V N. (1997) "Studies on sediment transport along kerela coast, southwest coast of India", *Indian Journal of Marine Sciences*, *Vol. 26*, pp.11-15

*IN PROCEEDINGS OF 25th HYDRO 2020, INTERNATIONAL CONFERENCE, NATIONAL INSTITUTE OF TECHNOLOGY ROURKELA, ODISHA, INDIA 26-28, March 2021, ISBN 978-93-90631-56-8*

Paper ID - 175

# Assessment of wave tranquillity and littoral drift studies using time dependent wave parameters to develop tourist harbour in Andhra Pradesh

Vighe K S[1], Barve K H[2], Ranganath L R[3], Agrawal J D[4]

[1]*Assistant Research Officer, Central Water and Power Research Station, Pune 411024, India*
[2]*Scientist 'B', Central Water and Power Research Station, Pune 411024, India*
[3] *Scientist 'D', Central Water and Power Research Station, Pune 411024, India*
[4] *Scientist 'E', Central Water and Power Research Station, Pune 411024, India*
*Email: ks.vighe@gmail.com, barvekh@gmail.com, praranga@yahoo.com, agrawal_jd@cwprs.gov.in*

## Abstract

Government of India envisages modernization of ports and development of coastlines to contribute India's growth under Sagarmala project. As a part of Sagarmala project developing small tourist harbour at Kakinada along the East coast of India. To check the feasibility of passenger jetty comprehensive studies of wave transformation and tranquility, assessment of littoral drift and Sedimentation are essential. The paper explains the assessment of wave tranquility and littoral drift studies using wave time series. MIKE 21-SW model was used for wave transformation studies with 69x70 km area. To estimate littoral movement along the coast it is necessary to have measured wave data. The measured wave data at Kakinada is not available. The yearly wave data from IMD offshore of Andhra Pradesh coast were analysed and a time series of one-year duration (2012 – 13) with wave height, wave period and wave direction were obtained. The wave time series obtained from IMD data was used as input for the wave transformation studies carried out using MIKE 21 SW model. At the two locations north of Kakinada bay and south of the bay both at -8m depth wave time series were derived from the results of the simulation of one-year duration. These time series of wave parameters were used for the littoral drift studies using LITPACK model. The wave data incorporated the temporal variations of the wave parameters nearshore hence the results are more realistic. The details of the method of the study and the results obtained shall be presented in the paper.

***Keywords:*** *Wave transformation, litdrift, time series, harbour*

## 1. Introduction

Government of India's flagship programme under Sagarmala project envisages modernization of ports to augment port-led development and to ensure that coastlines can be developed to contribute to India's growth. The vision is to transform the existing ports into modern world class ports and integrate the development of the ports, the industrial clusters and hinterland and efficient evacuation systems through road, rail, inland and coastal waterways resulting in ports becoming the drivers of economic activity in coastal areas.

The programme aims to promote port-led development in the country by harnessing India's 7,500km long coastline, 14,500km of potentially navigable waterways and strategic location on key international maritime trade routes. As part of the Central government's Sagarmala project, 36 projects have been proposed by the Andhra Pradesh government. In line with the above, Andhra Pradesh Tourism Development Corporation (APTDC) identified several locations where tourist harbours can be developed, out of which four locations in Andhra Pradesh viz., Kalingapatnam, Bheemunipatnam, Kakinada and Manginapudi have been considered in the first phase for development. The basic objectives of the proposal are creating tourism enhancing infrastructure, Development of leisure boating industry and facilitate cruise rides, Improvement in transportation of goods and public through sea, creation of additional employment. The feasibility of development of tourist harbour studies, considering the hydraulics, were carried out in CW&PRS. The mathematical modelling studies for wave tranquillity and littoral drift for the development of Kakinada tourist harbour are described in this paper.

Wave conditions considered for the wave tranquility and littoral drift studies are obtained from wave transformation studies. If there are structures like breakwaters wave propagation studies are carried out. In some cases, like the study of harbour near Sagar Island, West Bengal only wave transformation

studies were carried out successfully to assess wave conditions at the jetty locations. (A.M. Vaidya et al. 2014). The Kakinada tourist terminal is located inside the Kakinada bay beyond the Kakinada Port. Solid structures are not required for the protection of the terminal. Thus, only wave transformation studies are carried out and the wave conditions at the location are obtained.

Its s desirable to use measured wave data to study along shore sediment movement. However, such data is rarely available. Thus, the wave climate as represented in the percentage occurrence table of wave height and wave direction is generally used. Thus, wave conditions are representative of the wave height and direction bins. However, in the present study time dependent series of wave parameters is used as input for the littoral drift studies. This method and results are reported in details in this paper.

## 2. Site Conditions

### *2.1 Location and site condition*

Kakinada is on the east coast of India**,** it is protected by **t**he Hope Island from the open sea, as shown in Figure 1. Kakinada can be developed as a tourist place. Thus, development of harbour for passenger water terminal is proposed in Kakinada. The site inside the Kakinada bay beyond the present Kakinada Port as shown in the Figure1 was considered for further studies.

### *2.2 Wave data in deep sea*

The offshore wave data available at CWPRS data bank, for period 28/05/1999 to 25/11/2008 at six hourly intervals at location 792905.00 m Easting and 1874966.00 m Northing at -200 m depth were used for the studies (CWPRS Technical report no. 5242. 2015). This wave data information was used as input at the offshore end of the MIKE 21-SW model limits. The frequency distribution of wave heights from different directions during entire year for the above offshore data is given in Table 1. The corresponding rose diagram is presented in Figure 2. The predominant wave direction is South. These deep-water wave data were transformed using a spectral wave model MIKE21-SW to get the nearshore wave climate. For wave transformation studies, MIKE21-SW module of MIKE21 software was used for estimation of nearshore wave field in the fishing harbour. MIKE21 Spectral Wave (SW) model is one of the state-of-the art third generation spectral wind wave model.

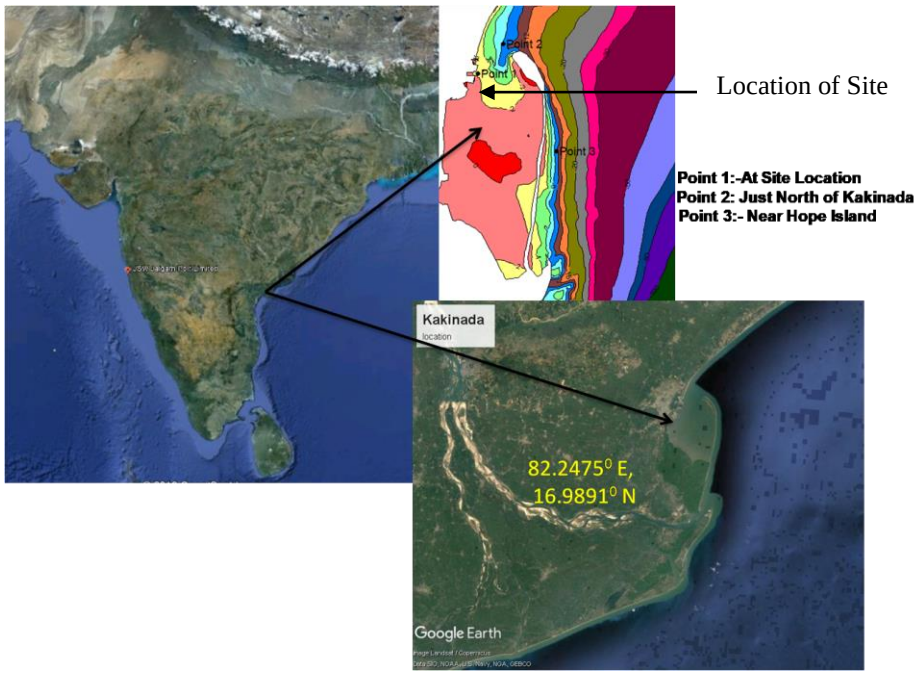



**Figure 1** Location map of proposed site at Kakinada

**Table 1** Percentage occurrence of wave height & direction off Kakinada for entire period (Jan-Dec)

| Wave Ht (m) | <0.5 | <1 | <1.5 | <2 | <2.5 | <3 | <3.5 | <4 | <4.5 | Total |
|---|---|---|---|---|---|---|---|---|---|---|
| Direction($^o$n) | | | | | | | | | | |
| 45 | 0 | 0 | 0.6 | 0.6 | 0.2 | 0.1 | 0 | 0 | 0 | 1.6 |
| 67.5 | 0 | 0.3 | 1.5 | 1 | 0.5 | 0.1 | 0.1 | 0 | 0 | 3.5 |
| 90 | 0.2 | 0.4 | 0.8 | 0.2 | 0.1 | 0 | 0 | 0 | 0 | 1.7 |
| 112.5 | 0 | 0.7 | 0.5 | 0.2 | 0 | 0 | 0 | 0 | 0 | 1.4 |
| 135 | 0.1 | 1 | 0.3 | 0.1 | 0 | 0.1 | 0 | 0 | 0 | 1.7 |
| 157.5 | 0.5 | 3.4 | 2.9 | 1 | 0.1 | 0 | 0 | 0 | 0 | 7.9 |
| 180 | 0.5 | 10.9 | 25.7 | 17.8 | 7 | 1.8 | 0.4 | 0.1 | 0 | 64.2 |
| 202.5 | 0 | 0.5 | 1.5 | 3.2 | 2.2 | 0.7 | 0.2 | 0 | 0 | 8.4 |
| 225 | 0 | 0.1 | 0.7 | 1.8 | 1.9 | 1.1 | 0.5 | 0.2 | 0.1 | 6.3 |
| 247.5 | 0 | 0 | 0.3 | 0.8 | 0.8 | 0.6 | 0.2 | 0.2 | 0 | 2.9 |
| Total | 1.2 | 17.4 | 34.9 | 26.8 | 12.9 | 4.6 | 1.5 | 0.6 | 0.1 | 100 |

The MIKE21-SW model simulates wave growth due to wind action, transformation due to refraction and shoaling resulting from depth variations, and decay due to white capping, bottom friction and wave breaking. The effects of wave-current interaction, non-linear wave-wave interaction, time-varying water depth and dissipation are also included within the model. The model is based on flexible mesh which allows for coarse spatial resolution for offshore area and high-resolution mesh in shallow water and at the coastline.

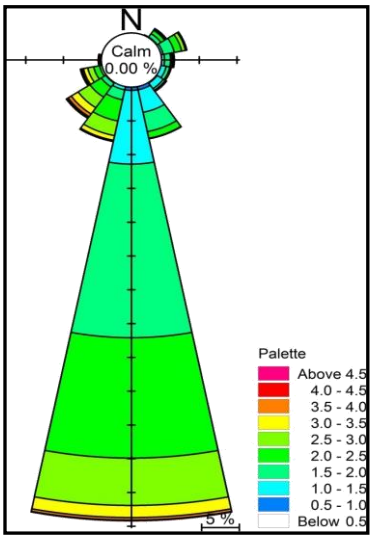



**Figure 2** Offshore wave rose diagram for entire year

## *2.3 Wave tranquility studies*

### *2.3.1 Method of studies*

To test whether the site is tranquil with respect to wave disturbance, wave height distribution at the site for the input wave conditions. The wave climate near the site can be simulated by conducting wave transformation studies followed by wave propagation studies near the harbour area or only conducting wave transformation studies. In the harbour with solid structures like breakwater and berths, the diffraction at tips of breakwater and reflections due to berths or breakwater are important parameters affecting the wave heights in the harbour area. Hence in this situation, the wave propagation studies are particularly required.

However, when there is no structure, diffraction and reflection need not be considered. In such scenario wave transformation studies including refraction, shoaling, Wave-wave interaction, frequency dispersion is sufficient to simulate wave climate in the area. The MKE21-SW model is capable of all

these phenomena. Thus, where there are no solid structures, simulation by MIKE 21-SW gives the desired wave height, wave direction and period accurately.

The development in the site and the in the vicinity does not have any solid structure. The influence of diffraction, due to the offshore breakwater, vanishes at a distance far from the area near the site. Hence the studies by MIKE21-SW give the wave height, direction and wave period near and at the site accurately (A.M. Vaidya et al. 2014). Thus, in the wave tranquillity studies for the development of Kakinada passenger terminal use of only MIKE 21-SW is appropriate. The MIKE21-SW model is used for wave transformation studies and the results are used to determine the tranquility at the terminal.

### *2.3.2 Wave transformation from deep water to nearshore region*

The nearshore wave climate at Kakinada was obtained by transforming the deepwater wave data using MIKE21-SW Model. Bathymetry in the model region of about 80 km by 50 km area was descreitized using unstructured mesh. The region up to -100 m depth is considered. The model area and bathymetry is shown in Figure 3.

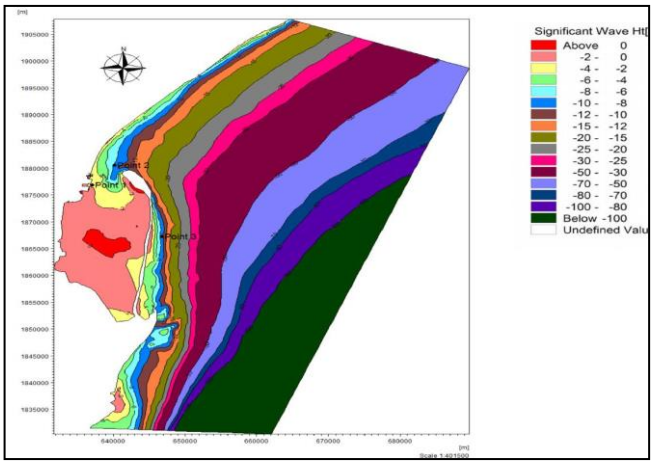



**Figure 3** Bathymetry for wave transformation from offshore to nearshore

Kakinada Port and the proposed passenger terminal are in the bay between Hope Island and shore. This area and the points where results are extracted and studied in detail are shown in Figure 4.

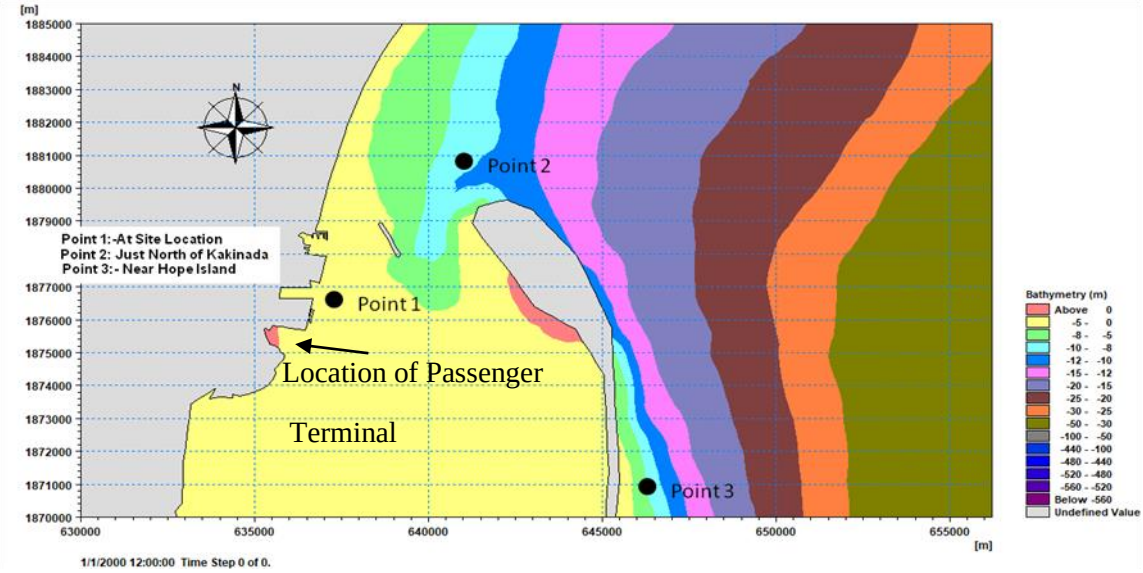
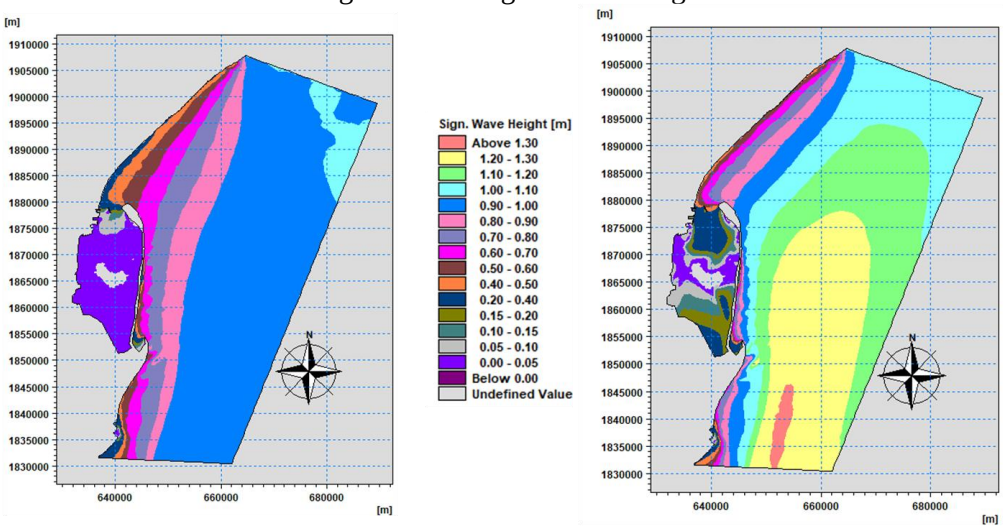


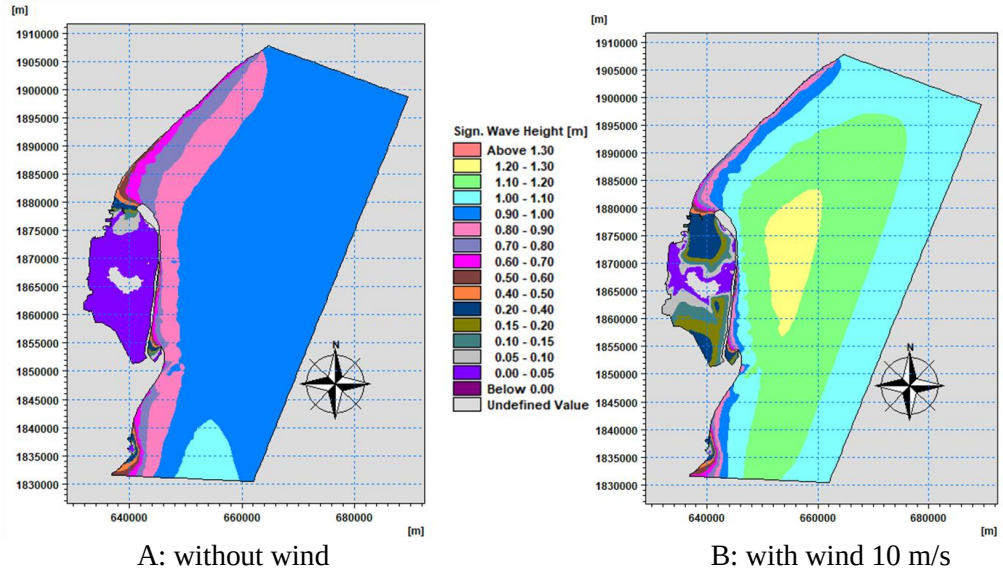

**Figure 4** Location of points for extraction of results

The analysis of IMD data indicated that the predominant wave directions are SSW, South, SSE and SE for 95% of the annual duration the wave heights will be less than 2.5m, 3.5m, 3.0m and 2.5m respectively. The wave transformation studies were performed using MIKE 21 SW and the wave conditions were simulated. The waves from NE and ENE directions are likely to enter the bay and reach the passenger terminal. Hence the wave approach from NE and ENE incident wave directions is simulated. The wave height distribution plots for direction of wave incidence from NE and East for the incident wave height 1.0 m are given in the Figures 5 and 6.




A: without wind B: with wind 10 m/s

**Figure 5** Wave height distribution for waves incident from the NE direction




A: without wind B: with wind 10 m/s

**Figure 6** Wave height distribution for waves incident from the East direction

**Table 2** Wave heights at the site location, without wind and the wind (10m/s)

| Incident Wave Direction | Incident Wave Height (m) | Wave Height (m) Without wind | Wave Height with wind (10m/s) |
|---|---|---|---|
| NE | 2.0 | 0.06 | 0.12 |
| ENE | 2.5 | 0.18 | 0.25 |
| East | 2.0 | 0.06 | 0.16 |
| ESE | 2.0 | 0.06 | 0.12 |

The Severe wave conditions are also tested by considering the wind of 10 m/s following the incident wave direction. With these conditions as well, the wave heights are less than or equal to 0.1m. The wave heights at the terminal for incident wave direction from NE, ENE, East and ESE with wave height

2.0 m, 2.5m, 2.0 m and 2.0 m respectively are tabulated in Table 2. Thus, in the severe weather conditions also the wave heights at the terminal will be less than 0.3m. Due to the sand bar and the Hope Island the area is protected from waves. The waves from SE to South are negligible. From the wave transformation studies, it is observed that the passenger terminal and the nearby area will be tranquil considering the tranquility limit of 0.3m, throughout the year.

## 3. Estimation of Littoral Drift Distribution

### *3.1 Wave transformation studies*

To estimate littoral movement along the coast it is necessary to have measured wave data. The measured wave data at Kakinada is not available. Thus, the derived wave data from wave transformation studies is used. Generally, the wave climate as described by the inshore percentage occurrence of wave height and direction distribution bins is used. If a time series of the wave parameters at the specified locations can be obtained from the wave transformation studies it is desirable. The time series represents the time dependent wave climate with better accuracy. In these studies, the wave height, wave direction and period time series is obtained from the wave transformation studies.

The yearly wave data from IMD offshore of Andhra Pradesh coast are analysed and wave height, wave period and wave direction time series of one-year duration (2012 – 13) was obtained. The IMD data represents the wave climate quite accurately. The wave time series at Kakinada coast is derived from the wave transformation study.

For the wave transformation studies regional model was setup on the large area encompassing Kakinada, Bheemunipatanam, Vishakhapatanam and Kallingapatanam. The area considered for MIKE21-SW model is shown in Figure 7. Bathymetry in the model region of about 400 km along the shore and 100 km across the shore was descreitized using unstructured mesh.

The annual time series of wave height, wave direction and wave period obtained from IMD data, was used as input at the offshore boundary. Simulated results from the wave transformation studies by MIKE21-SW matched well with the available wave data south of Kakinada. (CWPRS Technical report no.5242. 2015). The analysis of measured wave data near Vishakhapatanam and that obtained from the simulation indicated very good agreement. Thus, the regional model gave reliable results in the area. A typical wave vector plot on 11th September, 3:30pm of the simulation is shown in Figure 8.

The time series of wave parameters at the Point 2, just north of Kakinada bay and Point 3, near Hope Island as shown in Figure 4 were extracted. Both the points are at -8 m depth. These time series are used as wave climate time series for the littoral drift studies. To understand qualitatively the net drift direction, rose diagrams of the annual period at the points are prepared. The rose diagrams are shown in Figure 9 (A) and 9(B). Hope Island shields the north side from the wave attack from ESE to South wave directions. In the north of Kakinada wave approach is from the north of the normal to the shore, whereas on the Hope Island it is predominantly from south of the shore normal. This indicates the change in the net drift direction from North to South near Kakinada.

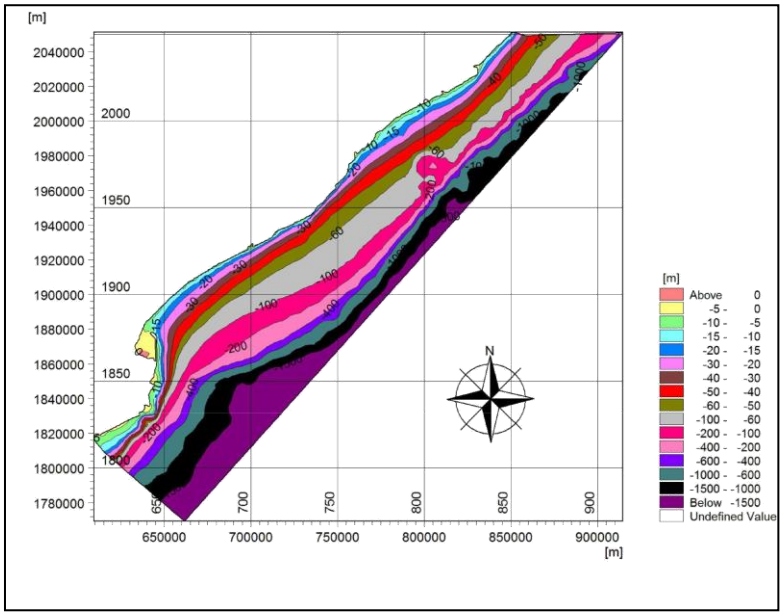



**Figure 7** Bathymetry for regional model for MIKE21-SW studies

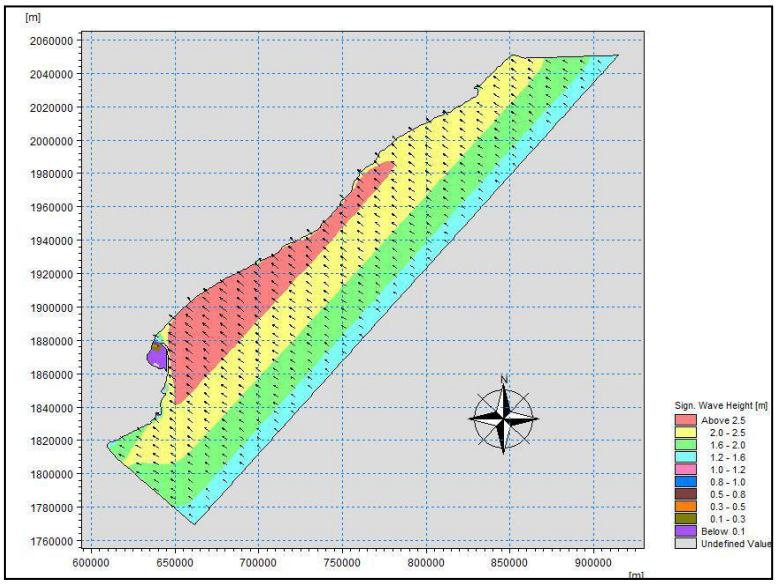
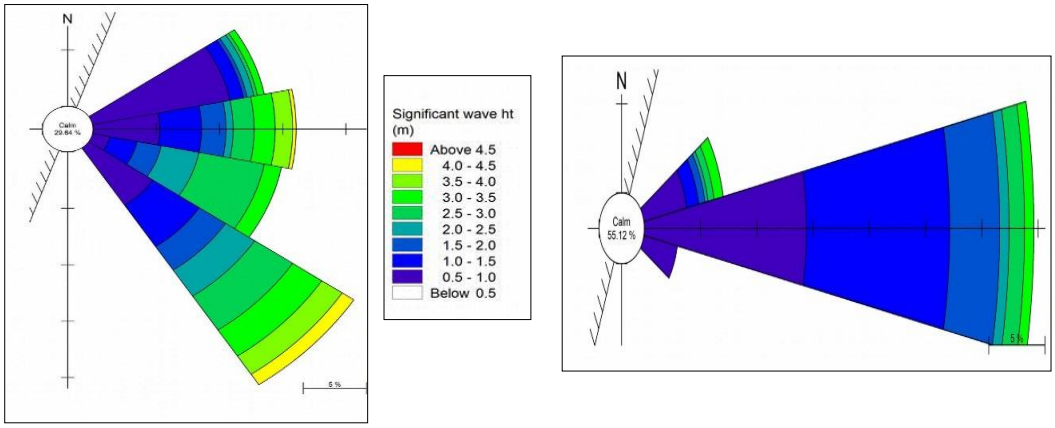



**Figure 8** Typical wave vector plot (11 September - regional model)




(A) On Hope island (B) North of Kakinada

**Figure 9** Annual wave rose diagrams

### *3.2 Littoral drift studies*

Mathematical model studies for estimation of littoral drift distribution were carried out using LITPACK model. LITPACK is a professional engineering software package for the modelling of non-cohesive sediment transport in waves and currents, littoral drift, coastline evolution and profile development along quasi-uniform beach. The longshore and cross-shore momentum balance equation is solved to give the cross-shore distribution of longshore current and setup. LITDRIFT calculates the net/gross littoral transport over a specific design period.

### *3.3 Estimation of littoral drift rate*

For estimation of littoral drift, the Kakinada region is divided in to two regions one towards the North of the mouth of the bay. Another region is the shore which is protected by the sand bar and Hope island from the wave attack from west south west to south wave directions. The littoral drift studies were done at the location from each region.

#### *3.3.1 Littoral drift at hope island shore*

LITDRIFT module of LITPACK software was used to estimate annual littoral drift rates and its distribution on the profile normal to the shoreline i.e. $110^0$N. Sea bed profile shown in Figure 10 near the Hope Island. The profile covers a distance of 2200 m extending up to about -10.2m depth contour (with respect to Chart Datum). The profile was discretized with grid size of 10 m. The wave climate time series was extracted from the regional model. The rose diagram obtained from the simulation is shown in Figure 9 (A). The model was run for annual nearshore wave climate. Annual northward and southward, transport rates were computed and are shown in Figure 10. The northward drift is plotted as negative while southward drift is plotted as positive. The northward, southward, net and gross transport rates are given in Table 3.Net transport in a year is of the order of 0.223 million cum and is towards north and gross transport is of the order of 2.64 million cum. The maximum transport occurs at about 225 m from the shore at around 1.5 m depth contour. The drift is moderate and no new structure will be constructed on the shore hence there will not be significant change in the shoreline.

**Table 3** Littoral transport rates (million $m^3$/year)

| Season | Northward | Southward | Net * | Gross |
|---|---|---|---|---|
| Annual | -1.431 | 1.208 | -.0.223 | 2.639 |

Note* For the Net Drift '-ve' Northward '+ve' Southward

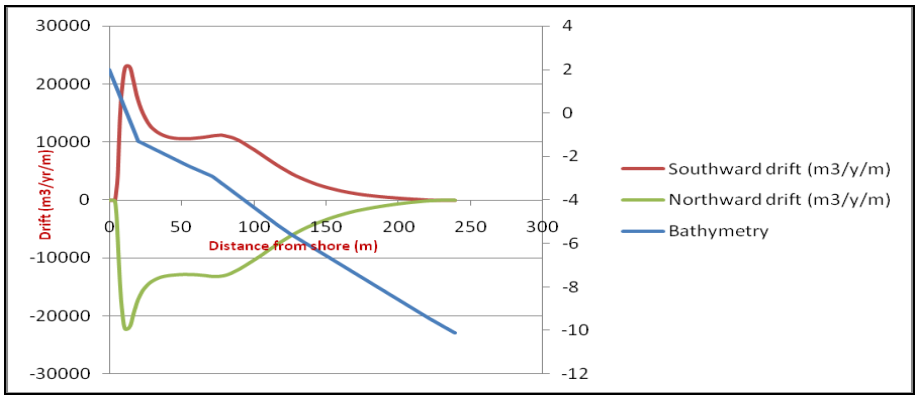



**Figure 10** Annual northern & southern littoral drift (Hope island)

#### *3.3.2 Littoral drift north of bay mouth*

Littoral drift was estimated just north of the mouth of the Kakinada Bay (Point 3). The Location is shown in the Figure 11. LITDRIFT module of LITPACK software was used to estimate annual littoral drift rates and its distribution on the profile normal to the shoreline i.e. $110^0$N. Sea bed profile shown in

Figure 11 near the North of Bay Mouth. The profile covers a distance of 2000 m extending up to about -8m depth contour (with respect to Chart Datum). The profile was discretized with grid size of 10 m. The wave climate time series was extracted from the regional model. The rose diagram obtained from the simulation is shown below Figure 9(B). The model was run for annual nearshore wave climate. Annual northward and southward, transport rates were computed and are shown in Figure 11. The northward drift is plotted as negative while southward drift is plotted as positive. The northward, southward, net and gross transport rates are given in Table 4.

**Table 4** Littoral transport rates (million $m^3$/year)

| Season | Northward | Southward | Net * | Gross |
|---|---|---|---|---|
| Annual | -0.536 | 0.9902 | 0.9434 | 1.037 |

Note* For the Net Drift '-ve' Northward '+ve' Southward

Net transport in a year is of the order of 0.9434 million cum and is towards south and gross transport is of the order of 1.037 million cum. The maximum transport occurs at about 250 m from the shore at around 1.6 m depth contour. The drift is moderate and no new structure will be constructed on the shore hence there will not be any change in the shoreline.

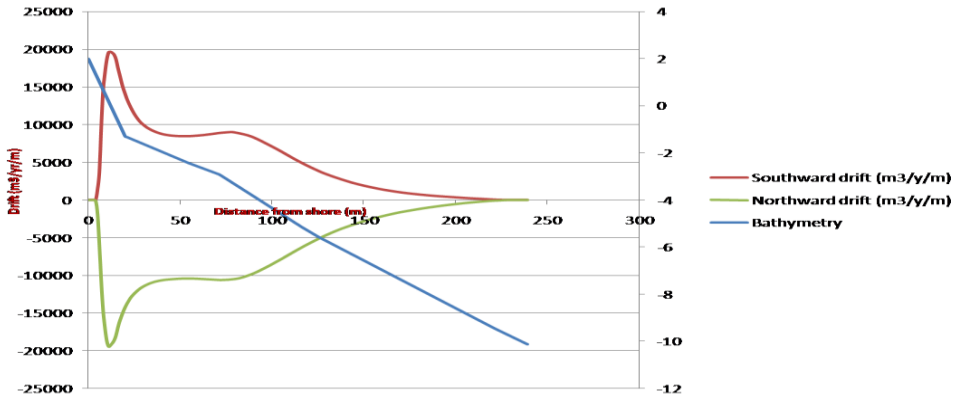



**Figure 11** Annual northern & southern littoral drift at point 3 (nearshore)

At both the locations there is a change in the net littoral drift direction. North of the bay the net drift is southward and on the Hope Island it is northward. This is due to the change in the wave climate because of the shielding effect of the Hope Island. The studies were carried out with time series of wave height, wave direction and wave period over one-year duration at the locations. Thus, the results are realistic and emulate the nature better.

## 4. Conclusions

1. The analysis of IMD data indicated that the predominant wave directions are SSW, South, SSE and SE for 95% of the annual duration the wave heights will be less than 2.5m, 3.5m, 3.0m and 2.5m respectively. The wave transformation studies were performed using MIKE 21-SW and the wave conditions were simulated. The waves from NE and ENE directions are likely to enter the bay and reach the passenger terminal. Hence the wave approach from NE and ENE incident wave directions is simulated. Table 3 shows that at the terminal the wave heights are below the tranquility limit.

2. For the wave transformation studies, regional model was setup on the large area encompassing Kakinada, Bheemunipatanam, Vishakhapatanam and Kallingapatanam was setup. The model region of about 400 km along the shore and 100 km across the shore was discretized using unstructured mesh from the IMD data, the annual time series of wave height, wave direction and wave period was obtained. The simulated results matched well with the available results south of Kakinada (CWPRS Technical report no. 5242. 2015). The analysis of measured wave data near Vishakhapatanam and the simulated wave data there indicated very good agreement. Thus, the regional model gave reliable results of wave height, wave direction and wave period, in the area.

3. The assessment of littoral drift was done using LITPACK. In the absence of measured wave data, the time dependent wave data near Kakinada extracted from the simulation of the regional model were used. The Hope Island area shoreline and the shore just north to the bay have different wave climates. Hence, the studies were done at two locations separately.

4. Littoral Drift at Hope Island Shore was carried out at the Point shown in the Figure 9 (A). Net transport in a year is of the order of 0.223 million cum and is towards north and gross transport is of the order of 2.64 million cum. The maximum transport occurs at about 225 m from the shore at around 1.5 m depth contour. The sediment transport is moderate and will not affect the shoreline.

5. Littoral Drift North of Bay Mouth was carried out at the Point shown in the Figure 9 (B). Net transport in a year is of the order of 0.9434 million cum and is towards south and gross transport is of the order of 1.037 million cum. The maximum transport occurs at about 250 m from the shore at around 1.6 m depth contour. The sediment transport is moderate and will not affect the shoreline.

6. The studies to assess wave climate at the site and estimation of littoral drift, indicated that at the proposed site for a small harbour/ passenger water terminal is safe. Hence, it is recommended that the passenger terminal may be developed.

## Acknowledgements

The authors wish to thank Shri A. K. Agrawal, Director, CW&PRS for his consistent support, encouragement and kind consent for publishing this paper. The authors acknowledge the guidance of Dr. J. D. Agrawal, Scientist – E, CW&PRS during the study.

## References

A.M. Vaidya, K.H. Barve, S. Kori and M.D. Kudale (2014). Mathematical modelling of short-wave propagation over a complex bathymetry. *Indian National Conference of Harbour and Ocean Engineering Goa.*
Mathematical model studies for shoreline changes near ONGC plant and pipe lines near Odalarevu village, East Govdavari, Andhra Pradesh (2015). *CWPRS Technical report no. 5242.*
Patil B. M., Manivanan R., Kanetkar C.N., Barve K. H. and Jha S. N. (2009). Simulation of shoreline changes to assess impact of proposed port. *National Conference on Hydraulics, Water Resources, Coastal and Environmental Engineering HYDRO 2009, CWPRS, Pune.*

*IN PROCEEDINGS OF 25th HYDRO 2020, INTERNATIONAL CONFERENCE, NATIONAL INSTITUTE OF TECHNOLOGY ROURKELA, ODISHA, INDIA 26-28, March 2021, ISBN 978-93-90631-56-8*

Paper ID - 176

# Numerical model studies for assessment of wave tranquillity and littoral drift for proposed passenger jetty in an inlet harbour at Kalingapatnam

Vighe K S[1], Sawant Rahul[2], Barve K H[3], Ranganath L R[4], Agrawal J D[5]

[1]*Assistant Research Officer, Central Water and Power Research Station, Pune 411024, India*

[2]*Research Assistant, Central Water and Power Research Station, Pune 411024, India*

[3]*Scientist 'B', Central Water and Power Research Station, Pune 411024, India*

[4] *Scientist 'D', Central Water and Power Research Station, Pune 411024, India*

[5] *Scientist 'E', Central Water and Power Research Station, Pune 411024, India*

*Email: ks.vighe@gmail.com, sawant.rahul333@gmail.com*

## Abstract

As part of the Central government's Sagarmala project, 36 projects have been proposed by the Andhra Pradesh government. In line with the above, Andhra Pradesh Tourism Development Corporation (APTDC) identified 39 beaches for developmental activities for promotion of tourism. Government of Andhra Pradesh has identified the Kalingapatnam as potential site for the development of a water transport facilities, catering to the needs of transport of material as well as passenger transport for commuters as well as tourist visiting the region. Kalingapatnam Beach is the place where river Vamsadhara empties into Bay of Bengal, it has one of the major beach sand deposits of the state. The present paper discusses the details of the Numerical model studies carried out by different module of MIKE21 software to assess the wave tranquillity and littoral drift for the proposed development in an inlet harbour at Kalingapatnam, to establish the feasibility from the hydraulics point of view. The proposed development consists of approach channel of width of 100 m, depth 5 m, turning circle of 200 m diameter dredged to -5.5 m, along with the northern and southern sand traps of -5.5 m depth, adjacent to the channel on the shore. The wave transformation studies carried out to obtain input wave conditions for wave tranquillity studies and nearshore wave climate for littoral drift studies. Further details of the study shall be presented in the full-length paper.

***Keywords:*** *Numerical Model, Wave Tranquillity, Littoral Drift, Inlet Harbour.*

## 1. Introduction

Government of India's flagship programme under Sagarmala project envisages modernization of ports to augment port-led development and to ensure that coastlines can be developed to contribute to India's growth. The vision is to transform the existing ports into modern world class ports and integrate the development of the ports, the industrial clusters and hinterland and efficient evacuation systems through road, rail, inland and coastal waterways resulting in ports becoming the drivers of economic activity in coastal areas.

The programme aims to promote port-led development in the country by harnessing India's 7,500 km long coastline, 14,500 km of potentially navigable waterways and strategic location on key international maritime trade routes. As part of the Central government's Sagarmala project, 36 projects have been proposed by the Andhra Pradesh government. In line with the above, Andhra Pradesh Tourism Development Corporation (APTDC) identified 39 beaches for developmental activities for promotion of tourism. 9 locations have been identified for the construction of jetties for facilitating cruise movement out of which four locations in Andhra Pradesh viz., Kalingapatnam, Bheemunipatnam, Kakinada and Manginapudi have been considered in the first phase for development. The basic objectives of the proposal are

- Creating tourism enhancing infrastructure.
- Development of leisure boating industry and facilitate cruise rides.
- Improvement in transportation of goods and public through sea.
- Creation of additional employment.

The prospective locations identified by the APTDC along the coast line for development under Sagarmala scheme is indicated in Fig. 1 while the location of the proposed Kalingapatnam site is indicated at Fig. 2.




**Figure 1** Locations under Sagarmala

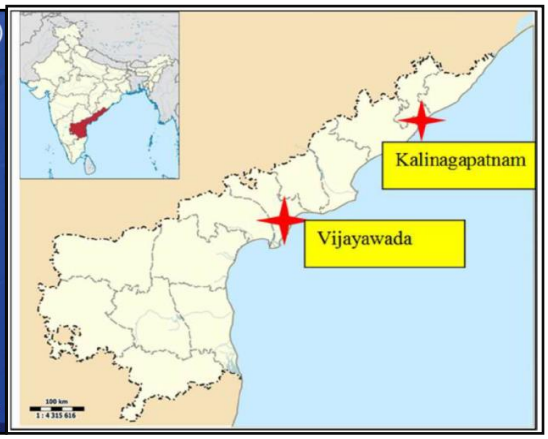



**Figure 2** Location of proposed site

The coastal region in and around Kalingapatnam is a fast-growing region over crowded by the various developments of industries and there is a great demand for transport of material from its main source as well as man power to this region from distance places within the state as well as outside the state.

Government of Andhra Pradesh has identified the Kalingapatnam as potential site for the development of a water transport facilities, catering to the needs of transport of material as well as passenger transport for commuters as well as tourist visiting the region in Phase I and big size vessels in the next phase of development based on the working experience. Kalingapatnam, a village in Srikakulam district of Andhra Pradesh, is located in North latitude of 18°19'27.70" N and East longitudes of 84° 7'39.57" E. It is located in Gara mandal of Srikakulam revenue division. It has one of the major beach sand deposits of the state. Kalingapatnam Beach is the place where river Vamsadhara empties into Bay of Bengal. The proposed location of jetty as indicated in the DPR for the Kalingapatnam is shown in Fig. 3.




**Figure 3** Proposed location of jetty in Kalingapatnam

## 2. Scope of Study

1. Mathematical model study of wave transformation to assess the wave conditions at the site for existing and proposed layout.
2. Mathematical model studies for littoral drift and shoreline changes to evaluate the effect in the near shore region of the proposed passenger jetty, navigation channel and sand trap.

The present paper discusses the details of the Mathematical model studies carried out to evaluate the wave tranquility and shoreline changes aspects due to the proposed passenger jetty and other infrastructure facilities at Kalingapatnam, Srikakulam district in Andhra Pradesh to establish the feasibility from the hydraulics point of view.

## 3. Methodology

The mathematical model studies were carried out using MIKE21 software using the Flexible Mesh, which is most suitable for creeks with meandering coastline.

The wave tranquility and shoreline changes studies are carried out in two stages.
1. Mathematical model studies to transform deep water wave climate to obtain nearshore wave climate and to assess the wave conditions in the vicinity of the jetty, with MIKE21-SW (Spectral Wave model).
2. Mathematical model studies to assess the shoreline changes due to the development, with Litdrift module of LITPACK software.

The details of the wave tranquility and shoreline changes studies for both existing and proposed conditions for the envisaged developments in Kalingapatnam are presented in this paper.

## 4. Mathematical Model Studies for Wave Tranquility

To test whether the site is tranquil with respect to wave disturbance wave conditions in the nearshore area are required. The wave climate near the site can be simulated by conducting wave transformation studies followed by wave propagation studies near the harbour area or only conducting wave transformation studies. In the harbour with solid structures like breakwater and berths, the diffraction at tips of breakwater and reflections due to berths or breakwater are important parameters affecting the wave heights in the harbour area. Hence in this situation, the wave propagation studies are particularly required.

However, when there is no structure, diffraction and reflection need not be considered. In such scenario wave transformation studies including refraction, shoaling, wave-wave interaction, frequency dispersion is sufficient to simulate wave climate in the area. The MIKE21-SW model is capable of all these phenomena. Thus, where there are no solid structures, simulation by MIKE21-SW gives the desired wave height, wave direction and period accurately.

In the area of development and in the vicinity of approach channel solid structure is not proposed. Hence the studies by MIKE21-SW give the wave height, direction and wave period near and at the site accurately. Thus, in the wave tranquility studies for the development of Kalingapatnam passenger terminal, use of MIKE21-SW only, is appropriate.

The MIKE21-SW model is used for wave transformation studies and the results are used to determine the tranquility at the terminal.

Mathematical model studies were undertaken to examine wave tranquility in Kalingapatnam harbour with the proposed developments by using MIKE21-SW model. The details of the studies are presented in this paper.

### *4.1 Offshore wave climate*

For studying wave tranquility, nearshore wave data is essential. Instrumentally observed wave data at the site over a period of several years, if available, is best suited for this purpose. However, if such data are not available, the nearshore wave climate can be obtained by transforming the offshore wave data to the nearshore location by using mathematical modelling technique. For this purpose, the wave

data observed by ships plying in the offshore region of between Latitude15-20 deg N and Longitude 80-85 deg E, reported by India Meteorological Department (IMD) during past 30 years were considered. It may be noted that the ship observed wave data closely correspond to the significant wave height. The wave data was analysed and the seasonal and annual percentage occurrence of wave heights and wave direction is obtained. The annual table is given in Table 1 and offshore wave rose plot for entire year shown in Fig. 4.

These deep-water wave data were transformed using MIKE21-SW model to get the nearshore wave climate at the harbour.

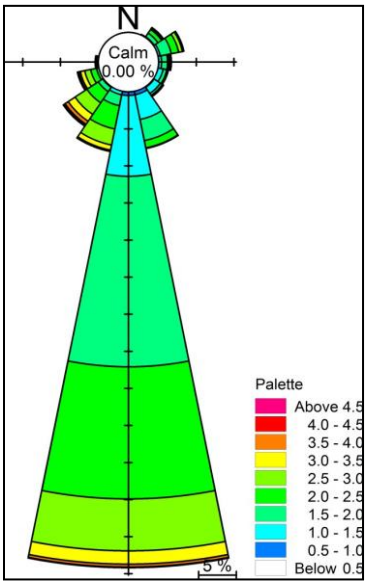



**Figure 4** Offshore rose diagram for entire year

**Table 1** Percentage occurrence of wave height & direction off Kalingapatnam for entire year (Jan-Dec)

| Wave Ht (m) | 0-0.5 | 0.5-1 | 1-1.5 | 1.5-2 | 2-2.5 | 2.5-3 | 3-3.5 | 3.5-4 | 4-4.5 | Total |
|---|---|---|---|---|---|---|---|---|---|---|
| Direction | | | | | | | | | | |
| 22.5 | 0.00 | 0.00 | 0.02 | 0.03 | 0.02 | 0.02 | 0.00 | 0.00 | 0.00 | 0.09 |
| 45 | 0.00 | 0.12 | 0.60 | 0.48 | 0.24 | 0.12 | 0.02 | 0.01 | 0.00 | 1.57 |
| 67.5 | 0.00 | 0.49 | 1.66 | 0.83 | 0.42 | 0.07 | 0.05 | 0.03 | 0.01 | 3.57 |
| 90 | 0.00 | 0.63 | 0.60 | 0.18 | 0.09 | 0.04 | 0.03 | 0.01 | 0.00 | 1.57 |
| 112.5 | 0.01 | 0.88 | 0.33 | 0.14 | 0.02 | 0.03 | 0.02 | 0.02 | 0.00 | 1.45 |
| 135 | 0.14 | 1.15 | 0.21 | 0.05 | 0.03 | 0.03 | 0.02 | 0.01 | 0.00 | 1.64 |
| 157.5 | 0.57 | 4.08 | 3.04 | 0.73 | 0.06 | 0.01 | 0.01 | 0.01 | 0.00 | 8.51 |
| 180 | 0.44 | 15.00 | 25.50 | 15.21 | 5.67 | 1.38 | 0.35 | 0.03 | 0.00 | 63.59 |
| 202.5 | 0.01 | 0.73 | 1.92 | 3.34 | 1.86 | 0.62 | 0.13 | 0.02 | 0.01 | 8.64 |
| 225 | 0.00 | 0.10 | 0.90 | 1.84 | 1.80 | 0.79 | 0.41 | 0.17 | 0.07 | 6.07 |
| 247.5 | 0.00 | 0.01 | 0.37 | 0.83 | 0.84 | 0.52 | 0.19 | 0.17 | 0.03 | 2.95 |
| 270 | 0.00 | 0.01 | 0.05 | 0.08 | 0.07 | 0.06 | 0.02 | 0.01 | 0.00 | 0.29 |
| 292.5 | 0.00 | 0.01 | 0.01 | 0.00 | 0.00 | 0.00 | 0.00 | 0.00 | 0.00 | 0.02 |
| 315 | 0.00 | 0.00 | 0.01 | 0.00 | 0.00 | 0.00 | 0.00 | 0.00 | 0.00 | 0.01 |
| 337.5 | 0.00 | 0.00 | 0.00 | 0.00 | 0.00 | 0.00 | 0.01 | 0.01 | 0.00 | 0.01 |
| 360 | 0.00 | 0.00 | 0.00 | 0.02 | 0.00 | 0.00 | 0.00 | 0.00 | 0.00 | 0.02 |
| Total | 1.17 | 23.21 | 35.21 | 23.75 | 11.11 | 3.70 | 1.26 | 0.48 | 0.12 | 100.00 |

The IMD data for 30 years between 15 to 20 degrees latitude and 80 to 85 degrees longitude was analysed to get offshore wave climate. The predominant directions are SSE, South and SSW with percentage occurrence of 8.51, 63.59 and 8.64. Maximum wave heights up to 4.0 m occur.

### *4.2 Tidal levels*

Tidal levels of Kalingapatnam are given bellow: (Admiralty Chart No. 7408)

**Table 2** Tidal levels

| | |
|---|---|
| Mean High Water Spring (MHWS) | +1.70 m |
| Mean High Water Neap (MHWN) | +1.30 m |
| Mean Sea Level (MSL) | +1.00 m |
| Mean Low Water Neap (MLWN) | +0.70 m |
| Mean Low Water Spring (MLWS) | +0.30 m |

## 5. Modelling Techniques

For wave transformation studies, module of MIKE21 software i.e. MIKE21-SW was used for estimation of nearshore wave field in the harbour. Brief description of this model is given below.

### *5.1 MIKE21-SW model*

As waves travel from deep sea to shallow coastal waters, they undergo changes in direction and height due to the processes of refraction and shoaling. The computation of wave transformation from deep to shallow coastal waters was carried out using MIKE21-SW model. MIKE21 Spectral Wave (SW) model is one of the state-of-the art third generation spectral wind wave model. The MIKE21-SW model simulates wave growth due to wind action, transformation due to refraction and shoaling resulting from depth variations, and decay due to white capping, bottom friction and wave breaking. The effects of wave-current interaction, non-linear wave-wave interaction, time-varying water depth and diffraction are also included within the model. The model is based on flexible mesh which allows for coarse spatial resolution for offshore area and high-resolution mesh in shallow water and at the coastline.

## 6. Wave Tranquility Studies

### *6.1 Wave transformation from deep water to nearshore region*

The nearshore wave climate at Kalingapatnam was obtained by transforming the deep-water wave data using MIKE21-SW Model. Model area considered for SW model is shown in Fig. 5. Bathymetry in the model region of about 16 km cross shore up to -58 m depth and 33 km along the shore area was discretized using unstructured mesh.

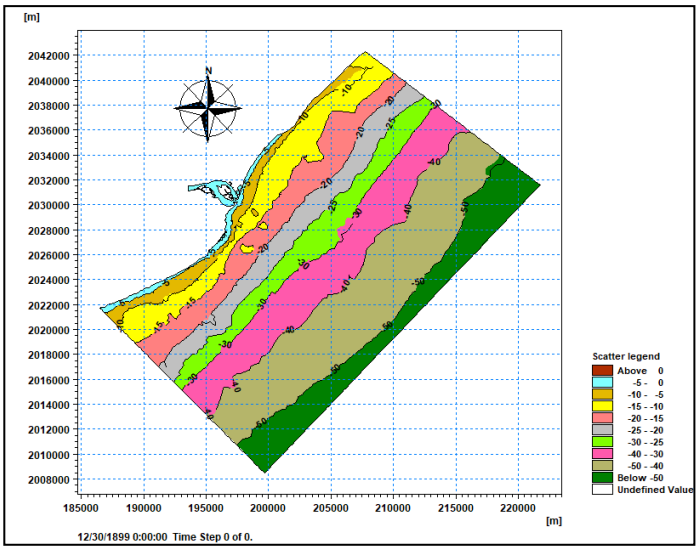



**Figure 5** Bathymetry for the wave transformation studies

Considering the offshore wave climate and the criterion of 98 percentile that is for only 2% of the duration in the entire year the waves may be more severe, the input wave conditions are selected (Table 3).

**Table 3** The input wave conditions for wave transformation studies

| Incident Wave Direction | Incident Wave Height |
|---|---|
| East | 1.5 m |
| ESE | 2.5 m |
| SE | 2.5 m |
| SSE | 3.5 m |
| South | 3.5 m |

The MIKE21-SW model was run with the input wave conditions given in Table 3, with wind forcing of 10 m/s speed from $140^0$ N direction (DPR 2016). The wave height distribution and wave vectors for the entire model area with incident wave height 3.5 m and incident direction SSE, which is the most predominant direction, is shown in Fig. 6 and the wave height distribution and wave vector plots in the vicinity of the existing condition for incident direction SSE is shown in Fig. 7.

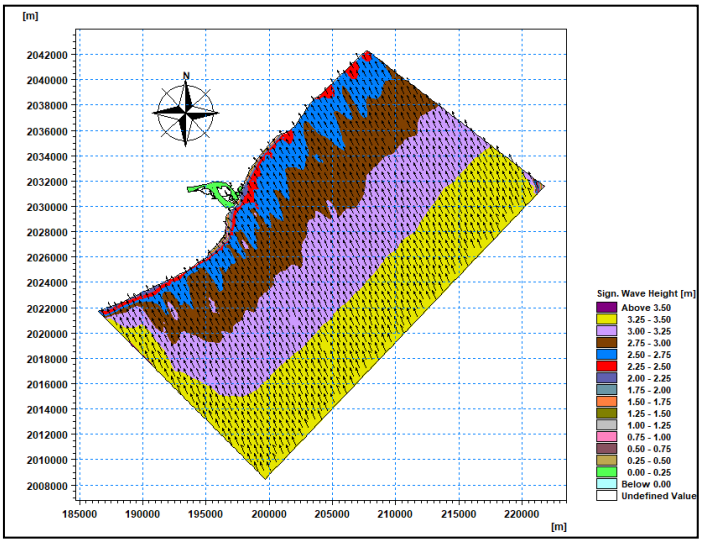



**Figure 6** Wave height distribution and wave vectors for waves incident from SSE direction with incident wave height 3.5 m on entire domain for existing condition

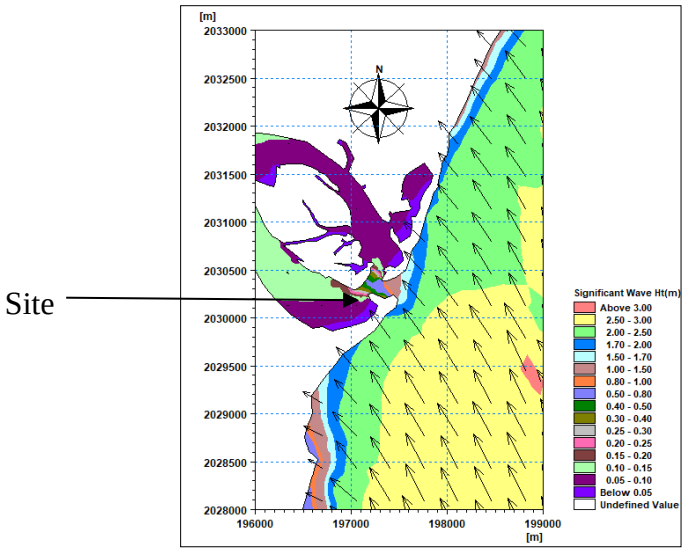



**Figure 7** Wave height distribution for waves incident from SSE direction with incident wave height 3.5 m for existing condition

The mouth opens in the east direction so there is a natural protection for the incident wave directions from SE to South. It is seen that the waves are unable to reach the site. For the incident wave directions of East, ESE, SE, SSE and South, the maximum wave height near the site are 0.1 m, 0.15 m, 0.15 m, 0.15 m and 0.15 m respectively. Also, the incident wave directions of East, ESE, SE and SSE are predominant directions. This wave climate is the most important input for the littoral drift studies.

The mouth opening has shifted from the northern part of the inlet to the southward direction and periodically mouth opening towards east was created. To allow the entry of boats at proposed passenger jetty, mouth opening should not be varying from time to time. So, layout consisting of -5.0 m deep channel and sand pits of depth -5.5 m is considered and the wave transformation studies to assess the wave tranquility at the development adjacent to the channel were carried out.

### *6.2 Wave tranquility studies in the area of development*

The drawing showing layout of the proposed facilities indicating the approach channel, turning circle and sand traps is at Fig. 8.

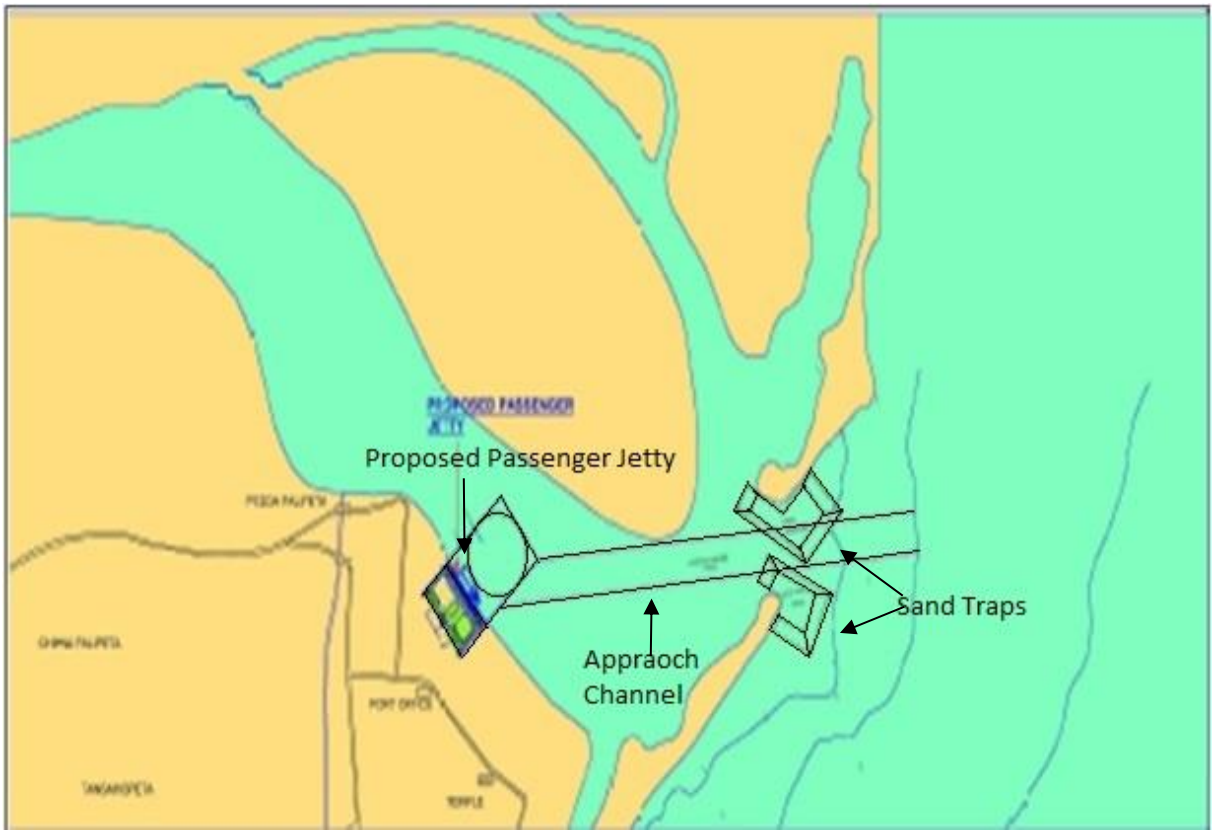



**Figure 8** Proposed layout at Kalingapatnam for APTDC

The approach channel with a width of 100 m and depth of 5.0 m below CD extending upto -5.0 m contour along with a turning circle of 200 m diameter dredged to 5.5 m CD has been incorporated in the model. In order to study the effectiveness of the Sand traps suggested on the northern and southern side of the mouth.

The model was then discretized with finite element mesh and bathymetry interpolated with the mesh. The mesh superimposed on the bathymetry for the proposed conditions is shown in Fig. 9.

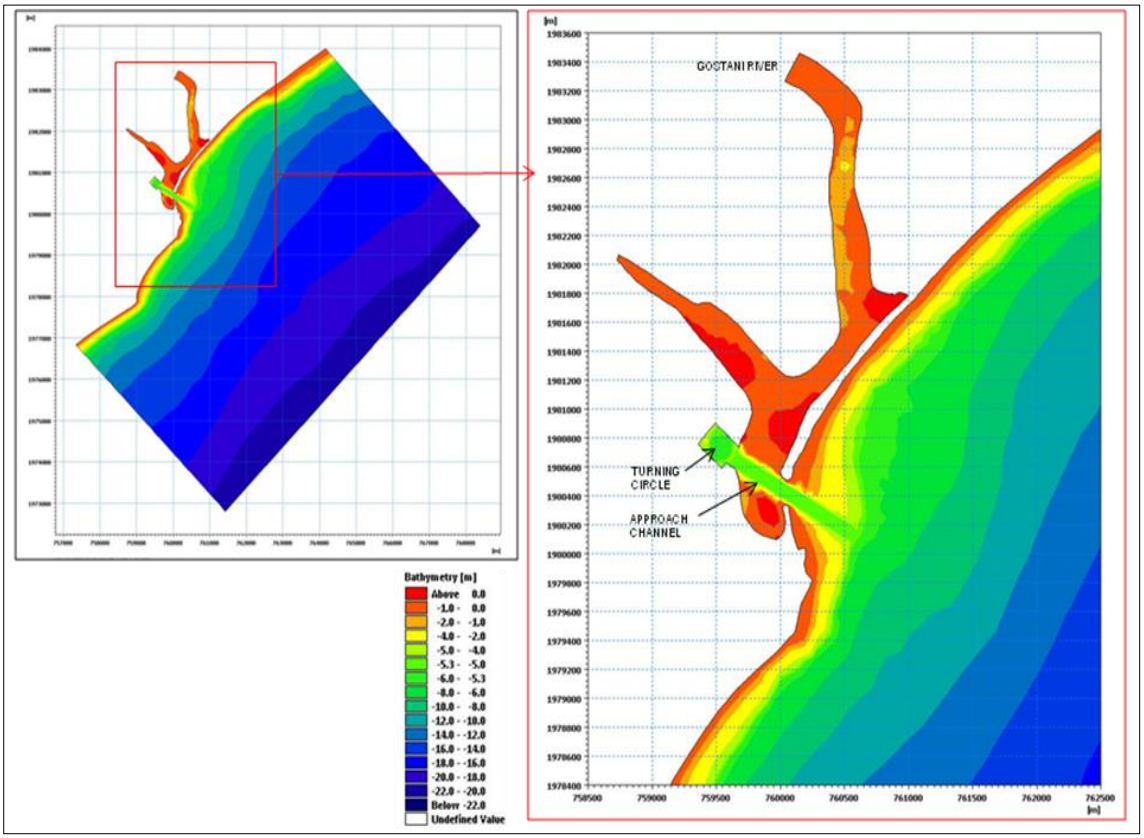



**Figure 9** Bathymetry for the proposed development

The wave transformation and tranquility studies with proposed layout are carried out with predominant incident wave directions and incident wave heights given in the Table 3. The channel is oriented towards East direction. The waves from East are minimal. For the directions from ESE to South there will be partial or total natural protection from the waves. The model was run including wind 10 m/s from 140 deg wind direction, as reported in the DPR. Wind direction matches the channel alignment. The incident wave heights of 1.5 m, 2.5 m, 2.5 m and 3.5 m corresponding to the East, ESE, SE and SSE incident wave direction, respectively are input at the model boundary. These input conditions correspond to severe weather.

The wave vector plots showing the wave height distribution for incident wave direction SSE in the vicinity of the site of development including the mouth of the inlet, channel, sand pits and at the jetty location is shown in Fig. 10.

The mouth opens in the east direction so there is a natural protection for the incident wave directions from SE to South. It is seen that the waves are unable to reach the site hence the site of development will be tranquil considering the tranquility limit of 0.3 m.

For the incident wave directions of East, ESE, SE and SSE the maximum wave height near the site is 0.15 m. The waves do not reach the site through the channel. Significant reduction in the wave heights in the sand pit region is observed for all the incident wave direction. Thus, the sediment will settle down in the sand pits. Though diffraction due to structures is not simulated in the MIKE21-SW, diffraction due to the side walls of the sand pits is considered, Diffraction is included using the phase-decoupled refraction-diffraction approximation proposed by Holthuijsen et al. (2003). The approximation is based on the mild-slope equation for refraction and diffraction, omitting phase information. It does therefore not permit coherent wave fields in the computational domain as in deterministic phase-resolving models such as Boussinesq type models.

The results indicate that at the jetty location the wave heights are less than 0.3 m which is the permissible wave tranquility limit. The proposed development will be safe from the wave tranquility point of view throughout the year. The inshore wave climate at the nearshore was obtained using these results.

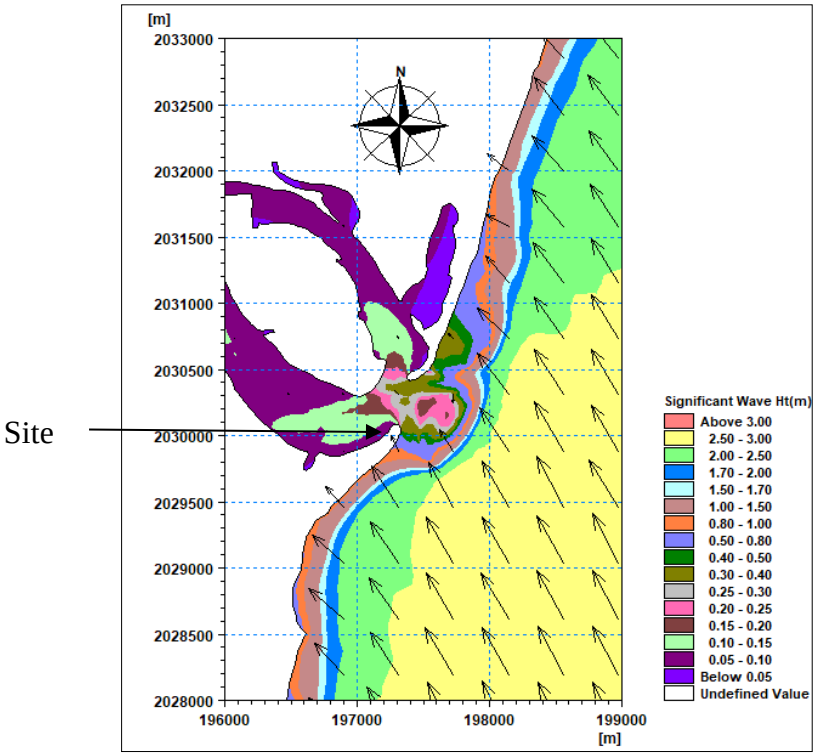



**Figure 10** Wave height and wave vector plot from SSE direction with incident wave height 3.5 m for proposed condition

## 7. Littoral Drift Studies

East coast of India is characterised by strong sediment movement along the shoreline. The rivers meeting the sea to form inlets bring sediments along with them. Hence in the inlets, sediment movement is observed. River Vamasdhara debouches in the inlet and the sea at Kalingapatnam. The Google images of the shoreline near Kalingapatnam are given below.

The image taken on 24/02/2013 shows that the mouth opening is at the northern part of the inlet. In 2015 the mouth has shifted southward. Then it seems that somewhere in early 2016 mouth opening towards east was created. The northward drift is clearly visible. This shows that there is considerable sand movement due to the sediment in the inlet and also due to the littoral drift northward.



**Figure 11** Google image of Kalingapatnam as on 24/02/2013, 15/03/2015 & 06/02/2016

The study of sediment movement along the shore is carried out by LITPACK model. A brief description of the capabilities of the model is as follows.

LITPACK software is used for computation of littoral drift and simulation of shoreline changes due to construction of the breakwaters or any development on the shoreline, or due to any break in the sediment movement such as in the case of inlet. LITPACK is a professional engineering software package for the modelling of non-cohesive sediment transport in waves and currents, littoral drift, coastline evolution and profile development along quasi-uniform beach.

The LITDRIFT module simulates the cross-shore distribution of wave height, setup and longshore current for an arbitrary coastal profile. It provides a detailed deterministic description of the cross-shore distribution of the longshore sediment transport for an arbitrary bathymetry for both regular and irregular sea states. The longshore and cross-shore momentum balance equation is solved to give the cross-shore distribution of longshore current and setup. Wave decay due to breaking is modelled, either by an empirical wave decay formula or by a model of Battjes and Janssen. LITDRIFT calculates the net/gross littoral transport over a specific design period. Important factors, such as linking of the water level and the beach profile to the incident sea state, are included.

The littoral drift along the Kalingapatnam coast is estimated using LITPACK software. There is a change in the shoreline orientation as seen from Fig. 12. To incorporate the changes, profile at location South 0 was considered. This profile is taken normal to the shoreline orientation. Littoral drift depends on the shoreline orientation and the near shore depth contours. Thus, the quantity of the drift changes with the orientation, and cross shore bathymetry. The wave climates are prepared by extracting wave parameters at the point just south of the inlet on the profile South 0 (197190 E, 2029300 N, -6.38 m depth).

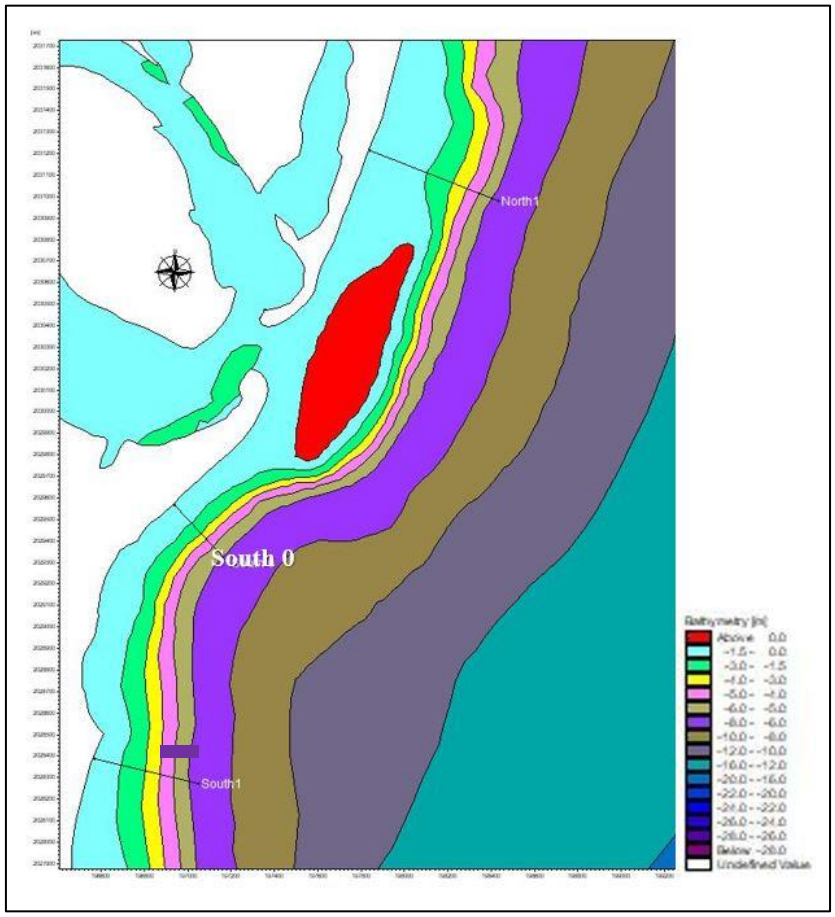



**Figure 12** Bathymetry near shoreline showing the profiles

### *7.1 Littoral drift at South 0 location*

LITDRIFT module of LITPACK software was used to estimate annual littoral drift rates and its distribution on the profile normal to the shoreline i.e. $130^0$ N. The profile covers a distance of 1050 m extending up to about -8.6 m depth contour. The profile was discretized with grid size of 5 m.

The ratio of wave height at the nearshore point (-6.13 m) to the incident wave height and inshore wave directions as shown in Table 4 are obtained from the wave transformation studies. The annual wave climate table and the rose diagram are presented in the Table 5 and Fig. 13.

**Table 4** Transformation from deep to shallow coastal water for South 0

| Sr. No. | Offshore Direction (Deg. N) | Inshore Direction (Deg. N) | Wave Height Ratio (Hi /Ho) |
|---|---|---|---|
| 1 | 67.5 | 109.427 | 0.809793 |
| 2 | 90 | 116.575 | 0.759964 |
| 3 | 112.5 | 130.252 | 0.818844 |
| 4 | 135 | 142.569 | 0.672714 |
| 5 | 157.5 | 147.824 | 0.54122 |
| 6 | 180 | 148.922 | 0.39498 |
| 7 | 202.5 | 147.272 | 0.310251 |
| 8 | 225 | 109.427 | 0.809793 |

**Table 5** Percentage occurrence of wave height & direction in Kalingapatnam for entire year South 0 (Jan-Dec)

| Wave Ht (m) | <0.5 | <1 | <1.5 | <2 | <2.5 | <3 | <3.5 | <4 | <4.5 | Total |
|---|---|---|---|---|---|---|---|---|---|---|
| Direction ($^o$N) | | | | | | | | | Calm | 8.7% |
| 112.5 | 0 | 1.1 | 1.3 | 0.4 | 0.1 | 0 | 0 | 0 | 0 | 2.9 |
| 135 | 0.6 | 4.4 | 4.2 | 0.2 | 0.1 | 0 | 0 | 0 | 0 | 9.5 |
| 157.5 | 1.8 | 48.3 | 26.5 | 2.2 | 0.1 | 0 | 0 | 0 | 0 | 78.9 |
| Total | 2.4 | 53.8 | 32 | 2.8 | 0.3 | 0 | 0 | 0 | 0 | 100 |

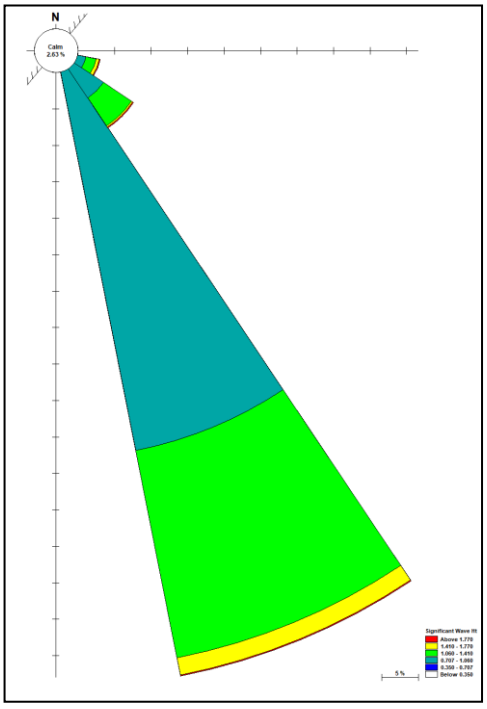



**Figure 13** Inshore wave rose diagrams at South 0

The model was run for annual period. Northward and southward, transport rates were computed and are shown in Fig. 14. The northward drift is plotted as negative while southward drift is plotted as positive. The northward, southward, net and gross transport rates are given in Table 6. Net transport in a year is of the order of 0.48 million cum and is towards north and gross transport is of the order of 0.52 million cum. The major sediment transport occurs in southwest monsoon. The maximum transport occurs at about 85 m from the low water level, at around 1.1 m depth contour. The net movement of sediment is moderate and towards north. This Northward movement of sediment will reach the inlet and hence will contribute in the formation of the sand bar which is seen in the Google images.

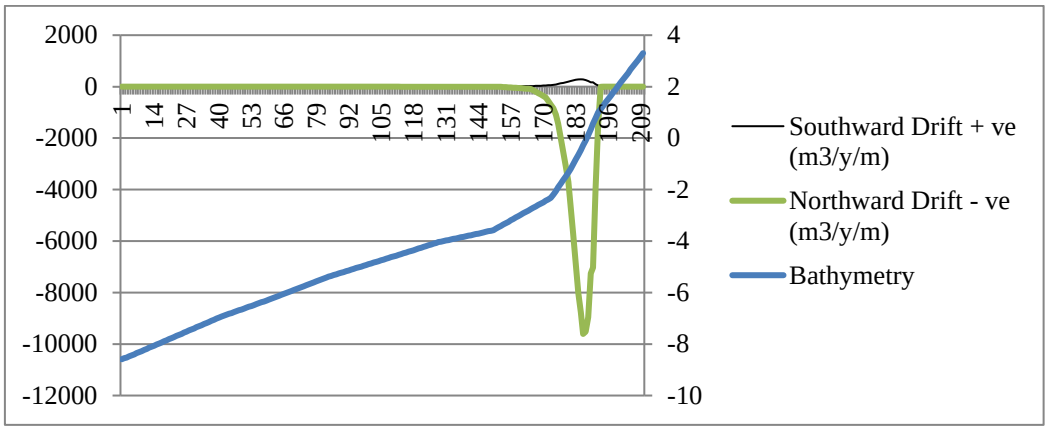



**Figure 14** Annual northern & southern littoral drift for entire year (South 0)

**Table 6** Littoral transport rates (million $m^3$/year) for South 0

| Season | Northward | Southward | Net * | Gross |
|---|---|---|---|---|
| Annual | 0.5 | 0.02 | -0.4812 | 0.52 |

Note*: For the Net Drift '-ve' Northward '+ve' Southward

## 8. Conclusions

1. The IMD data for 30 years between 15 to 20 degrees latitude and 80 to 85 degrees longitude was analysed to get offshore wave climate. The predominant directions are SSW, South and SSE with percentage occurrence of 8.51, 63.59 and 8.64. Maximum wave heights up to 4.0 m occur.

2. The Wave transformation studies with existing layouts were carried out with incident wave directions of ESE, EAST, SE, SSE and South with incident wave height 1.5 m, 2.5 m, 2.5 m, 3.5 m and 3.5 m respectively. It may be noted that 98 percent of the wave heights will be less than the selected wave heights. The results show that the jetty and development area is tranquil with respect to wave disturbance considering the permissible limit of 0.3 m.

3. The wave transformation studies with proposed layout was carried out for East, ESE, SE and SSE incident wave direction with bathymetry. The solid structure is not required for achieving wave tranquility at the jetty. Hence the studies with MIKE21-SW are sufficient to assess wave condition in the channel and the site. Though the waves approach inside through the channel but at the jetty location the wave heights are less than 0.3 m. Thus, the area of jetty will be tranquil throughout the year. Considering wave tranquility aspects, it is recommended that the harbour may be developed.

4. The orientation of the shoreline in the vicinity shows considerable variation. To study littoral drift, South 0 profile with the angles of the normal to the coast is considered. The LITPACK model was run for annual period. Annual northward and southward, transport rates were computed for this profile. The major sediment transport occurs in the southwest monsoon, contribution in the rest of the duration is less.

5. For the profile just South of the inlet at the head land, South 0, Net transport in a year is of the order of 0.48 million cum and is towards north and gross transport is of the order of 0.52 million cum. The major sediment transport occurs in southwest monsoon. The maximum transport occurs at about 85 m from the low water level, at around 1.1 m depth contour. The net movement of sediment is moderate and towards North. This Northward movement of sediment will reach the inlet and hence will contribute in the formation of the sand bar.

6. The channel is oriented in the east direction. The percentage of wave's incident from east is negligible. The flushing due to the waves will be minimal.

7. The sand pits will be able to arrest the littoral drift significantly. Hence, the layout with the sand pits as proposed is more suitable for the development from littoral movement considerations and wave tranquility as well.

## Acknowledgement

The authors wish to thank Shri A. K. Agrawal, Director, CW&PRS for his consistent support, encouragement and kind consent for publishing this paper. The authors acknowledge the guidance of Dr. J. D. Agrawal, Scientist – E, CW&PRS during the study.

## References

CWPRS Technical report no. 5639 (2018). Mathematical model studies for hydrodynamics and siltation for development of jetty at Kalingapatnam for APTDC.
Detailed project report (2016) for a passenger jetty at Kalingapatnam, Monarch surveyors and engineering consultants pvt. ltd.
Leo Holthuijsen, Agnieszka Herman, N. Booij (2003). Phase-decoupled refraction-diffraction for spectral wave models. *Coastal Engineering 49(4):291-305*.

*IN PROCEEDINGS OF 25th HYDRO 2020, INTERNATIONAL CONFERENCE, NATIONAL INSTITUTE OF TECHNOLOGY ROURKELA, ODISHA, INDIA 26-28, March 2021, ISBN 978-93-90631-56-8*

Paper ID - 177

# Wave Hindcasting and Storm Surge Analysis at Porbandar, Gujarat

Santosh Kori [1], Dr Prabhat Chandra [2]

[1] *Assistant Research Officer, CWPRS, Khadakwasla Pune, India -411024*
[2] *Scientist 'E', CWPRS, Khadakwasla Pune, India -411024*
*Email: kori.sk@cwprs.gov.in*

## Abstract

Storm surge can cause colossal damage to life, property and coastal infrastructure. Stability of coastal infrastructure depends on structural design that should withstand extreme wave conditions without significant damage. Determination of design wave height should be based on the statistical analysis of long-term extreme wave height measurements. Since the long-term measurements of extreme wave heights which occur during the storm conditions are not often available, the extreme value analysis is carried out using hindcast storm wave data for estimating the design wave conditions. This paper describes the numerical model studies carried out for estimation of extreme wave, surge and water level conditions during the cyclonic climate at the coast of Porbandar. Information of past 60 years of cyclones (1959-2019) was collected from the Indian Metrological Department and used for present wave hindcasting studies. A 100-year return-period wave height of 7.87 m was predicted at the Porbandar, from extreme value analysis of hindcast storm wave data. The storm surge analysis revealed that storm surge of 2.14 m may occur for return period of 1 in 100 years for Porbandar. The Water level data fitted in distribution functions to predict its value for different return period reveal that the water level of 6.05 m may occur for return period of 1 in 100 years for Porbandar.

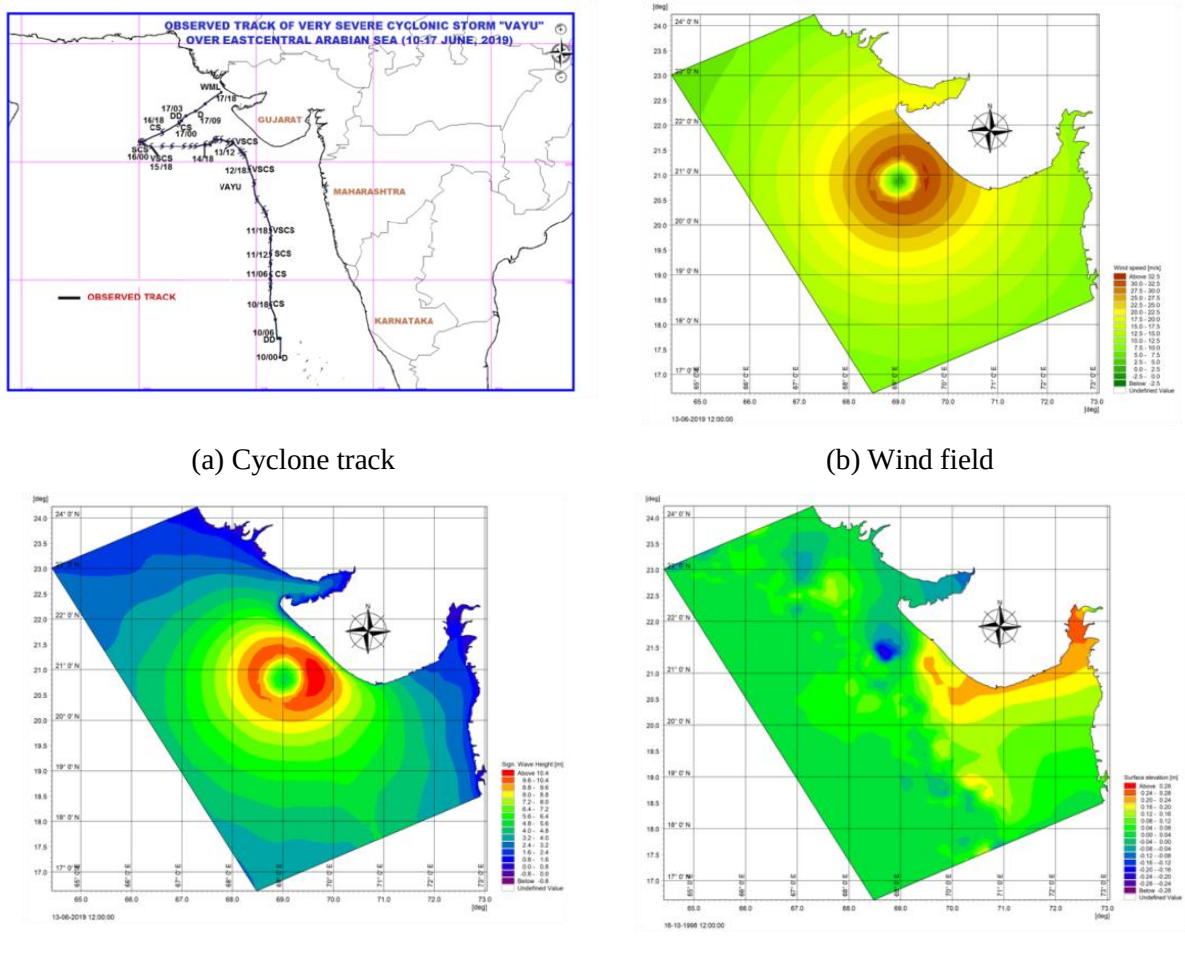
***Keywords:*** *Hindcasting; Storm; Extreme Value Analysis*

## 1. Introduction

Storm surge is the temporary rise in the water level at the coastline during the cyclone. Gujarat is one of the regions in India which is affected by storm surges associated with tropical cyclones. Porbandar is situated on the West Coast of Saurashtra facing the Arabian Sea at 21.63° North Latitude and 69.6° East Longitude. Porbandar was the seat of the eponymous princely state in British India. At present, it has an all-weather port with direct berthing facilities. The design wave height for any marine structure is the extreme wave height that a structure should withstand without significant damage. The determination of design wave height is site specific and depends on extreme wave climate at the site, life of the structure, risk, cost etc. Ideally, the determination of design wave height should be based on the statistical analysis of long-term extreme wave height measurements. There are various sources of wave data such as visually observed data, instrumentally recorded data and hindcast storm wave data. Since the long-term measurements of extreme wave heights which occur during the storm conditions are seldom available, the extreme value analysis is carried out using hindcast storm wave data for estimating the design wave conditions. This paper describes the numerical model studies carried out for estimation of extreme wave, surge and water level conditions during the cyclonic climate at the coast of Porbandar. The cyclone tracks along with information about its center location, Central Pressure, Maximum Wind speed and intensity were collected for the period 1959- 2019 from the IMD Daily Weather Reports, Synoptic Charts, e-cyclone atlas and cyclone bulletins for cyclones occurred in and around the Gujarat Coast. Wind field is generated by making use of the MIKE tools from the available details of cyclone track and pressure field from the IMD cyclone bulletins. Varying wind fields during the time domain of cyclone are computed with the help of Young and Sobey parametric model available in Mike tools. Generated wind fields were given as input to coupled flow model of MIKE 21 to obtain cyclonic wave and surface elevations. Extreme value analysis was carried out using EVA tool of MIKE 21.

## 2. Hindcasting of Strom Wave Data

Estimation of waves generated by the storms in the past is called Wave Hindcasting. Wave hindcasting is generally used to obtain storm wave data for extreme value analysis. Measured data is often not available during periods long enough to allow for the establishment of sufficient accurate estimation of extreme sea states. Wind and pressure data generated by a tropical cyclone can often be described by simple parametric models based on few parameters like position of the cyclone's eye, radius of the maximum winds, etc. The MIKE 21 FM coupled model developed by DHI, was used to simulate the cyclone generated waves and surges. The fully spectral formulation, which can simulate waves generated by complex wind fields during storms, was used for the wave hindcast study. Twenty five (25) cyclone tracks (period 1959 to 2019) were simulated. Figure 1, shows cyclone track, wind field, significant wave height and surface elevations for 2019 cyclone (Vayu).




(a) Cyclone track (b) Wind field

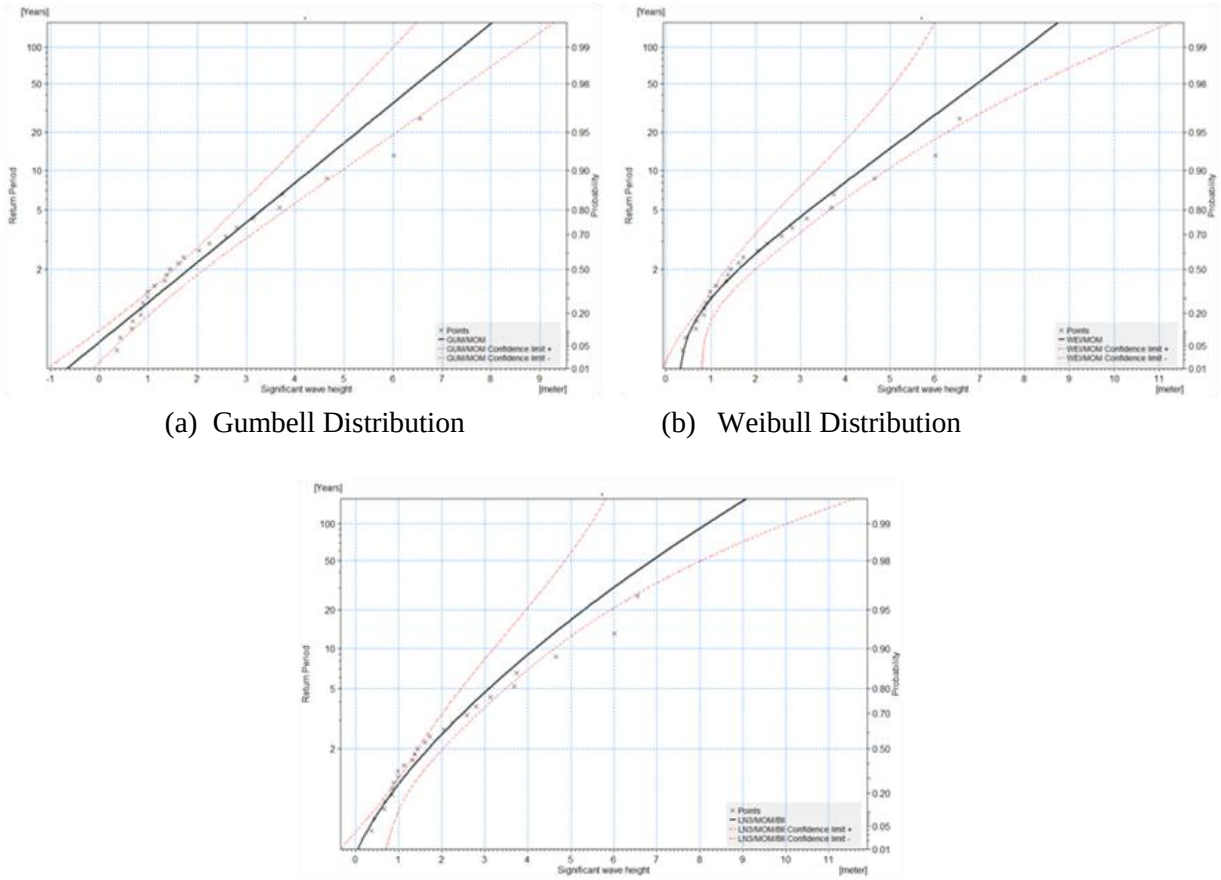
(c) Significant Wave Height (d) Surface Elevations

**Figure 1 :** Cyclone of June 2019

### 2.1 *Extreme Value Analysis of Strom Wave Data*

The return period is basic parameter in extreme value analysis, wherein for a specified return period, the wave height is predicted such that it is expected to occur once on the average during time span of return period. The statistical analysis for determination of various return period wave heights from the data set involves (Burcharth and Liu, 1994) hindcasting of storms data. The hindcasted wave data of storms for Porbandar were considered for extreme wave analysis. These data for a period of 60 years (1959-2019), represent the storm waves and were fitted to Gumbel, Weibull and Log-Normal distributions. MIKE 21 EVA was used for analysis. The plots of Gumbel, Weibull and Log-Normal

distributions are shown in Figure 2. Black line represents the best fit line and red lines show the confidence limits.




(a) Gumbell Distribution (b) Weibull Distribution

(c) Log-Normal Distribution

**Figure 2. :** Hindcast storm Wave data fitted to various distributions

Averages of each return period are shown in Table 1. The 100 - year return-period significant wave height off Porbandar in a water depth of (-) 10 m is predicted as 7.87 m.

**Table 1 :** Extreme Wave Heights on Porbandar Coast

| Return Period (Years) | Significant Wave Height (m) (-10 m) Water Depth |
|---|---|
| 10 | 4.27 |
| 25 | 5.63 |
| 50 | 6.80 |
| 100 | 7.87 |

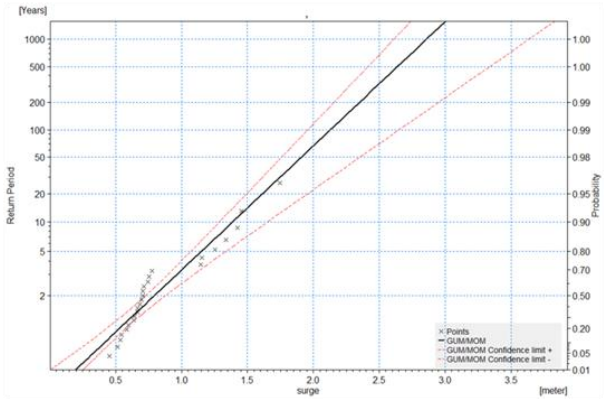
## 3. Strom Surge Hindcasting

Storm surge is the temporary rise in the water level at the coastline during the cyclone. This temporary rise in the water level takes place only when the cyclonic wind blows over the continental shelf and pushes the water against the coastline. Rise in the normal water level due to storm is called as “storm surge”. The storm surge at or near the shoreline is due to two main components viz. (a) inverted barometric pressure effect and (b) onshore wind stress effect. The values of the storm surge

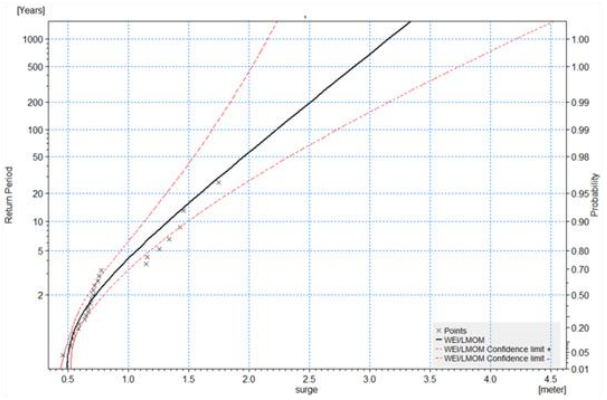
due to inverted barometric effect and due to wind stress were computed for all the storms. Total storm surge was computed by adding these two components.

### 3.1 *Extreme Value Analysis of Strom Surge Data*

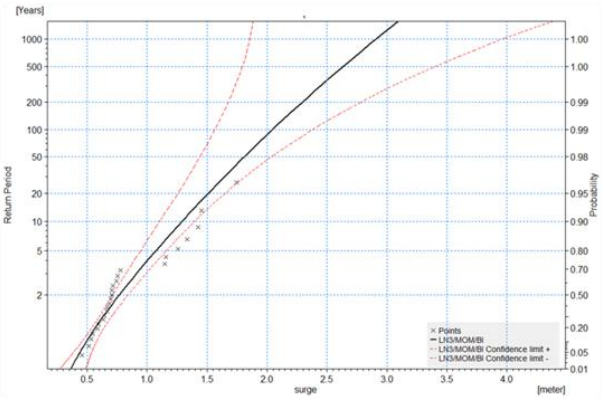
The storm surge data of 25 storms were considered for extreme value analysis. These data represent the actual storms over a period of 60 years (1959 to 2019) and were fitted to Gumbel, Weibull and Log-Normal distributions. The plots of Gumbel, Weibull and Log-Normal distributions for the storm surge at Porbandar are shown in Figure 3.




(a) Gumbell Distribution




(b) Weibull Distribution




(c) Log-Normal Distribution

**Figure 3. :** Hindcast storm surge data fitted to various distributions

Averages of these three values for each return period are shown in Table 2. The 100 - year return-period Strom Surge for Porbandar is predicted as 2.14 m.

**Table 2 :** Extreme Strom Surge at Porbandar

| Return Period (Years) | Strom Surge (m) |
|---|---|
| 10 | 1.34 |
| 25 | 1.63 |
| 50 | 1.85 |
| 100 | 2.14 |

## 4. Design Water Level

The design water level is the combination of tidal and non-tidal (Meteorological disturbances) components. Non-tidal components contributing to water level constitute of storm surge, sea level rise by climate change and other meteorological disturbances. Mean sea level, on a global scale, has been increasing over the past century, approximately 1.8 mm/yr due to the thermal expansion of the oceans and glacial melting. IPCC (2007) project an increase in mean sea level of between 0.18 and 0.59 m by the end of the 21st century, with the possibility of an additional 0.1 to 0.2 m due to ice sheet flow. Design water level for various return periods at Porbandar is given in Table 3.

**Table 3 :** Design water level for various return periods at Porbandar

| Return Period (Years) | Tide(m) | Strom Surge (m) | Climate Change (m) | Design Water Level(m) |
|---|---|---|---|---|
| 10 | 2.91 | 1.34 | 0.10 | 4.35 |
| 25 | 2.91 | 1.63 | 0.25 | 4.79 |
| 50 | 2.91 | 1.85 | 0.50 | 5.26 |
| 100 | 2.91 | 2.14 | 1.00 | 6.05 |

## 5. CONCLUSIONS

Based on studies carried out for wave hindcasting and storm surge analysis at Porbandar, the main conclusions are as below:

1. The storm Wave data fitted in distribution functions to predict its value for different return period reveal that significant storm wave of 7.87 m may occur for return period of 1 in 100 years for Porbandar at - 10 m depth
2. The storm surge data fitted in distribution functions to predict its value for different return period reveal that storm surge of 2.14 m may occur for return period of 1 in 100 years for Porbandar.
3. The Water level data fitted in distribution functions to predict its value for different return period reveal that Water level of 6.05 m may occur for return period of 1 in 100 years for Porbandar.

## Acknowledgements

Authors are grateful to Shri A. K. Agrawal, Director, Central Water and Power Research Station for his continuous encouragement and motivation during the course of studies and for granting permission to publish this paper.

## References

Burcharth, H. F., & Zhou Liu (1994), “On the Extreme Wave Height Analysis.” Hydro-port'94 (1994): 123–142
IPCC (2007), “Climate Change 2007, Impacts, Adaptation and Vulnerability”, Fourth Assessment Report of the Intergovernmental Panel on Climate Change.

*IN PROCEEDINGS OF 25th HYDRO 2020, INTERNATIONAL CONFERENCE,*
*NATIONAL INSTITUTE OF TECHNOLOGY ROURKELA, ODISHA, INDIA*
*26-28, March 2021, ISBN 978-93-90631-56-8*

Paper ID - 178

# IMPORTANCE OF OPTIMIZATION OF OVER LAPPING OF BREAKWATER AT FISHING HARBOUR ENTRANCE

R.K.Chaudhari[1], S.K. Kori[2], Dr. Prabhat Chandra[3]

[1]*Scientist 'B', CWPRS, Khadakwasla Pune,India -411024*
[2] *ARO, CWPRS,Khadakwasla Pune,India -411024*
[3] *Scientist 'E', CWPRS,Khadakwasla Pune,India -411024*
***Email:*** *rajeev_cwprs@yahoo.co.in*

## Abstract

Adequate wave tranquility at the berthing area and at entrance is an essential requirement for development of a fishing harbour. The wave disturbances at entrance and inside the harbour should be in limit which may further necessitate the need for construction of breakwaters. The overlapping of the breakwaters at the entrance of fishing harbour is to be designed suitably for safe navigation and maneurving of fishing vessels near the entrance. In the present paper, mathematical model studies for wave tranquility for development of a fishing harbour at Chethy in Alappuzha district of Kerala have been described. The proposed layout consisted of north and south breakwaters of the respectively of lengths 661m and 847m with entrance width of 150m. In order to reduce the wave height at the entrance and at the berth, the various alternatives for extension of south breakwater were studied using MIKE 21 BW. It is seen that with optimum 100m extension in the length of south breakwater, enough shelter area near the entrance for safe navigation of the fishing boats to the harbour is available and the significant wave height at operating berth is also reduced with total downtime from 35 days to about 9 days during the monsoon season.

***Keywords:*** *Fishing harbour, Wave Tranquility, Numerical model, Shoaling, Refraction*

## 1. Introduction

To overcome the growing needs of fisheries industry, all weather fishing harbours are required in the coastal states. In coastal state Kerala, fishing industry plays a very important role in the economy of the state. The Harbour Engineering Department (HED) Kerala has a proposal to develop a fishing harbour at Chethy in Alappuzha district of Kerala (Figure1). The proposed layout consisted of north and south breakwaters of the lengths of 661m and 847m respectively with entrance width of 150m (Figure2). Understanding nearshore waves is indispensable for the proper design and construction of coastal infrastructures. Waves attack coastal structure and infiltrate harbor entrance, generating disturbance in the sheltered waters. Hence, it is necessary to know beforehand the magnitude and direction of propagating waves to design the optimal layout of fishing harbor. The wave tranquility at the proposed harbour was assessed through the mathematical models. For the present studies, the transformation of wave height and wave direction from deep water to near shore at (-) 7m depth was done using spectral wave model MIKE 21-SW. The results indicated that the predominant directions at nearshore are from $220^0$ N to $300^0$ N with significant wave heights of upto 3.5m. Further, the wave propagation studies carried out using MIKE21- Boussinesq wave model. This model was used for the prediction of the wave field due to combined refraction diffraction of directional random waves in a harbor. Studies with the wave tranquility for proposed layout indicated that the wave height at berth would be higher than the permissible limit of 0.3m for almost 35 days in a year and the maximum significant wave disturbance at the entrance would be upto 1.5m. In order to reduce the wave height at the entrance and at the berth, the various alternatives for extension of south breakwater were studied using MIKE 21 BW and an optimum breakwater extension was evolved. The siltation pattern at the site was also taken into consideration while finalizing the layout. Littoral drift studies were also conducted and the suitability of the entrance was considered keeping in view this aspect too.
In this present paper, the details of the mathematical model studies for evolving a modified layout of fishing harbour at Chethy, Kerala have been described.

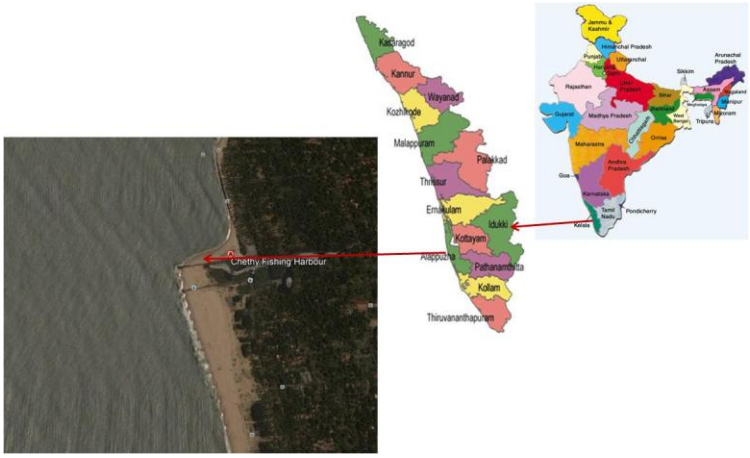



Figure1: Location of proposed Chethy Fishing harbour

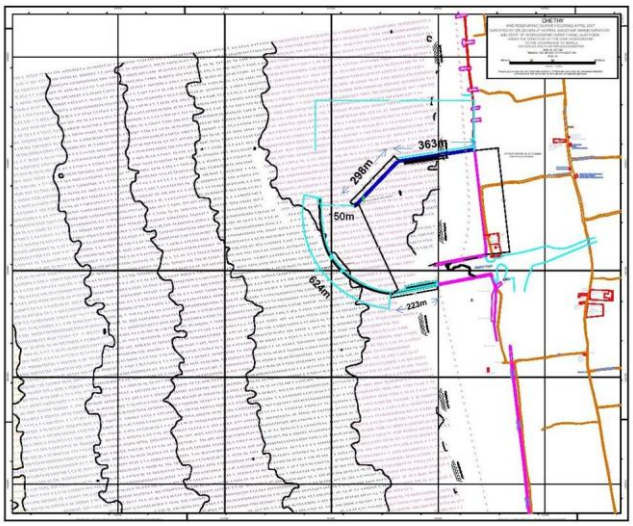



Figure2 : Proposed Layout of the Chethy Fishing Harbour

## 2. SITE CONDITIONS

Chethy fishing harbor is situated at $9^0$ 37' N longitude $76^0$ 17' E latitude in Alappuzha district in Kerala State at 40 km south of Kochi. A pair of training walls of length 280m upto about 1.5 to 2.0m depth in the year 2009 was constructed at the river mouth at Chethy to keep it open throughout the year. However, it was observed that the creek mostly remained closed due to the prevailing littoral drift except for July when the sufficient river discharges occur (Figure1). The tidal range at the Chethy is about 1m is considered for the studies. Wave is the single most important parameter which influences the layout of this harbour. In absence of measured wave data, the offshore wave data of 14 years from year 2001 to 2014 off Chethy fishing harbour, compiled by India Meteorological (IMD) as observed from ships plying in deep waters, were analyzed. This wave data information was considered at the offshore end of the model limits. The frequency distribution of wave heights for entire year for the above offshore wave data is presented in form of wave rose diagram in Figure 3. It could be seen from diagram that the predominant wave directions in deep water are from $230^0$N to $320^0$N with the maximum wave heights of 5 m. These deep water wave data were transformed using the mathematical model MIKE 21- SW to get the near-shore wave climate near the harbour entrance.

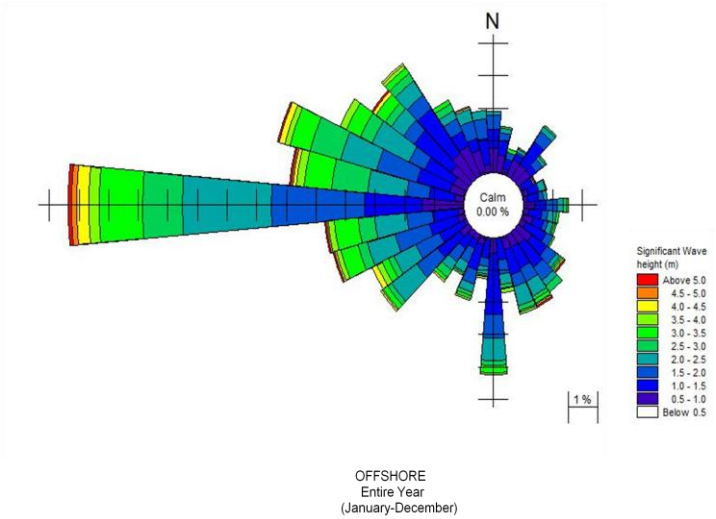



Figure3: Offshore Wave Rose Diagram for Entire Year

## 3. NUMERICAL MODELLING TECHNIQUES

For the evolving the optimized fishing harbour, mathematical models like MIKE 21 – SW, MIKE – 21 BW are used. These studies were mainly carried out in two following stages:

1. Transformation of wave height and wave direction from deep water to (-) 7m depth using MIKE 21-SW model.
2. Simulation of wave propagation in the harbour to obtain wave height distribution in the harbour to evolve suitable layout for safe operations of fishing boats, using MIKE21- BW model.

### *3.1 Transformation of wave height and wave direction from deep water to (-) 7m depth*

As waves propagate toward shore, a combination of shoaling, refraction, reflection, diffraction, and breaking effects modify the waveform and the wave characteristics will be very different from those in deep water. To get the wave conditions from offshore to nearshore at (-) 7m depth, the numerical model MIKE21-SW was used. This is a state-of-the-art third generation spectral wind wave model based on unstructured mesh. The model simulates the growth, decay and transformation of wind generated waves and swells in offshore and coastal areas. It takes into account refraction and shoaling of waves, which are important in the transformation of waves from offshore to inshore. It also includes physical phenomena of wave growth by action of wind, dissipation due to white-capping, dissipation due to bottom friction, and dissipation due to depth induced wave breaking. In the absence of measured wave data of at least one year near the proposed site of development, the nearshore wave climate at Chethy was obtained by transforming the ship observed deep water wave data using MIKE21-SW Model. Model area considered for MIKE 21-SW model is shown in Figure4. Bathymetry in the model region of about 85km X 170km area was descreitized using unstructured mesh. The model was run to obtain nearshore wave climate at the Inshore Point in (-) 7m depth contour. The wave directions and ratio of wave heights at (-) 7m depth to deep water wave height, with different directions of wave incidence at the offshore boundary are obtained. After applying the ratio to of deep water wave height and direction as shown in rose diagram (Figure 3) the frequency distribution of waves in (-) 7 m depth were obtained shown in table 1 and corresponding rose diagram (Figure 5).

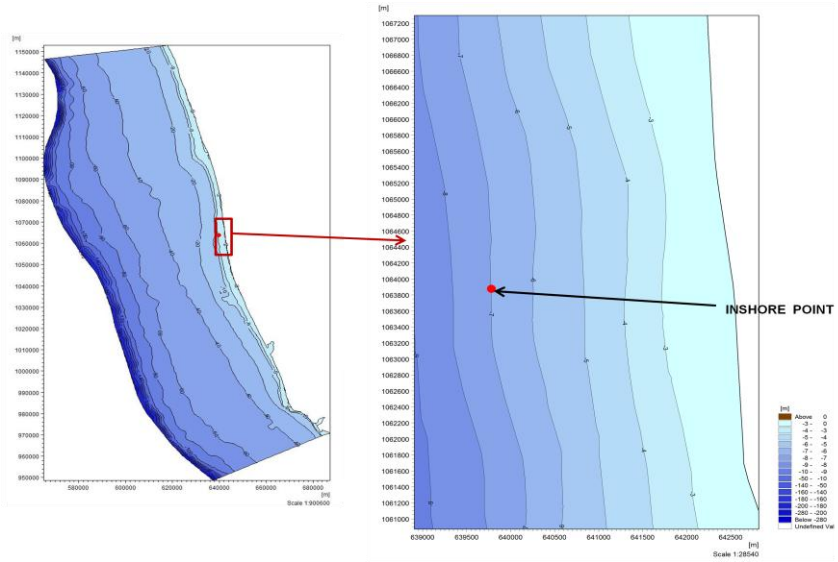



**Figure 4**: **Bathymetry for Wave Transformation from Offshore to Nearshore**

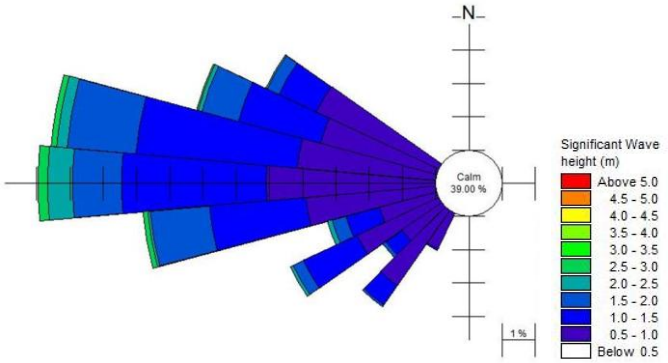



**Figure 5: Rose diagram at (-)7m depth (Year)**

**Table 1: Percentage Occurrence of Wave Height & Direction at Chethy in -7m Depth for Entire Period (Jan-Dec)**

| **Wave height (m)** | **0.5-1** | **1-1.5** | **1.5-2** | **2-2.5** | **2.5-3** | **3-3.5** | **Total** |
|---|---|---|---|---|---|---|---|
| **DIRECTION (deg N)** | | | | | | Calm% | **39.98** |
| **220** | 1.96 | 0.22 | 0 | 0 | 0 | 0 | **2.17** |
| **230** | 3.15 | 0.92 | 0.22 | 0 | 0 | 0 | **4.29** |
| **240** | 1.68 | 0.98 | 0.16 | 0.05 | 0 | 0 | **2.88** |
| **250** | 3.59 | 1.85 | 0.76 | 0.27 | 0.22 | 0 | **6.68** |
| **260** | 3.04 | 2.93 | 1.47 | 1.2 | 0.05 | 0.16 | **8.85** |
| **270** | 3.59 | 7.44 | 3.53 | 2.06 | 0.6 | 0.33 | **17.54** |
| **280** | 4.24 | 3.04 | 2.34 | 0.38 | 0.22 | 0.05 | **10.27** |
| **290** | 3.69 | 1.63 | 0.54 | 0.11 | 0.05 | 0 | **6.03** |
| **300** | 1.2 | 0.05 | 0.05 | 0 | 0 | 0 | **1.3** |
| | **26.13** | **19.07** | **9.07** | **4.07** | **1.14** | **0.54** | **100** |

On the basis of wave transformation studies, it is clear that waves are incident from $210^0$ N direction to $300^0$ N direction at -7m depth. Considering the layout of the breakwaters and opening of the proposed fishing harbour (Figure 2), there is adequate wave protection for the waves incident from the

directions between $210^0$ N to $260^0$ N. The predominant critical wave incident conditions lie in the quadrant $270^0$ to $300^0$ N quadrant. The following input wave conditions as shown in Table 2 were considered for simulation of wave propagation in the proposed harbour using MIKE 21-BW model at (-) 7m depth.

Table 2: Input Wave condition for MIKE 21 –BW Model

| Wave Direction (deg. N) | Peak Wave period Tp(sec) | Significant Wave Height (m) |
|---|---|---|
| 270 | 10 | 2.5 |
| 280 | 10 | 2.5 |
| 290 | 10 | 2.5 |
| 300 | 10 | 2 |

### *3.2 Model Simulations for wave propagation in the harbour:*

The permissible wave disturbance at the berthing place depends on the ship size, mooring and berthing system. A permissible limit of 0.3 m for wave heights in the habour is considered for this proposed development of fishing harbour keeping in view the size of fishing boats. The MIKE 21 BW simulations were carried out for layout proposed by HED Kerala and then to get improved tranquility the layout was optimized and again assessed wave tranquility through MIKE21 –BW. The Numerical model MIKE21-BW was used for studying the wave disturbances in the harbour. This model is based on time dependant Boussinesq equations of conservation of mass and momentum obtained by integrating the three-dimensional flow equations without neglecting vertical acceleration. They operate in the time domain, so that irregular waves can be simulated. These equations include nonlinearity as well as frequency dispersion. The frequency dispersion is included in the flow equations by taking into account the effect of vertical acceleration or the curvature of stream lines on pressure distribution. The model simulates the processes of shoaling, refraction, diffraction from breakwater tips and bed friction. It also takes into account partial reflections from the boundaries, piers and breakwaters (DHI-2005).

### *3.2.1 Boussinesq wave simulation for proposed by HED:*

The experiments were conducted to examine wave propagation in the harbour for layout proposed by the HED Kerala. This layout consisted of two breakwaters; 661m long Northern breakwater and 847m long Southern Breakwater (Measured from the tip of existing southern breakwater) with 150m wide harbour entrance as shown in Figure 6.

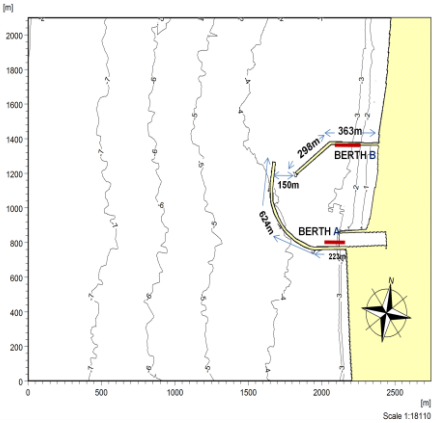



Figure6: Bathymetry of Proposed harbour showing Location of Berths

The model was simulated for the four incident wave directions obtained in wave transformation studies table 2. The wave height distribution in the harbour for the four most critical conditions are shown in Figs. 7 to 10 respectively.

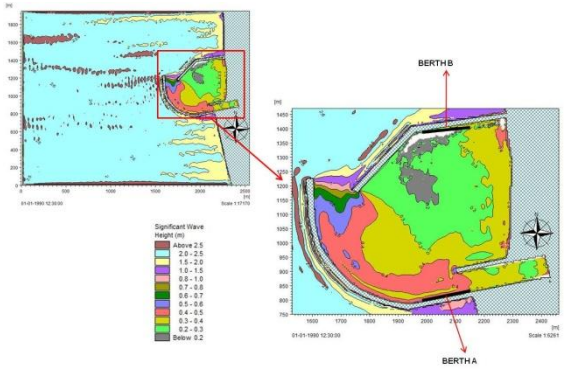



Figure 7: Wave Height Distribution Plot for Waves Incident from $270^0$ N Direction
(Incident Wave Height: 2.5m)

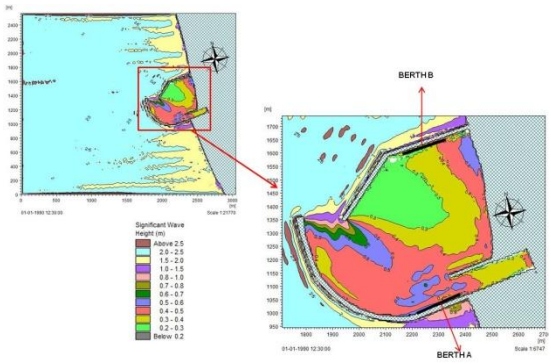



Figure 8: Wave Height Distribution Plot for Waves Incident from $280^0$ N Direction
(Incident Wave Height: 2.5m)

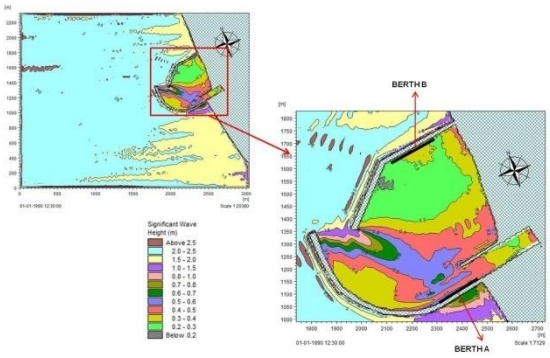



Figure9B: Wave Height Distribution Plot for Waves Incident from $290^0$ N Direction
(Incident Wave Height: 2.5m)

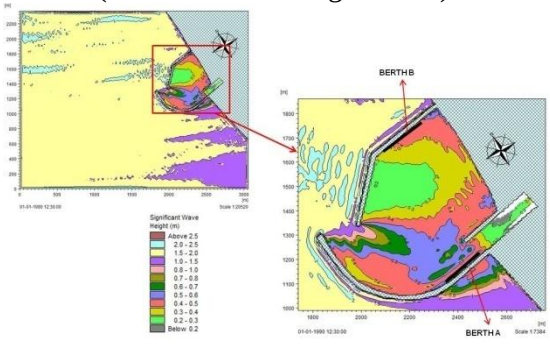



Figure10B: Wave Height Distribution Plot for Waves Incident from $300^0$ N Direction
(Incident Wave Height: 2.0m)

The permissible wave height in the harbour has been considered as 0.3 m for operations in the fisheries harbour. The average wave heights at berth A and Berth B and near the entrance are given in Table 3.

Table 3: Average Significant Wave Height in Proposed Chethy Fishing Harbour

| Incident Wave Direction/ Wave Height (m) | Average Wave Height Hs(m) | | |
|---|---|---|---|
| | At Berth A | At Berth B | Near Entrance |
| $270^0$N/2.5 | 0.5 | 0.3 | 1 |
| $280^0$N/2.5 | 0.5 | 0.3 | 1.5 |
| $290^0$N/2.5 | 0.5 | 0.3 | 1.5 |
| $300^0$N/2.0 | 0.5 | 0.4 | 1.5 |

It is seen from the simulations that at berth A, the significant wave height will be more then the permissible limits of 0.3m for almost 35 days in a year and this will generally occur during the monsoon season. The wave heights at berths B are generally in permissible limit of 0.30m except two to three days in the whole year. To achieve the desired tranquility for safe navigation of fishing boats a modified layout was evolved with optimum 100m extension in the south breakwater.

### *3.2.1 Boussinesq wave simulation for Modified layout(1oom extension in south breakwater):*

The MIKE21-BW simulations were conducted to examine wave propagation inside the harbour with extension in south breakwater by total 100m length as shown in Figure 11. The layout consists of two breakwaters; 661m long Northern breakwater and 947m long Southern Breakwater (Measured from the tip of existing southern breakwater) with 150m wide harbour entrance.

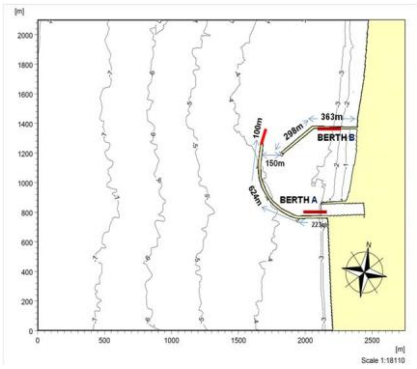



Figure11: Bathymetry of Proposed harbour showing Location of Berths with 100m extension in south breakwater

The wave height distribution in the harbour for the four predominant incident wave directions are shown in Figs. 12 to 15 respectively.

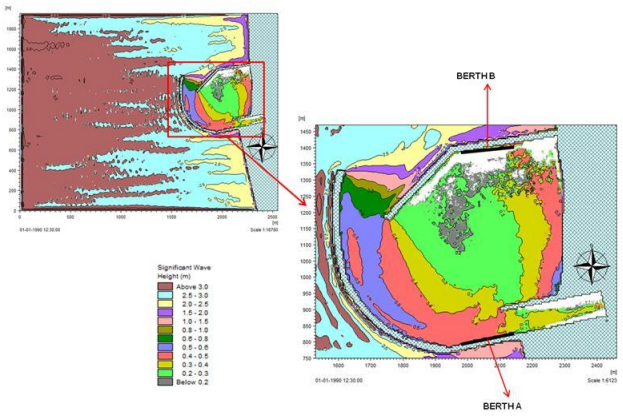



Figure 12: Wave Height Distribution Plot for Waves Incident from $270^0$ N Direction
(Incident Wave Height: 3.5m)

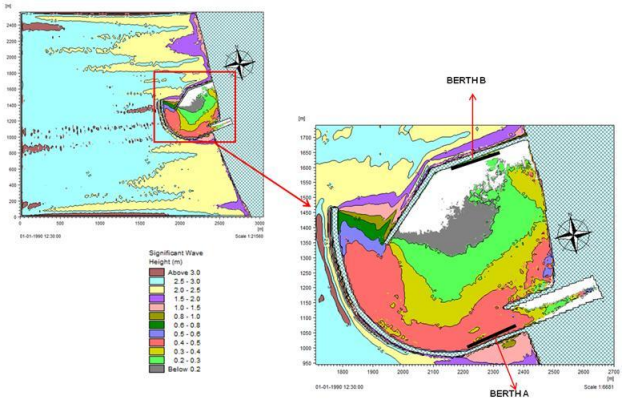



Figure 13: Wave Height Distribution Plot for Waves Incident from $280^0$ N Direction
(Incident Wave Height: 3.0m)

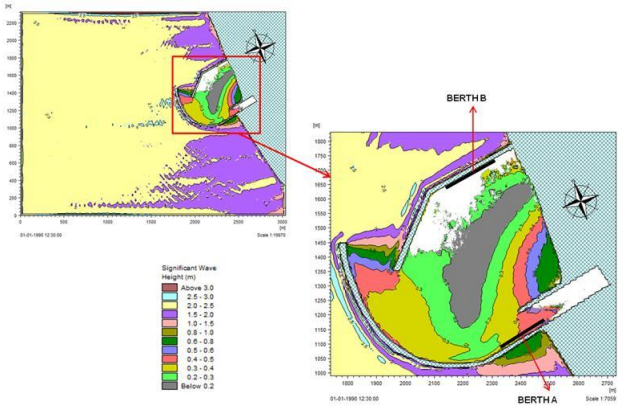



Figure14: Wave Height Distribution Plot for Waves Incident from $290^0$ N Direction
(Incident Wave Height: 2.5m)

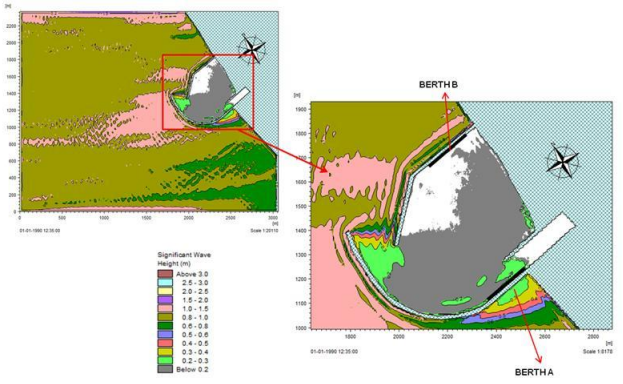



Figure 15: Wave Height Distribution Plot for Waves Incident from $300^0$ N Direction
(Incident Wave Height: 1.0m)

With modified layout simulations, it is observed that wave disturbance reduced to upto 0.7m near the entrance due to the extension of south breakwater by 100m and the downtime near berth A reduced to about 9 days. The comparisons of wave heights obtained from proposed and modified layout given in table 4.

Table 4: Significant Wave Height at Harbour Entrance of Chethy Fishing Harbour

| Incident Wave Direction/ Wave Height (m) | Range of Wave Height Hs(m) at Harbour Entrance | |
|---|---|---|
| | Harbour Layout proposed by HED | Modified Harbour Layout with 100m extension in South Breakwater |
| $270^0$N/3.5 | 0.9 to 1.0m | 0.6 to 0.7m |
| $280^0$N/3.0 | 1.0 to 1.5m | 0.5 to 0.6m |
| $290^0$N/2.5 | 1.0 to 1.5m | 0.5 to 0.6m |
| $300^0$N/1.0 | 1.0 to 1.5m | 0.4 to 0.5m |

It is seen from the fishing harbour layout that south breakwater overlapping at the mouth with extension of almost 100m length, will also provide enough shadow zone for the safety of fishing boats at time of entry to the fishing harbour. It is also seen that with 100m extension in the length of south breakwater, enough shelter area for safe navigation of the fishing boats to the harbour is available and the significant wave height at berth A is also considerably reduced with total downtime from 35 days to 09 days in a year during the monsoon season. It is clear that this modified layout will provide the shelter for fishing boats for entire year and safe navigation through the entrance.

## 4. CONCLUSIONS

The following conclusions derived from the present study are given as follow:

- Mathematical model studies for transformation of wave height and wave direction from deep water to (-) 7m depth using spectral wave model MIKE 21-SW indicated that predominant directions at (-) 7m depth are from $220^0$ N to $300^0$ N.
- Wave propagation studies carried out with MIKE21-BW model to assess the wave tranquility inside the fishing harbour indicated that, the proposed harbour layout (Figure2) is not adequate to provide proper shelter to the fishing boats at the mouth and also at berth A. The downtime would be about 35 days in a year at berth A and the maximum significant wave heights near the entrance would be more upto 1.5m.
- The modified layout with 100m extension in the south breakwater (Figure11) enables reduction in the wave heights near the entrance to upto 0.7m and downtime at berth A to about 9 days. This layout is recommended for development of fishing harbour.
- The area on the west of berth B on the proposed extension of North breakwater may also be considered for development of berth due to the availability of adequate wave tranquility throughout the year.

## ACKNOWLEDGEMENTS

Authors are grateful to Shri A.K. Agrawal, Director, Central Water and Power Research Station for her continuous encouragement and motivation during the course of studies and for granting permission to publish this paper.

## REFERENCES:

Danish Hydraulic Institute, 2005. MIKE 21 Boussinesq Wave Module, User Guide and Reference Manual.

*IN PROCEEDINGS OF 25th HYDRO 2020, INTERNATIONAL CONFERENCE, NATIONAL INSTITUTE OF TECHNOLOGY ROURKELA, ODISHA, INDIA 26-28, March 2021, ISBN 978-93-90631-56-8*

Paper ID - 179

# UTILIZATION OF NUMERICAL MODEL FOR SHORELINE CHANGES TO EVOLVE THE SUITABLE COASTAL PROTECTION WORK AT HOSABETTU, KARNATAKA

R.K.Chaudhari[1], S.K. Kori[2], Dr. Prabhat Chandra[3]

[1]*Scientist 'B', CWPRS, Khadakwasla Pune,India -411024*
[2] *ARO, CWPRS,Khadakwasla Pune,India -411024*
[3] *Scientist 'E', CWPRS,Khadakwasla Pune,India -411024*
***Email:*** *rajeev_cwprs@yahoo.co.in*

## Abstract

Coastline is dynamic morphological interface which responses to the external forces exerted by tides, waves and near shore currents. As a result, it causes movement of sediment along coastline and erosion or accretion may occur. Coastal erosion is also loss of land area due to action of waves, Currents, wind and gradual increase in the sea level due to global warming. This problem becomes much more serious when severe damages occur to the manmade structures viz. buildings and roads etc. in cities situated very near to coastal line. In order to protect the coastline to avoid this damage, suitable coastal protection measures are required. In this present paper, suitable coastal protection works have been suggested through the numerical modeling for shoreline changes. The site is situated in the open coast at Hosabettu, in Mangalore, Karnataka and subjected to high waves of upto 4.5 m associated with significant littoral drift. As a result, the severe erosion takes place in some of the stretches along the shoreline. Also, some important buildings have been totally demolished due to this severe erosion. In order to stabilize the shoreline near Hosabettu, suitable coastal protection measures were suggested through Numerical model LITPACK in the form of; sixteen groynes of length 50m and spacing 200m along the coastline or as an alternative, ten offshore breakwaters of 100m length each at 200m spacing. The suggested coastal protection works are expected to stabilize the eroding coast line at Hosabettu.

***Keywords:*** *Numerical model, Groyne, Offshore breakwater, Erosion , Accretion*

## 1. Introduction

India has very large coastline and the morphological changes near the shore region due to waves, tides and other environmental parameters cause changes in the coastline in form of erosion or accretion. In the present scenario, changes at coastline are also seen due to global warming and other natural calamities like storm and tsunami. It is observed that coastline at different places in India faces serious erosion. It is also noticed that the magnitude and nature of erosion change from place to place. However, in some places, temporary erosion takes place during the monsoon season and again built up of beach is restored during non monsoon season. Whereas, in some places, permanent erosion takes place and serious damages may occur to manmade monuments building roads etc. To mitigate this type of erosion, coastline is required to be protected as per the priority. Coastline near Hosabettu, Mangalore, Karnataka (Fig.1) faces serious erosion and some important buildings have been also demolished due to this. It is also seen from the recent Google images that a significant amount of erosion has taken place from previous year (Fig.2). In order to protect this vulnerable coast site from severe erosion, only hard measures such as groynes, seawall and offshore breakwater can be used. To evolve the suitable costal protection measures, the effect of these possible protections on the shore line can be assessed through numerical model. In the present study, the effect of putting a series of groynes and offshore breakwaters to save the coastline and for maintenance of beach, has been assessed through the Numerical Model LITPACK.

In the present paper, the details of the mathematical model studies using numerical model for evolving suitable coastal protection measures at Hosabettu, Mangalore, have been described.




**Fig.1 : Location Map of Hosabettu Site**




**Fig. 2 : Google Image showing the distoration in shoreline from last one year**

## 2. SITE CONDITIONS

Hosabettu site is situated at about 1.5 km north of New Mangalore Port at the latitude of 12.960021 degree and the longitude of 74.799665 degree as shown in Fig.1. The coastline at the site, consists of long, sandy beaches and is oriented in NNW-SSE direction. The nearshore bathymetry is steep with straight and parallel depth contours. The tidal range at Hosabettu is about 1.65m. Beaches at the site are having fine sand. The average value of $D_{50}$ (mm) from various sand samples is about 0.38mm and the same has been used for the model runs. Wave is a very important parameter which influences the littoral drifts that causes the erosion of coaslines. In absence of measured wave data, the offshore wave data of 14 years from year 2001 to 2014 off Hosabettu fishing harbour as observed by India Meteorological (IMD) from ships plying in deep waters, were analyzed. This wave data information was considered at the offshore end of the model limits. The frequency distribution of wave heights for

entire year for the above offshore wave data is presented in form of wave rose diagram in Figure 3. It could be seen that the predominant wave directions in deep water are from $220^0$ N to $360^0$ N with the maximum wave heights of 4.5 m. These deep water wave data were transformed using the mathematical model MIKE 21- SW to get the near-shore wave climate near the Hosabettu.

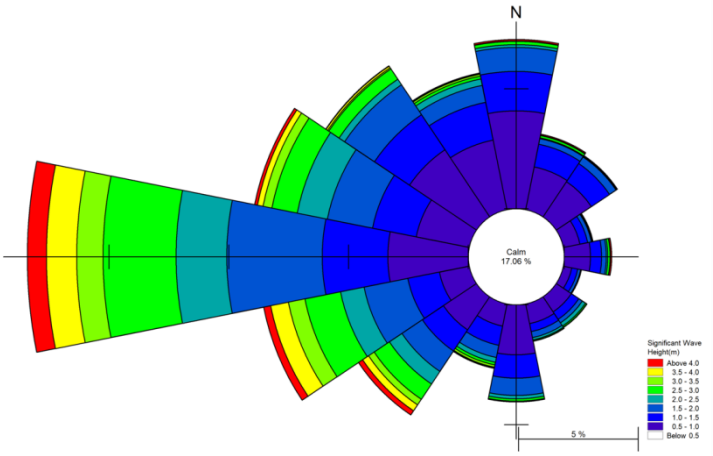



**Fig .3: Offshore Wave Rose Diagram for Entire Year**

## 3. NUMERICAL MODELLING TECHNIQUES

For evolving suitable coastal protection measures at Hosabettu, Mangalore, mathematical models like MIKE 21 – SW, LITPACK have been used. These studies were mainly carried out in two following stages:

1. Transformation of wave height and wave direction from deep water to (-) 10m depth using MIKE 21-SW model.
2. Estimation of Littoral drift distribution and simulation of shore line changes using LITPACK model.

### *3.1 Transformation of wave height and wave direction from deep water to (-) 10m depth*

As waves propagate toward shore, a combination of shoaling, refraction, reflection, diffraction, and breaking effects modify the waveform and the wave characteristics will be very different from those in deep water. To get the wave conditions from offshore to nearshore at (-) 10 m depth, the numerical model MIKE21-SW was used. This is a state-of-the-art third generation spectral wind wave model based on unstructured mesh. The model simulates the growth, decay and transformation of wind generated waves and swells in offshore and coastal areas. It takes into account refraction and shoaling of waves, which are important in the transformation of waves from offshore to inshore. It also includes physical phenomena of wave growth by action of wind, dissipation due to white-capping, dissipation due to bottom friction, and dissipation due to depth induced wave breaking. In the absence of measured wave data of at least one year near the proposed site of development, the nearshore wave climate at Hosabettu was obtained by transforming the ship observed deep water wave data using MIKE21-SW Model. Model area considered for MIKE 21-SW model is shown in Figure 4. Bathymetry in the model region of about 75 km X 60 km area was descreitized using unstructured mesh. The model was run to obtain nearshore wave climate at the Inshore Point in (-) 10 m depth contour. The wave directions and ratio of wave heights at (-) 10 m depth to deep water wave height, with different directions of wave incidence at the offshore boundary are obtained. After applying the ratio of deep water wave height and direction as shown in rose diagram (Figure 3), the frequency distribution of waves in (-) 10 m depth were obtained shown in Table 1 and corresponding rose diagram (Figure 5).

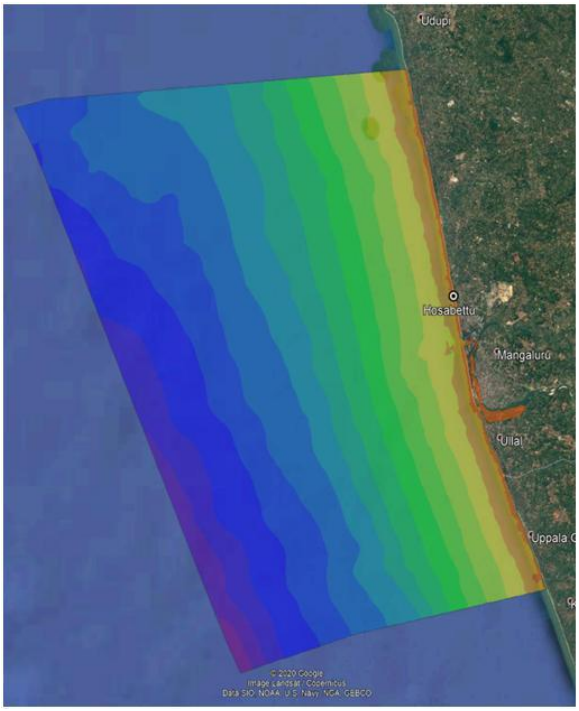



**Figure 4**: **Bathymetry for Wave Transformation from Offshore to Nearshore**

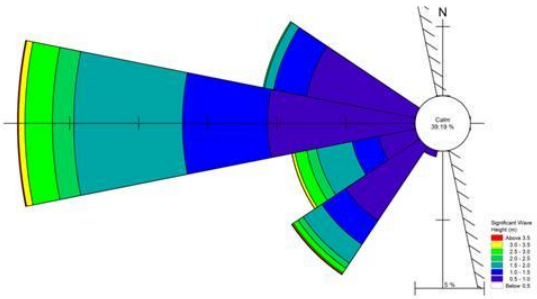



**Figure 5: Rose diagram at (-)10 m depth (Year)**

**Table 1: Percentage Occurrence of Wave Height & Direction at Hosabettu in (-)10 m Depth for Entire Period (Jan-Dec)**

| WAVE HEIGHT(m) | 0.-0.5 | 0.5-1 | 1-1.5 | 1.5-2 | 2-2.5 | 2.5-3 | 3-3.5 | 3.5-4 | Total |
|---|---|---|---|---|---|---|---|---|---|
| **DIRECTION (degN)** | | | | | | | | | |
| **202.5** | 4.97 | 0.44 | 0.02 | 0 | 0 | 0 | 0 | 0 | 5.43 |
| **225** | 4.74 | 6.46 | 2.07 | 1.63 | 0.44 | 0.42 | 0.08 | 0.06 | 15.9 |
| **247.5** | 0.61 | 2.74 | 1.94 | 2.63 | 0.73 | 0.88 | 0.21 | 0.02 | 9.76 |
| **270** | 2.13 | 10.68 | 6.17 | 7.86 | 1.55 | 1.99 | 0.46 | 0.08 | 30.91 |
| **292.5** | 22.3 | 8.07 | 2.42 | 0.67 | 0.1 | 0 | 0 | 0 | 33.56 |
| **315** | 4.43 | 0 | 0 | 0 | 0 | 0 | 0 | 0 | 4.43 |
| **Total** | 39.18 | 28.38 | 12.62 | 12.79 | 2.82 | 3.28 | 0.75 | 0.17 | 100 |

### *3.2 Estimation of Littoral drift distribution and simulation of shore line changes :*

Mathematical model studies for estimation of littoral drift distribution and simulation of shoreline changes were carried out using LITPACK model. LITPACK software was used for computation of littoral drift and simulation of shoreline changes due to construction of the breakwaters. LITPACK is a professional engineering software package for the modelling of non-cohesive sediment transport in waves and currents, littoral drift, coastline evolution and profile development along quasi-uniform beach (DHI 2014). The two modules of LITPACK i.e. LITDRIFT and LITLINE are used in the present study.

LITDRIFT module simulates the cross-shore distribution of wave height, setup and longshore current for an arbitrary coastal profile. It provides a detailed deterministic description of the cross-shore distribution of the longshore sediment transport for an arbitrary bathymetry for both regular and irregular sea states. The longshore and cross-shore momentum balance equation is solved to give the cross-shore distribution of longshore current and setup. Wave decay due to breaking is modelled, either by an empirical wave decay formula or by a model of Battjes and Janssen. LITDRIFT calculates the net/gross littoral transport over a specific design period. Important factors, such as linking of the water level and the beach profile to the incident sea state, are included. Wave climate is described in time series file in LITDRIFT. Each set of items in wave climate describe the characteristics of one wave incident and duration of wave incident is in percentage fraction of year. Thus, the total annual drift Qannual is sum of contributions from all wave incidents.

$$\text{Qannual} = \sum_{i=1}^{NSETS} Qs(i).Duration\ (i) \quad (1)$$

Where,
NSETS is the total number of wave incidents.
The annual drift Qannual is obtained when the total duration in the wave climate is one year.

LITLINE simulates the coastal response to gradients in the longshore sediment transport capacity resulting from natural features and a wide variety of coastal structures. LITLINE predicts the coastline evolution by solving a continuity equation for the sediment in the littoral zone. The influence of structures, sources and sinks is included. With jetties and breakwaters, the influence of diffraction on the wave climate is also included. The main equation in LITLINE is the continuity equation for sediment volumes expressed as

$$\frac{\partial \mathbf{yc(x)}}{\partial t} = -\frac{1}{\mathrm{h_{act}\,(x)}} \frac{\partial Q}{\partial x} + \frac{Q_{sou}\,(x)}{h_{act}\,(x)\Delta x} \quad (2)$$

Where,
Yc(x) is distance from baseline to coastline t is time
$h_{act}$ (x)is height of active cross-shore profile
Q(x) is longshore transport of sediment expressed in volume
x is the longshore position
Qsou (x) source/sink term expressed in volume/$\Delta x$
$\Delta x$ is longshore discretization step

#### *3.2.1 Estimation of Littoral Drift Rate*

LITPACK model was used to estimate annual littoral drift rates and its distribution on the profile. Normal to the shoreline i.e. $257^0$ N. Fig. 6 shows the cross shore profile near the Hosabettu and the same was used for drift computation.

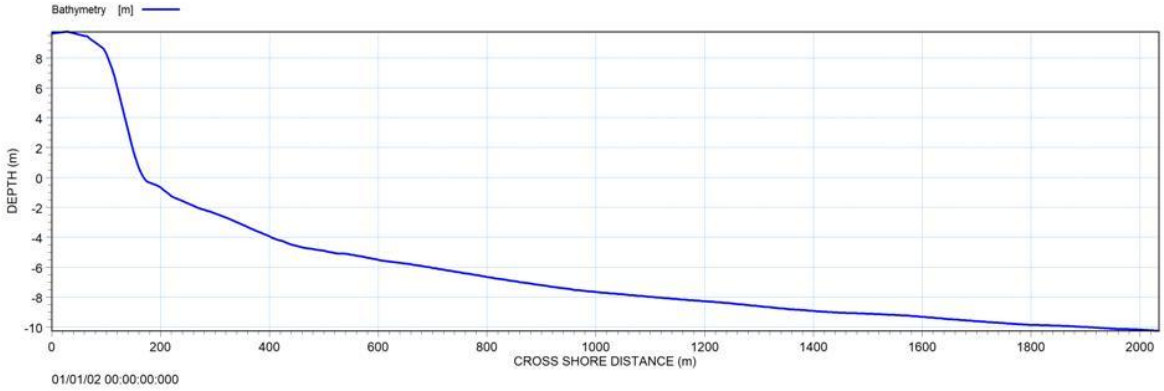



**Fig. 6: Cross shore Profile**

The profile covers a distance of 2.1 km extending up to about -10 m depth contour (with respect to chart datum) as shown in Fig. 9. The profiles were descretized with grid size of 5 m. Grain size distribution, fall velocity and roughness coefficient over the profile were required for computation of littoral drift. At the site, mean grain size is observed to be of the order of 0.34 mm. In the studies of Longshore sediment transport rates for the Indian Coast made by Chandramohan and Nayak in 1991, it is estimated that the northerly drift along the Mangalore coast is 3.62 × $10^5$ $m^3$/year and the southerly drift is 10.69 × $10^5$ $m^3$/year. Study by Jayappa K S (1996) reported net transport of 0.043 million cum toward South. In another study done by G.S. Dwarakish and K. Sankar Babu (2003), the average net alongshore sediment transport is estimated as 0.22 million cum toward South. In an estimate by Sanil Kumar (2006), annual net transport of 0.036 million cum toward South at Ullal was reported. Additionally, as seen from various Google earth images that the net drift is towards South and shorelines in the neighborhood of New Mangalore Port Trust (NMPT) does not show any long term trend of erosion or accretion. The model was calibrated using bed roughness to get the annual net transport of the order 0.045 x $10^6$ $m^3$/year. The model was run for annual nearshore wave climate given in Table 1. Annual northward and southward drift distribution across the cross shore profile is shown in Fig.7 and in Table 2. The northward drift is plotted positive as while southward drift is plotted as negative.

**Table 2:** Littoral Transport Rate ($m^3$)

| Northward | Southward | Net * | Gross |
|---|---|---|---|
| 153030 | 198870 | -45840 | 351900 |

Note*: '-ve' Southward '+ve' Northward for the Net Drift

Net transport in a year is of the order of 0.045 million cum and is towards South and gross transport is of the order of 0.35 million cum.

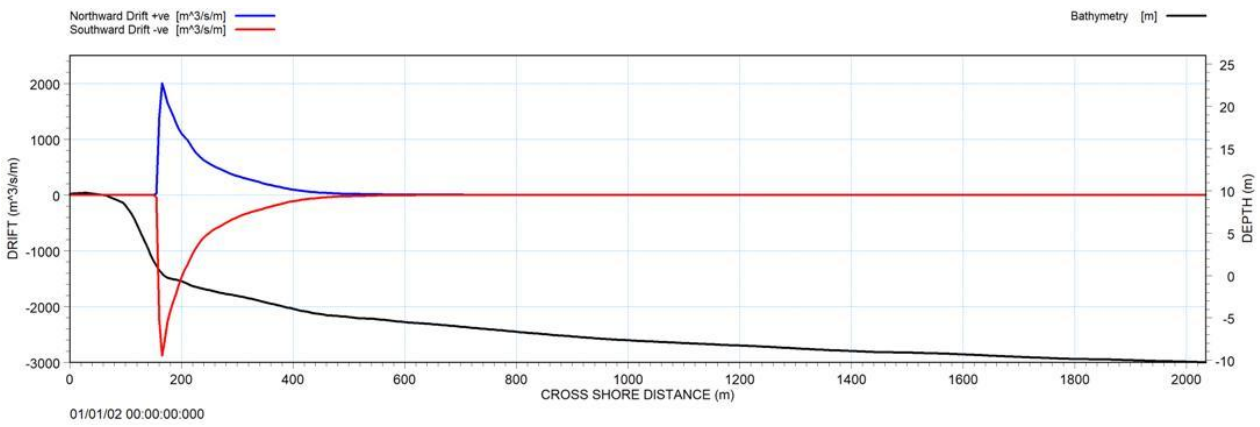



**Fig. 7: Cross shore Distribution of Northward and Southward Littoral Drift During Entire Year**

According to cross shore distribution plot (Fig. 7), the maximum transport occurs at about 20 m from the shoreline (i.e. High Water Line) at 0.24 m depth contour. The sediment transport occurs between 1.5 m and (-) 6.02 m depth contours

### *3.2.2 Shoreline Evolution*

In order to assess the impact of the shore connected breakwaters on the coastline, LITLINE module of LITPACK software was used. It may be noted that LITPACK is a 1-D model, in which the shore connected breakwaters are assumed as obstructions which are perpendicular to shoreline. The length of the shoreline considered for the studies is 6 km. It is divided into 1200 grid points of grid size 5m. In order to reduce the erosion on the Hosabettu shore for about 3 km stretch, two options viz., groyne fields and offshore breakwaters, were tested through model studies.

**OPTION-1**

For protection of shore at Hosabettu site, sixteen groynes in series with of 50 m length with 200 m spacing between them were considered for reducing erosion. The effect of the groynes has been assessed through the model studies as shown in Fig.8 below:

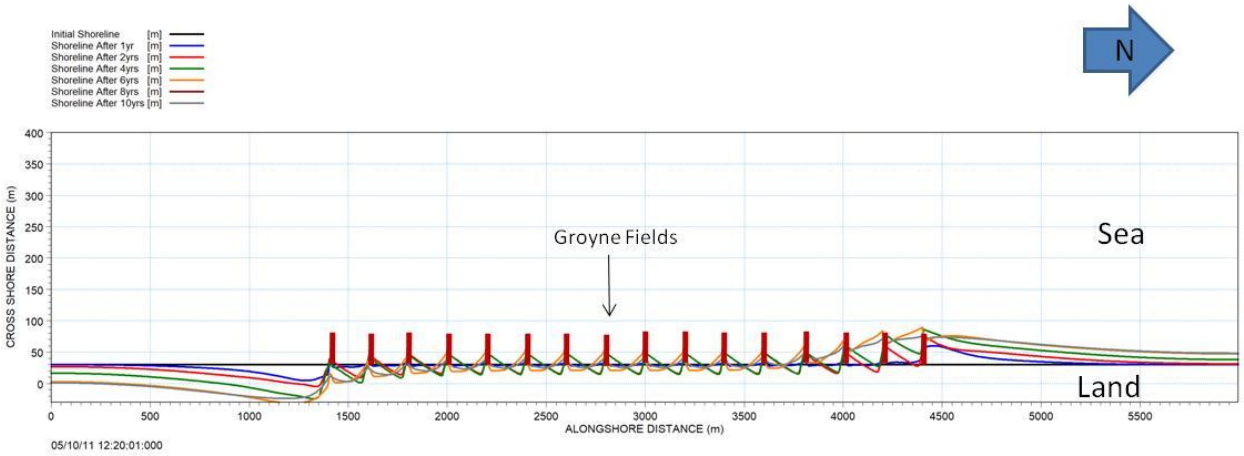



**Fig. 8: Effect on Shoreline changes with the sixteen groynes in series**

The model was run for 1, 2, 4, 6, 8 and 10 years with the proposed groyne field. An accretion of 8 m , 21 m, 29 m, 59 m, 46 m and 46 m on North groyne field was seen for 1, 2, 4, 6, 8 and 10 years respectively. After 6 years, by passing of sand would start. Accretion of 4 m, 11 m, 15 m, 25 m, 14 m and 14 m was seen between the groyne fields for 1, 2, 4, 6, 8 and 10 years respectively. Maximum 35 m erosion on south of groyne field was observed in 10 years.

**OPTION-2**

As shore protection measure, other option, a series of ten offshore breakwaters of 100 m length each with 200 m spacing between them at a distance of 120 m (- 2 m depth contour) from the shore was considered for reducing erosion. The model was run for 1, 2, 4, 6, 8 and 10 years with the proposed offshore breakwaters. The model output is shown in Fig .9 below.

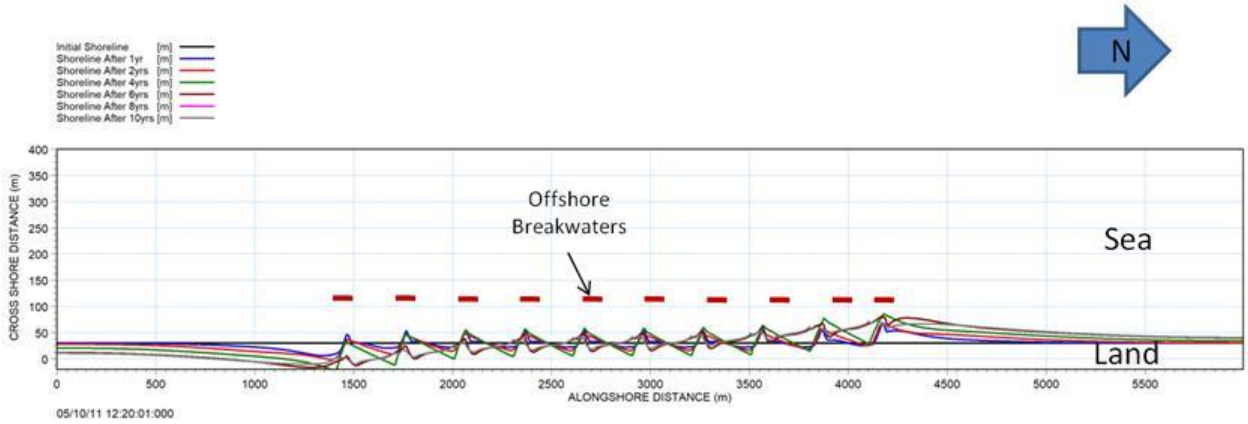



**Fig. 9: Effect of offshore breakwaters on the Shoreline**

Accretion of 34 m , 37 m, 55 m, 50 m, 36 m and 36 m on the Northern most offshore breakwater was seen for 1, 2, 4, 6, 8 and 10 years respectively. After 6 years, by passing of sand would start. Accretion of 14 m, 19 m, 19 m, 18 m, 11 m and 11 m was seen between the offshore breakwaters for 1, 2, 4, 6, 8 and 10 years respectively. Maximum 20 m erosion on south of offshore breakwaters was observed in 10 years.

## 4. CONCLUSIONS

The main findings of the Mathematical Model Studies for Shoreline Changes to evolve the suitable coastal protection work near Hosabettu are as below:

- The Wave transformation study indicates that the predominant wave directions at the near shore (-) 10 m depth are from $202.5^0$ N to $315^0$ N.
- LITDRIFT studies indicates that at the proposed site net sediment transport in a year is of the order of 0.045 million cum and is towards South and gross transport is of the order of 0.35 million cum.
- With the option of shore protection with the groyne fields (sixteen of 50 m length each with 200 m spacing), it was found that maximum 25 m of accretion would be between the groyne fields after 6 years.
- With the option of shore protection with offshore breakwaters ( ten each of 100 m length with 200 m spacing), it was found from studies that maximum 55 m of accretion would be between the shore and offshore breakwaters in 6 years
- Numerical models are efficient to assess the impact of coastal protection, it is cost effective and less time consuming, assessed protection layout can applied to protect the vulnerable coast site.

## ACKNOWLEDGEMENTS

Authors are grateful to Shri A.K. Agrawal, Director, Central Water and Power Research Station for her continuous encouragement and motivation during the course of studies and for granting permission to publish this paper.

## REFERENCES

Danish Hydraulic Institute, 2014. LITPACK, LITDRIFT (Longshore Currents and Littoral drift) , LITLINE (Coastline Evolution) Module, User Guide and Reference Manual

Chandramohan, P. and Nayak, B.U (1991). "Longshore Sediment Transport Along the Indian Coast"; Indian Journal of Marine Science; Vol 20; 110–114.

Jayappa K S (1996) "Longshore sediment transport along the mangalore coast west coast of India", Indian Journal of Marine Science Vol 25, June 1996, pp 157-159

Pravin D Kunte & B G Wagle (2001) "Littoral transport studies along west coast of India" Indian Journal of Marine Science Vol 30, June 2001, pp57-64

Reddy M P, Hariharan V and Kurian N P (1982), "Beach stability along the coast from Ullal to Thannirbhavi near Mangalore", Indian Journal of Marine Science Vol 11, December 1982, pp 327-332

V. Sanil Kumar, K. C. Pathak, P. Pednekar, N. S. N. Raju and R. Gowthaman (2006), "Coastal processes along the Indian coastline" Current Science, Vol. 91, No. 4, 25 August 2006

*IN PROCEEDINGS OF 25th HYDRO 2020, INTERNATIONAL CONFERENCE,*
*NATIONAL INSTITUTE OF TECHNOLOGY ROURKELA, ODISHA, INDIA*
*26-28, March 2021, ISBN 978-93-90631-56-8*

Paper ID - 180

# SHORELINE CHANGES STUDIES FOR DEVELOPMENT OF PASSENGER TERMINAL AT KASHID, MAHARASHTRA

Dr. Prabhat Chandra[1], R.K.Chaudhari[2], S.K. Kori[3],

[1]*Scientist 'E', CWPRS, Khadakwasla Pune,India -411024*
[2]*Scientist 'B', CWPRS,Khadakwasla Pune,India -411024*
[3]*ARO, CWPRS,Khadakwasla Pune,India -411024*
***Email:*** *rajeev_cwprs@yahoo.co.in*

## Abstract

Design of Passenger terminal is a complex process requiring consideration of site specific environmental parameters such as wave, current and tide, littoral movement etc. Many a times, the effect of these parameters on the coastline changes due to the construction of breakwaters is significant. Adequate area for maneuvering of passenger vessels and berthing place, adequate depth and tranquility are essential requirements for development of a passenger jetty. Sometimes littoral drift becomes single most parameter which affects the design consideration. The sediment movement (Littoral drift) at the site and impact of development of the Passenger terminal on the coastline can be effectively assessed using the numerical modeling. In the present paper, the impact of the passenger terminal on the shore line changes and morphological impact on the adjacent regions has been assessed using LITPACK studies. Littoral drift studies indicated that net littoral drift at the site of development is of the order of 10,000 cum only towards south. The simulations of shoreline changes carried out with LITLINE indicated that due to the construction of the breakwaters, there are no significant changes in the shore upto 5 years, but after 10 year less than 5 m accretion on north of the breakwater may occur which is almost negligible. The presence of rocky out crops on the north of breakwater would not allow any significant accretion or movement of sand. Consequently, the erosion on the south side of breakwater will too be negligible.

***Keywords:*** *Numerical model, Littoral drift, Passenger terminal, Breakwater, Layout*

## 1. Introduction

Water transport plays an important role in economic growth. It is the cheapest and most convenient mode of transport. Maharashtra state is having almost 35 creeks and rivers spread across 720 km long coast line. As per available information, approx. 15 million passengers in the coastal districts of state use Inland water transport annually. In order to promote the water transport, Maharashtra Maritime Board have a proposal of developing a passenger jetty at Kashid for ferry operations to boost tourism in this area. Kashid situated on the western cost of India in northern Konkan region of Maharashtra, is a tourist destination because of its beautiful beaches (Fig.1). It is proposed to operate the passenger jetty only during fair weather season for vessels having minimum draft of 3.0 m. The location is exposed to the incident waves from South quadrant to NW quadrant. The Kashid beach is located between two headlands located about 3.0 km apart. There is no sand movement visible on the north of north headland and on the south of south headland. Development of a passenger jetty surely enhances the clan transport facility. Passenger berth must be easily accessible from the sea to enable quick embarkation and disembarkation of passengers and it must be sheltered to avoid excessive vessel movement and offer convenience and comfort. To achieve this, two alternative layouts have been proposed considering the wave tranquility conditions. Alternative layout-1 consists of a total breakwater length of 780 m with shore connected arm of 550 m length and a 230 m long arm making an angle of $120^0$ to the shore connected arm. Alternative layout-2 consists of a breakwater of 770 m length with shore connected part of the breakwater is 540 m long with a 230 m long arm of breakwater making an angle of $110^0$ to it (Fig.2). Wave tranquility studies carried out for the fair weather (non monsoon season) indicated that the Alternative layout -1 can be operated during whole fair weather as the significant wave heights near the proposed passenger jetty would be less than the permissible limit of 0.30m. The Alternative layout -2 would have some days down time because of marginally higher wave heights at jetty for the waves incident from SW and WSW directions even during non monsoon season. The proposed layout will act as hindrance to littoral movement and may cause erosion or accretion at the coastline. The assessment of the impacts of the breakwater

construction on the shore line changes and morphological impact on the adjacent regions has been carried out for both alternative layouts using numerical model LITPACK. It is also seen that during the non monsoon season, the beach is almost fully developed but during the monsoon season, the beach gets eroded to some extent due to the high waves from SW and west directions and again gets developed during non monsoon season. This trend is also proved by the Google images of different seasons (Photos 1 & 2). It is also noticed that the sand movement at Kashid beach is oscillating between these two head lands. Beyond the headlands, the rocky out crop exists on both sides and no beach was observed to develop on either side of the head land. The bottom of the proposed breakwater is on the rocky outcrop having the length of about 100 m upto -1.5 m depth and width of almost 200 m at reduced level of +1.3 m. This rocky outcrop is behaving like natural breakwater at the development site and no sand movement is observed around this.

In this present paper, details of the impact of breakwater/ Jetty on the shorelines at Kashid beach has been assessed through numerical modeling.



**Fig. 1: Location Map Of Proposed Kashid Water Treminal at Kashid,Maharshtra India**

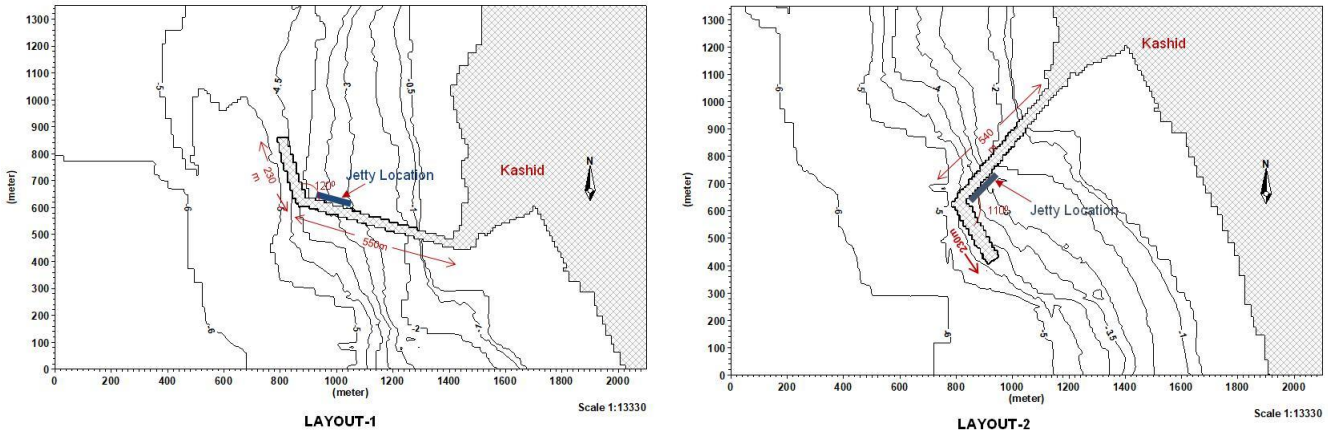



**Fig. 2: Two Proposed Kashid Water Treminals at Kashid, Maharshtra India**

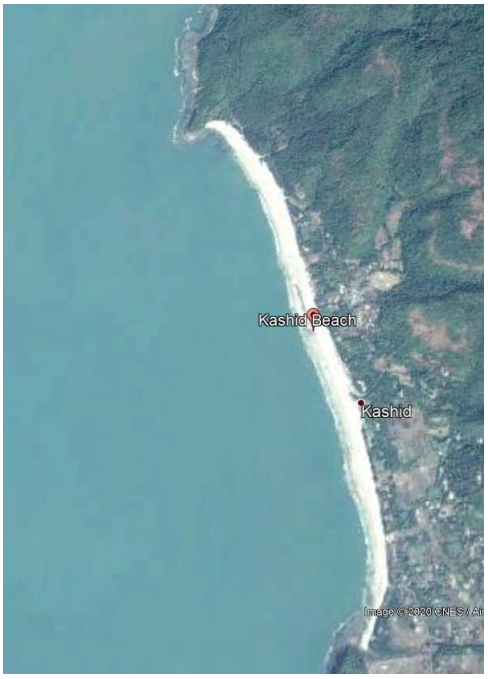



**Photo 1: Google Image during Non Monsoon Season**

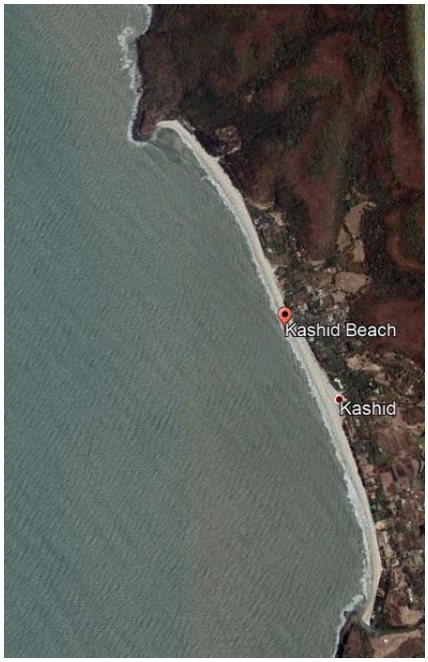



**Photo 2: Google Image during Monsoon Season**

## 2. SITE CONDITIONS

Kashid is situated at $18^0$ $27^{'}$' North and $72^0$ $53^{'}$ East on the west coast of India. The North side of proposed site is rocky crop and on the south side of it, the Kashid beach is situated. The wind at Kashid is moderate, mainly from SW direction having magnitude of about 5-10 m/s while the tidal range is 2.0 m resulting in weak currents. The beach expands between two head lands. It is seen that beach has been stable over the years. No littoral movement of sand is observed on the north and south sides of the existing beach. Beach is only eroding to some extent during the monsoon season and again building up during non monsoon. The coastline at the site, consists of long, sandy beach and is oriented in NW-SE direction and also having rocky portion in the north of head land. The average value of $D_{50}$ (mm) from various sand samples is about 0.224 mm and the same has been used for the model runs. Wave is a very important parameter which influences the littoral drifts that causes the erosion of coastlines. In absence of measured wave data, the offshore wave data of 14 years from 1986 to 2000 off Kashid, compiled by India Meteorological Department (IMD) from ships plying in deep waters, were analyzed. This wave data information was considered at the offshore end of the model limits. The frequency distribution of wave heights for entire year for the above offshore wave data is presented in form of wave rose diagram in Figure 3. It could be seen that the predominant wave directions in deep water are from $200^0$ N to $360^0$ N with the maximum wave heights of 4.5 m. These deep water wave data were transformed using the mathematical model MIKE 21- SW to get the near-shore wave climate near the Kashid.

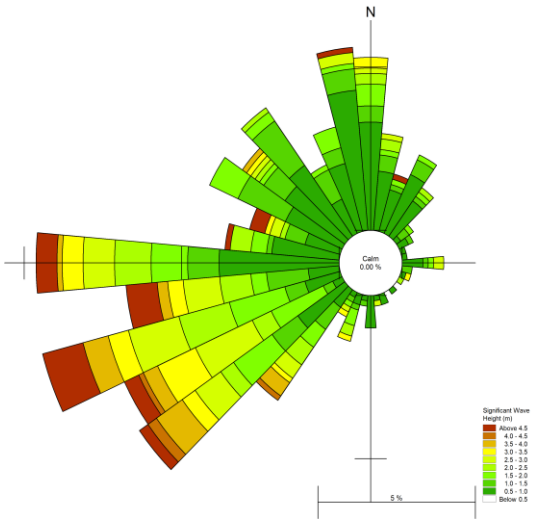



**Fig .3: Offshore Wave Rose Diagram for Entire Year**

## 3. NUMERICAL MODELLING TECHNIQUES

To get the impact of Passenger Jetty on coastline, mathematical models like MIKE 21 – SW, LITPACK have been used. These studies were mainly carried out in two following stages:

1. Transformation of wave height and wave direction from deep water to (-) 7 m depth using MIKE 21-SW model.
2. Estimation of Littoral drift distribution and simulation of shore line changes using LITPACK model.

### *3.1 Transformation of wave height and wave direction from deep water to (-) 7 m depth*

As waves propagate toward shore, a combination of shoaling, refraction, reflection, diffraction, and breaking effects modify the waveform and the wave characteristics will be very different from those in deep water. To get the wave conditions from offshore to nearshore at (-) 7 m depth, the numerical model MIKE21-SW was used. This is a state-of-the-art third generation spectral wind wave model based on unstructured mesh. The model simulates the growth, decay and transformation of wind generated waves and swells in offshore and coastal areas. It takes into account refraction and shoaling of waves, which are important in the transformation of waves from offshore to inshore. It also includes physical phenomena of wave growth by action of wind, dissipation due to white-capping, dissipation due to bottom friction, and dissipation due to depth induced wave breaking. In the absence of measured wave data of at least one year near the proposed site of development, the nearshore wave climate at Kashid was obtained by transforming the ship observed deep water wave data using MIKE21-SW Model. Model area considered for MIKE 21-SW model is shown in Figure 4. Bathymetry in the model region of about 100 km X 110 km area was descreitized using unstructured mesh. The model was run to obtain nearshore wave climate at the Inshore Point in (-) 7 m depth contour. The wave directions and ratio of wave heights at (-) 7 m depth to deep water wave height, with different directions of wave incidence at the offshore boundary are obtained. After applying the ratio of deep water wave height and direction as shown in rose diagram (Figure 3), the frequency distribution of waves in (-) 7 m depth were obtained shown in Table 1 and corresponding rose diagram (Figure 5).

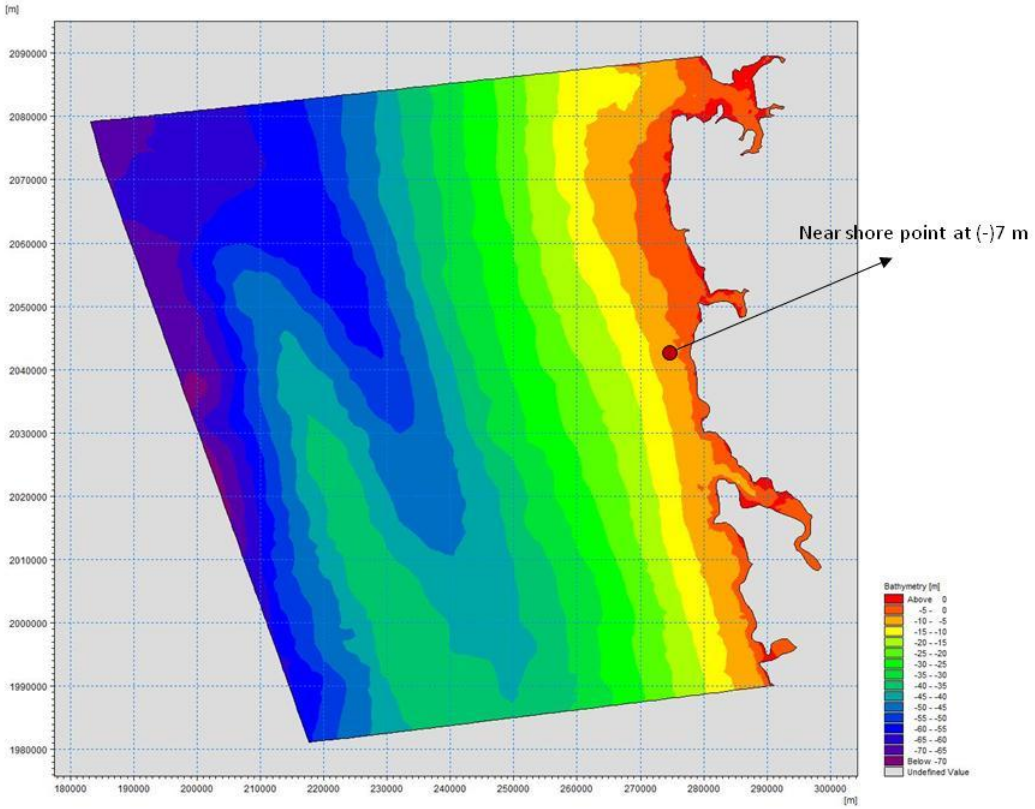



**Figure 4**: **Bathymetry for Wave Transformation from Offshore to Nearshore**

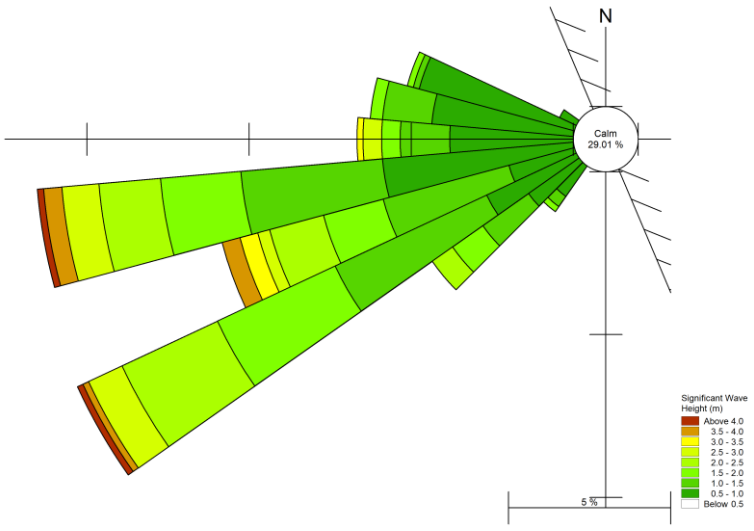



**Figure 5: Rose diagram at (-)7 m depth (Year)**

**Table 1: Percentage Occurrence of Wave Height & Direction at Kashid in (-) 7 m Depth for Entire Period (Jan-Dec)**

| Wave height (m) | 0.5-1 | 1-1.5 | 1.5-2 | 2-2.5 | 2.5-3 | 3-3.5 | 3.5-4 | 4-4.5 | Total |
|---|---|---|---|---|---|---|---|---|---|
| **DIRECTION** | | | | | | | | Calm% | 29.01 |
| 220 | 1.15 | 0.38 | 0.19 | 0 | 0 | 0 | 0 | 0 | 1.72 |
| 230 | 1.91 | 1.72 | 1.15 | 0.76 | 0 | 0 | 0 | 0 | 5.53 |
| 240 | 3.05 | 5.15 | 4.01 | 3.24 | 1.15 | 0 | 0.19 | 0.19 | 16.98 |
| 250 | 2.1 | 4.01 | 1.91 | 1.72 | 0.38 | 0.57 | 0.57 | 0 | 11.26 |
| 260 | 5.92 | 4.39 | 2.48 | 1.91 | 1.15 | 0 | 0.57 | 0.19 | 16.6 |
| 270 | 3.82 | 1.53 | 0.57 | 0 | 0.57 | 0.19 | 0 | 0 | 6.68 |
| 280 | 4.39 | 1.53 | 0.38 | 0 | 0 | 0 | 0 | 0 | 6.3 |
| 290 | 4.97 | 0.19 | 0.19 | 0 | 0 | 0 | 0 | 0 | 5.35 |
| 300 | 0.57 | 0 | 0 | 0 | 0 | 0 | 0 | 0 | 0.57 |
| Total | 27.86 | 18.89 | 10.88 | 7.63 | 3.24 | 0.76 | 1.34 | 0.38 | 100 |

### *3.2 Estimation of Littoral drift distribution and simulation of shore line changes :*

Mathematical model studies for estimation of littoral drift distribution and simulation of shoreline changes were carried out using LITPACK model. LITPACK software was used for computation of littoral drift and simulation of shoreline changes due to construction of the breakwaters. LITPACK is a professional engineering software package for the modelling of non-cohesive sediment transport in waves and currents, littoral drift, coastline evolution and profile development along quasi-uniform beach (DHI 2014). The two modules of LITPACK i.e. LITDRIFT and LITLINE are used in the present study.

LITDRIFT module simulates the cross-shore distribution of wave height, setup and longshore current for an arbitrary coastal profile. It provides a detailed deterministic description of the cross-shore distribution of the longshore sediment transport for an arbitrary bathymetry for both regular and irregular sea states. The longshore and cross-shore momentum balance equation is solved to give the cross-shore distribution of longshore current and setup. Wave decay due to breaking is modelled, either by an empirical wave decay formula or by a model of Battjes and Janssen. LITDRIFT calculates the net/gross littoral transport over a specific design period. Important factors, such as linking of the water level and the beach profile to the incident sea state, are included. Wave climate is described in time series file in LITDRIFT. Each set of items in wave climate describe the characteristics of one wave incident and duration of wave incident is in percentage fraction of year. Thus, the total annual drift Qannual is sum of contributions from all wave incidents.

$$\text{Qannual} = \sum_{i=1}^{NSETS} Qs(i).Duration\ (i) \quad (1)$$

Where,
NSETS is the total number of wave incidents.
The annual drift Qannual is obtained when the total duration in the wave climate is one year.

LITLINE simulates the coastal response to gradients in the longshore sediment transport capacity resulting from natural features and a wide variety of coastal structures. LITLINE predicts the coastline evolution by solving a continuity equation for the sediment in the littoral zone. The influence of structures, sources and sinks is included. With jetties and breakwaters, the influence of diffraction on the wave climate is also included. The main equation in LITLINE is the continuity equation for sediment volumes expressed as

$$\frac{\partial \mathbf{yc(x)}}{\partial t} = -\frac{1}{\mathrm{h_{act}\,(x)}} \quad \frac{\partial Q}{\partial x} + \frac{Q_{sou}\,(x)}{h_{act}\,(x)\Delta x} \qquad (2)$$

Where,
Yc(x) is distance from baseline to coastline t is time
$h_{act}$ (x)is height of active cross-shore profile
Q(x) is longshore transport of sediment expressed in volume
x is the longshore position
Qsou (x) source/sink term expressed in volume/$\Delta x$
$\Delta x$ is longshore discretization step

### *3.2.1 Estimation of Littoral Drift Rate*

LITPACK model was used to estimate annual littoral drift rates and its distribution on the profile normal to the shoreline i.e. $250^0$ N. Fig. 6 shows sea bed profile near the harbour which was used for drift computation. The profile covers a distance of 2 km extending up to about -6.5 m depth contour (with respect to chart datum).

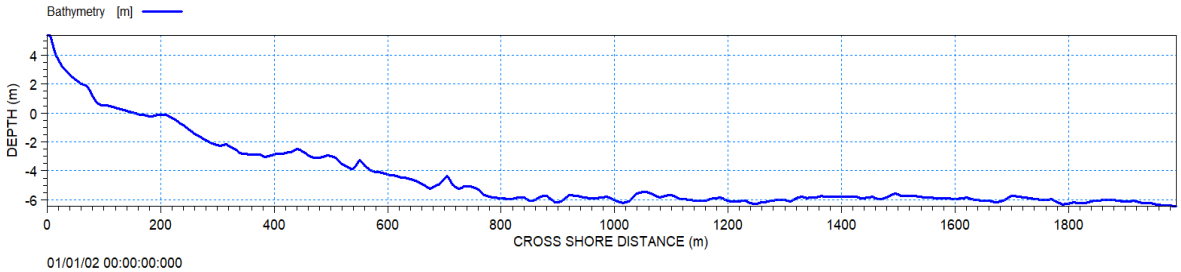



**Fig. 6: Cross shore Profile**

The profile was descretized with grid size of 5 m. Grain size distribution, fall velocity and roughness coefficient over the profile are required for computation of littoral drift. At the site, grain size is observed to be of the order of 0.04 mm to 0.224 mm. The model was run for annual nearshore wave climate given in Tables 2. Annual northward and southward drift distribution across the cross shore profile is shown in Fig. 7. The northward drift is plotted positive as while southward drift is plotted as negative.

**Table 2:** Annual Littoral Transport Rate ($m^3$)

| Northward | Southward | Net * | Gross |
|---|---|---|---|
| 60610 | 49690 | -10920 | 110300 |

Note*: '-ve' Southward '+ve' Northward for the Net Drift

Net transport in a year is of the order of 0.011 million cum and is towards south. According to cross shore distribution plot (Fig. 7), the maximum transport occurs at -0.86 m depth about 190 m from high water line total span will be 650 m it spread from shore at around 0.1 to -5.8 m depth contour. The net sediment transport at the site is very less as it seen from littoral drift studies. It is also confirmed by the paper at the journal of coastal Research, vol.8 No.4, 1992 by Chandramohan and Nayak that Maharashtra coast experiences negligible quantity of annual net transport and sediment movement spread in some nodal points. The net drift is in the southward direction is hardly about 10000 cum.

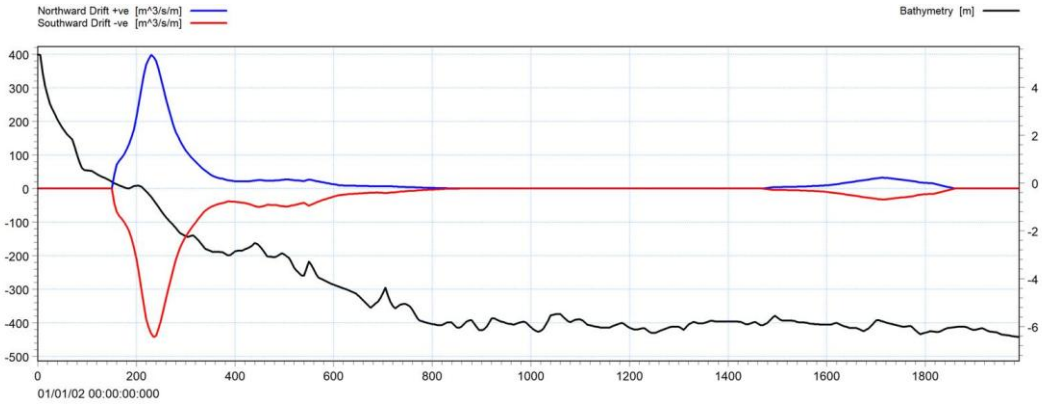


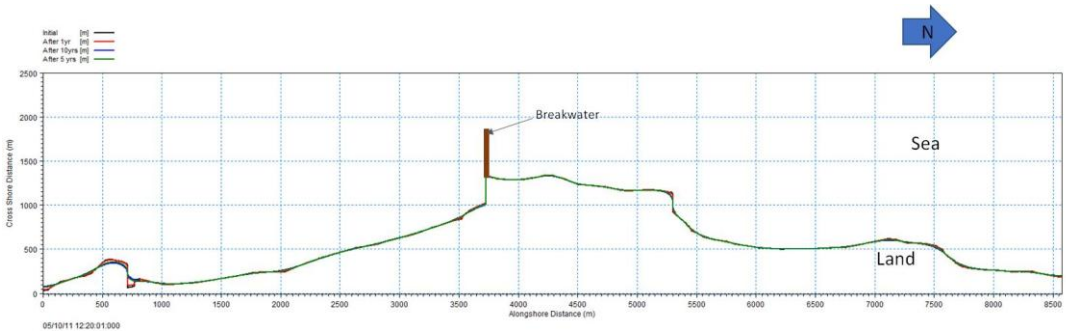

**Fig. 7: Cross shore Distribution of Northward and Southward Littoral Drift During Entire Year**

### *3.2.2 Shoreline Evolution*

In order to assess the impact of the shore connected breakwaters on the coastline, LITLINE module of LITPACK software was used. The length of the shoreline considered for the studies is 8.5 km, extending about 5.0 km towards north of the breakwater and about 3.5 km towards south of the breakwater. It is divided into 1700 grid points of grid size 5 m. One shore connected breakwater of length 550 m were included perpendicular to the shoreline. It may be noted that LITPACK is a 1-D model, in which the shore connected breakwaters are assumed as obstructions which are perpendicular to shoreline. Therefore projections of both the breakwaters for both the layout of length 550 m were considered in the simulation. The model was run for 1, 5 and 10 years with the proposed breakwater as shown in Fig 8.




(a)




**(b)**

**Fig. 8: (a) Google Image (b) Shoreline Evolution**

The simulation of shoreline changes indicate that due to the construction of the breakwaters, there are no significant changes in the shore upto 5 years, but after 10 year less than 5 m accretion on north of the breakwater may occur which is almost negligible. The presence of rocky out crops on the north of breakwater would not allow any significant accretion or movement of sand. Consequently, the erosion on the south side of breakwater will too be negligible.

Considering the wave tranquility studies and the trend of shore changes at the site, the layout - 1 (Fig. 2) will be more appropriate for proposed passenger jetty. There will not be any significant change in shoreline due to this proposed development. In the case of Layout-2, the wave climate of the Kashid beach would slightly change, particularly during the monsoon season due to the main arm of the breakwater. This may result in slightly less erosion of the beach during monsoon season but overall, there would not be any significant change in the beach profile on annual basis.

## 4. CONCLUSIONS

The main findings of the mathematical model studies carried out for predicting the shoreline changes due to the development of passenger terminal at the Kashid beach are:

1. The predominant wave incident at the nearshore at (-7) m depth are from $220^0$ N to $300^0$N.
2. Littoral drift at the site of development is very small. The net drift is of the order of 10,000 cum only, towards South.
3. The simulation of shoreline changes indicate that due to the construction of the breakwaters, there are no significant changes in the shore upto 5 years, but after 10 year less than 5 m accretion on north of the breakwater may occur which is almost negligible. The presence of rocky out crops on the north of breakwater would not allow any significant accretion or movement of sand. Consequently, the erosion on the south side of breakwater will too be negligible.
4. These studies were done by taking into account the development needs, planning consideration and the site condition of Kashid. It was found that layout with facing north direction is more suitable for operation of the passenger terminal in term of littoral movement during fair weather.

## ACKNOWLEDGEMENTS

Authors are grateful to Shri A.K. Agrawal, Director, Central Water and Power Research Station for her continuous encouragement and motivation during the course of studies and for granting permission to publish this paper.

## REFERENCES

Danish Hydraulic Institute, 2014. LITPACK, LITDRIFT (Longshore Currents and Littoral drift) , LITLINE (Coastline Evolution) Module, User Guide and Reference Manual

P Chandramohan, and B.U.Nayak, Dec 1994 ‘Longshore sediment transport model for the Indian west coast’ JCR vol.8 No.4, 775-757

R.K.Chaudhari , S Kulkarni, A.M Vaidya and M.D. Kudale, Dec. 2015 “ Wave Model studies for feasibility of Development of Passenger Jetty at Open Coast- A case study” Proceedings of HYDRO 2015 International, 20th Internatinanal Conference on Hydraulics water Resources and River Engineering ( 17-19 December 2015) organized by Departmenbt of Civil Engineering IIT Roorkee.

# Theme III

# Impact of Climate Change on Water Resources

*IN PROCEEDINGS OF 25th HYDRO 2020, INTERNATIONAL CONFERENCE, NATIONAL INSTITUTE OF TECHNOLOGY ROURKELA, ODISHA, INDIA 26-28, March 2021, ISBN 978-93-90631-56-8*

Paper ID - 016

# Effect of Climate Change on Precipitation for Bhopal, India

Priyank Agrawal[1], H. L. Tiwari[2] and Ankit Balvanshi[3]

[1,2&3] *Department of Civil Engineering, Maulana Azad National Institute of Technology, Bhopal, 462003, INDIA*
*Email: agrawal.priyank519@gmail. com Telephone/Mobile No.:+918989458261*

## Abstract

General Circulation Models (GCMs) have been widely used to simulate the current climate and predict future climate change at regional and global scales. GCM CanESM2 have been used to downscale the precipitation for Bhopal city, Madhya Pradesh, India. The SDSM (Statistical downscaling model) is used for downscaling of data. In this study baseline period from 1979-1995 and 1996-2005 is used in calibration and validation respectively. The GCM outputs were evaluated by Nash Sutcliffe Efficiency (N SE) and Coefficient of determination ($r^2$). Future series are generated for RCP 2.6, RCP 4.5, and RCP 8.5 for future period (2006-2035), future period (2036-2070) and future period (2071-2100) using CanESM2 data. Rate of change in precipitation has been compared in three future period for Bhopal city. The study of future simulations shows that there is change in Precipitation for Bhopal city.

***Keywords:*** *General Circulation Model (GCM); CanESM2; RCP 2.6; RCP 4.5; RCP 8.5.*

## 1. Introduction

Climate change is a major challenge in India to billion people in the 21st century for water, food security and welfare. There is uneven water distribution in many areas of India, from the drier north-west, where the precipitation is low, to the northeast, the highest precipitation zone in the world. In recent decades, India has undergone many catastrophic extremes. Based on scientists and scholars' work, increased levels of carbon dioxide (CO2) will drastically change the global climate in this century. Climate measure the typical pattern of weather variability for a long time in a given area. . Climate change is broadly defined as a statistically significant change in the mean or variability over a prolonged period. According to reports from the Intergovernmental Panel on Climate Change (IPCC), the supply of freshwater will be reduced by the middle of this century, especially in large rivers because of climate change. GCMs General Circulation models or Global Climate models are an important tool to assess Impacts of climate change on a variety of human and natural systems. General Circulation Models or Global Climate Models (GCMs) is one of the highest quality tools for global distribution of simple continental and wide-ranging climate parameters. However, these models cannot provide descriptions of regional climate conditions at various time and space levels. To acquire local surface weather from regional atmospheric variables, which are supplied by GCMs, Downscaling methods are created. Understanding the interplay of environment and water supplies will help scientists and policymakers reduce the adverse effects of global warming by developing effective scenarios.

### 1.1 *Objective of study*

Based on the challenges because of climate change effects on water resources, the aim of current study is to study the effect of climate change on Precipitation over Bhopal city, India. It includes- To Downscale the GCM model output by statistical downscaling technique using daily data Bhopal city.

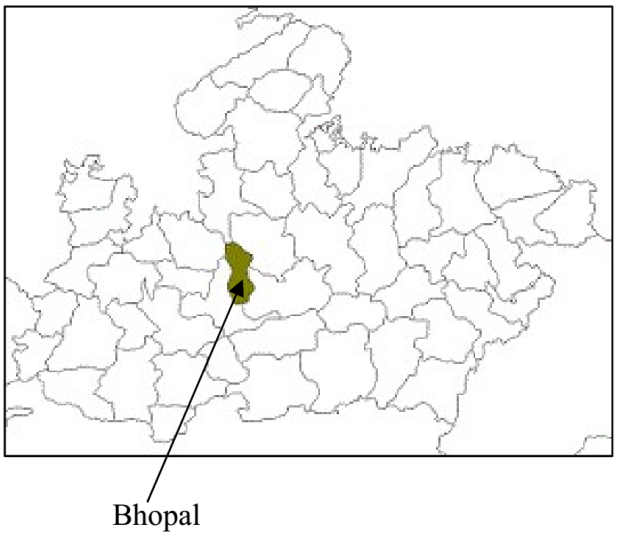
- To generate the future scenario based on GCM downscaled output for precipitation.
- Study of trend in Precipitation for Bhopal city.

## 2. Data and Method

### *2.1 Study Area*

*Bhopal*, It is the capital of the Madhya Pradesh and lies between latitude: 23.2599° N and longitude: 77.4126° E .With its various natural and artificial lakes, Bhopal is known as the City of Lakes and is also among the greenest cities in India. It has two lovely lakes, jointly known as the Bhoj Wetland. The Upper Lake and the Lower Lake are these lakes. The climate here is tropical.

Madhya Pradesh




(23.2599° N, 77.4126° E)

### *2.2 Data*

- ***Reanalysis data***

National Centre for Environmental Prediction (NCEP) reanalysis data collection has been used for the period January 1979 to December 2005.

- ***GCM Data***

The GCM chosen for this study is developed by Canadian Centre for Climate Modelling and Analysis (CCCMA), Canada, i.e. CanESM2 (Second generation Canadian Earth System Model). It is derived from the first-generation Canadian Earth System Model (CanESM1). The CanESM2 improves physical ocean part compared to CanESM1, since it has improved resolution and improved physical parameters. The atmospheric component of CanESM2 has 22 pressure levels with a resolution of 2.81° latitude by 2.81° longitude spatial (horizontal). The predictor variables are available for period from 2006-2100 for CanESM2 model. The key factor behind the selection of the CanESM2 model is the availability of SDSM-compatible data and the literature review. Furthermore, this model was commonly used for the statistical downscaling of climate variables across the Indian subcontinent. The gridded CanESM2 predictor variables for the nearest grid in the study area were directly downloaded from the website (http://climatescenarios.canada.ca/?page=pred- canesm2) of Canadian Centre for Climate Modelling and Analysis. The predictors are simulated under RCP2.6, RCP4.5, and RCP8.5 for CanESM2 model.

- Series of observed daily precipitation from 1979 to 2005 from (http://globalweather.tamu.edu/) has been used in this study.

### *2.3 Methodology*

Wilby and Dawson developed the *Statistical Down-Scaling Model (SDSM)* is used to construct c limate change scenarios over Bhopal city. Due to many advantages over dynamic methods, like low co st and more user friendly, the statistical tool SDSM is used. SDSM has been used in several experiments on impact assessments of climate change. Linear or nonlinear relationship is established between predictors and predictors using the regression method. The statistical downscaling approach thus depends heavily on empirical statistical relationships. Effortlessness and less computational demand for the regression statistical approach is the key preference point of this approach.

### *2.4 Model Evaluation*

The SDSM model performance is examined by the Coefficient of determination ($R^2$) and Nash- Sutcliffe efficiency (NSE). The efficiency of Nash-Sutcliffe provides normalised statistical data which determines the relative extent of the residual variance compared to measured data variance. NSE differs from -<» to 1.0, the values from 0.0 to 1.0 are accepted while values less than zero indicate prediction performance is worse compared to mean. NSE's highest potential value is 1.0, suggesting that model is perfect. The coefficient of determination ($R^2$) represents the proximity between the observed and modelled values.

## 3. Results and Discussion

### *3.1 Identification of predictors*

Predictors were defined on the basis on the relationship between predictors and predictand using correlation coefficient. The predictors finalized in the step screen variables are used in the step calibration model

**Table 1**: Predictors selected for Bhopal city

| Predictand | Predictors |
|---|---|
| Daily Precipitation | ncepp8zhgl,nceps500gl, ncepshumgl |

### *3.2 Calibration and Validation of SDSM*

In this analysis by using selected screen variables Calibration and validation is done for maximum temperature, minimum temperature and precipitation. For calibration the period from 1979-1995 is used and for validation the period from 1996-2005 is used.

### *3.4 Model Evaluation criteria for Bhopal*

The statistical measures Nash-Sutcliffe efficiency (NSE) and the Coefficient of determination ($R^2$) during calibration and validation obtained is fairly good for Bhopal city for precipitation are shown below

**Table 2**: NSE and $R^2$ for calibration and validation

| | Nash-Sutcliffe efficiency (NSE) | | Coefficient of determination ($R^2$) | |
|---|---|---|---|---|
| | Calibration | Validation | Calibration | Validation |
| Precipitation | 0.689 | 0.630 | 0.643 | 0.657 |

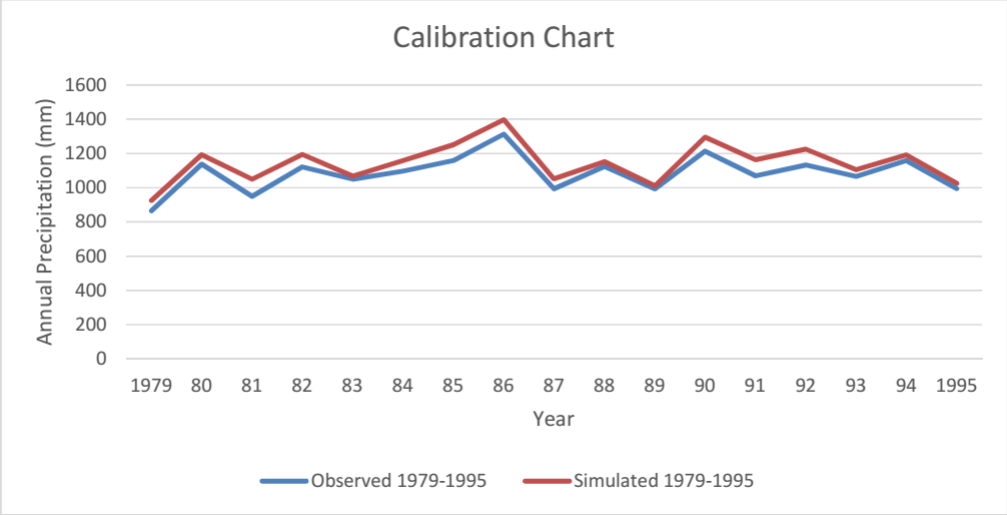



**Figure 1**: Calibration of annual precipitation

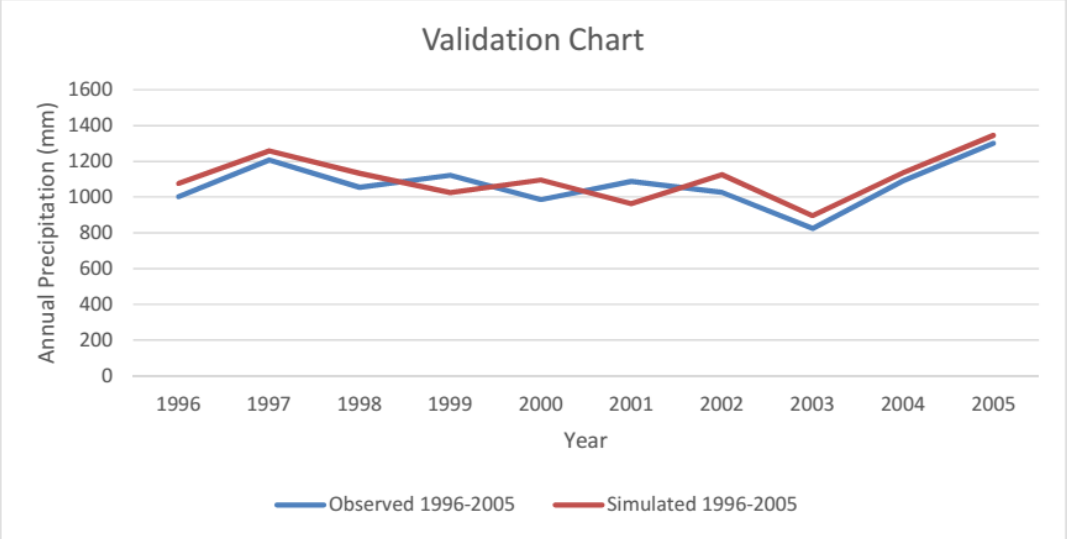



**Figure 2**: Validation of annual precipitation

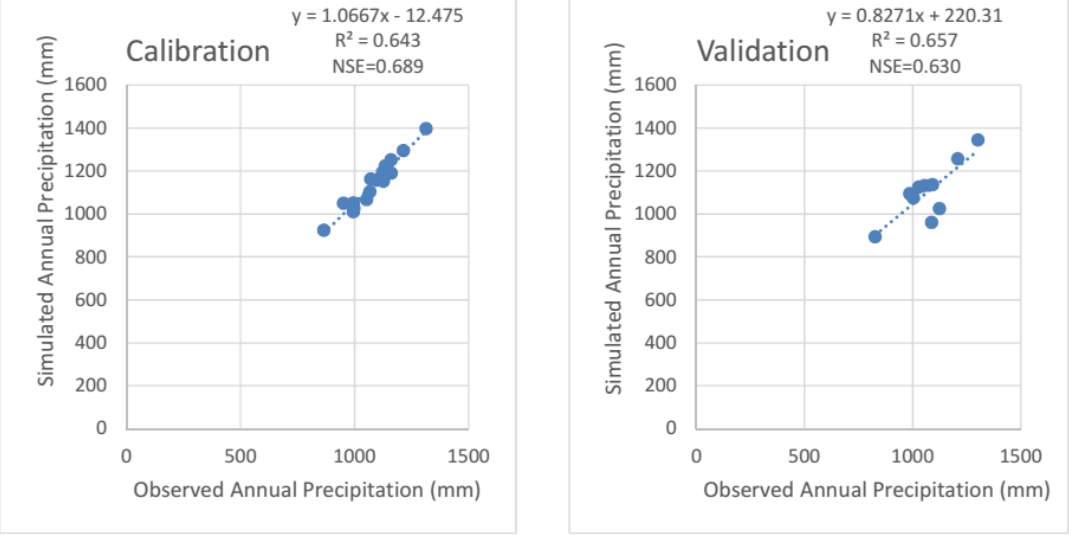



**Figure 3**: Values of NSE and $R^2$ for Calibration and validation for precipitation

### *3.5 Generation of Future series for CanESM2 RCPs*

The selected variables combination with calibrated parameters has been used for series generation synthetically for three future periods Future Period (2006-2035), Future Period (2036-2070) and Future Period (2071-2100) using gridded predictors obtained from Second generation Canadian Earth System Model (CanESM2) under the different RCPs (RCP 2.6, RCP 4.5, & RCP 8.5 ). The statistics including annual precipitation were computed.
The annual precipitation for all three periods Future Period (2006-2035), Future Period (2036-2070) and Future Period (2071-2100) for *Bhopal city* is seen in Figure below-

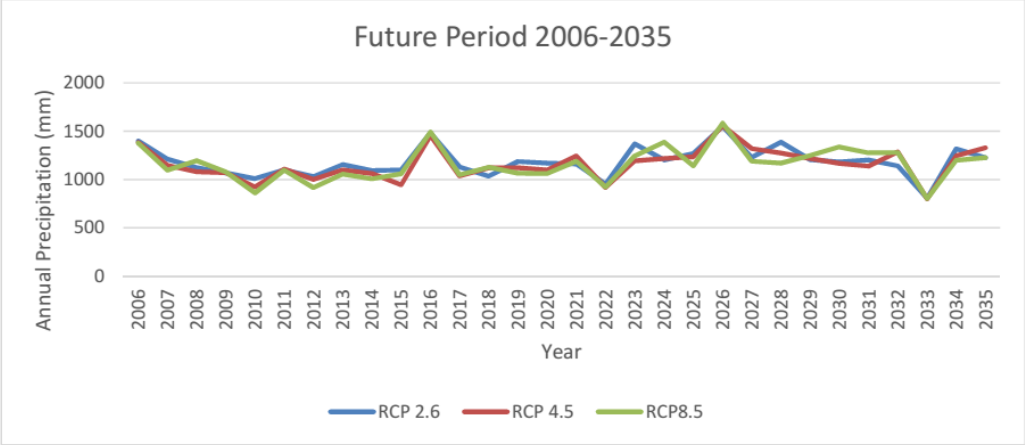



**Figure 4**: Comparison of annual generated precipitation for RCP 2.6, 4.5 & 8.5 for FP (2006-2035)

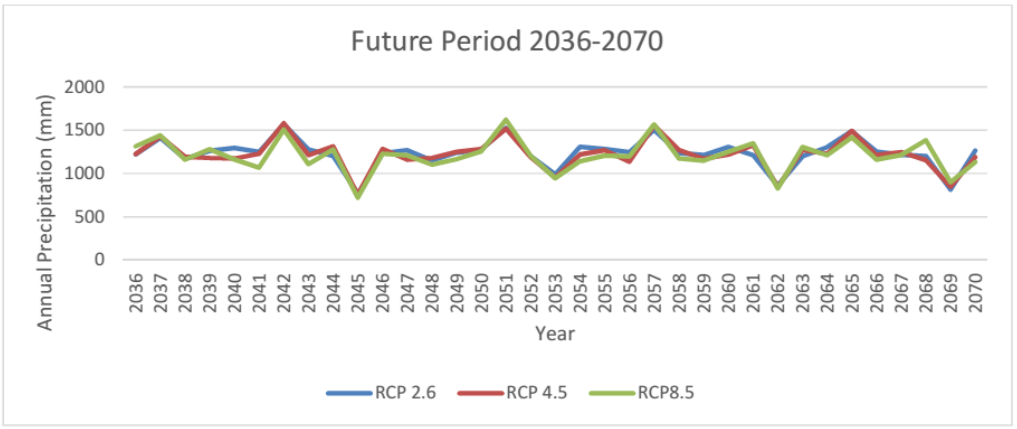



**Figure 5**: Comparison of annual generated precipitation for RCP 2.6, 4.5 &8.5 for FP (2036-2070)

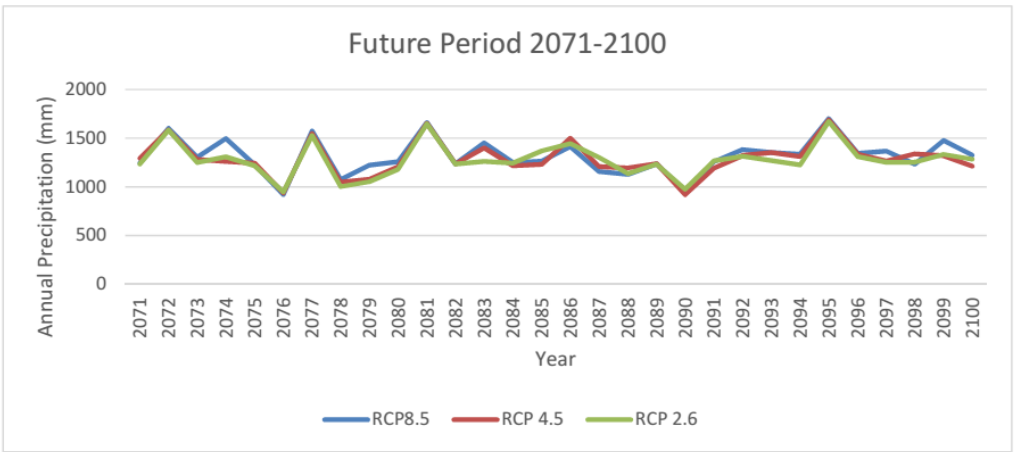



**Figure 6**: Comparison of annual generated precipitation for RCP 2.6, 4.5 &8.5 for FP (2071-2100)

From the analysis, it has been analysed that annual precipitation of *Bhopal city* increase for *RCP 2.6*by 9.71%, 14.40% and 21.797% for FP (2006-2035), FP (2036-2070) and FP (2071-2100) respectively. It increase for RCP 4.5 by 7.50%, 13.10% and 19.19% for FP (2006-2035), FP (2036-2070) and FP (2071-2100) respectively. And it increase for RCP *8.5* by 6.43%, 12.10% and 18.306% for FP (20062035), FP (2036-2070) and FP (2071-2100) respectively.

## 4. Summary and Conclusion

At the annual level, *precipitation* is expected to increase from future period (2006-2035) to future period (2071-2100) for all three RCPs (RCP 2.6, RCP 4.5 and RCP 8.5). If we assume that RCP 2.6 and their condition are prevalent in future then there is average increase is seen in precipitation which is approximate 9.71% to 21.797% from 2006 to 2100. If we assume that RCP 4.5 and their condition are prevalent in future then there is average increase is seen in precipitation which is approximate 7.50% to 19.19% from 2006 to 2100. If we assume that RCP 8.5 and their condition are prevalent in future then there is average increase is seen in precipitation which is approximate 6.43% to 18.306% from 2006 to 2100.

The National Environment Policy also argued that anthropogenic climate change has serious adverse effects on rainfall patterns in India, agricultural potential ecosystems, water resources, coastal resources and marine resources. Large-scale planning would clearly be required for adaptation measures to climate change impacts, so that the current results of future downscaling in precipitation can be used for water resource planning, basin management and enabling policy makers to identify adaptation and mitigation strategies that are robust to future uncertainties.

## References

Ali, S., Mishra, P. K., Islam, A., & Alam, N. M. (2016): Simulation of Water Temperature in a Small Pond Using Parametric Statistical Models- Implications of Climate Warming. *Journal of Environmental Engineering, 142(3),* 04015085.

Anandhi, A., Srinivas, V.V., Nanjundiah, R. and Kumar, N. (2008): Downscaling Precipitation to River Basin in India for IPCC SRES Scenarios Using Support Vector Machine. *International Journal of Climatology, 28,* 401-420

Arora, H., Ojha, C. S. P., & Kashyap, D. (2016): Effect of Spatial Extent of Atmospheric Variables on Development of Statistical Downscaling Model for Monthly Precipitation in Yamuna-Hindon India. *Journal of Hydrologic Engineering 1084-0699.*

Chen, H., Chong, Y.X. and Shenglian, G. (2012): Comparison and Evaluation of Multiple GCMs, Statistical Downscaling and Hydrological Models in the Study of Climate Change Impacts on Runoff. *Journal of Hydrology*, 36-45.

Crane, R.G. and Hewitson, B.C. (1998): Doubled $CO_2$ Precipitation Changes for the Susquehanna Basin: Downscaling From the Genesis General Circulation Model. *Int J Climatol; 18*, 65-76.

Das, J., and Umamahesh, N. V. (2015): Multisite Downscaling of Monsoon Precipitation over the Godavari River Basin under the RCP 4.5 Scenario. *World Environmental and Water Resources Congress* 1066-1075

Dibike, Y.B. and Coulibaly, P. (2005): Hydrologic Impact of Climate Change in the Saguenay Watershed: Comparison of Downscaling Methods and Hydrologic Models. *J Hydrol 307*, 145-163

Duhan, D. and Pandey, A. (2012): Statistical Analysis of Long-Term Spatial and Temporal Trends of Precipitation during 1901-2002 at Madhya Pradesh, India. *Atmospheric Research, 122,* 136-149.

Fowler, H. J.,Blenkinsop, S. and Tebaldi, C. (2007): Linking Climate Change Modelling to Impacts Studies: Recent Advances in Downscaling Techniques for Hydrological Modelling. *Int. J. Climatol. 27(12),* 1547-1578

Ghosh, S. and Mujumdar, P.P. (2006): Future Rainfall Scenario over Orissa with GCM Projections by Statistical Downscaling. *Current Science; 90(3),* 396-404.

Gosain, A.K., Rao, S. and Arora, A. (2011): Climate Change Impact Assessment of Water Resources of India, *Current Science; 101(3),* 356-371.

Goyal, M. K., & Surampalli, R. Y. (2018): Impact of Climate Change on Water Resources in India. *Journal of Environmental Engineering, 144(7), 04018054.*

Jaiswal, R.K., and Tiwari, H. L., (2015): Downscaling and Generation of Future Scenarios for Maximum Temperature in Upper Mahanadi Basin. *Int. J. Frontier Technol, 2(2),* 41-46

Karl, T.R., Wang, W.C., Schlesinger, M.E., Knight, R.W. and Portman, D. (1990): A Method of Relating General Circulation Model Simulated Climate to The Observed Local Climate. Part 1 Seasonal statistics. J. Climate, 3, 1053-79.

Mall, R.K., Gupta, A., Singh, R., Singh, R.S., and Rathore, L.S. (2006): Water Resources and Climate Change: An Indian Perspective. Current Science, 90(12), 1610-1626

Masui, T., Matsumoto, K., Hijioka, Y., Kinoshita, T., Nozawa, T., Ishiwatari, S., Kainuma, M. (2011): An emission pathway for stabilization at 6 Wm-2 radiative forcing. *Climatic Change, 109(1-2),* 59-76.

Mujumdar, P.P. and Ghosh, S. (2008): Modelling GCM and Scenario Uncertainty Using a Possibilistic Approach: Application to the Mahanadi River, India. *Water Resources Research. 44,* 1-15

Murphy, J.M. (1999): An Evaluation of Statistical and Dynamical Techniques for Downscaling Local Climate, *Journal of Climate, 12,* 2256-2284.

Pichuka, S., & Maity, R. (2016): Spatio- temporal downscaling of projected precipitation in the 21st century: indication of a wetter monsoon over the Upper Mahanadi Basin, India. *Hydrological Sciences Journal, 1—16.*

Rai, S. P., Sharma, N., & Wolf, A. T. (2019): Perceived Risk of Cooperation between India and Nepal on the Kosi River. *Journal of Water Resources Planning and Management, 145(9),* 05019012.

Rogelj, J., Meinshausen, M., & Knutti, R. (2012): Global warming under old and new scenarios using IPCC climate sensitivity range estimates. *Nature Climate Change, 2(4),* 248253.

Salmi, T., Maatta, A., Anttila, P., Ruoho-Airola, T., Amnel,l T. (2002): Detecting Trends of Annual Values of Atmospheric Pollutants by the Mann-Kendall test and Sen's Slope Estimates - the EXCEL Template Application MAKESENS: *Publications on Air Quality 31,* Finnish Meteorological Institute, Helsinki

Sen P. K. (1968): Estimates of the regression coefficient based on Kendall's tau. *Journal of American Statistical Association* 39, 13791389.

Stocker, T.F.D., Qin, G.-K., Plattner, M., Tignor, S.K., Allen, J., Boschung, A., Nauels, Y., Xia, V., Bex and P.M., Midgley (2013): Summary for Policymakers. In: Climate Change 2013: The Physical Science Basis. Contribution of Working Group I to the Fifth Assessment Report, AR5. *Intergovernmental Panel on Climate Change (IPCC).*

Thomson, A. M., Calvin, K. V., Smith, S. J., Kyle, G. P., Volke, A., Patel, P.,Edmonds, J. A. (2011): RCP4.5: A Pathway for Stabilization of Radiative Forcing By 2100. Climatic Change, 109(1-2), 77-94.

Van Vuuren, D. P., Stehfest, E., den Elzen, M. G. J., Kram, T., van Vliet, J., Deetman, S.,van Ruijven, B. (2011): RCP2.6: exploring the possibility to keep global mean temperature increase below 2°C. *Climatic Change, 109(1- 2), 95-116.*

Van Vuuren, D. P., Edmonds, J., Kainuma, M., Riahi, K., Thomson, A., Hibbard, K., Rose, S. K. (2011): The representative concentration pathways: an overview. *Climatic Change, 109(1-2),* 5-31.

Wilby, R.L., and Wigley, T.M.L. (1997): Downscaling General Circulation Model Output: A Review of Methods and Limitations. *Progress in Physical Geography, 21,* 530-548.

Wilby, R.L., Hay, L.E., and Leavesly, G.H. (1999): A Comparison of Downscaled and Raw GCM Output: Implications for Climate Change Scenarios in The San Juan River Basin, Colorado. *J. Hydrol., 225,* 67 - 91.

Winkler, J.A., Palutikof, J.P., Andresen, J.A., and Goodess, C.M. (1997): The Simulation of Daily Temperature Series from GCM Output. Part II: Sensitivity Analysis of an Empirical Transfer Function Methodology. *Journal of Climate 10,* 2514-2532.

Wood, A.W., Leung, L.R., Sridhar, V., and Lettenmaier, D.P. (2004): Hydrologic Implications of Dynamical and Statistical Approaches to Downscaling Climate Model Output. *Climatic Change, 62,* 189-216.

Xu, C.Y. (1999): From GCMs to River Flow: A Review of Downscaling Methods and Hydrologic Modelling Approaches. *Prog. Phys. Geogr. 23(1),* 57-77.

*IN PROCEEDINGS OF 25th HYDRO 2020, INTERNATIONAL CONFERENCE, NATIONAL INSTITUTE OF TECHNOLOGY ROURKELA, ODISHA, INDIA 26-28, March 2021, ISBN 978-93-90631-56-8*

Paper ID - 048

# A MORPHOLOGICAL COMPARISION OF TWO DIFFERENT CLIMATIC SETTINGS AND ITS SIGNIFICANCE ON THEIR SEDIMENT YIELD

Nirjharini Sahoo[1], Pradip Kumar Das[2] & Janhabi Meher[2]

*Dept. of Civil Engineering, Veer Surendra Sai University of Technology, Burla- 768018, India.*

*Email:nirjharini_sahoo@yahoo.co.in*

## ABSTRACT

Several parts of the world have been facing severe droughts and frequent floods due to climatic variables. For efficient management and adaptation measures, it is important to understand the relative effect of climate variability, morphometric variability on runoff, sediment erosion and sediment deposition. In the present study a comprehensive comparison of India's two major river basins, Budhabalanga and Nagavali belongs to two different climate settings is done on the basis of morphometric parameters, Land Use Land Cover (LULC) and soil texture. Budhabalanga river is situated in Odisha's Northern plateau zone have a catchment area of 4840 sq.km. and Nagavali river is of Eastern ghat zone have a catchment area of 9510 sq.km. These two rivers are very prone to flood in every year monsoon. In this study ASTER digital elevation model (DEM) data are used in Geographic Information System (GIS) environment for evaluation of linear, areal and relief aspects of morphological parameters. LULC map of India and soil map of world are used for respective study. To complete the study, runoff and sediment yield data (2010-2016) are collected from Central Water Commission (CWC). Based on the relation of sediment yield volume with these parameters sediment prone areas are identified. This study will be helpful to the concerned people/ departments in prediction of sediment yield, erosion of bank and will be useful in soil and water conservation process and plan strategies for any construction work.

***Key words:*** *Morphometric analysis,LULC, Soil Classification, Geographic Information System, Sediment yield.*

## 1. INTRODUCTION

Morphometric analysis is the estimation of geomorphologic parameters (linear aspect, areal aspect and relief aspect) of land. Hydrological behavior and soil erosion depend on geomorphologic parameters which determines the variation in earth's surface from past to present. A great step forward was made by Horton (1932) when he proposed general methods for the description of drainage basins characteristic. Morphometric analysis & prioritization of river drainage basin using remote sensing and GIS techniques have been attempted by no. of researchers (Pareta and Pareta (2012); Iqbal et. al. (2013); Kowsalya and Suresh (1014); Pophare and Balpande (2014); Guida et. al. (2016); Khakhlari and Nandy (2016); Mahala (2018)) and concluded that RS & GIS are most effective tools for morphometric analysis.

Soil erosion has been accepted as a serious problem arising from agricultural intensification, land degradation and possibly due to global climatic change, Yang et al. (2003). Not only the deposition of sediment transported by river into a reservoir reduces the reservoir capacity, but also sediment deposition on river bed and banks causes widening of flood plains during floods. Soil erosion is the most significant contributor of off-site ground water pollution on a global scale with most of the contaminants originating within an agricultural setting, Marsh and Grossa (1996).

The basins of Budhabalanga and Nagavali are considered to evaluate the degree of significance of morphometric parameters, LULC and soil characteristics on the sediment yield. These two basins belong to two different geographic conditions. So, the other morphological parameters those influence the sediment yield are analyzed to prioritize the sediment prone basin among the selected basin, for the present study.

## 2. STUDY AREA

The gauging stations Govindpur and Srikakulam are considered for Budhabalanga and Nagavali river basins for meteorological observation respectively. The Budhabalanga basin encompasses 4414.14 sq. km at Govindpur gauging station with the extension 18.277°N to 19.723° N and 82.889°E to 83.915°E. The Nagavali basin encompasses 9027.63 sq. km. at Srikakulam with extension 21.34°N to 22.352°N and 86.319° E to 86.939° E. The Figure. 1. Shows the location of study areas.

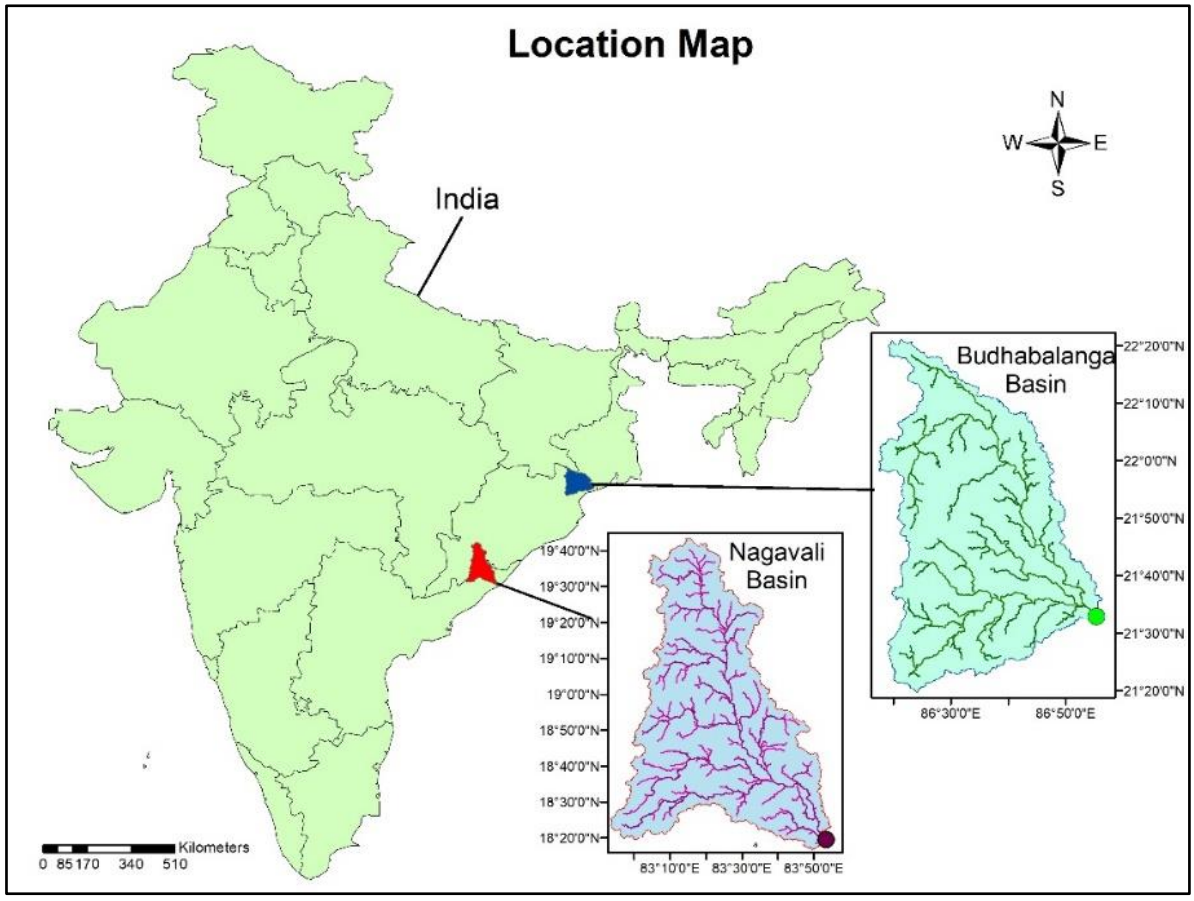



**Figure. 1.** Location map of the study areas

## 3. METHODOLOGY AND DATA ANALYSIS

### 3.1. *Discharge - Sediment Relationship*

Day wise sediment and discharge data was collected from (Central Water Commission) CWC. As the climate at study areas shows peak monsoon period from July to October, we have considered these four months data of 2010 to 2016 for the analysis. The maximum of sediment intensity (S in ton/$m^3$/s) of every month and the corresponding discharge (Q in $m^3$/s) of the study areas is plotted in Figure.2. It can be noted that the sediment intensity increases with increase in discharge, at the same time it can also be noted that for a constant discharge the intensity the sediment intensity at Nagavali is more than the same at Budhabalanga. This is why we have studied how with different characteristics of basin the sediment intensity changes.

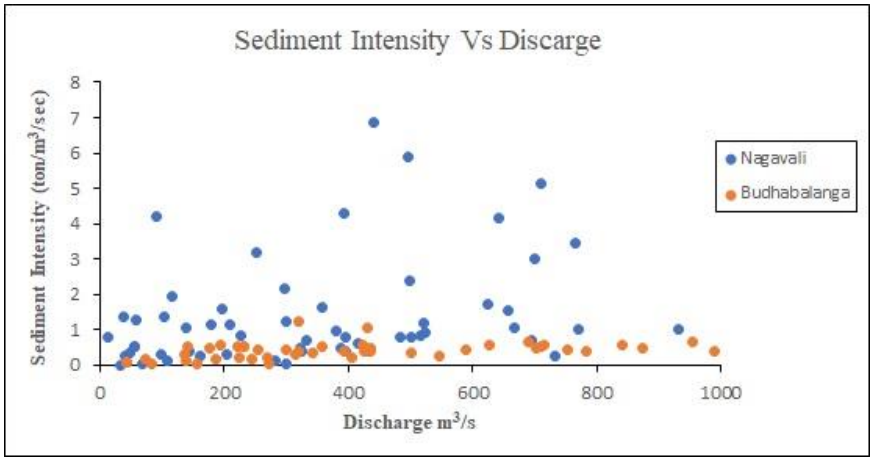



**Figure. 2.** Sediment vs Discharge of different basins

### 3.2. *Watershed delineation*

ArcGIS 10.3 software is used to fulfill the objectives of the study. In first step ASTER DEM data of the Budhabalanga and Nagavali basin is downloaded. Then the DEMS mosaic is done. The Dem is projected as WGS_1984_UTM_Zone_44N for the process of geo-referencing. Then process of watershed delineation is done by giving the Latitude and Longitude of the gauging stations.

### 3.3. *Morphometric analysis*

Morphometric analysis is a useful tool for watershed characterization. The study of morphometric analysis can be used to determine the ground water potential zones, water recharge sites, watershed delineation and geotechnical investigation in a watershed.
Primary parameters such as number of stream and length of the stream, area, perimeter, basin length etc. are derived from the thematic layers by using ArcGIS. Basically, morphometric analysis is done under three aspects; namely linear aspect, areal aspect and relief aspect. The three aspects are described below:

#### 3.3.1. *Linear aspect*

The characteristics of a stream and its tributaries from inlet to outlet are described by linear aspect parameters of morphometric analysis. The linear aspect parameters are [I] Stream order: it is delineated in ArcGIS which follows Strahler's stream ordering rule. According to Strahler's system of stream ordering, fingertip tributaries are taken as 1st order stream. Two 1$^{st}$ order streams combine to form a 2$^{nd}$ order stream. Two 2$^{nd}$ order streams combine to form a 3$^{rd}$ order stream and so on. [II] Stream number ($N_u$) is the total stream segments present in a particular order of stream is called as, calculated in ArcGIS. [III]Stream length ($L_u$) is the total length of stream order in a particular order of stream, calculated in ArcGIS. [IV] Mean stream length ($L_{um}$) is the ratio of the total stream length in a particular order to the total number of streams in that order. [V] Bifurcation ratio is a dimensionless parameter, shows the form of drainage basin. It is considered as the index of relief. Higher bifurcation ratio implies high runoff and low permeability of the drainage basin. It is also indicating the shape of the basin. High $R_b$ value is indicative of elongation shape of the basin and low $R_b$ value is indicative of circular shape of the basin. [VI] Stream length ratio is calculated by dividing mean stream length of one particular order and the mean stream length of next lower order. It is denoted by $R_L$. The higher value of stream length ratio indicates the formation of young geomorphic landforms along the area. Delineated stream order of the watersheds is shown in Figure.3.

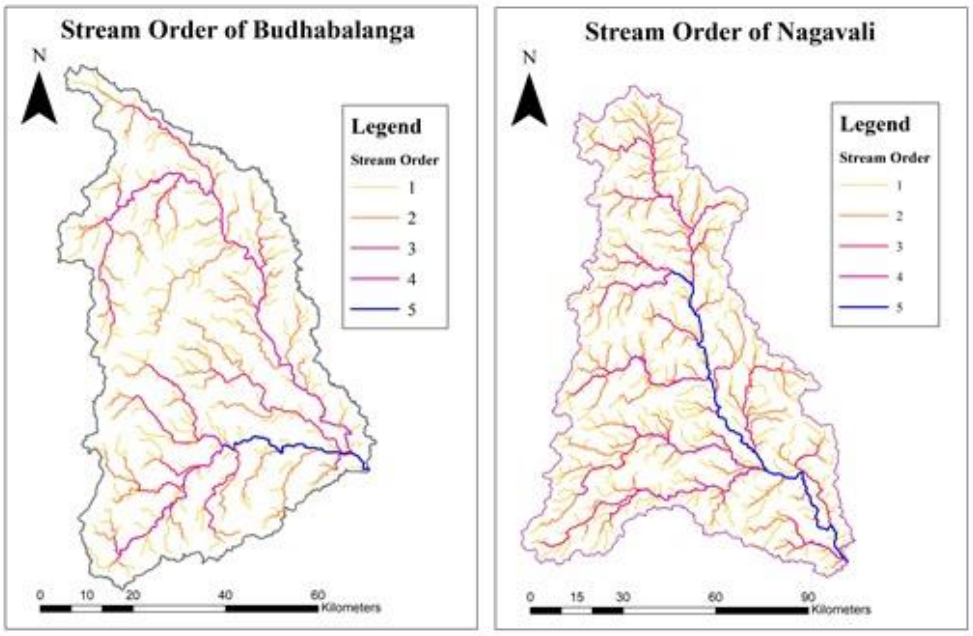



**Figure. 3.** Stream order of river basins

Computation of linear aspect parameters includes order of streams, stream number and stream length in a selected order, bifurcation ratio, mean bifurcation ratio, mean stream length etc. is tabulated in Table.1.

**Table 1.** Linear aspects of watersheds

| | Linear Parameters | | | Linear Aspects | | | | | |
|---|---|---|---|---|---|---|---|---|---|
| Formula | GIS | | | | Lum = Lu/Nu | Rb = Nu / Nu+1 | Rbwm= Rb (Nu+Nu+1) /(Nu+Nu1) | RL= Lu/Lu-1 | RLwm= RL(Lu+Lu+1) / (Lu+Lu1) |
| Sl. No. | Stream Order | No. of Streams (Nu) | Length of Stream in km (Lu) | Total length of all order stream (L) in km | Mean Stream Length (Lum) in km | Bifurcation Ratio (Rb) | Weighted Mean Bifurcation Ratio (Rbm) | Stream length Ratio (RL) | weighted mean Stream length Ratio (RLm) |
| Nagavali | 1st | 569 | 1828.56 | 3604.30 | 3 | 5.47 | 0.516 | | 0.549 |
| | 2nd | 104 | 879.872 | | 8.460 | 2.74 | | 0.48 | |
| | 3rd | 38 | 453.451 | | 11.933 | 4.75 | | 0.52 | |
| | 4th | 8 | 289.187 | | 36.148 | 8.00 | | 0.64 | |
| | 5th | 1 | 153.230 | | 153.230 | | | 0.53 | |
| Budhabalanga | 1st | 312 | 850.539 | 1807.17 | 3 | 5.20 | 0.549 | | 0.516 |
| | 2nd | 60 | 473.741 | | 7.896 | 3.75 | | 0.56 | |
| | 3rd | 16 | 266.337 | | 16.646 | 5.33 | | 0.56 | |
| | 4th | 3 | 172.236 | | 57.412 | 3.00 | | 0.65 | |
| | 5th | 1 | 44.325 | | 44.325 | | | 0.26 | |

### 3.3.2. *Areal Aspects*

Areal aspect is two-dimensional aspect, which depends on Basin perimeter (P), length ($L_b$) and area (A). The basin perimeter, length and area are calculated in ArcGIS. Basin area is an important factor in the morphometric analysis which relates to various factors. Areal aspect includes the drainage density, drainage texture, stream frequency, shape factors of basin etc. [I] Basin length ($L_b$): is the longest length of the basin, from farthest inlet point to the outlet point. [II] Drainage density ($D_d$): is the ratio of total stream length of a basin and the basin area. Higher drainage density indicates higher runoff, sparse vegetation and mountainous relief and lower drainage density indicates the higher infiltration. The factors affecting drainage density are geology and Land use/Land cover. Dd is shown in Figure. 4.

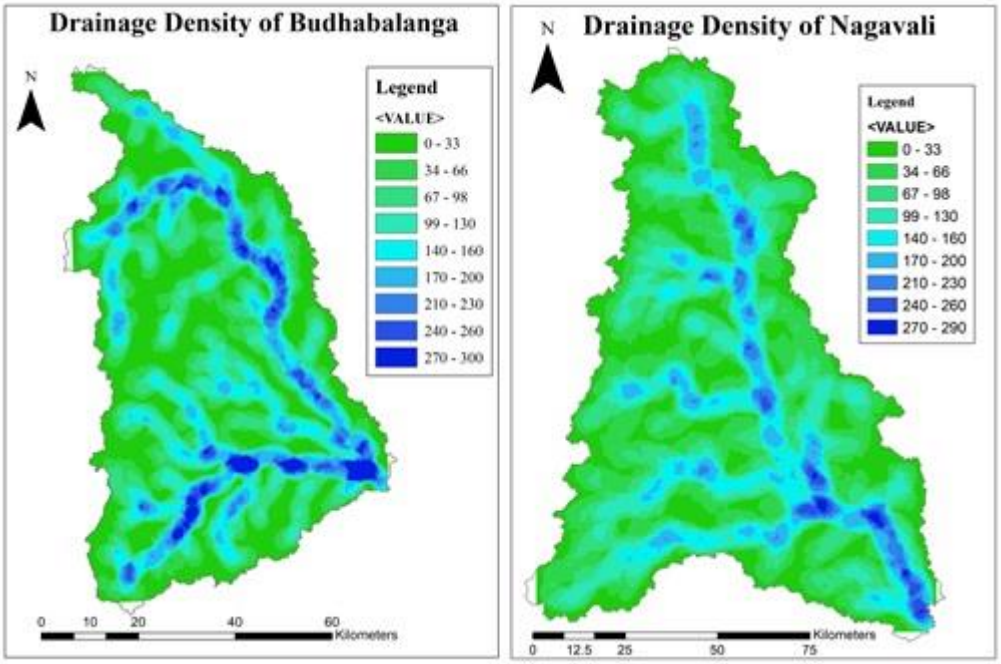



**Figure. 4.** Drainage density of watersheds

[III] Stream frequency ($F_s$): is the ratio of total stream number of the basin and the basin area. Stream frequency increases by increasing the numbers of streams, as a result drainage density also increases. [IV] Drainage Texture ($R_t$): is the ratio of total stream number present in a watershed to the selected watershed parameter. The drainage texture depends on natural factors, infiltration capacity and relief. [V] Length of Overland Flow ($L_g$): the length of stream on the surface before it joins a definite stream channel. $L_g$ is mostly influenced by both hydrologic and physiographic structures of the area. Higher value of $L_g$ indicates that the watersheds have longer flow paths which relates to higher infiltration and lower runoff. $L_g$ is half of the inverse of $D_d$. [VI] Infiltration Number ($I_f$): is the multiplication of $D_d$ and $F_s$. It indicates the infiltration property of the basin. Higher $I_f$ indicates the lower infiltration and higher runoff. [VII] Compactness Coefficient ($C_c$): is the ratio of basin perimeter and the circumference of circular area, whose area equals to the area of the basin. A circular watershed is the most hazardous because it will yield the shortest time of concentration before peak flow happens in the watershed. [VIII] Constant of Channel Maintenance (C): is the reciprocal of Dd. Higher C value indicates the high infiltration and low runoff. [IX]Form Factor ($R_f$): is estimated by dividing basin area and square of the basin length. It indicates the shape of the basin. Generally, $R_f$ ranges from 0.1 to 0.8. Lesser $R_f$ value indicates highly elongated nature of the basin and higher $R_f$ value i.e 0.8, indicates highly circular nature of the basin. [X] Circularity ratio

($R_v$): is obtained by dividing the area of the watershed to the area of the circle having same perimeter as the watershed. Generally, the value of Rc varies from 0 to 1. Lower value Rc indicates elongated nature of basin and the higher value indicates circularity nature of the basin. [XI] Elongation Ratio (Re): Elongation ratio varies from 0 to 1. Higher value of Re (> 0.9) indicates the circular shape of the watershed and lower value (< 0.7) indicates the elongation shape of the watershed. These parameters are calculated and tabulated in Table. 2.

### 3.3.3. *Relief Aspects*

Relief aspect is also called as three-dimensional aspect. It describes the physical characteristics of the basin. It includes Basin relief ($B_h$), Relief ratio ($R_h$), Relative relief ($R_r$) and Ruggedness number ($R_n$). [I]Basin Relief ($B_h$): is the difference between elevation of the highest point and the lowest point of the watershed. Higher basin relief indicates low infiltration and high runoff. It is calculated using DEM of basins. Reliefs of Budhabalanga and Nagavali watersheds are shown in Figure. 5.

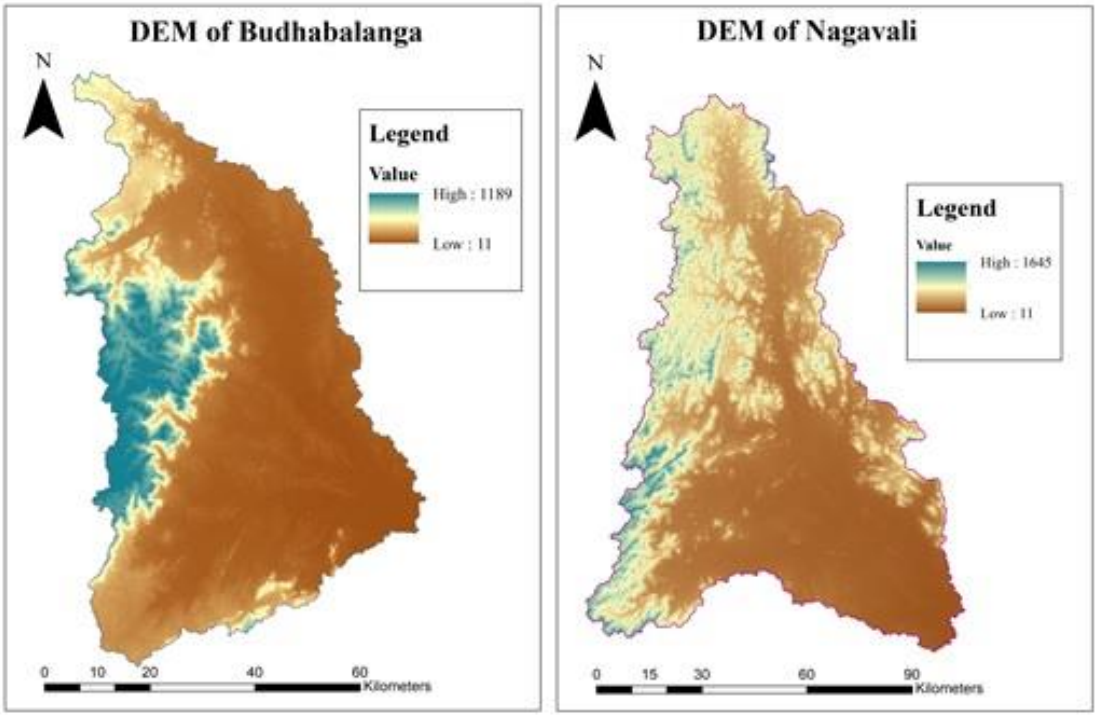



**Figure. 5.** DEM of watersheds showing highest and lowest elevation (Relief)

[II] Relief Ratio $R_h$ is obtained by dividing basin relief and the basin length. $R_h$ indicates the steepness of relief in the watershed and it signifies the intensity of soil loss process according to the slope of the watershed. Generally, $R_h$ increases with decreasing drainage area of the watershed. [III] Relative Relief ($R_r$): is obtained by dividing basin relief and the watershed perimeter. [IV] Ruggedness Number ($R_n$): $R_n$ is found by multiplying highest relief of basin and drainage density of the basin. Extremely higher $R_n$ shows the steeper slope of the basin as well as the longer slope. The slope percentage of the watersheds are shown in Figure 6. The slope of Nagavali is much higher than Budhabalanga as it is in Eastern ghat zone. The relief aspects of the watersheds are tabulated in Table 2.

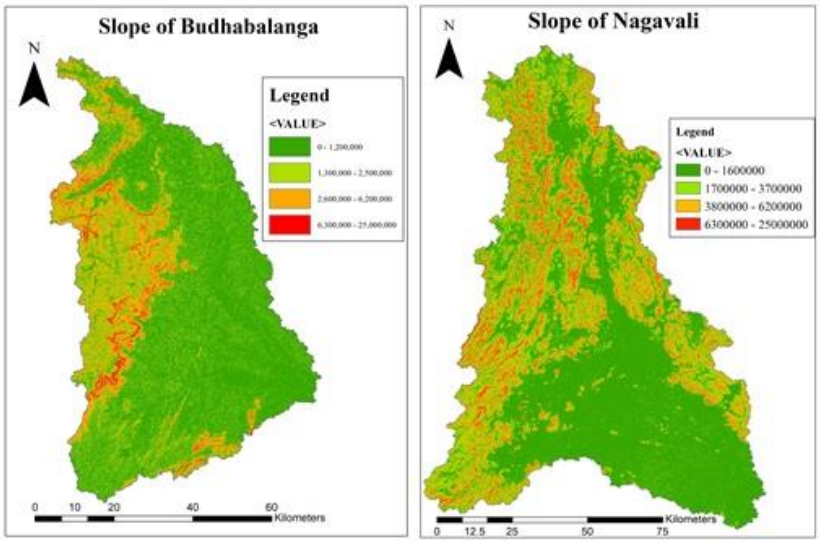



**Figure. 6.** Slope of watersheds

**Table 2.** Areal and relief aspects of watersheds

| Sl.No. | Parameters | Formula | Nagavali | Budhabalanga |
|---|---|---|---|---|
| 1 | Area (A) in sq.km | GIS | 9027.630 | 4414.144 |
| 2 | Perimeter (P) in km | | 734.640 | 618.227 |
| 3 | Basin length (Lb) in km | | 243.700 | 164.149 |
| 4 | Highest Elevation (Hh) in m | | 1645 | 1189 |
| 5 | Lowest Elevation (Hl) in m | | 11 | 11 |
| **Areal Aspect** | | | | |
| 1 | Drainage Density (Dd) | Dd = Lu /A | 0.399 | 0.409 |
| 2 | Length of Overland Flow (Lg) | Lg= 1/2*Dd | 0.200 | 0.205 |
| 3 | Stream Frequency (Fs) | Fs = Nu / A | 0.080 | 0.089 |
| 4 | Drainage Texture (Rt) | Rt = Nu / P | 0.980 | 0.634 |
| 5 | Infiltration Number (If) | If= Dd*Fs | 0.032 | 0.036 |
| 6 | Compactness Coefficient (Cc) | Cc=0.2821*P/A^0.5 | 2.181 | 2.625 |
| 7 | Constant of Channel Maintenance (C) | C=1/Dd | 2.505 | 2.443 |
| 8 | Form Factor (Rf) | Rf = A /Lb^2 | 0.152 | 0.164 |
| 9 | Circularity Ratio (Rc) | Rc=4πA/P^2 | 0.228 | 0.158 |
| 10 | Elongation Ratio (Re) | Re = (2/Lb)*{(A/π)^0.5} | 0.440 | 0.457 |
| **Relief Aspect** | | | | |
| 1 | Basin Relief(Bh) in m | Bh = highest elevation/lowest elevation | 1634 | 1178 |
| 2 | Relief ratio (Rh) | Rh= Bh/ Lb | 0.067 | 0.056 |
| 3 | Relative relief (Rr) | Rr = Bh/P | 0.002 | 0.002 |
| 4 | Ruggedness number (Rn) | Rn= Bh* Dd | 0.652 | 0.172 |

*3.4. LULC*

LULC map of the watersheds was taken from LULC map of India. The land use and land cover characteristics of soil tabulated in Table 3. Here we can note that the % crop land is nearly equal. The forest cover at Budhabalanga 12% more than Nagavali. The LULC map of the two watersheds is shown in Figure7.

**Table 3.** Land Use and Land Cover of watersheds

| | | Budhabalanga | | Nagavali | |
|---|---|---|---|---|---|
| **Sl.No** | **LULC_Classes** | **Area km²** | **Area (%)** | **Area km²** | **Area (%)** |
| 1 | Water Bodies | 56.20 | 1.27 | 781.29 | 8.66 |
| 2 | Barren land | 1.95 | 0.04 | 80.15 | 0.89 |
| 3 | Built-up land | 43.24 | 0.98 | 34.88 | 0.39 |
| 4 | Cropland | 2497.20 | 56.58 | 4452.5 | 49.33 |
| 5 | Shrubland | 182.21 | 4.13 | 1420.69 | 15.74 |
| 6 | Forest | 1632.93 | 37.00 | 2256.33 | 25.00 |

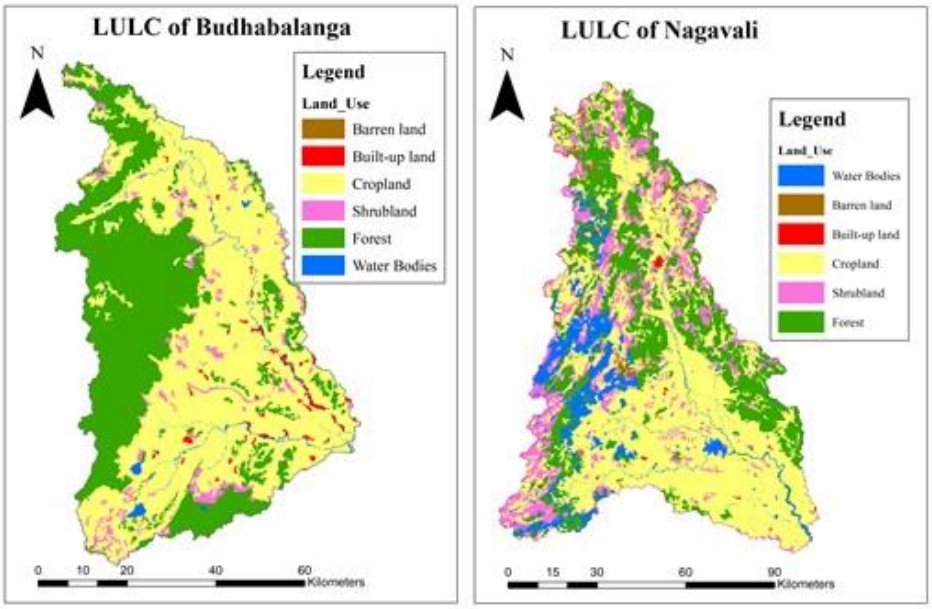



**Figure. 7.** LULC of watersheds

## 3.5. *Soil Classification of the Watersheds*

Soil map of the watersheds was taken from soil map of the world. The soil characteristics of the watersheds is tabulated in Table 4. Here we can note that the soil characteristics of Budhabalanga is loam by 99.7% of the watershed area where that is of Nagavali is clay_loam by 78.3% and loam by 21.6% of the total watershed area. The soil classification map of the two watersheds is shown in Figure 8.

**Table 4.** Soil classification of the watersheds

| Budhabalanga | | | | | Nagavali | | | | |
|---|---|---|---|---|---|---|---|---|---|
| **Sl No.** | **Soil Classes** | **Soil Texture** | **Area (in km$^2$)** | **% of Area** | **Sl No.** | **Soil Classes** | **Soil Texture** | **Area (in km$^2$)** | **% of Area** |
| 1 | 3819 | Loam | 26.36 | 99.7 | 1 | 3829 | Loam | 1946.73 | 21.6 |
| 2 | 3735 | Loam | 423.56 | | 2 | 3830 | Clay_Loam | 6393.90 | 78.3 |
| 3 | 6668 | Loam | 1753.60 | | 3 | 3754 | Clay_Loam | 670.60 | |
| 4 | 3729 | Loam | 2204.91 | | 4 | 3845 | Clay (light) | 8.14 | 0.1 |
| 5 | 6663 | Clay_Loam | 12.05 | 0.3 | | | | | |

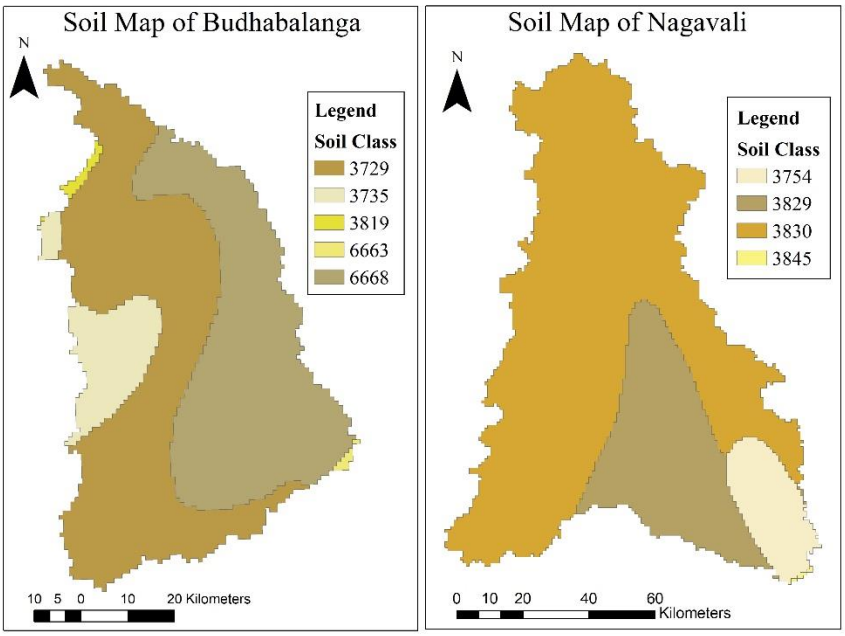



**Figure. 8.** Soil Classification of the Watersheds

## 4. DISCUSSION AND CONCLUSION

From the sediment intensity vs discharge graph, it can be noted that the Nagavali basin is sediment prone area in comparison to Budhabalanga. This may be due to various factors which we have come across through this study. From morphometric analysis, it is seen that the weighted mean bifurcation ratio (Rbm) and weighted mean stream length ratio (RLm) of the two watersheds are same whereas the total length of all order stream (L) of Nagavali is double that of Budhabalanga and from basin relief and percentage increase in slope, it can be noted that the slope of Nagavali is enough high than the Budhabalanga basin, these can be a reason of Nagavali's high flood susceptibility and high sediment disposing behaviour. From soil classification, Budhabalanga comes under loamy soil, whereas Nagavali comes under clay-loam soil which gives one more reason of Nagavali's openness to erosion and deposition. All these information's are very important for soil and water conservation process and plan strategies for any construction work.

## 5. REFERENCES:

Guida, D., Cuomo, A. and Palmieri, V. (2016) Using object-based geomorphometry for hydro-geomorphological analysis in a mediterranean research catchment". Hydrol. Earth Syst. Sci., 20: 3493–3509

Iqbal, M.,Sajjad, H., Bhat, F.A. (2013) Morphometric analysis of Shaliganga sub catchment, Kashmir valley, India using geographical information system. International Journal of Engineering Trends and Technology- Volume4 (1): 2231-5381

Khakhlari, M. and Nandy, A. (2016) Morphometric analysis of Barapani river basin in Karbi Anglong district, Assam. International Journal of Scientific and Research Publications, Volume 6 (10): 2250-3153.

Kowsalya, M. and Suresh, B. S. (2014) Quantitative geomorphological analysis of micro watersheds of Ghataprabha River sub-basin. International Journal of Advance Research in Science and Engineering, Vol. No.3 (2), ISSN:2319-8354.

Mahala, A. (2018) Drainage basin morphometric analysis of mountain-plain (Kosi, Bihar) and plateau-plain (Kangsabati, WB) regions of tropical environment: a comparative analysis. J. Ind. Geophys. Union, Vol. 22(4)

Pareta, K. and Pareta, U. (2012) Quantitative geomorphological analysis of a watershed of Ravi river basin, H.P. India. International Journal of Remote Sensing and GIS, Volume 1(1): 2277–9051

Pophare, A. M., Balpande, U. S. (2014) Morphometric analysis of Suketi river basin, Himachal Himalaya, India. J. Earth Syst. Sci. 123 (7): 1501–1515

Yang, D., Kanae, S., Oki, T., Koike, T., & Musiake, K. (2003) Global potential soil erosion with reference to land use and climate changes. Hydrological Processes, Vol. 17: 2913–2928.

*IN PROCEEDINGS OF 25th HYDRO 2020, INTERNATIONAL CONFERENCE, NATIONAL INSTITUTE OF TECHNOLOGY ROURKELA, ODISHA, INDIA 26-28, March 2021, ISBN 978-93-90631-56-8*

Paper ID - 091

# Sensitivity change of water deficit droughts on evapotranspiration methods in the Indian subcontinent

Femin C Varghese[1], Subhasis Mitra[1]

[1] *Department of Civil Engineering, Indian Institute of Technology Palakkad, Kerala-678623, India*
*Email: 101914002@smail.iitpkd.ac.in*
*Telephone/Mobile No.: +91 9495656893*

## Abstract

The choice of general circulation model (GCM) and reference evapotranspiration (ETo) estimation methods are crucial to projecting water deficit. Standardized Precipitation Evapotranspiration Index (SPEI) which is derived from water deficit also depends on choice of GCM and ETo estimation methods. In this study variance-based global sensitivity analysis will be used to evaluate relative sensitivity of projected changes in future water deficit (P-ETo) and SPEI to the choice of GCM and ETo estimation methods over parts of the Indian subcontinent. Two distinct periods are considered i.e. 2030-2060 and 2070-2100 for analysing the change in water deficit and droughts. To quantify the range and estimate the relative sensitivity of future projections to both factors, 7 GCMs and 11 ETo estimation methods are used. The 11 ETo methods are categorized into 4 major ETo methods based on temperature, radiation, mass transfer and combination. Results show that changes in future water deficit and droughts properties varies with regions and seasons. Overall, changes in water deficit droughts are more influenced by the choice of ETo, while GCM effects are more prominent for different regions. Result of this study indicate, the role of proper ensemble formation of GCMs and ETo estimation methods based on seasons and regions, to develop a robust range of future conditions for water resources planning.

***Keywords:*** *Standardized Precipitation Evapotranspiration Index, Global Sensitivity Analysis, Drought.*

## 1. Introduction

In the warming climate scenario, frequency, severity and extent of the extreme weather events are expected to change. A warming climate will lead to increases in evapotranspiration which can exacerbate droughts or amplified atmospheric moisture can lead to higher frequency of extreme rainfall events leading to floods (Sharma and Mujumdar 2017; Zhao and Dai 2017). Droughts are extreme climate events, caused by prolonged precipitation deficiency and temperature rise. For assessment of drought risk under a changing climate, drought projections are important. Changes in future precipitation and potential evapotranspiration are likely to affect future drought characteristics (Chang et al. 2016, Shi et al. 2020).

In India agriculture is the primary livelihood, and characteristics of extreme events have to be studied both spatially and temporally. Since the impacts of such extreme events are devastating towards agricultural and economic point of view, studies have been carried out to understand how their properties are projected to change in future. Different model projections, have uncertainties in projected climate variables, thus affecting drought tendencies. Evapotranspiration is the connection between energy balance and water balance and thus, helps in understanding the behaviour of climate. Different ETo estimation approaches can lead to a range of ETo values depending on the variables used (Wang et al. 2015).

The uncertainty in the projected drought occurrence thus may arise from the choice of GCMs and/or ETo estimation methods. In this study we aim to understand how sensitivity of drought properties vary with GCM and ETo estimation methods across different climate zones in India under a changing climate.

## 2. Dataset and methods

### *2.1 Data used*

The Indian subcontinent was divided over four climate zones (figure 1) derived from Koppen-Geiger climate classification (Kottek et al. 2006) for this study.

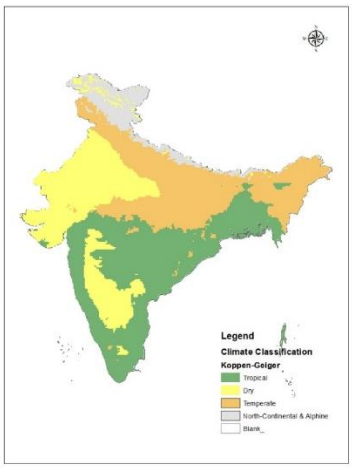



**Figure 1**: Climate region classification derived from Koppen-Geiger Classification

Seven GCMs from the Coupled Model Intercomparison Project 5 (CMIP5) archive have been selected for analysis that were found to perform well in capturing the South Asian summer monsoon (Ashfaq et al. 2017). These seven models also had all the climate variables required for most data-intensive ETo estimation methods. All the GCMs were re-gridded into $1^0$ x$1^0$ to have a common resolution. Table 1 provides the description of the GCMs used in this study.

**Table 1**: Description of GCMs

| Model | Institute | GCM grid(degree) |
|---|---|---|
| ACCESS 1 | Centre for Australian Weather and Climate Research (CAWCR) | 1.5 |
| CNRM-CM5 | Centre National de Recherches Meteorologiques | 1.4 |
| GFDL-ESM2G | Geophysical Fluid Dynamics Laboratory | 1.9 |
| GFDL-ESM2M | Geophysical Fluid Dynamics Laboratory | 2.2 |
| MIROC-ESM | Atmosphere and Ocean Research Institute (The University of Tokyo) | 2.2 |
| MIROC-ESM-CHEM | Atmosphere and Ocean Research Institute (The University of Tokyo) | 2.8 |
| MIROC5 | Atmosphere and Ocean Research Institute (The University of Tokyo) | 1.4 |

Climate variables for historical base period (1950-2005) and future period (2006-2100) under the RCP 8.5 trajectory for the rli1p1 ensemble were downloaded. For analysis, the future period was divided into two time periods: future 1 (2030-2060) and future 2 (2070-2100). The climate variables were used to estimate ETo values for different estimation methods and GCMs. Eleven reference evapotranspiration estimation methods (Blaney- Criddle, Hamon, Hargreaves, Kharrufa, Thornwaithe, Dalton, Meyer, Irmak-Rn, Irmak-Rs, Priestley-Taylor, and Penman-Monteith) mainly categorized based on

temperature, radiation, mass transfer and combination was used in this study (Table 2) (Xu and Singh 2001; Allen 1998).

**Table 2**: ETo estimation methods

| **Method** | **Equation** |
|---|---|
| Blaney-Criddle | $ETo = p(0.46T + 8.13)$ |
| Hamon | $ETo = 0.55{\delta_T}^2 P_t$ |
| Hargreaves | $ETo = 0.0135K_T S_o(T + 17.8)\sqrt{\delta_T}$ |
| Kharrufa | $ETo = 0.34pT^{1.3}$ |
| Thornwaithe | $ETo = 16 * \frac{L}{12} * \frac{N}{30} * 10 * \left(\frac{T_d}{I}\right)^{\alpha}$ |
| Dalton | $ETo = (0.3648 + 0.07223u)(e_s - e_a)$ |
| Meyer | $ETo = (0.375 + 0.05026u)(e_s - e_a)$ |
| Irmak-Rn | $ETo = 0.486 + 0.289R_n + 0.023T$ |
| Irmak-Rs | $ETo = -0.611 + 0.149R_s + 0.079T$ |
| Priestley-Taylor | $ETo = \alpha * \frac{\Delta}{(\Delta + \gamma)} * (R_n - G)/\lambda$ |
| Penman-Monteith | $\mathrm{ETo} = \frac{0.408\Delta(R_n - G) + \gamma * \left(\frac{900}{T+273}\right) * u_2 * (e_s - e_a)}{(\Delta + \gamma(1 + 0.34u_2)}$ |

Drought severity changes with marked increase in temperature, and thus an index accounting for temperature has been considered for this analysis (Wang et al. 2015; Su et al. 2018). Standardized Precipitation Evaporation Index (SPEI) is calculated using the water deficit (P-ETo) series which is fitted into a log-logistic distribution (Vicente-Serrano et al. 2010). The log logistic distribution can account for negative values in the D series, where D series is equal to the difference of precipitation and potential evapotranspiration. Parameters of log logistic distribution was obtained by L-moments method. The cumulative distribution function (CDF) of log logistic distribution for D series is given by

$$F(x) = [1 + \left(\frac{\alpha}{x - \gamma}\right)^{\beta}]^{-1} \quad (1)$$

Standardized values of F(x), will give the SPEI values. Since SPEI is a standardized variable, with mean equal to zero and standard deviation equal to one, we can be compared over space and time. Water deficit (P-ETo) and SPEI were estimated for both historical and future periods. Thereafter, the values were segregated based on the seasons: monsoon (June - September), autumn (October- September), winter (December to February) and summer (March- May) seasons. These seasons were classified based on India Meteorological Department (IMD) classification (Vardhan and Chowdary 2017). Changes in future were calculated by taking the difference of seasonal mean value for future 1 or future 2 from the historical base period.

### *2.2 Sensitivity Analysis*

The uncertainty of changes in future water deficit and SPEI, to the choice of GCMs and ETo estimation methods was studied using the variance based global sensitivity analysis (GSA) (Saltelli 2008). Given

a model $Y = f(X_1 X_2 \ldots X_k)$ where $X_i$ represents the factors considered. The conditional expectation $E(Y/Xi)$, is the average over $Y/Xi$, which shows the variance across $X_i$ values. Hence, the variance of conditional expectation can be considered as a measure of sensitivity. The first order sensitivity index is obtained as:

$$S_i = \frac{V[E(Y/Xi)]}{V(Y)} \quad (2)$$

where V(Y) is the total variance over all Xi. Si is a normalized index varying between 0 and 1, as the numerator varies between 0 and V(Y).

The first order sensitivity of projected changes in water deficit and SPEI to the choice of GCMs and ETo estimation methods was calculated over four climate regions for different seasons and both the future periods, to assess the comparative contribution of each of these factors in the future uncertainties.

## 3. Results and discussions

The uncertainty of changes in future water deficit droughts i.e., SPEI values were assessed using variance based global sensitivity analysis (GSA) across different climate regions over diverse seasons. The analysis shows the percentage contribution of individual factors responsible for uncertainty in future water deficit and drought projections.

Figure 2 shows the first order sensitivity analysis result of water deficit and SPEI values over different seasons and climate regions for future 1.

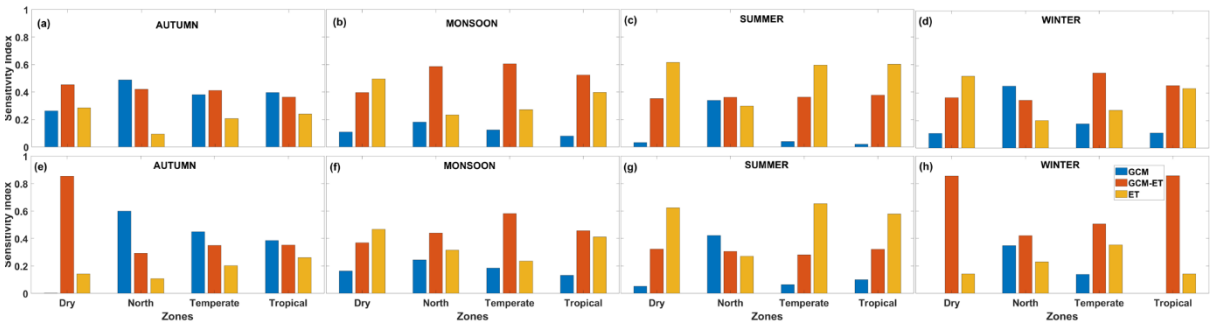



**Figure 2**: First order sensitivity analysis result of projected changes in water deficit (a, b, c, and d) and SPEI (e, f, g, and h) values for future 1

In the case of water deficit values in autumn season, all three variables, such as GCM, ETo methods and their interactions, contribute to uncertainty. Also, the contribution of ETo methods in the north zone is less compared to GCM and the interaction term. In the monsoon season ETo methods and interaction term indicate higher sensitivity values than GCM. And in the summer season, as the temperature is high, the sensitivity of the ETo methods is dominant. During the winter season, ETo methods and interaction term indicate higher sensitivity, but in the north zone, GCM shows higher sensitivity compared to ETo methods and interactions. Standardizing water deficit using SPEI values, changed the contribution of uncertainty among the three factors. In autumn season, the sensitivity of GCMs is relatively higher, but in the dry zone GCM has the least sensitivity. During the monsoon season GCM-ETo interaction and ETo estimation methods shows high sensitivity and the pattern is similar to water deficit. For summer, ETo methods shows higher sensitivity in both drought and water deficit, but in north zone GCM have high sensitivity values. In contrast to other seasons, during the winter season the interaction term contributed to higher uncertainty compared to GCM and ETo methods in drought and water deficit projections.

Figure 3 shows the sensitivity analysis for projected changes in water deficit and SPEI values for future 2. For water deficit, in the autumn season GCMs exhibited high uncertainty for north and temperate

zones. However, for monsoon and summer seasons, ETo methods and the interaction term contributed towards high uncertainty in water deficits. In winter season all the three factors (GCM, ETo and interaction) was found to be contributing to uncertainty. For droughts, autumn season have uncertainty contribution from all the three factors. While in monsoon season, interaction term imparts high uncertainty. During summer season ETo method contributed to high sensitivity, except in north zone. In the winter season all factors contribute to uncertainty, but interaction term shows high uncertainty for dry zone.

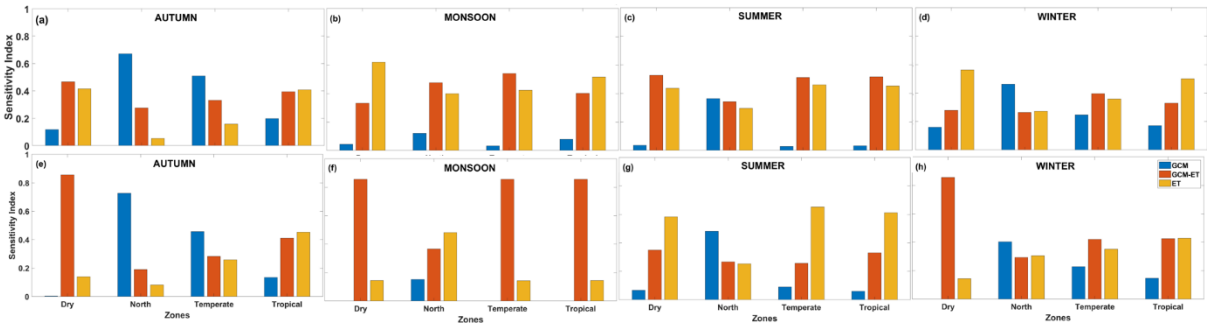



**Figure 3**: First order sensitivity analysis result of projected changes in water deficit (a, b, c, and d) and SPEI (e, f, g, and h) values for future 2

From future 1 to future 2, sensitivity of GCM, GCM-ETo interaction and ETo estimation methods varies for projected changes in water deficit and SPEI values over all seasons.

## 4. Conclusion

In the climate change scenario, the hydrological balance is affected with changes in future precipitation and evapotranspiration. This study helps in understanding the uncertainty involved in the estimation of future drought risk using PET based drought indices such as SPEI on the choice of GCMs or ETo estimation methods. For the projected changes in droughts during summer season, the source of uncertainty is dominant on ETo methods. While, uncertainty in GCM dominated during autumn season for both the future periods. Uncertainty during monsoon seasons was dominated by interaction term. And for winter season all the factors contributed to the uncertainty. This study shows that the sensitivity of the factors involved and the correct choice / set of GCMs and ETo estimation methods for different regions over different seasons are important for estimating the risk of drought when projecting climate variables in water resource planning.

## References

Allen, R. G., Pereira, L. S., Raes, D., and Smith, M.: Crop evapotranspiration: guidelines for computing crop water requirements, *FAO Irrigation and Drainage Paper 56*, 1998.

Ashfaq, M., Rastogi, D., Mei, R., Touma, D., Ruby Leung, L., 2017. Sources of errors in the simulation of south Asian summer monsoon in the CMIP5 GCMs. *Clim Dyn* 49, 193–223.

Chang, S., Graham, W.D., Hwang, S., Muñoz-Carpena, R., 2016. Sensitivity of future continental United States water deficit projections togeneral circulation models, the evapotranspiration estimation method, and thegreenhouse gas emission scenario. *Hydrol. Earth Syst. Sci.* 20, 3245–3261.

Kottek, M., Grieser, J., Beck, C., Rudolf, B., Rubel, F., 2006. World Map of the Köppen-Geiger climate classification updated. metz 15, 259–263

Saltelli, A. (Ed.), 2008. Global sensitivity analysis: the primer. John Wiley, Chichester, England; Hoboken, NJ.

Sharma, S., Mujumdar, P., 2017. Increasing frequency and spatial extent of concurrent meteorological droughts and heatwaves in India. *Sci Rep* 7, 15582.

Shi, L., Feng, P., Wang, B., Liu, D.L., Yu, Q., 2020. Quantifying future drought change and associated uncertainty in southeastern Australia with multiple potential evapotranspiration models. *Journal of Hydrology* 590, 125394.

Su, B., Huang, J., Fischer, T., Wang, Y., Kundzewicz, Z.W., Zhai, J., Sun, H., Wang, A., Zeng, X., Wang, G., Tao, H., Gemmer, M., Li, X., Jiang, T., 2018. Drought losses in China might double between the 1.5 °C and 2.0 °C warming. *Proc Natl Acad Sci* USA 115, 10600–10605.

Vardhan, D.H., Chowdary, S.Y.S., n.d. Annual Report 2017, INDIA METEOROLOGICAL DEPARTMENT MINISTRY OF EARTH SCIENCES 144.

Vicente-Serrano, S.M., Beguería, S., López-Moreno, J.I., 2010. A Multiscalar Drought Index Sensitive to Global Warming: The Standardized Precipitation Evapotranspiration Index. *Journal of Climate* 23, 1696–1718.

Wang, H., Chen, Y., Pan, Y., 2015. Characteristics of drought in the arid region of northwestern China. *Clim. Res.* 62, 99–113.

Wang, W., Xing, W., Shao, Q., 2015. How large are uncertainties in future projection of reference evapotranspiration through different approaches? *Journal of Hydrology* 524, 696–700.

Xu, C.-Y., Singh, V.P., 2001. Evaluation and generalization of temperature-based methods for calculating evaporation. *Hydrol. Process.* 15, 305–319.

Zhao, T., Dai, A., 2017. Uncertainties in historical changes and future projections of drought. Part II: model-simulated historical and future drought changes. *Climatic Change* 144, 535–548.

*IN PROCEEDINGS OF 25th HYDRO 2020, INTERNATIONAL CONFERENCE, NATIONAL INSTITUTE OF TECHNOLOGY ROURKELA, ODISHA, INDIA 26-28, March 2021, ISBN 978-93-90631-56-8*

Paper ID - 132

# Generation of Intensity-Duration-Frequency Curve for a River Basin in South Kerala by Incorporating Climate Changes

Lini R. Chandran[1], Aiswarya B. Babu[2], Krishna Priya S. B.[3], Sumina[4], Sini S. Nair[5]

[1]*Assistant Professor, Department of Civil Engineering, GEC Barton Hill, Thiruvananthapuram, 695035, India*
[2]*UG Scholar, Department of Civil Engineering, GEC Barton Hill, Thiruvananthapuram, 695035, India*
*Email:linisam@gmail.com Telephone/Mobile No.: +91 9447460832*

## Abstract

Global warming has a significant impact on frequency of extreme precipitation. It is one of the prominent factors which cause huge impact on drainage system by means of flooding. Intensity Duration – Frequency (IDF) curve plays a crucial role in designing robust drainage systems. Over the years it is seen that there is noticeable climate variability in many parts of the country. Hence to resist the impact of extreme precipitation we need to consider climate changes also by incorporating climate variable data in the IDF curve. In this study, IDF curves for the Neyyar river basin in Southern part of Kerala was generated using historical rainfall data from IMD for a period of 1955-2005 using Gumbel's distribution. This area was selected for the study as many major irrigation projects of the state are commissioned here. This IDF curve was compared with the standard IDF curve generated using the empirical relationship developed by Sherman C.W. (1931) and further modified by Bernard M. (1932) and the parameters suggested by Ram Babu (1979) and both the curves were found to follow the same pattern. The IDF curve was also developed for a period of 2006-2050 from the rainfall projected over the period from the multivariate linear regression model developed for each month. The projection of rainfall was performed using the predictor variables derived from the ICTP regional climate model (RegCM4). The NRMSE value of 0.08 obtained between the standard and projected IDF Curves shows that the curves developed by incorporating climate variables are more reliable than the standard curves for water resources applications.

***Keywords:*** *Extreme precipitation, Gumbel's distribution, Multivariate linear regression model, Intensity–Duration-Frequency Curve*

## 1. Introduction

The sustainability of infrastructure, ecosystems and public health depends on a predictable and stable climate. Thomas Vandal et al. (2018) suggested that key infrastructure required for the society are built to withstand specific levels of climate extreme and perform optimally in its expected conditions. Climate changes have significant impacts on the critical infrastructure. Most drainage systems are designed based on a long service life cycle of many decades. But the design standards existing now do not take the effect of climate change into consideration. Design of water resources infrastructures are based on Intensity-Duration-Frequency curves computed from historical data which essentially assumes that the historical statistics on extreme precipitation remain unchanged even for future use. Improving IDF curves to reflect the effect of climate has attracted a lot of attention in recent years and many researches are going on in this field. The method for future projection of IDF curves is based on the downscaled Global Climate Models (GCMs) or Regional Climate Models (RCMs).

The Intensity Duration Frequency curve shows the relationship between the rainfall intensity, the duration and the return period. Bhatt et al. (2014) generated IDF curves using daily rainfall data for different return periods in Bhadar river basin. There are two approaches to compute IDF curve. The first method is to make assumptions on the precipitation distribution and then use mathematical tools to derive a formula for IDF curve. Generalized Extreme Value (GEV) distribution is the most common one. The second method is based on empirical analysis. The empirical formula proposed by Sherman is used widely for this approach. Intensity Duration Frequency curves computed using historical rainfall data does not include the climate variables which are important in the current scenario. By incorporating the climate variables an accurate curve can be computed and projected, which helps in designing robust hydraulic structures.

In this study, IDF curves for the Neyyar River basin in Southern part of Kerala was generated using historical rainfall data from IMD for the period 1955-2005 using Gumbel's distribution (John A 2018). This IDF curve was compared with standard IDF curve generated using the empirical relationship developed by Sherman and further modified by Bernard and the parameters as suggested by Ram Babu and both the curves were found to follow the same pattern. The IDF curve was also developed for a period of 2006-2050 from the rainfall projected over the period using the multivariate linear regression model developed for each month. The projection of rainfall was performed using predictor variables derived from the ICTP regional climate model (RegCM4).

## 2. Study Area

The Neyyar River is the southernmost river of Kerala state. The river originates from Agastya Hills at about 1860 m above mean sea level. It flows down rapidly along falling terrain in the higher reaches and through almost flat terrain at the tail end. It flows in a southwesterly direction in the mountainous regions and then takes a westerly course into Lakshadweep Sea near Poovar. It has a total length of 56 km and the main tributaries of Neyyar are the Kallar and Karavalliar. The Neyyar river basin constitutes one of the major river systems in Thiruvananthapuram district of Kerala. It is an important terrain for biodiversity hot spot in Peninsular India. It lies between $8^0$ 15'N to $8^0$ 40'N and $77^0$ 00' E to $77^0$ 20'E. The basin has a total area of 483 sq. km covering 24 panchayats. The basin experiences a tropical climate. The mean annual temperature of the basin is $27.5^0$ C. The region usually receives maximum rainfall during the month of June and minimum rainfall during January. The mean monthly temperature varies from a maximum value of $33^0$ C during the months of March to May and to a minimum of $26^0$ C during June to November. Figure 1 shows the map of the Neyyar river basin.

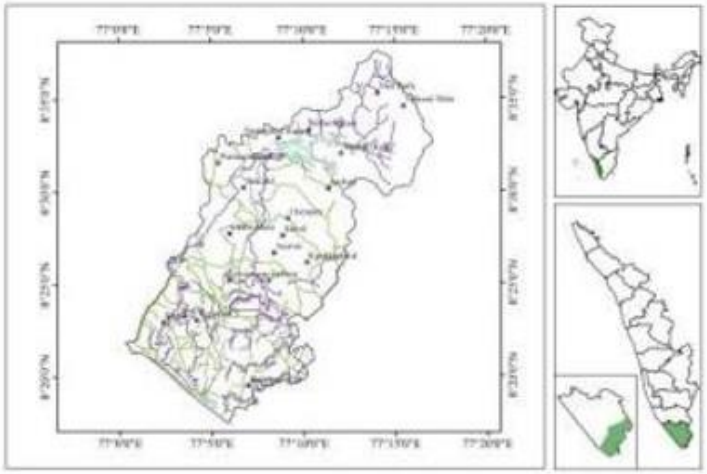


**Figure 1** Neyyar river basin

## 3. Materials and Methods

The data used for the study and the methodology adopted for IDF generation is detailed in the following sections.

### 3.1 *Data Used*

The data utilized for the study is rainfall data of Neyyar River Basin. Fifty years of daily rainfall data at 0.25° x 0.25° grids for the period from 1955 to 2005 were obtained from National Climate Centre, Indian Meteorological Department. For the projection of IDF Curve, future rainfall of the basin for forty five years (2006-2050) was predicted using predictor variables derived from the ICTP regional

climate model (RegCM4) with NOAAGFDL-GFDL-ESM2M as the driving model. Suitability of predictor variables used for regression analysis were ensured by performing correlation analysis between the predictors and predictand. The predictors from NCEP/NCAR reanalysis data set at $2.5^0$ spatial resolution were used for training and testing the multivariate linear regression model developed. Separate models were developed for each month for better accuracy in projection of the rainfall. The predictors from RCM were used for projecting the rainfall after plotting scatterplots between reanalysis predictors and RCM predictors.

### 3.2 *Gumbel's Extreme Value Distribution*

The Gumbel's Type I distribution is,

$$G(x;\mu,\beta) = \frac{1}{\beta} e^{\frac{x-\mu}{\beta}} e^{-e^{\frac{x-\mu}{\beta}}} \quad (1)$$

where μ is the location parameter and $\beta$ is the scale parameter.

It can be shown that the value of the random variable $X_T$ associated with a given return period, T, may be obtained from the following expression,

$$X_T = \bar{X} + K_T S \quad (2)$$

Where $\bar{X}$ is the mean of the observations (e.g., arithmetic average of the observations), and S is the standard deviation of the observations. The frequency factor associated with return period T, $K_T$, is given by,

$$K_T = -\frac{\sqrt{6}}{\pi}\left[0.5772 + \ln\left(\ln\left(\frac{T}{T-1}\right)\right)\right] \quad (3)$$

### 3.3 *Generation and Projection of IDF Curves*

IDF curves were generated for the observed rainfall data using Gumbel's distribution. The reanalysis data was used for developing regression equations for each month using multivariate linear regression model after identifying the best predictor variables through correlation analysis. Using these regression equations, future rainfall for forty five years from 2006-2050 were projected using the RCM data and IDF Curves were generated for this data using Gumbel's method.

Standard IDF Curves were generated for the empirical relationship developed by Sherman and further modified by Bernard utilizing the parameters suggested by Ram Babu (1979). The equation is given by-

$$i = \frac{K * T^a}{(t+b)^n} \quad (4)$$

where k, a, b and n are constants which depends on the geographical locations and i is the intensity of rainfall in cm/hr. Ram Babu (1979) provided the values of these constants and for the study region these values were given as K = 6.762, a = 0.1536, b = 0.5, n = 0.8158.

### 3.4 *Validation of IDF Curves*

Hu H. et al. (2019) measured the goodness of fit of IDF Curves using Normalized Root Mean Square Error (NRMSE).

Suppose $O_{i,p}$ is the intensity of rainfall with the time interval i and return period p from the standard IDF curve and $E_{i,p}$ is the same value computed from the projected IDF curve, for I={ 1 h, 2 h, 6h, 12h, 24h} and P = {2 years, 5 years, 10 years, 25 years,50 years, 100 years},

$$NRMSE = \sqrt{\frac{1}{|I|*|P|}\sum_{i\epsilon I, p\epsilon P}\left(\frac{O_{i,p}-E_{i,p}}{O_{i,p}}\right)^2} \quad (5)$$

Also, the percentage increase in rainfall can be calculated from historical and projected IDF curves using the equation-

$$Ratio = \frac{1}{|I|*|P|}\sum_{i\epsilon I, p\epsilon P}\frac{projected_{i,p}}{historical_{i,p}} \quad (6)$$

Where I={ 1 h, 2 h, 6h, 12h, 24h} and P = {2 years, 5 years, 10 years, 25 years,50 years, 100 years}

## 4. Results and Discussions

The selection of best predictor variables, development of regression equations and the development of IDF curves using projected rainfall are discussed in detail under this section.

### 4.1. *Identification of best predictor variables*

The accuracy of the regression model developed depends mainly on the selection of the optimum predictors influencing the predictand. The best predictors were identified by conducting correlation analysis between reanalysis data of predictors and the rainfall data obtained from IMD. The predictors selected from reanalysis data were vertical components of wind at various pressure levels namely V-wind at 850 hPa, V- wind at 500 hPa, V- wind at 200 hPa, U- wind at 850 hPa, horizontal components of wind at various pressure levels namely U- wind at 500 hPa, U- wind at 200 hPa, specific humidity, surface air temperature, air temperature at 500 hPa , air temperature at 850 hPa, geopotential height at 250 hPa, geopotential height at 500 hPa and mean sea level pressure. From the above listed predictors, it was found that six predictors are significant for the Neyyar basin. They are V- wind at 500 hPa, U-wind at 850 hPa, U- wind at 500 hPa, U- wind at 200 hPa, specific humidity and mean sea level pressure. The correlation coefficients for the predictors obtained with the predictand are shown in Table 1.

**Table 1** Correlation coefficients

| Sl no. | Predictor Variables | Correlation Coefficients |
|---|---|---|
| 1. | V Wind at 850 hPa | 0.075 |
| 2. | V wind at 500 hPa(x1) | 0.336 |
| 3. | V Wind at 200 hPa | -0.225 |
| 4. | U Wind at 850 hPa(x2) | 0.283 |
| 5. | U Wind at 500 hPa(x3) | 0.279 |
| 6. | U Wind at 200 hPa(x4) | -0.314 |
| 7. | Specific humidity (x5) | 0.389 |

| | | |
|---|---|---|
| 8. | Surface air temperature | -0.182 |
| 9. | Air temperature at 500 hPa | 0.151 |
| 10. | Air temperature at 850 hPa | -0.029 |
| 11. | Geopotential height at 250 hPa | 0.129 |
| 12. | Geopotential height at 500 hPa | -0.176 |
| 13. | Mean sea level pressure (x6) | -0.305 |

After smoothing the data, the maximum correlation coefficient obtained was 0.4. Variables with correlation coefficient greater than 0.3 were taken. Thereby 6 of the predictor variables were identified as the best predictor variables for the model development. These variables are shown in the table as x1 to x6.

### 4.2. *Development of regression equations*

Regression equations were developed using the above identified best predictors for a training period of 40 years from 1955-1995 and was tested for a testing period of 10 years from 1996-2005. The regression equations were developed on a monthly basis for all the 12 months using the rainfall data for each month over the training period using the six predictors found to influence the rainfall in the area. The regression coefficients for the model developed are given in Table 2.

**Table 2** Regression coefficients for the monthly models

| Month | Constant | X1 | X2 | X3 | X4 | X5 | X6 |
|---|---|---|---|---|---|---|---|
| January | 65.17 | 0.031 | _ | -0.058 | -0.016 | 174 | -0.0006 |
| February | 62.83 | 0.007 | 0.031 | 0.012 | -0.0081 | 171.3 | -0.0006 |
| March | 54.8 | 0.003 | 0.015 | 0.042 | -0.026 | 164.9 | -0.00054 |
| April | -1.359 | 0.207 | -0.034 | 0.140 | -0.054 | 156.5 | 0.00002 |
| May | 314.641 | 0.258 | 0.197 | 0.131 | 0.102 | 798.68 | -0.003 |
| June | -20.41 | 0.202 | 0.176 | 0.177 | 0.121 | 511 | 0.0002 |
| July | 357.9 | 0.152 | 0.247 | 0.069 | 0.016 | -121.7 | -0.0035 |
| August | 184.968 | 0.103 | 0.144 | 0.072 | 0.065 | 330.497 | -0.0018 |
| September | 344.289 | 0.316 | 0.113 | 0.152 | 0.154 | 419.75 | -0.0034 |
| October | 70.36 | 0.484 | -0.055 | 0.270 | 0.1008 | 1105 | -0.0007 |
| November | 197.027 | 0.320 | 0.266 | 0.127 | -0.059 | 877.023 | -0.002 |
| December | 31.215 | 0.160 | -0.069 | 0.114 | -0.699 | 470.337 | -0.0003 |

x1 : V- wind at 500hPa; x2 : U- wind at 850hPa; x3 : U- wind at 500hPa; x4 : U- wind at 200hPa; x5 : Specific Humidity; x6 : Mean Sea Level Pressure

### 4.3. *Overlapping of reanalysis and RCM data*

The accurate prediction of rainfall depends on selection of optimum climate variables. The regression equations were developed using the Reanalysis data. However, the projection of future rainfall was done by using RCM predictor data as future climate variable data is not available on the reanalysis database. RCM data is a simulated data set in contrast to Reanalysis data which are based on observed data from various observation platforms. Therefore, in order to use the RCM data for future projection using the developed model, it is mandatory to ensure that both the data sets follow the same pattern. For that a scatter plot of the Reanalysis data and RCM data of all the six best predictor variables were drawn with Reanalysis data on the X-axis and RCM data on the Y-axis. It was found that they both follow the same pattern. The scatterplots for all the predictor variables are shown in Figure 2.

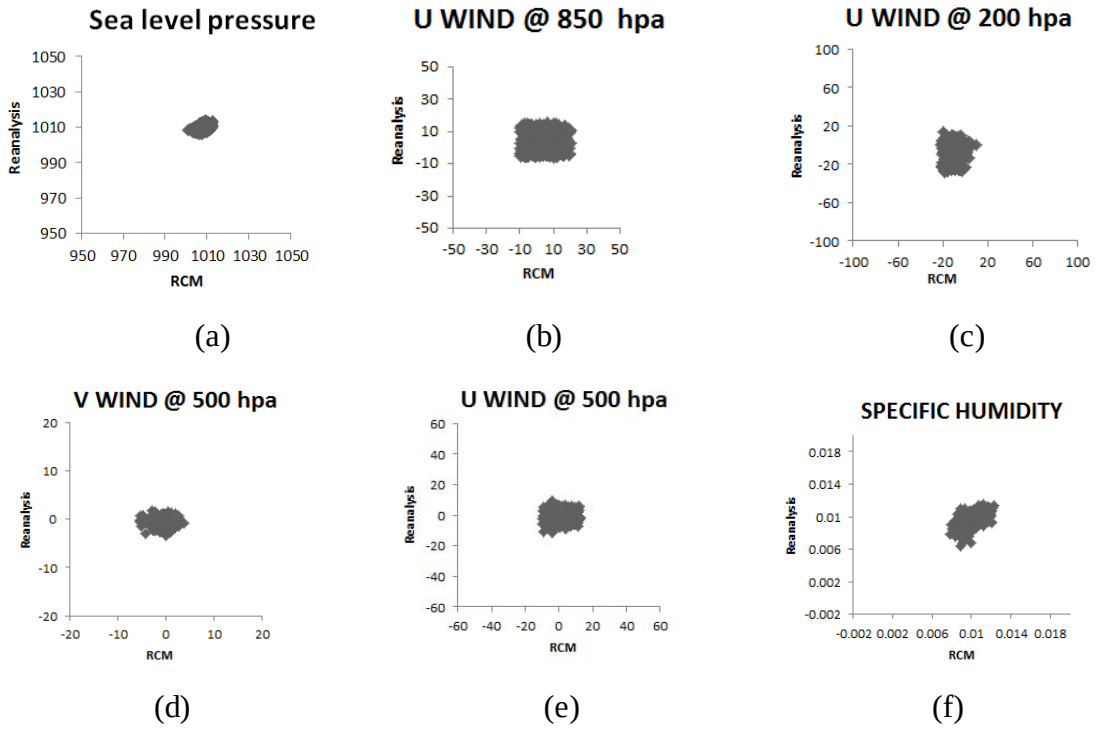



**Figure 2** Scatterplots of Reanalysis data and RCM data

Hence using RCM climate variable daily data, future daily rainfall for 50 years (2006-2050) were projected using the developed regression equations.

### 4.4. *Generation and projection of IDF curve*

From the daily rainfall measurements of Neyyar river basin, the cumulative value for the durations 1, 2, 6, 12 and 24 hours were obtained. The maximum values for each duration for each year from 1955-2005 was found out. By dividing the rainfall depths with the durations, the rainfall intensity in mm/hr was calculated. The mean and standard deviation of each of the durations were calculated. Using the frequency factor proposed by Benny M. and Brema J. (2019), the intensity corresponding to different return periods were calculated as given in Table 3. These values were used for generating the IDF Curves for Neyyar river basin for the historical rainfall data for a period of 1955-2005 as shown in Figure 3.

**Table 3** Intensity-Duration-Frequency relations obtained using Gumbel's method for historical rainfall data.

| | Intensity values (mm/hr) for return periods of | | | | | |
|---|---|---|---|---|---|---|
| Duration(hr) | 2 Years | 5 Years | 10 Years | 25 Years | 50 Years | 100 Years |
| 1 | 10.963 | 15.959 | 19.267 | 23.446 | 26.546 | 29.624 |
| 2 | 6.906 | 10.053 | 12.137 | 14.770 | 16.723 | 18.662 |
| 6 | 3.320 | 4.833 | 5.835 | 7.1008 | 8.039 | 8.972 |
| 12 | 2.092 | 3.044 | 3.675 | 4.473 | 5.065 | 5.652 |
| 24 | 1.317 | 1.918 | 2.315 | 2.817 | 3.190 | 3.560 |

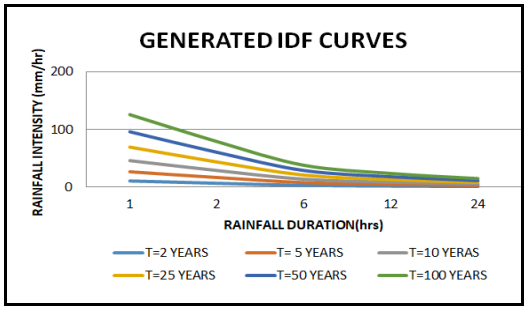



**Figure 3** Intensity-Duration-Frequency Curve for historical rainfall data using Gumbel's method.

Similarly, the intensity corresponding to various return periods were calculated for the projected rainfall for Neyyar river basin from 2006-2050 as shown in Table 4.

**Table 4** Intensity-Duration-Frequency relations obtained using Gumbel's method for predicted rainfall data.

| | Intensity values (mm/hr) for return periods of | | | | | |
|---|---|---|---|---|---|---|
| Duration(hr) | 2 years | 5 years | 10 years | 25 years | 50 years | 100 years |
| 1 | 124.568 | 124.882 | 125.09 | 125.352 | 125.547 | 125.741 |
| 2 | 78.473 | 78.670 | 78.802 | 78.967 | 79.090 | 79.212 |
| 6 | 37.725 | 37.821 | 37.884 | 37.963 | 38.022 | 38.081 |
| 12 | 23.765 | 23.825 | 23.865 | 23.915 | 23.952 | 23.989 |
| 24 | 14.971 | 15.009 | 15.034 | 15.065 | 15.089 | 15.112 |

The projected IDF Curves for Neyyar river basin were plotted as shown in Figure 4 using the calculated values.

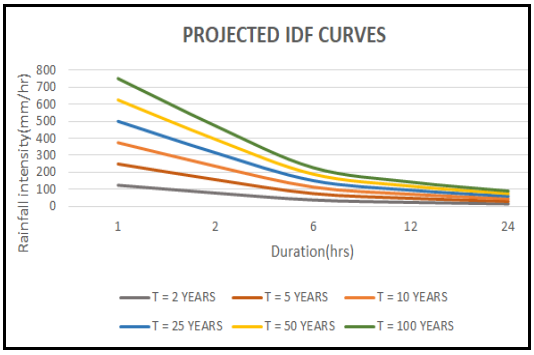



**Figure 4** Intensity-Duration-Frequency Curve for projected rainfall data using Gumbel's method.

Based on the empirical equation (4), the intensity values for various durations were obtained and the values are tabulated in Table 5.

**Table 5** Intensity-Duration-Frequency Relations obtained using Empirical Equations

| | Intensity values in mm/hr for return period of | | | | | |
|---|---|---|---|---|---|---|
| Duration(hr) | T=2 years | T=5 years | T=10 years | T=25 years | T=50 years | T=100 years |
| 1 | 54.028 | 62.198 | 69.185 | 79.64 | 88.588 | 98.541 |
| 2 | 35.615 | 41.0008 | 45.607 | 52.49 | 58.397 | 64.958 |
| 6 | 16.334 | 18.804 | 20.916 | 24.08 | 26.782 | 29.792 |
| 12 | 9.581 | 11.029 | 12.269 | 14.12 | 15.709 | 17.474 |
| 24 | 5.533 | 6.37 | 7.085 | 8.156 | 9.073 | 10.092 |

The standard IDF Curve for the region was developed and is shown in Figure 5.

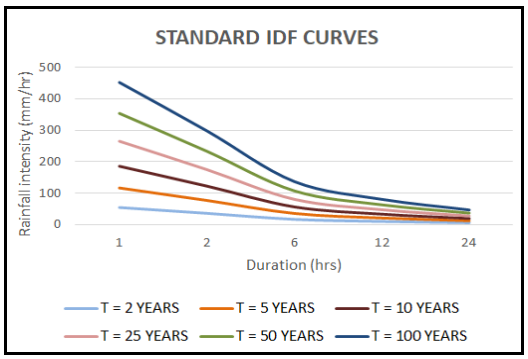



**Figure 5** Standard IDF Curve generated using Empirical Equation

The projected IDF curves developed by incorporating climate variables were overlayed on standard IDF curves generated using empirical equations as seen in Figure 6.

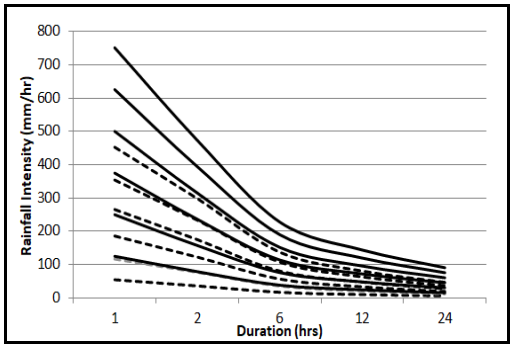



**Figure 6** Projected IDF Curves overlayed on Standard IDF Curves

The results obtained from Gumbel's distribution and empirical equations were almost the same as is evident in the figure where dotted lines represent standard IDF Curves and solid lines represent projected IDF Curves. Both curves were found to follow the same pattern.

### 4.5. *Validation of IDF Curves*

The NRMSE value between standard and projected IDF Curves were found to be 0.08 which is almost negligible. The percentage increase in rainfall found using equation (6) between historical IDF Curve and Standard IDF Curve was found to be 3.4%. But the percentage increase between historical IDF Curve and Projected IDF Curve was found to be 6.3%, which is almost double that of the rainfall predicted by the standard IDF Curve. Hence, the IDF Curve projected by incorporating climate variables is more accurate and reliable than the standard IDF Curve generated using the empirical equation.

## *5. Conclusion*

The IDF curves projected by incorporating climate variables were validated and was compared with the standard IDF curves generated using the empirical equation. Both the curves were found to follow the same pattern and the NRMSE value of 0.08 calculated between standard and projected IDF Curves shows their acceptability. However, the percentage increase in rainfall of the projected IDF Curves were almost the double that of the Standard IDF Curves. Hence, the IDF Curves projected by incorporating climate variables are more accurate and reliable than the standard IDF Curves and this shows that design of hydraulic structures using IDF curves made by incorporating climatic factors helps to increase their design life. For further work, the rainfall intensities obtained for different durations can be used to generate the flood hydrographs for design flood events. In usual cases, a flood of higher return periods is considered for hydrological design as floods of higher return periods cause more damages. Once the return period and the durations are fixed, the rainfall intensity can be estimated and used it to generate flood hydrograph.

## References

1. Benny M., Brema J. (2019). Development of Intensity Duration Frequency (IDF) Curves for Upper and Lower Kuttanad, Kerala. *International Journal of Engineering and Advanced Technology*. Vol.8, pp. 2249-8958.
2. Bernard M. (1932). Formulas for rainfall intensities of long duration. *Transactions of the American Society of Civil Engineers*. Vol.96, pp. 592-624.
3. Bhatt J., Gandhi H., Gohil K. (2014). Generation of Intensity Frequency Duration Curve using daily rainfall data for different return period. *Journal of International Academic Research for Multidisciplinary*. Vol. 2(2).

4. Hu H., Ayyub B.M., (2019). Machine learning for projecting extreme precipitation intensity for short durations in a changing climate. *Geosciences*. Vol. 9(5), 209.
5. John A., Brema J. (2018). Analysis of rainfall by Intensity Duration - Frequency (IDF) curves for Vamanapuram river basin, Kerala. *International Journal of Civil Engineering and Technology*. Vol. 9(7).
6. Ram Babu, Tejwani K.G., Agarwal M.C., Bhushan L.S. (1979). Rainfall Intensity-duration return period equations & nomograms of India. CSWCRTI, ICAR, Dehradun, India
7. Sherman C.W. ((1931). Frequency and intensity of excessive rainfall at Boston, Massachusetts. *Transactions of the American Society of Civil Engineers*. Vol. 95, pp.951-960.
8. Thomas Vandal, Evan Kodra, Auroop R. Ganguly. (2018). Intercomparison of machine learning methods for statistical downscaling: the case of daily and extreme precipitation. *Theoretical and Applied Climatology*. Vol. 137, pp.557-570.

*IN PROCEEDINGS OF 25th HYDRO 2020, INTERNATIONAL CONFERENCE, NATIONAL INSTITUTE OF TECHNOLOGY ROURKELA, ODISHA, INDIA 26-28, March 2021, ISBN 978-93-90631-56-8*

Paper ID - 152

# A review on Climate Change Impact Analysis using Statistical tools

Parth Sinroza[1*], Mohdzuned Shaikh [2]

[1]*P.G. Scholar, CED, L. D. College of Engineering, Ahmedabad (380015), Gujarat, India*
[2]*Assistant Professor, CED, L. D. College of Engineering, Ahmedabad (380015), Gujarat, India*
**Email:* pdsinroza@gmail.com

## Abstract

Science has shown that climate change is impacting every corner of the environment on our planet and the water cycle is no exception. Climate is considered to be the greatest challenge faced by mankind in the present era. It is therefore, very important to study the predictions and analyses of change in critical climate variables such as precipitation and temperature and to strategize parameters about the future management. It will also help to predict the special regions that are vulnerable to climate change which will give the future scenario of water resources. The main aim of this study is to provide a literature review and discuss about the researchers who carried out the study of climate change behaviour. Various techniques and tools have been employed by all the researchers to study rainfall and temperature analysis. Statistical methods are most widely used for this study.

***Keywords:*** *Climate change; precipitation and temperature analysis; statistical tools*

## 1. Introduction

Our environment is changing. Rivers overflow their borders. Due to drought and heavy storms the carefully tended crops failed. Forests turn into tinder. Huge glaciers fuse at an increasing pace. We've heard for decades about climate change. But now, in a warming world, we are seeing and witnessing the extreme weather that scientists have long warned us to expect. Cataclysmic events (storms, floods, and droughts) are happening more regularly all over the world. This isn't quite natural. And if we continue to pollute our climate, these incidents will only become more frequent and serious. This modern reality is all too frequently dismissed or ignored, given the vast amount of extreme weather events happening all over the globe. The public is receiving contradictory media reports on climate change and how we can fix it. Changing climate raises our chance of both heavy rain and prolonged droughts.

In several regions of the world, the spatial distribution of water supplies is unequal. The highest rainfall-receiving region on planet earth is India, from the drier northwest, where rainfall is scarce, to the north east (Goyal et al., 2018). Science has shown that climate change is impacting every corner of the environment on our planet, and the water cycle is no exception. Since the processes involved are heavily temperature dependent, changes in one would have effects on the other. Specifically, with global temperature continuously increasing at their highest levels in millions of years, things like water vapour concentrations, clouds, precipitation patterns, and stream flow patterns are all directly affected, all of which are linked to the water cycle. One of the most significant global issues addressed by scientists and researchers is global warming / climate change. The scientific community is concerned about this issue, as it could have a significant effect on natural and social processes at the local, regional and national level (Chinchorkar et al., 2018).

Climate change strengthens this process, as more water evaporates into the air as air temperature rises. Warmer weather can contain more water vapour which can lead to more violent rainstorms, causing significant problems in coastal areas around the world such as severe flooding. Yet, it's not over. Although some places experience heavy storms, some face more dry weather, and even drought. As a result, temperature rises, evaporation rises and soils dry out. Then, as rain arrives, much of the water flows into rivers and streams off the hard land and the soil remains dry. The outcome of which still greater soil evaporation and increased drought risk.

## 2. Climate Change Impacts

Climate change is considered as the greatest challenge faced by mankind in the twenty first century. Analyses and prediction of change in critical climatic variables like rainfall and temperature are, therefore, extremely important to develop strategies and make informed decisions about the future water allocation for different sectors and management of available water resources (Sarkar and Chicholikar, 2017). The hydrological cycle is primarily controlled by several rainfall parameters, humidity, temperature etc. So, a change (sudden or steady) in any of these parameters can influence the hydrological distribution on land. The shift occurring in these parameters can be sometimes difficult to identify even though an effective statistical test is used (Zbigniew W. Kundzewicz and Alice J. Robson, 2004).

When a trend is identified, the series of trends might suggest that certain type of climate change is taking place (Khan, 2001). Trend analysis is commonly used to identify and measure change in a hydro climatic time series. If a correlation (positive or negative) occurs among the dependent variable, such as, rainfall and time, the independent variable, a time series can be said to have trends.

From the observations of the climate change impact studies using Global Circulation Models (GCMs), it seems that collection of greenhouse gases in climate is the reason behind trend elements such as rise in temperature and precipitation. Climate change proof therefore may show positive or negative trends in hydro climate time series records (Khan, 2001).

## 3. Literature Review

Colin et al. (1999) analysed long term temperature data from two stations on the island of Cyprus, they collected the data and analysed to investigate the long-term changes in the diurnal temperature cycle with long term temperature records from Cyprus. They presented two main possible causes of these changes in the diurnal temperature range during the 20th century and also concluded that the heat island effect influences both minimum and maximum temperature, although it has a larger effect on the minimum temperature.

Kothawale and Rupa Kumar (2005) reported the substantial recent changes in the nature of trends, using updated data sets up to 2003, with special focus on the last three decades. They stated that All-India mean annual temperature has increased by 0.05 C/10yr for the period 1901–2003 and minimum temperature during the monsoon season have shown significant increasing trends during the recent period over almost all the regions, which is quite contrary to the their trends observed over the full data period .

The climate changes in India and search for robust evidences are issues of concern especially when it is known that poor people are very vulnerable to climate changes are studied (Dash et al., 2007). Their study was within the constraints imposed by the possible climate change and hydrologic regimes, suggested some adoptive measures and future research needs in India. They described that extreme temperature events have increased in the recent past. During the heat wave period from 19 May up to 10 June 2003, the highest daily maximum temperature in the country was observed in Andhra Pradesh instead of in the north west and central plains of India where it used to occur normally and rainfall pattern during different seasons indicate small increase during winter months of January and February, pre-monsoon months of March, April and May and post-monsoon months of October, November and December.

Mall et al. (2007) examined the potential for sustainable development of surface and groundwater resources within the constraints imposed by the possible climate change and hydrologic regimes, suggested some adoptive measures and future research needs in India and concluded that the Indian region is highly sensitive to climate change. The elements/sectors currently at risk are likely to be highly vulnerable to climate change and variability and uncertainties that exist in dealing with vulnerabilities associated with climate change and variability.

Sontakke et al. (2008) developed instrumental period summer monsoon (June–September) total rainfall series (1813–1995) for six homogeneous zones and all of India using 306 rain gauge stations. Alongwith the longest possible summer monsoon rainfall series (1813–2005), post-monsoon (October– December total) and annual rainfall series have also been developed for seven homogeneous zones: North Mountainous India (NMI), Northwest India (NWI), North Central India (NCI), Northeast India (NEI), West Peninsular India (WPI), East Peninsular India (EPI), South Peninsular India (SPI), and the whole country using data from 316 well-spread stations. They concluded that the post-monsoon (OND) rainfall over the South Peninsular India shows rising trend which appears to be due to rising trend in the SST of the oceans around the areas.

The trends of maximum atmospheric temperature, rainfall were analyzed for meteorological data of Anand district in Central Gujarat India by Chinchorkar et al. (2015). The long-term change in temperature, rainfall (Seasonal & Annual) has been analyzed by correlation and linear trend analysis. The increasing trend in MMAX temperature and decreasing trends in TMRF, TMRF (J-S), was observed and confirmed by Mann-Kendall trend test. It was observed that annual MMAX temperature has increased, the TMRF (J-S) showed statistically significant decreasing trend shows statistically insignificant decreasing trend during the last 41 years and was confirmed by Mann Kendall trend at 5% level of significance. The maximum temperature, rainfall during period 1970 to 2011 obtained from Department of Agricultural Meteorology, Anand was analyzed. It was observed that mean of maximum temperature shows increasing trend, total monthly rainfall and total monthly rainfall in the rainy season days shows decreasing trend in Anand of central Gujarat.

Recently, Sarkar and Chicholikar (2017) have proposed a study to verify the skills of LARS-WG (Long Ashton Research - Weather Generator), a statistical downscaling model, in simulating weather data in hot semi-arid climate of Saurashtra and analyzed, the future changes of temperature (maximum and minimum) and precipitation downscaled by LARS-WG based on IPCC SRA2 scenario generated by seven GCMs' projections for the near (2011-2030), medium (2046-2065) and far (2080-2099) future periods. Rajkot (22.3° N, 70.78° E) observatory of IMD, representing hot semi-arid climate of Saurashtra, Gujarat state was chosen for the study. Daily rainfall, maximum and minimum temperature data for the period of 1969-2013 have also been utilized in their study.

A comprehensive and detailed understanding and clear assessment of the impact of climate change on India’s water resources is provided by Goyal et al. (2018) which is required to reach a definitive conclusion and explanation of the trends to better inform policy actions. They reported that there has been a significant change in precipitation and temperature during 2000–2015 in India in comparison to the last 100 years.

Very recently, Rajeshwari and Rashmi (2019) have studied temperature and time series analysis. Auto Regressive Integrated Moving Average models have been grouped and used to perform short-term predictions on maximum and minimum temperature. They found the temperature and time series in Curitiba.

## 4. Conclusion

For India, there is no agreement on rainfall variability so far. It is not consistent with the degree and path of variability itself. Runoff signs are also mixed, with some basins showing increased runoff, while others suggest decreased flow. Studies using both statistical and dynamic downscaling approaches to track changes in runoff may be able to help create confidence in potential runoff estimates. The effects of land use and land cover changes and climate variability is hard to disaggregate. Through the use of hydrological models, numerous experiments around the world have been carried out to examine the changes in rainfall and water balance simultaneously due to climate change. In such works, socio-environmental changes such as land use changes have not been listed.

From all the literature reviewed in this study, it emerges that, not only globally, but also locally, climate change is now a serious problem. In this field, where not only scientists and engineers, but also social scientists, economists, environmentalists and policy makers put their best to deal with the problem, major research efforts are now being concentrated. It is here that statistical techniques and software help to explain whether the climate has changed in the past and, more importantly, whether the climate will change in the future. Much of the literature available has used trend detection techniques to estimate the degree of change, such as linear regression. It has now become easier to schedule adaptation to the predicted quantum of change by detecting various magnitudes of change as well. Analyses and prediction of change in critical climatic variables like rainfall and temperature are, therefore, extremely important. Based on the present study, we are trying to expand the research area by examining these parameters based on statistical analysis, selecting various districts that are vulnerable to climate change which will help to understand the future scenario of water resources.

## References

Chinchorkar S., Sayyad F., Vaidya V., Vyas P. (2015). Trend detection in annual maximum temperature and precipitation using the Mann Kendall test – A case study to assess climate change on Anand of central Gujarat. *MAUSAM, 66*, 1-6.

Chinchorkar S., Suryavansi S. B., Patel G. R. (2018). Assessment of Climate Change in Anand of Central Gujarat with reference to Temperature Fluctuation: A Case Study. *HortFlora Research Spectrum*, 7(1), 11-18.

Colin P., Silas M., Stylianos P., Pinhas A. (1999). Long term changes in diurnal temperature range in Cyprus. *Atmospheric Research, 51*, 85–98.

Dash S. K., Jenamani R. K., Kalsi S. R., Panda S. K. (2007). Some evidence of climate change in twentieth-century India. Climatic Change. *Climate Change, 85*, 299–321.

Goyal M., Surampalli R. (2018). Impact of Climate Change on Water Resources in India. *Journal of Environmental Engineering, 144 (7)*, 1-10.

Khan, A. R. (2001). Searching evidence for climatic change: Analysis of hydro-meteorological time series in the Upper Indus Basin, *IMWI Working paper no. 23*.

Kothawale D. R., Rupa Kumar K. (2005). On the recent changes in surface temperature trends over India. *Geophysical Research Letters, 32*, 1-4.

Mall R., Bhatla R., Pandey S. (2007). Water Resources in India and Impact of Climate Change. *Jalvigyan Sameeksha, 22*, 157-176.

Rajeshwari M., Rashmi P. (2019). Temperature and Time Series Analysis. *Journal of the Gujarat Research Society, 21(14)*, 1109-1112.

Sarkar J., Chicholikar J. (2017). Future Climate Change Scenario in Hot Semi-Arid Climate of Saurashtra, Gujarat by Using Statistical Downscaling by LARS-WG Model. *Mausam, 68(4)*, 589-596.

Sontakke N. A., Singh N., Singh H. N. (2008). Instrumental period rainfall series of the Indian region (AD 1813—2005) revised reconstruction, update and analysis. *The Holocene, 18(7)*, 1055–1066.

Zbigniew W. K., Alice J. R. (2004). Change detection in hydrological records—a review of the methodology. *Hydrological Sciences–Journal–des Sciences Hydrologiques, 49(1)*, 7-19.

*IN PROCEEDINGS OF 25th HYDRO 2020, INTERNATIONAL CONFERENCE, NATIONAL INSTITUTE OF TECHNOLOGY ROURKELA, ODISHA, INDIA 26-28, March 2021, ISBN 978-93-90631-56-8*

Paper ID - 370

# Climate Variability Influences on Seasonal Precipitation-Temperature Associations across Florida

Priyank J. Sharma[1], Ramesh S. V. Teegavarapu[2]

[1]*Postdoctoral Scholar, Department of Civil, Environmental and Geomatics Engineering, Florida Atlantic University, Boca Raton - 33432, Florida, USA.*
[2]*Professor, Department of Civil, Environmental and Geomatics Engineering, Florida Atlantic University, Boca Raton - 33432, Florida, USA.*
*Email: pjs230688@gmail.com, ramesh.teegavarapu@gmail.com*

## Abstract

Climate variability is found to exert varied influences on the meteorological processes across the globe depending upon the geographical location. The exploration of climate variability influences on hydroclimatic variables is key for effective water resources management. The space-time variability of precipitation and temperature is also influenced by large-scale oceanic-atmospheric oscillations, apart from local physiographic factors such as topography and land use. The current study focuses upon an investigation of influences of large-scale oceanic-atmospheric oscillations such as El Niño Southern Oscillation (ENSO) and Atlantic Multidecadal Oscillation (AMO) on seasonal precipitation-temperature (P-T) association for Florida, USA. The dry and wet seasons in Florida extends from November to April and May to October, respectively. The monthly precipitation and temperature data for the period 1950-2017 are analyzed to assess the changes in seasonal P-T correlations within two temporal windows (i.e., 1950-1983 and 1984-2017) using multiple rank-based association measures. The influence of ENSO and AMO phases, viz., El Niño and La Niña, and Warm AMO and Cool AMO, on variations in the P-T associations, are evaluated for the dry and wet seasons. A nonparametric test, the Mann-Whitney test, is used to evaluate the statistically significant differences in seasonal P-T associations between two temporal windows during ENSO and AMO phases. The results indicated the predominance of wet and hot conditions during the summer, while the prevalence of dry and cool conditions during the winter. Also, considerable variations in P-T associations are observed, wherein a positive shift in the P-T association is noticed in the recent period as compared to the earlier period.

***Keywords:*** *Climate variability, El Niño Southern Oscillation, Atlantic Multidecadal Oscillation, Nonparametric tests, Florida*

## 1. Introduction

The fluctuations in the sea surface temperatures (SSTs) govern the climate variability which modulates the hydroclimatology of a region. The climate variability impacts the intra-annual and inter-annual fluctuations in the hydroclimatic variables, such as precipitation, temperature, streamflow, etc., over a region. The coupled oceanic-atmospheric circulations namely El Niño-Southern Oscillation (ENSO), Indian Ocean Dipole (IOD), North Atlantic Oscillation (NAO), Pacific Decadal Oscillation (PDO), Atlantic Multidecadal Oscillation (AMO), and others have been found to influence the hydroclimatic variability at intra-annual and decadal time scales (Enfield et al. 2001; Almanaseer and Sankarasubramanian 2012; Ward et al. 2014; Goly and Teegavarapu 2014; Bothale and Katpatal 2016; Sharma et al. 2020; Gehlot et al. 2020). The current study is primarily focused on the assessment of the influences of AMO and ENSO on seasonal precipitation and temperature variability. The changes in the oceanic and atmospheric conditions of the tropical Pacific Ocean are jointly referred to as El Niño-Southern Oscillation (ENSO). The positive and negative phases of ENSO, which characterize the anomalously warm and cool SSTs in the tropical Pacific, are known as El Niño and La Niña, respectively. On the other hand, AMO is described as a pattern of Atlantic climate variability which is detected as a fluctuation in the sea surface temperatures over the North Atlantic Ocean (Enfield et al. 2001). Compared to the ENSO, which exhibits intra-annual variability (generally 2 – 7 years), the AMO shows multi-decadal variability (usually 20 – 40 years). The ENSO and AMO circulations may exert varied influences on the regional hydroclimatic variability based on the geographical position. For instance, drier (wetter) conditions are observed over the eastern (western) coast of the United States

during the El Niño. The present study aims to evaluate the influences of climate variability on seasonal P-T associations across two temporal windows for a tropical climatic region.

## 2. Methods

The Spearman's rank correlation measure is used to determine the strength of association between precipitation and temperature, whereas the Mann-Whitney is used to evaluate the statistically significant differences in the P-T association between two temporal windows.

### 2.1 *Spearman's rank correlation measure*

The Spearman's rank (SR) correlation measure assesses the strength of the monotonic association between precipitation and temperature. This is a nonparametric rank-based measure. The null and alternate hypothesis suggests the variables are not correlated (i.e., $\rho = 0$) and correlated (i.e., $\rho \neq 0$), respectively. The SR statistic is estimated as (Rousseau et al. 2018):

$$\rho = 1 - \frac{\sum_{j=1}^{N} D_j}{N(N^2 - 1)} \tag{1}$$

where $N$ is the number of bivariate observations and $D_j$ is the rank difference for the observation $j$.

### 2.2 *Kernel density estimates*

The kernel density estimation is a nonparametric smoothing approach used to estimate and compare the probability distributions of several datasets (Wilks 2011; Teegavarapu et al. 2013). The kernel density estimates can be viewed as a kind of continuous replacement for the discrete histograms. The kernel estimator adopts a kernel function for estimating the distance of each data point from the center and bandwidth parameter for smoothing. The kernel effectively smooths or interpolates the probabilities across the range of outcomes for a random variable such that the sum of probabilities equals one.

### 2.3 *Mann-Whitney test*

The Mann-Whitney (MW) test is employed to assess the changes in the median of two independent datasets. It is a nonparametric rank-based test wherein the null hypothesis evaluates that the two populations' medians are equal against the alternate hypothesis that the population medians are different. The MW test statistic ($Z_{MW}$) is estimated as:

$$Z_{MW} = \frac{U_1 - \bar{x}_u}{S_u} \tag{2}$$

where $U_1$ is estimated from the ranks assigned to the sample, $S_u$ and $\bar{x}_u$ denote the standard deviation and mean values to estimate the test statistic. More details on the MW test can be found in Teegavarapu et al. (2013).

### 2.4 *Methodology*

The present study is focused on assessing the changes in seasonal P-T associations across two temporal windows under the influence of climate variability. The point-based observations of daily precipitation and temperature are collected and aggregated to a seasonal time scale. Thus, time series of total precipitation and mean temperatures for dry and wet seasons are formulated for each station. Thereafter, the climate variability information is extracted by analyzing the SSTs of Niño 3.4 and north AMO regions to derive the warm and cool phases of ENSO and AMO, respectively. The P-T associations are evaluated using a nonparametric rank-based association measure, viz., Spearman's rank correlation, at

each station for both the seasons. The changes in the distribution of these correlations for different AMO and ENSO phases for both seasons are visualized using nonparametric kernel density estimates. The statistical significance in the P-T associations is derived using a nonparametric Mann-Whitney test. Hence, the influence of climate variability on seasonal P-T relationship over time is evaluated.

## 3. Case study domain and data sources

The methodology discussed in the previous section is applied to assess the changes in seasonal P-T association across Florida state during AMO and ENSO phases. The Florida state is situated in the southeastern United States on the North Atlantic coast. Florida is surrounded by the Atlantic Ocean to its east, the Caribbean Sea to its south, the Gulf of Mexico to its west and land mass in its north (see Figure 1). Florida is mainly delineated into two geographical zones, viz., the peninsular region and the continental or panhandle region (see Figure 1). The topographic variability across the state is minimal, with most regions being close to the coastline. Spatial variability in mean annual precipitation is observed across the state, ranging from 984 mm to 1638 mm (Teegavarapu et al. 2013). The precipitation and temperature also exhibit considerable temporal variability. Two major seasons are experienced in Florida, namely wet (summer) and dry (winter). The dry and wet seasons in Florida extends from November to April and May to October, respectively (Teegavarapu 2012). The Atlantic hurricanes largely influence the precipitation in the region.

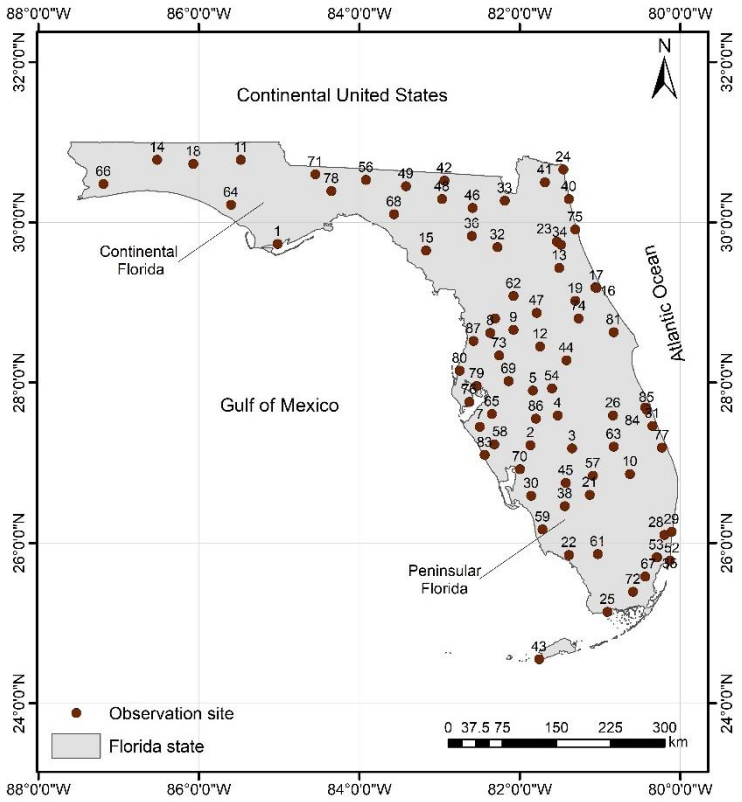



**Figure 1** Location of observation sites across Florida state

In the present investigation, the daily observed precipitation (P) and temperature (T) data are collected for 78 monitoring sites across the state from Florida Climate Center (FSU 2020). The average ($T_{avg}$), minimum ($T_{min}$) and maximum ($T_{max}$) temperatures at each station are analyzed. The daily data are collected for the period 1950 – 2017 and aggregated at monthly time scale for further analyses. The data is further divided into two temporal windows, viz., 1950-1983 and 1984-2017, and analyzed further for changes in P-T associations across them. These datasets have undergone quality check and the sites with fewer than 5% missing observations are included in the analysis. In addition to these datasets, the monthly sea surface temperatures (SSTs), characterizing the ENSO and AMO phases, are also collected.

The monthly SST of the Niño 3.4 region (5°N-5°S and 120°W-170°W) in the central Pacific is obtained from the National Centers for Environmental Protection (NCEP) (NECP, 2020) (www.origin.cpc.ncep.noaa.gov/, accessed November 2020). These SSTs are used to define the phases of ENSO, viz., warm (El Niño), cool (La Niña), and neutral. On the other hand, the monthly SST over the North Atlantic Ocean (0°N-65°N and 80°W-0°E) are used to describe the AMO phases, viz., warm and cool. The AMO SSTs for the period 1950-2017 are obtained from NOAA's Earth System Research Laboratory, Physical Sciences Division (https://www.psl.noaa.gov/data/timeseries/AMO/). The years associated with AMO and ENSO phases for both the temporal windows are described in Table 1.

**Table 1** Years associated with warm and cool phases of ENSO and AMO across two temporal windows

| Climate variability phase | Temporal window I (1950-1983) | Temporal window II (1984-2017) |
|---|---|---|
| Warm AMO | 1950 – 1969 | 1995 – 2017 |
| Cool AMO | 1970 – 1983 | 1984 – 1994 |
| El Niño* | 1951, 1953, 1957, 1958, 1963, 1965, 1966, 1968, 1969, 1972, 1977, 1979, 1982, 1983 | 1986, 1987, 1991, 1992, 1994, 1997, 1998, 2002, 2004, 2006, 2009, 2015, 2016 |
| La Niña* | 1950, 1954, 1955, 1956, 1964, 1970, 1971, 1973, 1974, 1975, 1976 | 1984, 1985, 1988, 1989, 1995, 1996, 1999, 2000, 2005, 2007, 2008, 2010, 2011, 2017 |

* *The remaining years were associated with the neutral ENSO phase.*

## 4. Results and Discussions

The spatial and temporal variability of precipitation and temperature across the Florida state is discussed. Further, the variability in the P-T associations under the influence of climate variability is also assessed.

### 4.1 *Climatology of the region*

The precipitation distribution across Florida shows considerable spatial and temporal variability, as shown in Figure 2. Higher precipitation is recorded during the wet season as compared to the dry season. The wet season precipitation variation is observed in the range 540 – 1170 mm, whereas during the dry season, the precipitation varies from 170 – 650 mm. Moreover, the peninsular region receives higher precipitation during the wet season, while the continental region (or the panhandle) receives higher precipitation during the dry season. The peninsular Florida receives rainfall from the local convective action due to proximity of large water bodies on its three sides. On the other hand, the panhandle receives frontal precipitation during the dry season also. The temperature variability is also considerable during dry and wet seasons. Higher average temperatures are experienced during the wet season uniformly across Florida, whereas comparatively milder temperatures are noticed during the dry season (see Figure 3). Thus, considerable seasonal variability in precipitation and temperature is observed across Florida, wherein the wet season shows wet and hot conditions and the dry season reflects dry and cool conditions.

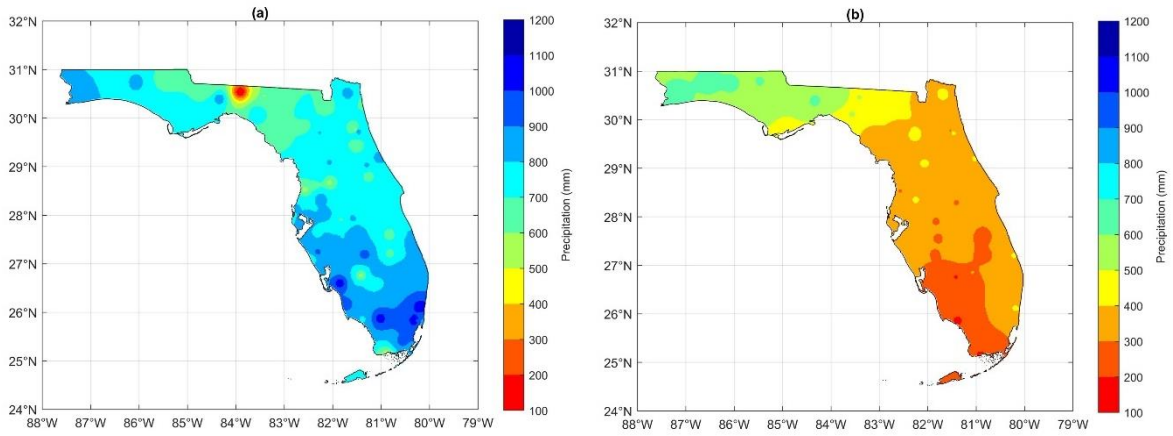



**Figure 2** Spatial variation of mean precipitation across Florida during (a) wet and (b) dry seasons

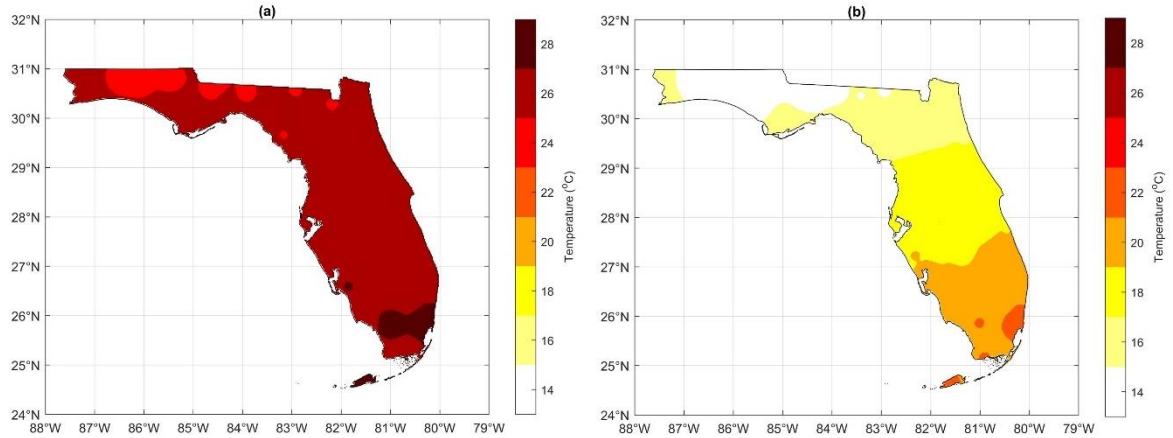



**Figure 3** Spatial variation of average temperature across Florida during (a) wet and (b) dry seasons

## 4.2 *Influence of climate variability on seasonal P-T associations*

In Florida, the dry season spans from November to April and the wet season ranges from May to October. The seasonal total precipitation and mean temperatures (i.e., maximum, minimum, and average) are derived from their respective observed daily values for each station and analyzed. The association of precipitation with $T_{max}$, $T_{min}$, and $T_{avg}$ for dry and wet seasons are estimated using Spearman's rank correlation measure. These P-T associations are evaluated for two temporal windows to assess the changes in the precipitation temperature relationship over time. Also, the influence of AMO and ENSO phases on these associations are evaluated. The distribution of these correlations for both the temporal windows are represented using kernel density estimates and compared.

The distribution of P-T correlations during the warm AMO phase are shown in Figure 4. From Figure 4, a positive correlation is observed between P and $T_{min}$, whereas a negative correlation is observed for P and $T_{max}$ for both wet and dry seasons. Also, an evident shift (towards the positive axis) in the P-$T_{max}$ correlation is observed in the recent period (1984-2017) as compared to the earlier period (1950-1983) during the wet season (see Figure 4(a)). Contrary to that, a decrease in P-$T_{min}$ correlation is noted in the recent period than the earlier period during the dry season (see Figure 4(e)). The Mann-Whitney test indicated statistically significant changes in the P-$T_{max}$ (wet season) and P-$T_{min}$ (wet and dry season) at a 5% significance level, as shown in Table 2.

The distributional changes in the P-T associations for cool AMO phase are shown in Figure 5. A negative (positive) correlation between P and $T_{max}$ (P and $T_{min}$) is observed during cool AMO for both dry and wet seasons, while the P-$T_{avg}$ correlations show widespread heterogeneity. The P-T associations

did not indicate much variability across the temporal windows for both dry and wet seasons. The MW test results also fail to reject the null hypothesis for all cases.

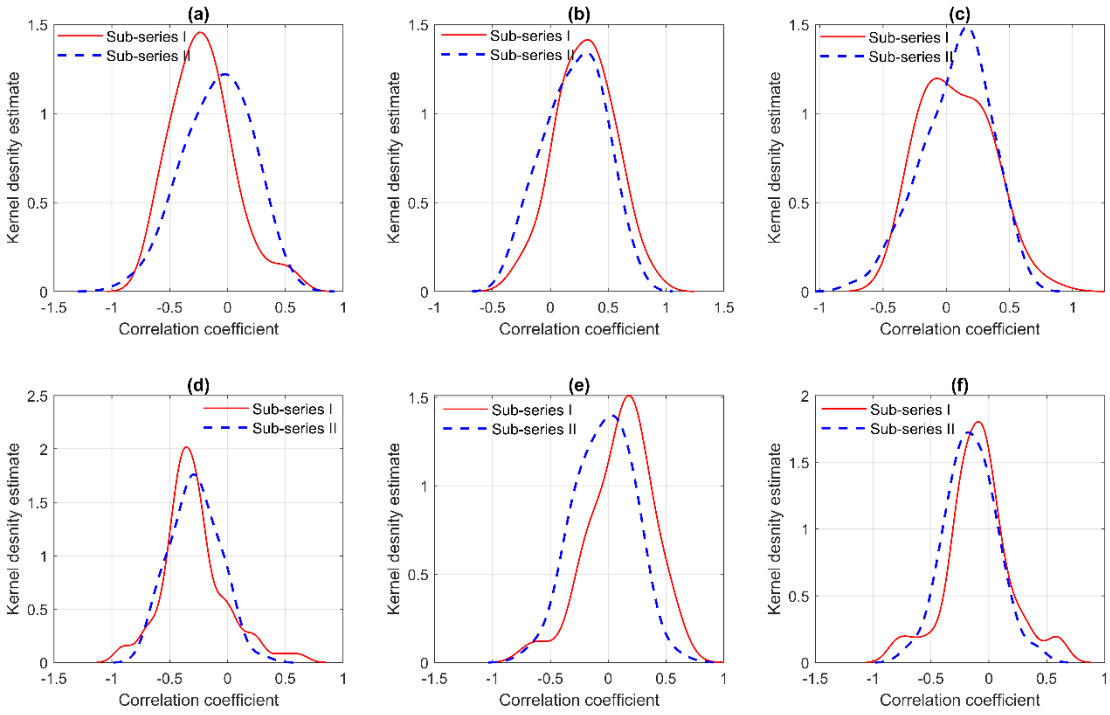



**Figure 4** Changes in P-T associations across two temporal windows, viz., 1950-1983 and 1984-2017, for dry and wet seasons during the warm AMO phase. *The upper and lower tiles represent the distributions of P-$T_{max}$ ((a) & (d)), P-$T_{min}$ ((b) & (e)), and P-$T_{avg}$ ((c) & (f)), for wet and dry seasons, respectively.*

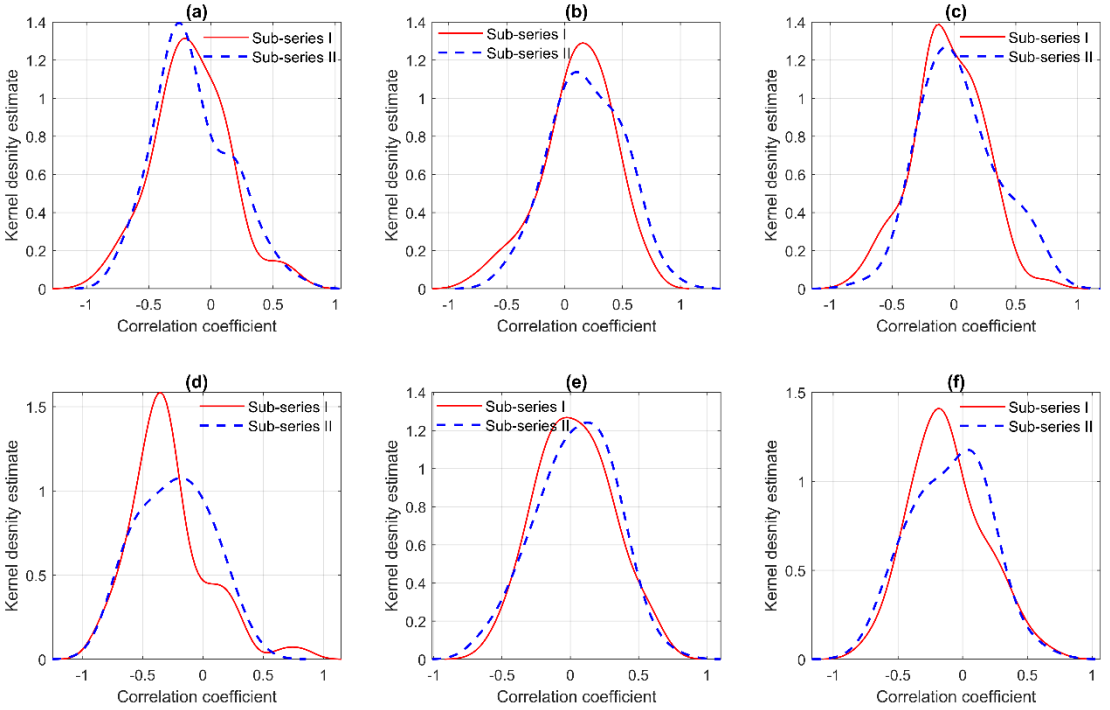



**Figure 5** Changes in P-T associations across two temporal windows, viz., 1950-1983 and 1984-2017, for dry and wet seasons during the cool AMO phase. [*Refer Figure 4 for description*]

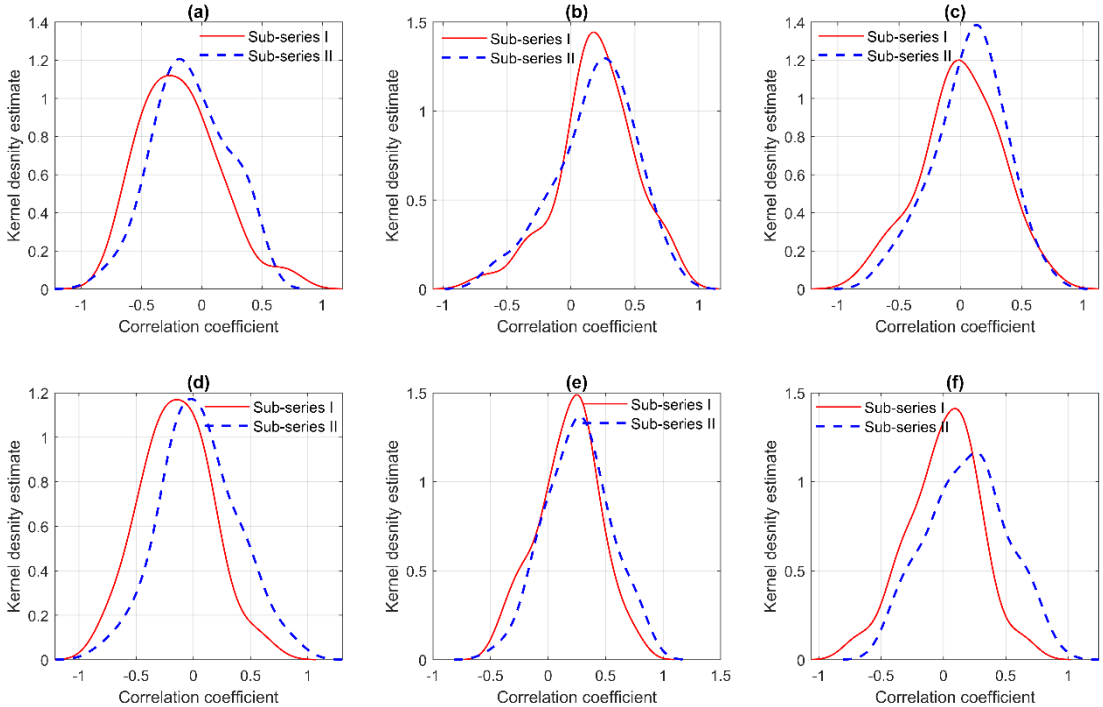



**Figure 6** Changes in P-T associations across two temporal windows, viz., 1950-1983 and 1984-2017, for dry and wet seasons during the El Niño phase. [*Refer Figure 4 for description*]

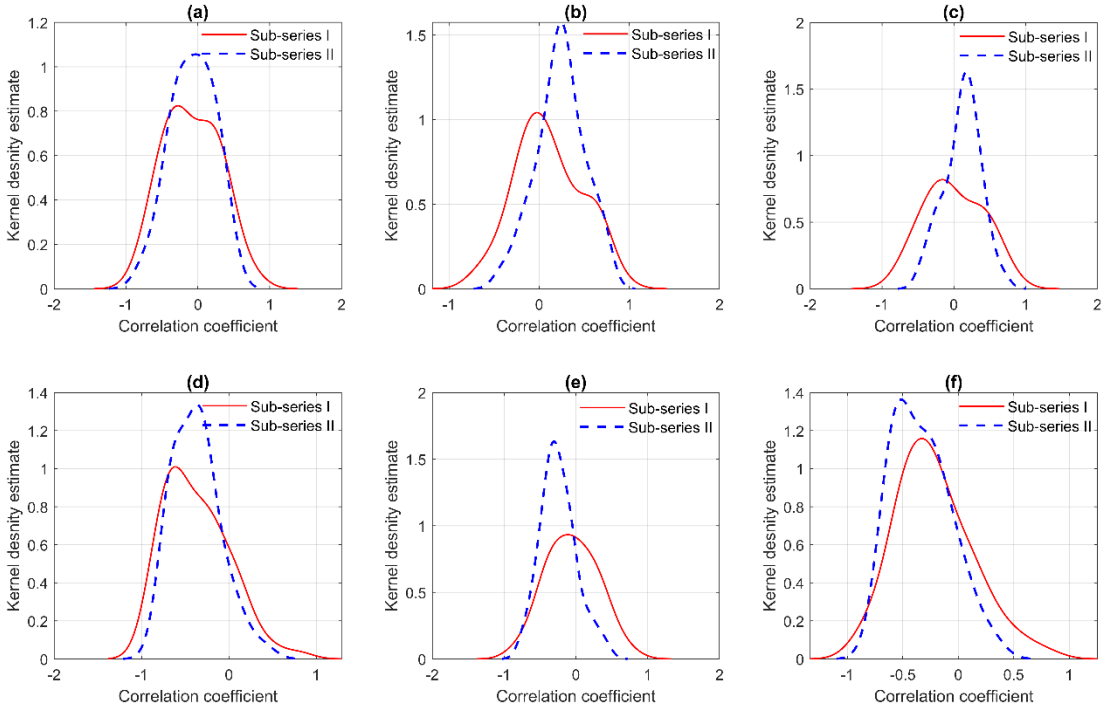



**Figure 7** Changes in P-T associations across two temporal windows, viz., 1950-1983 and 1984-2017, for dry and wet seasons during the La Niña phase. [*Refer Figure 4 for description*]

The variation in the P-T relationship across both the temporal windows during El Niño phase is shown in Figure 6. Like the AMO phase, positive and negative correlations are observed for P-$T_{max}$ and P-$T_{min}$ respectively for both dry and wet seasons. A positive shift in the P-$T_{max}$ relationship is noticed in the recent period than the earlier period during both dry and wet seasons (see Figures 6(a) and (d)). Also, a similar positive shift is noted for P-$T_{avg}$ correlation in the recent period during the dry season (see Figure

6(f)). The Mann-Whitney test also indicated that shifts in these correlations are statistically significant (see Table 2).

The changes in the seasonal P-T association during La Niña phase are shown in Figure 7. The P-$T_{max}$ and P-$T_{avg}$ show strong negative correlations during both seasons (wet and dry) and dry season respectively (see Figures 7(a), (d), and (f)). A positive (negative) P-$T_{min}$ relationship is observed in the wet (dry) season during La Niña phase. The P-$T_{min}$ and P-$T_{avg}$ correlations show a positive shift in the recent period for the wet season, while the P-$T_{min}$ and P-$T_{avg}$ display a negative shift in the recent period for the dry season. The MW test indicated a rejection of the null hypothesis for P-$T_{min}$ associations for both dry and wet seasons, while for P-$T_{avg}$ for the dry season (see Table 2). Thus, the individual influences of AMO and ENSO phases in modulating the seasonal P-T associations are found to be insignificant, except for La Niña. However, the P-T associations have shown a positive shift in the recent period as compared to the earlier period for both wet and dry seasons, except for P-$T_{min}$ and P-$T_{avg}$ for the dry season during La Niña.

**Table 2** Distribution similarity assessment of seasonal P-T correlations for AMO and ENSO phases using the Mann-Whitney test

| Season | Association between | *p*-value of Mann-Whitney test | | | |
|---|---|---|---|---|---|
| | | Warm AMO | Cool AMO | El Niño | La Niña |
| Wet | P & $T_{max}$ | **0.003** | 0.969 | **0.041** | 0.720 |
| | P & $T_{min}$ | **0.040** | 0.220 | 0.970 | **0.009** |
| | P & $T_{avg}$ | 0.748 | 0.184 | 0.164 | 0.051 |
| Dry | P & $T_{max}$ | 0.486 | 0.162 | **0.000** | 0.677 |
| | P & $T_{min}$ | **0.000** | 0.700 | 0.100 | **0.001** |
| | P & $T_{avg}$ | 0.084 | 0.537 | **0.000** | **0.031** |

***Bold faced*** *values indicate statistical significance at* $\alpha = 0.05$.

## 5. Conclusions

A detailed analysis of the influence of climate variability on seasonal P-T associations is undertaken in the present study. The precipitation and temperature exhibit considerable spatio-temporal variability across Florida. Wet and hot conditions prevail during the wet season, whereas dry and cool conditions are observed during the dry season. Also, the peninsular region receives higher rainfall during the wet season as compared to the dry season. A negative relationship between precipitation and maximum temperature is observed during both dry and wet seasons for both AMO and ENSO phases, whereas the precipitation displays a positive association with minimum temperature. Also, a positive shift in the P-$T_{max}$ and P-$T_{min}$ correlation is observed in the recent period (1984-2017) as compared to the earlier period (1950-1983), which is found to be consistent under the influence of climate variability. However, the P-$T_{min}$ and P-$T_{avg}$ display a negative shift in the recent period for La Niña phase. The positive shift in P-$T_{max}$ and P-$T_{min}$ correlations in the recent period indicate a predominant role of convection in inducing higher precipitation across Florida. The individual influences of climate variability show insignificant influences on the P-T associations across dry and wet seasons, however, their joint influences on seasonal P-T relationship can be explored further.

## References

Almanaseer, N., and Sankarasubramanian, A. (2012). Role of climate variability in modulating the surface water and groundwater interaction over the southeast United States. *Journal of Hydrologic Engineering*, 17(9), 1001-1010.

Bothale, R. V., and Katpatal, Y. B. (2016). Trends and anomalies in extreme climate indices and influence of El Niño and La Niña over Pranhita catchment in Godavari Basin, India. *Journal of Hydrologic Engineering*, 21(2), 05015023.

Enfield, D. B., Mestas-Nuñez, A. M., and Trimble, P. J. (2001). The Atlantic Multidecadal Oscillation and its relation to rainfall and river flows in the continental U.S. *Geophysical Research Letters*, 28(10), 2077-2080.

FSU (2020). https://climatecenter.fsu.edu/climate-data-access-tools/downloadable-data (accessed November 2020).

Gehlot, L. K., Jibhakate, S. M., Sharma, P. J., Patel, P. L., andTimbadiya, P. V. (2020). Spatio-Temporal Variability of Rainfall Indices and their Teleconnections with El Niño-Southern Oscillation for Tapi Basin, India. *Asia-Pacific Journal of Atmospheric Sciences*, 1-20.

Goly, A., and Teegavarapu, R. S. (2014). Individual and coupled influences of AMO and ENSO on regional precipitation characteristics and extremes. *Water Resources Research*, 50(6), 4686-4709.

NCEP (2020). National Centers for Environmental Protection (NCEP) (NECP, 2020). https://origin.cpc.ncep.noaa.gov/products/analysis_monitoring/ensostuff/ONI_v5.php (accessed November 2020).

Rousseau, R., Egghe, L., and Guns, R. (2018). *Becoming metric-wise: A bibliometric guide for researchers*. Elsevier-Chandos, Kidlington.

Sharma, P. J., Patel, P. L., and Jothiprakash, V. (2020). Hydroclimatic teleconnections of large- scale oceanic-atmospheric circulations on hydrometeorological extremes of Tapi Basin, India. *Atmospheric Research*, 235, 104791, 1-18.

Teegavarapu, R. S. V. (2012). *Floods in a Changing Climate: Extreme Precipitation*, Cambridge University Press, London.

Teegavarapu, R. S. V., Goly, A. and Obeysekera, J. (2013). *Influences of Atlantic Multi-decadal Oscillation on regional precipitation extremes*. Journal of Hydrology, 495, 74–93.

Ward, P. J., Jongman, B., Kummu, M., Dettinger, M. D., Weiland, F. C. S., and Winsemius, H. C. (2014). Strong influence of El Niño Southern Oscillation on flood risk around the world. *Proceedings of the National Academy of Sciences*, 111(44), 15659-15664.

Wilks, D. S. (2011). *Statistical methods in the atmospheric sciences* (Vol. 100). Academic press.

*IN PROCEEDINGS OF 25th HYDRO 2020, INTERNATIONAL CONFERENCE, NATIONAL INSTITUTE OF TECHNOLOGY ROURKELA, ODISHA, INDIA 26-28, March 2021, ISBN 978-93-90631-56-8*

Paper ID - 419

# Assessment of Climate Change for Generating Grid Wise Future Scenarios of Precipitation and Temperature Over Lower Godavari Sub Basin Maharashtra State, India.

Barokar Y. J.[1], Regulwar D.G.[2]

[1] *Assistant Professor, MGM's Jawaharlal Nehru Engineering College Aurangabad, Maharashtra State, India.*
[2] *Professor, Department of Civil Engineering, Government College of Engineering & Research, Avasari, Pune, Maharashtra State, India.*
*Email:* yogeshbarokar@gmail.com, regulwar@gmail.com

## Abstract

Climate change causes severe effect on human health, agricultural field, water resources sectors etc. Hence assessment of climate change is very important. There are different ways to assess the climate change. One of the way is 'Downscaling'. Downscaling is the way of finding climatic variables at local scale which are available at larger scale. Downscaling has two ways to perform, either by dynamical way or by statistical way. The work on downscaling has been classified into two groups, first one is work on finding different possible ways of downscaling and second one is work in which results of downscaling were used for prediction of effects of climate on different sectors. To perform downscaling in statistical way, we can use SDSM (Statistical Downscaling Model) software. This software predicts future values for climate variables by establishing relation between local scale variables and larger scale variables i.e. variables provided by GCM (General Circulation Models).

In the present study, we have used SDSM tool for a statistical downscaling of Temperature (Tmax, Tmin) and Precipitation over lower Godavari Sub basin Maharashtra State India (Latitude:19011', Longitude:76033').The National Centre for Environmental Prediction (NCEP) reanalysis dataset for the period 1961-2000 and GCM data of HadCM3 under A2a and B2a scenarios have been used. To get better results in downscaling, study has been carried out grid wise. For Temperature downscaling $0.50^0 \times 0.50^0$ grid resolution data have been used whereas for precipitation $0.25^0$ x $0.25^0$ grid resolution data have been used. Calibration and validation have been performed for each grid and results have been plotted. Results are plotted in three future series 2020s, 2050s and 2080s. All the variables i.e. Tmax, Tmin and Precipitation show increasing trends under A2a and B2a scenarios. The mean monthly values of these variables are compared. Highest increase have been noted for 2080s series and lowest increase have been recorded for 2020s series.

***Keywords:*** *SDSM, HadCM3, A2a, B2a, Tmax, Tmin, Precipitation*

## 1. Introduction

Change in climate occurs due to different reasons but one of the major affecting reason is increase in greenhouse gases. The concentration of $CO_2$ and other greenhouse gases are increasing day by day which is causing disturbance in the climate (Mahmood 2014). According to IPCC 4th assessment report, up to 2007 earth temperature has increased by 0.74 $^0$C since last 150 years, whereas 5th assessment report gives the increase in global average temperature is 0.85 $^0$C. Downscaling the climatic parameters help to study such changes in the climate.

### 1.1 *Downscaling*

Downscaling means converting high scale resolution data into finer scale resolution. Downscaling can be done in two ways, either by 'Dynamical downscaling' or 'Statistical Downscaling'. Dynamical downscaling can be carry out with the help of RCM (Regional Circulation Model) whereas in statistical downscaling, one statistical relation between Predictor and Predictand helps for downscaling the climate variables.

According to Wilby et.al. (2002), this statistical downscaling is based on certain assumptions as: a) Whatever predictors and predictands we use, they must have direct correlation for future period, b) Changes for predictor variable will be well characterized by GCMs.

### 1.2 Statistical Downscaling Model (SDSM)

Statistical downscaling model is the one which forms statistical relation between predictor and predictand. Such type of statistical relation helps to downscale the climatic variables for future series. In the study of Mahmood and Babel (2014) SDSM has been used and climate variables have been downscaled with application of bias correction for the trans-boundary region of Jhelum River. Huang et.al (2011) have used SDSM to downscale the climate parameters for basin of Yangtze River. In this study, future precipitation values for selected area have been predicted. Samadi et al (2011) have also used SDSM model for statistical downscaling in the prediction of precipitation and temperature for the area of Khorasan province.

In the present study, SDSM have been used for predicting the future values of temperature and precipitation over Lower Godavari Sub Basin Maharashtra State India. To achieve more accuracy, work has been carried out in grid wise manner. For Temperature downscaling, $0.50^0 \times 0.50^0$ grid resolution data have been used whereas for precipitation $0.25^0$ x $0.25^0$ grid resolution data have been used.

## 2. Experimental program

For the execution of present study, grid wise daily temperature and precipitation values have been obtained from Indian Meteorological Department (IMD), Pune for the period 1961-2000. GCM data of HadCM3 under A2a and B2a scenarios have been obtained from Canadian Climate Impact Scenarios (CCIS) site for the area Lower Godavari Sub Basin Maharashtra State India (Latitude:$19^0$11', Longitude:$76^0$33').

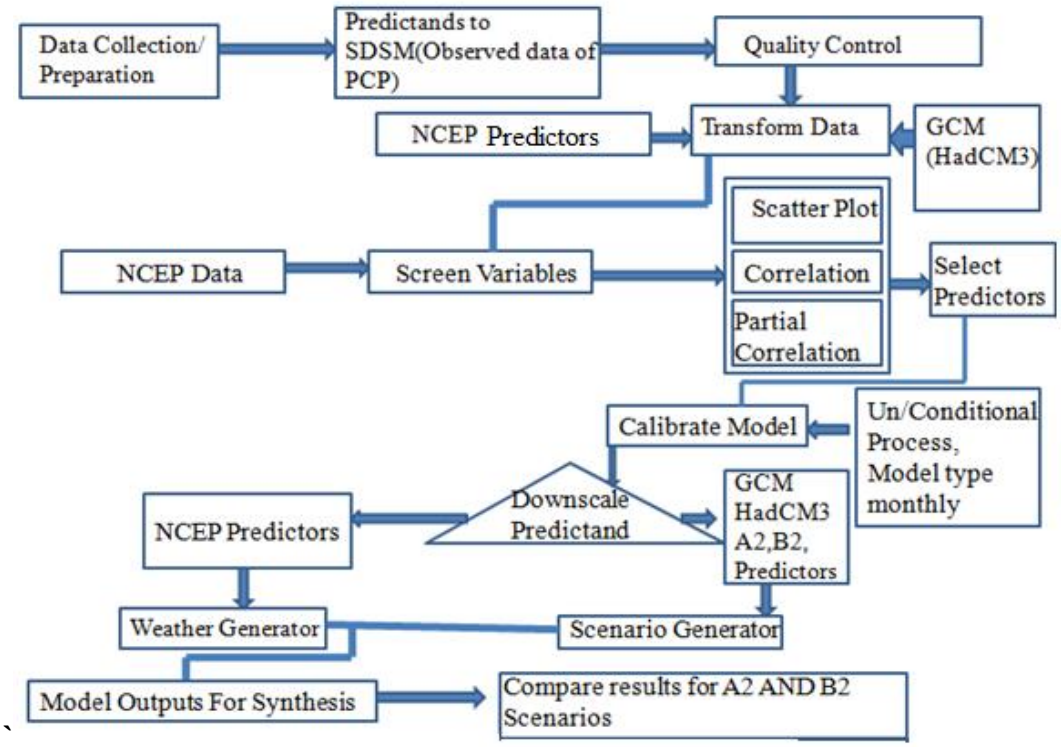



**Fig. 1 Flow Chart for SDSM Execution**

Statistical Down-Scaling Model (SDSM) was developed by Wilby and Dawson, this tool has been used in this study for prediction of precipitation and temperature values for future series over Lower Godavari Sub Basin Maharashtra State India.Working of SDSM is divided into different steps such as: a) Quality Control, b) Transforming Predictor data, c) Screen Variables, d) Model Calibration, e) Weather Generator, f) Finding statistics of the data in summary statistics menu, g) Compare results, h) Scenario generation etc. With the help of 'Quality Control', missing values can be identified in the input data, after that the input data can be transformed using 'Transformed Predictor data'. 'Screen Variable' helps to select the specific NCEP predictor values which gives more correlation values with our observed values which can be used for further analysis. After selecting the specific predictors and predictands, 'Model Calibration' helps to computes the parameters of multiple regression equations via an optimization algorithm. 'Weather Generator' use in verification of calibrated models. Based on the performance of these steps, suitable predictors under A2a an B2a scenarios can be selected and can be used for prediction of future series data under 'Scenario Generation' section

In this method of downscaling the amount of total PCP (Pi) downscaled on day 'i' is given by below equation

$$P_i^k = \beta_0 + \sum_{j=1}^{n} \beta_j \chi_i + e_i \quad \text{.....} \quad 1$$

Similarly the amount of total Temp. (t) downscaled on day 'i' is given by

$$U_i = \gamma_0 + \sum_{j=1}^{n} \gamma_j X_{ij} + e_i \quad \text{.....} \quad 2$$

Where $X_{ij}$ = Predictor values for selected predictors.

$e_i$ = Bias correction value.

$\gamma_0$ and $\beta_0$ = Intercept between predictor and predictand,

## 3. Result and Conclusions

### 3.1 Results for Calibration and Validation

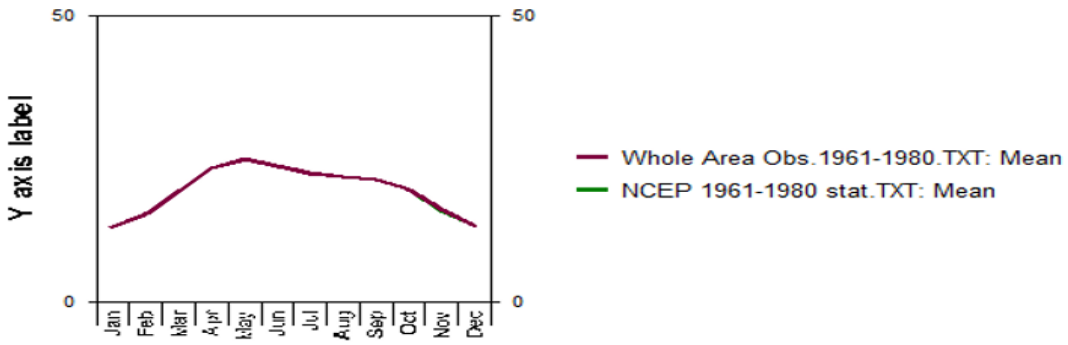



**Fig. 2 Graphical Comparison of Observed and Downscaled Mean Monthly Daily $T_{min}$ during Calibration (1961-1980) for Whole Area Results.**

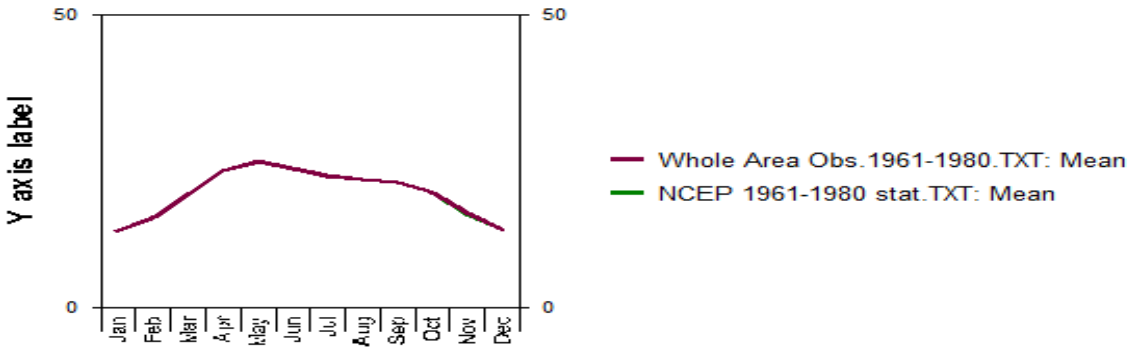



**Fig. 3 Graphical Comparison of Observed and Downscaled Mean Monthly Daily $T_{min}$ during Calibration (1961-1980) for Whole Area Results.**

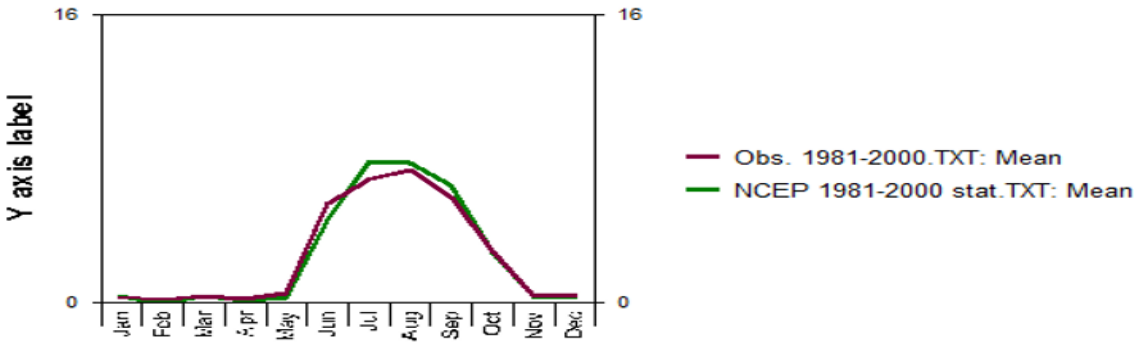



**Fig. 4 Graphical Comparison of Observed and Downscaled Mean Monthly Daily Precp. during Calibration (1961-1980) for Whole Area Results.**

Statistical results have been studied by finding coefficient of determination ($R^2$) between monthly mean daily observed and downscaled Tmax, Tmin and precipitation during validation period (1981-2000). The following table represents the coefficient of determination between monthly mean daily observed and downscaled Tmax, Tmin and precipitation for all grids and whole area.

**Table 1** Statistical Comparison of Observed and Downscaled Monthly Mean Daily Precipitation, Tmax and Tmin during Validation (1981-2000)

| Model | Variable | Grid No. | $R^2$ |
|---|---|---|---|
| | | 153 | 0.92 |
| | | 154 | 0.93 |
| | | 155 | 0.96 |
| | | 186 | 0.94 |
| | | 187 | 0.90 |

| | | | |
|---|---|---|---|
| HadCM3 | Precipitation | 188 | 0.97 |
| | | 190 | 0.93 |
| | | 191 | 0.99 |
| | | 192 | 0.94 |
| | | 193 | 0.98 |
| | | 194 | 0.97 |
| | | 195 | 0.92 |
| | | 196 | 0.98 |
| | | 226 | 0.90 |
| | | 227 | 0.93 |
| | | 228 | 0.95 |
| | | 229 | 0.96 |
| | | 230 | 0.98 |
| | | 233 | 0.97 |
| | | 234 | 0.88 |
| | | 265 | 0.87 |
| | | 266 | 0.92 |
| | | 267 | 0.93 |
| | | For whole area by taking average of observed data of all grids and executed in SDSM | 0.94 |
| | | 59 | 0.99 |
| | | 60 | 0.99 |
| | | 61 | 0.99 |
| | | 62 | 0.99 |
| | | 63 | 0.99 |

| | | | |
|---|---|---|---|
| HadCM3 | Tmax | 80 | 0.99 |
| | | 81 | 0.99 |
| | | For whole area by taking average of observed data of all grids and executed in SDSM | 0.99 |
| | Tmin | 59 | 0.99 |
| | | 60 | 0.99 |
| | | 61 | 0.99 |
| | | 62 | 0.99 |
| | | 63 | 0.99 |
| | | 80 | 0.99 |
| | | 81 | 0.99 |
| | | For whole area by taking average of observed data of all grids and executed in SDSM | 0.99 |

In above table, $R^2$ for all grids and whole area represents values > 0.80, it indicates good result during validation period. These results indicate the successful execution of calibration and validation during validation period of 1981-2000.

### 3.2 Comparing Grid-wise Average for Whole Area Results for Downscaled Values during Period 1961-2000

Statistical comparison between observed and downscaled Tmax, Tmin and Precipitation has been plotted during base line period (1961-2000) by finding coefficient of determination $R^2$.

**Table 2** Statistical Comparison between Observed and Downscaled Precp. , Tmax and Tmin during 1961-2000 for Grid Wise Average for Whole Area

| GCM-Scenario | Variable | $R^2$ for grid wise average for whole area during 1961-2000 |
|---|---|---|
| HadCM3 A2a | Precipitation | 0.96 |
| | Tmax | 0.97 |
| | Tmin | 0.99 |
| HadCM3 B2a | Precipitation | 0.96 |
| | Tmax | 0.97 |
| | Tmin | 0.99 |

The above table represents coefficient of determination between monthly mean daily observed and monthly mean daily downscaled Tmax, Tmin and Precipitation for base line period. Above table denotes, $R^2$ >0.90 for grid wise average results for whole area downscaling of Tmax, Tmin and precipitation during base line period (1961-2000), it indicates good correlation between observed and downscaled climatic parameters.

### 3.3 Change in Future Precipitation, Tmax and Tmin

Future change in monthly mean daily values of Precipitation, Tmax and Tmin with respect to base line period have been found out for different future series 2020s (2011-2040), 2050s (2041-2070) and 2080s (2071-2099). Grid wise average for whole area shows increasing results of change in precipitation under A2a as well as under B2a scenarios with HadCM3 model. Under A2a scenarios it gives values which vary from 0.21 to 0.78 mm and under B2a scenarios these values varies from 0.21 to 0.47 mm. In similar way it also shows increasing trends for change in future Tmax and Tmin. Future change in Tmax under A2a scenarios varies from 0.90 to $3.12^0$C and under B2a scenario it varies from 0.94 to $2.35^0$C for grid wise average results. Grid wise average results for Tmin also shows increasing trend for change in future monthly mean daily Tmin. Under A2a scenario it gives variable change from 0.25 to 1.54 $^0$C and under B2a scenarios it gives values in the range 0.31 to $1.05^0$C.

The following table indicates future change in monthly mean daily Tmax, Tmin and Precipitation under different scenario with respect to base line period 1961-2000.

**Table 3** Future Change in Monthly Mean Daily Tmax, Tmin and Precipitation under Different Scenario with Respect to Base Line Period 1961-2000

| Type | Model | Scenario | Future Series | Tmax $^0$C | Tmin $^0$C | Precp. Mm |
|---|---|---|---|---|---|---|
| Average of Grid Wise Results for Whole Area | HadCM3 | A2a | 2020s (2011-2040) | 0.90 | 0.25 | 0.21 |
| | | | 2050s (2041-2070) | 1.94 | 0.82 | 0.41 |
| | | | 2080s (2071-2099) | 3.12 | 1.54 | 0.78 |
| | | B2a | 2020s (2011-2040) | 0.94 | 0.31 | 0.21 |
| | | | 2050s (2041-2070) | 1.58 | 0.63 | 0.29 |
| | | | 2080s (2071-2099) | 2.35 | 1.05 | 0.47 |

## References

Huang J., Zhang J., Zhang Z.,Sun S. and Yao J. (2011) Simulation of extreme precipitation indices in the Yangtze River basin by using statistical downscaling method (SDSM), Theoretical and Applied Climatology, Springer Link, pp 325-343

Intergovernmental Panel on Climate Change (IPCC) (2001) Climate Change 2001—The Scientific Basis. Contribution of Working Group I to the Third Assessment Report of the Intergovernmental Panel on Climate Change.

IPCC (2007), General Guidelines on the Use of Scenario Data for Climate Impact and Adaptation Assessment Climate Change, Fourth Assessment Report of the Intergovernmental Panel on Climate Change

Mahmood R. and Babel M.S. (2014) Future changes in extreme temperature events using the statistical downscaling model (SDSM) in the trans-boundary region of the Jhelum river basin, Weather and Climate Extremes, Elsevier, doi.org/10.1016/j.wace.2014.09.001 2212.

Mahmood R. and Babel M.S. (2012) Evaluation of SDSM developed by annual and monthly sub-models for downscaling temperature and precipitation in the Jhelum basin, Pakistan and India, Theoretical and Applied Climatology, Springer, Vol 113,pp 27-44

Samadi S., Ehteramian K. and Sarraf B.S. (2011), "SDSM ability in simulate predictors for climate detecting over Khorasan province", The 2nd International Geography Symposium GEOMED2010, Elsevier, pp 741-749, doi:10.1016/j.sbspro.2011.05.193

Wilby, R.L., Dawson, C.W. and Barrow, E.M. (2002) SDSM—A Decision Support Tool for the Assessment of Regional Climate Change Impacts. Environmental Modelling & Software, 17, 147-159.

IN PROCEEDINGS OF 25th HYDRO 2020, INTERNATIONAL CONFERENCE,
NATIONAL INSTITUTE OF TECHNOLOGY ROURKELA, ODISHA, INDIA
26-28, March 2021, ISBN 978-93-90631-56-8

Paper ID - 420

# Effect of Climate Change on the Precipitation of Saraikela-Kharsawan District of Jharkhand by Statistical Downscaling Method

Nirup Sundar Mandal[1], Sanat Nalini Sahoo[2]

*1. M.Tech Scholar, National Institute of Technology, Rourkela – 769008*
*Email: nirupaiims@gmail.com*
*2.Professor, National Institute of Technology, Rourkela – 769008*
*Email: sahoosanat@nitrkl.ac.in*

## Abstract

Over the years, changing climate has been a matter of concern which has led to drastic changes in various climatic factors like precipitation, temperature, humidity etc. The state of Jharkhand receives a lower amount of precipitation when compared with other states of India. So the objective of the study was to predict the future rainfall of a district receiving moderate to low rainfall. The second generation of the Canadian Earth System Model (CanESM2) was the chosen Global Climatic Model for the study. The historical precipitation data of the district Saraikela-Kharsawan that was used to downscale was chosen from the 15 years span of 1981-1995.
The prediction of the monthly average precipitation was based on two separate Representative Concentration Pathways i.e., RCP4.5 and RCP8.5 with an aim to find out the precipitation from 2021 to 2090 considering whether the emission of greenhouse gas $CO_2$ will be controlled or will not be controlled in the upcoming years. The study proves that there is an increase of 16.5386% while considering RCP4.5 and a considerable increase of 24.2795% while considering RCP8.5 until the year 2090. By this study, there is a future scope of prediction of river flow, groundwater recharge, sedimentation etc for that particular district of Saraikela-Kharsawan.

***Keywords:*** *Precipitation, downscale, global climate model, greenhouse, representative concentration pathway*

## 1. INTRODUCTION

Global warming has been a serious concern for the scientist and engineers over the years as it has led to various climate changing issues especially due to the increase of greenhouse gases. Intergovernmental panel on climate change (IPCC) 2013, reports that there might be a rise of 1.4°C to 5.8°C temperature from the year 1990 to 2100 [1]. And such changes might also affect the other environmental factors like precipitation, humidity, wind speed etc. It is also been predicted that there shall be an increase of rainfall in the upcoming years until 2100.
The study on climate changes is done by the help of General Circulation Models or Global Climate Models (GCMs). It is a typical climatic model commonly used for weather forecasting, understanding the climate and forecasting climate change on the earth. A computational grid is employed over the earth where the grid points shall be close enough to develop a relationship between all kinds of physical, chemical and biological mechanisms and hence can be simulated well enough for the weather and climatic studies. Various types of GCM models are available which can be very useful for the particular study. Amongst all of them CanESM2 model was used for the prediction of the future precipitation.
CanESM2 is the second generation of the Canadian Earth System Model. CanCM4, a physically coupled atmosphere-ocean model coupled to a terrestrial carbon model (CTEM) and CMOC - an ocean-carbon model are the main constituents of the CanESM2 Global Climate Model. Government of Canada sponsored website of Canadian climate data and scenarios provide all the necessary data related to CanESM2 of any region on the earth. 26 climatic parameters having historical data of the years 1976-2005 is also provided by CanESM2. It also provides the future climatic data of the years 2006-2100 under three scenarios of Representative Concentration Pathways (RCPs) i.e., RCP2.6, RCP4.5 and RCP8.5.

The Central Water commission (CWC), Ministry ofWater Resources, River Development and Ganga Rejuvenation (now ministry of Jal Shakti) and the Indian Space Research Organization (ISRO) together on 3rd December 2008, initiated the memorandum of understanding on developing a platform which consists ofweb enabled Water Resource Information System which shall be popularly known as India-WRIS. This online platform India-WRIS provides essential surface water data on river monitoring, reservoirs, surface water quality, soil moisture, precipitation, minor irrigation tanks and evapotranspiration. It also provides groundwater data like the groundwater level and groundwater quality. And this data can be received from any available stations where the recording is done along with the suitable time step required by the user between any two possible dates from all the possible resources available.

The data available needs to be downscaled by taking information known at large scales for the predictions to be made at local scale. Downscaling can be done in two possible ways. Either by dynamical or statistical approach. Statistical Downscaling Model (SDSM) does the work in two steps. Firstly, a statistical relationship is developed between the large scale predictors and local variables. Secondly, the relationships developed, are applied to the output ofthe GCM experiments so as to simulate the future oflocal climatic characteristics.

When the rainfall ofLimbang River Basin was statistically downscaled under transitional climate by Tahir et al. (2017), it was found out that there was an increase of8.13% ofrainfall as per RCP2.6 scenario, 14.7% increase ofrainfall as per RCP4.5 scenario and drastic 40.6% increase ofrainfall as per RCP8.5 scenario from 2071-2100 with 1976-2005 as the base period [2]. Pichuka et al. (2017) have done their work on Bhadra Reservoir Basin and predicted the basin to experience increased events ofdaily extreme high inflow during the future period of2006-2035 when compared with a baseline period of1971-2000 due to increase ofthreshold value [3]. The same analysis can also be done by using SUFI-2 algorithm in SWAT-CUP and some other GCMs like CNRM-CM5. In Krishna River Basin, the analysis on CNRM-CM5 gave a prediction offuture rainfall to increase by 10% and 17% as per RCP4.5 and RCP8.5 scenarios respectively as claimed by Tirupathi et al. (2018) [4]. Sometimes, the amount ofrainfall in the future years may decrease. Soundharajan et al. (2016) proved that by using CMIP5 GCM on Pong Reservoir ofthe Beas Reservoir Basin. The reservoir inflow runoff reduced due to the reductions ofrainfall. But, the rise oftemperature has also resulted in the melting ofsnow and glaciers in the same basin which in turn again increases the inflow and thereby complements the effect of reduction of rainfall and nullifies its effect [5]. Anandhi et al. (2008) downscaled precipitation for IPCC SRES Scenarios using support vector machine (SVM). Potential predictors were chosen as the NCEP variables which are correlated to the precipitation and are also realistically simulated by CGCM3 whereas the predictand is chosen as monthly Thiessen weighted precipitation for the river basin for downscaling precipitation. The projected increase in precipitation is least for COMMIT scenario whereas it is high for A2 scenario. [6]. Gaur et al. (2018) applied physical scaling towards downscaling climate model precipitation data. Future precipitation projections that were downscaled well indicate increase in mean and maximum precipitation intensity and a decrease in the number of dry days. Also an increase in the frequency of short (1-day), moderately long (2--4 day), and long (more than 5-day) precipitation events is projected [7]. Aziz et al. (2018) have represented their work on analysis of statistical correlation for downscaled precipitation data and have given the conclusion that no strong statistical correlation existed between observed data with the reanalysed GCM data. A highest value of 0.18 could be obtained as a correlation coefficient between the predictors and predictands ofNCEP [8].

### 1.1 *Study Area*

From the formerly known princely states of Saraikela and Kharsawan, the district Saraikela - Kharsawan is one district ofthe state Jharkhand (India). It is one among all the 24 districts ofthe state situated between 85°30'14"E & 86°15'24"E longitudes and 22°29'26"N & 23°09'34"N latitudes covering an area of2724.55 sq. kilometers approximately. Saraikela-Kharsawan is bordered by East

Singhbhum District (Jharkhand) in the East, West Singhbhum district (Jharkhand), Khunti district (Jharkhand) & Ranchi district (Jharkhand) in the west, Purulia district (West Bengal) in the north and Mayurbhanj district (Odisha) in the south. The district also has an elevation range of 209 meters to 178 meters. The district faces typical Indian climate comprising of five seasons namely – summer, monsoon, autumn, winter and spring. Being located in one of the drier parts of Jharkhand, Saraikela-Kharsawan district receives a moderate rainfall during the monsoon.

**Table 1:** About Saraikela-Kharsawan Geography and Demography

| | |
|---|---|
| **Location** | Saraikela – Kharsawan (District) |
| **Headquarters** | Saraikela |
| **Division** | Kolhan |
| **Area** | 2724.55 sq. kilometers |
| **Average annual precipitation** | 1350 mm |
| **Rainfall Station** | Saraikela |
| **Popular Rivers** | Subarnarekha, Kharkai, Korkori |
| **Popular Dams & Reservoirs** | Chandil Dam & Reservoirs |
| **Population** | 10,65,056 |

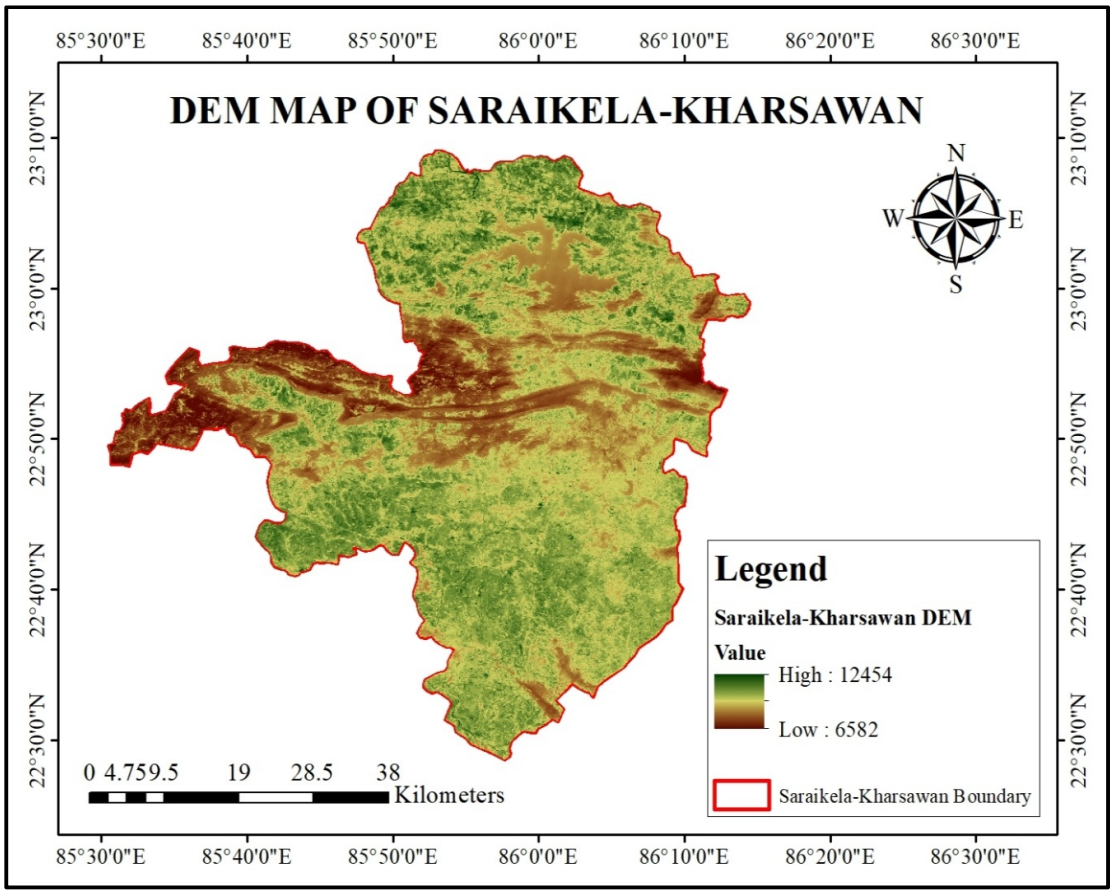



**Fig 1:** DEM Map of District Saraikela-Kharsawan

## 2. METHODOLOGY

Downscaling refers to the process of prediction of climate at local scales with reference to the available large scale information. Statistical Downscaling Model (SDSM) is a well known tool for making predictions and downscale climate data. Ordinary Least Square method is used for downscaling the data. The very initial step includes the screening of the variables to find the best suited ones from the available variables of NCEP-NCAR (1961-2005). This is analyzed for the P-value and Partial r value and the screened values are ensured to have zero or minimum P-value and maximum partial correlation (r) value. For this particular study, the chosen predictor variables for calibration after the screening were "ncepp500gl" and "ncepprcpgl" out of all the available 26 predictor variables. The scenario was generated as per CanESM2 and the precipitation for a period of 15 years (1981-1995) of District Saraikela-Kharsawan was modelled. The modelled past data was used to predict the monthly average precipitation for the district for all the future years i.e, 2021-2090 in a span of 15 years with each year taken as the central value of the span.

### *2.1 Screening of the Predictor Variables*

As per the Multiple Linear Regression (MLR), the most relevant atmospheric parameters are chosen based on the P-value and partial correlation (r) value. The parameters of the predictors must have a high partial correlation and a minimum P-value and then only can be chosen for the calibration. The chosen parameters for calibration after the screening were "ncepp500gl" and "ncepprcpgl" out of all the available 26 parameters of the predictor.

### *2.2 Calibration of Data*

The historical data that has been used for the calibration of precipitation of the district in the study is 1981-1995. Regression equation and Chow Test was fed to calculate for the calibration providing a conditional process as the sub-model. The calibration of the model was done for monthly output. Also, 20 histograms were created in this calibration process. The Ordinary Least Square (OLS) method was used to optimize the model instead of the other available method i.e., the Dual Simplex (DS) method as the latter is a slower method. The R-squared, Root Mean Square Error (RMSE) and Chow Test results were calculated for both the conditional and unconditional statistics with the autoregression applied. And this was done for all the 12 months from 1981 to 1995.

### *2.3 Future Prediction of Precipitation*

The prediction was made for the years 2021-2090 as per two scenarios of Representative Concentration Pathway of CanESM2 i.e., RCP4.5 and RCP8.5. The modelled data of the monthly averages was the input parameter and individually for each future year, monthly average precipitation was predicted as per both RCP4.5 and RCP8.5. This prediction was done by estimating the values for a period of 15 future years with the central year being the desired year whose prediction is to be done and such process was repeated for all the years from 2021-2090. The trend is analysed from the historical data of 1981-1995 which is the base for the quantitative analysis and prediction of the future trends. Simultaneously the data for the future precipitation is also formulated. Firstly, the prediction is done for the RCP4.5 scenario of CanESM2 where the emission is somehow controlled. Secondly, the prediction was made for the RCP8.5 scenario of CanESM2 where there is no control on emission.

## 4. RESULTS AND DISCUSSIONS

The results of the R-squared, RMSE and the Chow Test for both conditional and unconditional statistics are shown in Table 2. The predictor parameters so screened to be perfect for these tests are "ncepp500g"l and "ncepprcpgl". All these values are from the historical data of 1981-1995.

**Table 2:** Results of $R^2$, RMSE and Chow Test for Model Validation

| UNCONDITIONAL STATISTICS | | | |
|---|---|---|---|
| **Month** | **RSquared** | **RMSE** | **Chow** |
| January | 0.127 | 0.252 | 2.8520 |
| February | 0.150 | 0.302 | 0.6823 |
| March | 0.198 | 0.309 | 2.7133 |
| April | 0.192 | 0.363 | 1.9127 |
| May | 0.116 | 0.446 | 2.1072 |
| June | 0.132 | 0.413 | 1.6450 |
| July | 0.112 | 0.312 | 0.5762 |
| August | 0.067 | 0.335 | 0.8653 |
| September | 0.224 | 0.415 | 1.3606 |
| October | 0.204 | 0.398 | 1.7429 |
| November | 0.239 | 0.204 | 2.0726 |
| December | 0.193 | 0.180 | 1.6604 |
| Mean | 0.163 | 0.327 | 1.6825 |
| **CONDITIONAL STATISTICS** | | | |
| **Month** | **RSquared** | **RMSE** | **Chow** |
| January | 0.021 | 0.243 | 1.5304 |
| February | 0.015 | 0.321 | 1.4811 |
| March | 0.011 | 0.295 | 2.6388 |
| April | 0.008 | 0.317 | 1.3135 |
| May | 0.017 | 0.333 | 0.4238 |
| June | 0.001 | 0.436 | 2.7703 |
| July | 0.005 | 0.400 | 2.6327 |
| August | 0.002 | 0.385 | 3.7849 |
| September | 0.005 | 0.427 | 0.7838 |
| October | 0.004 | 0.349 | 0.2410 |
| November | 0.029 | 0.483 | 0.2809 |
| December | 0.286 | 0.330 | 0.0000 |
| Mean | 0.034 | 0.360 | 1.4901 |

The results of the prediction was based on two different Representative Concentration Pathways (RCPs) of CanESM2 i.e., RCP4.5 and RCP8.5. The historical data of 1981-1995 is modelled to find the future data of 2021-2090 and it is the predicted monthly mean precipitation for every single year between 2021-2090. It has been seen that there is a rise of 16.5386% of annual precipitation as per the RCP4.5 scenario and an abrupt rise of 24.2795% for the annual precipitation as per RCP8.5 until the year 2090. It was also interesting to find out that, despite of an overall rise of precipitation as per both the scenarios, the observed mean precipitation of April and May month has always been higher than the modelled precipitation of the same two months be it any scenario for the decade 2080-2090.

These results are shown and well represented in Table 4 (a) and 3 (b). Also a comparison showing the rise of the monthly average precipitation for each month of 2080 - 2090 is represented in the form of bar graphs.

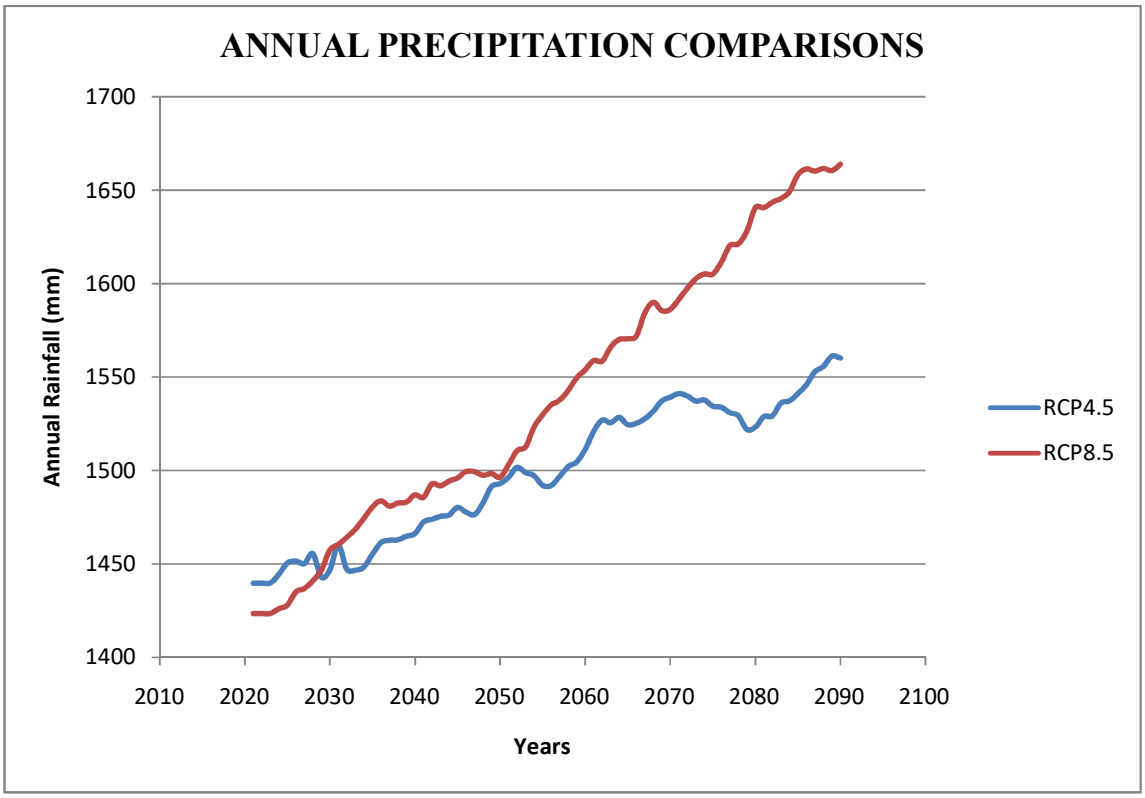



**Fig. 2:** Graph showing the comparison of Annual Precipitation as per RCP4.5 and RCP8.5.

**Table 3: Comparison between Observed and Predicted Rainfall for the year 2090**

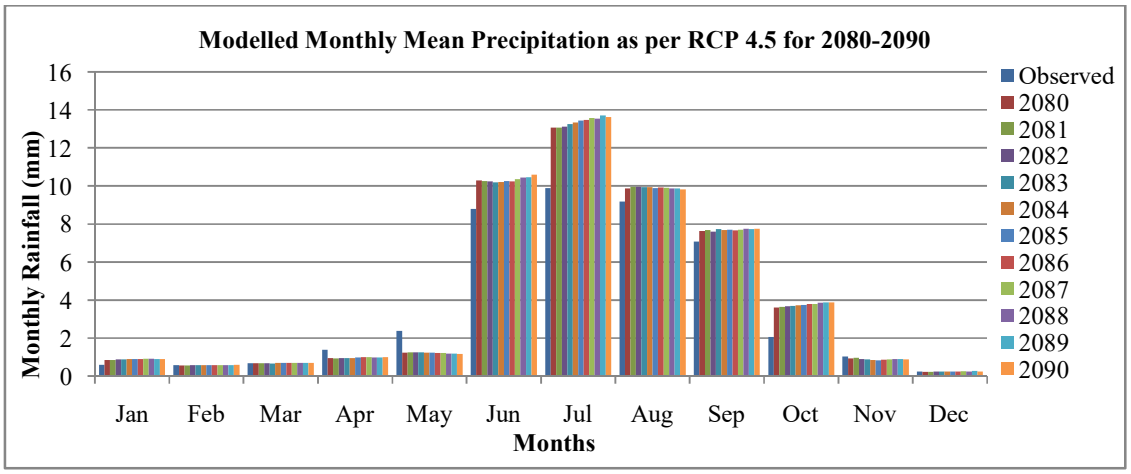
| Month | Observed (Mean) | RCP4.5_2090 (Mean) | RCP8.5_2090 (Mean) |
|---|---|---|---|
| **Jan** | 18.0359 | 27.537 | 31.6997 |
| **Feb** | 16.1222 | 16.2177 | 15.189 |
| **Mar** | 20.7545 | 21.1208 | 20.2586 |
| **Apr** | 41.2623 | 29.7709 | 28.2101 |
| **May** | 73.5433 | 36.0897 | 22.9303 |
| **Jun** | 263.763 | 317.964 | 334.252 |
| **Jul** | 306.04 | 422.047 | 473.078 |
| **Aug** | 284.666 | 304.12 | 304.579 |
| **Sep** | 212.383 | 232.173 | 228.973 |
| **Oct** | 64.0228 | 119.781 | 161.793 |
| **Nov** | 30.9273 | 25.9791 | 32.4378 |
| **Dec** | 7.22334 | 7.35341 | 10.3838 |
| **ANNUAL** | **1338.744** | **1560.15361** | **1663.7843** |
| | | *16.5386% RISE* | *24.2795% RISE* |

**Table 4 (a): Modelled Monthly Mean Precipitation as per RCP4.5 for 2080-2090**

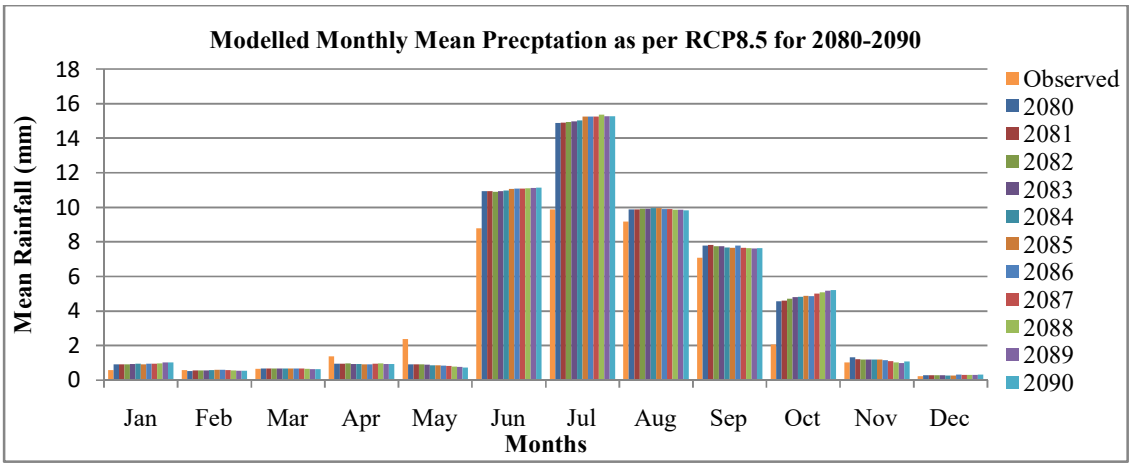
| Month | Observed | 2080 | 2081 | 2082 | 2083 | 2084 | 2085 | 2086 | 2087 | 2088 | 2089 | 2090 |
|---|---|---|---|---|---|---|---|---|---|---|---|---|
| Jan | 0.581804 | 0.836 | 0.835 | 0.865 | 0.875 | 0.893 | 0.888 | 0.889 | 0.898 | 0.909 | 0.892 | 0.888 |
| Feb | 0.575793 | 0.555 | 0.563 | 0.576 | 0.578 | 0.568 | 0.568 | 0.572 | 0.575 | 0.573 | 0.573 | 0.579 |
| Mar | 0.669501 | 0.665 | 0.672 | 0.663 | 0.658 | 0.683 | 0.679 | 0.681 | 0.691 | 0.683 | 0.692 | 0.681 |
| Apr | 1.37541 | 0.939 | 0.92 | 0.928 | 0.942 | 0.939 | 0.979 | 1.003 | 1.001 | 0.986 | 0.979 | 0.992 |
| May | 2.37237 | 1.238 | 1.251 | 1.259 | 1.259 | 1.215 | 1.216 | 1.212 | 1.206 | 1.173 | 1.176 | 1.164 |
| Jun | 8.7921 | 10.29 | 10.27 | 10.25 | 10.2 | 10.21 | 10.25 | 10.24 | 10.35 | 10.43 | 10.45 | 10.6 |
| Jul | 9.87225 | 13.07 | 13.06 | 13.11 | 13.25 | 13.33 | 13.44 | 13.47 | 13.57 | 13.55 | 13.69 | 13.61 |
| Aug | 9.18276 | 9.867 | 9.955 | 9.966 | 9.941 | 9.943 | 9.882 | 9.927 | 9.89 | 9.859 | 9.868 | 9.81 |
| Sep | 7.07944 | 7.622 | 7.672 | 7.591 | 7.721 | 7.68 | 7.695 | 7.66 | 7.693 | 7.745 | 7.722 | 7.739 |
| Oct | 2.06525 | 3.595 | 3.633 | 3.681 | 3.689 | 3.733 | 3.739 | 3.797 | 3.793 | 3.854 | 3.871 | 3.864 |
| Nov | 1.03091 | 0.922 | 0.952 | 0.894 | 0.878 | 0.841 | 0.832 | 0.861 | 0.868 | 0.887 | 0.88 | 0.866 |
| Dec | 0.233011 | 0.228 | 0.228 | 0.241 | 0.246 | 0.24 | 0.238 | 0.245 | 0.253 | 0.239 | 0.264 | 0.237 |

**Table 4 (b): Modelled Monthly Mean Precipitation as per RCP8.5 for 2080-2090**

| Month | Observed | 2080 | 2081 | 2082 | 2083 | 2084 | 2085 | 2086 | 2087 | 2088 | 2089 | 2090 |
|---|---|---|---|---|---|---|---|---|---|---|---|---|
| Jan | 0.581804 | 0.903 | 0.925 | 0.925 | 0.935 | 0.955 | 0.93 | 0.953 | 0.963 | 0.976 | 1.029 | 1.023 |
| Feb | 0.575793 | 0.521 | 0.554 | 0.557 | 0.561 | 0.572 | 0.592 | 0.587 | 0.577 | 0.563 | 0.538 | 0.542 |
| Mar | 0.669501 | 0.675 | 0.682 | 0.678 | 0.675 | 0.681 | 0.675 | 0.679 | 0.677 | 0.668 | 0.647 | 0.654 |
| Apr | 1.37541 | 0.967 | 0.968 | 0.975 | 0.94 | 0.934 | 0.926 | 0.929 | 0.961 | 0.968 | 0.947 | 0.94 |
| May | 2.37237 | 0.91 | 0.92 | 0.908 | 0.886 | 0.853 | 0.85 | 0.83 | 0.813 | 0.783 | 0.76 | 0.74 |
| Jun | 8.7921 | 10.93 | 10.94 | 10.91 | 10.93 | 10.97 | 11.05 | 11.08 | 11.09 | 11.11 | 11.13 | 11.14 |
| Jul | 9.87225 | 14.88 | 14.89 | 14.93 | 14.96 | 15.04 | 15.25 | 15.24 | 15.25 | 15.36 | 15.29 | 15.26 |
| Aug | 9.18276 | 9.887 | 9.884 | 9.932 | 9.919 | 9.955 | 9.961 | 9.914 | 9.906 | 9.853 | 9.846 | 9.825 |
| Sep | 7.07944 | 7.797 | 7.824 | 7.743 | 7.738 | 7.683 | 7.65 | 7.775 | 7.664 | 7.64 | 7.622 | 7.632 |
| Oct | 2.06525 | 4.565 | 4.6 | 4.713 | 4.798 | 4.829 | 4.876 | 4.873 | 5.003 | 5.077 | 5.18 | 5.219 |
| Nov | 1.03091 | 1.326 | 1.198 | 1.19 | 1.187 | 1.18 | 1.189 | 1.149 | 1.092 | 1.028 | 0.991 | 1.081 |
| Dec | 0.233011 | 0.282 | 0.272 | 0.28 | 0.272 | 0.27 | 0.267 | 0.315 | 0.288 | 0.299 | 0.303 | 0.335 |




**(a)**




**(b)**

**Fig. 3: (a)** Comparison Showing the Observed and Modelled Monthly Mean Rainfall as per RCP4.5 for 2080-2090 **(b)** Comparison Showing the Observed and Modelled Monthly Mean Rainfall as per RCP8.5 for 2080-2090.

## 4. CONCLUSIONS

The precipitation of the district Saraikela-Kharsawan has been downscaled and a prediction of the future precipitation has been done. The historical data of 1981-1995 has been the base for the quantitative approach applied in SDSM to predict the precipitation of the district for the future years of 2021-2090 under two different scenarios i.e., RCP4.5 and RCP8.5 of the CanESM2 model. It has been seen that there is an overall increase of rainfall for both the scenarios with RCP8.5 scenario resulting in the highest precipitation. Also, the precipitation of April and May, which was observed to be higher, has somehow shown a decrease of monthly mean precipitation be it any year or any scenario. So, for Saraikela-Kharsawan District, there will be less precipitation in summers in the future as per both RCP4.5 and RCP8.5 scenarios. But there will be an overall increase in precipitation in other months or seasons. Also, the annual precipitation will increase every year. The outcomes of this study could be helpful for the analysis of climate change effects on various other water resources of the district like the flow of Subarnarekha River and the capacity and sedimentation of Chandil Dam & Reservoir all being part of the same district.

## REFERENCES

[1] Kaspar F, Meinshausen M and Schulz M (2013) IPPC Introduction Climate Change 2013 Phys Sci Basis Contrib Work Gr 1 to Fifth Assess Rep Intergov Panel Clim Chang pp 1-90.

[2] Tahir T, Hashim A M, Yusof K W (2017). Statistical downscaling of rainfall under transitional climate in Limbang River Basin by using SDSM. IOP Conf. Series: Earth and Environmental Science 140 (2018) 01203. doi :10.1088/1755-1315/140/1/012037.

[3] Pichuka Subbarao, Prasad R Rajendra, Maity Rajib, Kunstmann Harald (2017). Development of a method to identify change in the pattern ofextreme streamflow events in future climate: Application on the Bhadra reservoir inflow in India. Journal of Hydrology: Regional Studies 9 (2017) 236–246. doi : 10.1016/j.ejrh.2016.12.084.

[4] Tirupathi Chanapathi, Shashidhar Thatikonda, Srinivasan Raghavan (2018). Analysis of rainfall extremes and water yield of Krishna river basin under future climate scenarios. Journal of Hydrology: Regional Studies 19 (2018) 287–306. doi : 10.1016/j.ejrh.2018.10.004.

[5] Soundharajan Bankaru-Swamy, Adeloye Adebayo J., Remesan Renji (2016). Evaluating the variability in surface water reservoir planning characteristics during climate change impacts assessment. Journal of Hydrology 538 (2016) 625–639. doi : 10.1016/j.jhydrol.2016.04.051.

[6] Anandhi Aavudai, Srinivas V. V., Nanjundiah Ravi S., Kumar D. Nagesh (2008). Downscaling precipitation to river basin in India for IPCC SRES scenarios using support vector machine. International Journal of Climatology, Int. J. Climatol. 28: 401–420 (2008). doi: 10.1002/joc.1529.

[7] Gaur Abhishek, Simonovic Slobodan P. (2018). Application of physical scaling towards downscaling climate model precipitation data. Theor Appl Climatol (2018) 132:287–300. doi : 10.1007/s00704-017-2088-7.

[8] Aziz Khairunnisa Sajidah Abdul, Shams Shahriar, Rahman Ena Kartina Abdul Rahman, Ratnayake Uditha (2018). An Analysis of Statistical Correlation for Downscaled Precipitation Data. Conference Paper · January 2018. doi : 10.1049/cp.2018.1559

*IN PROCEEDINGS OF 25th HYDRO 2020, INTERNATIONAL CONFERENCE, NATIONAL INSTITUTE OF TECHNOLOGY ROURKELA, ODISHA, INDIA 26-28, March 2021, ISBN 978-93-90631-56-8*

Paper ID - 421

# Ranking of CMIP6 based Global Climate Models for prediction of temperature in Godavari river basin

Narapareddi Manasa[1], K.C. Patra[2], M Uma Maheswar Rao[3]

*1, M.Tech. Scholar, Department of Civil Engineering, NIT Rourkela, Odisha 769008, India*
*Email: manasanarapareddi@gmail.com*
*2, Professor, Department of Civil Engineering, NIT Rourkela, Odisha 769008, India*
*Email: kcpatra@nitrkl.ac.in*
*3, PhD Scholar, Department of Civil Engineering, NIT Rourkela, Odisha 769008, India*
*Email: mahesh93.happy@gmail.com*

## Abstract

Climate change is emerging as one of the crucial problems to our environment as they would lead to negative effects on natural as well as human systems. To examine the climate change impact on a river basin, prediction of future climate is essential. Global Climate Models (GCMs), also known as the General Circulation Models are the most credible tools for modeling the climate change. In the present study, selection of suitable GCM to assess the performance of maximum temperature ($T_{max}$) simulation for Godavari river basin covering 28 points (with a grid resolution of 1° X 1°) is assessed. The observed and model historical temperature datasets cover the period from 2000-2019. Twelve Coupled Model Intercomparison Project – Phase 6 (CMIP6) GCMs (ACCESS-CM2, BCC-CSM2-MR, CanESM5, GISS-E2-1-G, FGOALS-g3, GFDL-ESM4, HadGEM3, IPSL-CM6A, MIROC-ES2L, MPI-ESM1, NESM3, UKESM1) are used for the climate variable ($T_{max}$) using five performance indicators. Performance indicators used are Correlation Coefficient (CC), Skill Score (SS), Absolute Normalized Mean Bias Deviation (ANMBD), Normalized Root Mean Square Deviation (NRMSD), Average Absolute Relative Deviation (AARD). GCMs are downscaled to finer spatial resolution before ranking them. Statistical downscaling technique is applied to eliminate the systematic biases in GCM simulations. Weights are determined using Entropy technique for each performance metric. Preference Ranking Organization Method of Enrichment Evaluation (PROMETHEE-2) and Compromise programming (CP) methods are utilized to rank the GCMs for the study area. Group decision making is an approach used to integrate the ranking techniques of GCMs to get a collective single rank. The results obtained suggest that MIROC-ES2L, HadGEM3, GFDL-ESM4, ACCESS-CM2 and FGOALS-g3 are the top five models that are suitable for prediction of maximum temperature for the Godavari river basin.

***Keywords:*** *GCM, CMIP6, Entropy method, PROMETHEE-2, Compromise Programming*

## 1. Introduction

Climate is defined as the average condition of the atmosphere mainly represented by the temperature and precipitation. Climate change is defined as an increase or decrease in the statistical properties of the climate variables. The changes in the greenhouse gases concentration and the radiative balance of the atmosphere will result in change of temperature and precipitation. Impact assessment studies of climate change on climate variables like precipitation, temperature, evaporation and runoff have become very important due to an increase in the frequency of floods and droughts. Change in temperature variable depicts adverse impact in terms of reservoir operation, water availability, irrigation, droughts, floods and other extreme events. Ongoing climate change have huge impacts on our systems and recent anthropogenic greenhouse gases emissions are the highest in recent times. The temperature at the Earth's surface in the last three decades when compared with any preceding decade considered since 1850 are more warmer.

In order to investigate the climate change of a region, climate data is considered from several global climate models (GCMs) which are effective tools to simulate present climate data and predict changes in future caused due to increase in greenhouse gas concentration. They are most advanced tools for studying the climate trends of past, present and future and also variability by simulating the climate system. GCMs are mathematical equations which are solved for 3D atmospheric grid with the help of high computing resources over a number of time steps. The resolution of GCMs is defined by the grid cell size. The GCM with small grid cell size will have high level of details and vice versa. GCM data

enable us to know climate change impact on environmental systems at global and regional scales. Initially, Intergovernmental Panel on Climate Change (IPCC) has provided the future climate datasets over the past decades. At present, World Climate Research Programme has been providing the data of Coupled Model Intercomparison Project – Phase 6 (CMIP6) which is the updated version of CMIP5 and CMIP3.

Considering from global to regional and to local catchment scales, the potential of GCMs to predict the temporal and spatial distributions of climate variables (temperature, precipitation etc) will decline. It also declines from annual to monthly to daily data frequency. Hence downscaling methods are used to derive the regional data from the global data. The two main approaches are dynamic downscaling and statistical downscaling. Dynamic downscaling approach uses very high resolution GCMs to produce an output model that is close to the nature condition. Statistical downscaling approach demonstrates a statistical relationship between the local scale variables called predictands and large scale climate variables called predictors.

Numerous studies are attempted for simulating GCMs for the validation of maximum temperature, minimum temperature, average temperature and precipitation all over the world. Perkins et al. (2007) used the skill score indicator which measures the resemblance between a observed and simulated(modelled) probability density function to find the suitability of GCMs to simulate $T_{max}$ and $T_{min}$ and precipitation. Srinivas Raju K and Nagesh Kumar D (2014) calculated weights of five performance indicators using Entropy method and Equal weight scenario. PROMETHEE-2 is employed to obtain the ranks of GCMs suitable for India. Srinivasa Raju K, Sonali P (2015) evaluated the performance of maximum and minimum temperature simulations by using three performance indicators and Compromise programming is used to rank the CMIP5 GCMs for India.

Accuracy of GCMs will decrease when used at finer scales (Xu 1999). This is due to the uncertainities like downscaling to regional or local levels and variability in simulations. Therefore, GCMs should be evaluated and GCM performance should be calculated before applying them to climate change studies. To identify the performance of GCMs, different performance measures have been developed (Pitman et al. 2012; Fordham et al. 2011; Knutti et al. 2010; Johnson and Sharma 2009; Gleckler et al. 2008). Five performance indicators are considered for assessing the performance of 12 GCMs from CMIP6. The GCMs selected are ACCESS-CM2, BCC-CSM2-MR, CanESM5, FGOALS-g3, GISS-E2-1-G, GFDL-ESM4, HadGEM3, IPSL-CM6A, MIROC-ES2L, MPI-ESM1, NESM3, UKESM1 for maximum temperature. Weights of the statistical performance metrics are calculated based on the non bias technique called as Entropy method. A distance based decision making technique called compromise programming (CP) and built-in preference function concept called Preference Ranking Organization Method of Enrichment Evaluation (PROMETHEE-2) are employed for the ranking of GCMs. Group Decision Making Technique is carried out on the ranking techniques to get a single combined rank. The objective of this study is to evaluate 12 CMIP6 models (i.e) ACCESS-CM2, BCC-CSM2-MR, CanESM5, FGOALS-g3, GISS-E2-1-G, GFDL-ESM4, HadGEM3, IPSL-CM6A, MIROC-ES2L, MPI-ESM1, NESM3, UKESM1 based on their performance indicators and also rank them for future projection of maximum temperature for the Godavari basin.

## 2. Study Area

Godavari is second longest river system after Ganga in India and is the largest in India in terms of its discharge, length and catchment. Other name of river Godavari is Dakshin Ganga. It drains the states of Andhra Pradesh, Chhattisgarh, Maharashtra, Telangana and Odisha as shown in Figure 1.

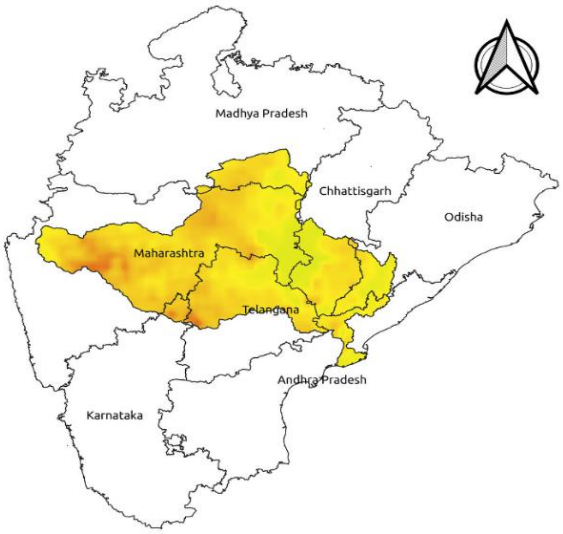



**Figure 1** Godavari river basin

The basin broadens over an area of 312,812km$^2$ which occupies nearly 10% of the total India's geographical area. Godavari river arises in the Western Ghats of central India near Nashik in Maharashtra which is 80km from the Arabian Sea. It first flows for a length of 1,465km in east direction across the Deccan Plateau and turns southeast to enter the districts of West Godavari and East Godavari district of Andhra Pradesh. It flows till it divides into two distributaries which widens into a large river delta in Rajamahendravaram at Sir Arthur Cotton Barrage. The Godavari river flows into the Bay of Bengal ultimately. The basin is enclosed between latitudes 16°19'37.76"N and 22°35'57.89"N, longitudes 73°31'10.45"E and 83°8'14.46"E. The location map is shown in Figure 2.

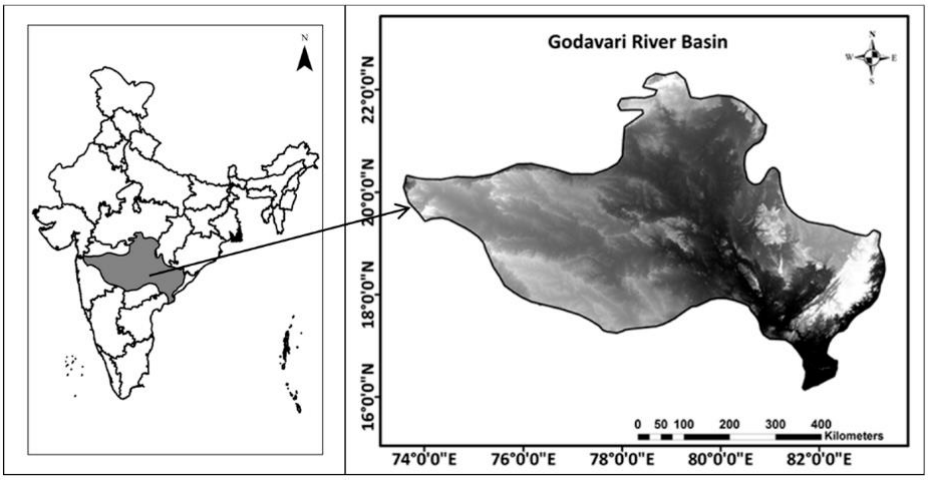



**Figure 2** Godavari river basin's location map

## 3. Data and Methodology

### *3.1 Data Collection*

For climate simulations, WCRP's (World Climate Research Programme) CMIP6 data of the twentieth century is considered. CMIP6 based GCMs providing monthly maximum temperature ($T_{max}$) are considered. Twelve dataset models of CMIP6 are considered for evaluation and are downloaded from clim4impact portal. The GCM models are considered in a way that it has historical data till 2015. Historical or observed gridded maximum temperature ($T_{max}$) data with a resolution of 1°X1° is obtained from power.larc.nasa.gov portal for a period of 2000-2019.

### *3.2 Downscaling*

GCMs generate data at a coarser resolution and hence downscaling methods are used to derive regional scale weather variables from global scale atmospheric predictor variables. Statistical downscaling methods are chosen over dynamic downscaling method as they render good fit to the observed data while being inexpensive and providing quick results.

Statistical downscaling method is carried out in SD-GCM V2.0 software by giving the inputs as station data and GCM data (.nc format). There are three methods of statistical downscaling namely Delta method, Empirical Quantile Mapping method (EQM) and Quantile Mapping method (QM) available in SD-GCM software. The root mean square error values of Delta method, EQM method and QM method are 0.145, 0.157 and 0. 168 respectively. Hence, Delta method is chosen for extracting the downscaled data as it has great correlation and least error as compared to EQM and QM methods.

### *3.3 Methodology*

Observed data is collected in 1°X1° resolution. GCMs are having different resolution. To judge the GCMs performance, all the GCMs are converted to the same resolution as that of IMD data. Climate Data Operator (CDO) is used to convert the GCM resolution to 1°X1° resolution. The process in explained in Figure 3 in the form of a flow chart.

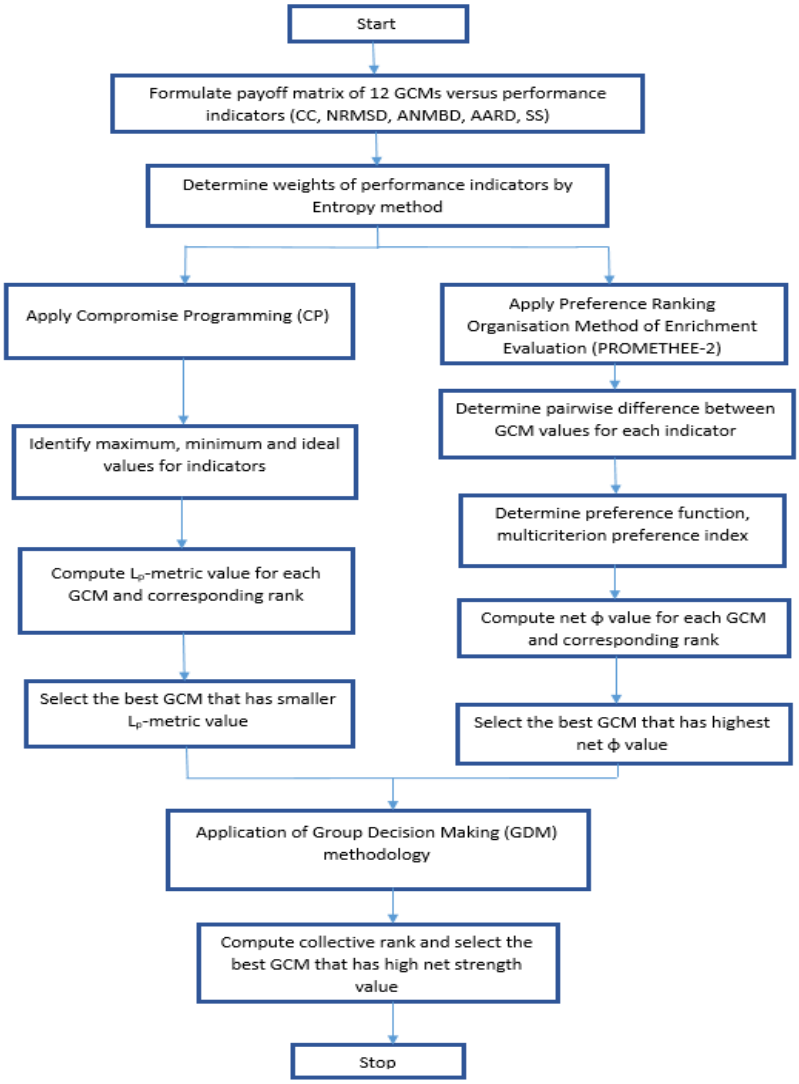



**Figure 3** Flow Chart of present study

### *3.4 Performance indicators or Statistical performance metrics*

SPMs or performance indicators are the estimate of a GCM to find how good the GCM data simulates the observed data. Based on the literature, five effective indicators are selected to find the association between the GCM and observed station datasets. The performance indicators chosen are correlation coefficient (CC), skill score (SS), absolute normalized mean bias deviation (ANMBD), normalized root mean square deviation (NRMSD) and average absolute relative deviation (AARD). These values are calculated for every GCM using the respective equations as appropriate.

Correlation coefficient is defined as how well the observed and model data correlates representing their strength. The correlation coefficient is given as

$$CC = \frac{\sum_{i=1}^{T}(x_i - x_{avg})(y_i - y_{avg})}{(T-1)\sigma_x \sigma_y} \quad (1)$$

where, $x_i$, $y_i$ are the observed and simulated model values; $x_{avg}$ and $y_{avg}$ are the average of observed and simulated values respectively; $\sigma_x, \sigma_y$ are the standard deviations of observed station and simulated model values respectively; T represents the entire number of observations.
If CC value is near to 1, it represents best performance of the model and if CC value is near to 0, it indicates poor model performance.

Normalized root mean square deviation (NRMSD) is defined as the ratio of square root of the average of square difference between the observed and model values to the average of the observed values. NRMSD is given as

$$NRMSD = \frac{\sqrt{(1/T)\sum_{i=1}^{T}(x_i - y_i)2}}{x_{avg}} \quad (2)$$

where, $x_i$, $y_i$ are the observed and simulated values; $x_{avg}$ is the average of observed station values; T represents the number of observations.

Absolute Normalized Mean Bias Deviation (ANMBD) is defined as the ratio of the average of difference between the observed and model values to the average of the observed values. ANMBD is given as

$$ANMBD = \left|\frac{(1/T)\sum_{i=1}^{T}(y_i - x_i)}{x_{avg}}\right| \quad (3)$$

where, $x_i$, $y_i$ are the observed station and model values respectively; $x_{avg}$ is the average of observed values; T represents the entire number of observations.

Average Absolute Relative Deviation (AARD) is the average of the absolute relative deviation (ARD) values. AARD is given as

$$AARD = \left(\frac{1}{T}\right)\sum_{i=1}^{T}|ARDi| \quad (4)$$

where $ARDi = \frac{|y_i - x_i|}{x_i}$

where, $x_i$, $y_i$ are the observed station and model values respectively; T represents the total number of observations.

Skill Score (SS) is an estimate of resemblance between the probability density function (PDF) of the observed and model values. It varies between zero and one.

If the observed and the model PDF simulates perfectly, the SS should be nearly 1. If they simulates poorly, the SS will be nearly 0. SS is given as

$$SS = (1/T)\sum_{i=1}^{nb} min(f_m f_o) \quad (5)$$

where, nb is the number of bins used to calculate the PDF (probability density function), $f_m$, $f_o$ are the frequencies of values in bin obtained from the observed and GCM values.

The performance indicator values for each GCM are calculated using the above mentioned equations and are given below in Table 1.

**Table 1** Performance indicators values obtained for 12 GCMs

| GCM | CC | NRMSD | ANMBD | AARD | SS |
|---|---|---|---|---|---|
| **ACCESS-CM2** | 0.622 | 0.114 | 0.000 | 0.100 | 0.691 |
| **BCC-CSM2** | 0.823 | 0.082 | 0.004 | 0.068 | 0.808 |
| **Can-ESM5** | 0.682 | 0.121 | 0.007 | 0.105 | 0.105 |
| **FGOALS-g3** | 0.703 | 0.101 | 0.000 | 0.090 | 0.090 |
| **GFDL-ESM4** | 0.787 | 0.107 | 0.001 | 0.084 | 0.084 |
| **GISS-ES-1-G** | 0.732 | 0.095 | 0.006 | 0.080 | 0.080 |
| **HadGEM3** | 0.835 | 0.078 | 0.001 | 0.063 | 0.063 |
| **IPSL-CM6A** | 0.805 | 0.085 | 0.003 | 0.067 | 0.067 |
| **MIROC-ES2L** | 0.797 | 0.085 | 0.000 | 0.071 | 0.071 |
| **MPI-ESM1** | 0.868 | 0.085 | 0.003 | 0.066 | 0.066 |
| **NESM3** | 0.744 | 0.105 | 0.001 | 0.091 | 0.091 |
| **UKESM1** | 0.772 | 0.089 | 0.002 | 0.076 | 0.076 |
| | Higher value is preferable | Lower value is preferable | Lower value is preferable | Lower value is preferable | Higher value is preferable |

### *3.5 Entropy method*

#### *3.5.1 Normalize the payoff matrix*

This is done to convert various indicators of different space to the indicators of same space.
Payoff matrix is formulated with GCM names as rows and performance indicators as columns. The normalized value is given as

$$\text{Normalized value}, k_{aj} = \frac{K_j(a)}{\sum_{a=1}^{T} K_j(a)} \quad (6)$$

where, $K_j(a)$ is the normalized value of indicator j for GCM a; a is the index of GCMs; the total number of GCMs are represented by T.

#### *3.5.2 Entropy for each indicator*

This method is used to measure the weights of each indicator. A payoff matrix i.e GCMs versus performance indicators is generated. Weights are determined without any bias which reduces the error and the variation in weights of indicators gives a clear view to understand the importance of them. These weights are used as an input for the CP and PROMETHEE-2 techniques.
The entropy for each indicator j is given as

$$En_j = \frac{-1}{ln(T)} \sum_{a=1}^{T} k_{aj}\, ln(k_{aj}) \text{ for } j=1,2,3,\ldots,J \quad (7)$$

where, a represents the index of GCMs; $k_{aj}$ is the normalized value; j is the number of indicators and entire number of GCMs are represented by T.

### *3.5.3 Degree of diversification*

It is a parameter calculated for each indicator to find the weight of the indicator and is expressed as

$$Dd_j = 1 - En_j \quad (8)$$

where, $En_j$ represents the entropy for each indicator j.

### *3.5.4 Normalized weight of performance indicators*

The weights of indicators is expressed as,

$$r_j = \frac{Dd_j}{\sum_{j=1}^{J} Dd_j} \quad (9)$$

where, $Dd_j$ is the degree of diversification assigned to indicator j.
The weight of each indicator acquired by entropy method using the equations (7), (8), (9) are shown below in Table 2.

**Table 2** Weights of performance indicators

| | CC | NRMSD | ANMBD | AARD | SS |
|---|---|---|---|---|---|
| $\boldsymbol{En_j}$ | 0.998398 | 0.996271 | 0.883903 | 0.994553 | 0.997172 |
| $\boldsymbol{Dd_j}$ | 0.001602 | 0.003728 | 0.116096 | 0.005446 | 0.002828 |
| $\sum_{j=1}^{J} \boldsymbol{Dd_j}$ | 0.129702 | 0.129702 | 0.129702 | 0.129702 | 0.129702 |
| $\boldsymbol{r_j}$ | **0.012354** | **0.028748** | **0.895099** | **0.0419945** | **0.021804** |

## *3.6 GCMs Ranking*

Multicriterion Decision Making Techniques (MCDM) are applied in order to rank the GCMs. In the present study, Compromise Programming (CP) and Preference Ranking Organization Method of Enrichment Evaluation (PROMETHEE-2) are applied to rank the GCMs.

### *3.6.1 Compromise Programming (CP)*

CP gives the ranking based on the least distance of value from an ideal measured value. Lower value of $L_p(a)$ indicates the suitable GCM. Distance measure Lp metric is expressed as

$$L_p(a) = \left[\sum_{j=1}^{J} r_j \left|k_j^* - k_j(a)\right|^p\right]^{\frac{1}{p}} \quad (10)$$

where, $k_j(a)$ is normalized value of indicator j for the GCM a; $k_j^*$ is normalized ideal value of the indicator j; $r_j$ is indicator weight, p is the distance measure parameter (p=1, linear and p=2, squared Euclidean distance measure).

Ranking of GCMs calculated by using compromise programming is given in Table 3

**Table 3** $T_{max}$ statistical performance metric values of GCMs, $L_p$ metric, Rank (CP)

| GCM | CC | NRMSD | ANMBD | AARD | SS | $L_p$ metric | RANK |
|---|---|---|---|---|---|---|---|
| ACCESS-CM2 | 0.6223 | -0.1141 | -0.0003 | -0.1004 | 0.6916 | 0.006585 | 9 |
| BCC-CSM2 | 0.8235 | -0.0825 | -0.0684 | -0.0684 | 0.8086 | 0.004623 | 7 |
| Can-ESM5 | 0.6826 | -0.1211 | -0.1057 | -0.1057 | 0.6666 | 0.009260 | 12 |
| FGOALS-g3 | 0.7033 | -0.1012 | -0.0905 | -0.0905 | 0.7541 | 0.004853 | 8 |
| GFDL-ESM4 | 0.7879 | -0.1075 | -0.0843 | -0.0843 | 0.8333 | 0.003018 | 5 |
| GISS-ES-1-G | 0.7325 | -0.0954 | 0.0800 | -0.0800 | 0.7333 | 0.007700 | 11 |
| HadGEM3 | 0.8358 | -0.0784 | -0.0639 | -0.0639 | 0.8916 | 0.001871 | 2 |
| IPSL-CM6A | 0.8050 | -0.0855 | -0.0678 | -0.0678 | 0.9458 | 0.002626 | 3 |
| MIROC-ES2L | 0.7977 | -0.0859 | -0.0711 | -0.0711 | 0.9291 | 0.001035 | 1 |
| MPI-ESM1 | 0.8686 | -0.0852 | -0.0666 | -0.0666 | 0.8375 | 0.003357 | 6 |
| NESM3 | 0.7445 | -0.1058 | -0.0918 | -0.0918 | 0.6583 | 0.006749 | 10 |
| UKESM1 | 0.7724 | -0.0890 | -0.0764 | -0.0764 | 0.8458 | 0.002981 | 4 |

### *3.6.2 Preference Ranking Organization Method of Enrichment Evaluation (PROMETHEE-2)*

This technique depends on the preference function concept $Pr_j(a,b)$. For each indicator, pairwise GCMs values difference is calculated. If the pairwise difference >0, the preference function is $Pr_j(a,b) = 1$, otherwise $Pr_j(a,b) = 0$. So, the matrix of preference function values are either 1 or 0. Weights estimated using Entropy method and preference function values are employed to calculate the Multicriterion Preference Index (MIPI). The diagonal values of the MIPI matrix will be 0 because of the comparison of GCM with itself.

MIPI is the weighted average value of the preference functions $Pr_j(a,b)$ considering all indicators. The MIPI is given as

$$MIPI = \pi(a,b) = \frac{\sum_{j=1}^{J} r_j Pr_j(a,b)}{\sum_{j=1}^{J} r_j} \quad (11)$$

where, $\pi(a,b)$ is the MIPI value with respect to GCM a; $Pr_j(a,b)$ represents the preference function values; $r_j$ is the weight of the indicator.

The values of MIPI calculated using equation (11) are presented in Table 4

**Table 4** Multicriterion preference index values

| | ACCESS-CM2 | BCC-CSM2 | Can-ESM5 | FGOALS-g3 | GFDL-ESM4 | GISS-ES-1-G | HadGEM3 | IPSL-CM6A | MIROC-ES2L | MPI-ESM1 | NESM3 | UKESM1 |
|---|---|---|---|---|---|---|---|---|---|---|---|---|
| ACCESS-CM2 | 0 | 0.895 | 0.987 | 0.895 | 0.895 | 0.895 | 0.895 | 0.895 | 0.895 | 0.895 | 0.916 | 0.895 |
| BCC-CSM2 | 0.104 | 0 | 1 | 0.104 | 0.083 | 1 | 0 | 0.041 | 0.083 | 0.028 | 0.104 | 0.083 |
| Can-ESM5 | 0.012 | 0 | 0 | 0 | 0 | 0 | 0 | 0 | 0 | 0 | 0.021 | 0.012 |
| FGOALS-g3 | 0.104 | 0.895 | 1 | 0 | 0.923 | 0.916 | 0.895 | 0.895 | 0 | 0.895 | 0.987 | 0.895 |
| GFDL-ESM4 | 0.104 | 0.916 | 1 | 0.076 | 0 | 0.929 | 0.895 | 0.895 | 0 | 0.895 | 0.971 | 0.907 |
| GISS-ES-1-G | 0.104 | 0 | 1 | 0.083 | 0.070 | 0 | 0 | 0 | 0 | 0 | 0.092 | 0 |
| HadGEM3 | 0.104 | 1 | 1 | 0.104 | 0.104 | 1 | 0 | 0.978 | 0.083 | 0.987 | 0.104 | 1 |
| IPSL-CM6A | 0.104 | 0.958 | 1 | 0.104 | 0.104 | 1 | 0.021 | 0 | 0.104 | 0.021 | 0.104 | 0.104 |
| MIROC-ES2L | 0.104 | 0.916 | 1 | 1 | 1 | 1 | 0.916 | 0.895 | 0 | 0.916 | 1 | 1 |
| MPI-ESM1 | 0.104 | 0.971 | 1 | 0.104 | 0.104 | 1 | 0.012 | 0.978 | 0.083 | 0 | 0.104 | 0.083 |
| NESM3 | 0.083 | 0.895 | 0.978 | 0.012 | 0.028 | 0.907 | 0.895 | 0.895 | 0 | 0.895 | 0 | 0.104 |
| UKESM1 | 0.104 | 0.916 | 1 | 0.104 | 0.092 | 1 | 0 | 0.895 | 0 | 0.916 | 0.104 | 0 |

Outranking index is calculated for GCM a as below

$$\varphi^{+}(a) = \frac{\sum_T \pi(a,b)}{T-1} \quad (12)$$

where, $\pi(a,b)$ is the MIPI value with respect to GCM a; T is the entire number of GCMs

Outranked index is calculated for GCM a as below

$$\varphi^{-}(a) = \frac{\sum_T \pi(b,a)}{T-1} \quad (13)$$

where, $\pi(b,a)$ is the MIPI value with respect to GCM b; T is the entire number of GCMs

Net ranking is calculated by using the equations (12) and (13) for GCM a and is given by

$$\varphi(a) = \varphi^{+}(a) - \varphi^{-}(a) \quad (14)$$

Ranking of the GCMs is done based on the value of $\varphi(a)$. Higher the value of $\varphi(a)$ indicates best GCM.

The ranks of GCMs obtained by PROMETHEE-2 are shown in Table 5.

**Table 5** Values of $\varphi^+(a)$, $\varphi^-(a)$, $\varphi(a)$, rank (PROMETHEE-2)

| GCM | $\varphi^+(a)$ | $\varphi^-(a)$ | $\varphi(a)$ | RANK |
|---|---|---|---|---|
| ACCESS-CM2 | 0.905 | 0.094 | 0.8109 | 1 |
| BCC-CSM2 | 0.239 | 0.760 | -0.5211 | 10 |
| Can-ESM5 | 0.004 | 0.996 | -0.9926 | 12 |
| FGOALS-g3 | 0.764 | 0.235 | 0.5288 | 3 |
| GFDL-ESM4 | 0.690 | 0.309 | 0.3802 | 4 |
| GISS-ES-1-G | 0.122 | 0.877 | -0.7543 | 11 |
| HadGEM3 | 0.588 | 0.411 | 0.1760 | 5 |
| IPSL-CM6A | 0.330 | 0.669 | -0.3396 | 9 |
| MIROC-ES2L | 0.886 | 0.113 | 0.7728 | 2 |
| MPI-ESM1 | 0.413 | 0.586 | -0.1731 | 8 |
| NESM3 | 0.517 | 0.410 | 0.1073 | 6 |
| UKESM1 | 0.466 | 0.462 | 0.0045 | 7 |

### *3.6.3 Group decision making (GDM) and Net strength*

GDM approach is opted as the ranking is done by two different methods. It is a procedure in which different ranking methods to calculate ranks are united to get a single ranking preference. Ranks are arranged in the decreasing order and then upper and lower portions are separated. The division is done based on the number of GCMs.

X = T / 2, when the GCMs count is even
Y = (T / 2) + 1 = X+1, when the GCMs count is odd

Strength and weakness are calculated for each GCM to find the net strength of GCM. The strength of GCM is given as

Strength of GCM a, $ST_a = \sum_{k=1}^{m} \sum_{z}^{X} (X - z + 1)\, q_{az}^{k}$ (15)

where the position in upper part considering from first position to $X^{th}$ position is represented by z; a represents the GCMs in upper part; k is ranking technique; $q_{az}^{k}$ = 1 if GCM's position is in z for k and otherwise its value is 0.

Weakness of GCM is given as

Weakness of GCM a, $WE_a = \sum_{k=1}^{m} \sum_{z=y}^{T} (z - Y + 1)\, q_{az}^{k}$ (16)

where the position in lower part considering from first position to the lower $Y^{th}$ position is represented by z; a represents the GCMs in lower part; k is the ranking technique; $q_{az}^{k}$ = 1 if GCM's position is in z for k and otherwise its value is 0.

Net strength of GCM is calculated using the equations (15), (16) and is given as

Net strength of GCM a, $NS_a = ST_a - WE_a$ (17)

Ranking is done based on the net strength values. Higher net strength represents best GCM.
Net strength and ranking values are given in Table 6.

**Table 6** Net strength and rank values of GCMs

| GCM | Net Strength | RANK |
|---|---|---|
| ACCESS-CM2 | 3 | 4 |
| BCC-CSM2 | -5 | 9 |
| Can-ESM5 | -12 | 11 |
| FGOALS-g3 | 2 | 5 |
| GFDL-ESM4 | 5 | 3 |
| GISS-ES-1-G | -10 | 10 |
| HadGEM3 | 7 | 2 |
| IPSL-CM6A | 1 | 6 |
| MIROC-ES2L | 11 | 1 |
| MPI-ESM1 | -1 | 7 |
| NESM3 | -3 | 8 |
| UKESM1 | 2 | 5 |

Net strength values for maximum temperature variable obtained from the Group Decision-Making technique are depicted in the Figure 4. Negative strength values are represented below the axis and positive strength values are represented above the axis. The highest positive strength is shown by MIROC-ES2L GCM which is given the first rank. The highest negative strength is shown by Can-ESM5 GCM which is given the least rank.

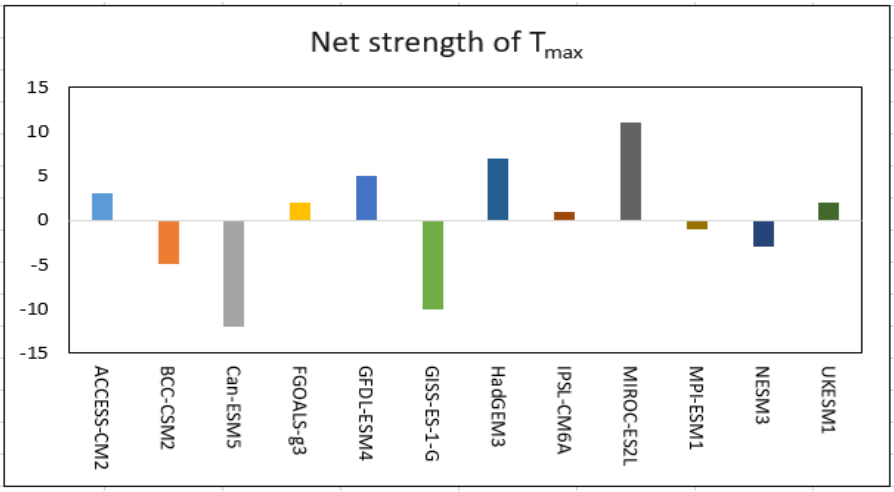



**Figure 4** GCMs net strength for $T_{max}$ (using GDM)

## 4 Results & Discussions

Mean monthly maximum temperature data is collected and the ranking procedure is done to find out the performance of individual GCMs using the techniques like CP and PROMETHEE-2. The number of indicators used to assess the performance are five. The ideal value for NRMSD, ANMBD and AARD is 0 and the ideal value for CC and SS is 1. Ranking is done individually using CP and Promethee-2 and then application of Group decision making (GDM) technique is done to get the combined GCMs ranking. In Compromise Programming technique, the GCM with the minimum $L_p$-metric based value is considered as the suitable model. From Table 3, it is observed that the minimum value is 0.001035 and hence the best GCM as per CP is MIROC-ES2L. The second suitable GCM is Had-GEM3 with $L_p$-metric of 0.001871 and third suitable GCM is IPSL-CM6A with $L_p$-metric of 0.002626.

In PROMETHEE-2, the GCM with maximum φ(a) value will be more suitable. From table 5, it is observed that the first best GCM is ACCESS-CM2 with φ(a) value of 0.8109. The second best GCM is MIROC-ES2L with φ(a) value of 0.7728 and the third best GCM is FGOALS-g3 with φ(a) value of 0.5288. It is also observed that GISS-ES-1-G and Can-ESM5 occupied 11th and 12th ranks in both the

methods. Group decision making (GDM) approach is applied for both the methods to get the collective ranks of the GCMs. Net strength values are calculated using the equations (15), (16), (17) and the best GCM will have more net strength. From the Table 6, it is observed that the first best GCM after GDM is MIROC-ES2L with a net strength of 11. The second and third best GCMs are HadGEM3 and GFDL-ESM4 with net strength values of 7 and 5 respectively. The fourth suitable GCM is ACCESS-CM2 with a net strength value of 3. It is observed that FGOALS-g3 and UKESM1 are having same net strength value of 2, so they both occupy the fifth position in suitability.

Table 7 represents the collective rank obtained by Group Decision-Making technique using Compromise Programming and Promethee-2 methods.

**Table 7** Ranking of GCMs

| RANK (GDM) | GCM |
|---|---|
| 1 | MIROC-ES2L |
| 2 | HadGEM3 |
| 3 | GFDL-ESM4 |
| 4 | ACCESS-CM2 |
| 5 | FGOALS-g3 |
| 5 | UKESM1 |
| 6 | IPSL-CM6A |
| 7 | MPI-ESM1 |
| 8 | NESM3 |
| 9 | BCC-CSM2 |
| 10 | GISS-ES-1-G |
| 11 | Can-ESM5 |

MIROC-ES2L GCM is the best suitable GCM for the Godavari river basin by considering the climate variable as maximum temperature. The observed and simulated data are compared from a period of 2000-2019 and the future temperature is predicted till 2030. This is shown in Figure 5.

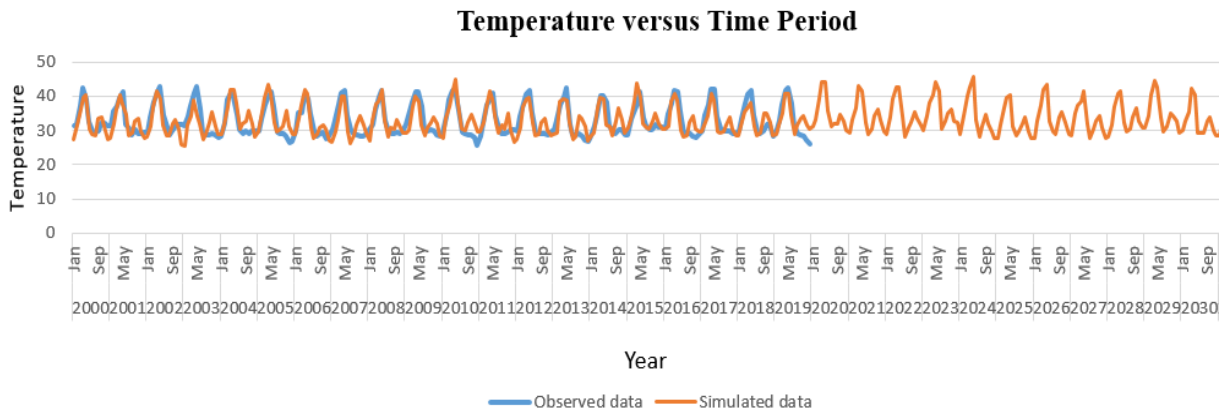



**Figure 5** Observed and simulated historical data, Future simulated data

## 5 Conclusion

Five performance indicators like NRMSD, ANMBD, AARD, CC, SS are utilized to assess the suitability of 12 GCMs with the maximum temperature, $T_{max}$ data for the Godavari river basin. Weights are determined using an unbiased Entropy method. The ranking is carried out on CMIP6 GCMs using CP and PROMETHEE-2 techniques.
From the present work, following conclusions are drawn.

- Increasing the number of indicators and decreasing the resolution will further give accurate results.
- Among the five indicators, ANMBD is the best performance indicator as it is given high importance because of its weight. This means that the indicators effect is significant on ranking of GCMs. The contribution of remaining indicators is less than 0.2.
- MIROC-ES2L, HadGEM3 and GFDL-ESM4 occupies the first 3 positions in ranking. We recommend the ensemble of all three GCMs.

## 6 Limitations

In this study, 12 models are taken into consideration but the study can be extended for remaining CMIP6 models so as to evaluate the ability of each model. The resulting ranking of GCMs vary with the further inclusion of GCMs, indicator and climate variable (precipitation, minimum temperature).

## 7 References

1. Brans JP, Vincke Ph, Mareschal B (1986) "How to select and how to rank projects: the PROMETHEE method". Eur J Oper Res 24: 228−238
2. Gleckler, P.J., Taylor, K.E., and Doutriaux, C. (2008). "Performance metrics for climate models." J. Geophys. Res., 113, D06104. doi:10.1029/2007JD008972.
3. Hashino T, Bradley AA, Schwartz SS (2007) Evaluation of bias-correction methods for ensemble streamflow forecasts. Hydrol Earth Syst Sci 11: 939−950
4. Johnson, F., and Sharma, A. (2009). "Measurement of GCM skill in predicting variables relevant for hydroclimatological assessments."J. Clim., 22, 4373–4382. doi: 10.1175/2009JCLI2681.1.
5. Kamworapan, S., &Surussavadee, C. (2019). Evaluation of CMIP5 global climate models for simulating climatological temperature and precipitation for southeast Asia. *Advances in Meteorology*, *2019*. https://doi.org/10.1155/2019/1067365.
6. Khan, N., Shahid, S., Ahmed, K., & Ismail, T. (2018). *Performance Assessment of General Circulation Model in Simulating Daily Precipitation and Temperature Using Multiple Gridded Datasets*. https://doi.org/10.3390/w10121793.
7. McMahon, T. A., Peel, M. C., &Karoly, D. J. (2015). Assessment of precipitation and temperature data from CMIP3 global climate models for hydrologic simulation. *Hydrology and Earth System Sciences*, *19*(1), 361–377. https://doi.org/10.5194/hess-19-361-2015
8. Raju, K. S., & Kumar, D. N. (2014). Ranking of global climate models for India using multicriterionanalysis. *Climate Research*, *60*(2), 103–117. https://doi.org/10.3354/cr01222.
9. Ruan, Y., Liu, Z., Wang, R., & Yao, Z. (2019). Assessing the performance of CMIP5 GCM's for projection of future temperature change over the lower Mekong Basin. *Atmosphere*, *10*(2). https://doi.org/10.3390/ATMOS10020093
10. Salman, S.A., Shahid, S., Ismail, T., Al-Abadi, A.M., Wang, X.-J., and Chung, E.-S. (2018b). "Selection of gridded precipitation data for Iraq using compromise programming." J. Meas., 132, 87–98. doi:10.1016/j.measurement.2018.09.047.
11. SrinivasaRaju, K., Nagesh Kumar, D. (2015). Ranking general circulation models for India using TOPSIS. *Journal of Water and Climate Change*, *6*(2), 288–299. https://doi.org/10.2166/wcc.2014.074
12. SrinivasaRaju, K., Sonali, P., &Nagesh Kumar, D. (2017). Ranking of CMIP5-based global climate models for India using compromise programming. *Theoretical and Applied Climatology*, *128*(3–4), 563–574. https://doi.org/10.1007/s00704-015-1721-6

*IN PROCEEDINGS OF 25th HYDRO 2020, INTERNATIONAL CONFERENCE, NATIONAL INSTITUTE OF TECHNOLOGY ROURKELA, ODISHA, INDIA 26-28, March 2021, ISBN 978-93-90631-56-8*

Paper ID - 463

# Climate change or land-use dominated streamflow variations: An empirical model-based contribution analysis of the Baitarani River Basin, India

Sushree Swagatika Swain[1], Ashok Mishra[2], Chandranath Chatterjee[3], Bhabagrahi Sahoo[4]

[1]*Research Scholar, School of Water Resources, Indian Institute of Technology Kharagpur, India*
[2]*Professor, Agricultural and Food Engineering Department, Indian Institute of Technology Kharagpur, India*
[3]*Professor, Agricultural and Food Engineering Department, Indian Institute of Technology Kharagpur, India*
[4]*Associate Professor, School of Water Resources, Indian Institute of Technology Kharagpur, India*
*Email:* sushreeswain1991@gmail.com

## Abstract

Streamflow, which is considered as the fundamental element of the basin-scale hydrological processes, is influenced by climate change (CC) and land-use transformations (LUT). Quantifying the relative impacts of the above drivers on streamflow variation has drawn significant attention from researchers nowadays. In this study, the relative contributions of CC and LUT for the Baitarani River Basin (BRB) of eastern India are estimated using two empirical approaches i.e. (i) the modified Double Mass Curve (DMC) method and (ii) the modified Slope Change Ratio of Accumulative Quantity (SCARQ) method. The statistical characteristics (trend, slope, and significance) of hydro-meteorological variables (precipitation, temperature, and streamflow) are studied for the study period (1979-2018) employing the Mann-Kendall test. The sequential Mann-Kendall test is applied to check the abrupt shift or break in the streamflow data series. Based on the outcomes of abrupt change analysis, the entire study period is divided into the reference period (1979-1994) and the impacted period (1995-2018). The results of the empirical methods showed that the relative impacts of the LUT ($\lambda_{LUT}$) are presiding over CC ($\lambda_{CC}$) on streamflow variations in the impacted period of the study area. Further, the SCARQ method is relatively convenient as compared to the DMC method since it is capable of estimating the relative influences of both the climatic factors i.e. the impact of precipitation ($\lambda_P$) and the impact of temperature ($\lambda_T$) on the streamflow variations. However, both the empirical methods are attributed to different sources of errors and uncertainty with individual advantages. Thus, the outcomes of this study can provide vital information regarding the relative vulnerability of the BRB streamflow to CC and LUT that is essential for the sustainable planning and management of future water resources.

***Keywords:*** *Climate change; Land-use transformations; DMC method; SCARQ method*

## 1. Introduction

The water resources management needs to be addressed by understanding the underlying concepts of variations in streamflow, the fundamental component of the hydrological cycle of a river basin, (Dey and Mishra 2017). Previous studies reveal that climate change and human interventions are two important factors that consequence in decreasing/ increasing streamflow worldwide (Legesse et al. 2003; Jones et al. 2006; Jiang et al. 2011; Zhang et al. 2013; Abeysingha et al. 2016). The effects of changing climate show the variations in meteorological variables (precipitation and temperature) that alter the patterns of soil moisture availability, evaporation as well as other components of the hydrologic cycle (Swain et al. 2020). Further, human interventions as a result of land-use changes, urbanization, irrigation, and dam/reservoir construction affect river basin-scale streamflow variations (Zhang and Lu 2009; Mishra et al. 2010; Wang and Hejazi 2011; El-Khoury et al. 2015). However, the impacts of climate change and human activities are regional (Ye at al. 2013).

Several studies reported the quantification of climate change and land-use alterations on streamflow variations all over the world ((Li et al. 2007; Yang et al. 2017; Saidi et al. 2018; Zhang et al. 2019; Li et al. 2020). The most adopted methods are categorized into an experimental method (Lee 1980; Bosch

and Hewlett, 1982), conceptual method (Budyko 1948; 1974; Tomer and Schilling 2009), analytical method (Schaake 1990; Milly and Dune 2002; Ma et al. 2010; Guo et al. 2014), and hydrological modeling method (Jones et al. 2006; Fan et al. 2010; Montenegro and Ragab 2010; Ma et al. 2010; Petchprayoon et al. 2010; Wang et al. 2013; Bu et al. 2018) along with their advantages and limitations (Dey and Mishra 2017). However, the validity of an appropriate method of contribution analysis is catchment specific (Wu et al. 2017; Zhai and Tao 2017). Thus, it is necessary to check data availability, reliability of developed methods, and catchment perspective (Dey and Mishra 2017).

Based on the above background, the policymakers need to pay attention to the outlined issues; i) How to deal with multiple break-points of streamflow using the change-point analysis method? ii) How to isolate the impacts of climate change and human activities in a data-scarce river basin? iii) Can the contributions of precipitation and temperature be quantified in streamflow variation? To address the above concerns, this study aims to isolate the potential contributions of climate change and land-use transformations using the DMC method and the SCRAQ method under the presence of multiple break-points in streamflow with the limitations of land-use land cover data availability.

## 2. Study area

The Baitarani River Basin (BRB) with an area of 12094 km$^2$ of eastern India is selected for this study. The study area (20°30′ N to 22°20′ N, 85°05′ E to 87°05′ E) travels a length of 355 km covering the major portions of Odisha with a small part of Jharkhand and drains into the Bay of Bengal along with the Brahmani River basin (BR). The primary water demand from BRB is agricultural irrigation. The land use and cover of the study area are dominated by agricultural land with forest areas (Swain et al. 2020). The type of soil varies from rich red loamy to gravely detritus (Paul et al. 2019). Human interventions like the Salandi dam is located in the middle of the basin. The detailed study area map is shown in Fig. 1.

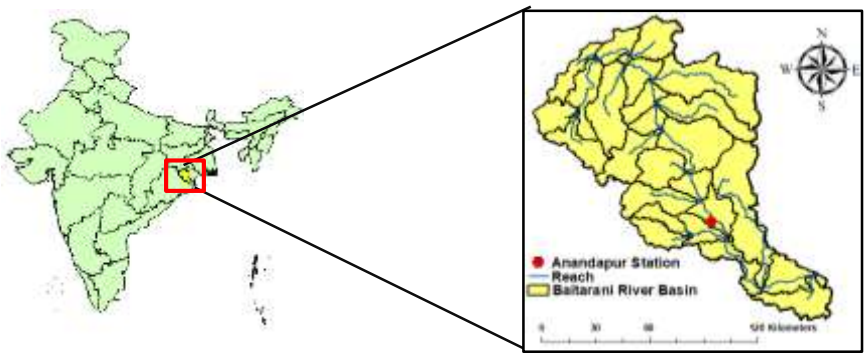



**Figure 1** Index map of BRB.

## 3. Data sources and processing

The data considered for this analysis are total annual precipitation, annual average mean temperature, and annual average streamflow. The gridded metrological data (precipitation, minimum temperature, and maximum temperature) are downloaded from the India Meteorological Department (IMD), Pune for the study period of (1979-2018). The obtained precipitation data series is of 0.25° resolution (Pai et al. 2014). However, to maintain uniform resolution, the obtained 1° temperature data is resampled to 0.25° employing the bilinear interpolation approach (Bisht et al. 2019). The observed daily-scale streamflow data series of the study period are collected from the Central Water Commission (CWC), Bhubaneswar for the Anandapur gauging station (21° 13′ N, 86° 7′ E). All the above hydro-

meteorological data series (precipitation, mean temperature, and streamflow) are averaged into an annual scale for further analysis.

## 4. Methodology

The whole study period is segregated into two sub-periods (reference period and impacted period) based on the sequential Mann-Kendall technique based abrupt change method. The statistical characteristics (trend, slope, and significance) of hydro-meteorological data series are studied for both the sub-period employing the Mann-Kendall test. The quantitative analysis of driving factors (CC and LUT) that affect streamflow variation are studied using two empirical approaches i.e. (i) the modified Double Mass Curve (DMC) method and (ii) the modified Slope Change Ratio of Accumulative Quantity (SCARQ) method. The aspects of the above approaches are outlined in the following sub-sections.

### *4.1 Trend and Break-point analysis*

The Mann-Kendall test (Mann, 1945; Kendall, 1975) is applied to detect the trends of hydro-meteorological data series at an annual scale. It is a statistical non-parametric analysis and a useful tool to address abnormalities in data series and reliability towards biased variables (Ye et al. 2013). The Mann-Kendall test statistic S of X time series with n samples is given by:

$$S = \sum_{i=1}^{n-1} \sum_{j=i+1}^{n} \mathrm{sgn}(x_j - x_i) \tag{1}$$

where $x_i$ and $x_j$ = sequential data values of observed data series while $i < j$; n = length of observed data-series data; and $\mathrm{sgn}(x_j - x_i)$ = sign of a function. The values of the sign function are as follows:

$$\mathrm{sgn}(x_j - x_i) = \begin{cases} 1 & if\ x_i > x_j \\ 0 & if\ x_i = x_j \\ -1 & if\ x_i < x_j \end{cases} \tag{2}$$

Further, the variance (S) and final Mann-Kendall static value (Z) is given as:

$$\mathrm{Var(S)} = \frac{n(n-1)(2n-5)}{18} \tag{3}$$

$$Z = \begin{cases} \dfrac{S-1}{\sqrt{Var(S)}} & if\ S > 0 \\ 0 & if\ S = 0 \\ \dfrac{S+1}{\sqrt{Var(S)}} & if\ S < 0 \end{cases} \tag{4}$$

Here, the Z values are assumed as normally distributed. The Mann-Kendall test is performed at a significance level of 0.05. when the absolute Z value is greater than 1.96, the determined trend is significant. The magnitude of the trend, Δ, is estimated by (Hirsch et al. 1982):

$$\sigma = Median\left[\frac{x_j - x_i}{j - i}\right] \quad for\ all\ i < j \tag{5}$$

Further, the existence and significance of the abrupt change in streamflow data series are checked using the sequential version of the Mann Kendall test (Sneyers 1990; Douglas et al. 2000; Modarres and Sarhadi, 2009). The sequential values of the statistic $u(d_j)$ are then calculated as:

$$u(\mathrm{d}_j) = \frac{d_j - E(d_j)}{\sqrt{Var(d_j)}} \tag{6}$$

where $\mathrm{E}(\mathrm{d}_j)$ and $Var(\mathrm{d}_j)$ are mean and variance of the test statistic, $\mathrm{d}_j$, given by

$$\mathrm{d}_j = \sum_{1}^{j} n_j \tag{7}$$

The terms of $u(\mathrm{d}_j)$ $(1 \leq \mathrm{j} \leq \mathrm{n})$ constitute a progressive series ($C_1$). The same method is then applied to the inversed series to get a regressive sequence ($C_2$). The intersection point of $C_1$ and $C_2$, located between the confidence interval is the point of abrupt changes in the observed streamflow data series.

### *4.2 Double Mass Curve (DMC) method*

The DMC method is generally used for evaluating the trend and consistency of long-term time series of hydro-meteorological data (Gao et al. 2011). Further, this method has been modified for the contribution analysis of CC and LUT (Zhang et al. 2018). The multiple linear regression-based traditional trend analysis technique of the DMC method is outlined as:

$$\sum_{i=1}^{n-1} R_{rp} = a \sum_{i=1}^{n-1} P_{rp} + b \sum_{i=1}^{n-1} T_{rp} + c \tag{8}$$

where $P_{rp}$, $T_{rp}$, and $R_{rp}$ are the cumulative precipitation (mm/a), temperature (°C/a), and streamflow ($m^3/s/a$), respectively of reference period (rp); a and b are regression coefficients, and c is the intercept. Cumulative streamflow is simulated for the impacted period (ip) using the cumulative precipitation and temperature of the reference period for further analysis. The contribution analysis steps are as follows:

$$\Delta R_T = R_{rp} - R_{ip} \tag{9}$$

$$\Delta R_{LUT} = R_{ip}^{obs} - R_{ip}^{Sim} \tag{10}$$

$$\Delta R_{CC} = R_{ip}^{Sim} - R_{rp}^{obs} \tag{11}$$

$$\lambda_{LUT} = \frac{\Delta R_{LUT}}{\Delta R_T} \times 100 \tag{12}$$

$$\lambda_{CC} = \frac{\Delta R_{CC}}{\Delta R_T} \times 100 \tag{13}$$

where $\Delta R_T$ is the streamflow variation between the reference period and impacted period; $\Delta R_{LUT}$ and $\Delta R_{CC}$ are average streamflow variation as a result of LUT and CC, respectively; $\lambda_{LUT}$ and $\lambda_{CC}$ are the potential impact of LUT and CC on streamflow variation.

### *4.3 Slope Change Ratio of Accumulative Quantity (SCARQ) method*

With the concept of slope change ratios of hydro-meteorological data series, the SCARQ method addresses the contributions of LUT ($\lambda_{LUT}$) along with precipitation ($\lambda_P$) and temperature ($\lambda_T$) which results in contributions of CC ($\lambda_{CC}$) (Liang et al., 2020). The procedures of the SCARQ method is given as:

$$\Delta R_T = \frac{\left|\Delta R_{rp} - \Delta R_{ip}\right|}{\Delta R_{ip}} \times 100 \quad (14)$$

$$\Delta P = \frac{\left|\Delta P_{rp} - \Delta P_{ip}\right|}{\Delta P_{ip}} \times 100 \quad (15)$$

$$\Delta T = \frac{\left|\Delta T_{rp} - \Delta T_{ip}\right|}{\Delta T_{ip}} \times 100 \quad (16)$$

where $\Delta R_T$ is the slopes of the linear relationship between cumulative streamflow ($m^3/s/a$) of reference period and impacted period; $\Delta P$ and $\Delta T$ are linear slopes of cumulative precipitation (mm/a) and temperature (°C/a), respectively.

$$\lambda_P = \frac{\Delta P}{\Delta R_T} \times 100 \quad (17)$$

$$\lambda_T = \frac{\Delta T}{\Delta R_T} \times 100 \quad (18)$$

$$\lambda_{CC} = C_P + C_T \quad (19)$$

$$\lambda_{LUT} = 100 - \lambda_{CC} \quad (20)$$

where $\lambda_P$, $\lambda_T$, $\lambda_{CC}$, and $\lambda_{LUT}$ are the potential impact of precipitation, temperature CC and LUT on streamflow variation.

## 5. Results and discussions

### *5.1 Variations in hydrological data series*

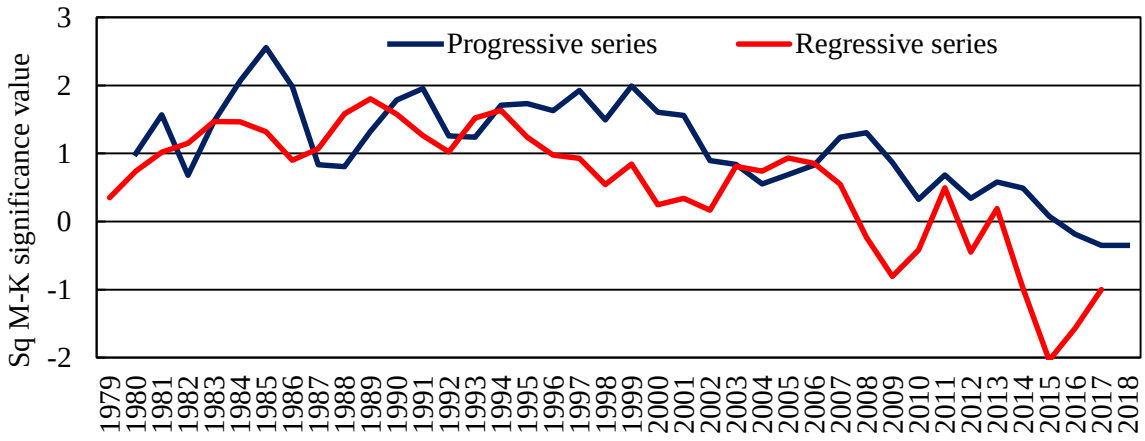



**Figure 2** Sequential Mann-Kendall results of annual streamflow in the Anandapur station of BRB.

The results of the sequential Mann Kendall test for hydrological data series (streamflow) are shown in Fig. 2. Multiple break-points are observed from the figure. The observed break-points are 1982, 1983, 1987, 1990, 1993, 1994, 2003, and 2006. However, the year 1994 has a maximum significance value (1.64) than other break-points. Thus, it is chosen as the abrupt change in the streamflow data series. Based on the sequential Mann-Kendall analysis, the entire study period (1979-2018) is divided into a reference period (1979-1994) and an impacted period (1995-2018). Similarly, the trend values, its

significance, and the slope values of the entire study period, reference period, and impacted period of the streamflow data series are studied applying the Mann-Kendall test from Table 1. All the tests are performed based on the 0.05 level of confidence.

### *5.2 Variations in meteorological data series*

The statistical variables (trend values, its significance, and the slope values) of the entire study period, reference period, and impacted period of the meteorological (precipitation and temperature) data series are studied using the Mann-Kendall test from Table 1. There is no significant trend in precipitation and streamflow data series. However, the total study period and the reference period of temperature data series showed a significant trend in BRB. Further, the slope values are negative for all the period of temperature data series. Thus, it is reasonable to consider precipitation and temperature as climate change factors in this study.

**Table 1** Summary of Mann-Kendall trend statistics of precipitation, temperature, and streamflow

| Variables | | Total study period | Reference period | Impacted period |
|---|---|---|---|---|
| Precipitation | p-value | 0.36 | 0.22 | 0.94 |
| | Δ | 16.88 | 13.95 | -37.46 |
| Temperature | p-value | **0.02** | **0.02** | 0.08 |
| | Δ | -0.05 | -0.06 | -0.05 |
| Streamflow | p-value | 0.74 | 0.09 | 0.22 |
| | Δ | 16.54 | 26.15 | 8.38 |

Note: Bold number indicates significance trends at 95% confidence level; p-value= Significance value; Δ= Slope value

### *5.3 DMC-based and SCARQ-based contribution analysis of CC and LUT*

Table 2 shows the contribution analysis of climate change impact and land-use changes on streamflow of impacted period using the DMC method and SCARQ method. According to the result of the DMC method, the potential impact of CC and LUT on streamflow variation of the BRB is accounted for -184.38% and 284.38% respectively for the impacted period. However, the SCARQ method is capable of addressing the contributions of precipitation and temperature on streamflow variation. The contributions of precipitation and temperature are found out to be -12.18% and -13.36% for the BRB. Similarly, the isolating impacts of CC and LUT are observed to be -25.54% and 125.54% in the impacted period. From both the method, it is clear that streamflow variation is more sensitive to land-use variations. Thus, LUT plays a major role in leading to the streamflow variations of the BRB.

**Table 2** Contribution (%) of CC and LUT on streamflow variations in the BRB

| Method | Streamflow variables ($m^3/s$) | | | Contributing factor (%) | | | |
|---|---|---|---|---|---|---|---|
| | $\Delta R_{CC}$ | $\Delta R_{LUT}$ | $\Delta R_T$ | $\lambda_P$ | $\lambda_T$ | $\lambda_{CC}$ | $\lambda_{LUT}$ |
| DMC | 12.39 | -19.11 | -6.72 | - | - | -184.38 | 284.38 |
| SCARQ | - | - | -9.09 | -12.18 | -13.36 | -25.54 | 125.54 |

## 6. Conclusions

Variations of climatic variables and land-use changes during the study period and their effects on streamflow of the impacted period of the BRB are analyzed in this study. The Mann-Kendall test and its sequential version are used to study the trend, its significance, and abrupt change in the precipitation, temperature, and streamflow data series. The DMC and SCARQ method is used to study the

contribution analysis of climate change and land-use transformations. The following conclusions are made from this study;

i. The abrupt change of streamflow data series using sequential Mann-Kendall technique showed multiple change points. However, the year 1994 with a high significance value is considered as the change point for this analysis.
ii. During the whole study period and the reference period, the temperature data series revealed a significant decreasing trend.
iii. Considering precipitation and temperature as climate change factors, the proposed SCARQ method is simple and advantageous to quantify the climate change impact and land-use transformations on long-term annual streamflow variations.
iv. Using both the DMC and the SCARQ methods, it is clear that land-use transformations play a vital role in streamflow variations in the present study area (BRB).
v. The above methods are capable of explaining the potential contributions of land-use transformations without considering any such data.

Though the above study gives a quantitative idea about the significant contributions of climate change and land-use alterations, it is necessary to validate the above analysis incorporating hydrological models that integrate climate data to topographic variations. Human interventions other than land-use transformations should be quantified to capture the real consequences of streamflow variations of a river basin.

## References

Abeysingha, N. S., Singh, M., Sehgal, V. K., Khanna, M., & Pathak, H. (2016). Analysis of trends in streamflow and its linkages with rainfall and anthropogenic factors in Gomti River basin of North India. Theoretical and applied climatology, 123(3-4), 785-799.

Bisht, D.S., Sridhar, V., Mishra, A., Chatterjee, C., Raghuwanshi, N.S. (2019). Drought characterization over India under projected climate scenario. Int. J. Climatol. 39 (4), 1889–1911.

Bosch, J. M., & Hewlett, J. D. (1982). A review of catchment experiments to determine the effect of vegetation changes on water yield and evapotranspiration. Journal of hydrology, 55(1-4), 3-23.

Bu, J., Lu, C., Niu, J., & Gao, Y. (2018). Attribution of runoff reduction in the Juma River basin to climate variation, direct human intervention, and land use change. Water, 10(12), 1775.

Budyko, M. I. (1948). Evaporation under natural conditions, Gidrometeorizdat, Leningrad. English translation by IPST, Jerusalem.

Budyko, M. I. (1974). Climate and Life, Academic Press, New York.

Dey, P., & Mishra, A. (2017). Separating the impacts of climate change and human activities on streamflow: A review of methodologies and critical assumptions. Journal of Hydrology, 548, 278-290.

Douglas, E. M., Vogel, R. M., & Kroll, C. N. (2000). Trends in floods and low flows in the United States: impact of spatial correlation. Journal of hydrology, 240(1-2), 90-105.

El-Khoury, A., Seidou, O., Lapen, D. R., Que, Z., Mohammadian, M., Sunohara, M., & Bahram, D. (2015). Combined impacts of future climate and land use changes on discharge, nitrogen and phosphorus loads for a Canadian river basin. Journal of environmental management, 151, 76-86.

Fan, J., Tian, F., Yang, Y., Han, S., & Qiu, G. (2010). Quantifying the magnitude of the impact of climate change and human activity on runoff decline in Mian River Basin, China. Water Science and Technology, 62(4), 783-791.

Gao, P., Mu, X. M., Wang, F., & Li, R. (2011). Changes in streamflow and sediment discharge and the response to human activities in the middle reaches of the Yellow River. Hydrology and Earth System Sciences, 15(1), 1-10.

Guo, Y., Li, Z., Amo-Boateng, M., Deng, P., & Huang, P. (2014). Quantitative assessment of the impact of climate variability and human activities on runoff changes for the upper reaches of Weihe River. Stochastic Environmental Research and Risk Assessment, 28(2), 333-346.

Hirsch, R. M., Slack, J. R., & Smith, R. A. (1982). Techniques of trend analysis for monthly water quality data. Water resources research, 18(1), 107-121.

Jiang, S., Ren, L., Yong, B., Singh, V. P., Yang, X., & Yuan, F. (2011). Quantifying the effects of climate variability and human activities on runoff from the Laohahe basin in northern China using three different methods. Hydrological Processes, 25(16), 2492-2505.

Jones, R. N., Chiew, F. H., Boughton, W. C., & Zhang, L. (2006). Estimating the sensitivity of mean annual runoff to climate change using selected hydrological models. Advances in Water Resources, 29(10), 1419-1429.

Kendall, M. G. (1975). Rank correlation measures (220 pp.). London: Charles Griffin.

Lee, R. (1980). Forest hydrology. Columbia University Press.

Legesse, D., Vallet-Coulomb, C., & Gasse, F. (2003). Hydrological response of a catchment to climate and land use changes in Tropical Africa: case study South Central Ethiopia. Journal of hydrology, 275(1-2), 67-85.

Li, L. J., Zhang, L., Wang, H., Wang, J., Yang, J. W., Jiang, D. J., ... & Qin, D. Y. (2007). Assessing the impact of climate variability and human activities on streamflow from the Wuding River basin in China. Hydrological Processes: An International Journal, 21(25), 3485-3491.

Li, S., Zhang, L., Du, Y., Zhuang, Y., & Yan, C. (2020). Anthropogenic impacts on streamflow-compensated climate change effect in the Hanjiang River Basin, China. Journal of Hydrologic Engineering, 25(1), 04019058.

Ma, H., Yang, D., Tan, S. K., Gao, B., & Hu, Q. (2010). Impact of climate variability and human activity on streamflow decrease in the Miyun Reservoir catchment. Journal of Hydrology, 389(3-4), 317-324.

Mann, H. B. (1945). Non-Parametric Tests against Trend. Econmetrica, 13, 245-259. Mantua, NJ, SR Hare, Y. Zhang, JM Wallace, and RC Francis (1997), A Pacific decadal.

Milly, P. C. D., & Dunne, K. A. (2002). Macroscale water fluxes 2. Water and energy supply control of their interannual variability. Water Resources Research, 38(10), 24-1.

Mishra, V., Cherkauer, K. A., Niyogi, D., Lei, M., Pijanowski, B. C., Ray, D. K., ... & Yang, G. (2010). A regional scale assessment of land use/land cover and climatic changes on water and energy cycle in the upper Midwest United States. International Journal of Climatology, 30(13), 2025-2044.

Modarres, R., & Sarhadi, A. (2009). Rainfall trends analysis of Iran in the last half of the twentieth century. Journal of Geophysical Research: Atmospheres, 114(D3).

Montenegro, A., & Ragab, R. (2010). Hydrological response of a Brazilian semi-arid catchment to different land use and climate change scenarios: a modelling study. Hydrological Processes, 24(19), 2705-2723.

Pai, D.S., Sridhar, L., Rajeevan, M., Sreejith, O.P., Satbhai, N.S., Mukhopadhyay, B. (2014). Development of a new high spatial resolution (0.25× 0.25) long period (1901–2010) daily gridded rainfall data set over India and its comparison with existing data sets over the region. Mausam 65 (1), 1–18.

Paul, P.K., Zhang, Y., Mishra, A., Panigrahy, N., Singh, R. (2019). Comparative study of two state-of-the-art semi-distributed hydrological models. Water 11 (5), 871.

Petchprayoon, P., Blanken, P. D., Ekkawatpanit, C., & Hussein, K. (2010). Hydrological impacts of land use/land cover change in a large river basin in central–northern Thailand. International Journal of Climatology, 30(13), 1917-1930.

Saidi, H., Dresti, C., Manca, D., & Ciampittiello, M. (2018). Quantifying impacts of climate variability and human activities on the streamflow of an Alpine river. Environmental Earth Sciences, 77(19), 690.

Schaake, J. C. (1990). From climate to flow. Climate change and US water resources., 177-206.

Sneyers, R. (1991). On the statistical analysis of series of observations (No. 143).

Swain, S. S., Mishra, A., Sahoo, B., & Chatterjee, C. (2020). Water scarcity-risk assessment in data-scarce river basins under decadal climate change using a hydrological modelling approach. Journal of Hydrology, 590, 125260.

Tomer, M. D., & Schilling, K. E. (2009). A simple approach to distinguish land-use and climate-change effects on watershed hydrology. Journal of hydrology, 376(1-2), 24-33.

Wang, D., & Hejazi, M. (2011). Quantifying the relative contribution of the climate and direct human impacts on mean annual streamflow in the contiguous United States. Water Resources Research, 47(10).

Wang, S., Zhang, Z., McVicar, T. R., Guo, J., Tang, Y., & Yao, A. (2013). Isolating the impacts of climate change and land use change on decadal streamflow variation: Assessing three complementary approaches. Journal of Hydrology, 507, 63-74.

Wu, J., Miao, C., Zhang, X., Yang, T., & Duan, Q. (2017). Detecting the quantitative hydrological response to changes in climate and human activities. Science of the Total Environment, 586, 328-337.

Yang, L., Feng, Q., Yin, Z., Wen, X., Si, J., Li, C., & Deo, R. C. (2017). Identifying separate impacts of climate and land use/cover change on hydrological processes in upper stream of Heihe River, Northwest China. Hydrological Processes, 31(5), 1100-1112.

Ye, X., Zhang, Q., Liu, J., Li, X., & Xu, C. Y. (2013). Distinguishing the relative impacts of climate change and human activities on variation of streamflow in the Poyang Lake catchment, China. Journal of Hydrology, 494, 83-95.

Zhai, R., & Tao, F. (2017). Contributions of climate change and human activities to runoff change in seven typical catchments across China. Science of The Total Environment, 605, 219-229.

Zhang, J. Y., Wang, G. Q., Pagano, T. C., Jin, J. L., Liu, C. S., He, R. M., & Liu, Y. L. (2013). Using hydrologic simulation to explore the impacts of climate change on runoff in the Huaihe River basin of China. Journal of Hydrologic Engineering, 18(11), 1393-1399.

Zhang, L., Nan, Z., Wang, W., Ren, D., Zhao, Y., & Wu, X. (2019). Separating climate change and human contributions to variations in streamflow and its components using eight time-trend methods. Hydrological Processes, 33(3), 383-394.

Zhang, S., & Lu, X. X. (2009). Hydrological responses to precipitation variation and diverse human activities in a mountainous tributary of the lower Xijiang, China. Catena, 77(2), 130-142.

Zhang, Z., Wan, L., Dong, C., Xie, Y., Yang, C., Yang, J., & Li, Y. (2018). Impacts of climate change and human activities on the surface runoff in the Wuhua River Basin. Sustainability, 10(10), 3405.

# Theme IV

# Hydraulic & Hydrologic Modelling

*IN PROCEEDINGS OF 25th HYDRO 2020, INTERNATIONAL CONFERENCE, NATIONAL INSTITUTE OF TECHNOLOGY ROURKELA, ODISHA, INDIA 26-28, March 2021, ISBN 978-93-90631-56-8*

Paper ID - 120

# Rainfall-Runoff Simulation in Mahi Bajaj Sagar Dam Catchment, India, Using HEC-HMS

Mr. Biltu Pal[1], Prof. Mahender Choudhary[2], Prof. Y.P. Mathur[2]

[1]*Research Scholar, Malaviya National Institute of Technoloy Jaipur, Jaipur 302017, India*
[2]*Faculty in Department of Civil Engineering, Malaviya National Institute of Technoloy Jaipur, Jaipur 302017, India*
*Email: 2018rce9505@mnit.ac.in*

## Abstract

Rainfall-runoff simulation is an essential step to estimate hydrological process and the water resources availability for a reservoir. This can aid in water resource management and planning. Mahi Bajaj Sagar Dam is one of the major water resource projects in the Mahi Basin. This study utilizes hydrological modeling system (HEC-HMS) for simulation of Mahi Bajaj Sagar Dam catchment to analyze the response of rainfall and runoff. Rainfall-runoff modelling helps in estimating inflows which is very essential to strategize water resources management. This model also incorporates ArcGIS extension HEC-GeoHMS which performs geospatial analysis and generates the hydrologic modeling inputs for the HEC-HMS model. SCS unit hydrograph method was used for runoff estimation. Daily precipitation data, temperature data. monthly evaporation data, elevation data, and curve number, which takes in to account the land use and soil characteristics of the watershed was used as model inputs for the HEC-HMS model. Then the calibrated model (period 2010-2014) was validated with data set of the period of 2015-2017 The performance of the models is assessed using different statistical indicators such as the Nash–Sutcliffe efficiency (NSE), Root mean square error (RMSE), Percent bias error (PBIAS), and the coefficient of determination ($R^2$). The results shows good relation with observed data. Thus, this study shows that HEC-HMS hydrological model can be used for rainfall-runoff simulation for long time period for reservoir operation planning and management.

*HEC-HMS; Rainfall; Runoff; HEC-GeoHMS; Reservoir Operation; LULC; ERDAS IMAGINE*

## 1. Introduction

The hydrological processes of a watershed are very complex. Usually they are governed by the meteorological conditions (e.g., precipitation, evapotranspiration, temperature, humidity and solar radiance), the physical characteristics (topography, soils, and land use and land cover), and socioeconomic development inside the watershed (Alipour, Shamsai, and Ahmady 2010; Easterling et al. 2000). Rainfall-runoff simulation is an essential step to estimate hydrological process and the water resources availability for a reservoir. Among the various natural resources, water is a key component for domestic water supply, agricultural production and power generation. Land-use planning, land management practices and Urbanization have adversely effect on surface runoff quantities for power generation, domestic water supply and agricultural production as well as ground water recharge. To overcome the related problems of water, reservoir operation policy should be made for multireservoir systems. In the study of streamflow, there are many types of hydrologic models are available such as SWAT (Soil & Water Assessment Tool), HEC-HMS (Hydrologic Engineering Center - Hydrologic Modeling System), VIC model, which has been developed by Liang et al. (1994) etc. The SWAT model was developed by the USDA–Agriculture Research Service (ARS) in the early 1990s (Arnold et al. 1998; Olivera et al. 2006) and it is mostly used for long-term hydrological simulation with respect to the effect of different land management practices on water, sediment, and chemicals in large complex watersheds with various conditions in soil, LULC, and management (Coutu and Vega 2007; Nguyen Khoi 2015; Zhu and Li 2014). The HEC-HMS model, on the other hand , was developed by the HEC of U.S. Army Corps of Engineers and it was designed primarily to simulate spatially distributed rainfall-runoff processes (e.g., runoff hydrographs resulting from a rain storm) in a watershed (Motevalli et al. 2012; Sintayehu 2015; Thu, Zin, and Khine 2019; Visweshwaran 2017). In other words, the HEC-HMS model takes into consideration of spatial distribution of topography, soils, and LULC. Therefore, the HEC-HMS model is appropriate to be used to study the impact of LULC change on the hydrology of a watershed. The objective of this study is aimed to simulate the rainfall runoff simulation

process for Mahi Bajaj Sagar Dam catchment with help of Arc Hydro (an ArcToolbox from ArcGIS),ERDAS Imagine ,HEC-GeoHMS (an extension from ArcGIS) and the HEC-HMS model.

## 2. Study Area

The Mahi Bajaj Sagar catchment is located between east longitudes 72˚15' to 78 ˚ 15′ and north latitudes 22 ˚ 0′ to 22 ˚ 40′ N respectively with watershed area of 6646 km$^2$. The elevation of the basin varies between 255 m to 605 m with respect to the mean sea level. The major soil types in the basin are black and red soils. The study area mostly covered by agricultural lands (78.5%) and forests (17.2%). Average mean annual rainfall data for Mahi Bajaj Sagar Catchment area is 964 mm and maximum and minimum rainfall are 359.8 mm and 2090 mm respectively.

## 3. Data Collection

**Table 1** Data used and their sources

| Data Type | Description | Resolution | Source |
|---|---|---|---|
| Topography map | Digital Elevation Model | 30m×30m | United States Geological Survey (USGS) |
| LULC map | Landsat OLI Images | 30m×30m | United States Geological Survey (USGS) |
| Soil map | Soil data | 1 km × 1 km | FAO, HWSD (Harmonized World Soil data) |
| Rainfall Data, Temperature Data | Daily Data (2007-2017) | (0.25 ˚ ×0.25˚) for Rainfall (1 ˚ ×1 ˚) for Temperature | Indian Meteorological Department (IMD) |
| Discharge Data | Daily Discharge (2007-2017) | Daily | Water Resources Department, Udaipur Region, Govt. of Rajasthan |

## 3.Methodology

### *3.1 HEC-HMS Basin Model Development using HEC-GEOHMS and Arc-Hydro tool*

The Geospatial Hydrologic Modeling Extension (HEC-GeoHMS) has been developed as a geospatial hydrology toolkit for engineers and hydrologists with limited GIS experience. HEC-GeoHMS uses ArcGIS and the Spatial Analyst extension to develop a number of hydrologic modeling inputs for the Hydrologic Engineering Center's Hydrologic Modeling System, HEC-HMS. It is widely used in rainfall-runoff simulation by taking losses, direct runoff, metrological, base flow and river routing and reservoir component into account. For the HEC-HMS input, basin model file was developed by using HEC-GeoHMS and Arc Hydro tool. HEC-GeoHMS, and Arc Hydro are the extension tool of ArcGIS which is useful to process the geospatial data and create input file for HEC-HMS model. Digital Elevation Model (DEM) was extracted for surface elevation and then it was filled before extraction of flow direction. Flow direction and flow accumulation were extracted for stream network processing. Here threshold value is kept as 400 km$^2$ for larger subbasin area. The total number of Mahi Bajaj Sagar watershed was divided into 5 (five) sub-basins, depending on gauging station. Here drainage point is calculated for defining the project point. The outlet point shapefile is created for watershed delineation. The length of river, slope of both river and basin, basin centroid, longest flow path, and centroidal flow path was computed and attributed in the basin and reach characteristics. The reach connects two junctions and the outflow joins the junctions. The outflow was determined at the outlet by applying the

loss model, runoff transform model and baseflow model. Muskingum method was used to route the flow from one junction to the other. To develop HMS process the detailed flowchart is given below

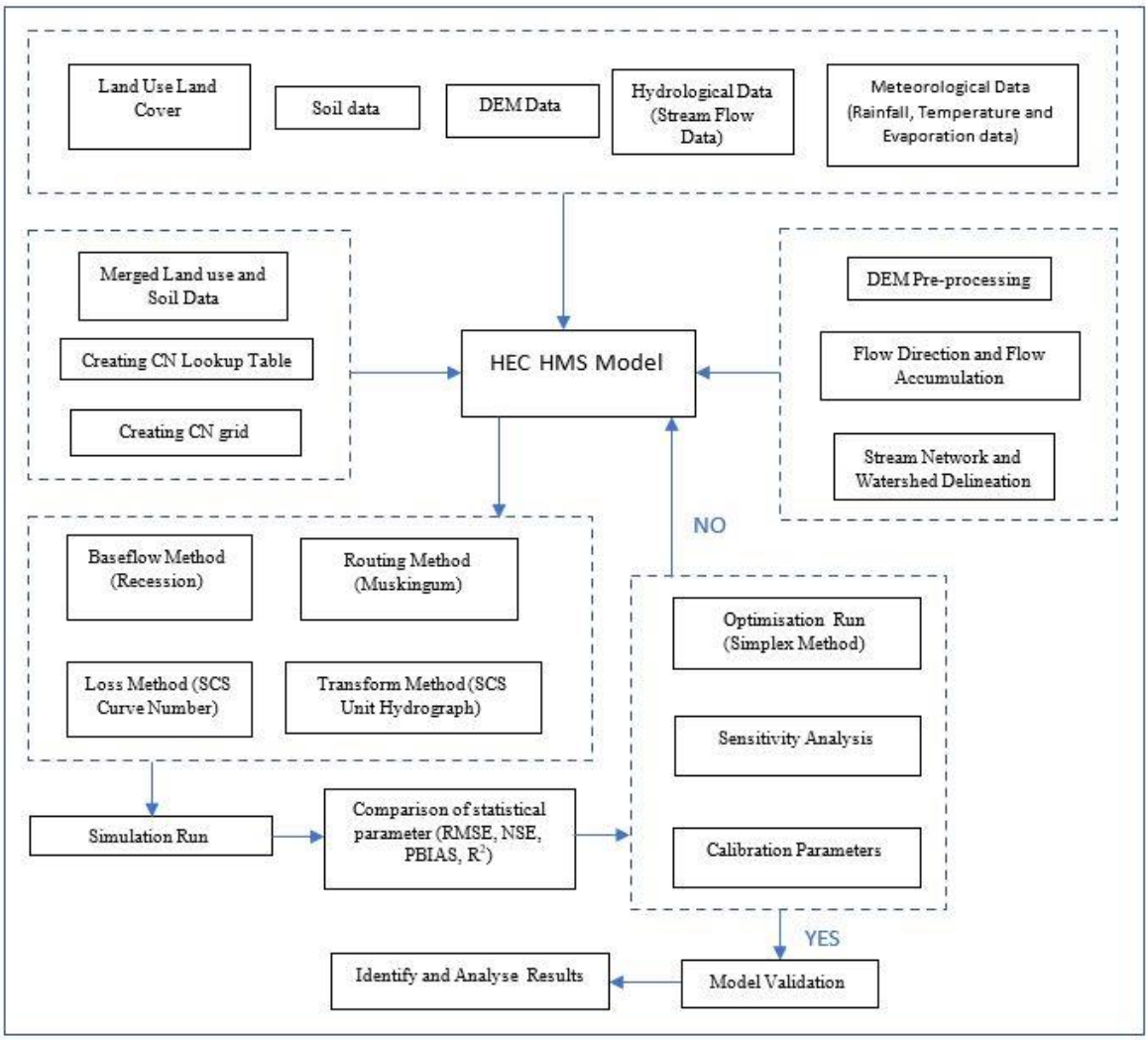



**Figure 1** Methodology flow chart for HEC HMS Model

To develop HMS process following was used based on the issues to be considered while selecting the methods.

### *3.1.1 Land use land cover*

Landsat OLI data was downloaded and image pre-processing including layer stacking, mosaics the images was done. Mahi Bajaj Sagar Catchment was first clipped from the Landsat OLI imagery of 2015 using the shapefile of the catchment boundary. Then image processing and enhancement was done by band and colour combination. The supervised classification have been selected with maximum likelihood classification. For this process signature files has been created with experience and knowledge of the data. For HEC-HMS model we have selected four classes namely agriculture, builtup, forest and water. For all the above operations were performed using Earth Resource Development Assessment System (ERDAS) Imagine 2013 and ArcMap 10.2 software packages. The flowchart of LULC preparation is given below

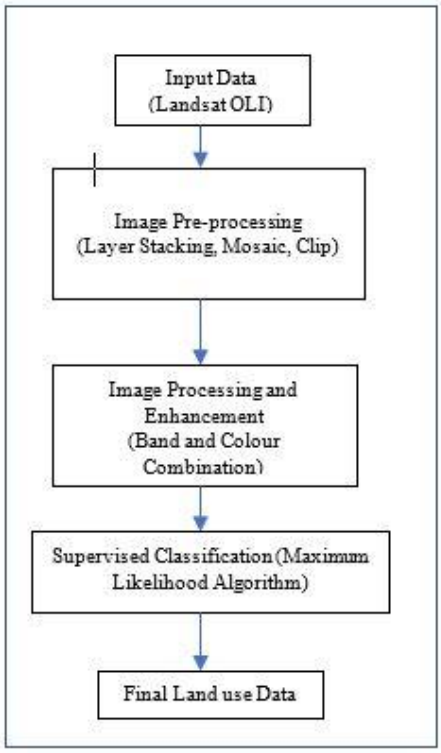



**Figure 2** Physical parameters processing using HEC-GeoHMS

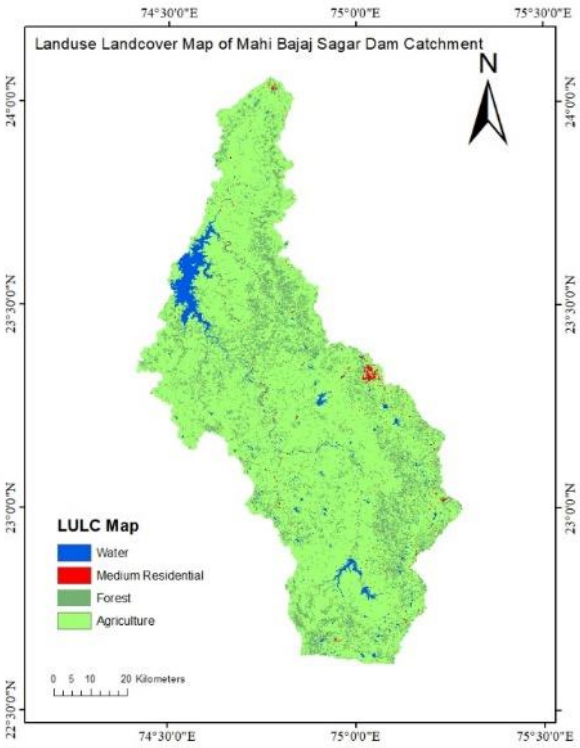



**Figure 3** LULC map of study area

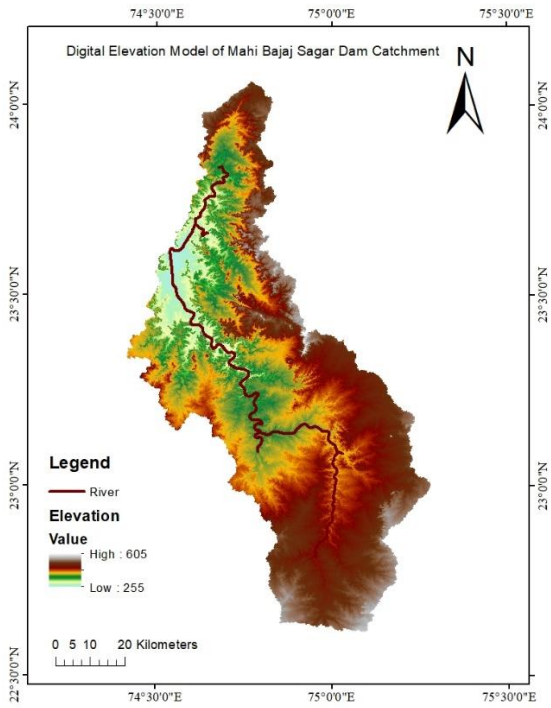



**Figure 4** DEM map of study area

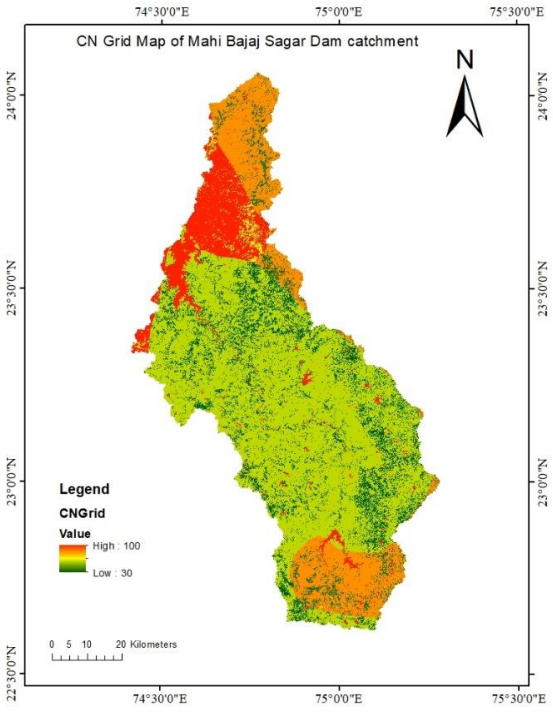



**Figure 5** CN Grid map of study area

### *3.2 HEC-HMS Modelling*

The centroid flow length, the longest flow length, basin slope and basin centroid were extracted for each basin. Different hydrologic nodes (HMS nodes) were assigned with in each sub-basin and an outlet was defined as shown in Figure 6 using the HEC-GeoHMS. All the HEC-HMS input of the study area assigned with basin name as W80, W90, W100, W110, W120, W130, W140 having J41, J46, J51 junction and R10, R30 and R50 are the name of assigned river. The schematic diagram of HEC-HMS is shown in Figure 6. HEC-HMS 4.6 is used here for modelling of study area as it was compatible with Arc-GIS 10.2 version. In this model SCS unit hydrograph is selected for transform method, SCS Curve Number is used for loss method, Muskingum parameter is used for routing method and recession is used for baseflow model. In our study area the available rain gauge station are four and temperature data is one. Monthly total evaporation data used for each subbasin. The HEC-HMS model was applied to the Subbasin of the Mahi Bajaj Sagar catchment at daily time steps.

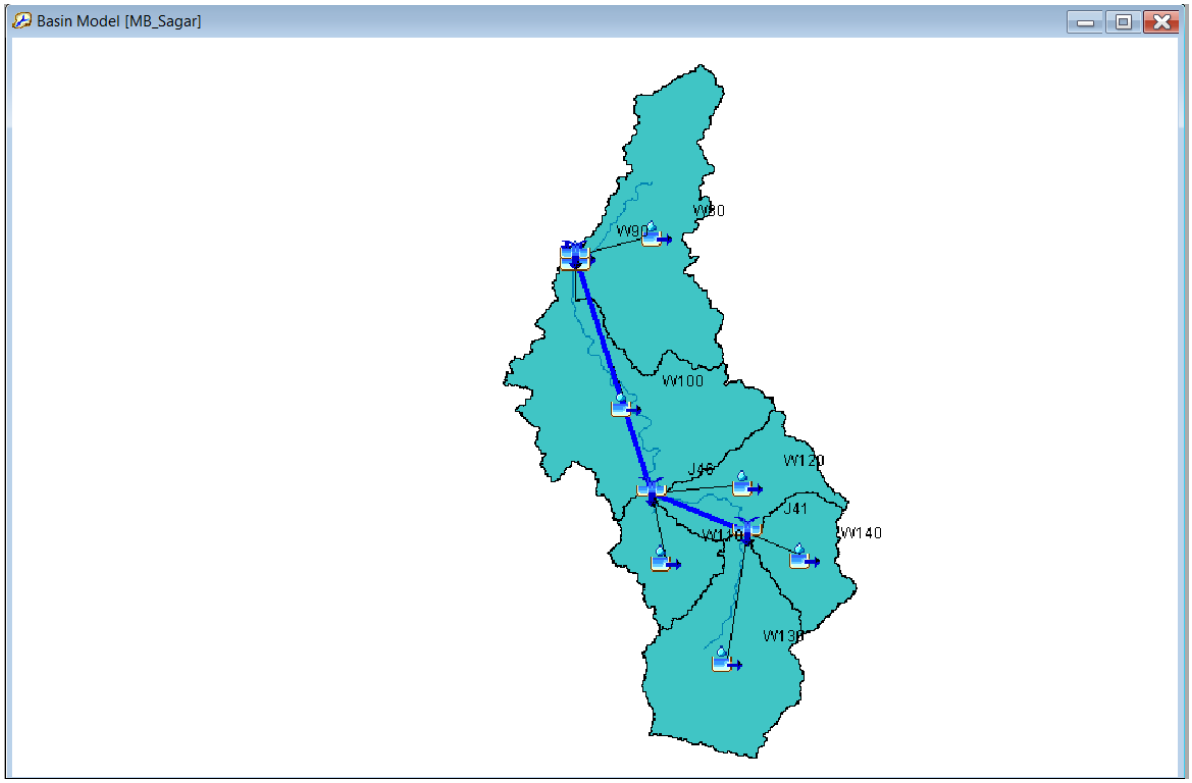



**Figure 6** HEC-HMS 4.6 Model for Mahi Bajaj Sagar catchment

### *3.3 Calibration and validation of HEC-HMS Parameters*

The model was calibrated with observed streamflow data at mahi Bajaj Sagar Dam outlet. Different Statistical indices like Nash-Sutcliffe efficiency (NSE), Percentage Bias (PBIAS), coefficient of correlation ($R^2$) and Root mean square error(RMSE) were used to check the reliability of the model. Different parameters were selected such as lag time, time of concentration, curve number ,Muskingum parameter (K and X) and ratio to peak discharge . The quality of the input data determines the capability of the calibrated hydrological model. HEC-HMS model was calibrated to develop a model which can simulate the peaks, time and volume similar to the observed data. Daily rainfall data and temperature data from 2010 to 2017 were used to simulate the direct runoff, peak flows and runoff volumes. Initial abstraction, lag time, were considered for the calibration in HEC-HMS.

These model parameters were estimated using the optimization algorithm available in HECHMS. Each parameter was modified and resultant simulation run, and observed stream flow were plotted and compared. Total 8 years of daily data were selected to calibrate and validate the model. The comparison of the initial parameters for calibration with the optimized parameter using HEC-HMS is shown in Table 2 and 3. The model was calibrated for 5 years then the optimized value is updated for validation period of 3 years.

**Table 2** Routing parameters used for calibration period

| Reach | Parameter | Unit | Initial Value | Optimized Value |
|---|---|---|---|---|
| R10 | Muskingum - K | HR | 7.4 | 5.959 |
| R30 | Muskingum - K | HR | 2.15 | 1.8836 |
| R50 | Muskingum - K | HR | 21 | 20.107 |
| R10 | Muskingum - Number of Sub reaches | | 2 | 2 |
| R30 | Muskingum - Number of Sub reaches | | 3 | 3 |
| R50 | Muskingum - Number of Sub reaches | | 3 | 3 |
| R10 | Muskingum - x | | 0.3 | 0.15046 |
| R30 | Muskingum - x | | 0.3 | 0.22726 |
| R50 | Muskingum - x | | 0.3 | 0.28346 |

**Table 3** Loss method parameters used for calibration period

| Sub-Basin Name | Parameter | Initial Value | Optimized Value |
|---|---|---|---|
| W140 | SCS Curve Number - Curve Number | 53.2269 | 56.9 |
| W130 | SCS Curve Number - Curve Number | 60.2442 | 48.819 |
| W120 | SCS Curve Number - Curve Number | 56.3427 | 47.985 |
| W110 | SCS Curve Number - Curve Number | 55.9071 | 51.624 |
| W100 | SCS Curve Number - Curve Number | 57.0141 | 56.795 |
| W90 | SCS Curve Number - Curve Number | 79.1424 | 58.493 |
| W80 | SCS Curve Number - Curve Number | 65.7855 | 51.767 |

## 4. RESULT AND DISCUSSION

The IMD gridded prepitation , temperature, average monthly evaporation data and observed discharge data for 8 years (2010-2017) were extracted and used for calibration and validation. In HEC-HMS there two method for calibration and validation namely as Optimization and Simulations runs. Before calibration, the initial value for different parameters were calculated and a sensitivity analysis was carried out to find out the most sensitive parameters in the model. The NSE and RMSE value were checked with each simulations and it is observed that the most sensitive parameters are SCS Curve

Number, Musking K, Muskingum X, Recession constant and number of Subreaches. SCS Curve Number depends on the soil type and Landuse pattern of the study area. Muskingum K,X are depends on the channel slope. After sensitivity analysis optimization technique is used in the model. Here Simplex method is used with maximum iteration 100 and torelerance value kept as 0.01. The objective function for the optimization process has been taken as minimization of RMSE for 8 years. The optimized value obtained by optimization runs applied to every subbasins. Then manual calibration has been done with the parameter values increased/decreased by +/- 5% to +/-30%. Figure 7 and figure 8 shows a comparison of simulated flow hydrograph at the outlet with the observed flow for 5 years of calibration period and 3 years of validation period. The final model had a good fit with the observed flow data. The reliability of the model while calibrating with different parameters were checked using different statistical indices.Here we have used four statistical index to evaluate the performance of the model. The first measure, RMSE is used to measure the error of prediction. The value was obtained as 0.48 for calibration period and 0.53 for validation period. The NSE value is used for to evaluates the efficiency of the modelled flow to observed flow. The second measures, NSE evaluates the efficiency of the modelled flow to observed flow. It is found to be 0.77 for calibration and 0.72 for validation in our model, which shows that its perfect match of simulated to observed flow. The coefficient of correlation showed a very good match with the observed and the simulated hydrograph for long period. The performance of the model can be compared using different statistical indices as shown in Table 8.

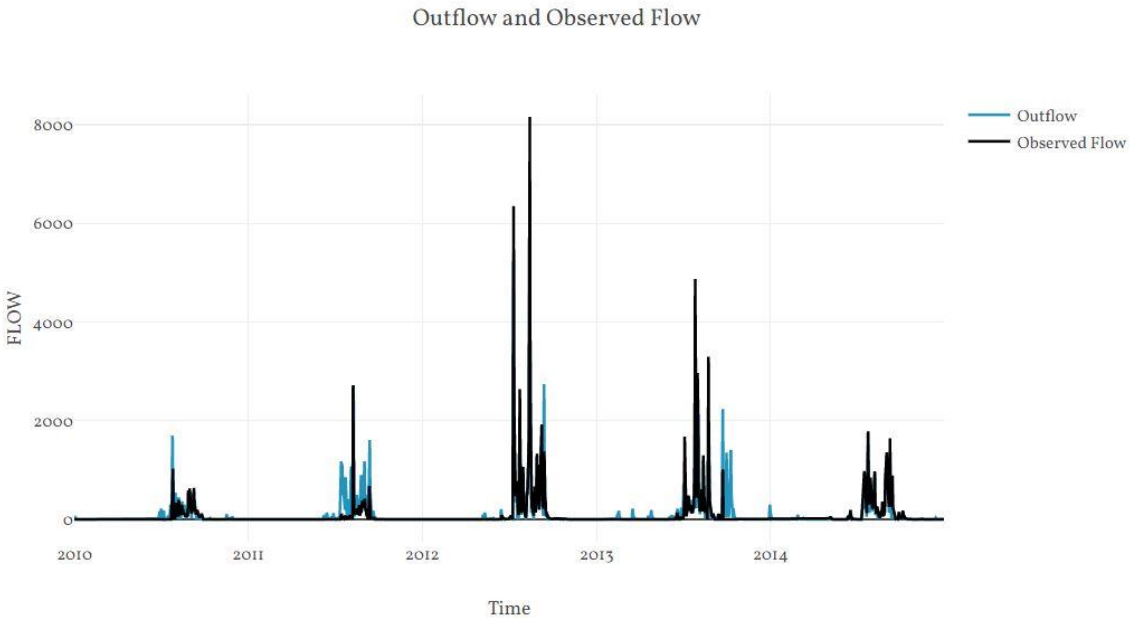



**Figure 7** Observed and simulated daily discharge hydrograph of Mahi Bajaj Sagar Dam catchment for calibration period(2010-2014)

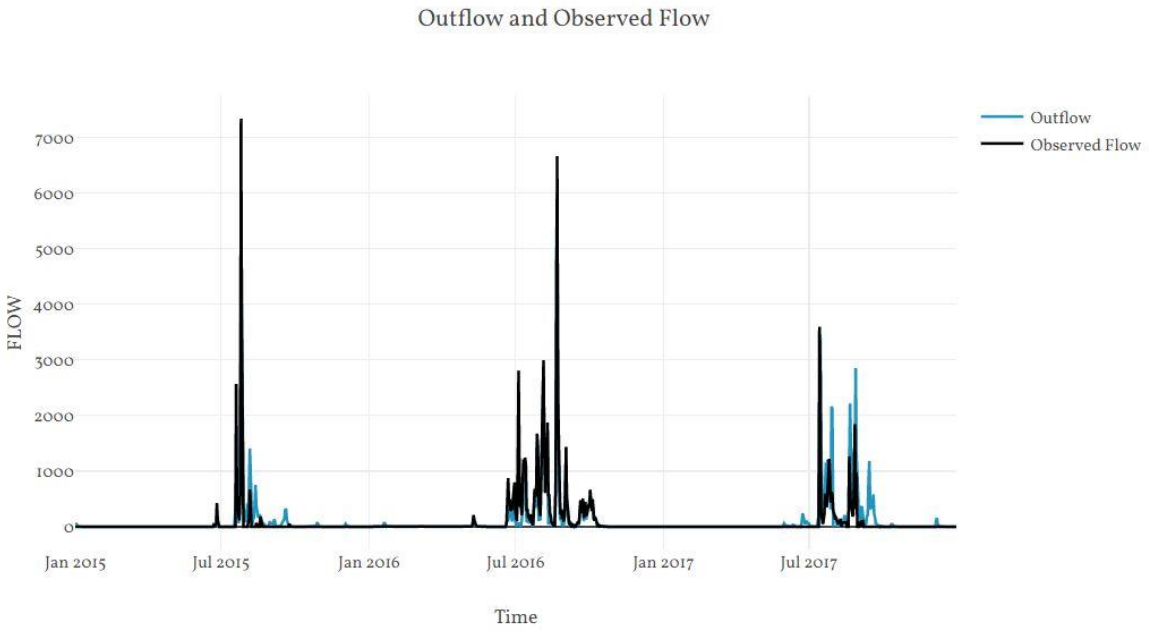



**Figure 8** Observed and simulated daily discharge hydrograph of Mahi Bajaj Sagar Dam catchment for validation period(2015-2017)

| Statistical Parameter | Calibration | Performance | Validation | Performance |
|---|---|---|---|---|
| RMSE | 0.48 | Very Good | 0.53 | Good |
| NSE | 0.77 | Very Good | 0.72 | Very Good |
| PBIAS | 22.45 | Satisfactory | 11.71 | Very Good |
| $R^2$ | 0.78 | Very Good | 0.72 | Very Good |

## 5. Conclusions

This study set out to simulate the rainfall-runoff model in Mahi Bajaj Sagar Dam Catchment, India, using HEC-HMS. This process is done with help of Arc-GIS software with extensions of Arc-Hydro and Hec-GeoHMS tools for watershed delineation with DEM and prepare the input file for HEC-HMS. Daily rainfall,temperature and monthly evaporation data used with LandUse landcover data for a period of 8 years(2010-2017). Curve Number grid is prepared with classified LULC data. For classification we have done maximum likelihood algorithm with help of ERDAS Imagine software. The model is then evaluated by Nash-Sutcliffe(NSE), root mean square error(RMSE), percent bias(PBIAS) and coefcient of determination ($R^2$ ). The results shows good relation with observed data. . Sensitivity analysis is done with simplex method of optimization with 100 simulations with 0.01 accuracy. After optimization the optimized value used for calibration and the result shows good relation with observed streamflow data. The NSE,RMSE and $R^2$ values for validation period are as 0.72,0.53 and 0.72, which shows very good relation with observed data(Boskidis et al.2012;Cameron et al.1997;Moriosi et al.2007;Singh et al.2005). Thus, this study shows that HEC-HMS hydrological model can be used for rainfall-runoff simulation for long time period for reservoir operation planning and management.

## Acknowledgements

The authors would like to thank officials of The Ministry of Water Resources, River Development and Ganga Rejuvenation for providing financial assistance. The work has been done under the INCCC Project on ‘‘Climate Change Impacts Studies for Rajasthan (Areas of Inland Drainage and Mahi Basin)”. Authors thank IMD for providing daily gridded data on rainfall and temperature. Authors also thank Water Resources Department, Udaipur Region, Govt. of Rajasthan and Mahi Bajaj Sagar Dam officials for providing daily streamflow data.

## References

Alipour, M. H., A. Shamsai, and N. Ahmady. 2010. A new fuzzy multicriteria decision making method and its application in diversion of water. Expert Systems with Applications 37 (12):8809–13. doi: 10.1016/j.eswa.2010.06. 023.

Arnold, J. G., R. Srinivasan, R. S. Muttiah, and J. R. Williams. 1998. Large area hydrologic modeling and assessment part I: Model development. Journal of the American Water Resources Association 34 (1):73–89. doi: 10. 1111/j.1752-1688.1998.tb05961.x.

Ateeq-ur Rauf and Abdul Razzaq Ghumman(2018). Impact Assessment of Rainfall-Runoff Simulations on the Flow Duration Curve of the Upper Indus River—A Comparison of Data-Driven and Hydrologic Models. *Water* **2018**, *10*(7), 876; **https://doi.org/10.3390/w10070876**

Belayneh Alemshet, Gashaw, Sintayehu(2020). Modeling Earth Systems and Environment; Heidelberg Vol. 6, Iss. 4, (Dec 2020): 2015-2032. DOI:10.1007/s40808-020-00792-z

Boskidis, I.; Gikas, G.D.; Sylaios, G.K.; Tsihrintzis, V.A. Hydrologic and water quality modeling of lower nestos river basin. Water Resour. Manag. 2012, 26, 3023–3051.

Cameron, A.C.; Windmeijer, F.A. An R-squared measure of goodness of fit for some common nonlinear regression models. J. Econom. 1997, 77, 329–342.

Coutu, W. G., and C. Vega. 2007. Impacts of land use changes on runoff generation in the East branch of the Brandywine Creek watershed using a GIS-based hydrologic model. Middle States Geographer 40:142–9.

Easterling, D. R., J. L. Evans, P. Y. Groisman, T. R. Karl, K. E. Kunkel, and P. Ambenje. 2000. Observed variability and trends in severe weather climate events: A brief review. Bulletin of the American Meteorological Society 81 (3):417–25. doi: 10.1175/1520-0477(2000)081 2.3.CO;2.

Garg, V., Aggarwal, S. P., Gupta, P. K., Nikam, B. R., Thakur, P. K., Srivastav, S. K., & Senthil Kumar, A. (2017). Assessment of land use land cover change impact on hydrological regime of a basin. Environmental Earth Sciences, DOI 10.1007/s12665-017-6976-z

Halwatura, D., & Najim, M. M. M. (2013). Application of the HEC-HMS model for runoff simulation in a tropical catchment. doi.org/10.1016/j.envsoft.2013.03.006

Hydrologic modeling system HEC-HMS user’s manual. Version 4.6. U.S. Army Corps of Engineers. Hydrologic Engineering Center.

Moriasi, D.N.; Arnold, J.G.; Liew, V.M.W.; Bingner, R.L.; Harmel, R.D.; Veith, T.L. Model evaluation guidelines for systematic quantification of accuracy in watershed simulations. Am. Soc. Agric. Biol. Eng. 2007, 50, 885–900

Motevalli, S., M. M. Hosseinzadeh, R. Esmaili, K. Derafshi, and S. Gharehchahi. 2012. Assessing the effects of land use change on hydrologic balance of Kan Watershed using SCS and HEC-HMS hydrological models – Tehran, IRAN. Australian Journal of Basic and Applied Sciences 6 (8):510–9.

Neekita Joshi , Astha Bista, Indira Pokhrel, Ajay Kalra4 and Sajjad Ahmad(2019). Rainfall-Runoff Simulation in Cache River Basin, Illinois, Using HEC-HMS. World Environmental and Water Resources Congress 2019.

Olivera, F., M. Valenzuela, R. Srinivasan, J. Choi, H. Cho, S. Koka, and A. Agrawal. 2006. ArcGIS-SWAT: a geodata model and GIS interface for SWAT. J Am Water Resour Assoc 42 (2):295–309. doi:10.1111/j.1752-1688. 2006.tb03839.x

Shunfu Hu & Prasanna Shrestha (2020): Examine the Impact of Land Use and Land Cover Changes on Peak Discharges of a Watershed in the Midwestern United States Using the HEC-HMS Model, Papers in Applied Geography, DOI: 10.1080/23754931.2020.1732447.

Singh, J.; Knapp, H.V.; Demissie, M. Hydrologic modeling of the Iroquois river watershed using HSPF and SWAT; Illinois State water survey contract report. J. Am. Water Resour. Assoc. 2005, 41, 343–360.

Tewodros M. Tena , Phenny Mwaanga and Alick Nguvulu(2019). Impact of Land Use/Land Cover Change on Hydrological Components in Chongwe River Catchmen Sustainability 2019, 11(22), 6415; https://doi.org/10.3390/su11226415t

Visweshwaran, R. 2017. Application of the HEC-HMS model for runoff simulation in the Krishna basin. Master's thes., National Institute of Technology Karnataka, Surathkal, India, 17 p.

Xu Liang Dennis P. Lettenmaier Eric F. Wood Stephen J. Burges.1994.A simple hydrologically based model of land surface water and energy fluxes for general circulation models. https://doi.org/10.1029/94JD00483

Zhang, H. L., Y. J. Wang, Y. Q. Wang, D. X. Li, and X. K. Wang. 2013. The effect of watershed scale on HECHMS calibrated parameters: A case study in the Clear Creek watershed in Iowa, US. Hydrology and Earth System Sciences 17 (7):2735–45. doi: 10.5194/hess-17-2735-2013.

Zhu, C., and Y. Li. 2014. Long-term hydrological impacts of land use/land cover change from 1984 to 2010 in the Little River Watershed, Tennessee. International Soil and Water Conservation Research 2 (2):11–21. doi: 10. 1016/S2095-6339(15)30002-2.

*IN PROCEEDINGS OF 25th HYDRO 2020, INTERNATIONAL CONFERENCE, NATIONAL INSTITUTE OF TECHNOLOGY ROURKELA, ODISHA, INDIA 26-28, March 2021, ISBN 978-93-90631-56-8*

Paper ID - 209

# Physics Based Hydrologic Model for Runoff Prediction in Lower Tapi Basin, India.

Shubham M. Jibhakate[1], P. V. Timbadiya[2], P. L. Patel[3]

[1] *Ph.D. Scholar, Department of Civil Engineering, Sardar Vallabhbhai National Institute of Technology Surat, Surat-395007, India*

[2] *Associate Professor, Department of Civil Engineering, Sardar Vallabhbhai National Institute of Technology Surat, Surat-395007, India. (Corresponding Author)*

[3] *Professor, Department of Civil Engineering, Sardar Vallabhbhai National Institute of Technology Surat, Surat-395007, India.*

*Email: shubhamjibhakate1771@gmail.com; pvtimbadiya@ced.svnit.ac.in; plpatel@ced.svnit.ac.in;*

## Abstract

The distributed hydrologic models are useful in prediction of runoff at the outlet of the catchment which makes it an important tool in water resources management and decision making. In the present study, the distributed physics based hydrologic model in MIKE SHE/MIKE 11 has been developed to simulate the overland flow, evapotranspiration (ET), unsaturated flow and channel flow processes in the Lower Tapi Basin (LTB) having area of 3,618 km$^2$ in India. The distributed model has been developed with cell size of 250 m spatial resolution with consideration of spatially lumped model parameters for vegetation and soil type across the basin. The appropriate value of overland flow resistance parameter (Manning's 'M'), vegetation properties such as leaf area index (LAI) and root depth (RD) for the existing land use land cover class (for Landsat data of 1995) were obtained from the literature. The model was calibrated for the observed streamflow data at Ghala stream gauging station for year 1990-1995 having wide range of climatic (Wet/normal/dry) condition. The performance of the calibrated model also evaluated by using split sampling (independent dataset) technique. The model performance is quantitatively assessed using statistical indicator (RMSE = 312.8 – 341.8 m$^3$/s and 119.5 – 130.7 m$^3$/s, $R^2$ = 0.89-0.80 and 0.98-0.97 and NSE = 0.87-0.77 and 0.94-0.84) on daily as well as monthly time scales respectively, during calibration and validation periods. The calibrated model would be useful in the prediction of runoff and water level along the river as well as Surat city located at the tail portion of the Lower Tapi River.

***Keywords:*** *Distributed physics based hydrologic model, Lower Tapi Basin, MIKE SHE etc.*

## 1. Introduction

Hydrological cycle is a combination of different complex hydrological processes treating all phases of earth's water (Chow et al. 1988). The relationship between phases of water such as precipitation, evapotranspiration, runoff, soil moisture, groundwater recharge can be effectively understood with the help of hydrological models. It is efficient in calculating the water balance of the catchment for a specific time period. The physics based distributed hydrological models describe the rainfall-runoff relationship of the catchment using mass and momentum equation, and extensively preferred due to their inherent limitations over the lumped and semi-distributed models which can take spatial heterogeneity of the catchment into account (Sun et al. 2007; Zang et al. 2008). Though distributed hydrological models demand the substantial set of climatic, surface and subsurface data while applying to the catchment scale.

The physics based fully distributed hydrological MIKE SHE model is originally derived from the SHE model (Abbott et al. 1986a, b). Development over the years, provide replacement of MIKE SHE river model with coupled 1D channel model i.e. MIKE SHE/MIKE 11 which is capable for both continuous and event-based modelling and widely used by the previous researchers. Refsgaard et al. (1997) describes the methodology and applications for integrated MIKE SHE/MIKE 11 model for Danubian Lowland and found integrated model performs better than individual model component. The water balance for the small watershed (6.49 km$^2$) of Kangsabati River catchment, West Bengal, India is calculated using MIKE SHE while minimizing the error in stream flow at the catchment outlet by Singh et al. (1999). Thompson et al. (2004) applied integrated MIKE SHE/ MIKE 11 model for simulation of groundwater and ditch water level for Elmley Marshes in southeast England. El-Nasr et al. (2005) found MIKE SHE model perform better than SWAT (semi-distributed model) in the prediction of river

discharge and accumulated runoff volume while applying it to Jeker River basin, Belgium. The developed MIKE SHE model successfully simulate the daily stream flows vis-à-vis specific storm events for small watershed in north western China by Zhang et al. (2008). Im et al. (2008) developed the MIKE SHE model for Gyeongancheon watershed in South Korea to evaluate the impact of land use change on catchment hydrology; found increase in total runoff and overland flow with change in non-urban area to urban area. Huang et al (2010) developed the MIKE SHE/MIKE 11 model for Tarim River basin in China considering the lumped model parameter over the catchment found RS (remote sensing) data shows better performance against the gauged data in the simulation of actual evapotranspiration. Rahim et al. (2012) performed the detailed water balance computation for Paya Indah wetland with the application of MIKE SHE and found satisfactory results. The groundwater and surface water interaction including climate change impact analyzed for mountain coast watershed of Cowichan using of MIKE SHE/MIKE 11 model and found decrease in amount of recharge and precipitation with increase in evapotranspiration by Foster and Allen (2015). Krishnaveni and Rajeshwari (2018) successfully simulate routing through the irrigation tank cascade system in Tamil Nadu with the application of MIKE SHE/MIKE 11. Loliyana and Patel (2019) developed MIKE SHE/MIKE 11 model for the prediction of soil moisture in Gopalkheda sub-catchment, India; found model performing better for gridded rainfall input against the station data. From past studies, it is evident that MIKE SHE/MIKE 11 integrated model is efficient and powerful tool in modelling different components of hydrological cycle.

The Tapi River was frequently flooded and caused disastrous situation generally in lower reaches of the river including Surat city. The Lower Tapi River experienced riverine flood in past, mostly due to reservoir releases from the Ukai Dam. The daily rainfall intensity is increasing with increase in maximum 1-day and 5-day extreme rainfall (1944-2013) for the LTB (Gehlot et al. 2020). Such significant rise in rainfall can generate large amount of runoff volume. The large runoff in addition to riverine flow could aggravate the flooding situation in LTB. Therefore, development of integrated rainfall runoff and hydrodynamic model would be helpful in efficient water resource and flood management in LTB. Thus, in present study MIKE SHE and MIKE 11 models are integrated for the development of rainfall-runoff model for the LTB.

## 2. Study Area and Data Source

The Tapi River is one of the largest westwards moving rivers in India after the Narmada River. It originates from Multai in Betul district of Madhya Pradesh covering about 700 km before meeting to Arabian Sea near the Surat city. The Tapi River has a total 65,145 $km^2$ area distributed over three different states viz. Madhya Pradesh, Maharashtra and Gujarat. The entire Tapi basin is divided into three sub-basins as (i) Upper Tapi Basin (UTB) from river origin to Hathnur (Near the confluence of Purna River with main Tapi River) (29,430 $km^2$). (ii) Middle Tapi basin (MTB) from Hathnur to Ukai Dam (32,097 $km^2$) and (iii) Lower Tapi Basin (LTB) from Ukai Dam to Arabian Sea (3,618 $km^2$). The Tapi basin consists of mainly black soil. The south-west monsoon is the major source of rainfall over the basin, starts by middle of June and withdraws by mid-October. The annual average rainfall for Tapi basin in the last 10 years is 870 mm and for Upper, Middle and Lower Tapi basin, it is 935.5 mm, 631.5 mm and 1,042.3 mm respectively (Jain et al. 2007). The present study area includes LTB having area of 3,618 $km^2$ with 128 km long river stretch. The Ukai Dam is the largest multipurpose project in Tapi basin, present on upstream of the study area. The project provides the irrigation facility to the surrounding area with partial flood control in the downstream area of the dam. The two control structures viz, Kakrapar Weir (with crest elevation of 48.78 m and weir coefficient 1.881) and Singanpur Weir (with crest elevation of 6 m and weir coefficient 1.666) are also present on the river at the chainage of 22.2 and 103.03 km respectively. The lateral inflow contribution is negligible as no major tributary enters to the study reach (Timbadiya et al. 2014). The detailed location of rainfall stations, weather stations and stream gauging stations across the study area shown in Figure 1.

The required data for the present investigation were collected from different relevant agencies responsible for the measurement and validation of the data. The topography of the study area is developed from the contours (vector) collected from different data sources considering their respective accuracy. The 20 m interval contours were digitized from Survey of India (SOI) toposheet for hilly and agricultural part of the basin, the 0.5 m surveyed contour for Surat-Hazira twin city were collected from

Surat Municipal Corporation (SMC) and 10 m contours were generated from Shuttle Radar Topographic Mission (SRTM) DEM for the remaining coastal part of the basin. The contours (vectors) from the different sources combined and converted to raster by using the spatial interpolation tool "Topo to Raster" in ArcGIS 10.6.1 (see Figure 1). The cross sections for the aforesaid river stretch were also collected from SMC. The Land Use Land Cover (LULC) classification is obtained from Landsat satellite imagery (February, 1995) in ERDAS IMAGINE 2010 in which agricultural land (28%) found to be dominated land class. The soil maps (1:2,50,000 scale; hard copy) collected from the National Bureau of Soil Survey and Land Use Planning (NBSS&LUP), Nagpur; found that clay is the major soil class across the study area. The station-based rainfall data on daily time scale for nine rain gauge stations were collected from India Meteorological Department (IMD), Pune; Central Water Commission (CWC), Narmada-Tapi division Surat and State water Data Centre (SWDC), Gandhinagar. The maximum as well as minimum temperature for Surat city and Ghala station were collected from IMD and CWC respectively. The other hydrologic/hydraulic data such as daily inflow, outflow from the Ukai Dam is collected from the Ukai Civil Circle. The daily discharge and water level at Ghala, Kakrapar and Nehru bridge were collected from CWC whereas, for the Mandavi gauging station it was collected from SWDC. The tidal levels at the Arabian Sea were monitored by Surat Irrigation Circle (SIC) during December 6, 2009 to January 5, 2010 which are synchronized with model simulation period to be used in the present study.

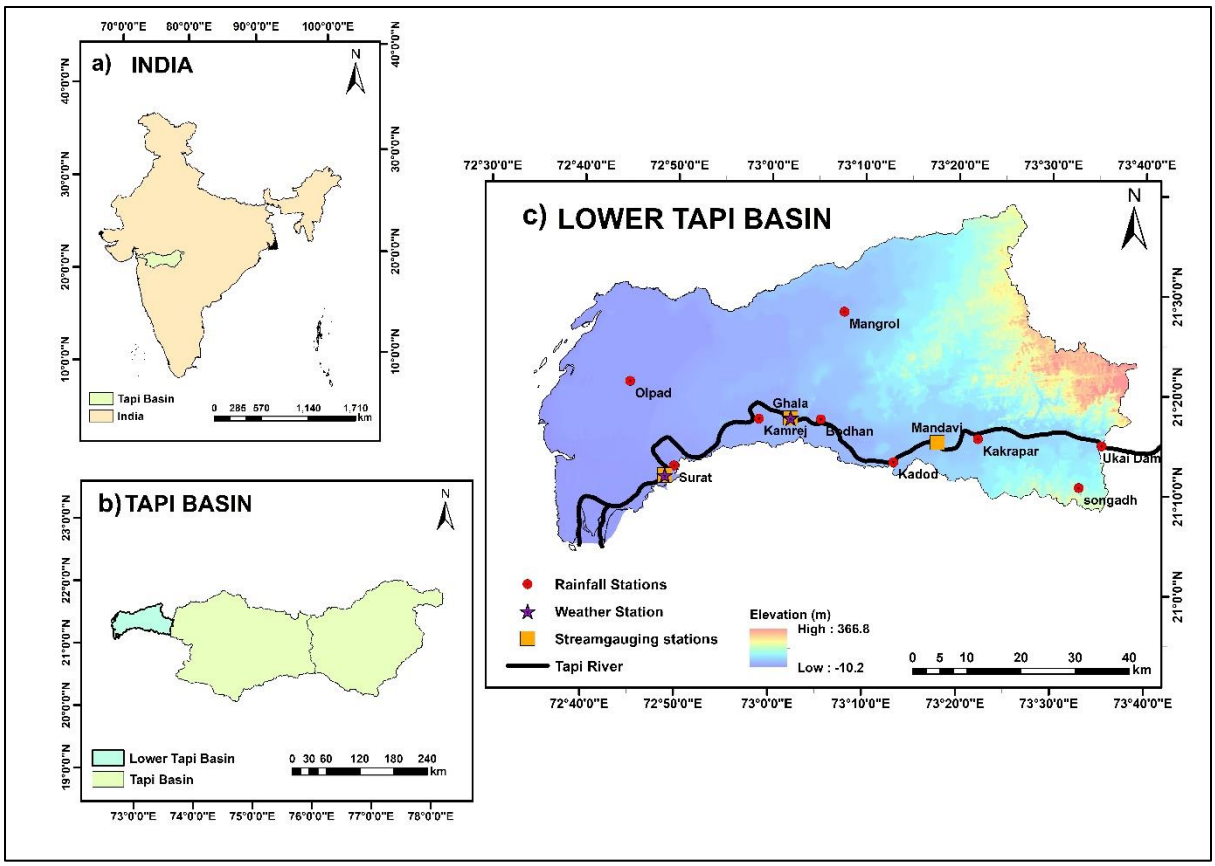



**Figure 1** Index Map of Lower Tapi Basin.

## 3. Description of the MIKE SHE Model

The MIKE SHE (Système Hydrologique Européen) is a fully distributed, physically based, deterministic hydrological model which capable of both continuous and event-based hydrological modelling (DHI 2016a). The water moment module of MIKE SHE systematically deals with the hydrological process of precipitation as input; losses in the form of interception, evapotranspiration (ET) and infiltration; overland flow over the catchment surface and flow through the unsaturated and saturated layers of the hydrologic system. In MIKE SHE/MIKE 11 integrated hydrological model, finite

difference approach (Diffusive approximation of 2D Saint-Venant equation) is used to solve the partial differential equation for the process of overland flow, evapotranspiration (Kristensen and Jensen's method), unsaturated flow (2-layer water balance method) and channel flow (Kinematic wave approximation of 1D Saint-Venant equations) (DHI 2016b).

## 4. Methodology

The methodology adopted in the present study i.e. development of distributed physics based hydrological model for the simulation of overland flow, ET, unsaturated flow and channel flow for LTB is given in Figure 2.

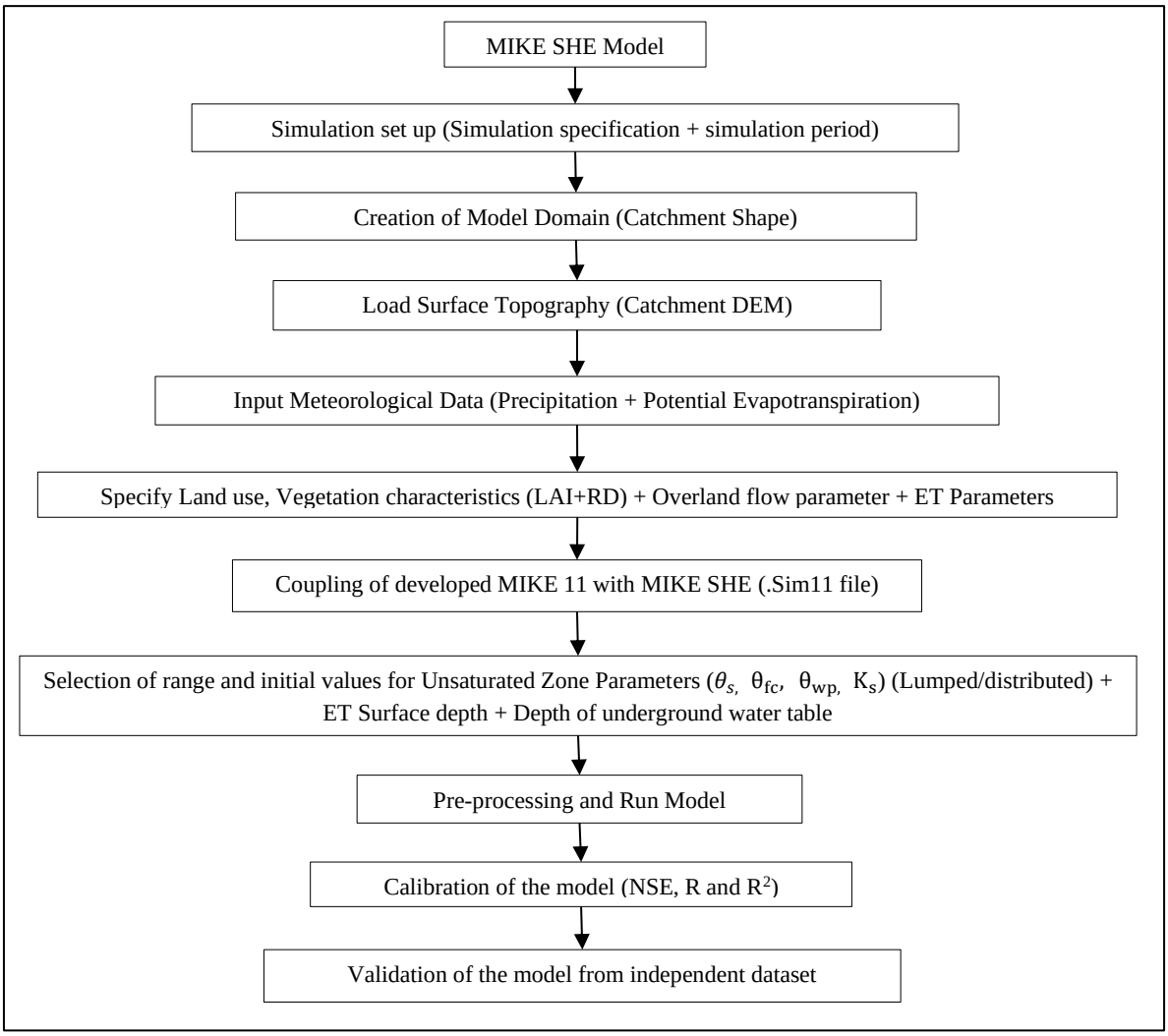



**Figure 2** Methodology adopted in the present study.

## 5. Model Development and Parameterization

The generated raster (DEM) (30 m) is used to represent the topography with model grid size of 250 x 250 m spatial resolution. The lumped type Thieseen Polygon method was adopted for the areal distribution of Precipitation and Potential Evapotranspiration (PET) across the basin. The PET for Surat and Ghala stations were calculated from temperature-based Hargreaves and Samini method as mentioned in Eq. (1). The surface roughness coefficient Manning's 'M' responsible for the horizontal movement of overland flow; Leaf Area Index (LAI) and Root Depth (RD) depend on existing cropping pattern and vegetation responsible for the calculation of actual evapotranspiration (AET) were obtained from the LULC classification. The respective values for different classes were taken from literature

(Chow et al. 1959; Kothyari et al. 2010; Loliyana and Patel 2018). The distributed dataset for the development of MIKE SHE/MIKE 11 model is shown in Figure 3 and weighted average values of LAI, RD and adopted Manning's 'M' given in Table 1. The 2-layered water balance method effective and recommended for the area with shallow water tables is used to model unsaturated flow in the present study. The MIKE SHE calculates the unsaturated flow only in vertical direction. The infiltration from rainfall (downward movement) within an unsaturated zone depends on the maximum water content at saturation ($\theta_s$), water content at field capacity ($\theta_{fc}$), water content at wilting point ($\theta_{wp}$) and saturated hydraulic conductivity ($K_s$) which need to be calibrated.

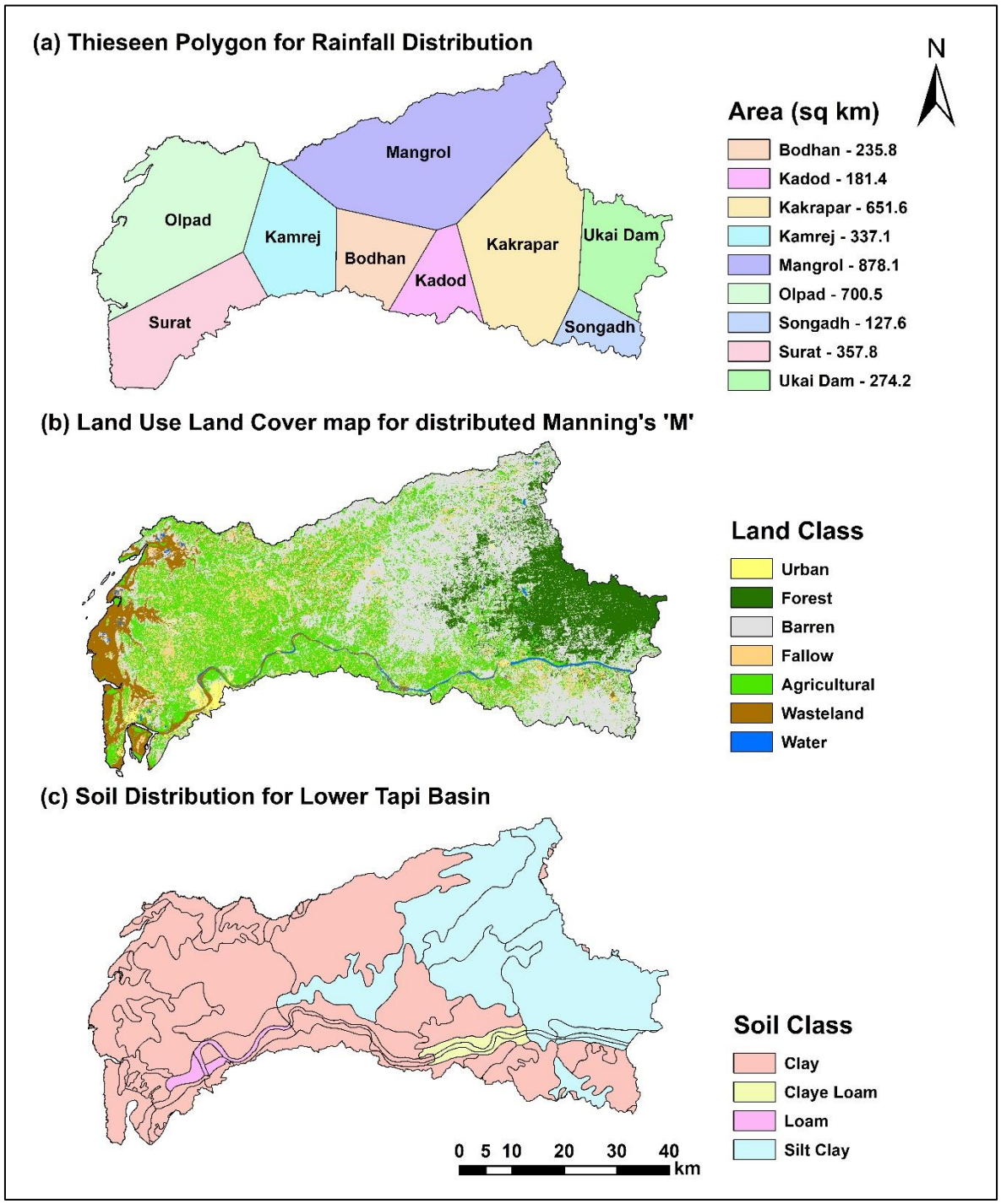



**Figure 3** Distributed data for the development MIKE SHE model (a) Rainfall distribution (b) Land use land cover map and (c) Soil classification for the LTB.

$$ET_o = 0.408 \times 0.0023 \times R_a\sqrt{T_D} \times (T_{mean} + 17.8) \quad (1)$$

Here, $R_a$= extra- terrestrial radiation (MJ m$^{-2}$ day$^{-1}$),
$T_D$ = temperature difference ($^o$C) and
$T_{mean}$ = mean daily air temperature ($^o$C).

**Table 1** LAI, RD and Manning's 'M' for Lower Tapi Basin

| Land use class | Area (%) | Manning's n ($m^{-1/3}s$) | Manning's M ($m^{-1/3}s$) | LAI | Wt. Avg of LAI | RD (mm) | Wt. Avg of RD |
|---|---|---|---|---|---|---|---|
| Agriculture | 28.1 | 0.035 | 28.57 | 5 | 1.40 | 1045 | 298.55 |
| Fallow | 11.4 | 0.040 | 25 | 1.5 | 0.17 | 650 | 162.5 |
| Water | 0.74 | 0.030 | 33.33 | 0 | 0 | 0 | 0 |
| Forest | 12.7 | 0.150 | 6.67 | 6 | 0.76 | 800 | 53.36 |
| Urban | 1.00 | 0.150 | 6.67 | 0 | 0 | 0 | 0 |
| Barren | 38.5 | 0.055 | 18.18 | 3 | 1.16 | 400 | 72.72 |
| Wasteland | 7.3 | 0.033 | 30.1 | 3 | 0.22 | 400 | 120.4 |
| **Total** | **100** | | | | **~3.75** | | **~710** |

The 1D channel flow model from Ukai Dam to Arabian Sea is developed in MIKE 11. The thalweg line of river is formed by joining the identical lowest points in all (190) cross sections. The daily outflow from Ukai Dam and daily average tide at Arabian sea is considered as upstream and downstream boundary conditions respectively. The channel roughness coefficient Manning's 'n' = 0.03 is adopted for the aforesaid stretch of the Lower Tapi River taken from previous studies (Timbadiya et al. 2014; Vora et al. 2018). The channel flow model in MIKE 11 coupled with the hydrological model in MIKE SHE to simulate the runoff across LTB. The distributed model is simulated for the lumped (spatially) model parameters across the basin. Total seven model parameters up-to unsaturated zone for the simulation of MIKE SHE/MIKE 11 model are considered in the present study.

## 6. Calibration and Validation of the Model

In the present investigation, the model parameters (vegetation, unsaturated zone) lumped over the study area and model calibrated using the data of the years 1990-1995 and validated for the data of year 1996-2000. The daily streamflow data at Ghala stream gauging station has been used for the model calibration. The auto-calibration tool in MIKE SHE based on the Shuffle complex evaluation algorithm (Madsen 2003) has been used to obtain the optimal values of seven model parameters shown in Table 2. The auto-calibration procedure is set for the single objective function i.e. overall agreement of shape of hydrograph, minimizing the Root Mean Square Error (RMSE). The initial values of the model parameters have been chosen from prevailing condition of the study area and relevant literature. The performance of the model under calibration stage for monsoon period of year 1990 and 1994 are shown in Figure 4 (a) and (b). Also, the simulated and observed streamflow during calibrated stage compared for 10-daily and monthly time scale (see Figure 5 (a) and (b). The performance of the model for calibrated parameter has also been evaluated using statistical indices such as co-efficient of determination ($R^2$), Nash Sutcliff Efficiency (NSE) from the comparison between observed and simulated streamflow at Ghala station are tabulated in Table 3.
The calibrated model parameters are validated using the independent data set at Ghala station for the period of 1996-2000. The performance of the model under validation comparing observed and simulated discharge for monsoon period of year 1998, 10-daily and monthly time scale are shown in Figure 6 (a), (b) and (c) respectively. The performance of the validated model using statistical indices given in Table 3. From calibration and validation, it is observed that, model is performing better in monthly and 10-daily scale compared to daily time scale in the prediction of peak flow.

**Table 2** Calibration of MIKE SHE parameters for daily streamflow data

| Components | Parameters | Unit | Range | Initial Value (Manual) | Calibrated Value |
|---|---|---|---|---|---|
| **Surface Zone and Stream Channel** | | | | | |
| Surface Roughness | Manning's M | $m^{-1/3}s$ | 6.67-33.33 (from Table 1) | - | - |
| Storage | Detention Storage ($D_s$) | mm | 00-5.0 | 2 | 1.75 |
| Channel Roughness | Manning's n | $m^{-1/3}s$ | 0.03 | - | - |
| **ET Zone** Vegetation | Leaf Area Index (LAI) (Average based on the land use) | - | from Table 1 | - | - |
| | Root Depth (RD) (Average based on the land use) | mm | from Table 1 | - | - |
| | Co-efficient of interception ($C_{Int}$) | mm | 0.01-0.1 | 0.02 | 0.038 |
| | ET surface Depth | m | 0.1-2.0 | 1.5 | 0.57 |
| **Unsaturated Zone** Soil (Lumped over area) | Moisture content at saturation ($\theta_s$) | - | 0.3-0.6 | 0.4 | 0.33 |
| | Moisture content at field capacity ($\theta_{fc}$) | - | 0.2-0.45 | 0.2 | 0.27 |
| | Moisture content at wilting point ($\theta_{wp}$) | - | 0.1-0.25 | 0.1 | 0.22 |
| | saturated hydraulic conductivity ($K_s$) | m/s | $1x10^{-8}$ - $1x10^{-5}$ | $1.2x10^{-6}$ | $4 x10^{-6}$ |

**Table 3** Performance of the developed model under calibration and validation

| | Calibration stage (1990-1995) | | | Validation stage (1996-2000) | | |
|---|---|---|---|---|---|---|
| | RMSE ($m^3$/sec) | $R^2$ | NSE | RMSE ($m^3$/sec) | $R^2$ | NSE |
| **Daily Flow** | 312.8 | 0.897 | 0.875 | 341.8 | 0.803 | 0.773 |
| **10-Daily Flow** | 151.03 | 0.978 | 0.956 | 155.1 | 0.948 | 0.872 |
| **Monthly Flow** | 119.5 | 0.981 | 0.944 | 130.7 | 0.979 | 0.836 |

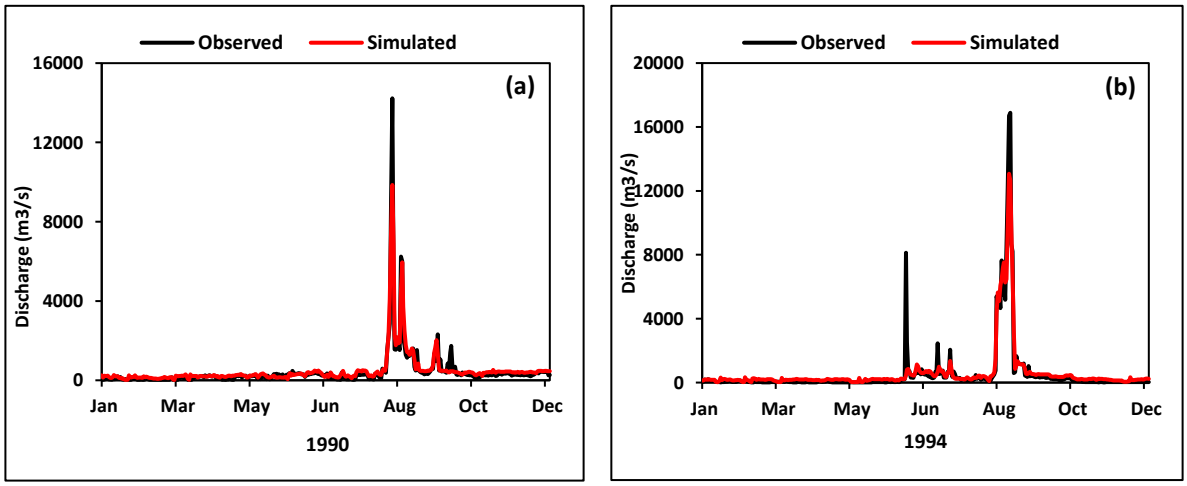



**Figure 4** Comparison of observed and simulated streamflow at Ghala station for Year (a) 1990 (b) 1994

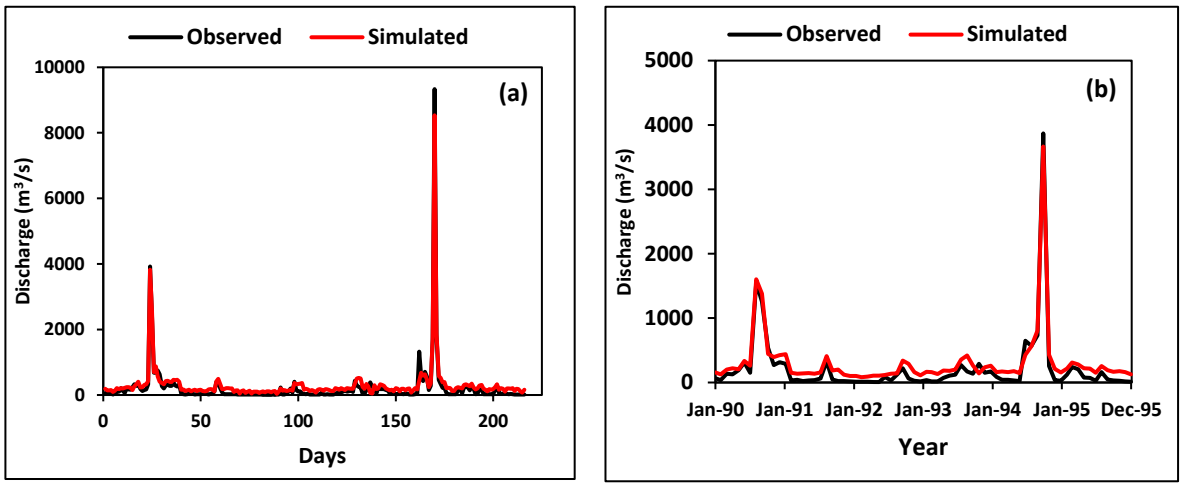



**Figure 5** Comparison of observed and simulated streamflow at Ghala station (a) 10-daily discharge (b) Monthly discharge for year 1990-1995

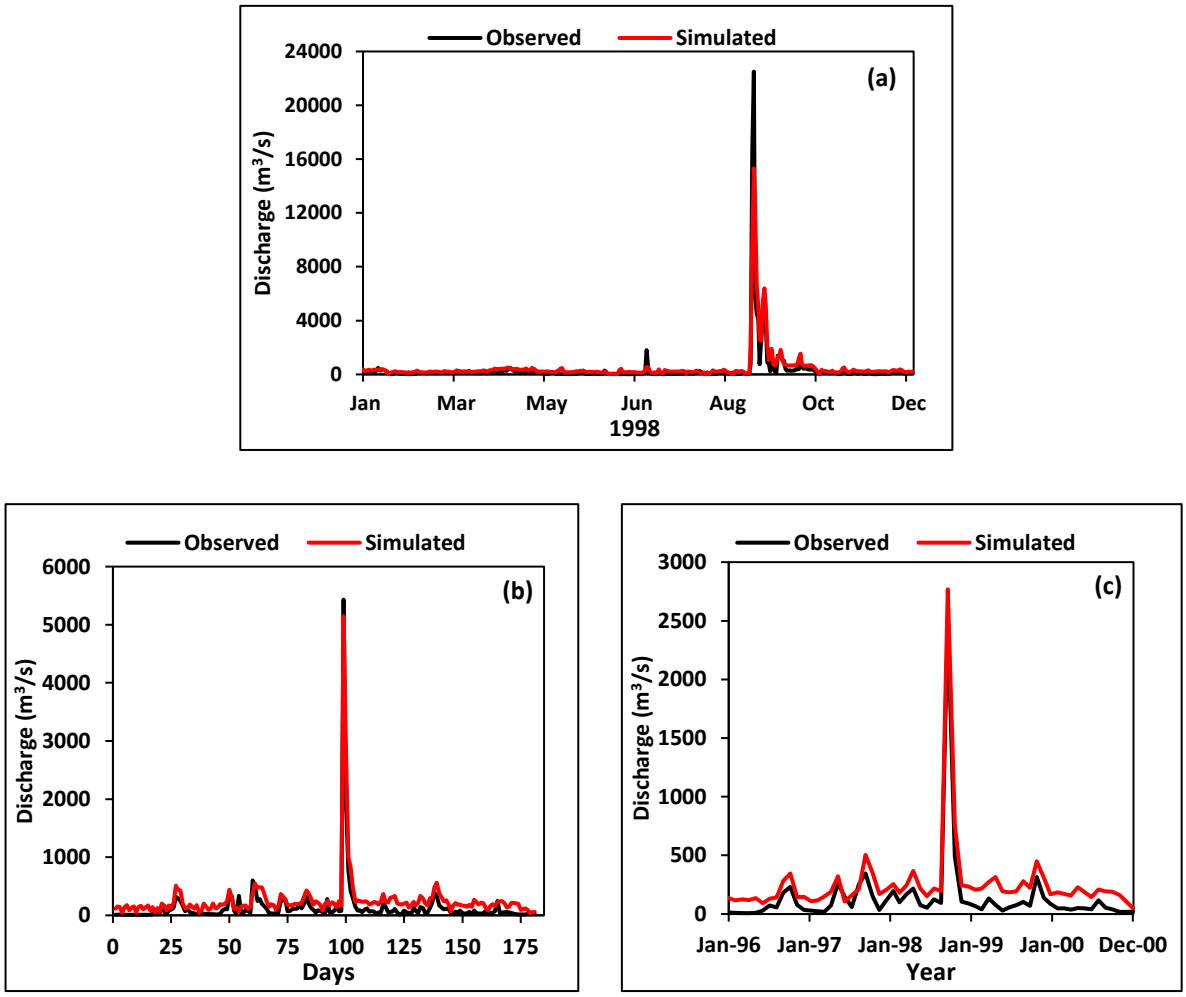



**Figure 6** Comparison of observed and simulated streamflow at Ghala station (a) monsoon period of year 1998 (b) 10-daily discharge (c) Monthly discharge for year 1996-2000

## 7. Conclusions

The distributed physics based hydrological model has been developed for the LTB (3,618 $km^2$) in MIKE SHE/MIKE 11 by considering the lumped (spatial) model parameters for the vegetation and unsaturated zone flow. The Manning's resistance parameter 'M' for overland flow and vegetation properties such as LAI and RD have been selected from existing LULC of the catchment. The performance of the calibrated model has been evaluated using the statistical indices by comparing observed and simulated discharge at Ghala stream gauging station, which have been found to be RMSE = 312.8 $m^3/s$, $R^2$ = 0.897 and NSE = 0.875 for daily time scale. The simulated discharge underpredicts the peak flow on daily time scale may be due to non-consideration of distributed subsurface parameters and saturated zone flow in the model. However, the model shows better performance at monthly time scale compared to 10-daily and daily time scale. The performance of the model under calibrated parameter has also been evaluated for independent data sets and found to be NSE = 0.773, $R^2$ = 0.803 for daily time scale as well as NSE = 0.872 - 0.836 and $R^2$ = 0.948 – 0.979 for 10 daily and monthly time scales respectively, which shows reasonably good agreement of observed data and with simulated values.

## Limitations of the study

In present study, unsaturated zone and vegetation parameters are considered as lumped (spatial) over the study area. However, the fully distributed hydrological model with inclusion of irrigation demand, existing cropping pattern and saturated zone flow with underground lithology, groundwater extraction for irrigation and industrial purpose is likely to give better results and comprehensive idea of the water balance within study area.

## Acknowledgment

The authors would like to acknowledge the financial support received from Indian National Committee on Climate Change (INCCC), Ministry of Jal Shakti, Department of Water Resources, River Development & Ganga Rejuvenation, Government of India for funding this research. The authors appreciate the infrastructural and necessary financial support provided by Centre of Excellence (CoE) on Water Resources and Flood Management, TEQIP-II, Ministry of Human Resources Development (MHRD), Government of India, for conducting the study reported in this paper. The authors duly grateful to India Meteorological Department (IMD), Pune; Central Water Commission (CWC) Surat; State Water Data Centre (SWDC) Gandhinagar; Ukai Civil Circle, Ukai; Surat Irrigation Circle (SIC), Surat; and Surat Municipal Corporation (SMC), Surat; National Bureau of Soil Survey and Land Use Planning (NBSS&LUP), Nagpur; Central Ground Water Board (CGWB), Ahmedabad and State Ground Water Data Center, Ahmedabad for providing the required data for the present study.

## References

Abbott, M. B., Bathurst, J. C., Cunge, J. A., O'Connell, P. E., and Rasmussen, J. (1986a). An introduction to the European Hydrological System—Systeme Hydrologique Europeen,"SHE", 1: History and philosophy of a physically-based, distributed modelling system. *Journal of Hydrology*, *87*(1-2), 45-59.

Abbott, M. B., Bathurst, J. C., Cunge, J. A., O'connell, P. E., and Rasmussen, J. (1986b). An introduction to the European Hydrological System—Systeme Hydrologique Europeen,"SHE", 2: Structure of a physically-based, distributed modelling system. *Journal of Hydrology*, *87*(1-2), 61-77.

Chow, V. T. (1959). *Open Channel Hydraulics*, McGraw-Hill. New York, 26-27.

Chow, V. T., Maidment, D. R., and Mays, L. W. (1988). *Applied Hydrology*, Mcgraw Hill, New York.

DHI (Danish Hydraulic Institute) (2016a) User guide and reference manual to MIKE 11: Modeling system for the rivers and channels. Software manual, DHI, Denmark.

DHI (Danish Hydraulic Institute) (2016b) User guide and reference manual to MIKE SHE: An Integrated hydrological modeling framework. Software manual, DHI, Denmark

El-Nasr, A. A., Arnold, J. G., Feyen, J., and Berlamont, J. (2005). Modelling the hydrology of a catchment using a distributed and a semi-distributed model. *Hydrological Processes: An International Journal*, *19*(3), 573-587.

Foster, S. B., and Allen, D. M. (2015). Groundwater—surface water interactions in a mountain-to-coast watershed: effects of climate change and human stressors. *Advances in Meteorology*, *2015*.

Gehlot, L. K., Jibhakate, S. M., Sharma, P. J., Patel, P. L., and Timbadiya, P. V. (2020). Spatio-Temporal Variability of Rainfall Indices and their Teleconnections with El Niño-Southern Oscillation for Tapi Basin, India. *Asia-Pacific Journal of Atmospheric Sciences*, 1-20.

Hargreaves, G. H., and Samani, Z. A. (1985). Reference crop evapotranspiration from temperature. *Applied Engineering in Agriculture*, *1*(2), 96-99.

Huang, Y., Chen, X., Li, Y., Willems, P., and Liu, T. (2010). Integrated modeling system for water resources management of Tarim River Basin. *Environmental Engineering Science*, *27*(3), 255-269.

Im, S., Kim, H., Kim, C., and Jang, C. (2009). Assessing the impacts of land use changes on watershed hydrology using MIKE SHE. *Environmental Geology*, *57*(1), 231.

Jain, S. K., Agarwal, P. K., and Singh, V. P. (2007). *Hydrology and water resources of India* (Vol. 57). Springer Science and Business Media.

Kothyari, U. C., Ramsankaran, R., Kumar, D. S., Ghosh, S. K., and Mendiratta, N. (2010). Geospatial-based automated watershed modeling in Garhwal Himalaya. *Journal of Hydroinformatics*, *12*(4), 502-520.

Krishnaveni, M., and Rajeswari, A. (2019). Flow Routing and Surface Water Balance Simulation of a Tank Cascaded Catchment Using Coupled MIKE SHE/MIKE 11 Modeling. *Journal of The Institution of Engineers (India): Series A*, *100*(1), 65-74.

Loliyana, V. D., and Patel, P. L. (2018). Performance evaluation and parameters sensitivity of a distributed hydrological model for a semi-arid catchment in India. *Journal of Earth System Science*, *127*(8), 117.

Loliyana, V. D., and Patel, P. L. (2019). Evaluation of soil moisture prediction for Gopalkheda sub-catchment, India. *ISH Journal of Hydraulic Engineering*, 1-10.

Madsen, Henrik, and Torsten Jacobsen. "Automatic calibration of the MIKE SHE integrated hydrological modelling system." *4th DHI Software Conference*. 2001.

Rahim, B. E. E., Yusoff, I., Jafri, A. M., Othman, Z., and Abdul Ghani, A. (2012). Application of MIKE SHE modelling system to set up a detailed water balance computation. *Water and Environment Journal*, *26*(4), 490-503.

Refsgaard, J. C. (1997). Parameterisation, calibration and validation of distributed hydrological models. *Journal of Hydrology*, *198*(1-4), 69-97.

Singh, R., Subramanian, K., and Refsgaard, J. C. (1999). Hydrological modelling of a small watershed using MIKE SHE for irrigation planning. *Agricultural Water Management*, *41*(3), 149-166.

Sun, G., Zhang, Z. Q., Zhou, G. Y., & Wei, X. H. (2007). Forest watershed hydrological simulation models: Concepts, use and application problems in China. Beijing Linye Daxue Xuebao *(Journal of Beijing Forestry University)*, *29*(3), 178-184.

Thompson, J. R., Sørenson, H. R., Gavin, H., and Refsgaard, A. (2004). Application of the coupled MIKE SHE/MIKE 11 modelling system to a lowland wet grassland in southeast England. *Journal of Hydrology*, *293*(1-4), 151-179.

Timbadiya, P. V., Patel, P. L., and Porey, P. D. (2014). One-dimensional hydrodynamic modelling of flooding and stage hydrographs in the lower Tapi River in India. *Current Science*, 708-716.

Vora, A., Sharma, P. J., Loliyana, V. D., Patel, P. L., and Timbadiya, P. V. (2018). Assessment and prioritization of flood protection levees along the lower Tapi River, India. *Natural Hazards Review*, *19*(4), 05018009.

Zhang, Z., Wang, S., Sun, G., McNulty, S. G., Zhang, H., Li, J., ... & Strauss, P. (2008). Evaluation of the MIKE SHE model for application in the Loess Plateau, China 1. JAWRA *Journal of the American Water Resources Association*, *44*(5), 1108-1120.

Zhang, Zhiqiang, Shengping Wang, Ge Sun, Steven G. McNulty, Huayong Zhang, Jianlao Li, Manliang Zhang, Eduard Klaghofer, and Peter Strauss. "Evaluation of the MIKE SHE model for application in the Loess Plateau, China 1." *JAWRA Journal of the American Water Resources Association* 44, no. *5* (2008): 1108-1120.

*IN PROCEEDINGS OF 25th HYDRO 2020, INTERNATIONAL CONFERENCE, NATIONAL INSTITUTE OF TECHNOLOGY ROURKELA, ODISHA, INDIA 26-28, March 2021, ISBN 978-93-90631-56-8*

Paper ID - 212

# IDENTIFICATION OF HYDROLOGICALLY EFFICIENT REGIONS IN SEMI-ARID YERLI SUB-CATCHMENT OF UPPER TAPI BASIN, INDIA.

Lalit Kumar Gehlot[1], P. L. Patel[2] and P. V. Timbadiya[3]

[1]*Research Scholar, Department of Civil Engineering, Sardar Vallabhbhai National Institute of Technology Surat, Surat - 395007, India.*
[2]*Professor, Department of Civil Engineering, Sardar Vallabhbhai National Institute of Technology Surat, Surat - 395007, India. (Corresponding Author)*
[3]*Associate Professor, Department of Civil Engineering, Sardar Vallabhbhai National Institute of Technology Surat, Surat - 395007, India.*
*Email: gehlot.lalit1994@gmail.com; plpatel@ced.svnit.ac.in; pvtimbadiya@ced.svnit.ac.in*

## Abstract

The spatial variations in the topography, land use and land cover (LULC), soil and climatic factors lead to spatial variability in the hydrological attributes. The regions of the catchment having high potential for hydroclimatic variables, i.e., rainfall, ground water recharge, surface runoff generation, baseflow, soil water content, water yield etc., and low potential for major loss, i.e., evapotranspiration, are identified as hydrologically efficient regions. In present study, Soil Water Assessment Tool (SWAT) has been used to simulate the hydrological variables for a semi-arid Yerli sub-catchment of Upper Tapi basin in India for period 1990-2013. The SWAT hydrologic model was developed using 30m SRTM DEM, LULC, derived from LISS-III satellite image, Global FAO-soil database, station-based observed weather data. The parametric global sensitivity analysis was carried out using Sequential Uncertainty Fitting (SUFI-2) and it has been observed that the monthly streamflow is more sensitive towards the ground water related processes, channelization of the generated overland flow and land management parameters in the sub-basins. The single site calibration (at Yerli station; period 1990-2005) and multisite validation (at Yerli and Gopalkheda stations; period 2006-2013) signify 'good' reliability of the model performance, indicated by the statistical parameters, i.e., ($R^2$> 0.73), (NSE > 0.68) and (PBIAS < ±15%). The principal component analysis of the space v/s representative/simulated hydrological variables resulted into three statistically significant principal components (PC) with explained variance of more than 85%. Using the combined ranking of the rotated PCs, 20 watersheds (out of 55), having more than 50% share of the study area, have been identified as the hydrologically efficient regions in the sub-catchment. The identified hydrologically efficient and inefficient regions would be useful in employing better water resources and agriculture management practices in the sub-catchment.

***Keywords:*** *Hydrologic modeling; Principal Component Analysis (PCA); SWAT; SUFI-2; Sensitivity and Uncertainty analysis.*

## 1. Introduction

The rapid industrial and population growth demands more fresh water resources and more alterations in the land management system. In addition to these, the climate change and variability have an edge in increasing water stress threats, particularly during summer season. The water resources planning and management may critically be optimized with understanding of spatio-temporal variability of various hydrologic processes. One cannot manage what one cannot measure (Eslamian et al. 2010), thus, measurement of water in hydrological processes is of almost importance, however, it is very costly option (Chiang et al. 2002). The fundamental understanding of hydrology and mathematical advancement permit to model hydrologic processes at regional scale to global scale. Modeling hydrological processes using available gauged data and a suitable hydrologic model enables understanding the watershed behavior. Depending upon the objective, availability of data, computational cost and model complexity, various researchers have used SWAT (Tan et al. 2020), HEC-HMS (Chu and Steinman 2009), MIKE-SHE (Loliyana and Patel 2018), VIC (Lettenmaier et al. 1999) etc. The SWAT model has been extensively used for various water resources related issues across the globe because of its simplicity, less computing efforts and readily available database (Arnold et al. 1998).

Despite the growth, the complexity and uncertainties involved in modeling hydrologic process requires crucial understanding of connections between the actual system and the mathematical formulations. These hydrological processes, being a part of global/region hydrological cycle, exhibits very high correlation among them. Such multivariate correlation issues are frequently encountered in hydroclimatic studies. The Principal Component Analysis (PCA) has been used to deal with multivariate correlation and multidimensional issues to get simplified representation of the complex problems. The PCA is used for hydrologic regionalization of watersheds (Chiang et al. 2002), hydrologic impact of dam (Matteau et al. 2009), hydrological classification of natural flow regimes (Belmar et al. 2011), clustering of geomorphic parameters into different components based on their physical significance (Sharma et al. 2015), multivariate sensitivity analysis (Xiao et al. 2017), climate change assessment (Tadić et al. 2019) etc. The present study proposes another application of PCA to identify the hydrologically efficient regions based on the strength/potential of the simulated hydrological variables using SWAT. The identification of such regions, particularly, in an agrarian based semi-arid basin will help planning sustainable utilization of the available water resources and efficient management for agricultural practices.

## 2. Material and Methods

### 2.1 *Study area and data sources*

The Tapi River is the sixth largest river of Peninsular India and second largest westward flowing river, originating at an elevation of 752 m near Multai, Betul, Madhya Pradesh and draining into the Arabian Sea. The Tapi river has total length of 724 km and drains area of 65,145 km$^2$ from West Central India. The Tapi basin has been divided into three sub-basins, viz. Upper Tapi (UTB), Middle Tapi (MTB) and Lower Tapi (LTB) basins. The major tributaries of the Tapi River are Purna (≈ 379 km) and Girna (≈ 346 km) Rivers, draining corresponding area of 18,490 km$^2$ and 10,061 km$^2$ respectively. The Purna sub-catchment, part of UTB, is situated between the Gwaligarh hills in north, the Ajanta and Satmala ranges in south, and the Mahadeo hills in east. The hydrological model developed in the present study is up to Yerli stream gauging site (see Fig. 1), which is attributed as Yerli sub-catchment here after. The index map of Yerli sub-catchment, digital elevation model (DEM) and location of rain gauge stations, weather stations and stream gauging stations are shown in Fig. 1. The major soil type in the study region is gently to very gently sloping deep loamy to clayey and nearly level to gently sloping deep black soils. The Yerli sub-catchment, from geological point of view, comprises of predominately impermeable and very poorly permeable Deccan basalts and permeable quaternary alluvial deposits.

The development of hydrological model requires topographical, land use and land cover (LULC), soil and hydroclimatic data etc. In present study, rainfall data of 15 rain gauges; temperature, wind speed and relative humidity data of four weather stations; and observed discharge data of three stream gauging stations have been used and their sources are enlisted in Table 1. The observed discharge data at Yerli has been used for calibration and validation of the model at monthly time step. The average annual rainfall in the Yerli sub-catchments and streamflow depth observed at the Yerli stream gauging station, during the period under consideration, has varied from 541.3 mm to 1168.3 mm while the streamflow depth ranges from 13.6 mm to 296.4 mm with their respective mean values of 827.2 mm and 110.3 mm. The average ratio of the streamflow depth to rainfall depth in the Yerli sub-catchment has been found to be 0.133.

### 2.2 *Methodology*

The availability of in-situ measured data of various hydroclimatic variables have been a challenging task, particularly in developing countries. The availability of these data help decision makers in planning sustainable use of the water resources potential. However, with availability of limited set of hydroclimatic variables, hydrologic model may be used to simulate the other key variables with fair degree of confidence. The degree of accuracy of these simulated variables primarily depends upon the

accuracy of the input data used, model structure and its capabilities. The present study undertakes the development of a hydrological model, Soil Water Assessment Tool (SWAT), to estimate other key hydrological variables with the use of available hydroclimatic and streamflow data. The methodology used in the present study is shown in Fig. 2.

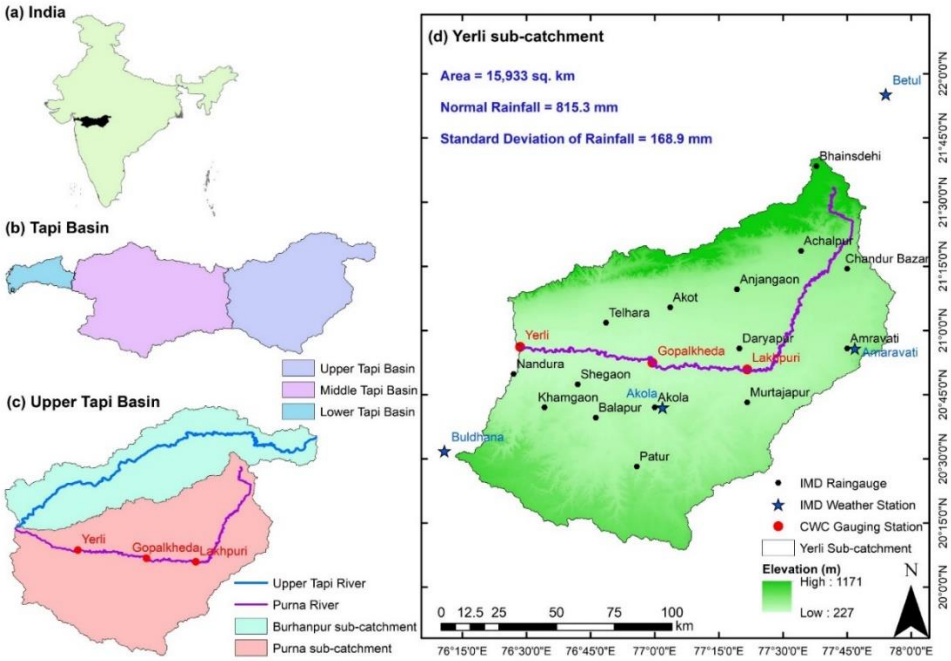



**Figure 1** Index map of Yerli sub-catchment

**Table 1** Data used in present study and their sources

| Data | Frequency/ Resolution | Period of data used | Source |
|---|---|---|---|
| Rainfall<br>Temperature<br>Wind Speed<br>Relative Humidity | Daily (station data) | 1988 - 2013 | India Meteorological Department (IMD), Pune |
| Streamflow | | | Central Water Commission (CWC), Surat Division |
| SRTM DEM | 30 m | 2000 | https://earthexplorer.usgs.gov |
| LULC Map | 23.5 m | 2009 | IRS-P6 LISS-III |
| Soil Map | 5,000 m | - | FAO-UNESCO global soil map http://www.fao.org |

The hydrologic models are widely used across the globe to inculcate the response of catchments, from watershed scale to basin scale, pertaining to varying physiographic and climatic conditions. The SWAT was primarily developed to understand the hydrologic response of the watersheds for different land use and management practices, later, extensively used by researchers to study the behavior of the watershed under different climatic scenarios (Arnold et al. 1998; Tan et al. 2020). The geographic information system (GIS) interface used for the present study is ArcGIS®10.6 and SWAT 2012 has been used for development of rainfall-runoff model. The calibration, parametric sensitivity analysis and overall uncertainty analysis is done using Sequential Uncertainty Fitting (SUFI-2) in SWAT Calibration and Uncertainty Program (SWAT-CUP) (Abbaspour 2013), followed by model validation. The key hydrologic parameters (including simulated variables) such as rainfall, evapotranspiration, ground water recharge, surface runoff, baseflow, soil water content and water yield etc. is simulated using the calibrated and validated SWAT model for each sub-basin. These variables were then processed using

PCA to derive statistically significant Principal Components (PCs). These PCs are used to derive the hydrologically efficient regions in the Yerli sub-catchment.

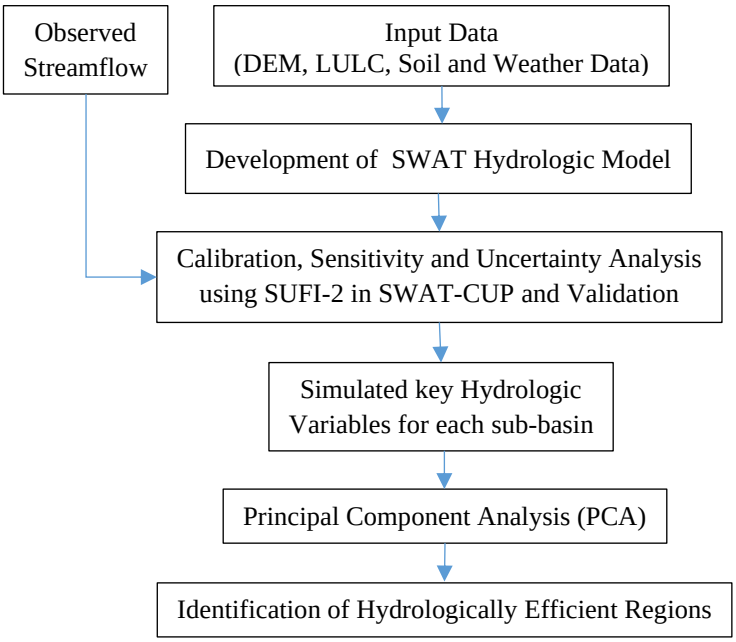



**Figure 2** Methodology used in the present study

## 2.3 *Development of SWAT model*

The quality and prediction accuracy of any hydrological model primarily depends on the quality and the resolution of the input data used for the model preparation. The horizonal and vertical resolution of SRTM DEM use in this study is ± 30 m and ± 16 m respectively. The source of DEM, its resolution and resampling technique used for its development have significant impact on the uncertainty in the simulated flow, erosion and nutrients from the catchments. The stream network threshold required to generate the stream network in the watershed also play significant role in defining the number of sub-watersheds. In the present study, the stream network has been generated using arbitrarily selected threshold value of 200 $km^2$ resulting in to the 55 watersheds in the Yerli sub-catchments (see Fig. 3(b)).

The LULC map of year 2009, Global FAO soil map and three slope classes have been used for the generation of the HRUs (see Fig. 3(c)-(e)). There are seven LULC classes identified, i.e., Deciduous forest (FRSD - 14.8%), Fallow land (AGRR - 7.8%), Scrub land (RNGB - 3.3%), Crop land (AGRL - 69.7%), Urban area (URMD - 0.8%), Rural area (URLD - 0.9%) and water bodies (WATR - 2.8%) (Loliyana and Patel 2018), where the bracketed codes are SWAT reference codes defined in database for various land use type. The soil map of Global FAO-soil database having spatial resolution of 5000 m has been used. The land slope has been classified into three classes, viz., 0 – 3%, 3 – 15% and more than 15% with their total percentage of 54.83%, 35.99% and 9.9% respectively of the areas of the basin. A HRU is a unique combination of the land use, soil, slope and management practices in a watershed. The hydrologic responses derived from these small-small HRUs are integrated by SWAT to predict the outflow and sediment yield at the catchment outlet(s). The percentage threshold values used for defining multiple HRU's are 5%/ 10%/ 10% respectively for land use/soil/ slope resulted into 409 no(s). of HRUs in the catchment.

Apart from the physiographic data, hydroclimatic data such as precipitation, temperature, wind speed, solar radiation and relative humidity are also required to generate the response of the catchment against these variables. Since the density of the rain gauge stations in the catchment is quite good as compared

to weather stations, the missing values in the observed rainfall were filled using Inverse Distance Weighing (IDW) method while the gaps in the observed daily weather data were replaced with -99.0. The SWAT model during calibration will replace those missing values using the simulated values of climate model with the help of weather generator inputs provided. The present study incorporates the use of readily available weather generator database developed from IMD daily gridded data of 85 years at spatial resolution of 1° × 1° (accessible on https://swat.tamu.edu/software/india-dataset).

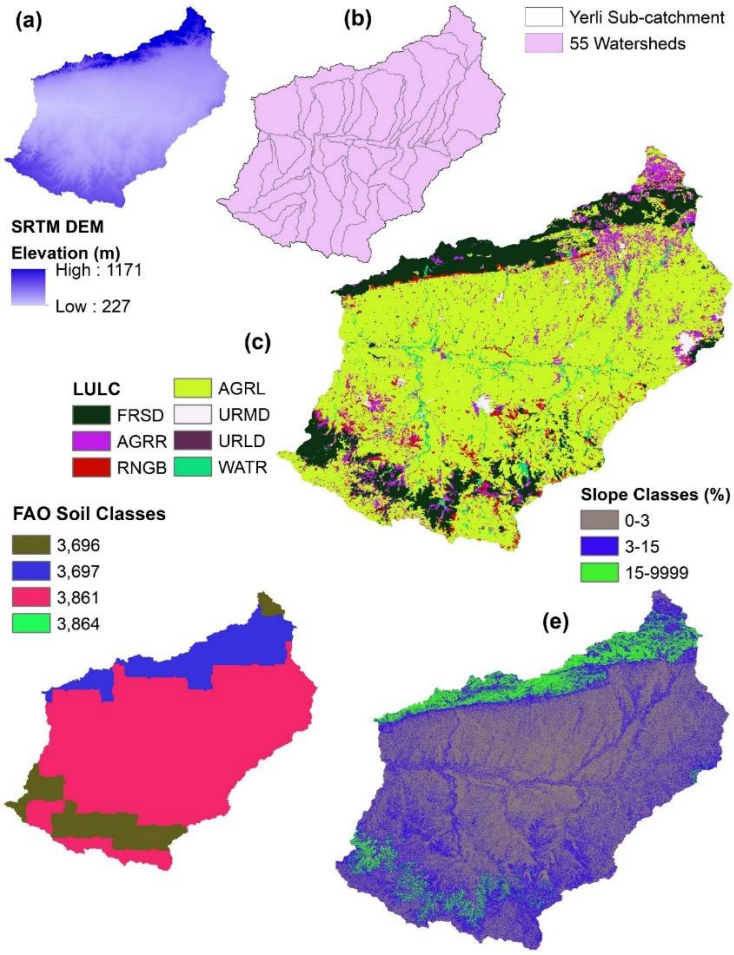



**Figure 3** SWAT Model inputs (a) SRTM DEM, (b) Delineated watersheds (55 Nos.), (c) Land use land cover (year 2009), (d) Global FAO-Soil, (e) Land slope classification.

The calibration and validation periods of the continuous hydrological models must be such that both the periods include wet years, normal years and dry years. Also, the statistical parameters calculated for both the periods must not have large scale deviations among them. The developed model in the present study has been calibrated and validated for the period 1990 – 2005 and 2006 – 2013 respectively such that both the periods includes high as well as low rainfall years. The simulated streamflow has been initially checked using coefficient of determination ($R^2$), wherein, $R^2 < 0.5$ indicates that the developed model needs to be re-evaluated. During calibration due care has to be taken that the model does not violet the water balance and the absolute physical ranges of the parameters used for the calibration.

## 2.4 *Principal component analysis (PCA)*

The variables associated with hydrological cycle have profound correlation among them. It necessarily states that a significant portion of information/variance is common among these variables. The PCA is

a multivariate statistical method, popularly used for dealing multicollinearity and curse of dimensionality, which orthogonally transforms original variables, using their correlation/covariance matrix, into principal components (PCs) (Wilks 2011). These PCs are linear combinations of all the original variables such that the first PC describes maximum variance and is independent to remaining PCs. For *n* variables, PCA results into *n* PCs with *n* Eigenvalues and *n*×*n* Eigenvector (also termed as loading). The Eigenvalues and Eigenvector represent the variance explained by each PC and corresponding weights to original variables respectively. The PCs with their Eigenvalue greater than 0.7 are considered statistically significant (Jolliffe 1972) and remaining PCs may be eliminated from further analysis. The statistically significant PCs may be rotated, preferably using varimax rotation method, to get the simplified loading structure (Wilks 2011).

## 3. Results and Discussions

### 3.1 *Model performance evaluation*

The hydrologic models consist large number of parameters which make modeling very complex. The parametric sensitivity analysis helps selection of key parameters primarily affecting the targeted hydrologic process(es). The sensitive parameters are one which considerably change the output/objective function with minor change in their input values. Another complexity in dealing with hydrologic models is the uncertainty in the simulated hydrologic variables. It is primarily a function of uncertainty in the model spatial inputs, model structure, weather parameters and observed target variables. The initial set of parameters, identified based on the literature and previous studies, for the calibration of the model are shown in Table 2. The sensitivity analysis of the tabulated parameters was performed using global sensitivity analysis. These parameters were varied within the defined range to assess the sensitivity of their relative change on the objective function and also the uncertainty in the model prediction. The parameters which were found non sensitive, for particular objective function, were fitted to their best estimated values and were removed from the next iteration. The best estimation range, fitted values, probability values and rank of sensitivity are shown in Table 2. The objective function plays a critical role in sensitivity analysis as well as the performance of the model, however, uncertainty in the predicted model is independent of the objective function defined.

**Table 2** Calibrated model parameter values, calibrated range and sensitivity rank

| Parameter | Fitted Value | Range | p-value | Rank |
|---|---|---|---|---|
| *V__CN2.mgt__FRSD* | 55.118 | 52.29 - 62.41 | 0.265 | 13 |
| ***V__CN2.mgt__AGRL*** | 64.474 | 58.28 - 67.22 | 0.000 | 6 |
| *V__CN2.mgt__AGRR* | 83.327 | 73.24 - 84.77 | 0.191 | 11 |
| *V__CN2.mgt__RNGB* | 61.701 | 58.55 - 67.21 | 0.974 | 27 |
| *V__CN2.mgt__URMD* | 86.185 | 84.71 - 89.03 | 0.158 | 9 |
| *R__SOL_AWC(1).sol__FRSD* | 1.166 | 0.98 - 1.48 | 0.906 | 26 |
| *R__SOL_AWC(1).sol__AGRL,AGRR, RNGB* | 1.078 | 1.01 - 1.39 | 0.311 | 16 |
| *R__SOL_K(1).sol* | 0.329 | 0.19 - 0.34 | 0.707 | 22 |
| *R__SOL_BD(1).sol* | -0.418 | -0.79 - -0.3 | 0.273 | 14 |
| ***V__ALPHA_BF.gw*** | 0.906 | 0 - 1 | 0.000 | 1 |
| ***V__GW_DELAY.gw*** | 5.054 | 0 - 38.57 | 0.000 | 4 |
| ***V__REVAPMN.gw*** | 417.702 | 0 - 459.79 | 0.000 | 5 |
| *V__ESCO.hru* | 0.284 | 0.23 - 0.32 | 0.710 | 23 |
| *V__EPCO.hru* | 0.576 | 0.49 - 0.59 | 0.282 | 15 |
| ***V__GWQMN.gw*** | 527.473 | 308.69 - 871.9 | 0.000 | 3 |
| *V__CH_COV2.rte* | 0.424 | 0.41 - 0.44 | 0.422 | 18 |
| *V__LAT_TTIME.hru* | 19.598 | 18.39 - 24.49 | 0.472 | 19 |
| *V__RCHRG_DP.gw* | 0.135 | 0.06 - 0.17 | 0.134 | 8 |
| *V__CANMX.hru__FRSD* | 85.149 | 39.24 - 97.73 | 0.838 | 24 |
| *V__CANMX.hru__AGRL* | 7.165 | 4.69 - 45.11 | 0.567 | 20 |
| *V__CANMX.hru__AGRR* | 19.313 | 2.98 - 55.68 | 0.197 | 12 |

| Parameter | Fitted Value | Range | p-value | Rank |
|---|---|---|---|---|
| *V__CANMX.hru__ANGB* | 80.893 | 30.68 - 92.05 | 0.166 | 10 |
| *R__OV_N.hru__AGRL* | -0.656 | -0.7 - -0.61 | 0.313 | 17 |
| *R__HRU_SLP.hru* | -0.511 | -0.65 - -0.42 | 0.578 | 21 |
| *R__CH_S2.rte* | -0.425 | -0.46 - 0.01 | 0.841 | 25 |
| ***R__CH_N1.sub*** | -0.273 | -0.35 - 0.11 | 0.012 | 7 |
| ***V__CH_K1.sub*** | 152.929 | 44.99 - 315.01 | 0.000 | 2 |
| *R__SOL_AWC(1).sol__URMD** | 0.624 | - | - | - |
| *R__SOL_AWC(1).sol__WATR** | -0.209 | - | - | - |
| *V__SURLAG.bsn** | 25.827 | - | - | - |
| *V__CH_N2.rte** | 0.067 | - | - | - |
| *V__CH_COV1.rte** | 0.460 | - | - | - |
| *R__LAI_INIT.mgt** | 0.042 | - | - | - |
| *R__OV_N.hru__FRSD** | 0.903 | - | - | - |
| *R__OV_N.hru__AGRR, RNGB** | 0.017 | - | - | - |
| *R__OV_N.hru__URMD** | -1.236 | - | - | - |

***Bold** faces represent the parameters sensitive at 5% level of significance.*
** indicates the parameters were fitted to the best estimates of previous iteration and were removed in the successive iteration.*

There are seven most sensitive parameters identified corresponding to the RSR objective function are *V__ALPHA_BF.gw*, *V__CH_K1.sub*, *V__GWQMN.gw*, *V__GW_DELAY.gw*, *V__REVAPMN.gw*, *V__CN2.mgt__AGRL* and *R__CH_N1.sub*. It can be observed form the Table 2 that *CN2* being the most sensitive parameter is found to be insensitive due to parameterization except in case of AGRL where it covers nearly 69.7% of the area of the basin. Also, it can be seen that the most of the sensitive parameters are related to the ground water (*.gw*) related processes, two are related to the sub-basin (*.sub*) channelization of the flow and one is related to the curve number (*.mgt*). The CN2 values indicates the runoff potential of the soil and the higher values are obtained for the urban areas, fallow land while least value is obtained for the deciduous forest land. The uncertainty assessment has been carried out in the present study using SUFI-2 which estimates P-factor and R-factors. The ideal calibration is the one which encapsulates the maximum observed values at minimum uncertainty band thickness. The ideal values of the P-factor and R-factor are 1 and 0 respectively. The P-factor and R-factor values obtained during calibration and validation period in the present study are 0.61 and 0.86; and 0.38 and 1.02 respectively.

The streamflow at Yerli station for monthly scale has been calibrated and the performance evaluation has been carried out at all three gauging stations, i.e., multisite validation with the help $R^2$, *NSE*, *PBIAS*, *MNS*, *RSR* and *RMSE* (see Table 3). The values of the performance indices $R^2$, *NSE* and *PBIAS* during the calibration period at Yerli are well within the range defined for a model to be very good (Moriasi et al. 2015). Along with the aforesaid indices, *MNS* (calculated using power 1, indicates sensitivity to the low flows) values are also greater than the 0.70 (0.55) during calibration (validation) indicating good (satisfactory) simulation of the low flow values. The *RSR* values during the calibration and validation were well below 0.5, indicating very good simulation of the peak flows and also the *RMSE* in the model in the prediction were well below the mean and standard deviation of the observed data. The performance of the model during validation process is also found to be very good for the monthly time scale. The simulated and observed flow hydrograph shows that the peaks during the calibration period were fairly simulated and concurrent with respect to the monthly rainfall (see Fig. 4). The high $R^2$ values indicates that the occurrence of the peak flow during observed and simulated are not having lag time among them. The probable reason behind over estimation of the peak flows during validation period can be the high mean and standard deviation of the annual mean rainfall, i.e., the wet years are more during validation period as compared to calibration period. The systematic over and underprediction of the flow during validation period can be one of the reasons behind the good $R^2$ values. The overestimated low flows show the inability to simulated the zero flows present in the observed data while the overestimated high flows are (prominently present during the validation period) due to the dominance of the wet regime during the validation period.

**Table 3:** Performance evaluation of model

| Performance Indicators | Calibration Period (1990 – 2005) | | | Validation Period (2006 – 2013) | |
|---|---|---|---|---|---|
| | ***Yerli*** | ***Gopalkheda*** | ***Lakhpuri**** | ***Yerli*** | ***Gopalkheda*** |
| $R^2$ | 0.89 | 0.73 | 0.84 | 0.90 | 0.87 |
| *NSE* | 0.89 | 0.68 | 0.83 | 0.86 | 0.84 |
| *RSR* | 0.33 | 0.56 | 0.40 | 0.37 | 0.39 |
| *MNS* | 0.71 | 0.55 | 0.66 | 0.68 | 0.69 |
| *PBIAS (%)* | 4.13 | 1.96 | 14.44 | -14.09 | -12.74 |
| *MAE ($m^3/s$)* | 20.69 | 15.44 | 6.85 | 28.86 | 19.11 |
| *RMSE ($m^3/s$)* | 41.01 | 33.88 | 13.91 | 51.13 | 38.46 |

** Data was available up to May, 2005.*

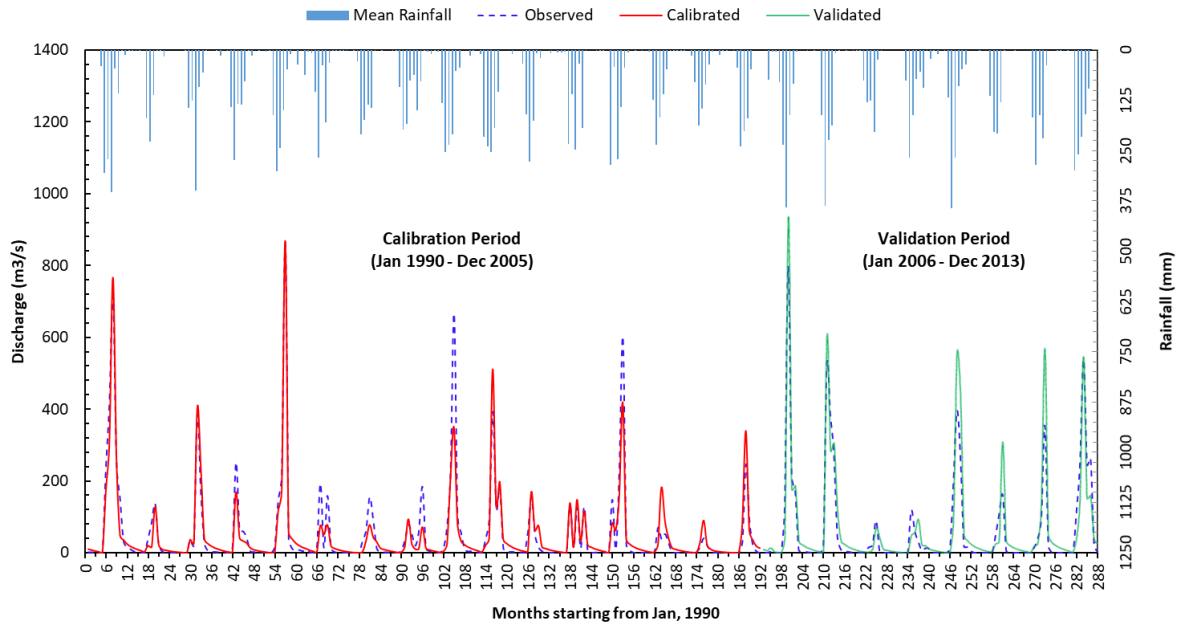



**Figure 4** Monthly observed and simulated discharge during calibration and validation period at Yerli

## 3.2 *Identification of hydrologically efficient regions*

The hydrologically efficient regions may be identified as the regions/watersheds of the basin/catchment having high potential for hydroclimatic variables, i.e., rainfall, ground water recharge, surface runoff generation, baseflow, soil water content, water yield etc., and low potential for major loss, i.e., evapotranspiration etc. The potential of the aforesaid variables may be considered to be the long-term average of in-situ measurements. In absence of the in-situ measurements, the simulated average values of these hydrological variables, from calibrated and validated SWAT model, for each watershed are considered. It is to be noted that these variables exhibit very high correlation among them, thus, their absolute values may be misleading due to significant duplication of information. However, the independent component (PCs) derived using PCA lead to true interpretation of their correlation/information structure. Three statistically significant PCs, identified based on Jolliffe (1972) criteria, with their rotated loading structure are shown in Table 4. The PC1 comprises precipitation, groundwater recharge, groundwater revap, baseflow and surface runoff as these variables are found to exhibit profound correlation (at 1% level of significance). The soil water content and water yield in the watersheds are grouped under PC3. These two PCs are very favorable for the agriculture dominated semi-arid Yerli (Purna) sub-catchment, thus, considered as PCs with positive effect. On other hand, PC2 comprising of evapotranspiration as major variable which withdraws water from an agrarian system as major loss. Therefore, the effects produced on the system by PC2 are considered negative.

**Table 4** Rotated loading values used for principal components

| Hydrologic variables | PC1 | PC2 | PC3 | Communality |
|---|---|---|---|---|
| *Precipitation* | **0.978** | 0.027 | -0.094 | 0.967 |
| *Evapotranspiration* | -0.030 | **0.956** | 0.037 | 0.915 |
| *Soil water content* | 0.365 | -0.390 | **-0.764** | 0.869 |
| *Groundwater Recharge* | **0.935** | -0.238 | -0.048 | 0.933 |
| *Groundwater Revap* | **0.875** | -0.304 | -0.086 | 0.865 |
| *Baseflow* | **0.841** | -0.088 | -0.013 | 0.716 |
| *Water yield* | 0.416 | -0.430 | **0.709** | 0.860 |
| *Surface runoff* | **0.811** | 0.053 | 0.173 | 0.690 |
| % variance explained (Total = 85.19) | 53.36 | 17.63 | 14.19 | |

The absolute loading values greater than 0.70 are considered significant and marked **bold** faced

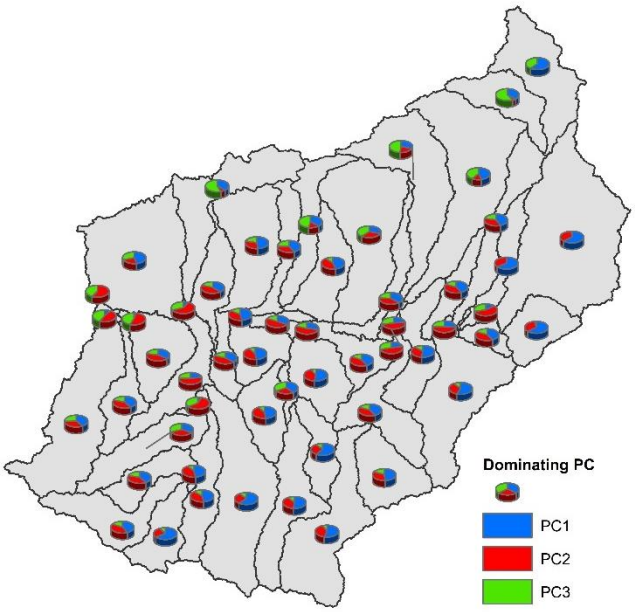



**Figure 5** Dominating principal components across 55 watersheds in Yerli sub-catchment

The spatial values of all three PCs are normalized between 0 to 1, where 0 representing the least dominance while 1 represent the prominent effect of the PC in that watershed. The dominating PCs, represented as a fraction, across 55 watersheds of Yerli sub-catchment are shown in Figure 5. It can be seen that the watershed lying on the foothills of Gwaligarh, Mahadeo and Ajanta and Satmala hill ranges are characterized by the dominating nature of PC1 and PC3, thereby indicating these watersheds have good potential for development of agricultural activities. The PC2 can be seen to have an edge over the other two PCs, especially, in middle portion of the Yerli sub-catchment. Based on the combined normalized values/ranking of the PCs, 20 major watersheds (out of 55), sharing more than 50% of the total area of the Yerli sub-catchment, can be identified as hydrologically efficient regions. The outcomes of the present study enable identification regions having good potential available for sustainable planning and management of agricultural activities, particularly in semi-arid region.

## 4. Conclusions

The key conclusion derived from the present study are as follows:

i. The SWAT model developed, calibrated and validated using SUFI-2 in SWAT-CUP, to simulate the key hydrological variables. The single site calibration and multisite validation signify 'good' reliability of the model performance, indicated by the statistical parameters, i.e., ($R^2$: 0.73-0.90), (NSE: 0.68-0.89) and (PBIAS %: ±1.96-14.44). The present study does not take into account

multisite and multivariable calibration and validation of hydrologic model. It may be considered as the limitation of the present study.

ii. The parametric global sensitivity analysis states the monthly streamflow is more sensitive towards the ground water related processes, channelization of the overland flow and land management.

iii. The study presents the application of Principal Component Analysis in identification of hydrologically efficient regions with the help of hydrological variables and 20 watersheds (out of 55), sharing more than 50% area of the Yerli sub-catchment, are identified as hydrologically efficient regions. The outcomes of the present study enable identification regions having good potential available for sustainable planning and management of agricultural activities, particularly in semi-arid region.

## Acknowledgement

The authors would like to acknowledge the Indian National Committee on Climate Change, Ministry of Jal Shakti, Department of Water Resources, River Development & Ganga Rejuvenation, Government of India (GoI) for providing funding for this research. The authors would also appreciate the infrastructural support provided by Centre of Excellence on 'Water Resources and Flood Management', TEQIP-II, Ministry of Education, GoI. All data disseminating agencies, i.e., India Meteorological Department, Pune, Central Water Commission, Surat Division and National Remote Sensing Centre, Hyderabad are duly acknowledged.

## References

Abbaspour, K. C. (2013). *SWAT-CUP 2012: SWAT calibration and uncertainty program—A user manual*. Dübendorf Switzerland: Eawag, Swiss Federal Institute of Aquatic Science and Technology

Arnold, J. G., Srinivasan, R., Muttiah, R. S., and Williams, J. R. (1998). Large area hydrologic modeling and assessment part I: model development 1. *JAWRA Journal of the American Water Resources Association*, *34*(1), 73-89.

Belmar, O., Velasco, J., and Martinez-Capel, F. (2011). Hydrological classification of natural flow regimes to support environmental flow assessments in intensively regulated Mediterranean rivers, Segura River Basin (Spain). *Environmental Management*, *47*(5), 992.

Chiang, S. M., Tsay, T. K., and Nix, S. J. (2002). Hydrologic regionalization of watersheds. I: Methodology development. *Journal of Water Resources Planning and Management*, *128*(1), 3-11.

Chu, X., and Steinman, A. (2009). Event and continuous hydrologic modeling with HEC-HMS. *Journal of Irrigation and Drainage Engineering*, 135(1), 119-124.

Eslamian, S., Ghasemizadeh, M., Biabanaki, M., and Talebizadeh, M. (2010). A principal component regression method for estimating low flow index. *Water Resources Management*, *24*(11), 2553-2566.

https://swat.tamu.edu/software/india-dataset accessed on April 02, 2019.

Jolliffe, I. T. (1972). Discarding variables in a principal component analysis. I: Artificial data. *Journal of the Royal Statistical Society: Series C (Applied Statistics)*, *21*(2), 160-173.

Lettenmaier, D. P., Wood, A. W., Palmer, R. N., Wood, E. F., and Stakhiv, E. Z. (1999). Water resources implications of global warming: A US regional perspective. *Climatic Change*, *43*(3), 537-579.

Loliyana, V. D., and Patel, P. L. (2018). Performance evaluation and parameters sensitivity of a distributed hydrological model for a semi-arid catchment in India. *Journal of Earth System Science*, 127(8), 117.

Matteau, M., Assani, A. A., and Mesfioui, M. (2009). Application of multivariate statistical analysis methods to the dam hydrologic impact studies. *Journal of hydrology*, *371*(1-4), 120-128.

Moriasi, D. N., Gitau, M. W., Pai, N., and Daggupati, P. (2015). Hydrologic and water quality models: Performance measures and evaluation criteria. *Transactions of the ASABE*, *58*(6), 1763-1785.

Sharma, S. K., Gajbhiye, S., and Tignath, S. (2015). Application of principal component analysis in grouping geomorphic parameters of a watershed for hydrological modeling. *Applied Water Science*, *5*(1), 89-96.

Tadić, L., Bonacci, O. and Brleković, T. An example of principal component analysis application on climate change assessment. *Theor Appl Climatol* 138, 1049–1062 (2019).

Tan, M. L., Gassman, P., Yang, X., and Haywood, J. (2020). A review of SWAT applications, performance and future needs for simulation of hydro-climatic extremes. *Advances in Water Resources*, 103662.

Wilks, D. S. (2011). *Statistical methods in the atmospheric sciences* (Vol. 100). Academic press.

Xiao, S., Lu, Z., and Xu, L. (2017). Multivariate sensitivity analysis based on the direction of eigen space through principal component analysis. *Reliability Engineering and System Safety*, *165*, 1-10.

*IN PROCEEDINGS OF 25th HYDRO 2020, INTERNATIONAL CONFERENCE, NATIONAL INSTITUTE OF TECHNOLOGY ROURKELA, ODISHA, INDIA 26-28, March 2021, ISBN 978-93-90631-56-8*

Paper ID - 224

# Activation of central channel in river Kosi, Bihar

Arun Kumar[1], Dr. R. G. Patil[2]

[1]*Scientist 'B', Central Water and Power Research Station, Pune – 411024, India*
[2] *Scientist 'E', Central Water and Power Research Station, Pune – 411024, India*
*Email: ak_cwprs@yahoo.co.in, rsrgp@rediffmail.com.*
*Telephone/Mobile No.: +91 9921667369, +919421051534*

## Abstract

Kosi river carries large amount of sediments which get deposited in the internal delta portion of Nepal and Bihar resulting in formation of braided river. The river keeps changing its course inside the restricted manmade embankments. It has shown greater affinity to flow along the line connecting the noses of spurs provided to push the flow away from the embankments. As the river is dynamic in nature, it poses frequent migration to either bank during passage of each flood. The migration of channels along the existing spurs and embankments causes concern to the engineers and danger of breaching of the embankments. Since, the embankments are composed of only consolidated soil without protection to its slope and other protective measures such as geofabric filter, launching apron, etc., at most of the reaches, there is a possibility of erosion of embankment, if left without managing such flow conditions. However, due to the presence of intermittent spurs, the attack over the embankment is restricted. The spurs being almost perpendicular to the embankments are helpful in managing flow conditions that are parallel to the embankment. But due to the formation of braded channels, there are formations of channels that tend to flow at critical angles towards the embankment bypassing the effect of spurs. During the floods of 2016, a channel developed which was directed towards the eastern Kosi embankment just upstream of Prakashpur in between spur at 27.88 km to 24.78 km upstream of Kosi barrage in Nepal portion. This caused major damage in the form of erosion to the nose and shanks of the nearby spurs. To train the river in order to minimize the attack on the said reach, studies were conducted in the existing mobile bed physical model at CWPRS to assess the efficacy and sustainability of the proposed channel in front of spurs at 27.88 km to 24.78 km, upstream of Kosi barrage. The project authorities proposed a pilot channel adjacent to the said reach over the shoal for activation thereby reducing the pressure of flow in the channel along the eastern embankment (left bank).

The model studies conducted indicated that proposed pilot channel was not able to absorb large quantity of discharge and was unable to reduce flow intensity in the channel adjacent to the eastern embankment and also will get silted up over the period. Alternatively, a channel on the right side of the said shoal was able to absorb large quantity of flow given some minor modifications. Hence, based on the studies, it was recommended to activate the existing channel on right side of the shoal opposite to the spurs from 27.88 to 25.25 km including streamlining in plan near the mouth, dredging/de-silting at the upstream junction and deepening of channel by about a meter over a length extending about a kilometer along the right side channel. In addition, the activation of right side channel was found to be efficient and sustainable if resistance to flow in the form of porcupine screens were provided in the parallel channel along the eastern embankment in addition to the above modifications. Based on the studies conducted and recommendations made by CWPRS, Pune, the project authorities carried out the river training works. It was seen in the subsequent years that after passage of each flood since 2017, the right channel got activated appreciably and is still trending to activate further. This resulted in gradual reduction of pressure along the eastern embankment near spur at 27.88 km to 24.78 km, upstream of Kosi barrage. The trend was also verified using the satellite imageries.

***Keywords:*** *Kosi river, Eastern Embankment, pilot channel, RCC porcupine, spurs, activation of channel.*

## 1. Introduction

River Kosi rises in the Himalaya and drains the foot hills to the west of Kanchenjunga in Nepal. It has seven tributaries namely, Sun Kosi, Tama or Tamba (copper) Kosi, Dudh Kosi, Indravati, Likhu River, Arun and Tamur. At about 10 km upstream of Barahkshetra in Nepal, Sun Kosi joins with the tributaries Arun and Tamur to be called as the Sapta Kosi. Further downstream, the river flows through a deep gorge across the lesser Himalayan range of Mahabharata Lake in a length of 10 km and exits into the plains near Chatra (Jha D. K. et al. 2013). After flowing for another 58 km, it enters the north Bihar near Bhimnagar. Finally, after flowing about another 260 km, it merges with river

Ganges near Kursela. The river carries large amount of sediments which get deposited in the internal delta portion of Nepal and Bihar resulting in formation of braided river. It has an exceptionally high sediment yield of 0.43 million tonnes/year/km$^2$ which is to be accommodated in a very narrow alluvial plains almost one-fifth of the upland area (Sinha Rajiv, 2009). The river keeps changing its course inside the restricted manmade embankments. It has shown greater affinity to flow along the line connecting the noses of spurs provided to push the flow away from the embankments. Some of the water management experts advocate 'living with flood' concept and some think of dealing with the flood locally and delink the flood problem from the dams (Jha D. K. et al. 2013). Kale V. S. (2008) describes that the August 2008 extreme event was a clear demonstration indicating that flood embankments or levees are only short-term measures and large dams can only control common moderate magnitude floods, but not the extreme ones. Galgali (1986) also emphasized that regular maintenance and constant vigilance are a pre-requisite for preventing breaching of flood embankments and levees. The engineers of the Kosi barrage project are working hard successfully for the last five decades and are undertaking various river training measures to protect the adjoining areas of Kosi flood plain by different river training techniques. However, Kosi being a dynamic river, it is a phenomenal task to tame the river having the naked embankments along most of the reaches. The population around the Kosi are indebted for the successful river management for so many years.

### *1.1 Study reach*

During the floods of 2016, a channel developed which was directed towards the eastern Kosi embankment just upstream of Prakashpur in between spur at 27.88 km to 24.78 km upstream of Kosi barrage in Nepal portion. This caused damage in the form of erosion to the nose and shanks of the nearby spurs. There was a possibility of further damage to left embankment, if left without any measures to tackle it. It needs to be either redirected away from the embankment or intensity has to be reduced or else the embankment has to be provided with protective sustainable armour. After considering these alternatives to train the river in order to minimize the attack on the said reach, the project authorities proposed a pilot channel adjacent to the said reach over the shoal (Figure 1) for activation thereby reducing the pressure of flow in the channel along the eastern embankment (left bank).

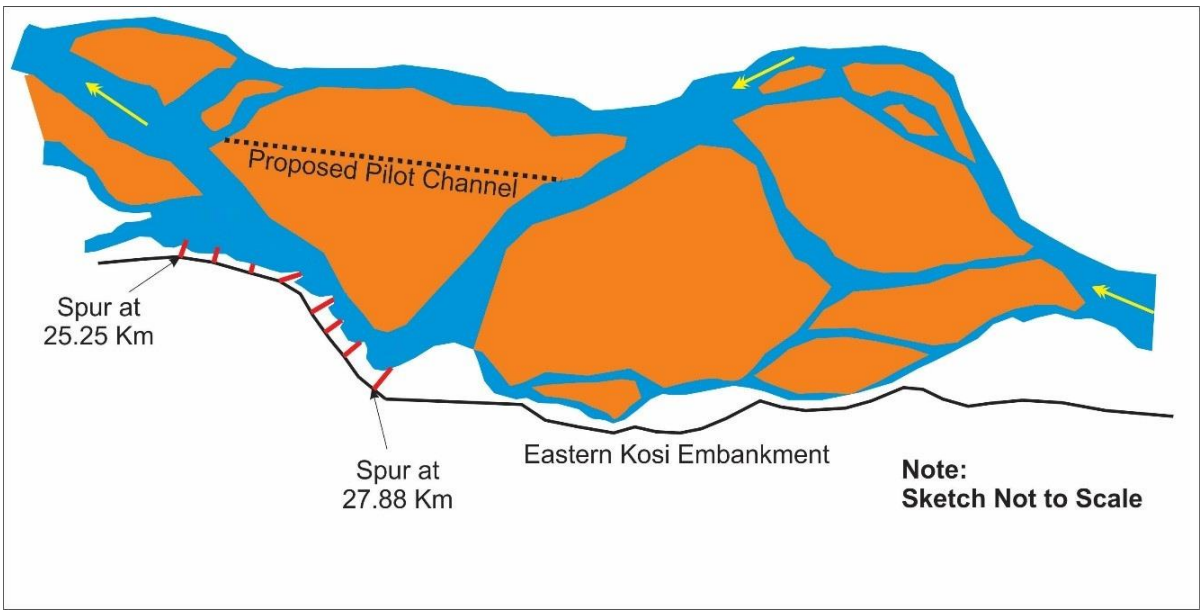



**Figure 1** Index plan showing study reach

To study efficacy and sustainability of the pilot channel proposal of the project authorities in front of spurs at 27.88 km to 24.78 km upstream of Kosi barrage, studies were conducted on the existing mobile bed physical model at CWPRS.

## 2. Model studies

The existing mobile bed model of river Kosi extending from Chatra up to 80 km downstream of Kosi barrage, built to a distorted scale of 1:70 (V) and 1:500 (H) was used to study the existing flow conditions and assess-cum-optimize the activated channel for its sustainability for longer period or any other alternative measures. The bed contours of Kosi River were reproduced in the model after reducing them to the horizontal (1: 500) and vertical (1:70) model scales. The bed sediments of river in the model were simulated using silt having mean size of $d_{50}$ = 0.26 mm. The existing structures across the river such as embankments, afflux bunds, approach bunds, guide banks, barrage, bridge and spurs have been reproduced in the model using cement mortar/wood. A standing wave flume on upstream and a Rehbock weir on downstream of model are provided for discharge measurement and verification. For downstream boundary condition, gauge was maintained at Kosi barrage for the respective discharges as per the gate operation schedules supplied by project authorities. The typical view of the dry model is presented in Photo 1.

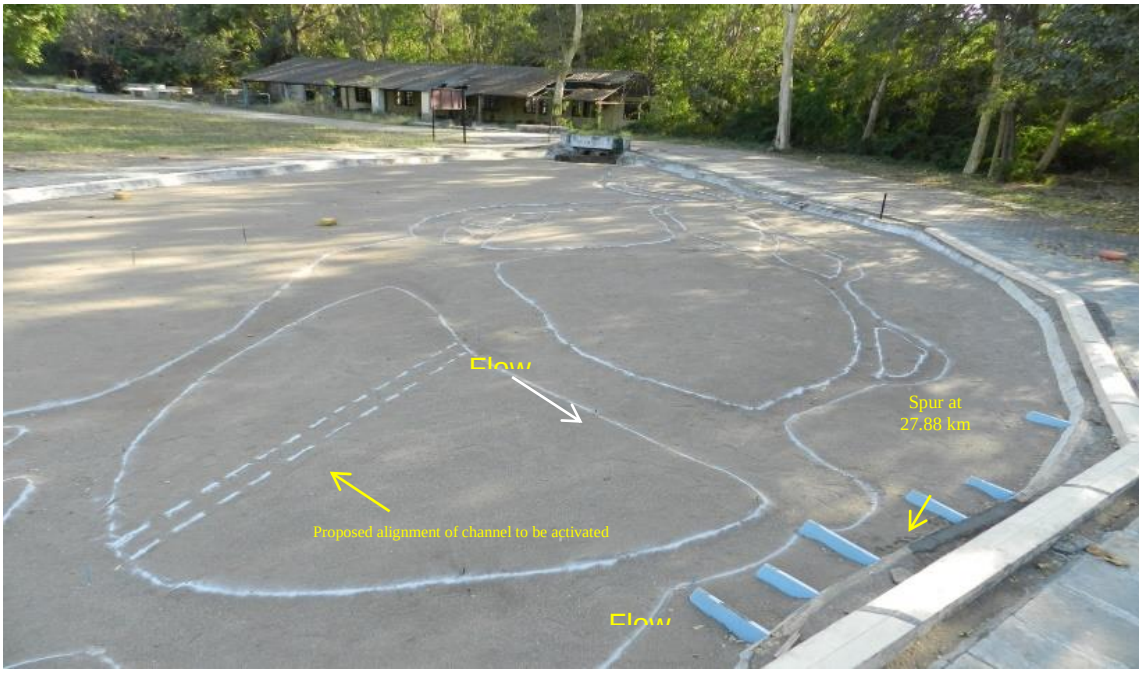



**Photo 1** Dry model showing proposed alignment of channel to be activated.

### 2.1 *Studies with existing condition*

After making arrangements in the model such as laying the prototype geometry by reducing it to model scale, injecting sediment flow at a rate of about 0.25 $m^3$/hr immediately up stream of the steadyreach (to qualitatively simulate the sediment flow conditions), maintaining the barrage pond for theflood discharges, etc., the model was run for two discharges namely 5,663 $m^3$/s and 14158 $m^3$/s which are annual discharge ranges. The flow velocities and water depth along the left bank in deep channel, in front of spur noses starting from spur at 27.88 km to spur at 25.25 km upstream of Kosi barrage were observed. Similarly, velocity and depth at 500 m interval from entry (mouth) to the exit of adjacent right channel along with the entry and exit point of proposed alignment of Pilot channel in deeper portion were also observed. The velocities/depth of flow/discharge intensities were measures in the model using Ott type current meter and depth of flow at the identified locations in the reach under consideration. The experiments on model indicated that the proposed Pilot channel alignment cuts across an existing shoal with average bed levels that did not carry any flow for a river discharge of 5,663 $m^3$/s. During the steady state discharge of 14158 $m^3$/s, the island (shoal) containing the proposed Pilot channel was submerged. However, due to insufficient depth of flow, sheet flow conditions prevailed and hence the depth and velocities along proposed Pilot channel could not be measured. The channel on the left (Eastern embankment side), just downstream of spur at 27.88 km was active. After about two hours of running the model with discharge of 14158 $m^3$/s, the discharge was gradually reduced to 5663 $m^3$/s and further brought to zero discharge. It is seen that a deep scour pockets developed in front of spurs at chainage 27.4 Km, 27.2 Km and 26.88 km indicating these spurs would be under attack during the floods (Photo 2).




**Photo 2** Deep scour pockets near spurs under post model run (Dry condition)

### *2.2 Studies for pilot channel*

The studies were repeated similar to the one conducted for existing condition after simulating Pilot Channel by modifying the bed as per the details given by the project authorities. The flow conditions observed in the model indicated that the Pilot Channel got activated at a slower pace as compared to the other existing natural channels on left and right side. Over a period of time during the model simulation, it was noticed that the mouth of the Pilot channel got silted up, resulting in slack flow through the Pilot channel. However, it was also seen that the channel got widened due to erosion of the banks and the sediments got settled in the deeper portion along the channel thereby aggrading the bed of the Pilot channel. Marginal reductions in the velocity along the eastern embankment side channel as well as marginal increase in velocity along right side channel of the proposed Pilot channel were noticed. During the steady state discharge of 14158 $m^3/s$, the discharge through the proposed Pilot channel significantly increased and the flow width increased as the time progressed indicating activation of this channel. However, the velocity/intensity of flow in the left channel (along the eastern embankment side) increased. This is mainly attributed to the induced attraction of flow towards the Pilot channel which resulted in further flow diversion to the existing channel on left side. Over the period of time, with the adjustment in flow cross section as a result of the deposition of sediments, the Pilot channel had reduced depth of flow and increased channel width. The deposition of silt was also noticed near the mouth of the right channel near inner left bank. Photo 3 and 4 shows the generalized flow patterns in the reach under consideration for a discharge of 5663 $m^3/s$ and 14158 $m^3/s$ after activation of the Pilot Channel.

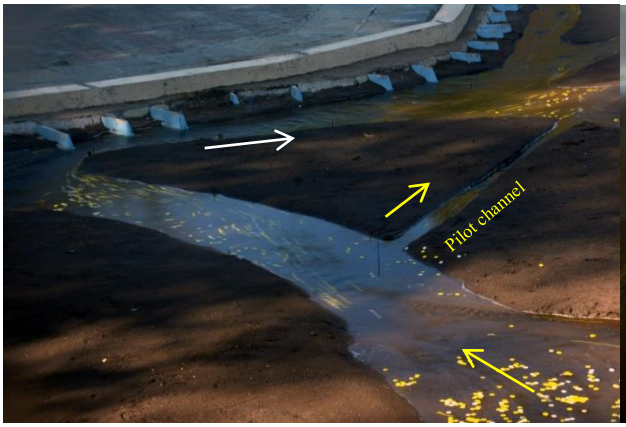



**Photo 3** Generalized flow pattern in the vicinity of proposed Pilot channel for discharge of 5663 $m^3/s$ with activation of Pilot channel.

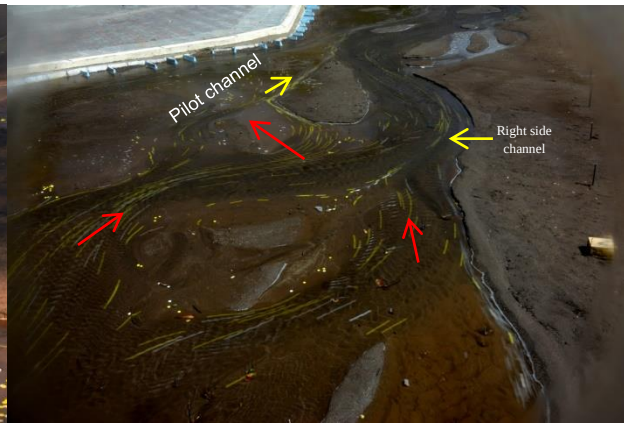



**Photo 4** Generalized flow patter in the vicinity of proposed Pilot channel for discharge of 14,158 $m^3/s$ with activation of Pilot channel.

### *2.3 Alternative proposal*

As per the model studies explained in the previous sections, the proposed Pilot Channel was not expected to activate on its own after initial activation by digging/dredging under the given flow conditions or have any major influence in reducing the flow intensity/velocity along the eastern embankment side channel. Geometric disposition of various existing channels on model showed that by increasing the resistance to the flow along the eastern embankment side channel, the possibility of right side existing channel (Western side) further getting activated will increase. Considering this aspects, the resistance to the flow was introduced by providing 3 rows of porcupines with a length of 150 m along the eastern embankment side channel starting from Spur at chainage 27.10 km and downstream at an interval of 200 m center to center by placing them in articulated manner as shown in Photo 5. Studies in this scenario indicated that for a discharge of 5,663 $m^3/s$ about 37-45% reduction in velocity was noticed along the eastern embankment side channel as compared to the earlier case of Pilot channel. Similarly, the increase in velocity and discharge intensity was observed along the right side main channel (Western side). With the discharge of 14158 $m^3/s$, similar flow conditions/ pattern was noticed. However, the tendency of severe erosion along the right bank of Western (right) side channel was also seen over the period of time in the model. Therefore, activating this channel by selective dredging near the mouth along with streamlining the right bank at entry would boost the discharge in this channel. This may eventually lead to reduction of flow velocity/ intensity in the eastern embankment side channel. The comparison of velocity along the eastern side and western side channels for the three different conditions are shown in Figures 2 and 3.

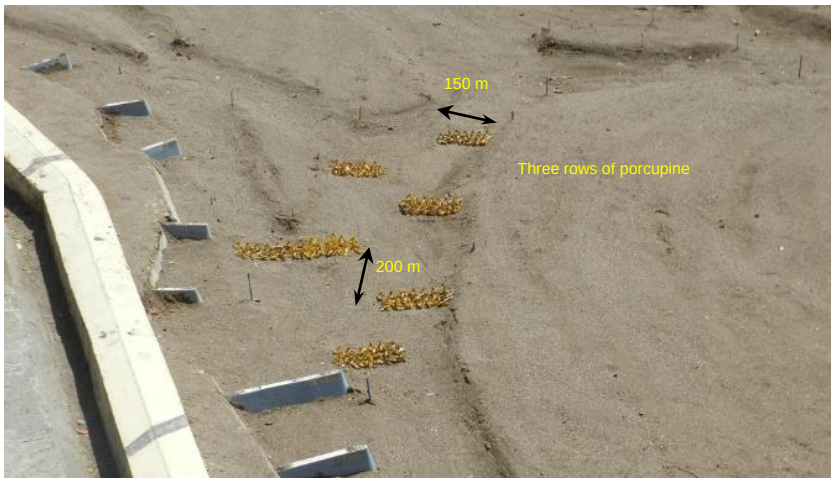



**Photo 5** Typical layout of porcupine screens along Eastern Embankment side channel

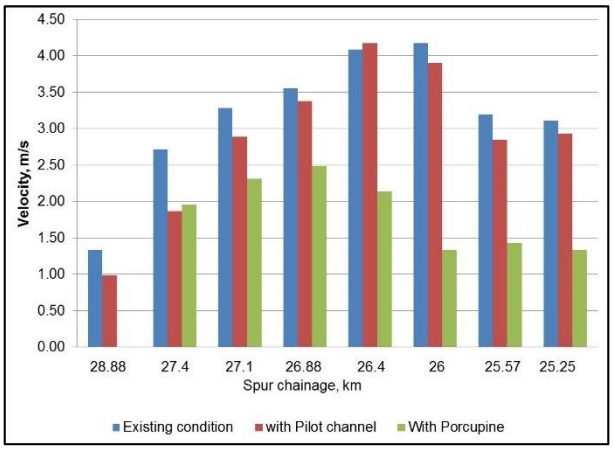



**Figure 2** Comparison of velocity along Eastern Embankment side (Left bank) channel

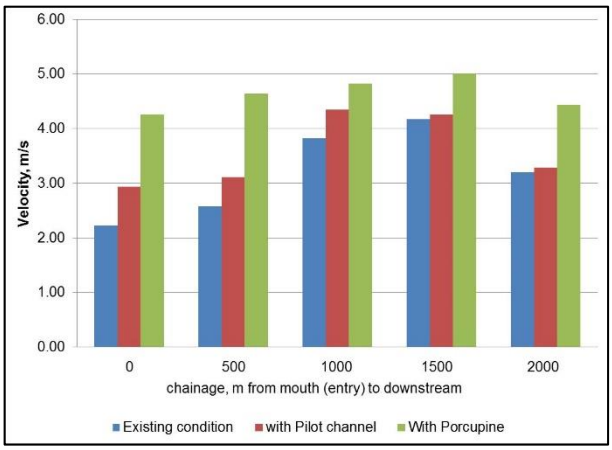



**Figure 3** Comparison of velocity along Western side (Right bank) channel

The Velocity and discharge intensity along different locations of the reach under consideration for different cases is given in Table 1 and 2.

**Table 1** Velocity and discharge intensity at different locations for discharge of 5663 $m^3/s$

| Along Eastern Embankment Side upstream of Kosi Barrage (Left Bank) | | | | | | | |
|---|---|---|---|---|---|---|---|
| | | Existing condition | | With Pilot channel | | With CWPRS proposal | |
| Sl. No. | Spurs at (Km) | Velocity (m/s) | Intensity ($m^3/s/m$) | Velocity (m/s) | Intensity ($m^3/s/m$) | Velocity (m/s) | Intensity ($m^3/s/m$) |
| 1 | 27.88 | 2.44 | 11.12 | 0.98 | 4.20 | * | * |
| 2 | 27.4 | 2.71 | 19.92 | 1.87 | 16.35 | 1.96 | 6.30 |
| 3 | 27.1 | 3.29 | 21.16 | 2.89 | 17.18 | 2.31 | 8.41 |
| 4 | 26.88 | 3.55 | 23.62 | 3.37 | 15.36 | 2.49 | 12.37 |
| 5 | 26.4 | 4.08 | 24.30 | 4.17 | 23.66 | 2.13 | 7.62 |
| 6 | 26 | 4.17 | 18.98 | 3.91 | 12.31 | 1.34 | 4.68 |
| 7 | 25.57 | 3.20 | 07.83 | 2.84 | 10.95 | 1.43 | 5.09 |
| 8 | 25.25 | 3.11 | 08.71 | 2.93 | 9.23 | 1.34 | 4.77 |
| Average values | | 3.32 | 27.23 | 2.87 | 13.66 | 1.63 | 6.16 |
| Proposed Pilot channel | | | | | | | |
| 1 | Entry (Mouth) | 1.25 | 5.68 | 2.49 | 6.10 | * | * |
| 2 | 1000 m | * | * | 0.89 | 2.19 | * | * |
| 3 | 2000 m | * | * | * | * | * | * |
| 4 | 3000 m | * | * | * | * | * | * |
| 5 | Exit | 1.51 | 7.21 | 0.98 | 3.44 | * | * |
| Right bank channel (Western side) | | | | | | | |
| 1 | Entry (Mouth) | 2.22 | 5.45 | 2.05 | 7.88 | 4.26 | 12.23 |
| 2 | 500 m | 2.58 | 9.02 | 3.73 | 15.66 | 4.64 | 21.12 |
| 3 | 1000 m | 3.82 | 14.70 | 4.08 | 20.58 | 4.82 | 16.88 |
| 4 | 1500 m | 3.91 | 12.31 | 4.62 | 16.15 | 5.01 | 13.67 |
| 5 | 2000 m | 3.20 | 8.73 | 4.26 | 13.42 | 4.44 | 13.98 |
| Average values | | 3.15 | 10.04 | 3.75 | 14.74 | 4.63 | 15.58 |
| Note: * Velocity not observed due to insufficient depth of flow/slack flow/no flow | | | | | | | |

**Table 2** Velocity and discharge intensity at different locations for discharge of 14,158 $m^3/s$

| Along Eastern Embankment Side upstream of Kosi Barrage (Left Bank) | | | | | | | |
|---|---|---|---|---|---|---|---|
| | | Existing condition | | With Pilot channel | | With CWPRS proposal | |
| Sl. No. | Spurs at (Km) | Velocity (m/s) | Intensity ($m^3/s/m$) | Velocity (m/s) | Intensity ($m^3/s/m$) | Velocity (m/s) | Intensity ($m^3/s/m$) |
| 1 | 27.88 | 1.54 | 9.18 | 2.22 | 6.22 | 2.98 | 12.08 |
| 2 | 27.4 | 1.72 | 16.14 | 1.96 | 13.43 | 2.89 | 16.17 |
| 3 | 27.1 | 2.28 | 21.56 | 2.87 | 16.09 | 3.02 | 17.13 |
| 4 | 26.88 | 2.43 | 23.81 | 2.67 | 21.46 | 3.32 | 21.12 |
| 5 | 26.4 | 2.93 | 20.52 | 3.67 | 24.41 | 3.61 | 24.01 |
| 6 | 26 | 3.51 | 20.87 | 3.51 | 13.50 | 4.17 | 21.90 |
| 7 | 25.57 | 4.44 | 23.30 | 3.82 | 14.16 | 4.57 | 17.60 |
| 8 | 25.25 | 3.15 | 16.55 | 3.64 | 15.04 | 3.82 | 13.36 |
| Average values | | 2.75 | 18.99 | 3.05 | 15.54 | 3.55 | 17.92 |
| Proposed Pilot channel | | | | | | | |
| 1 | Entry (Mouth) | 1.34 | 7.02 | 1.51 | 5.41 | * | * |
| 2 | 1000 m | * | * | 1.16 | 4.95 | * | * |
| 3 | 2000 m | * | * | 2.67 | 7.46 | * | * |
| 4 | 3000 m | * | * | 3.55 | 8.70 | * | * |
| 5 | Exit | 1.16 | 6.49 | 2.36 | 7.32 | * | * |
| Right bank channel (Western side) | | | | | | | |
| 1 | Entry (Mouth) | 2.05 | 7.88 | 3.11 | 7.18 | 5.24 | 27.49 |
| 2 | 500 m | 3.73 | 15.66 | 4.08 | 21.44 | 4.08 | 15.15 |
| 3 | 1000 m | 4.08 | 20.58 | 5.15 | 26.30 | 4.35 | 24.36 |
| 4 | 1500 m | 4.62 | 16.15 | 4.79 | 18.45 | 5.32 | 25.34 |
| 5 | 2000 m | 4.26 | 13.42 | 4.70 | 16.46 | 4.35 | 16.75 |
| Average values | | 3.75 | 14.74 | 4.4 | 17.97 | 4.67 | 21.82 |
| Note: * Velocity not observed due to insufficient depth of flow/slack flow/no flow | | | | | | | |

## 3. Discussion

The flow mainly concentrated along the channel adjacent to the eastern embankment between spurs at chainage 27.1 km to chainage 26 km for both the discharges under existing condition. As the sediment front formed near the mouth of proposed pilot channel, the flow intensity in pilot channel reduced which resulted in formation of sheet flow condition over the island of proposed Pilot channel and forming oblique flow towards the eastern embankment near spurs at chainage 26 km to 25.25 km. Considering the above facts, it was felt that activation of pilot channel by modifying the geometry near the mouth by deepening (Approximately 1 m) and widening as per the proposal of project authorities may encourage the diversion of flow through the pilot channel. However, the model studies indicated that the quantum of discharge through the pilot channel was low as compared to the main channels because the proposed alignment of Pilot channel is almost at right angle to the main river flow and the Pilot channel (20 m wide) is very small compared to the other adjacent channels which range between 200 m to more than a kilometer. Thus, the model studies for the proposed Pilot channel clearly indicated its ineffectiveness in mitigating or reducing the flow in the eastern channel which was the basic aim of the studies. Therefore, it was thought that activation of existing right side channel is a best way forward. Therefore, the right channel was modified at the entry of its mouth including dredging/desilting to some extent and providing resistance to flow along the eastern side channel with series of three rows of porcupine screens alternatively extending from right and left side of the eastern channel. The studies indicated that the western side channel (right side) was gradually activated. On the other part, the eastern side channel (Left side) started accumulating the sediments and hence, the attack towards the embankment and spurs were reduced. The Generalized flow pattern as shown in Photo 6 indicates the development of right channel. The successful development of this channel can also be noticed in the recent Google satellite imagery (Figure 4)



**Photo 6** Generalized flow pattern for a discharge of 14158 $m^3/s$ after placing the porcupine screens.




Post flood 2016 Post flood 2019

**Figure 4** Google explorer imagery of river Kosi near the study reach.

## 4. Conclusions

- The proposed Pilot channel is not able to absorb large quantity of discharge and is unable to reduce flow intensity in the channel adjacent to the eastern embankment, rather, the flow intensity increased.
- As the Pilot channel is almost at right angles to the upstream channel, it is drawing large quantity of sediment and is getting silted up, thereby it is not sustainable over the period.
- The activation of right side existing channel and effective introduction of resistance in the left side channel, effectively reduced the attack on the eastern embankment. However, regular maintenance of the nose/shank and embankment toe is also needed from chainage 27.88 km to 25.25 km.

**Acknowledgement**

The authors wish to express their deep sense of gratitude to Shri A. K. Agrawal, Director, CWPRS for his constant encouragement and valuable suggestions for writing this paper.

## References

CWPRS Technical report No. 5486 of April 2017, *Hydraulic model studies for activation of channel (in front of spur at 27.88 km to 24.78 km) in river Kosi, upstream of Kosi barrage, Bihar*.

Jha D. K. &. Tripathi V. K. (2013), *Kosi flood hazard & Disaster Management: A case study of Sapaul district*, published in National Geographical Journal of India; ISSN 0027-9374/2013/1500-1507, Vol.59,Pt.4, (pp387-404).

Galgali, V. G. (1986), *River training and flood regulation on the Kosi River*. Proceedings of the 53rd Research and Development Session, Bhubaneshwar, Orissa, October. New Delhi: Central Board of Irrigation and Power, pp.181-197

Kale V. S (2008), *Himalayan Catastrophe that Engulfed North Bihar*, Journal of Geological Society of India, Vol.72, pp.713-719

Sinha Rajiv (2009), *Dynamics of a river system – The case of the river Kosi in North Bihar*, e-Journal Earth Science India Vol.2 (I), pp. 33- 45 http://www.earthscienceindia.info/; ISSN: 0974 – 8350

*IN PROCEEDINGS OF 25th HYDRO 2020, INTERNATIONAL CONFERENCE, NATIONAL INSTITUTE OF TECHNOLOGY ROURKELA, ODISHA, INDIA 26-28, March 2021, ISBN 978-93-90631-56-8*

Paper ID - 244

# Development of a distributed physics hydrological model for prediction of inflows into Hathnur Reservoir from Main Tapi River in Upper Tapi basin, India.

Nikita Saptarishy[1], P. L. Patel [2]

[1]*P.G student, Department of Civil Engineering, Sardar Vallabhbhai National Institute of Technology, Surat, 395007, India.*

[2]*Professor, Department of Civil Engineering, Sardar Vallabhbhai National Institute of Technology, Surat, 395007, India. (Corresponding Author)*

*Email: niki.saptarishy@email.com; plpatel@ced.svnit.ac.in*

*Telephone/Mobile No.: +9I 8839870766; 9904003857*

## Abstract

The present study aimed at evaluating the performance of a deterministic physics-based distributed model, MIKE SHE coupled with MIKE 11 to have a good understanding of the occurrences of the overland flow and channel flow in the Burhanpur sub-catchment of Upper Tapi basin and predict inflows into the Hathnur reservoir. The catchment covers an area of 10,340 $km^2$ and has mountainous and steep topography with the deciduous forest as the dominant land cover class. A grid size of 500m x 500m has been used in the foregoing modeling. The distributed nature of the topography, land use class of the catchment, and meteorological data are given as inputs using the Shuttle Radar Topographic Mission (SRTM) Digital elevation model (DEM) of 30m resolution, IRS P6 LISS III, and station-based rainfall and potential evapotranspiration (PET) respectively. The integrated model has been calibrated against daily observations of stream flows at Burhanpur stream gauging station for four years from 1993-1996. The auto-calibration is performed using the AUTOCAL tool of DHI for minimizing the overall root mean square error of daily discharges. The calibrated parameters are validated using independent data of the years 1997-2000. The model performance indicators demonstrated that the model predicts satisfactorily stream flows at daily and monthly time scales (NSE=0.60-0.93, r=0.80-0.95) for calibration and validation periods for the Burhanpur sub-catchment. The model performance analysis indicates the usefulness of the model in predicting the inflows into the Hathnur reservoir.

***Keywords:*** *Hydrological model, Distributed physics-based, Burhanpur sub-catchment, MIKE SHE/MIKEII model*

## 1. Introduction

The hydrological cycle is a complex system with many interconnected components. These components of the hydrological cycle are all non-uniformly distributed spatially and temporally. Water-related issues such as floods, droughts cause serious damage to human life and property. Disastrous flood events have become more recurrent and severe because of the impact of change in the climate. Hydrological models are powerful tools for understanding, analyzing, and managing water resources. Hydrological models play a significant role in understanding the interaction between hydrological processes in a catchment for decision making for water management practices and mitigate catastrophic damage. Advancement in remote sensing and GIS tools can be helpful in the study of the hydrological system precisely. The models can be classified as conceptual and physics- based models based on the description of physical processes and lumped or distributed on the spatial description of the hydrological processes (Refsgaard 1996). The selection of the model depends on the availability of data and spatial features of the catchment. The Physics-based distributed models are better suited for characterizing the spatial variation in the basin considering changes in topography, land use land cover, and soil characteristics.

Water scarcity and a decreasing trend in streamflow is a major concern in the Tapi Basin in west- central India, which may be attributed to anthropogenic activities like rapid urbanization, increase in population, excessive groundwater extraction, and decrease in forest cover. There has been an increase in the percentage of the population living with the chronic water shortage in Tapi Basin, from 34% in the year 1981 to 63.2% in the year 2011(Sharma et al. 2019). The development of a modeling system to study the hydrology of the watershed is significant for the management of water resources in the basin. Refsgaard(1997) emphasized the significance of physics-based distributed models over lumped

conceptual models for modeling surface flow, saturated zone flow, and also modeling the effects of climate change and land-use changes on the hydrological processes in the catchment. Madsen(2003) developed a framework for model parameterization and calibration using MIKE SHE for Danish Karup Catchment (440 $km^2$) in Denmark and emphasized better performance results on a multi-objective calibration approach than a single objective. Sahoo et al. (2006) formulated the MIKE SHE model to study the hydrological response of the Manoa-Palola stream system in Oahu, Hawaii, USA. The study indicated the significant effect of Manning's roughness coefficient and the hydraulic conductivities of the saturated zone in determining flood peaks. Zhang et al. (2008) studied the usefulness of the MIKE SHE model for analyzing the rainfall-runoff mechanism in a small watershed in north-western china (12 $km^2$). The study concluded that model performance was better for continuous daily stream flows than individual storm events. Gupta et al. (2008) applied the integrated MIKE SHE/ MIKE11 model in the Damodar Irrigation Project, West Bengal, India to estimate the performance of the model on using remote sensing data and conventional data. The study concluded that remote sensing data give more definitive results for integrated models and should be used for practical and effectual results from distributed hydrological models. Wijeskara et al. (2013) used an integrated MIKE SHE/MIKE11 approach to analyze the effect on hydrological processes in the watershed due to past and future land-use changes. The study concluded an increase in overland flow and a decrease in evapotranspiration, baseflow, and infiltration with a rapid increase in urban areas and deforestation. Vo et al. (2016) analyzed the impacts of climate change on runoff in the Vu Gia Thu Mon catchment in Vietnam using the distributed MIKE SHE/MIKE11 model. The study concluded that the model performance can be enhanced using multi-site calibration, and emphasized that distributed models can satisfactorily assess the impact of climate change on hydrological processes. Loliyana and Patel (2018) applied the integrated MIKE SHE/MIKE11 model in the semi- arid sub-catchment of the Upper Tapi basin, India for the prediction of stream flows, groundwater level, and water balance. The sensitivity analysis concluded that saturation water content, field capacity, and hydraulic conductivity of saturated media significantly affect the volume of stream flows, peak flows, and groundwater level

In the present study, a Physics-based distributed approach has been developed for the Burhanpur sub-catchment of the Tapi River basin, India using an integrated MIKE SHE /MIKE 11 model to simulate streamflows in the catchment and predict runoff into Hathnur Reservoir from the Burhanpur sub-catchment. The model parameters have been auto-calibrated for the period 1993-1996. The calibrated model is simulated for independent data of the period 1997-2000. Model performance has been evaluated using various statistical indices.

## 2. **Study Area**

The present study area includes the Burhanpur sub-catchment (Origin of Main Tapi River to Hathnur Reservoir) of the Upper Tapi basin. The catchment covers an area of 10340$km^2$ and drains Maharashtra and Madhya Pradesh states. The sub-basin lies between 75°45'E to 78°30'E longitudes and 21°00'N to 22°00'N latitudes. The length of the Tapi River from the origin to the outlet at Hathnur Reservoir is 350 km. The sub-catchment is bounded by hilly ranges from two sides i.e Satpura ranges and Gwaligarh mountains from the North and south of the sub-catchment respectively. The catchment has steep topography with the elevation in the catchment ranging from 752m near Multai to 188m at the outlet of the catchment. The Upper Tapi river is characterized by high banks, narrow valleys, and gravely beds and descends in the plains of Burhanpur. The initial portions of the catchment area are covered by basaltic lava which is followed by alluvial deposits. The catchment receives 93% rainfall during the monsoon months (mid-June to mid-October), whereas scanty rainfall during the remaining eight months. There are two stream gauging stations along the Main Tapi river in the Burhanpur sub-catchment namely Dedtalai and Burhanpur. The catchment is predominantly covered by deciduous forest(55.82%) and agricultural land(36.60%). There is a total of 8 rain gauge stations and 3 weather stations in the Burhanpur sub-catchment. Figure1- shows the location of the rain gauge and discharge gauge stations. The input data required and the sources of data for the foregoing model is included in the Table-1.

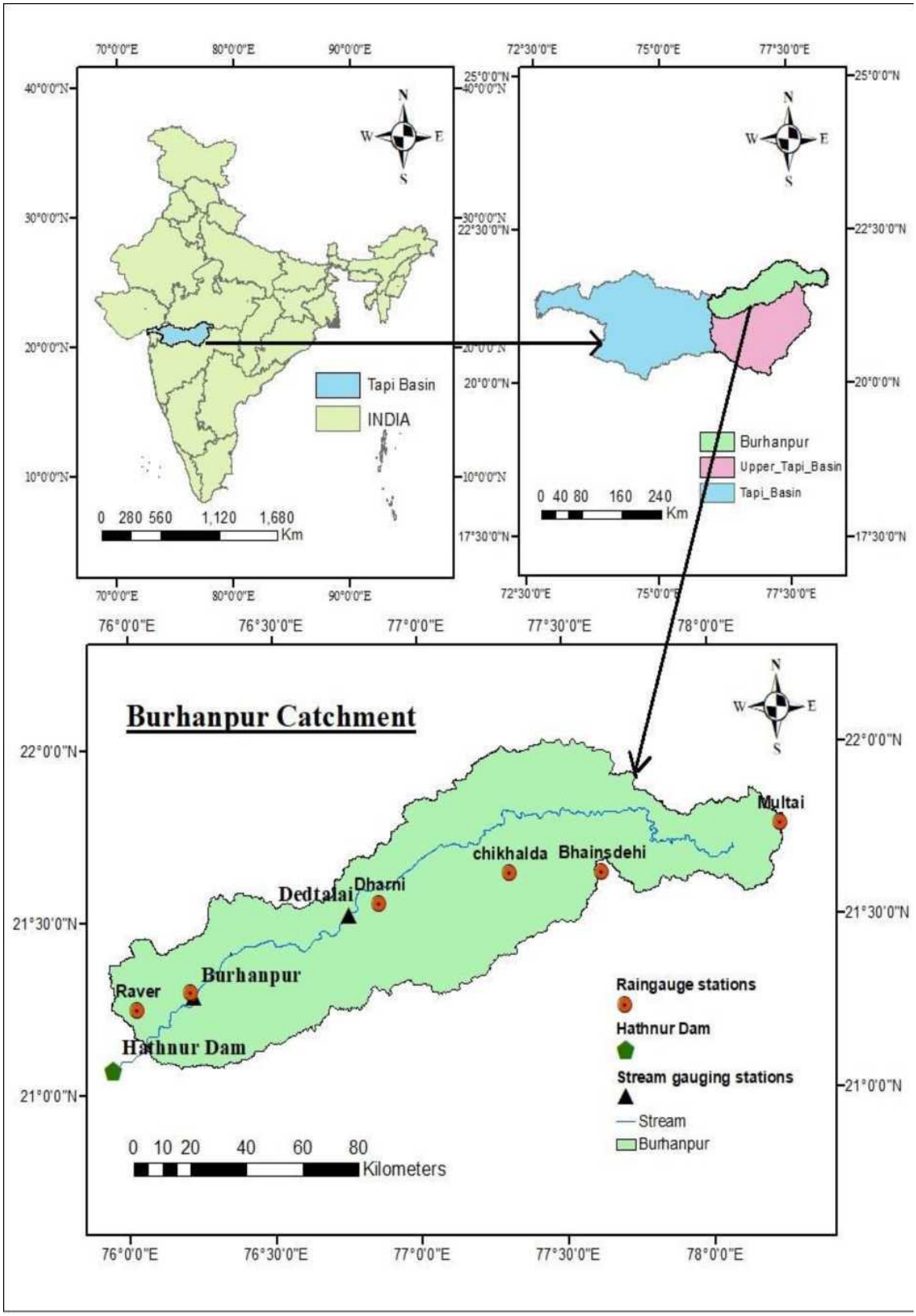



**Figure 1** Index map of study area

**Table 1**Input data for model development

| Input data | Description | Data source |
|---|---|---|
| Topography | Digitial Elevation models; Resolution:30m | Shuttle Radar Topographic Mission (SRTM) |
| Satellite Imagery | IRS P6 LISS-III Imagery; Resolution:23.5m | National Remote Sensing Centre, Hyderabad |
| Rainfall | 6 Rain gauge station data; Daily time series-1991-2000 | India Meteorological Department(IMD) |
| Discharge and water level | Dedtalai and Burhanpur Discharge and water level time series:1991-2000 | Central Water Commission(CWC) |
| Weather data | 3 weather station data; Daily time series-1991-2000 | India Meteorological Department(IMD) |

## 3. **Description of MIKE SHE/MIKE11 Model**

MIKE SHE (Systeme Hydrologique Europeen) is a physics-based distributed model developed by DHI Water & Environment (DHI, 2017). MIKE SHE includes all the important components in the hydrological cycle i.e., evapotranspiration, overland flow, unsaturated flow, groundwater flow, and integrates MIKE 11 to simulate channel flow. Figure-1 represents a schematic diagram of hydrological processes in the MIKE SHE/MIKE11 integrated model. MIKE 11 is a fully dynamic, one-dimensional modeling software for the simulation of flows in rivers, irrigation systems, and canals. MIKE 11 model calculates river discharge and water level at 'Q' and 'H' points respectively. In integrated MIKE SHE/ MIKE 11 the flow in different components is represented at the grid-scale with mathematic descriptions. The integrated model incorporates partial differential equations describing mass and momentum transfer for describing the process of Overland flow, flow in the unsaturated zone, and channel flow whereas the process of evapotranspiration and interception are simulated using an analytical solution. The saint Venant equations are solved numerically in two dimensions and one dimension for overland flow and channel flow respectively. The major input required for the development of the model includes spatial data, drainage network, soil characteristics, and meteorological data i.e precipitation and potential evapotranspiration (PET). Precipitation and PET data are given as input as spatially averaged using the Theissen polygon approach.

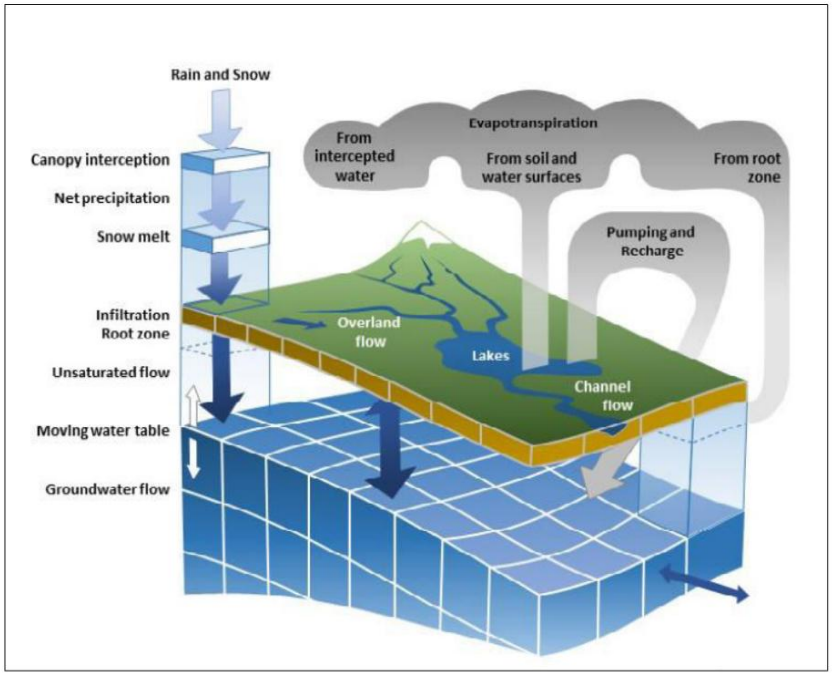



**Figure 2** Schematic diagram of MIKE SHE/MIKE11 model(DHI,2017)

The process of evapotranspiration in MIKE SHE is modeled in the following order: evaporation from plant canopy, ponding, and Evapotranspiration (ET) from the root zone. The AET is simulated using a two-layer water balance method (Yan and Smith 1994). Overland flow occurs when the rainfall over an area is more than the capacity of the infiltration of soil; the water gets ponded over the surface and thus results in sheet flow on the surface. In the present study 2D, diffusive wave approximation of Saint Venant's equation is used for simulation of overland flow. The flow in the unsaturated zone is solved using a two-layer balance method. The horizontal flow of water in the unsaturated zone is considered negligible.

## 4. Model Development

The rainfall-runoff model was developed for the Burhanpur sub-catchment using an integrated MIKE SHE/MIKE11 approach for the prediction of stream flows in the sub-catchment. In MIKE SHE the catchment is discretized into uniform grids of cell size 500m x 500m. The development of input files for the MIKE SHE model is carried out using ArcGIS 10.2.2. The Digital elevation model of 30m resolution is used for obtaining catchment shapefile and river network using ArcHydro tools of ArcGIS 10.2.2. Land use land cover maps are generated by supervised classification of IRS P6 LISS- III imagery of 2000, using ERDAS IMAGINE 10.0. The methodology adopted for the prediction of stream flows using MIKE SHE/MIKE11 is represented in Figure-3. In the model, major inputs include topography, meteorological data, vegetation characteristics, and land use land cover map. Potential evapotranspiration (PET) is calculated using the Penman-Monteith method (FAO)(Allen et. al 1998) using weather station data. Database prepared for the present study is included in Figure-4.

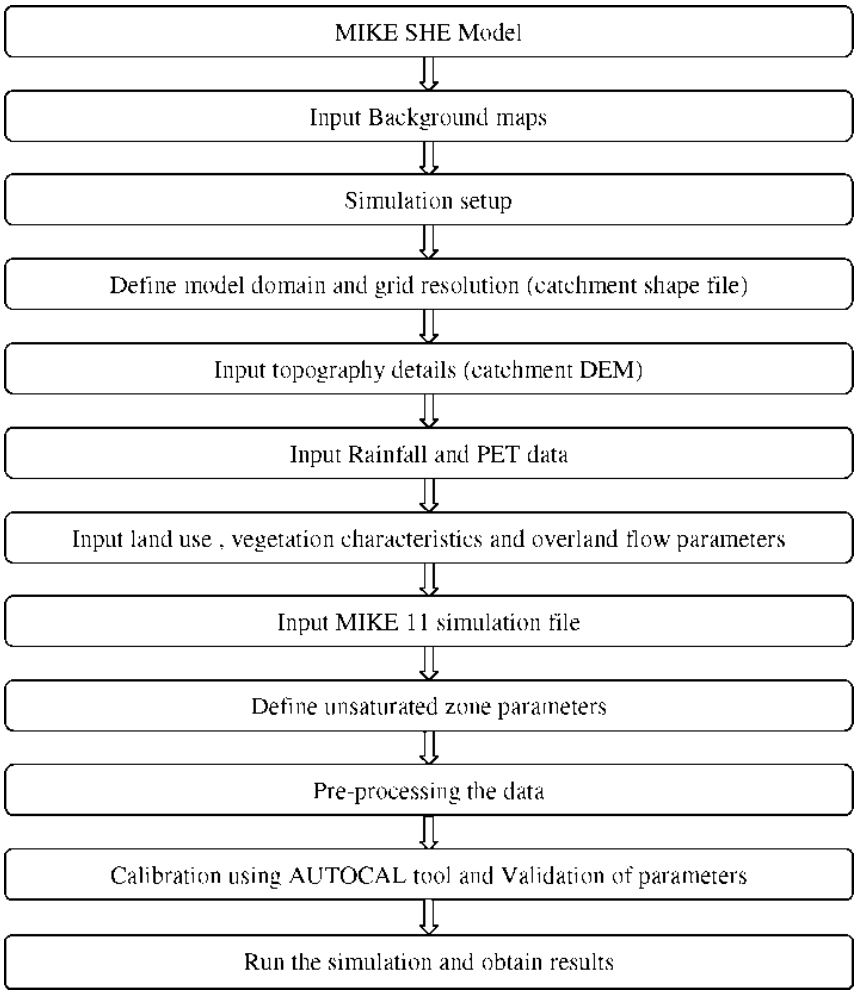



**Figure 3** Methodology adopted in present study

The computation of Actual evapotranspiration majorly depends on vegetative factors such as the Leaf area index (LAI) and Root Zone Depth (RD) i.e average root zone depth in the unsaturated zone in the catchment. The LAI and RD are given as input into the model, and the values of these parameters are selected based on land use land cover classification of the study area. Manning's M is given as input as distributed based on the different land use land cover of the catchment. The values of Manning's M (reciprocal of Manning's roughness coefficient ), LAI, and RD are obtained from Engman (1986), Chow (1959), Vieux et al. (2001), Loliyana and Patel(2018) for different land uses.

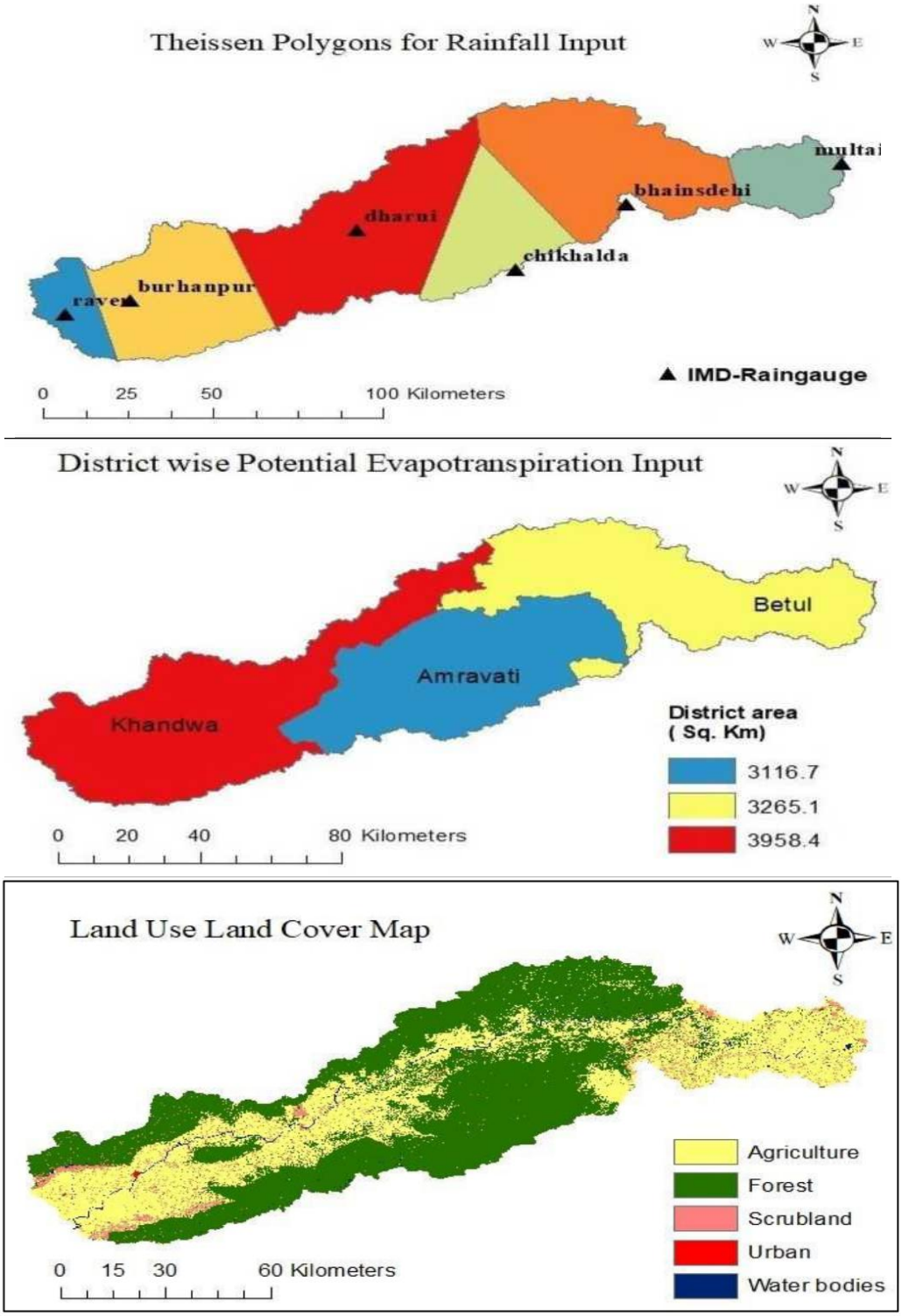



**Figure 4** Data for development of MIKE SHE model (a) rainfall (b) PET (c) land use characteristics

Weighted LAI and RD according to different land use land cover classes are calculated and given as input into the model as shown in Table-2.

**Table 2** Calculation of LAI, RD, and Manning's M for Burhanpur sub-catchment

| Land use class | Area(%) | LAI | Wt. Avg of LAI | Root Depth (mm) | Wt. Avg. of RD(mm) | Manning's 'M' |
|---|---|---|---|---|---|---|
| Agriculture | 36.60 | 4.8 | 1.757 | 700 | 0 | 28.57 |
| Water Bodies | 1.04 | 0 | 0.0 | 0 | 0 | 40 |
| Forest | 55.82 | 6 | 3.349 | 800 | 446.597 | 6.67 |
| Scrubland | 6.03 | 3 | 0.181 | 600 | 256.209 | 18.18 |
| Urban area | 0.50 | 0 | 0.0 | 0 | 36.204 | 66.7 |
| Total | | | 5.287 | | 739.011 | |

## 5. **Model Calibration**

The parameters of the MIKE SHE model, for simulation of flows at Burhanpur stream gauging station, are calibrated and validated for periods, 1993-1996 and 1997-2000 respectively. The calibration of the model is performed using the discharge data at Burhanpur stream gauging station. Model calibration has been performed using the AUTOCAL tool of the DHI package. The calibration is based on population evolution-based algorithm i.e. shuffle complex evolution algorithm. The auto-calibration is performed for a single objective function of minimizing the overall root mean square error (RMSE) of daily discharge or agreement of the shape of the flow hydrograph. The number of model evaluations was taken as 1000 for getting the set of optimal parameters. Estimated and calibrated parameters of the MIKE SHE model are given in Table-3.

**Table 3** Calibrated parameters of MIKE SHE/MIKE11 model for Burhanpur sub-catchment

| Component | Parameter | Unit | Range | Initial value | Calibrated value |
|---|---|---|---|---|---|
| Vegetation parameters | Leaf Area Index(LAI) | | 5.28 | 5.28 | - |
| | Root Depth(RD) | mm | 739.011 | 739.011 | - |
| | Cint | mm | 0.01-0.1 | 0.01 | 0.035 |
| | ET surface depth | m | 0.10-10 | 1 | 1.163 |
| Overland flow parameters | Manning's M | $m^{1/3}s^{-1}$ | 6.67-66.71 | - | - |
| | Detention Storage | mm | 0.00-5.00 | 0.50 | 2.29 |
| River | Manning's n | $m^{-1/3}s$ | 0.045 | 0.045 | - |
| Soil parameters | Moisture content at saturation | | 0.10-0.70 | 0.40 | 0.567 |
| | Moisture content at field capacity | | 0.10-0.60 | 0.20 | 0.438 |
| | Moisture content at wilting point | | 0.00-0.50 | 0.10 | 0.129 |
| | Saturated hydraulic conductivity | m/sec | $1x10^{-9}$-$1x10^{-2}$ | $1x10^{-6}$ | $0.26x10^{-7}$ |

From the calibration results, it can be observed that Cint i.e. maximum amount of water stored as interception can be 0.035mm, while the thickness of the capillary fringe is 1.163m in the catchment. The Detention storage over the surface (Ds) is 2.29mm. In the unsaturated zone, it can be observed that the saturated hydraulic conductivity of soil is low indicating clay and loam content in the soil. The maximum moisture content in the root zone is 0.567 indicating the amount of water available in the root zone for evapotranspiration and recharge to saturated zone, the maximum moisture content in the soil to meet the requirements of the plants is 0.438, and moisture content at the wilting point is 0.129 indicating the minimum amount of water required by plants not to wilt.

The performance of the model has been evaluated using statistical performance indices like the Coefficient of Determination ($R^2$), Root Mean Square Error (RMSE), and Nash Sutcliffe efficiency (NSE), as given in Table-4. The coefficient of Correlation stipulates the strength of a linear

relationship between simulated and observed discharge, whereas the Nash-Sutcliffe Efficiency indicates the efficiency of the model to simulate varying hydrographs for a stream gauging station.

**Table 4** Performance criteria for model evaluation

| Sr. No. | Statistical Indices | Equation | Optimal values |
|---|---|---|---|
| 1 | Root Mean Square Error (RMSE) | $RMSE = \sqrt{\frac{\sum_{i=1}^{n}(Q_i^{sim} - Q_i^{obs})^2}{n}}$ | 0 |
| 2 | Coefficient of correlation ( r) | $r = \sqrt{\frac{\sum_{i}^{n}(Q_i^{sim} - \bar{Q}^{obs})^2}{\sum_{i}^{n}(Q_i^{obs} - \bar{Q}^{obs})^2}}$ | 1 |
| 3 | Nash-Sutcliffe Efficiency (NSE) | $NSE = 1 - \frac{\sum_{i=1}^{n}(Q_i^{obs} - Q_i^{sim})^2}{\sum_{i=1}^{n}(Q_i^{obs} - \bar{Q}^{obs})^2}$ | 1 |

$Q_i^{sim}$, $Q_i^{obs}$ are simulated and observed runoff values respectively, $\bar{Q}^{obs}$ represents mean of observed runoff; n is the number of observed data points

## 6. Results and discussion

The model of performance using integrated MIKE SHE/MIKE11 for Burhanpur sub-catchment under calibration period for years 1993-1996 in daily and monthly scale are represented in Figure-5 and Figure-6. The performance of the model is evaluated using statistical indices such as RMSE, r, and NSE against observed and simulated runoff. The prediction performance indices of MIKE SHE/MIKE11 using calibrated parameters are shown in Table-5. The satisfactory model performance is indicated by the statistical performance indicators (RMSE=390m$^3$/sec, r=0.828, NSE=0.680). Figure-5 and Figure-6 show good agreement between observed and simulated runoff with the peak flows being slightly underestimated on a daily scale but show good agreement on a monthly scale.

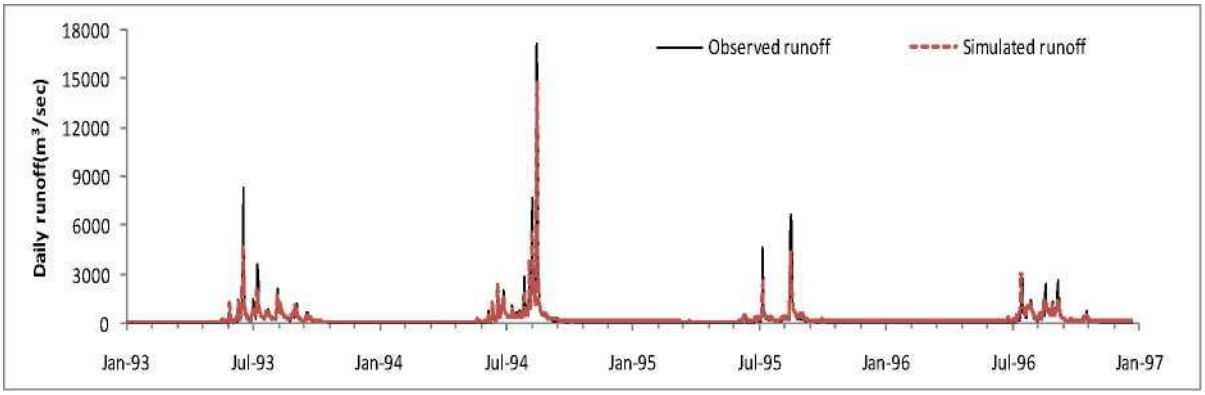



**Figure 5** Comparison of observed and simulated runoff under calibration period at daily scale

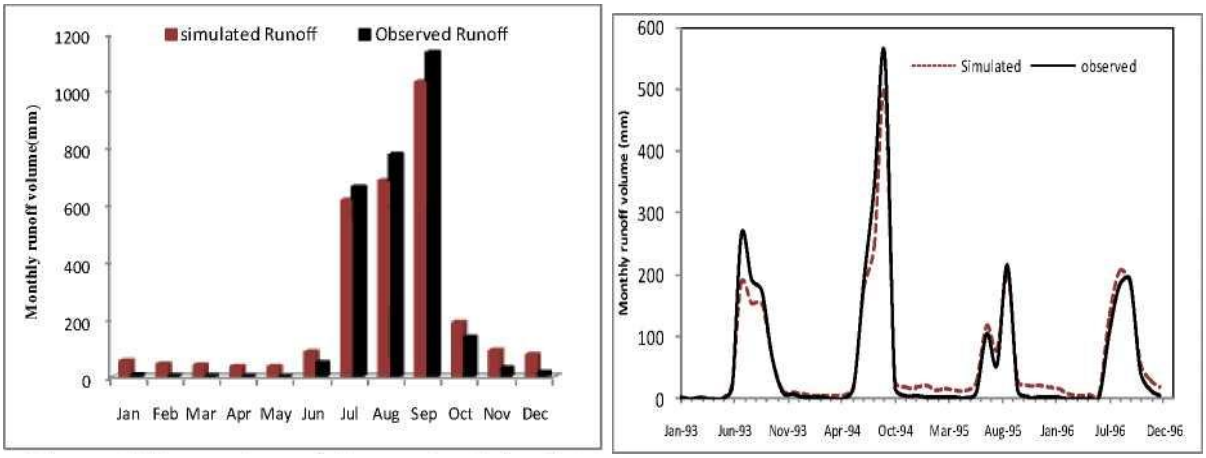



**Figure 6** Comparison of observed and simulated runoff under calibration period at monthly scale

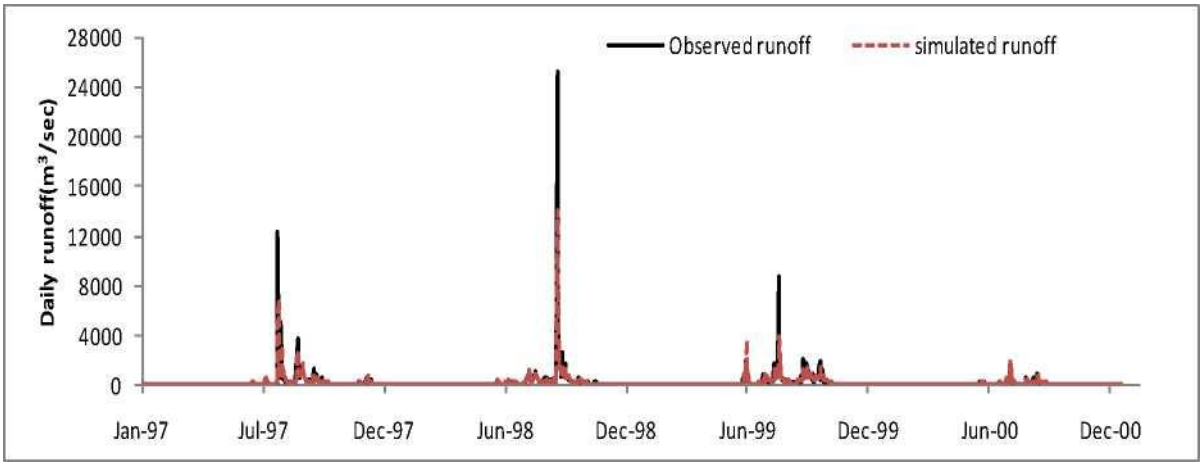



**Figure 7** Comparison of observed and simulated runoff under validation period at daily scale

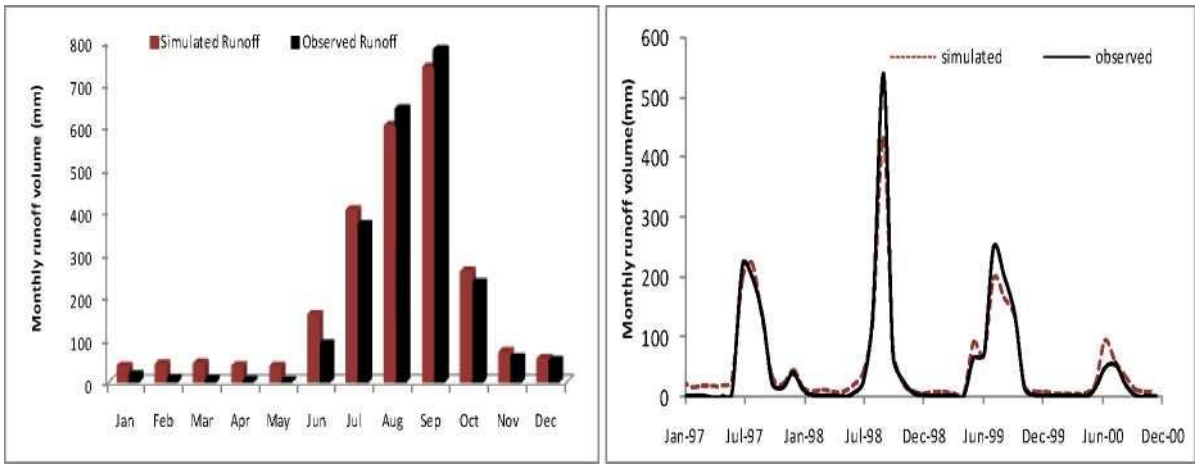



**Figure 8** Comparison of observed and simulated runoff under validation period at monthly scale

**Table 5** Performance of the developed model under calibration and validation

| Stream gauging site | Period | Daily | | | Monthly | | |
|---|---|---|---|---|---|---|---|
| | | RMSE ($m^3$/sec) | r | NSE | RMSE(mm) | r | NSE |
| Burhanpur | 1993-1996 | 390.788 | 0.828 | 0.680 | 23.368 | 0.986 | 0.935 |
| | 1997-2000 | 452.256 | 0.821 | 0.639 | 22.097 | 0.988 | 0.922 |

The performance of the calibrated MIKE SHE/MIKE11 model has been evaluated for streamflows at Burhanpur stream gauging station using independent data for the period 1997-2000. The daily and monthly flow hydrographs for the validation period 1997-2000 are represented in Figure-7 and Figure-8. The model performance is satisfactory as indicated by RMSE=452.256($m^3$/sec), r=0.821, NSE=0.639 on daily scale and RMSE=22.097(mm), r=0.988, NSE=0.922 on monthly scale. The simulated and observed hydrographs for the validation period show good agreement with slight underprediction of the peak discharges on a daily scale.

The hydrographs show the satisfactory performance of the model under the calibration and validation stage except for the peak flow event of 1998, which might improve by taking a longer calibration period and including extreme flood events in the calibration period. The overall runoff volume simulated under the calibration and validation stage is satisfactory however the low flow events are overpredicted by the model which maybe be attributed to MIKE SHE that does not allow a river to dry out. (Wang et al.2012). The model performance indices in the calibration period and the validation period are within acceptable limits (NSE > 0.60, r >0.80) (Wang et. al. 2012)(Moriasi et al. 2007). Moreover, the model gives good results for monthly time scales in both calibration and validation stages.

## 6. Conclusions

A hydrologic-hydrodynamic model for the prediction of inflow into the Hathnur reservoir has been developed for the Main Tapi River in the Burhanpur sub-catchment using MIKE11 and MIKE SHE. The calibration of the integrated model is carried out using the auto-calibration process for four years 1993-1996 while validation of the calibrated has been model carried out using independent data for the period 1997-2000. The statistical performance indices have been used to evaluate the performance of the model on comparing the observed and simulated discharge at the Burhanpur stream gauging site. The model performance indicators for the calibration period (NSE >0.680, r>0.828) indicate good agreement between the observed and simulated runoff for both daily and monthly scales. The performance of the model in the validation period gives satisfactory results with NSE>0.639 and r>0.821 at both daily and monthly scale. The overall integrated MIKE SHE/MIKE11 model is an asset for predicting the inflow into the Hathnur reservoir and would be very useful in decision making for water resources management in the catchment.

The limitations of the study including the future scope of work as mentioned below:

- The performance of the model can be improved by taking a longer calibration period and including extreme flood events in the calibration period.
- The performance of the model could be improved by incorporating computationally extensive Richard's equation for the descriptive understanding of flow in the unsaturated zone and incorporation of the saturated zone for understanding the movement of groundwater and contribution of baseflow in streamflow.
- Finer finite grid size may enhance the model performance, and distributed parameters like soil properties; leaf area index, and root zone depth may improve the performance of the model.

**Acknowledgment**: Authors are thankful to the '**Centre for Excellence on Water Resources and Flood Management**' developed using TEQIP-II World bank grant for accessing the computational facilities over there. Also, the authors are thankful to the Central Water Commission (CWC), Ministry of Jal Shakti, GOI, and India Meteorological Department (IMD) for providing useful data for the present investigation.

## References

Allen, R. G., Pereira, L. S., Raes, D. & Smith, M. (1998). Crop Evapotranspiration-Guidelines for Computing Crop Water Requirements. Irrigation and Drainage Paper No. 56, Food and Agriculture Organisation of the United Nations, Rome.

Chow, V. T. (1959). Open channel Hydraulics, 197 pp. Editions McGraw-Hill, New York.

DHI (Danish Hydraulic Institute). (2017a). MIKE 11 User and Reference Manual(Volume -II).

DHI (Danish Hydraulic Institute). (2017b). MIKE SHE User and Reference Manual(Volume -II).

Engman, E. T., (1986): Roughness coefficients for routing surface runoff. Journal of Irrigation Drainage Engineering, 112(1), pp. 39-53.

Gupta, P.K., Singh, R., Raghuwanshi, N. S., Dutta, S., and Panigrahy, S. (2008). "Effect of remotely sensed data on the Performance of a Distributed Hydrological Model: Case Study." Journal of Hydrologic Engineering, Vol. 13 (10), pp. 1-22.

Loliyana, V. D., and Patel, P. L. (2018). "Performance evaluation and parameters sensitivity of a distributed hydrological model for a semi-arid catchment in India." Journal of Earth System Science, Springer India, 127(8), 1-26.

Madsen, H. (2003). "Parameter estimation in distributed hydrological catchment modelling using automatic calibration with multiple objectives." Advances in Water Resources, Vol. 26(2), pp. 205-216.

Moriasi, D. N., Arnold, J. G., Liew, M. W. Van, Bingner, R. L., Harmel, R. D., and Veith, T. L. (2007). Model evaluation guidelines for systematic quantification of accuracy in watershed simulations. Trans ASABE 50(3):885-900.

Refsgaard, J.C., 1996. Terminology, modelling protocol and classification of hydrological model codes. In: Abbott, M.B., Refsgaard, J.C. (Eds.), Distributed Hydrological Modelling. Kluwer Academic, pp. 17-39.

Refsgaard (1997). "Parameterisation, calibration and validation of distributed hydrological models." Journal of hydrology, Vol.198, pp.69-97.

Sahoo, G. B., Ray, C., and De Carlo, E. H., (2006). "Calibration and validation of a physically distributed hydrological model, MIKE SHE, to predict streamflow at high frequency in a flashy mountainous Hawaii stream."

Journal of Hydrology, Vol. 327, pp. 433-465.
Sharma, P. J., Patel, P. L., and Jothiprakash, V. (2019). "Impact of rainfall variability and anthropogenic activities on streamflow changes and water stress conditions across Tapi Basin in India." Science of the Total Environment, 687, 885-897.
Vieux, B. E., (2001): Distributed hydrologic modeling using GIS, Kluwer Academic Publishers, Dordrecht, and The Netherlands.
Vo, N. D., and Gourbesville, P. (2016). "Application of deterministic distributed hydrological model for large catchment: A case study at Vu Gia Thu Bon catchment, Vietnam." Journal of Hydroinformatics, 18(5), 885904.
Wang, S., Zhang, Z., Sun, G., Strauss, P., Guo, J., Tang, Y., and Yao, A. (2012). "Multi-site calibration, validation, and sensitivity analysis of the MIKE SHE Model for a large watershed in northern China." Hydrology and Earth System Sciences, 16(12), 4621-4632.
Wijesekara, G. N., Farjad, B., Gupta, A., Qiao, Y., Delaney, P., and Marceau, D. J. (2013). "A comprehensive land-use/hydrological modeling system for scenario simulations in the Elbow River watershed, Alberta, Canada." Environmental Management, 53(2), 357-381.
Yan J and Smith K R 1994 Simulations of integrated surface water and ground water systems - model formulation; J. Am. Water Resour. Assoc. 30(5) 879-890.
Zhang, Z., Wang, S., Sun, G., Zhang, H., Li, J., Zhang, M., Klaghofer, E., and Strauss, P. (2008) "Evaluation of the MIKE SHE model for application in the Loess Plateau, China."Journal of the American Water Resources Association, Vol. 44(5), pp.1108-1120.

*IN PROCEEDINGS OF 25th HYDRO 2020, INTERNATIONAL CONFERENCE,*
*NATIONAL INSTITUTE OF TECHNOLOGY ROURKELA, ODISHA, INDIA*
*26-28, March 2021, ISBN 978-93-90631-56-8*

Paper ID - 258

# A comparison between flood models developed using topographical details from field survey and SRTM DEM using MIKE HYDRO River

Anju B[1], Drissia T.K[2], Nowshaja P.T[3]

[1]*Student, Government Engineering College Trichur, Thrissur-680009, India*
[2]*Senior Scientist, Centre for Water Resources Development and Management, Kozhikode-673571, India*
[3]*Associate Professor, Government Engineering College Trichur, Thrissur-680009, India*
*Email:* anjubtikkoti@gmail.com

## Abstract

The quality of terrain data and the cross sectional details of the river are very important factors influencing the modelling of flood. The main objective of the study is to compare the flood model developed using cross sections measured in the field and generated from the freely downloadable SRTM DEM using MIKE HYDRO River model and to analyse its effect. The study area considered for the analysis is Pamba River in Kerala. In this study, we utilize the time series of daily discharge and water level of different gauging station of Centre Water Commission at Kallooppara, Malakkara, Thumpamon and water level data of Thottappalli spillway, Measured cross sections in the field and SRTM DEM were used to generate the flood model for the for the period June to August 2010. The model is developed for three scenarios i) with surveyed cross sections, ii) cross section generated from DEM and iii) corrected DEM cross sections. The study shows good correlation between the outputs of the flood model developed using the surveyed cross section and the observed discharge. When the SRTM DEM is corrected with the observed elevation from MSL the model developed gives more comparable values to the model developed using surveyed cross sections than the uncorrected DEM. The correlation coefficient value ranges from 0.91 to 0.96 in all three cases. The model developed using DEM cross sections can be used for the simulation of one dimensional model when the measured cross sections were unavailable and it also make the study more economical.

***Keywords:*** *SRTM DEM; Pamba; MIKE HYDRO River; Flood modelling*

## 1. Introduction

A flood is an exceptionally high level of water in a river, typically the level at which the river overflows its banks and floods the adjacent area. The harm caused by floods is of great magnitude in terms of loss of life, property and economic loss due to disruption of economic activities. In order for an emergency evacuation plan to be planned and adequately executed, information about the flood must also be disseminated well in advance to the individuals likely to be affected (Alfiya et al.,2015). Flood occurs due to natural and anthropogenic reasons. In India, major causes of flooding include heavy precipitation, insufficient ability to control high flows within riverbanks, and silting of riverbeds. Furthermore, landslides leading to flow obstruction and changes in the course of the river, poor natural drainage, cyclones and extreme rainstorms / cloud bursts, snowmelt and glacial production are other factors (Alfiya et al., 2015). Human beings' influence has a significant effect on the occurrence of flood events. The frequency and magnitude of the flood has been elevated because of human intervention and causes many problems (Jayakumar, 2014). A detailed evaluation of the flood is important because of the severe change in the pattern of land use and rainfall trend.

The prediction of river stages plays an important role in the structural and non-structural measures of flood management (Rahman et al. 2011). The predictions are also useful to prepare the flood maps in river floodplains. The key outputs of flood modeling are flood inundation and hazard maps that are used to measure floodwater's magnitude, depth and velocity, all of which are critical for identifying and assessing areas at potential risk during a flood event (Mokhtar et al., 2018). Such maps form the basis for flood risk maps used to assess flood costs and impacts. Different one-dimensional (1D) hydrodynamic models, based on hydraulic routing, have been developed, calibrated, validated and successfully applied for flood forecasting and inundation mapping with rapid advances in computational technology and research in numerical techniques (Gharbi et al. 2016). These models

require detailed data on river geometry, which may not be available at the desired locations of river. In order to extract the river cross-sections, which describe the geometry of the river, a hydraulic model coupled with GIS uses the digital elevation model (DEM) (Manoranjan Kumar, 2018). A study was conducted by Ravindra.et.al (2020), for identify the flood vulnerability sites for high discharge release by barrage using MIKE HYDRO River. This study considered the variations in the physical shape of river. Another study was conducted by Mahsa et.al (2020) to Calibrate, validate the HD river model and evaluate the sensitivity of the model using MIKE HYDRO River. In the hydraulic model for the computation of water level and flow measurement, the extracted river cross-sections are then used and it is compared with the available field measured cross section. This will helps to find the use of DEM for the generation of cross sections of river at desired locations.

The worst floods occurred in Kerala in 2018 and 2019. The Pamba River is one of the flooding regions most affected in 2018. The river Pamba flows into Kuttanad, where flooding occurs even during regular precipitation. A detailed hydrodynamic study is very essential for the river Pamba which has not conducted so far. So there is a need for studying the pattern of flood in the study area.

## 2. Study area and data collection

The river Pamba is taken for the study. It originates from Pulachimala hills in Western Ghats. The total length of Pamba River is 176 km. The watershed lies between $9^0$ 10' to $9^0$ 40' in the north latitude and $76^0$15' to $77^0$ 20' east longitude (Padma Priya et al., 2015). The Pamba River enriches the lands of Pathanamthitta, Kottayam and Alappuzha Districts of Kerala covering an area of 2235 $km^2$. It flows through many places in the Pathanamthitta and Alappuzha districts, including Kuttanad, an important rice cultivation centre, before emptying into the Vembanad River. The entire catchment area is restricted to Kerala state and is surrounded on the east by the Western Ghats, and on the west by the Arab Sea. The river shares its northern boundary with the Manimala basin, while it shares its southern boundary with the Achankovil basin (Navnith. et al. 2016). The river stretch considered for the study is between the CWC gauging stations; Malakkara, Thumpamon, Kalloopara and Thottappally spillway as shown in the Figure 1.

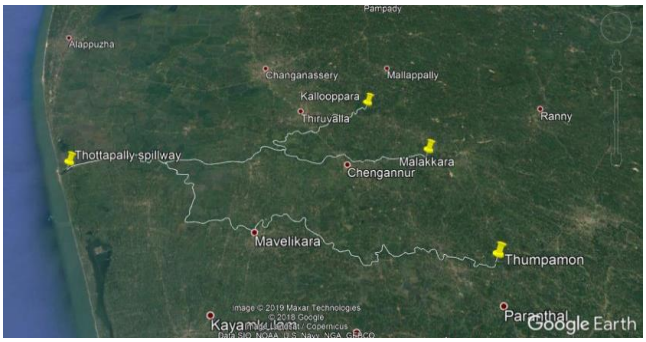



**Figure 1** location of Pamba river considered for the study in Google map view

The Pamba basin experiences good rainfall, moderate temperature and humid atmosphere. The average annual rainfall varies from 2276 mm to 4275 mm. The wind speed varies from 8.5 to 13.6 km/hr (CWC, 2017-2018). The approximate length of Pamba river considered for the study is 38 Km. The stretch of Manimala River and Achenkovil River considered for the study are 15 km and 63 km respectively. The Thottappally spillway consists of a 1310 m long, 365 m wide lead channel with a bridge cum regulator across the spillway channel (CWC, 2018).

The collection of data required for the research work is a very important step. Because if the collected data are accurate, the model developed closely resembles the real world situation. A significant collection of input data is needed for the operation of MIKE HYDRO River. The daily water levels and discharges data recorded in the upstream of the river is downloaded from the INDIA WRIS site. There are three Central Water Commission (CWC) stations Govt. of Kerala, in the upstream side of

the rivers. The observed water levels at different gauging stations at different years show that the water levels were high during the years 2007, 2010 and 2013. For this study, 2010 was chosen for the simulation of the model. Shuttle Radar Topography Mission digital elevation model (SRTM DEM) with spatial resolution of 30 m downloaded from USGS was used in the study. The cross sections are generated from MIKE HYDRO River model using DEM and the field measured cross sections are collected from Centre for water resource development and management, Kozhikode (CWRDM). The value of manning's coefficient were inferred based on the study conducted by IITM and CWRDM (2011).

## 3. Methodology

The main aim of the study is to generate flood extend and depth at each cross section of the river using DEM and it is compared with the field observed cross section. For the study to be made the identification of data required is the first step. Depending upon the work methodology, the relevant data required is to be identified and the sources for procurement of the same are to be explored and obtained. 1D modelling is carried out in MIKE HYDRO River software.

### 3.1 *MIKE HYDRO River*

It is a one-dimensional, unstable, non-uniform flow simulation model developed by the Danish Hydraulic Institute which solves the 1D hyperbolic dynamic Saint – Venant equations using an implicit six-point Abbott – Ionescu finite difference scheme (Alfiya, et. al., 2015).

1. Continuity equation

(1)

2. Momentum equation

(2)

The MIKE HYDRO River model is developed for three scenarios. First one for surveyed cross section, second one for cross section generated from DEM and the last one is for cross section generated from corrected DEM. The hydraulic model developed using MIKE HYDRO River to get the flood depth, water level and discharge at various location of the river. In all three cases, the model run separately and the results obtained are compared with each other. The flow chart of the methodology is given bellow.

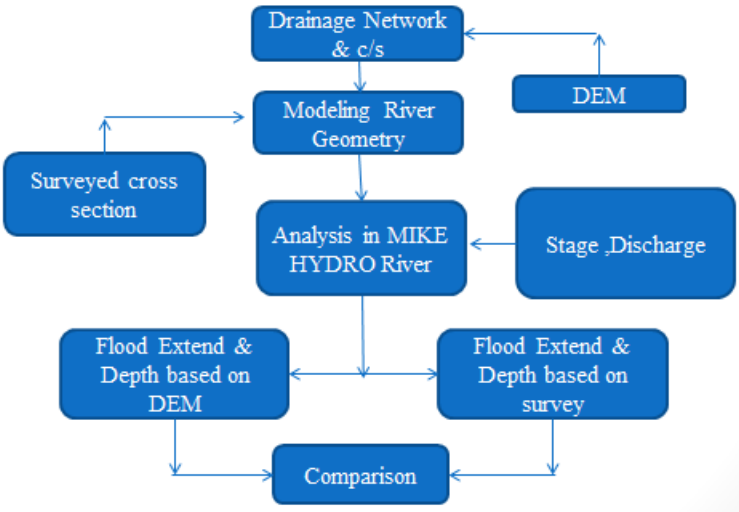



**Figure 2** flow chart of methodology

The MIKE HYDRO River setup requires mainly the creation of four modules. The first module is river network module. To setup hydrodynamic model, the river network of the rivers Pamba (0-38km), Manimala (0-15km), and Achenkovil (0-63km) have been considered. The river network has to be digitized using DEM data. For modelling purposes, flow direction is taken as positive and river type is taken as regular. Separate TOPO ID and BRS ID are given to each river in order identify them easily (DHI, 2017a).The second and most important module is river cross section module. In this study, there are three type of cross section modules were generated. One is generated from DEM, other is surveyed cross section last one is cross section generated from corrected DEM. The DEM cross sections were generated at the same locations of surveyed cross section as to compare them. There were 37 surveyed cross sections are available for the study. Then the cross section generated from DEM is compared with the surveyed cross section. After that, a correction is made on DEM with respect to the observed elevation from mean sea level (MSL). For this, the average difference of the elevations between the cross-section from the topographic survey and DEM are estimated and adjusted the elevation of the DEM. Then cross section from corrected DEM are also generated (DHI, 2017b).

Hydrodynamic parameter module is the third module. For a variety of variables used during hydrodynamic computation, the HD parameter editor provides the possibility of defining user-defined values. All parameters have default values in this editor and these values are considered to be good for obtaining satisfactory simulation results in most cases. The Manning's coefficient or bed resistance can be applied differently to various river reaches (DHI, 2017c).The last module is boundary condition module. The most important step of one dimensional HD model setup is the accurate definition of boundary conditions, including both upstream and downstream conditions. In this study we gave the time series of discharge of gauging stations as upstream boundary condition. The observed water level is taken as downstream boundary condition. For this we have to create dfs0 files of time series data (DHI, 2017a).

### 3.1.1 *Calibration of MIKE HYDRO River*

The hydrodynamic model can be calibrated using Manning’s coefficient n. initially the model was simulated using the default value of Manning’s roughness coefficient n as 0.033 in MIKE HYDRO River. The estimated water depth at the three rivers upstream was correlated with the respective observed values. Then the value of n is given different for each stretch of the river and again stimulates the model. To get a good agreement between the observed and stimulated water levels at upstream and downstream of the river, the Manning’s’ coefficient was calibrated to a uniform value. The observed water level in the downstream and upstream of the river is compared with the stimulated water level. The final value of the Manning’s coefficient of roughness was found to be within 0.03 to 0.06 ranges.

## 4. Result and Discussion

The cross sections of rivers were generated using DEM and corrected DEM in MIKE HYRO River. The comparison of cross sections generated from DEM and corrected DEM with the measured elevation from mean sea level is discussed here firstly. Then the calibration of MIKE HYDRO River results and the graphs of observed and stimulated water level graphs were shown. The output obtained from the MIKE HYDRO River in the form of flood depth, water level, and discharges are also obtained.

### 4.1 *Cross section*

The average water level difference of all the cross sections in each river between the generated cross sections from DEM and surveyed cross sections were calculated. Using the average difference from the surveyed cross section and DEM cross sections, the SRTM DEM of the study area is corrected. Then the cross sections generated from corrected DEM were also compared with the surveyed cross section. The river cross sections comparisons of all three rivers are shown below.

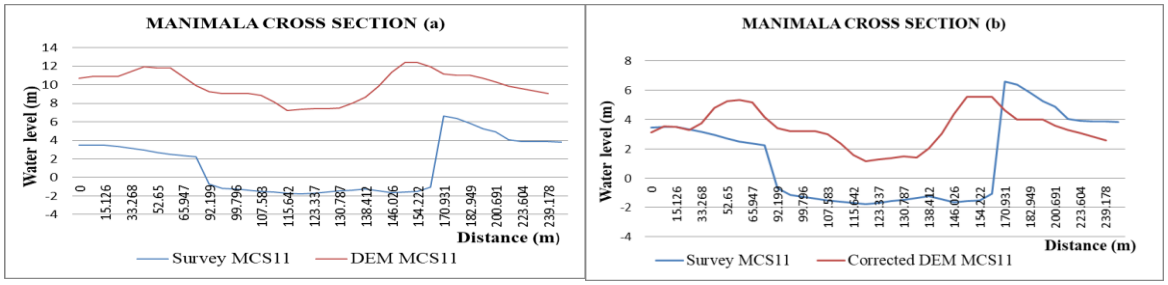



**Figure 3** Comparison of surveyed cross sections in Manimala River with a) DEM cross section b) Corrected DEM cross section

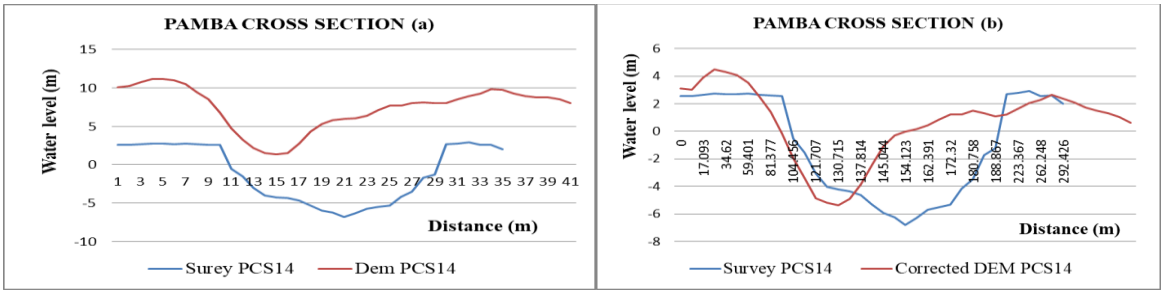



**Figure 4** Comparison of surveyed cross sections in Pamba River with a) DEM cross section b) Corrected DEM cross section

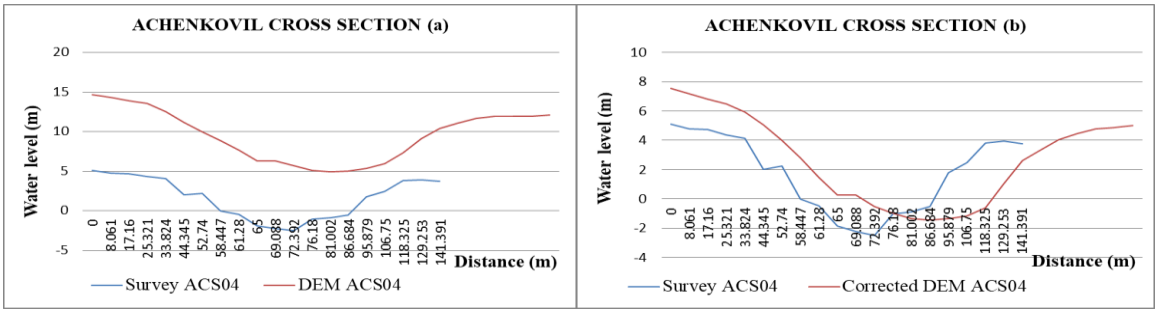



**Figure 5** Comparison of surveyed cross sections in Achenkovil River with a) DEM cross section b) Corrected DEM cross section

There was an average level difference of 6.78 m between the cross sections generated from SRTM DEM and surveyed cross section in Manimala River. When the DEM is corrected with observed elevation at mean sea level, the average level difference is reduced to 4.14 m. In Pamba River, the average level difference is 8.31m between the surveyed cross section and DEM cross section and the average water level difference is reduced to 4.01m, when the DEM is corrected with observed elevation from MSL. The same occurred in Achekovil River also. Initially, the average level difference is about 6.04m then, it is reduced to 3.23m.

### 4.1 *MIKE HYDRO River model- Calibration*

The MIKE HYDRO River was developed and simulated with default hydrodynamic parameters for surveyed cross section. Initially the manning's coefficient value is given as 0.033. Figure 6 shows the graph plotted with observed and simulated time series (TS) water level of Manimala, Pamba and Achenkovil Rivers.

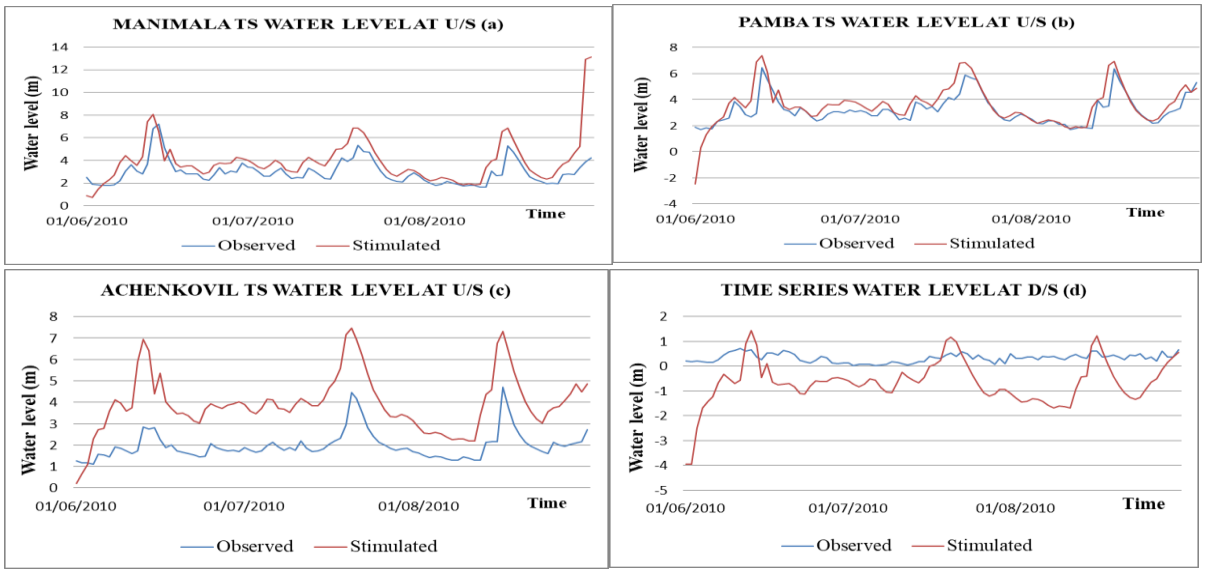



**Figure 6** Observed and simulated water level before calibration at a) Manimala River b) Pamba River, c) Achenkovil River d) Thottappally spillway

The model is calibrated by changing Manning's coefficient (n). It is changed for different stretches of different rivers, as the n value is not uniform throughout the length of the river. MIKE HYDRO River model was developed for three scenarios; i) with surveyed cross section ii) with cross section generated from SRTM DEM and iii) with corrected cross section from DEM. Using these values again run the model. Then the observed and simulated time series (TS) of water level at the upstream (U/S) become more close to each other as shown in Figures below.

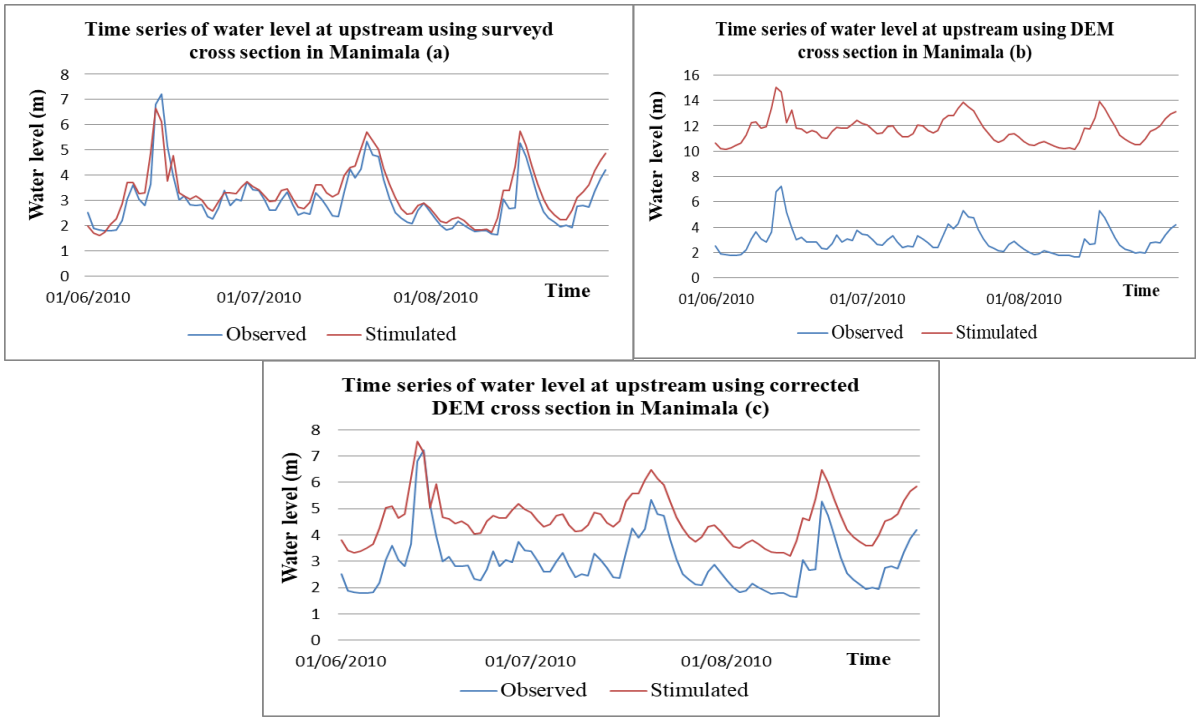



**Figure 7** Time series of water level at upstream in Manimala River using (a) Survey cross section (b) DEM cross section (c) Corrected DEM cross section

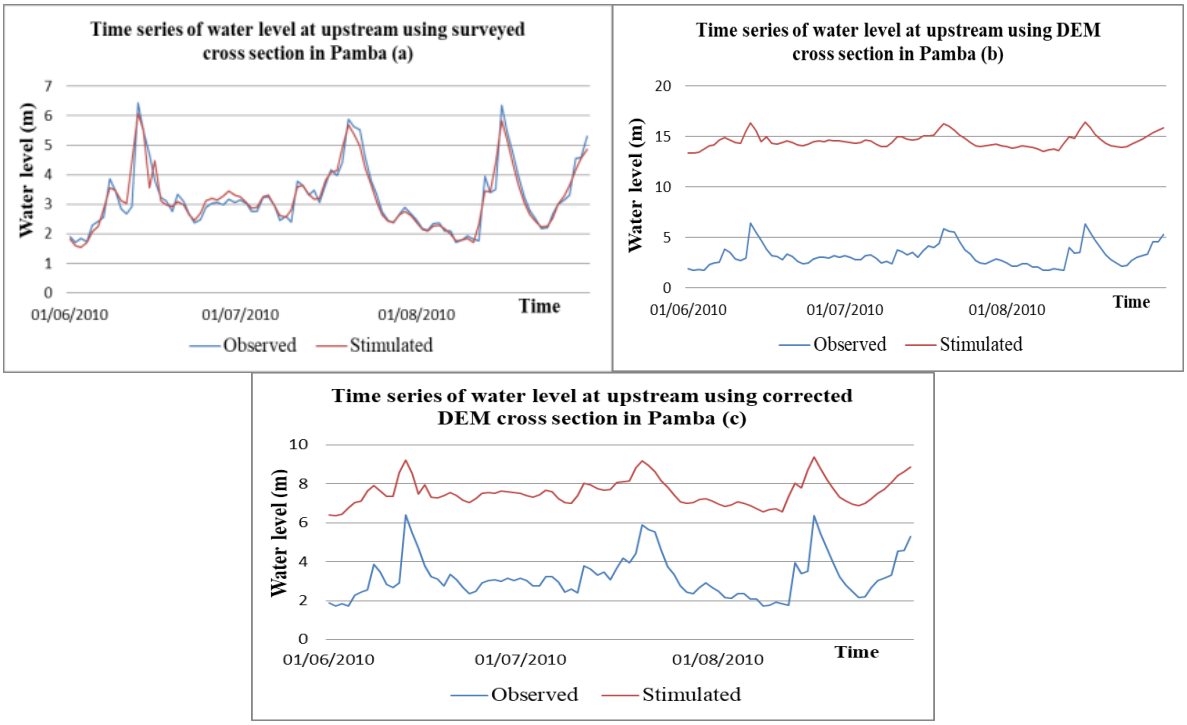



**Figure 8** Time series of water level at upstream in Pamba River using (a) Survey cross section (b) DEM cross section (c) Corrected DEM cross section

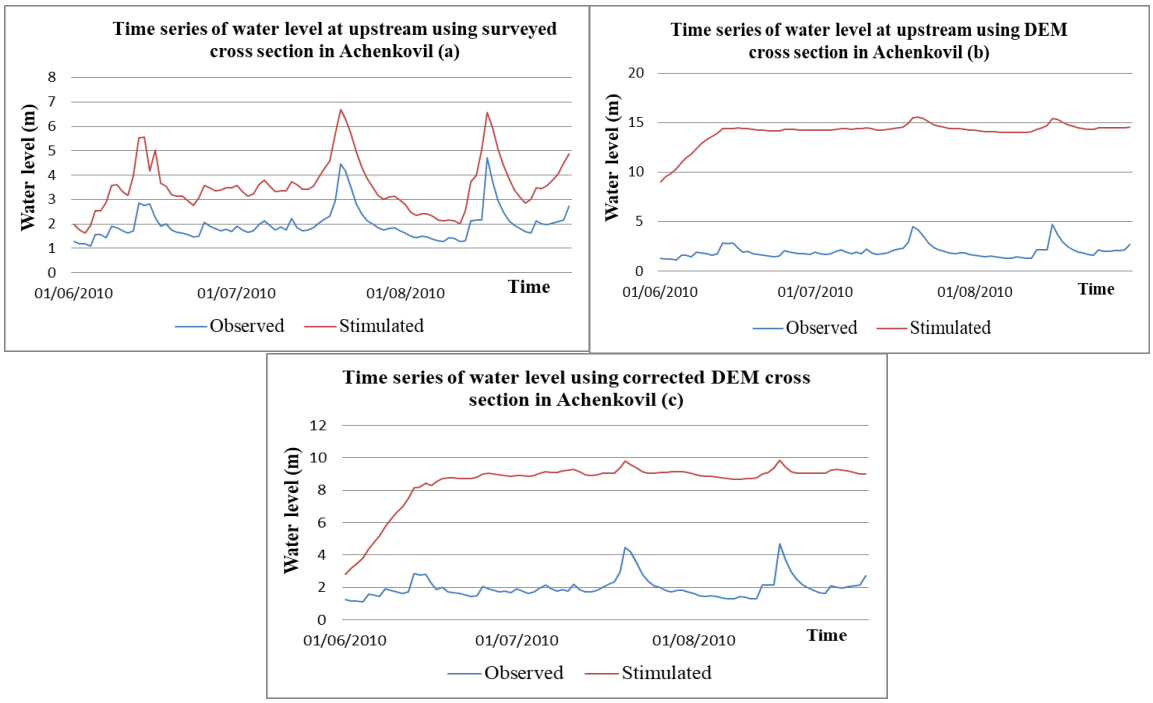



**Figure 9** Time series of water level at upstream in Achenkovil River using (a) survey cross section (b) DEM cross section (c) corrected DEM cross section

In all three rivers the observed values are more close to the simulated value from surveyed cross sections than the DEM cross section. In addition, when the corrected DEM is used for the simulation, the simulated value of water level became closer. The correlation coefficients obtained are given the Table 1.

**Table 1** Correlation coefficient values

| Points | Surveyed C/S | From DEM C/S | From corrected DEM c/s |
|---|---|---|---|
| Manimala | 0.931 | 0.941 | 0.941 |
| Pamba | 0.956 | 0.923 | 0.919 |
| Achenkovil | 0.935 | 0.529 | 0.388 |
| Thottappally | 0.969 | 0.969 | 0.969 |

In all three cases, we have obtained high values for correlation coefficient except for Achenkovil river.

### 4.1 *1D Model*

The 1D result of the MIKE HYDRO River for the three scenarios is described below. The flood depth, water level and discharge at different location of river are simulated for the three cases separately and compare the results obtained.

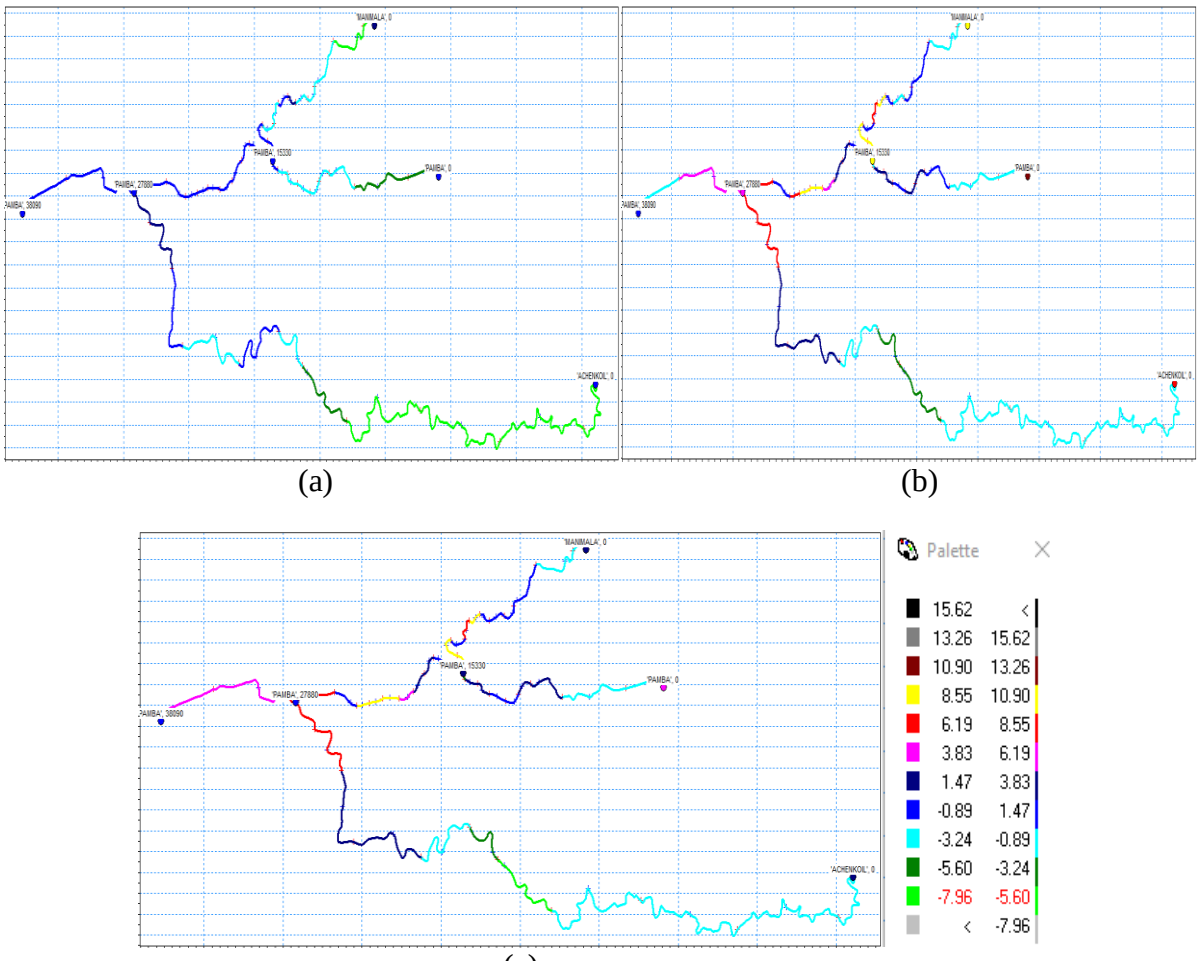



**Figure 10** Computed flood using (a) Survey cross section (b) DEM cross section (c) Corrected DEM cross section

The computed flood depth is indicated by using different colors s shown in the palette. . The maximum flood depth obtained by the model using surveyed cross section is in the range of 1.47 to

3.83 m. It shows high flooding in the range 1.47 to 3.83 m where Achenkovil river meets Pamba river. The model developed using DEM shows no flooding at the downstream end, which may not a correct depiction and the flood depth is higher than that from the model developed using surveyed cross section. In the case of the model developed using corrected DEM also the flood depth is more than the model developed using surveyed cross section. For the model, developed using DEM cross section and corrected DEM cross section have same maximum flood depth in the range of 8.55 to 10.90 m.

The maximam water level obtained by using surveyed cross section was in the rage of 1.48 m to 2.98 m. In the case of DEM cross section the range is between 11.96 m to 13.46 m. The water level simulated was reduced when the corrected DEM cross section was used for the simulation. Its value ranges from 4.47 m to 5.97 m. In all three cases the obtained discharges were in the same range and maximum value was in the range of 155.82 to 332.10 $m^3/s$.

## 5. Conclusion

The study is about the comparison of cross section obtained from DEM and surveyed cross section, and also the analysis of the results obtained by using these cross sections. At each cross section stage, discharge and flood depth values were obtained using the one dimensional model MIKE HYDRO River in three scenarios i.e., first one for surveyed cross section second for DEM cross section and the last one was corrected DEM cross section. . The water level and discharge simulated using observed cross section is very much comparable with the observed values. The correlation coefficient value obtained for the model developed using surveyed cross section were 0.93, 0.95 and 0.93, for the upstream of Manimala, Pamba, and Achenkovil respectively. The model developed using DEM cross section for Manimala, Pamba and Achenkovil gives correlation coefficient values as 0.94, 0.92, and 0.53 respectively. The obtained correlation coefficient values are slightly lesser for the model developed using corrected DEM cross section except for Achenkovil River. The downstream correlation coefficient values obtained for all the three cases were same.

The model developed using surveyed cross-section gives more accurate output, when compares with the model using DEM cross-sections. When the SRTM DEM is corrected with the observed elevation from MSL, the model developed gives more comparable values than the uncorrected DEM. Because the average water level difference between the DEM cross section and corrected DEM cross section with the surveyed cross section get reduced. The average water level difference for Manimala river cross section with the surveyed cross section was about 6.78 m and when the DEM was corrected, the water level difference is reduced to 4.14 m. The same trend is seen in Pamba and Achenkovil rivers also. In the same way the stimulated flood, water level and discharges from corrected DEM cross sections were also comparable with model developed using surveyed cross section. The simulated water levels from corrected DEM cross section have less difference with the observed water levels in the upstream and downstream of the river.

From the study, we can understand that, the model developed using DEM cross sections can be used for the simulation of one dimensional model when the measured cross sections were unavailable. We know that the measured cross sections are very rare and it is labour intensive and expensive work. Sometimes it is very difficult to measure the cross sections in the field due to obstrucles. In such cases, also we can depend on DEM cross sections which more economical compared to surveyed cross sections, provided the DEM shall be corrected with some observed elevation from mean sea level. The occurrence and intensity of flood has been increased now a day. So a detailed evaluation of the flood is needed. This study will help the water resources policy makers for arriving at suitable mitigation measures.

## 6. References

Alfiya S., Pradnya D., Dnyanedo B. (2015). Application of MIKE 11 for Flood Forecasting (A review). *International Journal of Modern Trends in Engineering and research*, 2(7), 520-530.

CWC (2018). Study report Kerala floods of August 2018. *Central Water Commission Hydrological Studies Organisation*, Government of India.

CWC (2019). Water year book of Central Water Commission, Bengaluru.

DHI. (2017a). MIKE HYDRO River, User guide, Danish Hydraulic Institute, Denmark.

DHI. (2017b). MIKE 11. A modelling system for Rivers and Channels, Reference Manual, Danish Hydraulic Institute, Denmark.

DHI. (2017c). MIKE 11. Rivers and Channels a short introduction – tutorial, Danish Hydraulic Institute, Denmark.

Gharbi M., Soualmia A., Dartus D., Masbernat L. (2016). Comparison of 1D and 2D Hydraulic Models for Floods Simulation on the Medjerda River in Tunisia. *Journal of Materials and Environmental Science*, 7 (8), 3017-3026.

IITM & CWRDM. (2011). Study for modernizing the Thanneer Mukkom bund and Thottappalli spillway for efficient water management in Kuttanad region, Kerala, Final report, Indian Institute of Technology Madras (IITM), Chennai and Centre for Water Resources Development and Management, Kozhikode, Kerala.

Jayakumar K.K. (2014). Rural and Urban Flooding in Kaveri Delta Controlling Factors and Vulnerability using GPS and Remote Sensing data. PhD Thesis. Bharathidasan University, Kombakonam.

Mahsa J.T.,Fernanda H.,Hong Z.,Graham J.,Yingying Y.(2020). Hydrodynamic modelling of a flood-prone tidal river using the 1D model MIKE HYDRO River: calibration and sensitivity analysis. *Environmental Monitoring and Assessment*, 192(97), 1-18.

Manoranjan Kumar. (2018). River flow simulation using MIKE11 and SRTM DEM data: Case of Mahanadi Delta region in India. *Annals of Plant and Soil Research*, 20(2), 130–138.

Mokhtar E. Pradhan B., Abd Halim Ghazali A.H., & Mohd Shafri H.Z. (2018). Assessing flood inundation mapping through estimated discharge using GIS and HEC-RAS model. *Arabian Journal of Geosciences*, 11, 1-20.

Navnith K.P., Kumaran,Damodaran Padmalal, RutaB. Limaye, Vishnu Mohan S., Tim Jennerjahn, PradeepG.Gamre. (2016).Tropical Peat and Peat land Development in the Floodplains of the Greater Pamba Basin, South-Western India during the Holocene. *Public Library of Science*, 11(5), 1-21.

Padma Priya T.V and Jane Mithra S. (2015). Socio-Economic Modeling of Pamba River Basin in Kerala State using Geospatial Technology. *International Journal for Innovative Research in Science & Technology*, 2(1), 1-17.

Rahman M., Arya D.S., Goel N.K., Anand Prakas Dhamy. (2011). Design Flow and Stage Computations in the Teesta River, Bangladesh, Using Frequency Analysis & MIKE 11 Modelling. *Journal of Hydrologic Engineering*, 16(2),176-186.

Ravindra K.S., Vasanta Govind Kumar V.,Srinivas P.,Rajesh n.(2020). Hydrodynamic modeling for identifying flood vulnerability zones in lower Damodar river of eastern India. *Ain shams engineering journal*, 11(4), 1-12.

*IN PROCEEDINGS OF 25th HYDRO 2020, INTERNATIONAL CONFERENCE, NATIONAL INSTITUTE OF TECHNOLOGY ROURKELA, ODISHA, INDIA 26-28, March 2021, ISBN 978-93-90631-56-8*

Paper ID - 269

# A Rainfall- Runoff Simulation Model for estimation of Floods for Purna River Basin Part of Upper Tapi Basin

Ankita Patel[1] , Prof. Darshan Mehta[2], Dr. S. M. Yadav[3]
[1]*Dr. S. & S.S. Ghandhy Gove. Eng. College, Surat and 395001, India*
[2]*Dr. S. & S.S. Ghandhy Gove. Eng. College, Surat and 395001, India*
[3]*Sardar Vallabhbhai National Institute of technology, Surat and 395007, India*
*Email: anki.pate116@gmail.com, darshanmehta2490@gmail.com*

## Abstract

Floods are the most widespread climate-related hazards in the world and affect more people around the world. Rainfall and subsequent runoff produced are the most important processes of hydrology. The aim of this research is to develop a rainfall runoff model for the Purna River basin (Upper Tapi). The objective of this study is to determine the runoff of Purna basin using Hydrologic Modelling System (HEC-HMS). Purna is one of important tributary of Tapi River. For the prediction of peak flow based upon the available historical precipitation data, land use condition, soil type and suitable routing method is selected. Digital elevation model was used to delineate the watershed. Using precipitation data hydrological model is developed in HEC-HMS. The main aim of this study is to develop modelling system for flood prediction for Purna basin. After optimization of the model result shows relatively close agreement between the simulated and observed flow values during the calibration period ($R^2$ = 0.95) and root mean square and mean absolute error are also low. So, this model helps to visualize the response of water systems due to changes in the land-use and meteorological events.

***Keywords:*** *Rainfall-Runoff, Purna river, Flood estimation, ARC-GIS, HEC-HMS*

## 1. Introduction

Flood have always been weather-related natural disasters, which have influenced human's life. The flood risks have also risen due to climate change and human interaction with the river systems. Human has been fighting with flood in different ways for a long time, but the fact must be accepted that flood is not fully controlled. Flood losses can be reduced by proper floodplain management. Watershed is natural hydrological unit that contributes to the storm runoff of a single watercourse which is classified on the basis of its geographical area. Water shortage in most of the water scarring area are caused by low or uneven rainfall pattern and not enough of capacity to conserve and manage the available natural rain-water. River runoff estimation which depends on rainfall is one of the prior requirements for planning and execution of water resource projects. Hydrologic modelling is a simplified representation of the real situation. Remotely sensed data offers useful and real-time spatial knowledge on natural resources and physical parameters. In this method remote sensing derived data can be well combined with the traditional runoff prediction data, this can aid in the planning of suitable soil and water conservation steps. [2]

The activities to estimate runoff volumes and flood peaks can be easily simplified by adopting a modelling concept and by understanding rainfall partitioning and the principal factors triggering runoff [14]. The type of the modelling approach normally depends on the purpose, data availability and ease of use [7]. Rainfall-runoff models are often used as a tool for a wide range of tasks, such as the modelling of flood events, the monitoring of water levels during different water conditions or the prediction of floods [3].HEC-HMS uses main three different models for each part of the runoff cycle which includes model for measuring runoff volume, for measuring direct runoff, and for measuring base flow. In which for every model run combines the model for basin, the model for metrological and the control specifications with the run options for results. It is a simple model and establishes a relationship between rainfall and runoff. [8]. These deterministic hydrologic models are classified into three major categories. Firstly, the lumped model, which assesses the catchment response simply at the outlet without obviously counting for an individual sub-basin's response. Secondly, the semi-distributed model, which is partly permitted to change in space with a division of the catchment into a number of sub-basins. The third

type of model is the distributed model, which permits its parameters to change in place at a resolution normally chosen by the client. Distributed hydrological models such as the European Hydrological System Model (MIKE-SHE) and Modular Modeling System (MMS), and semi-distributed models like the Hydrological Engineering Centre Hydrological Modelling System, Soil and Water Assessment Tool (SWAT),Topography Based Hydrological Model (TOPMODEL) and Hydrological Simulation Program-Fortran (HSPF) are developed for a runoff estimation based on the data availability and complexity of the hydrological systems. Hydrographs developed by HEC-HMS either directly or in conjunction with other software's are used for studies of urban drainage, water availability, future urbanization impact, flow forecasting, flood damage reduction, floodplain regulation, and systems operation [23] Therefore, the objectives of this study were: To develop the rainfall-runoff model and assess the runoff potential of the catchment; and to calibrate and validate the model and fix the corresponding calibrated values for future hydrological investigations in similar catchments within the basin and the nearby basins. The extraction of hydrologic information, such as flow direction, watershed boundaries, flow accumulation, and networks, from a DEM (digital elevation model) is through GIS applications. [1] The model is used in the Purna basin and its physical properties are used as model parameters. This study combined GIS with HEC-HMS, and analyse the model's suitability for the Purna Basin catchment.

## 2. Methodology

### *2.1 Study area*

Purna river watershed is the sub-basin of Upper tapi basin. Purna river is the principal tributary of the Tapi River. Purna river rises in the eastern Satpura Range of southern Madhya Pradesh, and flow westwards, draining Maharashtra's Marathwada, Vidarbha region before merging with the Tapi river. There are 15 major tributaries of Purna River. The purna meets the Tapi at Changdev Village in the Muktainagar Taluk of Jalgaon district in Northen Maharastra. It raises at the Gawilgarh hills at an elevation of 900m, North latitude 21° 38' 00" and East longitude 77° 36' 00" and flows in a south westerly direction for about 60 km. through hills and forests, where after it enters the purna plains. Purna drains a total geographic area of 18,929 Sq.km. Total length of Purna river is 379 km. The three stream gauging stations namely Gopalkheda, Lakhpuri, and Yerli gauging sites located at 229km, 226.7km and 299km respectively from the origin of the Purna River. There are 18 Rainguage stations available in Purna. [25]




**Figure 1** Purna river map

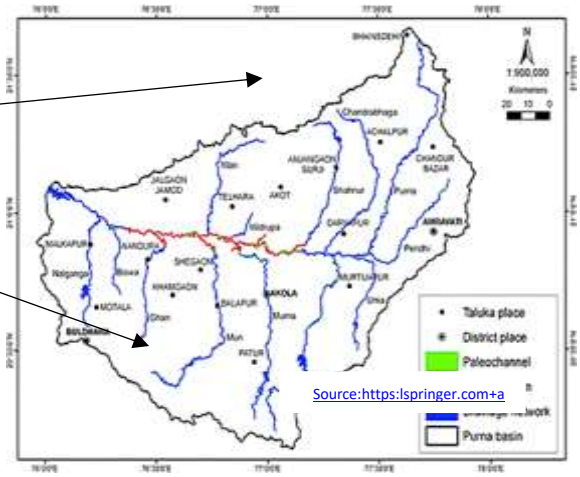



**Figure 2** Purna river Basin Drainage network

### *2.2. Data Collection*

Terrain data are SRTM DEM downloaded from https://bhuvan.nrsc.gov.in/ of year 2015. Hydrological data are Daily Rainfall, Discharge data of Lakhpuri and Gopalkheda site, Humidity, temperature, Manning's roughness, velocity, slope and water level data are collected from CWC, Surat.

### *2.3 Model development*

The information on physiographic characteristics of the watershed (elevation and slope) was extracted from a 30 m × 30 m resolution digital elevation model of the Purna Basin which was downloaded from the bhuvan site. The Geographic Information System (ArcGIS-Arcmap 10.1) interface of the HEC-GeoHMS model was used to further process the DEM data. Terrain pre-processing and basin processing tools were used to generate the characteristic parameters of the basin and input files for HEC-HMS.

#### *2.3.1 HEC-GeoHMS*

HEC-GeoHMS has been developed as a geospatial hydrological tool kits for hydrologist with less experience in GIS. It provides various program like Data Management, Terrain Processing, basin processing, Hydrologic parameter Estimation and HEC-HMS model Support, it help to create hydrologic input which directly used with HEC-HMS modeling. HEC-GeoHMS is an extension for ArcGIS and the spatial analyst extension. In this study we used HEC-GeoHMS version 10.1 as we have ArcGIS version 10.1. Terrain Processing: The first steps to develop HEC-GeoHMS project is Terrain Processing. In HEC-GeoHMS project additional eight dataset are required. First five data set are in form of grid layer (flow direction, flow accumulation, stream network, stream segmentation and watershed delineation) and net two dataset are in from of vector layer (watershed and stream**).** After that HEC-HMS project is created.

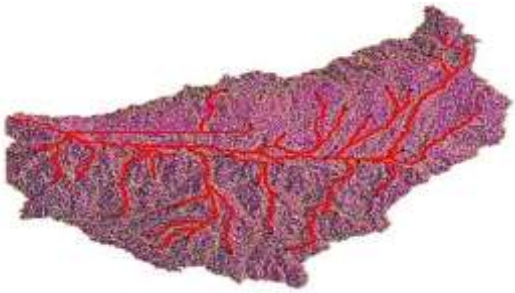


**Figure 3** Longest flow path tool result

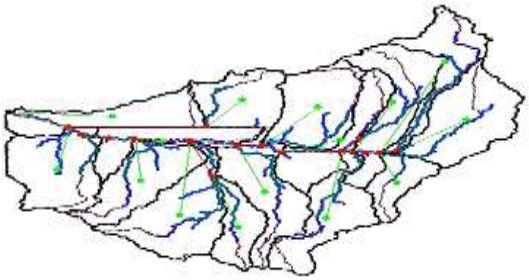


**Figure 4** Generated HEC-GeoHMS Purna Basin Project

#### *2.3.2 Creating LULC map*

Land use land cover (LULC) map used for the identify the basic change in the study area. We can find this that how much area was cover by the water, vegetation, forest, urbanization etc. by classify

the LULC map in different category. From Decadal land use and land cover classification across india 1985, 1995, 2005- Downloaded data LULC map was prepared in ARC-GIS. From FAO soil portal which gives the soil map of world. The soil map and purna basin map were selected for intersection, after intersection a map with new polygon representing the merged soil map was generated.

### *2.3.3 HEC-HMS Model*

The HEC-HMS model is used for large range of geographic areas and also for river basin water supplies, watershed runoffs and flood hydrology for the purpose of rainfall-runoff. US Army Corps of Engineers-Hydrologic Engineering Center (HEC) developed hydrological model (HEC-HMS).This model is conceptually semi- distributed and physically based model. This easily performs important tasks in relationto study of hydrology which includes losses, runoff transformation, routing of open channel, meteorological data analysis, rainfall runoff simulation and calculation of parameters . The methods selected for each component of the runoff process are- The SCS Unit hydrograph, Muskingum routing and Soil Conservation Service Curve Number as direct runoff, channel routing and runoff depth respectively.. [24]

1. Loss Model -HEC-HMS loss models usually measure the volume of the runoff by measuring the amount of water that is captured, invaded, deposited, evaporated, or occurred and subtracting it from the precipitation. For this analysis, the method of loss of the Soil Conservation Service number was chosen to estimate direct runoff from a design rainfall. It depends only on the curve number.

$$Pe = (P - Ia)\, 2\, P - Ia + S \quad (1)$$

where Pe -accumulated precipitation excess at time t (mm); P- accumulated rainfall depth at time t (mm); Ia - Initial abstraction (initial loss) (mm) = αS, α is 0.2 as a standard; S - potential maximum retention (mm), a measure of the ability of a watershed to abstract and retain storm precipitation.

$$S = \frac{25400}{CN} - 254 \quad (2)$$

where CN is curve number.

**Table 1**. Physiographic characteristics of the catchment

| Sr.No. | Station name | Sub-basin | HSG | Landscape | CN |
|---|---|---|---|---|---|
| 1 | Bhainsdehi | W720 | C | Forest | 73 |
| 2 | Yerli | W740 | C | Forest | 73 |
| 3 | Akola | W780 | D | Crop | 89 |
| 4 | Telhara | W790 | C | Crop | 85 |
| 5 | Edalabad | W850 | D | Forest | 79 |
| 6 | Chikhalda | W860 | D | Forest | 79 |
| 7 | Buldana | W900 | D | Crop | 89 |
| 8 | Nandura | W1010 | D | Crop | 89 |
| 9 | Amraoti | W1090 | D | Crop | 89 |
| 10 | Khamgaon | W1110 | C | Mixed forest+ Forest | 73 |
| 11 | Achalpur | W1120 | D | Cultivated crop | 89 |

| | | | | | |
|---|---|---|---|---|---|
| 12 | Shegaon | W1210 | D | Forest | 79 |
| 13 | Murtajpur | W1240 | D | Crop | 89 |
| 14 | Khamgaon | W1290 | C | Mixed forest | 73 |
| 15 | Balapur | W1320 | C | Forest | 73 |
| 16 | Patur | W1340 | C | Forest | 73 |

2. The Transform Model-The HEC-HMS transform prediction models simulate the cycle of direct runoff of excess precipitation on the watershed, and transform the excess of precipitation into point runoff. The Soil Conservation Service Unit Hydrograph model was used in this analysis to turn excess precipitation into runoff. This is a parametric model which is based on the Unit Hydrograph derived from measured runoff and rainfall data. Input for this method is Lag time ($T_{\text{lag}}$).

$$T_{\text{lag}} = 0.6\text{t}_\text{c} \tag{3}$$

where $T_{\text{lag}}$- Lag time, $T_c$ – Time of concentration both in minute. The time of concentration is calculated using the characteristics of the basin including length of reach and topography based on Kirpich formula

$$t_c = 0.0078\ \text{L}^{0.77}\ \text{S}^{-0.385} \tag{4}$$

where L- length of flow path in feet, S - slope in (ft/ft) Here S = Bed slope (0.436% for subbasin-1 and 0.01 to 0.1% for other)

3. Routing Model -Flood runoff becomes attenuated due to the effects of channel storage as it travels through the reach of the channel. For this attenuation the routing models available in HEC-HMS. The Muskingum routing method is a simple method in which calculation of the hydrograph of outflow at the downstream end of the channel reach from the upstream end of the inflow hydrograph is made. KQ - prism storage in the reach, K - proportionality coefficient, KX (I − Q) - volume of the wedge storage, where X is a weighting factor having a range of $0 \leq X \leq 0.5$. Now for X=0.25 Value of K from Muskingum graph is 9.32Hrs between two gauging site.

$$S = K\,[XI + (1 - X)\,Q] \tag{5}$$

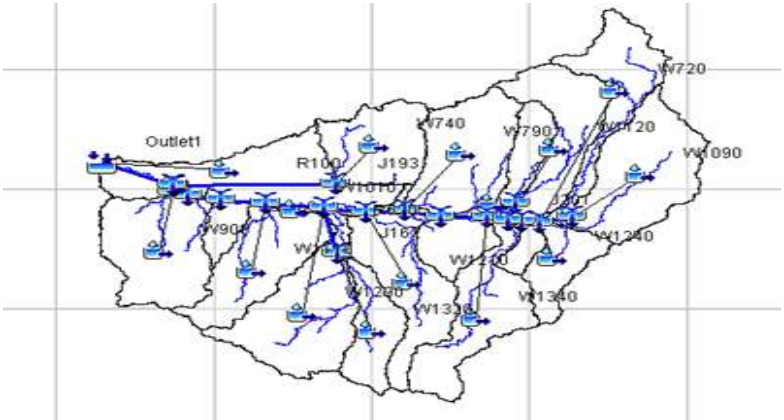



**Figure 5** Purna basin .hms file

After that all meteorological data- temperature, humidity, windspeed, Precipitation and observed discharge data are inputted in HEC-HMS.

## 3. Result and Discussion

### *3.1 LULC map and soil map*

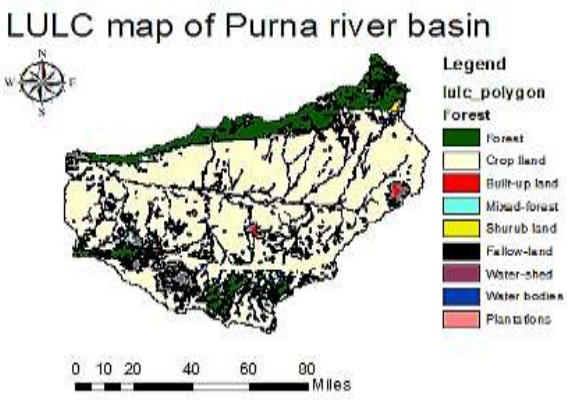



**Figure 6** LULC map of Purna river basin

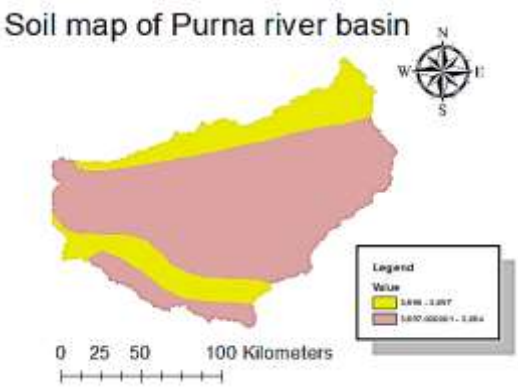



**Figure 7** Soil map of Purna river basin

Land use detail of Purna basin include area covered by crop land is 42.30%, forest land is 25.01%, mixed forest is 2.62%, shurub land is 8.81%, water bodies is 6.76%, fallow land is 4.74%, built up land is 1.90%, water-shed is 5.99%, and plantations is 1.87%. There are two type of soil in Purna basin -Vc and Bv. 1) Vc (Chromic Vertisols) are soils with a high proportion of swelling clays. These soil form deep wide cracks from the surface downward when they dry out, which happens in most years. Common local name is Black cotton soil in India. So this is D type soil. 2) Bv (Vertic Cambisols) is a soil with a beginning of soil formation. The horizon differentiation is weak. Cambisols are developed in medium and fine-textured materials. It is derived from a wide range of rocks, mostly in alluvial, colluvial and aeolian deposits. So, this is C type soil.

### *3.2 Model Calibration and Validation*

The process of modifying the model parameter value to obtain a fixed parameter value to find the best estimate of the observed discharge is known as the calibration of the model. In this study we used 2013,2014,2016,2017 data for the calibration of the model. The observed and simulated flow graph for all data and year is as below. In this study, the hydrological model results showed a reasonable fit between the model and the observations after optimization; the hydrographic shape and timing of the peaks matched well, although the model tended to overestimate the runoff before optimization. In most cases, the shape of the simulated hydrograph was accurately produced in the output of the model but the volume of runoff was overestimated in events 1,2, and 6 and also underestimated for the events (3, 4, and 5).

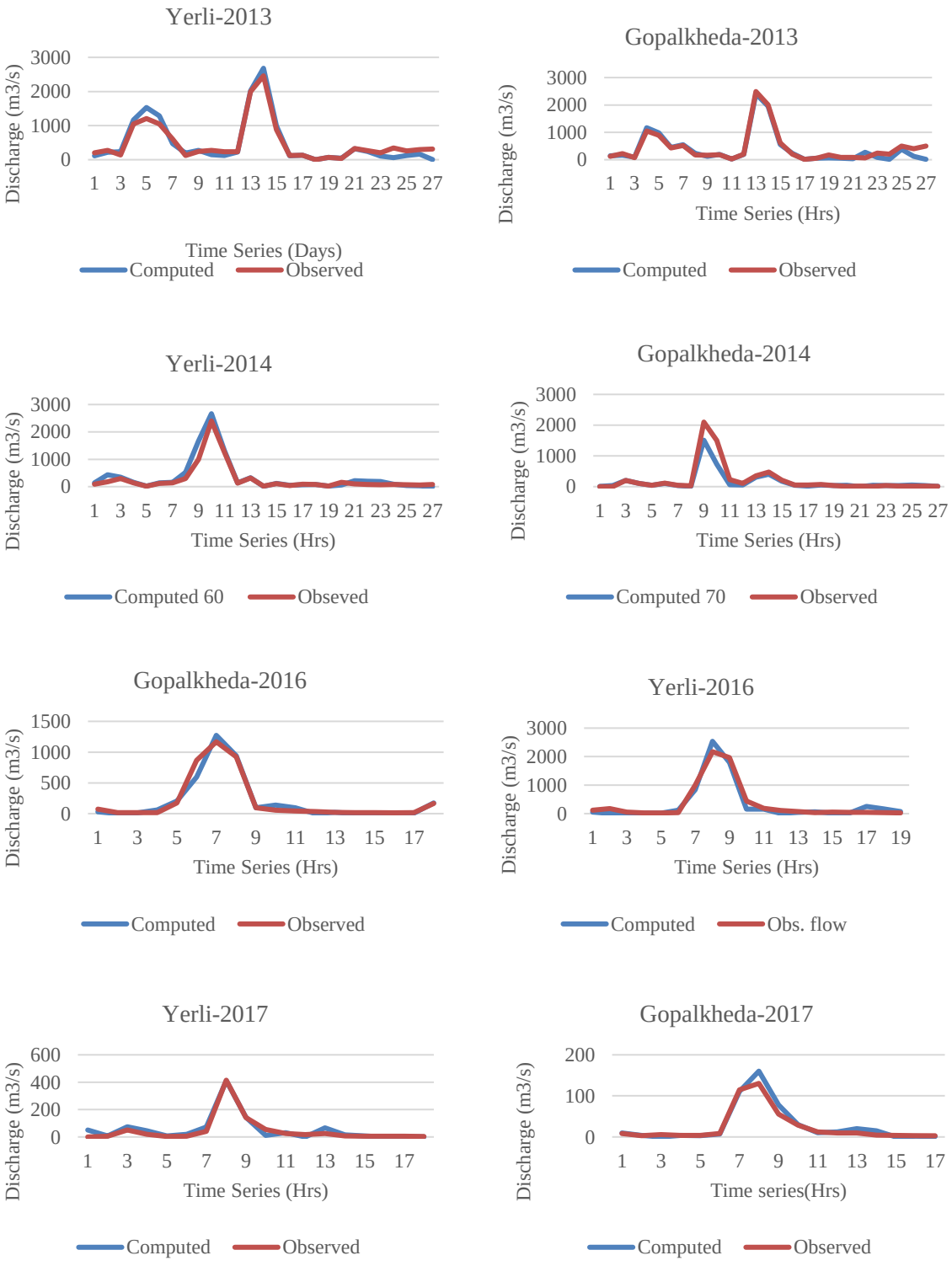
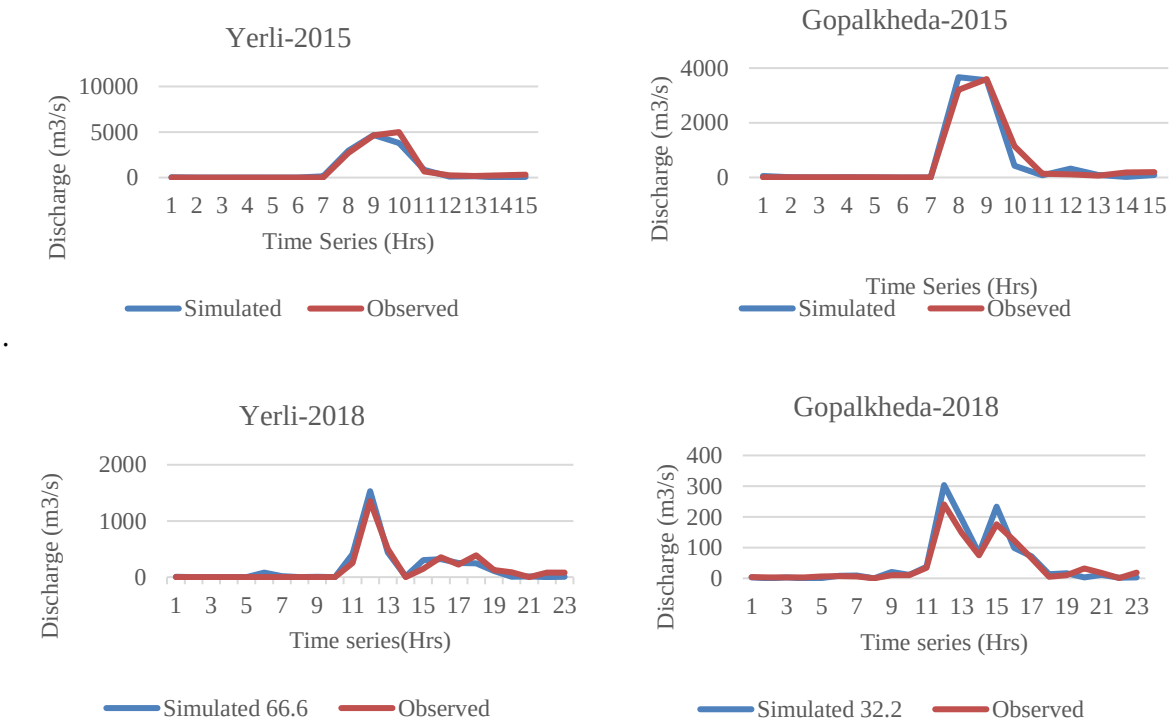



**Figure 8** Calibrated and observed hydrograph for Purna river watershed

Testing the model's ability to simulate the observed data for models other than those used for model calibration is known as model Validation. Validation of the model was done for event year 2015 and 2018 data by using optimized model parameters. Observed and simulated flow graph are shown as below

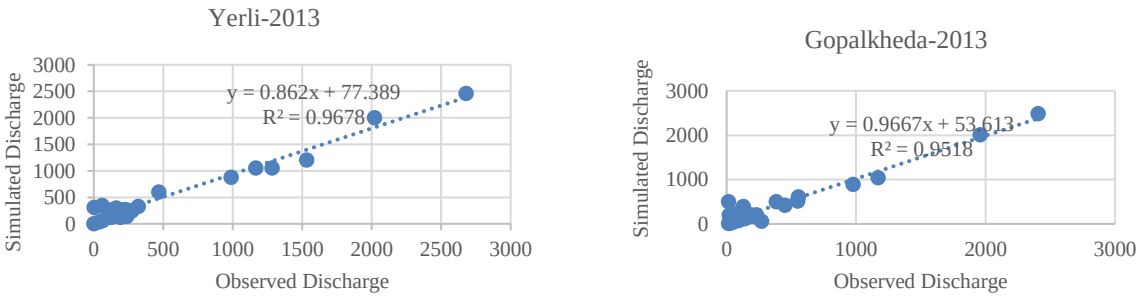



.

**Figure 9** Validated and observed hydrograph for Purna river watershed

The regression analysis is used to fit a linear model. In Linear regression calculation of an equation that minimizes the distance between the line and all data points is made. In general, the model fits the data well if the differences between the observed values and the predicted values of the model are small and unbiased. $R^2$ is a measure of statistics that shows how close the data is to the regression line. R^2 is always between 100 and 0%.

$$R^2 = \frac{\text{Explained variation}}{\text{Total variation}} \quad (6)$$



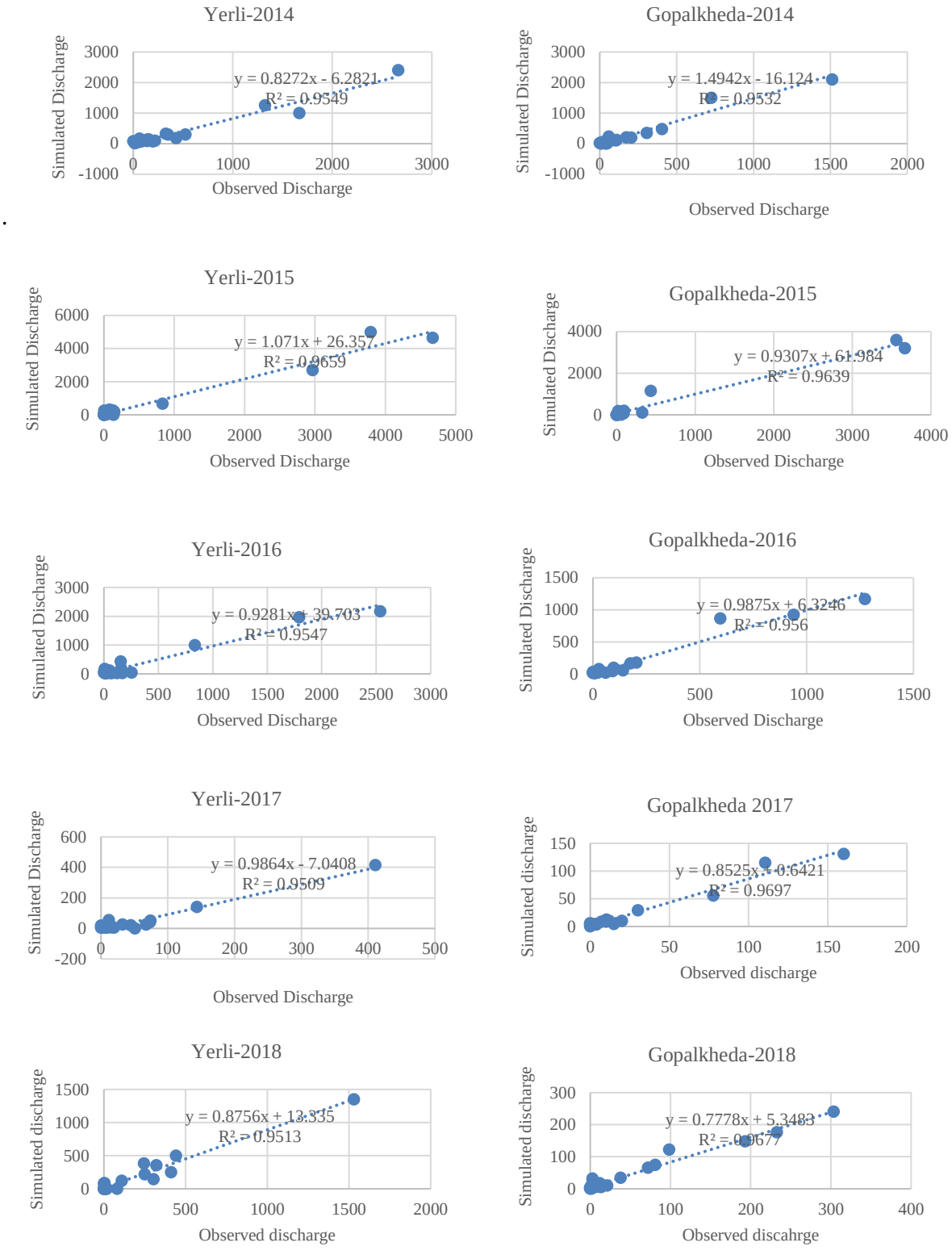



**Figure 10** Regression analysis graph of Purna river modelling result

The comparison of peak discharge between observed and simulated discharge and all errors is summarised as below.

1. Mean Absolute Error (RME):

$$\text{RME} = \frac{1}{n}\sum| Y_i - X_i | \quad (7)$$

where RE$i$ is relative error percent for each of events, $Y_i$ is observed peak discharge, and $X_{i_i}$ is computed peak discharge.

2. Root of Mean Square Error (RMSE):

$$\text{RMSE} = [\frac{1}{n}(\sum \text{SEi})]^{1/2}; \text{SE}i = (\text{Qop} - \text{Q cp})^2 \quad (8)$$

where RE$i$ is relative error percent for each of events, $Q$op is observed peak discharge, and $Q$cp is computed peak discharge.

3. Nash–Sutcliffe model efficiency coefficient (NSE) :

$$\text{NSE} = 1 - \frac{(\text{Qcp} - \text{Q op})^2}{(\text{Qop} - \text{Q mean})^2} \quad (9)$$

$Q$op is observed peak discharge, and $Q$cp is computed peak discharge.Nash–Sutcliffe efficiency can range from $-\infty$ to 1. An efficiency of 1 ($NSE = 1$) corresponds to a perfect match of modelled discharge to the observed data. Gopalkheda site

**Table 2** Result summary table of Gopalkheda site

| Year | Date | Simulated discharge ($m^3$/s) | Observed discharge ($m^3$/s) | NSE | $R^2$ | RMSE ($m^3$/s) | MAE ($m^3$/s) |
|---|---|---|---|---|---|---|---|
| 2013 | 1Aug | 2405.3 | 2489.9 | 0.982 | 0.9518 | 80.959 | 8.88 |
| 2014 | 23Jul | 1510.5 | 2100 | 0.832 | 0.9532 | 188.59 | 58.77 |
| 2015 | 6Aug | 3666.0 | 3598.1 | 0.958 | 0.956 | 233.86 | 23.56 |
| 2016 | 12Jul | 1272.7 | 1167.9 | 0.955 | 0.9639 | 72.82 | 3.594 |
| 2017 | 30Jul | 160.2 | 130.4 | 0.932 | 0.9697 | 9.67 | 3.183 |
| 2018 | 17Aug | 303.3 | 240.5 | 0.882 | 0.9677 | 22.2 | 5.5 |

Yerli site

**Table 3** Result summary table of Yerli site

| Year | Date | Simulated discharge ($m^3$/s) | Observed discharge ($m^3$/s) | NSE | $R^2$ | RMSE ($m^3$/s) | MAE ($m^3$/s) |
|---|---|---|---|---|---|---|---|
| 2013 | 2Aug | 2680.1 | 2457.8 | 0.943 | 0.9678 | 137.88 | 10.41 |
| 2014 | 23 Jul | 2663.7 | 2400 | 0.896 | 0.9549 | 158.38 | 62.92 |
| 2015 | 6Aug | 4695.3 | 4654.2 | 0.958 | 0.9547 | 336.59 | 86.91 |
| 2016 | 12Jul | 1791.6 | 1968.1 | 0.911 | 0.9659 | 143.61 | 15.78 |
| 2017 | 30Jul | 410.8 | 414.7 | 0.944 | 0.9509 | 22.49 | 7.772 |
| 2018 | 17Aug | 1529.7 | 1350.6 | 0.932 | 0.9513 | 76.29 | 6.99 |

This study's events were selected by comparing the runoff produced for the respective rainfalls. In the rainfall-runoff modelling the parameters and initial storage and fraction scale factor show a high variability and parameters of Muskingum routing (K and X) and curve number are constant in the all events. These results shows the impact of topography of the basin area, soil type detail, land use and other characteristics of the catchments. According to the result of the MAE as can be seen in result table, the error is relatively small for all flood events. The flood runoff is driven by excess infiltration under the condition of short but heavy rainfall, or by a mixture of infiltration and excess saturation under the condition of long-lasting rainfall of different intensity.

Outlet

**Table 4** Result summary table of Simulated Discharge and volume at outlet

| Year | Date | Gopalkheda | | Date | Yerli | | Date | Outlet | |
|---|---|---|---|---|---|---|---|---|---|
| | | Q ($m^3$/s) | Volume (mm) | | Q ($m^3$/s) | Volume (mm) | | Q ($m^3$/s) | Volume (mm) |
| 2013 | 1/8 | 2405.3 | 257.45 | 2/8 | 2680.1 | 126.76 | 2/8 | 5090 | 386 |
| 2014 | 23/7 | 1510.5 | 178.6 | 23/7 | 2663.7 | 124.5 | 23/7 | 4178 | 305 |
| 2015 | 6/8 | 3666.0 | 194.18 | 6/8 | 4695.3 | 124.11 | 6/8 | 8365 | 320 |
| 2016 | 12/7 | 1272.7 | 150.6 | 12/7 | 1791.6 | 105.6 | 12/7 | 3078 | 260 |
| 2017 | 30/7 | 160.2 | 39.01 | 30/7 | 410.8 | 9.18 | 30/7 | 575 | 50 |
| 2018 | 17/8 | 303.5 | 25.79 | 17/8 | 1529.7 | 36.78 | 17/8 | 1847 | 65 |

From table it is possible to conclude that runoff in most events is caused by the combination of infiltration and saturation excess due to strong intensity rainfall. The calculated RMSE and MAE error values in both total volume and peak flow between simulated and observed values in all pre-optimization simulations were very high, falling within the range of the peak flow between the absolute value of 500 to 1000 (m^3 / s). In light of this finding, a sensitivity analysis was carried out to determine the most sensitive parameter for methods of loss, transformation, and routing. It was noticed that the model's curve number, initial abstraction, and lag time were, respectively, more sensitive, less sensitive and insensitive parameters. After optimization, the values in this study were reduced to 5 to 350($m^3$/s) for the peak flow. The result is better for this model. The positive values indicate model underestimation bias in this statistic assessment test, and the negative values indicate model overestimation bias. Result table of both site show a relatively close agreement between the observed and simulated peak flow values at the period of calibration ($R^2$ = 0.956) after optimization. More specifically, Event of year 2015 had the highest MAE and RMSE. These might be due to high peak discharges in this year. Considering the Nash–Sutcliffe Efficiency (NSE) criteria, better results were obtained between the simulated and observed values, with a mean NSE value of 0.92. Therefore, the model performs well. Finally, the three statistical assessment criteria with mean values in this study showed good simulation between the estimated and observed values. The results of this study generally provide basic information on the extent of the total volume and peak flow generated in the catchment from the respective rainfall events, which in turn are useful for the planning, design and management of various water resources activities. This study would help in the proper management of Purna River catchment..

## 4. Conclusion

HEC-HMS has been used for rainfall runoff modeling of Purna sub-catchment of Tapi basin India. Real time Rainfall-runoff modelling process is carried out in this study for Purna river basin using HEC-HMS model and SCS-CN methods. Land use land cover map was generated which shows majority of land 42.30% is crop land. Soil map was generated which shows two types of soil class C & D. Watershed physical parameters such as Curve Number grid, Basin lag time, initial abstraction, maximum potential retention, flood wave traveling time (K), and weighted coefficient of discharge (X) have been used as input data in addition to stream flow and precipitation data. Curve Number was found for each sub-basin by using this two maps and NLCD class. Basin lag time and time of concentration for each sub-basin was calculated by using Kirpich equation. Muskingum constants K(hrs) and x=0.25 was finalised using Muskingum method and calibration of model. The rainfall-runoff simulation was conducted with the 2013,2014,2016 and 2017 rainfall data. The model was calibrated to optimize the parameters using 2013,2014,2016 and 2017 data. The model was validated for 2015 and 2018 data using optimized parameters. Among the watershed physical parameters used for rainfall runoff modeling of this study, flood wave travel time (K) and weighted coefficient of discharge (X) have been more sensitive and model calibration and validation were carried out. NSE and Regression value $R^2$ have been used for model performance evaluation. The model validation with optimized lag time values showed the RMSE and MAE reduced to 5 to 350($m^3$/s) for the peak flow. Very small difference between observed and simulated discharges for 2013 and 2018 year. Also, the comparison of observed and simulated hydrographs with high $R^2$ value (0.956) shows the capability of the model to be used in hydrologic simulation in Purna watershed. The final peak flow obtained from the model was nearly close to the observed peak flow for both site Gopalkheda and Lakhpuri. Discharge at outlet was estimated for all events. Performance of the model was also evaluated by regression analysis which gave Highest $R^2$ value 0.956 at Gopalkheda gauging site for year 2015. The value of MSE and RMSE is 23.56($m^3$/s) and 233.86 ($m^3$/s). So, from these result it can be seen that model is best suitable for year 2015. As model evaluation parameter gives the good answer so conclusion is made that existing rain gauge network is sufficient for flood forecasting. With these results one can conclude that HEC-HMS can be applicable in order to develop rainfall runoff modeling for the specified basin and computed flow can be represented the direct observed flow with further catchment investigation and modification. Reliable estimates of stream flow from a catchment are required to help policy makers to inform decisions on water planning and management. This runoff model helps to visualize the response of water systems due to changes in the land-use and meteorological events. For instance, the real-time flood forecasting and warning that is operational in many countries, utilizes the results of rainfall-runoff modeling. So far, these hydrological models also estimate flood frequencies, provide inputs for flood routing and inundation prediction. For the case of this study, the main target of rainfall runoff modeling was to obtain peak flood at the outlet of the Purna sub-catchment. Therefore, input – output relationships are relatively unique and the only mechanism dominates the runoff formation. Lastly, the methodologies developed in this research can also be applied in other ungauged catchments and similarly characterized regions.

## References

Abushandi, E., & Merkel, B. (2013). Modelling rainfall runoff relations using HEC-HMS and IHACRES for a single rain event in an arid region of Jordan. Water Resources Management, 27(7), 2391-2409.

Alexakis, D. D., Grillakis, M. G., Koutroulis, A. G., Agapiou, A., Themistocleous, K., Tsanis, I. K., ... & Retalis, A. (2014). GIS and remote sensing techniques for the assessment of land use change impact on flood hydrology: the case study of Yialias basin in Cyprus. Natural Hazards and Earth System Sciences, 14(2), 413-426.

Azam, M., Kim, H. S., & Maeng, S. J. (2017). Development of flood alert application in Mushim stream watershed Korea. *International Journal of Disaster Risk Reduction*, *21*, 11-26. doi:10.1016/j.ijdrr.2016.11.008

Basarudin, Z., Adnan, N. A., Latif, A. R. A., Tahir, W., & Syafiqah, N. (2014). Event-based rainfall-runoff modelling of the Kelantan River Basin. In IOP conference series: earth and environmental science (Vol. 18, No. 1, p. 012084). IOP Publishing.

Bose and AS Chandra, "WATERSHED DELINEATION AND STREAM NETWORK ANALYSIS UISNG GIS." International Journal of Watershed Engineering Hydrabad VOL – 1, ISSUE – 1,2014.

Choudhari, K., Panigrahi, B., & Paul, J. C. (2014). Simulation of rainfall-runoff process using HEC-HMS model for Balijore Nala watershed, Odisha, India. International Journal of Geomatics and Geosciences, 5(2), 253.Natarajan, S., & Radhakrishnan, N. (2019).

Derdour, A., Bouanani, A., & Babahamed, K. (2018). Modelling rainfall runoff relations using HEC-HMS in a semi-arid region: Case study in Ain Sefra watershed, Ksour Mountains (SW Algeria), *Journal of Water and Land Development*, *36*(1), 45-55. doi: https://doi.org/10.2478/jwld-2018-0005

Giuli, D., Baldini, L., & Facheris, L. (1994). Simulation and modeling of rainfall radar measurements for hydrological applications. In Recent Studies in Geophysical Hazards (pp. 109-122). Springer, Dordrecht.

Gumindoga, W., Rwasoka, D. T., Nhapi, I., & Dube, T. (2017). Ungauged runoff simulation in Upper Manyame Catchment, Zimbabwe: Application of the HEC-HMS model. Physics and Chemistry of the Earth, Parts A/B/C, 100, 371-382.

Haibo, M., Xin, D., & Wenjuan, C. (2018). Application of Synthetic Unit Hydrograph on HEC-HMS Model for Flood Forecasting. In MATEC Web of Conferences (Vol. 246, p. 01076). EDP Sciences.

Halwatura, D., & Najim, M. M. M. (2013). Application of the HEC-HMS model for runoff simulation in a tropical catchment. Environmental modelling & software, 46, 155-162.

Haque, Shammi, AKM Saiful Islam, GM Tarekul Islam, Mashfiqus Salehin, and Md Jamal Uddin Khan. "Event Based Flash Flood Simulation at Sunamganj using HEC-HMS."

Ibrahim-Bathis, K., & Ahmed, S. A. (2016). Rainfall-runoff modelling of Doddahalla watershed—an application of HEC-HMS and SCN-CN in ungauged agricultural watershed. Arabian Journal of Geosciences, 9(3), 170.

J. Joo, T. Kjeldsen, H.-J. Kim, H. Lee, A comparison of two event-based flood models (ReFH-rainfall runoff model and HEC-HMS) at two Korean catchments, Bukil and Jeungpyeong, KSCE J. Civ. Eng. 18 (2014) 330–343. http://dx.doi.org/ 10.1007/s12205-013-0348-3

Kishanlal Darji, Vidhi Khoklani, Dr. Indra Prakash, Khalid Mehmood (2019). Rainfall Runoff modelling Using HEC-HMS Model: An application of regression analysis. Journal of Emerging Technologies and Innovative Research (JETIR),6(5), 190.

Khaleghi, S., Mahmoodi, M., & Karimzadeh, S. (2015). Integrated application of HEC-RAS and GIS and RS for flood risk assessment in Lighvan Chai River. Int J Eng Sci Invent, 4(4), 38-45.

Latif, Muhamad Zulhilmi Abdul. "Simulation of Flood Event in Kelantan on December 2014 as Revealed by the HEC-HMS." *Journal of the Civil Engineering Forum* 4, no. 3 (2018): 215. https://doi.org/10.22146/jcef.34020.

Makkena, J. (2016). Modelling the hydrology of watershed by using HEC-HMS (Doctoral dissertation, Kelappaji College of Agricultural Engineering and Technology, Tavanur).

Mandal, S. P., & Chakrabarty, A. (2016). Flash flood risk assessment for upper Teesta river basin: using the hydrological modeling system (HEC-HMS) software. Modeling Earth Systems and Environment, 2(2), 59.

Masseroni, D., Cislaghi, A., Camici, S., Massari, C., & Brocca, L. (2016). A reliable rainfall–runoff model for flood forecasting: review and application to a semi-urbanized watershed at high flood risk in Italy. Hydrology Research, 48(3), 726-740.

Martin, O., Rugumayo, A., & Ovcharovichova, J. (2012). Application of HEC HMS/RAS and GIS tools in flood modeling: A case study for river Sironko–Uganda. Journal of Engineering, Design and Technology, 1(2), 19-31.

Mistry, A., Lodha, P. P., Prakash, I., & Mehmood, K. (2017). Estimation of direct runoff for purna river sub-basin, using SCS-CN method, Dangs District, Gujarat. Development, 4(4).

Mokhtari, E. H., Remini, B., & Hamoudi, S. A. (2016). Modelling of the rain–flow by hydrological modelling software system HEC-HMS–watershed's case of wadi Cheliff-Ghrib, Algeria. Journal of Water and Land Development, 30(1), 87-100.

Srivastava AK, Kale VM. Purna River, Maharashtra. InThe Indian Rivers 2018 (pp. 479-502) Springer, Singapore.

Water year book tapi 2016

IN PROCEEDINGS OF 25th HYDRO 2020, INTERNATIONAL CONFERENCE,
NATIONAL INSTITUTE OF TECHNOLOGY ROURKELA, ODISHA, INDIA
26-28, March 2021, ISBN 978-93-90631-56-8

Paper ID - 270

# Hydrodynamic challenges and role of physical model in evolving layout of boat landing facility at confluence of Elephanta deep and Nhava creek

A.A. Purohit[1], A. Basu[2], K.A. Chavan[3] and Dr. J.D. Agrawal[4]

[1]Scientist-D, Central Water & Power Research Station, Pune- 411024, India
[2]Scientist-B, Central Water & Power Research Station, Pune- 411024, India
[3]Research Assistant, Central Water & Power Research Station, Pune- 411024, India
[4]Scientist-E, Central Water & Power Research Station, Pune- 411024
Email: purohit_aa@cwprs.gov.in

## Abstract

Jawaharlal Nehru (JN) Port is developing a mega container terminal in Thane creek and as a social responsibility, development of boat landing jetty at the confluence of Elephanta deep/Nhava creek for the transport of passengers from Nhava Island to Mumbai is under consideration. JN port area is free from wave disturbance being well inside from the entrance to Arabian Sea. However presence of macro type of tides (range of 5 m), siltation; govern the hydraulic design criteria for waterfront facilities. The location of boat landing jetty is in hydrodynamically complex region wherein steep bathymetry varying from +1 m CD at entrance of Nhava Creek to -15 m CD at recently deepened navigational channel of JN Port exists. It causes change in the direction of flow, formation of dynamic eddies and flooding/drying of area in-front of jetty. As such to finalise the safe alignment of boat landing jetty, studies were carried out in a distorted physical model (Scale 1:400(H) & 1:80(V)). The flow patterns observed during tidal phase reveal that, current strengths are strong (1.27 m/sec-0.97 m/s during spring/neap tide), while its direction varies between $214^0$-$224^0$ N and also there are formation of dynamic eddies during few hours of ebb tide. Thus, original jetty alignment at $26^0$ N needs modification to $36^0$ N and reclamation on leeside of jetty further improves the flow field at jetty. Dredging up to 1.2 m depth below CD over an area of 2.5 ha, in front of jetty also improves the operability at the jetty.

***Keywords: Creek; Eddy; Hydrodynamics; Jetty; Tides***

## 1. Introduction

Among the maritime countries in the World, India has a long coastline of about 7,500 km and to serve the waterborne transport need of the country, it is having 12 major and about 200 minor/intermediate ports. The ports/shipping industry play a vital role in achieving sustainable growth of the country's trade/commerce and around 95 percent of India's trading by volume and 70 percent by value is accomplished through maritime transport. The major ports like Mumbai & Jawaharlal Nehru (JN) (situated on the west coast of India in Thane creek) had played a vital role in maintaining sustained growth of country's trade by developing minor/mega waterfront facilities. The JN port which handles almost 56% of the Container transshipment among all the major ports of the country has five dedicated container terminals along with a liquid cargo berth and shallow water berths to handle other commodities. The existing waterfront facilities of JN port does not face the problem of wave disturbance in view of their locations being well inside in the Thane Creek. However, due to the presence of macro- semidiurnal type of tidal phenomenon (tidal range of 5 m) in the region with ultra-wide estuarine entrance of about 10 km and water area extending 30-40 km north in Thane estuary, it contributes to large exchange of water mass in and out of the creek during flood/ebb phase of the tide. The ships plying from JN Port to the Arabian Sea makes the use of Main Navigational Channel in the Thane creek and is shared with Mumbai Port up to Butcher Island from offshore end. Recently deepening of entire main navigational channel (15-16 m depth below CD) has been completed by JN port. The local villagers from Nhava Island through small passenger boats ply up to Mumbai through beaching facility at Nhava headland and needs a safe berthing facility at Nhava creek entrance. Thus JN port as a social responsibility, proposes to construct a boat landing jetty at the confluence of Nhava creek and Elephanta Deep at Nhava island headland. The location plan of the boat landing jetty is shown in Figure 1.

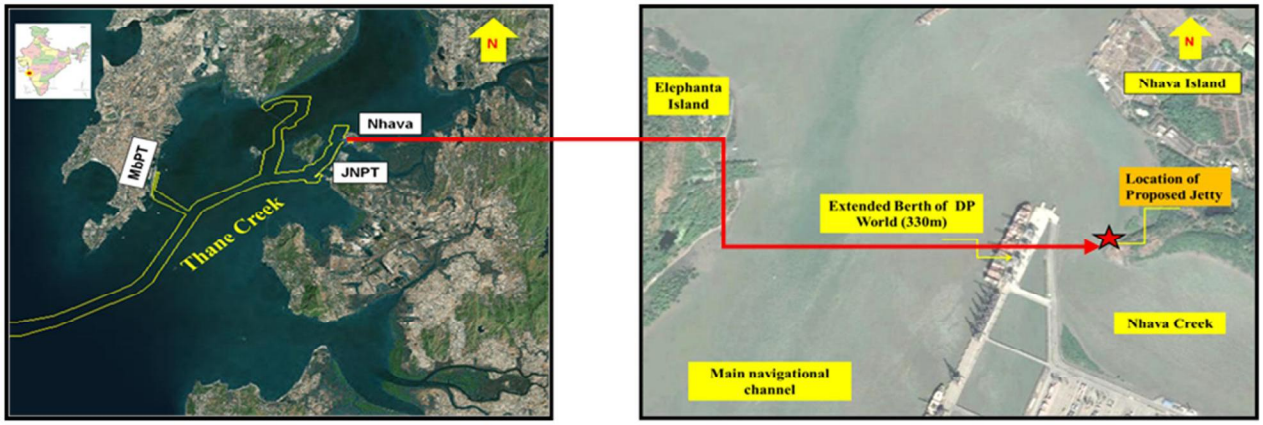



**Figure 1** Overall view of Thane creek and proposed location of boat landing jetty

## 2. Complexity at the entrance of Nhava creek

The location of proposed boat landing jetty at the headland of Nhava Island is not only in geographically complex region as shown in Figure 1 but also a challenging task to coastal engineer to make it feasible due to other hydrodynamic considerations. The hydrodynamic complexity of the region is mainly due to the presence of very steep bathymetry viz. +1 m CD near the jetty location and -15 m in the main navigational channel at the Elephanta deep along with presence of 160 m long guide bund at 10˚ N constructed to achieve safe berthing for 330 m long terminal (DP world). This constricts the tidal flow between bund and Nhava headland. Thus, presence of steep bathymetry at bund side, availability of no water during initial hours of flooding near the proposed jetty and drying during last hours of ebb tide (especially during spring tidal cycle) creates undesirable flow field in this region. It results in strong tidal current (about 1 - 1.7 m/sec during different phases of spring tide), dynamic eddy formation (during the ebb phases of tide) in the approaches towards the proposed jetty. Thus, to finalise the safe/suitable alignment of the proposed boat landing jetty, increase operability, proper simulation of flooding/drying of areas, dynamic eddy formation near the jetty location is essential. Therefore, hydraulic model studies were carried out in a distorted scaled (1:400(H) & 1:80(V)) physical model using Automatic tide generator.

## 3. Oceanographic data for study

The latest bathymetry, Oceanographic data (tide and current) are required for proper simulation of the prevailing flow conditions in the scaled model. The latest bathymetry data near the Nhava end was used to reproduce the bathymetry in and around the proposed jetty location at Nhava headland. The tidal data available at Apollo Bunder and current data in the Elephanta deep for a spring/neap tidal cycle (Year 2016) was used to carry out the model study and their locations are shown in Figure 2.

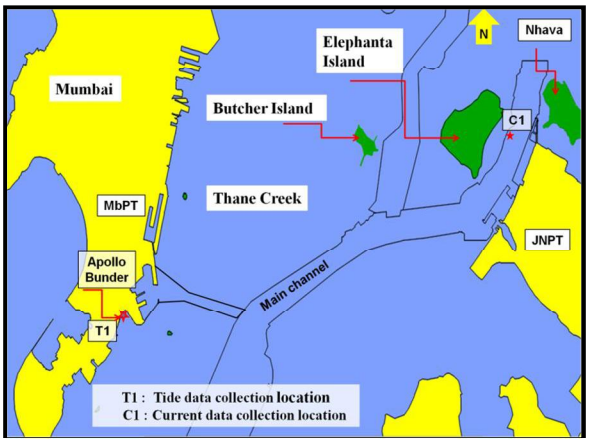



**Figure 2** Tide and current measurement locations

## 4. Hydraulic modeling

Physical hydraulic modeling has been used since ancient time for studying the complex near-shore hydrodynamic phenomena such as formation of eddy, flow separation, identification of siltation prone zones etc. and is a miniature reproduction of actual flow processes. The gravitational and inertia forces being dominant in tidal flow, the physical hydraulic tidal model works on the principles of Froude similitude (Hughes 1993). The Froude Number is described as follows:

$$\text{Froude Number, } F_r = \frac{\text{Inertial Force}}{\text{Gravitational Force}} \quad (1)$$

The present study was conducted in a distorted scaled model [1:400 (Horizontal scale) & 1:80 (Vertical scale)]. As per the Froude Similitude, the Velocity scale, "$V_r$" and Time Scale, "$T_r$" are given below.

$$V_r = \sqrt{d_r} = 8.994 \quad (2)$$

$$T_r = \frac{L_r}{d_r} = 44.7214 \quad (3)$$

### 4.1. *Description of physical model*

The physical model of Thane creek available at CWPRS, Pune is a distorted scaled model and is having horizontal scale of 1:400 and vertical scale of 1:80. It is a rigid bed model. This physical model has been used for several decades to study the layouts of various waterfront facilities and based on the studies the alignment of various jetties/berths, navigational channel etc. have been finalised and also shape of reclamations were evolved to have its minimal impact on nearby existing waterfront facilities. The total model area is around 150 m X 90 m and it represents about 2100 $Km^2$ area in prototype. In order to nullify the effect of local wind on flow field, the part of the model area where the major developmental activities took place, is covered by a shed (70 m X 45 m). The water is supplied to the model bed by three pumps (75HP). Automatic Tide Generating (ATG) system is used to generate the tidal flow in the model and water levels are measured by advanced Radar sensors. The location plan of the boat landing jetty in the model of Thane creek area is shown in Figure 3.

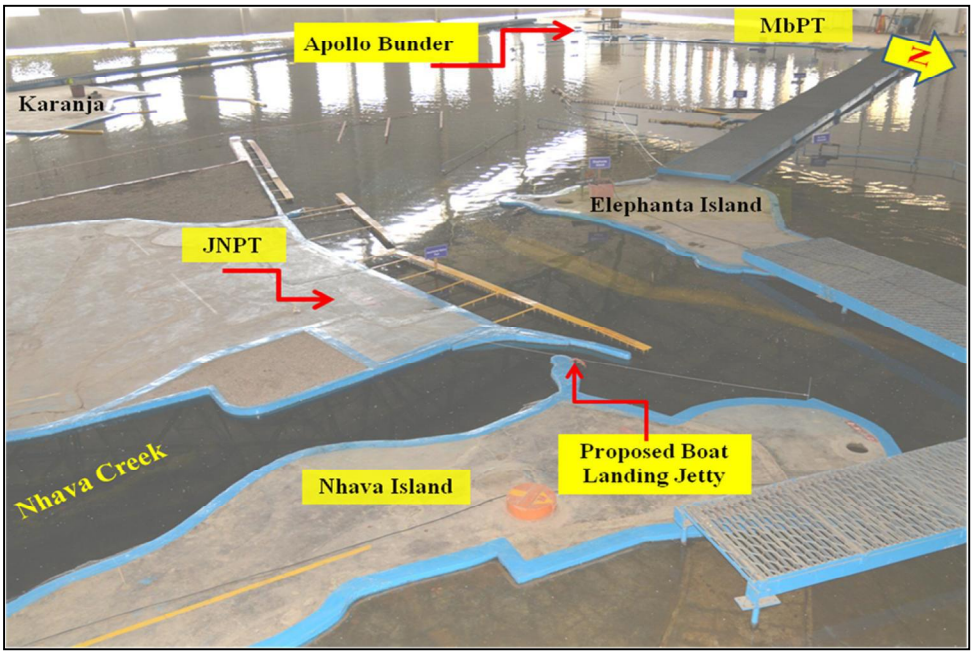



**Figure 3** Location of proposed boat landing jetty in physical model

### 4.2 *Tide generation system*

Automatic Tide Generating (ATG) system has been used to simulate the prevailing flow field in the model. The model is fitted with balanced radial gates resting on weirs and the gates are connected to a common shaft which is connected to a gear box. The gear box is driven by a stepper motor. The movement of stepper motor is controlled by motor drive, which is connected to the computer (Purohit et al. 2014). The desired water levels are fed into the computer, while the actual water level in the model is measured by a pressure transducer known as Rosemount sensor. At every time step ($\Delta t$), the computer compares the actual water level with desired level in the model and as per the requirement the radial gates are opened or closed to generate the tide in the model. The ATG system fitted for the model is shown in Figure 4.




**Figure 4** Automatic tide generating system in physical model

### 4.3 *Calibration of Model*

A tidal model is said to be calibrated when the flow conditions in model are in proportion to that in prototype and this can be achieved by comparing water levels and currents between prototype and model at desired location. The physical model of Mumbai Port was calibrated in terms of tide data for two tidal cycles (spring and neap) measured during non-monsoon (year 2016) at Apollo Bunder. The comparison of proto tide data (at Apollo Bunder) with the model data is given in Figure 5.

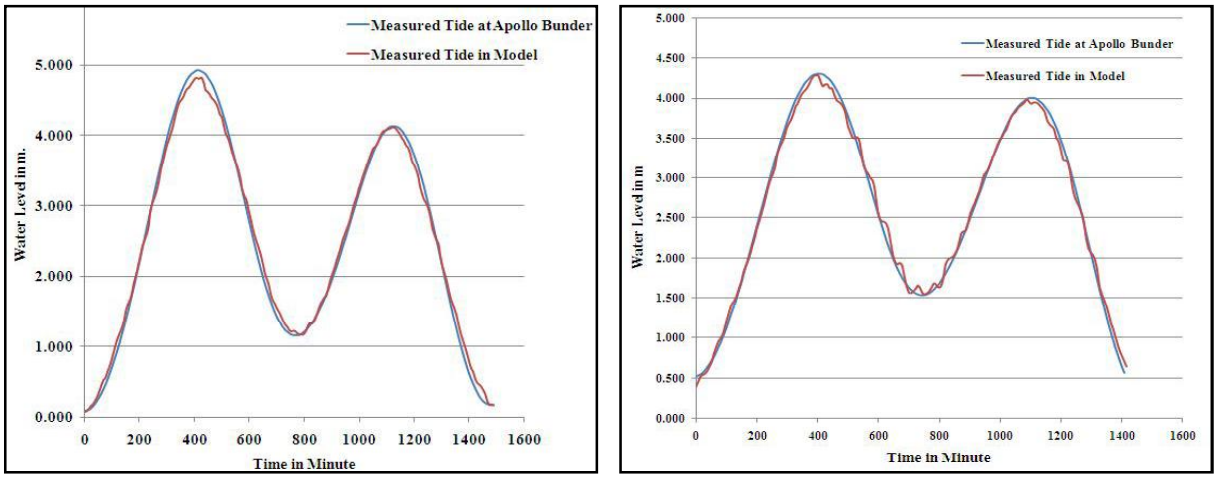
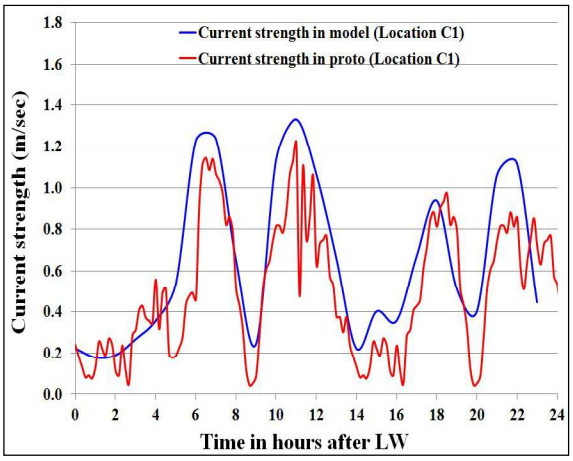
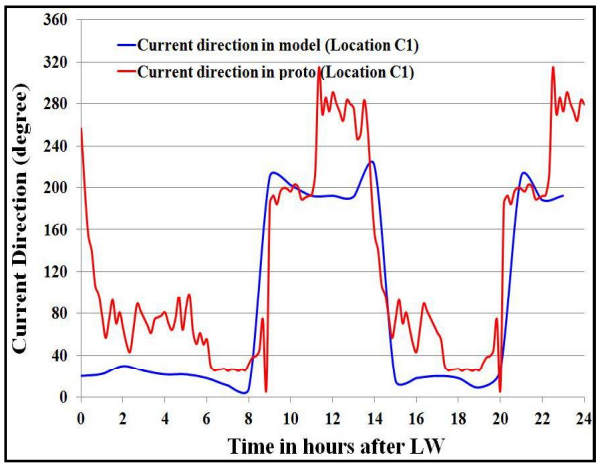



**Figure 5** Comparison of proto and model tide at Apollo Bunder

The current measurements in the model were carried out by digital image processing technique. In this technique, paper confetti was spread on the water surface. The confetti move with flow velocity and photographs of the flow were taken at known time interval for a specified exposure time using digital camera. The displacement of confetti in known time gives magnitude of current, while its direction is found by measuring the angle of flow lines with respect to North in the model. The calibration plots for current data measured in model and prototype are given in Figure 6. & 7.

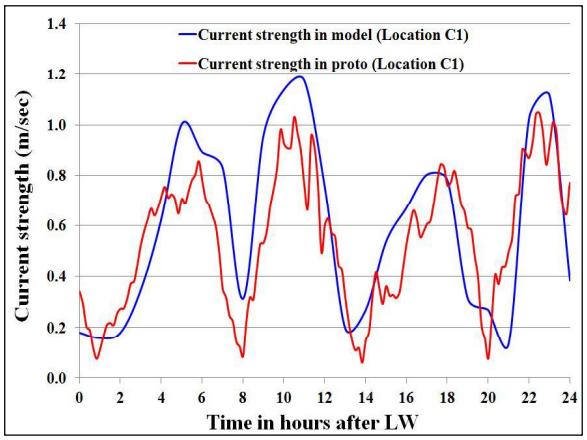



(Current Strength)

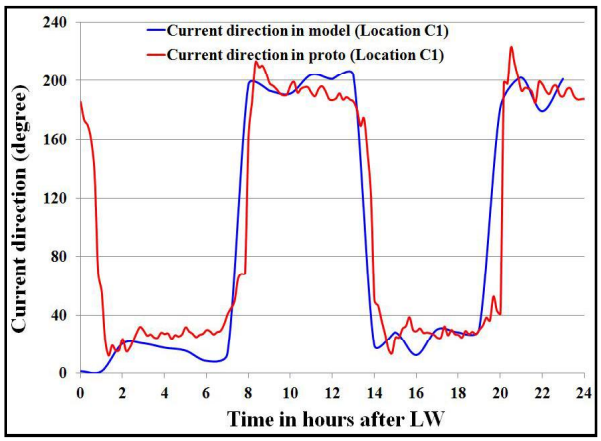



(Current Direction)

**Figure 6** Comparison of proto and model current at "C1" for spring tide




(Current Strength)




(Current Direction)

**Figure 7** Comparison of proto and model current at "C1" for neap tide

### 4.4 *Model studies under existing bathymetry condition*

The physical hydraulic model studies were carried out to assess the existing current pattern at the location of boat landing jetty proposed by project Authority at 26° N at Nhava headland. Also flow pattern near the Nhava creek entrance viz. flow lines, formation of eddies, flooding and drying zones during different stages of flood/ebb, both for spring and neap tidal conditions were studied. The proposed jetty location and wherein the current measurements (viz. locations "1" and "2") are carried out is shown in Figure 8. The approach to the location of the jetty at Nhava creek headland for the passenger boats is through hydrodynamically dynamic region, wherein tidal flow conditions are constantly varying at the entrance of Nhava. Thus measurement of current strength and direction along with locations of eddy formations during various phases of tide are essential to get information about dynamic behaviour of flow field over the entire tidal cycle.

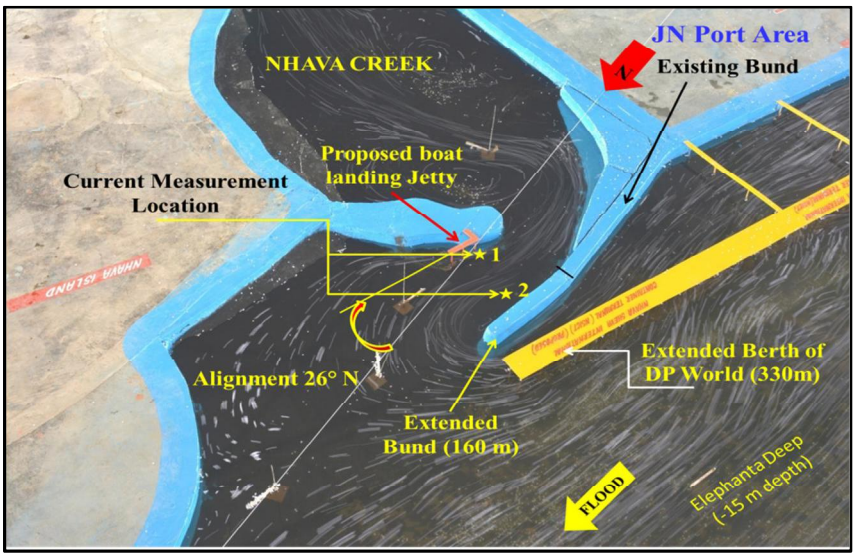
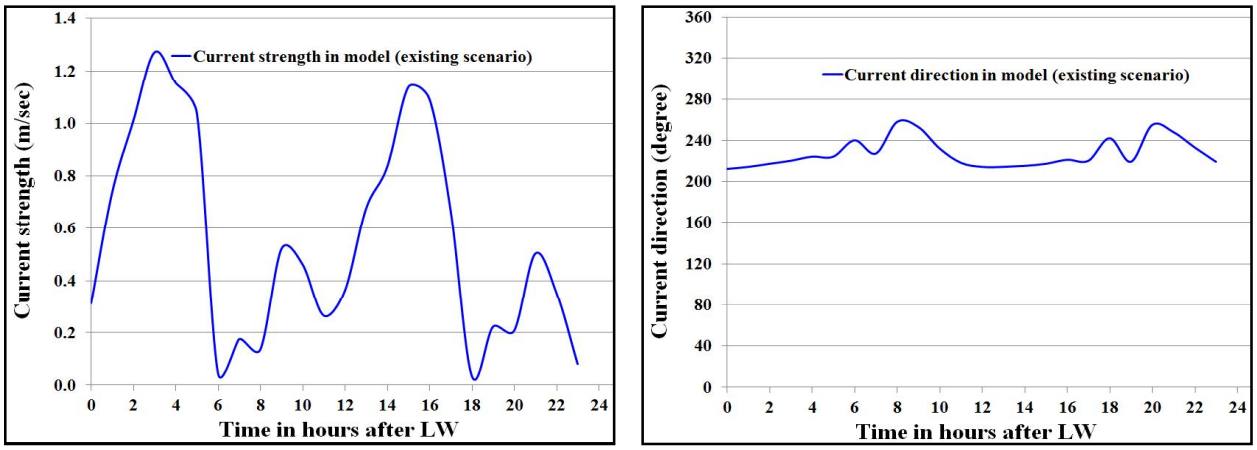


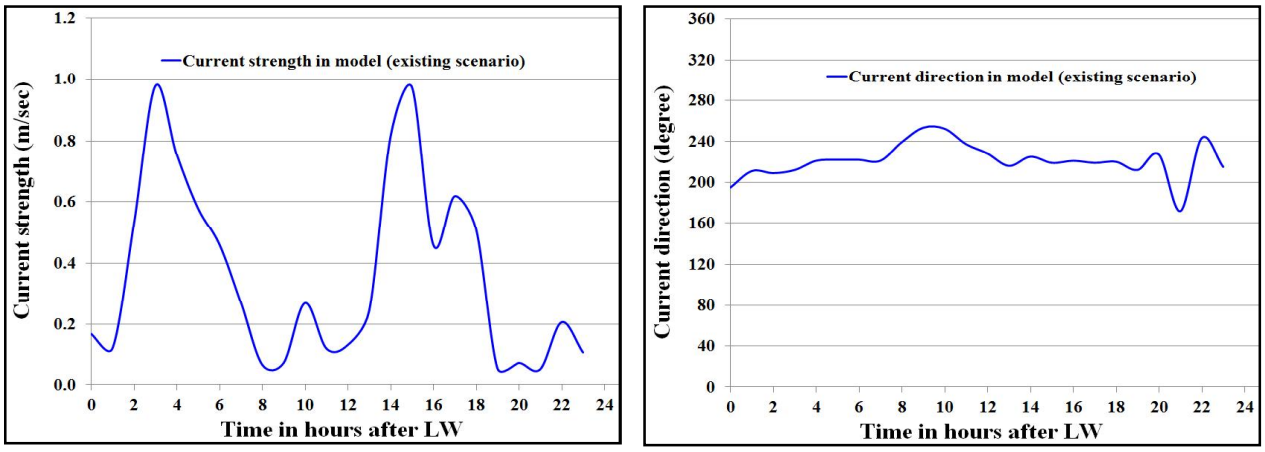

**Figure 8** Current measurement locations & flow pattern during 3rd hr. of flood tide (spring)

The current strength measured at proposed jetty location (1) during spring and neap tidal conditions are shown in Figure 9 and 10.




(Current Strength) (Current Direction)

**Figure 9** Measured current data for spring tide at the proposed jetty (location 1)




(Current Strength) (Current Direction)

**Figure 10** Measured current data for neap tide at the proposed jetty (location 1)

The study reveals that maximum strength of current during flood/ebb phase of tide is about 1.27 m/sec and 0.52 m/sec during spring tide whereas during neap tide, it is 0.97 m/sec and 0.27 m/sec. The current direction during flood/ebb tide varies from 214° - 224° N (36° N + 180°) for spring/neap tide. This is due to the fact that during ebb tide there is stagnation/wake zone at jetty face and the main flow passes away from jetty face (deeper depths prevailing between Nhava head and 160 m long guide bund constructed for guiding the flow for 330 m long container terminal of DP world). As the proposed alignment of the jetty was 26° N (given by JN port), it was decided to modify the alignment of the jetty to 36° N as shown in Figure 11 so that flow will remain almost parallel to the berthing face during flood/ebb phase of tide. The flow patterns observed indicates that during flood tide flow remains parallel to the modified aligned face of the berth (36° N) and the flow pattern observed during 3rd hour of flood tide (spring) is shown in the same Figure 11.

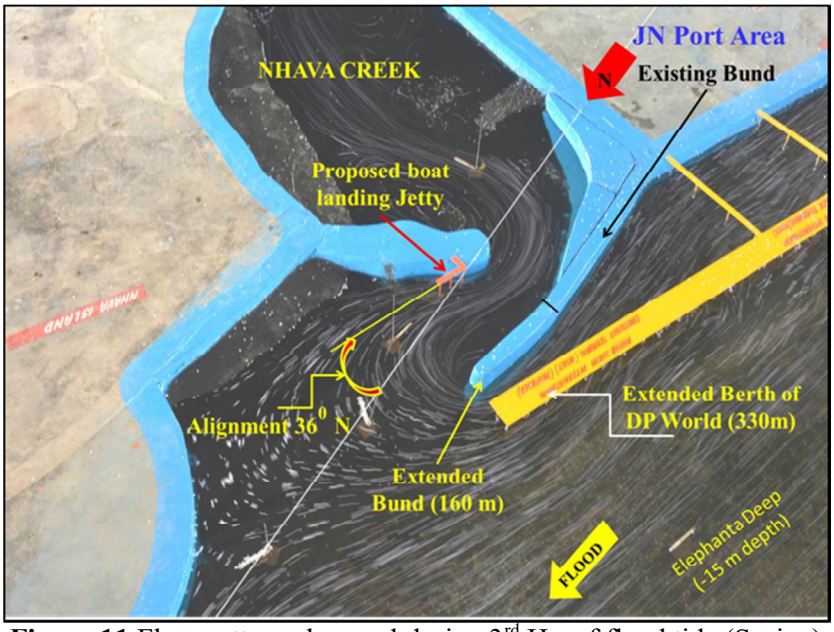



**Figure 11** Flow pattern observed during 3rd Hr. of flood tide (Spring)

The study also reveals that during initial two hours of ebb tide, the flow from the Nhava creek comes out at a very high speed of about 1.7 m/sec (location "2" referred in Figure 8) and meets the main channel at Elephanta deep. This is due to the steep gradient of seabed (Zone- "A" as shown in Figure 12) having bed levels of about 1 m above CD in Nhava creek and 15 m below CD in main navigational channel in Elephanta deep. The relatively shallow depths exist in Zone-"B".




**Figure 12** Various flow zones at Nhava creek entrance

As the ebb tide progresses the water mass in the zone- "B" gets reduced and at the same time the current strength in main navigational channel starts increasing from 2nd hour of ebb tide. Therefore from 3rd to 4th hour of ebb, the resultant of the flow field created by the water mass coming out of zone-"A" and the water mass flowing at an increased speed through main navigational channel as well as the reduced water mass in zone-"B" creates eddies near the proposed boat landing jetty during 3rd to 4th hour of ebb tide. The flow pattern observed during 3rd hour of ebb tide is shown in Figure 13.

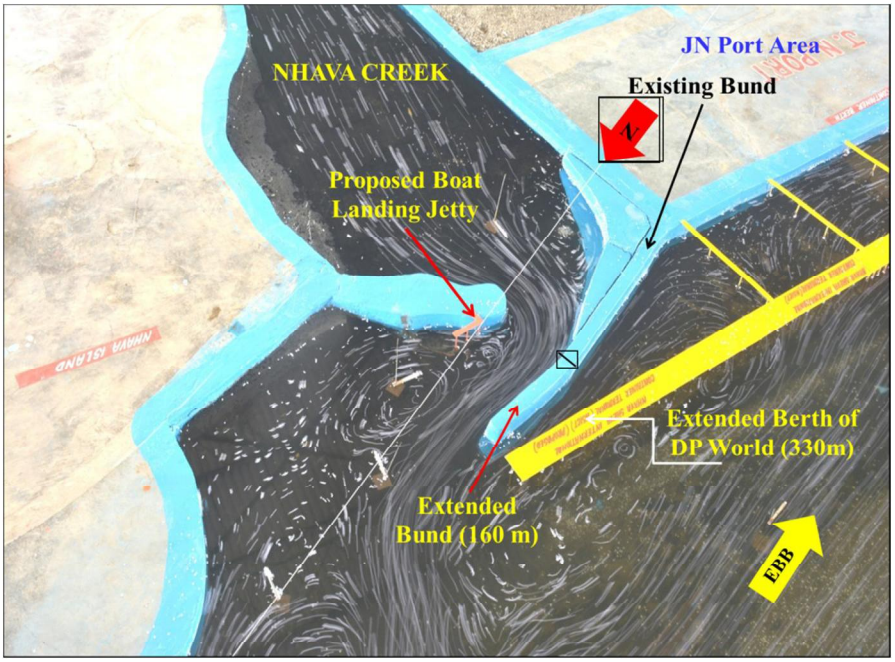



**Figure 13.** Flow pattern observed during 3rd hr. of ebb (neap)

These eddies are likely to create problem for the vessels/passenger boats berthed at the boat landing jetty. As such to avoid the eddy formation near the jetty, a flow guide structure in the form of reclamation was proposed on the leeside of jetty. Also due to non-availability of sufficient depths for plying of the boats during initial hours of flood towards proposed jetty an area of about 2.5 ha, was dredged to a depth of 1.2 m below CD to improve the operability at the berth. The model studies carried out for this combined scenario and the findings of the same are given in following section.

### 4.5 *Model studies with reclamation and dredging*

The physical hydraulic model studies were again carried out to study the flow field near the proposed jetty with the flow guide structure in the form of reclamation on leeside of boat landing jetty over area of about 3500 $m^2$ and dredging in front of jetty over an area of 2.5 ha, up to 1.2 m level below chart datum as shown in Figure 14. The dredging layout was decided in such a way that dredging area is almost parallel to the path of existing streamlines in front of jetty face. The model study reveals that during flood phase of spring/neap tide, flow starts entering into the Nhava creek region even at low tide and reaches up to boat landing jetty and thereafter when the tide levels starts rising, it further increases the water depth and will allow smooth entry of passenger boats up to jetty. Also due to the typical shape of the reclamation flow gets well guided near the jetty berth face and it remains parallel to the berthing face. Thus, dredging will be beneficial to increase operability of passenger boats during flood phase of the tide up to the boat landing jetty and reclamation will allow safe berthing.
The flow pattern observed during ebb phase of tide indicates that during initial hour of ebb tide, flow from the Nhava creek comes out at a very high speed of about 1.63 m/sec (location "2") through the steepest contour (Zone-"A") at the entrance of Nhava creek. However due to the typical shape of the reclamation the diameter/shape of the eddy which was getting formed under existing condition has now been happens to get modified in such a way that near the berthing face of the boat landing jetty, flow remains parallel to the berthing face as well as the current strength near the jetty also gets

reduced. This will create favorable flow condition for the vessels/boat berthed at the jetty. The plot of current strength/direction near the jetty (Location- "1") is given in Figure 15 & 16.

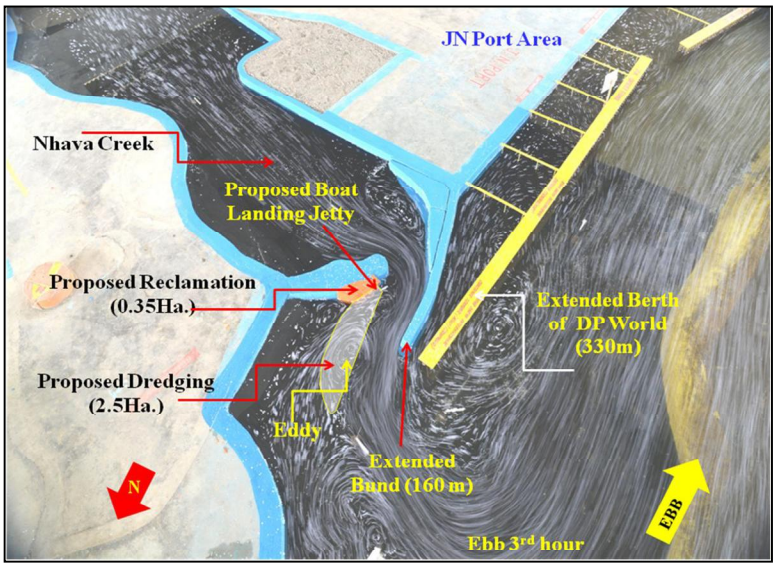
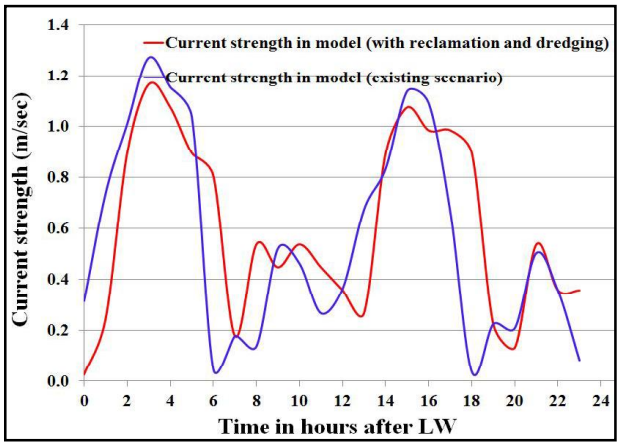
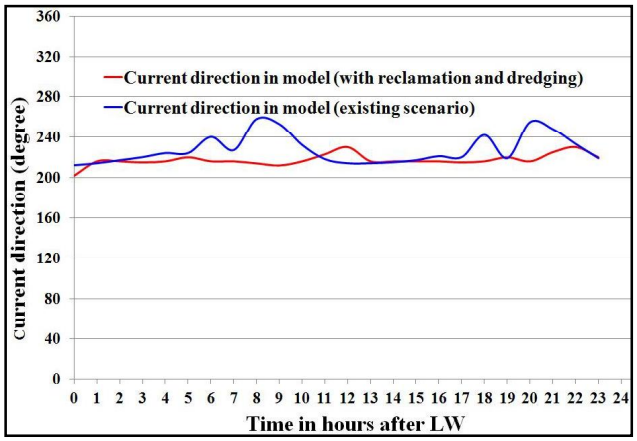



**Figure 14.** Flow pattern observed during 3rd hr. of ebb

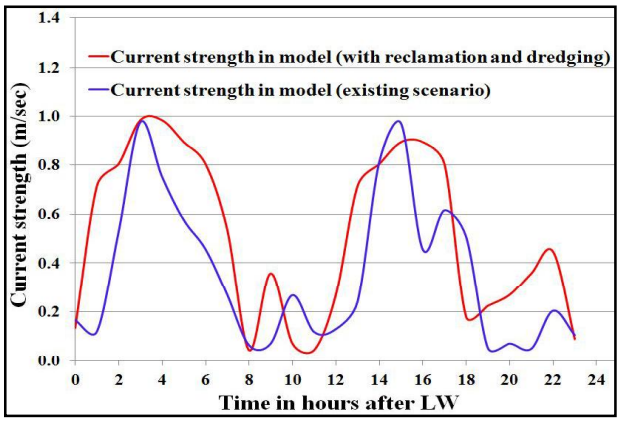



(Current Strength)

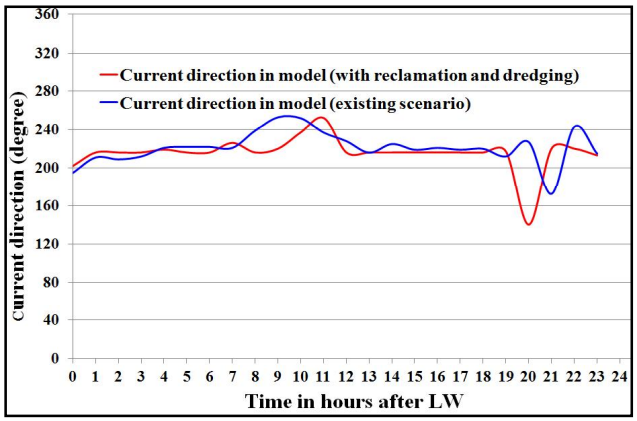



(Current Direction)

**Figure 15** Comparison of current strength at jetty (Location-1) for spring tide




(Current Strength)




(Current Direction)

**Figure 16** Comparison of current strength at jetty (Location-1) for neap tide

Based on the studies carried out, finalised alignment of 60 m long boat landing jetty, shape of reclamation covering area of 0.35 ha. on leeside of boat landing jetty and dredging up to 1.2 m depth below CD over 2.5 ha, area is shown in Figure 17.

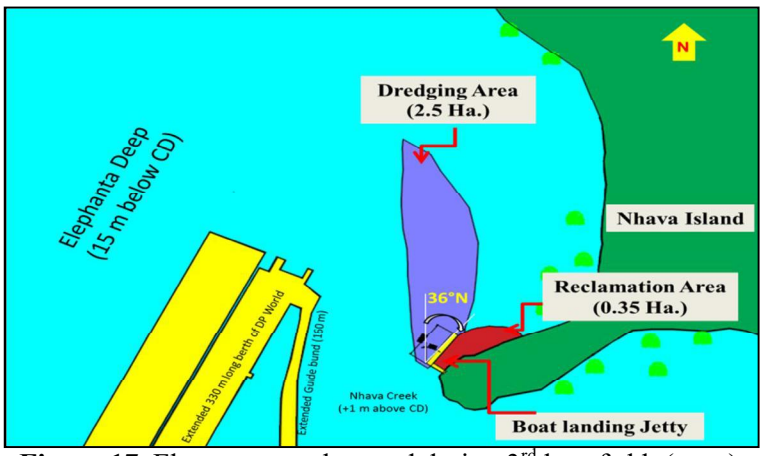



**Figure 17.** Flow pattern observed during 3rd hr. of ebb (neap)

## 5. Conclusions

Based on the studies carried out the following broad conclusions are drawn:

- The hydraulic model study reveals that at Nhava creek entrance the flow field is dynamic in nature with significant variation in current strength in various areas/zones, presence of dynamic eddy etc. The maximum current strengths during flood phase of spring/neap tides are 1.27 m/sec & 0.97 m/sec respectively at the jetty location. The current direction during flood varies from 214° - 224° N (36° + 180° N) at jetty head. As such the orientation of jetty needs to be modified to 36° N as against 26° N proposed earlier by project Authority.
- The model study also indicate that during 3rd to 4th hour of ebb tide, due to the resultant of the water mass coming out at a high speed (1.7 m/sec) through the steepest contour region at Nhava entrance (zone-"A"), water mass flowing at an increased speed through main navigational channel in Elephanta deep and the reduced water mass near the jetty head (zone "B"); eddies get formed near the proposed jetty. These eddies will create the problem for berthing of boats at the jetty head. As such as a remedial measure, flow guide structures in the form of reclamation on leeward side of jetty is studied to improve flow condition and is suggested to achieve safe berthing at jetty.
- The study carried out with flow guide structure in the form of reclamation reveals that during flood phase of tide, flow is guided due to the peculiar shape of the reclamation and flow remains parallel to the berthing face. Whereas during 3rd to 4th hour of ebb tide due to the complex flow field in Nhava creek entrance, eddies are seen to be formed away from the jetty. Also due to the typical shape of the reclamation the diameter/shape of the eddy gets adjusted in such a way that near the berthing face of the jetty, flow remains parallel to the berthing face as well as the current strength also gets reduced. Thus, it will create favorable flow condition at the boat landing jetty for the berthing of boats.
- The study also reveals that during initial two hours of flood tide required draft (1.0 m) was not available for the boats to ply/berth at jetty from the Nhava creek entrance. The dredging up to 1.2 m depth below CD over an area of about 2.5 ha, allow the boats of 1m draft to ply easily even during low waters and berthing is also safe.
- The physical model study plays an important role in evolving the remedial measures in the form of reclamation & dredging layout to offer a feasible solution for finalising the alignment of boat landing jetty proposed in complex hydrodynamic condition at the confluence of Elephanta deep and Nhava creek. This will not only allow safe berthing of boats at jetty during any tidal phase but also will improve operability even at low tide levels.

## References

Hughes, S.A. (1993). *Physical Models and Laboratory Techniques in Coastal Engineering.* World Scientific Publishing Co. Pte. Ltd., Singapore, 31-32.

Purohit, A.A, Vaidya, M.M, Basu, A, and Chavan, K.A (2014). Importance of Modelling in Fixing Orientation of Bund at the Mouth of Narrow Steeply Graded Creek for Safe Berthing in Macro Tidal Region. *International Journal of Scientific Engineering and Technology,* 46-51.

IN PROCEEDINGS OF 25th HYDRO 2020, INTERNATIONAL CONFERENCE,
NATIONAL INSTITUTE OF TECHNOLOGY ROURKELA, ODISHA, INDIA
26-28, March 2021, ISBN 978-93-90631-56-8

Paper ID - 281

# Hydrodynamic Modelling of Upper Tapi River, India

M. Sayan [1], P.V. Timbadiya [2]

[1]Former Post Graduate Student, Water Resource Engineering, Department of Civil Engineering, Sardar Vallabhbhai National Institute of Technology, Surat 395007, Gujarat, India
Email: sayanmesariya@gmail.com

[2]Associate Professor, Department of Civil Engineering, Sardar Vallabhbhai National Institute of Technology, Surat 395007, Gujarat, India
Email: Email: pvtimbadiya@ced.svnit.ac.in

## ABSTRACT

The prediction of River stage and discharge is required for effective flood management by adopting some structural and non-structural measures. The present study addresses the development of one-dimensional Hydrodynamic model using MIKE 11 software to simulate hydraulic characteristics of flow for Upper Tapi River between Dedtalai to Hathnur gauging station having reach length of 120 km. The calibration of the unsteady simulation model was performed for the flood event of the year 1994 with the due consideration of upstream (flood hydrograph) and downstream (water levels) boundary conditions to estimate the optimum value of the roughness coefficient. The comparison between the time series of simulated and observed water levels at the intermediate station, i.e., Burhanpur, was conducted to estimate the optimum value of the Manning's coefficient. The performance of the aforesaid developed model was also assessed using the standard performance indices such as Root Mean Square Error (RMSE) and Coefficient of Determination ($R^2$). The calibrated model was also validated using the independent flood events of the year 1998 and 2015. In addition, the rating curve was established using the simulated results of the developed model, which can be used in future to predict the discharge at the section based on river stage. The energy slope obtained from the MIKE 11 result file was used to estimate the stream power and the energy lost during the flood. The stream power obtained for the flood year 1994 was enough to move the small size boulders along the Upper Tapi River.

**Keywords:** *Hydrodynamic modelling, MIKE 11, Upper Tapi River, Manning's roughness coefficient, Rating curve, Stream power.*

## 1. INTRODUCTION

In recent decades, India has observed rapid population growth, which is the primary reason for modifications in land-use patterns, atmospheric temperatures, flood plains, drainage, etc. In addition, the effects of global warming have resulted into heavy storm, high precipitation intensity, seawater level rise, etc. (Nandalal, 2009). The major losses of property and lives have been observed worldwide every year due to flooding conditions. While this is a natural phenomenon, human activities in the catchment and flood plains influences the severity of the floods. Various anthropogenic behaviours often increase the impermeability of the earth's surface, thereby reducing the infiltration capacity and produces more runoff. Floods can rarely be prevented, but the severity of the flood can be minimized by embracing absolute preparedness for the flood (Rahman et al., 2011). The construction of reservoirs and dams, diversions, floodway, increasing conveyance capacity through channel expansion, channel deepening, channel realignment, and Riverbank protection are the effective precautionary structural measures. The non-structural flood measures such as land use regulations, flood warning, flood forecasting, etc. plays an important role for alleviating not only the catastrophic consequences but also the environmental contamination. Out of this, the flood prediction (forecasting) plays a significant role (Nandalal, 2009). The rapid revolution in the field of computational technology has been observed nowadays and various ranges of hydraulic models i.e. one dimensional (1D), two dimensional (2D), three dimensional (3D) and coupled schemes are being prepared for the water level predictions. Out of these, one dimensional model is very common and adopted globally due to its speed of calculation, ease of parameterization and representation of the hydraulic structure in the flow domain. The one dimensional hydrodynamic models are reasonably precise than hydrological routing, since hydrodynamic models compute and update the flow discharge and water level simultaneously in the time domain and thus provide more

reliable results for the analysis of unsteady flow during propagation in the River channel (Kamel, 2008). MIKE 11 HD model is a one dimensional hydrodynamic modelling tool for Rivers and channels developed by Danish Hydraulic Institute (DHI) with the MIKE zero graphical interface. The aforesaid unsteady non uniform simulation model which solves the 1D hyperbolic dynamic saint Venant equation using a six-point Abbot Ionesco finite difference scheme for the calculation of discharge and water levels. (DHI, 2014). Various studies have been carried out for the development of hydraulic modelling using MIKE 11 HD model for the forecasting of the water level and area inundated. Chatzispiroglon et al., 2006; Kamel, 2008; Majewski, 2008; Nandlal, 2009; Pramanik et al., 2009; Delphi et al, 2010; Timbadiya et al., 2014 a; have been proved to be quite efficient.

The Tapi River is the second largest west flowing River in the Indian peninsula which is frequently influenced by large floods and causes considerable loss of life and property in the lower regions. The severe floods with discharge of 17,027 $m^3/s$ and 25,261 $m^3/s$ were reported at Burhanpur station in the years 1994 and 1998 respectively, which necessitates the need to mitigate the floods. The present study had intended to discuss the following objectives:

a) The development of the hydrodynamic model for the Upper Tapi River between Dedtalai and Hathnur stream gauging station using MIKE 11 HD model.
b) The estimation of optimum value of Manning's roughness coefficient for the Upper Tapi River by calibrating the hydrodynamic model for the year 1994.
c) The validation of the developed aforesaid model using the independent event of the year 1998 and 2015.
d) Establishment of the stage discharge relationship along the River from the developed model.
e) Estimation of stream power and energy expended during the flood at Burhanpur gauging station to assess the geomorphic preparedness of the flood.

## 2. STUDY AREA AND DATA COLLECTION

### 2.1 *Description of study reach*

The Tapi River is India's second largest River that flows from East to West. The River begins at the Multai, situated at 752 meters above sea level in the Betul district of Madhya Pradesh. The River length of the Tapi River is around 725 km and along its path, it flows through three states namely Madhya Pradesh, Maharashtra and Gujarat and ultimately meets the Arabic ocean. After traveling 282 km distance in Madhya Pradesh, the River arrives in Maharashtra and travels 228 km after that it eventually flows in Gujarat state which meets to the Arabian sea. The Tapi Basin is located between the longitudes of 72°31'E to 78°20'E and the latitudes of 20°24'N to 21°52'N (Jain et al., 2007). The Tapi basin is comprised of three sub catchments, i.e., Upper, Middle and Lower Tapi basin. Upper Tapi basin covers the total area of 29430 km2 ranging from the Betul district to Hathnur dam. Middle Tapi basin covers the total area of 25,320 km2 starting from Hathnur reservoir to Gidhade station. Lower Tapi basin covers relatively small area of 10395 km2 ranging from Gidhade station to the Arabic ocean (Jain et al., 2007). The present study addresses the study of the Upper Tapi basin that located between the 75°55'E to 78°17'E (longitude) and 20°05'N to 22° 03'N (latitude). Upper Tapi basin is composed of two sub catchments: (1) The Purna sub catchment and (2) The Burhanpur sub-catchment (Kale et al., 1994). The Burhanpur sub catchment is located between east longitude of 75°56' 43''E to 78°15'40'' E and north latitude 21°06'57'' N to 21°47'43''N. The length for the present study is 120 km lying in the upper Tapi basin from Dedtalai to Hathnur stream gauging stations as shown in Figure 1.

### 2.2 *Geometric and hydrological data collection*

The topographical data i.e., cross sections were acquired from the Central Water Commission (CWC), Gov. of India for the development of the hydrodynamic model. The most recent 13 surveyed cross sections along the River were acquired between the Dedtalai and Hathnur reservoir with its longitude, latitude, River bank points, chainages along the River, RL of benchmark, etc. The daily time series of

discharge and water levels for the year 1994 and 1998 were collected from the CWC, Govt. of India recorded at Dedtalai and Burhanpur gauging station. For the validation of the model, the time series of discharge and water level for the year 2015 was obtained from the water year book issued by CWC (Central Water Commission, 2016). For this present study, the flow hydrograph at Dedtalai (upstream boundary condition) and water level (downstream boundary condition) at Hathnur were considered to simulate the aforesaid model.

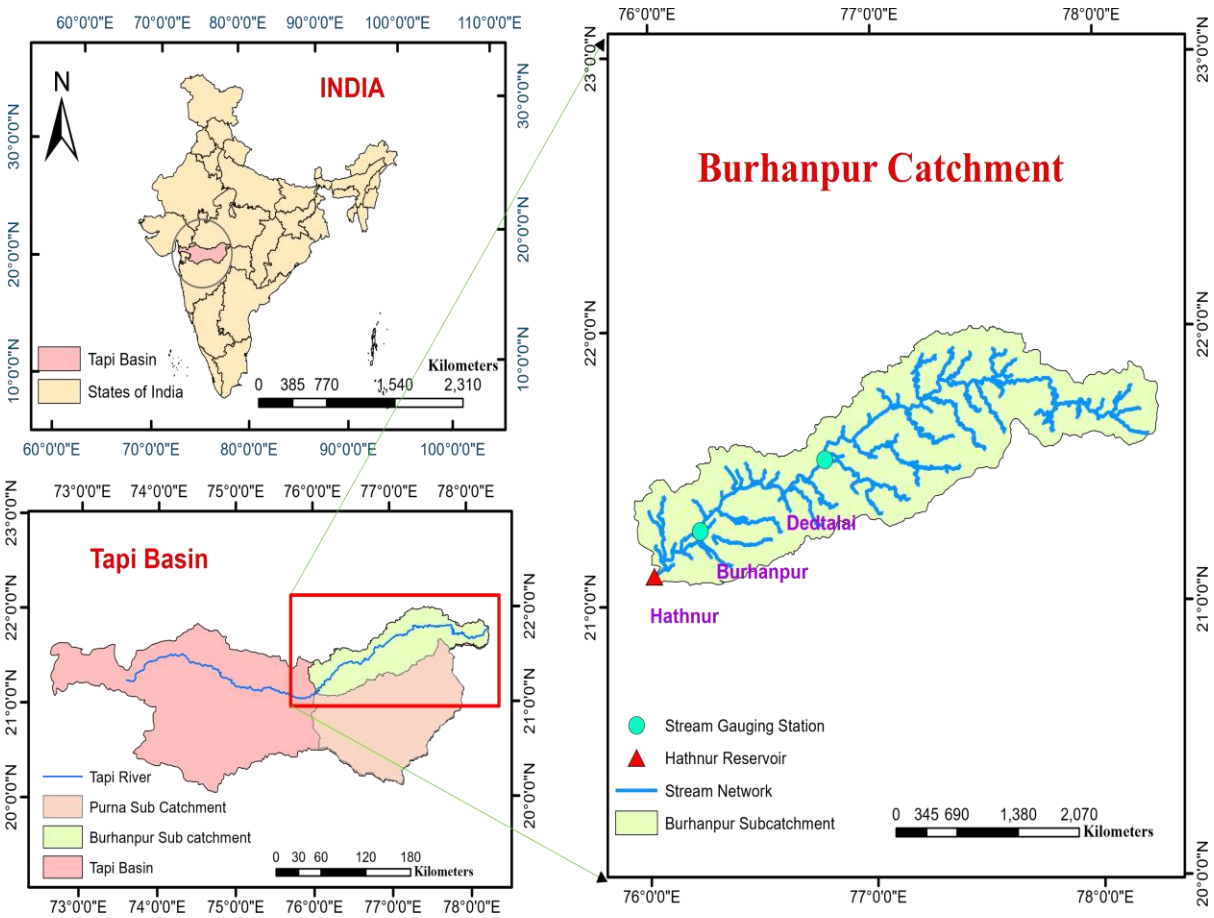



**Figure 1.** Index map of the Study Area

## 3. METHODOLOGY

The approach adopted in the present research work to develop a one dimensional hydrodynamic model for the Upper Tapi River is shown conceptually by schematic chart in Figure 2.

### 3.1 *Numerical scheme*

MIKE 11 HD model is a 1D hydrodynamic modelling tool for Rivers and channel with the MIKE zero graphical interface, which has been developed by Danish Hydraulic Institute (DHI) and it is a one dimensional, unsteady, simulation model which solves the 1D hyperbolic dynamic Saint Venant equation using the six-point Abbott Ionescu finite difference scheme (DHI, 2014). The system employs a staggered grid solution for the finite differential equations using a double sweep algorithm. Furthermore, the module in an open channel can consider both subcritical and supercritical flow conditions.

### 3.2 *Hydrodynamic modelling*

The implementation of the model requires the River network geometry, series of cross sections, hydrodynamic parameters and boundary conditions. The subsequent paragraphs illustrate the concise description of the numerical scheme used in the model, development of River geometry, boundary conditions, and hydrodynamic parameters.

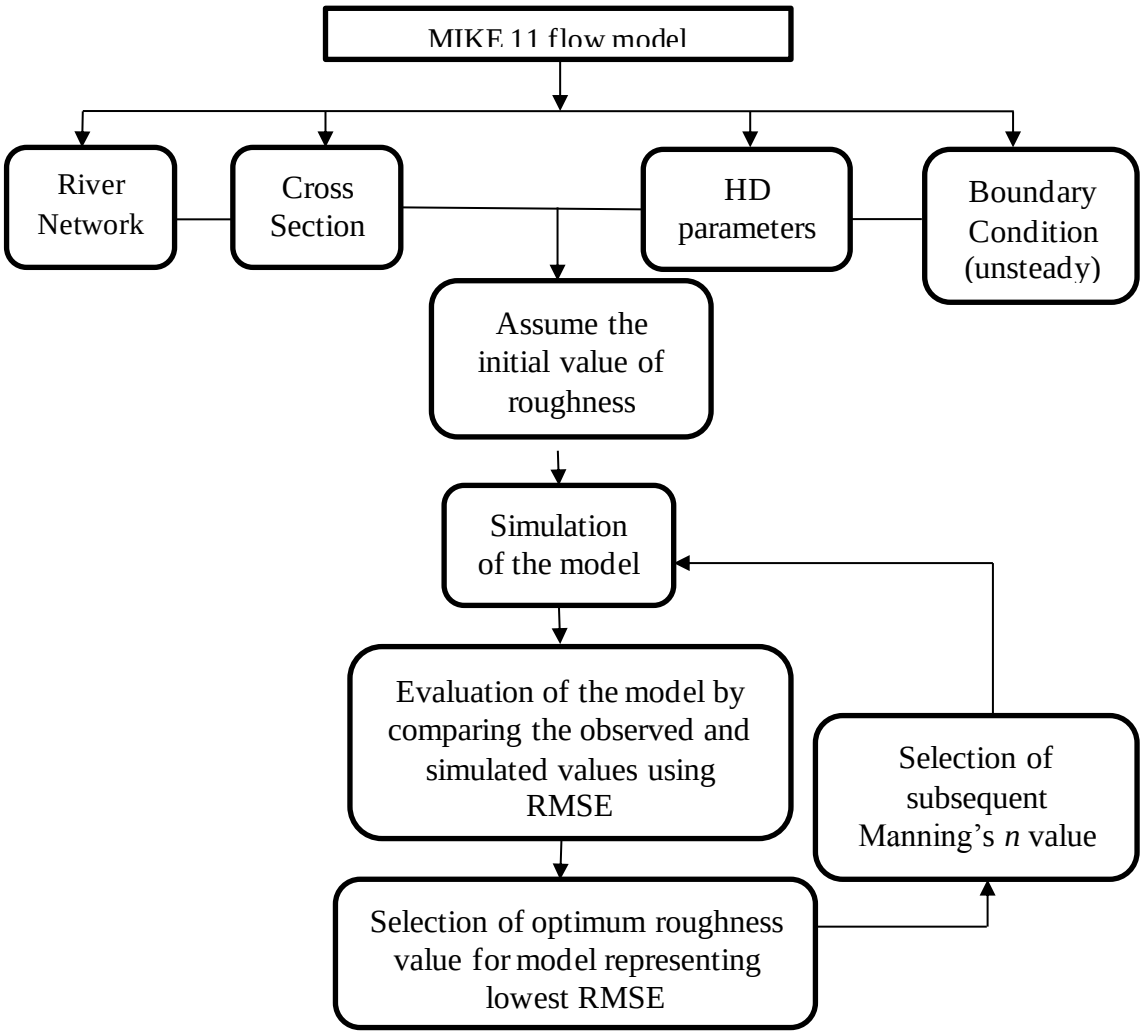



**Figure 2.** Methodology used for Model Development

#### 3.2.1 *River network*

The River network was prepared using the network editor tool available in the MIKE 11 between two stream gauging stations. i.e., Dedtalai and Hathnur Dam. The Tapi River traverses the 120 km long route between the Dedtalai to Hathnur dam which is shown in the Figure 3 which represents the study area for this presented study. The longitudinal profile of the study reach at thalweg line is presented in Figure 5 including the left and right bank levels.

#### 3.2.2 *Cross sections*

The 13 surveyed cross sections between the Dedtalai and Hathnur have been used for this present study.

The intervals between these surveyed cross sections were situated in the range from 4km to 12 km. The chainages were obtained using the Arc GIS 10.3 extension using the latitude and longitude. The markers were defined for left bank and right bank accordingly. The Figure 4 represents the cross section profile including left and right bank at Dedtalai stream gauging station.

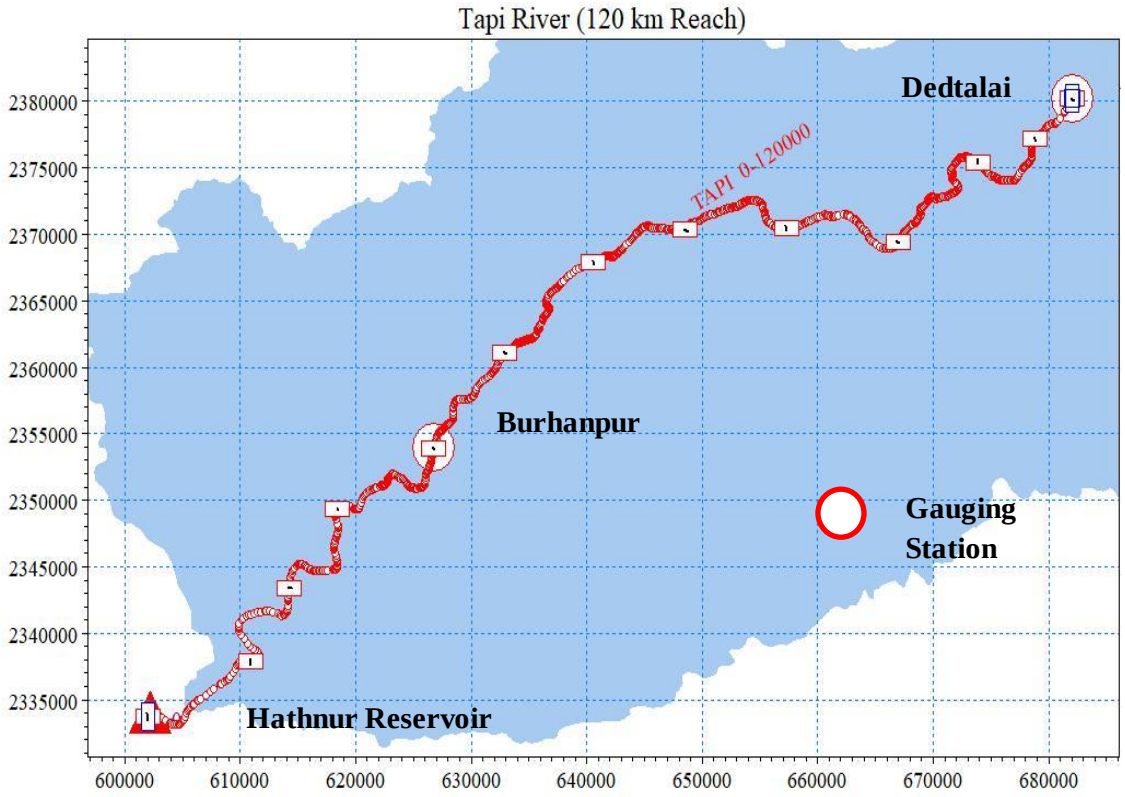



**Figure 3**. River Network Edited in MIKE 11

### **3.2.3** *Boundary conditions*

The boundary conditions are the most significant parameter for the development of the model because inappropriate selection of the boundary conditions may lead to erroneous results and the predictions made through simulation model may be become unrealistic. For this present study, the flow hydrograph at Dedtalai (upstream boundary condition) and water level (downstream boundary condition) at Hathnur were considered to simulate the aforesaid model.

### **3.2.4** *Hydrodynamic parameters*

The Tapi River flowing in the Burhanpur catchment exhibit gentle slope hence, fully dynamic equations were used for the simulation. The simulation editor is used for integration and exchange of information between each of the individual data editor. It provides the linkage between the network and other MIKE 11 editors. All the files required for HD model were updated in the simulation editor tool with the simulation time step of 1 day and the calculation timestep of 5 second. The spatial interval of 1000m was taken.

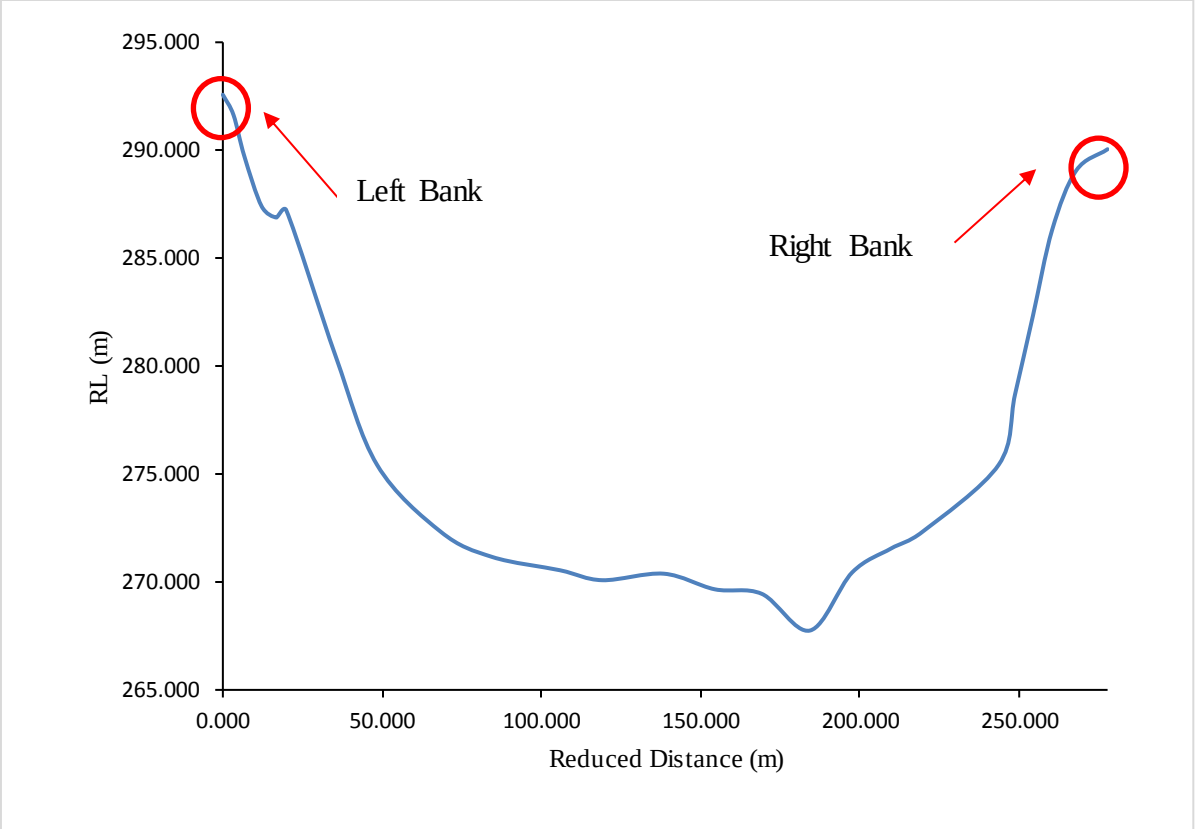



**Figure 4.** Cross Section at Dedtalai (zero chainage)

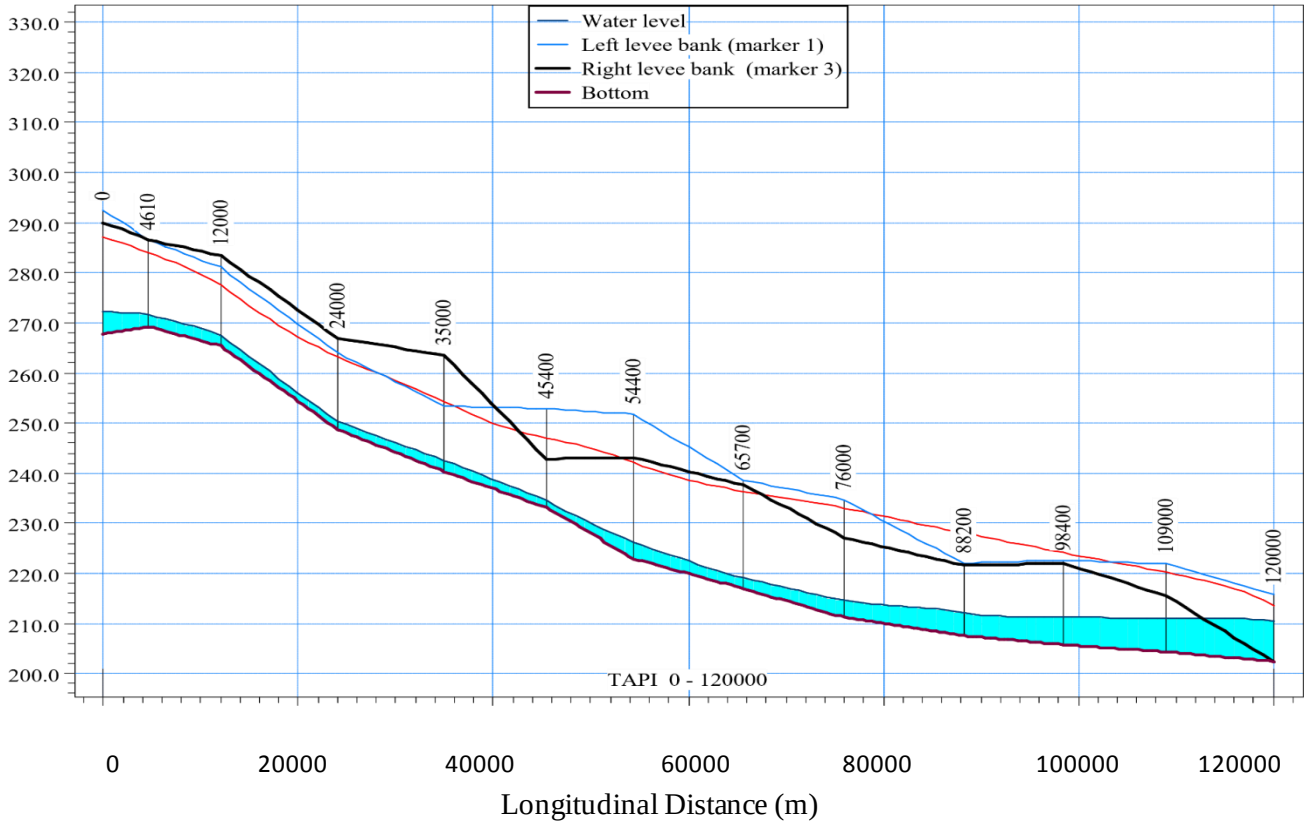



**Figure 5**. Longitudinal Profile of the River

## 4. CALIBRATION OF THE MODEL

The method for calibration and validation requires two independent data sets. One data set is required for acquiring the optimum value of independent coefficients and second data set is required to validation of the calibrated model. Usually, the model calibration is performed manually by trial & error method to ensure the least deviation from the actual observed value of the past data (Timbadiya et al., 2014b). The optimized value of the Manning's roughness coefficient by comparing the observed and simulated water level was obtained to minimize the deviation between the observed and simulated values.

For this present study, MIKE 11 HD model has been calibrated using flood event of the year 1994. The trial values of Manning's '*n*' were selected in the range of 0.025 to 0.04 and the performance of simulated model was assessed by comparing the observed water level at Burhanpur station. The most relevant Manning's '*n*' which satisfies the criteria of RMSE, and $R^2$ was considered as optimal value for this reach. From Table 1, it can be clearly observed that The Manning's *n* of 0.035 gives the value of RMSE value of 0.813 m. The coefficient of collinearity ($R^2$) was found to be 0.934 which gives the results in permissible limits which can be clearly seen in Figures 6 and 7. So, the value of Manning's n can be taken as 0.035 for further analysis.

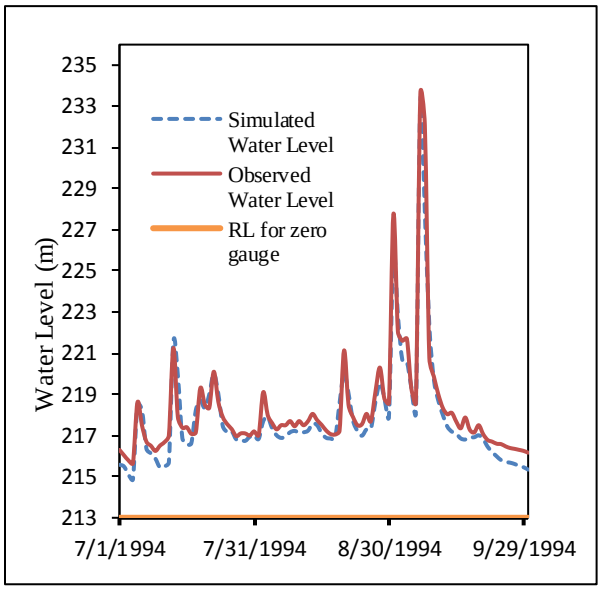



**Figure 6**. Observed and Simulated Water Level at Burhanpur for Flood year 1994

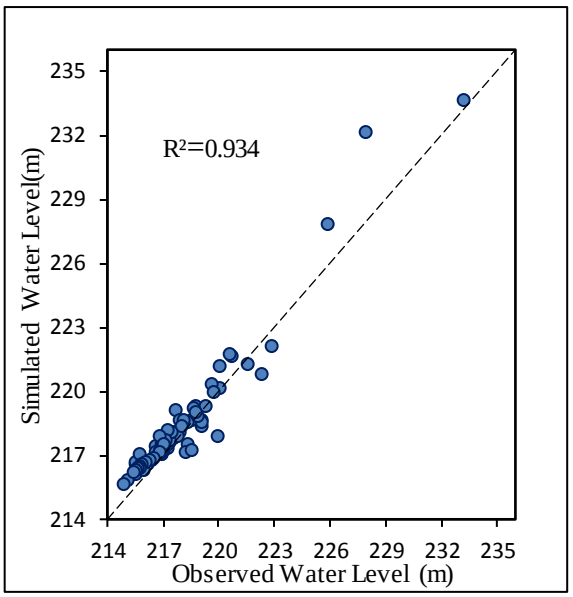



**Figure 7**. Scatter Plot of Daily Water Level at Burhanpur for year 1994

**Table 1.** Root Mean Square Error(m) compared using water level for calibration and validation of the one dimensional model

| Simulation | Year | Manning's '*n*' for Burhanpur station | RMSE in water level (m) |
|---|---|---|---|
| Calibration | 1994 | n= 0.025 | 1.23 |
| | | n= 0.03 | 1 |
| | | n= 0.035 | 0.813 |
| | | n= 0.04 | 0.942 |
| Validation | 1998 | | 0.897 |
| | 2015 | | 0.74 |

## 5. VALIDATION OF THE MODEL

The calibrated model was utilized to simulate the flow for year 1998 and 2015. The observed and simulated water levels were compared at the intermediate stream gauging station Burhanpur for 1998 flood event. The maximum discharge in the year of 1998 was observed 25,261m$^3$/s with the corresponding water level of 238 m. The developed model was validated with the year 1998 and the performance evaluation was carried out using the RMSE and $R^2$ value and it was found to be 0.897 and 0.921 respectively as shown in Figure 8 and 9.

The performance evaluation of the model was also carried out using one more independent event of the year 2015. The maximum discharge and the corresponding water level were observed 12,938 m$^3$/s and 230.3 m respectively. The results obtained from the model was compared with the observed water level and RMSE and $R^2$ value were found 0.79 and 0.97 respectively (Refer Figure 10 and 11).

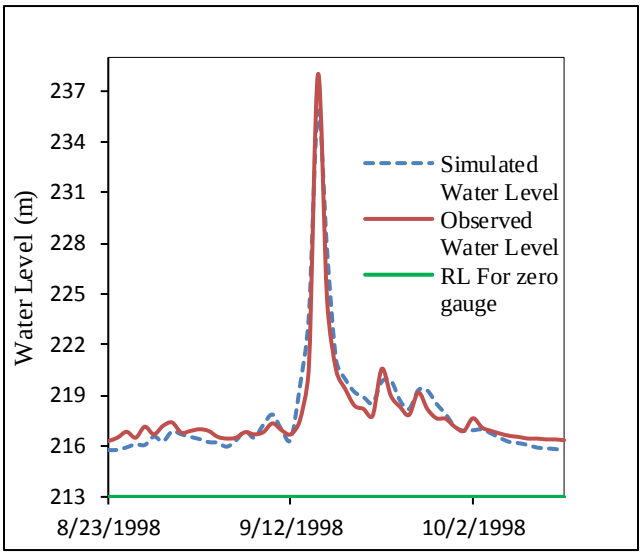



**Figure 8**. Observed and Simulated Water Level at Burhanpur for Flood year 1998

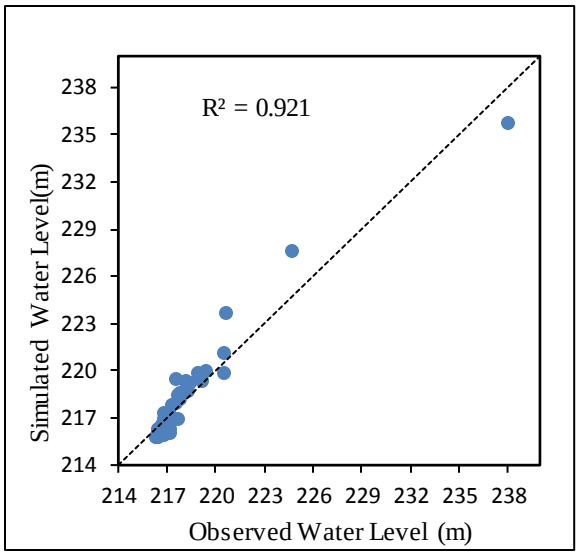



**Figure 9**. Scatter Plot of Daily Water Level at Burhanpur for year 1998

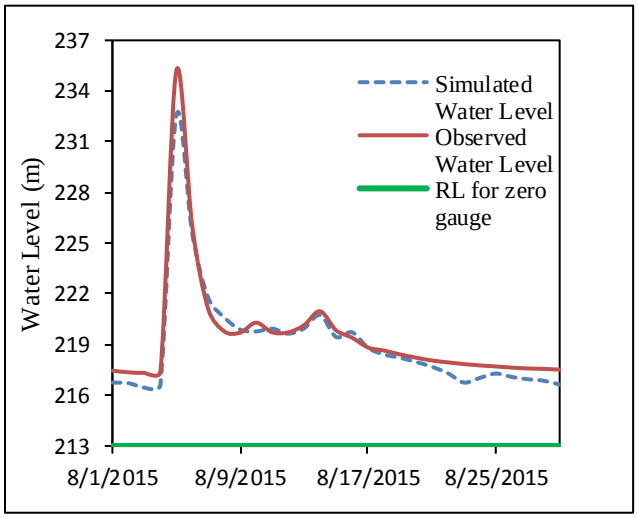



**Figure 10**. Observed and Simulated Water Level at Burhanpur for Flood year 2015

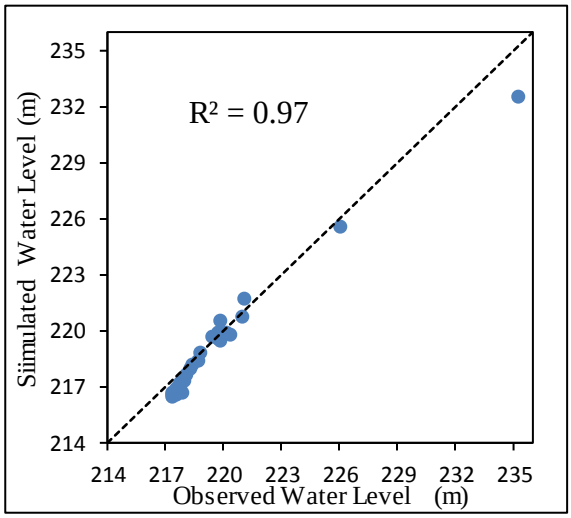



**Figure 11**. Scatter Plot of Daily Water Level at Burhanpur for year 2015

## 6. RESULTS AND DISCUSSIONS

The development of the 1D unsteady flow simulation HD model using MIKE 11 for the prediction of the water level and discharge for the required location. The model was calibrated for the year 1994 to get the optimum value of the Manning's n for the further analysis. The calibrated value was obtained as 0.035 due to its minimum deviation from the observed values. The model was validated with the independent events of year 1998 and 2015. The calibration of model for the year 1994 shows the value of RMSE and $R^2$ as 0.813 and 0.934 respectively. The validated model for year 1998 shows the value of RMSE and $R^2$ as 0.897 and 0.921 respectively. The model developed for the year 2015 gave the satisfactory results with the value of RMSE and $R^2$ as 0.74 and 0.97.

### 6.1 *Prediction of stage discharge curve in the upper tapi river*

The magnitude of discharge is required for hydraulic and hydrologic analysis but the continuous record of the flow over the channel is typically impractical and unfeasible. River stage can be measured continuously and very quickly. The prediction of discharge with respect to measured stages at the location of the bridge requires the establishment of the stage discharge curve. For the derivation of the rating curve, water level (y) acts as an independent variable and discharge (Q) acts as a dependent variable.

The rating curves were developed from the simulated results of model at the Burhanpur gauging station. The results obtained by the MIKE 11 are used for the development of the rating curve due to its minimum deviation from the observed results as shown in Figure 12.

The equation of rating curve can be given as below:

$$Q = 10.05\ (G - a)^{2.4915} \qquad (1)$$

where G = water level in m, Q= discharge in $m^3/s$, a= gauge reading corresponding to zero discharge.

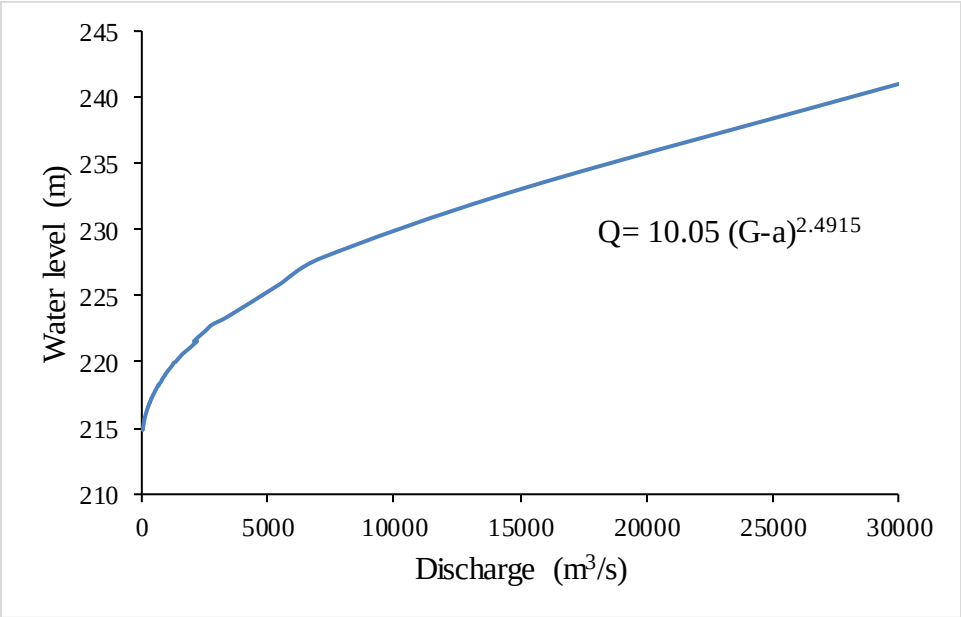



**Figure 12.** Rating curve (Q-h relationship) at Burhanpur station

The obtained stage discharge curve can be useful for the prediction of the discharge along the Upper Tapi River for different return periods. The rating curve plays an important role for the deciding the height of hydraulic structures, design of flood protection structures, flood inundation mapping, etc.

### 6.2 *Stream power calculation*

The flood power can be defined in terms of the discharge and channel geometry with the following equation:

$$\omega = \frac{\gamma QS}{W} \tag{2}$$

Here, $\omega$ is the unit stream power in W/m$^2$; $\gamma$ represents the weight density of water (9800 N/m$^2$); Q represents the discharge (m$^3$/s): S represents the energy slope and W stands for the top width (m).

The changes in the River channel geometry can be experienced when the flood power exceeds the threshold value. The theoretical estimates designate that the minimum unit stream power requires to move the cobbles (> 64mm), boulders having size of 256 mm and 512 mm are 15.54,90.38 and 217.97 W/m$^2$ respectively (Kale and Hire, 2007).

Also, the total energy expended in joules can be computed by obtaining the area under the stream power graph. The slope energy slope obtained from the MIKE 11 output file was used for the calculation of the stream power calculation. The peak stream power was obtained for the year 1994 at the Burhanpur gauging station was found to be 225.7 W/m$^2$ as shown in Figure 13. The peak stream power for the year of 1998 was found to be 303.96 W/m$^2$.

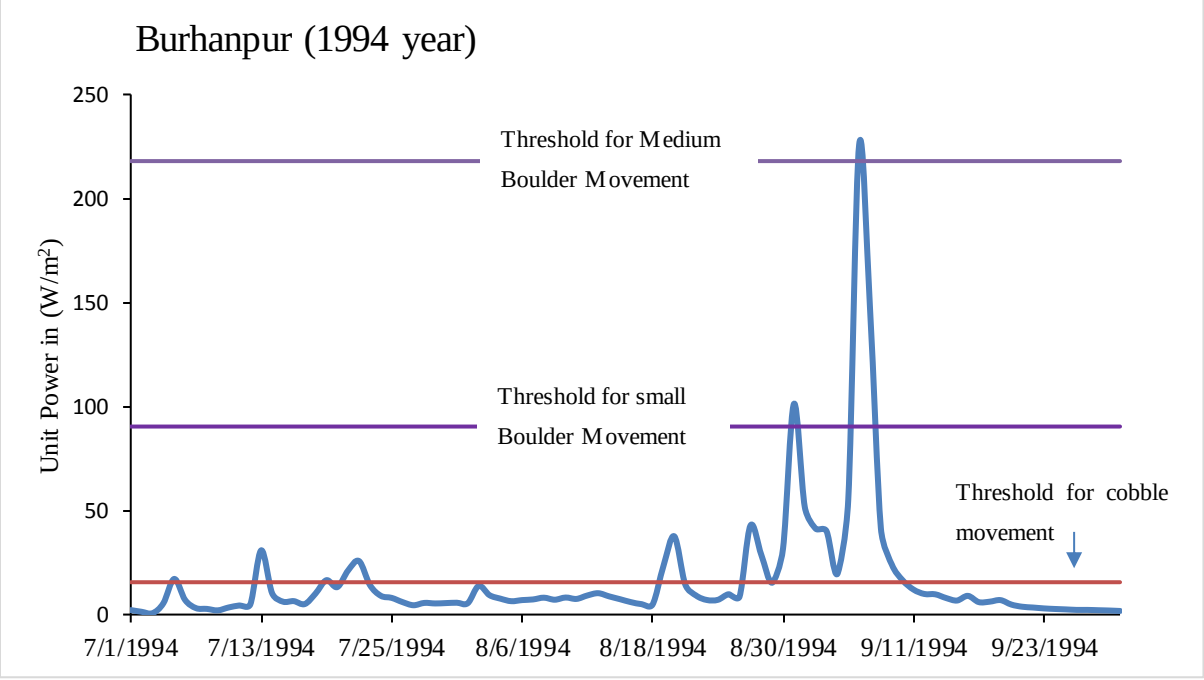



**Figure 13.** Time Series of Unit Stream Power for Flood of year 1994 at Burhanpur

## 7. CONCLUSIONS

The development of the MIKE 11 hydrodynamic model was carried out for the year of 1994 and validated with the year of 1998 and 2015 flood data. Following conclusions were derived from the present study:

a) Calibration of the one dimensional hydrodynamic model using MIKE 11 reveals that the optimum value of roughness coefficient can be taken as 0.035 for the Upper Tapi reach.
b) The performance evaluation was carried out using statistical parameters such as RMSE, $R^2$ to compare the observed and simulated water levels which gave satisfactory results.
c) The stage discharge relationship is developed at Burhanpur station using the simulated values which can be helpful in future for the flood prediction.
d) The stream power for the flood of year 1994 is computed to be 225.7 W/m$^2$ which is enough for movement of small boulders at Burhanpur station.

## ACKNOWLEDGEMENT

The authors are thankful to the Central Water Commission (CWC), Ministry of Water Resources, River Development and Ganga Rejuvenation, Govt. of India for providing necessary data required for the study. The authors also thankful to Centre of Excellence (CoE) on "Water Resources and Flood Management", SVNIT-Surat under TEQIP-II for the resourceful help and infrastructural support.

## REFERENCES

Central Water Commission (2016). "Tapi Basin. Ministry of Water Resources, River Development and Ganga Rejuvenation", Government of India, New Delhi.

DHI, MIKE 11: "A modelling system for Rivers and channels". Reference Manual. Danish Hydraulic Institute, Denmark, 2014.

Jain, S. K., Agarwal, P. K., & Singh, V. P. (2007). "Hydrology and water resources of India *" Springer*, ISBN: Vol. 1(4020), pp. 522-545

Kale, V. S., Ely, L. L., Enzel, Y., and Baker, V. R. (1994). "Geomorphic and hydrologic aspects of monsoon floods on the Narmada and Tapi Rivers in central India". *International journal of Geomorphology and Natural Hazards* Vol. 42, pp. 157-168.

Kale, V. S., and Hire, P. S. (2007). "Temporal variations in the specific stream power and total energy expenditure of a monsoonal River": The Tapi River, India. *Geomorphology*, Vol, 92(3), pp. 134-146.

Kamel, A. H. (2008): "Application of a hydrodynamic mike 11 model for the Euphrates River in Iraq". *Slovak Journal of Civil Engineering*, Vol.3(3), pp: 1-7.

Majewski, W. (2008). "Urban flash flood in Gdańsk-2001; solutions and measures for city flood management". *International Journal of River Basin Management*, Vol. *6*(4), pp. 357-367.

Nandalal, K. D. W. (2009). "Use of a hydrodynamic model to forecast floods of Kalu River in Sri Lanka". *Journal of Flood Risk Management*, Vol. *2*(3), pp. 151-158.

Pramanik, N., Panda, R. and Sen, D. (2009), "One dimensional hydrodynamic modelling of River flow using DEM extracted River cross-section". *Water Resources Management* (2010) Vol. 24: pp. 835–852.

Rahman, M. M., Arya, D. S., Goel, N. K. and Dhamy, A. P. (2011), "Design flow and stage computations in the Teesta River, Bangladesh, using frequency analysis and MIKE 11 Modelling". *Journal of Hydrologic Engineering* Vol. 16, pp. 176–186.

Timbadiya, P. V., Patel, P. L., and Porey, P. D. (2014a), "One-dimensional hydrodynamic modelling of flooding and stage hydrographs in the lower Tapi River in India". *Current Science* Vol.106: pp. 708-716.

Timbadiya, P. V., Patel, P. L., and Porey, P. D. (2014b). "A 1D–2D coupled hydrodynamic model for River flood prediction in a coastal urban floodplain". *Journal of Hydrologic Engineering*, Vol. *20*(2), pp. 50-147.

*IN PROCEEDINGS OF 25th HYDRO 2020, INTERNATIONAL CONFERENCE, NATIONAL INSTITUTE OF TECHNOLOGY ROURKELA, ODISHA, INDIA 26-28, March 2021, ISBN 978-93-90631-56-8*

Paper ID - 312

# Optimization of common energy dissipator for the two-tier spillway – A case study

Bhate R.R[1]., Amit Kulhare[1],Dr. Bhajantri M.R.[2]
[1]*Scientist'B', CWPRS, Pune – 411024,INDIA*
[2]*Scientist'E', CWPRS, Pune – 411024,INDIA*

*Email: ravindra.bhate@gmail.com, akulhare@live.com*
*Telephone/Mobile No.: +91 9960900137, +91 9271242149*

## Abstract

Siang Lower H. E. Project is a run-of-the-river scheme located on Siang River in East Siang district of Arunachal Pradesh. It is proposed to construct 86 m high and 709.48 m long concrete dam. The spillway has to perform dual functions of disposing the flood as well as flushing the sediments. Due to the geological constraints, the power house has to be accommodated in the dam body. This made the space for the spillway to pass the design flood restricted. Hence, the spillway arrangement envisaged was unique, consists of two-tier spillway comprising overflow ogee spillway on the top tier and sluice spillway in bottom tier. A common energy dissipator in the form of stilling basin was provided for both overflow and sluice spillways due to corresponding high tail water. The stilling basin provided was acting as a typical hydraulic jump basin when only sluice spillway is operated; but, it will act as plunge pool for the overflow spillway operation. For both spillways operating the design was hydraulically complex as there was interaction of flow at the junction of exit of the lower and upper spillways. The design becomes more complicated as the power house is provided adjacent to the spillway and interaction between the flow in the stilling basin and tail race channel is envisaged. The design of these structures cannot be standardized and mainly governed by site specific conditions. Physical model investigations are required for optimizing the hydraulic behaviour of the energy dissipation arrangement. This paper describes the hydraulic model studies conducted at CWPRS, Pune, which played an important role in enhancing the overall performance of spillway and energy dissipator by incorporating various modifications to the sluice roof & bottom profile, overflow spillway profile, length & elevation of the stilling basin, end sill etc. The details of model studies conducted on 1:55 scale 2-D sectional and 1:100 scale 3-D comprehensive models for improving the overall performance of common energy dissipator is described in the paper.

***Keywords:*** *Two tier spillway; Overflow spillway; Sluice Spillway; Ski-jump bucket; Stilling Basin*

## 1. Introduction

Himalayan rivers pose some of the greatest challenges in construction of hydropower projects. Any river project in the Himalayas must evolve within the context of land use practices and natural phenomena like monsoon hydrology, the complex geology and the severe sediment transport. In the Himalayan region mountainous terrain, narrow gorges, steep gradients, young/fragile geology, high level of seismicity and excessive silt load are a few factors which influence the river systems Harnessing these rivers to generate the much needed electricity by constructing hydraulic structures in such inclement conditions is a real challenge to the engineers. In search of new potential sites on the tributaries of mighty Bramhaputra, one may face challenges like narrow valleys and high discharges with very high head available for power generation. Accommodation of low level Breastwall spillways having adequate capacity is a big challenge due to narrow topography and fragile geology. Such situation led to consideration of some innovative type of spillway design like multitier spillways. In this type of spillway arrangement, the lower level sluices are provided to handle both sediments and flood. The size of low level opening has a structural tab due to forces on gates due to very high head and large pier thickness. Therefore, it is necessary to provide another set of spillway at an adequate higher location to tackle for the remaining flood. This makes the hydraulic system complex.

Thus, the design of spillway and energy dissipator becomes very involved, requiring extensive model studies. The present paper describes the hydraulic model studies carried out to optimise the effective energy dissipation system provided for two tier spillway.

## 2. Details of project

Lower Siang H.E. Project, on Siang river in Arunachal Pradesh is a proposed project where the designers have thought of two level spillways with hydraulic jump type stilling basin as energy dissipator. Figure 1 shows the location of the project. The project is essentially for hydropower generation. It is proposed to construct an 86 m high and 709.48 m long concrete dam. The project envisages generation of 2700 MW of power utilizing a net head of 55 m. The power intakes are located in the body of the dam. The discharge in excess of power generation requirements will be passed over the spillways. The spillway structure proposed is a unique one. There are two tiers to the spillway. An ogee overflow spillway is proposed as the upper tier and sluice spillway as the lower tier. Each block of a spillway comprises of a 20 m span overflow spillway and two 7 m span sluice spillways separated by 6 m thick piers. One block on the left side spillway will have two diversion sluices of dimensions 7 m x 10 m. Thus, there are overall 8 spans of overflow and 14 spans of sluice spillways. Figures 2 and 3 show the cross section and upstream elevation of the original design of spillways. The spillways together are designed to cater a discharge of 60,115 $m^3/s$. This translates to a discharge intensity of about 300 $m^3/s/m$ on the sluice spillway and about 192 $m^3/s/m$ on the overflow spillway. Initial design envisages a common stilling basin type energy dissipator for both the spillways. The sluice spillway has to dispose off sediments likely to be deposited in the vicinity of the power intakes at least twice every year – one during the onset of monsoon and second during the receding phase of the monsoon. This in turn will impose an unusual duty on the hydraulic jump stilling basin to function satisfactorily in terms of energy dissipation and sediment disposal simultaneously during floods. Design guidelines are not readily available for such kind of hydraulic structure. Thus it is necessary to optimise the design by the way of physical hydraulic modelling.

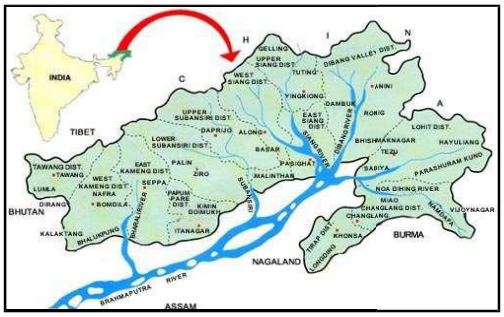



**Figure 1**Index map of project

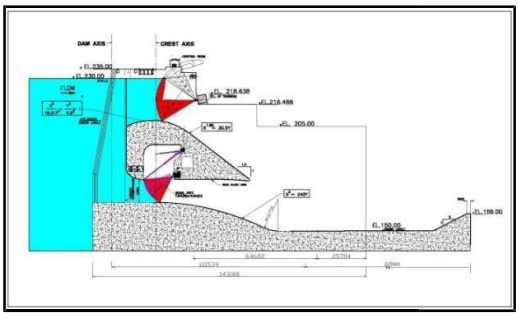


**Figure 2**Cross section of spillway (Original Design)

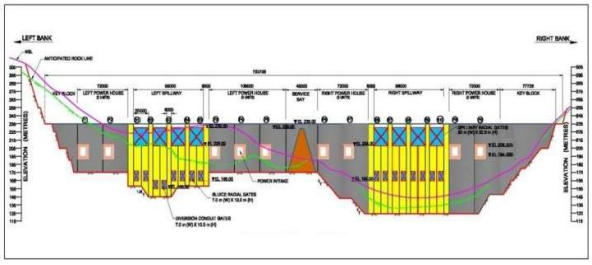


**Figure 3** Upstream elevation of spillway




**Photo 1** View of 1:55 scale 2-D model

## 3 Physical model studies

Hydraulic model studies for optimising the design of energy dissipation system were conducted on 1:55 scale 2-D sectional model and 1:100 scale 3-D comprehensive model. 2-D sectional model was constructed to a geometrically similar scale of 1:55 in a glass sided flume. One block containing one full span of overflow spillway and two spans of sluice spillway with stilling basin were incorporated in the model. Overflow and sluice spillways, piers and radial gates were fabricated in Perspex and PVC foam sheet. Stilling basin was constructed in brick masonry and the surface was plastered in smooth cement and painted with enamel paint. Photo 1 shows the view of the model. Necessary arrangements were made for measurement of discharge, pressures and water levels.

### *3.1 Studies on 2-D model for the performance of the energy dissipator for various discharges*

#### *3.1.1 Only sluice spillway operating with gates fully open*

It was observed that the spillway passes a discharge of 32,215 $m^3/s$ at FRL El. 230 m. The discharge intensity of 329 $m^3/s/m$ for this condition is one of the highest ever encountered. The corresponding tail water at El. 189 m was extremely high and the resulting flow condition in the stilling basin was very wavy with oscillating waves of the order of 5 -10 m due to low Froude number resulting in low energy dissipation. The back flow due to high tail waters was entering nearly half the length of the sluice. Thus, it was found that the performance of the hydraulic jump stilling basin was not satisfactory. Photo 2 shows the performance of the spillway and energy dissipator for this condition.



**Photo 2**Flow condition for sluice spillway operating at FRL El. 230 m with gates fully open

#### *3.1.2 Both sluice and overflow spillways operating at FRL El 230 m*

The combined flow through the sluice and overflow spillways was observed to be 61,500 $m^3/s$ at FRL El 230 m. The major concern in this flow is the interaction of the jets from the overflow spillway and the sluice spillway. The flow from the sluice spillway was greatly affected due to the flow from overflow spillway, the discharge intensity of which is 200 $m^3/s/m$. This flow induced unsteady flow in the sluice to travel further upstream and to drown the trunnion of the radial gate under the influence of the high tail water at El 203 m. Even for this condition, the hydraulic jump is oscillatory or pulsating with huge waves of the order of 5-10 m generated in the stilling basin. Excessive residual energy was seen to pass downstream. Photo 3 depicts the flow conditions on the spillway and in the stilling basin.



**Photo 3** Flow condition for both spillways operating at FRL El. 230 m with gates fully open Two aspects of flow are of concern here:

1. Interaction of the jets in the vicinity of the sluice outlet is not favourable. Hence a mechanism has to be devised to prevent the interaction at the sluice outlet and to guide the flow from the overflow spillway to a point downstream of the sluice opening.
2. The stilling basin here is a typical case of high discharge intensity and low Froude Number. As evident from literature for Froude numbers between 2.5 and 4.5, an oscillating form of jump occurs, the entering jet intermittently flowing near the bottom and then along the surface of the downstream channel. This oscillating flow causes objectionable surface waves which were seen to be carried considerably beyond the end of the basin. Stilling basins to accommodate these flows are the least effective in providing satisfactory dissipation.

### *3.1.3 Modified design of energy dissipation arrangement*

Taking due cognizance of the results, the modifications in the energy dissipation arrangement were considered. Sequent depths were calculated assuming the stilling basin invert at El. 150 m, 145 m and 140 m. for sluice spillway and for overflow spillway. Both the jump height and tail water curves were plotted as in figure 4

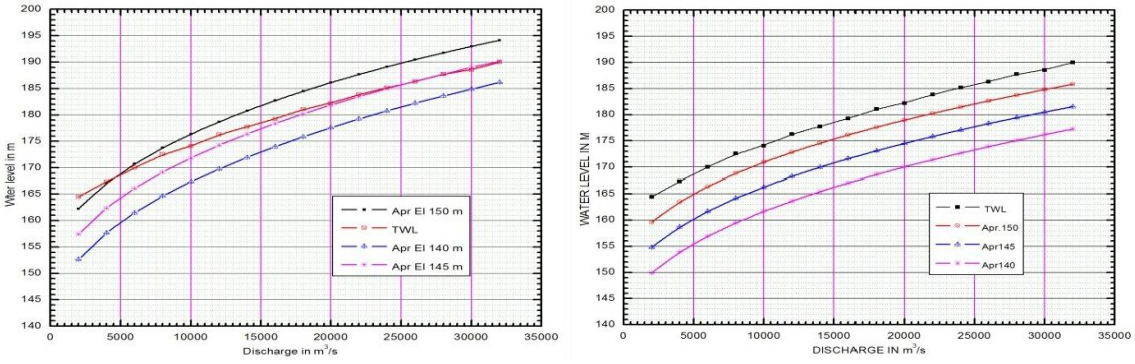



**Figure 4** Jump height curve vs TWL curve for sluice and overflow spillways

It can be seen that the tail water level almost matches the jump height curve for EL. 145 m for Q >= 20000 $m^3/s$. For lower discharges, it is above the sequent depth for Invert El. 145 m. This

ensures stable jump formation for all discharges. For invert level El .140 m, TWL is always above the jump height curve. The curves for overflow spillway indicates drowned jump for all the levels. But as the flow coming from overflow spillway produces unfavourable flow conditions downstream of spillway, it was proposed to provide the flip bucket at the end of the overflow spillway which will impinge into the pool formed in the basin due to end sill. The basin will act as hydraulic jump dissipator for sluice spillway and as a plunge pool for the flow entering from overflow spillway. The length of stilling basin provided was 220 m which is approximately 6 times $D_2$. An end sill of height 13 m was designed based on *I.S.-4997* and downstream ground level. Based on the performance of original design and sequent depth calculations, following changes were incorporated in the modified design of energy dissipation arrangement:

a. Stilling basin to be lowered by 5 m and 10 m to El 145 m and 140 m respectively.
b. Introduction of a flip at El 185 m to direct the jet away from the exit of sluice and improve the flow conditions in the stilling basin. The flip will have a radius of 30 m and an exit angle of 10 degrees.
c. End sill elevation to be changed to El 153 m from the existing level of 159 m.

Various combinations of stilling basin inverts and end sill levels were tested on the hydraulic model studies for effective performance of energy dissipation arrangement. For stilling basin with invert level El. 145 m and end sill El. 162 m, the flow conditions in the stilling basin were found to be wavy and oscillating. Energy dissipation due to hydraulic jump was found to be poor. The performance of the energy dissipator was found to be improved with further decrease of invert to El 140 m along with end-sill with top at El 153 m considering downstream river bed. For the original design of the spillways, interaction of jets in the vicinity of the sluice spillway outlet was not satisfactory / acceptable. Also, the oscillating jump in the stilling basin caused objectionable surface waves which travelled further downstream. Lowering the stilling basin apron by 10 m improved the flow conditions in the stilling basin. Hence, this design, as shown in figure 5, was adopted for further studies. Introduction of a flip for overflow spillway at El. 185 m improved the flow conditions in the vicinity of the sluice spillway outlet. For higher discharges of the order of Q=40,000 $m^3/s$ the dissipation

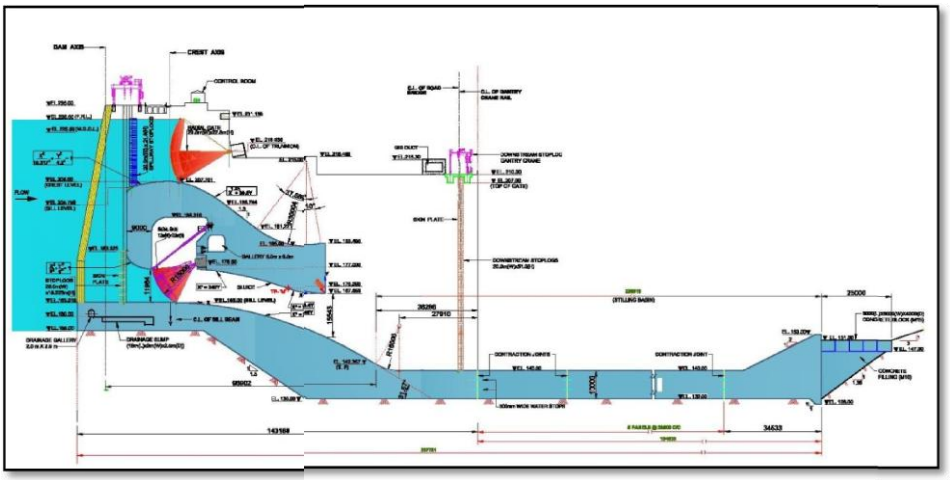


**Figure 5** Adopted design of spillway and Energy dissipator




**Photo 4** Flow condition for both spillways operating passing PMF with gates fully open

is mainly due to formation of jump for flow through sluice spillway and due to impingement of water jet coming through overflow spillway with the pool of water. This also helps in reduction of oscillatory waves in the stilling basin. Photo 4 depicts the flow conditions in the energy dissipation system while passing probable maximum flood.

### 3.2 Studies on 3-D comprehensive model

The spillway design finalised based on 2-D model studies was reproduced in the 3-D model. The studies were carried out for performance of energy dissipator for sluice and overflow spillway and its interaction with adjoining tail race channels. The 3-D comprehensive model incorporated left bank spillway, five units of power house structure with draft tube arrangements, tail race channels and stilling basin downstream of the spillway. River reach up to 1200 m upstream and 700 m downstream of the dam axis was reproduced with smooth cement plaster. During the construction of phase – II spillway, two coffer dams upstream and downstream are proposed for diverting the main river flow towards the left bank spillway. A diversion channel with an El. 155.0 m was also reproduced to divert the lean period discharge towards the diversion sluices. Upstream protection wall and coffer dam with its top at El. 229 m and downstream protection wall and coffer dam at its top at El. 190 m were also reproduced in brick masonry finished with cement plaster. Photo 5 and 6 shows the 3-D comprehensive model.

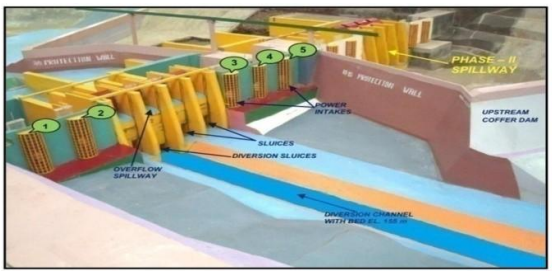



**Photo 5** Upstream View of the Model




**Photo 6** Downstream View of the Model

#### *3.2.1 Performance of stilling basin and flow conditions downstream of spillway*

Studies were conducted to assess the performance of stilling basin and the flow conditions downstream of spillway for the entire range of discharges up to the design diversion discharge of 28,500 $m^3/s$ for various conditions. It was seen that the flow conditions were tranquil in the tail race channels and the stilling basin, when all five power intake units are operating with design discharge of 604.44 $m^3/s$ for each unit at MDDL El. 225.5 m without spillway operation. The flow conditions were observed for the different operating combinations and found to be predominantly tranquil for all the conditions. Stagnation in the stilling basin zone and forward flow were seen in both the tail race channels except a mild return flow along the downstream protection wall. Photo 7 shows the flow conditions. Flow condition were observed in the stilling basin for the condition of only overflow spillway with all units operating with passing discharge of 13,667 $m^3/s$ at MDDL El. 225.5 m. The performance of stilling basin was satisfactory as the flow was contained within the divide walls of the stilling basin as depicted in photo 8. Hence, the flow condition in both the tail race channels remained unaffected by the spillway operation. The flow was seen evenly distributed across the width of stilling basin having a uniform velocity of the order of 5 to 6 m/s at the downstream of stilling basin.




**Photo 7** Flow Conditions

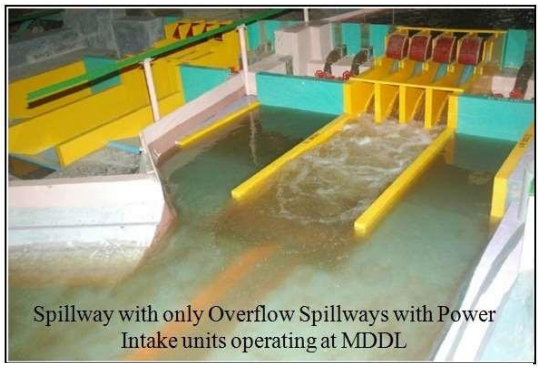



**Photo 8**Flow Conditions Downstream

Based on the various observations, it was suggested to maintain the water level in the stilling basin lower than El. 180 m, so that there are no return flow condition along the downstream protection wall through right tail race channel, which will also help in avoiding the pounding effect due to return flow and falling over stilling basin close to the draft tube outlet. To observe the above flow condition, the discharge of 18,000 $m^3/s$ was maintained by operating all sluices fully open and partial and equal gate opening of 4.45 m of overflow spillway without operation of intakes. Photo 9 shows the flow condition downstream of spillway for the same. It was observed that the flow conditions were tranquil on either sides of stilling basin in the tail race channels, when all five power intake units with design discharge (604.44 $m^3/s$ for each unit) are operating at MDDL El. 225.5 m with sluice spillway fully open (excluding diversion sluices) for corresponding discharge of 16,560 $m^3/s$. Return flows with wave formation were seen along the downstream protection wall and stagnation in front of draft tube wall on right side in the tail race channel. Heavy fluctuations of the order of 4 to 5 m of the water level were seen along the divide wall in the stilling basin. Intermittent spilling of water over the divide walls was seen. Photo 10 shows the flow conditions.

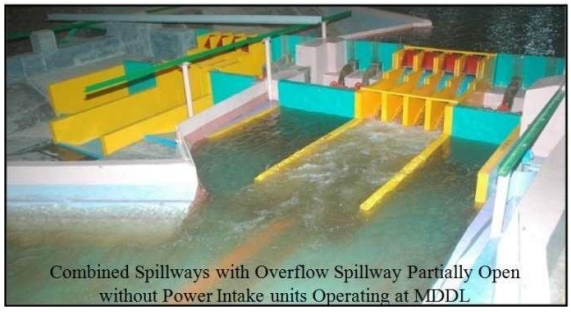



**Photo** 9 Flow Conditions Downstream

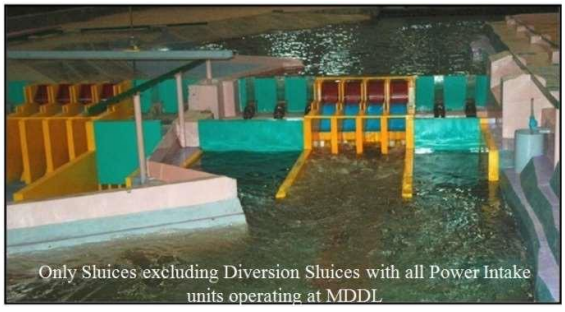



**Photo 10** Flow Conditions Downstream

When both sluice as well as overflow spillways (excluding diversion sluices) were operated at MDDL El. 225.5 m along with all five power intake units, there was mixing of flow due to the intersection of flows coming from sluice and overflow spillways causing fluctuations in the stilling basin for discharge of 27,265 $m^3/s$. Outflow from the spillway hits the downstream protection wall; as a result of this, flow turns towards the tail race channel of the central power house catering the outflow of three units to be made functional in the Phase-I commissioning. As the water starts moving backwards its flow velocity reduces sharply due to enlargement of area of flow. Due to reduction in the velocity head, the water level rises. This return flow hits back the downstream wall of the central power house housing the three units and takes towards the stilling basin. This water after traversing the width of the tail race channel laterally drops into the stilling basin thereby causing a very heavy pounding effect in this region. It was suggested to consider the raising of the height of divide in the initial portion so that the lateral flow could be restricted. Photo 11 shows the flow conditions downstream of spillway for all five power intakes and both spillways operating excluding diversion sluices. However, it was observed for simultaneous operation of sluice and overflow spillways that the waves in the stilling basin is reduced. For higher discharges the waves in the stilling basin were moderate due to intense mixing of jets. Thus, the overall performance of the stilling basin is satisfactory. Photo 12 depicts the flow condition downstream of spillway for this combined spillways operation at RWL El. 226.28 m without power units operating.

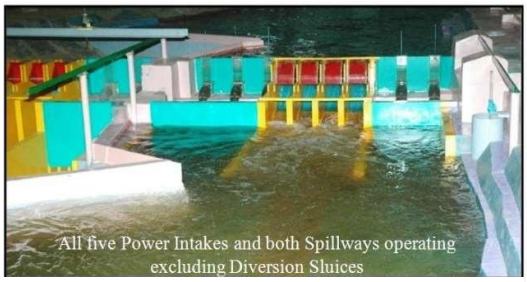



**Photo 11**Flow Conditions Downstream




**Photo 12**Flow Conditions Downstream

## 4. Conclusions

- For the original design of the spillways, interaction of jets in the vicinity of the sluice spillway outlet was not satisfactory / acceptable. Also, the oscillating jump in the stilling basin caused objectionable surface waves which travelled further downstream.
- This was the typical case of high discharge intensity and low Froude number stilling basin. To improve the energy dissipation various options were tested on the 2-D model
- Lowering the stilling basin apron by 10 m to El. 140 m improved the flow conditions in the stilling basin while passing the discharge through sluice spillway.
- Introduction of a flip for overflow spillway at El. 185 m nullified the the effect of blocking of sluice spillway outlet due to overflow spillway discharge. This improved the flow conditions in the vicinity of the sluice spillway outlet and reduced the oscillatory waves in the basin due to jet impingement at the surface of the water pool.
- Hydraulic model studies played decisive role in optimizing the design of spillway and energy dissipator for this unique project.

## Acknowledgements

The authors are grateful to Director, CWPRS for encouragement and permission to publish this paper. The authors are also thankful to the project and design engineers from M/s.Jaypee Hydro and M/s. WAPCOS Ltd. for constant interaction during the course of studies. The help of all the staff in conducting the studies and compiling the data is gratefully acknowledged.

## References

CWPRS (2012), Technical Report No. 4933. Hydraulic model studies for spillway of Siang Lower hydroelectric project, Arunachal Pradesh, 1:55 scale 2-D sectional model

CWPRS (2012), Technical Report No. 5006. Hydraulic model studies for spillway of Siang Lower hydroelectric project, Arunachal Pradesh, 1:100 scale 3-D comprehensive model

CWPRS (2008). Technical Memorandum on research into factors which influence hydraulic design of breast wall / sluice spillways

# Theme V

# RS/GIS Application for Water Resources Management

*IN PROCEEDINGS OF 25th HYDRO 2020, INTERNATIONAL CONFERENCE, NATIONAL INSTITUTE OF TECHNOLOGY ROURKELA, ODISHA, INDIA 26-28, March 2021, ISBN 978-93-90631-56-8*

Paper ID - 019

# STUDY ON VEGETATION AND RAINFALL PATTERN FOR THE STATE OF MAHARASHTRA

M L Harshavardhan[1], Anirban Mandal[2]

[1]*M.Tech Student, Civil Engineering Department, VNIT, Nagpur, 440010, India*
[2]*Associate Professor, Civil Engineering Department, VNIT, Nagpur, 440010, India*
*Email: mlharshavardhan8@gmail.com*

## ABSTRACT

Land use / Land cover pattern has been changing with civilization. The rainfall pattern changed significantly in the recent years. Dense vegetation is one of the significant factors that affecting the rainfall and vice versa. The present study pertains to the impact of dense vegetation on the local rainfall pattern in the state of Maharashtra. The area of very dense forest in Maharashtra is 8,027 sq.km and also increase in water bodies near forest area 432 sq.km from the year 2005 to 2015 as per reports published by Forest survey of India in the year 2017. This indicates that there is some relation between dense vegetation and rainfall. Filter Normalized Difference Vegetation Index (NDVI) data of Ocean Color Monitor (OCM2) sensor of IRS-P4 OCEANSAT-2 has been collected. The data have been classified into seven classes based on NDVI range using ArcGIS. The NDVI analyses showed there is an increase in vegetation initially and then it is decreased. The rainfall data have been collected from CHRS portal. The rainfall and NDVI data were analyzed using correlation analysis. Conclusion shows that there is a change in rainfall pattern with a decrease in vegetation.

***Keywords:*** *NDVI, Rainfall, NDVI classification, Correlation, ArcGIS*

## 1. INTRODUCTION

Human development and increasing population, changing the dimension of the earth's surface. Which in return leads to change in the Land use / Land cover and also we have to increase food production. In India agriculture is mostly dependent on the monsoon. Hydrological cycle (rainfall) is dependent on the earth's surface. To understand the change in earth system vegetation change is the important parameter. The vital information about the earth's surface can be extracted from the remote sensing imaging over a wide area. It has the broad range of objective capability and cost effective data collection for regional and large areas. There are several methods used to quantify the vegetation. One of the methods is vegetation index differencing, which is widely used to extract the information related to vegetation changes.

Vegetation fraction enhances the distinction between vegetation and barren ground. Influence of illuminating conditions is less affected, however it is sensitive to the ground optical properties(Baret & Guyot, 1991). Normalized Difference Vegetation Index (NDVI) is one of the important methods proposed by Rouse et al. (1974). This index is adaptive to green vegetation(Sellers, 1985); it allows to predict agricultural crops ((Tucker & Sellers, 1986);(Bullock, 1992) and rainfall in semi-arid regions ((Kerr et al., 1989), (Nicholson et al., 1990a)). NDVI can be implemented in the different aspects such as Vegetation dynamics (Wellens, 1997), change detection (Minor et al., 1999) and Land use /Land cover classification (Geerken et al., 2005).

Regardless of the cultivated and physical vegetation the development process is affected by rainfall, temperature etc.., (Li et al., 2000; (Zhang et al., 2003); (Ding et al., 2007); (Nicholson et al., 1990b); (Schmidt & Gitelson, 2000). One of the study by India Meteorological Department on the impact of deforestation on similar rainfall revealed that deforestation increases with a decrease in the rainfall. Studying the relationship between the vegetation and rainfall with the spatial variability, which enables to forecast the progressive status of the development. Rainfall is affected by many complex climatic factors. Temperature is also one of the important climatic factors that affects the rainfall pattern.

Normalized Difference Vegetation Index (NDVI) data have been collected from the BHUVAN portal. Rainfall in the given study area is highly unpredictable due to the influence of different parameters like temperature, wind, pressure etc. Rainfall data have been collected from the CHRS Portal. Temperature data collected from NOAA Portal. NDVI data have been classified using ArcGIS software. Similarly Rainfall and Temperature data are classified according to the NDVI data using ArcGIS software. The data are collected and analyzed using correlation analysis. This analysis is used to predict Rainfall using Vegetation and Temperature as a tool. This study shows that the parameters i.e. Rainfall, vegetation and temperature are interdependent in the forest zone.

### *1.1 Study area*

The selected study area is Maharashtra, India, located centre and along the west coast of peninsular India. It extends between 22° 1' 44.5" N to 15° 36' 24.46" N latitudes and 72° 38' 34.55" E to 80° 54' 16" E longitudes, covering an area of 307982.5 km2. It is the third largest state in India in terms of area. Physical features of the state are Deccan plateau, Satpura hills and Konkan coastline covered by the Western Ghats. It is the third largest state in India in terms of area.
Climatic conditions of the state are typically with hot, cold and monsoon climate. Summer (March to May) is extremely hot having temperature rises from 22 °C to 43 °C. During monsoon (June to September) July is the wettest month with more downpour and winter (October to February) a cool, dry spell occurs with temperature 12 °C to 34 °C

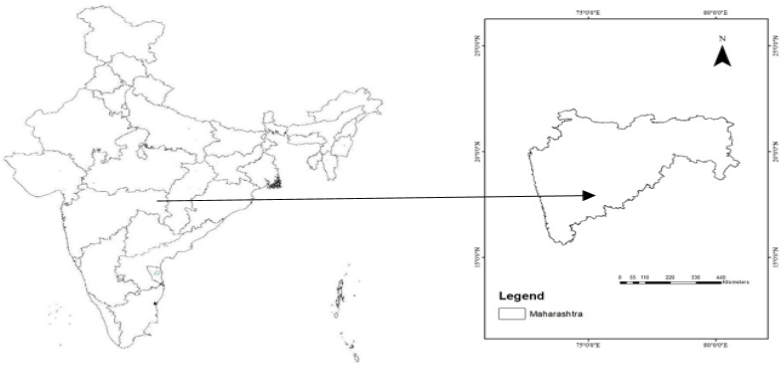



**Figure 1** Location map of the study area

Classification according to Champion and Seth, there are five types of forest. Southern Tropical Thorn Forests with low rainfall, Southern Tropical Dry Deciduous Forests it occupied most of the areas in the state. Southern Tropical Moist Deciduous Forests which contain bamboo, teak etc. Southern Tropical Semi-Evergreen Forests which are present in Western Ghats. Littoral and Swamp Forests protect coastal line.

Mumbai, the capital of Maharashtra is also known as the financial capital of India. There are 66 notified special economic zones while 24 zones are approved according to the Directorate of industries Government of Maharashtra. The location map of study area shown in figure 1.

### *1.2 Criteria behind the selection of the study area*

It is chosen based on data over uncontrolled extraction of water resource (both surface water and ground water) for various purposes, including agriculture, domestic and industrial. The surface water and ground water depend on the rainfall. Forest plays a crucial role in the conservation of water, as vegetation and other trees reduce runoff and increase percolation in the soil by enhancing the water regime in the soil. As per the Indian State of Forest report of 2017, the increase in the water bodies near the forest area between 2002 and 2015 of Maharashtra state is 432 sq.km which is the top among the states in the country. Hence, this is an area with interesting character and also the procedure of statistical modelling can be used for many other similar situations and can be related to many parts of the country which may contribute to the rainfall study.

## 2. METHODOLOGY

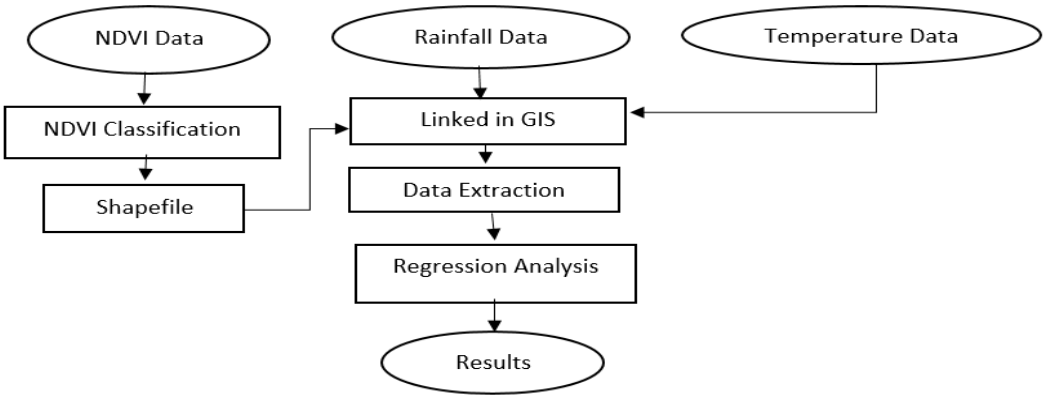



**Figure 2** Flow chart of the methodology adopted

### *2.1 Data Collection*

Monthly NDVI data products from Oceansat 2 satellite is collected from BHUVAN portal maintained by National Remote Sensing Centre and ISRO by using OCM2 (ocean color monitor) with GAC (Global Area Coverage) sensor. PERSIANN CCS (PERSIANN Cloud classification system) satellite rainfall products from CHRS portal developed by the Center for Hydrometeorology and Remote Sensing (CHRS) at the University of California, USA, which is based on TRMM (Tropical Rainfall measuring mission) and ground radar observations. Temperature data collected from physical sciences laboratory of NOAA portal maintained by the United states Department of commerce.

### *2.2 Data pre-processing*

It is necessary that the NDVI data be summed up by the raster calculator to get yearly data and then clipped to get the study area. Raw data of NDVI in DN values have to be converted using the conversion rule given by NRSC (National Remote Sensing Centre, India). Subsequently to reclassify based on density classes and is re-projected to World Geodetic System (WGS) 1984 UTM ZONE 44N.

### *2.3 Normalized difference vegetation index (NDVI)*

It is important to access and identify the vegetation for the present study. Basically living green plants absorb solar radiation for photosynthesis and emit radiation in the Infra-red band. This is the main principle of NDVI. Clouds and snow are radiated by red bands. NDVI values are ranging from -1 to 1. For the water bodies NDVI values are negative. Soils NDVI values are within the limit of 0.2 to 0.3. For the plants and vegetation, it ranges from 0.3 to 0.8.

NDVI is calculated using the formula

$$NDVI = \frac{bNIR + bRED}{bNIR - bRED}$$

Here bNIR is infra-red band, bRED is red band.

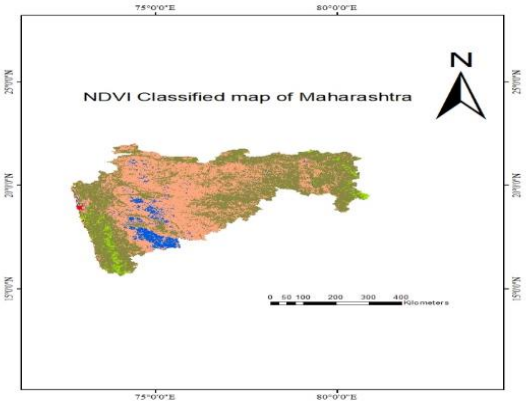
### *2.4 NDVI classification*

Base on categorization, NDVI comprise of 6 classes that are non-vegetation, lowest dense, lower dense, moderate dense, dense, and highest dense (Zaitunah et al., 2018) as given in Table 1. NDVI classified map of Maharashtra are shown in the figure 3.

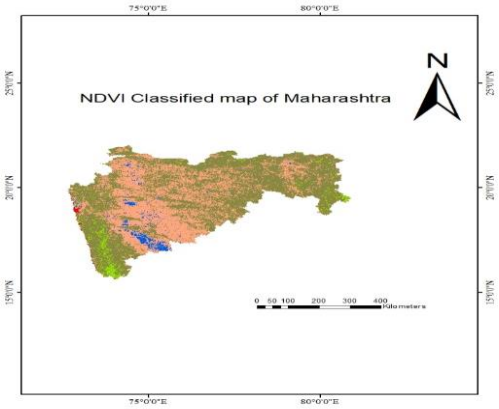
**Table 1** NDVI classification based on density class

| Sl.no | Type of vegetation class | NDVI values |
|---|---|---|
| 1 | Lowest vegetation | 0 to 0.15 |
| 2 | Lower vegetation | 0.15 to 0.30 |
| 3 | Moderate vegetation | 0.3 to 0.45 |
| 4 | Higher vegetation | 0.45 to 0.6 |
| 5 | Highest vegetation | 0.6 to 1.0 |
| 6 | Non vegetation | <0 |
| 7 | Error* | Other than -1.0 to 1.0 |

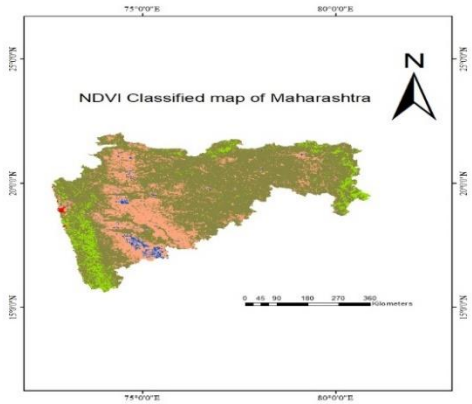
*Error may occurs due to clouds or atmospheric effects



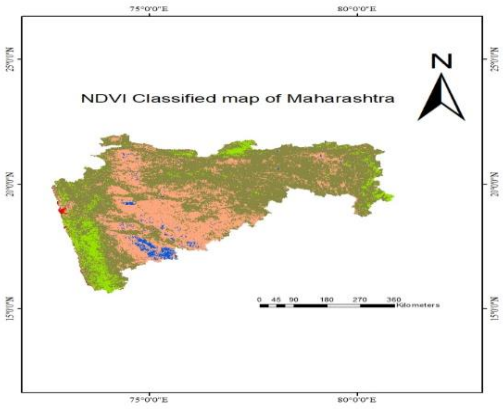

**a. 2012**



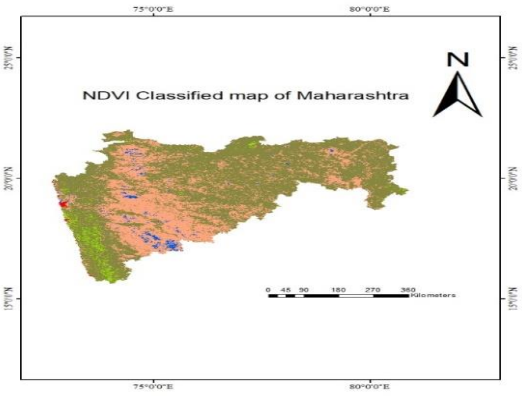

**b. 2013**



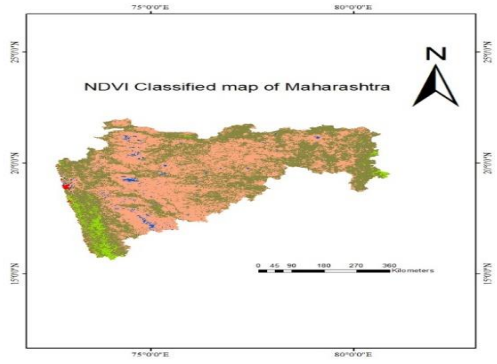

**c. 2014**



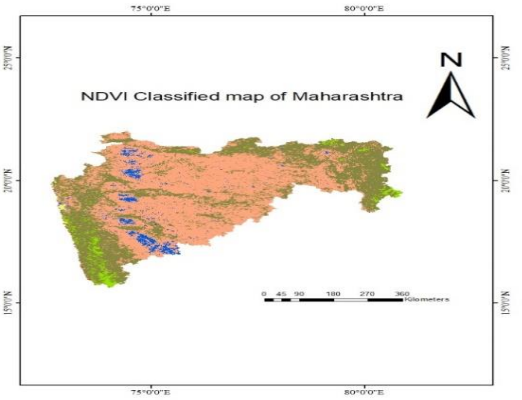

**d. 2015**




**e. 2016**




**f. 2017**




**g. 2018**

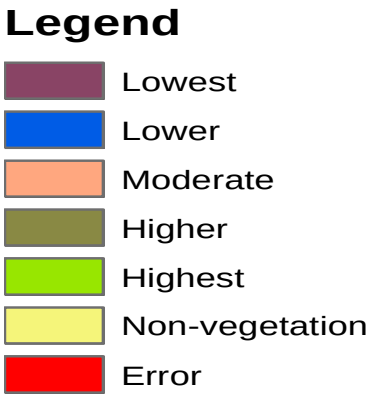
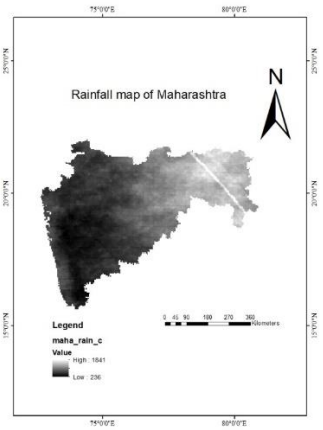


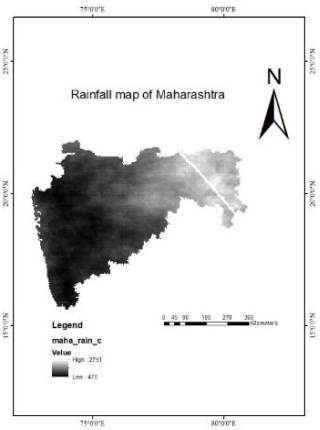

**Figure 3** NDVI Classified maps of Maharashtra (2012 to 2018)

### *2.5 Rainfall data*

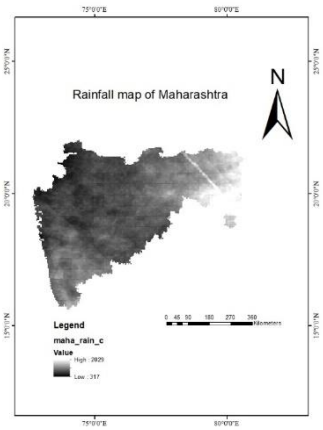
Yearly rainfall data from 2012 to 2018 are collected in TIFF format of India and it is clipped to require area as shown in the figure 4. The study area has to be divided into different zones to extract the data separately.



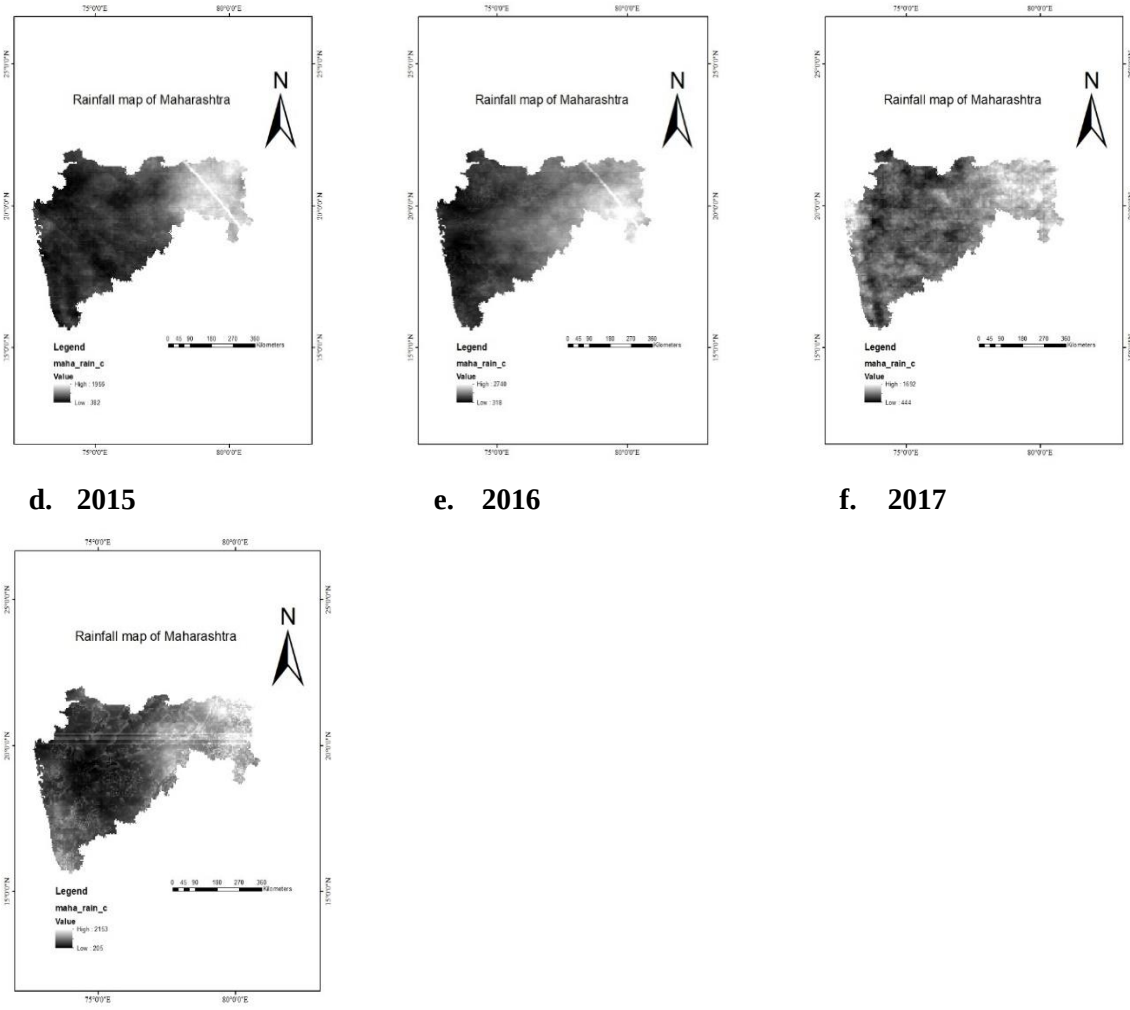

**a. 2012**




**b. 2013**




**c. 2014**




**d. 2015** **e. 2016** **f. 2017**

**g. 2018**

**Figure 4** Rainfall maps of Maharashtra (2012 to 2018)

### *2.6 Temperature data*

Yearly temperature data from 2012 to 2018 are collected in netCDF format as per coordinates of the study area. Using ArcGIS, obtained data are converted into Raster format and then it is clipped to the study area. Thus, data are extracted for the different zones.

### *2.7 Hypothesis development for Regression analysis*

Rainfall is affected by various climatic variables, but in the main study focus is given on the vegetation (forest cover) and temperature. Two hypothesis are drawn to analyse the effect on the rainfall parameter.
$H_0$: Vegetation and temperature doesn't affect the rainfall parameter.
$H_1$: Vegetation and temperature affect the rainfall parameter.
Extracted rainfall data from ArcGIS, NDVI and Temperature are taken as the inputs for regression analysis. By using data solver in MS excel, the R square value and P value are calculated.

## 3. RESULTS AND DISCUSSION

The Rainfall data, NDVI data and Temperature data obtained from ArcGIS are analysed and validated.

### *3.1 Data extracted from ArcGIS*

### *3.1.1 Rainfall*

Average annual rainfall of the study area from 2012 to 2018 are compared with the average annual normal rainfall given by IMD (Indian meteorological department). Table 2 showing rainfall in 2013 is higher than the normal rainfall, but in the remaining years significantly less. Rainfall again increasing from 2016 in each zone separately.

**Table 2** Rainfall data in different zones

| | RAINFALL (mm) | | |
|---|---|---|---|
| YEAR | ZONE 3 | ZONE 4 | ZONE 5 |
| 2012 | 675.1299 | 794.3151 | 663.1076 |
| 2013 | 1026.104 | 1194.471 | 1041.995 |
| 2014 | 702.0085 | 765.8896 | 847.4757 |
| 2015 | 703.462 | 813.1942 | 726.6524 |
| 2016 | 897.7263 | 973.8681 | 645.2109 |
| 2017 | 876.2237 | 926.7019 | 897.1353 |
| 2018 | 744.5033 | 899.6486 | 983.5401 |

### *3.1.2 NDVI*

Table 3 shows the NDVI data in different zones which is compared with the ISFR (Indian State of Forest reports) from 2013 to 2019. In 2014 and 2015 data of zone 5 which is very much larger than the usual data. In the study area bamboo and teak trees are large in number as the rainfall in 2013 is more than normal. It would have triggered the growth of these trees and also agricultural production in the state at comparatively higher in those years. Remaining years, it is somewhat higher than the normal.

**Table 3** NDVI data in different zones

| | NDVI AREA (sq.km) | | |
|---|---|---|---|
| YEAR | ZONE 3 | ZONE 4 | ZONE 5 |
| 2012 | 132659.8 | 152196.7 | 8327.389 |
| 2013 | 118196.6 | 171434.5 | 9888.151 |
| 2014 | 70119.61 | 211564.3 | 21836.96 |
| 2015 | 90238.75 | 186740.5 | 24303.52 |
| 2016 | 100550.3 | 194812.7 | 6759.248 |
| 2017 | 147567.3 | 146022.7 | 9155.69 |
| 2018 | 172029 | 117331.6 | 8455.78 |

### *3.1.3 Temperature*

Temperature data are compared with IMD (Indian meteorological department) data. The study area has the mixed type of climate temperature in three seasons' winter, summer and monsoon. The temperature difference in between the zones is varying from 1K to 3K. In all zones temperature increased by 1K from 2012 to 2018. This may be due to the development of infrastructure or Roads and transport or Pollution etc..,

## *3.2 Trend Analysis*

Trend analysis is performed to predict the future pattern. In this study linear trend analysis is used.

### *3.2.1 NDVI data*

Figure 5 shows Year wise bar charts are drawn from NDVI data to establish the trend based on the linear trend analysis. In 2013 rainfall is more as shown to increase of Zone 5 in 2014. In 2015 it decreases in Zone 3. The predicted values show that there is a maximum decline in zone 5, slight decline in zone 4 and incline in zone 3. These results show that very dense forest, converting into dense and open forest by linear trend analysis. The bar chart of NDVI data for zone 3 decreased from 2012 to 2014 and then again increased from 2014 to 2018. This is due to heavy rainfall in 2013 vegetation of zone 3 is grown in 2014 and in 2015 it intern converted to zone 4 and zone 5. The bar chart of NDVI data for zone 4 showing the highest in 2014 as a result of heavy rainfall in 2013. In 4 years, it decreased by 50%. It shows that moderate dense forest is being affected very badly. The bar chart of NDVI data for zone 5 shows highest in 2015. This led to increase in the rainfall again in 2017. In 2014, 2015 and 2016 the average annual rainfall is lesser than the normal rainfall. However ISFR reports that water bodies near the forest cover is increased. It is for complete zone 5 which covers very dense and some parts of moderate dense also.

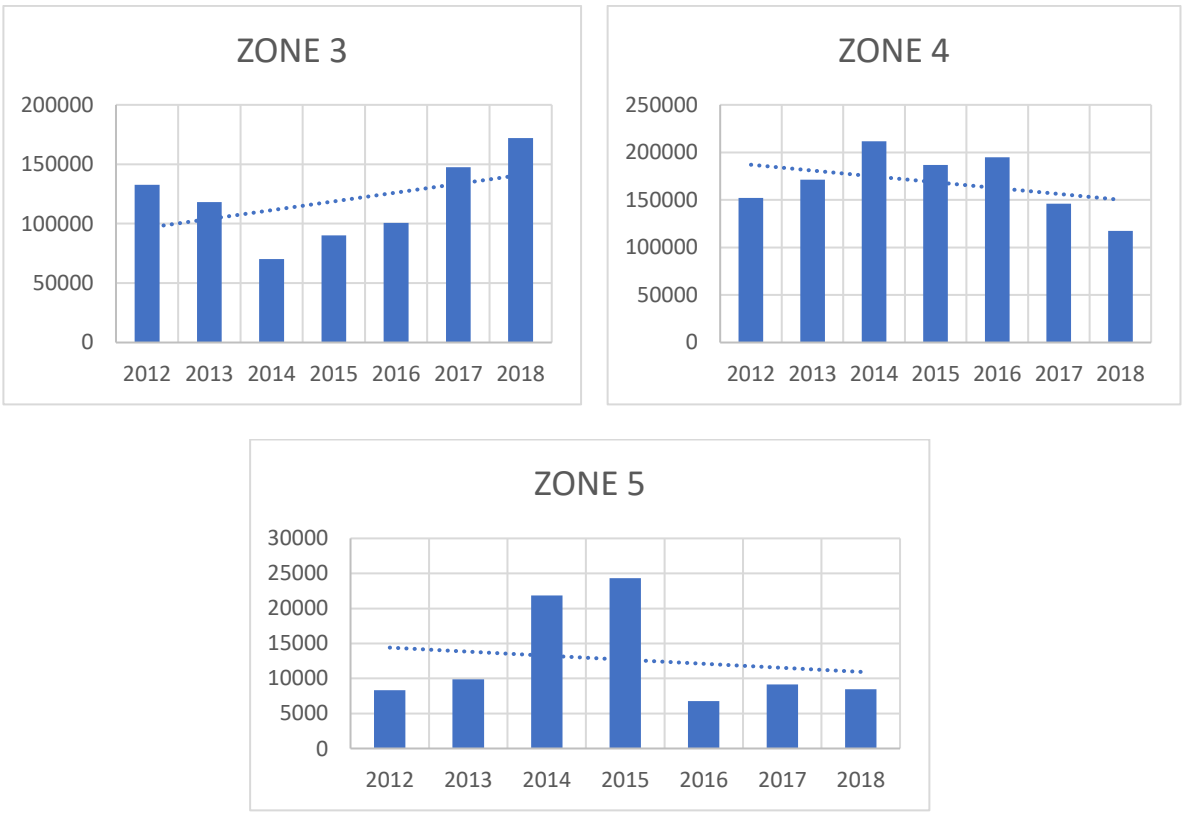



**Figure 5** Chart showing Year wise NDVI data in zone 3,4 and 5 of the study area

### *3.2.2 Temperature data*

Future values of the temperature are estimated by using linear trend analysis. Future estimates are almost same in all the zones. The average annual Temperatures are increasing in all the zones.

### *3.3 Regression analysis*

Regression analysis is carried out for dependent variable rainfall and independent variables Vegetation data (NDVI) and Temperature. The regression statistics of rainfall in zone 3 has $R^2$ value 0.48 which is less than 50% probability. Based on this rainfall, it doesn't exhibit have any relationship with dependent parameters. One more reason may due to lack of a sufficient number of data. The regression statistics of rainfall in zone 4 has $R^2$ value is 0.36 which is less than 50% probability. Number of observations is

less and also adjusted $R^2$ value tends to zero. It shows rainfall doesn't have any relationship with dependent parameters. The regression statistics of rainfall in zone 5 has $R^2$ value of 0.36 and adjusted $R^2$ value 0.61 both values are higher than 50% probability. This is sufficient enough to establish the relationship between independent parameter rainfall and the dependent parameters vegetation and temperature.

### *3.4 Regression Model*

The regression statistics of rainfall in zone 3 and 4 have $R^2$ value are 0.48 and 0.36 respectively, which indicates very less probability to establish any relationship. By thumb rule, minimum of 50% probability is required. For zone 5, $R^2$ value 0.74 which (Hair et al. 2011 &2013) is acceptable to establish the relationship between dependent and independent variable. Table 4 shows the regression model for different zones of which Zone 3 and Zone 4 are not acceptable, whereas Zone 5 is acceptable.

**Table 4** Regression Model for different zones

| Regression Analysis | | | | |
|---|---|---|---|---|
| Zone | Dependent Variable | Independent Variable | Regression Model | $R^2$ value |
| 3 | Rainfall | NDVI, Temp | $Y=-0.00049X_1+46.95287X_2-13232.5$ | 0.477104 |
| 4 | Rainfall | NDVI, Temp | $Y=-7*10^{(-5)}X_1+49.5736X_2-13990.7$ | 0.359385 |
| 5 | Rainfall | NDVI, Temp | $Y=0.024263X_1+158.2233X_2-47124.7$ | 0.742106 |

Good $R^2$ value doesn't imply good model. There may exists multitude problem. To address multitude problem Hypothesis testing is conducted. From the hypothesis testing P values are obtained. P values in zone 3 and zone 4 for all the parameters are close to 1. In the regression analysis model, the p values by thumb rule is taken as less than 0.05. But here the sample size is less than 30. It can be defined by taking the significance level as 0.01 according to (Parker & Berman, 2003). So from the above table, we cannot make the future prediction as the values are greater than 0.01. So null hypothesis $h_0$ is accepted. In Zone 3 and Zone 4, Vegetation and temperature doesn't affect the rainfall parameter. For zone 5, P values are acceptable so null hypothesis is rejected. In zone 5, Vegetation and temperature affect the rainfall parameter. We can predict only for the zone 5 as both P value and $R^2$ are satisfied.

**Table 5** P Value

| Zone | 3 | 4 | 5 |
|---|---|---|---|
| Intercept | 0.14918 | 0.242847 | 0.029715 |
| NDVI Area | 0.75138 | 0.971641 | 0.064886 |
| Temp | 0.132531 | 0.21611 | 0.028094 |

The quality of the General linear model of the regression analysis is defined by the measurement of the coefficient ($R^2$) value for the given data points. The $R^2$ value is good for zone 5, therefore the linear equation is obtained by dependent variables i.e. Vegetation and Temperature.

## 4. CONCLUSIONS

From the study it is observed that the regression analysis is effective in modelling for rainfall parameter. GIS provides easy access to user to study the NDVI data, Temperature data and rainfall data to present results graphically. The primary objective is to assess the vegetation, rainfall and temperature in the study area and establish the correlation. The main conclusion from the study is

- Future prediction of rainfall data using Regression model for zone 5 (Forest cover) 2023 and 2028 are1037.54343mm and 1167.84930mm respectively

We can finally conclude that the rainfall is directly proportional to the Vegetation and temperature in zone 5 (forest cover) based on Regression analysis.

In the present study general linear model is adopted to forecast the rainfall in the study area of Maharashtra. The accuracy of the methods depends on the accuracy of rainfall data, vegetation data and temperature data which also require a full depth knowledge in Statistics. In this study Regression analysis is used and verified with Hypothesis testing P value. The forecast of the Rainfall gives the sustainable management of dependent parameters. The study could be extended further to assess the rainfall pattern with the other climatic factors.

## REFERENCES:

Baret, F., & Guyot, G. (1991). Potentials and limits of vegetation indices for LAI and APAR assessment. *Remote Sensing of Environment*, *35*(2–3), 161–173. https://doi.org/10.1016/0034-4257(91)90009-U

Bullock, D. G. (1992). Crop rotation. *Critical Reviews in Plant Sciences*, *11*(4), 309–326. https://doi.org/10.1080/07352689209382349

Ding, M., Zhang, Y., Liu, L., Zhang, W., Wang, Z., & Bai, W. (2007). The relationship between NDVI and precipitation on the Tibetan Plateau. *Journal of Geographical Sciences*, *17*(3), 259–268. https://doi.org/10.1007/s11442-007-0259-7

Geerken, R., Zaitchik, B., & Evans, J. P. (2005). Classifying rangeland vegetation type and coverage from NDVI time series using Fourier Filtered Cycle Similarity. *International Journal of Remote Sensing*, *26*(24), 5535–5554. https://doi.org/10.1080/01431160500300297

Kerr, Y. H., Imbernon, J., Dedieu, G., Hautecoeur, O., Lagouarde, J. P., & Seguin, B. (1989). NOAA AVHRR and its uses for rainfall and evapotranspiration monitoring. *International Journal of Remote Sensing*, *10*(4–5), 847–854. https://doi.org/10.1080/01431168908903925

Nicholson, S. E., Davenport, M. L., & Malo, A. R. (1990a). A comparison of the vegetation response to rainfall in the Sahel and East Africa, using normalized difference vegetation index from NOAA AVHRR. *Climatic Change*, *17*(2–3), 209–241. https://doi.org/10.1007/BF00138369

Nicholson, S. E., Davenport, M. L., & Malo, A. R. (1990b). A comparison of the vegetation response to rainfall in the Sahel and East Africa, using normalized difference vegetation index from NOAA AVHRR. *Climatic Change*, *17*(2–3), 209–241. https://doi.org/10.1007/BF00138369

Parker, R. A., & Berman, N. G. (2003). Sample Size: More Than Calculations. *American Statistician*, *57*(3), 166–170. https://doi.org/10.1198/0003130031919

Schmidt, H., & Gitelson, A. (2000). Temporal and spatial vegetation cover changes in Israeli transition zone: AVHRR-based assessment of rainfall impact. *International Journal of Remote Sensing*, *21*(5), 997–1010. https://doi.org/10.1080/014311600210399

Sellers, P. J. (1985). International Journal of Remote Sensing Canopy reflectance, photosynthesis and transpiration. *International Journal of Remote Sensing INT. J. REMOTE SENSING*, *68*(68), 1335–1372. http://www.tandfonline.com/action/journalInformation?journalCode=tres20%5Cnhttp://dx.doi.org/10.1080/01431168508948283

Tucker, C. J., & Sellers, P. J. (1986). Satellite remote sensing of primary production. *International Journal of Remote Sensing*, *7*(11), 1395–1416. https://doi.org/10.1080/01431168608948944

Wellens, J. (1997). Rangeland vegetation dynamics and moisture availability in Tunisia: An investigation using satellite and meteorological data. *Journal of Biogeography*, *24*(6), 845–855. https://doi.org/10.1046/j.1365-2699.1997.00159.x

Zaitunah, A., Samsuri, Ahmad, A. G., & Safitri, R. A. (2018). Normalized difference vegetation index (ndvi) analysis for land cover types using landsat 8 oli in besitang watershed, Indonesia. *IOP Conference Series: Earth and Environmental Science*, *126*(February 2018), 012112. https://doi.org/10.1088/1755-1315/126/1/012112

Zhang, H., Links, P. H., Ngsee, J. K., Tran, K., Cui, Z., Ko, K. W. S., & Yao, Z. (2004). Localization of Low Density Lipoprotein Receptor-related Protein 1 to Caveolae in 3T3-L1 Adipocytes in Response to Insulin Treatment. *Journal of Biological Chemistry*, *279*(3), 2221–2230. https://doi.org/10.1074/jbc.M310679200

*IN PROCEEDINGS OF 25th HYDRO 2020, INTERNATIONAL CONFERENCE, NATIONAL INSTITUTE OF TECHNOLOGY ROURKELA, ODISHA, INDIA 26-28, March 2021, ISBN 978-93-90631-56-8*

Paper ID - 036

# Estimation of surface heat fluxes using Remote Sensing Method

Ankan Jana[1], Prof. Mahesh Kumar Jat[2], Prof. Mahender Choudhary[2]

[1]*PhD scholar, Dept of Civil Engineering MNIT, Jaipur, Rajasthan-302017, India*
[2]*Professor, Dept of Civil Engineering MNIT, Jaipur, Rajasthan-302017, India*
*Email: 2018rce9507@mnit.ac.in*
*Telephone/Mobile No.: +91 9163226097*

## Abstract

Surface heat fluxes are most important parameters to investigate the interaction between surface and atmosphere. The main goal of this study is to calculate the surface energy fluxes with remote sensing data based on remote sensing algorithm to solve the energy balance equation on each data pixel. Surface Energy Balance Algorithm for Land (SEBAL) was developed by Bastiaanssen et al., (1998) is used for the study. Landsat OLI image for 19th February 2015 and 17th February 2020 are selected for the study. Cloud free image is necessary for the algorithm. Visible, near infrared and thermal infrared bands are used from Landsat OLI image. The surface energy fluxes are estimated by partitioning of available energy at the surface between Sensible Heat flux (H) and Latent Heat Flux (LE). The method is based on the hot (dry) and cold (wet) pixel selection and heat fluxes of that pixels. Reference evapotranspiration and wind speed are collected from CLIMWAT 2.0 provided by FAO. Results indicate that SEBAL method can be used for calculating surface heat fluxes at pixel level and for determination of its spatial distribution.

***Keywords:*** *Surface Heat flux, SEBAL, Remote Sensing*

## 1. Introduction

A reliable quantification of surface heat fluxes is crucial in many agro-meteorological, hydrological applications and climate change studies, like agricultural water management or drought monitoring etc. (Anderson et al., 2011; Castellvi and Oliphant, 2017). Surface heat flux components are net radiation ($R_N$), soil heat flux (G), sensile heat flux (H) and latent heat flux (LE). Net radiation reflects the total energy over the surface coming from the Sun and soil heat flux represents the heat absorbed to the ground. Accurate measurement of heat flux components is necessary. Sensible heat flux and latent heat flux corresponds to the heat transfer between surface and atmosphere with the process of convection or conduction because of difference in temperature between them. Sensible heat flux helps to compensate the sharp change in temperature for regulating the regional climate through the absorption of heat energy by surface from the atmosphere and release of heat energy to the atmosphere. Information about sensible heat flux is important for modelling and monitoring other energy balance components, including net radiation, latent heat flux and ground heat flux (Mito et al., 2012). Increasing the latent heat energy over sensible heat energy induces local evaporative cooling (Davin and De Noblet-Ducoudrè, 2010). Variations in surface heat fluxes impacts on the atmospheric circulation and climate change, which have significantly influenced the surface energy budget (Ge et al., 2019).

Different techniques to estimate surface heat fluxes have advanced regarding method, instrumentation, and computation. There have direct measurements, using eddy covariance techniques (ECTs), large aperture scintillometers (LASs) or surface renewal analysis (SRA). Those ground measurement instrument have advantage to provide measurement at different atmospheric levels (Petropoulos et al., 2009). However, those methods have been conveyed to have various limitations, including precision errors, need for decent expertise and high cost, with further limited to intensive field experiments (Watts et al., 2000) and sometime instrument failure. Point data measurement by flux instrument cannot describe the spatial variations in surface heat fluxes. These methods also provide estimates of surface heat fluxes with low spatial and temporal resolution. Instead of these methods, the use of mathematical models has drawn mixed results despite the similarity in input variables (Allen et al., 2005). Satellite remote sensing has provided major advances in understanding the climate system and its changes, by quantifying processes and spatio-temporal states of the atmosphere, land, and oceans. In the last two decades, surface energy balance methods have demonstrated their utility in modeling water availability

using diagnostic retrievals of energy fluxes from in situ or remote sensing data, especially data acquired in the thermal infrared (TIR) region (Kalma et al., 2008).

Remote sensing-based surface energy balance models can be divided in two categories: single-source energy balance model and duel source energy balance model. In single source energy balance model soil and vegetation are considered in a combined energy budget. Whereas soil and vegetation are separately analyzed in duel source energy balance model. Single source energy balance models are Surface Energy Balance Algorithm for Land (SEBAL; Bastiaanssen et al., 1998), Simplified surface energy balance index (S-SEBI; Roerink et al., 2000), Surface Energy Balance system (SEBS; Su 2002), Mapping evapotranspiration at High Resolution with Internalized Calibration (METRIC; Allen et al., 2007), Operational Simplified Surface Energy Balance (SSBop; Senay et al., 2013). Duel source energy balance models are Two source model (TSM; Norman et al., 1995), Two source time integrated model (TSTIM; Anderson et al., 1997), Atmosphere land exchange inverse (ALEXI; Mecikalski et al., 1999), Duel temperature difference (DTD; Norman et al., 2000), Enhanced two source Evapotranspiration model for land (ETEML; Yang et al., 2015). Those remote sensing-based algorithms mainly used for evapotranspiration (ET) estimation (Sun et al.,2011; Papadavid et al., 2013; Rahimi et al 2014; Kundu et al., 2018). Within those Algorithms SEBAL is most popular and used by many researchers (Silva et al., 2019).

SEBAL algorithm has been used worldwide for determination of evapotranspiration in water balance studies, irrigation requirements, lake energy balance etc. (Bastiaanssen et al., 2005; Papadavid et al., 2017). Surface heat fluxes can be calculated as residual to determine of evapotranspiration using SEBAL algorithm (Bastiaanssen et al., 2000). This algorithm has high level of accuracy to measure evapotranspiration and surface heat flux components. Anchor pixels (hot and cold) selection is the most sensitive part of the calculation. Accurate selection of anchor pixel is necessary for accurate result. There was very less amount of work available, which have used SEBAL algorithm to determine surface heat fluxes. Bastiaanssen et al., (2000) used SEBAL algorithm for determination of latent heat flux and sensible heat flux in an irrigated area. Zahira et al., (2009) used SEBAL algorithm outputs to justify the results of their work. Schirmbeck et al., (2018) used SEBAL model to evaluate energy balance in a humid subtropical crop area. But the accuracy of SEBAL algorithm for surface heat flux estimation is still not verified properly. In this study, SEBAL algorithm has been used to determine the surface heat fluxes. Sensible heat flux has influences to regulate the surface temperature. The main objective of the study to determine the efficiency of the SEBAL algorithm to calculate the surface heat fluxes.

## 2. Materials and Methods

SEBAL algorithm has been used to determine surface heat fluxes. Landsat OLI satellite data has been used for the study. Landsat OLI image has 30 m spatial resolution with 16-day repeat cycle. Cloud free Landsat image of 147-43 path-row on 19th February 2015 and 17th February 2020 selected for the study. Cloud create errors in calculation. Cloud free data is necessary calculation. Wind speed and reference evapotranspiration is collected from CLIMWAT 2.0 provided by FAO.
ASTER 30 m digital elevation model (DEM) has been used in this study.

Detailed methods SEBAL algorithm shown in figure 2. The general equation used in SEBAL is

$$\lambda ET = R_n - G - H \quad (1)$$

Where, $\lambda ET$ is the latent heat flux(W/m$^2$), $R_n$ is the net radiation at surface (W/m$^2$), G is the soil heat flux (W/m$^2$) and H is the sensible heat flux (W/m$^2$).

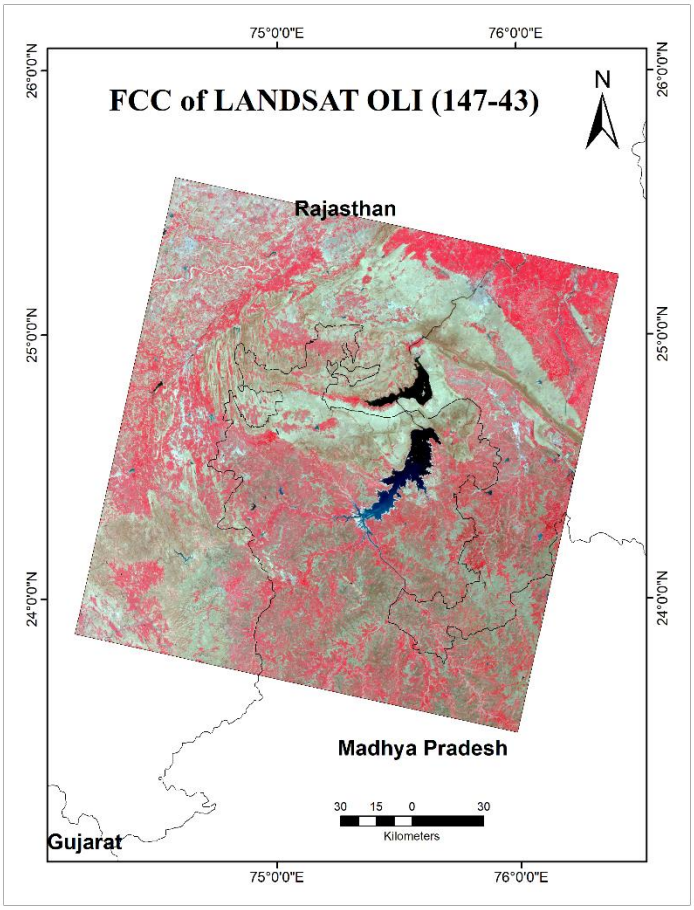



Figure1: False colour composite (FCC) Landsat OLI image (147-43)

The net radiation ($R_n$)

Net radiation is calculated using albedo and atmospheric transmissivity for each pixel. Shortwave and longwave radiation is used. The net instantaneous radiation per unit area is calculated as (Bastiaanssen et al., 1998)

$$R_n = (1-\alpha)R_{S\downarrow} + R_{L\downarrow} - R_{L\uparrow} - (1-\epsilon_0)R_{L\downarrow} \quad (2)$$

Where, $\alpha$ is surface albedo, $\epsilon_0$ is thermal surface emissivity, $R_{S\downarrow}$ incoming shortwave radiation, $R_{L\downarrow}$ incoming longwave radiation, $R_{L\uparrow}$ outgoing longwave radiation.

Surface albedo is the ratio of solar electromagnetic radiation reflected from the surface of the soil and plant to the incoming radiation. It is the average reflectance of the sun's spectrum .it is a unitless quantity value ranges from 0 to 1. And vary based on the land cover. Liang (2000) developed a series of algorithms for calculating albedo from various satellite sensors. Surface albedo can be calculated using following equation:

$$\alpha = \frac{\alpha_{toa} - \alpha_{path_radiance}}{\tau_{SW}^2} \quad (3)$$

Where, $\alpha_{path_radiance}$ is the average of the part of solar incident radiance for all bands, which has been scattered to the sensor before reaching ground level. Its values range from 0.025 to 0.04, which has

been suggested as 0.03 for SEBAL (Bastiaanssen 2000). $\alpha_{toa}$ is top of the atmospheric albedo. $\tau_{SW}$ is atmospheric transmissivity.

$$\alpha_{toa} = \sum(W_\lambda \times \rho_\lambda) \quad (4)$$

Where, $\rho_\lambda$ corrected reflectance for each band, $W_\lambda$ weighting coefficients for each band.

Atmospheric transmissivity is defined as the fraction of the incident radiation that is transmitted by the atmosphere and it represents the effects of absorption and reflection occurring with the atmosphere.

$$\tau_{SW}^2 = 0.75 + (2 \times 10^{-5} \times z) \quad (5)$$

Where, z is the height of the meteorological station from the mean sea level (Bastiaanssen et al., 1998).

Incoming shortwave radiation ($R_{S\downarrow}$):

The flux of direct and diffuse solar radiation that actually reaches the ground assuming clear sky conditions at the time of imaging is calculated using following equation.

$$R_{S\downarrow} = G_{SC} + \cos\theta + d_r + \tau_{SW} \quad (6)$$

Where, $G_{SC}$ is the solar constant (1367 W/m$^2$), $\theta$ is the incident angle obtained from satellite image header file, $d_r$ is the inverse of the square relative distance of the earth to the sun.

Outgoing longwave radiation ($R_{L\uparrow}$):

The reflected longwave radiation flux is calculated using Stefan-Boltzman relation.

$$R_{L\uparrow} = \epsilon_0 \times \sigma \times T_S^4 \quad (7)$$

Where, $\epsilon_0$ is the broadband surface emissivity, $\sigma$ is the Stefan-Boltzman constant ($5.67\times10^{-8}$ W/m$^2$/K$^4$) and $T_S$ is the surface temperature in Kelvin. Surface temperature is calculated using the plank equation (Bastiaanssen et al., 2005).

$$\epsilon_0 = 0.85 \times (-ln\tau_{SW})^{0.09} \quad (8)$$

$$T_S = \frac{K_2}{ln\left(\frac{\varepsilon_{NB} K_1}{R_c} + 1\right)} \quad (9)$$

Where, $R_c$ is the corrected thermal radiance of the surface and $\varepsilon_{NB}$ is the narrowband surface emissivity. $K_1$ and $K_2$ are constant value acquired from satellite metadata.

Incoming long wave radiation ($R_{L\downarrow}$):

This radiation is thy flux of thermal radiation from the atmosphere to downwards. It is also calculated using Stefan-Boltzman relation.

$$R_{L\downarrow} = \epsilon_0 \times \sigma \times T_a^4 \quad (10)$$

Where, $T_a$ is the temperature of the air near the surface, which is replaced by a cold pixel temperature.

Soil Heat Flux (G)

The heat transfer rate inside the soil and vegetation by molecular convection. Temperature, vegetation index and net surface radiation is used to calculate soil heat flux.

$$\frac{G}{R_n} = \frac{T_S}{\alpha}(0.0038\alpha + 0.0074\alpha^2)(1 - 0.98NDVI^4) \quad (11)$$

Where, $T_S$ is surface temperature ($^0$C) and NDVI is the Normalized Differential Vegetation Index (Sun et al., 2011).

Sensible heat flux (H):

The sensible heat flux is the heat transfer to the air by molecular convection due to temperature difference between the air and the surface is calculated as (Bastiaanssen et al., 2000):

$$H = (\rho \times C_p \times dT)/r_{ah} \quad (12)$$

Where, $\rho$ is the air density(kg/m$^3$), $C_p$ air specific heat(1004J/kg/K), dT is the temperature difference ($T_1$-$T_2$) at height $z_1$and $z_2$($^0$K) and $r_{ah}$ is the aerodynamic resistance against heat transfer(s/m).

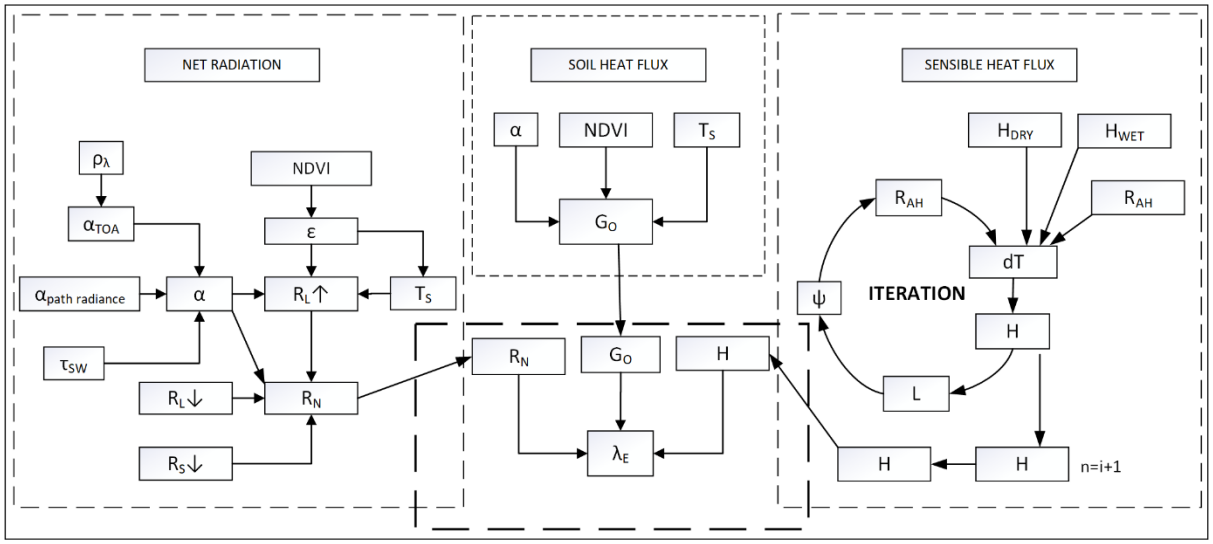



Figure 2: Methodology chart for full SEBAL algorithm

## 3. Results and Discussion

Surface heat fluxes for 19th February 2015 and 17th February 2020 were computed using SEBAL algorithm. Landsat OLI satellite data was used. Erdas Imagine 10.5 has been used for model preparation and calculation. SEBAL algorithm were applied in many areas mainly to determine the evapotranspiration with good accuracy (Bastiaanssen et al., 2005). Selection of anchor pixel has an important role to determine the heat fluxes accurately (Bhattarai et al., 2016; Silva et al., 2019). The net radiation is the total net energy in the surface energy budget. Net radiation was calculated using eq.2. Surface albedo ($\alpha$) is one the main input for net radiation estimation. Weight coefficients for different bands of Landsat OLI data used for $\alpha$ given in the table1. According to Allen et al., (2002), the net radiation values should be within the range 100-700 W/m$^2$ depending on the location and the time of overpass. Our results also within the range. The net radiation is directly associated with incoming long-wave and short-wave radiation. These two parameters are correlated with surface temperature. Soil heat flux is the rate of heat storage in soil and vegetation due to conduction. Sensible heat flux is the rate of heat loss to the air by convection and conduction, due to a temperature difference. The sensible heat flux (H) is a function of the temperature gradient, surface roughness, and wind speed. Latent heat flux is the rate of latent heat loss from the surface due to evapotranspiration. Latent heat flux is calculated using eq.1.

Table1: Weight coefficients used for albedo calculation (Jaafar and Ahmed, 2020)

| Sensor | Blue band | Green Band | Red Band | Near-infrared band | Shortwave-infrared band 1 | Shortwave-infrared band 1 |
|---|---|---|---|---|---|---|
| Landsat OLI | 0.246 | 0.146 | 0.191 | 0.304 | 0.105 | 0.008 |

Surface temperature is a most important parameter for estimation of surface heat fluxes. For 19th February 2015 surface temperature vary from 293.304 K minimum to 316.665 K maximum. For 17th February 2020 surface temperature range from 293.136 K minimum to 315.672 K maximum. For selection of cold pixel, we used NDVI value greater than 0.4 and surface temperature less than the median of the temperature. For selection of hot pixel, we use SAVI value between 0.18 to 0.3 and temperature greater than median of temperature. Aerodynamic resistance ($r_{ah}$) and temperature difference (dT) are main two input to calculate H. Atmospheric stability condition is necessary to determine $r_{ah}$ and dT. Mohin Obukhov stability theory has been applied here for correction of stability error. Six iterations have been done here to reach instability. Final H is calculated using final $r_{ah}$ and dT. After calculation of H, latent heat flux ($\lambda ET$) has been calculated using eq.1. The value of $r_{ah}$ for hot pixels is low, caused the more release of sensible heat to the atmosphere. Thus, the surface temperature at hot pixels is high. High temperature difference between surface and air temperature is justified for low $r_{ah}$. The high $r_{ah}$ over cold pixel because the energy is available for evapotranspiration.

Table2: Instantaneous parameters and heat flux during Landsat overpass at hot and cold pixels

| Parameter | Unit | 19-Feb 2015 | | 17-Feb 2020 | |
|---|---|---|---|---|---|
| | | Hot pixel | Cold pixel | Hot pixel | Cold pixel |
| NDVI | | 0.277 | 0.708 | 0.268 | 0.767 |
| SAVI | | 0.190 | 0.505 | 0.187 | 0.502 |
| Surface albedo | | 0.232 | 0.178 | 0.238 | 0.172 |
| Surface emissivity | | 0.951 | 0.962 | 0.951 | 0.962 |
| Surface temperature | K | 313.440 | 300.851 | 312.494 | 298.365 |
| Outgoing longwave radiation | $Wm^{-2}$ | 520.913 | 447.212 | 514.609 | 432.547 |
| Net radiation | $Wm^{-2}$ | 396.287 | 515.304 | 380.398 | 542.530 |
| Soil heat flux | $Wm^{-2}$ | 87.636 | 55.033 | 82.862 | 43.608 |
| LET | m | 0 | 460.271 | 0 | 498.921 |
| Sensible heat flux | $Wm^{-2}$ | 308.65 | 0 | 297.536 | 0 |

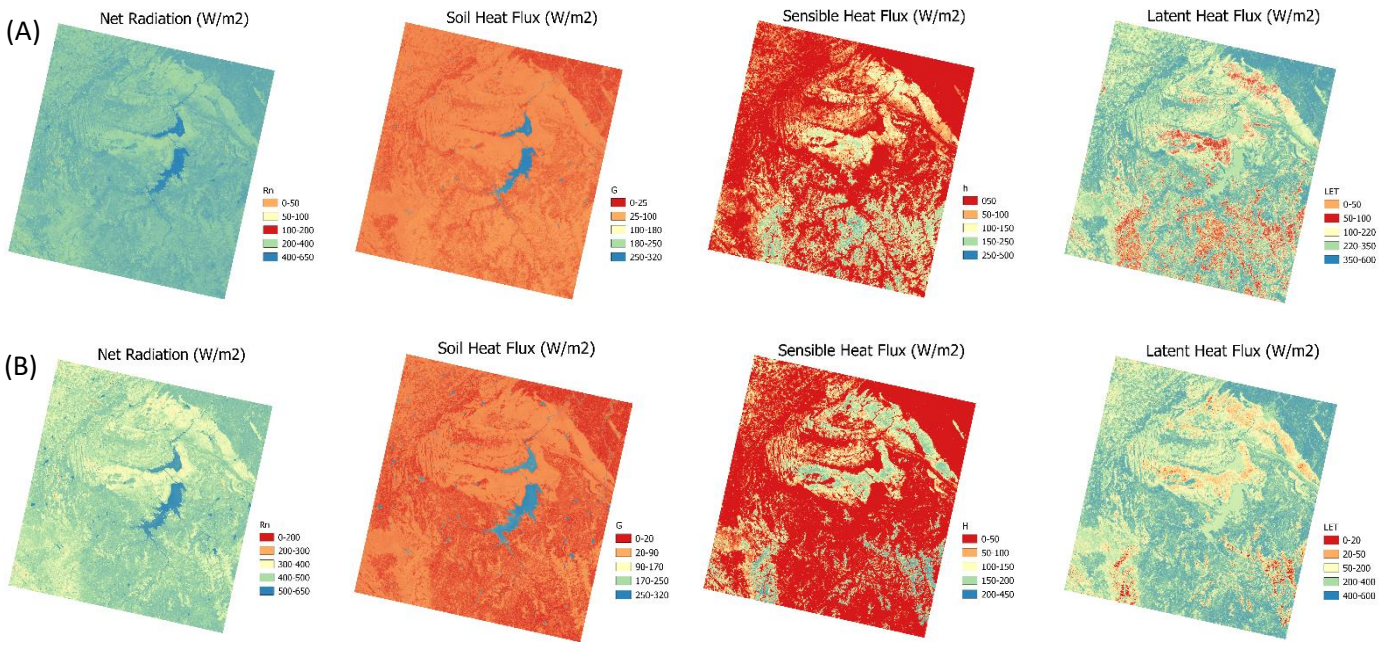



Figure3 Spatial distribution of net radiation flux (Rn), soil heat flux (G), sensible heat flux (H), and latent heat flux (LE) (A) 19th February 2015 (B) 17th February 2020

The spatial patterns of latent heat and sensible heat flux estimated using SEBAL model with Landsat data are shown in Figure 3. Sensible heat flux is higher for barren and rocky area. Latent heat flux is higher for vegetation area. Different Surface energy flux and other required parameter for calculation is shown in table 2 for hot and cold pixels.

## 3. Conclusions

SEBAL algorithm has been applied with Landsat OLI data for 19th February 2015 and 17th February 2020. Net radiation is higher for vegetated area and lower for barren area. Sensible heat flux is higher over barren area and lower over vegetated area.

This study has demonstrated that remote sensing algorithm and data can be applied to determine the surface heat fluxes. The spatial variation of the surface heat fluxes can also be measure with remote sensing data. SEBAL algorithm is suitable for arid region.

Due to unavailability of field data validation work has not been done. Further, the results will be validated with the field observed sensible heat flux data. The algorithm can be modified using different module for determination of net radiation and other component and can also be applied over humid area.

## References

Allen, R.G., Tasumi, M. and Trezza, R. (2007). Satellite-based energy balance for mapping evapotranspiration with internalized calibration (METRIC)—Model. *Journal of irrigation and drainage engineering*, *133*(4), 380-394.

Allen, R.G., Tasumi, M., Morse, A. and Trezza, R. (2005). A Landsat-based energy balance and evapotranspiration model in Western US water rights regulation and planning. *Irrigation and Drainage systems*, *19*(3-4), 251-268.

Allen, R.G., Tasumi, M., Trezza, R., Waters, R. and Bastiaanssen, W. (2002). Sebal (surface energy balance algorithms for land). *Advance Training and Users Manual–Idaho Implementation, version*, *1*, 97.

Anderson R G et al 2011 Biophysical considerations in forestry for climate protection Front. Ecol. Environ. 9 174–82

Anderson, M.C., Norman, J.M., Diak, G.R., Kustas, W.P. and Mecikalski, J.R. (1997). A two-source time-integrated model for estimating surface fluxes using thermal infrared remote sensing.

Bastiaanssen, W.G. (2000). SEBAL-based sensible and latent heat fluxes in the irrigated Gediz Basin, Turkey. *Journal of hydrology*, *229*(1-2), 87-100.

Bastiaanssen, W.G., Menenti, M., Feddes, R.A. and Holtslag, A.A.M. (1998). A remote sensing surface energy balance algorithm for land (SEBAL). 1. Formulation. *Journal of hydrology*, *212*, 198-212.

Bastiaanssen, W.G.M., Noordman, E.J.M., Pelgrum, H., Davids, G., Thoreson, B.P. and Allen, R.G. (2005). SEBAL model with remotely sensed data to improve water-resources management under actual field conditions. *Journal of irrigation and drainage engineering*, *131*(1), 85-93.

Bhattarai, N., Shaw, S.B., Quackenbush, L.J., Im, J. and Niraula, R. (2016). Evaluating five remote sensing based single-source surface energy balance models for estimating daily evapotranspiration in a humid subtropical climate. *International journal of applied earth observation and geoinformation*, *49*, 75-86.

Castellví, F. and Oliphant, A.J. (2017). Daytime sensible and latent heat flux estimates for a mountain meadow using in-situ slow-response measurements. *Agricultural and Forest Meteorology*, *236*, 135-144.

Davin, E.L. and de Noblet-Ducoudré, N. (2010). Climatic impact of global-scale deforestation: Radiative versus nonradiative processes. *Journal of Climate*, *23*(1), 97-112.

Ge, N., Zhong, L., Ma, Y., Cheng, M., Wang, X., Zou, M. and Huang, Z. (2019). Estimation of Land Surface Heat Fluxes Based on Landsat 7 ETM+ Data and Field Measurements over the Northern Tibetan Plateau. *Remote Sensing*, *11*(24), 2899.

Jaafar, H.H. and Ahmad, F.A. (2020). Time series trends of Landsat-based ET using automated calibration in METRIC and SEBAL: The Bekaa Valley, Lebanon. *Remote Sensing of Environment*, *238*, 111034.

Kalma, J.D., McVicar, T.R. and McCabe, M.F. (2008). Estimating land surface evaporation: A review of methods using remotely sensed surface temperature data. *Surveys in Geophysics*, *29*(4-5), 421-469.

Kundu, S., Mondal, A., Khare, D., Hain, C. and Lakshmi, V. (2018). Projecting Climate and Land Use Change Impacts on Actual Evapotranspiration for the Narmada River Basin in Central India in the Future. *Remote Sensing*, *10*(4), p.578.

Liang, S. (2001). Narrowband to broadband conversions of land surface albedo I: Algorithms. *Remote sensing of environment*, *76*(2), 213-238.

Mecikalski, J.R., Diak, G.R., Anderson, M.C. and Norman, J.M. (1999). Estimating fluxes on continental scales using remotely sensed data in an atmospheric–land exchange model. *Journal of Applied Meteorology*, *38*(9), 1352-1369.

Mito, C.O., Boiyo, R.K. and Laneve, G. (2012). A simple algorithm to estimate sensible heat flux from remotely sensed MODIS data. *International journal of remote sensing*, *33*(19), 6109-6121.

Norman, J.M., Kustas, W.P. and Humes, K.S. (1995). Source approach for estimating soil and vegetation energy fluxes in observations of directional radiometric surface temperature. *Agricultural and Forest Meteorology*, *77*(3-4), 263-293.

Norman, J.M., Kustas, W.P., Prueger, J.H. and Diak, G.R. (2000). Surface flux estimation using radiometric temperature: A dual-temperature-difference method to minimize measurement errors. *Water Resources Research*, *36*(8), 2263-2274.

Papadavid, G., Hadjimitsis, D.G., Toulios, L. and Michaelides, S. (2013). A modified SEBAL modeling approach for estimating crop evapotranspiration in semi-arid conditions. *Water resources management*, *27*(9), 3493-3506.

Papadavid, G., Neocleous, D., Kountios, G., Markou, M., Michailidis, A., Ragkos, A. and Hadjimitsis, D. (2017). Using SEBAL to Investigate How Variations in Climate Impact on Crop Evapotranspiration. *Journal of Imaging*, *3*(3), p.30.

Petropoulos, G., Carlson, T.N., Wooster, M.J. and Islam, S. (2009). A review of Ts/VI remote sensing based methods for the retrieval of land surface energy fluxes and soil surface moisture. *Progress in Physical Geography*, *33*(2), 224-250.

Rahimi, S., Gholami Sefidkouhi, M.A., Raeini-Sarjaz, M. and Valipour, M. (2015). Estimation of actual evapotranspiration by using MODIS images (a case study: Tajan catchment). *Archives of Agronomy and Soil Science*, *61*(5), 695-709.

Roerink, G.J., Su, Z. and Menenti, M. (2000). S-SEBI: A simple remote sensing algorithm to estimate the surface energy balance. *Physics and Chemistry of the Earth, Part B: Hydrology, Oceans and Atmosphere*, *25*(2), 147-157.

Schirmbeck, J., Fontana, D.C. and Roberti, D.R., 2018. Evaluation of OSEB and SEBAL models for energy balance of a crop area in a humid subtropical climate. *Bragantia*, *77*(4), 609-621.

Senay, G.B., Bohms, S., Singh, R.K., Gowda, P.H., Velpuri, N.M., Alemu, H. and Verdin, J.P. (2013). Operational evapotranspiration mapping using remote sensing and weather datasets: A new parameterization for the SSEB approach. *JAWRA Journal of the American Water Resources Association*, *49*(3), 577-591.

Silva, A.M., da Silva, R.M. and Santos, C.A.G. (2019). Automated surface energy balance algorithm for land (ASEBAL) based on automating endmember pixel selection for evapotranspiration calculation in MODIS orbital images. *International Journal of Applied Earth Observation and Geoinformation*, *79*, 1-11.

Su, Z. (2002). The Surface Energy Balance System (SEBS) for estimation of turbulent heat fluxes. *Hydrology and earth system sciences*, *6*(1), 85-99.

Sun, Z., Wei, B., Su, W., Shen, W., Wang, C., You, D. and Liu, Z. (2011). Evapotranspiration estimation based on the SEBAL model in the Nansi Lake Wetland of China. *Mathematical and Computer Modelling*, *54*(3-4), 1086-1092.

Watts, C.J., Chehbouni, A., Rodriguez, J.C., Kerr, Y.H., Hartogensis, O. and De Bruin, H.A.R. (2000). Comparison of sensible heat flux estimates using AVHRR with scintillometer measurements over semi-arid grassland in northwest Mexico. *Agricultural and Forest Meteorology*, *105*(1-3), 81-89.

Yang, Y., Su, H., Zhang, R., Tian, J. and Li, L. (2015). An enhanced two-source evapotranspiration model for land (ETEML): Algorithm and evaluation. *Remote sensing of Environment*, *168*, 54-65.

Zahira, S., Abderrahmane, H., Mederbal, K. and Frederic, D. (2009). Mapping latent heat flux in the western forest covered regions of Algeria using remote sensing data and a spatialized model. *Remote Sensing*, *1*(4), 795-817.

*IN PROCEEDINGS OF 25th HYDRO 2020, INTERNATIONAL CONFERENCE, NATIONAL INSTITUTE OF TECHNOLOGY ROURKELA, ODISHA, INDIA 26-28, March 2021, ISBN 978-93-90631-56-8*

Paper ID - 037

# Assessment of grape crop acreage using geospatial technique for command area of Palkhed reservoir (Maharashtra)

Shraddha Kuwar[1], Sunil Gaikawad[1], Makarand Kulkarni[1],

[1]*Resources Engineering Center, Maharashtra Engineering Research Institute, Dindori Road, Nashik-4, Water Resources Department, Government of Maharashtra, India*

*E mail: - mak6980@yahoo.co.in*

## Abstract

Realistic acreage estimation of cash crop like grape in the service area of irrigation projects is essential. The existing practices of crop measurement are tedious, time consuming and sometimes causes errors in measurement. Geospatial technique provides quick, accurate and cost effective method for crop acreage estimation. This technique was adopted to estimate grape crop acreage in Palkhed irrigation command area which is rich in grape cultivation. Normally, for separating grape from other crops, multi-dates satellite images of 2 different periods, are analysed. In the present study, satellite images of two different period viz. December 2019, February 2020 were used to estimate grape crop acreage.

The work of grape crop acreage estimation at village level comprises of two components. First one is remote sensing and the other is GIS. Remote sensing part covers the selection of appropriate satellite images, their analysis, pre and post analysis ground truth. The GIS part covers the collection of village maps / cadastral map, their geo-referencing, vectorisation and then rasterisation of maps and overlaying of these raster maps to extract the land use statistics at village level. ERDAS IMAGINE, a standard image analysis software is being used for these studies. The paper presents in brief the methodology adopted, utility and importance of this technique for acreage estimation of grape crop area.

***Keywords:*** *Grape; Remote Sensing; Palkhed; Command; Analysis; Methodology*

## 1. Introduction

Grapes (Vitisvinifera) are one of the most consumed fruit crop worldwide. Grapes are believed to introduced into the northern part of India by the Persian invaders in 1300 AD by the Christian missionaries, it was introduced in Salem and Madurai districts of Tamil Nadu around 1832 AD. Grape is known as the Queen of the fruits as it is treasure of the health benefitting nutrients. India ranks 9$^{th}$ position in grape production (Shikamany, 2001; Gade et al., 2014). The grapes are one of the most important fruit crops in India. In India grape is grown in tropical, Sub tropical and temperate zones mainly for table purpose. Normal grape harvest season starts in February and continuous up to end of April. Grape is strictly and regularly irrigated perennial crop. For flood irrigation, 5-7 days during summer, 8-10 days during winter and 15-20 days during rainy season – interval is maintained. Among the fruit crops grown in India grape occupies the first position in terms of area and production. Grape cultivation in India is a popular agribusiness in some states.Besides heavy investment, it requires close attention and careful nursing. The important Grape growing states in India are Maharashtra, Karnataka, Tamil Nadu, Andhra Pradesh and Punjab. As Nashik called 'Grape Capital of India', the majority of farmers in Nashik district are leading producer of Grape crop in Maharashtra. Present study utilizes data of Resourcesat – IIA (IRS-2A) satellite. It has LISS III sensor, which operates in four spectral bands. IRS-2A multi spectral data is very useful in deriving crop information at different levels.

Hence the aim of this study is to develop a new mapping approach that will capture both the spatial and spectral reflectance properties of Grape plantations to separate them from other land cover features.

## 2. Objectives

i. To identify and measure grape crop in the command area of the Palkhed project.
ii. To generate village-wise statistics for the grape crop area.

## 3. Study area

The Kadwa river originates and flows through Dindori taluka of Nashik district. The Palkhed dam built in 1975 across the kadwa river which is located 30 km away from Nashik city. This area is situated in the basin of Godavari basin. The maximum height of the dam is 19 meters. The dam site is located at Lattitude $20^0$ 10' 00" N Longitude $73^0$ 54' 00" E. The command area of Palkhed reservoir is located in Nashik, Ahmadnagar & Aurangabad district. Three talukas from Nashik, one taluka from Ahmadnagar and one taluka from Aurangabad district which includes total 136 villages.

## 4. Data used

### 4.1 *Field data*

i) Index map of reservoir along for precise geographiclocation of study area.
ii) Salient features of the command area.
iii) Toposheet of Palkhed Reservoir and command area.
iv) List of villages falling under command area of Palkhed reservoir.

### 4.2 *Satellite data*

The details of the satellite data selected for study are shown in Table 1 and data received from National Remote Sensing Centre, Hyderabad.

**Table 1** Dates of pass for satellite data

| Satellite | Sensor | Path/Row | Date of pass |
|---|---|---|---|
| Resource-sat-2A | LISS III | 95/58 | 20/12/2019 |
| Resource-sat-2A | LISS III | 95/58 | 06/02/2020 |

### 4.3 *Digital village maps from Maharashtra Remote Sensing Application Centre (MRSAC)*

The digital Village Maps in vector form for Dindori, Kopargaon, Niphad, Yeola, Vaijapur talukas have been used.

## 5. Methodology

The methodology adopted is briefly described under two themes as follows:
1) **Remote sensing** for analysis of satellite data.
2) **GIS Analysis** for preparation of village level data base and output extraction.

### 5.1 *Remote sensing*

#### 5.1.1 *Selection of satellite data*

First image of initial period of the crop year selected is December month and the second image is month of February. In the present study it is decided to map the grape crop standing in December

2019 to May 2020, which is harvested during December 2019 to February 2020. Selection of satellite data is done on Grape crop cycle.

### 5.1.2 *Subseting area of interest*

The full satellite image is cut in such a way that it contains only the study area as shown in figure 1 which help for manipulation of data in order to simplify the analysis process.

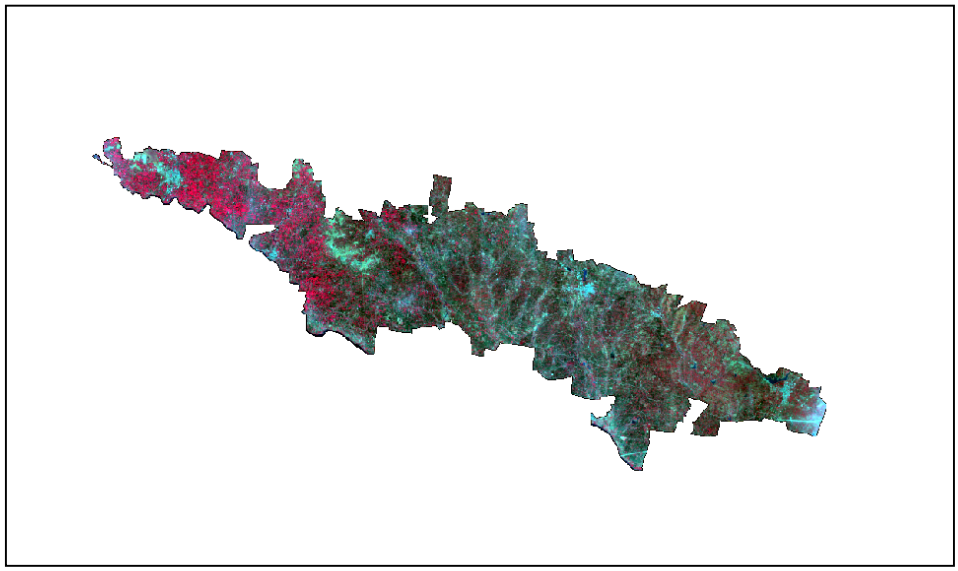


**Figure 1** Subset of study area

The visually seen urban and vegetation patches are substracted from the subset as shown in figure 2 as to avoid mixing of classes.

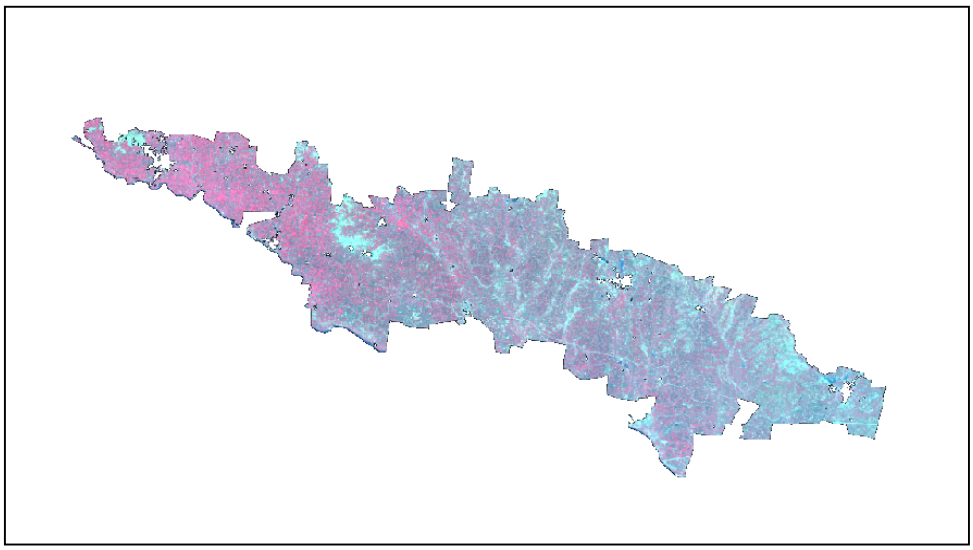


**Figure 2** Urban and vegetation substracted from subset

### 5.1.3 *Field visit for ground truth verification*

To carry out the supervised classification of satellite image ground truthing activity is a prime activity. As in supervised classification the location of land cover types ie. Ground features should be known prior. Hence in ground truthing activity the samples are collected in such a way that the whole area of interest should be covered uniformly and the samples are taken for each and every surface

features actually present in the field. More samples collected gives the confidence for the analysis which help to achieve better accuracy. The handheld GPS receivers are used to collect the surface features in the format of point, line and polygon. For every class these collected point, line and polygon features are overlay on the subset of satellite image which is shown in figure 2 and supervised analysis of image is carried. The same process is adopted for the collection of ground truthing data for the second image.

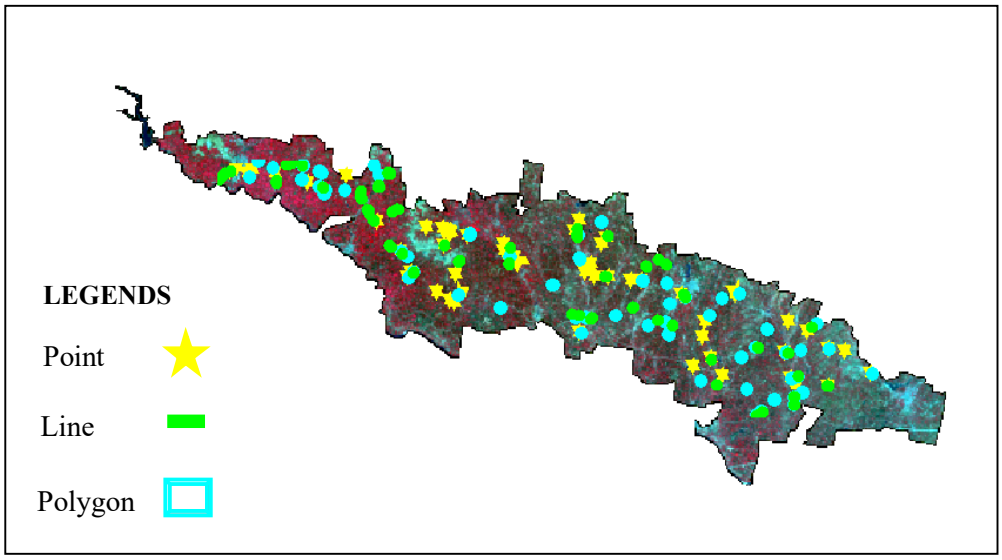



**Figure 3** Collected ground truth features (GPS data) overlaid on subset of satellite image of command area of Palkhed reservoir

### 5.1.4 *Classification and Analysis of Satellite Data*

Classification of two images as shown in figure 4 and figure 5 are done by using supervised classification technique. Maximum Likelihood Classification (MLC) techniques have been applied for the images. In supervised classification technique, the location of land cover types should be known a priori to carry out the classification of an image. The areas of each land cover types are known as training sets or samples. These training site samples are collected during the field visit for each class and marked on the subset and by using all these classes the supervised classification of image carried out. Digital values of the pixels of evenly distributing training samples and standard class signatures are used for classification of satellite image in seven classes.

Land use land cover classes

i) Dark red/ pink –Confirmed grape.
ii) Cyan–Barren.
iii) Dark purple – other crops.
iv) Gray–Fallow.
v) Mix pixel –Urban.
vi) Red–Vegetation.
vii) Blue-Water in lakes and river.

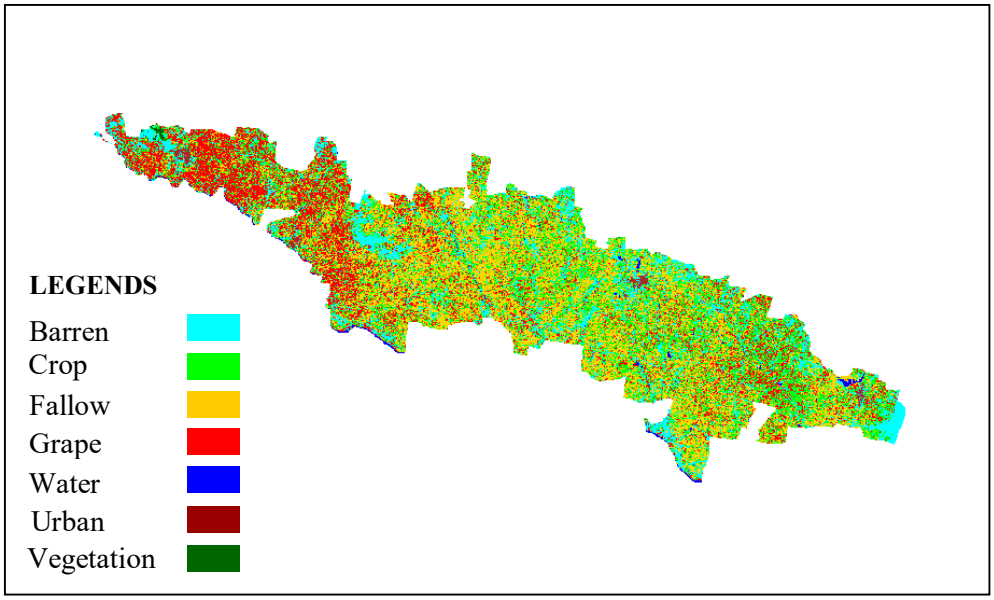



**Figure 4** First supervised image

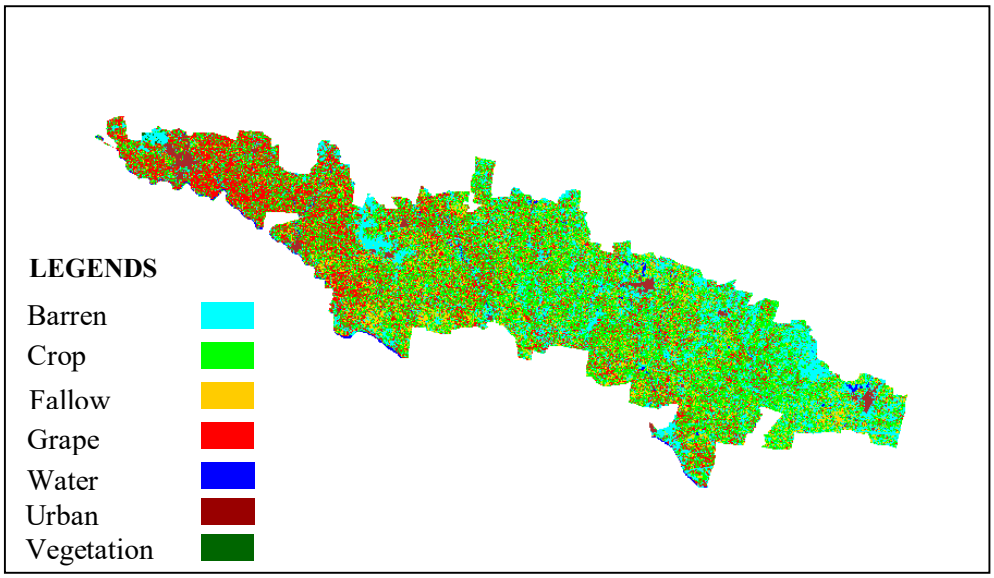



**Figure 5** Second supervised image

To prepare a composite classified image, a MATRIX image as shown in figure 6 is created from the two supervised classified images. This matrix image contains 324 (18 X 18) possible combinations of classes.

In this matrix image each and every class checked and common class from both the images are selected. Recoding of that matrix as shown in figure 7 is done and and reduced to following seven classes.

Class 1- Barren, Class 2- Crop, Class 3- Fallow land, Class 4 - Grape, Class 5- Water, Class 6- Urban, Class 7- Vegetation.

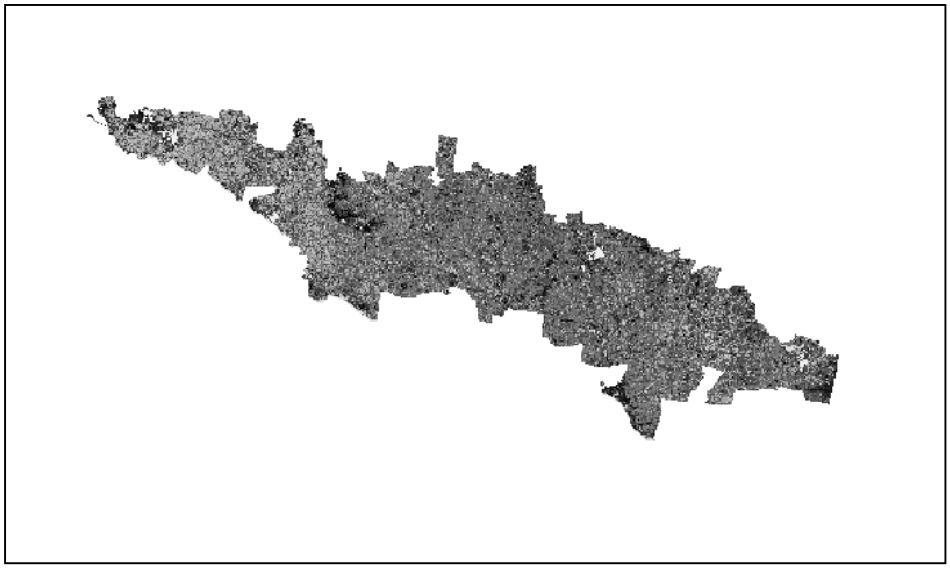


**Figure 6** Matrix image

This recoded image is the final recoded image which is used for generation of area statistics.

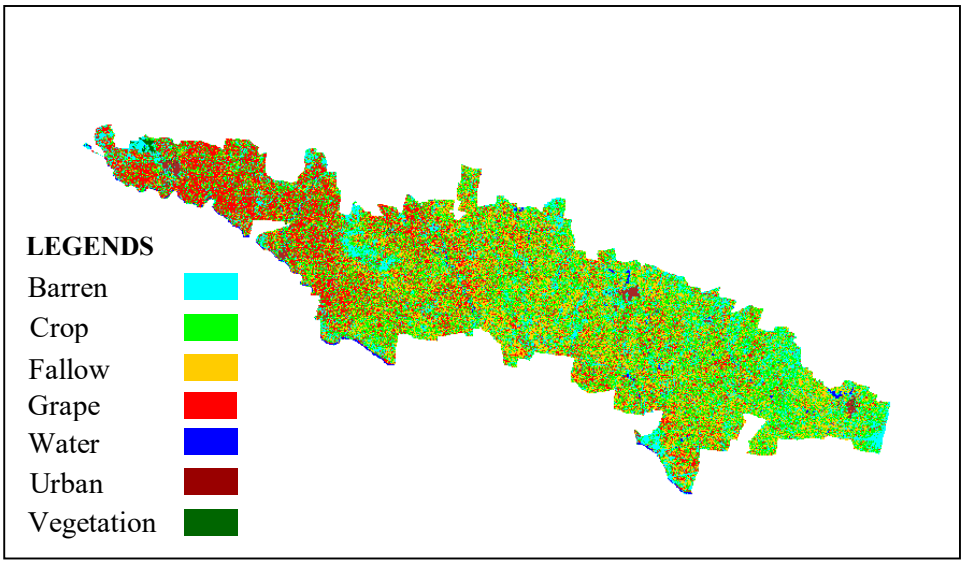



**Figure 7** Final recoded image

## 5.2 *GIS analysis*

### 5.2.1 *Digital Village Maps*

For accurate village-wise estimation of grape crop, accurate maps of villages are required. For the purpose of present studies the extracting of area under grape crop through village boundaries has been done in vector module of ERDAS IMAGINE 2010. Digital village maps in vector form of villages in Dindori, Niphad, Yeola, Kopargaon and Vaijapur talukas have been used for village-wise statistics generation.

### 5.2.2 *Generation of Area Statistics*

Recoded composite image showing the land use classes is prepared. The village-wise statistics of areas land uses in each village is obtained using summary module of GIS analysis. Data is edited in MS Excel to present in a tabular form.

## 6. Results

The area statistics given in tabular form as shown in table 2 as well as in pie chart as shown in figure 8.

**Table 2** Summary of results

| Sr. No. | Name of Taluka | No. of Villages | Area of Taluka in command (Ha) | Total Grape Crop Area (Ha) | Percentage of Grape Crop |
|---|---|---|---|---|---|
| 1 | Dindori | 02 | 1887.299 | 829.902 | 43.973 |
| 2 | Niphad | 55 | 18921.947 | 3227.655 | 17.058 |
| 3 | Yeola | 55 | 44665.430 | 6681.614 | 14.959 |
| 4 | Kopargaon | 19 | 43679.920 | 15553.273 | 35.607 |
| 5 | Vaijapur | 05 | 7771.368 | 419.803 | 5.402 |
| **Total** | | **136** | **116925.965** | **26712.247** | **22.845** |

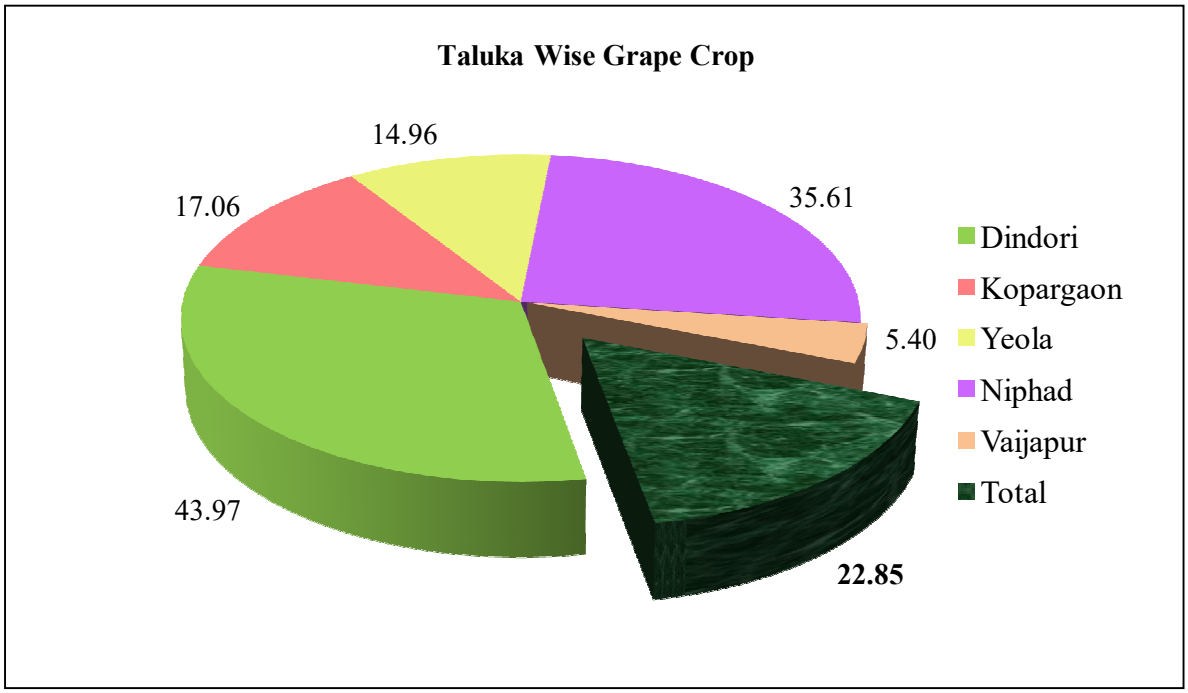



**Figure 8** Pie Chart Showing Percentage of Grape Crop of Command Area of Palkhed Reservoir in Nashik District

## 7. Discussion and conclusion

i. The methodology adopted using the geospatial technique with two season images of LISS III sensors is used to give fairly accurate results at village level Grape crop. The village level database prepared in this study can be used for periodical mapping of grape crop as well as for any other mapping.
ii. The 50% of the collected signature samples used for classification whereas remaining 50% samples used for validation purpose with which 95% of accuracy is achieved.
iii. It is to conclude that average of 22.845 % of grape crop is assessed in command area of Palkhed reservoir which lies in Nashik district.
iv. The methodology adopted in this study can be definitely adopted for acreage estimation of perennial crops.

## References

National Horticulture Board, India 2010-11.
Murasoli. M* and Jambulingam S, IJRSR Vol. 7, Issue, 10, pp. 14040-14044, October, 2016
P. S. Roy, R. S. Dwevedi, D. Vijayan, Remote Sensing Applications, National Remote Sensing Centre.
N. R. Sonawane, S. A. Gaikwad, M. M. Kulkarni, Sugarcane Acerage Estimation In Pravara Left Bank Canal Command Area In Maharashtra Using Remote Sensing & GIS Technique, 9IMIC on Micro Irrigation For Modern Agriculture(Jan- 2019).
Technical report on “Measuring Village Level Grape Crop Under Command Area Of Palkhed Reservoir Project, Using Satellite Remote Sensing Technique ”by MERI, Nashik- 2020.

*IN PROCEEDINGS OF 25th HYDRO 2020, INTERNATIONAL CONFERENCE, NATIONAL INSTITUTE OF TECHNOLOGY ROURKELA, ODISHA, INDIA 26-28, March 2021, ISBN 978-93-90631-56-8*

Paper ID - 038

# Hydro-cover Mapping by Remote Sensing and GPS Technology: A case study of Nashik District, Maharashtra, India.

Santosh Wagh[1], Makarand Kulkarni[2] and Anita Morkar[3]

[1] *Sub Divisional Engineer, Resources Engineering Center, MERI, Nashik-422004, Maharashtra, India.*
[2] *Executive Engineer, Resources Engineering Center, MERI, Nashik-422004, Maharashtra, India.*
[3] *Junior Scientific Assistant, Resources Engineering Center, MERI, Nashik-422004, Maharashtra, India.*
*Email: sanganwagh@yahoo.co.in*

## Abstract

Hydro-cover maps are essential for many water resources as well as environmental applications. Accurate information of hydro-cover is important for flood prediction, monitoring and relief etc. The information of hydro-cover is difficult to produce using traditional survey techniques because water bodies can be fast moving as in floods, tides and storms etc. Remotely sensed data provide a means of delineating water boundaries over a large area on the date of pass of satellite. Hydro-cover mapping from satellite images remain a challenging task due to sensor limitations, the presence of clouds, topographic and atmospheric conditions etc. Various water body mapping approaches have been developed to extract water bodies from multispectral images.

The objective of this study is to identify and map hydro-cover using remote sensing technique. This paper proposes a supervised classification methodology for hydro-cover mapping at district level. Resourcesat-II satellite of LISS-III sensor (23.5m) resolution have been used for this study. The post-monsoon and pre-monsoon statistics for the water year 2019-2020 have been generated for Nashik district. About 450 ground truthing sets in the form of point, line and polygon using handheld GPS instruments are collected from various tahasils in Nashik district for analysis and validation purpose. The accuracy of the method is tested using ground truthing information. The proposed method produces the accurate results. The geographical area of Nashik district is 15530 sq.km. Hydro-cover area estimated in post-monsoon is 36985 ha that is around 2.38% of the geographical area and hydro-cover area estimated in pre-monsoon is 10518 ha that is around 0.68 % of the geographical area. The result discussed in this paper will provide fundamental information to state as well as local authorities for the protection and restoration of hydro-covers and conservation of natural ecosystem in Nashik district.

***Keywords:*** *Hydro-cover, Remote Sensing, Supervised Classification, Ground Truthing.*

## 1. Introduction

Two third of the word is surrounded by water bodies. Hydro cover is the area that is temporarily or permanently covered with water. As a result of rapid urbanization, increase in population, technical growth, economical growth and various anthropogenic activities more and more waste materials are discharged into natural sources of water bodies (Rajinikanth et.al 2000). The natural resources are now depleting very fast causing serious environmental problem. Hydro cover is one of the most important parameter play crucial role in hydrological cycle. Water body performs some useful function in the maintenance of overall balance of nature. Hence to maintain ecological balance, it is imperative to preserve water bodies and to make it fit for various purposes. The effective management and protection of water bodies is urgently needed, and accurate and comprehensive water body classification maps and spatio-temporal change information are very important for ecological protection and local government decision (Fang, et.al 2016). Due to scarcity of rainfall in various region assessment of water spread in district level is most important. Remote sensing technique proves to be cost effective and accurate for doing spatially large area. Remote sensing technique for hydro cover assessment is essentially based on mapping of water-spread areas at the time of satellite over pass. Remote sensing is the major source of spatial information about the Earth's surface cover and contribution (SAC, ISRO, Ahmedabad Technical Report, 2010) Different sensors capture abundant information regarding the Earth, which can be used by scientists that are interested in monitoring spatial information in a timely manner (Guo, et.al 2017). Issue in water body mapping is the size of water body. Water body in urban areas are usually small and are very much complex which

result in considerable amount of mixed pixels. High resolution imagery reduce the number of mixed land water pixel, which increases the accuracy in the delineation of water boundaries (Jakovljevic, et.al , 2018). The accuracy of water body mapping is also affected by high level of suspended soilds, nutrients and various pollutants which change the spectral signature compared to those of unpolluted areas (Jakovljevic, et.al , 2018). This paper focuses on identification of water bodies using supervised classification technique. Since the delineation of water body is still challenging for small water bodies and dependent on spatial resolution and availability of data. The objectives of this paper are: (1) To establish the method for hydro cover mapping at district level. (2) To generate taluka-wise hydro cover statistics of Nashik district for post monsoon and pre monsoon for the year 2019. (3) To carry out spatial and temporal analysis of hydro cover of Indian Remote Sensing satellite data.

## 2. Study area and data used

### 2.1 *Study area*

Study area includes Nashik district. Nashik is located between $19^0$ 35' to $20^0$ 52' North latitude and between $73^0$ 15' to $74^0$ 56' East Longitude at Northwest part of the Maharashtra state. It is at 565 m above mean sea level. The western slope of the Ghats is drained by several rivers, including the Daman-Ganga River, which drains westwards to the Arabian Sea. The larger eastern portion of the Nashik district, which lies on the Deccan Plateau, is open, fertile, and well cultivated. The Godavari River originates in the district and drains east towards the Bay of Bengal. Kadwa and Darna, are tributaries of the Godavari. Girna River and its tributary flow eastward through fertile valleys into the Tapi River. (Document Collector office, Nashik) The index map of Nashik district is shown in figure 1.

(Source: ISRO, Bhuvan)




**Figure 1** Index map of Nashik district, Maharashtra

## 2.2 *Materials*

### 2.2.1 *Satellite data*

National Remote Sensing Centre, Hyderabad website has been browsed to prepare a list of dates of satellite pass over the Nashik district for the year 2019. The list of cloud free satellite images have been prepared for the both pre monsoon and post monsoon period. Resourcesat II satellite data have been finalized and used for the analysis. These images cover the total area of interest. The details of satellite pass are given in Table 1.

**Table 1** Dates of pass for satellite data

| Satellite | Sensor | Path | Row | Date of pass for pre monsoon | Date of pass for post monsoon |
|---|---|---|---|---|---|
| Resourcesat-II | LISS-III | 94 | 58 | 06/05/2019 | 08/12/2019 |
| Resourcesat-II | LISS-III | 95 | 58 | 11/05/2019 | 13/12/2019 |
| Resourcesat-II | LISS-III | 95 | 59 | 11/05/2019 | 13/12/2019 |
| Resourcesat-II | LISS-III | 96 | 58 | 16/05/2019 | 24/11/2019 |

### 2.2.2 *SOI topo sheet*

Survey of India(SOI) topo sheets of 1:50000 scales have been used for geo-referencing of satellite images for study area. These details are as given in Table 2.

**Table 2** Details of SOI topo sheet used

| Sr.No | Toposheets | Number |
|---|---|---|
| 1 | 46H5 to 46H15 | 11 |
| 2 | 46L1 to 46L15 | 11 |
| 3 | 46I10 to 46I13 | 3 |

## 2.3 *Methods*

There are several methods and models available for mapping hydro cover by satellite remote sensing technique. The models such as Normalized Difference Vegetation Index (NDVI), Normalized Difference Water Index (NDWI), Modified Normalized Difference Water Index (MNDWI) and Normalized Difference Pond Index (NDPI) are available for water area extraction. The mentioned above models have their own limitations. Such as in NDVI water features covered with vegetations are not highlighted, in NDWI some of the urban or built up area get mixed with water class, in MNDWI seasonal vegetation covered with water cannot be identified and in NDPI some of the slopes, shadow portions now classified as water. (Manohar, et.al., 2015) The methods such as unsupervised and supervised classification are regularly used to extract water features.

In this paper supervised classification method is used for identifying and mapping large as well as small water bodies. Supervised classification method proved to be more sensitive method for detecting water bodies. However supervised classification method requires a prior knowledge about the number of classes and spectral signature attribute to each class in the scene. The extensive ground truthing was done for classifying the pre and post monsoon images. The overview of the steps and methodology comprises the following components.

i) Data loading, Merging and Geo-referencing of satellite data.

ii) Demarcation of district boundary on 1:50,000 scale topo-sheets.

iii) Ground truth collection for supervised classification.

iv) Classification of pre monsoon and post monsoon images.

v) Refinement of classification based on field data collection

vi) Taluka-wise statistics generation.

vii) Preparation of report and district level pre monsoon and post monsoon maps.

## 3. Results and Discussion

### 3.1 *Images of colour composite*

To classify remotely sensed images, different colour compositions are used. The natural or true colour composite is a combination of visible spectrum of blue, green and red bands. Natural colour composite of bands resemble closely what the naked eyes can recognize as a true colour. Water in dark blue to black, vegetation in green, bare soil in brown and built up in gray. While for classification technique false color composition of images are used. In false colour composition images presence of water resemble as black dark, vegetation as red, built up in shades of cyan etc.

### 3.2 *Field visit and ground truth collection*

Remote sensing techniques require certain amount of field observation called “ground truth” in order to convert pixel data into meaningful information. Such work involves visiting a number of sites. The data dictionary was created for recording the field information. The location of the features is recorded using the Hand held GPS shown in figure 2. The standard proforma was used to record the field data. Field photographs are also taken during the field visit. (REC, MERI, Technical Report, 2020)

The first field visit and ground truth was conducted by team of this institute from 12th March 2020 to 17th March 2020. GPS readings were taken with the help of Trimble Juno Handheld GPS device and simultaneously latitude /longitude values have been recorded during the visit. Almost 129 point feature, 14 line feature and 6 polygon features, total 149 features from 5 talukas i.e Nashik, Dindori, Chandwad, Sinnar and Igatpuri of Nashik district have been collected.




**Figure 2** Handheld GPS for recording field data

Similarly the second field visit and ground truth was conducted by team of this institute from 8th June 2020 to 16th June 2020. GPS readings were taken with the help of Trimble Juno Handheld GPS device and simultaneously latitude /longitude values have been recorded during the visit. Almost 116 point feature, 3 line feature and 1 polygon features, total 120 features from 5 talukas i.e Peth, Surgana, Kalwan, Trimbakeshwar and Niphad of Nashik district have been collected. The team has visited natural as well as man-made different water retaining structures. With the above data a total of 269 features from 10 talukas in Nashik district have been collected. The overlay of ground truth collection on study area is shown in figure 3. (REC, MERI, Technical Report, 2020)

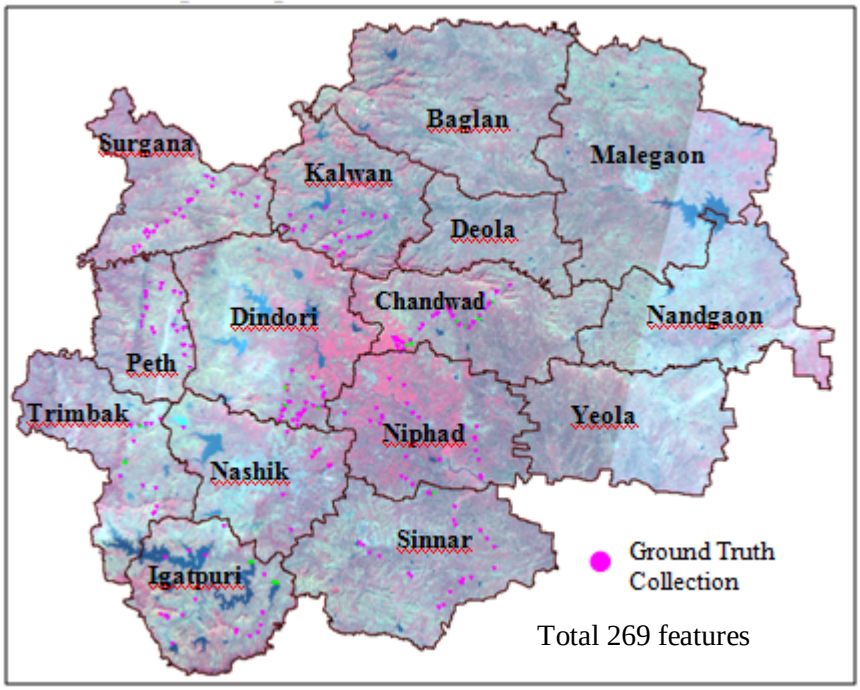



**Figure 3** Field visit and ground truth data collection on satellite image

### 3.3 *Image classification*

These collected features are used for supervised classification of pre monsoon and post monsoon images. The collected features are now exported in shape file which is overlaid on mosaic false colour composite images of pre monsoon and post monsoon for generating signature sets. Similarly signature of forest, built up, barren, fallow, vegetation, crop, scrub, shadow has been generated and images are now classified in these nine different classes. The sole purpose of this research report was to generate statistics of hydro cover in Nashik district. Therefore the classes other than water class are clubbed in one class and name it as other class.

### 3.4 *Accuracy Assessment*

In this process total 245 points, 17 lines and 7 polygon features are used during supervised classification technique. Then the accuracy assessment is carried out for talukas in which ground truthing is not done by verification of supervised classified image with Google Earth data. In these process random 10 locations i.e two locations per talukas are cross checked and validated. Out of total 10 cross checked features, 9 classified features are matching with the google earth data. In this regard the accuracy of the work is found out to be 90%. The following table 2 shows the classification accuracy.

**Table 2** Details of classification accuracy (post monsoon)

| Sr. No | Taluka | Village | Latitude (Deg, Min, sec) | Longitude (Deg, Min, sec) | Google Earth Feature | Classified Feature |
|---|---|---|---|---|---|---|
| 1 | Malegaon | Kashti | 20 35 43.01 N | 74 28 19.06 E | Farm Pond | Water |
| 2 | | Hatane | 20 39 13.97 N | 74 33 32.11 E | Farm Pond | Water |
| 3 | Nandgaon | Dahigaon | 20 15 42.04 N | 74 40 02.89 E | Farm Pond | Non-Water |
| 4 | | Bhalur | 20 13 26.98 N | 74 33 49.14 E | Farm Pond | Water |
| 5 | Baglan | Deolane | 20 37 33.85 N | 74 16 41.84 E | Farm Pond | Water |
| 6 | | Vanoli | 20 39 03.24 N | 74 09 27.12 E | Farm Pond | Water |
| 7 | Deola | Vithewadi | 20 30 40.88 N | 74 09 27.56 E | River Water | Water |
| 8 | | Shrirampur | 20 26 10.15 N | 74 11 35.99 E | Water Body | Water |
| 9 | Yeola | Angangaon | 20 02 25.00 N | 74 27 50.98 E | Water Body | Water |
| 10 | | Andarsul | 19 59 28.03 N | 74 34 08.90 E | Farm Pond | Water |

### 3.5 *Taluka-wise hydro-cover statistics and maps (post monsoon)*

Hydro cover statistics followed by hydro cover map for each taluka in post monsoon and pre monsoon is given to have a fairly good idea about the distribution pattern and density of hydro cover in the taluka. Following Table 3 and 4 gives the statistics of hydro cover in post monsoon and pre monsoon respectively. Similarly Figure 4 and 5 shows the hydro cover maps in post monsoon and pre monsoon of Nashik district for the year 2019.

**Table 3** Taluka-wise hydro cover area (post monsoon)

| Taluka | Geographic Area (Sq.Km) | Hydro cover Area (Ha) | % of total Hydro cover Area | % of Taluka Geographic Area |
|---|---|---|---|---|
| Baglan | 1453 | 1066.12 | 2.89 | 0.73 |
| Chandwad | 953 | 975.05 | 2.65 | 1.02 |
| Deola | 548 | 416.67 | 1.13 | 0.76 |
| Dindori | 1319 | 5346.72 | 14.51 | 4.05 |
| Igatpuri | 867 | 9503.54 | 25.79 | 10.96 |
| Kalwan | 864 | 1606.87 | 4.36 | 1.86 |
| Malegaon | 1818 | 5390.84 | 14.63 | 2.97 |
| Nandgaon | 1087 | 2900.22 | 7.87 | 2.67 |
| Nashik | 891 | 3331.41 | 9.04 | 3.74 |
| Niphad | 1049 | 1323.07 | 3.59 | 1.26 |
| Peth | 557 | 318.01 | 0.86 | 0.57 |
| Sinnar | 1344 | 1284.42 | 3.49 | 0.96 |
| Surgana | 821 | 197.68 | 0.54 | 0.24 |
| Trimbakeshwar | 900 | 2685.66 | 7.29 | 2.98 |
| Yeola | 1059 | 507.39 | 1.38 | 0.48 |
| **Total** | **15530** | **36853.67** | **100.00** | **2.37** |

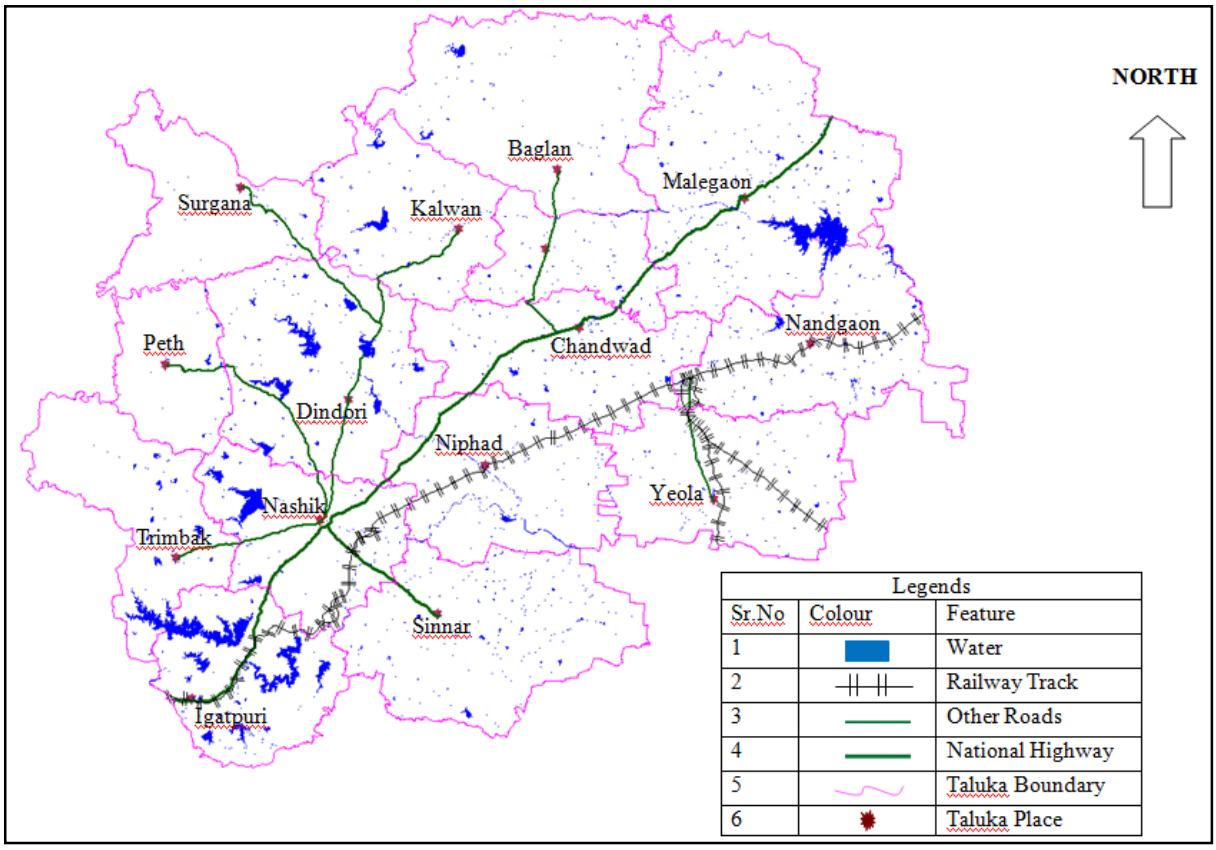



**Figure 4** Hydro-cover maps of Nashik district (post monsoon) year 2019.

**Table 4** Taluka-wise hydro cover area (pre monsoon)

| Taluka | Geographic Area (Sq.Km) | Hydro cover Area (Ha) | % of total Hydro cover Area | % of Taluka Geographic Area |
|---|---|---|---|---|
| Baglan | 1453 | 255.80 | 2.43 | 0.18 |
| Chandwad | 953 | 25.23 | 0.24 | 0.03 |
| Deola | 548 | 12.33 | 0.12 | 0.02 |
| Dindori | 1319 | 1095.78 | 10.43 | 0.83 |
| Igatpuri | 867 | 3250.83 | 30.93 | 3.75 |
| Kalwan | 864 | 438.39 | 4.17 | 0.51 |
| Malegaon | 1818 | 1197.56 | 11.39 | 0.66 |
| Nandgaon | 1087 | 1034.84 | 9.85 | 0.95 |
| Nashik | 891 | 1622.02 | 15.43 | 1.82 |
| Niphad | 1049 | 348.13 | 3.31 | 0.33 |
| Peth | 557 | 80.06 | 0.76 | 0.14 |
| Sinnar | 1344 | 57.37 | 0.55 | 0.04 |
| Surgana | 821 | 5.18 | 0.05 | 0.01 |
| Trimbakeshwar | 900 | 1026.95 | 9.77 | 1.14 |
| Yeola | 1059 | 59.62 | 0.57 | 0.06 |
| **Total** | **15530** | **10510.09** | **100.00** | **0.68** |

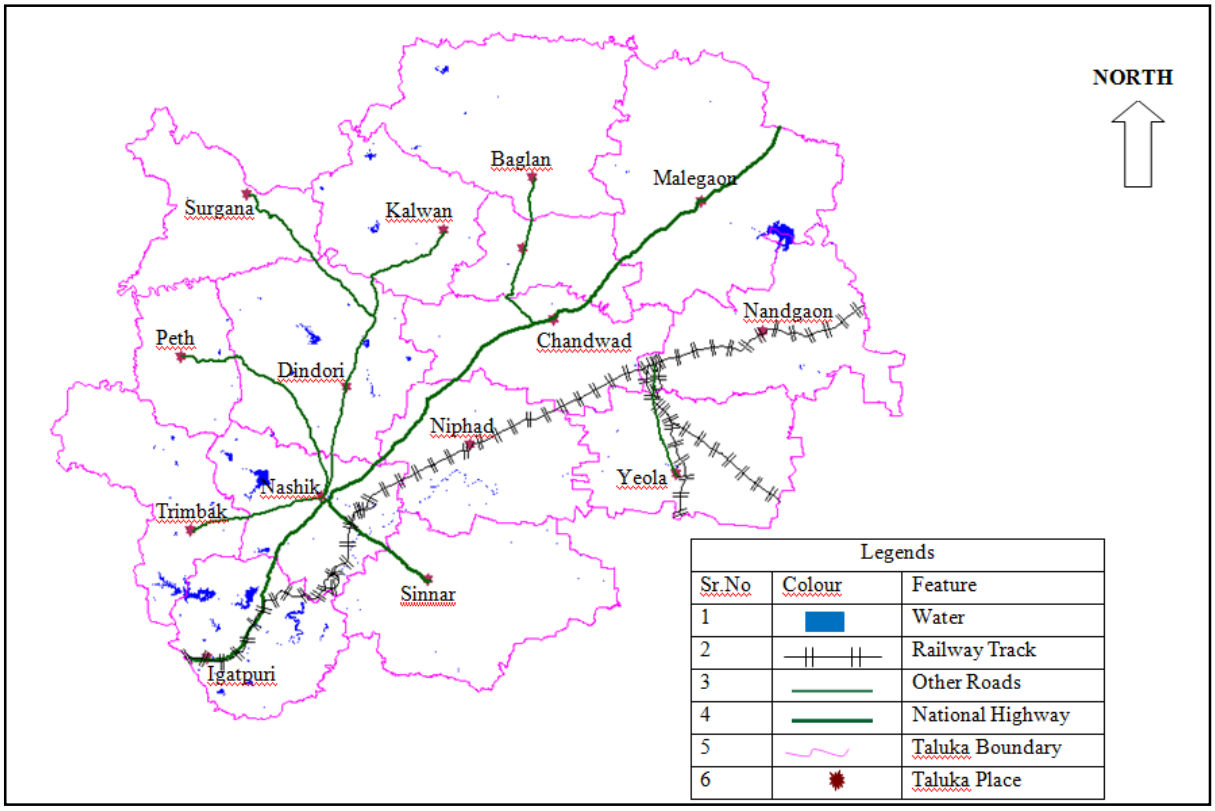



**Figure 5** Hydro-cover maps of Nashik district (pre monsoon) year 2019.

### *3.6. Limitations*

Hydro cover area less than 24mx24m cannot be identified and mapped because of the resolution of LISS-III image is 23.5m. Classification with higher resolution images i.e LISS-IV with 5.8 m resolution is not possible for larger area like district, region and state because of the non availability of images at regular interval fallow land with more water content is also get mixed with water pixel classification. Shadow portion of hilly areas gives same reflection as of water.

## 4. Conclusions

A bar chart is prepared to show the comparison of hydro cover area in pre monsoon and post monsoon in the year 2019 for Nashik district. Figure 6 shows the comparative bar chart of pre and post monsoon hydro cover area in Nashik district for the year 2019. From the study following conclusions are made.

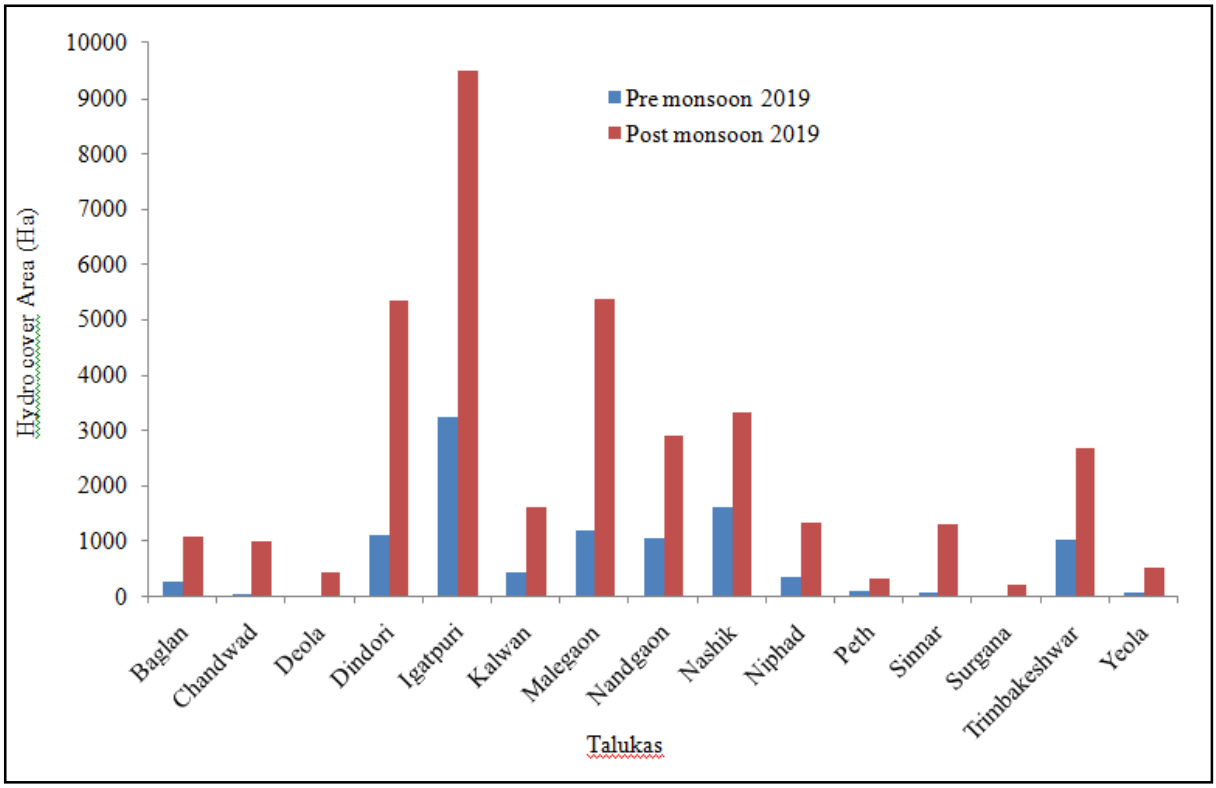



**Figure 6** Pre monsoon and post monsoon taluka wise distribution of hydro cover area of Nashik district, year 2019.

Hydro cover area in Nashik district as per geographical area in post monsoon is 2.37% and in pre monsoon it is 0.68%. In post monsoon the hydro cover in each taluka as per percent of total district hydro cover area ranged from as 0.54% (Surgana Taluka) to 25.79% (Igatpuri Taluka). The hydro cover in talukas as per geographic areas varied from 0.24% (Surgana Taluka) to 10.96% (Igatpuri Taluka). Dindori, Igatpuri, Malegaon, Nandgaon, Nashik and Trimbakeshwar are hydro cover rich talukas contributing more than 5 percent of total hydro cover area of the Nashik district. In pre monsoon the hydro cover in each taluka as per percent of total district hydro cover area ranged from as 0.05% (Surgana Taluka) to 30.93% (Igatpuri Taluka). The hydro cover in talukas as per geographic areas varied from 0.01% (Surgana Taluka) to 3.75% (Igatpuri Taluka). Dindori, Igatpuri, Malegaon, Nandgaon, Nashik and Trimbakeshwar are hydro cover rich talukas contributing more than 5 percent of total hydro cover area of the Nashik district. The result of this study will provide fundamental information to state as well as local authorities for the protection and restoration of hydro-covers and conservation of natural ecosystem in Nashik district.

## References

*A Research Report on Hydro Cover Assessment of Nashik District, Maharashtra, Through satellite Remote Sensing (2020).* Resources Engineering Centre, Maharashtra Engineering Research Institute, Water Resources Department, Govt. of Maharashtra.

Fang, C., Tao, Z., Gao, D., and Wu, H. (2016). Wetland mapping and wetland temporal analysis in the Nanjishan wetland using Gaofen one data. *Annales of GIS, 22(4),* 259-271.

Guo, M., Li, J., Sheng, C., Xu, J., and Wu, L. (2017). A review of wetland remote sensing. *Sensors, 17 (777),* 2-36.

Jakovljevic, G., Govedarica, M., and Alvarez-Taboada, F. (2018). Waterbody mapping: a comparison of remotely sensed and GIS open data sources. *International Journal of Remote Sensing*, 1-29.

Manohar, K. (2015). Report on *Automatic extraction of water features at multi scale*. Indian Institute of Remote Sensing, Indian Space Research Organization, Department of Space, Govt. of India, Dehradun, India.

*National Wetland Atlas , Maharashtra(2010).* Space Application Centre, Indian Space Research Organization, Ahmedabad.

Rajnikanth, R., and Ramchandra, T. (2000). Effective wetland management using GIS. *In proceedings of National Conference on Geoinformatics 2000, School of Civil Engineering, PSG College of Technology, Coimbatore, Nov 17th and 18th 2000*, 262-275.

https://villageinfo.in/maharashtra/nashik.html

https://nashik.gov.in/document/collector-office-nashik-2

*IN PROCEEDINGS OF 25th HYDRO 2020, INTERNATIONAL CONFERENCE, NATIONAL INSTITUTE OF TECHNOLOGY ROURKELA, ODISHA, INDIA 26-28, March 2021, ISBN 978-93-90631-56-8*

Paper ID - 070

# Impact of land use land cover on the response of the Mahanadi river basin in a sub-basin scale using SWAT

Shasanka Sekhar Barik[1], Dr. Janhabi Meher[2], Laxmipriya Mohanty[3]

*[1]Research scholar, [2,3]Assistant Professor, Department of Civil Engineering, Veer Surendra Sai University of Technology, Burla, 768018, India*

*Email: shasanka.96@gmail.com, janhabimeher@gmail.com, kajal.laxmi16@gmail.com*

## ABSTRACT

Land use activities, development and management of water resource are interdependent and thus land use/land cover (LULC) change has significant impacts on water quantity such as surface runoff, groundwater, over a range of temporal and spatial scales. The land-water interactions need to be addressed to determine whether they represent the best available information and supports decision making processes for developmental activities in a sustainable way. This article has focused on the hydrological modelling of the Mahanadi river basin on sub-basin scale which is situated in the states of Odisha & Chhattisgarh in India. In this article, the hydrological modelling has been done using "SWAT (Soil & Water Assessment Tool)" along with GIS interface. The data used in this study are the Digital Elevation Model (DEM), Land Use Land Cover (LULC), Soil, rainfall, relative humidity, wind speed, temperature, solar radiation. At first, the basin was delineated into various sub-basins. Then four sub-basins were considered and further delineated to generate smaller sub-basins. Then the newly generated smaller sub-basins were further divided into HRUs (Hydrological Response Units) based upon unique land use, slope & soil data combinations. Runoff was simulated separately for each of the four sub-basins. By using SWAT-CUP, the parameters sensitive to runoff were pinpointed & their optimized values were taken into consideration for model calibration. The simulated values were validated against field values. Here SWAT was used to simulate the impact of land use pattern, soil type, slope class & different weather conditions on runoff in a sub-basin scale. Model performance was administered or each of the five sub basins using the Nash–Sutcliffe model efficiency coefficient (NSE). The model efficiency was found to be satisfactory for both calibration phase validation phase within the SWAT model. It was found that cultivation land and urbanisation appear to be major environmental stressors affecting local water resources at the sub basin scale. As a result, increased runoff, decreased percolation, and increased evapotranspiration has a detrimental impact on the Mahanadi River Basin. This study can motivate the policymakers and experts to formulate and implement appropriate and sustainable response strategies to minimize the undesirable effects of land use land cover changes.

***keywords:*** *SWAT, HRU, SWAT-CUP, DEM, LULC, NSE*

## 1.introduction

Land-use change is a very important issue considering global dynamics and their response to hydrologic characteristics of soil and water management in a catchment. The assessment of variation of Land-use and Land cover uses on natural hydrology is essential for the development of sustainable water resource strategies. The impacts of LULC change are likely to be severe in developing countries due to lack of adaptability. Developing countries where agriculture serves as the backbone of the economy and ensure the wellbeing of people, the adverse effects of land use land cover change are diverse. Many river basins in India, where drastic LULC change has taken place in the last century, have been facing adverse reoccurring hydro meteorological extremes such as floods and droughts in the recent times. The future climate and LULC changes within the basin are the vital reasons for such changes within the hydrological regime. In addition to this, the developmental activities pursued throughout the country are expected to put additional stress on future water availability. Hence there is a need to understand and point out the impact of such changes on water resources availability, so as to

develop suitable adaptation strategies. Stream flows are sensitive to land use change i.e. minor change in land use causes major changes to stream flows.

Hence it is necessary to pinpoint the effect of variations in land use land cover pattern up on the runoff properties of a particular neighbourhood in sub-basin levels. Therefore, knowledge of changes in LU/LC is becoming much more important from both ecological and economical point of view. This type of analysis can be performed efficiently by employing watershed simulation models combined with GIS framework. Watershed replication through SWAT demands a lot of attributes including land use and land cover classification, soil texture classification & slope specification. With the incorporation of satellite imageries, both from Indian sources as well as from foreign sources, it becomes easier to extract the land use and land cover data of a particular area, which helps in modelling small watersheds accurately.

### *1.1 Objectives of the Study*

The objective of this study is intended to focus and scrutinize the influence of land use and land cover patterns on the response of the Mahanadi river basin in a sub-basin scale. This research work deals with the calculation of streamflow and preparation of hydrological model using the SWAT model.

## 2. Study Area and Data Collection

The study area includes four sub basins from upper Mahanadi river basin. The gauging stations are Simga, Basantpur, Rajim, Jondhra.

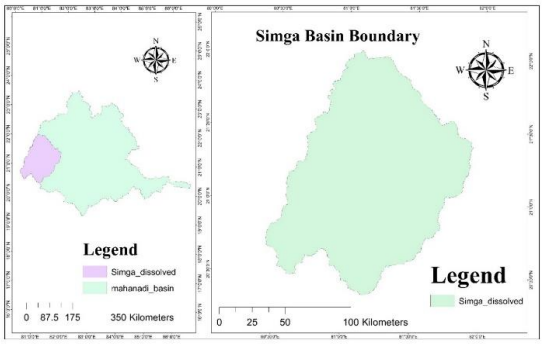



**Fig 2.1** Basin boundary of Simga basin

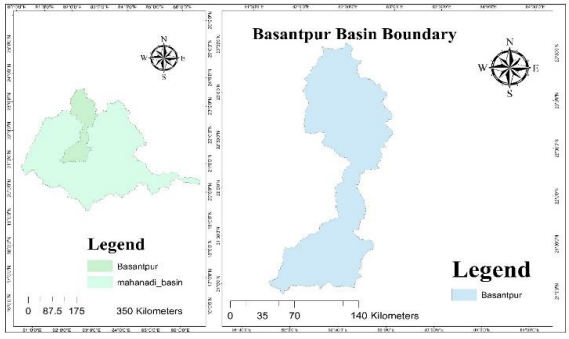



**Fig 2.2** Basin boundary of Basantpur basin

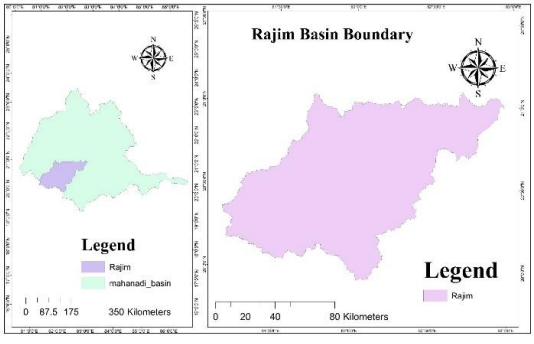



**Fig 2.3** Basin boundary of Rajim basin

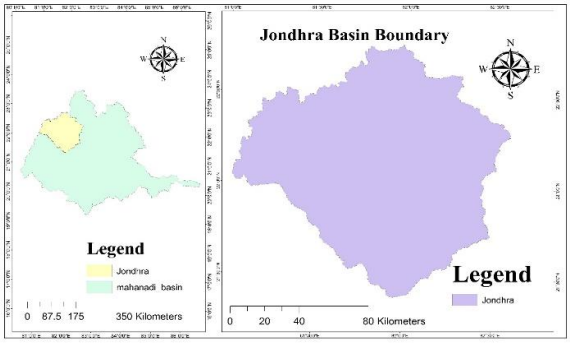



**Fig 2.4** Basin boundary of Jondhra basin

### *2.1 Location and Extent of the Basin*

Mahanadi is a significant river in East Central India. The Mahanadi river basin extends over an area of 1,41,589 square km which is almost 4.3% of the total geographical area of the country. It also has a total course of 858 kilometers. It is present between 80° 30' to 86° 50' east longitudes and 19° 21' to 23° 35' north latitudes. The river flows mainly through the states of Odisha and Chhattisgarh. The river basin spans over 11 parliamentary constituencies of Chhattisgarh, 13 parliamentary constituencies of Odisha, 1 constituency each of Madhya Pradesh, Maharastra & Jharkhand.

| Subbasin name | Latitude Range | Longitude Range | Outlet Gauging Station | Area in Sq.Km | % age of Total Basin Area |
|---|---|---|---|---|---|
| Simga | 20°15'-22°0'N | 80°23'-81°54'E | Simga | 16,616.2 | 11.74 |
| Basantpur, | 20°52'-23°30'N | 81°45'-89°0'E | Basantpur | 9865.94 | 6.97 |
| Rajim | 19°55'-21°5'N | 81°7'30"-82°55''E | Rajim | 8,374.92 | 5.91 |
| Jondhra | 21°0'-22°45'N | 81°6'-82°34''E | Jondhra | 14208.03 | 10.03 |

**Table 2.1** Study area details in Mahanadi River basin

### *2.2 Data Collection*

#### *2.2.1 Digital Elevation Model*

A digital elevation model (DEM) is a three dimensional representation of a terrain's surface created from the elevation data of the terrain. This is used for drainage or flood modelling, land-use studies, geological applications, planetary science and other applications. In this study DEM of 1 arc-second resolution was considered and extracted from Shuttle Radar Topography Mission (SRTM) data set of USGS. Then the DEM was projected in to WGS 1984 UTM zone 45N coordinate system for watershed delineation in SWAT.

#### *2.2.2 Land Use Land Cover*

Different land use and management patterns have significant impacts on water, soil and various other natural resources. In this study, land use land cover data of the study area is essential for HRU definition and runoff simulation in order to perform the hydrological analysis of the basin. Land use land cover data from MODIS LP DAAC Data Pool of USGS Earth explorer has been used for this study.

#### *2.2.3 Soil Data*

Soil is one of the major components of natural ecosystem. The texture of soil is determined by the relative proportion of three kinds of soil mineral particles known as sand, silt, and clay. Various properties of soil such as porosity, infiltration, permeability, water-holding capacity, and susceptibility to erosion are significantly influenced by soil texture. The soil data for this study area has been extracted from the FAO data set.

#### *2.2.4 Hydro meteorological Data*

The hydro meteorological data consists of discharge data, weather data and the spatial information of the gauging stations. In this study, the discharge data and spatial information of the gauging stations were obtained from Central Water Commission (CWC). The weather data including precipitation, temperature, solar radiation, relative humidity & wind speed were collected from global weather data set.

## 3. Methodology

SWAT (Soil and Water Assessment Tool) is a river basin, or watershed scale model evolved by US Department of Agriculture along with Agricultural Research service (ARS), Texas. This model has been developed to enumerate the commands of various land management scenarios up on agricultural chemical yields, water and sediments in small, large & complex watersheds with respect to various land use pattern, soil and different management scenarios over a long period of time. The model is computationally efficient and uses readily available input datasets thereby enabling users to analyse long term impacts. SWAT is a conceptual model which operates on a daily time step. SWAT can be used to simulate a lone watershed or many hydrologically connected watersheds. Each watershed is initially delineated in to various sub basins as per the stream network and then the sub basins are further divided in to small Hydrological Response Units (HRUs) with respect to the land use, soil distributions and slope classes. Then weather data is provided so as to simulate the field conditions. The model was simulated from 2000-2010 by taking three years as warmup period.

### *3.1 Hydrological processes in SWAT*

Water balance is the driving force for simulation of hydrology. To accurately predict the flow, the hydrologic cycle is simulated by the model from 2000-2010 to confirm the scenario. Simulation of hydrology of a watershed can be divided into two major parts.

- ✓ The land phase of hydrologic cycle (controls the amount of water, sediment & pesticide loading to the main channel in each sub basin.)
- ✓ The water/routing phase of hydrologic cycle (Controls the movement of water, sediment, nutrients & pesticides through channel network)

#### *3.1.1 Land Phase of Hydrologic Simulation*

The land phase of hydrologic simulation is performed by SWAT with respect to water balance equation.

$$SW_t = SW_0 \pm \sum_{i=1}^{t}(R_{day} - Q_{surf} - E_a - W_{seep} - Q_{gw}) \quad \text{Eqn. (3.1)}$$

Where,

$SW_t$ represents the final soil water content in mm $H_2O$
$SW_0$ represents the initial soil water content in mm $H_2O$
$t$ represents the time in days
$R_{day}$ represents the amount of precipitation on day $i$ in mm $H_2O$
$Q_{surf}$ represents the amount of surface runoff on day $i$ in mm $H_2O$
$E_a$ represents the amount of evapotranspiration on day $i$ in mm $H_2O$
$W_{seep}$ represents the amount of water entering the vadose zone on day $i$ in mm $H_2O$
$Q_{gw}$ represents the amount of return flow or base flow on day $i$ in mm $H_2O$

The delineation of watershed in to sub basins and further sub division in to HRUs makes it possible for the SWAT model to assess the condition effectively for various land use patterns, soil types and slope. Runoff is assessed for each HRU and then it is routed to get the total runoff for the entire watershed. This helps in analysing the water balance effectively with a greater accuracy.

#### *3.1.2 Routing Phase of Hydrologic Simulation*

SWAT follows two methods for routing.

a) Variable storage method
b) Muskingum river routing method

As there is no reservoir taken in to consideration in the study area, the Muskingum routing method was further used for simulation.

### *3.2 Hydrology Modelling*

As the precipitation starts falling, it might get intercepted by the vegetation canopy or reach the ground surface without any interception. Then the water will infiltrate in to the soil profile or will be turned in to surface runoff. The runoff will join to the nearby stream with in a very short period of time. However, the infiltrated water will be held in the soil profile and later gets used by plants or slowly joins to the stream network by seepage.

#### *3.2.1 Surface Runoff*

When the rate of precipitation falling on the ground is way more than the rate of infiltration, the excess water that flows over the soil is known as surface runoff. SWAT uses two methods namely "SCS curve number method" and the" Green & Ampt infiltration method" in order to assess the surface runoff. The SCS curve number depends up on land use, antecedent moisture content and permeability of the soil. The Green & Ampt infiltration method takes in to account the wetting front metric potential and effective hydraulic conductivity in order to determine the surface runoff. For daily time steps, SWAT uses SCS curve number method and for hourly time steps, SWAT uses the Green & Ampt infiltration method.

In the current project SCS curve number method has been used as there are a lot of readily available daily data that are used as inputs. The SCS curve number equation is as follows.

$$Q_{surf} = \frac{(R_{day} - I_a)^2}{(R_{day} - I_a + S)} \qquad \text{Eqn. (3.2)}$$

Where,

$Q_{surf}$ represents the rainfall excess in mm $H_2O$

$R_{day}$ represents the rainfall depth for the day in mm $H_2O$

$I_a$ represents the initial abstractions which includes surface storage interception and infiltration prior to runoff in mm $H_2O$

$S$ represents the retention parameter in mm $H_2O$

#### *3.2.2 Soil Hydrologic group*

There are 4 hydrologic groups based up on the infiltration properties of the soil. A hydrologic group can be defined as the group of soil having similar infiltration properties under identical moisture conditions. The soils can be arranged in groups of A, B, C & D based upon their properties.

Class A: The soils which belongs to this class have high infiltration rate. These soils consist of sands or gravels and shows high rate of water transmission.

Class B: The soils which belongs to this class have a moderate infiltration rate. These soils show moderate rate of water transmission.

Class C: The soils which belongs to this class have a low infiltration rate. These soils show a low rate of water transmission.

Class D: The soils which belongs to this class have a very very low infiltration rate. This class consist of soils having permanent water table, high swelling potential and impervious layer. This class of soil show a low rate of water transmission.

The soil type in this study area is known as Cambisol. This soil comes under class B and poses 5 layers

### *3.3 Sensitivity Analysis, Calibration & Validation of SWAT Model*

#### *3.3.1 Sensitivity Analysis*

SWAT model poses a huge number of parameters for hydrological modelling. For simulation purpose, the input parameters must be selected as per the process requirement and they should be kept in a realistic range of uncertainty. The first and foremost step in calibration and validation is to identify the parameters that are most sensitive to the model. In sensitivity analysis, the main focus is to reduce the number of parameters. A parameter is considered to be sensitive, when a small change in the parameter leads to significant change in model output value. Sensitivity analysis helps in decreasing the computational time for the simulation by reducing the number of non-influential input parameters. SWAT provided various algorithms to execute uncertainty analysis. In this study SUFI2 (Sequential Uncertainty Fitting version 2) algorithm was used. SUFI2 algorithm supports two type of sensitivity analysis namely One-at-a-time sensitivity and Global sensitivity analysis. These two types of sensitivity analysis may produce different results since sensitivity of one parameter depends up on the value of other parameters. In this study, one-at-a-time sensitivity analysis was performed to point out the influential parameters and then Global sensitivity analysis was performed for the influential parameters to determine their ranks.

##### *3.3.1.1 One-at-a-time Sensitivity Analysis*

As the name suggests, this type of sensitivity analysis is done for a single parameter at a time thereby keeping the values of other parameters constant. This type of analysis helps in determining the sensitivity of output to a small change in the input parameter value. In this project the objective function used for the calibration was NSE (Nash Sutcliffe Efficiency).

##### *3.3.1.2 Global Sensitivity Analysis*

As the name suggests, this type of sensitivity analysis is done for every parameter at once. This analysis uses t-value & p-values in order to determine the sensitivity of every single parameter. The t-value indicates the measure of the sensitivity whereas, p-value indicates the significance of the sensitivity. This type of sensitivity analysis requires a high number of simulations.

#### *3.3.2 Model Calibration & Validation*

Model calibration is a procedure which is performed in order to parameterize the model for a set of desirable local conditions. Model calibration is done to minimise the uncertainty. In order to perform the calibration process, the values of input parameters were adjusted with in the uncertainty range and the simulated values were compared with the observed values. SUFI2(Sequential Uncertainty Fitting version 2) algorithm was used for calibration process. Then the manual calibration was performed for the parameters which were physically wrong. In this study each of the 4 sub basins were calibrated from 2003-2007. Once the model is calibrated, it needs to be authenticated against the observed values. In this study each of the 4 sub basins were validated from 2008-2010.

## 4. Results And Discussion

### *4.1 SWAT Output results*

After providing certain input data such as DEM, Land use, Soil types, Slope & weather conditions, the SWAT model processes all this information and gives various output. The output contains precipitation, lateral flow, surface runoff, ground water, evapotranspiration, water yield and many more. In order to analyse the discharge in a particular basin, it is necessary to have the observed discharge values of the particular basin. The observed discharge data can be accessed through a gauging station corresponding to the basin to be analysed. In this research the discharges for the considered sub basins were separately simulated for a period of 11 years. Then the observed discharge values of each sub basin for the same time period were recorded from CWC (Central Water Commission).

The total sub basin load of flow for Simga, Basantpur, Rajim , Jondhra basin were found to be 381.59 cumec,194.56 cumec,186.5 cumec & 323.82 cumec respectively. In case of Simga basin, it is

observed that the surface runoff is excessive in the areas of croplands and urban areas. In case of Basantpur basin, it is observed that the surface runoff is excessive in the areas of croplands and barren lands. In case of Rajim basin, it is observed that the surface runoff is excessive in the areas of croplands and barren lands. In case of Jondhra basin, it is observed that the surface runoff is excessive in the areas of croplands.

### *4.2 Model Parameter Uncertainty & Sensitivity Analysis*

The sensitivity analysis was performed separately for each of the four basins considered by taking the discharge as variable. This was performed prior to calibration process. In sensitivity analysis, the parameters that significantly affects the model output are pointed out so as to minimise the computation time in calibration phase. In this research nine significant parameters for discharge analysis are selected. They are R_SOL_AWC.sol; R_SOL_K.sol; R_OV_N.hru; V_CH_N2.rte; V_CH_K2.rte; V_ALFA_BF.gw; V_GW_REVAP.gw; V_ESCO.hru and V_CANMX.hru.

### *4.3 Manual Calibration Results*

The model performance was assessed by statistical comparison of observed and simulated discharge data separately for all the four basins considered.

#### *4.3.1 NSE (Nash Sutcliffe efficiency) Coefficient*

There are plenty of statistical parameters, which can be adopted to analyse various hydrological models. Particularly NSE model has been highlighted by the American Society of Civil Engineers as an effective parameter for analysing hydrological conditions. The NSE indicates deviation from unity of the ratio of the square of the difference between the observed and simulated values and the variance of the observations. The range of NSE coefficient is from -∞ to 1. The value 1 indicates a perfect agreement between observed and simulated values. For NSE values that are negative or too much close to 0, the model prediction is considered to be poor or unacceptable. The NSE value is represented as follows.

$$NSE = 1 - \frac{\sum_{i=1}^{n}(O_i - S_i)^2}{\sum_{i=1}^{n}(O_i - O_{mean})^2} \qquad \text{Eqn. (4.1)}$$

Where,

$O_i$ represents the observed value

$S_i$ represents the simulated value

$O_{mean}$ represents the observed mean

$n$ represents the total number of data

| VALUES | PERFORMANCE CLASSIFICATION |
|---|---|
| 0.75 < NSE ≤ 1.00 | Very good |
| 0.65 < NSE ≤ 0.75 | Good |
| 0.50 < NSE ≤ 0.65 | Satisfactory |
| 0.40 < NSE ≤ 0.5 | Acceptable |
| NSE ≤ 0.4 | Unsatisfactory |

**Table 4.1** Statistical Performance Table

From the observed and simulated data, the NSE value was found to be 0.54 for Simga basin, 0.43 for Basantpur basin, 0.52 for Rajim basin & -0.17 for Jondhra basin. After analysis from the table, it was noted that the model for Basantpur is acceptable & models for Simga and Rajim are satisfactory. However, the model for Jondhra basin is unsatisfactory.

### *4.4 Validation*

Once the parameters are calibrated for the time period of 2003 to 2007, it needs to be validated. In this research, the validation period has been considered from 2008 to 2010. The value of NSE was found to be 0.54 & 0.49 for Simga basin, 0.43 & 0.42 for Basantpur basin, 0.48 & 0.43 for Rajim basin and -0.17 & -0.15 for Jondhra basin respectively for both calibration and validation. This implicates that there is a good relation between calibration and validation data. However, it was also observed that there is some inconsistency between observed and simulated data. This inconsistency is due to non-availability of discharge data of certain days from corresponding gauging stations. The statistical measures indicate an acceptable correlation between the observed and simulated values.

## 5. Conclusions and Future Scope

### *5.1 Conclusions*

In this research, SWAT model was incorporated to simulate discharge in four sub basins of Mahanadi river basin. The prime intention of this research was to simulate and assess the discharge of Mahanadi river in a sub basin scale. GIS interface was adopted in order to prepare various geospatial data which were in turn used as inputs for the SWAT model. The availability of not so exact data inputs moderately affected the model simulation. The parameters used for sensitivity analysis and model calibration were identified from certain published literatures.The developed models for each of the four sub basins were calibrated for a period of 5 years (2003-2007) by considering a period of 3 years (2000-2002) as warm up period. Then the models were validated for a period of 3 years (2008-2010). The observed discharge data for the above mentioned periods were collected from CWC annual reports.The value of NSE was found to be 0.54 & 0.49 for Simga basin, 0.43 & 0.42 for Basantpur basin, 0.48 & 0.43 for Rajim basin and -0.17 & -0.15 for Jondhra basin respectively for both calibration and validation.The statistical measures indicate an acceptable correlation between the observed and simulated values for all the sub basins except for Sundergarh, Jondhra & Kantamal. The performance of the models in validation phase indicated that the parameters selected in calibration phase were able to represent the hydrological scenario in the river basin. It was noted that suitable and accurate input data is highly essential in order to obtain an excellent fit between observed and simulated data. In the present study, It was noted that Crop lands and barren lands generally produce more runoff than any other land use classes.

### *5.2 Future Scope of the Research*

This study attempts to assess and analyse the discharge variable of the Mahanadi river hydrology at a sub basin scale using SWAT model. There are a lot of rivers and corresponding basins in India, which are yet to be analysed at a reduced scale, in order to study the structure and response of river hydrology to various natural as well as manmade scenarios. This study might draw the attentions of other researchers to study and analyse many other Indian rivers in reduced scale so as to magnify and visualise the structure and response of river hydrology restricted to an indigenous location. This small scale analysis will help in developing unique management practices that can be adopted only for the particular location.

## References

1. Wenming Nie, Yongping Yuan, William Kepner, Maliha S.Nash, Michael Jackson, Caroline Erickson (2011). Assessing impacts of Landuse and Landcover changes on hydrology for the upper San Pedro watershed. Journal of Hydrology, Volume 407, Issues 1–4, Pages 105-114.
2. Tekalegn Ayele, Woldesenbet, Nadir Ahmed Elagib, Lars Ribbe', Jürgen Heinrich (2016). Hydrological responses to land use/cover changes in the source region of the Upper Blue Nile Basin, Ethiopia. Science of The Total Environment, Volume 575, Pages 724-741.

3. Santosh Babar and H. Ramesh (2015). Streamflow Response to Land Use–Land Cover Change over the Nethravathi River Basin, India. Journal of Hydrologic Engineering, Volume 20, Issue 10.
4. Priyamitra Munoth and Rohit Goyal (2019). Impacts of land use land cover change on runoff and sediment yield of Upper Tapi River Sub-Basin, India. International Journal of River Basin Management, Volume 18, 2020 - Issue 2.
5. Sushil Kumar Himanshu, Ashish Pandey & Prabin Shrestha (2017). Application of SWAT in an Indian river basin for modeling runoff, sediment and water balance. Environmental Earth Sciences 76, Article number: 3.
6. Navneet Kumar, Bernhard Tischbein, Jürgen Kusche, Mirza Kaleem Beg & Janos J. Bogardi (2017). Impact of land-use change on the water resources of the Upper Kharun Catchment, Chhattisgarh, India. Regional Environmental Change volume 17, pages 2373–2385.
7. Nirmal Kumar, Sudhir Kumar Singh, Vikram Gaurav Singh & Bloodless Dzwairo (2018). Investigation of impacts of land use/land cover change on water availability of Tons River Basin, Madhya Pradesh, India. Modeling Earth Systems and Environment volume 4, pages295–310
8. N Sajikumar , R S Remya (2014). Impact of Land Cover and Land Use Change on Runoff Characteristics. Journal of environmental management, volume 161,pages 460-468.
9. Chunhao Zhu and Yingkui Li (2014). Long-term hydrological impacts of land use/land cover change from 1984 to 2010 in the Little River Watershed, Tennessee. International Soil and Water Conservation Research, Vol. 2, No. 2, pp. 11-22.
10. Laurent Ahiablame, Tushar Sinha, Manashi Paul, Jae-Hyung Ji, Adnan Rajib (2017). Streamflow response to potential land use and climate changes in the James River watershed, Upper Midwest United States. Journal of Hydrology: Regional Studies, volume 14, pages 150-166.
11. Dao Nguyen Khoi, Vu Thi Thom (2015). Parameter uncertainty analysis for simulating stream flow in a river catchment of Vietnam. Global Ecology and Conservation, volume 4, pages 538-548.
12. Vaibhav Garg, Bhaskar Ramchandra Nikam, Praveen Kumar Thakur, Shiv Prasad Aggarwal, Prasun Kumar Gupta, Sushil Kumar Srivastav (2019). Human-induced land use land cover change and its impact in hydrology. Hydro Research, volume 1, pages 48-56.
13. Rafael A. Almeida, Silvio B. Pereira, Daniel B. F. Pinto (2018). Calibration and validation of the swat hydrological model for the Mucuri river basin. Engenharia Agrícola, volume 38, pages 55-63.
14. K.C.Abbaspour, E. Rouholahnejad, S. Vaghefi, R. Srinivasan, H.Yang, B. Klove (2015). A continental-scale hydrology and water quality model for Europe: Calibration & uncertainty of a high-resolution large-scale SWAT model. Journal of Hydrology, volume 524, pages 733-752.
15. K. Venkatesh, H. Ramesh (2018). Impact of land use land cover change on run off generation in Tungabhadra river basin. ISPRS Annals of the Photogrammetry, Remote Sensing and Spatial Information Sciences, Volume IV-5.
16. Pakorn Petchprayoon, Peter D. Blanken, Chaiwat Ekkawatpanit and Khalid Hussein (2010). Hydrological impacts of land use/land cover change in a large river basin in central–northern Thailand. International journal of climatology, volume 30, pages 1917–1930.
17. Faiza Hallouz, Mohamed Meddi, Gil Mahe, Salaheddine Alirahmani, Abdelkader Keddar (2018). Modelling of discharge and sediment transport through the SWAT model in the basin of Harraza (Northwest of Algeria). Water Science, volume 32, page 79-88.
18. Wubishet Tadesse, Stephanie Whitaker, William Crosson, Constance Wilson (2015). Assessing the Impact of Land-Use Land-Cover Change on Stream Water and Sediment Yields at a Watershed Level Using SWAT. Open Journal of Modern Hydrology, volume 5, pages 68-85.
19. Limin Zhang, Xianyong Meng, Hao Wang and Mingxiang Yang 2 (2019). Simulated Runoff and Sediment Yield Responses to Land-Use Change Using the SWAT Model in Northeast China. Water 2019, 11, 915; doi:10.3390/w11050915
20. Muhammad Adnan, Shichang Kang, Guoshuai Zhang, Muhammad Saifullah, Muhammad Naveed Anjum and Ayaz Fateh Ali (2019). Simulation and Analysis of the Water Balance of the Nam Co Lake Using SWAT Model. Water 2019, 11, 1383; doi:10.3390/w11071383.
21. Charles Gyamfi, Julius Musyoka Ndambuki, Ramadhan Wanjala Salim (2016). Application of SWAT Model to the Olifants Basin: Calibration, Validation and Uncertainty Analysis. Journal of Water Resource and Protection, volume 8, pages 397-410.
22. Charles Gyamfi, Julius M. Ndambuki and Ramadhan W. Salim (2016). Hydrological Responses to Land Use/Cover Changes in the Olifants Basin, South Africa. Water 2016, 8, 588 doi:10.3390/w8120588.

*IN PROCEEDINGS OF 25th HYDRO 2020, INTERNATIONAL CONFERENCE, NATIONAL INSTITUTE OF TECHNOLOGY ROURKELA, ODISHA, INDIA 26-28, March 2021, ISBN 978-93-90631-56-8*

Paper ID - 102

# Comparison of Land Surface Temperature for Bare soil from MODIS and ASTER data

Sreelakshmi C V[1] and Jairaj P G[2]

[1]*Post Graduate Scholar, Dept. of Civil Engineering, College of Engineering Trivandrum, Kerala, 695016, India*

[2]*Professor, Dept. of Civil Engineering, College of Engineering Trivandrum, Kerala, 695016, India*

*Email: cvsreelakshmi@cet.ac.in ; jairaj@cet.ac.in*

*Mobile No.: +91 9747206006 ; +91 9847241141*

## Abstract

Land Surface Temperature (LST) is known as the radiative skin temperature of the surface of earth and it has a major role in water balance and surface energy of earth. LST has wide applications in different fields like evapotranspiration, climate change, urban climate and environmental studies. Ground based measurements of LST is not practically possible, but satellite sensors in the region of thermal infrared are used for LST estimation. The Moderate Resolution Imaging Spectroradiometer known as MODIS, having a good temporal and spatial resolution is one of the commonly used sensor for land surface temperature monitoring. The product of collection 6 MODIS (C6) LST is now accessible for the public users and has been refined for bare soil pixels. This study compares the MODIS C6 LST product's accuracy in three study areas of bare soil lands. The calculated RMSE and bias of the temperature differences ($MODIS_{LST}$ - $ASTER_{LST}$) between MODIS C6 LST and ASTER LST indicates that the accuracy of MODIS C6 LST has notably improved, than the collection 5 MODIS (C5) LST. Effect of seasons over the accuracy of LST showed that RMSE and bias of the differences ($MODIS_{LST}$ - $ASTER_{LST}$) between the MODIS C6 LST and the ASTER LST during summer season is higher than that of winter season. This may be attributed to the high amount of water vapour column in the atmosphere in summer season, since the standard LST or emissivity algorithm of ASTER is poor in compensating the atmospheric effects in the presence of higher amount of water vapour in the atmosphere.

***Keywords:*** *Land Surface Temperature, MODIS, ASTER*

## 1. Introduction

Land Surface Temperature (LST) plays a critical role in determining the radiative energy budget of the Earth's surface. Monitoring and understanding of LST along with its connection to changes produced by human are important for predicting and modeling changes in environment due to variability in climate and for many other applications like vegetation monitoring, hydrology, geology etc. It is the main input to land surface models for soil moisture estimation, drought monitoring and evapotranspiration estimattion. According to Planck's law as the temperature increases the total radiative energy emitted by the land surface also increase and it is the theory behind the remote sensing of LST. LST is often referred to as the skin temperature, or radiometric temperature and it is a direct measures how the Earth would feel to the touch, whether it is hot or cold . For a dense vegetation LST will be the temperature of the leaves of the canopy while for bare soil it is the temperature of the few micrometers of the top soil surface.

Ground based measurements of LST in global and regional level is not possible practically. So satellites in the thermal infrared (TIR) region are used to measure LST. The MODIS, aboard the aqua and terra satellites, with a good spatial and temporal resolution, is the one of the most widely used and important sensor for land surface temperature monitoring. The product has different datasets with a spatial resolution ranging from 1 km as well as temporal resolution ranging from day to month.

The MODIS LST products on the Aqua and Terra platforms are collections C4, C4.1, C5, and C6 in which C6 is recently revised and progressed one with much quality. C6 products are undergone three refinements compared to that of previous MODIS LST products. Two coefficient sets for night and day time retrieval of LST, are added to the split window algorithm to refine over the bare soil in warm and hot bare soil zones (WAHBSZs) of 38ºS to 49.5ºN latitudes. The differences in land

surface emissivity (LSE) of the band 31 and band 32 are adjusted in the WAHBSZs over bare soil pixels and day/night algorithm incorporated with split window algorithm for LST and LSE retrieval in the WAHBSZs. Based on the temperature and the radiance method a lots of studies have already been done over different sites including grassland, bare soil, cropland, silt playa etc to validate MODIS LST product. Validation results shows that the MODIS C5 LST product is accurate over most of the sites other than the bare soil sites (Wan, 2014). Over semiarid and arid areas the accuracy of the MODIS C5 LST product is significantly underestimated.

To assess the accuracy of the MODIS C6 LST under different surface conditions we used the Advanced Spaceborne Thermal Emission Reflection Radiometer, known as ASTER LST as reference LST data. The seasonal variation in accuracy of MODIS C6 LST is also evaluated taking the same reference.

## 2. Experimental program

### *2.1 Study area*

Three study areas were selected in this study, which includes the bare soil surfaces of different surface and atmospheric conditions. The study areas are located in North America (Great Basin Desert), Northern Africa (Sahara) and South America (Atacama). The basis of selecting the three areas is they are relatively large bare soil surfaces and are located over different continents. Figure 1 is the geolocations of the three areas. The informations of the three areas are shown in Table 1.

**Table 1** Information of study areas

| | Area | Continent | Climate Type | Longitude & Latitude |
|---|---|---|---|---|
| 1 | Great Basin Desert | North America | Temperate continental climate | 113º-116ºW, 39º-42º N |
| 2 | Sahara Desert | North Africa | Tropical desert climate | 11º-14º E, 22º-25º N |
| 3 | Atacama Desert | South America | Mild coastal climate | 67º-70º W, 24º-26º S |

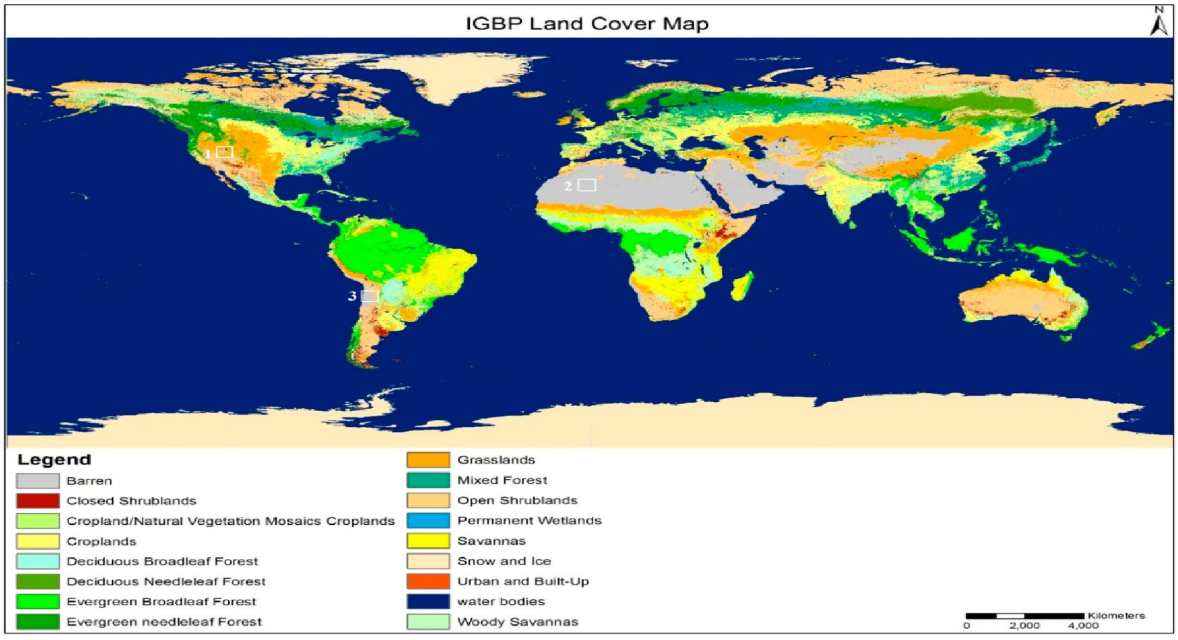



**Figure 1** Geolocation of three study areas

### *2.2 Data used*

The study used two MODIS and one ASTER products. The product descriptions are given in the following sections.

#### *2.2.1 MODIS LST product*

MODIS is an important instrument aboard the Aqua (EOS PM-1) and Terra (EOS AM-1) satellites. Aqua and Terra were launched on 18 th December 1999 and 4 th May 2002, respectively. The Terra satellite passes from north to south across the equator in the morning (approximately 10:30 a.m. local solar time), similarly Aqua passes from south to north over the equator in the afternoon (approximately 10:30 a.m. local solar time). Aqua MODIS and Terra MODIS are capable of viewing the whole surface of earth in every 1 to 2 days. They acquire datas in 36 spectral bands. The MOD11A1 Version 6 product which provides daily Land Surface Temperature per pixel used in this study. It's spatial resolution is about 1000 m and geographic dimension of 1200 km x 1200 km. LST was calculated from MODIS 31 and 32 bands of brightness temperatures by the generalized split window algorithm.

#### *2.2.2 MODIS land cover type product*

The Version 6 (V6) Aqua and Terra MODIS Land Cover Type (MCD12Q1) data product gives land cover types globaly in every year and contains five different schemes of land cover classification. This MCD12Q1 V6 data is generated by the supervised classifications of MODIS Aqua and Terra reflectance data. The scheme of land cover, described by the International Geosphere Biosphere Programme (IGBP), is used for the identification of bare soil with IGBP ID = 16. It has a spatial resolution of 500 m. So it is resampled from 500 m to 1000 m to agree with the MOD11A1 spatial resolution.

#### *2.2.3 ASTER LST product*

The Advanced Space borne Thermal Emission and Reflection Radiometer (ASTER) is a leading multispectral imager. ASTER was launched by NASA's Terra spacecraft on December 1999. It can cover a broad region in the spectra with14 bands ranging from the visible region to the thermal infrared region with high radiometric, spectral and spatial resolution. The spatial resolution varies as the wavelength varies, such that 15 m for the visible and near infrared , 30 m for the short wave infrared, and 90 m for the thermal infrared (TIR). Every ASTER scene can cover of 60 x 60 km area with a 16 days repeat cycle.
The ASTER Surface Kinetic Temperature (AST_08) which is generated using the five TIR bands between 8 and 12 μm spectral range is used in this study as a references to assess the MODIS LST product's accuracy. It contains surface temperatures for the land areas at a spatial resolution of 90 m. This product is derived using Temperature/Emissivity Separation algorithm.

### *2.3 Methodology*

MODIS C6 products and ASTER LST products are downloaded using NASA earthdata search tool in HDF format and GeoTIFF format respectively for different study area and for different seasons (summer, spring and winter). The downloaded MODIS data products are converted from HDF format to GeoTIFF format using ERDAS IMAGINE 2013. MODIS image is obtained in sinusoidal coordinate system and ASTER image in UTM coordinates itself. So MODIS image is reprojected to WGS 1984 UTM zone 11 N for Great Basin Desert, WGS 1984 UTM zone 32 N for Sahara desert and WGS 1984 UTM zone 19 S for Atacama desert. For pixel wise comparison of LST both the images should have same spatial resolution. ASTER image is resampled from 90 m to 1000 m resolution to compensate the spatial resolution of MODIS image using bilinear resampling.

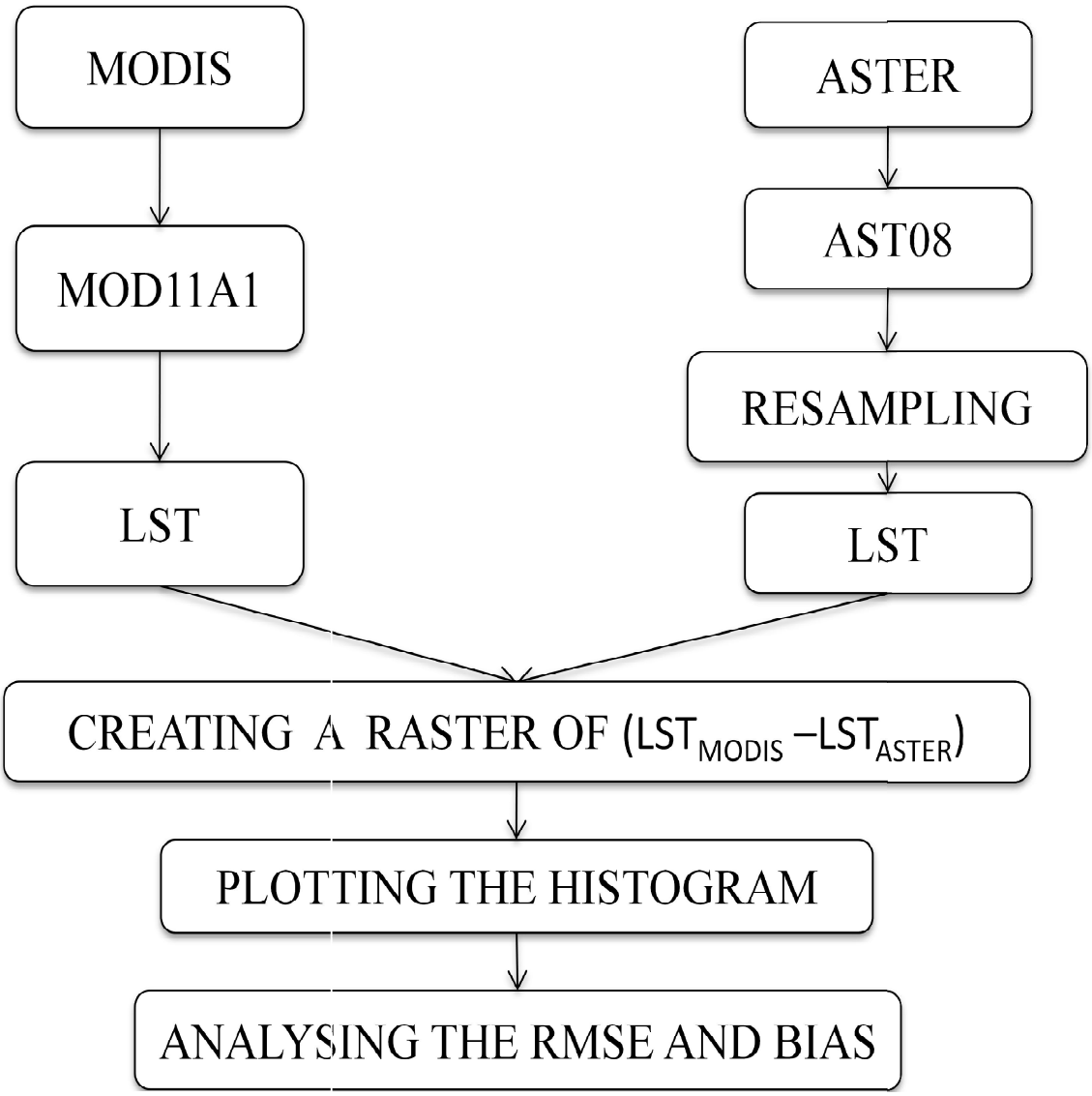



**Figure 2** Workflow of LST comparison

Bilinear resampling method is useful for continuous data and it executes a bilinear interpolation. In this, based on a weighted distance average of the four nearest input cell of the central cell, the new value of the central cell is determined. Study areas are clipped from the images. The pixel value range for MODIS image is 7500 to 65535. To convert it into LST value in Kelvin it is multiplied by a scale factor of 0.02 using Math tool in ArcMap and converted into integer.

The range of pixel value for ASTER image is 200 to 3200 and it is multiplied by the scale factor of 0.1 and its values also converted into integer. The scaled image is shown in figure 3. Using these two rasters a new raster of differences ($MODIS_{LST} - ASTER_{LST}$) between MODIS C6 LST and ASTER LST is created which is shown in figure 4. The attribute tables of the new raster ($LST_{MODIS} - LST_{ASTER}$) is exported to MS Excel for further calculations. Histograms are created to show the pixel wise LST differences and frequency. The bias and RMSE is calculated to compare the accuracy of MODIS C6 LST to the MODIS C5 LST. The figure 2 shows the path followed for comparing the LST values and accuracy.

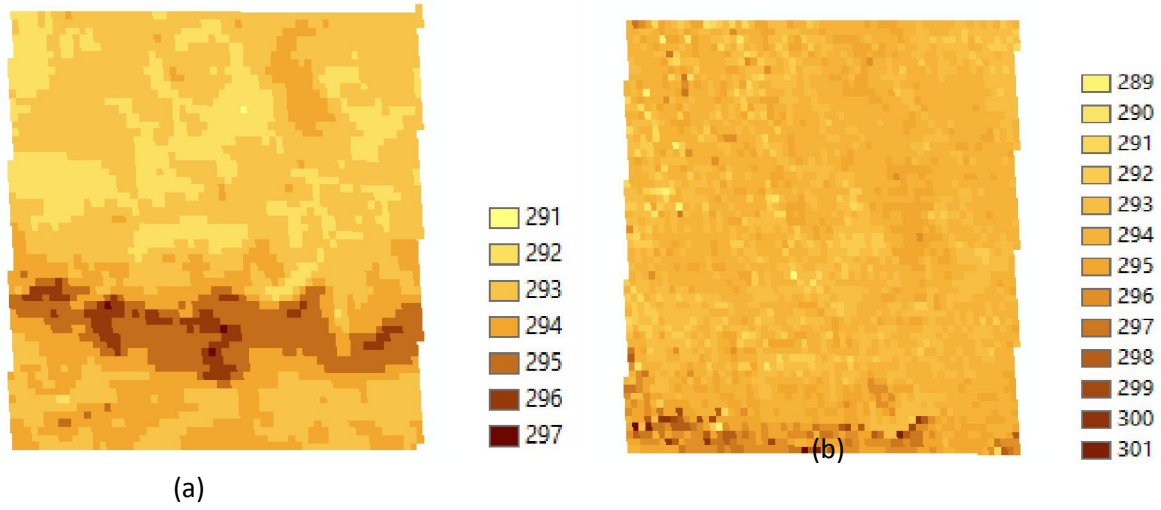



**Figure 3 (a)** Scaled MODIS LST data (LST in K), **(b)** Scaled ASTER LST data (LST in K)

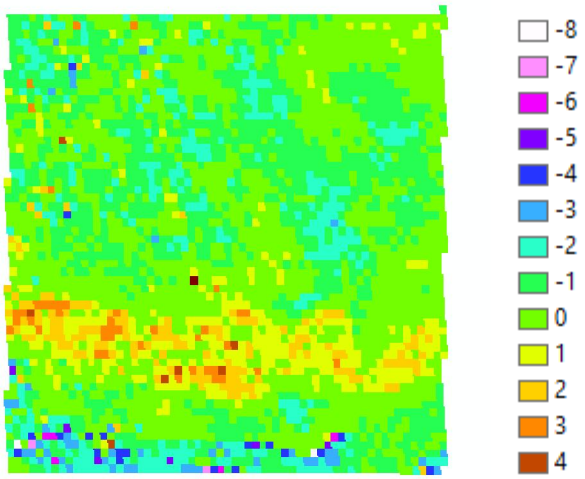



**Figure 4** Raster of LST differences ($MODIS_{LST}$ –$ASTER_{LST}$)

### *2.4 Results and Discussions*

The detailed analysis of the study was done sequentially. LST data of both MODIS and ASTER were studied in detail and LST vales were obtained after processing the image. A new raster of differences ($MODIS_{LST}$ –$ASTER_{LST}$) between MODIS LST (C6) and ASTER LST was created. Histograms are used to compare the pixel values and RMSE and bias are calculated to check the accuracy of MODIS C6 LST data.

#### *2.4.1 Results for the Great Basin Desert*

Figure 5 is the histograms swowing the differences ($MODIS_{LST}$ – $ASTER_{LST}$) between MODIS C6 LST and ASTER LST over Great Basin desert for summer (a), spring (b) and winter (c) seasons. The RMSE and bias of the MODIS C6 LST differences varies from 0.92 to 0.94 K and -0.06K to -0.14K respectively compared to the ASTER LST. It is less than the RMSE and bias of the MODIS C5 LST , which is 0.94K and -0.63K (Duan et al., 2017).

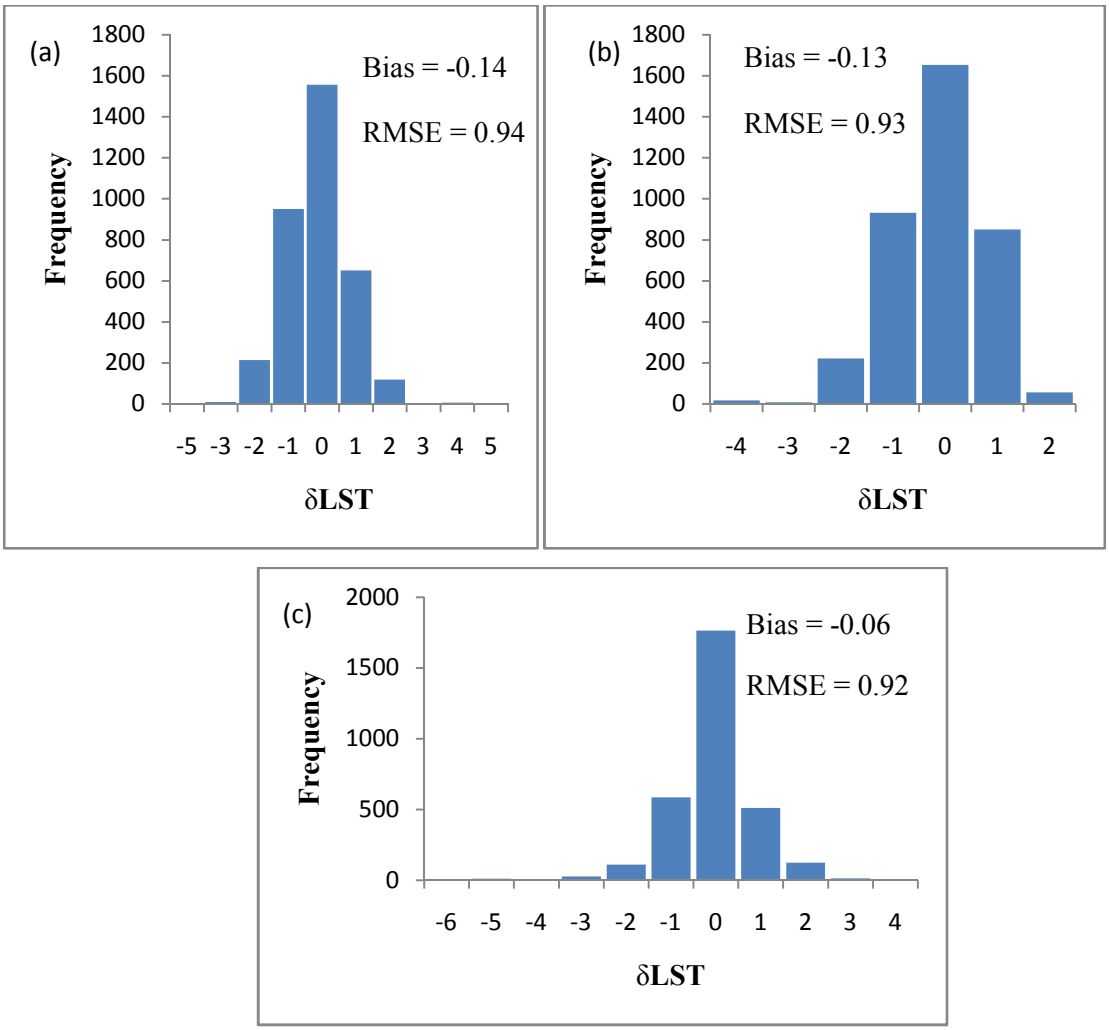



**Figure 5** Histograms showing the differences ($MODIS_{LST}$ –$ASTER_{LST}$) between the LST of MODIS C6 and ASTER over Great Basin desert:(a) summer, (b) spring, and (c) winter seasons

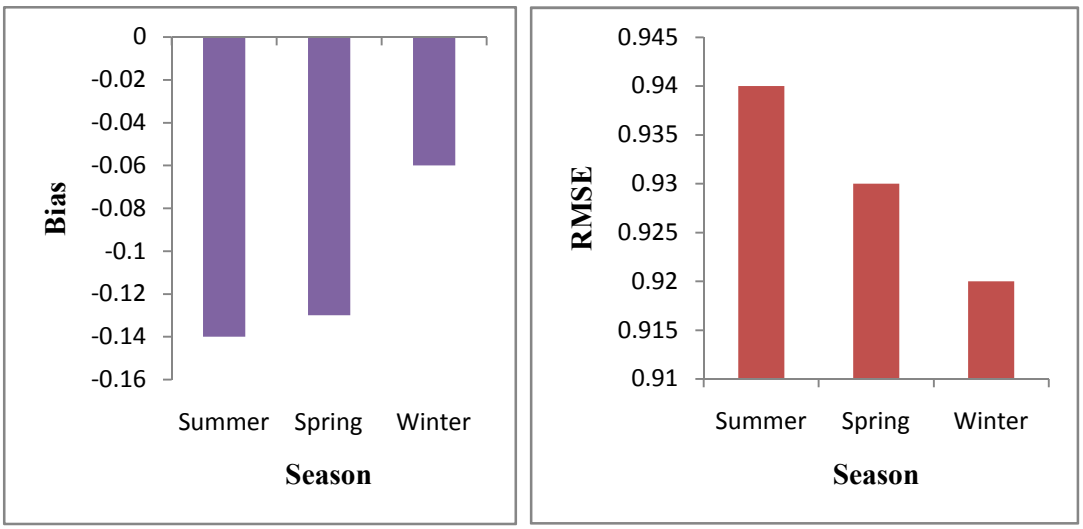



**Figure 6** RMSE and Bias of the differences ($MODIS_{LST}$ –$ASTER_{LST}$) between the LST of MODIS C6 and ASTER over Great Basin desert

To evaluate the effects of seasons on the LST product's accuracy, the RMSE and bias of the differences ($MODIS_{LST}$ – $ASTER_{LST}$) between the MODIS C6 LST and the ASTER LST are calculated over Great Basin desert. The results are shown in figure 6. It is clear that the RMSE and bias in summer and spring are higher than that in winter for the MODIS C6 LST .

*2.4.2 Results for the Sahara Desert*

Figure 7 displays the differences ($MODIS_{LST}$ – $ASTER_{LST}$) between the MODIS C6 LST and ASTER LST over Sahara desert for three different seasons. Compared to the accuracy of the MODIS C5 LST with a bias of -3.8 K and RMSE of 4.2 K (Duan et al., 2017 ) accuracies of the MODIS C6 LST are unquestionably improved. It has a bias varying from -2.8 K to -0.09 K and the RMSE varying from 3.5 K to 1.3 K. Analysis of the seasonal effects on the accuracy of LST product which is shown in figure 8 indicates that absolute RMSE and bias are obtained in summer for the MODIS C6 LST .

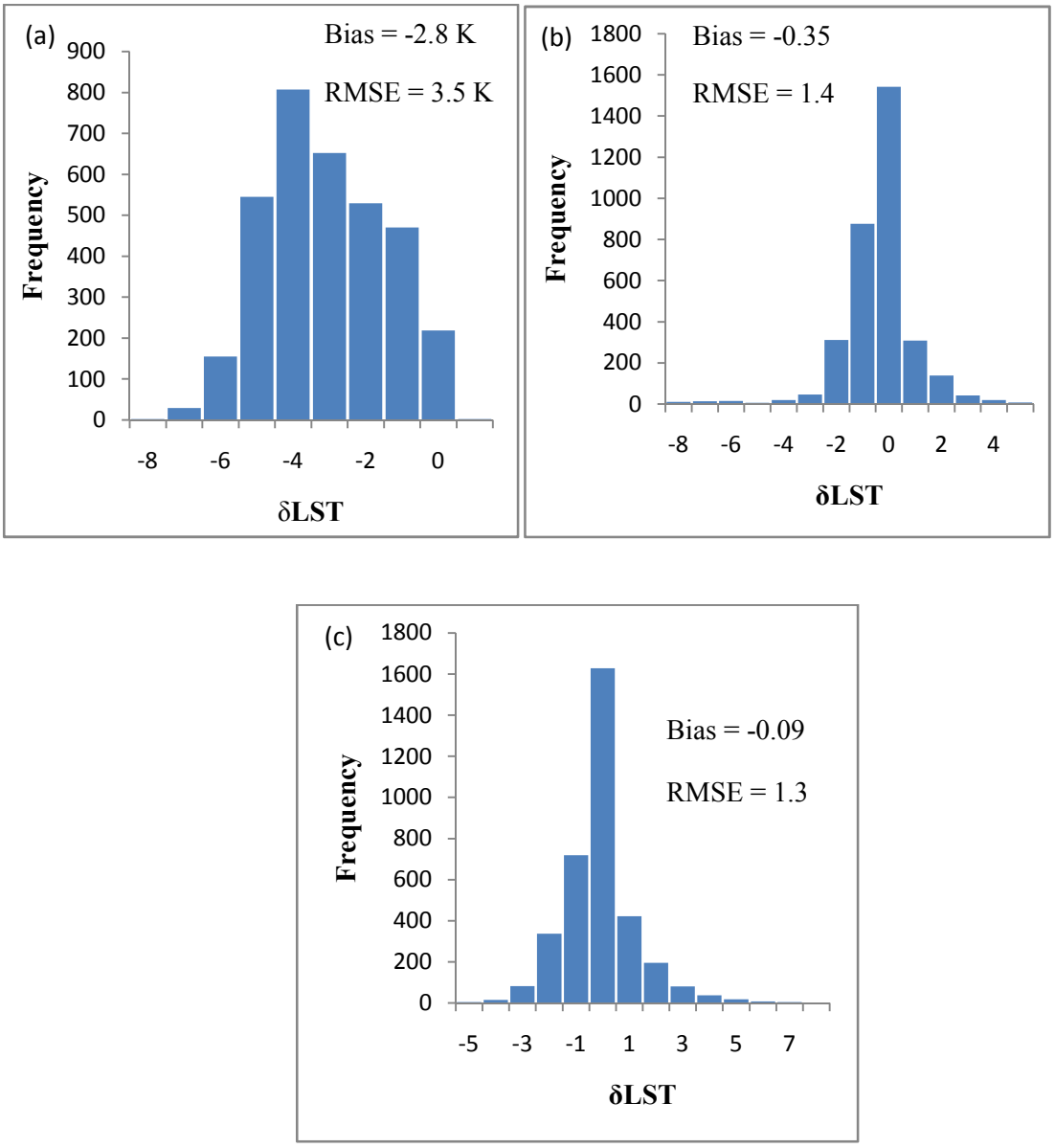



**Figure 7** Histograms of the differences ($MODIS_{LST}$ –$ASTER_{LST}$) between LST of the MODIS (C6) and ASTER over Sahara desert: (a) summer, (b) spring, and (c) winter seasons

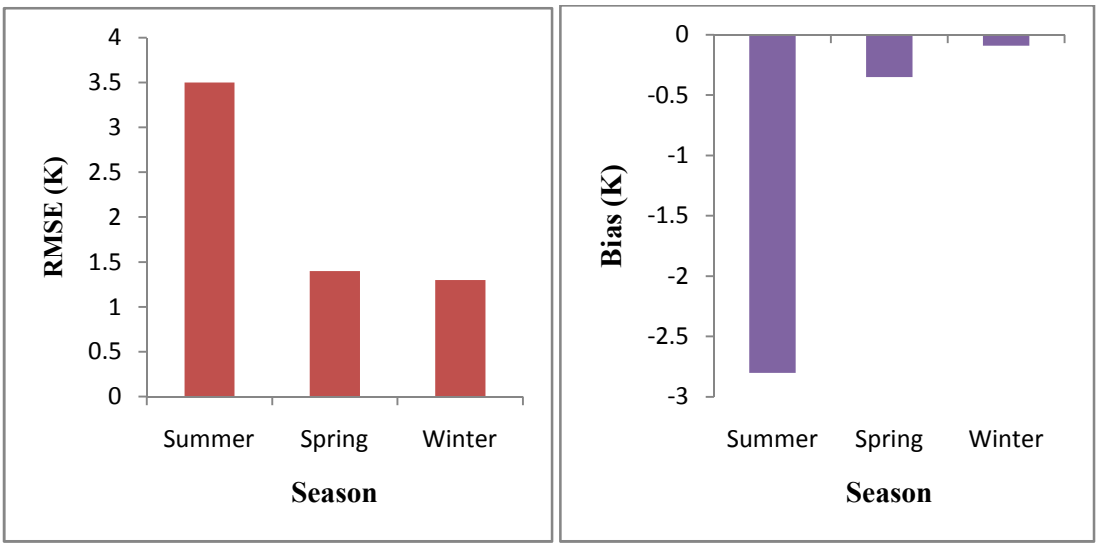



**Figure 8** RMSE and Bias of the differences ($MODIS_{LST}$ –$ASTER_{LST}$) between LST of the MODIS (C6) and ASTER over Sahara desert.

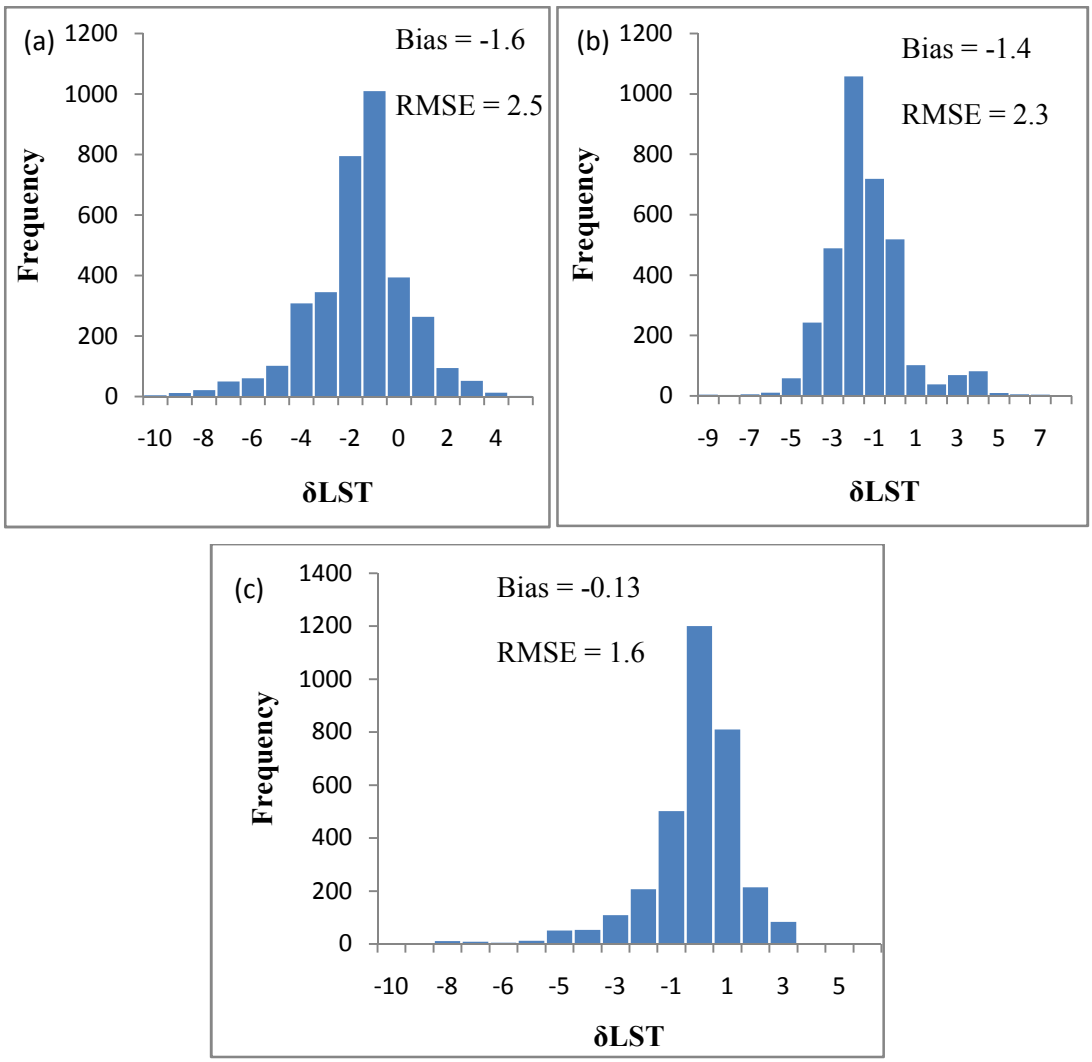



**Figure 9** Histograms of the differences ($MODIS_{LST}$ –$ASTER_{LST}$) between the LST of MODIS C6 and ASTER over Atacama desert: (a) summer, (b) spring, and (c) winter seasons

### *2.4.3 Results for the* Atacama Desert

The differences ($MODIS_{LST}$ –$ASTER_{LST}$) between the MODIS C6 LST and ASTER LST over Atacama desert are shown in figure 9. Considering the ASTER LST, here the bias of the differences in LST is -2.8 K (Duan et al., 2017 ) for the MODIS C5 LST while it varies from -1.6 k to -0.13 K for the MODIS C6 LST. Similarly the RMSE of the differences in LST is 3.1 K (Duan et al., 2017) for the MODIS C5 LST while it varies from 2.5 K to 1.6 K for the MODIS C6 LST . Figure 10 shows the analysis of the effects of seasons on the LST product's accuracy, and calculated RMSE and bias of the ($MODIS_{LST}$ –$ASTER_{LST}$) between the MODIS C6 LST and the ASTER LST over Atacama desert. Here also the winter season shows less bias and RMSE value when summer season has high bias and RMSE.

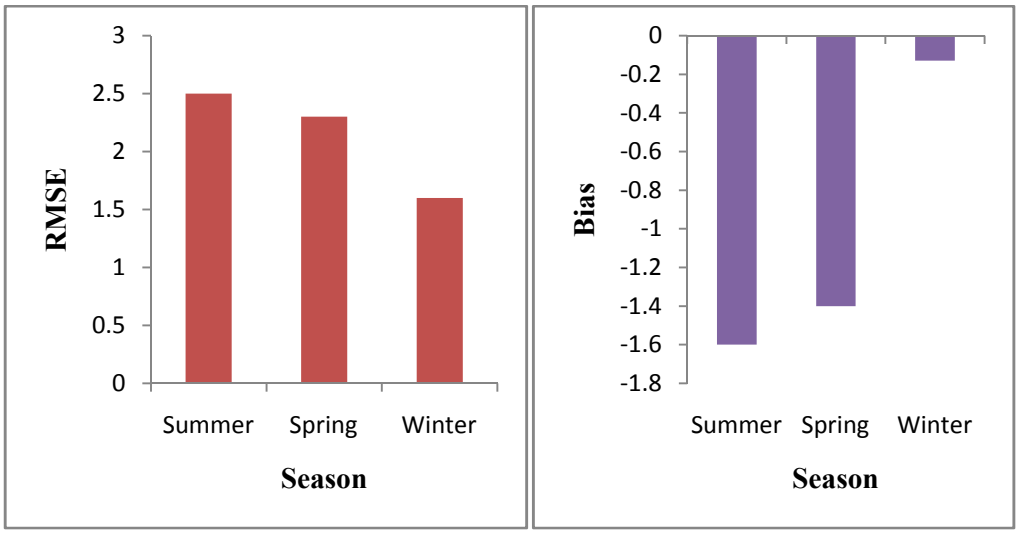



**Figure 10** RMSE and Bias of the differences ($MODIS_{LST}$ –$ASTER_{LST}$) between LST of the MODIS (C6) and ASTER over Atacama desert.

## 3. Conclusions

LST is the one of the key parameter controlling the physical, chemical and biological process of earth. Now the MODIS C6 LST product is accessible for the users. So determining the accuracy of the MODIS C6 LST product will be a benefit in facilitating the use of the LST product in a lots of operations. There are developments in the MODIS C6 LST product compared to the MODIS C5 LST product, over bare sois.

To assess the accuracy of the MODIS C6 LST product over the surface of bare soil a comparison strategy was adopted taking the reference as ASTER LST. The MODIS LST products are analysed with the ASTER LST product over the surfaces of bare soil in three study areas having differenrt surface and atmospheric condition. Considering the MODIS C5 LST, the accuracy of the MODIS C6 LST was undoubtedly advanced. The RMSE and bias of the differences of the MODIS C6 LST and ASTER LST ranges from 0.92 to 3.5 K and -0.06 to – 2.8 K respectively. It is much less than that of the RMSE and bias of differences of the MODIS C5 LST and ASTER LST.

Effect of seasons on the accuracy of LST product showed that RMSE and bias of the differences ($MODIS_{LST}$ –$ASTER_{LST}$) between the MODIS C6 LST and the ASTER LST during summer season higher than the other seasons. For summer season bias ranges from – 0.14 to – 2.8 K while for winter season it is from -0.09 to - 0.13 K and RMSE ranges for summer season is 0.94 to 3.5 K while that for winter season is 0.92 to 1.6 K. The column water vapour (CWV) is high in summer season and low in winter season. Due to this high amount of CWV highest absolute RMSE and bias are obtained

in summer season because the ASTER standard LST or emissivity algorithm has complication in rectifying these effects during the case of relative high atmospheric water vapour content.

## References

Duan, S.B., Li, Z. L., Cheng, J., Leng, P. (2017) .Cross-satellite comparison of operational land surface temperature products derived from MODIS and ASTER data over bare soil surfaces. *ISPRS Journal of Photogrammetry and Remote Sensing,* 123, 1-10

Jacob, F., Petitcolin, F., Schmugge, T., Vermote, E., French, A., Ogawa, K. (2004). Comparison of land surface emissivity and radiometric temperature derived from MODIS and ASTER sensors. *Remote Sensing of Environment* 90, 137 -152

Tonooka, H. (2001). An atmospheric correction algorithm for thermal infrared multispectral data over land-A water vapor scaling method. *IEEE Transactions on Geoscience and Remote Sensing.* 39, 682-692

Wang, K., Liang, S. (2009). Evaluation of ASTER and MODIS land surface temperature and emissivity products using long-term surface longwave radiation observations at SURFRAD sites. *Remote Sensing of Environmen.t* 113, 1556 -1565

Wan, Z., Li, Z.-L., (2008). Radiance-based validation of the V5 MODIS land-surfacetemperature product. *International Journal of Rmote Sensing*. 29, 5373–5395

Wan, Z., (2014). New refinements and validation of the collection-6 MODIS landsurface temperature/emissivity product. Rem. Sens. Environ. 140, 36–45

Zhengming Wan. (2013). New refinements and validation of the collection 6 MODIS land surface temperature/emissivity product. *Remote Sensing of Environment* 140, 36 - 45

https://earthdata.nasa.gov/

*IN PROCEEDINGS OF 25th HYDRO 2020, INTERNATIONAL CONFERENCE,*
*NATIONAL INSTITUTE OF TECHNOLOGY ROURKELA, ODISHA, INDIA*
*26-28, March 2021, ISBN 978-93-90631-56-8*

Paper ID - 164

# HYDROLOGICAL GEOPHYSICAL AND GIS APPROACH IN DELINEATION OF SUITABLE ARTIFICIAL RECHARGE SITE

**Rolland Andrade**

*Central Water & Power Research Station, Pune, 411024, India*
*Email: andrade.rolland@gmail.com*

## ABSTRACT

Potable groundwater availability is one of the prime global issues of the 21st century, apart from food security and environmental degradation. In the recent past, several provinces in India have faced severe scarcity of potable groundwater. In view of the same, several projects have been initiated to augment the depleting ground water resources by harvesting surface runoff and recharge the groundwater aquifer system. One of the most feasible strategies available to overcome the scarcity problem in drinking water sector is by adopting suitable water harvesting and artificial recharge strategy. Water harvesting and artificial recharge are two important scientific interventions to remediate most of the drinking water scarcity problems. Suitable site delineation is one of the prime requisite for implementing water harvesting and recharge structures. Geo-hydrological studies, Geophysical investigation and application of GIS are the major tools for the above said purpose. In this paper the author has attempted to emphasize the significance of surface geophysical investigation followed by infiltration tests, tracer studies, GIS etc., at various site locations with few significant case studies from southern province of India.

***Keywords:*** *Infiltration test, resistivity investigation, Artificial Recharge, GIS.*

## 1. Introduction

Scarcity of water in the drinking water sector is turning out to be a major cause of concern in India. With growing population, unsustainable lifestyle and urbanization, the demand for potable water and stress on groundwater aquifer has increased many folds in the recent past. Indian subcontinent has been subdivided into different climate zones based on several factors like precipitation, wind, solar radiations, humidity etc. The monsoon in India is highly inconsistent as the amount of rainfall varies from heavy to scanty in different provinces of India. The average annual rainfall in India is about 125 cm, which is sparsely, distributed over 3.1 million $km^2$ area. Of the total quantum of rainfall, only about one-fourth of which is actually usable, whereas the rest is lost as surface runoff and evaporation loss. Since historic time the natural water bodies like lakes, ponds, river and tanks have been fulfilling the needs of the inhabitants of the particular province. Unfortunately, with time due to negligence and greed of the increasing population, fresh water resources have witnessed a considerable decline in their water quality and quantity. There is a drive to conserve maximum quantum of water which is otherwise lost as surface runoff into usable form for basic human needs, several strategies have been adopted to harness the same. Numerous government schemes are implemented in the recent times towards sustainable groundwater development and quality management through water harvesting and artificial recharge strategy development (CGWB report, 2011).

Several integrated projects are executed to improve the quality and quantity of groundwater through aquifer recharge and sustainability. Infiltration recharging system (IRS) is the most widely adopted water harvesting scheme for enhancing in-situ groundwater aquifer quality and quantity. The basic aspects which are considered during the implantation of such scheme are:

- Moving the surface water through the vadoze zone.
- Making the water move through the aquifer away from the infiltration recharge site.

A systematic planning and understanding of the cause of problem in the site area i.e. Geology, geomorphology, lithology, aquifer depth, source of water, rainfall etc., is necessary. In order to implement or execute IRS, the following area characteristics are essential to be known i.e. soil characteristics, subsurface geology, and depth to aquifer etc. (Rolland & Balamurugan, 2020). In this paper the author tries to emphasis the authenticity of geophysical investigation, geological understanding through remote sensing (Land use and land cover (LULC) map, Soil map, Geomorphology map, lineament map etc.) and also the engineering design of recommended recharge structures (Rolland & Rangarajan, 2012). Few distinctive attempts made towards sustainable groundwater development schemes in semi-arid climate zones of central and southern Indian sub-continent; are referred as case studies and the same can always be extended for groundwater recharge and sustainability measures in similar geological/geomorphological terrain and climatic conditions.

## 2. Water Scarcity – A Need for Harvesting

India has experienced water scarcity and drought like scenario in the recent past and similar such conditions are alarmingly increasing with space and time. Water scarcity, if not controlled, will affect the food production, biodiversity and the environmental balance. According to the National Environment Policy (NEP) 2006: "India's freshwater resources consist of the single most important class of natural endowments enabling its economy and its human settlement patterns. The freshwater resources comprise the river systems, groundwater, and wetlands. Each of these has a unique role and characteristic linkages to other environmental entities (Mo.E.F, 2006:28)". Over a period of few decades, surface water sources have drastically failed to meet the rising demands of water supply in urban areas; groundwater reserves are being tapped and over-exploited resulting into decline in groundwater levels and deterioration of groundwater quality. Such precarious situation needs an immediate attention and may be rectified by recharging the depleted aquifers through proper understanding of the subsurface and appropriate water harvesting measures. Hence, the need for implementing such measures is necessary to ascertain that precipitation over any province is conserved entirely by utilizing it for recharging the groundwater aquifers or storing it for direct use (Rolland, 2016).

## 3. Natural Recharge Scenario in India

Measurements towards natural recharge estimation carried out in about 20 basins, distributed over the various climatic, physiographic, geologic and geomorphic zone in the country, suggest that about 5 to 10 percent of the seasonal rainfall is contributed as annual recharge in the peninsular hard rock regions, whereas in the alluvial areas, about 15 to 20 percent of the rainfall is contributed to ground water (Athavale et.al., 1992). Since, past few decades several parts of India are reportedly showing signs of over-exploitation and consequently depletion in water level and deterioration in its quality. The annual replenishable groundwater resource of India is 433 billion cubic metre (bcm) and net annual groundwater availability is 399 bcm. The annual groundwater draft for 2004 was 231 bcm. Thus the overall stage of groundwater development is 58%. Out of 5723 assessment units in the country, 4078 are 'safe' and 839 are 'overexploited' (Rana Chatterjee and Raja Ram Purohit, 2009). Artificial recharge strategy has been adapted largely in such situations to augment the ground water reserves by transferring the surface water to the aquifers during the monsoon months and using this water in lean period.

## 4. Groundwater Status in India

The Annual Replenishable Ground Water Resources depends on major contribution from rainfall (about 68% in India) and from other sources like viz. canal seepage, return flow from irrigation, recharge from tanks, ponds, and water conservations structures taken together is 32%. Central Groundwater Board (CGWB), Government of India had initiated a prime activity of Ground Water

Regime Monitoring, with a basic objective of recording information on ground water level and its quality through representative sampling in space and time, through a wide network of ground water observation wells located all over the Country. The result of the study initiated by CGWB has revealed that the general depth to water level ranges from 5 to 10 m bgl (below ground level) in India (Rolland & Balamurugan, 2020). There are several provinces, were there is acute problem of physical unavailability of groundwater, natural contaminant problem like enrichment of Fluo ride, Arsenic, and Iron etc. Several remedial measures to overcome such acute problem have been adopted by non-gazetted organizations, State and Central Government organizations. The best suitable approach found is water harvesting and artificial recharge.

## 5. Surface Studies for Site Characterization

### 5.1 *Geophysical investigation*

Several geophysical methods have been deployed since late 1915 in groundwater studies, of which the electrical method has shown a wider approach and better applicability. Basically, there are two types of procedures involved in electrical resistivity survey, of which resistivity profiling is adopted to understand qualitatively the nature of sub-surface, were as vertical resistivity sounding (VES) quantifies the resistivity variation with depth and thickness (Gangadhar Rao, T., 1999). Both these methods are quite often used together, in groundwater exploration (Klaus Knödel et. al, 2007). Electrical resistivity of a formation is dependent upon (i) porosity, (ii) degree of saturation / water conductivity and (iii) resistivity of rock matrix. The objectives behind resistivity method are as follows:

a) Inferring the litho-stratigraphical variation(s) and determining the thickness of subsurface layers at a point of measurement – Vertical electrical sounding (VES).
b) Lateral resistivity variation(s) in sub-surface features – Profiling.

Resistivity measurements are normally carried out by injecting current through two current electrodes (C1 and C2) and measuring the resulting voltage difference through pair of potential electrodes (P1 and P2). From the current (I) and voltage (V) values, an apparent resistivity ($\rho a$) value is calculated with k is the geometric factor, which depends on the arrangement of the four electrodes.

$$\rho a = k\ V / I \quad \ldots\ldots\ldots\ldots\ldots\ldots\ldots\ldots (1)$$

The depth of investigation in a direct current electrical method for schlumberger configuration was assessed to be 0.125 x L (distance between two active electrode), as per Roy and Apparao, 1971. Resistivity survey gives us a picture of the subsurface resistivity distribution, and to convert the resistivity picture into a geological layer, some knowledge of typical resistivity values for different types of subsurface materials and the geology of the area surveyed, is important (Keller and Frischknecht 1966; Daniels and Alberty 1966).

### 5.2 *Hydrological Investigation*

Infiltration is an important process of water movement through the unsaturated zone from the ground surface. The process can be best described through the Green-Ampt model (Green-Ampt, 1911). The rate of movement of water through the soil is called the infiltration rate. Factors controlling the movement of water into the soil are soil porosity, permeability, capillary action and gravitational drainage. The infiltration rate as per the Green Ampt model can be expressed as

$$q = \left(\frac{\sqrt{2}}{2} * \tau^{-1/2} + \frac{2}{3} - \frac{\sqrt{2}}{6} * \tau^{1/2} + \frac{1-\sqrt{2}}{3} * \tau^{1}\right) * K_s \quad \ldots\ldots\ldots\ldots (2)$$

Where q is the infiltration rate (cm/h) $K_s$ is saturated hydraulic conductivity (cm/h), and τ is related to time as:

$$(\tau) = \frac{t}{[t]+[X]} \quad \ldots\ldots\ldots\ldots\ldots\ldots\ldots\ldots\ldots\ldots\ldots\ldots (3)$$

and

$$X = \frac{(h_s - h_f) * (\Theta_s - \Theta_0)}{K_s} \quad \ldots\ldots\ldots\ldots\ldots\ldots\ldots\ldots (4)$$

Where'$t$' is time, '$h_s$' is ponding depth, or capillary pressure head at the ground surface (cm), $h_f$ is capillary pressure head at the wetting front (cm), '$\Theta_s$' is saturated volumetric water content and '$\Theta_0$' is initial volumetric water content. From the above derivation of equation 2, 3 and 4 it is clear that as time becomes large, the '$\tau$' in equation (3) becomes 1 and the infiltration rate is equal to the saturated hydraulic conductivity (Rolland & Balamurugan, 2020).

## 6. Application of Remote Sensing and GIS

Remote sensing is one of the versatile tool used in the groundwater exploration studies by hydrologists and geologists. Yet, hydrogeological analysis of any satellite imagery is a difficult task, since "groundwater by it's very nature is not available for direct observation" (Fransworth et al., 1984; Gupta et al., 1989; Waters et al., 1990; Balamurugan et al., 2017). An integrated approach is required for groundwater exploration, especially of hard rock aquifer systems, due to the involved heterogeneity of the mentioned aquifer systems. Many researchers have utilized remote sensing techniques in order to delineate the potential groundwater zones in the hard rock terrain (Anbazhagan, 1993; Gustafsson, 1993; Ramasamy et al., 1996; Saraf, 1998). To generate exact details specifically on structure, geomorphology and lithology from Indian Remote sensing Satellite (IRS) data for exploration of groundwater, digital enhancement techniques are used (Krishnamurthy and Srinivasan, 1995; Krishnamurthy et al., 1996; Rao et al., 1996). In hard rock terrains, these structural features are often observable on remote sensing data, in the form of vegetation, topography, drainage, or even soil tonal anomalies. Usually, in lineament mapping for groundwater exploration, the common assumption is that these features represent fracture concentrations in vertical zones (Lattman, 1958). As stated by Herman Bouver (2002) in one of his own articles, "Artificial recharge systems are engineered systems where surface water is put on or in the ground for infiltration and subsequent movement to aquifers to augment groundwater resources".

## 7. Artificial Recharge and Concept

The sub-surface reservoirs are complex but technically feasible alternatives for storing surplus monsoon run off. The sub-surface geological formations may be considered as "*storehouse*" for accommodating surplus surface water from vivid sources. Besides suitable lithological condition, the sub-surface storage should also possess favorable geological structures and physiographic units, whose dimensions and shape will allow retention of substantial volume of water in porous and permeable formations. The basic requirements for recharging the ground water reservoir are:

a) *Source Water Availability*: It is basically assessed in terms of surplus monsoon run off, which as per present water resource development scenario goes unutilized. This component can be assessed by analyzing the monsoon rainfall pattern, its frequency, number of rainy days, and maximum rainfall in a day and its variation in space and time.
b) *Identification of Area*: Implementation of suitable artificial recharge strategy is site specific and even the replication of the same technique to a similar area is dependent on the local hydrogeological and hydrological setup.
c) *Hydrogeological Aspects*: Knowledge of geology and hydrological features of the area is necessary for adequately selecting the site and the type of recharge structure. The basic data essential for understanding the site scenario is LULC, Soil, Slope, Drainage pattern etc., and all these maps can be prepared with the help of GIS and Remote Sensing.
d) *Surface Geophysical Information*: Based on surface investigation(s) using appropriate geophysical method, certain parameters like hydraulic boundaries, inflow and outflow of

waters, storage capacity, porosity, hydraulic conductivity, transmissivity, natural discharge of springs, natural recharge, depth of the aquifer, tectonic boundaries etc. can be deduced. The aquifers best suited for artificial recharge are those which have high vertical hydraulic conductivity while their horizontal hydraulic conductivity is moderate.

There are many methods of artificially increasing ground water supplies, which may be classified in two broad groups:

a) *Direct Method(s):* in which water from nearby surface water source is conveyed or stored in-situ at places above the aquifer areas, where it is made to percolate and recharge the ground water.

b) *Indirect Method(s):* are those, in which, the transfer of surface water is induced or it takes place as a consequence of a human activity which is not specifically aimed at recharging the aquifers. Induced recharge is affected by locating the ground water abstraction wells near influent streams. The second type of indirect recharge is that arising out of seepage from stream or canal or lake beds and return flow from irrigation.

### 7.1 *Case Histories of Artificial Recharge Strategy Adopted For Drinking and Agriculture Sector of India*

The construction of new check dams in certain parts of India have actually improved the livelihoods of people by helping them in increasing the income generated by them through agricultural activities, due to the availability of water (Tomar 2005; Shiferaw et al. 2006; Bhattacharya, 2010; Kulkarni et al. 2011; Hossein et al., 2014). The construction of such check dams have also helped to revive the agricultural activities in the region that is especially vulnerable to disasters. Check dam construction has actually led to an increase in income generated from agricultural activities, according to Redlich (2010). All across Asia and Africa, studies have confirmed the utility and role of artificial recharge wells as well as check dams in fast forwarding the economic growth of regions by accelerating groundwater recharge and therefore benefitting the society at large. The concept of artificial recharge towards augmentation of ground water reservoir and also to provide sustainable groundwater development measures are being implemented in different hydrogeological setup. A few typical case histories in Indian context are elaborated under this article.

#### 7.1.1 *Case: 1 – Artificial recharge strategy for In-Situ dilution of Fluoride in Nalgonda, Andhra Pradesh (A.P) for drinking water purpose.*

A pilot scale study was done in a micro-water shed area of ~2-3sqkm in Narayanpur Mandal of Nalgonda district. Nalgonda district is one of the fluoride endemic areas in Andhra Pradesh. The objective was to locate and construct appropriate source for drinking water for supply to villages, also to sustain the same in terms of quality and quantity. Based on integrated geophysical, remote sensing and hydrological investigation suitable site for source well creation was identified. Also the water (ground & surface) quality analysis was done periodically to create a base line reference before implementing artificial recharge and water harvesting strategies in the study area as seen in Figure. 1. Integrated geophysical investigation revealed the sub-surface information like depth to basement, weathered zone thickness and presence of natural barriers like dykes etc. Hydrological and tracer investigation confirmed the continuity of a single unconfined aquifer system in the area. Periodic analysis of water quality showed presence of Fluoride (F) both in surface and in groundwater ranging from 2.8 to 3.5ppm, existing at a higher range as compared to Bureau of Indian Standard (BIS) norms. Appropriate sites were selected for construction of artificial recharge structures like check dams, levees and percolation tanks, based on geophysical studies, soil tests, tracer studies and other hydrological investigations. Shallow depth bore wells were drilled at every recharge structure to assess the efficacy of the structure with time. The groundwater samples were collected for laboratory analysis to ascertain enhancement in water quality after construction of these structures over a period of 3 hydrological cycles. Fluoride analysis showed that the concentration was brought down to

1.3ppm due to in-situ dilution. The study concluded that appropriate site allocation for recharge structure in integration with geophysical, hydrological and tracer studies can cause in-situ dilution and subsequently improve the quality of groundwater to that of drinking water standards. Presently similar pilot scale study is running successfully for over a period of 6 years near Gurkanipalli in Chittor district.

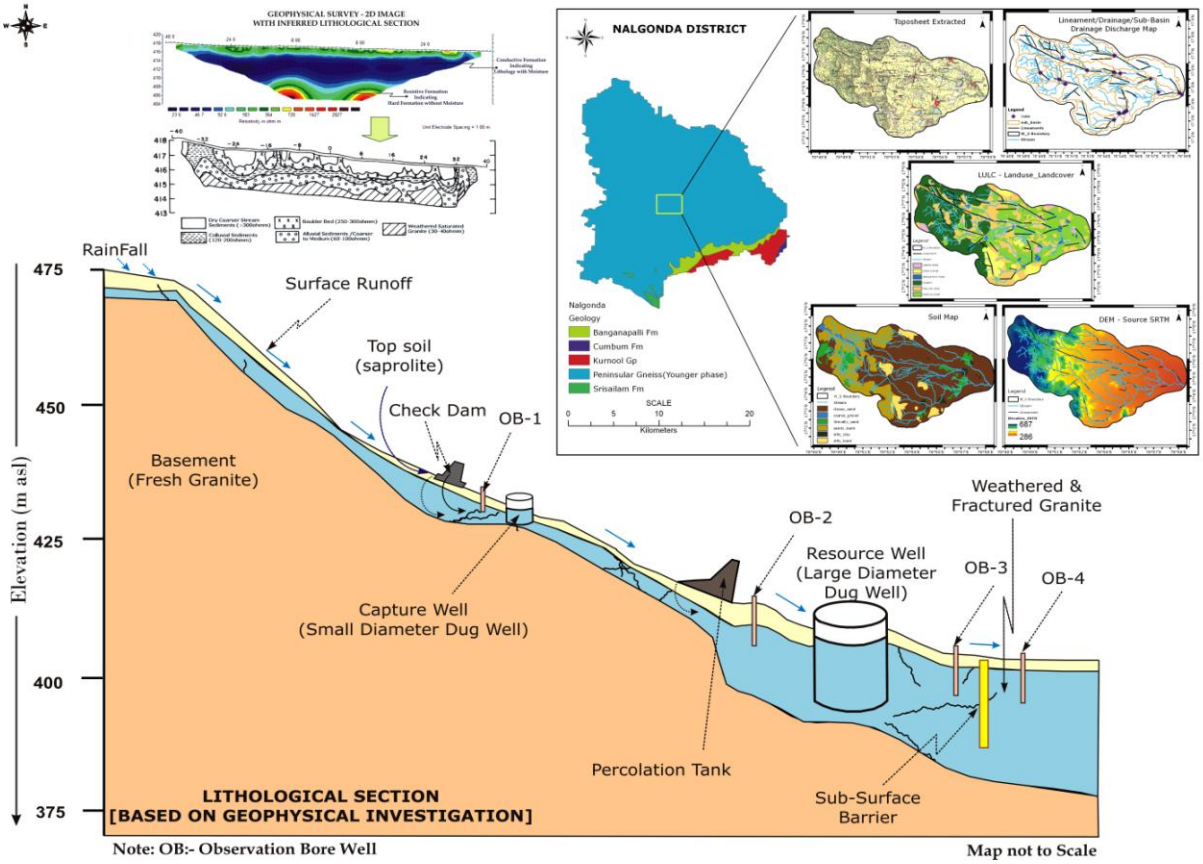



**Figure 1** Recharge well for in-situ dilution of fluoride in Nalgonda, Andhra Pradesh, India

*7.1.2 Case: 2 – Artificial recharge through In-tank bore well recharge near Ujjain district, Madhya Pradesh for sustenance and enhancement of agriculture practice.*

Percolation tanks are water storage structures which are especially constructed in hard rock areas for inducing recharge to the aquifers. Artificial recharge through percolation tanks is practiced in many of the southern states of India. Though, the maximum potential of these tanks in recharging the shallow aquifer is obtained in the year of construction, the efficiency decreases over the time due to siltation, shallow water table development in the ponding area and inadequate development of ground water utilization in the influence area. The preference and adaptation of borehole irrigation by farmers in recent times necessitates replenishment of the deeper semi-confined aquifers (fracture zones). The indirect recharging of fractured aquifer zones through shallow aquifer replenishment achieved by percolation tanks. The recharge potential is controlled by the interconnection of shallow aquifer with deeper aquifers and as well as inter linking of fractures. An experiment on recharging the deeper aquifers (high transmissivity zones) through in-tank borehole artificial recharge method was attempted on a pilot scale in a basaltic terrain were multi-storied aquifer system exists. A borehole with a diameter of 150 mm was drilled inside the percolation tank near to the bund at a suitable site after detailed geophysical surveys. Borehole logging was used for confirming the depth and thickness of fractured zones encountered while drilling. Plain casing was maintained upto the depth of fractured

basaltic aquifer. A filter bed of dimension 2m X 2m was erected around the borehole in such a way that only filtered water entered the borehole continuously as shown in Figure.2. It was expected that the water stored in the percolation tank after the monsoon would percolate through the filter media and recharge the aquifer directly. A continuous water level logger was installed to monitor the recharge rate through water level fluctuation and the total quantification was made at the end of the experiment. The casing of the borehole above the ground was raised to a level such that it remained always above the flood escape level of the tank. This also facilitated escape of air entering into the borehole through recharge water. The results of the experiments have shown the utility of this technique in augmenting surface runoff and enhancing the aquifer performance during the lean period, which was reflected in the total area of cultivation before and after the study within a span of 3 hydrological cycles.

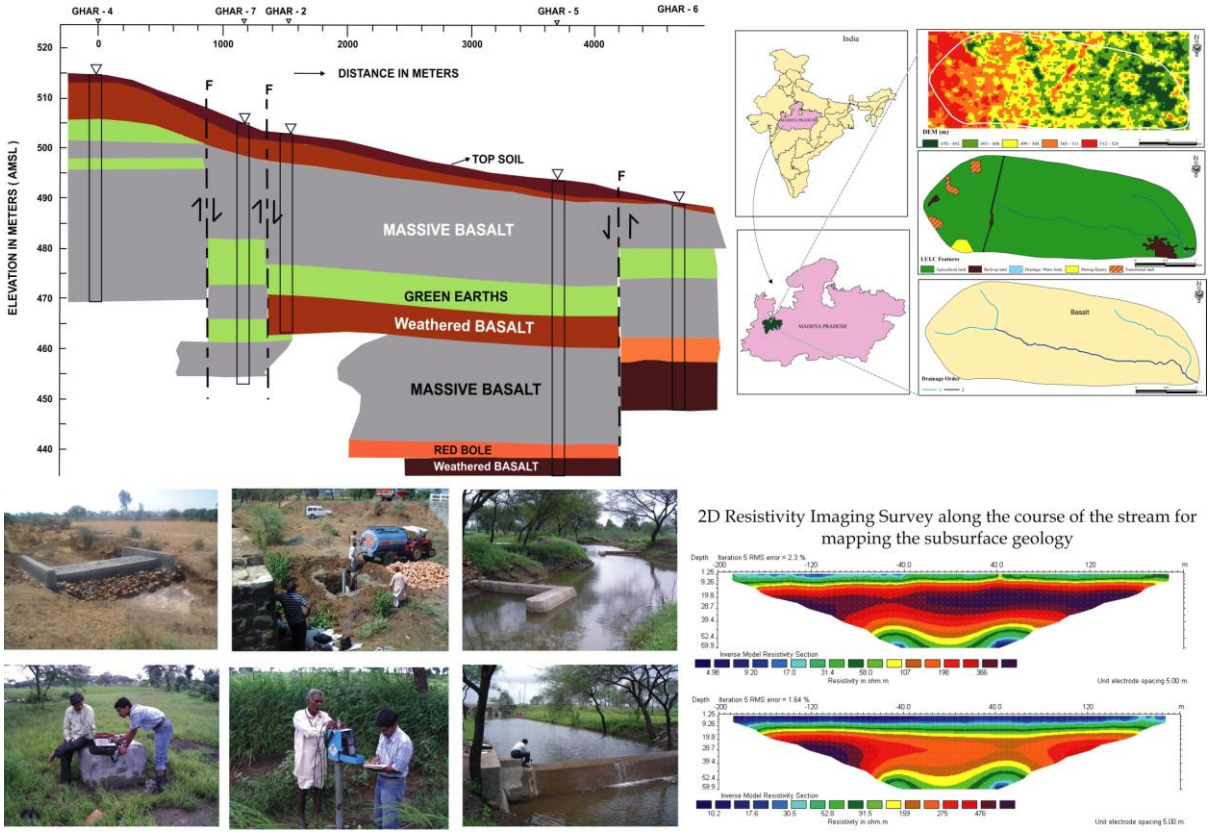



**Figure 2** Artificial Recharge through in-tank bore well near Ujjain District, Madhya Pradesh, India

*7.1.3. Case: 3 – Artificial recharge through recharge cum filter chamber and Gabbion structure across perennial stream near Agali and Vazhikadavu Gram Panchayath for sustaining drinking water source.*

Two distinct gram panchayath in Palakkad and Mallapuram districts of Kerala are considered under this case study wherein sites were delineated based on GIS mapping. Further surface geophysical investigations (electrical resistivity survey) were carried out with closer current electrode separation along with hydrological tests like water level measurements, infiltration studies etc. to ascertain site feasibility and response of recharge structures.

(a) ***Agali Gram panchayath*** *(Site: Priyadarshini Kukkampalayam)*
Resistivity investigation was conducted near the seasonal stream cutting the road and downstream of a check dam. Based on integrated geophysical, remote sensing and hydrological investigation and also interactions with local residents it was learned that the stream carried base flow all the time and it was

felt that a dug well may be able to cater the need(s) of people through gravity siphoning. Based on investigation results rectangular source well with dimension 5x4x5 m was recommended, with the length cutting across the base of groundwater flow direction as shown in Figure. 3. To sustain the drinking water source site, a recharge cum filter chamber strategy was formulated and recommended to tap the groundwater flow. After implementing the recommended structures, pump test was conducted to check the response of the shallow aquifer to induced recharge.

*(b)* ***Vazhikadavu Gram panchayath*** *(Site: Anamary):*
In the similar lines of that of *Priyadarshini Kukkampalayam*, resistivity investigations were conducted near to the forest land and adjacent to a seasonal stream. Geophysical, remote sensing and hydrological investigation revealed an overburden (alluvium with weathered charnokite) of 8 m thick followed by very hard substratum. Also, the interpreted aquifer zone exhibited very low resistivity, probably due to intercalation of clayey material with weathered charnockite. It was expected that, with the present subsurface scenario, the water flow to the well from the stream would be moderate due to poor permeability of the surrounding formation. In order to increase the permeability of the shallow zone in the near vicinity of the dug well, a filter bed was proposed with a width of 1.5 m as shown in Figure. 3. Gabbion structure of length 9 m and height 1.8 m was recommended across the stream on the upstream of the dug well site in order to harvest the baseflow water drained by the stream in the post monsoon period and recharge the shallow aquifers. Apart from this, the vertical flow near the well was designed to be diverted through the filter bed surrounding the well site with pebble/cobble bed and porous concrete top. Based on resistivity investigations results at each site as discussed, suitable / appropriate water harvesting and recharge structures were recommended. Similarly, several other sites from different gram panchayath were investigated, which depicted the judicious approach of integrated geophysical, remote sensing and hydrological investigation in site selection for various recharge structures towards sustaining those sites.

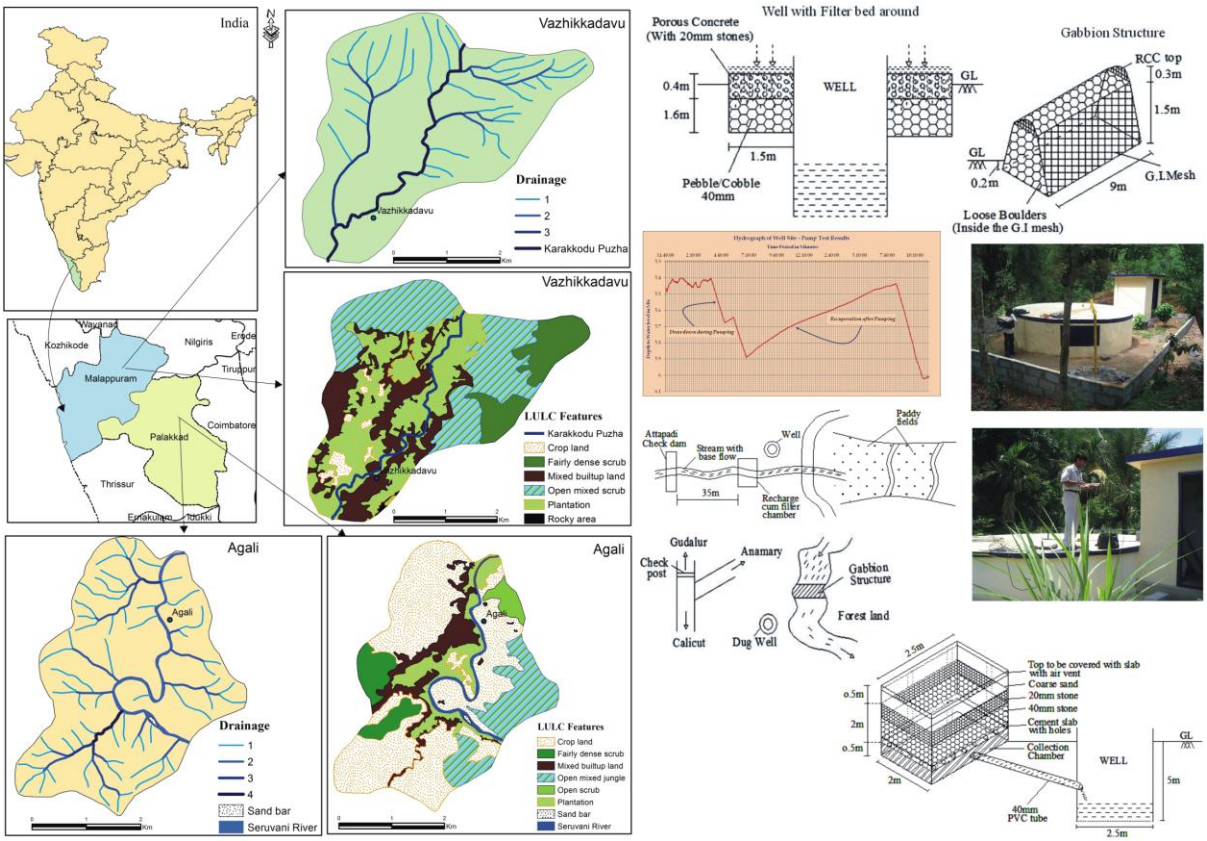



**Figure 3** Recharge measures recommended based on Geophysics, GIS and Hydrological tests at Priyadarshini Kukkampalayam and Anamary sites at Kerala

## 8. CONCLUSIONS

Delineation of suitable artificial recharge site in order to harvest the surface runoff and induce the same into groundwater regime is a complex process, which demands proper and detailed understanding of the subsurface. Based on GIS and geophysical investigation, appropriate sites are delineated for implementing recharge strategy. Hydrological studies are necessary to be conducted to ascertain these recharge sites for its site feasibility. All the case studies discussed in this paper, pertains to different geological terrain, where the integrated approach of geophysical, hydro-geological and GIS studies have been implemented. Similar strategy can be adopted at any given site to achieve effective outcome in enhancing the groundwater recharge and its sustenance.

*Acknowledgement*

The author is thankful to Shri A.K.Agrawal, Director CWPRS, for promoting this publication. The author is also thankful to groundwater replenishment group, NGRI for their support in field investigation.

## References

Anbazaghan, S., 1993. Integrated groundwater study in drought prone Pennagaram, Dharampuri district. Tamilnadu. *Bulletin of the Indian Geologists Association*, v.26:2, pp.117-123

Athavale RN, Rangarajan R, MurlidharanD (1992). Measurement of natural recharge in India. Jour. *Geol. Soc. India*, 39: 235-244.

Balamurugan, Guru., Karthiki, Seshan, Somnath, Bera., (2017). Frequency ratio model for groundwater potential mapping and its sustainable management in cold desert, India. *Journal of King Saud University - Science*, pp. 333-347.https://doi.org/10.1016/j.jksus.2016.08.003

Bhattacharya, A.K., 2010. Artificial ground water recharge with a special reference to India. *Int. J. Res. Rev. Appl. Sci.* 4, 214–221.

CGWB Report (2011) - Select case studies Rainwater Harvesting and Artificial Recharge, http://mahenvis.nic.in/Pdf/Report/report_nrmc_water%20harvesting.pdf.

Daniels, F. and Alberty,R.A. 1966. Physical chemistry, John Wiley & Sons,Inc.

Fransworth, R.K., Barrett, E.C., and Dhanju, M.S., 1984. Application of remote sensing to hydrology including groundwater. UNESCO, Paris, IHP Project AlS.

GangadharRao, T., (1999). Training course on Sustainable drinking water source creation through integrated geohydrological approaches – Groundwater Exploration Techniques, National Geophysical Research Institute, pages 1-294.

Green, W.H. and G. Ampt. 1911. Studies of soil physics, part I –the flow of air and water through soils. *J. Ag. Sci.* 4:1-24.

Gupta, A.K., Ganesh, Raj, K., and Yogarajan, N., 1989. Use of digital techniques of remotely sensed data for geological applications – a review. *International Conference on Image Processing, Singapore* (unpub).

Gustaffson, P., (1993). High resolution satellite data and GIS as a tool for assessment of groundwater potential in semi arid area. *In: Proceedings of 9th Thematic conference on Geological remote sensing, Pasadena, California, USA*, pp.123.

Herman Bouwer, 2002. Artificial recharge of groundwater: hydrogeology and engineering.

Hossein, Hashemi, Ronny, Berndtsson, Magnus, Persson, 2014. Artificial recharge by floodwater spreading estimated by water balances and groundwater modelling in arid Iran. *Hydrol. Sci. Jour.* 60 (2), 336–350. http://dx.doi.org/10.1080/02626667.2014.881485.

Keller, G.V. and Frischknecht, F.C. (1966) Electrical Methods in Geophysical Prospecting. Pergamon Press, Oxford.

Klaus Knödel, Gerhard Lange and Hans-Jürgen Voigt., "Environmental Geology", *Handbook of Field Methods and Case Studies*, 2007, ISBN: 978-3-540-74669-0, 1-1193.

Krishnamurthy, J., and Srinivasan, G.,1995. Role of geological and geomorphological factors in groundwater exploration - A study using IRS LISS data. *International Journal of Remote Sensing*, v.16:4, pp.2595 – 2618.

Krishnamurthy, J., Venkateskumar, K.N., Jayaraman, V., and Manivel, M., (1996). An approach to demarcate groundwater potential zones through remote sensing and Geographica1 Information System. *International Journal of Remote Sensing*, v.17:10, pp.1867-1884.

Kulkarni Himanshu, Sunderrajan Krishnan, P.S.V.S., 2011. India's Groundwater Challenge and the Way Forward. Economic and Political Weekly vol xlvi no 2, 37–45.

Lattman, L.H., 1958. Technique of Mapping Geological Fracture and Lineaments on Aerial Photographs. Photogrammetric Engineering, v.19:4, pp.568-576.

Ministry of Environment and Forest (MoEF) (2006) National Environment Policy 2006. Ahmedabad: Center for Environment Education, pp. 28.

Ramasamy, SM., Anbazhagan, S., and Moses Edwin. J., 1996. Control of Fracture Systems in Artificial Recharge with Special Reference to Crystalline Aquifer System in Tamil Nadu. In: SM.Ramasamy (Ed). *Trends in Geological Remote Sensing*, Rawat Publishers, Jaipur, pp. 274 – 280.

Rana Chatterjee and Raja Ram Purohit (2009), Estimation of replenishable groundwater resources of India and their status of utilization, *Current Science*, Vol. 96, no. 12, 25 June 2009.

Rao, K.G., Narasimha, R. and Prabhu, A. (1996). Estimation of drag coefficient at low wind speeds over the monsoon trough land region during MONTBLEX-90. *Geophysical Research Letters 23: doi: 10.1029/96GL02368. issn: 0094-8276.*

Redlich, C., 2010. Check dam impact assessment, Report byASA (Action for Social Advancement). Available via http://www.asaindia.org/pdf/Socio- economic% 20impact%20 Check%20 Dams %20in %20Nagda, %20Ujjain%20District%20 Case%20study %20of% 2 0farmers. pdf.Cited 12 September 2013.

Rolland Andrade and Rangarajan.R, (2012), "Runoff Estimation and Potential Recharge Site Delineation Using AHP (*Analytic Hierarchy Process*)", *Go-carto International Journal.*

Rolland Andrade, "Suitable water harvesting measures for managing drinking water scarcity in different provinces of India", *Journal of Hydrogeology and Hydrologic Engineering*, 2016, 5:2.

Rolland Andrade and Balamurugan Guru "Recharge site delineation through integrated geophysical hydrological and GIS approach – A basic understanding with case studies from Indian sub-continent", Groundwater for Sustainable Development, V.10, 100343, February 2020.

Roy, A., and Apparao, A., 1971, Depth of investigation in direct current methods: Geophysics, 36, 943–959.

Saraf, A.K., and Chaudhary, P.R., 1998. Integrated remote sensing and GIS for groundwater exploration and identification of artificial recharges sites. *International Journal of Remote Sensing*, v.19:10, pp.1825-1841.

Shiferaw, B., Anupama, G.V., Nageswara Rao, G.D., Wani, S.P., 2006. Socioeconomic characterization and analysis of resource-use patterns in community watersheds in semi-arid India.: *International Crops Research Institute for the Semi-Arid Tropics*. 2 (1), 44 pp.

Tomar, S., Nair, S. 2005. Adaptive Policies Community Case Study: Participatory Watershed Management in Maharashtra, India, The Adaptive Policies Project, Project Report No.IDRC2005 GW 24. Available via http:// www.iisd. org /climate /canada/adaptive_policy. asp. Cited 20 October 2014.

Waters, P.D., Greenbaum, P.L., Smart, P. and Osmaston, H. (1990). *Applications of Remote Sensing to Groundwater Hydrology*, *Remote Sensing Reviews*, v.4:2, pp.223-264.

*IN PROCEEDINGS OF 25th HYDRO 2020, INTERNATIONAL CONFERENCE, NATIONAL INSTITUTE OF TECHNOLOGY ROURKELA, ODISHA, INDIA 26-28, March 2021, ISBN 978-93-90631-56-8*

Paper ID - 219

# Estimation of Soil Loss from Bagmati River Basin using RUSLE model and GIS Technique

Mani Kumar Singh[1], Vivekanand Singh[2]

[1]*PG student, Dept. of Civil Engineering, National Institute of Technology Patna, Patna, Bihar, 800005, India*
[2]*Professor, Dept. of Civil Engineering, National Institute of Technology Patna, Patna, Bihar, 800005, India*
*Email: manikumarsingh9135@gmail.com,vsingh@nitp.ac.in*

## Abstract

**S**oil loss has become a major issue these days that take place from pasture, barren land and from other practices. Bagmati, a tributary of the River Ganga, is a perennial river of Nepal and India. During monsoon it carries heavy discharge with huge amount of sediment, which is eroded from the hilly region of the basin. After emerging from the hills, their slope gradually becomes flatter towards the plains, thereby reduces the velocity, resulting in deposition of sediment on river beds. This reduces the carrying capacity of river and flood water overtops the bank causing inundation of the adjoining areas, which causes loss of life, property, environment etc. By knowing the soil loss prone area proper planning for soil conservation can be done in appropriate time. Soil loss leads to the loss of sediments and also reduces the fertility of agricultural land, so its estimation is very important.

In this study, RUSLE method has been used to estimate the soil loss and to prepare the soil loss map of Bagmati river basin. The various factors of RUSLE model have been computed using ARCGIS Map along with Remote Sensing and GIS tools. The map of these factors - rainfall erosivity (R), soil erodibility (K), slope length and steepness (LS), cover management (C) and conservation practice (P) have been prepared using ArcGIS. Based on these data, loss maps have been prepared for the years 2013 and 2014 using RUSLE model. The soil loss for year 2013 and 2014 were 727.236 t/ha/yr and 889.33 t/ha/yr, respectively.

***Keywords:*** *Soil loss; RUSLE; ArcGIS; Bagmati River Basin*

## 1. Introduction

Land depletion by soil loss is a worldwide fact that results in the loss of the top surface soil having higher percentage of nutrients. Soil loss causes very harmful effect on environment. Plants growth reduces due to loss of top fertile soil. Due to top soil loss, the impenetrable soil layer is exposed and it reduces the supply of water to the plants. Soil erosion is about 2.1 billion hectares. The land area affected by soil detachment is approximately 1100 Mha because of water erosion and 550 Mha due to wind erosion (Saha 2003). Conservation of soil is very important due to which agricultural land is converted into barren land. Agricultural sector is highly affected by the loss of soil in India. Soil losses from catchment, carried by river and finally deposited on the bed of the river and in the reservoirs etc. (Thomas et al. 2017). Thus, its conservation and management is very important for the human being.

From 130 million hectares of land in India (Kothari 1994), approximately 45% of the overall geographical region are highly affected by soil erosion. It occurs mainly by gorge and gully, farmland changing, agricultural wasteland, sandy field and water logging. Soil losses from river catchment submerge in the river and results in increase of water level and sedimentation level of the river (Tundu et al. 2018). The reduction in soil productivity has significant environmental issue for the world and devastating for the country economy (Ganasri and Ramesh 2016).

Water is one of the primary factor of soil degradation and more vulnerable if land is not adequately used. Soil loss is also affected by land use pattern. The area having high vegetation growth rate leads to less loss soil due to water or wind. It has been observed that in forest areas soil loss rate is very low (Prasannakumar et al. 2011). Soil loss is very high in barren land. Some researchers have studied on soil erosion considering the factors - runoff erosivity, surface erodibility, slope steepness and vegetation cover, which has more impact on soil loss. For the prevention of soil loss mainly

restoration of vegetation and proper support practices are needed to be done. Various soil loss models are given by the researchers to estimate soil loss. Researchers have made effective attempts on soil degradation concept (Nearing et al. 2005). Remote sensing and GIS technologies have been used in earlier decades to measure the soil loss on the watershed, even at a field level (Pham et al. 2018). Many soil loss models with varying degrees of complexity have been given by researchers. The Universal Soil Loss Equation (USLE), which was developed by Wischmeier and Smith in (1965), is one of the commonly used mathematical models for estimating sheet and rill erosion. USLE was developed mainly for estimating soil loss in agricultural land and the area having sloppy topography.

In this study, RUSLE model is used for estimating soil loss in Bagmati catchment. This model detects soil losses using a pixel-by-cell (Shinde et al. 2010), which is very successful in trying to locate the soil loss in wide areas. Field data, Landsat image 8 of study area have been taken from earth explorer and processed by using remote sensing and GIS technique as suggested by Fernandez et al. 2003. DEM (Digital Elevation Model) has been included as an input for determination of soil loss. The geometrical distribution of the annual rate of soil loss was determined by incorporating variables of geo-environment in a GIS method based on Raster. The map of RUSLE parameters and soil loss map of Bagmati river catchment have been prepared using ARCGIS.

## 2. Study area

The Bagmati River is one of the perennial river of Nepal and India. The Bagmati River originates from Shivpuri range at latitude 27º47' N and longitude 85º17' E and about 16 km North East of Kathmandu at an elevation of 1500m above MSL in Nepal and meets in Kosi River at Badlaghat in India, which join river Ganga. Length of Bagmati River is about 589 km out of which 195 km is in Nepal and 394 km is in Bihar state of India. It comes in Adhwara group which covers total drainage area of 14,384 $km^2$. Drainage area in Bihar is 6500 $km^2$. It is one of the main river in Bihar known for its large stream and it becomes destructive during monsoon season. It has many tributaries among them Lakhande, Lalbakeya and Adhwara group of rivers are major tributaries. The average rainfall of Baghmati Adhwara group is 1255 mm.

## 3. Methodology and data used

### 3.1 *Catchment area delineation*

DEM image of the Bagmati river basin has been downloaded from the earth explorer. Shape file of the catchment area has been delineated using ArcGIS 10.3. DEM contains drainage pattern as well as the different elevation which is shown in Fig. 1.

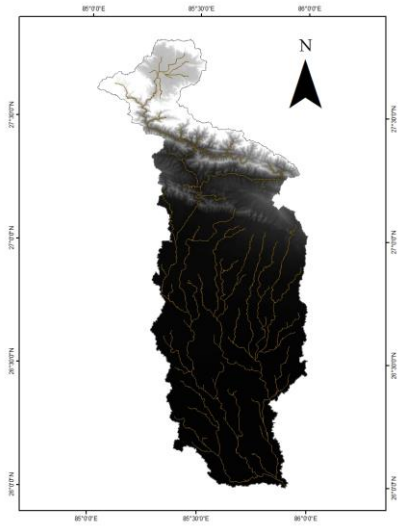



**Figure 1** DEM of the study area

### 3.2 *Estimation of RUSLE parameters*

Annual soil loss has been estimated using the RUSLE model. The expression for the RUSLE model is as follows:

$$A = R \,.\, K \,.\, LS \,.\, C \,.\, P \quad (1)$$

Where,
A: represents average annual soil loss which is conjunction of all parameters and its unit is t/ha/yr.
R: represents rainfall erosivity factor and its unit is $MJ.mm.ha^{-1}hr^{-1}$.
K: represents soil erodibility factor and its unit is $t.ha.hr.MJ^{-1}mm^{-1}$.
LS: represents slope topographic factor which has no dimension.
C: represents cover management factor which is no dimension.
P: represents support practice factor which is no dimension.

### 3.3 *Rainfall erosivity factor (R)*

#### 3.3.1 *Weather data*

Meteorological data such as rainfall, temperature, wind speed, relative humidity etc. have been collected for the five years from the Nasa Meteorological Site. The average annual rainfall has been taken by the average of five years.

#### 3.3.2 *Estimation of R factor*

Rainfall erosivity factor shows the impact of rainfall intensity on soil loss and requires detailed rainfall data for its calculation (Wischmeier and Smith 1978). Rainfall erosivity factor has been computed as product of storm kinetic energy times the maximum 30 m storm depth and summed for all storm in a year. One of the expressions derived by Singh et al. which can be used for the entire Indian region has been used.
Empirical formula used for this study:

$$R=79+0.363P \quad (2)$$

Where, P is the average rainfall in mm.

### 3.4 *Soil erodibility factor (K)*

#### *3.4.1 Soil data*

Soil classification map of entire world has been obtained from FAO DSMW (Digital soil map of the world). From this map percentage of sand, silt, clay and organic content are obtained. By the use of this soil data of study area is extracted with the help of GIS technique.

#### *3.4.2 Estimation of K factor*

The soil erodibility factor (K) is a description of the inherent erodibility of a particular soil type (Guboin et al. 2006). By knowing the soil type in the area direct value of soil erodibility factor can be computed using table, here data obtained from FAO has been taken and by using equation of Williams.

$$K=f_{csand} \,.\, f_{cl\text{-}si} \,.\, f_{org} \,.\, f_{hisand} \quad (3)$$

Where,

$f_{csand}$: Factor that lowers the K indicator in soil with high coarse-sand content and higher for soils with little sand.
$f_{ci-si}$: Gives low soil erodibility factors for soils with high clay to silt ratios.
$f_{org}$: reduces K values in soils with high organic content.
$f_{hisand}$: lowers K values $f_{pr}$ soils with extremely high sand content.
$f_{csand}$: [0.2+0.3exp {-0.256ms (1-msil/100)}]
$f_{cl-si}$: (msil/mc+msil)^0.3
$f_{org}$: (1-0.25 orgc/(orgc+exp (3.72-2.95 orgc))
$f_{hisand}$: (1-(0.7 (1-ms/100))/(1-ms/100)+exp (-5.51+22.9(1-ms/100)).

### 3.5 *Slope length and steepness factor (LS)*

Slope length and steepness factor are combined together and termed as Topographic factor (LS). The LS factor represents a ratio of soil loss under given condition to that of study area with standard slope steepness of 9 % and slope length of 22.6 m. The LS factor is computed using Moore and Wilson (1992), which is modified form of empirical equation of Wischmeier and Smith (1978).

LS = power ("flowaccu" cellsize/22.1, 0.4) power (sin ("slopedeg" 0.01745)/0.09, 1.4) 1.4 (4)

### 3.6 *Cover management factor (C)*

Factor, C is significant for the control of soil loss risk and it shows the effect of management and cropping practices. Landsat image 8 of the study area has been obtained from Earth Explorer. The information about NDVI (Normalized Difference Vegetation Index) has been obtained from this image. NDVI gives difference in green vegetation coverage. The range of NDVI is from -1 to +1. By the obtained value of NDVI, C factor has been obtained using equation given by (Durigon et al. 2014).

$$C= (-NDVI+1)/2 \quad (5)$$

$$NDVI= (NIR-RED)/(RED+NIR) \quad (6)$$

Where,
NIR- (band 5) spectral reflectance in the near infrared band.
RED- (band 4) spectral reflectance in the red band.

For the calculation of NDVI, Landsat image which was downloaded from Earth explorer and band 4 and band 5 was used.

### 3.7 *Support practice factor (P)*

It is defined as the ratio of soil loss of given conservation practices to the soil loss obtained from up and down the slope. Here, P factor is obtained through Landsat images by computing slope degree in ArcGIS and type of farming done nearby the catchment area. Table given by (Shin 1999**)** has been taken for P factor value. Value of P factor depends upon the type of farming practices done in the study area. Mainly contour farming has been done nearby the study area.

**Table 1** Support practice factor as per agricultural practices

| Slope% | Contouring | Strip cropping | Terracing |
|---|---|---|---|
| 0.0-7.0 | 0.55 | 0.27 | 0.10 |
| 7.0-11.3 | 0.60 | 0.30 | 0.12 |
| 11.3-17.6 | 0.80 | 0.40 | 0.16 |
| 17.6-26.8 | 0.90 | 0.45 | 0.18 |
| >26.8 | 1.00 | 0.50 | 0.20 |

### 3.8 Flow chart of methodology

The flow chart for the estimation of RUSLE parameters has been given in Figure 2.

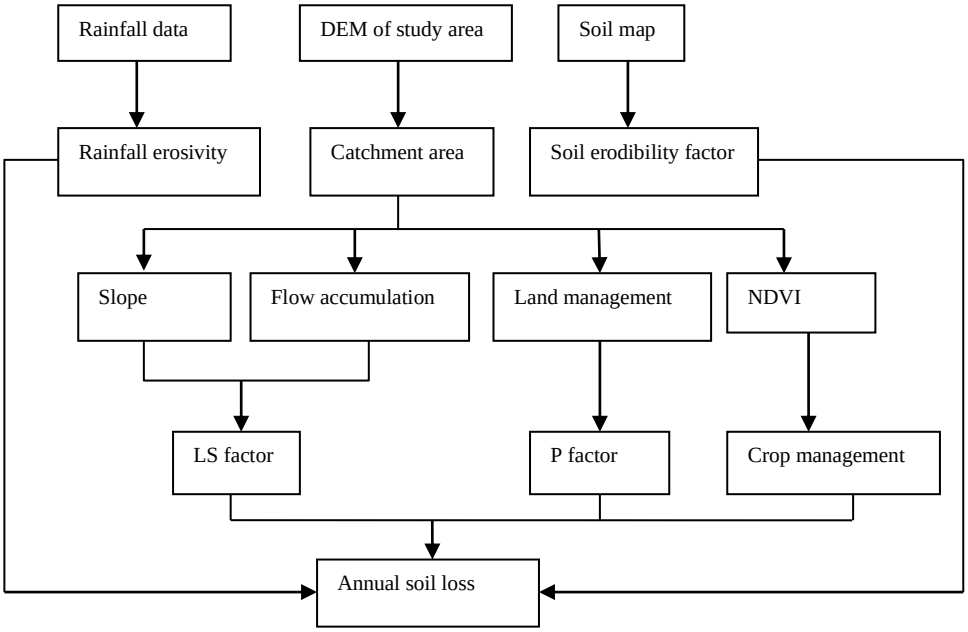



**Figure 2** Flow chart for estimation of RUSLE parameters

## 4. Results and discussion

Based on rainfall data rainfall erosivity map has been prepared and shown in Fig. 3. Rainfall Erosivity factor has the large variation, which ranges from 499.19 to 1300.3 MJ.mm/ha.h.yr. K factor ranges from 0.10 t.ha.hr.MJ$^{-1}$mm$^{-1}$ to 0.169 t.ha.hr.MJ$^{-1}$mm$^{-1}$ which has been shown in Fig. 4. Low value of K factor indicates rock area in Bagmati river catchment. LS factor plays key role in soil loss process. The LS values have been computed and shown in Fig. 5. The LS factor ranges from 0 to 93.61 and its value is less for most of the region. C factor map has been prepared by using NDVI. NDVI values varies from -0.17861 to 0.555. The values of C factor ranges from 0 to 0.58 and 0.22 to 0.59 for the years 2013 and 2014 and shown in Fig. 6 and Fig. 7, respectively. The value of C factor is high in the region with less vegetation cover or forest areas and less for the region having high vegetation cover. In general, P factor lies between 0 to1. P factor with 0 represents good soil loss resistance and 1 represents less soil loss resistance. Figure 8 shows the P factor value ranges from 0.55 to 1. The major area is having less value of P factor it means soil loss resistance is more in that area.

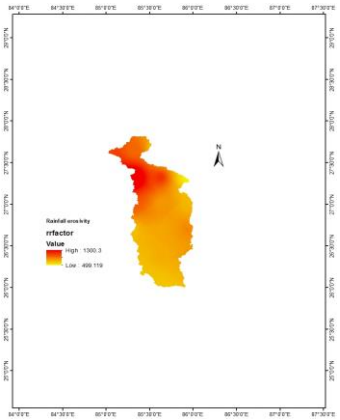


**Figure 3** R factor

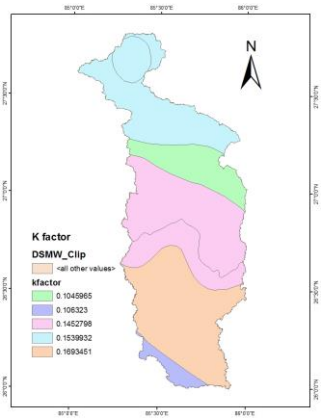



**Figure 4** K factor

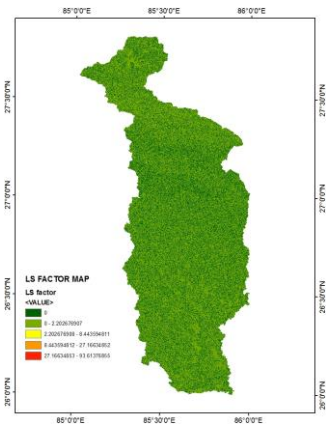



**Figure 5** LS factor

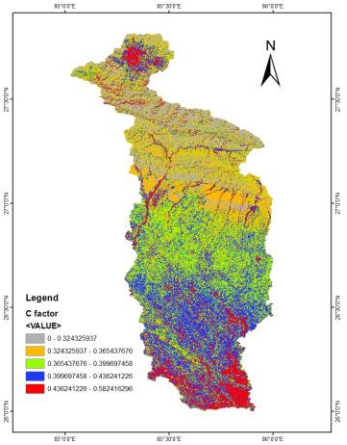



**Figure 6** C factor of 2013

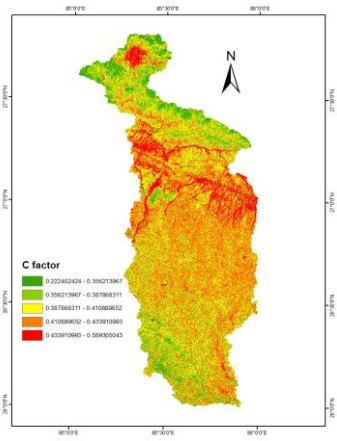



**Figure 7** C factor of 2014

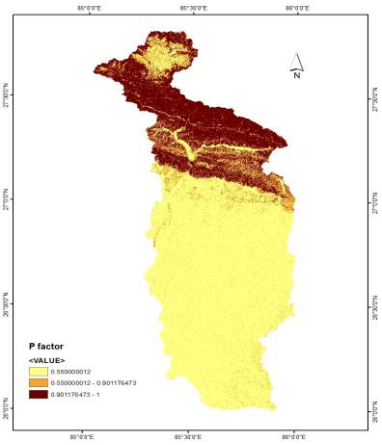



**Figure 8** P factor map

### 4.1 *Soil loss map*

All the parameters of RUSLE model have been computed and Eq (1) is used to compute the soil loss and to prepare the soil loss map. Rainfall erosivity factor (R), Soil erodibility factor (K), Slope length and steepness factor (LS) and Support practice factor have been taken constant. The cover management factors of two years have been taken to show the effect of this on soil loss map. C factor value ranges from 0 to 0.58 and from 0.22 to 0.58 in the years 2013 and 2014, respectively. Soil loss map for the years 2013 and 2014 have been shown in Fig. 9 and Fig. 10, respectively. Soil loss ranges from 0 to 727.236t/ha/yr and from 0 to 889.33t/ha/yr in year in years 2013 and 2014, respectively. Annual average soil loss is more in year 2014 than 2013 because of less vegetation cover in this year.

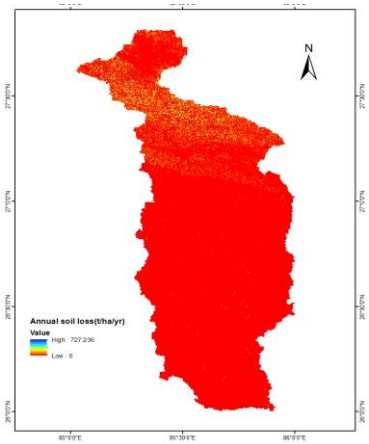



**Figure 9** Soil loss map of 2013

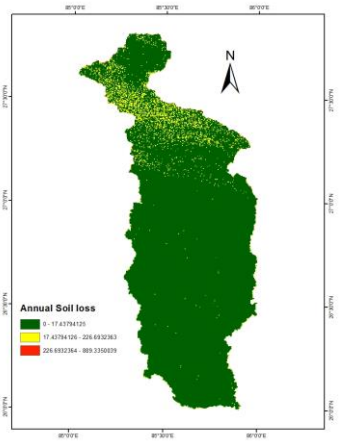



**Figure 10** Soil loss map of 2014

## 5. Conclusions

In this study, average annual soil loss of Bagmati river catchment has been computed using RUSLE model. The parameters of the RUSLE have been computed using ARCGIS and soil loss map has been prepared based on these parameters. The annual average soil loss of Bagmati river catchment for the year 2013 and 2014 were 727.236 t/ha/yr and 889.33 t/ha/yr, respectively. Soil loss depends on factors like rainfall, slope, soil type, cover management, support practices but the effect of soil loss has also been seen due to change in cover management factor. It has been found that soil loss increase with the increase in C factor. The rate of soil loss was uneven in the Bagmati river catchment. It can be concluded that the RUSLE is suitable model for the estimation of soil loss in any river catchment as it gives more realistic result. More vegetation should be grown in the river catchment so that soil loss can be minimized and conserved.

## References

Biswas, S.S., and Pani, P. (2015). Estimation of soil erosion using RUSLE and GIS techniques: A case study of Barakar river basin, Jharkhand, India. *Earth system Environment 1:42.*

Durigon, V.L., Caravalho, D.F., Antunes, M.A.H., Oliveira, P.T.S. and Fernandes, M.M. (2014). NDVI time series for monitoring RUSLE cover management factor in a tropical watershed. *International Journal of remote sensing*, 35 (2), 441-453.

Fayas, C.M., Abeysingha, N.S., Nirmanee, K.G.S., Samaratunga, D. and Mallawatantri, A. (2019). Soil loss estimation using RUSLE model to prioritize erosion control in KELANI river basin in Sri Lanka. *International soil and water conservation research* 7, 130-137.

Fernandez, C., Wu, J.Q., Mccool, D.Q. and Stockle, C.O. (2003). Estimating water erosion and sediment yield with GIS, RUSLE and SEDD. *Journal of soil and water Conservation* 58 (3), 128-136.

Fu, G., Chen, S. and Mccool, D. K. (2006). Modelling the impacts of no-till practice on soil erosion and sediment yield with RUSLE, SEDD and ArcView GIS. *Soil and Tillage Research*, 85(1-2), 38-49.

Ganasri, B.P., and Ramesh, H. (2015). Assessment of soil erosion by RUSLE model using remote sensing and GIS- A case study of Nethravathi Basin. *Geoscience Frontiers* 7, 953-961.

Jha, M.K., and Paudel, R.C. (2010). Erosion predictions by empirical models in a mountainous watershed in Nepal. *Journal of spatial hydrology* 10 (1), 89-102.

Kayet, N., Pathak, K., Chakrabarty, A. and Sahoo, S. (2018). Evaluation of soil loss estimation using the RUSLE model and SCS-CN method in hillslope mining areas. *International Soil and Water Conservation Research* 6, 31-42.

Kothyari, U.C., Tewari, A.K., and Singh, R. (1994). Prediction of sediment yield. *Journal of irrigation and drainage engineering* 6, 1122-1131.

Nearing, M.A., Jetten, V., Baffaut, C., Cerdan, O., Courtier, A., Heranandez, M., Bissonnais, Y., Nichols, M.H., Nunes, J.P., Renschler, C.S., Souchere, V. and Vanoost, K. (2005). Modelling response of soil erosion and runoff to changes in precipitation and cover. *Catena* 61, 131-154.

Pandey, A. (2019). Alternative land use in the Sone command area using remote sensing and GIS techniques. *A thesis report of civil engineering department*, National Institute of technology, Patna.

Pham, T.G., Degener, J., and Kappas, M. (2018). Integrated universal soil loss equation (USLE) and geographical information system (GIS) for soil erosion estimation in a sap basin: Central Vietnam. *International soil and water conservation research.*

Prasannakumar, V., Vijith, H., Abinod, S. and Geetha, N. (2011). Estimation of soil erosion risk within a small mountainous sub-watershed in Kerala, India, using Revised Universal Soil Loss Equation (RUSLE) and geo-information technology. *Geoscience Frontiers.*

Raghunath, J. (2002). Potential erosion map for Bagmati basin using Grass GIS. *Proceeding of the open source GIS-GRASS user conference.*

Saha, S.K. (2003). Water and wind induced soil erosion assessment and monitoring using remote sensing and GIS. *Satellite remote sensing and gis application in agricultural metrology*. 315-330.

Shinde., Vipul., Tiwari, K.N. and Singh, M. (2010). Prioritization of microsheds on the basis of soil erosion hazard using remote sensing and geographic information system. *International journal of water resources and environmental engineering* 2 (3), 130-136.

Shin, G.J. (1999). The analysis of soil erosion analysis in watershed using GIS. *Department of Civil engineering, Gang-won National University.*

Thomas, J., Joseph, S., and Thrivikramji, K.P. (2017). Assessment of soil erosion in a tropical mountain river basin of the southern Western Ghats, India using RUSLE and GIS. *Geoscience Frontiers*.

Tundu, C., Tumbare, M.J., and Onema, J.M.K. (2018). Sedimentation and its impact /effects on river system and Reservoir water quality: case study of Mazowe Catchment, Zimbabwe. *International Association of Hydrological Sciences*, 377, 57-66.

Wischmeier, W.H., and Smith, D.D. (1978). Predicting rainfall erosion losses: A guide to conservation planning. *Agriculture handbook* 282.

Yin, S., Xie, Y., Liu, B., and Nearing, M.A. (2015). Rainfall erosivity estimation based on rainfall data collected over a range of temporal resolutions. *Hydrology Earth system science*, 19, 4113-4126.

Yesuph, A.Y., and Dagnew, A.B. (2019). Soil erosion mapping and severity analysis based on RUSLE model and local Perception in the Beshillo catchment of the Blue Nile basin, Ethiopia. *Environmental systems research*, 8-17.

*IN PROCEEDINGS OF 25th HYDRO 2020, INTERNATIONAL CONFERENCE, NATIONAL INSTITUTE OF TECHNOLOGY ROURKELA, ODISHA, INDIA 26-28, March 2021, ISBN 978-93-90631-56-8*

Paper ID - 235

# STUDIES FOR PROPOSED BANK PROTECTION WORKS ALONG EXISTING GHATS OF NIRA AND BHIMA RIVERS AT NIRA NARSINGPUR, MAHARASHTRA-A CASE STUDY

Jotsana G. Ambekar[1], B. Raghuram Singh[2], Dr. R. G. Patil[3]

[1]*Research Assistant, Central Water and Power Research Station, Pune - 411024, India*
[2]*Scientist 'C', Central Water and Power Research Station, Pune - 411024, India*
[3]*Scientist 'E', Central Water and Power Research Station, Pune - 411024, India*
*Email:jotsana.ambekar@rediffmail.com, banothuraghu@yahoo.com, patil.rg@cwprs.gov.in*

## Abstract

River Nira joins River Bhima near village Nira Narsingpur, Indapur Taluka, Pune district, Maharashtra. The famous Sri Laxmi narasimha temple is located at the confluence of these rivers. There are five ghats along these rivers for use of devotees and village people. Two ghats are on left bank of River Nira and two ghats are on right bank of River Bhima and one ghat is at the confluence. These ghats were constructed long back using black stone with provision of steps articulated over the sloping banks of the rivers. These ghats are working as a slope protection and are protecting the banks from erosion. Due to undermining of foundation, ghats have disturbed at few locations. In order to strengthen the ghats from further erosion/damage, Executive Engineer, PWD, Pune east approached CWPRS with a proposal of renovating the existing ghats. Project authorities proposed stone crated gabions for slope protection works and a vertical gabion wall for toe protection at the edge. The studies were conducted for verification of proposed protection works and necessary modifications were suggested wherever necessary. The proposed design of gabion wall for toe protection was found to be safe against overturning, sliding and bearing. The design of proposed slope protection works as per the given hydraulic parameters of river and in terms of river training methods appeared to be safe and was recommended to be adopted for the protection of ghats along River Nira and River Bhima.

***Key words:*** *Gabion wall, erosion and scouring, Geo-fabric filter, Toe wall, launching apron, etc.*

## 1. Introduction

Nira is a river flowing through the Indian state of Maharashtra. It is a tributary of Bhima river and flows through Pune and Solapur districts and then joins river Bhima at Nira Narsingpur, Indapur Taluka, Pune district, Maharashtra. Sri Laxmi narasimha temple is located at the triangular land portion between the confluence of Nira and Bhima Rivers as shown in Fig. 1. The temple is a family deity in Maharashtra and people in large numbers visit the Temple. At the confluence of these rivers, Sangam ghat was constructed with basalt stone in the year 1605 by Trimalpal Dhadji Mudhoji. It is learnt that the banyan trees and construction of stepped stones of sangam ghat were protecting the area near confluence of Rivers Bhima and Nira from bank erosion. Other ghats namely Dashkriya ghat and Laxmi ghat along left bank of Nira River and Kewada ghat and Sambar ghat along right bank of Bhima River were also constructed for easy access to the devotees/village people. The old ghats were found to have been disturbed at few locations due to undermining of bed of the foundation. In order to strengthen and beautify the ghats from further erosion/damage, Executive Engineer, PWD, Pune East approached CWPRS with a proposal of renovating the existing ghats. [Technical report No. 5682 of CWPRS].

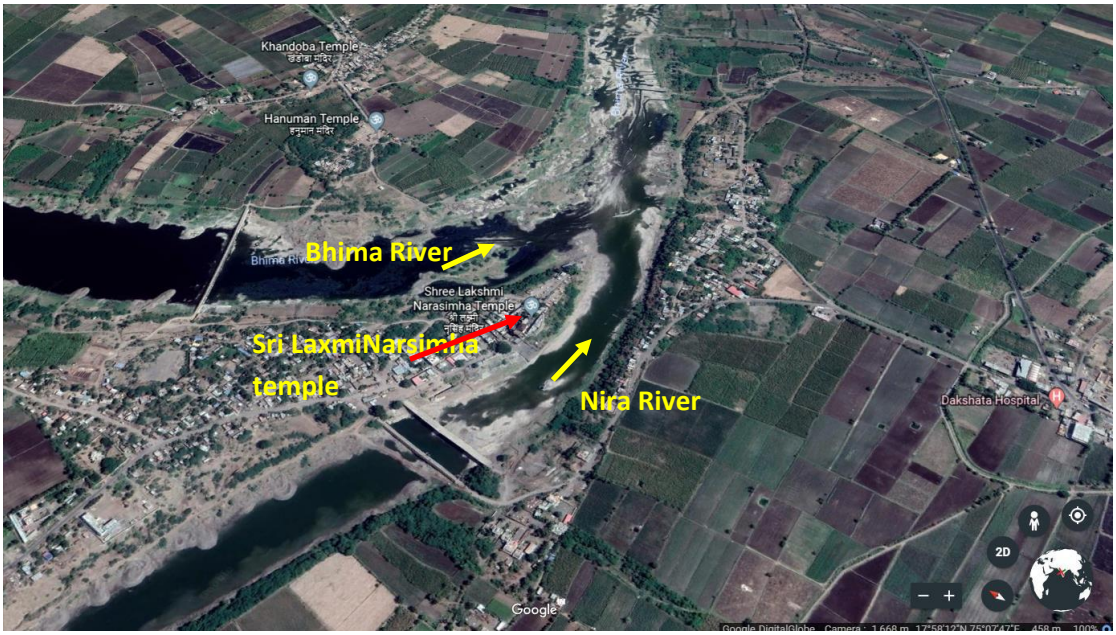



**Figure 1** Satellite imagery of study reach showing confluence of Nira and Bhima Rivers

## 2. Site inspection

Joint site inspection was carried out by the officials of CWPRS, Pune and Public Works Department, Indapur sub division along the banks of Nira and Bhima River. It was noticed that Sri Laxmi Narsimha temple and Laxmi ghat are situated along the left bank of River Nira. The Ghat was constructed by black stone steps sloping towards river from its bank. This ghat was seen to be working as a slope protection and is protecting the bank from erosion. River Nira is joining River Bhima near Sagam ghat. The existing Sambar ghat was constructed on right bank of Bhima River immediately downstream of K. T. Weir. Kewada ghat is also constructed on right bank of River Bhima around 500 m downstream of K. T. weir. In most of the places, rock outcrop along the banks of both the rivers were observed. During site visit, it was noticed that the construction of a road bridge is under progress across River Bhima downstream of K. T. weir as shown in Fig. 2.

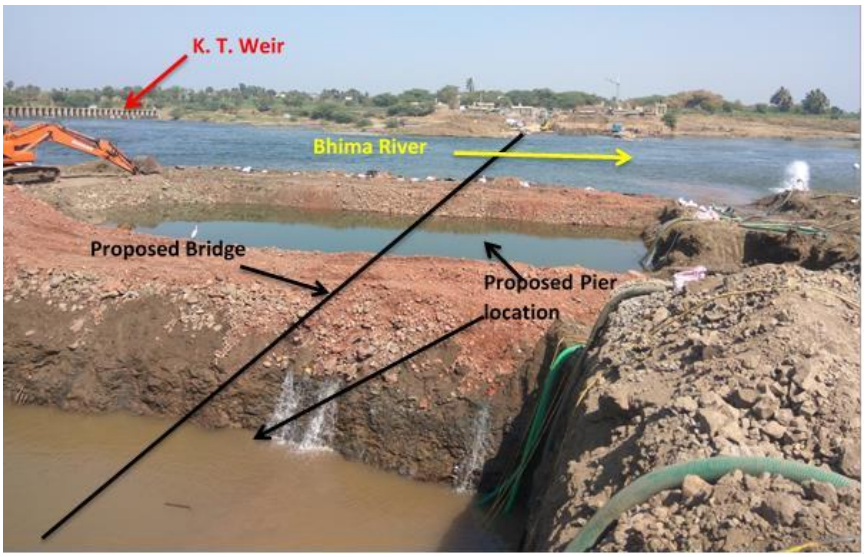



**Figure 2** Alignment of under construction Road Bridge across River Bhima downstream of K. T. weir

## 3. Analysis of data

The data supplied by the PWD Sub Division, Indapur was analyzed by CWPRS and the following points were noted.

- Nira and Bhima River are flowing in the reach with a longitudinal slope of around 1 in 228 and 1 in 287 respectively.
- Nira River width (bank to bank) varies from 210 m to 400 m in the study reach.
- Bhima River is having more or less uniform width (bank to bank) of about 350 m along the study reach.
- Discharge of Bhima River is high as compared the discharge of Nira River.
- Flow velocity of Nira River is slightly higher than that of Bhima River.

## 4. Proposed protection works

The proposed protection works are presented in Figure 3 (plan). The main aim is to provide protection works together with provision of access to river water in the form of ghats to the people. The provision contains berm/ plain land for resting/garden development along with sloping/ steps to go down to the river. The water is expected to be accessible even during the lean season water levels. There is proposal to construct a weir across the River Bhima after the confluence that will ensure availability of water throughout the year in both Nira and Bhima river limbs. The bank beatification/ protection works will be divided into rectangles of suitable sizes. The protection work consists of provision of Gabion mattresses along the periphery of rectangles together with loose stones filled inside the rectangular space. Stone crated Gabion mattresses are of 0.5 m thickness and at the centre loose stone pitching of 0.5 m thickness is proposed. It seems there is proposal to develop gardens for beatification. Such development is extended till the low water level so that the water is accessible for the devotees for religious purposes round the year. The end of the protection works towards river is in the form of near vertical gabion wall of 5 to 7 m height that is rested below on the non-erodible hard soil strata. Non-woven geotextile is proposed below the gabion wall only and is not proposed below gabion mattresses or loose stone filling. The overall development envisages slope protection and development along the slope of the bank. However, end wall of gabion encroaches the river water way to a minor extent and it is acceptable. This will not cause any major problem to the river flow conditions.

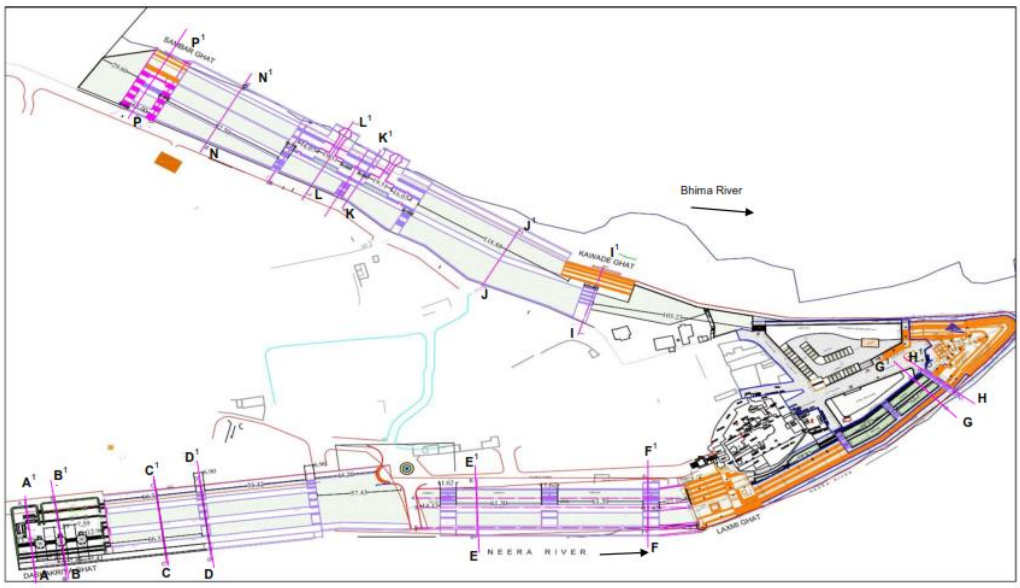



**Figure 3** Plan of proposed protection works along Nira River and Bhima River

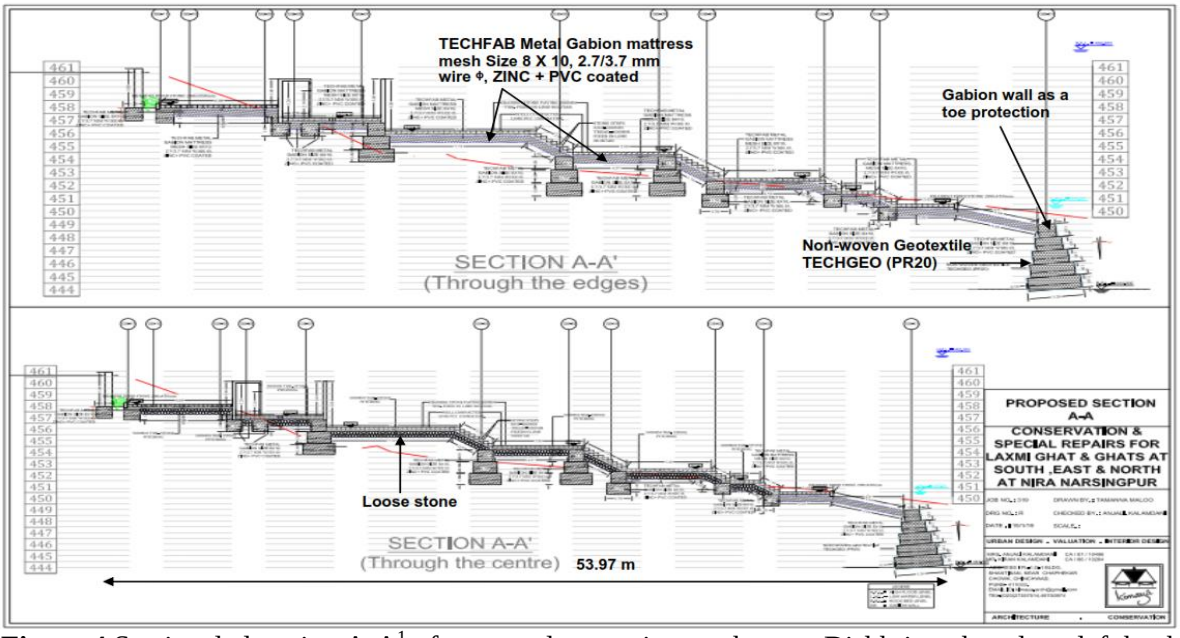



**Figure 4** Sectional elevation A-A[1] of proposed protection works near Dishkriya ghat along left bank of River

## 5. Desk studies

The analysis was made for the necessity of gabion and other protection works. The end protection in the form of near vertical gabion wall was checked for the safety, it was found to be safe against overturning, sliding and did not exceed the bearing capacity of the substrata. The requirement of thickness of gabions was verified by using average velocity (average of bank velocity and velocity at the central portion) of River Bhima and River Nira. To account for the turbulence near the protection work the average velocities adopted were increasing by 10%, for the computation of the thickness of protection works in sloping portion. The computations indicated the necessity of 0.5 m thick gabion mattresses for both Bhima and Nira Rivers. Hence, the designed gabion mattress of thickness 0.5 m and 0.5 m loose stone filling in sloping portion is found to be necessary and sufficient. The drawings provided do not explicitly indicate to the provision of Geofabric filter below all the protection works. It is again made clear that the Geo fabric filter shall be provided below all these works including gabion mattresses, loose stone filling, toe walls and end gabion wall. The geofabric filter shall be continuous. The filter joints either will have sufficient lap lengths or reduced lap length with proper stitching. Since the protection works do not encroach into the water way and are proposed to be constructed mostly along the existing slope of the bank, it is considered to be satisfactory from the point of not causing any afflux or change in flow behaviour.

The protection works have to be connected to the guide bunds/abutments of existing or under construction structures such as bridges or weirs. It is recommended to properly connect these protection works with the guide bunds or abutments with smooth streamlined alignment in plan so that the flow is not disturbed leading to formation of vortices or cause blockage of water way. It is understood that a KT weir is proposed downstream of the confluence of the two rivers with its crest at RL. 450.50 m. To protect the proposed bank protection development, it is suggested to stop the sand mining activity for the time being. However, in future after the construction of K. T. weir there is possibility that sand may get collected in the area and may pose problem, as it may occupy the depth presently available for water. The area may be monitored and remedial measures may be undertaken by allowing controlled sand mining that does not lead to failure of the bank protection works. The encroachments of these protection works are less than 15% of the total width of the cross section at that section as shown in Table 1. Hence the proposed protection works are seems to be safe at this location. Total 9 cross sections of Bhima River at an interval of 100 m were supplied by project authority. The encroachment of proposed protection works are ranging from 6.77% to 17.16% as

shown in Table 2. The percentage of encroachment is slightly higher than the permissible limit i.e., 15%. The proposed protection works are not completely blocking the cross section. Hence the proposed protection works along right bank of River Bhima may not be creating considerable afflux and may not affect the flow conditions near the existing ghats.

## 6. Discussions of results

Based on the data supplied by PWD Sub Division, Indapur, desk studies were carried for the proposed protection works along right bank of River Bhima and along left bank of River Nira. As per the designs of project authorities, a 0.5 m thick techfab metal gabion mattress was designed for slope protection as shown in Figure 4. Khandki stone of 200 mm thick fixed in lime mortar was designed as a flooring over the gabion mattress which gives aesthetic view to the ghats. The designed thickness of gabion mattress and loose stone crates i.e., 0.5 m is safe as per the analysis. Gabion wall of height 5 m to7 m is used as toe protection. This gabion wall was designed with steps with bottom width of 3 m to 4 m and top width of 1 m. The design of gabion wall against sliding, overturning, bearing was checked and found to be safe against these aspects. Gabion wall bottom shall be placed at least 50 cm below the non-erodible hard soil strata depending on site conditions. The protection works have to be connected to the guide bunds/ abutments of existing or under construction structures such as bridges or weirs. It is recommended to properly connect these protection works with the guide bunds or abutments with smooth streamlined alignment in plan so that the flow is not disturbed leading to formation of vortices or cause blockage of water way.

It is learnt from the site visit that the sand mining was being practiced along the River Nira. It seems the river had achieved a sediment balance with this extraction of sand from the river bed. However there is a proposal to build a KT weir across river Bhima downstream of the confluence with its crest at RL. 450.50 m. This development along with stopping of the sand mining as proposed in the area after the construction of bank protection works in future may lead to collection of sand/silt in the area. Hence, it is advised to monitor the development and sand mining may be allowed in controlled manner later so that the bank protection works are not disturbed while allowing for sufficient depths of water in the area for religious and other purposes. The sand mining restriction as indicated in Figure 5 may be imposed later. However, sand mining may be banned with immediate effect till proper assessment after the construction of the K. T. weir.

**Table 1** The percentage of encroachments of proposed protection works along left bank of Nira River

| S. No | SECTIONS ALONG NIRA RIVER | WIDTH OF THE RIVER (m) | LENGTH OF THE PROTECTION WORKS (m) | % of Encroachment |
|---|---|---|---|---|
| 1. | A-A$^1$ | 400 | 53.97 | 13.5 |
| 2. | B-B$^1$ | 400 | 55.25 | 13.81 |
| 3. | C-C$^1$ | 400 | 55.18 | 13.79 |
| 4. | D-D$^1$ | 400 | 54.15 | 13.53 |
| 5. | E-E$^1$ | 380 | 33.77 | 8.86 |
| 6. | F-F$^1$ | 380 | 44.33 | 11.66 |
| 7. | G-G$^1$ | 310 | 20.66 | 6.66 |
| 8. | H-H$^1$ | 310 | 19.36 | 6.25 |

**Table 2** The percentage of encroachments of proposed protection works along right bank of Bhima River

| S. No | SECTIONS ALONG NIRA RIVER | WIDTH OF THE RIVER (m) | LENGTH OF THE PROTECTION WORKS (m) | % of Encroachment |
|---|---|---|---|---|
| 1. | I-I$^1$ | 350 | 23.71 | 6.77 |
| 2. | J-J$^1$ | 350 | 53.53 | 15.29 |
| 3. | K-K$^1$ | 350 | 45.79 | 13.08 |

| | | | | |
|---|---|---|---|---|
| 4. | L-L[1] | 350 | 56.01 | 16.0 |
| 5. | M-M[1] | 350 | 50.82 | 14.52 |
| 6. | N-N[1] | 350 | 54.94 | 15.69 |
| 7. | O-O[1] | 350 | 56.42 | 16.12 |
| 8. | P-P[1] | 350 | 60.08 | 17.16 |

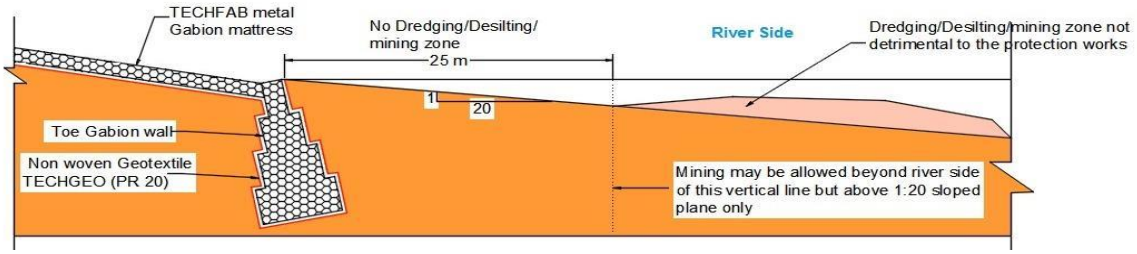



**Figure 5** Dredging/Mining restrictions for protecting river bank/ embankment protection works

## 7. Conclusion

Based on the desk studies for verification of the proposed bank protection works along existing ghats of River Nira and River Bhima, following are the conclusions:

- The proposed protection works along River Bhima and River Nira are not affecting the effective waterway of the Rivers.

- The proposed design of gabion wall for toe protection is safe against overturning, sliding and bearing capacity of the substrata.

- The thickness of gabion mattress and loose stone filling may be adopted as 0.5 m along the banks of Nira and Bhima Rivers. The loose stones of 0.5 m thickness may be sufficient and the site engineers are advised to monitor the bank protection works with loose stone during the flood. Necessary corrective measure could be undertaken if there is any disturbance in the loose stones.

- The depth of toe wall may be restricted if hard rock strata are encountered before the required depth and the gabion walls may be embedded in a trench of 0.5 m depth inside the non-erodible hard sub-strata for safety. This could be decided by the site engineers.

- The suitable geo-fabric filter as per the IS code is necessary to be provided below the entire protection works including gabion mattress, loose stone filling and gabion end walls. While placing geo-fabric filter below the protection works, care may be taken to place 15 cm thick layer of sand below the filter and also 15 cm thick sand layer above the filter (sandwiching the geo-fabric filter between sand layers) to avoid rupture of filter material. The joints shall have sufficient lap lengths or stitching may be provided to avoid openings.

- The stone crates may have to be filled up with graded stones so that maximum density is achieved and crates are efficient in arresting the high velocity flow approaching the protection works of ghat.

- The loose stone pitching at the centre part of rectangular portion of the protection works maybe filled with one man stones (larger than 300 mm size) and monitor this portion for any disturbance after the passage of flood. It is advised to take up maintenance work if there is any disturbance of these stones every year after the flood.

- The protection works have to be connected to the guide bunds/ abutments of existing or under construction structures such as bridges or weirs. It is recommended to properly connect these

protection works with the guide bunds or abutments with smooth streamlined alignment in plan so that the flow is not disturbed leading to formation of vortices or cause blockage of water way.

- During the site inspection, sand mining was noticed along the banks of River Nira near Dashkariya ghat. The sand mining activity shall be controlled by the local authorities and may follow the guide lines given in Figure 5 for the safety of all structures in the reach under consideration.

- Factory made crates should be preferably used for protection works. The crate should be tied to each other on sloping portion. The size of stones to be used for filling crates should be preferably 125 mm – 225 mm. Angular stones are desirable to minimize the porosity in crates and also increase the density of crates.

- The restoration and maintenance of existing protection works are needed to avoid further damage to the banks. Provision may be made for maintaining the proposed bank protection works annually, before the monsoon.

- To drain the storm water collected in the country side, proper storm water drainage facility such as culverts/pipes along with non-return flap gates on the river side should be provided. The dimensions of such vent/pipes and numbers may be designed based on the hydrological features of the catchment area which can be assessed by the project authorities.

## 8. References

Technical Report No. 5682 of CWPRS, "Desk studies for verification of proposed bank protection works along existing Ghats of left bank of Nira and right bank of Bhima Rivers at Nira Narsingpur, Maharashtra", March 2019.
IS 14458 (Part 1): 1998 "Retaining wall for Hill area - Guidelines"

*IN PROCEEDINGS OF 25th HYDRO 2020, INTERNATIONAL CONFERENCE, NATIONAL INSTITUTE OF TECHNOLOGY ROURKELA, ODISHA, INDIA 26-28, March 2021, ISBN 978-93-90631-56-8*

Paper ID - 411

# Assessment of Water Balance Components in the Genale River Basin, Ethiopia Using SWAT Model

**Tufa Feyissa Negewo[1], Arup Kumar Sarma[2]**

*[1]PhD Research Scholar, Department of Civil Engineering, IIT Guwahati, Assam, India 781039*
*[2]Professor, Department of Civil Engineering, IIT Guwahati, Assam, India 781039*
*E-mail:tufa1886@gmail.com, aks@iitg.ac.in*
*Telephone/Mobile No.: +97662972431*

## Abstract:

To utilize water resources sustainably, understanding the quantity and quality of water resources in spatial and temporal variation is essential. Assessment of water availability is a vital aspect for planning, exploring, and management of water resources in the catchment for every country, especially for developing one. This study was initiated to evaluate various water balance components in the Genale River Basin, Ethiopia using physically-based semi-distributed Soil and Water Assessment Tool (SWAT) model. The data used in this study was included spatial data (Land use/cover, soil type, and digital elevation model) and temporal data (meteorological/daily climate and discharge data) for analyzing water balance components in the catchment. The delineated Genale watershed (54,942Km$^2$) contained 25 sub-basins that encompassing 464 Hydrologic Response Units (HRUs). The calibration and validation of streamflow were performed from (1998-2007) and (2008-2012), respectively, using SUFI-2 at watershed outlet on Monthly basis. The model performance revealed curve number (CN2.mgt), available water capacity of the soil layer (SOL_AWC.sol), and saturated hydraulic conductivity (SOL_K.sol) are sensitive parameters to runoff respectively. Nash–Sutcliffe efficiency (NSE) for calibration and validation period was 0.77 and 0.71, and the coefficient of determination ($R^2$) obtained was 0.82 and 0.80 during calibration and validation, respectively, which indicate satisfactory model performance in both cases on Monthly basis. From the simulation results, sub-basins located at upstream of the watershed, particularly sub-8 and 12 contained high water yield potential, while the low amount was recorded in the middle and downstream sub-basins. The soil water content, evapotranspiration, groundwater recharge from shallow/deep aquifer overshadowed in the Genale watershed. The reason is due to the type of scuttered bushland cover, infrequent occurrence of rainfall events, and sometimes rise in temperatures in the dry seasons with a high speed of wind energy. Then, the decision-maker will enable sustainable management and identify the high potential area of water to recommend water resources planning and management practice.

***Keywords:*** *Water yield; SWAT; sensitivity analysis; SWAT-CUP; Genale watershed*

## 1. Introduction

Truly water is a unique resource given to mankind from the nature. For the comprehensive development and sustainability of any country, pre-eminent development and utilization of water resources are of a significant concern (Bagstad et al., 2013). For planning and management of water resources in the basins, water availability assessment is an important aspect. Evaluation of different water balance components of hydrologic cycle is necessary for planning and management of a river catchment (Gupta et al, 2020; N'Dri et al, 2019).

Indeed, the burgeoning demand/change in water quality and quantity in the watershed was primarily due to population growth, increased productive activities, environmental deterioration of water bodies, decreased rainfall, changes in land-use land cover, increasing influx of chemicals from agricultural activities/non-point sources of pollution, urban expansion, and un proper watershed management practice held in the study area (Espinosa, 2016). This way contributed to the extent of water scarcity in several regions of the planet.

The integration between runoff/rainfall models and geographic information systems was emerged out as an essential tool that allows the simulation of hydrological processes at river basin scales and helps in the management of water resources where the problem of water scarcity is occurred. The study grants insight into the assessment of water balance components through various water balance models for various watersheds. There are various kinds of models; like empirical, conceptual, physically based model or lumped, semi-distributed and distributed model based on data dependence and applicability,

time bound, parameters used, and model algorithm in simulation of physical processes (Gupta et al, 2020). Models that have frequently applied at the watershed scale include the Hydrologic Simulation Program Fortran (HSPF; Bicknell, 2001) and Soil and Water Assessment Tool (SWAT) (Arnold et al., 1998). So, it gave an impression opportunity to extend the present work to water quality in the future studies. Among these models, the reason to choose SWAT model is emerged out as one of the abstract used models in the world, showing acceptable results in several applications, (De Medeiros, 2019), (Ouallali et al.,2020) and (Ayivi & Jha,2018).

The study was used by delineating the different watersheds using Remote Sensing and ArcGIS, interfaced with SWAT model in estimating the runoff, lateral flow, evapotranspiration, soil water content, groundwater recharge, and water yield. Identifying and assessing water balance components of the catchments will help to prepare a future plan for the water resources development and management (Gupta et al. 2020; (Healy et al. 2007). A comprehensive, semi-distributed, physically based model like (SWAT-model) is always been the primary choice of the modelers when dealing with complex issue like assessment of water balance components of the basins. The SWAT model has been convinced as an effective/efficient model to study hydrological impacts around the world which can be used for understanding the effects of current and future development and management activities. These model uses different empirical and complex physical-based mathematical formulae to represent major components of hydrological system (Gupta et al, 2020; N'Dri et al, 2019; Ayivi & Jha,2018).

In this research work, the Specific objectives of the SWAT model are, to calibration/validation of the model, sensitivity analysis in the Genale watershed to simulate streamflow and evaluating the spatial and temporal variability of water balance components to understand the status of water resources in the area. Understanding of the water balance components of the Genale basin is essential for water sectors & decision-makers because it will suggest them to better plan, know high potential sub-basins, manage and protect water resources of the area.

## 2. Materials and methodology

### *2.1 Description of the study area*

The study area is located on the Genale watershed with 54,941.583 $Km^2$ of the part of Genale Dawa River, situated in the South-Eastern part of Ethiopia and joins with Dawa River at the border with Somalia (Dolo Ado) (4° 10'N, 42° 04'E) to become the Juba River. In the Genale River Basin, a total of 484 HRUs were created and scattered among 25 sub-basins. The annual mean of precipitation experienced in the area 809mm distribution of rainfall in the watershed is 300 to 1302mm per year. The daily max and min temperatures are 34.5$^0$C and 8.6$^0$C, respectively, with a daily average of 19$^0$C.

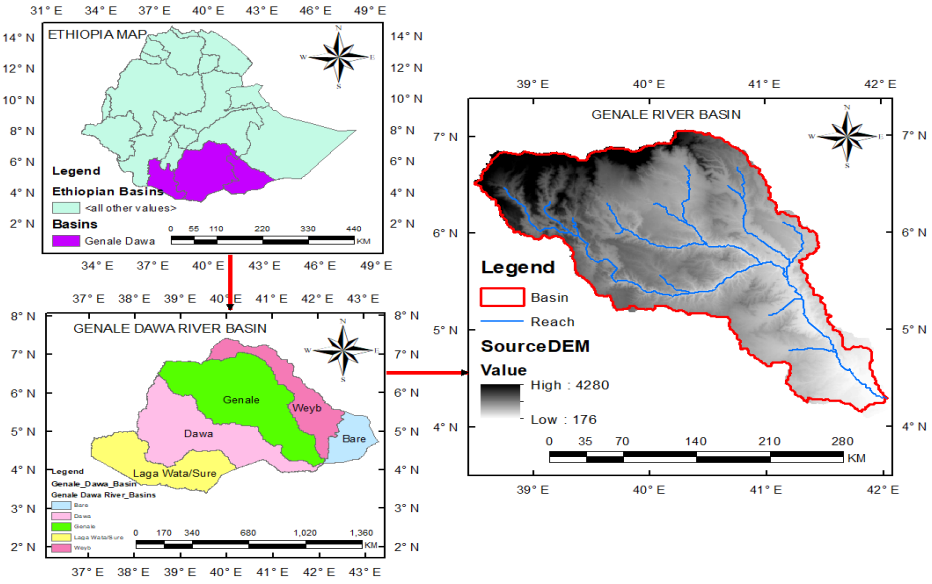



**Fig. 1** shows the delineated watershed of the study area extracted from Ethiopia map.

### *2.2 Description of the SWAT model*

The SWAT (Soil and Water Assessment Tool) hydrological model was advanced in the 1990s by the United States Department of Agriculture (USDA). It is a mechanism-based and spatially semi-scattered hydrological model or flexible tool in different parts of the world, designed to calculate and route water, sediments, management practices and nutrient-point sources of pollution from individual sub-basins through the mainstream watersheds towards its outlet resulting from changes in land use/cover in the river basins (Arnold et al., 1998). In general, SWAT simulates the hydrological cycle and water balance in the catchment using this equation:

$$SW_t = SW_o + \sum_{i=1}^{t}\left( R_{day} - Q_{sur} - E_a - W_{seep} - Q_{gw} \right) \quad (1)$$

Where; $SW_t$ = Final soil water content on a day i (mm/day), $SW_o$ = Initial soil water content on day i (mm/day), t = time in days, $R_{day}$ = amount of precipitation on day i (mm/day) ,$Q_{sur}$ = amount of surface runoff on day i (mm/day), $E_a$ = amount of evapotranspiration on day i (mm/day), $W_{seep}$ = amount of water entering the vadose zone from the soil profile on day i (mm/day), $Q_{gw}$ = amount of return flow on day i (mm/day). The SWAT model uses the soil conservation service curve number (SCS-CN) approach to evaluate surface run-off which illustrate run-off to soil type, land use/cover, slope classes, and management practices and is computationally effective (Arnold et al., 1995). The model estimates the streamflow in the sub-basins as a result of the total daily rainfall using the Soil Conservation Service (SCS) curve number (CN) method as follows:

$$Q_{Surface} = \frac{\{R_{Day-0.2S}\}^2}{\{R_{Day+0.8S}\}} \quad (2)$$

The retention parameter(S) and prediction of lateral flow by SWAT model expressed as;

$$S = 25.4(1000/CN - 10) \quad (3)$$

Where; S=drainable volume of soil water per unit area of saturated thickness(mm/day), CN= curve number. Water yield within a watershed has evaluated by the model based on the equation;

$$W_{YLD} = Q_{Surface} + BF - T_{Loss} = Q_{Surface} + Q_{GW} + Q_{LAT} - T_{Loss} \quad (4)$$

Where; WYLD = water yield (mm), $Q_{Surface}$ = surface runoff (mm), $Q_{LAT}$ = lateral flow contribution to stream(mm), $Q_{GW=}$ groundwater contribution to streamflow (mm), and $T_{Losses}$ = the transmission losses (mm) from tributary in the HRU through the bed. Water balance is the main propulsive force behind every process in the SWAT model as a result of its effects on plant development and the movement of sediments, nutrients, pesticides, and pathogens within the watershed region (Neitsch et al.,2011). Typically, the application of the SWAT model convoluted five mains: (a) watershed delineation and streams network generation, (b) combination of DEM, soil data and land use/cover data and create slopes classes, (c) creating HRU (Hydrological response unit) definition, (d) combination of climate data (e) run the simulation (**Fig. 2**).

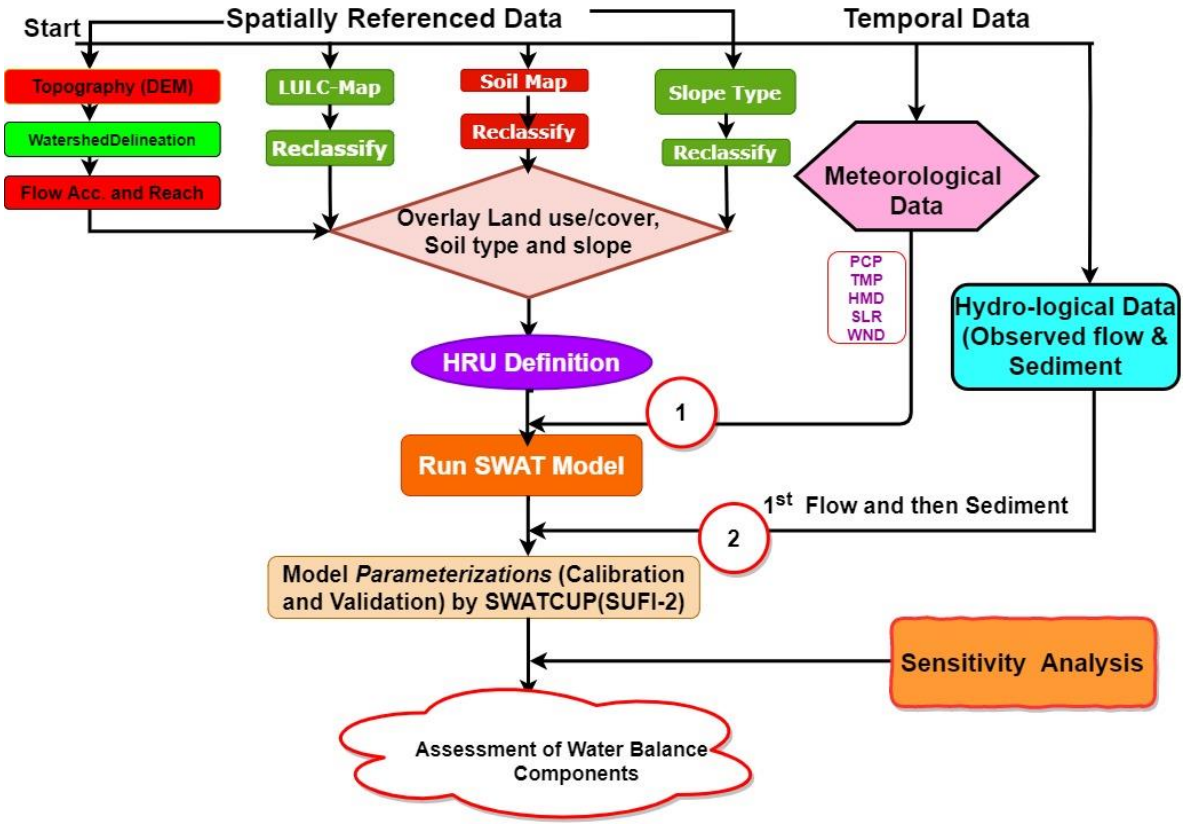



**Fig. 2** Steps of the implementation of the SWAT model for the study area

### *2.3 Analysis of SWAT input data*

Digital elevation model was downloaded from USGS Earth Explorer (http://earthexplorer.usgs. gov/) SRTM (Shuttle Radar Topography Mission) 90m*90m and used for watershed delineation, sub-basin, slope calculation/ classification and extract stream networks. The spatial land use/cover collected from the Ethiopian Ministry of water, irrigation, and electricity (MoWIE) GIS department of the year 2001 used for SWAT input, and the dominant land use/cover is range brushland (RNGB) accounts about 71% of the area. The soil map/type used in this study is from the Food and Agricultural Organization (FAO) Digital Soil Map of the World (http://www.fao.org/geonetwork/srv/en/metadata at the scale 1/5000000 for 2007. The soil data that integrated into the SWAT model are: the available water content, the texture, the hydraulic conductivity, the apparent density of the different soil layers and the dominant soil type in the study watershed was Rc19-bc-204 (Calcaric Regosols), and it accounts about 40% of the catchment.

The climate data required for this paper has taken from the National Meteorological Agency of Ethiopia, http://www.ethiomet.gov.et/etms. These data subsist of precipitation, max and min temperatures, wind energy, solar radiation, and relative humidity on daily time and covered the period from 1995 to 2012 for 16 stations. The discharge data has taken from the Ethiopian Ministry of water, irrigation, and electricity (MoWIE) Hydrology department gauged Genale @ Halwen station about 25km upstream of the outlet, transferred to the outlet, and arranged for SWAT language for the period from 1998-2012 on Monthly basis.

### *2.4 SWAT-CUP(SUFI-2) Description*

The automatic calibration and validation adjustment in the SWAT model achieved using the SWAT-CUP (SUFI-II) public user software developed by (Abbaspour et al.,2007). The SWAT-CUP has interfaced with five algorithms: (1) sequential uncertainty fitting (SUFI-2, (2) generalized likelihood

uncertainty estimation (GLUE), (3) parameter solution (ParaSol), (4) Markov chain Monte Carlo (MCMC), and (5) particle swarm optimization (PSO) (Moriasi et al.,2007).
In this finding, the analysis of sensitivity, calibration/validation, and was conducted using the SUFI-2 algorithm because this algorithm needs less simulation number, faster and one of the most used in the automatic calibration of model for several basins in the semi-arid region like Genale River Basin.

### *2.4.1 Assessment of Performance criteria for the model*

Nash-Sutcliffe efficiency (NSE), PBIAS, and Coefficient of determination ($R^2$) has been used as the efficiency criteria to evaluate the performance of models the Genale watershed. The first three objective functions mainly used for both daily and monthly streamflow/sediment calibration–validation uncertainty analysis.

Coefficient of Determination ($R^2$)

$$R^2 = \frac{[\sum_{i=1}^{n}(Q_{si}-Q_{sm})(Q_{oi}-Q_{om})]^2}{\sum_{i=1}^{n}(Q_{si}-Q_{sm})^2 \sum_{i=1}^{n}(Q_{oi}-Q_{om})^2} \quad (5)$$

Where, $Q_{si}$ is the simulated value, $Q_{oi}$ is the measured value, $Q_{om}$ is the average observed value and $Q_{sm}$ is an average simulated value? Nash Sutcliffe Efficiency (NSE).

$$NSE = 1 - \frac{\sum_{i=1}^{n}(Q_{oi}-Q_{si})^2}{\sum_{i=1}^{n}(Q_{oi}-Q_{om})^2} \quad (6)$$

where, $Q_{oi}$ is the observed, $Q_{si}$ is the simulated, and $Q_{om}$ is the observed discharge.

Percent Bias (PBIAS); $PBIAS = 100\% \times \frac{\sum_{i=1}^{n}(Q_{oi}-Q_{si})}{\sum_{i=1}^{n} Q_{oi}}$ (7)

## 3. Results and discussions

The model built with DEM, soil type, land use/cover, and slope characteristics for the Genale River Basin, which composed of 25 sub-basin, 484 HRUs with the drainage area of 54,942Km$^2$ at outlet located about 25km upstream of Dolo Ado boarder.

### *3.1 Model parameter sensitivity analysis*

In a sensitivity analysis of the model, SCS curve number (CN2.mgt), available water capacity of the soil layer (SOL_AWC.sol), and saturated hydraulic conductivity (SOL_K.sol) are the most sensitive parameters for runoff estimation. However, model efficiency also influenced by the reliability of spatial and temporal data.

**Table: 1** Fitted values and rank of parameters used in the SWAT model calibration/validation (1998-2012).

| Parameter Name | Description of the parameter | Range value | Fitted value | p-value | t-stat | Rank |
|---|---|---|---|---|---|---|
| CN2.mgt | SCS runoff curve number | 35-98 | -0.176 | 0.0 | -42.55 | 1 |
| SOL_AWC.sol | Available water capacity of the soil layer | 0-1 | 1.0 | 0.004 | 2.912 | 2 |
| SOL_K.sol | Saturated hydraulic conductivity | 0-2000 | 0.566 | 0.122 | -1.548 | 3 |
| SOL_BD.sol | Moist bulk density | 0.9-2.5 | 0.984 | 0.20 | 1.28 | 4 |
| ALPHA_BF.gw | Baseflow alpha factor (days). | 0-1 | 0.570 | 0.21 | -1.26 | 5 |
| REVAPMN.gw | Threshold depth of water in a shallow aquifer for "revap" to occur (mm) | 0-500 | 408.6 | 0.308 | -1.02 | 6 |
| GW_REVAP.gw | USLE support practice factor | 0-1 | 1.2 | 0.489 | -0.69 | 7 |
| ESCO.hru | Soil evaporation compensation factor | 0-1 | 0.27 | 0.65 | -0.45 | 8 |
| HRU_SLP.hru | Average slope steepness | 0-1 | 0.578 | 0.72 | 0.354 | 9 |
| SURLAG.bsn | Surface runoff lag time | 0.05-24 | 0.072 | 0.96 | -0.05 | 10 |

A parameter with a larger absolute value of t-stat is more sensitive to flow. The p-value gives the relevance of the sensitivity. Thus, when p-value is close to zero, then the sensitivity of the parameter is a priority (Table 1).

### *3.2 Calibration/ validation*

Calibrated parameters and the fitted values are final notes for modeler from the calibration action & performance in the calibration/ validation period for streamflow mimicked well the respective rainfall in the given span. **Table 2** shows the acceptable range for the performance of the model in light of calibration and validation process.

**Table: 2** Model Performance acceptable range assessment during calibration and validation period.

| R2 | NSE | PBIAS | RSR | Rating | Reference |
|---|---|---|---|---|---|
| 0.75-1 | 0.75-1 | <10% | 0-0.5 | very good | (Abbaspour et |
| 0.65-0.75 | 0.65-0.75 | 10-15% | 0.5-0.6 | good | al.,2007) |
| 0.5-0.65 | 0.5-0.65 | 15-25% | 0.6-0.7 | satisfactory | |
| <0.5 | ≤0.5 | >25% | >0.7 | unsatisfactory | **(**Moriasi et al.,2007) |

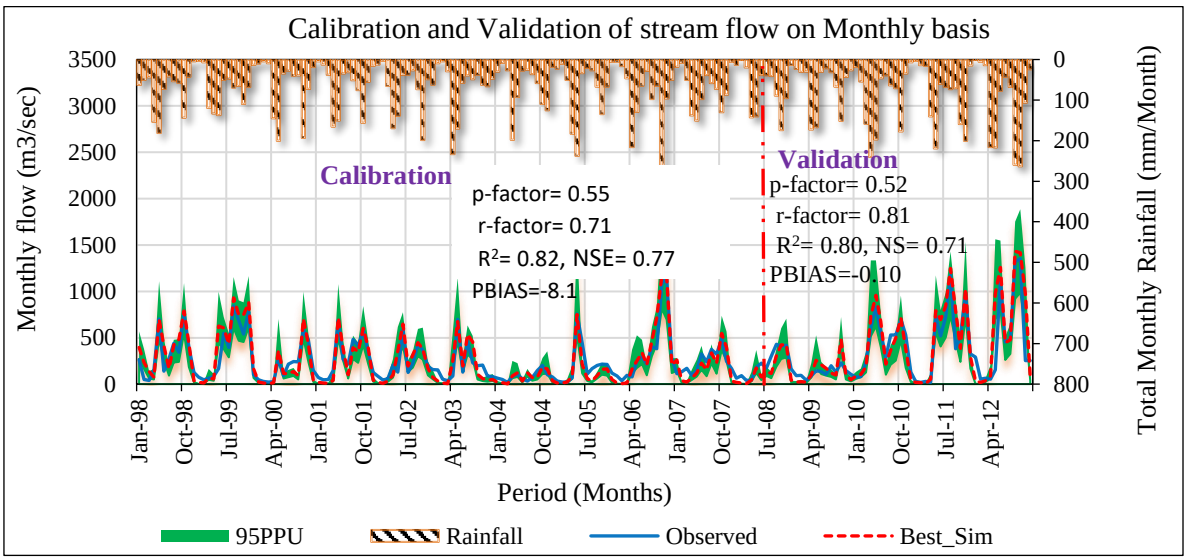



**Fig. 3** Monthly calibration and validation (1998-2012) for Genale River Basin at Genale Halwen.

The calibration was done from 1998 to 2007 & validation period from 2008 to 2012 and the model performance shows satisfactory agreement between the observed and simulated flow **(Fig. 3).** The calibrated/validated model also responded to the rainfall with the respective months.

### *3.3 Estimation of water balance components in the watershed*

Water balance is actually a representation of the net flow of water in and out of the system in hydrological process. Precipitation is accounted as the most significant inflow component. The most significant outflow components of water balance include: surface runoff, lateral flow, evapotranspiration and groundwater recharge. The water balance is a pattern of "book-keeping" of a catchment or reservoir where all critical components are considered for a specific duration of time. Water balance is the best approach to determine the availability of water in various parts of the hydrological cycle and modification in between these components. The calibrated/validated SWAT model predicted a very crucial water balance components in the catchment. Water yield is one of the critical parameters predicted by the model for adequate water management and planning of the study area. **Table 3** shows the simulated water balance components in the Genale catchment.

**Table: 3** Summary of monthly water balance components simulated for base periods (1998-2012).

| S.no | Water Balance Components | Amount (mm) |
|---|---|---|
| 1 | Precipitation | 851.5 |
| 2 | PET-Potential Evapotranspiration | 1,937.7 |
| 3 | ET-Actual Evapotranspiration | 405.4 |
| 4 | SURQ=Surface runoff | 48.79 |
| 5 | LATQ- Lateral flow contribution to streamflow | 3.2 |
| 6 | Percolation= GW_RCHRG+ Capillarity | 394.44 |
| 7 | GW_Q=Return flow/Discharge of the shallow aquifer contributes to streamflow | 374.7 |
| 8 | Revap from shallow aquifer/ Capillarity | 0.2 |
| 9 | DA_RCHRG-Deep aquifer recharge | 19.72 |
| 10 | Stream flow= SURQ+Base flow | 426.69 |
| 11 | Base flow=LATQ+GW_Q | 377.9 |
| 12 | GW_RCHRG- Recharge entering shallow and deep aquifers during time step | 394.42 |

The annual mean of the distinctive water balance components in each sub-basin between 1998 and 2012, are shown in **Fig. 4**. The Soil water content, actual evapotranspiration, and groundwater contribution to streamflow (from shallow aquifer) contributed a high percentage. In comparision, surface runoff, deep aquifer recharge, and lateral flow represented a low percentage relative to the other water balance components **(Fig. 4).** From the analysis, it might have winded up that evaporation loss is one of the significant loss components in the water balance of the Genale River Basin. Soil water content is the highest in the catchment which accounts 36% and the actual evapotranspiration is among the parameter that contributes to the greatest water loss in the basin (21%). Groundwater flow contributes 18% while surface runoff is low (2%) **(Fig. 4)**.

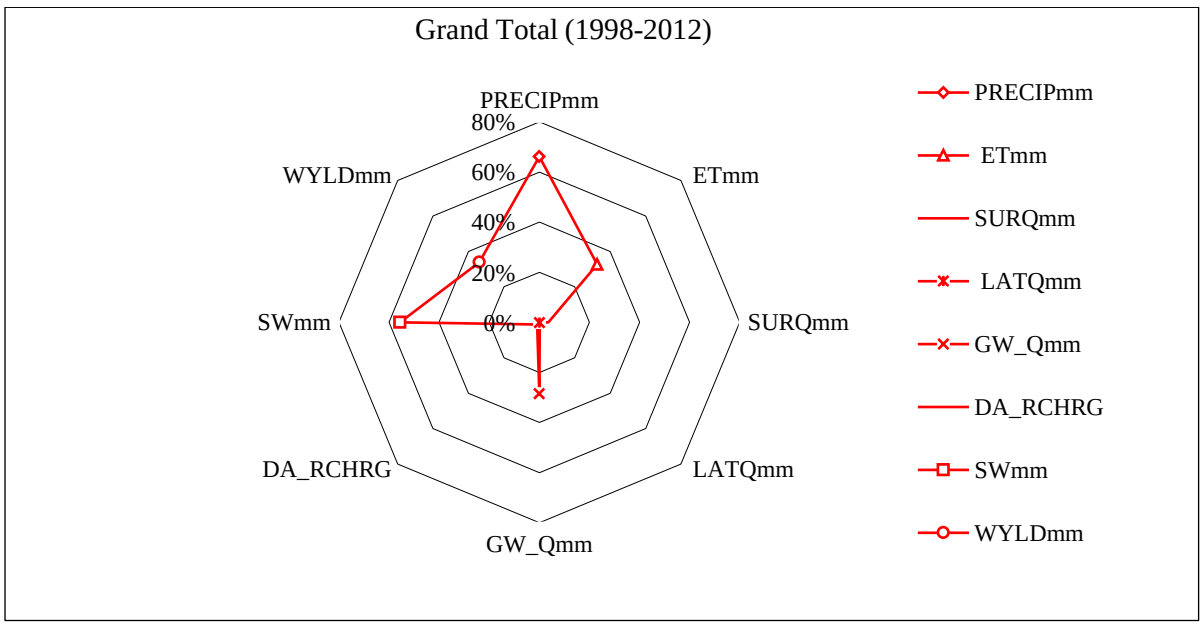



**Fig. 4** Predicted water balance components for some simulated years in the Genale watershed (1998-2012).

Expressed as; (PRECIP-Precipitation, ET-Actual evapotranspiration, SURQ-Surface runoff, LATQ-Lateral flow, GW_Q-Groundwater contribution to streamflow (mm H2O) from the shallow aquifer (Return flow), DA_RCHG-Deep aquifer recharge (mm H2O), SW- Soil water content (mm H2O) all in mm.

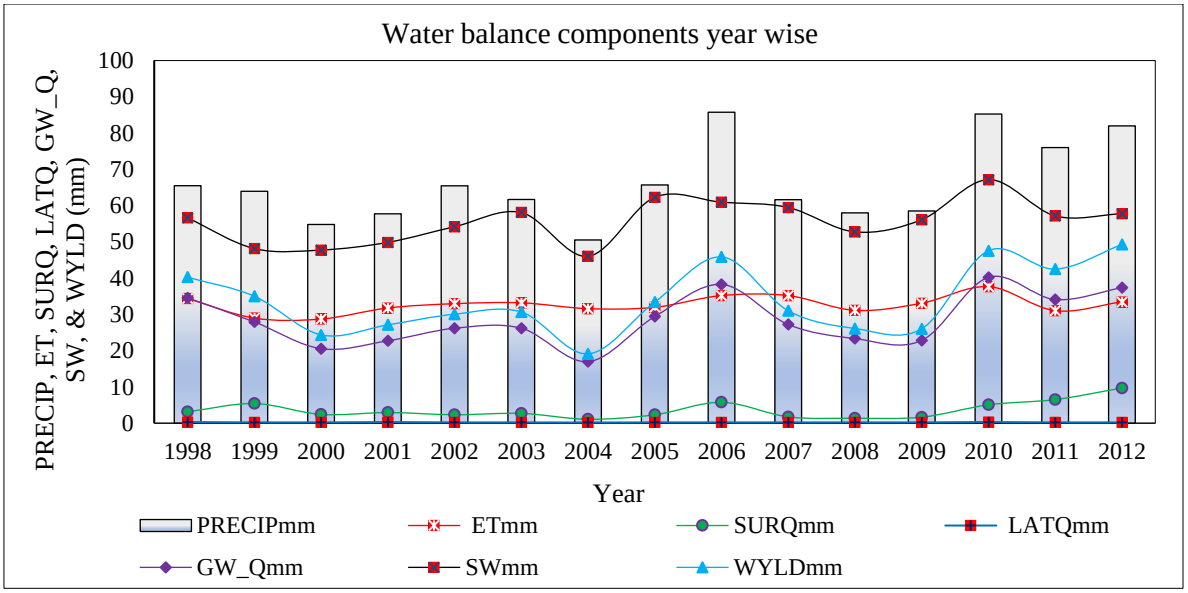



**Fig. 5** Temporal disparity rate of simulated water balance components and water yield in Genale watershed (1998-2012).

From different components of simulated water balance, the rate of water yield was higher in 2006 & 2010 and promisingly decreasing from 1998 to 2000 following the precipitation pattern.

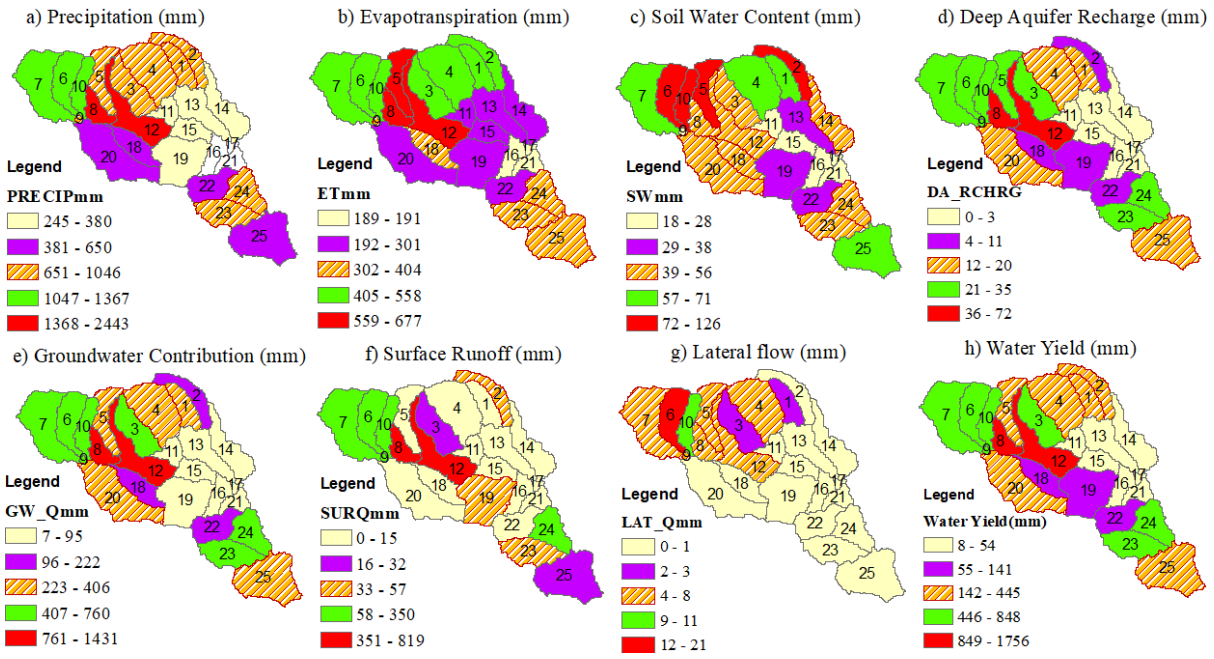



**Fig. 6** Assessment of water balance components spatially within the sub-basins (1998-2012).

The spatial distribution of the water balance components in each sub-basin, is disciplined by the type of land use, soil type, slope classes and quantity of precipitation in the area. As we have seen from **Fig. 6** most of the water balance components are higher in value at the upstream of watershed. In contrast, sub-basin located downstream reflects low amounts of water balance components in the watershed. The soil water content, evapotranspiration, groundwater recharge from shallow/deep aquifer overshadowed in the Genale watershed. Mainly due to the type of range scrub cover and less occurrence of rainfall events that increase in the study area and sometimes rise in temperatures principally in the dry seasons with high speed of wind energy. Regarding water yield, the predicted values by the SWAT model was varied from 8 mm up to 1756 mm with an average value equal to 456.2 mm and sub-8 and 12 are the sub-basins with highest water yield production (**Fig. 6**).

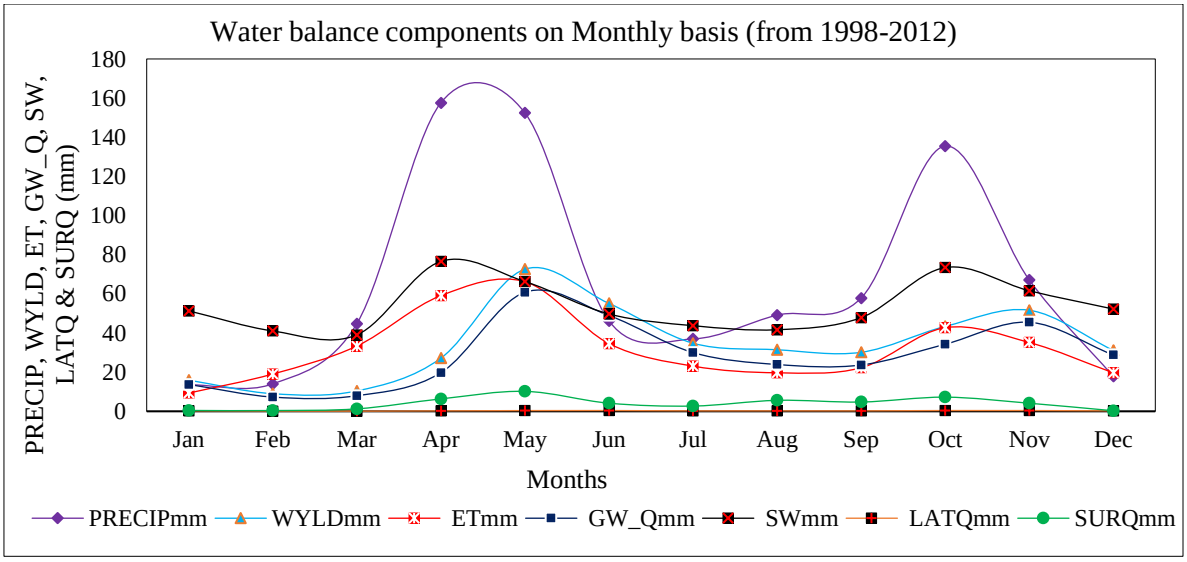



**Fig. 7** Monthly mean values of water balance components (1998-2012)

Monthly water balance components analysis would provide an estimate of the water distribution and which could further be utilized for the better water management plans and development. It was executed over the period of 1998–2012. **Fig. 7** represents the monthly distribution of the seven water balance components, i.e. precipitation, surface runoff, water yield, groundwater flow, soil water content, lateral flow, and evapotranspiration, indicates that major portion of components occurred mostly in the monsoon months and followed the precipitation graph.

## 4. Conclusions

The SWAT model for the Genale catchment was built up and exported in the SWAT–CUP application for sensitivity, calibration (1998-2005), and validation (2006-2012) using the SUFI2 optimization technique. The sensitivity analysis enabled that the SCS curve number (CN2.mgt), available water capacity of the soil layer (SOL_AWC.sol) and saturated hydraulic conductivity (SOL_K.sol) are the most sensitive parameters for runoff estimation.

The NSE & $R^2$ for calibration and validation period indicated satisfactory model performance in both cases on Monthly basis. The calibrated/validated SWAT model was used to evaluate the water balance components (all incoming & outgoing) over 1998-2012. Soil water content, actual evapotranspiration, and groundwater contribution to streamflow (from shallow aquifer) overshadowed in the basin. In contrast, surface runoff, deep aquifer recharge, and lateral flow represented a low percentage relative to the other water balance components. From this work, the evaporation loss is one of the significant loss components in the water balance of the Genale River Basin. The reason is, type of range scrub/bushland cover, infrequent occurrence of rainfall events in the study area and sometimes significant solar radiation (rise in temperatures principally in the dry season). The maximum value of water balance components was recorded in upstream side of watershed while low value was resulted in middle and downstream sub-basins.

Within the catchment, sub-basins with high surface runoff and groundwater were the most water yielded sub-basins to which the local authority government should give the earliest priority while looking for water resources project exploring, planning, and management practice for the basin.

## References

Abbaspour, K. C., Vejdani, M., Haghighat, S., & Yang, J. (2007, December). SWAT-CUP calibration and uncertainty programs for SWAT. In MODSIM 2007, international congress on modeling and simulation, modeling, and simulation society of Australia and New Zealand (pp. 1596-1602).

Arnold, J. G., Srinivasan, R., Ramanarayanan, T. S., & Bednarz, S. T. (1998). Large area hydrologic modeling and assessment part II: model application 1. JAWRA Journal of the American Water Resources Association, 34(1), 91-101.

Arnold, J. G., Williams, J. R., & Maidment, D. R. (1995). Continuous-time water and sediment-routing model for large basins. Journal of Hydraulic engineering, 121(2), 171-183.

Ayivi, F., & Jha, M. K. (2018). Estimation of water balance and water yield in the Reedy Fork-Buffalo Creek Watershed in North Carolina using SWAT. International Soil and Water Conservation Research, 6(3), 203-213.

Bagstad, K. J., Semmens, D. J., Waage, S., & Winthrop, R. (2013). A comparative assessment of decision-support tools for ecosystem services quantification and valuation. Ecosystem Services, 5, 27-39.

Bicknell, B. R., Imhoff, J. C., Kittle Jr, J. L., Jobes, T. H., Donigian Jr, A. S., & Johanson, R. C. (2001). Hydrological simulation program–FORTRAN (HSPF): User's Manual for Version 12. US Environmental Protection Agency, Athens, GA.

De Medeiros, I. C., da Costa Silva, J. F. C. B., Silva, R. M., & Santos, C. A. G. (2019). Run-off–erosion modelling and water balance in the Epitácio Pessoa Dam river basin, Paraíba State in Brazil. International journal of environmental science and technology, 16(7), 3035-3048.

Espinosa, V., & Rivera, A. (2016). First line of defense: Innate cell-mediated control of pulmonary aspergillosis. Frontiers in microbiology, 7, 272.

Gupta, A., Himanshu, S. K., Gupta, S., & Singh, R. (2020). Evaluation of the SWAT Model for Analysing the Water Balance Components for the Upper Sabarmati Basin. In *Advances in Water Resources Engineering and Management* (pp. 141-151). Springer, Singapore.

Healy, M., Newe, T., & Lewis, E. (2007). Efficiently securing data on a wireless sensor network. In Journal of Physics: Conference Series (Vol. 76, No. 1, p. 012063). IOP Publishing.

Moriasi, D. N., Arnold, J. G., Van Liew, M. W., Bingner, R. L., Harmel, R. D., & Veith, T. L. (2007). Model evaluation guidelines for systematic quantification of accuracy in watershed simulations.Transactions of the ASABE, 50(3), 885-900. Tical documentation version 2009. Texas Water Resources Institute.

N'Dri, W. K. C., Séverin, P., Jourda, J. P., & Kouamé, K. J. (2019). Application of SWAT to Estimate Water Balance in the Aghien Lagoon Basin, South-East of Côte d'Ivoire. *International Journal of Science and Research*, *8*(10).

Neitsch, S. L., Arnold, J. G., Kiniry, J. R., & Williams, J. R. (2011). Soil and water assessment tool theoretical documentation version 2009. Texas Water Resources Institute.

Ouallali, A., Briak, H., Aassoumi, H., Beroho, M., Bouhsane, N., & Moukhchane, M. (2020). Hydrological foretelling uncertainty evaluation of water balance components and sediments yield using a multi-variable optimization approach in an external Rif's catchment. Morocco. Alexandria Engineering Journal, 59(2), 775-789.

USGS Earth Explorer (**http://earthexplorer.usgs. gov/)SRTM** (Shuttle Radar Topography Mission) large basins. *Journal of Hydraulic engineering*, *121*(2), 171-183. Food and Agricultural Organization (FAO) Digital Soil Map of the World **(http://www.fao.org /geonetwork/srv/en/metadata** at the scale 1/5000000 for 2007

# Theme VI
# River Hydraulics

*IN PROCEEDINGS OF 25th HYDRO 2020, INTERNATIONAL CONFERENCE, NATIONAL INSTITUTE OF TECHNOLOGY ROURKELA, ODISHA, INDIA 26-28, March 2021, ISBN 978-93-90631-56-8*

Paper ID - 011

# EXPERIMENTAL INVESTIGATION OF FRICTION FACTOR IN ALLUVIAL CHANNEL

Anurag Sharma[1], Nikhitha Elsa Sam[2], Asmita Tanwani[3], Hardipsinh Jadeja[4], Bimlesh Kumar

[1]*Assistant Professor, Department of civil engineering, NIT Rourkela, India*
[2]*Student, Department of civil engineering, IITRAM, Ahmedabad-380026, India*
[3]*Student, Department of civil engineering, IITRAM, Ahmedabad-380026, India*
[4]*Student, Department of civil engineering, IITRAM, Ahmedabad-380026, India*
[5]*Professor, Department of civil engineering, IIT Guwahati, India*

*Email: sharmaan@nitrkl.ac.in*

## Abstract

As a Civil Engineer, hydraulic engineering is a fundamental stream which is concerned with flow and fluid properties for better design parameters of a hydraulic structure. However, the flow of water varies from topography to cross-section of the channel or reservoir. For a prismatic channel or a non-prismatic channel, one of the important aspects is the bed resistance acting in the channel. The formulas developed in recent year, are empirically or graphically derived on the basis of one dimensional analysis. In this work, we developed empirical formula with the help of observed data. This formula establishes relation between Friction Factor, Shear Reynolds Number and Froude Number. As a river engineer, head loss of river is easily found by the friction factor which will be get through this equation. Also, we have been comparing our result with other developed formula through various parameters like Mean Squared Error, Nash-Sutcliffe efficiency, Index of Agreement, etc.

***Keywords:*** *Friction Factor; Shear Reynolds Number; Froude Number*

## 1. Introduction

For flow through an open channel, various parameters need to be properly studied and taken into account. Such as the cross section of the channel, properties of fluid, settlement characteristic, type of bed form, resistance to flow. A precise and accurate equation is needed for tabulating the friction factor value in an open channel for safe and reasonable design of a hydraulic structure, watershed, and flood studies. However till date, due to the complexity of resistance varying from place to place due to different parameters like skin distortion, surface distortion, form drag and local acceleration, the empirical formulas derived so far differs. Normally, friction factor formulated by Fanning (1896), stated the following:

$$\lambda = \frac{\tau_0}{\frac{1}{2}\rho v^2} \tag{1}$$

Where λ is friction factor, $\tau_0$ is wall shear stress, ρ is fluid density, v is free stream velocity. The difficulty arises in predicting friction factor value in alluvial channel because the flow boundary in alluvial channels is not fixed but continually deform-able through mutual interaction between the flow and bed. Friction factor is defined as ratio between wall shear stress and force required to flow fluid.

### 1.2 Literature Review

Over time, as a fixed and accurate formula for tabulating the value of friction factor is not yet formed, a number of empirical formulas were developed for the tabulation of friction factor in an open channel. Due to the complexity of various parameters affecting the friction factor in a fluid, researcher studied and predicted empirical formulas for calculating the friction factor in a fluid. Some of them are as follows in Table 1.

**Table 1** Friction Factor Formulas

| Sr. No | Authors | Equation | Notation |
|---|---|---|---|
| 1. | Strickler (1923) | $n = \frac{D_{50}^{1/6}}{21.1}$ | $D_{50}$ = bed material size of sampling location.<br>g = Gravitational force<br>n = Gauckler-Manning coefficient |
| 2. | keulegan (1938) | $\frac{u}{u_*} = 6.25 + 5.75 \ln\left(\frac{R}{k_s}\right)$ | R = hydraulic radius<br>$k_s$ = Nikuradse roughness constant = 2*$D_{50}$<br>$u_*$ = shear velocity<br>u = velocity in x-direction |
| 3. | Coles (1956) | $\frac{u}{u_*} = \frac{1}{k} \ln\left(\frac{y u_*}{\mu}\right) + 5.1$ | $u_*$ = shear velocity<br>u = velocity in x-direction<br>k = Von Karaman constant<br>y = depth of flow<br>s = channel bed slope.<br>μ = kinematic viscosity |
| 4. | Thompson & Cambell (1979) | $\lambda = \left(2 * \left(1 - \frac{0.1 k_s}{R}\right) * \log_{10}\left(\frac{12R}{k_s}\right)\right)^{-2}$ | R = hydraulic radius<br>$k_s$ = Nikuradse roughness constant = 4.5*$D_{50}$<br>λ = friction factor |
| 5. | Griffiths (1981) | $\frac{1}{\sqrt{\lambda}} = 1.98 \log\left(\frac{R}{D_{50}}\right) + 0.76$ | $D_{50}$ = bed material size.<br>R = hydraulic radius<br>λ = friction factor |
| 6. | Sarma et al (1983) | $\frac{u}{u_*} = 8.3\left(\frac{y u_*}{\mu}\right)^{1/7}$ | $u_*$ = shear velocity<br>u = velocity in x-direction<br>μ = kinematic viscosity<br>y = lateral distance from side wall |
| 7. | Bruschin (1985) | $n = \left(\frac{D_{50}^{1/6}}{12.38}\right)\left(\frac{RS}{D_{50}}\right)^{1/7.3}$ | $D_{50}$ = Bed material size of sampling location.<br>R = hydraulic radius<br>S = channel bed slope<br>n = Gauckler-Manning coefficient |
| 8. | Swamee (1993) | $u = u_*\{(\frac{\gamma}{u_* y})^{\frac{10}{3}} s + [k^{-1}.\ln(1 + \frac{9u_* y}{\gamma + 0.3\varepsilon})]\}$ | $u_*$ = shear velocity<br>u = velocity in x-direction<br>k = Von Karaman constant<br>y = depth of flow<br>$\epsilon$ = Roughness Height |
| 9. | Rice et al (1998) | $n = 0.029(D_{50}S)^{0.147}$ | $D_{50}$ = Bed material size of sampling location.<br>S = channel bed slope<br>n = Gauckler-Manning coefficient |
| 10. | Julien (2002) | $n = 0.062 D_{50}^{\frac{1}{6}}$ | $D_{50}$ = Bed material size of sampling location.<br>n = Gauckler-Manning coefficient |
| 11. | Lee & Ferguson (2002) | $\frac{1}{\sqrt{\lambda}} = 1.48\left(\frac{R}{D_{84}}\right)^{1.8}$ | $D_{84}$ = Bed material size of sampling location.<br>R = hydraulic radius<br>λ = friction factor |
| 12. | Pagliara & Chiavaccini (2006) | $\sqrt{\frac{8}{\lambda}} = \log(S^{-2.5}\frac{R}{D_{84}}) + 2.8$ | R = hydraulic radius<br>$D_{84}$ = bed material size of sampling location.<br>s = channel bed slope<br>λ = friction factor |

For the development of friction factor, many researchers developed empirical formulas for different conditions. Cheng-lung Chen's study (1991) on the Unified Theory on Power Laws for Flow resistance analyzed two main formulas; for smooth and rough flows based on the widely accepted logarithmic formula for velocity profile and Darcy-Weisbach's friction factor. He took into account Reynold's number, relative roughness and Hazen-Williams Constant to formulate an empirical equation. Also Strickler (1923) equation was developed to determine Manning's roughness for gravel bed rivers. Strickler equation takes into account $D_{50}$ as the median size of the material found in the soil sample. The assumptions taken into account by Strickler were that the roughness considered varied from smooth polished cement to stones of head size. Keulegan (1938) studied the principles of

flow in circular pipes and applied the studied principles to the theoretical development of open channel turbulent flows. The formula he developed is under the assumption that resistance to flow in a rough channel is the same as to the flow in pipe with same hydraulic radius and degree of roughness. He took into account $D_{50}$ as the sample size of the material passing through 50mm sieve and hydraulic radius as the functions of the formula. Later Vanoni (1941) derived another formula which takes into account the shear velocity, initial velocity Von Karman constant and the cross sectional area of the flow. Similar to Vanoni equation, Yang (2004) derived an empirical formula which considered all the parameters as that to the Vanoni's equation but only with the additional function of channel bed slope and also α which is a constant value depending on the value of Reynold's number. Here α is the dip correction factor. Schlichting. H (1979) derived the following equation:

$$\frac{V_{\max}-V}{V*}=-\frac{1}{k}*\ln(\frac{y}{\delta}) \tag{2}$$

However later Coles (1956), in his study of Law of wake in turbulent boundary layer added a wake term on the right hand side of the Schlichting equation. His equation considered following as the function of friction factor, shear velocity, initial velocity, Von Karman constant, depth from free surface, channel bed slope, cross sectional area and also two new parameters as Coles's wake function and wake parameter. Coles studied and derived an empirical formula on the basis of experimental data. He studied the mean velocity profile excluding the effects of turbulence in the flow and derived the formula for calculating the friction flow. Thompson and Campbell (1979) studied the hydraulics of large channel paved with boulders. As a part of his study, he crosschecked the authenticity of Nikuradse roughness factor. In his study he recommended the average size of the boulder and the effect of friction factor with respect to the boulder size in the channel. Gabor Takacs (2015) states that friction factor is a function of Reynolds Number and the pipe roughness. Also, the roughness condition of a pipe section or of a channel bed plays a very important role in determining the channel flow conditions. Kumar (2011) observed that flow resistance is not affected by only Reynold's number and roughness condition but also Froude's number.By comparing predicted values and empirical values of friction factor. From Subramanya (2014) gave friction factor equation:

$$\lambda=\frac{8*(u*)^2}{\nu^2} \tag{3}$$

### 1.3 Objective

Although previous studies explored friction factor in the open channel flow, the issue of predicting friction factor in alluvial channels with sufficient accuracy is of great interest to hydraulic engineers.

In the present study, we will develop a resistance equation empirically for an alluvial channel by using a big database of flume experimental observations. Also, we will perform a comparative analysis to ascertain prediction ability of different friction factor equations based on statistical criteria.

## 2. Experimental Program

In the present work, experimental data have been taken from Sharma et al. (2019). Experiment was conducted in a large tilting flume with dimensions of 17.24 m in length, 1m in width, and 0.72m in deep as per shown in Figure 1. The flow depth in the channel was measured with digital point gauge attached to a moving trolley. Main Flow discharge in channel was measured by using the flow depth over the rectangular notch at the downstream collection tank.

The characteristics of sediment and flow parameters used in study are shown in Table 2, where $D_{50}$ is the median size of sediment, $y$ is depth of flow, $S_f$ is friction slope, $u_*$ is shear or friction velocity, $u_{avg}$ is flow velocity, $R$ is hydraulic radius, $\lambda_{obv}$ is friction factor.

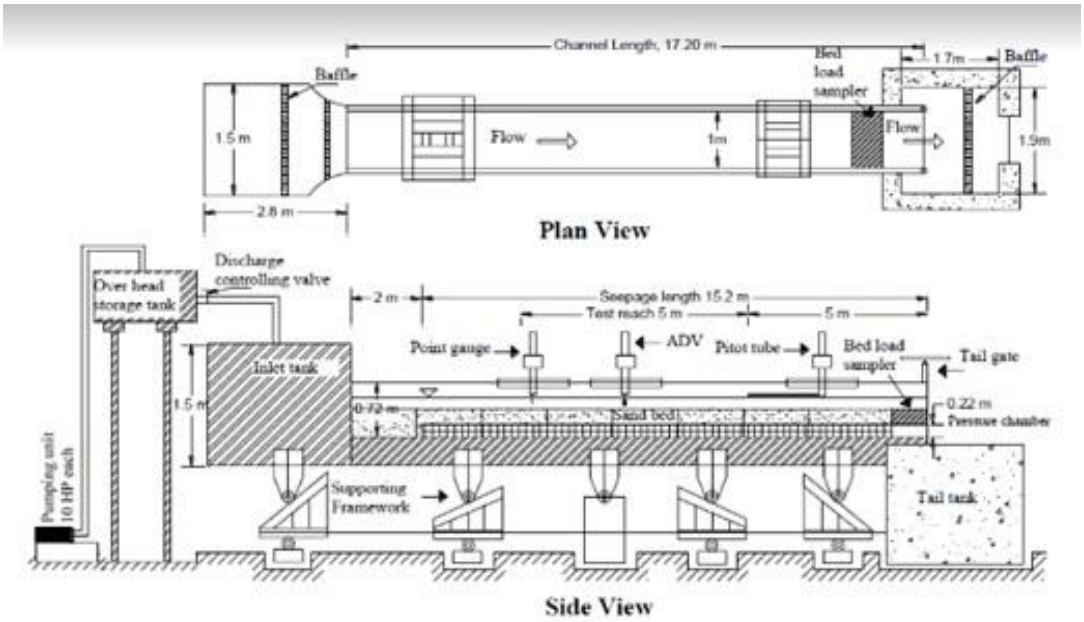



**Figure 1** Flume

**Table 2** Range of parameters

| $y$ (m) | $S_f$ | $u_*$(m/s) | $D_{50}$ (m) | $R$ (m) | $u_{avg}$ (m/s) | $\lambda_{obv}$ |
|---|---|---|---|---|---|---|
| (0.105 - 0.129) | (4.3E-05 - 0.00018) | (0.00621 - 0.01287) | (0.00042 - 0.0005) | (0.08678 - 0.10254) | (0.30768 - 0.45282) | (0.0031797 - 0.0066116) |

## *2.1 Results And Discussion*

### *2.1.1 Empirical formulation of friction factor*

In the present work, the friction factor was measured during experimental runs. In order to find the effect of flow parameters on the friction factor, a proper non-dimensional study was done for the friction factor. The friction factor is a function of various factors given in equation (4).

p

$$\lambda = f(Q, \rho, s_f, \mathrm{p}, \mathrm{D}_{50}, \upsilon, g, y) \tag{4}$$

Equation (4) can be transformed into velocity term.

$$\lambda = f(v, \rho, s_f, \mathrm{p}, \mathrm{D}_{50}, \upsilon, g, y) \tag{5}$$

Equation (5) converted into non-dimensional term

$$\lambda = f(\mathrm{Re}^*, Fr) \tag{6}$$

Where ,

$$\mathrm{Re}* = \frac{v^* \times \mathrm{D}_{50}}{\upsilon}$$

$$v^* = \sqrt{g \frac{\mathrm{A}}{\mathrm{p}} s_f}$$

$$Fr = \frac{v}{\sqrt{gy}}$$

The friction factor λ was assumed to be proportional to logarithmic of the parameters.

$$\lambda = a * \ln\left(\frac{b}{\mathrm{Re}_*^{\,c}} + \frac{c}{Fr^{d}}\right) \tag{7}$$

The experimental data sets were used to evaluate the values of empirical co-efficient a, b, c, and d. The predicted friction factor equation is:

$$\lambda = 0.208 \ln\left(\frac{2}{\mathrm{Re}_*^{\,0.145}} + \frac{1.251}{Fr^{0.083}}\right) \tag{8}$$

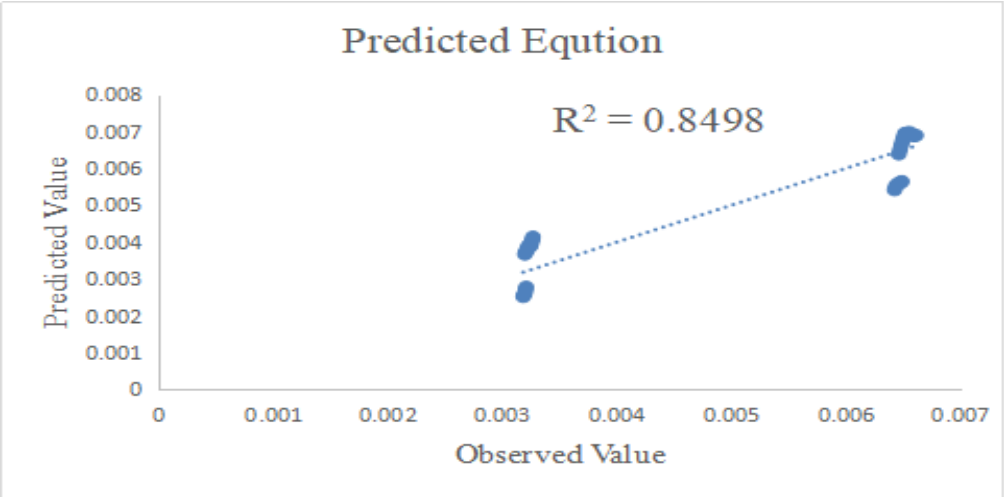



**Figure 2** Observed and Predicted Value of Friction Factor

Figure 2 shows the friction factor prediction value with the observed data. The performances of predicted equation (8) satisfy with the observed values.

### *2.1.2 Efficiency Criteria*

The efficiency criteria are designed to measure the accuracy of equation. To check the credibility of the empirical formula developed from the observed data, we take into consider following efficiency criterion.

### 2.2.3 *Co-efficient of Determination ($R^2$)*

Co-efficient of determination is proportion of dependent variable that is predicated from in-dependent variable. It is normally varies from 0 to 1. On the basis of data given in Table 3 and Fig 2, 3, 4, regression analysis of our developed formula generated an accuracy of 0.8498, which is far better than Rice et al (1998). From the comparison with other equations in table, this accuracy of indicates that our equation correlates with the observed equation.

**Table 3** Co-efficient of Determination of various equations

| Various Equation | Co-efficient of Determination ($R^2$) |
|---|---|
| Strickler | -1.435 |
| Kuelegun | -85.71 |
| Coles | -92.92 |

| | |
|---|---|
| Thomson and Cambell | -80.61 |
| Griffiths | -67.76 |
| Sarma et al | -36 |
| Bruching | 0.0422 |
| Swamee | -158.1 |
| Rice | 0.1653 |
| Julian | -1.435 |
| Lee | -0.326 |
| Pagliara and Chiavaccini | -9.168 |
| Predicted Equation | 0.8498 |

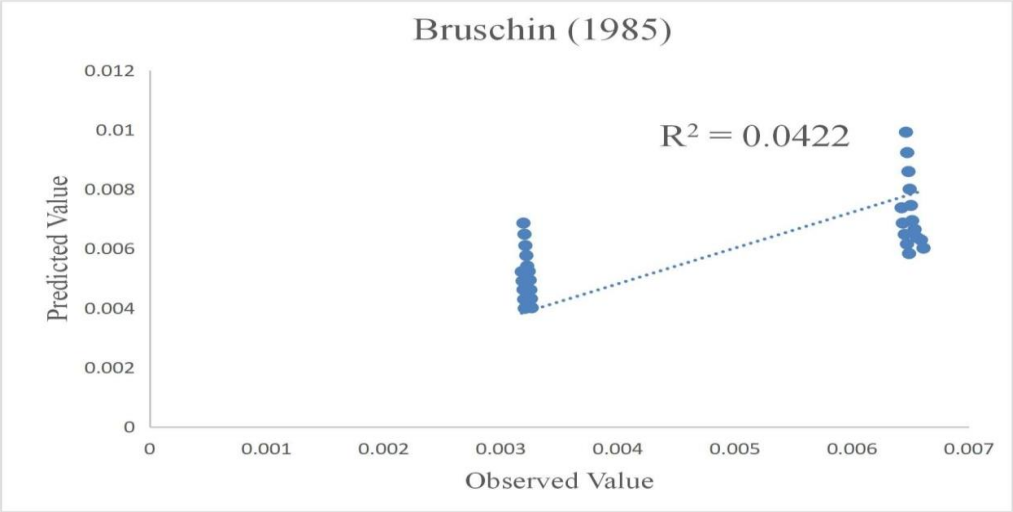



**Fig 3** Comparison between observed value and Bruschin (1985)

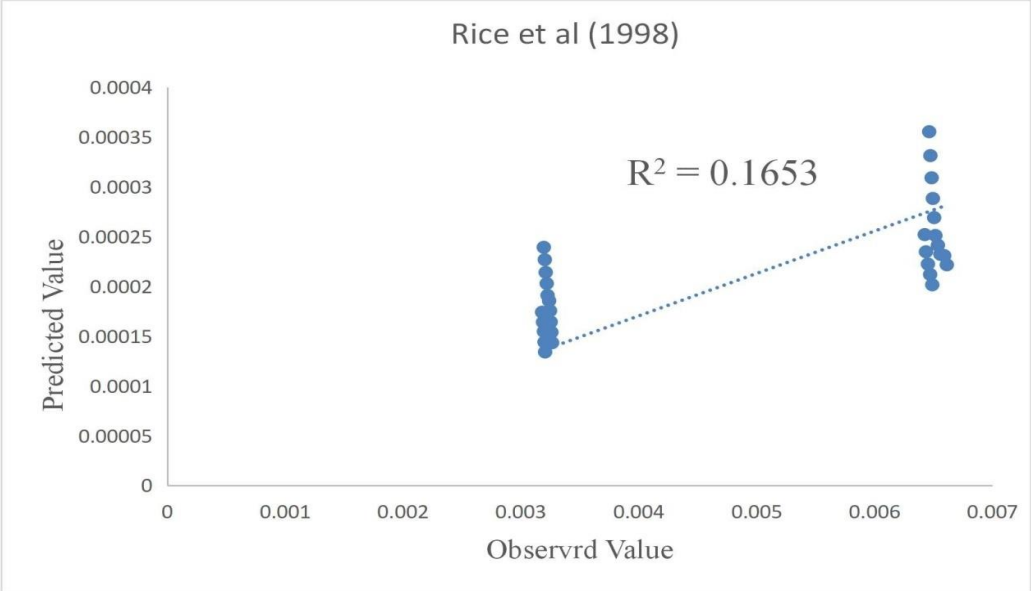



**Fig 4** Comparison between observed value and Rice at el (1998)

### 2.2.4 *Nash-Sutcliffe efficiency (E)*

Nash–Sutcliffe efficiency can be used to quantitatively describe the accuracy of predicted. Nash–Sutcliffe efficiency can range from $-\infty$ to 1.

$$E = 1 - \frac{\sum_{i=1}^{n}(O_i - P_i)^2}{\sum_{i=1}^{n}(O_i - \bar{O})^2} \quad (9)$$

Were, $O_i$ is observed value, $P_i$ is predicted value and $\bar{O}$ is mean of observed value.

**Table 4** Nash-Sutcliffe efficiency of various equations

| Various Equation | Nash-Sutcliffe efficiency (E) |
|---|---|
| Strickler | -0.4333 |
| Kuelegun | -0.3779 |
| Coles | -718.0692 |
| Thomson and Cambell | -0.7847 |
| Griffiths | -3.3264 |
| Sarma et al | -41.4696 |
| Bruching | -0.1716 |
| Swamee | -3946.1402 |
| Rice | -7.9539 |
| Julian | -0.5024 |
| Lee | -8.7673 |
| Pagliara and Chiavaccini | -858.5120 |
| Predicted Equation | 0.8627 |

By the comparison with other equation in Table 4, value of this parameter indicates that our equation very well correlates with the observed equation.

### 2.2.4 *Mean Squared Error (MSE)*

Mean Squared Error gives the average of the square of difference between the actual and the predicted value. Mean Squared Error is always non-negative, and values closer to zero are better.

$$MSE = \frac{1}{n}\sum_{i=1}^{n}(O_i - P_i)^2 \quad (10)$$

**Table 5** Mean Squared Error of various equation

| Various Equation | Mean Squared Error (*MSE*) |
|---|---|
| Strickler | 3.85994E-06 |
| Kuelegun | 3.71064E-06 |
| Coles | 1.93646E-03 |
| Thomson and Cambell | 4.80609E-06 |
| Griffiths | 1.16511E-05 |
| Sarma et al | 1.14371E-04 |
| Bruching | 3.15522E-06 |
| Swamee | 1.06296E-02 |
| Rice | 2.41129E-05 |
| Julian | 4.04600E-06 |
| Lee | 2.63035E-05 |
| Pagliara and Chiavaccini | 2.31467E-03 |
| Predicted Equation | 3.69744E-07 |

From the data given in Table 5, our equation is more accurate with the observed value among the other equations.

### 2.2.5 *Index of Agreement ($I_d$)*

Index of Agreement developed by Willmott and Wicks (1981), is a dimensionless value which predicts the accuracy of predicted equation. The range of Index of Agreement is 0 to 1.

$$I_d = 1 - \frac{\sum_{i=1}^{n}(O_i - P_i)^2}{\sum_{i=1}^{n}\left(\left|P_i - \overline{O}\right| + \left|O_i - \overline{O}\right|\right)^2} \quad (11)$$

**Table 6** Index of Agreement of various equations

| Various Equation | Index of Agreement ($I_d$) |
|---|---|
| Strickler | 0.5785 |
| Kuelegun | 0.4927 |
| Coles | 0.0671 |
| Thomson and Cambell | 0.5118 |
| Griffiths | 0.4642 |
| Sarma et al | 0.2169 |
| Bruching | 0.7266 |
| Swamee | 0.0306 |
| Rice | 0.3891 |
| Julian | 0.5987 |
| Lee | 0.3774 |
| Pagliara and Chiavaccini | 0.0677 |
| Predicted Equation | 0.9628 |

Tabulated value of our equation in Table 6 indicates that our equation correlates with the observed equation.

### 2.2.6 *Mean Absolute Percentage Error (MAPE)*

Mean Absolute Percentage Error also known as Mean Absolute Percentage Deviation (MAPD) gives accuracy in percentage.

$$MAPE = \frac{100}{n}\sum_{i=1}^{n}\left|\frac{O_i - P_i}{O_i}\right| \quad (12)$$

**Table 7** Mean Absolute Percentage Error of various equations

| **Various Equation** | **Mean Absolute Percentage Error** |
|---|---|
| Strickler | 27.5722 |
| Kuelegun | 45.4982 |
| Coles | 1043.5339 |
| Thomson and Cambell | 48.9773 |
| Griffiths | 82.3526 |
| Sarma et al | 260.5835 |
| Bruching | 37.1457 |
| Swamee | 2411.4799 |
| Rice | 95.2589 |
| Julian | 44.3692 |
| Lee | 99.9989 |
| Pagliara and Chiavaccini | 1102.0439 |
| Predicted Equation | 13.4413 |

Obtained result in Table 7 shows that our equation is precise and accurate in compare to any other equations.

## 3. Conclusions

The empirical equations derived so far by various scholars take into account parameters like Manning's co-efficient, cross sectional area of flow, hydraulics radius and so on. Although previous studies explored friction factor in the open channel flow, the problem of predicting friction factor in alluvial channels with non uniform particles with sufficient accuracy is of great interest to hydraulic engineers. Therefore, in the predicted equation proposed in the present study, the various parameters which would likely affect the friction factor value in a channel is considered. The different parameters taken into account are discharge, friction slope, bed width, kinematic velocity, shear velocity, hydraulic radius, observed flow resistance, discharge and median size of settlement; all these parameters when expressed as a non dimensional number can be expressed as Shear Reynold's Number, Froude's Number and as ratio of depth of flow and median size of settlement. The regression analysis performed on the predicted equation generates Co-efficient of Determination ($R^2$) to be 0.8498, Nash-Sutcliffe efficiency (E) to be 0.8627, Mean Squared Error (MSE) to be 3.69744E-07 and Index of Agreement ($I_d$) to be 0.9628.

Further to check the accuracy of our predicted equation in the present study, observed values of friction factor derived so far in previous literature were compared. It was found that the values of equation derived by previous researchers do not meet the required accuracy and are not within the range, whereas our predicted equation meets all the required accuracy and criteria.

## References

1. Bruschin, J. (1985). Discussion of " Flow Depth in Sand-Bed Channels " by William R. Brownlie (July, 1983). *Journal of Hydraulic Engineering, 111*(4), 736-739. doi:10.1061/(asce)0733-9429(1985)111:4(736)
2. Chen, C. (1991). Unified Theory on Power Laws for Flow Resistance. *Journal of Hydraulic Engineering, 117*(3), 371-389. doi:10.1061/(asce)0733-9429(1991)117:3(371)
3. Coles, D. (1956). The law of the wake in the turbulent boundary layer. *Journal of Fluid Mechanics, 1*(2), 191-226. doi:10.1017/s0022112056000135
4. Dey, S. (2014). *Fluvial Hydrodynamics Hydrodynamic and Sediment Transport Phenomena*. Berlin, Heidelberg: Springer Berlin Heidelberg. doi:https://doi.org/10.1007/978-3-642-19062-9
5. Fanning, J. T. (1896). *A practical treatise on hydraulic and water-supply engineering: Relating to the hydrology, hydrodynamics, and practical construction of water-works, in North America*. New York: D. Van Nostrand.
6. Griffiths, G. A. (1981). Stable-channel design in gravel-bed rivers. *Journal of Hydrology, 52*(3-4), 291-305. doi:10.1016/0022-1694(81)90176-1
7. Julien, P. Y. (2002). *River mechanics*. Cambridge: Cambridge University Press.
8. Keulegan, G. H. (1938). Laws of turbulent flow in open channels. *Journal of Research of the National Bureau of Standards, 21*(6), 707-741. doi:10.6028/jres.021.039
9. Krause, P., Boyle, D. P., & Bäse, F. (2005). Comparison of different efficiency criteria for hydrological model assessment. *Advances in Geosciences, 5*, 89-97. doi:10.5194/adgeo-5-89-2005
10. Kumar, B. (2011). Flow resistance in alluvial channel. *Water Resources, 38*(6), 745-754. doi:10.1134/s009780781106008x
11. Lee, A. J., & Ferguson, R. I. (2002). Velocity and flow resistance in step-pool streams. *Geomorphology, 46*(1-2), 59-71. doi:10.1016/s0169-555x(02)00054-5
12. Milhous, R. T. (1973). *Sediment transport in a gravel-bottomed stream* (Doctoral dissertation, Oregon State University, 1973). Corvalis, Oregon: Oregon State University.
13. Pagliara, S., & Chiavaccini, P. (2006). Flow Resistance of Rock Chutes with Protruding Boulders. *Journal of Hydraulic Engineering, 132*(6), 545-552. doi:10.1061/(asce)0733-9429(2006)132:6(545)
14. Rice, C. E., Kadavy, K. C., & Robinson, K. M. (1998). Roughness of Loose Rock Riprap on Steep Slopes. *Journal of Hydraulic Engineering, 124*(2), 179-185. doi:10.1061/(asce)0733-9429(1998)124:2(179)
15. Sarma, K. V., Lakshminarayana, P., & Rao, N. S. (1983). Velocity Distribution in Smooth Rectangular Open Channels. *Journal of Hydraulic Engineering, 109*(2), 270-289. doi:10.1061/(asce)0733-9429(1983)109:2(270)

16. Sharma, A., Herrera-Granados, O., & Kumar, B. (2019). Bedload transport and temporal variation of non-uniform sediment in a seepage-affected alluvial channel. *Hydrological Sciences Journal*, *64*(8), 1001-1012. doi:10.1080/02626667.2019.1615621
17. Strickler, A. (1923). Contributions to the Question of a Velocity formula and Roughness Data for Streams, Channels and Closed Pipelines, translated by T. *Roesgan and WR Brownlie. Translation T-10, WM Keck Lab of Hydraulics and Water Resources, California Inst. Tech., Pasadena, CA*.
18. Swamee, P. K. (1993). Generalized Inner Region Velocity Distribution Equation. *Journal of Hydraulic Engineering*, *119*(5), 651-656. doi:10.1061/(asce)0733-9429(1993)119:5(651)
19. Takács, G. (2015). *Sucker rod pump handbook*. Amsterdam: Gulf Professional Publishing.
20. Thompson, S. M., & Campbell, P. L. (1979). Hydraulics Of A Large Channel Paved With Boulders. *Journal of Hydraulic Research*, *17*(4), 341-354. doi:10.1080/00221687909499577
21. Vanoni, V. A. (1941). Velocity distribution in open channels. Civil Engineering. ASCE 11(6), 356- 357.
22. Willmott, C. J. (1981). On The Validation Of Models. *Physical Geography*, *2*(2), 184-194. doi:10.1080/02723646.1981.10642213
23. Yang, S., Tan, S., & Lim, S. (2004). Velocity Distribution and Dip-Phenomenon in Smooth Uniform Open Channel Flows. *Journal of Hydraulic Engineering*, *130*(12), 1179-1186. doi:10.1061/(asce)0733-9429(2004).

*IN PROCEEDINGS OF 25th HYDRO 2020, INTERNATIONAL CONFERENCE,*
*NATIONAL INSTITUTE OF TECHNOLOGY ROURKELA, ODISHA, INDIA*
*26-28, March 2021, ISBN 978-93-90631-56-8*

Paper ID - 047

# Effect of dense streambank vegetation with steep sloping riverbanks on Manning's roughness coefficient of 0.11 in hydraulic model studies

Ashish A. Doshi[1], Pramod B. Deolalikar[2]

[1]*Director, Infraplan Hydraulic Laboratory (IHL), Village Chandkhed, Tal. Maval, Dist. Pune 410506, India.*
[2]*Independant Hydraulic Consultant, former Joint Director, CWPRS, Salil, Chintamani nagar, Sahakar nagar No.2, Pune 411009, India.*
*Email – ashishdoshi@infraplan.in*

## Abstract

The Manning's Roughness Coefficient (n) is a major hydraulic parameter which extensively affects the estimation of velocities and consequently the water surface elevations along any water conductor system. The assessment of n value involves many uncertainties, as its estimation is based on literature, judgement and most importantly the slope of the water conductor system. Project reach is characterized with the highly vegetated steep sloping banks of the river. The riverbanks are mainly rainforests, densely vegetated with high trees and bushes. Riverbed is consisting of gravels, rocks and large boulders. The river slope is around 1 in 100 at the river reach under consideration. The daunting task as per the contract was to calibrate the hydraulic model of the river by reproducing the 'n' value of 0.11 (Prototype) for riverbank rainforests. Various alternatives were carried out to match these high friction values in the 3D comprehensive hydraulic as well as 2D mathematical model. The 'n' value in hydraulic model was then arrived based on the results of calibration. It was observed that, these high friction values do not affect much on the composite Manning's 'n' value of the river reach, especially due to the steep slope of the river. This paper represents the results of these studies and recommendations for steep river flows.

***Keywords*** *- Manning's roughness, streambank vegetation, River model calibration, steep sloping rivers*

## 1. Introduction

Principal of conservation of energy of flow as stated by Bernoulli considers the frictionless and incompressible fluid, in which the sum of the potential head, the pressure head and the kinetic head is the same for all points. Based on this, later Chazy derived the formula for calculating flow velocity, considering the resistance of the channels. He assumed a constant frictional value, due to limited data availability. Later investigations showed that frictional value is not constant but depends on the characteristics of the channel. Further, immense contribution in this regard is provided by many scientists namely; Kutter, Manning, Bazin, Kennedy, Lindley, Lacey, etc. Manning's formula is most popular due to its simplicity and applicability in most cases. Manning considered the frictional value to be dependent upon roughness and hydraulic radius, thereby simplifying the computations. Manning's formula is used extensively to predict the velocities and water surface elevations for various flood scenarios. Choice of the correct roughness coefficient, remains a subjective and most challenging task during the analysis of any water conductor system. The project reach under consideration is characterized with densely vegetated and wide river banks having steep side slopes. The river is also having steep gradient. Very sparse literature is available in this regard and choice of Manning's roughness coefficient becomes a factor which induces uncertainty in the predicted behaviors of the floods. Assuming the correct roughness coefficient and reproducing it in the laboratory on a scale model was the challenging task which need to be tackled in the current project. The problem was tackled by implementing a scientific approach by calibrating the river model. Both mathematical and physical models were built and the friction was analyzed in both the models. This paper discussed the procedure and the results obtained from the studies.

## 2. Manning's Roughness coefficient

One the most commonly used equations governing Open Channel Flow is known as the Manning's Equation. It was introduced by the Irish Engineer Robert Manning in 1889 as an alternative to the Chezy

Equation. The Manning's equation is an empirical equation that applies to uniform flow in open channels and is a function of the channel velocity, flow area and channel slope. Frictional resistance to the stream discharges is dependent upon flow-impending characteristics of stream channel and stream banks. Collective effect of these roughness characteristics retards the flow and is represented by a Manning's roughness coefficient in Manning's equation.

The procedure for estimating Manning's roughness coefficient (n value) is generally subjective, and the accuracy is largely dependent on a hydrologist's or engineer's experience in estimating these values over a wide range of hydraulic conditions. Even experienced hydrologists sometimes have difficulty in assessing accurately all the factors that contribute to flow resistance [Coon]. Manning's roughness coefficient is a major factor which affects the velocity and water surface calculations in any river reaches, and at the same time involves lot of uncertainty. In the following sections, few methods are discussed briefly, which are available to estimate the roughness values.

## *2.1. Estimation of Roughness values*

A lot of field data is required to confirm the selected values. In the absence of field data, the traditional approach is to predict the roughness value based on either of the following methods, which are subjective in nature. The various methods available and assumptions are discussed below.

### *2.1.1. Calibrated Photographs*

In this approach the Engineer uses calibrated photographs of the river reaches of known or measured 'n' values to associate hydraulic roughness values with conditions observed and anticipated in the Project reach. Chow (1959), Barnes (1967) and Aldridge & Garrett (1973) are the dominant sources of calibrated photographs. They represented photographs and cross-section of typical river and creeks and their representative 'n' values.

### *2.1.2. Acrement and Schneider (1989)*

They have summarized the procedure in "Guide for selecting Manning's Roughness coefficient for natural channels and flood plains". The most important factors that affect the selection of channel 'n' value are; a) The type and size of material that compose the bed and banks of the channel and b) The slope of the channel. Cowan (1956) developed a procedure for estimating the effects of these factors for determining the value of 'n' for a channel. The value of 'n' may be computed as follows.

$$N = (n_b+n_1+n_2+n_3+n_4)\, m$$

where;

$n_b$ = Base value of n for a straight, uniform, smooth channel in natural materials.
$n_1$ = Degree of irregularity
$n_2$ = Variation in Channel cross-section
$n_3$ = Effect of Obstructions
$n_4$ = Amount of Vegetation
m = meandering ratio (upto 1.2)

The modifying values for the various factors were developed from the analysis of 40 to 50 small and medium size channels, with top width less than 60 feet. Therefore, use of these adjustment values, is questionable for large channels, in which the hydraulic radius exceeds 15 ft, and large adjustments are required generally for narrow channels. As vegetation adjustment values are for vegetation that is uniformly distributed and not limited to streambank alone.

## *2.2. Factors affecting roughness*

'William F Coon', have published a report on the "Estimates of Roughness Coefficients for selected natural stream channels with vegetated banks in New York". This report is prepared by U.S. Geological

Survey in 1995. The following paragraph discuss the important aspects of this report pertaining to project study area. Roughness value has a good correlation with Hydraulic Radius R, Slope Sf, Streambed particle size and Relative smoothness, (R/d50). Other good correlated pairs are; Energy gradient and water surface slope, Stream top width and wetted perimeter, hydraulic radius and mean depth. The various relationships are discussed below in brief.

### *2.2.1. Relation between n and R*

Channels with low relative smoothness (R/d50 < 5), generally are in mountain streams with high gradients and large median bed particle size. The n value decreases rapidly for such streams with increasing depth and approach an asymptotic value as bank-full flow is approached, as shown by Sargent (1979) and Jarrett (1984). At higher depth flexible vegetation seem to bend and thus provides less resistance. On narrow (top width < 60 ft), low gradient channels (S<0.002) with less streambank vegetation, the n value is expected to increase with increasing depth, at least to the point of vegetation submergence.

### *2.2.2. Relation between n and Energy Gradient*

Hydraulic roughness increases with the increase in slope gradient, in general. Further, slope could be more reliable estimator of n value than size of bed material. In high gradient channels slope can exert a controlling effect on the n value, that can obscure the effect of streambank vegetation.

### *2.2.3. Streambank Particle size and Relative Smoothness*

Benson and Dalrymple (1967) have shown that, wide channels (top width > 100 ft) with R/d50 < 5 and bank-full stages as well as narrow channels with little or no streambank vegetation, following relation exists. All other factors, remaining constant, the hydraulic roughness of a channel will increase with an increase in bed particle size.

### *2.2.4. Streambank Vegetation*

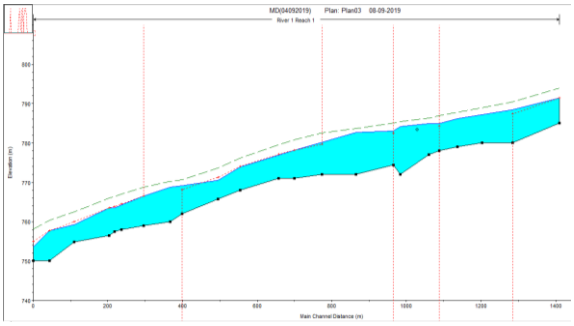
The narrow channels, normally less than 100 ft wide, require larger adjustments in n values for vegetation. Wide channels with no substantial channel bottom vegetation would require negligible adjustments, if any. The graphs of n against R values presented in “Station descriptions, hydraulic data and channel photographs for the 21 study sites” indicate that, bank vegetation has no measurable effect on the roughness coefficient of streams, that are wider than 100 ft and that have wetted perimeter less than 25% vegetated. At study sites where stream widths are less than 63 ft, vegetation that covers are more than 25% of the wetted perimeter causes the roughness coefficient to increase by as much as 0.005 during non-growing (vegetation) season and additional 0.002 to 0.012 during the growing (vegetation) season. The values for streambank vegetation adjustment for one site (East Branch Ausable River at Au Sable Forks), where the top width is about 200 ft and wetted perimeter is more than 30% vegetated, appears to range from 0.005 to 0.009. The n value computed is in the range of 0.055 to 0.057. The higher roughness coefficient values are generally adopted for the overbanks and floodplains with dense vegetation. The n values can vary from range of 0.1 to 0.4. These values are related with flatter slopes of overbanks / floodplains, with high degree of resistance to flow by vegetation.

### *2.2.5. Scale effects and Roughness*

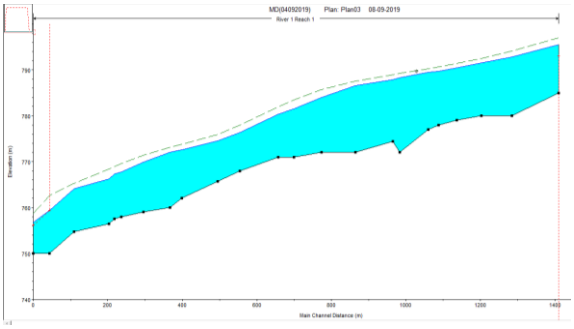
In the physical model, scale effects increase with reduction in scale. The scale effects normally have a damping effect, resulting in a higher frictional effects. Thus, sometimes reducing the roughness by ignoring geometric roughness similarity can result in an identical friction coefficient in both the model and real-world prototype, despite different Reynold number, resulting in a compensation of scale effects. (Heller, et al, 2011).

### *2.3. Effects of n value on water surface profiles*

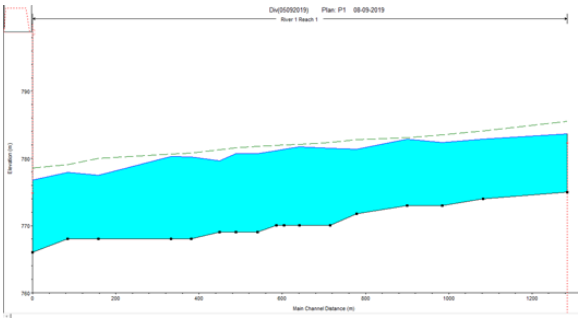
Following comparison shows the water surface profiles predicted for the different n values assumed, for different river slopes. It is clearly evident that higher n values will result in lower velocities and higher water surface elevations. Depending on the flow depths and velocities, the predicted flow regime can vary from super-critical to sub-critical, for higher n values. Hence, the correct assumption of n value is very important.



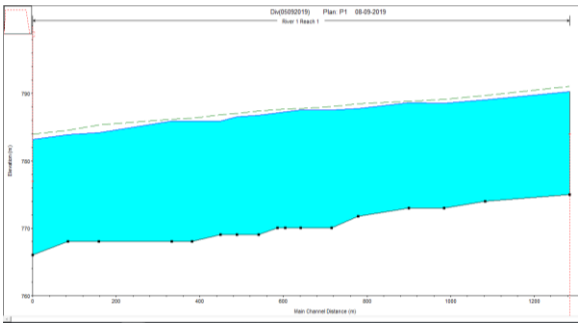
i-a) n value = 0.06



i-b) n value = 0.1



ii-a) n value = 0.04



ii-b) n value = 0.08

Figure 1 – Water surface profiles obtained in Hec-RAS model for different n values

## 3. Project reach

The project is located in tropical rainforest in mountainous terrain. The highest flood discharge estimated for 1 in 2 year return period is 1000 cumec and that of 1 in 500 year flood frequency is around 3100 cumec. The yearly average discharge is around 15 cumec. Powerhouse is envisaged to be operated for a design discharge of 20 cumec. The longitudinal slope of the river bed is around 1 in 100 at the project reach. The water depth of the 1 in 200 year flood is around 8 to 12 m and stream width of around 50 to 70 m. The river has wide banks with highly vegetated forest cover.

### *3.1. Riverbed*

The riverbed consists of gravel, rock and boulders with a diameter up to 5 m, however most boulders are of less than 1 m in diameter. The riverbanks are lined with rock (steep slopes), boulders, trees and bushes. Size and shape of the cross sections vary occasionally. Dredged channels, considerable bed roughness and moderately sloughed side slopes can be identified. Almost no vegetation is observed inside the riverbed. The typical condition can be seen in the Figure 1 below. The partial roughness coefficients derived from these descriptions (according to Arcement and Schneider 1989) yield an overall roughness coefficient of 0.05, which was adopted by project authorities for the river channel bed which is in good conformity with Barnes (1967) and Chow (1959).

### *3.2. Streambanks*

Floodplains are typically characterized with the steep slopes covering tall trees of more than 15 to 20m height, which are very densely vegetated. The vegetation of the floodplains mostly consists of medium to large trees. Firm soil with slight surface irregularities can be found. Few obstructions such as downed trees and flood debris are present. Ground cover consists of weeds and small undergrowth. The typical streambank can be seen in the Figure 2 below. This leads to an estimated roughness coefficient of 0.11 by the project authorities. There are some patches of the mountains covered by medium size weeds and bushes. For the areas of the flood plains with a dominating characteristic of smaller vegetation, such as growing bushes, a roughness coefficient of 0.06 was estimated by project authorities, which is in good conformity with Barnes (1967).



**Figure 2** - Riverbed channel showing large boulders




**Figure 3** – Densely vegetated steep sloping riverbanks

Conclusively the project domains was divided into three different types of landscapes with their characteristic Manning coefficients;

- Bushlands: 0.06
- Rainforest: 0.11
- Riverbed: 0.05

## 4. Model studies

A comprehensive, geometrically similar, three-dimensional model on Froudian similitude for a scale of 1:40, for assessing the performance of proposed Dam Spillway was constructed. A river reach of 900 m upstream and 500 m downstream of dam axis was reproduced in the model. As per the contract the requirement was first to construct the river portion in the reach and calibrate it for the given discharges and water levels. The pre-defined water levels were established in the physical model by adjusting the friction. The various alternatives were tested to reproduce the high friction values in the model. In the second step the spillway structure would be fixed inside the calibrated river model to assess its impact and hydraulic behavior.

### *4.1. Mathematical model*

LiDAR survey was carried out for entire project area and contours were obtained. Bathymetry survey of the project area was carried out. The bathymetry survey was used for the river bed whereas LiDAR survey prevailed for the streambanks. Cross sections were worked out from these surveys using GIS software. The horizontal extend for the project domain was selected to be about 4 km of the river length. The dam structure was placed roughly in the middle of the respective domain. For the finalization of the horizontal extend, requirements for the inlet and outlet boundary condition had to be met. For the inlet boundary condition, a river section with a relatively flat slope was chosen, so as to assures subcritical inlet boundary conditions. The river section for the outlet was chosen by a relatively steep slope in the area in order to assure supercritical outlet boundary conditions in the simulation. In order to take into account, the different landscapes and therefore different Manning coefficients, an analysis of satellite recordings was carried out. By this analysis the surrounding area of the river could be divided into regions with bushland and areas with growing trees. Manning coefficients of 0.06 for bushlands and 0.11 for forest areas were applied. For the riverbed itself a value of 0.05 was selected for the corresponding Manning coefficient.

### *4.2. Procedure for Calibration of the physical river model*

The adopted methodology for the calibration of the physical model was as follows;

- The physical models was calibrated based on the results of the mathematical models. This calibration was carried out without structures in the riverbed in order to ensure that the impact of the structures on the rivers is properly assessed.
- The calibration consisted of various trials which were carried out by using various materials such as coarse sand, sandpaper, gravels, pebbles, acrylic teeth, etc. or any other suitable material, to increase the friction of the river bed and banks. During the trials, the roughness values applied in different areas of the mathematical model were recreated in the same areas in the physical models.
- It was pointed out that shallow obstacles, commonly used to reproduce high roughness values in physical models, will lose their impact with increasing water depth to the contrary of trees as stream bank vegetation, which obstruct water flows all the way up to their crown. It was therefore required to employ obstacles in the physical model that capture this effect over the entire water level range. To achieve this, plastic or aluminum rods of up to 40 cm length may be used as obstacles. It was expected that the high friction of rods may distort flow conditions and thus may result in excessive roughness values. To counteract this, the density of rods was varied such as to achieve the desired water levels.
- The upstream and downstream water levels at the start and end of the physical model domains were adopted according to the numerical model results for the different discharges to be calibrated.

- This procedure was carried out in an iterative manner until a satisfactory similarity between the physical and mathematical models was achieved. The similarity was proven by comparing the Manning roughness coefficients' as per numerical and physical models as well as by comparing water levels in control sections.
- The calibration was done sequentially for the 10-years return flood (1500 cum/sec), the 200-years return flood (2500 cum/sec), corresponding to the design flood, and the 500-years return flood (3000 cum/sec), corresponding to the safety flood. The riverbeds were calibrated for the 10-years return flood first. Materials used in this first calibration phase to reproduce the riverbed, bushland and trees roughness, and thus to increase friction, were retained for the next calibration phase which was performed for the next higher flow. Additional materials required to increase the friction for the next phase were applied only in areas where they don't impact the water levels calibrated in the previous phase. This procedure was repeated until the highest flood discharge was calibrated.
- After the calibration process of the river beds and banks, the dam models were installed in the river models and further detailed experiments were carried out.

### *4.3. Reproduction of the high friction in physical model*

River channel bed and banks were marked on the river cross sections as per the survey data. The areas of different roughness values were identified and marked on the model. Pebbles and grit were used to reproduce the high friction in the river bed channel. The size and density of the pebbles and grit was varied as per requirement. For the reproduction of model trees, steel rods of 8 mm diameter were installed vertically on river bed, and the plastic leaves were tied to it. This arrangement is removable and fast. Further, spacing of trees could be altered as per requirement very quickly. Even the density of the leaves of the trees can be adjusted vertically, which again adds to the friction. Further at areas where bushlands were to be reproduced on the river banks, again the pebbles and grit were used. Figure 4 shows the roughness raster alongside the photographs of reproduction of high friction in the river model. Various trials were carried out to understand the effect of friction and the desired water levels were successfully achieved in the model. At first the 10-year return flow was calibrated, followed 200-year and 500-year return floods. Spillway and power intake structures were installed after the calibration process was completed, by excavating the river bed and removing the trees in the vicinity. Further hydraulic model studies were conducted for analyzing discharging capacity, energy dissipation at the downstream, gates and power house operations, etc.

## 5. Results and Discussions

Following observations were made from this exercise;

- In the first step trials were made to evaluate the water levels in the river model without any friction applied. When the inlet and outlet boundary conditions are maintained, it was observed that, the water levels in-between drop below the expected levels by large extent. The flow shoots up at curves and bends of river and the main controlling factor is longitudinal slope of the river. The high velocity flow is being concentrated along the center line of the river. The water levels observed at the banks are well below the expected levels.
- Various trails were carried out, by changing the density of trees and changing the plaster roughness on riverbed, for finding the best match for all three discharges. The current arrangement as shown in photographs in Figure 4, shows a good match for all three discharges. It is noted that, very high-density trees are required at some places, to reproduce the desired water levels.
- Considerably higher water levels are observed at near the banks after reproducing high friction. Without friction the flow in the river is observed to be concentrated at some locations. Friction has helped in avoiding these flow concentrations, and the flow is observed to be streamlined. The difference in the flow conditions can be observed in the Figure 5.
- Water levels were compared from mathematical and physical model for all the cross sections. The examples are shown in Figure 6 for various cross sections along the length of the river. It can be seen from the comparison of graphs, that the water surface profiles are matching quite very well. Further it was observed that, water surface patterns at cross-sections are getting exaggerated in the physical model, especially at curves and bends, due to scale effects.

- For the river reach under consideration, the average composite roughness value (Manning's roughness coefficient, n) was estimated to be 0.05 for 10-year return period flood, whereas it was 0.055 for the 200-year and 500-year return period flood.
- The trees on the streambanks have resulted in higher water levels near the banks. There is not much effect on the water levels and velocities in the central portion of the river. The maximum flow is passing through the central portion of the river due to high velocities and large cross-sectional area.
- As the maximum flow is passing through the central portion of the river, the flow velocities do not differ considerably.
- The flow is being controlled mainly due to the higher slope gradient of the river and the vegetation on the banks have very limited effect on the average flow velocities and flow depths except near the banks.
- As such when the spillway structure was installed along with the power intake structure, a good reservoir is formed on the upstream of spillway for the length of around 120 m. The flow conditions are completely governed by the operation of gates. Comprehensive experiments were conducted for the spillway to analyze the overall flow conditions. It was observed that, due to the steep slope of the river, very high momentum of the flow passes through the spillway, generating high velocities.

## 6. Conclusion and Recommendations

From the above experiments and calibration studies, it was concluded that;

- Higher Manning's roughness coefficient (n) values were observed on the flatter gradient, whereas n value decrease with the increase in river slope.
- With the increase in discharge, n values observed to increase marginally for the river reach under consideration.
- Friction has little or negligible effect on the overall flow conditions, especially in the presence of spillway structure. The higher friction has negligible effect on the upstream water levels and these are totally controlled by the gate operations.
- High gradient of the river is the controlling factor in the absence of the spillway structure and friction has limited effect.
- The water levels in the vicinity of the river banks varied considerably due to the frictional effects along the streambank. However, it has very negligible effect on the flow velocities as the maximum flow is passing through the center of the river channel.
- Composite Manning's Roughness Coefficient ('n') value should be restricted to maximum 0.06 for reproduction of the higher friction in the model for the wide and steep sloping banks and steep gradient rivers.

## References

George J Acrement Jr, and Verne R. Schneider, 1989. Guide for selecting Manning's roughness coefficients for Natural channels and floodplains, U.S. Geological Survey water-supply paper 2339.

Harry H. Barnes Jr (1967), Roughness Characteristics of Natural Channels by Colour photographs and descriptive data for 50 stream channels for which roughness coefficient have been determined. U.S. Geological Survey water-supply paper 1849.

Henderson F. M., 1966, '*Open channel flow*' Macmillan Publication.

Robert D. Jarrett (1985). Determination of Roughness Coefficients for streams in Colorado, U.S. Geological Survey, Water-Resources Investigations Report 85-4004.

Ven te Chow, 1959, '*Open Channel Hydraulics*, McGraw-Hill Publication.

William F. Coon (1995). Estimates of Roughness Coefficients for selected natural stream channels with vegetated banks in New York by, U. S. Geological Survey open file report 93-161.

M. Fathi-Moghadam, M. Kashefipour,N. Ebrahimi, S. Emamgholzadeh, Nov 2011. Physical and numerical modeling of Submerged vegetation roughness in Rivers and Floodplains, Artical in Journal of Hydrologic Engineering.

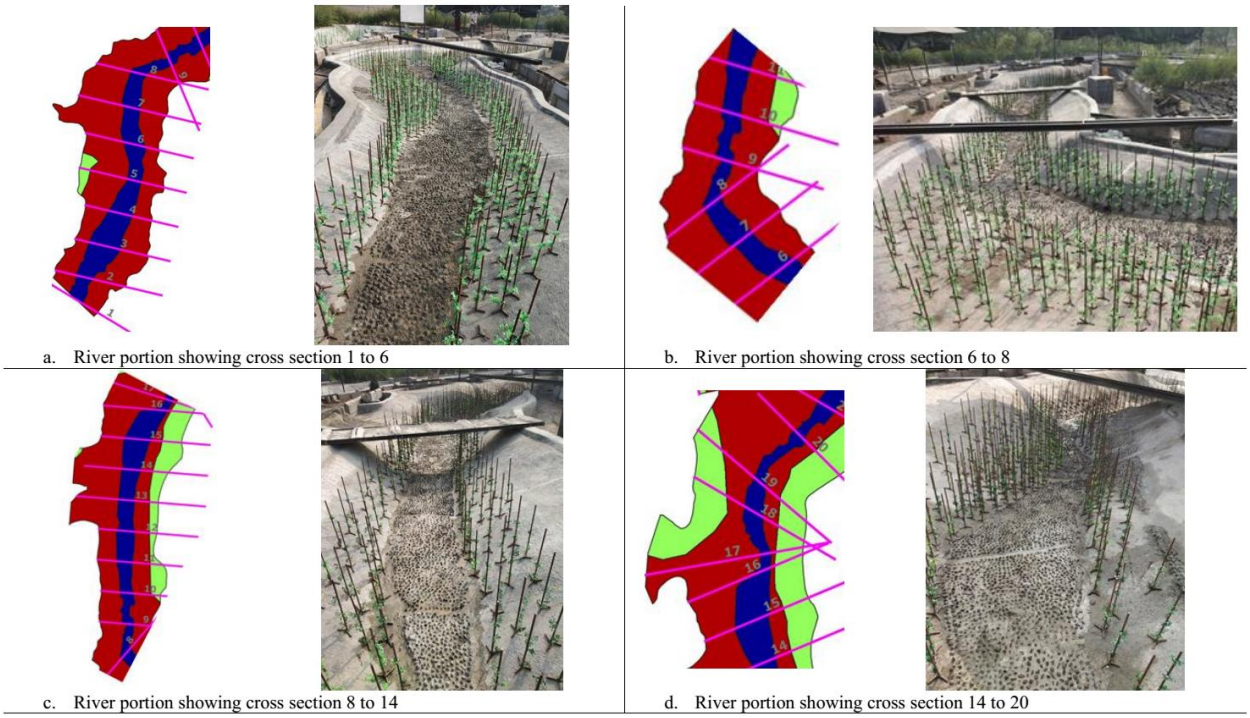



**Figure 4** Reproduction of high friction, pebbles and grit was used in the river bed and tress were modelled in the river banks




**Figure 5** Effect on the flow conditions due to high friction (such as tall trees) at the stream banks.

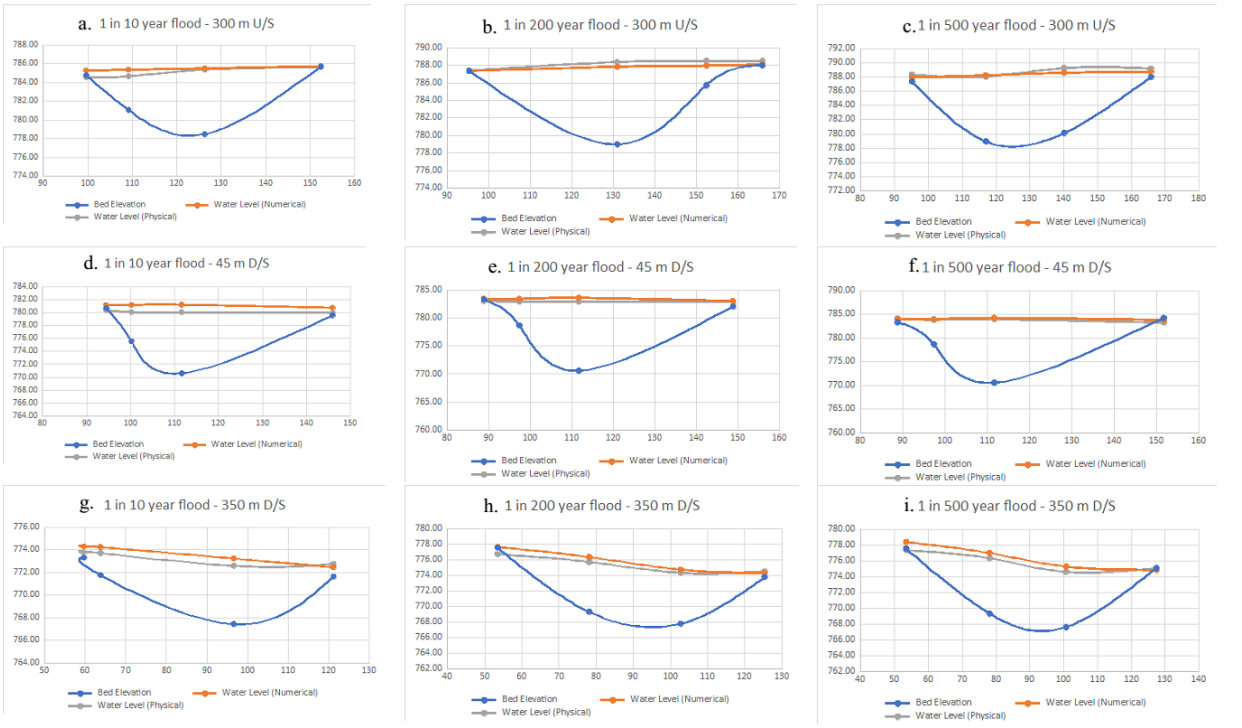



**Figure 6** Graphs showing comparison of water surface profiles obtained from Mathematical and Physical model.

*IN PROCEEDINGS OF 25th HYDRO 2020, INTERNATIONAL CONFERENCE, NATIONAL INSTITUTE OF TECHNOLOGY ROURKELA, ODISHA, INDIA 26-28, March 2021, ISBN 978-93-90631-56-8*

Paper ID - 087

# Discharge predictions of meandering river using artificial neural networks

Tushar Khankhoje[1], Susmita Ghosh[2]

[1]*Research Scholar, Dept. of Civil Engineering, National Institute of Technology (NIT), Silchar, Assam, 788010, India*

[2]*Assistant Professor, Dept. of Civil Engineering, National Institute of Technology (NIT), Silchar, Assam, 788010, India*

*Email: susmita@civil.nits.ac.in*

## Abstract

For streams the most important parameter is the discharge. It is essential to establish rating curve well in advance. But the discharge prediction problem lies for meandering rivers where the influence of the curved geometry (due to erosion/deposition) is highly pronounced, may lead to flood problem on its banks, e.g. Barak river. ANN model was used to address this problem. Sinuosity values were extracted from remote sensing tool. Knowing the monthly head and discharge values of past 13 years, it would predict the future values of discharge for this river. Four parameters as input variables viz. head, slope, sinuosity of the current month as well as the previous month's discharge, one output variables i.e. current month's discharge was considered. The impact of learning rate of the developed ANN model was examined on the basis of performance indices like RMSE, coefficient of correlation, coefficient of determination. In the present study, the ANN model was developed using data sets of Barak river (Annapurna Ghat gauging site). It can be useful for better planning of flood warning system.

***Keywords:*** *Discharge prediction; ANN; sinuosity; remote sensing*

## 1. Introduction

For a given stream, the rate of flow, known as discharge is the most important parameter to know its nature and general behavior. The stage and discharge obey a certain relationship which is represented as a rating curve (Sahoo and Ray, 2005). The discharge mainly depends upon factors like head (flow depth), bed slope, area of flow, wetted perimeter, roughness parameters (coefficients). According to certain equations, the discharge can be calculated from the flow parameters as well as channel geometry (Sapkale, 2014). These are mainly Manning's equation, Chezy's equation, Darcy Weisbach equation, etc. These are valid only for straight channels, not for bent or curved channels (Dash and Khatua, 2016).

The discharge through any channel depends upon channel geometry parameters like those mentioned above, as well as nature of the surface (roughness coefficient). Its value is derived from various factors which offer resistance to flow (Coon, 1995), in which, 'm' represented the correction factor due to meandering. An empirical formula was given by Khatua et al. (2013) after performing stage-discharge experiments using channels of different sinuosity indices in the laboratory. Especially if its extent is large, channel bends may cause huge variation from the normal results of calculating the discharge. So, an accurate model needs to be established to study the contribution of meandering to the discharge of the stream.

### 1.1 *Meandering Rivers and its Parameters*

The rivers usually do not flow perfectly straight. Due to the presence of sediment load (as a consequence of continuous erosion and deposition) in alluvial rivers, one of its banks undergoes erosion and the other one sedimentation. This process continues with time. A stage comes when the river geometry is significantly changed from its original straight course. This is known as meandering of rivers (Barman and Goswami, 2015). Slowly the river follows a sinuous or S-curve which grows large with time. There are various undesirable effects of meandering near to its banks and the riparian life (Aswathy et al., 2007). The extent of meandering can be determined w.r.t parameters like

sinuosity and radius of curvature, criteria for sinuosity is shown in Table 1. These are explained in further sections.

### 1.2 *ANN as a Prediction Tool*

ANN is a tool which is recently being introduced for solving very complex input-output relations (Karunanithi et al., 1994). The word 'Artificial Neural Network' comes from biological neural networks in which there are trillions of unit cells (called neurons), which perform learning operations in the human brain (Maier and Dandy, 1996). The idea of ANN is to mimic the human brain upto certain extent. There are various applications of ANN. In many practical problems, where we don't know the actual underlying process, ANN has the solution based on past dataset. ANN can be utilized for solving various on-field problems accurately, where other techniques may fail (Kumar et al., 2016). There are mainly 2 types of ANN learning, i.e. supervised learning & unsupervised learning. In the former case, we have known values of input-output, which is applicable in this project.

For using ANN, we need computer platforms, as manual calculations take long time and efforts. MATLAB is very convenient Software to code ANN back propagation algorithm. Solving matrices is very simple in MATLAB. ANN has its inputs, outputs, weight values which can be represented in matrix form and fed to MATLAB directly.

## 2. Study Area and Data Collection

### 2.1 *Study Area*

In a broad sense, the area of the river 'Barak' lying within the Cachar district of the state of Assam is considered for this research. The Barak river, as the name suggests, is derived from two words i.e. 'Bodo' meaning big or high and 'Bak' means bends. Therefore it is certainly a river of high bends or in simple words we call it as a highly meandering river. The river originates from the Manipur hills named as the 'Mukru River'. After passing through various North-Eastern states of India i.e. Manipur, Meghalaya, Mizoram and Assam, it reaches Bangladesh. Ultimately the river drains into the Bay of Bengal at Bangladesh. The path of flow of the river is shown in Figure 1.

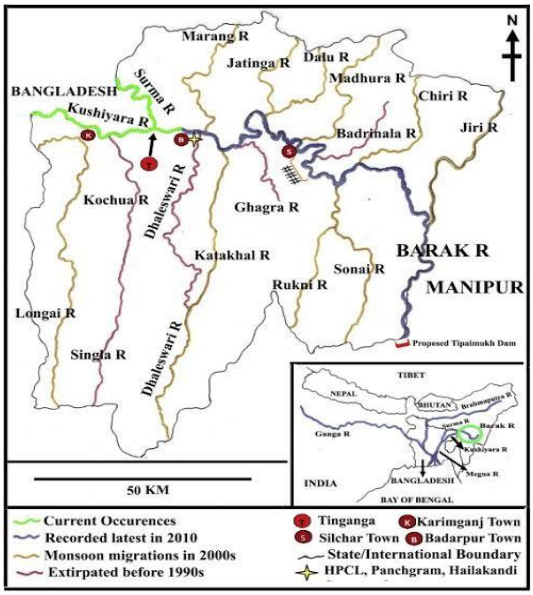



**Figure 1** Barak river and its tributaries (Source:https://imgs.mongabay.com/wpcontent/uploads/sites/30/2019/04/29075112/Barak-map.jpg)

There are mainly two gauging stations at this river lying within the district of Cachar. These are mainly the Annapurna Ghat and the Badarpur Ghat station. Some other sites are also available to measure the flow rate of this river. The gauging sites measure the water levels as well as the discharge passing across the section. The Annapurna ghat gauging site lies near the Silchar railway station and as shown in the Figure 2. Its location is given as 24°49'58"N latitude and 92°47'24"E longitude.




**Figure 2** Annapurna ghat and its adjacent flow path
(Source: Google map)

## 2.2 *Data Collection*

In this work, field data as well as map data was collected, both through a different medium. The role of the past dataset almost decides the accuracy of the prediction as well as efficient use of the program (Tayyab et al., 2016). So care was of utmost importance during the data collection and its proper organization in a standardized form (Riad et al., 2003). The use of Microsoft Excel is quite easy and robust so as to put the data in a well organized manner. Two methods of data collection were adopted as per its type. These are as mentioned in the below sub-sections.

### 2.2.1 *Field or observed dataset*

As we know, the discharge is primarily a function of flow depth (or simply the hydraulic head). Along with it, the stream flow depends upon channel geometry i.e. area of flow, wetted perimeter, slope of the energy line (bed slope in case of uniform flow), roughness coefficients (Petrovszki et al., 2014). If we calculate on monthly basis, all the parameters have to be available in the form of monthly average (or total). In our case of research, we had the data available from the gauging site, i.e. Annapurna Ghat station. The 'Water Resources Department' of Silchar division had provided the past data as monthly values. A total of 13 years data was obtained from the month of January, 2006 to December, 2018. The 'Average monthly head' and the 'Total monthly discharge' dataset were obtained from the department. In this way the number of data points we had with us was 13 x 12 = 156.

### 2.2.2 *Map data*

The two other parameters affecting the discharge of such rivers are the bed slope as well as sinuosity. The sinuosity index (S) of a meandering river is defined as the ratio of curved length to straight length between two points along its length (Friend and Sinha, 1993). There are various definitions of sinuosity index given by different researchers, according to the type of length data available to us. In this work, the sinuosity is calculated as the ratio of stream length (Lm) to valley length (S) (Friend and Sinha, 1993). Let us consider Figure 3:

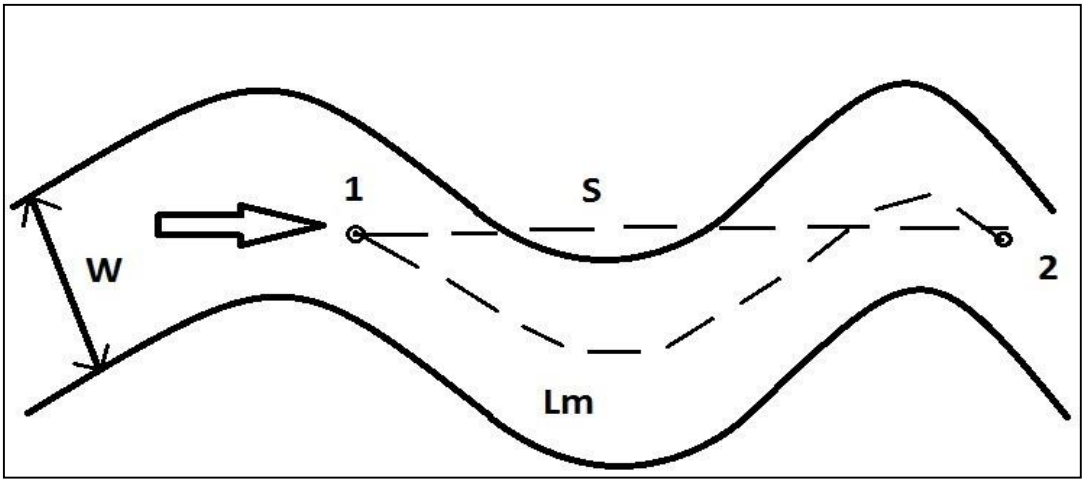



**Figure 3** Schematic diagram of sinuosity

In this case, S = valley length between 1 & 2 (length of meandering axis) and Lm = stream length between 1 & 2 (centre-line length).

This formula is valid only if the stream length is greater than 20 times the bankful width (Rosgen, 2007). For this we found bankful width using Google Earth software as shown in Figure 4. Bankful width, b came out to be 249m, hence 20b = 4980m. Whereas the minimum stream length considered (l) was 6.35 km or 6350 m. As l > 20b, hence our minimum length criteria was satisfied.




**Figure 4** Bankful width of river

**Table 1** Channel classification based on sinuosity index

| Sinuosity Index | Types of River Path |
|---|---|
| 1 | Straight channel |
| 1-1.5 | Sinuous channel |
| >1.5 | Meandering channel |

Barak river is considered as a meandering river. Its sinuosity needs to be studied as an extent of meandering for flow predictions. The use of satellite images has made it very easy to extract important features of the ground. With the help of Google Earth software, we have found out the two

parameters i.e. sinuosity and slope which affects the discharge as shown in Figure 5 and Figure 6 respectively.




**Figure 5** Topographic representation of sinuosity

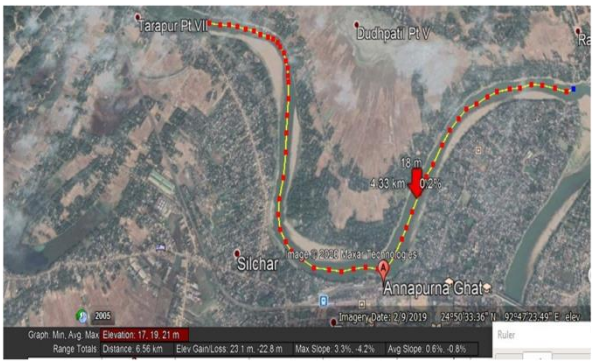



**Figure 6** Slope representation in Google Earth

## 3. ANN Model Setup

### 3.1 *General*

In this chapter, the computational features are described which are used for setting up the ANN model in MATLAB. The basics of how the data is arranged and fed into the back propagation network are explained further. The selection of input and output along with the hidden layer characteristics are described at the end.

### 3.2 *Backpropagation Network Flow Diagram*

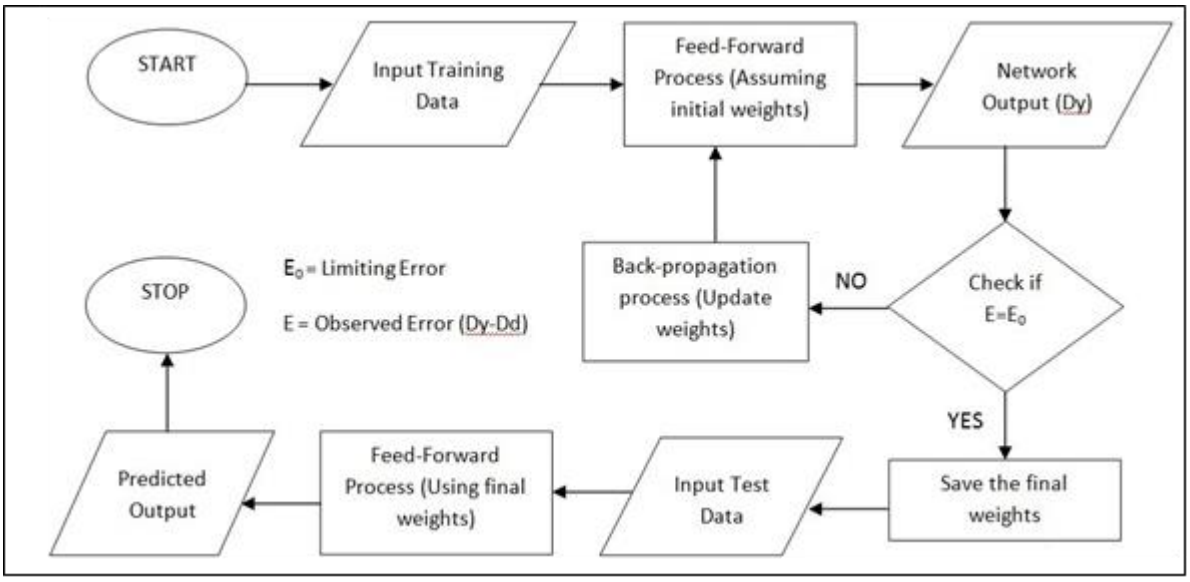



**Figure 7** Flow chart of backpropagation network

The process involved in the complete working of this network can be visualized by the block-diagram as shown in Figure 7 and is explained as follows:

#### 3.2.1 *The feed-forward process*

The first and foremost step of this network is the input of known dataset. This data is transformed as the output after assuming initial weights and finding the network output (Guru and Jha, 2019).

### 3.2.2 *Comparison of network output and desired output*

The first attempt of weight assumption never gives the desired output but certain error. This error is squared up and its gradient w.r.t. initial weights, is determined (Alvisi *et al*., 2005).

### 3.2.3 *The backpropagation process*

Using the gradients as calculated above, a portion of the error is transferred backwards (right to left) and distributed according to their weights. New updated weights are obtained (Kisi, 2004). It completes one cycle of FFBP. Repeat all the above steps until the error reaches a certain limiting value (minima). The final weights are saved and used for other unknown Inputs for which output is to be predicted.

## 3.3 *Matrix Approach of Input-Output*

For a given point in the loop, the dimension of 1st weight matrix (input to hidden layer) is 'h x 4' and that of input being '4 x 1'. So the product of the two would be 'h x 1'. It is the input of hidden layer. Using the activation function, this is transformed into output of hidden layer (having same dimensions 'h x 1'). The next weight matrix (hidden to output layer) should have the dimensions '1 x h'. Therefore the product of this weight matrix and output of hidden layer will give us the input of output layer (1 x 1). Using a linear transfer function, we get the network output (same dimension 1 x 1, or simply '1'). This can be further extended for more no. of hidden layers. But in our case, one hidden layer was sufficient.

## 3.4 *Equations for BPN*

For solving the backpropagation network, some system equations are put into the frame, as internal process of ANN. Although a black-box model, some governing equations are used for the learning of the system. These are as shown from eqn.1 to 9:

$$\frac{\partial E}{\partial Wij} = \delta j * xi \tag{1}$$

$$o'j = oj * (1 - oj) \tag{2}$$

$$\varphi'j = (1 - \varphi j) * (1 + \varphi j) \tag{3}$$

$$\varphi'j = \varphi j * (1 - \varphi j) \tag{4}$$

$$ej = (oj - tj) \tag{5}$$

$$\delta j = ej * o'j \tag{6}$$

$$\delta j = \sum(\delta j * wj) * \varphi'j \tag{7}$$

$$\Delta wij = \alpha * \frac{\partial E}{\partial Wij} \tag{8}$$

$$w'ij = wij + \Delta wij \tag{9}$$

Here, $e_j$=absolute error at jth output node, $w_{ij}$=weight of ith node of hidden layer to jth node of output layer, $x_i$=input signal at the ith node, $\delta_j$=a factor for back-propagation error at jth node, E=sum of squared error at output layer, Δwij=small change in weight between ith hidden node and jth output node, $\varphi_j$=weighted sum of inputs at the jth hidden node, $\varphi'_j$=derivative of $\varphi_j$ in the jth hidden node,

$o_j$=network output at the jth output node, $o'_j$=derivative of $o_j$ in the jth output node, $t_j$=target output at the jth output node and $\alpha$=learning rate.

### 3.5 *Backpropagation Network Parameters*

#### 3.5.1 *Input-Output Parameters*

The dependency of hydraulic head (flow depth) with the discharge is well known. So, one of the factors is the head. Now, the slope of hydraulic gradient line (HGL) is another factor. But for uniform flow, water surface slope is same as bed slope as well as that of HGL. Keeping the channel geometry as constant, we try to find out the influence of sinuosity to the discharge. As mentioned previously, the roughness parameter is itself involved in discharge by different standard formulas. The bending of river causes additional loss in flow. This loss is incorporated in sinuosity. The resulting ANN structure is shown in Figure 8. For our network, 4 parameters were selected as inputs, as mentioned below.

Inputs
i. Average monthly head (current month)
ii. Previous month's discharge
iii. Sinuosity index (current month)
iv. Slope of water level (current month)

Only one parameter was selected as output of the network i.e. current month's discharge.

#### 3.5.2 *No. of Hidden Layers*

With more no. of hidden layers, the no. of weights will increase. Hence, for the same accuracy of work, more training patterns would be required. But doing so also increases the overall efficiency of the network (more no. of weights refers to more accuracy in general). Having a limited no. of data points (i.e. 156 in total), we opt for only one hidden layer in this network The no. of nodes in the hidden layer was also selected based on the data available for training the network and accuracy desired. The no. of nodes in the hidden layer should be between no. of input and output nodes i.e. between 1 and 4, and in no case exceed twice the no. of input nodes (i.e. 4x2=8) (Karsoliya, 2012). So we have taken 3 hidden nodes.

#### 3.5.3 *Activation Function*

For the conversion of input at any node into the output, there are some specifications which are to be maintained like the range of values, linearity or non-linearity, the operator and many other aspects of network. The function which transforms the nodal input into the output, with a suitable range, is known as the activation function. It acts as a bridge between the input and its corresponding output. The main significance of this function is to add non-linearity to the network, which makes the artificial neural network an upper hand over conventional methods of regression. The activation function is layer specific, i.e. for each layer one may adopt a different function for improving the performance as required by the user. Table 2 shows how to deal with different layers in terms of activation function.

**Table 2** Some commonly used Activation Functions

| Activation Function | Formula | Range |
|---|---|---|
| Linear | y = x | (-∞,+∞) |
| Absolute | y = \|x\| | [0, +∞) |
| Sigmoid | $y = \frac{1}{1+e^{-x}}$ | (0,1) |
| Tanh | $y = \frac{e^{x}-e^{-x}}{e^{x}+e^{-x}}$ | (-1,+1) |
| ReLU | Max (0, x) | [0, +∞) |

Here, x = net input to the node and y = transformed output at the node. In our case, for two layers the activation function has been used as given below:

i. For hidden layer : sigmoid activation function
ii. For output layer : absolute activation function

The choice of activation function depends upon the complexity of the problem. For linear approach, one can adopt a linear function. In this case, the hidden layer becomes insignificant.

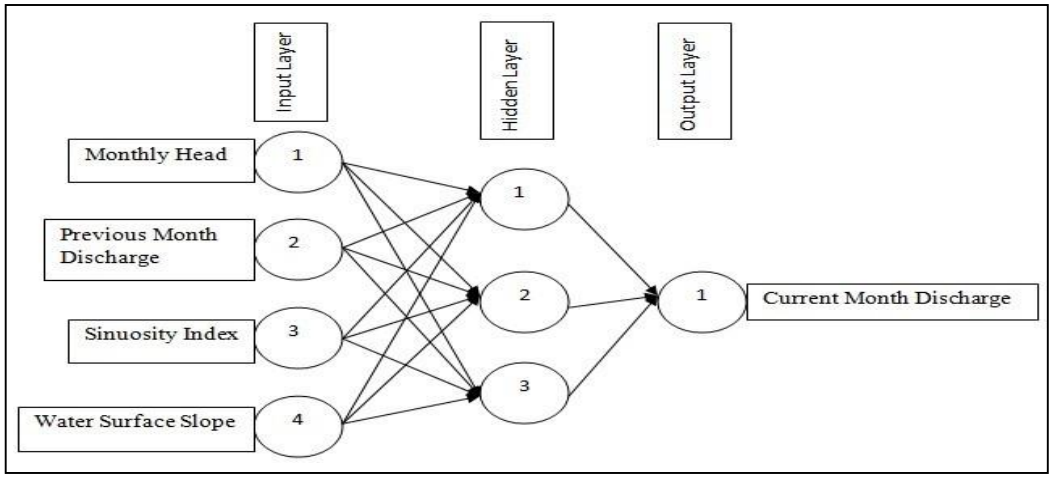



**Figure 8** Proposed ANN architecture

### 3.5.4 *Training and Testing Dataset*

For this network we had a total of 152 data patterns (13 years monthly data). There is a certain minimum no. of patterns which are required as a training set. The minimum no of training data should be 10 times the total no. of weights in the network (Abu Mostafa, 1995). In this network, having a total of 15 unknowns (weights), at least 150 training sets were required. So we have adopted a convenient value of 120 sets for training our network, rest of them for testing it. So 77% data was taken for training and 23% data for testing the network.

### 3.5.5 *Learning Rate*

The rate with which improvement of the network weights takes place is known as the learning rate, denoted as 'α'. Keeping a conformable ANN architecture as constant, value of α was varied by small steps i.e. 0.08, 0.09, 0.10, 0.11, 0.12 and 0.13, and the results were compared.

## 4. Results and Discussions

After running the ANN model with all the training and testing set, we get the following parameters which describes about the model in a statistical way. The various evaluation parameters were calculated using eqn.10 to 12. Here, x = observed discharge (cumecs) = Qo, y = predicted discharge (cumecs) = Qp and n = no. of data points. The performance evaluation parameters were obtained as shown by the Table 3.

### 4.1 Performance Evaluation

i. Root mean square error (RMSE) = $\sqrt{\frac{\sum(y-x)^2}{n}}$ (10)

ii. Coefficient of correlation (r) = $\frac{n\sum(xy)-(\sum x)(\sum y)}{[\sqrt{(N\sum(x^2)-(\sum x)^2}*\sqrt{(N\sum(y^2)-(\sum y)^2)}]}$ (11)

iii. Coefficient of determination = $r^2$ (12)

**Table 3** Performance Evaluation

| | Validation Set | | | | | | Training Set |
|---|---|---|---|---|---|---|---|
| α | 0.08 | 0.09 | 0.10 | 0.11 | 0.12 | 0.13 | 0.11 |
| RMSE | 3.65921 | 2.76659 | 2.20154 | 1.39194 | 1.61923 | 2.74808 | 1.43676 |
| r | +0.99903 | +0.99965 | +0.99994 | +0.99998 | +0.99912 | +0.99890 | +0.99997 |
| $r^2$ | 0.998061 | 0.99930 | 0.99988 | 0.99996 | 0.998241 | 0.997801 | 0.99994 |

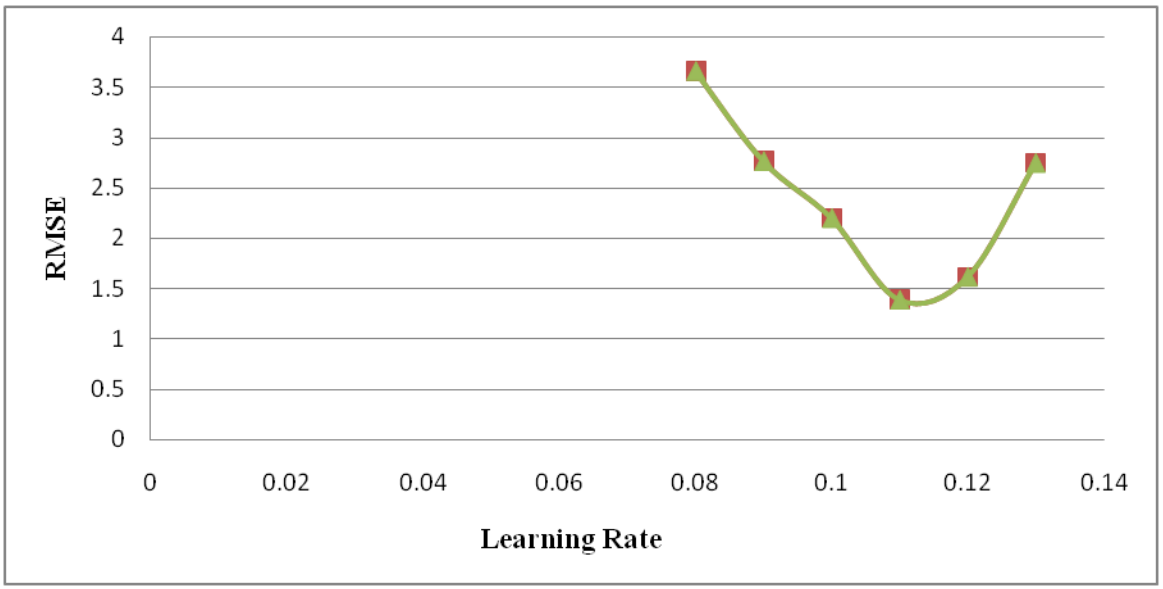



**Figure 9** Learning rate v/s RMSE curve

The general behavior of the results can be plotted as scatter diagrams as shown in Figure 9. Here, the RMSE shows a falling trend and then crossing the extreme point, it rises again. In Figure 10, correlation coefficient was plotted against the learning rate. It rises initially and then goes on falling again, the optimal rate being 0.11. Same as for correlation coefficient, determination coefficient showed a rising and then falling behavior shown by Figure 11.

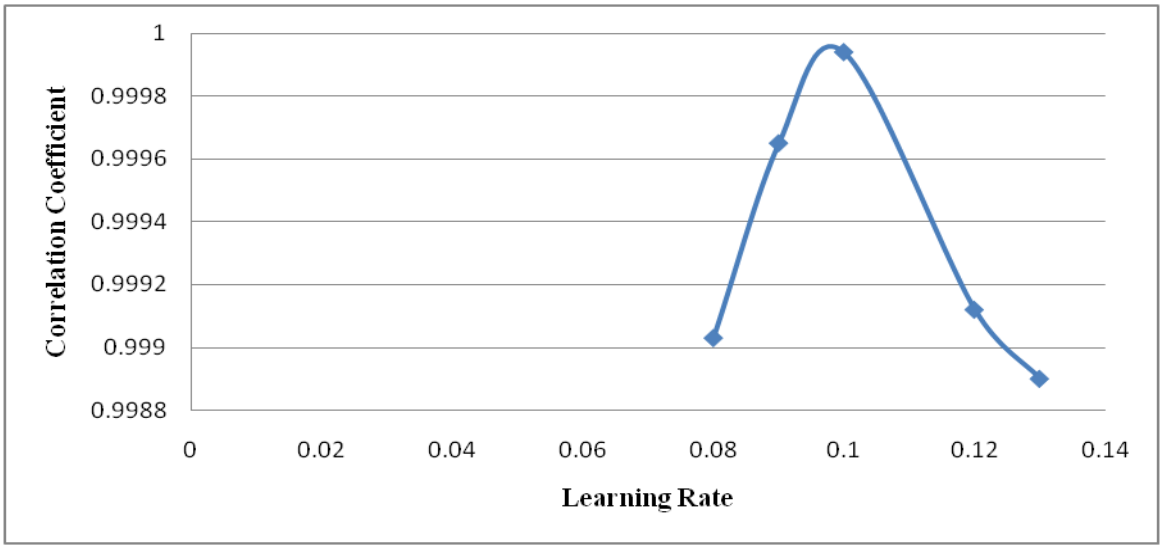



**Figure 10** Learning rate v/s correlation coefficient curve

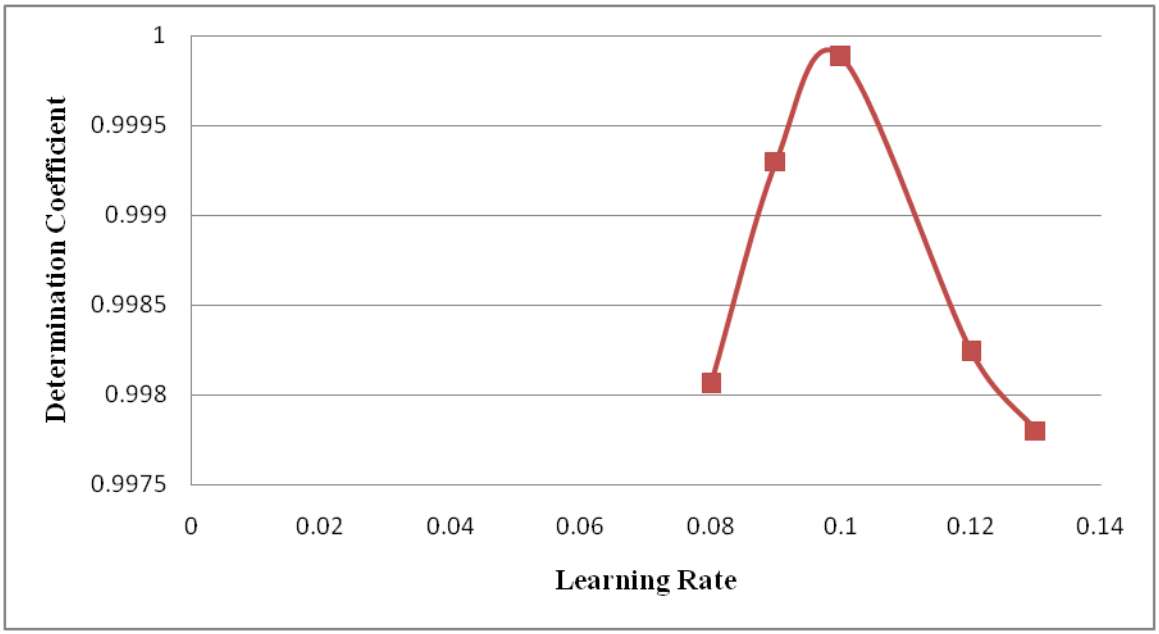



**Figure 11** Learning rate v/s determination coefficient curve

As the no. of iterations are increased from about 600 to 850 (keeping $\alpha$=0.11), the error falls down rapidly to about 1.39 as shown in Figure 12. But further increase of no. of iterations decreases the error gradually (almost negligible amounts). So, this much no. if iterations are not significant as it takes a lot of time for training the network.

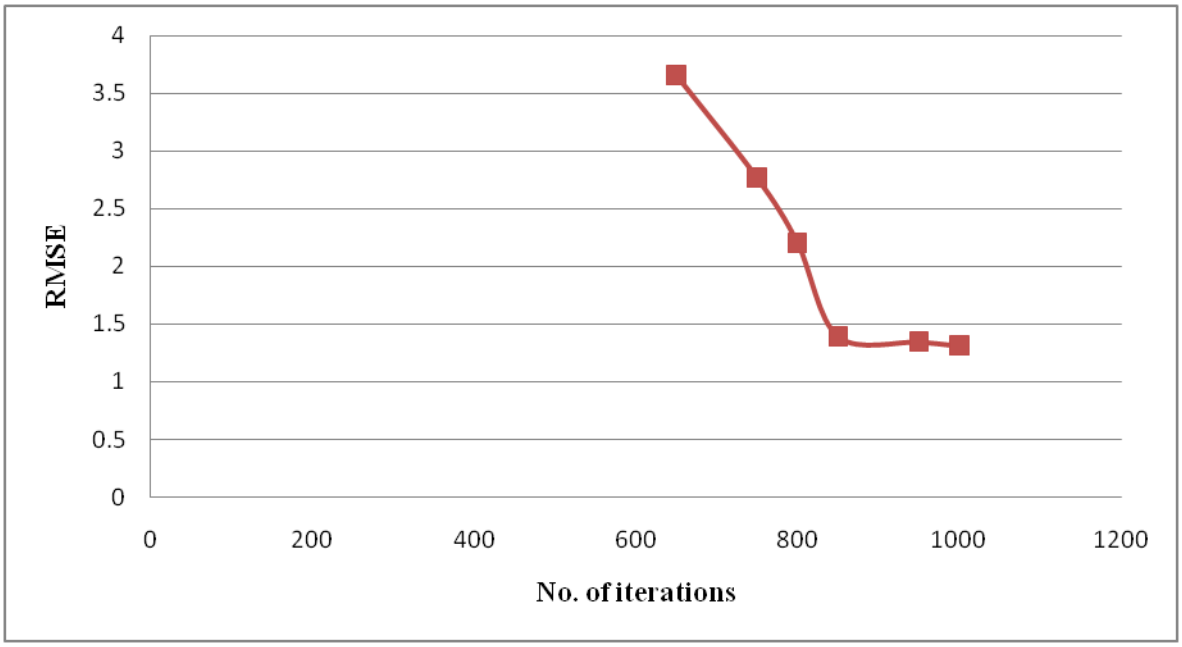



**Figure 12** RMSE v/s no. of iterations curve

By performing a run on training set and validation set, with a learning rate of 0.11, we get the best performance results:

1. RMSE = 1.39194 cumecs
2. Coefficient of correlation (r) = +0.99998
3. Coefficient of determination ($r^2$) = 0.99996

### 4.2 Discussions

As we can see by increasing the rate of learning, the RMSE goes on decreasing and after a certain trough point (point of minima), it again increases. Same was observed for coefficient of correlation (r) and determination ($r^2$). The optimal learning rate was obtained as 0.11. After certain no. of iterations, error reduction was insignificant so this was our stopping criteria. It can be interpreted in the following two ways:

i. At lower learning rates, the network tends to become too slow and training time required is more.
ii. At higher rates, the calculations become inaccurate and show oscillatory behaviour, i.e. it tends to move around the minima but never stops at the very point of minima.

So, to maintain a balance between the accuracy and time, we stop after 850 iterations with a learning rate of 0.11.

## 5. Conclusions

It is found that for a given network and type of data available, we can design a specific ANN network having a certain no. of input, output and hidden nodes as well as having an optimal learning rate. With an RMSE < 5, $r \approx +1$ & $r^2 \approx 1$, we have obtained a reliable result. So, this network can be used for similar cases to predict the discharge of such (sinuous) rivers. The use of satellite images has made it very simple for extracting important features of flow without much effort.

Using the artificial neural networks, there are so many problems that can be made simpler using the rightly programmed algorithm. It depends upon the situation in hand, data types, time of operation, accuracy needed (although compromising with time), etc. The biggest development in this world has been going on for the application of 'Artificial Intelligence'. So one needs to cope up with the current issues related to AI and make ethical use of the modern technology.

## Acknowledgements

The authors are thankful to the Water Resources Department, Silchar for its valuable contribution towards the work by providing the average monthly head & discharge data. Without their efforts this work would not have been possible at all.

## References

Abu-Mostafa Y. S. (1995). Financial market applications of learning from hints. *Neural Networks in the Capital Markets*, 221-232.

Alvisi S., Mascellani G., Franchini M. and Bardossy A. (2005). Water level forecasting through fuzzy logic and artificial neural network approaches. *Hydrology and Earth System Sciences*, 10, 1-17.

Aswathy M. V., Vijith H. and Satheesh R. (2007). Factors influencing the sinuosity of Pannagon river, Kottayam, Kerala, India: An assessment using remote sensing and GIS. *Environ Monit Assess*, 138, 173-180.

Barman P. and Goswami D. C. (2015). Evaluation of sinuosity index of dhansiri (south) river channel and bank erosion, Assam in GIS. *International Advanced Research Journal in Science, Engineering and Technology*, 2(5), 111-114.

Coon W. F. (1995). Estimates of roughness coefficients for selected natural stream channels with vegetated banks in New York. U.S. *Geological Survey Open-File Report*, 93-161.

Dash S. S. and Khatua K. K. (2016). Sinuosity dependency on stage discharge in meandering channels. *Journal of Irrigation and Drainage Engineering*, 142(9).

Friend P. F. and Sinha R. (1993). Braiding and meandering parameters. *Geological Society London Special Publications*.

Guru N. and Jha R. (2019). Application of soft computing techniques for river flow prediction in the downstream catchment of Mahanadi river basin using partial duration series, India. *Iranian Journal of Science and Technology, Transactions of Civil Engineering*.

Karsoliya S. (2012). Approximating number of hidden layer neurons in multiple hidden layer BPNN architecture. *International Journal of Engineering Trends and Technology*, 3(6), 714-717.

Karunanithi N., Grenney W. J., Whitley D., and Bovee K. (1994). Neural networks for river flow predictions. *Journal of Computing in Civil Engineering*, ASCE, 8(2), 201-220.

Khatua K. K., Patra K. C., Nayak P. and Sahoo N. (2013). Stage-discharge prediction for meandering channels. *International Journal of Computational Methods and Experimental Measurements*, 1(1), 80-92.

Kisi O. (2004). River flow modelling using artificial neural networks. *Journal of Hydrologic Engineering*, 9(1), 60-63.

Kumar P. S., Praveen T. V. and Prasad M. A. (2016). Artificial neural network model for rainfall-runoff-a case study. *International Journal of Hybrid Information Technology*, 9(3), 263-272.

Maier H. R. and Dandy G. C. (1996). The use of artificial neural networks for the prediction of water quality parameters. *Water Resources Research*, 32(4), 1013-1022.

Petrovszki J., Timar G. and Molnar G. (2014). Is sinuosity a function of slope and bankfull discharge? – A case study of the meandering rivers of the Pannonian basin. *Hydrology and Earth System Sciences Discussions*, 11, 12271-12290.

Riad S., Mania J., Bouchaou L. and Najjar Y. (2003). Rainfall-runoff model using an artificial neural network approach. *Mathematical and Computer Modelling*, 40, 839-846.

Rosgen D.L. (2007). A stream classification system. *Journal of the American Water Resources Association*, 44(3), 782-792.

Sahoo G.B. and Ray C. (2005). Flow forecasting for a Hawaii stream using rating curves and neural networks. *Journal of Hydrology*, 317, 63-80.

Sapkale J. B. (2014). Human interferences and variations in sinuosity index of Tarali channel, Maharashtra, India. *Indian Journal of Research*, PARIPEX, 3(5), 36-37.

Tayyab M., Zhou J., Zeng X. and Adnan R. (2016). Discharge forecasting by applying artificial neural networks at the Jinsha river basin, China. *European Scientific Journal*, 12(9), 108-127.

*IN PROCEEDINGS OF 25th HYDRO 2020, INTERNATIONAL CONFERENCE, NATIONAL INSTITUTE OF TECHNOLOGY ROURKELA, ODISHA, INDIA 26-28, March 2021, ISBN 978-93-90631-56-8*

Paper ID - 122

# Investigation of the Issues in the Inter Linking of Rivers: A Case Study for Godavari-Krishna Link Indira Sagar Polavaram Project

Gurusamy B. T[1], Vasudeo A. D[2], Gautam N.R[3], Godbole S. P[4] and Ghare A. D[5]

[1]*Research Scholar, Department of Civil Engineering VNIT, Nagpur-440010, India*
[2]*Associate Professor, Department of Civil Engineering VNIT, Nagpur-440010, India*
[3]*Asst Professor, Department of Civil Engg, Priyadarshini Bhagwati College of Engg, Nagpur-440024, India*
[4]*Assistant Professor, Dr. Ambedkar Institute of Management Studies and Research, Nagpur-440010, India*
[5]*Professor, Department of Civil Engineering VNIT, Nagpur-440010, India*
[1]*guru19april2009@gmail.com*, [2]*avasudeo@yahoo.com*, [3]*nimita_gautam@yahoo.com*,
[4]*snehal_prakash1@rediffmail.com and* [5]*adghare@yahoo.co.in*

## Abstract

Government is working and surviving on the basic principle of Interlinking of People in the form of collecting tax from people in order to provide products, facilities and services to the peoples and thereby to create Synchronous and Harmonious living environment with the characteristics of Concrete Society rather than Aggregate Society. Accordingly in the name of Interlinking of Rivers, collecting water from some Rivers and transferring water to other rivers becomes the basic Characteristics of a Government in order to create a Balance between Flood and Drought across the Time and Space domains of the nation and thereby to convert the existing Aggregate Basins into a Concrete Basin having high Resilience to the impact of Climate Change and that of Population Growth. Anyhow the observation in the last two decades shows the existence of a lot of Issues in the form of Criticism and Resistance against the implementation of National River Linking Projects (NRLP) of India designed based on the principle of Inter Basin Water Transfer (IBWT). This Review paper focuses on the investigation of various such Specific Issues including that of flora and fauna existing over one of the Peninsular Components of the NRLP of India named as Godavari-Krishna Link Indira Sagar Polavaram Project having the Idea Conceived since the year 1941, during the British Colonial Period. In addition various General Issues existing over the Interlinking of Rivers using NRLP of India have also been presented. Various quantitative Benefits including Irrigation Command Area benefits of this Indira Sagar Polavaram Link Project motivating towards successful implementation have also been explored. The Technical Characteristics such as Hydraulic and Hydrologic Characteristics including Flood handling capacity of this Link Project have been analyzed. The Flood Submergence Characteristics of the Godavari River with and without this link Project have been compared for both the cases of Upstream and Downstream sides of the Polavaram Dam.

***Keywords:*** *Concrete Basin versus Aggregate Basins; NRLP of India; Issues and Benefits of IBWT; Hydraulic & Hydrologic Characteristics; Godavari-Krishna Link Indira Sagar Polavaram Project;*

## 1. Introduction

According to the basic Theory of Fluid Mechanics, by the Characteristics of Potential Distribution Function (Φ), the Flux flow per unit area (u) in x direction is given by the formula ($\partial\Phi/\partial x = - u$) while the direction of Flux flow is towards the direction of decrease in Potential. The Flux flow distribution function (Ψ) also called as Stream Function is completely characterized by Φ function (Streeter, 1958). Assuming the Potential Quantity (Φ) as the Authority exercised by an entity X, the Flow Quantity (Ψ) becomes the Responsibility placed over the entity X. Based on many Management Theories, the Authorities and Responsibilities are represented as two sides of same Coin because one cannot exist without the other (DuBrin, 2009). Accordingly the Flux Flow from points of high potential towards the points of low potential can be assumed as a natural process. Hence the Diversion of water from the Surplus River Basin having high Per Capita Water Availability (Φ) towards Deficit River Basin having Low Per Capita Water Availability using a set of IBWT (Ψ) based National River Linking Projects (NRLP) of India, becomes the natural Process of Water Resources Management to Balance the Flood and Drought in Space and Time Domain across any Geographical Region of India.
The interlinking of Economy in the name Globalization Policy facilitates the Flow of Products and Services across the Boundary of a Country from the Source of High Availability towards the Destination Point of Demand across the World. The Figure 1 shows the positive impact of interlinked Economy or Globalization policy implemented by China and India from 1978 and 1991 respectively.

Similar increase in Per Capita GDP can be expected with the implementation of interlinking of Rivers using IBWT based NRLP of India by increased utility of runoff loss water.

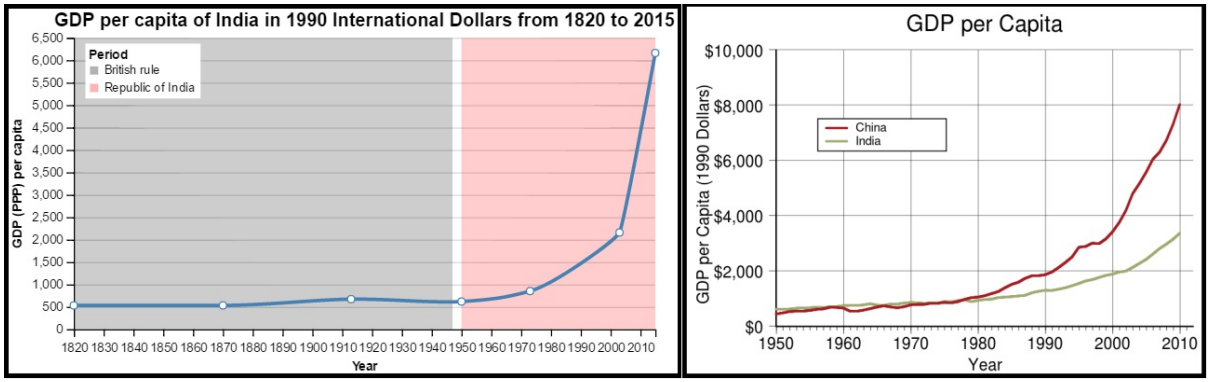



**Figure 1** Sharp Growth in Per Capita GDP produced by Interlinking of Economy and Motivating towards Interlinking of Rivers (Maddison, 2010)

Many Literatures including Markus (2019) have presented about the possibilities of severe variations in the pattern of precipitation and thereby causing for Extreme Flood and Drought produced because of the future predicted Climate Change Scenarios. The existence of Water Storage/Diversion and Conveyance Structures across the Basins in the form of Reservoirs and IBWT based Interlinking Canals will be highly useful to balance the Flood and Drought across the Time and Space axis in order to increase the Resilience of the Basin for withstanding the impact of Flood and Drought variations produced by Climate Change.

By comparing the Physical Bearing Strength Characteristics of Coarse and Fine aggregates (Coduto, 2001) with that of Concrete produced by interlinking those aggregates using Cement, the bearing Strength of the Concrete (Shetty, 2010) has been observed to be more than 10 times that of aggregates. Hence it can be expected that the Resilience in the form of Climate Change Withstanding Capacity of the Canal Interlinked Concrete Basin produced by the IBWT based NRLP of India to be relatively higher than that of isolated Aggregate Basins practicing Closed Water Economy. Hence an attempt has been made to investigate the Issues and Benefits of Interlinking of Rivers in India along with a specific focus to the proposed Godavari – Krishna Link Indira Sagar Polavaram Project.

## 2. Materials and Methods

It was the Idea developed during British Colonial period in India before 1947, in the form of interlinking of populated areas using First Indian Railways near the localities of Mumbai, Chennai etc. (IRFCA, 2011) and Waterways including Buckingham Canal along the East coast of India (MoT, 1957), may be in order to ensure more degree of control over the people or otherwise to increase the facilities required for the development of East India Company or the peoples. Accordingly the Idea of Interlinking of Rivers in India was developed by Sir Arthur Cotton one of the British Hydraulic Engineer at least 120 years back nearly around 1881 with the purpose of development of Inland Waterways (Elizabeth, 2005). Sir Arthur Cotton had also developed basic frame work for the construction of Cotton Barrage across Godavari River near Dowleswaram, Prakasam Barrage across Krishna River near Vijayawada, and also he constructed the Upper Dam in Mukkombu and lower dam near Anaikarai both across Cauvery River to enhance the performance of existing Kallanai Dam having age more than 1500 years (Christopher, 2008). These works across Godavari, Krishna and Cauvery Rivers nearby to east coast line provides evidence for the plan of Interlinking of Rivers to have an age more than 120 years.

After the Formation of Government of India since the year 1947, the first proposal in the year 1972 as in Figure 2 in the name of "National Water Grid" was introduced by Dr. K L Rao, a well-known three times Central Minister of Irrigation and Power during 1963-1973 (Lok Sabha, 2016). According to

Amarasinghe (2008), it was a Crude Proposal to interconnect Ganga and Cauvery from a point near Patna across Ganga. A few years later another Proposal had been submitted by Captain D. J. Dastur in the year 1977 as shown in Figure 2 to construct high level Canal network interconnecting many Rivers (Joshi, 2013). In order to increase the utility of available water and to balance the Flood and Drought in time and Space Domain across India, Ministry of Water Resources, Government of India had Formulated a National Perspective Plan (NPP) in the year 1980 for the transfer for Water from Surplus Basins to Deficit Basins in the name of Inter Basin Water Transfer (IBWT) Links (MoWR, 1980). Further National Water Development Agency (NWDA) was developed by 1982 to assist the Ministry of Water Resources towards Planning, Designing, Implementation and Management of NPP based NRLP of India. Based on the NPP the IBWT Links had been classified into Two Components such as Himalayan Components and Peninsular Components as in Figure 1 (NWDA, 2018). The Feasibility Studies Report of many of such Links based on priority position had been prepared by NWDA and kept available online to the public. These materials have been used in the investigation of Issues and Benefits of Interlinking of Rivers across India with the Specific consideration of Godavari-Krishna Link Indira Sagar Polavaram Project.

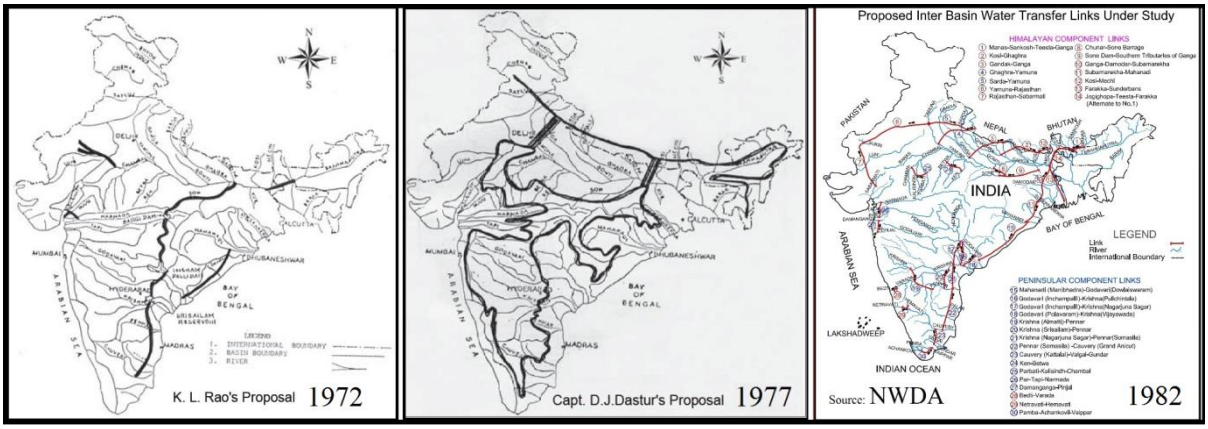



**Figure 2** Evolution of National River Linking Projects of India (NWDA, 2018 and Joshi, 2013)

The digital elevation Model (DEM) data obtained using NASA Shuttle Radar Topographic Mission (SRTM) and distributed free of Charge by United States Geological Survey (USGS), with 90m (3Sec) resolution and provided by Consortium for Spatial Information of the Consultative Group for International Agricultural Research (CGIAR-CSI, 2020), has been used for the Analysis of Submergence area corresponding to the FRL of the proposed Polavaram Dam. Longitudinal Bed Slope on the upstream and downstream sides of the proposed Submergence area has also been determined using these Data. The River Basin Boundaries from micro watershed Level to Region Level along with drainage networks in vector file format, provided by the HydroSHEDS database (Hydrological data and maps based on SHuttle Elevation Derivatives) have been used for the preparation of relative location and elevation profiles of the Godavari-Krishna Link (Lehner, 2008).

The Cross Section details at different gauging locations of the Godavari River had been obtained from the Discharge Year Book Publications of the Central Water Commission (CWC, 2018). In order to compare the Discharge carrying Capacity of the Godavari River between the upstream and downstream sides of the Submergence area, the Standard Manning's Formula have been adopted (Manning, 1891). To determine the Submergence Volume using the Contour Map of the Submergence Area, the average area occupied between two consecutive contours and multiplied by the contour interval had been used as adopted by Crawford (2008). Towards the Justification of the IBWT based National River Linking Projects of India, the Basin wise annual average runoff loss data and latest updated Water Assessment Reports published by CWC of India have been used (CWC, 2019). The annual Water Transfer Volume and Water allocation Procedure along with the Technical specification of the Indira Sagar Polavaram Project as approved by the Godavari Water Disputes Tribunal (GWDT, 1980) have been adopted for this Investigation.

Various Technical issues including Hydraulic and Hydrologic aspects of the Project have been considered as a major focus in this Review Paper and other issues involving Social, Ecological, Environmental and Economic aspects of the Project have only been highlighted while the Agricultural aspects involving the actual distribution of Irrigation Water Demand across the Command Area have not been considered.

## 3. Results and Discussions

According to FAO (2014), the achievement of SDGs, demands for the balanced development of Water, Food and Energy Sectors across a Geographical Region. In order to ensure such a balanced development, the distribution of Water Availability should be balanced with that of Population. As presented by Amarasinghe (2005), the East Flow River Regions, present in the South of Godavari Basin covers a 16% of India's Land Area and 17% of India's Population, but drains only 6% of Indian Water Resources. This shows a spatial imbalance and any transfer of Water from Godavari towards south side basins using various IBWT Links as shown in Table 1 is justified as a process of balanced development demanded by Water-Food-Energy Nexus Concept. The observed average annual runoff loss data for the last 30 years of Godavari Basin is compared with that of Krishna, Pennar and Cauvery Basin as shown in Figure 3. The distribution of Estimated Per Capita Water Availability across the Basins of East Flow Rivers Region is shown in Figure 4.

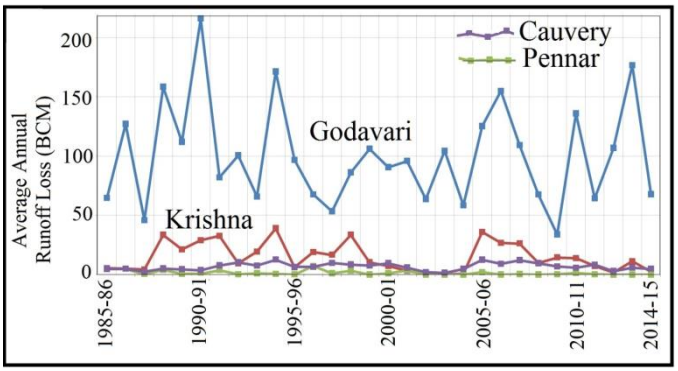



**Figure 3** Annual Average Runoff Loss Observations Motivating IBWT from Godavari Basin towards Krishna-Pennar-Cauvery Basins (CWC, 2019)

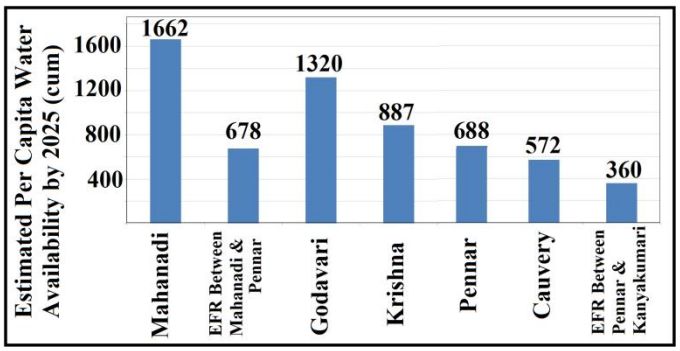



**Figure 4** Estimated Per Capita Water Availability across the Basins of East Flow Rivers Regions by the year 2025 (CWC, 2019)

Accordingly Mahanadi and Godavari Basins have been considered as Water Surplus Basins with respect to other basins in the East Flow Rivers Region such as Krishna, Pennar, Cauvery, etc. In order to reduce such an imbalance over East Flow Rivers Region, a set of IBWT based NRLP of India in the name of Peninsular Components had been proposed by NWDA (2010) as shown in Table 1. Using this Table 1, the typical annual volume of Diversion and actual Water Transfer has been compared with the estimated average annual water availability of the corresponding Basins.

As shown in the Table 1, any transfers of Water from Krishna towards Pennar and Cauvery have been substituted by proposed three Godavari-Krishna links. Again the transfer of water from Godavari to

Krishna is substituted by corresponding transfer of Water from Mahanadi to Godavari. Hence the Basic Objectives of the IBWT projects as shown in Table 1 are to utilize the very high Runoff loss water existing in the Godavari and Mahanadi Basin towards the locations of Water Demand existing over entire East Flow Rivers Region of India.

**Table 1** Comparison of Average Annual Diversion and Transfer Volume with Water Availability of selected Peninsular Components of IBWT based NRLP of India (NWDA, 2010 and CWC, 2019)

| IBWT Link | Water Availability of Source Basin (MCM) | Water Availability of Destination Basin (MCM) | Diversion Volume (MCM) | Transfer Volume (MCM) |
|---|---|---|---|---|
| Mahanadi - Godavari | 73000 | 117740 | 9182 | 4046 |
| Godavari (Icchampally) Krishna (Nagarjunasagar) | 117740 | 89040 | 16426 | 14200 |
| Godavari (Icchampally) – Krishna (Pulichintala) | | | 4370 | 0 |
| Godavari (Polavaram) – Krishna (Vijayawada) | | | 5325 | 2265 |
| Krishna (Almatti) – Pennar (Kalvapalli) | 89040 | 11000 | 1980 | 871 |
| Krishna (Srisailam) – Pennar (Somasila) | | | 2310 | 2095 |
| Krishna (Nagarjunasagar) Pennar (Somasila) | | | 12146 | 8426 |
| Pennar (Somasila) – Cauvery (Grand Anicut) | 11000 | 27670 | 8565 | 3855 |

Because the actual water Transfer is at a level of 10% of the Water Availability, Any Ecological and Environmental Issues produced because of the IBWT Projects need to be attributed towards the Storage and Submergence Reasons and not to be attributed for Water Transfer Reasons. Storage and Submergence is common for both in-basin and inter-basin Water Distribution. Without Storage and possible Submergence, River water cannot be diverted towards the point of Demand. The Development of Any Geographical Regions in the form of GDP growth depends on the Effective utilization of the basic input Resources Materials including Water in collaboration with other sectors in order to increase the productions of Products and Services. The Economic Feasibility of all these IBWT based Projects have been analyzed by NWDA and kept available to the public. Hence any efforts in the form of Projects to utilize the Runoff Loss Water with Economic viability and capacity to satisfy SDGs need to be motivated or encouraged towards Economic Development of a Region.

The Idea of Polavaram Project in the Name of Ramapadasagar Project, a Report had been presented by Shri L. Venkatakrishna Iyer, the Chief Engineer for Irrigation, during the Madras Presidency of British Colonial period in the year 1941. In the Name of Indira Sagar Polavaram Project, after many revisions in the years 1976, 1978 and 1982, a revised Report prepared with the agreement of neighboring States, had been presented by CWC in the year 1986. Accordingly the FRL and MWL of the Project had been decided as 45.72 m (150.00 feet) accommodating the Submergence and other issues of the neighboring States (WRD, 1986). The Godavari Water Disputes Tribunal (GWDT) had been constituted by Government of India on 10-04-1969 to solve the water sharing issues among the States. As per GWDT award in the year 1980, an annual transfer of 80 TMC (2265 MCM) from Polavaram to Krishna River had been approved (GWDT, 1980). The planned annual diversion from the Reservoir is 5325 MCM and after meeting the Enroute demand in the form of Irrigation, Domestic, Industrial and losses the remaining 2265 MCM will get transferred to Krishna River (NWDA, 2010). The Location and elevation profile of the Godavari (Polavaram)-Krishna (Vijayawada) Link Canal is shown in Figure 5. This IBWT based Godavari-Krishna Link Indira Sagar Polavaram Project had been declared as a National Project on 01-03-2014 along with Andhra Pradesh Reorganization Act 2014 and fully funded by Central Government of India and also under Accelerated Irrigation Benefits Programme (AIBP) (Lok Sabha, 2019 and MoWR, 2018). Accordingly, after the bifurcations of the Andhra Pradesh State into Telangana and Revised Andhra

Pradesh, in the year 2014, the seven mandals of the Telangana State was reunited and merged with Andhra Pradesh just for the purpose of smooth and successful implementation and operation of the Polavaram Project. This is because of the major Submergence area of the Project being present over the Seven Mandals merged with Andhra Pradesh as in Figure 6.

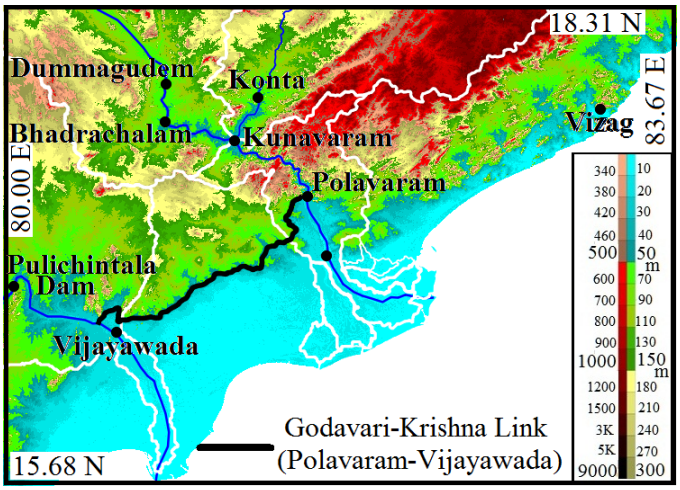



**Figure 5** Locations and Elevation Profile of Godavari – Krishna IBWT Link from Polavaram to Vijayawada (Lehner, 2006 and NWDA, 2010)

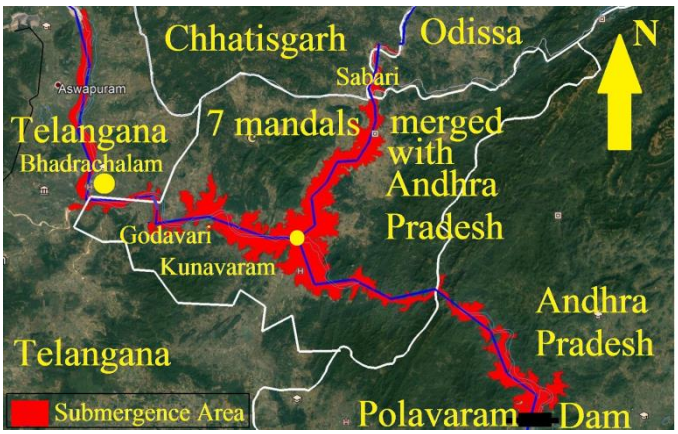



**Figure 6** Location of Submergence Area at FRL 45.72 m of Polavaram Project across Seven Mandals merged with AP from Telangana State

At the FRL of 45.72m the Gross Storage Capacity (GSC) and Live Storage Capacity (LSC) have been reported to be equal to 5511 MCM and 2130 MCM respectively along with the Submergence area as 637sq.km. The Gross Command Area (GCA) and Culturable Command Area (CCA) benefits of the Godavari-Krishna Link (Right Main) Canal having length 174 km and capacity 453 Cumec have been reported as 162691 ha and 139740 ha respectively. The CCA of Left Main Canal with Capacity 250 Cumec and aligned towards Visakhapatnam is 174978 ha. The planned water supply to the steel and other industries present in Visakhapatnam using Left Main Canal is 664 MCM. The Hydraulic Design of the Storage Structure has been reported with necessary consideration for 50 years of Sedimentation and Reservoir Operation Procedure in order to accommodate the Flood discharge safely. The proposed Hydro Power capacity of 960 MW will be fully utilized only during monsoon season and with a firm power generation of 80 MW across the year with the annual planned Power Generation of 2369.43 million Units. Necessary procedure and steps to be implemented in order to get clearance from Forest and Environmental Departments along with Criteria for handling Rehabilitation and Resettlements issues have also been prescribed in the Reports prepared by NWDA (2010). Polavaram Project Authority (PPA) had been created by Government of India to execute the Project and also to obtain above Clearances including all court cases. More than 10000 crore had been incurred up to March 2018 towards the implementation of the Project (MoWR, 2018). Expected Arial View Image

of the Polavaram Project is shown in Figure 7. Location of Additional Command Area Benefits has also been presented using Rose Colour in Figure 7.

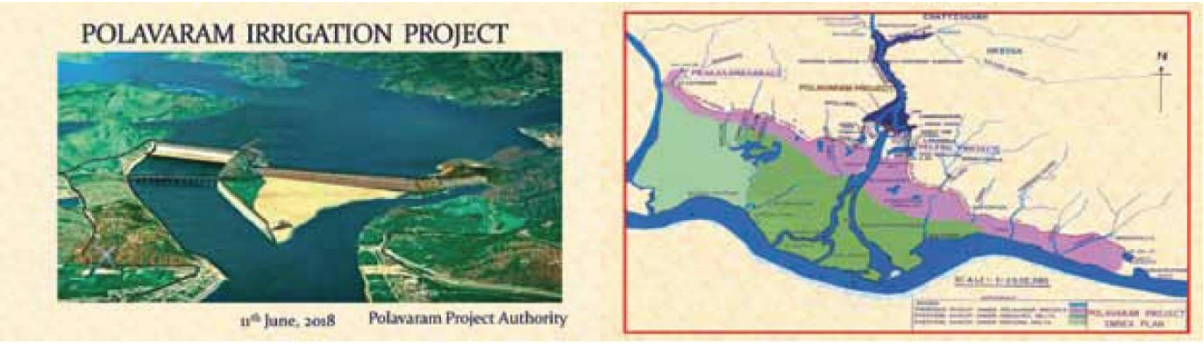



**Figure 7** Expected Arial View Image and Location of Additional Command Area of the Polavaram Project Under Construction (MoWR, 2019)

Based on the Flood Inundation Map of Godavari River Published by Andhra Pradesh State Development Planning Society (2019), for the Flood Discharge of 73283 Cumec estimated as 50 Year Flood, there is no Flood Submergence Area reported in between Papikondalu Gorge Section and Dowleswaram for a length of more than 75 km as shown in Figure 8. The Criteria of Delta Region Flood Submergence below Dowleswaram is not the same as that as Flood Submergence on the upstream side of Papikondalu Gorge Section. This can be realized by comparing the Water Level Buildup Phenomena for Kunavaram region on the upstream side of Papikondalu Gorge and the Delta Region on the downstream Side of Dowleswaram during a given Flood Scenario on 16-August-1986 as shown in Table 2. For the Same Flood Discharge without a Dam at Polavaram the water level buildup above Danger Level at Kunavaram had been observed as more than five times that of Dowleswaram. Hence Flood Submergence depth at Kunavaram is higher than that of Dowleswaram.

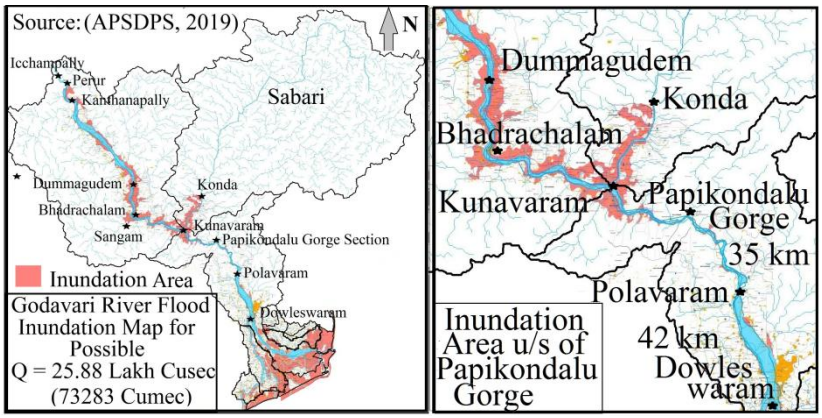



**Figure 8** Inundation Map for a Flood Discharge of 73283 Cumec across Godavari Lower Sub Basin (APSDPS, 2019)

**Table 2** Comparison of Water Level Buildup from Bhadrachalam to Dowleswaram (CWC, 2018)

| Gauging Location/Site | Danger Level (m) | Highest Flood Level (HFL) in m | (HFL – Danger Level) in m |
|---|---|---|---|
| Bhadrachalam | 48.77 | 55.66 on 16-08-1986 | 6.89 |
| Kunavaram | 39.24 | 51.30 on 16-08-1986 | 12.06 |
| Dowleswaram | 16.08 | 18.36 on 16-08-1986 | 2.28 |

The DEM details of Kunavaram Flood Submergence Region as shown in Figure 9 shows that the Submergence Region is having Natural Reservoir/Tank like Storage Space bounded by Elevated Land on the circumference of the Natural Reservoir along with Papi Hills on the East side with only Narrow outlet through Papikondalu Gorge section having relatively a very narrow flow width less than 300 m. This is also delineated using Figure 10 presenting the Submergence Area/Map produced by the proposed Polavaram Dam at a FRL of 45.72m. The Submergence between Papikondalu Gorge

Section and Polavaram is not because of the Flood but due to the proposed Polavaram Dam. But on the upstream side of the Gorge Section the land gets submerged temporarily with the Flood water even without a Dam at Polavaram. The possible reasons for such Flood Submergence have been analyzed and presented with the use of Figure 11 through Figure 14.

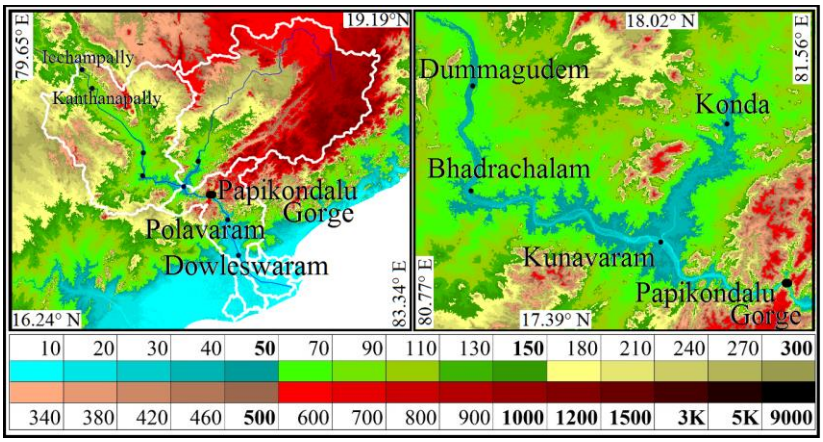



**Figure 9** DEM details of Possible Low Lying Submergence Area on the upstream side of Papikondalu Gorge Section across Godavari Lower Sub Basin (SRTM Data: CGIAR-CSI, 2020)

As shown in Figure 11 there is a sharp decrease in longitudinal bed slope on the downstream side of Kunavaram compared with that of upstream side. Based on SRTM DEM data the bed slope in between Bhadrachalam and Kunavaram Section 1in 3500 and that in between Kunavaram and Polavaram is 1 in 14000. According to Manning formula keeping other thing constant, when the bed slope is reduced by 4 times the discharge carrying capacity will get reduced by two times. This becomes the First possible reason for Flood Submergence at Kunavaram.

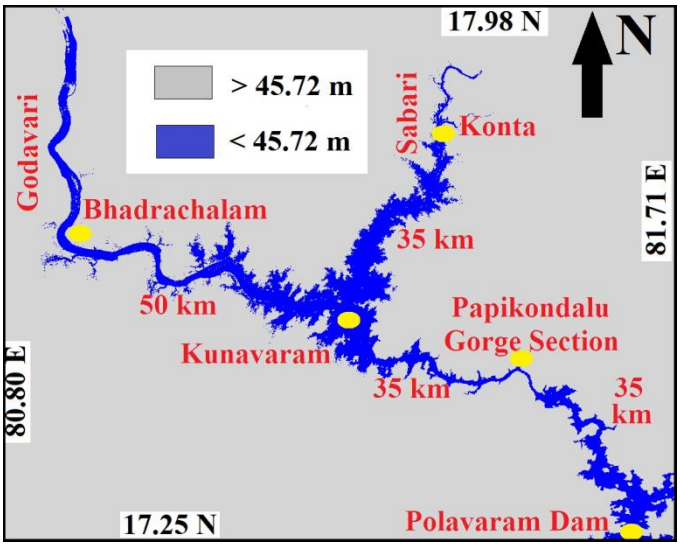



**Figure** 10 Natural inland Low Lying Submergence Area bounded by Papikondalu Gorge Section with Narrow Outlet less than 300 m width

Figure 12 shows the variation of submergence area and submergence volume on the upstream side of Papikondalu Gorge Section as a function of water level at Kunavaram. Up to the danger flood level of 39.24 m the Submergence volume is less than 1000MCM. But in between 40m and 51m water level buildup the storage volume is estimated to be more than 5000 MCM. Existence such natural Floodplain land of area more than 500 sq.km at a level of 40-51m becomes the second possible reason for the flood Submergence. The Cross Section areas at different locations of Godavari River from Perur to Polavaram have been compared using Figure 13. The flow width at Gorge section is less than 300m when compared to more than 1500 m at other upstream and downstream locations of Godavari

River. The obstruction produced by the Papikondalu Gorge Section in the form of natural Venturiflume becomes the third possible reason towards water level buildup on the upstream side of Gorge Section.

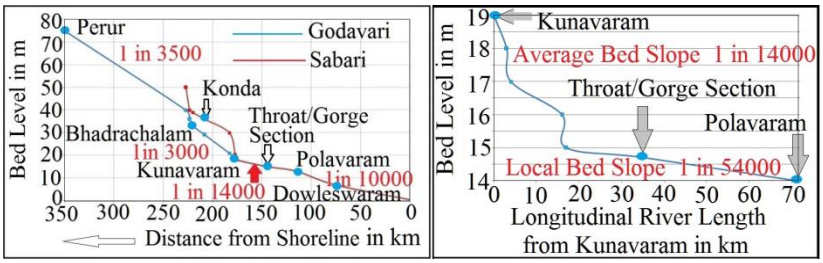



**Figure 11** Longitudinal Bed Slope profile across Godavari Lower Sub-Basin from Perur to Polavaram (SRTM Data Source: CGIAR-CSI, 2020)

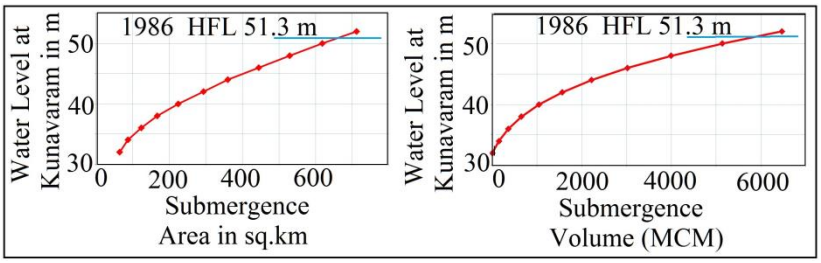



**Figure 12** Static Submergence Area and Volume corresponding to Kunavaram Water Level on the upstream side of Papikondalu Gorge Section (Lehner, 2006)

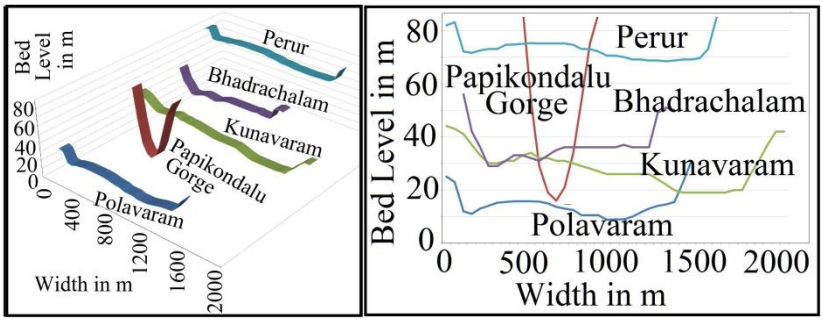



**Figure 13** Comparison of Cross Section of Godavari River from Perur to Polavaram with respect to Papikondalu Gorge Section (CWC, 2018)

The Water Level Buildup Phenomena along the length of Godavari River between Perur to Polavaram has been compared graphically for different Flood Discharge Scenario as shown in Figure 14. It can be observed that for flood Discharge less than 20000 Cumec, the Water Level profile follows the bed level profile. When the Discharge increases there is Sharp Water Level Buildup at Kunavaram Section relative to other sections of the River. This Phenomena of Water Level Buildup is also supported by flood Scenario observed on 22 August 2018 and reported that when the peak water level is less than the Danger Level at locations both upstream side Bhadrachalam and downstream side Dowleswaram, the Peak water level at Kunavaram had been observed above Danger Level (CWC, 2018).

The Bach Water Level Profile of the Submergence Area on the upstream side of the proposed Polavaram dam site, have been analyzed by Rai (2018), for both the cases of with and without the Dam using Hydrologic Engineering Center-River Analysis System (HEC-RAS) based one dimensional mathematical model and the typical result obtained for the case of without embankment have been presented as shown in Figure 15. This Result shows that for a Flood discharge of 101940 Cumec the water level buildup in Kunavaram is just 1.51m (51.25m-49.74m) higher than that without Dam. From the Figure it can be interpreted that the Flood Submergence effect in the upstream side of Papikondalu Gorge is less sensitive to the Dam Constructed at Polavaram.

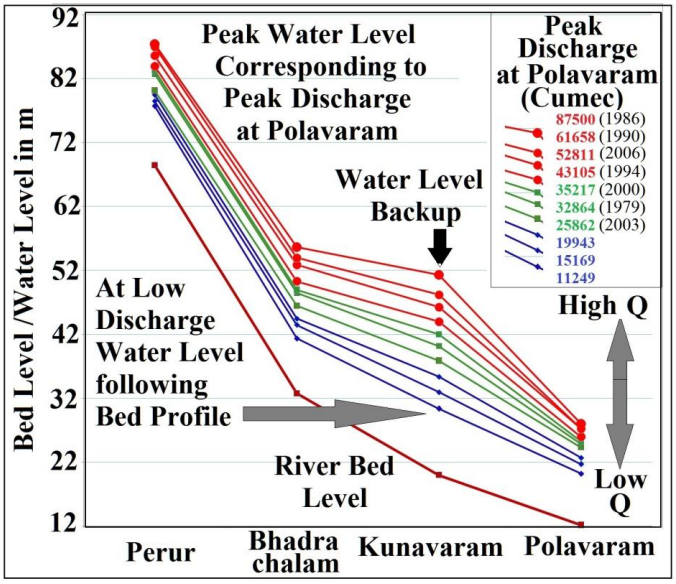



**Figure 14** Comparison of Peak Water Level Buildup around the Kunavaram Submergence Region corresponding to historical Polavaram Peak Discharge (CWC, 2018)

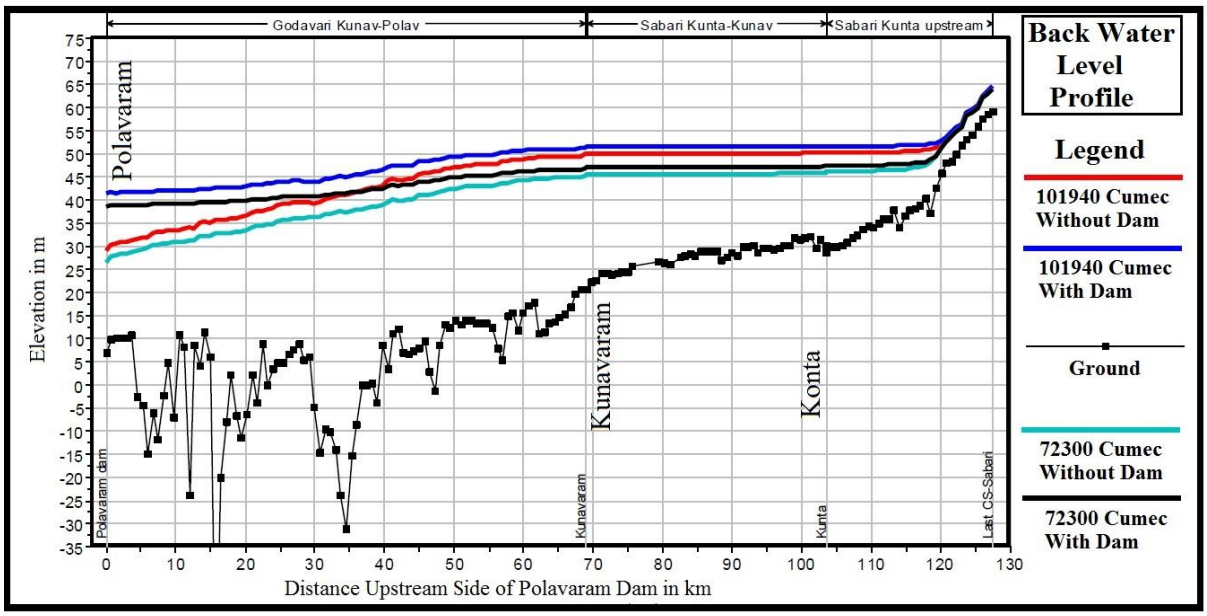



**Figure 15** Back Water Profile of Submergence Area of Polavaram Project with and without Dam (Rai, 2018)

Any Economic Development Activity on the Floodplain land will cause for the corresponding increase in Flood Damage Risk. Without Polavaram Dam the Submergence on the upstream side of Papikondalu Gorge Section is temporary only during Flood Season. With Polavaram Dam, these Regions is permanently allocated for Storage Purpose and hence further economic development activities inside these floodplain land will get reduced causing for the reduction of Flood Damage Risk of the Flood Prone Region on the upstream side of the Papikondalu Gorge Section.

Using the Flood Routing Characteristics of a Reservoir and by efficient operation of the Reservoir, a typical LSC of 1000 MCM can be used to attenuate the Peak discharge of a Flood Wave of one day duration at least by 10000 Cumec. Hence the 2130 MCM Live Storage Capacity of the proposed Polavaram Project can be effectively used to attenuate a Peak Discharge of Flood Wave of even Two days Duration by a magnitude of at Least 10000 Cumec. Hence it can be expected that with the effective Utilization of Existing Flood Warning System across Godavari Basin (CWC, 2018) along

with the Storage capacity of the Polavaram Project, the Flood Damage Risk on the Flood Prone Delta Region of the Godavari River downstream side of Dowleswaram as shown in Figure 8, will get reduced. Issues in the form of Possibilities of Polavaram Dam Failure had been raised by Rao (1983) and Shivaji Rao (2013) citing the reason as insufficient design of Spillway to handle a Flood discharge of more than 110000 Cumec in the name of 500 Year and 1000 Year Flood. Because of the possibilities of such Flood, the Polavaram Projects keeps the downstream side Population of more than 50 Lakhs under Risk. Anyhow compared to the Spillway width (Width 550m) specified by Rao (1983), the Current Design Parameters of Spillway (Width 754 m) (NWDA, 2010) is an improved version with more safety Level. According to WRD (1986), the design Flood Discharge is 102000 Cumec and Spillway Width is 1128.40m. Hence the Safety of Dam Wall needs to be ensured with the provision of enough Factor of Safety even for 1000 Year Flood Discharge Cases.

It can be assumed that when the Ecological Equilibrium of flora and fauna of a river system had been maintained or survived during the season of minimum discharge of unobstructed River, by maintaining minimum discharge called Environmental Flow, it can be made possible to protect the Ecological Equilibrium even with the obstruction structures in the Form of Dam along with the provision of facilities for upward migration of species. Hence to store water using Dams in order to satisfy the demand of increasing population, along with the assurance for minimum downstream side flow and facilities for upwards migration of species may be considered as sufficient procedure to protect flora and fauna of a River system.

## 4. Conclusions

Water in the River or Lower / higher order Stream is passing through the steepest flow path representing the valley line of the Basin, and hence it does not have the capacity to flow through the point of Demand unless the water gets diverted by using a Diversion Structure constructed across the River. Therefore the water in the River can be considered as Available Water but not the Commendable Water. In order to convert the available water into usable/ commendable water it is always necessary to create Storage, Diversion, Conveyance and Distribution type Hydraulic Structures across the Basin. With the help of Diversion and Conveyance Structures the Commendable Capacity of Available water can be increased based on the level of Diversion. Any such diversion involves corresponding Storage and Submergence Area in the upstream sides of the Obstructions. The destination point towards which the water gets diverted may be within the Basin or outside the Basin. The issues generated because of the Submergence or Diversion is common for both the cases of inside or outside the Basin. Hence such Issues need not to be called as IBWT issues. The Real IBWT issue is the percentage of annual volume of water diverted from a given River basin to the adjacent River basin. The IBWT concept is to transfer water from Surplus Basin towards Deficit Basin. This is the natural process. Because any flux including Water has the natural tendency to flow from a point of High Potential towards low Potential with a flow magnitude based on the reluctance/resistance of the flow path. This is similar to the basic concept of a Government in the form of collecting high percentage income tax from high income group peoples in order to produce Products and Services to the Public. The current income tax percentage in India is at level of 0%, 10%, 20% and 30% based on the Annual Income Level. All the National River Linking Projects have been designed to divert less than 10% of the Annual Available Water in the Source Basin considered as Surplus Basin. Even for low income group people the tax paid at 10% level is not considered as vulnerable and also it is used for the development of the Society. Similarly the Water Transferred from the Surplus Basin is not to be considered as a loss because it provides Benefits and return Revenue to the Source Basin in the name of Reward. Hence any Environmental and Ecological Problems realized as a consequence of the Storage and Diversion Structures across a River cannot be attributed to Issue of IBWT based National River Linking Projects which involves only less than 10 % Diversion of Annual Available volume of Water from the Source Basin. Anyhow, the Current Water Sharing Strategy is to share some fixed volume of Water per year rather than fixed percentage of Available Water. Because the Annual Water Availability is not a Certain Parameter, the Transfer of Fixed volume of Water during the year of Low Water Availability is likely to be highly painful to the peoples of Source Basin. Hence similar to the

Income Tax formula, a fixed Percentage as Water Transfer rather than a Fixed Quantity as Water Transfer may create more Satisfaction in the form high water Transfer during the Year of high Water Availability and vice versa.

A River Basin is an idealized model of the existing physical Entity on the Earth Surface in order to characterize and understand or appreciate the natural Hydrological Processes. Such understanding can help us to utilize the natural Water Resources efficiently to achieve the Sustainable Development Goals (SDGs) that have been recommended as Global objectives by World Health Organization (WHO, 2003) and that of India by National Institution for Transforming India (NITI, 2018). The concept of Integrated Water Resources Management (IWRM) have been recommended by Global Water Partnership (GWP, 2000) to achieve SDGs and also adopted by World Meteorological Organization (WMO, 2009), in order to ensure integrated development of all Sectors in collaboration with Water Sector. Hence a self-sustained and self-reliant independent River Basin with Closed Water Economy is not to be assumed as a component of the IWRM. According to National Water Policy of India (MoWR, 2012), and IWRM Guidelines of Central Water Commission of India (CWC, 2016) a Basin need to be considered as a basic unit for the Planning, Development and Management of Water Resources using the principles of IWRM, rather than considering a Basin to have a Closed Water Economy. Hence realizing interconnected River Basins having the characteristics of a Concrete Entity can be considered as the basic principle of IWRM to achieve SDGs and to promote GDP by fully utilizing the Water Economy of the Country.

Based on the Provisions in the Article 246 of the Constitution of India, the Water is the State Subject according to Entry 17 of the State List II subject to the condition/provision based on Entry 56 of the Central Union List I. According to the eleventh Report of Standing Committee on Water Resources (Lok Sabha, 2008), the Parliament can utilize the Power/ Facilities of Entry 56 of Union List I through an enactment, which empowers the Union so that the process of Implementation and Maintenance of IBWT based National River Linking Projects can be Regulated and Controlled. According to Mazumder (2003), by Amendment of Indian Constitution, Water Subject can be brought under Concurrent List III. The National Highway Networks are being developed and maintained by the Central Government of India while the State Highways and other District Roads are being developed and maintained by State Governments. Similarly the Rivers can also be classified into National Rivers (say Higher order Stream passing through two or more States) and State Rivers (Lower order Streams). Using an enactment utilizing the Power of Entry 56 of List I, the Authority over Water can be shared between State and the Central Government. Accordingly once the Water enters into the National River which represents higher order main stream that water will becomes the property of Central Government and the State will lose its Authority over the Water. Such Enactment may force the State Government to develop more water Harvesting Structures across the Watersheds of Low Level catchments so that the Water entering into the National Rivers will get reduced or minimized. Such Strategy can indirectly work to reduce the Runoff Loss into the National River and thereby reducing the Impact of Flood. Such Enactment can also facilitate the successful implementation of the IBWT projects connecting the National River Portions of the Indian Rivers.

A Surplus Basin may have Deficit Watershed present somewhere inside the Basin. Particularly the Ganga basin considered as Water Surplus Basin includes Bundelkhand Region which has been reported as Water Deficit Drought prone Area by many publications including Thomas (2016) and located on the downstream side Ken and Betwa Sub basins. And hence the Average Water Availability of a basin estimated based on the Runoff Loss at the Terminal site may not represent the actual distribution of Water Availability across the Basin. Because all IBWT based NRLP of India is based on the Criteria of Surplus Basin and Deficit Basin, in order to ensure proper in-basin Water Resource Management (WRM) Practices in collaboration with inter-basin WRM practices, the Water Availability Distribution (in MCM per sq.km) at all Watershed and Catchment Levels by accounting runoff loss at all gauging sites needs to be estimated and to be kept available to the public for planning of efficient Water Management Practices at all levels of the Management across the Basin.

Unlike other normal Reservoir Characteristics, in case of Polavaram Project, the Reservoir Storage space is located well above 70 km on the upstream side of the Polavaram Dam. The existence of Narrow pass Gorge Section having width less than 300m and a length more than 6 km in between the Dam and Storage Reservoir, increases the complexity of Hydraulic Conditions in order to Characterize the Submergence and Water Level buildup Phenomena of the Storage Reservoir having length of more than 120 km from Polavaram Dam to Bhadrachalam. Hence the construction of Computational Fluid Dynamics (CFD) based Simulation Model by accommodating the exact Hydraulic and Hydrologic Characteristics of the Polavaram Project is likely to be useful to determine exact dynamic Water Level Buildup and Submergence Characteristics of the Storage Reservoir for different combinations of the inflow Flood Wave and corresponding Reservoir operation Strategy. Such Simulation experiment on the CFD based Simulation Model can be used to determine the optimum Reservoir operation Strategy for a given inflow Flood Wave Scenario or otherwise such Simulation Experiment can be used to determine the factor of safety of the different Reservoir operation Strategies to handle the given inflow Flood Wave Scenario.

Because of the Existence of Natural Dam in the Form of Papikondalu Gorge Section on the upstream side of Polavaram Dam, even with the Polavaram Dam Failure, the peak Discharge Level is likely to be limited by the Gorge Section having natural flood attenuation Capacity. Hence the impact of Flood on the downstream side of Dowleswaram is virtually because of the natural Flood Discharge and less influenced by the Polavaram Dam failure. And also, because of the Width of Flow more than 3000 m in the downstream side of Dowleswaram, it can be expected that even with Dam Failure, the Vulnerability for Flood is likely to be less due to the possibly low Submergence Depth in the Delta Regions. Hence, a Computational Fluid Dynamics based Simulation Studies need to be carried out in order to determine the Flood Propagation Pattern as well as Dynamic Scenario of Submergence Characteristics in the Downstream Side of Polavaram dam for a Possible Discharge of 500 and 1000Year Floods with a typical value nearly 150000 Cumec.

## Acknowledgement

The research facilities that have been provided by the administration of VNIT, Nagpur, the water resources data that have been published by USGS, United Nations Organizations and Government of India through its sub-divisional organizations such as CWC, CGWB, NWDA, IMD, NRSC and WRIS along with the financial supports provided by MHRD and Various Services such as Web, Google Earth, Wikipedia & Search Engines available through internet communications, are acknowledged.

## References

Amarasinghe et al. 2005, “Spatial variation in water supply and demand across river basins in India”, Research Report 83, International Water Management Institute Colombo, Sri Lanka
http://www.iwmi.cgiar.org/Publications/IWMI_Research_Reports/PDF/pub083/RR83.pdf
Amarasinghe U.A and Sharma B.R, 2008, “Strategic analyses of the National River Linking Project of India”, series 2 Proceedings of the Workshop on Analyses of Hydrological, Social and Ecological Issues of the NRLP, Sri Lanka: International Water Management Institute. ISBN: 978-92-9090-694-0
APSDPS, 2019, “Flood Inundation Map for Godavari River”, Andhra Pradesh State Development Planning Society, Planning Department, Government of Andhra Pradesh, India
http://www.apsdps.ap.gov.in/pages/publications/river/rivers/index.html#
CGIAR-CSI, 2020, “SRTM 90m DEM Version 4”, Consortium for Spatial Information (CGIAR-CSI) of the Consultative Group for International Agricultural Research (CGIAR), http://srtm.csi.cgiar.org/srtmdata/
Christopher V. H, 2008 “South Asia: An Environmental History”, ABC-CLIO, pp. 33 ISBN 978-1-85109-925-2
Coduto Donald P, 2001, “Foundation design: principles and practices”, Upper Saddle River, N.J.: Prentice Hall. ISBN 0135897068 OCLC 43864336
Crawford, W. G. 2008. Construction Surveying and Layout, 3rd Edition, Indiana: Creative Construction Publishing Inc. ISBN-13: 978-0964742116
CWC, 2016, “Guidelines for Integrated Water Resources Development and Management”, Central Water Commission, Ministry of Water Resources, Rivers Development and Ganga Rejuvenation, Government of India, New Delhi http://cwc.gov.in/sites/default/files/IWRM_Guidelines.pdf

CWC, 2018, "Godavari Basin - Discharge Year Book", Central Water Commission, Ministry of Water Resources, Government of India, http://cwc.gov.in/sites/default/files/admin/10BGBWYB17-18.pdf
CWC, 2018, "Flood Forecasting Appraisal Report Godavari Basin-2018", Lower Godavari Division, Godavari Circle, Hyderabad, Central Water Commission, Ministry of Water Resources Government of India. http://cwc.gov.in/sites/default/files/kgbouser/kgbo/FF%20Appraisal%20report_2018_godavari%20Cicle.pdf
CWC, 2019, "Reassessment of water availability in basins using space inputs", Central Water Commission, Ministry of Water Resources, Government of India, http://cwc.gov.in/sites/default/files/main-report.pdf
CWC, 2019, "Reassessment of Water Availability in India Using Space Inputs", Volume I and II, Basin Planning & Management Organization, Central Water Commission, India. http://cwc.gov.in/sites/default/files/volume-i-compressed.pdf
CWC, 2019, "Water and Related Statistics-2019", Central Water Commission, Ministry of Water Resources, Government of India, http://cwc.gov.in/sites/default/files/water-and-related-statistics-2019.pdf
DuBrin, Andrew J. (2009). Essentials of management (8th Ed.), Mason, OH: Thomson Business &Economics. ISBN 978-0-324-35389-1 https://www.worldcat.org/oclc/227205643
Elizabeth H and William D, (2005), General Sir Arthur Cotton his life and work, Asian Educational Services, New Delhi, ISBN 81-206-1829-7
FAO, 2014, "The Water-Energy-Food Nexus-A new approach in support of food security and sustainable agriculture", Food and Agriculture Organization of the United Nations, http://www.fao.org/3/a-bl496e.pdf
GWDT, 1980, "The Report of the Godavari Water Disputes Tribunal Volume I and II", Godavari Water Disputes Tribunal, Ministry of Energy and Irrigation, Government of India, New Delhi https://irrigationap.cgg.gov.in/img/tribunaryDisputes/GWDT%20AWARD.pdf
GWP, 2000, Integrated Water Resources Management. Global Water Partnership Technical Advisory Committee, Background Paper No. 4 https://www.gwp.org/globalassets/global/toolbox/publications/background-papers/04-integrated-water-resources-management-2000-english.pdf
IRFCA, 2011, "India's First Railways", Indian Railways Fan Club https://www.irfca.org/docs/history/india-first-railways.html
Joshi N. M, 2013, "National River Linking Project of India", Hydro Nepal, Issue no. 12 pages (13-19)
Lehner, B., Verdin, K., Jarvis, A. (2006): HydroSHEDS Technical Documentation. World Wildlife Fund US, Washington, DC. http://hydrosheds.cr.usgs.gov.
Lok Sabha Secretariat, 2008, "Eleventh Report of Standing Committee on Water Resources-Inter Linking of Rivers", Government of India, https://eparlib.nic.in/bitstream/123456789/63626/1/14_Water_Resources_11.pdf
Lok Sabha Secretariat, 2016, "Council of Ministers 1947-2015", Government of India, New Delhi https://eparlib.nic.in/bitstream/123456789/759802/1/Council_of_Ministers_English.pdf
Lok Sabha Secretariat, 2019, "First Report of Standing Committee on Water Resources-Demands for Grants", Government of India, http://164.100.47.193/lsscommittee/Water%20Resources/17_Water_Resources_1.pdf
Maddison A (2010). Statistics on World Population, GDP and Per Capita GDP, 1-2008 AD (Horizontal file, copyright Angus Maddison, university of Groningen) http://www.ggdc.net/maddison/oriindex.htm
Manning, R. (1891). "On the flow of water in open channels and pipes" Transactions of the Institution of Civil Engineers of Ireland 20: 161–207.
Markus M et al. 2019, "Extreme Floods and Droughts under Future Climate Scenarios", Water, MDPI, 11, 1720; doi: 10.3390/w11081720 https://www.mdpi.com/2073-4441/11/8/1720/pdf
Mazumder S K, 2003, " Interlinking Indian Rivers-Issues and Challenges", Proceeding of the National Conference on Hydraulic and Water Resources Engineering, HYDRO-2003, organized by ISH and CW&PRS, Pune, India. http://profskmazumder.com/PDF/Ref_73.pdf
MoT, 1957, "Estimate Committee Sixty-First Report-Inland Water Ways", Ministry of Transport, Lok Sabha Secretariat, Government of India, https://eparlib.nic.in/bitstream/123456789/5047/1/ec_1_61_1957.pdf
MoWR, 1980, "National Perspective Plan for water resources development", Government of India, New Delhi http://nwda.gov.in/content/innerpage/click-more.php
MoWR, 2012, "National Water Policy", Ministry of Water Resources, Government of India, New Delhi http://mowr.gov.in/sites/default/files/NWP2012Eng6495132651_1.pdf
MoWR, 2018, "Annual Report 2017-18", Ministry of Water Resources, River Development and Ganga Rejuvenation, Govt of India, http://jalshakti-dowr.gov.in/sites/default/files/Annual_Report_MoWR_2017-18.pdf
MoWR, 2019, "Annual Report 2018-19", Ministry of Water Resources, Government of India, New Delhi http://jalshakti-dowr.gov.in/sites/default/files/Annual_Report_MoWR_2018-19_Eng.pdf.pdf
NITI Aayog, SDG India Index Base Line Report 2018, National Institution for Transforming India, Government of India, https://niti.gov.in/writereaddata/files/SDX_Index_India_21.12.2018.pdf
NWDA, 2010, "Feasibility Studies Reports for the Peninsular Components of NRLP of India", National Water Development Agency, Ministry of Water Resources, Government of India. http://nwda.gov.in/content/innerpage/feasibility-studies.php

NWDA, 2018, "Annual Report 2017-18", National Water Development Agency, Ministry of Water Resources, Rivers Development and Ganga Rejuvenation, Government of India, New Delhi http://nwda.gov.in/upload/uploadfiles/files/Annual.pdf

Rai N and Manish, 2018, "Backwater Study for Polavaram Irrigation Project", Compendium of Technical Papers, Volume-2, International Dam Safety Conference – 2018, Thiruvananthapuram, Kerala, India https://damsafety.in/ecm-includes/PDFs/Conference/IDSC2018/Compendium_Vol-2.pdf

Rao K L, 1983, "Indian Express News dated 01-05-1983", Central Minister for Irrigation and Power (1963-1973), Government of India, https://sites.google.com/site/profshivajirao/1-5-83klrao.jpg

Shetty M S, 2010, "Concrete Technology Theory and Practice", S Chand and Company Ltd, New Delhi, India

Shivaji Rao T, 2013, Hydraulic Details of Polavaram Project", Former Director, Center for Environmental Studies, GITAM University, Visag, India https://sites.google.com/site/profshivajirao/polavaramdamimages-4

Streeter V L, 1958, "Fluid Mechanics", International Student Edition, McGraw-Hill Book Company, New York

Thomas, et al. (2016), "Drought indicators-based integrated assessment of drought vulnerability: A case study of Bundelkhand droughts in India" Natural Hazards DOI 10.1007/s11069-016-2149-8

WHO, "World Summit on Sustainable Development: Key Outcomes, Challenges and Opportunities for Health and Sustainable Development. World Health Organization 2003 https://apps.who.int/iris/bitstream/handle/10665/42786/9241590955.pdf?sequence=1&isAllowed=y

WMO, 2009, "Integrated Flood Management Concept Paper", World Meteorological Organization, CH-1211 Geneva 2, Switzerland, ISBN 978-92-63-11047-3 https://library.wmo.int/doc_num.php?explnum_id=9811

WRD, 1986, "Polavaram Project Report", Water Resources Department, Government of Andhra Pradesh, India https://irrigationap.cgg.gov.in/wrd/static/approjects/polavaramnew.html

*IN PROCEEDINGS OF 25th HYDRO 2020, INTERNATIONAL CONFERENCE, NATIONAL INSTITUTE OF TECHNOLOGY ROURKELA, ODISHA, INDIA 26-28, March 2021, ISBN 978-93-90631-56-8*

Paper ID - 143

# MEMS Based Remote Operated Bed Profiler for River Model

M. Selva Balan[1] , Pratiksha Mete[2], Ruchita Pagar[3], Harshada Shelkande[4], Dipali Bangar[5]

[1] *Scientist D, Instrumentation and Control Dept., CWPRS, Khadakwasla, Pune-411024, India*
*Email: instcwprs@gmail.com*

[2] *B.Tech in E&TC, Vishwakarma Institute of Technology, Pune-411037, India*

[3] *B.Tech in E&TC, Vishwakarma Institute of Technology, Pune-411037, India*

[4] *B.Tech in E&TC, Vishwakarma Institute of Technology, Pune-411037, India*

[5] *B.Tech in E&TC, Vishwakarma Institute of Technology, Pune-411037, India*

## Abstract

The MEMS based Remote Operated Bed Profiler for River Model helps in illustrating river bed by collecting the sensor data and transmitting it through a wireless transmission technique. The wireless transmission protocol RF used in the project provides a sufficient range. This range can be varied using an antenna. This makes the model unique and easy to use. The 3-axis MEMS sensor is used to measure the acceleration and rotation which then helps to get details about the river bed. The MEMS accelerometer and gyroscope are used to get the acceleration and rotation of the bot where it is mounted. It uses I2C/SPI communication in order to communicate to Arduino. By using the angle tilt of the particular axis towards the surface, we can convert this angle measurements into height (distance) in Arduino. The sensed data in arduino is then send to the remote location using an RF transmitter. The received data at the remote location is then saved in the form of a ".csv" file. Also, a Graphical User Interface is used to get pictorial view of the data..

***Keywords:*** *Bed Profiler, MEMs, RF Transmission, Contour, Bot, GUI.*

## 1. Introduction

The bed profiling of river model is challenging task when it comes to collecting data precisely and remotely. This task can be done by developing a system using a MEMS Accelerometer and gyroscope sensor in order to get the illusion of the river bed in numeric format. The system is meant to sense the acceleration and rotation of the moving vehiclebot where the MEMs is mounted. The main objective is to run the bot at constant speed and continuously collect the sensor data. Sending this sensor data to the remote location makes system more reliable, for that a wireless RF transmission module is getting used. RF module is capable to provide a good range of transmission with flexibility. The transmitted data when received at the receiving end is converted and stored in a readable .csv file. The data file could be further used to manipulate the data to give the graphical user interface so to analyze various parameters.

### 1.1 *Literature Review*

Make small changes in governing equation and discretization technique reconstruct the river bed topography from known free surface area. The governing equation for forward and inverse problems are very similar so that both of them use similar discretization process to solve problem is presented in [1]. Hydraulic geometry have parameters like width, depth, cross sectional area, meander length, and other hydraulic variables like mean slop, friction, and mean velocity. These parameters depends on many factors such as discharge and type of bed material. Due to soil erosion on one side sedimentation happens on other side it is known as the instability of river geometry. Solving instability of river geometry analysis the meandering characteristics by using Acoustic Doppler Current Profiler presented in [2]. River vegetation is one of reason for cause of flooding. It is also barrier for water flowing naturally. To deal with this problem use camera and photo modeler scanner software for photogrammetric data processing. It gives the practicalities of deriving the three dimensional surface topography and water surface velocity of a dynamic and flowing water surface. This technique is flexible and applied in both the flume and field presented in [3]. For small area collection of data of seabed or riverbed parameter and their characterization are boring and time

consuming task. There for mathematical model system design for seabed or riverbed. This system is based on the acoustic behaviour of river and river bed presented in [4].

Study purpose of river bed topography and parameter which effect to river bed, river bed profiler system introduce by using Arduino, Ultrasonic and Bluetooth model. It is low cost and compatible presented in [5]. The challenges faced during waterway communication in navigation, Bangladesh introduce a system which is underwater riverbed 3D mapping system. They used the ultrasonic transducer and microcontroller. They used colour codes in mapping system for easy analyzing data or parameters presented in [6]. In flushing experiment study the degree of undercut of the riverbed under the action of clear water scouring. Water level in the sanding part first decrease and then stabilized. Water level in middle section of sanding first increase and then decrease. For the outlet part water level is stable. In the experiment rate of sediment transport in river is large at initial stage and then decrease. Presented in [7].

Minimum cost, less energy consumption, good precision and moderate speed have great importance in the embedded market, hence designing an embedded system with minimum cost, minimum energy consumption, high accuracy and moderate processing speed are kept in the first priorities. Hence, the designed system is enhanced by using MEMs sensor and RF transmission to get real data with increased accuracy, transmission speed and provides efficient data transmission

## 2. Proposed System (Methodology)

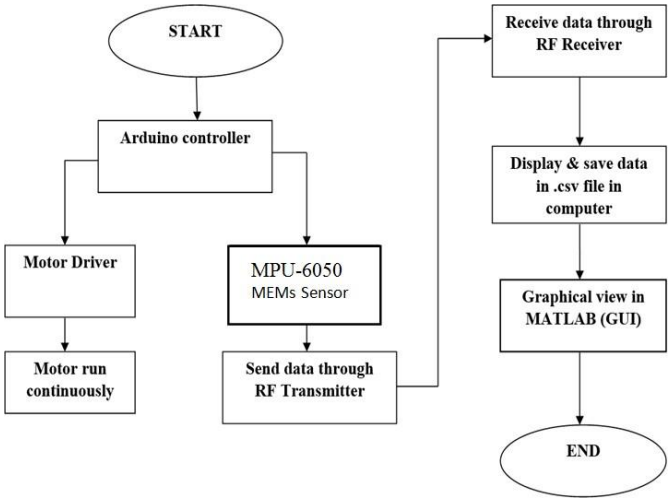



**Figure 1** Flow chart

The proposed system is an embedded module that consists of an autonomous bot which travels at a constant speed, an Arduino, a 3-axis MEMs accelerometer and gyroscope present in MPU6050 placed on the bot, RF modules placed at both transmission and reception end, etc. A bot made using dc motors and Arduino runs continuously at a constant speed on the bridge. As soon as the bot starts running, the sensor module gets activated and the MPU6050 (accelerometer & gyroscope) sense the rotation and the acceleration of the bot cause by the profiler of the bed. The data from the MPU is translated to get the degree(from gyroscope) and force in g(from accelerometer). The translated data then send through the RF wireless communication protocol .The another end of the RF receiver has the arduino which log the data into the ".csv" file using Tera Term software. To get visualization of the data the Graphical User Interface has been build. A GUI is made with the help of MATLAB which take ".csv" file as an input. The ".csv" file contains the orientation information of the bot in 3 axis X, Y, Z. This x, y, z input data is first gridded using some gridding techniques like linear, nearest, natural and cubic gridding methods. Then, the contour plots are plotted.

**Gridding methods:**
1. Linear Gridding:

Linear interpolation is a simple technique used to estimate unknown values that lie between known values. The concept of linear interpolation relies on the assumption that the rate of change between the known values is constant and can be calculated from these values using a simple slope formula. Then, an unknown value between the two known points can be calculated using one of the points and the rate of change.

2. Nearest Gridding:
   Nearest gridding is also called as closest gridding.
   Each grid node is simply assigned the value of the closest control point.
3. Natural Gridding:
   The natural gridding algorithm interpolates grid values by weighting neighbour data points based on proportionate areas. It uses weighted average of the neighbouring observations
4. Cubic Gridding:
   The interpolated value at a query point is based on cubic interpolation of the values at neighbouring grid points in each respective dimension. Grid must have uniform spacing, though the spacing in each dimension does not have to be the same. Requires at least 4 points in each dimension.

Using this gridded data, the contour lines are plotted which connects the same data point giving the curvy line through the dots. This contour line plot is used to observe the undulations along the path of the bot moving in the river field.

**Mathematical Manipulation:**

MPU-6050 module is a 3-axis sensor. It is used to take orientation of the object mounted on 3D space.The 3-axis helps us to find the change in acceleration.

If force F is applied for mass then the displacement X is occure by amount of x with acceleration A.

By applying force conservating equation (Newton Law).

$$F= mA =Fs = Kx\ mA = Kx\ A=F(x)$$

Acceleration is the function of displacement.

Initially, the rest position readings of all the 3-axis is taken.

Ex: Xrest=analogRead(sensorpinX)
Yrest=analogRead(sensorpinY)
Zrest=analogRead(sensorpinZ)

Then when the bot starts running, the rest position readings are subtracted from the actual readings which in turn gives the change in acceleration readings in all 3-axis.

Ex.Xread=analogread(sensorpin)-Xrest
Yread=analogread(sensorpin)-Yrest
Zread=analogread(sensorpin)-Zrest

This acceleration is further converted into Velocity and distance.

Also, the profile plots for each line are plotted.

### *2.1 Block Diagram*

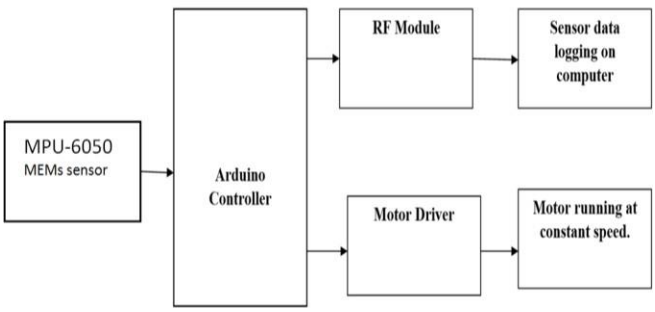



**Figure 2** Block Diagram

It mainly consists of following blocks:

1. Arduino UNO:



**Figure 3** Arduino Uno

Arduino Uno is a microcontroller board based on 8-bit ATmega328P microcontroller. Along with ATmega328P, it consists other components such as crystal oscillator, serial communication, voltage regulator, etc. to support the microcontroller. Arduino can be used to communicate with a computer, another Arduino board or other microcontrollers. In this project, the two Arduino boards are placed at the transmitting and receiving end. The data from the accelerometer sensor is taken using Arduino and transmitted to the receiving Arduino through RF transmission.

2. MPU6050 MEMs sensor

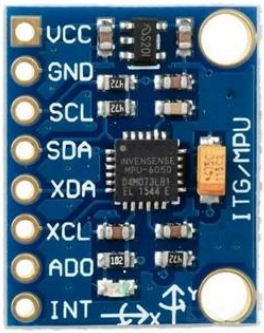



**Figure 4** MPU6050 MEMs sensor

The MPU6050 is a Micro Electro-Mechanical Systems (MEMS) which consists of a 3-axis Accelerometer and 3-axis Gyroscope inside it. This helps us to measure acceleration, velocity, orientation, displacement and many other motion related parameter of a system or object. Sensor data is extracted and manipulated using the x, y and z-axis tilt. Initially, the rest position readings of all the 3-axis is taken. Then when the bot starts running, the rest position readings are subtracted from the actual readings which in turn gives the change in acceleration readings in all 3-axis.

Accelerometer measures acceleration by measuring change in capacitance . It's micro stucture consist a mass attached to a screen which is confined to move along one direction and fixed outer plates. So when an acceleration in the particular direction will be applied the mass will move and the capacitance between the plates and the mass will change. This change in capacitance will be measured process and it will correspond to the particular acceleration.

3. RF Module




**Figure 5** RF Module

An RF module (short for radio-frequency module) is a (usually) small electronic device used to transmit and/or receive radio signals between two devices. In an embedded system it is often desirable to communicate with another device wirelessly. Rf module uses ASK digital modulation technique where amp of carrier changes with respect to digital input signal. RF signals can travel even when there is an obstruction between transmitter & receiver. Transmission through RF is better than IR (infrared). Firstly signal through RF can travel larger distances making it suitable for longer range applications. RF propagation occurs at the speed of light and does not need a medium like air in order to travel. Here, RF transmitter receiver module is used to transmit the distance data over the distance of 100m.

4. L298n motor driver & motors

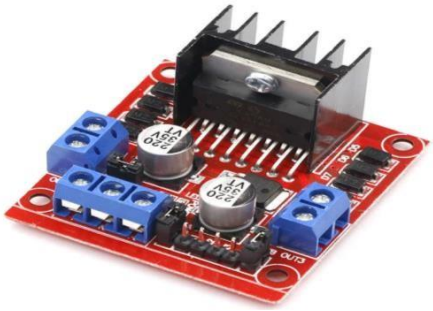


**Figure 6** L298n motor driver

The L298N is a dual H-Bridge motor driver which allows speed and direction control of two DC motors at the same time. The module can drive DC motors that have voltages between 5 and 35V, with a peak current up to 2A. It is a high voltage, high current dual full-bridge driver de-signed to accept standard TTL logic level sand drive inductive loads such as relays, solenoids, DC and stepping motors. Two enable inputs are provided to enable or disable the device independently of the in-put signals .The emitters of the lower transistors of each bridge are connected together rand the corresponding external terminal can be used for the connection of an external sensing resistor. An additional Supply input is provided so that the logic works at a lower voltage.

### *2.2 Hardware Requirements*

- Arduino uno
- MPU-6050 module
- RF module
- L298n motor driver & motors

### *2.3 Software Requirements*

- Arduino
- Proteus for simulation
- Tera term for .csv generation
- Matlab for GUI

### *2.4 Advantages*

- Stores the data at one place which is easily accessible to the user
- Robust And Compatible
- Continuous data transmission
- Efficient in non-range zones

### *2.5 Applications*

- Survey of River Topography
- Planning of building of structures across the river.
- Emergency Flow control and Diversion planning.
- For deeper study and even education regarding river- bed profiler.
- Predicting effect on water level due to various experiments.

## 3. Results

Data sensing & transmission:
The elevation of the bot travelling on the river field calculated using MEMS sensor is sent to the remote room through RF communication.

Data reception:
This received information or data is extracted in the form of an excel file using a software called TeraTerm.

**GUI**

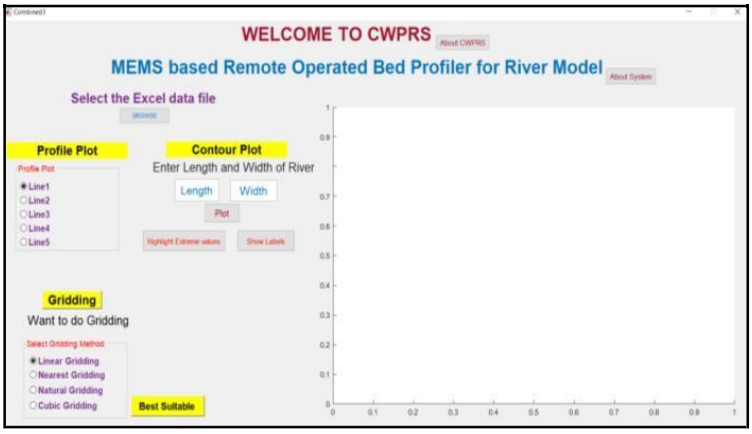



**Figure 7** Gridding plot

1. As the GUI is made in MATLAB, this excel data file(.csv) is converted into MATLAB file (.mat).
   This file contains the elevation information of the bot which includes the length, width of the river and the depth information.
   For example:
   Bot travelled on a rectangular patch of length 100cm and width 50cm. And the corresponding depth (undulation) values in mm.
   The bot travels 50cm for each length value of the total 100cm length.
2. First the GUI layout is designed which includes the user input section, buttons and figures.
3. Then, the data in .mat file is loaded into the MATLAB software as column vectors.
4. The .mat file includes 3 columns length, width and depth.

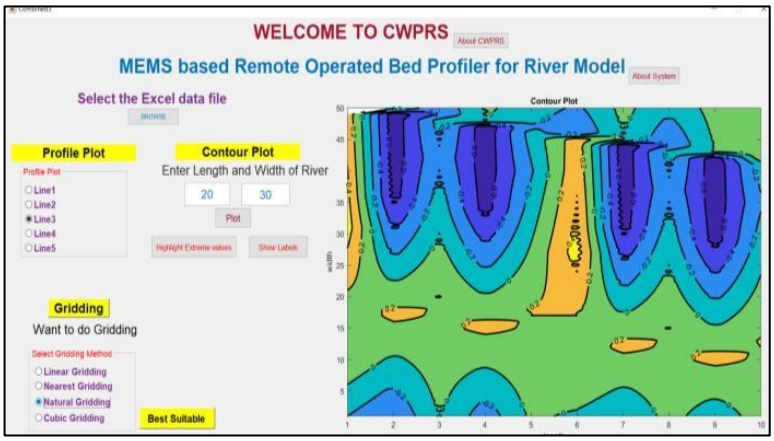



**Figure 8** Gridding plot

This input data is first gridded using some gridding techniques like linear, nearest, natural and cubic gridding methods.
Gridding is the process whereby a set of irregularly distributed points are converted to a regularly spaced grid. Grids are used to model and map structures such as the seabed, reservoir layers etc.
Amongst all the gridding techniques, Natural gridding is found to be more appropriate. It takes the weighted average of the neighbouring values.

5. The contour function in MATLAB needs it's input parameters as matrix. So, This column vectors are converted into matrix using meshgrid function. Then this data is plotted as a contour plot using MATLAB's inbuilt command.

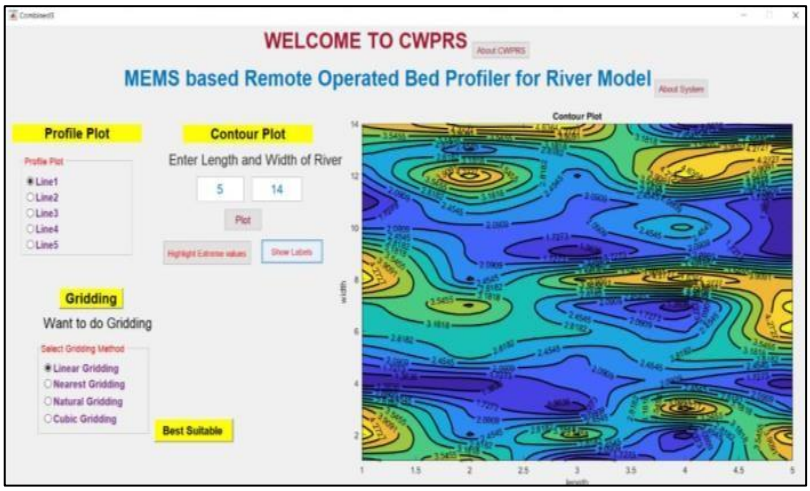



**Figure 9** Contour plot

A contour is a imaginary line joining points of equal elevation. Contour lines are used to understand the nature of the ground surface of a region.
It accepts the user input. User can enter the length(X) and width(Y) dimensions of the river and the GUI arranges the data according to this length and width dimensions and plots the contour.
The above figure shows the contour plots of the data.

6. Also, the profile plot for each line acquired by the sensor is drawn as shown in fig.10 below. The system acquires mm level variation due to the technology and can wirelessly transmit data to the

logger system. The software is developed in Matlab to have line plot as well as the contour plots by applying different gridding methods.

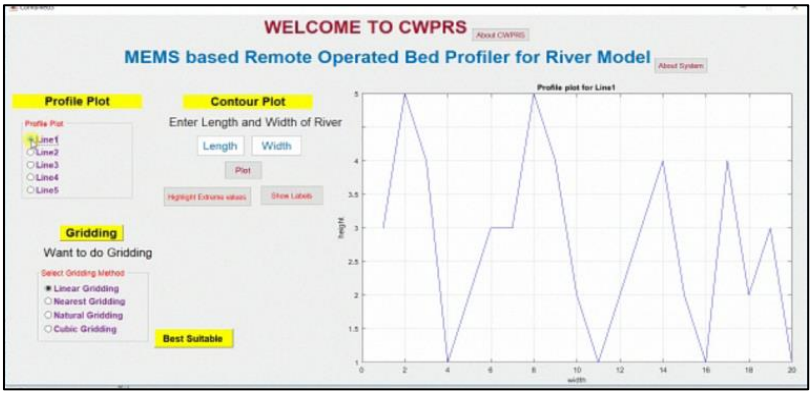



**Figure 10** Profile plot

The above figure shows the profile plot for one line.



**Figure 11** Profile plot in real use

## 4. Conclusion

The system acquires three axis movement in 0.01 degree accuracy and hence small changes in model before and after dam flushing is modelled. This is an important parameter in river training works. This system is effective where continuous monitoring river parameters is to be carried out. RF propagation does not need any physical medium to travel, therefore high speed data transmission is achieved. Also, as the output data is extracted to an .csv file, the data can be used for building the GUI which further can be used to analyze the river parameter.

**Acknowledgement**
We thank the Director of CWPRS for providing necessary facilities at CWPRS to carry out the experiment. We also thank our college Vishwakarma Institute of Technology for supporting us in the MATLAB simulation and guidance throughout the project.

## References

[1] A. F. Gessese, M. Sellier, E. Van Houten, G. Smart, "Reconstruction of river bed topography from free surface data using a direct numerical approach in one-dimensional shallow water flow" presented at "IOP Publishing", Published 6 January 2011.

[2] Asst. Prof. Dr. Mohammed Shaker Mahmood, Asst. Prof. Dr. Kareem R.Almurshedi,
Zaid Nori Hashim, "Hydraulic Geometry Relationships for Meadring River in Al Abbasia Reach in Euphrates River" presented at "International Journal of Engineering Research & Technology (IJERT)", Issue 3, March 2014.

[3] J.H. Chandler, E. Ferreira, R.Wackrow, K Shiono, "Water Surface And Velocity Measurement- River And Flume" presented at "ResearchGate Publication", June 2014.

[4] Soorya Gayathri J, N. Dayakar, Haneesh Sankar T P, "Mathematical Modelling of Ultrasonic System for Riverbed Identification and Classification" presented at "International Journal of Engineering Research & Technology (IJERT)", Issue 12 December 2016.

[5] Aniket Mangale, Santosh Nagargoje, Vikram Pansare, "River-Bed Profiler System" presented at "International Journal of Advance Engineering and Research Development"
Issue 6 June 2017.

[6] Navan Tanjeem Hossain, Rahat Mahmood Khan, Saifur Rahman, Dr. Md. Ziaur Rahman Khan, "Design of an Underwater Riverbed 3D Mapping System for Navigation in Bangladesh" presented at "Proceedings of TENCON 2018 - 2018 IEEE Region", 31 October 2018.

[7] Cheng Xiaobing, "Study on the Riverbed Evolution under the Condition of Clear Water Flushing" presented at "2019 International Conference on Civil and Hydraulic Engineering IOP Publishing", 2019

[8] Aditi Awasthi,Dr.S.S.Lokhande,M.Selva Balan "Reservoir Characteristics Classification using Acoustic Signal Processing" , publised in "IJSTE" issue 01 July 2016.

[9] Anjali Ghadage, Salva Balan , Sushama Shelke " Performance Analysis Different Filters for Noise Removal of Underwater Bathymetric Data" publised in "IJAIEM" issue 03 March 2014.

[10] Pooja Gavande, Dr.R.S.Kawitkar, M.Selva Balan, "Classification of Underwater Objects using Acoustic Techniques" publised in "IJECS" issue 03 January2011.

*IN PROCEEDINGS OF 25th HYDRO 2020, INTERNATIONAL CONFERENCE, NATIONAL INSTITUTE OF TECHNOLOGY ROURKELA, ODISHA, INDIA 26-28, March 2021, ISBN 978-93-90631-56-8*

Paper ID - 286

# Hydrodynamic Modelling of Middle Tapi River Using MIKE 11

K. B. Baladaniya [1], P. L. Patel [2], P. V. Timbadiya[3]

[1]*Former Post Graduate Student, Water Resource Engineering, Department of Civil Engineering, Sardar Vallabhbhai National Institute of Technology, Surat 395007, India*
[2]*Professor, Department of Civil Engineering, Sardar Vallabhbhai National Institute of Technology, Surat 395007, India*
[3]*Associate Professor, Department of Civil Engineering, Sardar Vallabhbhai National Institute of Technology, Surat 395007, India*
*Email: kalpeshb1701@gmail.com*
*Telephone/Mobile No.: +91 9974751216, +91 8160440659*

## ABSTRACT

The severe losses of property and lives are observed every year due to flooding conditions across the globe. The events of flood are invariably being considered as natural phenomenon, however, anthropogenic activities in the catchment and flood plains affect the severity of the events. The prediction of stage-discharge hydrograph in the river is required for effective flood management for adopting various structural and non-structural measures. The present study addresses the development of one-dimensional (1-D) Hydrodynamic model using MIKE 11 software to simulate hydraulic characteristics of flow for Middle Tapi River. The calibration of the unsteady simulation model was performed for the flood events of the years 1998, 1999, 2002, 2003, 2004 and 2005 with the due consideration of upstream and downstream boundary conditions to estimate the optimum value of the Manning's roughness coefficient of the river bed. The upstream and downstream boundary conditions in the calibrated model was taken as flood hydrograph and water levels, respectively. The performance of the calibrated model was determined by comparing the simulated and observed water levels at the intermediate stream gauging stations. With the help of standard performance indices such as Root Mean Square Error (RMSE), Nash-Sutcliffe efficiency (NSE) and Coefficient of Determination ($R^2$). The calibrated model was also validated using the independent flood events of the years 2006 and 2007. The performance of developed model during validation period was found to be satisfactory, with RMSE and NSE of 0.975 m and 0.966 m, 0.980 and 0.861, respectively.

***Keywords**: Hydrodynamic modelling, MIKE 11, Middle Tapi River, Manning's roughness coefficient.*

## 1. Introduction

In recent decades, India has observed rapid population growth, which is the primary reason for modifications in land-use patterns, atmospheric temperatures, flood plains, drainage, etc. In addition, the effects of global warming have resulted into heavy storm, high precipitation intensity, seaw ater level rise, etc. (Nandalal 2009). However, the events of the flood are a natural phenomenon but still the anthropogenic activities affect the flood plains and hence, also influences the severity of damages due to flooding conditions. Various anthropogenic behaviors often increase the impermeability of the earth's surface, thereby reducing the infiltration capacity and produces more runoff. Floods can rarely be prevented, but the severity of the flood can be minimized by embracing absolute preparedness for the flood (Rahman et al. 2011). The various effective structural measures to mitigate the damages due to flood events are the construction of reservoirs and dams, diversions, floodway, or by increasing conveyance capacity through channel expansion, channel deepening, channel realignment, and riverbank protection. The non-structural flood measures such as land use regulations, flood warning, flood forecasting, etc. plays an important role for mitigating not only the catastrophic consequences but

also the environmental contamination. Out of this, the flood prediction (forecasting) plays a significant role (Nandalal 2009). The rapid evolution in the field of computational technology has been observed nowadays and various ranges of hydraulic models i.e. one dimensional (1D), two dimensional (2D), three dimensional (3D) and coupled schemes are being prepared for the water level predictions. Out of these, one dimensional model is very common and adopted globally due to its speed of calculation, ease of parameterization and representation of the hydraulic structure in the flow domain. The one-dimensional hydrodynamic models are reasonably precise than hydrological routing, since hydrodynamic models (HD) compute and update the flow discharge and water level simultaneously in the time domain and thus provide more reliable results for the analysis of unsteady flow during propagation in the river (Kamel 2008). MIKE 11 HD model is a one-dimensional hydrodynamic modelling tool for rivers and channels developed by Danish Hydraulic Institute (DHI) with the MIKE zero graphical interface. The aforesaid unsteady non uniform simulation model which solves the 1D hyperbolic dynamic Saint Venant equation using a six-point Abbot Ionesco finite difference scheme for the calculation of discharge and water levels. (DHI, 2014). The various studies have been carried out for the development of hydraulic models using MIKE 11 HD modelling tool for the forecasting of the water level and inundation of flood plain area. (Le Ngo et al. 2008; Kamel 2008; Majewski 2008; Nandalal 2009; Pramanik et al. 2009; Delphi et al. 2010; Timbadiya et al. 2014a)have been proved to be quite efficient.

The Tapi River is the second largest west flowing river in the Indian peninsula which is frequently influenced by large floods and causes considerable loss of lives and properties in the lower Tapi river sub-catchments. The present study had intended to discuss the following objective of developing the hydrodynamic model for the Middle Tapi River between Sukwad to Sarangkheda stream gauging station 40.5 km river length using MIKE 11 HD model.

## 2. STUDY AREA AND DATA COLLECTION

### 2.1 *Description of study reach*

The Tapi River is the second largest west flowing river in India after Narmada. The River Tapi is also known as Tapti and Surya Putri. Tapi River originates in Madhya Pradesh from Multai forest in Betul district. The elevation at the beginning is about 752 m with respect to mean sea level. The complete length of the Tapi River from source to the meeting point at the ocean is 724 km. It flows 282 km through M.P., 228 km passes through Maharashtra and 214 km passes through Gujarat to merge into the Arabian Sea at Dumas. The Tapi basin is having a total catchment area of 65145 sq. km out of which 79.1% of the area is in Maharashtra, 15% of the area is in Madhya Pradesh and 5.9% of the area is in Gujarat. There are several tributaries located on either bank of Tapi River. Among them, 14 are major tributaries which are having approximately 50 km or more length. There are 4 major tributaries the Gomai, the Vaki, the Aner and the Arunavati which connects the Tapi River on the right bank, and 10 major tributaries the Amravati, the Nesu, the Panjhara, the Sipna, the Bori, the waghur, the Girna, the Mona, the Purna and the Buray connects the main channel from left bank. Among all these tributaries, 45 percent of the total basin area is contributed by two major tributaries namely the Purna and the Gima. The total basin area of Tapi is almost 2% of the entire geographic area of India. The basin boundaries are located between the latitudes of 20°5’ N to 22°3’ N and longitudes of 72°35’ E to 78°17’ E. The shape of the basin is elongated having 587 km of extreme length from west to east and 210 km of extreme width from south to north. The entire, Tapi basin area is further distributed into three sub-basins: Upper Tapi Basin from origin to Hathnur dam site (29,430 sq. km), Middle Tapi Basin from Hathnur dam site to Ukai dam site (32,925 sq. km) and Lower Tapi Basin from Ukai dam site to the Arabian Sea (2,790 sq. km). The river length for the present study is 40.5 km lying in the Middle Tapi basin from Sukwad to Sarangkheda stream gauging stations as shown in Figure 1.

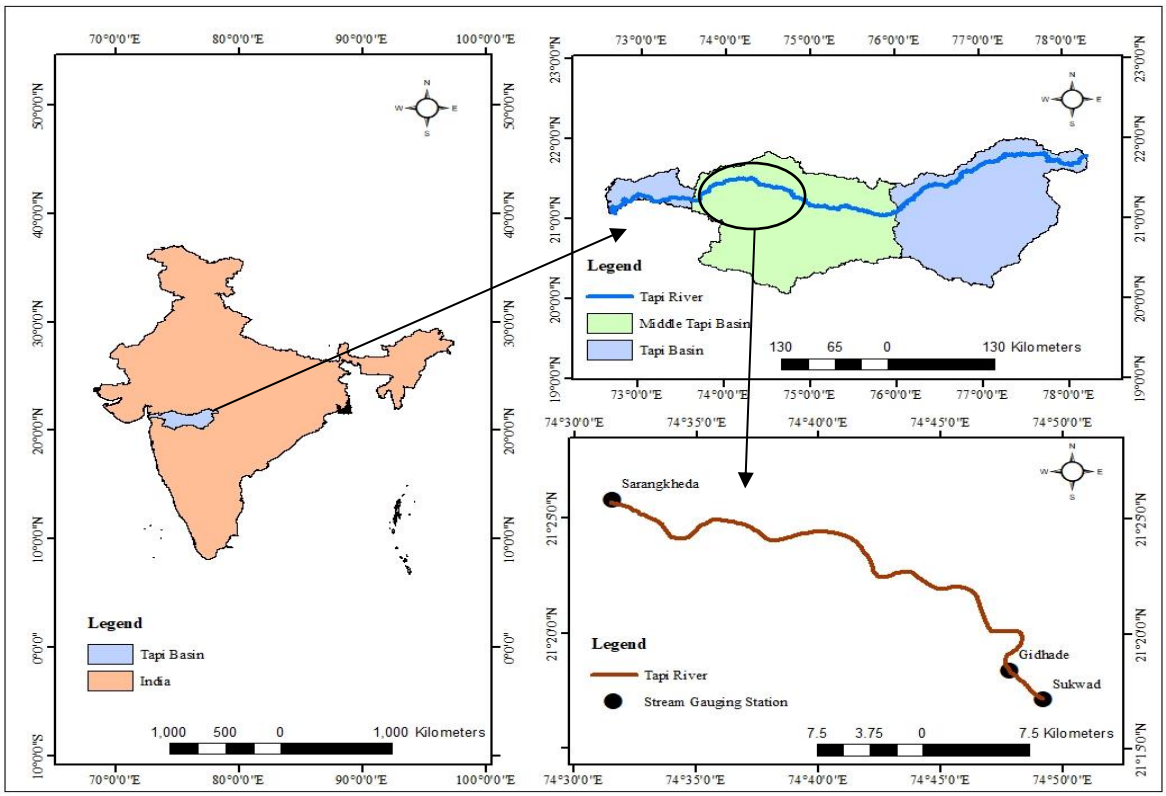



**Figure 1.** Index map of the Study Area

### 2.2 *Geometric and hydrological data collection*

The river geometry data i.e., cross sections were acquired from the Central Water Commission (CWC), Govt. of India for the development of the hydrodynamic model. The most recent six surveyed cross sections along the river were acquired between the Sukwad to Sarangkheda with its longitude, latitude, river bank points, chainages along the river, RL of benchmark, etc. The daily time series of discharge and water levels for the years 1998 to 2007 were collected from the CWC and HDUG, Govt. of India and Nashik recorded at Sukwad, Gidhade and Sarangkheda stream gauging station. For this present study, the flow hydrograph at Sukwad (upstream boundary condition) and water level (downstream boundary condition) at Sarangkheda were considered to simulate the aforesaid model.

## 3. METHODOLOGY

The approach adopted in the present research work to develop a one-dimensional hydrodynamic model for the Middle Tapi River is shown conceptually by schematic chart in Figure 2.

### 3.1 *Numerical scheme*

MIKE 11 HD model is a 1D hydrodynamic modelling tool for Rivers and channel with the MIKE zero graphical interface, which has been developed by Danish Hydraulic Institute (DHI) and it is a one dimensional, unsteady, simulation model which solves the 1D hyperbolic quasi linear Saint Venant equation using the six-point Abbott Ionescu finite difference scheme (DHI, 2014). The system employs

a staggered grid solution for the finite differential equations using a double sweep algorithm. Furthermore, the module in an open channel can consider both subcritical and supercritical flow conditions.

### 3.2 *Hydrodynamic modelling*

The implementation of the model requires the river network geometry, series of cross sections, hydrodynamic parameters and boundary conditions. The subsequent paragraphs illustrate the concise description of the numerical scheme used in the model, development of river geometry, boundary conditions, and hydrodynamic parameters.

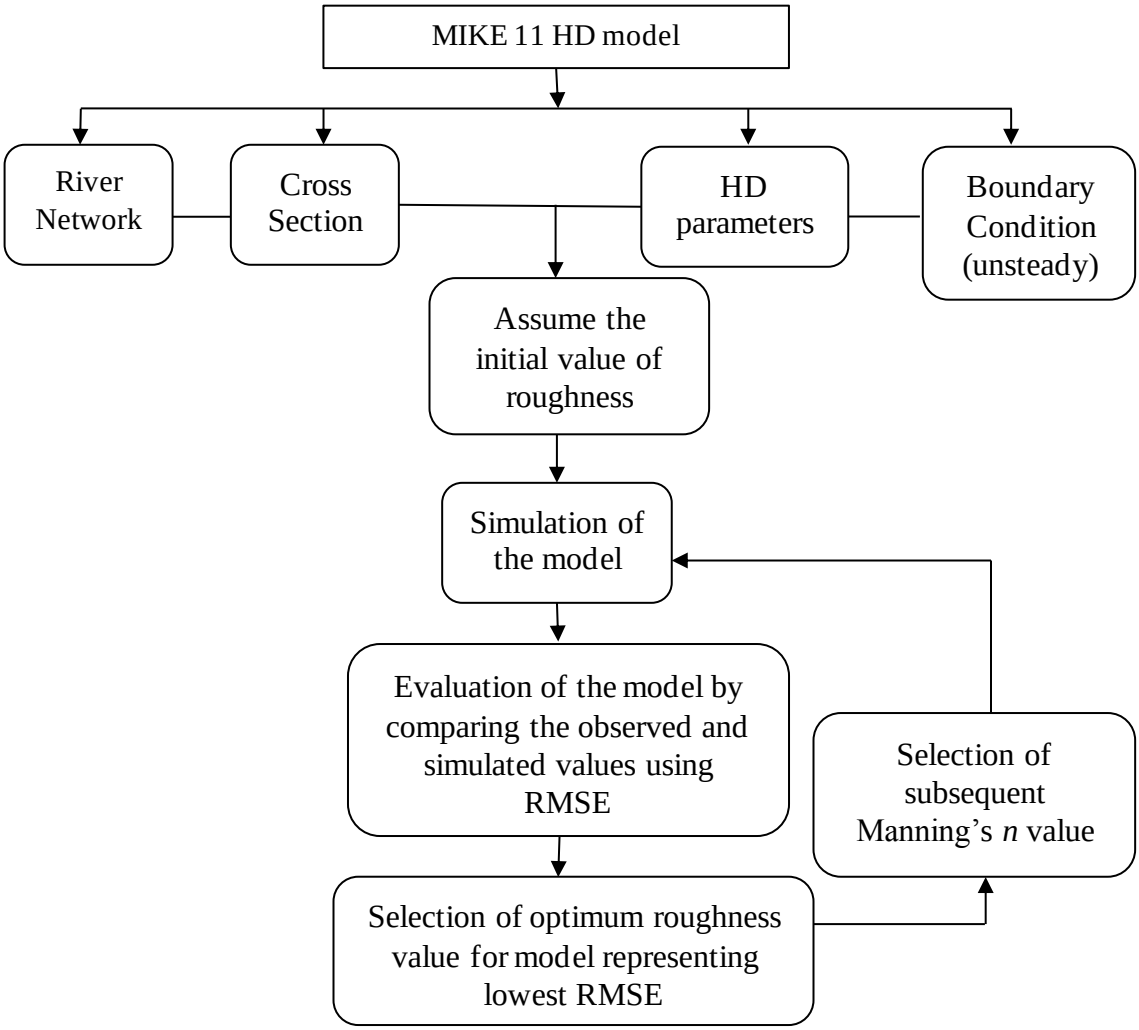



**Figure 2.** Methodology used for Model Development

#### 3.2.1 *River network*

The river network was prepared using the network editor tool available in the MIKE 11 between two stream gauging stations. Sukwad and Sarangkheda. The Tapi River traverses the 40.5 km long route between the Sukwad to Sarangkheda which is shown in the Figure 3. The longitudinal profile of the study reach at thalweg line is presented in Figure 4 including the left and right bank levels.

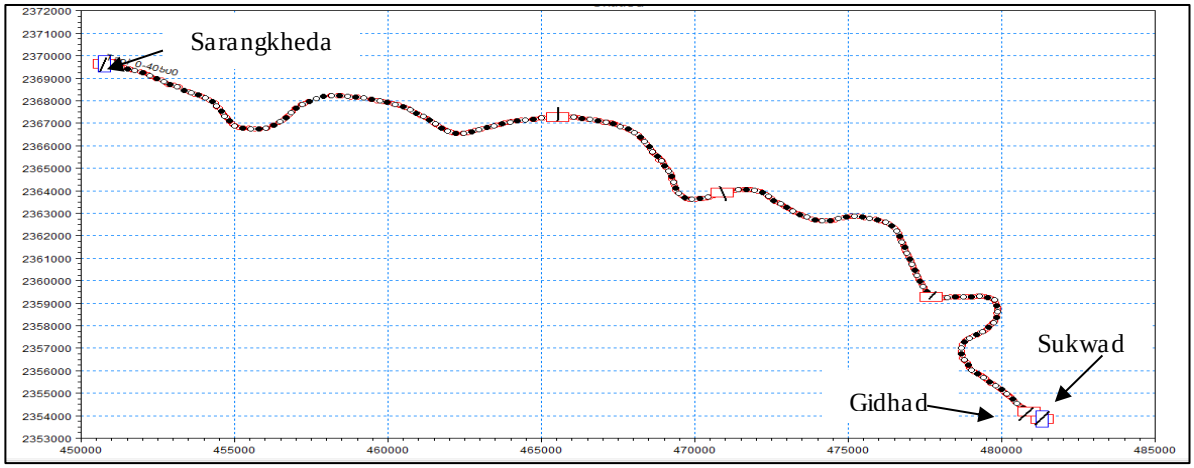



**Figure 3.** River Network for Middle Tapi River from Sukwad to Sarangkheda, stream gauging stations

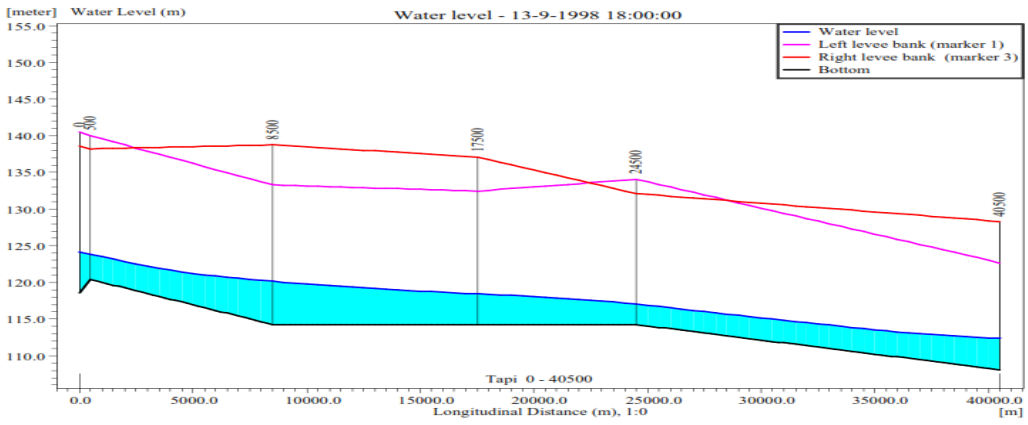



**Figure 4.** Longitudinal Profile of the River

### 3.2.2 *Cross sections*

The six surveyed cross sections between the Sukwad to Sarangkheda have been used for this present study. The intervals between these surveyed cross sections were in the range from 0.5km to 16 km. The chainages were obtained using the Arc GIS 10.3 extension using the latitude and longitude. The markers were defined for left bank and right bank accordingly. The Figure 5 represents the cross-section profile including left and right bank at Sukwad stream gauging station.

### 3.2.3 *Boundary conditions*

The boundary conditions are the most significant parameters for the model development because inappropriate selection of the boundary conditions may lead to erroneous results and the predictions made through simulation model may be become unrealistic. For this present study, the flow hydrograph at Sukwad (upstream boundary condition) and water level (downstream boundary condition) at Sarangkheda were considered to simulate the aforesaid model.

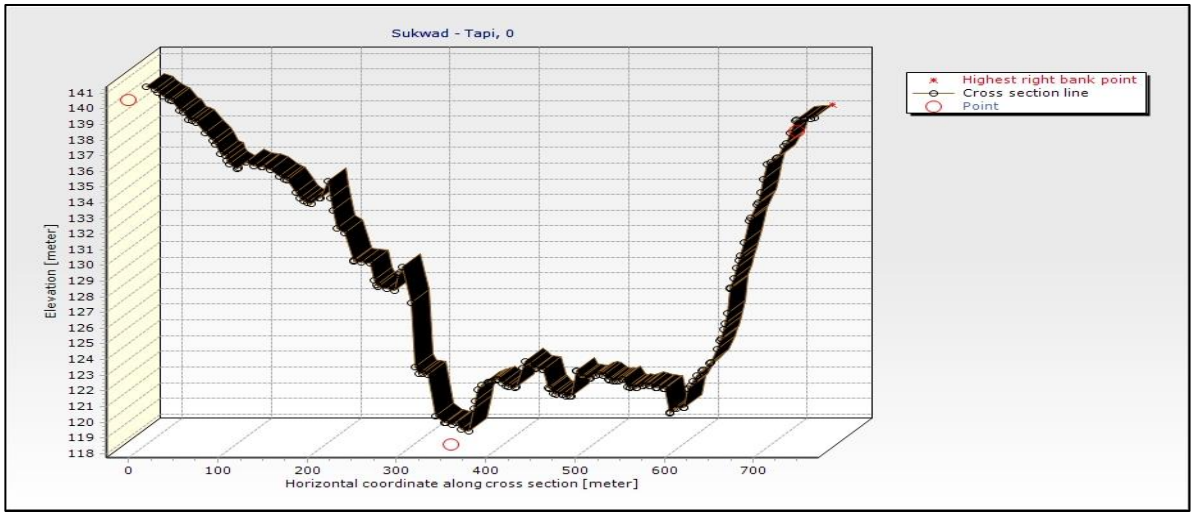



**Figure 5.** Cross section in MIKE 11 at chainage (0.00 km chainage at Sukwad)

### 3.2.4 *Hydrodynamic parameters*

The Middle Tapi River exhibit gentle slope hence, fully dynamic equations were used for the simulation. The simulation editor is used for integration and exchange of information between each of the individual data editor. It provides the linkage between the network and other MIKE 11 editors. All the files required for HD model were updated in the simulation editor tool. The time step for simulation was taken as 5 sec. The results of the simulations were stored at the time interval of 60 minutes. According to Courant-Friedreich-Lewy condition, for the stable numerical calculations, the grid spacing of 500m was taken.

## 4. ANALYSIS OF DATA

### 4.1 *Calibration of the model*

The method for calibration and validation requires two independent data sets. One data set is required for acquiring the optimum value of independent coefficients and the other data set is required to validate the calibrated model. Usually, the model calibration is performed manually by trial & error method to ensure the least deviation from the actual observed value of the past data (Timbadiya et al. 2014b). The optimized value of the Manning's roughness coefficient by comparing the observed and simulated water level was obtained to minimize the deviation between the observed and simulated values.

In present study, the MIKE 11 has been calibrated for Manning's 'n' using flood events of years 1998, 1999, 2002, 2003, 2004 and 2005. The trial values of Manning's n were selected in the range of 0.15 to 0.45, and the performance of simulated model were assessed by comparing the observed water levels at Gidhade stream gauging station. The Root Mean Square Error (RMSE), NSE and $R^2$ were used to compare the adequacy of simulated results with corresponding observations. The performance of the model in simulation of stage at Gidhade Stream gauging station for aforesaid years are shown in Table 1.

The simulated and the observed values of water level at Gidhade stream gauging station were compared for the validated model in 1998, 1999, 2002, 2003, 2004 and 2005 independent flood events which can

be seen in Figures 6(a) and 6(f). The scatters plot of hourly water level using 1D hydrodynamic model at Gidhade stream gauging station for the respective years are shown in Figures 7(a) and 7(f).

**Table 1** Calibrated Manning's n value corresponding RMSE and NSE

| No | Year | n | RMSE (m) | NSE |
|---|---|---|---|---|
| 1 | 1998 | 0.028 | 0.658 | 0.975 |
| 2 | 1999 | 0.031 | 0.596 | 0.943 |
| 3 | 2002 | 0.039 | 0.508 | 0.969 |
| 4 | 2003 | 0.017 | 1.616 | 0.698 |
| 5 | 2004 | 0.036 | 0.845 | 0.671 |
| 6 | 2005 | 0.056 | 0.465 | 0.839 |

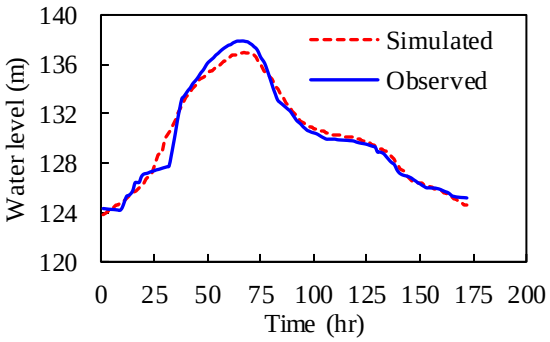



**Figure 6(a)** Comparison observed and simulated water levels for n = 0.028 at Gidhade stream gauging station year 1998

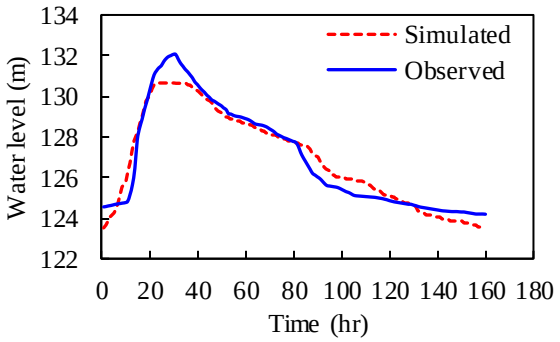



**Figure 6(b)** Comparison observed and simulated water levels for n = 0.031 at Gidhade stream gauging station year 1999

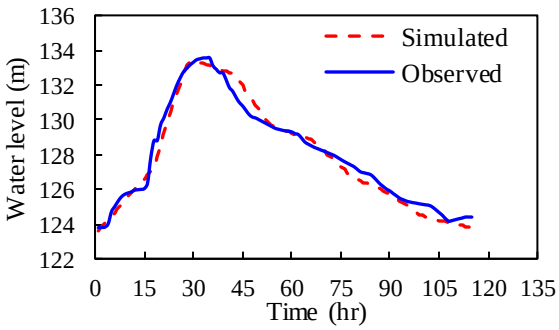



**Figure 6(c)** Comparison observed and simulated water levels for n = 0.039 at Gidhade stream gauging station year 2002

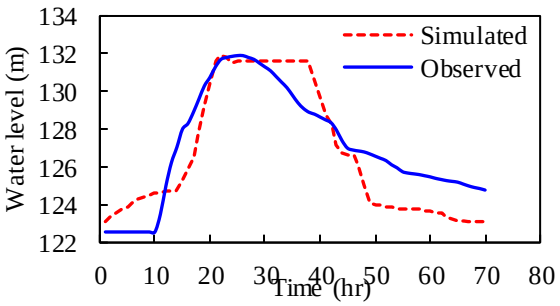



**Figure 6(d)** Comparison observed and simulated water levels for n = 0.017 at Gidhade stream gauging station year 2003

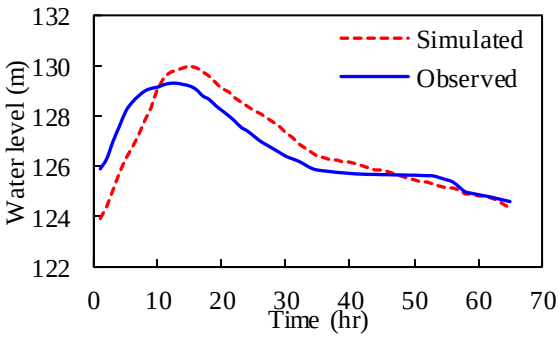



**Figure 6(e)** Comparison observed and simulated water levels for n = 0.036 at Gidhade stream gauging station year 2004

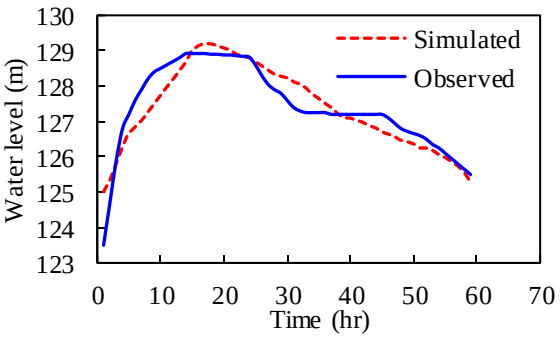



**Figure 6(f)** Comparison observed and simulated water levels for n = 0.056 at Gidhade stream gauging station year 2005

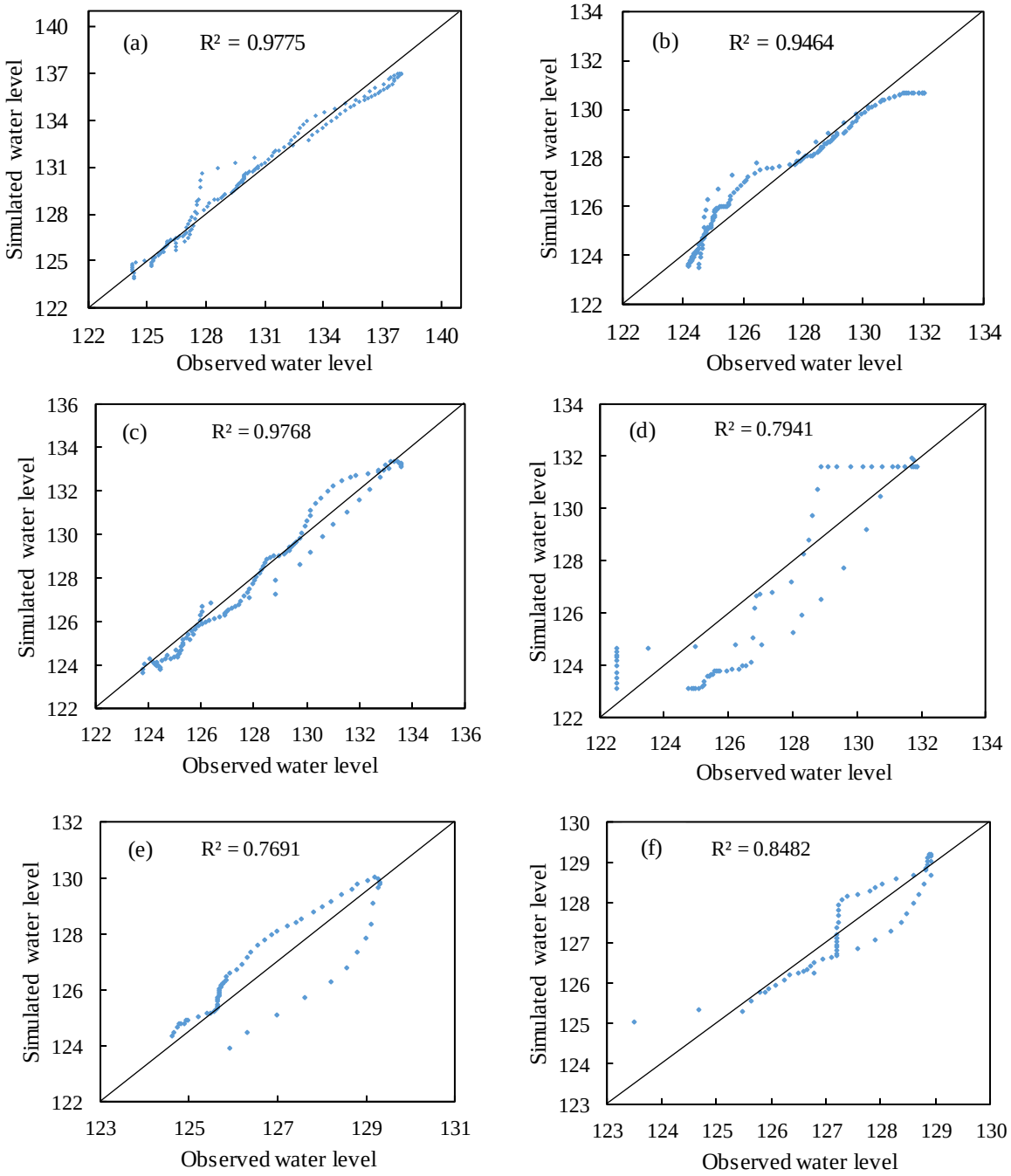



**Figure 7(a)-7(f)** Scatter plot of hourly water level using 1D hydrodynamic model at (a) 1998 (b) 1999 (c) 2002 (d) 2003 (e) 2004 (f) 2005

## 4.2 Validation of the model

The model has been validated for independent flood events in the year 2006 and 2007. The calibrated model has been able to simulate satisfactorily the flood stages at Gidhade stream gauging station for both year 2006, 2007. Here, the optimal value of Manning's 'n' for the validation of calibrated model was taken as the mean value of calibrated Manning's 'n' (n = 0.034). The performance evaluation was carried out using the RMSE and NSE are shown in Table 2. The simulated and the observed values of water level at Gidhade stream gauging station were compared for the validated model in 2006 and 2007

independent flood events which can be seen in Figures 8(a) and 8(b). The scatters plot of hourly water level using 1D hydrodynamic model at Gidhade stream gauging station for the respective years are shown in Figures 9(a) and 9(b).

**Table 2** Validated Manning's n value corresponding RMSE and NSE

| No | Year | n | RMSE (m) | NSE |
|---|---|---|---|---|
| 1 | 2006 | 0.034 | 0.975 | 0.966 |
| 2 | 2007 | 0.034 | 0.980 | 0.861 |

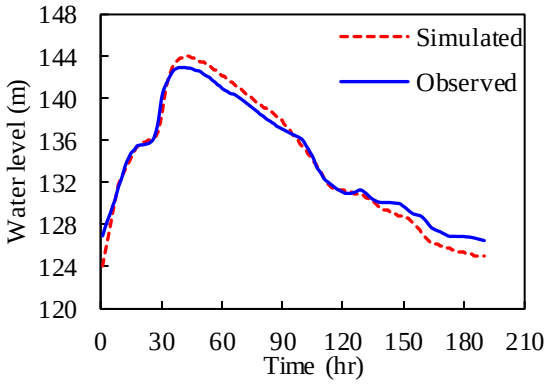



**Figure 8(a)** Comparison observed and simulated water level for validated Manning's n at Gidhade stream gauging year 2006

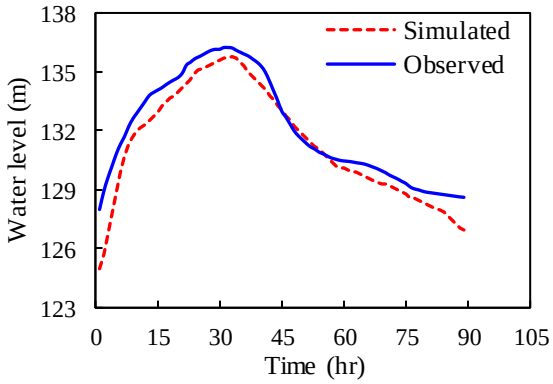
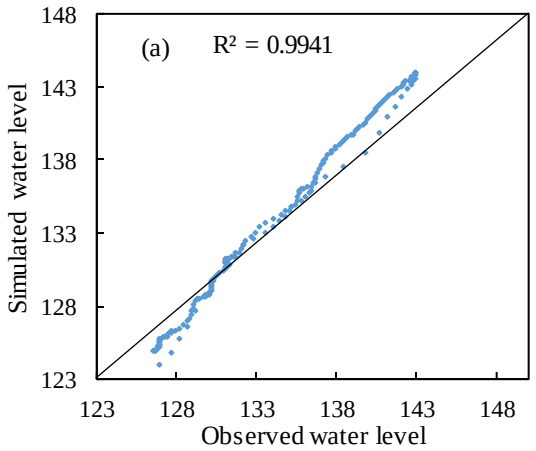
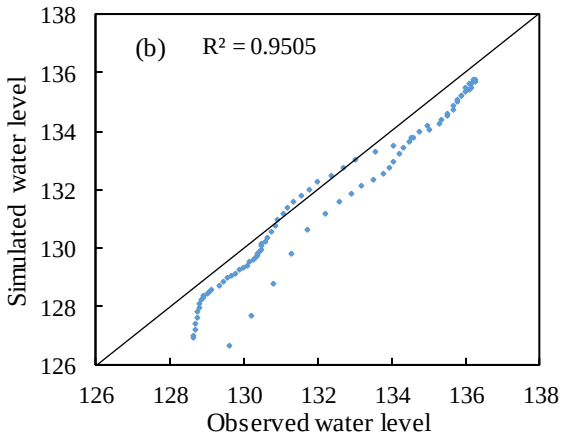



**Figure 8(b)** Comparison observed and simulated water level for validated Manning's n at Gidhade stream gauging year 2007




**Figures 9(a) – 9(b)** Scatter plot of hourly water level using 1D hydrodynamic model at (a) 2006 (b) 2007

## 5. CONCLUSIONS

The development of the MIKE 11 hydrodynamic model was carried out for the years of 1998, 1999, 2002, 2003, 2004 and 2005, and validated with the year of 2006 and 2007. flood data. Following conclusions were derived from the present study:

a) Calibration of the one-dimensional hydrodynamic model using MIKE 11 reveals that the optimum value of roughness coefficient can be taken as 0.034 for the Middle Tapi reach.
b) The calibration of model for the years 1998, 1999, 2002, 2003, 2004 and 2005 shows the value of RMSE, NSE and $R^2$ as 0658, 0.596, 0.508, 1.616, 0.845 and 0.465; 0.975, 0.943, 0.969, 0.698, 0.671 and 0.839; and 0.97, 0.94, 0.97, 0.79, 0.76 and 0.84 respectively.

c) The validated model for year 2006 and 2007 shows the value of RMSE, NSE and $R^2$ as 0.975, 0.980; 0.966, 0.861; and 0.99, 0.95 respectively.
d) The performance evaluation was carried out using statistical parameters such as RMSE, NSE and $R^2$ to compare the observed and simulated water levels which gave satisfactory results. The developed 1D HD model can be used for routing the flood at various location along the length of Middle Tapi River.

## ACKNOWLEDGEMENT

The authors are thankful to the Central Water Commission (CWC), Ministry of Water Resources, River Development and Ganga Rejuvenation, Govt. of India and Hydrology Data User Group (HDUG), Nashik for providing necessary data required for the study. The authors are also thankful to Centre of Excellence (CoE) on "Water Resources and Flood Management", SVNIT-Surat under TEQIP-II for the resourceful help and infrastructural support.

## References

Central Water Commission (2016). "Tapi Basin. Ministry of Water Resources, River Development and Ganga Rejuvenation", Government of India, New Delhi.

DHI, MIKE 11: "A modelling system for Rivers and channels". Reference Manual. Danish Hydraulic Institute, Denmark, 2014.

Delphi, M., Shooshtari, M. M., and Zadeh, H. H. (2010). "Application of diffusion wave method for flood routing in Karun River". *International Journal of Environmental Science and Development*, 1(5), pp. 43-52.

Kamel, A. H. (2008): "Application of a hydrodynamic mike 11 model for the Euphrates River in Iraq". *Slovak Journal of Civil Engineering*, Vol.3 (3), pp: 1-7.

Le Ngo, L., Madsen, H., Rosbjerg, D., and Pedersen, C. B. (2008). "Implementation and comparison of reservoir operation strategies for the Hoa Binh reservoir, Vietnam using the MIKE 11 model". *Water Resources Management*, 22(4), pp. 457-472.

Majewski, W. (2008). "Urban flash flood in Gdańsk-2001; solutions and measures for city flood management". *International Journal of River Basin Management*, Vol. *6*(4), pp. 357-367.

Nandalal, K. D. W. (2009). "Use of a hydrodynamic model to forecast floods of Kalu River in Sri Lanka". *Journal of Flood Risk Management*, Vol. *2*(3), pp. 151-158.

Pramanik, N., Panda, R. and Sen, D. (2009), "One dimensional hydrodynamic modelling of River flow using DEM extracted River cross-section". *Water Resources Management* (2010) Vol. 24: pp. 835–852.

Rahman, M. M., Arya, D. S., Goel, N. K. and Dhamy, A. P. (2011), "Design flow and stage computations in the Teesta River, Bangladesh, using frequency analysis and MIKE 11 Modelling". *Journal of Hydrologic Engineering* Vol. 16, pp. 176–186.

Timbadiya, P. V., Patel, P. L., and Porey, P. D. (2014a), "One-dimensional hydrodynamic modelling of flooding and stage hydrographs in the lower Tapi River in India". *Current Science* Vol.106: pp. 708-716.

Timbadiya, P. V., Patel, P. L., and Porey, P. D. (2014b). "A 1D–2D coupled hydrodynamic model for River flood prediction in a coastal urban floodplain". *Journal of Hydrologic Engineering*, Vol. *20*(2), pp. 50-147.

*IN PROCEEDINGS OF 25th HYDRO 2020, INTERNATIONAL CONFERENCE, NATIONAL INSTITUTE OF TECHNOLOGY ROURKELA, ODISHA, INDIA 26-28, March 2021, ISBN 978-93-90631-56-8*

Paper ID - 293

# SIMULATION OF CHANNEL BED LEVEL VARIATION AND ITS EXPERIMENTAL VALIDATION

G. Yatirajulu[1] and P. V. Timbadiya[2]

[1]*Post Graduate, Department of Civil Engineering, Sardar Vallabhbhai National Institute of Technology Surat, Surat - 395007, India.*

[2]*Associate Professor, Department of Civil Engineering, Sardar Vallabhbhai National Institute of Technology Surat, Surat - 395007, India.*

*Email: yatirajulu1994@gmail.com; pvtimbadiya@ced.svnit.ac.in*

## Abstract

Aggradation and degradation in the alluvial channels are natural phenomena formed mainly near the structures such as bridge piers, abutments, etc. in the river. A study on aggradation and degradation is required to prevent damage to these structures. Experiments were conducted in the laboratory flume with sediment overloading to study the bed and water level variations of uniform sediments under uniform flow condition by Soni et al. (1980), Rehman et al. (2010) and Andharia et al. (2018). In the present study, a one-dimensional semi coupled Hydrodynamic model with Sediment transport module was developed in MIKE 11 using the data from the above three study. The bed level and water level variations were computed using Meyer Peter Muller (MPM) sediment transport function in the aforesaid model. The model developed was used to predict the transient bed and water levels corresponding to 15, 30 and 40-minutes time intervals for the test run U-1 (Soni et al. 1980) and also for 15, 30, 60 and 120-minutes time intervals corresponding to the test run A-1 (Andharia et al. 2018). The transient bed levels corresponding to 1, 2, 3 and 4-hour time intervals from the beginning of sediment overloading for the test run -1 (Rehman et al. 2010) was also predicted using the model. The comparison between simulated and experimental results of bed and water level variation was evaluated and found satisfactory.

***Keywords:*** *Aggradation; Degradation; Sediment Overloading; Hydrodynamic Model; Sediment Transport Module; MIKE 11*

## 1. Introduction

The agents like running water, wind, ground water, etc. configure the shape of earth surface. Under natural conditions, a river carries water, sediment and at particular location, it meets the sea. The results of landforms are due to aggradation, degradation process or combination of both. The evolution of an alluvial river is subjected to pressure from many factors including water and sediment discharges, structure of channels, heat, and properties of sediments. If these conditions remain unchanged for a sufficiently long time, a state of equilibrium will enter the flow. Hydrodynamic modeling is an efficient method to compute flow and sediment transport in a river. It can be modelled as 1D, 2D or 3D according to the extent and need of study. Many approaches to understand the basic processes of flow-by-flow sediment erosion, transport and deposition in a river and to predict the transient bed and water surface profiles analytically under assumed boundary conditions (Ranga Raju and Garde, 2000) have been performed. Zhang and Kahawita (1987) developed the numerical model to compute elevation of bed and sediment discharge using non-linear parabolic equations. Bhallamudi and Chaudhry (1991) presented a 1D bed level variation model for unsteady gradually varied open channel flow to determine aggradation due to sediment overloading using explicit MacCormack numerical scheme. The Manning's roughness coefficient and Colby type power function of velocity were used in the model for estimation of resistance and sediment transport rates respectively. Bizzi et al. (2014) developed a semi coupled 1D mobile bed hydro morphological model using explicit finite difference scheme. MIKE 11 is a fully dynamic 1D modelling software package which is used for modelling complex river networks. The equations incorporated, for variation of the bed level are derived based on experiments with uniform flow condition and uniform grain size distribution for non-cohesive material. These are solved using six-point Abbott Ionescu scheme (1967). It is important to check and validate the applicability of these equations for real field problems wherein the flow is neither uniform nor is the bed material uniform. Hence, an attempt has been made here to check and validate the available total load equation in the MIKE 11 on the basis of its performance

of the flume in the laboratory. The results are useful to understand the mechanism of the bed level variation adopted in the simulation engine of MIKE 11.

The objectives of the present study are:

a) Development of one-dimensional semi coupled numerical model for aggrading channels, due to overloading of uniform sediments using the data of Soni et al. (1980, run U-1), Rahman et al. (2010, run U-1) and Andharia et al. (2018, run A-2).
b) Evaluation of performance of the developed numerical model with a given sediment transport function by comparing the bed levels in aggrading channels due to sediment overloading, obtained from the numerical model and the experimental results of the aforesaid three studies.

## 2. Experimentation

### 2.1 *Experimental setup and data collection of Soni et al. (1980)*

Soni et al. (1980) conducted experiments to collect the data of transient bed and water surface profiles under assumed boundary conditions. The experiments have been carried out in a flume in the hydraulics laboratory of University of Roorkee. The experimental set-up consists of 30 m long, 0.5 m deep, and 0.2 m wide recirculating flume. The sand of median diameter 0.32 mm and geometric standard deviation of 1.30 was used to form the bed material. After establishing uniform flow conditions for a given discharge and slope, the sediment supply rate was increased to a predetermined value by continuously feeding excess sediment at upstream end of the flume at a constant rate. The bed and water surface profiles were recorded using point gauge with a flat bottom at every 2.5 m at an interval of 10 to 20 min. The aggradation experiments were conducted using two discharges, 4 l/s and 7 l/s. The rate of sediment addition was varied from (0.30 to 4.0) $q_t$. The slope ranges from 0.00212 to 0.00652 under different rates of sediment addition.

### 2.2 *Experimental setup and data collection of Rehman et al. (2010)*

The experiments were conducted in a 12 m long, 1 m wide and 0.61 m deep recirculatory tilting flume located in the Hydraulics and River Engineering Laboratory of the Bangladesh University of Engineering and Technology, Dhaka. Sixteen test runs were performed in the laboratory channel with uniform sediment bed having median diameter 0.285 mm for the aggradation processes. Colby type power law velocity function was used in the numerical model with the coefficient derived from the experimental data. The 1D numerical model for prediction of bed level variation was developed using explicit finite difference scheme and tested with the above experimental data. It was noted, during the numerical computation, that full length of aggradation did not occur within the channel length.

### 2.3 *Experimental setup and data collection of Andharia et al. (2018)*

The experiments were carried out using tilting and recirculating flume at the Advanced Hydraulics Laboratory in Civil Engineering department at SVNIT, Surat. The flume has a length of 15 m, width 0.89 m and 0.6 m depth. A portion of 2 m was provided at the upstream for stilling the freely falling water. Two honeycombed perforated plates were provided to reduce the excessive wave effect of the water and to straighten the flow. A coarse gravel was provided for a length of 3m before the working section, for the development of the flow. A sediment trapper was provided at downstream of the working section to accumulate the sediment in the form of bed load. A tail gate was provided at the end of the flume to regulate the flow depth at the working section that helps to maintain uniform depth throughout the flume. A semi-coupled 1D numerical model was developed to compute bed and water levels of aggrading channels due to the overloading of sediments.

**Table 1** Experimental data of some researchers

| Experimental. Run no. | da (mm) | Flow Discharge ($m^3$/s) | Flow depth (m) | Mean flow velocity (m/s) | Water Surface slope (%) | Bed load transport rate× $10^{-6}$ (m2 /s) | $\Delta q_s / qs_0$ | Time interval of runs (min) |
|---|---|---|---|---|---|---|---|---|
| A2 Andharia et al. | 0.707 | 0.0263 | 0.0785 | 0.377 | 0.25 | 0.36 | 4 | 15, 30, 60, 120 |
| U-1 Soni et al. | 0.32 | 0.004 | 0.050 | 0.400 | 0.356 | 1.2 | 4 | 15,30, 40 |
| U-1 Rahman et al. | 1 | 0.285 | 0.02 | 0.07 | 0.286 | 0.022 | – | 60,120, 180,240 |

## 2.4 *MIKE 11 software*

MIKE 11 is a software developed by Danish Hydraulic Institute (DHI), Denmark. It is a modelling package capable of using kinematic, diffusive and fully dynamic wave model. It has various modules including sediment transport, advection, dispersion, Eco lab, etc. The governing equations based on conservation of mass and momentum of water and conservation of mass of sediments for 1D flow in alluvial channels has been used in the numerical model of MIKE 11. These equations have been solved using an implicit finite difference numerical scheme (Abbot and Ionescu, 1967).

Meyer–Peter and Muller (MPM) equation (1948) has been used as the sediment transport function here. The MPM proposed following relation (Equation 1 and 2) for bed load transport of sediments.

$$\phi = 8\,(\,\tau_*' - 0.047)^{\,3/2} \tag{1}$$

$$\phi = \frac{q_B}{\Upsilon_s}\sqrt{\frac{\rho_f}{\rho_s - \rho_f}}\left(\frac{1}{gd^3}\right)^{1/2} \tag{2}$$

Where, $\phi$ is dimensionless bed load transport function (volumetric rate per unit channel width-Einstein's function), $\tau_*'$ is dimensionless grain shear stress ($\tau_0'/\Delta\Upsilon_s d$), $\tau_0'$ is effective shear stress related to grain resistance ($N/m^2$), $R_b'$ is hydraulic radius related to grains ($Un'/\sqrt{S})^{3/2}$ in which n' is Manning-Stickler roughness coefficient corresponding to grain roughness $d_{90}^{1/6}$ /26.0); $d_{90}$ is sediment size such that 90 % of the material, by weight, is finer than this size, $q_B$ is rate of bed load transported per unit width, by weight, (N/s/m).

## 2.5 *Methodology*

Continuous flows of varying magnitudes are simulated using a one-dimensional semi coupled Hydrodynamic model with Sediment transport module in MIKE 11 using the data from the above three researchers. The discharge hydrograph and sediment transport rate has been used as two upstream boundary condition. The water levels have been used as downstream boundary condition. The methodology used for simulating continuous flows in MIKE 11 has been described using a flowchart as shown in Figure 1.

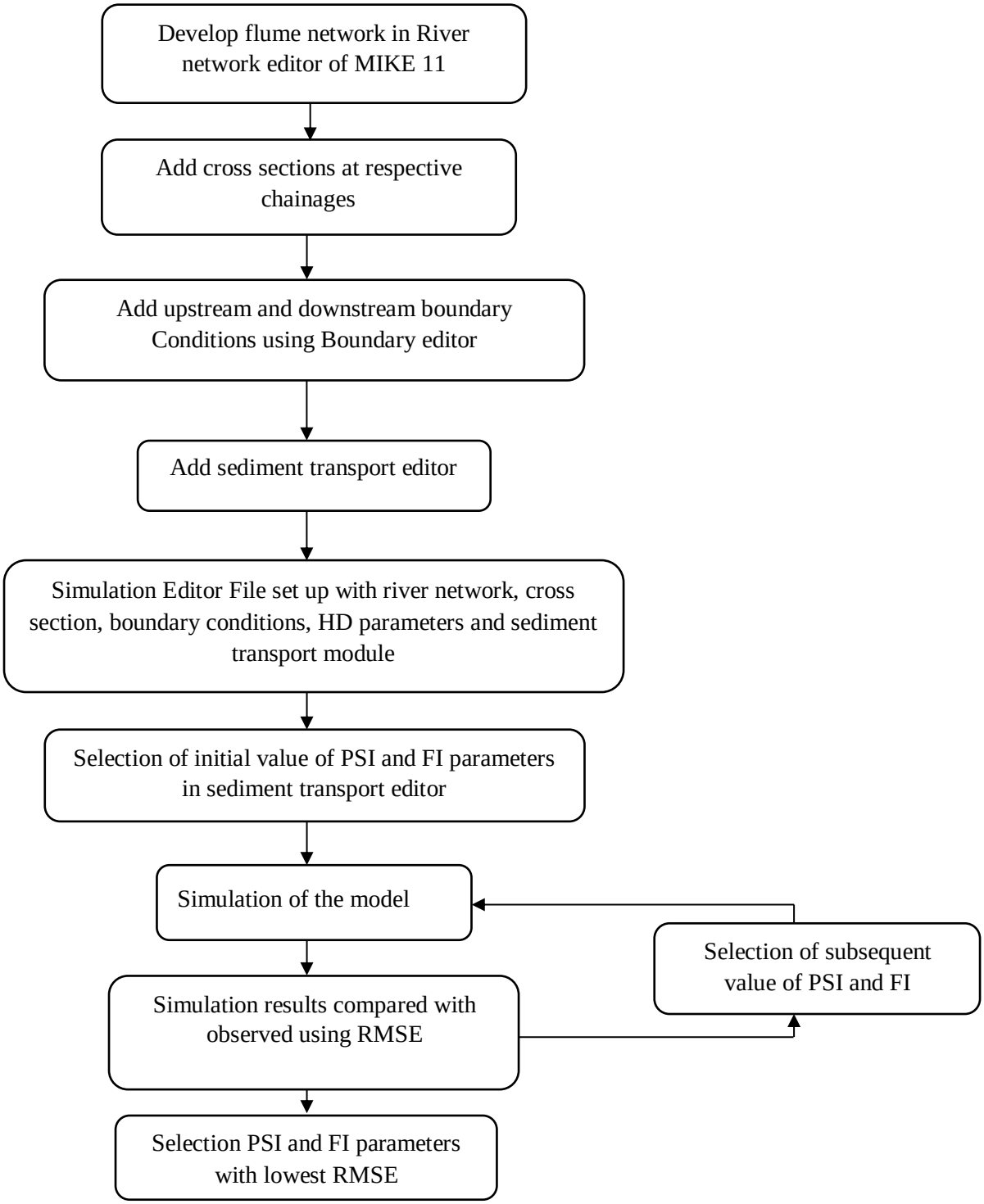


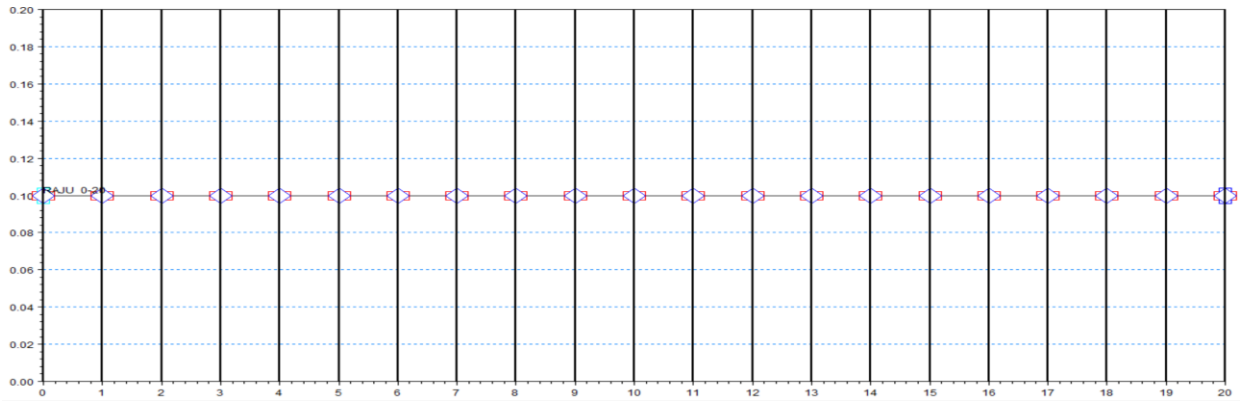

**Figure 1** Methodology for calibration of 1D HD and ST model in MIKE 11

## 2.6 *Model development*

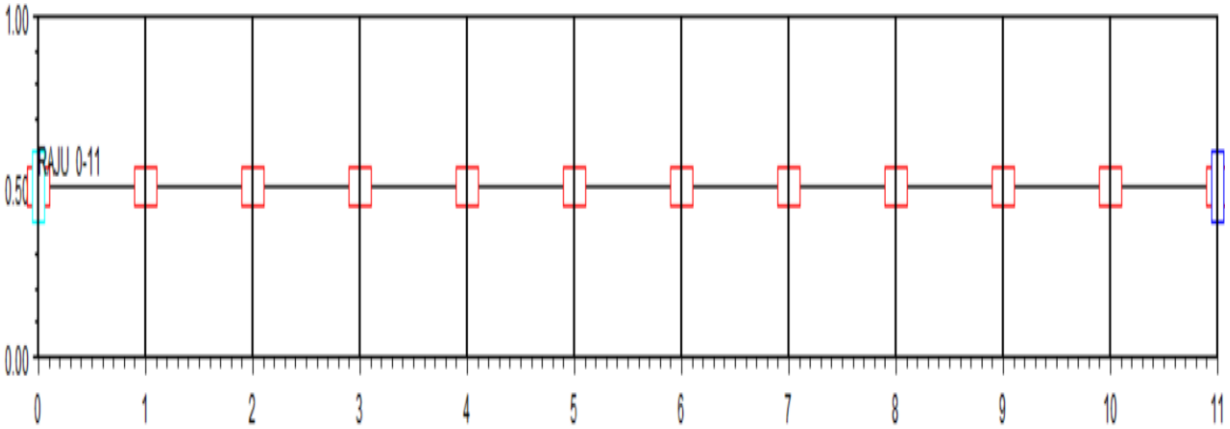
The model has been developed in MIKE 11 from the experimental data of Soni et al. (1980), Rahman et al. (2010) and Andharia et al. (2018)

### *2.6.1 River network editor*

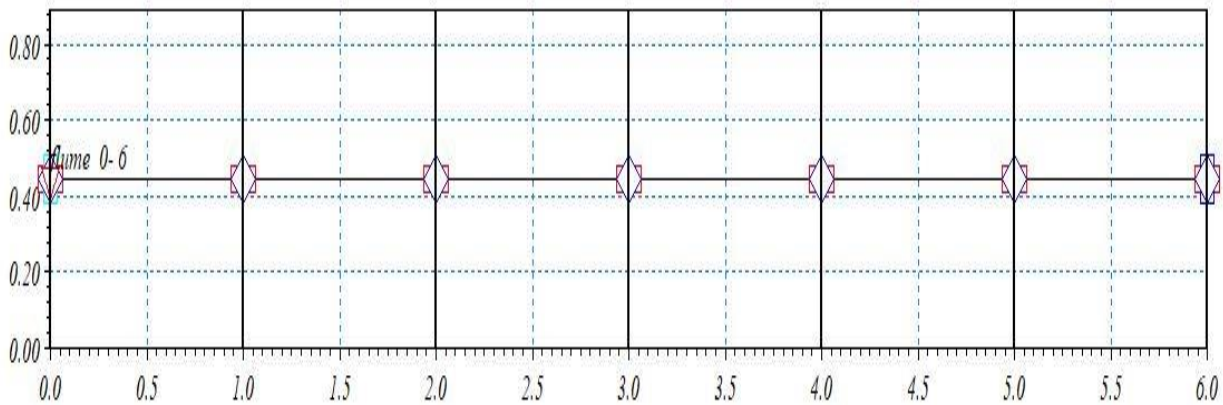
The flume network of 20 m has been prepared for the experimental data of Soni et al. (1980), 11 m for the experimental data of Rahman et al. (2010) and 6 m for the experimental data of Andharia et al. (2018) using Network editor in MIKE 11. A $\Delta x$ of 0.5 m has been provided as distance grid. The plan of the flumes is shown in figure 2.



(a)




(b)




(c)

**Figure 2** The flume network edited in MIKE 11 a) Soni et al. 1980; b) Rehman et al. 2010; c) Andharia et al. 2018

### *2.6.2 Cross section editor*

The cross sections of the flume consist of 21 sections for the data of Soni et al. (1980), 12 sections for Rehman et al. (2010) and 7 sections for the experimental data Andharia et al. (2018). These have been provided using the cross-section editor of MIKE 11.

### *2.6.3 Boundary conditions*

A constant discharge hydrograph and sediment transport have been given as the upstream boundary condition in the form of time series. Similarly, time series file of constant water level has been given as the downstream boundary condition for the data of above three researchers.

### *2.6.4 Sediment transport editor*

The properties of the sediment i.e. arithmetic mean size, standard deviation and Meyer Peter Muller transport function are entered according to the data of the above three researchers. All files are linked to the simulation file.

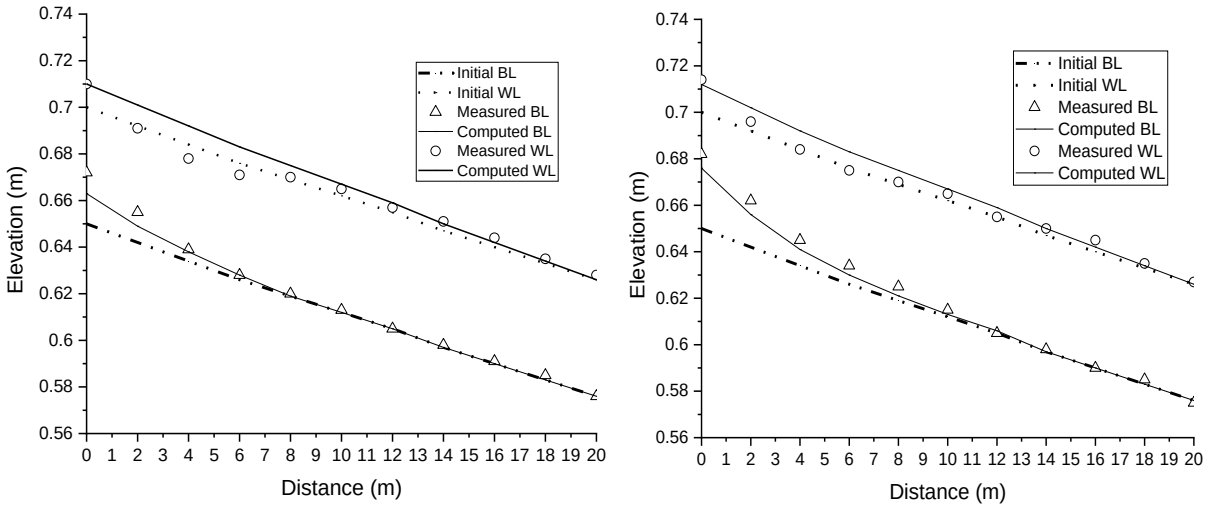
### *2.6.5 Hydrodynamic parameters and simulation file*

Higher order fully dynamic wave equations have been set for simulation. The simulation time step has been set as 0.1 second for improving accuracy and the results have been stored at an interval of 1 minute for the data of above three researchers. All files are linked to the simulation file.

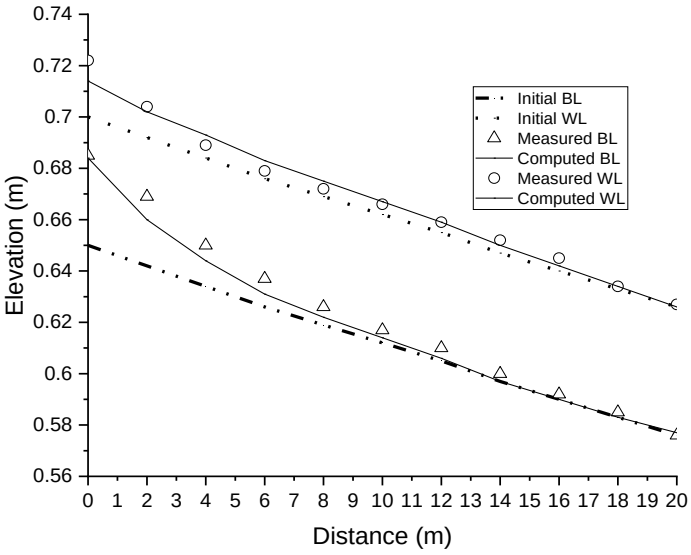
## *2.7 Results and discussion*

### *2.7.1 Results of developed model using the data of Soni et al. (1980), Rahman et al. (2010) and Andharia et al. (2018)*

The performance of model developed for bed level (BL) variations in aggrading channels due to overloading of sediments using Meyer Peter Muller (MPM) sediment transport function has been validated using the experimental data of Soni et al. (1980) (Figure 3), Rehman et al. (2010) (Figure 4) and Andharia et al. (2018) (Figure 5).




(a) (b)




(c)

**Figure 3** Computed and measured bed (BL) and water level (WL) profiles for run U-1 (Soni et al.). a) Time = 15 minutes (RMSE = 0.34 cm for bed level); b) Time = 30 minutes (RMSE = 0.35 cm for bed level); c) Time = 40 minutes (RMSE = 0.44 cm for bed level).

**Table 2** Statistical parameters of bed level and water surface profiles using data of Soni et al. (1980) and scheme data of MIKE 11

| Sr No | Transient time(min) | Relative Error | | % Error | | MASE (m) | | MSE(m) | | RMSE (m) | |
|---|---|---|---|---|---|---|---|---|---|---|---|
| | Run U - 1 | BL | WL | BL | WL | BL | WL | BL | WL | BL | WL |
| 1 | 15 | 0.003 | 0.006 | 0.310 | 0.690 | 0.002 | 0.0046 | 0 | 0.0004 | 0.0034 | 0.022 |
| 2 | 30 | 0.004 | 0.005 | 0.440 | 0.539 | 0.0028 | 0.0036 | 0 | 0.0002 | 0.0035 | 0.015 |
| 3 | 40 | 0.005 | 0.003 | 0.59 | 0.371 | 0.0037 | 0.0025 | 0 | 0.0001 | 0.0044 | 0.011 |

*BL: Bed Level; WL: Water Level; MASE: Mean Absolute Standard Error: MSE: Mean Square Error; RMSE: Root Mean Square Error.

The distribution of sediment along the longitudinal direction in the numerical model is less compared to the experimental data. The bed levels are under predicted and water levels are over predicted by the model. The results obtained are almost the same by using different sediment transport functions. This may be because MIKE 11 is suitable for rivers where the area is more to stabilize the flow.

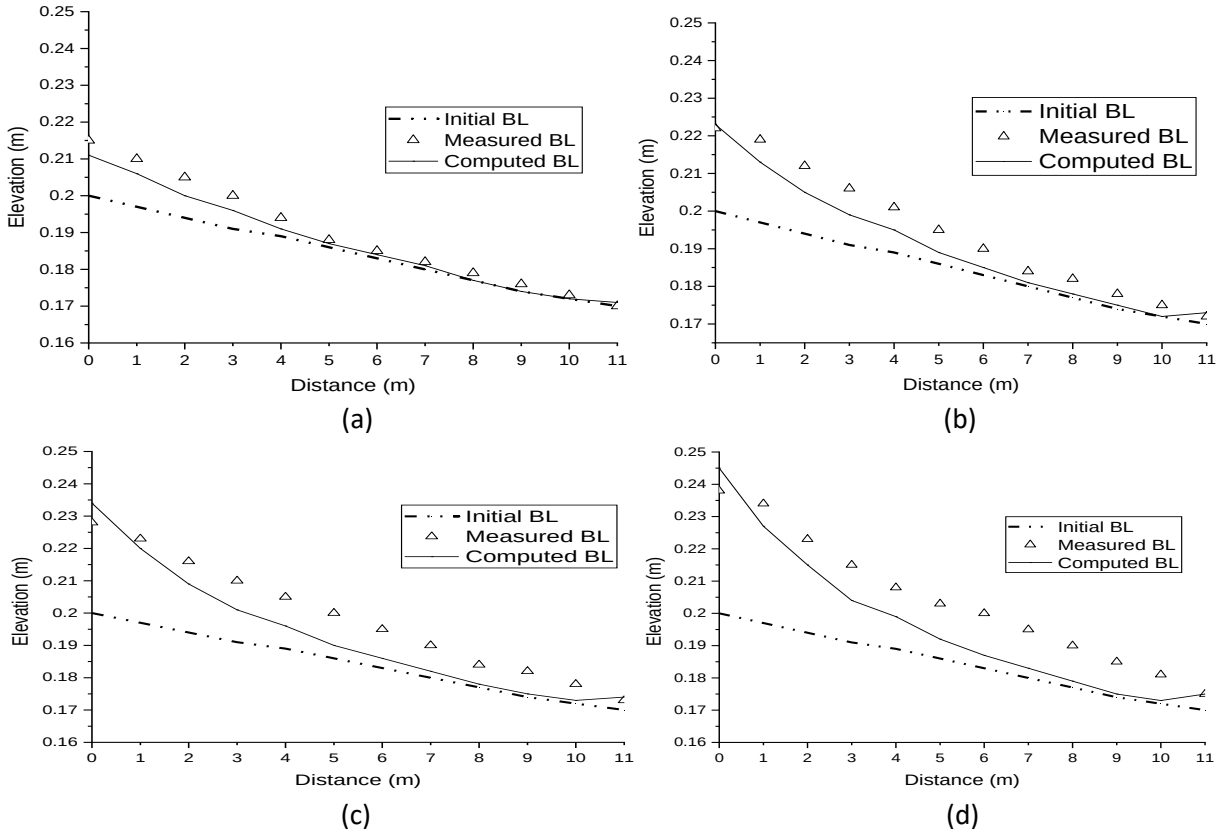



**Figure 4** Computed and measured bed and water level profiles for run U-1 (Rehman et al. 2010). a) Time = 1-hour (RMSE = 0.29 cm for bed level); b) Time = 2-hour (RMSE = 0.47 cm for bed level); c) Time = 3-hour (RMSE = 0.71 cm for bed level); d) Time = 4 hour (RMSE = 0.95 cm for bed level).

**Table 3** Statistical parameters of bed level and water surface profiles using data of Rehman et al. (2010) and scheme data of MIKE 11

| Transient time (Hours) Run U – 1 | Relative Error in BL | % Error in BL | MASE (m) in BL | MSE(m) in BL | RMSE (m) in BL |
|---|---|---|---|---|---|
| 1 | 0.0127 | 1.2721 | 0.0025 | 0.0000 | 0.0029 |
| 2 | 0.0219 | 2.1994 | 0.0043 | 0.00002 | 0.0047 |
| 3 | 0.0335 | 3.3511 | 0.00666667 | 0.00005 | 0.0071 |
| 4 | 0.0438 | 4.3875 | 0.00891667 | 0.0000 | 0.0095 |

The bed and water levels are under predicted in the numerical model compared to the results of experimental data. The aggrading profile of bed gradually decreases from upstream to 90% of the length of the flume. It forms an aggrading profile again near to the downstream of the flume.

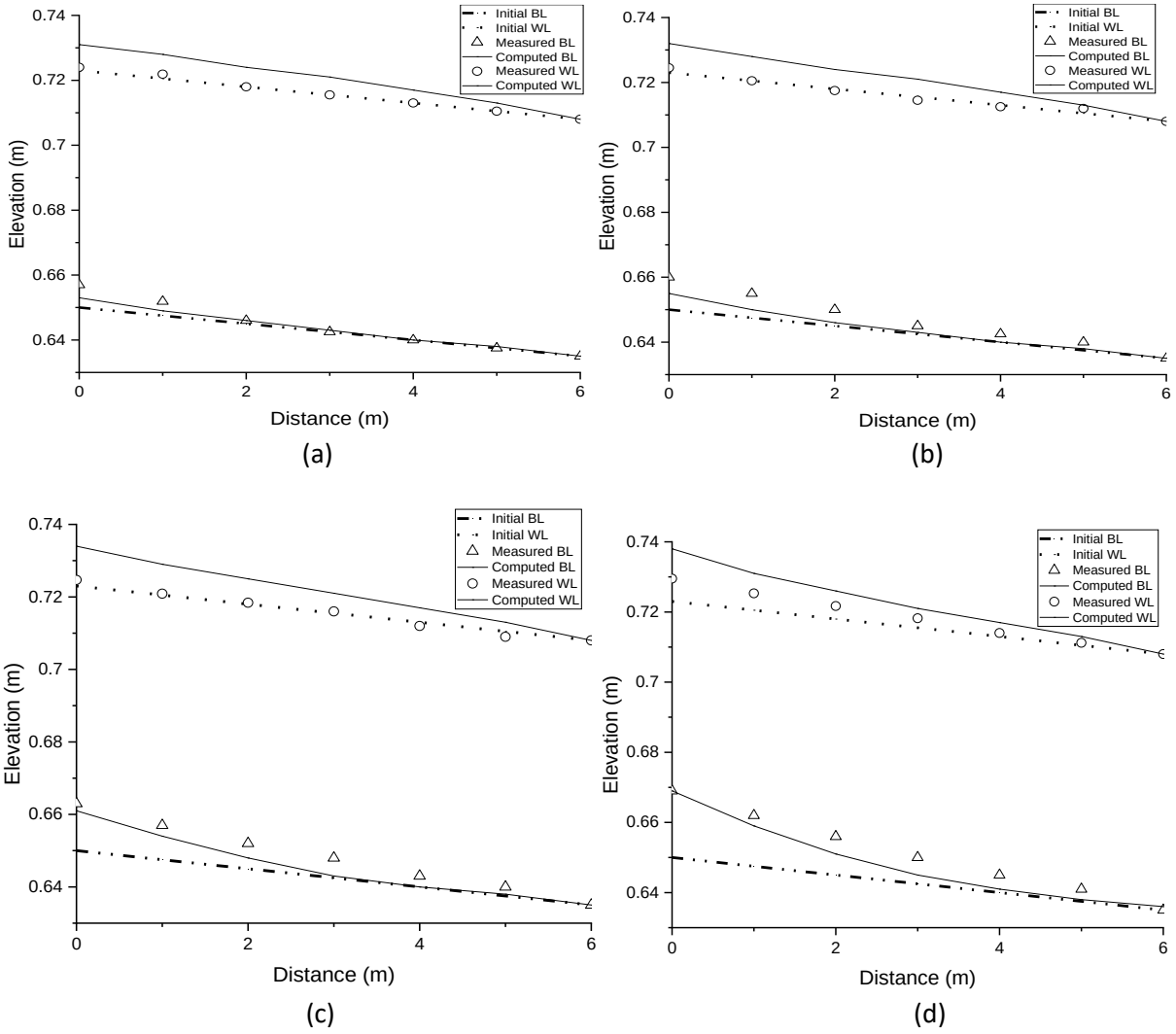



**Figure 5** Computed and measured bed and water level profiles for run U-1 (Andharia et al. 2018). a) Time = 15 minutes (RMSE = 0.19 cm for bed level); b) Time = 30 minutes (RMSE = 0.34 cm for bed level); c) Time = 60 minutes (RMSE = 0.31 cm for bed level); d) Time = 120 minutes (RMSE = 0.35 cm for bed level).

**Table 4** Statistical parameters of bed level and water surface profiles using data of Andharia et al. (2018) and scheme data of MIKE 11

| Sr No | Transient time(min) Run A - 2 | Relative Error BL | Relative Error WL | % Error BL | % Error WL | MASE (m) BL | MASE (m) WL | MSE(m) BL | MSE(m) WL | RMSE (m) BL | RMSE (m) WL |
|---|---|---|---|---|---|---|---|---|---|---|---|
| 1 | 15 | 0.002 | 0.006 | 0.17 | 0.619 | 0.0011 | 0.004 | 0 | 0 | 0.0019 | 0.005 |
| 2 | 30 | 0.004 | 0.007 | 0.45 | 0.666 | 0.0029 | 0.005 | 0 | 0 | 0.0034 | 0.005 |
| 3 | 60 | 0.004 | 0.008 | 0.42 | 0.756 | 0.0027 | 0.005 | 0 | 0 | 0.0031 | 0.006 |
| 4 | 120 | 0.005 | 0.005 | 0.46 | 0.516 | 0.003 | 0.004 | 0 | 0 | 0.0035 | 0.004 |

The model computes the bed and water levels satisfactorily with the flow parameters used by Andharia et al. (2018). The bed levels are predicted same as the experiment data but water levels are over predicted by the model. The performance of the developed model has been found to be better with the data of Andharia et al. (2018) compared to the data of other researchers.

## 3. Conclusions

A one-dimensional numerical model has been developed for prediction of bed level variations in aggrading channels due to over loading of uniform sediments under uniform flow condition using the data of Soni et al., Rehman et al. and Andharia et al. (2018). The model developed using MIKE 11 simulating the bed level variation satisfactory. The study presented shows the capability of the MIKE 11 sediment transport module in simulation of bed level variation.

## Acknowledgements

Authors would like to thank Centre of Excellence (CoE) on 'Water Resource and Flood Management' financed by TEQIP-II for giving vital infrastructural bolster and monetary help to do this work.

## References

Abbott, M. B., and Ionescu, F. (1967). On the numerical computation of nearly horizontal flows. *Journal of Hydraulic Research*, *5*(2), 97-117.
Andharia, B. R., Patel, P. L., Manekar, V. L., and Porey, P. D. (2018). Numerical and experimental studies in prediction of bed levels of aggrading channels. *Current Science*, *114*(8), 1697-1708.
Bhallamudi, S. M., and Chaudhry, M. H. (1991). Numerical modeling of aggradation and degradation in alluvial channels. *Journal of Hydraulic Engineering*, *117*(9), 1145-1164.
Bizzi, S., Dinh, Q., Bernardi, D., Denaro, S., Schippa, L., and Soncini-Sessa, R. (2015). On the control of riverbed incision induced by run-of-river power plant. *Water Resources Research*, *51*(7), 5023-5040.
Chow, V. T., Maidment, D. R., and Mays, L. W. (1988). *Applied hydrology*. McGraw-Hill, New York.
Colby, B. R. (1964). Discharge of sands and mean-velocity relationships in sand-bed streams. *U.S. Geological Survey Professional Paper 462-A*, US Geological Survey, Washington, DC.
Danish Hydraulic Institute (DHI). (2008). *MIKE 11- A modelling system for rivers and channels reference manual*, Hørsholam, Denmark.
Engelund, F., and Hansen, E. (1967). *A monograph on sediment transport in alluvial streams*. Teknisk Forlag Publications, Denmark.
Garde, R. J., and Raju, K. R. (2000). *Mechanics of sediment transportation and alluvial stream problems*. New Age Publications, New Delhi.
Meyer-Peter, E., and Müller, R. (1948). *Formulas for bed-load transport. Proceedings*, Second Congress IAHR, Stockholm, Sweden.
Rahman, M. A., and Matin, M. A. (2010). Numerical modeling of bed level changes of alluvial river. *Journal of Civil Engineering*, *38*(1), 53-64.
Soni, J. P., Ranga Raju, K. G., and Garde, R. J. (1980). Aggradation in streams due to overloading. *Journal of Hydraulic Engineering*, *106*(1), 117-132.
Zhang, H., and Kahawita, R. (1987). Nonlinear model for aggradation in alluvial channels. *Journal of Hydraulic Engineering*, *113*(3), 353-368.

*IN PROCEEDINGS OF 25th HYDRO 2020, INTERNATIONAL CONFERENCE, NATIONAL INSTITUTE OF TECHNOLOGY ROURKELA, ODISHA, INDIA 26-28, March 2021, ISBN 978-93-90631-56-8*

Paper ID - 298

# Water security assessment of Karuvannur watershed - Current and future scenario

Anjana Ramesh[1], Reeba Thomas[2]

[1]*PG Scholar, Dept. of Civil Engineering, Government Engineering College, Thrissur, 680009, Kerala, India*
[2]*Associate Professor, Dept. of Civil Engineering, Government Engineering College, Thrissur, 680009, Kerala, India*
*Email: anjanarameshs10@gmail.com*

## Abstract

Water security is referred as the availability of sufficient amount of water of good quality to boost all ecosystem services with a tolerable level of water related risks, whereas water scarcity is defined as the ratio of water demand over water availability and it is used as an indicator of water security (Giri et al. 2018). The water security in a watershed may get adversely affected due to the changes in climate and landuse pattern, population growth, developmental activities etc. Since the balance between water demand and water availability has reached life-threatening levels in many regions, the gravity of water security issue can be gauged by compartmentalising various kinds of water demands and available sources. Hence the present and future water security assessment based on the classification of the available water into blue and green water is done in this paper, since it gives a clear picture about the effects of human intervention on freshwater resources. Future landuse and climate are predicted using CLUE-S and SDSM 4.2.9 models respectively and the crop water requirement is assessed using CROPWAT. The different components of blue and green water are calculated by modeling the watershed in ArcSWAT and water security is assessed separately under present and future condition. It is observed that water security diminishes at an alarming rate due to climatic and landuse changes. The severity of the problem is even more in the case of green water as increased demand for water in food production is expected in the future.

***Keywords:*** *Water security; CLUE-S; SDSM; ArcSWAT; CROPWAT*

## 1. Introduction

The demand for fresh water, which is vital for supporting life on earth, is increasing globally at a rapid rate and in many parts of the globe, the balance between water demand and water availability has reached life-threatening levels. This global crisis has already affected nearly one-sixth of the total population in the world and according to the Food and Agricultural Organization of the United Nations, two-third of the global population will be facing water scarcity by 2025. So, water security assessment is the first step to tackle such problems so as to find out a practical solution.

Water security is defined as “an acceptable level of water related risks to humans and ecosystems, coupled with the availability of water of sufficient quantity and quality to support livelihoods, national security, human health, and ecosystem services” (Bakker 2012), whereas water scarcity is defined as the shortage in the amount of water required to meet all the demands in a region. Water scarcity, which is obtained as the ratio of water demand over water availability, is used as an indicator of water security (Giri et al. 2018). The water security in a watershed gets adversely affected due to the changes in the precipitation patterns, increased frequency of drought and flood, changes in the landuse pattern and climate, population growth etc. The gravity of water security issue can be gauged by tagging various kinds of water demands and available sources.

Allocation and use of different water sources can be done by colour coding like blue and green water. Blue water refers to the surface water and ground water, which is directly available for human consumption, whereas green water refers to the portion of precipitation that is available to the vegetation in the form of soil moisture and also the portion that reaches the atmosphere as evapotranspiration. This classification will give a better picture on the efficient use of the evaporative flow from rainwater stored in the soil versus the efficient use of groundwater and surface water

resources (Falkenmark 1995). Hence the present and future water security assessment based on the classification of the available water into blue and green water is done in this paper. This gives a clear picture about the effects of human intervention separately on components of freshwater resources.

Models such as CLUE-S and SDSM 4.2.9 are used to predict future landuse and climate respectively and CROPWAT is used to assess the crop water requirement. The different components of blue and green water are calculated by modeling the watershed in ArcSWAT and water security is assessed separately under present and future condition.

### 1.1 *Literature review*

The main objective of this study is to assess the present and future water security of Karuvannur watershed in terms of both blue and green water. Various researches dealing with the concept of blue and green water, hydrologic modeling, crop water requirement, climate prediction and landuse prediction have been reviewed and recorded.

The concept of classifying water into blue and green water was put forward by Falkenmark (1995). He has defined green water as the portion of rainfall that infiltrates into the root zone of plants which is used for biomass production and blue water is that which is stored in lakes, aquifers etc. He also explained the importance of considering green water in water resources management which was often ignored in the earlier studies (Falkenmark 2008). Jewitt (2006) also stated the importance of blue and green water classification in the planning and management of water resources. According to him, the hydrological linkages between blue and green water flows and their representation in water resources management and planning needs greater attention. Liu and Yang (2009) suggested that, in order to assess global water scarcity, an accurate estimate of global water uses with high spatial resolution is essential. They studied the importance of green water in both crop production and food trade calls for a better management of green water, in addition to blue water. Sulser et al. (2010) analyzed the alternative water futures using a combined green and blue water accounting framework. They found that accounting explicitly for green water resources broadens the scope of options for decision-makers trying to improve agricultural production. Veettil and Mishra (2016) used a hydrological modeling framework for evaluating the spatio-temporal variability of blue and green water and to quantify the water security. They incorporated both climatic & anthropogenic factors.

Wilby and Dawson (2004) developed a tool known as Statistical Downscaling Model (SDSM) based on the linear multiple regressions for the climate prediction. SDSM and LARS-WG were used to forecast climate in 2050 and 2090 by Koch and Cherie (2013). Tukimat et al. (2017) analysed the changes in irrigation water demand in an intensive irrigated area of Malaysia under climate change scenario using SDSM. Miao et al. (2014) used land use prediction model CLUE-S and hydrological model SWAT to simulate Non-Point Source (NPS) pollution load in future. Thus with the help of SDSM and CLUE-S models, it is possible to replicate the future hydrological scenario realistically.

Zhao et al. (2015) used SWAT model and the Mann–Kendall method to investigate the spatiotemporal variations of blue and green water resources under different landuse change, agricultural irrigation expansion and climate variability scenarios during the 1980s –2000s for the Weihe River Basin. Liuying et al. (2018) made a comprehensive assessment on the spatio-temporal trend of Blue Water (BW) and Green Water (GW) in Ohio River Basin over the past 80 years (1935–2014), and from thereon, quantifies the combined as well as relative contributions of climate and land use changes using SWAT, Mann-Kendall and Theil-Sen statistical. Giri et al. (2018) used an integrated modelling framework consisting of SWAT loosely coupled with an agent based probabilistic land use conversion model to analyse how the factors affecting blue versus green water security vary both spatially and temporally.

### 1.2 *Study Area*

The Karuvannur river basin in the Thrissur district of Kerala State is chosen as the study area. The main stream of the river is 48 kilometers long and it drains an area of 1,054 square kilometer. The river originates from the Western Ghats (Pumalai Hills) and the two main tributaries of the river are Manali and Kurumali. The Chimony and Muply are the two sub tributaries of the Kurumali. The location map of the study area is shown in figure 1.

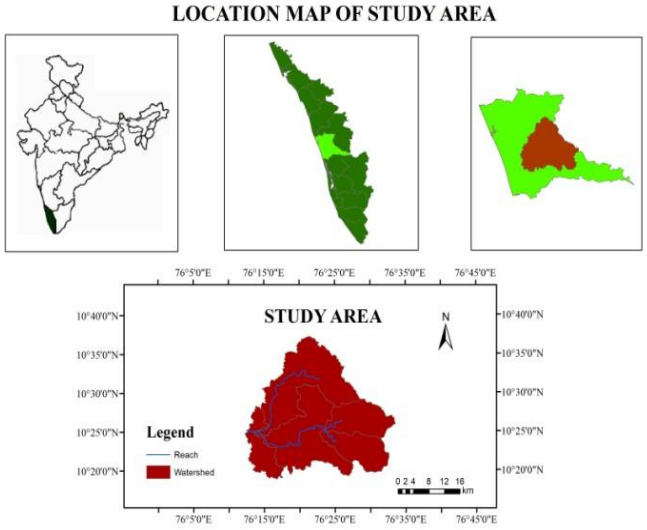



**Figure 1** Location map of study area

Karuvannur River provides potable water to numerous Panchayats in the Thrissur District. It has an annual utilizable water resource of 623 million cubic meters of which the net utilizable surface and ground water resources are 519.8 million cubic meters and 103.2 million cubic meters respectively. The average annual precipitation in the low land, midland and highland of the river basin is calculated to be 2858 mm, 3011mm and 2851 mm respectively.

## 2. Methodology

ArcSWAT (Soil and Water Assessment Tool) is used to model the hydrologic processes in the study area and to calculate the different components of blue and green water. The study area is modeled using SWAT for three different decades (1983-1992, 1993-2002 and 2003-2013). The various input data required in SWAT are spatial data which includes the Digital Elevation Model (DEM), land use map and soil map of the study area and meteorological data like daily precipitation, maximum and minimum air temperature, river discharge, relative humidity, wind speed and solar radiation along with the prevailing agricultural management practices.

The model is calibrated for a period from 2006 to 2008 and validated for a period from 2009-2011. From the output of the calibrated SWAT model of the study area, the various components of blue and green water are obtained. Blue water is computed as the sum of water yield and groundwater storage. Green water is estimated as the sum of initial soil moisture available to the plants and the soil evapotranspiration.

The total irrigation water requirement is computed using CROPWAT. Data required in CROPWAT includes soil map, maximum and minimum temperature, wind speed, relative humidity and sunshine, crop data and soil data. The estimated irrigation water requirement is compared with the blue water

available. Population data of the study area is also used to determine the domestic water demand. Green water demand, which is the actual evapotranspiration, is obtained from the SWAT output.

Present water security in the study area is assessed in terms of blue and green water scarcity. Blue water scarcity is the ratio of the blue water demand over blue water available. While calculating the blue water availability, environmental flow requirement should also be considered. Environmental flow requirement is the minimum flow that is required to sustain the ecological balance. This is applicable to both surface water as well as ground water. It is obtained from Global Environmental Flow Information System, IWMI. Similarly, green water scarcity is calculated as the ratio of green water demand and green water available. Knowing the blue and green water scarcity values, temporal variations of blue and green water security for the three decades are generated.

In order to assess the future water security, future climate and landuse are to be forecasted. Statistical Downscaling Model (SDSM) 4.2.9 is used to predict the future climate in the watershed. The datasets used for downscaling the meteorological parameters are GCM Output Data and NCEP/NCAR Reanalysis Data. Daily data for meteorological parameters like temperature, precipitation, relative humidity, wind speed, sunshine and evaporation are required. For the prediction of climate data, observed climate data for a period from 1983 to 2013 is used. Calibration is carried out for a period of 23 years from 1983 to 2000 and validation for a period from 2001 to 2005.

CLUE-S (Conversion of Land Use and its Effects at Small regional extent) is used to predict the future landuse of the study area. The landuse map of 1985 is chosen as the initial landuse map. Calibration is performed for the year 1995 and validation for 2005. Kappa statistic is used to compare the observed and simulated maps during calibration and validation. The calibrated model is used to predict the landuse map for the year 2050.

The forecasted climate and landuse map are used to run the calibrated ArcSWAT model for the study area and the future components of blue and green water are obtained from the SWAT model output. Using the predicted climate data, future irrigation water requirement for crops are computed using CROPWAT. Water security in the study area under future condition is assessed using the blue and green water availability computed from the output of ArcSWAT model modeled for future climate and landuse and using the blue and green water demand computed from the projected population of the study area and the predicted irrigation water requirement.

## 3. Results and discussions

The result obtained from the study includes the forecasted climate and landuse, the irrigation water requirement and the simulation results from the hydrologic model of the study area.

Using the calibrated model, the future climate is forecasted using SDSM. In order to study the seasonal variation in blue and green water security, assessment of the same is made for four seasons. For this, the winter season is taken from December to February, summer season from March to May, southwest monsoon season from June to August, north east monsoon season from September to November. Daily maximum and minimum temperatures show an increasing trend in all seasons. Figure 2 and 3 shows the seasonal variation of maximum and minimum temperature respectively. There is an increasing trend in rainfall during South-west monsoon and decreasing trend during North-east monsoon. Figure 4 shows the seasonal comparison of rainfall. Solar radiation also shows an increasing trend in all the seasons. During North-east monsoon, humidity shows a decreasing trend while for all other seasons, an increasing trend is seen. Wind speed shows an increasing trend in all seasons except South-west monsoon. Fig.5, Fig.6 and Fig.7 shows the seasonal variation of solar radiation, humidity and wind speed respectively.

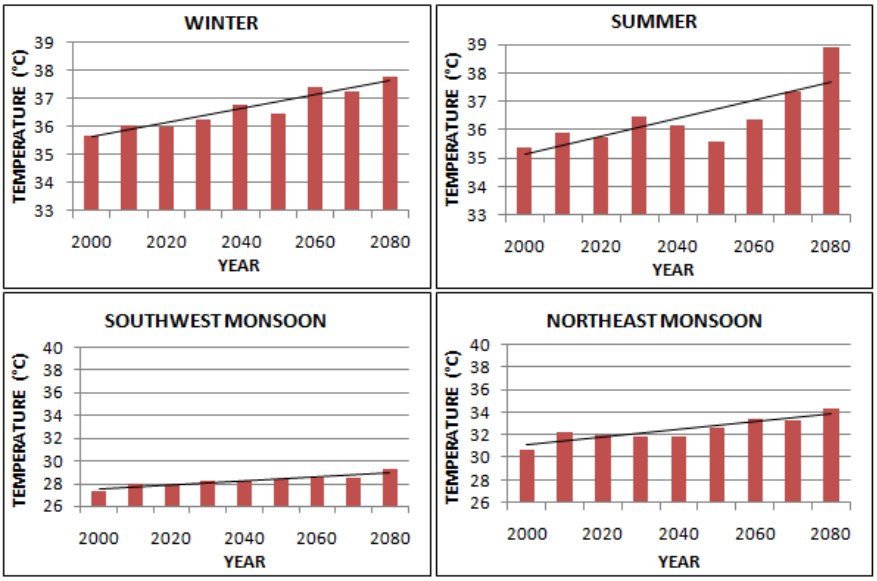



**Figure 2** Seasonal variation of maximum temperature

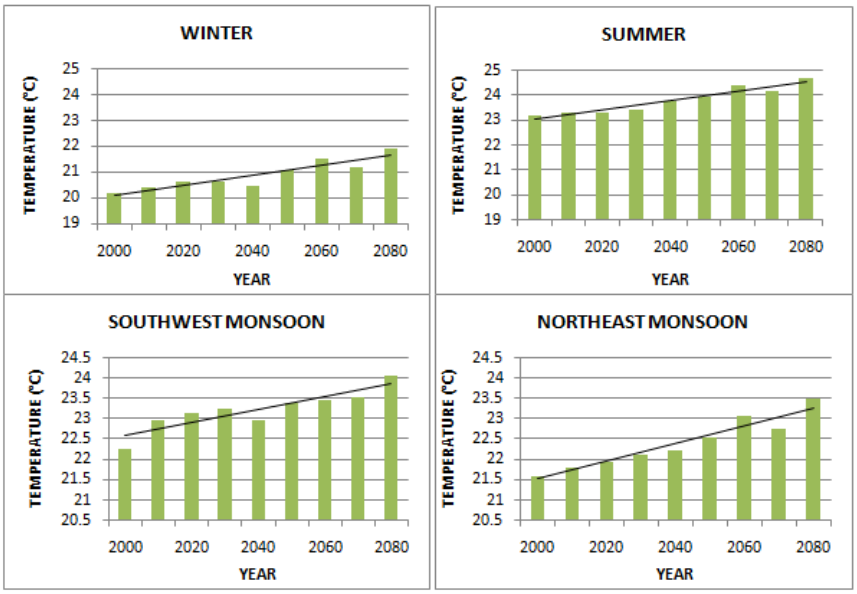



**Figure 3** Seasonal variation of minimum temperature

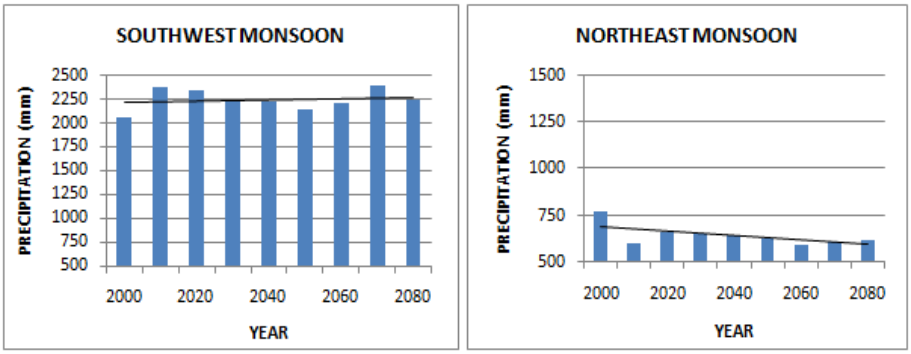



**Figure 4** Seasonal variation of rainfall

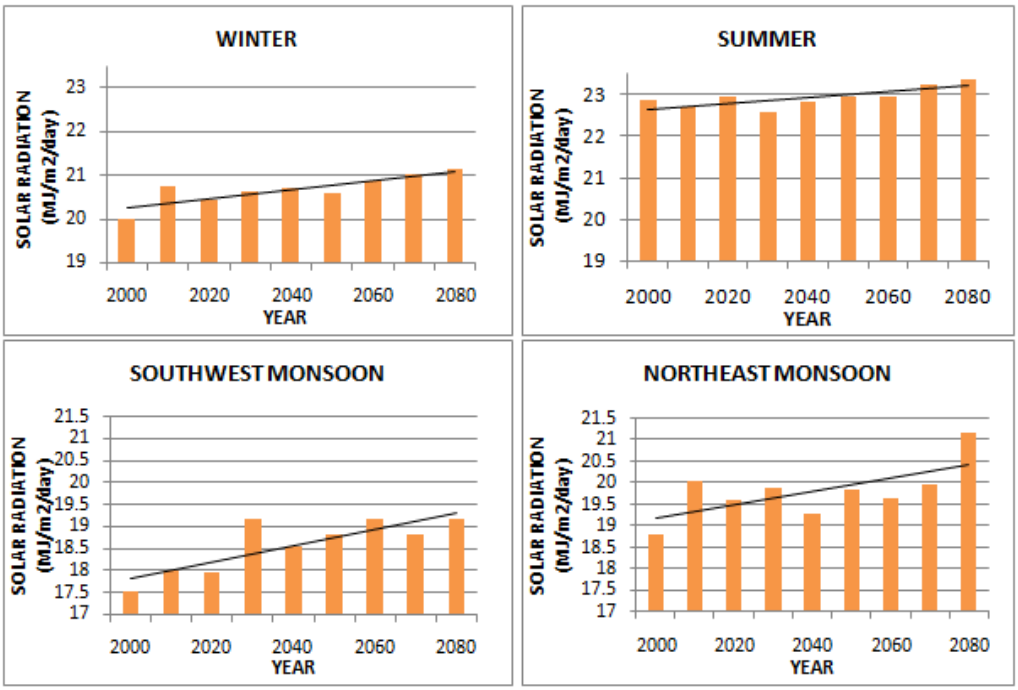



**Figure 5** Seasonal variation of solar radiation

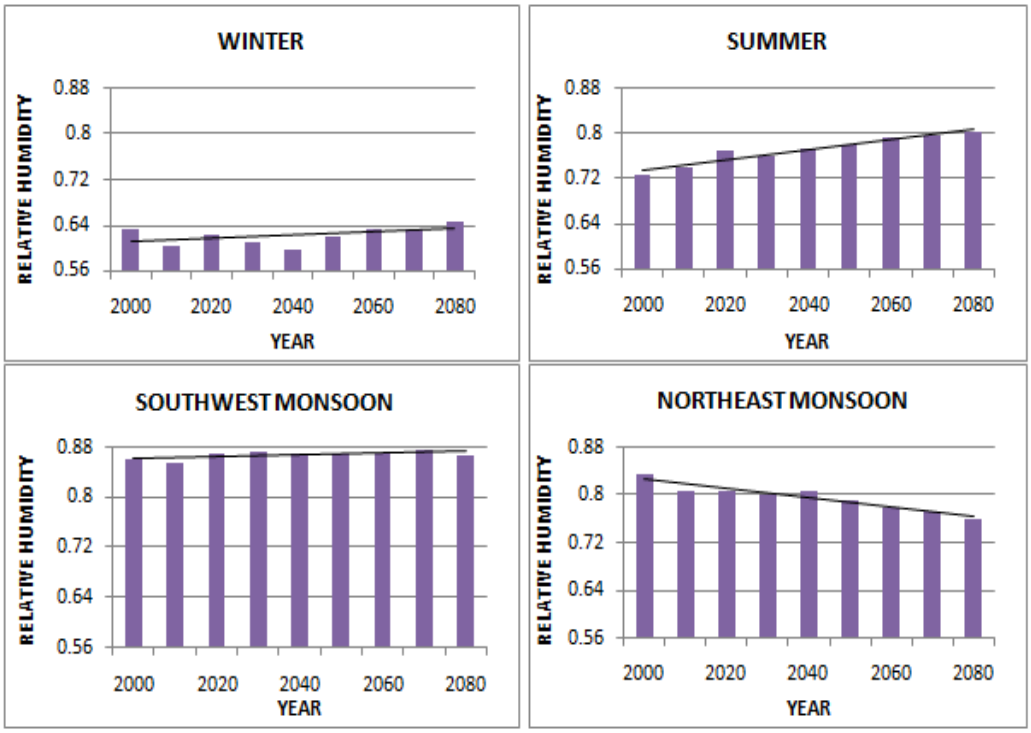



**Figure 6** Seasonal variation of relative humidity

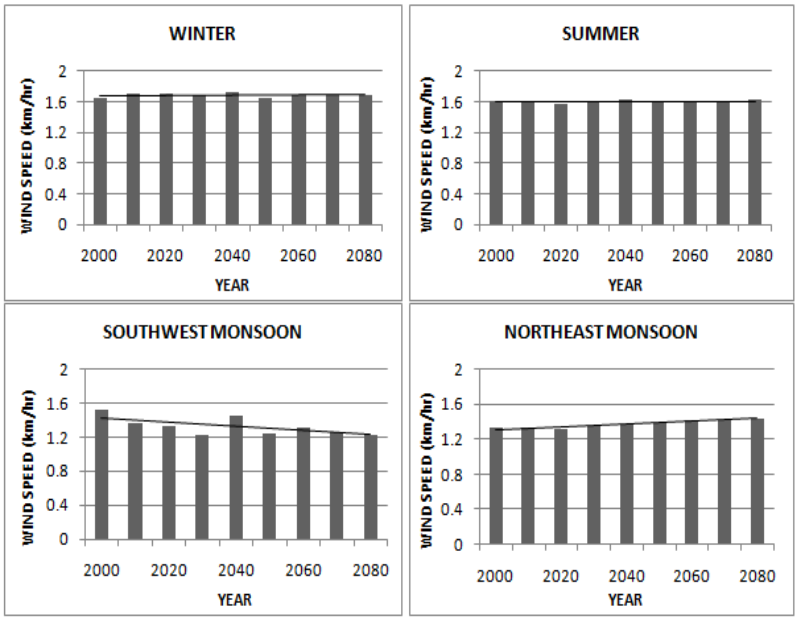



**Figure 7** Seasonal variation of wind speed

After the climate prediction, the landuse map for the year 2050 is forecasted using the validated CLUE-S model. Simulated landuse map for the year 2050 shows a very significant increase in the percentage of built-up area. Plantation area also increased. There is a decrease in the area of forest, agriculture and water body. Figure 8 shows the forecasted landuse map for the year 2050.

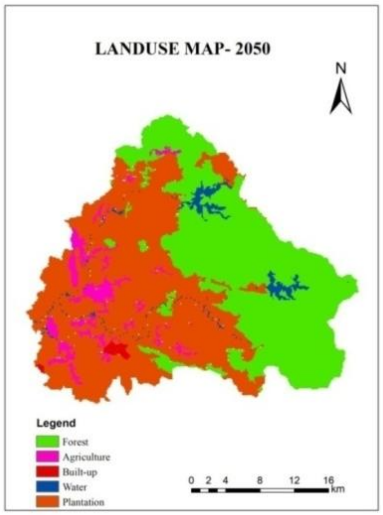



**Figure 8** Forecasted landuse map for the year 2050

The irrigation water demand for the major crops in the study area is calculated for the decades 1990s, 2010s, 2030s and 2050s. This irrigation water requirement is used in the calculation of blue water demand. Fig.9 shows the comparison of irrigation water requirement over different decades.

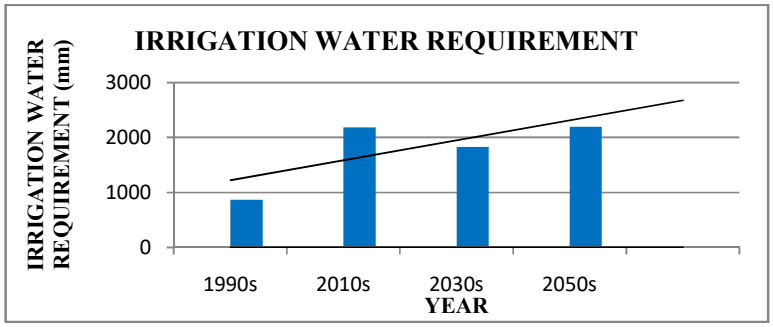



**Figure 9** Comparison of irrigation water requirement over different decades

The hydrologic modeling of the study area is done using ArcSWAT. After performing calibration and validation, the model is made to suit the conditions of the study area. Temporal variation of blue and green water is calculated for different decades (1990s, 2010s, 2030s and 2050s) from the SWAT model output. Annual and seasonal variation in blue water availability and demand is determined and water security is assessed yearly. Since there is excess water during the South-West and North-East monsoon period, seasonal study is limited to pre-monsoon (summer season- March to May) and post –monsoon (winter season -December to February). For easiness, decadal average is calculated and presented as shown in Table 1. Similarly decadal average of green water scarcity is also done. It is observed that both blue and green water scarcity tend to increase over the years and will cross the limit in the near future. Figure 10 shows the comparison of water scarcity over different decades. Also it can be observed that the throughout the study period, green water scarcity bears an alarming rate in comparison to blue water.

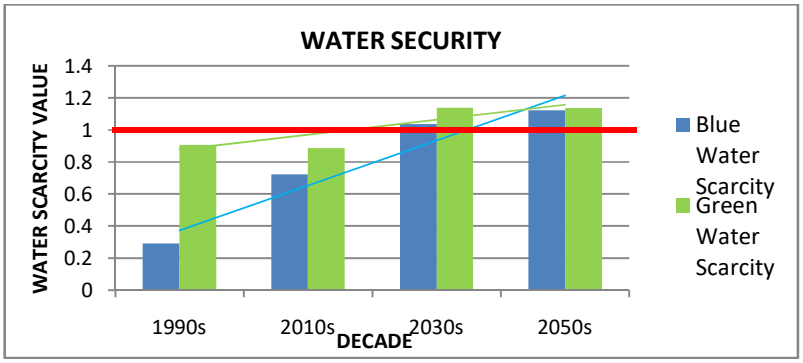



**Figure 10** Comparison of water security in terms of scarcity values over different decades

**Table 1** Blue and green water security in terms of scarcity values over the decades

| Decade | Blue Water | | | Green Water | | |
|---|---|---|---|---|---|---|
| | Average Annual Availability (mm) | Average Annual Demand (mm) | Scarcity | Average Annual Availability (mm) | Average Annual Demand (mm) | Scarcity |
| 1990s | 3274.63 | 955.69 | 0.29 | 928.76 | 843.21 | 0.91 |
| 2010s | 3155.95 | 2281.60 | 0.72 | 928.73 | 822.97 | 0.89 |
| 2030s | 2875.31 | 2764.72 | 1.04 | 681.70 | 776.40 | 1.14 |
| 2050s | 2067.22 | 2322.73 | 1.12 | 722.25 | 820.90 | 1.14 |

From the table, it is clear that for all the decades, green water scarcity value is greater than blue water scarcity value. In 1990s and 2010s, both blue and green water is secure (i.e., no scarcity) whereas in 2030s and 2050s, the scarcity value is greater than 1, indicating scarcity of both blue and green water. The blue water scarcity value shows an increase of 43.4% and 55.4% in 2030s and 2050s respectively when compared to 2010s and green water scarcity value shows an increase of 28.5% and 28.3% in

2030s and 2050s when compared to 2010s. Fig.11 shows the seasonal comparison of blue and green water scarcity and Table 2 shows the blue and green water scarcity values for monsoon season over the decades.

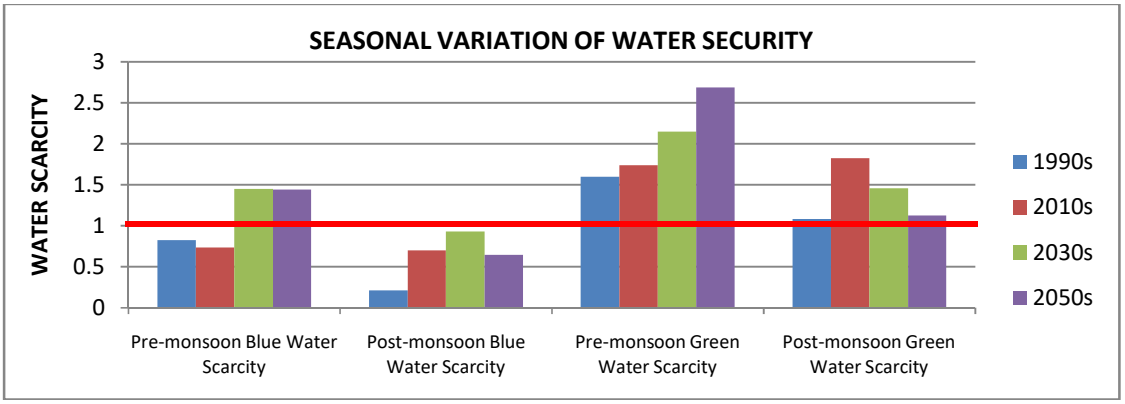



**Figure 13** Seasonal comparison of blue and green water scarcity

**Table 2** Pre-monsoon and post-monsoon blue and green water security in terms of their scarcity values for different decades

| Decade | Pre-monsoon | | | | | |
|---|---|---|---|---|---|---|
| | Blue Water | | | Green Water | | |
| | Average Annual Availability (mm) | Average Annual Demand (mm) | Scarcity | Average Annual Availability (mm) | Average Annual Demand (mm) | Scarcity |
| 1990s | 127.69 | 105.10 | 0.82 | 62.86 | 99.74 | 1.60 |
| 2010s | 148.75 | 109.53 | 0.74 | 44.85 | 77.99 | 1.74 |
| 2030s | 83.17 | 120.57 | 1.45 | 37.92 | 81.51 | 2.15 |
| 2050s | 85.01 | 122.61 | 1.44 | 34.37 | 92.41 | 2.69 |
| Decade | Post-monsoon | | | | | |
| | Blue Water | | | Green Water | | |
| | Average Annual Availability (mm) | Average Annual Demand (mm) | Scarcity | Average Annual Availability (mm) | Average Annual Demand (mm) | Scarcity |
| 1990s | 193.01 | 41.35 | 0.21 | 80.45 | 87.12 | 1.08 |
| 2010s | 67.34 | 46.99 | 0.70 | 44.86 | 81.72 | 1.82 |
| 2030s | 56.00 | 52.01 | 0.93 | 48.87 | 71.37 | 1.46 |
| 2050s | 90.24 | 58.51 | 0.65 | 62.29 | 70.00 | 1.12 |

From the table, it is clear that, both blue and green water is less secure during the pre-monsoon season compared to post-monsoon season. Considering the case of blue water, blue water is secure during all the decades during the post monsoon whereas during the pre-monsoon season, blue water is not secure in the 2030s and 2050s. In the case of green water, it is not secure in both pre-monsoon and post-monsoon season in all the decades. In pre-monsoon season, blue water scarcity value shows an increase of 76.1% and 75.2% in 2030s and 2050s when compared to 1990s while green water scarcity value shows an increase of 8.7%, 34.36% and 68.05% in 2010s, 2030s and 2050s respectively when compared to the 1990s. In the post-monsoon season, green water scarcity value shows an increase of 68.2%, 34.85% and 3.8% in 2010s, 2030s and 2050s when compared to 1990s.

## 4. Conclusions

In order to assess the current and future water security of the study area, hydrologic modeling of the study area is performed in ArcSWAT and the various components of blue and green water is identified. The water demand for various decades is found out using the projected population of the study area and irrigation water requirement obtained from CROPWAT model. Future climate is

forecasted using SDSM 4.2.9 and it is observed that SDSM is able replicate the observed values well. Precipitation showed an increasing trend in Southwest and decreasing trend in Northeast monsoon season. This reflects their adverse effects in the form of flooding in monsoon season and drought in summer season. Maximum temperature, minimum temperature and solar radiation show an increasing trend in all the seasons. Wind speed shows an increasing trend in all seasons except South-west monsoon whereas relative humidity shows increasing trend in all seasons except North-east monsoon. Simulated landuse map for the year 2050 showed that built-up area showed the largest increase (54.82%) in area. From the comparison of blue and green water availability with their demands, it is clear that both blue and green water scarcity tend to rise in the future. In 1990s and 2010s, both blue and green water is secure, whereas in 2030s and 2050s, they are not. The blue water scarcity value shows an increase of 255.19% and 284.9% in 2030s and 2050s respectively when compared to 1990s and green water scarcity value shows an increase of 25.45% and 25.19% in 2030s and 2050s in comparison to 1990s. On seasonal comparison, although blue and green water seems secure currently; the future scenario is not giving promising results. Blue water scarcity value shows an increase of 76.1% and 75.2% in 2030s and 2050s when compared to 1990s while green water scarcity value shows an increase of 34.36% and 68.05% in 2030s and 2050s respectively when compared to the 1990s in the pre-monsoon season. In the post-monsoon season, blue water is secure in all the decades whereas green water shows scarcity. The green water scarcity value shows an increase of 68.2%, 34.85% and 3.8% in 2010s, 2030s and 2050s when compared to 1990s. In all the cases, green water scarcity value exceeds the blue water scarcity. Therefore more attention is to be given to preserve and optimize the use of green water. It is observed that water stress escalates sharply due to climate change and increased demand for water. The situation may become more severe if sustainable water conservation and management plans are not implemented soon.

## References

Bakker, K. (2012). Water security: Research challenges and opportunities. *Science, 337*(6097), 914–915.

Falkenmark, M. (1995). Coping with water scarcity under rapid population growth. *Paper Presented at Conference of SADC Ministers, Pretoria, South Africa,* 23-24.

Falkenmark, M. (2008). Peak water: Entering an era of sharpening water shortage. *Stockholm Water Front,* 3-4.

Giri, S., Arbab, N.N., and Lathrop, R.G. (2018). Water security assessment of current and future scenarios through an integrated modeling framework in the Neshanic river watershed. *Journal of Hydrology, 563*, 1025-1041.

Jewitt, G. (2006). Integrating blue and green water flows for water resources management and planning. *Physics and Chemistry of the Earth, 31*, 753–762.

Koch, M., and Netsanet (2013). SWAT- modeling of the impact of future climate change on the hydrology and the water resources in the Upper Blue Nile river basin, Ethiopia. *International Conference on Water Resources and Environmental Research.*

Liu, J., and Yang, H. (2010). Spatially explicit assessment of global consumptive water uses in cropland: Green and blue water. *Journal of Hydrology, 384*, 187–197.

Liuying, D., Rajib, A., and Merwade, V. (2018). Large scale spatially explicit modeling of blue and green water dynamics in a temperate mid-latitude basin. *Journal of Hydrology, 562*, 84-102.

Miao, L., Chunlin, L., Yuanman, H., Fengyun, S., Yanyan, X., and Tan, C. (2014). Combining CLUE-S and SWAT models to forecast land use change and non-point source pollution impact at a watershed scale in Liaoning province, China. *Chinese Geographical Science, 24*, 540-550.

Sulser, T. B., Ringler, C., Zhu, T., Msangi, S., Bryan, E., and Rosegrant, M. W. (2010). Green and blue water accounting in the Ganges and Nile basins: Implications for food and agricultural policy. *Journal of Hydrology, 384*, 276–291.

Tukimat, N. N. A., Harun, S., and Shahid, S. (2017). Modeling irrigation water demand in a tropical paddy cultivated area in the context of climate change. *Journal of Water Resource Planning and Management, 143*, 1-8.

Veetil, A. V., and Mishra, A. K. (2016).Water security assessment using blue and green water footprint concepts. *Journal of Hydrology, 542*, 589-602.

Wilby, R. L., and Wigly, C. (2012). SDSM 4.2-A decision support tool for the assessment of regional climate change impacts. *A Consortium for the Application of Climate Impact Assessments.*

Zhao, A., Zhu, X., Liu, X., Pan, Y., and Zuo, D. (2016). Impacts of land use change and climate variability on green and blue water resources in the Weihe River Basin of northwest China. *Catena, 137*, 318-327.

*IN PROCEEDINGS OF 25th HYDRO 2020, INTERNATIONAL CONFERENCE, NATIONAL INSTITUTE OF TECHNOLOGY ROURKELA, ODISHA, INDIA 26-28, March 2021, ISBN 978-93-90631-56-8*

Paper ID - 307

# EVALUATING PERIODIC CHANGES OF RIVER DISCHARGE CARRYING CAPACITY: A CASE STUDY OF LOWER TAPI RIVER

Vineela Nandam[1], Patel P. L.[2]

[1]*DST-Inspire Fellow, Civil Engineering Department, Sardar Vallabhbhai National Institute of Technology, Surat, Surat 395007, India*

[2]*Professor, Civil Engineering Department, Sardar Vallabhbhai National Institute of Technology, Surat, Surat 395007, India*

*Email: vineela.nandam65@gmail.com , premlalpatel1966@gmail.com*

## Abstract

The dynamic equilibrium of natural rivers is getting altered significantly due to natural or human induced activities along the rivers, viz. excessive inflow of sediments from the catchments in the form of land slide, construction of hydraulic structures like storage dams and weirs or barrages, sand mining activities on the river bed and encroachment of flood plains. Ever since the construction of Ukai dam across Tapi river in the year 1972, the flow characteristics in the downstream of the river got altered, thereby, impacting the carrying capacity of the river. The coastal flood plain of Surat city has witnessed six major flood events after the construction of Ukai dam. The periodic changes of carrying capacity of Tapi river was evaluated by considering the discharge at Ghala stream gauging station (located at 37 km upstream of Surat city and at 65 km downstream of Ukai dam) and water levels at the Nehru bridge in the Surat city over a period of 1978–1994. It is noticed that, for warning level (+8.5m) at Nehru bridge, the carrying capacity was estimated to be 5.15, 4.91, 5.08 and 4.15 lacs cusecs during the period 1978 – 88, 1980 – 90, 1982 – 92 and 1984 – 94 respectively. The carrying capacity of Tapi river in Surat city was estimated to be approximately 8.5 lacs cusecs at the time of dam construction. From aforesaid values, it can be inferred that, after the construction of Ukai dam, the river carrying capacity got reduced to less than half by 1994. The possible reason for such drastic capacity reduction could be due to, morphological changes in the Tapi river, inadequate discharge in the river to flush the sediments deposited during tidal currents and encroachments in the river floodplains.

***Keywords:*** *Tapi river, Carrying capacity; Ukai dam; Surat city; Capacity curves*

## 1. Introduction

Reduction in river discharge carrying capacity can be related to increase in flood frequency. The Surat city is located on coastal floodplain of Lower Tapi River, which has been in the influence of major floods in the past during the years 1727, 1776, 1782, 1829, 1837, 1872, 1944, 1959, 1968, 1970, 1994, 1998, 2006 and 2013 (Kale and Hire 2004; and Timbadiya et al. 2014; Vora et al. 2018). A recent flood in the year 2006 is considered as major flood post Ukai dam construction. The present study aims to quantify changes occurred in lower Tapi river's discharge carrying capacity after construction of Ukai dam in the year 1972 by making use of stage – discharge relationships during 1978 to 1994.

Human induced activities along the rivers aids in aggravating risks associated with occurrence in events. Construction of controlled structures across the rivers, sand mining activities in the riverbed, thereby changes in cross-sections, encroachments in the flood plains changes river's natural regime. In some cases, the downstream of hydraulic structure is left dry during non-monsoon periods, where environmental flows are absent leading to abrupt changes in bed levels and in addition to prevailing floodplain encroachments. The Tapi basin is identified as one of the nine basins in India that is to be given due consideration to protect its aquatic biodiversity. Also, the river has been categorized as "strongly affected" by "flow fragmentation and regulation" by constructing dams across the river (Nilsson et al. 2005; Jain and Kumar 2014). Patel et al. (2020) simulated 1D hydrodynamic model of lower Tapi river and it indicated that the carrying capacity at the Surat city is less than 24,081 cumecs for against the discharge of 25,768 cumecs released from Ukai dam. A significant increase in extreme rainfall events has been observed in the Lower Tapi basin and in upstream of Ukai dam (Gehlot et al. 2020). Also, it is reported that the major flood occurred in the year 2006 is due to increase in rainfall,

heavy releases from the Ukai dam and high tide condition. The reduced carrying capacity of a river under exposure to such a combination may turn out to be a catastrophic event.

An Ukai dam which is constructed in the year 1972 is one of the major water resource structures across the Tapi river and is located at 110 km upstream of Surat city. From Table 1, it is clearly seen that carrying capacity of Tapi River is reduced significantly in the post dam period, particularly in the recent years. For example, a river discharge of 43,891 $m^3/s$ caused a water level of 12.08 m during the flood of year 1968, while a similar water level of 12.40 m was attained at much lower discharge of 25,768 $m^3/s$ during the flood year 2006.

**Table 1** Historic floods and corresponding water levels in Surat city *[source: Vora et al. (2018)]*

| Year | Peak flood discharge ($m^3/s$) | Water level at Nehru Bridge (m) | Remarks |
|---|---|---|---|
| 1942 | 24,355 | 10.56 | - |
| 1944 | 33,527 | 11.32 | - |
| 1945 | 28,996 | 11.09 | - |
| 1949 | 23,842 | 10.49 | - |
| 1959 | 36,642 | 11.55 | - |
| 1968 | 43,891* | 12.08* | - |
| 1970 | 37,208 | 11.02 | - |
| 1978 | 12,459$^{\$}$ | 8.59 | Post-Dam period |
| 1979 | 9,345 | 8.22 | Post-Dam period |
| 1994 | 14,866 | 10.10 | Post-Dam period |
| 1998 | 19,057 | 11.40 | Post-Dam period |
| 2006 | 25,768$^{\#}$ | 12.40$^{\#}$ | Post-Dam period |
| 2013 | 12,257 | 9.70 | Post-Dam period |

**maximum values corresponding to prior dam construction; #maximum values corresponding to post-dam period; $Ukai dam outflows corresponding to post-dam period*

Jain et al. 2007 stated that the design discharge carrying capacity of Surat was 24,070 cumecs (8.5 lac cusecs) at the time of Ukai dam construction. The present value was mentioned to be 11,320 cumecs (4 lac cusecs). There is a necessity to identify the causes and to quantify the changes more explanatory concerning river flow carrying capacity as the flow has become controlled ever since construction of Ukai dam. Therefore, the objective of this study is to evaluate periodic changes of river discharge carrying capacity that occurred after construction of Ukai dam using stage – discharge data collected from Central Water Commission.

## 2. Materials and Methods

### 2.1 *Study area*

The Tapi River which is the second largest west flowing river in peninsular India originates from Multai in the Betul district of Madhya Pradesh and flows towards west to meet the Arabian Sea at 8 km from Surat city. The Lower Tapi Basin (LTB) has watershed area of 3749 $km^2$ and it lies between 72º30’ to 72º40’ East longitudes and 21º00’ to 21º40’ North latitudes. The length of Tapi River, 127 km downstream of Ukai reservoir, is considered as Lower Tapi River (LTR). The Ukai reservoir, which is constructed in the year 1972, is located at 110 km (Timbadiya et al. 2011) upstream of the Surat city (Figure 1). The reservoir regulates the flow in the downstream reaches for meeting irrigation, municipal and industrial demands including partial flood control during the monsoon. No major tributaries enter the Tapi river in the downstream of Ukai reservoir (Timbadiya et al. 2014). Towards the downstream of Ukai reservoir, there are two water resources structures namely Kakrapar weir, and Singanpore weir in the Surat city. The stream gauging sites: Mandavi, Ghala, Khator bridge and Nehru bridge are stationed along the river for measuring stage and (or) discharge of the river flow. The mean annual temperature in LTB is 27.1ºC (Sharma et al. 2019). The South-West Monsoon contributes to about 87.4% of mean annual rainfall in the entire Tapi basin. On an average, the LTB receives about 1040

mm of rainfall (PMP Atlas, 2015). The South-West monsoon sets in by the mid of June and withdraws by the first week of October.

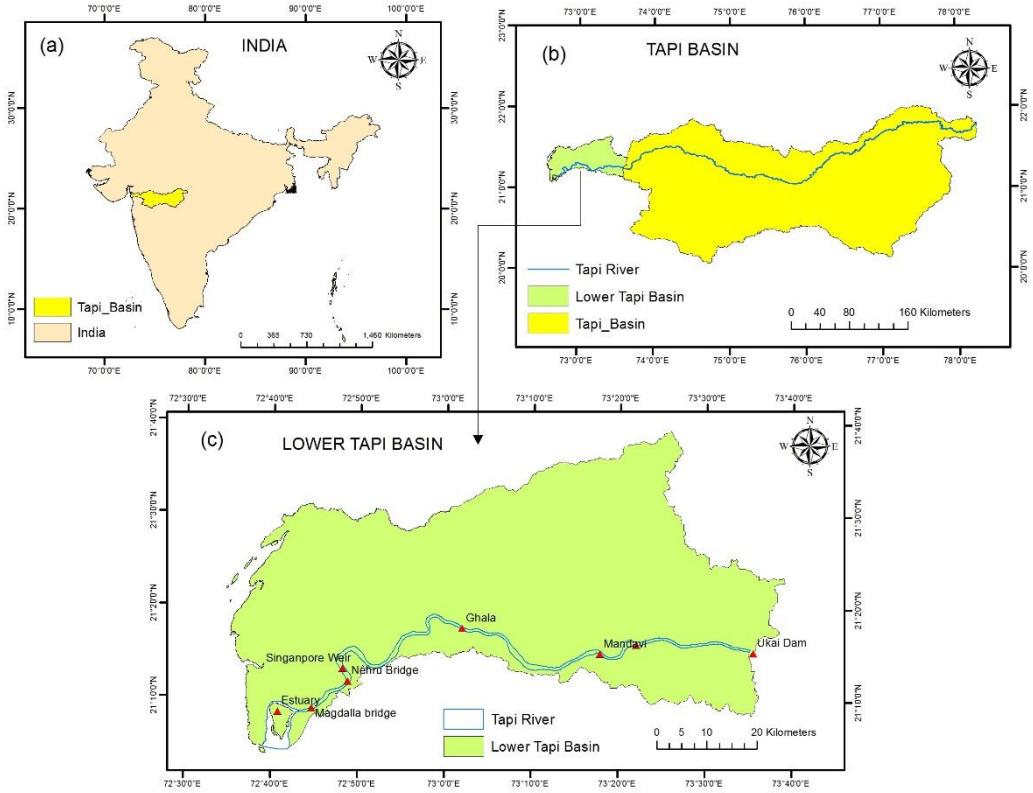



**Figure 1** Index map showing the geographic location of Lower Tapi River and stream gauging stations

The topographic terrain of LTB is almost flat. The coastal plains in Gujarat has alluvial clays with a black soil layer on its top (PMP Atlas, 2015). The dominant land use classes in the Lower Tapi basin are agriculture and forest lands. The Surat city originated in the banks of river Tapi. An area of 326.52 $km^2$ falls under Surat Municipal Corporation. It is evident from the census data of India that in the year 2001, Surat district has maximum growth rate of 47.01%. Since 1971, population growth rate of Surat Municipal Corporation continued to be on the higher side (1971-63.75%, 1981- 64.65%, **1991- 93.00%**, 2001-62.38% and 2011- 83.53%). The Nehru bridge in the Surat city is the stage measurement site.

## 2.2 *Data sources*

Discharge and water levels at Ghala stream gauging (Ghala SG) site from 1978 – 1994 and the corresponding water levels at Nehru bridge for the same time period in the Surat city were collected from Central Water Commission (CWC), Tapi division, Surat. No regulatory structures were constructed in between the two stations considered in the above time period. In the year 1995, Singanpore weir was constructed in the upstream of Nehru bridge and hence, the flow became regulated.

## *2.3 Methodology*

The present study is aimed to quantify the river discharge carrying capacity at Surat city. It can be achieved by establishing a relation between discharge at a stream gauging site and the corresponding water levels at the Surat city. Prior in doing so, the stability of the stream gauging site (Ghala SG site) was checked by plotting rating curves. The power fit equations were then generated by keeping discharge at stable SG as independent variable and the corresponding stage values at the Surat city's

Nehru bridge as a dependent variable to find fluctuations if any. From the graphs plotted, the discharge with respect to warning and danger levels were traced to understand the temporal changes in river flow carrying capacity.

## 3. Results and Discussion

To quantify river flow carrying capacity at Surat city, two stream gauging stations were chosen on Lower Tapi river, one in the Surat city and the other in the upstream of Surat city i.e., Ghala SG station. Ghala SG site is located at nearly 37 km in the upstream with respect to Surat city's Nehru bridge.

### 3.1 *Rating curves of Ghala SG site*

Initially, stability of rating curve at Ghala SG site was checked to derive water level changes if any at Nehru bridge to compute river discharge carrying capacity at Surat city. Based on data availability, for comparison, four rating curves were generated from the data sets available from 1978 – 1994, by applying sliding at every two years. In doing so, any drastic change in rating curve may be captured. The stage-discharge curves of Ghala SG site for over a period of 16 years (from 1878 – 1994) were plotted (Figure 2).

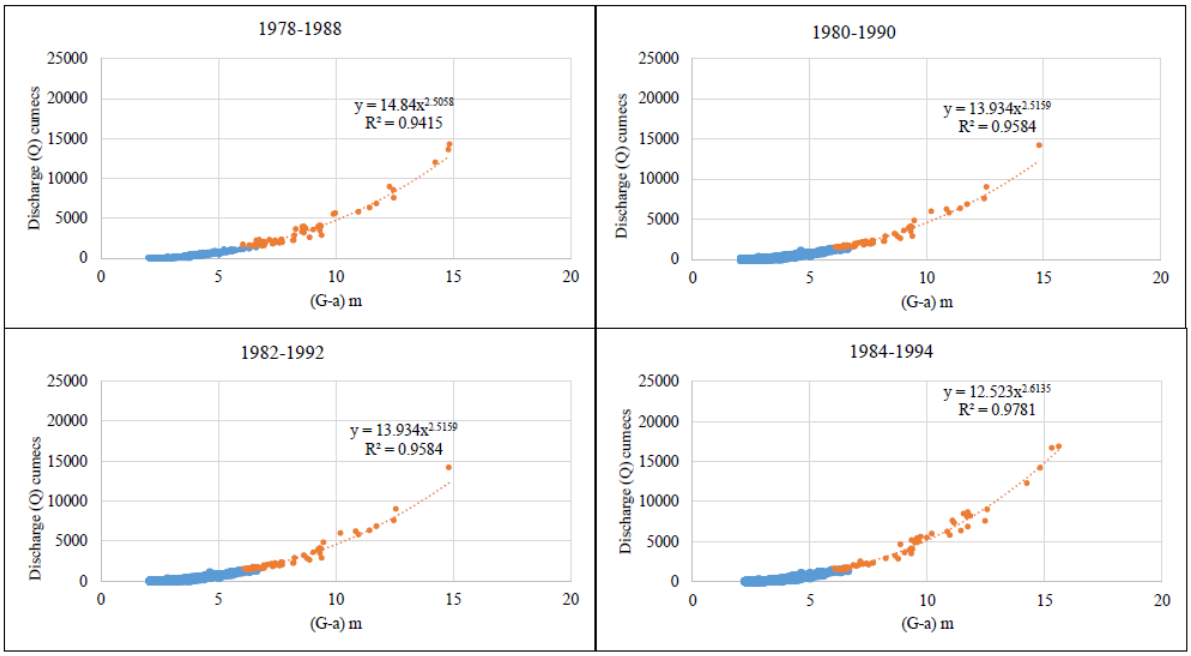



**Figure 2** Stage – Discharge curves of Ghala SG station (*Blue coloured data points correspond to low discharge)*

The discharge greater than 1405 cumecs was considered as threshold based on field experience, which contributes significantly in quantifying the river discharge carrying capacity. The results showed any change in the rating curves plotted in the time period considered. Also, the graphical representation of cross-section of Ghala stream gauging site for years 1980 and 1991 in Figure 3 depicts the stability of cross-section.

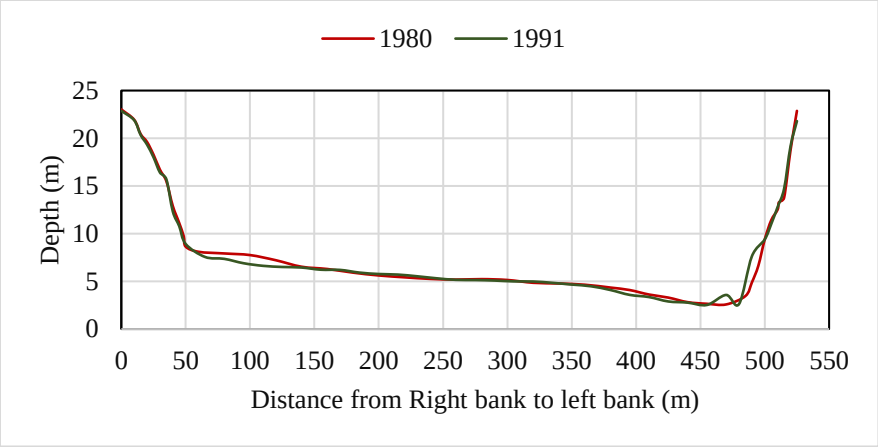



**Figure 3** Graphical representation of cross-section of Ghala SG site in the year 1980 and 1991

### 3.2 *River discharge carrying capacity at Surat city*

In a view to explain the changes in river flow carrying capacity, the discharge data of Ghala SG station and the corresponding water levels at Nehru bridge were used. The water levels at Nehru bridge are recorded during monsoon period. The data recorded since 1978 to 1994 was undertaken on decadal basis as datasets of 1978-88, 1980-90, 1982-92 and 1984-94. The low flows (< 0.5 lacs cusecs or < 1406 cumecs) were ignored as they have least or no contribution in finding river discharge carrying capacity. The respective water levels were plotted against discharge values. The power fit Equations (1), (2), (3) and (4) were generated, each corresponding to decades 1978-88, 1980-90, 1982-92 and 1984-94 respectively. As the stability of Ghala SG site was checked, the discharge corresponding to Ghala SG site was taken to be independent variable and the water level at Nehru bridge as dependent variable.

$$y = 0.3086\, Q^{0.3528} - 0.5875 \quad (1)$$

$$y = 4.684\, Q^{0.1477} - 10.67 \quad (2)$$

$$y = 35.29\, Q^{0.04625} - 46.45 \quad (3)$$

$$y = 0.6714\, Q^{0.3033} - 3.018 \quad (4)$$

where, ‘y’ is water level (m) at Nehru bridge and ‘Q’ is discharge at Ghala SG site. The equations generated are valid only for high flows (defined as Q > 0.5 lacs cusecs for our study). The coefficient of determination and RMSE values of the thus generated equations are shown in Table 2.

**Table 2** Performance indicators for discharge vs water level equations

| Description | 1978-88 | 1980-90 | 1982-92 | 1984-94 |
|---|---|---|---|---|
| **R square** | 0.73 | 0.81 | 0.83 | 0.90 |
| **Adjusted R square** | 0.71 | 0.80 | 0.83 | 0.89 |
| **RMSE (m)** | 0.80 | 0.70 | 0.66 | 0.64 |

The water level at Nehru Bridge is considered as water level of Surat city. The warning and danger levels of Surat city are 8.5 m and 9.5 m, respectively. Ideally, the river carrying capacity should be related with safe water level, beyond which water starts overflowing from either side of the banks. Hence, the discharge corresponding to 8.5 m water level was considered to evaluate river flow carrying capacity at Surat city. The values pertaining to warning level and danger level for the four time periods showed any changes, but, from 1982-92 to 1984-94, the discharge carrying capacity was dropped by

2648.27 cumecs and 5402.5 cumecs respectively, denoting a change and decrease in river flow carrying capacity.

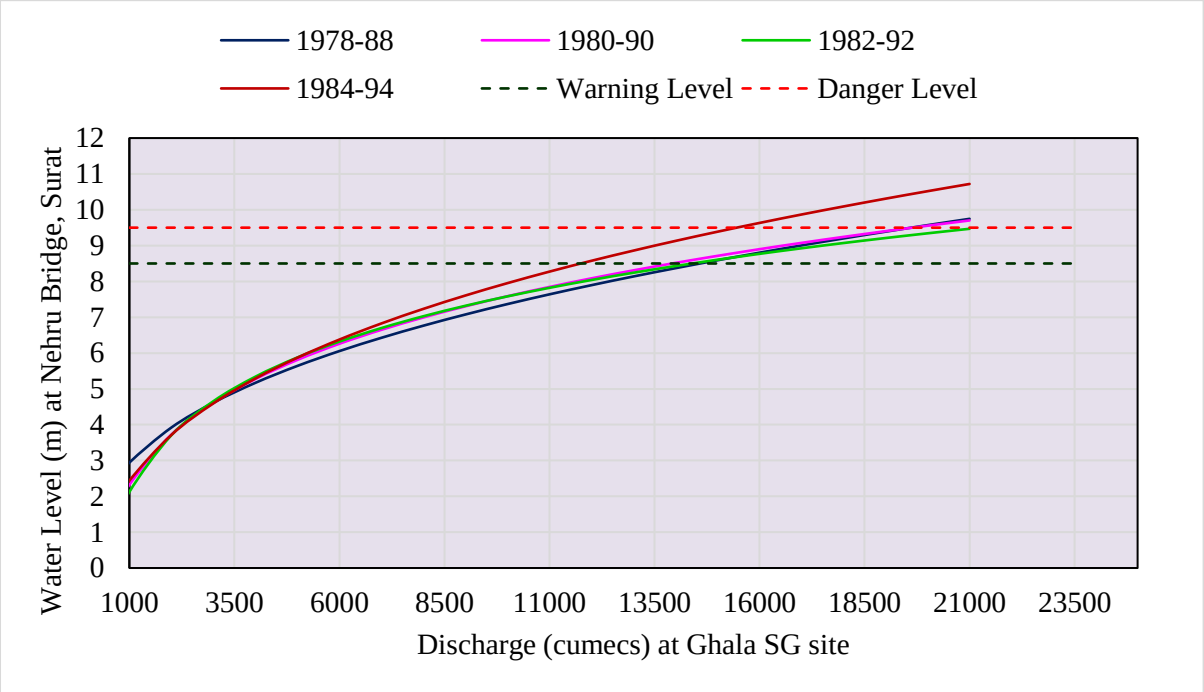



**Figure 4** Capacity curves of Tapi river in between Ghala SG site and Surat city's Nehru bridge

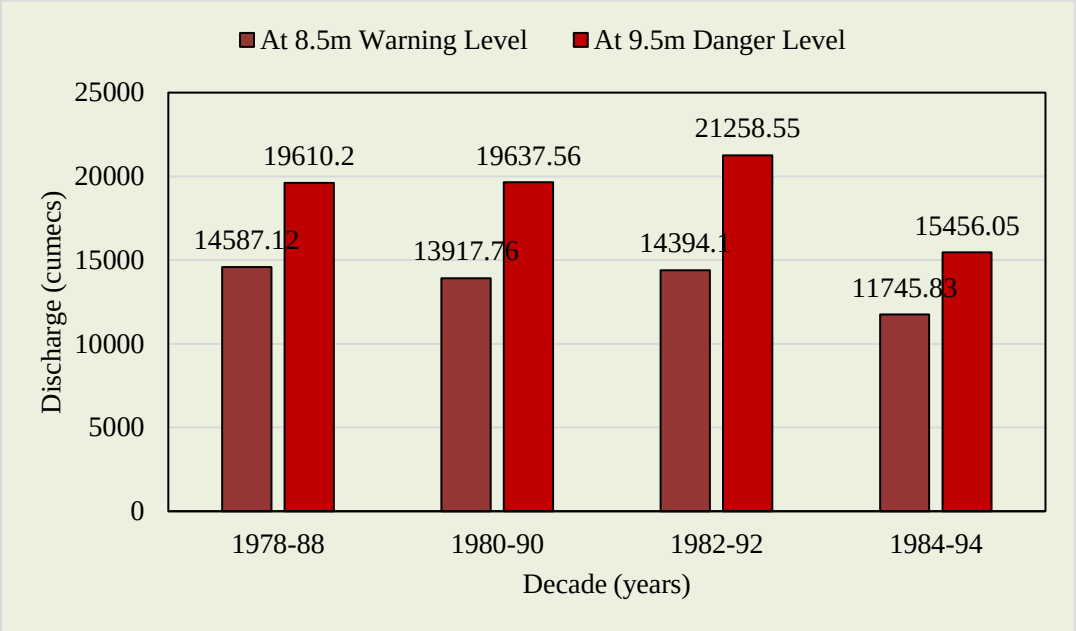



**Figure 5** River flow carrying capacity at warning and danger levels in Surat city

The carrying capacity of lower Tapi river was estimated to be 8.5 lacs cusecs (i.e., 24,070 cumecs) when Ukai dam was constructed. From the assessed capacity curves, it is very much evident that the carrying capacity of Tapi river calculated at Surat city dropped down to 11,745 cumecs (~ 4 lacs cusecs) by year 1994.

## 4. Conclusion

In the present study, the Tapi river discharge carrying capacity at Surat city was found to be decreasing. The key conclusions obtained from the analysis are:

- The stage-discharge curves of Ghala stream gauging site tend to show insignificant change during the period from 1978 to 1994. Also, the cross sections of this site when plotted for the years 1980 and 1991 showed any abrupt changes. Therefore, the site may be considered as stable.
- The graph plotted between discharge at Ghala SG site and corresponding water levels at the Surat city's Nehru bridge when considered only high flows (defined as > 0.5 lacs cusecs or 1406 cumecs) indicated a reduction in flow carrying capacity to 11,745.3 cumecs for the latest period (1984 – 1994). Therefore, the discharge carrying capacity of Lower Tapi river has been found to be decreased.
- According to Jain et al. 2007, the safe river carrying capacity was estimated to be 24,070 cumecs (8.5 lacs cusecs) after construction of Ukai dam, and the value was dropped to 11,745.3 cumecs (~ 4 lacs cusecs). In the year 1995, Singanpore weir was constructed in the upstream of the Nehru bridge. Hence, the flow became regulated.

The possible reasons for such drastic reduction in the Tapi river flow carrying capacity may be due to changes in river morphology after construction of Ukai dam, absence of environmental flows to flush off the sediments deposited during tidal currents and may be due to human intervention in floodplains, which needs further investigation.

## Acknowledgment

The first author would like to acknowledge *Department of Science and Technology, Ministry of Science and Technology, Government of India* for the financial support vide their letter no. DST/INSPIRE Fellowship/2018/[IF180589] dated July 24, 2019. The authors are grateful to the infrastructural support provided in Centre of Excellence (CoE) on "Water Resources and Flood Management", TEQIP-II, *Ministry of Human Resources Development (MHRD), Government of India*, for conducting this research.

## References

Central Water Commission and India Meteorological Department (2015). PMP Atlas – Narmada, Tapi, Sabarmati, and Luni river systems and rivers of Saurashtra and Kutch regions including Mahi final report.

Gehlot, L.K., Jibhakate, S.M., Sharma, P.J. Patel, P. L., and Timbadiya, P. V. (2020). Spatio-Temporal Variability of Rainfall Indices and their Teleconnections with El Niño-Southern Oscillation for Tapi Basin, India. *Asia-Pacific Journal of Atmospheric Science* (2020).

Jain, S. K., Agarwal, P. K., and Singh, V. P. (2007). Hydrology and water resources of India. *Springer Science & Business Media.* (Vol. 57).

Jain, S. K., and Kumar, P. (2014). Environmental flows in India: towards sustainable water management. *Hydrological Sciences Journal*, *59*(3-4), 751-769.

Kale, V. S., and Hire, P. S. (2004). Effectiveness of monsoon floods on the Tapi River, India: role of channel geometry and hydrologic regime. *Geomorphology*, *57*(3-4), 275-291.

Nilsson, C., Reidy, C. A., Dynesius, M., and Revenga, C. (2005). Fragmentation and flow regulation of the world's large river systems. *Science*, *308*(5720), 405-408.

Patel, D., Srivastava, P., Singh, S. K., Prieto, C., Bray, M., and Han, D. (2018). Flood hydrodynamic modelling of river discharge carrying capacity-A case study of the Tapi river 2006 flood in Surat city of India. *EGUGA*, 1406.

Sharma, P. J., Patel, P. L., and Jothiprakash, V. (2019). Impact of rainfall variability and anthropogenic activities on streamflow changes and water stress conditions across Tapi Basin in India. *Science of the total environment*, *687*, 885-897.

Timbadiya, P. V., Patel, P. L., and Porey, P. D. (2011). HEC-RAS based hydrodynamic model in prediction of stages of lower Tapi River. *ISH Journal of Hydraulic Engineering*, *17*(2), 110-117.

Timbadiya, P. V., Patel, P. L., and Porey, P. D. (2014). One-dimensional hydrodynamic modelling of flooding and stage hydrographs in the lower Tapi River in India. *Current science*, 708-716.

Vora, A., Sharma, P. J., Loliyana, V. D., Patel, P. L., and Timbadiya, P. V. (2018). Assessment and Prioritization of Flood Protection Levees along the Lower Tapi River, India. *Natural Hazards Review*, *19*(4), 05018009.

*IN PROCEEDINGS OF 25th HYDRO 2020, INTERNATIONAL CONFERENCE, NATIONAL INSTITUTE OF TECHNOLOGY ROURKELA, ODISHA, INDIA 26-28, March 2021, ISBN 978-93-90631-56-8*

Paper ID - 339

# Study of unsteady flow parameters and hysteresis effect in a simple channel under unsteady flow condition

S.Sahoo[1] K.Devi[2] J.R.Khuntia[3] K.K.Khatua[4]

[1]*PhD Research Scholar, Civil Engineering Department, National Institute of Technology, Rourkela,769008,India*

[2]*Associate Professor, Civil Engineering Department, VJIT, Hyderabad, 500075, Telengana, India*

[3]*Assistant Professor, Civil Engineering Department, St. Martin's Engineering college, Secunderabad, 500100, Telangana, India*

[4]*Professor, Civil Engineering Department, National Institute of Technology, Rourkela,769008, India*

[1]*Email: sarjatisahoo1991@gmail.com* (Corresponding Author)

*Mobile Number: +91 8895632739*

## Abstract

Flows in the natural rivers and channels are often unsteady. Rivers in flood are characterized by unsteadiness of the flow. Various field studies show that when flood passes in a river, the bed load movement, the suspended-load distributions, as well as the river processes are different from those in steady flow. Therefore, it is very important to understand the behavior of unsteady open channel flow and to predict the flood passage and the river processes. Some researchers proposed some parameters called unsteady flow parameters to understand the behavior of unsteady flow. However, there are very less literatures available on the study of unsteady flow parameters. In this present study, experimentations on a simple open channel is performed under unsteady flow condition to investigate the various parameters of unsteady flow. Two hydrographs are passed through the rectangular flume with a fixed rigid grass bed under two different inlet conditions. Flow hydrograph and depth hydrographs are plotted for both the different inlet conditions. The hysteresis effect of stage-discharge ($h \sim Q$) rating curve between rising and falling limbs is also studied for the present hydrographs. To study more about the hysteresis effect in unsteady flow another data sets of Bombar (2016) has been considered and stage-velocity curves are presented. In the present study, three unsteady flow parameters have been considered. A total of nine hydrographs were studied including the present hydrographs and data of other researchers. It has been observed that the rising and falling limbs in hysteresis plots are closer to each other in experiments having low unsteadiness whereas the limbs are more separated in experiments having high unsteadiness.

***Key Words:*** *Unsteady Flow, Simple Channel, Hydrograph, Unsteady Flow Parameter, Hysteresis effect*

## 1. INTRODUCTION

Flows in the natural rivers and channels are often unsteady. Rivers in flood are characterized by unsteadiness of the flow. Various field studies show that when flood passes in a river, the bed load movement, the suspended-load distributions, as well as the river processes are different from those in steady flow. So, it is very important to understand the behavior of unsteady open channel flow and to predict the flood passage and the river processes. Naturally the river cross-section is usually composed of a deep main channel and adjacent shallow flood plains. When there is a single flood plain on the either side of the main channel then this is called as an asymmetric compound channel. If flood plains of equal width are present on the both side of the main channel, it may be called as a symmetric compound channel and if the width of the flood plains is not same, it may be an unsymmetrical compound channel. The floodplain may be a wetland and is frequently a wild life

habitat. Flow in a compound channel is very complicated. Townsend (1967), Knight and Demetriou (1983), Knight and Sellin (1987), and Wormleaton and Merrett (1990) pointed out that at a low floodplain depth the large velocity difference between the main channel and the floodplain induced a strong shear layer and a lateral momentum transfer across the interface between the main channel and the floodplain. It is often observed in rivers that the discharge *Q(t)* does not show a single curve against the flow depth *h(t)* but shows a loop diagram in unsteady open-channel flows; a peak discharge appears before a time of peak depth (French 1985). The peak of the flood wave attenuates along the channel and a hysteresis occurs in the stage-discharge curve (Tingsanchali 1976, 1988; Cunge et al. 1980; Yen 1987). Stephenson and Kolovo-poulos (1990) and Abida and Townsend (1992) both noticed the effect of the lateral momentum transfer to the unsteady flow prediction. Because of the difficulties in measurement, studies on unsteady open-channel flow are rare. There are many experimental works have been performed on simple channels to study the unsteady flow process. However, for compound channel cases, the study of unsteady flow is very rare. So, the object of this work to perform experimentation in compound channel as well as simple channel to investigate the flow parameters and study the behavior of those parameters under unsteady flow condition.

## 2 METHODOLOGY

### 2.1. Unsteadiness Parameters

Some of the parameters which describe the unsteadiness of flow are discussed below.

- It is useful to define an outer-variable parameter that characterizes the effects of unsteadiness on velocity profiles and turbulence in open-channel flows. Takahashi (1969) proposed the following parameter to analyze the one-dimensional hydraulic equation of flood waves.

$$\lambda = \frac{V_s}{c.sin\theta} \quad (1)$$

In which

$$V_s = \frac{h_p - h_b}{T_d} \quad (2)$$

where $T_d$ = duration from the base discharge to the peak discharge in flood. The subscripts *b* and *p* denote the "base" and "peak" values, respectively. The parameter $\lambda$ implies the ratio of the rising speed $V_s$ of water surface to the vertical component of celerity *c* of long waves. Nezu and Nakagawa (1991) have used the value of $\lambda$ as an unsteadiness parameter. However, this parameter is not suitable to compare unsteady flows over smooth beds with those over rough beds, because the values of bed slope $S_b = sin\theta$ are quite different between the two. Therefore, Nezu and Nakagawa (l993b) have proposed the following parameter $\alpha'$ that correlates with the pressure gradient *dPldx:*

$$\alpha' \equiv \frac{1}{U_c}\frac{\partial h}{\partial t} \cong \frac{1}{U_c}\frac{h_p - h_b}{T_d} = \frac{V_s}{U_c} \quad (3)$$

Where $U_c$ is the convection velocity of the turbulent eddies and is roughly equal to $(U_b + U_p)/2$.

- An unsteady parameter $\lambda_{um}$ proposed by Tominaga et al. (1994) to control the rising limb of a model flood so that it acted like a real flood. The unsteady parameter was defined as

$$\lambda_{un} = \frac{h_p - h_b}{t_p S_0 \sqrt{g h_p}} \quad (4)$$

Their experiments were conducted in a compound channel having a relative width between 1.2 and 3.5. The unsteady parameter value of those experiments was less than 1.0. It was suggested that a stronger $\lambda_{un}$ and wider floodplain would produce better condition for the observation of the overbank flow and inundating process in a compound channel.

$h_p$ = water depth at peak of a flood

$h_b$ = water depth of steady uniform base flow

$g$ = gravitational acceleration

$t_p$ = peak time of model flood

$S_0$ = average slope of channel

- Another parameter called skewness parameter was proposed by Wang et al. (1997) and also recently used by Khuntia et al. (2018) which is given by

$$\eta = \frac{T_r}{T_f} \quad (5)$$

where $T_r$ and $T_f$ are the duration of time for rising and falling limbs

## 3. EXPERIMENTAL SETUP AND DESCRIPTION OF HYDROGRAPH RUNS

- The experiments were carried out in a 12m long, 0.6m wide and 0.6m deep recirculating, rectangular, tilting flume in the Hydraulics Laboratory of Civil Engineering department.
- For supplying water into the experimental channels, a large reinforced cement concrete (R.C.C) overhead tank was constructed on the upstream side of the flume inside the laboratory.
- A volumetric tank was built at the downstream end of the flume for measuring the discharge of each flow depth. A large underground sump located outside was used for maintaining continuous water supply to the overhead tank. A pump of 10 HP capacity was used to carry out the experiments, which also maintained the recirculation system of water.
- A stilling chamber fitted with an adjustable head gate and flow strengtheners are provided in the entrance region of the flume to maintain the flow uniform entering the channel.
- On the downstream side of the channel, an adjustable tailgate is fitted to control depth of flow and to maintain the uniformity of the flow throughout the length of the channel.
- An electromagnetic flow meter is fitted with inlet pipe at upstream to measure the flow discharges.
- A longitudinal slope ($S_0$) of approximately 1.2cm in 10m was set and kept unchanged throughout the experimental program. The picture of the experimental channel is shown in Fig 2.
- The unsteady flow was established in the channel by passing two hydrographs over the fixed rough bed.
- This was done by one cycle of experiments with two steps (i.e. for getting rising and falling limb of hydrograph). For rising limb, the flume pipe inlet valve was opened and the constant head tank was filled with water by the pump continuously. When water reaches the full height of the overhead tank, the motor was stopped.
- To make the falling limb of hydrograph, water was fully allowed to pass through the experimental channel up to the time when the constant head tank gets empty. But, in this case,

some amount of flow was still available in the channel which was fixed as the base flow. Geometry and roughness parameters of the experiment are given in table 1.

**Table 1.** Geometry and roughness parameters for this experiment

| Sl No | Item Description | Parameters |
|---|---|---|
| 1 | Channel type | Straight |
| 2 | Geometry of channel section | Rectangular |
| 3 | Channel base width ($b$) | 0.6m |
| 4 | Depth of channel | 0.6m |
| 5 | Bed Slope ($S_0$) | 0.0012 |
| 6 | Length of flume | 12m |
| 7 | Nature of surface bed | Dense rigid grass |
| 8 | Flow condition | Un-steady |
| 9 | Manning's $n$ of bed material | 0.0304 |

- Two hydrographs were made to pass over the channel and the discharges were measured with the help of flow meter fitted with the inlet pipe of the channel. The pictures of the flow meter and the display unit are shown in Fig 3.
- For the first hydrograph (Hydrograph-1), the inlet valve was opened full and for the second hydrograph (Hydrograph-2), the inlet valve was opened three rounds. (The valve takes 3.25 number of rounds to full open)
- The corresponding data for each variable was then ensemble-averaged and smoothened.



**Fig 2**: Photograph of the experimental channel

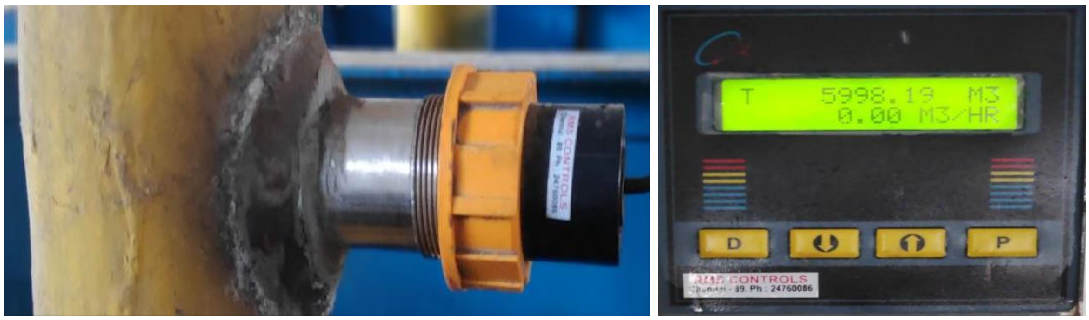



**Fig 3**: Photograph of Flow meter and display unit of flow meter




**Fig 4**: Photo of overhead tank

## 4 RESULTS AND DISCUSSIONS

### 4.1. Presentation of Hydrographs

Two hydrographs were investigated during the experimentation. The flow and depth hydrographs under unsteady flow run has shown in Fig. 5. The hysteresis effect of stage-discharge ($h \sim Q$) rating curve between rising and falling limbs is illustrated in Fig. 6.

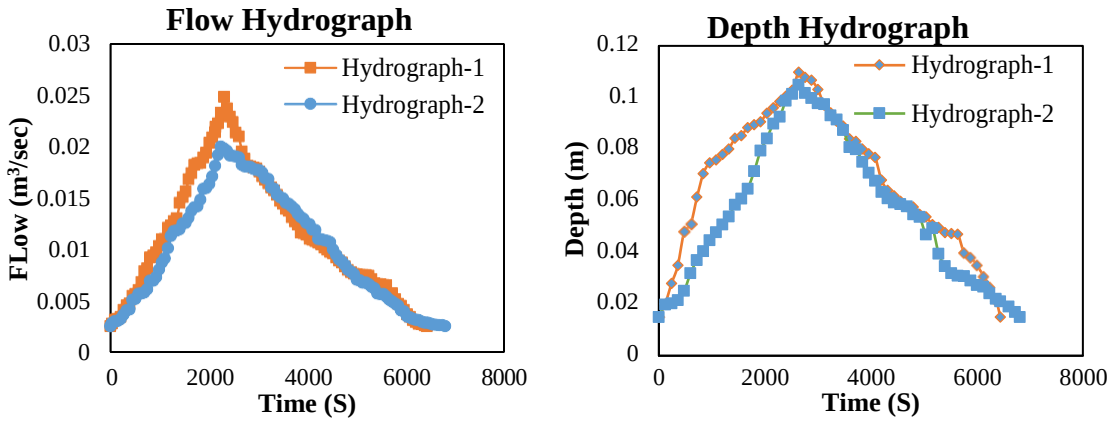



**Fig. 5.** Flow and Depth hydrographs for the present experiment

### 4.2. Hysteresis Effect

Fig. 6 represents the hysteresis effect observed in both the hydrographs.

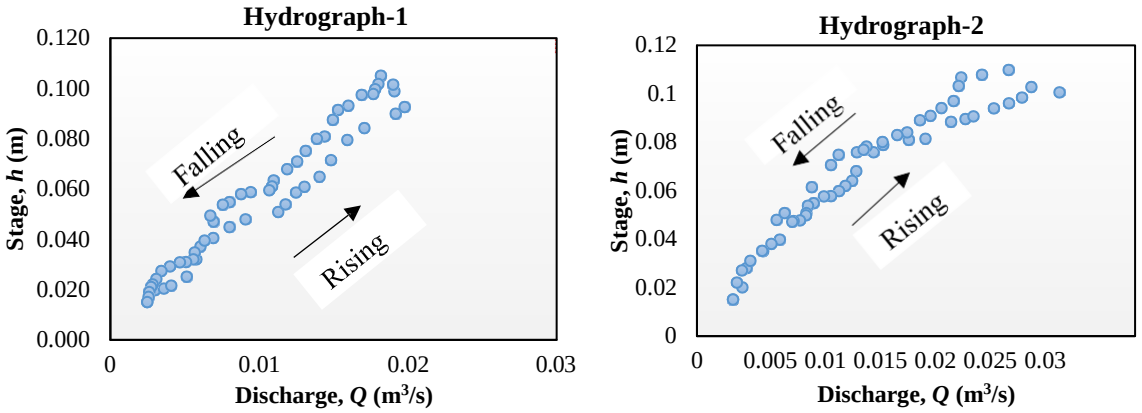



**Fig. 6.** Hysteresis effect in stage-discharge curve for present study

- To study more about the hysteresis effect in unsteady flow another data sets of Bombar (2016) has been considered and stage-velocity curves are presented in Fig. 7.

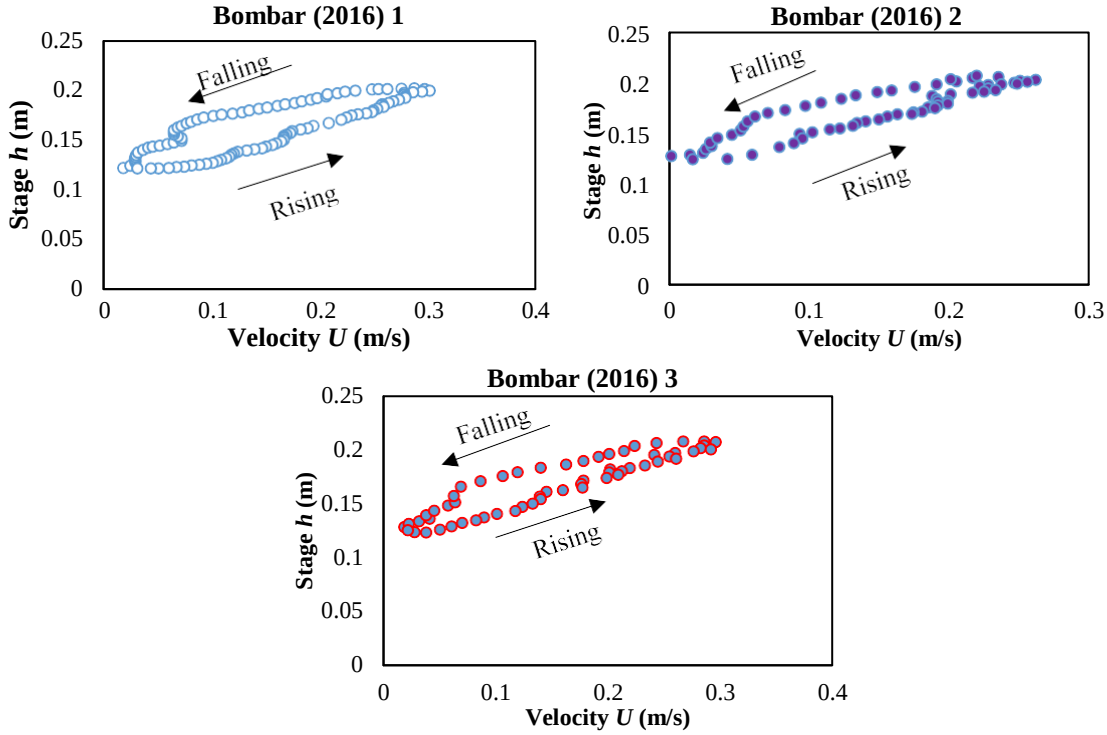



**Fig. 7.** Hysteresis effect in stage- velocity curve for Bombar (2016)

### 4.3. Unsteady flow parameters

In the present study, three unsteady flow parameters have been considered. A total of nine hydrographs were studied including the present hydrographs and data of other researchers. All the hydrograph properties are given in table 2.

**Table 2. Properties of hydrographs under different unsteady flow cases**

| Data Set | Base flow ($m^3/s$) | Peak Flow ($m^3/s$) | Water depth in | Water depth at | Time duration for rising | Time duration for falling |
|---|---|---|---|---|---|---|

| | | | base flow (m) | peak (m) | limb ($T_r$) (Sec) | limb($T_f$) (Sec) |
|---|---|---|---|---|---|---|
| Hydrograph-1 | 0.0025 | 0.02 | 0.015 | 0.11 | 2310 | 4130 |
| Hydrograph-2 | 0.0025 | 0.0248 | 0.015 | 0.105 | 2250 | 4560 |
| Khuntia et al. (2018) | 0.0025 | 0.028 | 0.015 | 0.114 | 2040 | 4440 |
| Bombar (2016) 1 | 0.00206 | 0.0388 | 0.1216 | 0.201 | 194 | 218 |
| Bombar (2016) 2 | 0.00206 | 0.0384 | 0.1216 | 0.2057 | 282 | 230 |
| Bombar (2016) 3 | 0.00206 | 0.0393 | 0.1216 | 0.208 | 553 | 210 |
| Tu and Graf (1993) | 0.0243 | 0.11868 | 0.1116 | 0.2298 | 48 | 59 |
| Song and Graf (1995)-1 | 0.05815 | 0.08924 | 0.1079 | 0.1364 | 65 | 66 |
| Song and Graf (1995)-2 | 0.04837 | 0.09235 | 0.1424 | 0.1859 | 29 | 51 |

The unsteady flow parameters $\alpha'$, $\lambda_{un}$, $\eta$ are calculated using equations 3, 4 and 5 and presented in table 3.

**Table 3. Values of unsteady flow parameters used**

| Data Set | $\alpha'$ | $\lambda_{un}$ | $\eta$ |
|---|---|---|---|
| Hydrograph-1 | 0.000126 | 0.03299 | 0.56 |
| Hydrograph-2 | 0.000134 | 0.03284 | 0.49 |
| Khuntia et al. (2018) | 0.000141 | 0.03824 | 0.46 |
| Bombar (2016) 1 | 0.002729 | 0.07286 | 0.89 |
| Bombar (2016) 2 | 0.00205 | 0.05248 | 1.23 |
| Bombar (2016) 3 | 0.001062 | 0.02734 | 2.63 |
| Song and Graf (1995)-1 | 0.000441 | 0.12634 | 0.98 |
| Song and Graf (1995)-2 | 0.002152 | 0.74050 | 0.57 |
| Tu and Graf (1993) | 0.004027 | 0.82004 | 0.82 |

### 4.4. Discussion

Bombar (2016) observed that the rising and falling limbs are close to each other for Exp3 in which the unsteadiness is small whereas for Exp1, the limbs become further apart, because of high unsteadiness (Fig.7). This distance between the limbs depends on the unsteadiness of the hydrograph as mentioned by Graf and Altınakar (1998). Same phenomenon was also observed in Fig. 6 for present cases as the rising limb and falling limbs were more nearer for Hydrograph-2 when compared to Hydrograph-1 however the unsteady parameter range ids 10 times lower from the Bombar (2016) results.

## REFERENCES

1. Abida, H., & Townsend, R. (1992). A numerical model for routing floods through compound channels. In *Hydrocomp' 92, Proceedings of the International Conference on Interaction of Computational Methods and Measurements in Hydraulics and Hydrology, Budapest, Hungary* (pp. 115-122).
2. Ahmadi, M. M., Ayyoubzadeh, S. A., Namin, M. M., & Samani, J. M. V. (2009). A 2D numerical depth-averaged model for unsteady flow in open channel bends. *Journal of Agricultural Science and Technology*, *11*(4), 457-468.
3. Bao, W., Zhou, J., Xiang, X., Jiang, P., & Bao, M. (2018). A hydraulic friction model for one-dimensional unsteady channel flows with experimental demonstration. *Water*, *10*(1), 43.
4. Becker, L., & Yeh, W. W. G. (1972). Identification of parameters in unsteady open channel flows. *Water Resources Research*, *8*(4), 956-965.
5. Bombar, G. (2016). Hysteresis and Shear Velocity in Unsteady Flows. *Journal of Applied Fluid Mechanics*, *9*(2).
6. Cunge, J. A., Holly, F. M., & Verwey, A. (1980). Practical aspects of computational river hydraulics.
7. Farhadi, H., Zahiri, A., Hashemi, M. R., & Esmaili, K. (2019). Incorporating a machine learning technique to improve open-channel flow computations. *Neural Computing and Applications*, *31*(3), 909-921.
8. French, R. H. (1985). Open-channel hydraulics. McGraw-Hili Inc., New York, N.Y.
9. Graf, W. H. and M. S. Altınakar (1998). Fluvial Hydraulics, John Wiley & Sons Inc.
10. Graf, W. H., & Qu, Z. (2004). Flood hydrographs in open channels. In *Proceedings of the Institution of Civil Engineers-Water Management* (Vol. 157, No. 1, pp. 45-52). Thomas Telford Ltd.
11. Hashemi, M. R., Abedini, M. J., & Malekzadeh, P. (2007). A differential quadrature analysis of unsteady open channel flow. *Applied Mathematical Modelling*, *31*(8), 1594- 1608.
12. Hu, J., Yang, S., & Fu, X. (2012). Experimental investigation on propagating characteristics of sinusoidal unsteady flow in open-channel with smooth bed. *Science China Technological Sciences*, *55*(7), 2028-2038.
13. Khatua, K. K., Patra, K. C., & Mohanty, P. K. (2011). Stage-discharge prediction for straight and smooth compound channels with wide floodplains. *Journal of hydraulic Engineering*, *138*(1), 93-99.
14. Khuntia, J. R., Devi, K., Proust, S., & Khatua, K. K. (2018). Depth-averaged velocity and bed shear stress in unsteady open channel flow over rough bed. In *E3S Web of Conferences* (Vol. 40, p. 05071). EDP Sciences.
15. Knight, D. W., & Demetriou, J. D. (1983). Flood plain and main channel flow interaction. *Journal of Hydraulic Engineering*, *109*(8), 1073-1092.
16. Knight, D. W., and Sellin, R. H. J. (1987). ‘‘The SERC flood channel facility.’’ J. Instn. Water and Envir. Mgmt., 1(2), 198–204.
17. Krishnappan, B. G., & Altinakar, M. S. (2006). Numerical Modeling of Unsteady Flows in Rivers. *Encyclopedia of Hydrological Sciences*.
18. Lai, C. J., Liu, C. L., & Lin, Y. Z. (2000). Experiments on flood-wave propagation in compound channel. Journal of Hydraulic Engineering, 126(7), 492-501.
19. Lee, K., Firoozfar, A. R., & Muste, M. (2017). Monitoring of unsteady open channel flows using the continuous slope-area method. *Hydrology and Earth System Sciences*, *21*(3), 1863-1874.

20. Majdalani, S., Chazarin, J. P., & Moussa, R. (2019). A New Water Level Measurement Method Combining Infrared Sensors and Floats for Applications on Laboratory Scale Channel under Unsteady Flow Regime. *Sensors*, *19*(7), 1511.
21. Mrokowska, M. M., Rowiński, P. M., & Kalinowska, M. B. (2015). Evaluation of friction velocity in unsteady flow experiments. *Journal of Hydraulic Research*, *53*(5), 659-669.
22. Nezu, I. (1991). Turbulent structure over dunes and its role on suspended sediments in steady and unsteady open-channel flows. In *Proc. of Int. Symp. on Transport of Suspended Sediments and its Mathematical Modeling* (pp. 165-189). IAHR.
23. Nezu, I., Kadota, A., & Nakagawa, H. (1997). Turbulent structure in unsteady depth-varying open-channel flows. Journal of Hydraulic Engineering, 123(9), 752-763.
24. Nezu, I., & Nakagawa, H. (1993). Turbulence in open-channel flows, IAHR monograph series. *AA Balkema, Rotterdam*, 1-281.
25. Retsinis, E., Daskalaki, E., & Papanicolaou, P. (2018). Hydraulic and Hydrologic Analysis of Unsteady Flow in Prismatic Open Channel. In *Multidisciplinary Digital Publishing Institute Proceedings* (Vol. 2, No. 11, p. 571).
26. Song, T. C., & Graf, W. H. (1996). Velocity and turbulence distribution in unsteady open- channel flows. *Journal of Hydraulic Engineering*, *122*(3), 141-154.
27. Stephenson, D., & Kolovopoulos, P. (1990). Effects of momentum transfer in compound channels. Journal of hydraulic engineering, 116(12), 1512-1522.
28. Takahashi, H. (1969). Theory of one-dimensional unsteady flows in a prismatic open channel. *Annu Dis Prev Res Inst Kyoto Univ Kyoto Japan B*, *12*, 515-527.
29. Tingsanchali, T., & Ackernann, N. L. (1976). Effects of overbank flow in flood computations. Journal of the Hydraulics Division, 102(ASCE# 1226).
30. TOMINAGA, A., NAGAO, M., MIO, N., & LIU, J. (1994). Hydraulic Characteristics of Flood Waves Passing Compound Channels. *PROCEEDINGS OF HYDRAULIC ENGINEERING*, *38*, 443-448.
31. Townsend, R. D. (1967). ‘‘An investigation of turbulence characteristics in a river model of complex cross-section.’’ *J. Inst. Civ. Engrs.*, London, 155–175.
32. Treske, A. (1980). *Experimentelle Überprüfung numerischer Berechnungsverfahren von Hochwasserwellen*. na.
33. Tu, H., Graf, W. H., & Tamai, N. (1993). Unsteady Open-Channel Flow-Its mean structure and suspended sediment load transport.
34. Venutelli, M. (2011). Analysis of dynamic wave model for unsteady flow in an open channel. Journal of Hydraulic Engineering, 137(9), 1072-1078.
35. Wang, L., Cuthbertson, A., Pender, G., & Zhong, D. (2019). Bed load sediment transport and morphological evolution in a degrading uniform sediment channel under unsteady flow hydrographs. *Water Resources Research*.
36. Wang, Z., Lin, B., & Nestmann, F. (1997). Prospects and new problems of sediment research. *Int. J. Sediment Res*, *12*(1), 1-15.
37. Wheaton, J. M., Brasington, J., Darby, S. E., Kasprak, A., Sear, D. and Vericat, D. (2013). Morphodynamic signatures of braiding mechanisms as expressed through change in sediment storage in a gravel-bed river. Journal of Geophysical Research, Earth Surface 118(2), pp. 759–779.
38. Woolhiser, D. A., & Liggett, J. A. (1967). Unsteady, one-dimensional flow over a plane- The rising hydrograph. *Water Resources Research*, *3*(3), 753-771.
39. Wormleaton, P. R., and Merrett, D. (1990). ‘‘An improved method of calculation of steady uniform flow in prismatic main/flood channel plain sections.’’ J. Hydr. Res., 28,157–174.
40. Yen, C. L. (1987). ‘‘Subsidence of peak flow in open channel with storage area.’’ J. Hydr. Res., 16(4), 309–326.

# Theme VII

# Coastal and Ocean Engineering

*IN PROCEEDINGS OF 25th HYDRO 2020, INTERNATIONAL CONFERENCE, NATIONAL INSTITUTE OF TECHNOLOGY ROURKELA, ODISHA, INDIA 26-28, March 2021, ISBN 978-93-90631-56-8*

Paper ID - 081

# NUMERICAL MODEL STUDIES TO ASSESS THE MORPHOLOGICAL CHANGES DUE TO COASTAL FRONT DEVELOPMENT- A CASE STUDY

B.Krishna[1] G.A.Rajkumar[2] Karthikeyan.M[3] L.R. Ranganath[4] J.D Agrawal[5]

[1]*Scientist B, Central Water and Power Research Station, Pune- 411 024, India*

[2] *Scientist B, Central Water and Power Research Station, Pune- 411 024, India*

[3]*Research Assistant, Central Water and Power Research Station, Pune- 411 024, India*

[4]*Scientist D, Central Water and Power Research Station, Pune- 411 024, India*

[5]*Scientist E, Central Water and Power Research Station, Pune- 411 024, India*

*Email: krishna07_boora@yahoo.co.in*

## Abstract

Modernization of ports and port-led development will lead to India's economic growth. The Industrial clusters and hinterland and efficient evacuation systems through road, rail, inland and coastal waterways resulting in Ports becoming the drivers of economic activity in coastal areas. Along the East Cost of India in Andhra Pradesh State series of passenger jetties are proposed under Sagarmala project to promote tourism in the state which in turn would generate revenue and employment. Safe berthing and maneuvering facilities for passenger cruise require proper alignment of jetty and approach channel. The sedimentation in and around the development area should be optimal so that the project is techno-economic viable and should be conducive to all weather operations. Optimization of layout of a harbour in an inlet on East Coast of India which is generally characterized by steep bed slopes, high magnitude of littoral drift and severe wave climate with rivers debouching sediments into Bay of Bengal, is an engineering challenge. The present paper describes a case study in which mathematical model studies was carried out by using MIKE 21 software to study hydrodynamics and morphological changes in the vicinity of proposed passenger jetty. The model limits considered for the studies about 2 km on either side of the Gostani River mouth at Bheemunipatnam and extended to a depth -21.0 m CD in the offshore. The study include simulation of hydrodynamics for different tidal conditions for the existing condition to calibrate with the field data and then the calibrated model is run for the proposed conditions to find out the changes in the hydrodynamics and morphology in and around the proposed passenger jetty.

***Keywords:*** *Hydrodynamics, Morphology, approach channel, Passenger jetty.*

## 1.0 Preamble

Indian government recognized the importance of water led development and launched its flagship programme of "Sagarmala" envisaging modernization of ports and development of coastlines which contribute India's growth. As a part of Sagarmala project, series of passenger jetties were proposed along the coast line of Andhra Pradesh to promote tourism in the state as shown in Fig.1.




**Figure 1** Locations under Sagarmala Scheme




**Figure 2** Location of Proposed Site

The present study describes the mathematical model studies carried out to evaluate the feasibility of a passenger jetty proposed to be developed at Bheemunipatnam coast of Andhra Pradesh for promotion of tourism (Fig. 2). Needless to say, before planning any waterfront development it is essential to understand the behavior of hydrodynamics and morphological changes in the proposed region which help in arriving at establishing the feasibility of the proposal and thereby facilitate the optimization of its design.

## 2.0 Introduction

Bheemunipatnam is a village in Visakhapatnam district of Andhra Pradesh located in North latitude of 17.9075˚ N and East longitudes of 83.4270˚ E and the beach is the place where Gostani River empties into Bay of Bengal. Bheemunipatnam is located 95 km towards west from District headquarters Vishakhapatnam. The proposed site is located inside the creek formed by the Gostani river debouching in the sea. The coast in this region is oriented along 40° N. At the Gostani river mouth, owing to various coastal processes there are island formations inside the river coarse and spit development at river - mouth along the shore providing a good tranquil region for the development of passenger jetty. The proposed location of jetty at Bheemunipatnam is shown in Fig. 3.

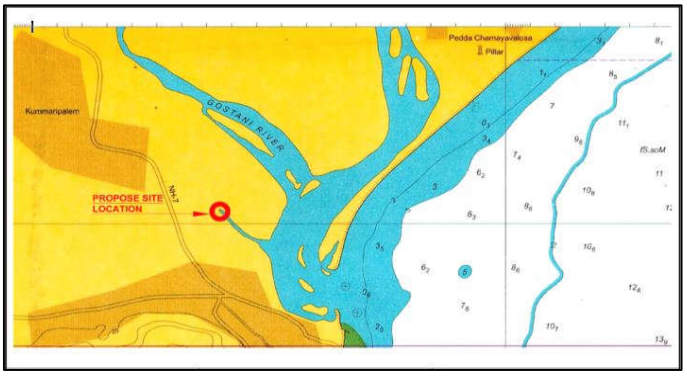



**Figure 3** Proposed Location of Jetty in Bheemunipatnam

## 3.0 Methodology

The 2-dimensional hydrodynamic model MIKE-21 with Flexible Mesh was used for simulating the flow field in the model area. The tidal hydrodynamics plays a major role in planning any developments in the coastal area. The simulation of the tidal hydrodynamics for different tidal conditions for the existing conditions would be carried out and is calibrated with the observed field data. The calibrated model then would be simulated to evaluate the tidal hydrodynamics for the proposed conditions. The changes in the flow field for proposed conditions would be evolved using these studies. The results of the hydrodynamic studies would then be coupled with the sand transport model to predict the sedimentation rates. Sediment transport is simulated considering both tide and wave induced currents. These studies help in evaluating the changes in the hydrodynamics and siltation aspects and predict the probable zone of siltation and erosion for the proposed conditions.

## 4.0 Data Analysis

The field data collected during December 2017 is used for carrying out the model studies. The locations of field data collection and field data collected are shown in Fig.4.

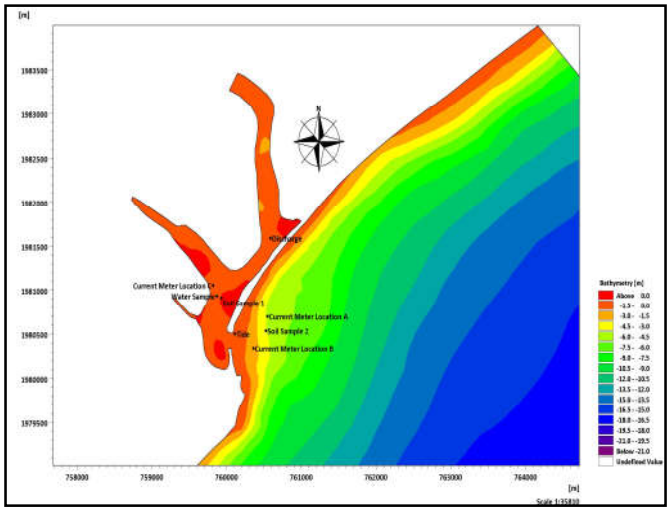


**Figure 4** Locations of Field data Collection

### 4.1 *Bathymetry*

The bathymetric data for the offshore region has been obtained from the C-MAP and Admiralty charts and the area specific bathymetry as supplied by the project authorities for the near shore region was used for preparation of bathymetry for computational model.

### 4.2 *Tide & Current*

The tides in the Bheemunipatnam region are of the semidiurnal type with diurnal inequality i.e. characterized by occurrence of two high and two low waters every day. There is marked inequality in the levels of the two low waters in a day. The water levels with respect to chart datum at Bheemunipatnam are as under:

**Table 1** Tide level w.r.t CD

| | |
|---|---|
| MHW Spring | + 1.70 |
| MHW Neap | + 1.30 |
| MSL | + 1. m |
| MLW Neap | + 0. 0 m |
| MLW Spring | + 0.30 |

The tidal data was collected from 04.12.2017 to 18.12.2017 covering both spring and neap tides. The tidal plot at the observed location is shown in Fig. 5.

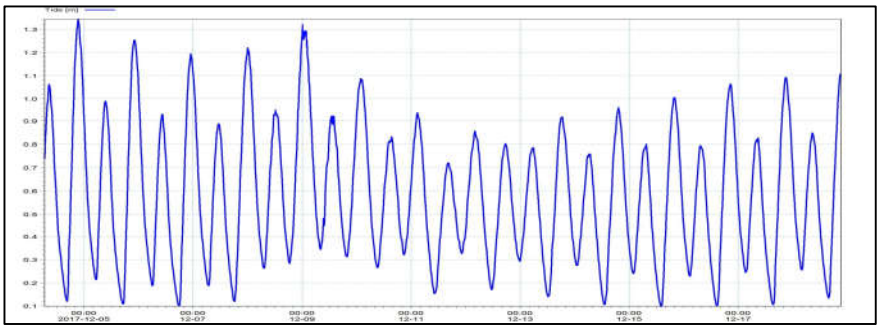


**Figure 5** Observed Tide at the Creek

Coastal currents along the east coast are unidirectional beyond 5 m depth contour, that the coastal currents near proposed site change the direction seasonally. From February to July, the currents are towards North and from August to January they are towards South. Even though the flow during flood and ebb are unidirectional in the offshore, the reversal of flows exists inside the creek during a tidal cycle. The model simulations were also carried out for both the seasons considering appropriate tidal flow directions.

A large volume of tidal flux gets exchanged in and out of creek during tidal cycle resulting in tide induced currents during flood and ebb tide. The velocity data has been simultaneously collected in tandem with the tidal data, at three locations viz., Point A (Offshore), Point B (Offshore) and Point C (inside creek) during the period from 04.12.2017 to 18.12.2017. The velocity plots for the above three locations showing the magnitude of the current is shown in Fig. 6.

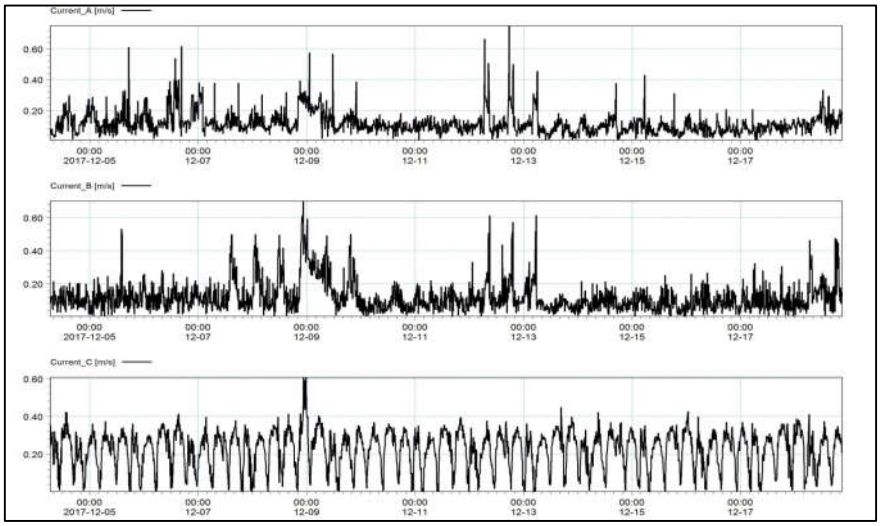



**Figure 6** Strength of the Current at Points A, B and C

### 4.3 *Sediment and Bed Sample*

Water samples were collected at one location inside the creek during the spring on 18.01.2018 and during neap tides on 25.01.2018 respectively. The silt charge is found to vary from 1000 mg/lit to 1350 mg/lit during the spring tide while it varied from 5400 mg/lit to 9500 mg/lit during the neap tide. In order to understand nature of the bed material, bed sample was collected at two locations viz., Point 1 (Creek) and Point 2 (Offshore- Near Mouth) were analyzed for grain size distribution. The particle size distribution is shown in below table and its analysis for the two locations is indicated in Fig. 7. The $D_{50}$ for the locations for Point 1 and Point 2 has been found to be 0.18 mm and 0.14 mm respectively.

**Table 2** Particle Size Distribution

| S. No. | Location | Particle Size Distribution % | | | | | |
|---|---|---|---|---|---|---|---|
| | | Clay | Silt | Sand | | | Gravel |
| | | | | Fine | Medium | Coarse | |
| 1 | Point 1 | 0.3 | 3.6 | 83.7 | 13.1 | 0 | 0 |
| 2 | Point 2 | 0.5 | 3.3 | 83.2 | 12.9 | 0 | 0 |

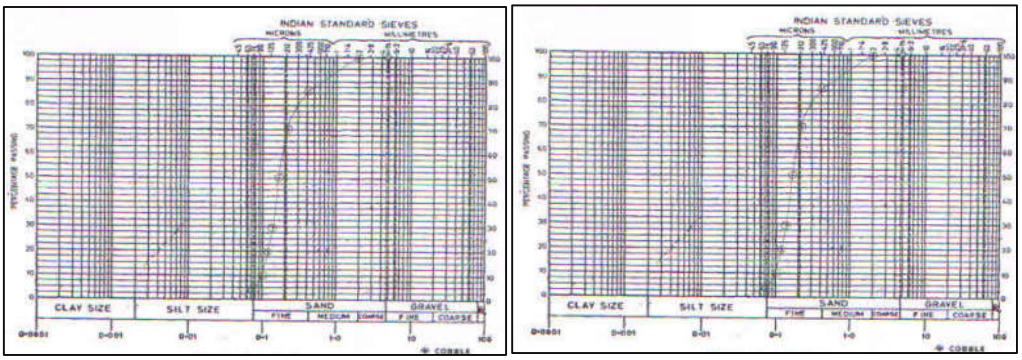



**Figure 7** Particle Size Distribution for Point 1 and Point 2

## 5.0 Mathematical Model – Existing Condition

The mathematical model domain developed and considered for the present studies extends 2 kms on either side of the river mouth and is extended to a depth of about -21.0 m CD in the offshore which is about 7 km from the shore. The total model domain covers an extent of an area of about 4 km x 8 km. The area of interest i.e. in the creek, near the proposed site and considerable area extending on either side of the mouth of the creek has been fine meshed for carrying out the studies and visualizing the results more comprehensively, while the offshore domain has been discretised into coarser mesh. The entire model domain has been discretised into about 3219 elements and 1816 nodes. The bathymetry for the model domain obtained from the field survey, CMAP and the Admiralty charts has been interpolated with the mesh generated. The bathymetry so generated for the existing conditions of the model domain is shown in Fig. 8 and the grid superimposed on the bathymetry is shown in Fig. 9.

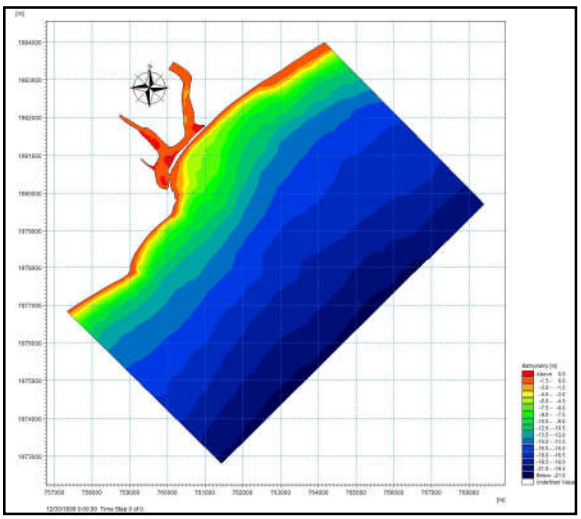


**Figure 8** Bathymetry for the Model Domain (Existing condition)

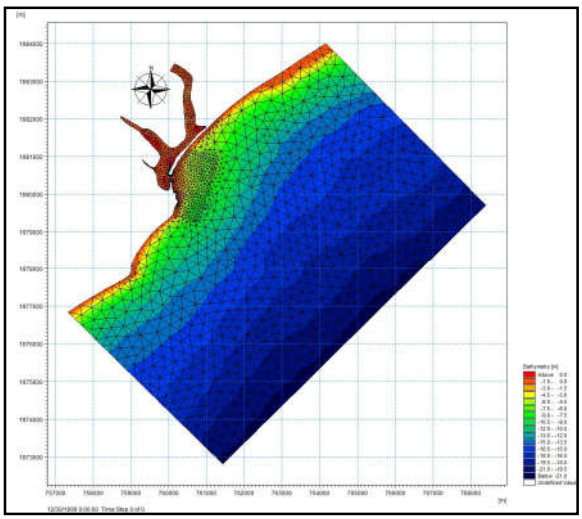


**Figure 9** Bathymetry with Mesh for the Model (Existing condition)

### 5.1 *Simulation of Flow Field for Existing Condition*

Fig. 10 shows the bathymetry and the boundary conditions considered for the flow simulations for the existing conditions of the model domain. It could be seen that there are three open boundaries AB, CD and EF where flow conditions are required to be defined. The AB, and EF represent Northern and Southern model boundaries in the offshore region respectively while the boundary CD represents the

model boundary truncated in the Gostani river in the creek. The Boundary FA has been assumed to be parallel to the flow and treated as boundary with no cross flow.

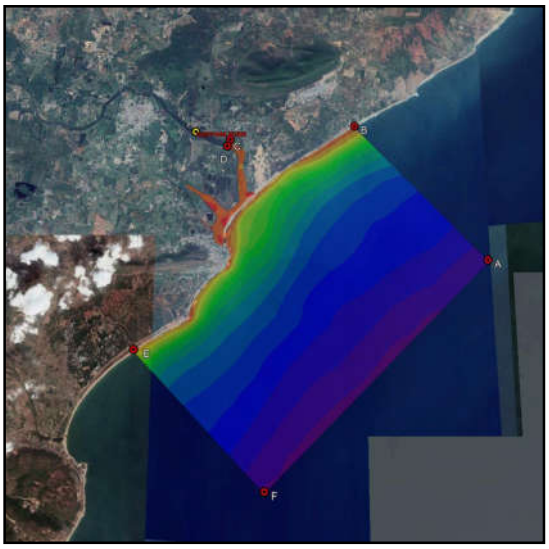


**Figure 10** Boundary Conditions for the Model Domain

The simulations were carried out for number of tidal cycles to generate hourly variations in the flow conditions during the tidal cycle for both the flow conditions viz., Northward and Southward flow directions. The flow conditions for the existing conditions during peak ebb and peak flood for Spring tide for Southward flow directions are shown in Fig. 11 and Fig. 12 respectively.

It could be seen that the flow is unidirectional in the offshore, both during flood and ebb, during above flow conditions. The length of the vector shows the magnitude of velocity while the arrowhead shows the direction of flow. From the above figures it can be observed that the flow is generally parallel to the coast line.

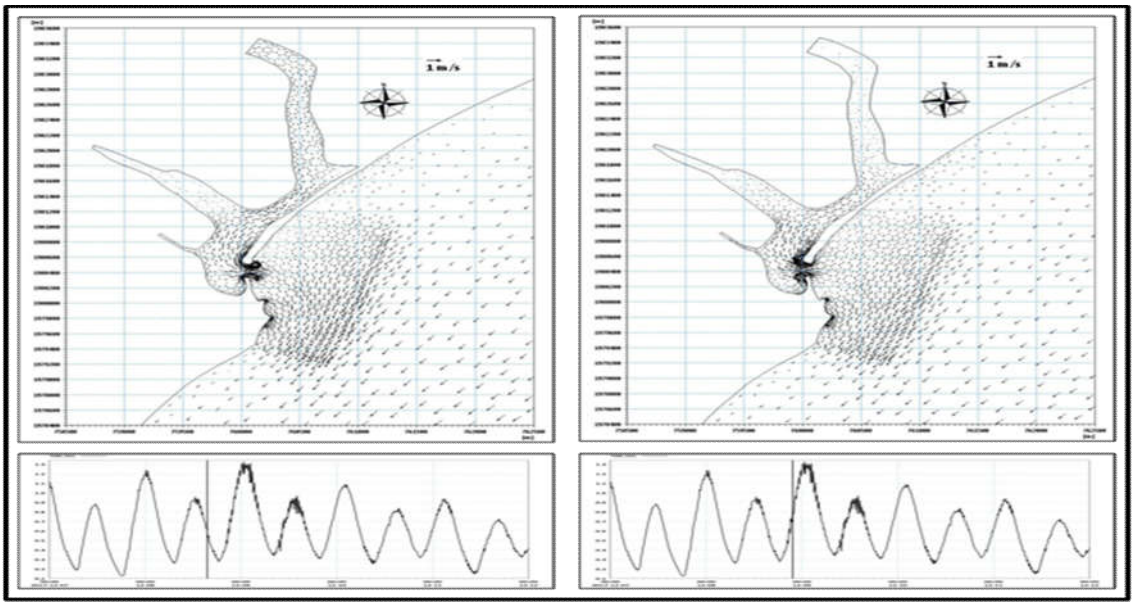


**Figure 11** Flow field in Existing Condition- Southward flow (Peak Ebb and Peak Flood)

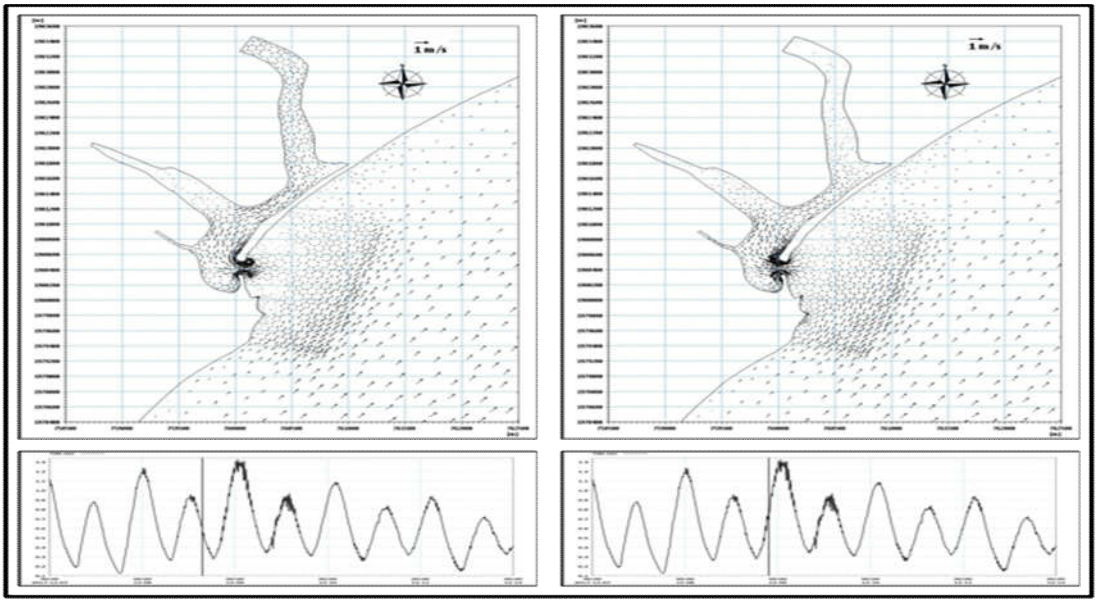


**Figure 12** Flow field in Existing Condition- Northward flow (Peak Ebb and Peak Flood)

However, the currents in the creek are basically tide induced with reversal of flow during flood and ebb phase of the tide. During the flood phase of the tide, the sea water will enter the creek from the sea while during the ebb phase, the water from the creek will return to the sea along with the discharge available in the river. The model thus simulated is calibrated for predicted velocities by the model with the observed field data at site. The comparison of currents is shown in Fig.13.

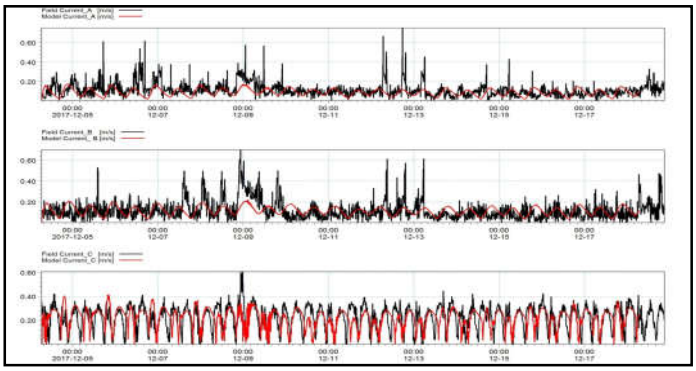


**Figure 13** Comparison of Currents (Field Vs. Model)

From the figures it can be seen that observed (field data) and computed velocities as well as water levels compare well. Thus, it can be inferred that the model is well calibrated with respect to water levels and velocities for the study area under consideration.

### 5.2 *Sediment Transport Model – Existing Condition*

Silt/sediment is being carried by tidal currents and the strength of this current at any instant in space and time is responsible for siltation in coastal creeks. The morphology study was carried out using MIKE 21 ST Module The above calibrated hydrodynamics model coupled with the sediment module will be run to evaluate the probable siltation in the model domain. The sediment model requires suspended sediment concentrations that are prevalent at the site. The water samples have been collected during the field data collection and were analyzed for suspended sediment concentrations as already discussed in the earlier paragraphs has been used in the model to simulate the silt model. The

Visakhapatnam Coast is subjected to the vagaries of two monsoons viz., South-West (SW) Monsoon during June to October and North-East (NE) monsoon from November to February. The period from March to May is considered as pre-monsoon. The sediment model after simulation gives deposition rates at different locations in the model domain. Fig. 14 show the sediment deposition pattern in the model domain as well as in the creeks, as obtained from the silt model for southward and northward flow conditions respectively.

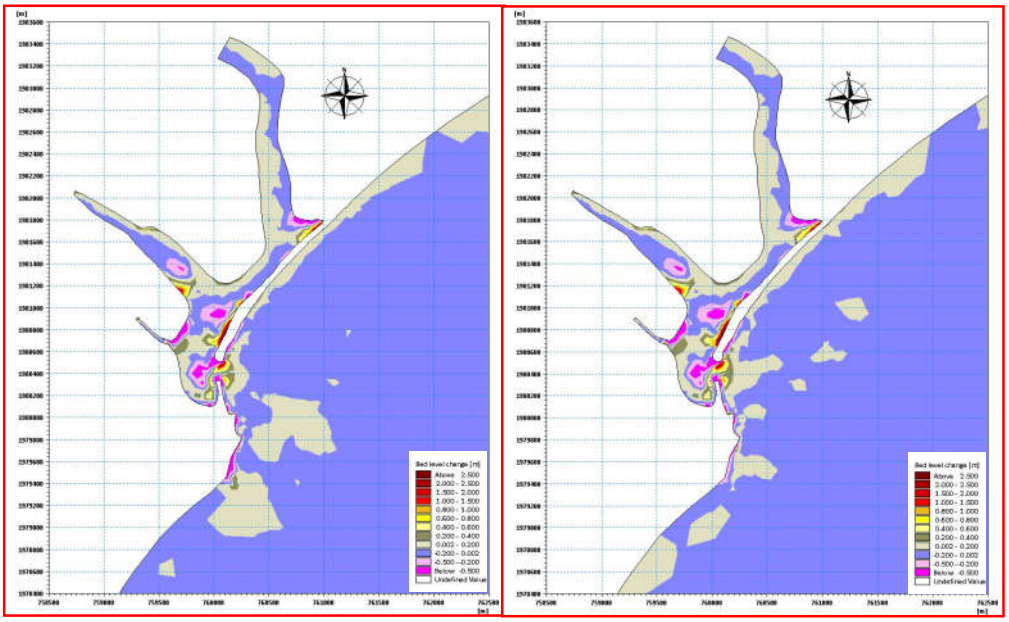


**Figure 14** Sedimentation Pattern in Existing Condition (Southward flow and Northward Flow)

## 6.0 Mathematical Model – Proposed Condition

The model calibrated for existing conditions is used for evaluating the hydrodynamics and siltation aspects by incorporating the proposed conditions. The proposal consists of approach channel with a width of 100m and depth of 5.0m below CD extending into offshore up to -5.0m contour along with a turning circle of 200 m diameter dredged to 5.5 m below CD with Northern, Southern sand traps which are incorporated in the model. The bathymetry of the domain for the proposed condition is shown in Fig.15. The model was then discretised with finite element mesh and bathymetry interpolated with the mesh.

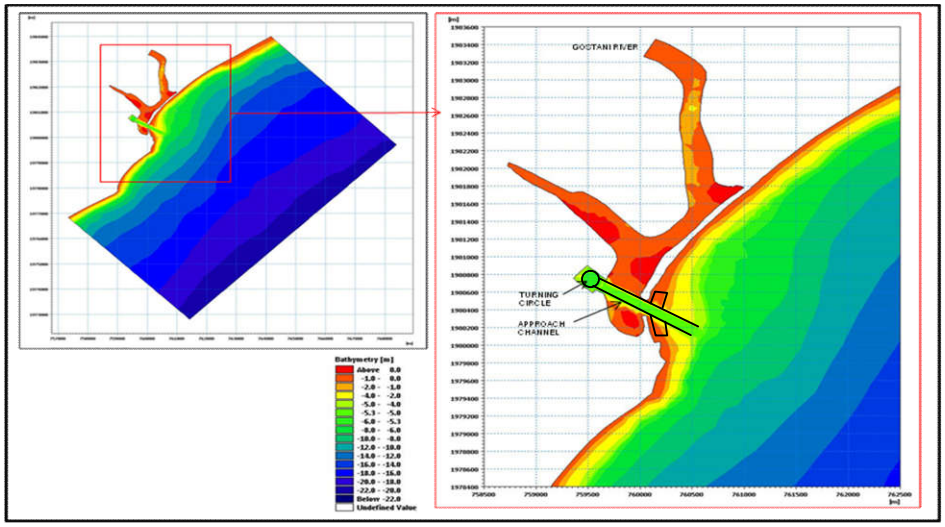



**Figure 15** Bathymetry of the Mathematical Model Domain-Proposed Condition

### 6.1 *Simulation of flow field for Proposed conditions*

The model thus calibrated for existing conditions is used for evaluating the hydrodynamics and siltation aspects by incorporating the proposed conditions. The drawing showing layout of the proposed facilities indicating the approach channel, turning circle and sand traps is at Fig. 16.

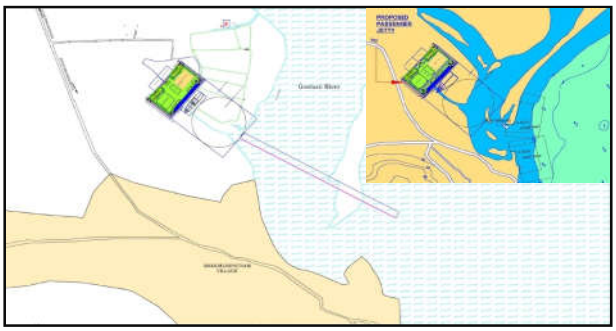


**Figure 16** Proposed Layout at Bheemunipatnam for APTDC

The simulations were carried out for number of tidal cycles to generate hourly variations in the flow conditions during the tidal cycle for both the flow conditions viz., Northward and Southward flow directions. The flow conditions for the proposed conditions during peak ebb and flood for Spring tide for Southward and Northward flow directions are shown in Fig. 17 and Fig. 18 respectively.

Due to the proposed development there is significant change in the velocities in the turning circle and approach channel leading from the jetty to the mouth of the creek, as compared to existing conditions, owing to deepening of the channel below its existing regime depth. The velocities in channel near to turning circle witnessed reduction in velocities as compared to existing conditions. This reduction in velocities will result in increase in sedimentation in these pockets/ areas. The velocities in the sand trap locations and in the offshore indicate a considerable drop in velocities as compared to existing conditions indicating probable deposition of sediments in these areas. Same trend is observed for the northward flow also.

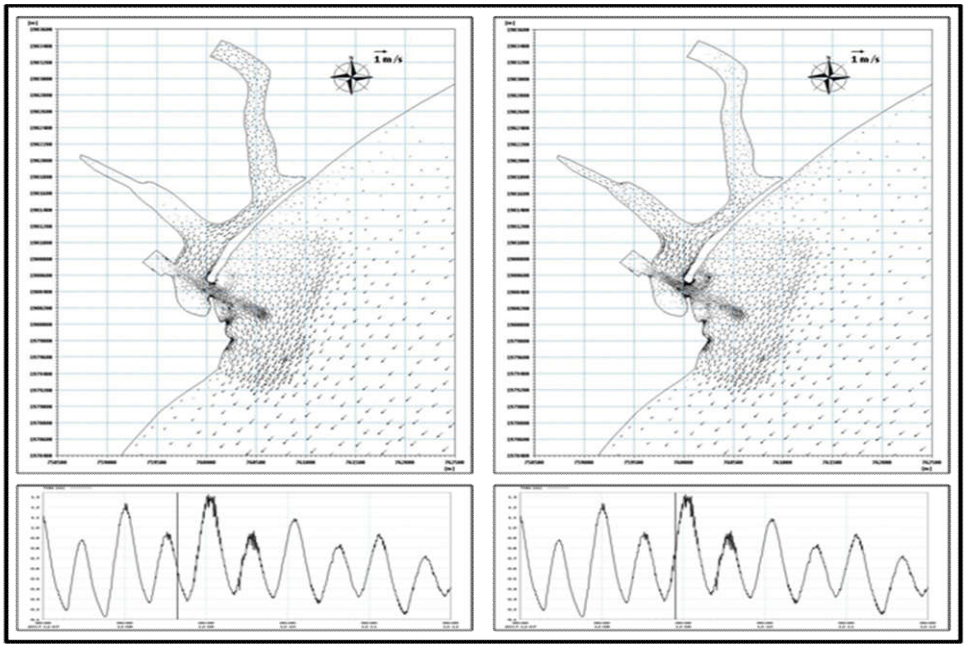


**Figure 17** Flow field in Proposed Condition- Southward flow (Peak Ebb and Peak Flood)

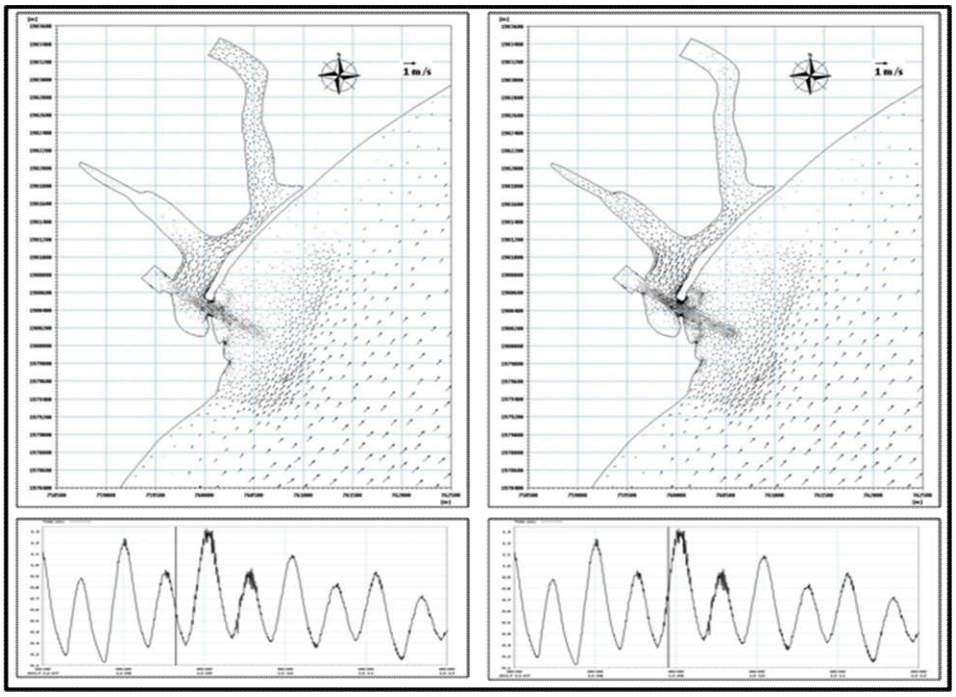


**Figure 18** Flow field in Proposed Condition- Northward flow (Peak Ebb and Peak Flood)

### 6.2 *Sediment Transport Model – Proposed Condition*

The sediment model was then run for proposed conditions for southward and northward flow directions. Fig.19 shows the sediment deposition pattern in the model domain as well as in the creeks, as obtained from the silt model.

From the results it is quite evident that there is increased deposition of sand in the approach channel and turning circle during southern flow conditions as compared to northern flow conditions which is primarily due to huge freshet discharge during monsoon carrying considerable sediments during the southern flow conditions and also due to reduction in velocities due to deepening of the channel and turning circle.

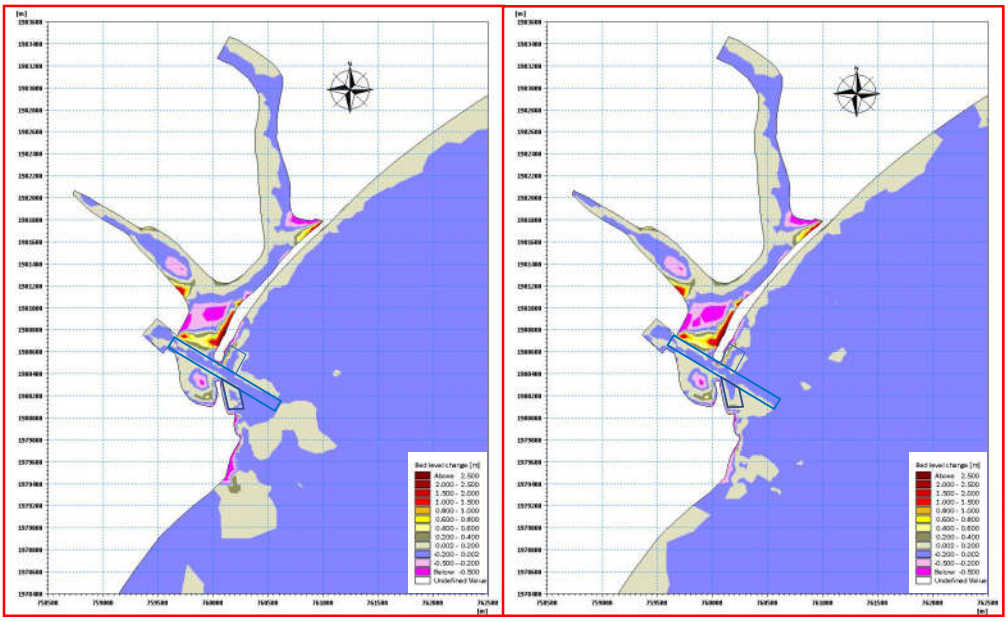


**Figure19** Sedimentation Pattern in Proposed Condition (Southward flow and Northward Flow)

The results of Sand transport model show that the sand traps are significantly effective in arresting the sediments in the approach channel and turning circles. It is observed that there is deposition of sand to the extent of 3000 $m^3$ and 10000 $m^3$ per annum in the turning circle and approach channel respectively. The sand traps located at Northern and Southern side of the mouth of the creek experience a deposition of 100000 $m^3$ and 120000 $m^3$ annually.

## 7.0 Conclusions

From the model studies it is observed that for the existing conditions the velocities are comparatively weak in the creek ranging from 0.1 to 0.3 m/s when compared to at the entrance of the mouth of the creek where it is of the order of 0.6 m/s. The velocities are of the range of 0.3 to 0.4 m/s in the offshore region. Due to the proposed developments the velocities in the turning circle and approach channel leading from the jetty to the mouth of the creek, there is significant change in the velocities as compared to existing conditions owing to deepening of the channel below its existing regime depth. For the existing conditions the sand transport model predicts deposition inside the creek area which can be attributed to weak strength of the currents and for the proposed conditions it is quite evident that the sand traps are significantly effective in arresting the sedimentation in the approach channel and turning circle. It is observed that there is deposition of sand to the extent of 3000 $m^3$ and 10000 $m^3$ per annum in the turning circle and approach channel respectively with the sand traps. The sand traps located at Northern and southern side of the mouth of the creek experience a deposition of 100000 $m^3$ and 120000 $m^3$ annually. Siltation is continuous process it is suggested that the periodical maintenance dredging is required to be carried out at regular intervals to maintain the required depths in the approach channel and turning circle. Mathematical model when complemented with the appropriate field data will be an efficient tool, to carry out studies for evaluating the changes in the hydrodynamics and siltation aspects for various proposals and renders an excellent platform for predicting the siltation rates effectively.

## Acknowledgement

Authors acknowledge the support, encouragement and facilities provided by the Director, CWPRS for publishing this paper.

## Reference

1) A Technical Report No.5673 on Mathematical Model Studies for hydrodynamics and siltation for development of Jetty at Bheemunipatnam for APTDC.
2) A Technical Report No. 5738 on Mathematical Model Studies for Assessment of Wave Tranquility and shoreline Changes for the development of jetty at Bheemunipatnam for APTDC.

*IN PROCEEDINGS OF 25th HYDRO 2020, INTERNATIONAL CONFERENCE, NATIONAL INSTITUTE OF TECHNOLOGY ROURKELA, ODISHA, INDIA 26-28, March 2021, ISBN 978-93-90631-56-8*

Paper ID - 184

# Historical and Future Sea Level Rise at Major Indian Ports

Priyen Somaiya[1] Raghavendra G Patil[2] M C Deo[3]

*Department of Civil Engineering, Indian Institute of Technology Bombay*

[1]193040058@iitb.ac.in [2]patilraghu23@gmail.com [3]mcdeo@civil.iitb.ac.in

## Abstract

Considering that India has a large port infrastructure spread across its 7000 km of coastline it becomes necessary to estimate the sea level rise (SLR) likely to be impacted by the effect of climate change at its major port locations. Although a good number of studies assessing historical India-specific data exist, those comparing them with rigorous future projections from the general circulation models are few in number and owing to various uncertainties in the predictions involved they need further confirmation. This study is aimed in this direction and it provides an evaluation of SLR at 11 major Indian ports as per historical tide gauge observations as well as from satellite-based measurements. Such SLR estimates are further compared with SLR values projected into the future and up to the end of the present century as per a medium global warming scenario called representative concentration pathway (RCP) – 4.5. The projected SLR data are based on an existing algorithm that scales the global SLR with the local one empirically. The results show that the recently collected satellite data are indicative of an accelerated growth of SLR than the one estimated from the past long-term tide gauge data; however, both these rates are likely to be much exceeded in future and could go beyond 5 mm/year at some major ports.

***Keywords:*** *Sea Level Rise; Climate Change; Major Ports*

## 1. Introduction

One of the major impacts of global warming on oceans and at the coasts is the change in global as well as regional mean sea level (MSL). At regional or local scale such change can affect planning of the entire coastal infrastructure including coastal defense and harbor operations. As the MSL rises, additional land area gets flooded, wave attack becomes stronger, salinity ingress into the land increases, plants and animal habitats get displaced, and harbor operations are hindered. Further, tidal currents can become stronger and tidal asymmetry can increase (Wachler et al., 2020).

The sea level rise (SLR) could be of global or regional type (in 100 km scale) or local type (in 10 km scale). The SLR has both spatial and temporal variations. The MSL's are routinely recorded over the world through instruments of tide gauge and radar altimeter aboard satellites. These can also be estimated from dynamic ice flow models or from climate models. An averaged value of all these records yields global mean sea level (GMSL). The sea level change can be of 'steric' type resulting from thermal and salinity changes, of 'eustatic' type caused by land-based ice melting and resulting additional volume of water or of 'isostatic' type arising out of the rebound of earth's surface that was earlier under ice in the ice age.

The human induced or anthropogenic greenhouse gas emissions produce excess heat in the climate system out of which about 90% is absorbed in the oceans while remaining 10 % is spent in warming the land and atmosphere which in turn results in melting ice on land and on sea (Church et al. 2011b; 2013). The heat absorption in the ocean significantly enhances the upper ocean heat content due to which surface water undergoes thermal expansion. The long-term changes in MSL and consequent SLR have been studied since last several decades over the world and also along the Indian seas. The global trend in SLR however is not be same as the regional one and the deviations can be very significant at many places (Church et al., 2013). Hence regional or local level evaluations of SLR are important.

There are many reasons for the spatial changes in SLR. An important contributor in this regard is Glacial Isostatic Adjustment (GIA). The GIA indicates the still rebounding and deforming part of the solid earth

that was once under heavy loads of ice during the ice age. This is accompanied by change in earth's rotation and gravitational field and along with water redistribution it further causes spatial SLR patterns (Mitrovica et al., 2011). Spatial SLR variations are also caused by thermal and salinity changes. Such changes are more in warmer regions which absorb more heat since as the latter depends on the temperature itself (Saenko et al., 2015). The regional SLR can be expected to differ by an amount of the order of 30 % than the GMSL because of the regional ocean processes including land subsidence and thermal expansions as per Oppenheimer et al., (2019). Of recent origin, the high amount of water consumption due to increasing agricultural, industrial and domestic usage have caused high regional rise, although storage of land water through dam construction and resulting reduction in flow of fresh water into the oceans had earlier seen to reduce the SLR to some extent. (Wada et al. 2017). Added to this are variations in the land water storage because of weather phenomena of El-Nino Southern Oscillation (ENSO) (Fasullo et al.,2013).

The studies on historical as well as future SLR at oceanic as well as regional and local levels for India have been carried out since late 1980's and starting from an initial work of Emery and Aubrey, (1989) they continue to the recent ones of Kundu et al. (2014), Unnikrishnan et al.(2015), Ramachandran et al. (2017),Black et al. (2017) and Krishnan et al.(2020). The past tide gauge data analysis by some investigators shows that the SLR in Indian Ocean (rather than at the port locations) was in between 1.06 mm/year to 1.75 mm/year during 1874 to 2004 and consistent with the global SLR spanning the years 1880 to 2009. Some of the past investigators have reported that the altimeter data since 1992 estimated SLR of the order of 3.28 mm/year in the Indian Ocean, again consistent with the Global MSL change. (Unnikrishnan et al., 2006, Unnikrishnan and Shankar, 2007, Church and White, 2011).

Recently, Patil and Deo (2019; 2020) evaluated futuristic SLR along major ports of India using medium and most severe warming scenario. These studies used tide gauge and general circulation model (GCM) data to obtain past and future SLR. The present work goes beyond these studies and looks at the tide gauge-based and GCM projections of SLR in light of historical satellite altimeter data. Thus, the aim of this work is to determine SLR at major Indian ports through tide gauge, altimeter as well as futuristic GCM data.

## 2. The Methodology

### *2.1 The data used*

This study employs three types of data, namely, tide gauge and satellite for past periods and GCM based data for the future time period at 11 major port locations around the Indian coastline. Figure1 shows the locations of these ports. Out of these sites, the ports of Kandla, Mumbai, Mormugao, Mangalore and Cochin are sited along the west coast while those of Tuticorin, Chennai, Vizag, Paradip and Haldia lay along the east coast of the Indian peninsula. The remaining Port Blair is in Bay of Bengal and off the east coast. Two additional major ports of Jawaharlal Nehru and Ennore could not be considered separately as required data were not available there. However, these ports are very close to Mumbai and Chennai respectively and can be considered to share similar SLR information.

The data bank of Permanent Service for Mean Sea Level (PSMSL, 2020a, 2020b), contributed by tide gauge authorities over the world is used here (https://www.psmsl.org/data/obtaining/). It gives monthly and annual averages at around 2000 locations distributed over the entire world. These measurements are relative to a land bench mark. To this, vertical land movements known either from global positioning system (GPS) measurements or from modeling have to be added to get the absolute values. The received data are first subjected to initial quality checks, forming so called Metric Data. These are then bench-marked with local land, forming revised local reference (RLR) data for subsequent applications. Such bench-mark is arbitrarily taken as 7 m below the MSL. (Woodworth and Player, 2003). For the purpose of knowing the long-term trends at least 40-year long record was recommended by Douglas (2001).

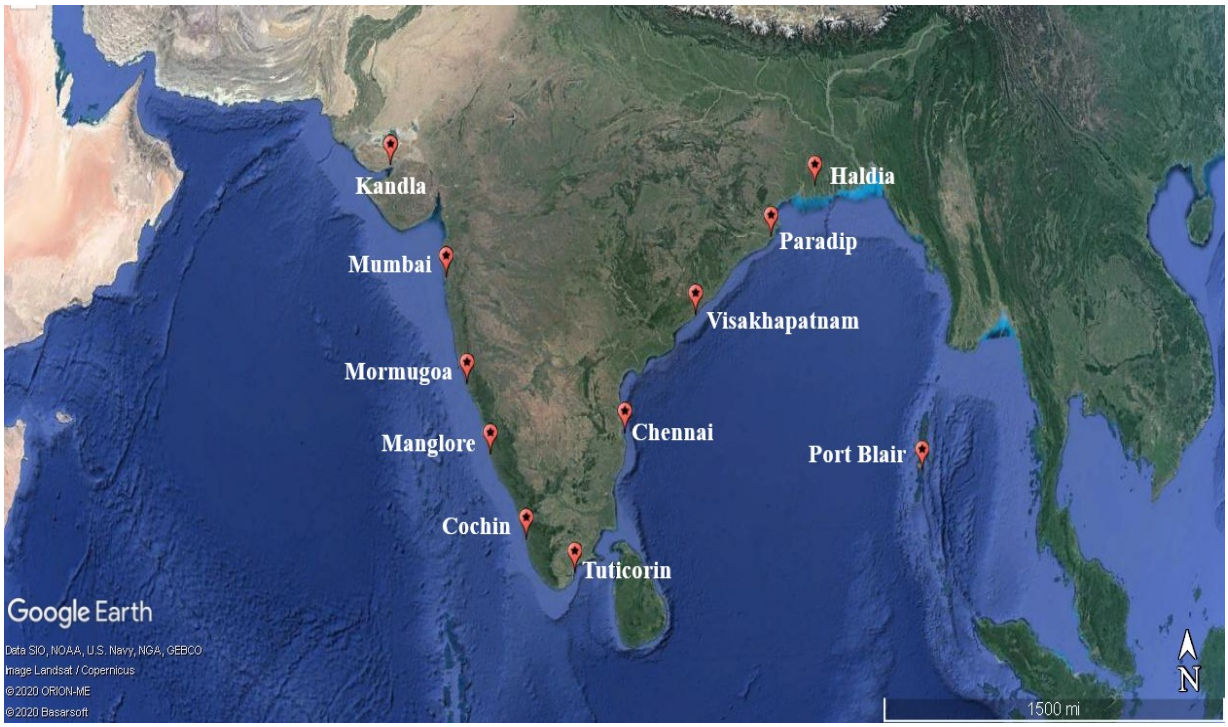



**Figure 1** Location of Indian Major Ports (Image Landsat/Copernicus © 2020 ORION-ME)

The earlier tide gauges were of mechanical recording type while the present ones are electronic - either of pressure gauge or of radar gauge types. The pressure sensors measure height of water column through pressure measurements which are converted into the depth of water using the hydrostatic relationship. The radar gauge works on the principle of travel time difference of radio pulses sent from an aircraft. The measurements are filtered for waves and tides to get MSL. PSMSL includes 27 Indian sites but only 6 have more than 40 years data.

As against the above tide gauge data the satellite data started flowing in since 1992, initially from TOPEX/Poseidon and later from Jason -1. -2 and -3. Satellites send a radio pulse to ocean surface from where it returns and by knowing the travel time difference the distance of the water surface from the satellite can be calculated. At the same time the distance of the satellite from the geoid surface (or hypothetical surface of earth's gravity) is also sensed and the difference between these two distances gives the sea level from the geoid surface (Acker et al. 2014). These data used herein are in the form of monthly averages given at the spatial resolution of 1°x 1°and over the period of January 1993 to March, 2018. The MSL data sets are available with Glacial Isostatic Adjustment (GIA), Inverse Barometric (IB) and seasonal (annual/ semi-annual) corrections. The GIA causes small but systematic contribution to altimetry estimates and they are typically in the range of -0.15 mm/year to 0.50 mm/year (Tamisiea, 2011). In this study the MSL data corrected for GIA, IB and seasonal variations are used.

Apart from the above-mentioned historical information, the futuristic data of MSL generated from GCMs are used. There are a large number of GCMs developed by researchers from all over the world. Each model essentially encapsulates the climate system into differential equations representing conservation of mass, momentum, energy and some other laws, and solves them using numerical methods with appropriate initial and boundary conditions. However, the use of a different sub-process modeling, their parameterization technique, initial and boundary conditions, together with use of alternative modeling parameters, numerical schemes and observational assimilation data gives varying outcome of climate parameters. Hence certain type of averaging of all GCMs, like simple or weighted or quantile-based, is required.

In this work we have used the proprietary SimCLIM algorithm and data base in which a median quantile of 28 GCMs was used as it avoids too small or two high values. (Krishnamurti et al., 2013).

Further, the GCM data of low resolution needs to be brought down to regional high-resolution level by downscaling – either process based or data driven. Instead, in the SimCLIM algorithm a special pattern matching technique is used in which the local level MSL anomaly, or the difference between the future (2080-2100) and past (1986-2005) time slices, is tagged with the corresponding global level difference. Thus, for any given latitude and longitude, the monthly sea level anomaly from its long-term mean, *SL*, is calculated as:

$$Z = \frac{(Z_{2090} - Z_{1995}) + \Delta GSLR}{\Delta GSLR} \quad (1)$$

Where, $Z_{2090}$ = local mean anomaly during 2080-2100, $Z_{1995}$ = local mean anomaly during 1986-2005 as per local past data; $\Delta GSLR$ = (global mean anomaly during 2080-2100) – (global mean anomaly during 1986-2005).

## *2.2 Data analysis*

### *2.2.1 SLR using tide gauge data*

The available tide gauge data of varying durations as seen in the first two columns of Table 1 were downloaded from the PSMSL website (https://www.psmsl.org/data/obtaining/). The third column of this Table shows the completeness of the data and as can be seen, most of the locations had good data recovery. A linear regression was fitted to these data in excel base and SLR rate was determined (column 4). To this value, the GIA and VLM corrections (columns 5 and 6) at each location were added. It can be seen that GIA correction was much smaller than the VLM changes and that at all sites the VLM was positive or that the land was raising. The GIA and VLM corrected SLR is given in the last column. From this it can be noticed that the Chennai port area exhibits a falling trend (most probably due to the highest VLM) while all others show a rising one. The maximum rate of 1.91 mm/year was seen at Haldia port. These rates were found to match (within 95 % confidence level) with NOAA's SLR rates (https://tidesandcurrents.noaa.gov/sltrends/ sltrends_global_country.html?gid=1269). The maximum rate is seen at Haldia while the minimum one was observed at Chennai.

In the past, Unnikrishnan and Shankar (2007) had analyzed the tide gauge data at several stations located in the northern part of the Indian Ocean and noted consistency in the trends of station specific records with the global ones. The corrected SLR for Arabian Sea and Bay of Bengal were within 1 to 2 mm/year in comparison with the global SLR after correcting it with modeled values of GIA. At Mumbai and Vizag, the average SLR was noticed by them as 1.29 mm/year varying in between 1.06 mm/year to1.75 mm/year. Shankar and Shetye (1999, 2001) had reported considerable inter-annual and decadal variability among the northern IndianOcean data due to large scale wind and salinity variations and further, Shankar (2000) observed that the SLR variability was changing from east to west coast due to salinity and seasonal differences. Chowdhury and Behera (2015) analyzed tide gauge and satellite data at some Indian coastal stations and found large variations in the estimates of the trend of MSL at local and regional/global scales.

**Table 1** SLR rate from tide gauges (Note: The GIA corrections were obtained from Peltier GIA data sets from https://www.psmsl.org/train_and_info/geo_signals/gia/peltier/)

| (1) | (2) | (3) | (4) | (5) | (6) | (7) |
|---|---|---|---|---|---|---|
| Location | Time period of data | Completeness of data in % | Relative SLR rate in mm/year | GIA correction | VLM correction | SLR corrected mm/year |
| Kandla | 1950-2015 | 79 | 1.809 | 0.461 | 1.39 | 0.88 |
| Mumbai | 78-2015 | 89 | 0.834 | 0.348 | 1.11 | 0.072 |
| Mormugao | 1969-2015 | 70 | 1.629 | 0.263 | 0.79 | 1.102 |
| Mangalore | 1976-2015 | 74 | 2.083 | 0.241 | 0.61 | 1.714 |
| Cochin | 1939-2013 | 89 | 1.432 | 0.177 | 0.75 | 0.859 |
| Tuticorin | 1964-2014 | 56 | 0.619 | 0.26 | 0.78 | 0.099 |
| Chennai | 1960-2015 | 62 | 0.818 | 0.271 | 2.25 | -1.161 |
| Vizag | 1937-2013 | 86 | 1.19 | 0.246 | 1.27 | 0.166 |
| Paradip | 1966-2015 | 77 | 1.993 | 0.277 | 1.64 | 0.63 |
| Haldia | 1970-2015 | 94 | 2.607 | 0.347 | 1.04 | 1.914 |
| Port Blair | 1916-1964 | 29 | 2.157 | -0.017 | 1.47 | 0.67 |

### *2.2.2 SLR Using Altimeter Data*

As mentioned earlier, the altimeter data from satellites: TOPEX/Poseidon, Jason-1, Jason-2 and Jason-3 were used to obtain the SLR trend from 1993 to 2018 from the Commonwealth Scientific and Industrial Research Organization (CSIRO, 2020) website (https://www.cmar.csiro.au/sealevel/sl_data_cmar.html). Unlike the site specific tide gauge data these measurements were averages over a wide area (1°x 1°grid size) around the ports. Trends were drawn after correcting the observations for GIA and IB affecting the sensing during cyclonic periods. Examples of the trend lines are given in Figures 2 and 3 that pertain to the ports of Mumbai and Chennai while the coordinates of the regions near the ports, GIA and IB corrections for each one of them and the corrected SLR rate are given in Table 2.

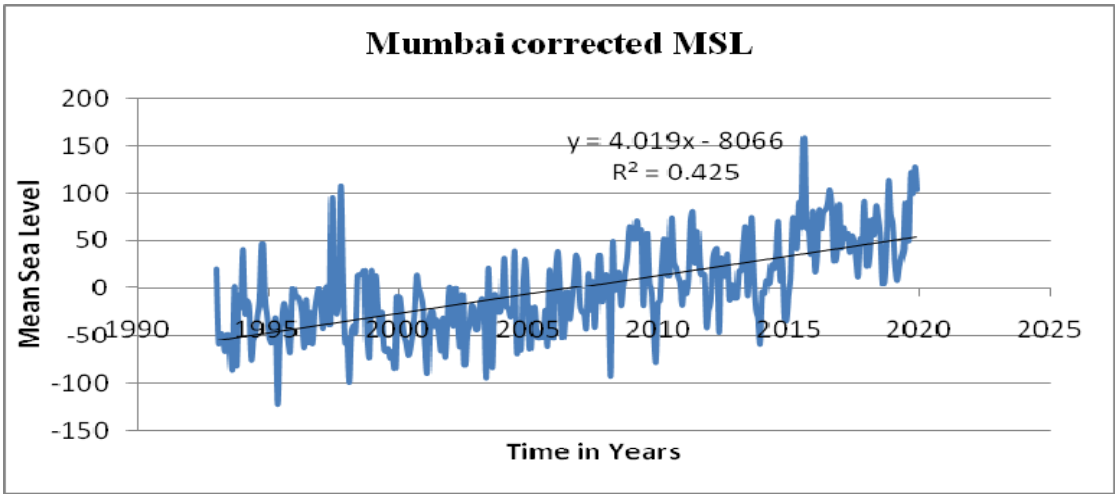



**Figure 2** Altimeter based MSL trend at Mumbai

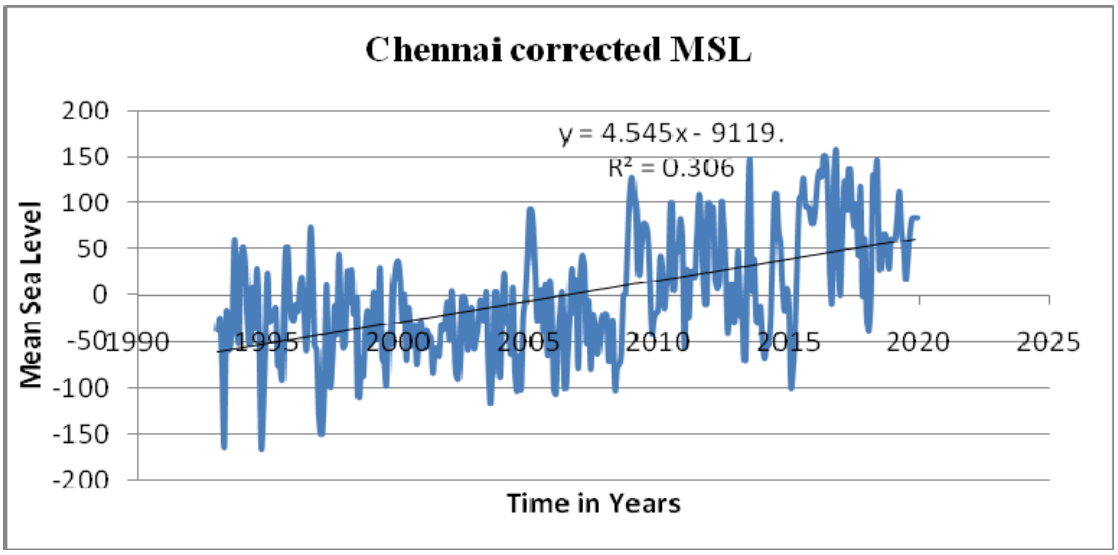



**Figure 3** Altimeter based MSL trend at Chennai

**Table 2** SLR near the major ports during 1993-2018

| Location | Latitude (°N) | Longitude (°E) | GIA and IB correction (mm) | Corrected SLR (mm/year) |
|---|---|---|---|---|
| Chennai | 13 | 81 | -0.696 | 4.54 |
| Mumbai | 19 | 73 | -0.613 | 4.02 |
| Cochin | 10 | 76 | -0.653 | 4.64 |
| Kandla (Dwarka) | 22 | 69 | -0.808 | 3.85 |
| Haldia | 2 | 88 | -0.532 | 5.13 |
| Mangalore | 13 | 74 | -0.468 | 4.44 |
| Mormugao | 5 | 74 | -0.484 | 4.41 |
| Paradip | 0 | 87 | -0.874 | 4.93 |
| Port Blair | 12 | 93 | -0.282 | 3.84 |
| Tuticorin | 9 | 79 | -0.596 | 5.07 |
| Vizag | 7 | 83 | -0.816 | 5.64 |

The maximum SLR rate was observed at Visakhapatnam (Vizag) port which was 5.64 mm/yr while the minimum one of 3.84 mm/year was seen at Port Blair (and also nearly sameat Dwarka, near the Kandla port). The satellite-based rates appear much higher and different than the earlier tide gauge-based ones and this could be due to the difference in available sample sizes and methods of data collection, namely, in-situ and remote sensing averages over large spatial domains. None the less it does show accelerated rate of SLR since recent past. This observation confirms the earlier one in Unnikrshnan et al. (2015).

The available altimeter data collected all over the world ($65^0$ N to $65^0$ S latitude and $0^0$ to $359^0$ longitude) from 1993 to 2018 with a grid resolution of $1^0$ x $1^0$ were available on the web page of Commonwealth Scientific and Industrial Research Organization (CSIRO) web page (https://www.cmar.csiro.au/sealevel/sl_data_cmar.html).These data are corrected for GIA, IB corrections as well as seasonal variations. The downloaded data were plotted in excel base and linear SLR trend was fitted. The resulting Figure 4 shows that the global SLR trend was 3.51 mm/year for a period of 1993 to 2018.

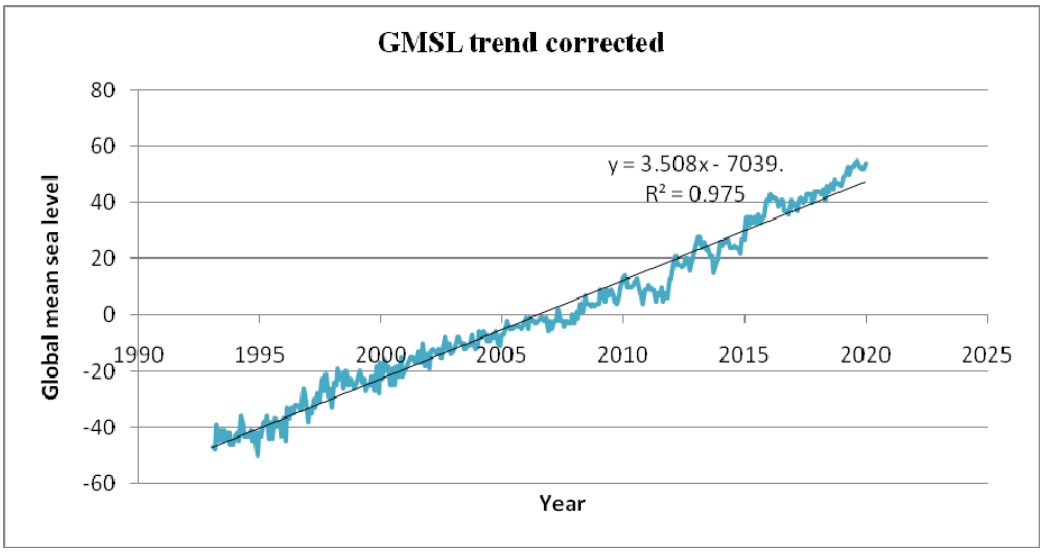



**Figure 4** Global Mean Sea Level trend

As per Church et al. 2011a, b, 2013) the globally averaged trend of SLR over last 25 years (up to 2017) was 3.3 (+/-) 0.5 mm/year for which the ice melt contributed more than the thermal expansion in recent times. At regional level and in general, thermal expansion-based change was found to be dominant; however, at some locations like Bay of Bengal, salinity differences were also seen by the authors as important contributors of the regional variations.

According to Oppenheimer et al. (2019) the GMSL is increasing and also accelerating since last few decades; the latter being due to large pouring of water onto the oceans by melting glaciers and ice sheets. Thus, while it was 1.4 mm/year during 1901-1990, it grew up to 3.6 mm/year during the period of 2005-2015 as seen from tide gauge and satellite altimeter data. According to the authors the future SLR evaluated as per all four warming scenarios is slated to increase further, depending more on the global warming scenarios and typically, by the year 2100 the SLR rate could be in the range of 10-20 mm/year.

When the global mean SLR was compared with the SLR trend around the Indian coastline, it was seen that the SLR rate around the Indian coastline was much higher than the global mean rate and further, at some places like Haldia and Vishakhapatnam it was more than 50% of the global average. However, this comparison has limitation in that apart from different sample sizes, while the tide gauge data are station specific the altimeter data are large spatial averages. Nonetheless the differences may seem reasonable.

As per Unnikrishnan et al. (2016), the satellite-based measurements from 1992 to 2016 show the global MSL rise of 3.4 with (+/-) 0.4 mm/year of standard error. Authors found that the recent SLR rate was much higher than the past. They also noted generally good correlation between satellite and tide gauge data.

### *2.2.3 SLR using Projected Data*

While the SLR rates from tide gauges and altimeters discussed earlier were for the historical period, the future SLR rate was determined in this study from the SLR scenario generator of the SimCLIM tool box (SimCLIM, 2003). The base year was taken as 1995 for the evaluation of SLR. The medium warming pathway of RCP-4.5 was used. The high sensitivity (upper 90% percentile of GCM ensemble) SLR data corrected for VLM at each port was subjected to the linear trend analysis. The result of SLR rates is shown in Table 3. As can be seen the rate of the SLR varied in between 3.40 mm/year (Chennai) and 5.16 mm/year (New Mangalore) across all the ports.

**Table 3** Projected SLR Rate

| Sl. No. | Port | Latitude (˚N) | Longitude (˚E) | SLR rate Corrected with VLM (mm/year) |
|---|---|---|---|---|
| 1 | Kandla Port | 23.008 | 70.187 | 4.76 |
| 3 | Mumbai Port | 18.948 | 72.844 | 5 |
| 4 | Mormugao Port | 15.411 | 73.8 | 5.03 |
| 5 | New Mangalore Port | 12.933 | 74.821 | 5.16 |
| 6 | Cochin Port | 9.955 | 76.268 | 5.12 |
| 7 | Tuticorin Port | 8.756 | 78.179 | 5.11 |
| 8 | Chennai Port | 13.082 | 80.292 | 3.4 |
| 10 | Visakhapatnam Port | 17.683 | 83.24 | 4.22 |
| 11 | Paradip Port | 20.254 | 86.701 | 4.05 |
| 12 | Haldia Port | 22.018 | 88.067 | 4.7 |
| 13 | Port Blair Port | 11.623 | 92.727 | 4.45 |

SLR projections have also been made in the Inter-Government Panel on Climate Change (IPCC)'s AR5 report and this indicates future SLR for different warming scenarios up to the year: 2100 resulting from the Climate Model Inter-comparison (CMIP) modeling effort of World Climate Research Program (Taylor et al., 2012).Such rise encompasses effects of thermal and salinity expansions, melting of glaciers, melting of ice sheets and ice caps, changes in land water storage. According to these estimates and subject to modeling uncertainties, for the medium scenario called representative concentration pathway (RCP)-4.5 the GMSL rate would be on an average 6.10 mm/year by the year 2100. Further, as per the worst scenario of RCP 8.5, the total SLR will be in the range of 58 to 98 cm relative to the baseline period of 1986-2005 (Taylor et al., 2012).

### *2.2.4 Inter-comparison across the three datasets*

An inter-comparison across the three data sets as above is shown in Figure 5. This shows that the projected SLR will be higher at all west coast sites and also at Tuticorin on the east, but it will be smaller at the rest of east coast locations. There is fair amount of closeness between the historical satellite based and projected GCM based rates, although at the west coast ports (and also at Port Blair at the eastern offshore) the projected rates were higher and vice versa at the east coast ports. The historical tide gauge data however showed much less rate than the satellite based historical as well as the projected rates.

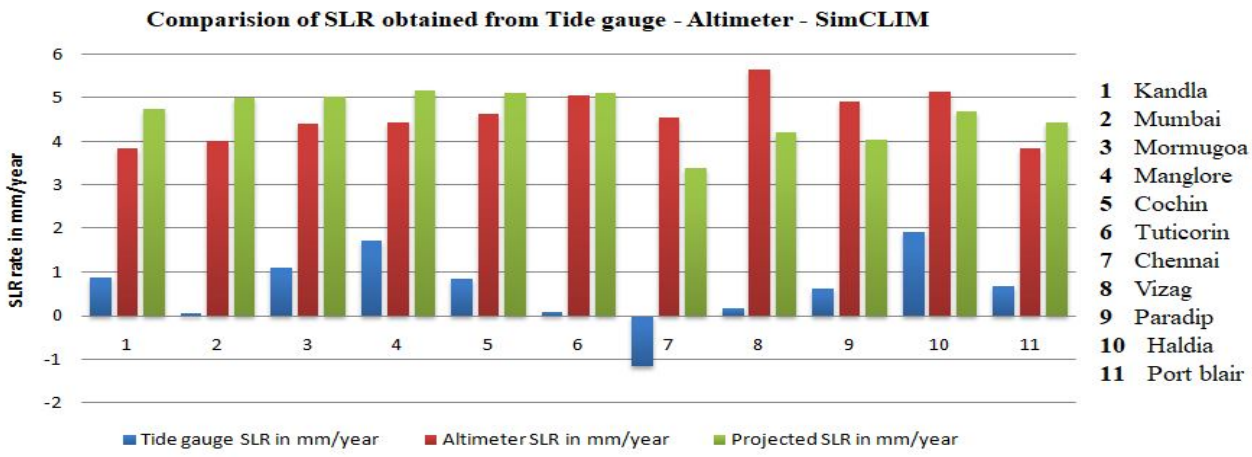



**Figure 5** Corrected SLR comparison obtained from Tide gauge - Altimeter – SimCLIM

## 3. Conclusio

The rate of sea level rise derived from the historical data indicated that at all major ports the SLR rate was positive, except at Chennai. It was the maximum in value at Haldia (1.91 mm/year) and minimum in value at Tuticorin (0.10 mm/year). The tide gauge at Chennai showed a negative trend of -1.16 mm/year due to probably very high rate of VLM.

As against the long-term site-specific historical data of tide gauges, the relatively short term and recent spatially averaged satellite-based sea level data showed that the SLR rate everywhere was positive and much higher than the tide gauge data. It varied from 3.84 mm/year at Port Blair (almost same at Kandla) to 5.64 mm/year at Vizag port. It thus appears that sine last 25 years or so the SLR rate had accelerated upwards at all major ports of India.

The historical SLR rate around the Indian coastline was much higher than the globally averaged one and further, at some places like Haldia and Vishakhapatnam it was more than 50% of the global average. The SLR projections based on an ensemble GCM showed that by the turn of this century the SLR rates at the major Indian ports will vary from 3.40 mm/year (at Chennai) to 5.16 mm/year (at New Mangalore).

An inter-comparison across the three data sets as above indicated a fair amount of closeness between the historical satellite based and projected GCM based rates, although at the west coast ports (and also at Port Blair at the eastern offshore) the projected rates were relatively higher and vice versa at the east coast ports. The historical tide gauge data however showed much less rate than the satellite based and also than the projected rates.

## References

Acker, J., Williams, R., Chiu, L., Ardanuy, P., Miller, S., Schueler, C., Vachon, P. W., and Manore, M. (2003). Remote sensing from satellites. *In: Meyers, R. A. (Ed.), Encyclopedia of Physical Science and Technology*, third ed. Academic Press, New York.

Black, K. P., Baba, M., Kurian, N. P., Urich, P., Narayan, B., Stanley, D. O., & Mathew, J. (2017). *Climate change adaptation guidelines for coastal protection and management in India. ADB TA-8652 IND*.

Chowdhury, P., & Behera, M. R. (2015). A study on regional sea level variation along the Indian coast. *Procedia Engineering*, *116*, 1078-1084.

Church, J. A., & White, N. J. (2011a). Sea-level rise from the late 19th to the early 21st century. *Surveys in geophysics*, *32*(4), 585-602.

Church JA, White NJ, Konikow LF, Domingues CM, Cogley JG, Rignot E, Gregory JM, VandenBroeke MR, Monaghan AJ, Velicogna I (2011b) Revisiting the Earth's sea-level and energy budgets from 1961 to 2008. *Geophys Res Lett* 38: L18601.https://doi.org/10.1029/2011GL048794.

Church JA, Clark PU, Cazenave A, Gregory JM, Jevrejeva S, Levermann A, Merrifield MA, Milne GA, Nerem RS, Nunn PD, Payne AJ, Pfeffer WT, Stammer D, Unnikrishnan AS (2013) *Sea level change*. In: Stocker TF, Qin D, Plattner G-K, Tignor M, Allen SK, Boschung J, Nauels A, Xia Y, Bex V, Midgley PM (eds) Climate change 2013: the physical science basis. Contribution of working group I to the fifth assessment report of the intergovernmental panel on climate change. Cambridge University Press, Cambridge, United Kingdom and New York, NY, USA

CSIRO (2020). *Altimeter data.* The Commonwealth Scientific and Industrial Research Organization. https://www.cmar.csiro.au/sealevel/sl_data_cmar.html on 13/05/2020.

Douglas, B. C. (2001). Sea level change in the era of the recording tide gauge. *International Geophysics* 75, 37-64.

Emery, K. O., & Aubrey, D. G. (1989). Tide gauges of India. *Journal of Coastal Res. 1989.* 489-501.

Fasullo, J. T., Boening, C., Landerer, F. W., & Nerem, R. S. (2013). Australia's unique influence on global sea level in 2010–2011. *Geophysical Res. Lett. 40*(16), 4368-4373.

Krishnan R., Sanjay J., Gnanaseelan C., Mujumdar M., Kulkarni A. and Chakraborty S. (2020). Assessment of Climate Change over the Indian Region - *Ministry of Earth Sciences, Government of India.* Springer https://doi.org/10.1007/978-981-15-4327-2.

Krishnamurti, T. N., Kishtawal, C. M., Zhang, Z., Larow, T., Bachiochi, D., Williford, E., Gadgil,

S. &Su ndran, S. (2000). Multimodel ensemble forecasts for weather and seasonal climate. *J. Clim*.13, 4196–4216. (doi:10.1175/1520-0442(2000)013!4196: MEFFWAO2.0.CO;2)

Kundu, S., Mondal, A., Khare, D., Mishra, P. K., and Shukla, R. 2014.Shifting shoreline of Sagar Island Delta, India. *Journal of Maps,* 10(4), 612–619.

Mitrovica J X, N. Gomez, E. Morrow, C. Hay, K. Latychev, M. E. Tamisiea (2011). On the robustness of predictions of sea level fingerprints. Geophy. J. Intern. 187 (2), 729-742.

Oppenheimer, M., Glacovic, B., Hinkel, J., Van De Wal, R., Magnan, A., Abd-Elgawad, A., Cai, R., Cifuentes-Jara, M., Deconto, R., Ghosh, T., Hay, J., Isla, F., Marzeion, B., Meyssignac, M., Sebesvari, Z. (2019). Sea-level rise and Implications for low lying islands, coasts and communities. *Special report on the ocean and cryosphere in a changing climate* (SROCC).

Patil R G and M C Deo (2019). Future rise in sea levels and impact on shorelines at the Indian Ports. Hydro-2019 International Conference, Hotel Marriot, Hyderabad, Dec. 18-20, 2019. ISBN 978-93-8935-484-3. Vol. I, pp 327-336.

Patil R G, M C Deo. (2020). Forthcoming. Sea Level Rise and Shoreline Change under the Changing Climate at a Series of Locations along the Indian Coastline. ASCE Journal of Waterways, Port, Coastal and Ocean Division. DOI:10.1061/(ASCE)WW.1943-5460.0000586.

PSMSL (2020a) Permanent Service for Mean Sea Level, "Tide gauge data", https://www.psmsl.org/data/obtaining/ on 09/02/2020.

PSMSL (2020b) Permanent Service for Mean Sea Level. "Peltier GIA data sets", https://www.psmsl.org/train_and_info/geo_signals/gia/peltier/ on 01/07/2020.

Ramachandran, A., Khan, A. S., Palanivelu, K., Prasannavenkatesh, R., &Jayanthi, N. (2017). Projection of climate change-induced sea-level rise for the coasts of Tamil Nadu and Puducherry, India using SimCLIM: a first step towards planning adaptation policies. *J. of Coast. Conserv*. 21(6), 731-742.

Saenko, O. A., Yang, D., Gregory, J. M., Spence, P., and Myers, P. G. (2015). Separating the influence of projected changes in air temperature and wind on patterns of sea level change and ocean heat content. *J, of Geophy, Res.: Oceans*, *120*(8), 5749-5765.

Shankar, D., & Shetye, S. R. (1999). Are interdecadal sea level changes along the Indian coast influenced by variability of monsoon rainfall? *J. of Geophy. Res. Oceans,* 104(C11), 26031-26042.

Shankar, D. (2000) Seasonal cycle of sea level and currents along the coast ofIndia, *Current Science*, *78*(3), 279 – 288.

Shankar, D., & Shetye, S. R. (2001). Why is mean sea level along the Indian coast higher in the Bay of Bengal than in the Arabian Sea? *Geophy. Res. Lettt.* 28(4), 563-565.

SimCLIM systems, (2003) *User's Manual. SimClim,* New Zeeland https://www.climsystems.com/slr-cities-app/technical/#data-and methods

Tamisiea, M. E. (2011). Ongoing glacial isostatic contributions to observations of sea level change. *Geophy. J. Intern.*, *186*(3), 1036-1044.

Taylor, K. E., Stouffer, R. J., & Meehl, G. A. (2012). An overview of CMIP5 and the experiment design. *Bulletin of the Amer. Met. Soc*., 93(4), 485-498.

Unnikrishnan, A. S., Kumar, K. R., Fernandes, S. E., Michael, G. S., &Patwardhan, S. K. (2006). Sea level changes along the Indian coast: Observations and projections. *Cur. Sc.* 362-368.

Unnikrishnan A S and D. Shankar. (2007). Are sea-level-rise trends along the coasts of the north Indian Ocean consistent with global estimates? *Global Planet. Change*: 57(3-4); 2007; 301-307.

UnnikrishnanA S, Nidheesh A G, Lenagaigne M L, (2015). Sea level rise trends off the Indian coasts during the last two decades. *Curr. Sc.* 108. 5 966-971.

Unnikrishnan A S (2016). Is sea level rising? *Quarterly News Letter of Ocean Society of India* 3, 3, Nov. 2016.

Wachler, B., Seiffert, R., Rasquin, C., & Kösters, F. (2020). Tidal response to sea level rise and bathymetric changes in the German Wadden Sea. *Ocean Dyn.*, 1-20.

Wada Y., J. T. Reager, B. F. Chao, J. Wang, Min-Hui Lo, C. Song, Y. Li and A. S. Gardner. (2017). Recent Changes in Land Water Storage and its Contribution to Sea Level Variations. *Surveys in Geophy.* 38 (1), 131-152.

Woodworth P L and R. Player. (2003). The Permanent Service for Mean Sea Level: An Update to the 21st Century. *J. of Coast. Res.* 19(2). pp. 287-295

IN PROCEEDINGS OF 25th HYDRO 2020, INTERNATIONAL CONFERENCE,
NATIONAL INSTITUTE OF TECHNOLOGY ROURKELA, ODISHA, INDIA
26-28, March 2021, ISBN 978-93-90631-56-8

Paper ID - 190

# STABILIZATION OF INLET AND RESTORATION OF RIVER MOUTH IN PUTHIYANGADI

**V.B.Sharma**[1] **Shivani Sahu**[2] **VaibhavKonde**[3] **Prabhat Chandra**[4]

[1]*Scientist B, Mathematical Modelling in Coastal Engineering, Central Water and Power Research Station, Pune – 411 024, IndiaEmail: vipin_bihari@yahoo.com*
[2]*Scientist B, Mathematical Modelling in Coastal Engineering, Central Water and Power Research Station,Pune – 411 024, India*
[3]*Research Assistant, Mathematical Modelling in Coastal Engineering, Central Water and Power Research Station, Pune – 411 024, India*
[4]*Scientist E, Mathematical Modelling in Coastal Engineering, Central Water and Power Research Station,Pune – 411 024, India*

## ABSTRACT

The alongshore sand movement which occurs in both, northward and southward directions, depending upon the wave conditions, is mainly responsible for choking the mouth of estuaries / rivers either partially or completely depending upon the river discharge conditions.The Proposed mini fishery harbour site ($12^0$ 01’ 08’’N and $75^0$ 14’ 05”E) is located at Puthiyangadi, Kerala on the west coast of India. This development area is about 1.10 km south from the Perumba river mouth. This river mouth is used by the fishermen but it is unstable in nature due to the prevailing drift conditions. Net drift in this area is towards south which partially blocks the river mouth causing large inconvenience to fishermen for the movement of their boats. In this regard, the Project Authority suggested one training work of about length 600m on the southern side of river mouth. The hydrodynamic and sedimentation studies carried out at CWPRS indicated that the proposed layout would block the southward drift causing huge sedimentation at the river mouth.

Further, a modified layout was recommended consisting of two converging training works (breakwaters) on either bank of the river mouth with total length of about 560m, about 40 m less than the proposed length of single training work. It was also observed that with the modified layout, the velocity at the river mouth would increase by about 45% which would help in flushing the sediments. It was found that with the proposed layout with two training works on either bank of the river mouth, the suitable hydraulic conditions at the entrance of river would be maintained and the mouth would keep open throughout the year.

***Keywords: Hydrodynamics, Siltation, Tidal current, wave induced currents and river mouth***

## 1. INTRODUCTION

The movement of sediments along the coastal regions of the land has always been a problem in development of Ports and harbours. The sediment material mainly from the; sea bed, erosion and accretion of the shore and from the rivers discharging into the sea, contribute for the sediment that moves along the coast. Coastal sediment movement along shore is mainly due to the action of the waves (Eaton, 1950; Johnson, 1919). This sediment is major cause of shifting of river mouth and sometimes chocking of river mouth during fair weather condition for non-perennial rivers. The proposed fishing harbour is influenced by Perumba river mouth which is about 1 km north of proposed site. The study area ($12^0$ 01’ 08’’N and $75^0$ 14’ 05”E) is located on the west coast of India as shown in Figure 1. It is an open beach and presently beach landing is resorted for the fish catch. Net drift in the area is towards south causing partial closing of river mouth. It was proposed by project authorities to construct a 600m long

breakwater on the southern side of the bank to deflect the flow away from fishing harbour as shown in Figure 2.




**Figure 1: Location Map of Site**

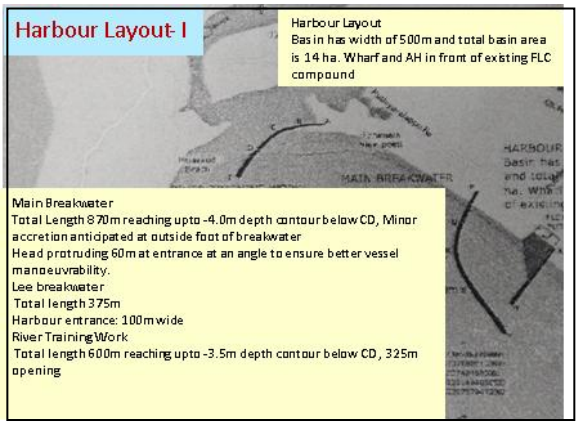



**Figure 2:Proposed Layout**

Perumba river mouth during monsoon and during fair weather is shown in Figure 3. A sand bar can be noticed during fair weather condition which partially chocks the river mouth. The high currents in the river during monsoon period wash away the sand bar and mouth gets widened. In order to maintain the unstable Perumba river mouth, the optimum length and alignment of the training works have been evolved as per the prevailing drift and flow conditionsusing MIKE21 HD/MT software




**Figure 3: Perumba river mouth during monsoon and non-monsoon periods**

## 2. Data Analysis

For the model studies of tidal hydrodynamics and siltation, the data required are mainly; bathymetry, tidal data, sediment characteristics, suspended sediment concentration, wind and currents. In this study, field observed near shore region bathymetry is amalgamated with offshore region obtained from C-MAP software as shown in Figure 4. The bathymetry covers an area of 38kmX 57km extending up to-55m depth contour which includes part of Perumba River.

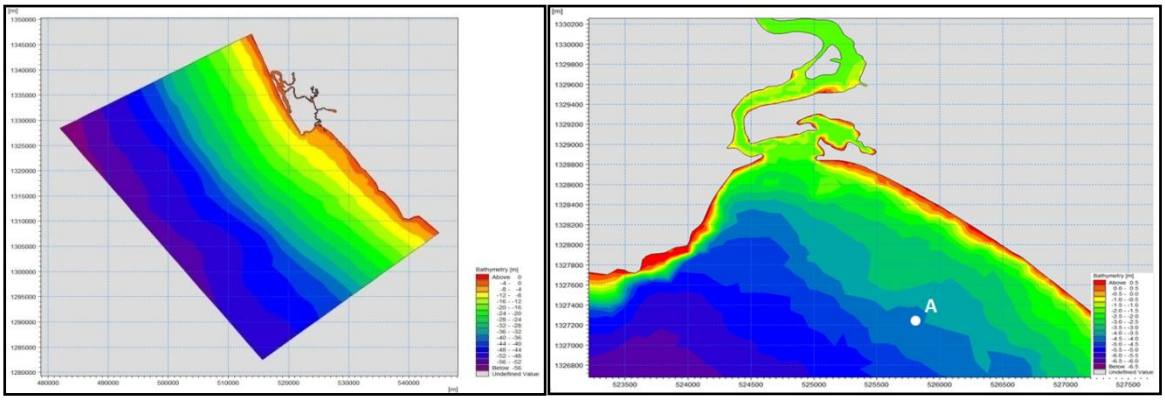



**Figure 4: Existing bathymetry at the proposed site and observation point 'A'**

Predicted tide at the study region is semidiurnal with pronounced diurnal inequality having considerable difference in the tidal ranges and the elevation of low waters and high waters in the successive tidal cycles. The spring tidal range is about 1.2 m while neap tidal range is 0.4 m as shown in Figure 5.

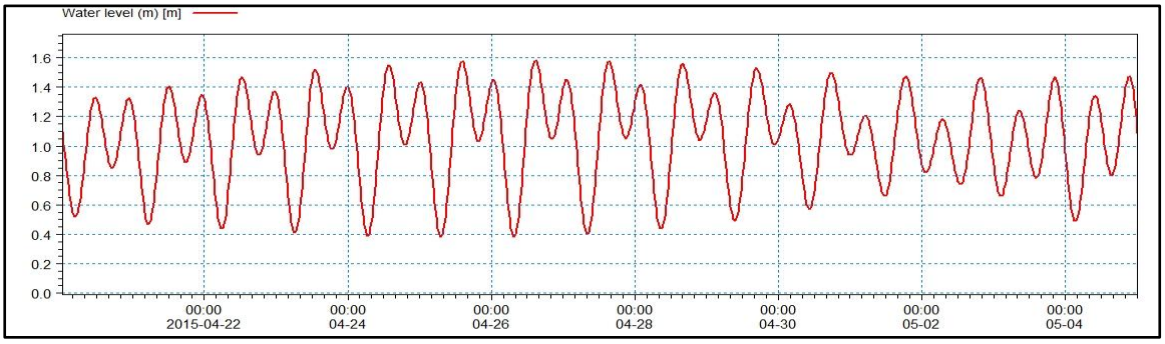



**Figure 5: Predicted Tide at Puthiyangadi Fishing Harbour**

Perumba river peak discharge data in monsoon period is about 80 $m^3/s$ while during non-monsoon, it is about 10 $m^3/s$. This river discharge data was supplied at river boundary to simulate hydrodynamic condition in the river stretch.The suspended sediment concentration near the fishery harbour location varies between 50 mg/l to 300 mg/l. The mean grain size $D_{50}$ of the river bed material is of the order of 0.15 mm.

## 3. MODELING APPROACH

Two Dimensional hydrodynamic model, MIKE 21 HD and mud transport Model, MIKE 21 MT are used to simulate flow field and transport of sediment in existing as well as proposed conditions of fishery harbour for predetermined boundary conditions. The Hydrodynamic Module is based on the numerical solution of the two- dimensional shallow water equations integrated over the depth and assumed to be incompressible ReynoldsaveragedNavier-Stokesequations. The governing equations of the MT module are essentially based on Mehta et al. (1989). In MIKE-21 HD model, turbulence modelling is included in the momentum equations in the terms containing laminar stresses and Reynolds stresses. It can be either used as a constant in the horizontal stress terms or by using the Smagorinsky's formulation (1963) to express sub-grid scale transports by using an effective eddy viscosity related to characteristic length scale (Lily, 1989).

The wave induced radiation stresses are the depth integrated and wave averaged excess momentum fluxes due to waves as defined by Longuet-Higgins and Stewart (1964). Radiation stresses are responsible for set-up, set-down and longshore current in the near shore zone. This approach is used in MIKE-21 SW model to simulate radiation stresses.

The cohesive sediment transport module or mud transport (MT) module deals with the movement of mud in a fluid and the interaction between the mud and thebed. The transport of the mud is described by equation given byTeisson, 1991.

The two dimensional depth averaged sediment transport model (MIKE- 21MT/AD) takes into account conservation of mass of sediment, depth averaged velocities, longitudinal dispersion coefficient, lateral diffusivity, settling velocity, critical deposition stress, and critical erosion stress for the given sediment. Flocculation of mud particles is described as function of suspended sediment concentration as given by Burnt 1986. The numerical values of these parameters were modified within their ranges such that the prevailing sedimentation in the existing approach channel is achieved.

## 4. MODEL CALIBRATION

The proposed site is influenced by both tides and waves and accordingly the related tide and wave hydrodynamics have to be simulated in the model using MIKE-21 HD and MIKE-21 SW model. The HD Model was simulated considering both monsoon and non-monsoon conditions. In this region, waves are mainly approaching from SW direction ($210^0$N to $270^0$ N). Significant wave height of 2.5 m from the quadrant southwest to west has been considered in the Spectral Wave(SW) model for simulation during the year. The hydrodynamic HD model was simulated after imposing appropriate boundary conditions. Observed tide with appropriate phase lag at sea boundary and an observed river discharge were supplied at Perumba river boundary.

The model was simulated in the existing condition for 15 days to covers both spring and neap tide. The simulations were repeated by changing model hydraulic parameters until the computed values matched with the field observed data. Calibration of currents at location ‘A’ is shown in Figure 6. It could be seen from figure that the magnitude of simulated currents matches well with prototype data. The calibration is reasonably good and currents are very weak in the region.

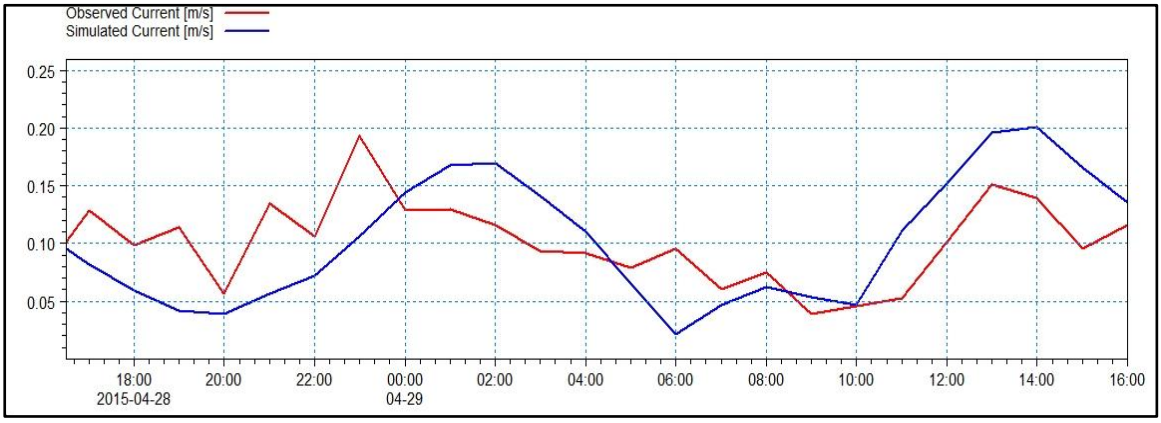



**Figure 6: Current data calibration in offshore region**

Flow fields during peak flood and ebb in non-monsoon period are shown in Figure 7. The arrow head of vector shows the direction of flow while its magnitude is denoted by its length on the length scale. It could be seen that flow along the shoreline is unidirectional while reversal of flow is taking place in rest of the model area.

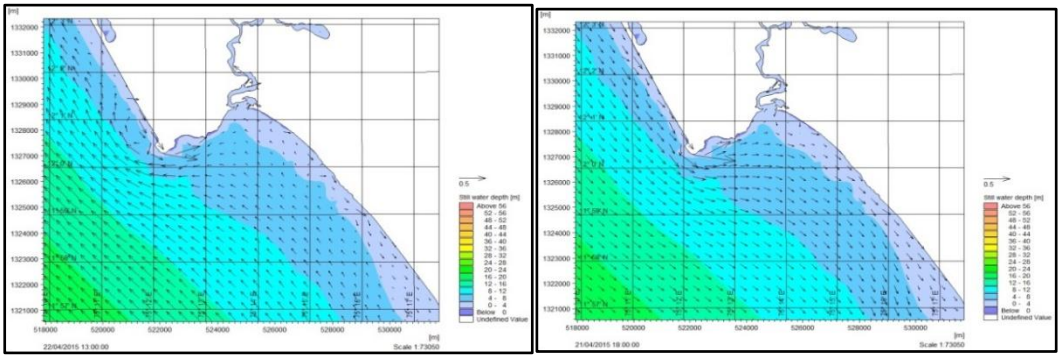


**Figure 7: Velocity Vector Plot in Existing Condition (Non-monsoon period)**

Model was simulated for monsoon period. River discharge hydrograph was provided as boundary condition at the river boundary about 8 km upstream of river mouth. Currents at inside the river location are 1.5m/s while during non-monsoon period, it is 0.6 m/s. These currents erode the sand bar at the river mouth. Flow fields during peak flood and ebb during monsoon period are shown in Figure 8.

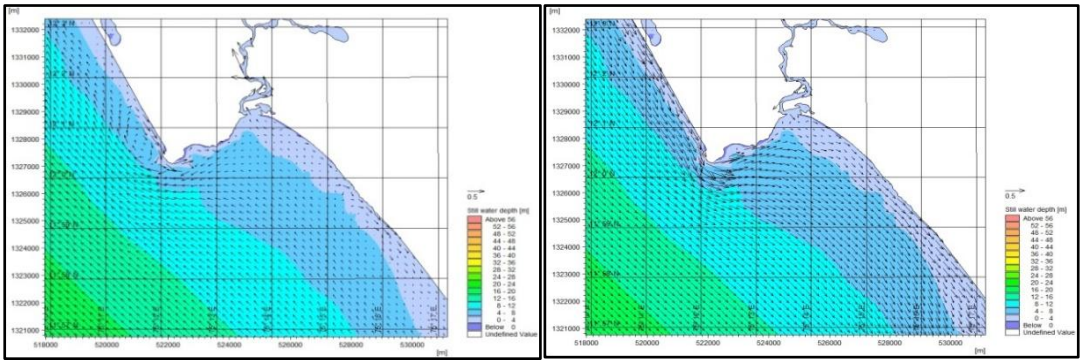


**Figure 8: Velocity Vector Plot in Existing Condition (Monsoon period)**

Sediment model was calibrated in the vicinity of river mouth using MIKE-21 MT model during fair weather. Sedimentation pattern is shown in Figure 9. It could be seen that sedimentation pattern matches well with prevailing sedimentation in Figure 3.

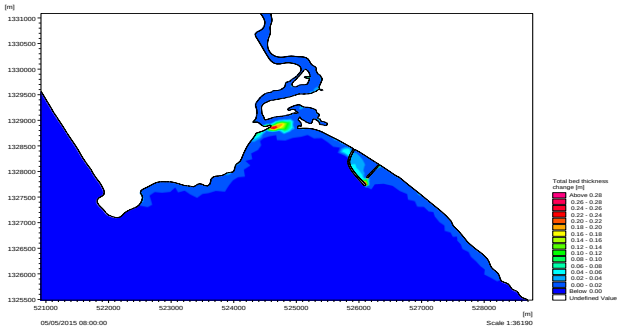


**Figure 9: Sedimentation Pattern in Existing Condition at River Mouth (Calibration)**

## 5. MODEL EXPERIMENTS

Proposed layout (Figure -2) was incorporated in the model and model was simulated for both hydrodynamics and sedimentation without changing the parameters of model for which model has been calibrated. The studies shows that the proposed training work at the river inlet of length 600m at southern side of bank completely blocks the southward sand movement resulting in complete closure of river mouth. Typical plot of sedimentation is shown in Figure 10. This proposalwas discarded and experiments were carried for a new proposal with two training works on either side of bank mouth. The idea is to arrest the southward drift and to increase the flushing velocities at the inlet.

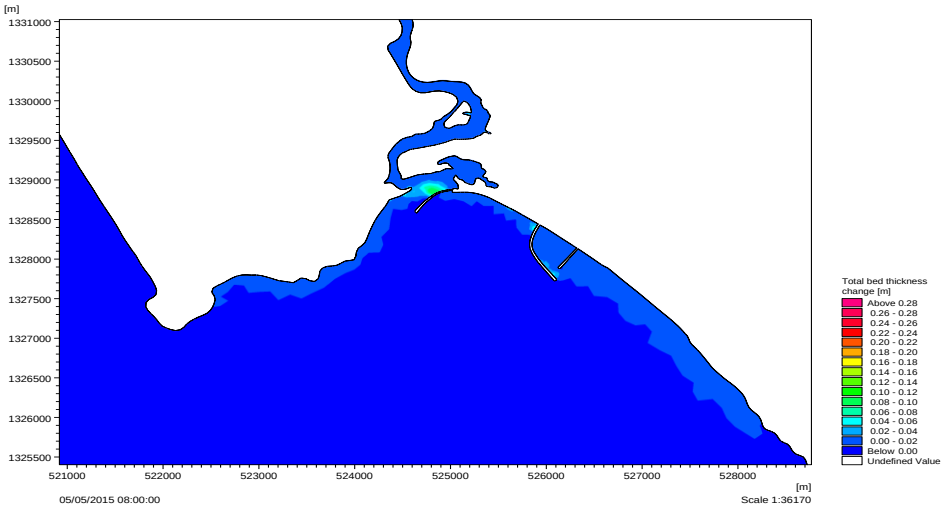



**Figure 10: Sedimentation Pattern in Proposed Condition at River Mouth**

Hence, a comprehensive layout with two converging breakwaters (training works) at the mouth of river, as shown in Figure 11, has been evolved to overcome this problem. The root of two breakwaters rest at 420 m apart at mouth of river which converges to 190 m at the tip of breakwaters. The tip of northern breakwater of length 365 m lies at -3.2 m depth contour while the tip of southern breakwater of length 210 m lies at -2.1 m depth contour.

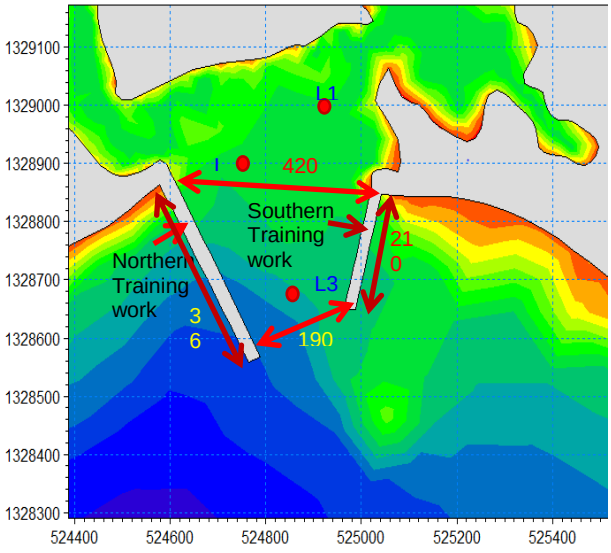



**Figure 11: Proposed River Training Works at River Mouth**

Proposed layout was incorporated in the model and it was simulated for 15 days during both monsoon and non-monsoon. The changes in flow fields were computed every time step of 30 sec and results are recorded at every 30 minutes time interval. Flow pattern during Peak flood and peak ebb (during monsoon and non-monsoon) are shown in Figure 12 and Figure 13 respectively.

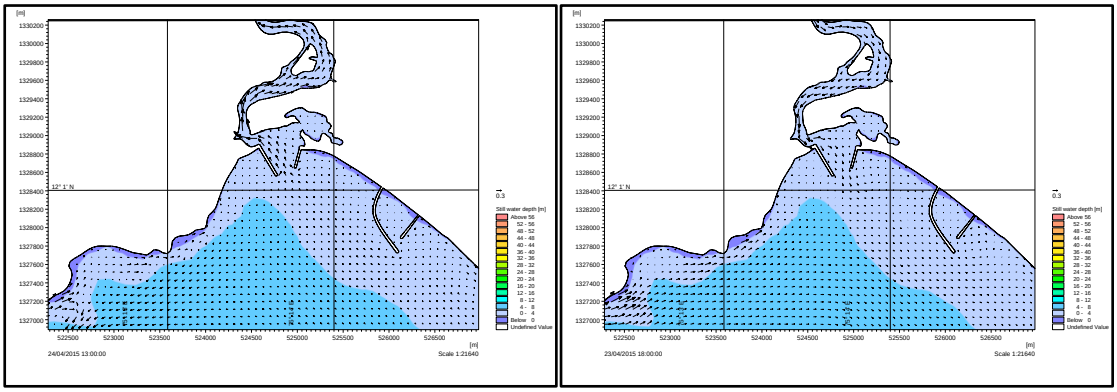


**Figure 12: Flow field during peak of flood and ebb (Non-Monsoon period)**

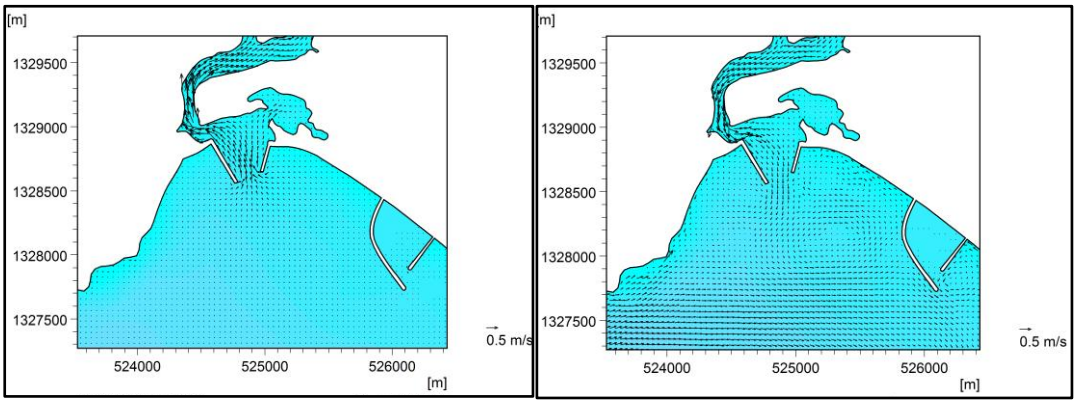



**Figure 13: Flow field during peak flood and ebb(Monsoon period)**

The currents were monitored at 2 locations and compared with existing condition. The locations are marked in Figure 14.

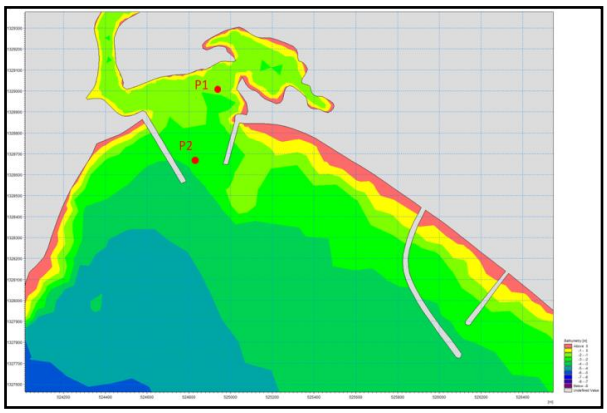



**Figure 14: Locations points at river mouth for comparison of flow behaviour**

It could be observed from the figure 15 that at location P1, velocity drops down by about 60% in this layout, which would be beneficial for movements of boat/trawlers in the river and at location P2, and velocity increases by 45% from 0.20 m/s to 0.35 m/s due to constriction of flow between breakwaters.This increase in velocity at location P2 would not allow the sediment to settle at the mouth and hencetheriver mouth would remain open throughout the year.

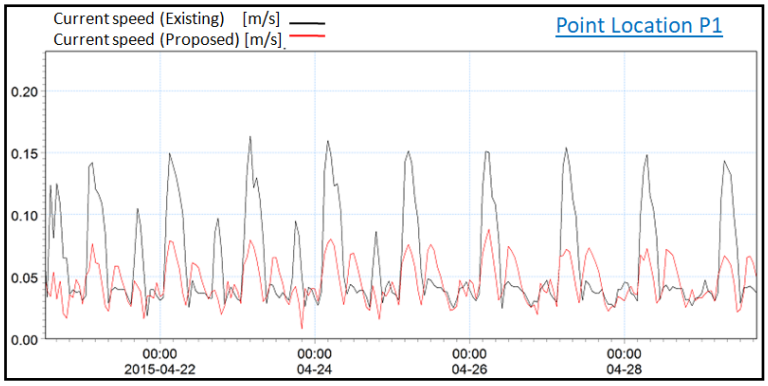



**Figure 15: Comparison of Currents at P1 Location**

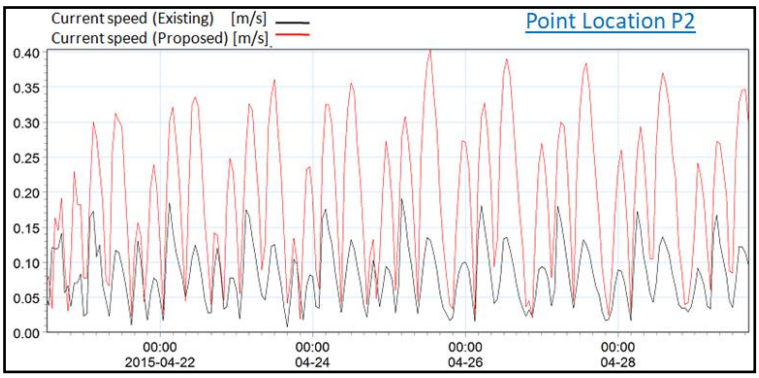



**Figure 16: Comparison of Currents at P2 Location**

Model was simulated for sediment transport for 15 days. The sedimentation pattern is shown in Figure 17. It could be seen from figure that there will be sedimentation on either side of breakwater root and shoal would also be formed at the location marked. It can be seen from figure that the river mouth will remain open through the year.

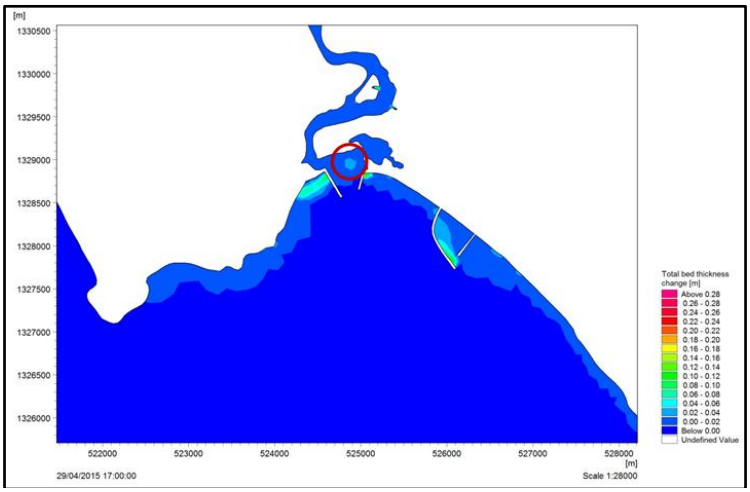



**Figure 17: Sedimentation Pattern for Proposed layout**

## 6. RESULTS AND DISCUSSION

The currents in the offshore are of the order of 0.2 m/s. Single breakwater of 600m length as proposed by project authority would block the river mouth and during monsoon period the area upstream of river mouth would get inundated. In order to avoid choking of river mouth during the fair weather condition, a modified layout was studied with two training works on either bank of the river mouth. It was found that thislayout would be beneficial for maintaining hydraulic conditions at the entrance of river which will keep the mouth open throughout the year. The tip of the proposed training work has been kept at about -3.0m depth which would avoid bypassing of the littoral drift in the inlet area and the overall length of two training works ( 570m long) is also marginally less than the single training work ( length 600m ) proposed by the Project authorities.

## 7. CONCLUSIONS

- The wave induced currents play major role in bringing sediment in suspension which gets deposited at the river mouth and sand bar is formed.
- Proposed layout with two training works on either bank of the river mouth will be beneficial for both fishing harbor point of view and maintaining hydraulic conditions at the entrance of river which will keep the mouth open throughout the year.

## 8. ACKNOWLEGDMENT

Authors are thankful to Shri A. K. Agrawal, Director, Central Water and Power Research Station, Pune for his kind consent for publishing this paper.

## REFERENCES

Eaton R.O., (1950). "Littoral Processes on Sandy Coasts" Proc. First Conf. of Coastal Engineering pp. 140-54.

Burnt, N., 1986 Field settling velocities of estuary muds. In: Estuarine cohesive sediment Dynamics, Edited by Mehta, A J Spring – Veriag, Berlin, Heidelberg, New York, Tokyo, 126-150

Johnson, D. K., (1919). "Shore Processes and Shoreline Development", John Wiley & Sons, 584 pp.

Longuet-Higgins, M. S., & Stewart, R. W., 1964, August. Radiation stresses in water waves; a physical discussion, with applications. In Deep Sea Research and Oceanographic Abstracts (Vol. 11, No. 4, pp. 529-562). Elsevier.

Lilly, D. K., 1989, February. The length scale for sub-grid-scale parameterization with anisotropic resolution. In Annual Research Briefs, 1988 (Vol. 1, pp. 3-9)

Mehta, A.J., Hayter, E.J., Parker, W.R., Krone, R.B. and Teeter, A.M., 1989. Cohesive sediment transport. I: Process description. Journal of Hydraulic Engineering – ASCE 115 (8), 1076–1093.

MIKE 21 (2014). Scientific background, DHI, Denmark.

Smagorinsky, J., 1963. General circulation experiments with the primitive equations: The basic experiment. Monthly weather review, 91(3), 99-164.

Teisson, C., 1991. Cohesive suspended sediment transport: feasibility and limitations of numerical modelling. Journal of Hydraulic Research 29 (6), 755–769.

TR No.5693 (2019). Mathematical Model Studies for hydrodynamics and siltation in the mini fishing harbour at puthiyangadi, kerala, CWPRS, Pune, India.

*IN PROCEEDINGS OF 25th HYDRO 2020, INTERNATIONAL CONFERENCE, NATIONAL INSTITUTE OF TECHNOLOGY ROURKELA, ODISHA, INDIA 26-28, March 2021, ISBN 978-93-90631-56-8*

Paper ID - 194

# RESTORATION OF TIDAL CREEK INLET FOR NAVIGATION USING PILE JETTY - A CASE STUDY

**Shivani Sahu**[1] **Jiweshwar Sinha**[2] **Vaibhawi Roy**[3] **Prabhat Chandra**[4]

[1] *Scientist B,* [2]*Scientist D,* [3]*Research Assistant and* [4]*Scientist E*

*Central Water and Power Research Station, Pune 411 024, India*

*Email:sahushivani.cwprs@outlook.com*

## ABSTRACT

In this study, a depth-averaged numerical model has been developed using MIKE 21 FM software to study tidal circulation in creek inlet located at Satpati, Maharashtra in West coast of India. The creek area is facing sedimentation problem due to meagre and irregular tidal circulation in the inlet. Numerical experiments of tidal circulation are carried out for probable restoration of the creek inlet with partial replacement of the existing 170 m long solid passenger jetty on the south bank of the river with the semi-piled jetty having 18 numbers of piles each of 1 m diameter. The alignment of the proposed jetty is modified to streamline flow conditions near the jetty head for making ferries more suitable for berthing at the jetty. Computed results are validated with field observations. Model results in experimental scenarios indicated that flow conditions in the creek channel near the piled jetty have been improved with maximum flow velocity to be of the order of 0.3 m/s. As no freshwater discharge conditions have been considered, the results are appropriate for dry season only.

***Keywords: Fishing harbour, Tide, wave induced currents, creek inlet and navigational channel.***

## 1. INTRODUCTION

Coastal processes are the mechanisms that operate along a coastline, which remain in a dynamic state and nature behaves to maintain it in equilibrium condition. The coastal zone is the part of the land surface influenced by continuously changes in dynamic interaction between the ocean and the land. Tides, waves, wind and current are responsible for continuous tidal exchange through an inlet in the creek. The irregular tidal circulation causes sedimentation in inlet regions. The process of sediment transport can change the topography of the bed level of inlet area.

A number of researchers have studied the mathematical modelling for better understanding and analyzing the problems of coastal engineering. Ershadi et al. (2012, 2013) examine the effect of waves, wind and tidal current on sediment transport in Bassaidu fishefy port, Qeshm and Tiyab Port, Iran by using MIKE21 HD model. Movement of sediment load and its pattern of transportation along near shore coastal water is a very important phenomenon to be assessed by Hossain (2016) for different sectors of coastal Engineering to develop and understand the physical processes responsible for shaping the ongoing evolution of the coast and to develop the management strategies to deal the impact of human activities on the coastal zone. Zavattero (2016) develop a suitable methodology to build 2D surface water flow model, including sediment transport in the lower Var valley, France, using MIKE 21 FM. In addition, any unsuitable anthropogenic development in such regions may cause accretion and erosion. Such developments are harmful in maintaining the balance in natural processes and also cause hindrance to the safe movement of boats /trawlers etc.

In the present paper, a 2-D mathematical model has been developed using MIKE – 21 FM software for tidal hydrodynamics to study the probable effect of replacement of Solid jetty

with a Semi solid pile jetty in the creek inlet located at Satpati, Maharashtra. The study area (Lat 19° 43' N and Long 72° 42' E) is situated at about 100 km north of Mumbai, India. Location map of the area is shown in Fig.1. From the figure, it can be seen that considerable amount of silt is deposited near the entrance of creek as well as inside the creek.




**Fig.1: Location map of the study area**

It is further seen that post construction of 170 m long passenger solid jetty on south bank of the creek opposite to 600 m long passenger jetty, siltation problem in creek region aggravated enormously as shown in Fig. 2. It can also be noticed that 170 m long passenger jetty normal to the shore on the south bank of the creek causes obstruction to the tidal flow into the creek as flow is getting diverted away from the southern bank of the creek where berthing of fisheries boats are done.




**Fig. 2: Present status of the study area**

In order to regulate tidal circulation in the creek, it is proposed to replace the 90 m length of the existing solid jetty with a piled jetty keeping the remaining 80 m part of the jetty as solid as shown in Fig. 3.

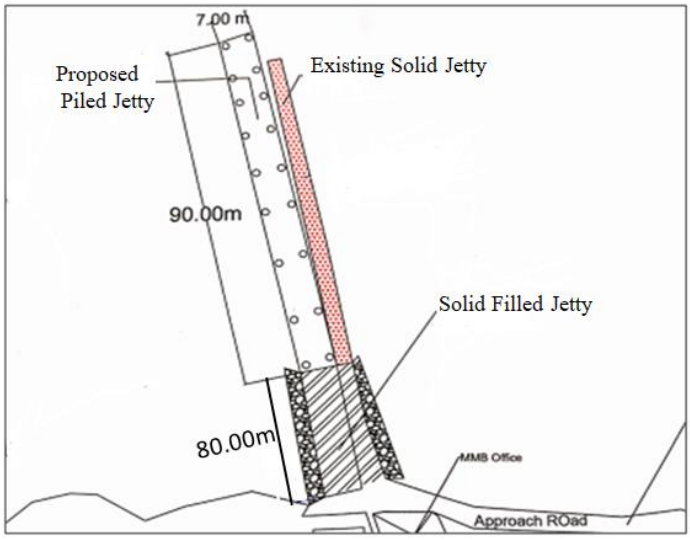



**Fig. 3: Layout of proposed semi piled Jetty in place of solid jetty**

In the present paper, the detailed mathematical model studies have been presented to assess the flow and sedimentation conditions as a result of change in the configuration of jetty.

## 2. DATA ANALYSIS

For the model studies of tidal hydrodynamics, the data required are mainly bathymetry, tidal conditions, bed characteristics, wind and currents. In this study, field observed near shore region bathymetry is amalgamated with offshore region obtained from C-MAP software as shown in Fig. 4.

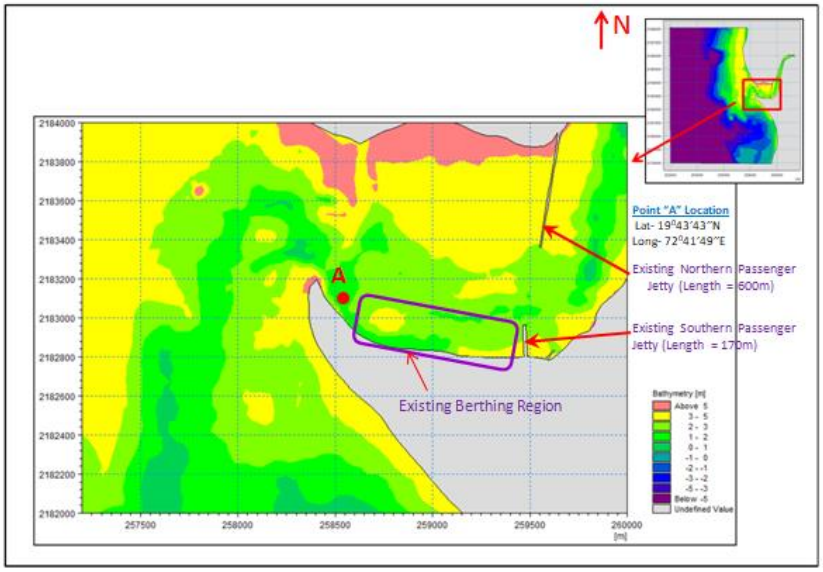



**Fig. 4: Bathymetry of Model area and observation point 'A'**

The bathymetric data reveals that shallow depths of the order of +1 m above CD persist near the creek inlet. Depths more than +2 m above CD are available near berthing zone of fishing vehicles on the southern bank inside the creek. Shallower portion near the creek inlet are apparently visible in the figure. It is reported that there exists a shallower inlet channel of water depths of the order of +0.0 m through which tidal water generally enters into the creek

region even during low tides. Maximum depths of the order of -2.0 m are available near the inlet mouth of the creek. It can also be observed that offshore contours beyond -12 m depth CD are mostly parallel to the shoreline; whereas depth contours upto -1.0 m CD falling close to shoreline near inlet mouth of creek indicates significant siltation in the region. From the figure, it is also be seen that most of the areas in the creek inlet and the region inside the creek have been silted up, which require suitable measure such selective dredging to be adopted for its revival for berthing and navigation purposes.

Predicted tide at the study area (Satpati) is semi-diurnal in nature as shown in Fig. 5. The analysis of tidal data reveals that spring tidal range of 5.5 m and neap tidal range of 2.0 m is generally prevailing at the site. Grain size distribution of bed samples at open sea near the study area indicated that bed materials were mainly composed of coarse silt to silty-clay having mean grain size $D_{50}$ ranging between 0.005 mm and 0.1 mm (Caldwell and Edmonds, 2014).

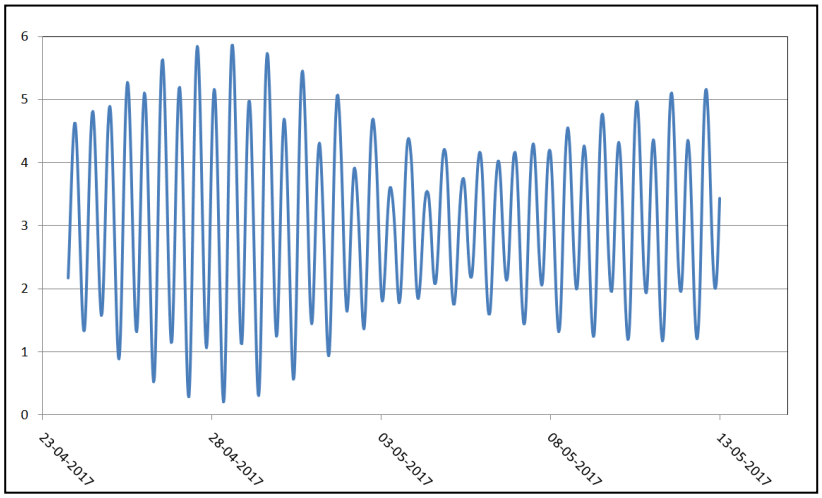



**Fig. 5: Predicted Tidal level at Satpati site**

## 3. MODELING APPROACH

Mathematical models usually describe a system by a set of variables and a set of equations that established relationship between the variables. Those models have advancement to a point where they are considered to be an effective tool for simulation natural phenomena in coastal regions. In order to compute the hydrodynamics of water body in terms of velocity and water level fluctuations, MIKE-21HD model has been used for simulating hydrodynamics while MIKE-21 SW (Short Wave) model has been used to simulate wave induced stress which is input to MIKE -21 HD Model. MIKE-21 HD model is based on the numerical solution of two- dimensional incompressible Reynolds averaged Navier-Stokes equations invoking the assumptions of Boussinesq and of hydrostatic pressure. The spatial discretization of the primitive equations is performed using a cell-centred finite volume method (MIKE 21, 2014).

## 4. MODEL VALIDATION

Hydrodynamic model simulations under the prevailing conditions at the study area are carried out. It could be seen in model bathymetry (refer Fig. 4) that there are three open boundaries at the east, north and south directions in open sea region, and a boundary in the upstream of the creek. No cross flow flux is provided at the west boundary. Validation parameters such as bottom roughness coefficient, eddy viscosity are adjusted and simulations are repeated by changing these parameters until computed current value matches well with the field observed data.

The computational model considered for tidal flow simulations covers the creek region and the extended portion up to -12 m contours in the offshore region. Location of current observation 'A' at the site is also shown in Fig. 4. The model area is discretized into a number of triangular grids with flexible mesh. The study area is mainly influenced by tides and accordingly the hydrodynamic model is simulated tidal boundary conditions with appropriate phase lag at various boundaries. The model is simulated for one month continuously covering both spring and neap tides.

For calibration of the model, the model boundaries and other model parameters (eddy viscosity 0.28; bed resistance 40 m1/3/s) are adjusted in such a way that simulated tidal currents at the offshore region in the model would be generated up to the order of 0.45 m/s. Quantitatively current magnitude of observed and computational current at Location 'A' is matching well as shown in Fig. 6. However, peak current during the model simulation obtained at the creek inlet is of the order of 1.0 m/s.

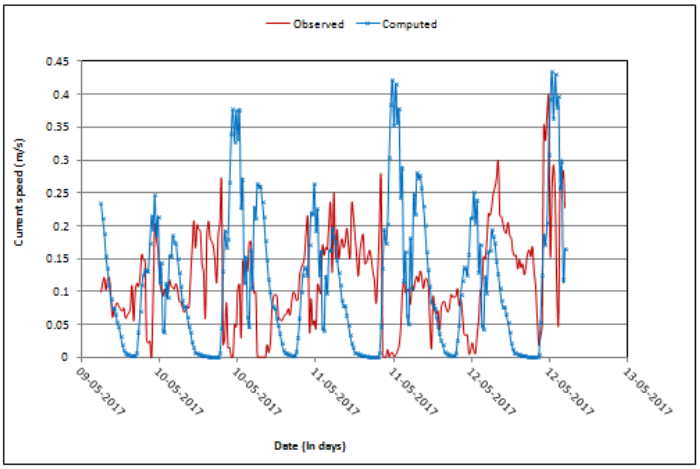



**Fig. 6: Comparison of current speed at Location 'A'**

## 5. MODEL EXPERIMENTS

The calibrated model is used for the experiment with the proposal of replacing the part of solid jetty with a piled jetty, incorporated in the local model bathymetry under the existing site condition as shown in Fig. 7. In the proposed scenario total 18 piles having 1m diameter each, are incorporated in the model. Out of 170 m length, 80 m is covered by the solid portion and the remaining 90 m with pile structures. The width of jetty/ berthing face would be about 7.0 m. The structure was oriented properly based on the flow field prevailing at the jetty location in the site. In order to assess hydrodynamic change in the study area due to the

proposed condition, coupled models were simulated for a period of 30 days under the prescribed calibrated boundary conditions. Effect of wave propagation in the form of wave radiation stresses was also considered in the model simulations.

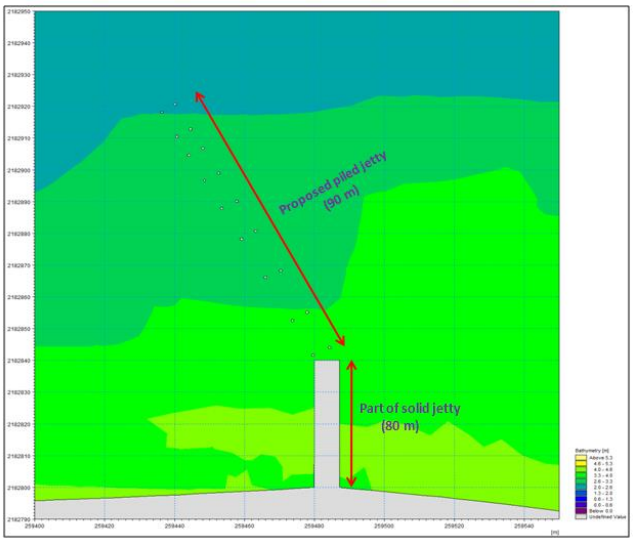
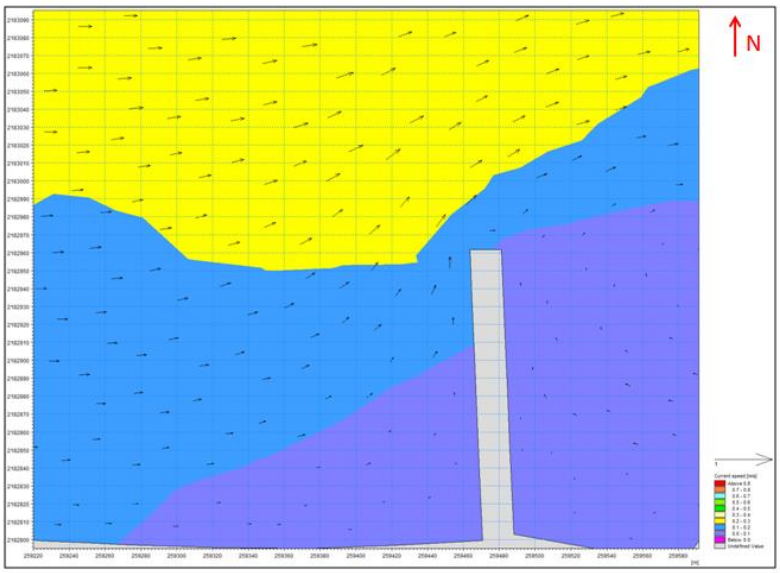


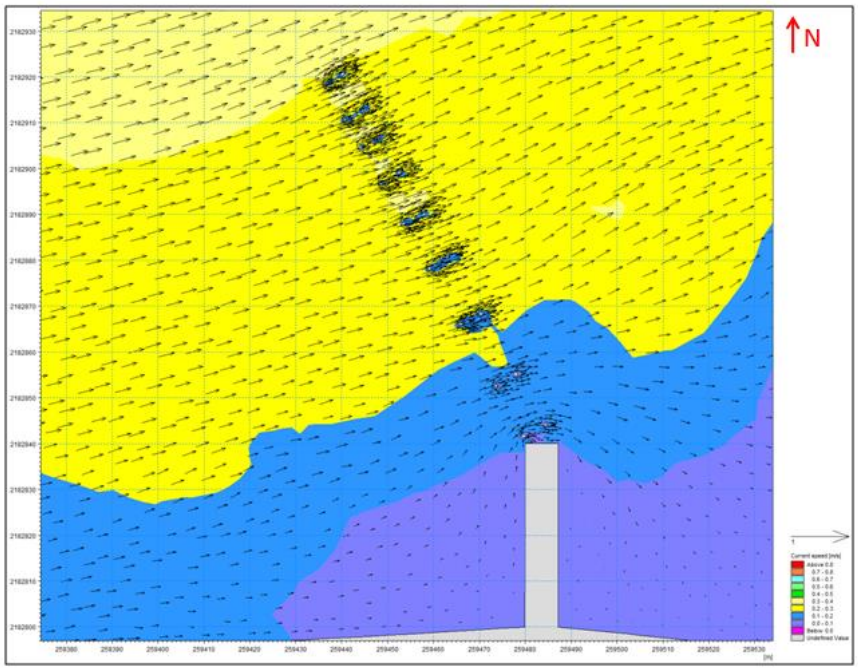

**Fig.7: Part of Bathymetry with Piled jetty**

## 6. RESULTS AND DISCUSSION

Instantaneous flow field near the jetty region is shown in Figs. 8 (a-b). Flow field with solid jetty in the creek is presented in the Fig. 8(a), whereas flow field with semi piled jetty is presented in Fig. 8(b). From the figures it can be noticed that flow depth near the semi piled jetty is comparatively more than that of solid jetty. Current speed near the solid jetty is the order of 0.1 m/s and on both sides of the jetty there exist stagnation of water with no currents at all. The current speed all around the pile jetty is found to be of the order of 0.25 m/s, which is about 2.5 times more than that of the solid jetty. It is also noticed that near the pile jetty head, the flow is streamlined and the current speed increased up to the order of 0.35 m/s.




(a) With 170 m solid jetty




(b) With semi piled jetty (90 m piled & 80 m solid)

**Fig. 8: Flow pattern in model area near jetty location**

## 7. CONCLUSIONS

Based on the present studies undertaken for tidal hydrodynamics, following conclusions are drawn:

1) Flow velocity is streamlined through the gap of piers of piled jetty.
2) Magnitude of current speed near the piled jetty is increased from 0.1 m/s to 0.25 m/s which regulate the flow in the jetty region.
3) Water level inside the creek region is fluctuating with tide and there does not exist stagnation of water during low tide.
4) The piled jetty is found to be suitable as there is no stagnation of water occurring near the jetty resulting into the restoration of navigation in the creek.
5) Dredging of channel in the creek region would also be required.

## 8. ACKNOWLEGDMENT

The authors are grateful to Shri A.K. Agrawal, Director, CWPRS for his guidance and constant encouragement during the course of study. The authors express their deep gratitude for according permission to publish this paper.

## REFERENCES

Caldwell R.L., Edmonds D.A.(2014), A numerical modelling study of the effects of sediment properties on deltaic processes and morphology, journal of Geophysics Research: Earth surface 119(5),961-982,2014.

Ershadi S., Arasteh M. and M. Tajziehchi (2013). Numerical Modelling of Flow Pattern Changes in Tidal Inlet of TIYAB Port, Research Journal of Environmental and Earth Sciences 5(11): 691-702.

Hossain, S. (2016). Application of mathematical model to assess sediment movement pattern along nearshore coastal water, J. Earth Science and Engineering, 177-182.

MIKE 21 (2014). Scientific background, DHI, Denmark.

TR No.5582 (2018). Mathematical model studies for tidal hydrodynamics and siltation for proposed development of training wall at inlet of Satpati (Maharashtra), CWPRS, Pune, India.

Uddin M., Alam , J.B., Khan , Z.H., Hasan , G.M. J. and Rahman , T. (2014) Two Dimensional Hydrodynamic Modelling of Northern Bay of Bengal Coastal Waters . Computational Water, Energy, and Environmental Engineering, 140-151.

*IN PROCEEDINGS OF 25th HYDRO 2020, INTERNATIONAL CONFERENCE, NATIONAL INSTITUTE OF TECHNOLOGY ROURKELA, ODISHA, INDIA 26-28, March 2021, ISBN 978-93-90631-56-8*

Paper ID - 200

# Estimation of Wave Loads on Deck Structures at Indian Ports in a Changing Climate

Akhila Padmajan[1], Rameeza Moideen[2], Manasa Ranjan Behera[3]

[1]*Department of Civil Engineering, Indian Institute of Technology Bombay, Mumbai, 400076, India*
[1]akhilapadmajan@gmail.com; [2]rameezasindoora@gmail.com; [3]manasa.rb@gmail.com

## Abstract

Coastal structural damage has been a serious issue in past decades due to changes in various ocean environmental parameters and increased frequency of extreme events. The present study focuses on the estimation of wave loads on typical coastal deck structures at major Indian ports in a changing climate scenario. The percentage changes in wave height and sea level rise (SLR) due to climate change at the end of the design life of the structures were considered from the recent past studies. The vertical and horizontal impact forces on deck structures are computed using suitable method suggested by Xu (2015). The effect of climate change has been investigated by applying the future ocean climate characteristics, such as future wave height conditions and sea level rise scenarios. The computed impact forces are compared with the current ocean state impact force estimation to assess the percentage change due to climate change. The impact forces are estimated on the deck structures located at different airgaps that may arise under the rising sea level condition. Overall, the study concluded that there is a significant change in impact forces on coastal deck structures due to climate change, where the percentage change varies with varying airgaps and port location. The vertical force is increasing for smaller air gaps only whereas horizontal force increases for increasing air gaps. Thus, it is necessary to consider the increasing impact forces for design of future deck structures at port facilities and along coastal locations.

***Keywords:*** *Wave Load; Coastal deck; Ports; Climate change; Sea level rise; Extreme events; Airgap*

## 1. Introduction

Intergovernmental Panel on Climate Change (IPCC) has defined climate change as the change in the state of climate that can be identified using statistical tests and that persists for an extended period, typically decades or longer (IPCC 2019). Climate change has become a major focus of attention of the scientific community because of its potential hazards and impacts on our environment in the near future. The impacts on global climate change due to the green house effects on the Earth's surface require assessment and adaptation for the future of our society.

The average air and ocean temperatures over the Earth is increasing due to global warming as an impact of natural long-term cycles as well as man made changes (Church et al. 2001; IPCC 2007). It is found that since the mid-1970s, the average surface temperature has increased by about 1°F and the current warming rate is about 0.29°F per decade (Deepthi and Deo 2010). Both the melting of ice in the Arctic regions and changes in the wind pattern are induced by global warming. The major effects due to these changes are rise in sea level and increased intensity and frequency of extreme events.

Ocean environment is highly susceptible due to the impact of climate change. Although, coastal vulnerability assessments focus mainly on SLR, it is not the only physical process of concern to coastal communities. As pointed out by various authors (Bengtsson et al. 2006; Weisse and Von Storch 2010), the greenhouse effects and the complex interactions of atmospheric processes may produce changes in near-surface wind and pressure patterns, which, in turn, can affect the pattern of all the wave parameters. In the coastal region of East Anglia (UK), wave statistics are sensitive to the trend in sea level rise. For nearshore points, the increase of the mean sea level alters not only extreme wave heights but also the frequency of occurrence of extreme wave conditions (Chini et al. 2010).

The evidence of anthropogenic climate change is widely accepted in the scientific community and many of the observed changes for the period 1950 onwards are unprecedented from over decades to centuries (Stocker et al. 2013). Climate change signals were detected in the North Atlantic, Equatorial Pacific and Southern Ocean in the current decade of 2010 – 2020. The studies showed that these changes in climate are detectable in 60% of the global ocean area until 2060. Also, reversible changes were expected in more than 3% of ocean area (Dobrynin et al. 2015). A general trend of increasing wind speed, wave height, sea level rise, etc., are found throughout the globe. At the 99$^{th}$ percentile, wave height is increasing at the rate of 0.5% per year (Young et al. 2011) and the global mean sea level rises at the rate of 3.1 ± 0.7 mm/year with an accelerating tendency (Timmermann et al. 2010). The climate change not only cause increase in the rate but also significantly cause reduction in certain areas.

Chowdhury et al. (2019) presented a study along the Indian coastline for two different time slices 2011-2040 and 2041-2070 using an ensemble of five general circulation models (GCMs) under RCP 4.5 emission scenario. Mean annual significant and maximum wave heights are projected to increase along much of the Indian coast. East coast is expected to experience much higher waves compared to the west coast. The SLR along the west coast is somewhat higher than the global one, which could be due to typical changes in future circulation patterns around the Indian coastline. The study presented an initial contribution towards the climate change impacts in Indian Ocean region.

Although a large number of works have been done to assess the impacts of climate change on various ocean environmental parameters, their direct effect on the wave load on coastal deck structures have been relatively less studied.

Wave loading on decks of coastal structures is a complex non-linear phenomenon, which may affect the structural integrity and reliability. The wave conditions in coastal waters are different from those in the ocean and on the open sea. The wave-induced water particle velocities and accelerations are stronger in the coastal waters, which interact over the width of a deck span with corresponding variations in wave forces (Marin and Sheppard 2009). Interaction of surface waves with the coastal deck is a complex problem, involving fluid–structure interaction, wave breaking, and overtopping. Possible submergence of the deck and entrapment of air pockets between girders can increase destructive forces and add to the complexities of the problem. Even though significant effort has been devoted to the development of predictive methods for wave loads on vertical structures such as piles, seawalls, etc., horizontal, bridge span like structures have received little attention (Denson 1980).

Most studies focused on the adaptation of in-service phase, which includes repair and retrofit measures to prevent the damage caused due to the impacts of climate change. Mondoro et al. (2018) reviewed about the current challenges on bridge management due to the anthropogenic and natural climate changes. The various complexities of climate change and potential measures for the adaptation, repair and retrofit were outlined. Some methodologies including stochastic and robust optimization methods for planning under uncertainty due to the impacts of climate changes were also discussed. Rather than this measure, more potential efforts can be made in the calculation of wave loads during the design phase to mitigate these effects of climate change.

A recent study was done regarding the vertical impact force on coastal bridge deck by generating a solitary wave to represent the extreme wave conditions using REEF3D and analysed the effects of various parameters like increasing wave height, girder spacing and girder depth on the peak vertical impact force (Moideen et al. 2019). The present study goes beyond these studies and aims to evaluate the increase in wave impact forces on a typical coastal deck structure due to the effects of climate change at specific locations near the major ports along the Indian coast. The impact forces are calculated with future ocean climate characteristics, such as future wave height and sea level rise scenarios and are compared with the current ocean state impact forces to assess the percentage change due to climate change. The study is done for all the major Indian port locations and different airgaps that may arise under rising sea level condition.

## 2. Methodology

### 2.1 *Selection of Method*

The wave-deck interaction is a very complicated process which involves various structural complexities and wave conditions. There are various theoretical formulations which have already been developed to estimate the wave load on coastal deck structures.

The existing theoretical approaches established by McConnell et al. (2004), Douglass et al. (2006), Cuomo et al. (2007), AASHTO (2008) and Yim et al. (2011) were studied in detail and compared on the basis of various parameters. Various aspects such as, considering inertia forces in the estimation of wave force; comparison of the results of wave forces to the values obtained from the numerical methods (Xu 2015); applicability in case of solitary waves; applicability in case of submerged conditions of the deck and considering hydrodynamic effects in the estimation of wave forces. It was understood that these methods could predict wave induced forces on coastal deck structures other than solitary waves. McPherson (2008) proposed a method to better assess solitary wave forces that is comparable to process based numerical model results.

Xu (2015) reported that the method proposed by McPherson (2008) performs better since the overtopping water on deck and the hydrostatic force due to water at the back side of the deck are considered in this method. But it is also evident that the hydrodynamic effects should be considered by taking into the account of the effects of wave period, wave types and water particle velocities near the structure in order to obtain more realistic results and incorporate the impacts of climate change. Xu (2015) suggested an improved version of the method proposed by McPherson (2008) by including hydrodynamic effects in order to make more reliable predictions for solitary wave forces on bridge decks.

### 2.2 *Locations of Study*

The impacts of climate change on various ocean environmental parameters showed a general trend of increasing wave heights, sea level rise and increased frequency of extreme events even though a decreasing trend is found at some locations. Hence, these effects are more region specific and needs to be evaluated at concerned locations.

India has a vast coastline of approximately 7500 km. The developmental activities in the coastal regions especially the port locations provide a significant contribution to the economic development of the country. Thus, the major port locations all along the Indian coast were considered for this study. A total of 12 locations near the 12 major ports were chosen for this study out of which 6 locations are in the west coast and the other 6 locations are in the east coast of India. The locations considered for this study near the major ports are shown along the Indian coast in Figure 1. The latitude, longitude and all the important wave parameters at these locations along with the relative sea level rise (SLR) and the percentage change in wave height from the previous studies done on the impacts of climate change on various ocean environmental parameters at these locations are given in Table 1.

### 2.3 *Estimation of Wave Loads*

The vertical and horizontal wave impact forces are calculated at these locations using the method suggested by Xu (2015). The total vertical impact force is a combination of hydrostatic force, buoyancy due to the bridge volume, force due to air entrapment inside the chambers and the uplift force. The hydrostatic force is calculated by subtracting the overtopping water on the top of the deck. The total horizontal impact force is a combination of hydrostatic force at the front and trailing edge of the deck and the drag force. The equations used in the estimation of wave impact forces are given in equations (1) to (12). Some of the parameters used in this method are illustrated in Figure 2.

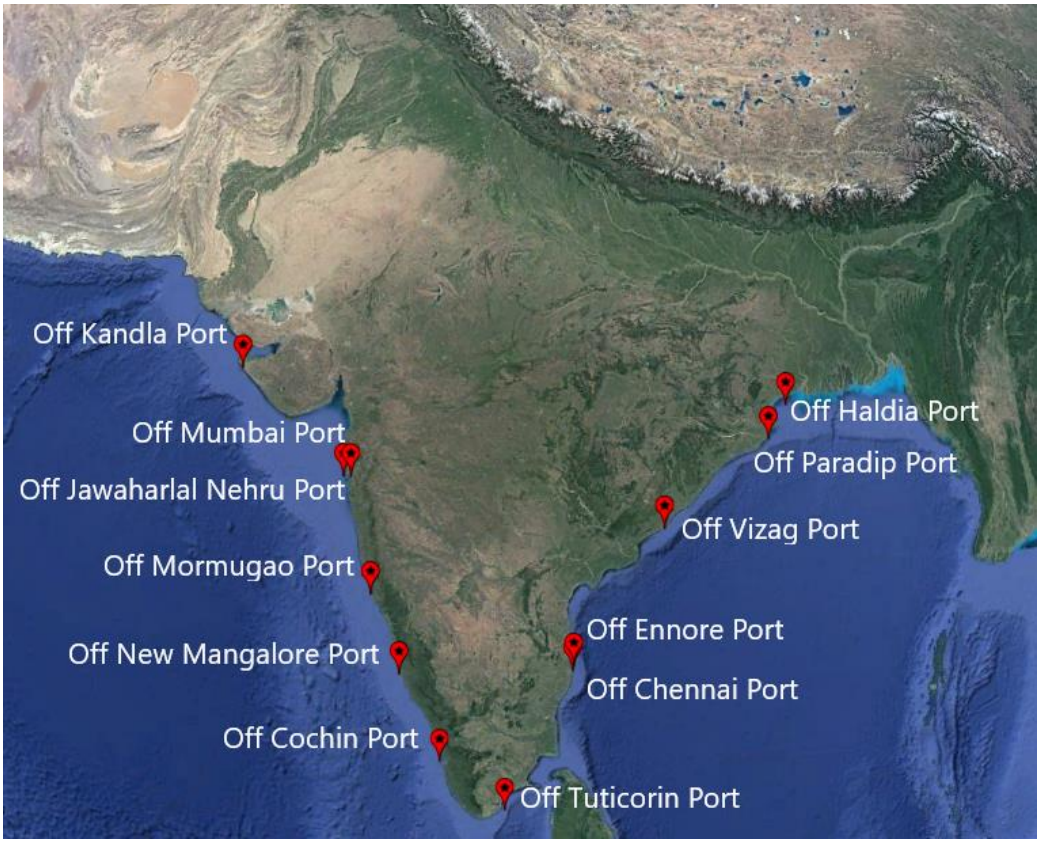



**Figure 1** The locations considered for the study shown along the Indian coast (Source: Google Earth Pro)

**Table 1** Important parameters at the study locations (Source: Patil 2019)

| Sl. No | Location | Latitude (°N) | Longitude (°E) | Water Depth (m) | Design Significant Wave Height, $H_s$ (m) | Breaking Wave Height, $H_b$ (m) | Percentage Change in $H_s$ (%) | Relative SLR (mm/yr) |
|---|---|---|---|---|---|---|---|---|
| 1 | Kandla Port | 22.083 | 69.083 | 19 | 4.06 | 0.83 | -5 | 6.15 |
| 2 | Jawaharlal Nehru Port | 18.943 | 72.708 | 15 | 2.64 | 0.37 | 20 | 6.10 |
| 3 | Mumbai Port | 18.943 | 72.708 | 15 | 2.64 | 0.43 | 20 | 6.10 |
| 4 | Mormugao Port | 15.333 | 73.750 | 20 | 3.8 | 0.67 | 40 | 5.82 |
| 5 | New Mangalore Port | 12.833 | 74.750 | 17 | 3.85 | 0.67 | 20 | 5.77 |
| 6 | Cochin Port | 10.018 | 76.119 | 18 | 3.54 | 0.65 | 10 | 5.87 |
| 7 | Tuticorin Port | 8.417 | 78.250 | 20 | 3.54 | 0.46 | 45 | 5.89 |
| 8 | Chennai Port | 13.217 | 80.349 | 18 | 5.54 | 0.84 | 18 | 5.63 |
| 9 | Ennore Port | 13.217 | 80.349 | 18 | 5.54 | 0.84 | 18 | 5.61 |
| 10 | Vizag Port | 17.550 | 83.206 | 18 | 5.04 | 0.97 | 45 | 5.49 |
| 11 | Paradip Port | 20.250 | 86.750 | 20 | 4.54 | 0.92 | 45 | 5.70 |
| 12 | Haldia Port | 21.296 | 87.388 | 13 | 2.69 | 0.31 | 25 | 5.76 |

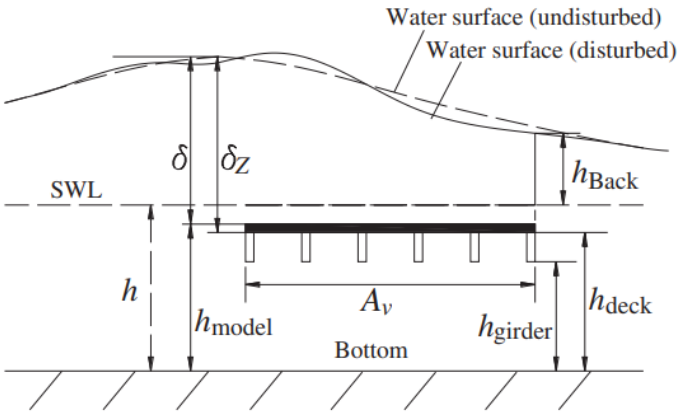



**Figure 2** Definition sketch proposed by Xu (2015) for the parameters used in the method

$$F_v = F_{hydrostatic} + F_{bridge} + F_{air\ entrapment} + F_l \quad (1)$$

$$F_v = \Upsilon\delta_z A_v - F_w + \Upsilon Vol_{bridge} + (N-1)\frac{1}{2}\Upsilon\delta_G A_G + 0.5 * \rho C_l A_v u^2 \quad (2)$$

If the SWL is below the top of the deck and no overtopping water exists i.e., $h + \eta_{max} \leq h_{model}$

$$F_w = 0 \quad (3)$$

If the SWL is below the top of the deck but overtopping water exists, i.e., $h \leq h_{model} < h + \eta_{max}$

$$F_w = C_w \Upsilon \delta A_v \quad (4)$$

If the SWL is above the top of the deck, i.e., $h > h_{model}$

$$F_w = C_w \Upsilon \delta A_v + \Upsilon(h - h_{model})A_v \quad (5)$$

$$F_h = F_{hydrostatic_front} - F_{hydrostatic_back} + F_D \quad (6)$$

If the front girder is partially submerged, i.e., $h_{girder} < h + \eta_{max} < h_{model}$

$$F_{hydrostatic_front} = 0.5 * (\eta_{max} + h - h_{girder}) H_{bridge} L_{bridge} \Upsilon \quad (7)$$

If the front girder is fully submerged, i.e., $h + \eta_{max} > h_{model}$

$$F_{hydrostatic_front} = 0.5 * [(\eta_{max} + h - h_{girder}) + (\eta_{max} + h - h_{model})] H_{bridge} L_{bridge} \Upsilon \quad (8)$$

If the back girder is above the water, i.e., $h + h_{back} < h_{girder}$

$$F_{hydrostatic_back} = 0 \quad (9)$$

If the back girder is partially submerged, i.e., $h_{girder} < h + h_{back} < h_{girder} + H_b$

$$F_{hydrostatic_{back}} = 0.5 * (h + h_{back} - h_{girder})^2 L_{bridge} \Upsilon \quad (10)$$

If the back girder is fully submerged, i.e., $h + h_{back} > h_{girder} + H_b$

$$F_{hydrostatic_{back}} = 0.5 * (2h + 2h_{back} - h_{girder} - h_{model}) H_{bridge} L_{bridge} \Upsilon \quad (11)$$

$$F_D = 0.5 * \rho C_D A_h u^2 \quad (12)$$

where, $F_l$ is the uplift force; $F_D$ is the drag force; $C_D$ and $C_l$ are the drag and lift coefficients, respectively, and they are typically taken as 1.0 in this study; N is the number of girders; $C_w$ is an empirical factor to facilitate the consideration of the water on deck and is taken as 0.6 when $h \leq h_{model}$ and 0.7 when $h > h_{model}$; $h_{back}$ is the possible water height above the SWL at the trailing edge of the bridge deck and it is related to the effective wave length, the wave height, the water depth, the wave speed and the geometry of the bridge superstructure and its value ranges from 0.4 m (for smaller wave heights) to 0.8 m (for higher wave heights); and u is taken as the horizontal velocity of the water particle at the SWL located at the section of the wave crest and at the level of object for subaerial and submerged cases, respectively.

The water particle velocity u of the solitary wave of the second-order (Sarpkaya & Isaacson 1981) is expressed in equation (13)

$$\frac{u}{\sqrt{gd}} = \varepsilon \operatorname{sech}^2 q + \varepsilon^2 \operatorname{sech}^2 q \left\{\frac{1}{4} - \operatorname{sech}^2 q - \frac{3}{4}\left(\frac{s}{d}\right)^2 (2 - 3\operatorname{sech}^2 q)\right\} \quad (13)$$

where, $\varepsilon = \frac{H}{d}$; $q = \frac{\sqrt{3\varepsilon}}{2d}\left(1 - \frac{5}{8}\varepsilon\right)(x - ct)$; $s = y + d$; d is the still water depth, H is the wave height and y is the distance from the SWL and is negative if it is in the same direction with the gravitational acceleration. Hence, the wave celerity can be calculated as in equation (14)

$$\frac{c}{\sqrt{gd}} = 1 + \frac{1}{2}\varepsilon - \frac{3}{20}\varepsilon^2 \quad (14)$$

The effect of climate change has been introduced by considering the future ocean environmental characteristics. The percentage changes in wave height and sea level rise (SLR) due to climate change at the end of the design life of the structures at the major Indian port locations were considered from the recent past study done by Patil (2019). After introducing the climate change impacts on wave height and sea level rise, the impact forces are calculated again to estimate the percentage changes occurring in these forces due to climate change at all the major port locations. Further, the study is extended to calculate the variation in wave impact forces on the deck structures located at different airgaps that may arise under the rising sea level condition.

## 2.4 *Results and Discussions*

The vertical and horizontal wave impact forces on the deck structure with and without the climate change impact and the percentage changes in these forces due to the climate change were calculated at different airgaps between the bottom of the deck and the SWL for each study locations. The increase in wave force due to climate change impacts for different values of airgaps between the bottom of the deck and the SWL is more drastic in case of horizontal force as compared to the vertical force. These general trends showed an exception in case of the location near the Kandla Port in which both the vertical and horizontal wave forces tend to decrease due to the impacts of climate change since this location is expected to experience a decrease in wave height due to climate change.

An example for the plots showing the variation in vertical and horizontal wave impact forces due to climate change and their percentage changes by varying the airgap between the deck and the SWL that pertain to the New Mangalore Port is shown in Figure 3 and Figure 4, respectively while the tabulated results are given in Table 2. It is evident from the plots that an increase in vertical impact force was observed at this location for smaller airgaps but later observed a decrease in this force for further higher values of airgaps due to the impacts of climate change. But in case of horizontal impact force at this location, an increase in impact force was observed for all the values of airgaps.

The bar chart comparison of the variation in vertical and horizontal wave impact forces due to climate change at varying airgaps at all the considered locations are shown in Figure 5 and Figure 6,

respectively. It is clearly evident from the results that the variation in both the vertical and horizontal wave impact force due to the impacts of climate change is more drastic in case of east coast than west coast. The maximum variation in the vertical impact force is observed at Paradip port at an air gap of 4 m whereas the maximum variation in the horizontal impact force is observed at Tuticorin port at an air gap of 5 m. The general trends showed an exception in case of Kandla Port in which both the vertical and horizontal wave forces tend to decrease due to the impacts of climate change since this location is expected to experience a decrease in wave height due to climate change.

**Table 2** Variation in wave force due to climate change by varying airgap at a location near the New Mangalore Port

| Sl. No | Air Gap (m) | Vertical Force | | | Horizontal Force | | |
|---|---|---|---|---|---|---|---|
| | | Without Climate Change (kN) | With Climate Change (kN) | Percentage Change (%) | Without Climate Change (kN) | With Climate Change (kN) | Percentage Change (%) |
| 1 | 0.5 | 31217.66 | 38448.48 | 23.16 | 8767.18 | 11159.81 | 27.29 |
| 2 | 1.0 | 28923.98 | 36154.80 | 25.00 | 8767.18 | 11159.81 | 27.29 |
| 3 | 2.0 | 24215.90 | 31516.38 | 30.15 | 6961.41 | 9950.68 | 42.94 |
| 4 | 3.0 | 19387.10 | 26687.58 | 37.66 | 4491.68 | 7609.89 | 69.42 |
| 5 | 4.0 | 25543.82 | 21858.78 | -14.43 | 2794.05 | 5094.89 | 82.35 |
| 6 | 5.0 | 37615.82 | 27026.80 | -28.15 | 1536.55 | 3323.70 | 116.31 |

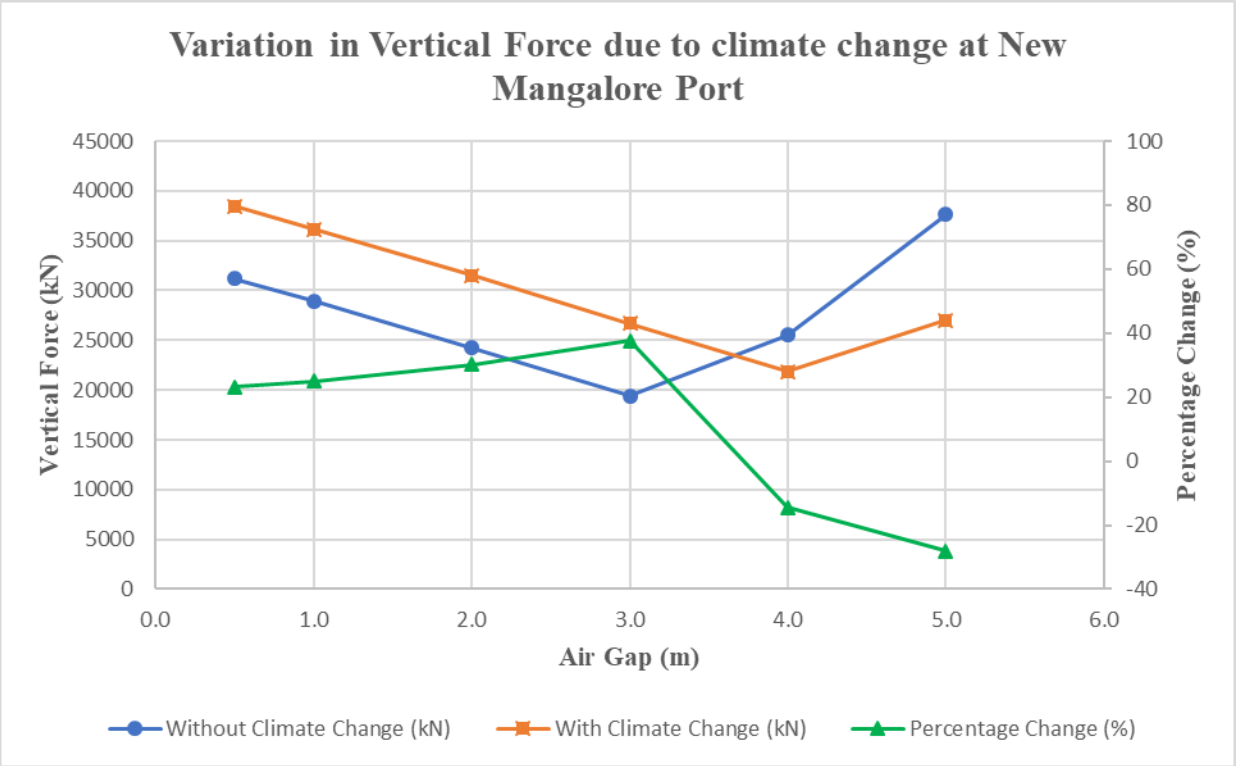



**Figure 3** The plot showing the variation in vertical force due to climate change by varying airgap at a location near the New Mangalore Port

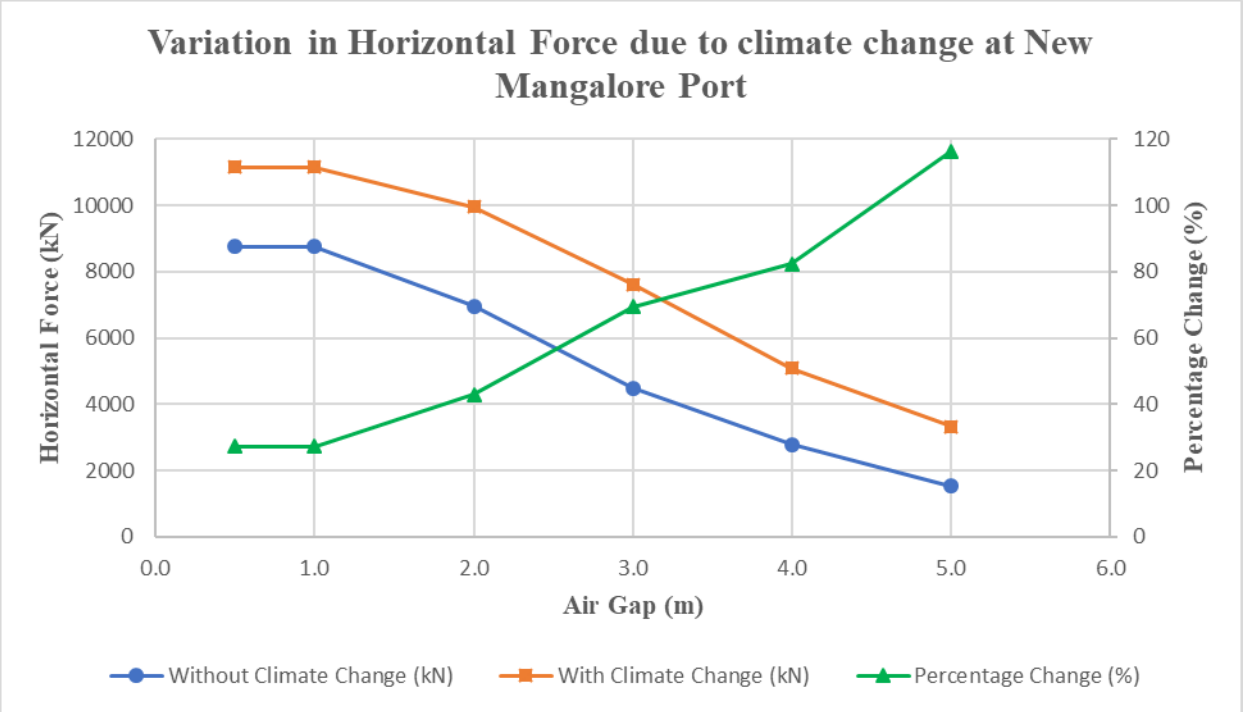



**Figure 4** The plot showing the variation in horizontal force due to climate change by varying airgap at a location near the New Mangalore Port

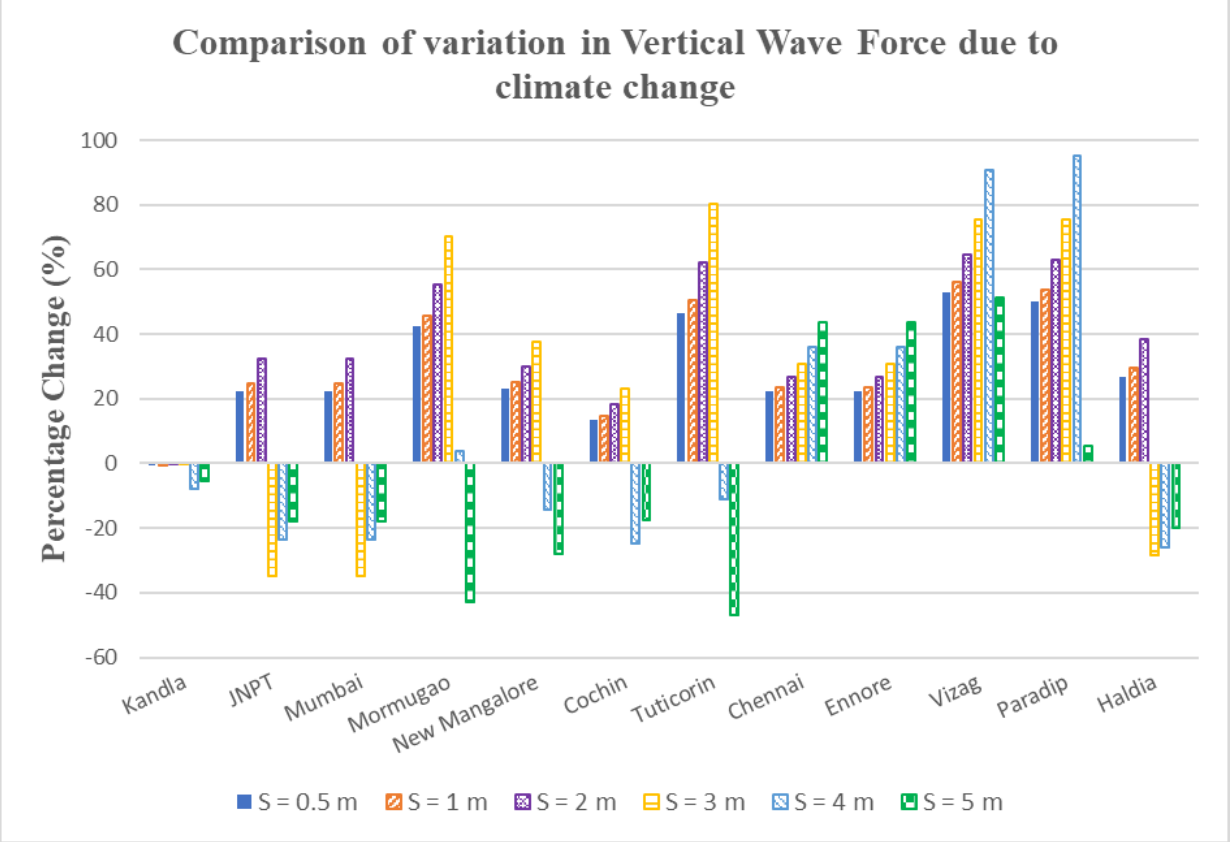



**Figure 5** The bar chart comparison of the variation in vertical force due to climate change by varying airgap at all the considered port locations

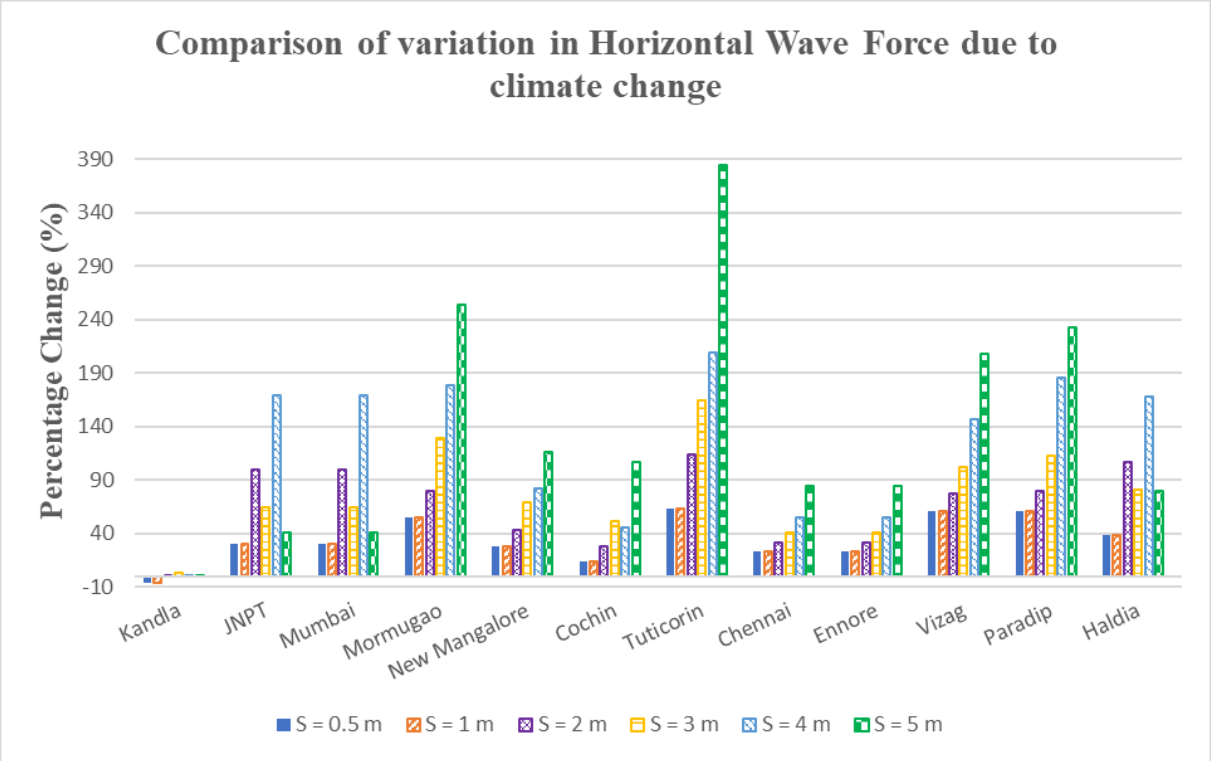



**Figure 6** The bar chart comparison of the variation in horizontal force due to climate change by varying airgap at all the considered port locations

## 3. Conclusions

The expected variation in vertical and horizontal impact forces on deck structures at Indian ports due to climate change over a period of 50 years were estimated. An extended parametric study was also done to analyse this variation under different airgap scenarios. The following conclusions were drawn from the present study:

- An increase in vertical impact force was observed due to the impacts of climate change for smaller airgaps and later observed a decrease in this force due to climate change for further higher values of airgaps between the bottom of the deck and the SWL.
- In case of horizontal impact force, an increase in this force was observed due to the impacts of climate change for all the values of airgaps.
- The increase in vertical impact forces due to climate change with varying airgaps for elevated structures is not much evident as compared to the increase in horizontal forces.
- The increase in wave impact force due to the impacts of climate change for different values of airgaps is more drastic in case of horizontal force as compared to the vertical force.
- These general trends showed an exception in case of the location near the Kandla Port in which both the vertical and horizontal impact forces tend to decrease due to the impacts of climate change since this location is expected to experience a decrease in wave height due to climate change.

Overall, the study shows that there is a significant change in the vertical and horizontal wave impact forces on the costal deck structure due to climate change, even though, the percentage change could vary with varying airgaps and with different locations. Thus, it is necessary to account for the changing

climate impact on the ocean parameters while designing the structure for future projects and even while retrofitting the existing structures.

## References

AASHTO (American Association of State Highway and Transportation Officials). (2008). *Guide Specifications for Bridges Vulnerable to Coastal Storms*. The AASHTO code, Washington D.C.

Bengtsson, L., Hodges, K. I., and Roeckner, E. (2006). Storm tracks and climate change. *Journal of Climate*, *19*(15), 3518-3543.

Yim, S. C., Boon-Intra, S., Nimmala, S. B., Winston, H. M., Azadbakht, M., & Cheung, K. F. (2011). *Development of a guideline for estimating tsunami forces on bridge superstructures* (No. OR-RD-12-03). Oregon. Dept. of Transportation. Research Section.

Chini, N., Stansby, P., Leake, J., Wolf, J., Roberts-Jones, J., & Lowe, J. (2010). The impact of sea level rise and climate change on inshore wave climate: A case study for East Anglia (UK). *Coastal Engineering*, *57*(11-12), 973-984.

Chowdhury, P., Behera, M. R., and Reeve, D. E. (2019). Wave climate projections along the Indian coast. *International Journal of Climatology*, *39*(11), 4531-4542.

Church, J. A., Gregory, J. M., Huybrechts, P., Kuhn, M., Lambeck, K., Nhuan, M. T., Qin, D. and Woodworth, P. L. (2001). Changes in Sea Level, in: J. T Houghton, Y. Ding, D.J. Griggs, M. Noguer, P.J. Van der Linden, X. Dai, K. Maskell, and C.A. Johnson (eds.): Climate Change 2001: The Scientific Basis: Contribution of Working Group I to the Third Assessment Report of the Intergovernmental Panel.

Cuomo, G., Tirindelli, M., and Allsop, W. (2007). Wave-in-deck loads on exposed jetties. *Coastal Engineering*, *54*(9), 657-679.

Deepthi, R., and Deo, M. C. (2010). Effect of climate change on design wind at the Indian offshore locations. *Ocean Engineering*, *37*(11-12), 1061-1069.

Denson, K. H. (1980). *Wave forces on causeway-type coastal bridges: Effects of angle of wave incidence and cross-section shape* (No. MSHD-RD-80-070 Final Rpt.).

Dobrynin, M., Murawski, J., Baehr, J., and Ilyina, T. (2015). Detection and attribution of climate change signal in ocean wind waves. *Journal of Climate*, *28*(4), 1578-1591.

Douglass, S. L., Chen, Q., Olsen, J. M., Edge, B. L. and Brown, D. (2006). *Wave forces on bridge decks*. Final Report for U.S. Department of Transportation, Federal Highway Administration, Office of Bridge Technology, Washington D.C.

https://www.ipcc.ch/site/assets/uploads/2019/01/SYRAR5-Glossary_en.pdf retrieved on 2020/09/05

IPCC (2007). *Climate change 2007-impacts, adaptation and vulnerability: Working group II contribution to the fourth assessment report of the IPCC*. Vol. 4. Cambridge University Press, 2007.

Marin, J., and Sheppard, D. M. (2009). Storm surge and wave loading on bridge superstructures. *Structures Congress 2009: Don't Mess with Structural Engineers: Expanding Our Role*, 1-10.

McConnell, K., Allsop, W., Allsop, N. W. H., & Cruickshank, I. (2004). *Piers, jetties and related structures exposed to waves: guidelines for hydraulic loadings*. Thomas Telford Press, London, 148

McPherson, R. L. (2008). *Hurricane induced wave and surge forces on bridge decks*. Master's thesis, Texas A & M University.

Moideen, R., Ranjan Behera, M., Kamath, A., and Bihs, H. (2019). Effect of girder spacing and depth on the solitary wave impact on coastal bridge deck for different airgaps. *Journal of Marine Science and Engineering*, *7*(5), 140.

Mondoro, A., Frangopol, D. M., and Liu, L. (2018). Bridge adaptation and management under climate change uncertainties: A review. *Natural Hazards Review*, *19*(1), 04017023.

Patil, R. G. (2019). *Climate Change Impact on Ocean Parameters around the Indian Coastline*. Master Thesis Project Report, Indian Institute of Technology, Bombay.

Sarpkaya, T., & Isaacson, M. (1981). *Mechanics of wave forces on offshore structures*. New York, NY: Van Nostrand Reinhold.

Stocker, T. F., Qin, D., Plattner, G. K., Tignor, M., Allen, S. K., Boschung, J., and Midgley, P. M. (2013). Climate change 2013: The physical science basis. *Contribution of working group I to the fifth assessment report of the intergovernmental panel on climate change*, 1535.

Timmermann, A., McGregor, S., and Jin, F. F. (2010). Wind effects on past and future regional sea level trends in the southern Indo-Pacific. *Journal of Climate*, *23*(16), 4429-4437.

Weisse, R., and Von Storch, H. (2010). Past and future changes in wind, wave, and storm surge climates. In *Marine Climate and Climate Change*, Springer, Berlin, Heidelberg, 165-203

Xu, G. (2015). *Investigating Wave Forces on Coastal Bridge Decks*. LSU Doctoral Dissertations. 1468.

Young, I. R., Zieger, S., and Babanin, A. V. (2011). Global trends in wind speed and wave height. *Science*, *332*(6028), 451-455.

IN PROCEEDINGS OF 25th HYDRO 2020, INTERNATIONAL CONFERENCE,
NATIONAL INSTITUTE OF TECHNOLOGY ROURKELA, ODISHA, INDIA
26-28, March 2021, ISBN 978-93-90631-56-8

Paper ID - 204

# Effect of wave steepness on wave overtopping discharge of an emerged quarter-circle breakwater

Vishwanatha Mane[1]*, Subba Rao[2], A.Vittal Hegde[3]

[1*]*Research Scholar, Department of Water Resources and Ocean Engineering, National Institute of Technology Karnataka, Surathkal – 575 025. India, Email: vishwanathmanel@gmail.com*
[2]*Professor, Department of Water Resources and Ocean Engineering, National Institute of Technology Karnataka, Surathkal – 575 025. India, Email: surakrec@gmail.com*
[3]*Professor (Retd.), Department of Water Resources and Ocean Engineering, National Institute of Technology Karnataka, Surathkal – 575 025. India, Email arkalvittal@gmail.com*
**Corresponding author, Email: vishwanathmanel@gmail.com*

## Abstract

A breakwater is a structure that is commonly used in ports and harbour to protect from the onslaught of perennially hitting ocean waves. There are different types of breakwater structures developed so far by various researchers, in which Quarter circle breakwater (QBW) is also one such innovation. In the present investigations, the physical model studies are conducted on emerged non-perforated and sea-side perforated QBW with varying percentages of perforation using the wave flume available in the in Marine Structures Laboratory of Water Resources and Ocean Engineering Department, National Institute of Technology Karnataka, Surathkal, India. A model scale of 1:30 is used, along with a range wave climate of the Mangalore coast in the Karnataka state of India. The wave overtopping discharge is measured by varying wave characteristics & depth of water(d). The data gathered is analyzed by plotting non-dimensional graphs depicting the variation of $q/gH_iT$ with varying percentages of perforations (p) for values of wave steepness ($H_i/gT^2$). It is observed that the dimensionless wave overtopping discharge ($q/gH_iT$) increases with an increase in wave steepness ($H_i/gT^2$). Also, it is found that an increase in the percentage of perforation, wave overtopping discharge ($q/gH_iT$) is decreased.

***Keywords:*** *Quarter circle breakwater, incident wave steepness, wave overtopping discharge, percentage of perforations.*

## 1. Introduction

Breakwaters are one of the essential harbour structures constructed to withstand and dissipate the dynamic energy due to the action of the waves. Due to the fast-growing needs of humanity and advances in technology, different varieties of breakwaters are being developed. Quarter circle breakwater (QBW) is one such innovation derived from the basis of the semicircular breakwater. The first QBW model was developed in the Peoples Republic of China.

QBW with perforations possess advantages of caisson as well as perforated breakwaters such as low weight, require fewer materials, suited for poor soil conditions, easily transported, handled, and placed at the site, aesthetically pleasing, cost-effective, eco- friendly and stable. The most crucial benefit of QBW is the reduction in the volume of concrete as well as rubble mound foundation, because of the smaller bottom width (Binumol 2017).

## 2. Literature review

Bruce et al. (2007) investigated a major programme of 2D model test trials to establish enhanced the effect of unevenness or permeability on overtopping. Specifically, the objective was to determine the relative difference in overtopping behavior for various types of armour units leading to roughness factors for the database and for use in the neural network prediction of overtopping. It is noticeable

that in almost all cases, the wave period influences the overtopping, a more extensive wave period gives more overtopping, though the result is not very significant.

Jiang et al. (2008) studied the performance of QBW by comparing the hydraulic performances of SBW and QBW under similar hydraulic conditions. The authors had conducted a 2D (vertical) wave numerical model and physical model studies. From their research, they stated that wave overtopping in submerged conditions, they found high flow velocity and vortexes near the rear walls of QBW. It was due to the top sharp corner and sudden expansion of the flow field around QBW.

Dhinakaran et al. (2008) conducted tests to investigate the reflection characteristics, runup, hydrodynamic pressures, horizontal and vertical forces on the sea-side perforated SBW models with 7%, 11%, and 17% perforations due to the action of random waves. The variations of $K_r$ for SBW7, SBW11, and SBW17 for $h_w/h_t$ ratios equal to 0.6, 0.7, and constant $h_r/h_t$ (ratio of rubble mound height to total structure height ) equal to 0.18 were analyzed. The results indicate that $K_r$ increases with the increase in $h_w/L$ for all the $h_w/h_t$ and decreases with the increase in perforations from 7% to 11%. Experiments on runup were analyzed and shown that the runup ($R_u/H_s$, $R_u$ = runup and Hs = significant wave height) decrease with the increase in $h_w/h_t$ and also decrease with the increase in the percentage of perforations from 7% to 11%.

Binumol et al. (2015) conducted physical proto-type model studies on QBW with different radius and different S/D ratio. The authors found that the wave runup, which is dimensionless, increases with an increase in wave steepness for all values of $h_s/d$ and $d/gT^2$. Another observation was that $R_u/H_i$ diminishes with the increase in the water depth parameter ($d/gT^2$). It is expected that because of the high depths of water, the influence of curvature is more pronounced, and this results in the lower runup.

Binumol et al. (2017) Binumol et conducted experiments in a two-dimensional monochromatic wave flume on a sea-side perforated quarter-circle breakwater model. The data collected was analyzed by plotting the non-dimensional graphs of the reflection coefficient, $K_r=H_r/H_i$ for various values of wave steepness, $H_i/gT^2$, and R/H. It was observed that Kr increased with an increase in wave steepness, and when the freeboard ($h_c$) increased, then the reflection coefficient also increased. That is, if water depth increases, then the $K_r$ value decrease because, for smaller water depths, waves encountered were relatively vertical. Hence, fewer perforations were encountered and more reflection, whereas for more considerable water depths, waves met a more perforated surface due to the curvature effect and less $K_r$ value.

Oztunali Ozbahceci & Bilyay (2018) investigated the effect of crest parameters on the wave overtopping for armored slopes with crown walls. A series of hydraulic model experiments were explicitly conducted to investigate how the armor crest freeboard relative to the crown wall freeboard affects the wave overtopping rate. From his results indicate that while the armor crest freeboard lower than the crown wall freeboard is giving larger overtopping, higher armor crest freeboard is reducing the overtopping. However, this reduction is not the same as the reduction due to the increase in the crown wall freeboard. The reason may be the porosity of the armor crest. Also, he proposed a new correction factor is to describe the change in the wave overtopping due to the armor crest freeboard by using his experimental results.

Ramesh N et al. (2019) developed Multi-Layer Perceptron (MLP) and Radial Basis Function (RBF) networks for the prediction of hydrodynamic characteristics of QBW. Goodness-of-Fit (GoF) test using the Kolmogorov–Smirnov (KS) test statistic is applied for checking the adequacy of MLP and RBF networks to the experimental data. The authors suggested that the GoF test results and values of MPIs indicated the MLP is better suited amongst two systems adopted to evaluate the hydrodynamic performance of QBW.

Mane et al. (2019) conducted laboratory investigations to study the wave overtopping characteristics of an emerged quarter-circle breakwater. The experiments were conducted for impermeable and sea-side perforated QBW models with varying S/D ratios at a radius of 0.45m with two water depths. Finally, the authors concluded that as the wave steepness increases, the dimensionless wave overtopping discharge also increases. But the wave overtopping discharge decreases with an increase in relative freeboard.

## 3. Experimental setup and dimensional analysis

For the investigations, QBW models of the radius (R = 0.45m) and percentage of perforations chosen 0%, 5%, and 20% for the study. The BW model dimensions are chosen to satisfy the condition that the model will have emerged at all water depths (0.40m, 0.425m, and 0.45m). Figures 1 and 2 show the cross-sections of non-perforated (p = 0%) and perforated (p = 5% and 20%) QBW models. The planned model of BW consists of two parts, the bottom concrete slab and the top quarter-circle shaped caisson. Galvanized Iron (GI) sheet of 0.002m thickness is used to fabricate the quarter circle caissons of radius 0.50m. The GI sheet is fixed to the slab with the help of stiffeners made up of flat plates. Then BW model was placed over the rubble mound foundation of thickness 0.05m. The breakwater model is placed in the flume at a distance of 30m from the wave generator flap (Figure 3).

The factors taken into consideration under the investigations are $R$, the radius of structure; $h_s$, the height of the structure; $D$, the diameter of perforations; $q$, wave overtopping discharge; $d$, water depth; $L$, wavelength; $H_i$, incident wave height; $T$, wave period; $\rho$, the mass density of water; $g$, acceleration due to gravity. The dimensional analysis is carried out using Buckingham's π theorem. The analysis yields the following non-dimensional $\pi$ terms: Dimensionless wave overtopping discharge $(q/gH_iT)$, Incident wave steepness parameter $(H_i/gT^2)$, Depth parameter $(d/gT^2)$, Dimensionless freeboard $(R_c/H_i)$, and percentage of perforations $(p)$.

The wave probes arranged at suitable spacing will record the wave specific characteristics. Wave overtopping will be measured as the amount of water overtopped over the structure and which is collected in the water collecting tray. Also, the burst of five waves is taken to obtain five overtops depending on the condition. Hence overtop per wave is calculated by dividing the total volume of water by the number of waves overtopped. The overtopping discharge is generally calculated in $m^3/s$ per m width of the breakwater.

The QBW models are tested with the existing facilities of the wave flume and to suit the wave parameters of the Mangalore coast, Karnataka, India (Dattatri 1993). In the laboratory with the wave flume, the regular wave of heights ranging from 0.02m to 0.24m and period ranging from 0.8 s to 4 s can be generated. So for the present study, a geometrically similar scale of 1:30 is to be used. In the current investigation, as cited in Table 1. regular waves of different wave periods, different wave heights are produced.

**Table 1** Range of parameters

| Sl. No. | Parameters | Experimental Range |
|---|---|---|
| 1 | Incident wave height, $H_i$ (m) | 0.08, 0.10, 0.12, 0.14, 0.16 |
| 2 | Water depth, d (m) | 0.40, 0.425, 0.45 |
| 3 | Time period, T (secs) | 1.4, 1.6, 1.8, 2.0, 2.2 |
| 4 | The radius of the structure (m) | 0.45 |
| 5 | Percentage of perforation (%) | 0, 5, and 20 |
| 6 | The diameter of perforation (m) | 0.016 |

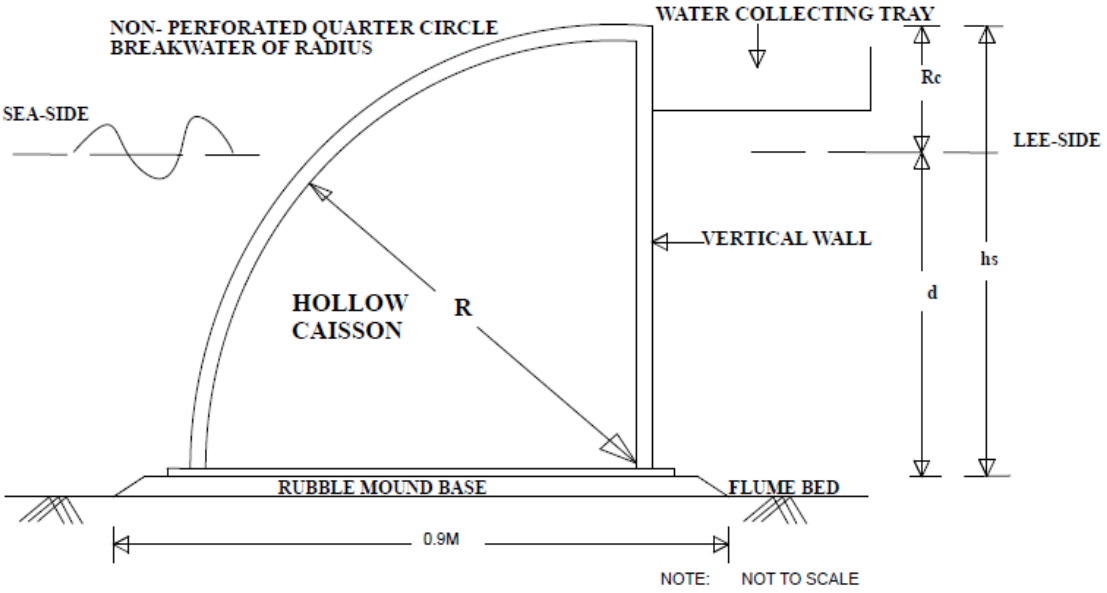



**Figure** 1 Typical cross-section of a Non-perforated QBW

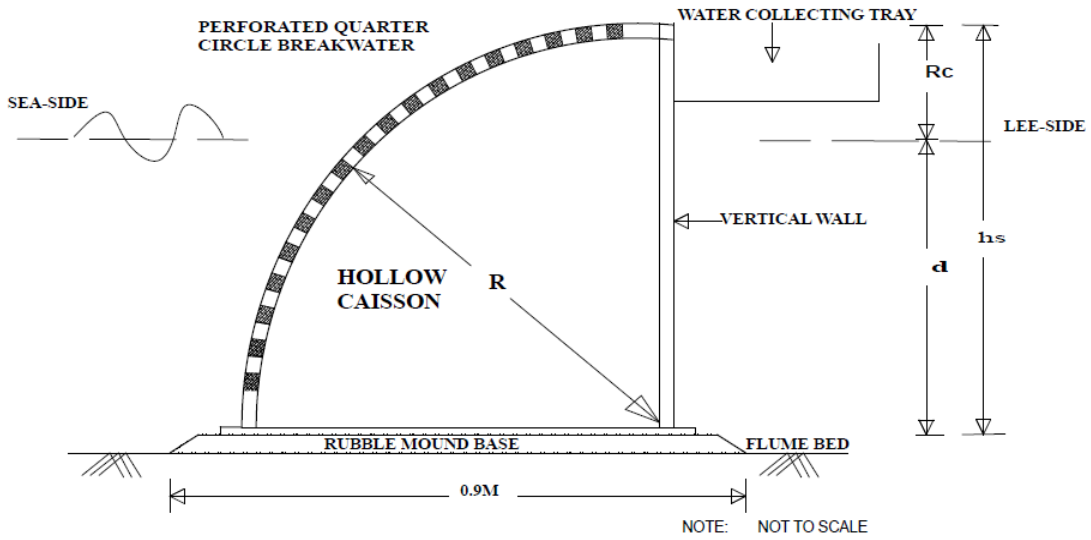



**Figure 2** Typical cross-section of a sea-side perforated QBW

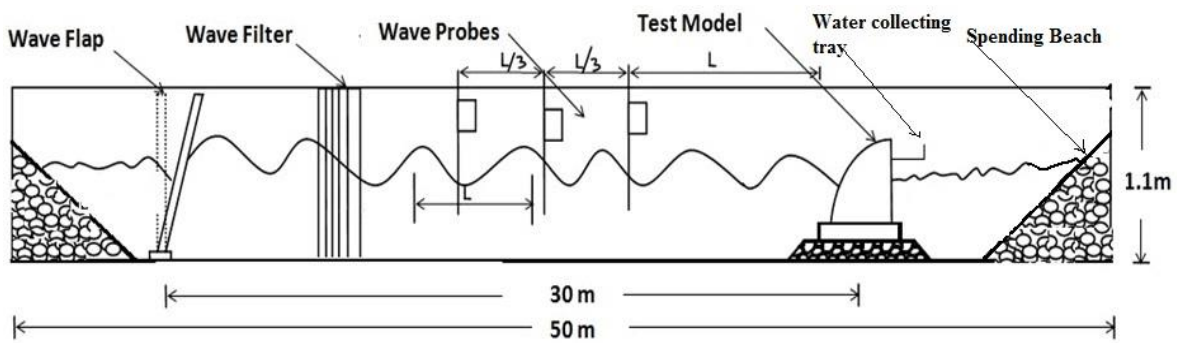



**Figure 3** Longitudinal section of the wave flume arrangement

## 4. Results and discussion

The present investigation deals with the study of the effects of wave steepness on the wave overtopping discharge of an emerged non-perforated and perforated QBW. The research work is conducted on quarter circular breakwater models in a two-dimensional regular wave flume. During the investigation, observations are made on the wave overtopping performance of an emerged quarter circular breakwater for different water depths, wave heights, and wave periods. Three breakwater models are investigated, one non-perforated and two perforated, with percentages of perforation of 5% and 20%.

### 4.1 *Analysis and interpretation of experimental data*

The data collected is expressed in non-dimensional quantities. The wave height and the wave period data are obtained using the EMCON's lab wave-recorder software. The inputs to this software are measured by the water surface elevation by the three-wave probes. The data was analyzed for spikes by a MATLAB program. The incident wave was then decomposed by the method proposed by Isaacson (1991). An overtopped wave will be measured as the amount of water overtopped over the structure and collected in the water collecting tray. The amount of wave overtopping discharge is measured in $m^3/s$ per meter width of the breakwater, but in practical applications, it may be quoted as liters per second per meter width of the breakwater.

A thorough study is carried out to analyze the variation of dimensionless wave overtopping discharge parameter ($q/gH_iT$) with incident wave steepness ($H_i/gT^2$) for different percentage of perforations (p). Different ranges of dimensionless depth parameter ($d/gT^2$) values used in the present study are 0.0095 to 0.0234, 0.0090 to 0.0221, and 0.0084 to 0.0208. The graphs are drawn using non-dimensional parameters to study the effect of wave steepness influencing variables on the non-perforated (p = 0%) and perforated (p = 5% and 20%) QBW model. In Figures 4 to 6, the trend line is shown, which is polynomial of order 2. The results obtained from the experimental works and discussion on the same are presented.

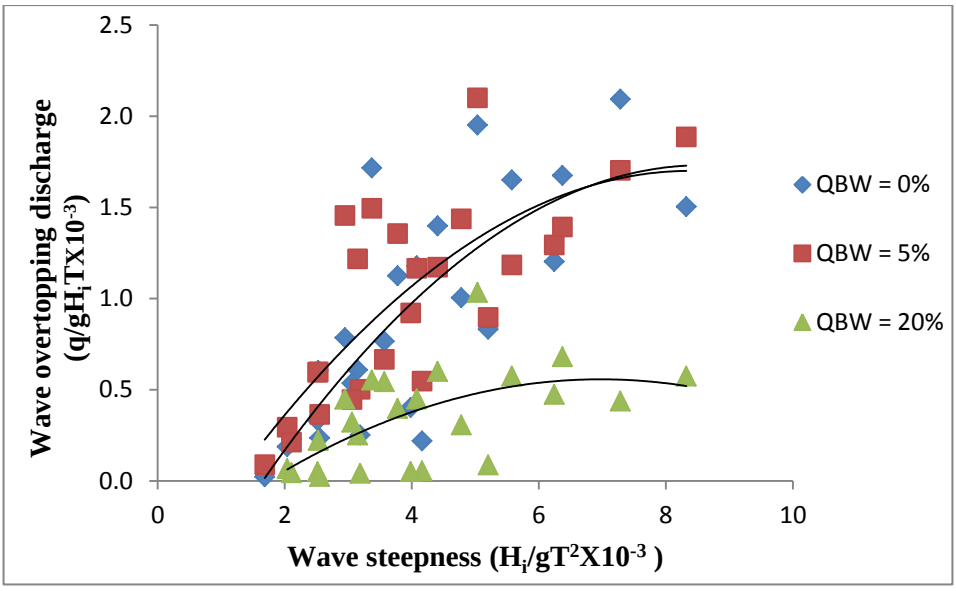



**Figure 4** Variation of $q/gH_iT$ with $H_i/gT^2$ for $d/gT^2$ = 0.0095 to 0.0234

### 4.2 *Effect of wave steepness ($H_i/gT^2$) on dimensionless wave overtopping discharge ($q/gH_iT$) for an emerged QBW*

The variation of dimensionless wave overtopping discharges ($q/gH_iT$) with wave steepness ($H_i/gT^2$) for different percentages of perforation (p) values and depth parameters ($d/gT^2$) was plotted. From figures 4 to 6, it was observed that the dimensionless $q/gH_iT$ increases with an increase in $H_i/gT^2$ for all values of p and $d/gT^2$. This was because as wave height increases, there is an increase in wave energy, and hence overtopping increases with an increase in wave steepness. Further, it was observed that $q/gH_iT$ decreases with the increase in the depth parameter ($d/gT^2$). This was because at higher water depths, the effect of curvature is more pronounced, and this results in lower overtopping rates.

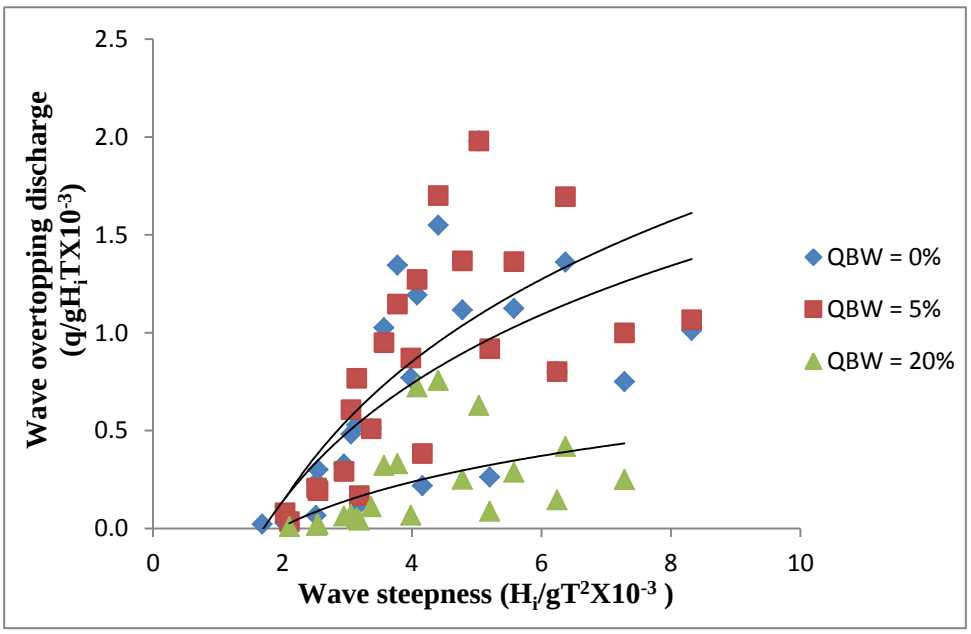



**Figure 5** Variation of $q/gH_iT$ with $H_i/gT^2$ for $d/gT^2$ = 0.009 to 0.0221

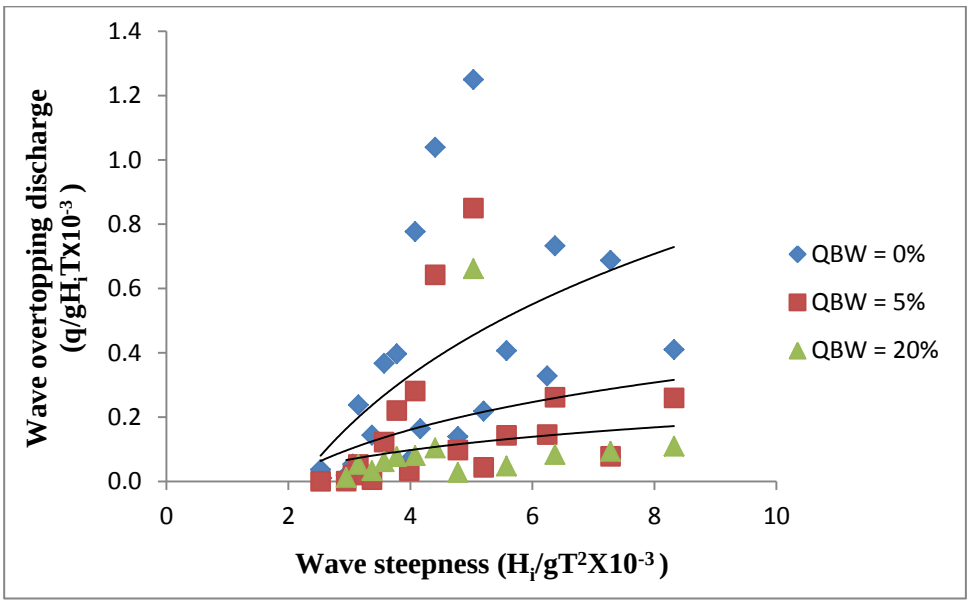



**Figure 6** Variation of $q/gH_iT$ with $H_i/gT^2$ for $d/gT^2$ = 0.0084 to 0.0208

The variation of dimensionless $q/gH_iT$ with wave steepness for $d/gT^2$ varying from 0.0095 to 0.0234 is shown in figure 4. The dimensionless $q/gH_iT$ ranges from $0.02\times10^{-3}$ to $2.19\times10^{-3}$ for p = 0%, from $0.02\times10^{-3}$ to $1.98\times10^{-3}$ for p = 5%, and from $0.01\times10^{-3}$ to $1.25\times10^{-3}$ for p = 20% perforations. The variation of dimensionless $q/gH_iT$ with wave steepness for $d/gT^2$ varying from 0.009 to 0.0221 is shown in figure 5.The dimensionless wave $q/gH_iT$ ranges from $0.02\times10^{-3}$ to $2.09\times10^{-3}$ for p = 0%, from $0.02\times10^{-3}$ to $1.90\times10^{-3}$ for p = 5%, and from $0.01\times10^{-3}$ to $0.86\times10^{-3}$ for p = 20% perforations.

The variation of dimensionless $q/gH_iT$ with wave steepness for $d/gT^2$ varying from 0.0084 to 0.0208 is shown in figure 6. The dimensionless wave $q/gH_iT$ ranges from $0.02\times10^{-3}$ to $1.03\times10^{-3}$ for p = 0%, from $0.01\times10^{-3}$ to $0.76\times10^{-3}$ for p = 5%, and from $0.01\times10^{-3}$ to $0.66\times10^{-3}$ for p = 20% perforations. It has been observed that the greater number of perforations dissipate more amount of incident wave energy, and thus less water is overtopped. From all these figures 4 to 6, it is clear that the dimensionless wave overtopping discharge increases with an increase in wave steepness and decreases with an increase in depth parameter. As the steepness of the wave increases, the wave growth takes place to form a steeper wave, and hence greater is the amount of water overtopped.

## 5. Conclusions

The study involved investigations of wave overtopping discharges on the physical models of the emerged sea-side perforated and non-perforated quarter-circle breakwater subjected to regular waves of different heights and periods. Based on the analysis of the results of the present study, the following conclusions are drawn.

It is observed from the present study that an increase in the percentage of perforations results in decrease dimensionless wave overtopping discharge. Also, the dimensionless wave overtopping discharge increases with an increase in wave steepness and decreases with an increase in depth parameter. The values of $q/gH_iT$ are higher for non-perforated QBW when compared with perforated QBW, due to less dissipation of wave energy in the non-perforated breakwater. The percentage of reduction in $q/gH_iT$ for 5% perforated QBW is varied from 5% to 27%. Similarly, the rate of decrease in $q/gH_iT$ for 20% perforated QBW is varied from 23% to 57%.

## Acknowledgments

The authors are thankful to the Director, National Institute of Technology Karnataka (NITK), Surathkal, and also to the Head, Department of Water Resources and Ocean Engineering, NITK, Surathkal for the encouragement and facilities provided to carry out the investigations, and also for the permission granted to publish the results.

### Notations

The following symbols are used in this paper:

| | |
|---|---|
| d | = depth of water; |
| D | = diameter of perforation; |
| g | = acceleration due to gravity; |
| $h_s$ | = Height of structure; |
| $H_i$ | = Incident wave height; |
| L | = Wave length; |
| p | = Percentage of perforation; |

Q = Overtopping volume;

R = Radius of structure;

T = Wave period;

ρ = Mass density of water;

$d/gT^2$ = Depth parameter;

$H_i/gT^2$ = Incident wave steepness;

$q/gH_iT$ = Overtopping discharge; and

## References

Binumol, S., Subba Rao, and Arkal Vittal Hegde. (2015). "Runup and Rundown Characteristics of an Emerged Seaside Perforated Quarter Circle Breakwater." *Aquatic Procedia* 4(ICWRCOE): 234–39. http://dx.doi.org/10.1016/j.aqpro.2015.02.032.

Binumol, S., Subba Rao, and Arkal Vittal Hegde. (2017a). "Wave Reflection and Loss Characteristics of an Emerged Quarter Circle Breakwater with Varying Seaside Perforations." *Journal of The Institution of Engineers (India): Series A* 98(3): 311–15.

Binumol, S, Subba Rao, and Arkal Vittal Hegde. (2017b). "Sliding stability analysis of emerged quarter-circle breakwater with varying sea-side perforations." *Indian Journal of Geo-Marine Sciences*, Vol. 46(07), pp 1428-1435.

Bruce, Tom, Jentsje van der Meer, Leopoldo Franco, and Jonathan M. Pearson. 2007. "A Comparison of Overtopping Performance of Different Rubble Mound Breakwater Armour." 4567–79, 1705, ICCE 2006.

Dattatri, J. 1993. "Waves off Mangalore Harbour - West Coast of India." *Journal of Waterway, Port, Coastal and Ocean Engineering* ASCE, 99(2): 39–57.

Dhinakaran, Govindasamy, Vallam Sundar, Renganathan Sundaravadivelu, and Kai Uwe Graw. 2008. "Hydrodynamic Characteristics of Seaside Perforated Semicircular Breakwaters Due to Random Waves." *Journal of Waterway, Port, Coastal and Ocean Engineering* 134(4): 237–51.

Isaacson, Michael. 1991. "Measurement of Regular Wave Reflection." *Journal of Waterway, Port, and Ocean Engineering* 117(6): 553–69.

Jiang, X.-L., H.-B. Gu, and Y.-B. Li. 2008. "Numerical Simulation on Hydraulic Performances of Quarter Circular Breakwater." *China Ocean Engineering* 22(4).

Oztunali Ozbahceci, Berguzar, and Engin Bilyay. 2018. "Effect of the Armor Crest Freeboard Relative to the Crown Wall Freeboard on Wave Overtopping for Simple Rubble Mound Slopes." *Ocean Engineering* 169(September): 511–28. https://doi.org/10.1016/j.oceaneng.2018.09.043.

Vishwanatha Mane, Subba Rao, A.Vittal Hegde. (2019). "Laboratory investigations on the wave overtopping characteristics of an emerged quarter-circle breakwater." *International Conference on Hydraulics, Water Resources, Coastal engineering (ISH-HYDRO)*, Osmania University, Hyderabad, 18- 20. December 2019, pp. 406-413.

*IN PROCEEDINGS OF 25th HYDRO 2020, INTERNATIONAL CONFERENCE, NATIONAL INSTITUTE OF TECHNOLOGY ROURKELA, ODISHA, INDIA 26-28, March 2021, ISBN 978-93-90631-56-8*

Paper ID - 222

# Numerical Modelling for Wave Transformation along the Ratnagiri Coast-Case Study

Pranav Vaishampayan[1], Amol S. Borkar[2], Varun Khengare[3], Ketan Jadhav[4], Abhishek Deshmukh[5], Prof. Shilpi Bhuinyan[6], Dr. Prabhat Chandra[7]

[1,3-5]*Student, Civil Engineering, AISSMS COE, Pune-411001, India*
[2]*Scientist 'B', Central Water and Power Research Station, Pune-411024, India*
[6]*Assistant Professor, Department of Civil Engineering, AISSMS COE, Pune-411001, India*
[7]*Scientist 'E', Central Water and Power Research Station, Pune-411024, India*
*Email: pranav8pm@gmail.com, newamol_borkar@rediffmail.com*

## Abstract

Wave transformation from deep shore to the near shore is a composite process. Generally, near shore wave climate along the coast is not readily available. The present investigation covers obtaining the near shore wave climate near Bhagwati breakwater close to Ratnagiri coast along West coast of India by using the Numerical MIKE-21 SW (Spectral Wave) model. The maximum tidal range at the site is about 2.3 m and the site is exposed to waves from SW to NW directions. The deep offshore data as obtained from Indian Meteorological Department (IMD) was utilized to derive the nearshore wave conditions at the Bhagwati Breakwater at (-)10 m depth. The model results were also compared with the measured wave data at (-)15 m near site of Bhagwati breakwater. The results from the MIKE-21 Spectral wave model studies show that the predominant waves after transformation from deep to near fall between the sector 225° N to 315° N i.e. the site is exposed to predominant waves from SW, WSW, West, WNW, and NW directions. The significant waves of height of about 2.5m waves reach at (-)10 m depth. The analysis of the statistical parameters of waves and wave direction shows a reasonably good match between the model and the observed data except some minor difference in the angles. The studies will be very useful for providing input conditions for future port development scheme at Bhagwati bunder for ascertaining the detailed wave tranquility conditions.

***Keywords:*** *Wave transformation; offshore wave data; near-shore wave data; numerical modelling.*

## 1. Introduction

Information on wave climate is of paramount importance for the planning and execution of ocean engineering projects and for the proper management of the coastal zone. The morpho-dynamics of the littoral zone is controlled by the wave climate, as waves are the principal source of input energy into this zone. To design various structures and plan their construction a clear picture of the maximum wave forcing and wave climate should be available. There is a fairly sharp optimum cost of design for coastal structures. Without a fairly good estimate of wave conditions, it would be nearly impossible to come close to this optimum and the cost would unnecessarily increase. Since most of the coastal or marine structures are designed for a long life time, long-term wave data is essential to account for the variability of waves during their life time. Of late, the wave data requirements have gone up further as ocean waves have been accepted as a potential alternate renewable source of electrical energy.

Ratnagiri has a long coastline and beaches. Commercial fishing and shipping, and coastal zone development are activities that are affected by ocean surface waves. For these activities, knowledge of the coastal wave climate is critical. Wave data is generally not available at the site or depth required. Hence numerical models are used for calculating wave propagations from deep water to surf zone. The study addresses this issue through the use of spectral wave model to derive nearshore wave climate

## 2. Methodology

The coastal processes are first necessary to understand and they are then well defined by numerical modelling techniques. In the absence of measured near shore data of the study location, offshore wave data was collected by Indian Meteorological Department (IMD) as their ships ply in the offshore region off Ratnagiri. The data was then transformed by MIKE 21-SW model to get near-shore wave climate.

The model is developed by Danish Hydraulic Institute (DHI), Denmark and study was carried out at Central Water and Power Research Station (CWPRS).

## 3. Site Conditions

The study has been carried out near Bhagwati bunder which is located on the West coast of India, Ratnagiri District, Maharashtra. To the West of Bhagwati bunder, Bhagwati breakwater facing N-S direction of approximate length 0.45 km is situated. The incoming waves will be calculated at the Bhagwati breakwater tip which is at 17° 0' 6.192" N latitude and 73° 16' 7.392" E longitude.

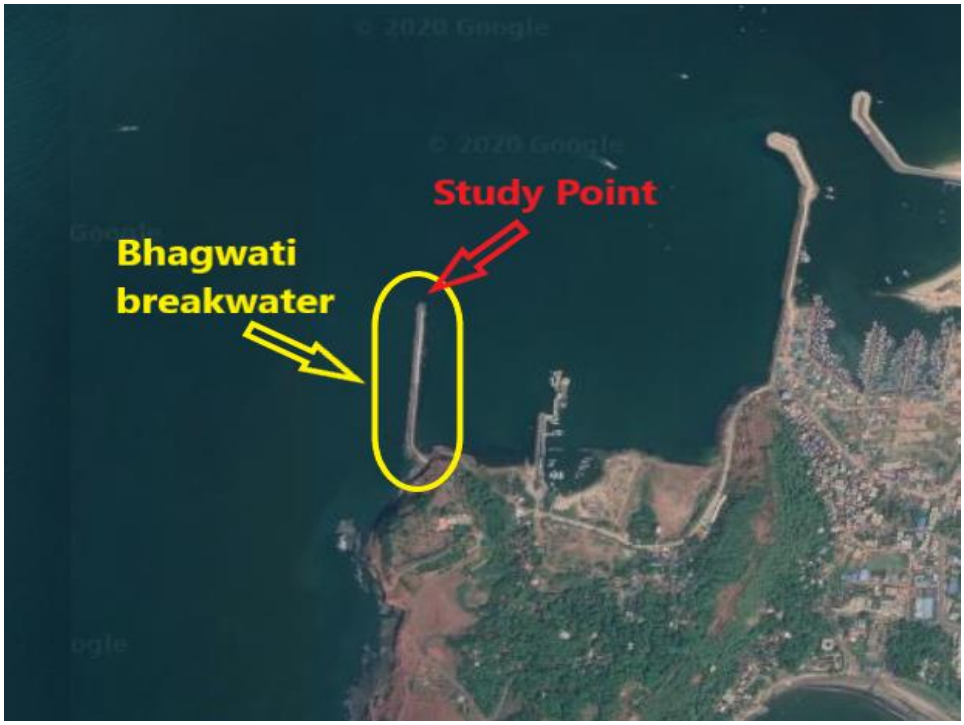



**Figure 1:** Bhagwati breakwater and Study Point

### *3.1 BATHYMETRY*

The term "bathymetry" originally refers to the ocean's depth relative to sea level, although it has come to mean “submarine topography,” or the depths and shapes of underwater terrain. The accuracy of all numerical simulations primarily depends on how accurately the bathymetry is generated. The bathymetry for the simulation of waves are generated from MIKE C-MAP. Bathymetry generated from database (xyz coordinate i.e. latitude and longitude with depth values) of C-MAP is shown in figure 2.

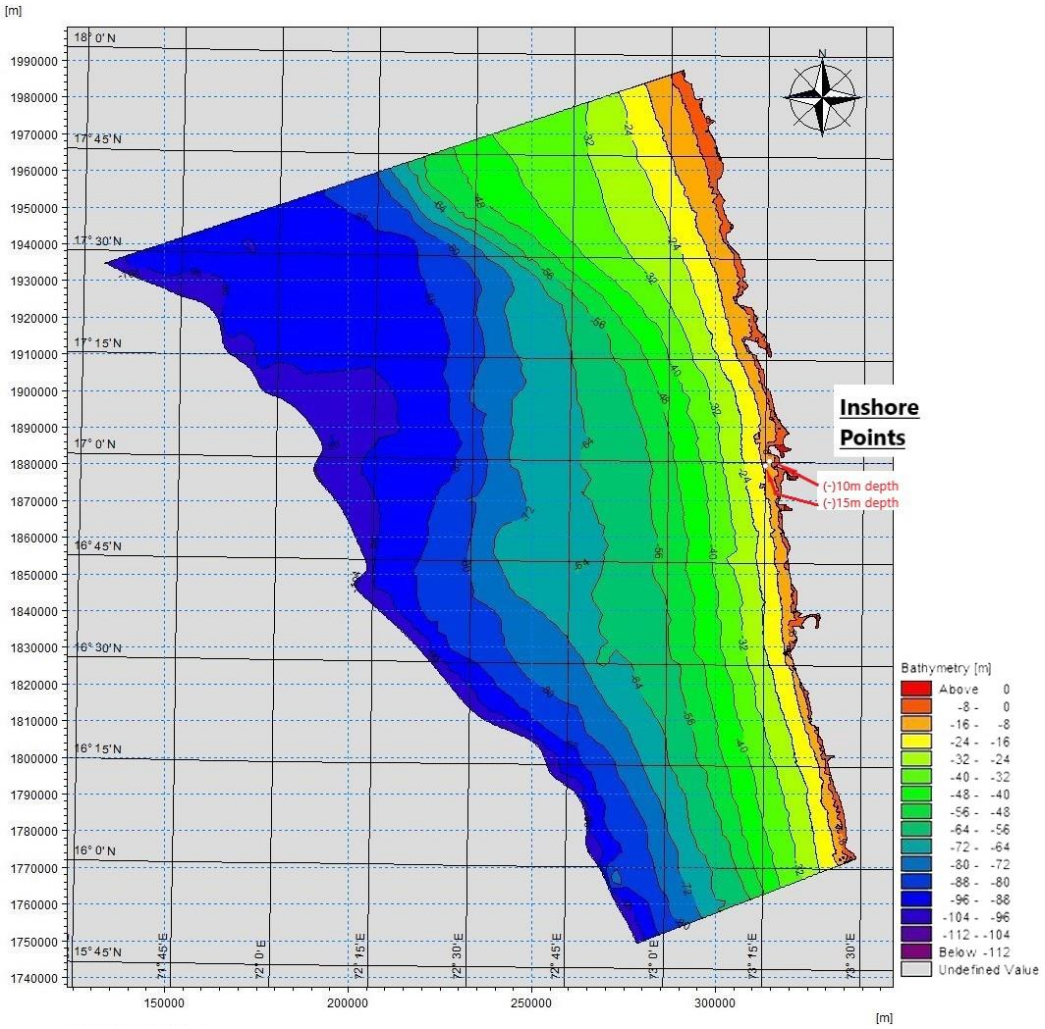



**Figure 2:** Bathymetry used for Spectral Wave Model

### *3.2 DATA Source*

Data used in this study is taken from Indian Meteorological Department (IMD) and Indian National Centre for Ocean Information Services (INCOIS). The data for the study was requested from INCOIS and was utilized for project and research work. INCOIS has deployed various wave rider buoys around the coastline of India, taking measurements at that particular location. Our source of information is from the wave rider buoy located at Ratnagiri at (-)15m depth and 16° 58' 37.2" N latitude and 73° 15' 18" E longitude.

### *3.3 TIDAL Levels*

The tidal levels near Ratnagiri were taken from nautical charts. They were measured at 16° 59' N and 73° 18' E and are shown in table below: -

**Table 1:** Tidal Levels

| Water levels | Height above datum |
|---|---|
| Mean Higher High water (MHHW) | 2.3m |
| Mean Lower High water (MLHW) | 2.1m |
| Mean Higher Low water (MHLW) | 1.2m |
| Mean Lower Low water (MLLW) | 0.5m |
| Mean Sea Level (MSL) | 1.5m |

## 4. Model Setup and Wave Transformation

Setting up the model is actually another way of saying transforming real world events and data into a format which can be understood by the numerical model. Thus, generally speaking, all the data collected have to be resolved on the domain selected.

To set up the MIKE-21 SW model the following steps are taken.
a) Grid Generation- the grid generation process is undertaken by the MIKE Zero. The model domain, depicted in figure 3 is approximately 100-kilometre-wide and 220-kilometre-long, between latitude 15°45′ N to 18° N and longitude 71°30′ E to 73°30′ E. In this process a two-dimensional (flexi triangular mesh and depth averaged) grid represents the study. Coarser mesh was used for offshore and finer mesh for nearshore.

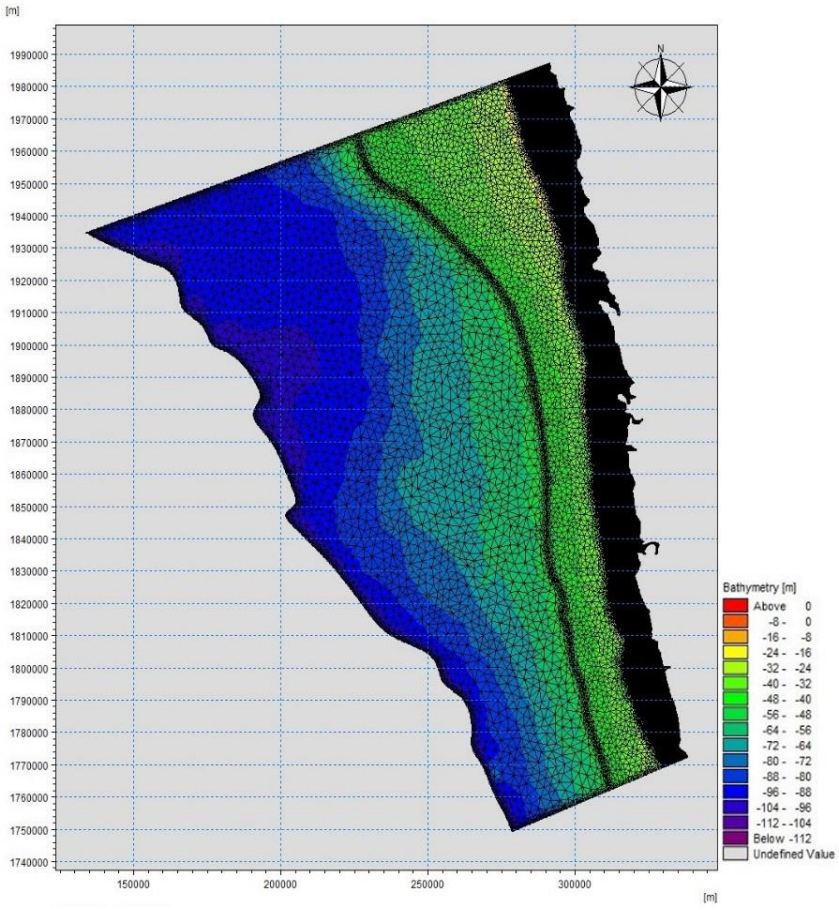



**Figure 3:** Bathymetric Mesh used for SW Modelling

b) Wave Transformation from Offshore to Nearshore-
The simulation of wave transformation from offshore (at -100m depth contour) to near shore is done using MIKE 21-SW model. It is done for two separate nearshore points which are

i) At Study site location- the wave is transformed from (-)100m depth contour (offshore) to (-)10m depth contour (nearshore) which is the tip of the Bhagwati breakwater located at 17° 0' 6.192" N and 73° 16' 7.392" E.
ii) At Wave rider buoy location- the wave is transformed from (-)100m depth contour (offshore) to (-)15m depth contour (nearshore) which is the location of the wave rider buoy deployed by INCOIS located at 16° 58' 37.2" N and 73° 15' 18" E.

For defining the boundary conditions, the boundary data used in this modelling exercise is taken form Indian Meteorological Department (IMD). A Significant wave height of 5m and mean wave period of 8 sec were transformed from offshore location to the nearshore points along all 16 directions.

## 5. Results and Discussion

### *5.1 CORRECTNESS of the Simulated Data*

The calibrated model was first used to hindcast the wave climate at the wave rider buoys location deployed by INCOIS near Ratnagiri. The results have been scrutinized and a concise overview of the results were obtained. The aim of this calibration was to prove that the study carried out at Bhagwati breakwater tip procured correct results as the measured data by the wave rider buoy and simulation done by software at the rider location gave similar outputs. Also, both the output locations i.e. wave rider buoy and Bhagwati breakwater tip are close to each other. The figures shown below are the outputs at the wave rider buoy location.

#### *5.1.1 MEASURED INCOIS Data*

The wave rose diagram shown in fig.4 represents the wave data provided by INCOIS through their wave rider buoy located at Ratnagiri.

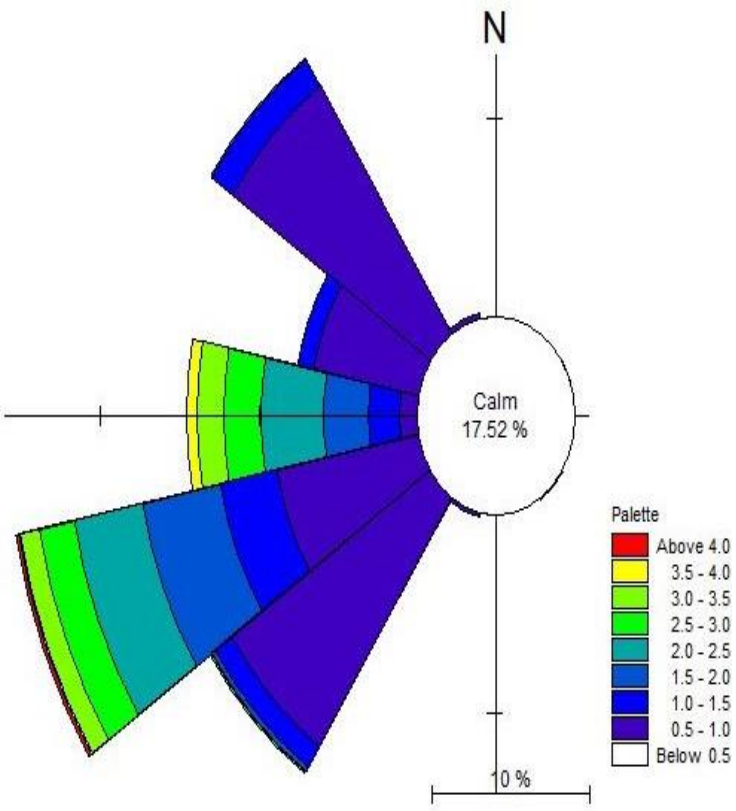



**Figure 4:** Wave Rose diagram at (-)15m depth- INCOIS

### *5.1.2 SIMULATED Data.*

The offshore data provided by IMD was simulated to obtain the nearshore wave climate at the INCOIS wave rider buoy location which is shown in the form of wave rose diagram in fig.5.

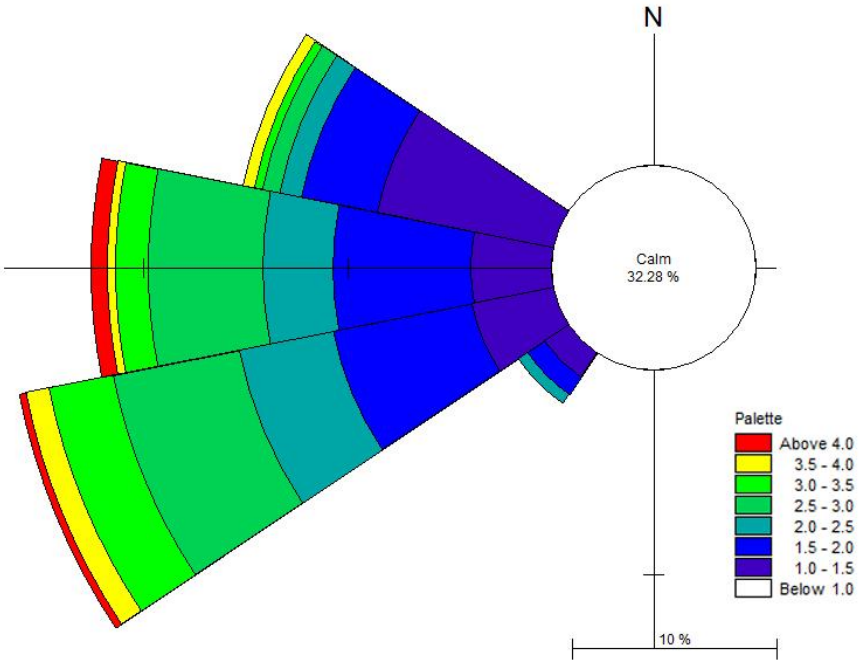



**Figure 5:** Inshore Wave Rose Diagram at (-)15m depth- IMD

By observing figures 4 & 5 we can say that the measured wave data and calibrated wave data of the wave rider buoy are similar in terms of incoming waves direction. However, there are some differences in terms of frequency of occurrences along directions and wave heights. The differences might be due consideration of different time series data of IMD and INCOIS, dynamically changing climate, global warming, etc. This also may be due to the high input values given to the software as a factor of safety and for future consideration. Therefore, the differences can be overseen and the correctness of the study is proved successfully.

### *5.2 NEARSHORE Wave Climate of Site*

Due to the lack of nearshore wave climate data at Bhagwati breakwater tip, IMD offshore data was used for simulation, done by using MIKE 21-SW model and the required nearshore wave climate was obtained. The output of the simulated data of the study site can be seen in wave rose diagram fig.6

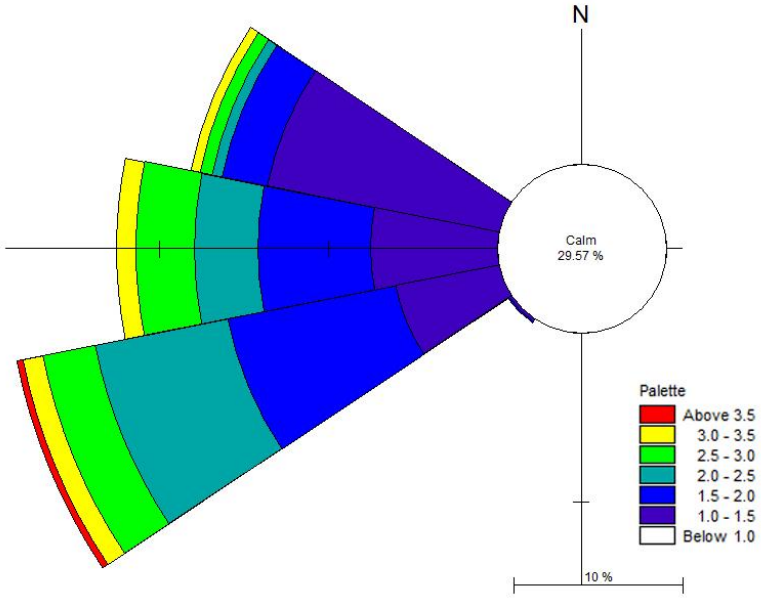



**Figure 6:** Inshore Wave Rose Diagram at (-)10m depth

## 6. Conclusion

Bhagwati bunder location was chosen to check the nearshore wave climate in the region, and help the port authorities to achieve tranquility condition in their area by using the data and carrying out the further required studies.

In this present study wave climate of South Maharashtra (Ratnagiri) coast was estimated with the help of a third-generation Spectral wave model MIKE 21-SW. The model was first hindcasted with measured wave rider buoy data, nearshore Ratnagiri and then the wave climate near Bhagwati bunder was simulated to get the nearshore data. The major conclusions drawn from the study are as below.

The predominant directions of incoming waves at (-)10m depth are from WSW, W and WNW during entire year with percentage of occurrence of 30%, 24.5% and 27% respectively. Around 30% wave are calm waves as they are between 0-0.5m height. However, no wave marching near the tip of Bhagwati breakwater is greater than 3.5 m height.

## Acknowledgement

The authors are grateful to Dr. Mrs. V. V. Bhosekar, Director, CWPRS, Pune for her consistent support, encouragement and kind consent for publishing this paper.

## References

1. Butterworth-Heinemann (1999). Waves, Tides and Shallow Water Processes, 2nd edition. Oxford, Open University.
2. Danish Hydraulic Institute (DHI), Denmark, 2017. MIKE 21 SW Model- User Guide and Reference manual.

*IN PROCEEDINGS OF 25th HYDRO 2020, INTERNATIONAL CONFERENCE,*
*NATIONAL INSTITUTE OF TECHNOLOGY ROURKELA, ODISHA, INDIA*
*26-28, March 2021, ISBN 978-93-90631-56-8*

Paper ID - 243

# Effect of Marine Growth on Wave Loading on Small Diameter Tubular Structural Members

Sarath Suresh[1], Rameeza Moideen[2], Manasa Ranjan Behera[3]

[1]*Department of Civil Engineering, Indian Institute of Technology Bombay, Mumbai, 400076, India*
[1]saraths96@gmail.com; [2]rameezasindoora@gmail.com; [3]manasa.rb@gmail.com

## Abstract

Offshore structural installations are the backbone of key industries such as Oil & Gas and Wind Energy. These structures are subjected to harsh environmental loads and conditions that are not encountered by any land-based structures. Marine growth resulting in excess hydrodynamics loading is the major concern for all these structures. These marine growths, typically classified as hard and soft growth, alter various aspects of the structural member such as its thickness and surface roughness. The variation in these parameters can drastically affect the wave forces acting upon them, causing loading that was not intended or expected during the design phase. The present study aims at computing the additional wave loading that occurs on an offshore structural member, particularly small diameter tubular members, due to the presence of naturally occurring marine growth. To estimate the effect of marine growth, a typical structural member is divided into user-specified number of zones with varying degrees of growth thicknesses. A GUI tool is developed based on the modified Morison's equation using MATLAB that calculates the wave forces on these structural members. A detailed investigation is carried out by varying different parameters affecting the wave force due to marine growth such as member diameter, varying marine growth thickness along depth and member inclination. The study concludes that the presence of marine growth causes an accompanying increase in the wave loading, with a sample case of a 70 mm thick uniform marine growth yielding a ~26% increase in the wave loading. The variation in member parameters such as its inclination and diameter also caused corresponding changes in the wave loading, the effect of each being tabulated and explained as part of the study. Thus, the study helps to comprehend the magnitude of the change in wave loading due to marine growth and the need for its accurate estimation during the design phase of the structure.

***Keywords:*** *Offshore Structure; Marine Growth; Wave Loading; Morison's Equation, GUI*

## 1. Introduction

Ever since the offshore platforms were constructed in the early 1900's, the impact of marine growth on the structural members is of great interest to researchers all around the globe. Marine growth refers to various kinds of fouling organisms that grow on submerged members over a period of time. Offshore structures, due to their very nature, provide highly favourable conditions for the growth of these organisms. Marine growth is typically classified into three categories (Jusoh and Wolfram 1996), namely hard growth, soft growth, and weeds. Hard growth refers to organisms such as barnacles, oysters, mussels, and tubeworms. Soft growth includes corals, sponges, seaweeds, and algae. Weeds are characterised by their long and flapping bodies. They are also called kelp and are distinct from the other categories due to their much larger size.

This growth constitutes an increase in the structural mass of the members. It also alters the hydrodynamic properties of the structural members, such as its diameter and surface roughness, which leads to an increase in the wave loading. According to various tests conducted on offshore installations in the North Sea, typical values of growth thickness of around 100 mm at depths between +2 m to -40 m, and 50 mm to 20 mm below -40 m of depth were found. Marine growth was determined to take around 2 to 8 years to attain its maximum thickness. Further, no amount of appreciable growth was seen on the members above +2m from the waterline.

The presence of marine growth alters the hydrodynamic coefficients $C_d$ and $C_m$, which are used to compute the drag and inertia force on the tubular members. However, there is a large variation up to 60% in the recommended values of these coefficients by various design codes namely, Llyods R.S, Det Norske Veritas, the Bureau Veritas, etc. (Theophanatos 1988). Furthermore, it was noted that different types of marine growth affected the hydrodynamic coefficients in different ways. For instance, the

presence of hard growth like barnacles increases $C_d$ while decreasing $C_m$. However, certain types of flexible, soft growth, such as flapping weeds, increases both $C_d$ as well as $C_m$.

Another potential issue with the presence of marine growth on offshore structural members is its effect on the fatigue life and the natural frequency of the structure. It was revealed that the fatigue life of the structure also showed a decrease of 38% for 150 mm thick marine growth and as much as 54% for a thickness of 250 mm (Heaf 1979). This reduction in fatigue life is considered to be the most worrying of the effects of marine growth since fatigue failure of a structure often leads to extremely dangerous operating conditions of the offshore structure. Additionally, the presence of marine growth was also determined to cause a reduction in the structural natural frequencies (especially in the local-mode natural frequencies) by around 24% and 40% for growth thicknesses of 100mm and 200mm, respectively (Fevåg 2012).

Various control measures have been proposed over the years to keep the marine growth in check (Jusoh and Wolfram 1996). Controlling the growth is done through the use of Anti-fouling agents, which can be further classified as Toxic and Non-Toxic Anti-fouling agents. Toxic Anti-fouling involves the use of biocides that are detrimental to the growth of marine organisms. Some of the techniques involved are Anti-fouling paints, gelcoats, and copper-nickel alloy coatings. All of these work through the introduction of free copper ions into the surrounding water, making it poisonous for the marine organisms. Non-toxic Anti-fouling uses methods that make the surface of the structural member unsuitable for settling of the marine organisms. The surface of the member is made slippery through the application of oil-based fouling release coatings. However, due to the relatively high operation expenses of these methods, manual removal of marine growth is the more commonly adopted cleaning strategy. Various removal techniques such as the use of anti-fouling hoops utilising pressurised water jets, scrapper devices, rotating cutters etc, are used to forcibly remove the marine growth layer present on the structural member.

Hence the need to have a thorough understanding of the effects of marine growth on offshore structural members is ever-present. The present study aims at understanding the effect of marine growth on the wave forces that acts on the structural members and develop a simple GUI tool to compute the wave loading due to marine growth. Further, the developed tool is used to investigate the effect of wave loading on various tubular member specifications with varying marine growth scenarios.

## 2. Methodology

The methodology involved in determining the excess wave force due to marine growth on small diameter structural members comprises the following steps:

1. Selection of an appropriate Wave Theory
2. Selection of suitable hydrodynamic co-efficient values, i.e., $C_d$ and $C_m$.
3. Application of Morison's equation

### 2.1. *Selection of Wave Theory*

The selection of a wave theory depends on many factors, and no wave theory is capable of accurately predicting the state of the fluid under all conditions. The suitability of a particular wave theory to provide a good understanding of the wave particle kinematics depends on the conditions and properties of the wave/oscillatory flow it is applied to. For instance, the kinematics of a very steep wave near its breaking is not well understood by any wave theory. In practice, the wave theory most suitable to the given fluid conditions is selected for design purposes. Airy's wave theory, also known as the Linear wave theory, is preferred for small steepness waves. This theory also holds good for multi-directional sea states and when the structural member is such that the inertial forces are dominant over the drag forces. Stokes fifth order theory is one that gives adequate results in deep water and is good for predicting particle kinematics. For steep waves and when the water depth is shallow, wave theories such

as the Solitary wave theory and the Cnoidal wave theory give better results. Experimental studies by Sarpkaya and Issacson (1981), have established a guideline for the selection of the most suitable wave theory. Fig.1. shows the guide chart that was developed for this purpose. The intersection point of the known non-dimensional quantities ($H/gT^2$) & ($d/gT^2$) determines the appropriate wave theory to be used, where H, d & T are the Wave height, depth and Time period respectively. Linear wave theory is adopted for the present study to compute the wave kinematics and wave forces on small diameter tubular members in a multi-directional, deep sea state. However, Stokes 2nd and 3rd order wave theory can be adopted for more detailed analysis.

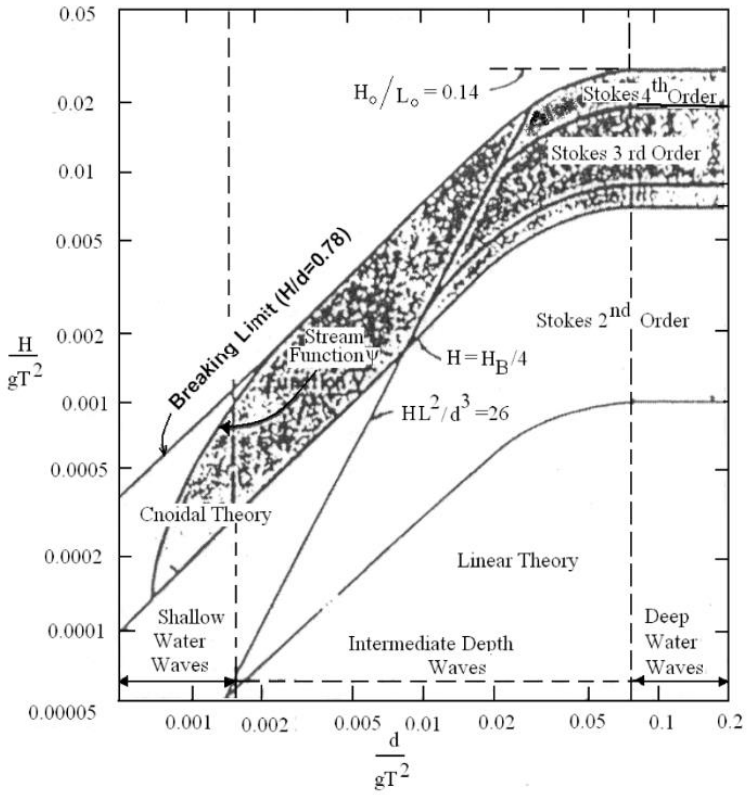



Figure 1. Selection of wave theory (Sarpkaya and Issacson, 1981)

## 2.2. *Selection of Hydrodynamic Coefficients*

The force coefficients $C_d$ and $C_m$, required in the calculation of the wave force, depends mainly on the wave theory chosen and the Reynolds number ($R_e$). Generally, for smooth cylinders, the flow separation from Laminar to the Turbulent flow regime occurs at a relatively high Reynolds number of $10^5$. Even for much higher RN values, the point of flow separation remains almost the same. Hence, the values for $C_d$ remains a constant. However, for roughened cylinders, as in the case of cylinders with marine growth, flow separation occurs at a much lower RN due to the increased friction. This causes the $C_d$ value to increase considerably. The inertial co-efficient $C_m$, also changes slightly with an increase in roughness and Reynolds number.

In reality, the value of the coefficients varies widely with the sea state and flow parameters. In fact, $C_d$ and $C_m$ values can change slightly over a single wave cycle. For design purposes, various wave theories suggest different values for $C_d$ and $C_m$, as given in Table 1. The range in values for $C_d$ is to account for any effects that are introduced by the added roughness and the change in the Reynolds number.

Table 1. $C_d$ and $C_m$ values for different wave theories

| Wave Theory | $C_d$ | $C_m$ | Comments | Reference |
|---|---|---|---|---|
| Linear Theory | 1.0 | 0.95 | Mean values for ocean wave data on 13-24in cylinders | Wiegel, et al. (1957) |
| | 1.0-1.4 | 2.0 | Recommended design values based on statistical analysis of published data | Agerschou and Edens (1965) |
| Stokes 3rd order | 1.34 | 1.46 | Mean Values for oscillatory flow for 2-3in cylinders | Keulegan and Carpenter (1958) |
| Stokes 5th order | 0.8-1.0 | 2.0 | Recommended values based on statistical analysis of published data | Agerschou and Edens (1965) |

In this study, $C_d$ & $C_m$ values of 1.0 and 2.0 are taken for load calculation without marine growth, and 1.4 and 2.0 are taken when marine growth is considered.

### 2.3. *Application of Morison's Equation*

The wave forces are calculated using the modified Morison's equation for inclined tubular members. This equation is suitable for small diameter structural members, which is defined as members having diameters less than 0.15 times the design wavelength of the wave. For inclined members, the force normal to the member axis ($F_n$) is taken for design considerations. The normal force is computed by considering the normal components of the particle velocity and acceleration vectors.

$$F_n = C_m \rho \frac{\pi D^2}{4} a_n + C_d \rho \frac{D}{2} |V_n| V_n \quad [1]$$

where,

- $V_n$ and $a_n$ are the normal components of the velocity and acceleration vectors.
- $\rho$ is the density of the oscillating fluid.
- $C_m$ & $C_d$ are empirical, hydrodynamic coefficients obtained through experimental data.
- $D$ is the diameter of the body.

The normal components of velocity and acceleration are determined as follows:

$$V_n = V_{nx}\hat{\imath} + V_{ny}\hat{\jmath} + V_{nz}\hat{k} \quad [2]$$

$$a_n = a_{nx}\hat{\imath} + a_{ny}\hat{\jmath} + a_{nz}\hat{k}$$

where

$$\begin{Bmatrix} V_{nx} \\ V_{ny} \\ V_{nz} \end{Bmatrix} = \begin{bmatrix} 1 - c_x{}^2 & -c_x c_y & -c_x c_z \\ -c_x c_y & 1 - c_y{}^2 & -c_y c_z \\ -c_x c_z & -c_y c_z & 1 - c_z{}^2 \end{bmatrix} \begin{Bmatrix} V_x \\ V_y \\ V_z \end{Bmatrix} \quad [3]$$

and

$$\begin{Bmatrix} a_{nx} \\ a_{ny} \\ a_{nz} \end{Bmatrix} = \begin{bmatrix} 1 - {c_x}^2 & -c_x c_y & -c_x c_z \\ -c_x c_y & 1 - {c_y}^2 & -c_y c_z \\ -c_x c_z & -c_y c_z & 1 - {c_z}^2 \end{bmatrix} \begin{Bmatrix} a_x \\ a_y \\ a_z \end{Bmatrix} \quad [4]$$

where

- $V_{nx}, V_{ny}, V_{nz}$ and $a_{nx}$, $a_{ny}, a_{nz}$ are the axial components of the normal velocity and acceleration vectors.
- $V_x, V_y, V_z$ and $a_x$, $a_y, a_z$ are the axial components of the velocity and acceleration vectors in line with the wave direction.
- $c_x, c_y, c_z$ are the direction cosines of the unit vector $\bar{c}$ along the member axis. These are the cosines of the angles made by the unit vector and the three axes.

Since the Linear Wave Theory is used, the following relations are used to determine the horizontal and vertical particle velocities, $u, w$ and accelerations $\dot{u}, \dot{w}$:

$$u = \frac{\pi H \cosh\left(k(d+z)\right)}{T \sinh(kd)} \cos\left(kx - \omega t\right) \quad [5]$$

$$w = \frac{\pi H \sinh\left(k(d+z)\right)}{T \sinh(kd)} \sin\left(kx - \omega t\right)$$

$$\dot{u} = \frac{2\pi^2 H \cosh\left(k(d+z)\right)}{T^2 \sinh(kd)} \sin\left(kx - \omega t\right) \quad [6]$$

$$\dot{w} = \frac{2\pi^2 H \sinh\left(k(d+z)\right)}{T^2 \sinh(kd)} \cos\left(kx - \omega t\right)$$

where

- $H$ is the design wave height.
- $k = \frac{2\pi}{L}$ is the wavenumber where $L$ is the wavelength.
- $d$ is the water depth at site.
- $z$ is the depth at which the particle velocity and acceleration are to be calculated.
- $\omega$ is the angular velocity
- $t$ is the time instant at which the velocity and acceleration are calculated.

## 3. Development of GUI tool for wave load estimation

A program was written using MATLAB to compute the wave load on the structural member. User inputs such as the member and wave properties and marine growth characteristics are taken through an Input GUI and the total wave force acting on the member is provided as the output. Provisions to subdivide the structural member into user-specified number of zones with varying marine growth thicknesses is provided. This is done in order to better simulate the real-life growth case, wherein the marine growth is often distributed non-linearly throughout the length of the member. The growth thickness is often the highest closer to the waterline and decreases with increase in the water depth. Force diagram along the various axes are also plotted. The algorithm followed to determine the wave load due to the marine growth is given in Figure 2. The tool thus developed is capable of determining the wave load in the presence of marine growth for a structural member of any orientation.

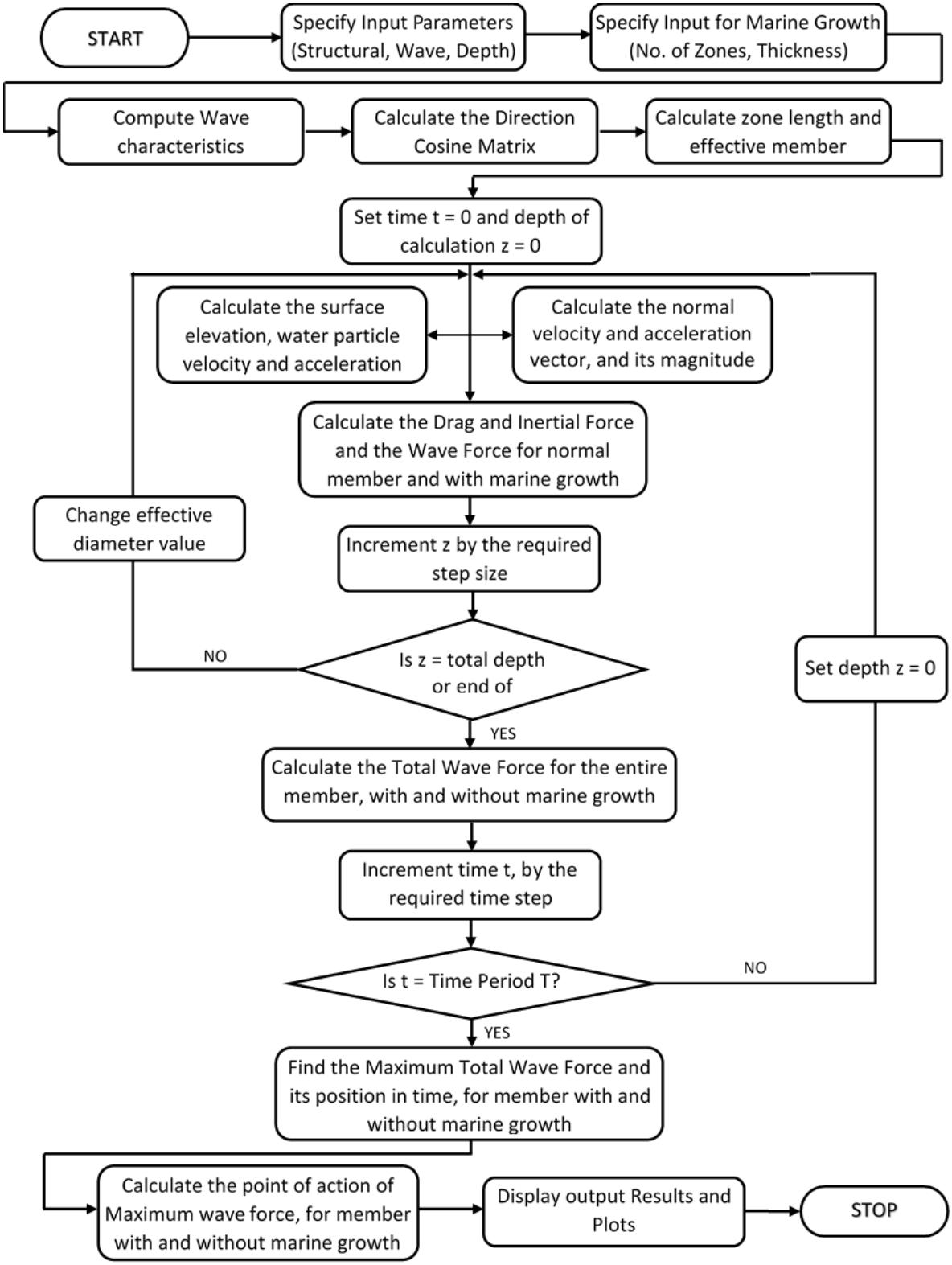



Figure 2. Flowchart of the algorithm followed for programming the GUI Tool

The detailed algorithm is as follows:

i. Obtain the input parameters from the user, such as:
   - The co-ordinates of member end points A and B.

- Wave characteristics such as wave height, wave period and water depth.
- The diameter of the member.
- The number of zones of marine growth.
- The growth thickness values for each zone.

ii. Assign values to known parameters such as $C_d$, $C_m$, with and without marine growth, and the density of water.

iii. Compute the wave characteristics such as:
- Wavelength, L (An implicit function that has to be solved iteratively)
- wavenumber, k
- angular velocity, ω
- length of the member, $l_m$
- Constants C and K present in the Morison's equation for members without marine growth and with marine growth.

iv. Calculate direction cosines $C_x$, $C_y$, and $C_z$ of the member and create the matrix with the direction cosines as per the Morison's equation.

v. Discretize the member into length segments of unit length.

vi. Determine the sea surface elevation, eta(t) for the current time instance to account for the increase in the surface level due to the passage of the wave.

vii. For each segment of unit length, calculate the horizontal and vertical water particle velocities $u, w$, and accelerations $a_x, a_z$ according the Linear wave theory, accounting for the instantaneous sea surface elevation eta(t). Assign velocity and acceleration in the direction transverse to wave action i.e., v and $a_y$ as zero. (Eqn. 5, 6)

viii. Calculate the normal velocity vector, $V_n$ and normal acceleration vector, $a_n$ by multiplying the velocity vector $[u, v, w]$ and acceleration vector $[a_x, a_y, a_z]$ with the direction cosine matrix calculated in step iv. (Eqn. 3, 4)

ix. Calculate the magnitude of the normal velocity vector $|V_n|$ as $\sqrt{V_n * V_n'}$

x. Calculate the drag and inertial wave force components in the x, y and z direction for the unit length of the member as: (Eqn. 1)

- $F_D = C * |V_n| * V_{nx,ny,nz}$
- $F_I = K * a_{nx,ny,nz}$

xi. Also calculate the drag and inertial force components along x, y and z direction for the case of marine growth. For each zone of marine growth change the member diameter by adding the corresponding growth thickness to the original member diameter.

xii. Calculate the Wave Force acting on each section of unit length by adding the Inertial and Drag force components. This is to be done for both the normal member and for the member with marine growth. $F_T = F_D + F_I$

xiii. Repeat steps v to xii for various time instances, t = 0 to t = T, where T is the time period of the wave.

xiv. Determine the Total Force acting on the entire member, with and without marine growth for each time instance by using the trapezoidal method of numerical integration.

xv. Determine the value and position in time of the maximum total wave force acting on the member, with and without marine growth, for x, y, and z directions.

xvi. Calculate the point of action of this maximum total wave force along the x, y, and z direction as the centroid of the force diagram.

xvii. Display the Maximum Total Force value and the point of action of wave force value for each axis as the output. Also plot the force diagram for the time instant of maximum force along the x, y and z directions for the member with and without marine growth.

A sample input-output setup using the tool for a vertical member of length 30m, diameter 1.2m, in a water depth of 25m, subjected to a wave of height 6m and time period 6s with a uniform marine growth thickness of 70mm is given in Figure 3 and 4.

| Member End Point Coordinates (m) | | | | Wave Properties | | |
|---|---|---|---|---|---|---|
| A | X | 0 | | Wave Height (m) | Time Period (s) | Water Depth (m) |
| | Y | 0 | | 6 | 8 | 25 |
| | Z | 0 | | | | |
| B | X | 0 | | Marine Growth Input | | |
| | Y | 0 | | | | |
| | Z | 30 | | Number of Zones | | Zone 1 Thickness (mm) |
| Member diameter (m) | | 1.2 | | 1 | | 70 |

Figure 3. Input for the sample calculations

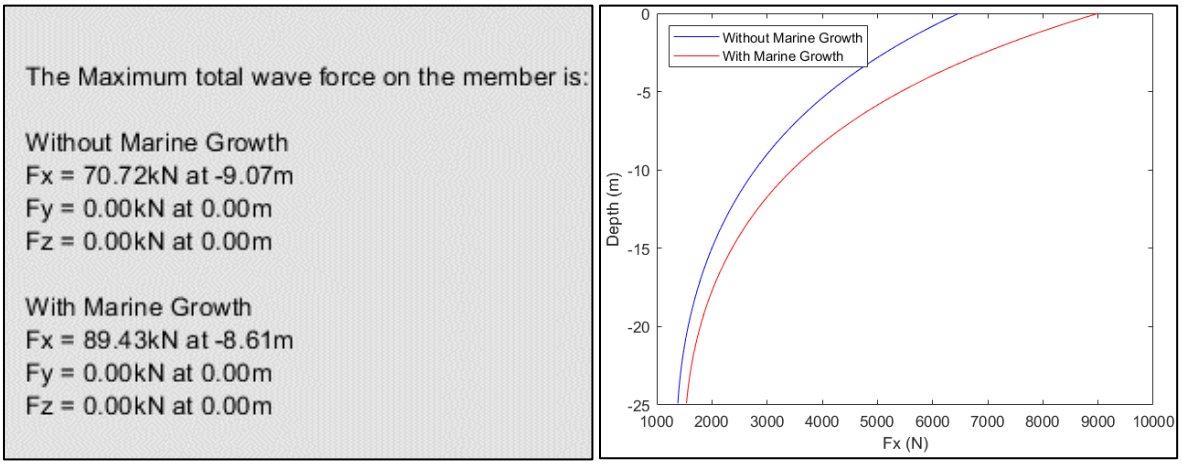



Figure 4. Output Results from tool and plot of wave force diagram for t = 0.9s

## 4. Parametric Study and Results

A parametric investigation is conducted to get a better grasp of the extent of the wave force on the structural member and the effect of the marine growth on this wave force. Various parameters like the member diameter, inclination, marine growth thickness and so on are varied and the wave forces are calculated using the tool.

### 4.1 *Effect of member diameter on wave force*

The wave force acting on a vertical member was calculated for various member diameters starting from 0.5m to 1.5m, in 0.1m increments. The member length was kept at 20m, the wave height as 3m, with time period of 7s and water depth of 17m for all cases. The wave force diagrams for various member diameters, is shown in Figure 5.

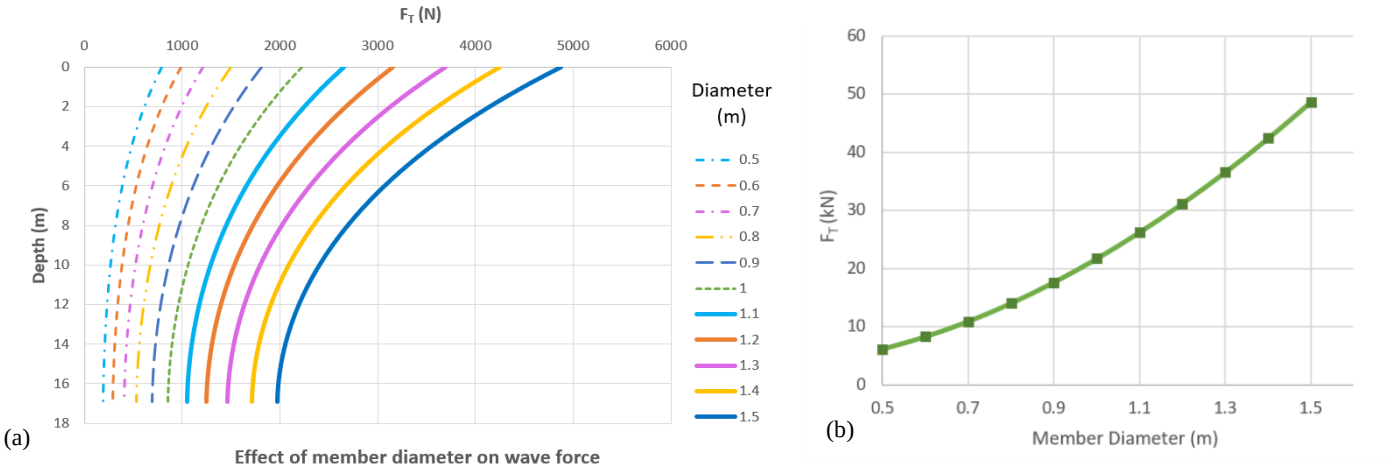



Figure 5. (a) Variation of wave force diagram with increase in member diameter from 0.5m to 1.5m, in increments of 0.1m. (b) Variation of total resultant force with member diameter.

It can be observed from the wave force diagram that the wave force is increasing rapidly with the increase in the diameter of the members. This is expected since both the drag component and the inertial component of the wave force is directly proportional to the member diameter.

## 4.2 *Effect of Uniform Marine Growth on Wave Force*

The presence of marine growth on the structural member increases the wave loading. In order to understand the extent of this effect, the wave force on the same vertical member for varying thickness of marine growth applied uniformly was calculated. The wave force for marine growth thickness starting from 40mm to 140mm, in 10mm increments is shown in Figure 6.

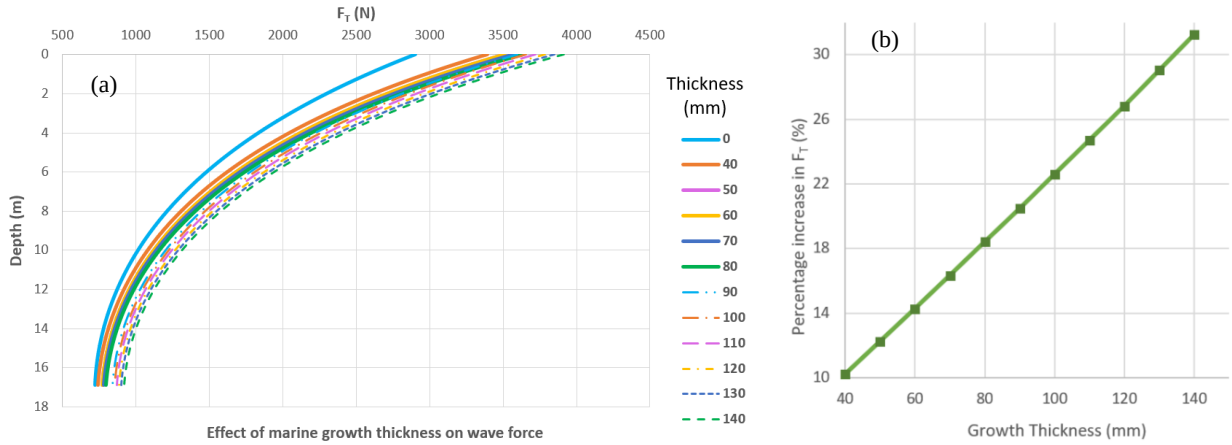



Figure 6. (a) Wave force diagram for varying marine growth thicknesses. (b) % increase in wave force vs marine growth thickness

It can be seen that as the marine growth thickness increases, the wave force acting on the member also increases. This increase is significantly more at the waterline and decreases with depth. The average percentage increase in wave force due to marine growth was found to vary linearly with increase in the growth thickness.

## 4.3 *Zonal Variation of Marine Growth*

In real world scenario, the marine growth on the structural members is not uniform throughout its length. The growth thickness is large near the waterline, attaining its maximum thickness about 2-3m below the waterline, and then decreases in thickness with increasing depth of water. In order to simulate this, a vertical member of 1m diameter and length 20m, subjected to a wave of height 3m, time period 6s

and water depth of 18m, was subdivided into 6 zones of varying marine growth thicknesses as shown in Figure 7. The resulting wave force diagram is shown below in Figure 8.

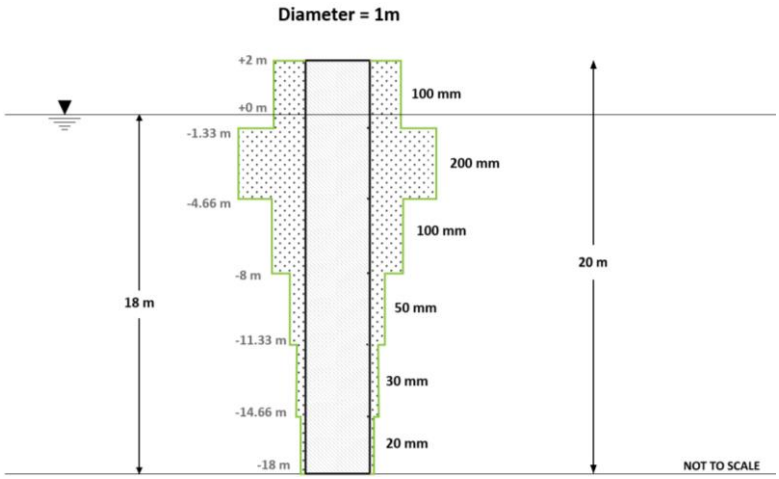
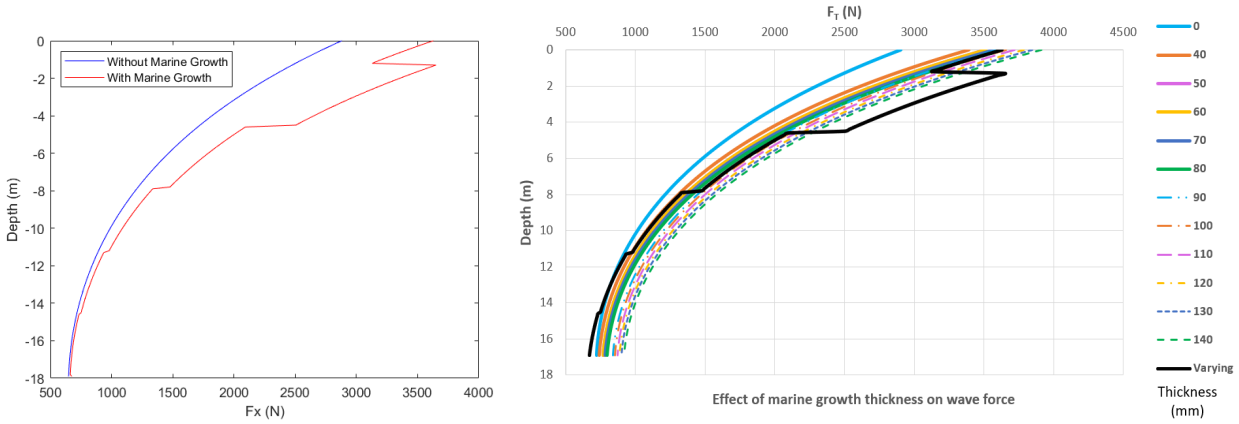



Figure 7. Schematic diagram of the zonal marine growth on the member




(a) (b)

Figure 8. (a) Wave force diagram with and without marine growth in zones. (b) Comparison of wave force diagram for marine growth applied uniformly and in zones.

It was found that the wave force increases or decreases with a corresponding increase or decrease in the marine growth thickness. The maximum total wave force increased from 23.63kN to 29.00kN, corresponding to an increase of 22.73%. Also, the percentage increase in wave force is maximum towards the waterline, since the growth thickness was higher. Furthermore, the point of action of wave force was found to shit upwards towards the waterline from -6.96m to -6.03m. This shift in the point of action of wave force would result in an increase in the turning moment acting on the foundation of the structure.

## 5. Conclusions

The following Conclusions were drawn from this study:

- The wave force on a small diameter tubular member is maximum at the waterline and decreases as water depth increases.
- The increase in the member diameter increases the wave force. This was attributed to the dependency of both the inertial and drag component of the wave force on the member diameter.

- The application of marine growth was found to cause a noticeable increase in the wave forces. Increase in the marine growth thickness causes an increase in the wave force. This increase in the wave force was found to be linearly dependant on the growth thickness.
- It was also found that the percentage increase in the wave force was highest at the waterline and that it decreased with depth. The average percentage increase in total wave force, however, varied linearly with growth thickness.
- Upon applying the marine growth in various zones with varying thicknesses, it was found that the point of application of wave force was shifting upwards towards the waterline. This would lead to increased rotational moments on the foundation of the structure as well as higher fatigue load on the structure.

## References

Agerschou, H. A., & Edens, J. J., (1965). Fifth and first order wave-force coefficients for cylindrical piles. *In Proceedings Santa Barbara specialty conference*, *ASCE*, 219-248.

Fevåg, L. S. (2012). Influence of marine growth on support structure design for offshore wind turbines (*Master's thesis*, *NTNU – Trondheim*, 109pp).

Heaf, N. J., (1979). The effect of marine growth on the performance of fixed offshore platforms in the North Sea. *In Offshore Technology Conference (OTC)*, 256-270.

Jusoh, I., & Wolfram, J., (1996). Effects of marine growth and hydrodynamic loading on offshore structures. *Jurnal Mekanikal*, 1(1), 77-98.

Keulegan, G. H., & Carpenter, L. H., (1958). Forces on cylinders and plates in an oscillating fluid. *Journal of research of the National Bureau of Standards*, 60(5), 423-440.

Theophanatos, A., (1988). Marine growth and the hydrodynamic loading of offshore structures, *Doctoral dissertation, University of Strathclyde*, 276 pp.

Sarpkaya, T., Isaacson, M., & Wehausen, J. V., (1982). Mechanics of Wave Forces on Offshore Structures. *ASME. J. Appl. Mech*, 49(2), 466–467.

Wiegel, R. L., Beebe, K. E., & Moon, J., (1957). Ocean wave forces on circular cylindrical piles. *Transactions of the American Society of Civil Engineers*, 124(1), 89-113.

IN PROCEEDINGS OF 25th HYDRO 2020, INTERNATIONAL CONFERENCE,
NATIONAL INSTITUTE OF TECHNOLOGY ROURKELA, ODISHA, INDIA
26-28, March 2021, ISBN 978-93-90631-56-8

Paper ID - 261

# Performance evaluation of detached breakwater in Poonthura coast using Boussinesq wave approach

Aleena Elsa Mathew, Ram Kumar J, Satya Kiran Raju[1],Sridhar Muddada[2], M V Ramanamurthy[1]

[1]*National Centre for coastal research, NIOT Campus, Velachery-Tambaram Main road, Pallikarnai, Chennai, India*
[2]*National institute of Ocean Technology,Velachery-Tambaram Main road, Pallikarnai, Chennai, India*
*Email:* aleenamundackal@gmail.com

## Abstract

Poonthura coast located at the southwest part in Kerala, has been undergoing severe chronic erosion. A series of detached breakwater was proposed to prevent erosion at Ponnthura coast, Trivandrum. This study analyses the hydrodynamic performance of these artificial reefs using an interactive coastal wave simulation tool, Celeris. It is a hybrid finite volume-finite difference based code that solves the extended Boussinesq equation for modeling the near shore wave transformation. The proposed configuration of structure at Ponnthura coast includes five detached reef at a distance of 125m from the shore with the crest of the structure placed at charted datum. The design height of reef is 6m with a length of 100m and a spacing of 50m between individual reefs. The model is setup with a domain extending 9.5km along the coast and 11 km across with a structured mesh of size 5m. The boundary along the east is considered as open and forced by input wave parameters and the lateral boundaries were chosen to reduce the reflections into the domain. The average significant wave heights were found from the wave data collected by NIOT at 50m depth during 2018.The model was run with and without the structure and results were compared for changes in wave height. The differences in wave heights with and without reef were quantified. With most of the wave energy getting reflected or diffracted due to the reefs, only a small portion of wave energy reaches the protected coastal stretch. It was observed that most of the waves propagating through the 50m gaps were laterally spreading, resulting in dissipation of wave energy through diffraction. The relation of wave height and alongshore transport suggest a reduction in the erosion and hence the proposed structure will satisfy its intended purpose.

***Keywords:*** *Detached breakwater; Celeris; Open source Boussinesq wave model; Poonthura*

## 1. Introduction

Wave action is one of the primary drivers of coastal erosion. Increasing wave action in recent decades has seen the development of coastal structures that protect a beach from further erosion by reducing the wave energy. The structure slope, width and crest height can control the wave transmission to an extent. The wave transmission is dependent on the diffraction and the wave energy entering the leeside of the structure. The commonly used structures in India include seawalls, groins, rubble mount breakwater and detached breakwater especially the south-west part of India.

Kerala, located at the south-west part of India has a very dynamic coast of about 570km, the entirety of which, is prone to erosion (Sanil Kumar et.al., 2006). The Trivandrum coast had the maximum erosion zones in Kerala (NCSCM,2011) and Poonthura, Trivandrum was identified as an erosion hotspot.

National Institute of Ocean Technology (NIOT) tested different shore protection schemes using numerical model studies to suggest suitable protection measures for Poonthura coast. A series of detached breakwaters was suggested by National Institute of Ocean Technology, Chennai from their studies. The Poonthura coast was to be protected with five offshore detached reefs. The reef was suggested to dissipate the wave energy and reduce the amount of wave energy at the coast. The reef dimensions were determined after taking into consideration a number of factors including the field condition. As proposed by Seiji, Uda, Tanaka (1987), for no erosion on the lee side of the gap the following equation is used:

$$\frac{Lg}{X} < 0.8 \qquad (1)$$

Where,
Lg is the length of the segment
X is the proposed spacing

The length of each segment is chosen to be 100m based on the results of calculation based on the method proposed in the Shore protection Manual (SPM, 1984), Gourlay (1981) and Ahrens and Cox and also taking into consideration the field conditions.

The breakwater was proposed at a distance of 125m from the shore. The crest of the structure is placed at the charted datum. The design height of the reef is 6m.Each segment of the structure is placed at a distance such that the gaps are designed to not to let significant wave energy through it so as to cause erosion of the coastline at the lee side.Hence the gap should be less than 100m. So the gap was fixed at 50m.

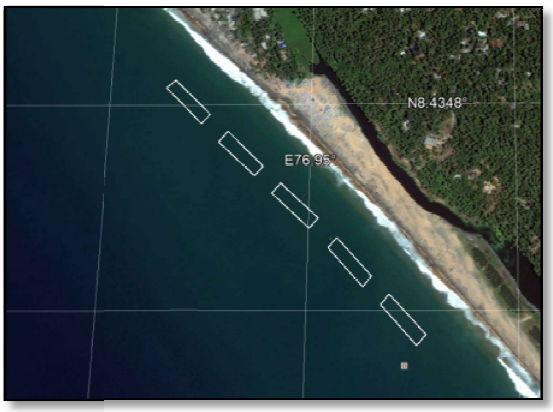



**Figure 1** Proposed detached breakwater at Poonthura coast

The effectiveness of the designed reef structure for the area was studied using the open source hybrid finite volume finite difference Boussinesq model, Celeris. The Boussinesq equation is commonly applied to simulate short waves. Even though the Non-linear shallow water equation is less expensive than Boussinesq equation for computation using CPU cores, Celeris take advantage of the direct3D library for GPU based computation which makes the simulations run faster in real-time, less expensive and also doesn't require any third party software to be installed for running the model. The finite volume wave modeling solvers along with the smoothening schemes enhances the robustness of the model. (Kurganov et.al., 2007)

The GUI of Celeris enables numerical and physical parameters to be changed while the model is running. This Windows-OS based model requires minimum preparation with inputs including bathymetry and wave data. The model enables to render photorealistic images and colour-maps which results in better visualization of results.

Celeris BW model is capable of taking into account the following physical phenomena:

i. Reflection
ii. Refraction
iii. Diffraction
iv. Breaking of waves
v. Wave run-up
vi. Wave generated by underwater landslides
vii. Rip and longshore currents
viii. Wave current interaction

The extended Boussinesq equations by Madsen and Sorensen (1992) are used as wave solvers for a hybrid finite volume–finite difference scheme.

This paper mainly aims to assess the effectiveness of the proposed offshore detached breakwater using the open source Boussinesq wave model, Celeris.

## 2. Methodology

Poonthura coast is located at the south-west part of Kerala. It is located at about 6km south of Trivandrum. The proposed structure was imported to the open source Boussinesq-Wave (BW) model, Celeris for modeling the wave transformation. Celeris solves the extended Boussinesq equation based on hybrid finite volume-finite difference method. Being an interactive coastal wave simulation tool with embedded GUI, it is effective in modeling the near shore wave transformation. Celeris uses the power of GPU to run the numerical model as well as to concurrently visualize the results. The main features of the software include:

- Its fast computation speed
- The interactivity of the model
- The ability to change physical and numerical parameters while model is running
- Photorealistic rendering option

The model is setup with a domain extending 11km along the coast and 9.5km across, with a structured mesh of size of 5m. Two model setups were prepared. First model set up is with the structure and second model set up is without the structure. The height of the reef is taken to be 6m with a length of 100m and a spacing of 50m between individual reefs.

Model bathymetry was generated from field data collected by National Institute of Ocean Technology. Additional requirements were obtained from C-Map electronic charts provided as a part of MIKE modeling suite. The CFL criteria was satisfied and the boundary along the east is considered as open and driven by wave parameters, whereas the northern and southern boundaries, called the lateral boundaries, will let the waves pass out of the domain without reflections. The minimum, maximum and average significant wave heights were found from the wave data collected by NIOT at 50m depth during 2018. Additional wave conditions were also considered and 2m wave was forced from the offshore boundary. The simulation was run for 2m wave height.

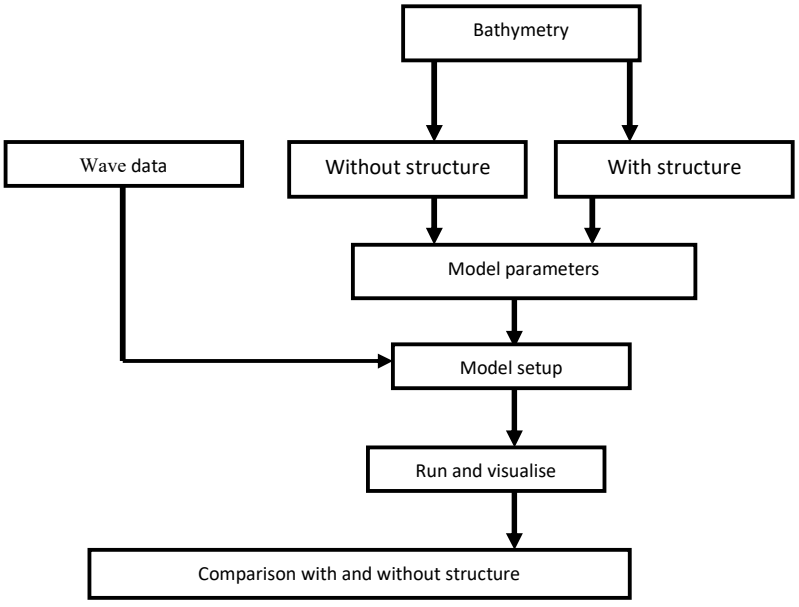



**Figure 2** Flow chart of methodology

The model uses the extended Boussinesq equations by Madsen and Sorensen (1992) equation. The equations for 2DH flow:

$$\begin{bmatrix}\eta\\ P\\ Q\end{bmatrix}_t + \begin{bmatrix}P\\ P^2/h\\ PQ/h\end{bmatrix}_x + \begin{bmatrix}Q\\ PQ/h\\ Q^2/h\end{bmatrix}_y + \begin{bmatrix}0\\ gh\,\eta_x + \psi 1 + f1\\ gh\,\eta_y + \psi 2 + f2\end{bmatrix} = 0 \quad (2)$$

Where,
η is the free surface elevation measured from the still water surface elevation
h is the total water depth, P and Q are the depth-integrated mass fluxes in x and y directions, respectively
g is the gravitational acceleration coefficient
f1 and f2 are the bottom friction terms
ψ1 and ψ2 are the modified dispersive terms
Subscripts x and y denote spatial differentiation, with respect to the corresponding direction
Subscript t denotes temporal differentiation.

For d = 0, the extended Boussinesq equations, reduces to the NLSW equations. In areas where the still water surface elevation is not defined, such as on lands above the sea level, we set d = 0, so the solver automatically switches to NLSW equations

By applying, h= w-b, the above equation changes to

$$Ut + F(U)x + G(U)y + S(U) = 0 \quad (3)$$

Where,
w is the water surface elevation
b is the bottom elevation measured from a fixed datum
U is the conservative variables vector
F(U) and G(U) are the advective flux vectors
S(U) is the source term which includes bottom slope, friction, and dispersive terms

The model was run with and without the structure respectively and the advantage of the GPU model is reflected in the runtime of 30mins. The results of selected locations were written into the gauge file. The files were post processed using Matlab.

## 4. Result

A regular mesh was created for the Poonthura coast with a domain extending 11km along the coast and 9.5km across with a mesh size of 5m and a 2m wave was forced at the boundaries. It was ensured that the CFL criteria is satisfied. The model was run and the results were written into the gauge file. The results were analyzed and plotted. The model was run for two cases, with and without structure. The structure was placed at 125m from the coast with five segments having a length of 100m each. The spacing between the segments was chosen as 50m.

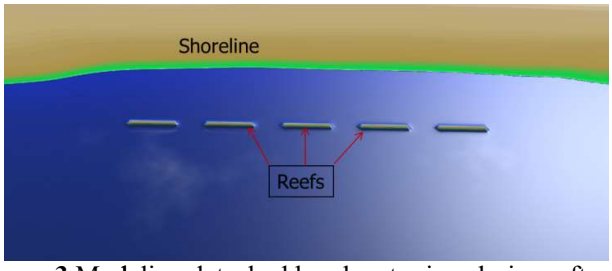



**Figure 3** Modeling detached breakwater in celeries software

The result file was preprocessed using Matlab and the model results of the two cases were compared for changes in the wave height. The change in wave heights for different conditions, averaged over the simulation, at locations around the reef system. The performance evaluation of the detached breakwater was studied. The propagation of waves in the vicinity of the structure is shown in figure. The red color indicates highest water elevation and blue indicates the lowest with yellow in between.

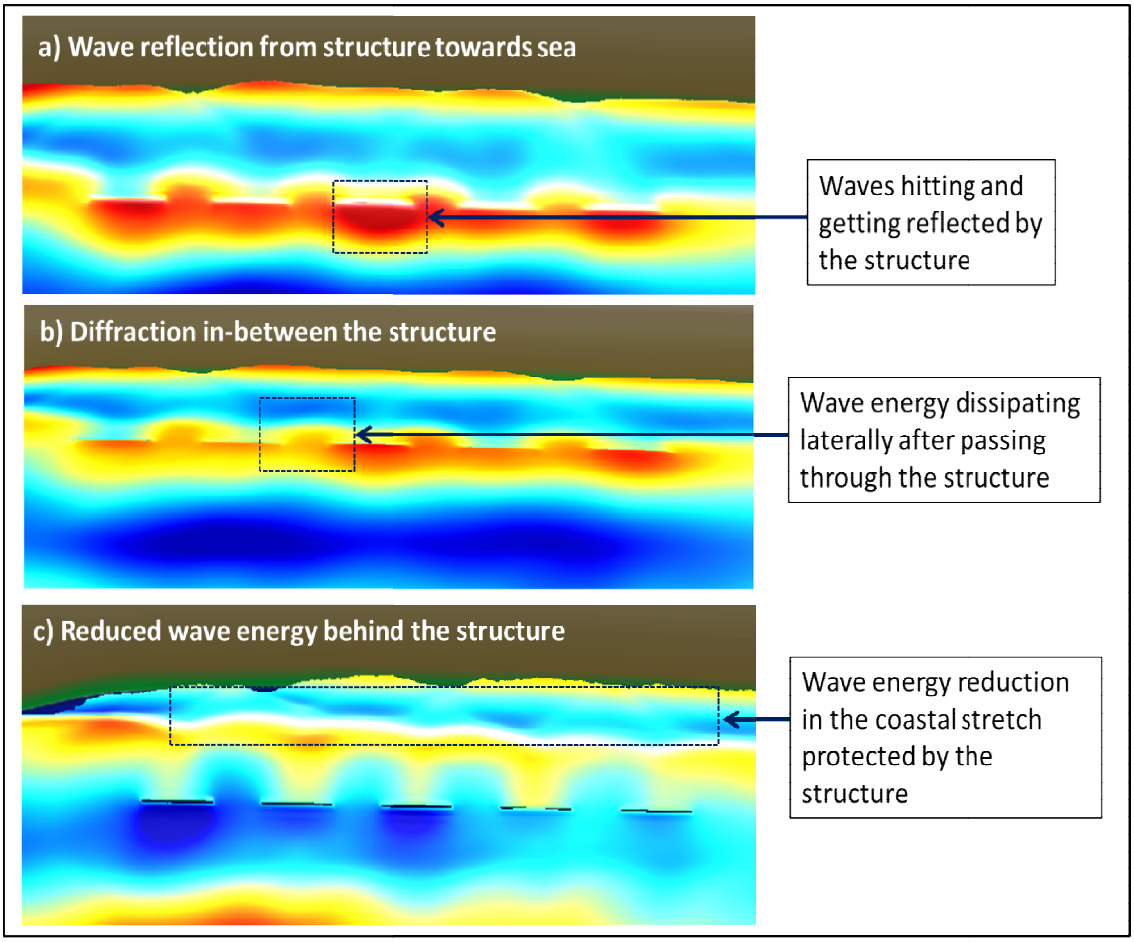



**Figure 4** Propagation of waves near the detached breakwater at Poonthura coast

From Figure (a) it can be seen that just in front of the structure at seaward side there is an increase in wave height. This is due to the reflections caused by the structure. In Figure (b), the waves can be seen propagating through the 50m gaps and then laterally spreading, resulting in dissipation of wave energy through diffraction. With most of the wave energy getting reflected or diffracted due to the reefs, only a small portion of the wave energy reaches the protected coastal stretch as can be seen in Figure (c).

The difference in wave heights with and without the presence of the reefs were quantified as,

$$\%\ change = \left(\frac{wave\ height\ with\ structre - wave\ heig\quad without\ structure}{wave\ height\ withou\ \ structure}\right) X100 \qquad (4)$$

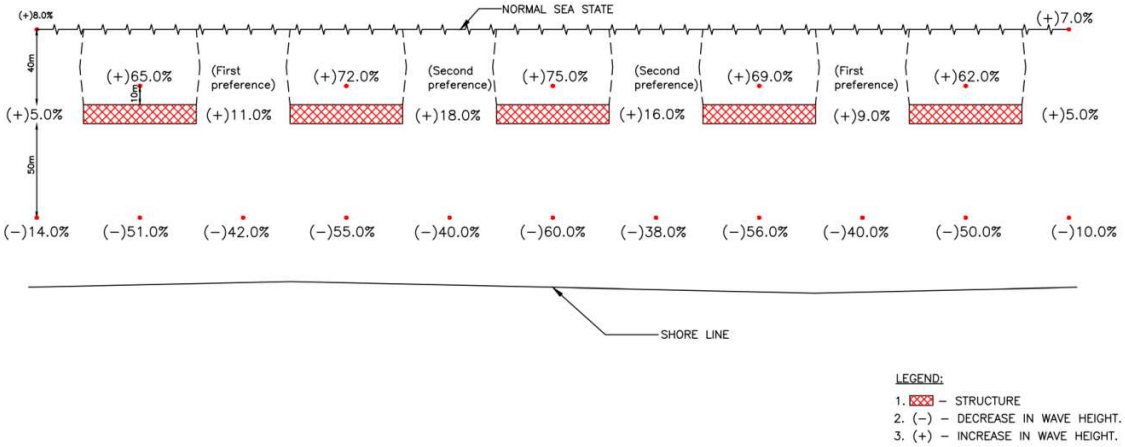



**Figure 5** Quantification of change in wave height near to the reef

It can be seen that an increase of 60% to 75% in wave heights takes place within 10m seaward of the structure. This is due to wave reflections and is as expected. However the effect of reflections die down when one move further seaward and it is barely felt at around 40m seaward of the structure, so any navigation should be avoided on the seaward side of reef and over the reef. There are 4 gaps between the 5 reefs. The percentage increase in wave height in these gaps varies between 9% and 18%. The two central gaps experience a higher value compared to the two end gaps and hence the end gaps should preferred as first choice for navigation purposes. Still, the central gaps experience an increase of less than 20% and also can be used for navigation. The percentage changes near the shoreline are all negative, meaning decrease in wave heights. The value varies from 40% to 60% with points directly behind the structure experiencing a higher reduction compared to points landward of the gaps. With the rate of longshore transport (capacity to erode) proportional to wave height raised to the power of 2.5-3, the reduction in wave height near the shore will help in formation of a stable beach.

The wave power is an important parameter in coastal engineering as it can give an idea of the sediment transport potential of the waves. The reef system should ideally reduce the wave power near the coast in order to reduce sediment transport and in turn erosion. When waves from these directions encounter the reef system they could propagate only through the gaps. This causes a lateral movement of wave crusts, called diffraction. The phenomenon is desirable as it dissipates wave energy

## 5. Conclusions

Poonthura coast was severely affected due to erosion and a series of detached breakwater was suggested at the coast. The performance of this detached breakwater in the Poonthura coast was studied using extended boussinesq wave approach in this paper. The open source software celeris is used for the study. The model was mainly run for two cases, with and without the structure for a wave of height 2m. The wave heights were compared with and without the structure and the percentage reduction was determined. It was found that the wave heights tend to reduce at the leeward side of the structure. As expected the wave height is increasing at the seaside of the structure due to reflection of waves from the structure. Some waves are getting diffracted through the gaps between the structures due to which the wave height is increasing between the structures. Reduction in wave height will imply a reduction in wave energy and could lead to subsequent reduction in the erosion at the coast.

## 6. References

Ali TA (2003) New methods for positional quality assessment and change analysis of shoreline features. Ohio State University, Columbus, p 156

Bakker WT, Klein Breteler EAJ, Roos A (1970) The dynamics of a coast with a groin system. In: Proceedings. 12th conference on coastal engineering, pp 1001–1020

Fassardi C. (2004) "The transformation of deep water wave hindcasts to shallow water",Proceedings of 8th International Workshop on Wave Hindcasting and Forecasting-2004, North Shore, Hawaii,(2004).

Galvin C. J. and Eagleson P. S. 1965, Experimental study of long-shore currents on a plane beach: U. S. Army Corps of Engineers, Coastal Engineering Research Center, TM-10.

Griggs, G.B. The impacts of coastal armoring. Shore Beach 2005, 73, 13–22.
Ranasinghe, R.; Turner, I.; Symonds, G. Shoreline response to multi-functional artificial surfing reefs:
A numerical and physical modelling study. Coast. Eng. 2006, 53, 589–611

Hameed T.S., Ramana Murty M.V. (2007): "Long-term shoreline change along the south central Kerala coast". In: Proceedings of the INCHOE 2007, Mangalore, Vol. II, pp. 761–768

J. C. W.Berkhoff (1972), Computation of combined Refraction Diffraction, Proc. thirteenthth International conference in Coastal engg:, Vancouver, Canada, pp-471-490.

Komen G.J., Cavaleri L., Donelan M., Hasselmann K., Hasselmann S., Janssen PAEM (1994): "Dynamicsand modelling of ocean waves". Cambridge University Press, Cambridge, 560 pp.

Kurian N. P., Rajith K., Shahul Hameed. T. S., Sheela Nair L., Ramana Murthy M. V., Arjun S., Shamji V. R. (2009): "Wind waves and sediment transport regime off the south-central Kerala coast, India". Natural Hazards 49:2, 325–345.

Kurian N.P., Ramachandran K.K., Sheela Nair L., Thomas K.V., Shahul Thomas, K.V., Kurian, N.P., Sundar, V., Sannasiraj, S.A., Badarees, K.O., Saritha, V.K., Abhilash, S., Sarath, L.G., Srikanth, K. (2010): "Morphological changes due to coastal structures along the southwest coast of India". Proceedings on Joint Indo-Brazil Workshop, 125–133 pp.Young IR (1999) Wind generated ocean waves. In: Bhattacharyya R, McCormick ME (eds) Oceanengineering book series, vol 2. Elsevier, Amsterdam, p. 306.

Madsen, P.A. and Sørensen, O.R. 1992. A new form of the Boussinesq equations with improved linear dispersion characteristics. Part 2. A slowly-varying bathymetry. Coastal engineering. 18, 3–4 (1992), 183–204.

Mendonça, A.; Fortes, C.; Capitão, R.; Neves, M.; Carmo, J.S.A.D.; Moura, T. Hydrodynamics around an Artificial Surfing Reef at Leirosa, Portugal. J. Waterw. PortCoastal OceanEng. 2012, 138, 226–235

National Centre for Sustainable Coastal Management (NCSCM) (2011) Shoreline change assessment for Kerala coast. Fact sheet, p 6

P.A.Madsen,O.R.Sørensen,Coastal Eng.18(1992)183–204.

Parvathy.K.G, Deepthi I Gopinath & Noujas V. (2013) "Wave Transformation along Thiruvananthapuram Coast using MIKE 21", in Proc. National Conference of Ocean Society of India (OSICON'13), Role of Ocans in Earth System, Baba M & Jayachandran K V (Eds), pp 193197.

P.A. Work, J.M. Kaihatu,**Wave transformation at Pensacola Pass, Florida**
Journal of Waterways, Port, Coastal and Ocean Engineering, 123 (6) (1997), pp. 314-321

R.G. Dean, R.A. Dalrymple Coastal processes with engineering applications, Cambridge University Press, United Kingdom (2002), p. 475

Sanil Kumar, V.; Pathak, K.C.; Pednekar, P.; Raju, N.S.N.; Gowthaman, R. Coastal processes along the Indian coastline. *Curr. Sci.* 2006, *91*, 530–536.

Shamji, V.R., Shahul Hameed, T.S., Kurian, N.P., Thomas, K.V., 2010. Application of numerical modelling for morphological changes in a high-energy beach during the south-west monsoon. Current science 98 (5), 691-695

Swamy G. N., Varma P. U., Abraham Pylee, Rama Raju V.S., Chandra Mohan P. (1979), "Wave Climate off Trivandrum (Kerala)", Indian Journal of Marine Science 12(3), 127-133

Tavakkol, S. 2019. Interactive and Immersive Coastal Hydrodynamics. University of Southern California.

Tavakkol, S. and Lynett, P. 2017. Celeris: A GPU-accelerated open source software with a Boussinesq-type wave solver for real-time interactive simulation and visualization. Computer Physics Communications. 217, (2017), 117–127. DOI:https://doi.org/10.1016/j.cpc.2017.03.002.

Tavakkol, S. and Lynett, P. 2016. Opportunities for interactive, physics-driven wave simulation using the boussinesq-Type model, celeris. Proceedings of the Coastal Engineering Conference (2016).

Thomas KV, Kurian NP, Sundar V, Sannasiraj SA, Badarees KO, Saritha VK, Abhilash S, Sarath LG, Srikanth K (2010) Morphological changes due to coastal structures along the southwest coast of India. In: Proceedings, Indo-Brazil Workshop, pp 125–133

Thomas KV, Kurian NP, Shahul Hameed TS, Sheela Nair L, Srinivas R (2013) Shoreline management plan for selected location along Kerala coast. Report submitted to ICMAM Project Directorate, MoES. Centre for Earth Science Studies, Thiruvananthapuram, p 308

T.L. Walton Jr, R.O. Bruno,**Long-shore transport at a detached breakwater, Phase-II**
Journal of Coastal Research, 65 (9) (1989), pp. 667-668

Vieira, B.F.V. Wave Hydrodynamics in Coastal Stretches Influenced by Detached Breakwaters. Master's Thesis, Civil Engineering, University of Minho, Guimarães, Portugal, 2014
V.S. Kumar, K.C. Pathak, P. Pednekar, N.S.N. Raju, R. Gowthaman, Coastal processes along the Indian coastline,Current Science, 91 (4) (2006), pp. 530-536

USACE. 1984, Shore Protection Manual, Coastal Engineering Research Center, Vicksburg, Mississippi, Vol. 1.

*IN PROCEEDINGS OF 25th HYDRO 2020, INTERNATIONAL CONFERENCE, NATIONAL INSTITUTE OF TECHNOLOGY ROURKELA, ODISHA, INDIA 26-28, March 2021, ISBN 978-93-90631-56-8*

Paper ID - 416

# Behaviour of Rubberized concrete when subjected to exposure along coastal zone

Bejay Kumar Yadav[1], Showmen Saha[2]

[1]*Research Scholar, Dept. of Civil Engineering, NIT Durgapur, West Bengal 713209, India*
[2]*Professor, Dept. of Civil Engineering, NIT Durgapur, West Bengal 713209, India*
*Email: bejay.nitd@gmail.com*
*Telephone/Mobile No.: +91 8145910018*

## Abstract

It has always been a challenge to maintain and protect the structures in and around the coastal area. Concrete which is one of the mostly used material for construction has many limitations when exposed to coastal environment. Rubberized concrete is continuously evolving as a sustainable concrete by minimizing the use of river sand in concrete and utilizing scrap tires in place of fine and coarse aggregate. In this study, behavior of rubberized concrete was studied in coastal environment to assess its suitability for construction along coastal area. Rubberized concrete (M30) was made by utilizing waste scrap tires in the form of fine aggregate, replacing river sand by 7.5%. This optimum percentage was taken after the result of strength studies which showed that strength decreased below the minimum strength criteria when crumb rubber percentage was increased beyond 7.5%. The concrete samples were then subjected to curing for 28 days, and also some samples were cured up to 150 days along the coast of Visakhapatnam, Andhra Pradesh. Experimental tests like Compressive strength, split tensile strength, water absorption, sorptivity, electrical resistivity and chloride ingression test were conducted. The test results indicated that water absorption, sorptivity, electrical resistivity and chloride ingression tests of rubberized concrete were comparatively less than conventional M30 mix subjected to same exposure condition. This gives an idea that rubberized concrete can perform better and give better durability in coastal environment. The strength result obtained were comparatively less than normal M30 mix but were well above the minimum strength criteria.

***Keywords:*** *Rubberized concrete; Coastal environment; Sorptivity; electrical resistivity.*

## 1. Introduction

Indian tire industry has become an integral part of the auto sector, contributing about 3% to manufacturing GDP and 0.5% of total GDP directly. It had increased from Rs 30,000 crores in year 2010-11 to Rs 59,500 in 2017-18. Trucks and Buses tires is the major contributor by about 55% of total revenue generated by the manufacturing of tires(Akshay Satija, Apollo, Balakrishna, Bias ply, Bias tyre, n.d.) Every year the Indian tire production increases by about 10-12% and, an equal amount of tyre are being discarded annually, creating major environmental problems. The trend of increasing tyre market and its regional distribution in India is shown in **Error! Reference source not found.** and **Error! Reference source not found.**, respectively. Moreover, India's waste tire account for about 6-7% of the global total(Mishra, 2016). Thus it can be observed that globally, disposal of scrap tire has become a major issue. The main problem with the recycling of waste tire is the complexity of materials. Tires for different vehicle are made with a mixture of natural and synthetic rubbers along with various combination of structural reinforcing elements like metals and chemical additives. So separation of different tires with different properties and their recycling through different process is a tedious and costly job.

Attempts are being made to recycle and use waste scrap tires in various industries. In the context of civil engineering also, presently, many research is being done to include waste scrap tires in the form of crumb and chips in place of fine and coarse aggregate.

For the first time, tire chips were used as aggregate in concrete, and its effect on concrete behavior was found. The result showed that tire chips prevented the brittle failure of concrete and improved ductility. However, the compressive strength drastically reduced(Neil N. EldinAhmed

SenouciAhmed Senouci, n.d.) The key findings obtained from a study done by replacement of rubber chips in the percentage of 2.5-7.5 % in concrete indicated that depth of chloride penetration decreased and resistance to acid attack and macro-cell corrosion significantly improved(Thomas et al., 2015). The main reason for the reduction in strength of concrete was found to be due to the hydrophobic nature of the rubber particle. This property of tire chips leads to imperfect bonding between the rubber particles and cement paste. A study was conducted to improve the performance of rubber concrete by employing different surface treatments with NaOH and Silane Coupling Agent. The result indicated an increase in mechanical performance and long-term durability of rubber concrete when treated with NaOH(Guo et al., 2017).

In this present study an attempt is made to find out the behavior of crumb rubber concrete when exposed to coastal zone.

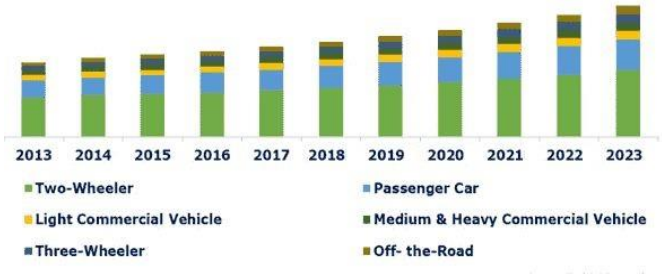



Figure 1: Tire market future in India

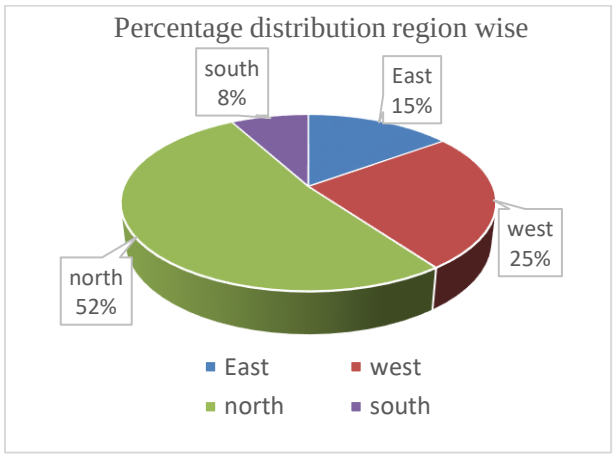



Figure 2: Tire market distribution in India

## 2. Experimental program

### 2.1 *Materials and Mix proportions*

The raw materials used in the study are Ordinary Portland cement 43 grade, conforming to IS: 8112-2013(Bureau of Indian Standard(BIS), 2013). The specific gravity was noted as 3.15. Normal consistency of the cement was 35%, initial and final setting time was 90 min and 175 min respectively. The properties of cement were measured as IS: 8112-2013 and (IS-4031 (Part II), 1999). The sand used was obtained from the banks of river Damodar, confirming to zone II as per IS: (383, 1970). The specific gravity of sand was 2.63 and fineness modulus 2.85. Coarse aggregate used was a mix of 10 mm and 20 mm in the ratio of 40:60 having an average specific gravity of 2.63. The particle size distribution is shown in **Error! Reference source not found.**. The physical properties of aggregates were measured according to (IS 2386- Part III, 1963). Scrap vehicle tire were ground into sizes between 0.075 to 2.36 mm. The specific gravity of crumb rubber was found

to be 1.1. M30 grade concrete was mixed as per IS: 10262-2009(Bureau of Indian Standards, 2009) and (IS 456, 2000). Water-cement ratio adopted was 0.42. Crumb rubber was used as a partial replacement for fine aggregate in the proportion varying from 0 to 15% in multiple of 2.5%. The crumb rubber obtained was first soaked in 1 N NaOH solution and then washed with clean water for about an hour and air-dried at room temperature. The main purpose of washing with NaOH is to improve the interfacing bond between crumb rubbers and cement paste by etching the surface of rubber crumb(Kashani et al., 2018) and (Guo et al., 2017). Fly-ash was used as 5% replacement to cement. The properties of fly-ash, fine aggregate and coarse aggregate are given in **Error! Reference source not found.**, **Error! Reference source not found.**and **Error! Reference source not found.**. The details of the mix is shown in **Error! Reference source not found.**. Particle size distribution is shown in Fig 3.

Table 1: Physical properties of cement, fly-ash

| Physical Properties | Cement | Fly-ash |
|---|---|---|
| Color | Grey | Grey (blackish) |
| Specific gravity | 3.15 | 2.13 |
| Fineness modulus | - | 1.42 |

Table 2: Chemical composition of Cement and Fly-ash

| Chemical composition | Cement % | Fly-ash % |
|---|---|---|
| Silica | 34 | 58 |
| Alumina | 5.5 | 28.3 |
| Calcium oxide | 63 | 2.25 |
| Ferric oxide | 4.4 | 3.45 |
| Magnesium oxide | 1.26 | 0.32 |
| Sulphur | 1.92 | 0.07 |
| Potassium oxide | 0.48 | 1.26 |
| Loss on ignition | 1.3 | 4.17 |

Table 3: Physical properties of Fine and coarse aggregate

| Physical Properties | Fine aggregate | Coarse aggregate |
|---|---|---|
| Bulk density(kg/m$^3$) loose | 1610 | 1460 |
| Bulk density(kg/m$^3$) compacted | 1790 | 1680 |
| Specific gravity | 2.63 | 2.63 |
| Water absorption | 0.95 | 0.92 |
| Fineness modulus | 2.85 | 2.32 |

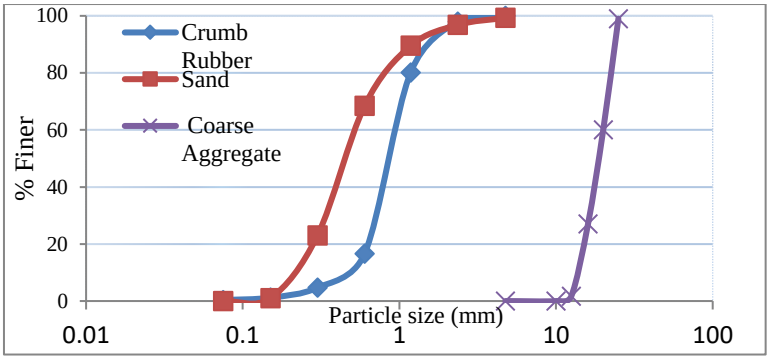



Figure 3: Particle size distribution

Table 4: Mix proportion of concrete used in study

| Mix | % by weight CR + FA | Gravel (kg/m$^3$) | Sand (kg/m$^3$) | Rubber (kg/m$^3$) | Cement (kg/m$^3$) | Fly-ash (kg/m$^3$) | w/c |
|---|---|---|---|---|---|---|---|
| 0R | 0 + 0 | 1283 | 711 | 0 | 380 | 0 | 0.42 |
| 0RF | 0 + 5 | 1283 | 711 | 0 | 361 | 19 | 0.42 |
| 2.5R | 2.5 + 0 | 1283 | 693.23 | 17.77 | 380 | 0 | 0.42 |
| 2.5RF | 2.5 + 5 | 1283 | 693.23 | 17.77 | 361 | 19 | 0.42 |
| 5R | 5 + 0 | 1283 | 675.45 | 35.55 | 380 | 0 | 0.42 |
| 5RF | 5 + 5 | 1283 | 675.45 | 35.55 | 361 | 19 | 0.42 |
| 7.5R | 7.5 + 0 | 1283 | 657.68 | 53.32 | 380 | 0 | 0.42 |
| 7.5RF | 7.5 + 5 | 1283 | 657.68 | 53.32 | 361 | 19 | 0.42 |
| 10R | 10 + 0 | 1283 | 639.9 | 71.1 | 380 | 0 | 0.42 |
| 10RF | 10 + 5 | 1283 | 639.9 | 71.1 | 361 | 19 | 0.42 |
| 12.5R | 12.5 + 0 | 1283 | 622.13 | 88.87 | 380 | 0 | 0.42 |
| 12.5RF | 12.5 + 5 | 1283 | 622.13 | 88.87 | 361 | 19 | 0.42 |
| 15R | 15 + 0 | 1283 | 604.4 | 106.6 | 380 | 0 | 0.42 |
| 15RF | 15 + 5 | 1283 | 604.4 | 106.6 | 361 | 19 | 0.42 |

## 2.2 *Casting and Testing of test specimens:*

### *2.2.1 Compressive and split tensile strength test*:

The purpose of a compressive strength test is to find the crushing strength of hardened concrete. Cubes of size 150 mm x 150 mm x 150 mm were cast for compressive strength and cylinders of 150 mm dia and 300 mm height were cast for carrying out split tensile test. Compressive strength and split tensile strength test was done as per IS: 516 (Bureau of Indian Standards, 2004) after 7, 28, 56, 90, 120 and 150 days of curing using Compression Testing Machine of capacity 3000kN. The average strength of three specimen was recorded as the strength of that particular mix.
The split tensile strength of the specimen is calculated using the formulae:

$$\mathbf{T = 2P/\pi dL}$$

Where T is split tensile strength, P is the maximum load applied, L is the length of the specimen, d is the diameter of the specimen.

### *2.2.2 Electrical resistivity:*

The electrical resistivity test was conducted on cube specimens cast and cured in normal and marine environment. The test was conducted at different intervals starting after just 24 hr from casting to a period of 150 days. The current was passed through the cube specimens on which a conductor was attached on its opposite faces which were connected to the electrical terminals at the time of conducting tests. A voltage of 30V was applied and the current passed was measured in mA. From the value of current passed and voltage applied, Resistance is calculated using formulae V = I R, and resistivity is calculated as q = RA/L. The setup is shown in Fig 4.



Figure 4: Electrical resistivity test setup

### *2.2.3 Water absorption and sorptivity test:*

The specimen used for water absorption had a dimension 100 mm dia x 50 mm height cylinder. The specimens were cured for 28 days before performing the water absorption test. For each mix, three specimen were tested. After the curing period, the specimens were oven-dried for 24 hours at 110º C till the mass became constant. The weight was noted as W1. Again the samples were immersed in water for 48 hours, and the weight was noted as W2. (Antil et al., 2014; Thomas et al., 2015; Yilmaz & Degirmenci, 2009)

$$\% \text{ Water absorption} = [ (W2 - W1) / W1 ] \times 100$$

Sorptivity is the property of a material to absorb and transmit water by capillarity. It can be determined by measuring the capillary rise absorption rate on a material. The specimen used for sorptivity was the same as that used in water absorption test, 100 mm dia x 50 mm height cylinders. After 28 days of curing the concrete specimen are taken and oven-dried at a temperature of 110º C until the weight becomes constant (W1)(Gesolu & Güneyisi, 2011; Pandi & Ganesan, 2015). The specimens are then kept in a tray and water is poured into it such that the water level is not more than 5mm above the base. The flow of water from the peripheral surface is prevented by sealing it with some non-absorbent coating. The samples placed in water for sorptivity is shown in Fig 5. The amount of water absorbed in the time period of 30 minutes is measured by weighing the specimen (W2).

$$\text{Sorptivity} = I/t^{1/2}$$

$$\text{Where } I = [ ( W2 - W1) / A\gamma ]$$

A is the cross-section area of the specimen through which water penetrates. γ is the density of water.



Figure 5: Sorptivity test

### *2.2.4 Chloride ingression test:*

Chloride ingression test was conducted on specimens exposed along the coastal zone as well specimens cured in normal environment at different age. A 5mm dia hole was drilled into the specimens and pulverized concrete sample was collected at different depths from the surface. Potentiometric titration test was conducted on these samples to find out the percentage of chloride content.

## 3. Result and Analysis

### 3.1 *Strength Results*

Based on the tests results obtained from compressive and split tensile tests conducted on cube and cylindrical specimens and exposed to normal water curing and sea water curing, it was observed that there was gradual decrease in both compressive as well as tensile strength, Fig 6 and Fig 7, with increasing amount of crumb rubber. It was also observed that concrete mix containing fly-ash gave slightly better results than mix without fly-ash content. From the compressive tests results it can be concluded that crumb rubber concrete with sand replacement percentage up to 7.5% and containing 5% fly-ash content reached strength value above 30MPa, design strength value of M30 mix. Thus, crumb rubber concrete containing rubber percentage up to 7.5% can be advantageously used. Tensile test results obtained were also comparatively better for replacement percentage up to 7.5% by weight.

The test results of rubberized concrete 7.5RF-NW, 7.5RF-SW, 0RF-NW and 0RF-SW mix were compared to find the effect of coastal zone exposure on strength of concrete. Fig: 8 and Fig: 9 shows the percentage reduction and pattern of reduction in compressive strength due to exposure in coastal zone. From Fig 8 it can be observed that in normal concrete (NC-NW and NC-SW) the strength variation was higher when the specimens were exposed to coastal zone and this variation showed an exponential pattern with increase in age, Fig 9. However rubberized concrete (RF-NW and RF-SW) showed a minor reduction in strength, from Fig 8 and Fig 9, it can be observed clearly.
Thus overall, from these strength tests results and graphical comparison it can be concluded that rubberized concrete can give better performance than normal concrete when exposed to coastal environment.

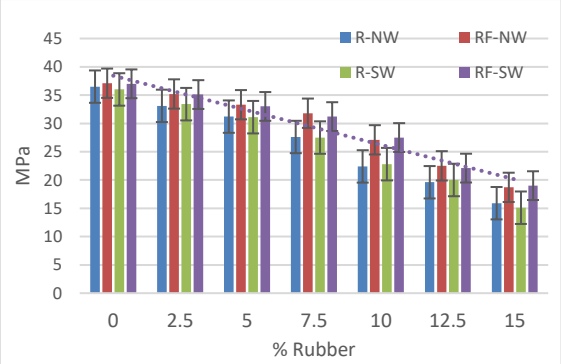



Figure 6: Compressive strength test results

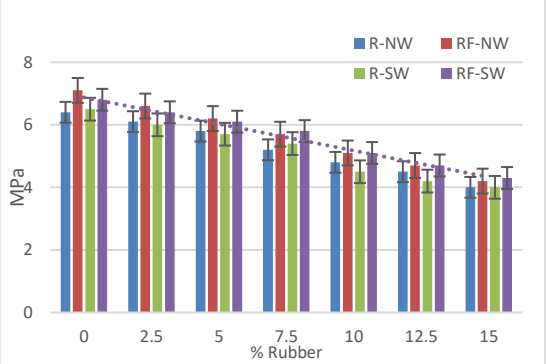



Figure 7: split tensile strength test results

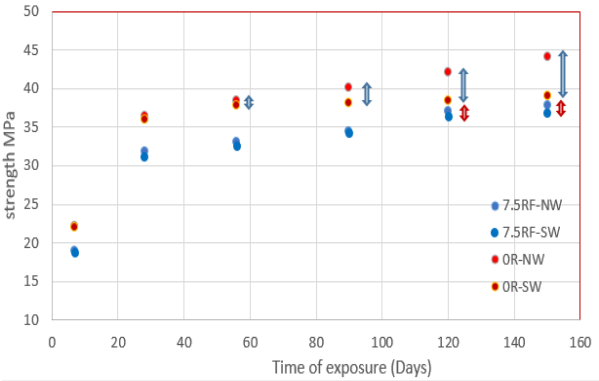



Figure 8: compressive strength comparison

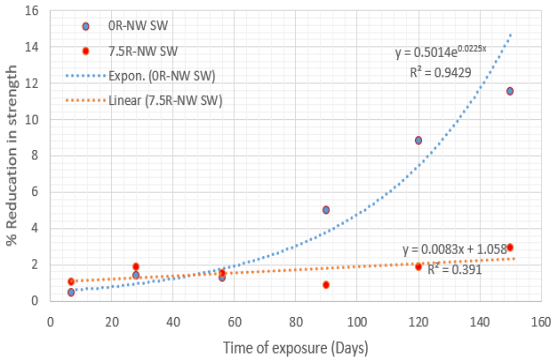



Figure 9: Pattern of variation in strength

### 3.2 *Electrical resistivity*

Fig 10 and Fig 11 shows the tests results of electrical resistivity on concrete specimens. It was observed that resistivity was more for rubberized concrete as compared to normal concrete. Specimens containing 7.5% rubber content and specimens with zero rubber content were compared (Fig 10 and Fig 11). The value of resistivity increased with increase in exposure time. In the initial stages i.e up to 28 days of exposure (Fig 11), rubberized concrete showed good conductivity rather than resistivity, the reason may be that rubberized concrete takes time to dry internally and the water content present might have helped in conductivity. However, it was observed that at later stages (after 60 days of exposure) the resistivity of rubberized concrete increased with increase in exposure condition. When the specimens of concrete kept in normal environment were compared with those exposed to coastal zone, it was noted that specimens exposed to coastal zone offered less resistivity comparatively to specimens kept in normal environment condition. The reason may be that salt particles may have deposited on the surface and in the voids present in concrete and have helped in conductivity of current through it. From the test results value obtained it can be concluded that rubberized concrete proved to offer better resistivity than normal concrete even when exposed to aggressive environment along coastal zone.

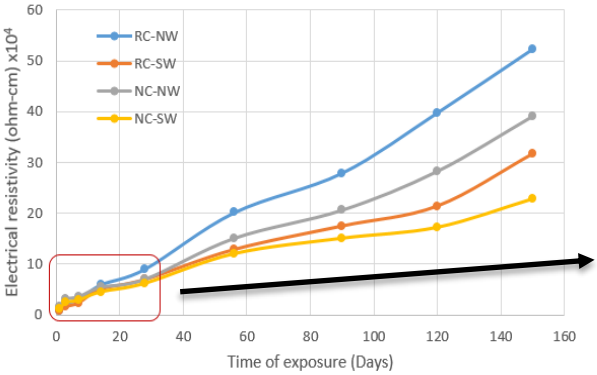



Figure 10: Electrical resistivity test results

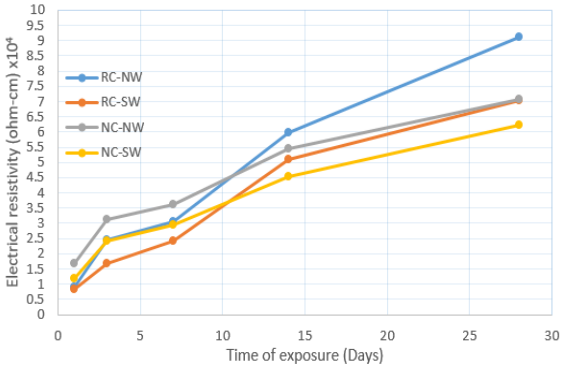



Figure 11: Electrical resistivity up to 28 days

### 3.3 *Water absorption and sorptivity*

Fig 12 and Fig 13 shows the test results obtained from water absorption test and sorptivity tests. It was observed that water absorption and sorptivity increased gradually for both normal concrete and rubberized concrete specimens which were exposed along coastal zone, however the specimens which were cured and kept in normal environment showed consistently decreasing rate of water absorption and sorptivity with increase in time of exposure. But in both the cases (normal environment exposure and coastal zone exposure) rubberized concrete specimens showed lower water absorption and sorptivity as compared to specimens of normal concrete. This behavior may be due to the fact that in rubberized concrete, fine crumb rubber particles block the inter-connected voids and prevent the transportation of water particles into the concrete. Moreover rubber particles being elastic and hydrophobic in nature blocks and prevents adhesion of water molecules into the concrete voids. In case of specimens exposed to coastal zone the increase in both water absorption and sorptivity may be because of settlement of salt particles layers on and into the voids of concrete which may have caused higher amount of absorption and also increased rate of sorptivity.

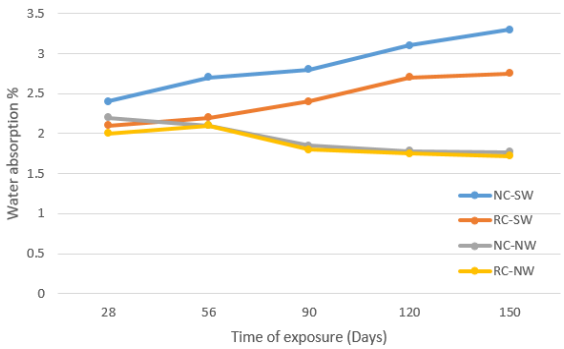



Figure 12: water absorption result

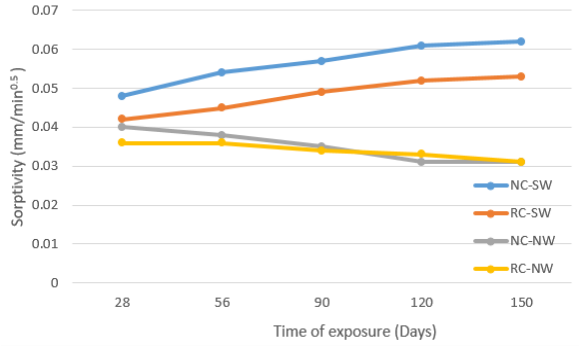



Figure 13: sorptivity test results

### 3.4 *Chloride ingression*

Fig 14 shows the chloride ion depth penetration determined by potentiometric titration test at 56 days. It was observed that with increase in depth the chloride percentage by mass reduced. From the results obtained and from the graphical plot it can be concluded that rubberized concrete showed lower amount of chloride ingression as compared to conventional concrete without any rubber content. Both in normal and marine environment exposure rubberized concrete performed better than normal concrete in resisting chloride ingression. This behavior of rubberized concrete mainly attributes to the fact that fine rubber particles which are hydrophobic in nature block the interconnected voids making the concrete more impermeable and resistant to chloride ingression.

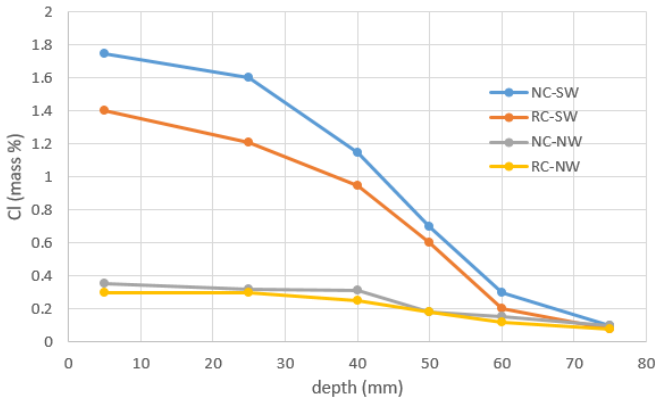



Figure 14: Chloride ingression test results

## 4. Conclusions

Based on the experimental investigation conducted in the present study, the following conclusions can be highlighted:

1. Strength of concrete decreased gradually with increase in percentage of crumb rubber content. Mix containing fly-ash showed better performance than other mixes. It was observed that up to 7.5% sand can be replaced with crumb rubber advantageously without much sacrifice in the compressive and tensile strength. The decrease in the strength is mainly attributed due to lack of adhesion between rubber particles and cement paste. Also rubber particles being soft, cracks initiate quickly along the boundary of the rubber particles, accelerating the failure of concrete.
2. It was observed that when concrete was exposed along the coastal zone, conventional concrete showed higher percentage of reduction in strength than crumb rubber concrete with increase in time of exposure. Fig: 8 and Fig: 9 shows the variation of strength in conventional and crumb rubber concrete. In conventional concrete with 0% crumb rubber, the percentage of reduction in strength was very less up to 28 days but it showed and exponential increase in percentage reduction of strength from 90 days to 150 days of exposure. However, rubberized concrete showed very little and linear variation in reduction of strength with exposure condition along coast, which makes it suitable for use along coastal areas.
3. Electrical resistivity test results are shown in Fig: 10 and Fig 11. It was observed that rubberized concrete showed better resistivity than conventional concrete at later stages, the reason being rubber particles act as insulators and also due to the fact that fine rubber particles block the voids and reduces permeability and porosity in hardened concrete. However, in the initial stages up to 28 days it was observed that rubberized concrete showed higher conductivity and this may be due to the fact that crumb rubber concrete takes more time to dry internally and gain strength and the presence of water particles in the inter-connected voids might have increased the conductivity.
4. Samples exposed in coastal zone showed higher conductivity, which may be due to the reason that salt particles gets deposited on the surface and into the voids and increases the conductivity in concrete.
5. Water absorption and sorptivity tests showed similar pattern of results in which conventional concrete exposed to coastal zone showed higher value of water absorption and rate of transportation of water into concrete (sorptivity). This is due to the fact that salt particles gets deposited on the surface and into the voids which absorbs more water. Higher value of water absorption and sorptivity reduces the durability of concrete. Rubberized concrete on other hand showed lower rate of sorptivity and water absorption making it suitable for concreting in coastal zones.
6. Chloride ingression tests depicted that rubberized concrete has higher resistance to chloride penetration than conventional concrete. This is because the fine crumb rubber blocks the interconnected path in concrete making the concrete less permeable. Also the rubber particles are immune to chloride action, thus increasing the durability aspect of concrete.

Overall, it can be concluded that rubberized concrete performs better in coastal exposure conditions that conventional concrete. From the water absorption, sorptivity, electrical resistivity and chloride ingression tests it can be observed that rubberized concrete can have better durability than conventional concrete when exposed along coastal zone.

## References:


383, I. (1970). Specification for Coarse and Fine Aggregates From Natural Sources for Concrete. In *Bureau of Indian Standards,New Delhi* (pp. 1–24).

Akshay Satija, Apollo, Balakrishna, Bias ply, Bias tyre, C. (n.d.). *The Indian Tyre Industry, Key Players & The Road Ahead*. https://www.alphainvesco.com/blog/understanding-the-indian-tyre-industry/

Antil, Y., Verma, E. V., & Singh, E. B. (2014). Rubberized Concrete Made with Crumb Rubber. *International Journal of Science and Research*, *3*(5), 2012–2014.

Bureau of Indian Standard(BIS). (2013). *IS: 8112 – 1989, Specification for 43 grade Ordinary Portland Cement* (p. 17).

Bureau of Indian Standards. (2004). Method of Tests for Strength of Concrete. In *IS : 516 - 1959 ( Reaffirmed 2004 )* (p. New Delhi,India). https://doi.org/10.3403/02128947

Bureau of Indian Standards. (2009). Guidelines for concrete mix design proportioning. In *Is 10262 : 2009* (p. New Delhi,India).

Gesolu, M., & Güneyisi, E. (2011). Permeability properties of self-compacting rubberized concretes. *Construction and Building Materials*, *25*(8), 3319–3326. https://doi.org/10.1016/j.conbuildmat.2011.03.021

Guo, S., Dai, Q., Si, R., Sun, X., & Lu, C. (2017). Evaluation of properties and performance of rubber-modified concrete for recycling of waste scrap tire. *Journal of Cleaner Production*, *148*, 681–689. https://doi.org/10.1016/j.jclepro.2017.02.046

IS-4031 (Part II). (1999). Methods of Physical Tests for Hydraulic Cement- Determination of Consistency of Fineness By Blaine Air Permeability Method. In *Bureau of Indian Standards, New Delhi*.

IS 2386- Part III. (1963). Method of Test for aggregate for concrete. Part III- Specific gravity, density, voids, absorption and bulking. In *Bureau of Indian Standards, New Delhi* (p. (Reaffirmed 2002)).

IS 456. (2000). Plain and reinforced concrete- Code of practice. In *Bureau of Indian Standards,New Dehli* (pp. 1–114).

Kashani, A., Ngo, T. D., Hemachandra, P., & Hajimohammadi, A. (2018). Effects of surface treatments of recycled tyre crumb on cement-rubber bonding in concrete composite foam. *Construction and Building Materials*, *171*, 467–473. https://doi.org/10.1016/j.conbuildmat.2018.03.163

Mishra, L. (2016, July). Turning waste tyre into ‘green steel.’ *The Hindu- Business*. https://www.thehindu.com/business/Turning-waste-tyre-into-‘green-steel’/article14518524.ece

Neil N. EldinAhmed SenouciAhmed Senouci. (n.d.). Rubber-Tire Particles as Concrete Aggregate. *Journal of Materials in Civil Engineering 5(4)*, *5*(4), 478–496. https://doi.org/10.1061/(ASCE)0899-1561(1993)5:4(478)

Pandi, K., & Ganesan, K. (2015). Effect of water absorption and sorptivity on durability of ground nut shell ash mortar. *International Journal of Earth Sciences and Engineering*, *8*(6), 2687–2692.

Thomas, B. S., Gupta, R. C., Mehra, P., & Kumar, S. (2015). Performance of high strength rubberized concrete in aggressive environment. *Construction and Building Materials*, *83*, 320–326. https://doi.org/10.1016/j.conbuildmat.2015.03.012

Yilmaz, A., & Degirmenci, N. (2009). Possibility of using waste tire rubber and fly ash with Portland cement as construction materials. *Waste Management*, *29*(5), 1541–1546. https://doi.org/10.1016/j.wasman.2008.11.002

# Theme VIII

# Hydraulic & Hydrologic Modelling

*IN PROCEEDINGS OF 25th HYDRO 2020, INTERNATIONAL CONFERENCE, NATIONAL INSTITUTE OF TECHNOLOGY ROURKELA, ODISHA, INDIA 26-28, March 2021, ISBN 978-93-90631-56-8*

Paper ID - 035

# Mathematical model studies for construction of Temporary Pile bridge for erection of a Flyover bridge across an estuarine river

Uday B. Patil[1], Prabhat Chandra[2]

[1]*Scientist 'B', Central Water and Power Research Station, Khadakwasla, Pune 411 024, India*
[2]*Scientist 'E', Central Water and Power Research Station, Khadakwasla, Pune 411 024, India*
*Email: udaybpatil@gmail.com, patil.udayb@cwprs.gov.in*

## Abstract

Mumbai Metropolitan Region Development Authority (MMRDA), Mumbai has undertaken construction of an overhead Flyover Bridge, a connector across Mithi River just upstream of Mini Confluence, to link the area of 'G' Block and Mahim Nature park through Eastern Express Highway (EEH) as part of Mumbai Urban Town Planning (MUTP) Scheme to improve the traffic condition and accessibility to BKC at chainages 3.40 km from Mahim Causeway Bridge. On the basis of the studies conducted for the proposed Flyover Bridge at CWPRS in July 2014, the project authority accepted the proposal of 2.20 m diameter of Pier with minimum clear waterway width of 50 m having total length as 210 m. The present studies pertain to one dimensional mathematical model studies conducted to assess the effect on the hydraulic conditions due to the erection of Temporary Pile Bridge structure of 1.0 m diameter with 7.5 m c/c to be subsequently used to facilitate construction of Piers of the Flyover Bridge. The clusters of 28 Temporary Piles are proposed to be laid across Mithi River throughout the span of 210 m. The studies were carried out for unsteady state discharge condition in the model for rainfall event of 100 year return period with storm duration of 6 hours having Daily Maximum Rainfall of 570 mm based on analysis of latest Isopluvial maps of IMD. On simulation of Temporary Pile Bridge in mathematical model for four proposals as per the stages of construction of Piers, the maximum water level observed upstream of bridge location is (+) 5.66 m CD with marginal afflux of 0.01 m which is safe from hydraulic point of view.

***Keywords:*** *Temporary Pile Bridge, afflux, return period, Isopluvial, linear waterway*

## 1. Introduction

The Mumbai Metropolitan Region Development Authority (MMRDA), Mumbai has planned and proposed an overhead Flyover Bridge, a connector across Mithi River just upstream of Mini Confluence, to link the area of 'G' Block and Mahim Nature park through Eastern Express Highway (EEH) as part of Mumbai Urban Town Planning (MUTP) Scheme to improve the traffic condition and accessibility to BKC at chainage 3.40 km from Mahim Causeway Bridge. The One Dimensional Mathematical Model Studies for the proposed connector i.e. Flyover Bridge were already conducted at CWPRS in the year 2014. The said studies were conducted for three different proposals of different diameter of pier for the 100 years return period flood with storm duration of 6 hours based on the latest Isopluvial Map provided by IMD (October 2008) through MMRDA. Finally, based on CWPRS recommendations, MMRDA approved the proposal of 2.20 m diameter Pier with minimum clear waterway width of 50 m. The center to center to distance between the piers is 52.50 m with four spans across the Mithi River having total length as 210 m. The MMRDA has now taken up the implementation of an elevated connector through its design and construction by commencing the construction work of Temporary Pile Bridge to facilitate the erection of Piers of proposed Flyover Bridge. The present studies for the Temporary Pile Bridge for erection of pier of a connector have been conducted using 1 - D mathematical model.

The MMRDA provided detailed cross sections covering the flood plain widths of about 500 m on either side of banks of the Mithi River and readily available rainfall data recorded at Santacruz and Coloba rain gauge stations of the IMD. The index plan showing the location of proposed Flyover Bridge and Temporary Pile Bridge is shown in Figure 1. The studies were conducted with public domain software for one dimensional mathematical model by using Hydrologic Engineering Centre of U.S. Army Corps of Engineers, USA which was designed and developed River Analysis System (HEC-RAS) (HEC-RAS,

2005) which is an integrated package of hydraulic analysis program, in which the user interacts with the system through the use of Graphical User interface (GUI).

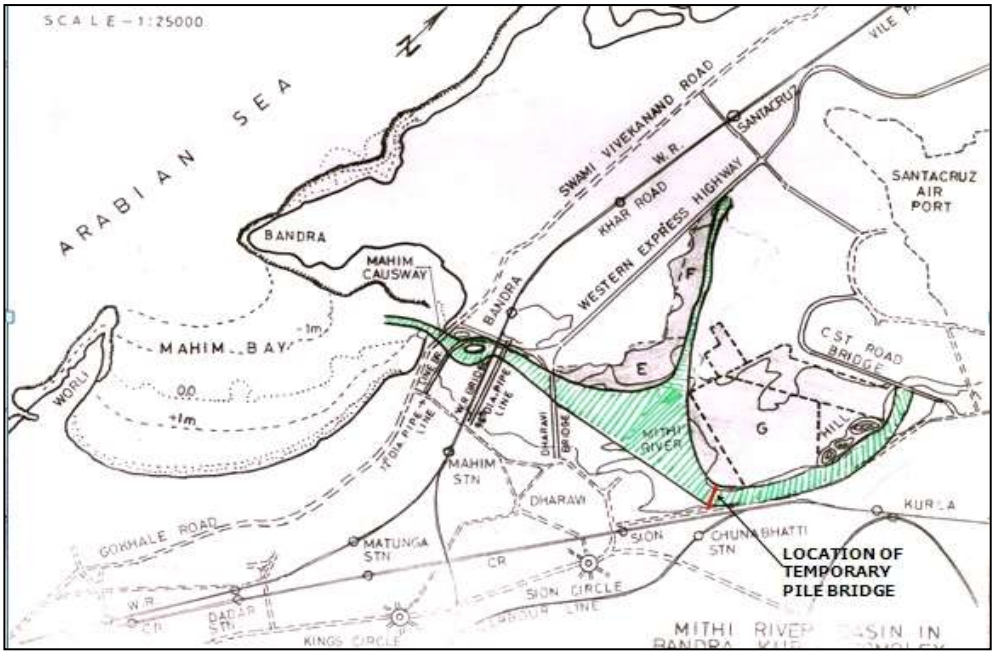



**Figure 1** Index plan showing the location of proposed Flyover Bridge and Temporary Pile Bridge

## 2. The Study Area of Mithi River Basin

The physical characteristics of the river are most important parameters viz., general configuration of the land, the nature of the surface strata etc. are investigated before undertaking any estuarine river engineering study. The salient physical characteristics of Mithi River are briefly described as below.

### 2.1 *Physiographic characteristics of the Mithi River*

The Mithi River originates in the hills east of the Sanjay Gandhi National Park. It carries the overflow from Tulsi -Vihar-Powai Lake system and runoff from its catchments. The river is of short length of 17.922 km, which flows from its origin as Vihar Lake and joins the Arabian Sea near the Mahim Bay. The river has widely varying bed gradients in different reaches. The river flows southward upto Sion and then westwards to join Mahim Bay. The tidal reach in the river is about 7 km from Mahim Bay upto Air India complex. The total catchment area of Mithi River basin is 7295 ha which also includes the 907 ha area of a major tributary, the Vakola Nalla system and 70 ha of Mahim bay. The catchment area of Mithi River basin was divided into six sub-catchments. Bed gradients of different reaches of the river were computed based on cross sectional data of the year 2005 for the Mithi River and that of the year 2001 for the Vakola Nalla. The two dams have been constructed in the upper reaches, one at Vihar Lake on the main river and the other one at Powai Lake on a tributary of the Mithi River. These dams were constructed to supply drinking water to Mumbai city. Mithi River is an estuarine river having influence of tides in the entire period of the year as well as fresh water discharges in its major portion during monsoon periods.

### 2.1 *Physiographic characteristics of the Vakola Nalla*

The major tributary of the Mithi River is the Vakola Nalla. The nalla flows in the areas of Vile Parle (E), Prabhat Colony at Santacruz (E), Khar and part of Bandra (E). The Nalla originates from north of Santacruz downstream airport, passes through the airport to Prabhat Colony then continues south across CST and through Kole Kalyan University campus to join Mithi river. The length of the nalla is about 3.8 km and average bed levels is (+) 3.0 m above Chart Datum (CD). The catchment area as reported in BRIMSTOWAD report (BRIMSTOWAD, 1993) is 907 ha. Presently, the existing widths and bed levels are much less than the design conditions. The cross sectional data of the year 2001 was used for the present study. The catchment area of Mithi river basin is shown in Figure 2 as produced in the BRIMSTOWAD project report.

## 3. Prototype Data Used For Model Studies

### 3.1 *Cross section geometry and creek system network*

The cross sectional data along the entire length of Mithi river was collected and furnished by the project authority, MMRDA, Mumbai after the deluge of 26th July 2005, surveyed in 2005 from Mahim causeway (chainage 0.00 km) to Vihar lake (chainage 17.922 km) without the flood plain widths and post deluge in 2007, surveyed in 2007 covering the flood plain widths of approximately 500 m on either side of banks. The Mahim bay portion was reproduced from bathymetry survey of the year 1994, conducted by Maharashtra Maritime Board.

### 3.2 *Currentmeter observations*

The maximum velocity observed at the Mahim Causeway during non-monsoon period was 2.2 m/sec and that during the monsoon period was enhanced up to 3.3 m/sec due to freshet discharges as observed in year 2003. This data was further used for calibration of model.

### 3.3 *Tidal data*

The tide at Mumbai is of mixed type having considerable inequality in consecutive tidal ranges approximately matching low water levels after 25 hours duration. During the spring tide, the tidal range is about 5.06 m and during neap, it is 2.87 m. The Tides are semi-diurnal (12 hr 15 min) or diurnal period of 25 hours for mixed tide prevalent at Mumbai. All the levels are with respect to Tidal Datum (Chart Datum). The spring tide was observed on 06/06/2016 during the consecutive three days from 05/06/2016 to 07/06/2016. The spring tide at Bandra point in the month of June 2016 having HWL as 5.00 m and 0.30 m as LWL having tidal range of 4.70 m was used in the form of stage hydrograph for the present study.

### 3.4 *Hydrological data*

The rainfall data provided by MMRDA for period of 55 years cycle covering from 1950 to 2005 was used and analyzed statistically to derive Daily Maximum Rainfall for different periods at Santacruz raingauge station. The frequency analysis of the daily maximum rainfall data series at Santacruz was carried out using the Extreme Value Type -I (EV-I) distribution commonly known as Gumbel Distribution as standard distribution for frequency analysis.

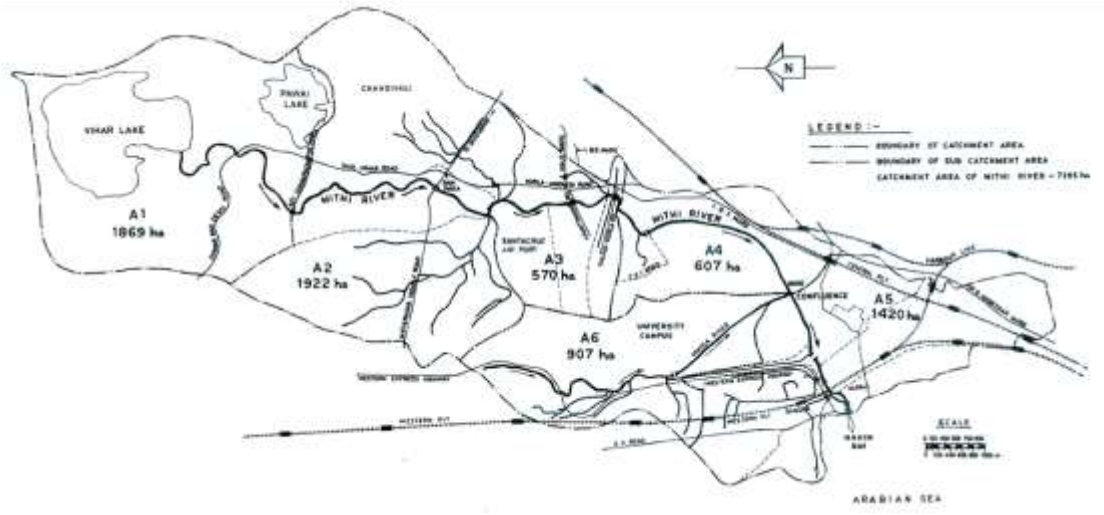



**Figure 2** Catchment area of Mithi river basin

Further, the MMRDA had furnished the latest Isopluvial Maps published in October 2008, based on which the analysis was carried out to arrive at refined and new value of Daily Maximum Rainfall for different returns periods. The 100 year return period flood having Daily Maximum Rainfall of 570 mm based of analysis of latest Isopluvial Maps (October,2008) was used in the model studies.

### 3.5 *Details and data of the proposed Temporary Pile Bridge*

The Engineering Division of MMRDA had provided and submitted the details of proposed Temporary Pile Bridge indicating span and diameter of piles across Mithi River. The MMRDA on the basis of CWPRS recommendations has finalized the layout of a connector having clear linear water way as 50 m with 2.20 m diameter of pier of Flyover bridge. The construction of Temporary Pile Bridge was used for the erection of Pier of the proposed connector or flyover to link the area of 'G' Block and Mahim Nature Park. The Circular temporary piles driven vertically down sufficiently below the river bed to counteract the weight of entire Gantry girder, Service road and vehicular traffic moving over the service road along with moving working staff. The temporary pile has been driven from Pier P-5 to P-9 aligned in the river cross section. The diameter of pile is 1.00 m spaced centre to centre at a distance of 7.50 m. The width of service road platform is 6 m. The size of the Gantry Girder is 15 m X 27 m, which will be mainly used for erection and driving the Pier of the proposed flyover bridge. The above proposal was studied using the one dimensional mathematical model from hydraulic point of view only to observe the hydrodynamic parameters across the section upstream and downstream of Temporary Pile Bridge location.

## 4. One Dimensional Mathematical Model Studies for Different Proposals

The One Dimensional Mathematical Model Studies were carried out using the HEC-RAS (HEC-RAS, 2005) Software for hydrodynamic conditions under different combinations of rainfall events and spring tidal condition covering the stretch of Mithi river from Mahim causeway (Ch.0.00 km) to J. V. L. Road (Ch.13.959 km) including sea portion of Mahim Bay (0.50 km) downstream of Mahim causeway.

The analysis of prototype data in respect of water levels, velocities, cross sections of the Mithi River and the Vakola Nalla, rainfall events corresponding 100 year return periods were used as boundary conditions. There are three open boundaries described as stage hydrograph, a spring tide, applied at the




**Figure 3** Location plan of the proposed Fly over Bridge and Temporary Pile Bridge

downstream of the Mahim Causeway, flood hydrograph applied at upstream end of the Vihar-Powai Lakes and Vakola Nalla. Also, the internal boundaries as lateral flows of the storm water drains from different locations are introduced along the Mithi River. The HEC-RAS system is capable of modeling one dimensional unsteady flow through a full network of open channels. The unsteady flow components were developed for subcritical flow regime calculations. The physical laws which govern the flow of water in a stream are expressed in terms of mathematical expressions as continuity equation and momentum equation.

Continuity Equation: Conservation of mass for a control volume states that the net rate of flow into the volume be equal to the rate of change of storage inside the volume. The final form of continuity equation is as follows

$$\frac{\partial Q}{\partial t} + \frac{\partial Q}{\partial x} - q_1 = 0 \qquad (1)$$

Where, $Q$ = Discharge; $q_1$ = lateral inflow per unit length; A = total cross sectional flow area; $x$ = distance along the channel; $t$ = time

Momentum Equation: Conservation of momentum for a control volume states that net rate of momentum entering the volume (momentum flux) plus the sum of all external forces acting on the volume is equal to the rate of accumulation of momentum.

$$\frac{\partial Q}{\partial t} + v\frac{\partial Q}{\partial x} + gA\frac{\partial z}{\partial x} + gAS_f = 0 \qquad (2)$$

Where, $S_f$ = slope of the energy grade line (friction slope); $A_i$ = wetted cross sectional area;

v = velocity through area; $\frac{\partial z}{\partial x}$ = water surface slope

### 4.1 *Geometry of the Mithi river basin and the model configuration*

The Mithi river basin geometry produced in the model was as described below and schematization is shown in Figure 4. The spacing between cross section is about 100 to 120 m along the length of river. The Mithi river basin is divided into three reaches as described below.

- Reach 1 - Mithi River – M.V. Road to Upstream of Mini Confluence -
  Chainage 13.289 km to 6.310 km - total cross sections 60 No.
- Reach 2 - Mithi River - Upstream of Mini Confluence (MC) upto Mahim bay –
  Chainage 6.214 km to 0.00 km- total cross sections 54 No.
- Reach 3 -Vakola Nalla, major tributary of Mithi River-
  Chainage 0.345 km to 2.40 km- total cross sections 7 No.

The hydraulic structures details such as bridges, culverts etc. are simulated in the model using limited available data received from project authority.

### 4.2 *Generation of flood hydrograph*

The flood hydrographs were generated using the most popular method as the rational method. In an American literature, the method was first mentioned in 1889 by Kuichling for a determination of peak runoff for sewer design in New York (Smart and Herbertson, 1992).The rational method is used in most engineering offices.

An important formula for determining the peak runoff rate, the rational method is characterized by:

- consideration of the entire drainage area as a single unit,
- estimation of flow at the most downstream point only,

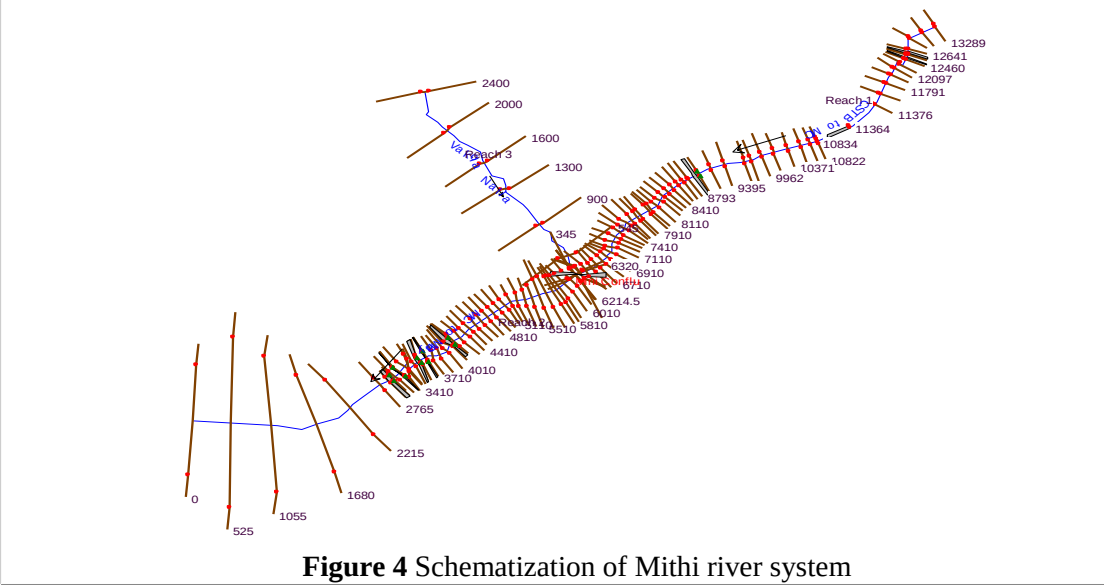



**Figure 4** Schematization of Mithi river system

- the assumption that the rainfall is uniformly distributed over the drainage area.

The Rational method follows the assumptions that:

- the predicted peak discharge has the same probability of occurrence (return period) as the used rainfall intensity
- runoff coefficient is constant during the rainstorm, and
- the recession time is equal to the time of rise or peak .

When the storm continues beyond the time of concentration, every part of the catchment would be contributing to the runoff at the outlet and therefore it represents condition of Peak Runoff. The peak runoff rate corresponding to this condition is given by the formula,

$$Q_p = 0.275 * C * I * A \quad (3)$$

Where, $Q_p$ = Design Peak runoff rate in $m^3$ /sec; C = the runoff coefficient of the watershed which allows for catchment losses; $I$ = rainfall intensity for the design return period and for a duration equal to the " time of concentration" in mm/hour ; A = drainage area of the watershed in $km^2$

### 4.3 *Model studies with Temporary Pile bridge for erection of Flyover bridge at chainage 3.40 km from Mahim causeway 'Without Widening of Existing Five Bridges'*

The one dimensional mathematical model studies were carried out keeping in view, that the Connector (Flyover Bridge) structure can be tested considering the smallest span being the most critical from hydraulic point of view and pier dimension out of three proposals envisaged by MMRDA, which will offer more resistance to hydrodynamic parameters viz maximum water level, channel velocity, safe discharge passing within the structure, etc. Calibrating of the mathematical model for water levels and discharge conditions was carried out separately for non-monsoon season and monsoon season. Thus the model was proved under non-monsoon condition before conducting the model studies for different proposals. Considering the above criteria, the Proposal having Span of 210 m linear waterway, was adopted for testing the hydrodynamic conditions which has 1.00 m diameters of 28 piles spaced at 7.50 m c/c. The bridge structure was tested for 100 year return period having daily maximum rainfall of 570 mm. The geometry of the river system includes the configuration of Temporary Pile Bridge for proposal along with the initial five existing bridges without widening condition. The Figures 5 show the configuration of Temporary Pile bridge for a span of 210 m c/c with total 28 Piles from Pier P-5 to P-9 aligned in cross section.

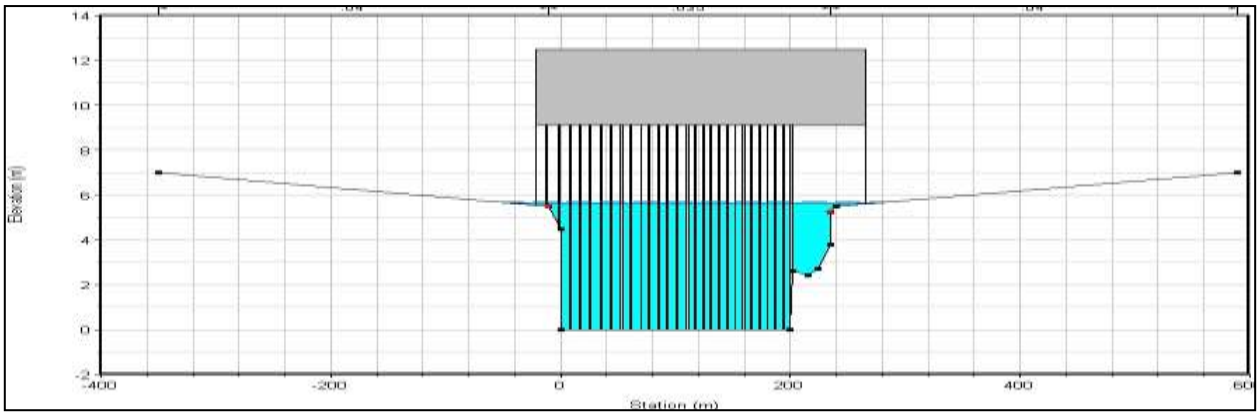



**Figure 5** Configuration of Temporary Pile Bridge for span of 210 m with 28 piles

The geometry of the river system includes the configuration of proposed flyover bridge with the initial five existing bridges 'Without Widening' condition. It is observed from the simulations and table below that the maximum flood water level near the proposed location of Temporary Pile Bridge without widening of existing initial five bridges would rise to (+) 6.28 m (CD) and channel velocity was dampened to 0.46 m/s as compared to the upstream near Kurla Court area having velocity 0.65 m/s. There is no afflux observed at this location. The mathematical model simulation results obtained are analyzed and the hydrodynamic parameters viz. maximum flood water level, channel velocity and the channel flow

area are depicted in Table 1. The Figure 6 shows the longitudinal profile of Maximum Flood water Level along Mithi River with Temporary Pile Bridge (Without Widened condition of Existing Bridges) for 100 Year return period.

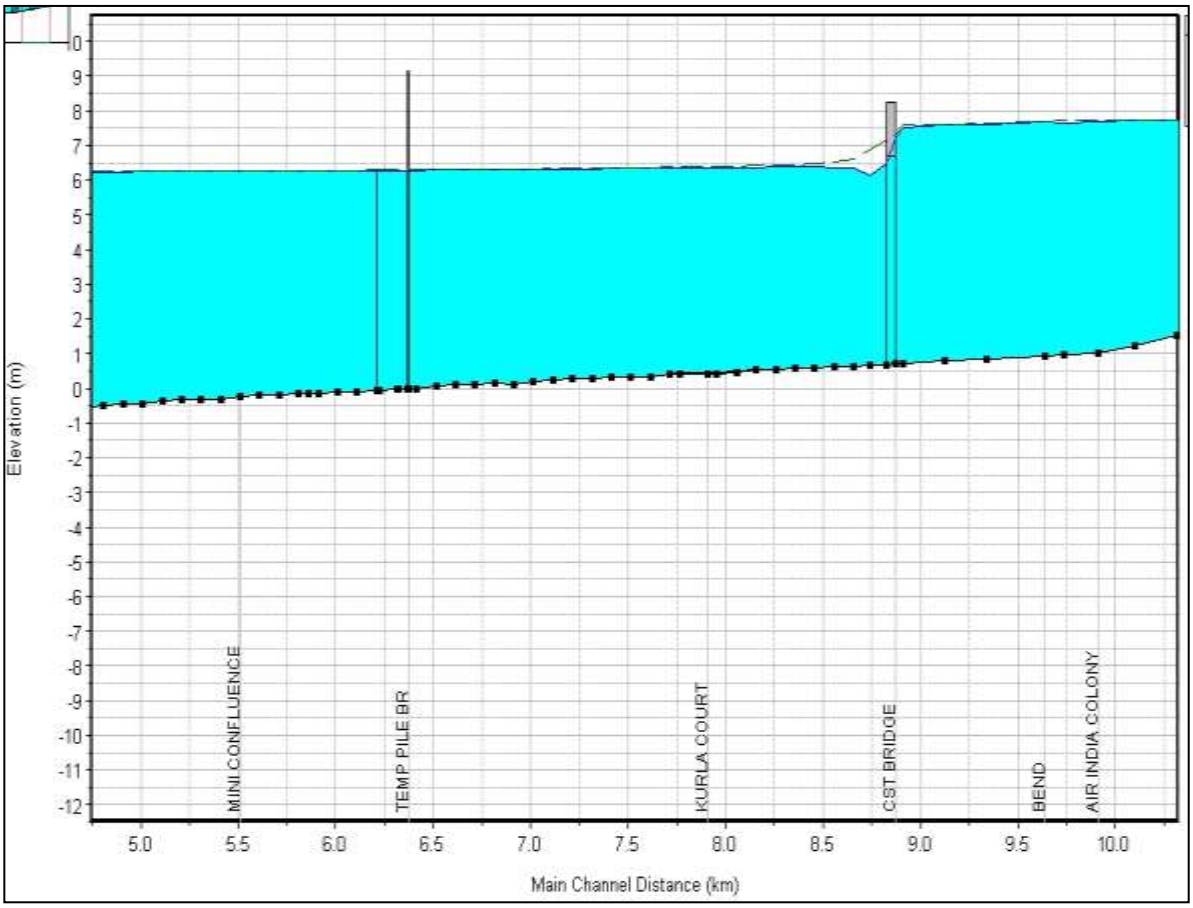



**Figure 6** Longitudinal profile of Maximum Flood Water Level along Mithi River with Temporary Pile Bridge (Without Widened condition of Existing Bridges) for 100 Year return period

**Table 1** Maximum Flood water level with possible top width proposal with existing initial five bridges (Without Widening Condition of Five Bridges)

| Return Period : 100 Year | | Daily Maximum Rainfall : 570 mm ( Isopluvial Map, Oct 2008) | HWL : 5.00 m LWL : 0.30 m Tidal Range : 4.70 m | | |
|---|---|---|---|---|---|
| Sl. No. | Chainage from MCB (km) | Location | MMRDA POSSIBLE TOP WIDTH PROPOSAL | | |
| | | | Maximum Water Level (m) | Channel Velocity (m/s) | Channel Flow Area ($m^2$) |
| 1 | 3.400 | Temporary Pile Bridge : Upstream | 6.28 | 0.46 | 1396 |
| | | Downstream | 6.28 | 0.46 | 1399 |

### 4.4 *Model studies with Temporary Pile Bridge at chainage 3.40 km from Mahim causeway 'With Widening of Existing Five Bridges'*

The mathematical model studies were carried out using the Temporary Pile Bridge proposal and its geometry includes initial Fives bridges 'With proposed widening'. The proposed linear waterway for the five existing bridges was used as mentioned in Municipal Corporation of Greater Mumbai (MCGM) drawing under title prototype data as "Widened Bridges" proposal. The mathematical model simulations have been carried out for proposal and the results thus obtained were analyzed and the hydrodynamic parameters viz. maximum flood water level, channel velocity and the channel flow area are presented in Table 2.

These results are pertaining to proposal in which 28 nos. of Temporary piles are simulated in model studies having span of 210 m. The Maximum Flood water profile for different reaches of Mithi River for the "Widened Condition of five Bridges" along with Temporary Pile is shown in Figure 7. It is observed from the table and the figure that there is reduction in maximum water level in the order of 0.60 m and increase in the channel velocity by 0.20 m/sec due to the reduction in channel flow area at the proposed location as compared to condition of existing bridges without proposed widening. The maximum water level obtained near the location of Temporary Pile bridge is (+) 5.67 m (CD). There is an afflux of 0.01 m hardly at the location which is not harmful and safe from hydraulics. There is no change in the channel velocity on the upstream and downstream side of the Temporary Pile Bridge location which is 0.66 m/s. This increased channel velocity will help faster draining of the flood waters and flushing the sediments downstream. There is negligible afflux formation on upstream side of proposed flyover bridge.

**Table 2** Maximum Flood water level with Temporary Pile Bridge with Widening

| Return Period : 100 Year | | Daily Maximum Rainfall : 570 mm ( Isopluvial Map, Oct 2008) | HWL : 5.00 m LWL : 0.30 m Tidal Range : 4.70 m | | |
|---|---|---|---|---|---|
| Sl. No. | Chainage from MCB (km) | Location | MMRDA POSSIBLE TOP WIDTH PROPOSAL | | |
| | | | Maximum Water Level (m) | Channel Velocity (m/s) | Channel Flow Area ($m^2$) |
| 1 | 3.400 | Temporary Pile Bridge: Upstream | 5.67 | 0.66 | 1249 |
| | | Downstream | 5.66 | 0.66 | 1247 |

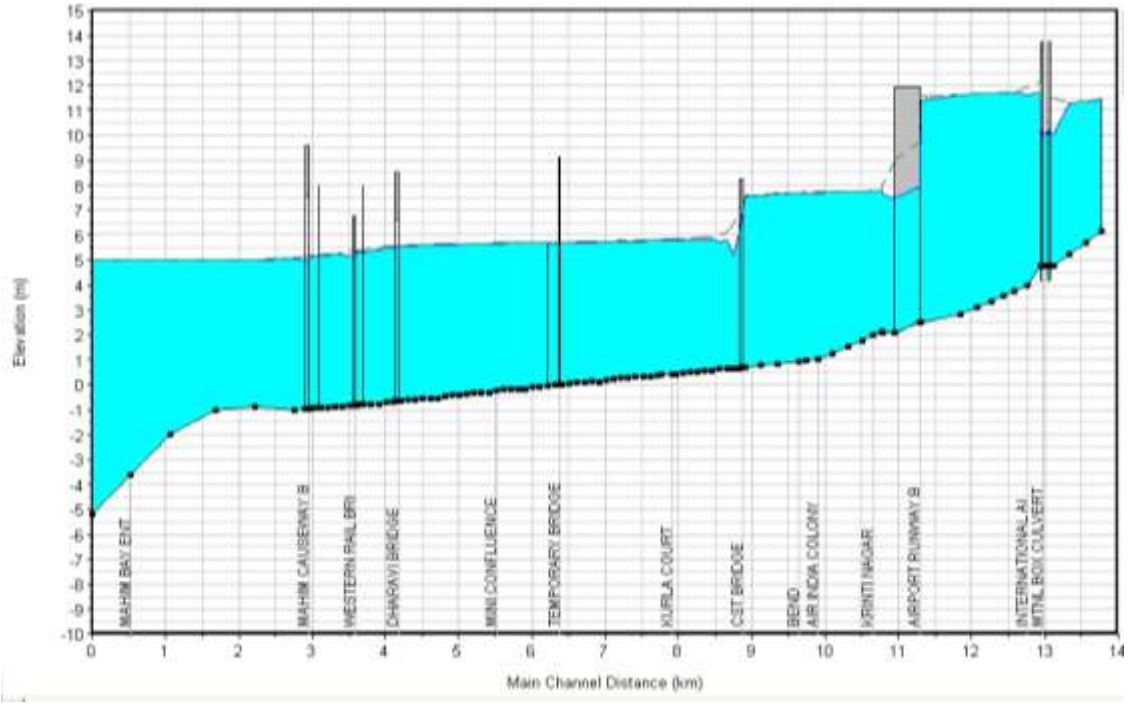



**Figure 7** Longitudinal profile of maximum flood water level along Mithi river with proposed Flyover Bridge (with widened condition of existing bridges)

## 5. Conclusions

- The mathematical model studies for Proposal (Pier P-5 to P-9, Span 210 m, 28 Piles) indicated that there would be marginal afflux (0.01 m) formed on upstream side of Temporary Pile Bridge site which is safe from hydraulic point of view.
- It is also recommended that after the completion of erection of Piers (Pier P-5 to P-9) of proposed connector/ flyover bridge, the Temporary Piles Bridge structure (28 Piles) should be removed immediately to keep the river cross section free from cluster of piles which may create hindrance to free passage of flow during monsoon season on downstream side to avoid the formation of afflux and back water effect on upstream side.
- It is advisable to widen the initial five bridges including Mahim Causeway up to Dharavi bridge as per drawing / proposal submitted by MCGM for safe disposal of flood waters during monsoon season.

## Acknowledgement

The authors are thankful to the Shri A.K. Agarwal, Director, CWPRS for providing direction to this work. The authors are thankful to the project authorities for providing the prototype data.

## References

BRIMSTOWAD Project Report, (1993), Brihanmumbai Mahanagarpalika, “Master Planning For Greater Bombay Storm Drainage And Sewer Rehabilitation”.
CWPRS Technical Report No. 5196, (2014),” Mathematical Model and Desk Studies for Proposed Flyover Bridge Across Mithi River Just Upstream of Mini Confluence, Mumbai”.
HEC-RAS, (2005), U.S. Army Corps of Engineers, Washington, D.C.
Smart, P., Herbertson, J.G., (1992), “Drainage Design”, Springer Science+Business Media, LLC, New York.

*IN PROCEEDINGS OF 25th HYDRO 2020, INTERNATIONAL CONFERENCE, NATIONAL INSTITUTE OF TECHNOLOGY ROURKELA, ODISHA, INDIA 26-28, March 2021, ISBN 978-93-90631-56-8*

Paper ID - 125

# EVALUATION OF RUN-OFF AND IT'S IMPACT ON CONFLUENCE OF TRIBUTARY DUE TO RAPID URBANIZATION IN SHIPRA RIVER BASIN

**Dr. Munendra Kumar1 and Mr. Jaganniwas2**

*1 Associate professor, Delhi Technological University, Delhi, India*

*2 Ph.D Student, Delhi Technological University, Delhi, India*

*E-mail: munendrakumar@dtu.ac.in, jaganniwas827@gmail.com*

Indore & Ujjain are the major towns in the Shipra River Basin and the same is experiences the flash flood every year. The Shipra River is a tributary of Chambal River and it consists of around 5600 Sqkm. The Shipra River originates from Indore district, Madhya Pradesh Malwa Plateau and travel around 214 KM upto the confluence point of Chambal River. Around 20 no of towns and 1047 no of villages comes under this river basin. The Land use changes have been calculated over a period with satellite Image of Shipra River Basin and increase in built-up area has been calculated of urban and Rural area. The built-up area has been increased by 8-10% and run-off has been increased by 15-20% from year 2005-2016. The complete river Basin has been divided into thirteen sub-catchment to know the change in built-up area. The rainfall data of 30 years from rain-gauge stations have been analyzed and the rainfall intensity has been adopted for calculations of Run-off in sub-catchments wrt change in land use over a period. In depth analysis has been made known to the run-off at the confluence point of the stream. It has been observed that contributing runoff is increasing over the period due to changes in pervious surface to impervious surface. The width of the stream is fixed in some places and at some places has been encroached. Due to rapid urbanization, the time of concentration and lag time has been reduced drastically and value of runoff coefficient has been increased. The flash flood received at the outlet of main drain/ drainage channel and the same is connected with tributaries. The flash flood received in tributary from urban area and rural area in the same time and flooding conditions created by River Basin. The carrying capacity of streams is not sufficient to cater the complete flood and same is spread in the surrounding area. The flood affects the Urban property as well as agriculture. Now a day, the flood is happening in most of part of India. It is most important that complete river basin should be studied considering all factors i.e. Urbanization effect, agriculture area, etc. and same will help for the design of urban drainage.

**Keyword:** Land use, Urban Development, Runoff

## 1. INTRODUCTION

Now a days, the flood is become normal phenomena during rainy season. In last few years, the number floods and scale of flood sharply increased in India. Every year in rainy season, the large number of flood occurred in most of the cities of India. According to data presented in India 2018, India lost 1808 life and suffered loss of worth Rs 957 billions. Government of India's data shows that from 1951-2011, on an average the flood claims 1653 lives lost year year.

Experts/researcher wants that the effective and structured flood management is urgently required to handle these challenges. Accordingly, the author studies the increase in built-up area due to rapid urbanization in Shipra River Basin.

## 2. OBJECTIVE OF STUDY

This study aim to identify the change in built-up area over a period due to rapid urbanization in Shipra River Basin. Due to change in built-up area, the run-off increases at the confluence point of river basin.

## 3. STUDY AREA

The Ujjain and Indore city experience the extreme floods year. The Shipra River, Madhya Pradesh, India basin has been selected as the project area for study.

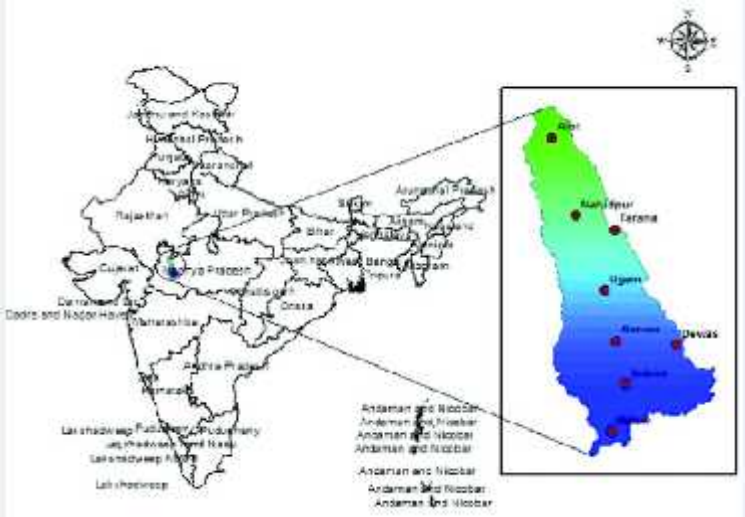


**Figure-1**: Location Map

The Shipra River is a tributary of Chambal River and it consists of around 5679 Sqkm. The Shipra River originates from Indore district, Madhya Pradesh Malwa Plateau and travel around 214 KM through four district Dewas Ujjain Indore and Ratlam upto the confluence point of Chambal River. Around 20 no of towns and 1047 no of villages comes under this river basin. The average annual rainfall is about 931.87 mm. he Land use changes have been calculated over a period with satellite Image.

## 4. DATA PREPARATION

The Landsat data was used for studying of land use changes for Shipra River Basin The Landsat-8 with-7 bands 30 m resolutions for year 2019 and Landsat-5 with-7 bands 30 m resolutions for 2002 were downloaded from the USGS website.

Survey of India (SOI) toposheets at 1:50000 were used for identification of land pattern of built-up area long with the Google image.

The processed image was downloaded from google. The image was re-sampled, Geo-corrected.

## 5. METHODOLOGY

The re-sampled, Geo-corrected was downloaded from google. The image was pre-proceed in ENV software. The toposheet and google image was used for supervised classifications. Image has been classified for five classes i.e. Built-up, Barren Land, Water body, Agriculture Land and Forest. Multi-temporal satellite image was used for classifications. The different band combinations were made for identifications of various features from image. Training sample (signature value) was created for identifications of similar pixels.
In all software the supervised classifications features are available i.e. Maximum Likelihood classifications, support vector machine, neural network etc. For landuse classifications, the support vector machine classifications were used.

Landuse map was created for year 2000 and 2020 for Shipra river basin.

## 6. ACCURACY ASSESSMENT:

The accuracy assessment has been done for both images and the following accuracy was obtained.

- Land Classification for Year 2000
  - Over All Accuracy-92%
  - Kappa Accurancy-0.84

- Land Classification for Year 2020
  - Over All Accuracy-94%
  - Kappa Accurancy-0.86

## 7. ANALYSIS OF LANUSE IN SHIPRA RIVER BASIN

Landsat-8 image for year 2020 and Landsat-5 image for year 2000 were used for LULC classifications using supervised classifications. Total 20 numbers of towns and 135 numbers of villages lie inside the project area. The built-up area for Shipra river basin has been calculated using the satellite images. It has been observed that built-up area has been increased by 5.08% and the pervious land has been reduced by 5.49% from 2000 t0 2020. The increase in urban area is due to conversion of land from Agriculture, Forest, Fallow land etc. into Built-up area. The detail of landuse has been presented in table 1:

**Table 1:** Change in Last land from 2000 to 2020

| S. No. | Description | 2000 | 2020 | Change in Percentage |
|---|---|---|---|---|
| 1 | Built-up | 155.170947 | 436.82607 | 5.08% |
| 2 | Barran Land | 599.342794 | 797.51322 | 3.57% |
| 3 | Water Body | 39.891091 | 62.440262 | 0.41% |
| 4 | Agriculture Land | 4747.93047 | 4237.9711 | -9.19% |
| 5 | Forest | 3.835631 | 11.403228 | 0.14% |
| | **Total** | **5546.17** | **5546.15** | 0.00% |

The complete Shipra river basin has been divided into eight sub-catchments and landuse changes has been calculated basin wise. The increase in built-up area in sub-catchment has been presented in table 2 & 3:

**Table 2:** Sub-catchment Landuse for 2000

| S. No. | Description | Catchment for Year 2000 | | | | | | | | |
|---|---|---|---|---|---|---|---|---|---|---|
| | | 1 | 2 | 3 | 4 | 5 | 6 | 7 | 8 | Total |
| 1 | **Built-up** | 0.58 | 1.24 | 2.50 | 2.98 | 22.76 | 8.99 | 102.57 | 13.55 | 155.17 |
| 2 | **Barren Land** | 55.71 | 61.66 | 127.45 | 7.12 | 107.62 | 38.15 | 109.68 | 91.96 | 599.34 |
| 3 | **Waterbody** | 1.78 | 7.74 | 4.04 | 0.12 | 15.09 | 0.34 | 6.12 | 4.66 | 39.89 |
| 4 | **Agricultural Land** | 273.80 | 295.39 | 447.92 | 196.47 | 1358.40 | 531.65 | 945.43 | 698.86 | 4747.93 |
| 5 | **Forest** | | | | | 1.83 | | 2.01 | | 3.84 |
| | **Total** | **331.87** | **366.03** | **581.90** | **206.69** | **1505.71** | **579.13** | **1165.81** | **809.04** | **5546.17** |

**Table 3:** Sub-catchment Landuse for 2020

| S. No. | Description | Catchment for Year 2020 | | | | | | | | |
|---|---|---|---|---|---|---|---|---|---|---|
| | | 1 | 2 | 3 | 4 | 5 | 6 | 7 | 8 | Total |
| 1 | **Barran Land** | 60.23 | 70.60 | 102.36 | 13.48 | 199.43 | 60.84 | 136.36 | 154.21 | 797.51 |
| 2 | **Buit-up** | 4.53 | 5.94 | 13.37 | 12.15 | 53.22 | 34.50 | 237.97 | 75.14 | 436.83 |
| 3 | **Waterbody** | 1.84 | 8.21 | 5.98 | 0.67 | 21.07 | 2.53 | 12.53 | 9.60 | 62.44 |
| 4 | **Agricultural Land** | 264.69 | 279.72 | 459.00 | 180.39 | 1226.68 | 480.92 | 776.54 | 570.03 | 4237.97 |
| 5 | **Forest** | 0.57 | 1.56 | 1.19 | 0.00 | 5.29 | 0.33 | 2.40 | 0.06 | 11.40 |
| | **Total** | **331.87** | **366.03** | **581.90** | **206.69** | **1505.70** | **579.12** | **1165.81** | **809.04** | **5546.15** |

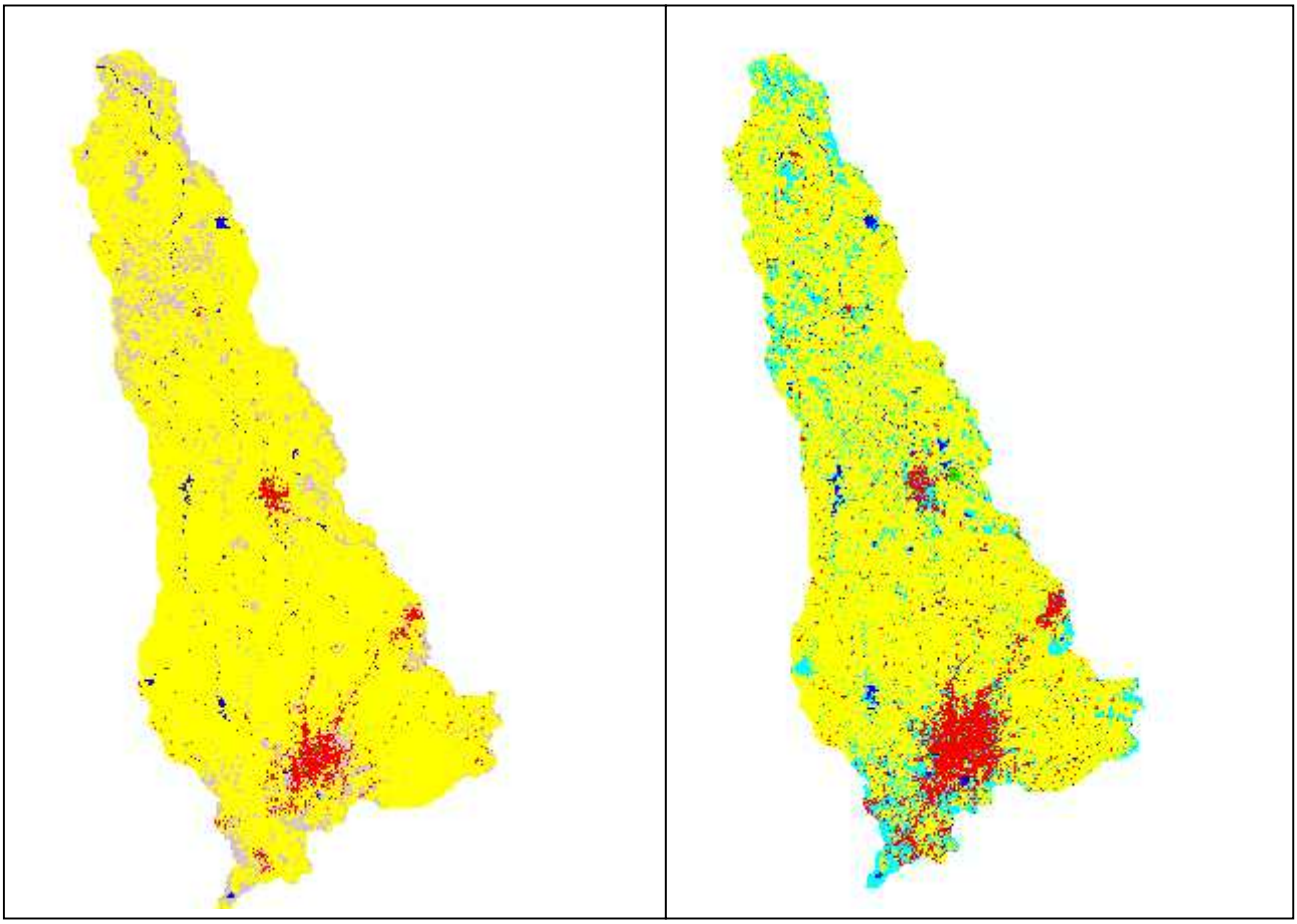


**Figure-2**: Showing Landuse Map for Year 2000 & 2020




**Figure-3:** Showing Sub-catchment of Shipra River Basin

## 8. RAINFALL DATA

The daily rainfall data from 1970 to 2016 was collected from Water Resources, Government of Madhya Pradesh. The daily rainfall data for 2003, 2005 and 2006 was missing. The maximum daily rainfall data was analysed and same was converted into houly data emplying the IMD formula

Pt=P24 (t/24)

t:- time duraion in minutes

P24: Daily rainfall vlaue in minutes

Pt:-Rainfall of t mins durations in mm

The IDF cuver generated for 1:5 year return period and rainfall intensity 0f 281.6 mm has been calculated. Same intensity has been utilized for further calculations of run-off.

## 9. ANALYSIS OF RUN-OFF

The run off co-efficient has been taken from CPHEEO manual on Storm Water Drainage System (August-2019), Government of India. The run-off coefficient value is given below:

- Built-up Area – 0.90
- Pervious Area – 0.2

The cumulative run-off co-efficient has been calculated based on above given run-off co-efficients.The run-off has been calculated for year 2000 and year 2020.The data has been presented in table:

**Table 4:** Sub-catchment wise discharge

| Description | Catchment | | | | | | | |
|---|---|---|---|---|---|---|---|---|
| | 1 | 2 | 3 | 4 | 5 | 6 | 7 | 8 |
| I (mm/hr) | 281.6 | 281.6 | 281.6 | 281.6 | 281.6 | 281.6 | 281.6 | 281.6 |
| **Year 2000** | | | | | | | | |
| Run-off coefficient | 0.20 | 0.20 | 0.20 | 0.21 | 0.21 | 0.21 | 0.26 | 0.21 |
| Discharge ($m^3$/sec) | 522.37 | 579.42 | 924.05 | 339.67 | 2480.21 | 955.24 | 2385.47 | 1339.88 |
| **Year 2020** | | | | | | | | |
| Run-off coefficient | 0.21 | 0.21 | 0.22 | 0.24 | 0.22 | 0.24 | 0.34 | 0.27 |
| Discharge ($m^3$/sec) | 543.98 | 605.16 | 983.56 | 389.88 | 2646.98 | 1094.91 | 3126.85 | 1677.13 |
| Increase in discharge ($m^3$/sec) | 21.61 | 25.74 | 59.50 | 50.21 | 166.77 | 139.67 | 741.37 | 337.26 |

It has been observed from anaysis of data that the discharge is increasing year to year due to repid urbanizations. The discharge has been increase in shipra river basin from 9526 cumecs to 11068 cumecs.

## 10. RESULT AND DISCUSSIONS

It has been observed that contributing runoff is increasing over the period due to changes in pervious surface to impervious surface.

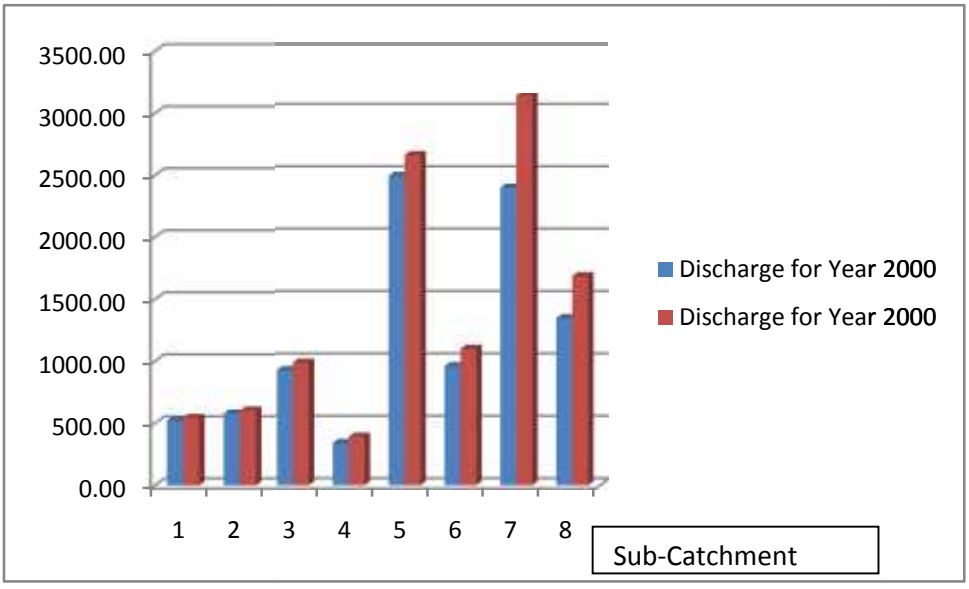



**Figure-4:** Showing Graph Discharge ($m^3$/s) vs sub-catchments

Overall discharge has been increase in shipra river basin from 9526 cumecs to 11068 cumecs. The discharge has been calculated considering that the water will be infiltrate and some water will be retain in retention body for initial rain but the quantity of discharge will increase when .the soil will saturate and retention body will be fully filled. The value of run-off co-efficient will not be same as taken in calculations.

The width of the stream is fixed in some places due to encroachment. Due to rapid urbanization and modifications in agriculture fields, the time of concentration and lag time has been reduced drastically and value of runoff coefficient has been increased. The flash flood received at the outlet of main drain/ drainage channel and the same is connected with tributaries. The flash flood received in tributary from urban area and rural area in the same time and flooding conditions created in River Basin. The carrying capacity of streams is not sufficient to cater the complete flood and same is spread in the surrounding area. The flood affects the urban property as well as agriculture. Now a day, the flood is happening in most of part of India. It is most important that complete river basin should be studied considering all factors i.e. Urbanization effect, agriculture area, etc. and same will help for the fixation of return period and run-off-co-efficient for urban drainage.

## REFERECES

1. Bramhe, V. S., Ghos, S. K., and Garg, P. K., Extraction of Built-up Area by Combining Textural Features and Special Indices From Landsat-8 Multispectral Image, The Internaltional Archives of the Photogrametry, Remote Sensing and Spatial Scieence, Volume XLII-5, 2018

2. David C. F., Return Period–Dependent Rational Formula Coefficients for Two Locations in Texas. Journal of Irrigation and Drainage Engineering ASCE, Vol. 142, Issue 9 (September 2016)

3. Debu Mukharji, "Effect of Urbanization on Flood- A review with Recent Flood in Chennai (India)" IJESRT, July, 2016

4. Drainage Master Plan of NCR Delhi 2016, Department of Civil Engineering, IIT Delhi, India

5. Laura Casas Cardona, "Analysis of Urban Catchment for Flood Return Period Assessment", Master Thesis, 2016.

6. HE, Chunyang, Shi, Peijun, XIE, Dingyong and Zhao, Yuanyuan, Improving the normalized Difference Built-up Index to Map Urban Built-up Areas using a Semiautomatic Segmentation Apporach, Remote Sensing Letters, Vol-1, No-4, December 2010, 213-221

7. Nirjan Dhakal and Theodore G. Cleveland. Return Period Adjustment for Runoff Coefficients Based on Analysis in Undeveloped Texas Watersheds, ASCE, 2013

8. P. E. Jope, Development of Rainfall Intensity Duration Frequency Curves for Mumbai City, India, Journal of Water Resource and Protection, 2016, 8, 756-765

9. Salih, Abdelrahim, Classification and Mapping of Land Cover Types and Attributes in Al-Ahsaa Oasis, Eastern Region, Saudi Arabia Using Landsat-7 Data, Journal of Remote Sensing & GIS, 2018

10. Sewerage and Sewage Treatment Manual, 2013, Government of India

11. Xu, Hanqlu, Extract of Urban Buit-up Land Features from Landsat Imegery Using a Thematic Oriented Index Combinations Technique, Photogrammetric Engineering & Remote Sensing, Vol. 73 No-12, December, 2007, pp 1381-1391

12. Yueling W and Xiaoliu. Land use/cover change effects on floods with different return periods: a case study of Beijing, China. Frontiers of Environmental Science & Engineering, October 2013, Volume 7, Issue 5, pp 769–776

*IN PROCEEDINGS OF 25th HYDRO 2020, INTERNATIONAL CONFERENCE, NATIONAL INSTITUTE OF TECHNOLOGY ROURKELA, ODISHA, INDIA 26-28, March 2021, ISBN 978-93-90631-56-8*

Paper ID - 128

# SELECTION OF THE OPTIMAL DESIGN RUN-OFF COEFFICIENT FOR URBAN DRAINAGE SYSTEM

**Dr. Munendra Kumar[1] and Mr. Jaganniwas[2]**

*1 Associate professor, Delhi Technological University, Delhi, India*

*2 Ph.D Student, Delhi Technological University, Delhi, India*

*E-mail: munendrakumar@dtu.ac.in, jaganniwas827@gmail.com*

## ABSTRACT

The design of urban drainage system has been established in Storm Water Manuals and International Standards. The design of storm drainage network is mainly depends upon the Run- off co-efficient, rainfall intensity and return period. The planning and design of new or existing drainage infrastructure should be designed in such a way so that localized flooding and harmful environmental impacts should not be occurred, but it is very difficult to accommodate all parameters in the design. Therefore, the evaluation of design run-off is most important in any drainage scheme. Due to rapid urbanization, increase in impervious, the flooding in Urban areas has become increasingly common in recent decades in India. Almost all cities in India have been developed adjacent to the river in unplanned manner. The run-off co-efficient plays a vital role in run of a catchment. The runoff coefficient has also been calculated over a period 2000 to 2020 and the result shows that built-up area has been increased by 72%. The urban infrastructure development in term of imperviousness level, the cumulative run-off coefficient has been increased from 0.3 in 2000 to 0.36 in 2020. The value of the runoff coefficient arranged in ascending order and plotted on a graph and it shows the strong relationship an increase in runoff coefficient. The storm water drainage designed for complete development of catchment in term of urbanization by considering the runoff coefficient and return period. In this paper, it has been recommended that runoff coefficient and return period should be considered in such a way so that urban catchment should be capable to cater the urban flood.

**Keyword:** Land use, Urban Development, Runoff coefficient

## 1. INTRODUCTION

The design of urban drainage system has been established in Storm Water Manuals and International Standards. The design of storm drainage network is mainly depends upon the Run- off co-efficient, rainfall intensity and return period. The planning and design of new or existing drainage infrastructure should be designed in such a way so that localized flooding and harmful environmental impacts should not be occurred, but it is very difficult to accommodate all parameters in the design. Therefore, the evaluation of design run-off is most important in any drainage scheme. Due to rapid urbanization, the flooding in Urban areas has become increasingly common in recent decades in India. Almost all cities in India have been developed adjacent to the river in unplanned manner. The run-off co-efficient plays a vital role in urban catchment.

The exact evaluation of run-off coefficient is very important for calculation of run-off. Over the period, the value run-off coefficient increases. Accordingly, the run-off coefficient has been evaluated by dividing the planning area of Ujjain Town, Madhya Pradesh, India in sub-catchment.

## 2. OBJECTIVE

The main objective of Author is to observe the change in run-off coefficient over a period in urban catchment. The Planning area has been divided into small watershed and pattern for increase of built-up area studied. The saturation limit of run off coefficient has been calculated for urban catchment using Landsat data.

## 3. STUDY AREA

Shipra River is passing through the Ujjain Town and all small tributaries join this river. The run-off from Ujjain planning area fall under the Shipra River. The Ujjain town is located at 23.179o N and 75.7849o E. Most of time town is flooded in rainy season due to rapid urbanizations.



**Figure 1:** Locaion Map of Study Area

## 4. DATA PREPARATION

The Landsat data was used for studying of land use changes for Shipra River Basin The Landsat-8 with-7 bands 30 m resolutions for year 2020 and Landsat-5 with-7 bands 30 m resolutions for 2000 were downloaded from the USGS website.

Survey of India (SOI) toposheets at 1:50000 were used for identification of land pattern of built-up area long with the Google image.

The processed image was downloaded from google. The image was re-sampled, Geo-corrected.

## 5. METHODOLOGY

The re-sampled, Geo-corrected image was downloaded from google. The image was pre-proceed in ENV/QGIS software. The toposheet and google image was used for supervised classifications. Image has been classified for five classes i.e. Built-up, Barren Land, Water body, Agriculture Land and Forest. Multi-temporal satellite image was used for classifications. The different band combinations were made for identifications of various features from image. Training sample (signature value) was created for identifications of similar pixels.

In all software the supervised classifications features are available i.e. Maximum Likelihood classifications, support vector machine, neural network etc. For landuse classifications, the support vector machine classifications were used.

Landuse map was created for year 2000 and 2020 for Ujjain Planning Area.

## 6. ACCURACY ASSESSMENT:

The accuracy assessment has been done for both images and the following accuracy was obtained.

- Land Classification for Year 2000
  - Over All Accuracy-92%
  - Kappa Accurancy-0.84

- Land Classification for Year 2020
  - Over All Accuracy-94%
  - Kappa Accurancy-0.86

## 7. DISCUSSIONS ON LANDUSE DATA

The landuse map has been calculated for year 2000 and year 2020 for Ujjain Planning area. The detail of Landuse is shown in table below:

**Table 1:** Landuse Data for Year 2000 & 2020

| Type of Area | Area-2000 (Sqkm) | Area-2020 (Sqkm) |
|---|---|---|
| Built-up | 17.87 | 30.81 |
| Barren Land | 16.12 | 32.97 |
| Waterbody | 2.19 | 3.99 |
| Agricultural Land | 113.97 | 79.26 |
| Forest | 1.84 | 4.96 |

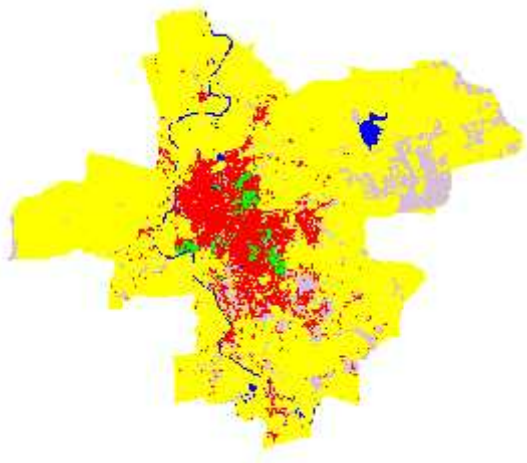


**Figure 2:** Showing the Landuse Map of Year 2000

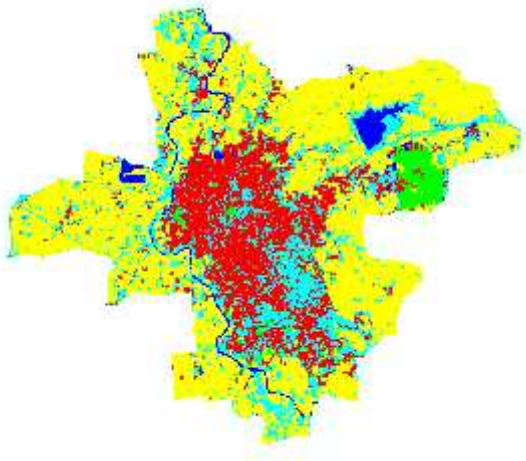


**Figure 3:** Showing the Landuse Map of Year 2020

It has been observed that overall built-up area has been increased by 72% from year 2000 to 2020.

## 8. ANALYSIS OF RUNOFF COEFFICIENT WRT SUB-CATCHMENTS

The Ujjain planning area has been divided into 32 small watershed area. Twelve number of watershed lie at boundary of planning area and same has been discarded from analysis of landuse and landcover study. The figure below is showing the sub-catchments of planning area.



**Figure 4:** Showing Sub-catchments of Ujjain Planning Area

**Table 2:** Showing the Run-off Coefficent for sub-catchements

| S. o. | Cumulative Run-off Coefficient-2000 | Cumulative Run-off Coefficient-2020 | Percentage Change in Run-off Coefficient |
|---|---|---|---|
| 1 | 0.25 | 0.28 | 12% |
| 2 | 0.25 | 0.27 | 8% |
| 3 | 0.26 | 0.31 | 19% |
| 4 | 0.28 | 0.36 | 29% |
| 5 | 0.27 | 0.28 | 4% |
| 6 | 0.44 | 0.54 | 23% |
| 7 | 0.25 | 0.32 | 28% |
| 8 | 0.25 | 0.27 | 8% |
| 9 | 0.26 | 0.34 | 31% |
| 10 | 0.35 | 0.46 | 31% |
| 11 | 0.63 | 0.68 | 8% |
| 12 | 0.28 | 0.28 | 0% |
| 13 | 0.26 | 0.29 | 12% |
| 14 | 0.48 | 0.59 | 23% |
| 15 | 0.25 | 0.27 | 8% |
| 16 | 0.25 | 0.37 | 48% |
| 17 | 0.26 | 0.27 | 4% |
| 18 | 0.30 | 0.45 | 50% |
| 19 | 0.26 | 0.34 | 31% |
| 20 | 0.25 | 0.27 | 8% |

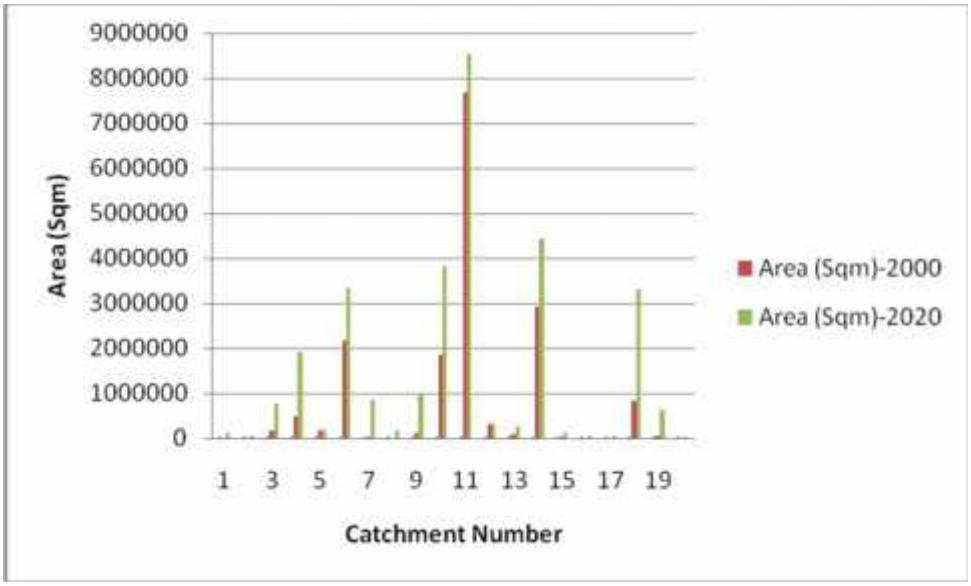



**Figure 6:** Showing the Run-off Coefficent for sub-catchements

The value of the runoff coefficient arranged in ascending order for year 2000 and plotted on a graph and it shows the strong relationship an increase in runoff coefficient.

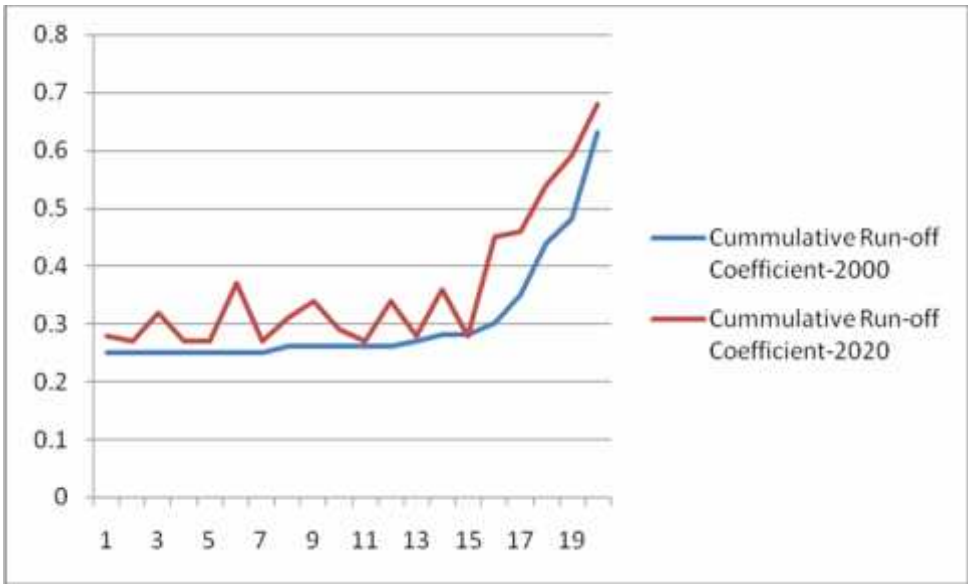



**Figure 5:** Showing the Run-off Coefficent for sub-catchements arranged in incerasing order

It has been oberved that 0.68 is maximum value of run-off coefficient for sub-catchmen. So the same valve may be the sturation limit for development in Urban area. The run-off coefficient has been calculated based on Landsat data. The exact value may be calcualted based on actual survey or high resolution data.

## 9. DISCUSSIONS AND CONCLUSION

The result plotted on graphs shows that maximum value of run-off coefficient obtained in various sub-catchements is 0.68. We can assume that maximum value achieved for rub-off coefficient is stauration limit. In Such a way, all sub-catchment will achive the same run-off catchement over a peiod.

During design of urban storm Drainage, the run-off coefficient and return period shuld be adjested in such a way so that drainage network should be capable to cater the flood. As per author, the run-off coefficient should be taken based on actual landuse pattern sub-catchmnet wise and retrun perod should be adjested in individual sub-catchemnt.

## REFERECES

1. Bramhe, V. S., Ghos, S. K., and Garg, P. K., Extraction of Built-up Area by Combining Textural Features and Special Indices From Landsat-8 Multispectral Image, The Internaltional Archives of the Photogrametry, Remote Sensing and Spatial Scieence, Volume XLII-5, 2018

2. David C. F., Return Period–Dependent Rational Formula Coefficients for Two Locations in Texas. Journal of Irrigation and Drainage Engineering ASCE, Vol. 142, Issue 9 (September 2016)

3. Debu Mukharji, “Effect of Urbanization on Flood- A review with Recent Flood in Chennai (India)” IJESRT, July, 2016

4. Drainage Master Plan of NCR Delhi 2016, Department of Civil Engineering, IIT Delhi, India

5. Laura Casas Cardona, "Analysis of Urban Catchment for Flood Return Period Assessment", Master Thesis, 2016.

6. HE, Chunyang, Shi, Peijun, XIE, Dingyong and Zhao, Yuanyuan, Improving the normalized Difference Built-up Index to Map Urban Built-up Areas using a Semiautomatic Segmentation Apporach, Remote Sensing Letters, Vol-1, No-4, December 2010, 213-221

7. Nirjan Dhakal and Theodore G. Cleveland. Return Period Adjustment for Runoff Coefficients Based on Analysis in Undeveloped Texas Watersheds, ASCE, 2013

8. P. E. Jope, Development of Rainfall Intensity Duration Frequency Curves for Mumbai City, India, Journal of Water Resource and Protection, 2016, 8, 756-765

9. Salih, Abdelrahim, Classification and Mapping of Land Cover Types and Attributes in Al-Ahsaa Oasis, Eastern Region, Saudi Arabia Using Landsat-7 Data, Journal of Remote Sensing & GIS, 2018

10. Sewerage and Sewage Treatment Manual, 2013, Government of India

11. Xu, Hanqlu, Extract of Urban Buit-up Land Features from Landsat Imegery Using a Thematic Oriented Index Combinations Technique, Photogrammetric Engineering & Remote Sensing, Vol. 73 No-12, December, 2007, pp 1381-1391

12. Yueling W and Xiaoliu. Land use/cover change effects on floods with different return periods: a case study of Beijing, China. Frontiers of Environmental Science & Engineering, October 2013, Volume 7, Issue 5, pp 769–776

*IN PROCEEDINGS OF 25th HYDRO 2020, INTERNATIONAL CONFERENCE,*
*NATIONAL INSTITUTE OF TECHNOLOGY ROURKELA, ODISHA, INDIA*
*26-28, March 2021, ISBN 978-93-90631-56-8*

Paper ID - 186

# MATHEMATICAL MODEL STUDIES FOR SURGE ANALYSIS OF HALDI PURANI LIFT IRRIGATION SCHEME

G.V.R.Murthy[1] , V.S. Telgote[2] , Y.N.Srivastava[3]

*1 Scientist 'B', CWPRS, Pune-411024, India*
*2 Assistant Research Officer, CWPRS, Pune-411024, India*
*3 Scientist 'E', CWPRS, Pune-411024, India*
*Email: bgumma@yahoo.com, vishaltelgote@gmail.com*

## Abstract

Lift irrigation schemes carry water by means of pumps from the water source to the main delivery chamber, which is situated at the top most point in the command area from where water is laid to the distribution system. The capacity of pumps is fixed depending upon the duty point head and discharge. The main advantage of the lift irrigation is the minimal land acquisition and water losses. Lift irrigation schemes are useful where the distribution points of land are at higher level. The pressure transients often occur in lift irrigation due to power failure, pump start-up and shut-down operations, sudden valve closure and check-valve slam. CWPRS has taken up the hydraulic transient analysis of Haldi Purani Lift Irrigation Scheme, Maharashtra. The primary objectives of surge analysis are to determine the transient pressures and to suggest surge control devices for an acceptable level of protection against hydraulic transients.

The Haldi Purani Lift Irrigation Scheme project is located on the River Wainganga in Gadchiroli district of in Maharashtra. This scheme envisages lifting of water from River Waingangā by means of three vertical turbine pumps with rated discharge of 0.733 $m^3/s$ (each). Pumps were followed by a manifold, a rising main of 1.2 m diameter and 5.34 km length and a deliver chamber. The total static lift was 21 m.

Based on the hydraulic transient studies of the rising main during power failure, protective devices in the form of air valves of ten numbers and air vessel of 150 $m^3$ capacity was suggested to control maximum and minimum transient pressure in the rising main.
***Keywords:*** *Pressure transients*, Finite difference, Surge analysis, Transient control devices

## 1.0 Introduction

Lift irrigation schemes have assumed significance owing to their unique features of their adaptability even in the regions where the topography does not permit gravity flow of irrigation from rivers and streams. Last five decades have witnessed the mammoth development of lift irrigation duly impacting the agricultural economy of the country. This method of irrigation envisages lifting water from perennial sources of rivers with heavy electric pumps and distributed through pipe line to nearby fields within its command area. The pressure transients often found to occur in various water supply schemes of Municipal Corporations, Lift Irrigation Schemes, Thermal Power Stations etc. basically due to power failure, main breaks, pump start-up and shut-down operations, sudden valve closure, check-valve slam, etc. Failing to provide adequate transient protection may result in water column separation and catastrophic failure of piping network.

The primary objectives of transient analysis are to determine the values of transient pressures that can result from flow control operations and to establish the design criteria for system equipment and devices (such as control devices and pipe wall thickness) so as to provide an acceptable level of protection against system failure. Because of the complexity of the equations needed to describe transients, numerical computer models are used to analyze transient flow hydraulics.

Pressure transient can be avoided through systematic pipeline assessments and protection. Accurate assessment of pressure transients caused by different operating scenarios, based on the pipeline length, profile and configuration of the water conductor system, exact pipeline material, fluid properties, and rate of change of the flow, possible contents of dissolved gases in the water, equipment type and location is

needed. In view of above, transient analysis of water conducting systems for lift irrigation schemes assumes importance.

Ideally, a hydraulic system design involves adequate investigation, specification of equipment and operational procedures to avoid undesirable transients. Following are two existing possible strategies for controlling transient pressures:

a) To control minimum pressures
   Air vessels, Air inlet valves, One-way tanks, Pump inertia
b) To control maximum pressures
   Air vessels, Relief valves, Anticipator relief valves, Pump bypass valves, Lower pipeline velocity

The transient analysis of the water conductor system is carried out using WH-2 software, which uses explicit finite difference approach for calculating time varying flow and pressure during a time step at each boundary. The present paper mainly focuses on the importance of providing the protection devices to control the adverse effects due to transient pressures occur in the piping system and also optimizing the transient control devices in the piping network. A case study of Haldi Purani Lift Irrigation Scheme, Maharashtra is also discussed to highlight the necessity of transient analysis.

## 2.0 Water hammer effects

Water hammer could be potentially dangerous if the pumping system is not properly designed with necessary safety devices. In a pumping system, the water hammer caused by a mains power failure to the pump motors, is generally most severe.

This causes a down surge pressure wave to travel along the pumping main to the delivery reservoir at the velocity of sound close to 1000 m/Sec. On reaching the delivery reservoir, this wave is reflected back to the pump. When the pump speed drops so low that it hardly develops any head, then reversal of flow from delivery reservoir to pump might take place. After each pump a 0.6 m diameter non-return valve (NRV) has been provided. NRV remains open during forward flow, and depending on its design it may close upon flow reversal.

Depending upon the rate of change of velocity, the magnitude of pressure rise would vary. During the down surge the negative pressure formed may drop down to the vapor pressure of water. This would cause the water to vaporize and form a cavity at some intermediate point in the pipe, which could increase in size. The continuum of water inside the pipe is separated from the cavity, a phenomenon known as “column separation”. Upon reversal in pressure during wave propagation, the positive pressure causes cavities to collapse within a very short interval of time. Thus, the two separated water columns would collide with each other, leading to uncontrollable bursting pressures.

After tripping of power, owing to the moment of inertia the pump and motor rotor would continue to rotate in the same direction for some more time. The liquid column in the pipeline owing to its momentum would also continue to flow in the forward direction. Both these motions contribute to keep the NRV disc open. Eventually, the speed of the pump would start dropping down and the forward moving liquid column would momentarily come to rest. Thereafter, the liquid column would have tendency to flow in the reverse direction. Depending on the design of the valve, the disc of NRV may close at this point of time or near about them, which is also affected by factors like inherent characteristics of the valve, damper, springs, or other devices to control the rate of closure, etc. Hence, the exact event at which the disc fully closes is an important parameter, which needs to be furnished by the manufacturer accurately.

The primary aim of providing a non-return valve (NRV) after each pump is to prevent the reversal of flow of water from the delivery chamber of the sump in the event of failure of power supply to the pumps. In a situation where a number of pumps are operating in parallel and if one of the pumps fails, then it is

possible that the high head flow delivered by other working pumps would rush to the suction side through the failed pump. It would cause reverse rotation at a high speed and consequent damage to the failed pump. However, the provision of NRV after each individual pump would prevent such a happening. Reversal of flow of water from the high head delivery reservoir if allowed to take place uncontrolled can cause reverse runaway of pumps and could cause damage to them. Provision of NRV avoids such reversal of flow of water. NRV also helps in keeping the rising main filled with water by its self-acting closure which prevents further draining of water to sump.

During normal functioning the pumps are delivering water into the rising main. The disc of the NRV is hinged at one end and the momentum of the forward flow keeps it open. The drop in head developed by pumps following tripping of power supply and consequent drop in steady state forward velocity of flow has been discussed earlier. Under equilibrium of its own weight, hydrodynamic lift, bearing friction and buoyancy force the disc starts closing. Normally, NRV is designed to close when the flow in the rising main is about to reverse or a small amount of reverse flow is established. This may be seen from Figure-5, (Wylie and Streeter; 1993) [17]. It shows the behavior of an "ideal valve" which closes when the forward velocity (in rising main) is just zero. It also shows an acceptable closure when a small amount of reverse flow is established.

## 3.0 Formulation

The mathematical model of unsteady flows of compressible liquid in elastic pipe is expressed by the set of two partial differential equations of the first order of hyperbolic type, i.e. a momentum equation (1), stating the dynamical equilibrium of the liquid particles in the cross section of pipe, and the continuity equation (2) derived from the mass conservation of the elastic fluid particles during their flow through an elastic pipe.

Momentum equation:

$$\frac{\partial H}{\partial x} = (-)\frac{1}{gA}\cdot\frac{\partial Q}{\partial t} + f(Q) \tag{1}$$

Continuity equation:

$$\frac{\partial H}{\partial t} + \frac{a^2}{gA}\cdot\frac{\partial Q}{\partial x} = 0 \tag{2}$$

The momentum and continuity equations form a set of non-linear, hyperbolic, partial differential equations which cannot be solved by hand. The partial differential equations (PDE) are quasi linear and hyperbolic because the coefficient of PDE are constant but losses due to friction are non linear. A numerical method with an initial condition and two boundary conditions are needed. For a water distribution system, there are many more parameters needed for solving the water hammer problem and every branch of the system requires an additional boundary condition. External boundary conditions take on the form of a driving head, or a flow leaving the system. Internal boundary conditions arise in the form of nodal continuity, energy loss between points, head across valves, pumps, and more.

The complexity of the problem requires the use of modeling software. The most general and exact technique for solving the Euler and Continuity equations of unsteady flow in pipe systems is the method of characteristics which converts the partial differential equation into ordinary differential equations whose validity is constrained to a set of characteristic curves, related to the velocity of the travelling wave. Typically, the method of finite differences is then applied to discretise the equations (temporally and spatially). Finally, for numerical calculation an iterative procedure, known as predictor-corrector method has been applied.

In this method of characteristics, liquid is assumed to be slightly compressible if density changes only slightly with finite changes in pressures. It is also assumed that changes in conduit cross sectional area due to finite changes in pressure are finite but small. With these assumptions, the wave speeds is finite,

but at the same time both area of conduit and density of liquid can be assumed as constants in the calculations.

## 4.0 Methodology of Surge Analysis

The transient conditions can be analyzed using the computer program WH-2.7, which uses explicit finite difference method for calculating time varying flow and pressure during a time step at each boundary and each conduit section of the water conductor system using the method of characteristics (MOC).

All the data in respect of the system pertaining to passive elements like pipes, fittings, etc. and active elements like pumps and NRVs was sought from the Project Authorities. Based on the input data received, the following iterative procedure shall be followed:

- Prior to calculation of transient – state conditions in a system, it is necessary to determine the initial steady - state conditions. These conditions must be consistent with the boundary conditions and with the transient flow equations. Otherwise disturbances will be induced at every node where the conditions are inconsistent. This may be done by running the program for two or three computational time intervals. The discharge and pressures should not be modified in the system except at and near the boundary nodes where the boundary conditions are to be changed, eg. Opening or closing the valves, load acceptance or rejection, power failure etc.
- Carry out computation of maximum and minimum pressures without any protective device and examine necessity of providing it.
- Carry out computation of maximum and minimum pressures with few air valves at a particular nodes distributed along the rising main and examine necessity of providing optimum nos. of air valves and examine the likely extent of pressure fluctuations.
- Carryout water hammer analyses of the system with air vessel in position at a particular node, air valves distributed along the rising main and examine the likely extent of pressure fluctuations.
- If the protection is found to be inadequate, another location and/or higher size of air-vessel are tried. The vertical location of air vessel at a particular chainage, is also varied to assess the effect on water hammer pressures.
- If the protection is found to be adequate, the volume of air-vessel is slightly reduced, the position along the length is kept the same and iteration is taken to examine the pressures.
- Minor adjustments are also carried out in elevation of air vessel, initial position of water level in air vessel and initial pressure of air (as related to the static pressure at the specified point), and each time the pressures are reassessed.
- The entire procedure is repeated till the least volume of air-vessel leading to acceptable positive and negative pressures is obtained.

## 5.0 Results and Discussions

The study of Haldi Purani Lift Irrigation Scheme, Maharashtra is presented to highlight the necessity of transient analysis. This scheme envisages lifting of water from river Wainganga in near village Haladimal in Chamorshi Taluka district of Gadchiroli in Maharashtra State to the distribution point (i.e. 5340 m away from the lift point) by means of pumping to irrigate 4127 hectare Land in Chamorshi Taluka. The distribution point is approximately 5340 m away from the lift point.

The lift irrigation scheme for pumping water from the river Waiganga to the delivery chamber comprises a forebay, a sump, a pumping station with three vertical turbine pumping units, three delivery pipes of 600 mm diameter, one manifold and a rising main of 1200 mm dimeter and 5340 m long. The total discharge of two pumps is 2.199 $m^3/s$ and total static lift from pump sump to delivery chamber is 32.2 m

### 5.1. *Transient Analysis without any Protection Devices*

The surge analyses were carried out without using any protective devices on water conductor. From the analysis the results are graphically depicted in figure-1. Unacceptable low pressures are observed at all locations of the water conductor which clearly indicates the need of transient controlling devices.

### 5.2. *Transient Analysis with air valves*

**Case 1:** In this case, air valves were provided at 8 selected locations at higher elevation of water conductor. The results are graphically depicted in Figure-2. At certain locations unacceptable low pressures are observed in the pipeline which clearly indicates need to provide more air valves.

**Case 2:** In this case, air valves were provided at 10 selected locations of higher elevation of rising main. The results are graphically depicted in Figure - 3. Unacceptable low pressures are not observed at any locations of the pipeline except at a chainage of 10 m which clearly indicates no need to provide any more air valve. But the positive pressures are not in the acceptable limits. It clearly indicates that the need of a surge protection device like Air vessel (capable to control the maximum and minimum pressures) to be incorporated to alleviate such surge pressures. And also in case of malfunctioning of any of the 10 air valves, severe, unacceptable pressure conditions in the pipeline may result. In view of this, further analyses were carried out using air vessels in combinations with 10 air valves.

### 5.3. *Transient Analysis with air valves- 10 Nos. and air vessel – 1 No.*

**Case 1:** A horizontal cylindrical air vessel of diameter 3.0 m and a capacity of 200 $m^3$ was provided along with air valves at 10 selected locations of rising main. The vertical distance between the centerline of air vessel and the centerline of rising main was kept at 3.0 m. The results are computed in the critical case which is tripping off all pumps and presented in Figure - 4. It is observed that the maximum, minimum transient pressures are well within the acceptable limits. Subsequently, an air vessel of lower capacity was attempted.

**Case 2:** In this case, a horizontal air vessel of reduced capacity of 150 $m^3$ was provided. From the Figure 5, it is observed that both the maximum and minimum pressures are acceptable. It is an important requirement that after the down surge the air vessel should hold sufficient quantum of water and should not get drained completely. In this case, the minimum water level reached in the air vessel, after the down surge, is EL 174.14 m whereas the initial or steady state water level to be maintained in the air vessel is at EL 175.16 m. Hence, the air vessel does not get drained completely and has sufficient reserve of water volume. For further reduced size of air vessel, the results are not found in acceptable limits. Hence air vessel of 150 $m^3$capacity 3.0 m diameter and 21.231 m straight lengths (excluding dished ends), is finalised. Figure 6. shows the details of air vessel dimensions and other salient features of the scheme.

## 6.0 Conclusion

Based on surge analysis for Haldi Purani Lift Irrigation Scheme, number of air valves was initially optimized and further analyses were carried out to arrive at optimum size of air vessel along with air valves in the rising main. A total of ten air valves of the "Kinetic air valve" type, conforming to IS 14845:2000[2] and one air vessel optimized capacity of 150 $m^3$ are provided. From the point of view of longevity, the air vessel shall be internally coated with paint or with hot molten zinc after sand blasting. The air vessel should be designed not only for the rated positive pressures i.e. 10.0 kg/ $cm^2$ or 100 mwc but also for full vacuum i.e. typically for (–) 1 kg/ $cm^2$.

To conclude it can be reiterated that surge analysis would help and provide excellent platform to the field engineers to design water conductors for different lift irrigation projects.

## Acknowledgement

The authors are thankful to Shri.A.K. Agarwal, Director, CW&PRS for his constant encouragement and kind permission to publish the paper.

## References

Chaudhry, M.H. (2014). Applied Hydraulic Transients (3rd Edition), Litton educational Publishing Inc., Van Nostrand Co, New York

Piping Handbook by Crocker and King.

Wylie, E.B., and Streeter V.L. (1993). Fluid transients in systems, Prentice-Hall, Englewood Cliffs, N.J.

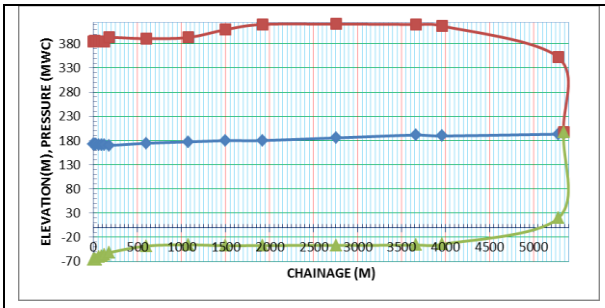



**Figure 1** Surge analysis without any protection

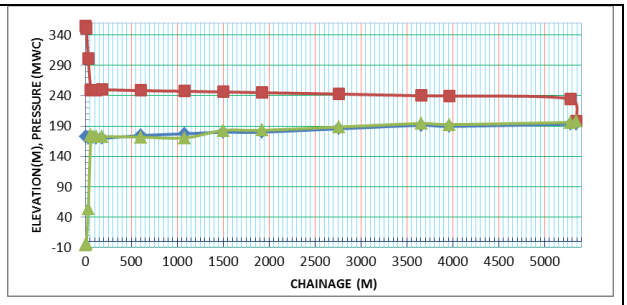



**Figure 2** Surge analysis with Air Valves – 8 Nos.

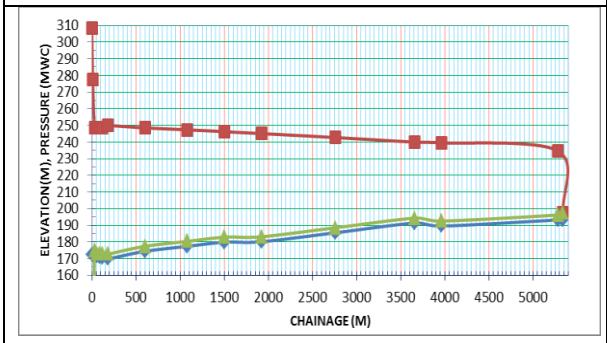



**Figure 3** Surge analysis with Air Valves – 10 Nos.

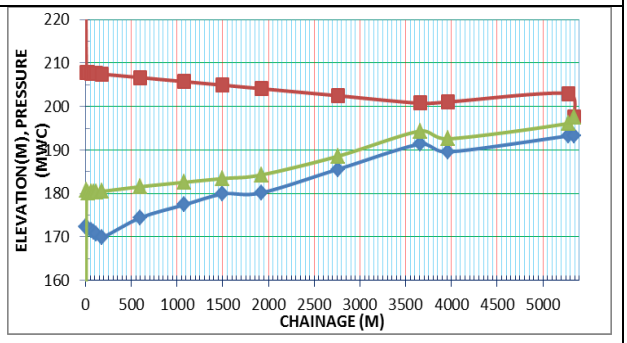



**Figure 4** Surge analysis with Air Valves – 10 Nos. and One Air Vessel of 200 $m^3$

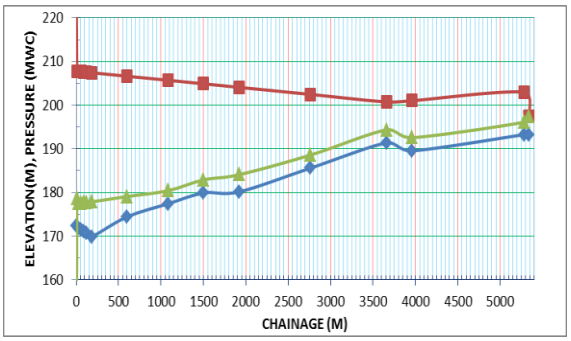



**Figure 5** Surge analysis with Air Valves – 10 Nos. and One Air Vessel of 150 $m^3$

Vessel Of

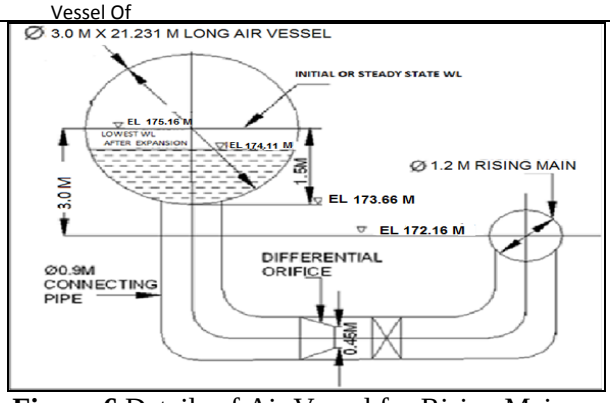



**Figure 6** Details of Air Vessel for Rising Main

Surge analysis of Rising Main of Haldi Purani Lift Irrigation Scheme for Various Cases

IN PROCEEDINGS OF 25th HYDRO 2020, INTERNATIONAL CONFERENCE,
NATIONAL INSTITUTE OF TECHNOLOGY ROURKELA, ODISHA, INDIA
26-28, March 2021, ISBN 978-93-90631-56-8

Paper ID - 205

# UTILITY OF PHYSICAL WAVE MODELS FOR DEVELOPMENT OF FISHING HARBOURS – A CASE STUDY FOR MOPLA BAY

*Sudheer S. Chavan[1]  Hradaya Prakash[2]  Dr. Prabhat Chandra[3]*

*[1]Scientist 'B', [2] Scientist 'D', [2] Scientist 'E'*
*Central Water & Power Research Station, Khadakwasla, Pune,*
*411 024, India*

*Email: sudheertask@rediff.com*

## ABSRACT

The present study emphasizes on the utility of physical wave model for establishing wave tranquility conditions in fishing harbour at Mopla bay, Kerala on the west coast of India. The full harbour was constructed in 1999 with south breakwater of 360m length and north breakwater of 500m length. Physical wave model studies were conducted at CWPRS for the existing layout of the fishing harbour at Mopla bay, using 3-D physical rigid bed model (Scale G.S. of 1/100) facility equipped with the servo-hydraulic computer based Random Sea Wave Generation (RSWG) system and Data Acquisition System (DAS) with SCADA control. The permissible limit for the wave tranquility was considered as 0.30m for berthing operations at fishing wharfs/ berths located in the harbour basin. The wave tranquillity studies were conducted for incident waves from critical SSW direction and South directions. It was observed that mainly diffracted waves from tip of main breakwater approach berthing area of fishing harbour. The adequate wave tranquillity was observed at fishing wharfs, berths, turning circle inside the harbour basin except marginal increase in wave height upto 0.40m at old wharf and hatchery which are located along main breakwater and exposed to the harbour entrance. The loss of operational days at old wharf would be about 3-4 days in monsoon which is insignificant. Physical wave model studies revealed that there is no need of further extension of breakwater/s of fishing harbour since desired tranquillity prevails in fishing harbour for its operation throughout the year.

***Keywords***: *Wave tranquility, harbour, breakwater, berth, wharf, diffraction*

## 1. Introduction

A number of minor/intermediate ports and fishing harbours are coming up on open sea coast and estuarine region. The wave tranquility aspects are very important for berthing operations in ports and fishing harbours. The breakwater length and alignment are required to be optimized for providing safe sheltered harbour areas. Mopla bay fishing Harbour is located in Kannur District on Kerala Coast at Longitude $75^0$ 22' E and Latitude $11^0$ 51' 40" ( Fig.1). Mopla bay is a small bay with width about 1.2Km and with maximum depths of about 5m. The construction of main breakwater i.e south breakwater of 360m length and leeward north breakwater of 500m length was over in the year 1999. Since no dredging was carried out, heavy siltation occurred inside the harbour. The existing harbour facilities are shown in Fig. 2. The physical wave model studies for the existing layout of Mopla fishing harbour, were conducted at CWPRS to assess wave tranquility conditions for the predominant incident waves from different directions. The physical wave model studies were conducted at geometric similar scale of 1/100 in a three dimensional model tray equipped with the Random Sea Wave Generation (RSWG) facilities. The permissible limit for the wave tranquility was considered as 0.30 m for berthing operations at Fishing wharfs/ berths located in the harbour basin. The existing harbour basin with bathymetry is shown in Fig. 3 and the site photograph of Mopla bay fishing harbour in Photo 1.

The present paper describes the physical wave model studies conducted for the development of fishing harbour in Mopla bay, Kerala.




**Figure 1** Location Plan of Fishing harbour at facilities Mopla Bay, Kerala

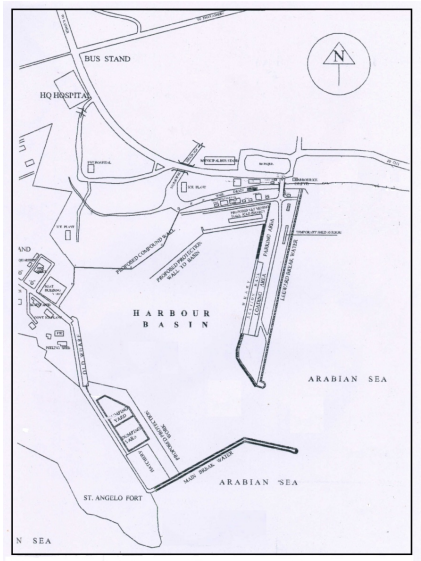



**Figure 2** Existing Harbour

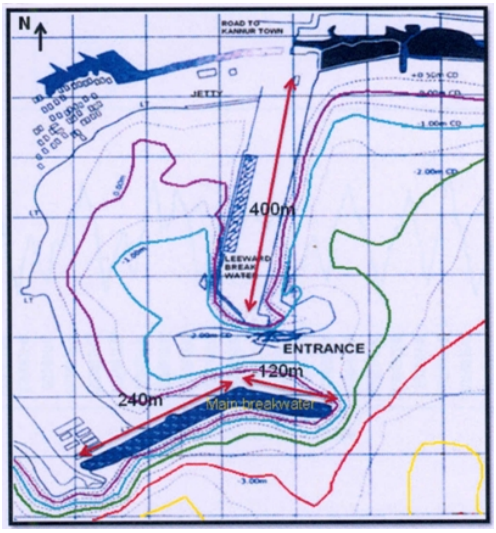



**Figure 3** Depth contours in the existing fishing habour at Mopla bay



**Photo 1** The existing Layout of Fishing harbour fishing habour at Mopla bay

## 2. Data analysis

Analysis of data is the most important part of model studies as the results are dependent upon the accuracy of data. The basic inputs for wave model studies are bathymetry data, wave and tidal data.

### 2.1 *Wave data*

The wave data was supplied by the project authorities at -8m and -10m depth contour for SW monsoon (June to September), NE monsoon (October to January), non-monsoon (February to May) and annual period (January to December). These wave data have been analyzed by CWPRS and it was found that waves coming from South to SSW (South of South-West) quadrant are more predominant in South-West monsoon season. The Significant wave height (Hs) 2m will hardly exceed 2 days in a year from South direction and the Significant wave height (Hs) 2.5 m will hardly exceed 2.5 days in a year from SSW direction. The Significant wave period for incident waves from the South direction is

considered as 10 sec and the Significant wave period for incident waves from the SSW direction is considered as 7 sec during physical wave model studies.

Considering the configuration of opening and the existing breakwater layout, the following predominant incident significant wave conditions were adopted for wave tranquility studies:

**Table 1** Input Wave Conditions for Wave Tranquility Studies

| Incident Wave Direction | Significant Wave Height (m) |
|---|---|
| SSW | 2.0 |
| South | 2.5 |

### *2.2 Bathymetry Data*

The bathymetry was reproduced in the model to the scale as a rigid bed using hydrographic survey chart of December 2015 (Fig. 3) as provided by the Project Authorities. The contours are more or less parallel to coastline and the tip of existing breakwaters are at -1.0 m depth contour. At the entrance of the harbour, a deep channel can be observed (Fig.3) adjacent to north breakwater tip and siltation is observed adjacent to the southern breakwater.

### *2.3 Tide and current data*

The observed tide data provided by the project authorities at Mopla bay is shown in Fig.4. The tidal ranges are of the order of 1.55 m and 0.63 m respectively during spring and neap tides.

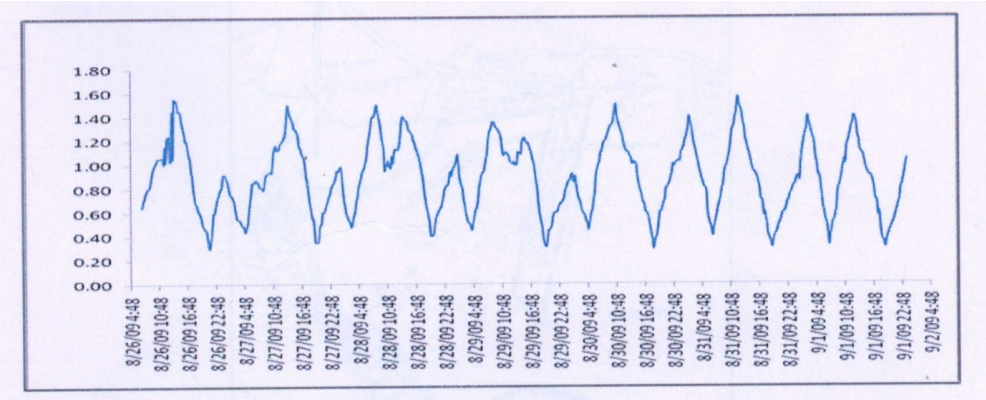



**Figure 4** Observed Tide at Mopla bay

The currents data available at CWPRS shows that the magnitude of current in Mopla bay area varies from 0.3-0.35 m/s during the year.

## 3. Physical wave model studies

### *3.1 Physical wave model*

The physical wave model studies were conducted for fishing harbour at Mopla Bay at geometric

similar (G.S.) scale of 1:100 based on Froudian similarity with Random Sea Wave Generation (RSWG) system with SCADA control and multichannel data acquisition system. Model tray is housed in the Multi Purpose Wave Basin (MPWB) hangar of size 75m x 60m at CWPRS and the wave generators and data acquisition system control cabin are as shown in Photos 3, 4 and 5. Two wave paddle units of 10.5 m each have been used for generating incident waves from incident in the model which corresponds to about 3.2 km long water face (wave front) in proto and one wave paddle 14.3 m in the model for South direction corresponding to 2.14 km in proto. Power to wave paddles is supplied by the hydraulic power pack unit by creating required hydraulic pressures as per the input wave generation signal. Hydro Servo Actuator system is used for random sea wave generation. This RSWG system has the facilities for generation of waves in a frequency range of 0.3 – 3.0 Hz in model, significant waves of up to 10.0 cm and water depths of up-to 25.0 cm in model.



**Photo 2** Multipurpose Wave Basin hangar



**Photo 3** View of Wave generators



**Photo 4** View of RSWG Control and DAS Cabin with SCADA System

The crest level of the existing breakwaters were kept at (+) 5.5 m (C.D) and crest level of fishing wharf, old wharf, berths, reclamations were kept at (+) 4.5m (C.D.). The experiments were conducted at high water level. The wave tranquility conditions were studied for the existing condition of fishing harbour with basin dredged to (-) 3.0m (C.D.). The approach channel for fishing harbour with average width about 90m was dredged to (-) 3.0 m depth in the physical model. The approach channel was extended beyond the tip of main breakwater up-to -3.0 m contour to a length about 210 m. The matching of the wave spectrum for the two incident wave directions SSW and South are shown in Figs. 5 and 6.

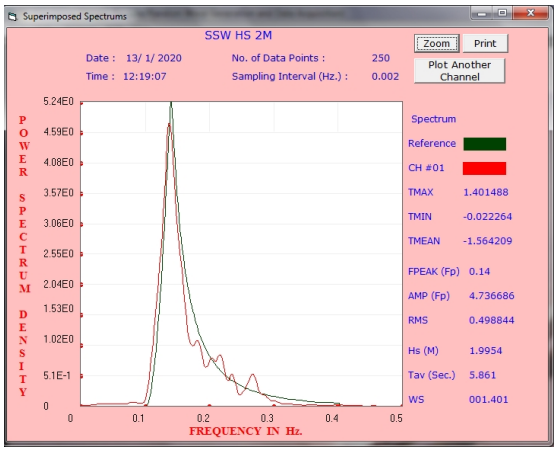



**Figure 5** Matching of wave spectrum in the Model for incident SSW Direction Direction (Hs 2.0m, Fp 0.14 Hz)

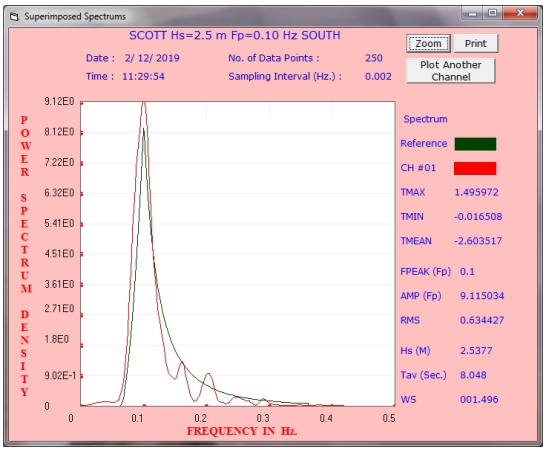



**Figure 6:** Matching of wave spectrum in the Model for incident South Direction (Hs 2.5m, Fp 0.1 Hz)

### *3.2 Wave tranquility for Existing Condition of Fishing harbour*

#### *3.2.1 Incident Waves from SSW Direction*

During model studies for incident SSW waves (Hs = 2.0m, Fp = 0.14Hz), it was observed that mainly diffracted waves in monsoon are approaching at the tip of the South(Main) breakwater and approaching at entrance opening with slight wave attenuation. Waves get further attenuated and reach the fishing harbour. The wave disturbance at the tip of the main breakwater was observed to be 0.70 m and reduces to 0.60 m at the entrance opening. The wave disturbance in the turning circle area was observed as 0.50 m. The wave disturbance at the start of fishing wharf located on the lee side of North breakwater was observed as 0.25 m and wave disturbance was observed as 0.20 m at the end of wharf near the root of the North breakwater. The wave disturbance in front dumping yard and hatchery was observed to be 0.35 m. The wave disturbance in front of the old wharf located along the main(South) breakwater was observed to be 0.30 m. The wave tranquility conditions observed during the model studies are shown in Photo 6.

#### *3.2.2. Incident Waves from South Direction*

During model studies for incident Southerly waves (Hs = 2.5 m, Fp = 0.10 Hz) under the existing condition fishing harbour basin dredged to (-) 3.0 m, it was observed that both direct as well as diffracted waves in monsoon are approaching at the tip of the South(Main) breakwater and approaching at entrance opening with slight wave attenuation. Waves get further attenuated and reach the fishing harbour. The wave disturbance at the tip of the main breakwater was observed to be 0.85 m and reduces to 0.70 m at the entrance opening. The wave disturbance in the turning circle area was observed as 0.60 m. The wave disturbance at the start fishing wharf located on the lee side of North breakwater was observed as 0.30 m and wave disturbance was observed as 0.25m at the end of wharf near the root of the North breakwater. The wave disturbance in front dumping yard and hatchery was observed to be 0.40 m. The wave disturbance in front of the old wharf located along the main (South) breakwater was observed to be 0.35 m. The wave tranquility conditions observed during the model studies is shown in Photo 7. The results of wave tranquility conditions envisaged during the model studies for the existing condition of fishing harbour for both the incident waves from SSW and South direction are shown in Fig. 7.

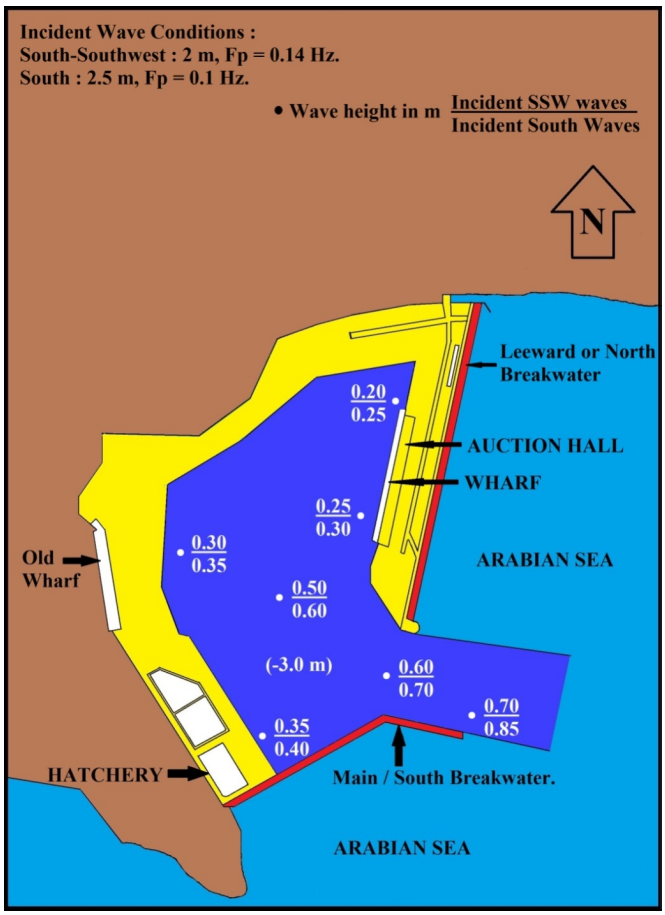



**Figure 7** Wave Tranquility Conditions for fishing harbour at Mopla bay for incident wave from SSW (Hs 2.0 m, Tp 7 sec ) and South ( Hs 2.5 m, Tp 10 sec )

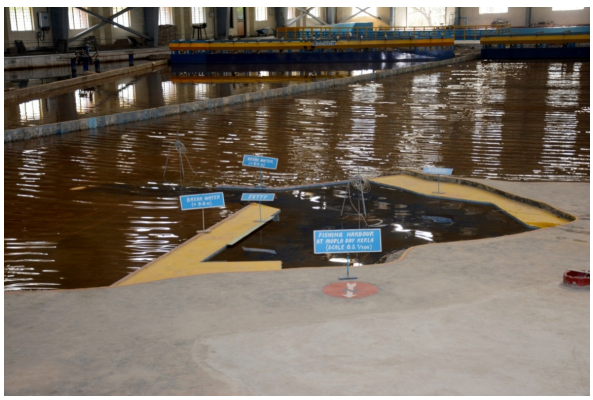


**Photo 5** View of the incident waves from SSW direction (Hs 2.0m Fp 0.14 hz)



**Photo 6** View of the incident waves from South direction (Hs 2.5m Fp 0.1 hz)

The wave disturbances obtained in the physical wave model for above two incident wave conditions have been tabulated in Table 2. The physical wave model studies indicated that the adequate wave tranquillity was observed at fishing wharfs, berths, turning circle inside the harbour basin except marginal increase in wave height upto 0.40 m at old wharf and hatchery which are located along main breakwater and exposed to the harbour entrance. The loss of operational days at old wharf would be about 3 - 4 days in monsoon which is quite insignificant. The physical wave model studies also revealed that there is no need of further extension of either of two breakwaters/s of fishing harbour since desired tranquillity prevails in fishing harbour for its operation.

**Table 2** Physical wave model results for Incident Waves SSW (Hs = 2.0m, Tp = 7 sec) and South (Hs = 2.5 m, Tp = 10 sec)

| Sl. No. | Location | **Incident waves from SSW (Hs = 2.0m, Tp = 7 sec)** | **Incident waves from South (Hs = 2.5m, Tp = 10 sec)** |
|---|---|---|---|
| 1 | Tip of Main (South) Breakwater | 0.70 | 0.85 |
| 2 | Entrance of harbour | 0.60 | 0.70 |
| 3 | Dumping yard and Hatchery along Main Breakwater | 0.35 | 0.40 |
| 4 | Old Wharf | 0.30 | 0.35 |
| 5 | Fishing wharf along North or lee breakwater (near entrance) | 0.25 | 0.30 |
| 6 | Fishing wharf along North or leeward breakwater (at the end) | 0.20 | 0.25 |

## 4. Conclusions

1. The analysis of the wave data and the configuration of Mopla bay fishing harbour established that the most critical and predominant incident waves to be considered for the physical model studies are from SSW (Hs = 2.0m, Tp = 7 sec) and South (Hs = 2.5m, Tp = 10 sec) directions.

2. The physical wave model studies were conducted for existing layout of fishing harbour ( Fig.2) at Mopla bay using 3-D model with geometric similar scale of 1/100 using random sea wave generation system with multiple data acquisition system at CWPRS.

3. The physical model studies for wave tranquility indicated that adequate wave tranquility would be achieved at all berths and fishing wharf located on lee side of Leeward or Norh breakwater. The wave disturbances in front of old wharf and dumping yard located along main breakwater which are exposed to the entrance opening of the harbour are exceeding wave tranquility limit of 0.30m for both the incident wave directions viz. SSW and South. There would be about loss of 3-4 operational days in monsoon which is quite insignificant.

5. The physical wave model is very useful tool for realistic simulation of complicated wave patterns in the bay and near berths/ jetties.

## Acknowledgements

The authors are thankful to Shri A.K. Agrawal, Director in-charge, Central Water and Power Research Station, Pune for his kind permission to publish this paper.

*IN PROCEEDINGS OF 25th HYDRO 2020, INTERNATIONAL CONFERENCE,*
*NATIONAL INSTITUTE OF TECHNOLOGY ROURKELA, ODISHA, INDIA*
*26-28, March 2021, ISBN 978-93-90631-56-8*

Paper ID - 208

# 'Acquisition of depth profile using bathymetry survey near left bank spillway and proposed additional spillway of Hirakud dam, Odisha - A case study'

**M.S. Bist[1] Ajay Sonawane[2] Ajit Singh[3] J. K. Singh[4] M. Selva Balan[5]**

[1] *Scientist-C, Central Water & Power Research Station (CWPRS), Pune-411024, India*
[2] *Assistant Research Officer, Central Water & Power Research Station (CWPRS), Pune-411024, India*
[3] *Research Assistant, - Central Water & Power Research Station (CWPRS), Pune-411024, India*
[4] *Scientist-B, Central Water & Power Research Station (CWPRS), Pune-411024, India*
[5] *Scientist- D, Central Water & Power Research Station (CWPRS), Pune-411024, India*
*Email: msbist1974@gmail.com*

## ABSTRACT

The Hirakud Dam is constructed across Mahanadi river situated at upstream of Burla town situated in Sambalpur district, Odisha. The project was constructed with the objective to control the floods besides catering the needs of irrigation and hydro power generation. The Chief Engineer, Dam Safety, Secha Sadan Unit-V, Bhubaneswar has requested CWPRS to conduct hydrographic survey for getting the profiles at given Easting and Northing locations for 1.5 km on left bank of Hirakud dam including reservoir portion in front of the proposed additional spillway of the left bank. This cross-section depth profile is needed to construct model at CWPRS for additional spillway studies.

The survey was taken up at RL 183.82 m. The bathymetry survey was conducted as per model requirement study area that includes total thirty nine cross sections with a 50 meter grid interval. A motorized fiber boat was used for survey work. The SyQuest Bathy DF-500 single beam dual frequency echo-sounder was used for water depth measurement with an accuracy of 10 mm for 210 KHz frequency. The position of boat in the reservoir was logged with GPS R110 model, Hemisphere make. The GPS unit consisting of receiver antenna for catching satellite signal was used in DGPS mode with beacon correction. By DGPS mode the location of the boat can be obtained with accuracy in sub meter. The depth and position data was stored in a laptop through a 4 port serial RS 232 to USB convertor. The logged data in the laptop was processed using HYPACK navigation software.

After editing and filtering the raw data using HYPACK software the analyzed data was plotted for the 39 cross sections consisting of 70 depth profiles using different software such as Q-GIS Surfer, Global Mapper etc. These cross section depth profiles obtained through bathymetric survey would be utilized in the hydraulic model at CWPRS for carrying out the additional spillway studies of Hirakud dam.

***Key Words*: *Bathymetry, DGPS, Echo-sounder, HYPACK, Surfer.***

## 1. INTRODUCTION

Hirakud Dam Project is in operation since 1957 constructed on the Mahanadi river in Odisha state. The dam is mostly used for controlling the flood, catering to the need of irrigation demands of the region and generation of power supply. The view of Hirakud dam is shown in Photo. 1. The project authority decided to conduct proposed additional spillway studies of Hirakud dam by constructing model in CWPRS, Pune. In this regard the Chief Engineer, Dam Safety, Secha Sadan Unit-V, Bhubaneswar had requested CWPRS to conduct hydrographic survey for getting the profiles at given Easting and Northing locations for 1.5 km on left bank of Hirakud dam including reservoir portion in front of the proposed additional spillway of the left bank. These cross-section depth profiles are needed to construct model at CWPRS for additional spillway studies.

For plotting the depth profile of the required cross-section CWPRS team conducted the bathymetric survey during June 2019 at Hirakud dam. Integrated Bathymetry system (IBS) ( CWPRS Technical Report No. 5760, Dec. 2019) was used for this purpose which consists of dual frequency echo-sounder (210 Khz and 33 Khz) for measuring the water depth and a Global Positioning System (GPS) for finding the accurate location of boat moving on the predefined grid lines. The data (depth and position) collected is logged in real time mode in laptop with survey software at site. Data processing and calculations are done by proven algorithms inbuilt in the software at the time of doing analysis.



**Photo 1** Hirakud dam upstream view.

## 2. COMPONENTS AND METHODOLOGY

This bathymetric survey was carried out with a boat equipped with the ultrasonic single beam dual frequency echo sounder, Mobile GPS system with beacon correction and a lap-top for logging the data. The IBS system used during survey consists of the following components:

i) Single beam echo sounder, SyQuest Bathy Make - DF 500 model (Single beam echo sounder Manual).
ii) GPS make Hemisphere R110 model with DGPS mode using beacon (GPS R110 receiver Manual).
iii) Data collection laptop with Hypack software (Hypack Manual) used for real time bathymetry data acquisition.

The survey was carried out in a motorized fiber boat. The eco-sounder sensor with special fixture was fitted on one side of the boat for depth measurement. The GPS antenna was mounted on boat for receiving the satellite signal and for establishing accurate boat position, GPS was used with beacon correction. The depth and position data was logged in real time mode in laptop with survey software. The survey boundary data of existing left bank spillway and proposed additional spillway is shown in Fig.2 and 3 respectively. The Hypack survey software was used for fixing of grid lines and interfacing of bathymetry equipment and GPS for logging position longitude, latitude (x, y), and water depth (z) values at required interval/grid. The boat was fitted with Hemisphere GPS taking beacon

correction from nearby reference station. The echo sounder was calibrated for its accuracy before using it.

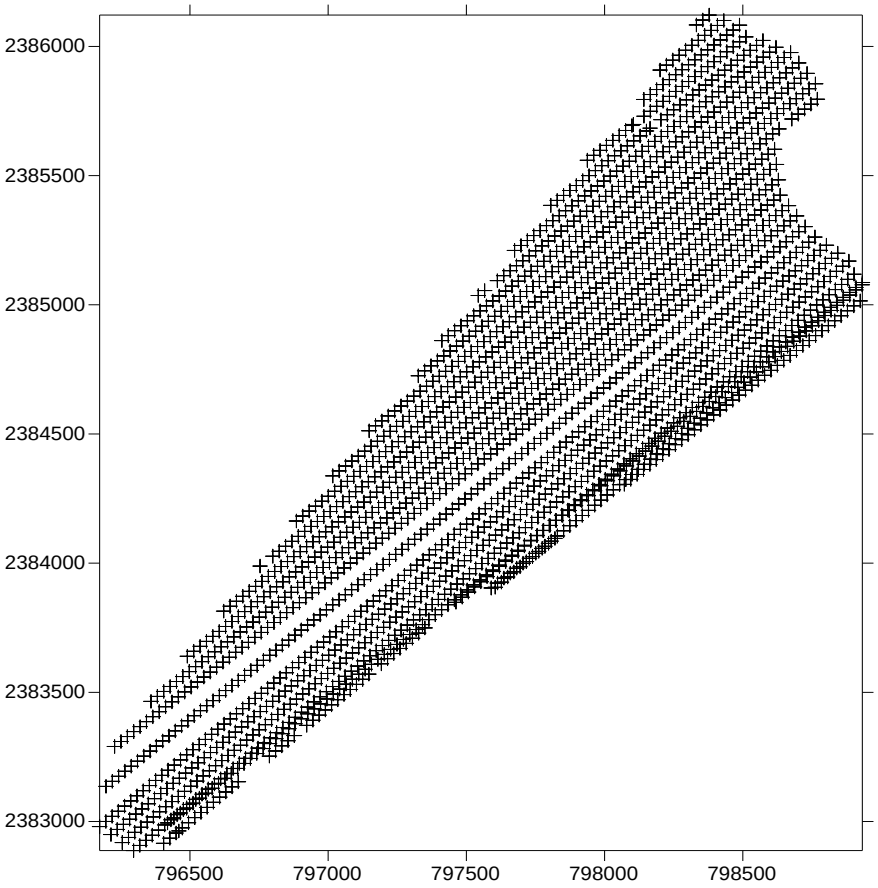



**Figure 2** Left side existing spillway data logging points (lat. and long.) during survey

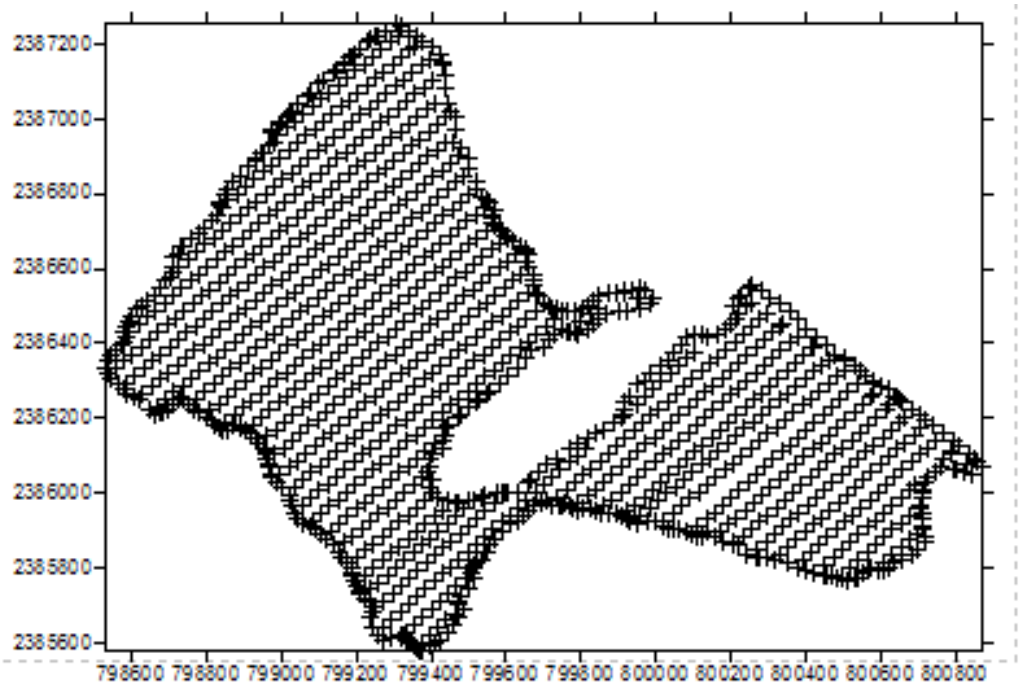



**Figure 3** Data logging points (lat. and long.) in front of proposed additional spillway.

In order to create an accurate cross section profile, the position information is required to be accurately measured along with the depth data in a straight survey line. A survey is carried out based on the pre survey process before collecting the position and depth data using a survey boat as shown in Fig.4. Pre survey includes assigning the proper coordinate system for the Differential Global Positioning System, setting the data logging protocol, zone, coordinate system etc. Similarly the echo sounder as shown in Fig. 5 also needs to be calibrated for the sound velocity and multipath noise data. Boat navigation is also controlled by the software so that boat tracks the grid line accurately while logging the data. The bathymetric survey was carried out during the month of June 2020.



**Figure 4** Equipment Boat set up



**Figure 5.** Eco sounder

The survey area of left side existing spillway and proposed spillway is shown in Fig 6 and Fig. 7.




**Figure 6** Left bank Survey cross- section line in front of existing spillway




**Figure 7** Surveyed cross section lines in front of proposed additional spillway.

The same has been verified by running the boat on the actual cross sections at site. After confirmation, the actual survey lines were drawn and data was collected on the required cross-sections. The bathymetry data collection was completed. The river water level was at 183.82 m RL. The survey boat was taken on the survey lines drawn on left and right side of the island behind the dam wall. The left side is where additional spillway is proposed.

## 3. RESULTS AND ANALYSIS

The purpose of the bathymetry survey was to plot the depth profile at fixed 39 cross sections in front of left spillway and proposed additional spillway. During the survey, it was observed that the maximum depth in the left side of island (proposed spillway portion) was 12 meters and in the existing left side spillway was up to 30 meters.

After processing the data using various software such as Surfer / Navisoft, Autocad (Auto CAD Manual), etc. the different graphs and drawings have been plotted which include survey line boundary, cross-section depth profile, depth cross-section drawing showing depth value marked at an interval of 3m on the grid lines. During survey cross-section data was logged near existing left bank spillway and proposed additional spillway on left bank. The cross scetions profiles of left existing spillway and proposed additional spillway bank were made. One of the cross section on Goggle image and depth profile is shown in Fig. 8 and Fig. 9 respectively.




**Figure 8** Cross section line of bathymetry survey

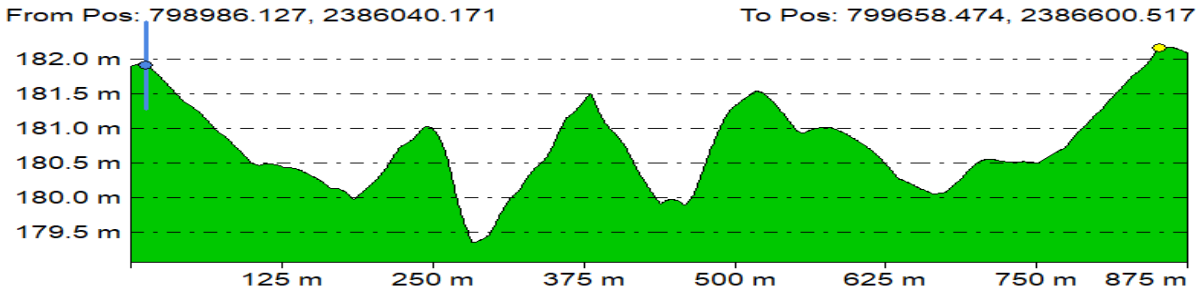



**Figure 9.** Profile plot of line 52 (800m from dam axis in left side portion)

## 4. CONCLUSIONS

The data was collected at 39 cross sections between the dam axis to upstream approx. one kilo meter which included the required cross sections. The collected data was edited and filtered using HYPACK and analyzed using AutoCAD, Surfer. The cross section depth profiles were generated as required by the project which would be used in the constructed physical model at CWPRS and for study of proposed additional spillway at Hirakud dam.

## 5. ACKNOWLEDGEMENT

The authors are thankful to Shri A K Agrawal, Director, CW&PRS for guiding them and giving his consent for publishing this paper. Our sincere gratitude to Dr. Prabhat Chandra, Scientist-E who encouraged us during the preparation of this paper. Our sincere thanks are due to Shri Er.

Jyotiramaya Rath, Chief Engineer & Basin Manager, Upper Mahanadi Basin, Burla, Shri Himanshu Mishra, Executive Engineer, Additional Spillway Division, Hirakud, Shri Jitray Boskey, A.E.E of Hirakud dam for their kind co-operation and support during survey work at Hirakud site. The service of M/s. Global Marine Infratech Pvt. Ltd, Bhubaneshwar is duly acknowledged for their support in data collection activities.

## REFERENCES

Auto CAD Manual, Source: www.autodesk.com
CWPRS, Pune Technical Report No. 5760, December, (2019). Hydrographic survey (Depth profile) near left bank spillway and proposed additional spillway of Hirakud Dam, Odisha.
GPS R110 Series Receiver Manual, Source: http://hemispheregnss.com
Hypack Manual, Source: https://www.hypack.com
Single beam echo sounder, Manual SyQuest Bathy Make - DF 500 model. Source: ttps://www.syqwestinc.com/ media /bathy- 500df/b500df-syq-web.pdf

*IN PROCEEDINGS OF 25th HYDRO 2020, INTERNATIONAL CONFERENCE, NATIONAL INSTITUTE OF TECHNOLOGY ROURKELA, ODISHA, INDIA 26-28, March 2021, ISBN 978-93-90631-56-8*

Paper ID - 220

# MORPHOLOGICAL CHANGES AROUND SOGAL CHANNELOF DEENDAYAL PORT, GUJARAT IN THE APPROACHES

Chaudharee B.B[1], Hradaya Prakash[2], Dr.Prabhat Chandra[3]

[1]*Scientist B, Central water and Power Research Station Pune-411024,India*
[2]*Scientist D, Central water and Power Research Station Pune-411024,India*
[3]*Scientist E, Central water and Power Research Station Pune-411024,India*

*Email: chaudhareebb@gmail.com*

## Abstract

All weather Deendyal port trust (DPT) formerly known as Kandla Port Trust, was established in 1949. The hydraulic model studies and analysis of hydrographic surveys are being carried out at CWPRS regularly to optimize the dredging strategy. The existing Sogal channel has been in operation since 1984 starting with a depth of 3.7m and is divided in different segments in the form of Buoy number 12 -13 to Buoy number 4. The hydrographic surveys of the 350m wide approach channel having side slope of 1:5 consisting of a bend portion starting from Buoy number 12-13 to buoy number 8A-9A for different years (from the period 1984 to till date) have been analysed rigorously to assess the morphological changes in the vicinity of Sogal channel. The depth of the channel has been progressively increased from 3.7 m to about 9.0 m at present, with minimum quantity of maintenance dredging as a result of recommendations from hydraulic model studies (both physical and mathematical models) at CWPRS. The critical areas for dredging have been identified and zone wise dredging strategy has been suggested. Further, an empirical equation to predict the morphological changes in the approach channel at Kandla has been formulated on the basis of the prototype data base available at CWPRS. This empirical equation is valid for site specific for the soil classification in the channel with mean grain size of about 0.08mm.

***Key words:*** *hydrographic survey, model, morphology, prototype, Sogal channel*.

## 1. Introduction

Deendayal Port formerly known as Kandla Port is an all weather natural port. It is located at the head of Gulf Kutchch on the west coast of India at about 120 km east of the entrance to the gulf of Kutchch 23$^{o}$ 10 ’ N latitude 70$^{o}$ 10’ E longitude as shown in figure 1. Morphology of Sogal channel is more or less stable with very marginal changes. The monitoring and planning of dredging planning for Sogal channel has not only resulted in optimizing the maintenance dredging but also in progressive improvement of depths along the channel. The navigational channel is the main stream for the ship transportation. Recently, this channel has been deepened to -9.0 meter and made two way channel with increase in base width from 300 m to 350 m. Sogal channel starts from 9 meter counter and this channel has total length of 13 km which consist of straight length of 7 km from 9 meter contour to bend and curved portion is having length of about 4200 meter.

Earlier Kandla port were considering the dredging quantity Zone-wise, at present zone does not exist also Bouy no 12-13 and bending portion of Bouy no.8-9 alignment of navigational channel is as shown in figure 2. The development of navigational channels for ports located in large tidal ranges above 7 meter, generally involves continuous maintenance dredging in the Sogal channel. Deendayal port trust is improving the depths along the Sogal channel to cater to allow higher draft vessels.

In the present paper, the analysis of the hydrographic surveys during the period 2014-2018 in the bend portion of Sogal channel has been presented and suitable recommendations have been provided.

In general the criteria to choose the navigational channel are

A. Specific& fixed geographic area within a water body or series of water bodies that has been authorized for navigation by some group or organization.
B. The effect of shoal on navigation channel due to detached area of any material except rock the depths over it area danger to surface navigation similar continental or insular shelf features of great depth.
C. Sinkage and trim of a vessel in a navigation channel depend on the factors that control the pressure distribution along the vessel hull.

D. Navigation channel requires designing the dimension, beam & width of a ship, the bed material site condition wind wave & tides are the governing force.




Fig 1. Google view of Deendayal Port

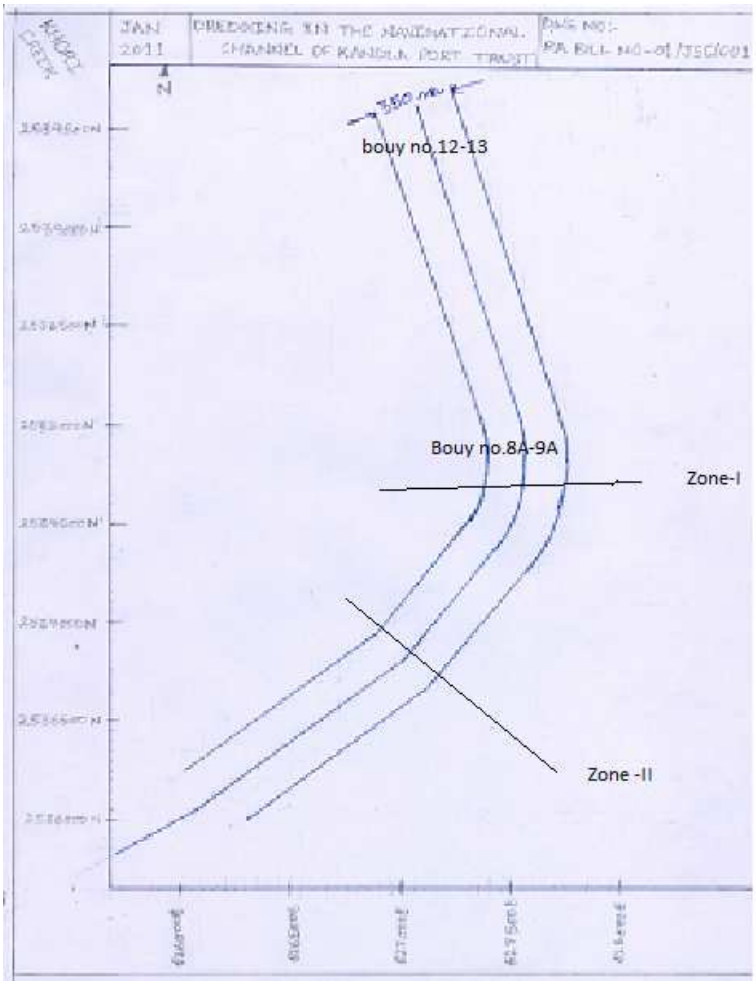



Fig. 2. Navigational Channel under Study

## 2. Methodology

The studied portion of the Sogal channel is divided in 42 cross sections numbered as 01 to 42 having distance of one hundred meter at the centre of channel. The depth in each cross section is measured at an interval of 25m across the channel totaling 350m base width of Sogal channel with side slope of 1:5 except at the curved portion of the channel. Imaginary line at the center of Sogal channel has been drawn to be considered as reference line. Data collected on monthly basis i.e. January to December and starting from 2014 to 2018 at about 250m on both sides of this centre reference line has been considered for analysis in the present study for morphological changes. Thus, about 4200 graphs were prepared to see the behavior of individual section. Typically cross section number 38 for the month of May 2016 is shown in Figure 3 with proposed channel. This graph shows that dredging in this cross section is hardly required any dredging or with minor change.

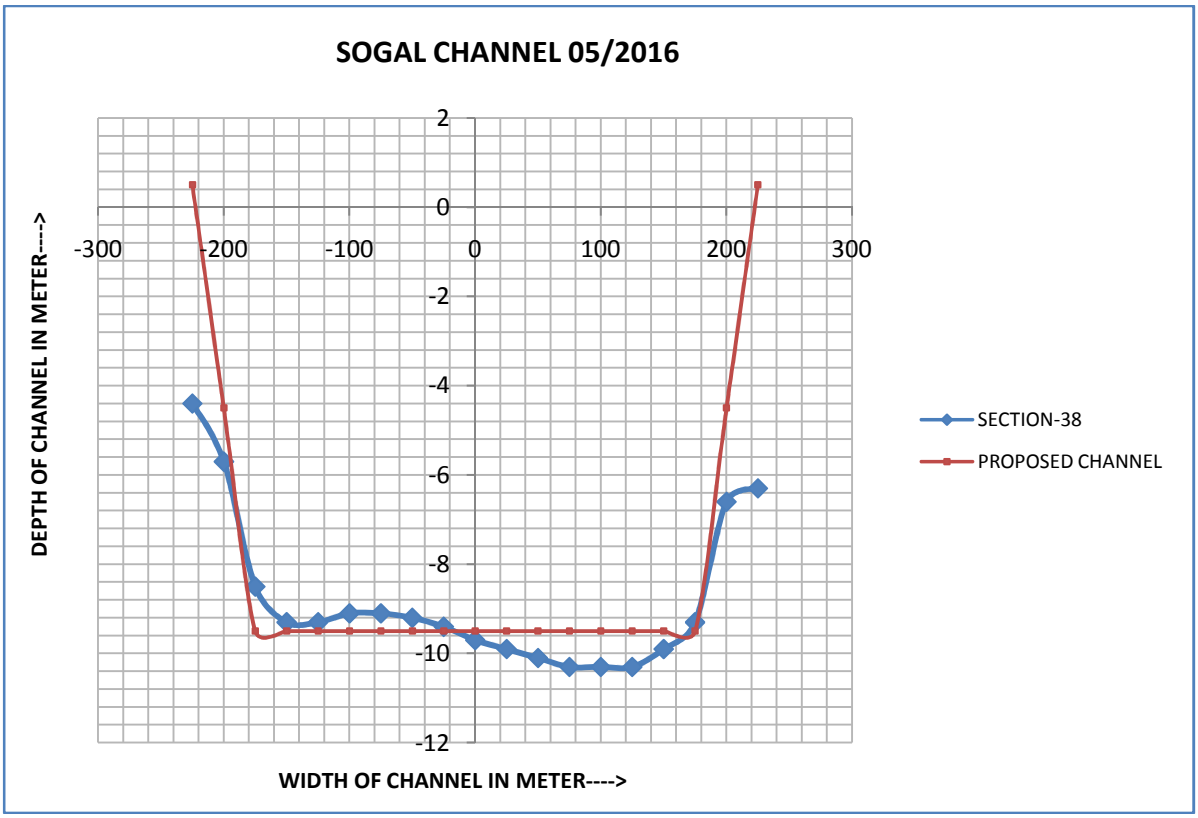



Fig. 3. Variation of depth with proposed channel.

## 3. Analysis of Data

The collected data by project authority was analyzed in the curved and critical portion of Sogal channel having length of 4200 meters. In the present study, the data starting from 2014 to 2018 has been considered when depth of channel was increased from 8.5 to 9.5 meter. Overall 1277 data along the central line of channel has been considered for the analysis. Now, it is found that the derived equation by regression or trial and error method as well. The following equation (2) has arrived which covers total data in ±25% band width and almost 96% data in ±10%band width.
$R^2 = 0.145$, where R is correlation coefficient and can be given as

$$R = \frac{n(xy)-(\sum x)(\sum y)}{\sqrt{[n\sum x^2-(\sum x)^2][n\sum y^2-(\sum y)^2]}} \quad (1)$$

In the Sogal channel depth is variable parameter, therefore, an attempt was made to predict the dredging quantity with respect to depth. Initially ratio of depth to average depth in the base width

=350m of the channel was considered with respect to a ratio of annual dredging quantity to monthly dredging quantity. Following equation has been arrived based on regression analysis.

$$PDQr = 1.47Dr - 0.46 \quad (2)$$

(Where PDQr = Predicted dredging quantity/Observed Dredging quantity, (non-dimensional)
Dr = Depth/average depth (dimensionless) in cross section of base width of 350 meter.)

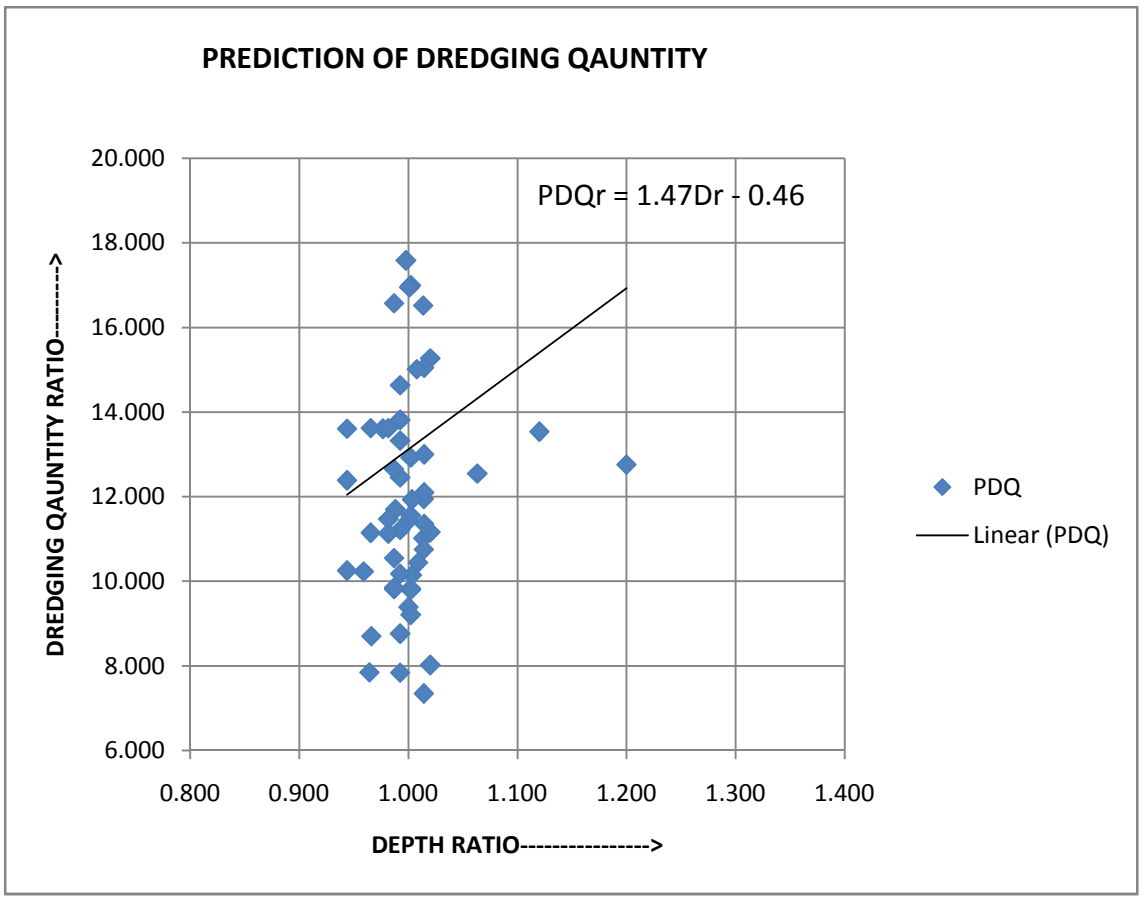



Fig. 4. Variation of Depth with Dredging Quantity

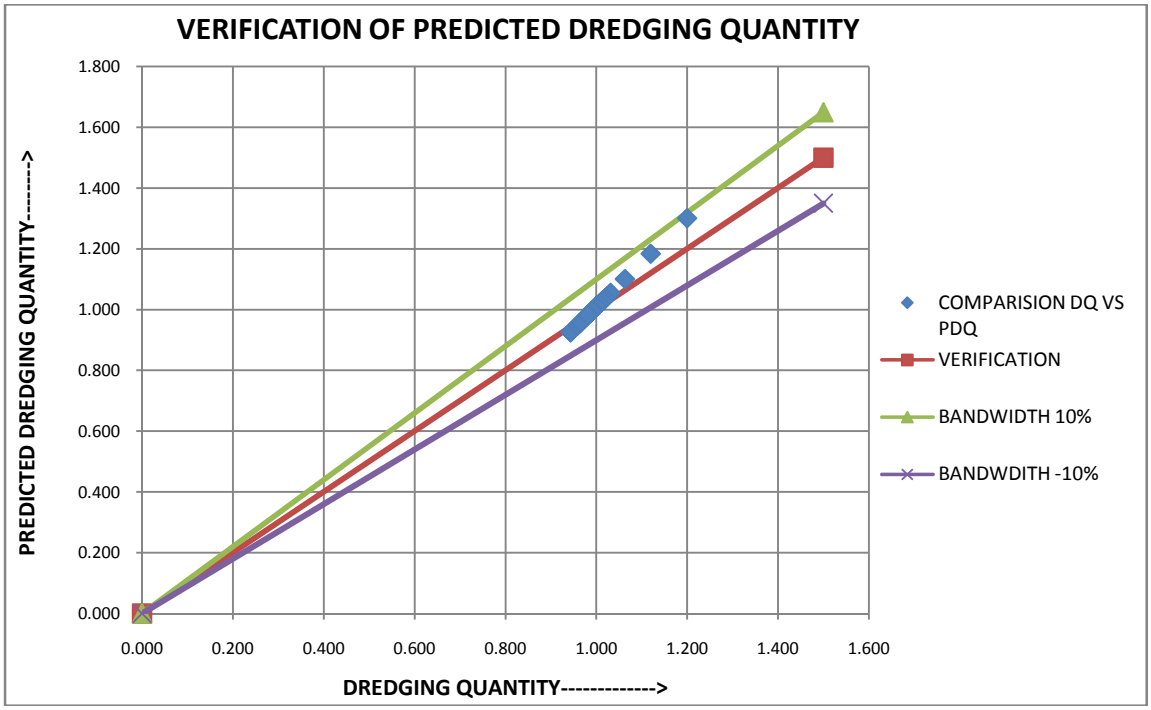



Fig. 5. Predicted dredging quantity Variation with Dredging Quantity in Sogal Channel

Comparison of the predicted quantity with actual dredging quantity is shown in Fig. 5. This graph shows that hundred percent data is covered in ±10% bandwidth and having correlation coefficient =100%.

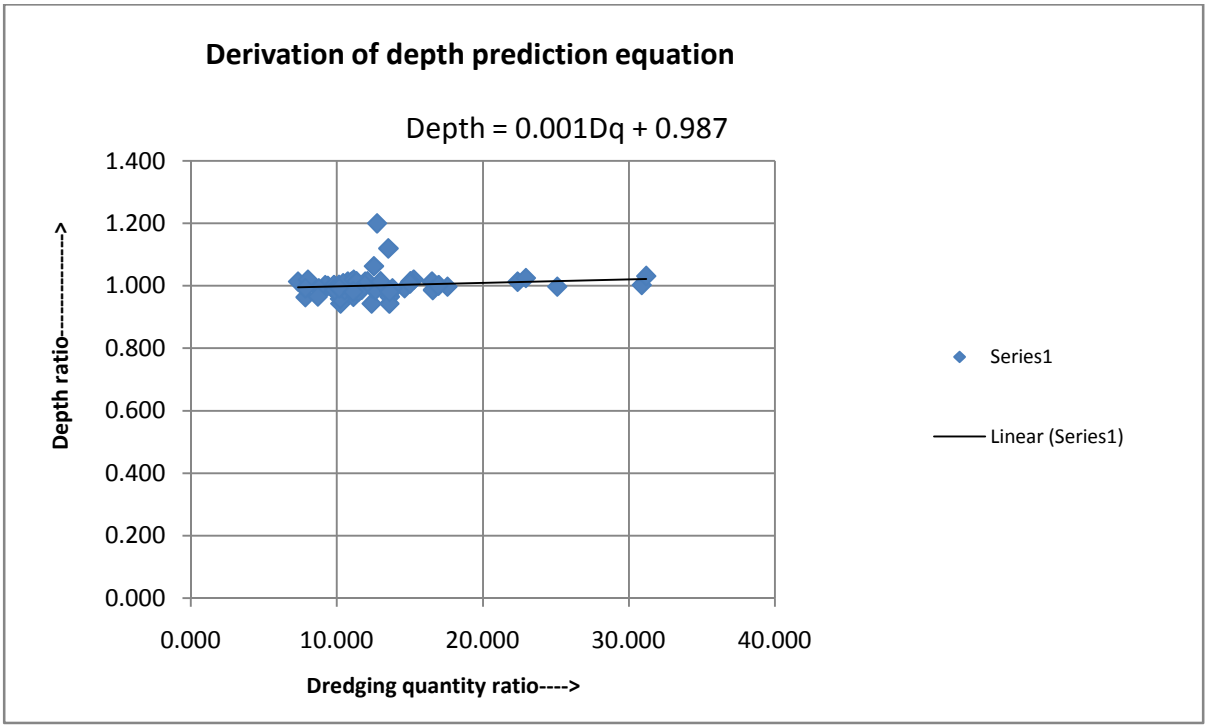



Fig. 6. Prediction of depth with Dredging Quantity Sogal Channel

Sometimes the dredging quantity is required to predict based on available depth therefore an attempt was made to correlate depth with dredging quantity. The following equation has been arrived after regression analysis as shown in Fig.6.

$$\text{Depth} = 0.001\text{Dqr} + 0.987 \quad (3)$$

(Where Dqr= dredging quantity ratio=monthly dredging quantity/annually dredging quantity)

It can be seen from the following Fig.6 that the predicted value with observed values are making $45^0$ curve which shows good prediction. The validity of this graph is checked with other data of Deendayal port.

Table no.1

| Equation number | Value of $R^2$ |
|---|---|
| 1 | 0.145 |
| 2 | 0.021 |
| 3 | 0.021 |

The equation number 1 has $R^2$ value 0.145 whereas equation number 2 & 3 having $R^2$ value same i.e.0.021. The $R^2$ values are shown in table number 1for the equation number 1-3.

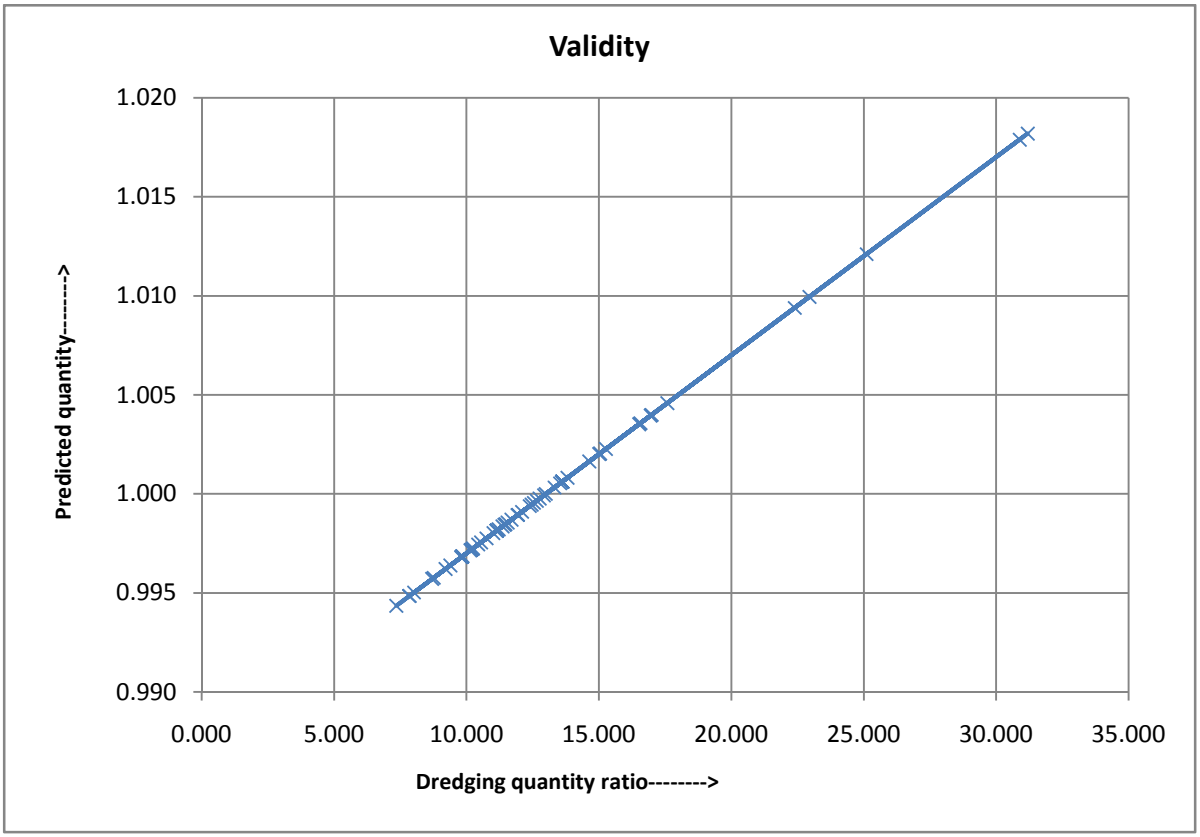



Fig. 7. Validity for the prediction of depth with Dredging Quantity Sogal Channel

## 4. Conclusions

1. The empirical equation number (3) has been received after regression analysis of the observed dredging data starting from 2011-2018. This empirical equation has hundred percent data covered in ±10% bandwidth and having correlation coefficient =100%.
2. The regular monitoring and analysis of dredged surveys of Soga channel was done at CWPRS which resulted achieving depth of more than 9 m in the navigational channel.

3. An empirical equation to predict the Morphological changes in the Sogal channel at Deendayal Port (Kandla) has been formulated on the basis of the prototype data base available at CWPRS.
4. This empirical equation is valid for site specific for the soil classification in the channel with mean grain size of about 0.08mm.
5. Equation number 2 shows that there is minor change towards decreasing dredging quantity.
6. This equation is valid geographically at Deendayal Port (Kandla) but can be checked for other Ports too.
7. The Equation number 3 can predict the dredging quantity for the required average dredging depth.

## Acknowledgement

Authors acknowledge Shri A. K. Agrawal, Director, CWPRS for his continues guidance and encouragement.

## References

Bathymetric data of Sogal channel starting from year 2011 to 2018 on monthly basis. (96 months)

CWPRS (2020), Morphological changes around Sogal Channel in the approaches to Deendayal Port (Kandla) during 2011-2018, CWPRS Khadakwasla Pune-24. P-39.

Ramesh N, Berde, Chuadharee, B.B and Purandare, U.V, (2004) Morphological behavior of large range Tidal Creek: A case study Hydro 2004 VNIT, Nagpur. pp-418-423.

*IN PROCEEDINGS OF 25th HYDRO 2020, INTERNATIONAL CONFERENCE, NATIONAL INSTITUTE OF TECHNOLOGY ROURKELA, ODISHA, INDIA 26-28, March 2021, ISBN 978-93-90631-56-8*

Paper ID - 450

# WAVE SIMULATION FOR OPTIMISATION OF BREAKWATER LAYOUT – A CASE STUDY

Smt.Alkananda Pardeshi [1], Amol Borkar[2] , Banwari Lal Meena[3], Dr. Prabhat Chandra[4]

*[1]Scientist-D, [2] Scientist-B,[3] Scientist-B ,[4]Scientist-E*
*Central Water and Power Research Station, Pune-411024, India*
*Email: abpardeshi82@yahoo.co.in*

## Abstract

The wave data analysis and studies are of fundamental importance for any coastal development especially on the open coast. Wave tranquility plays vital role for deciding the layouts of breakwaters to obtain the suitable operational conditions for berthing etc. Numerical modeling is an efficient tool for wave simulation. This paper presents the wave tranquility aspect for optimization of breakwater layout by using numerical model technique for a site specific fishing harbour proposal at Kasargod located at the upstream of inlet gut of the River Chandragiri at Kasargod, Kerala on the west coast of India. Under the existing condition, with two training works at site, the problems were faced by the fishermen while maneuvering their trawlers /boats due to high wave actions, adverse flow conditions near the entrance and wave breaking at low tides. In order to ease the difficulties of fishermen, Mathematical wave model studies were conducted to evolve an offshore breakwater of 730m length which would provide adequate wave tranquility. From the considerations of cost, economy and convenience in construction, the proposal of offshore breakwater was modified and further optimized with the help of studies conducted at CWPRS. In offshore region, waves approach with the maximum significant wave height of the order of 4.5 m. The offshore wave data were transformed to a nearshore location by applying MIKE 21 SW model. The optimum layout of breakwater of 700m length was evolved to effect suitable wave tranquillity near the entrance and further inside throughout the year against the proposed 895 m length by using MIKE 21 BW model. The present paper describes the methodology and optimization of breakwater layout from wave tranquility point of view by using MIKE21 BW/SW model.

*Keywords: Wave tranquility, Deep sea waves, Jetty, Numerical modeling, Predominant wave directions.*

## 1. Introduction

Nearshore wave transformation is a complex coastal process of shoaling, refraction, diffraction, reflection, and energy dissipation due to bed friction and breaking contributing variation in the wave height, period and direction. The specific case of Kasargod Fishing Harbour located at the upstream of inlet gut of the River Chandragiri at Kasargod, Kerala was selected for the wave transformation studies. It is situated at the right bank ( Lat $12^0$ 28' 32.71" N & Long $74^0$ 59' 36.14" E ) in the backwaters of the river Chandragiri ( Fig.1). The distance between fishing harbour from the mid of inlet gut is about 700 m whereas the second harbour is about 450 m north of the mid of inlet gut. The mouth ( gut ) had kept on shifting all the time as observed over the years.

Earlier studies recommended the construction of a structure consisting of parallel training works spaced 120m centre to centre aligned east-west to maintain the inlet with minimum siltation at site which were constructed in the year 2010-11 ( Fig.2 ). Thereafter, in the year 2015, a channel in between the training works was dredged. During 2018, it was reported that fishermen were facing difficulties due to sedimentation in the channel, wave and current actions near the entrance of the channel while maneuvering their trawlers /boats through the channel.




**Figure 1** Location map of Kasargod site

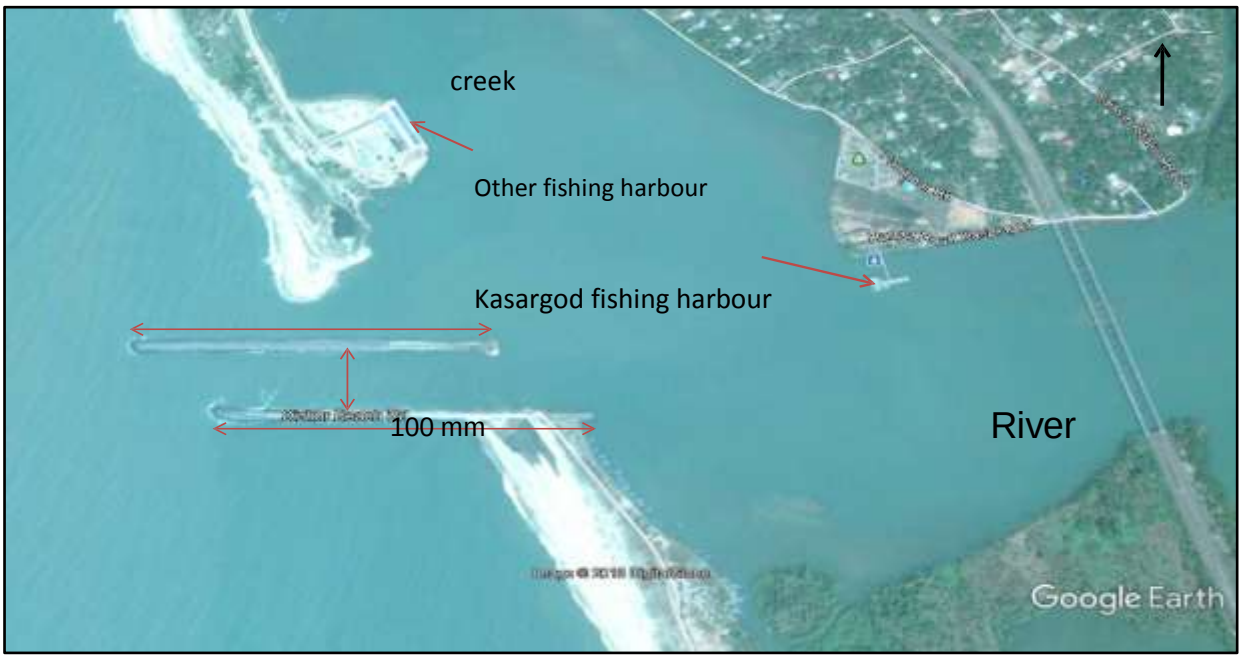



**Figure 2** Fishing harbours and Intake channel with parallel training works

In order to ease the difficulties of fishermen, it was proposed to evolve the suitable breakwater structure and /or extend the lengths of training works and their configuration as well to provide necessary wave tranquillity at the entrance and the suitable flow conditions.

Mathematical wave model studies were conducted to evolve an Optimised offshore breakwater of 730m length and additionally 120m extension of south breakwater ( Fig. 3 ). With a view to understand the wave transformation an area of 6.9 km by 4.5 km schematized with 5m grid size were considered. The simulations were carried out using MIKE21- BW model for critical predominant wave directions with corresponding wave heights. This layout would provide adequate wave tranquillity throughout the year near the entrance and would also be suitable from the considerations of flow conditions and siltation.

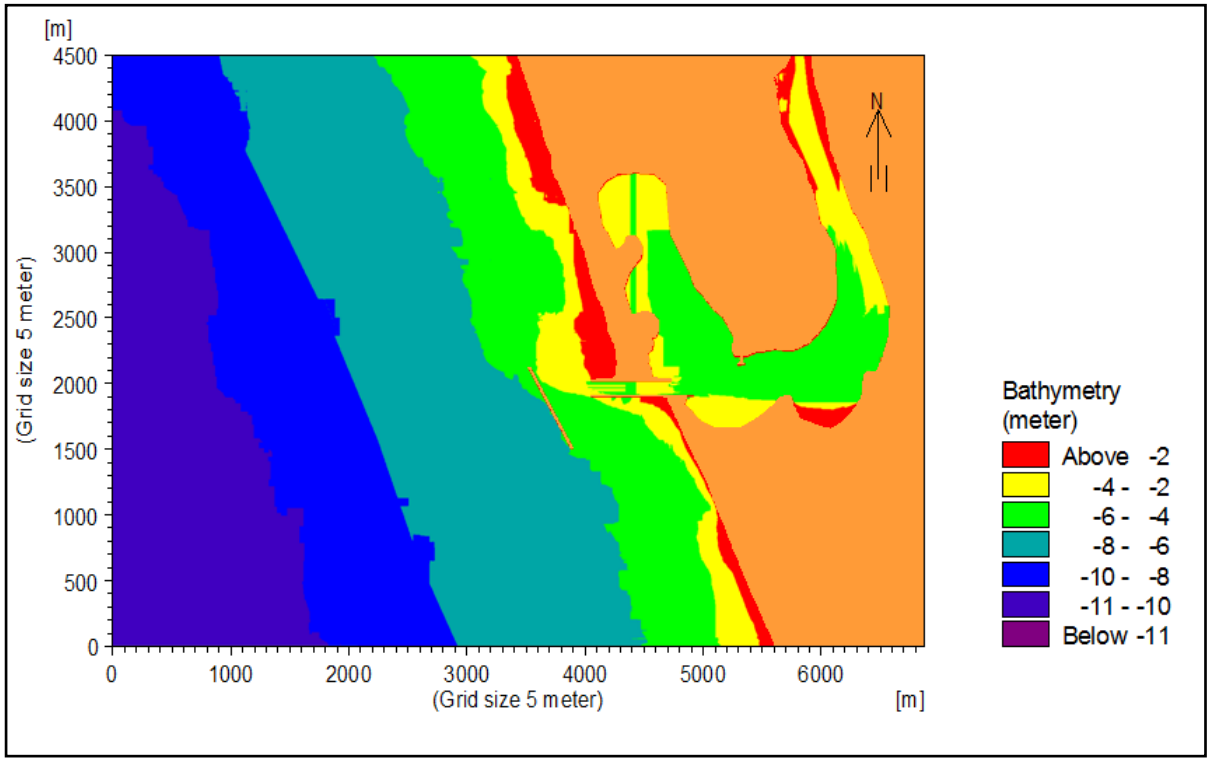



**Figure 3 :** Bathymetry of offshore breakwater For MIKE21 BW Model

As the project authority apprehended about the high cost of offshore breakwater, proposal of shore connected breakwater of total length 895m ( 745m curved plus 150m straight extension ) along the existing northern breakwater was initiated. The idea was to limit the wave disturbances to 0.50m near the entrance for safe maneuverability of the vessels. Since the direction of net drift is from north to south, this alignment would be suitable from littoral drift consideration as it would have towards the south direction. The fishermen conveyed their concern about the safe entry into the navigational channel due to the prevailing high waves particularly during the monsoon season. The proposed shore connected breakwater alignment suited their navigational requirements in principle. appropriate layout of the extension of the proposed breakwater was decided to be finalized based on mathematical model studies in order to provide protection against the waves and minimize the effect of currents and siltation near the channel entrance.

In the present study numerical simulations of waves in the deep waters as well as shallow waters have been carried out using MIKE 21 models to evolve the optimum length and alignment of breakwater.

## 2. odelling Techniques

Winds, waves and bathymetry are the major oceanographic parameters required for wave modeling. Wave climate plays a significant role in understanding the coastal environment. Wave height, wave period and wave direction are the important wave parameters. Nowadays, numerical modeling is powerful tool for the study of sea waves. Numerical models are mathematical models that use suitable numerical time-stepping procedure to obtain the models behavior over time. For wave transformation studies, two modules MIKE21- SW model and MIKE21- BW (BOUSSINESQ WAVE )[1]were used for estimation of near shore wave field and wave penetration in the terminal area respectively. Brief description of these models is given below.

### 2.1 *MIKE21-SW Model*

As waves travel from deep sea to shallow coastal waters, they undergo changes in wave direction and wave height due to the processes of refraction and shoaling. The MIKE21-SW model simulates the growth, decay and transformation of wind generated waves and swells in offshore and coastal areas. It involves directional decoupled parametric formulation, which is based on a parameterization of the wave action conservation equation. The parameterization is made in the frequency domain by introducing the zeroth and first moment of the wave action spectrum. The discretisation of the governing equation in geographical and spectral space is performed using cell-centered finite volume method. In the geographical domain, an unstructured mesh technique is used. The time integration is performed using a fractional step approach where a multi-sequence explicit method is applied for the propagation of wave action.

### 2.2 *MIKE21-BW Model*

Mathematical model MIKE 21-BW is based on time dependent Boussinesq equations of conservation of mass and momentum obtained by integrating the three-dimensional flow equations without neglecting vertical acceleration. They operate in the time domain, so that irregular waves can be simulated. These equations include nonlinearity as well as frequency dispersion. The frequency dispersion is included in the flow equations by taking into account the effect of vertical acceleration and the curvature of stream lines on pressure distribution. The model simulates the processes of shoaling, refraction, diffraction from breakwater tips and bed friction. It also takes into account partial reflections from the boundaries, piers and breakwaters.

## 3.0 Specific Case study

### 3.1 *Transformation of deep sea wave data*

Engineers are usually confronted with insufficient or no wave data when performing studies in remote or under developed coastal areas. Measurements at the site of interest would be the most adequate source of data, but these are often expensive , Hence In absence of instrumentally measured data, the nearshore wave climate is obtained by transforming the offshore wave data to a near shore location of the study area with the help of MIKE 21- SW model. Model area considered is about 60 km X 51 km schematized by triangular mesh ( Fig. 4 ). This area has been extracted from C-MAP in offshore region,

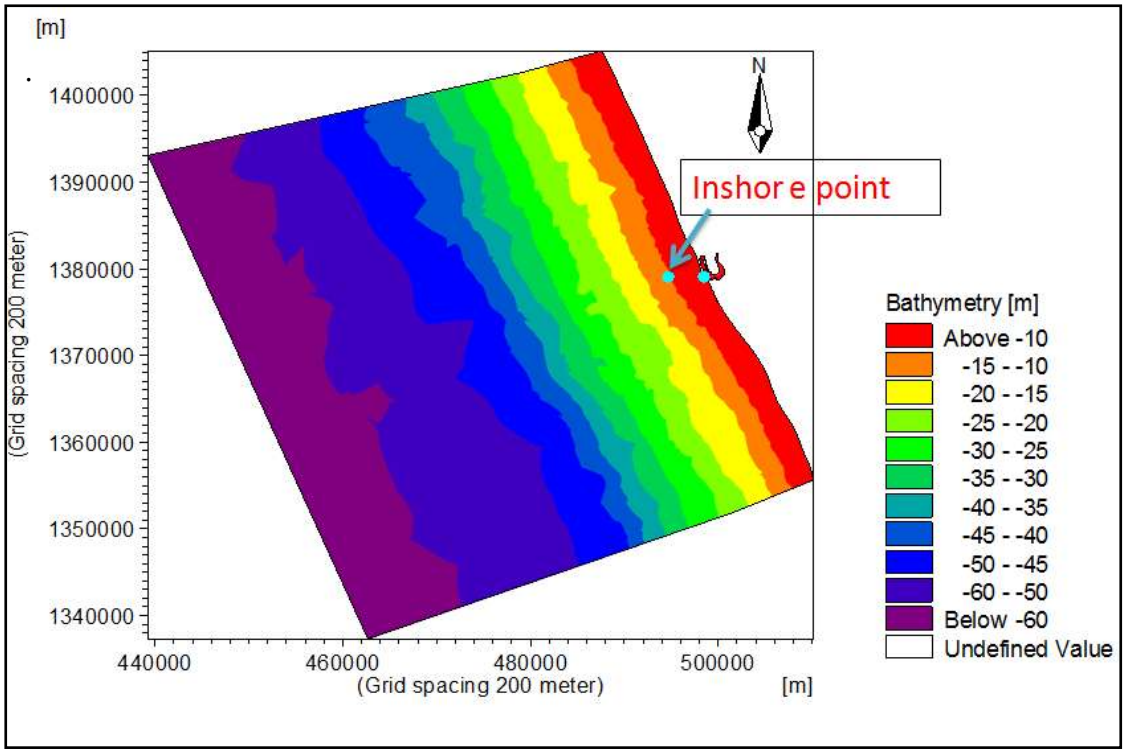
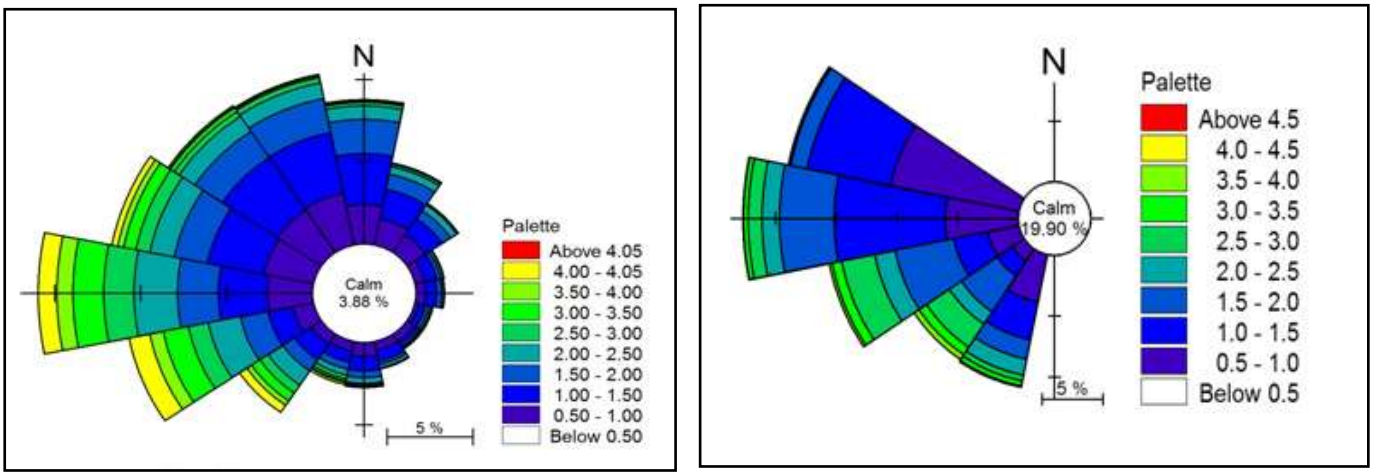



**Figure 4** Bathymetry for MIKE21 BW Model - existing condition




**(a) :** Offshore **(b):** Nearshore

**Figure 5** Wave rose diagram for entire year

At offshore boundary Waves approach predominantly from NNW, NW, WNW, WEST, WSW,SW, SSW with the maximum significant wave height of the order of 4.5 m (Fig 5a). With this wave conditions simulations were carried out by using MIKE21-SW model. It is observed that at near shore region, waves approachs predominantly from SSW, SW, WSW, West and WNW directions with percentage of

occurrence of 11%, 11% , 16%, 23% , 21% and Wave height of 2m, 2.5m, 2.5m,3m, 1.5m respectively for the annual period having the maximum wave height of the order of 3.5m ( Fig. 5b ).

### 3.2 *Wave propagation inside the harbour area*

The accuracy of all numerical simulations primarily depends on how accurately the bathymetry is generated. The near shore bathymetry data provided by project was superimposed on the bathymetry taken from C-Map to cover the model region. The simulations of model were carried out for following three cases using MIKE21 BW model for all the predominant directions at offshore boundary.

Case I. Existing condition with staggered training works in position.

Case II Modified layout by extending the northern breakwater in a semicircle of 300m radius

Case III. Optimisation of extended northern breakwater

#### **3.2.1** *Studies with Case I*

The experiments were conducted to examine the wave propagation in the harbour area for existing condition with only staggered training works in position. The bathymetry for the simulation of waves was generated by considering an area of 7.5km by 4.5 km discretised with a grid size of 3 m by 3 m ( Fig.6 ). The simulations were carried out using MIKE21 BW model for all the predominant wave directions at offshore boundary of the area with corresponding wave heights.

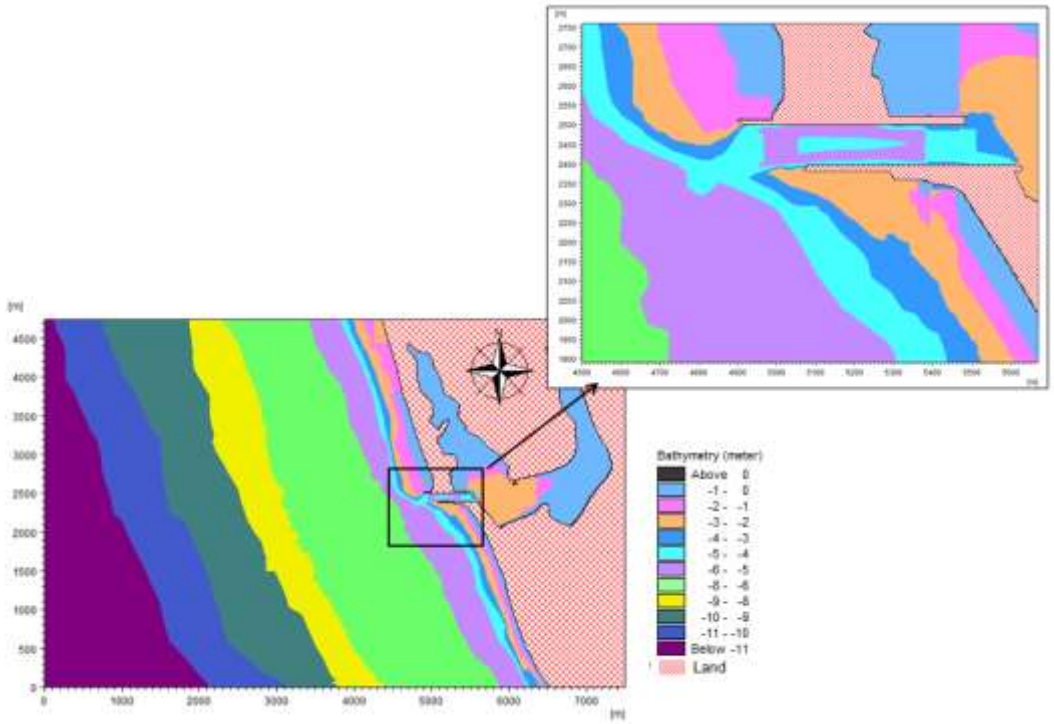
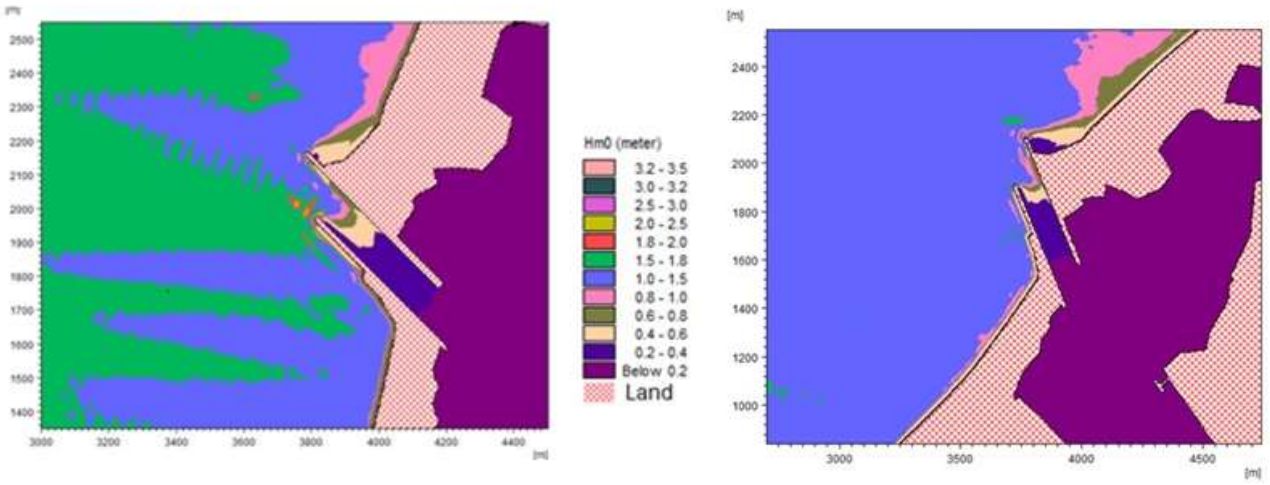



**Figure 6** Bathymetry for MIKE21-BW Model - Existing condition

Average wave heights at various locations are summarized in Table 1 and significant wave height distribution plot ( Fig. 7a and 7b ). From the results it can be seen that Wave heights observed at the entrance of the channel are in the range of 0.6m to 1.8 m which is far more than the permissible limit of 0.50 m.

**Table 1** Significant wave heights at the entrance of the channel

| Incident wave direction / wave height (m) | Range of Significant wave height (m) At entrance of the channel |
|---|---|
| SSW / 2.0 m | 1.0 to 1.5 |
| SW / 2.5m | 1.0 to 1.55 |
| WSW / 2.5m | 1.0 to 1.8 |
| W / 3.0m | 1.0 to 1.8 |
| WNW / 1.5m | 0.5 to 0.95 |




**(a)** SW direction (H=2.5m) **(b)** SSW direction (H=2.0m)

**Figure 7** Wave height distribution under existing conditions

### 3.2.2 *Studies with Case II*

After conducting trials with different layouts, a layout of extending the northern breakwater in a semicircle of 300m radius of total 895m long ( 745m curved plus 150m straight extension ) with breakwater tip 1 (Lat $12^0$ 28' 31.06" N & Long $74^0$ 58' 38.39" E) and tip 2 (Lat $12^0$ 28' 10.83" N & Long $74^0$ 58' 50.47" E) was evolved in order to provide adequate wave tranquility conditions near the entrance of the channel and in the gut area. The south training work was also extended by about 120m to match the tip of northern training work. The areas of 7.5 km by 4.5 km were schematized with 3m grid size was

considered ( Fig. 8). The simulations were carried out using MIKE21 BW model for most critical predominant wave directions from SSW and SW with corresponding wave heights. Average wave heights at various locations are summarized in Table 2 and significant wave height distribution plot ( Figs. 9a and 9b)

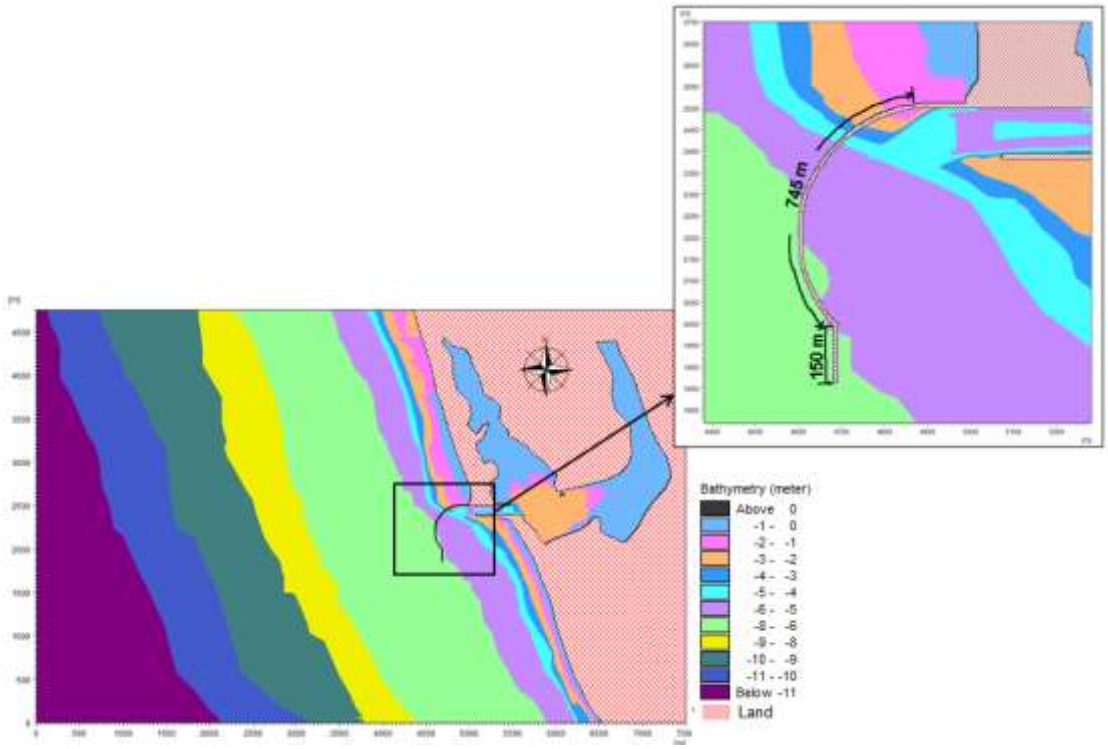
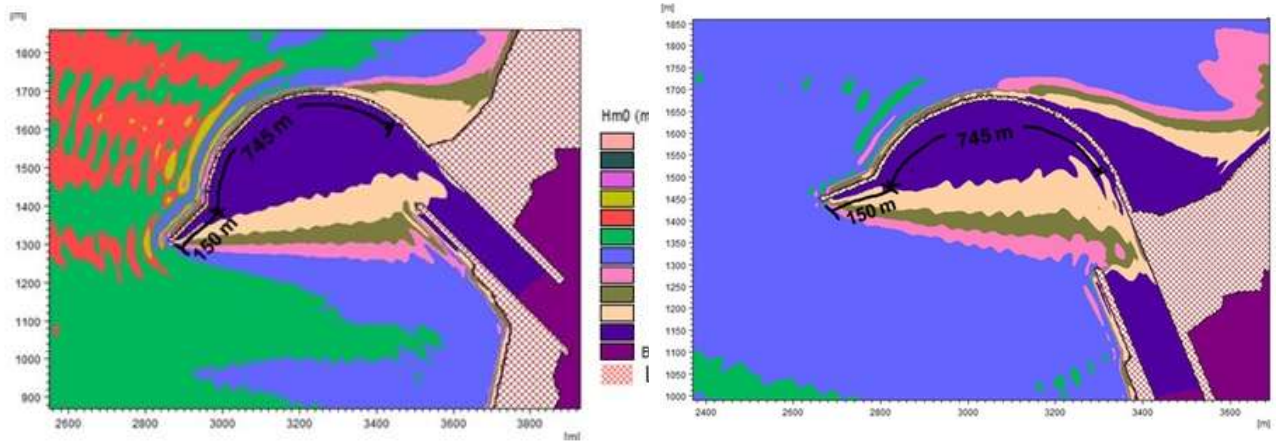



**Figure 8** Bathymetry of the extended northern breakwater layout

From the results, it can be seen that the significant wave heights at entrance of the breakwater are within the limit of permissible wave height of 0.50m for incidence from all critical wave directions .Hence, the proposed layout of extension of northern breakwater of length 745 m provides adequate tranquility near the entrance and in the harbour round the year. This layout needs to be further optimized to minimize the cost of the project.

**Table 2** Significant wave heights at the entrance of the channel

| Incident wave direction / wave height (m) | Range of Significant wave height (m) At entrance of the channel |
|---|---|
| SSW / 2.0 m | 0.6-.1.0 |
| SW / 2.5m | 0.40-0.58 |




(a) SW direction(H=2.5m) **(b)** SSW direction (H=2.5m)

**Figure 9** Wave height distribution for extended northern breakwater layout

### 3.2.3 *Studies with Case III*

The radius of the curvature of the extension of northern breakwater and its total length is required to be modified to most effective layout based on cost and tranquillity /littoral barrier for the harbour entrance After conducting different trials a layout of 700 m was finalised. The areas of 7.5 km by 4.5 km were schematized with 3m grid size ( Fig 10 ). The simulations were carried out using MIKE21-BW model for all predominant wave directions with corresponding wave heights.

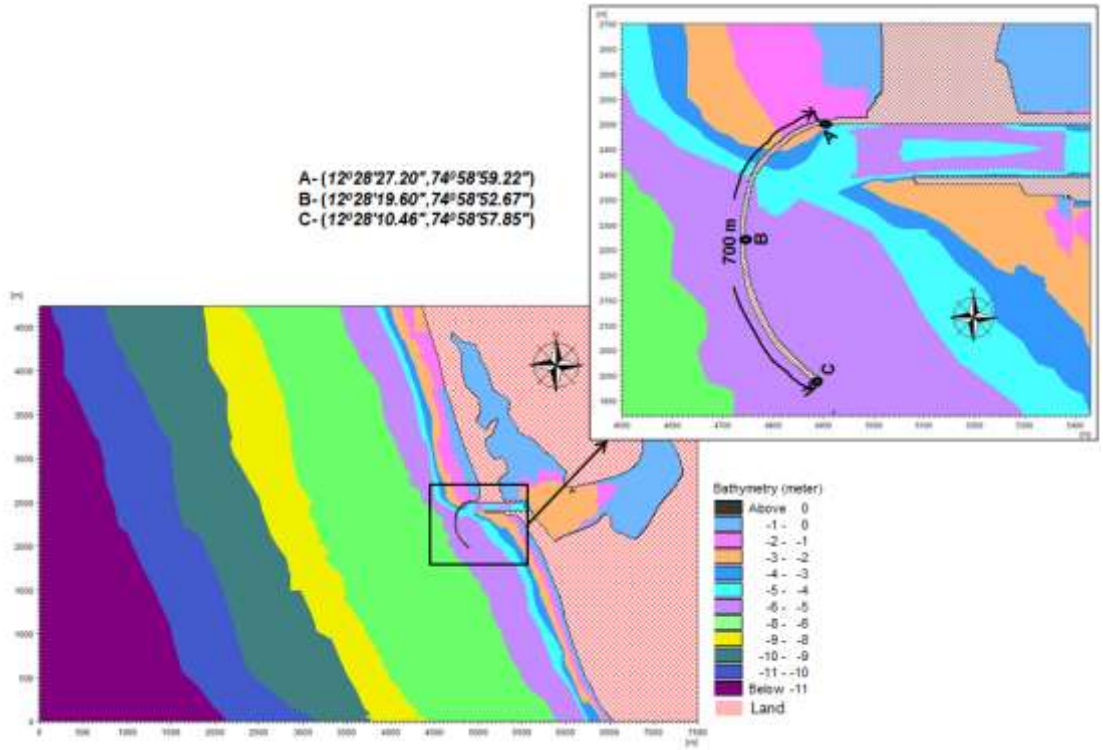
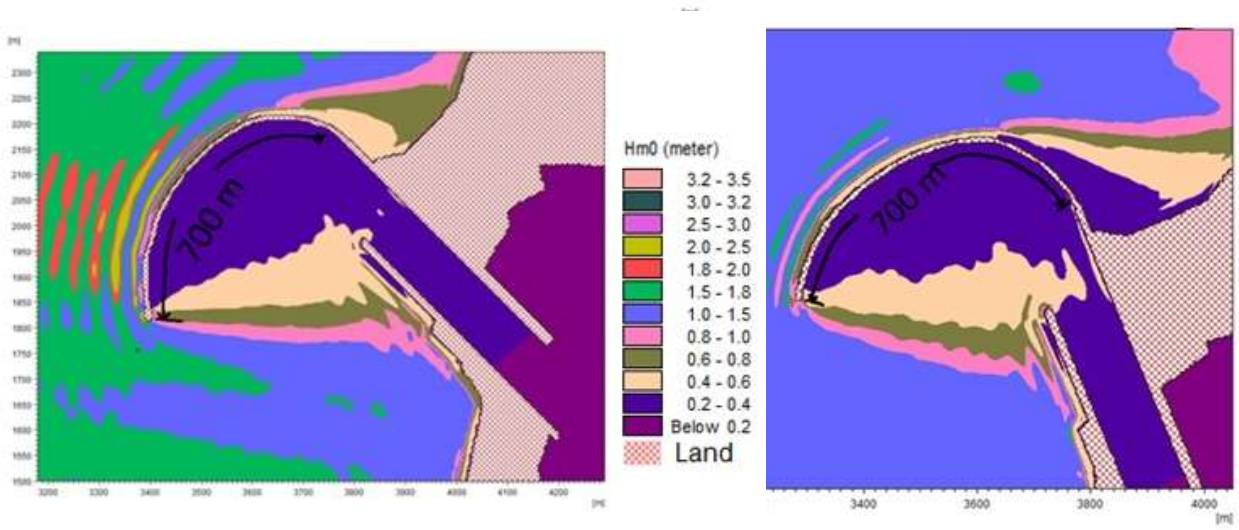



**Figure 10** Bathymetry of Optimised northern breakwater layout

Average wave heights at various locations are summarized in Table 3 and significant wave height distribution plots ( Figs11a and 11b ).The results shows that the significant wave heights at entrance of the breakwater are within the limit of permissible wave height of 0.50m for incidence from all wave directions.

**Table 3** Significant wave heights at the entrance of the channel

| Incident wave direction / wave height (m) | Range of Significant wave height (m) At entrance of the channel |
|---|---|
| SSW / 2.0 m | 0.45-0.51 |
| SW / 2.5m | 0.37-0.50 |
| WSW / 2.5m | 0.25-0.32 |
| W / 3.0m | 0.30-0.35 |
| WNW / 1.5m | 0.12-0.15 |




**(a)** SW direction(H=2.5m) **(b)** SSW direction (H=2.5m)

**Figure11** Wave height distribution of Optimised northern breakwater layout

## 5 . Conclusions

Detailed wave tranquility studies using mathematical modeling techniques to assess the wave tranquility inside the harbour were carried out for optimizing the breakwater layout, since breakwaters are very costly structures. The main conclusions from the studies carried out for Optimisation of breakwater at Kasargod Port have been drawn as below:

- The present paper describes the methodology and optimum layout evolved through the studies which would be helpful for planning the fisheries harbour with reference to specific case.

- The studies carried out with Optimum layout with 700 m long breakwater (Fig. 11) to minimize the cost of the project indicated that wave heights are in the range of permissible limit at the entrance of the channel for all the incidence wave directions. Hence it is possible to operate the port for round the year.

- With optimization, the length of the breakwater is reduced to 700m from total length of 895m ( 745m curved length plus 150m extension towards south ) suggested by project, which is cost effective solution. It would also be suitable from the considerations of flow conditions and siltation.

- Wave propagation inside the harbour is an interesting example of combined refraction and diffraction sophisticated numerical model like MIKE21-SW and MIKE21-BW provide accurate tool for simulation of such complex phenomena. Since, Fisheries play an important role in the economy of India.

## ACKOWLEDGEMENTS

The authors are thankful A.K. Agrawal, Director, Central Water and Power Research Station (CW&PRS) Pune, for the encouragement and permission to publish this paper.

## REFERENCES:

1 MIKE 21 BW user guide (Boussinesq wave module).

2 Technical Report No. 5742 of (October 2019) of Central water and power research station Khadkwasla Pune 24, on “Mathematical model studies to assess the impact of extension of breakwater at Kasargod fishery harbour, Kerala..”

IN PROCEEDINGS OF 25th HYDRO 2020, INTERNATIONAL CONFERENCE,
NATIONAL INSTITUTE OF TECHNOLOGY ROURKELA, ODISHA, INDIA
26-28, March 2021, ISBN 978-93-90631-56-8

Paper ID - 492

# Numerical Simulation of Pool Characteristics Formed at Vertical Drops by Volume of Fluid Method

Pranaya Keshari Nahak[1], Adwaith Gupta[2]

[1,2]*Paanduv Applications Private Limited, 124 Parwana Nagar, Bareilly, Uttar Pradesh-243122, India*
*Email: pranayanahak@gmail.com, adwaith1990@gmail.com*
*Telephone/Mobile No.: +91 8791470881*

## Abstract

The pool characteristics at the vertical drops play an important role in water and environmental applications such as dam/spillway designs for minimizing loss to the downstream structures. While detailed experimental work is reported earlier providing insights to the dynamics of vertical drops under varying upstream conditions, a detailed numerical investigation appears to be missing from the literature. In this paper, we report the results generated from an elaborate set of numerical simulations for the dynamics of a vertical drop. The numerical results are then validated against the previously reported experimental results. Vertical drops have a complex water-air interface. Such flows are called free surface flows and require special numerical treatment at the interface for accurately capturing the flow dynamics, such as pool characteristics. Volume of Fluid (VOF) is a well-known numerical technique for estimating the free surface flows accurately. Additionally, turbulence plays an important role in intermixing of the downstream water pool and the falling jet. In this research, we use OpenFOAM's interFoam solver that uses the VOF method and buoyancy modified k-Omega SST turbulence model for capturing the turbulence. We have found that OpenFOAM can be used in fairly accurately predicting the flow dynamics of the pool formed at the vertical drops and by extension can be potentially applied to various water and environmental applications.

***Keywords:*** *Vertical Drop; Pool Characteristics; VOF; RANS; free surface flow; turbulence; numerical solution*

## 1. Introduction

Drops are the features of a lot of civil engineering designs e.g, in irrigation systems where the drops are made in order to decrease the slope of the channel. Apart from that there are natural phenomena such as river erosion in which vertical drops are formed spontaneously. Generally, in such structures, energy loss occurs due to the turbulent mixing of the falling jet and the water pool formed. A series of experimental studies have been conducted in the past regarding this matter. Moore and White [8] discussed the basics of the drop hydraulics, especially the energy loss at the base of the drop. Later, White came up with some theoretical findings [12] for this which was again changed by Gill [4]. Some empirical solutions in terms of some non-dimensional number, such as Drop Number, D are presented by Rand [11] for studying the flow behaviors of vertical drop. All the studies conducted earlier were with some assumptions. As a result, there is some lacunae in predicting some characteristics. Later Rajaratnam et al. [9] did some experimental work in more detail by studying the pool characteristics along with the energy loss mechanism.

White [8] made some assumptions in his work such as the included angle and the momentum flux of the jet do not change by the presence of the pool, the water enters in the pool with a constant velocity and energy loss at the drop structures is due to intermixing of the pool water with the jet etc. Gill [4] made several improvements upon the work of White and found the inaccuracies of the assumptions made by White. But Gill assumed that there is no energy loss in the water pool formed which is not true. Later, Rajaratnam et al. [9] did some experiments and found out the validity of all assumptions made e.g., falling jet has varying velocity which invalidates the equal kinetic energy assumption made by White [8]. The extensive experimental work by Rajaratnam et al. [9] led to study of various flow characteristics in detail which made this present work possible to study the drop mechanism in greater depth numerically. The interFoam solver is used while studying the drop

phenomena which is based on the 'Volume of Fluid Method' developed by Noh & Woodward in 1976 [10]. But the first journal publication is in the name of Hirt and Nichols [5]. The performance of the interFoam has been validated accurately by Deshpande et. al. [3] has been found to be successful for many inertia and surface tension dominated flows. In this study, the buoyancy modified k-ω SST turbulence model is used for predicting the turbulent eddy viscosity. There are two important features of this turbulence model i.e., and the selection of k-ω SST model and the included buoyancy term. The k-ω SST model is proved to be superior in comparison to other available RANS turbulence models. The k-ε model has its stability issue with the transport equation of the turbulent kinetic energy dissipation rate, ε which becomes singular in the viscous sublayer region and the k-ω model is dependent on the freestream value of ω strongly. The k-ω shear stress transport model becomes independent of the freestream ω value and is devoid of stability issues as that of k-ε and it is so because of blending the advantage of both the turbulence models. The details regarding this can be found in ref. [6]. Secondly, the in-house turbulence models available in the OpenFOAM were developed only for single phase models. In multiphase simulations, the buoyancy changes suddenly at the interface region and this led to addition of the buoyancy term in the transport equation of turbulent kinetic energy by Devolder et al. [1]. Surprisingly, this led to significant drop in the turbulent eddy viscosity as compared to other turbulence models. The details regarding the advantage of this model can be found in ref. [1, 2]. In this work, the pool characteristics such as the recirculation zone, the dimensions of the formed pool etc. are studied in depth.

## 2. Numerical Model and Implementation

The numerical study of the pool characteristics at the vertical drop is studied in the interFoam solver in OpenFOAM Software. In the experimental configuration, two drop heights were studied,i.e., 25 cm and 62 cm with different critical depth of flow, Yc. For the simulation purpose, four cases for 25 cm drop height and 3 cases of 62 cm drop height were investigated in total. The interFoam solver uses the volume of fluid method as a prime asset for doing the multiphase simulation. The two phases are air and water as obvious for the study. The basic equations which constitute the 'volume of fluid' method are the momentum equation, the continuity equation and the transport equation for the phase fraction, α There is loss of energy due to turbulent mixing in the region of the pool and the falling water jet. Hence, all the constitutive equations are solved in Reynolds Averaged Navier Stokes (RANS) modelling.
The continuity equation:

$$\frac{\partial u_j}{\partial x_j} = 0 \tag{1}$$

The momentum equation:

$$\frac{\partial \rho u_i}{\partial t} + \frac{\partial \rho u_i u_j}{\partial x_j} = -\frac{\partial p}{\partial x_i} + \frac{\partial (\tau_{ij} + \tau_{t_{ij}})}{\partial x_j} + \rho g_i + f_{\sigma i} \tag{2}$$

where u represents velocity, $g_i$ represents the acceleration due to gravity, $p$ is the pressure and $\tau_{ij}$ and $\tau_{t_{ij}}$ are the viscous and turbulent stress tensors and $f_{\sigma i}$ represents the surface tension vector.
The density ρ is defined as

$$\rho = \alpha\rho_1 + (1-\alpha)\rho_2 \tag{3}$$

where, α is the phase fraction, $\rho_1$ and $\rho_2$ are the densities of two phases.
The transport equation of the interphase is represented as follows:

$$\frac{\partial \alpha}{\partial t} + \frac{\partial \alpha u_j}{\partial x_j} = 0 \tag{4}$$

In the regions of mixing, the turbulent kinetic energy and its dissipation rate plays a significant role in determining the flow characteristics. Hence, accurate prediction is one of the prime objectives. The available turbulence models for determining the turbulent eddy viscosity are not meeting the expected flow behavior. The buoyancy modified kOmegaSST turbulence model [1] worked pretty well comparatively.

The transport equations for the buoyancy modified k- ω SST model are as follows:

$$\frac{\partial \rho k}{\partial t} + \frac{\partial \rho u_j k}{\partial x_j} - \frac{\partial}{\partial x_j}[\rho(\nu + \sigma_k \nu_t)\frac{\partial k}{\partial x_j}] = \rho P_k + G_b - \rho\beta^* \omega k \tag{5}$$

$$\frac{\partial \rho \omega}{\partial t} + \frac{\partial \rho u_j \omega}{\partial x_j} - \frac{\partial}{\partial x_j}[\rho(\nu + \sigma_w \nu_t)\frac{\partial \omega}{\partial x_j}] = \frac{\gamma}{\nu_t}\rho G - \rho\beta\omega^2 + 2(1 - F_1)\rho\frac{\sigma_{w2}}{\omega}\frac{\partial k}{\partial x_j}\frac{\partial \omega}{\partial x_j} \tag{6}$$

$$P_k = min\,(G,\ 10\beta^*\omega k)$$

$$G = \nu_t \frac{\partial u_i}{\partial x_j}\left(\frac{\partial u_i}{\partial x_j} + \frac{\partial u_j}{\partial x_i}\right) \tag{7}$$

$$\nu_t = \frac{a_1 k}{max\,(a_1\omega, SF_2)}$$

$$G_b = -\frac{\nu_t}{\sigma_t}\frac{\partial \rho}{\partial x_j} g_j \tag{8}$$

where, $k$ is the turbulent kinetic energy, $P_k$ is the production term of $k$, $\nu$ is the kinematic viscosity, $\nu_t$ is the turbulent kinematic viscosity, $\omega$ is the specific dissipation rate, $G_b$ is the buoyancy term, S is the mean strain rate of flow, $\beta^*$=0.09, $a_1 = 0.31$, $\sigma_t = 0.85$. $F_1$ and $F_2$ are blending functions.The appropriate values of other constants such as $\beta, \gamma, \sigma_k, \sigma_w$ can be found in ref. [1].

For carrying out the study in detail, the dimensions are fetched from all the available scaled images from the Appendix section of the thesis by Chamani et al. [7] and the velocity fields are extracted from the image and implemented as input. It is a completely two-dimensional study. For implementing the velocity profile in the inlet with ease, a new boundary condition was developed in the OpenFOAM environment named as 'ExpDataCentricVectorBC' (https://gitlab.com/pranayarin/inletdatamonitoredbc). Accordingly, the pressure boundary condition was set to Neumann type at the entry of water in the domain. As the flow is supercritical at the outlet, it was necessary to set the boundary condition to Neumann type for both velocity and pressure. For the drop height of 25 cm cases, the mesh resolution was 0.25 cm for all the subcases while for the sub-cases of 62 cm drop height, a little coarser mesh was preferred for the simulation. Slip boundary condition was applied at all the walls owing to its materialistic nature. Ventilated drops are one of the key aspects of the study and necessary provisions were made in the mesh to account for the effect. Constant pressure and zero gradient velocity boundary conditions were implemented at those ventilations.

## 3. Results and discussion

Total seven cases are simulated considering both the drop heights. Different characteristics of the pool and the narrow base water stream are studied with respect to the non-dimensional critical depth of the flow, Yc/H. The flow behavior of different regions e.g., upstream and downstream are studied with necessary caution. When the water flows downwards from the drop in the form of a water jet, a pool builds up very slowly between the falling jet and the vertical drop. After achieving a certain shape and flow behavior, it nearly doesn't change. Hence, for getting a statistically stationary

state, all the simulations are run at least for 10 seconds and then the time averaged data are obtained for next 10 seconds. The pool heights and lengths of different cases were non-dimensionalized with respect to the drop height and studied against the non-dimensional critical depth of flow.

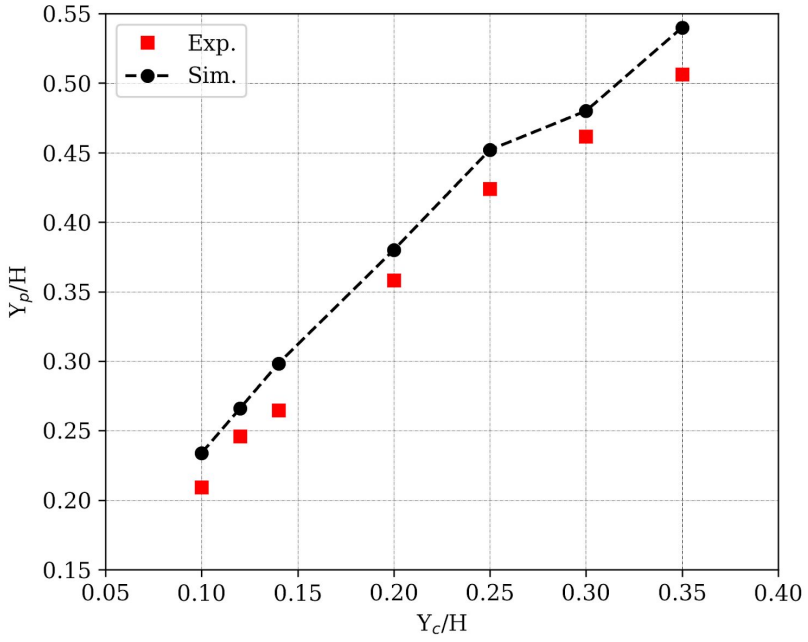



**Figure 1**. Plot of nondimensional pool height v/s nondimensional critical depth

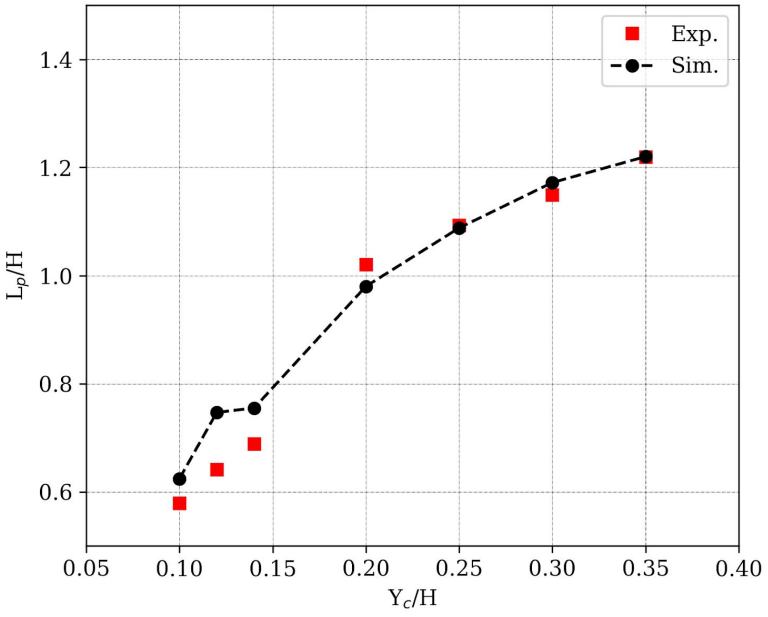



**Figure 2**. Plot of nondimensional pool length v/s nondimensional critical depth

With the increase in the non-dimensional critical depth, the pool length and height both increases as shown in fig. [1, 2]. This means that with the increase in the volume flow rate at the inlet, the amount of water accumulating in the pool also increases and this leads to increasing pool length and height. However, the amount of rise decreases with the same increase in non-dimensional critical

depth in case of the pool length as shown in fig. [2] and the simulation results of the pool length captured this behavior quite satisfactorily.

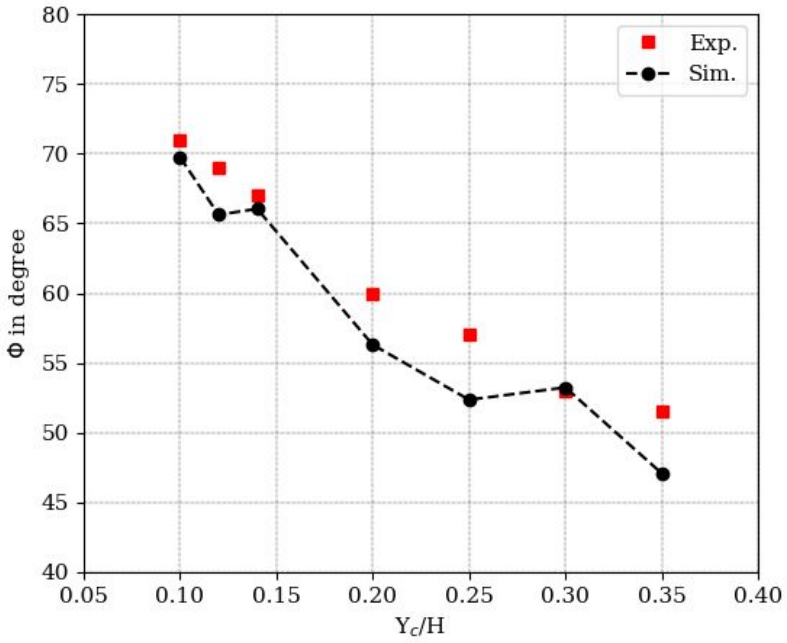



**Figure 3**. Plot of the included angle v/s the nondimensional critical depth

The falling jet and the pool upper surface create an angle at the point of initial meeting and this angle is termed as the included angle, $\Phi$ . From the figure [3], it is evident that with the increase in the non-dimensional critical flow depth, $Y_c/H$, the included angle decreases. This is due to the fact that with increase in the volume flow rate, the momentum and inertia associated with the water upstream makes the water jet fall at a little longer distance and as a result of which, the included angle magnitude decreases. In the simulated results, for some instances, there is very little under prediction and this is due to slightly lower velocity prediction at the edge of the drop upstream.

In figure [4], the primary pool recirculation zone is rotating in the clockwise direction. The in-house turbulence models available in the OpenFOAM were not able to predict the recirculation behavior quite accurately. In fact, in some instances, the recirculation was in the opposite direction to that achieved in the experiment. This is quite unphysical owing to the over prediction of the turbulent kinematic viscosity in the multiphase interface region. However, with the buoyancy modified kOmegaSST turbulence model, the recirculation zone was predicted with some great confidence. As shown in literature [7], a very small secondary recirculation zone should also be present, but again its size depends on the inlet flow characteristics and the drop height etc. According to Rajaratnam et al. [9], there is extensive mixing between the sliding jet and the pool which is clearly evident in fig. [5].

After the falling jet hits the horizontal base wall, a narrow stream of water flows in the opposite direction to the formed water pool. It is interesting to note that the pool depth is always more as compared to the base narrow water stream depth as shown in fig. [5] and it is observed in all the cases. The horizontal momentum with which the sliding jet moves changes after it hits at the bottom and the narrow flow at the base carries most of the kinetic energy. This leads to reduced depth at the downstream and comparatively larger depth at the pool side.

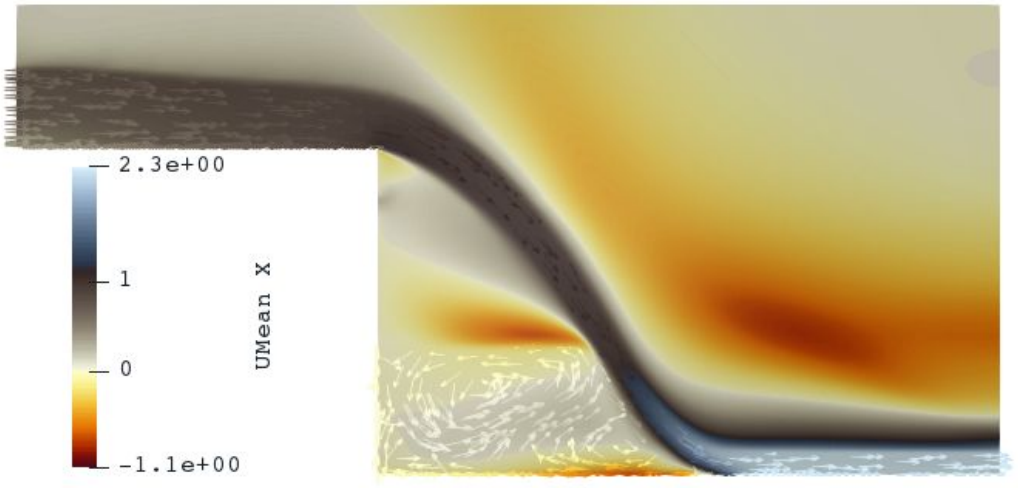



**Figure 4.** Contour plot of time averaged velocity in x-direction ,Ux in m/s for the case of Yc/H=0.2 with 25 cm drop height. The arrowheads show the velocity direction at a particular spatial position.

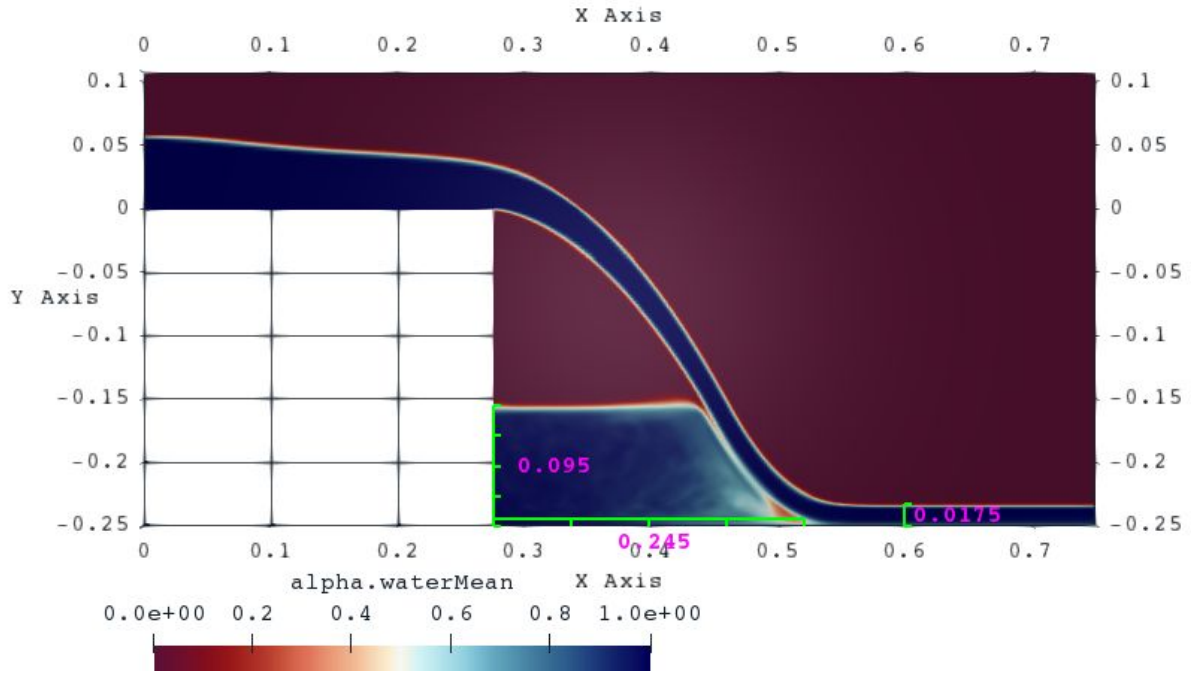
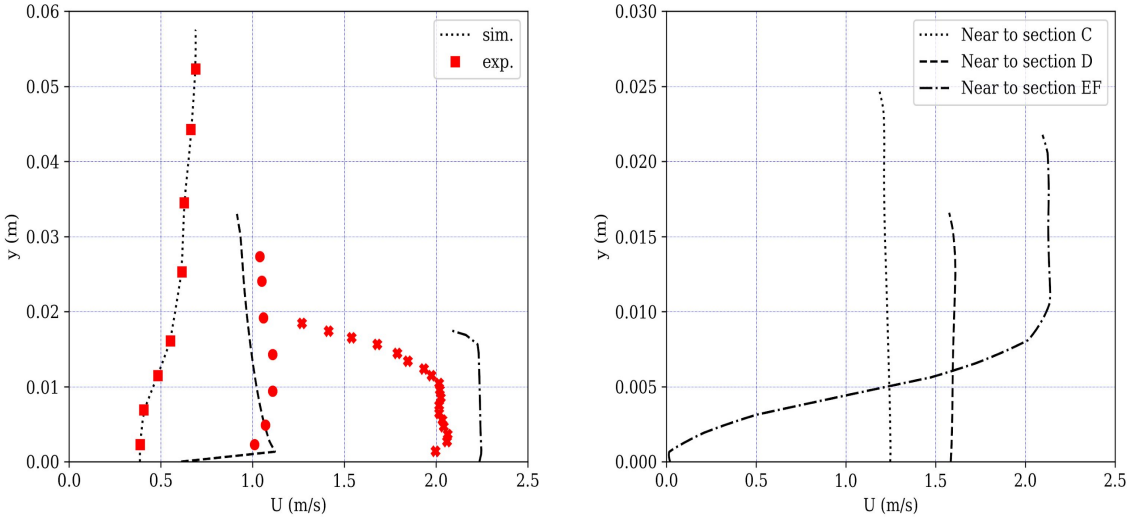



**Figure 5**. The phase fraction contour of water for the case of Yc/H =0.2 with 25 cm drop height. The measured pool height, length and the base height is shown in this figure.

For the case of Yc/H =0.2, the flow velocities are predicted at different sections and plotted and compared to that given by Rajaratnam et al. [9]. As mentioned earlier, a slightly underpredicted velocity profile at the edge can be seen in fig. [6 (a)]. The base velocity prediction is also off upto some extent. As there is slight variation of the include angle, pool length etc., getting the exact location of the section planes is not possible. Hence, a possible nearest location is chosen and predicted profiles are shown in figure [6 (b)]. It is interesting to observe that the predicted velocity profiles are quite similar as predicted experimentally by the Rajaratnam et al. [9]. A neat pictorial idea about the location of the section C, D, E and F can be found in ref. [9]. In fig. [6 (b)], a non-uniform velocity profile is obtained for the section EF. This clearly indicates the momentum exchange

between the sliding jet and the pool by shear. This also gathers the evidence for the loss of energy in the pool by turbulent mixing.




(a) (b)

**Figure 6.** In (b), the simulated (black lines) velocity profiles are plotted against the experimental data (red scatter marks). These are plots at locations of inlet, at the edge of the drop and at the base from left to right. In (a), only the simulated results are plotted for various locations of the falling jet. section C, D, EF are basically positioning from the top of the falling jet to the base of the jet near to striking the bed consecutively. These velocity profiles are of Yc/H = 0.2 with 25 cm drop height case.

## 4. Conclusion

In this paper, the pool characteristics at the drops is studied numerically in interFoam solver with the help of the buoyancy modified kOmegaSST turbulence model. Various pool characteristics such as its length, height and the included angle are studied thoroughly and found to be in good agreement. The attempt to replicate the pool characteristics and the velocity profiles of the falling and the sliding jet are in good agreement with the experimental data. This numerical setup can be used for simulating the vertical drop studies and other free surface flow studies. As the water stream at the base downstream is a very critical region due to its very narrow depth and the supercritical flow behavior, it needs a separate precise study and can be rendered as a future study.

## References

1. Brecht Devolder, Pieter Rauwoens, Peter Troch, Application of a buoyancy-modified k-ω SST turbulence model to simulate wave run-up around a monopile subjected to regular waves using OpenFOAM®, Coastal Engineering, Volume 125, 2017, Pages 81-94, ISSN 0378-3839, https://doi.org/10.1016/j.coastaleng.2017.04.004.

2. Brecht Devolder, Peter Troch, Pieter Rauwoens, Performance of a buoyancy-modified k-ω and k-ω SST turbulence model for simulating wave breaking under regular waves using OpenFOAM®, Coastal Engineering, Volume 138, 2018, Pages 49-65, ISSN 0378-3839, https://doi.org/10.1016/j.coastaleng.2018.04.011.

3. Deshpande, S. S., Anumolu, L., & Trujillo, M. F. (2012). Evaluating the performance of the two-phase flow solver interFoam. Computational science & discovery, 5(1), 014016.

4. GILL, M. A., Hydraulics of Rectangular Vertical Drop Structures. Journal of Hydraulic Research, Vol. 17, No. 4, 1979, pp 289-302.

5. Hirt, C.W.; Nichols, B.D. (1981). "Volume of fluid (VOF) method for the dynamics of free boundaries". Journal of Computational Physics. 39 (1): 201–225. Bibcode:1981JCoPh..39..201H. doi:10.1016/0021-9991(81)90145-5

6. Menter, F.R., 1993. Zonal two equation k-ω turbulence models for aerodynamic flows. In: 23rd Fluid Dyn. Plasmadynamics, Lasers Conf. American Institute of Aeronautics and Astronautics, Reston, Virigina. https://doi.org/10.2514/6.1993-2906.

7. Mohammad R. Chamani, Jetflow on stepped spillways and drops (Thesis), University of Alberta

8. MOORE, W. L., Energy Loss at the Base of Free Overfall. Transactions, ASCE, Vol. 108, 1943, pp 1343-1360.

9. N. Rajaratnam & M.R. Chamani (1995) Energy loss at drops, Journal of Hydraulic Research, 33:3, 373-384, DOI: 10.1080/00221689509498578

10. Noh, W.F.; Woodward, P. (1976). "SLIC (Simple Line Interface Calculation). In proceedings of 5th International Conference of Fluid Dynamics, edited by A. I. van de Vooren & P.J. Zandbergen". Lecture Notes in Physics. 59: 330–340. doi:10.1007/3-540-08004-x_336

11. RAND, W., Flow Geometry at Straight Drop Spillways. Proceedings, ASCE, Vol. 81, 1955, Paper 791, pp 1-13.

12. WHITE, M. P., Discussion of Moore (1943), Transactions, ASCE, Vol. 108, 1943, pp 1361-1364.

*IN PROCEEDINGS OF 25th HYDRO 2020, INTERNATIONAL CONFERENCE, NATIONAL INSTITUTE OF TECHNOLOGY ROURKELA, ODISHA, INDIA 26-28, March 2021, ISBN 978-93-90631-56-8*

Paper ID - 507

# Impact of deforestation and urbanization on extreme temperature and humidity over Brahmani River Basin

Ratnakar Swain

*Assistant Professor, Department of Civil Engineering, National Institute of Technology, Rourkela, Odisha, India, E-mail: swainrk@nitrkl.ac.in*

## Abstract

Urbanization and industrialization responsible for change in land use/land cover (LULC) which plays a vital role in studying its impact climate change parameters. The aim of this study is (i) to determine time-series of land use/land cover (LULC) map of the eastern India's Brahmani River Basin that experienced a fast increase in industrialization and deforestation in the recent decade; (ii) Impact of LULC change on extreme Temperature and humidity. The supervised classification method is followed herein to classify the study area with delineated classes such as water bodies; sand; barren/crop land; forest area and built-up area. The study reveals that the major land cover in the study area is dense forest which decreases from 71.70% to 14.85% from year 1975 to 2018. The second major category of land is barren/crop land, which was increased by 30% due to development in agricultural technology, irrigation facilities. The third category of land cover is built-up area which increases by 32.73% from year 1975–2018 due to man-made activities. The least area covered by water bodies which is fifth category of land cover was 0.33% in the year 1975 increased to 1.65% in the year 1999 due to the construction of Rengali Dam and Samal Barrage but subsequently decreased to 0.87% in 2018. Hence, it is verified that the industrialization and development activities cause heavy deforestation in the catchment. It is also found that the decrease in about 56.85% of forest land in just 38 years causes the average maximum temperature and minimum temperature increased to 4.8% and 3.19%, respectively. The relative humidity is found to be decreased by 11.5%. Hence, LULC change especially, deforestation need an urgent control measure to stop global warming and climate change.

***Keywords*****:** *LULC; Remote sensing; Brahmani River Basin; temperature; humidity.*

## 1. troduction

Remote sensing data is useful because of its repetitive coverage and real time data acquisition. The digital data in the form of satellite imageries; therefore, enable to accurately compute as Figure and use and Land cover categories help in maintain spatial data infrastructure The aims of this study are to produce a land use/land cover (LULC) map for two of the states in India that experienced a fast increase of urban population in the recent decades (Odisha and Chhattisgarh) at different years in order to detect changes that have taken place particularly in the built-up land and subsequently to analyze the urban sprawl of the different time periods and to predict the urban area growth in the same over a given period (1975–2018). Multispectral land use and land cover classification has found a great deal of applications in agricultural assessment, forest management, urban planning, ecological monitoring and water resource information collection (Hord 1982). Land cover serves as an important source of information for both the scientific and business communities, and remote sensing represents a cost-effective method to generate land cover information. The ability to analyse remote sensing data is important because it allows changes in earth's surface to be monitored as they occur (Comber et al., 2005; Townshend 1992).

Many studies have been conducted by several authors across the globe and concluded that the disturbance in the LULC highly impact the regional climate condition (Takahashi et al., 2010; Xiao et al., 2010; Strengers et al.2010; Lawrence and Chase 2010; Swain and Sahoo, 2015). Herein, the Brahamni River Basin of Odisha state of Eastern India is chosen due to various anthropogenic activities over the last 4-5 decades. Especially after the construction of Rengali Dam in the Brahmani River, there is huge

agricultural activities which disturb the LULC of the basin. Moreover, the vast industrial set up in the basin also the prime reason of human settlement which are responsible for deforestation and vegetation change (Swain and Sahoo, 2017a, 2017b). In this study, the LULC changes have been studied over the last four decades. Impact of the LULC changes is verified with the change in climate change parameters like extreme temperature, extreme daily rainfall pattern and extreme relative humidity. In the last, the peak streamflow at Jenapur a downstream gauging station in the Brahmani River is analyzed.

## 2. ethodology

Satellite image re-processing prior to the detection of change is immensely needed and has a primary unique objective of establishing a more direct affiliation between the acquired data and biophysical phenomena (Coppin et al., 2004). Data were preprocessed in ERDAS IMAGINE 12 model for geo-referencing, mosaicking and sub-setting of the images on the basis of Area of Interest (AOI). All satellite data were studied by assigning per-pixel signatures and differentiating the watershed into five classes on the bases of the specific Digital Number (DN) value of different landscape elements. The delineated classes were Crop land, Sand, water bodies, Built-up areas, Deciduous Broad Leaf Forest are identified in the study area. A satisfactory spectral signature is the one ensuring that there is 'minimal confusion' among the land covers to be mapped (Gao and Liu, 2010). After that maximum likelihood algorithm was used for supervised classification of the images. ERDAS IMAGINE allows an unlimited number of layers or bands of data to be used for one classification. The procedure to carryout supervised classification using ERDAS IMAGINE is described in **Fig. 1**. In the supervised classification technique, the maximum likely hood algorithm will classify the image based on the training sets provided by the user based on his field knowledge. The training data given by the user guides the software as to what types of pixels are to be selected for certain land cover type such as (i) Barren/Crop land; (ii) Sand; (iii) Water bodies; (iv) Built up areas; (v) Dense Forest.

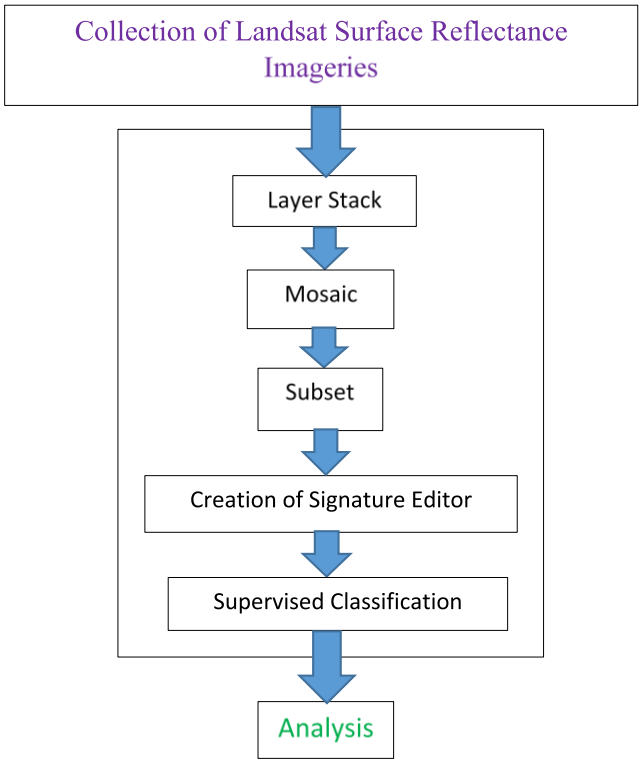
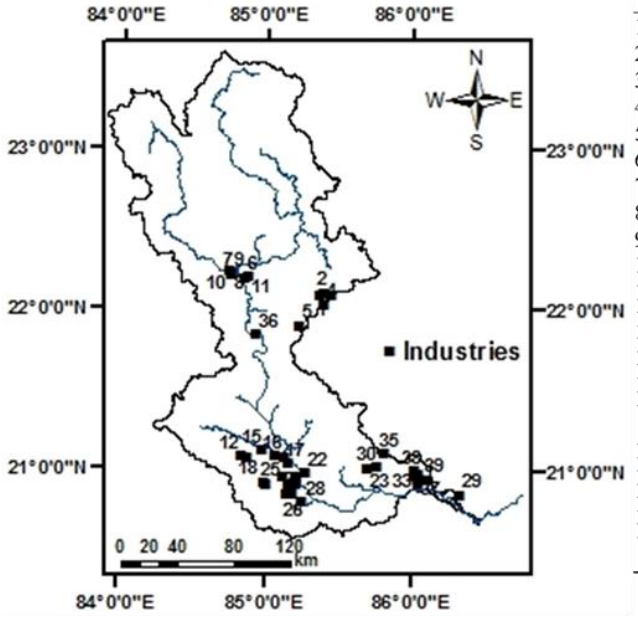



**Figure 1** Flow Chart of supervised LULC Classification.

## 3. Study Area and Data Collection

Herein, the Brahmani River Basin, the second largest river of Odisha is considered for the study due to vast industrialization and deforestation of its catchment. The Brahmani River is formed by the confluence of the Sankh and South Koel rivers, near the major industrial town of Rourkela at 22 15'N and 84 47'. After flowing through the districts such as Cuttack, Anugul, Jajpur, Kendrapara and Sundargarh, the Brahamani River forms a delta with the Baitarani River near Bay of Bengal. However, if its constituent rivers are included its length extends to about 799 kilometers (496 mi), of which 541 kilometers (336 mi) are in Orissa. It has a catchment area of about 39,033 square kilometers (15,071 square mi) in Odisha alone. There are 37 major industries in the Brahmani River basin (Fig.2). The Landsat satellite images of the study area were collected from USGS Earth Explore website <https://earthexplorer.usgs.gov/>. The 0.50 lat-long gridded daily meteorological data for the study area for the same period were also collected from the Climate Forecast System Reanalysis (CSFR), India. The daily scale meteorological variables of maximum temperature, minimum temperature, rainfall, relative humidity was downloaded for the study period from 1979 to 2014 <https://climatedataguide.ucar.edu/climate-data/climate-forecast-system-reanalysis-cfsr>.




| | |
|---|---|
| 1- I K I W L | 20- I.W.S.S Mcl |
| 2- Essel Mining and Industries Ltd | 21- Bharatpur Coal Mines |
| 3- JSPL Pellet Plant | 22- Rana Sponge Iron Ltd. |
| 4- TISCO Plant, Joda | 23- Sukinda Chromite Mine |
| 5- Essel Mining & Industries Ltd | 24- Talcher Thermal Power Corporation |
| 6- Slag Dumping Area | 25- Jindal steel & Power ltd |
| 7- Poly Refractories Pvt Ltd | 26- NALCO |
| 8- Britannia Industries Ltd | 27- NALCO CPP |
| 9- Utkal Metalics Ltd | 28- Bhusan Steel |
| 10- Ifgl Refractories Limited | 29- Ferochrome plant |
| 11- RSPL | 30- KVK Nilachal Power Pvt. Ltd |
| 12- Machhakuta Coal Mine | 31- Kathpal Chromite Mine |
| 13- MCL | 32- Jindal steel |
| 14- NTPC Kanhia | 33- TATA steel |
| 15- Jindal India Thermal Power Limited | 34- Maithan ispat ltd |
| 16- OPCL 25 MW Power Plant | 35- IFCAL |
| 17- Bindal Sponge Ltd | 36- Daitari Ore Mines |
| 18- Monnet Power Plant | 37- B.R Iron Sponge Plant |
| 19- Fertilizer Corporation of India Ltd. | |

**Fig. 2**: Location of major industries over Brahmani River Basin (Swain and Sahoo, 2017b).

## 4. Result and Discussion

### *4.1 LULC classification*

The classified images obtained after pre-processing and supervised classification which are showing the land use and land cover of the study area are shown in **Fig. 3**. The maroon color represents the built-up area, dark Green color represents the Forest area, and Blue color shows the water bodies, yellow color shows the crop land & white shows the sand. A supervised algorithm was used to derive land cover and land use map in the study area based on natural grouping and by ERDAS imagine.

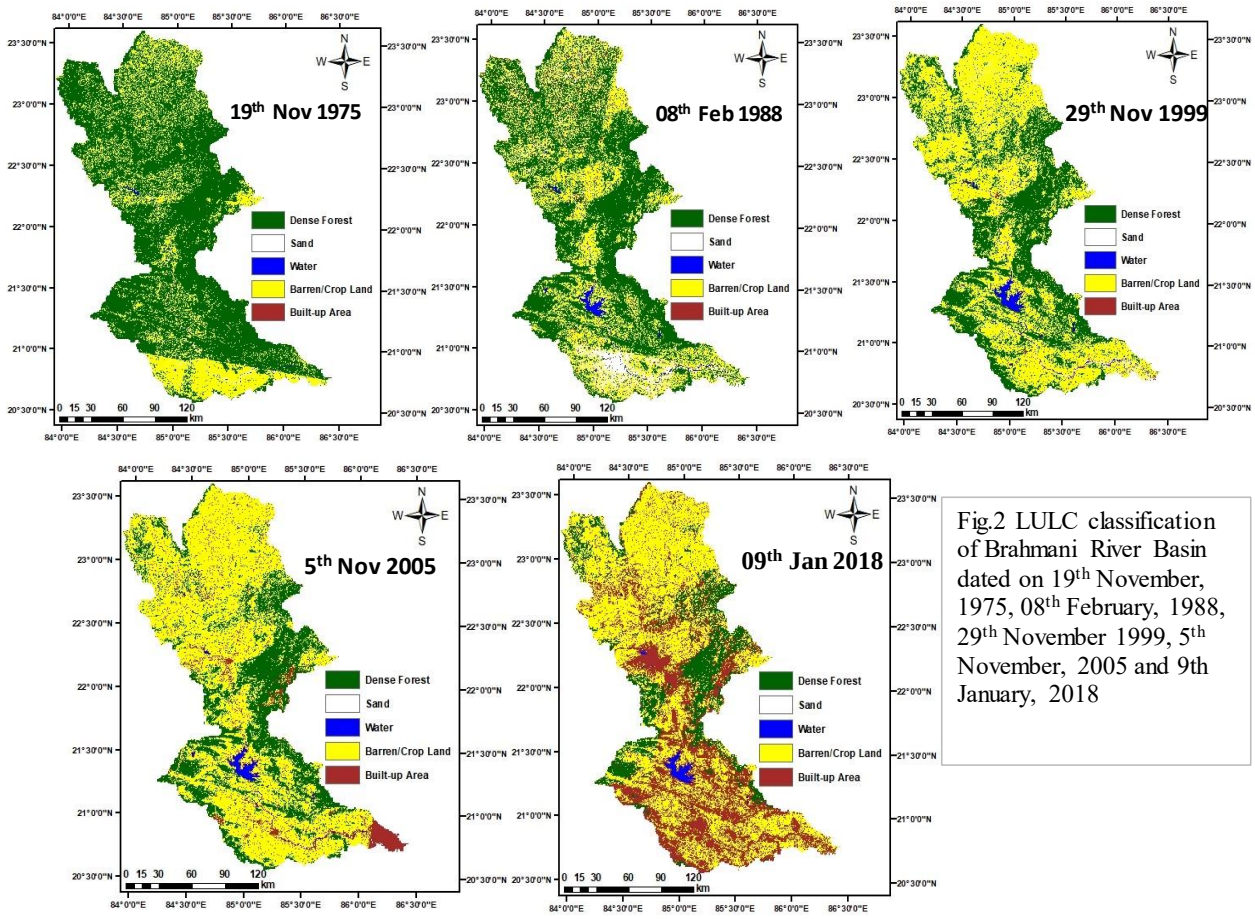



Fig.2 LULC classification of Brahmani River Basin dated on 19th November, 1975, 08th February, 1988, 29th November 1999, 5th November, 2005 and 9th January, 2018

The areas under each classification was calculated in km$^2$ and expressed in percentage (%). The areas under water bodies, sand, barren/crop land, forest area, built up area were subsequently entered in the table along with their respective dates. Classified images depict spatial distributional pattern of land use/cover of the Bramhani basin for the year 1975-2018. These data reveal that in 1975, about 71.70% (29,517 km$^2$) of area were under forest, 27.41% (11,284 km$^2$) under crop/barren land, 00.00% (0 km$^2$) under built-up land and 0.33% (134.34 km$^2$) under water body and 0.56% (230.30 km$^2$) under sand. During 1988 the area under these land categories was found about 14.85% (22,369 km$^2$) forest, 34.7% (14,273 km$^2$) crop/barren land, 7.13% (2933 km$^2$) sand, 2.69% (1105.29 km$^2$) built-up land and 1.11% (457.63 km$^2$) water body. Whereas in 1999 it was found that about 39.39% (16,205 km$^2$) belongs to forest, 54.79% (22,538 km$^2$) crop/barren land, 2.87% (1182 km$^2$) sand, 1.3% (532.96 km$^2$) built-up land and 1.65% (679 km$^2$) water body. During 2005 the area of deep forest was 29.18% (10,836 km$^2$), the area of crop/barren land 62.06% (23,044 km$^2$), the area of sand 0.12% (45.89 km$^2$), area of built-up land 7.49% (8454 km$^2$) and 1.13% (562.49 km$^2$) under water body. During 2018 the area under these land categories was found about 54.38% (5514 km$^2$) under forest, 51.46% (19,107 km$^2$) under crop/barren land, 0.08% (31.40 km$^2$) sand, 32.73% (12153 km$^2$) under built-up land and 0.87% (322.46 km$^2$) under water body.

### *4.2 LULC analysis*

The LULC change from year 1975 to 2018 is shown in **Fig. 4-5.** Figure 1 shows that the area of dense forest was high in 1975 i.e., 71.70%, eventually it was decreasing in a linearly to only 14.85% at the current time period. So there is a huge loss of vegetation, and ultimately it has a great impact on the

climate and rainfall. Also, it is clear from the table that in 1975 the water bodies are only 0.33% of the total area but it is somehow increased to 1.65% in 1999 due to the construction of Rengali Dam and Samal Barrage. Then it is again decreased to 0.87% in current time period. The area of sand was only 0.56% in 1975 and it reached to a pick of 7.13% in 1988 and it is again decreased to 1.13% and 0.08% in 2005 & 2018 respectively.

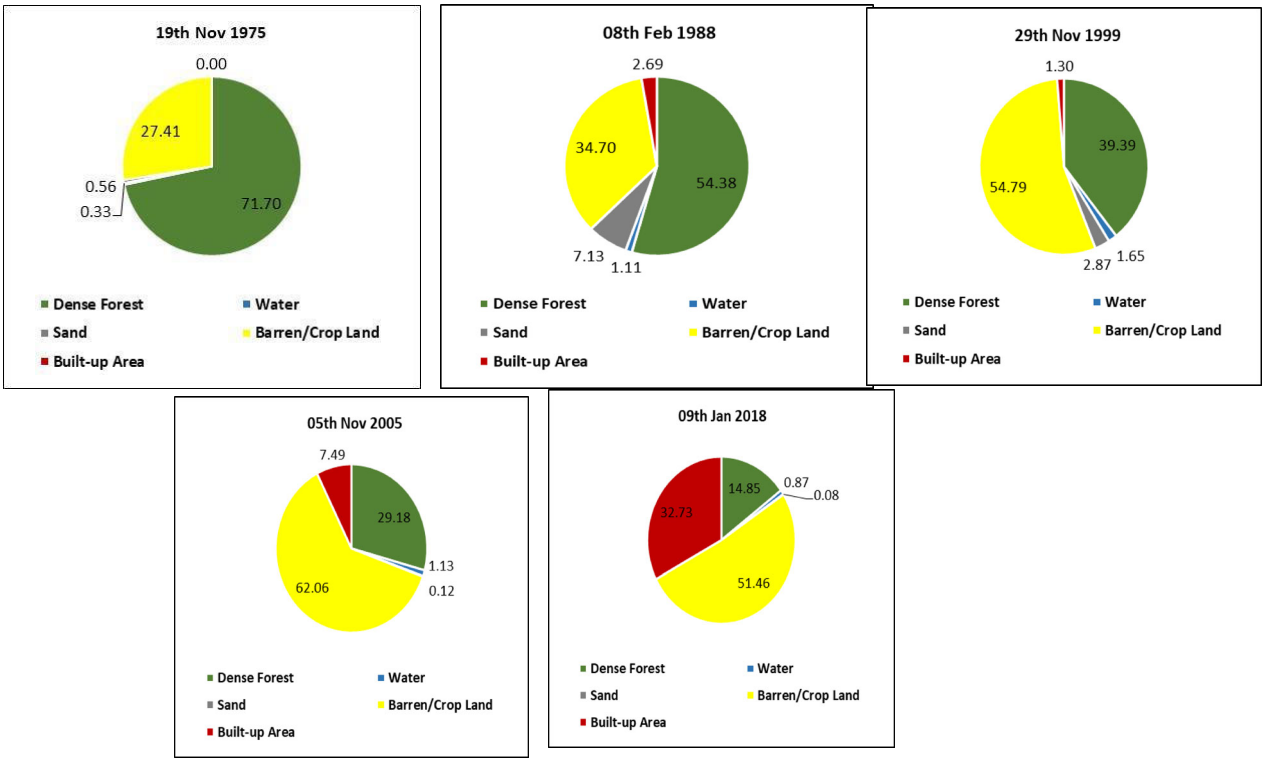



**Figure 4** Representation of LULC changes of Brahmani River Basin (%)

There was only 27.41% of crop land in 1975 due to the lack of irrigation facilities but subsequently it increased to 62.06% in 2005. It is also clear from the table that there is a negligible portion of residential or built up areas in1975, but it increased in a steadily to 2.69% in 1988. And there is again a fall in built up area in 1999 i.e., from 2.69 to 1.30%. Thereafter it increased to 7.49% in 2005 and at the current stage it is 32.73%. The various graphs were also plotted for the change in the parameters of land cover with respect to the time period.

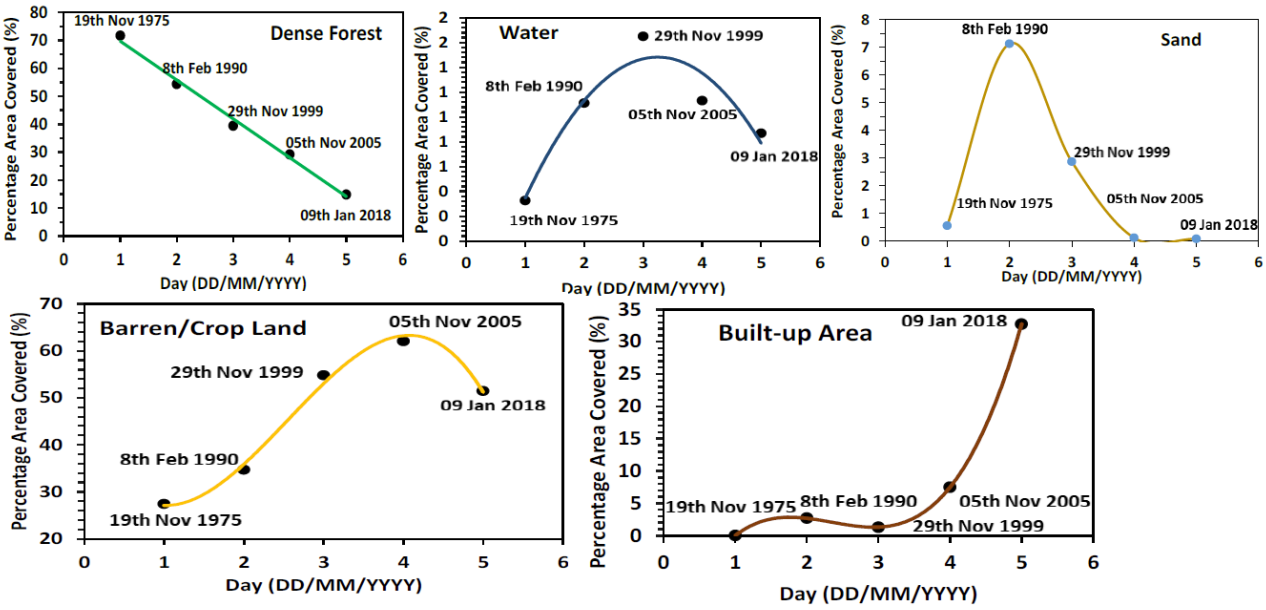


**Figure 5** Graphical representation of change in different land cover from 1975 to 2018.

### 4.3. Analysis of change in climate change parameters

It is clear from the above analysis and from Table-3 that the area of dense forest was very high in 1975 i.e., 71.70%, eventually it is decreasing in a linear manner to only 14.85% at the current time period. So, this indicates a very negative impact on our environment. So, there is a huge loss of vegetation, and ultimately it has a great impact on discharge, temperature, rainfall and relative humidity which we can see from the above graphs. Due to the rapid increase in deforestation between these 33 years, the average maximum temperature is increased to 4.8% and that for average minimum temperature is 3.19%. The relative humidity is increased by 11.5%. The discharge which is affected by both change in forest area and rainfall is increased to 37.5%. So, there is a huge loss of vegetation, and ultimately it has a great impact on discharge, temperature, rainfall and relative humidity which we can see from the above graphs. Due to the rapid increase in deforestation between these 33 years, the average maximum temperature is increased to 4.8% and that for average minimum temperature is 3.19%. The relative humidity is increased by 11.5%.

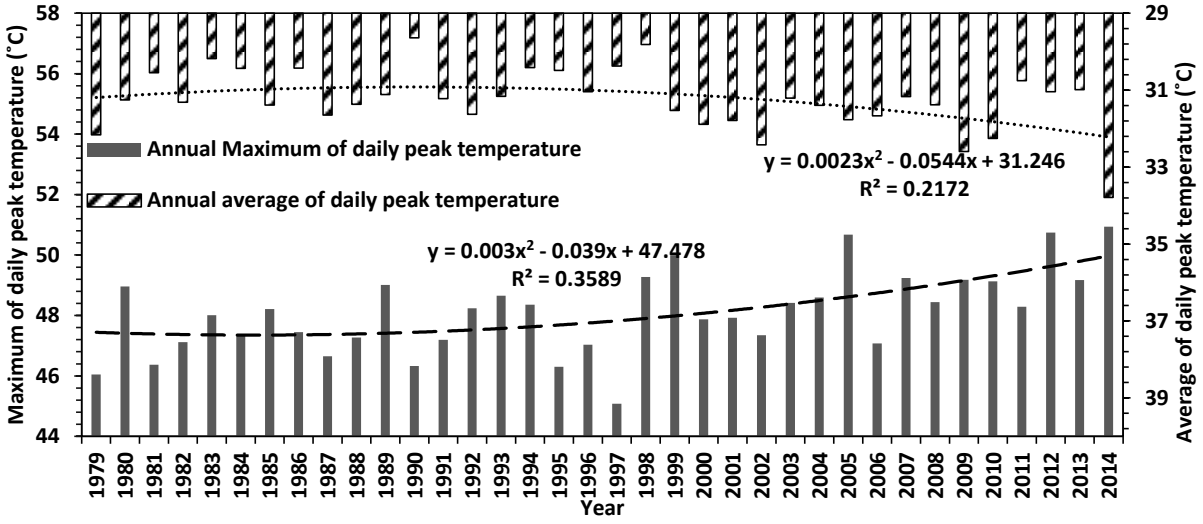



**Fig. 5:** Change in maximum and average of daily peak temperature (˚C) over the years 1979-2014.

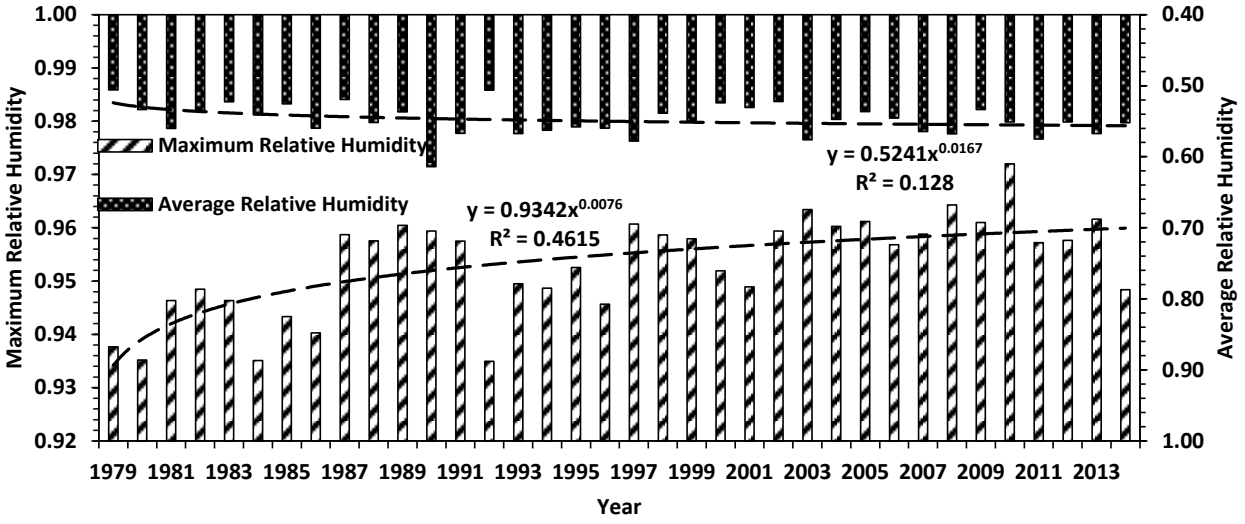



**Fig. 6:** Change in Maximum and average of daily relative humidity (%) over the years 1979-2014

## 5. Conclusion

The study conducted in one of the development blocks of Bramhani river catchment in Odisha state (India) advocates that multi temporal satellite imagery plays a vital role in quantifying spatial and temporal phenomena which is not possible to attempt through conventional mapping. The study reveals that the major land use in the study area is dense forest. The area under dense forest decreased by 57% due to increase in urbanization & agriculture. The second major category of land in the study area is barren/crop land, which was increased by 30% due to development in agricultural technology, irrigation & transportation facilities etc. The third major category of land in the study area is built up area which is increasing by 32.73%. During the study period (i.e., 1975–2018), built up area has been increased due to advancement of communication, transportation, agricultural activities. The area under fourth category of land, i.e., the sand has increased at the first stage by 6.57%& in the later stage it is decreased by 7.05%. Hence, the present study proves that remote sensing technology can be efficiently used for the spatio-temporal changes in catchment cover no cost and in real time. From this study we clearly found the decrease in about 56.85% of forest land in just 38 years and its serious impact on climate, temperature, rainfall, relative humidity and discharge by analyzing the previous 35 years data. So, we have to stop the rapid deforestation and to increase afforestation to reduce the unwanted weather change and hence to reduce global warming and other calamities.

## Acknowledgement

The authors would like to thank the USGS research team for allowing us to download the surface reflectance products of Landsat from their website <http://www.earthexplorer.usgs.gov>.

## References

Comber, A., Fisher, P., & Wadsworth, R. (2005). What is land cover? Environment and Planning B: Planning and Design, 32(2), 199-209.
Coppin P, J. (2004). Digital Change Detection Methods in Ecosystem Monitoring: A Review. International Journal of Remote Sensing, 25(9), 1565.

Gao, J., & Liu, Y. (2010). Determination of land degradation causes in Tongyu County, Northeast China via land cover change detection. International Journal of Applied Earth Observation and Geoinformation, 12(1), 9-16.
Lawrence PJ, Chase TN. 2010. Investigating the climate impacts of global land cover change in the Community Climate System Model (CCSM). International Journal of Climatology 30: 2066–2087.
Strengers B, M¨uller C, Schaeffer M, Haarsma R, Severijns C, Gerten D, Schaphoff S, van den Houdt R, Oostenrijk R. 2010. Assessing 20th century climate–vegetation feedbacks of land-use change and natural vegetation dynamics in a fully coupled vegetation– climate model. International Journal of Climatology 30: 2055–2065.
Swain, R. and Sahoo, B. (2015). Variable parameter McCarthy-Muskingum flow transport model for compound channels accounting for distributed non-uniform lateral flow. Journal of Hydrology, Elsevier, 530, 698-715, doi: 10.1016/j.jhydrol.2015.10.030.
Swain, R. and Sahoo, B. (2017a). Mapping of heavy metal pollution in river water at daily time-scale using spatio-temporal fusion of MODIS-Aqua and Landsat satellite imageries, Journal of Environment Management, Elsevier, 192, 1-14, doi: 10.1016/j.jenvman.2017.01.034.
Swain, R. and Sahoo, B. (2017b). Improving river water quality monitoring using satellite data products and a genetic algorithm processing approach. Sustainability of Water Quality and Ecology, Elsevier, 9-10, 88-114, https://doi.org/10.1016/j.swaqe.2017.09.001.
Takahashi HG, Yoshikane T, Hara M, Takata K, Yasunari T. 2010. High-resolution modelling of the potential impact of land-surface conditions on regional climate over Indochina associated with the diurnal precipitation cycle. International Journal of Climatology 30: 2004–2020.
Townshend, J. R. (1992). Improved global data for land applications. A proposal for a new high-resolution data set. Report of the Land Cover Working Group of IGBP-DIS. Global Change Report (Sweden).
Xiao C, Yu R, Fu Y. 2010. Precipitation characteristics in the Three Gorges Dam vicinity. International Journal of Climatology 30: 2021–2024.

# Theme IX

# Flood Forecasting and Management

*IN PROCEEDINGS OF 25th HYDRO 2020, INTERNATIONAL CONFERENCE, NATIONAL INSTITUTE OF TECHNOLOGY ROURKELA, ODISHA, INDIA 26-28, March 2021, ISBN 978-93-90631-56-8*

Paper ID - 014

# Flood Frequency Analysis Using Gumbel's Distribution Method: A Case Study of Sita River, Karnataka, India.

Soumya S Nyamathi[1], Dwarakish G.S[2]

[1]*M.Tech (Research) Student, Department of Water Resources and Ocean Engineering, National Institute of Technology Karnataka (NITK), Surathkal, Mangaluru-575025, India.*
[2]*Professor, Department of Water Resources and Ocean Engineering, National Institute of Technology Karnataka (NITK), Surathkal, Mangaluru-575025, India.*
*Email: soumyanyamathi@gmail.com*
*Telephone/Mobile No.: +91 9739011593*

## Abstract

Estimation of Peak Flood Discharge for a desired return period is a pre-requisite for planning, design and management of hydraulic structures like barrages, dams, spillways, bridges, etc. The main objective of the study was to carry out the Flood Frequency Analysis for the Sita River, one of the West flowing rivers in Karnataka, using the discharge data of Avershe gauging station. The Gumbel method was used to model the annual maximum discharge of the river from Avershe Weir for a period of 13 years, from 2003 to 2015. The mean instantaneous flow in the river is 548.23 $m^3/s$ with a return period of about 2.5 years. The $R^2$ value of 0.9783 obtained from the regression analysis, indicates that the Gumbel's distribution is suitable for predicting the expected flow in the river. Hence, using the Gumbel's distribution analysis, the flood with different recurrence intervals were also computed, which will be useful for future storm management in the area.

***Keywords:*** *Flood Frequency Analysis; Gumbel distribution method; Sita River; Regression Analysis; Peak flood discharge; Return periods.*

## 1. Introduction

In the planning and design of water resources projects, engineers and planners are often interested to determine the magnitude and frequency of floods that will occur at the project areas. Besides the rational method, unit hydrograph method and rainfall-runoff models method, frequency analysis is one of the main techniques used to interpret a record of events to predict the future probabilities of occurrence and estimate the magnitude of a flood event corresponding to a specific return period (Bhagat 2017). Flood Frequency Analysis (FFA) is the estimation of how often a specified flood event will occur. Before the estimation is carried out, analysis of the stream flow data plays a crucial role in order to obtain a probability distribution of floods (Ahmad et al. 2011). FFA is most commonly used by hydrologists worldwide in the planning and design of water resources projects and consists of estimating flood peak quantities for a set of non-exceedance probabilities. Reliable flood frequency forecasts are essential for floodplain management; to protect the public, mitigate flood-related costs to government and private entities, for planning and designing hydraulic systems, and evaluating hazards related to the creation of flood plains (Tumbare 2000).

FFA involves the fitting of a probability model to the sample of annual flood peaks recorded throughout the observation, for a catchment of a given region. Further, the model parameters established can then be used to predict the extreme events of large recurrence interval. The main objective of the study was to conduct the Flood Frequency Analysis for the Sita River using the discharge data of Avershe discharge gauge station. The Gumbel distribution was used to model the annual peak discharge data of Sita River from 2003 to 2015. The results of the analysis generated from the study gives detailed information of likely flow discharge to be expected in the Sita river catchment for the various return periods based on the observed data. This information will be useful for engineering purposes while designing structures in or near the river that may be affected by the flood as well as in planning and designing the flood structure to protect against the expected events (Izinyon and Igbinoba 2011).

## 2. Study Area and Data Product

Sita River originates in the Western Ghats of Karnataka state at an altitude of 980 m above mean sea level at Kutrikal Gudda and covers an area of 1408.33 km$^2$ lying between latitude 13º8'23"N to 13º35'36"N latitude and 75º11'22"E to 74º 41' 27"E longitude (Figure 1). It flows south-westerly from the origin for about 82 km and then joins Swarna-Madisal River near Hangarkatte and finally flow together into Arabian Sea at Kodi-Bengre, Udupi. The major tributaries of Sita River are Goli hole, Honakal halla, Kollangar hole, Koodluthirtha hole, Nemar hole and Achladi hole. The catchment receives higher rainfall of about 4500 mm annually. In the Sita River, the flow is regulated by Avershe discharge gauge station. The discharge data used for the flood frequency analysis was collected from the Central Water Commission (CWC), Bengaluru for a time period of 13 years (2003-2015).

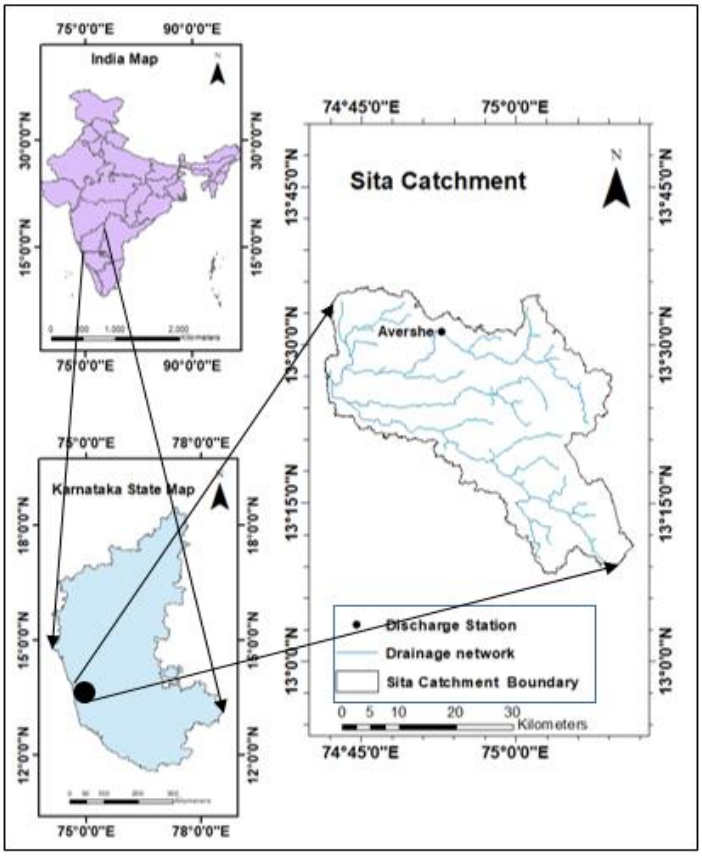



**Figure 1**: Location map of the Sita River Catchment

## 3. Methodology

Gumbel's distribution is one of the most widely used probability distribution functions for predicting extreme values in hydrological and meteorological studies for prediction of flood peaks, maximum rainfalls and maximum wind speed (Zelenhasic 1970; Shaw 1983; Haan 1997; Solomon and Prince 2013, Chow 1988). Gumbel defined flood as the largest of the 365 daily flows and the annual series of flood flows constitute a series of largest values of flows. The discharge data of Avershe discharge gauging station, from 2003-2015 was considered for the flood frequency analysis applying the Gumbel's distribution. The equation used for Gumbel's distribution with a return period T is given as follows:

$$X_T = \bar{X} + K.\sigma_X \quad (1)$$

where, $\sigma_X$ = Standard deviation of the Sample Size N

K = Frequency Factor, which is expressed as, $K = \frac{Yt - Yn}{Sn}$ (2)

in which $y_t$ = reduced variate, a function of T and is given by

$$Y_t = -[\ln . \ln(\frac{T}{T-1})] \quad (3)$$

$Y_n$= reduced mean, $S_n$= reduced standard deviation.

Depending on the sample size, the values of $Y_n$ and $S_n$ are selected from Gumbel's Extreme Value Distribution. The above equations are used to estimate the flood magnitude corresponding to a given return period based on annual flood series.

The various steps to estimate the design flood for a specific return period is given as follows:

1. The discharge data was assembled from 2003 to 2015 and the sample size N was noted. The peak discharge values were arranged in descending order and here the annual flood value is the variate X. The mean and standard deviation for the given data was calculated.
2. From the Gumbel's Extreme Value distribution table, the appropriate values for $Y_n$ and $S_n$ are considered depending on the sample size.
3. Compute $Y_T$ for given return period T using equation (3).
4. From $Y_n$, $S_n$ and $Y_t$, compute frequency factor K using equation (2).
5. Determine the required magnitude of flood with a return period T using equation (1).

It is important to verify if the observed flood data collected in the catchment fit Gumbel's distribution or not. To achieve this, the observed data was arranged in descending order and then assigning the return period for each flood event; the reduced variate corresponding to each flood was computed. A graph of the reduced variate and magnitude of the flood is plotted on ordinary graph paper. The Gumbel's distribution is said to be a good fit for the observed flood data, if an eye fits this plot suggests a straight line.

## 4. Results and Discussion

The peak flood discharge for a return period of 2, 5, 10, 25, 50, 100 and 200 years was estimated using the Gumbel's distribution. The method was used to model the annual maximum discharge of the river Sita from Avershe discharge station for a period of 13 years (2003 to 2015). The Gumbel's distribution analysis was conducted and the results obtained are shown in Table 1. Also a graph of reduced variate v/s flood peak was plotted (Figure 2).

**Table 1:** Computation Table.

| Year | Peak Discharge (cumecs) | Peak Flood in Descending order (cumecs) | Order (m) | $S_x^2$ | Return Period, $T_r$ | Reduced Variate Y |
|---|---|---|---|---|---|---|
| 2003 | 338.3 | 943.8 | 1 | 156468.9 | 14 | 2.60 |
| 2004 | 544.0 | 806.5 | 2 | 650442.3 | 7 | 1.86 |
| 2005 | 616.5 | 680.2 | 3 | 69484.96 | 4.67 | 1.42 |
| 2006 | 462.7 | 616.5 | 4 | 36100 | 3.5 | 1.08 |
| 2007 | 545.4 | 555.7 | 5 | 15500.25 | 2.8 | 0.81 |
| 2008 | 806.5 | 545.4 | 6 | 5055.21 | 2.33 | 0.58 |
| 2009 | 555.7 | 544 | 7 | 136.89 | 2 | 0.36 |
| 2010 | 422.9 | 477.7 | 8 | 4583.29 | 1.75 | 0.16 |
| 2011 | 680.2 | 462.7 | 9 | 6609.69 | 1.56 | -0.02 |
| 2012 | 477.7 | 422.9 | 10 | 3003.04 | 1.4 | -0.22 |
| 2013 | 389.9 | 389.9 | 11 | 5299.84 | 1.27 | -0.43 |
| 2014 | 943.8 | 343.5 | 12 | 6304.36 | 1.17 | -0.66 |
| 2015 | 343.5 | 338.3 | 13 | 2662.56 | 1.07 | -0.97 |

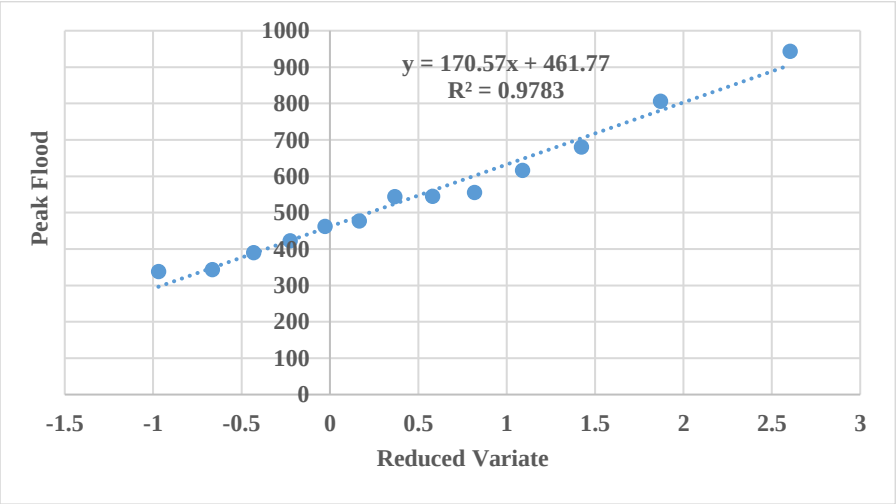



**Figure 2** Graph of Reduced Variate v/s Peak Flood for Sita River.

The above results show that the maximum flow of 943.8 $m^3/s$ was recorded in 2014 while the lowest flood flow of 338.3 $m^3/s$ was recorded in 2003. The 13-year mean instantaneous flood flow is 548.23 $m^3/s$. From the regression analysis, $R^2$ value of 0.9783 was obtained, which indicates that Gumbel's distribution is suitable for predicting the expected flow in the river. Hence, using the Gumbel's distribution analysis, the floods with different recurrence intervals were also computed. The results show the expected floods in the river reach for return periods of 2years, 5years, 10years, 25years, 50years, 100years and 200years (Table 2).

**Table 2** Computation of Expected Flood along Sita River.

| Return Period T in years | Reduced Variate, $Y_t$ | Frequency Factor, K | Expected Flood in cumecs |
|---|---|---|---|
| 2 | 0.36 | -0.15 | 521.27 |
| 5 | 1.49 | 0.98 | 723.51 |
| 10 | 2.25 | 1.74 | 859.52 |
| 25 | 3.19 | 2.68 | 1027.75 |
| 50 | 3.9 | 3.39 | 1154.82 |
| 80 | 4.38 | 3.87 | 1240.73 |
| 100 | 4.6 | 4.09 | 1280.10 |
| 200 | 5.29 | 4.78 | 1403.59 |

## Conclusions

The Flood Frequency Analysis was conducted for the Sita River, one of the West flowing rivers in Karnataka, using the discharge data of Avershe gauging station. The Gumbel method was used to model the annual maximum discharge of the river from Avershe Weir for a period of 13 years, from 2003 to 2015. The mean instantaneous flow in the river was 548.23 $m^3/s$ with a return period of about 2.5 years. The $R^2$ value of 0.9783 was obtained from the regression analysis, indicates that the Gumbel's distribution is suitable for predicting the expected flow in the river. Hence, using the Gumbel's distribution analysis, the flood with different recurrence intervals were also computed, thus can be useful for the future storm management in the area. This prediction of the flood can be utilized in the designing of important hydraulic structures and bridges in the river reach. Also in case of extreme floods, emergency evacuation of people can be carried out well in advance.

## References

C. T. Haan. (1997). Statistical Methods in Hydrology. Iowa State University Press, Ames, Iowa. I '. Haefner, *Journal of Water*.

Chow, V. T., Maidment, R., Mays, L. W. (1988). *Applied Hydrology*. McGraw Hill Book Company, Singapore.

Izinyon, O. C. and Igbinoba E. (2011). Flood Frequency Analysis of Ikpoba River Catchment at Benin City using Log Pearson Type III distribution", *Journal of Emerging Trends in the Engineering and Applied Sciences, 2 (1),* 50-55.

J. R. Stedinger and R. M. Vogel. (2013). *Frequency analysis of extreme events*. Handbook of Hydrology, McGraw-Hill, New York, 3(10).

Nirman Bhagat. (2017). Flood Frequency Analysis Using Gumbel's Distribution Method: A Case Study of Lower Mahi Basin, India. *Journal of Water Resources and Ocean Science*, *6(4)*, 51-54.

N. Mujere. (2011). Flood frequency analysis using the Gumbel distribution. *International Journal on Computer Science and Engineering (IJCSE)*, 3, 2774- 2778.

O. Solomon and O. Prince. (2013). Flood Frequency Analysis of Osse River Using Gumbel's Distribution. *Civil and Environmental Research*, 3(10), 55-60.

Shaw, E. M. (1983). *Hydrology in Practice*. Van Nostrand Reinhold, UK.

Tumbare, M. J. (2000). *Mitigating floods in Southern Africa*. Paper presented at the 1st WARSFA/WaterNet Symposium: Sustainable Use of Water Resources, 1-2 November, Maputo.

U. N. Ahmad, A. Shabri, and Z. A. Zakaria. (2011). Flood frequency analysis of annual maximum stream flows using L-Moments and TL-Moments. *Applied Mathematical Sciences*, 5, pp. 243– 253, 2011.

Zelenhasic, E. (1970). *Theoretical Probability Distributions for Flood Peaks*. Colorado University Press, Colorado.

*IN PROCEEDINGS OF 25th HYDRO 2020, INTERNATIONAL CONFERENCE, NATIONAL INSTITUTE OF TECHNOLOGY ROURKELA, ODISHA, INDIA 26-28, March 2021, ISBN 978-93-90631-56-8*

Paper ID - 066

# Investigating the role of streamflow forecasts to mitigate floods in the delta region of Mahanadi River basin

Amina Khatun[1], Chandranath Chatterjee[1], Bhabagrahi Sahoo[2]

[1]*Agricultural and Food Engineering Department, IIT Kharagpur, Kharagpur 721302, India*
[2]*School of Water Resources, IIT Kharagpur, Kharagpur 721302, India*
*Email: aminakhatun9286@gmail.com*
*Telephone/Mobile No.: +91 9609775450*

## Abstract

Floods affect millions of people all around the globe annually. About 7.5 million hectares of area is affected by floods in India every year causing severe destruction to life and property. In this study, major source of flooding in the Mahanadi River basin in the recent past was analyzed. The releases from the Hirakud reservoir were routed to the Mundali gauging site using a calibrated and validated MIKE 11 HD model. The contribution of the middle reaches at Mundali were obtained by subtracting the routed releases from the observed discharges at Mundali. A flow duration curve analysis at Mundali for the $Q_5$ threshold level was performed to identify the years receiving significant flow from the Hirakud reservoir. Critical analysis of observed discharges in these years revealed that high floods in the delta reaches of the basin occurred due to significant contribution from the reservoir releases during 2001 and 2011. High correlation (0.748) between inflow to Hirakud and its releases indicated that most of the incoming flows were released on the same day without storage. Analysis of the inflow-outflow and reservoir level maintained at the Hirakud reservoir during the monsoon season of the years receiving high floods indicated that inflow forecasts to the reservoir with sufficient lead time could have helped in systematic release of the storage prior to the flood event. This would have aided to keep storage capacity of the reservoir available for storing further high inflows. Hence, forecasted reservoir inflows can be attributed to play a vital role in preventing havoc created by floods in the downstream reaches of large river basins with tropical pluvial regime. This study can provide an insight to the planners and decision makers in design and management of structural flood control measures.

***Keywords:*** *Flood forecasting; MIKE 11 HD; flow duration curve; floods; Mahanadi River basin*

## 1. Introduction

Flood hazards can be significantly reduced by structural as well as non-structural measures. Since structural flood control measures are not always feasible, it is generally favoured to adopt non-structural measures to further reduce flood risk in the downstream areas. Streamflow forecasting and early warning systems serve as one of the inexpensive and most widely used non-structural flood management strategy in many river basins worldwide. Reliable inflow forecasts into a reservoir with a sufficient lead-time could serve for effective flood management. Several studies employed runoff modelling to forecast inflows from the catchment upstream to a reservoir (Bürger et al. 2009; Odiyo et al. 2012; Valipour et al. 2013; Shah and Mishra 2015; Mosavi et al. 2018; Yao et al. 2019). In a rapidly changing climate, the current reservoir operating rules are found to be ineffective for flood control in the downstream areas. It has now become imperative to incorporate both upstream and downstream effects to develop/modify the flood control operating rules of a multipurpose reservoir.

Heavy rainfall in the Upper Mahanadi River basin generates high floods in the upstream catchment, which the reservoir often unable to store leading to severe floods in the middle and the delta region of the basin (Parhi et al. 2012). Based on historical gridded precipitation records over the whole Mahanadi River basin, Jena et al. (2014) observed that the increase in extreme rainfalls in the middle reaches has resulted in incidents of extreme flooding in the basin. Several other studies (Mujumdar and Ghosh 2008; Raje and Mujumdar 2009; Mondal and Mujumdar 2012) have also shown changes in precipitation regimes in the future climate projections, which could make plausible changes in flood trends in this basin. Further, a few studies (Pattanayak et al. 2017; Mondal and Mujumdar 2012) reveal changes in flood regimes during the post-1980s in the basin which cannot be solely explained by the natural variability, but also strongly attributed to the anthropogenic effects. Recently, Ganguli et al. (2019) have

shown an apparent delay in the mean flood dates at a large number of gauges in the Upper Mahanadi River basin. However, none of these studies so far have assessed the role of inflow forecasts to the Hirakud reservoir with sufficient lead time in managing the high floods in the delta region of the river basin.

## 2. Materials and methods

### *2.1 Study Area and Data used*

The Mahanadi River basin (Fig. 1) lies in eastern India with a total area of 1,41,589 km$^2$ geographically extending mostly over the two states of Chhattisgarh (53%) and Odisha (46%). The basin is governed by south-west monsoon season from June to October with an average annual rainfall of 1572 mm. The entire river basin can be divided into three parts namely, the Upper basin, the Middle basin and the Delta region by the Hirakud dam and the Mundali weir (upstream of the Naraj gauging site). The Upper and Middle basins have geographical areas of 83,400 km$^2$ and 48,700 km$^2$, respectively. The delta region extends over an area of 9,489 km$^2$ which is highly flood prone (Jena et al. 2014). Extreme precipitation in the upper and middle reaches of the basin accompanied by peak releases from the Hirakud dam leads to major floods occurring in the delta region (Jena et al. 2014).

The details of data collected for this study are listed in Tables 1.

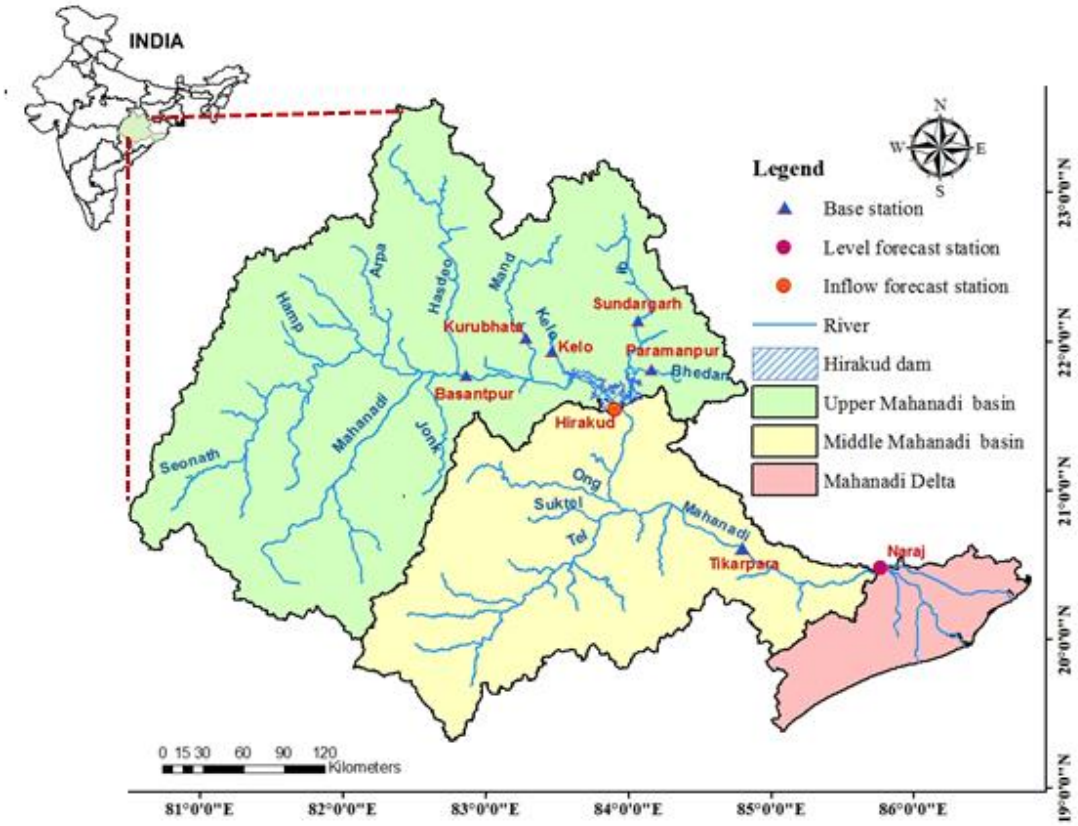



**Figure 1** Index map of the Mahanadi River basin showing CWC flood forecasting network

**Table 1** Details of Hirakud reservoir, Mundali gauging station and geospatial data

| Sl. No. | Data | Temporal resolution | Data period (Year) | Data source |
|---|---|---|---|---|

| | | | | |
|---|---|---|---|---|
| 1 | Hirakud reservoir data (Reservoir elevation, inflow and outflow) | Daily | 2000-2011 | HDC, Burla, Odisha |
| 2 | Mundali gauging station data<br>i) Water level and<br>ii) Rating curve | Daily<br>- | 2000-2011<br>- | DoWR (Prachi Division), Odisha. |
| 3 | SRTM 90 m DEM (Catchment delineation) | - | - | https://earthexplorer.usgs.gov |

### *2.2 Methodology*

Releases from the Hirakud reservoir were routed to the Mundali gauging site using a calibrated and validated MIKE 11 HD model. The contribution from the middle reaches at Mundali gauging site were obtained by subtracting the routed releases from the observed discharges at Mundali. A flow duration curve analysis at Mundali for the $Q_5$ threshold level was performed to identify the years receiving significant flow from the Hirakud reservoir. Also, to critically analyze the variation of inflow and outflow, Pearson's correlation coefficient (r) between observed discharge ($Q_5$) at Mundali and routed (lagged) Hirakud releases; and Hirakud releases ($Q_5$) and lagged Hirakud inflow were computed. The workflow is presented in a flowchart as follows:

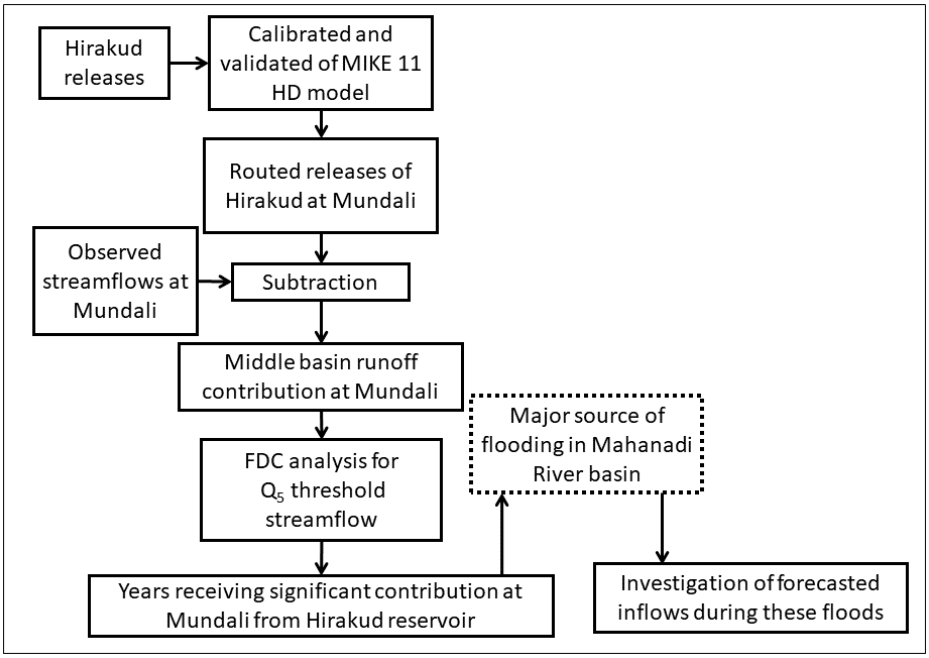



**Figure 2** Flowchart showing the methodology used in this study

## 3. Results

### *3.1 Flow-Duration Curve Analysis*

The daily releases from the Hirakud reservoir for 12 years (2000-2011) was fed into the calibrated and validated hydrodynamic module of MIKE11 model (MIKE11 HD) to route the flows from the outlet of Hirakud reservoir to the Mundali gauging site (hereafter, termed as MGS). The streamflow contribution of the middle reaches of the Mahanadi River basin at the MGS was then obtained by subtracting the routed releases of Hirakud reservoir from the daily observed discharges at the MGS. The $Q_5$ flows (the flow magnitude that can be expected to be equalled or exceeded 5% of time; 95$^{th}$ percentile) is considered as the threshold for high flows at the MGS that would flow to the delta region of the river basin. The $Q_5$ flow is computed from the flow-duration curve of observed discharges at the MGS and

was found to be 16507 $m^3/s$. Separate line graphs were plotted for the observed discharges and contribution from the middle reaches during the monsoon season at the MGS for the years 2000 to 2011 showing the $Q_5$ threshold (Fig. 3). Figure 3 also shows the flood magnitudes (28,400 $m^3/s$ and 35,000 $m^3/s$, respectively) mitigated by the existing structural (embankment system) and the proposed non-structural measures. From Figure 3, it can be seen that in all the years except 2000 and 2002, the discharges at MGS during the monsoon season has exceeded the high flow threshold. Moreover, significant contribution from the Hirakud releases during 2001, 2003, 2004, 2005 2006, 2007, 2008, 2009, 2010 and 2011 (exceeding high flows threshold) was found. However, very high flows (> 35,000 $m^3/s$) during the years 2001, 2003, 2006, 2008 and 2011 were observed. The observed discharges at MGS of these five years were critically analyzed and found that in the year 2001 and 2011, the floods had occurred because of the contribution from the Hirakud releases (Fig. 3). From the inflow-outflow plots (Figs. 4-5) of the Hirakud dam, during these years large inflow to the reservoir was observed. There was a time lag of 1 day between the peak inflow and outflow from the Hirakud dam during the 2001 flood (Fig. 4). As the reservoir level was way below the Full Reservoir Level (FRL), this high inflow could have been stored and released later on to prevent downstream floods (Fig. 6). In contrast, the high flows into the Hirakud reservoir during the 2011 flood were released immediately without storage into the reservoir (no lag between peak inflow and outflow) (Fig. 5). In this case, inflow forecasts to the reservoir could have helped in systematic release of the storage prior to the flood event to keep storage capacity of the reservoir available for storing the high inflows (Fig. 7).

### *3.2 Correlation Analysis among High Flow Conditions at Upstream, Downstream and Reservoir Releases*

Linear correlation (Pearson's correlation coefficient 'r') between observed high flows (above $Q_5$) at the MGS and routed releases from the Hirakud reservoir with time lag of 0 to 5 days; and between Hirakud releases (above $Q_5$) and time lagged inflow from 0 to 5 days into the Hirakud reservoir are shown in Table 2. Moderate correlation (r = 0.497) between the former was obtained on the 2nd day lag which is also the translation time of the released flows from the reservoir to the MGS. Also, high correlation (0.748) between inflow to Hirakud (with no lag) and its releases reveals that most of the incoming flows into the reservoir are released on the same day without storage.

**Table 2** Correlation coefficient at different lag times

| Correlation between | Lag (Days) | | | | | |
|---|---|---|---|---|---|---|
| | 0 | 1 | 2 | 3 | 4 | 5 |
| Observed discharge ($Q_5$) at Mundali vs routed (lagged) Hirakud releases | 0.260 | 0.385 | 0.497 | 0.479 | 0.324 | 0.182 |
| Hirakud releases ($Q_5$) vs lagged Hirakud inflow | 0.748 | 0.460 | 0.267 | 0.078 | -0.053 | -0.024 |

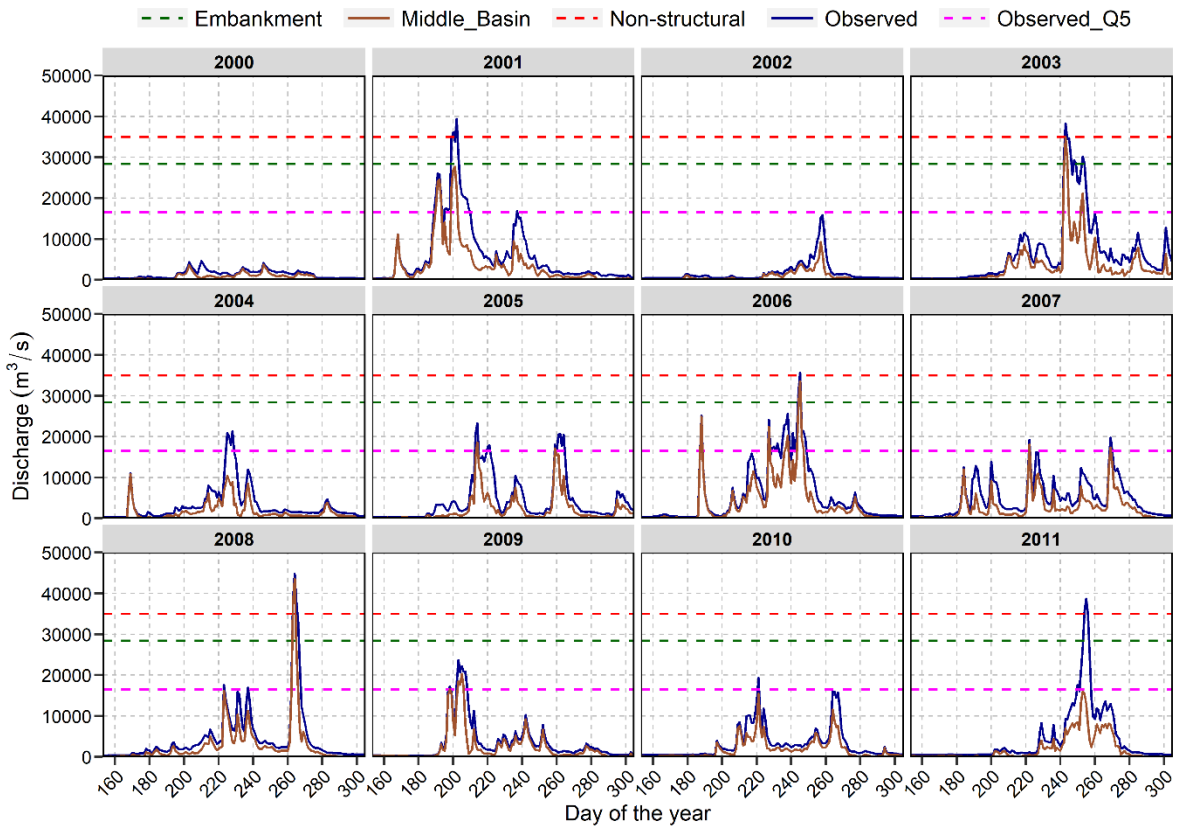



**Figure 3** Twelve years (2000-2011) of historical observed discharge at Mundali and contribution from middle reaches at Mundali gauging station during monsoon season. Pink dotted line shows the high flow ($Q_5$) threshold, green dotted line shows the flood protection magnitude by embankment system (28,400 m3/s) and red dotted line shows the flood protection magnitude by the proposed non-structural measures (35,000 m3/s))

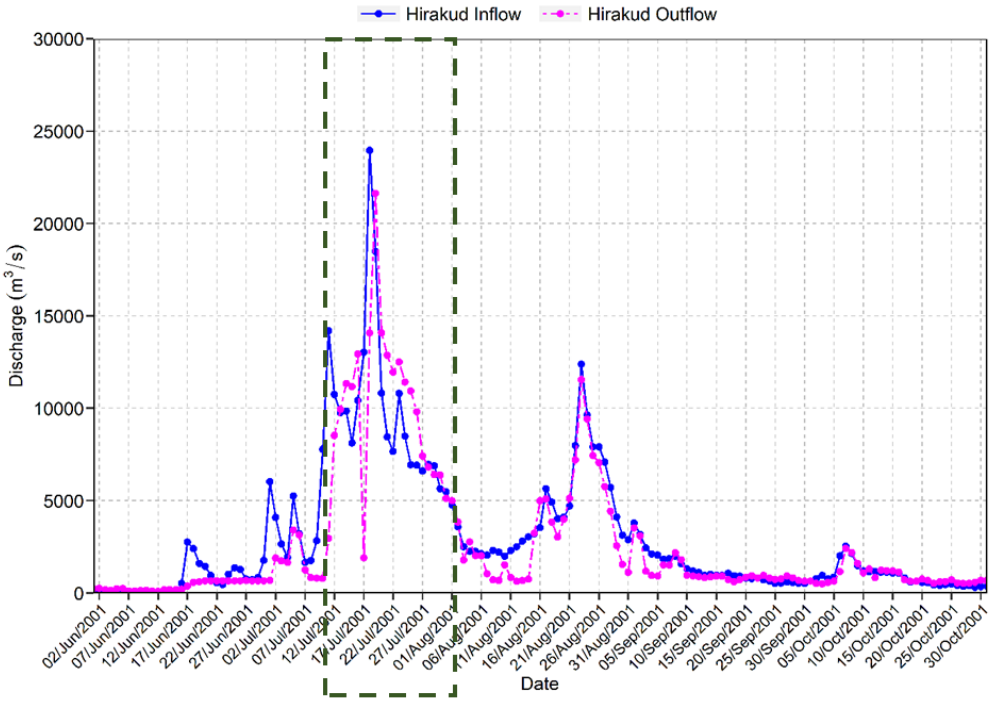



**Figure 4** Inflow to and outflow (releases) from Hirakud reservoir during the monsoon season of 2001

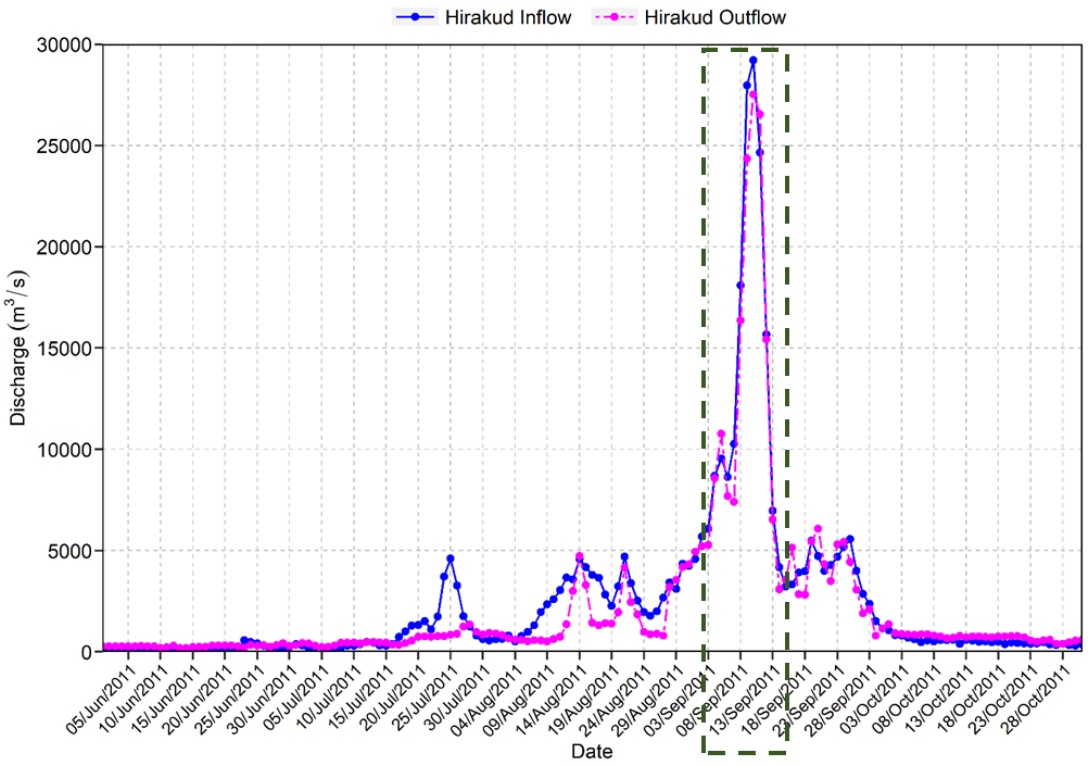



**Figure 5** Inflow to and outflow (releases) from Hirakud reservoir during the monsoon season of 2011

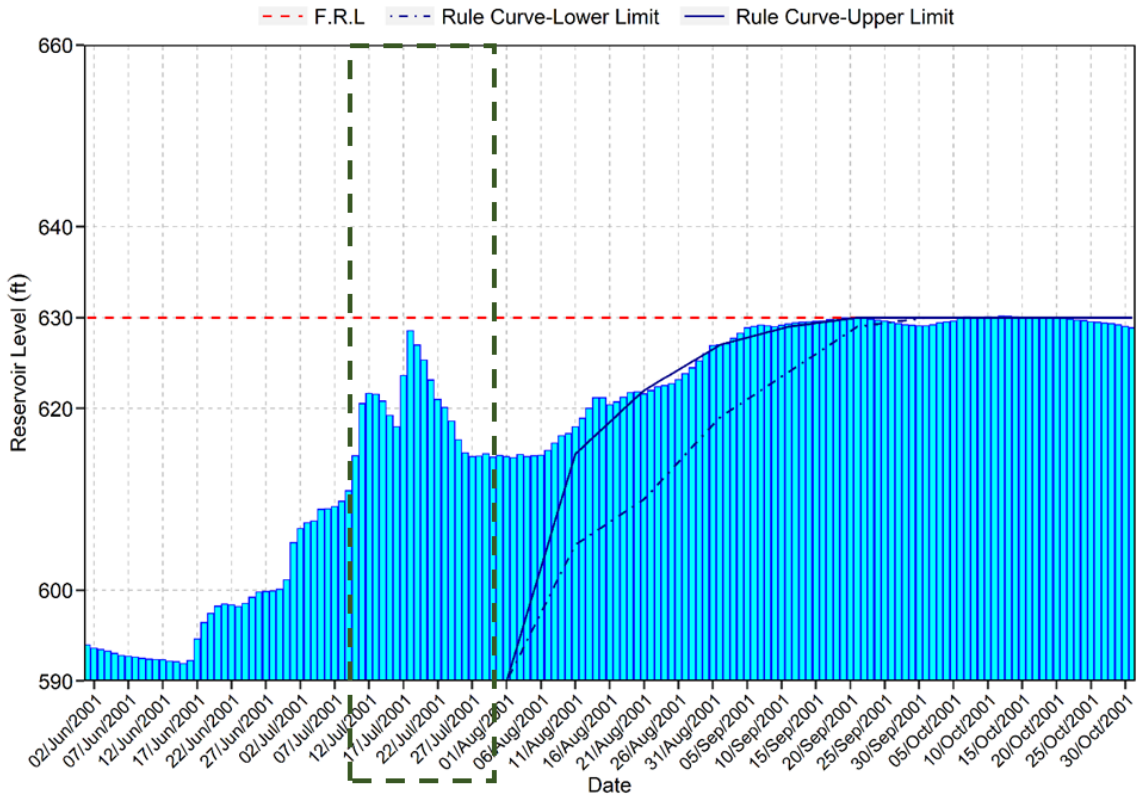



**Figure 6** Hirakud reservoir level during the monsoon season of 2001

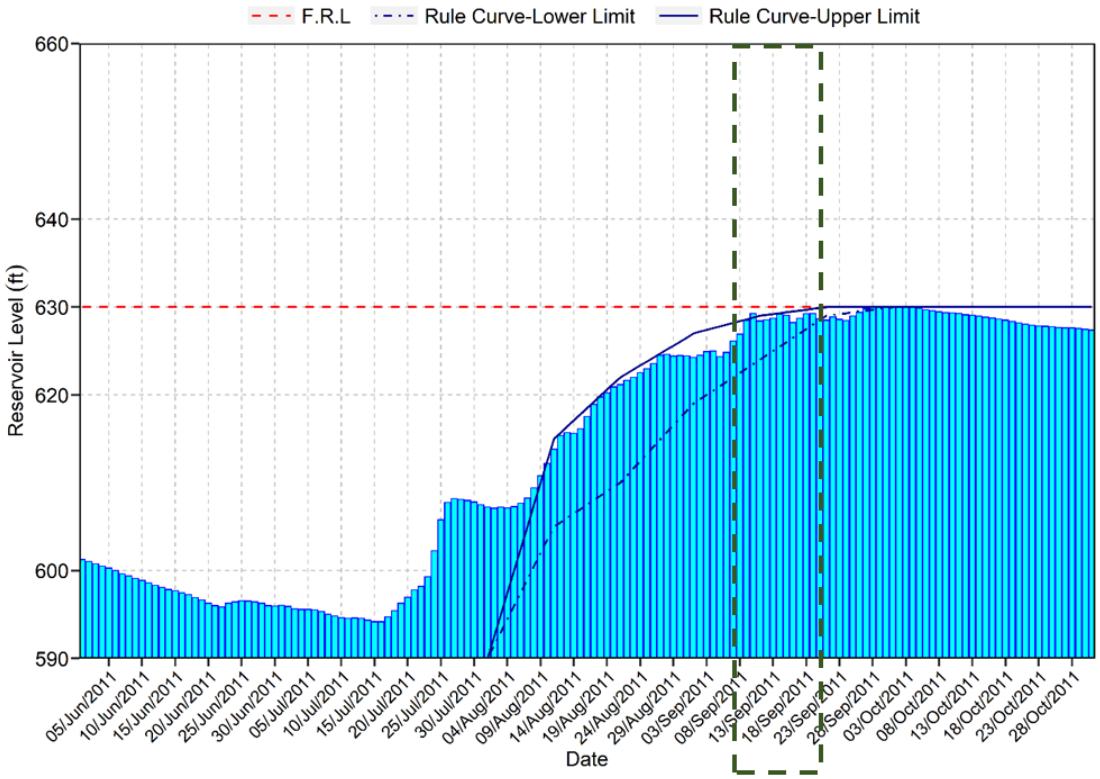



**Figure 7** Hirakud reservoir level during the monsoon season of 2011

## 4. Conclusions

The conclusions drawn from this study area as follows:

i. There was significant contribution from the reservoir releases to the observed discharges of the Mundali gauging site in the years 2001 and 2011. This indicates that the high floods in the delta reaches of the basin during these years (2001 and 2011) occurred mainly due to the reservoir releases.

ii. Correlation analysis revealed that there was high correlation (r = 0.748) between inflow to Hirakud and its releases. This indicates that most of the incoming flows to the reservoir were released on the same day without storage.

iii. Analysis of the inflow-outflow and reservoir level maintained at the Hirakud reservoir during the monsoon season of the years receiving high floods (2001 and 2011) indicated that inflow forecasts to the reservoir with sufficient lead time could have helped in systematic release of the storage prior to the flood event.

This study points towards the fact that reliable inflow forecasts to the reservoir with sufficient lead time could have aided to keep storage capacity of the reservoir available for storing further high inflows. Thus, forecasted reservoir inflows can be attributed to play a vital role in preventing flood hazards in the downstream reaches of large river basins. This study can provide an insight to the planners and decision makers in management of large dams in India for flood prevention and management.

## References

Bürger, G., Reusser, D., and Kneis, D. (2009). Early flood warnings from empirical (expanded) downscaling of the full ECMWF Ensemble Prediction System. *Water Resources Research*, *45*(10).

Ganguli, P., Nandamuri, Y. R., and Chatterjee, C. (2019). Analysis of persistence in the flood timing and the role of catchment wetness on flood generation in a large river basin in India. *Theoretical and Applied Climatology*, 1-16.

Jena, P. P., Chatterjee, C., Pradhan, G., and Mishra, A. (2014). Are recent frequent high floods in Mahanadi basin in eastern India due to increase in extreme rainfalls?. *Journal of Hydrology*, *517*, 847-862.

Mondal, A., and Mujumdar, P. P. (2012). On the basin-scale detection and attribution of human-induced climate change in monsoon precipitation and streamflow. *Water Resources Research*, 48(10).

Mosavi, A., Ozturk, P., and Chau, K. W. (2018). Flood prediction using machine learning models: Literature review. *Water*, *10*(11), 1536.

Mujumdar, P. P., and Ghosh, S. (2008). Modeling GCM and scenario uncertainty using a possibilistic approach: Application to the Mahanadi River, India. *Water Resources Research*, *44*(6).

Odiyo, J. O., Phangisa, J. I., and Makungo, R. (2012). Rainfall–runoff modelling for estimating Latonyanda River flow contributions to Luvuvhu River downstream of Albasini Dam. *Physics and Chemistry of the Earth, Parts A/B/C*, *50*, 5-13.

Parhi, P.K., Mishra, S.K., Singh, R. and Tripathy, V.K. (2012). Floods in Mahanadi river basin, Orissa (India): a critical review. *India Water Week, Water, Energy and Food Security: Call for Solutions. 10–14 April 2012*, New Delhi.

Pattanayak, S., Nanjundiah, R. S., and Kumar, D. N. (2017). Linkage between global sea surface temperature and hydroclimatology of a major river basin of India before and after 1980. *Environmental Research Letters*, *12*(12), 124002.

Raje, D., and Mujumdar, P. P. (2009). A conditional random field–based downscaling method for assessment of climate change impact on multisite daily precipitation in the Mahanadi basin. *Water Resources Research*, *45*(10).

Shah, R. D., and Mishra, V. (2015). Development of an experimental near-real-time drought monitor for India. *Journal of Hydrometeorology*, *16*(1), 327-345.

Valipour, M., Banihabib, M. E., and Behbahani, S. M. R. (2013). Comparison of the ARMA, ARIMA, and the autoregressive artificial neural network models in forecasting the monthly inflow of Dez dam reservoir. *Journal of Hydrology*, *476*, 433-441.

Yao, C., Ye, J., He, Z., Bastola, S., Zhang, K., and Li, Z. (2019). Evaluation of flood prediction capability of the distributed Grid-Xinanjiang model driven by weather research and forecasting precipitation. *Journal of Flood Risk Management*, *12*, e12544.

IN PROCEEDINGS OF 25th HYDRO 2020, INTERNATIONAL CONFERENCE,
NATIONAL INSTITUTE OF TECHNOLOGY ROURKELA, ODISHA, INDIA
26-28, March 2021, ISBN 978-93-90631-56-8

Paper ID - 088

# Flood risk assessment and mapping using AHP: A case study in Thuthapuzha river basin, Kerala

Athira K[1], Sarmistha Singh[2]

[1]Research scholar, Dept. of Civil Engineering, IIT Palakkad, Kanjikode, Palakkad, Kerala-678623, India
[2]Assistant Professor, Dept. of Civil Engineering, IIT Palakkad, Kanjikode, Palakkad, Kerala-678623, India
Email: [1]102004001@smail.iitpkd.ac.in, [2]sarmistha@iitpkd.ac.in

## Abstract

Flood is one of the most destructive natural hazards which distresses substantial damages to mankind, infrastructures, agronomic and economic systems. Flood risks have been assessed with the combination of hazard and vulnerability index which extensively used as a vital tool for the formulation of flood management strategies. The main objective of this study is to comprehend the probability and magnitude of the occurrence of flood hazards and the extent of vulnerability to flood in order to map the risk zones in Thuthapuzha river basin (Kerala) using Multi-Criteria Analysis (Analytic Hierarchy Process-AHP). The concerned area of study is one the main tributary of Bharathapuzha where the river has changed its course by collapsing the river banks during the 2018 however; it has never been investigated in terms of flood risk assessment. In this study, the flood hazard map is prepared using meteorological and topographical parameters whereas vulnerability map is prepared using demographic and infrastructural parameters.

***Keywords:*** *Flood Risk; AHP; Vulnerability; Hazard; River Basin; Kerala*

## 1. Introduction

Floods are among the most recurring and destructive natural hazards, impacting upon human lives and cause severe damage throughout its floodplain. In Kerala, the rainfall is controlled by two monsoon seasons, namely south-west and north-east monsoon. Around 90% of rainfall is received during these seasons (June to December) (Gosh et al. 2018). Heavy precipitation events during monsoon season causes havoc river discharge. The continuous and heavy rainfall that occurs in the steep and undulating terrain finds its way into the main rivers through numerous streams and water courses. Recently the frequency of occurrence of flood events increases significantly, due to the variability of climatic conditions (Guhathakurta et al. 2011).

Recently many studies are carried out to evaluate the flood risk at different levels with the help of GIS. Multi criterion based statistical method is one of such approaches which is a cost effective and efficient tool to identify and quantify the flood risk in terms of hazard and vulnerability (Ouma and Tateishi 2014). Hazard can be defined as a probability of occurrence of a potentially destructive phenomena for a given time period and area while vulnerability is the most crucial component of risk that determines whether or not exposure to a hazard constitutes a risk that may actually result in a disaster (Gosh et al. 2018; Sanyal and Lu 2006). Due to the dense concentration of population and infrastructure development, vulnerability increases. Presence of industries, waste treatment plants, sewage systems, etc., cause post flood hazards which affect the health of people who live in flood encroachment areas. Flood hazard and vulnerability incorporate the effect of meteorological, topographical, demographic and infrastructural parameters (Sanyal and Lu 2005; Masood and Takeuchi 2012; Aydin and Uysal 2014; Barman et al. 2016). Several research works have already shown the reliability of Multi-Criteria Analysis while preparing composite environmental risk at local and regional level (Sanyal and Lu 2006; Meyer and Hasse 2009; Ouma and Tateishi 2014; Danumah et al. 2016; Ghosh et al. 2016; Sharma et al. 2018).

Bharathapuzha is the second-longest River with a length of 209 km and the second-largest river basin of Kerala (4400 km$^2$). Kannadipuzha, Gayathripuzha, Kalpathipuzha and Thuthapuzha rivers are the main tributaries of Bharathapuzha river and it became a support system for over 4.5 million people and more than four hundred thousand hectares of agriculture (Nikhil and Azeez 2010). Around 42% of annual discharge of Bharathapuzha is contributed by Thuthapuzha (Nikhil and Azeez 2009). Several studies have been carried out in Bharathapuzha River Basin on various characteristics like water quality, runoff characteristics etc (Manjula and Warrier (2019)). Dinesan et al. (2004) addressed the water availability and the status of water demands in the watershed. The present study aims to comprehend the probability and magnitude of the occurrence of flood hazards and the extent of vulnerability to flood in order to map the risk zones in Thuthapuzha river basin (Kerala) using Multi-Criteria Analysis (Analytic Hierarchy Process-AHP).

## 2. Study area

Thuthapuzha river basin is the sub watershed of Bharathapuzha river which is located 10°50′–11°15′ north and 76° 05′–76°40′ east covering major part of Palakkad and south-west side of Malappuram district (figure 1). It is a sixth-order sub-basin of Bharathapuzha covering an area of about 1018 km$^2$ and 63 km in length (Warrier and Manjula 2014). Kuntipuzha, Nellipuzha, Kanhirapuzha and Thuppanadpuzha are the major tributaries draining to the catchment area. The major towns situated on the banks of the river are Palakkad, Parli, Ottapalam, Shoranur, Pattampi, Thrithala, Kudallur, Thiruvegappura, Pallipuram and Kumpidi. The average annual precipitation in Thuthapuzha river basin is 3830 mm and average annual discharge is 1750 million cubic meters.

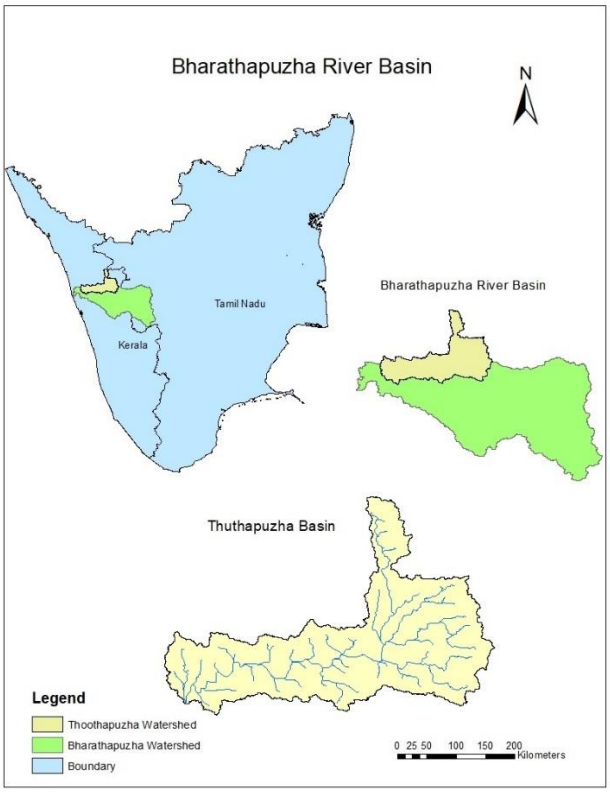



**Figure 1** Location of Thuthapuzha basin

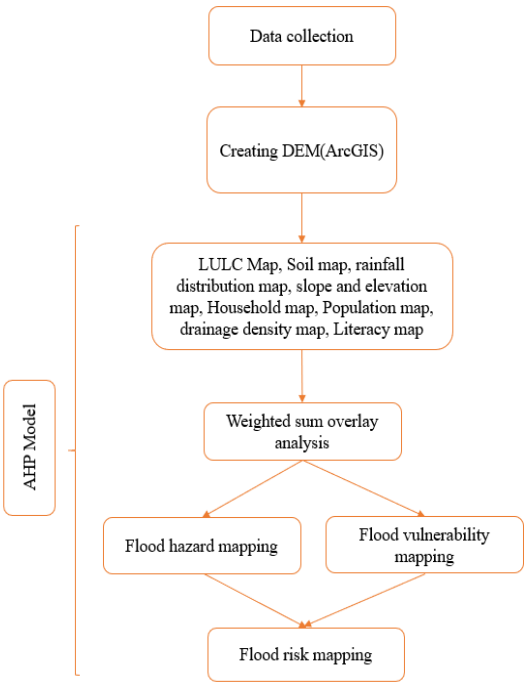



**Figure 2** Methodology

## 3. Data and methodology

### 3.1 data used

Flood risk assessment requires meteorological, topographical, demographic and infrastructural data. Aster Digital Elevation Model (DEM) data of 30m resolution, collected from Earth Data Search NASA has been used in this study for creating slope and elevation maps whereas LANDSAT images have been used for land use map preparation. Gridded rainfall data of $0.25^0$* $0.25^0$ resolution was collected from Indian Meteorological Department Pune and the soil data was obtained from Soil Conservation and Survey of Kerala. Data regarding population, household density and literacy were collected from the census of India.

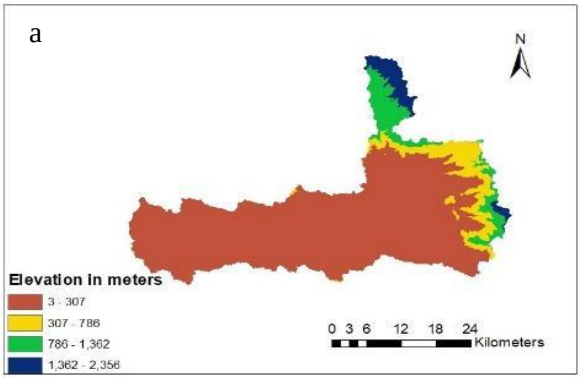
### 3.2 Methodology

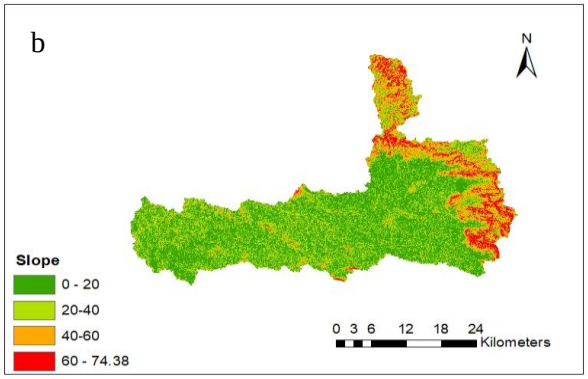
In this study GIS based spatial multi-criteria analysis was carried out to determine the flood risk areas. Factors associated with the flooding were selected as hazard and vulnerability parameters. Spatial distribution of selected parameters was carried out using Geographic Information System (GIS).

3.2.1 *Flood hazard parameters*

Flood hazard refers to the potential of a given flood to threaten human life and property (Smith 1996). It can be defined as a probability of occurrence of a potentially destructive phenomena for a given time period and area. Flood hazard mapping can be carried out using meteorological and topographical parameters. In this context, five hazard parameters have been selected namely, elevation, slope, soil type, drainage density, and rainfall pattern.

Slope and elevation are the important factors for determining the direction and amount of surface runoff or subsurface drainage reaching a site (Dai et al. 2002). Elevation of an area controls the flood risk whereas slope determines the amount of rainfall that reaches to the stream. Similarly, the type of soil governs the infiltration rate while the amount of runoff increases with increase in drainage density. The rainfall pattern has a significant role among all the aforementioned parameters and the intensity of rainfall has been found to be directly proportional to the intensity of flood (Gosh et al. 2018).



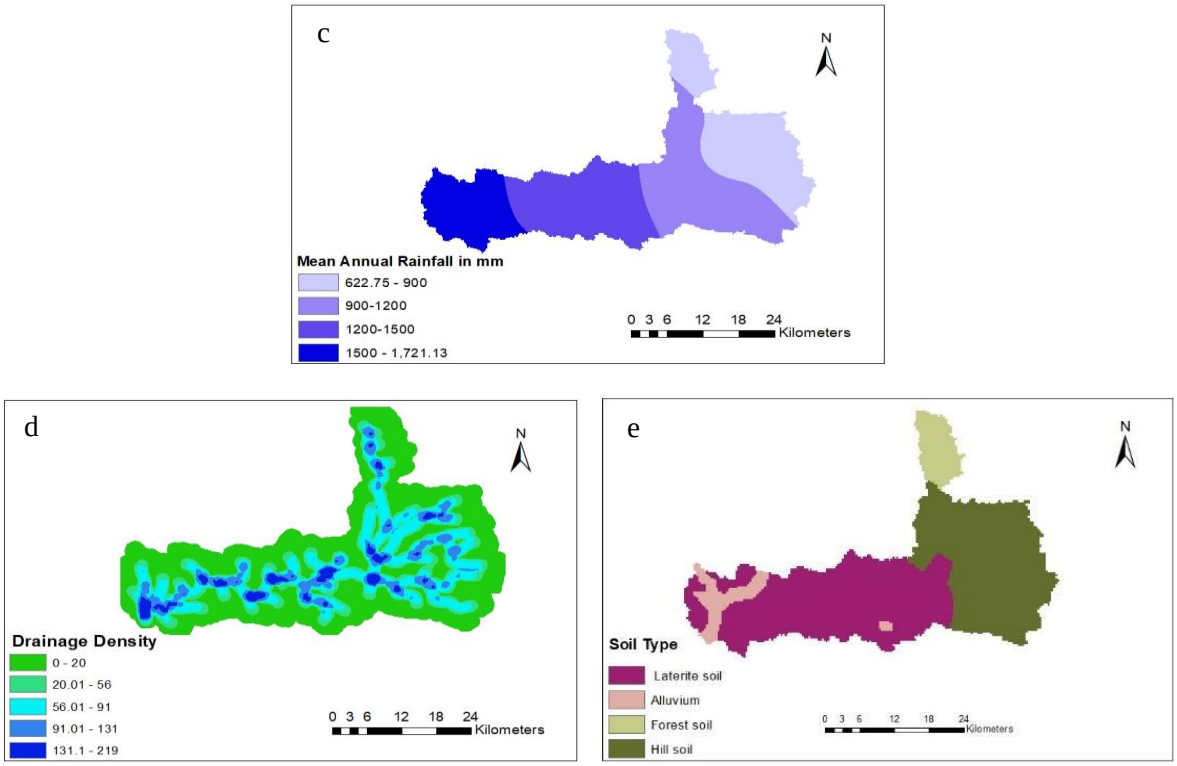
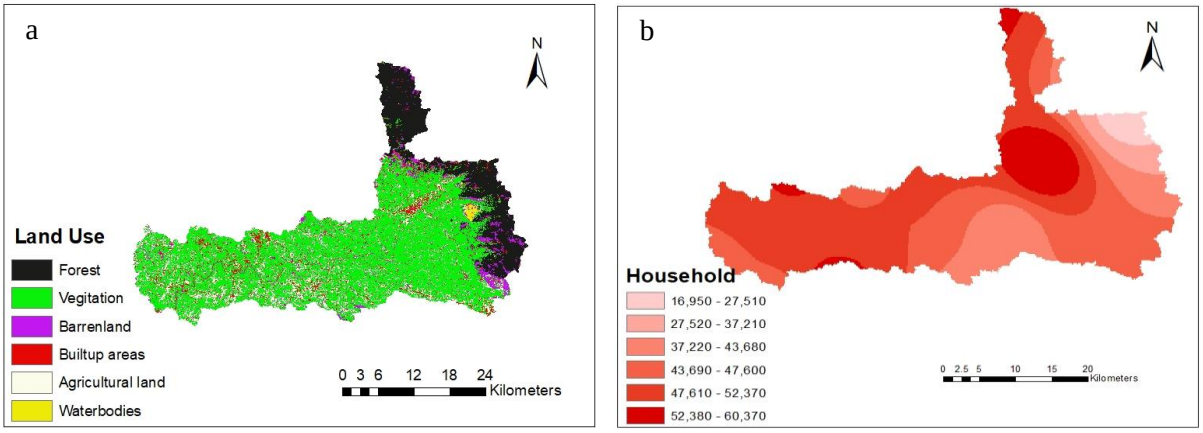



**Figure 3** a) elevation, b) slope, c) rainfall, d) drainage density, e) soil type map

3.2.2 *Vulnerability parameter*

Vulnerability can be stated as the level of foreseeable consequences of a natural phenomenon on issues and is the most crucial component of risk assessment that determines whether exposed to a hazard causes a risk or not (Mate 2001). Flood vulnerability assessment incorporates the effect of demographic and infrastructural parameters of the study area. In this study, household density, population, literacy in percentage and land use are used as vulnerability indicators.



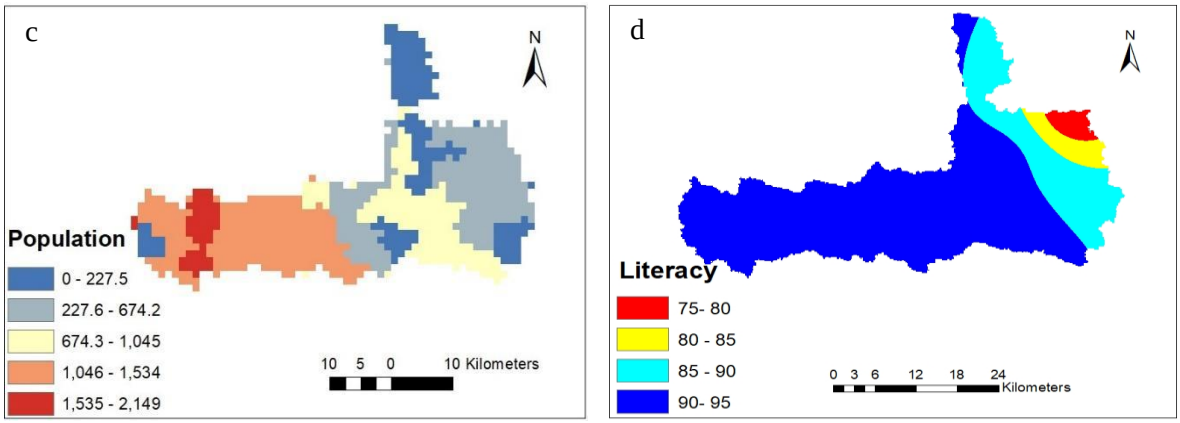



**Figure 4** a) land use b) household density c) population d) literacy

3.2.3. *Analytical hierarchy process (AHP)*

AHP is a semi-quantitative decision-making value judgment approach that serves the objectives of the decision maker. AHP has a hierarchical structure of the criteria, which provides a better emphasis on specific criteria and sub-criteria when allocating the weights. In the application of multi-criteria decision analysis, the analytic hierarchy process, which is a structured technique for dealing with complex decisions, was applied in structuring the flood causative factors (Ouma and Tateishi 2014). The procedure was developed by Saaty in 1980 to compute required weighting factors with the help of preference matrix where all relevant criterions are compared against each other with reproducible preference factors which is illustrated in table 1.

**Table 1** Scale of preference between parameters

| Intensity importance | Description |
|---|---|
| 1 | Equal importance |
| 3 | Moderate importance |
| 5 | Strong importance |
| 7 | Very strong importance |
| 9 | Extreme importance |
| 2, 4, 6, 8 | Intermediate values |
| Reciprocals | Inverse comparison |

Steps in AHP can be summarised into four classes;

1. Construction of the decision hierarchy
2. Determination of the relative importance of attributes and sub-attributes
3. Evaluation of the each alternative and calculation of its overall weight for each attribute
4. Check the consistency of the subjective evaluations

Decision is decomposed into independent elements to construct a decision hierarchy. Then each pair of attributes have subjectively evaluated on a nine-point scale. Further, weight is calculated for each attribute and its sub-attribute based on pairwise comparisons and later, logical consistency of these evaluations is tested. In AHP, a pair-wise comparison method is used to derive the priorities for the criteria in terms of their importance in achieving the goal. In this study, AHP was used to give weights for both the hazard and vulnerability factors.

The flood index model can be stated as following:

$$FH = \sum_{i=1}^{n} W_i R_i \quad (1)$$

$FH =$ Flood hazard index or Flood vulnerability index, $W_i$ is the weight and $R_i$ is the rank of $i^{th}$ parameter.

A pairwise comparison matrix has been made for which, each factor was rated against every other factor by assigning relative importance value ranges between 1 and 9 (Table 2 and 3).

$$A = (a_{ij})_{n*n} = \begin{matrix} a_{11} & a_{12} & a_{13} \\ a_{21} & a_{22} & a_{23} \\ a_{31} & a_{32} & a_{33} \end{matrix} \quad a_{ii} = 1,\ a_{ij},\ = 1/a_{ij} \quad (2)$$

After pairwise evaluation, priority vectors were computed which is the normalized Eigenvector of the matrix. The calculations were done by dividing each column by corresponding sums. Later average values of each row were computed and used as weights in objective hierarchy for calculating flood hazard and flood vulnerability. The relative weights for hazard and vulnerability are provided in the last column of Table 2 and 3.

**Table 2** Comparison matrix for flood hazard

| Parameter | Elevation | Slope | Rainfall | Drainage density | Soil | Relative weights |
|---|---|---|---|---|---|---|
| Elevation | 1 | 2 | 5 | 3 | 7 | 0.44 |
| Slope | 0.5 | 1 | 2 | 3 | 5 | 0.26 |
| Rainfall | 0.2 | 0.5 | 1 | 2 | 4 | 0.15 |
| Drainage density | 0.33 | 0.33 | 0.50 | 1 | 3 | 0.11 |
| Soil | 0.143 | 0.2 | 0.25 | 0.33 | 1 | 0.05 |

**Table 3** Comparison matrix for flood vulnerability

| Parameter | Population | Household | Lu | Literacy | Relative weights |
|---|---|---|---|---|---|
| Population | 1 | 2 | 3 | 7 | 0.48 |
| household | 0.5 | 1 | 4 | 5 | 0.33 |
| LU | 0.33 | 0.25 | 1 | 3 | 0.13 |
| literacy | 0.14 | 0.2 | 0.33 | 1 | 0.06 |

Saaty (1980) proposed a consistency index (CI) to measure consistency of a comparison matrix and it can be calculated by the following equation.

$$CI = \frac{\lambda_{max} - n}{n-1} \quad (3)$$

where, $\lambda_{max} =$ largest Eigenvalue and $n$ is the dimension of the matrix.

Consistency ratio (CR) was used to check the consistency of a random matrix and was calculated as the ratio of the CI and the random index (RI) as shown in Table 4. If CR is greater than 10%, then it indicates the judgement was wrong and need to revise the pairwise comparison.

$$CR = \frac{CI}{RI} \quad (4)$$

**Table 4** RI for hazard and vulnerability

| N | 1 | 2 | 3 | 4 | 5 | 6 |
|---|---|---|---|---|---|---|
| RI (for hazard) | 0 | 0 | 0.58 | 0.9 | 1.12 | 1.24 |
| RI (for vulnerability) | 0 | 0 | 0.58 | 0.9 | 1.12 | 1.24 |

Five parameters were considered for hazard mapping and four parameters for vulnerability mapping. In this investigation, the values for CI and CR are found to be 0.056 and 0.049, respectively for hazard (RI= 1.12), and 0.061 and 0.068, respectively for vulnerability (RI= 0.9). Consistency ratios for both cases were found to be within the permissible limit and the values were used to prepare hazard and vulnerability maps on a GIS platform (Figure 5a and 5b).

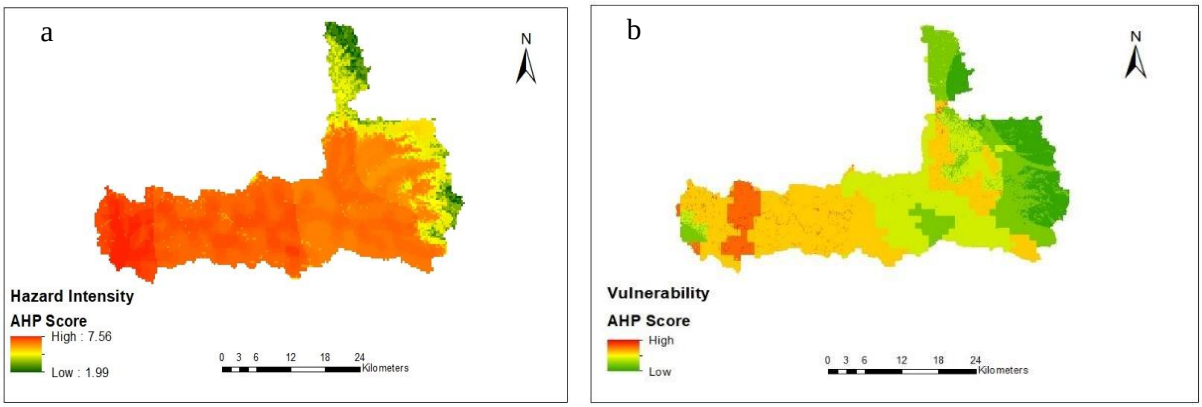



**Figure 5** a) Spatial distribution of hazard map b) Spatial distribution of vulnerability map

From the spatial distribution of hazard (Figure 5a), it is found that the intensity of flood hazard was very severe in western side of the basin. Major parts of the basin found to have low elevation and low slope, which caused high risk hazard in this area. The North-East part including Attappadi and Mannarkad were at relatively higher elevation where the risk has varied from low to moderate. Central to western parts of the study area have been observed to be vulnerable to moderate to high flood.

Vulnerability assessment incorporates the parameters like population, LU, household and literacy rate which collectively increases the flood vulnerability. Ottapalam, Patambi and Thrithala regions of the Thuthapuzha basin are most vulnerable to flood (Figure 5b) as population density and infrastructure development are high in these regions (Figure 4 a-c). It can be inferred that the places with high population density and infrastructures are more susceptible to flood.

3.2.4 *Flood risk mapping*

Risk assessment is very important in disaster management to understand the functional relationship that exists within hazard, vulnerability and flood risk. Flood risk can be calculated as a product of hazard and vulnerability (equation 5). Flood risk area identification and zoning map was prepared on an ArcGIS platform using a raster calculator (spatial analyst tool).

$$Risk = Hazard * Vulnerability \quad (5)$$

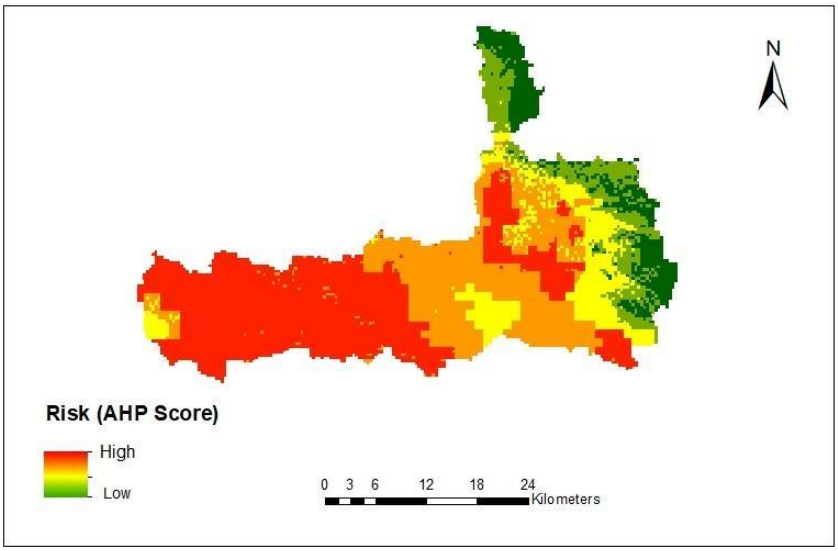



**Figure 6** Spatial Pattern of flood risk

During monsoon season, Thuthapuzha was flooded and water rose up to 2.5m, the river banks collapsed and river changed its course and many depressions were formed in the river bed (Kerala state biodiversity board 2018). Low lying areas like Kuttipuram, Pattambi, and Thrithala, Pulamanthole, etc., are under high risk. Spatial pattern of flood risk is presented in Figure 6.

## 3. Conclusions

In this study, a multi criteria analysis-based approach was used to analyse the flood risk of Thuthapuzha sub-basin. Flood risk map is a combination of flood hazard map (includes precipitation, slope, elevation, soil type and drainage density data) and vulnerability map (comprises population, household density, land-use and literacy data). In recent years, Thuthapuzha sub-basin has experienced frequent floods during monsoon season. Based on this analysis, it was found that low elevated areas are severely affected by flood hazards due to the high concentration of population, changes in the precipitation pattern and improper flood management policies. AHP based studies are efficient and cost effective, which generate a complete risk map through efficient valuation of associated parameters. Furthermore, this type of study can be implemented at district and basin level which will help in development of more comprehensive risk maps and better assessment of risk associated with river flood.

## References

Aydın, S., Uysal, S. (2014). Risk assessment of coastal erosion of Karasu coast in Black Sea. *journal of coastal conservation*, 18,673–682.

Barman, N.K., Chatterjee, S., Paul, A.K. (2016.) Estimate the coastal vulnerability in the Balasore Coast of India: a statistical approach. *Modeling Earth Systems and Environment*, 2,20.

Danumah, J.H., Odai, S.N., Saley, B.M., Szarzynski, J., Thiel, M., Kwaku, A., Kouame, F.K., Akpa, L.Y. (2016). Flood risk assessment and mapping in Abidjan district using multi-criteria analysis (AHP) model and geoinformation techniques, (cote d'ivoire). *Geoenvironmental Disasters*, 3:10.

Dinesan, V.P., Anitha, A.B., Gopakumar. R. (2004). Water resources scenario of Bharathapuzha River Basin. *Proceedings of industrial environmental conference*, pp 36–48.

Gosh, A., Kar, S.K. (2018). Application of analytical hierarchy process (AHP) for flood risk assessment: a case study in Malda district of West Bengal, India. *Natural Hazards*. 94:349–368.

Guhathakurta, P., Sreejith, O.P., Menon, P.A. (2011). Impact of climate change on extreme rainfall events and flood risk in India. Journal of Earth System Science 120(3), 359–373.

Manjula. P., Warrier. C.U. (2019). Evaluation of water quality of Thuthapuzha Sub-basin of Bharathapuzha, Kerala, India. *Applied Water Science* 9:70.

Masood, M., Takeuchi, K. (2012). Assessment of flood hazard, vulnerability and risk of mid-eastern Dhaka using DEM and 1D hydrodynamic model. *Natural Hazards* 61, 757–770.

Meyer, V., Haase, D. (2009). A multicriteria flood risk assessment and mapping approach. *Flood Risk Management: Research and Practice.*

Nikhil Raj, P.P., Azeez PA (2012) Trend analysis of rainfall in Bharathapuzha river basin, Kerala, India. *International Journal of Climatology* 32, 533–539.

Nikhil Raj, P.P., Azeez, P.A. (2009). Spatial and temporal variation in surface water chemistry of a tropical river, the river Bharathapuzha, India. *Current Science* 96(2), 245–251.

Ouma, Y.O., Tateishi, R. (2014). Urban Flood Vulnerability and Risk Mapping Using Integrated Multi-Parametric AHP and GIS: Methodological Overview and Case Study Assessment. *Water* 6, 1515-1545.

Saaty, T. L. (1980). The Analytic Hierarchy Process: Planning, Priority setting, Resource allocation. Mc Graw-Hill, New York, 19.

Sanyal, J., Lu, X.X. (2006). GIS-based flood hazard mapping at different administrative scales: A case study in Gangetic West Bengal, India. *Singapore Journal of Tropical Geography*, 27, 207–220.

Sharma, S.V., Roy, P.S., Chakravarthi, V., Rao, S.G. (2018). Flood risk assessment using multi-criteria analysis: a case study from Kopili River Basin, Assam, India. *Geomatics, Natural Hazards and Risk.* 9(1), 79–93.

Smith, L.M., Winkley, B. R., (1996). The response of the Lower Mississippi River to river engineering. *Engineering Geology*, 45, 433–455.

*IN PROCEEDINGS OF 25th HYDRO 2020, INTERNATIONAL CONFERENCE, NATIONAL INSTITUTE OF TECHNOLOGY ROURKELA, ODISHA, INDIA 26-28, March 2021, ISBN 978-93-90631-56-8*

Paper ID - 097

# Application of *L*-Moment based Regional Flood Frequency Analysis for Krishna River Basin

Amit Kumar Singh[1], Sagar Rohidas Chavan[2]

[1]*Department of Civil Engineering, Indian Institute of Technology, Ropar, India*
[2] *Department of Civil Engineering, Indian Institute of Technology, Ropar, India*
*Email: amit.19cez0016@iitrpr.ac.in*

## Abstract

Flood is one of the worst and costliest natural disaster which results in great loss of mankind and nature. Design flood estimates are desired at locations of interest along the river network. Design flood estimation becomes a difficult task when historical streamflow records are not available at the locations of interest, famously known as ungauged locations. *L*-moment based Regional Flood Frequency Analysis (RFFA) helps in estimating design flood estimates at ungauged locations. In this paper, RFFA was applied to catchments in Krishna River basin. In RFFA, hydrologically similar regions were identified through a Global K-means clustering algorithm. Discordant sites were recognized with the help of discordancy measure. Subsequently, homogeneity test was performed to make regions homogeneous in terms of their flood response. Finally, leave-one-out-cross-validation (LOOCV) was used investigate the performance of formed regions in predicting design flood estimates. Results indicated that RFFA can be effective for reliable prediction of design flood estimates in Krishna River Basin.

***Keywords:*** *L-moment; Global K-means; discordancy measure*

## 1. Introduction

Floods are the hydrological extremes which are caused due to extreme precipitation. The mechanism of conversion of extreme precipitation to extreme flow i.e. flood in a catchment is governed by the physical characteristics of the catchments. Flood is considered as one of the worst and costliest natural disaster which results in great loss of mankind and nature. Reliable estimates of magnitude and frequency of flood events i.e. flood quantiles are required for effective planning and management of flood hazard. Flood magnitudes and their frequencies are needed for successful operation and economical design, of pivotal hydraulic structures such as dams, reservoirs and spillways, bridges, small culverts, urban drainage systems, flood plain zoning, economic evaluation of flood protection projects etc.

Traditionally, practitioners seek flood quantiles at locations of interest which are either ungauged or sparsely gauged. Researchers addressed this issue of estimation of flood quantiles at ungauged locations through Regional Flood Frequency Analysis (RFFA) (e.g., Wallis and Wood 1985, Acreman, M.C. and Sinclair, C.D. 1986, Farquharson et al. 1992, Rao and Hammed 1997, Smith 2014; Cassalho 2018). In RFFA, computation of flood quantiles involves 2 steps. First step comprises grouping of hydrologically similar catchments into a number of groups/clusters/regions in terms of physical and climatic characteristics/attributes. This procedure is known as a regionalization. A variety of regionalization approaches are in use for identifying regions, and each approach has its strengths and limitations. The various approaches viz. method of residuals (MOR), canonical correlation analysis (CCA) (Cavadias, 1990; Cavadias et al., 2001), region of influence (Burn, 1990a,b; Zrinji and Burn, 1994), hierarchical approach (Gabriele and Arnell, 1991; Zrinji and Burn, 1996) and cluster analysis (Mosley (1981), Burn (2000), Srinivas (2006) etc. ) are widely used. Hosking and Wallis (1997) suggested five different approaches for forming regions viz. geographical convenience, subjective partitioning, objective partitioning, cluster analysis, and multivariate methods. Cunnane (1988), GREHYS (1996) presented detailed comparisons of the various regional estimation methodologies for RFFA. Overview of RFFA can be found in past research (e.g., Dawdy, 2012; Hosking and Wallis,1995; Rao and Hamed, 2000). Clustering is one of the most preferred approaches for regionalization (Burn, 1997). Number of clusters can be determined using various cluster validity indices such as Dunn index (Dunn, 1973), Davies-Bouldin index (Davies and Bouldin,

1979), average silhouette index (Rousseeuw, 1983) etc. An overview of clustering approach is found in Regionalization of Watersheds: An Approach Based on Cluster Analysis (Rao, A.R., Srinivas, V. V.). Once the hydrologically similar regions are formed, they are tested for homogeneity in terms of predictand i.e. flood quantiles. Subsequently, regional growth curve for the region/cluster is used to determine the probability distribution of ungauged catchment following the Index flood method (Dalrymple (1960).

There are many characteristics that the region should posses to ensure the effective information transformation to an ungauged location. This can be achieved by ensuring formation of homogeneous region in terms of predictand (i.e., flood quantile). The importance of regional homogeneity has been demonstrated by many researchers (e.g. Lettenmaier et al., 1987; Stedinger & Lu, 1995). Further, the region should be sufficiently large to provide an effective estimate of extreme event. Reed et al., (1999) suggested that the region should be sufficiently large enough, so that a 5T rule can be invoked to predict effective estimates of floods for T year return period.

The remainder of the paper provides brief description of the study region and data used in section 2. This is followed by section 3 describing background on Probability Weighted Moments with *L*-moment calculations and section 4 where, procedure for identification of the homogeneous region. Subsequently, section 5 demonstrates the application of RFFA on Krishna River Basin. Finally, concluding remarks are made in section 6.

## 2. Description of the Study Region and Data used

The **Krishna River** is the fourth largest river in terms of water inflows and catchment area in India, after the Ganga, Godavari and Brahmaputra. The river is almost 1,288 kilometers long. The river is also called Krishnaveni and is one of the major sources of irrigation for the states like- Maharashtra, Karnataka, Telangana and Andhra_Pradesh. It comprises a cathcment area of 258,948 $Km^2$ and annual discharge of 69.8 $km^3$/year (Kumar et al. 2005). The river originates in the Western Ghats of Maharashtra and Karnataka, drains the Deccan Plateau, and discharges into the Bay of Bengal.

In this study, the attributes and the flow record from 30 gauged sites from Krishna Basin were considered. Two physiographic attributes (Drainage Area, Elevation), and one meteorological variable (mean annual precipitation) are extracted for cluster analysis/regionalization by using GIS. The location attributes, latitude and longitude, were also considered in the cluster analysis to identify regions that are geographically contiguous. Of the five attributes selected for cluster analysis, only drainage area was transformed by using logarithmic transformation. Then, each of the five attributes was rescaled using transformations presented in Table 1 (Srinivas, 2005). Equal weight was assigned to all the attributes implying equal importance is given to all the features.

**Table 1. Transformation of site characteristics**

| Site characteristic, Y | Cluster variable, X |
|---|---|
| Drainage basin area($km^2$) | Y = (1/5)*log(X) /s.d.(log X) |
| Elevation(m) | Y = (1/5)*X/s.d.(X) |
| latitude (deg) | Y = (1/5)*X/s.d.(X) |
| longitude (deg) | Y =(1/5)* X/s.d.(X) |
| Precipitation(mm) | Y = (1/5)*X/s.d.(X) |

## 3. Background on Probability Weighted Moments

Probability weighted moment of a random variable X with cumulative distribution function F(.) were defined by Greenwood et al. (1979) to be the quantities

$$M_{p,r,s} = E[X^p\{F(X)\}^r\{1 - F(X)\}^s \quad (1)$$

The useful important cases of probability weighted moment are $\alpha_r = M_{1,0,r}$ and, $\beta_{1,r,0}$. For a distribution having quantile function $x(u)$

$$\alpha_r = \int_0^1 x(u)(1-u)^r du, \quad (2)$$

$$\beta_r = \int_0^1 x(u)(u)^r du, \quad (3)$$

The unbiased estimator of $\beta_r$ is

$$b_r = n^{-1}\binom{n-1}{r}^{-1} \sum_{j=r+1}^{n} \binom{j-1}{r} x_{j:n} \quad (4)$$

which on expansion gives the general expression as

$$b_r = n^{-1} \sum_{j=r+1}^{n} \frac{(j-1)(j-2)\ldots(j-r)}{(n-1)(n-2)\ldots(n-r)} x_{j:n} \quad (5)$$

$L$-moment was introduced by Hosking in 1990 and being adopted by many researchers worldwide (Hosking and Wallis, 1997) over last two decades. $L$-Moments are certain linear combinations of the element of an ordered sample contain information about the location, shape and scale of the distribution from which sample is being drawn. The sample estimates of the $L$ moment are as shown below:

$$l_1 = b_0 \quad (6)$$
$$l_2 = 2b_1 - b_0 \quad (7)$$
$$l_3 = 6b_2 - 6b_1 + b_0 \quad (8)$$
$$l_4 = 20b_3 - 30b_2 + 12b_1 - b_0 \quad (9)$$

where, $b_0$, $b_1$, $b_2$, and $b_3$ are the unbiased estimators and $l_1$, $l_2$, $l_3$ and $l_4$ are first four sample $L$-moment estimates.

Coefficient of $L$-variation $L$-$CV$ (t) is shown as below:

$$t = \frac{l_2}{l_1} \quad (10)$$

L moment ratio $t_3$ ($L$-Skewness) and $t_4$ ($L$-Kurtosis) is as shown below:

$$t_r = \frac{l_2}{l_1} \quad r = 3,4,.. \quad (11)$$

In above mention quantities, the location parameter $l_1$ can take any value as it is the mean of the distribution, the scale parameter $l_2 \geq 0$, for a distribution that takes only positive value the coefficient of variation ($L$-$CV$) ranges from 0 to 1 and $L$-moment ratio satisfies $|t_r| < 1$ for all $r \geq 3$. The sample $L$-moments are asymptotically unbiased and robust to outliers.

## 4. Identification of the homogeneous region

The aim of this step is to form groups of sites that approximately satisfy the homogeneity condition, that is, the sites frequency distributions are identical apart from a site-specific scale factor. The criteria used for grouping is Cluster Analysis. The goal of clustering is to identify the sites with similar characteristics in a cluster and differ from other clusters.

First step in regional flood frequency analysis is to check the data are appropriate for performing regional flood frequency analysis. The Mann Kendall test is performed to check the trend present in the data set and the site with significant trend at 5% significance level is removed (Cassalho et al., 2018). The discordance measure (Hosking & Wallis 1997) used for the screening for RFFA. A discordancy measure is useful to identify sites with gross error in their data or those which are grossly discordant with the region as a whole.

To estimate discordancy values for sites in region, the sites are considered as points in three dimensional space and sample *L*-moment ratio (*L-CV*, *L*-Skewness, and *L*-Kurtosis).Centroid of the region is regarded as a point depicting average of sample L-moment ratio of the sites in the region. Any point that is far away from the centroid of the region is flagged as discordant.

Let $N_R$ represent the number of sites in a region. Further, let $u_i = \left[t^{(i)}\ t_3^{(i)}\ t_4^{(i)}\right]^T$ be a vector containing $t$,$t_3$, and $t_4$ values of site $i$ in the region, where the superscript T denotes transpose of a vector. The discordancy statistic for site $i$ is defined as:

$$D_i = \frac{1}{3} N_R (u_i - \bar{u})^T S^{-1} (u_i - \bar{u}) \quad (13)$$

$$\bar{u} = \frac{\sum_{i=1}^{N_R} u_i}{N_R} \quad (14)$$

$$S = \sum_{i=1}^{N_R} (u_i - \bar{u})\,(u_i - \bar{u})^T \quad (15)$$

$\bar{u}$ is the unweighted group average of the *L*-moment ratios

$S$ is a covariance matrix

The critical values for discordancy measures with respect to number of sites are mentioned in table (2).

**Table 2. Critical values for the discordancy statistics**

| $N_k$ | Critical value of $D_i$ | $N_k$ | Critical value of $D_i$ |
|---|---|---|---|
| 5 | 1.333 | 11 | 2.632 |
| 6 | 1.648 | 12 | 2.757 |
| 7 | 1.917 | 13 | 2.869 |
| 8 | 2.140 | 14 | 2.971 |
| 9 | 2.329 | ≥15 | 3.000 |
| 10 | 2.491 | | |

After the discordant sites being removed, the data is tested for regional homogeneity and goodness of fit measure to find the homogeneous region and best fitted distribution over the region. The regional homogeneity tests are developed to examine whether the between-site dispersion of the sample LMRs for the group of sites under consideration is larger than the dispersion expected in homogeneous region. A large number of realizations ($N_{sim}$=500) of the region are simulated from a kappa distribution fitted to regional average LMRs: $l_1^R, t^R, t_3^R, and\ t_4^R$. The data simulated at any site in the region is serially independent and the data simulated at different sites in the region are not cross correlated. For each region V (weighted standard deviation of the at site sample *L-CVs*), $V_2$ (weighted average distance from the site to the group weighted mean in the two dimensional space of *L-CV* and *L*-Skewness), and $V_3$ (weighted average distance from the site to the group weighted mean in the two dimensional space of *L*-skewness and *L*-kurtosis) are computed.

$$V = \left\{ \sum_{i=1}^{N_R} n_i (t^i - t^R)^2 \Big/ \sum_{i=1}^{N_R} n_i \right\}^{1/2} \quad (16)$$

$$V_2 = \sum_{i=1}^{N_R} n_i \left\{ (t^{(i)} - t^R)^2 + (t_3^{(i)} - t_3^R)^2 \right\}^{1/2} \Big/ \sum_{i=1}^{N_R} n_i \quad (17)$$

$$V_2 = \sum_{i=1}^{N_R} n_i \left\{ (t_3^{(i)} - t_3^R)^2 + (t_4^{(i)} - t_4^R)^2 \right\}^{1/2} \Big/ \sum_{i=1}^{N_R} n_i \quad (18)$$

where

$$t^R = \sum_{i=1}^{N_R} n_i t^{(i)} \Big/ \sum_{i=1}^{N_R} n_i \quad (19)$$

$$t_3^R = \sum_{i=1}^{N_R} n_i t_3^i \Big/ \sum_{i=1}^{N_R} n_i \quad (20)$$

$$t_3^R = \sum_{i=1}^{N_R} n_i t_3^i \Big/ \sum_{i=1}^{N_R} n_i \quad (21)$$

The regional average mean $l_1^R$ is set to 1. For examine the estimates of a region three heterogeneity measure (HMs) are used:

$$H_1 = \frac{(V - \mu_V)}{\sigma_V} \quad (22)$$

$$H_2 = \frac{(V_2 - \mu_{V_2})}{\sigma_{V_2}} \quad (23)$$

$$H_3 = \frac{(V_3 - \mu_{V_3})}{\sigma_{V_3}} \quad (24)$$

A region can be regarded as 'acceptably homogeneous' if HM $< 1$, 'possibly homogeneous' if $1 \leq HM < 2$, and 'definitely heterogeneous' if $HM \geq 2$ (Hosking and wallis, 1997).

Further, the goodness of fit measure is applied to check the best fitted distribution. The test of goodness of fit should judge how well the $L$-Skewness and $L$-Kurtosis of the fitted distribution match the regional average $L$-skewness and $L$-kurtosis of the observed data. The $Z$ statistic is give as

$$Z^{Dist} = (t_4^R - \tau_4^{Dist}) / \sigma_4 \quad (25)$$

where, $\tau_4^{Dist}$ is $L$ kurtosis of fitted distribution and $\sigma_4$ denotes the standard deviation of $t_4^R$.

Declare the fit to be adequate if $Z^{Dist}$ is sufficiently close to zero, a reasonable criterion being $|Z^{Dist}| \leq 1.64$.

## 5. Application of RFFA to study area

The effectiveness of RFFA in estimating flood quantiles at ungauged locations, RFFA was applied to Krishna River basin. The peak flood data of 30 sites at Krishna river basin along with five different attributes viz. latitude, longitude, drainage area, elevation and Mean annual precipitation, has been used. The summary of the attributes is shown in Table 3.

**Table 3. Details of attributes used in present study for regionalization**

| Attributes Name | Range over 30 sites | | Mean | Standard Deviation |
|---|---|---|---|---|
| | Minimum | Maximum | | |
| Drainage Area ($km^2$) | 690 | 251360 | 41138 | 72592.51 |
| Mean Annual Precipitation (mm) | 346.0 | 901.7 | 530.8 | 174.17 |
| Elevation (m) | 12.0 | 756.0 | 356.7 | 209.82 |
| Latitude ($^oN$) | 15.47 | 17.42 | 16.43 | 0.55 |
| Longitude ($^oE$) | 74.47 | 80.62 | 77.36 | 2.04 |

Considering a significance level of 5%, the nonparametric test of Mann–Kendall was applied to the 30 sites. Based on this test, five historical series were classified as non-stationary as significant trend were present in those sites, so excluded for the further study. The remaining 25 sites went through discordant test and none of the sites are found to be discordant as none of the site having discordant value more than 3. Assuming all the 25 sites as a homogeneous region, heterogeneity test were performed. The heterogeneity measure $H_1$ found to be 10.24, which is significantly higher than critical value. A region is deemed to be homogeneous if $H_1$ is less than the critical value of 2, failing which the region can further be divided into various sub regions. The Global K- means algorithm (Jintao Han and Haiming Li (2019)) is invoked for the formation of region and Davies-Bouldin Index was used to arrive at optimum number of cluster. The global K-means algorithm resulted in formation of 3 regions, of which region 1 contains 7 sites, region 2 contains 10 sites and region 3 contains 8 sites. The region is so divided that each region should follow either of 3T rules or 5T rules for estimation of flood quantiles. Now each region is also checked for discordancy which revealed that region 1 and region 2 do not have discordant sites but there is one discordant site in region 3 with the value of 2.61 which is greater than the critical value for discordancy (i.e. 2.14 for a region with 8 sites). The discordant site is removed from further analysis.

The heterogeneity test is performed over each region as mention in section 4 and the entire region is found to be homogeneous with $H_1$ value of 1.02, 0.41, and 1.20 for region 1, region 2 and region 3 respectively. It is worth mentioning that Hosking and Wallis (1997) recommend the use of the measure H rather than $H_2$ and $H_3$, since the last two can likely provide false homogeneity classification as they are more sensitive, especially for regions with fewer sites. The summary of the heterogeneity test is provided in table 4. NS represent number of sites in the region and RS represent the region size in station year.

**Table 4. Summary of the final region for study area**

| Region | NS | RS | Heterogeneity Measures | | | Region Type |
|---|---|---|---|---|---|---|
| | | | $H_1$ | $H_2$ | $H_3$ | |
| 1 | 7 | 229 | 1.02 | 0.71 | 0.88 | Homogeneous |
| 2 | 10 | 368 | 0.41 | 1.56 | 2.89 | Homogeneous |
| 3 | 7 | 167 | 1.20 | 1.49 | 0.56 | Homogeneous |

Taking into account all the sites within a region, the best PDF fitted were chosen based on the $Z^{DIST}$ statistic (refer Table 5). GLO, GEV, GNO, PE3, and GPA stand for the probability density functions (PDFs) of generalized logistic, generalized extreme values, generalized normal, person Type 3, and generalized Pareto, respectively. An adequate fit is obtained when $|Z^{DIST}| \leq 1.64$. On evaluation of $Z^{DIST}$ we can clearly see that GEV, GNO, PE3 and GPA is adequate fit for region 1 but the closeness of GPA to 0 with the value of 0.06 represents the best fit for region 1 is GPA distribution. Similarly for region 2 and region 3 it can be said that the best fit are GEV and PE3 distribution respectively.

**Table 5. Goodness-of-fit results along with the average *L*-skewness and *L*-kurtosis**

| Region | Regional Average | | | $Z^{DIST}$ statistic | | | | |
|---|---|---|---|---|---|---|---|---|
| | t | $t_3$ | $t_4$ | GLO | GEV | GNO | PE3 | GPA |
| 1 | 0.552 | 0.423 | 0.230 | 1.85 | 1.47 | 0.60 | -0.90 | 0.06 |
| 2 | 0.346 | 0.152 | 0.146 | 1.85 | -0.20 | -0.33 | -0.86 | -4.63 |
| 3 | 0.337 | 0.180 | 0.106 | 2.99 | 1.69 | 1.47 | 0.97 | -1.26 |

Figures 1, 2 and 3 show the *L*-moment ratio diagram for visual assessment of best fit distributions for the regions.

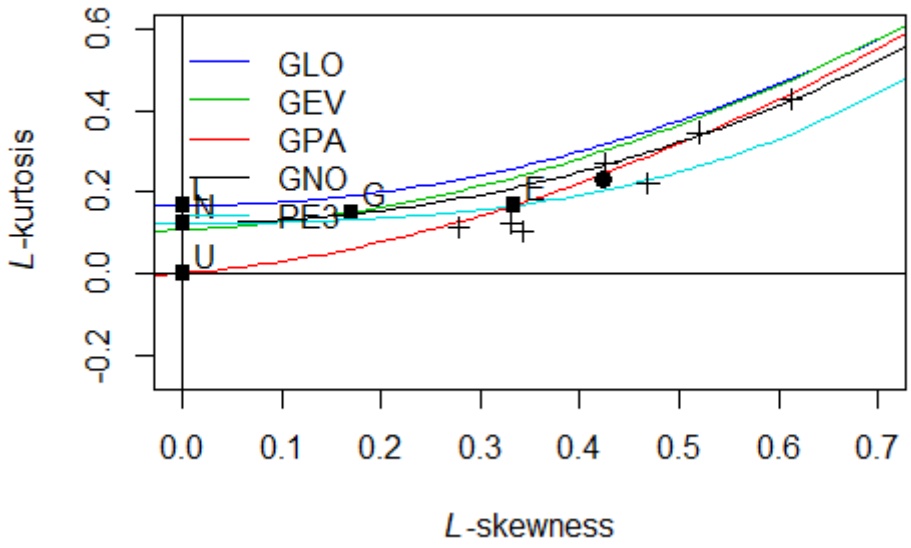



**Figure 1.** *L*-moment Ratio diagram of Region 1

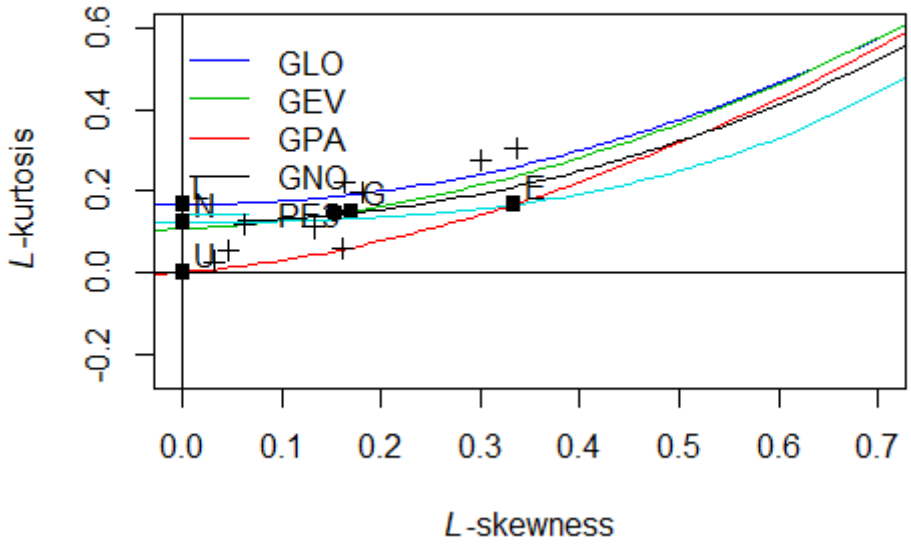



**Figure 2.** *L*-moment Ratio diagram of Region 2

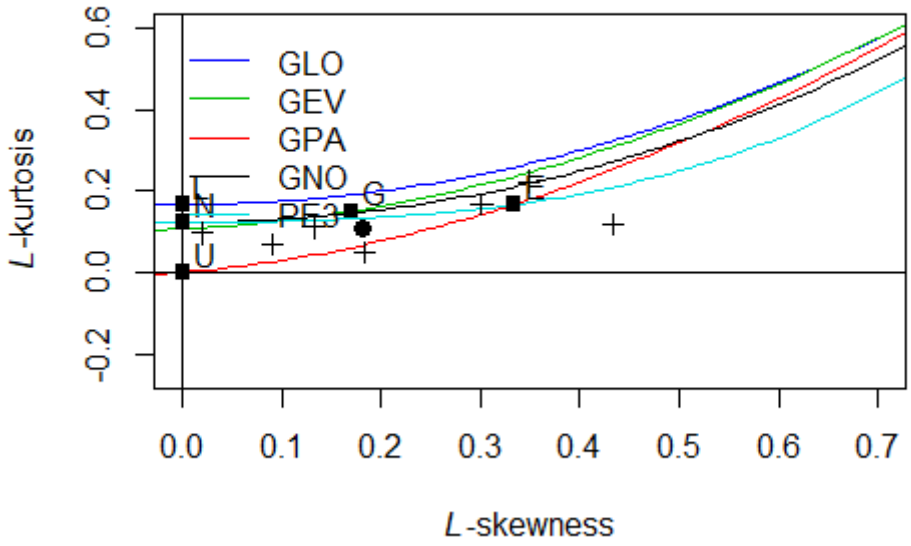



**Figure 3.** *L*-moment Ratio diagram of Region 3

### 5.1 Construction of Regional growth factor

The regional parameters of the best fitted distribution for regions 1, 2, and 3 are tabulated in table 6,

**Table 6. Parameter of the best fitted distribution in defined region**

| Region | Best fitted parameter | Parameter of the distribution | | |
|---|---|---|---|---|
| 1 | GPA | $\xi$=0.00038 | α=0.80963 | k=-0.19006 |
| 2 | GEV | $\xi$=0.71756 | α=0.51289 | k=0.02752 |
| 3 | PE3 | $\mu$=1.00 | $\sigma$=0.62012 | $\gamma$=1.09401 |

After the parameters of a distribution are estimated, quantile estimates which corresponds different return period may be computed. As it is known that, the return period is related to probability of non-exceedance (F) by the relation

$$F = 1 - \frac{1}{T}$$

The graph between non-exceedance probability and growth factor of fitted distribution is shown in figure 4. The graph for all the 3 region are merged into a single figure to visualize the behavior of growth factor by using the parameter estimated from goodness of fit test. The blue line in the graph shows the growth factor for region 1, black line is growth factor curve of region 2 and the red line is for region 3. The growth factor curve of region 2 and region 3 is almost similar, even having two different distributions with different parameter. Table 7 shows the growth factor at different return period.

**Table 7. Growth factor over a range of Return Period**

| Region | Return Period(T) | | | |
|---|---|---|---|---|
| | 25 | 50 | 75 | 100 |
| 1 | 3.59 | 4.70 | 5.41 | 5.96 |
| 2 | 2.28 | 2.61 | 2.80 | 2.93 |
| 3 | 2.28 | 2.60 | 2.78 | 2.91 |

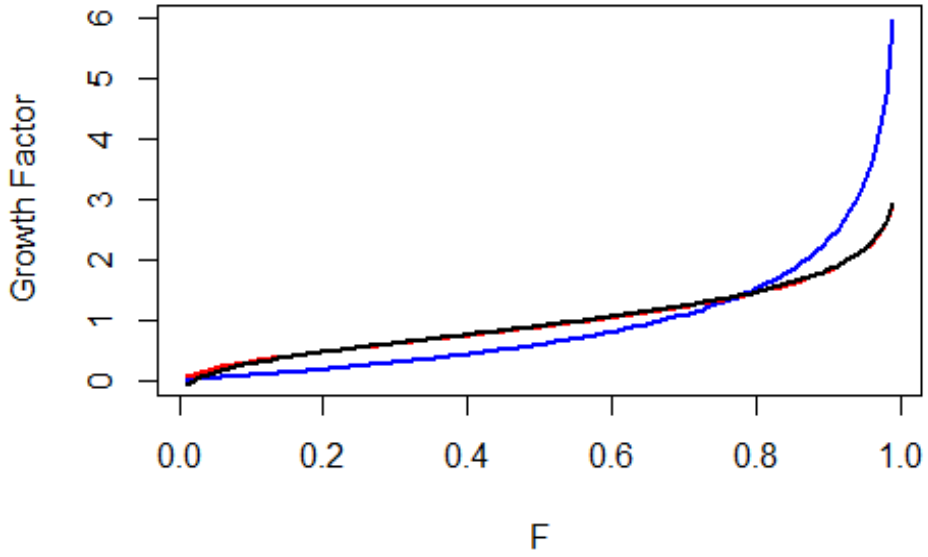



**Figure 4.** Regional growth factor

### 5.2 Performance assessment by leave-one-out cross-validation

The effectiveness of the region is assessed using leave one out cross validation procedure. In this procedure one site out of N sites in a region is considered as ungauged (considered for testing). The information from the remaining sites is used for training the model. The goal of cross-validation is to test the model's ability to predict new data that was not used in estimating it, in order to flag problems like over fitting or selection bias and to give an insight on how the model will generalize to an independent dataset (i.e., an unknown dataset, for instance from a real problem). In the present study, the LOOCV approach is performed on the region formed using Global K-Means algorithm. Firstly the generalized linear model is applied over all the three regions. For region 1 and region 3 Adjusted R square is 0.90 and 0.92 respectively which is acceptable where as region 2 gave the value of adjusted R square of 0.84 for generalize logistic model.

The comparison of regional quantile estimates of un-gauge site with at-site quantile estimates is performed. Two performance measure were used for comparison: Relative Bias (R-bias), Absolute Relative Bias (AR-bias)

$$R - bias(T) = \frac{1}{N}\sum_{m=1}^{N}\left\{\frac{\hat{Q}_m^R - \hat{Q}_m^a}{\hat{Q}_m^a}\right\} \times 100 \quad (26)$$

$$AR - bias(T) = \frac{1}{N}\sum_{m=1}^{N}\left|\frac{\hat{Q}_m^R - \hat{Q}_m^a}{\hat{Q}_m^a}\right| \times 100 \quad (27)$$

where, $\hat{Q}_m^R$ and $\hat{Q}_m^a$ represents regional and at-site estimates of T year quantile of predictand at site m.

The results indicated that the error R-bias and AR-bias is reasonable; hence, the RFFA is effective in estimation of ungauged flood quantiles in Krishna basin.

**Table 8. Performance measure**

| Region | Percentage R-Bias | | | | Percentage AR-Bias | | | |
|---|---|---|---|---|---|---|---|---|
| | T=25 | T=50 | T=75 | T=100 | T=25 | T=50 | T=75 | T=100 |
| Region 1 | 6.14 | -2.69 | 7.31 | 7.90 | 19.6 | 25.6 | 28.4 | 30.84 |
| Region 2 | 17.8 | 21.1 | 23 | 24.4 | 42.35 | 47.47 | 50.4 | 52.43 |
| Region 3 | 5.45 | 6.96 | -3.35 | -6.05 | 32.57 | 39.05 | 41.76 | 45.81 |

## 6. Conclusion

In the present study, a complete RFFA based on *L*-moment is carried out on 30 sites of Krishna river basin. Five basins were deleted initially as there is presence of significant trend and one site is deleted based on discordant test. Global K- means clustering algorithm is used to subdivide the region as all regions together gave high value of heterogeneity. Using *L*- moment based algorithm GPA, GEV and PE III distribution is selected as best fit distribution for region 1, region 2, and region 3 respectively. After analyzing the result of goodness of fit test one can use PE III or GNO distribution for all the three sites as it is in the range of $|Z^{DIST}|$. Growth curve were fitted using the best fit distribution and one can observe that the growth curve of region 2 and region 3 is overlapping over each other.

The Global K-means clustering algorithm, applied in this study, was reasonably efficient in the identification of catchments with similar hydrological and physical characteristics, and DB index verified the optimal number of clusters. On the basis of study the following conclusion were drawn.
(i) Initial screening of data is an important task to obtain good quality of results.
(ii) Regional frequency analysis based on the homogeneous region can be considered as reliable tool to obtain ungauged flood quantiles
(iii) It was observed that the graph for growth curve of region 2 and 3 coincide each other even though they are having different distribution. It can be concluded that two regions with different distribution may show similar characteristics but they can't be merge together as it will induce heterogeneity

The performance of the regionalization was examined by analyzing homogeneity test results and the error between locally and regionally estimated mean annual flood values for the different return periods using the LOOCV. Results indicated that RFFA can be effective for reliable prediction of design flood estimates in Krishna River Basin.

## References

Andrew Smith, (2014). Regional flood frequency analysis at the global scale. *water resources research.*
A. Ramachandra Rao, and V.V. Srinivas (2006). Regionalization of watersheds by hybrid-cluster analysis, *Journal of Hydrology* 318 (2006) 37–56
Betül Saf. (2008). Regional Flood Frequency Analysis Using L-Moments for the West Mediterranean Region of Turkey. *Water Resour Manage* DOI 10.1007/s11269-008-9287-z
Burn, D. H. (1990). Evaluation of regional flood frequency analysis with a region of influence approach. *Wat. Resour. Res.* 26(10), 2257-2265.
Burn, D. H. (1997). Catchment similarity for regional flood frequency analysis using seasonality measures. *J. Hydrol.* 202, 212-230.
Burn, D. H.. Zrinji, Z. & Kowalchuk, M. (1997). Regionalization of catchments for regional flood frequency analysis. *J. Hydrol. Engng ASCE* 2(2), 76-82.
Carolina Lauro,(2018). Regional flood frequency analysis in the central-western river basins of Argentina, *River Res Applic.* 2018;1–13.
Cassalho et al.,(2018). Regional flood frequency analysis using L-moments for geographically defined regions: An assessment in Brazil, *J. Flood Risk Management* DOI: 10.1111/jfr3.12453
Donald H. Burn and N. K. Goel (2000). The formation of groups for regional flood frequency analysis. *Hydrological Sciences-Journal~des Sciences Hydrologiques*, 45( Î ) February
Greenwood, J. A., Landwehr, J. M., Matalas, N. C. and Wallis, J. R.(1979). Probability weighted moments: Definition and relation to parameters of several distributions expressible in inverse form. *Water Resour. Res*. 15, 1049–1054.
Gingras, D., Adamowski, K., 1992. Coupling of nonparametric frequency and L-moment analysis for mixed distribution identification. *Water Resour. Bull*. 28 (2), 263–272

Gingras, D., Adamowski, K., 1993. Homogeneous region delineation based on annual flood generation mechanisms. *Hydrol. Sci. J. 38* (2), 103–121.

Hosking, J. R. M. and Wallis, J. R. (1986). The value of historical data in flood frequency analysis. *Water Resour. Res*. 22(11), 1606–1612.

Hosking, J. R. M (1990). L-moments: Analysis and estimation of distributions using linear combinations of order statistics. *J. Royal Stat. Soc., Series* B,52, 105–124.

Hosking, J. R. M. and Wallis, J. R (1997). Regional Frequency Analysis – An Approach Based on L-moments. *Cambridge University Press, New York*.

Jakob, D., Reed, D. W. & Robson, A. J. (1999). Choosing a pooling-group, chapter C6. In: Flood Estimation Handbook, vol. 3, Statistical Procedures for Flood Frequency Estimation. *Institute of Hydrology, Wallingford, UK.*

Jintao Han and Haiming Li (2019). Initial Value Filtering Optimizes Fast Global K-Means. *Journal of Computer and Communications*, 2019, 7, 52-62

Manish Kumar Goyal and Vivek Gupta, (2014). Identification of Homogeneous Rainfall Regimes in Northeast Region of India using Fuzzy Cluster Analysis, *Water Resour Manage* (2014) 28:4491–4511

Rakesh Kumar , C. Chatterjee ,Sanjay Kumar, A. K. Lohani and R. D. Singh (2003). Development of regional flood frequency relationships using l-moments for middle Ganga plains subzone 1(f) of India. *Water Resources Management* 17: 243–257, 2003.

Rakesh Kumar, & C. Chatterjee, (2005). Regional flood frequency analysis using l-moments for North Brahmaputra region of India. *Journal of Hydrological Engineering*, 10(1), 1–7. https://doi.org/10.1061/(ASCE)1084-0699(2005) 10:1(1)

R. Bharath and V. V. Srinivas, (2014). Regionalization of extreme rainfall in India. *Int. J. Climatol*. 35: 1142–1156 (2015)

Rao and Hamed. (2000). Flood frequency analysis. *CRC Press, Boca Raton London, New York, Washington, D.C.*

Tom Micevski,(2014). Regionalisation of the parameters of the log-Pearson 3 distribution: a case study for New South Wales, Australia. *Hydrol. Process*. 29, 250–260 (2015)

Viglione, A., Laio, F., and Claps, P. (2007). A comparison of homogeneity tests for regional frequency analysis. *Water Resour. Res., 43(3),* W03428.

*IN PROCEEDINGS OF 25th HYDRO 2020, INTERNATIONAL CONFERENCE, NATIONAL INSTITUTE OF TECHNOLOGY ROURKELA, ODISHA, INDIA 26-28, March 2021, ISBN 978-93-90631-56-8*

Paper ID - 202

# Assessment of floodplain mapping of Ulhas River basin using HEC-RAS 1D/2D hydraulic simulation

Sachin Bhere[1], M. Janga Reddy[1]

[1]*Department of Civil Engineering, Indian Institute of Technology Bombay, Mumbai-400076, INDIA*
*Email: studentsachinbhere@gmail.com*

## Abstract

The study presents flood modeling and floodplain mapping of Ulhas River basin, Maharashtra using HEC-HMS, HEC-RAS model along with ArcGIS's GeoRAS for floodplain visualization. The focus of the work is to find out the suitability of the HEC-RAS model for simulating water surface profiles of the Ulhas River basin for the different return periods. The Ulhas River is a west-flowing river that originated in the Western Ghat and home of about 10 million people and the six major municipal corporations of the Mumbai Metropolitan Region (MMR). The average annual rainfall of about 2500 mm along with the rapidly changing land-use makes Ulhas River basin more vulnerable to the floods. The urban and pavement area is increased by 145 Sq. Km and the broadleaf forest is shrinking by 142 Sq. Km in the basin since year 2001. Also, the mixed forest, wasteland, evergreen forest, and plantations decreased. For flood plain mapping, the SRTM's DEM of 1 arcminute used for the river cross-section. The IDF curve is calculated using IMD, Kothari Grade, and Modified Kothari Grade formulas for different return periods and incorporated in the HEC-RAS model for floodplain mapping. The analysis of floodplain mapping shows around 3.5 times of the area of natural flow of the river inundated and vulnerable to the flood for 100-year return period, mostly the Urban built-up and agricultural land of Badlapur Municipal corporation. The simulation of the 2019's flood shows a good correlation when compared with the ground survey and Landsat 8 images.

***Keywords:*** *Flood; HEC-RAS; Floodplain mapping; Ulhas River.*

## 1. Introduction

Floods are one of the disastrous extreme hydrological events responsible for the thousands of casualties worldwide and the billion US dollars of economic damage. The flood's impact is so devastated that it is one of the critical reasons for people's migration. Most of the ancient civilization has come to an end due to such extreme hydrological events. Many institutions warned about the increasing intensities and frequencies of such extreme events due to climate change and anthropogenic reasons. The extent of the flood can be determined by calculating the amount of excess water overflowing from the water bodies' natural flow, but the flood complexity lies in the different reasons and the factors affecting the floods and understanding that floods can be divided based on the location, frequency, and the intensity. Urban floods can cause majorly due to anthropogenic reasons, and on the other hand, some floods in the river basin happed as a part of the natural cycle. Some of the long-term factors like climate change, land-use changes, and river morphological changes affect the flood intensities and their impact on the region. Reservoir operation, snowmelt, and extreme rainfall are also significant reasons for the floods. The extreme rainfall events cause flood events and further intensified due to anthropogenic reasons like rapid urbanization, poor drainage infrastructure, which is not designed considering the climate change extremes, and the informal settlement makes the people more vulnerable to flood events and to push people and business into poverty and the debt trap.

The Ulhas river basin is located at the western Maharashtra, India which drains 4670 Km2 approximately and the river is 120 Km long flows in the western direction, originated in the western ghat. The watershed is expanded from longitude 72°55’ north to 73°50’ north and latitude 18°45’ east to 19° 40’ east. The annual rainfall in the basin is about 2500 mm. The average slope of the basin is 10.61°. The Large Part of the Ulhas River basin is covered with the dispersed vegetation and the upstream of the Ulhas basin has a steep slope and the topographic slope reduces towards the west or the coast of the Arabian sea (Das and Pardeshi 2018). The average slope of the basin is 5.79% with a standard deviation of 7.79%. The maximum slope is towards the east side of 72.49%. The Major part of the basin is covered with the sequestered hills whose elevation is lower than 500 Meter (Das 2019b). The Ulhas basin is home of around 10 million people as per the 2011 census in 6 major municipal

corporations like Thane, Kalyan-Dombivili, Ulhasnagar, Bhiwandi-Nijampur, Badlapur and Ambernath which makes it most populated district in the country and any small natural calamity can lead to massive social and economic disaster. (Das 2019a; Das and Pardeshi 2018; Kim et al. 2019; Patel et al. 2017) The flooding is very frequent in the basin due to its location in the high monsoon region. Dr. Rakesh Kumar, Head of National Environmental and Engineering Research Institute (NEERI) says that due to unplanned urbanization the 25-year floods are coming at 10-year frequencies, and also climate change increases the frequencies of the flood. The Planning officials are requesting for the revised flood lines for new building sanction. In flood line of 17.5 Meter is crossed 10 times from the year 1991.

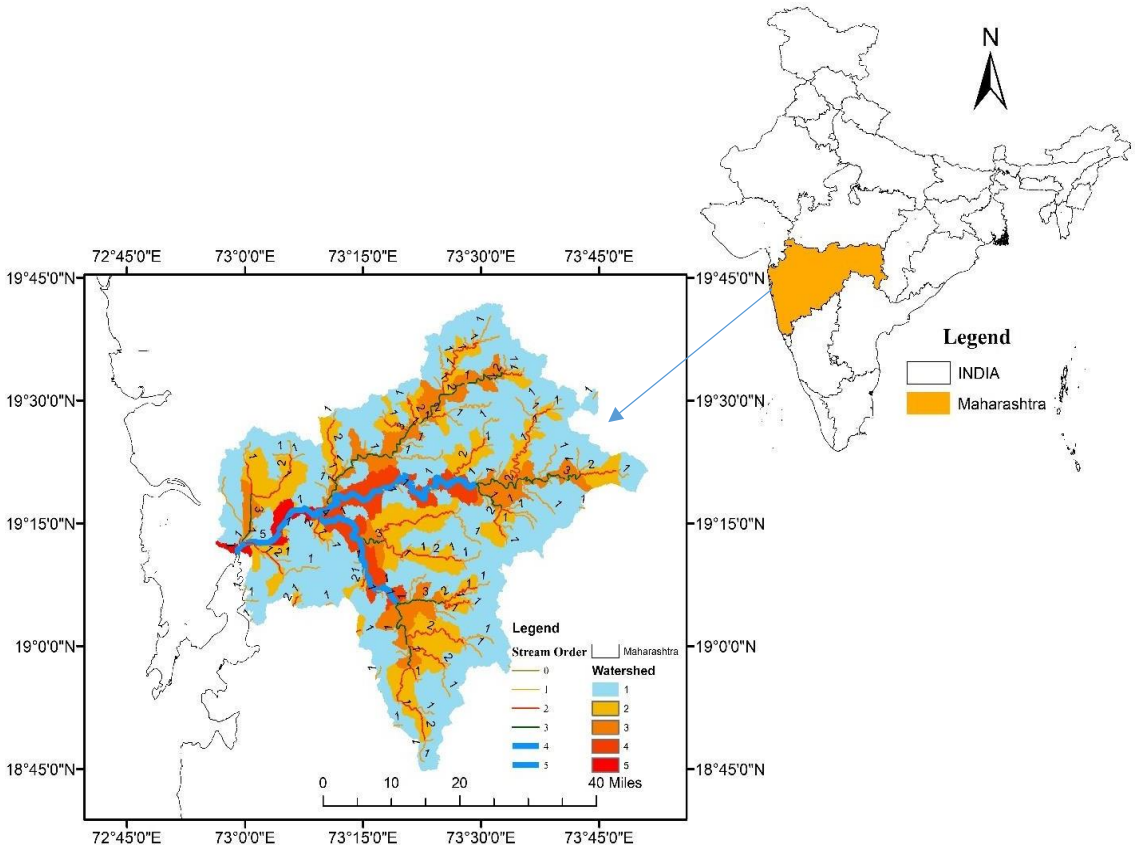



**Figure 1** Study Area of Ulhas River Basin

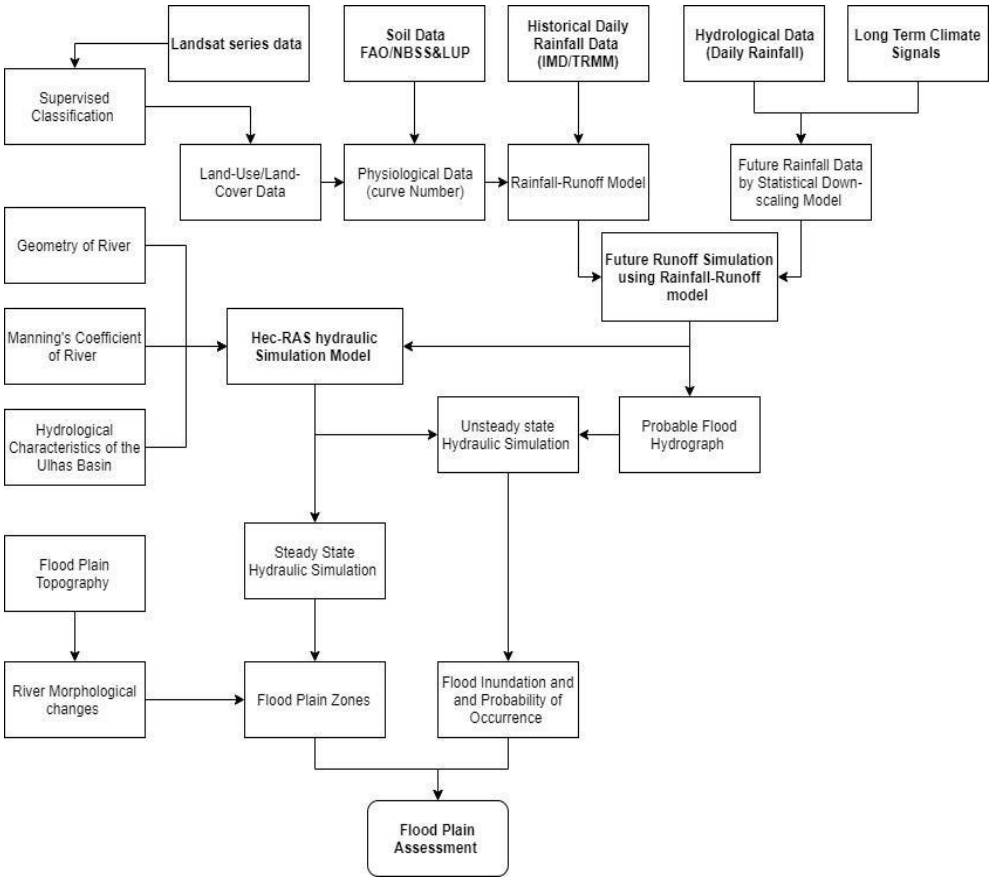
The Ulhas basin can be classified geographically into three parts as steep escarpment of western ghat with a slope of more than 20%. The gentle slope or pediment in the central part with a slope ranging from 2% to 10% and the Arabian Sea coastal low land area with a slope less than 2% (Das and Pardeshi 2018) and The Basalt rock is predominant in the Ulhas basin. The study area is situated in the Monsoon climatic region with heavy rainfall in the month of June to September and the rest of the year, the basin is in dry climatic condition. The Annual Rainfall in the basin is more than 2500 mm and the temperature ranges from 12°C to 45°C. The elevation of the basin is 0 Meters near the low land coastal area of the Arabian Sea and it reaches about 1472 Meters at the east side of the basin at the Western ghat. These physical parameters and characteristics influence the hydrological and hydraulic properties of the Ulhas basin. (Doke et al. 2018).

The Paper divided into two sections as data and methodology, which include the data used for model development for flood plain analysis and methodology of flood quantification using HEC-HMS and HEC-RAS and Conclusions as the outcome of the model as flood plain.

## 2. Data and Methodology:

For understanding the flood extent the basin characteristics are important to known and study i.e. slope of the basin, streamflow, soil types, Land use and Land cover data for curve number and other climatic information about the basin (Das 2019b; Liu and De Smedt 2005; Mohamed and El-Raey 2019; Nguyen et al. 2016),. To delineate the watershed of the Ulhas River the digital elevation map of SRTM 30M resolution is downloaded from the United States geographic survey (USGS) earth explorer website. https://earthexplorer.usgs.gov/. Land use and Land cover data are generated by the multispectral data of the Landsat 8 OLI\TIRS sensor. The LULC data is created by a supervised classification method. The daily Rainfall data of the Indian Meteorological Department (IMD), Pune, and TRMM daily Precipitation is used. The satellite rainfall product TRMM_3B42 is TRMM (TMPA) Rainfall Estimate 3 hour 0.25-degree x 0.25 degree V7 (Huffman 1997; Huffman et al. 2007). The TRMM is the combination of the passive microwave measurement from a polar-orbiting satellite and infrared measurement from a geostationary satellite (Li et al. 2009).

| Data Type | Resolution |
|---|---|
| Digital Elevation Map | 1 arc-Minute (30 Meter) |
| Land-Use/Land- Cover data | 1 arc-Minute (30 Meter) and 100 Meter (1985, 1995, 2005, 2015, 2019) |
| Daily Rainfall Data (Observed) | 0.25 X 0.25 (1901 to 2019) |
| Radar based Rainfall Data | 0.25 X 0.25 (1997 to 2019) |
| Discharge Data (Bhatsa, Badlapur, Pise and Kolhar station) | Daily Discharge 23/06/1998 to 31/10/2009 |
| Soil Data | 3 arc-Minute and 100 M x 100 M |
| Flood Inundation Maps | 100 M x 100 M |



To simulate the discharge over Ulhas basin the IMD precipitation data is used which is of spatial resolution of 0.25° X 0.25°. The Ulhas river basin is divided into 16 sub basins, 12 junctions and 10 reaches using HEC-GeoHMS tool. The elevation is process to get the flow accumulation, flow direction and to delineate the watershed the ARC-Hydro tool is used. The daily rainfall data of five metrological stations are used between the years 1975 to 2018. For loss parameters the curve number method is used in the HMS tool and the surface parameter is assigned as initial storage as 1% and maximum storage volume as 7In and then the parameters are optimized for maximum discharge using the Simplex method. The Muskingum method is used as a routing parameters with the Muskingum 'K' constant as 7 Hr and 'X' as 0.2. The simulated discharge is then compared with the observed flow data of Badlapur-hydro station. The HEC-RAS mode is run by incorporating the HEC-HMS discharge.

The elevation is processed to get the flow accumulation, flow direction and to delineate the watershed the ARC-Hydro tool is used. The daily rainfall data of five metrological stations are used between the years 1975 to 2018. For loss parameters, the curve number method is used in the HMS tool and the surface parameter is assigned as initial storage as 1% and maximum storage volume as 7In, and then the parameters are optimized for maximum discharge using the Simplex method. The Muskingum method is used as a routing parameter with the Muskingum 'K' constant as 7 Hr and 'X' as 0.2. The simulated discharge is then compared with the observed flow data of Badlapur-hydro station. For validating the simulated discharge, the validation is done for the year 2018 with the daily observed data of Badlapur hydro-station. In the HMS tool, the Badlapur hydro-station is located at the junction J129. The junction J129 is located on the reach R430 and the sub-basins W920 and W900. The curve number method is used for loss parameters in the HMS tool and the surface parameter is assigned as initial storage as 1% and maximum storage volume as 7In and then the parameters are optimized for maximum discharge using the Simplex method. The Muskingum method is used as a routing parameter with the Muskingum 'K' constant as 7 Hr and 'X' as 0.2. The simulated discharge is then compared with the observed flow data of Badlapur-hydro station. Using the optimization tool of HEC-HMS the discharge is optimized using the Simplex method for 100 maximum Iterations with 0.01 Tolerance. The following table shows the optimization parameters, its initial value, and optimized value.

| Elements | Parameters | Unit | Initial Values | Optimized Value |
|---|---|---|---|---|
| **R430** | Muskingum - K | HR | 7 | 9.1161 |
| **R450** | Muskingum - K | HR | 7 | 8.8988 |
| **W980** | Simple Surface - Initial Storage | % | 1 | 1.2402 |
| **W980** | Simple Surface - Max Storage | IN | 7 | 8.4642 |
| **W950** | Simple Surface - Initial Storage | % | 1 | 1.1781 |
| **W950** | Simple Surface - Max Storage | IN | 7 | 8.0297 |
| **W940** | Simple Surface - Initial Storage | % | 1 | 1.1161 |
| **W940** | Simple Surface - Max Storage | IN | 7 | 7.5952 |
| **W930** | Simple Surface - Initial Storage | % | 1 | 1.054 |
| **W930** | Simple Surface - Max Storage | IN | 7 | 7.1606 |
| **W920** | Simple Surface - Initial Storage | % | 1 | 0.99191 |
| **W920** | Simple Surface - Max Storage | IN | 7 | 6.7261 |
| **W900** | Simple Surface - Initial Storage | % | 1 | 0.92983 |
| **W900** | Simple Surface - Max Storage | IN | 7 | 6.2915 |
| **R430** | Muskingum - x | | 0.2 | 0.0677504 |
| **R450** | Muskingum - x | | 0.2 | 0.0562589 |
| **R430** | Muskingum - Number of Subreaches | | 1 | 1 |
| **R450** | Muskingum - Number of Subreaches | | 1 | 1 |

For the simple surface method, the initial storage is assumed to be 1% and the maximum storage is 7 IN for the watersheds. In routing parameters the Muskingum - X value is considered as 0.2 for the reach R450 and R430. The Muskingum - K value for the reach is considered as 7 hours and then it optimized for the discharge at the junction J129 which is Badlapur hydro-station. The table below shows the

optimized values for different parameters in HEC-HMS. These optimized values are used for calculating the magnitude of the peak events for the Ulhas river basin form year 1975 to 2018 to check the impact of land-use changes on the runoff.

## 3. Results and Discussion

The Land-use/Land-cover over the 20 years changed in the Ulhas river basin as the pavement area is increased in the cost of land which helps to decreases the surface runoff. The average rainfall-runoff coefficient before 20 years was 0.395 which increase to 0.42 and due to that, the overall discharge is increased by 6.0976%. The rainfall days are shrinking which makes more intense rainfall events which lead to higher flood frequencies.(Ramesh & Goswami, 2007) The urban and pavement area is increased by 145 Sq. Km and the broadleaf forest is shrinking by 142 Sq. Km in the basin. Also, the mixed forest, wasteland, evergreen forest, and plantation is decreased. The water bodies, shrubland, and cropland are increased. The Ulhas basin is home of around 10 million people as per the 2011 census in 6 major municipal corporations like Thane, Kalyan-Dombivili, Ulhasnagar, Bhiwandi-Nijampur, Badlapur and Ambernath which makes it most populated district in the country and any small natural calamity can lead to massive social and economic disaster.(Ahn & Kim, 2019; Das, 2019; Das & Pardeshi, 2018; Patel et al., 2017) The flooding is very frequent in the basin due to its location in the high monsoon region. Dr. Rakesh Kumar, Head of National Environmental and Engineering Research Institute (NEERI) says that due to unplanned urbanization the 25-year floods are coming at 10-year frequencies and also climate change increases the frequencies of the flood. The Planning officials are requesting for the revised flood lines for new building sanction. In flood line of 17.5 Meter is crossed 10 times from year 1991(Times of India, Lack of flood lines laid Badlapur low, 26th August 2019).

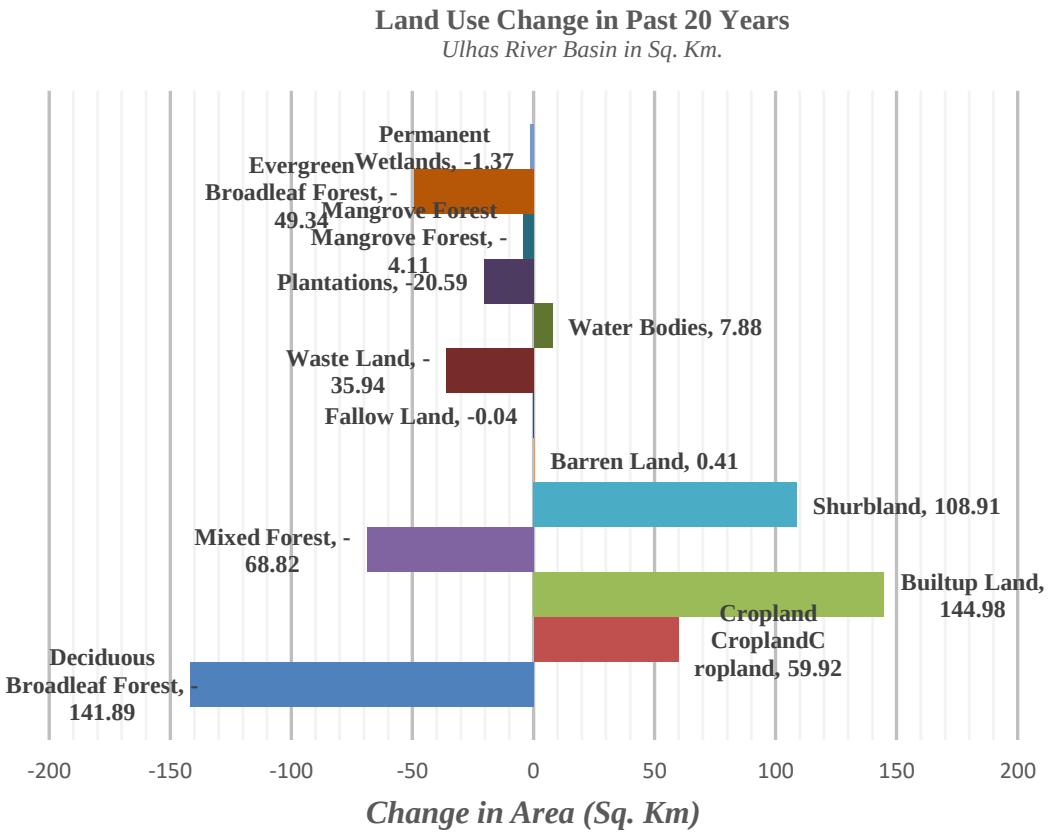
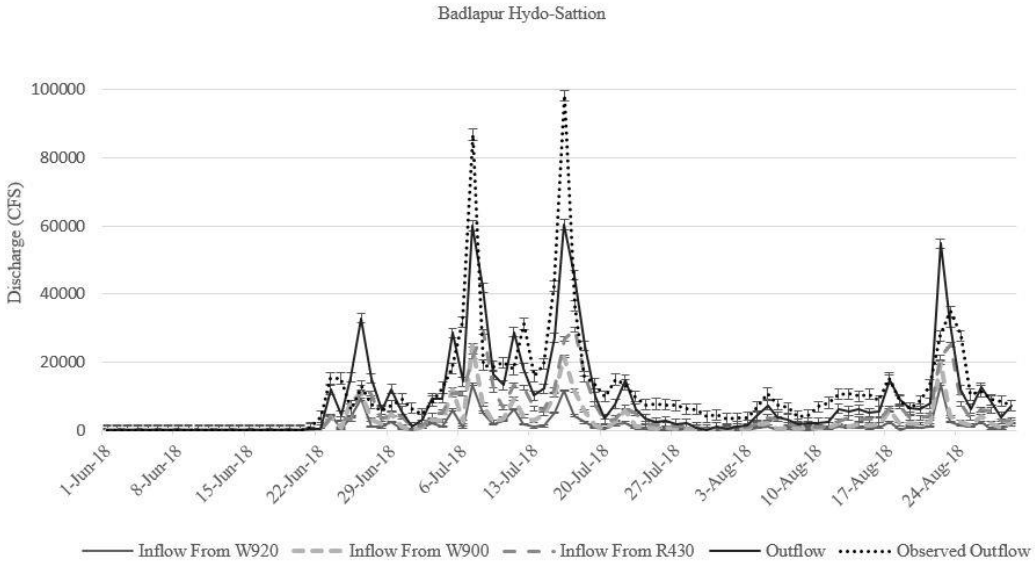



Fig:

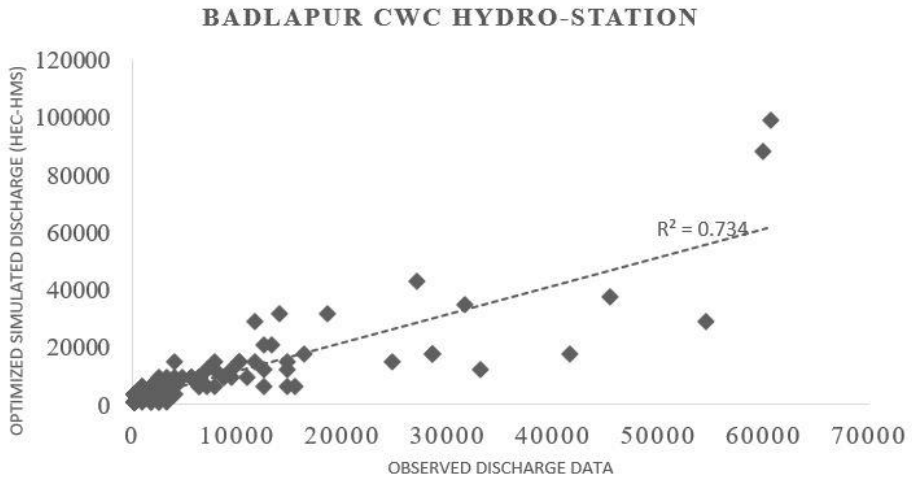
In the HMS tool, the Badlapur hydro-station is located at the junction J129. The junction J129 is located on the reach R430 and the sub-basins W920 and W900. The graph below shows the Inflow and outflow at Badlapur Hydro-station. To simulate the discharge over Ulhas basin the IMD precipitation data is used which is of the spatial resolution of 0.25° X 0.25°. The Ulhas river basin is divided into 16 sub-basins, 12 junctions, and 10 reaches using the HEC-GeoHMS tool. The optimized results show a satisfactory correlation (Wagner et al., 2016) of 0.73 with simulated and observed values of the discharge at the J129.




The above graph represents the inflow and outflow at the junction J129 which is the only observation station of the Ulhas river basin for validating maintained by the central water commission (CWC). The graph include the outflow from the junction and inflow of the sub basins W920 and W900 which contribute to the reach R430 and junction J129. The simulated outflow is matches with the observed outflow of the Badlapur hydro-station. The good correlation can achieve with the good degree of filed data and the stream coefficients(El Alfy, 2016; Thakur et al., 2017).

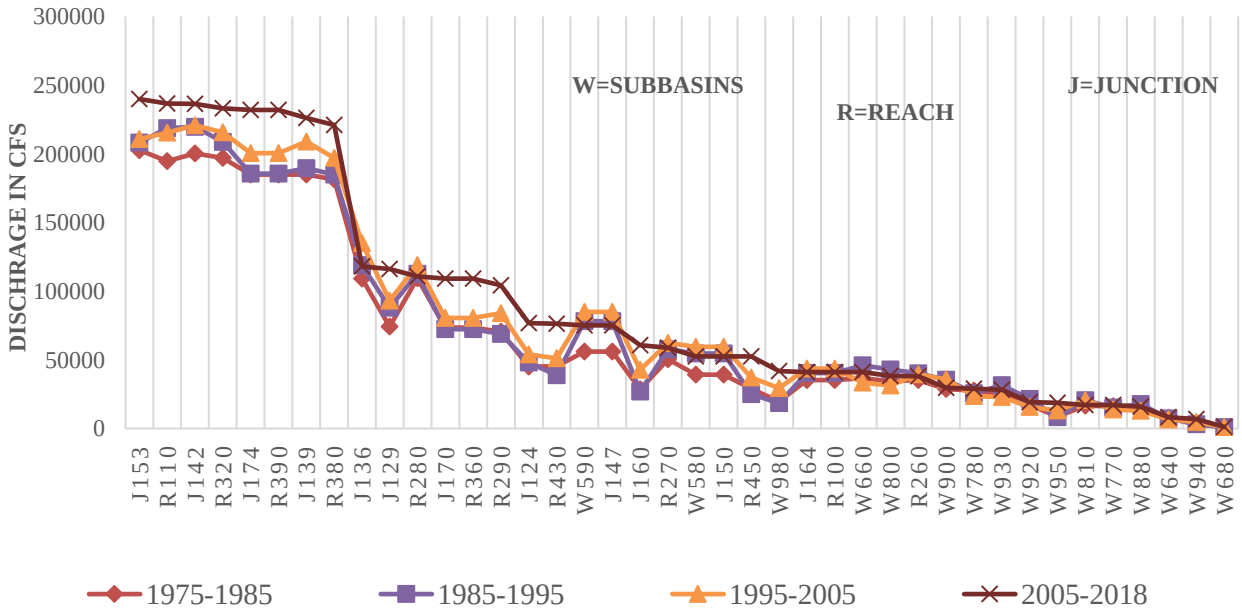
The simulating the discharge at the junction the simple surface parameter is consider with the initial assumption of 1% initial storage and 7 In as maximum storage. For losses the SCS CN is used and the routing parameter is set by the Muskingum method. The above graph represents the significant amount of correlation with the observed outflow and simulated discharge using HEC-HMS. The figure below is the correlation of the observed and optimized simulated discharge. The correlation coefficient i.e. $R^2$ value is 0.734 which shows the good performance of the model.

The graph 3 represents the magnitude of the peak events of each hydrologic components like sub basins, junctions and reaches in the Ulhas river basins. The peak events are calculated from year 1975 to 2018 with the help of daily rainfall data from the Indian meteorological department, Pune. The rainfall runoff model is generated with help of HEC-HMS to identify the impact on the peak events occur in the Ulhas river basin. The graph clearly shows the magnitude of the peak events is increasing from the year 1975 to 2018. The upper line represent the magnitude of the peak events from year 2005-2018 which is higher than the magnitude of the peak discharge in the years 1975-1985. The magnitude is increasing from the year 1975 to 2018 because of change in land use changes in the Ulhas river basin. The change in magnitude of peak events are due to either change in rainfall magnitude or change in the curve number because the runoff is proportional to the curve number. Over the years Ulhas river basin faces the massive changes in the land use due to its location and development of the housing and industrial projects and as a result the area of pavement is increased with the significant rate and the runoff is increased which leads to the flash floods and high magnitude of the peak discharge.




The figure below also shows the junction and reaches who suffer a lot or generate maximum runoff compare to the other hydrologic elements are the most vulnerable regions in the Ulhas river basin. The junction J153, J142, J174 located at the most dense populated region of Thane Municipal Corporation. Similarly the J139 is located at the populated area of Kalyan-Dombivili Municipal corporation and J129 located at the Badlapur and all the locations are consider as the sub-urban area which are going to change due to the high demand of houses and industry around them.

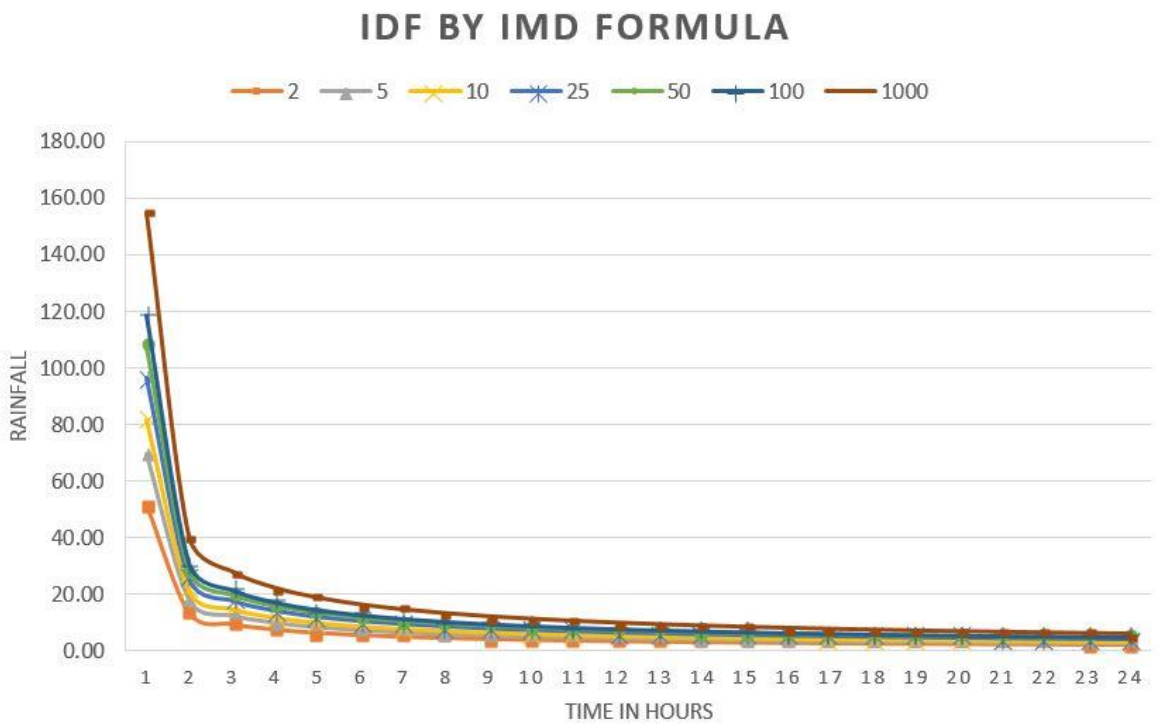
The reach R110, R320, R390 and R380 also located at the highly dense populated regions The Graph (A) below represents the rainfall which is responsible for the peak discharge over the Ulhas river basin from the year 1970 to 2018. The rainfall data is obtained from the gridded IMD, Pune data of spatial resolution of 0.25° X 0.25°. The values below are the mean of the five rainfall stations over the Ulhas river basin. The trend line shows slightly increasing trend but not significant to observe. The slope of the trend line is positive 0.0007 which isn't the significant slope to observe. On comparing the rainfall with the change in magnitude of peak discharge the rainfall is not playing significant role.



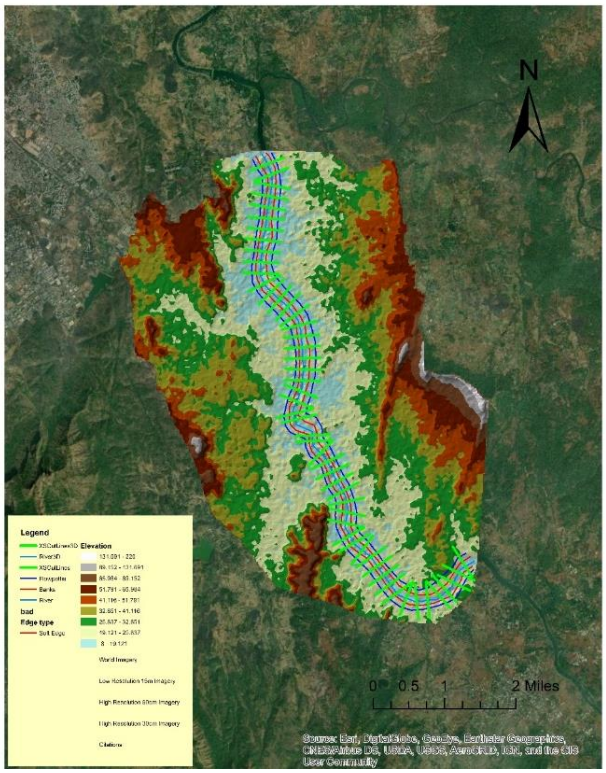
Modeling and management of the floods under changing climate is important for the design of many hydrological structure which are based on the maximum water discharge during floods. The analysis of the floods is also important to understand the degradation of the quality of the water, losses of life during the disaster and the other socio-economical losses. The Intensity-Duration-Frequency Curve provides the information of the relationship between the rainfall intensity, its duration and the return period of the rainfall which is important for the analysis of the floods and its probable return period. The IDF can be determine by different methods and some of the methods are describing below.

IDF by Indian Metrological Department (IMD) method:

| **T** | **2** | **5** | **10** | **25** | **50** | **100** | **1000** |
|---|---|---|---|---|---|---|---|
| **KT** | -0.1643 | 0.71946 | 1.30456 | 2.04385 | 2.59229 | 3.13668 | 4.93552 |
| **XT (mm/Day)** | 148.888 | 200.403 | 234.51 | 277.604 | 309.574 | 341.308 | 446.166 |
| **Rainfall Intensity (mm/hr)** | 6.20368 | 8.35011 | 9.77124 | 11.5668 | 12.8989 | 14.2212 | 18.5902 |
| **0** | **2** | **5** | **10** | **25** | **50** | **100** | **1000** |
| **1** | **51.67** | **69.55** | **81.39** | **96.34** | **107.44** | **118.45** | **154.84** |
| **2** | 13.42 | 18.06 | 21.13 | 25.01 | 27.89 | 30.75 | 40.20 |
| **3** | 9.41 | 12.66 | 14.82 | 17.54 | 19.56 | 21.57 | 28.20 |
| **4** | 7.49 | 10.08 | 11.80 | 13.96 | 15.57 | 17.17 | 22.44 |
| **5** | 6.32 | 8.51 | 9.96 | 11.79 | 13.15 | 14.50 | 18.95 |
| **6** | 5.53 | 7.44 | 8.71 | 10.31 | 11.49 | 12.67 | 16.56 |
| **7** | 4.94 | 6.65 | 7.79 | 9.22 | 10.28 | 11.33 | 14.81 |
| **8** | 4.49 | 6.05 | 7.07 | 8.37 | 9.34 | 10.30 | 13.46 |
| **9** | 4.13 | 5.56 | 6.51 | 7.70 | 8.59 | 9.47 | 12.38 |
| **10** | 3.84 | 5.16 | 6.04 | 7.15 | 7.97 | 8.79 | 11.49 |
| **11** | 3.59 | 4.83 | 5.65 | 6.69 | 7.46 | 8.22 | 10.75 |
| **12** | 3.38 | 4.54 | 5.32 | 6.29 | 7.02 | 7.74 | 10.12 |
| **13** | 3.19 | 4.30 | 5.03 | 5.95 | 6.64 | 7.32 | 9.57 |
| **14** | 3.03 | 4.08 | 4.78 | 5.66 | 6.31 | 6.95 | 9.09 |
| **15** | 2.89 | 3.89 | 4.55 | 5.39 | 6.01 | 6.63 | 8.67 |
| **16** | 2.77 | 3.72 | 4.36 | 5.16 | 5.75 | 6.34 | 8.29 |
| **17** | 2.65 | 3.57 | 4.18 | 4.95 | 5.52 | 6.08 | 7.95 |
| **18** | 2.55 | 3.43 | 4.02 | 4.76 | 5.30 | 5.85 | 7.64 |
| **19** | 2.46 | 3.31 | 3.87 | 4.58 | 5.11 | 5.63 | 7.37 |
| **20** | 2.37 | 3.19 | 3.74 | 4.42 | 4.93 | 5.44 | 7.11 |
| **21** | 2.30 | 3.09 | 3.61 | 4.28 | 4.77 | 5.26 | 6.88 |
| **22** | 2.22 | 2.99 | 3.50 | 4.15 | 4.62 | 5.10 | 6.66 |
| **23** | 2.16 | 2.90 | 3.40 | 4.02 | 4.48 | 4.94 | 6.46 |
| **24** | 2.10 | 2.82 | 3.30 | 3.91 | 4.36 | 4.80 | 6.28 |




The HEC-GeoRAS is an extension to the Arc-GIS to create the geometry of the river. The HEC-GeoRAS helps to determine the Stream center line, Banks and flow path center line. The geometry of the river system is digitized using the elevation map. For this study the 30-meter ASTER Digital Elevation Model (DEM) is used and then it was converted into the Triangulated integrating network. The cross section is drawn at the specific interval to the river, bank and flow path. The river geometry is then import into the HRC-RAS.



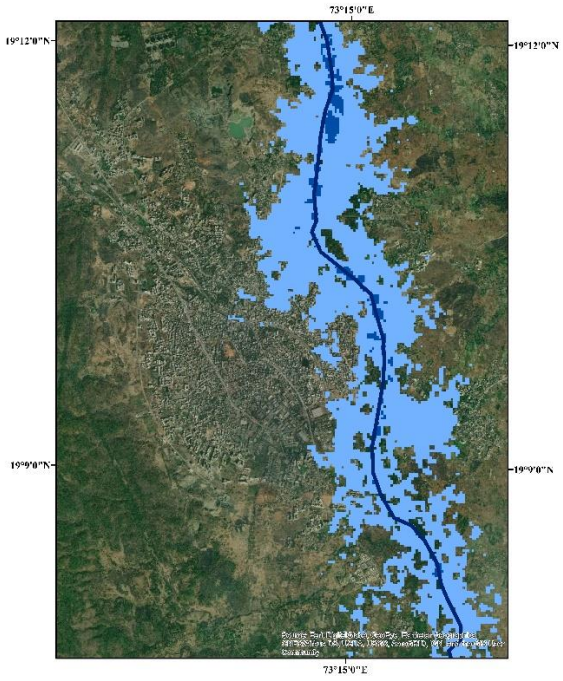
After importing the geographic data of the river in HEC-RAS, the manning's Constant is applied to the stream and the discharge is assign to the river which was derived from the HEC-HMS.

| Cross-Section | River Station | Left Bank Station | Right Bank Station | Cross-Section | River Station | Left Bank Station | Right Bank Station |
|---|---|---|---|---|---|---|---|
| **1** | 18807.13 | 1254.003 | 2471.325 | 20 | 9620.739 | 1820.407 | 3310.696 |
| **2** | 18197.04 | 1252.789 | 2507.645 | 21 | 9057.419 | 1544.619 | 3129.331 |
| **3** | 17709.45 | 1476.247 | 2640.945 | 22 | 8484.9 | 1660.827 | 2914.272 |
| **4** | 17150.18 | 1409.547 | 2742.52 | 23 | 8011.586 | 1659.121 | 3017.126 |
| **5** | 16695.7 | 1443.373 | 2754.068 | 24 | 7538.576 | 1672.408 | 3099.606 |
| **6** | 16294.14 | 1443.373 | 2793.865 | 25 | 7150.425 | 1755.052 | 3258.858 |
| **7** | 15906.31 | 1456.004 | 2742.684 | 26 | 6595.381 | 1669.816 | 3139.993 |
| **8** | 15387.35 | 1594.226 | 2746.26 | 27 | 6126.121 | 1585.433 | 3099.639 |
| **9** | 14915.51 | 1573.491 | 2773.491 | 28 | 5620.299 | 1679.134 | 3265.453 |
| **10** | 14426.1 | 1928.15 | 3290.748 | 29 | 5014.109 | 1322.736 | 3034.318 |
| **11** | 14006.99 | 1746.982 | 2797.408 | 30 | 4518.572 | 1566.798 | 3284.613 |
| **12** | 13555.28 | 1874.344 | 2995.636 | 31 | 3853.479 | 1592.848 | 3109.252 |
| **13** | 13201.92 | 2234.252 | 3495.473 | 32 | 3436.912 | 1808.694 | 3418.143 |
| **14** | 12537.06 | 1571.161 | 3160.4 | 33 | 3006.69 | 1692.979 | 3295.112 |
| **15** | 11957.19 | 1459.941 | 2736.056 | 34 | 2448.347 | 1433.104 | 2961.188 |
| **16** | 11468.43 | 1359.121 | 2652.559 | 35 | 1789.92 | 1731.857 | 3267.651 |
| **17** | 11028.96 | 1813.681 | 3245.21 | 36 | 1168.013 | 1773.589 | 3070.079 |
| **18** | 10583.44 | 2664.042 | 4083.137 | 37 | 668.7075 | 1126.87 | 2291.864 |
| **19** | 10197.78 | 2378.182 | 3785.105 | 38 | 248.7827 | 1778.117 | 2832.218 |

After preprocessing in the HEC-RAS, the water surface and flood analysis is done using the HEC-GeoRAS. In HEC-GeoRAS the water surface is generated along with the floodplain delineation. In HEC-RAS the steady and unsteady analysis is performed separately to perform the flood plain delineation.

The Following maps shows the 25 year and 100-year flood inundation map derived with help of HEC-RAS and HEC-GeoRAS.



## 4. Conclusion

The study shows the land use changes are affecting the magnitude of the peak discharge by significant amount. The findings are focused on the change in the characteristics of the flood over the Ulhas river basin using HEC-HMS, Arc-Hydro tool and HEC-GeoHMS. The area covered with the forest and shrub is converting into built-up land due to rapid urbanization and the industrialization. The paved surface is increased by 6.079% which is significantly high for the basin where average rainfall is above 93.25 Inches. The Magnitude of the discharge is increasing by 5.465 $M^3/S$ per year. The maximum change in the magnitude of peak discharge is observed at the junction J153 which is located at the Kasarwadwali, Thane Municipal Corporation. This area is densely populated which makes it most vulnerable in the Ulhas River basin. The maximum changes is also observed at the junction J153, J142 and J129 which is located at the Kalyan and Badlapur, a sub-urban region of Mumbai Metropolitan Region (MMR) which is developing at the alarming rate. The maximum changes in the land use is also observed at the Kalyan Municipal Corporation and Badlapur Municipal Corporation. The characteristics and the frequency of the flood can be analyzed with help of this study to help the planning and rehabilitation of flood prone regions in MMR. The study also involves the analysis of the Intensity-Duration-Frequency (IDF) by three methods i.e., IMD, Kothyari and Modified Kothyari Grade method. The overall rainfall for 100 year return period is about 125 mm per hour and 250 to 175 mm per hour which shows the differences by different methods in the values of probable rainfall density. The Modified Kothyari Grade over predict the rainfall intensities for higher return period than other two methods i.e., IMD and Kothyari method. For smaller return period like 2, 5, 10 and 20 the intensities show the resemblance.The mapping of the flood is done using the HEC-RAS. The projected discharge from the HEC-HMS is used to determine the area under flood and the inundation map is created. After preprocessing in the HEC-RAS, the water surface and flood analysis is done using the HEC-GeoRAS. In HEC-GeoRAS the water surface is generated along with the floodplain delineation. In HEC-RAS the steady and unsteady analysis is performed separately to perform the flood plain delineation.

## References

Ahn, K. H., & Kim, Y. O. (2019). Incorporating climate model similarities and hydrologic error models to quantify climate change impacts on future riverine flood risk. *Journal of Hydrology*, *570*(June 2018), 118–131. https://doi.org/10.1016/j.jhydrol.2018.12.061

Das, S. (2019). Geospatial mapping of flood susceptibility and hydro-geomorphic response to the floods in Ulhas basin, India. *Remote Sensing Applications: Society and Environment*. https://doi.org/10.1016/j.rsase.2019.02.006

Das, S., & Pardeshi, S. D. (2018). Morphometric analysis of Vaitarna and Ulhas river basins, Maharashtra, India: using geospatial techniques. *Applied Water Science*, *8*(6), 1–11. https://doi.org/10.1007/s13201-018-0801-z

El Alfy, M. (2016). Assessing the impact of arid area urbanization on flash floods using GIS, remote sensing, and HEC-HMS rainfall-runoff modeling. *Hydrology Research*, *47*(6), 1142–1160. https://doi.org/10.2166/nh.2016.133

Patel, D. P., Ramirez, J. A., Srivastava, P. K., Bray, M., & Han, D. (2017). Assessment of flood inundation mapping of Surat city by coupled 1D/2D hydrodynamic modeling: a case application of the new HEC-RAS 5. *Natural Hazards*, *89*(1), 93‑130. https://doi.org/10.1007/s11069-017-2956-6

Thakur, B., Parajuli, R., Kalra, A., Ahmad, S., & Gupta, R. (2017). Coupling HEC-RAS and HEC-HMS in Precipitation Runoff Modelling and Evaluating Flood Plain Inundation Map. *World Environmental and Water Resources Congress 2017: Hydraulics and Waterways and Water Distribution Systems Analysis - Selected Papers from the World Environmental and Water Resources Congress 2017*, 240 251. https://doi.org/10.1061/9780784480625.022

*IN PROCEEDINGS OF 25th HYDRO 2020, INTERNATIONAL CONFERENCE, NATIONAL INSTITUTE OF TECHNOLOGY ROURKELA, ODISHA, INDIA 26-28, March 2021, ISBN 978-93-90631-56-8*

Paper ID - 249

# Flood Inundation Mapping of Chalakkudy River using HEC RAS

Jeslin Jose A [1], Dr. Sumam K S [2]

[1]*M Tech, WR&HI, Dept of Civil Engineering, GEC Thrissur 680009, Kerala, India*
[2]*Associate Professor, Dept of Civil Engineering, GEC Thrissur 680009, Kerala, India*
*Email:* [1] *jeslin23@gmail.com ,* [2] *sumam@gectcr.ac.in*

## Abstract

Flood mapping with respect to discharge or water level through the river is a pre requirement for any flood disaster management, evacuation or rehabilitation plan. Flood, that occurred in Kerala during 2018, known as flood of the century causes loss of lives, properties and massive destruction to infrastructure. Chalakudy town, located near the bank of Chalakkudy river, was one of the most affected area during the flood. The flood mapping for a selected stretch on either banks of Chalakkudy river including the town is performed to understand the flood severity and the inundation depth. In order to account the meandering nature of the river, a two dimensional model is taken for flood inundation study using HEC RAS The flood inundation map is prepared and validated by site investigation.

***Keywords:*** *flood mapping, Kerala flood, inundation map*

## 1. Introduction

A flood is an overflow of a large amount of water beyond its normal limits, submerges land that is usually dry. It is considered to be the most frequent type of natural disaster. Heavy rainfalls, snowmelts, tropical cyclones or tsunami can cause flood. Floods may end up in widespread destruction includes loss of life, damaging the personal property or creating critical public health issues. More than 2 billion people are affected worldwide by flood which occurred from the year 1998 to 2017. People, who live in floodplains, non-resistant buildings, or with lack of warning systems and awareness of flood hazard, are most vulnerable to floods (World Health Organization- Floods). Recently high intense floods are increasing in number because of unpredictable climatic changes- the intensity and frequency of extreme precipitation is also expected to increase further- in future.

### 1.1. *Flood routing*

In hydrology, flood routing is a technique for assessing flood hydrographs at a river section by using flow data at one or more upstream sections. Flood routing and hydrograph generation form the key elements of a watershed hydrologic model. Study of problems like flood prediction, flood control, reservoir design and spillway design inevitably requires flood routing. Routing methods can be broadly classified into reservoir routing and channel routing on the basis of applications. Impact of a flood wave entering a reservoir is studied in reservoir routing to understand the variations in reservoir elevation and outflow discharge; considering volume-elevation characteristic of the reservoir and the outflow elevation relationship for the spillways and other outlet structures in the reservoir. The transition in hydrograph shape is studied in channel routing as it flows down a river. By considering a channel reach and an input hydrograph, channel routing aims to predict the flood hydrograph at different parts of the channel stretch.

The routing methods can be broadly classified into hydrologic routing and hydraulic routing. Hydrologic routing methods use the equation of continuity for computations. The basic consideration in this method is inflow minus storage gives the outflow. Hydraulic routing method employs both the continuity equation and equation of motion of unsteady flow. The basic equation used in hydraulic routing are Saint-Venant equations, which gives a better definition for unsteady flow than the hydrologic methods (Subramanya, 2013). The invention of modern high speed digital computers has given rise to many intelligent softwares than can solve numerical problems of flood routing, so that one can easily determine the flood extend and flood depth at specified locations by knowing the inflow hydrograph.

### 1.2. *Flood in Kerala*

The recent flood in Kerala that occurred due to extreme downpour from 8th August 2018 is known to be the worst flood in the state in nearly a century. Over 483 people died, and 14 are found to be missing during the disaster. About a million people were evacuated. According to CWC, from June 1st to August 19th in 2018, Kerala experienced abnormally heavy rainfall than any year. Rainfall was about 42 % more than normal rainfall (CWC, 2018). As per the recent studies (Mishra et al., 2018; IIRS, 2018) continuous and extreme precipitation events in Kerala, resulted in a huge surface runoff; filling all reservoirs, which were already almost full. The dams were forced to release a huge quantity of water in a short duration, resulting in splashing and destruction of downstream areas.

The persistent and extreme rainfall happened in Kerala during August 2018 affected all aspects of human lives including socioeconomic conditions, transportation, infrastructure, agriculture, livelihood etc. The Government of India had declared the flood as a Level 3 Calamity, or "calamity of a severe nature". All 14 districts of the state were placed in red alert. According to the Government of Kerala, one-sixth of the total population of Kerala had been directly affected by the floods and related incidents. Chalakudy town was one of the most effected towns in that flood. Chalakudy, like many parts of Kerala, had been underwater for three days. At least four people in the town lost life during the flood.

### 1.3. *Need for the study*

Flood as a natural disaster causes huge losses to lives and infrastructure. Preparation of flood inundation maps based on the peak discharge (of previous floods) will be very useful for disaster management in future. When flood inundation maps are prepared, it will be helpful to conduct the flood studies, which are necessary for real-time evacuation/ emergency action. The flood maps can be used to create a priority based evacuation plans in advance. Also mapping the flood is very important for future references and planning. This paper attempts to prepare the flood inundation map of the study area using HEC RAS.

## 2. Methodology

Methodology adopted in this study is summarized as a flow chart and is given below.

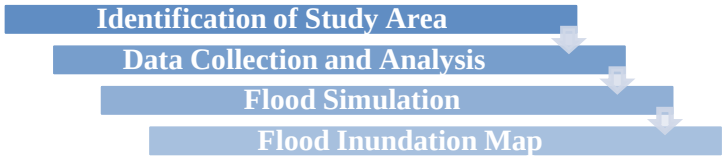



**Figure 1** Flow chart showing Methodology

### 2.1. *Identification of study area*

**Chalakudy** municipal town situates on the banks of Chalakudy river in Thrissur District of Kerala. It is functioning as the headquarters of Chalakudy taluk. Chalakudy lies on NH 544 and located about 30 km south of Thrissur town and 47 km north of Cochin city. Chalakudy Market is an important place for trade in the district.

**Chalakudy river** is a tributary of Periyar River, and also it is the fifth largest river in Kerala having length of about 145.5 km. It flows through three districts in Kerala; Palakkad, Thrissur and Ernakulam. Even though Chalakudy river is a tributary of the Periyar, for all practical studies it is treated as a separate river by Government or other agencies. Chalakudy river has a catchment area of 1,704 $km^2$, with 1,404 $km^2$ in Kerala and 300 $km^2$ in Tamil Nadu (Maya K. 2005).

Chalakkudy was one of the most effected regions in the flood of 2018. From 14th to 18th August 2018, Chalakudy city, located on the right bank of Chalakudy River faced a massive destruction due to heavy flood. Chalakudy market itself had of a loss of more than 300 crores due to drowning of food grains stored for the upcoming festival – Onam. Further in 2019 also there was heavy rainfall in Chalakudy area but it was not ended up in heavy floods as in 2018. The occurrence of flood in consequent years indicates its chance in future. So in consideration of the flood occurred in 2018, Chalakudy was selected as the study area. Figure 2 shows the major areas of town during flood in 2018.



**Figure 2** Impact of flood in Chalakudy in 2018
[Oline news/youtube of Mathrubhumi, Times of India, Malayala Manorama Newspapers]

For disaster management of probable floods in future, flood inundation maps of the area (Chalakudy) will be helpful. Flood routing software HEC RAS that can be downloaded from the website of US Army Corps of Engineers is widely used for flood inundation studies across the world. Chalakudy town is located at upstream of the river gauging station of Central Water Commission (Arangaly gauging site). At upstream, State Irrigation Board has a gauging station in Chalakudy River, but it is too far from the town. Also, the data of state irrigation department's gauging station located at Vettilapara is not available due to interstate water conflicts. So, in order to study the flood inundation and flood extend of the area, the discharge at upstream location of Chalakudy town is required. Since it is not available, it was accomplished by using reverse routing technique.

## 2.2. *Data collection and analysis*

Shape file of Chalakkudy watershed was collected from the website of Kerala Land Use board www. kslublris.com - Land Use Information System. This shape file will help to confine the other files to a required region alone, making computations simpler. Digital elevation model (DEM) is a three-dimensional representation of a terrain's xyz coordinates, each point showing the location and elevation. DEMs were used to assess terrain attributes like slope, aspect and height of any point. The DEM used in this study was downloaded from USGS-Earth Explorer with a 30 m x 30 m resolution. River Gauging station selected for the study is Arangaly station of Central Water Commission (CWC), which is located downstream of Chalakkudy town in Chalakkudy River. The data from this station was collected from CWC Office Coimbatore and Bangalore. Discharge data from the gauging station include the observed and interpolated flow values in $m^3/s$ for the year 2018; hydrograph for the period is shown in Figure 3. The peak of the hydrograph is observed from 12th August to 23rd August 2018; this period is selected for the modeling. Also the details regarding the Arangaly station like location, coordinates are obtained from Water Year Book, CWC (2017-2018).

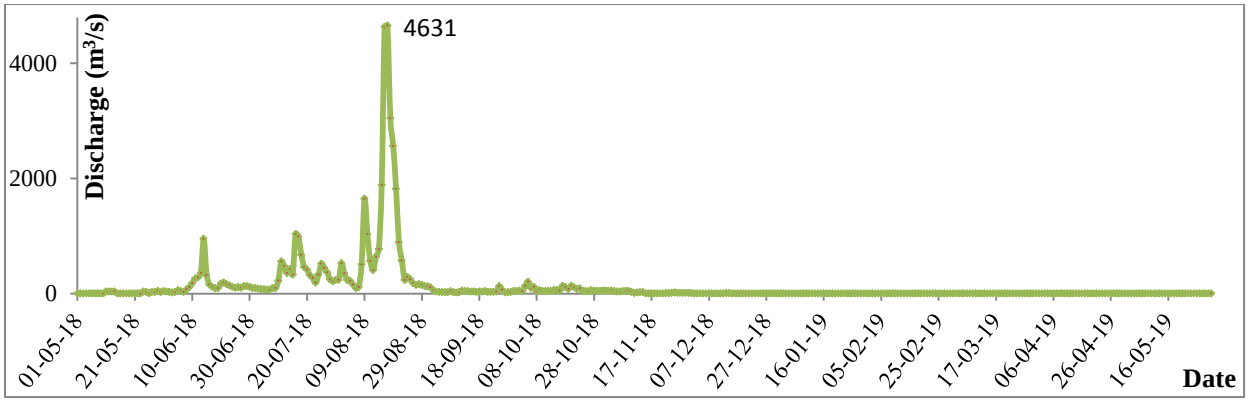



**Figure 3** Hydrograph from May 2018 to May 2019

### 2.3. *Flood Routing and map*

The flow routing software used in this study is HEC RAS. Input data required for executing HEC-RAS are cross section data, boundary conditions, Manning's value etc. Upstream and downstream conditions are provided for flow modeling. Flow in a river is modeled with required computational time steps. Results obtained from HEC-RAS are depth, velocity and water surface elevation. Flow chart showing various steps performed in this project is shown in Figure 4.

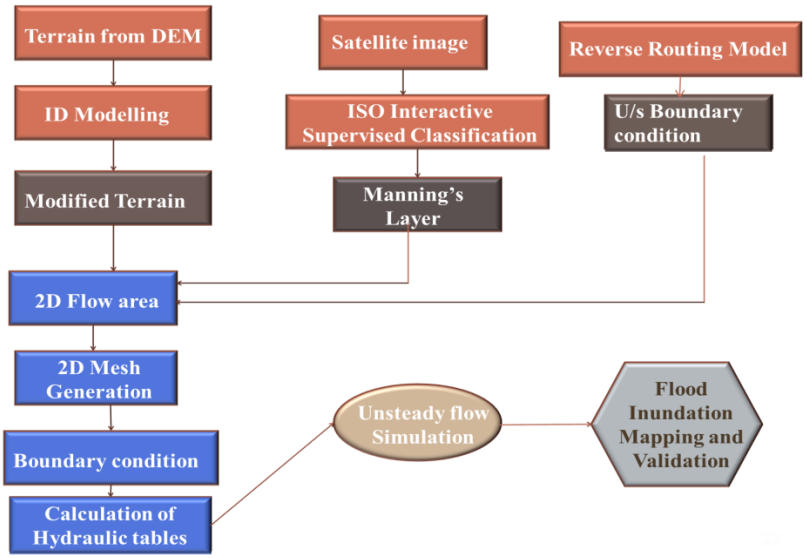



**Figure 4** Flow chart for flow modeling in HEC RAS

## 3. MODELLING IN HEC RAS

### 3.1. *One Dimensional Modeling*

HEC RAS software was used for the one dimensional modeling of Chalakkudy River. The RAS Mapper which is also a GIS Tool within HEC RAS is a dedicated interface for visualization and processing of geospatial data. Before geometry generation, it is necessary to create the basic conditions to develop geospatial features like terrain.

#### 3.1.1. *Terrain*

The DEM of Chalakkudy Basin was used to create terrain in the RAS Mapper. The terrain of Chalakkudy Watershed is shown in Figure 5. Elevation of the terrain varies from 0 to 1600. Grey colour indicates places with highest range of elevation and yellow to blue colour indicates places with lowest elevation. The river flows from highest to lowest elevation i.e right to left as shown in the Figure 5.

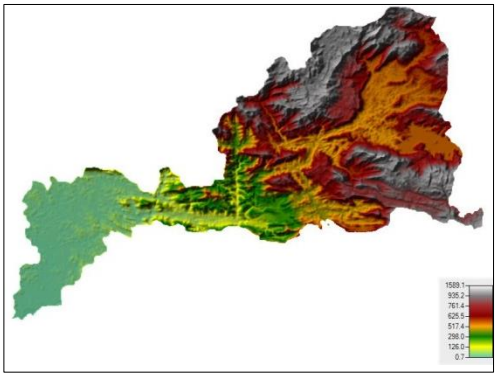


**Figure 5** Terrain of Chalakkudy Watershed

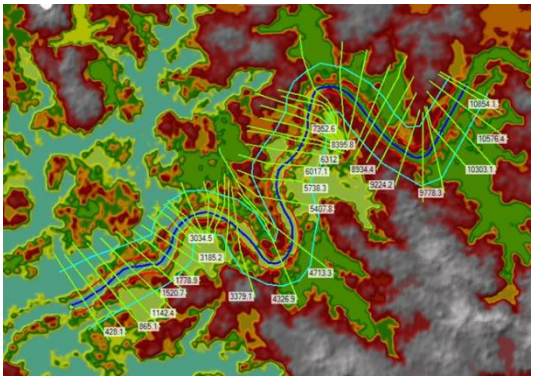


**Figure 6** River Geometry

### 3.1.2. *Geometry*

River Geometry was created in RAS Mapper that includes river centerline, bank lines, flow paths and Cross sections as shown in Figure 6. Google satellites map layer and Google hybrid map layer helped in that process. River centerline is seen in blue colour, bank lines in red colour, flow paths in cyan and cross section lines in green colour.

### 3.1.3. *Manning's value*

Manning's value indicates the roughness or resistance to the flow. Usually, channels have low Manning's value than the banks owing to high resistance. On banks the water is prevented from free flow and more water infiltrates into the soil. In this study, for one dimensional modeling, the channel section was assigned with a Manning's value of 0.035 and the banks were assigned a Manning's value of 0.06.

### 3.1.4. *Boundary Condition*

At upstream end of the reach, the boundary condition selected is hydrograph, predicted using reverse routing technique (Figure 7) and the downstream condition provided is the normal depth, by choosing friction slope value as 0.01. The value is selected based on the average slope of the channel. After providing the boundary condition the model was run for unsteady simulation with a computational time step of 30 seconds.

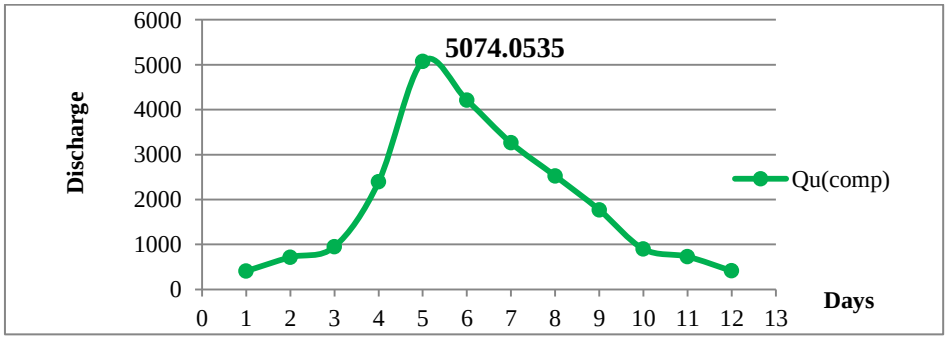



**Figure 7** Inflow Hydrograph

### 3.1.5. *Output*

Unsteady flow simulation was carried out and the output was seen to be in a scattered manner as in Figure 8. Even the flow in the river is not continuous manner. This was an erroneous result which necessitates the modification of terrain. The USGS DEM was filled using hydrology toolset in ARC GIS and then used for creating the terrain. Geometry, Manning's Value and boundary conditions were provided as in the previous case. By performing unsteady simulation on the filled DEM the output could be seen in a more satisfactory level (Figure 9).

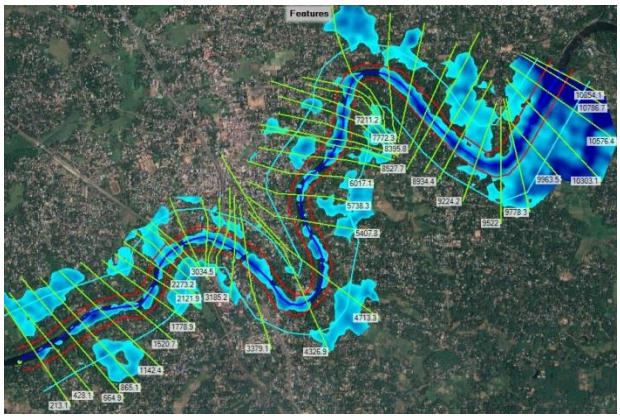



**Figure 8** I D Model output

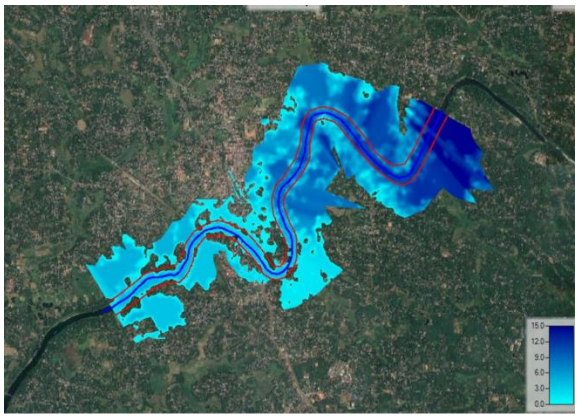


**Figure 9** I D Model output with filled DEM

While performing one dimensional simulation in HEC RAS, it was observed that straight reaches of rivers are more suitable for ID modeling. Because, to model a region on the banks of a river, sufficient numbers of the cross section lines should span over the entire region to determine the flood extent. Due to the excessive meandering property of the study reach of the Chalakudy River, the cross sections will either get congested or get intersected resulting in computational errors. Hence, two dimensional model of the study area is selected for further study.

## 3.2. *Two Dimensional Modeling*

### 3.2.1. *Modified Terrain*

A main problem that comes across hydraulic modelling is that, in the channel region, the terrain data do not always include the actual terrain underneath the water surface (HEC-RAS 2D Modeling User's Manual 2016). The RAS Mapper feature in advanced versions can be used to create a terrain model for the channel region using the cross sections and interpolation surface. This can be combined with the general terrain model to create improved terrain model for the study area. The geometry for the terrain modification that includes river centreline, bank lines, flow paths, cross section line and cross section interpolation surface, is shown in Figure 10 and the different images showing terrain before and after modification is shown in Figure 11 a to d.

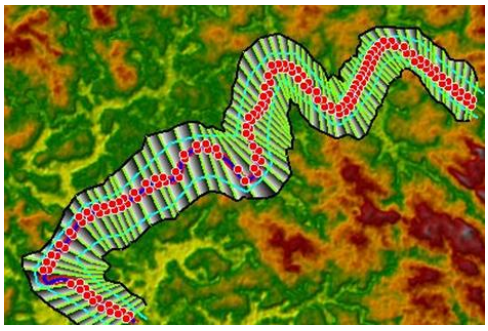


**Figure 10 -** Geometry for terrain modification

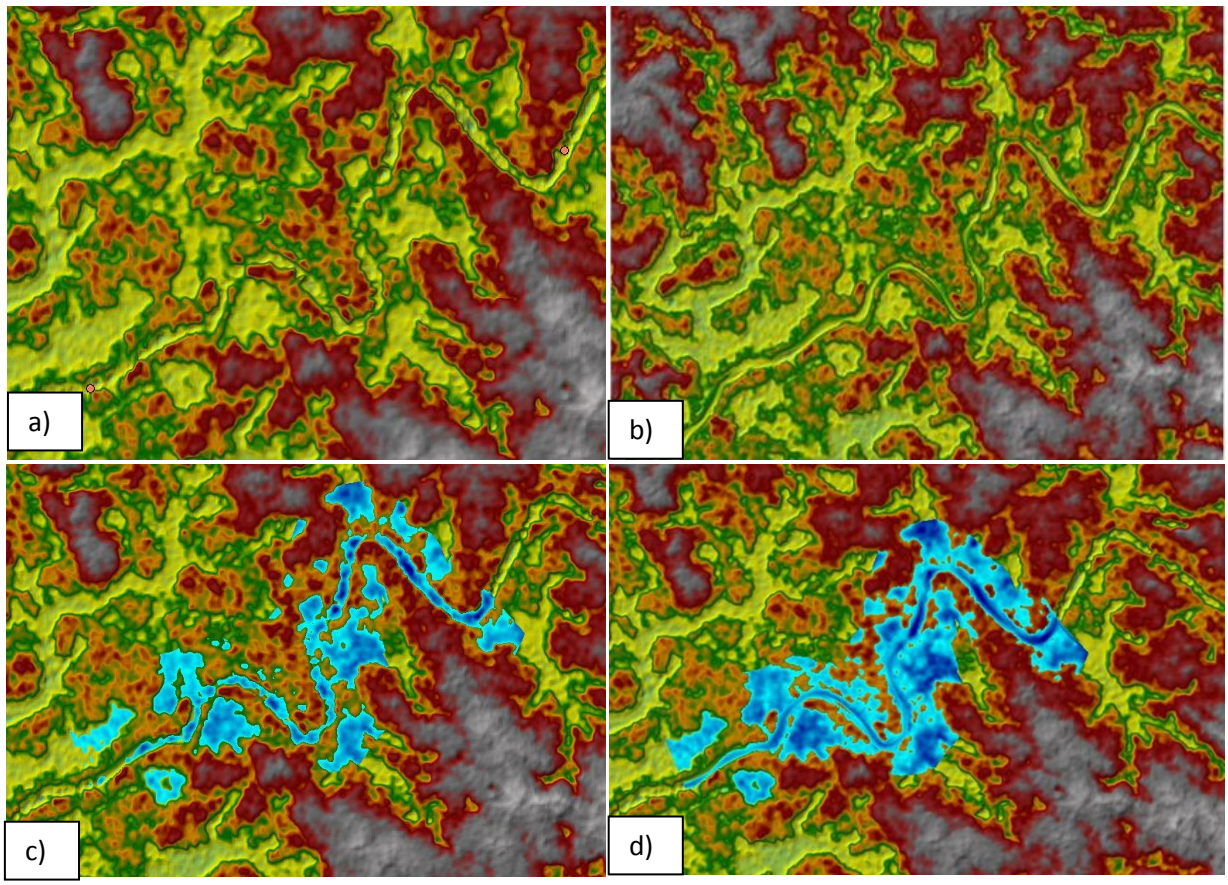



**Figure 11** Terrain Modification a) Actual terrain b) Modified terrain c) Output in actual terrain d) Output in modified terrain

### 3.2.2. *Manning's layer*

In 2D HECRAS model, the manning's values are assigned to specific land classes by creating land use polygon layer. Land use land classification map was prepared using 'Image Classification' tool set available in HEC RAS. The training samples were created by adopting minimum 10 locations for each class. Based on the training samples the ISO interactive supervised classification was performed. The land use map thus created was then converted to polygon shape file using 'Raster to Shape file' tool. The shape file layer was then organized using the tool 'dissolve'. The Land use land classification shape file was then imported to HEC RAS as Manning's layer. Manning's values were assigned to each class according to HEC RAS User's Manual as shown in figure 12. Manning's layer created from LULC shape file is shown in figure 13 with underlying terrain data.

mannings layer

| Color | Value | Name | Default Manning's n |
|---|---|---|---|
| | 0 | nodata | |
| | 1 | water body | 0.04 |
| | 2 | thick vegetation | 0.15 |
| | 3 | built up area | 0.015 |
| | 4 | agricultural area | 0.035 |
| | 5 | others | 0.06 |
| | 6 | barren land | 0.025 |

**Figure 12** Land class and assigned Manning's value

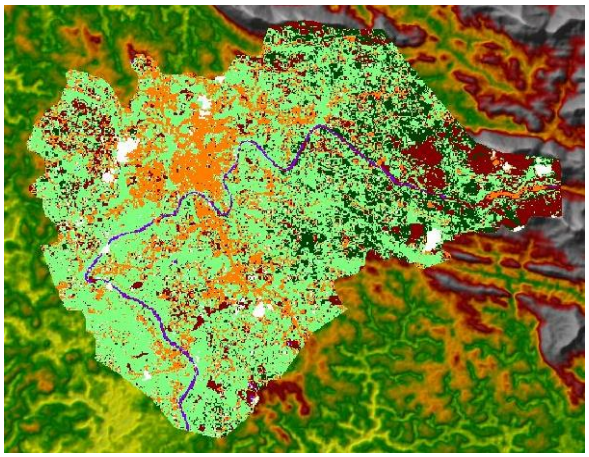


**Figure 13** LULC Map imported to HEC RAS

### 3.2.3. *Geometry- 2D flow area and mesh generation*

Most important geometry in 2D model is boundary polygon. A polygon is drawn covering the entire area of Chalakudy that is to be modeled, using '2D Flow Area' tool. After creating the flow area polygon, the 2D mesh is generated inside the polygon using the 'edit 2d flow area' button in Geometry editor. The computation point spacing for dx and dy direction is given as 50. The value indicates square meshes with sides 50 m. At the edges HEC RAS itself adjusts the shape of the mesh elements so as to match dx and dy requirements given. The total number of mesh generated is 34682. 2D Flow area, mesh generated, upstream and downstream boundary lines are shown in figure 14.

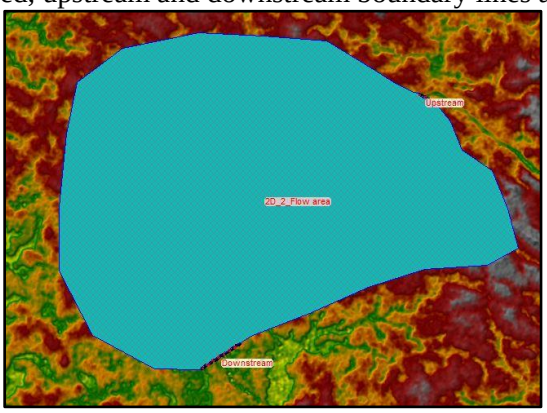



**Figure 14** 2D Flow area, mesh and boundary lines

### 3.2.4. *Boundary conditions and unsteady simulation*

Flow hydrograph is given as upstream boundary condition and normal depth is given as downstream boundary condition. The hydrograph predicted through reverse routing method forms the upstream flow boundary as in previous case. Normal depth is chosen as downstream condition by adopting friction slope value 0.01, which is based on average slope of river bed. In order to get a better result, the normal depth is provided at about 6 km downstream of actual downstream station at Arangaly. The boundary conditions were added as input data for unsteady flow simulation. Computational time step chosen was 30 seconds, based on Courant stability number which is approximated to 0.6.

### 3.2.5. *Output*

Regarding a flood inundation study the flow depth is the most important output. The flow depth corresponding to the given conditions was obtained as output from HEC RAS as shown in figure 15. The inundation depth varies from 0 to 20 m. Higher depths are observed in the channel and it reduces on banks. The terrain elevation is the most important factor that determines the flood inundation. Some regions remain dry even after they are found surrounded by flood water. This is due to high elevation of those regions. On banks, the flood inundation is maximum in the agricultural areas specifically paddy fields which have a low elevation compared to other regions.




**Figure 15** HEC RAS output –Depth

### 3.3. *Validation*

Validation of the flood inundation map which was the output of HEC RAS 2D simulation is important to check the applicability of the procedure adopted in the study. Site verification was unable to complete due to the Covid 19 pandemic situation in study area. The validation study was limited to published works, online flood maps and telephonic survey. Following are the main validation studies.

#### 3.3.1. *Published work*

In a study conducted by Jean et al (2019), a flood map of Meloor Panchayath which comes on left bank of Chalakkudy river was published. The shape of inundation map suits to the map obtained from RAS Mapper. Refer to figure 15 and 16.

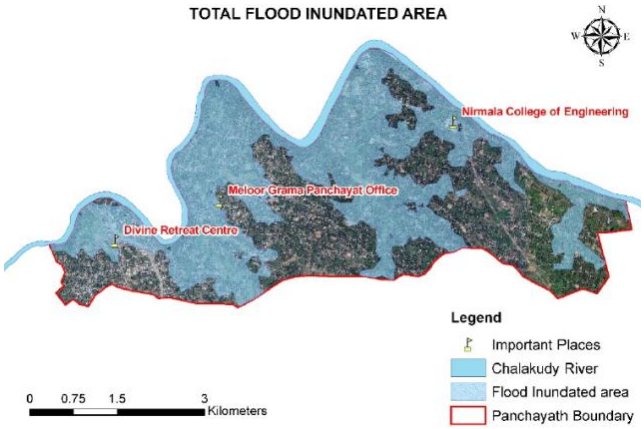



**Figure 16-**Flood Map [Jean et al.]

#### 3.3.2. *Online flood maps*

Flood maps of entire world are available at various websites on internet. One of them is www.floodmap.net. The flood map of study area is selected from floodmap.net and compared with RAS output. It is observed that the areas with major flood inundation are same in two figures (figure 15 and 17)

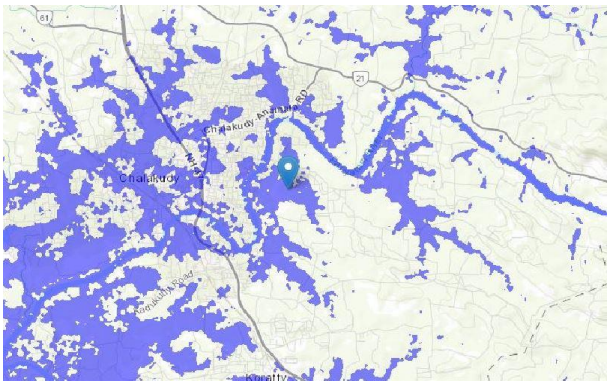



**Figure 17** Flood map [floodmap.net]

#### 3.3.3. *Telephonic survey/You Tube*

Due to Covid 19 Pandemic situation it was impossible to conduct a site survey in the study area. A telephonic survey was conducted to major institutions/shops/government offices and the inundation depth was enquired. The You Tube videos of news reports during August 2018 also give some information related to depth of flood inundation. The flood depth reported at these places in comparison with the RAS output is given in table 1. From the table it can be observed that result

obtained from HEC RAS is comparable with that of depth information collected through telephonic survey. A maximum variation of 1 m is only observed. Police station which was not affected by flood in 2018 (telephonic survey) was also not inundated by water level computed by HEC RAS. This forms a keystone for validation.

**Table 1.** Comparison of flow depth with field values

| Site | Depth as per Telephonic Survey/You Tube | Depth in m | Depth From HEC RAS | Difference |
|---|---|---|---|---|
| Arangaly station | 9.2 m | 9.2 | 9.634 | 0.434 |
| Chalakudy Market | 10.5 feet to 8.5 feet | 3.2 to 2.6 | 3.266 | 0.066 |
| Private bus stand | 1.5 person | 2.52 | 2.610 | 0.09 |
| KSRTC bus stand | 5.25 feet | 1.6 | 2.545 | 0.945 |
| BRD Car showroom | 12 feet | 3.675 | 3.795 | 0.12 |
| Carmel H S S | 2.34 m | 2.34 | 2.473 | 0.133 |
| Divine retreat centre | 10 feet | 3.05 | 3.895 | 0.845 |
| SH College | 9 feet | 2.74 | 2.944 | 0.204 |
| Govt ITI Chalakudy | 9 feet | 2.74 | 2.500 | 0.24 |
| Chikkus Curtains | 3 feet | 0.914 | 1.075 | 0.161 |
| St James Hospital | First floor | 4 | 4.284 | 0.284 |
| Police station | Not affected | 0 | 0 | 0 |
| St. Mary's Church | 2 feet | 0.609 | 0.648 | 0.039 |
| ESI Dispensary | First floor | 3.5 | 3.408 | 0.092 |
| Modi Bakers | First floor | 3.5 | 3.422 | 0.078 |
| | | | Error | 8.56 % |

## 4. Conclusions

The study aimed to prepare a flood inundation map for one of the most flood effected city in Kerala during the flood of 2018. Following are the conclusions arrived from this study.

- One dimensional flood modeling is limited in the study area because of the excessive meandering nature of the river at selected reach.
- Two dimensional model was found to be better for the study area to account the meandering nature of the river. Wider bank stretch is considered for the flood inundation study. With 2D simulation, model could predict the flood inundation map with an error of 10 %. The validation of the prepared flood inundated area was carried out through telephonic survey, news reports and published works. Some areas which were not affected by flood, were also not inundated in the simulated model, forms an important keystone for validation.

### 4.1. *Limitations of the study*

- Kerala flood of 2018 was an unexpected flood; called as Flood of Centaury, debated with thousands of reasons like dam release, flood plain encroachment etc. This study only considered the huge discharge through the river as the reason for flood.
- This study is limited to 12 km of a river (Chalakudy) whose actual length is 145 km.
- The Resolution of DEM used in the study is 30 m x 30 m, is also affecting the accuracy.
- Covid 19 pandemic situation also created certain limitations on the site investigation for the validation of flood inundation map.

### 4.2. *Scope for future work*

An extended study of entire Chalakudy basin or entire Kerala itself may be done for proper flood managements plans in future. Maps of buffer zones for various water levels in the river can also be prepared. Priority based evacuation plans can be prepared by considering like shortest routes, location based rehabilitation plans etc.

## References

1. Centre water commission, Govt. of India (2018). Study Report Kerala floods 2018.
2. HEC-RAS 2D Modeling User's Manual 2016, Version 5.0, U.S. Army Corps of Engineers Hydrologic Engineering Center, Davis, California, USA.
3. https://www.who.int/health-topics/floods- World Health Organization
4. Indian Institute of Remote Sensing and Indian Space Research Organization (2018), Hydrological Study of August 2018 Kerala Floods using Remote Sensing, Modeling and Geospatial tools, Govt. of India, Dehradun.
5. Jean, J., Kanga,S., and Suraj, K.S., (2019) Kerala Flood 2018: Flood Mapping by Participatory GIS approach, Meloor Panchayat, *International Journal on Emerging Technologies*, 10(1), 197-205
6. Maya K., (2005) Studies on the nature and chemistry of sediments and water of Periyar and Chalakudy rivers, Kerala, India, Ph.D. Thesis, Cochin University of Science and Technology, Kerala, India.
7. Mishra, V., Aadhar, S., Shah, H., Kumar, R., Pattanaik, D.R., and Tiwari, A.D. (2018), The Kerala flood of 2018: Combined impact of extreme rainfall and reservoir storage, *Hydrology and Earth System Science.*
8. Subramanya, K., (2013) Engineering Hydrology, Tata McGraw-Hill Publishers, 4th edition.
9. Water Year Book, June 2017– May 2018, West Flowing Rivers Basin, Volume I, Stream Flow & Suspended Sediment Data, CWC.

*IN PROCEEDINGS OF 25th HYDRO 2020, INTERNATIONAL CONFERENCE,*
*NATIONAL INSTITUTE OF TECHNOLOGY ROURKELA, ODISHA, INDIA*
*26-28, March 2021, ISBN 978-93-90631-56-8*

Paper ID - 291

# Non-stationary Flood Frequency Analysis of West flowing Rivers of Kerala usingBayesian Inference Approach

Anjitha U.G.[1], Meera G.Mohan[2], Adarsh S[3], Gopakumar R[4]

[1]*Post Graduate Student, Dept. of Civil Engg., Govt Engineering College Thrissur, PIN-680 009, India*
[2]*Research Scholar, TKM College of Engineering, Kollam, PIN-691 005, India*
[3]*Asso. Professor, Dept. of Civil Engg., TKM College of Engineering, Kollam, PIN-691 005, India*
[4]*Professor, Dept. of Civil Engg., Govt Engineering College Thrissur, PIN-680 009, India*
*Email: meeragmohan90@gmail.com*
*Telephone/Mobile No.: +91 8289834503*

## Abstract

Climate change has become a global concern over the past few decades and it has got a critical impact on hydrological cycle. Climatic changes display a general tendency to amplify hydrologic extremes and the hydraulic infrastructure should be capable to cope with such changes. Current practice of infrastructure design uses the hydrologic tools like flood frequency curves developed based on stationary assumption of hydrological data. Such a practice may lead to the underestimation of flood quantiles under non-stationarity of hydrologic data resulting from climatic changes. Development of non-stationary frequency analysis models is gaining popularity to avoid the failure of critical infrastructure under a changing environment. This paper presents the application of Bayesian Inference Approach (BIA) for the flood frequency analysis of 14 hydrologic stations ofwest flowing rivers of Kerala, India.The annual maximum stream flow was idealized to follow Log-Pearson Type III distribution with time varying parameters estimated in a Bayesian interface. From the analysis it was found that, the data of stations Ayilam and Perumanur were experiencing significant non-stationarity (> 25%) in the most likely estimates of discharges irrespective of the return period, over the stationary counterparts. The study showed that there exists a wide variability in the percentage change in non-stationary over the stationary estimates of flood quantiles in the state, for different return periods. The longer return period estimates show high degree of non-stationarity over the shorter return period estimates throughout the state, while the effect of non-stationarity is found to be significant even in the lower return periods at few locations. In general, it can be concluded that non-stationarity must be accounted for the design with longer return period applications (> 200 year) in all locations, while it must be accounted for smaller return period design (< 50 year) applications in few selected locations.

***Keywords:*** *Climate change; hydrologic extremes; infrastructure; non-stationarity; flood frequency; return period*

## 1. Introduction

Urbanization and anthropogenic activities have profoundly affected the environment and climate all over the world. Climate change has had extreme impacts in India over the past few years. The rise in average global temperatures has led to a worrying trend of excessive rainfall, causing extreme weather events, particularly floods. Flood Frequency Analysis (FFA) is an essential approach used widely in evaluating the occurrence probabilities of flood events. Traditional FFA methods usually assume stationarity of hydrological data, implying that floods in certain years are independent and identically distributed. Current infrastructure design concepts to deal with flooding and precipitation are based on local flood frequency curves. These curves are developed using historical streamflow data based on the assumptions that the occurrence of precipitation patterns and distributions are spatially similar within the drainage area and remain unchanged (stationary) throughout the life span of the infrastructures. i.e. concept of stationarity is used. However, climate change is expected to alter the intensity, duration or frequency of climatic extremes over time. Hence, the development of non-stationary flood frequency analysis models is gaining popularity in the field of hydro-climatology, because of recent evidences in climate change.

Various researches are being done in non-stationary frequency analysis in regard with stream flow, rainfall, temperature and so on considering time and climate as covariates (Cheng et al. 2014), Mondal and Mujumdar (2015), Ray and Goel (2019), Ouarda and Charron 2019). These studies differ in the approaches followed and datasets used in developing frequency curves in a non-stationary environment. Cheng et al. (2014) in their study developed a framework for estimating stationary and non-stationary return levels, return periods and risks of climatic extremes implemented in the form of a software package NEVA. Cheng and AghaKouchak (2014) proposed a generalized framework for estimating non- stationary IDF curves and their uncertainties using Bayesian inference. The study considered linear variation of location parameter of GEV distribution for developing IDF curves and the proposed method provided the lower and upper bound of estimated intensity values.

Mondal and Mujumdar (2015) presented the first application of non-stationary statistical modelling of intensity, duration and frequency of extreme rainfall over India. They analyzed the changes in extreme rainfall characteristics over India using a high resolution daily gridded dataset. Ray and Goel (2019) presented a case study to demonstrate a methodology for FFA considering non-stationarity of annual maximum flood series of six gauging sites from Narmada River Basin, India. The influence of climate indices and the effect of reservoir constructions on the Narmada River Basin have been included as external covariates. It was concluded that due to non-stationarity, the return level flood value increased substantially with time and may create problems for the old structures, which were designed using traditional FFA assumptions of stationarity.

Sarhadi and Soulis (2017) developed time-varying extreme rainfall intensity duration frequency curves for 911 stations from United States and Canada. The time trend and the Southern Oscillation (SOI) were used as covariates to model non-stationary conditions, various combinations of non-stationary models may be imposed in terms of the location and the scale parameters in the time-varying GEV distribution. To characterize the uncertainty of time-varying IDF curves, a Bayesian Markov chain Monte Carlo (MCMC) approach is incorporated into the non-stationary GEV model in the fully time-varying risk assessment framework. Ouarda and Charron (2019) developed a non-stationary frequency model integrating trends and climate variability by introducing covariates in the distribution parameters. Two case studies are considered in the present work, first case study deals with annual flood flows and second case study deals with extreme temperatures, both in the province of British Columbia, Canada.The addition of climate indices in the shape parameter of the non-stationary GEV model with a temporal trend on the scale parameter has resulted in improved goodness-of-fit in a flood flow case study.

The return level and return period estimates can be used in hydrology and climate studies to assess the risk (probability of occurrence) of extremes. Return period, which is also referred as recurrence interval, provides an estimate of the likelihood of any event to occur in a year. Return periods (RP) are used to convey the risks of rate events more effectively than simply stating the probabilities.Even though some studies have been conducted in India, they were centered on some specific stations (Mondal and Mujumdar 2015; Ray and Goel 2019).In this study, 14 stations covering the longest west flowing rivers of Kerala over different districts were considered for analysis. Annual maximum stream flow data set was used to develop stationary as well as non-stationary flood frequency curves. It was fit toLog-Pearson Type III distribution and the parameters were estimated using Bayesian Inference Approach (BIA)in order to find the spatial distribution of flood quantiles over Kerala under stationary and non-stationary conditions.

## 2. Methodology

FFA is a technique used by hydrologists to predict flow values corresponding to specific return periods or probabilities along a river. The flood frequency curve is used to relate flood discharge values to return periods to provide an estimate of the intensity of a flood event. The discharges are plotted against return periods using either a linear or a logarithmic scale.

Using annual peak flow data that is available for a number of years, FFA is used to calculate statistical information such as mean, standard deviation and skewness which is further used to create

frequency distribution graphs. The best frequency distribution is chosen from the existing statistical distributions such as Gumbel, Normal, Log-normal, Exponential, Weibull, Pearson and Log-Pearson. After choosing the probability distribution that best fits the annual maxima data, flood frequency curves are plotted. These graphs are then used to estimate the design flow values corresponding to specific return periods which can be used for hydrologic planning purposes. Flood frequency plays a vital role in providing estimates of recurrence of floods which is used in designing structures.

The major part of the study includes Non-stationary Flood Frequency Analysis of West flowing Rivers of Kerala using Bayesian Inference Approach. It aims to develop stationary as well as non-stationary flood frequency curves and to study spatial distribution of flood quantiles over Kerala under stationary and non-stationary conditions. In a Bayesian approach $DREAM_{(ZS)}$ algorithm estimates the extreme value parameters with a Monte Carlo Markov Chain (MCMC) approach for global optimization over the parameter space. It includes posterior probability intervals (uncertainty bounds) of estimated return levels through Bayesian inference, with its inherent advantages in uncertainty quantification. The software presents the results of non-stationary extreme value analysis using various exceedance probability methods. Non-stationary (NST) frequency analysis can improve the statistical representation of observed flood peak distributions compared to stationary (ST) analysis. This allows the parameters of the distribution to capture trends in flood frequencies. The estimation of presence of non-stationarity, computation of stationary and non-stationary LPIII parameters from annual peak discharge data through Bayesian inference was done using MATLAB.

### *2.1Log-Pearson type-III distribution*

In the present study, Log Pearson Type III (LP-III) probability distribution was applied for FFA. LP-III distribution has been widely and frequently used in hydrology and for hydrologic frequency analysis (Pawar and Hire (2018) and Sathe et al (2012)). The probability density function (PDF) and cumulative distribution function (CDF) of the log-Pearson type-III distribution are defined in (Hosking and Wallis, 1997) as:

If $\gamma \neq 0$, let $\alpha = 4/\gamma^2$ and $\xi = \mu - 2\sigma/\gamma$

If $\gamma > 0$ then,

$$F(x) = G\left(\alpha, \frac{x-\xi}{\beta}\right)/\Gamma(\alpha) \tag{1}$$

$$f(x) = \frac{(x-\xi)^{\alpha-1} e^{-(x-\xi)/\beta}}{\beta^{\alpha}\Gamma(\alpha)} \tag{2}$$

If $\gamma = 0$ the distribution is normal and

$$F(x) = \Phi\left(\frac{x-\mu}{\sigma}\right) \tag{3}$$

$$f(x) = \Phi\left(\frac{x-\mu}{\sigma}\right) \tag{4}$$

If $\gamma < 0$ then,

$$F(x) = 1 - G\left(\alpha, \frac{x-\xi}{\beta}\right)/\Gamma(\alpha) \tag{5}$$

$$f(x) = \frac{(\xi-x)^{\alpha-1} e^{-(\xi-x)/\beta}}{\beta^{\alpha}\Gamma(\alpha)} \tag{6}$$

Where $\mu$ is the location parameter, $\sigma$ is the scale parameter and $\gamma$ is the shape parameter.

A time dependent mean to account for NST in the Pearson Type III (PIII) distribution used

$$\log_{10}(Q) \approx PIII(\mu_t, \sigma, \gamma) \tag{7}$$

Where $Q$ signifies the annual maximum discharge, $t$ denotes time, and $\mu_0$, $\sigma$ and $\gamma$ characterize the mean, standard deviation, and skewness of the PIII distribution, respectively. The $\log_{10}$-transformation stabilizes the variance of the annual peak discharges and makes the transformed data more amenable to the PIII distribution. A simple linear trend for the mean of the PIII distribution

$$\mu_t = \mu_0 + \alpha t \tag{8}$$

where $\mu_0$ signifies the intercept and α is the slope of $(t, \mu_t)$ relationship. The value of $\mu_0$ is equivalent to the PIII mean of the first year of the discharge record. If flood peaks are assumed to be stationary then $\alpha = 0$ suffices in equation (2) and the resulting model simplifies to the ST PIII distribution. The use of a linear time-dependency of the LPIII mean in equation (8) is rather convenient and simplistic.

### *2.2Bayesian Inference*

The methodology used for parameter estimation, likelihood function, prior distribution and MCMC simulation using DREAM$_{(ZS)}$ algorithm in BIA is based on Luke et. al.(2017).

#### *2.2.1 Parameter Estimation*

The ST LPIII parameters $\theta_s = (\mu, \sigma, \gamma)$ and the NST LPIII parameters, $\theta_n = (\mu_0, \sigma, \gamma, \alpha)$ are inferred. More complex trends are not considered than the simple linear model, due to the uncertainity introduced by additional parameters. Here Bayesian inference and MCMC simulation with the DREAM$_{(ZS)}$ algorithm is adopted to estimate the posterior distribution of NST and ST parameters. Under the Bayesian approach for parameter estimation, Baye's theorem is used to calculate the posterior density of parameter values.

$$p(\theta_j|X, M_j) = \frac{p(\theta_j|M_j)L(\theta_j|X, M_j)}{p(X|, M_j)} \tag{9}$$

Where $p(\theta j|X,Mj)$ represents the posterior density of parameter vector $\theta j$, given the fitting period $X$, and the model of interest, $Mj$. The subscript j denotes competing model classes and here it is $s$ and $n$, which stands for the ST and NST models respectively. Here $p(\theta j|,Mj)$ represents the prior density of $\theta j$ given model and $L(\theta j|X,Mj)$ represents the likelihood of parameter values $\theta j$, given $X$ and model. The denominator is known as the marginal likelihood or evidence. The evidence is obtained through integration over the parameter space.

$$p(X|, M_j) = \int p(\theta_j|M_j)L(\theta_j|X, M_j)d\theta_j \tag{10}$$

Bayesian parameter estimation does not necessarily require the value of $p(X|,Mj)$ since parameter inference can be made from the unnormalized density.

$$p(\theta_j|X, M_j) \propto p(\theta_j|M_j)L(\theta_j|X, M_j) \tag{11}$$

when MCMC methods are used to sample from the posterior. Equation (3.7) is used to estimate the posterior density of both $\theta j$ from the data.

#### *2.2.2 Likelihood Function*

Conceptually $L(\theta j|X,Mj)$ represents how plausible a parameter combination is after observing $X$, which quantifies the information content of the data. Specifically, $L(\theta j|X,Mj)$ is the probability density of $X$ according to $M_j$ with parameterization $\theta j$. For the parameter inference procedure, the likelihood function is defined as

$$L(\theta_j \mid X, M_j) = \prod_{i=1}^{n} p(X_i \mid \theta_j, M_j) \quad (12)$$

Where $n$ is the number of observations in the fitting period, and $X_i$ represents the $i^{th}$ observation.

*2.2.3 Prior distributions*

While $L(\theta j|X,Mj)$ represents the plausibility of $\theta j$ after considering the data, $p(\theta j|,Mj)$ represents knowledge of $\theta j$ before the data are considered. Often, $p(\theta j|,Mj)$ is referred to as the prior. The prior represents an analyst's knowledge of $\theta j$ before any data are collected, which is described mathematically by the joint probability of the parameters within $\theta j$. The formal inclusion of prior knowledge about $\theta j$ in the parameter inference process is unique to Bayesian inference. The choice of priors is subjective, but it allows the analyst to use information other than the data for parameter inference. For uninformative, yet proper priors, the marginal priors for $\mu$, $\mu_o$, $\sigma$, and $\alpha$ were specified as a uniform distribution, $U(a,b)$, where $a$ and $b$ represent the lower and upper bounds of the uniform priors, respectively. Our primary reason for using bounded priors is algorithmic efficiency. Indeed, such prior enhances considerably the convergence speed of the $DREAM_{(ZS)}$ algorithm

*2.2.4 MCMC Simulation With $DREAMZ_{(ZS)}$ Algorithm*

The posterior distribution of $\theta s$ and $\theta n$ can be approximated using MCMC simulation with the $DREAMZ_{(ZS)}$ algorithm. Sampling methods such as MCMC are required for most applications of Bayes theorem, since $p(\theta j|X,Mj)$ is often analytically intractable. Essentially, MCMC methods provide a sample from the posterior distribution, and parameter inference is made from the generated sample. From the values obtained for the stationary and non-stationary cases return level v/s return period and density of return level for different return periods are plotted for the selected stations and inferences are made for it.

## 3. Study area

For this study to be conducted, daily discharge data for 14 hydrologic stations of west flowing rivers of Kerala, India was collected from Water Resource Information System, WRIS (www.indiawris.gov.in). The collected data is sorted out to get the annual maximum discharge data. Table- 1 below shows the chosen stations for the study.The annual maximum streamflow data for the record length greater than 25 years was used for the analysis.

**Table 1** Details of 14 hydrological stations over Kerala

| Sl. No. | District | River | Station | Opening date | Closing date |
|---|---|---|---|---|---|
| 1 | Ernakulam | Muvattupuzha | Kalampur | 23/06/1986 | 31/12/2018 |
| 2 | Ernakulam | Periyar | Neeleswaram | 16/03/1971 | 31/12/2018 |
| 3 | Ernakulam | Muvattupuzha | Ramamangalam | 25/04/1978 | 31/12/2018 |
| 4 | Kannur | Valapatnam | Perumannur | 26/06/1985 | 31/12/2015 |
| 5 | Kasaragod | Payaswani | Erinjipuzha | 25/06/1985 | 31/12/2018 |
| 6 | Kollam | Kallada | Pattazhy | 01/06/1973 | 31/12/2018 |
| 7 | Malappuram | Bharathapuzha | Kumbidi | 08/01/1979 | 31/12/2018 |
| 8 | Malappuram | Pulanthode | Pulamanthole | 17/02/1986 | 31/12/2018 |
| 9 | Palakkad | Bharatapuzha | Pudur | 02/09/1985 | 31/12/2018 |
| 10 | Pathanamthitta | Manimala | Kalloppara | 19/06/1985 | 31/12/2018 |
| 11 | Pathanamthitta | Pamba | Malakkara | 19/06/1985 | 31/12/2018 |
| 12 | Pathanamthitta | Achankoil | Thumpamon | 28/01/1978 | 31/12/2018 |
| 13 | Thiruvanathapuram | Vamanapuram | Ayilam | 18/12/1978 | 31/12/2011 |
| 14 | Thrissur | Periyar/ Chalakudi | Arangali | 27/04/1984 | 31/12/2018 |

## 4. Results and Discussions

The daily streamflow data was collected from 14 stations of west flowing rivers of India and the annual maximum stream flow was computed. Flood frequency curves were developed for both stationary and non-stationary condition for all the stations. Analysis was done by comparing stationary and non-stationary curves of return level v/s return period for all stations. i.e., NS model was developed by linearly varying location parameterand constant scale parameter. The ST and NST comparison plot of Ayilam station is shown in Figure 1. 95% confidence intervalcurve was also computed for each of them. It is worth noting that the uncertainty bounds are much wider for most of the non-stationary metrics relative to the uncertainty in stationary cases. Wider uncertainties in the design quantiles under non-stationary also question the reliability and can serve to increase the cost of the flood protection without increasing the level of protection.

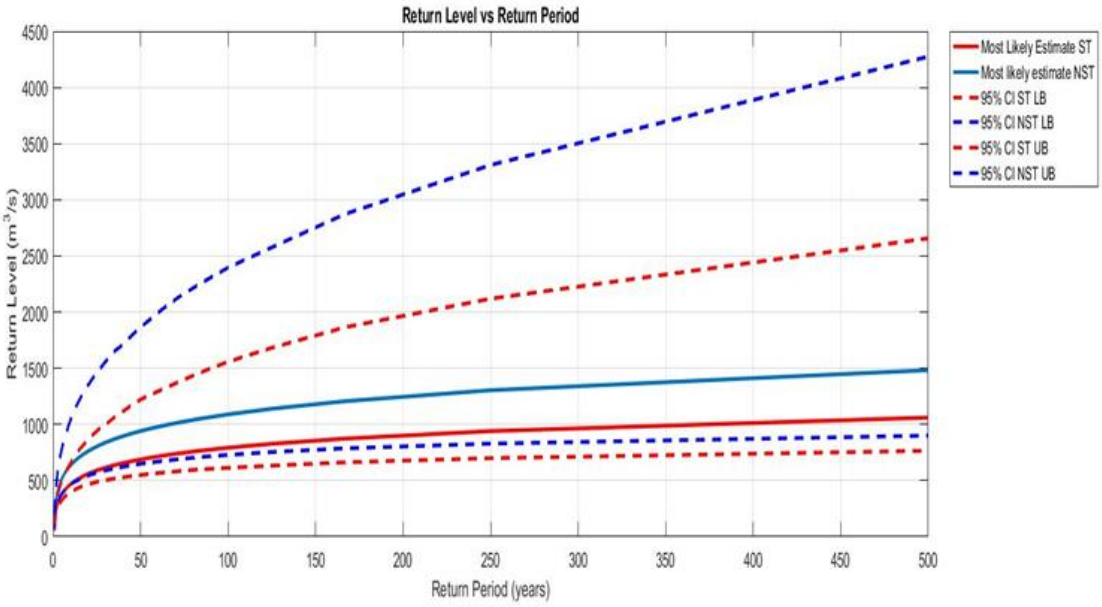



**Fig 1** ST and NST plot for Ayilam station

The percentage variations (PV) of return levels for each case were calculated for all the chosen stations as shown in Table 2.The comparison of ST and NST return levels for different return periods with a linear trend in the location parameter and constant scale parameter was plotted. From the results obtained it can be seen that stationary values are lower than all of the corresponding non-stationary values for data of all stations except for Malakkara and Pattazhy.It can also be noted that the percentage variation with respect to stationary and non-stationary values is decreasing as the return periods increases. Ayilam station shows highest percentage variation of more than 40% while Perumanur station shows a variation above 25%. Erinjipuzha, Kalloopara, Neeleswarm, Malakkara, Pattazhy and Ramamangalam show a percentage variation greater than 10% in most of the return periods. For Pudur station, the NS estimates exceed over 25% only for return period of 500. i.e., at this station NS becomes relevant only for designs accounting a return period of 500.

Malakkara and Pattazhy stations showed a very different pattern from others, as stationary estimates were found to be more than the NS estimates for different return levels. Due to this change in PV from other stations, a Mann Kendell Trend analysis test (Mann, 1945 and Kendall 1975) was carried out to assess the significance of trend in the hydrological time series. In this study, a confidence interval of 95% was considered, hence if the z-value so obtained after M-K test was greater than 1.96, the station was considered to be non-stationary. Ayilam and Perumannur stations indicated a positive trend with z values greater than 1.96 while all other stations showed a no signficance pattern of trend. It was also noticed that Malakkara and Pattazhy stations showed a negative trend. Hence it may be stated that the stationary estimates were more than the NST estimates

for different return levels due to the presence of negative trend.The positive and negative PV gives a clear idea about non-stationary return level estimate and stationary estimate for various return levels. The application of the NST LPIII model to stationary discharge records can lead to overestimation of flood peaks, and hence over engineered structures. Also, falsely selecting the ST model could lead to under designed infrastructure and potential disaster.

**Table 2** Percentage variations of NST and ST return levels for different return periods

| RP | | Ayilam | Perumanur | Erinjipuzha | Kalloopara | Pattazhy | Neeleswaram | Malakkara | Kumbidi | Arangali | Pudur | Thumpamon | Ramamangalam | Kalampur | Pulamanthole |
|---|---|---|---|---|---|---|---|---|---|---|---|---|---|---|---|
| 50 | ST | 147.20 | 1013.37 | 496.63 | 372.14 | 165.11 | 1120.08 | 615.30 | 814.16 | 361.13 | 64.61 | 211.49 | 653.74 | 650.53 | 309.48 |
| | NST | 217.35 | 1294.34 | 557.99 | 415.73 | 139.69 | 1235.64 | 531.77 | 869.10 | 373.21 | 65.47 | 227.10 | 729.67 | 701.26 | 336.36 |
| | PV | 47.66 | 27.73 | 12.36 | 11.71 | -15.39 | 10.32 | -13.58 | 6.75 | 3.34 | 1.32 | 7.38 | 11.61 | 7.80 | 8.68 |
| 100 | ST | 176.73 | 1170.92 | 578.19 | 428.10 | 205.69 | 1431.34 | 709.45 | 1004.86 | 431.27 | 70.45 | 253.96 | 737.27 | 736.19 | 383.82 |
| | NST | 254.92 | 1470.24 | 648.01 | 477.21 | 170.88 | 1289.86 | 604.97 | 1086.54 | 449.99 | 72.27 | 271.75 | 830.45 | 795.83 | 415.67 |
| | PV | 44.24 | 25.56 | 12.08 | 11.47 | -16.92 | 10.97 | -14.73 | 8.13 | 4.34 | 2.58 | 7.01 | 12.64 | 8.10 | 8.30 |
| 150 | ST | 202.78 | 1296.18 | 649.55 | 474.54 | 244.04 | 1605.59 | 790.34 | 1175.51 | 493.45 | 77.97 | 291.19 | 806.54 | 806.41 | 450.97 |
| | NST | 288.16 | 1609.33 | 726.55 | 527.86 | 200.52 | 1441.22 | 668.86 | 128004 | 517.82 | 80.94 | 311.12 | 912.29 | 872.61 | 486.89 |
| | PV | 42.11 | 24.16 | 11.85 | 11.24 | -17.83 | 11.40 | -15.37 | 8.89 | 4.94 | 3.81 | 6.85 | 13.11 | 8.21 | 7.97 |
| 200 | ST | 228.75 | 1410.46 | 720.32 | 518.58 | 284.63 | 1781.29 | 869.38 | 1347.56 | 555.75 | 87.79 | 328.11 | 872.24 | 872.71 | 519.23 |
| | NST | 321.45 | 1735.84 | 804.27 | 575.58 | 232.05 | 1594.03 | 732.13 | 1473.89 | 585.53 | 92.27 | 350.37 | 988.49 | 944.48 | 558.92 |
| | PV | 40.53 | 23.07 | 11.65 | 10.99 | -18.47 | 11.75 | -15.79 | 9.37 | 5.36 | 5.10 | 6.78 | 13.33 | 8.22 | 7.64 |
| 300 | ST | 288.56 | 1641.35 | 882.41 | 612.92 | 386.83 | 2193.98 | 1046.44 | 1749.45 | 700.39 | 120.56 | 412.49 | 1013.35 | 1014.42 | 680.62 |
| | NST | 398.76 | 1990.90 | 981.67 | 676.86 | 312.23 | 1953.54 | 876.82 | 1921.39 | 741.73 | 130.41 | 440.80 | 1147.55 | 1096.15 | 727.92 |
| | PV | 38.19 | 21.30 | 11.25 | 10.43 | -19.28 | 12.31 | -16.21 | 9.83 | 5.90 | 8.17 | 6.86 | 13.24 | 8.06 | 6.95 |
| 500 | ST | 1061.33 | 3088.01 | 2979.48 | 1442.95 | 2716.7 | 8608.08 | 3065.71 | 7198.58 | 2683.42 | 11087.92 | 1446.92 | 2298.57 | 2326.82 | 3037.44 |
| | NST | 1483.49 | 3614.67 | 3235.43 | 1523.70 | 2338.5 | 7622.76 | 2764.09 | 7398.83 | 2766.37 | 15948.89 | 1616.10 | 2371.13 | 2400.41 | 3085.58 |
| | PV | 39.78 | 17.06 | 8.59 | 5.60 | -13.92 | 12.93 | -9.84 | 2.78 | 3.09 | 43.84 | 11.69 | 3.16 | 3.16 | 1.58 |

The return level estimates for 50 and 100 year return period of Ayilam station is shown in Fig 2 and 3. Likewise, it was plotted for all stations. The distribution of the discharge densities for 50 and 100 year return level under ST and NST models were also compared and the same is indicated in Table 3.

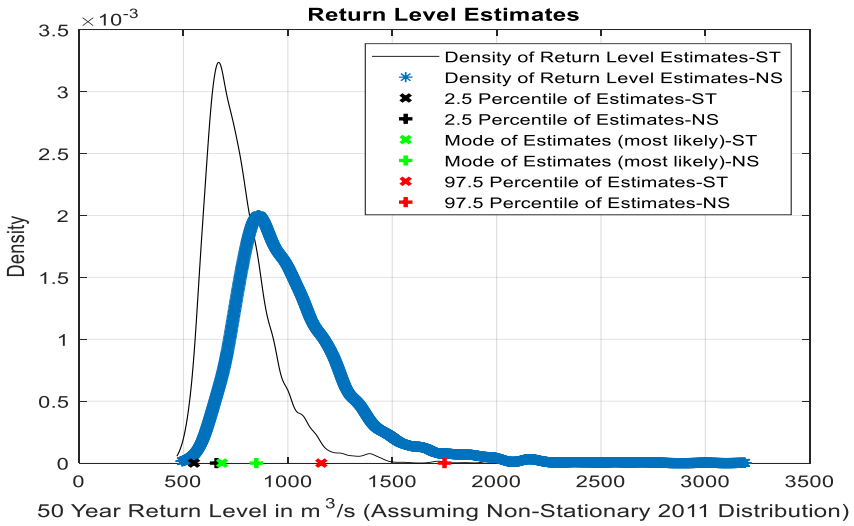



**Fig 2** Return level estimates of Ayilam for 50 year RP

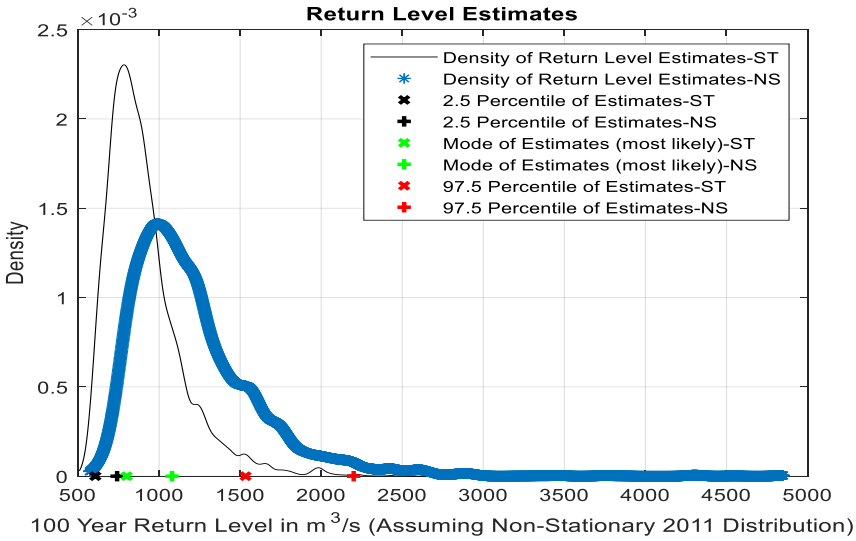



**Fig 3** Return level estimates of Ayilam for 100 year RP

**Table 3** Discharge density estimates for different return periods (2.5 and 97.5 percentile)

| | | ST 2.5 | ST 97.5 | ST-ME | NS 2.5 | NS 97.5 | NS-ME |
|---|---|---|---|---|---|---|---|
| **Ayilam** | RP 50 | 550.43 | 1160.40 | 684.79 | 658.64 | 1750.50 | 848.72 |
| | RP 100 | 606.54 | 1533.36 | 800.06 | 740.86 | 2200.25 | 1080.27 |
| **Perumanur** | RP 50 | 2290.17 | 3722.70 | 2579.33 | 2504.15 | 4419.45 | 3117.59 |
| | RP 100 | 2381.15 | 4350.10 | 2746.59 | 2581.63 | 5187.04 | 3253.89 |
| **Kalloopara** | RP 50 | 958.51 | 1655.20 | 1106.01 | 972.79 | 1785.00 | 1204.90 |
| | RP 100 | 1032.49 | 1858.01 | 1214.35 | 1063.69 | 2041.70 | 1290.53 |
| **Malakkara** | RP 50 | 1788.55 | 3395.08 | 2143.01 | 1484.48 | 3356.83 | 1876.01 |
| | RP 100 | 1962.00 | 4201.75 | 2456.63 | 1677.81 | 4165.67 | 2145.29 |
| **Kumbidi** | RP 50 | 3586.15 | 7825.39 | 4582.00 | 3496.13 | 8716.25 | 4811.27 |
| | RP 100 | 4157.61 | 9939.29 | 5341.29 | 3989.74 | 10837.16 | 5542.11 |
| **Arangali** | RP 50 | 1349.10 | 2876.70 | 1693.30 | 1318.40 | 3187.30 | 1750.50 |
| | RP 100 | 1542.70 | 3660.90 | 1986.10 | 1552.30 | 4014.00 | 2051.30 |
| **Pudur** | RP 50 | 487.63 | 15237.65 | 4524.99 | 467.17 | 3746.97 | 1149.28 |
| | RP 100 | 631.25 | 31511.12 | 5367.02 | 641.83 | 9248.41 | 3487.40 |
| **Thumpamon** | RP 50 | 779.14 | 1616.88 | 955.58 | 740.22 | 1795.45 | 947.60 |
| | RP 100 | 858.58 | 1894.44 | 1109.39 | 848.67 | 2087.94 | 1119.21 |
| **Ramamangalam** | RP 50 | 1532.57 | 2430.18 | 1753.26 | 1612.78 | 2546.12 | 1922.40 |
| | RP 100 | 1651.80 | 2897.31 | 1938.90 | 1709.45 | 2884.02 | 2052.67 |
| **Kalampur** | RP 50 | 816.14 | 1869.30 | 1049.86 | 785.24 | 1833.14 | 1064.12 |
| | RP 100 | 929.59 | 2536.28 | 1207.94 | 891.22 | 2376.21 | 1270.00 |
| **Pulamanthole** | RP 50 | 1430.64 | 3378.08 | 1867.21 | 1410.58 | 4041.02 | 1922.92 |
| | RP 100 | 1652.70 | 5029.87 | 2157.80 | 1579.56 | 5176.85 | 2304.64 |
| **Erinjipuzha** | RP 50 | 1573.65 | 3254.72 | 1940.79 | 1622.53 | 3716.25 | 2167.89 |
| | RP 100 | 1754.79 | 3986.33 | 2260.20 | 1839.91 | 5093.11 | 2409.45 |
| **Neeleswaram** | RP 50 | 4067.67 | 6799.56 | 4880.12 | 3385.45 | 7440.21 | 4439.00 |
| | RP 100 | 4487.34 | 9601.46 | 5647.23 | 3789.11 | 10320.22 | 5024.35 |
| **Pattazhy** | RP 50 | 961.70 | 2583.55 | 1341.78 | 741.62 | 2362.79 | 1003.21 |
| | RP 100 | 1149.37 | 3824.90 | 1629.33 | 889.70 | 3272.68 | 1324.11 |

In the case of density of return level estimates, most of the stations showed a greater value for non-stationarity cases at 2.5 and 97.5 percentiles than stationary values. Malakkara and Pattazhy station showed a different pattern, i.e, stationary values were greater than non-stationary estimates. This may be due to the negative trend followed by the streamflow of these stations. Some stations like Kumbidi, Arangali, Pulamanthole and Neeleswaram showed a greater value for stationary 2.5 percentile when compared to non-stationary 2.5 percentile. Mode of estimate value for 100 year return period was greater than 50 year return period.

## 5. Conclusions and Recommendations

This study developed stationary and non-stationary flood frequency curves, using annual maximum discharge data prepared from daily data of 14 stations in Kerala. The NS flood frequency curves for the west flowing rivers of Kerala are developed by considering the linear variation of location parameter using Bayesian Inference Approach. From the obtained results and their interpretations, it was identified that, there exist significant non-stationary behavior of annual maximum stream flow data at different locations across the state. By conducting such analysis, the following conclusions were obtained:

- From the analysis, it is observed that, Ayilam and Perumanur data are experiencing very high levels of non-stationary behavior (greater than 35% under estimation for Ayilam and 25 % for Perumanoor, consistently for all return periods, over the stationary case)
- There exit a wide variability in percentage change in NST over ST estimates of flood quantiles in the state, for different return periods. Arangali, Pudur, Thumpamon, Kalampur and Kumdidi are showing variation around 5-10%, while Erinjipuzha, Kalloopara, Neeleswaram, Pattazhy and Ramamangalam stations showing 10-15% variation for some return periods . This necessitates that the choice of NS case can be based on type of structure and location
- Ayilam and Perumanoor portrayed a significant trend in annual maximum flow displaying the highest percentage change in NST estimates over the ST estimates irrespective of return period. Malakkara and Pattazhy station showed a very different pattern from others, as stationary estimates were found to be more than the NST estimates for different return levels. All the other stations displayed reasonably high percentage change (over 10-15 %) in NS estimates over stationary estimates for some return periods.
- Non-stationarity must be accounted for the design with longer return period applications (> 200 year) in all locations, while it must be accounted for smaller return period design (< 50 year) applications as well in few selected locations.

Based on the study, it can be recommended that future research should focus on the evaluation of predictions derived from promising NS models. Better models can be developed by incorporating more stations in both local and national levels for getting a clear idea of the presence of non-stationary over Kerala as well as India. NS flood frequency analysis can be carried out by focusing other distribution parameters namely scale and shape parameter as well by considering covariates. Research can also be extended to generating various models considering different statistical distributions and interpretation techniques.

## References

Cheng, L. and AghaKouchak, A. (2014). Non-stationary precipitation intensity- duration frequency curves for infrastructure design in a changing climate, *Scientific Reports, 4*, 7093.doi:10.1038/srep07093

Cheng, L., AghaKouchak, A., Gilleland, E. and Katz, R.W. (2014) Non-stationary Extreme Value Analysis in a Changing Climate, *Climatic Change*, 127(2), 353-369

Hosking, J.R.M. and Wallis, J.R.(1997). Regional Frequency Analysis. Cambridge University Press, Cambridge

Kendall, M.G. (1975). Rank Correlation Methods, 4th edition, Charles Griffin, London.

Luke, A., J. A. Vrugt, A. AghaKouchak, R. Matthew, and B. F. Sanders (2017). Predicting nonstationary flood frequencies: Evidence supports an updated stationarity thesis in the United States, *Water Resources Research*, 53, 5469–5494, doi:10.1002/2016WR019676.

Mann, H.B. (1945). Non-parametric tests against trend, *Econometrica*, 13:163-171

Mondal, A. and Mujumdar P.P. (2015). Modeling non-stationarity in intensity, duration and frequency of extreme rainfall over India, *Journal of Hydrology*, *521*, 217-231

Obeysekera, J., and Salas, J. D. (2014).Quantifying the Uncertainty of Design Floods under Nonstationary Conditions. *Journal of Hydrology Engineering, 19(7)*, 1438–1446. doi:10.1061/(asce)he.1943-5584.0000931

Ouarda, TBMJ, Charron C. (2019) Changes in the distribution of hydro-climatic extremes in a non-stationary framework. *Scientific Reports* 9, 8104

Pawar.U. and Hire.P. (2018).Flood Frequency Analysis of the Mahi Basin by using Log Pearson Type –III Probability Distribution.*Hydrospatial Analysis*, 2(2), 102 – 112.

Ray, L.K. and Goel, N.K. (2019). Non-stationary frequency analysis of extreme rainfall events across India.*ASCE, Journal of Hydrologic Engineering*, Vol. 24, Issue 8.

Sarhadi, A. and Soulis E.D. (2017) Time-varying extreme rainfall intensity-duration- frequency curves in a changing climate, *Geophysical Research Letters*, *44*, doi:10.1002/2016GL072201

Sathe. B. K., Khire. M. V. and Sankhua. R. N. (2012). Flood Frequency Analysis of Upper Krishna River Basin catchment area using Log Pearson Type –III Distribution. *IOSR Journal of Engineering*. ISSN: 2250 – 3021, Vol 2, Issue 8, PP 68 - 77

*IN PROCEEDINGS OF 25th HYDRO 2020, INTERNATIONAL CONFERENCE, NATIONAL INSTITUTE OF TECHNOLOGY ROURKELA, ODISHA, INDIA 26-28, March 2021, ISBN 978-93-90631-56-8*

Paper ID - 458

# Web Interface for Random Sea Wave Generation and Data Acquisition System for Hydraulic Physical Model Studies

Vinay Jagadeesh[1], R.S. Erande[2]

[1]*Undergraduate, Dept. of Computer Science and Engineering, PES University, Bangalore - 560085, India.*

[2]*Scientist B, Central Water and Power Research Station, Pune - 411024, India.*

*Email: vjagadeesh1998@gmail.com*

## Abstract

Random sea wave generation is an extremely important method used for modelling and development of shallow basin physical wave models in coastal engineering for planning of ports and harbours. For generating random sea waves and data acquisition in models, an electro-hydraulic based wave generation system including a Programmable Logic Controller (PLC), servo controller, multi-channel capacitance wave height recorder, Supervisory Control and Data Acquisition (SCADA), differential pressure filtering system and a wave board assembly is extensively used. Random Sea Wave Generating (RSWG) Systems are used to simulate prototype sea conditions in laboratory like wave flumes for studying of maritime structures namely breakwaters, sea walls and shallow basin wave models for finalisation of port layouts and berthing alignments. For ease of accessing the model experimental results from a remote location with internet facility, a web interface has been developed using tools such as Python and JavaScript, making it easier to access the data and results for the modelling studies. This eliminates the need to physically access the data from the model each time when any studies being carried out. By doing so experts in the field can guide the laboratory experiments remotely thus saving their time and as well timely completion of studies can be achieved. The main tools used for this are Python, JavaScript, HTML and plotting libraries such as Plotly (for JavaScript) and matplotlib (for Python). This paper elaborates on the web interface created to view the data collected from the physical models with additional features added such as zooming in and saving as an image to be printed, etc.

***Keywords:*** *Random sea wave generation, hydraulic physical model, data acquisition system, web interface*.

## 1. Introduction

Physical models have played a pivotal role in the advancement of coastal engineering design problems. It gives an insight into complex hydrodynamic regime and aids in providing reliable and economic design solutions. Most of the present developments are the outcome of the laboratory experiments and to large extent even the theoretical developments have relied on laboratory experiments. In modelling condition it is possible to vary the parameter as and when required by the user at his discretion and hence more useful in assessing the extreme/critical event conditions and optimising the coastal structure design. Also the physical interaction with water in a physical model will lead to intuitive thinking about the wave hydrodynamic processes and thus a sophisticated physical model will be of great use in understanding wave hydrodynamic processes.

The complex wave hydrodynamic processes such as refraction, shoaling, diffraction, breaking, reflection etc. make the near shore wave dynamics complex and since some of these processes are simultaneous the numerical simulation of all these processes is difficult. Hence there are many

limitations for assessing wave characteristics through mathematical modelling techniques. While understanding the behaviour of wave during its propagation from deeper contours towards harbour basins it is evident to understand these complexities. Further theoretical development in this direction obviously needs laboratory verifications. A sophisticated physical model with random wave generating, computerised wave data acquisition and analysing facilities will serve as a very useful tool for this purpose.

Wave generating techniques in laboratory have evolved from time when limited technology was available to the present, where capabilities of wave generation and computers have exceeded the current understanding of the wave hydrodynamic processes. In regular wave models waves are generated by moving the wave board with required amplitude and period. It generates a train of unidirectional waves with wave crests parallel to wave board. These waves confirms well with linear wave theory, which is widely accepted and used in coastal engineering. Most physical models of coastal engineering involve forces resulting from gravity waves. In nature these wave are random and thus it is appropriate to simulate random waves with a close approximation to natural conditions with due care for minimising the laboratory effects that could influence the experimental out come.

Hydraulic servo systems were used for generating random waves by establishing increased control over the movement of the wave board. Through these developments it was possible to generate 2-D random waves for coastal engineering model studies.

### *1.1 Model Description:*

Random Sea Wave Generating Systems (RSWG) are used to simulate prototype sea conditions in laboratory.The wave boards are driven by electro-hydraulic servo system. Electro-hydraulic servo control system consists of servo controller, servo-valve, servo actuator, wave board and hydraulic power supply. The servo controller receives analog command signal from the micro processor and generates error signal by comparing it with a feedback signal obtained from the displacement transducer. The error signal from servo amplifier is converted into a current suitable for driving a servo-valve, which in turn controls oil flow to the actuator and hence the displacement. There are two main components of the RSWG & DAQ system, the wave generating equipment and the data acquisition equipment.

I. Wave Generating equipment:

a. Power Pack unit: A 50HP power pack is designed using Gilbert. at.el. design curves. It consists i) fluid tank ii) air breather iii) oil level gauge iv)level switch/magnetic float switch v) temperature switch vi) Pressure compensated variable displacement axial flow piston pump etc.

b. Servo-Mechanism Servo Valve and Actuator: A bidirectional flow control valve converts the electrical signal in to a horizontal movement of Actuator rod. The hydraulic power of the actuator drives the wave board to move the water column to and fro to generate waves of desired height and period.

c. Differential Pressure Filtering system:The method of filtration will be selected to suit each application, since the conditions of using hydraulics vary widely. Filtration has no direct bearing on power transmission, but is essential for the maintenance and good performance of the system. It may be carried out on the full or partial flow through the system, i.e. all the fluid in a given path will flow through a full flow filter or, with partial flow, some of the fluid is by passed through the filter, the remainder passing directly to the system. Filtration may be applied at any of the three main regions of

system: (a) at pump inlet between reservoir and pump, (b) in the pressure line between pump and actuator or (c) in the exhaust line between actuator and reservoir.

d. Wave Board Assembly: It is a fabricated steel structure used for generation of waves in water basin. Reciprocating motion of servo-actuator piston rod causes Wave flaps to oscillates like a pendulum about pivoted circular hallow beam. The weight of the moving mass is optimized to minimize effects of inertia forces while Wave flaps are oscillating by designing a hallow beam.

II. Data Acquisition equipment:

a. Multi-channel Capacitance Wave Height Recorder: Wave height is measured using capacitance type wave probes and signal conditioner. These eight channel wave height recorder and its wave probes are designed, developed and manufactured in CWPRS. The capacitance type wave height sensors are enamelled copper wire type. The copper wire and water acts as two conductors separated by the enamel dielectric. The surface area of the copper wire changes with change in water level fluctuations. Variation due to change in the water level (column) thus gives the change in capacitance, which in turn provide change in the voltage. The probe is excited by AC signal and voltage output from the bifilar winding which is amplified and filtered for high frequency components and fed to multi-channel ADC in the USB module.

b. SCADA Controlled Electro-Hydraulic Servo System:The wave generation is accomplished by moving the wave boards, which are aligned in the wave basin. A piston type wave board is used because of its simplicity and it is mainly used for shallow water waves. The wave boards are driven by electro-hydraulic servo system. Electro-hydraulic servo control system consists of servo controller, servo-valve, servo actuator, wave board and hydraulic power supply. The driving wave train is fed to the servo controller which in turn controls the opening and closing of the servo valve depending on the samples in the wave train. Operation of servo valve enables the high pressure fluid from the hydraulic power supply to flow in and out of the servo actuator. The movement of the piston in the servo actuator cylinder due to fluid flow in turn moves the wave board, which is connected to the piston rod of the servo actuator.

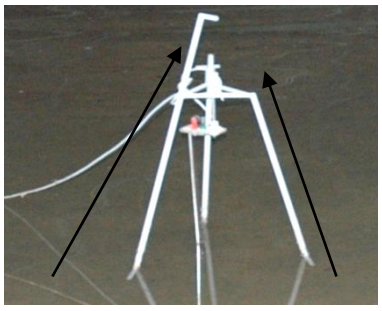


**Figure 1**Capacitance wave height recorder (CWHR)

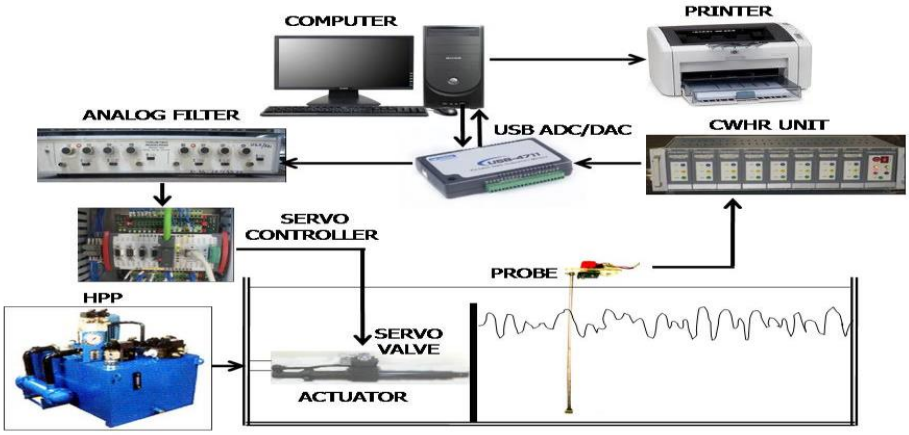



**Figure 2** Random Sea Wave Generation and Data Acquisition System

### *1.2 Driving/acquired time series:*

#### a. Driving Time Series:

The data required for plotting the driving and acquired time series are stored in a .dat file which is then stored as a Python list and manipulated to extract the required readings. It also has a calibration factor value which is required for plotting the acquired time series.
The driving time series is a graph derived from wave synthesis software to simulate sea state condition for defined wave parameters. It defines voltage Vs time wave profile to be generated in the model. From this graph we can also plot the acquired time series by multiplying each reading with the calibration factor.

The Python code for plotting the driving series is as follows:

Code 1:

```
from datetime import datetime as dt
import webbrowser as browser
from os import getcwd as current_working_directory, path
defread_file(filename):
try:
withopen(filename, 'r') as f: rawText = f.read().splitlines()
return rawText
exceptExceptionas e:
print(f"Exception Caught. {e}")
returnNone
filename = path.join(current_working_directory(), "THAatv01.dat")
```

```
rawData = read_file(filename)

ifnot rawData: exit(1)

headers = rawData[:3]

data = [float(datapoint) for row in rawData[3:-1] for datapoint in
row.split()]

footer = float(rawData[-1])

place, hs = headers[0].split(maxsplit=1)

time = dt.strptime(headers[1], '%d %m %Y %H:%M:%S')

freq, length, channel = headers[2].split(maxsplit=2)

freq, length = float(freq), int(length)

x = [round(i * freq, 2) for i inrange(length)]

y = data

savefilename = path.join(current_working_directory(),  f"{place}.html")

withopen(savefilename, 'w') as f:

print(f'<!DOCTYPE html><html lang="en"><head><script
src="https://cdn.plot.ly/plotly-latest.min.js"></script></head><body><div
id="lineChart"></div><script>var trace1 = {{x: {x},y: {y},mode: "lines"}};var
data = [trace1];Plotly.newPlot("lineChart", data, {{}},
{{}});</script></body></html>', file=f)

browser.open_new_tab(savefilename)
```

On execution, this code creates a HTML file and opens it in the default browser of the system. The screenshots from this HTML page is attached below:

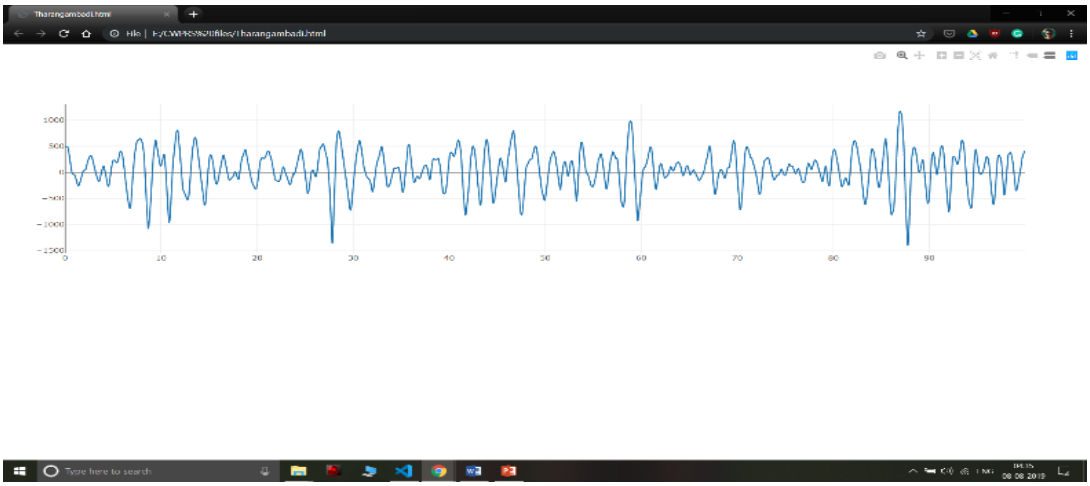


**Figure 3** HTML page created from code 1

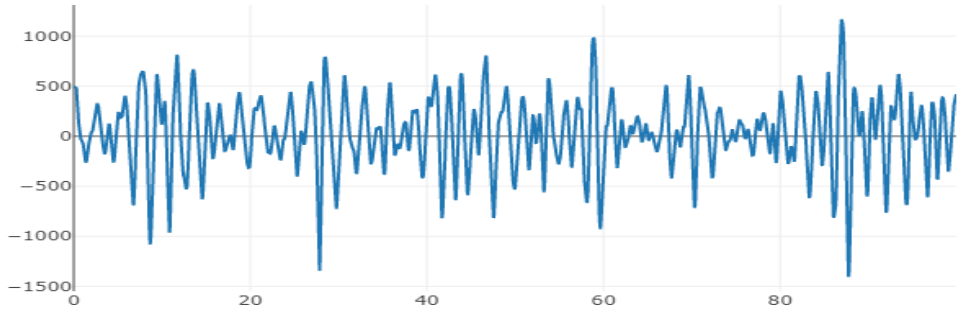



**Figure 4**PNG file downloaded

From the HTML page created as shown in Figure 3, we can access the displayed graph which has a few features in built (which can be accessed from the right hand top corner of the webpage) with the plotly library for JavaScript such as:

i. Selecting a particular part of the graph to be zoomed in to.
ii. An option to save the graph as a PNG image which will save a file (Figure 4) in the downloads folder of the computer and can be printed or shared more easily if required.
iii. Hovering over a point on the graph to pop-up the readings for that particular point.
iv. Being able to reset the axes to default after zooming in to a particular part of the graph, etc.

Alternatively, another Python script can be executed which will directly produce a high definition image of the required graph if required for printing purposes.
This code has been implemented with the use of the matplotlib plotting library for Python.

The code (*Code 2*) and the output image have been attached below:

*Code 2:*

```
from datetime import datetime as dt

import webbrowser as browser

from os import getcwd as current_working_directory, path

import matplotlib.pyplot as plt

defread_file(filename):

try:

withopen(filename, 'r') as f: rawText = f.read().splitlines()

return rawText

exceptExceptionas e:

print(f"Exception Caught. {e}")

returnNone
```

```
filename = path.join(current_working_directory(), "data.dat")

rawData = read_file(filename)

ifnot rawData: exit(1)

headers = rawData[:3]

data = [float(datapoint) for row in rawData[3:-1] for datapoint in
row.split()]

footer = float(rawData[-1])

place, hs = headers[0].split(maxsplit=1)

time = dt.strptime(headers[1], '%d %m %Y %H:%M:%S')

freq, length, channel = headers[2].split(maxsplit=2)

freq, length = float(freq), int(length)

x = [round(i * freq, 2) for i inrange(length)]

y = data

fig = plt.figure(figsize=(20, 10))

axes = fig.add_axes([0.1, 0.1, 0.8, 0.8])

axes.plot(x, y)

plt.ylabel("Voltage in mV")

plt.xlabel("Time in sec")

plt.title(f"{place}{time}")

plt.show()

savefilename = path.join(current_working_directory(),  f"{place}.html")

withopen(savefilename, 'w') as f:

print(f'<!DOCTYPE html><html lang="en"><head><script
src="https://cdn.plot.ly/plotly-latest.min.js"></script></head><body><div
id="lineChart"></div><script>var trace1 = {{x: {x},y: {y},mode: "lines"}};var
data = [trace1];Plotly.newPlot("lineChart", data, {{}},
{{}});</script></body></html>', file=f)
```

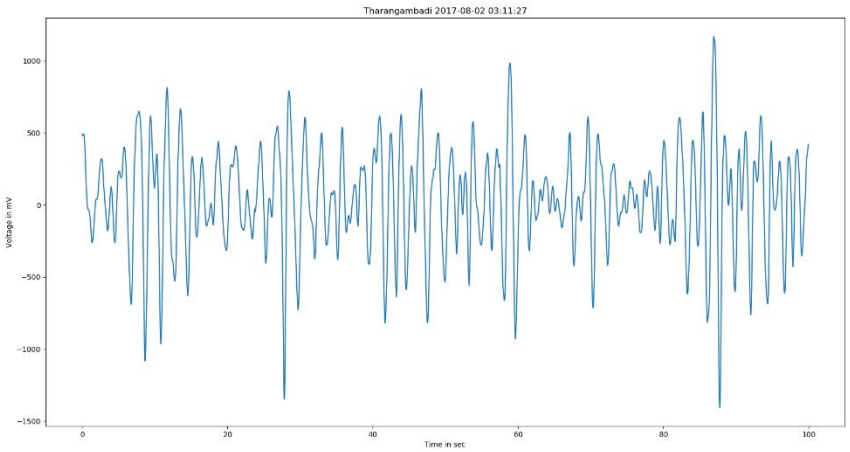



**Figure 5** Output for Code 2 (High definition image for printing)

**b. Acquired Time Series:**

If each reading from the driving time series is multiplied with the calibration factor and then plotted, we get the acquired time series. The output for which is as follows:

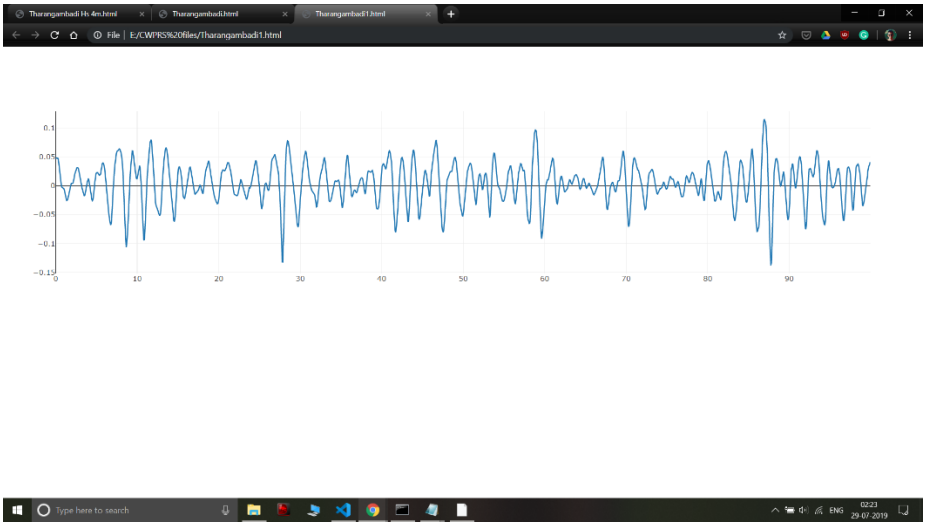


**Figure 6**Acquired time series

The graph hence acquired is of the wave height in meter vs time in seconds which can be viewed in Figure 4 and has the same features as the driving time series graph in Figure 1.

### *1.3 Reference/acquired spectrums:*

The data required for plotting the reference and acquired spectrums are stored in two separate .dat files. Both of which are stored as Python lists in the code and then manipulated to extract the required readings from the list.

The code for the plotting of the 2 graphs has been integrated into one and is as follows:

*Code 3*

```
from datetime import datetime as dt

import webbrowser as browser

from os import getcwd as current_working_directory, path


defread_file(filename):

    try:

        withopen(filename, 'r') as f: return f.read().splitlines()

    exceptExceptionas e:

        print(f"Exception Caught. {e}")

        raise e

# ------------ASP--------------

filename = path.join(current_working_directory(), "THAasp01.dat") # filepath

rawData = read_file(filename) # Simply read the files into a list of each line

headers = rawData[:3] # first 3 lines are headers

data = [float(datapoint) for row in rawData[3:-12] for datapoint in
row.split()] # 4th to 13th last line is data. make it in one list

footers = rawData[:-12] # last 12 lines are footers

place, hs = headers[0].split(maxsplit=1) # separate out headers

d_, m_, y_, H_, M_, S_ = map(int, headers[1].replace(':', ' ').split())  #
separate out date

date = dt(2000 + y_, m_, d_, H_, M_, S_) # date object if needed

sampling_interval, no_of_samples, channel_number =
headers[2].split(maxsplit=2) # separate out headers

sampling_interval, no_of_samples = float(sampling_interval),
int(no_of_samples) # cast headers into their types


x1 = [round(i * sampling_interval, 2) for i inrange(no_of_samples)] # scaling
x axis according to sampling interval

y1 = data # our data for y axis

# ------------RSP--------------

filename = path.join(current_working_directory(), "THArsp01.dat") # filepath
```

```
rawData = read_file(filename) # Simply read the files into a list of each line

headers = rawData[:3] # first 3 lines are headers

data = [float(datapoint) for row in rawData[3:] for datapoint in row.split()]
# 4th to last line is data. make it in one list

reference_spectrum = headers[0] # separate out headers

d_, m_, y_, H_, M_, S_ = map(int, headers[1].replace(':', ' ').split()) #
separate out date

date = dt(2000 + y_, m_, d_, H_, M_, S_) # date object if needed

sampling_interval, no_of_samples, theoretical = headers[2].split() # separate
out headers

sampling_interval, no_of_samples = float(sampling_interval),
int(no_of_samples) # cast headers into their types

x2 = [round(i * sampling_interval, 2) for i inrange(no_of_samples)] # scaling
x axis according to sampling interval

y2 = data # our data for y axis

savefilename = path.join(current_working_directory(),  f"{place}{hs}.html") #
HTML file name

withopen(savefilename, 'w') as f:

    print(f'<!DOCTYPE html><html lang="en"><head><script
src="https://cdn.plot.ly/plotly-latest.min.js"></script></head><body><div
id="lineChart"></div><script>acquired={{x:{x1},y:{y1},mode:"lines"}};reference
={{x:{x2},y:{y2},mode:"lines"}};data=[acquired,reference];Plotly.newPlot("line
Chart",data,{{}},{{}});</script></body></html>', file=f) # write data in HTML
file

browser.open_new_tab(savefilename) # Open HTML file
```

This code produces an HTML webpage and opens it with the default browser on the system.
It has the graphs for both, the acquired spectrum (Trace 0 in blue colour) and the reference spectrum (Trace 1 in orange colour) superimposed on to the same axes.

The screenshots for the output of *Code 3* are as attached below:

Figure 7 shows the acquired spectrum while figure 8 shows the reference spectrum.

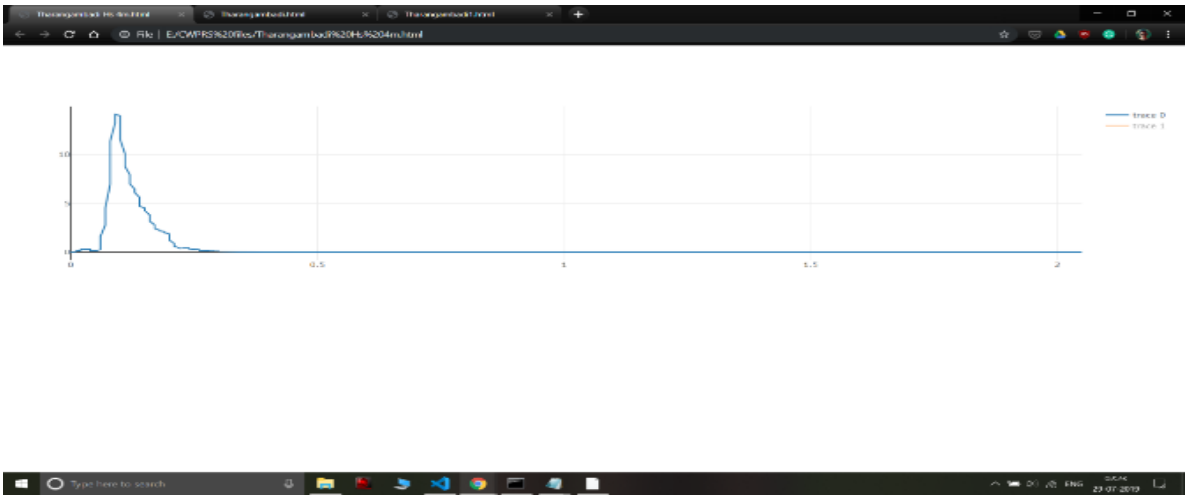


**Figure 7**Acquired spectrum

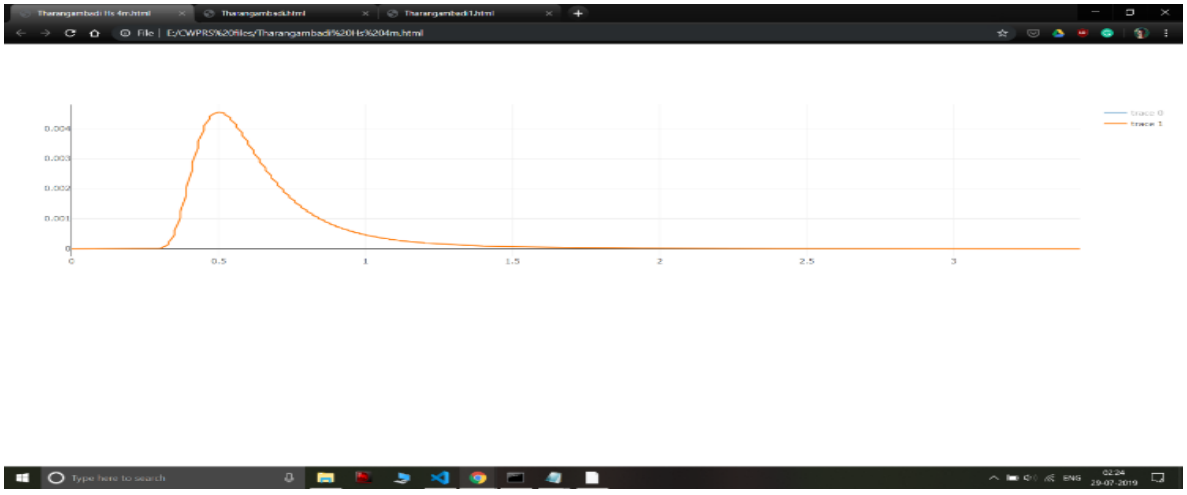


**Figure 8**Reference spectrum

In addition to the features mentioned for the graph in *Figure 1*, these graphs can also be displayed separately or together according to the requirements of the user, this can be toggled by clicking on the required plot once which will select it and display it. If clicked again, this will deselect that particular plot and hide it accordingly.

## 3. Conclusion:

By resorting to web based data interference in the hydraulic physical model it is possible for the field experts to control the model experiments from a remote place without their physical presence hence they don't need to access the model every time for model study data. This will be vital for receiving the opinions of experts during model studies from time to time. Hence it will help in avoiding expensive mistakes in the model studies by carrying out the least amount of trials possible. This also saves lot of cost in model studies since the cost of the studies is proportional to the time of model running. Having the ability to access the graphs and data online makes it very convenient for modelling domain experts to collaborate especially during situations where meeting in person is not possible. This is one more step ahead in the modernisation of hydraulic physical model studies in the modern era of computerisation.

**Acknowledgement:**

The authors are thankful to the Director CWPRS, Pune for permitting to carry out the mini project and senior officers at CWPRS for permitting to utilise the experimental data and equipment for the purpose of this project. Also thankful to the Chairperson of Computer Science department and Vice Chancellor PESU Bangalore for granting permission to publish the paper in the conference.

**References:**

Funke E. R. & Mansard E.P.D., 'On the Synthesis of Realistic Sea States in a Laboratory', National Research Council, Canada, Laboratory Technical Report No LTR-HY-66

Gilbert G., Thomason D.M. & Brewer A.J., *Design Curves for Regular and Random Wave Generators*, Hydraulic Research Station, Wallingford. UK, Technical report No. INT-81.

Steven A. Hughes (1993, 2005). "Physical models and laboratory techniques in coastal engineering" *World Scientific., Advanced series on ocean engineering-Vol.7.*

Dalrymple R A (1985) "Introduction to physical models in coastal engineering," *Ed., A A Balkema, Rotterdam*, The Netherlands.

I Berenguer et al (1986) "Mathematical and physical wave disturbance modelling complimentary tools' *20th Coastal engineering conference proceedings ,ASCE.*

Y Goda (1999) "Random seas and design of maritime structures" *World Scientific., Advanced series on ocean engineering*-Vol.15.

IAHR working Group on Wave Generation and Analysis "List of Sea-State Paramweters" *Journal of waterway, port,coastal,ocean engineering*, Vol.115, No.6,(1989)ASCE.

*Learn JavaScript Visually*by Ivelin Demirov

*JavaScript and JQuery: Interactive Front-End Web Development* by David McFarland

*Learning Python Data Visualization* by Chad Adams

*IN PROCEEDINGS OF 25th HYDRO 2020, INTERNATIONAL CONFERENCE, NATIONAL INSTITUTE OF TECHNOLOGY ROURKELA, ODISHA, INDIA 26-28, March 2021, ISBN 978-93-90631-56-8*

Paper ID - 462

# 2-D Flash Flood Modelling of Vamasadhara River basin

R. Venkata Raman[1], V.S. Jeyakanthan[1] , Y.R. Satyaji Rao[1] and T. Vijay[1]

[1]*Delatic Regional Centre, National Institute of Hydrology, Kakinada – 533 003, India*
*Email: venkataramana_1973@yahoo.co.in*

## Abstract

The Vamsadhara river basin is situated between the Mahanadi and Godavari river basins of south India. The total catchment area of Vamsadhara river basin, upstream to the point where it joins the Bay of Bengal, The river originates from the border at Thuamul Rampur in Kalahandi District and Kalyansinghpur in Rayagada district in Odisha and travels for a distance of about 254 km. The total catchment area of the river basin is 10,830 sq.km, Vamsadhara river basin occupies 8,015 sq.km in Odisha and the remaining 2,815 sq.km in Andhra Pradesh and lies within the geographical co-ordinates of $18^0$ 15' to $19^0$ 55' north latitudes and $83^0$ 20' to $84^0$ 20' east longitudes. Vamsadhara river is a non-perennial river so the only source of flow was rainfall. The basin is influenced by the south-west monsoon during the months of June to October, and by occasional cyclones due to the formation of depression in the Bay of Bengal. Highest rainfall was recorded in the basin during 2006 monsoon season over the period of 50 years from 1971-2020 and the river was over flooded which caused lots of losses either economic or loss of life. In this paper, the methodological approach was adopted, focused on the hydrologic modelling through the Hydrologic Engineering Centre Hydrologic Modelling System (HEC-HMS) and the hydrodynamic modelling wit Hydrologic Engineering Centre River Analysis System (HEC-RAS). The aim of this study was flood inundation behavior of vamsadhara river basin during extreme flood event in 2006 year. HEC HMS model output results are used in the hydrodynamic model (HEC-RAS) to simulate the flash flood. Hourly rainfall data downloaded from (CHRS) and simulated flash flood using 2-Dimentional HEC RAS. 2-D HEC RAS model was simulated by using output results of HEC HMS hourly runoff depth/excess rainfall and simulated results of Gunbupur and Kashinagar GD station ($R^2$ are 0.766 and 0.777) are well match with observed data. Flash flood model is very useful for flood warning system by generating pre-flood inundation maps and decision makers.

***Keywords:*** *Flash Flood, Rainfall, Model, Runoff, Simulation*

## 1. Introduction

Flash floods have been defined as weather related events that follow the causative storm events in a short period of time. The emphasis on the term flash, in flash floods explains how the raising water levels in the drainage network after the onset of rains leave extremely short time for warning and rapid response. In many cases, such basins respond rapidly to intense rainfall because of steep slopes and impermeable surfaces, saturated soils, or because of anthropogenic induced alterations to the natural drainage systems. Rainfall- runoff/flood correlation is a complex phenomenon to represent in the mathematical form. Rainfall runoff process involves many parameters either it may be physical features of the catchment or climatological parameters. In the real-world system rainfall runoff process is influenced by each and every physical characteristic of the catchment and to generalize all the physical characteristics of the catchment is really a difficult task. Consider the infiltration phenomenon which has direct influence on the runoff process, but when we observe the infiltration at different sites in the catchment, it comes out to be wide range of infiltration rates. In case of lumped hydrological model, representation of such a wide range of values is difficult because parameter values are to be averaged for the particular catchment. Hydrologic models are useful for the simulation of rainfall-runoff process and the hydraulic models are useful for analysis of the runoff flow in the river and its distribution.

Flash floods, with little or no warning of time, cause more deaths than slow-rising riverine floods. Flooding areas are used for socio-economic activities results in a variety of negative impacts. The magnitude of adverse effects depends on the vulnerability of the socio-economic activities, density of the population and the frequency, intensity and extent of flooding. Providing advanced warning for these types of situations can be challenging due to the combination of meteorological and other factors. A flood forecasting could help in indicating reservoir inflows that could lead to alerting the overtopping of dams.

The high variability of precipitations (Moussa et al., 2007) along with topography influence and spatial distribution of soil and land use properties makes hydrological processes largely variable both in time and space (Pilgrim et al., 1988). Flash floods are extreme catchment responses with high peak discharge often produced by severe localized thunderstorms. They are one of the most destructive hazards in the Mediterranean region and have caused casualties and billions of euros of damages in France over the last two decades (Gaume et al., 2009). These events often reveal aspects of hydrological behaviour that either were unexpected on the basis of weaker responses or highlight anticipated but previously unobserved behavior (Delrieu et al., 2005). Characterizing the response of a catchment during flash flood events thus may provide new and valuable insight into processes for extreme flood response and their dependency on catchment properties and flood severity (Borga et al., 2008). In the literature, several approaches are proposed for flash flood events modelling and/or prediction, each with its specificities depending on perception and parameterization of the dominant hydrological processes (Moussa et al., 2007; Saulnier and le Lay, 2009; Braud et al., 2010; Roux et al., 2011). These models often take advantage of available data in order to assign spatially distributed forcing as well as distributed catchment parameters. However, increasing model complexity can lead to over parameterization and equifinality problems because of high dimensionality and multi-modal response surface. As a result, parameter values might not be identifiable in the calibration process (Beven, 1989). Sieber and Uhlenbrook (2005) have highlighted that sensitivity analysis (SA) can not only identify the most important parameters but also contribute to understanding and improving the structure of hydrologic model. The Hydrologic Engineering Centers Hydrologic Modeling System (HEC-HMS) is a popularly used watershed model to simulate rainfall runoff process. Several studies have been conducted using the HEC-HMS model in different regions under different soil and climatic conditions. Chu and Stenman (2009) used HEC-HMS model for both event and continuous hydrological modelling in Monalack watershed in west Michigan. HEC-HMS model has also been used to simulate rainfall-runoff process with geo-informatics and atmospheric models for flood forecasting and early warnings in different regions of the world (Abed et al., 2005; Hu et al., 2006; Yusop et al., 2007; Dzubakova, 2010; Ali et al., 2011;Yener et al., 2012; Arekhi, 2012; Majidi and Shahedi, 2012; Halwatura and Najjim, 2013). The model was found accurate in spatially and temporally predicting watershed response in event based and continuous simulation as well as simulating various scenarios in flood forecasting and early warnings. For prediction of the floods in Romagna river basin in Italy, Pistocchi and Mazzoli (2002) completely integrated HEC- HMS and HEC-RAS model as a part of the decision support system.

## 2. STUDY AREA

Vamsadhara River is a significant east flowing river between Godavari and Mahanadi which meanders between north-eastern Andhra Pradesh and southern Odisha. Vamsadhara River Basin is prone to frequent floods with an area of 10,830 sq. km. It lies between 18°15' N and 19°57' N latitude and 83°25' E and 84°57' E longitude as shown in figure 1. The Vamsadhara River originates in the southwest part of Balagad village in the Pulbhani district of Odisha. The River confluences into the sea at Kalingapatnam after traversing a distance of 254 km in both the states.Major tributaries of Vamsadhara are Chauldua Nadi, Poladi Nadi, Gangudu River, Sanna Nadi, Pedda Gedda and Mahendratanaya joins the main Vamsadhara river before entering into the sea at Kalingapatnam in Srikakulam District.The river flows over three districts namely Srikakulam, Rayagada and Gajapati. Flash floods represent forecast and detection challenges because they are not always caused simply by meteorological phenomena. Flash floods occur when specific meteorological and hydrological conditions exist together. Although heavy rainfall is usually a factor, a given amount and duration of

rainfall may or may not result in a flash flood, depending on the hydrologic characteristics of the watershed where the rain is occurring.

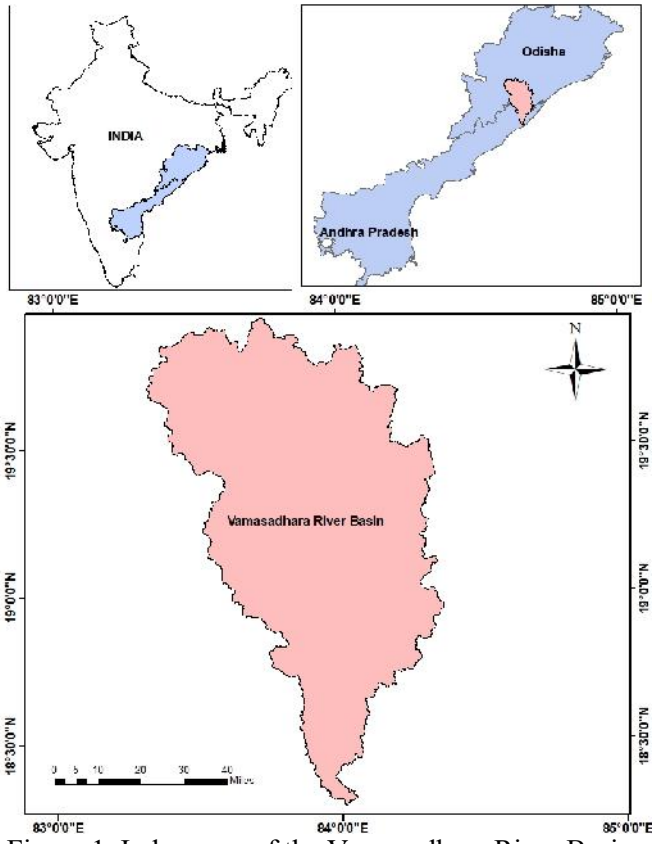



Figure 1. Index map of the Vamasadhara River Basin.

## 3. Methodology

The current study proposes by coupling the hydrological model HEC HMS (the Hydraulic Engineering Center hydrological model System) with the hydrodynamic model HEC-RAS (the Hydraulic Engineering Center River Analysis System) by employing rainfall as an input. The geospatial Hydrological Modeling Extension (HEC geoHMS) uses ArcGIS and spatial Analysts to develop several hydrological inputs, analyzing digital terrain information, HEC GeoHMS transforms the drainage paths and watershed boundaries into a hydrologic data structure that presents the watershed response to precipitation. Rainfall-runoff modelling would be performed using the HEC HMS model by importing results from HEC-GeoHMS. The physical representation of watershed would be accomplished with a basic model.

Flood simulations are typically based on a two-step process in which a hydrological model is first used to route the flood and determine expected flow hydrographs at the site of interest. The peak flow from this flood routing analysis is then included as a typical input into a steady flow hydraulic model, such as the U.S. Army Corps of Engineers HEC-RAS model, to determine the corresponding flood levels that would be expected along river reaches extending through populated areas. U.S. Army Corps of Engineers' public domain HEC-RAS (River Analysis System) model now offers flood forecasters with adjusts modelling capability. Specifically, HEC-RAS has been expanded to include an unsteady flow modelling component which, although not capable of handling highly dynamic flows such as dam break and ice jam release events, is more than adequate for the application of open water flood forecasting. Given that the HEC-RAS is so widely used in practice, virtually all water resources engineers have some familiarity with it. Furthermore, as it is the standard tool for floodplain delineation studies, most government agencies responsible for flood forecasting already have HEC-RAS models of the river reaches affecting the populated areas within their jurisdiction. For anyone who has used HEC-RAS in this capacity, the unsteady modelling component will be an easy

extension. HEC-RAS is a hydraulic model that is composed of three 1D hydraulic examination modules designed for 1) steady flow water surface profiles, 2) Unsteady flow simulation for 1D and 2-D and 3) Sediment transport, movable boundary computations. Ordinary geometric data modelling and geometric and hydraulic calculation sub-modules are implemented in all three of these models. Apart from these three models for hydraulic research, the model also includes many hydraulic planning utilities that can be used after the fundamental water surface contours are programmed

## 4. Results and discussion

In the proposed study hydrological model HEC HMS (Hydraulic Engineering Centre Hydrological Model System) with hydrodynamic model HEC-RAS (Hydraulic Engineering Centre River Analysis System) would be integrated by employing rainfall as an input. As per Central Water Commission (CWC) report Vamsadhara river basin falls in flood prone area in the sub zone 4(A) of the Andhra region. Accordingly, ASTER 30 m resolution digital elevation model (DEM) was downloaded from Earth Explorer (USGS WEB site) as shown in figure 2. ArcGIS extension HEC-GeoHMS terrain processing tool is used to delineation of the basin boundary, sub basins and drainage network as shown in figure 3. Landsat 8 image January 2019, Land use and land cover (LU/LC) were performed as shown in Figure 4 and Figure 5. Soil maps of the river basins were generated using NBSS, Nagpur soil map to estimate the losses parameters. Daily discharge data were collected from India-WRIS and rainfall collected from IMD and hourly data from CHRS data portal. Estimated all the input parameters of the HEC HMS model and simulated the runoff for peak flood year 2006 monsoon season. Calibrated results are well match with peak flow as shown in the figure 6 and 7 at Gunupur GD station and Kashinagar GD station in figure 8 and 9.

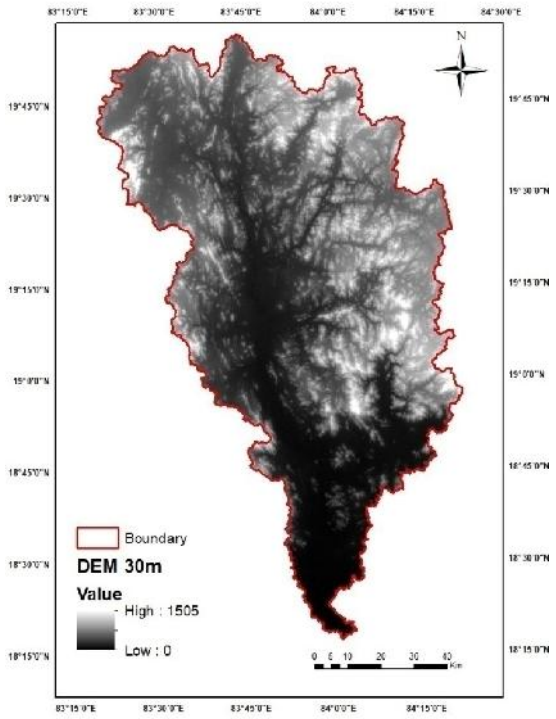



Figure 2. ASTER 30 m resolution digital elevation model (DEM) of the Vamasadhara river basin

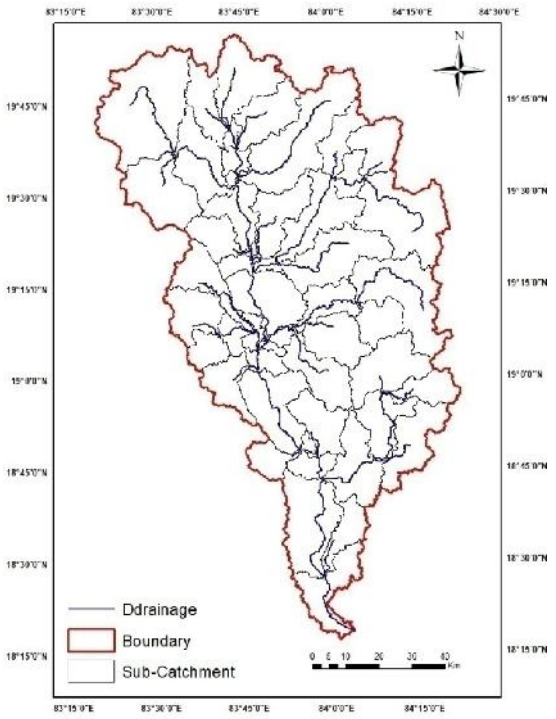



Figure 3. Basin boundary, sub basins and drainage network of the Vamasadhara river basin

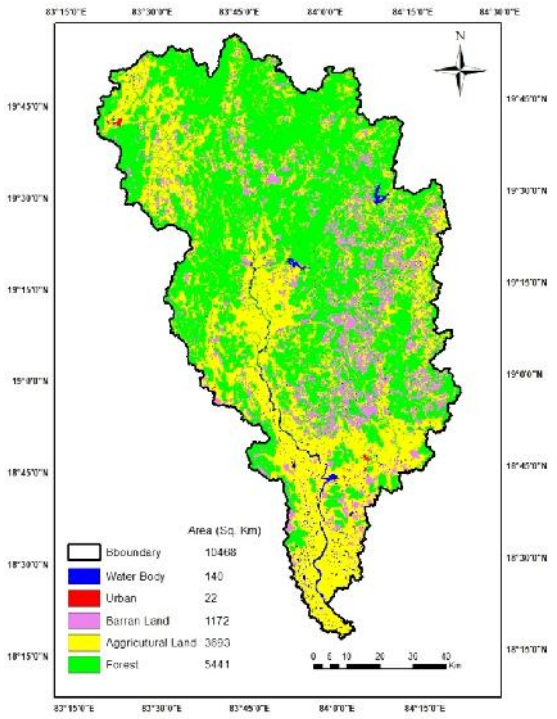



Figure 4. Classification of LULC of the Vamasadhara river basin.

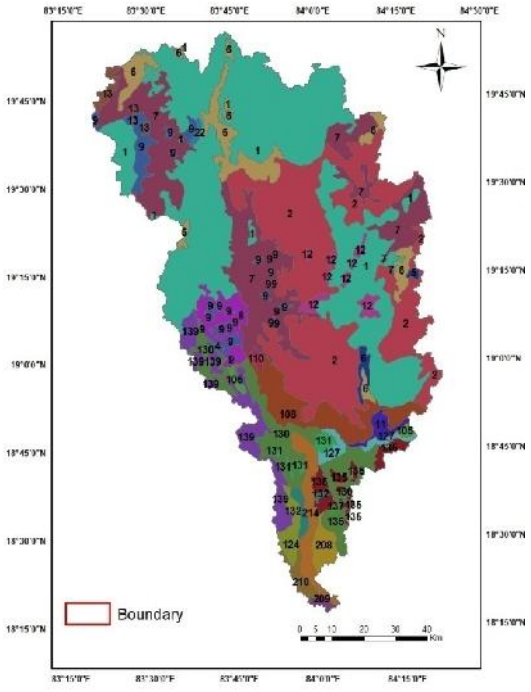



Figure 5. NBSS soil map of the Vamasadhara river basin.

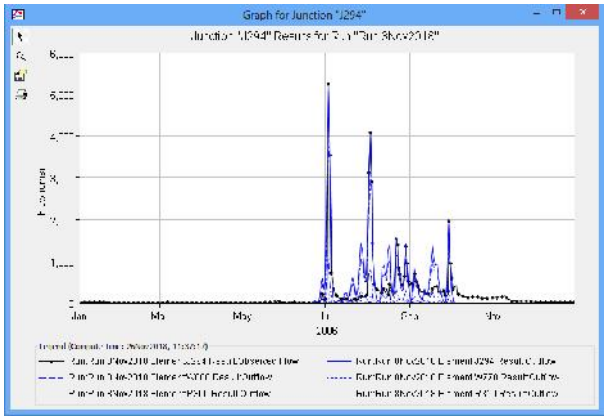



Figure 6. HMS simulated results compared with observed flow at Gunupur GD station of the Vamasadhara River basin.

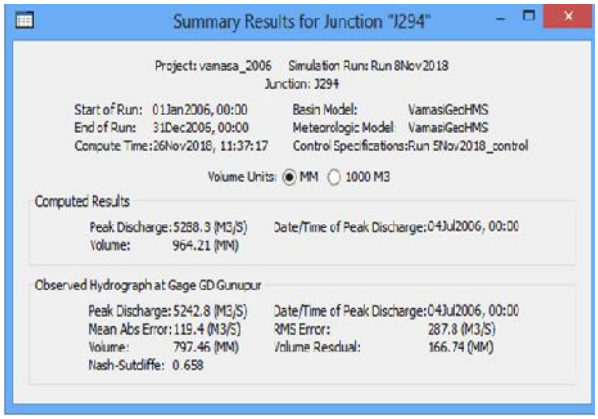



Figure 7. HMS model calibration results at Gunupur GD station of the Vamasadhara River basin.

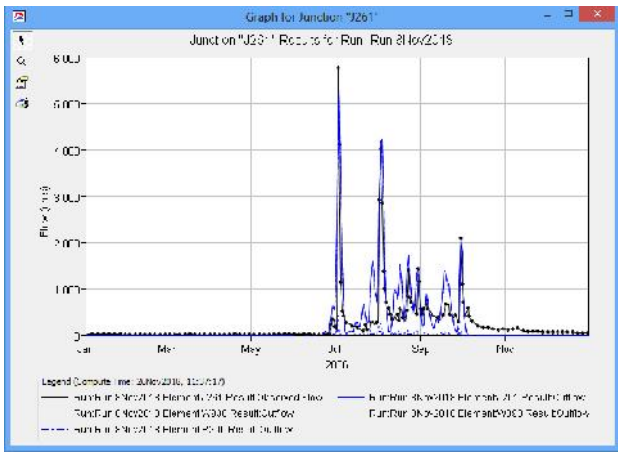



Figure 6. HMS simulated results compared with

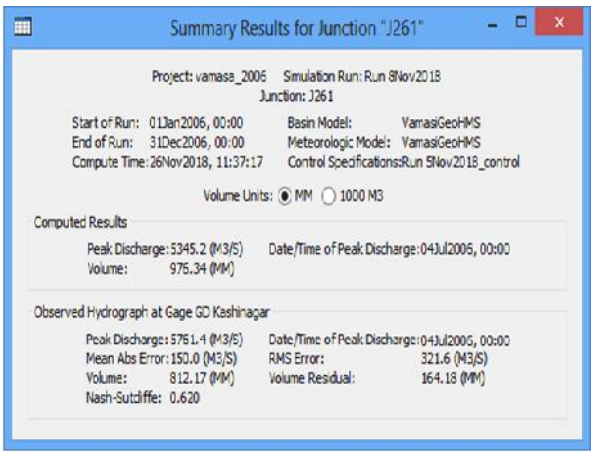



Figure 7. HMS model calibration results at

observed flow at Kashinagar station of the Vamasadhara River basin.

Kashinagar GD station of the Vamasadhara River basin.

Imported terrain data is used for creating the 2D flow area within the geometry editor and the total numbers of 536381 cells were made over the 2D river flow area within the river basin, as shown in Figure 10. Each cell size 500m × 500m was used for the analysis with the computational time interval of 1 hour with the output interval of 1 hour. The small-time interval and small cell size selection are better for getting good results though the simulation takes more time to complete. For the unsteady flow analysis in HEC-RAS, the initial conditions of the river were assumed to be wet even though the default mode of HEC-RAS simulation is dry. Considering this condition, at the initial process, HEC-RAS will fill up the mesh till the warm-up time and then the simulation will be done with that filled cells of the river as open channel flow using diffusion wave equation considering the finite volume approximation. Before analysing HEC-RAS, the hydraulic properties of each section should be assigned. HEC-RAS has the capability of creating hydraulic properties of each computed cell mesh. Those hydraulic properties are based on the provided geometric terrain data and provided manning's n value land cover.

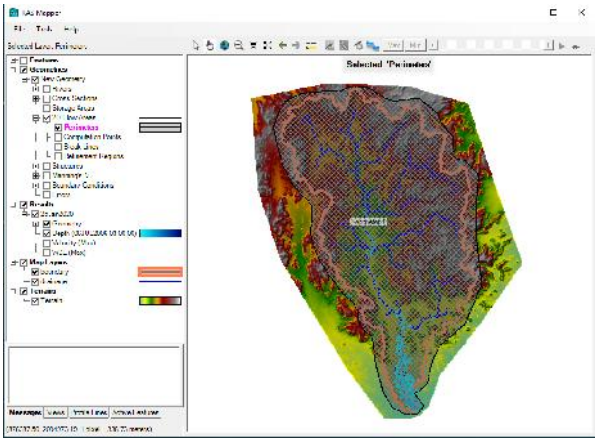


Figure 10. HEC RAS model setup of the Vamsadhara River basin.

Using the HEC HMS model simulated excess precipitation or runoff depth was used as an input to the HEC RAS model simulating for flash flood. Simulated HEC RAS model results from calibration with the observed flow at Gunupur and Kashinagar of Vamsadhara river basin from 1st Jan 2006 to 31st Jan 2006,are shown in Figures 11 and 12. The scattered plot coefficient of determination ($R^2$) was found to be 0.766 at Gunupur and 0.777 at Kashinagar which are shown in Figures 13 and 14. From the analysis, the correlation between observed and simulated flow has been found satisfactory. From the HEC-RAS analysis, the time variation of the result of unsteady flow analysis was obtained. The water depth, water velocity and water surface elevation within the time series is found to be maximum when there was maximum flow, though, the location of the maximum value of each result got varied over the reach with time. The maximum water depth of the basin for forecasting the flash flood is given in Figure 15. The location is dependent upon the cell properties and associated geometry.

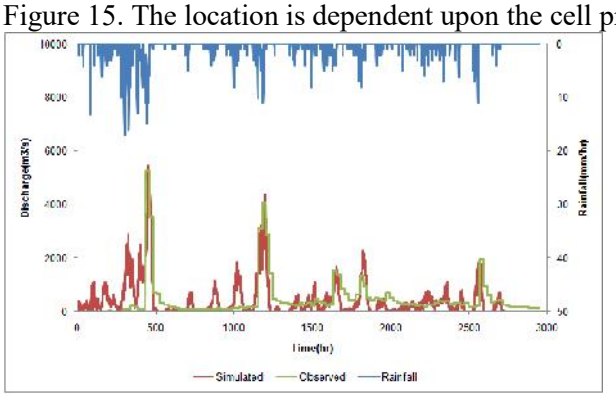



Figure 11. HEC RAS model simulated results results with observed flow at Gunupur GD station

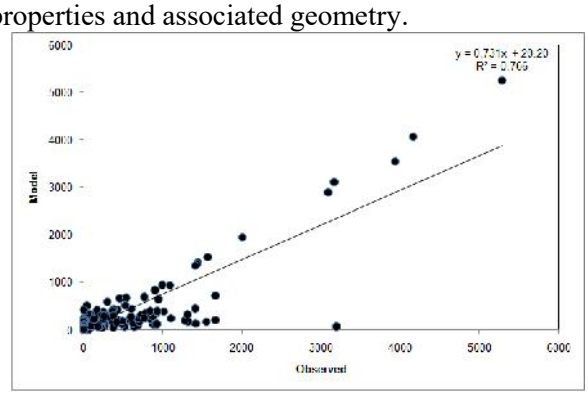



Figure 12. Scattered plot at Gunupur GD station of the Vamsadhara River basin.

of the Vamsadhara River basin.

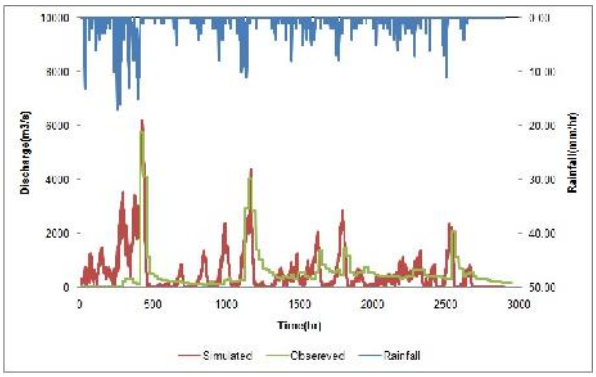



Figure 13. HEC RAS model simulated results with observed flow at Kashinagar GD station of the Vamsadhara River basin.

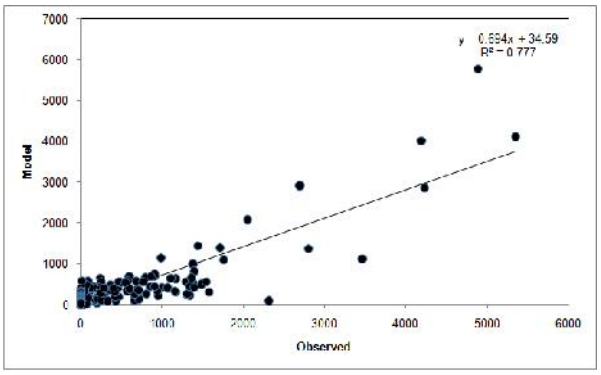



Figure 14. Scattered plot at Kashinagar GD station of the Vamsadhara River basin.

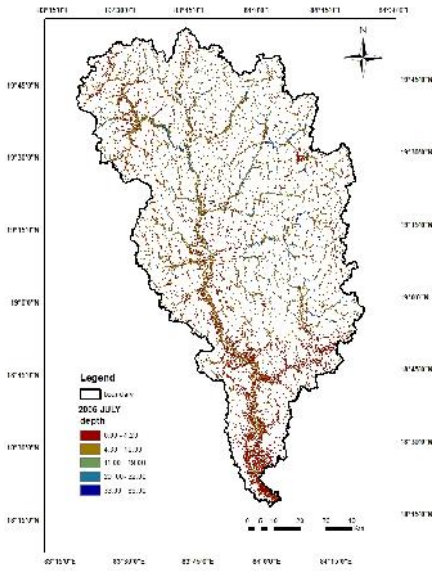



Figure 15. Flash Flood inundation map of peak flood 2006 monsoon season of Vamasadhara River basin with maximum depth of water with variable time.

## 3. Conclusions

In this paper, the hydrological model HEC-HMS (Hydraulic Engineering Center - Hydrological Model System) and hydrodynamic model HEC-RAS (Hydraulic Engineering Center - River Analysis System) is proposed to be integrated to forecast flash flood using rainfall as an input. The input parameters of the HEC-HMS model have been estimated. The simulated runoff has been calibrated with observed flow data of Vamsadhara River Basin. HEC-HMS model output results (Runoff depth) have been used as an input in the 2D hydrodynamic model (HEC-RAS) to simulate the flash flood for Gunupur GD site and Kashinagar GD site.The simulated 2-D HEC-RAS Model results compared with observed flow data and coefficient of determination ($R^2$) is around 0.766 for Gunupur and 0.777 for Kashinagar GD stations are well match with observed flow. Flash flood model is very useful for flood warning system by generating pre-flood inundation maps and decision makers.

**Acknowledgement:**

Authors are thankful to Dr J. V. Tyagi, Director, NIH, Roorkee and Dr. Sudhir Kumar Scientist ‘G’ and Coordinator, DRC, Kakinada for their encouragement to submit the paper.

## References

Abed, N. A., Abdulla, F. and Khyarah, A. A. (2005), GIS-hydrological models for managing water resources in the Zarqa River basin. *Environmental Geology*, 47, pp 405–411.

Arekhi, S. (2012), Runoff modelling by HEC-HMS Model (Case Study: Kan watershed, Iran). *International Journal of Agriculture and Crop Sciences* 4(23), pp 1807-1811.

Beven, K.(1989), Changing ideas in hydrology – The case of physicallybased models. *Journal of. Hydrology*., 105, 157–172.

Borga, M., Gaume, E., Creutin, J. D., and Marchi, L. (2008) Surveying flash floods: gauging the ungauged extremes. *Hydrol. Process*., 22, 3883–3885.

Braud, I., Roux, H., Anquetin, S., Maubourguet, M.-M., Manus, C., Viallet, P., and Dartus, D. (2010) The use of distributed hydrological models for the Gard 2002 flash flood event: Analysis of associated hydrological processes, *Journal of. Hydrology* .394, 162–181.

Delrieu, G., Ducrocq, V., Gaume, E., Nicol, J., Payrastre, O., Yates, E., Kirstetter, P.-E., Andrieu, H., Ayral, P.-A., Bouvier, C., Creutin, J.-D., Livet, M., Anquetin, S., Lang, M., Neppel, L., Obled, C., Parent-du-Chˆatelet, J., Saulnier, G.-M., Walpersdorf, A., andWobrock,W.(2005) The Catastrophic Flash-Flood Event of 8–9 September 2002 in the Gard Region, France: A First Case Study for the C´evennes–Vivarais Mediterranean Hydrometeorological Observatory. *Journal Hydrometeorol*. 6, 34–52.

Gaume, E., Bain, V., Bernardara, P., Newinger, O., Barbuc, M., Bateman, A., Blaskovicov´a, L., Bl¨oschl, G., Borga, M., Dumitrescu, A., Daliakopoulos, I., Garcia, J., Irimescu, A., Kohnova, S., Koutroulis, A., Marchi, L., Matreata, S., Medina, V., Preciso, E., Sempere-Torres, D., Stancalie, G., Szolgay, J., Tsanis, I., Velasco, D., and Viglione, A.(2009). A compilation of data on European flash floods. *Journal Hydroogy*. 367, 70–78.

Halwatura, D. and Najjim, M. M. M. (2013), Application of the HEC-HMS model for runoff simulation in a tropical catchment. *Environmental Modeling and Software*.46 (2013) pp 155-162.

Hu, H. H., Kreymborg, L. R., Doeing, B. J., Baron, K. S. and Jutila, S. A. (2006). Gridded Snowmelt and Rainfall-Runoff CWMS Hydrologic Modeling of the Red River of the North Basin. *Journal of Hydrologic Engineering*. Vol. 11. 2. DOI:10.1061/(ASCE)1084-0699(200611:2(91).

Majidi, A. and Shahedi, K. (2012). Simulation of Rainfall-Runoff Process Using Green-Ampt Method and HEC-HMS Model (Case Study: Abnama Watershed, Iran). *International Journal of Hydraulic Engineering*, 1(1), pp 5-9.

Moussa, R., Chahinian, N., and Bocquillon, C. (2007). Distributed hydrological modelling of a Mediterranean mountainous catchment – Model construction and multi-site validation. Jornal of Hydrology. 337, 35–51.

Pilgrim, D. H., Chapman, T. G., and Doran, D. G. (1988). Problems of rainfall-runoff modelling in arid and semiarid regions. *Hydrological Science Journal*. 33, 379–400.

Pistocchi and Mazzoli. P., (2002). Use of HEC-RAS and HEC-HMS Models with ArcView for Hydrologic Risk Management. *iEMSs2002 Congress Proceedings*. Lugano. pp 91-100.

Roux, H., Labat, D., Garambois, P.-A., Maubourguet, M.-M., Chorda, J., and Dartus, D. (2011). A physically-based parsimonious hydrological model for flash floods in Mediterranean catchments. , *Nat. Hazards Earth Syst. Sci*. 11, 2567–2582, doi:10.5194/nhess-11-2567-2011.

Saulnier, G.-M. and le Lay, M. (2009). Sensitivity of flash-flood simulations on the volume, the intensity, and the localization of rainfall in the C´evennes-Vivarais region (France). *Water Resource Research*. 45, W10425, doi:10.1029/2008WR006906.

*IN PROCEEDINGS OF 25th HYDRO 2020, INTERNATIONAL CONFERENCE, NATIONAL INSTITUTE OF TECHNOLOGY ROURKELA, ODISHA, INDIA 26-28, March 2021, ISBN 978-93-90631-56-8*

Paper ID - 490

# Flood Resistant and Amphibious Houses: An Overview

Dev Vrat Singh[1], Saurabh Agnihotri[1], Javed Alam[2] and Mohd. Muzzammil[3]

[1]*B.Techfinal year student, Civil Engineering Department, AMU, Aligarh-202002, India*

[2]*Professor, Civil Engineering Department, AMU, Aligarh-202002, U.P, India E-mail: javedalamced@gmail.com*

[3]*Professor, Civil Engineering Department, AMU, Aligarh-202002, U.P, India E-mail: muzzammil786@rediffmail.com*

## Abstract

Among all the natural disasters that the country faces, river floods are the most frequent and often the most devastating. Floods are sources of large scale destruction and are among the most common natural hazards causing extensive damage to infrastructure, economy and devastation to human settlements. Recurring flood losses have handicapped the economic development of both developed and developing countries. It takes several months or even years before the community comes to the pre-flood level. So floods are a natural and inevitable phenomenon of life in almost all the states of India. India is highly vulnerable to floods having more than 40 MHA flood prone area. The frequency and intensity of floods have grown in the country over the years mainly due to the increase in the encroachment of floodplains of rivers and extreme events of precipitation. A solution to this problem has to be put forward to mitigate the flood havocs by constructing Amphibious and Flood Resistant Houses. In this paper, an attempt is made to put forward an overview of Flood Resistant and Amphibious Houses and suggest the measures to be adopted in the design of such houses with an eye on new techniques developed in different parts of the world.

*Keywords: Amphibious houses; flood resistant houses; natural hazard; precipitation*

## 1. Introduction

Flood is a natural hydrological phenomenon causing extensive damage to infrastructure, public and private services, the environment, the economy and devastation to human life. Its occurrence is usually the result ofvarious meteorological events. Through geophysical studies, it has been found that more than 1.5 billion people on our planet reside on the riverside and coastal flood plains where they produce 1/3 of world's food production (Sinha et al., 1999). Floods vary in degree of severity in terms of aerial extent, magnitude and in-depth. Depending upon the severity, they are referred to as minor, medium and major floods. In a minor flood, inundation may or may not be due to over banking, but in a major flood, flooding is caused by the overbanking of rivers and lakes. The overbanking of rivers may result in breaks of dikes, levees, dams and other protective structures. The flood may also be due to uncontrollable releases of impounded water from reservoirs. Flood mitigation is a way to be well prepared to avoid heavy losses. The loss of life and properties can be reduced if the preparation is done well in advance. Irrespective of all the protective works, the danger of floods cannot vanish. The flood losses are costing several billion US dollars annually worldwide (Kundzewicz and Takeuchi, 1999). The flood protection works can be categorized into structural and non-structural measures. Dams, dikes, floodways, reservoirs for flood control etc comes into the structural measure category whereas efficient flood fore-casting warning system, following laws and regulation, awareness raising etc comes under the nonstructural measures.

In India, more than 12% of the total geographical area lies in a major flood prone zone. India is a peninsular country as it is surrounded by ocean from three sides namely the Arabian Sea in the west, the Bay ofBengal in the east and Indian ocean in the South (Ahmad et al., 2016). The monsoon season lasts between June and September and about 80 to 90% of the annual rainfall occurs in this season. The major flood prone areas in India are river banks and deltas ofRavi, Yamuna, Gandak, Sutlej, Ganga, Ghaggar, Kosi, Teesta, Brahmaputra, Mahanadi, Mahananda, Damodar, Godavari, Mayurakshi, Sabarmati and their tributaries. Cyclones can cause floods in Andhra Pradesh, Orissa and Tamil Nadu. The monsoon rain causes heavy rainfall and flooding in the southern & eastern parts of the country. There are many methods available for the estimation of floods. For some sites with lesser available data or sites with no data available at all, regional flood frequency analysis can be used (Alam et al. 2015, 2016)

In order to protect residents from floods and rising seawater, alternative design options for coastal residents should be implemented. It is necessary because as much as 90% of the 100 largest cities are located near the sea. These cities have large amounts of water in the form of lakes, rivers, canals, harbour.

Flood is a natural hydrological phenomenon causing extensive damage to infrastructure, public and private services, the environment, the economy and devastation to human life. Its occurrence is usually the result ofvarious meteorological events. Through geophysical studies, it has been found that more than 1.5 billion people on our planet reside on the riverside and coastal flood plains where they produce 1/3 of world's food production (Sinha et al., 1999). Floods vary in degree of severity in terms of aerial extent, magnitude and in-depth. Depending upon the severity, they are referred to as minor, medium and major floods. In a minor flood, inundation may or may not be due to over banking, but in a major flood, flooding is caused by the overbanking of rivers and lakes. The overbanking of rivers may result in breaks of dikes, levees, dams and other protective structures. The flood may also be due to uncontrollable releases of impounded water from reservoirs. Flood mitigation is a way to be well prepared to avoid heavy losses. The loss of life and properties can be reduced if the preparation is done well in advance. Irrespective of all the protective works, the danger of floods cannot vanish. The flood losses are costing several billion US dollars annually worldwide (Kundzewicz and Takeuchi, 1999). The flood protection works can be categorized into structural and non-structural measures. Dams, dikes, floodways, reservoirs for flood control etc comes into the structural measure category whereas efficient flood fore-casting warning system, following laws and regulation, awareness raising etc comes under the nonstructural measures.

In India, more than 12% of the total geographical area lies in a major flood prone zone. India is a peninsular country as it is surrounded by ocean from three sides namely the Arabian Sea in the west, the Bay ofBengal in the east and Indian ocean in the South (Ahmad et al., 2016). The monsoon season lasts between June and September and about 80 to 90% of the annual rainfall occurs in this season. The major flood prone areas in India are river banks and deltas ofRavi, Yamuna, Gandak, Sutlej, Ganga, Ghaggar, Kosi, Teesta, Brahmaputra, Mahanadi, Mahananda, Damodar, Godavari, Mayurakshi, Sabarmati and their tributaries. Cyclones can cause floods in Andhra Pradesh, Orissa and Tamil Nadu. The monsoon rain causes heavy rainfall and flooding in the southern & eastern parts of the country. There are many methods available for the estimation of floods. For some sites with lesser available data or sites with no data available at all, regional flood frequency analysis can be used (Alam et al. 2015, 2016)

In order to protect residents from floods and rising seawater, alternative design options for coastal residents should be implemented. It is necessary because as much as 90% of the 100 largest cities are located near the sea. These cities have large amounts of water in the form of lakes, rivers, canals, harbour.

A new house for the coast side and riverside should be designed to withstand the rising seawater and frequent floods. One such solution is flood resistant and Amphibious Houses. The flood resistant house is raised on some supports which should be sufficiently strong enough to bear the load of the structure and forces acting by the flood water and have ample space for the passage of flow in case of a flood. Amphibious housing is a dwelling type that rests on land but is capable of floating during the flood. The solution will also include waterproof material and protection of vital utilities, design of buoyant foundation, vertical guidance pole attached to the foundation, which provides resistance from the lateral force caused by wind and water.

In the present paper, an attempt is made to put forward an overview of Flood Resistant and Amphibious Houses and suggest the measures to be adopted in the design of such houses with an eye on new techniques developed in different parts of the world.

## 2. Flood Resistant Houses

Flood resistant houses can be categorized by their foundations and their relationship to the water. These include terp houses, housing on piles and floating houses.

### *2.1 Terp Houses*

Terp, by definition, refers to a large artificial earthwork mound created to provide safe ground in the event of a rise in water levels. The earliest terp houses have been discovered in the Netherlands, believed to be built around 500 B.C. The daily routines of the inhabitants were disturbed by the tides from the nearby rivers, and hence the need for such type of housing. These terps were intended to keep a house dry and provide enough space for cattle and food storage. They could be as high as 15 metres from the ground level. Later on, the connection of these mounds to prevent the flooding of their lands led to the formation of permanent dyke systems. Such dwellings have also been found in southern parts of Denmark and the north-western parts of Germany (Dirk Meier, 2006).

### *2.2 Housing On Pile*

Housing on piles includes the houses built on top of concrete, steel or wooden piles. They can be found in shallow water, coastal areas, or lakes. They are constructed in regions where changes in the water level can be predicted. These houses typically rest 2-5 metres above the ground and have been used throughout the world as a means of protection from high water level.

The use of timber piles in construction has a long history. Remains of piles found in Switzerland have been dated back to the bronze and stone age. Even in the present day and age, timber piles continue to be one of the leading types of driven piles. The use of timber in pile foundations is because of 2 factors: ready availability in certain regions and timber being a renewable resource. Being light in weight compared to other types of piles, it is easy to handle and cut. These piles, if properly treated, can have a very long life.
Concrete piles can be precast or cast-in-situ. They can also be reinforced, prestressed or plain. One significant advantage over other types of piles is that they do not corrode (steel piles) or decay (wooden piles). Precast concrete piles are shaped and moulded according to shape, length and size. Cast-in-situ piles are poured into holes in the ground where a rod has been previously driven and removed. Figure 1 shows a house on concrete piles.
Steel pilings can be formed into many different shapes. The most common steel pile types usually have rolled circular, X-shaped or H-shaped cross-sections. They are very strong and are great for driving especially in firm soil. They can be easily cut off. They can also be easily joined by welding. Steel pilings can last a long time but they are prone to corrosion, especially when submerged in water.

### 2.3 Houseboats

Houseboats, by definition, are boats, meant to be used as houses. These types of buildings, in their nature and construction, mimic a land-based property with the exception of being buoyant enough to withstand the forces of water.
In India, houseboats are used as accommodation for tourists. They are very common in the backwaters of Kerala and on the Dal Lake in Srinagar, J&K. The houseboats in the backwaters of Kerala are primarily used for leisure trips. They are 18-21 m in length and 4.5 m wide in the middle. Wooden planks, used in the construction of hulls, are held together by ropes. Unlike the houseboats of Kerala, the ones in Dal Lake are moored and only serve as hotels for tourists.

## 3. Amphibious Housing

Houses capable of resting on land during the dry season and floating during rising water levels are known as amphibious houses. During a rise in water levels, as in the case of floods, the house is lifted by water. A system of pontoons or a hollow basement type structure is adopted to ensure that the house remains dry. The structure returns to its original position, once the water level recedes (Anne Loes Nillesen, 2011). Figure 2 shows an amphibious house before and after the flood.

Amphibious houses may resemble houseboats however, there are some important differentiating factors. The basement of an amphibious house, being hollow, is exposed when there is no water. Thus, the base has to be concealed. The biggest difference between the two is their connection to the land. Typically amphibious houses are designed where water levels are moderate but are rarely prone to extreme flooding therefore all utility services can be connected to the municipal pipes whereas houseboats must contain all utilities within the structure (S. and Hamburg, 2005). Examples of these houses can be found throughout the Netherlands most notably the Maasbommel water-dwelling situated along the River Maas (Dirk Meier, 2006). Figure 3 shows Amphibious Houses along rivers.

### 3.1 Basic Principle of Construction

Generally, there are two basic principles for making floating houses. First is the pontoon principle in which one makes a solid platform, lighter than the water and the other based on the ship in which a hollow concrete box is created which is open on the top. The pontoon principle has the benefit of its use in shallow water, compared to the hollow concrete box while the concrete box has the benefit of higher space utilization within as a part of the building. Both types of floating houses are connected with a flexible connection to the quay, so the houses can rise with the water when the tide changes. When needed the floating system can be moved elsewhere at short notice without leaving any scar to the environment. Instead, a new house can be placed into the old situation which makes it the most sustainable and durable way to build.
The house is sited within a wet dock comprising retaining walls and base slab. When flooding occurs the dock fills with water and the house rises accordingly. Similarly, when the water subsides, houses come down. All the pipes, ducts and wires for water, gas, electricity and sewage disposal in such amphibious homes are flexible, designed to remain functional even when the house rises several metres from its usual position. Amphibious homes that rest on land are also built for rising conditions. (Soni et al. 2013)

### 3.2 Challenges to Amphibious Housing

Providing services in a floating house is a challenge which includes water supply, electricity and toilets. Therefore, green building concept has to be followed in the floating houses which use non-conventional resources for energy, make use of waste products, and recycle the water. Net-zero energy buildings are more useful as they do not require additional energy from external sources and total energy demand is met from on-site generation power. Normally solar panels are provided for the energy requirements. Due to aesthetic requirements as well as energy efficiency, roof gardens are also becoming popular. Other measures include incinerating toilets to bum waste and filtration units for drinking water collected from rainstorms. (Elizabeth Victoria Fenuta, 2010)

### 3.3 Low-Cost Solutions in Use

Fig 4 shows a makeshift houseboat that was constructed for a low cost of Rs 1.5 lacs. It uses a galvanised steel frame along with Fiber roof material. The wall is made up ofFRP and the base is made up of wood. Below the base, the buoyant force is provided by an interconnected system of plastic drums. This frame is further surrounded by used car tires, as shown in the picture, that provides additional stability to the houseboat. Such a structure can float during floods and remain stable on the ground during the dry seasons.

### 3.4 High-Cost Solutions in Use

Traditional floating houses, normally houseboats, were built in various countries in the places prone to floods, near coastlines and on the lakes and rivers. In Australia, especially on the Murray River and the sunny coastline of Queensland, there are many motorised pontoon based houseboats with two or more bedrooms, some of them even have multi-storeyed structures. Houseboats are also in Lake Eildon in Victoria and in Hawkesbury River near Sydney. Similarly, floating houses/houseboats are

available in Canada, Germany, Hong Kong, Laos, New Zealand, Serbia, UK, USA, Thailand and India. In India, houseboats have been traditionally constructed in Kashmir and Kerala. Houseboats are also very popular for recreational activities for groups of people of all ages for residential purposes, it is Holland where houses are designed, constructed and are in high demand. (Olthuis et al. 2010)
Floating houses are now constructed which float only during floods. Thus, there are two types of floating houses, one which permanently floats and others that float only during floodwaters, otherwise get placed on the ground, particularly during the dry season when there is no water. Some houses which were constructed on stilts or piles due to safety requirements during floods in many parts of the world and in India too, like in West Bengal, Assam and other parts, are not floating houses in true sense. Floating houses in true sense are those which do not require a foundation and are based on the principle of buoyancy. The base of the structure needs to be such that it helps in floating as well able to take the dead load of the house, live load and other loads to be encountered by the house. Thus the house may be constructed on boats, hollow pipes, lightweight pads and similar materials which help in the floating as well taking up loads. Flotation Systems now being used include log floats, solid Styrofoam encased in rubber, foam-filled steel pontoons, positive concrete, concrete ferrocement pontoons, concrete and foam, wood and foam, polyethylene shell with solid core polystyrene block moulded inside, fibreglass etc.

## 4. Need of Floating Houses In India

India has a huge coastal area as well as large flood-prone areas like Bihar, Assam and in many other states where almost every year, the public face difficulty due to floods and loss of lives and property takes place. In this case, the principle of construction of floating houses is adopted in which the houses would rise during floods and subside down during dry conditions, loss of lives and property can be avoided. Simple techniques based on telescopic arrangements should be designed according to requirements. (Soni et al. 2013) Therefore, research and development can be taken up as model projects for developing such designs. In the starting, lifeline buildings in the flood-prone areas can be constructed with such techniques. These buildings will function even during periods when they remain cut off due to floods and have no external electricity and water.

In the islands and coastal areas, such houses will certainly be adopted sooner or later and thus Indian architects and designers should start getting expertise in this field to design such houses. Floating houses can also be built for tourists who would love to stay in such houses and India can generate considerable revenue from the same.

## 5. Material Analysis

Materials of the structure play an important role in the amphibious dwellings. Since the structure is near the water, the salt in the water will cause the materials to corrode. Designers should take a special concentration on the selection of the material. Some of the materials are EPS blocks, pontoons and bamboo.

### 5.1 BPS Blocks

Expanded Polystyrene (EPS) or Extruded Polystyrene (XPS) is a Geofoam that is manufactured into large lightweight blocks. The blocks vary in size but are mostly in 2m x 0.75m x 0.75m. This geofoam is a lightweight void fill. It is used in many applications such as lightweight fill, green roof fill, compressible inclusions, thermal insulation and sometimes it is used in drainage also. The cross-sectional geometry of an individual tube typically has simple geometric shapes. The overall cross-section of the assembled bundled tubes resembles a honeycomb that gives its name. Figure 8 shows EPS blocks.

## 5.2 Pontoons

Pontoons is an air-filled structure providing for buoyancy. Polystyrene is commonly used as the core material in floating docks and pontoons. It is cost-effective, has good floatation properties and is easy to cut into custom pontoon profiles. Polystyrene can be used for both concrete and vinyl encasing of pontoons. (Gregory P. Tsinker, 2004). Figure 9 shows houses built on pontoons.

## 5.3 Bamboo

Bamboo will be of most appeal to consumers interested in using natural and renewable resources. Unlike trees, which require at least 20 years to mature, a bamboo stalk can be repeatedly harvested every five or six years. In India, they are found growing naturally in almost all parts of the country except Kashmir. In India, they are found in the following states- Arunachal Pradesh, Assam, Manipur, Meghalaya, Mizoram, Nagaland, Sikkim, Tripura and West Bengal (Forest Survey of India, 2017). Other areas rich in bamboo are the A&N Islands, Chhattisgarh, Madhya Pradesh and the Western Ghats. When compared to hardwood, bamboo is slightly more resistant to water damage. And bamboo is slightly harder than many hardwoods, giving it somewhat better resistance to scratches and dents.



**Figure 1** Pile housing to protect against flash floods



**Figure 2** Before and after scenario of amphibious house



**Figure 3** Amphibious Houses along rivers



**Figure 4** Low-Cost amphibious house



**Figure 5** A floating house

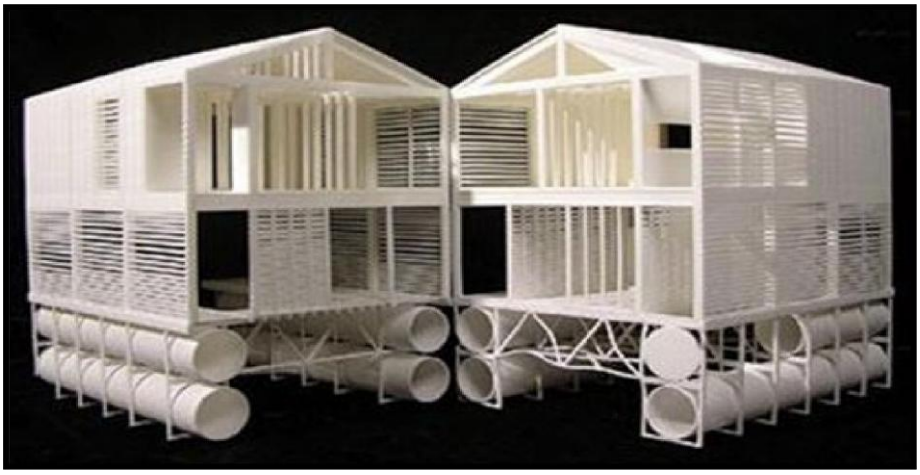


**Figure 6** House on steel platform pontoon structure

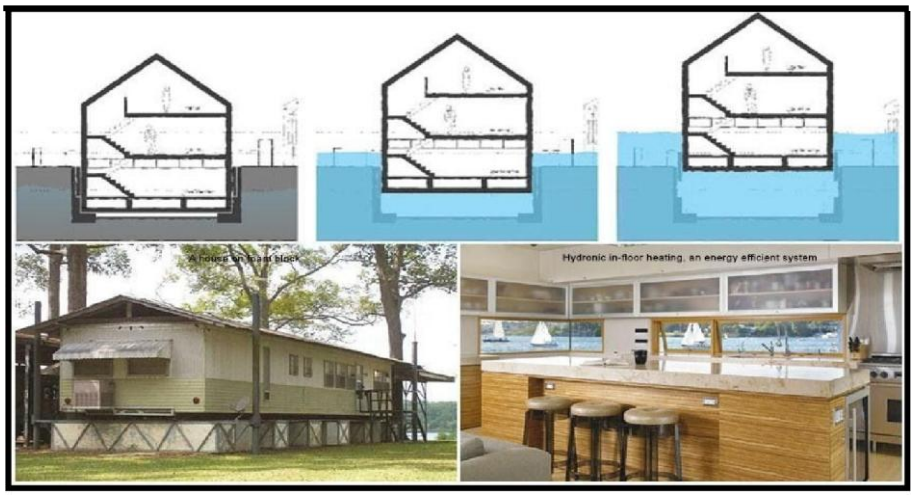



**Figure** 7 Self Elevating House

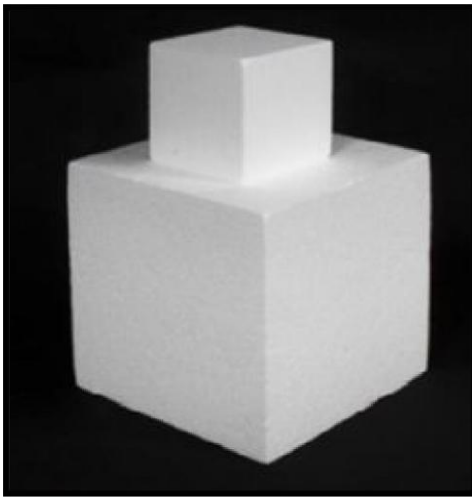


**Figure 8** EPS Blocks



**Figure 9** Houses built on pontoons

References

Ahmad S, Khan MK and Saqib M (2016). Flood Resistant Houses. Journal of Construction Engineering, Technology & Management; 6(3): 54-56

Alam J, Muzzammil Mand Khan MK (2015). Regional flood frequency analysis for some Indian catchments. In: 20th International conference on Hydraulics, Water resources and river engineering, HYDRO 2015, IIT Roorkee, 17-19 December 2015

Alam J, Muzzammil M and Khan MK (2016). Regional flood frequency analysis: comparison of L-moment and conventional approaches for an Indian catchment. ISH Journal of Hydraulic Engineering, 22(3): 247- 253.

Anne Loes Nillesen (2011). Amphibious Housing In The Netherlands Architecture And Urbanism On The Water.

Nai0l0 Publishers. ISBN: 9789056627805

Bamboo Resources of the Country (2017)- Forest Survey of India. Ministry of Environment & Forests, Government oflndia

Dirk Meier (2006), Die Nordseekuste : Geschichte einer Landschaft (in German), Heide: Boyens, ISBN 978-3-8042-1182-7

Eli zabeth Victoria Fenuta (2010). Amphibious Architectures: The Buoyant Foundation Project in Post-Katrina New Orleans. UWSpace.

Gregory P. Tsinker (2004). Port Engineering: Planning, Construction, Maintenance, and Security. John Wiley &

Sons. ISBN: 978-0-471-41274-8.

Olthuis, Koen, and David Keuning (2010). Float!: Building on water to combat urban congestion and climate change. Amsterdam: Frame. ISBN:978-9-077-17429-6

S. and Hamburg (2005), Amphibious houses: Dutch answer to flooding: Build houses that swim - DER SPIEGEL

ONLINE

Sinha, Anil & Sharma, K. Vinod (1999), Culture of Prevention, Government of India, Ministry of Agriculture, Natural Disaster Management Division, New Delhi

Soni, KM and Soni, Piyush (2013). Floating and Moving Houses, Journal of Indian Buildings Congress, XX (2),

17-22

What is EPS?- Expanded Polystyrene Australia < http://epsa.org.au/abo ut-eps /eps-in-buildin g/block/ >

ZW Kundzewicz, K Takeuchi (1999). Flood protection and management, Hydrological Sciences Journal 44(3)

# Theme X

# Urban Water Management

*IN PROCEEDINGS OF 25th HYDRO 2020, INTERNATIONAL CONFERENCE, NATIONAL INSTITUTE OF TECHNOLOGY ROURKELA, ODISHA, INDIA 26-28, March 2021, ISBN 978-93-90631-56-8*

Paper ID - 008

# Assessing flow parameters in sand nalla in the vicinity of mouda STPP of NTPC, Maharashtra

N.A.Sonawane[1], Kuldeep Malik[2], Ku.Madhavi Gajre[3],M.K.Pawar[4]

[1&2] *Scientist-B, CWPRS, Khadakwasla, Pune-411024*

[3] *Research Assistant, CWPRS, Khadakwasla, Pune-411024*

[4] *Scientist-E, CWPRS, Khadakwasla, Pune-411024*

*Email:* kuldeep.cwprs@gmail.com

## ABSTRACT

NTPC Limited has set up Super Thermal Power Station at Mouda in Nagpur district, Maharashtra. Construction of both stages of the project is over and all the units have been commissioned with Ash dyke for stage-I in function. The construction of Ash dyke stage-II is under progress. Just adjacent to Lagoon-I of 70 acres, Sand Nalla, a tributary of Kanhan River is flowing. The alignment of dyke of Lagoon-I, on left side, at some places, is located very close to Sand Nalla. During the monsoon in 2018, Sand Nalla was flooded due to heavy rainfall in the month of August 2018 in Nagpur district. The flood water of Sand Nalla was temporarily stagnating at Stage-II dyke area and some part of newly constructed dyke was also eroded.

1-D mathematical model studies were conducted using HEC-RAS software by reproducing about 34kmreach of Sand Nalla. Water levels and velocities were computed for different ranges of discharges in the river. A very small rise in water level of the order of about 0.21 m was observed due to provision of stage-II Ash dyke. This occurred mainly due to reduction in natural flow area and as result water rushed in to a village located on the left. Based on the analysis of results of mathematical model study and observations during the site inspection, a flood protection wall around the affected village with suitable provision to drain rainwater was recommended. The protection measures in the form of stone crates over a suitable synthetic filter were also recommended to the upcoming stage-II ash dyke as well as river bank where ever agriculture fields were very close to the river bank to minimize erosion.

***Keywords:*** *Ash dyke, Bank erosion, Discharge, Lagoon, Protection wall, Stone crate Velocity*

## 1. Introduction:

NTPC Limited has set up Super Critical Thermal Power Station at Mouda in Nagpur district, Maharashtra. The project site is located at about 32 km east of Nagpur between the right bank of Sand Nalla and left bank of Kanhan river. The project comprises of two stages; Stage-I (2 x 500 MW) and Stage-II (2 x 660 MW). All the units have been commissioned and are under production. Ash dyke for Stage-I has already been constructed and functional. The work of Ash dyke Stage-II has also been taken up and is under progress. Total area of Stage-II Ash dyke is spread across 282 acres which comprises of Lagoon-I (70 acres), Lagoon-II (50 acres) and Lagoon-III (151 acres). On the left north side of Lagoon-I, Sand Nalla (a tributary of Kanhan river) is flowing. As per Layout of alignment of starter dyke of Lagoon-I, at some places, distance between Sand Nalla and outer embankment of Ash dyke is very less.During the monsoon in 2018, there was a flood in Sand Nalla due to continuous heavy rainfall from 19 to 21 August 2018, in the surrounding area of Mouda plant and Nagpur district. It was noticed that flood water of Sand Nalla was temporarily stagnating at Stage-II dyke area and some part of newly constructed Dyke was eroded. Similar situation was also occurred during 2014.Average bed slope in Sand Nalla is about 1 in 7500 to 1 in 8000. Average width is about 40-50 m. It is a non-perennial small river which mostly flows during rainy season.Indexmap of Mouda Thermal Power Stationshows the layout of ash dykes with respect to Sand Nalla (Figs.1 and 2).

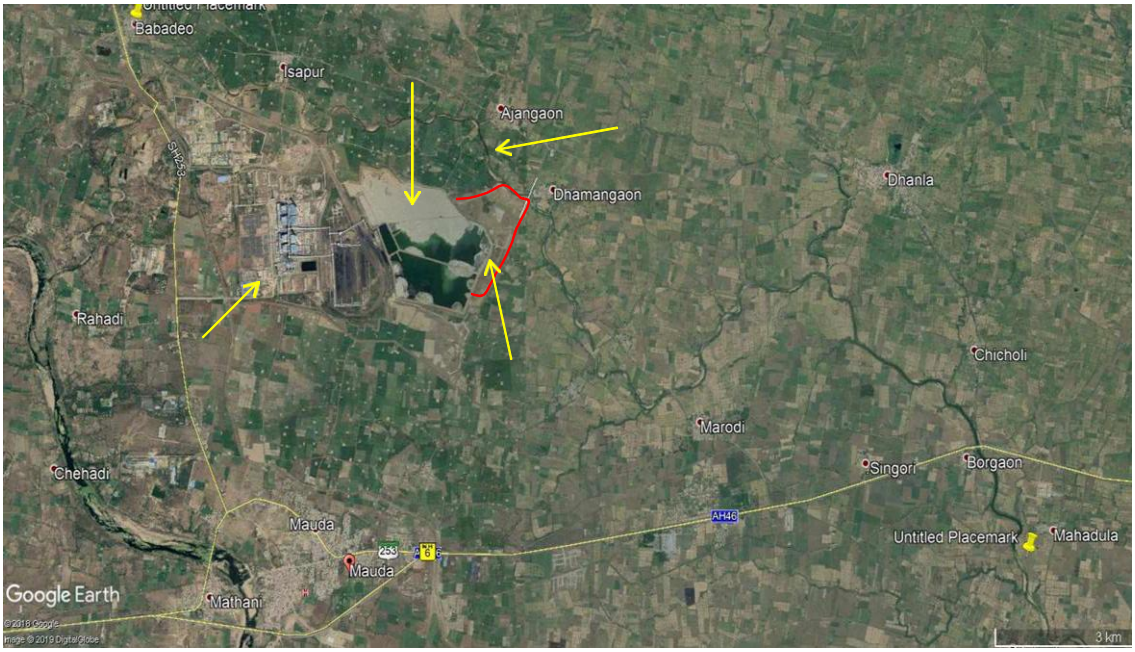



Fig.1: Index Map of Mouda STPS

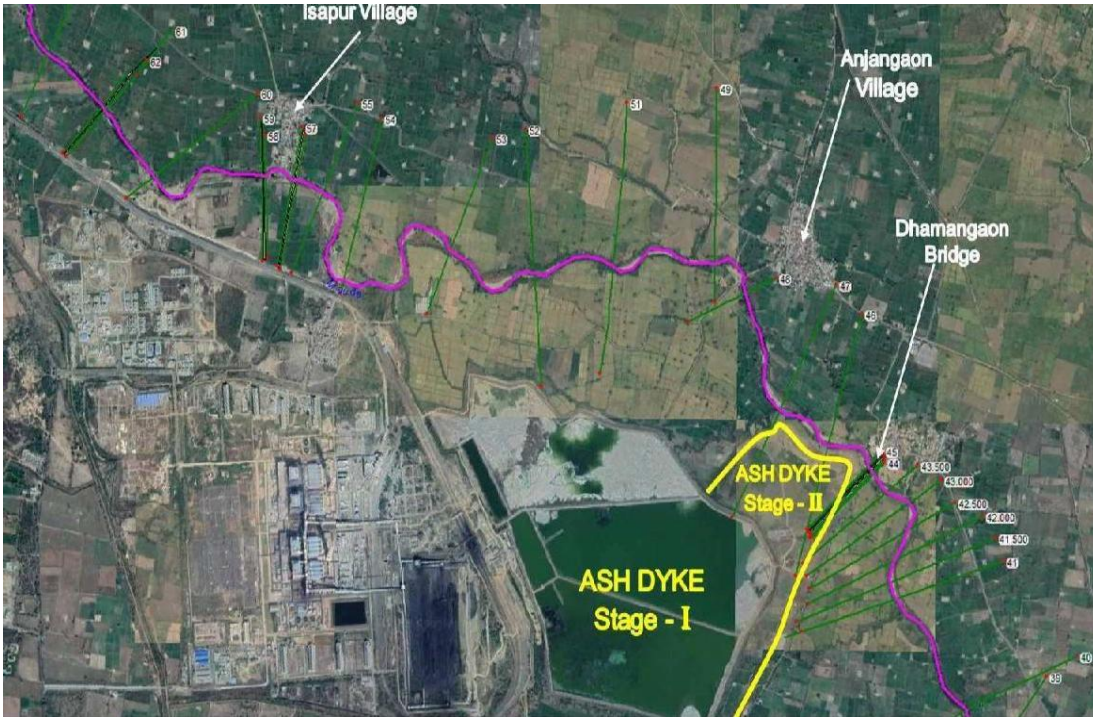



Fig.2: A close view of Ash dykes with respect to Sand Nalla

## 2. Data for studies

To carryout study for the estimation of water level and velocity in a stream, topographical and hydraulic data along with details of all existing and proposed structures in the river course are required. Following data was available for the study:

**2.1** The cross section data of Sand Nalla from Tarsa village in upstream of Dhamangaon to its confluence in the downstream with Kanhan River which covers a distance of about 38 km. Cross section details in the form of point levels were available at an interval of about 500 m in general for a total reach and at 100 m interval in the vicinity of structures. A typical cross section of Sand Nalla in the vicinity of Dhamangaon road bridge is shown in Fig.3.

**2.2** The hydrological data such as rainfall in Mouda Tehsil for a period of 2 years i.e.2017 and 2018 and flood level at Dhamangaon bridge and flood hydrographs from earlier studies.

**2.3** Data of salient features of the existing structures which helped in reproducing structures in the mathematical model.

**2.4** Ground levels and alignment of the proposed Stage-II Ash dyke.

**2.5** Ground levels along the periphery of Dhamangaon village.

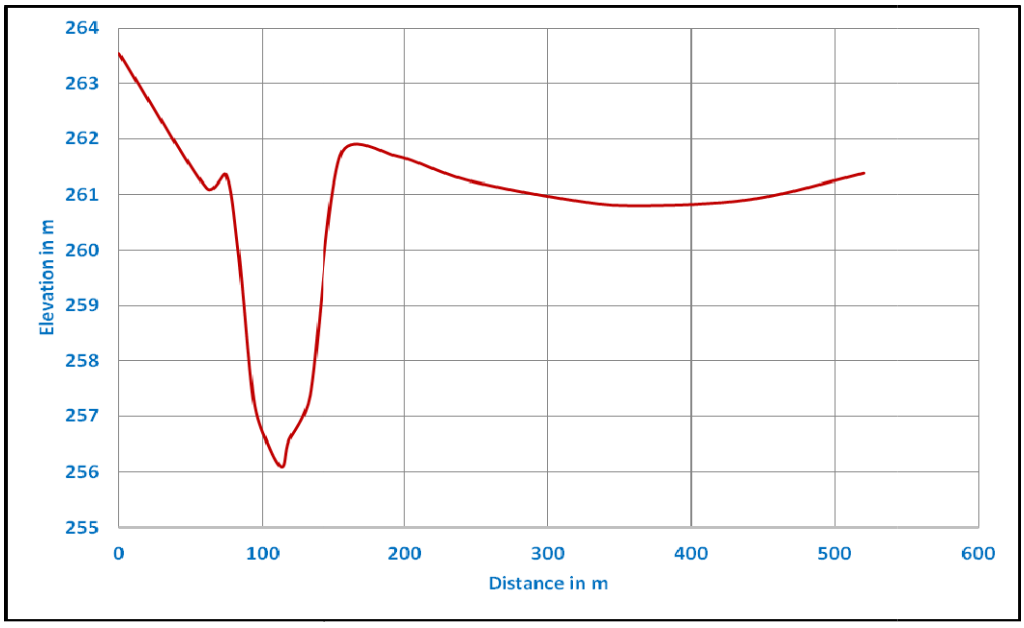



**Fig.3:** A cross section of Sand Nalla in the vicinity of Dhamangaon

## 3. Field observations

To get familiar with the site conditions, obstructions to the flow and state of existing structures, site was visited along with project engineers well conversant with the project site.

During the site inspection it was witnessed that many small structures were constructed across Sand Nalla for water conservation and irrigation purposes both upstream and downstream of Dhamangaon village. It was observed that many of these structures were causing obstruction to flow due to clogging/siltation etc. (Photo 1). The flow area of Sand Nalla within the banks was very less varying from 150 $m^2$ to 350 $m^2$ in the upstream of Dhamangaon at different locations. It was seen that the alignment of Stage-II Ash dyke was located very close to the right bank of Sand Nalla on the other side of which Dhamangaon village is located. It was observed that the construction of dyke had been started and it was raised about 0.50 m above average ground level. It was also seen that on the right

over bank, the raised dyke was partly eroded during high flood of 2018 as shown i Photo 2. The average width of Sand Nalla from bank to bank near Dhamangaon was about 40-50 m. The average bed level of Sand Nalla just upstream of Dhamangaon Bridge was about 55.00 m. The bed material of the stream consisted of fine silt along with clay mixed coarse sand.

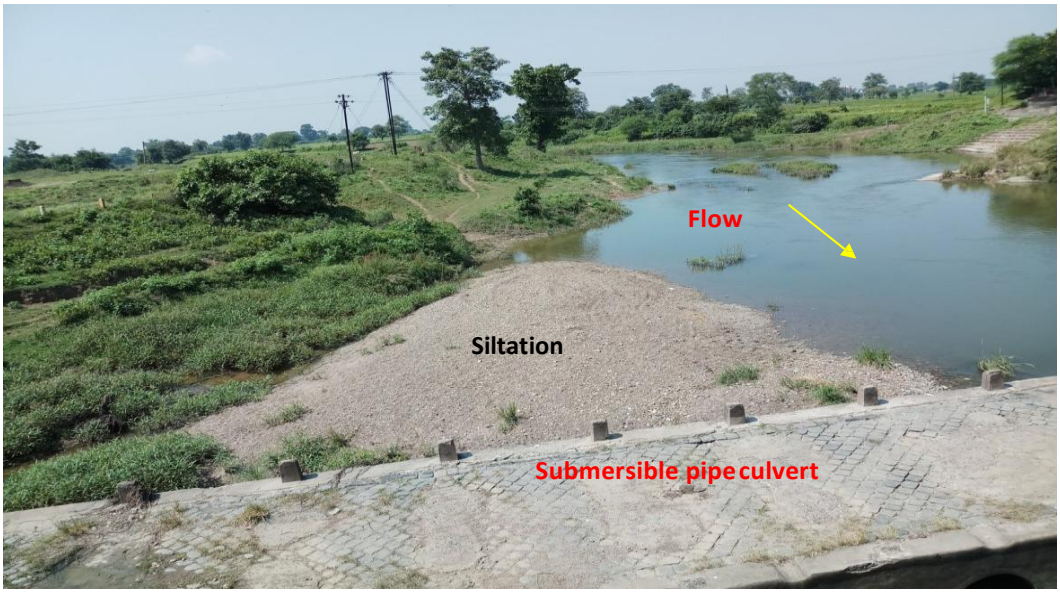



**Photo 1:** Abandoned pipe culvert upstream of Dhamangaon Road Bridge

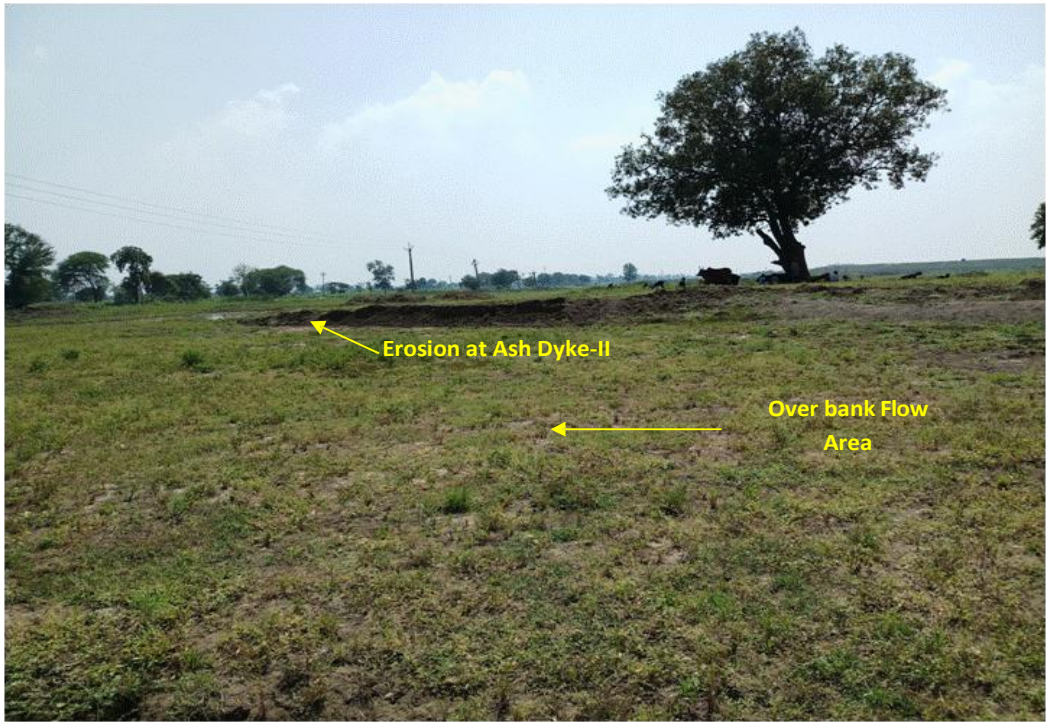



**Photo 2:** Erosion at under construction Stage-II Ash Dyke

## 4. Mathematical Model Studies

The one dimensional mathematical model HEC-RAS is used for the study. The accuracy of any prediction or simulation technique generally depends on the extent and quality of data available for representing the prototype topography and boundary conditions. Gauge discharge (G-Q) data for a period of about 15-20 years in the river reach of interest is required for better confirmation. The Sand Nalla is a small tributary of River Kanhan and detailed G-Q data in the river reach under studies was not available. However, a known water level near the Dhamangaon bridge for a observed flood of 2018 corresponding to 1020 $m^3/s$ was, therefore, used for calibration of the model.

### *4.1 Schematisation of Sand Nalla*

The topographical reach of Sand Nalla from Tarsa village about 14 km upstream of Dhamangaon Bridge to its confluence with Kanhan river in downstream was reproduced in the model. It covered a river reach of about 34 km. The flow area of Sand Nalla was schematized as shown in Fig. 4. All existing structures viz. bridges, bandharas, pipe culverts, check dams etc. were also reproduced in the model. At few locations cross-sections were developed with the help of Google image (due to paucity of data) considering levels of available upstream and downstream sections.

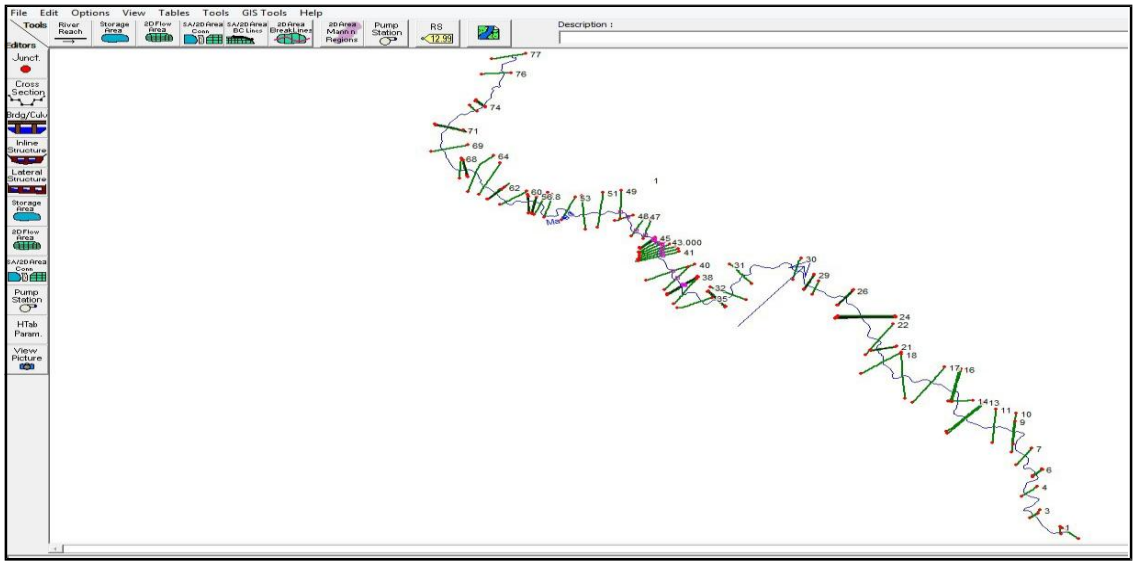



**Fig.4:** Schematization of Sand Nalla in HEC-RAS

### *4.2 Upstream Boundary Condition*

Different discharge hydrographs with 853$m^3/s$ and 1020 $m^3/s$(100 year return period discharge)as peak value were applied at the upstream boundary of the model.

### *4.3 Downstream Boundary Condition*

The normal depth condition with water surface slope as 1 in 8130 (S=0.000123) was applied at the downstream boundary considering the average thalweg slope in the study reach.

### *4.4 Model Calibration and Validation*

The most important parameters in the calibration of one-dimensional mathematical models are channel boundary roughness and channel width at water surface. Average value of 0.025 was adopted for bed and banks considering character of bed and bank material and observations at the site.

For the calibration run, observed flood discharge of1020$m^3$/s was applied at the upstream boundary with normal depth of 0.000123 as downstream boundary. Model simulation for this discharge stage gave a very close agreement between the water levels observed at Dhamangaon Bridge in the proto and in the model. Thus the model was considered to be calibrated and validated.

### *4.5 Study conditions*

Studies were conducted for following conditions

- Major hydraulic structures viz. check dams, pipe culverts and bridges reproduced within the study reach.
- Existing bed conditions at site without Stage-II dyke.
- After construction of Stage-II dyke
- Enhancing flow area of Sand Nalla by modifying/deepening river cross-sections in the vicinity of Dhamangaon
- After construction of flood protection wall around Dhamangaon.
- Providing Levee on left bank in different stretches.

### *4.6 Model Simulations*

After the calibration studies, model simulations are done for the all the conditions mentioned above for different discharges. The peak value (1020 $m^3$/s) corresponding to hydrograph of 100 year frequency daily rainfall of 250 mm for 6 hour storm was considered as the most vulnerable condition for the flooding in the vicinity of affected reach and bank erosion in Sand nalla as well as at stage-II dyke. Model simulations are also carried out for the same rainfall with 12hour storm generating peak flood of 853 $m^3$/s.

Water levels and velocities computed with the aid of mathematical model for different conditions with and without Stage-II Ash dyke are presented in Table-1for maximum flood discharge of 1020 $m^3$/s. Water levels observed after providing Levees along the left bank in different reaches are also shown in the Table-1. Water level profile for a typical critical condition is shown in figure 5 and velocity distribution along a cross-section in affected reach is presented in figure 6. Profile of ground levels and flood level along the flood protection wall around Dhamangaon village is plotted in figure 7 and alignment of the wall is shown in figure 8.

.

Attempts were also made for providing more flow area for the passage of flood by removing existing culvert upstream of existing high level bridge at Dhamangaon village, providing a pipe culvert with 6 nos. of 900 mm diameter pipes in the approach road of Dhamangaon bridge (where flood water overtopped the road during the flood of year 2018) and dredging a 100 m wide channel in the downstream of this culvert to join river in the downstream. Providing additional flow area reduced the flood level at the location of Stage-II Ash dykes. However, it increased the average velocity to 1.69 m/s in the affected area. However, it was not found feasible at the field level due to difficulty of acquiring additional land from the existing cultivable agriculture fields. Therefore, this alternative is not discussed in detail in the paper.

**Table-1:** Water levels and velocities for different conditions

| Chainage length in m from d/s boundary | Location | Lowest Bed Level (m) | Water Surface Elevation in m | | | Channel Velocity m/s | | | Levee level (m) | Bank levels (m) | Water Surface Elevation in m with | | |
|---|---|---|---|---|---|---|---|---|---|---|---|---|---|
| | | | Exist. Bed | Modified Bed | | Exist. Bed | Modified Bed | | | | Levee from cs 46 to 37 | Levee from cs 46 to 42.5 | Levee from cs 45 to 42.5 |
| | | | | With Dyke | Dyke + Flood Wall | | With Dyke | Dyke + Flood Wall | | | | | |
| 21367.1 | Anjangaon | 256.5 | 263.2 | 263.42 | 263.24 | 2.35 | 1.98 | 2.67 | 263.72 | 262.50 | 263.44 | 263.43 | 263.42 |
| **20428.1** | **249 m u/s of Dhamangaon** | **255.9** | **262.7** | **262.63** | **262.68** | **0.85** | **1.53** | **1.10** | **263.17** | **261.56** | **262.49** | **262.45** | **262.64** |
| 20163.0 | Dhaman-gaonBridge U/S | 256.1 | 262.6 | 262.54 | 262.59 | 1.02 | 0.99 | 1.00 | 263.07 | 261.5 | 262.59 | 262.55 | 262.55 |
| 20146.8 | Dhaman-gaonBridge D/S | 256.0 | 262.1 | 262.09 | 262.26 | 1.33 | 1.26 | 1.19 | 262.62 | 260.9 | 262.26 | 262.10 | 262.10 |
| 18279.5 | NawegaonCulvert_U/s | 255.5 | 260.4 | 260.41 | 260.68 | 1.50 | 1.50 | 1.58 | 260.91 | 259.21 | 260.45 | 260.41 | 260.41 |
| 18271.2 | NawegaonCulvert_D/s | 255.3 | 260.4 | 260.35 | 260.63 | 1.46 | 1.46 | 1.49 | 260.85 | 259.17 | 260.33 | 260.35 | 260.35 |
| 18262.9 | Under const Bridge-U/s | 255.1 | 260.4 | 260.36 | 260.64 | 1.34 | 1.34 | 1.37 | 260.86 | 259.23 | 260.34 | 260.36 | 260.36 |
| 18254.6 | Under const Bridge-D/s | 254.9 | 260.4 | 260.35 | 260.63 | 1.26 | 1.26 | 1.30 | 260.85 | 259.28 | 260.33 | 260.35 | 260.35 |
| 18237.9 | Nawegaon | 254.5 | 260.4 | 260.36 | 260.64 | 1.11 | 1.11 | 1.12 | 260.86 | 259.23 | 260.35 | 260.36 | 260.36 |

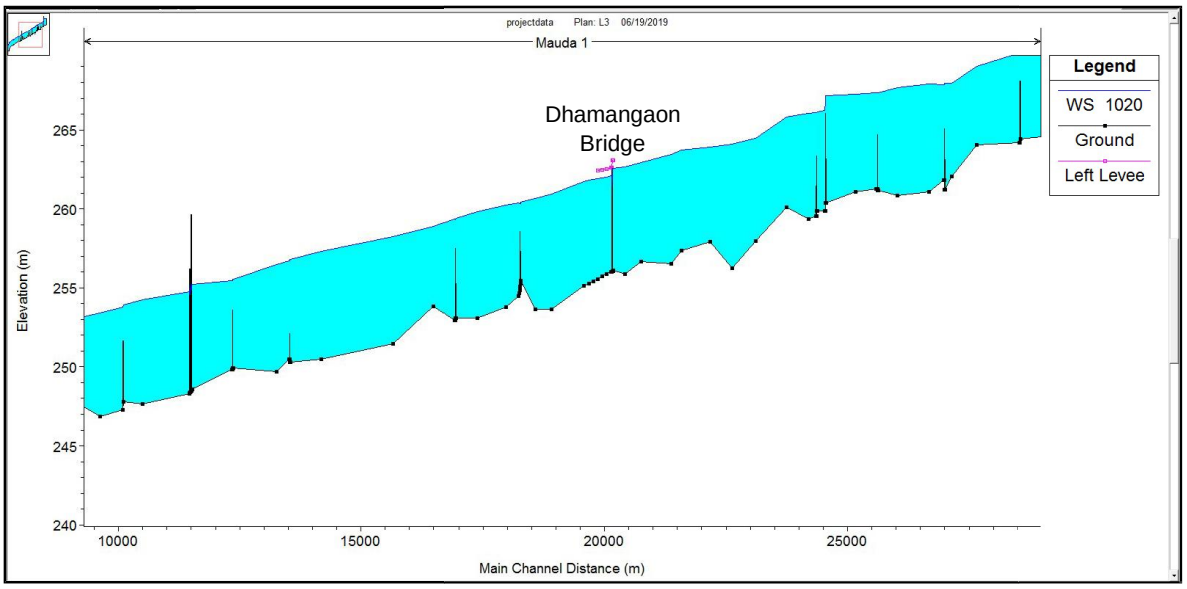



**Fig. 5:** Water surface profile from 10 km upstream to 10 km downstream of Dhamangaon village for Q= 1020$m^3$/s with Stage-II Dyke and Flood protection walls

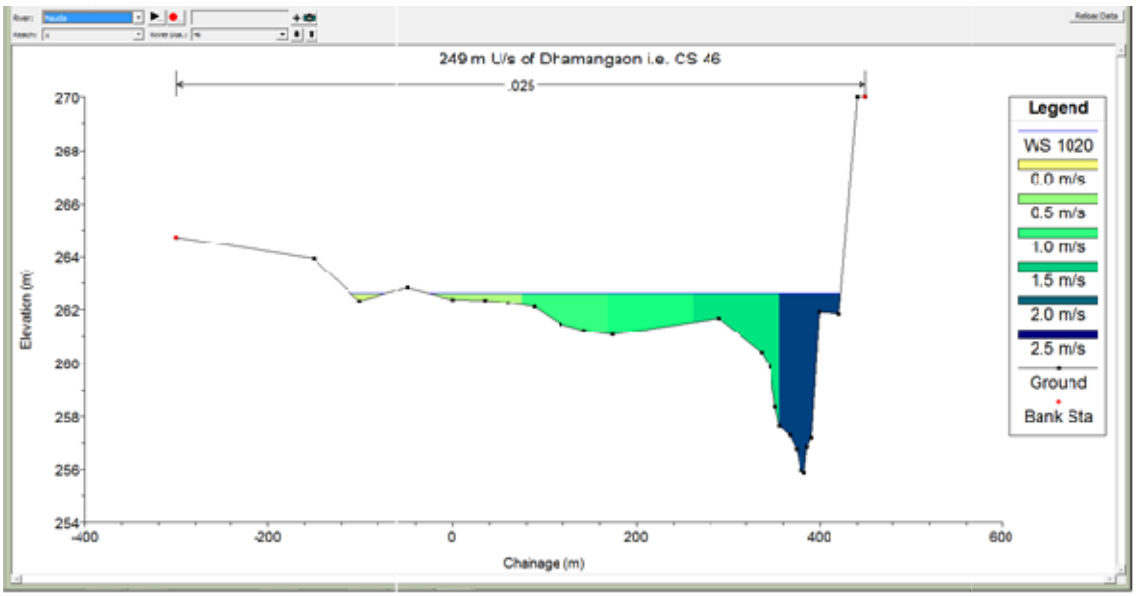



**Fig. 6**: Velocity Distribution at 249 m upstream of Dhamangaon(CS.46) for a Discharge of 1020 $m^3$/s

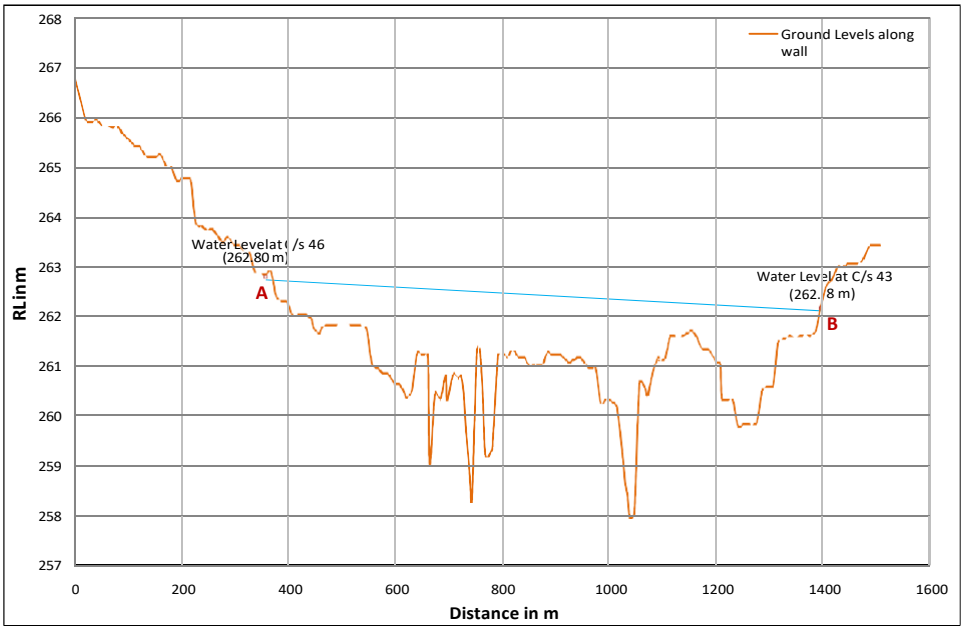



**Fig.7:** Ground levels along the proposed alignment of flood protection wall

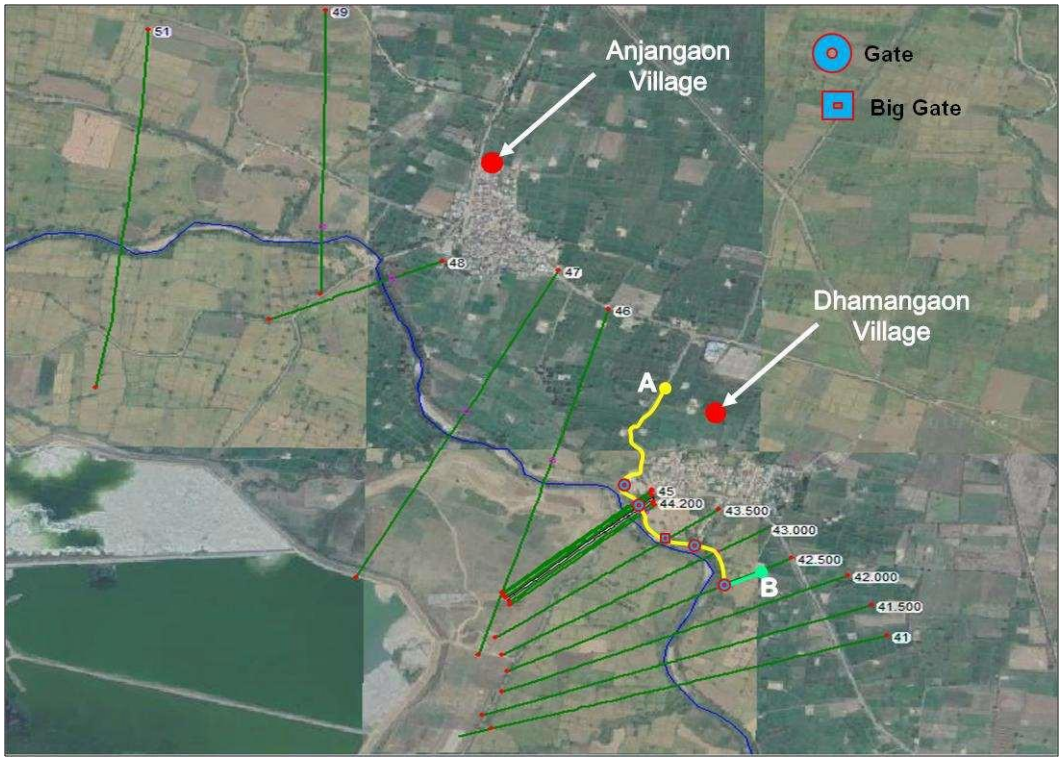



**Fig.8:**Proposed alignment of flood protection wall

## 5.0 Discussions

It was observed that in the existing condition Sand Nalla has flow area in river channel varying from 150 $m^2$ to 350 $m^2$ in the vicinity of affected area. With the present bed slope of about 1 in 1100 m in the vicinity, it can accommodate discharge up to 400 m3/s without overflowing on the over bank portions. Discharge of 1020 m3/s will spill over the low level banks and spread in the low lying areas of surrounding villages without construction of Stage-II dyke. Dredging in the deep channel of Sand Nalla may not result in increasing its carrying capacity to a great extent due to presence of many structures provided all along the reach in the form of low level bridges, bandharas etc. However, removal of old low level bridge along with silted material, upstream of Dhamangaon bridge may help in reducing water level at low discharge conditions and also avoid sedimentation in study reach.

Water levels and velocities computed with the aid of mathematical model were compared for different conditions with and without Stage-II Ash dyke as given in Table-1for maximum flood discharge of 1020 $m^3/s$ and it was found that there was only marginal increase in water level of the order of 0.21 m at 249 m upstream of Dhamangaon village (CS. No. 46) due to construction of Stage-II Ash dyke. However, the average velocity was increased from 0.8 m/s to 1.35 m/s. Water level profile for a typical critical condition is shown in figure 5 and velocity distribution along a cross-section in affected reach is shown in figure 6.

.

It is inferred that maximum velocity of 2.42 m/s is generated near Stage-II dyke at cross-section No. 46 (Fig.6). Bank protection measures in the form of stones in crates over suitable synthetic filter up to a level of RL 263.50 m will be required at the locations of higher velocities along the Dyke to safeguard against the erosion due to flood. A suitable length of apron will also be required for the toe protection of Ash dyke.

The construction of flood wall for the safety of Dhamangaon village is considered from the road joining Ajangaon and Dhamangaon in the upstream, along left bank of Sand nalla up to 300 m downstream of Dhamangaon road bridge and a closure wall in the downstream to avoid entry of flood water from river side as well as from upstream overbank portion or the downstream. It is evident from the ground levels along flood protection wall that there are many low-level points indicating the presence of natural drains towards the Sand nalla. Suitable control measures at these locations will be required to avoid entry of flood water from these locations and drainage of excess water towards Sand nalla.

## 6. Conclusions

Based on the site inspection, analysis of data and mathematical model studies, following conclusions are made:

- In the existing condition, Sand Nalla can accommodate discharges only up to 400 $m^3/s$ without overflowing on the over bank portions.
- Old defunct low level bridge upstream of Dhamangaon road bridge should be removed along with silted material.
- Comparison of Water levels and velocities with and without Stage-II Ash dyke computed with the aid of mathematical model for flood discharge of 1020 $m^3/s$ showed that there was only marginal increase in water level of the order of 0.21 m at 249 m upstream of Dhamangaon village due to construction of Stage-II Ash dyke.
- The average velocity in its vicinity however increases from 0.8 m/s to 1.35 m/s at 249 m upstream of Dhamangaon village due to provision of Stage-II Ash dyke.
- It was inferred from the velocity distribution that maximum velocity of 2.42 m/s was generated near Stage-II dyke at 249 m upstream of Dhamangaon village. Bank protection measures in the form of stones in crates over suitable synthetic filter up to a level of RL. 263.50 m are therefore

required at the locations of higher velocities along the Dyke to safeguard against the erosion during flood.

- Crates of size 0.5m X 0.5 m X 0.5 m are sufficient up to the velocity of 3 m/s. Size of stones to be used for filling inside the crates should be 23 kg or more.
- To avoid erosion at the toe of Dyke a minimum 4 to 5 m wide apron of the same crate size should also be provided over suitable synthetic filter.
- To avoid entry of flood waters in the affected area, a flood protection wall is considered from the road joining Ajangaon and Dhamangaon up to 300 m downstream of Dhamangaon Road Bridge. In addition to it, a closure wall in the downstream is also suggested to avoid entry of flood water from the downstream.
- The top level of flood protection wall should be kept at RL. 263.2 m in the upstream to RL. 262.7 m in the downstream.
- Natural drainages from Dhamangaon village to Sand Nalla should be provided with one-way flow type of gates to allow drainage of rainwater into the Sand Nalla after the flood recedes.

**Reference:** CWPRS Technical Report No. 5720 of July 2019

IN PROCEEDINGS OF 25th HYDRO 2020, INTERNATIONAL CONFERENCE,
NATIONAL INSTITUTE OF TECHNOLOGY ROURKELA, ODISHA, INDIA
26-28, March 2021, ISBN 978-93-90631-56-8

Paper ID - 073

# Morphometric Analysis of Trident Campus of Budhani in Madhya Pradesh

Jitendra Yadav[1], Ruchi Khare[2] Jyoti Sarup[3]

*1 MTech Student ,Civil, MANIT, Bhopal, India 462007*
*2 Associate Professor, WRE, MANIT, Bhopal India 462007*
*3 Professor, Civil, MANIT, Bhopal, India 462007*
*Email: ruchif4@rediffmail.com*
*Telephone/Mobile No.: +91 9425607454*

## Abstract

Morphometry means measurement and analysis of the configuration of earth and different landforms of it. In the present work morphometric analysis of Trident Campus at Budhani, M.P. is done by using Arc Hydro tool. Trident is the famous textile and paper industry, one of its campus is located at 22o46'10.53" N. 77o40'03.30" E at RL of 311 m from mean sea level (MSL) in western part of the Madhya Pradesh. It receives moderate rainfall of about 900 to 1000mm. Different linear, ariel and relief parameters are evaluated to analyze the quantitative evaluation of watershed drained by Narmada river

The study of Trident Campus drainage basin revealed that it is 5th order drainage basin of dendrite drainage pattern. Total number of streams are 609. For first order stream the stream segment length is maximum and decreases as the stream order increases. The drainage density (Dd) of the study area is 13.32 km/km$^2$ which indicates that the area has not been significantly affected by structural disturbances, whereas the drainage frequency (i.e., 161.54) and the very coarse drainage texture (i.e., 62.78) indicate low relief and porous, permeable rocks underneath the ground surface. This study is helpful to utilize the water resources of Trident campus for sustainable development of the area.

***Keywords:*** *drainage density, stream order, circularity ratio, arial aspect, relief aspects*

## 1. Introduction

Morphometry is the measurement and mathematical analysis of the configuration of the earth's surface, shape and dimension of its landforms (Jyoti et al , 2011 and Radhakrishnan et al 2014 ). Remote Sensing and GIS techniques are useful and efficient tools for delineating, updating and morphometric analysis of the drainage basin. It is very useful for hydrological investigation, identification of groundwater potential zones, ground water arrangement geomorphology and watershed characteristics. Many researchers i.e, Magesh et al. (2011), Guzhaa et al (2018), Machiwal et al (2018) successfully utilized these tools to derive morphometric parameters. In the present paper effort has been made to derive drainage network from SRTM DEM by using ARC HYDRO tool. Different linear, aerial and relief parameters are calculated and analysed. The study will be useful for the groundwater management of Trident Group watershed.

### *1.1 Study Area*

The present study area Trident Campus in Bhudni village in Sehore district of Madhya Pradesh between the parallels of North latitudes 22o45'19" and 22o46'08" and the meridians of east longitudes77o38'51" and 77o40'30". Trident Group with 3774795 m2 of area and 16808 population according to 2011 census. The normal rainfall of Bhudni village is 1239.6 mm. The highest rainfall i.e. 1412.3 mm received at Sehore. The district is surrounded in the North by the district of Guna, in the East by Vidisha and Raisen, in the South by Hoshangabad and Dewas and in the West by Shajapur and Rajgarh. In general, the district is covered with black cotton soils that cover nearly three fourth of the area. The Deccan Basalts occupy this portion. The remaining portion has red-yellow mixed sandstone, shale, and gneiss soils. The alluvial soils are found along the river courses.




**Figure1:** Location details of Trident Campus

## 2. Methodology

In the present study area, morphometric analysis of the watershed is done by using remote sensing and Arc GIS 10.5. For morphometric study of the area DEM is taken from http://earthexplorer.usgs.gov website. The watershed is delineated using the Arc GIS Hydro Tool on DEM. Then various steps which are followed to delineate the drainage network in the watershed are shown in Fig.2. Morphometric parameters are computed using standard formulae (Horton 1932, 1945). The fundamental parameter is derived from the drainage layer: stream length, area, perimeter, number of streams and basin length. Based on the formulae suggested by Horton (1932) the values of morphometric parameters namely; stream length, bifurcation ratio, drainage density, stream frequency, shape factor, elongation ratio, texture ratio, circularity ratio and compactness constant are calculated. Slope map and aspect are also drawn by using the spatial analysis tools for better interpretation of the land surface.

## 3. Formulae and Definitions

Various morphometric parameters which include linear, aerial and relief aspects of Trident Group drainage basin are as follows:

### 3.1 Linear Aspects

The network which has the single outlet through which the water and sediment of the system are transported is defined as drainage network. The order of the outlet stream is the highest order of the basin and considered as the order of the basin.

According to Strahler's [Horton (1945), Strahler (1952) method, which is a slight modification of Horton 's system, the smallest, unbranched finger tip streams are known as 1st order, the confluence of two 1st order channels creates a 2nd order channel section, two 2nd order streams join together to form a 3rd order section, and two 3rd order streams join together to form the 4th order, and so on.

### 3.1.1. Stream Length (Lu)

It is the total length of the stream of the individual order. Generally the stream length is highest for the first order stream and it decreases as the order of the stream increases.

### 3.1.2. Stream Length Ratio ($R_L$)

It defined as the ratio of the mean length ($L_{mu}$) of the stream of a given order to the mean length of the streams of the next lower order ($L_{mui}$-1).It is calculated for each pair. It signifies the variations in slope and topography of the watershed

$$L_{mu}= \frac{Lu}{Nu} \quad (1)$$

$$R_L=\frac{Lm}{Lmui-1} \quad (2)$$

**Bifurcation Ratio ($R_B$)**is the ratio of number of stream present in the given order (Nu) to number of segment of next higher order(Nu+1). The bifurcation ratio of large basins is the average bifurcation ratios of all stream orders within it.

$$R_B=\frac{Nu}{Nu+1} \quad (3)$$

**Basin length ($L_B$)** is measured as the longest dimension of the basin parallel to the principle drainage line.

**3.2 Aerial Aspects** is an aspect of two dimensions. It is defined as the total area projected over to a horizontal plane that contributes overland flow to the channel segment of the given order, and includes all lower order tributaries. Different parameters related to aerial aspects are drainage texture, drainage density, form factor, stream frequency, circularity ratio, elongation ratio and length of overland flow.

**Drainage density ($D_d$)** (Horton, 1932) shows the condition of the drainage system of a watershed. High drainage density results from weak or impermeable subsurface material, sparse vegetation and mountain relief, and low drainage density indicates that the basin was not significantly affected by structural disturbance (Strahaler, 1964).

$$Dd= L_M/A \quad (4)$$

Number of stream segments per unit area is referred to as Stream Frequency or Channel Frequency or Drainage Frequency (Fs) [Horton, 1945] Stream frequency is related to the lithological characteristics of watershed. If total number of streams are $N_M$

$$Fs= N_M/A \quad (5)$$

**Drainage texture ratio (T)** is defined as total number of stream segments of all orders per perimeter length of that area (Horton, 1932).

$$T= N_M/P \quad (6)$$

Where P is the perimeter of water shed. It depends on the lithology, infiltration capacity and relief aspect of the area.

**Form Factor ($F_F$)** is defined as the ratio of the basin area to the basin length (Lb). It represents the flow density and shape of the basin (Horton, 1932).

$F_F = A/L^2_B$ (7)

**Circulatory Ratio (Rc)** is the ratio of a basin area to the area of circle having the same circumference as the perimeter of the basin. [Miller, 1953]. It signifies the shape of the basin.

$Rc = 4\pi A/P^2$ (8)

**Elongation ratio (Re)** is the ratio of diameter of a circle of the same area as the basin to the maximum basin length.

$$Re = \frac{\sqrt{\frac{A}{\pi}}}{LB} \quad (9)$$

**Length of overland flow ($L_G$)** is independent variables which affect both hydrological and physiographical development of drainage basins. It is the length of the water on the ground surface before it is changed into definite channels.

$L_G = 1/2D_d$ (10)

**Constant channel maintenance (C) is inverse of drainage density (Schumm, 1956).**

**$C = 1/D_d$** (11)

**3.3. Relief Aspects** In morphometric analysis the concept of relief shows the third dimension i.e, elevation or height. The terms basin relief, relative relief, ruggedness number are associated with it.

**Basin Relief (H)** is the elevation difference of the highest and lowest point of the valley floor. It is an important characteristic to understanding the geomorphic processes and landform characteristics.

**Relief ratio (Rf)** is the ratio between the total relief of a basin and the longest dimension of the basin parallel to the main drainage line (Schumm, 1956). It shows the overall steepness of a drainage basin. It is used to indicate the of intensity of erosion processes operating on the slope of the basin. Relief ratio increases with decrease in drainage area and size of drainage basin (Gottschalk, 1964).

$R_r = H/L_B$ (12)

**Ruggedness Number (RH)** combines slope steepness with its length. It is defined as the product of maximum basin relief and drainage density

$RH = H * D_d$ (13)

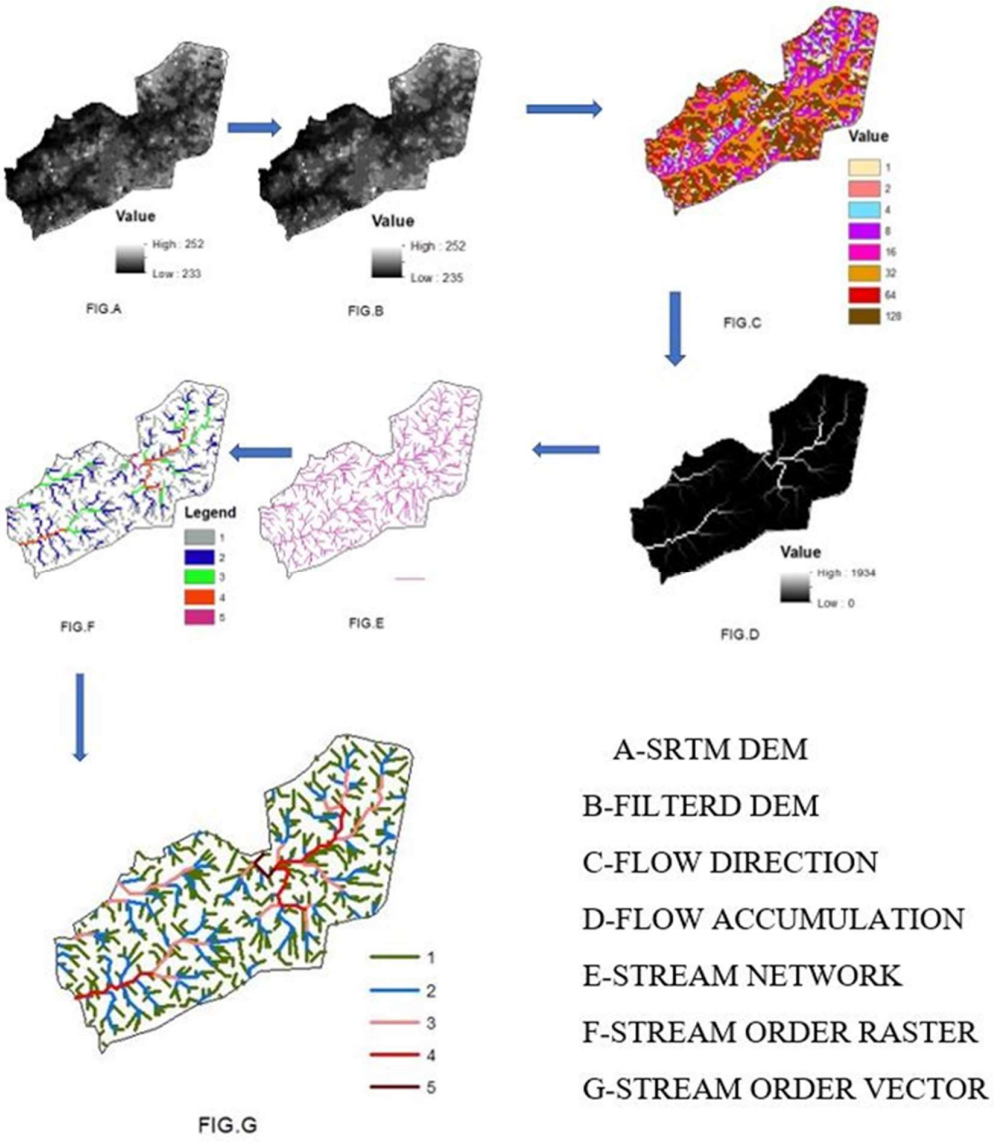
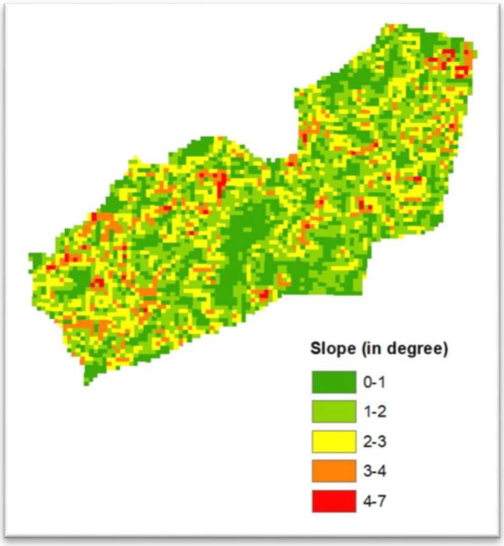



**Figure 2;** Methodology of Delineation of Drainage Network

## 4. Result and Discussion

The morphometric studies of Trident Campus include linear, aerial and relief parameters of the area. Analysis of slope of the watershed is also an important parameter in geomorphologic studies. Slope map of the watershed shows that the slope of the watershed varies in between 1 to 7 as shown in figure 3. Aspect of the area is shown in figure 4; it denotes the direction to which the slope faces on the basis of the majority of raster cells. It is clear that most of the slopes are towards north in the Trident Campus Basin.



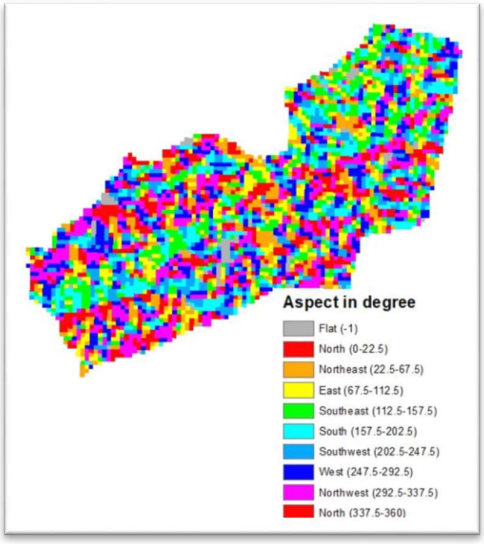




**Figure 3;** Slope map of Trident Campus **Figure 4;** Aspect map of Trident Campus

Various linear aspects of the campus area are calculated and shown in Table 1. It can be seen that the highest order of the stream in Trident Campus is 5. The stream number of first order stream is 349 which decreases with increase in order of the stream. The total length of the stream in the Trident Campus is 50.21 Km. The value of stream length ratio is having increasing trend towards higher order stream. The bifurcation ratio depends on the geology and lithology of the basin. It is seen that values bifurcation ratios are different for different stream orders because they are associated with the development of basin. The value of bifurcation ratio shows that drainage network of the basin is not influenced by geological structures.

**Table 1;** Linear Morphometric Parameters

| Stream order | Stream Length (km) | Mean Stream Length | Stream Length ratio | Mean Bifurcation Ratio | Length of overland Flow | Basin perimeter (km) | Basin length (km) |
|---|---|---|---|---|---|---|---|
| 1 | 32.25 | 0.092 | | | | | |
| | | | 0.75 | | | | |
| 2 | 10.68 | 0.069 | | | | | |
| | | | 1.06 | | | | |
| 3 | 4.62 | 0.073 | | 2.93 | 0.037 | 9.7 | 1.56 |
| | | | 0.85 | | | | |
| 4 | 2.29 | 0.062 | | | | | |
| | | | 0.84 | | | | |
| 5 | 0.37 | 0.053 | | | | | |
| Total | 50.21 | 0.349 | | | | | |

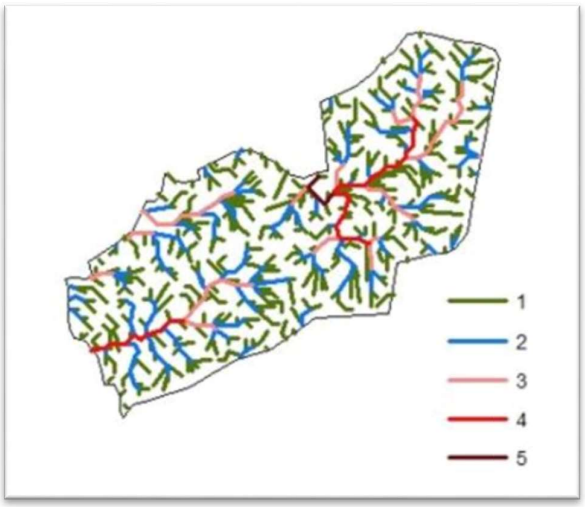



**Figure 5;** Stream Order Details of Trident Campus

Aerial parameters of Trident Campus is shown in Table 2 .The low drainage density of the area shows that this area is not much influenced by structural disturbances. The value of stream frequency obtained as per Horton,1945 is 161.54. The values of form factor and shape factors for the basin are 1.55 and 0.702 respectively which shows that area in Trident Campus is elongated and it experiences lesser peak flows.

**Table 2**; Aerial Morphometric Parameters

| Sr. No. | Parameter | Calculated value |
|---|---|---|
| 1 | Drainage Area (A) | 3.77 Km2 |
| 2 | Drainage Density (DD) | 13.32 |
| 3 | Drainage Frequency (FS) | 161.54 |
| 4 | Texture Ratio (T) | 62.78 |
| 5 | Circularity Ratio (RC) | 0.5035 |
| 6 | Form Factor (RF) | 1.55 |
| 7 | Elongation Ratio (RE) | 0.702 |
| 8 | Length of Overland Flow (LG) | 0.037 |
| 9 | Constant Channel Maintenance | 0.075 |

Relief Aspects of the campus area are shown in Table 3. It is found that the Relief ratio of this area is 10.89 and Ruggedness number is 226.44 which indicates average relief and steep to moderate slope of Trident Campus Drainage basin.

**Table 3;** Relief Aspects of Trident Campus

| Sr. No. | Parameter | Calculated Value |
|---|---|---|
| 1 | Maximum Basin Height (Z) | 252 m |
| 2 | Minimum Basin Height (Z) | 235 m |
| 3 | Basin Relief (H) | 17 m |
| 4 | Relief Ratio (RF) | 10.89 |
| 5 | Ruggedness Number (RH) | 226.44 |

## 5. Conclusion

GIS technique is an efficient tool in morphometric analysis for hydrological studies of drainage basins. Trident Campus is a 5th order drainage basin and shows a regular drainage pattern. The lower orders streams dominate the basin. The stream segment length is maximum for first order stream and decreases with increasing stream order ( Gebre et al,2015, Mallick et al,2014].The drainage density (Dd) of study area is.Low drainage density (i.e, 13.32 km/km2) indicates that the basin has not been much affected by structural disturbances while drainage frequency and very coarse drainage texture specifies low relief and porous, permeable rocks beneath the ground surface (Guzhaa et al, 2018),. The formation of streams in the basin area is affected by rainfall, groundwater discharge. The elongated shape of the basin indicates the low and delayed discharge of runoff and medium relief of the terrain. The study is very useful for planning and management of Trident Campus drainage basin.

## References

Gebre, T., Kibru, T., Samuale, T., & Taye., G. (2015). Analysis of watershed attributes for water resources management using GIS: The case of Chelekot micro-watershed, Tigray, Ethiopia. *Journal of Geographic Information System*, 7(2), 13 (Article ID: 55674).
\

Guzhaa, A. C., Rufinoa, M. C., Okoth, S., Jacobsa, S., & Nobregae, R. L. B. (2018). Impacts of land use and land cover change on surface runoff, discharge and low flows: Evidence from East Africa. *Journal of Hydrology: Regional Studies*, 15, 49–67.

Horton, R. E. (1932). Drainage basin characteristics. *Transactions of the American Geophysical Union*, 13, 350–361.

Jyoti Sarup, M. K. & Khatediya V, (2011) Delineate groundwater prospect zones and identification of artificial recharge sites using geospatial technique. *International Journal of Advance Technology & Engineering Research (IJATER)*, 1, (1).6-20.

Krishnamurthy, J., Venkatesa Kumar, N., Jayaraman, V., & Manivel, M. (1996). An approach to demarcate ground water potential zones through remote sensing and a geographical information system. *International Journal of Remote Sensing*, 17(10), 1867–1884.

Machiwal, D., Jha, M. K., & Mal, B. C. (2011a). Assessment of groundwater potential in a semi- arid region of India using remote sensing, GIS and MCDM techniques. *Water Resources Management*, 25(5), 1359–1386.

Radhakrishnan.D, Ramamoorthy. P (2014) Delineation of Groundwater Recharge Potential zones in Mailam Block, Villupuram district, Using GIS, *International Journal of Water Research* 2 (2), 71-75.

Magesh, N. S, Chandrasekar, N, & Soundranayagam, J. P. (2011a). Morphometric evaluation of papanasam and manimuthar watersheds, parts of western ghats, tirunelveli district, tamil nadu, india: a gis approach. Environmental Earth Sciences, 64, 373–381.

Mallick, J., Singh, C.K., Al-Wadi, H., Ahmed, M., Rahman, A., Shashtri, S., Mukherjee, S. (2014). Geospatial and geostatistical approach for groundwater potential zone delineation. Hydrol Processes. doi:10.1002/hyp.10153

*IN PROCEEDINGS OF 25th HYDRO 2020, INTERNATIONAL CONFERENCE, NATIONAL INSTITUTE OF TECHNOLOGY ROURKELA, ODISHA, INDIA 26-28, March 2021, ISBN 978-93-90631-56-8*

Paper ID - 161

# A STUDY OF GREYWATER REUSE SYSTEM FOR AN URBAN HOUSEHOLD

Susen Sinha[1],Dr. Sandeep Kr. Chouksey [2]

[1]*M.Tech scholar WRD&IE, NIT Raipur, Raipur 492010, India*
[2]*Assistant Professor, NIT Raipur, Raipur 492010, India*
*Email: susen.sinha@gmail.com*

## Abstract

With the rise in urbanization and simultaneous increase in population, India and the world is facing a problem of water stress situation. So, we must look for conservation and effective utilization of our present water resources like reusing of Greywater.

GW is part of sullage water accounting 60-70% of water consumed in urban homes. They are less contaminated, can be reused back in non-portable household activities after treatment. This study bring a sight on an effective and affordable technique of treatment of GW. Focus of the study was on optimization of EC and filtration treatment method coupled with other techniques like magnetic seperation. The whole system treatment is automated using micro-controllers. This model proves to have shorter and continuous process time of around 60 minutes. The model requires less foot print, no human intervention and consumes energy of 0.514kWh/$m^3$ for reusing 1364 litres of GW by an Indian urban household.

The effluent after treatment through EC has removal efficiency of Alkalinity (68.8%), Turbidity (80.3%), TDS (68.96%), BOD (64.5%), COD (68.2%) and bacterial removal efficiency of T.C (91.4%). This effluent after further treatment through filtration can be used for toilet flushing, sprinkling in gardens. The major challenge was determining the size of collection and EC chamber tank and controlling the flow of water continuous without lag. This task of designing is calculated using step algorithm and controlling of flow dynamics is managed by placing pumps, valves and sensors which are controlled by micro-controller. The feasibility and cost analysis of this model have given a positive result.

***Keywords:*** *Greywater, Electrocoagulation, Tube Settler, Automated control system*

## 1. Introduction {Main Headings [Times New Roman, 12pt + Bold]}

Whole world is suffering from water crisis. It has become a big concern for the whole world. In India, on an average 600 million population are affected by water scarcity as reported by NITI Aayog (2018) .

In several other towns and cities water resources are shrinking and depleting due to continuous townships and increase in population. International Water Management Institute (IWMI) has predicted that by 2025 in India out of three one will have water shortage [2].

Resources are limited and uneven distributed and at the same time urbanization and and population are increasing rapidly. So the question arises how this extra resources are gong to come to support these population sustainably. This question makes us to use the available resources efficiently. GW reuse seems to be one of the feasible solution for the sustainable usage of water.

### 1.1 About Greywater and its Treatment Technology

Grey water is a sullage water coming out of homes other than toilet waste . Waste water discharged from home are of two types- Black and Grey water. GW has got its name due to relatively grey in colour with comparatively less contaminants concentration than Black water.

Treatment process/Technologies reported are classified into five categories based on type of treatment.

They are:-

A. Simple treatment (coarse filtration and disinfection).

B. Physical treatment (sand filter, adsorption and membrane).

C. Biological treatment (aerated filters, RBC, MBR).

D. Extensive treatment (constructed wetlands).

E. Chemical treatment (chemical or EC).

Advantages and limitations associated with different technologies are presented in Table 1.

**Table 1**: List of GW reuse technologies- Efficiency and limitation

| S.no | Type of treatment | Efficiency | conclusion |
|---|---|---|---|
| 1. | Filtration[10,11,12,13]<br>Sand + Gravel + A.C + Plastic media | TSS = 53-93%, BOD = 89-98%, COD = 37.94%, oil & grease = 97%, E.Coli = 100% | Influent:- low strength GW, reused for toilet flush and irrigation. HRT 8-24 hours for large scale. Uneconomical in cities. Frequent clogging of media. |
| 2. | Chemical treatment-<br>a) coagulation + sand filter + activated carbon[7]<br>b) EC + disinfection[6] | Both combinations- BOD < 9mg/lit (50%),<br>SS < 9 mg/lit (100%),<br>Turbidity < 4 NTU,<br>E.Coli = no residual | HRT = around 20 and 40 minutes. |
| 3. | MBR (combination of Biological + Microfiltration and Ultrafiltration system)[8,18,19,20] | COD = 45, 49, 70 and 93% for MWCO of 400, 200, 30 and 0.2 kDa respectively.<br>Turbidity = 92, 94, 97 and 98%. BOD = 56% for UF<br>FC = upto 99% | Fouling is the major issue. Fouling after 120 minutes of operation in UF with GW. Fouling problem increased linearly with conc.of organic matter.<br>Used in urban areas, small foot print.<br>High capital and operating cost, complicated process, longer HRT upto 19 hours. |
| 4. | Biological treatment<br>a) RBC[21,22<br>b) SBR[14,15,16] | a) TSS = 9-12%, BOD = 27-53%, COD = 21-61%, FC = 88.5-99.9%<br>b) BOD = 90-98%, COD | a) Continuous power is required, lag period before operational.<br>b) Like activated sludge process, each process is sequenced in batches in the |

| | | | |
|---|---|---|---|
| | c) UASB[23,24] | = 90-98%, TN = 80%<br><br>c) BOD = upto 67%, COD = 38-79%, Oil&Grease = 83.7%, TN = 24.5%, TP = 10-39% | same tank.Initial and operating cost high.<br><br>c) Produces better settleable sludge, higher process time. |
| 5. | Extensive treatment like constructed wetlands like Reed Beds, Ponds. Plants used in them with species like (*alisma*, *iris*, *typha*, *metha*, *canna*, *thalia*, *lysimachia*, *lytrum*).[25,26] | BOD residual < 10 mg/lit, Turbidity < 8 NTU, SS < 13 mg/lit, Poor removal of micro-organisms. | HRT of 4.5 days. Cheap with low capital and operating cost. Eco-friendly. Larger foot print. |

In this article, physical and chemical treatment have been combined for the treatment of GW. As compared to other chemical treatments EC is more simpler, easy to operate and offers better perform ance.

This article is focussed on modelling of GW reuse system in a continuous mode. We reported a de-centralised system of sewer collection for a urban house-hold [DWMS]. An automated treatment system using EC process. At last an indirect conclusion is being drawn on cost and feasibility analysis.

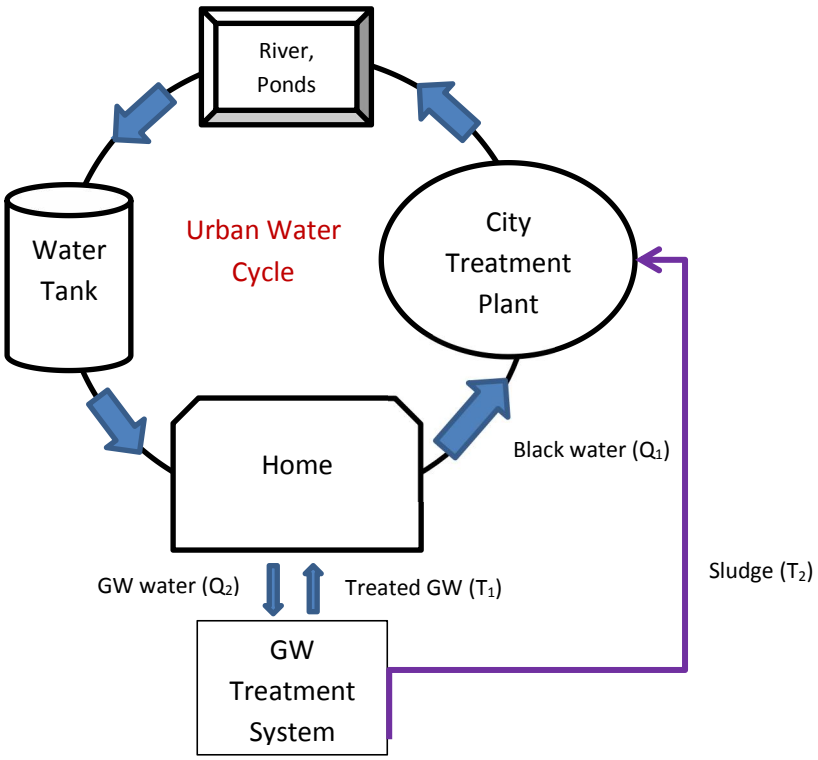



**Figure 1:-** Proposed Urban Water Cycle system.

### 1.1.1 *Electrocoagulation*

It is a physical treatment process that uses both electro-chemistry and basic chemical coagulation.. Basically, EC is based on three mechanism: -

(1) Electrolytic reactions at electrodes.

As electric current passes through electrodes present in aqueous solution either of the following reactions takes place (Here we have used Iron (Fe) electrodes):-

a)

At anode-

$Fe\ (s) \rightarrow Fe^{2+}\ (aq) + 2\ e^-$

$Fe^{2+}\ (aq) + 2\ OH^-\ (aq) \rightarrow Fe(OH)_2\ (s)$

At cathode:

$2\ H_2O\ (l) + 2\ e^- \rightarrow H_2\ (g) + 2\ OH^-\ (aq)$

Hence: $Fe\ (s) + 2\ H_2O\ (l) \rightarrow Fe(OH)_2\ (s) + H_2\ (g)$

or, b)

At anode:

$4\ Fe\ (s) \rightarrow 4\ Fe^{2+}\ (aq) + 8\ e^-$

$4\ Fe^{2+}\ (aq) + 10\ H_2O\ (l) + O_2\ (g) \rightarrow 4\ Fe(OH)_3\ (s) + 8\ H^+\ (aq)$

At cathode:

$8\ H^+\ (aq) + 8\ e^- \rightarrow 4\ H_2\ (g)$

Hence: $4\ Fe\ (s) + 10\ H_2O\ (l) + O_2\ (g) \rightarrow 4\ Fe(OH)_3\ (s) + 4\ H_2\ (g)$

Where,

(aq) = aqueous solution, (g) = gas, (s) = solid, (l) = liquid, ($e^-$) = electron, Fe = iron

(2) Coagulant formation (metal hydroxides) in the solution.

Metal hydroxides like $Fe(OH)_2$ (s), or $Fe(OH)_3$ (s) make coagulants

(3) Adsorption of dissolved or colloidal particles in solution with the hydroxides.

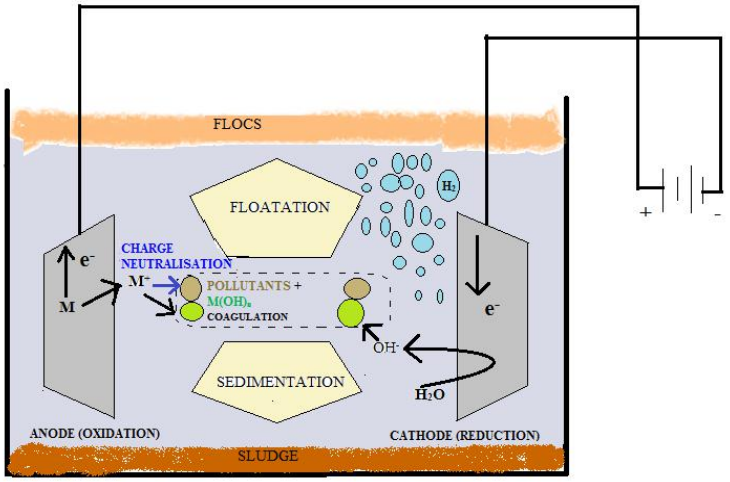



**Figure 2:-** Picture depicting the process of EC.

### 1.1.2 *Sequent Peak Method*

Sequent Peak method is a procedure used for determining the volume of tank/reservoir for the continuous inflow and outflow volumes.The basic conservation of mass equation or the basic storage equation is applied for determining the capacity.

### 1.1.3 *Tube settler*

A tube settler has been proposed to be fitted in Settling tank to increase the Removal efficiency. It increases the surface area of the settling tank.

## 2. Experimental program

### 2.1 *Quantification of Greywater*

The data was taken indirectly by the reading the decrease in level of water in water tank in a day. The total quantity per day = change in level of water x area of the tank.

- Water consumption was studied for four months from August to December.

Data was taken on one of non-weekend days and weekend days of a week. This study was conducted for each week in a month..
The average water usage was recorded as 1224 litres per day for 7 persons. Average Greywater produced = 123 lpcd.

**Table 2:** Monthly water consumption during Weekend and Non-Weekend days.

| | Monthly water consumption | | | | | | | | | |
|---|---|---|---|---|---|---|---|---|---|---|
| | week 1 | | Week 2 | | Week 3 | | week 4 | | | |
| Month | Weekend | Non-weekend | Weekend | Non-weekend | Weekend | non-weekend | Weekend | Non-weekend | Mean | S.D |
| August | 1256 | 1208 | 1314 | 1229 | 1293 | 1220 | 1306 | 1217 | 1255.375 | 40.4349 |
| Septem | 1247 | 1153 | 1250 | 1125 | 1173 | 1204 | 1237 | 1152 | 1192.6 | 45.450 |

| | | | | | | | | | | |
|---|---|---|---|---|---|---|---|---|---|---|
| ber | | | | | | | | | 25 | 4 |
| October | 1106 | 1134 | 1147 | 1188 | 1233 | 1113 | 1160 | 1077 | 1144.75 | 46.24864863 |
| November | 1120 | 1109 | 1138 | 1225 | 1141 | 1101 | 1148 | 1173 | 1144.375 | 37.26908068 |
| December | 1092 | 1106 | 1148 | 1099 | 1125 | 1116 | 1183 | 1089 | 1119.75 | 29.94891484 |

The present study of water usage for different domestic purposes was done indirectly:-

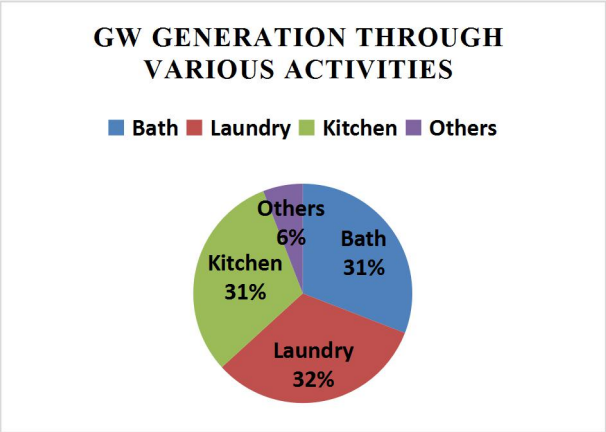



**Figure 3:-** Chart showing the percentage contribution of GW through various household activities.

## 2.2 *Characterization studies*

Raw greywater quality was studied as obtained from different sources. BOD and COD are majorly coming from kitchen and Laundary, and both these sources have similar biological quality result in terms of TC. Pollutants in Kitchen Greywater consists of milk, dal, vegetable and chicken curries, and oils.

**Table 3:-** GW quality analysis from a different sources.

| | **GW characteristics from different sources** | | | | | | | | | |
|---|---|---|---|---|---|---|---|---|---|---|
| **Parameters** | **Unit** | **Laundry** | | | | **Kitchen** | | | **GW** | |
| pH | | 8.25/26.6°c | 9.21/26.3°c | 9.43/25.3°c | 8.7/25.81°c | 7.76/25.4°C | 7.71/27.6°C | 7.63/25.5°C | 8.6/25.8°C | 9.42/26.3°c |
| Alkalinity | mg/lit | 800 | 850 | 850 | 800 | 700 | 750 | 700 | 900 | 800 |
| Turbidity | NTU | 104.2 | 131 | 127 | 135.2 | 216 | 273 | 257 | 148.6 | 153.8 |
| Hardness | mg/lit | | | | | | | | 950 | 1050 |
| | | | | | | | | | | |
| TDS | mg/lit | 1380 | 1476 | 1484 | 1424 | 788.4 | 821.3 | 875 | 985 | 973 |
| Conductivity | µs/cm | 752/26.5°c | 876/26.5°c | 814/25.5°c | 783/26°c | 365/21.9°c | 322/26.5°c | 341/25.3°c | 764/26.1°c | 821/26.5°c |
| BOD | mg/lit | 670 | 710 | 780 | 670 | 840 | 890 | 770 | 710 | 690 |

| | | | | | | | | | | |
|---|---|---|---|---|---|---|---|---|---|---|
| COD | mg/lit | 1560 | 1740 | 1770 | 1630 | 2350 | 2420 | 2280 | 1540 | 1555 |
| COD/BOD | | 2.3283 58209 | 2.4507 04225 | 2.2692 30769 | 2.4328 35821 | 2.7976 19048 | 2.7191 01124 | 2.9610 38961 | 2.1690 14085 | 2.253623 188 |
| Total colifor m | MPN/ 100lit | | | $3.9 \times 10^3$ | | | $4.2 \times 10^3$ | | $3.6 \times 10^3$ | |
| Fecal colifor m | MPN/ 100lit | | | 380 | | | | | 440 | |

## 2.3 *EC Reactor*

The laboratory setup of EC unit was of cylindrical tank of dimensions 22 cm diameter and 22 cm height. The effective volume was 7 liters. The iron electrodes of size 15 × 9.5 $cm^2$, 4 in numbers were arranged in parallel combination, at a spacing of 5 cm. The unit was operated at voltage of 12V through a DC source. It was operated for 45 minutes.

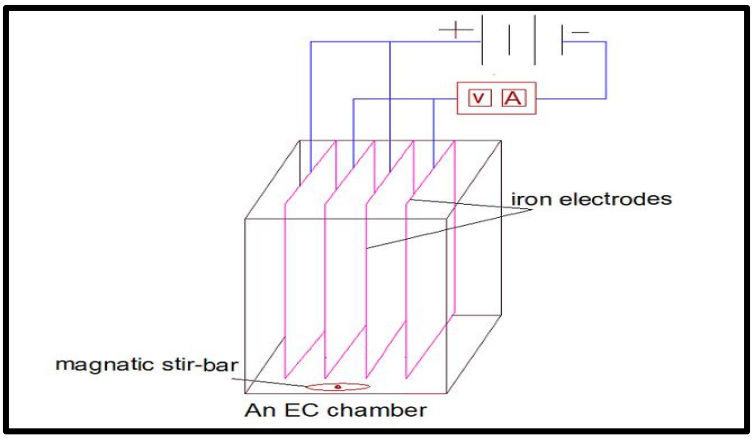



**Figure 4:-** An experimental setup of an EC unit.




**Figure 5:-** An Experimental apparatus of ac EC process.

**able 4:-** Performance in terms of removal efficiency of the EC process for the given GW sample.

| Removal efficiency of EC unit | | | | |
|---|---|---|---|---|
| | | **Untreated** | **Treated** | **% removal** |
| **Parameters** | **Unit** | | | |
| pH | | 9.4/26.35 °c | 8.24/25.6°c | |
| Alkalinity | mg/lit | 800 | 250 | 68.8 |
| Turbidity | NTU | 153.8 | 30.3 | 80.3 |
| Hardness | mg/lit | 1050 | 300 | 71.4 |
| Conductivity | µs/cm | 821 | 213 | 74 |
| TDS | mg/lit | 973 | 302 | 68.96 |
| | | | | |
| BOD | mg/lit | 690 | 245 | 64.5 |
| COD | mg/lit | 1555 | 495 | 68.2 |
| COD/BOD | | 2.253623188 | | |
| Total coliform | MPN/100lit | $3.6 \times 10^3$ | 310 | 91.4 |
| Fecal Coliform | MPN/100lit | 440 | | |

## 3. Conclusions

GW reuse is one the most promising way, as concluded by this study. Water consumption study in a typical Indian household resulted an average usage of 1235 liters per day. Around 65-70% of this is low contaminant water which can be reutilized for non human contact purposes. Volume of collection Tank as calculated is 300 litres.

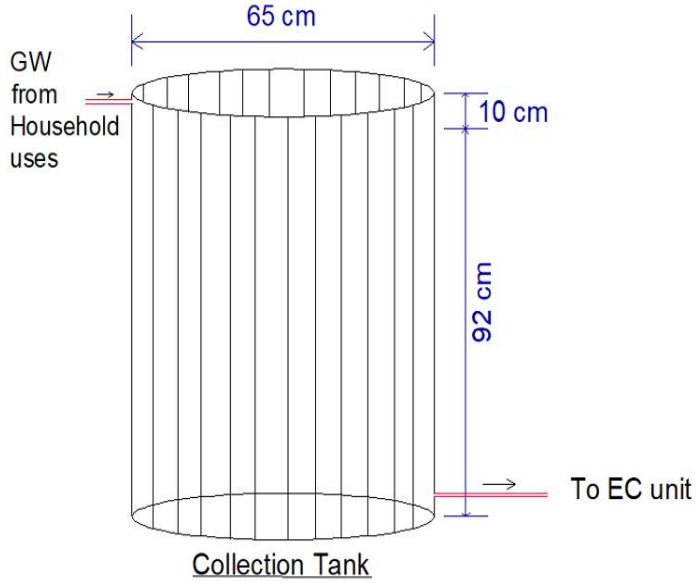



**Figure 6:-** Sketch of Circular Collection Tank.

The model presented in this study is fully automatic, overall less process time (45 minutes) and no human handling needed.
The electric potential across each electrode is calculated as 18 V and current = 0.9 A with 8 no of electrodes each of size 20 cm (b) × 15 cm (h) are there with a spacing of 7 cm.

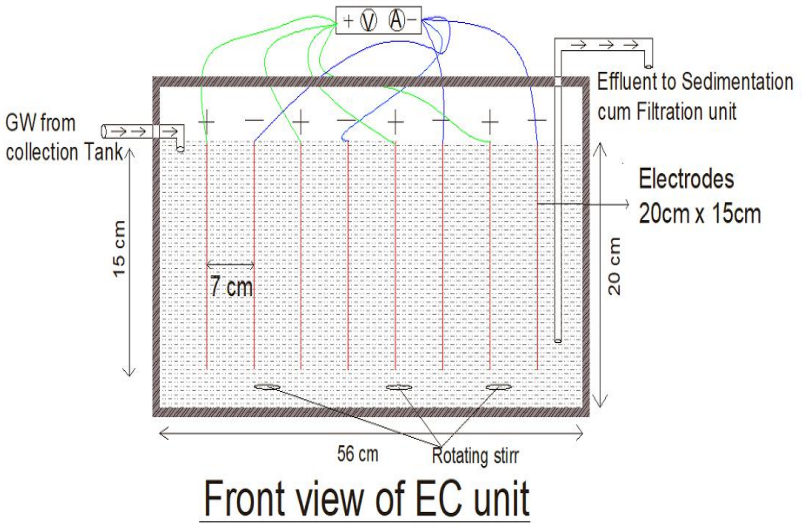



**Figure 7:-** Sketch showing the Front View of the EC unit.

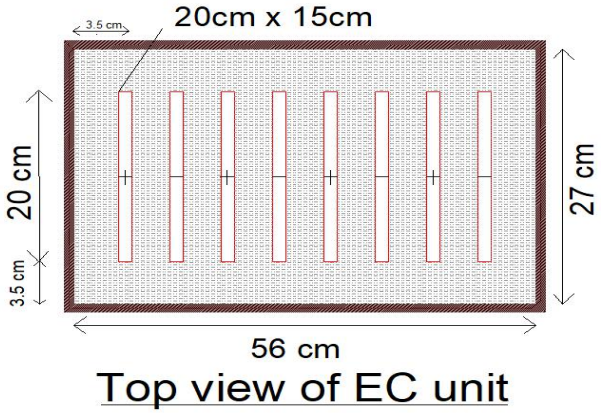



**Figure 8:-** Sketch showing the Top View of the EC Unit.

Energy consumption came out as 0.51 kWh/m$^3$ with COD removal efficiency as 68.2%. 60% to 65% of the water consumed are reused at the energy requirement of 1.458 kWh per day. Tube Settler has been studied which decrease the settling time and foot print area of the sedimentation tank.

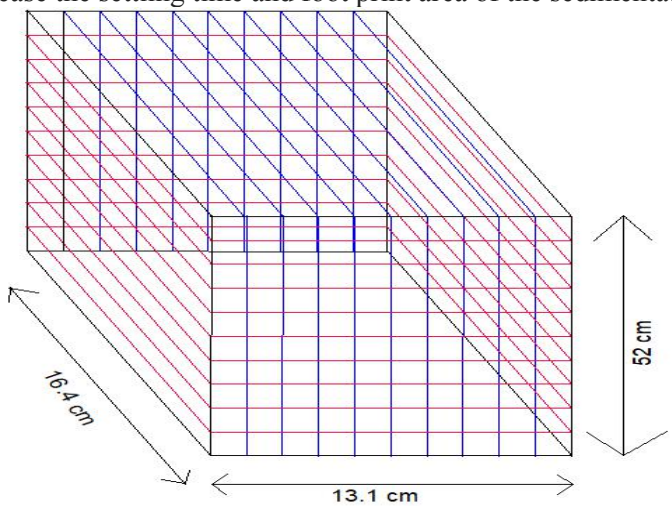



**Figure 9:-** Sketch of the Tube Settler with total of 20 tubes along length and width.

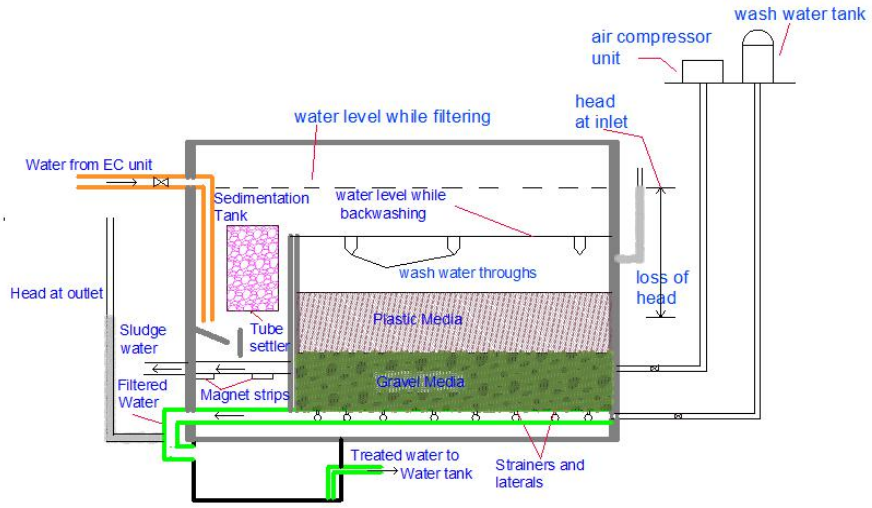



**Figure 10:-** Sketch of the Sedimentation cum Filtration Unit.

The EC unit is automated using Arduino microcontroller with each pump at inlet and outlet of collection tank and a water level sensor.

Supply system aided with this treatment technique have shown 15% to 79% costlier and convert 24% to 62% of water consumed as reusable w.r.t to boring system in houses. If water tariff is more than Rs 34/kL, this proposed UW system is cost effective converting 62% of the water consumed as reusable. However, a subsidy of more than 10% on water bill will make this system cost effective at tariff rate Rs 24/kL.If this GW is reused for Toilet flushing only this system has shown cost saving of 15.3% and 17% for two studied tariff rates. This EC process as studied in this project has proved to be quite effective and feasible, however further biological treatment is required for making treated GW under standard quality recommendations.

## References

1. Aayog, N.I.T.I., 2018. Composite water management index. National Institution for Transforming India, GOI.
2. Al-Hamaiedeh, H. and Bino, M., 2010. Effect of treated grey water reuse in irrigation on soil and plants. *Desalination*, *256*(1-3), pp.115-119.

3. Atanasova, N., Dalmau, M., Comas, J., Poch, M., Rodriguez-Roda, I. and Buttiglieri, G., 2017. Optimized MBR for greywater reuse systems in hotel facilities. Journal of Environmental Management, 193, pp.503-511.

4. Abdel-Shafy, H.I., Al-Sulaiman, A.M. and Mansour, M.S., 2015. Anaerobic/aerobic treatment of greywater via UASB and MBR for unrestricted reuse. Water Science and Technology, 71(4), pp.630-637.

5. Borin, M., Cossu, R., Lavagnolo, M.C. and Gandini, M., 2004. Phytotreatment of greywater with yellow water addition from an aesthetic approach. In Proc. of the International Conference On-Site wastewater treatment and recycling (Vol. 12).

6. Belhout,D.,Ghernaout,D.,Djezzar-Douakh,S.andKellil,A., 2010. Electrocoagulation ofraw water of Ghrib Dam (Algeria) in batch using aluminium and iron electrodes.De.salination and Water Treatment, 16(1-3), pp.1-9.

7. Belhout, D., Ghernaout, D., Djezzar-Douakh, S. and Kellil, A., 2010. Electrocoagulation of a raw water of Ghrib Dam (Algeria) in batch using aluminium and iron electrodes. Desalination and Water Treatment, 16(1-3), pp.1-9.

8. Donner, E., Eriksson, E., Revitt, D.M., Scholes, L., Lützhøft, H.H. and Ledin, A., 2010. Presence and fate of priority substances in domestic greywater treatment and reuse systems. Science of the Total Environment, 408(12), pp.2444-2451.

9. Dalahmeh, S.S., Pell, M., Vinnerås, B., Hylander, L.D., Öborn, I. and Jönsson, H., 2012. Efficiency of bark, activated charcoal, foam and sand filters in reducing pollutants from greywater. Water, Air, & Soil Pollution, 223(7), pp.3657-3671.

10. Edwin, G.A., Gopalsamy, P. and Muthu, N., 2014. Characterization of domestic gray water from point source to determine the potential for urban residential reuse: a short review. Applied Water Science, 4(1), pp.39-49.

11. Finley, S., Barrington, S. and Lyew, D., 2009. Reuse of domestic greywater for the irrigation of food crops. Water, air, and soil pollution, 199(1-4), pp.235-245.

12. Friedler, E., Yardeni, A., Gilboa, Y. and Alfiya, Y., 2011. Disinfection of greywater effluent and regrowth potential of selected bacteria. Water Science and Technology, 63(5), pp.931-940.

13. Gross, A., Wiel-Shafran, A., Bondarenko, N. and Ronen, Z., 2008. Reliability of small scale greywater treatment systems and the impact of its effluent on soil properties. International Journal of Environmental Studies, 65(1), pp.41-50.

14. Gilboa, Y. and Friedler, E., 2008. UV disinfection of RBC-treated light greywater effluent: kinetics, survival and regrowth of selected microorganisms. Water research, 42(4-5), pp.1043-1050.

15. Garg, S.K., 1999. Environmental engineering. Water Supply Eng, 1, pp.261-2.

16. Hernández Leal, L., Temmink, H., Zeeman, G. and Buisman, C.J., 2010. Comparison of three systems for biological greywater treatment. Water, 2(2), pp.155-169.

17. Huelgas, A. and Funamizu, N., 2010. Flat-plate submerged membrane bioreactor for the treatment of higher-load graywater. Desalination, 250(1), pp.162-166.

18. Hernández Leal, L., Temmink, H., Zeeman, G. and Buisman, C.J., 2010. Comparison of three systems for biological greywater treatment. Water, 2(2), pp.155-169.

19. Hashimoto, Y., Takashima, H. and Jayamohan, S., 2019. Application of roughing filter to pre-treat 1,000 NTU raw water for slow sand filter. Water Practice and Technology, 14(2), pp.355-364.

20. H.A. Moreno-Casillas, D.L. Cocke, J.A.G. Gomes, P. Morkovsky, J.R. Parga, E. Peterson, Electrocoagulation mechanism for COD removal, Sep. Purif. Technol.56 (2007) 204–211.

21. IS 1172:2002, Code of Basic Requirements for Water Supply, Drainage and Sanitation by Bureau of Indian Standards.

22. IS 10500:2002, Indian Standard Drinking water specifications by Bureau of Indian Standards.

23. IS 1622:1981, Methods of Sampling and Microbiological Examination of Water by Bureau of Indian Standards.

24. IS 3025: Part 1, 2, 4, 5, 9, 10, 14, 15, 16, 17, 18, 19, 20, 21, 22, 23, 24, 25, 26, 31, 32, 38, 44, 51, 58, 68 , Methods of sampling and test (Physical And Chemical) for water and wastewater by Bureau of Indian Standards.

25. International Water Management Institute (IWMI), 2003. Water Policy Briefifing—8. Jeppersen B., Solley, D., 1994. Domestic Greywater Reuse: Overseas Practice and its Applicability to Australia. Urban Research Association of Australia, Brisbane City Council, Research Report No. 73.

26. Krishnan, V., Ahmad, D. and Jeru, J.B., 2008. Influence of COD: N: P ratio on dark greywater treatment using a sequencing batch reactor. Journal of Chemical Technology & Biotechnology: International Research in Process, Environmental & Clean Technology, 83(5), pp.756-762.

27. Khan, R. and Jhariya, D.C., 2017. Groundwater quality assessment for drinking purpose in Raipur City, Chhattisgarh using water quality index and geographic information system. Journal of the Geological Society of India, 90(1), pp.69-76.

28. Karichappan, T., Venkatachalam, S. and Jeganathan, P.M., 2014. Optimization of electrocoagulation process to treat grey wastewater in batch mode using response surface methodology. Journal of Environmental Health Science and Engineering, 12(1), p.29.

29. Lin, C.J., Lo, S.L., Kuo, C.Y. and Wu, C.H., 2005. Pilot-scale electrocoagulation with bipolar aluminum electrodes for on-site domestic greywater reuse. Journal of environmental engineering, 131(3), pp.491-495.

30. Lamine, M., Bousselmi, L. and Ghrabi, A., 2007. Biological treatment of grey water using sequencing batch reactor. Desalination, 215(1-3), pp.127-132.

31. Marriaga-Cabrales, N. and Machuca-Martínez, F., 2014. Fundamentals of electrocoagulation. Peralta-Hernández, JM, Rodrigo-Rodrigo, MA & Martínez-Huitle, CA In: Evaluation of Electrochemical Reactors as a New Way to Environmental Protection, Kerala: Research Signpost, pp.1-16.

32. Mandal, D., Labhasetwar, P., Dhone, S., Dubey, A.S., Shinde, G. and Wate, S., 2011. Water conservation due to greywater treatment and reuse in urban setting with specific context to developing countries. Resources, Conservation and Recycling, 55(3), pp.356-361.

33. Ni'am, M.F. and Othman, F., 2014. Experimental design of electrocoagulation and magnetic technology for enhancing suspended solids removal from synthetic wastewater. International Journal of Science and Engineering, 7(2), pp.178-192.

34. Ni'am, M.F. and Othman, F., 2014. Experimental design of electrocoagulation and magnetic technology for enhancing suspended solids removal from synthetic wastewater. International Journal of Science and Engineering, 7(2), pp.178-192.

35. Ottoson, J. and Stenström, T.A., 2003. Faecal contamination of greywater and associated microbial risks. Water research, 37(3), pp.645-655.

36. Oteng-Peprah, M., Acheampong, M.A. and deVries, N.K., 2018. Greywater characteristics, treatment systems, reuse strategies and user perception—a review. Water, Air, & Soil Pollution, 229(8), p.255.

37. Pidou, M., Memon, F.A., Stephenson, T., Jefferson, B. and Jeffrey, P., 2007, September. Greywater recycling: treatment options and applications. In Proceedings of the Institution of Civil Engineers-Engineering Sustainability (Vol. 160, No. 3, pp. 119-131). Thomas Telford Ltd.

38. Šostar-Turk, S., Petrinić, I. and Simonič, M., 2005. Laundry wastewater treatment using coagulation and membrane filtration. Resources, Conservation and Recycling, 44(2), pp.185-196.

*IN PROCEEDINGS OF 25th HYDRO 2020, INTERNATIONAL CONFERENCE, NATIONAL INSTITUTE OF TECHNOLOGY ROURKELA, ODISHA, INDIA 26-28, March 2021, ISBN 978-93-90631-56-8*

Paper ID - 239

# ALIGNMENT OF RRTS RAILWAY BRIDGE ACROSS RIVER YAMUNA FOR DELHI-GHAZIABAD- MEERUT CORRIDOR AT NEW DELHI-A CASE STUDY

S. S. Kerimani[1], S. P. Hedaoo [2], R. G. Patil [3]

[1]*Scientist 'C', Central Water and Power research station, Pune, India, PIN- 411024*
[2]*Asst. Research officer, Central Water and Power research station, Pune, India, PIN- 411024*
[3]*Scientist 'E', Central Water and Power research station, Pune, India, PIN- 411024*
***Email:*** *shivanandkerimani@yahoo.co.in,siddharth_hedaoo@rediffmail.com, rsrgp@rediffmail.com*

## Abstract

Delhi being a capital city of India has an important strategic, political and ever demanding community role. The city has grown on both the banks of river Yamuna which is basically meandering alluvial river. The river Yamuna flows through highly urbanized corridor of Delhi. Due to continuous growth of the city, the basic need of efficient transportation is a prime issue. With the increasing number of such structures across the river in a relatively short reach length in National Capital Region (NCR) of Delhi, assessment of flooding conditions, back water effect of one structure on other and sediment equilibrium studies using physical model has become one of the essential requirement.

The National Capital Region Transport Corporation (NCRTC), a joint venture Company of Govt. of India and participating State Governments has proposed to connect Delhi with various nodal towns in NCR through eight Regional Rapid Transit System Corridors. Delhi-Ghaziabad-Meerut RRTS corridor is the first corridor which is being taken up for the implementation by NCRTC. Being a high speed, high capacity rail based commuter transit system; RRTS will drastically reduce the travel time between various towns of NCR. However, considering river morphology and minimal disturbance to the river regime, the NCRTC has proposed to convey RRTS bridge alignment entirely over elevated piers across river Yamuna, with distance varies from 418.94 m to 376.50 m from the existing right to left guide bunds upstream of the DND road bridge between existing upstream fixed boundaries of guiding bunds with fixed water way of 636.00 m. The studies were undertaken by CWPRS on existing model of river Yamuna at Delhi. This paper deals with various hydraulic parameters such as optimum span of bridge piers, safe deck level, orientation of bridge axis, afflux on upstream side, maximum expected scour and its back water effect.

***Keywords:*** *Waterway, Scour, Afflux, Guide bunds, Embankments etc.*

## 1. Introduction

River Yamuna originates from the Yamunotri glacier at an elevation of 3320 m from mean sea level and further flows through the National capital territory (NCT) of Delhi. The NCT of Delhi is surrounded on the Northern, Western and Southern sides by Sonepat, Rohtak and Gurugram districts respectively of Haryana and in the eastern side by the Gaziabad district of Uttar Pradesh. The width of river between banks/embankments of the river varies from 1.0 km to 4.5 km. It traverses a distance of approximately 1400 km before joining the river Ganga at Allahabad. Nearly 30 km of the river form a common boundary between Himachal Pradesh and Uttar Pradesh. The Chambal, the Hindon, the Ken, the Sahibi etc., are some of the tributaries of River Yamuna.

Delhi, the capital of India and one of the most populous and important cities was originally established on the western bank, now the development has taken place along both the banks of the river Yamuna. The river enters National Capital Territory (NCT) of Delhi near village Palla in the North after a journey of about 425 km and leaves at Jaitpur in the South after a distance of about 50 km.

The National Capital Region Transport Corporation (NCRTC) has proposed to connect Delhi with various nodal towns in NCR through eight Regional Rapid Transit System (RRTS) Corridors. Three corridors namely Delhi-Meerut, Delhi-Panipat and Delhi-Alwar have been prioritized for implementation in the first phase. Out of these three prioritized corridors, Delhi-Ghaziabad-Meerut RRTS corridor is the first corridor which is being taken up for implementation by NCRTC. In this regard NCRTC had approached CWPRS for the conduct of hydraulic model studies to assess the

hydraulic parameters of the proposed RRTS Bridge. Accordingly, the studies were carried out on existing model of River Yamuna Figure 1 constructed to a horizontal scale of 1:300 and vertical scale of 1:60 covering a river reach from Palla to Jaitpur updated with available cross sections data of post monsoon 2013.

This paper deals with the physical model studies carried out for RRTS railway bridge alignment with distance varies from 418.94 m to 376.50 m from the existing right to left guide bund upstream of the DND road bridge between existing upstream fixed boundaries of guiding bunds with fixed water way of 636.00 m across river Yamuna at Delhi.

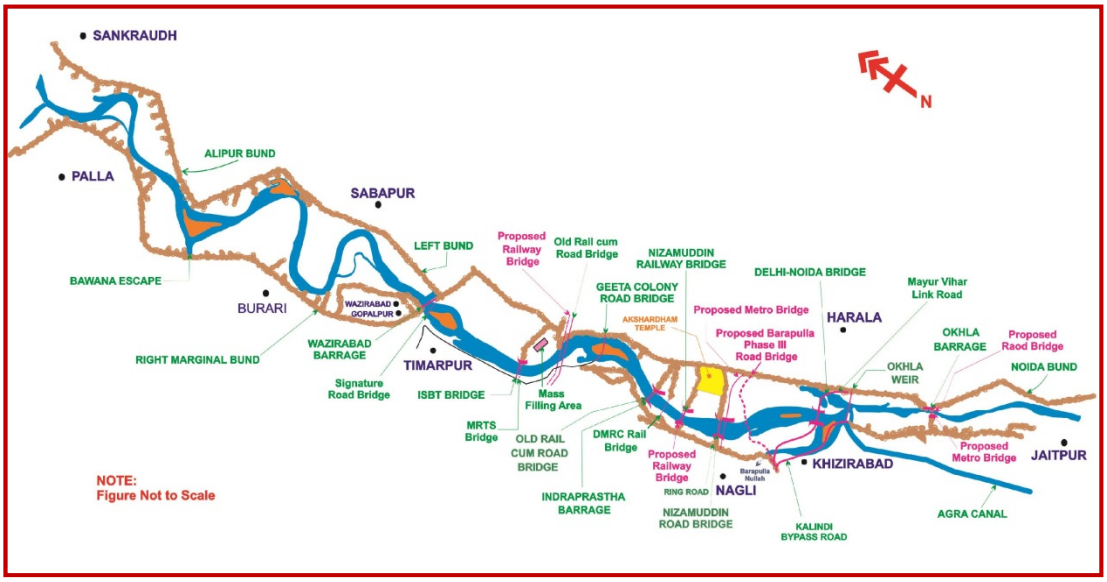



**Figure 1** Plan of River Yamuna at New Delhi

## 2. Model

The existing mobile bed model of River Yamuna at Delhi constructed to a horizontal scale (Lr) of 1:300 and a vertical scale (Dr) of 1:60, covering a river reach of 50 km from Palla to Jaitpur was utilized for model studies. The model reach including deep channels, shoals, spill portion and various existing bridge structure etc., for the reach from Palla to Jaitpur was laid as per the latest post monsoon 2013 survey data given by WAPCOS. In order to reproduce proper bed movement and roughness, the model bed is provided with sand having mean diameter ($D_{50}$) of 0.34 mm. The model discharge is measured using standing wave flume provided at the upstream inlet and is also verified at downstream using Rehbock weir. The model from Palla to Jaitpur was proved by comparing the water levels observed on the model at various gauge locations with the prototype values Figure 2.

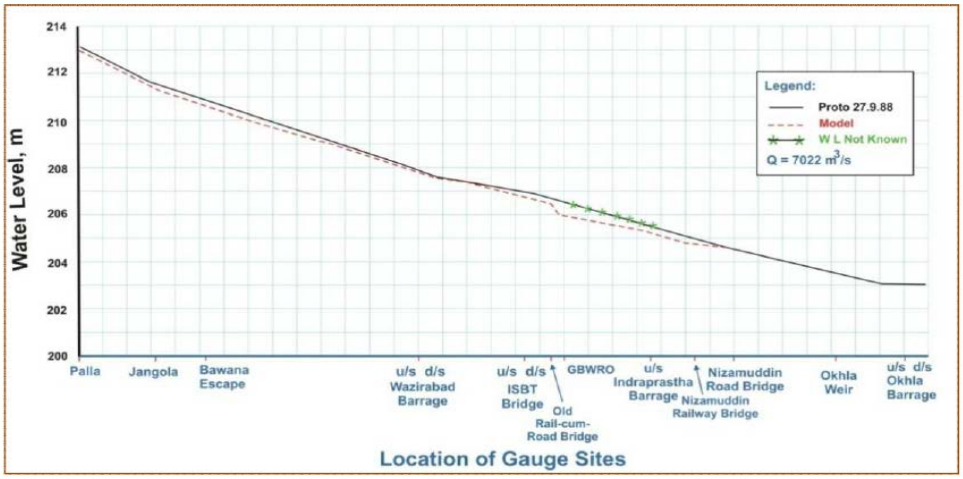



**Figure 2** Model prototype conformity for Discharge (Q= 7022 $m^3/s$)

## 3. Model studies

The model studies were carried out for the three different discharge conditions of 7,022 $m^3/s$ (maximum discharge observed in 1988 at Wazirabad Barrage), 9,910 $m^3/s$ (design discharge considered for ISBT bridge and bridge proposed subsequently on Yamuna) 12,750 $m^3/s$ (check flood for substructures, foundation and protection works suggested by Central Water Commission). In order to establish flood slope and to record water levels at various locations, All the existing structures such as Wazirabad barrage, under construction signature bridge, ISBT Road Bridge, MRTS railway bridge, old rail-cum-road bridge, Geeta colony road bridge, Indraprastha barrage, Lok Nayak Sethu, DMRC bridge (ITO), proposed and existing Nizamuddin railway bridge, Nizamuddin road bridge, Japan bridge, Metro rail bridge, Barapulla elevated road bridge, Noida road bridge, Okhla weir and barrage, Metro rail bridges and road bridge were reproduced on the model.

Available prototype gauge discharge data observed at Wazirabad barrage, rail-cum-road bridge, Nizamuddin road bridge and Okhla barrage are available information regarding behaviour of river and flow pattern observed during different discharge stages in the river were used for verification of the model. Proving studies were carried out based on the gauge discharge data of river Yamuna of 1988 flood. The maximum discharge in Yamuna at Delhi occurred in 1988 was 7,022 $m^3/s$. Discharge equivalent to 7,022 $m^3/s$ (maximum discharge observed at Wazirabad barrage in 1988) was let into the model and by controlling the gauge upstream of the Okhla weir as per the gauge discharge curve, water levels were observed at various gauge locations. Water levels observed on the model were in close agreement with the prototype values. It was noticed that in the river reach from Palla to Okhla barrage, the 1988 flood slope has been reproduced fairly well on the model. In addition, the model had indicated identical pattern of meandering particularly upstream of Wazirabad barrage upto Palla, where no control structure exists. In view of this, the model was considered as "proved".

Initially studies carried out with drawing indicated that the proposed bridge was parallel to the DND road bridge at a distance of 430 m upstream of DND bridge and experiment completed. However, the project authorities changed the alignment of the bridge as shown in Figure 3 due to the requirement of making the flow perpendicular to the bridge and requirement of mole head of the guide bund. CWPRS carried out the model studies with modified alignment that is not parallel and the distances varies from 418.94m to 376.50 m from NOIDA road bridge upstream. Hence, experiments were continued with modified alignment without and with bridge in position.

### 3.1 Studies under existing conditions with modified alignment

Studies were initially carried out for the existing conditions of river without reproducing the proposed road bridge. The modified alignment of the proposed bridge was identified and marked on the model as per the drawings in Figure 3 due to the requirement of making the flow perpendicular to the bridge and requirement of mole head of the guide bund supplied by the project authorities. Existing condition experiments were carried out for three river discharges i.e. 7,022 $m^3/s$, 9,910 $m^3/s$ and 12,750 $m^3/s$ independently after stabilising the model bed. Velocity, depth of flow and water levels were measured at various locations. Water levels and maximum velocities observed at proposed RRTS bridge axis and computed discharge intensities relevant to the studies are given in Table 1. Photos 1, 2 and 3 depict flow pattern along the proposed RRTS bridge site for the existing conditions for river discharges of 7,022 $m^3/s$, 9,910 $m^3/s$ and 12,750 $m^3/s$ respectively.

**Table 1** Maximum water level, velocity and discharge intensity under Existing condition, with bridge in position distances varies from 418.94 m to 376.50 m not parallel to NOIDA Road Bridge.

| Discharge $m^3/s$ | Existing Condition | | | With bridge in position with modified alignment | | | Afflux |
|---|---|---|---|---|---|---|---|
| | At bridge axis | | | At bridge axis | | | |
| | WL (m) | Max. Vel. (m/s) | Max. Discharge intensity ($m^3/s/m$) | WL (m) | Max. Vel. (m/s) | Max. Discharge intensity ($m^3/s/m$) | Bridge axis (m) |
| 7022 | 205.68 | 1.86 | 13.70 | 205.80 | 1.91 | 13.80 | 0.12 |
| 9910 | 206.46 | 2.60 | 25.33 | 206.64 | 2.60 | 25.70 | 0.18 |
| 12750 | 206.88 | 2.94 | 26.29 | 207.10 | 3.06 | 27.10 | 0.22 |

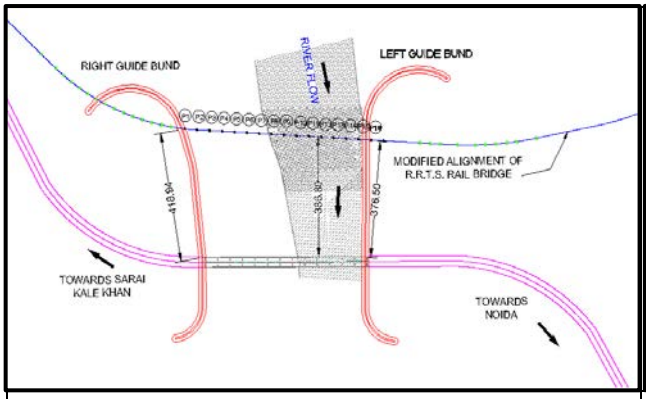



**Figure 3** Details of modified RRTS bridge alignment

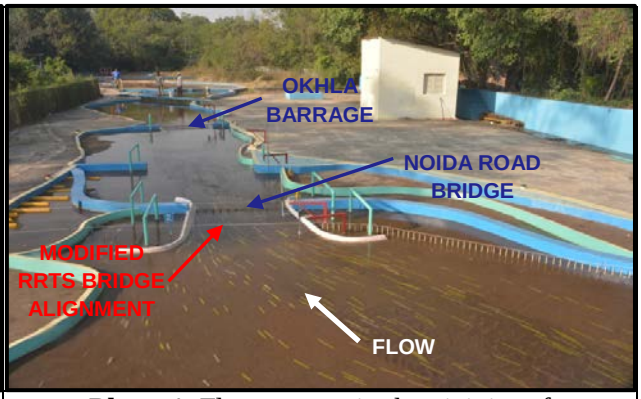



**Photo 1.** Flow pattern in the vicinity of proposed RRTS bridge site under existing condition (Q = 7,022 $m^3/s$)

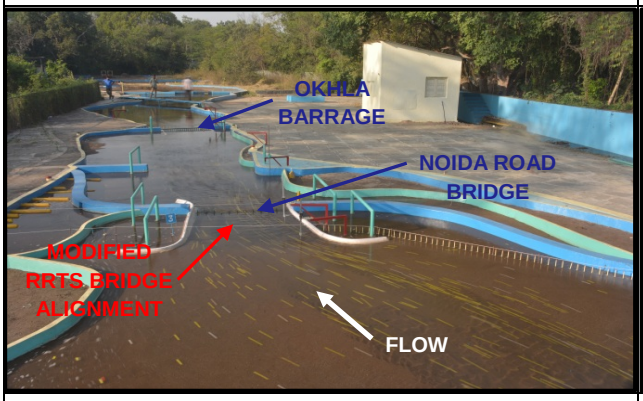



**Photo 2.** Flow pattern in the vicinity of proposed RRTS bridge site under existing condition (Q = 9,910 $m^3/s$)

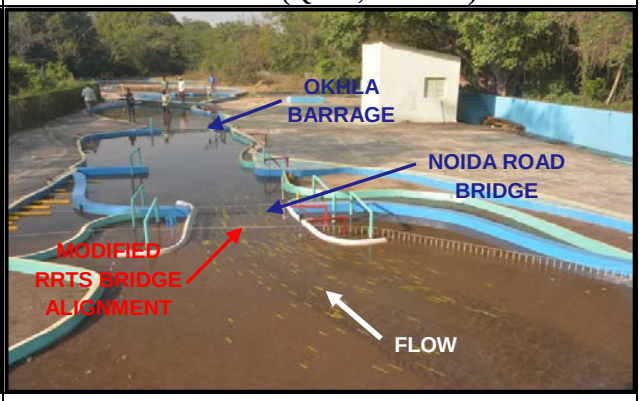



**Photo 3.** Flow pattern in the vicinity of proposed RRTS bridge site under existing condition (Q = 12,750 $m^3/s$)

### 3.1 Studies with modified RRTS Railway Bridge in position

The proposed RRTS railway bridge was reproduced on the model as per the modified alignment supplied by the project authority. The RRTS bridge alignment not parallel to DND road bridge and varies from 418.94 m to 376.50 m from the existing right to left guide bund upstream of the DND road bridge. The various details of piers, foundations and the general arrangements remained same as shown in Figure 4. Experiments were carried out for three river discharges i.e. 7,022 $m^3/s$, 9,910 $m^3/s$ and 12,750 $m^3/s$ independently after stabilising the model bed. Velocity, depth of flow and water levels were measured at various locations. Water levels and maximum velocities observed at proposed RRTS bridge axis and computed discharge intensities relevant to the studies are given in Table 1.

Photos 4, 5 and 6 depict flow pattern along the proposed RRTS2 bridge site for the existing conditions for river discharges of 7,022 $m^3$/s, 9,910 $m^3$/s and 12,750 $m^3$/s respectively.

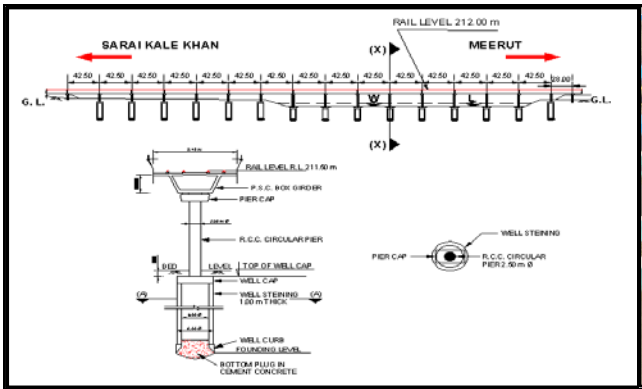



**Figure 4** Plan and sectional elevation of proposed RRTS bridge piers

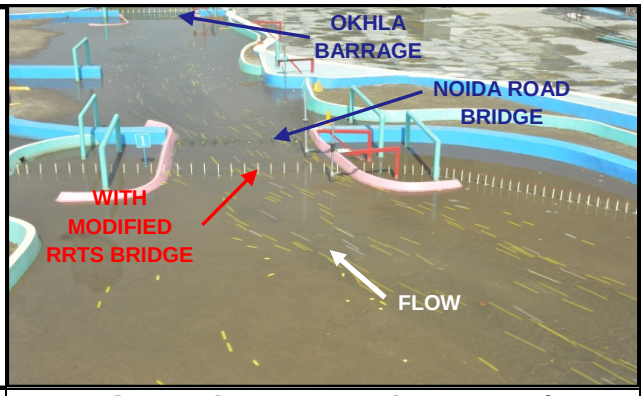



**Photo 4** Flow pattern in the vicinity of proposed RRTS bridge (Q = 7,022 $m^3$/s)

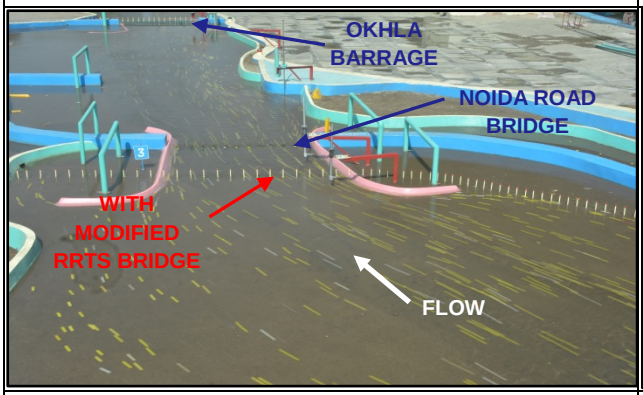



**Photo 5** Flow pattern in the vicinity of proposed RRTS bridge (Q = 9,910 $m^3$/s)

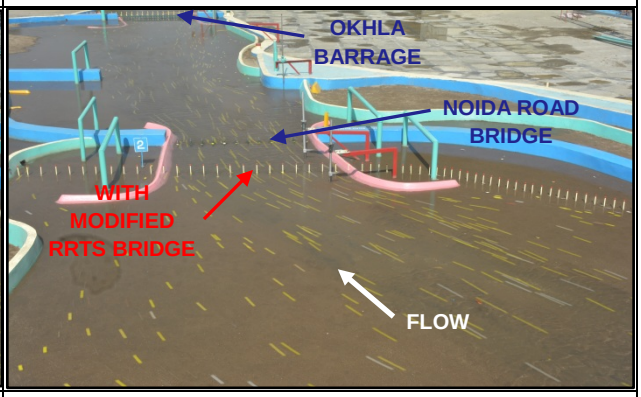



**Photo 6** Flow pattern in the vicinity of proposed bridge (Q = 12,750 $m^3$/s)

## DISCUSSION OF RESULTS

The RRTS Railway Bridge is proposed to be constructed about 418.94 m to 376.50 m upstream of the existing DND Road Bridge. The DND Bridge is having a water way of 552.50 m (42.50 X 13) between the two existing Guide bunds including pier widths. The guide bunds of this existing DND Bridge are extending upstream beyond the alignment of proposed bridge. The existing DND Road Bridge, downstream of proposed RRTS Railway Bridge are located within a distance of about 376.5 m. Because of the provision of guide bunds for DND Bridge, the river is held between the fixed boundaries in this reach. Hence, no major morphological change is expected in the reach of the river due to the construction of the proposed RRTS Bridge. Moreover, the model studies indicated that the proposed bridge is not inducing any change in the flow behaviour near the reach of guide bunds of the DND Bridge. The flow through the proposed bridge and downstream DND bridge is satisfactory and is well distributed within the given water way.

Velocities and discharge intensities obtained under existing conditions were analysed to understand the flow pattern in the vicinity. Under existing conditions, maximum velocities and discharge intensities observed along the proposed RRTS bridge axis were 1.86 m/s and 13.70 $m^3$/s/m respectively for a discharge of 7,022 $m^3$/s; 2.60 m/s and 25.33 $m^3$/s/m respectively for a discharge of 9,910 $m^3$/s and 2.94 m/s and 26.29 $m^3$/s/m respectively for a discharge of 12,750 $m^3$/s. with bridge in position, maximum velocities and discharge intensities observed along the proposed RRTS bridge

axis were 1.91m/s and 13.80 $m^3$/s/m respectively for a discharge of 7,022 $m^3$/s; 2.60 m/s and 25.70 $m^3$/s/m respectively for a discharge of 9,910 $m^3$/s and 3.06 m/s and 27.10 $m^3$/s/m respectively for a discharge of 12,750 $m^3$/s.

The water levels observed at proposed bridge axis with the discharge of 7,022 $m^3$/s, 9,910 $m^3$/s were RL 205.80 m, RL 206.64 m respectively and the same for the check flood of 12,750 $m^3$/s was RL 207.10 m. It is advised to adopt proper free board as per Indian Standard and accordingly set the deck level of the bridge.

The model studies indicated that the bridge with 8 m diameter wells and piers diameter of 2.5 m would cause an afflux of 12, 18, 22 cm at proposed bridge axis for the discharges of 7,022 $m^3$/s, 9,910 $m^3$/s and 12,750 $m^3$/s respectively. The afflux is found to be negligible (immeasurable) at a distance of about 1.70 km from the proposed bridge axis for discharge of 12750 $m^3$/s.

The model studies indicated that the afflux created by the bridge reduces to immeasurable values at a distance of about 0.90 km, 1.45 km and 1.70 km for the discharges of 7,022, 9,910 and 12,750 $m^3$/s respectively.

It is observed that the position of two piers are coming exactly on the toe of the existing left and right guide bunds, extra care should be taken during construction of the bridge foundation and raising of the pier/well.

## 4.0 Conclusions

Based on the studies carried out for river discharge of 7,022 $m^3$/s, 9,910 $m^3$/s and 12,750 $m^3$/s on the updated Yamuna river model at CWPRS, using post flood 2013 survey data, the following recommendations/ conclusions are made:

- The modified alignment of proposed RRTS railway bridge is proposed to be constructed about 418.94 m to 376.50 m upstream of the existing DND road bridge is found to be hydraulically satisfied in respect of river morphology. The construction of proposed RRTS Bridge will not cause any major change in the river regime in the reach under consideration. The proposed bridge will not induce any changes in the flow that pose difficulties to the downstream bridge.
- The maximum water level observed at the proposed bridge site is about RL 207.10 m with modified bridge alignments with river discharge 12,750 $m^3$/s. The project authorities are advised to decide the deck level by taking sufficient free board according to the relevant Indian Standard.
- Considering the likely maximum discharge intensity of 27.10 $m^3$/s/m, the deepest scour level is expected to extend up to about RL 179.66 m and after providing for grip length of about 1/3$^{rd}$ of the maximum scour depth below HFL, the founding level may be provided at RL 170.51 m.
- The model studies indicated that the bridge with 8 m diameter wells and piers diameter of 2.5 m would cause an afflux of 12, 18, 22 cm at proposed bridge axis for the discharges of 7022 $m^3$/s, 9910 $m^3$/s and 12750 $m^3$/s respectively.
- Maximum velocities and maximum discharge intensities are expected to be about 2.60 m\s and 13.80 $m^3$/s/m, 2.60 m/s and 25.70 $m^3$/s/m and 3.06 m\s and 27.10 $m^3$/s/m for a discharge of 7,022 $m^3$/s, 9,910 $m^3$/s and 12,750 $m^3$/s respectively at the proposed bridge axis.
- The afflux created by the bridge reduces to immeasurable values at a distance of about 0.90 Km, 1.45 Km and 1.70 Km for the discharges of 7,022 $m^3$/s, 9,910 $m^3$/s and 12,750 $m^3$/s respectively.
- It is observed that the model studies that the position of two piers are coming exactly on the toe of the existing left and right guide bunds, extra care should be taken during construction of the bridge.

## 5.0 References

CWPRS Technical report No. 5675 of February 2019 “Hydraulic model studies for proposed Delhi-Ghaziabad-Meerut Corridor of RRTs bridge cross river Yamuna on upstream of DND road bridge at New Delhi”.

Melville, B.W. (1997), “ Pier and Abutment scour’ Integrated approach,” Journal of Hydraulic Engineering, ASCE, 123(2), PP 123-136.

River Behaviour Management and training CBIP Publication No. 60, New Delhi. Vol-I

Smith, D.W. (1977). “Why Do Bridges Fail?” Civil Engineering, ASCE, November 1977.

## ACKNOWLEDGEMENT

We wish to express our deep sense of gratitude to Shri A.K. Agarwal, Director, CWPRS for constant encouragement and valuable suggestions during the course of this studies and kind permission given for publishing this paper.

*IN PROCEEDINGS OF 25th HYDRO 2020, INTERNATIONAL CONFERENCE, NATIONAL INSTITUTE OF TECHNOLOGY ROURKELA, ODISHA, INDIA 26-28, March 2021, ISBN 978-93-90631-56-8*

Paper ID - 256

# Issues and Challenges of the Urban Water Supply System in Ethiopia: A Case Study of Dire Dawa

Bahar Adem Beker[1] and Mitthan Lal Kansal[2]

*Department of Water Resources Development and Management, Indian Institute of Technology Roorkee, Roorkee 247667, India*

*Email*: baharwsee@gmail.com[1], mlk@wr.iitr.ac.in[2]

## Abstract

Cities around the world are facing critical potable water supply deficits due to population growth, hydroclimatic changes, and urbanization, especially in developing countries like Ethiopia. Although Ethiopia is often referred to as the water tower of Africa, no Ethiopian city receives a 24x7 pipe water supply. Water supply is only for a few hours a day. This study investigates the challenges of the Urban Water Supply System (UWSS) of Ethiopia, particularly in Dire Dawa city, and proposes possible solutions. For this purpose, primary and secondary data were collected from different sources to identify the status of the existing water system. The water utility has been drilling several boreholes to increase the water supply, but still, it has not been able to satisfy the water requirements at different times. A significant portion of the city (about 23 percent) does not have an adequate water supply. Further, the city water supply system has poor water quality affecting the public health and has several limitations of institutional capacity to build an improved and efficient water supply system. In order to model and simulate the existing water distribution network (WDN), a hydraulic modeling tool (WaterGEMs V8i) along with ArcGIS, is applied. It has been noticed that the WDN has issues related to high pressures in some locations and low velocities in some other parts. In order to manage the WDN effectively, it is recommended to computerize the network so that the various conditions/ stressors can be simulated and analyzed. Further, it is essential to plan and manage the system efficiently and effectively by way of improving the technical capacity of the existing system, and by way of good governance and better water policy.

***Keywords;*** *Challenges of urban water; Dire Dawa; Water Distribution Network; Water supply system; WaterGEMs*

## 1. Introduction

Next to air, potable water, and food are the basic requirements for every human being. Water plays a significant role in both economic and social development. The availability of adequate and safe water and sanitation is inextricably related to public health and better living standards for any society. Lack of sufficient wholesome water and poor sanitation services leads to the spread of diseases, which are responsible for the deaths of millions of people around the world, particularly in developing countries like Ethiopia (Toubkiss 2006). Study indicates that about 80 percent of all diseases and over one-third of deaths in developing countries are water-associated. One-tenth of each person's productive time is spent tending to diseases related water (WHO and UNICEF 2017).

Over the years, the accessibility of water sources throughout the world has become an increasing challenge due to depletion. These challenges are aggravated by population growth and urbanization. A recent study has shown that 2.1 billion people globally lack of potable water in their homes. Among those people, 844 million do not have basic drinking water services in their homes, 265 million spend half an hour for collecting water per round trip, and 159 million people drink water directly from surface water, such as streams and ponds (WHO 2017). Out of the 844 million people who do not have access to safe and potable drinking water in the world, 325 million (43 percent) of them live in Sub-Sahara Africa (SSA). In SSA, two out of five people have not accessed potable water (WHO and UNICEF 2017). From 35 countries globally below the UN Millennium Development Goal (MDG) of access to water for all, 26 are located in SSA, including Ethiopia (WHO 2017). UN-Habitat (2012) indicates that less than half of the populations in the urban centers of Latin America, Asia, and Africa have water piped systems within their homes. However, in Africa, up to 150 million urban residents, representing up to 50 percent of the urban population, do not have adequate water supply and sanitation services,

according to UN-Habitat. Ethiopia ranks as one of the lowest countries in SSA and the entire world regarding access to the potable water supply (Banerjee et al. 2008).

Despite Ethiopia being touted as one of the fastest developing countries in the world, it ranks very low in regards to providing safe drinking water and improved sanitation services to its people. The main challenges of the municipal Water Supply System (WSS) in Ethiopian cities, particularly in Dire Dawa, include urbanization, high water demand, and its mismanagement, water supply shrinking, water quality deterioration, low functionality of the existing WSS components (technical problems), limitation in institutional capacity, and lack of proper planning. The objectives of this study are to assess the issues and challenges of the UWSS in Ethiopia, particularly in Dire Dawa, and to propose a possible solution for those challenges. Such research is necessary to properly manage water in developing countries where equitable water distribution remains a challenge (Dayal et al. 2018). Rising issues of water availability exacerbate challenges that stem from mismanagement of water sources due to rapid population growth and looming climate change (Swain 2018). This study focuses on researching challenges and proposing possible solutions to alleviate the problem of the UWSS in Ethiopia, particularly in Dire Dawa that did not study yet, is both necessary and timely.

## 2. Issues and Challenges of Urban Water Supply System in Ethiopia

### *2.1 Cities and towns in Ethiopia*

The Ethiopian Central Statistic Authority (CSA) estimated that about 79.7 percent of the Ethiopian population would be living in rural areas and the remaining 20.3 percent in urban centers by the year 2020 (CSA 2016). The population living in cities is growing at around 5 percent per year, which is more than twice the growth rate for the country as a whole, according to Ethiopian (CSA) data. In 2017, there were 22 urban centers or cities in Ethiopia with a population of more than 100,000: one city (Addis Ababa) with more than a million people, seven cities with populations ranging from 100,000 to 1 million people, and 129 towns with populations ranging from 20,000 to 100,000 (Table 1). The fundamental criteria to categorize and classify cities and towns are population size, density, diversification of economic activities, and availability of infrastructure & services. Table 1 indicates the trend of cities and towns in Ethiopia from 1960 to 2017 based on the size of the population criteria. It has six settlement hierarchy and ten categories based

**Table 1** Town and city size distribution in Ethiopia (1960-2017)

| S.No. | Settlement Hierarchy | Class (Categories) | Population Range | Year | | |
|---|---|---|---|---|---|---|
| | | | | 1960 | 2007 | 2017 |
| 1 | Super large Cities | I | 1,000,000+(above) | 0 | 0 | 1 |
| 2 | Large Cities | II | 500,000-999,999 | 0 | 0 | 0 |
| 3 | Medium- Cities | III | 200,000-499,999 | 1 | 3 | 7 |
| 4 | Large towns | IV | 100,000-199,999 | 0 | 8 | 14 |
| | | V | 50,000-99,999 | 0 | 15 | 39 |
| 5 | Medium- Town | VI | 20,000-49,999 | 5 | 61 | 90 |
| | | VII | 10,000-19,999 | 5 | 145 | 212 |
| 6 | Small Town | VIII | 5,000-9,999 | 20 | 209 | 294 |
| | | IX | 4,999-2,000 | 43 | 325 | 393 |
| | | X | less than 2,000 | 310 | 161 | 202 |
| | | | **Total** | **384** | **927** | **1252** |

(Source: CSA survey of 1960; CSA Census of 1984, 1994 and 2007;
https://www.ethiovisit.com/ethiopia/ethiopia-regions-and-cities.html)

### *2.2 Urban water supply system and its challenges in Ethiopia*

Although Ethiopia is one of the fastest-growing countries globally, it is one of the least countries in terms of providing safe drinking water and sanitation for their people. However, the population accessed

portable water in Ethiopia has been growing compared to the previous decade; still, many people have no clean water in their homes. In 1990, only 17 percent of Ethiopia's population had access to clean water. According to the Ethiopian Ministry of Water, Irrigation, and Electricity (MoWRE 2017), national average urban and rural water supply coverage reached 68 percent (51.8 million) and 55 percent (10.6 million) in 2017, respectively. Also, per capita demand (PCD) is minimum compared to other countries. In urban areas, the PCD ranges 40 to 100 liters per person per day (LCD) and 25 LCD at a maximum distance of 1 km from the supply point in rural areas as MoWRE data.

Although Ethiopia is often mentioned as a water tower in Africa, only 65.5 percent of its population has access to clean water in the urban center of Ethiopia (MoWRE 2017). No cities provided a 24x7 water supply in any Ethiopian city. Water supply is limited to a few hours a day. Water supply systems face significant challenges in most urban centers in Ethiopia. The most critical challenges are:

- A considerable shortfall in the adequacy of the water supply;
- Lack of enhancement of existing and new WSS to ensure quality, safety and reliability;
- Low operation and maintenance capacity, which reduces the functionality of systems, an average non-functionality rate of 11 percent was reported by MoWIE (2016) ;
- Freshwater contamination and degradation of raw water (Low water quality) in Ethiopian cities are exacerbated by industrial emissions and water contamination from different effluents;
- Mismatch of the new water supply infrastructure which meets the rapidly growing population;
- The institutional capacity limitations to manage the water utility effectively, and lack of skilled human resources;
- High Non-Revenue Water (NRW), which is estimated between 25-60 percent of the water distributed (MoWIE 2016);
- Low demand management and
- Lack of efficient planning for alleviating the existing and future challenges of the UWSS.

Also, Table 1 shows the urban water supply problem and population in large Ethiopian cities. The demand for water in cities is greater than that of water supply. Additionally, Table 1 indicates the source and the main problem associated with the water source. The main problems are low water supply, water pollution, raw water hardness, high concentrations of $NO_3$ and fluoride, reduced water flow during drought, etc.

**Table 2** Glimpse of water sources in some large cities of Ethiopia

| City | Class (Category) | Population (2020) | Water Source | The problems of Water Source |
|---|---|---|---|---|
| Addis Ababa | I (Super large city) | 4,794,000 | 67.9% is groundwater (deep well), and the rest are surface water from Legedadi, Dire, and Gefersa dams or reservoir | Industrial and domestic pollution of raw water & only 67% of water demand is satisfied by sources |
| Dire Dawa | III (Medium- city) | 408,000 | 96.4% is deep wells (from Sabian, Boran & Tome well fields), and the rest is from legedol spring | Raw water hardness, high concentration of $NO_3$, and pollution of the wellfield from domestic waste. The source is only satisfied 77% of the demand |
| Gonder | III (Medium- city) | 362,000 | 84% is from surface water (reservoir constructed in river Angereb) & the rest are from a deep well | Reduction of a water source during the dry season and high erosion from mountain to dam |

| | | | | |
|---|---|---|---|---|
| | | | (Zewdu, 2010). | |
| Mekele | II (large- city) | 524,000 | Groundwater ( deep Wells) and surface water (river) | Heavy industry and domestic waste are the potential risks to the water source, causes for water contamination and degradation of raw water. |
| Hawassa | III (Medium- city) | 319,000 | Surface water (River "CADO" , two spring sources (Loke and Ambo spring), and ten boreholes (deep well) are the main water sources. | Contamination and pollution of water source from industrial and domestic waste. |
| Bahar-Dar | III (Medium- city) | 348,500 | Two springs and deep wells located at different parts of the city. | Reduction of a water source during the dry season (particularly spring water) |
| Adama | III (Medium- city) | 378,000 | Surface water(from the awash river) & groundwater(well field). | The high content of fluoride in raw water (deep well) and pollution of surface water(Awash river) from both industrial and domestic waste. |

(source: https://www.macrotrends.net/cities, United Nations population projections, and https://aawsa.gov.et/?lang=en,)

## 3. Dire Dawa water supply system and challenges

### *3.1 Description of the study area and the existing water supply system*

Dire Dawa, the study area, is one of the largest and oldest urbanized centers in Ethiopia. It has nine districts (*kebeles*) that cover an area of 1216 sq.km. It is located in the Awash basin in the eastern lowlands of Ethiopia with the geographical location of 41° 50' to 41° 52' latitude and 9° 34' to 9° 35' longitudinal direction (Figure 1) and 458 km far from the capital city of Addis Ababa. Dire Dawa has an elevation ranging from 1130 to 1335 m with a mean elevation of 1160 m above mean sea level (DWSSA, 2014). Steep hills and slopes are found in the south of the city, whereas moderate and gentle slopes are found in the north. According to the Central Statistic Authority of Ethiopia, the population of Dire Dawa in 2019 was estimated to be 394,024.

The construction of Dire Dawa's modern WSS is historically linked to the Ethio-Djibouti railway line. The first piped water supply in Dire Dawa was constructed by the French operating company (Ethio-Djibouti Railways) that built the Ethio-Djibouti Railway to connect Addis Ababa and Djibouti. The water supply was constructed in the year 1914 using Lega Hare (locally called Legedol) spring as a water source (MS Consultancy, 2015). As the city expanded and the population substantially increased over the next several decades, the single water source from Legedol became insufficient to alleviate the demand for water. In 1992, the former Dire Dawa Water Supply and Sewerage Authority (DWSSA) agreed to work with a Canadian consulting firm, Associated Engineering Service Limited (AESL) to study and design a new water supply system. AESL designed and implemented a water supply system that served the population in Dire Dawa (around 173,000) for ten years. However, the water supply system continued to expand over the years to meet increasing demands and resolve water scarcity problems.

Dire Dawa's current water source is the groundwater from the three wellfields (Sabian, Boren, and Tome), deep well located in the city, and the Legedol spring, which has a total production capacity of 54,061$m^3$/day. Two collector tanks, two transfer tanks, and eight service reservoirs are located in different parts of the city. Water pumped from collecter (transfer) tanks to service reservoirs located at high elevation in the corners of the city and then distributed to end-users through gravity. From an operational perspective, the existing WDN of Dire Dawa is divided into three pressure zones, with 887 nodes and 1135 pipes. The entire WDN has a 185.56 km long pipeline, with the pipe diameter varying between 50 and 700 mm (PVC, DI, and GS).

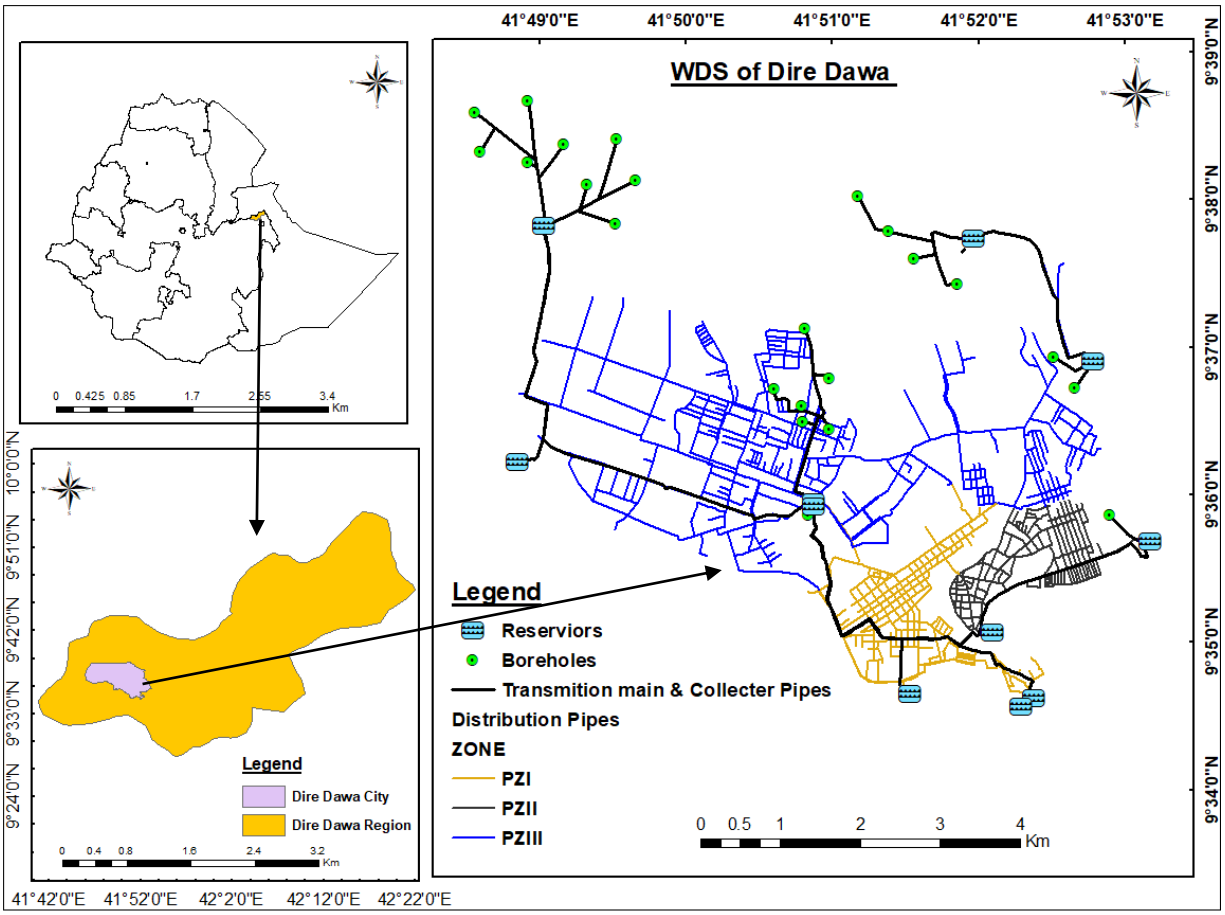



**Figure 1** Map of the study area

### *3.2 Issues and challenges of water supply system in Dire Dawa*

This study has two parts: (1) investigating the different challenges of Dire Dawa's water system supply and technical issues of WDN, and (2) proposing a possible strategy and solution. For this purpose, both primary and secondary data were collected from various sources. Field observations of the study area, including water source, reservoir, pumping station, and tanks, were performed. Further, interviews with selected water users, experts (engineers, operation and maintenance workers), and decision-makers (managers of water utility) of DWSSA were conducted to assess the status and various problems of related to WSS. Secondary data were collected from various sources (e.g, DWSSA and MoWIE) include; the WSS design document, study reports of the water utility, maps of the study area, different layout maps of the WDN, and etc

Sustainable and reliable water supply in a city requires careful consideration of all factors that affect the entire system from the point of water sources up to the consumer's delivery end. The challenges are complex and technical, financial, and institutional capacity to control against unsafe practices. In this

study, the challenges were categorized under water supply coverage (adequacy), water quality, technical and institutional issues, and more elaborate one by one.

### *3.2.1 Water quantity (supply) issues*

In the city of Dire Dawa, water shortage is increasingly creating constraints for the population. Water demand is rising due to population growth and economic developments; while on the other hand, the volume of water produced has been decreasing due to hydroclimatic change. The current water supply is too low to meet the demand, and also it does not supply some areas in the distribution network. The existing WSS of the city has reached a stage where it cannot fulfill the current demand for many sectors of the city. The current water supply is satisfying only 77 percent of Dire Dawa's residents.

### *3.2.2 Water quality issues*

Dire Dawa's water is supplied exclusively from groundwater that is highly polluted (UN-Habitat 2010). Analysis of water samples taken from groundwater shows that Nitrate ($NO_3$) concentration exceeds the allowable limits (35.5-109.5 mg/l). Also, bicarbonate (Ca-$HCO_3$ type) concentration with total dissolved solids is high, ranging from 400 to 640 mg/l (DWSSA 2003). The increase in nitrate concentration is attributed to contamination by organic pollutants arising from waste generated within the wellfield and from the catchments, mainly from the pit latrines around the wells. Additionally, according to previous groundwater assessments, Mintasenot (2011), the water quality in Dire Dawa is generally low, and the water has a hardness. The water type is Ca-$HCO_3$ and Ca- Mg-$HCO_3$ and also has high chlorides. The interaction with other factors, such as pH and alkalinity, water with hardness more than 200 mg/l can cause scale accumulation in the system and lead to excessive soap consumption and subsequent scum formation, leading to clogging pipes.

### *3.2.3 Institutional issues*

The absence of proper monitoring systems and low operation & maintenance capacity is among the main institutional problems in DWSSA. A complicated information sharing system can be better achieved through a regular monitoring process with a continual reporting system. However, water supply management is lacking this, and thus, monitoring systems and the technical data are not available for reliable decision-making. Further, the necessary facilities required for the engineer (expertise) and technical workers are not available with sufficient amount and quality. In some stations, the pumping system is operated by a non-skilled person. Such practices are worsening the DWSSA's liability and causing unsustainable service provision. Other institutional problems are lack of skilled human resources, weak customer services and management, inconvenient methods of bill settlement in the office, a low number of branch offices, and over-centralization of activities.

### *3.2.4 Technical issues*

Field observations indicated that some wells had been abandoned due to various technical reasons. It may be due to the declining productivity attributable to the over-pumping of groundwater beyond the natural recharging rates. During the field visit, I observed that the Dwellings and pump switchboards are placed hazardously in Sabian pumps house without regard to the accepted standards and safety regulations of the Ethiopia Electic Power Cooperation (EEPCo). The booster stations have contained various electromechanical system components to facilitate the water distribution process. As observed, most controlling instrumentations are inoperative, pumps have low efficiencies below the technical requirements, and pump delivery pipelines are significantly leaking the water. Generally, the overall plant operating situations are not ensuring the reliability of the water distribution systems.

Furthermore, various control valves and fittings are supplied to the deep well, and collector pipelines are very old in some areas. In a particular area, pipelines that distribute water to the end-user are connected from the main transmission line before reaching the reservoir, which has a technical problem in the overall network. Due to the current settlement trend, most of these pipeline routes are surrounded by residential areas. Such conditions expose the pipes to damage during the new housing construction process and can lead to leakage with possible access for pollutants. These conditions can also lead to

diminishing returns due to illegal connections and the reduction of pressure. Additionally, most pipe fittings and the control valves are inoperative due to prolonged service life; it has not been in a condition to fulfill their functional requirements.

However, the new expansion of WSS has been carried out for boosting water supply and improves the network coverage, stilt; the newly constructed system has not been appropriately linked with the old system. This may ultimately lead to unmanageable pipeline leakage and high NRW, resulting in economic failures to the DWSSA. Additionally, the entire experiences of DWSSA have been focus only on achieving the hardware (expansion works such as pipes, tanks, pumps, wells, etc.). In contrast, the software components have not been adequately developed to solve the operation & maintenance challenges. However, the system has monitored the bulk water using the SCADA system; the WDN has not been controlled and monitored using this system entirely. Other detailed technical issues related to WDN are investigated using hydraulic modeling and simulation of the system.

### *3.3 Hydraulic simulation of existing WDN*

#### *3.3.1 Modeling of the WDN in GIS*

In this study, ArcGIS was utilized to build modeling of the water distribution network and to prepare all necessary data for hydraulic simulations. The existing water distribution map of the network obtained from the DWSSA was validated through field visits to the study area. The validated network map was then scanned and imported to ArcGIS for georeferencing and digitalization. The layers of water distribution components (pipes, junctions, tanks, reservoirs, pumps, and valves) were created in ArcGIS. The input parameters, namely the pipe diameter and pipe material (pipe roughness), was added to the attribute table and documented in the ArcGIS database. The other characteristics of hydraulic elements such as pumps, tanks, and valves were also transferred to the attribute table. Only pipes with a diameter above 90 mm in the networks were considered for the model. The model builder tools play a crucial role in WaterGEMs V8i as they import and export data between ArcGIS and the model (Bentley Sys. Inc, 2014). Further, different layers of network data such as diameters, elevation, pipe roughness, valves, tanks, and reservoirs are synchronized in the WaterGEMs V8i model. After the constructed model is transferred to the hydraulic software (WaterGEMs V8i), the water demand and other necessary data are assigned for further analysis.

The average water consumption reached 80 LCD in the city (Ramana and Chekka 2018). The baseline demand for each node is allocated based on the water consumption of the node. The flow distribution method that involves lump-sum water demand distributed among the service area is used for allocating the baseline demands (Giustolisi and Todini 2009; Cross 1936). Thiessen polygons are generated for each node to estimate the population under each service polygon, based on the population density data. After incorporating the entire necessary data into the hydraulic model, the simulation is performed to predict the hydraulic characteristics of the WDN. The final step is the calibration of the model, which intends to improve the accuracy of the models.. Zone I of the WDN has been facing many problems compared to the other zones and could be representing the problems of WDN as a whole, therefore thus was selected for hydraulic modeling and simulation.

#### *3.3.2 Identification of a technical problem using the hydraulic simulation of the WDN*

A hydraulic model is a tool for determining how the system responds to the real system (Jeffrey and Gilbert 2004). Today, water distribution modeling and simulation are essential parts of designing and operating WDN to serve communities reliably, efficiently, and safely. The hydraulic parameter (velocity in the pipe, pressure, head loss, and water flow) output of the model simulation indirectly indicates the problem area of the WDN by comparing its value with the standard. Both extended period simulation (EPS) and steady-state analyses (SSA) are conducted to characterize the hydraulic parameters (pressure at each node, flow velocity in the pipes, and head loss). An EPS is carried out using the demand pattern collected from DWSSA. The result in Figure 2 shows the nodal pressure and velocity in pipes for the WDN in the steady-state analysis (SSA). The simulation output indicates problematic areas (nodes and pipes) where the hydraulic parameter (pressure and velocity) is beyond the recommended value. High

pressure and low velocity are observed at various nodes and pipes in WDN. The results in Figure 2 revealed that many pipes (58 out of 134 pipes) have a velocity value that is lower than the recommended minimum velocity (0.3m/sec). Low velocity of flow in a pipeline can be a reason for the accumulation of silt and water quality deterioration in the pipes, leading to minimizing the network performance of the WDN (Walski 2003).

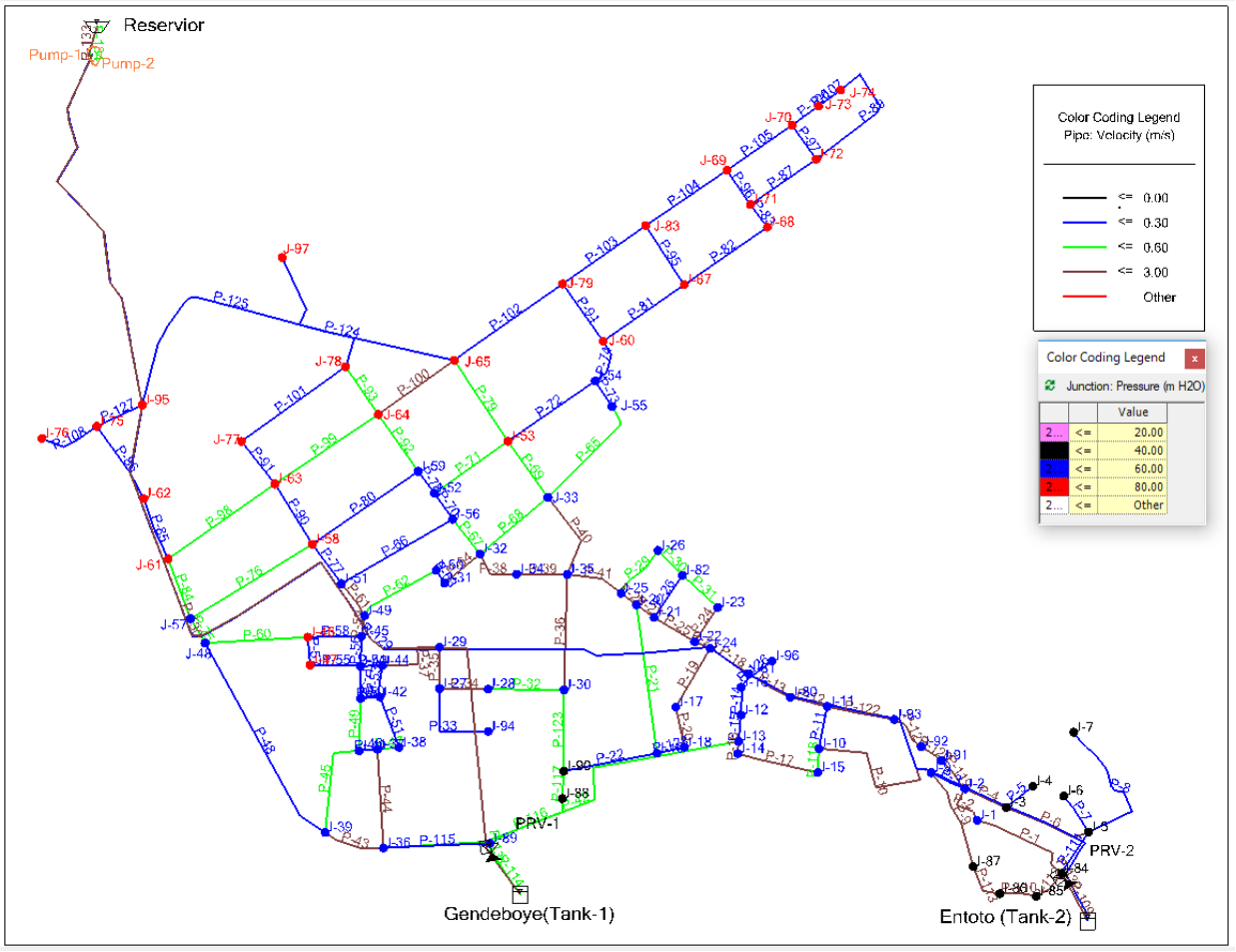



**Figure 2** Hydraulic simulation results of WaterGEMs V8i (in SSA) of the WDN

The oversized diameter of the pipe could be the main reason for the minimum flow velocity in the pipe. The EPS indicates lower velocity in the pipes observed at minimum hourly demands (particularly at midnight) when the base flow in the pipe is very low. Inversely the maximum velocity is observed at peak hourly demand during morning time.

Furthermore, a significant number of demand nodes (26 out of 97 nodes) are found to have a pressure value higher than the maximum allowable limit (60m). The maximum pressure is observed at nodes of lower elevation. Such high pressure can be the main reason for the significant leakage problem in the pipes, leading to pipe bursts and water loss. Also, high pressure above the maximum standard limit at the nodes may be a cause of low-performance of the networks. The values of pressure in the network fluctuate with time. Higher pressure for all nodes is observed at midnight of the minimum demand. The lowest nodal pressure is observed at the peak demand during morning time.

## 4 Possible strategy and solution

### *4.1 Efficient planning of UWSS*

Nowadays, the urban population is growing by 80 million people every year. The global population is projected to be 10 billion in the year 2050. Currently, more than 50 percent of people live in an urban

center. With an ever-increasing global population and with populations continually migrating to cities for better economic opportunities and living standards, the effective planning of urban water supply becomes an increasingly important part of integrated urban infrastructure planning and development. The UWSS plan must include a comprehensive and accurate identification of all options to meet the specified service standards, including options based on non-asset solutions. It should also be a simple process that balances the needs of the service with infrastructure, operation, maintenance, finance, and environmental alternatives. The purpose of the plan is to identify defined service levels, and short, medium, and long-term service need to achieve social, environmental, and financial outcomes. Evaluate options to provide defined results; determining a good strategy for low-cost financial, social, and environmental outcomes (bottom three), and communicating the planning results to decision-makers is among other planning objectives. The efficient water supply planning process is shown in Figure 3. It is displayed as linear. Such planning has nine key process steps.

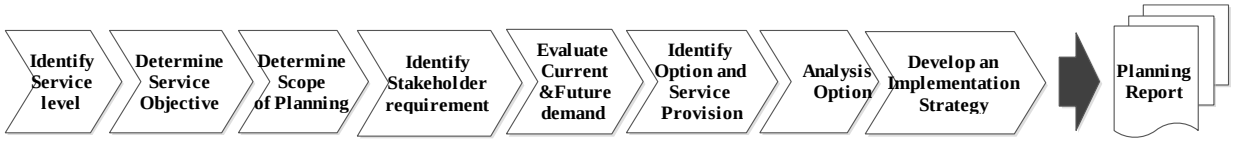



**Figure 3** The elements of an effective planning process of WSS

### *4.2 Apply demand and water management strategy*

Current and future water demand management strategies from the service provider should be given serious attention to mitigating the challenges associated with WSS adequacy. Once implications are increasing from time to time, the strategies may need to be re-evaluated. Additionally, the sustainability of managing demand over the long term can be considered. It is necessary to focus on water resource sustainability by encouraging demand management approaches and an unaccountable water reduction strategy. Demand management strategies have two parts: the Demand Reduction Strategy (DRS) and Supply Rationalization Strategy (SRS). DRS includes charging of water, education campaigns, water restrictions, installing water-saving equipment, bathroom self-replacement program, toilet retrofits, water audits, water-saving equipment (appliances), rainwater harvesting, and outdoor water audits. SRS includes customer metering, water loss reduction, leakage inspection and maintenance, accurate measurement, pressure reduction, re-use, and recycling of wastewater.

### *4.3 Increasing water productivity and non-conventional waters sources*

Water recycling and re-use is aimed at increasing water productivity. Many water-stressed cities are treated wastewater for irrigation or other purposes. A few cities, such as Singapore and Windhoek, have developed systems to recycle wastewater (Van Rensburg 2016). However, direct drinking use of the treated water still faces emotional and psychological barriers (Leong 2016). Another technology like desalination is used in those cities to increase supply; however, it is more energy-intensive than water recycling and not adapted for developing counties like Ethiopia

### *4.4 Institutional and organizational reform*

Many pressures, states, and influences are the result of administrative failures at many levels of government (Phel-West 2017), and institutional and organizational reforms are needed. Private sector participation and decentralized governance are suggested as solutions. However, the current water policy and management are complex. It is crucial to adapt to new perspectives, concepts, and frameworks such as adaptation and transformation, social education, self-organizing systems, and informal networks. Finally, it is essential to Promote institutional and organizational development and support reform of the urban water and sanitation sector through capacity building, knowledge sharing, and promotion of partnerships.

### *4.5 Monitoring the WDN using an advanced and computerized system*

One-of the challenges of WDN is the lack of monitoring and controlling entire system using advanced and computerized ways for proper operation of WSS components. So that is vital to apply SCADA (supervisory, control, and data acquisition) system. The SCADA system is a computer-based system that gathers and analyzes the period of knowledge to trace (real-time), monitor, and manage WDN. UWSS is a complex system composed of many different operational components, including pumps, motor, flow meter, sensor, and control valves. The system can be monitored, controlled, and supervised from a central location. The systems include sensors (hydraulic and water quality) and controllers (directly interface with the managed systems so that it is significant to resolve the problems that appear during operation and maintain the normal functioning of the entire WDN.

### *4.6 Installing PRV and replacing the pipes at the critical area*

High pressure and low pressure at nodes are a reason for reducing the hydraulic performance of the WDN. High pressure above recommended values (62m) is cause for pipe burst that leads to loss of water and for pipe failure. Whereas, low-pressure at a demand node decreases the amount of water delivered for the consumer. Installing pressure regulating values (PRV) at critical points is significant to minimize and regulate the problem related to the high pressure at anodes. Simultaneously, low velocity in the pipes is resolved by redesigning the system and changing some pipes in a problematic area with the recommended diameter size.

Overall, the issues, challenges, and the proposed solutions of UWSS are summarized in Table 3 shown below.

**Table 3** Summary of urban water supply system challenges and its possible solution

| Category of Issues | Problems (Challenges) of UWSS | Possible Solution |
|---|---|---|
| Water supply (adequacy) issue | • A shortfall in the adequacy of the water supply,<br>• low water supply coverage,<br>• Reduction of a water source during the dry season. | • Increasing water productivity and non-conventional waters sources using re-use and recycling of water,<br>• Expansion of the water supply system<br>• Conservation of supplied water, apply rainwater harvesting system and groundwater recharge |
| Water quality issue | • Pollution and contamination of water source,<br>• Lack of proper water treatment facilities,<br>• The high concentration of Physco-Chemical parameters in both raw and distributed water | • Proper domestic & Industrial wastewater treatment,<br>• Apply Anti-pollution laws and regulations at local, state, and international levels,<br>• Minimizing the storm runoff<br>• Uses both effective local and advanced water treatment techniques |
| Technical issue | • High non-functionality (failure) rate of WS components,<br>• The poor performance of WDN in delivering potable water to the end-user at the required pressure and available amount in every place and time,<br>• High Non-Revenue water (illegal connection & water loss) | • Regular operational and maintenance of the system,<br>• Monitoring & controlling the real-time WSS using a SCADA system<br>• Replacing the old WSS components (Upgrading the network),<br>• Apply leakage management (Active leakage control, pressure management, infrastructure management, and f repair). |

| | | |
|---|---|---|
| Institutional and Governance issue | • Lack of organized water utility and institution administration<br>• Poor urban water policy<br>• Lack of skilled human resources<br>• Lack of sufficient decentralized office and billing center | • Enhancing accountable, efficient, responsive, and sustainable water institution<br>• Improving coordination and integration within the organizational structure for water management<br>• stimulate changes in policy and practice in urban water management within the institution<br>• Improving skilled human resources through continuous capacity building |
| Planning of UWSS | • Lack of efficient technical and institutional planning of UWSS | • Develop the planning system that is a comprehensive and exact identification of all options to meet the defined service levels, including options based on non-asset solutions. |

## 5. Conclusions

This study is aimed at assessing the main challenges of the urban water supply system in Ethiopian cities, particularly in Dire Dawa, and proposing the solution. Both primary and secondary data were collected and used to analyze Dire Dawa's water supply system challenges. Technical problems related to the WDN were investigated through hydraulic modeling and simulation by coupling advanced hydraulic modeling tools (WaterGEMs V8i) with GIS. No cities in Ethiopia have access to piped water 24x7 water supply. Moreover, Dire Dawa has been experiencing potable water supply inadequacy in both quantity and quality. Even if the water utility has expanded its service by drilling many boreholes, the water demand has not been satisfied, and 23 percent of the population in Dire Dawa does not have access to an adequate amount of potable water. The main challenges of Dire Dawa's water supply system are low water supply coverage, low water quality, technical problems, and institutional capacity limitations. Besides, the distribution network is facing challenges, with high pressures (26 nodes out of 97), especially in low elevation areas and low velocities (58 pipes out of 134) in the pipes, in other parts of WDN. Therefore, to solve these challenges, it is vital to develop improved policies and planning for an effective water supply system, apply a demand management strategy, find alternative water sources, computerizes the system, installing PRV, and replace the pipes at the critical area, which altogether, would improve the capacity of the water supply system.

## 6. References

Banerjee, S., Skilling, H., Foster, V., Briceño-Garmendia, C., Morella, E. and Chfadi, T. (2008). *Africa-Ebbing water, surging deficits: urban water supply in sub-Saharan Africa*.World Bank. Washington.

Bentley Systems Incorporated. (2014). WaterCAD/GEMS V8i,.Water Distribution Design, and Modeling, Fundamentals, Version V8i (SELECT series 5).

Cross H. (1936). *Analysis of flow in networks of conduits or conductors*.The University of Illinois at Urbana Champaign, College of Engineering. Engineering Experiment Station, Urbana, Illinois.

CSA. (2016). *Federal Democratic of Ethiopia Office of Population Census Commission Central Statistics Agency, Population and Housing Census of Ethiopia Natural Statistical Summary Report*, Addis Ababa. Ethiopia.

Dayal, D., Swain S., Gautam, A., Palmate, S., Pandey, A., Mishra, S. K. (2019). Development of ARIMA Model for Monthly Rainfall Forecasting over an Indian River Basin. *In World Environmental and Water Resources Congress 2019, ASCE;* 264-271.

Dire Dawa Water Supply and Sewerage Authority. (2014). *Final Dire Dawa water supply and sanitation design review report*, Dire Dawa, Ethiopia.

DWSSA (2003). *Dire Dawa Water supply and sewerage (DWSSA) report document. Groundwater assessment of Dire Dawa feasibility study*, Dire Dawa, Ethiopia.

Giustolisi, O., and Todini, E. (2009). Pipe hydraulic resistance correction in WDN analysis. *Urban Water Journal*, 6(1);39-52.

Jeffrey, A., and Gilbert, P. (2004). "*Practical Design of Water Distribution Systems*." Retrieved from https://pdhonline.com/courses/c182/c182content.pdf.

Khatri, K., Vairavamoorthy, K., and Porto, M. (2008). Challenges for urban water supply and sanitation in developing countries.In *Water for a Changing World-Developing Local Knowledge and Capacity* (pp. 93-112). CRC Press.

Leong, C. (2016). A lived-experience investigation of narratives: recycled drinking water. *Int. J. Water Resour. Res.* 32 637–49.

MS Consultancy (2015). Final Design Review and Detail Design Preparation of Dire Dawa Water Supply Project, Volume – I, Dire Dawa, Ethiopia

Mintasenot, T. (2011). *Design Review and Detail Design preparation of the 2nd phase of Dire Dawa Water Supply and Sanitation Project*: *Ground Water Investigation, Well Field, and Borehole Sitting*. Dire Dawa, Ethiopia.

MoWIE. (2017). *Ministry of Water, Irrigation, and Electricity: Annual report of urban water supply and sanitation document.* Addis Ababa, Ethiopia.

MoWIE. (2016). *Ministry of Water, Irrigation, and Electricity: Annual report of urban water supply and sanitation document.* Addis Ababa, Ethiopia.

Pahl-Wostl, C., (2017). An evolutionary perspective on water governance: From understanding to transformation Water Resour. Manage. 31 2917–32.

Ramana, G., and Chekka, V. (2018) Validation and examination of existing water distribution networks for a continuous supply of water using EPANET. *Water resources management 32*(6):1993-2011.

Swain, S., Verma, M. K., & Verma, M. K. (2018). Streamflow estimation using SWAT model over Seonath river basin, Chhattisgarh, India. *In Hydrologic Modeling* (pp. 659-665). Springer, Singapore.

Toubkiss, J. (2006). *Costing MDG Target 10 on water supply and sanitation: Comparative analysis, obstacles, and recommendations.* Paris: World Water Council/World Water Forum.

UN-HABITAT. (2012). United Nations Centre for Human Settlements Water and Cities. Kyoto. Japan, https://www.un.org/press/en/2003/hab184.doc.htm.

UN-HABITAT. (2010). Water for African Cities. Dire Dawa City Programme, retrieved on 25 September 2010 from https://mirror.unhabitat.org/content.asp?typeid=19&catid=499&cid=3210

UNICEF. (2017). Drinking water, sanitation, and hygiene data base. Retrieved from https://data.unicef.org/topic/water-and-sanitation/drinking-water/.

Van Rensburg, P. (2016). Overcoming global water re-use barriers: the Windhoek experience Int. J. Water Resour. Dev. 32 622–36.

Van Rooijen, D. B. (2009). Urban growth, wastewater production, and use in irrigated agriculture: a comparative study of Accra, Addis Ababa, and Hyderabad. 24, 53-64.

Walski, T.M., Chase, D.V, Savic, D.A, Grayman, W., Beckwith, S., and Koelle, E. (2003*). Advanced water distribution modeling and management*.Civil and Environmental Engineering and Engineering Mechanics Faculty Publications, University of Dayton.

WHO. (2017). *Progress on drinking water, sanitation, and hygiene: 2017 Update and SDG Development global baseline study*, Retrieved from http://www.unwater.org/new-publication.

WHO and UNICEF. (2017). *WHO/UNICEF Joint Monitoring Programme 2017 report*. Retrieved from http://www.unwater.org/new-publication-who unicef-joint-monitoring-programme-2017-report/.

Zewdu, A. (2010). Assessment Of Water Supply In Gondar Town, Ethiopia: Challenges And Prospects. Journal of RJSSM : Volume: 08, Number: 06,

https://aawsa.gov.et/?lang=en

https://www.ethiovisit.com/ethiopia/ethiopia-regions-and-cities.html).

https://www.macrotrends.net/cities.

*IN PROCEEDINGS OF 25th HYDRO 2020, INTERNATIONAL CONFERENCE, NATIONAL INSTITUTE OF TECHNOLOGY ROURKELA, ODISHA, INDIA 26-28, March 2021, ISBN 978-93-90631-56-8*

Paper ID - 275

# Evolutionary Optimization Techniques for Optimal Design of Water Distribution Networks

S. N. Poojitha[1], Gagandeep Singh[2], V. Jothiprakash[3]

[1]*Research Scholar, Department of Civil Engineering, Indian Institute of Technology Bombay, Powai, Mumbai, Maharashtra 400076, India*

[2] *Former Post Graduate Student, Department of Civil Engineering, Indian Institute of Technology Bombay, Powai, Mumbai, Maharashtra 400076, India*

[3]*Professor, Department of Civil Engineering, Indian Institute of Technology Bombay, Powai, Mumbai, Maharashtra 400076, India*

*Email: vprakash@iitb.ac.in*

## Abstract

The design of water distribution networks (WDN) is familiar as a non-deterministic polynomial-time hard problem. To handle such problems effortlessly, the optimization tool with both the exploration and exploitation features is a primary requisite. In the present study, an efficient and effective optimization tool, the Genetic algorithm (GA) is considered. Different variants of GA are formulated considering three different selection mechanisms and by incorporating an elitism operator to these models. The working mechanism of GA variants is demonstrated considering the well-established WDN benchmark problem, Blacksburg Network (BLN). From the results of the analysis, it is observed that all the GA variants are efficient in converging to the feasible optimal solutions for BLN. Especially, the GA models with the truncation and tournament selection mechanisms are successful in converging to an optimal solution which is consistent with the results reported in the literature. When the number of successful trials out of 50 is considered, the GA variants are found to be less robust with only a maximum of three successful trials. Though all the GA variants considered in the study are efficient in exploiting the existing information with the parent chromosomes, GA is found to be less diversified. Considering the results of the present study, we suggest, any improvement that enhances the exploration capabilities of GA is futuristic.

***Keywords:*** *Exploitation; Exploration; Genetic Algorithm; Selection mechanism; Water distribution Network*

## 1. Introduction

Water distribution network (WDN) is an essential infrastructure for the adequate supply of potable water to the communities. They are of complex networks with interconnected components that have to be chosen from the commercially available options, which make the solution set intractable. While enumeration of all the possible solutions become exhaustive, the solution set consists of discrete feasible options besides the infeasible ones. Due to these complexities, the WDN design problem is familiar as a combinatorial optimization problem. And is also well recognized as a non-linear deterministic polynomial-time hard problem (Yates et al., 1984).

For designing WDNs optimally, for decades, various optimization techniques have been used. These include both the deterministic and stochastic based optimization techniques (Alperovits and Shamir 1977; Simpson et al. 1994; Sherali et al. 2001; Suribabu 2010; Poojitha et al. 2019 to name a few). Stochastic optimization techniques gained more attention due to their exploration and exploitation capabilities. The exploration capabilities aid in diversified search and the exploitation helps in intensifying the search around the best feasible solutions (Blum and Roli 2003). In the present study, the main objective is to minimize the design cost of the WDN. The best feasible solution is the one with the minimum design cost and satisfying the minimum pressure head requirement ($H_{min}$) at the demand nodes.

In the present study, the variants of the Genetic algorithm (GA), a bio-mimic evolutionary algorithm that is studied widely in various research fields are considered. To demonstrate their application, for the optimal design of WDNs, Blacksburg Network (BLN) is considered. The methodology of the proposed study, details of the BLN, and the results obtained along with the conclusions drawn from the present study are discussed in the following sections.

## 2. Methods and Methodology

### 2.1 *Genetic Algorithm and its Variants*

The success of GA lies in their adaptation i.e. exploiting the accumulated information in finding the unknown initial search space. The initial search spaces thus found guides the subsequent searches to the useful subspaces. In the present study, six variants of GA are considered, namely: i) GA with Truncation method of selection (GA-1), ii) GA with Tournament method of selection (GA-2), iii) GA with Roulette wheel method of selection (GA-3), iv) Elitist GA with Truncation method of selection (EGA-1), v) Elitist GA with Tournament method of selection (EGA-2), vi) Elitist GA with Roulette wheel method of selection (EGA-3). The elitism operator aids in saving a certain percentage of elite (best) solutions to replace the same percentage of worst (with high fitness value) ones, at the end of every generation. With the execution of this operator, the best available information is retained without being distorted by the subsequent GA operators.

Similar to the other evolutionary-based algorithms, GA starts with the randomly generated population set (in the present study, the size of the population is considered as 100). The fitness value for the chromosomes in the population is estimated and then, the chromosomes undergo a selection mechanism. As discussed earlier, three selection mechanisms are considered for different variants of GA. In the Roulette wheel method of selection, the more weightage is given to the best solutions (Hancock, 1997). In the Truncation method, at every generation, the chromosomes are arranged in the decreasing order of their fitness values, and a certain percentage of chromosomes at the top list is truncated (Hancock, 1997). In the present study, the truncation probability is considered as 0.5. In the Tournament selection mechanism, at every trial of the tournament, the best chromosome from the randomly chosen set is retained (Hingee and Hutter, 2008). Once the best solutions are regenerated from the population set, the crossover operator is carried out. In the present study, a single point crossover is considered with a crossover probability of 0.9. Once the offsprings are reproduced from the parent chromosomes, they undergo a mutation operator where a random gene from a randomly chosen chromosome is mutated. In the present study, mutation probability is considered as 0.2. Thus, the chromosomes evolve through with GA operators over generations. In the present study, the generation size is considered as the termination criteria and is considered to be 800 in the present study. All the GA's parametric values are fixed by conducting the sensitivity analysis, where, while estimating the optimal value for a single parameter, the others are kept constant. The flowchart gives a clear picture of the GA mechanism and is shown in Figure 1.

### 2.2. *Methodology*

Using the GA mechanism, the major aim of the present study is to minimize the design cost, '*DC*' of WDN, by assuming that all the essential details of the network are known prior. Thus, mathematically, the objective function is defined as

$$Minimze\ DC = \sum_{i=1}^{n} f(d_i, l_i) + PF$$

where $d_i$ and $l_i$ are the diameter and length of $i^{th}$ pipe. *PF* is the penalty function. In the present study, the static penalty function is considered, where the penalty multiplier is fixed through the sensitivity analysis. In the present case, through sensitivity analysis, for the minimum head violation, the *PM* is found to be $10^5$ and for the maximum head violation, it is 7000. The continuity and energy-based governing equations are taken care of by the simulation model, EPANET software (Rossman 2000). Thus, for optimally designing WDNs, the Simulation model in the combination of optimization technique, GA is considered. The code for which is written in MATLAB, and is combined with the simulation model, EPANET, using MATLAB -EPANET toolkit.

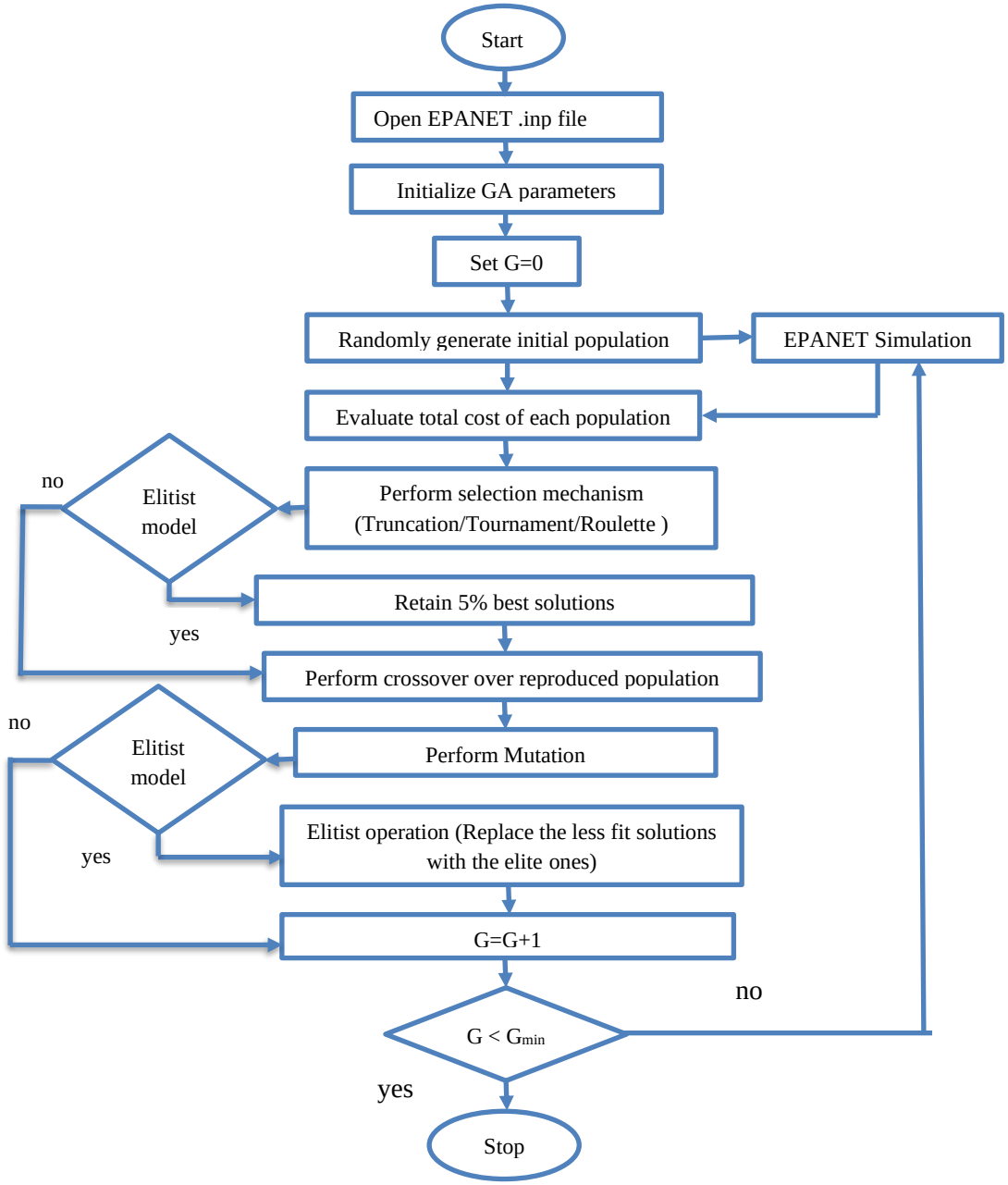



**Figure 1. Flow chart showing the mechanism of GA variants formulated in the present study**

### 2.2 *Benchmark Water Distribution Network, Blacksburg Network (BLN)*

Blacksburg Network (BLN) is first introduced by Sherali et al. (2001). It's a looped network with intermediate branches as shown in Figure 2, consisting of 35 pipes that are interconnected with 30 demand nodes. A source reservoir with a fixed head of 715.56m (CWS, Exeter) supplies BLN. It is a rehabilitated WDN, where, out of 35 pipes, only 23 pipes need to be re-designed. The remaining 12 pipes are the ones with known diameter and are highlighted in red color as shown in Figure 2. As there are 14 commercially available diameters, the total solution space formed by the BLN network with 23 design variables is $14^{23}$.

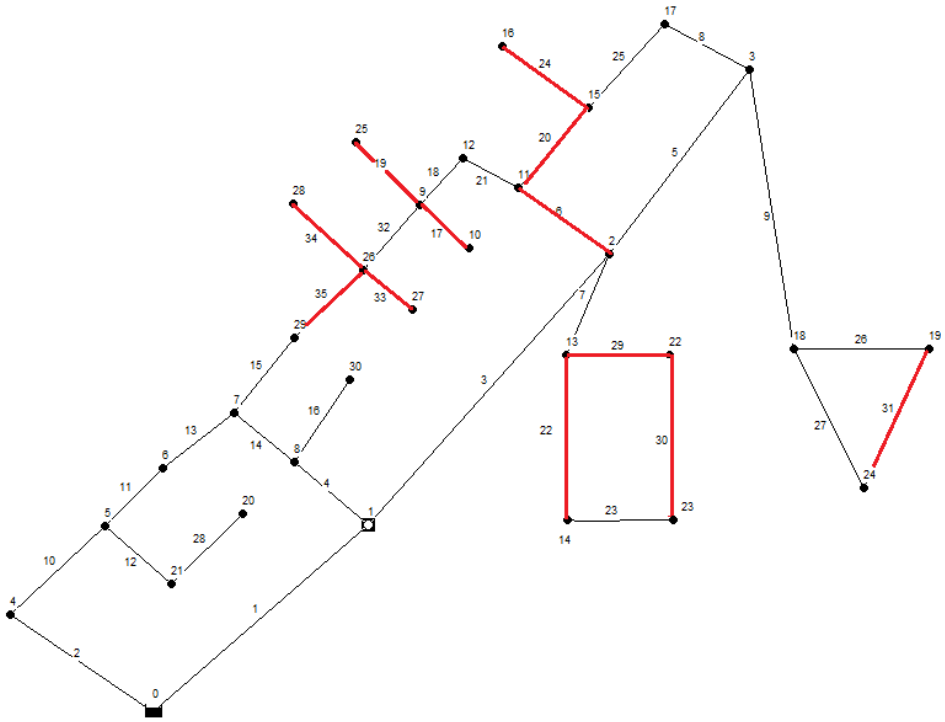


**Figure 2. The layout of the Blacksburg network (BLN)**

The complete nodal and commercially available diameters details for BLN are tabulated in Table 1 and is available in the centre of water system (CWS), benchmark problems, University of Exeter. In the present study, instead of taking the reservoir head as 659.28 m (as presented in CWS), it is considered as 715.56 m due to the insufficiency of head available for the demand delivery.

## 3. Results and Discussion

All six GA variants formulated in the present study are validated using BLN. Each of the six models is run for 50 trials and the performance reported by each model in each trial is recorded. It is observed that all the variants of GA are successful in converging to the possible minimum feasible design cost for BLN. The results are presented in Table 2. Here it is interesting to note that except for elitist and non-elitist models using the Roulette wheel method of selection, every other model is successful in converging to the best feasible optimal design cost of $ 59027 which is consistent with the previous studies. Whereas the models with the Roulette wheel method of selection are successful in

converging to a slightly higher design cost, yet the feasible ones as shown in Figure 3 and reported in Table 2. Figure 2 presents the bar chart comparing the minimum and average functional evaluations for all the GA variants formulated in the present study.

The details of the head available at every demand node of BLN corresponding to the optimal design cost obtained using the GA variants are reported in Table 3. It is observed that the pressure head available at the demand nodes meets the design criteria and lies within the minimum and maximum required pressure head ranges as presented in Table 1.

**Table 1. Nodal details and commercially available diameter set for BLN**

| Node Details | | | | Commercially available set of diameters | |
|---|---|---|---|---|---|
| **Node no** | **Demand (GPM)** | **Hmin (m)** | **Hmax (m)** | **Dia. (mm)** | **cost ($/m)** |
| 1 | 52.11 | 30.00 | 62.99 | 25.4 | 0.52 |
| 2 | 50.58 | 30.00 | 65.73 | 50.8 | 2.1 |
| 3 | 25.77 | 30.00 | 69.09 | 76.2 | 4.72 |
| 4 | 13.84 | 30.00 | 59.18 | 101.6 | 8.4 |
| 5 | 53.65 | 30.00 | 62.84 | 152.4 | 18.9 |
| 6 | 51.73 | 30.00 | 66.65 | 203.2 | 33.6 |
| 7 | 200.58 | 30.00 | 67.26 | 254 | 52.5 |
| 8 | 11.35 | 30.00 | 67.26 | 304.8 | 75.59 |
| 9 | 10.77 | 30.00 | 72.59 | 355.6 | 102.89 |
| 10 | 52.11 | 30.00 | 69.09 | 406.4 | 134.39 |
| 11 | 100.77 | 30.00 | 63.60 | 457.2 | 170.09 |
| 12 | 27.11 | 30.00 | 72.44 | 508 | 209.98 |
| 13 | 100.77 | 30.00 | 64.36 | 558.8 | 254.08 |
| 14 | 25.77 | 30.00 | 62.38 | 609.6 | 302.37 |
| 15 | 51.54 | 30.00 | 61.92 | | |
| 16 | 52.11 | 30.00 | 60.55 | | |
| 17 | 10.38 | 30.00 | 72.74 | | |
| 18 | 103.65 | 30.00 | 62.08 | | |
| 19 | 52.11 | 30.00 | 60.40 | | |
| 20 | 10.96 | 30.00 | 63.29 | | |
| 21 | 51.35 | 30.00 | 62.84 | | |
| 22 | 11.73 | 30.00 | 62.08 | | |
| 23 | 51.54 | 30.00 | 58.27 | | |
| 24 | 102.50 | 30.00 | 51.71 | | |
| 25 | 51.54 | 30.00 | 70.00 | | |
| 26 | 52.50 | 30.00 | 75.64 | | |
| 27 | 50.96 | 30.00 | 74.88 | | |
| 28 | 25.58 | 30.00 | 75.94 | | |
| 29 | 41.92 | 30.00 | 69.39 | | |
| 30 | 51.35 | 30.00 | 68.48 | | |

The computational results in terms of minimum and average computational evaluations are presented in Table 4. It is observed that the GA-1 model is successful in converging to an optimal design cost of $ 59027 at 129th generation requiring a minimum functional evaluation of 12900. Next to GA-1, the GA-2 model converged faster requiring a minimum of 14600 functional evaluations. GA-3 and its elitist model, EGA-3, failed in converging to the optimal solution of $ 59027. These two models converged to a sub-optimal cost of $ 59952. When elitist models are considered, EGA-I is successful in converging to an optimal cost with less computational evaluations. However, when comparing the EGA models with GA models, it is observed that EGA models required more functional evaluations for convergence.

**Table 2. The optimal diameter set for BLN using GA variants**

| Pipe No | Length (m) | Dia. (mm) | | | | | |
|---|---|---|---|---|---|---|---|
| | | GA1 | EGA1 | GA2 | EGA2 | GA3 | EGA3 |
| 1 | 415.44 | 203.2 | 203.2 | 203.2 | 203.2 | 254 | 254 |
| 2 | 59.13 | 152.4 | 152.4 | 152.4 | 152.4 | 25.4 | 76.2 |
| 3 | 558.4 | 203.2 | 203.2 | 203.2 | 203.2 | 203.2 | 203.2 |
| 4 | 46.02 | 50.8 | 50.8 | 50.8 | 50.8 | 152.4 | 101.6 |
| 5 | 270.66 | 152.4 | 152.4 | 152.4 | 152.4 | 152.4 | 152.4 |
| 6 | 47.24 | 76.2 | 76.2 | 76.2 | 76.2 | 76.2 | 76.2 |
| 7 | 94.18 | 76.2 | 76.2 | 76.2 | 76.2 | 76.2 | 76.2 |
| 8 | 213.06 | 25.4 | 25.4 | 25.4 | 25.4 | 25.4 | 25.4 |
| 9 | 350.83 | 152.4 | 152.4 | 152.4 | 152.4 | 152.4 | 152.4 |
| 10 | 334.67 | 152.4 | 152.4 | 152.4 | 152.4 | 25.4 | 76.2 |
| 11 | 176.17 | 152.4 | 152.4 | 152.4 | 152.4 | 76.2 | 25.4 |
| 13 | 28.96 | 101.6 | 101.6 | 101.6 | 101.6 | 76.2 | 50.8 |
| 14 | 127.71 | 25.4 | 25.4 | 25.4 | 25.4 | 152.4 | 152.4 |
| 15 | 63.4 | 101.6 | 101.6 | 101.6 | 101.6 | 76.2 | 101.6 |
| 16 | 33.53 | 50.8 | 50.8 | 50.8 | 50.8 | 50.8 | 50.8 |
| 18 | 17.98 | 25.4 | 25.4 | 25.4 | 25.4 | 50.8 | 25.4 |
| 21 | 250.85 | 25.4 | 25.4 | 25.4 | 25.4 | 25.4 | 25.4 |
| 23 | 116.43 | 25.4 | 25.4 | 25.4 | 25.4 | 25.4 | 25.4 |
| 25 | 307.54 | 25.4 | 25.4 | 25.4 | 25.4 | 25.4 | 25.4 |
| 26 | 124.36 | 101.6 | 101.6 | 101.6 | 101.6 | 101.6 | 101.6 |
| 27 | 359.97 | 25.4 | 25.4 | 25.4 | 25.4 | 25.4 | 25.4 |
| 28 | 34.44 | 25.4 | 25.4 | 25.4 | 25.4 | 25.4 | 25.4 |
| 32 | 82.6 | 76.2 | 76.2 | 76.2 | 76.2 | 76.2 | 76.2 |
| **Cost ($)** | **59027** | **59027** | **59027** | **59027** | **59027** | **59952** | **60512** |

**Table 3 Nodal heads corresponding to the optimal designs of GA variants**

| Nodes | H (m) | | | | | |
|---|---|---|---|---|---|---|
| | GA1 | EGA1 | GA2 | EGA2 | GA3 | EGA3 |
| 1 | 56.14 | 56.14 | 56.14 | 56.14 | 56.45 | 57.34 |
| 2 | 51.96 | 51.96 | 51.96 | 51.96 | 52.29 | 53.17 |
| 3 | 52.96 | 52.96 | 52.96 | 52.96 | 53.29 | 54.17 |
| 4 | 56.71 | 56.71 | 56.71 | 56.71 | 41.25 | 55.61 |
| 5 | 46.98 | 46.98 | 46.98 | 46.98 | 38.65 | 42.80 |
| 6 | 45.85 | 45.85 | 45.85 | 45.85 | 50.14 | 43.83 |
| 7 | 41.59 | 41.59 | 41.59 | 41.59 | 53.30 | 46.34 |
| 8 | 53.96 | 53.96 | 53.96 | 53.96 | 58.51 | 50.00 |
| 9 | 36.11 | 36.11 | 36.11 | 36.11 | 34.48 | 40.78 |
| 10 | 32.56 | 32.56 | 32.56 | 32.56 | 30.93 | 37.24 |
| 11 | 42.80 | 42.80 | 42.80 | 42.80 | 43.18 | 44.05 |
| 12 | 30.26 | 30.26 | 30.26 | 30.26 | 34.12 | 34.52 |
| 13 | 39.66 | 39.66 | 39.66 | 39.66 | 39.99 | 40.87 |
| 14 | 37.68 | 37.68 | 37.68 | 37.68 | 38.00 | 38.89 |
| 15 | 41.28 | 41.28 | 41.28 | 41.28 | 41.65 | 42.53 |
| 16 | 39.74 | 39.74 | 39.74 | 39.74 | 40.12 | 40.99 |
| 17 | 46.55 | 46.55 | 46.55 | 46.55 | 46.90 | 47.78 |
| 18 | 43.49 | 43.49 | 43.49 | 43.49 | 43.82 | 44.70 |
| 19 | 39.45 | 39.45 | 39.45 | 39.45 | 39.78 | 40.66 |
| 20 | 43.08 | 43.08 | 43.08 | 43.08 | 34.75 | 38.90 |
| 21 | 46.88 | 46.88 | 46.88 | 46.88 | 38.56 | 42.71 |
| 22 | 37.28 | 37.28 | 37.28 | 37.28 | 37.60 | 38.48 |
| 23 | 33.43 | 33.43 | 33.43 | 33.43 | 33.76 | 34.64 |
| 24 | 30.40 | 30.40 | 30.40 | 30.40 | 30.73 | 31.61 |
| 25 | 33.48 | 33.48 | 33.48 | 33.48 | 31.84 | 38.15 |
| 26 | 44.07 | 44.07 | 44.07 | 44.07 | 42.49 | 48.79 |
| 27 | 43.28 | 43.28 | 43.28 | 43.28 | 41.70 | 48.00 |
| 28 | 44.37 | 44.37 | 44.37 | 44.37 | 42.79 | 49.09 |
| 29 | 39.41 | 39.41 | 39.41 | 39.41 | 37.84 | 44.14 |
| 30 | 52.69 | 52.69 | 52.69 | 52.69 | 57.24 | 48.73 |

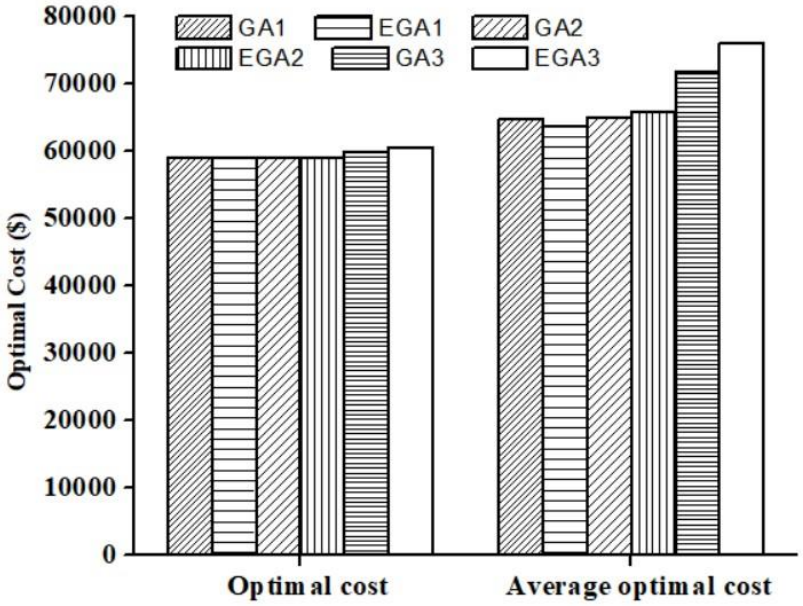



**Figure 3. Optimal and average optimal cost obtained for BLN with all the variants of GA**

**Table 4. Computational results of GA variants**

| Methods | Optimal cost obtained ($) | Generation number | Minimum number of function evaluations | No. of times optimal solution obtained in 50 trials | Percentage of the solution space explored |
|---|---|---|---|---|---|
| GA1 | 59027 | 129 | 12900 | 1 | 5.61882E-21 |
| EGA1 | 59027 | 249 | 24900 | 3 | 1.08456E-20 |
| GA2 | 59027 | 146 | 14600 | 2 | 6.35928E-21 |
| EGA2 | 59027 | 357 | 35700 | 2 | 1.55497E-20 |
| GA3 | 59952 | 715 | 71500 | 0 | 3.11431E-20 |
| EGA3 | 59952 | 705 | 70500 | 0 | 3.07075E-20 |

## 4. Conclusions

In the present study, three GA variants with different selection mechanisms, Truncation, Tournament, and Roulette wheel method of selection are formulated. In addition to these models, by incorporating the elitism operator, three more GA models, thus, in total, six variants of GA are formulated. To validate their performance, these models are used for optimally designing BLN. From the results, it is observed

that except for GA models with the Roulette wheel method of selection, remaining all models are successful in converging to the optimal design cost of $ 59027. And the GA model with the Truncation method excelled in converging to this optimal cost with less functional evaluations, followed by the GA model with the Tournament method selection. And also, it is observed that elitist models are less computationally efficient when compared to the non-elitist models. Overall, when the success rate, i.e., the number of successful trials out of 50 trials is considered, it is observed that the maximum success rate is six and that is with EGA-II. This indicates that the GA variants developed are not that robust. The plausible reason for this can be the imbalance between the exploration and exploitation features of GA. Therefore, based on the computational results, the present study, suggests any improvement given improving the exploration capabilities of GA is most futuristic.

## References

Alperovits, E., and Shamir, U. (1977). Design of optimal water distribution systems. *Water Resources Research*, 13(6), 885–900.

Blum, C., and Roli, A. (2003). Metaheuristics in Combinatorial Optimization: Overview and Conceptual Comparison. *ACM Computing Surveys*, 35(3): 268–308.

Hancock, P., J., B. (1997). Selection: A Comparison of Selection Mechanisms. *Handbook of Evolutionary Computation*, In T. Back, D.B. Fogel, and Z. ¨ Michalewicz (eds.), Bristol and New York: Institute of Physics Publishing and Oxford University Press, 212-227.

Hingee, K., and Hutter, M. (2008). Equivalence of probabilistic tournament and polynomial ranking selection. *Neural and Evolutionary Computing, Proceedings of 2008 Congress of Evolutionary Computations, CEC 2008*, 564-571.

Rossman, L. A. (2000). EPANET 2 Users Manual. *US Environmental Protection Agency*, Washington, D. C., USA, EPA/600/R-00/057.

Sherali, H., Subramanian, S., and Loganathan, G. V. (2001). Effective relaxations and partitioning schemes for solving water distribution network design problems to global optimality. *Journal of Global Optimization*, 19(1), 1–26.

Simpson, A. R., Dandy, G. C., and Murphy, L. J. (1994). Genetic algorithms compared to other techniques for pipe optimization. *Journal of Water Resources Planning and Management*, 120(4), 423–443.

Yates, D. F., Templeman, A. B. & Boffey, T. B. (1984). The computational complexity of the problem of determining least capital cost designs for water supply networks. *Engineering Optimization*, 7 (2), 143–155.

*IN PROCEEDINGS OF 25th HYDRO 2020, INTERNATIONAL CONFERENCE, NATIONAL INSTITUTE OF TECHNOLOGY ROURKELA, ODISHA, INDIA 26-28, March 2021, ISBN 978-93-90631-56-8*

Paper ID - 292

# Water Urbanism: Strategies for stormwater management through rainfall-runoff analysis using SCS-CN method and GIS in watersheds of Ajmer, Rajasthan

Aspruha Swain[1], Prof. Ashwani Kumar[2]

[1]*Student, Masters in Urban Planning, CEPT University, Ahmedabad 380009, India*
[2]*Associate Professor, Faculty of Planning, CEPT University, Navrangpura, Ahmedabad 380009, India*
*Email: aaspruhaa@gmail.com*
*Telephone/Mobile No.: +91 7978124865*

## Abstract

The ancient settlements grew ensuring the concerns of the regional water systems since beginning of human civilization. In recent times the cities expanded through planning mechanisms like Development Plans, that accommodates rapid growth of population and economic needs often ignoring the hydrological dynamics of the region. As a result, water scarcity or urban flooding are the most common impacts of urbanization and land use changes being observed in and around the cities. As the cities are expanding, there is continuous pressure on water resources.

In the context of water scarce regions, the efficient system for water harvesting, storage, use conservation, management and regulation systems are necessary for survival and growth of the cities. Many traditional Indian cities including Jaipur, Jodhpur, Ajmer, Bundi etc. during the medieval times demonstrate the use of efficient water management methods at city scale. In-spite of the rich history of water management, with the current demographic, urbanization trends and loss of local water sources, scarcity of water; can have disrupting influence on their economic growth, social harmony, and liveability. Thus, it is essential to find strategies to ensure that the cities are resilient to the challenges of water scarcity, droughts and floods; making the transitioning of cities more urgent. The current Global concepts of Water-sensitive Urban Design (WSUD), Sustainable Drainage Systems (SuDS), Green Infrastructure (GI), Integrated Urban water Management (IUWM) etc. are being taken up by many Indian cities at various levels to conserve, preserve and manage their water resources through planning.

This study attempts to demonstrate strategies for stormwater management through rainfall-runoff analysis based on the natural water regime especially for the cities falling in the water scarce region. The city of Ajmer, falls under the water-scarce region of Rajasthan, to the east of Aravalli ranges, receiving unpredictable rainfall. It also faces challenges of water shortage and urban flooding. The total area covered for the study is 767 sq.km, which falls within three river basins, such as, Sekhawati river basin in the north, Luni river basin in the west and Banas in the east. Six watersheds are identified within the study area using DEM file from USGS website in ArcGIS and the widely used method of surface runoff, i.e., SCS-CN is applied to calculate the watershed-wise surface runoff volume. Finally, strategies are identified for every watershed to conserve as well as preserve the surface water-runoff for fulfilling the non-domestic needs of water in the city.

***Keywords:*** *urbanization; water-scarce regions; rainfall-runoff analysis; stormwater management; hydrologic modelling*

## 1. Introduction

Land use and climate are two key factors that directly affect catchment hydrology, and the segregation of their impact is crucial for land use planning and water resource management (Li, Liu, Zhang, & Zheng, 2009). Researchers have explored the connection between land use and hydrology to understand the natural hydrological system (Leopold, 1968)(Dwarakish & Ganasri, 2015)(Wijesekara et al., 2012). Thus, any type of land use directly affects the use of water in a given area and, consequently, the hydrology of that area (Moors & Dolman, 2003). These studies express the knowledge in terms that a planner can use to test alternatives during planning process.

Planning according to the watersheds of an area can prove to be very crucial to eliminate the different water-related problems including water as resource as well as service. Urban planning based on watersheds is an effective acknowledgement of the watershed as a system that refers to anything that

occurs within it, directly or indirectly affects the quality of the rivers and the quality of the water, and thus affects all the other elements that constitute this system (Schussel & Nascimento Neto, 2015). A watershed is defined as a land area that drains all the streams and precipitation to a common source. With the increasing urbanization, there is also the increase in water stress. Effective stormwater management can prove to be useful in adding up to one of the sources of water supply for the urban areas in the upcoming years.

The understanding of rainfall and runoff is essential for evaluation of surface water availability as these are the significant contributors to the surface water resources as well as groundwater recharge. There are many methods offered for the rainfall-runoff modelling. The SCS-CN method, developed by US Soil Conservation Services (SCS) in 1969, is a simple, reliable and consistent perceptual method for estimating the direct runoff depth based on the intensity of storm precipitation (Subramanya, 2009). Many researchers have used the GIS-based SCS-CN method for estimating the runoff in the watersheds of South Indian districts like Pappiredipatti watershed of the Vaniyar sub basin (Satheeshkumar, Venkateswaran, & Kannan, 2017); Nilgries District, Tamilnadu (Viji, Prasanna, & Ilangovan, 2015)etc. The Rainfall-Runoff analysis by the globally accepted SCS-CN (Soil Conservation Service-Curve Number) method gives us the watershed-wise runoff as well as runoff volume for estimating the required measures to be taken at city level to achieve water sensitivity.

### 1.1 *Rationale for the study and selection of study area:*

The arid regions especially have the highest potential of being in drier conditions with the rapid urbanization. Thus, managing their water sector is more crucial for it's present as well as future development. The main purpose of undertaking this research is to investigate into the possibilities of managing the stormwater through various strategies in the arid regions that can help in preventing the urban flooding occurrences due to unpredictable rainfall and also add up to one of the sources of water supply to the water-scarce cities of these regions.

According to the Köppen's climate classification, the majority of Rajasthan comes under the Hot Desert (BWh) and the remainder of the state comes under the Hot Semi-Arid (BSh); so, the state climate varies from arid to semi-arid. Research have shown that Rajasthan is among regions with the highest vulnerability to climate and the lowest potential for adaptation (Hooda, 2013).

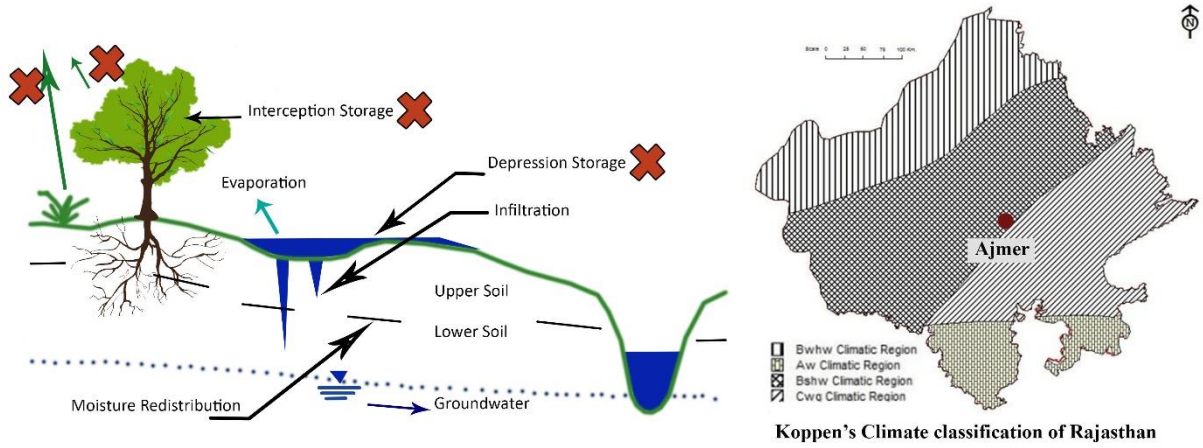



**Figure 1 (a)** Conceptual diagram of arid zone hydrology **(b)** Koppen's climate classification for Rajasthan; Source: ("Climatic Regions of Rajasthan | RajRAS - Rajasthan RAS," n.d.)

The city of Ajmer, falls in the borderline of arid as well as semi-arid region of Rajasthan, facing increasing variation in the intensity and frequency of temperature and rainfall that has affected the city's water availability (TERI, 2010). Moreover, Ajmer being selected among one of cities under the Smart city Mission of the Government of India, has been attracting investments in water resource sector, making the city suitable as a case for the study.

## 1.2 *Description of the Study area*

Ajmer is situated in the core of Rajasthan, upon the crib of Aravalli mountain range ("India Smart Cities," n.d.). It is surrounded by three hills of Aravalli Ranges i.e. Nag hills, Madar hills and Taragarh hills located at average 486.0 MSL. In the northwest direction, Anasagar forms the natural boundary. Area of the ADA limits (Study area) is 767.24 sq.km; with a population of 2,52,332 (excluding AMC). AMC limits (City area) measures to 88.90 sq.km; with a population of 5,42,321 (DCH Census, 2011). Ajmer is a low-density city with an inner center of very high density, with population density of around 50,000 people/ sq.km, while the City's gross average density is 5,750 people/sq.km. There were 45 wards in Ajmer in 1991 but in 1995 the wards were increased to 55 and the population of 45 wards was redistributed to 55 wards, which was again redistributed into 60 wards in 2019 (Price Water Coopers, 2009).

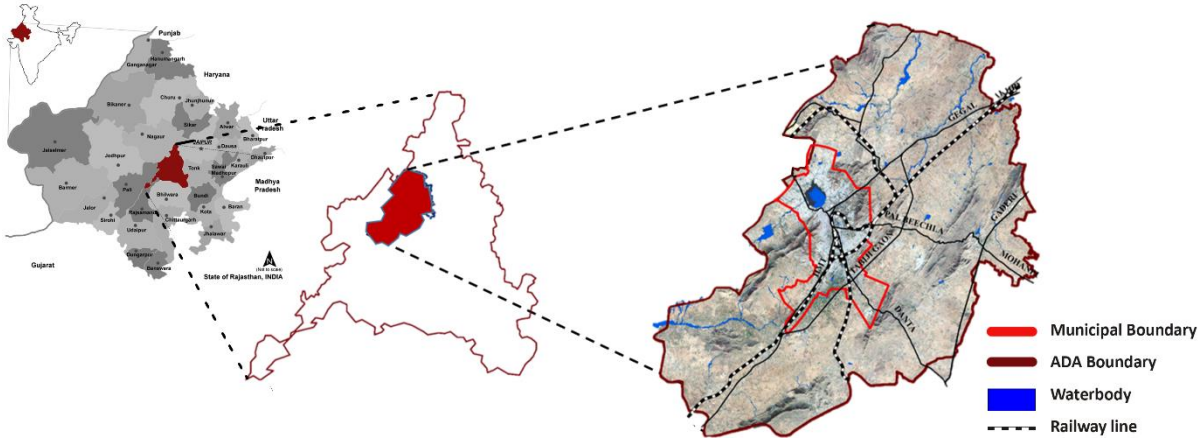



**Figure 2** Location of the study area generated by Author in ArcGIS with the data collected from "ADA (Ajmer Development Authority)".

## 1.3 *Methods and Data collection*

**Topography:**
The city resides upon higher elevation ranging from 322 to 837 meters above mean sea level (Figure:3). Thus, the rainwater flows away from the city and the accumulation is very low. The rain that falls on Nashirabad side, finds it's way through Chambal into Bay of Bengal and the rain of other side (west of Aravalli hills) is discharged from Luni river to Gulf of Kutch.

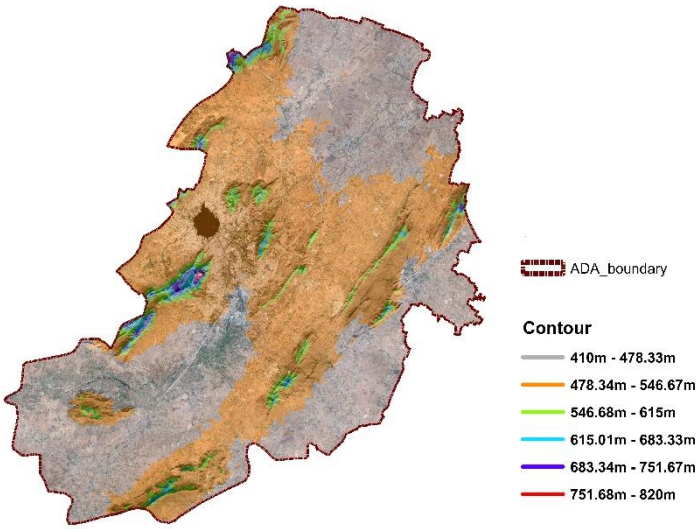



**Figure 3** Topography and contour; DEM data obtained from USGS website and generated in ArcGIS by Author

**Climate:**
The climate data has been collected from the Irrigation Department of Ajmer. Ajmer enjoys relatively moderate climate in the state with average humidity is 57 percent and daily temperature ranging from 26.90 degree C to 39.40 degree C during May, while 7.60 degree C to 22.50 degree C during January, the coldest month ("India Smart Cities," n.d.). It has mean annual rainfall of 558.63mm recorded between the years 1973 to 2018 (data assembled from water.rajasthan.gov.in). The rainfall in the region is very erratic.

The city recorded maximum rainfall of 1200.4mm in 1975 leading to severe floods. The recent flooding was recorded in 2019 by the Central flood cell of Rajasthan.

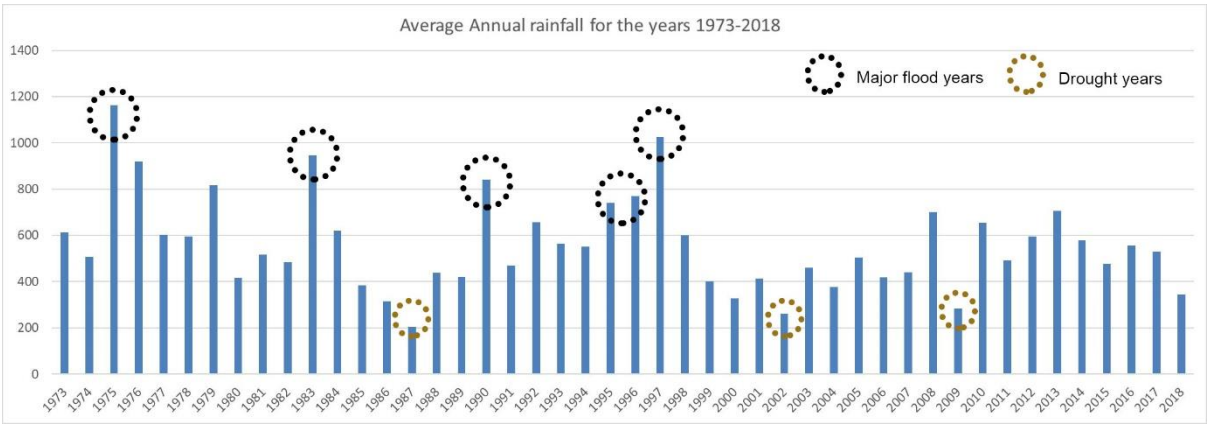



**Figure 4** Rainfall Data from the year 1973 to 2018; Data collected from "water.rajasthan.gov.in", generated by Author

There are three raingauge stations located within the ADA limits and three just outside the limits, from which the Pisangan and Gegal stations receive higher annual rainfall than other stations. The annual rainfall considered for the calculation are: average annual rainfall values of the four rain-gauge stations namely, Pisangan, Ajmer, Gegal, and Shreenagar falling within ADA limits. Meterologically, drought classification is based on the deficiency of rainfall, i.e., 25% or less is normal, 25%-50% is moderate and more than 50% is considered as severe drought condition. The city faces drought like situations every four years and according to the officials the water supply during those years are catered through government aided and private tankers. According to the notion, 2021 is predicted to be a drought year for the city, so it is necessary to preserve the incoming surface-runoff during the rains, where there has been seen erratic flash floods since 2008 in the city. The stormwater water can thus be added to one of the source of water supply for the city.

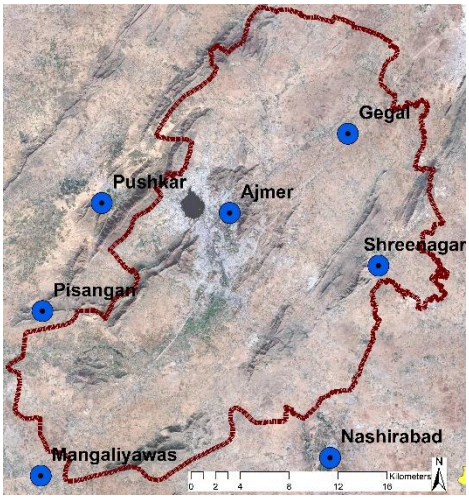



**Figure 5** Rain-gauge stations (Source: "water.rajasthan.gov.in") in and around the ADA limits, mapped in ArcGIS.

**City's available water resource:**

Out of all the lakes and streams, only Anasagar lake and Foysagar lake are the major water storage lakes of the city. Anasagar serves as wastewater lake, while the foysagar lake stores water during the rains. Currently, all the water needs of the city are met by the water drawn from the Bisalpur dam, situated 115 kms away to the southeast of Ajmer city.

**Delineating the watersheds within the study area:**

To estimate the total runoff volume available for the study area, stream network and watersheds are identified within the area with the DEM file available in USGS site in ArcGIS. For this, we first identified the river basins that the streams connect to. The three river basins; Luni in the west, Sekhawati in the north and Banas in the east, fall within the ADA limits (refer Figure: 6). The Luni basin is known for it's recurrence of floods which

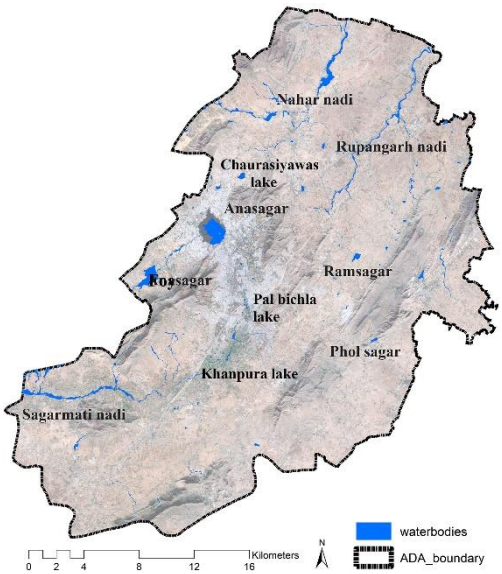



**Figure 6** Recognized waterbodies of Ajmer within the ADA limits. Source: "ADA"

has affected many cities of Rajasthan including Ajmer (1975, 1983, 1990, 1995, 1996, 1997).

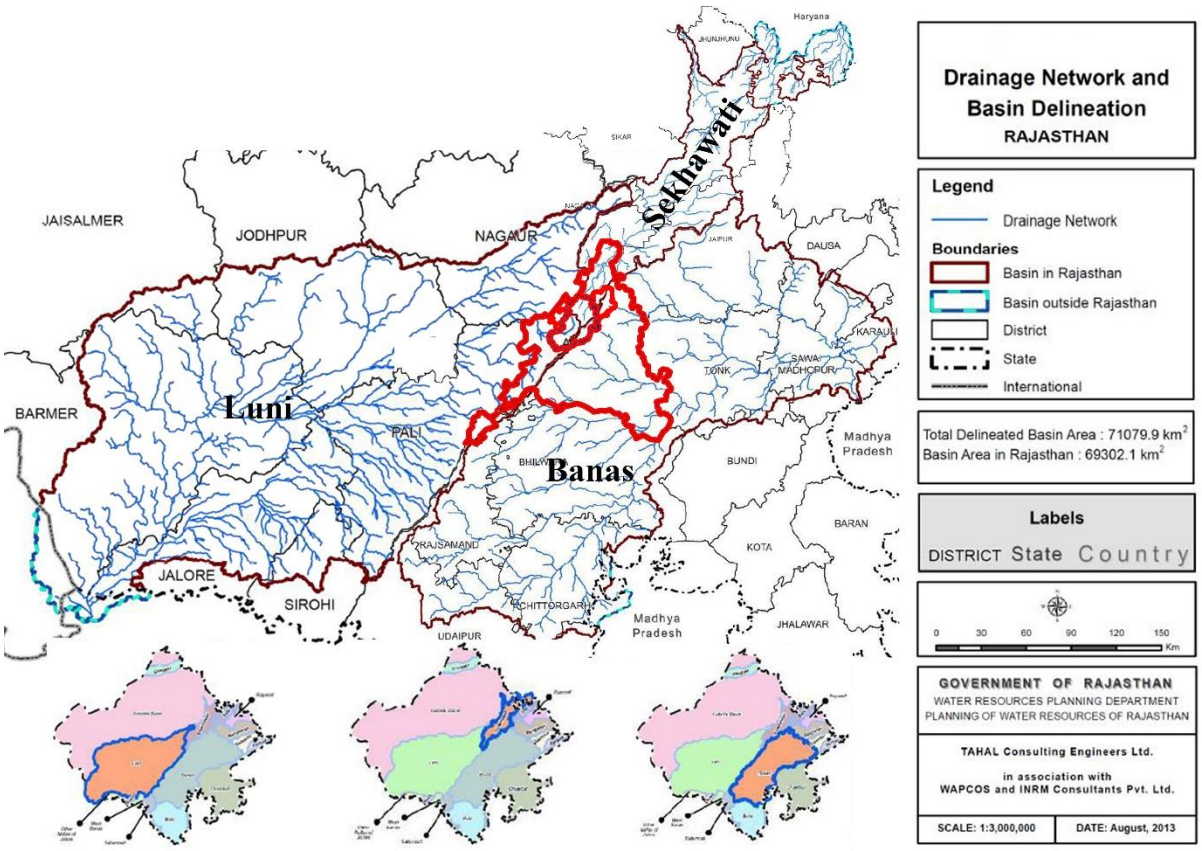



**Figure 7** River basins falling in ADA limits and Ajmer; Collated maps from the data collected.: Source: "http://water.rajasthan.gov.in/"

So, five watersheds form from the pour points (Figure: 8) taken in ArcGIS upon the 5th and 6th order streams within the ADA boundary. The areas other than these five watersheds are taken as 'Other watershed'.

Area of watersheds,
Watershed 1: **24,656.10** Ha

Watershed 2: **9,110.94** Ha

Watershed 3: **17,049.65** Ha

Watershed 4: **6,836.19** Ha

Watershed 5: **5,263.30** Ha

Other watershed: **13,808.24** Ha

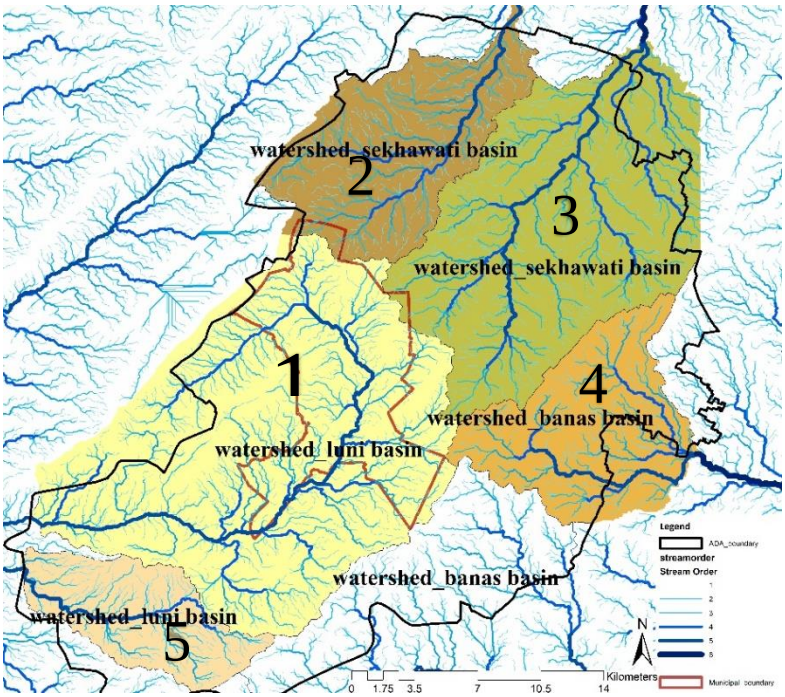



**Figure 8** Watershed delineation-DEM file from USGS site; map generation in ArcGIS by author

**Land Use / Land Cover Database for Dissemination through Bhuvan:**

The geo-spatial database on "Land Use/ Land Cover (Third Cycle) in 1:50,000 scale" is prepared using three season Resourcesat-2 ortho rectified LISS-III data of 2015-16. Entire database is prepared by NRSC, ISRO under Natural Resources Census (NRC) Project of National Natural Resources Repository (NRR) Programme with the participation of 29 State Remote Sensing Centers spread over entire country. The webmail services in the bhuvan website is extracted through QGIS software to convert the link to GeoTiff file for delineation of the land uses. The website contains the land-uses of years 2005-06, 2011-12 and 2015-16. For this study, the 2015-16 land-use data has been used for calculation.

*'Wms link used for 2015-16 LULC (Bhuvan website):*
*URL - "https://bhuvan-vec2.nrsc.gov.in/bhuvan/wms"*
*version - 1.1.1*
*layer - "lulc: RJ-LULC50K-1516"*

Five kinds of land uses are finalized for the map generation and further calculation. The area of each landuse within the study area calculated in ArcGIS is as follows:

**Built**: 7424.12 Ha

**Wasteland**: 12451.27 Ha

**Waterbody** (river/stream): 2193.16 Ha

**Agriculture**: 41152.55 Ha

**Forest**: 13503.33 Ha

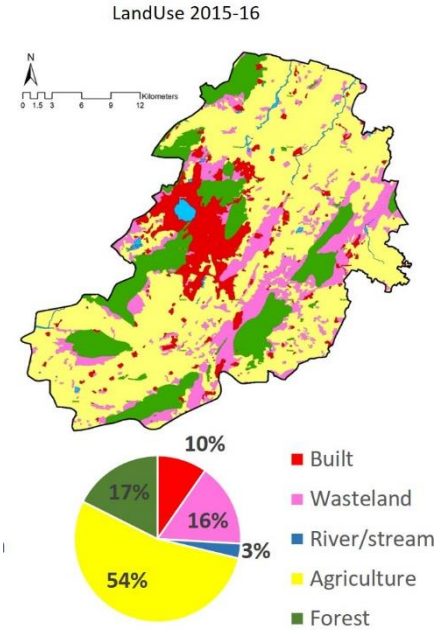



**Figure 9** LandUse 2015-16 map with percentage distribution pie chart

**Soil Characteristics:**

The study area has the aquifer systems as Alluvium, Schist and Genesis. The soil texture types of the study area include fine loam, course loam and loamy skeletal; which fall under the hydrological soil group of Sandy loam and loam. The map in Figure: 10 shows various soil types within ADA limits.

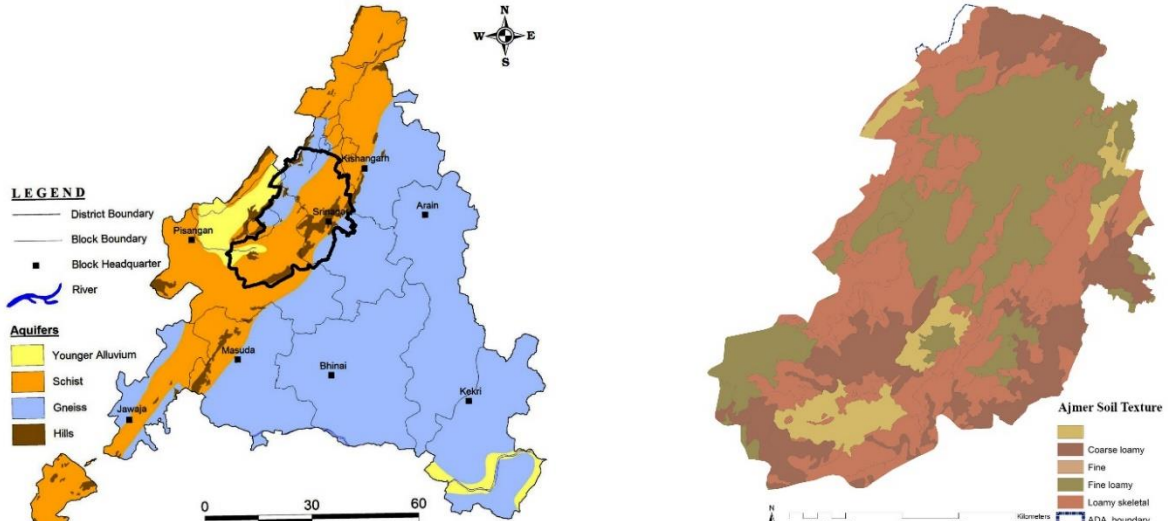



**Figure 10** Aquifer system and soil texture characteristics within the study area. Source: "WD&SC, Ajmer"

## 2. SCS-CN Model

The SCS-CN method, developed by US Soil Conservation Services (SCS) in 1969, is a basic, accurate and consistent procedural method for estimating the direct runoff depth based on the intensity of storm precipitation. It depends on only one parameter, CN. It is currently a well-established process, widely accepted for use in the USA and in many other countries (Subramanya, 2009). The SCS-CN approach is based on the equation of the rainfall's water balance over a defined time interval.

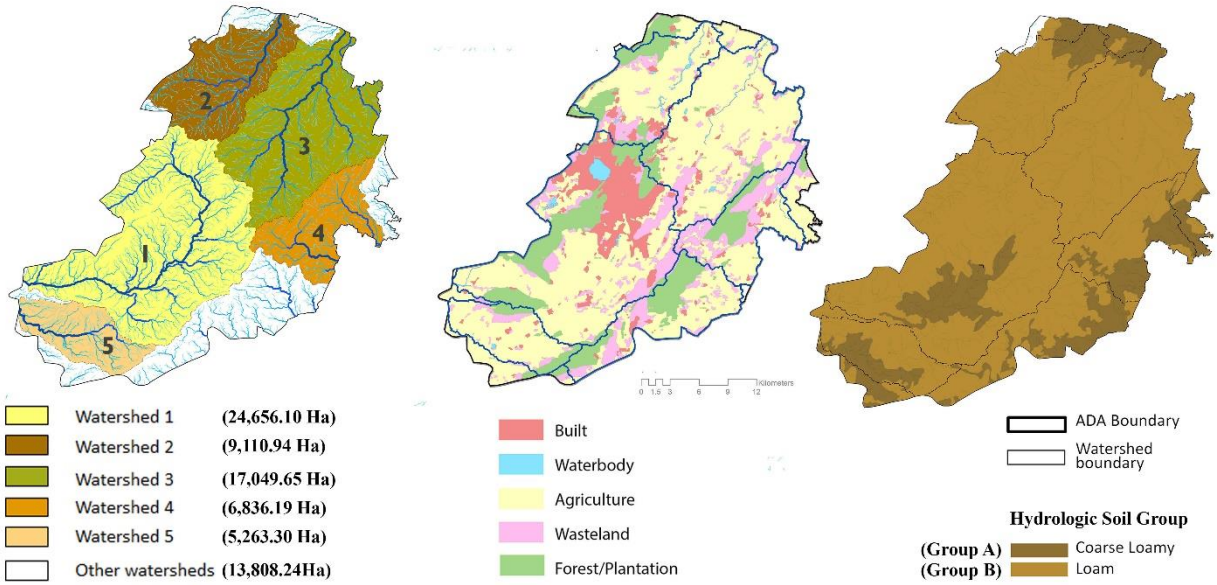



**Figure 11** Maps according to the parameters needed for SCS-CN method of runoff calculation ((a)Watersheds, (b) Landuse & (c) Hydrological soil group); generated by Author in ArcGIS.

The various steps are involved in the following manner as follows:

The Land-cover map is obtained from the Bhuvan web map services, and soil types from the Watershed development and soil conservation department of Ajmer, Digital Elevation model (DEM) derived from USGS website and Rainfall data collected 1973-2018 from the link provided by the Irrigation department of Ajmer. The various steps are involved to define the watershed boundary and catchment area, for which Curve number is calculated. The soil types collected from WD and SC department are converted to hydrological soil groups like A and B, according to their infiltration capacity (data collected from Groundwater Department (GWD) of Ajmer). Superimposing the landuse map (refer Figure:11) on the hydrologic soil groups maps, catchment-wise landuse percentages are calculated through polygons in ArcGIS for each soil type. Finally, the curve number is assigned to each landuse.

*CURVE NUMBER (CN):* The parameter S representing the potential maximum retention depends on the catchment's soil-vegetation-land use complex and also on the preceding soil moisture condition in the catchment just before the rainfall event commences. For convenience, the US Soil Conservation Services (SCS) expressed S (in mm) in terms of the dimensional parameter CN (the curve number) in functional application (Raju R., Raju G., & M., 2018). This CN curve number depends on:

- Soil type
- Land use cover
- Antecedent Moisture condition.

For Indian condition, the form S is the potential maximum retention and it is given by,

**S = (25400/CN) - 254**,
where CN can be taken from the SCS handbook of hydrology (NEH-4), section-4 (USDA 1972). Now the equation preferred for the study area is

**Q (Gathered runoff in mm) = (P - 0.3S)$^2$ / P + 0.7S** .....for soils other than black soil

Thus, the runoff from each watershed is calculated according to the value of CN. Here, based on rate of final infiltration and runoff probability, soils are graded into four groups A, B, C and D. Soil group A and B are identified for the study area.

*ANTECEDENT MOISTURE CONDITION (AMC):* AMC is considered when the previous rainfall is small and high when the prior rainfall has been significant to the model rainfall level. AMC II in watershed is basically an average state of moisture for modeling purposes. Runoff curve numbers from LU/LC and soil type taken for normal conditions (AMC II) and dry conditions (AMC I) or wet conditions (AMC III), comparable curve numbers (CN) are calculated. Curve values recognized for AMC-II (USDA 1985), are identified for Ajmer city (according to the data collected from Ground Water Department) for calculations. Since under AMC II, CN II values are directly taken from the prescribed SCS table and soil group A and B are identified (refer Figure: 10) from the data collected (Subramanya, 2009). In SCN-CN method, Antecedent moisture condition of the soil plays a very significant role because the CN number varies according to the soil, which is considered when estimating runoff depth.

**Table 1** Table on Hydrological Soil groups as distinguished by SCS-CN Method and highlighted, are the ones used for the study area. The values considered for the study are obtained from "WD&SC, Ajmer".

| Hydrological Soil Group | Group | Infiltration Rate (mm/hr) | Soil Texture |
|---|---|---|---|
| | **A** | **High >25** | **Sand, Loamy sand, or Sandy loam** |
| | **B** | **Moderate 12.5-25** | **Silt loam or loam** |
| | C | Low 2.5-12.5 | Sandy clay loam |
| | D | Very Low <2.5 | Clay loam, Silty clay loam, Sandy clay, Silty clay or clay |

**Table 2** AMC classes, as distinguished by SCS-CN Method and highlighted boxes are the ones used for the study. The values considered for the study are obtained from "GWD, Ajmer".

| ANTECEDENT MOISTURE CONDITION CLASSES | AMC-Class | Dormant season(mm) | Growing Season(mm) | Condition |
|---|---|---|---|---|
| | I | < 12.7 | <35.6 | Dry soil but not the wilting point |
| | **II** | **12.7-27.9** | **35.6-53.3** | **Average conditions** |
| | III | >27.9 | >53.3 | Saturated soils, heavy rainfall or light rainfall |

For the city of Ajmer, the soil groups A and B (as mentioned in SCS-CN method) that have soil texture as sandy loam and loam respectively are related according to the soil texture data obtained from the Watershed Development and Soil Conservation Department of Ajmer. Then, The Antecedent moisture condition (AMC) of soil of the city, as per the data obtained from the Ground Water department of Ajmer, is found to be within the range of 12.7mm to 27.9mm in the dormant season and 35.6mm to 53.3mm in the growing season, which falls under the AMC - II type of the SCS-CN method. Finally, from the identified site-specific Hydrological soil groups and AMC classes tables of SCS-CN method, the landuse wise Curve Number type is finalized for the study area, i.e., CN II.

**Table 3** Runoff Curve Numbers [CN II] for hydrologic soil cover complexes [Under AMC-II Conditions] identified for the study area from the prescribed SCS table

| Land-Use | Soil Type | CN II value | Soil Type | CN II value |
|---|---|---|---|---|
| **Built** | B | 86 | A | 77 |
| **Waterbody** | B | 100 | A | 100 |
| **Agriculture** | B | 75 | A | 65 |
| **Wasteland** | B | 80 | A | 71 |
| **Forests/Plantation** | B | 40 | A | 26 |

The landuse areas are divided into watershed-wise percentages for the watershed-wise runoff calculations. According to the method, watershed-wise monthly runoff and runoff volume of the year 2015 (normal year), 2018 (dry year) and 2019 (flood year) is calculated. For the city of Ajmer, monthly runoff is calculated with monthly rainfall data of the year 2018 as well as of the year 2015 (with same landuse for both years from bhuvan) to compare the both years' runoff. As the rainfall data of 2019 is not available for the whole year, the year's rainfall calculation is done based on the fortnightly flood report of Rajasthan flood cell, which gives the days of heavy precipitation in the city that caused the flooding. The rainfall of 2019 is as per the maximum rainfall days mentioned in the fortnightly report (15 June to 15 September 2019), on 17 August (145mm), 27 and 28 July(130mm).

According to the method, the determination of the CN value for a watershed is a function of soil characteristics, hydrologic condition and cover or land use. CN values for Hydrological soil cover (Under AMC-II conditions) for Indian conditions are given. For watersheds with multiple soil types or land uses, an area-weighted CN is calculated. The calculation of the year 2018 of watershed 1 is demonstrated below to show the process of carrying out the runoff volume calculation.

**Table 4** The monthly rainfall data as collected from "water.rajasthan.gov.in and Irrigation department, Ajmer"

| | Jan | Feb | Mar | Apr | May | June | July | Aug | Sept | Oct | Nov | Dec |
|---|---|---|---|---|---|---|---|---|---|---|---|---|
| **2015 (mm)** | 15.5 | 2.6 | 50.2 | 1.0 | 0.0 | 41.0 | 178.0 | 188.0 | 2.0 | 0.0 | 0.0 | 0.0 |
| **2018 (mm)** | 0.0 | 0.0 | 0.0 | 0.0 | 0.0 | **33.0** | 98.0 | 105.2 | 107.3 | 0.0 | 0.0 | 0.0 |

Month **June**, Year **2018**
AMC II Type
For Watershed 1:

**Table 5** CN II values as per the Land-use and hydrological soil group percentages for watershed 1, calculated by Author in ArcGIS according to CN II values of SCS-CN method

| **LandUse** | **Percentage** | **Soil group B (loam)** | | | **Soil group A (Course loam)** | | |
|---|---|---|---|---|---|---|---|
| | % (Total) | % (bifurcated) | CN II | Product I | % (bifurcated) | CN II | Product II |
| **Built** | 21 | 20 | 86 | 1720 | 1 | 77 | 77 |
| **Waterbody** | 3 | 2.8 | 100 | 280 | 0.2 | 100 | 20 |
| **Agriculture** | 46 | 28 | 75 | 2100 | 18 | 65 | 1170 |
| **Wasteland** | 12 | 11 | 80 | 880 | 1 | 71 | 71 |
| **Forest** | 18 | 17 | 40 | 680 | 1 | 26 | 26 |
| Total: | **100** | | | **5660** | | | **1364** |

Monthly Rainfall: 33mm (June)
Average CN = (Product I + Product II) / 100 = 7,024/100 = 70.24
S = (25400/Avg. CN) – 254 = 107.61

Run off, Q = (((P-0.3 x S) x (P-0.3 x S)) / (P+0.7 x S)) = **0.004716 mm**, for P > 0.3s (soils other than black soil)……(1)

Area of Catchment (in Ha) : 24656.10
Thus, Runoff Volume = Area of Catchment x 10 x Q = **1162.90 Mm$^3$** ……(2)

**Table 6** Table with watershed-wise rainfall-runoff volume calculations, calculated by Author

| Year /Month | Watershed 1 (cu.mm) | Watershed 2 (cu.mm) | Watershed 3 (cu.mm) | Watershed 4 (cu.mm) | Watershed 5 (cu.mm) | Other Watersheds (cu.mm) |
|---|---|---|---|---|---|---|
| | Soil group A: 31%, rest B | Soil group A: 13%, rest B | Soil group A: 8%, rest B | Soil group A: 42%, rest B | Soil group A: 36%, rest B | Soil group A: 80%, rest B |
| **2015** | | | | | | |
| March | 630367.64 | 235989.2 | 908365.79 | 114463.01 | 74712.24 | 36161.81 |
| June | 160968.30 | 60980.77 | 382220.34 | 17995.09 | 50461.54 | 9023.5 |
| July | 20665296.7 | 7653835.6 | 16536124 | 5346422.3 | 7872322.4 | 4017766.32 |
| August | 22702857.3 | 10061809 | 18026338 | 5895577.3 | 8804796.9 | 4436303.93 |
| **Total/yr** | **44.16 Mm$^3$** | **18 Mm$^3$** | **35 Mm$^3$** | **11.37 Mm$^3$** | **16.76 Mm$^3$** | **8.53 Mm$^3$** |
| **2018** | | | | | | |
| June | 1162.90 | 559.98 | 91497.89 | - | - | - |
| July | 6142878.88 | 2279931.8 | 5590088.2 | 1489933.9 | 1696111.5 | 1093963.4 |
| August | 7261084.78 | 2693998 | 8689208.9 | 1780693 | 1584287.4 | 1312736.9 |
| Sept | 7596986.61 | 2818365 | 6730607 | 1868378.6 | 2253246 | 1378807.32 |
| **Total/yr** | **21.02 Mm$^3$** | **7.8 Mm$^3$** | **21.10 Mm$^3$** | **5.13 Mm$^3$** | **5.53 Mm$^3$** | **3.8 Mm$^3$** |

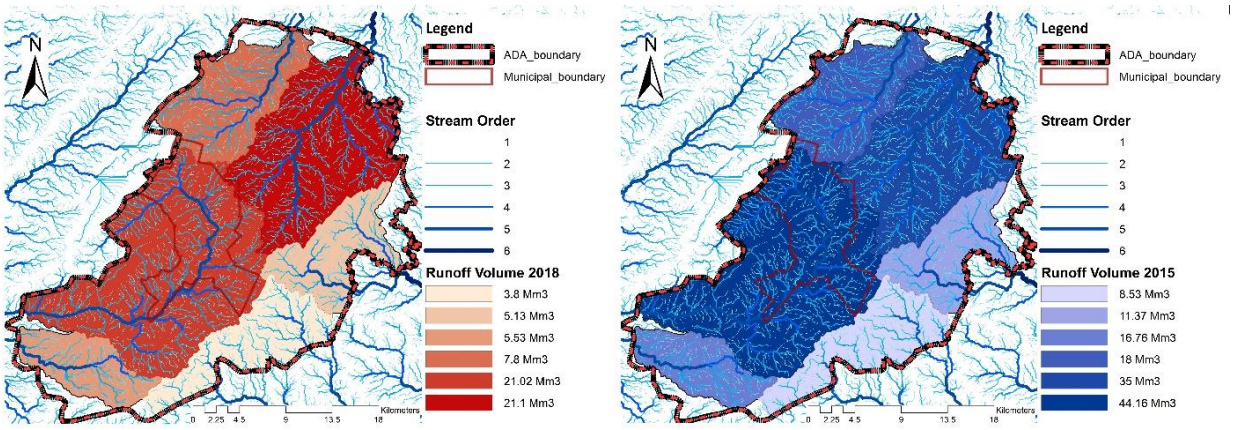



**Figure 12** Watershed-wise runoff volume map, generated in ArcGIS by Author

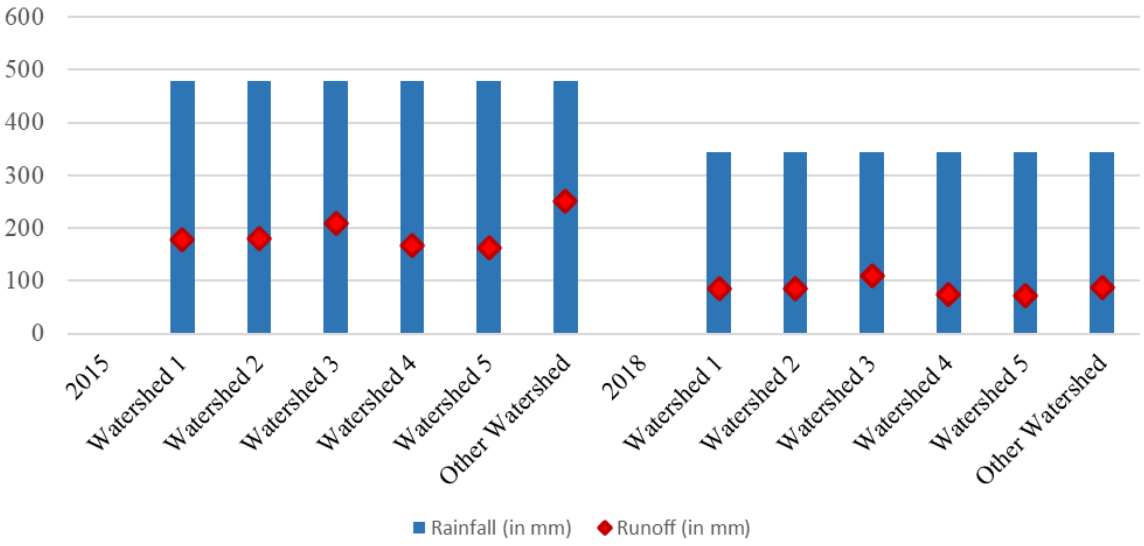
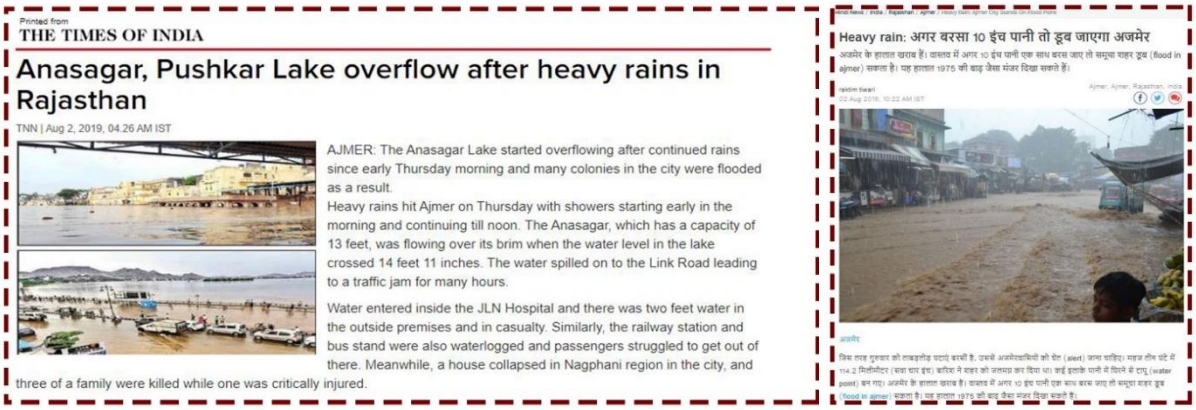



**Figure 13** Watershed-wise rainfall-runoff graph, generated by Author

The calculated monthly runoff and yearly runoff volume for 2018, comparing the values with 2015 for each watershed shows that the 1st and 3rd watersheds are recorded as the major runoff catchments of the city. Similarly, when the rainfall of 2019 is calculated as per the maximum rainfall days of the fortnightly report, on 27 and 28 July, in only two days, the runoff volume of watershed 1 came to be 22.84 Mm3. Thus, from the above rainfall-runoff analysis, the recommendations are intended to be given in the watersheds that are crucial for consideration.

## 3. Strategies Identified

For future Flash flood years: (Minimizing runoff volume through planning and managing the city according to it's watersheds).
To think of minimizing the runoff volume, it is necessary to know the quantity of water flowing or accumulating in the ADA limits during the rain. The devastation was enormous due to the flash flood in the year 2019 (Figure: 14) and hence the following measures can be taken at various levels by assessing the current scenario of encroachment and flash flood issues in ADA limits. There are few streams like Sagarmati nadi, Nahar nadi and Rupangarh nadi that flow from the ADA limits; while many artificial lakes and tanks like Anasagar (4.7 MCM), Foysagar, Phoolsagar (4.88 MCM) etc. have been built to store the rainwater as well as excess water during floods; but, those are not sufficient to prevent flash floods in the city due to low storage capacity.


Printed from
THE TIMES OF INDIA

Anasagar, Pushkar Lake overflow after heavy rains in Rajasthan

TNN | Aug 2, 2019, 04.26 AM IST

AJMER: The Anasagar Lake started overflowing after continued rains since early Thursday morning and many colonies in the city were flooded as a result.
Heavy rains hit Ajmer on Thursday with showers starting early in the morning and continuing till noon. The Anasagar, which has a capacity of 13 feet, was flowing over its brim when the water level in the lake crossed 14 feet 11 inches. The water spilled on to the Link Road leading to a traffic jam for many hours.

Water entered inside the JLN Hospital and there was two feet water in the outside premises and in casualty. Similarly, the railway station and bus stand were also waterlogged and passengers struggled to get out of there. Meanwhile, a house collapsed in Nagphani region in the city, and three of a family were killed while one was critically injured.

Heavy rain: अगर बरसा 10 इंच पानी तो डूब जाएगा अजमेर

**Figure 14** Newspaper clippings showing the intensity of the rains, resulting in flooding in the year 2019; Source: ("Ajmer records very heavy rains of 114 mm, normal life comes to a halt | Skymet Weather Services," n.d.; "Anasagar, Pushkar Lake overflow after heavy rains in Rajasthan | Jaipur News - Times of India," n.d.)

Thus, the following strategies are identified to curb the future urban flood issues:

- Additional potential areas or series of ponds/tanks in the watersheds from luni basin for harnessing the flood water in the identified watershed with maximum runoff volume (mainly watershed 1 with the whole city area within it) and the water can be used for non-potable purposes.

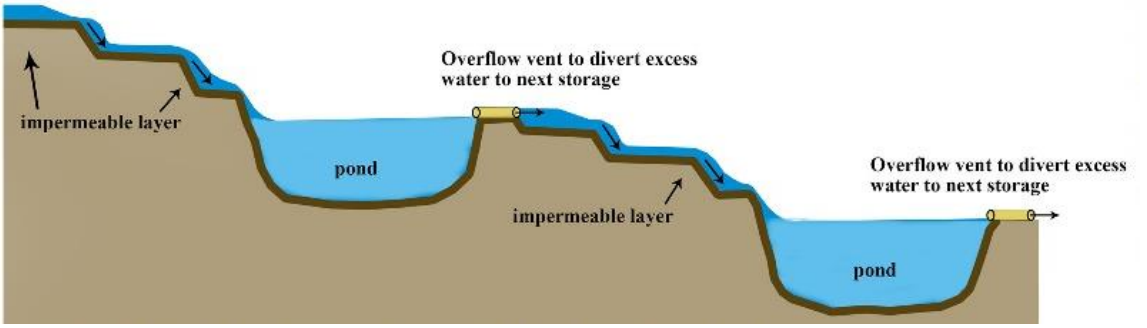



**Figure 15** Conceptual diagram of the interlinking reservoirs, drawn by Author

- The suggested locations of the various proposed wetlands or freshwater ponds or check-dams are mapped (Figure: 16). The check-dams in the watersheds can help in flood mitigation, water conservation, irrigation and soil conservation. The probable locations of check-dams is proposed according to the land-use, watersheds and topography. Since the Anasagar is already treated as wastewater lake in the city, thus constructed wetlands locations are identified in the watershed 1. Freshwater reservoirs are given in the streams other than the stream connecting the Anasagar lake.

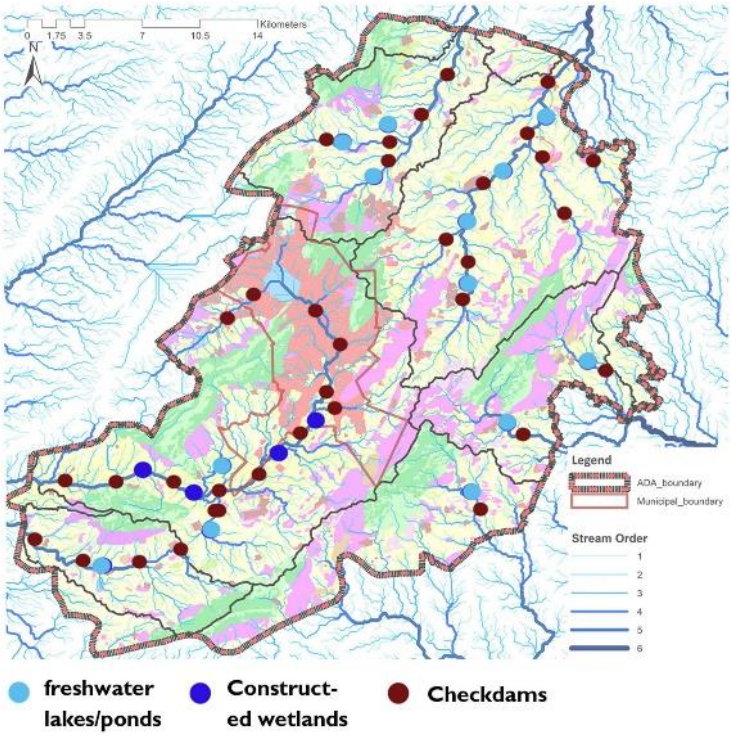



**Figure 16** Watershed-wise catchments map with the suggested locations of the freshwater lakes/ponds, constructed wetlands and check-dams; generated in ArcGIS by Author

## 4. Results and Discussion

Even though, historically, the Ajmer city is said to have an efficient system of rainwater collection through interlinked catchments (lakes), many have dried up in the recent years including foysagar lake or are choked with solid waste. Over the time the interlinked catchment system has declined due to the illegal settlements like slums and urban sprawl, that has added to the increasing impervious surfaces. These factors reduced the rainwater accumulation in the previously designed reservoir, which in turn is leading to urban floods since the past few years. Thus, this needs to be taken care, to prevent the future prospects of flooding in the city due to heavy rains.

The SCS-CN method proves to be a very rational method to calculate the rainfall-runoff data of the city. All the spatial data has been collected from the respective Authorities of Ajmer and only the DEM file has been extracted from the USGS website. The values of Antecedent Moisture condition, Hydrologic Soil groups has been collected from the respective departments of Ajmer. The runoff volume calculated through the SCS-CN method gives a good idea of identifying the major runoff watersheds, where the interventions have been suggested.

## 5. Conclusions and Recommendations

From the above experimentation and data analysis, following conclusions are arrived at:

- Watershed 1(luni basin), 2 and 3 (sekhawati basin) are the major runoff catchments with high surface runoff volume in the dry (year: 2015), normal (year: 2018) and severe (year: 2019) rains (refer Figure: 12).
- Presently, the city's rainwater harvesting system is non-functional due to drying of the streams or the natural drainage lines being choked with solid waste.
- Interventions such as potential areas or series of ponds/lakes, constructed wetlands and check-dams are required to conserve the rainwater for the future use.
- Also, it is observed that since 2008, the flash flood occurrence in the city has hiked every alternate year, leading to damage of properties in the city; which has yet to be looked upon by the officials of the city.

Among the many possible measures to make the city more sustainable and resilient from water related hazards, the co-ordination among the relevant departments under the leadership of Planning department of the city (i.e. Ajmer Development Authority) is crucial to curb the situation of recurring flash floods.

It is also recommended that the soil conservation measures like contour trenches, staggered contour etc. could be taken up by the Watershed development and soil conservation department to improve the percolation of water into the ground and meet the moisture content of the soil. Also, the Planning department can coordinate the strategies while planning for the city through integrating the water concerns in the Development Plan and in building bye-laws for provision of Rain Water Harvesting structures and green cover area of each plot proposed to be developed in the city.

This will not only change the scenario of frequent flood into the well managed storm water, but also will change the water governance in more coordinated and regulated manner. These measures provide for the overall long-term gain for the city to evolve as a water sensitive city.

## Acknowledgements

The authors are thankful to CEPT University, Ahmedabad [India] for this allowing this study as Directed Research Project and providing the needed financial support for carrying out the field work. We are deeply and sincerely indebted to experts and faculty members at Faculty of Planning, CEPT University, for their guidance and valuable suggestions during the study. We would also like to extend my gratitude towards the officials of Ajmer Smart City Limited (Urban Planner) and Ajmer Nagar Nigam, Officials of Public Health and Environment Department(Govt of Rajasthan), Officials of Water Resources Department (Irrigation circle-Govt or Rajasthan), Groundwater department (GWD) =-Govt. of Rajasthan, Watershed development and Soil conservation department (for providing the information on the digital maps and Agriculture Department (Ajmer) for their considerate co-operation for giving the required data , information sheets, maps and sharing their knowledge. Lastly, our heartfelt gratitude to HYDRO 2020 for giving us this opportunity to share our work with larger research community.

## Abbreviations

**AMC**: Antecedent Moisture Condition; **ADA**: Ajmer Development Authority; **CN**: Curve Number; **HSG**: Hydrological Soil Group; **MSL**: Mean Sea Level; **NRCS**: Natural Resources Conservation Service; **SCS**: Soil Conservation Service; **SCS-CN**: Soil Conservation Service-Curve Number; **US-SCS**: United States Soil Conservation Service; **GWD**: Groundwater Department; **WD&SC**: Watershed Development and Soil Conservation Department; **ASCL**: Ajmer Smart City Limited; **ANN**: Ajmer Nagar Nigam; **DCH**: District Census Handbook.

## References

***Websites***

A parsimonious watershed model - preview & related info | Mendeley. (n.d.). Retrieved September 22, 2020, from https://www.mendeley.com/catalogue/f2eff1e0-a36a-309c-ac9d-2afa232be0f5/

After flooding the city of Ajmer yesterday, rains to continue in Rajasthan until August 7 | Skymet Weather Services. (n.d.). Retrieved October 19, 2020, from https://www.skymetweather.com/content/monsoon-in-india/after-flooding-the-city-of-ajmer-yesterday-rains-to-continue-in-rajasthan-until-august-7/

Ajmer records very heavy rains of 114 mm, normal life comes to a halt | Skymet Weather Services. (n.d.). Retrieved October 19, 2020, from https://www.skymetweather.com/content/weather-news-and-analysis/ajmer-records-very-heavy-rains-of-114-mm-normal-life-comes-to-a-halt/

Annual Rainfall. (n.d.). Retrieved October 17, 2020, from http://water.rajasthan.gov.in/content/water/en/waterresourcesdepartment/WaterManagement/IWRM/annualrainfall.html#

Bhuvan | Thematic Data dissemination | Free GIS Data | OGC Services | Clip and Ship. (n.d.). Retrieved October 22, 2020, from https://bhuvan-app1.nrsc.gov.in/thematic/thematic/index.php

India Smart Cities. (n.d.). Retrieved October 19, 2020, from http://indiasmartcities.com/STATES/RAJASTHAN/AJMER.html

Rajasthan: Four killed due to heavy rainfall in Ajmer | Ajmer News - Times of India. (n.d.). Retrieved October 19, 2020, from https://timesofindia.indiatimes.com/city/ajmer/four-killed-due-to-heavy-rainfall-in-ajmer/articleshow/70485302.cms

Progress Reports : Ministry of Housing and Urban Affairs, Government of India. (n.d.). Retrieved October 19, 2020, from http://mohua.gov.in/cms/progress-reports.php

Rajasthan receives 30 per cent lesser rainfall compared to 2019; 25 districts get deficit rainfall | Jaipur News - Times of India. (n.d.). Retrieved October 19, 2020, from https://timesofindia.indiatimes.com/city/jaipur/rajasthan-receives-30-percent-lesser-rainfall-compared-to-2019-25-districts-get-deficit-rainfall/articleshow/77322789.cms

Water news: Water crisis in the offing for Jaipur and Ajmer. (n.d.). Retrieved October 19, 2020, from https://www.indiawaterportal.org/news/water-news-water-crisis-offing-jaipur-and-ajmer

Urban Water Supply in Rajasthan: Problems and Prospects on JSTOR. (n.d.). Retrieved October 19, 2020, from https://www.jstor.org/stable/4401678?seq=1

Kannan, M., & Chouhan, B. P. (n.d.). *Asian Review of Social Sciences Impacts of Urbanization on Land Use Pattern and Environment: A Case Study of Ajmer City, Rajasthan*. Retrieved from https://www.researchgate.net/publication/340378936

***Books or articles***

Al-Juaidi, A. E. M. (2018). A simplified GIS-based SCS-CN method for the assessment of land-use change on runoff. *Arabian Journal of Geosciences*, *11*(11). https://doi.org/10.1007/s12517-018-3621-4

Ajmer records very heavy rains of 114 mm, normal life comes to a halt | Skymet Weather Services. (n.d.). Retrieved October 19, 2020, from https://www.skymetweather.com/content/weather-news-and-analysis/ajmer-records-very-heavy-rains-of-114-mm-normal-life-comes-to-a-halt/

Anasagar, Pushkar Lake overflow after heavy rains in Rajasthan | Jaipur News - Times of India. (n.d.).

Retrieved January 1, 2021, from https://timesofindia.indiatimes.com/city/jaipur/anasagar-pushkar-lake-overflow/articleshow/70489225.cms

Chung, W. H., Wang, I. T., & Wang, R. Y. (2010). Theory-based SCS-CN method and its applications. *Journal of Hydrologic Engineering*, *15*(12), 1045–1058. https://doi.org/10.1061/(ASCE)HE.1943-5584.0000281

City, U. S. (2016). The Smart City Challenge Stage 2 Smart City Proposal Udaipur. *Government of India*, (7), 113. Retrieved from http://smartcities.gov.in/upload/uploadfiles/files/NDMC_SCP.pdf

Climatic Regions of Rajasthan | RajRAS - Rajasthan RAS. (n.d.). Retrieved December 31, 2020, from https://www.rajras.in/climatic-regions-of-rajasthan/

Dwarakish, G. S., & Ganasri, B. P. (2015). Impact of land use change on hydrological systems: A review of current modeling approaches. *Cogent Geoscience*, *1*(1). https://doi.org/10.1080/23312041.2015.1115691

Hooda, S. M. (2013). *Water Assessment - Potential for Private Intervention*. 140. Retrieved from www.ifc.org

India Smart Cities. (n.d.). Retrieved October 19, 2020, from http://indiasmartcities.com/STATES/RAJASTHAN/AJMER.html

Leopold, L. (1968). Hydrology for Urban Land Planning - A Guidebook on the Hydrologic Effects of Urban Land Use. *Geological Survey Circular*, *554*, 1–21. Retrieved from http://enviro.lclark.edu/resources/Tryon/Water/Hydrology.pdf

Li, Z., Liu, W. zhao, Zhang, X. chang, & Zheng, F. li. (2009). Impacts of land use change and climate variability on hydrology in an agricultural catchment on the Loess Plateau of China. *Journal of Hydrology*, *377*(1–2), 35–42. https://doi.org/10.1016/j.jhydrol.2009.08.007

Moors, E. J., & Dolman, A. J. (2003). Land-Use Change, Climate and Hydrology. In *Global Environmental Change and Land Use* (pp. 139–165). https://doi.org/10.1007/978-94-017-0335-2_6

Price Water Coopers. (2009). Government of Rajasthan. *Monthly Review*, *10*(2), 1–20.

Raju R., S., Raju G., S., & M., R. (2018). Estimation of Rainfall Runoff using SCS-CN Method with RS and GIS Techniques for Mandavi Basin in YSR Kadapa District of Andhra Pradesh, India. *Hydrospatial Analysis*, *2*(1), 1–15. https://doi.org/10.21523/gcj3.18020101

Satheeshkumar, S., Venkateswaran, S., & Kannan, R. (2017). Rainfall–runoff estimation using SCS–CN and GIS approach in the Pappiredipatti watershed of the Vaniyar sub basin, South India. *Modeling Earth Systems and Environment*, *3*(1), 1–8. https://doi.org/10.1007/s40808-017-0301-4

Schussel, Z., & Nascimento Neto, P. (2015). Urban planning based on watersheds: From theoretical debate to municipal management. *Ambiente e Sociedade*, *18*(3), 137–152. https://doi.org/10.1590/1809-4422ASOC838V1832015

Subramanya, K. (2009). *Engineering Hydrology* (3rd Editio). Tata Mc-Graw Hill.

TERI. (2010). *Draft Rajasthan State Action Plan on Climate Change*. Retrieved from https://nicra-icar.in/nicrarevised/images/State Action Plan/Rajasthan-SAPCC.pdf

Viji, R., Prasanna, P. R., & Ilangovan, R. (2015). Gis based SCS - CN method for estimating runoff in Kundahpalam watershed, Nilgries District, Tamilnadu. *Earth Sciences Research Journal*, *19*(1), 59–64. https://doi.org/10.15446/esrj.v19n1.44714

Wijesekara, G. N., Gupta, A., Valeo, C., Hasbani, J. G., Qiao, Y., Delaney, P., & Marceau, D. J. (2012). Assessing the impact of future land-use changes on hydrological processes in the Elbow River watershed in southern Alberta, Canada. *Journal of Hydrology*, *412–413*, 220–232. https://doi.org/10.1016/j.jhydrol.2011.04.018

*IN PROCEEDINGS OF 25th HYDRO 2020, INTERNATIONAL CONFERENCE, NATIONAL INSTITUTE OF TECHNOLOGY ROURKELA, ODISHA, INDIA 26-28, March 2021, ISBN 978-93-90631-56-8*

Paper ID - 309

# TRANSIENT ANALYSIS FOR WATER SUPPLY PIPELINEFOR POKARAN VILLAGES

Jyothi Prakash A, Naidu M. S. R, Abdul Rahiman P.M, and Patil R.G.

*Central Water and Power Research Station, Khadakwasla, Pune-411024, India*
*E-mail: jp.cwprs@gmail.com*

## Abstract

The sudden stoppage of pumps often cause alternating high pressure changes in long water supply pipelines, which result in back flow, negative pressures, column separation and excessively high pressures in pipelines. The resulting pressure variation may lead to damage of piping system. Transient analysis is essential to verify design and operation of piping systems and to determine maximum and minimum pressures acting on pipeline at various time intervals along the pipeline to prevent damage. Based on the transient analysis anti surge devices are installed at optimized locations on rising mains to protect the pipeline against surge pressures. This paper presents a transient analysis based on method of characteristics for water supply project of public health engineering department, Jodhpur, Rajasthan. It envisages drawing of water from Indira Gandhi Main Canal for drinking water supply to 106 villages of Jaisalmer district. The provision of anti-surge devices like air vessels, zero velocity valves, one way surge tank for this project are considered to be uneconomical for smaller diameter pipelines with small flow rate. Hence, it was considered to provide air valves alone for safeguarding system components against surge pressures due to power failure of pumps. Studies were conducted to optimise number of air valves and their location on rising main for each pumping scheme. The results showed that provision of air valves alone for all the rising mains at different chainages of the pumping schemes mitigated the water hammer pressures.

***Keywords:*** *Water hammer; anti surge devices; maximum pressure; minimum pressure*

## 1. Introduction

Villages in Jaisalmer district of Rajasthan are facing severe drinking water scarcity. The state government under its Public Health Engineering Department has embarked on a massive drinking water mission drawing water from Indira Gandhi Main Canal (IGMC) for supply to 106 villages of Jaisalmer district. CWPRS has taken up the study of transient analysis for the pumping systems and suggesting suitable protection devices in each rising main of this water supply scheme for the purpose of safe operation of pumping lines (CWPRS Technical Report).

The waterhammer pressures can be maintained within reasonable limits by using suitable pipe diameter and material or by the installation of proper anti-surge devices. Generally, the pressurised pipelines with a length of more than 100 m are prone to waterhammer phenomena. Hence, the economical way to address this phenomenon is to design pipeline systems with appropriate protection devices. The type of anti-surge device mainly depends on the geometrical and hydraulic characteristics of the system. The provision of anti-surge devices like air vessels, zero velocity valves, one way surge tank are considered to be uneconomical for smaller diameter pipelines with small flow rate. Hence, the pipelines of the water supply project of public health engineering department, Jodhpur, Rajasthan are analysed with an emphasis on use of air valves as a safety device to mitigate waterhammer pressures. This paper presents the transient analysis conducted to optimise number of air valves and their location on each rising main by using customised software, which is based on Method of Characteristics (Wylie et al. 1993).

## 2. Water supply project for Pokaran villages

The water supply project of PHED, Jodhpur, Rajasthan envisages drawing of water from Indira Gandhi Main Canal (IGMC) for drinking water supply to 106 villages of Jaisalmer district Water is drawn through closed gravity conduit from IGMC through off takes leading to the Clear Water Reservoirs (CWR). The pumps are installed near the CWR to pump the water to Elevated Service Reservoir (ESR) for further supply to the villages as shown in Figure 1. All the pump houses are provided with centrifugal pumps of capacity varying from 11 kW to 37 kW. They draw water from sump with input water sourced from gravity main through CWR. The water is pumped through rising mains (14 No's) of diameter varying from 150 mm to 250 mm, flow rate varying from 21.64 $m^3$/hr to 158.93 $m^3$/hr discharging into ESR which are at a distance varying from 2 Km to 14.22 Km long approximately. Further supply to corresponding villages is through gravity pipelines from ESR. All the delivery lines are connected with isolation valves and NRV for safeguarding pumping system. PHED has made provision for air valves for the purpose of air release during filling / power failure. The layout of system of reservoir CWR-pumping station, butterfly valve, NRV, rising main and ESR is similar in all the schemes. However, the lengths and sizes of various components/equipments are different. Figure 2 shows the photographs of gravity main line, CWR, Pump house and ESR.

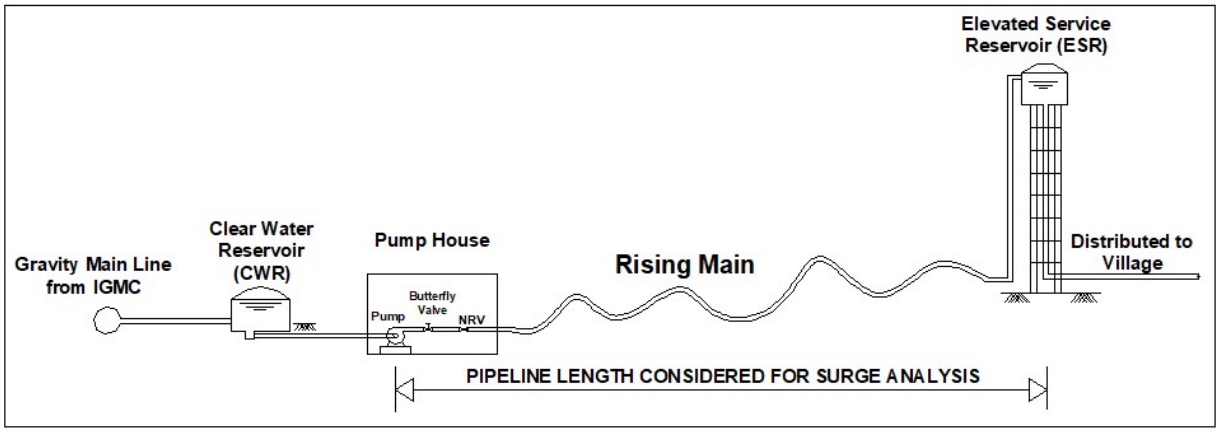



**Figure 1** A typical configuration of pumping system of water supply project of Pokaran villages, Rajasthan




**Figure 2**Photographs showing(a) gravity main line (b) CWR (c) Pump house (d) ESR

### 2.1. *Input data of pipeline*

The data for each conduit of the pipeline such as diameter, length, thickness and wave speed; suction and delivery reservoir levels are given in Table 1. The computational time interval ($\Delta T$) is calculated by using L/(aN), in which L = conduit length, a = wave speed and N= number of reaches on the shortest conduit. Reflection time of wave for water hammer response transferring back after the pump failure is 2L/a (Wan et al. 2018). Based on this, the simulation time is calculated. But, the simulation time is considered as 200

seconds for all the pumping schemes to achieve the stability. Alignment data of the rising mains for the pumping schemes were fed to the program as per the L-sections provided by the project authorities.

**Table 1** Details of pipelines and elevation of reservoirs

| Pumping Scheme (PS) | Length (m) | Diameter (m) | Thickness (mm) | Type and Class of pipe | Wave speed (m/s) | Suction Reservoir EL (m) | Delivery Reservoir EL (m) |
|---|---|---|---|---|---|---|---|
| PS #1 | 12450 | 0.150 | 6.0 | Ductile Iron/K9 | 1000 | 253.80 | 263.40 |
| PS #2 | 8775 | 0.150 | 6.0 | Ductile Iron/K9 | 1000 | 251.80 | 263.40 |
| PS #3 | 12650 | 0.125 | 5.0 | Ductile Iron/K7 | 1000 | 251.80 | 250.04 |
| PS #4 | 9325 | 0.250 | 5.3 | Ductile Iron/K7 | 1000 | 242.70 | 270.12 |
| PS #5 | 7600 | 0.150 | 5.0 | Ductile Iron/K7 | 1000 | 240.73 | 277.43 |
| PS #6 | 12800 | 0.200 | 5.0 | Ductile Iron/K7 | 1000 | 240.73 | 293.22 |
| PS #7 | 13870 | 0.200 | 5.0 | Ductile Iron/K7 | 1000 | 237.64 | 273.38 |
| PS #8 | 7050 | 0.150 | 5.0 | Ductile Iron/K7 | 1000 | 237.64 | 245.50 |
| PS #9 | 14220 | 0.125 | 5.0 | Ductile Iron/K7 | 1000 | 242.44 | 247.20 |
| PS #10 | 11100 | 0.200 | 5.0 | Ductile Iron/K7 | 1000 | 203.79 | 230.04 |
| PS #11 | 7770 | 0.200 | 5.0 | Ductile Iron/K7 | 1000 | 208.39 | 239.22 |
| PS #12 | 2000 | 0.250 | 5.0 | Ductile Iron/K7 | 1000 | 256.53 | 270.07 |
| PS #13 | 3675 | 0.200 | 5.0 | Ductile Iron/K7 | 1000 | 256.53 | 270.07 |
| PS #14 | 3845 | 0.200 | 5.0 | Ductile Iron/K7 | 1000 | 252.68 | 253.19 |

### *2.2. Input data of pump*

To simulate a transient process of a pumping system, the input data of pumps are necessary to be given correctly. Table 2 shows the input data of pumps for various pumping schemes. The pump needs to provide the head difference between upstream and downstream reservoir levels and extra energy to overcome the friction along the pipeline. Therefore after pump failure, the water will flow back and push the pumps to inverse. To ensure the pumps are not damaged due to rapid reverse flow, an NRV is provided on rising main, immediately after the pump delivery. The closure time of NRV is taken as 2 seconds as per its closing characteristics.

**Table 2** Details of pump

| Pumping Scheme (PS) | Head (m) | Discharge ($m^3$/hr) | Power (kW) | Speed (RPM) | Efficiency (%) | Moment of Inertia (KG-$M^2$) |
|---|---|---|---|---|---|---|
| PS #1 | 103.8 | 57.31 | 30.0 | 1450 | 69 | 2.08 |
| PS #2 | 94.29 | 57.42 | 30.0 | 1450 | 69 | 2.02 |
| PS #3 | 82.08 | 23.54 | 11.0 | 2950 | 60 | 0.17 |
| PS #4 | 42.18 | 47.92 | 15.0 | 1450 | 62 | 1.51 |
| PS #5 | 79.64 | 57.35 | 22.0 | 1450 | 69 | 1.17 |
| PS #6 | 74.06 | 39.17 | 15.0 | 2950 | 70 | 0.25 |
| PS #7 | 80.0 | 77.44 | 22.0 | 1450 | 64 | 1.56 |
| PS #8 | 45.9 | 45.9 | 18.5 | 1450 | 69 | 1.16 |
| PS #9 | 57.61 | 21.64 | 11.0 | 2920 | 59 | 0.16 |
| PS #10 | 102.8 | 60.12 | 30.0 | 1450 | 68 | 2.08 |
| PS #11 | 55.47 | 37.98 | 15.0 | 1460 | 60 | 1.19 |
| PS #12 | 37.62 | 75.06 | 15.0 | 2920 | 73 | 0.38 |
| PS #13 | 36.7 | 75.06 | 15.0 | 2920 | 73 | 0.38 |
| PS #14 | 35.92 | 158.93 | 30.0 | 1470 | 81 | 2.11 |

Generally, normal performance curve of a pump represents the characteristics at rated rotational speed, which cannot be used for hydraulic transients. The complete characteristics curve of a pump represents the complex relationship among the various parameters such as Dynamic head, discharge, and shaft torque at varying

rotational speed (Wan et al. 2011). This curve describes the pump operation in a dimensionless form with reference to rated conditions of the pump at its best efficiency point, expressed in $F_H$ and $F_B$ as shown in Figure 3 is used in the analysis.

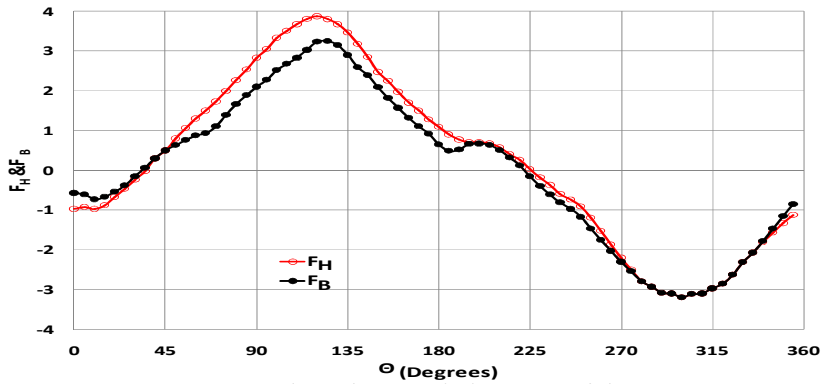



**Figure 3**Complete characteristic curve of the pump

## 3. Methodology of transient analysis

The transient analysis was carried out by using customised software available with CWPRS, which is based on Method of Characteristics (MOC) to solve the water hammer problems. MOC is a popular method for handling hydraulic transients, which converts the two partial differential equations of continuity and momentum into four ordinary differential equations. These equations are solved numerically using finite difference techniques (Streeter and Lai, 1962).

### *3.1. Analysis of conditions*

Sudden stoppage of pumps in the system induces reverse flow in the rising main while NRV closes as per its characteristics. Due to this event, the rising main from NRV to ESR is subjected to the possible water hammer pressures. Hence, in every case, the transient analysis was conducted for the rising main from NRV to ESR for critical operating condition of power failure and sudden stoppage of pumps in the system.

Following conditions are considered:

- *Analysis without safety devices*: The analysis is carried out to find out maximum and minimum pressures existing in the rising mains of the pumping schemes.
- *Analysis with safety devices*: The analysis is carried out to find out the effect of safety devices on maximum and minimum pressures for rising mains of the pumping schemes.

### *3.2. Limiting conditions of water hammer pressures*

The allowable maximum operating pressure for the pumping schemes PS #1 and PS #2 of ductile iron (K9) class type is 7.7 MPa and similarly for remaining pumping schemes of ductile iron (K7) class type is 1.25 MPa as per IS 8329-2000. The extent to which pressure inside the pipe may be allowed to fall below atmospheric pressure is governed by its structural integrity and column separation. Theoretically, column separation may occur at normal temperature at 0.3 mwc absolute pressure or when pressure inside the pipe has dropped down by 9.7 mwc below atmospheric pressure (assumed to be 10 mwc). However, the structural considerations do not allow such a low pressure to be attained; it is a general practice to limit this well above this value for practical considerations (Mohite and Morankar 2015).

### *3.3. Analysis procedure*

Data pertaining to the pumping system as provided by the project authorities for various pipelines are input to the program. The following iterative procedure is adopted to carry out the transient analysis:

- Model the piped network for all the pipelines case by case in software platform.
- Perform transient analysis of the network without any protective device.
- Check for steady state conditions for validity of data and to detect possible errors.
- Check the maximum and minimum pressures developed in the pipelines, if it exceeds the limiting values, select a suitable safety device to mitigate the surge pressures.
- Perform transient analysis of the network with air valves distributed along the rising main and examine the likely extent of pressure fluctuations.
- If the protection is found to be inadequate, additional air valves are tried.
- The entire procedure is repeated till acceptable pressures in pipeline are obtained.

## 4. Results and discussions

Objective of surge analysis is to provide optimum number of air valves and also ensure reliable operation of the system during starting and stopping of pumps. At first, water hammer analysis for the all schemes was carried out without any safety devices for pipeline, which is denoted as case-1 for every pumping station. Results of the analysis are given in Table 3. Figure 4 shows the temporal propagation of pressure wave in pipeline without safety devices for all the pumping schemes, corresponding graphical variation of extreme dynamic head along the pipeline is shown in Figure 6. It is observed from the results that for rising mains of pumping schemes PS #1 and PS #2, the maximum pressures are 104.55m (1.03MPa) and 104.04m (1.02MPa) respectively, which are within the acceptable level of 7.7 MPa, where as for pumping schemes PS #3 to PS #14, the maximum pressures are within the acceptable level of 1.25 MPa.

**Table 3** Maximum and minimum pressures of all the pumping schemes

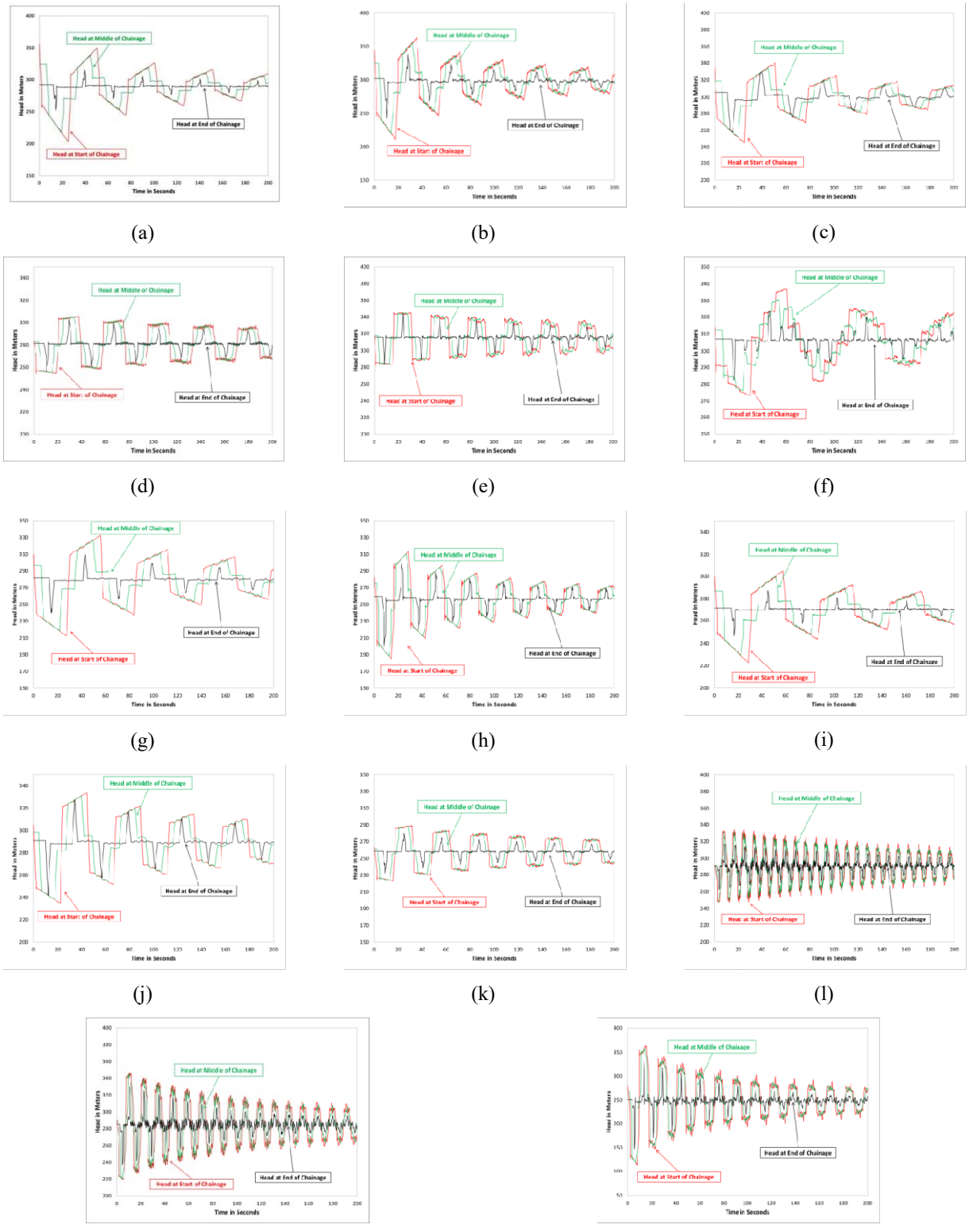
| Pumping Scheme (PS) | Without Protection (Case 1) | | | With Protection (Case 2) | | | |
|---|---|---|---|---|---|---|---|
| | Maximum Pressure | | Minimum Pressure (m) | No of Air Valves | Maximum Pressure (m) | | Minimum Pressure (m) |
| | (m) | (MPa) | | | (m) | (MPa) | |
| PS #1 | 104.55 | 1.03 | -54.37 | 10 | 104.55 | 1.03 | -4.72 |
| PS #2 | 104.04 | 1.02 | -29.59 | 10 | 104.04 | 1.02 | -3.85 |
| PS #3 | 93.04 | 0.91 | 3.47 | 10 | 93.04 | 0.91 | 3.47 |
| PS #4 | 52.8 | 0.52 | 10.77 | 9 | 52.8 | 0.52 | 10.77 |
| PS #5 | 114.01 | 1.12 | 38.7 | 8 | 114.01 | 1.12 | 38.7 |
| PS #6 | 80.68 | 0.79 | 10.14 | 10 | 80.68 | 0.79 | 10.14 |
| PS #7 | 74.52 | 0.73 | -31.24 | 9 | 74.65 | 0.73 | -4.77 |
| PS #8 | 47.15 | 0.46 | -51.17 | 8 | 47.15 | 0.46 | -3.98 |
| PS #9 | 66.39 | 0.65 | -17.19 | 10 | 66.39 | 0.65 | 1.15 |
| PS #10 | 120.88 | 1.18 | 31.13 | 10 | 120.88 | 1.18 | 31.13 |
| PS #11 | 80.3 | 0.79 | 5.06 | 8 | 80.3 | 0.79 | 5.06 |
| PS #12 | 51.73 | 0.51 | -6.45 | 4 | 46.86 | 0.46 | -1.94 |
| PS #13 | 105.19 | 1.03 | -33.92 | 7 | 90.59 | 0.89 | -2.86 |
| PS #14 | 106.24 | 1.04 | -136.01 | 6 | 35.21 | 0.34 | -4.54 |

The minimum pressures for pumping schemes PS #3, PS #4, PS #5, PS #6, PS #10 and PS #11 are within the acceptable level, where as for pumping schemes PS #1, PS #2, PS #7, PS #8, PS #9, PS #12,PS #13 and PS #14,the pressures values has gone below the acceptable level. Hence, safety devices are required to be

installed in these rising mains to mitigate the surge pressures. The provision of anti-surge devices like air vessels, zero velocity valves, one way surge tank are considered to be uneconomical for smaller diameter pipelines with small flow rate. Hence, the pipelines of this water supply project are analysed with an emphasis on use of air valves as a safety device to mitigate waterhammer pressures. Air valves also required to provide in rising mains to facilitate filling and draining purposes for pipelines with acceptable pressures without safety devices. Hence, the analysis is repeated with provision of anti surge devices mainly air valves in these pumping schemes, which is denoted as case-2.Studies are carried out with different number of air valves at different locations to optimize their location and number. The iterative procedure of surge analysis was repeated with different number of air valves as above, which is very difficult to present here as the analysis is voluminous. The final case, which happens to be an optimum number of air valves provided for arresting surge pressures and also to facilitate filling and draining purposes are presented here. Figure 5 the temporal propagation of pressure wave in pipeline with safety devices for all the pumping schemes, Corresponding graphical variation of extreme dynamic head along the pipeline is shown in Figure 7. It is observed from the results that, the minimum pressures of the pipelines for all the pumping schemes are within acceptable limits with provision of air valves on rising mains at different chainages as given in Table 4.

**Table 4** Location of Air Valves on rising main

| Pumping Scheme (PS) | Air Valve Number and Chainage (m) | | | | | | | | | |
|---|---|---|---|---|---|---|---|---|---|---|
| | AV 1 | AV 2 | AV 3 | AV 4 | AV 5 | AV 6 | AV 7 | AV 8 | AV 9 | AV 10 |
| PS #1 | 50 | 300 | 600 | 1250 | 2950 | 3700 | 4150 | 6150 | 7600 | 9650 |
| PS #2 | 750 | 1525 | 2350 | 3175 | 4100 | 5200 | 5650 | 6425 | 7000 | 7675 |
| PS #3 | 800 | 1900 | 2300 | 3550 | 4500 | 5300 | 6500 | 7800 | 8300 | 9500 |
| PS #4 | 625 | 1825 | 2775 | 3675 | 4900 | 5925 | 6850 | 7825 | 8650 | - |
| PS #5 | 450 | 1325 | 2800 | 3925 | 4850 | 5925 | 6325 | 7250 | - | - |
| PS #6 | 425 | 1375 | 3500 | 4400 | 5400 | 6650 | 7650 | 8575 | 10100 | 11750 |
| PS #7 | 10 | 800 | 2100 | 3300 | 5500 | 7800 | 9450 | 11500 | 13300 | - |
| PS #8 | 50 | 375 | 1725 | 2600 | 3600 | 4700 | 5525 | 6600 | - | - |
| PS #9 | 425 | 1825 | 3800 | 5750 | 6800 | 8200 | 9725 | 11000 | 11850 | 12400 |
| PS #10 | 650 | 1950 | 2425 | 3400 | 4500 | 5350 | 6150 | 7500 | 8950 | 9650 |
| PS #11 | 600 | 1300 | 2900 | 3500 | 4700 | 5500 | 6575 | 7500 | - | - |
| PS #12 | 50 | 175 | 850 | 1425 | - | - | - | - | - | - |
| PS #13 | 10 | 225 | 1050 | 2000 | 2425 | 2700 | 2925 | - | - | - |
| PS #14 | 10 | 20 | 1445 | 1995 | 2995 | 3370 | - | - | - | - |




(a) (b) (c)

(d) (e) (f)

(g) (h) (i)

(j) (k) (l)

(m) (n)

**Figure 4** Pressure wave in pipeline without safety device for pumping schemes (a) PS #1 (b) PS #2 (c)PS #3(d) PS #4 (e) PS #5 (f) PS #6 (g) PS #7 (h) PS #8 (i) PS #9 (j) PS #10 (k) PS #11 (l) PS #12 (m) PS #13 (n) PS #14

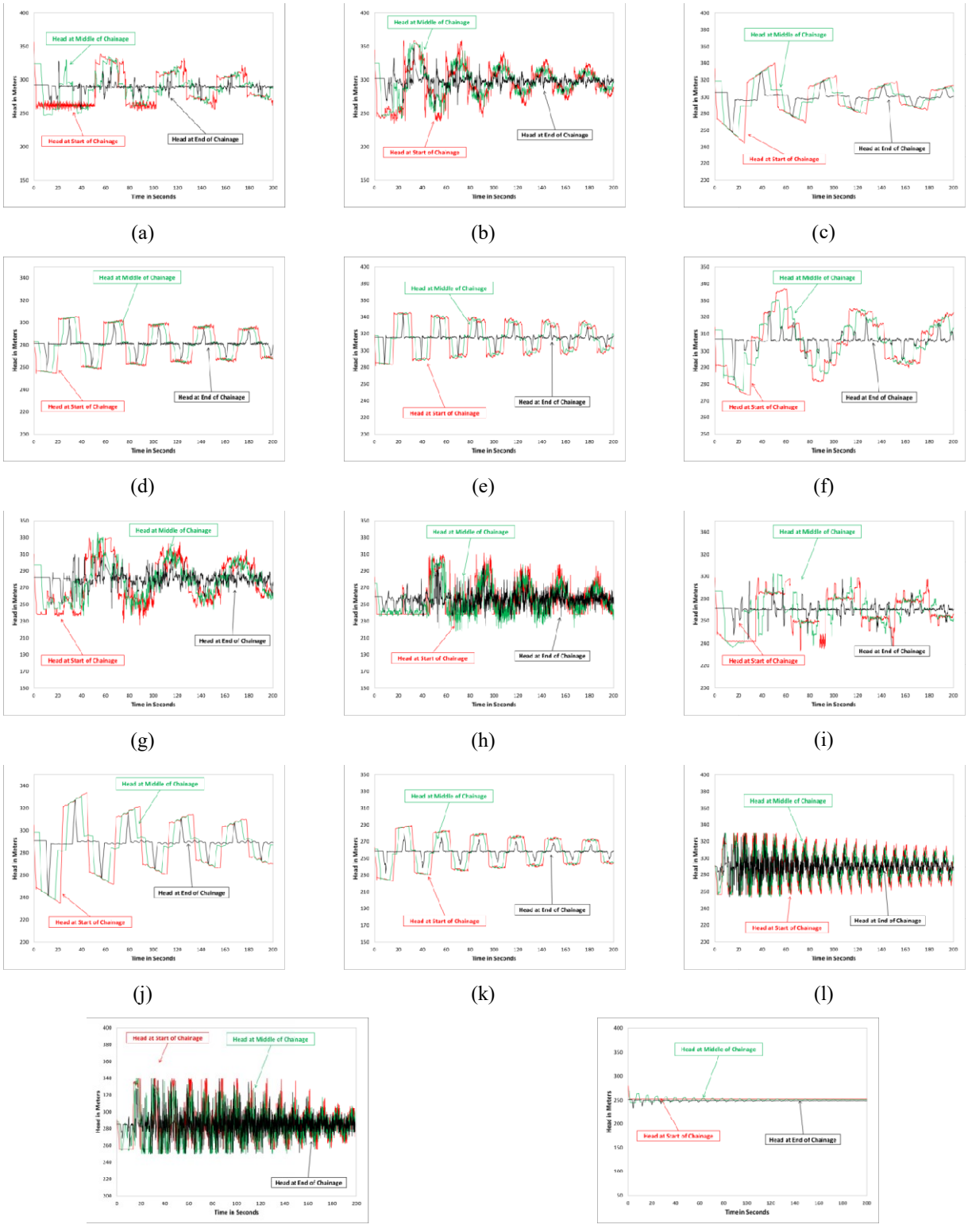



**Figure 5** Pressure wave in pipeline without safety device for pumping schemes (a) PS #1 (b) PS #2 (c) PS #3 (d) PS #4 (e) PS #5 (f) PS #6 (g) PS #7 (h) PS #8 (i) PS #9 (j) PS #10 (k) PS #11 (l) PS #12 (m) PS #13 (n) PS #14

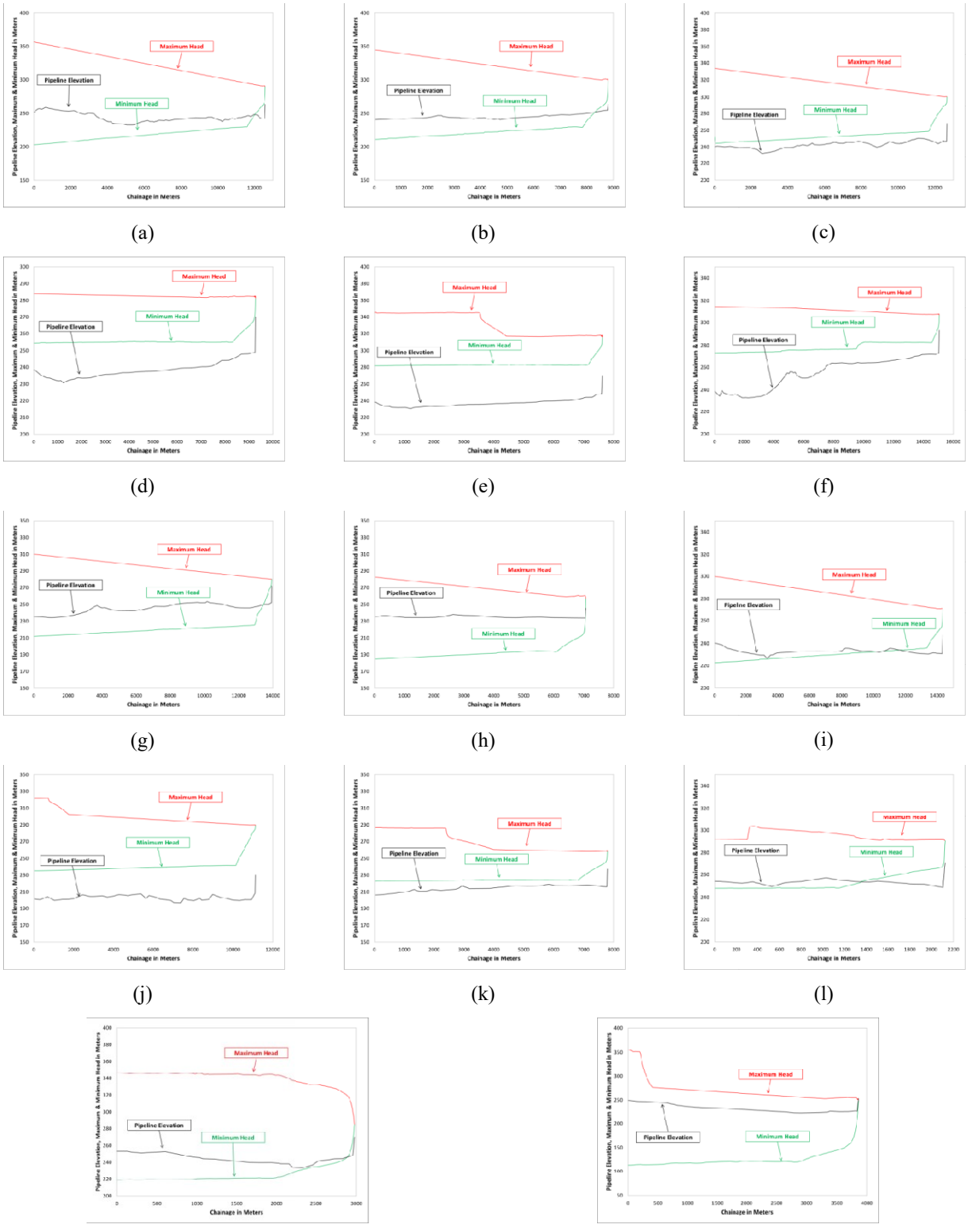



**Figure 6**Extreme dynamic head along the pipeline without safety device for (a) PS #1 (b) PS #2 (c) PS #3 (d) PS #4 (e) PS #5 (f) PS #6 (g) PS #7 (h) PS #8 (i) PS #9 (j) PS #10 (k) PS #11 (l) PS #12 (m) PS #13 (n) PS #14

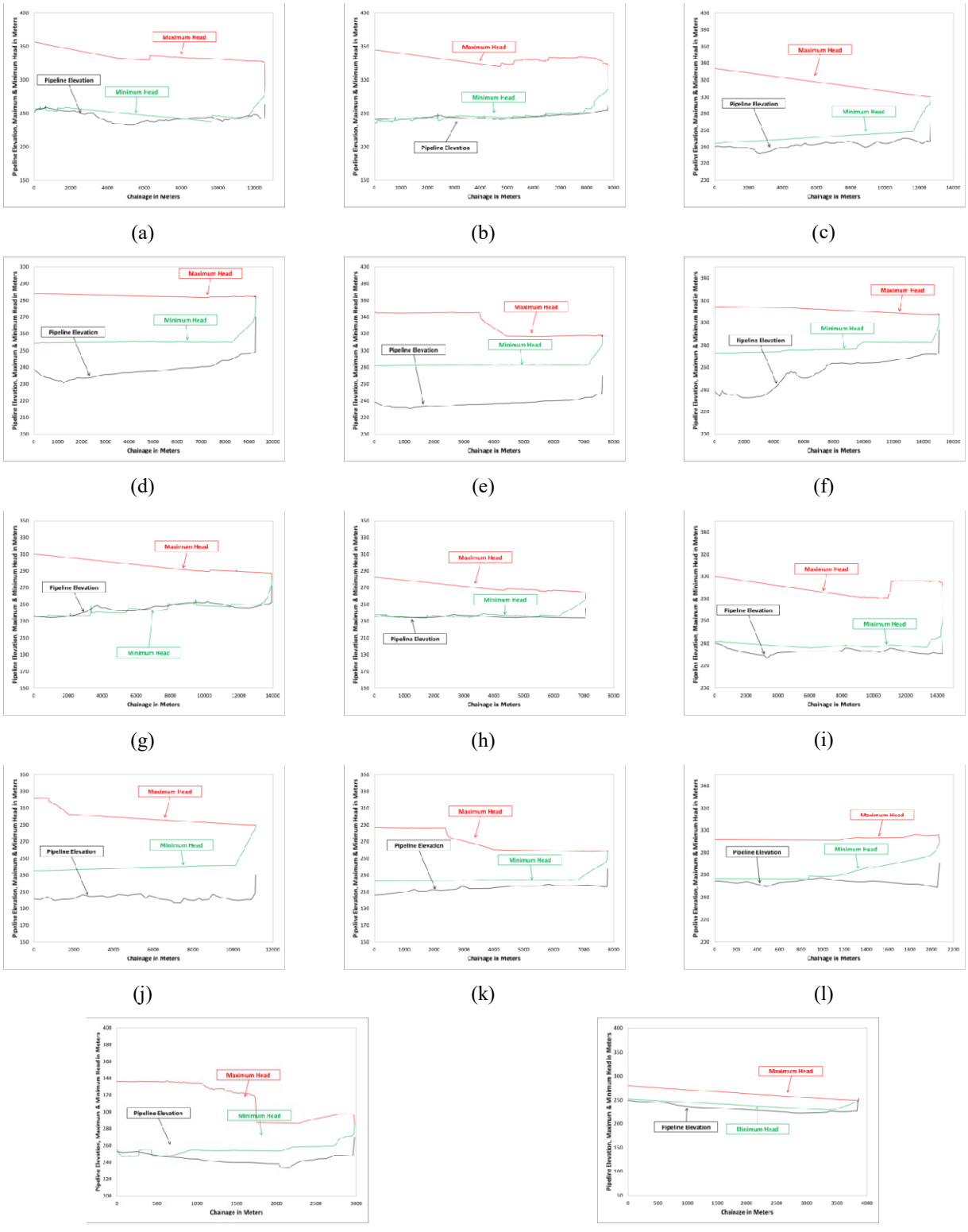



**Figure 7** Extreme dynamic head along the pipeline withsafety device for (a) PS #1 (b) PS #2 (c) PS #3 (d) PS #4 (e) PS #5 (f) PS #6 (g) PS #7 (h) PS #8 (i) PS #9 (j) PS #10 (k) PS #11 (l) PS #12 (m) PS #13 (n) PS #14

## Conclusions

In this study, the transient analysis was conducted to mitigate the water hammer pressures in the pipelines of the pumping schemes containing the pumps, reservoirs, valves and pipelines. After carrying out the analysis for the pumping schemes, without safety devices and with safety devices for critical power failure and sudden stoppage of pumps, the following conclusions are drawn:

- The maximum pressures for rising mains of all pumping schemes are within the acceptable level without any safety devices.
- For pumping schemes PS #3, PS #4, PS #5, PS #6, PS #10 and PS #11, the minimum pressure values are within the acceptable level without any safety devices.
- For Pumping schemes PS #1, PS #2, PS #7, PS #8, PS #9, PS #12,PS #13 and PS #14,the minimum pressures values have gone below the acceptable level of -10m.These minimum pressures are brought to acceptable limits with provision of air valves on rising mains at different chainages.
- Air valves are also required to provide on rising mains to facilitate filling and draining purposes for all the pumping schemes.
- For smaller diameter pipelines with smaller flow rates, only air valves are sufficient to control the minimum pressure in rising mains.
- The pumping systems of water supply project of PHED, Pokaran needs protective devices in the form of air valves.

## Acknowledgements

We wish to express our deep sense of gratitude to Shri A. K. Agrawal, Director CWPRS for his constant encouragement.

## References

CWPRS Technical Report, TR No. 5752, 2019.*Surge analysis for rising mains of water supply project of Pokaran villages, Rajasthan through M/s Mahaveer Infraengineering Pvt Ltd*.

Mohite, S. G., and Morankar, D.V. (2015). Hydraulic Transient: Lift Irrigation Scheme. *International Journal of Computational Engineering Research,* 5 (6), 71-78.

Wan, W., and Huang, W.(2011).Investigation on complete characteristics and hydraulic transient of centrifugal pump. *Journal of Mechanical Science and Technology,* 25, 2583.

Wan, W., Zhang, B., and Chen, X. (2018).Investigation on Water Hammer Control of Centrifugal Pumps in Water Supply Pipeline Systems. *Energies, 12, 108.*

Wylie, E.B., Streeter, V.L., and Suo, L. (1993).*Fluid transients in systems*.Prentice Hall, USA.

*IN PROCEEDINGS OF 25th HYDRO 2020, INTERNATIONAL CONFERENCE, NATIONAL INSTITUTE OF TECHNOLOGY ROURKELA, ODISHA, INDIA 26-28, March 2021, ISBN 978-93-90631-56-8*

Paper ID - 454

# Traditional stormwater management system in watershed of wetland, a study and overview of "Dong" systems in wetland fringe villages of Assam

Anushri Barman[1], Dr. Ramakar Jha[2]

[1]*Department ofArchitecture, NIT Patna, Bihar, Patna 800005, India*
[2]*Profe ssor,Department of Civil Engineering.NIT Patna, Bihar, Patna 800005,lndia*
*Email: anushribarman@nitp.ac.in*

## Abstract

Storm water management is the process of dealing with rainwater for a better habitable space in a best possible way. This process is essential whether it is a flood prone area or a drought prone area. An intelligent drainage system is required to ensure the current amount of water to exit either as runoff or Sub surface infiltration into the ground. A good storm water drainage system should be enforced to prevent flood like situations when there is a condition with maximum rainfall in monsoons and water table rises to ground. The state of Assam receives more than 2000 mm rainfall annually and 80% of rainfall in monsoons causing 9% of total area getting submerged . While managing stormwater it is very crucial to recognize and assess the amount of water that flows as surface runoff, groundwater infiltration and evaporation. While in special conditions where the daylight hours reduced to average 4.8 hours from 12 hours of daylight per day in monsoon the expected evaporation rate is comparatively very slow. The soil is sandy clay and the infiltration rate is very less in flatter slopes. In such cases the only way to manage storm water is a significant surface drainage system with combination of Sheet and Channel flow. This crucial condition is being manipulated by traditional people with their traditional knowledge system and practices passing through generations with observation and experimentation. This paper will discuss about how the rural Assam villages use traditional practices of stormwater drainage system with a series of "Khaal and Dongs" through the entire settlement exiting them to nearby waterbody, as one can say wetlands are the sponges to refrain from flood like situations. This case study of villages in fringe areas of Sorbhog Beel wetlands with detail study of parameters considered in the system deriving successful runoff of water hence preventing flood in wetland upland areas. This study has been done to contribute in future research of traditional knowledge of pertaining a good storm water management system through drainage system in watershed area.

***Keywords:*** *Traditional System, Stormwater management, Watershed, Drainage, Runoff, swale.*

## 1. Introduction

Stormwater runoff is the water from storm that moves on the ground by gravity and flows into streams, rivers, ponds, lakes and oceans or we can say natural waterbody. Subsurface runoff of stormwater is the water that infiltrates and moves through the soil horizontally and vertically where the rate of movement is affected by soil permeability and usually occurs at much slower rates. Measures that have been developed to control, store and treat stormwater runoff from developed settlements for the purpose of reducing flooding or removing pollutants while enhancing environmental qualities can be referred as Best management practices. Integration of specific management devices into the existing development pose a challenge to site planners, water engineers and landscape architects. This demands a need of framework for overall drainage design concept which could include understanding the existing hydrological characteristics, engineering of the proposed system which will establish size, storage capacity, discharge and infiltration rates.

### *1.1 Human settlements and Storm water management*

The stormwater management has the primary concern of dealing with storm water run-off to remove it as quickly as possible from a developed site to maximize local conveyance and protection. A more recent approach of stormwater management in watershed planning and management has been seen as a cost effective and environmentally beneficial in terms of controlling runoff and protecting water quality. Controlling stormwater runoff at different watershed with sub watershed levels through land use planning policies, management and design provides nonstructural and preventive solutions as well more cost-effective practice (Strom et al). The engineered approach to stormwater management on a site by site basis has primarily resulted in relatively expensive, maintenance intensive engineered structural

solution. Human settlements have a profound impact on existing natural drainage systems which typically result in increased number of impervious surfaces (roofs, streets etc). The consequences of these surface changes are numerous but primarily rooted in the fact that developed sites lose much of their natural stormwater storage capacity. The increased rate and volume of runoff become too great for the existing drainage system to handle which changes the environmental condition resulting from changes in the stormwater drainage pattern. There is an increase in flood potential due to increase in peak flow rates, decreased groundwater supply due to reduced infiltration, increased soil erosion and sedimentation. The modern stormwater management technique considers not only the quantity of the stormwater but it also gives equal attention to the quality and amenity of the stormwater which provides methods that allow source control to handle the quality and quantity of the runoff at local level. These approaches are named differently: 'Sustainable (urban) drainage systems' (SUDS), 'low impact development' (LID) or 'best management practices' (BMPs) (Fletcher et al., 2015). Their purpose is to reduce the runoff volume, to provide natural ground water recharge, to minimise the flood risk, to minimise the erosion risk, to reduce the stormwater pollutant concentration, to enhance the biodiversity, to safeguard water and air quality, to decrease the stormwater treatment and pipe capacity costs, and to increase the amenity and aesthetic value of the developed areas. (Jotte et al)

The purpose of managing runoff is to ameliorate safety and health hazards, including flooding and property damage, stagnation, earth slides and reduce soil bearing capacity; to increase the usability of areas through the elimination of unwanted water; to provide better growing condition for plants by increasing soil aeration and to prevent erosion by reducing the rate of flow and volume of runoff (Strom et al).The components of storm water management systems are swale, culvert, catch basins, rain inlet, area drain, trench drain, retention and detention basins, infiltration basins, sediment basins. Whereas in rural areas it could rely on "open drainage system" comprising of swales, gutters, channels and culverts and detention, retention, sedimentation or infiltration basins. Grassed channel, dry swale, biofilter are all included in the term "swale" for it represents an open channel system of series of vegetated practices to treat stormwater (Jotte et al).

### *1.1.1 Traditional drainage system in wetland watershed of Assam*

The traditional drainage system of Assam resembles few of the Open drainage system followed as engineered solutions. The swales can resemble with dongs and retention detention ponds can be considered as Khaal in rural Assam. Swales are traditional basic open-drainage systems which are able to remove stormwater-borne pollutants (Fardel et al.2018). The Dongs are open man made manually dug channels by rural inhabitants of the settlements as a meant for storm water runoff. Culverts are also seen in places where there are crossings with roads and settlements. A series of networks of these Dongs (open drains/swales), Culverts, Retention and detention basins which are linked to natural drainage system associated with wetland nearest to settlement can be seen in watershed areas (Figure 1). Here The dongs can be explained as open channels natural or manmade carries water for stormwater drainage or irrigation purpose.

**The study area and details:** Sorbhog Beel wetland is one of the most significant riverine wetlands in Barpeta district of Assam. It is situated towards north of Sorbhog town with geographical coordinates as 26° 30' O" North, 90° 52' O" East. The area is characterised by almost plain topography with the highest elevation of200 m. The Soil is partly sandy, Sandy-loamy and alluvial. The climate is mild and pleasant round the year and the maximum and minimum temperatures recorded for the district are 35°C and 7°C respectively. The area receives an average annual rainfall of 1715 mm. The air is highly humid throughout the year and during rainy season, the relative humidity is about 90 percent. The Lake is surrounded by rural settlement who are socioeconomically engaged in different agricultural, fishing activities with the lake. Kamargaon Villages in the North, Pampara and Kayastha gaon in the east and Sukanjani on west site and Sorbhog village on southern side. It is an oxbow lake formed by Beki River of its east. Study has been conducted in Kamargaon Village which is a main watershed of the wetland. Primary study along with secondary study in form of literature has been conducted and correlated. The study site has been observed and recorded different physical attributes related to stormwater drainage system. The sizes of drains, the settlement areas, depth and width of different drains has been physically

marked and recorded on site. For collecting information about the working of the drainage system village experts have been interviewed with onsite observation.

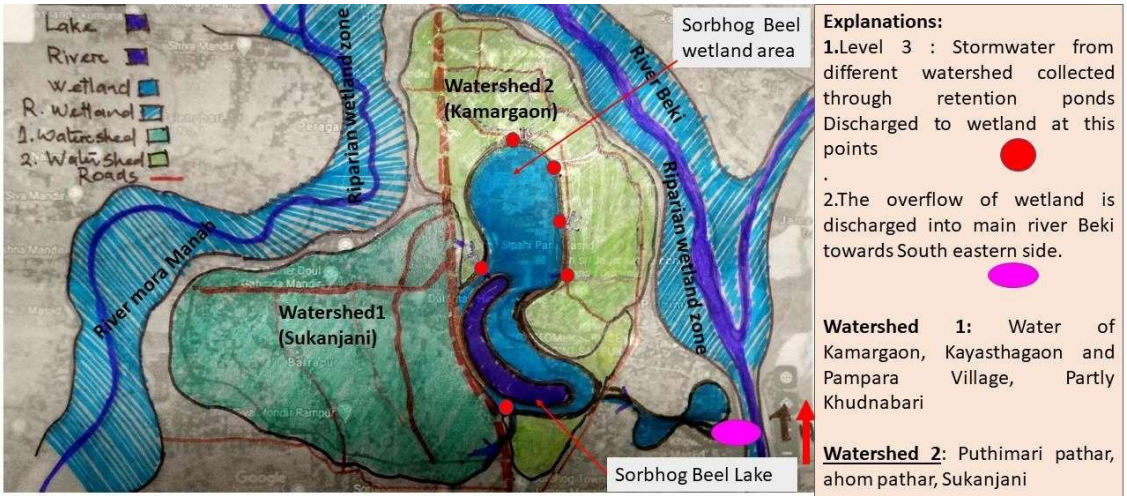



**Figure 1:** Watershed areas ofSorbhog Beel wetlands

A watershed-based study approach has been conducted to record the different parameters of existing drainage system. The study of the site was done from watershed to sub watershed with details of stormwater drainage system in household level. The main catchment area of the site is the land between the two rivers Mora Manah on west and Beki in the east. The Lake receives 60% of its water from Sukanjani village watershed (Watershed 1) and rest 40 % from Kamargaon and Kayasthagaon village sub watershed (watershed 2). The whole drainage system has a continuous flow of water. The water from agricultural fields get accumulated through sheet flow and channelized through wider open channel or swale and enters into the lake through a larger stream of water called as "Kurar Dong" near west side of the lake (watershed 1). The water from the dwelling areas also meets this Kurar Dong through different channels. The Junction Points of different channels are wider and called as "Khaal" as it increases the capacity of water it can retain as shown in Figure 2.These Retention "Dongs" are also surrounded by Bamboo plantations along the edges partly planted by local inhabitants and few are part of the water ecosystem which helps in preventing bank erosion and stop surface sedimentation of these open channels.

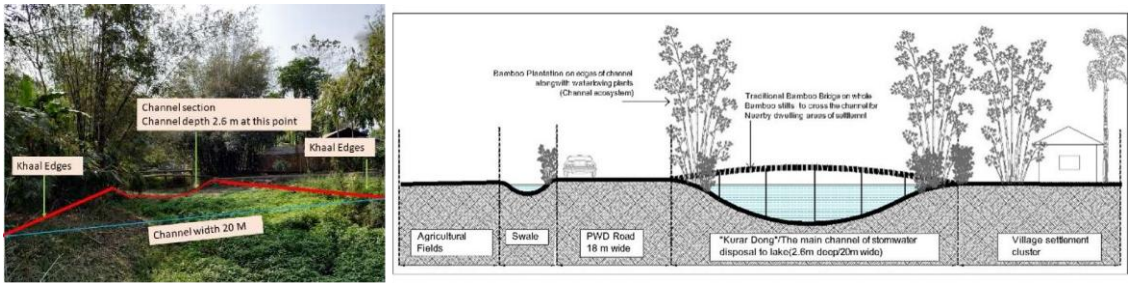



**Figure 2:** Kurar Dong: Image and section showing Main Channel carrying stormwater of Sukanjani

The other watershed that is Kamargaon and Kayasthagaon villages contributes 40% of the water of the lake. The Kamargaon watershed disposes its water through two points, one on its northern side "Gorkhuli" (deep field) area and another towards eastern side near Jamadarbari Pathar. The interconnected drains of varied sizes finally terminate at these channels or retention ponds and overflow into the wetland areas. The retention ponds that can hold water for the pre monsoon period and can be used in irrigation also as shown in Figure3.




**Figure 3** Stormwater Collecting in main retention ponds before disposing in Main wetland

**Methodology:** The stormwater management of the Sorbhog Beel wetland system can be segregated into 3 main level of interventions as explained in Figure 4. The main steps of stormwater drainage are in the system of collection, conduction and disposal. Collection is a process of collecting or accumulating stormwater from the surfaces, conduction is the process of transportation of collected water through any form of conduction systems and disposal of stormwater is the process of discharging storm water into any natural waterbody or into the ground. The steps of storm water disposal can be seen well through these three levels of interventions of manmade and natural structure.

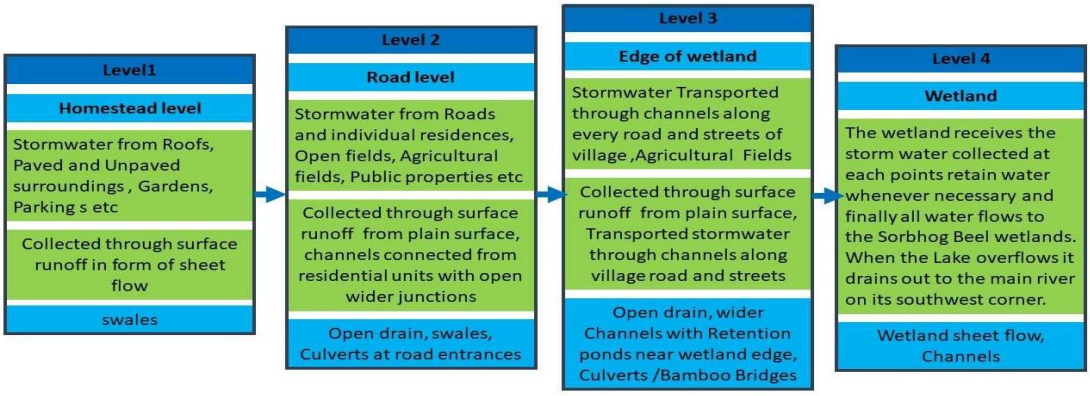
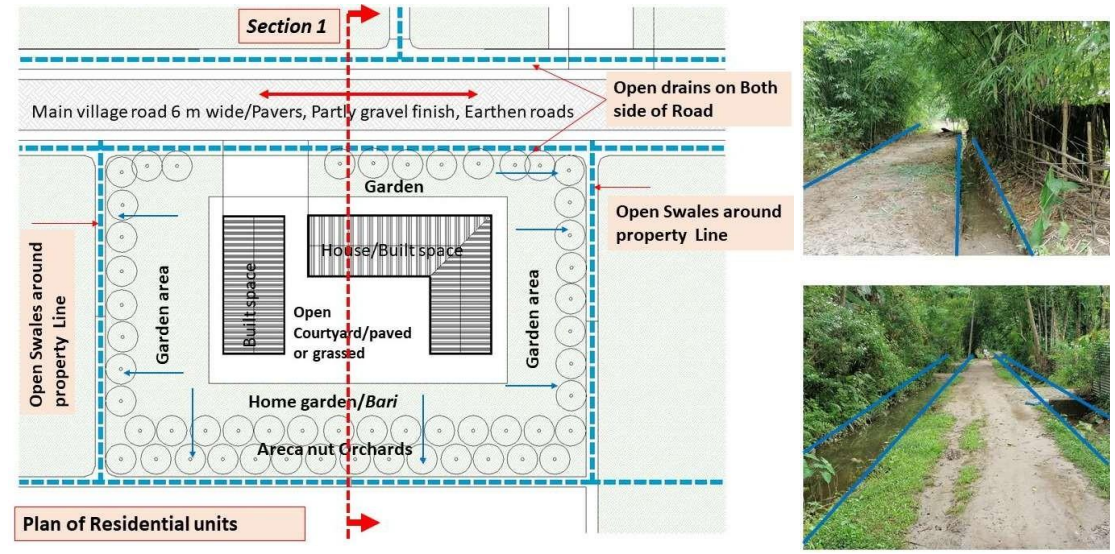



**Figure 4** Level of intervention Stormwater Management system of Sorbhog Beel Watershed

**Observation and Result:** The first level of intervention is at homestead level. The habitable areas are the foremost part of this level of intervention. The water collected from roof, paved and unpaved surfaces of dwelling units and individual gardens are collected and transported further through open swales surrounding the boundary walls or around each dwelling unit's property line. The channel around the property line helps in draining out water further and also gives a prominent property boundary as the materials used for boundary walls are bamboo which is the only suitable and easily available construction material for local inhabitants (Figure 5).

The second intervention has been made by collecting and transporting these stormwaters of individual residential units further to the next point with wider channels along village roads and streets. The sizes and dimensions also vary from residence level to street level, Refer Table 1. As the expected volume of storm water is increased the channels sections are also noticed to be increased. The older drain can be seen as an adaptation of nature with action of water hence it achieved a natural ecosystem with growth of water loving plants and also few of aquatic animals like fish, frogs etc which also help in pollution reduction, infiltration and slow stormwater flow (Figure 6)

The third level of intervention has been made for collection of stormwater from household through channels along roadside and discharging and merging these channels into wider channels or "Khaal" as similarly working as retention ponds before final discharge of these collected water into main lake area, Refer Figure 3.These retention ponds allows water to retain for some time and can be used for irrigation purpose also but when there is a condition of overflow the water passes through culvert or channels and is discharged into the main wetland area of lake.



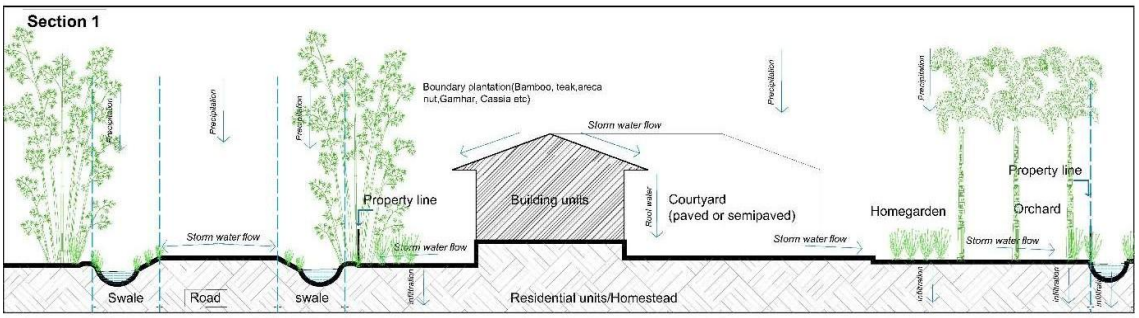




**Figure 5** Plan and Sections showing drainage of typical residential units of settlements

**Table 1** Hierarchy of drains at different intervention level

| Level | Details | Width of channel in meters | Depth of Channel |
|---|---|---|---|
| | Open swales around Residential boundary | 1 to 2 | Max lm |
| 2 | a. Main PWD Road 8 m wide | 3 to 5 | Max 2.6 m/Usually 1.6 m from road level |
| | b. village Panchayat roads connecting PWD road 6m wide | 1.2 to 3 | .9 to 1.5 |
| 3 | Retention ponds at the discharge points to wetlands | 5 to 20 | 2.6 to 3m |

The fourth stage of intervention is following the natural system of drainage. The water is collected in wetlands which are bare fields or partly under paddy cultivation. The wetland has the capacity of storing water of the entire monsoon season of the village which has been collected through intelligent conduction system of"Dongs" from each and every point of the different sub watershed of the wetland catchment area. In case of peak discharge where monsoon rainfall exceeds and it is near flooding condition, the water from the wetland's overflows through a natural channel that was partly cleared

through human interventions falls into River Beki which flows in eastern side of the Lake. The village has not yet flooded by stormwater.

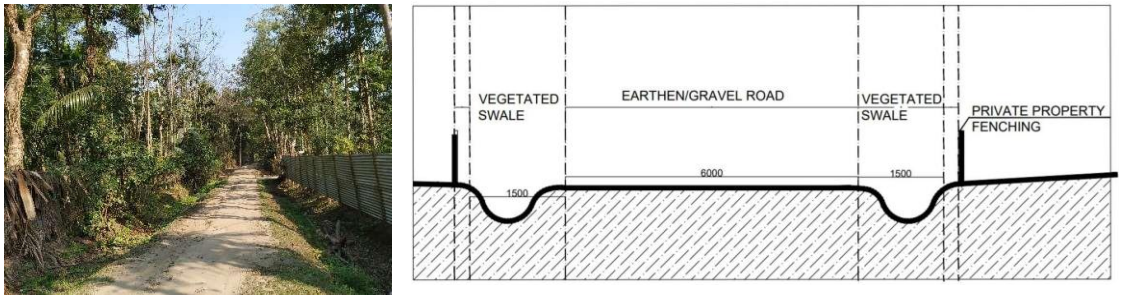



**Figure 6** Image showing vegetated swale along both side of road with Typical section

## 2. Experimental program

The experiment has been caried out calculating the designed storm water channel section and existing swale size of each homestead system. Refer to Figure 4 which is a typical example of homestead in residential settlements. A calculation for proposed stormwater drainage system has been done and compared with the existing system of drainage adopted by traditional system. For designing Drainage of the typical site, the calculated area of homestead is l 500sqm, the highest rainfall in the month of July during last 50 years is 0.5 lm, hence the volume of rainfall in the area is 765 cubic meters. The required length of the Drain is 162 considering the rainfall is uniformly distributed towards its perimeter, the area of drain needed is 4.7 square meter. To design a drain section the depth of drain is taken as 1.5 as considering safety and maintenance considerations, the expected width of drain will be 3.1 m. So the calculated designed section drainage section of swale is 3.1 mXl.5 m but it is observed to be 2m X 1.5m on site which means less water than desired will be carried out by the channels. Practically the existing section of swale is well accommodating the storm water runoff and no flooding is there on site. This raises a point of water through its infiltration into ground is also a parallel process along with runoff as the site has 70% of vegetated surface around it.

## 3. Conclusions

The continuous system of swales of varied size and retention ponds to drain out storm water into the wetland area has become the lifeline of its inhabitants. The swales (Dongs) has its own ecosystem developed through ecological succession once it is constructed. Though while construction it is of rectangular section but with time once water flows in it, it achieves it's own shape that is saucer shape or trapezoidal shape with growth of aquatic plants and animals within it. In due course of time it becomes a merged landscape of the settlement. The growth of plants in swales slow down the runoff speed and hence helps in groundwater recharge. Few plants also help in reducing pollution through the action of roots and shoots are in Phytostabilization, Rhyzodegradation, Phytoextraction, Phytodegradation, Phytovolatilization and Phytofiltration. The growth of certain plants like Fems, Colocasia, Banana, Altemanthera etc are also used by local inhabitants as a source of food and vegetable. Fishing in these dongs has become a recreational activity for local inhabitants and also a source of food. Once, the peak rainy season is over these dongs can also be used for irrigation of the fields, by stopping further water flow through earthen berms placed cross sectionally in swales which can be easily removable. The retention ponds are also used similarly for fishing, collecting plant food and also for irrigation in dry seasons. Summarily this traditional system could give an alternative for SUD system(Sustainable urban drainage system) of storm water management which is equally capable of reduction of runoff volume, promotion of natural ground water recharge which minimises the flood and erosion risk, reduce the stormwater pollutant concentration, enhance the biodiversity, safeguard water and air quality, decrease the stormwater treatment and pipe capacity costs, and to increase the amenity and aesthetic value of the developed areas.

## References

Fardel A, Peyneau Bechet B, Lakel A& Rodriguez F (2018). Analysis of swale factors implicated in pollutant removal efficiency using a swale database. *Environmental Science and Pollution Research volume 26, pages]287- 1302(2019).*

Jotte L, Raspati G, Azrague K (2017). Review of storm water management Practices, *Klima 2050 Report No* 7.

Strom S, Nathan K, Woland J, Site Engineering for Landscape Architects, 6th Edition, 2013

Yang L, Liu Y (2011) Economy, Environment and Agricultural Sources, *The Impact of Air Pollution on Health*

*IN PROCEEDINGS OF 25th HYDRO 2020, INTERNATIONAL CONFERENCE,*
*NATIONAL INSTITUTE OF TECHNOLOGY ROURKELA, ODISHA, INDIA*
*26-28, March 2021, ISBN 978-93-90631-56-8*

Paper ID - 477

# AN OVERVIEW OF DAM FAILURE AND IT'S ANALYSIS METHODS

**Umesh Meena[1]*, Kishanjit Kumar Khatua[2]**

*[1]Post Graduate Student, National Institute of Technology, Rourkela*
*[2]Professor, Department of Water Resources Engineering, National Institute of Technology, Rourkela, Odisha, 769008, India*
**Corr. Author: meenaumesh26@gmail.com*

## Abstract:

A dam is an obstruction that restricts the flow of water. In the present scenario, it has become very important and necessary to store water for the fulfillment of human needs. Dams do not only reduce the chances of flood but also provide water for many activities such as agricultural use, domestic use, industrial use, hydropower generation and navigational activities. As we all know that dams are massive structures thus, they carry risk of failure too. Failure of a dam creates disaster in the downstream of a valley causing loss of human life as well as loss of properties. Therefore, it is now become important to carry out studies to understand the behavior of the flood wave resulting from dam failure and to identify how much area have been breached because of dam failure. It would be very helpful in making an emergency action plan to reduce the loss of property and to evacuate human population. We cannot prevent the flood resulting from dam failure, but we can minimize the losses by adopting proper methods of evacuation. In this paper we have reviewed the results obtained from various numerical models and inundation mapping. We have also discussed about some of the hydraulic models which have been used for dam break study.

**Keywords: Dams, floods, numerical models, hydraulic models, inundation mapping.**

## 1. Introduction

The modelling of dam failures is an important study for maintaining better functioning and safety of dams. A dam is basically an obstruction that prevents the movement of water to downstream of a hill or valley of a place. These massive structures are very important part of any nations infrastructure which provides drinking water, irrigation, flood control, water supply, navigation, hydropower, and amusement benefits. The first built dams were gravity dams, these dams are straight made of stone brick(masonry), concrete that resists the load of water by means of weight. We found the signs of first ever dam built by Egyptians. The dam was known as Sadd el-Kafara, which means "Dam of Pagans. The dam was 37ft tall ,348ft wide at the crest and 265ft at the bottom. The first ever dam was made up of rubble masonry walls on outside and pouring of 10000 tons of gravel and stone had been done. A cover of limestone applied to resist the erosion and wave action of the dam. The cement had not been applied over the dam because of the shear weight of the structure which was sufficient to ensure stability of the structure.

The second kind of dam that had been built was an earth dam called Nimrod's dam in Mesopotamiya around 2000 BC. The earthen dams are massive dams resemble to gravity. The major difference between the two was that the earthen dams are made of soil. In the study of potential dam failure, the two most important tasks are the estimation of outflow hydrograph of the reservoir and routing of that hydrograph through the downstream valley for determining the consequences of dam failure. Ever since the first dam was built there are many dam failures have been occurred.

In spite of fact that we have advance technologies, design methodologies and construction techniques, failure of dam still occurs. Studies have been carried out on various failure of dams occurred in India and all over the world. These studies indicate that dam failure causes huge loss of life and property.

To carry out the flood management and evacuation of the population at risk effectively, emphasis to be given on analyzing the flood behavior and preparation of an emergency action plan to minimize the effect of flood. All these can be done by analyzing the major floods that have been recorded till now. For analyzing the flood event we need numerical and hydrodynamic models. The function of numerical models is to simulate the dam break and flood event based on various parameters. Thus, numerical models play a very important role to analyze the flood phenomenon and for the preparation of risk management and emergency action plan.

## 2. Purpose of Dam Break Study:

The goal of dam failure study is to critically analyze the dam breach parameters and evaluation of their suitability for application in future dam failure studies prediction equations . Dam break study is a major concern since the ancient times to ensure safety of the public. Dam break have been happening since the ancient times, but at that time there were no advance technologies to predict the dam failure possibilities of a dam. Therefore, it has now become an essential requirement to analyze the effect of dam failure to reduce the loss of life and minimizing the risk from individual structures.

The first law based on dam break was introduced in France in 1968 following the Malpasset dam failure. This is the first European law on Dam break. Since then many countries have made mandatory for all dam owners to establish guidelines for assessment. After the introduction of first European law in 1968, Indian Government has also been made it mandatory to submit application for environmental clearance in respect of river valley projects. The flood resulting from dam failure will have magnitude far more than the most natural flood events. The variation of flow will be different for natural flood events and the flood that occurs due to dam breach.

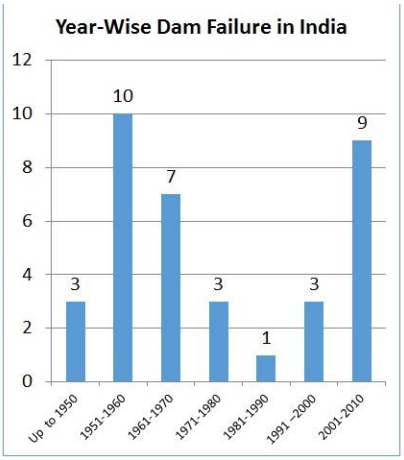
Thus, dam break modelling studies carry out separately for preparing the risk management and disaster management plan. There are various parameters and key information are required to perform the dam break modelling process. The major purpose of dam break modelling is simulation of movement of dam break flood wave downstream of the valley that would resulting from dam failure. Some of the important parameters which are required within flood zone are listed below:

- Breach formation time
- Peak discharge
- Duration of flooding
- Peak water level-extent of inundation

## 3. Dam Failure in India

India's first dam known to have been built is Kallanai (also known as Grand Anicut). It's an ancient dam that has been built across the kaveri river which flows from Tiruchirapalli district to Thanjavur district. The dam was originally built by king Karikalan of the Chola Dynasty. The dam was located at a distance of 45 km from Thanjavur, 15 km from Tiruchirapalli. The major function of the dam was to divert the waters of the kaveri across the fertile delta region for irrigation. Ever since the construction of India's first dam India has recorded many dam failures. The first dam break recorded in India was Tigra dam that had been built on Sank river in 1916 in Madhya Pradesh. The dam failure occurred during a flood event on August 4, 1917. The 86 feet high dam impounded a massive storage volume of 106041 acre-feet. On August 4, 1917, the water surface elevation rose to a historic level and overtopped the dam by about one foot from abutment to abutment. While undergoing the overtopping event two of the spillway monoliths had been moved several hundred feet downstream of the dam. The dam failure resulting in an uncontrolled release of the reservoir. The major cause of failure is sliding of sections of the gravity dam along the untreated, stratified foundation. The development of excessive uplift pressures creating tension at the heel of the dam likely contributed to ability of the dam to slide.

Recent dam failure that has been occurred in India was in Tiware dam situated in Ratnagiri district of Maharashtra. The dam has been breached in July 2, 2019 night flooding seven villages and swept away 20 people. The dam failure has now become a threat to public life and property. According to central water commission that hosts the central Dam safety organization, breaching due to flooding lead to the largest number of dam failures. The total number of dam failures that has been occurred in India, 44% of them were failed due to the result of breaching like Tiware dam. India has built around 5202 dams, out of which 35% are in Maharashtra, which is highest among all states.



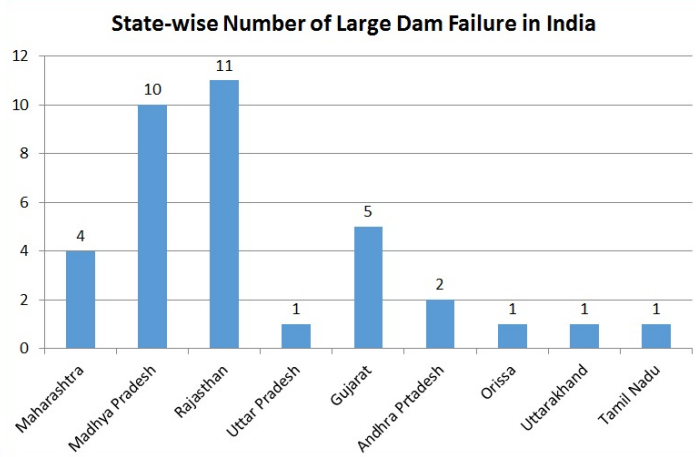




**Figure 1: Year-Wise Dam Failure in India; Figure 2: State-Wise Number of Large Dam Failures in India.**

### 3.1 Types of Dam Failures

#### 3.1.1 Embankment Dam Failures/ Earth Dam Failures

Since the earth dams are the oldest and mostly used dams in ancient times. There are many possibilities of earth or embankment dam failures. Usually , the superficial inspection of the dam is made but the owners and maintenance personnel should be aware of some prominent types of failures. These failures can be grouped into three general categories: overtopping, seepage, structural failure . Below is the brief discussion of each type of failures-

**a. Overtopping Failures**: It is the major kind of failure that takes place in an earthen dam. These failures result from the erosive action of water on the embankment. Generally , erosion happens when we observe uncontrolled flow of water near or adjacent to the dam. The earthen embankment s are designed in such a way that they are not t o be overtopped therefore they are susceptible to erosion. If erosion has started during the period of overtopping, it becomes almost impossible to stop it.

**b. Seepage Failures**: Seepage is the process by which liquid leaks through a permeable or porous material. All the embankment or earth dams leak to some extent. Seepage is the result of water moving or percolating gradually through the foundation of the dam. This is not the serious situation and can be controlled if measures are taken to contro l the movement of water under the dam. If seepage becomes uncontrollable and it is continuously eroding soil from embankment or dam foundation then it will result in failure of the dam. Generally , the process of erosion of embankment soil starts at downstr eam of the dam, this continuously works towards the reservoir eventually developing a path or way to the reservoir and this phenomenon is known as piping. Piping is taken place from upstream to downstream under the foundation of dam. We can easily recognize piping by an increased flow rate at the downstream near the embankment or a whirlpool at the surface of the reservoir. After observing the seepage phenomenon, the supervisors must take care of the dam in order to avoid the failure. After seepage, if we o bserve whirlpool or eddy at upstream of the water surface of the dam then failure of the dam may follow.

We can avoid the failure only if we are able to control the piping. Along with overtopping, fully developed piping is virtually impossible to control and will result in failure. Apart from piping, seepage can also cause dam failure. Seepage can cause dam failure in ways like saturating the embankment results in weakening of the dam or by rising the internal pressure within the embankment. But it is very difficult to determine the saturation and internal pressure within the dam without proper Instrumentation.

**C. Structural Failure:** Here we will talk about the dams other than embankment or earthen dams. These are non -earthen embankment dams made up of con crete, masonry or other materials and does not consist soil matrix. Of the total dam failures occurred till now, 30 percent of them have been attributed to structural failures. The general reason behind structural failure is shear failure which results in sliding.

**A) Foundation Slide**: When foundation of dam consists of soft soils such as fine silt, soft clay etc. in such cases the entire dam may slide over the foundation. Sometimes, we may find seams of fissured rocks, shales or soft clay under the foundation and dam may slide over some of them, resulting in failure of dam. In such type of failure, top of embankment gets cracked and sub-slides, the lower slope moves outward forming large mud waves near the heel. Excessive pore water pressure in confined seams of sand and silt or hydrostatic pressure developed due to consideration of seams of fissured rocks, soft clay or shales embedded between sands or silts may reduce the shear strength of the soil, leading to the failure of the dam foundation without warning. Loose sand foundations may fail by the liquefaction or flow slides.

**B) Slide in Embankments**: When slopes of the embankment too steep for the strength of the soil, may results in dam failure because of sliding. The most critical condition of the slide of u/s slope is sudden drawdown of the reservoir. When the reservoir is full then d/s slope will most likely to slide. The upstream slope failure hardly leads to catastrophic failures, but d/s slope failures are very serious. These failures generally occur due to development of excessive unaccounted pore pressures which may reduce the shearing strength of the soils.

### 3.1.2 Different Modes of Failures of Gravity Dams:

a. **Overturning/Rotation about the toe**: If resultant of all the forces acting on dam at any of its sections passes outside the toe then there may be chances that dam shall rotate and overturn about the toe but practically such a situation shall not arise because dam will fail much earlier by compression.

b. **Compression/Crushing**: This is the condition when compressive stresses produced may exceed the permissible stresses and dam may fail by then failure of its materials.

c. **Tension:** Generally, masonry and concrete dams are designed in such a way that no tension is developed anywhere in the dam because these materials cannot withstand sustained tensile stresses and if dam may subjected to these stresses then material of dam may finally crack. When a tension crack develops at the heel then crack width loose contact with bottom foundation and finally becomes ineffective. Hence effective width at dam base reduces and it will increase maximum compressive stress at toe. The process continues and effective base width goes on decreasing and compressive stress at toe goes on increasing, eventually results in failure of the toe by direct compression. Hence, we can say that tension crack itself does not fail the structure, but it leads to the failure of the structure by producing excessive compressive stresses.

d. **Sliding**: Sliding or shear failure in gravity or masonry dams occurs when the net horizontal force at the base of the dam exceeds the frictional resistance developed at that level.

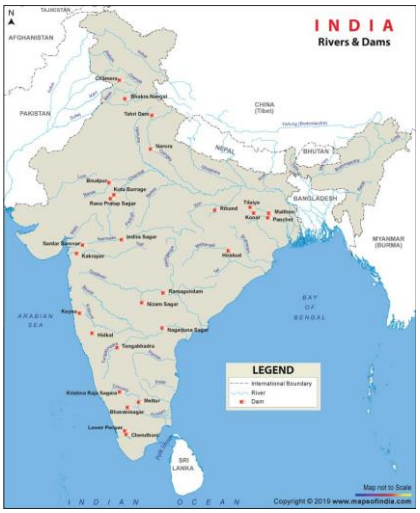



**Figure 3: Map of Major Dams of India**

## 4. Dam Break Modelling Process:

In dam break modelling process, we need numerical models to carry out the dam break study and flood routing. The study may be one dimensional, two dimensional or combination of both. When we increase channel width or flow becomes non- channelized, then accuracy of 1-dimensional models decreases. Hence, two dimensional models are more accurate and reliable while carrying out flood plain study. Mathematical modelling of dam break flood is carried out by one dimensional or 2-dimensional analysis. In one dimensional analysis we calculate the magnitude of flood, I.e., the discharge and level of water, variation of discharge and water level with time and velocity of flow through breach. The objective of most dam breach studies is to predict the flooding conditions and resulting loss of life. Talking about 2-dimensional analysis, we get additional information about the inundated area and variation of velocities and surface elevation can also be predicted. We use one dimensional analysis when the valley is long and narrow and flood wave characteristics over a large distance from the dam are of main concern. On the contrary, when the valley broadens in the downstream of the dam then in such a case large area would be flooded and 2-dimensional analysis becomes necessary. One dimensional analysis for dynamic routing consists of two partial differential equations derived by Barre De Saint Venant in 1871. These two equations are:

(a) Conservation of mass/continuity equation

$$(\partial Q/\partial X) + \partial (A + A0) / \partial t - q = 0$$

(b) Conservation of momentum equation

$$(\partial Q/\partial t) + \{\partial (Q2 /A)/\partial X\} + g A ((\partial h/\partial X) + Sf + Sc) = 0$$

Where Q = discharge; A = active flow area; $A_0$ = inactive storage area; h = water surface elevation; q = lateral outflow; $S_f$ = friction slope; X = distance along water way; t = time; Sc = expansion contraction slope and g = gravitational acceleration.

## 5. Types of Models for Dam Break Study

The models that have been used till now to carry out dam break study and flood inundation mapping are described below:

**(a) DAMBRK** model was developed by National Weather Services, USA in 1984. It predicts dam breach wave formation and progression of wave in downstream. The main features of this model are ability to describe dam break mode temporarily and geometrically, computation of outflow hydrograph of breach section and ability to route outflow through a downstream channel. DAMBRK model will be very helpful in finding potential influenced area. Thus, allowing users to input geometric and temporal data to accurately predict initial breach wave.

**(b) FLDWAV** model was developed as a replacement to DAMBRK model. It was developed by the National Weather Services, USA. It has wave front tracking for more accuracy and less computational time is required. This is designed basically to model rapid flood events from large precipitation event and it considers terrain and properties of material at different time interval. It also has secondary function of predicting flow through hydrological structures and river basins. This model can perform dam break analysis, pumping stations, flood predictions and other rapid flood events.

**(C) FLO-2D** model was developed in 1989. This model is based on MUDFLOW. It can predict flood hazard, mudflow, debris flow over alluvial river. It basically uses grid system for the determination of roughness coefficient, flow path and area. We can also estimate discharge based on depth of flow over each sector and summing up all sector on all the four sides of grid. The accuracy of FLO-2D model is dependent on data available and density of grid system.

**(d) SMPDBK** was developed by NWS I.e., National Weather Services, USA. This model was developed as a simplified version of DAMBRK. This model suits good for obtaining dam break risk and dam classification. Contrary to DAMBRK, this model is quick and easy to use and it does not require many parameters. The results provided by this model is similar as compared to DAMBRK. There is no need of a high specification computer to run the model. It is effective and efficient model to simulate the dam break and to prepare risk management plan.

**(e) Danish Hydraulic Institute (DHI) MIKE 11** is an advance and new generation software consist of Windows integrated graphical user interface. It is a 32 bit and 64 bit which have fast computation speed compared to previous versions of Mike. This software is user friendly, one dimensional tool for the dam break studies which simulates flood waves, water quality in channels or water bodies, sediment transportation, etc. Some of the major features of Mike 11 is that it is an integrated modular structure which consists various modules like hydrology, water quality model, cohesive sediment transport, non-cohesive sediment transport, rainfall-runoff model, hydrodynamic model and flood forecasting model.

One of the core module of Mike 11 package is hydrodynamic module which simulates unsteady flow in open channel. In this software, implicit finite difference method is used for simulation.

**(f) Danish Hydraulic Institute (DHI) Mike 2** is based on 2-dimensional modelling approach for 2D free surface flows and it performs study on Newtonian fluids over initial dry terrain. DHI Mike 2 is mostly preferred for 2-dimensional simulation of flow in rivers and estuaries. The model is very helpful for subcritical, supercritical and mixed flow conditions. We can also use it in designing of overland flood modelling, inland flooding, coastal and offshore structures. Mike 2 uses finite difference method for solving the numerical solution of the 2-dimensional shallow water equations.

**(g) Hydraulic Engineering Centre's River Analysis System (HEC-RAS)**: This software is designed for interactive use in a multitasking environment. This software is developed by the USACE (United States Army Corps of Engineers). In the old versions of HEC-RAS one dimensional flow simulation is possible only using full Saint Venant equation. In the new version which had arrived in February 2016, RAS model which has ability to perform 2D hydrodynamic unsteady flow routing using Saint Venant equation. In this HEC-RAS model diffusion wave equation was introduced to simulate the flow in river channels and flood and flood plains. This model was considered as an effective model for predicting downstream flooding effects by dam break analysis. The breach information and breach geometry are used as an input data to simulate the dam breach model by using the HEC-RAS model. Based on the consequences of an upstream event, the HEC-RAS model simulates the resulting flood wave generated. This model is very useful for mixed flow analysis, off channel and on channel reservoir storages and dam break modelling.

## 6. DAM BREACH PARAMETERS & PEAK FLOW PREDICTION EQUATIONS

Dam breach parameters have been classified into two categories- first one is geometric parameters and second one is hydrographic parameters and Shape and size of breach comes under geometric parameters. The second one is hydrographic parameters. Peak outflow rate and time of failure are defined by hydrographic parameters. The equations which are mostly used for the prediction of dam breach parameters have been described below:

### (a) Average Breach Width Equations:

**Von Thun & Gillette (1990)**

$B = 2.5h_w + C_b$ Where $C_b$= reservoir coefficient depending upon size of reservoir;

$h_w$ = height of water above breach bottom in m.

**Froehlich (2008)**

$B = 0.27K_0V_w^{1/3}$ Where, $K_0$=1.3, for overtopping;

$K_0$=1.0, for piping.

**(b) Peak Flow Equations:**

**Froehlich (1995q)**

$$Q_p = 0.607(V_w^{0.295} h_w^{1.24})$$

**Pierce (2010)**

$$Q_p = 0.038(V_w^{0.475} h_w^{1.09})$$

Where, $V_w$ = volume of water above breach bottom in $m^3$;

$h_w$ = height of water above breach bottom in m.

**(C) Failure Time Equations:**

**Von Thun and Gillette (1990)**

a. $t_f = 0.015hw$, for highly erodible

$t_f = 0.015h_w + 0.25$, for erosion resistant

**In terms of breach width**

b. $t_f = B / (4h_w + 61)$, for highly erodible;

$t_f = B / (4h_w)$, for erosion resistant

**Froehlich (2008)**

$$t_f = 0.0176\{V_w/(gH_b^2)\}^{1/2},$$

where $H_b$ = height of breach in m;

$V_w$ = volume of water above breach bottom in $m^3$.

## 7. Conclusion:

From the literature review carried out it was found that Mike 11, HEC RAS are the efficient tool which provides accuracy and reliability as well. Dam failure causes damage to structures, interruption to normal social and economic activities, loss of life. The losses occur due to flood mainly depends on velocity of flood, flood duration and inundation depth. On the basis of flood parameters, we can classify consequences as major, minor or moderate. Flood inundation map is generated with the help of Mike 21. Based on the results obtained from Mike 21, a risk management and rapid action plan are prepared for the unexpected dam break event. This will help to assign the responsibility to respective authorities such as dam owners, fire services, police and disaster management team.

Dam breach study also helpful in estimating the damage to property and loss of human life as a result of dam failure. Therefore, it has now become very important and necessary to carry out the detailed analysis of dam failure to study the effects of flood wave generated and to prepare inundation maps. After the dam breach, we need an emergency action plan for the evacuation of the population at risk. For that we prepare inundation maps, after that we select an appropriate model. Selection of the model can be done by analyzing the study area, accuracy of the model and dam breach parameters available.

## References:

[1]. Ankita Sawai, Dhananjay Singh Shyamal, Laukush Kumar, Dam Break Analysis - Review of Literature

[2]. A. Shahraki, A. Zadbar, M. Motevalli and F. Aghajani. Islamic Azad University, Central Tehran Branch, Tehran, Iran. Modeling of Earth Dam Break with SMPDBK Case Study of Bidekan Earth Dam

[3]. Data of Indian Dam failures, Central Water Commission, Government of India

[4]. DHI. MIKE FLOOD: 1D-2D Modelling User Manual; DHI Water and Environment: Horsholm, Denmark, 2009.

[5]. Froehlich, David C., (1995). "Peak Outflow from Breached Embankment Dam". ASCE Journal of Water Resources Planning and Management, Volume 121, Issue 1, January 1995, pages 90-97.

[6]. Heloisa Yang, Matt Haynes, Stephen Winzenread, and Kevin Okada (1999). The history of Dams.

[7]. History of Indian dams, Wikipedia

[8].Hydrologic Engineering Centre, (2010a). "HECRAS River Analysis System, Hydraulic Reference Manual", CPD-69. U.S. Army Corps of Engineers, Hydrologic Engineering Centre, 609 Second Street, Davis, CA.

[9]. Indian dam maps, Maps of India (2019)

[10]. Sunil Kumar, Anil Jaswal, Ashish Pandey, Nayan Sharma. Dam break study and inundation mapping
using hydraulic models and GIS. International Research Journal of Engineering and Technology.

[11]. Indian dam maps, Maps of India (2019)

[12]. Risk Assessment Report of Kanhar Barrage Project in Garhwa District, Jharkhand, Mantec Consultants Private Limited, Noida.

[13]. S.K. Garg, Irrigation Engineering and Hydraulic Structures (Khanna Publications)

[14]. Sunil Kumar, Anil Jaswal, Ashish Pandey, Nayan Sharma. Dam break study and inundation mapping using hydraulic models and GIS. International Research Journal of Engineering and Technology.

[15]. Tony L. Wahl, Hydraulic Engineer, Bureau of Reclamation, Denver, CO, twahl@usbr.gov, DAM BREACH MODELING – AN OVERVIEW OF ANALYSIS METHODS.

[16]. U.S. Department of the Interior Bureau of Reclamation Technical Service Center Hydraulic Investigations and Laboratory Services Group Denver, Colorado. Evaluation of Erodibility-Based Embankment Dam Breach Equations.

[17]. U.S. Army Corps of Engineers, "Engineering and Design–Hydrologic Engineering Requirements for Reservoirs,"EM 1110-2-1420, 31 October 1997. 12

[18]. US Army Corps of Engineers, "HEC-RAS River Analysis System, Applications Guide Version 3.1," Hydrologic Engineering Center, November 2002.

[19]. US Army Corps of Engineers, "HEC-RAS River Analysis System, User's Manual Version 4.0 Beta," Hydrologic Engineering Center, November 2006.

[20]. Wahl, Tony L., (1988). "Prediction of Embankment Dam Breach Parameters", A Literature Review and Needs Assessment, Water Resources Research Laboratory, U.S. Department of the Interior, Bureau of Reclamation, Dam Safety Office, 1988.

# Theme XI

# Watershed Management

*IN PROCEEDINGS OF 25th HYDRO 2020, INTERNATIONAL CONFERENCE, NATIONAL INSTITUTE OF TECHNOLOGY ROURKELA, ODISHA, INDIA 26-28, March 2021, ISBN 978-93-90631-56-8*

Paper ID - 012

# Variability analysis of hydrological parameters of Faridabad district (Haryana state)

Mridula Sharma[1]and Arun Goel[2]

[1]*M.Tech Student, Department of Civil Engineering, National Institute of Technology, Kurukshetra, Haryana-136119 India;*

[2]*Professor, Department of Civil Engineering, National Institute of Technology, Kurukshetra, Haryana-136119,India;*

*e-mails: mridula0995@gmail.com, drarun_goel@yahoo.co.in*

## Abstract

Hydro-geological parameters and land-use pattern of any region vary with space & time and have a profound impact on the groundwater resource of any region. Faridabad district, an industrial town of Haryana state is situated in south eastern part of Haryana and is a part of National Capital Region (Delhi-NCR) has been considered in this study. Some regions in Faridabad district have undergone ground water level declination recently and this pressure is attributed to ground water being the principal resource for irrigation in this district. The monthly and meteorological data for 37 years ranging from 1981-2018 was collected from the NASA website and later on it was arranged season wise namely monsoon, pre monsoon, post monsoon rabi (POMR) and post monsoon kharif (POMK). The ground water level data for 17 years (2000-2017) was accessed through CGWB website.

In this paper, an attempt has been made to analyse seasonal trends of hydrological parameters of the region including Precipitation, Temperature at 2m, Wind Speed at 2m and Relative Humidity at 2m along with ground water levels by using Mann-Kendall test and Sen's slope estimation techniques on the basis of MAKESENS excel template. The mean & standard deviation values of the hydrological parameters along with Mann Kendel test static 'Z' and Sen's slope 'Q' have been calculated and subsequently graphs are plotted for the purpose of trend analysis. It is expected that results of this study can be implemented for water availability studies in any region with similar climatic conditions for management of water resources at local and regional level.

**KEYWORDS** *Rainfall, Ground Water, Trend analysis, Hydrological parameters, Mann-Kendall Test, Faridabad.*

## 1. Introduction

The understanding of variations in trends of hydrological parameters and their inter-relationship can play a key-role in planning and maintaining a sustainable environment. Kumar et al. (2010) examined month to month, seasonal and yearly patterns of precipitation utilizing month to month precipitation information of one hundred thirty five years (1871– 2005) for thirty sub-divisions (sub-districts) in

India and expressed that regarding level of mean per 100 years, states of Punjab and Haryana saw a huge escalating pattern in the annual precipitation. Krishan et al. (2015) conducted the trend detection analysis of rainfall for 17 districts of Punjab including Patiala, Sangrur and Mansa which fall in Ghaggar basin and shown an increasing rainfall trends in annual, monsoon, pre-monsoon and post-monsoon seasons.

Whereas Kumar et al. (2015) divided Haryana state into three zones and stated that the yearly typical precipitation value differed from 389.4 to 815.0 mm and noted an apparent diminishing pattern in precipitation from north east to south west Haryana. Also, as per, Rainfall Statistics of India-2016 (2017), both Haryana and Punjab remained in Deficient/ Large Deficient category of rainfall at least for three of the seasons as well as annually.

Moreover, far ground water studies, Rodell et al. (2009) examined the perceptions from NASA's GRACE i.e. Gravity Recovery and Climate Experiment and observed that subterranean water was declining at a mean rate of $4.0 \pm 1.0$ cm/year proportional stature of water ($17.7 \pm 4.5$ $km^3$ $yr^{-1}$) in the Indian states of Punjab, Haryana, Rajasthan and capital, N.Delhi and more than 109 km3 of ground water vanished during August 2002 and October 2008, double the volume of India's biggest surface water repository, the Upper Wainganga in the state of Madhya Pradesh. In spite of the fact that there were no unordinary drifts in precipitation. Another examination combined satellite GRACE's information with hydrological models for excluding common variations and inferred that the area lost ground water at a rate of $54 \pm 9 km^3$/year during April, 2002 and June, 2008. It is expected to be the biggest rate of groundwater depletion in any approximately similar-sized locale of the world. Its plausible commitment to sea level ascent is probably comparable to that due to melting of Alaskan ice sheets. This pattern, if continued to sustain, will prompt a noteworthy water emergency in the area when this exhaustible asset gets depleted.

Sharma and Goel (2018, 2019, 2020) & Sharma (2019) and Pathak et al.(2019) inferred that there is a clear and alarming declination in ground water levels and although some decrease in local rainfall trends is also observed but decline in rainfall is not the only and prominent cause of such a sharp decline in ground water level. It is likely to be attributed to indiscriminate pumping of ground water for irrigation and other demands. Therefore, a need to explore rainfall vis-a-vis ground water trends in greater detail is felt since, such a study is expected to pave way for estimation of sustainable pumpage of ground water and play a vital role in accessing the scope of artificial groundwater recharge structures for mitigating the adverse impact of rainfall variability on groundwater (Ionut et al. 2020) . Moreover, in order to gain additional edge in gaining insights, trend analyses of factors like temp at

2m, wind speed at 2m and relative humidity at 2m have also been done along with analysis of depth to ground water level and rainfall in the present study.

## 2. Study Area

Faridabad districtof Haryana, as shown in Fig.1, is situated in south eastern part of Haryana and is located between 27° 39', 28°31' N latitude and 76°40' and 77°32' E longitudes. In the northdirection it is surrounded by Delhi and in the east of Uttar Pradesh state. On the North Western border of Faridabad, of Mewat and on the western border lies Gurgaon district of Haryana.

The total geographical area of the district is estimated as 2151 $km^2$ and the district is divided in two Blocks namely Faridabad and Ballabgarh with Faridabad town being the head-quarter of the district. The district is mainly drained by the river Yamuna and its climate can be classified as tropical steppe, semiarid and hot also which is mainly characterized by the extreme dryness of the Air except during the monsoon period. Some regions in Faridabad district have undergone ground water level declination recently and this pressure is attributed to ground water being the principal resource for irrigation in this district.

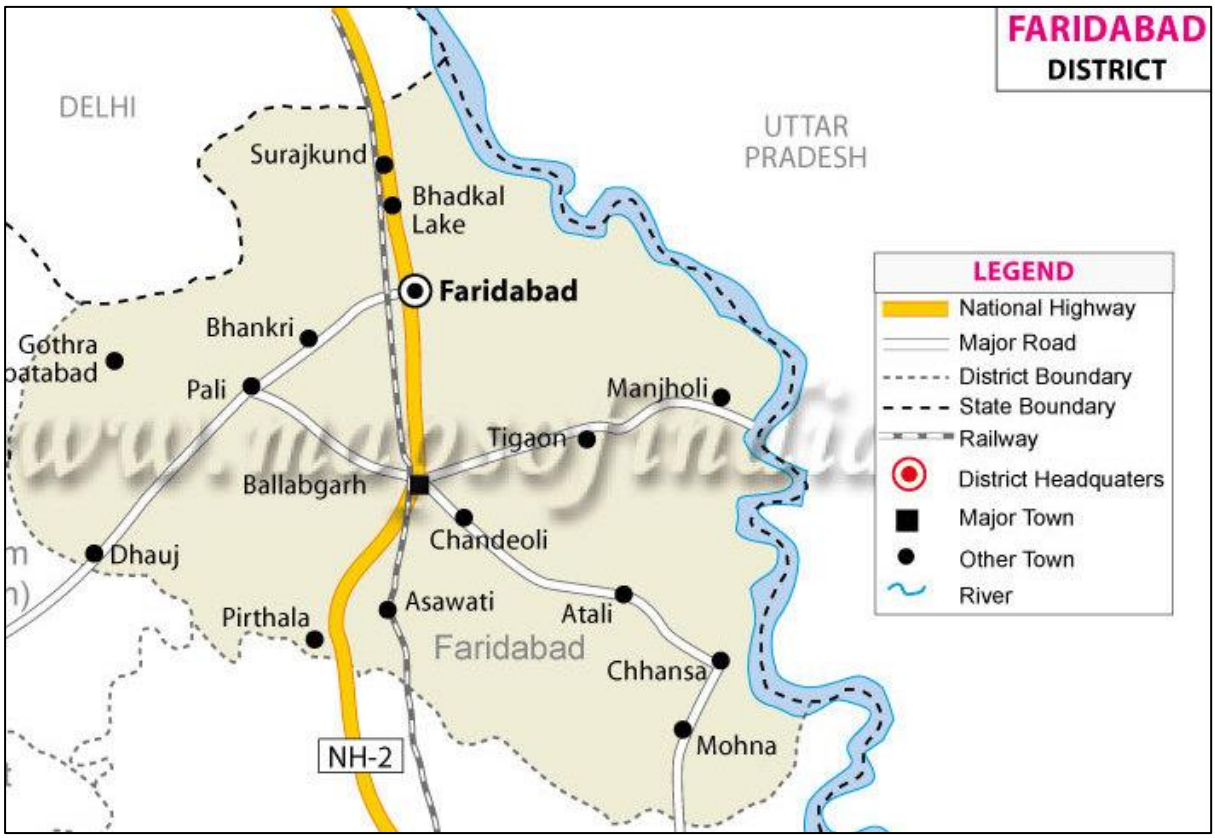



**Figure 1.** Map of Faridabad District.

## 3. Methodology

The monthly and annual meteorological data for a period of 37 years (1981-2018) was accessed from NASA's data access too and then the data was calculated and arranged season-wise. The year was divided into four seasons of three months: (a) Post Monsoon Rabi from January to March and abbreviated as PoMR, (b) Premonsoon season from April to June, (c) Monsoon Season from July to September and (d) Post Monsoon Kharif from October to December and abbreviated as PoMK.

The data corresponding to four seasons monsoon, pre-monsoon, post-monsoon rabi (PoMR) and post-monsoon kharif (PoMK) depth to ground water level below ground (m bgl) for a period of 22 years (1996-2018) was accessed from Central Ground Water Commission's website.

The sorted seasonal hydrological data of all five parameters was used to calculate average values and standard deviations and perform trend analysis which required use of Mann–Kendall Test and Sen's slope estimator is statistical analysis which was completed using MAKESENS excel template. The positive values of Mann Kendall test statistic Z represents inclining trend and vice-versa and the value of Sen's slope Q value represents the quantity of increasing or decreasing trend (Jain & Kumar 2012).

The mean and standard deviation values of the hydrological parameters along with values of Mann-Kendall Test statistic Z and Sen's slope Q are tabulated for all the hydrological parameters as mentioned above so that the trend of these parameters can be compared rationally. Moreover, graphical representation of trends for precipitation and depth to groundwater level has also been done.

## 4. Analysis of Trends

The hydrological parameters have been analysed statistically for district Panchkula. The results are tabulated in Table 1 and Table 2 and trends for hydrological parameters are plotted in Fig 2-6.

### *4.1 Precipitation*

The average and standard deviation (SD) values of the precipitation data for the period (years 1981-2017) in District Faridabad are (1.812162, 0.468758); (0.556847; 0.362271); (1.288739, 0.737964); (5.083874, 1.596706) and (0.282162, 0.308423) reported as Annual, PoMR, Premonsoon, Monsoon and PoMK. Also, as is evident, the average annual precipitation in the region is noted as 1.81216 mm/day. In terms of seasons, the highest rainfall, as expected, was noted in monsoon season as 5.08387 mm/day and the lowest was noted in PoMK as 0.28216 mm/day.

The Mann-Kendall test statistic indicates that precipitation trends for the period of 37 years were monotonic upward during monsoon and premonsoon but were decreasing during PoMR and PoMK. These trends were resonated by Sen's slope estimator which indicated that monsoon rainfall increased

by a slope of 1.8% and premonsoon rainfall had an upward slope of 0.9%. However, precipitation tended to be decreasing equally during PoMR and PoMK, each with a slope of -0.2%.

### *4.2 Temperature at 2m*

The average and standard deviation (SD) values of Temperature at 2m for the period 1981-2017 in District Faridabad are (25.84892, 0.609088); (18.36072, 0.976904); (33.80099, 1.057771); (30.58793, 1.2832) and (20.52631, 0.868714) reported as Annual, PoMR, Premonsoon, Monsoon and PoMK. Seasonally, highest average temperature was 33.8009°C in premonsoon and lowest was 18.3607°C in PoMR. The Mann-Kendall Z statistic was positive for every season except monsoon in which temperature showed a monotonic decreasing trend of slope -1.8% according to Sen's slope estimator. Also, temperature increased with a slope of magnitude 0.7%, 0.6% and 0.3% during PoMR, premonsoon and PoMK.

**Table 1.** Average and Standard deviations of Hydrological parameters of Faridabad District.

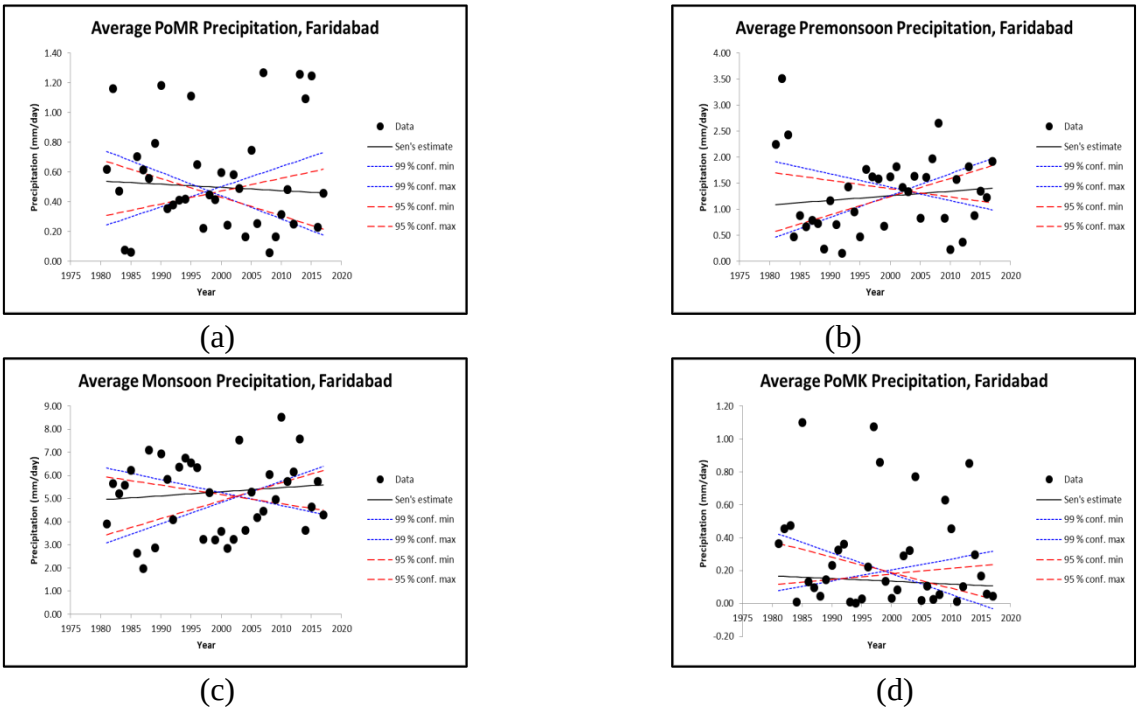
| **Time Series** | **Precipitation** | | **Temperature at 2m** | | **Wind Speed at 2m** | | **Relative Humidity at 2m** | | **Depth to Ground water level** | |
|---|---|---|---|---|---|---|---|---|---|---|
| | **Avg** | **SD** | **Avg** | **SD** | **Avg** | **SD** | **Avg** | **SD** | **Avg** | **SD** |
| Annual | 1.81216 | 0.468758 | 25.8489 | 0.609088 | 1.95351 | 0.120927 | 39.7554 | 4.995269 | 17.0412 | 6.795851 |
| PoMR | 0.55684 | 0.362271 | 18.3607 | 0.976904 | 1.84117 | 0.160309 | 33.5466 | 6.80858 | 14.1495 | 5.450613 |
| Premonsoon | 1.28873 | 0.737964 | 33.8009 | 1.057771 | 2.46252 | 0.214419 | 23.9621 | 5.497214 | 19.0159 | 7.381511 |
| Monsoon | 5.08387 | 1.596706 | 30.5879 | 1.2832 | 1.98837 | 0.202626 | 63.5604 | 9.286519 | 16.2442 | 4.287252 |
| PoMK | 0.28216 | 0.308423 | 20.5263 | 0.868714 | 1.52144 | 0.132971 | 37.7245 | 9.524401 | 18.7554 | 5.869552 |

**Table 2.**Mann-Kendall Test and Sen's Slope Estimator values for trends of Hydrological Parameters of Faridabad District.

| **Parameters** | **Precipitation** | | **Temperature at 2m** | | **Wind Speed at 2m** | | **Relative Humidity at 2m** | | **Depth to Ground Water Level** | |
|---|---|---|---|---|---|---|---|---|---|---|
| **Time series** | **Test Z** | **Q** | **Test Z** | **Q** | **Test Z** | **Q** | **Test Z** | **Q** | **Test Z** | **Q** |
| PoMR | -0.42 | -0.002 | 0.52 | 0.007 | -3.05** | -0.008 | 0.67 | 0.111 | 3.34*** | 0.742 |
| Premonsoon | 0.77 | 0.009 | 0.38 | 0.006 | -1.67+ | -0.006 | 2.41* | 0.196 | 3.05** | 0.863 |
| Monsoon | 0.65 | 0.018 | -1.16 | -0.018 | -2.35* | -0.007 | 0.95 | 0.162 | 2.28* | 0.394 |
| PoMK | -0.65 | -0.002 | 0.20 | 0.003 | -2.30* | -0.005 | 1.14 | 0.211 | 2.73** | 0.791 |

***trend at 0.1% level of significance; **trend at 1% level of significance

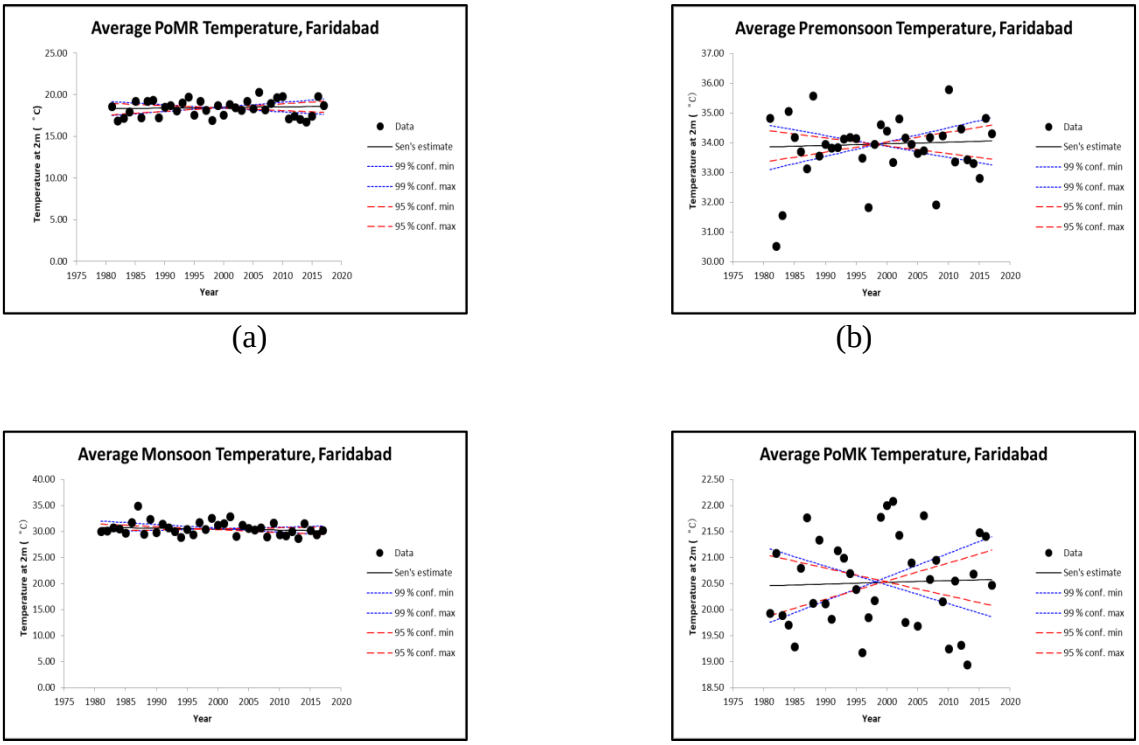
*trend at 5% level of significance; + trend at 10% level of significance




(a) (b)

(c) (d)

**Figure 2.** Variation in trend of Average Precipitation in Faridabad District (from 1981 to 2017) for (a) PoMR, (b) Premonsoon, (c) Monsoon and (d) PoMK season.




(a) (b)

**(c)** **(d)**

**Figure 3.** Variation in trend of Average Temperature at 2m in Faridabad District (from 1981 to 2017) for (a) PoMR, (b) Premonsoon, (c) Monsoon and (d) PoMK season.

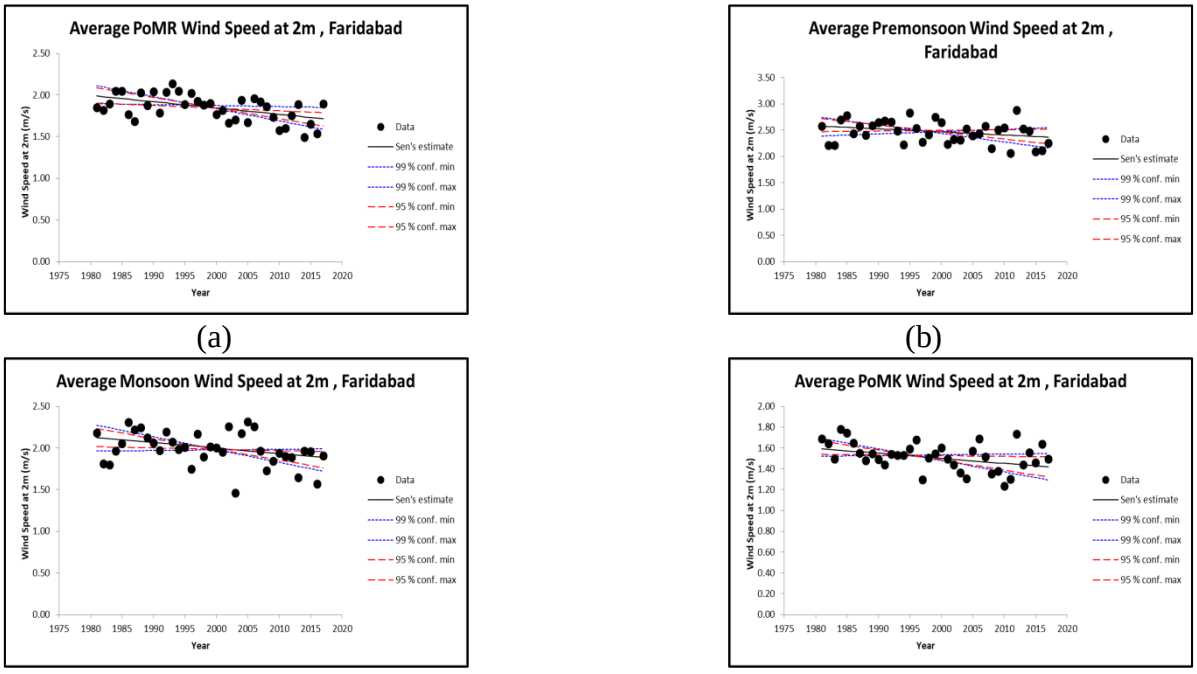



**Figure 4.** Variation in trend of Average Wind Speed at 2m in Faridabad District (from 1981 to 2017) for (a) PoMR, (b) Premonsoon, (c) Monsoon and (d) PoMK season.

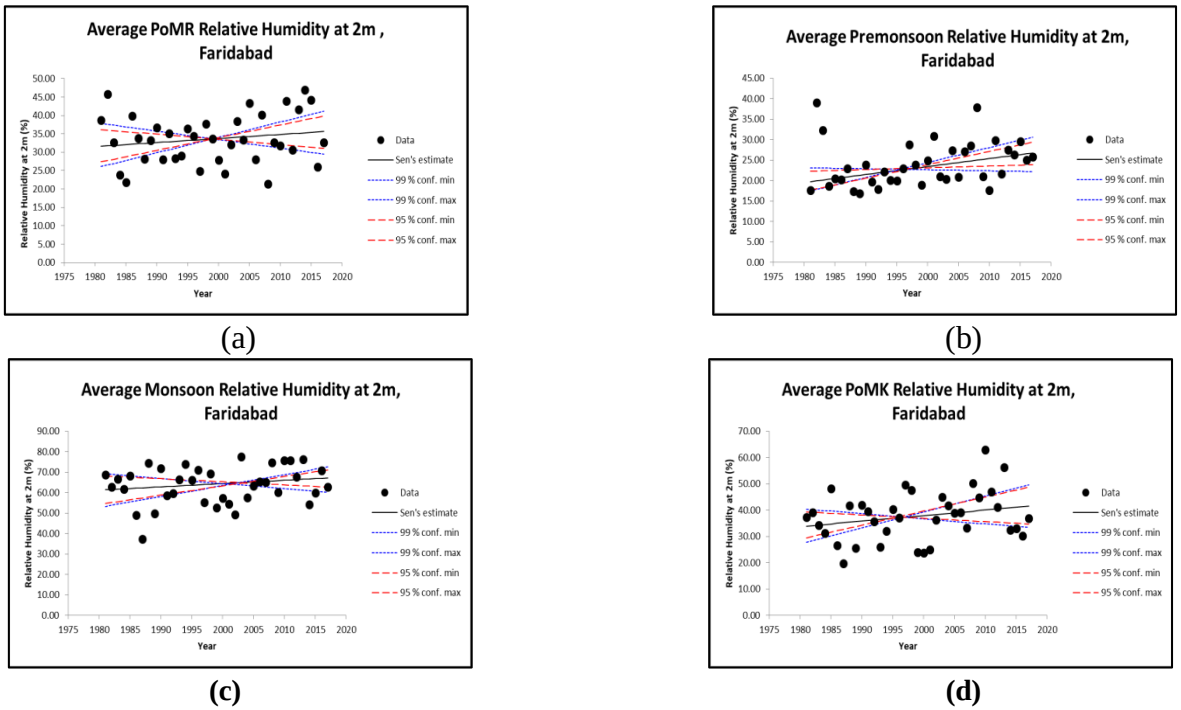



**Figure 5.** Variation in trend of Average Relative Humidity at 2m in Faridabad District (from 1981 to 2017) for (a) PoMR, (b) Premonsoon, (c) Monsoon and (d) PoMK season.

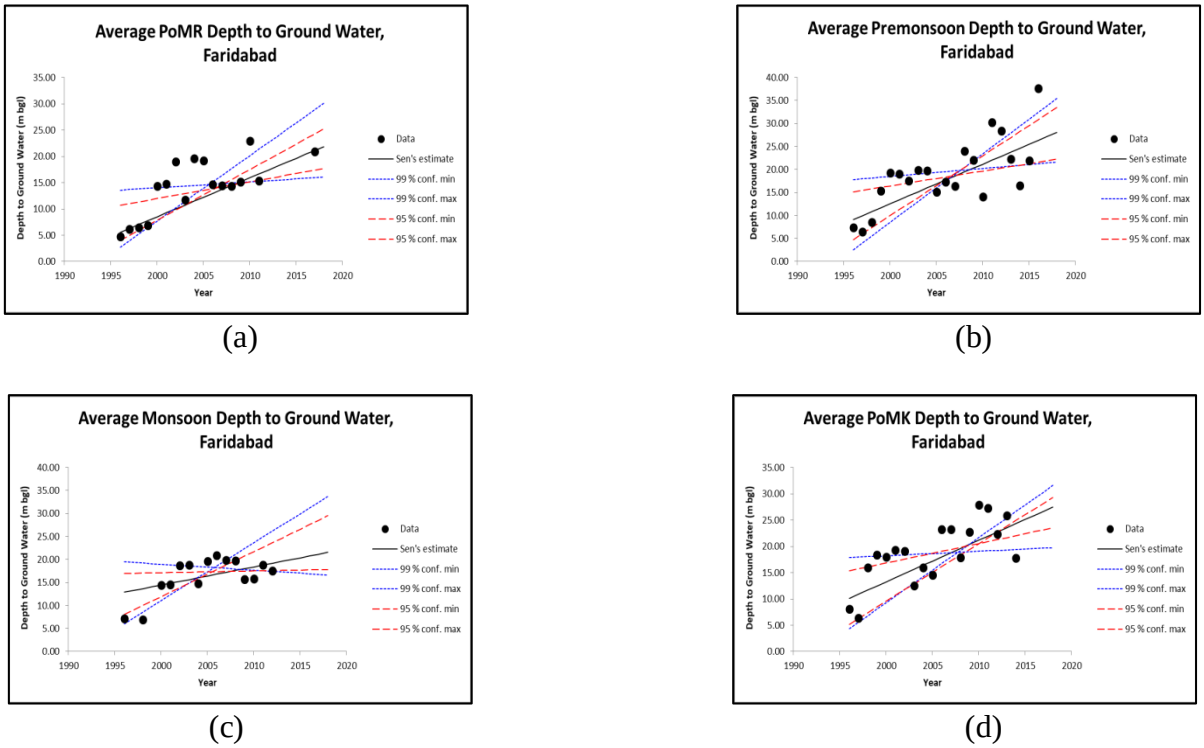



**Figure 6.** Variation in trend of Average Depth to Ground Water Level in Faridabad District (from 1996 to 2017) for (a) PoMR, (b) Premonsoon, (c) Monsoon and (d) PoMK season.

### *4.3 Wind Speed at 2m*

The mean and standard deviation values of Wind Speed at 2m for the period 1981-2017 in District Faridabad are (1.953514, 0.120927); (1.841171, 0.160309); (2.462523, 0.214419); (1.988378, 0.202626) and (1.521441, 0.132971) reported as Annual, PoMR, Premonsoon, Monsoon and PoMK. Also, as is evident, the maximum and minimum wind speed of 2.46252 m/sec and 1.52144 m/sec were noted for premonsoon and PoMK seasons respectively.

According to Mann-Kendall test, the wind speed trends were monotonic downward for every season with a significance level of 1%, 10%, 5% and 5% for PoMR, premonsoon, monsoon and PoMK respectively. Moreover, the most decreasing Sen's slope of magnitude 0.8% was observed for PoMR season and that for premonsoon, monsoon and PoMK was reported as 0.6%, 0.7% and 0.5% .

### *4.4 Relative Humidity at 2m*

The mean and standard deviation values of Relative Humidity at 2m for the period 1981-2017 in District Faridabad are (39.75541, 4.995269); (33.54667, 6.80858); (23.96216, 5.497214); (63.56045, 9.286519) and (37.72459, 9.524401) reported as Annual, PoMR, Premonsoon, Monsoon and PoMK. It is noted that the relative humidity was maximum in monsoon season with an average value of

63.5604% and minimum in premonsoon season with a value of 23.9621%. The relative humidity was found to be increasing for all the seasons, especially, during premonsoon, when the Mann-Kendall Z took the positive value of 2.41 with the significance level of 5%.

Further, as per Sen's slope estimator, the maximum upward slope of 21.1% was observed in PoMK and the minimum upward slope of 11.1% was observed in PoMR season. Also, the inclining slope of 19.6% and 16.2% was observed for premonsoon and monsoon season respectively.

### *4.5 Depth to Ground Water Level*

The mean and standard deviation values of depth to ground water level for the period 1981-2017 in District Faridabad are (31.52865, 5.556832); (31.62883, 5.333071); (33.40715, 5.181196); (33.26904, 4.406571) and (32.45842, 4.114574) reported as Annual, PoMR, Premonsoon, Monsoon and PoMK. The water level was deepest during premonsoon when it was observed to be 19.0159 m bgl and least average depth to water table was 14.1495 m bgl in PoMR season.

The Mann-Kendall test statistic indicated a prominent increase in depth to ground water level with a significance of 0.1%, 1%, 5% and 1% in PoMR, premonsoon, monsoon and PoMK respectively. The Sen's slope estimator highlighted that the depth to water increased the most during premonsoon with a slope of 86.3% and the least inclining slope of 39.4% was observed during monsoon season. Also, a slope of 74.2% and 79.1% was observed during PoMR and PoMK seasons respectively.

## 5. Conclusions

This study is focussed on statistical determining and monitoring four seasonal trends (premonsoon, monsoon, PoMR, PoMK) in hydrological parameters to understand the effect of climate change for an industrial city, Faridabad district, Haryana state. In this context, the results of the study have demonstrated that the rainfall increased during premonsoon and monsoon seasons and decreased with marginal slopes during PoMR and PoMK. The temperature at 2m increased for every season except monsoon whereas the wind speed at 2m showed decreasing slopes during all the seasons. Moreover, the depth to ground water increased considerably in all the seasons with a very high slope, indicating depletion of ground water resource due to high development rate, climate change effect on hydrological parameters and insufficient efforts towards groundwater recharge. This type of study would be quite helpful in effective and efficient management of available water resources of the area having similar conditions as of Faridabad district, Haryana, India.

## References

Ionut, Minea, Daniel Boicu and Oana-Elena Chelariu (2020), "Detection of Groundwater Levels Trends Using Innovative Trend Analysis Method in Temperate Climatic Conditions". *Journal of Water*, 2020, Vol. 12, pp 2129-2030.

Krishan G, Chandniha S. K, Lohani A. K. (2015). "Rainfall Trend Analysis of Punjab, India Using Statistical Non-Parametric Test." *Current World Environment*, 10(3).

Kumar, V., Jain, S. K. & Singh, Y. (2010)."Analysis of long-term rainfall trends in India." *Hydrol. Sci. J.* 55(4), 484-496.

Kumar, V., Niwas R. and Khichar, M.L. (2015). "Rainfall Zone and Its Trend Analysis in Haryana Using GIS." *Journal ofAgricultural Physics*. Vol. 15, No. 1, pp. 63-68.

Pathak, A.A.; Dodamani, B.M (2019), "Trend Analysis of Groundwater Levels and Assessment of Regional Groundwater Drought: Ghataprabha River Basin, India". Nat. Resour. Res., 28, 631–643.

Rodell M., Velicogna I. and Famiglietti J.S. (2009). "Satellite-based estimates of groundwater depletion in India." *Nature*. Vol.460, 999–1002.

Sharma M. and Goel A. (2018), "A Review of Rainfall and Ground Water Level Trends of Kurukshetra, Haryana'' *ASMMCE-2018 Proceedings,* NIT Jallandhar, Nov., pp 716-721.

Sharma M. and Goel A. (2019), "Trend analysis of hydrological parameters of two agrarian districts of Haryana, India, International Conference on Differential equations and control problems: Modelling, analysis and computations, June, IIT Mandi.

Sharma M (2019) "Study of Hydrological Parameters of selected Districts in Haryana", *M Tech thesis* NIT Kurukshetra.

Sharma M. and Goel A. (2020), "Analysis of Trends of Hydrological Parameters of Gurugram District, Haryana (India)." *International Journal of Water and Energy*, Vol. 63, No 2, pp 35 – 41.

Sharad K. Jain and Vijay Kumar (2012). Trend analysis of rainfall and temperature data for India, Current Science, Vol. 102, No. 1, pp 37-49

*IN PROCEEDINGS OF 25th HYDRO 2020, INTERNATIONAL CONFERENCE, NATIONAL INSTITUTE OF TECHNOLOGY ROURKELA, ODISHA, INDIA 26-28, March 2021, ISBN 978-93-90631-56-8*

Paper ID - 057

# *Comparison of spatial interpolation methods for filling missing observations in daily rainfall data*

C Reshma[1], R. Arunkumar[1]

[1]*Department of Civil Engineering, National Institute of Technology Calicut, NIT Campus PO, 673601, Calicut, Kerala*

*Email: reshmanarayananc@gmail.com*

## Abstract

Precipitation data is one of the main inputs for water-related research. However, there exits gaps (missing values) in the observed data series due to various reasons. To fill the missing observations in rainfall data, different spatial interpolation methods are available. Spatial interpolation techniques are also suitable in obtaining the spatial distribution of precipitation in areas where a sufficient number of rainguage stations are not available or the available stations are not evenly distributed. The current study involves the identification of the best method of spatial interpolation among four different interpolation methods, amounting to twelve different interpolation schemes in estimating missing rainfall data. In this study, the Koyna river basin located at Maharashtra, India was selected as a typical region. The performance of different methods in estimating the daily precipitation of the region was evaluated through a set of three error measures, Mean Bias Error (MBE), Mean Absolute Error (MAE) and Root Mean Square Error (RMSE) and using a cross-validation procedure. The comparative study demonstrated that the choice of different interpolation method yields significantly different results. Out of the twelve methods analyzed, Kriging with spherical variogram was found to provide best results with MBE, MAE and RMSE values as -4.06 mm, 2.67 mm and 8.33 mm respectively. The other methods that were found to perform reasonably well were Kriging with exponential and circular variograms, trend surface of degree n =1 etc.

***Keywords:*** *Rainfall Data; Missing Observations; Spatial Interpolation*

## 1. Introduction

The availability of reliable climate data is fundamental for proper planning, design, efficient operation and management of water resources systems (Legates and McCabe, 1999; Chen et al. 2010; Wagner et al. 2012; Borges *et al.*, 2016; da Silva *et al.*, 2019) as well as represents a critical input for developing diverse models dealing with environmental and ecological studies as well as agronomy (da Silva *et al.*, 2019). Being the primary source of inland water resources, rainfall has the greatest impact on environment. As such, rainfall represents a climate variable of extreme socioeconomic importance, directly related to the development and growth of crops and decision making for water management (Hoogenboom, 2000; da Silva *et al.*, 2019). Therefore, the availability of rainfall information plays an important role in hydrological modelling, water resources management and disaster mitigation (Silva,*et al.*, 2007; Suhaila *et al.*, 2008; di Piazza *et al.*, 2011; Keblouti *et al.*, 2012; Wagner *et al.*, 2012; Sridhar *et al.*, 2013; Seong and Sridhar, 2017; Venkata Rao *et al.*, 2020). In this respect, the accurate representation of spatial precipitation is very important in terms of the success of the hydrological studies (Chen *et al.*, 2017; İçağa and Taş, 2018; Xiangyu *et al.*, 2020). However, observation stations that provide the precipitation data have spatial limitations on installation and numerous shortages or disconnections occur in precipitation data because of missing of data from electrical shutdowns, machine failures, and program errors in the process of observing the data Suhaila *et al.*, 2008; Yoo, 2019). The results of the hydrological and meteorological models could be influenced by considering the incomplete series of rainfall records as an input in the analysis, which means the estimation of missing rainfall values becomes a more important task and the suitable methods to replace the missing values are always a main interest in hydrological and meteorological studies Suhaila *et al.*, 2008). Generally traditional weighting and data-driven methods can be used for estimating rainfall data; while regression, artificial neural networks and time series analysis belong to the latter, the former methods are given by a class of spatial interpolation techniques (di Piazza *et al.*, 2011). Spatial interpolation is a method in which values of a variable are estimated in a region surrounded by the available sampling

points allowing for spatially explicit mapping of the variable behaviour (da Silva *et al.*, 2019). A wide range of interpolation methods are available, which can be classified in two categories: the deterministic methods such as inverse- distance weighting and non- linear interpolation such as spline techniques and the stochastic interpolation methods of the kriging family (Wagner *et al.*, 2012; Mendez and Calvo-Valverde, 2016; Chen *et al.*, 2017; da Silva *et al.*, 2019). Each methods advantages and disadvantages depend strongly on the characteristics of the data set: a method that fits well with some data can be unsuitable for a different set of data (Keblouti *et al.*, 2012). The main objective of the current study is to evaluate the performance of different interpolation schemes in the determination of daily precipitation for Koyna river basin located at Maharashtra, India.

## 2. Materials and methods

### 2.1 *Study area and data used*

The area selected for current study is Koyna river basin, a sub-basin of Krishna river basin situated in Satara district, Maharashtra, India. The Koyna river basin extends between the latitude of 17º 07′ 55″ - 17º 57′ 50″ N and longitude of 73º 33′ 15″ - 74º 11′ 10″ E. This river basin generally trends north - south and covers an area of 2,036 km$^2$. The location of the Koyna river basin along with nine rain- gauge stations in the watershed is shown in Figure 1. Daily rainfall data of these nine stations located in the study area has been chosen in this study. From the whole rainfall time series, one month of data is taken to study the applicability of various spatial interpolation schemes. This data is shown in Figure 2.

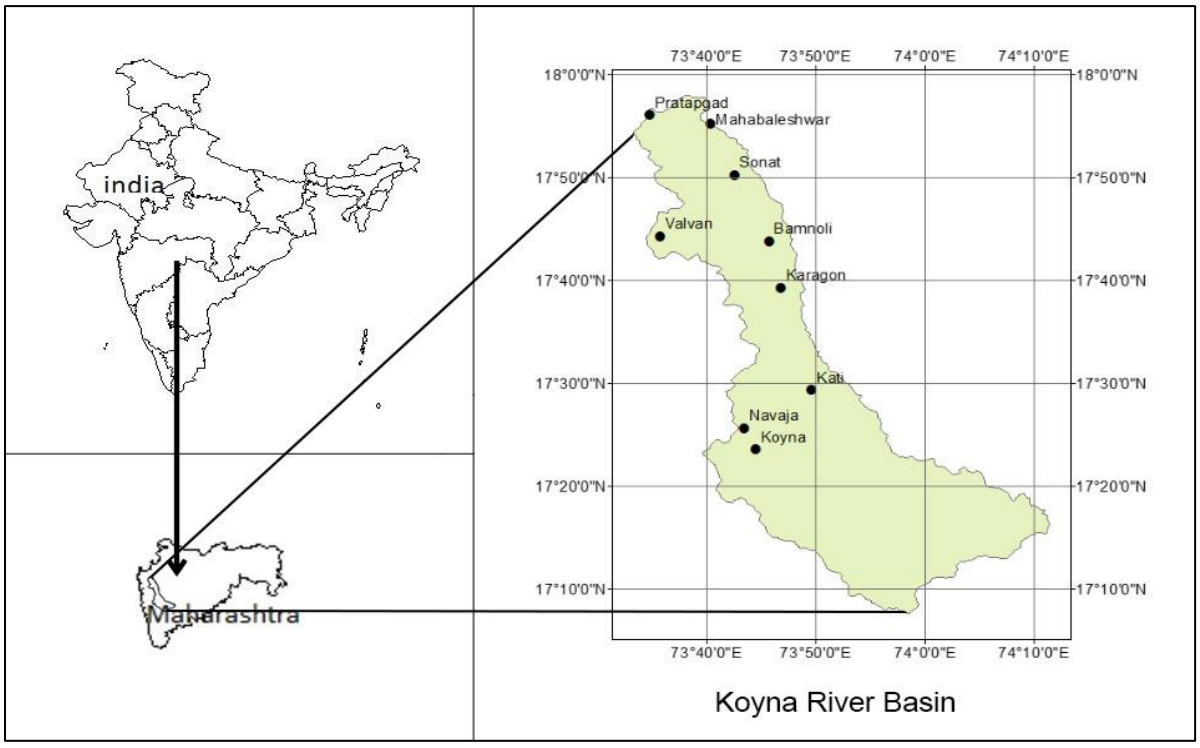



**Figure 1** Koyna River basin

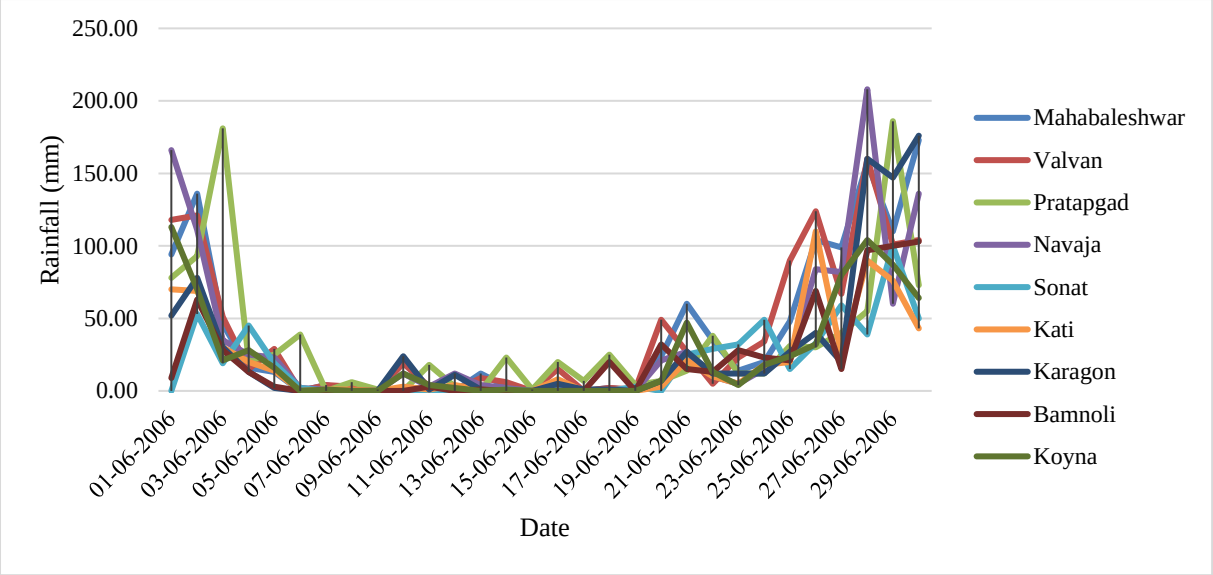



**Figure 2** Observed rainfall at the nine rainguage stations

## 2.2 *Spatial interpolation methods*

Spatial interpolation is a process that employs mathematical techniques to yield estimates (as precise as possible) of the values of a given variable within a region, in places where no real measurements have been performed (da Silva *et al.*, 2019). Spatial interpolation methods use the points with known values of the variable of interest to estimate the values at other points where the value of the variable of interest is not available. In general, interpolation methods assume that the value at a given place is more similar to the values measured at neighbouring sample points than the values of the most distant sample points (da Silva *et al.*, 2019). This section briefly introduces the four interpolation methods used in this study.

### 2.2.1 *Inverse distance weighting*

Inverse distance weighting is a deterministic method of spatial interpolation. It is widely used for the estimation of missing data in hydrology (Chen *et al.*, 2017). The inverse distance weighting method is based on the proximity of the neighboring stations or surrounding stations to the target station Suhaila *et al.*, 2008). The farther the position of the surrounding station from the station, i.e. the sample point of interest, lower its influence on the interpolation value. IDW mainly depends on the inverse of the distance between the station of interest and the surrounding stations. In this study three interpolation schemes based on IDW, with powers 2,3, and 4 has been compared. Let r = (x, y) be the position of an arbitrary point within the interpolation region, the IDW formula is given by

$$F(r) = \sum_{k=1}^{N} W(r_k) f(r_k) \quad (1)$$

where $F(r)$= interpolated value at the point r; N =total number of observations (rain gauge stations in the current study); $f(r_k)$ = value observed at the $k^{th}$ station at $r_k = (x_k, y_k)$; and $W(r_k)$= weight or relative contribution of station $r_k$ on the interpolated value. The weight is given by,

$$W(k_r) = \frac{d_k(r)^{-p}}{\sum_{k=1}^{N} d_k(r)^{-p}} \quad (2)$$

where $d_k(r)$the distance between points r and rk and p isd p is the specified power.

### 2.2.2 *Kriging*

The kriging method belongs to the category of geostatistical methods which depends on the statistical relationship among the sample points. In kriging method mathematical function is fitted to the selected sample points to determine the output value for the station of interest. It is based on the idea that values measured at near locations tend to be statistically more related than values measured at other locations (Tveito, Wegehenkel and Van Der Wel, 2006; Borges *et al.*, 2016). Kriging is a multistep process; it includes exploratory statistical analysis of the data, variogram modelling, and creating the surface. A variogram or covariance function provides a method for quantifying the spatial correlation which is then incorporated in the spatial model. The empirical semivariogram function used to obtain the weights is given by the equation,

$$\gamma(h) = \frac{1}{2N(h)} \sum_{k=1}^{N(h)} [f(r_k) - f(r_k + h)]^2 \quad (3)$$

where $N(h)$ is the number of sample pairs, $f(r_k)$ and $f(r_k + h)$ separated by a distance h. The empirical function $\gamma(h)$ is then fitted to a specific functional form (da Silva *et al.*, 2019) such as circular, spherical, exponential, exponential and linear. Even though different kriging versions exists, the current study is limited to ordinary kriging which works under the following condition.

$$\sum_{k=1}^{N} W(r_k) = 1 \quad (4)$$

In this work, all the aforementioned variograms are used.

### 2.2.3 *Spline*

The spline method is a deterministic interpolation method which belong to the Radial Basis Functions (RBF) group in which smooth surfaces are calculated from data points (Tveito, Wegehenkel and Van Der Wel, 2006; Borges *et al.*, 2016). In spline method a smooth surface passing exactly through the sample points is fitted under the assumption that the overall surface curvature is minimized. There are two spline types namely Regularized and Tension. In Regularized type of spline, a smooth gradually changing surface is generated with values that may lie outside the data range, where in tension type of spline the values are more closely constrained. In this method for surface interpolation, the following equation is used.

$$S(x, y) = T(x, y) + \sum_{k=1}^{N} \lambda_K R(r_k) \quad (5)$$

where $\lambda_K$ are the coefficients found by solving the system of linear equations relating the values at the known sample points and $T(x, y)$ and $R(r_k)$ are functions defined differently for the different types of spline.

For regularized spline $T(x, y)$ is given by,

$$T(x, y) = a_1 + a_2 x + a_3 y \quad (6)$$

where $a_1$, $a_2$, $a_3$ are the coefficients obtained by solving the system of linear equations. $R(r_k)$ is given by

$$R(r_k) = \frac{1}{2\pi}\left(\frac{r^2}{4}\left[\ln\left(\frac{r}{2\tau}\right) + c - 1\right] + \tau^2\left[k_o\left(\frac{r}{\tau}\right) + c + \ln\left(\frac{r}{2\pi}\right)\right]\right) \quad (7)$$

where r is the distance between the point and sample, $\tau^2$ is the weight parameter the value of which, used in this study is 0, $k_o$ is the modified Bessel function, and c is a constant equal to 0.0577215.

For the Tension spline, $T(x, y)$ is given by

$$T(x, y) = a_1 \quad (8)$$

where $a_1$ is a coefficient found by the solution of a system of linear equations. $R(r_k)$ is given by

$$R(r_k) = \frac{1}{2\pi\phi^2}\left[\ln\left(\frac{r\phi}{2}\right) + c + k_o(r\phi)\right] \quad (9)$$

where $\varphi^2$ is the weight parameter, the value of which is set to 0 in this study.

### 2.2.4 *Trend surface analysis*

The trend surface analysis is a deterministic method of interpolation. In this method a polynomial fit is developed for the data through a multiple regression process between the observed values and the geographic location of the sample points (da Silva *et al.*, 2019). This method allows to control the order of the polynomial used to fit the surface. In this study the order of the polynomial used is restricted to one and two.

$$F(r) = \sum_{\rho=0}^{n}\sum_{i=0}^{\rho}\sum_{j=0}^{\rho-1} c_{i,j,\rho} x^i y^j + \varepsilon \quad (10)$$

where n= polinomial order; $\varepsilon$= stochastic error term; and coefficients $c_{i,j,\rho}$ are determined through least square fitting by minimising the sum of stantard deviations from the trend surface.

$$S = \sum_{K=1}^{N}[F(r_k) - f(r_k)]^2 \quad (11)$$

In the present study, the performance of a total of twelve interpolation schemes corresponding to the four mentioned methods is evaluated. The method used for the evaluation of the interpolation techniques is introduced in the following section.

### 2.3 *Evaluation of spatial interpolation methods*

To identify the best suited spatial interpolation method for determining missing rainfall data the study area, a cross validation procedure is adopted. The cross validation procedure was implemented following Borges *et al.*, (2016), Chen *et al.*, (2017), and da Silva *et al.*, (2019). One of the sample points, i.e. rain gauge stations is removed from the data set. Then the value of rainfall at that particular station is estimated using the spatial interpolation methods. Finally, the estimated value of rainfall at the station is compared with the actual measured values. Comparison of the estimated and observed values is accomplished with the aid of error measures. The error measures used in this study are Mean Bias Error (MBE), Mean Absolute Error (MAE), and Root Mean Square Error (RMSE). The interpolation methods are ranked based on these three criteria to identify the most accurate one for the study area considered. The performance measures are given by,

Mean Bias error or simply bias is the difference between observed and estimated values. MBE gives a general idea about the direction of the error or bias and it is affected by the fact that positive and negative estimates can cancel out. The value of MBE ranges from -∞ to ∞. MBE is given by,

$$MBE = \frac{1}{M}\sum_{l=1}^{M}[f(r_l) - F(r_l)] \quad (12)$$

where M = number of chosen observations (total no. of days considered) at the test point chosen for cross validation, i.e. $r_{=}$ (x, y), $f(r_l)$ = value of rainfall observed at test point at a particular day l, and $F(r_l)$ = value estimated at point r for the particular day l.

Mean Absolute Error provides the average error of estimation. It is the arithmetic average of absolute error. The value of MAE ranges from 0 to ∞. Since the value of MAE will be always positive, it doesn't provide information regarding the direction of the error. But it is considered as a robust performance measure of interpolation methods (da Silva *et al.*, 2019).

$$MAE = \frac{1}{M}\sum_{l=1}^{M}|f(r_l) - F(r_l)| \quad (13)$$

Root Mean Square Error is the square root of the average of squared difference between the measured and estimated observations. The value of RMSE also ranges from 0 to ∞. For both MAE and RMSE lower values are desirable. RMSE is sensitive to large errors. Its value is amplified with the presence or large errors, since the errors are squared.

$$RMSE = \sqrt{(\frac{1}{M}\sum_{l=1}^{M}[f(r_l) - F(r_l)])} \quad (14)$$

This where M = number of chosen observations (total no. of days considered) at the test point chosen for cross validation, i.e. $r_= (x, y)$, $f(r_l)$ = value of rainfall observed at test point at a particular day l, and $F(r_l)$ = value estimated at point r for the particular day l.

## 2.4 *Results and discussions*

The boundaries of the Koyna watershed was extracted from SRTM DEM and the daily rainfall data for the nine rainguage stations in the catchment are collected. Among the nine rainguage stations, the data at the Koyna station was excluded and it was estimated using the twelve interpolation schemes of the four interpolation methods, IDW, Kriging, Spline and Trend surface analysis. Figure 3 shows the actual measured values of rainfall and the values estimated by the different interpolation schemes. The resulting values of rainfall from the interpolation is then compared with the actual measured values using three different performance measures namely MBE, MAE, and RMSE. Based on these three criteria the performance of the interpolation schemes is ranked to find the best suitable method. Table 1 gives the performance of the interpolation schemes based on these error measures.

Considering the MBE values the general direction of the errors were found to be negative, which implies that all the spatial interpolation schemes overestimated the missing rainfall values. Kriging with Gaussian semivariogram model was found to perform the best with the least value of MBE, i.e. -0.24, where Kriging with Linear semivariogram model performed the worst with MAE equal to -11.07. While comparing the performance using MBE, the range of error was found to be between 2.67 and 4.49, with Kriging with Spherical semivariogram model and IDW with power 3 being the best and worst performed interpolation schemes. The RMSE value was found to be varying between 8.33 and 24.64. Kriging with Spherical variogram model gave closer values and Trend surface analysis with degree of the polynomial equal to 2 gave least closer values.

The performance of all the interpolation schemes were ranked based on all these error measurers. Kriging with Spherical semivariogram model was ranked 1 where trend surface analysis with degree of the polynomial equal to two ranked 12. Among IDW schemes, the one with power equal to one performed the best. Also, Regularised Spline was found to perform better than the Tension Spline.

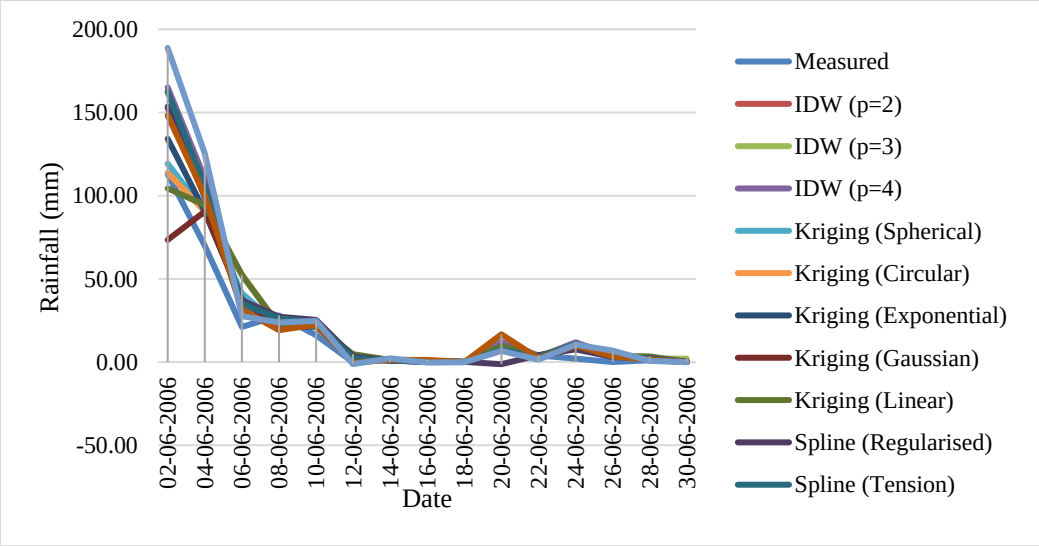



**Figure 3** Measured and estimated rainfall

**Table 1** Performance measures of interpolation methods

| | Performance Measures | | | |
|---|---|---|---|---|
| Interpolation Methods | MBE (mm) | MAE (mm) | RMSE (mm) | RANK |
| Inverse Distance Weighting | | | | |
| Power p =1 | -7.05 | 3.90 | 14.69 | 8 |
| p = 2 | -8.28 | 4.44 | 52.41 | 11 |
| p = 3 | -8.43 | 4.49 | 17.79 | 10 |
| Kriging | | | | |
| Spherical | -4.06 | 2.67 | 8.33 | 1 |
| Circular | -4.53 | 2.87 | 10.26 | 3 |
| Exponential | -4.40 | 3.06 | 9.39 | 2 |
| Gaussian | -0.24 | 3.64 | 32.71 | 5 |
| Linear | -11.07 | 3.28 | 11.07 | 6 |
| Spline | | | | |
| Regularized | -6.29 | 4.09 | 14.32 | 7 |
| Tension | -7.70 | 4.35 | 16.59 | 9 |
| Trend | | | | |
| Degree n =1 | -5.92 | 3.71 | 12.88 | 4 |
| n = 2 | -9.91 | 5.91 | 24.64 | 12 |

## 3. Conclusion

The performance of four spatial interpolation methods (twelve distinct schemes) in estimating missing rainfall data for Koyna river basin, Maharashtra, India was studied. The following conclusions can be drawn from the study:

1) The study demonstrated that the choice of different interpolation methods for estimating the missing rainfall data will yield significantly varying results.
2) For the chosen study area and data considered, Kriging with Spherical semivariogram model provided the best results. The other methods found to perform reasonably well were Kriging with Exponential and Circular semivariogram models and Trend surface analysis with degree of polynomial equal to 1.

## References

Borges, P. de A. *et al.* (2016) 'Comparison of spatial interpolation methods for the estimation of precipitation distribution in Distrito Federal, Brazil', *Theoretical and Applied Climatology*, 123(1–2), pp. 335–348. doi: 10.1007/s00704-014-1359-9.

Chen, T. *et al.* (2017) 'Comparison of spatial interpolation schemes for rainfall data and application in hydrological modeling', *Water (Switzerland)*, 9(5), pp. 1–18. doi: 10.3390/w9050342.

Hoogenboom, G. (2000) 'Contribution of agrometeorology to the simulation of crop production and its applications', *Agricultural and Forest Meteorology*, 103(1–2), pp. 137–157. doi: 10.1016/S0168-1923(00)00108-8.

İçağa, Y. and Taş, E. (2018) 'Aylık Yağışın Konumsal Dağılımının Modellenmesinde Farklı Enterpolasyon Yöntemlerinin Karşılaştırmalı Analizi', *Doğal Afetler ve Çevre Dergisi*, 90(272), pp. 89–103. doi: 10.21324/dacd.387061.

Keblouti, M., Ouerdachi, L. and Boutaghane, H. (2012) 'Spatial interpolation of annual precipitation in Annaba-Algeria - Comparison and evaluation of methods', *Energy Procedia*. Elsevier B.V., 18, pp. 468–475. doi: 10.1016/j.egypro.2012.05.058.

Legates, D. R. and McCabe, G. J. (1999) 'Evaluating the use of "goodness-of-fit" measures in hydrologic and hydroclimatic model validation', *Water Resources Research*, 35(1), pp. 233–241. doi: 10.1029/1998WR900018.

Mendez, M. and Calvo-Valverde, L. (2016) 'Assessing the Performance of Several Rainfall Interpolation Methods as Evaluated by a Conceptual Hydrological Model', *Procedia Engineering*. The Author(s), 154, pp. 1050–1057. doi: 10.1016/j.proeng.2016.07.595.

di Piazza, A. *et al.* (2011) 'Comparative analysis of different techniques for spatial interpolation of rainfall data to create a serially complete monthly time series of precipitation for Sicily, Italy', *International Journal of Applied Earth Observation and Geoinformation*. Elsevier B.V., 13(3), pp. 396–408. doi: 10.1016/j.jag.2011.01.005.

Seong, C. and Sridhar, V. (2017) 'Hydroclimatic variability and change in the Chesapeake Bay watershed', *Journal of Water and Climate Change*, 8(2), pp. 254–273. doi: 10.2166/wcc.2016.008.

da Silva, A. S. A. *et al.* (2019) 'Comparison of interpolation methods for spatial distribution of monthly precipitation in the state of pernambuco, Brazil', *Journal of Hydrologic Engineering*, 24(3), pp. 1–11. doi: 10.1061/(ASCE) HE.1943-5584.0001743.

Silva, R. P. De, Dayawansa, N. D. K. and Ratnasiri, M. D. (2007) 'A COMPARISON OF METHODS USED IN ESTIMATING MISSING RAINFALL DATA R. P. De Silva 1 , N.D.K. Dayawansa 1 and M. D. Ratnasiri 1', *University of Peradeniya*, (May), pp. 101–108.

Sridhar, V., Jin, X. and Jaksa, W. T. A. (2013) 'Explaining the hydroclimatic variability and change in the Salmon River basin', *Climate Dynamics*, 40(7–8), pp. 1921–1937. doi: 10.1007/s00382-012-1467-0.

Suhaila, J., Sayang, M. D. and Jemain, A. A. (2008) 'Revised spatial weighting methods for estimation of missing rainfall data', *Asia-Pacific Journal of Atmospheric Sciences*, 44(2), pp. 93–104.

Tveito, O. E., Wegehenkel, M. and Van Der Wel, F. (2006) *THE USE OF GEOGRAPHICINFORMATION SYSTEMS IN CLIMATOLOGY AND METEOROLOGY Final Report COST Action719*.

Venkata Rao, G. *et al.* (2020) 'Spatio-temporal analysis of rainfall extremes in the flood-prone Nagavali and Vamsadhara Basins in eastern India', *Weather and Climate Extremes*. Elsevier B.V., 29(January), p. 100265. doi: 10.1016/j.wace.2020.100265.

Wagner, P. D. *et al.* (2012) 'Comparison and evaluation of spatial interpolation schemes for daily rainfall in data scarce regions', *Journal of Hydrology*. Elsevier B.V., 464–465, pp. 388–400. doi: 10.1016/j.jhydrol.2012.07.026.

Xiangyu, Z., Chao, Z. and Jinyan, Y. (2020) 'Quantitative Analysis of Impact of Climate Variability and Human Activities on Water Resources Change in Suzhou City', in IOP Conference Series: Earth and Environmental Science. doi: 10.1088/1755-1315/435/1/012015.

Yoo, J. H. (2019) 'Optimal Exponent Values of Distance and Elevation Based on Hourly Rainfall Data in the Modified Inverse Distance Method', Journal of Hydrologic Engineering, 24(10), pp. 1–10. doi: 10.1061/(ASCE)HE.1943-5584.0001823.

*IN PROCEEDINGS OF 25th HYDRO 2020, INTERNATIONAL CONFERENCE, NATIONAL INSTITUTE OF TECHNOLOGY ROURKELA, ODISHA, INDIA 26-28, March 2021, ISBN 978-93-90631-56-8*

Paper ID - 133

# An Environment Concerned Risk Based Approach for Evaluating Watershed Health

Smaranika Mahapatra[1], Madan K. Jha[2]

[1]*Research Scholar, Agricultural and Food Engineering Department, Indian Institute of Technology Kharagpur, Kharagpur-721302, India*
[2]*Professor, Agricultural and Food Engineering Department, Indian Institute of Technology Kharagpur, Kharagpur-721302, India*
*Email: smahapatra44@gmail.com*

## Abstract

Evaluating the health of a watershed helps water managers and planners in prioritizing zones to formulate proper plans and efficient management strategies for ensuring sustainable water management. Yet, it has not attracted the attention of researchers, especially in developing countries. Also, the environmental flow (e-flow) concept has not been considered till now for assessing the health status of a river basin. To address these limitations, the present study was carried out in Rushikulya River Basin, a sub-tropical humid river basin of Eastern India. For assessing the health of the study area, two meteorological and hydrological criteria, viz., 'standardized precipitation index' (SPI), and 'monthly streamflow' for the period of 1990-2016 were selected. SPI of the whole basin was calculated at a monthly time scale. Further, three risk-based indicators, i.e., reliability, resilience, and vulnerability were calculated and combined to develop an 'integrated watershed health indicator' (IWHI). In the context of SPI, the threshold value was taken as that obtained for 'normal' condition, while 'monthly e-flow' was considered as the threshold for streamflow to assess the health of the river basin from a hydrological point of view. The e-flow was calculated by 'Flow Duration Curve Shifting' technique. Based on 'SPI', the related reliability and resilience of the whole river basin are found to be decreasing over the years with an increased vulnerability. However, the risk indicators corresponding to streamflow show an insignificant increasing trend over the years. The analysis revealed that the overall basin health was found to be in a bad state having mean IWHI value below 0.5 with being in the worst state (IWHI = 0) for 11 years. The methodology adopted and the results obtained in this study can provide the water managers and decision-makers a practical idea of the overall health status of a river basin from an ecohydrological context for developing an efficient water management plan.

***Keywords:*** *Integrated watershed health indicator; risk-based indicators; environmental flow; FDCS; SPI.*

## 1. Introduction

Along with rapid rise in the global population and related consumptions, unsustainable practices and policies are undermining the precious natural resources, thus threatening the ecosystem and human health. As a consequence, the dwindling land and fresh water resources put vast challenges before the water managers to deal them effectively in a sustainable way. In the past, demand-centric and the related wrong water management decisions taken have led to an unsecure and unsustainable world, rather, our environment has been greatly affected to the point in terms of dried rivers, exploited groundwater and severe pollution (Cosgrove and Loucks 2015), which further puts detrimental impact on us only in long run. Balancing human and environmental needs can be a possible solution in this direction and should be given an immediate attention (UNFPA 2001).

Integrated watershed management is one of the most widely adopted technology, aimed at protecting the environment, i.e., enhancing the productivity of soil, crops and conserving the water resources while benefiting the dependent habitats and livelihoods. Protecting the waters within the catchments is one of the key components of the strategies adopted in watershed management (Ahn and Kim 2017b).

Watersheds go through different levels of degradations with varying acceptable ranges related to different hydro-climatic, environmental or socio-economical aspects. Therefore, multiple watersheds within a catchment need to be brought within one framework that can aid watershed managers in effective decision making in terms of resource allocation or conservation in the whole catchment (Hoque *et al.* 2012). So, for implementation of effective watershed management strategies, spatial and temporal trends of the watershed health should be assessed so that strategic management priorities can be set at watershed level.

Generally, watershed health assessment includes some of the key components such as natural environment, hydrology, water quality, and aquatic communities (Ahn and Kim 2017b). In the recent past, some of the studies (Hoque *et al.* 2012; Sanchez *et al.* 2015; Ahn and Kim 2017a, 2017b; Hazbavi and Sadeghi 2017; Sadeghi and Hazbavi 2017; Alilou *et al.* 2019) have tried different approaches for watershed health assessment by using different indicators and highlighted the importance of this crucial analysis for effective watershed management. For example, Hoque et al. (2012) evaluated watershed health using stream-water quality data at different monitoring points within the Cedar Creek watershed in northeast Indiana, USA. The analysis revealed that the Cedar Creek watershed tends to be in compliance with respect to selected pesticides, ammonia and total phosphorus, while the watershed was found to be susceptible in violating sediment standards. Sanchez et al. (2015) employed streamflow, sediment, and nutrient load as the health indicators in the Saginaw River watershed in Michigan by using a rainfall-runoff model, Soil and Water Assessment Tool (SWAT) and the socioeconomic measures of communities by spatial-clustering techniques and confirmatory-factor analysis. Similarly, Ahn and Kim (2017a) determined watershed health, vulnerability and recovery potential for the Han River basin in South Korea using six major components, including the watershed landscape, stream geomorphology, hydrology, water quality, aquatic habitat conditions, and biological conditions. On the other hand, Hazbavi and Sadeghi (2017) have evaluated watershed health considering only the hydrologic criteria such as rainfall and streamflow, while Sadeghi and Hazbavi (2017) evaluated watershed health in relation to standardized precipitation index only.

From the pertinent literature review, it is clear that watershed health evaluation, which is a primary key step in watershed management plans, has not gained popularity in India, though some studies carried out in several countries. Additionally, in all those past studies, environmental flow concept has not been considered while incorporating streamflow criteria in evaluating watershed health. Environmental flow (e-flow) is defined as the quantity, quality and timing of streamflow maintained in a river reach for sustainable fresh water, and the dependent habitat and ecosystem services (Tharme 2003). Thus, e-flow should be considered as a key threshold while evaluating watershed health from hydrologic point of view. Furthermore, risk based indicators, i.e., reliability, resilience and vulnerability, primarily proposed by Hasimoto et al. (1982), were applied in only few watershed health assessment studies, whereas vastly used in other water resources problems such as reservoir water supply studies. To address these issues, this study was carried out in a river basin, located in Eastern India, for evaluating the temporal pattern of basin health using risk based indicators.

## 2. Data and methodology

### 2.1 *Overview of the study area and data collection*

The area selected for the present study is Rushikulya River Basin (RRB), which is a part of the East Flowing Rivers (EFR) between Mahanadi and Pennar rivers (Fig. 1). The river Rushikulya is one of the major rivers of Odisha state. It originates from the Rushimala hills near Daringibadi village of Kandhamal district at an elevation of about 1200 m above the mean sea level (MSL) along the eastern slope of the Eastern Ghats and drains into the Bay of Bengal in the east. This river basin lies between 19°07′ N and 20°19′ N latitude, 84°01′ E and 85°06′E longitude having total geographical area of about 7013 km$^2$.

The basin is characterized by 'sub-tropical' climate with an average annual rainfall of 1336 mm. About 80% of the annual rainfall is received during mid-June to October-end. The maximum and minimum temperatures of the basin are 45°C and 12°C, respectively and the relative humidity ranges from 80 to 90%. The soils in the study area are mostly clay and loam. As to the land use/land cover, a major part of the basin is covered by forest and agricultural land. Forest area, located mostly in Eastern Ghats, covers about 44% of the total basin area and about 34% of the basin is agricultural land. About 2% of the basin is covered by water bodies.

For this study, gridded rainfall data (0.25º×0.25º) was collected from India Meteorological Department, India. Additionally, daily streamflow data of the Rushikulya river at Purushottampur gauging station (at outlet) was collected for 26 years (1990-2016) from Central Water Commission (CWC), Bhubaneswar, Odisha.

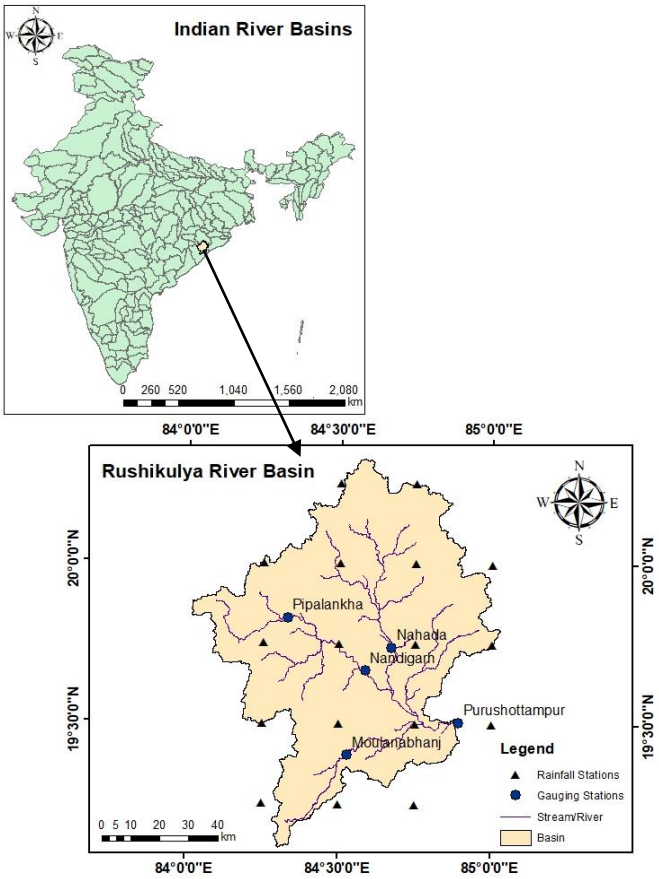



Fig. 1. Location of the study area and the hydro-meteorological stations.

## 2.2 *Calculation of Standardized Precipitation Index (SPI)*

In this study, 1-month scale SPI was calculated using monthly rainfall by assuming that rainfall follows a gamma type distribution. The monthly rainfall data at each station were aggregated to river basin scale. All these calculations were done in *R* software. The SPI values are generally classified into 'near normal ($0.99 < SPI < -0.99$)', 'moderately dry ($-1.0 < SPI < -1.49$)', 'severely dry ($-1.5 < SPI < -1.99$)' and 'extremely dry ($SPI < -2.0$)' conditions (Mckee *et al.*, 1993).

### 2.3 *Environmental flow estimation using Flow Duration Curve Shifting technique*

Flow Duration Curve Shifting (FDCS) method is based on the use of a flow duration curve, a cumulative distribution function of monthly flow time series. The flow duration curve (FDC) was derived from a monthly streamflow time series. To maintain a certain level of environmental protection, six environmental management classes (EMCs) are prescribed in the original method such as: unmodified or natural condition (class A and B), moderately modified ecosystems (class C), largely modified ecosystems (class D) and seriously and critically modified ecosystems (class E and F). FDC for each EMC was determined by lateral shift of original FDC to left along the probability axis to preserve the general pattern of the flow variability with every shift. Thereafter, a spatial interpolation procedure was used to convert the obtained FDCs to monthly environmental flow time-series.

### 2.4 *Assessment of the basin health*

For assessing the health/sustainability of the study area, two criteria, viz., 'standardized precipitation index' (SPI) and 'minimum monthly flow' (at Purushottampur) for the period of 1990-2016 were selected because of their easy accessibility in most of the river basins and their high importance. Health of the basin was calculated using risk-based indicators, i.e., reliability, resilience and vulnerability. Brief description about these indicators is given below.

*Reliability* is the probabilistic measure of a system being in a satisfactory state (Hasimoto *et al.* 1982). In other words, it is the probability of $X_t \in S$, where $X_t$ is value of a variable at any time t and S indicates the satisfactory stage of the given system. From the time series, reliability can be computed as follows:

$$Reliability = 1 - \left[\frac{\sum_{j=1}^{M} d(j)}{N}\right] \quad (1)$$

where *d (j)* is the duration of $j^{th}$ failure event, *M* is the number of failure events and *N* is the total number of events.

*Resilience* is defined as the probability of the system that can return to a satisfactory state after the failure state as quickly as possible. This is a conditional probability, which can be alternatively defined as the ratio of the probability of transition from the unsatisfactory to the satisfactory stage and the probability of failure. Thus, resilience can be expressed mathematically as:

$$Resilience = \frac{1}{\left[\frac{\sum_{j=1}^{M} d(j)}{M}\right]} \quad (2)$$

Vulnerability is a measure of severity of a failure event, once it has occurred. Vulnerability can be calculated as follows:

$$Vulnerability = \frac{1}{M}\sum_{t=1}^{N}\left\{\left[\frac{X(t)-T(t)}{T(t)}\right]H[X(t)-T(t)]\right\} \quad (3)$$

where X*(t)* is the observed criteria during $t^{th}$ time step, *M* is the number of failure events and *T* is the corresponding value of the threshold value for the criteria. *H* is the Heaviside function, a step function, ensuring involvement of failure events only in the calculation of vulnerability.

The values of reliability and resilience vary from 0 to 1, while vulnerability can be of high value

depending on the severity of the failure event. In the context of SPI, the threshold value was taken as 0 (normal condition) and the monthly EFR assessed from FDCS technique (EMC 'C') was considered as the threshold for 'minimum monthly flow' to assess the health of the river basin from a hydrological point of view. 'SPI' values above -0.99 and river discharge above the EFR values were considered as the safe events. All of these indices were standardized to overcome their incompatibilities among the criteria considered in the study. Thereafter, an integrated watershed sustainability indicator or health indicator (IWHI) was computed as the geometric mean of all the standardized indices. Thus, IWHI varies between 0 to 1; 0 indicates worst state of the basin and 1 indicates that the basin is at its best state.

## 3. Results and discussion

### 3.1 *SPI*

Time series of the calculated values of SPI-1 (at 1-month time scale) are presented in Fig. 2. It is revealed that the SPI values of Rushikulya river basin vary from -3.05 to 3.20 over the years. The basin experiences extreme drought with SPI value of -3.05 in the April month of 1999. However, the trend observed in the SPI values of the study area is slightly decreasing (almost stable), which is statistically insignificant with p-value of 0.10 as revealed from Mann-Kendall trend test.

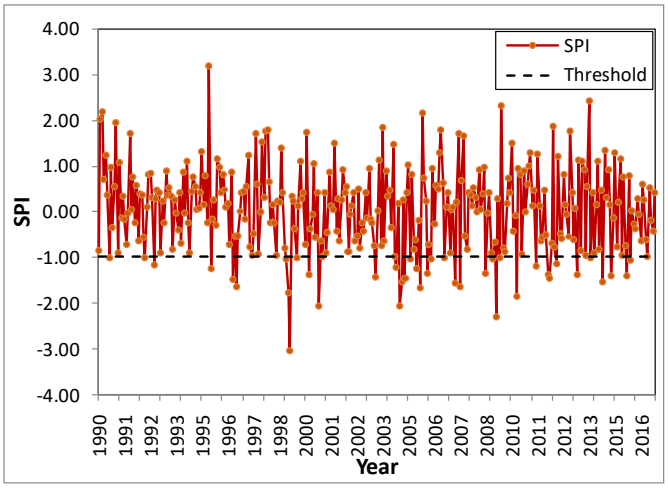
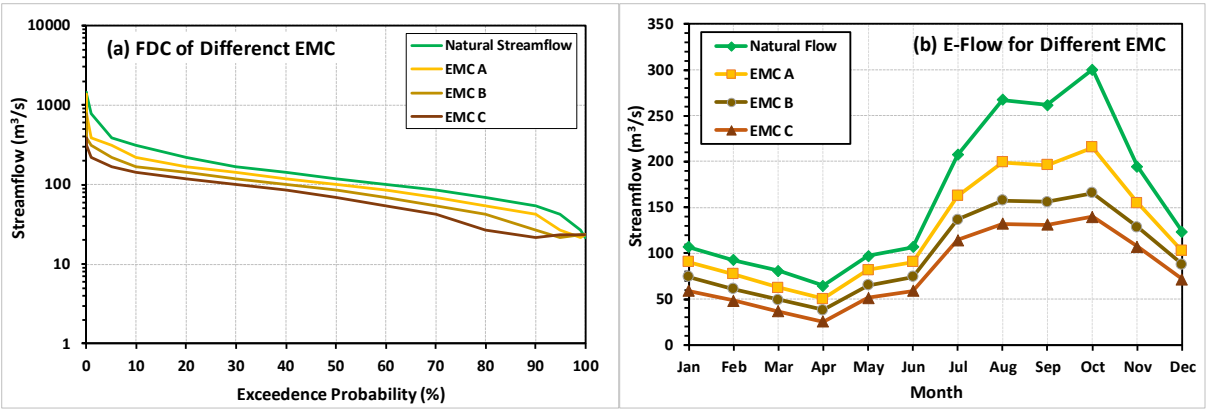



Fig. 2. Temporal variation of standardization precipitation index of the river basin.

### 3.2 *Environmental flow*

The FDC generated from the naturalized streamflow values, called reference FDC was shifted along the probability axis to generate FDCs for EMC 'A', 'B', and 'C' and they are shown in Fig. 3(a).



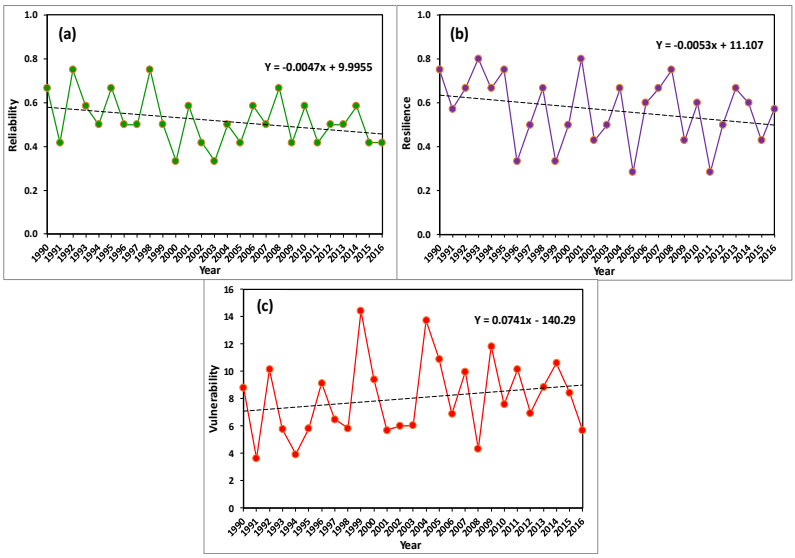

Figs. 3. (a) Flow duration curves for reference (natural streamflow) and EMC A, B and C conditions; (b) Environmental flows estimated by 'FDCS technique'.

The generated FDCs were then used to estimate environmental flow for EMC 'A', 'B', and 'C' scenarios by spatial interpolation technique and they are presented in Fig. 3(b). It is clearly shown that the monthly environmental flow series estimated for three EMCs mimic the pattern of natural flow series having maximum value in October and minimum flow in April for all three EMCs. The mean EFRs estimated for EMC 'A', 'B' and 'C' are 123.59±58.41, 99.60±46.24 and 81.21±41.01 $m^3/s$, respectively. The FDCS technique assigns about 78, 63 and 51% of the MAR for EMCs 'A', 'B' and 'C', respectively for ecological preservation. As there is an acute water shortage in the study area, EMC 'C' of FDCS technique can be adopted for ecological preservation.

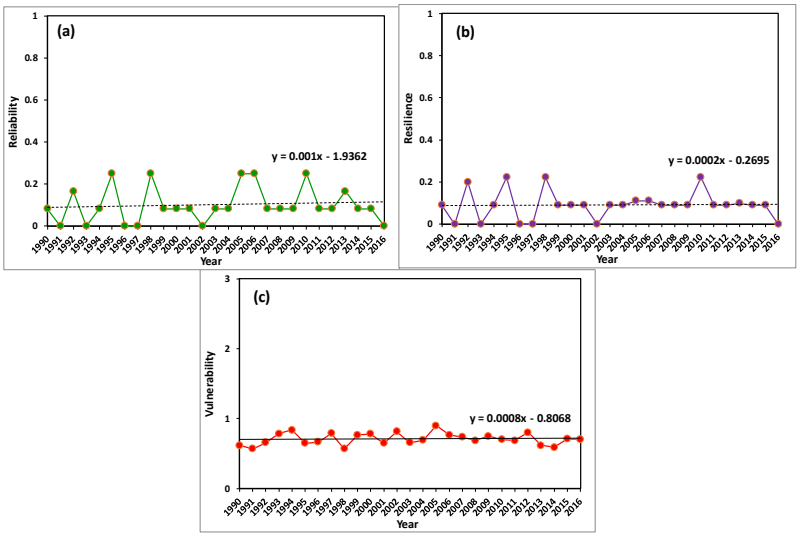
### 3.3 *R-R-V Indicators and Watershed Health*

On the other hand, the trend observed in the corresponding reliability and resilience for the SPI criteria is decreasing and an increasing trend is obvious in vulnerability values for the basin [Figs. 4(a-c)]. Reliability and resilience for the whole basin fluctuate from 0.33 to 0.75 with a mean of 0.52±0.11 and from 0.29 to 0.80 with a mean of 0.57±0.15, respectively [Figs. 4(a,b)]. On the other hand, vulnerability of the basin has a mean value of 8.04±2.83, varying from 3.63 to 14.42 [Fig. 4(c)].

Further, results of the analysis for the 'minimum monthly flow' criteria are shown in Figs. 5(a-c). The analysis revealed that all the indices show slightly increasing but insignificant trends over the years. As compared to the indices calculated for 'SPI', all the indices related to 'minimum monthly flow' have consistently small values of reliability and resilience showing that minimum flow required for ecological functioning of the river is not maintained due to prevailing water scarcity in the area.




Figs. 4(a-c). Temporal variation of risk-based indices (a) reliability (b) resilience, and (c) vulnerability for 'SPI' criteria in the Rushikulya River basin.




Figs. 5(a-c). Temporal variation of risk-based indicators (a) reliability (b) resilience, and (c) vulnerability for 'minimum monthly flow' criteria in the Rushikulya River basin.

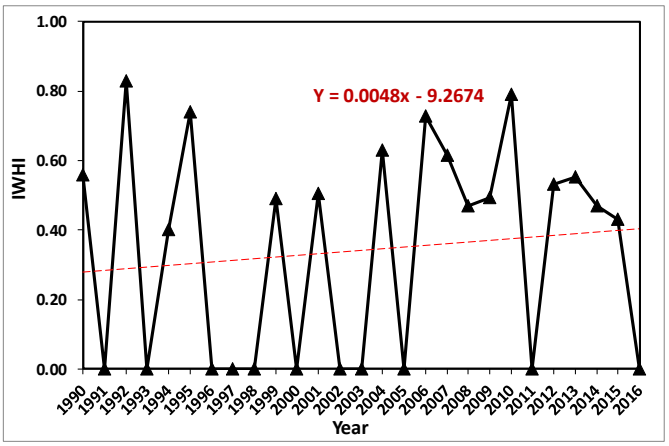



Fig. 6. Temporal variation of integrated health index for the Rushikulya River basin.

During 1990-2016, IWHI of the basin ranges from 0 to 0.80 (Fig. 6). The analysis reveals that the basin experiences its worst state having IWHI as '0' in 11 years, while the basin was in good state (IWHI = 0.6-0.8) in six years during 1990-2016. Overall, an increasing trend in basin health with a mean of 0.34±0.31 is observed for the basin. However, the increasing trend is not statistically significant at 5% level of significance. Thus, it can be inferred that the overall basin health has been in a bad state from the drought and stream health prospective.

## 4. Conclusions

This study shows the importance of including 'environmental flow' as the threshold while assessing the watershed health. In this study, the applicability of risk-based indicators has also been shown in assessing basin health in a single framework from the aspects of drought and stream health. Based on the analysis, the major conclusions drawn are as follows:

- SPI values of the basin vary from -3.05 to 3.20 over the years.
- The environmental flow requirements of the Rushikulya river at the outlet is 123.59 $m^3/s$ (78% of MAR), 99.60 $m^3/s$ (61% of MAR) and 81.21 $m^3/s$ (51% of MAR), for the EMC 'A', 'B', and 'C' conditions, respectively.
- Based on 'SPI' criteria, the analysis revealed that SPI related reliability and resilience of the whole river basin is degrading over the years with increased drought vulnerability.
- All the risk-based indices related to 'minimum monthly flow' have consistently smaller values revealing that the minimum flow required for ecological functioning of the river has not been maintained due to prevailing water scarcity in the area.
- During 1990-2016 period, the whole basin health was found to be in the 'worst state' (IWHI = 0) in 11 years, while it was in the 'good state' (IWHI = 0.6-0.8) in six years from the drought and stream health prospective. Overall, it can be concluded that the basin health is not good as indicated by the lesser mean value of IWHI of 0.34 (<0.5).

Such type of study can be extended to sub-watershed scale for investigating the spatial watershed health which in turn will help in prioritizing the spatial basic units while implementing watershed management action plans or planning any resource allocations among the users for achieving eco-hydrological sustainability for future generations.

## References

1. Ahn S, Kim S. 2017a. Environmental Modelling & Software Assessment of watershed health , vulnerability and resilience for determining protection and restoration Priorities. *Environmental Modelling and Software* DOI: 10.1016/j.envsoft.2017.03.014
2. Ahn SR, Kim SJ. 2017b. Assessment of integrated watershed health based on the natural environment , hydrology , water quality , and aquatic ecology. *Hydrology and Earth System Sciences* **21**: 5583–5602
3. Alilou H, Rahmati O, Singh VP, Choubin B, Pradhan B, Keesstra S, Saeid S, Hamidreza S. 2019. Evaluation of watershed health using Fuzzy-ANP approach considering geo- environmental and topo-hydrological criteria. *Journal of Environmental Management* **232** (November 2018): 22–36 DOI: 10.1016/j.jenvman.2018.11.019
4. Cosgrove WJ, Loucks DP. 2015. Water management: Current and future challenges and research directions. **51**: 4823–4839 DOI: 10.1002/2014WR016869.Received
5. Hasimoto T, Loucks DP, Stedinger JR. 1982. Reliability , resiliency , robustness , and vulnerability criteria for water resource systems
6. Hazbavi Z, Sadeghi SHR. 2017. Watershed health characterization using reliability – resilience – vulnerability conceptual framework based on hydrological responses. **1537** (June): 1528–1537 DOI: 10.1002/ldr.2680
7. Hoque YM, Tripathi S, Hantush MM, Govindaraju RS. 2012. Watershed reliability , resilience and vulnerability analysis under uncertainty using water quality data. *Journal of Environmental Management* **109**: 101–112 DOI: 10.1016/j.jenvman.2012.05.010
8. Mckee TB, Doesken NJ, Kleist J. 1993. The relationship of drought frequency and duration to time scales. (January): 17–22
9. Sadeghi SH, Hazbavi Z. 2017. Spatiotemporal variation of watershed health propensity through reliability-resilience-vulnerability based drought index ( case study : Shazand Watershed in Iran ). *Science of the Total Environment* **587**–**588**: 168–176 DOI: 10.1016/j.scitotenv.2017.02.098
10. Sanchez GM, Nejadhashemi AP, Zhang Z, Marquart-pyatt S, Habron G, Shortridge A. 2015. Environmental Modelling & Software Linking watershed-scale stream health and socioeconomic indicators with spatial clustering and structural equation modeling. **70**
11. Tharme RE. 2003. A global perspective on environmental flow assessment: Emerging trends in the development and application of environmental flow methodologies for rivers. *River Research and Applications* **19** (5–6): 397–441 DOI: 10.1002/rra.736

IN PROCEEDINGS OF 25th HYDRO 2020, INTERNATIONAL CONFERENCE,
NATIONAL INSTITUTE OF TECHNOLOGY ROURKELA, ODISHA, INDIA
26-28, March 2021, ISBN 978-93-90631-56-8

Paper ID - 169

# Surface Water Balance Study of River Sarada

JAGANNATH PATRO [1] Dr. VAZEER MAHAMMOOD [2]
[1] Research Scholar, jagannathpatro@gmail.com
[2] Professor, prof.vmahammood@andhrauniversity.edu.in
Civil Engineering Department, Andhra University, Visakhapatnam-530 003, AP, India

## Abstract

The Inter-basin water transfer, proposed in India, for transfer of water from a surplus river basin to adjacent deficit river basins, in the monsoon months of a year needs Water Balance Study of the donor river basin to be done. The surplus or deficit of a basin is decided based on the Water Balance Study of the basin, by taking into account the observed discharge data, upstream utilization, import & export, existing & future needs for irrigation, domestic, industrial, hydropower uses & regeneration, etc. The water availability studies are to be carried out in two parts viz., surface water availability and ground water availability. The surface water availability studies are to be carried out sub-basin wise and at diversion points. The necessary input data may be rainfall data, observed discharge data, upstream utilization, import and export of water, etc., needed to work out the dependable yields and to bring out the diversion proposals, accordingly. The Surface Water Balance study of the river *Sarada* in *Andhra Pradesh* is carried out basing on the gauge discharge data of the river and its water utilization. In due course of the study, the daily discharge data, missing over a period of 28 years from 1989-2017 despite availability of gauge data, was filled/ completed. The Surface Water Balance of the river Sarada on completion of the filled discharge is observed to be surplus, based on the water year approach.

***Keywords:*** *Sarada river, Gauge Discharge data, missing discharge data filling, Surface Water Balance study*

## 1. Introduction

### 1.1 *Water*

The oldest human civilization flourished on the river banks because water is one of the five Elements of nature and is essential for human existence. History indicates that civilization starts thriving where water is available in plenty. The common perception was that water is an infinite resource. Today, the competition for water resources is most intense. To avoid a global water crisis, farmers will have to strive to increase productivity to meet growing demands for food, while industry and cities should find ways to use water more efficiently. Successful agriculture is dependent upon farmers having sufficient access to water. However, water scarcity is a critical constraint for agriculture and industries in many parts of the world.

Water represents our priceless asset, which must be fully harnessed to meet the minimum needs of all the habitants. Proper harnessing of water resources can bring about food security and conservation of natural resources, eventually leading to either total removal or minimization of hunger, malnutrition, poverty among the weaker sections of population and unemployment among the youth. Due to inadequate water conservation and unsustainable water use, the water scarce basins are currently spread in many parts of the country (Desai *et al*, 2005).

### 1.2 *Water Balance Study*

Mutreja (1986) stated 'Water Balance' as the book-keeping of water of a basin or region in relation to the components of the entire hydrologic cycle or part thereof, carried over a specified period of time,

generally, one year. The Water Balance Study is necessary to evaluate the net available water resources in a river basin, both surface and subsurface and to assess the existing water utilization pattern and practices.

Subramanya (1984) stated the advantage to consider a 'Water year' for hydrologic study. A Water year is one beginning from the time when the precipitation exceeds the average evapotranspiration losses in which, a complete cycle of climatic changes is expected and hence the water budget will have the least amount of carry over. In India, June 1 is the beginning date of a water year which ends on May 31 of the following calendar year. Hence the current study is carried out with water year as a unit.

The surplus or deficit of a basin is decided based on the Water Balance Study of the basin, by taking into account, the observed discharge data, upstream utilization, import and export, existing and future needs for irrigation, domestic, industrial, hydropower uses and regeneration etc. (Hasan, 1992).

Water balance estimation is essential to make agriculture sustainable in view of increasing population, domestic use, industrial purpose and agriculture activities (Krishnaiah, 2014).

The water availability studies are to be carried out in two parts viz., surface water availability and ground water availability. The surface water availability studies are to be carried out sub-basin wise and also at diversion points. In this paper, only the Surface Water Balance Study had been considered.

### 1.3 *Sarada River*

The Sarada River is one of the minor rivers that drains the area between Eastern Ghats and Bay of Bengal in the North Eastern coastal area of Andhra Pradesh, India. The entire Sarada river basin is situated in the Visakhapatnam District of Andhra Pradesh. The basin approximately lies in between the Latitudes $17^0$25' & $18^0$17' and Longitudes $82^0$30' & $83^0$05'. It is surrounded by Anakapalli Minor Drainages and Naravagedda Minor Basin on the Eastern side; Sileru river basin, a tributary to Godavari on the Northern side and Varaha River basin on the Western side. The coast line of Bay of Bengal in this region is to the North Eastern direction of the basin. The basin covers an area of about 2629.03sq.km (area upto last irrigation source) lying entirely in Visakhapatnam District of the re-organized Andhra Pradesh State. The maximum length of the basin from East to West is 62.70 kilometer and from North to South is about 95.00 kilometer.

The river Sarada is an east following river taking its rise in the Eastern Ghats near Lakshmipuram village of Chodavaram taluk on the Eastern Coast of Andhra Pradesh. It traverses Chodavaram, Anakapalli and Yelamanchili Taluks of Visakhapatnam District due South upto Anakapalli, South Western direction from Anakapalli to Melupaka and thereafter again in Southern direction until it joins the sea. The river is not perennial, being only a hill stream and is characterized by occasional floods it receives.

### 1.4 *Data Filling*

According to the Hydrology Project Training Module (Nov'99), the process of filling in the missing discharge values is generally referred to as 'completion'. The missing discharge data of any basin is required to be completed/filled to go ahead with the Water Balance Study.

The discharge values 'Completion' needs to be carried out with the discharge values based on interpolation or other observations at the same station. It must be recognized that values estimated from other gauge stations are inherently less reliable than values properly measured. Doubtful original values will therefore be generally given the benefit of the doubt and will be retained in the record with a flag.

Where no suitable neighboring observations or stations are available, missing values will be left as 'missing' and incorrect values will be set to 'missing'.

## 2. Sarada River & its Gauge Discharge Data

### 2.1 *Sarada River*

The Gauge Discharge (G-D) data of any G-D station on a river is necessary to study the Water Balance Study of the river. The Water Balance Study of the river Sarada was proposed to be carried out to determine the water surplus status, or otherwise, of the river. The basin map of Sarada river is shown in ***Figure 1*** below:

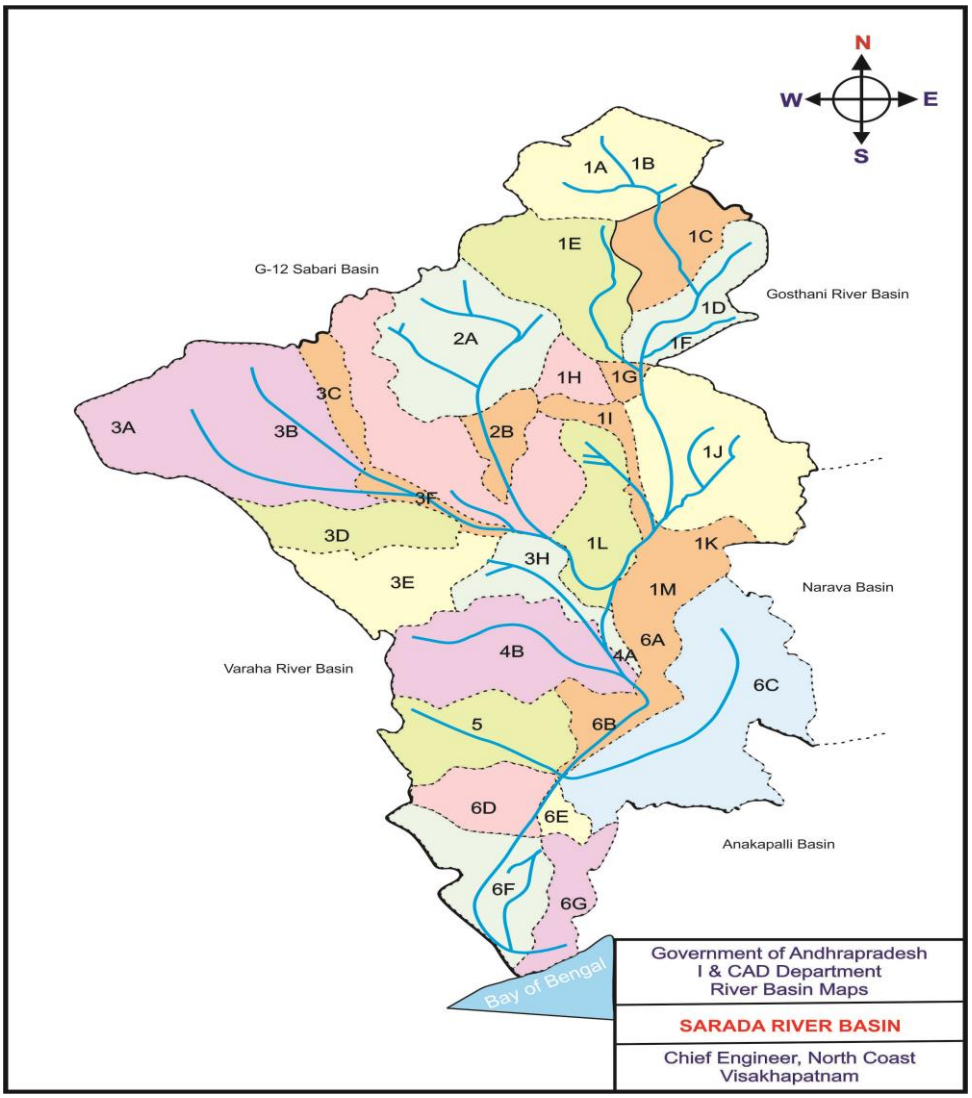



**Figure 1.** Sarada River Basin [Courtesy: Irrigation Profile of NC dist. of AP, CE, I&CAD, NC, 2014]

The river Sarada takes its rise in the Ananthagiri Reserved forest area of Eastern Ghats, the upper reaches lying in hilly and Zamindari Area. The main Sarada river originates at about +144.08m above MSL in the hill ranges of Chodavaram Taluk.

Many hill streams join the river and the river flows for a distance of 45.00kilometer and falls in short distances. After 45.00km, it flows almost in plain country. The bed level at 45.00km is about +106.68m. At 45.00km of its traverse, one major stream originating in Madugula Zamindari hill ranges joins Sarada river on its right side. At 6.40km downstream of this confluence, another stream Isukagedda flowing in South-Eastern direction joins Sarada river. At 77.00km i.e., about 26.00km downstream of the confluence of Isukagedda, another major stream Pedderu joins Sarada river on the right side at about MSL+36.58m. Thus, the average bed fall works out to 2.15m per kilometer. The whole course of the river and its tributaries upto 78.40km lies within Chodavaram and the bed fall in this taluk will be about 0.95m per kilometer. From 98.00km, it enters Yelamanchili Taluk. After flowing for a length of about 4.82km, i.e., at 101.00km at Gokivada Regulator, the river divides into two branches, one is called Sarada river and another Gokivadagedda and flows South wards until it reaches the Sea. The Sarada river joins the Varaha river near Bangarammapalem just before emptying into the Bay of Bengal.

The basin has been classified into 6 sub-basins viz., (1) Upper Sarada, (2) Bodderu Nadi, (3) Tacheru and Pedderu, (4) Vedurla Gedda, (5) Mamidivakagedda and (6) Lower Sarada. These sub-basins are again sub-divided into 33 minor sub-basins as indicated in Basin Plan for receiving the yield, utilization and balance of potential accurately. Malagedda is another minor stream rising in the Kasimkota Zamindari Forest area at level +445m. This consists of two streams, Seshugedda and Edlagedda joining near Yelamachili and directly flows upto sea where it joins Sarada and Gokivadagedda at the fag end and thus the contribution of the same for Sarada river is nil.

The Sarada basin is influenced by seven Rain gauge stations, viz., (1) Yelamanchili, 2) Anakapalli, 3) Chodavaram, 4) Narsipatnam, 5) Pulaparti, 6) Tulabada and 7) Srungavarapukota.

There is no possibility of generation of power as the quantum of supply in the hilly range is not sufficient. Hence this area has to entirely depend upon Machkund Hydro-electric power for domestic consumption and for small scale industries. The duty considered is 8 Ac/Mcft for irrigation in the whole basin. The entire catchment of the basin is classified into good or average according to the nature of the country.

### 2.1.1 *Major Projects*

The following are the major projects in the Sarada River basin:
a. Raiwada Reservoir Project on Sarada River
b. Pedd ru Reservoir Project on Pedderu Tributary
c. Konam Reservoir Project on Bodderu Tributary

### 2.1.2 *Groynes/Anicuts*

The Groynes/Anicuts in the Sarada River basin are as below:
1. Thagarampudi Groyne 2. Seethanaragaram Groyne, 3. Thumpala Groyne, 4. Cherlopalem Groyne, 5. Yellaiah Groyne, 6. Nagulapalli Groyne, 7. Godari anicut, 8. Kasimadum Groyne, 9. Veduruparthi Groyne, 10. Ugginapalem Groyne, 11. Perantalapalem Groyne, 12. Narasapuram anicut and 13. okivada anicut.

## 2.2 *Gauge Discharge Data*

To carry out the Water Balance Study of the Sarada River, the Gauge Discharge Data of the River for about 30 years was obtained from the Central Water Commission (CWC), Bhubaneswar.

After study of the available Gauge Discharge data of the G-D station on the river, a number of discharge values were found missing on several dates due to non-observation or loss on recording or transmission. These missing discharge data were to be filled to go ahead with the volume assessment and subsequently, the Water Balance Study of the river basin.

### 2.3 *Gauge Discharge Data Filling/Completion*

The Gauge Discharge Data for the Sarada River in between 1988 to 2017 was obtained from Mahanadi & Eastern Rivers Organization (M&ERO) of the Central Water Commission (CWC), Bhubaneswar.

The obtained daily gauge discharge data was organized on Water Year basis, i.e., from June of any year to May of the succeeding year. It was observed that several discharge data were missing against the available gauge data of the day.

The discharge data of a total of *1714 days* were found missing against the gauge on the corresponding dates, i.e., the missing data accounted for about *16.8%* of the data set of *10227 days for 28 Water years*, starting 1989-90 through 2016-17. This data needed to be filled/completed to arrive at a reasonable gauge discharge data set for the total period and subsequently take up the Water Balance Study.

The missing discharge data was completed basing on Patro and Mahammood's (2019) study which concluded that *the mean of minimum & maximum of observed discharge values for the particular gauge, would best represent the discharge data for that particular gauge***.** Subsequently, the Water Balance Study was carried out.

## 3. Methodology of the Water Balance Study

### 3.1 *Study area*

The water availability studies are to be carried out in two parts viz., Surface Water availability and Ground Water availability. The surface water availability studies are to be carried out sub-basin wise and also at diversion points. In this paper, only the Surface Water Balance Study of the Sarada river basin at the Raiwada reservoir had been considered, on monthly basis in the Water year approach.

The Raiwada Reservoir is a reservoir on the Sarada river, with the following details (Irrigation Profile of North Coastal districts of AP, CE, I&CAD, NC, 2014):

| | |
|---|---|
| Dam type | : Masonry gravity dam |
| Weir shape | : Ogee type weir |
| Length of the dam | : 5.75km |
| Tank Bund Level (TBL) of the dam | : +117.0m |
| Full Reservoir Level (FRL) | : +114.0m. |
| Storage Capacity at FRL | : 102 Million Cubic Metre (MCM) |
| Live Storage Capacity | : 92.6MCM |
| Ayacut under the reservoir | : 21,344 Acres (Ac) |

### 3.2 *Parameters for Water Balance Study*

The surplus water in a basin/sub-basin or at diversion point may be determined by taking into account the availability, import, existing and future needs for irrigation, domestic, industrial, hydro-power uses and

regeneration etc. (Hasan, 1992). In the Indian context, if the irrigation needs are considered such that 60% or more of the cultivable area is irrigated in a basin, the surplus water of such a basin may be reasonably considered as surplus for transfer outside the basin.

The parameters considered for the water balance calculation purposes are as follows (Krishnaiah, 2014):

1. The inflow into the reservoir.
2. The water supply for irrigation.
3. The water supply for drinking water purposes to adjacent areas.
4. The evaporation losses from the reservoir.
5. Water for Downstream uses & natural balance.

## 3.3 *Water Balance Study Methodology*

### 3.3.1 *Reservoir inflow*

The average month-wise water inflow into the reservoir was assessed after completion of the missing discharge data for the water years from 1989-90 to 2016-17. The volume of water inflow is shown in the **Table 1** below:

**Table 1.** Month-wise Water inflow in river from 1989-90 to 2016-17

| Month | Total Volume in 28 years (MCM) | Average monthly discharge (cumec) | Average Monthly inflow (MCM) |
|---|---|---|---|
| Jun | 617.20 | 255.13 | 22.04 |
| Jul | 928.76 | 383.91 | 33.17 |
| Aug | 1679.65 | 694.30 | 59.99 |
| Sep | 4069.77 | 1682.28 | 145.35 |
| Oct | 5351.12 | 2211.94 | 191.11 |
| Nov | 3190.57 | 1318.86 | 113.95 |
| Dec | 1015.93 | 419.95 | 36.28 |
| Jan | 714.96 | 295.54 | 25.53 |
| Feb | 203.53 | 84.13 | 7.27 |
| Mar | 272.65 | 112.70 | 9.74 |
| Apr | 204.62 | 84.58 | 7.31 |
| May | 707.24 | 292.35 | 25.26 |
| **Total** | **18956.00** | | **677.00** |

Gross release in reservoirs is assumed as 80% of the live storage capacity of the reservoirs. Thus, total likely utilizable resources do take into account likely reduction in utilizable surface water resource due to reservoir sedimentation which is estimated to be about 20% of total live storage capacity by year 2050.

### 3.3.2 *Irrigation water*

The total ayacut under the reservoir is 15344 Acres of precarious wet land and 6000 Acres of dry ayacut, to be converted into wet land. Accordingly, for the duty of 8Ac/Mcft, the total volume of water to be supplied for the sole crop in the year amounts to 75.52MCM from the period October to January, which was distributed equally, monthly, to arrive at the Irrigation water supplies.

### *3.3.3 Drinking water supply*

The water supply from the Sarada river to Visakhapatnam district for drinking water purpose @27Million Gallon per Day (MGD) works out to 0.102 MCM per day. The monthly quantity is calculated accordingly to arrive at the monthly drinking water supply to the areas adjacent to the river basin.

### 3.3.4 *Evaporation losses*

The mean monthly values of the Evaporation depth of water in Visakhapatnam District and the Raiwada Reservoir water levels obtained from the Water Resources Information Systems (WRIS), India were applied to the extent of water in the reservoir as per the Area Elevation table of the Raiwada Reservoir to arrive at the monthly water evaporation from the reservoir. The mean monthly evaporation volumes are depicted in **Table 2** below:

**Table 2.** Mean monthly evaporation losses from Raiwada Reservoir

| Month | Reservoir Water Level (m) | | | | Water Extent as per Area Elevation Curves (Ha) | Evaporation depth (mm) | Evaporation loss (MCM) |
|---|---|---|---|---|---|---|---|
| | 2017 | 2018 | 2019 | Average level | | | |
| Jun | 109.97 | 109.97 | 104.425 | 108.12 | 673.41 | 68.7 | 13.87 |
| Jul | 109.98 | 109.97 | 105.55 | 108.50 | 696.07 | 80.0 | 17.27 |
| Aug | 109.97 | 107.875 | 112.32 | 110.06 | 810.20 | 94.6 | 23.76 |
| Sep | 112.68 | 105.78 | 109.85 | 109.44 | 761.23 | 82.1 | 18.74 |
| Oct | 113.54 | 105.77 | 113.53 | 110.95 | 885.88 | 62.3 | 17.12 |
| Nov | 112.96 | 102.18 | 113.34 | 109.49 | 764.87 | 31.0 | 7.11 |
| Dec | 112.57 | 103.30 | 112.895 | 109.59 | 772.56 | 22.8 | 5.46 |
| Jan | 111.51 | 103.30 | 112.45 | 109.09 | 735.73 | 24.6 | 5.61 |
| Feb | 110.88 | 103.30 | 111.75 | 108.64 | 705.79 | 26.2 | 5.22 |
| Mar | 109.96 | 103.31 | 110.76 | 108.01 | 666.94 | 28.3 | 5.85 |
| Apr | 109.97 | 103.31 | 109.85 | 107.71 | 647.92 | 34.6 | 6.73 |
| May | 109.97 | 103.30 | 109.46 | 107.58 | 638.61 | 43.8 | 8.67 |
| | | | | | **Total evaporation volume (MCM)** | | **135.42** |

### 3.3.5 *Downstream uses & natural balance*

The water to be left to flow to downstream for downstream river flow, utilization in riparian area, to maintain the natural ecological balance and aqua life is considered as 20% of mean monthly water inflow volume.

The monthly outflows are arrived at by summation of the above 4 parameters and the cumulative monthly outflows are arrived at, for the Water year starting June.

The graph showing the values of the mean monthly inflows and outflows from the Raiwada reservoir are shown below in the **Figure 2** below.

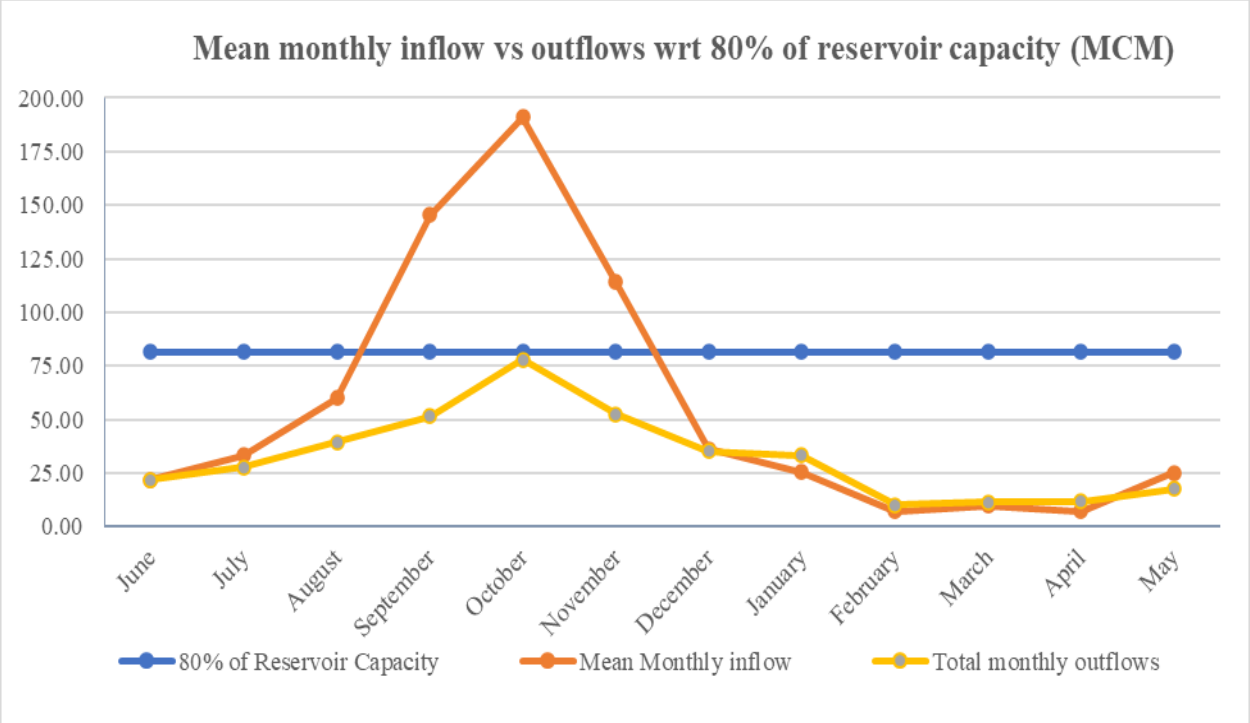



**Figure 2.** Mean monthly inflow vs outflows wrt 80% of reservoir capacity (MCM)

### 3.4 *Surplus water assessment*

The following steps are implemented to carry out the Water Balance Study:

- The mean monthly water inflow volume was assessed from the Gauge Discharge data after data completion of the missing discharge data, on Water year basis.
- The monthly outflows were assessed as the cumulative of the water supplied for irrigation & drinking water supply to adjacent areas, evaporation losses and the water to be left in the natural course of river flow, for maintaining the downstream uses and natural balance of the river.
- The cumulative monthly volumes of inflows and outflows were calculated.
- The monthly difference of the cumulative water inflow and cumulative water outflow was arrived at, to assess the quantum of surplus water in each month.
- 80% of the reservoir's total capacity, offsetting for sedimentation and dead storage, is deducted from this surplus water in each month. This surplus water in the last month of the Water year, i.e, May, is considered as the surplus water in the basin, as it completes the whole cycle of the water accounting. Further, this methodology ensures, theoretically, that the reservoir is always full.
- The Water Balance Study of the Sarada river at Raiwada reservoir is shown in **Table 3** below.

## 4. Results

According to the methodology cited at para 2.3 above, the missing discharge data in the G-D data of the river Sarada obtained from CWC, Bhubaneswar for the period from 1989-2017 had been filled/ completed. Subsequently, the Water inflow volume of the river had been assessed. With the assessment of the monthly outflows, the Water Balance Study of the Sarada river at Raiwada reservoir had been taken up as per the methodology detailed at para 3.3 and 3.4 above.

From these calculations, the following are observed:

**Table 3.** Water balance of Sarada river at Raiwada reservoir after completion of missing discharge values

| Month | 80% of Raiwada Reservoir Capacity | Mean Monthly inflow | Cumulative mean monthly inflows | Water supply to Vizag | Irrigation supply | Evaporation losses | Downstream uses & natural balance (@20% inflow) | Total water outflows | Cumulative mean monthly outflows | Cumulative Balance water | Surplus water over Reservoir Capacity |
|---|---|---|---|---|---|---|---|---|---|---|---|
| **1** | **2** | **3** | **4=∑3** | **5** | **6** | **7** | **8=3x20%** | **9=5+6+7+8** | **10=∑9** | **11=4-10** | **12=11-2** |
| **June** | 81.55 | 22.04 | **22.04** | *3.69* | *0* | *13.87* | *4.41* | **21.97** | 21.97 | 0.07 | 0.00 |
| **July** | 81.55 | 33.17 | **55.21** | *3.81* | *0* | *17.27* | *6.63* | **27.72** | 49.69 | 5.53 | 0.00 |
| **August** | 81.55 | 59.99 | **115.20** | *3.81* | *0* | *23.76* | *12.00* | **39.57** | 89.26 | 25.94 | 0.00 |
| **September** | 81.55 | 145.35 | **260.55** | *3.69* | *0* | *18.74* | *29.07* | **51.50** | 140.76 | 119.79 | 38.24 |
| **October** | 81.55 | 191.11 | **451.66** | *3.81* | *18.88* | *17.12* | *38.22* | **78.03** | 218.79 | 232.87 | 151.32 |
| **November** | 81.55 | 113.95 | **565.61** | *3.69* | *18.88* | *7.11* | *22.79* | **52.47** | 271.27 | 294.34 | 212.79 |
| **December** | 81.55 | 36.28 | **601.89** | *3.81* | *18.88* | *5.46* | *7.26* | **35.41** | 306.68 | 295.22 | 213.67 |
| **January** | 81.55 | 25.53 | **627.43** | *3.81* | *18.88* | *5.61* | *5.11* | **33.41** | 340.09 | 287.34 | 205.79 |
| **February** | 81.55 | 7.27 | **634.70** | *3.44* | *0* | *5.22* | *1.45* | **10.12** | 350.21 | 284.49 | 202.94 |
| **March** | 81.55 | 9.74 | **644.43** | *3.81* | *0* | *5.85* | *1.95* | **11.61** | 361.82 | 282.61 | 201.06 |
| **April** | 81.55 | 7.31 | **651.74** | *3.69* | *0* | *6.73* | *1.46* | **11.88** | 373.70 | 278.04 | 196.49 |
| **May** | 81.55 | 25.26 | **677.00** | *3.81* | *0* | *8.67* | *5.05* | **17.54** | 391.23 | 285.77 | 204.22 |
| **Total surplus water transferable from the basin in a year (Mm3)** | | | | | | | | | | | **204.22** |

*All figures are in MCM*



*IN PROCEEDINGS OF 25th HYDRO 2020, INTERNATIONAL CONFERENCE, NATIONAL INSTITUTE OF TECHNOLOGY ROURKELA, ODISHA, INDIA 26-28, March 2021, ISBN 978-93-90631-56-8*

- ✓ The mean annual water inflow into the reservoir across the water year, from the 28 water years G-D data, is 677MCM or 0.677 Billion Cubic Metre (BCM).
- ✓ The yearly outflow of water is observed to be 391MCM.
- ✓ The water balance in a water year in excess of 80% of the total reservoir capacity is observed to be 204MCM
- ✓ The Water Balance graph is shown in the **Figure 3** below.

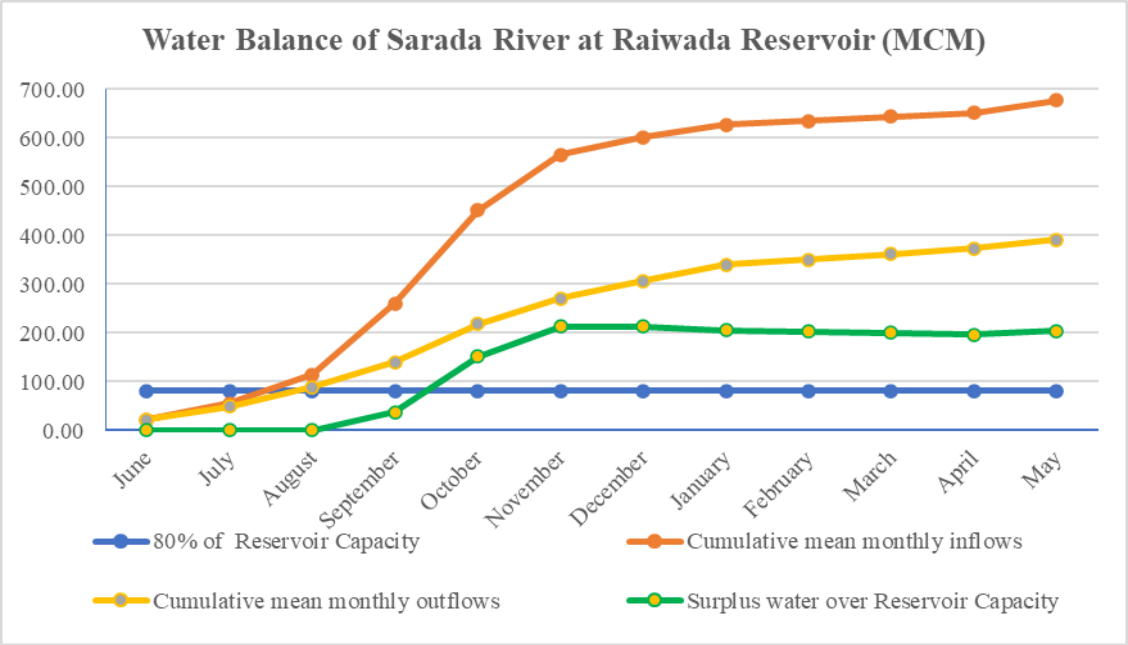



**Figure 3.** Water Balance of Sarada River at Raiwada Reservoir

## 5. Conclusions

The average annual surplus water in the river Sarada with a catchment area of about 2630sq.km at the Raiwada reservoir situated on the river from the study of the historical Gauge Discharge data of 28 years starting 1989 through 2017 is observed to be 0.204BCM. The basin can hence be concluded as Water surplus basin.

## References


- Chief Engineer, I&CAD, Govt. of AP, North Coast, Visakhapatnam (2014). *Irrigation profile North Coastal Districts of Andhra Pradesh.*
- Desai, V.R., Ghosh, S.N., and Patro, J. (2005). *Natural Water Grid – Its Objectives and Challenge*. Indian Society of Hydraulics (ISH) Journal of Hydraulic Engineering, 11(1), March, pp. 1-10.
- Hasan, Z. (1992). Inter-basin Water Transfers, *Seminar on Irrigation Water Management (WMF)*, New Delhi, pp. 124-137.
- Krishnaiah, Y.V. (2014). Water Balance Estimation in the Papagni River Basin, India. *The Indian Journal of Spatial Science*, pp. 70-76.
- Patro, J., Desai, V.R. (2004). River Interlinking For Flood Moderation In Lower Godavari Basin. *Proceedings of HYDRO–2004, National Conference on Hydraulics & Water Resources*, Nagpur, pp. 59-65.
- Patro, J., Mahammood, V. (2019). Completion of Discharge Data of River Sarada. *Proceedings of HYDRO – 2019, International Conference on Hydraulics & Water Resources*, Secunderabad, pp. 1286-1293.
- *https://indiawris.gov.in/wris/#/Reservoirs*

*IN PROCEEDINGS OF 25th HYDRO 2020, INTERNATIONAL CONFERENCE, NATIONAL INSTITUTE OF TECHNOLOGY ROURKELA, ODISHA, INDIA 26-28, March 2021, ISBN 978-93-90631-56-8*

Paper ID - 181

# Analysing the Response of Meteorological Droughts on Stream Flow in the Pennar River Basin

Arunav Nanda[1*], Dr. Bhaskar R. Nikam[2], Dr. Vaibhav Garg[2], Dr. S.P. Aggarwal[3]

[1]*M.Tech in Water Resources, Indian Institute of Remote Sensing, Dehradun-248001, India*
[2]*Scientist, Water Resources Department, Indian Institute of Remote Sensing, Dehradun-248001, India*
[3]*Group Head, Water Resources Department, Indian Institute of Remote Sensing, Dehradun-248001, India*
** Corresponding author: arunavnanda7@gmail.com*
*Telephone/Mobile No.: +91-6370541377*

## Abstract

Meteorological drought is a natural calamity characterized by lack of precipitation for a longer time period. The onset of drought occurs from the first category and evolves into other categories in the following manner: Meteorological, Agricultural, Hydrological and Socio-economic. In simpler terms, the meteorological drought propagates into other aspects of hydrological regimen such as soil moisture, groundwater, and stream flow. Is there any pathway by which it propagates? Does a strong relationship exist between meteorological drought and other parameters? These are the questions researchers are trying to answer globally. The response of basis towards meteorological drought may vary for different climatic zones, so in the present study, an attempt has been made to studies the impact of meteorological droughts on hydrological regime of Pennar River basin located in India. The meteorological drought is identified and characterized using advanced meteorological drought index, Standardized Precipitation-Evapotranspiration Index (SPEI). The daily gridded meteorological data obtained from India Meteorological Department was used to estimate SPEI for the period 1988 to 2018. To assess the impact of meteorological drought on stream flow of Pennar Basin, hydrological modelling using the Variable Infiltration Capacity (VIC) model was employed to compute discharge at the outlet of the basin. The validation of hydrological model was done with the observed discharge values at the outlet obtained from India-Water Resources Information System (India-WRIS; https://indiawris.gov.in/wris). The impact of meteorological drought on discharge of the Pennar River was analyzed by estimating Standardized Runoff Index (SRI) on a monthly time scale and correlating the SRI with SPEI for different drought events occurred in the basin during year 2008 to 2018. It was observed that the discharge values were lower for the drought hit periods when compared with normal periods. The impact of meteorological drought on stream flow appeared to vary with combination of severity, persistence, coverage and location of drought occurrence. The present attempt of using hydrological model for assessment of impact of meteorological drought on hydrological regime of a basin enabled the possibility of analyzing hydrological droughts, caused due to meteorological drought, at ungagged parts of the basin as well.

*Keywords: Meteorological drought; Variable Infiltration Capacity model, SPEI, SRI, SPI*

## 1. Introduction

Drought is an event where there is extended periods of water shortages (can either be surface water, ground water or atmospheric water). This phenomenon has no pre-defined timescale of its occurrence, persistence and difficult to determine its spatial extent. Due to its slow onset and propagation, its effect is variable at different place and time. According to World Meteorological Organization (2014), it can be defined as "slow onset phenomena caused due to lack of rainfall." It is the final product created by the combination of complex interplay in between natural precipitation of varying space & time scales and aggravated by water demand by humans and ineffective water distribution and usage. It has severe impact on various aspects of societies in different ways and also categorized as the most far-reaching disaster leading to hardships to millions of people. Unlike other natural hazards that cause structural damages and injury to humans, drought is different as compared to them. It is caused by the cumulative effect of deficient precipitation that is followed by a trail of its impacts on varying space and time scales.

The drought can be categorized into 4 different types according to Wilhite and Glanz (1985) i.e., Meteorological, Agricultural, Hydrological and Socio-economic. The following figure describes the process of propagation of drought categories.

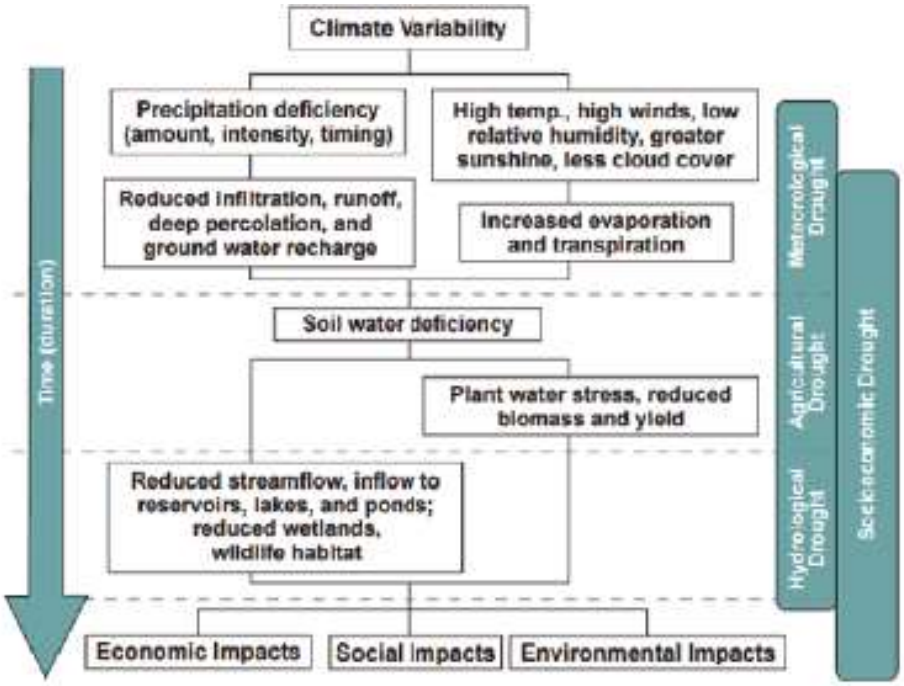



Figure 1.1 Different categories of drought

Meteorological drought can be defined in terms of the magnitude of deficiency in precipitation and its duration. Agricultural drought correlates the impact of meteorological drought to that of agricultural impacts such as differences in reference and actual evapotranspiration,

Although there are various approaches to monitor and quantify drought events, the indices approach is used worldwide as the best method. They are defined as the 'the typical numerical representations of drought severity, assessed using climatic or hydro-meteorological inputs. They aim to measure the qualitative state of droughts on a given landscape for a given time period.' They help in simplification of complex relationship between various drought monitoring parameters and provide easily interpretable results. They also provide quantitative information regarding the duration, severity and location of drought events.

The traditional drought indices which were used for quantifying drought events relied solely on a single parameter and neglected other climatological parameters like temperature, humidity, windspeed, etc. which do play a significant role. So, there is a need to explore and identify better meteorological drought index that addresses the drawback of the traditional indices. Thus, SPEI (Standardized Precipitation Evapotranspiration Index) is used in this study for characterizing and impact assessment of meteorological drought events as it takes into account the effect of reference evapotranspiration as well as precipitation during computation of meteorological drought index. Furthermore, it was found to be superior and more effective in monitoring meteorological drought events as compared to other meteorological drought indices.

For this study, the emphasis was made on assessing the severity and area affected due to the occurrence of drought events. In order to categorize the drought events, three different drought classes were taken into account based on the severity namely: Moderate, Severe and Extreme drought. Furthermore, the percentage of area under drought in these three categories were also taken into account. This helped in obtaining information regarding the different types of drought events that have occurred and its effect on hydrological parameters.

There is a lack of understanding on the altercations of the meteorological drought events and anthropogenic interventions on the hydrological regimen of a river basin due to lack of long-term water use data. To resolve this issue, a land surface model such as VIC (Variable Infiltration Capacity) hydrological model is employed in this study to simulate the water and energy fluxes by taking into account various hydrological parameters in the water cycle. This helps in assessment of future or historic drought characteristics for any region (Kang and Sridhar, 2017).

## 2. Study area

The Pennar river basin lies in between east longitudes of 77º04'E and 80º10'E and north latitudes of 13º16'N and 15º52'N. The total catchment area is around 55,213 km2 which is about 1.7% of the total geographical area of India. It is bounded on the north by the Erramala range, on the east by the Nallamala and Velinkoda ranges of the Eastern Ghats, on the south

by the Nandidurg hills and on the west by the narrow ridge separating it from the Vedavati valley of the Krishna river basin. The study area maps can be seen in Figure 2.1

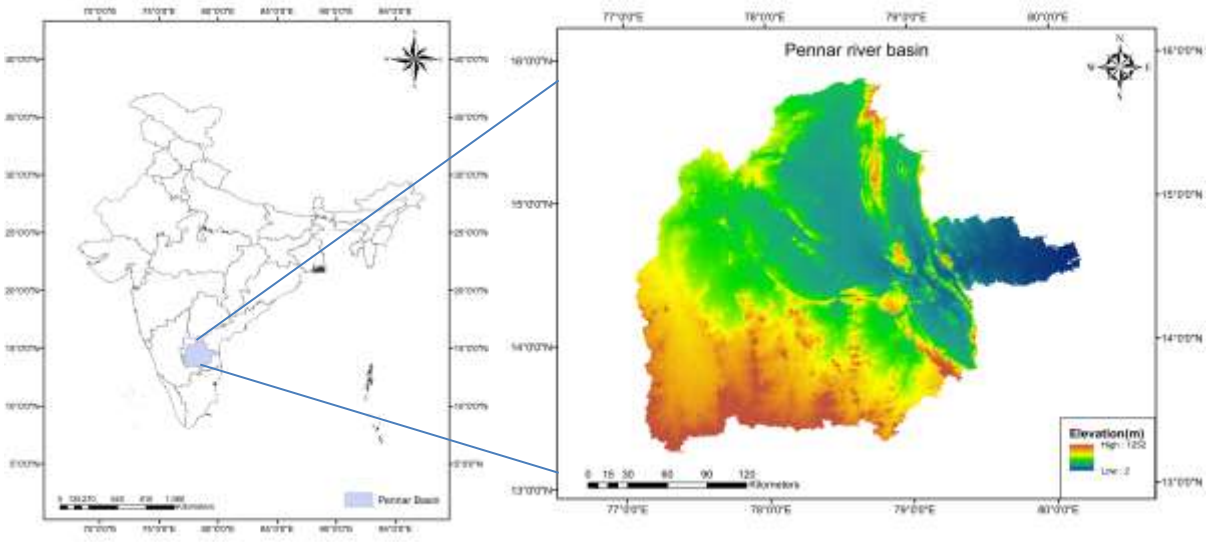



Figure 2.1 Location map of Pennar river basin

## *2.1 Pennar river*

The Pennar river originates from the Chennakesava Range of Nandi hills in Chikkaballapur district of Karnataka state and runs north and east through the states of Karnataka and Andhra Pradesh to empty into the Bay of Bengal in Nellore district of Andhra Pradesh. It is 597 kilometers long, with a drainage basin covering 55,213 $km^2$, from which 6,937 $km^2$ lies in Karnataka and about 48,276 $km^2$ lies in Andhra Pradesh.

This basin is located in the rain shadow region of the Eastern Ghats and receives an average annual rainfall of 500 mm. The river is seasonal in nature, its major source of water being from the rains. Therefore, it appears like small stream during the drought events. The major tributaries of Pennar river are Jayamangali, Kunderu and Sagileru from the north, and Chitravathi, Papagni and Cheyyeru from the south.

## *2.2 Topography and Geology*

The Pennar river along with its tributaries covers part of the southern Deccan plateau, including most of the Rayalseema region of Andhra Pradesh and part of Karnataka. The Kolar plateau forms the divide between the Pennar basin and those of the Kaveri, Ponniyar and Palar rivers

to the south. The Pennar drains the northern portion of the plateau, which includes parts of Kolar and Tumkur districts in Karnataka.

### *2.3 Climate*

The catchment receives rainfall during the south-west and north-east monsoon. The rainfall during the non-monsoon period is not significant. The north-east monsoon (October to January) provides a little precipitation but the predominant rain falls when the southwest monsoon (June through September) occurs. Post monsoon cyclonic activity in the Bay of Bengal during September and October produces an increased rainfall in the coastal region. The mean rainfall within the basin varies between 550 mm around Anantpur area to 900 mm around Nellore.

### *2.4 Soil and Land Use*

The important soil types found in the basin are red soil, black soil, sandy soil and mixed soil. The culturable area of the basin is about 3.54 M-ha which is about 1.8% of the culturable area of the country.
Under major land uses in the Pennar basin, forests account for 21% of the area whereas nearly 12% area falls under barren land. Net sown area is 36% of the total basin area while total culturable area is about 55%. In the basin, double crops are taken over very small, about 1.66 % area.

## 3. Materials and Methodology

The various materials which were used for this study are listed as follows:

- Indian Meteorological Department (IMD) gridded daily precipitation and temperature datasets from 1951 to 2018.
- Food and Agriculture Organization (FAO) Harmonized World Soil Database v1.2
- Indian Space Research Organization Geosphere Biosphere Program (IGBP) Land Use Land Cover (LULC) data
- Pennar river observed discharge data
- Digital Elevation Model (GTOPO30)

The flowchart showcasing the methodology used for this study is shown below:

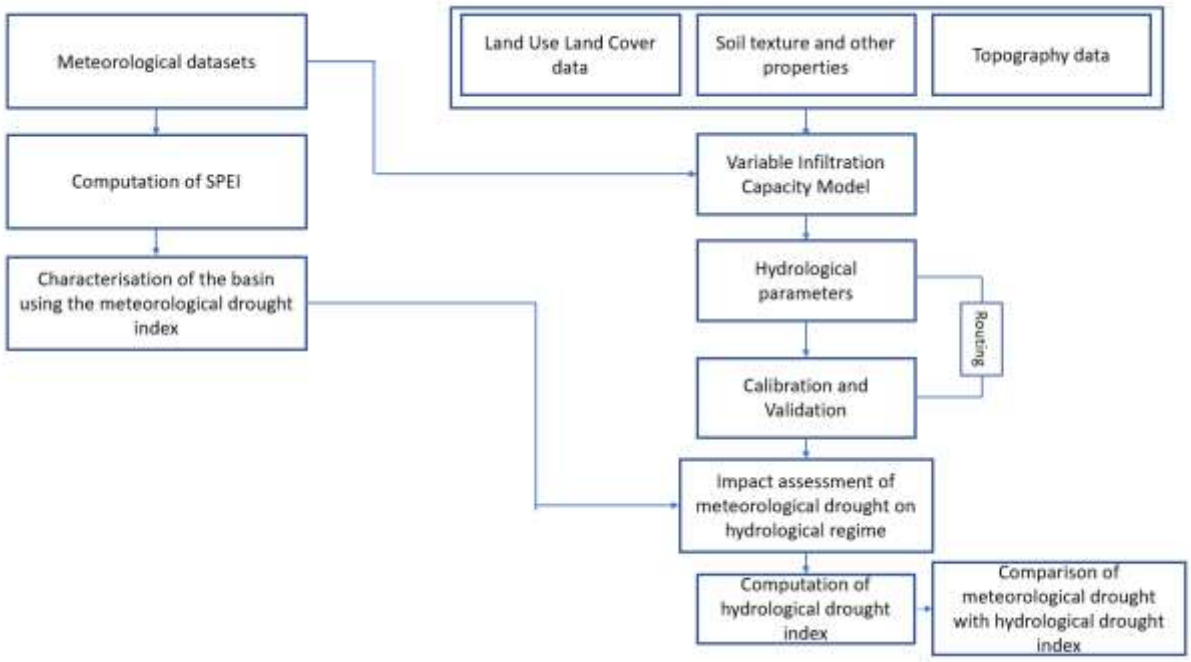



Figure 3.1 Methodology flowchart

### *3.1 Computation of SPEI*

The IMD gridded rainfall and temperature datasets which were available from 1988 till 2018 on daily time scale were used for computation of SPEI. The temperature datasets which had a spatial resolution of (1º x 1º) were resampled to match with the spatial resolution of precipitation datasets (0.25º x 0.25º). The computation of SPEI was carried out in monthly time scale and the procedure for its computation is described below:

The SPEI combines the precipitation and temperature datasets. It takes into account the monthly difference between precipitation and reference evapotranspiration which denotes a simple climatic water balance. The computation of reference evapotranspiration incorporates several parameters and several of these parameters are difficult to be measured. For this reason, the Thornwaite method (Thornthwaite, 1948) is employed to compute the monthly PET (reference evapotranspiration) values. Following this method, the monthly PET (mm) is obtained by

$$PET = 16K\left(\frac{10 * T}{I}\right)^{m} \tag{3.1}$$

where, T is the mean-monthly temperature (°C); I denote heat index, that can be computed as the summation of 12 monthly values, which can be computed by using the formula as shown:

$$I = \left(\frac{T}{5}\right)^{1.514} \tag{3.2}$$

where, m is a coefficient which depends on I: $m = 6.75 \times 10^{-7} I^3 - 7.71 \times 10^{-5} I^2 + 1.79 \times 10^{-2} I + 0.492$; and K denotes the correction factor which is a function of month and latitude as can be seen in the following equation

$$K = \left(\frac{N}{12}\right)\left(\frac{ND}{30}\right) \tag{3.3}$$

where ND denotes the number of days in a month and N denotes the maximum duration of sunshine hours, computed using

$$N = \left(\frac{24}{\pi}\right) * \omega_S \tag{3.4}$$

where $\omega_s$ is the hourly angle of the sun rising, which is calculated using

$$\omega_S = \arccos\left(-\tan\varphi \ \tan\theta\right) \tag{3.5}$$

where, φ denotes latitude in radians and δ denotes solar declination in radians, calculated by

$$\delta = 0.4093\sin\left(\frac{2\pi J}{365} - 1.405\right) \tag{3.6}$$

where, J is the average Julian day of a month.

With a value for PET, the difference between the precipitation P and PET for the month i is calculated using

$$D_i = P_i - PET_i \tag{3.7}$$

which provides a simple measure of the water surplus or deficit for the analysed month.

The probability distribution function for different values of D using log-logistic distribution is

$$F(x) = [1 + (\frac{\alpha}{x - \gamma})^{\beta}]^{-1} \tag{3.8}$$

The SPEI value can easily be obtained by the classical approach of the standardized value of F(x)

$$SPEI = W - \frac{(C_0 + C_1 W + C_2 W^2)}{1 + d_1 W + d_2 W^2 + d_3 W^3} \tag{3.9}$$

where,

$$\mathrm{W} = [-2\ln(P)]^{0.5} \quad \text{for P} < 0.5 \tag{3.10}$$

and $P$ denotes the probability to exceed a value of D which is determined, $P = 1 - F(x)$. In cases when P > 0.5, then the value of $P$ is replaced by $(1 - P)$ and the resultant sign of SPEI is reversed. The constants used in the above equations are $C_0 =$ 2.515517, $C_1 =$ 0.802853, $C_2 =$0.010328, $d_1 =$1.432788, $d_2 =$0.189269,and $d_3 =$0.001308(Abramowitz, 1974). The average value of SPEI is 0, and the standard deviation is 1. The values generated

for SPEI are standardized and can be compared with other meteorological drought indices. The value of SPEI if zero indicates a value that corresponds to 50% of the cumulative probability of *D* in log-logistic distribution(Vicente-Serrano et al., 2010; Aadhar and Mishra, 2018).

### *3.2 Characterization of SPEI over Pennar river basin*

The monthly SPEI maps generated were later on reclassified into eight different classes as per the severity of drought events as shown in Table 3.1 . This reclassification converted the index values into these different classes. A drought event was said to have occurred if the index values fell in either of the three drought classes i.e., Moderate, Severe or Extreme drought.

Table 3.1 Classification of meteorological drought

| INDICES VALUE RANGE | CLASSIFICATION |
|---|---|
| 10 to 2 | Extremely wet |
| 1.99 to 1.5 | Severely wet |
| 1.49 to 1 | Moderately wet |
| 0.99 to 0 | Normal condition (wet) |
| 0 to -0.99 | Normal condition (dry) |
| -1 to -1.49 | Moderate drought |
| -1.5 to -1.99 | Severe drought |
| -2 to -10 | Extreme drought |

After reclassification, the number of pixels in each class of drought for each month were computed which was later on used to calculate the percentage of area under each severity category of drought events. The percentage of area under each drought class was computed by

$$Percentage\ of\ area\ \ under\ drought(P_d)\ =\ \left(\frac{n_d}{N}\right) X\ 100 \tag{3.11}$$

$$Percentage\ of\ area\ not\ under\ drought(P_{nd}) = (100 - P_d) \tag{3.12}$$

where, $n_d$is the number of pixels under the drought category and N is the total number of pixels in the river basin. This provided information regarding how much percentage of area of each sub-basin was under meteorological drought in each month.

### *3.3 Hydrological modelling of Pennar river basin*

The daily hydrological simulations of Pennar basin were carried out using the three soil-layered VIC (VIC-3L) hydrological model in order to study the impact of meteorological drought events on the hydrological regime. The Pennar basin was transformed into 0.25º x 0.25º (27.5km x 27.5km) grid size. The masking of Pennar basin and grid map was done to

identify the active grids to be used as inputs for the model. The Variable Infiltration Capacity (VIC) is a semi-distributed hydrological model that can work in both water balance and surface energy balance mode and can easily incorporate sub-grid variations of land surface parameters and display it effectively. It also accounts for multiple soil layers data with variable infiltration values and non-linear base flow information in it. It also has a routing part which estimates streamflow using linear transfer function for the river basin. The calibration and validation of the daily streamflow simulations were carried out using observed discharge data at gauging station located in the river basin.

### *3.4 Impact assessment of meteorological drought on hydrological regime*

The various drought events that have occurred in the Pennar river basin were categorized into different classes and sub-classes by the use of characterization table (Table 3.1). The VIC (Variable Infiltration Capacity) hydrological model was used to generate model discharge values for Pennar river on a monthly time scale which was later on calibrated and validated using observed station discharge data. The discharge data obtained at the outlet point of the Pennar river basin was chosen for assessing the impact of meteorological drought events.
For assessing the impact of meteorological drought events, the discharge values were grouped into two different classes namely Model and Observed discharge datasets. In case of model discharge datasets, the discharge values of the outlet point of the Pennar basin obtained from running the VIC hydrological model was used while in case of observed discharge datasets, the discharge datasets obtained from the gauging station located in the outlet of Pennar river basin was used. It must be taken into account that the VIC hydrological model represents river discharge values in the natural flow conditions without taking any anthropogenic interventions into account while in case of the observed river discharge datasets, all the anthropogenic intervention activities like reservoirs, dams, irrigation water supply and industrial water usage are taken into account.

### *3.5 Computation of Hydrological drought Index for Pennar river basin*

The model and observed discharge values were later on used to compute the Streamflow Drought Index (SDI). The SDI is a hydrological drought index that uses monthly discharge values as input and the procedure for its computation is described below:
Initially, the monthly river discharge values are fitted into a gamma distribution.
The equation of 2-parameter gamma distribution is given by:

$$f(x) = \left(\frac{1}{\beta^{\alpha}\,\Gamma(\alpha)}\right) x^{\alpha-1} e^{-\left(\frac{x}{\beta}\right)} \tag{3.13}$$

where α and β are shape and scale parameters respectively. The function $\Gamma(\alpha)$ is given by:

$$\Gamma(\alpha) = \int_0^{\infty} x^{\alpha-1} e^{-x} dx \tag{3.14}$$

The cumulative probability distribution function is then computed by using the above parameters and is given by:

$$G(x) = \int_0^x f(x)dx \tag{3.15}$$

Since the gamma function is undefined for x = 0 and a precipitation distribution may contain zeros, the cumulative probability becomes:

$$H(x) = q + (1 - q)G(x)$$

where q is the probability of zero values.
The cumulative probability H(x) is then transformed to the standard normal random variable z with mean zero and variance of one, which is the value of the SDI given by (Myronidis et al., 2018; McKee, 2012):

$$z = SPI = -\left(t - \frac{(c_0 + c_1 t + c_2 t^2)}{(1 + d_1 t + d_2 t^2 + d_3 t^3)}\right) \quad \text{for} \quad 0 < H(x) < 0.5 \tag{3.16}$$

$$z = SDI = +\left(t - \frac{(c_0 + c_1 t + c_2 t^2)}{(1 + d_1 t + d_2 t^2 + d_3 t^3)}\right) \quad \text{for} \quad 0.5 < H(x) < 1 \tag{3.17}$$

where,

$$t = \sqrt{\ln\left(\frac{1}{(H(x))^2}\right)} \quad \text{for} \quad 0 < H(x) < 0.5 \tag{3.18}$$

$$t = \sqrt{\ln\left(\frac{1}{(1 - H(x))^2}\right)} \quad \text{for} \quad 0.5 < H(x) < 1 \tag{3.19}$$

and the value of the various constants taken in the above equations are (Abramowitz, 1974):
$c_0 = 2.515517$, $c_1 = 0.802583$, $c_2 = 0.010328$, $d_1 = 1.432788$, $d_2 = 0.189269$ and
$d_3 = 0.001308$
This index helps in the identification of the hydrological drought events that have occurred in the Pennar river basin as well as quantify the severity of the drought events. The characterization table for SDI is similar to that of the SPEI ranges used for characterizing SPEI.

## 4. Results and Discussions

The SPEI index were computed for the study area from 1988 till 2018 on a monthly scale and was used to showcase all the meteorological drought events that have occurred in Pennar river basin. Due to lack of a standardized characterization for drought events, the drought severity classes (Moderate, Severe and Extreme) and the percentage of area under each drought severity classes were used to chalk up a characterization table. These tables were used for characterizing the meteorological drought events that have occurred in the Pennar river basin. In order to generate monthly river discharge values for the study area, the VIC hydrological model was used. The input forcing file for running the VIC hydrological model were created and the model was run on a daily time step from 1990 till 2018 using the water balance mode. The daily fluxes from the VIC hydrological model were routed to generate monthly discharge

values for the study area. The model was calibrated and validated using the observed and model discharge values. It was taken into consideration that the outlet point of a river basin is best representative for the impact assessment of meteorological drought events on hydrological regime. The river discharge values were categorized into two groups: Model and Observed discharge values. The discharge values obtained were averaged out for each class and sub-class of meteorological drought events and the percentage reduction in discharge was represented in the form of boxplots. The hydrological drought index SDI (Streamflow Drought Index) was computed by using both observed and model discharge values and were compared with the meteorological drought events in order to assess the relationship between both the drought types.

### *4.1 Generation of meteorological drought index (SPEI)*

Using the algorithm mentioned in Section 3.1, the SPEI maps were computed for the Pennar river basin from 1988 till 2018 on a monthly scale. The computation of SPEI was carried out using daily gridded precipitation and temperature datasets and can be seen in the following figures:

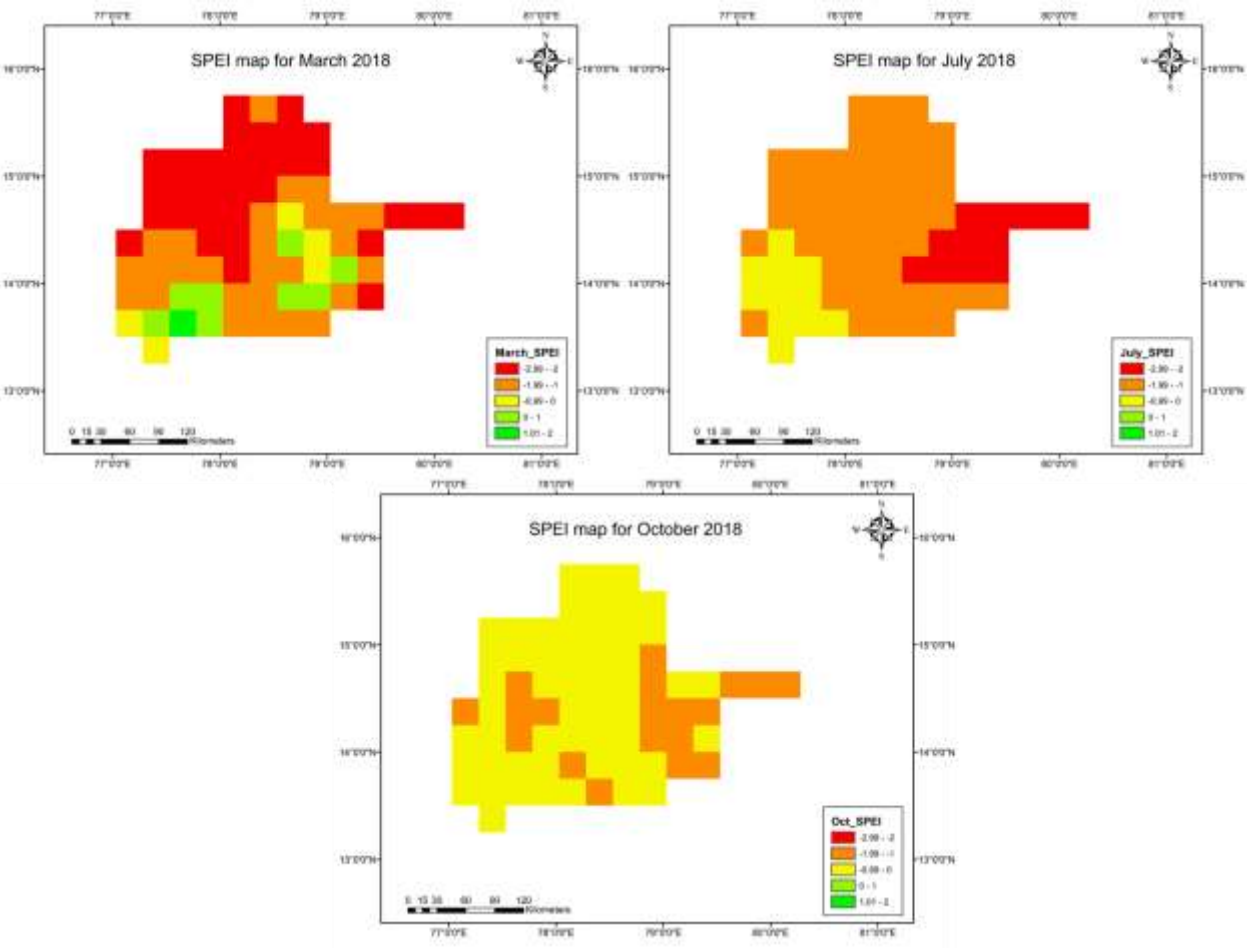



Figure 4.1 SPEI maps of Pennar river basin in March, July and October 2018

### *4.2 Characterization of Meteorological drought events over the study area*

The SPEI gridded maps were reclassified into eight different classes based on Table 3.1. A drought event was said to have occurred if the SPEI values fell either under "Moderate" drought or "Severe" drought or "Extreme" drought or any combination of these three categories. The number of pixels in each category were extracted and was used for analysis. After characterizing the meteorological drought events in terms of severity and percentage of area affected, a further characterization was carried out. A drought event that may occur over a river basin is found to be a composite event i.e., it involves combinations of different severity and percentage area affected and grouping them into a single class is erroneous. Different combinations of severity and percentage of area drought events will have different impacts. Thus, further characterization of drought events was carried out by assigning thresholds to percentage of area affected and severity of the drought events as seen in Table 4.1

Table 4.1 Categorization of meteorological drought events into major categories

| Category of drought | Total Percentage area under drought (%) |
|---|---|
| 0 | 0-6 |
| 1 | 7-26 |
| 2 | 27-50 |
| 3 | 51-75 |
| 4 | 76-100 |

Table 4.2 Sub-categorization of meteorological drought events

| Drought Sub-category | Contribution of Moderate Drought (%) | Contribution of Severe Drought (%) | Contribution of Extreme Drought (%) |
|---|---|---|---|
| **a** | >=0 & <=30 | >=0 & <=30 | >=0 & <=30 |
| **b** | >=0 & <=30 | >=0 & <=30 | >30 & <=68 |
| **c** | >=0 & <=30 | >=0 & <=30 | >68 & =<100 |
| **d** | >=0 & <=30 | >35 & =<68 | >=0 & <=30 |
| **e** | >=0 & <=30 | >30 & =<68 | >30 & =<68 |
| **f** | >=0 & <=30 | >35 & =<68 | >68 & =<100 |
| **g** | >=0 & <=30 | >68 & =<100 | >=0 & <=30 |
| **h** | >=0 & <=30 | >68 & =<100 | >30 & =<68 |
| **i** | >30 & <=68 | >=0 & <=30 | >=0 & <=30 |
| **j** | >30 & <=70 | >=0 & <=30 | >30 & =<68 |
| **k** | >30 & <=68 | >30 & <=68 | >=0 & <=30 |
| **l** | >30 & <=68 | >30 & <=68 | >30 & <=68 |

| | | | |
|---|---|---|---|
| **m** | >68 & =<100 | >=0 & <=30 | >=0 & <=30 |

This characterization table was chalked out keeping in mind all the possible combinations of the drought events. In these tables, the sub-categories are represented in the form of alphabets while the rest of the column represent the percentage contribution of each severity classes of drought events.

The following table showcases the number of drought months in the Pennar river basin for each month for the whole study time period. The 'Annual' column is the sum of all the drought events that have occurred in all the months. The category column refers to the major drought categories.

Table 4.3 Total number of drought events

| Category | Annual | Jan | Feb | Mar | Apr | May | Jun | Jul | Aug | Sep | Oct | Nov | Dec |
|---|---|---|---|---|---|---|---|---|---|---|---|---|---|
| 0 | 577 | 55 | 53 | 54 | 54 | 45 | 45 | 45 | 46 | 36 | 44 | 50 | 50 |
| 1 | 112 | 6 | 6 | 4 | 5 | 9 | 14 | 11 | 9 | 14 | 10 | 11 | 13 |
| 2 | 48 | 2 | 2 | 3 | 2 | 6 | 4 | 5 | 4 | 9 | 7 | 2 | 2 |
| 3 | 39 | 2 | 2 | 1 | 3 | 4 | 3 | 2 | 3 | 8 | 4 | 4 | 3 |
| 4 | 40 | 3 | 5 | 6 | 4 | 4 | 2 | 5 | 6 | 1 | 3 | 1 | 0 |

Table 4.4 Total number of drought events in each sub-category

| Category | Annual | Jan | Feb | Mar | Apr | May | Jun | Jul | Aug | Sep | Oct | Nov | Dec |
|---|---|---|---|---|---|---|---|---|---|---|---|---|---|
| 0 | 577 | 55 | 53 | 54 | 54 | 45 | 45 | 45 | 46 | 36 | 44 | 50 | 50 |
| 1.m | 77 | 6 | 6 | 3 | 0 | 3 | 13 | 12 | 6 | 11 | 9 | 5 | 3 |
| 2.i | 1 | 0 | 0 | 0 | 0 | 0 | 0 | 1 | 0 | 0 | 0 | 0 | 0 |
| 2.k | 1 | 0 | 0 | 0 | 0 | 0 | 1 | 0 | 0 | 0 | 0 | 0 | 0 |
| 2.m | 45 | 1 | 2 | 3 | 2 | 6 | 3 | 4 | 4 | 9 | 7 | 2 | 2 |
| 3.i | 2 | 0 | 0 | 0 | 0 | 0 | 0 | 0 | 1 | 0 | 0 | 0 | 1 |
| 3.m | 36 | 2 | 2 | 1 | 3 | 4 | 2 | 2 | 2 | 8 | 4 | 4 | 2 |

| | | | | | | | | | | | | | |
|---|---|---|---|---|---|---|---|---|---|---|---|---|---|
| 4.b | 3 | 0 | 2 | 1 | 0 | 0 | 0 | 0 | 0 | 0 | 0 | 0 | 0 |
| 4.c | 3 | 0 | 0 | 0 | 2 | 1 | 0 | 0 | 0 | 0 | 0 | 0 | 0 |
| 4.d | 7 | 2 | 0 | 0 | 1 | 0 | 2 | 1 | 1 | 0 | 0 | 0 | 0 |
| 4.e | 2 | 0 | 1 | 1 | 0 | 0 | 0 | 0 | 0 | 0 | 0 | 0 | 0 |
| 4.g | 4 | 0 | 0 | 2 | 0 | 0 | 1 | 0 | 0 | 0 | 1 | 0 | 0 |
| 4.i | 1 | 0 | 0 | 0 | 0 | 0 | 0 | 1 | 0 | 0 | 0 | 0 | 0 |
| 4.k | 11 | 0 | 2 | 2 | 0 | 0 | 0 | 3 | 2 | 1 | 1 | 0 | 0 |
| 4.m | 11 | 0 | 0 | 2 | 1 | 3 | 0 | 0 | 3 | 0 | 1 | 1 | 0 |

From the above tables it can be seen that the total percentage of area under meteorological drought was found to be within 65 in most of the cases and decreased with subsequent increase in the percentage area. In all of the meteorological drought events, the contribution of 'Moderate' severity drought category was found to be the highest as evident from the fact that most of the meteorological drought events had occurred in 'm' sub-category. Furthermore, the distribution of the meteorological drought events in the basin was found to be non-uniform and varied for each categories and sub-categories.

### *4.3 Hydrological simulation of the river basin*

Observed discharge data from Nellore gauging station were available for the study area in the India-WRIS portal. The VIC hydrological model was used to assess the river discharge values for Pennar river basin. The daily flux files generated from the hydrological model were routed to compute the monthly discharge values which were later on compared with the observed discharge data in order to calibrate and validate the model. In order to improve the efficiency of the model, certain soil parameters in the forcing files were modified and the model was rerun with the modified soil parameter file. The calibration process is carried out with the assumption of the fact that there might be some errors in the soil parameter forcing file that needs to be rectified in order to improve the relationship between observed and model discharge values.

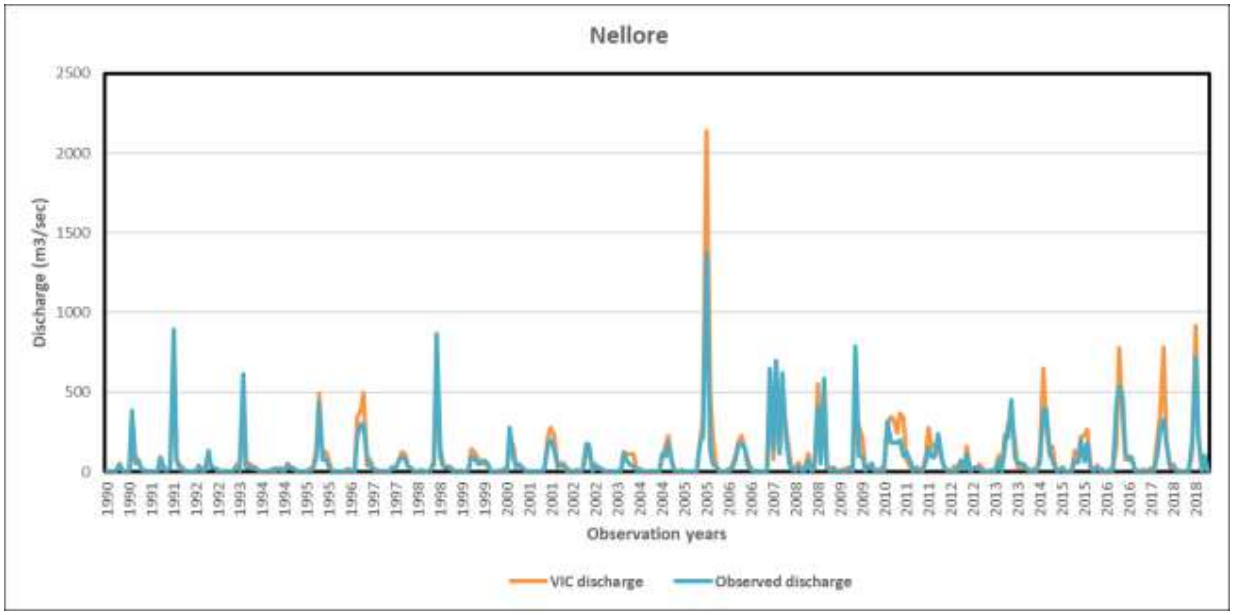



Figure 4.2 Plot between monthly and observed discharge values for Pennar river basin from 1990 till 2018

The time period for the calibration of the model was considered from 1990 till 2005 while it was validated from 2006 till 2018. To check the accuracy between the model and observed discharge values, the Nash-Sutcliffe efficiency (NSE) and coefficient of determination ($R^2$) were used. The closer the value of NSE and $R^2$ is to 1, the better the model results are. The NSE and Coefficent of determination for the calibration and validation phase is shown in Table

Table 4.5 The Nash-Sutcliffe efficiency and Coefficent of Determination of the model

| | **NSE** | **R2** |
|---|---|---|
| Calibration years (1990-2005) | 0.752 | 0.73 |
| Validation years (2006-2018) | 0.73 | 0.71 |

The soil parameter values for the best calibrated phase were found to be $b_{inf}$ = 0.43, $D_s$ = 0.02, $W_s$ = 0.91, $d_1$ = 0.3, $d_2$ = 1.3, $d_3$ = 1.33. For model discharge simulation, the model was run on the water balance mode. The model and observed discharge were later on used to assess the impact of meteorological drought on the river discharge values.

### *4.4 Impact of meteorological drought events on river discharge*

The impact assessment of meteorological drought events on both observed and model discharge values were analysed. In VIC hydrological model, the effects of anthropogenic interventions on river discharge values are completely ignored while that is taken into account in case of observed discharge values. The average discharge values for non-drought conditions for each month were computed. In order to quantify the effect of meteorological

drought events, the percentage reduction in discharge values due to each meteorological drought events were computed both for modelled and observed discharge values. These are represented below in the form of boxplots. The boxplots are a standardized way of showcasing how the datasets are distributed by taking into account 5 parameters such as Minima, First quartile, Mean/Median, Third quartile and Maxima.

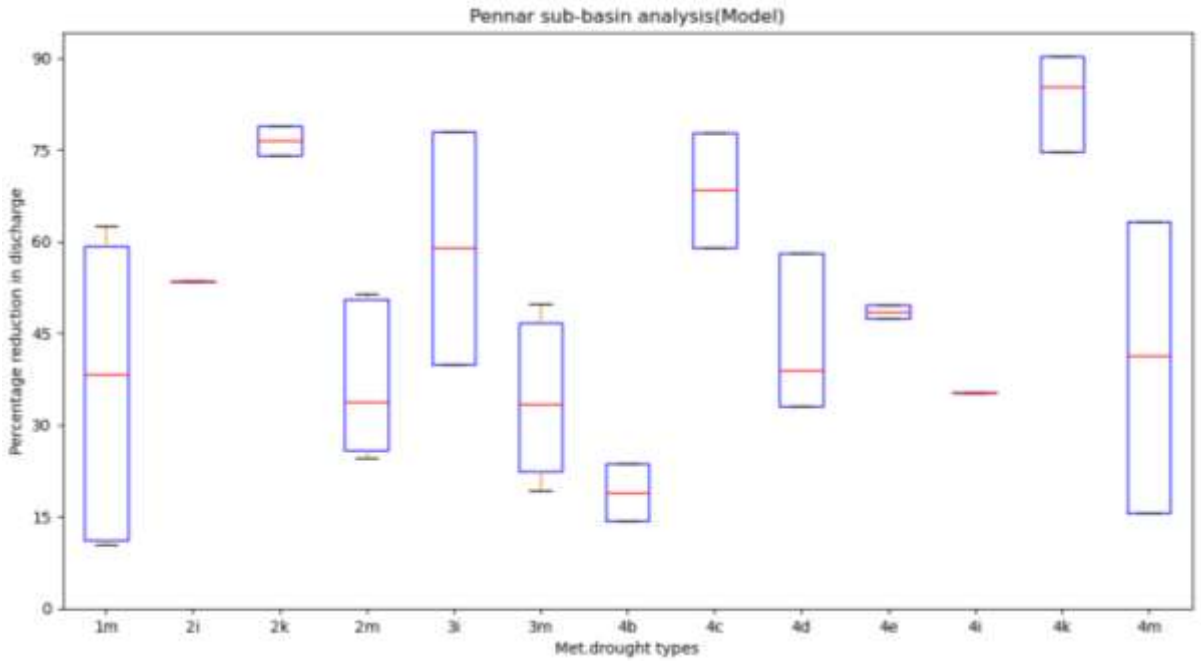



Figure 4.3 Boxplot for Pennar river basin using VIC hydrological model data

The percentage reduction in average discharge due to due to occurrence of each category of meteorological drought events can be visualized in the above boxplots. In the boxplots, the boxes contain about 80% of the data. The red line represents the mean/median value while the black ticks on each boxplots represent the maxima and minima values of the datasets. The orange whiskers represent the variability in the upper and lower quartiles. It can be seen that the maximum reduction in discharge occurred in '4.k' category i.e., around 90% while the minimum reduction occurred in the '1.m' category i.e., around 11%. The percentage reduction ranges in the model discharge was found to be 11-62 % for Category '1', 25-79 % for Category '2', 18-77 % for Category '3' and 15-90 % for Category '4' of meteorological drought events.

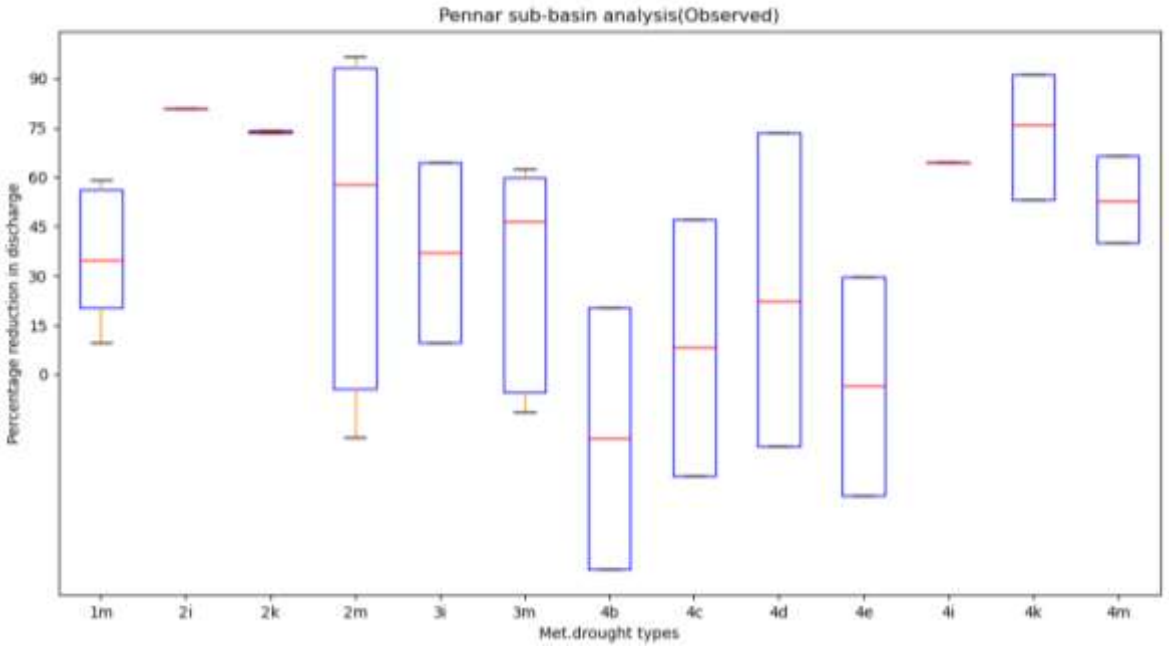



Figure 4.4 Boxplot for Pennar river basin using observed discharge data

Similarly, as seen in case of boxplots made using observed discharge data, the maximum percentage of discharge reduction was seen for Category '2.m' i.e., about 93% while minimum percentage of discharge reduction was seen in Category '1.m' and Category '3.i' i.e., around 10%. There are also some instances when the percentage reduction in discharge values are found to be negative. This occurred due to the fact that the natural flow regimen is obliterated by the anthropogenic intervnetions. Furthermore, this also explains why there is maximum reduction in river discharge value due to a Category '2' drought event. The average percentage reduction in discharge values due to Category '1' drought event is around 10-60 %, for Category '2' is around 0-93 %, for Category '3' is around 10-61 % and for Category '4' is around 0-90 %.

## *4.5 Computation of hydrological drought index and comparison with meteorological drought index*

The comparison of meteorological drought events with the average discharge values helped gain information regarding the response variation in discharge values both in model as well as observed datasets towards different meteorological drought events. Now, in order to showcase how each meteorological drought event affected the hydrological regimen in each month, the hydrological drought index was computed i.e., the Streamflow Drought Index (SDI). The values of SDI are in the same scale as that of the SPEI.

The time series of SDI for Pennar river basin is shown in Figure

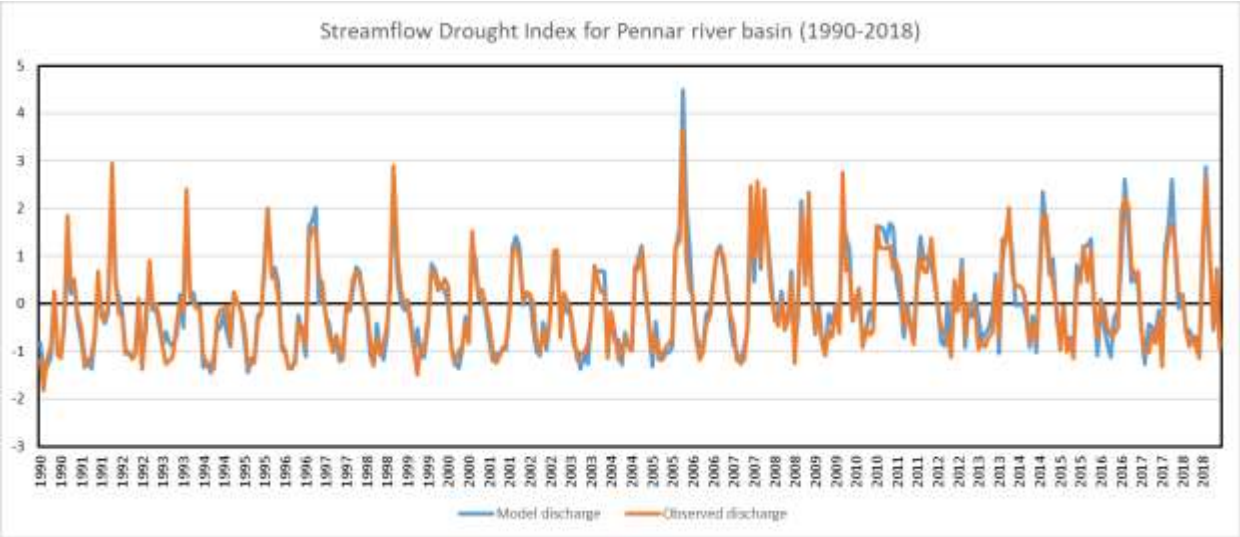



Figure 4.5 Streamflow Drought Index for the Pennar river basin

These tables were generated for Pennar river basin from 1990 till 2018. In these tables, the SDI values are provided for each month and the corresponding occurrence of meteorological drought event along with its severity is also shown.

Figure 4.6 Table showing SDI for Pennar sub-basin from 1990-1998. The colored boxes represent the meteorological drought events of different severity

| Years | Types | Jan | Feb | Mar | Apr | May | Jun | Jul | Aug | Sept | Oct | Nov | Dec |
|---|---|---|---|---|---|---|---|---|---|---|---|---|---|
| 1990 | Mod | -0.810 | -1.458 | -1.335 | -1.117 | 0.246 | -0.939 | -1.150 | -0.482 | 0.992 | 0.215 | 0.464 | 0.344 |
| | Obs | -1.186 | -1.817 | -1.172 | -0.899 | 0.270 | -1.078 | -1.126 | -0.336 | 1.841 | 0.407 | 0.517 | -0.189 |
| 1991 | Mod | -0.789 | -1.332 | -1.170 | -1.373 | -0.699 | 0.515 | -0.152 | -0.415 | -0.186 | 2.426 | 0.427 | 0.141 |
| | Obs | -0.538 | -1.213 | -1.279 | -1.068 | -0.689 | 0.687 | -0.296 | -0.327 | -0.068 | 2.939 | 0.557 | -0.227 |
| 1992 | Mod | -0.146 | -0.947 | -1.049 | -1.905 | -1.033 | 0.109 | -1.367 | -0.136 | 0.459 | -0.141 | -0.113 | -0.485 |
| | Obs | -0.243 | -1.062 | -1.007 | -1.161 | -1.062 | 0.107 | -1.375 | -0.480 | 0.904 | -0.031 | 0.004 | -0.304 |
| 1993 | Mod | --0.881 | -0.585 | -0.814 | -0.908 | -0.665 | 0.193 | -0.504 | 1.968 | 0.172 | 0.237 | -0.080 | -0.051 |
| | Obs | -0.903 | 1.274 | -1.192 | -1.133 | -0.429 | -0.018 | -0.173 | 2.399 | 0.126 | 0.022 | -0.093 | -0.085 |
| 1994 | Mod | -1.330 | -1.249 | -1.457 | -1.067 | -0.558 | -0.500 | -0.189 | -0.637 | -0.893 | 0.209 | 0.001 | -0.148 |
| | Obs | -1.082 | -1.275 | -1.241 | -1.376 | -0.304 | -0.109 | -0.096 | -0.047 | -0.806 | 0.254 | 0.005 | -0.177 |
| 1995 | Mod | -0.780 | -1.432 | -1.136 | -1.154 | -0.242 | -0.232 | 0.832 | 2.007 | 0.588 | 0.753 | 0.400 | -0.971 |
| | Obs | -0.492 | 1.314 | -1.280 | -1.255 | -0.367 | -0.181 | 0.674 | 1.987 | 0.540 | 0.585 | 0.116 | -0.831 |
| 1996 | Mod | -1.031 | -1.336 | -1.375 | -1.154 | -0.246 | -0.655 | -1.103 | 1.617 | 1.741 | 2.021 | 0.008 | 0.453 |
| | Obs | -0.975 | -1.345 | -1.313 | -1.258 | -0.419 | -0.479 | -0.917 | 1.332 | 1.588 | 1.554 | 0.606 | 0.267 |
| 1997 | Mod | -0.263 | -0.392 | -1.017 | -0.682 | -1.206 | -0.944 | -0.033 | -0.157 | 0.282 | 0.764 | 0.678 | 0.044 |
| | Obs | -0.217 | -0.693 | -0.991 | -0.659 | -0.952 | -1.172 | -0.022 | -0.085 | 0.522 | 0.682 | 0.558 | 0.093 |
| 1998 | Mod | -0.263 | -1.078 | -1.306 | -0.410 | -0.983 | -1.171 | -0.679 | 0.473 | 2.274 | 0.535 | 0.037 | -0.129 |
| | Obs | -0.084 | -0.771 | -1.259 | -0.735 | -1.075 | -0.848 | -0.483 | 0.278 | 2.891 | 0.991 | 0.296 | 0.024 |

From analysing the time series datasets of SDI, it can be seen that there were instances when the occurrences of meteorological drought coincided with that of hydrological drought events

while in some cases it doesn't. Furthermore, there is a certain time lag between the occurrence of meteorological and hydrological drought events which was found to be inconsistent in nature. These tables showcase how the river discharge value were affected due to the occurrence of various meteorological drought events. The colour code as shown in the above table is as such, the yellow boxes, represents Category '1' of meteorological drought events, the light orange represents the Category '2' of meteorological drought events, the darker orange represents the Category '3' of meteorological drought events while the red boxes represents the Category '4' of meteorological drought events.

The hydrological drought index values were found to remain negative for most of the time period as seen in the above table. In order to test the validity of SDI, it was compared with the past events of occurrence of flood or drought events in the Pennar river and the results were found to be consistent with the observations.

## 5. Conclusion

From the above study, it was found that there have been around 239 instances of meteorological drought events that have occurred in Pennar river basin from 1988 till 2018. The percentage of contribution of "Moderate' category of drought severity was found to be the highest than any other category. The VIC hydrological model was calibrated and validated using observed discharge datasets from Nellore gauging station on a monthly scale with the soil calibration parameters being $b_{inf}$ = 0.43, $D_s$ = 0.02, $W_s$ = 0.91, $d_1$ = 0.3, $d_2$ = 1.3, $d_3$ = 1.33 respectively. With increase in severity and percentage of area under meteorological drought, the percentage reduction in discharge values also increased in case of model discharge data while that was not the trend noticed in case of observed discharge data which showcases how the anthropogenic interventions have made the relationship between meteorological and hydrological droughts more unpredictable and complex. The basin was found to be prone to hydrological drought events for most of the months.

## 6. References

Thakur, P.K., Nikam, B.R., Garg, V., Aggarwal, S.P., Chouksey, A., Dhote, P.R., Ghosh, S., 2017. Hydrological Parameters Estimation Using Remote Sensing and GIS for Indian Region: A Review. Proc. Natl. Acad. Sci. India Sect. A Phys. Sci. 87, 641–659. https://doi.org/10.1007/s40010-017-0440-z

Thornthwaite, C.W., 1948. An Approach toward a Rational Classification of Climate. Geogr. Rev. 38, 55–94. https://doi.org/10.2307/210739

Tigkas, D., Vangelis, H., Tsakiris, G., 2012. Drought and climatic change impact on

streamflow in small watersheds. Sci. Total Environ. 440, 33–41. https://doi.org/10.1016/j.scitotenv.2012.08.035

Tsakiris, G., Pangalou, D., Vangelis, H., 2007. Regional drought assessment based on the Reconnaissance Drought Index (RDI). Water Resour. Manag. 21, 821–833. https://doi.org/10.1007/s11269-006-9105-4

Tsakiris, G., Vangelis, H., 2005. Establishing a drought index incorporating evapotranspiration. Eur. Water 9, 3–11.

UCLA Experimental Surface Water Monitor for the Continental U.S. [WWW Document], n.d. URL http://www.hydro.ucla.edu/SurfaceWaterGroup/forecast/monitor/index.shtml (accessed 6.8.20).

USGS EROS Archive - Digital Elevation - Global 30 Arc-Second Elevation (GTOPO30) [WWW Document], n.d. URL https://www.usgs.gov/centers/eros/science/usgs-eros-archive-digital-elevation-global-30-arc-second-elevation-gtopo30?qt-science_center_objects=0#qt-science_center_objects (accessed 9.7.20).

Van Lanen, H.A.J., 2006. Drought propagation through the hydrological cycle. IAHS Publ.

Vicente-Serrano, S.M., Beguería, S., López-Moreno, J.I., 2010. A multiscalar drought index sensitive to global warming: The standardized precipitation evapotranspiration index. J. Clim. 23, 1696–1718. https://doi.org/10.1175/2009JCLI2909.1

Wang, A., Lettenmaier, D.P., Sheffield, J., 2011. Soil Moisture Drought in China, 1950–2006. J. Clim. 24, 3257–3271. https://doi.org/10.1175/2011JCLI3733.1

Water Cycle | Science Mission Directorate [WWW Document], n.d. URL https://science.nasa.gov/earth-science/oceanography/ocean-earth-system/ocean-water-cycle (accessed 7.25.20).

Wieder, W.R., Boehnert, J., Bonan, G.B., Langseth, M., 2014. Regridded Harmonized World Soil Database v1.2. Data set. Available on-line [http//daac.ornl.gov] from Oak Ridge Natl. Lab. Distrib. Act. Arch. Center, Oak Ridge, Tennessee, USA.

https://doi.org/10.3334/ORNLDAAC/1247

Wong, G., van Lanen, H.A.J., Torfs, P.J.J.F., 2013. Probabilistic analysis of hydrological drought characteristics using meteorological drought. Hydrol. Sci. J. 58, 253–270. https://doi.org/10.1080/02626667.2012.753147

Wood, E.F., Lettenmaier, D.P., Liang, X., Lohmann, D., Boone, A., Chang, S., Chen, F., Dai, Y., Dickinson, R.E., Duan, Q., Ek, M., Gusev, Y.M., Habets, F., Irannejad, P., Koster, R., Mitchel, K.E., Nasonova, O.N., Noilhan, J., Schaake, J., Schlosser, A., Shao, Y., Shmakin, A.B., Verseghy, D., Warrach, K., Wetzel, P., Xue, Y., Yang, Z.L., Zeng, Q.C., 1998. The project for intercomparison of land-surface parameterization schemes (PILPS) phase 2(c) Red-Arkansas River basin experiment: 1. Experiment description and summary intercomparisons. Glob. Planet. Change 19, 115–135. https://doi.org/10.1016/S0921-8181(98)00044-7

Wood, E.F., Lettenmaier, D.P., Zartarian, V.G., 1992. A land-surface hydrology parameterization with subgrid variability for general circulation models. J. Geophys. Res. Atmos. 97, 2717–2728. https://doi.org/10.1029/91JD01786@10.1002/(ISSN)2169-8996.GCC1

Wu, J., Chen, X., Yao, H., Gao, L., Chen, Y., Liu, M., 2017. Non-linear relationship of hydrological drought responding to meteorological drought and impact of a large reservoir. J. Hydrol. 551, 495–507. https://doi.org/10.1016/j.jhydrol.2017.06.029

Zargar, A., Sadiq, R., Naser, B., Khan, F.I., 2011. A review of drought indices. Environ. Rev. 19, 333–349. https://doi.org/10.1139/a11-013

Zhao, L., Lyu, A., Wu, J., Hayes, M., Tang, Z., He, B., Liu, J., Liu, M., 2014. Impact of meteorological drought on streamflow drought in Jinghe River Basin of China. Chinese Geogr. Sci. 24, 694–705. https://doi.org/10.1007/s11769-014-0726-x

Zhao, L., Wu, J., Fang, J., 2016. Robust Response of Streamflow Drought to Different Timescales of Meteorological Drought in Xiangjiang River Basin of China. Adv. Meteorol. 2016, 1634787. https://doi.org/10.1155/2016/1634787

*IN PROCEEDINGS OF 25th HYDRO 2020, INTERNATIONAL CONFERENCE, NATIONAL INSTITUTE OF TECHNOLOGY ROURKELA, ODISHA, INDIA 26-28, March 2021, ISBN 978-93-90631-56-8*

Paper ID - 253

# Estimation of Peak Flood Discharge for Ungauged Catchments By Hydrometeorological Approaches

C. Srishailam[1*] N. Vivekanandan[2] R.G. Patil[3]

[1]*Scientist-C, Central Water and Power Research Station, Pune 411024, Maharashtra*
[*]*E-mail: srisaila2@rediffmail.com*
[2]*Scientist-B, Central Water and Power Research Station, Pune 411024, Maharashtra*
*E-mail: anandaan@rediffmail.com*
[3]*Scientist-E, Central Water and Power Research Station, Pune 411024, Maharashtra*
*E-mail: rsrgp@rediffmail.com*
[*]*Telephone/Mobile No.: +91 20 2410 3279*

## Abstract

Estimation of Peak Flood Discharge (PFD) for ungauged catchments is required in hydrological practices and also one of the important parameters for design of hydraulic structures, river protection works, development of integrated water resources management projects, etc. This can be achieved by adopting hydrometeorological approaches such as flood frequency analysis, rational formula, envelope curves and Synthetic Unit Hydrograph (SUH) method. In this paper, as the catchments of the study area are ungauged, PFD is estimated by using rational formula for the catchments with catchment area less than 25 km$^2$ and SUH method for the catchments with catchment area more than 25 km$^2$. For both rational formula and SUH method, rainfall depth becomes an important parameter, which can be estimated through extreme value analysis by fitting of Gumbel distribution to the Annual Maximum Series (AMS) of rainfall data. Parameters of the distribution are determined by maximum likelihood method and used for estimation of rainfall. Goodness-of-Fit tests viz., Anderson-Darling and Kolmogorov-Smirnov are applied for checking the adequacy of fitting Gumbel distribution to the AMS of rainfall data. The paper illustrates the procedures adopted in estimation of PFD for the ungauged catchments of Suketi Khad by hydrometeorological approaches, and the results obtained thereof.

***Keywords:*** *Extreme value analysis; Gumbel distribution; Maximum likelihood method; Peak flood discharge; Rational formula; Synthetic unit hydrograph*

## 1. Introduction

Estimation of Peak Flood Discharge (PFD) for ungauged catchments is required in hydrological practices and also one of the important parameters for the design of hydraulic structures, river protection works, development of integrated water resources management projects, etc. This can be achieved by adopting hydrometeorological approaches such as flood frequency analysis, rational formula, envelope curves and Synthetic Unit Hydrograph (SUH) method. For gauged catchments, flood frequency analysis that involves fitting probability distribution to the Annual Maximum Series (AMS) of discharge data is widely adopted for estimation of PFD whereas envelope curves are used when the catchment characteristics are available. For ungauged catchments, rational formula is used for estimation of PFD for the catchments with catchment area less than 25 km$^2$ whereas SUH method is adopted for the catchments with catchment area more than 25 km$^2$ (Mohammed and Azhar, 2017).

For ungauged catchments, stream flow data is not available for estimation of PFD. For such cases, the 24-hour maximum rainfall is an important parameter for estimation of PFD. This can be achieved through Extreme Value Analysis (EVA) that involves fitting probability distribution to the AMS of 24-hour or 1-day rainfall that is derived from the observed rainfall data. If hourly rainfall data is not available then the 24-hour maximum rainfall can be obtained by multiplying the 1-day maximum rainfall with 1.15 and the derived rainfall value is used for estimation of PFD. During the past, number of studies on estimation of PFD for ungauged catchments has been carried out by different researchers. Ramirez (2000) carried out the study on estimation of PFD by SUH for 20 watersheds located in the Appalachian Highlands. Jena et al. (2005) adopted the SUH for estimation of design flood for water resources project in Baitarani basin, Odisha. Natakusumah et al. (2011) carried out the study on derivation of flood hydrograph of the Cibatarua river basin by SUH. Priyanka Kumari and Goel (2015) adopted SUH for flood estimation for rivers of Saurashtra Region contributing into Gulf

of Khambhat. Kim and Mun-Ju Shin (2018) estimated the relationship between the runoff coefficient, intensity of rainfall, and curve number, and then utilized the relationship to calculated the peak flow using the rational method for ungauged catchments. Reddy et al. (2019) carried out the study on flood estimation at ungauged catchments of western catchments of Karnataka, West coast of India by adopting five different methods viz., CWC (Central Water Commission) approach, Snyder method, SCS (Soil Conservation Service) method, Gamma Distribution and hybrid model. They also found that Hybrid model satisfies the Unit Hydrograph criterion whereas, traditional methods of Snyder, SCS, CWC-SUH and CWC dimensionless methods require manual adjustments of the characteristics points and have a significant degree of subjectivity and trial and error. Andrea et al. (2020) carried out the study on comparison of design peak flow estimation methods for ungauged basins in Iran. They found that the CWC-SUH approach gives better results than other methods. However, the studies reported didn't suggest applying a particular method for estimation of PFD for ungauged catchments. In this context, an attempt has been made to estimate the PFD for ungauged catchments of Suketi Khad using rational formula and SUH method, and the results are presented in the paper. The methodology adopted in estimation of PFD using hydrometeorological approaches (viz., rational formula and SUH method) are briefly described in the following sections.

## 2. Methodology

### 2.1 *Gumbel (or Extreme Value Type-I) distribution*

Out of a number of probability distributions, the Extreme Value Type-I, commonly known as Gumbel, is widely applied for EVA of rainfall and hence used. The Cumulative Distribution Function (CDF) of the Gumbel distribution is given as below:

$$F(x) = e^{-e^{-(x-\alpha)/\beta}}, x > 0,\ \beta > 0 \quad \ldots (1)$$

where, $\alpha$ and $\beta$ are the location and scale parameters of the distribution (Gumbel, 1985). The estimators $(\hat{\alpha}$ *and* $\hat{\beta})$ of the parameters are determined by maximum likelihood method and also used to estimate the Extreme Rainfall (ER) for different return periods from $x_T = \hat{\alpha} + Y_T\hat{\beta}$ wherein $Y_T = -ln(-ln(1-(1/T)))$ is called as a reduced variate for a given return period $T$ (year).

$$\hat{\alpha} = -\hat{\beta} ln\left[\sum_{i=1}^{N} exp(-x_i/\hat{\beta})/N\right] \quad \ldots (2)$$

$$\hat{\beta} = \bar{x} - \left[\sum_{i=1}^{N} x_i\, exp(-x_i/\hat{\beta})\Big/\sum_{i=1}^{N} exp(-x_i/\hat{\beta})\right] \quad \ldots (3)$$

$$SE(x_T) = (\hat{\beta}/\sqrt{N})(1.15894 + 0.19187Y_T + 1.1Y_T^2)^{0.5} \quad \ldots (4)$$

where, $x_i$ is the observed data of i$^{th}$ sample, $\bar{x}$ is the average of observed data, $N$ is the sample size and $x_T$ is the ER for a given return period ($T$). The lower and upper confidence limits (*LCL* and *UCL*) of the estimated ER at 95% level are obtained from the linear expressions viz., *LCL=ER-1.96(SE)* and *UCL=ER+1.96(SE)*. Here, *SE* is the Standard Error of the estimated ER.

### 2.2 *Goodness-of-Fit tests*

GoF tests viz., *AD* and *KS* tests statistic are applied for checking the adequacy of fitting of Gumbel distribution (Zhang, 2002) to the AMS of observed data. Theoretical descriptions of GoF tests statistic are given as below:

$$AD = (-N) - (1/N)\sum_{i=1}^{N}\{(2i-1)\,ln(Z_i) + (2N+1-2i)\,ln(1-Z_i)\} \quad \ldots (5)$$

$$KS = \underset{i=1}{\overset{N}{Max}}\,(F_e(x_i) - F_D(x_i)) \quad \ldots (6)$$

where, $Z_i = F(x_i) = (i-0.44)/(N+0.12)$ for $i=1,2,3,\ldots,N$ with $x_1 < x_2 < \ldots < x_N$, $F_e(x_i)$ is the empirical CDF of $x_i$, $F_D(x_i)$ is the derived CDF of $x_i$ by Gumbel distribution. The theoretical values of *AD* and *KS* tests statistic for different sample size ($N$) at 5% or 1% significance level are available in the technical note on 'Goodness-of-Fit Tests for Statistical Distributions' by Charles Annis (2009). If the computed values of GoF tests statistic by Gumbel distribution are less than its theoretical values at the desired significance level (either at 5% or 1%), then the distribution is found to be acceptable for EVA of rainfall at that level.

## 2.3 *Approaches for estimation of PFD*

For the present study, rational formula and SUH method is adopted for estimation of PFD though many approaches or methods available. The procedures adopted in rational formula and SUH method are given as below.

### 2.3.1 *Rational formula*

Rational formula is adopted for estimation of PFD for ungauged catchments with catchment area less than 25 km$^2$, which is given as below:

$$q = (0.278)CiA \quad \ldots (7)$$

where, $q$ is the PFD (m$^3$/s), $C$ is runoff coefficient, '$i$' is the rainfall intensity (mm/hour) and $A$ is the catchment area (km$^2$).

### 2.3.2 *SUH method*

A systematic and sustained collection of hydrometeorological data for selected catchments in different climatic zones is required for estimation of PFD. Based on the data collected, the physiographic parameters viz., catchment area, length of the longest stream, length of the longest stream closer to the centre of gravity to the point of study and equivalent stream slope are computed by delineating the catchments of the study area using ArcGIS software.

**Table 1.** Empirical equations used in determination of SUH parameters

$$q_p = 1.048\left(t_p\right)^{-0.178}$$

$$t_p = 2.498\left(LL_c / S\right)^{0.156}$$

$$W_{50} = 1.954\left(LL_c / S\right)^{0.099}$$

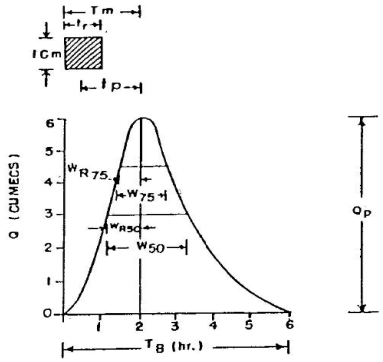
$$W_{75} = 0.972\left(LL_c / S\right)^{0.124}$$

$$WR_{50} = 0.189\left(W_{50}\right)^{1.769}$$

$$WR_{75} = 0.419\left(W_{75}\right)^{1.246}$$

$$T_B = 7.845\left(t_p\right)^{0.453}$$

$$Q_p = q_p * A \quad \text{and} \quad T_m = t_p + 0.5$$




Parameters of SUH (Snyder, 1938)

where,

| | | |
|---|---|---|
| $A$ | = | Catchment area (km$^2$) |
| $L$ | = | Length of longest main stream along the river course (km) |
| $L_c$ | = | Length of longest stream from centre of gravity (km) |
| $S$ | = | Equivalent stream slope (m/km) |
| $t_p$ | = | Time to peak or the basin lag (hour) |
| $t_r$ | = | Unit rainfall duration adopted in a specific study (hour) |
| $q_p$ | = | Peak flood (m$^3$/s) of UH per unit area (km$^2$) |
| $W_{50}$ | = | Width of the UH at 50% of $Q_p$ (hour) |
| $W_{75}$ | = | Width of the UH at 75% of $Q_p$ (hour) |
| $WR_{50}$ | = | Width of the rising limb of the UH at 50% of $Q_p$ (hour) |
| $WR_{75}$ | = | Width of the rising limb of the UH at 75% of $Q_p$ (hour) |
| $T_B$ | = | Time base of the UH (hour) |
| $T_m$ | = | Time from the start of rise to peak of unit hydrograph (hour) |
| $T_D$ | = | Design storm duration (hour) |
| $Q_p$ | = | Peak flood of UH (m$^3$/s) |

By using the physiographic parameters, the SUH parameters were determined from the empirical equations (Table 1) to derive the 1-hour SUH based on CWC (1994) Flood estimation report for Western Himalayas-Zone 7. In the process, the ordinates of the unit hydrograph are adjusted in such a way that the total volume of direct runoff is adjusted to 1cm depth over the catchment (Sathe et al., 2012).

## 3. Application

### 3.1 *Study area and data used*

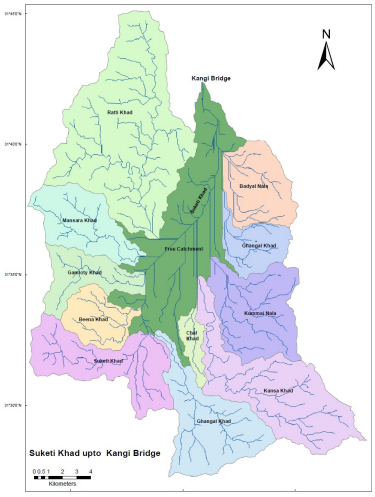



**Figure 1.** Location map of the SCs of Suketi Khad upto Kangi Bridge

In this paper, a study on estimation of PFD for ungauged catchments of Suketi Khad by EVA of rainfall and SUH method was carried out. The Suketi Khad is one of the main tributary of Suketi River Basin (SRB), which is located in the Mandi district of Himachal Pradesh, India. It encompasses a central intermontane valley and surrounding mountainous terrain in the Lower Himachal Himalaya. The SRB encompasses an area of 1710 km$^2$ with an altitude ranging from 754 m to 2052 m. Geographically, the study area falls between the longitudes 76$^o$ 48' to 77$^o$ 00' E and latitudes 31$^o$ 29' to 31$^o$ 45' N. From the topography of the SRB, it is noted that the Sub-Catchments (SCs) of Suketi Khad, as given in Figure 1, contributes flow to the SRB (Verma et al., 2012). Figure 1 shows the location map of the SCs of Suketi Khad upto Kangi Bridge.

## 4. Results and Discussions

### 4.1 *EVA of rainfall*

For EVA of rainfall, the daily rainfall data observed at Sundernagar site for the period 1969 to 2018 was used. The Annual 1-day Maximum Rainfall (AMR) data series derived from the daily rainfall data was used for EVA. Figure 2 presents the time series plot with descriptive statistics of the AMR of Sundernagar site.

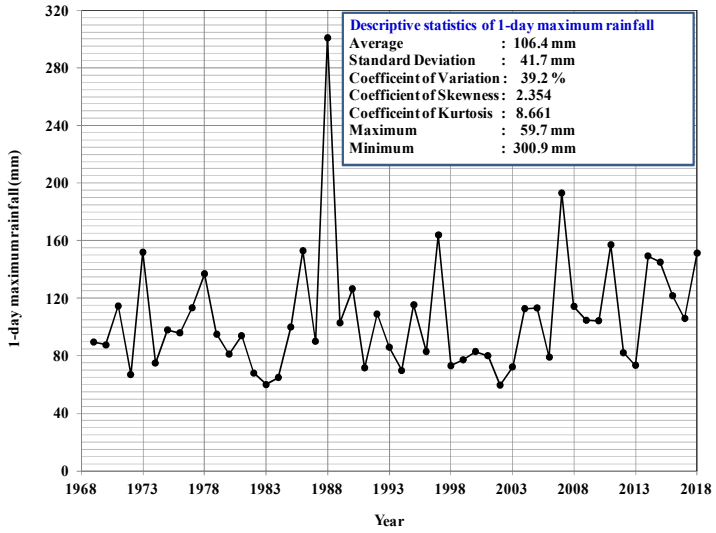



**Figure 2.** Time series plot with the descriptive statistics of the observed AMR

By applying the procedures of Gumbel distribution, as described above, the parameters of the distribution were determined and used for estimation of ER. Table 2 gives the ER estimates with confidence limits (*ER±1.96SE*) for different return periods at 95% level for Sundernagar site whereas the plots are presented in Figure 3. The 24-hour maximum rainfall was computed by multiplying the estimated 1-day maximum rainfall with 1.15 and also presented in Table 2.

### 4.2 *Analysis based on GoF tests*

By using the procedures of GoF tests, as described above, *AD* and *KS* tests statistic values of Gumbel distribution were computed as 0.455 and 0.082 respectively. From GoF tests results, it is noted that

the computed values are less than its theoretical values (i.e., 0.757 for *AD* and 0.178 for *KS*) at 5% level and at this level both GoF tests are supported the use of Gumbel distribution for EVA of rainfall for Sundernagar site.

**Table 2.** Estimated 1-day and 24-hour maximum rainfall using Gumbel distribution

| Return period (year) | 1-day maximum rainfall (mm) | Confidence limits of ER (mm) at 95% level | | 24-hour maximum rainfall (mm) |
|---|---|---|---|---|
| | | Lower | Upper | |
| 2 | 99.4 | 91.0 | 107.9 | 114.3 |
| 5 | 128.9 | 115.9 | 141.8 | 148.2 |
| 10 | 148.4 | 131.7 | 165.0 | 170.7 |
| 20 | 167.0 | 146.7 | 187.4 | 192.1 |
| 25 | 173.0 | 151.4 | 194.5 | 199.0 |
| 50 | 191.2 | 165.9 | 216.6 | 219.9 |
| 75 | 201.9 | 174.3 | 229.4 | 232.2 |
| 100 | 209.4 | 180.3 | 238.5 | 240.8 |
| 200 | 227.4 | 194.6 | 260.3 | 261.5 |
| 500 | 251.3 | 213.4 | 289.2 | 289.0 |
| 1000 | 269.3 | 227.5 | 311.1 | 309.7 |

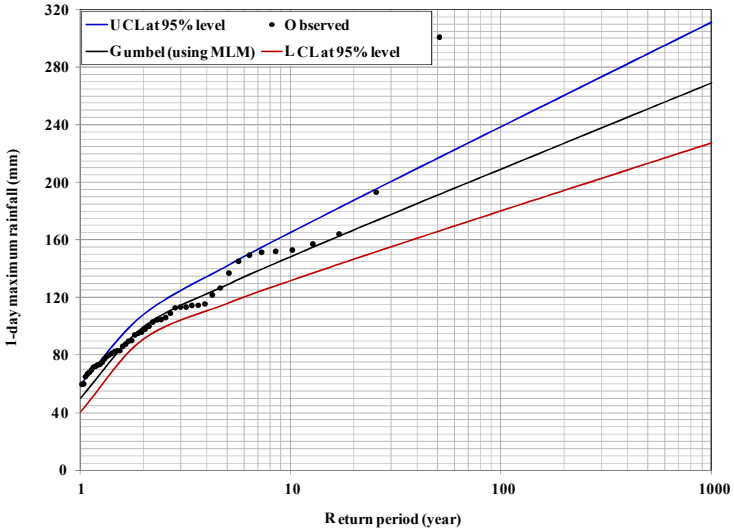



**Figure 3.** Plots of estimated 1-day maximum rainfall with confidence limits using Gumbel distribution and observed data

## 4.3 *Estimation of PFD for ungauged catchments*

### 4.3.1 *Estimation of PFD by rational formula*

From the analysis of catchment characteristics, the design storm duration is considered as 1-hour for Chal Khad, Sekar Khad, Beena Khad, Gamloty Khad, Bhadyal Nallah and free catchment. Based on the procedure, as given in CWC Report (1994) titled 'Flood estimation report for Western Himalayas-Zone 7', the 1-hour distributed rainfall for Sundernagar for various return periods was computed from the estimated 24-hour maximum rainfall by using conversion factor as given in Figure 4 and are presented in Table 3. This 1-hour distributed rainfall was used as input (rainfall intensity) for estimation of PFD for various SCs of Suketi Khad.

**Table 3.** 24-hour maximum and 1-hour distributed rainfall for different return periods

| Rainfall series | Extreme rainfall (mm) | | | |
|---|---|---|---|---|
| | 25-year | 50-year | 75-year | 100-year |
| 24-hour maximum | 199.0 | 219.9 | 232.2 | 240.8 |
| 1-hour distributed | 84.6 | 93.4 | 98.7 | 102.3 |

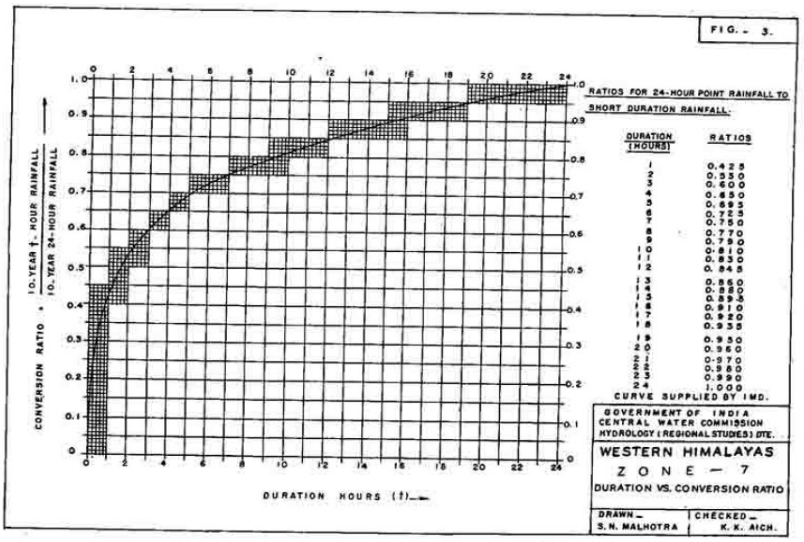



**Figure 4.** Conversion factor for computation of distributed rainfall for shorter duration

By considering topography and general land use character of the catchments, the value of the C was considered as 0.50 for all ungauged catchments while computing the PFD. As the catchement area of SCs of Suketi Khad, as given in Sr. No. 1 to 5 of Table 4, are less than 25 km$^2$, the PFD at these catchments was estimated by rational formula and the results are presented in Table 4. Also, from Table 4, it is noted that the catchment area of free catchment is 65.18 km$^2$, which is the total catchment area of six minor tributaries with its catchment area vary from 10 km$^2$ to 15 km$^2$ that contributes flow to SRB. By considering the said aspect of free catchment, PFD at free catchment was also computed by rational formula and the results are presented in Table 4.

**Table 4.** Estimated PFD (m$^3$/s) for different return periods given by rational formula

| Sr. No. | Name of the sub-catchment | Catchment area (km$^2$) | Peak flood discharge (m$^3$/s) | | | |
|---|---|---|---|---|---|---|
| | | | 25-year | 50-year | 75-year | 100-year |
| 1 | Chal Khad | 6.37 | 75.41 | 83.34 | 88.00 | 91.27 |
| 2 | Sekar Khad | 15.43 | 182.65 | 201.87 | 213.17 | 221.08 |
| 3 | Beena Khad | 16.15 | 191.18 | 211.29 | 223.11 | 231.40 |
| 4 | Gamloty Khad | 18.44 | 218.28 | 241.25 | 254.75 | 264.21 |
| 5 | Bhadyal Nallah | 24.39 | 288.72 | 319.09 | 336.95 | 349.46 |
| 6 | Free catchment | 65.18 | 771.57 | 852.74 | 900.46 | 933.91 |

### 4.3.2 *Estimation of PFD by SUH method*

The 24-hour maximum rainfall of Sundernagar site, as given in Table 3, was used for estimation of PFD by SUH method based on CWC (1994) Flood estimation report for Western Himalayas-Zone 7. By using Survey of India Toposheets, DEM (Digital Elevation Model) of National Remote Sensing Centre (NRSC) and Google Earth of the region of the SCs of Suketi Khad, the catchments of Hind Khad, Kummai Khad, Mansara Khad, Kansa Khad, Ratti Khad and Suketi Khad were delineated and used. The catchment characteristics of SCs of Suketi Khad were extracted with the aid of ArcGIS software and are presented in Table 5. The physiographic and SUH parameters of the SCs were determined by using the empirical equations (Table 5) and also used for estimation of PFD. By using the SUH parameters, the SUH of SCs of Suketi Khad were derived and presented in Figure 5.

## 4.4 Derivation of flood hydrograph

By considering the procedures described in CWC (1994) guidelines, various factors viz., design storm duration, base flow, loss rate and areal rainfall involved in computation of the ordinates of the flood hydrograph of SCs are presented in Table 6. By using the physiographic and SUH parameters, and the factors considered in computation of PFD, the 25-year, 50-year, 75-year and 100-year return period PFDs for SCs of Suketi Khad were computed and are presented in Table 7. The estimated PFDs were used to derive the flood hydrographs for the said SCs and presented in Figures 6 to 11.

**Table 5.** Physiographic and SUH parameters of SCs of Suketi Khad

| Parameters | Hind Khad | Kummai Khad | Mansara Khad | Kansa Khad | Ratti Khad | Suketi Khad |
|---|---|---|---|---|---|---|
| Physiographic parameters | | | | | | |
| Catchment Area ($km^2$) | 36.77 | 35.19 | 26.08 | 51.56 | 93.24 | 35.02 |
| Length (km) | 12.64 | 11.64 | 13.14 | 27.04 | 20.38 | 13.50 |
| $L_c$ (km) | 8.17 | 6.76 | 7.82 | 16.96 | 8.89 | 6.13 |
| Slope (m/km) | 38.55 | 37.20 | 47.64 | 36.18 | 11.39 | 41.61 |
| SUH parameters | | | | | | |
| $q_p$ ($m^3/s$) | 0.87 | 0.87 | 0.87 | 0.83 | 0.82 | 0.87 |
| $t_p$ (hour) | 2.91 | 2.81 | 2.82 | 3.71 | 3.85 | 2.78 |
| $t_r$ (hour) | 3.00 | 3.00 | 3.00 | 4.00 | 4.00 | 3.00 |
| $W_{50}$ (hour) | 2.15 | 2.10 | 2.11 | 2.51 | 2.57 | 2.09 |
| $W_{75}$ (hour) | 1.10 | 1.07 | 1.07 | 1.33 | 1.37 | 1.06 |
| $WR_{50}$ (hour) | 0.73 | 0.70 | 0.71 | 0.96 | 1.00 | 0.70 |
| $WR_{75}$ (hour) | 0.47 | 0.45 | 0.46 | 0.60 | 0.62 | 0.45 |
| $T_D$ (hour) ($T_D$=1.1*$t_p$) | 3.20 | 3.09 | 3.10 | 4.08 | 4.23 | 3.06 |
| $T_B$ (hour) | 13.00 | 13.00 | 13.00 | 15.00 | 15.00 | 13.00 |
| $Q_p$ ($m^3/s$) | 31.86 | 30.69 | 22.73 | 42.78 | 76.88 | 30.59 |
| Q ($m^3/s$) | 102.22 | 97.83 | 72.50 | 143.34 | 259.21 | 97.36 |

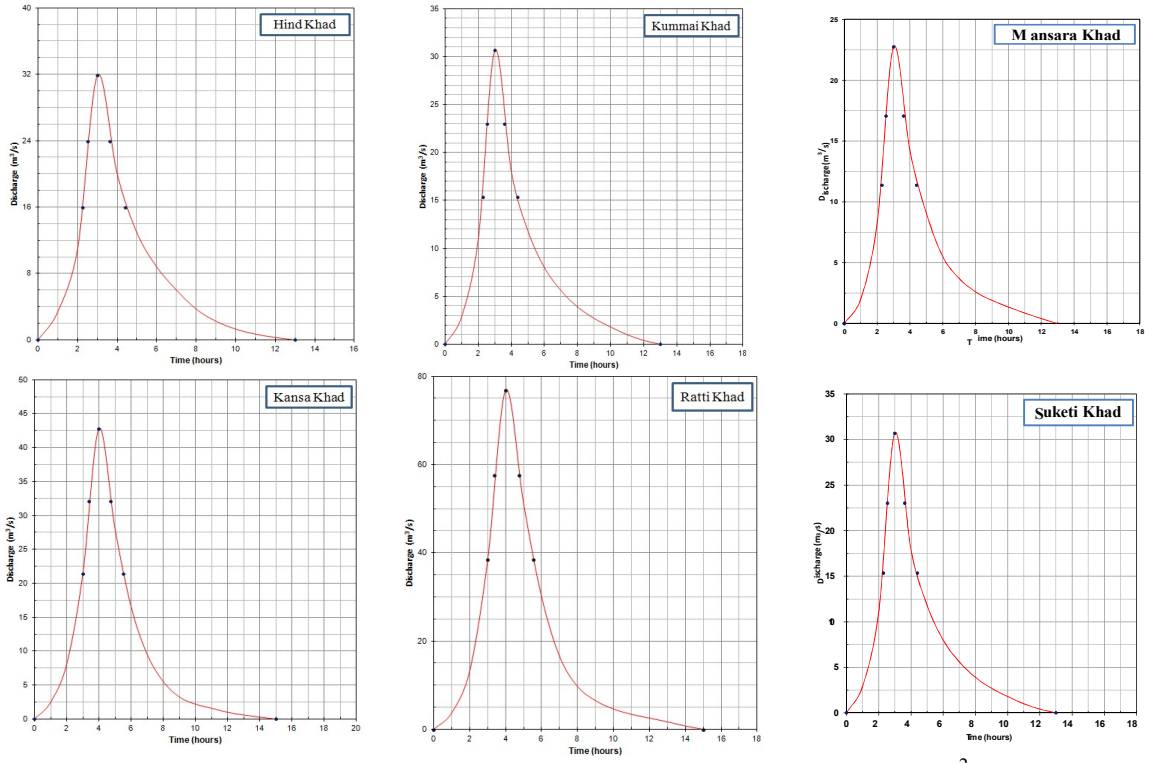



**Figure 5.** SUH for the SCs with catchment area more than 25 $km^2$

**Table 6.** Factors considered in computation of PFD and derivation of flood hydrograph

| Parameters | Hind Khad | Kummai Khad | Mansara Khad | Kansa Khad | Ratti Khad | Suketi Khad |
|---|---|---|---|---|---|---|
| Design storm duration (hour) | 3.00 | 3.00 | 3.00 | 4.00 | 4.00 | 3.00 |
| Base flow ($m^3/s$) | 1.84 | 1.76 | 1.30 | 2.58 | 4.66 | 1.75 |
| Loss rate (mm) | 2.00 | 2.00 | 2.00 | 2.00 | 2.00 | 2.00 |
| Areal rainfall (mm) for different return periods | | | | | | |
| 25-year | 116.2 | 116.3 | 117.1 | 124.5 | 120.7 | 116.4 |
| 50-year | 128.4 | 128.6 | 129.4 | 137.6 | 133.4 | 128.6 |
| 75-year | 135.6 | 135.8 | 136.7 | 145.3 | 140.9 | 135.8 |
| 100-year | 140.7 | 140.8 | 141.8 | 150.7 | 146.1 | 140.8 |

**Table 7.** Estimated PFD ($m^3/s$) estimates for different return periods given by SUH method

| Sr. No. | Name of the sub-catchment | Peak flood discharge ($m^3/s$) | | | |
|---|---|---|---|---|---|
| | | 25-year | 50-year | 75-year | 100-year |
| 1 | Hind Khad | 315.3 | 349.6 | 369.8 | 384.0 |
| 2 | Kummai Khad | 301.1 | 333.9 | 353.1 | 366.6 |
| 3 | Mansara Khad | 226.6 | 251.2 | 265.7 | 275.9 |
| 4 | Kansa Khad | 425.2 | 472.0 | 499.5 | 518.7 |
| 5 | Ratti Khad | 741.8 | 823.5 | 871.6 | 905.2 |
| 6 | Suketi Khad | 300.3 | 333.0 | 352.2 | 365.6 |

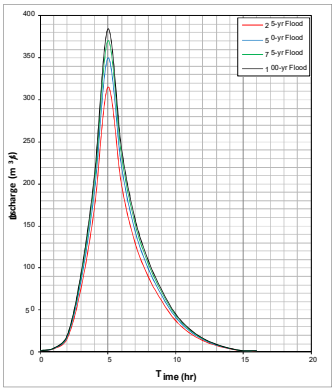



**Figure 6.** Flood hydrograph for different return periods of Hind Khad

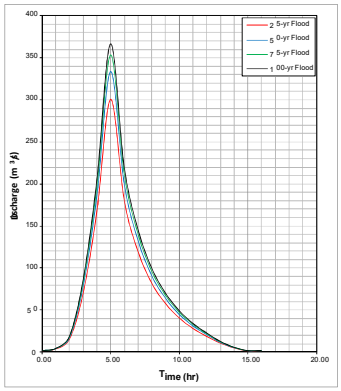



**Figure 7.** Flood hydrograph for different return periods of Kummai Khad

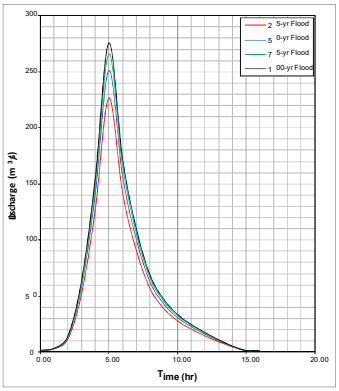



**Figure 8.** Flood hydrograph for different return periods of Mansara Khad

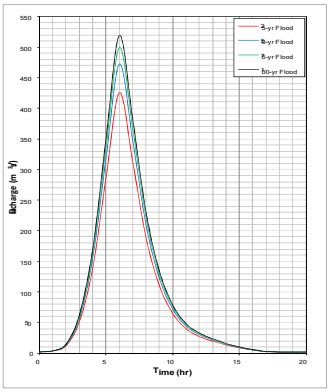



**Figure 9.** Flood hydrograph for different return periods of Kansa Khad

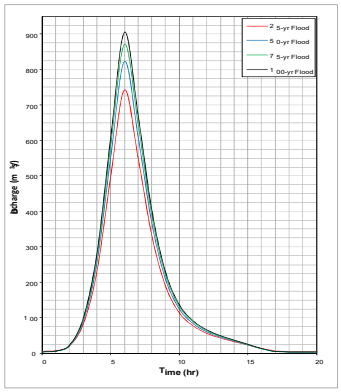



**Figure 10.** Flood hydrograph for different return periods of Ratti Khad

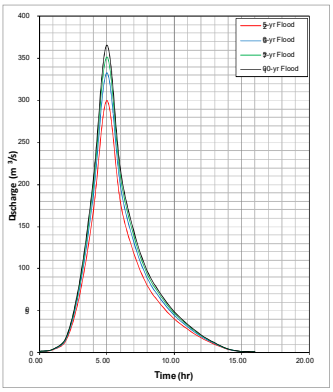



**Figure 11.** Flood hydrograph for different return periods of Suketi Khad

## 5. Conclusions

The paper presented a study on estimation of PFD for ungauged catchments of Suketi Khad upto Kangi Bridge. For this purpose, EVA of daily rainfall of Sundernagar site by Gumbel distribution and estimation of PFD by hydrometeorological approaches was carried out. On the basis of the results obtained from the study, some of the conclusions were drawn and summarized as given below:

- GoF tests results supported the use of Gumbel distribution for EVA of rainfall of Sundernagar.
- From the fitted curves of the estimated rainfall, about 98% of the observed AMR data are within 95% confidence limits of the estimated 1-day maximum rainfall.
- The computed 25-year, 50-year, 75-year and 100-year return period 24-hour maximum rainfall at Sundernagar site are 199.0 mm, 219.9 mm, 232.2 mm and 240.8 mm respectively.
- By considering topography and general land use character of the catchments, the value of the C was considered as 0.50 for Chal Khad, Sekar Khad, Beena Khad, Gamloty Khad, Bhadyal Nallah and free catchment while computing the peak flood by rational formula.

- The design storm duration was considered as 3-hours for Hind Khad, Kummai Khad, Mansara Khad and Suketi Khad catchments and 4-hours for Kansa Khad and Ratti Khad catchments.
- The estimated 25-year, 50-year, 75-year and 100-year return period PFD at Mansara Khad by SUH method are noted to be lower than the corresponding values of Hind Khad, Kummai Khad, Kansa Khad, Ratti Khad and Suketi Khad.

The study suggested that the estimated PFDs at various SCs of Suketi Khad upto Kangi Bridge, as given in Tables 4 and 7, could be used for design of hydraulic structures, river protection works and development of integrated water resources management projects.

## Acknowledgment

The authors are grateful to Shri A.K. Agrawal, Scientist-E & Director In-charge, Central Water and Power Research Station, Pune for encouragement during the course of the study and also according permission to publish this paper.

## References

Andrea, P., Shahla, A., Touraj, S., and Bahram, S. (2020). Comparison of design peak flow estimation methods for ungauged basins in Iran. *Hydrological Sciences Journal, 65(*1*)*, 127-137.

CWC (1994). Flood estimation report for Western Himalayas-Zone 7. Central Water Commission (CWC) Report No.: WH/22/1994, New Delhi, 1994.

Gumbel, E.J. (1960). Statistic of Extremes, Columbia University Press, New York.

Charles Annis, P.E.(2009). Goodness-of-Fit tests for statistical distributions.

Jena, J., Sahu, G.C., Prasad, C.V., Ray, G.P., and Das, A.K. (2005). Derivation of an equation for estimation of design flood for water resources project in Baitarani Basin (Odisha). Proceedings of Annual Conference of Institution of Engineers (India), Bhubaneswar, Odisha.

Kim, N.W., and Mun-Ju Shin (2018). Estimation of peak flow in ungauged catchments using the relationship between runoff coefficient and curve number. *Water*, *10(*11*),* 1-22.

Mohammed, S., and Azhar, H. (2017). Estimation of design flood at Kol dam using hydrometeorological approach. *International Journal of Environmental Sciences and Natural Resources*, *4(*1*),* 1-6.

Natakusumah, D.K., Hatmoko, W., and Harlan, D. (2011). A general procedure for developing a synthetic unit hydrograph based on mass conservation principle, Development of ITB-1 and ITB-2 synthetic unit hydrograph method. *International Seminar on Water-Related Risk*, 15-17 July 2011.

Priyanka Kumari and Goel, N.K. (2015). Flood estimation for rivers of Saurashtra region contributing into Gulf of Khambhat. *International Journal of Engineering Research and Technology*, *3(*3*),* 1-5.

Ramirez, J.A. (2000). Prediction and modelling of flood hydrology and hydraulics, Cambridge University Press, London, UK, 34pp.

Reddy, N.A., Jeya Kumar, S., Subba Rao., and Nagaraj, M.K. (2019). Flood estimation at ungauged catchments of western catchments of Karnataka, West coast of India. *ISH Journal of Hydraulic Engineering, 25(3)*, 325-335.

Sathe, B.K., Khir, M.V., and Sankhua, R.N. (2012). Rainfall analysis and design flood estimation for Upper Krishna River basin catchment in India. *International Journal of Science and Engineering Research, 3(*8*),* 1074-1084.

Snyder, F.F. (1938). Synthetic unit graphs: Transactions. *American Geophysics Union, 19(*1*),* 447-454.

Verma, N., Khanduri, K., and Singh, P. (2012). The study of drainage patterns of Suketi river basin for the proper environmental planning, Mandi district, Himachal Pradesh, India. *International Journal of Environmental Sciences, 2(*3*),* 1575-1584.

Zhang, J. (2002). Powerful goodness-of-fit tests based on the likelihood ratio. *Journal of the Royal Statistical Society, Series B: Statistical Methodology, 64(*2*),* 281–294.

*IN PROCEEDINGS OF 25th HYDRO 2020, INTERNATIONAL CONFERENCE, NATIONAL INSTITUTE OF TECHNOLOGY ROURKELA, ODISHA, INDIA 26-28, March 2021, ISBN 978-93-90631-56-8*

Paper ID - 266

# FLOOD ROUTING IN A RIVER BY MODIFIED PUL'S METHOD

Souvick Kumar Shaw[1] Prof. Kishanjit Kumar Khatua[2]

*1 M.Tech Scholar in Water Resources Engineering, Nit Rourkela .*

*2 Associate Professor in Civil Engineering (Water Resources Engineering, Nit Rourkela*

*Email: souvickshaw@gmail.com, kkkhatua@yahoo.com*

## ABSTRACT

Flood Routing is the technique of determining the Flood Hydrograph at a section of a river by utilizing the data of flood flow of one or more upstream sections . The hydrologic analysis of problems such as flood protection, flood forecasting, reservoir design and spillway design usually include flood routing . The flood flow in a river is basically a Gradually Varied Unsteady Flow (GVUF) . The inflow hydrograph used can be applied for different flood events by adjusting its parameters accordingly. Hydrologic Routing is performed here by using Modified Pul's Method /Level Pool Method. It is based on continuity equation. HEC -HMS software is used to simulate the routing process on Kol Dam, Himachal Pradesh where the inflow hydrograph is taken on Sutlej River. The maximum flood has come with a intensity of 80$m^3$/sec on 01Jan 2018 and the volume is worked out to be 9806.4 $m^3$ .Also Peak discharge was coming to be 69.8$m^3$/sec on 02Jan 2018 , peak storage 4.8404 $Mm^3$ and also peak elevation was at 102.0 m . The discharge volume is coming to be 9700.6 $m^3$.

***Key Words** : flood protection , flood forecasting , reservoir design and spillway design , HEC-HMS , attenuation, lag , GVUF , Modified Pul's Method.*

## Introduction :

A flood is an unusually high stage in a river, normally the level at which the river overflows its banks and inundates the adjoining area. The damages caused by floods in terms of loss of life, property, and economic loss due to disruption of economic activity are all too well known. The design of bridges, culvert waterways and spillways for dams and estimation of scour at a hydraulic structure are some examples wherein flood-peak values are required.

### 1. FLOOD ROUTING METHODS:

Flood Routing methods can be broadly classified by two approaches :

1. Reservoir Routing 2. Channel Routing

In Reservoir routing the effect of a flood wave entering a reservoir is studied. Knowing the volume-elevation characteristic of the reservoir and the outflow-elevation relationship for the spillways and other outlet structures in the reservoir, the effect of a flood wave entering the reservoir is studied to predict the variations of reservoir elevation and outflow discharge with time.

In Channel routing the change in the shape of a hydrograph as it travels down a channel is studied. By considering a channel reach and an input hydrograph at the upstream end, this form of routing aims to predict the flood hydrograph at various sections of the reach. Information on the flood-peak attenuation and the duration of high-water levels obtained by channel routing is of utmost importance in flood-forecasting operations and

flood-protection works.

Attenuation is a reduction of the peak flow due to dispersion of the flood wave over that interval of time. Flood translation or time lag is referred as the movement of a flood wave through a channel without attenuation caused by the time of travel of the flood wave between the two points. Keeping the peak discharge constant, the delay of the hydrograph occurs in observation points. This routing technique is used to analyze the effects of a channel on a hygrograph's peak flow and travel time. Inflow hydrograph and the channel characteristic data are needed for routing in a channel.

***1.1*** *Hydrologic Flood Routing Method* : Hydrologic routing methods employ essentially the equation of continuity, on the other hand hydraulic methods use continuity equation along with the equation of motion of unsteady flow hence better than hydrologic methods. Hydraulic routing is based on the solution of partial differential equations of unsteady overland flow. Saint-Venant equations are used for its solution.

Basic Equations : $I-Q=dS/dt$ …….(1)

Where , I= Inflow Rate , Q= Outflow Rate , dS/dt= Rate of change in storage.

Alternatively in a small interval of time Δt , the difference between the total inflow volume and total outflow volume gives the change in total storage .

$$I_{avg}\,\Delta t-Q_{avg}\,\Delta t=\Delta S \quad \text{…….(2)}$$
$$I_{avg}\,\Delta t-Q_{avg}\,\Delta t=S_2-S_1 \quad \text{…….(3)}$$

Where $S_1$ is the initial storage and $S_2$ is the final storage in the channel for a given reach of the channel .

There are three types of method in hydrological routing:

1. Level Pool Method (Modified Pul's Method)
2. Goodrich Method
3. Muskingum Method .

### ***1.1.1*** *Level Pool Method (Modified Pul's Method) :*

$$I_{avg}\,\Delta t-Q_{avg}\,\Delta t=S_2-S_1 \quad \text{……(Basic Continuity Equation)}$$

$$(I_1+I_2)/2+(Q_1+Q_2)/2= S_2-S_1 \quad \text{……(4)}$$

By rearranging we get , $(I_1+I_2)/2 +( S_1-Q_1\Delta t/2)= ( S_2+Q_2\Delta t/2)$ ……..(5)

Then a graph is plotted by taking Storage $[(S+Q\Delta t)/2]$ and Outflow (Q) in the abcessia and elevation as ordinate as given below and the routing can be completed .

### ***1.1.2*** *Goodrich Method* :

$I_{avg}\,\Delta t-Q_{avg}\,\Delta t=S_2-S_1$ ……(Basic Continuity Equation)

$$(I_1+I_2)/2+(Q_1+Q_2)/2= S_2-S_1$$

By rearranging we get , $(I_1+I_2) +( 2S_1/\Delta t -Q_1)= ( 2S_2/\Delta t +Q_2)$……..(6)

Then a graph is plotted by taking Storage [(2S)/ Δt +Q] and Outflow (Q) in the abscissa and elevation as ordinate as given below and the routing can be completed .

### *1.1.3 Muskingum Method* :

The Muskingum method is a routing method of flood, used widely. A direct relationship between the reservoir storage and the out flow is taken into consideration for it's development. Two parts of storage within a reach are present in Muskingum method; they are prism storage and wedge storage. When the water is in steady motion, the storage is known as the prism storage. The one is the storage under actual flow surface.

- *Prism Storage :*

It is the volume that would exist if the uniform flow occurred at the downstream depth, i.e. the volume formed by an imaginary plane parallel to the channel bottom drawn at the outflow section water surface.

- *Wedge Storage* **:**

It is the wedge-like volume formed between the actual water surface profile and the top surface of the prism storage.

The total storage in the channel is a function of both inflow as well as outflow and is given by the equation below :

$S =K[XI^m +(1-X)Q^m]$…….(7)

Where , K is known as storage time constant i.e travelling time of the flood wave along the channel . X is the Weighting factor which is varying from 0to 0.5 .

- Values of X = 0.2 to 0.3 are the most common for natural streams; however, values of 0.4 to 0.5 may be calibrated for streams with little or no flood plains or storage effects.
- A value of X = 0.5 would represent equal weighting between inflow and outflow and would produce translation with little or no attenuation.

m is taken as 0.6 for rectangular channel and 1 for all natural channels .

Considering , the natural channel , equation (7) can be modified as

$S =K[XI+(1-X)Q]$…….(8)

From equation (8) the storage value at the time of j and j+1is written below

$S_j =K[XI_j+(1-X)Q_j]$…….(9)

$S_{j+1}=K[XI_{j+1}+(1-X)Q_{j+1}]$…….(10)

If the value of X is zero , the equation becomes S=KQ…….(11)

Equation (11) gives the Total storage for linear reservoir .

Collecting similar terms and simplifying , we get ,

$Q_{n+1}=C_oI_{n+1} +C_1I_n + C_2Q_n$…….(12)
Equation (12) is known as the Muskingum equation in general .

Where , $C_o = (-KX+0.5\Delta t)/(K-KX+0.5\Delta t)$

$C_1 = (KX+0.5\Delta t)/(K-KX+0.5\Delta t)$

$C_2 = (K-KX-0.5\Delta t)/(K-KX+0.5\Delta t)$

$$\mathbf{C_o + C_1 + C_2 = 1}$$

## 1.2 Some features related to the topic :

***1.2.1*** *Rating curve* : In hydrology, a rating curve is a graph of discharge versus stage for a given point on a stream, usually at gauging stations, where the stream discharge is measured across the stream channel with a flow meter.

The development of a rating curve involves two steps. In the first step the relationship between stage and discharge is established by measuring the stage and corresponding discharge in the river. And in the second part, stage of river is measured and discharge is calculated by using the relationship established in the first part. Stage is measured by reading a gauge installed in the river. If the stage-discharge relationship does not change with time, it is called permanent control. If the relationship does change, it is called shifting control. Shifting control is usually due to erosion or deposition of sediment at the stage measurement site. Bedrock-bottomed parts of rivers or concrete/metal weirs or structures are often, though not always, permanent controls.

If G represents stage for discharge Q, then the relationship between G and Q can possibly be approximated with an equation:

$Q= Cr(G-a)^{\beta}$……(17)

Where , Cr and **β** are the rating curve constant and a is the gauge corresponding to zero discharge .

The parameter **β** is typically in the range of 2.0 to 3.0 when a stream is flowing under section control, and in the range of 1.0 to 2.0 when a stream is flowing under channel control.

***1.2.2*** *Stage hydrograph* : The hydrograph resulting from water depth with variation of time is used as either in upstream boundary or in downstream boundary.

## *1.3.About The Software Used : HEC-HMS (Hydrological Engineering Centre for Hydrologic Modelling System )*

The Hydrologic Modelling System (HEC-HMS) is designed to simulate the precipitation-runoff processes of dendritic drainage basins. HEC-HMS is a product of the US Army Corps of engineers

research and development program and is produced by the Hydrologic Engineering centre (HEC). HEC-HMS simulates Precipitation-Runoff and routing processes both natural and controlled. It includes many hydrologic analysis procedures such as event infiltration, unit hydrographs, and hydrologic routing. HEC-HMS also includes procedures necessary for continuous simulation including evapotranspiration, snowmelt, and soil moisture accounting. Supplemental analysis tools are provides for model optimization, forecasting stream flow, depth-area reduction, assessing model uncertainity, erosion and sediment transport, and water quality.

The HEC-HMS features a integrated work environment including a database, data entry utilities, computation engine, and results reporting tools. A graphical user interface allows the user seamless movement between the different parts of the software. Simulation results are stored in HEC-DSS( Data Storage System).

## 2. *PROBLEM STATEMENT*

The Reservoir has the following elevation, discharge and storage relationship:

| Elevation (m) | Storage ($10^6$) $m^3$ | Storage ($1000m^3$) | Outflow ($m^3$/sec) |
|---|---|---|---|
| 100.00 | 3.350 | 3350 | 0 |
| 100.50 | 3.472 | 3472 | 10 |
| 101.00 | 3.880 | 3880 | 26 |
| 101.50 | 4.383 | 4383 | 46 |
| 102.00 | 4.882 | 4882 | 72 |
| 102.50 | 5.370 | 5370 | 100 |
| 102.75 | 5.527 | 5527 | 116 |
| 103.00 | 5.856 | 5856 | 130 |

When the reservoir level is at 100.50m , the following flood hydrograph entered the reservoir :

| Time | Discharge($m^3$/sec) |
|---|---|
| 0 | 10 |
| 6 | 20 |
| 12 | 55 |
| 18 | 80 |
| 24 | 73 |
| 30 | 58 |
| 36 | 46 |

| | |
|---|---|
| 42 | 36 |
| 48 | 27.5 |
| 54 | 20 |
| 60 | 15 |
| 66 | 13 |
| 72 | 11 |

Route the Flood by using Modified Puls Method(Level Pool Method) by using HEC-HMS software .

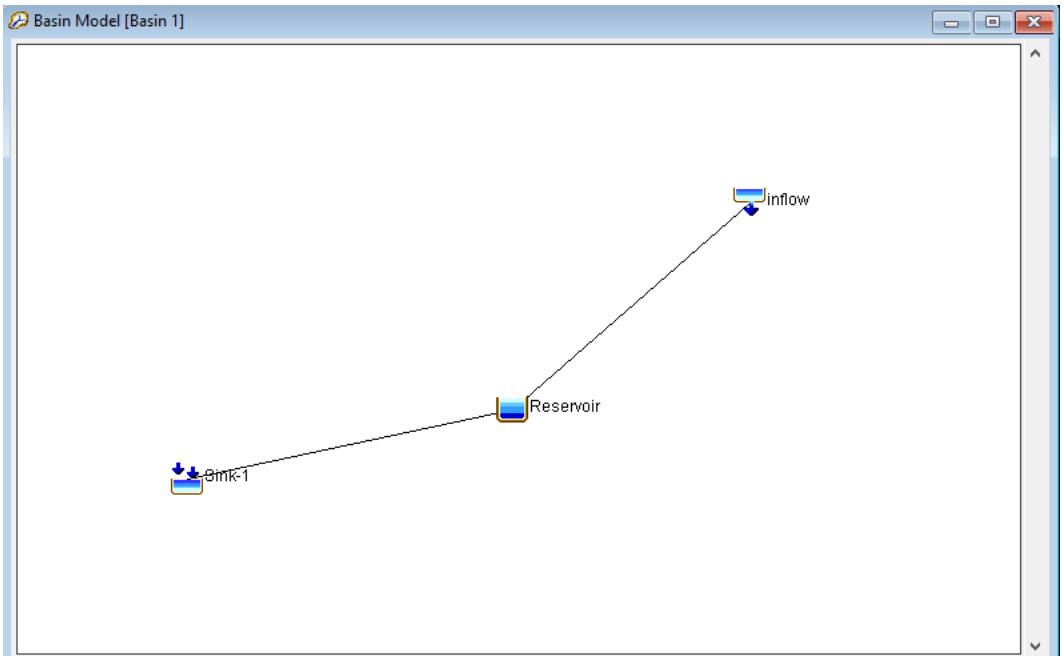


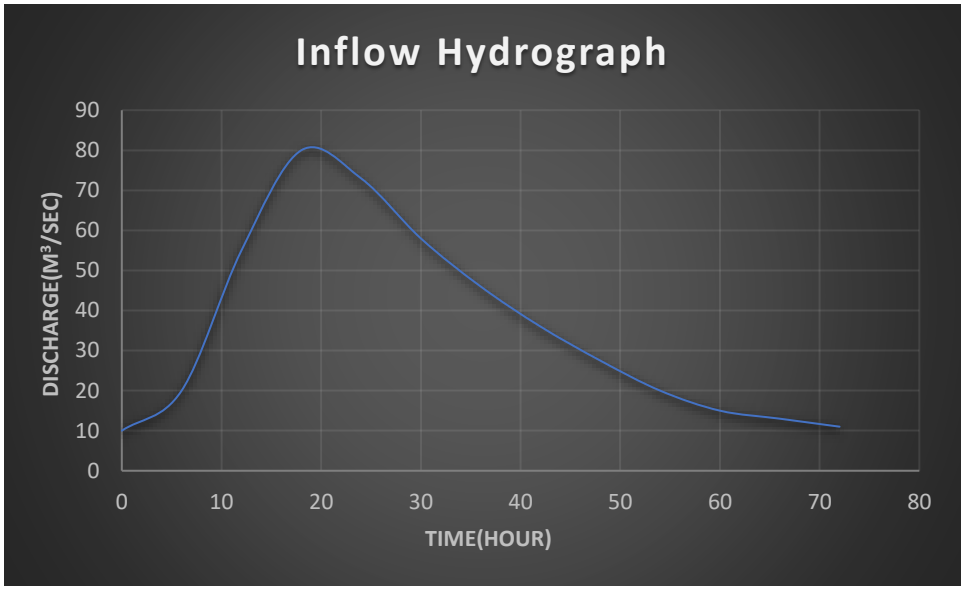

Fig.7

**RESULTS OBTAINED:**

***Global Summary*** :

| Hydrologic Element | Peak Discharge ($m^3$/sec) | Time of Peak | Volume (1000$m^3$) |
|---|---|---|---|
| Inflow(Sutlej River) | 80 | 1Jan2000,18.00 | 9806.4 |
| Reservoir 1(Kol Dam) | 69.8 | 2Jan2000,00.00 | 9700.6 |
| Sink1(D/S of dam) | 69.8 | 2Jan2000,00.00 | 9700.6 |

***Results for Inflow*** :




**Results for Reservoir** :

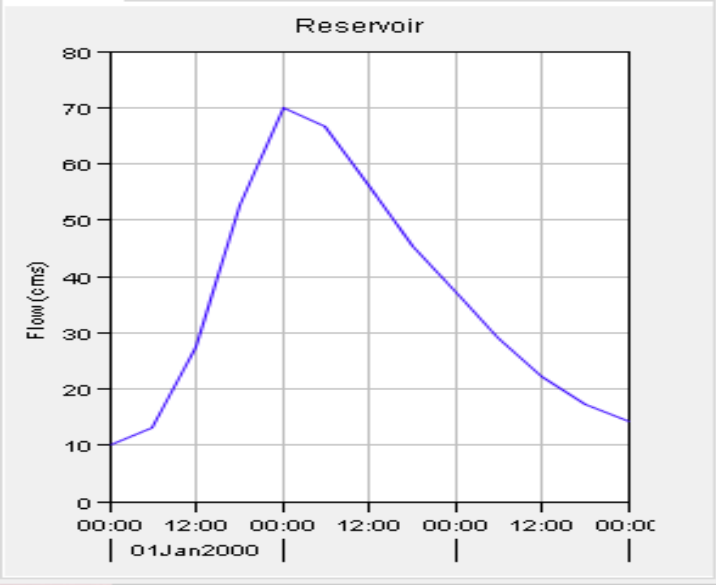
1. *Summary Table* :

| | | | |
|---|---|---|---|
| Peak Inflow: | 80.0 (M3/S) | Date/Time of Peak Inflow: | 01Jan2000, 18:00 |
| Peak Discharge: | 69.8 (M3/S) | Date/Time of Peak Discharge: | 02Jan2000, 00:00 |
| Inflow Volume: | 9806.4 (1000 M3) | Peak Storage: | 4840.4 (1000 M3) |
| Discharge Volume: | 9700.6 (1000 M3) | Peak Elevation: | 102.0 (M) |

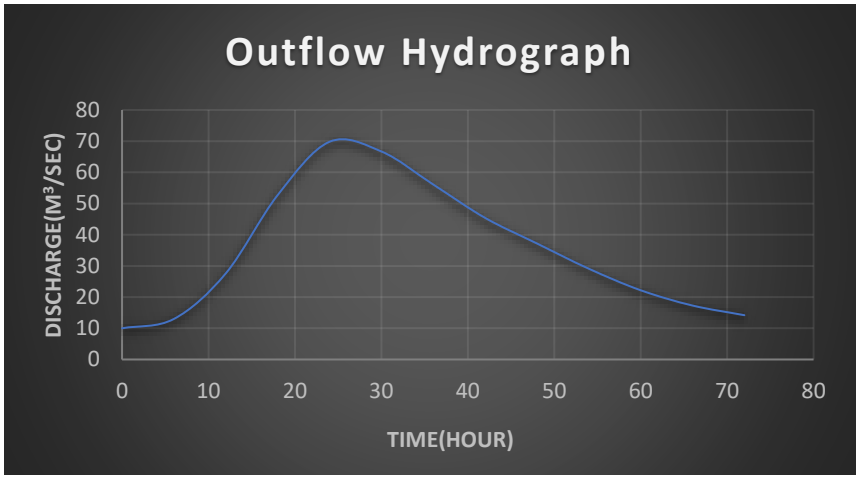
2. *Time Series Table* :

| Date | Time | Inflow (M3/S) | Storage (1000 M3) | Elevation (M) | Outflow (M3/S) |
|---|---|---|---|---|---|
| 01Jan2000 | 00:00 | 10.0 | 3472.0 | 100.5 | 10.0 |
| 01Jan2000 | 06:00 | 20.0 | 3547.9 | 100.6 | 13.0 |
| 01Jan2000 | 12:00 | 55.0 | 3919.8 | 101.0 | 27.6 |
| 01Jan2000 | 18:00 | 80.0 | 4511.1 | 101.6 | 52.7 |
| 02Jan2000 | 00:00 | 73.0 | 4840.4 | 102.0 | 69.8 |
| 02Jan2000 | 06:00 | 58.0 | 4780.5 | 101.9 | 66.7 |
| 02Jan2000 | 12:00 | 46.0 | 4577.2 | 101.7 | 56.1 |
| 02Jan2000 | 18:00 | 36.0 | 4366.8 | 101.5 | 45.4 |
| 03Jan2000 | 00:00 | 27.5 | 4161.2 | 101.3 | 37.2 |
| 03Jan2000 | 06:00 | 20.0 | 3958.3 | 101.1 | 29.1 |
| 03Jan2000 | 12:00 | 15.0 | 3782.4 | 100.9 | 22.2 |
| 03Jan2000 | 18:00 | 13.0 | 3658.4 | 100.7 | 17.3 |
| 04Jan2000 | 00:00 | 11.0 | 3577.8 | 100.6 | 14.2 |

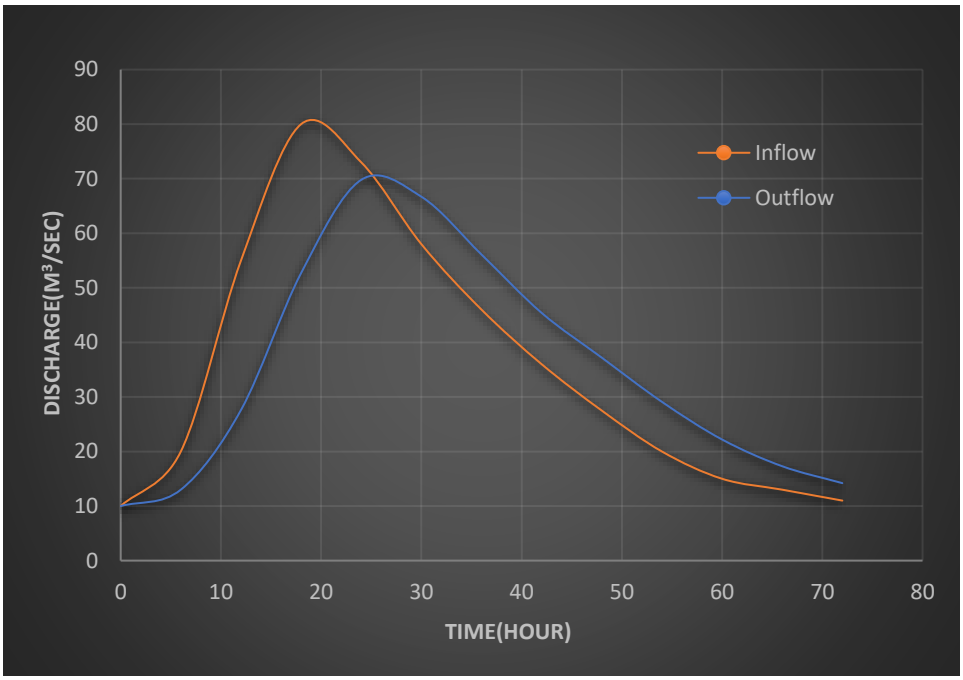
3. *Outflow* :




4. *Outflow Hydrograph :*



*5.Combined Inflow and Outflow Hydrograph :*




**Conclusion** : The following Flood is routed by using the inflow hydrograph and subsequently the outflow hydrograph is obtained . The base flow is 10$m^3$/sec . The attenuation is coming to be 10.2 $m^3$/sec and the lag is 6hours (Approx.) . We can also obtain the storage -elevation -time relationship . The maximum flood has come with a intensity of 80$m^3$/sec on 01Jan 2018 and the volume is worked out to be 9806.4 $m^3$ .Also Peak discharge was coming to be 69.8$m^3$/sec on 02Jan 2018 , peak storage 4.8404 $Mm^3$ and also peak elevation was at 102.0 m . The discharge volume is coming to be 9700.6 $m^3$ . HEC-HMS software is very popularly used software in the field of water resources engineering for solving several real life practical problems . This particular method of flood routing i.e. Modified Puls Method is accurately performed by this software and the results obtained can be very helpful for water resource management , flood management , possible modifications to be taken to avoid the damages due to flood . The only disadvantage of this work is that the data collected is for very small duration of time that's why it can't be possible to obtain several nos. of outflow hydrograph at different sections at the D/s section of the dam .

*IN PROCEEDINGS OF 25th HYDRO 2020, INTERNATIONAL CONFERENCE,*
*NATIONAL INSTITUTE OF TECHNOLOGY ROURKELA, ODISHA, INDIA*
*26-28, March 2021, ISBN 978-93-90631-56-8*

Paper ID - 276

# Wastewater Management through Water Drainage System: A Case Study

Jagpreet Singh Kamboj[1], Vaibhav Chaturvedi[1], Mahesh Patel[1]

[1]*Dr. BR Ambedkar National Institute of Technology, G.T. Road, Amritsar Bypass, Jalandhar, 144011, India*
*Email: vaibhavc.gg.19@nitj.ac.in*
*Telephone/Mobile No.: +91 9316 141 590*

## Abstract

Wastewater drainage and treatment prevails as one of the major contemporary problems in urban areas. The growing infrastructure constantly accrues stress on the already present wastewater drainage and treatment systems. One of the major problems has been the waterlogging of regions because of improper drainage. This problem worsens due to rainwater runoff in the low-lying area during the rainy season. This papers aims at developing a holistic methodology to cater the problems caused by ineffective drainage system by designing a drainage and treatment system for Dr. BR Ambedkar National Institute of Technology, Jalandhar. Rainfall pattern has been studied for the place to ensure the effectiveness of the drainage system during the peak stress. Sanitary wastewater and Stormwater runoff have both been taken into consideration to calculate the effective diameter of drainpipe and other important parameters. The study also suggests the use of Moving Bed Biofilm Reactor (MBBR) over other types of treatment plants through suitable comparison. Wastewater consists of a dynamic mixture of the contaminant in different environments; however, it can be treated similarly for institutions similar to that in the case study.

***Keywords:*** *Drainage; MBBR; rainwater; wastewater; sewage*

## 1. Introduction

Drainage is a mechanism in which water is accumulated and delivered to the treatment plant or disposed of to a water boy if contamination is poor. Either soil drainage or sub-surface drainage can be used for water drainage. In surface drainage, water is gathered from the earth's surface and transferred by open or closed drains. In sub-surface drainage, water is collected from below the earth's surface and transported in pipes. In any building job, water drainage should be granted the utmost priority. Incorrect drainage can destroy the foundation and create unhygienic conditions in the surroundings. Water deposited on roads can affect the roadway surface or cause subgrade damage. Wastewater treatment has not been known across decades. In most street communities and throughout metropolitan areas, polluted water has been depleted which significantly impacts the natural environment.

Millions of citizens worldwide do not have access to clean and sanitary water (H.0, 2003). Around 40% of the world's people lack basic sanitation and sanitation is usually even lower in developing countries. This improper management for sanitation leads to many diseases. The World Health Organization reports that 2,1 million humans suffer annually from diarrhoea. Collection, storage and disposal are three main elements of a treatment system.

Moreover, about 60 million US residents utilize all sorts of water management systems at the field, while around 20 million use the conventional septic tank process. Basic sewage networks have already become Iraqi waste management systems in ancient Mesopotamia, where vertical shafts have conveyed waste to the cesspools. In the Indus Valley culture, much as structures prevailed in modern India, Pakistan and some area of Afghanistan. In the Middle Ages, the drainage networks created by the Romans fall into a waste panel and were regularly vacated by 'rackers' who also marketed them to farmers outside the city as fertilizers. In the mid-19th century, new sanitation schemes were introduced owing to poor sanitary standards as a consequence of heavy industrialization and urbanization. Kaur et al. (2017) carried out the study in regards to the reasons responsible for the depletion of groundwater level in Punjab. Occupying 1.57% of the geographical area in India, Punjab is predominantly an agricultural state with a cropping intensity of 198%. The state of development and management of resources pertaining to groundwater has an excessive bearing on determining the future of agriculture

in the state. Groundwater trends, various reasons for the decline of GWT and policy initiatives have been discussed. Apart from suggesting multiple measures, the emphasis has been said on organizing pubic participatory movements to raise awareness regarding the resources of the state. Anggraini et al. (2015) carried an investigation aiming to find the effect of effective grain size on the removal of particles in the performance of slow sand filtration. Slow sand filtration despite being one of the oldest methods of filtration remain in the rage. Five Plexiglas columns of 125mm diameter were built for investigation of media size influence on particle removal. Those columns were under observation for six weeks. In turbidity removal and particle removal all five filters performed satisfactorily but concerning the size passing through the filter and maintaining their grain to stay inside the filter bed, filtration system with d10 equal to 0.26mm and 0.40mm performed exceptionally well.

According to Geoffrey F. Readin (1997), a sewerage system breakdown may result in waterlogging of surrounding areas, excessive-high sewer flow rates due to leakage, groundwater contamination, or widespread damage resulting from collapse or sewer destruction. A rational sewage management technique is indispensable in mitigating the causes of failure of sewage systems. To satisfy the self-cleaning velocity of the sewer pipes, the new per capita water supply is not even capable of meeting the necessary per capita demand of 135 litres (Saravanane et al., 2014).

Moreover, the world's first municipal sanitation schemes were found in the days of Harappa and Mohenjo-Daro (Webster, 1962). Households were attached to sewage canals, and runoff didn't explicitly spill through street sewers without being treated beforehand. Bricks and cut stones may fill the sewer lines, which were presumably cleared during repairs and cleaning. While Rome's water system was still claimed to be one of the ancient world's wonders shown in fig 1, they have less effect on wastewater treatment. Romans also regulated the water cycle from storage to disposal when they invented the very first distributed sanitation services, providing simultaneous rain harvesting networks and sewage treatment disposal systems. Romans discovered that spring water had a higher consistency for human use than seawater bodies, which was of low quality, but also realized that surface water could be used for other purposes. Besides, wastewater from spas was reused to drain outhouses prior drainage into the sewer system and then into the Tiber River (Jones 1967). The paper aims to undertake a case study for wastewater management that can be established for various institutes for wastewater management through the water drainage scheme.

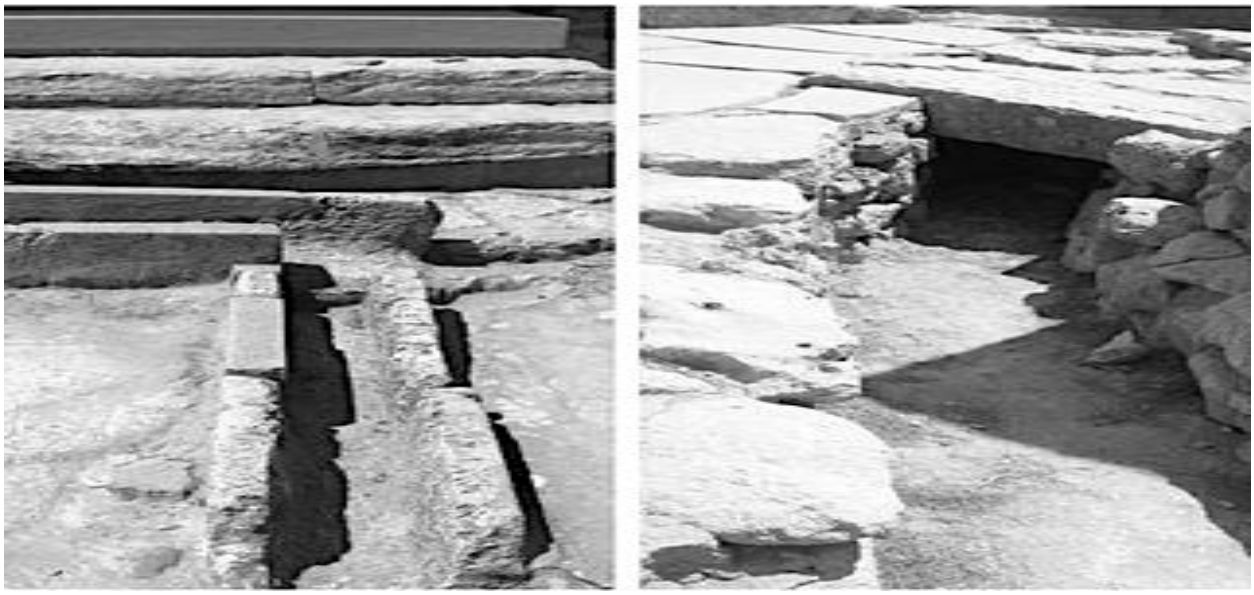


**Figure 1** Rom's water management system (Jones, 1967)

## 2. Hydraulic Design and Analysis

The following formula known as the rational formula is used for calculation of runoff water for highway drainage-

$$Q = 0.028CIA \quad (1)$$

Where:
Q is the maximum runoff in m3 per sec.
C is a constant depending upon the nature of the surface.
I is the critical intensity of the storm in mm per hour occurring during the time of concentration.
A is the catchment area in km2

### *2.1 Determination of Runoff*

For the purpose of determination of runoff, detailed study of the rainfall patterns is indispensable. Table 1 contains the monthly rainfall data for the city of Jalandhar. It can be seen that the maximum rainfall generally occurs in the month of August, with maximum of 301 mm in August, 2008. Hence, for a total catchment area of the Mega Hostel (i.e. 0.03km2) and surface runoff coefficient as 0.604, a net runoff discharge of 0.307m3/sec is obtained and used.

**Table 1** Monthly Rainfall Data for Jalandhar

| Year | Jan | Feb | March | April | May | June | July | August | Sept. | Oct. | Nov. | Dec. |
|---|---|---|---|---|---|---|---|---|---|---|---|---|
| 2008 | 11.3 | 3.4 | 0.0 | 43.1 | 7.0 | 195.7 | 123.9 | 301.0 | 23.0 | 14.0 | 0.0 | 2.2 |
| 2009 | 5.50 | 18.40 | 19.4 | 30.1 | 3.9 | 6.2 | 282.3 | 165.9 | 74.8 | 0.90 | 8.0 | 0.0 |
| 2010 | 5.20 | 3.9 | 1.4 | 1.8 | 1.6 | 12.3 | 251.2 | 82.0 | 136.1 | 3.6 | 0.0 | 14.2 |
| 2011 | 4.5 | 13.6 | 5.2 | 5.8 | 6.2 | 84.4 | 159.8 | 212.8 | 73.6 | 0.0 | 0.0 | 5.8 |
| 2012 | 93.7 | 1.8 | 3.2 | 13.9 | 0.20 | 1.90 | 91.0 | 79.2 | 107.5 | 0.70 | 0.0 | 6.2 |
| 2013 | 6.4 | 84.2 | 10.3 | 6.0 | 7.4 | 166.3 | 117.5 | 151.8 | 34.7 | 5.5 | 2.6 | 1.2 |
| 2014 | 4.0 | 18.4 | 16.4 | 11.0 | 6.9 | 6.1 | 95.3 | 40.0 | 84.3 | 10.2 | 0.0 | 18.7 |
| 2015 | 22.5 | 40.0 | 64.9 | 40.8 | 24.4 | 30.6 | 65.0 | 40.3 | 44.5 | 3.0 | 0.0 | 0.0 |
| 2016 | 10.6 | 8.9 | 27.1 | 1.3 | 14.0 | 26.8 | 131.5 | 136.4 | 15.2 | 2.4 | 0.5 | 0.0 |
| 2017 | 31.0 | 3.3 | 22.1 | 17.7 | 25.7 | 87.1 | 76.2 | 161.5 | 18.5 | 0.0 | 6.1 | 16.3 |
| 2018 | 12.4 | 8.6 | 3.5 | 13.5 | 5.6 | 75.5 | 132.4 | 94.4 | 315.5 | 0.9 | 0.1 | 1.3 |

### 2.2 *Determination of Wastewater Discharge*

This involves sewage accessing the wastewater system from different causes such as defective irrigation pipes, crack joints, bad pipe ties, broken manhole walls, etc. Figure 2 represents the weekly variation of the wastewater entering the sewer from the area under study. The wastewater generation during the wet periods and the dry periods have been presented and taken into consideration to maintain the self-cleaning velocity during the dry periods and to keep the velocity of flow lower than the limiting velocity during the wet periods. Also, the number of students present in the various hostels are given in Table 3.

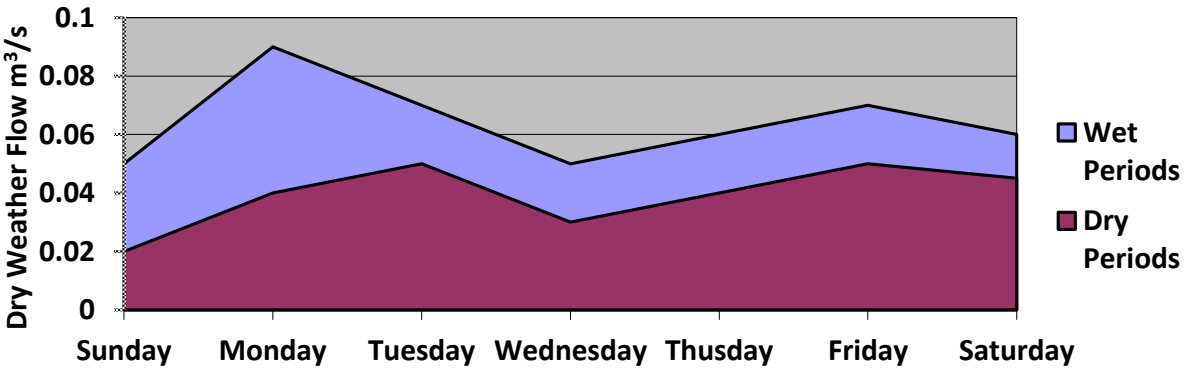



**Figure 2** Weekly presentation of wastewater during wet and dry periods

**Table 3** Number of Students in the different hostels of the campus

| Hostel Name | NO. of Students |
|---|---|
| BOYS HOSTEL 1 | 370 |
| BOYS HOSTEL 2 | 370 |
| BOYS HOSTEL 3 | 147 |
| BOYS HOSTEL 4 | 170 |
| BOYS HOSTEL 5 | 165 |
| BOYS HOSTEL 6 | 152 |
| BOYS HOSTEL 7 & 7E | 398 |
| MEGAHOSTEL | 1487 |
| Total | 3259 |

The daily water use for various activities in the premises have been presented in Table 4. According to the standard per capita water usage of 165l/da, of which 80% comes out as wastewater in the sewers, the total wastewater discharge can be obtained as 4,30,188 litre per day.

**Table 4** Average quantities of water used in different activities

| **Types of domestic waste** | **Average use (l)** |
|---|---|
| Shower | 45 |
| Kitchen Sink | 35 |
| Wash Basin | 15 |
| Toilet Flushing | 33 |
| Laundry | 30 |
| Others | 7 |
| Total | 165 |

## 2.3 *Calculation of diameter pipe*

- According to IS:1742-1983, Gradient of 1 in 57 has to be provided for the required flow
- Minimum Allowable Velocity of is 0.6 m/sec
- Maximum Allowable Velocity is 2.5 to 3.0 m/sec.

$$D = 1.548 * \left[\frac{NQ}{S^{0.5}}\right]^{0.375} \quad (2)$$

- Keeping the value of Q as 0.1375m$^3$/sec and slope as 1 in 57, i.e. 0.01754, Mannings constant 0.015.
- The diameter of pipe required is 434 mm, So a sewer pipe of 500 mm diameter can be used which is commercially available in the market.

### *2.4 Calculation of velocity of flow*

$$\left[\frac{1}{N}\right] * \left[\frac{D}{4}\right]^{0.66} * S^{0.5} \quad (3)$$

Using the above equation, velocity during full flow is 2.20 m3/sec which is greater than the self-cleaning velocity of the pipe. Velocity is lower than the scouring velocity of the pipe. Hence the design velocity is taken as 2.20 m3/sec.

## 3. Wastewater Treatment

The contemporary treatment plant in NIT Jalandhar is 0.5 MLD and work is underway to expand the treatment plant to 1.5 MLD after completion. The wastewater characteristics were determined and are given in Table 2.

**Table 2** Wastewater Characteristics

| *Analysis Parameter* | *units* | *Waste Water type Concentration* |
|---|---|---|
| *5-days Biochemical Oxygen Demand* | *mg/l* | *350* |
| *Chemical Oxygen Demand* | *mg/l* | *740* |
| *Total Oxygen Demand* | *g/m$^3$* | *250* |
| *Suspended Solid* | *g/m$^3$* | *450* |
| *Volatile Suspended Solids* | *g/m$^3$* | *320* |
| *Alkalinity* | *eqv/m$^3$* | *37* |
| *pH* | | *7.6* |

### *3.1 Use of MBBR (Moving Bed Film Reactor) in the treatment plant*

In the early 1980s, these types of reactors were first used. It usually has a plastic transporter aeration tank. The aeration tank allows the biofilm to expand on the surface, and its density is the same as that of the ocean. The aquatic treatment plant MBBR consists of an aeration tank that is much like an active sludge tank that has several special plastic carriers providing a surface for the biofilm where it can expand. These plastic carriers are constructed of a specific form of fibre, the density of which is around 1g/cm3 water. An example of this type of substance with a water-like consistency is HDPE(High-Density Polyethylene) with density around 0.95.
This carrier is combined by aeration device into the water tank. It is used to provide a strong relation with the substrate with the incoming waste water and the biomass contained in the carriers as shown in figure 2. The plastic carrier must be vigilant that aeration does not escape and a sieve is present on the

outlet of the aeration tank. For the higher biomass concentration in a bioreactor, hybrid MBBR method is also often used while suspended. It is not possible to use a basic MBBR strategy in this case. There are also anaerobic MBBRs which are commonly used to treat industrial water because of the high concentration of toxins. Today the aerobic, also known as methanogenic MBBR, is used for aerobic treatment of wastewater.

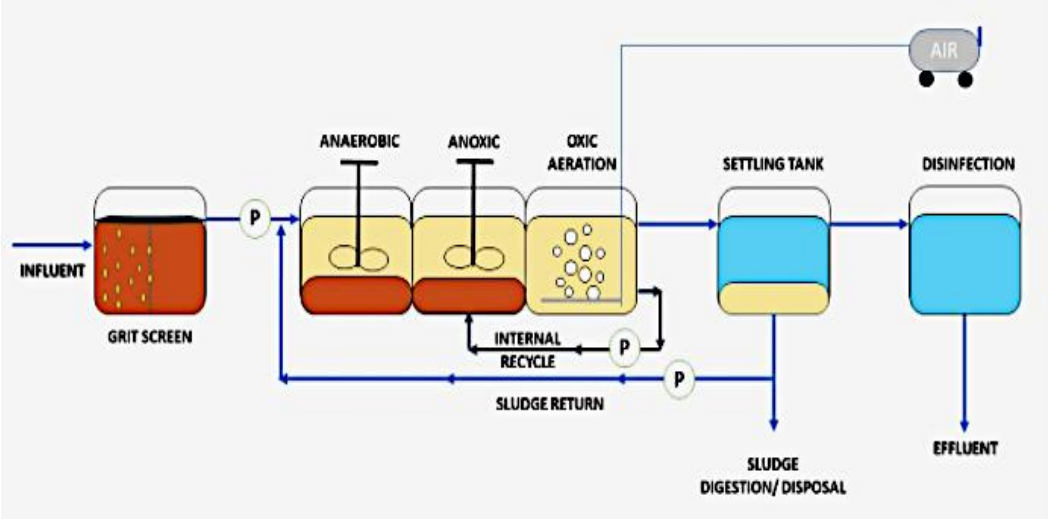



**Figure 3.** MBBR treatment plant

MBBR technique is a method of biofilm. Other processes use biofilm for wastewater disposal that uses membranes, biological aeration filter and biological filter. The MBBR method is a biofilm operation. Such forms of biofilm water treatment processes are classified as the trickling filter, biological contactor spinning and aerated filter. Biofilm processes need less space than other processes, such as the activated sludge process. The explanation behind this is that the biomass is heavily dispersed, which allows the efficiency more effective and reduces reliance on final sludge separation. The critical issue with Biofilm processes is that there is a problem of biological obstruction, and as a consequence of this pore's obstruction, there is a major head loss. Another benefit is that MBBRs do not need active sludge for each cycle so they can be reused for several cycles.

## 4. Discussion

Many advanced economies experience government interference in environmental decisions like the identification of sites as well as other building and organizational aspects. The required institutions and applied laws should help even the most sophisticated technologies to achieve optimum productivity. Many times millions of dollars and millions are expended on constructing and obtaining accurate construction details. Replication of active projects is adequate, but the framework should be tailored to local circumstances and environmental conditions in particular. The institution structure must also enable adaptation of the strategy to meet evolving global, regional and local objectives.
Moving Bed Film Reactor are commonly used where pre-activated sludge treatment is used to improve the device output and power. Compared to the form of water treatment plant MBBRs in our case provide some benefits over others, as this allows a full elimination of solids, the area used for that type of plant is smaller than other plants. It can treat vast volumes of water without washing the plant. Besides that, this treatment plant is cost-effective and reliable. As calculated, a treatment plant of 1MLD costs roughly 15-16 ruptures which is slightly less than other treatments taking into consideration the size of the treatment needed.

## 5. Conclusion

Management solutions for social, educational, environmental and economic circumstances within the goal region should be site-specific. One of most suitable technology is the commercially affordable, sustainable and socially acceptable technology. This paper contains different details obtained from the hostels and the weather cycle in Jalandhar. Different styles for irrigation pipes and their slopes and forms. The research aims to control and handle wastewater. And as we note, the number of students in our hostels is growing over time. In exchange, the volume of wastewater produced would therefore rise, meaning that the amount of wastewater generated and even the sizes and configuration of pipes will have to be researched.

This study recommends the usage of the MBBR treatment plant type in compliance with our requirements and the capability we demand. In future, though, it will be appropriate to review the treatment plant to develop the technologies and properties of wastewater, and it is suitable. Environmental knowledge and accountability are key to preventing and mitigating environmental impacts in the institutes and the government, by implementing a more effective approach to waste management that are crucial factors for managing the use of resources.

## References

Anggraini, A. K., S. Fuchs, and A. Silva. (2015). Investigation on slow sand filtration performance: influence of effective grain size on the particle removal. *Anais do 7th Eastern European Young Water Professionals Conference*.

Baweja, S., Aggarwal, R., Brar, M., & Lal, R. (2017). Groundwater depletion in Punjab, India. *Encyclopedia of Soil Science*, Third Edition: Three Volume Set, 5.

Ho, G. (2004). Small water and wastewater systems: pathways to sustainable development? *Water Science and Technology*, 48(11-12), 7-14..

Jones, D. Earl. "Urban hydrology-a redirection." *Civil Engineering* 37.8 (1967): 58.

Saravanane, R., Ranade, V. V., Bhandari, V. M., & Rao, A. S. (2014). Urban Wastewater Treatment for Recycling and Reuse in Industrial Applications: Indian Scenario. *Industrial Wastewater Treatment, Recycling and Reuse*, 283-322.

Webster, C. (1962). The sewers of Mohenjo-Daro. *Journal (Water Pollution Control Federation)*, 116-123..

WHO (World Health Organization), 2002. *Environmental Health*. Eastern Mediter- ranean Regional Center for Environmental Health Activities (CEHA).

IN PROCEEDINGS OF 25th HYDRO 2020, INTERNATIONAL CONFERENCE,
NATIONAL INSTITUTE OF TECHNOLOGY ROURKELA, ODISHA, INDIA
26-28, March 2021, ISBN 978-93-90631-56-8

Paper ID - 317

# River discharge estimation using SARIMA model and OLS regression from satellite altimetry data –A case study of Amazon River

Raviraj Dave [1], Udit Bhatia [2]

[1]Research Scholar, Indian Institute of Technology Gandhinagar, Palaj, Gandhinagar, Gujarat -382355, India
[2]Assistant Professor, Indian Institute of Technology Gandhinagar, Palaj, Gandhinagar, Gujarat -382355, India
Email: dave_raviraj@iitgn.ac.in

## Abstract

River discharge estimation has a vital role in infrastructure planning, flood mitigation. However, the number of stream gauges is decreasing globally, which is seen significantly in developing countries, which made streamflow estimation difficult. Here we propose a Seasonal Autoregressive Integrated Moving Average (SARIMA) time series model, which can be a potential alternative for conventional methods such as hydraulic modeling, velocity-area method, etc. for discharge estimation. The present study demonstrates the use of the SARIMA model for long term river discharge (2007-2011) forecast with (1971-2011) discharge data at the Fazenda Vista Alegre station in the Amazon river. The Relative Root-Mean-Square Error (RRMSE), Relative Root-Mean-Absolute Error (RRMAE), and coefficient of determination ($R^2$) values of the model are 0.154, 0.120, and 0.89, respectively. For poorly gauged rivers, discharge can be estimated from the satellite altimetry water level. Here Optimized Least-Square (OLS) regression is used to obtain best-fit values for the relation between water level (H) and Discharge (Q) from the Envisat (RA-2) altimetry water level observations. This analysis shows the potential of altimeter data in a poorly gauged river basin as its regression equation can help quantify discharge only using altimeter data. The RRMSE, RRMAE, and $R^2$ values of regression are 0.261, 0.297, and 0.83. The result shows that the SARIMA model produced estimated Q shows good prediction fitting and can be used for long-term forecasting. Whereas for the poorly gauged river, the discharge estimation from satellite altimetry data shows good prediction and can be employed for discharge estimation.

***Keywords:*** *Discharge estimation, SARIMA Model, Satellite Altimeter, OLS regression, Amazon river*

## 1. Introduction

River discharge (Q) plays a crucial role in water resource management and flood mitigation. The accurate forecasting of river discharge provides the information for disparate water resource planning, such as designing hydraulic structures, reservoir operation management and irrigation. Therefore, there is a need for long-term discharge forecasting.

Forecasting of discharge or any hydrological process is often done using two broad categories of models. These two broad categories are processed based models and data-driven models. Processed based models of estimating discharges are Lumped conceptual models, hydrologic or hydrodynamic models (Anderson et al., 2004) , Manning's equation method (Sichangi et al., 2016) and velocity area method. However, these all methods required catchment specific information with sufficient knowledge of principles of energy. Unavailability of an adequate amount of data in these models can lead to poor discharge estimation. Whereas the data-driven models, which include Artificial neural network (ANN), Support vector machine (SVM) and time series models, namely, Autoregressive (AR), Moving average (MA), Autoregressive moving average (ARMA), Autoregressive integrated moving average (ARIMA) and Seasonal autoregressive integrated moving average (SARIMA) models. The data-driven method provides liberty while using the inherent relationship of input and output with data without considering the internal physical process. The last decade shows the increasing use of the data-driven models, especially time series models (Pektaş and Kerem Cigizoglu, 2013; Tadesse and Dinka, 2017; Valipour et al., 2012; Wang et al., 2014).

The earlier studies of the runoff forecast started with the application of simple and multiple regression technique (Kisiel, 1969). The (Box et al., 2011) shown the approach for modeling time series for estimating the rainfall and discharge. It involves a four-step process: Identification, estimation,

diagnostic, verification and forecasting. Several researchers have adopted this univariate approach without focusing on other parameters (Wang et al., 2008). The hydrological parameters such as precipitation and runoff tend to show the trend in the data, and the ARIMA models of time series are widely used in these domains as they help remove the trends term and stationarity terms converts nonstationary time series to stationary time series (Valipour et al., 2012; Wang et al., 2014). However, some of the researchers have not considered the seasonality involved in the forecasting of hydrological data while using time series models (Han et al., 2010; Toth et al., 2000). The SARIMA models considered as among the best statistical linear type model as it also takes account the seasonality involved in the hydrological parameters (Tadesse and Dinka, 2017; Valipour, 2015). In this study, we used SARIMA model for estimation of river discharge in the Amazon river.

The number of stream gauges worldwide is decreasing significantly in the developing countries over the past few decades; that's where the remote sensing data comes to aid the cause for forecasting the hydrological parameters. (Dubey et al., 2015; Hossain et al., 2014; Sichangi et al., 2016). This remote sensing data, such as satellite altimetry data, can estimate water level depth in the rivers and be used as a proxy to estimate the discharge. The forecasting of Q by constructing the relationship between the satellite altimeter depth and river discharge through the rating curve can be crucial when there is a lack of in-situ measurements. We estimated the river discharge using satellite altimetry data by assimilating the remote sensing data with ground measurements.

In this paper we present two approaches for river discharge forecasting: (1) data driven SARIMA model and (2) through satellite altimeter data.

## 2. Region of study and Data

The Amazon river is the greatest in South America. The Amazon river has the largest drainage basin amongst all rivers in the world. The Amazon river length is 6400km, which makes it the second-largest river in terms of size. We used Fazenda Vista Alegre station in the Amazon river basin as a study area (Figure 1) situated in the basin's central part. The station's geographical location is $4.9596^0$ S, $60.0496^0$ W. The station is located in the Madeira river- a tributary of the Amazon river.




**Figure 1** Area of study depicting the Amazon basin boundary and ground observation stations. The Fazenda Vista Alegre station is highlighted with red dotted box

The ground observed daily river discharge (Q), and ground observed water level depth data from 1971-2010 at the Fazenda Vista Alegre station in Amazon catchment is collected from the SO-HYBAM (Amazon basin water resources observation service) ( https://hybam.obs-mip.fr/ ). This station data is used to set up the SARIMA model. We used the ENVISAT altimetry (RA-2) water level depth data from 2002-2010 (http://hydroweb.theia-land.fr ). RA-2 products are based on the Geophysical Data

Record (GDR). The RA-2 product consists of location, data and output retracted at 18 Hz. The ENVISAT data has a temporal resolution of 35 days.

## 3. Material and Methods

The flowchart of the methodology is shown in (Figure 2). At first, we applied the SARIMA model to forecast the long-term river discharge data. In the second scenario, we used the regression model to estimate the river discharge from satellite altimeter data. The detailed steps of the methods are shown in subsequent sections.

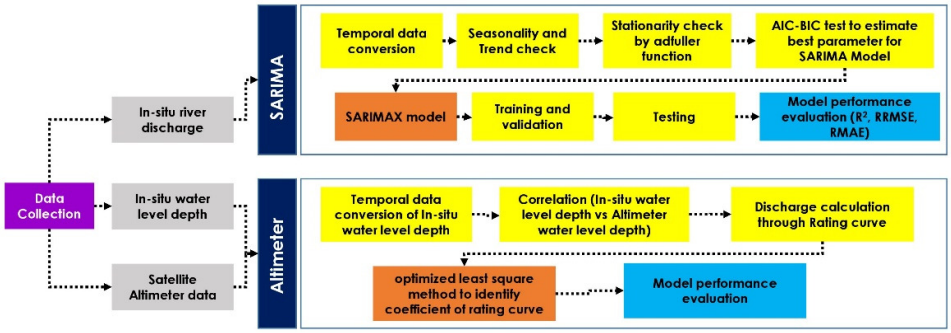



**Figure 2** Overview of the modeling framework. The methodology consists of (a) The SARIMA framework for discharge forecasting and (b) Satellite altimeter based discharge forecasting.

### 3.1 *SARIMA Model for river discharge forecasting*

SARIMA models are extensions of ARIMA models to take care of seasonality terms involved in hydrological parameters. The SARIMA model consists of two terms that are seasonal and non-seasonal. The SARIMA model is presented as SARIMA (p,d,q)(P, D, Q, S). The first part represents the non-seasonal component and the second part describes the seasonal component.

$$\psi(B^s)\theta(B)(1-B^s)^D(1-B)^d x_t \;=\; \emptyset(B^s)\varphi(B)\varepsilon_t \qquad (1)$$

where,
$\psi$ = Moving average (MA) parameters of seasonal component
$\theta$ = Moving average (MA) parameters of nonseasonal component
$\emptyset$= Autoregressive (AR) parameters of seasonal component
$\varphi$ = Autoregressive (AR) parameters of nonseasonal component
B= backward operator
$B(x_t) = x_{t-1}$
$\varepsilon_t$= Independent random variable
$(1-B)^d$ = d$^{th}$ non-seasonal variable
$(1-B^s)^D$= D$^{th}$seasonal variable
p and P = AR components
q and Q = MA components
d and D = difference terms

#### 3.1.1 *Exploratory data analysis*

The Box-jenkins approach (Box et al., 2011) to model the univariate time series is considered in this study. To fit the stochastic time series model, the data should be stationary. To forecast the annual Q, daily data is converted to monthly data. First, we checked the seasonality and trend by plotting the average monthly time series data and calculating 10-year moving averages from 1971 to 2010.

### 3.1.2 *Model parameter identification*

To check the stochastic time-series stationarity, we performed an Augmented dickey fuller (ADF) test. The ADF test is part of a unit root test, which is often used for checking stationarity. ADF test is defined as (Equation 2).

$$x_t = c + \beta t + \alpha\, x_{t-1} + \emptyset_1\, \Delta x_{t-1} + \emptyset_2\, \Delta x_{t-2} + \ldots + \emptyset_p\, \Delta x_{p-1} + \varepsilon_t \quad (2)$$

where,
β= coefficient of time trend
p= lag order

After checking the stationarity, to estimate the best fit values of (p,d,q) and (P, D, Q, S), Autocorrelation function (ACF) and partial autocorrelation function (PACF) is used to estimate the model parameter graphically. To be more precise while selecting the parameter, we also calculated the Akaike information criteria (AIC) and Bayesian Information Criteria (BIC). The low values of AIC and BIC indicate better model parameter values compared to the other models. The AIC and BIC calculated using (Equation 3) (Aike, 1974; Stone, 1979)

$$AIC = -2ln(L) + 2k \quad (3)$$

$$BIC = -2ln(L) + 2ln(N)k$$

where,
L= likelihood value
N= number of recorded measurement
k= number of estimated parameters

### 3.1.3 *Calibration, Validation and Testing*

We split our data set into 80% calibration, 10% validation and 10% testing. The best-estimated SARIMA model parameters from the calibration data set are applied to the validation data set. We used a walk forward approach while cross-validating the model parameters. The model's performance is evaluated using three model performance criteria: coefficient of determination ($R^2$), relative mean absolute error (RMAE) and relative root mean squared error (RRMSE). Residuals values of the validation are also checked for validation results.

After validation, we applied the selected SARIMA model parameters on a testing data set to evaluate the model's appropriateness.

## 3.2 *Regression model for river discharge forecasting from satellite altimeter data*

Ground observed water level data and Envisat (RA-2) satellite altimeter derived water level data from 2002 -2010 is plotted simultaneously to check the appropriate value of satellite altimeter derived water level depth (H). After that, a power law is fitted between the altimeter water level depth data and the ground observed Q. We used the rating curve equation to derive the relationship between Q and H (Equation 4).

$$Q = a \times H^b \quad (4)$$

Where,
Q = observed river discharge
H= Altimeter derived water level depth
a and b = regression parameters

The optimized least square regression is used to derive the regression parameters. The model performance is evaluated using the coefficient of determination ($R^2$), Relative mean absolute error (RMAE) and Relative root mean squared error (RRMSE).

$$R^2 = 1 - \frac{RSS}{TSS}$$

$$RMAE = \frac{1}{Q}\left[\frac{1}{n}\sum_{i=1}^{n} |\widehat{Q}_i - Q_i|\right] \quad (5)$$

$$RRMSE = \frac{1}{Q}\left[\sqrt{\frac{1}{n}\sum_{i=1}^{n}(\widehat{Q}_i - Q_i)^2}\right]$$

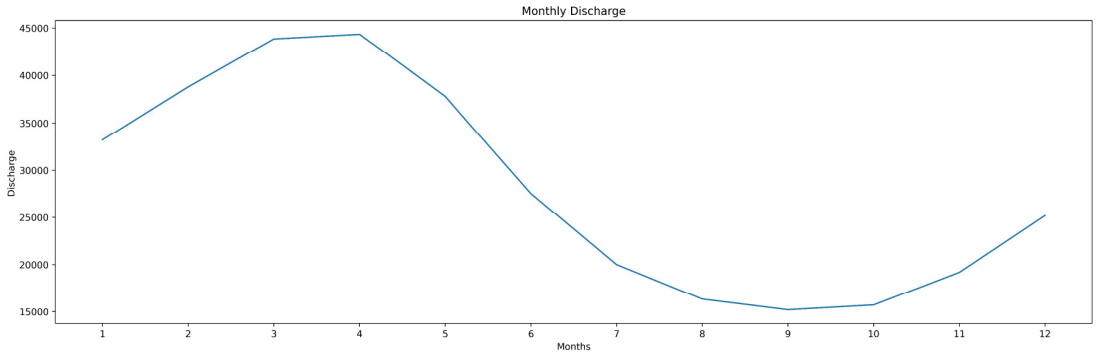
Where,
RSS= sum of squares of residuals
TSS = total sum of squares
n= Number of data points
Q= Observed value
$\widehat{Q}$ = Predicted value

## 4. Results

### 4.1 *SARIMA Model*

#### 4.1.1 *Stationarity check and model selection*

We performed Exploratory data analysis (EDA) and calculated the mean monthly discharge variation from 1971-2010. It shows seasonality as the discharge is high from March to May and low from June to November (Figure 3(a)). Ten years of moving average is calculated to check the trend and it is showing a negative trend. The (Figure 3(b)) shows the negative trend and average Q decreased 1250 m3/s in the duration of 40 years.



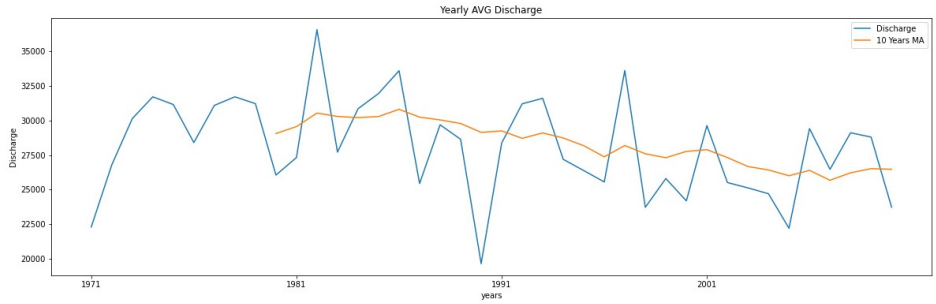



**Figure 3** Exploratory data analysis: (a) mean average monthly discharge and (b) 10 year moving average discharge

We performed the stationarity check using the ADF test. The p-value obtained from the test was less than 5%, which indicates that the stochastic time series for Q is stationary. The time series have shown interesting behavior as the negative autocorrelation observed at lag six and it is repeating in an interval of 12. The same behavior is seen in the PACF but in a positive direction (Figure 4). This is due to the seasonal change, so the first seasonal difference of 1 with s=12 is taken and again, we plot the ACF and PACF to estimate the other SARIMA model parameters (Figure 5).

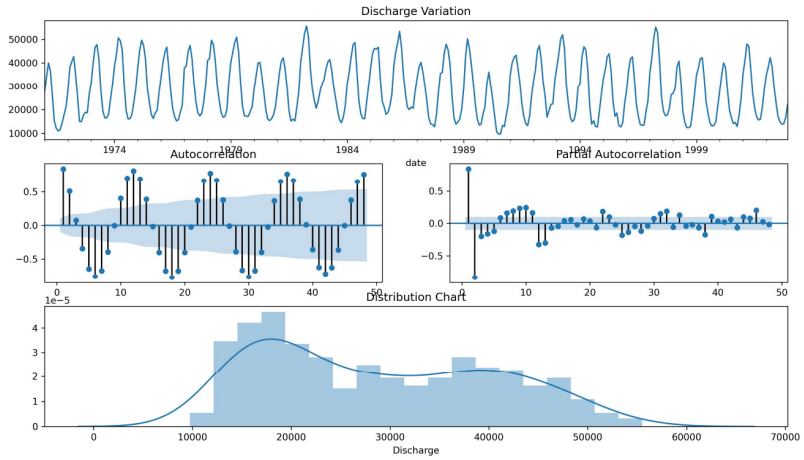



**Figure 4** ACF and PACF plots for estimating SARIMA model

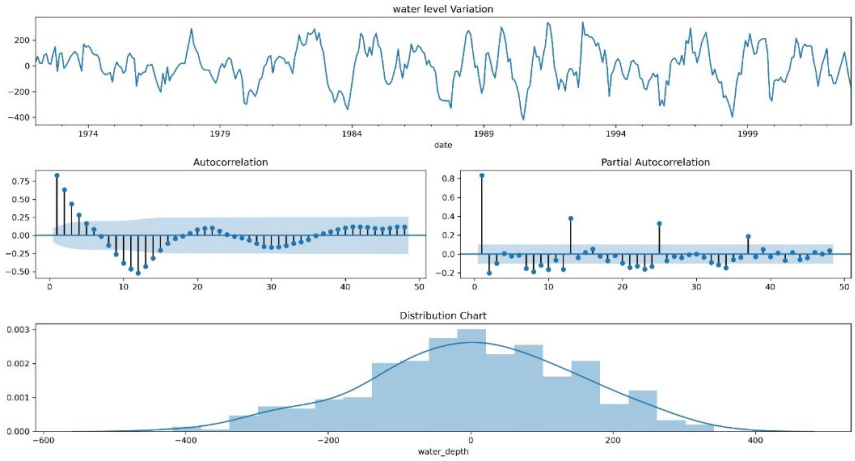



**Figure 5** ACF and PACF plots for estimating SARIMA model after seasonal differencing

The ACF and PACF plot (Figure 5) indicates the order of (p, d, q) and (P, D, Q, S) as (1,0,1) and (0,1,1,12) respectively. AIC and BIC test further verify these model parameters as it also produces the lowest value for the order mentioned above.

### 4.1.2 *Model performance*

We validated the result by implementing the SARIMA (1,0,1) (0,1,1,12) on validation data set. The model performance criteria shown good fitting as the $R^2$, RMAE and RMSE values are 0.92, 0.070 and 0.924, respectively. To evaluate the result, we generated four graphs indicating the (1) current and predicted values through time, which shows good fitting, (2) error vs. predicted value, which shows the linear distribution, (3) The QQ plot indicating the distribution of errors in our case we found out that plot shows the normal pattern with very fewer outliers and (4) Autocorrelation plot of residuals to check it falls under the confidence interval. (Figure 6(d)) shows that all the residual of autocorrelation falls under the confidence interval.

After validating the model parameters, we performed the SARIMA model on the testing data set. The testing shows the appropriate fitting as the $R^2$, RMAE and RMSE values shows 0.89, 0.120 and 0.154, respectively (Figure 7).

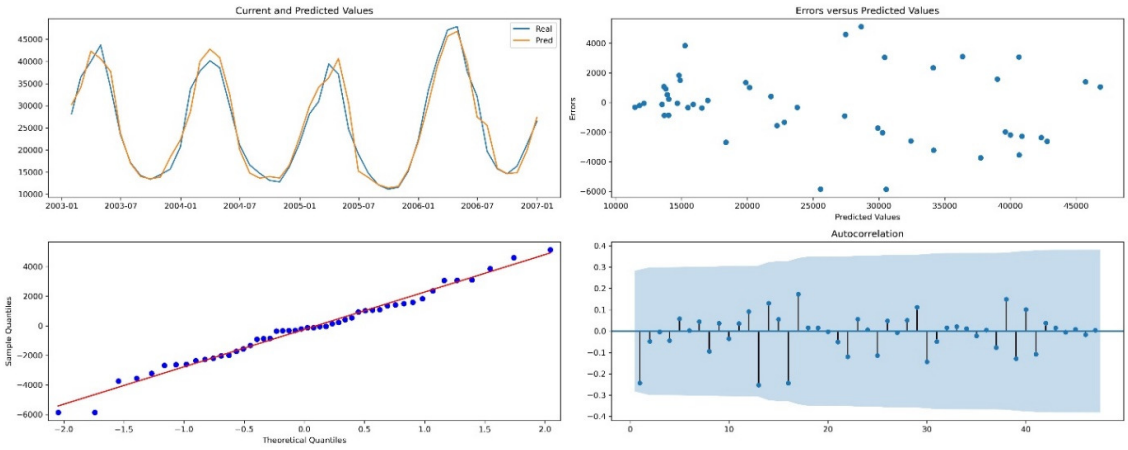



**Figure 6** SARIMA model on validation data set (a) current and predicted values shows the model appropriateness as there is good fitting between observed and predicted value, (b) Errors Vs predicted values shows the linear distribution, (c) QQ plot representing the distribution of errors and with it's ideal distribution and (d) Autocorrelation of residuals

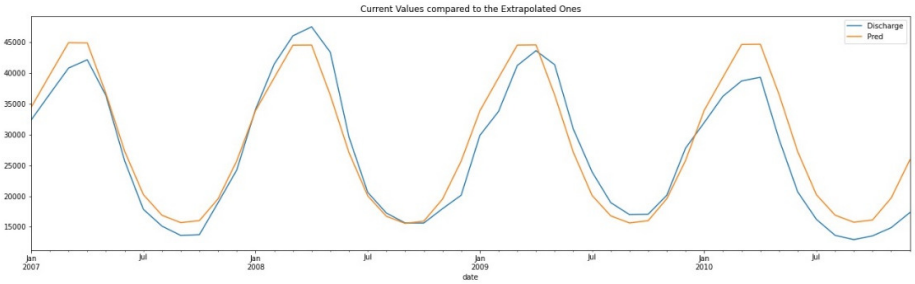



**Figure 7** SARIMA model on testing data set showing the fitting between the observed and predicted values of discharge

### 4.2 *Altimeter based discharge forecasting*

First, we calculate the correlation between Ground observed water level depth and altimeter based water to understand the behavior of altimeter based water level depth with the ground condition. The correlation value shows a high correlation between these two data sets, as the correlation coefficient turned out to be 0.99 (Figure 8). These show that we can use the altimeter data as the proxy of ground observation when there is less availability of in-situ measurements.

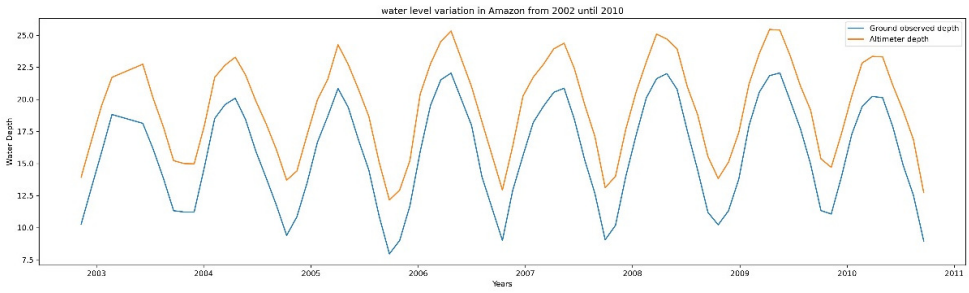



**Figure 8** Correlation between Altimeter water level depth and ground station observed water level depth

We plot the observed discharge (Q) and altimeter water level depth (H) to understand the relationship between them and they show exponential relationship (Figure 9).

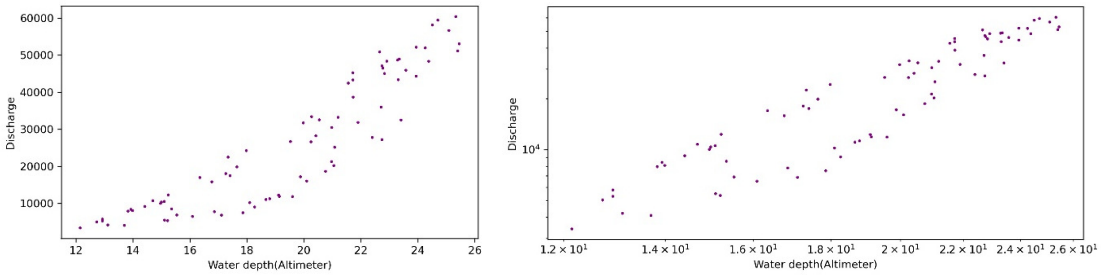



**Figure 9** Q vs H on standard scale (left), Q vs H on log-log scale (Right)

We used the rating curve method approach to estimate the regression parameters (Equation 4). The using optimized least square regression method is used and the regression parameter values a and b are 0.359 and 3.698, respectively (Figure 10). The regression model's performance is evaluated using $R^2$, RMAE and RMSE, which are 0.83, 0.261 and 0.297, respectively.

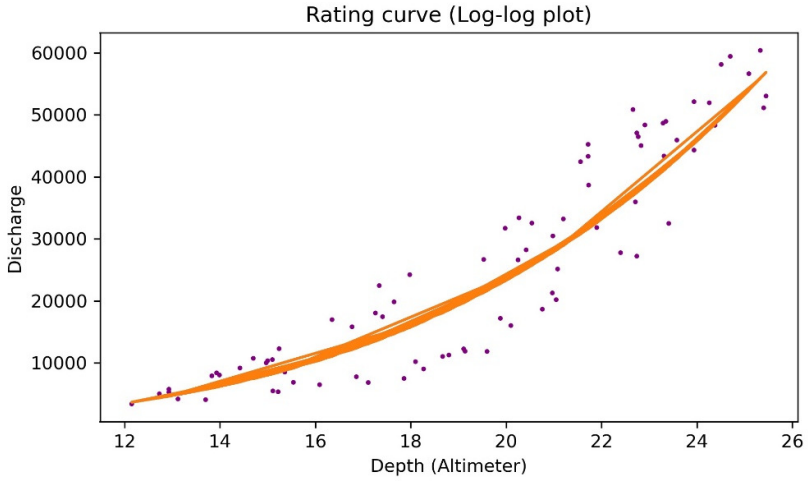



**Figure 10** Rating curve fitting using OLS regression

**Table 1** Model performance

| Model | $R^2$ | RMAE | RMSE |
|---|---|---|---|
| SARIMA (Validation) | 0.92 | 0.070 | 0.924 |
| SARIMA (Testing) | 0.89 | 0.120 | 0.154 |
| OLS regression | 0.83 | 0.261 | 0.297 |

## 5. Conclusion and Discussion

The forecasting of river discharge always plays a crucial role in the future planning of hydraulic structures and flood mitigation strategies. Simultaneously, the accuracy improvement of these hydrological forecasting, mainly long term forecasting, is important and complex. The time series model such as ARIMA and SARIMA can reduce the catchment specific data requirement and provide accurate prediction while using a data-driven approach. ARIMA model is widely used for these forecasting types, but SARIMA models can significantly improve the ARIMA-based forecasting models. The SARIMA model used during this study has given good prediction results and the SARIMA model can be implemented in the long term forecasting.

Developing nations face enormous challenges for discharge forecasting as the less data availability and the reduction in ground observation station. The remote sensing data, such as satellite altimetry, provides good forecasting results and can be used as an alternative approach in the data-scarce region. This study shows that satellite altimeter data show good prediction fitting.

The result of this analysis allows several meaningful inferences, which can make the impact of discharge forecasting. First, the SARIMA time series model can be effectively used for long-term forecasting and can be implemented where specific catchment data are not available. The second one is in the data-scarce region, or poorly gauged rivers, the satellite altimeter data can be used for river discharge prediction.

## References

Aike, H.A.I. (1974), A New Look at the Statistical Model Identification.
Anderson, M.L., Chen, Z.Q., Kavvas, M.L. and Feldman, A. (2004), Coupling HEC-HMS with atmospheric
Aike, H.A.I. (1974), A New Look at the Statistical Model Identification.
Anderson, M.L., Chen, Z.Q., Kavvas, M.L. and Feldman, A. (2004), Coupling HEC-HMS with atmospheric

models for the prediction of watershed runoff, *Joint Conference on Water Resource Engineering and Water Resources Planning and Management 2000: Building Partnerships*, Vol. 104 No. 4, pp. 312–318.

Box, G.E.P., Jenkins, G.M. and Reinsel, G.C. (2011), *Time Series Analysis: Forecasting and Control*, Vol. 734, John Wiley & Sons.

Dubey, A.K., Gupta, P.K., Dutta, S. and Singh, R.P. (2015), An improved methodology to estimate river stage and discharge using Jason-2 satellite data , *Journal of Hydrology*, Vol. 529 No. December 2017, pp. 1776–1787.

Han, P., Xin, P., Yu, S. and Zhu, D.H. (2010), Drought forecasting based on the remote sensing data using ARIMA models, *Mathematical and Computer Modelling*, Elsevier Ltd, Vol. 51 No. 11–12, pp. 1398–1403.

Hossain, F., Siddique-E-Akbor, A.H., Mazumder, L.C., Shahnewaz, S.M., Biancamaria, S., Lee, H. and Shum, C.K. (2014), Proof of concept of an altimeter-based river forecasting system for transboundary flow inside Bangladesh, *IEEE Journal of Selected Topics in Applied Earth Observations and Remote Sensing*, Vol. 7 No. 2, pp. 587–601.

Kisiel, C.C. (1969), *Time Series Analysis of Hydrologic Data*, *Advances in HYDROSCIENCE*, Vol. 5, ACADEMIC PRESS, INC., available at:https://doi.org/10.1016/b978-1-4831-9936-8.50007-6.

Pektaş, A.O. and Kerem Cigizoglu, H. (2013), ANN hybrid model versus ARIMA and ARIMAX models of runoff coefficient, *Journal of Hydrology*, Vol. 500 No. 2013, pp. 21–36.

Sichangi, A.W., Wang, L., Yang, K., Chen, D., Wang, Z., Li, X., Zhou, J., et al. (2016), Estimating continental river basin discharges using multiple remote sensing data sets, *Remote Sensing of Environment*, The Authors, Vol. 179, pp. 36–53.

Stone, M. (1979), Comments on Model Selection Criteria of Akaike and Schwarz Author ( s ): M . Stone Source : Journal of the Royal Statistical Society . Series B ( Methodological ) , 1979 , Vol . 41 , Published by : Wiley for the Royal Statistical Society Stable, Vol. 41 No. 2, pp. 276–278.

Tadesse, K.B. and Dinka, M.O. (2017), Application of SARIMA model to forecasting monthly flows in Waterval River, South Africa, *Journal of Water and Land Development*, Vol. 35 No. 1, pp. 229–236.

Toth, E., Brath, A. and Montanari, A. (2000), Comparison of short-term rainfall prediction models for real-time flood forecasting, Vol. 239, pp. 132–147.

Valipour, M. (2015), Long-term runoff study using SARIMA and ARIMA models in the United States, *Meteorological Applications*, Vol. 22 No. 3, pp. 592–598.

Valipour, M., Banihabib, M.E. and Behbahani, S.M.R. (2012), Parameters estimate of autoregressive moving average and autoregressive integrated moving average models and compare their ability for inflow forecasting, *Journal of Mathematics and Statistics*, Vol. 8 No. 3, pp. 330–338.

Wang, H.R., Wang, C., Lin, X. and Kang, J. (2014), An improved ARIMA model for precipitation simulations, pp. 1159–1168.

Wang, J., Du, Y.H. and Zhang, X.T. (2008), Theory and application with seasonal time series, Nankai University Press, Chinese.

IN PROCEEDINGS OF 25th HYDRO 2020, INTERNATIONAL CONFERENCE,
NATIONAL INSTITUTE OF TECHNOLOGY ROURKELA, ODISHA, INDIA
26-28, March 2021, ISBN 978-93-90631-56-8

Paper ID - 390

# Distribution, Trend, and Concurrence of Meteorological, Hydrological and Agricultural Droughts over Madhya Pradesh, India

Vikas Poonia[1] and Manish Kumar Goyal[2]

[1]*Research Scholar, Discipline of Civil Engineering, Indian Institute of Technology, Indore, India, 453552*
[2]*Associate Professor, Discipline of Civil Engineering, Indian Institute of Technology, Indore, India, 453552*
*Email:* vgpcivilengineer@gmail.com
*Mobile No.: +918112210590*

## Abstract

Drought assessment is crucial to mitigate its adverse impact, especially in areas where risk is more due to changing climate. However, most of the studies deal with one or a couple of droughts and the absence of integration of meteorological, hydrological, and agricultural droughts in terms of frequency, concurrence, and evolution process, especially in Madhya Pradesh. In this study, we estimate the meteorological, hydrological, soil moisture, and vegetation droughts over Madhya Pradesh using the standardized precipitation index (SPI), standardized runoff index (SRI), standardized soil moisture index (SSI) and vegetation drought index (VCI) during the period 1982-2013 respectively. The study investigates the spatio-temporal distribution of droughts, individually and concurrently. Further, drought trend analysis is carried out in terms of their extent, duration, and frequency. Finally, we proposed a decentralized Blockchain-based disaster management framework to enhance and improve the existing drought management system and facilitates the disaster victims to get their relief as fast as possible. Examinations indicate that soil moisture and hydrological droughts are more extreme related to other drought types over Madhya Pradesh. Moreover, 90% of concurrent droughts include soil moisture drought as a major part. This study facilitates a comprehensive approach to better understand the dynamic characteristics of all major droughts and their complex interaction from various perspectives over Madhya Pradesh, and thus provides useful insights for policymakers to develop effective strategies for drought mitigation and sustainable ecosystem management in the state.

***Keywords:*** *Drought Concurrence, Drought Evolution, Drought Extent, Drought Severity.*

## 1. Introduction

Drought is one of the dangerous natural hazards that has taken billions of life (Keyantash & Dracup, 2002; Wilhite, 2005). It is very difficult to understand the beginning and end of the drought event (Wilhite, 2000). Droughts are defined with respect to deficiency of precipitation, runoff, or soil moisture (Hisdal and Tallaksen, 2000). Broadly, they are divided into 3 categories, meteorological, hydrological, and agricultural droughts (National Commission on Agriculture, 1976). In the present study, agricultural drought is divided into two parts (soil moisture and vegetation drought). In the past, various drought indices have been used to monitor drought conditions such as SPI(McKee et al., 1993); vegetation condition index, VCI(F. N. Kogan, 1995), etc. Each of the drought indices has its own merits and demerits. For further details, various studies can be referred (Heim, 2000; Zargar et al., 2011). Table 1 describes the specific thresholds to categorize drought severity.

Kogan (1997) observed that approximately 50% of the earth's surface is sensible towards drought conditions. India is on top of the list of drought-prone country in the world, where (Mishra and Singh, 2010) suggests that drought is occurring in every three years in the past 50 years. Nagarajan (2003) observed that some parts of Gujarat and Rajasthan have experienced extreme droughts. In the changing climate (2050-2099), it is estimated that droughts are exaggerated in the peninsular and central northeast part of India (Ojha et al., 2013). Some of the possible reasons such as unusually high temperatures or unknown monsoon conditions (Nagarajan, 2003). Mallya et al., (2015) suggested that

drought frequency and severity are likely to follow increasing trend during 1972-2014 related to the 1936-71 period. In a recent study, vegetation drought over India is also estimated in the changing climatic variables such as temperature and precipitation (Jha et al., 2019). The literature review suggests that only meteorological drought is focused, however, there is a lack of integration of all major droughts. Hence, a combined study is required to witness the crucial relationship among major drought types.

**Table 1** Classification of drought indices based on severity (Source: (Svoboda et al., 2002))

| S. No. | Drought Severity | SPI, SRI, SSI | VCI | Category |
|---|---|---|---|---|
| 1. | Abnormally Dry | -0.50 to -0.79 | 0.45 to 0.36 | D0 |
| 2. | Moderate Drought | -0.80 to -1.29 | 0.26 to 0.35 | D1 |
| 3. | Severe Drought | -1.30 to -1.59 | 0.25 to 0.16 | D2 |
| 4. | Extreme Drought | -1.60 to -1.99 | 0.15 to 0.06 | D3 |
| 5. | Exceptional Drought | -2.00 or less | 0.00 to 0.05 | D4 |

Therefore, the present study examines all major droughts and their distribution alone as well as concurrently over Madhya Pradesh. It provides a joint approach to comprehend all major drought types using temporal and spatial distribution and their concurrence over Madhya Pradesh during 1982-2013. This study provides useful insights to policy-makers to design an effective framework to reduce drought risks at a regional scale. In the end, we present a decentralized Blockchain-based disaster management framework to enhance and improve the existing drought management system and facilitates the disaster victims to get their relief as fast as possible.

## 2. Materials and Methods

In the present study, most widely used drought indices such as standardized precipitation index (SPI), vegetation condition index (VCI), standardized soil moisture index (SSI) and standardized runoff index (SRI) to monitor all major drought types over Madhya Pradesh. All these drought indices are computed at monthly scale using precipitation, runoff, soil moisture and NDVI datasets for meteorological, hydrological, soil moisture and vegetation drought respectively.

### *2.1. Data used*

For the meteorological drought condition, the standardized precipitation index is computed using SPI. For SPI computation, daily precipitation is derived from the Indian Meteorological Department (IMD) at a spatial resolution of 0.5°*0.5°. The runoff and soil moisture data are derived from Modern-Era Retrospective analysis for Research and Applications, Version 2 (MERRA-2) product. Runoff and soil moisture data are available at a spatial resolution of 1/2°*2/3°. Finally, the NDVI data is downloaded from Global Inventory Modeling and Mapping Studies (GIMMS). NDVI dataset is a remote sensing dataset which is a good indicator of vegetation and greenness condition. To match the resolution f precipitation dataset, the runoff, soil moisture, and vegetation dataset are regridded to 0.5°*0.5°. Table 2 describes the data used and the sources used in the present study.

**Table 2** Data used and their sources

| Data | Source | Original Resolution | Final Resolution |
|---|---|---|---|
| Precipitation | Indian Meteorological Department (IMD) | 0.5°*0.5° | 0.5°*0.5° |

| | | | |
|---|---|---|---|
| Runoff and Soil Moisture | Modern-Era Retrospective analysis for Research and Applications, Version 2 (MERRA-2) | 1/2°*2/3° | 0.5°*0.5° |
| NDVI | Global Inventory Modeling and Mapping Studies (GIMMS) | 1/12°*1/12° | 0.5°*0.5° |

### *2.2. Frequency, duration, spatial extent and temporal extent*

Drought frequency can be defined as number of drought events in a decade, however, this study computes drought frequency for eleven years. The spatial extent shows the area (in%) under drought in the given time period. It can be defined as the ratio of number of grids experiencing droughts to the total count of grids in the study area.

$$\text{Areal Extent} = \frac{\text{Number of grid cells experiencing drought conditions}}{\text{Total number of grid cells in the study area}} \quad (1)$$

The temporal extent can be defined as counting the number of years that each grid cell experiencing drought during the given period 1982-2013. In case of concurrent drought, two or more than drought indices are taken together at the same time. Mean duration of each drought in the decade can be defined as the ratio of total duration time to the drought concurrence numbers.

$$\text{Mean Duration} = \frac{\text{Total duration time}}{\text{Drought concurrence numbers}} \quad (2)$$

Four most widely used drought indices i.e., SPI, VCI, SSI, and SRI are used to monitor drought conditions. After drought characterization, their spatio-temporal distribution is examined. Further, drought trend is examined in terms of frequency, areal extent, and mean duration. Finally, concurrent droughts are quantified in the present study.

## 3. Results and Discussions

### *3.1. Drought analysis*

For the primary examination, the major droughts are estimated using two criteria i.e., first is maximum spatial extent and second is severity. Figure 1 presents the major droughts based on both criteria over Madhya Pradesh during the period 1982-2013. From the investigation, it was observed that soil moisture and hydrological droughts are more extreme based on severity as compared to the other two drought types. A similar finding was observed in case of the maximum spatial extent criteria of major droughts.

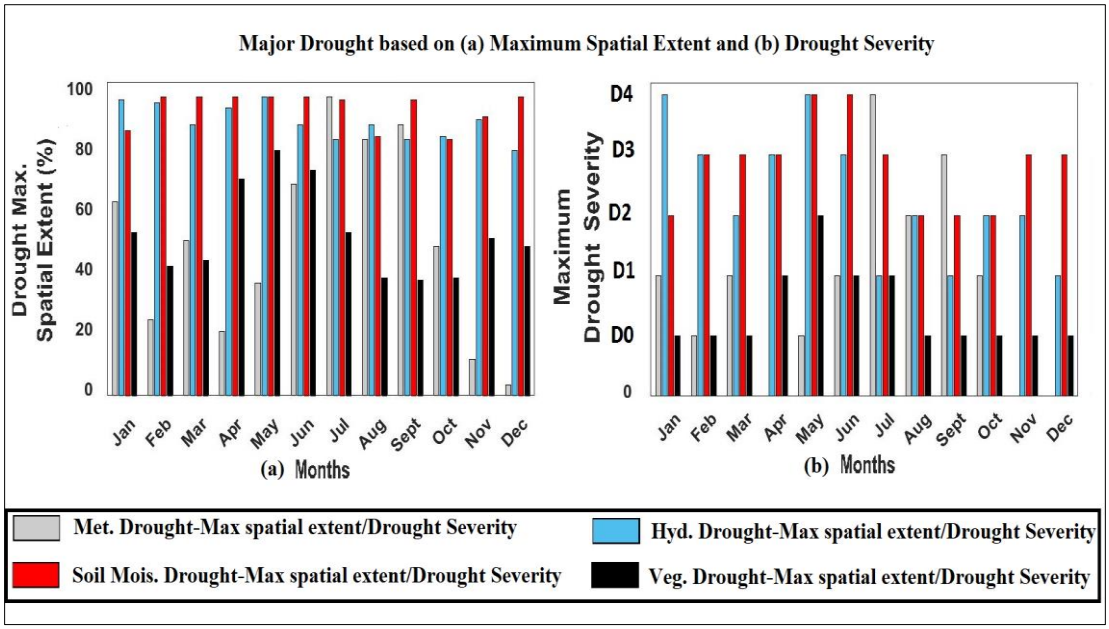



**Figure 1** Major Droughts based on (a) maximum spatial extent and (b) drought severity

### *3.2. Temporal extent*

Figure 2 illustrates the temporal extent at each pixel of the study area for monsoon and non-monsoon season during the period 1982-2013 for all major drought types. From the investigation, I was observed that meteorological droughts mostly occur during the monsoon season. Whereas soil moisture and hydrological drought do not show any remarkable seasonal variation in the temporal extent. However, vegetation drought illustrates the heterogeneous distribution as compared to the above three drought types over Madhya Pradesh during 1982-2013.

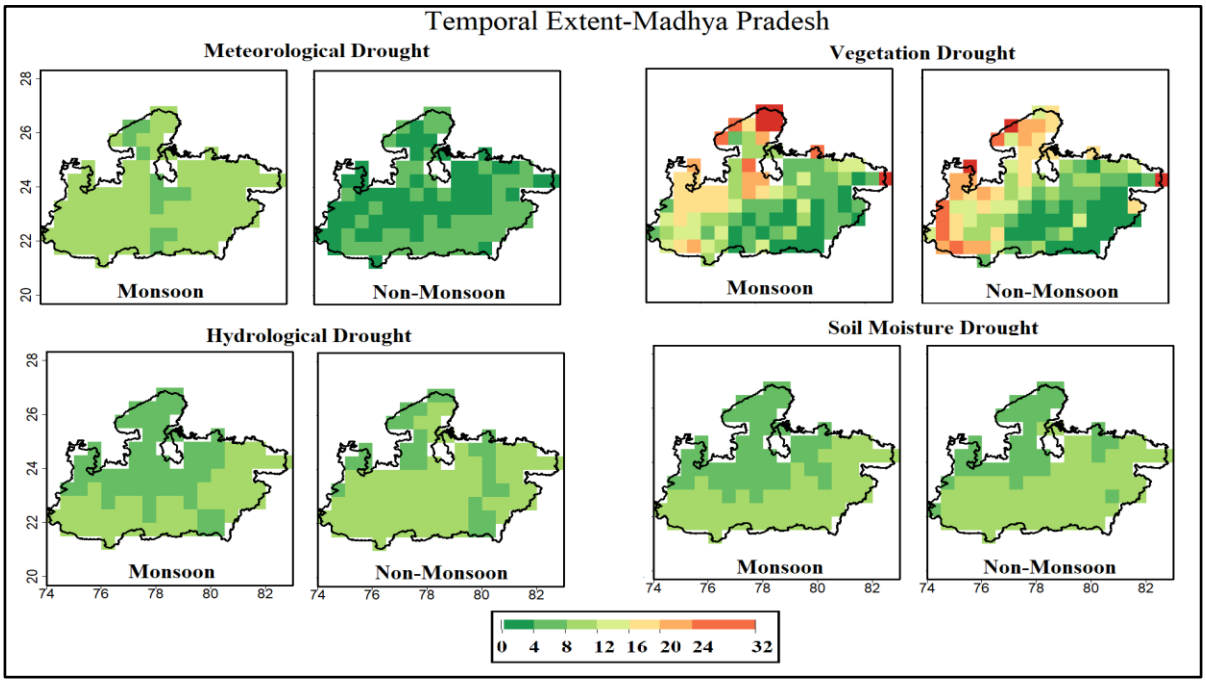



**Figure 2** Temporal Extent of droughts (1982-2013)

### *3.3. Drought trend in terms of mean duration, frequency and mean areal extent.*

Figure 3 presents the drought trend in terms of mean duration, frequency, and mean duration for all four drought types. For comparison, the time period 1982-2013 is further divided into three subparts i.e., 1982-1992, 1993-2003, and 2004-2013. In the topmost part of Figure 3, the mean duration trend is illustrated vegetation drought indicates the increasing trend from 1982-1992 to 2004-2013. However, all other three drought types show a decreasing trend from 1982-1992 to 2004-2013. All these three droughts exhibit a reduction from 1.5 months to 1.17 months for meteorological droughts, 2.4 months to 1.67 months for hydrological droughts, and 3.56 months to 1 month for soil moisture droughts from 1982-1992 to 2004-2013 respectively.

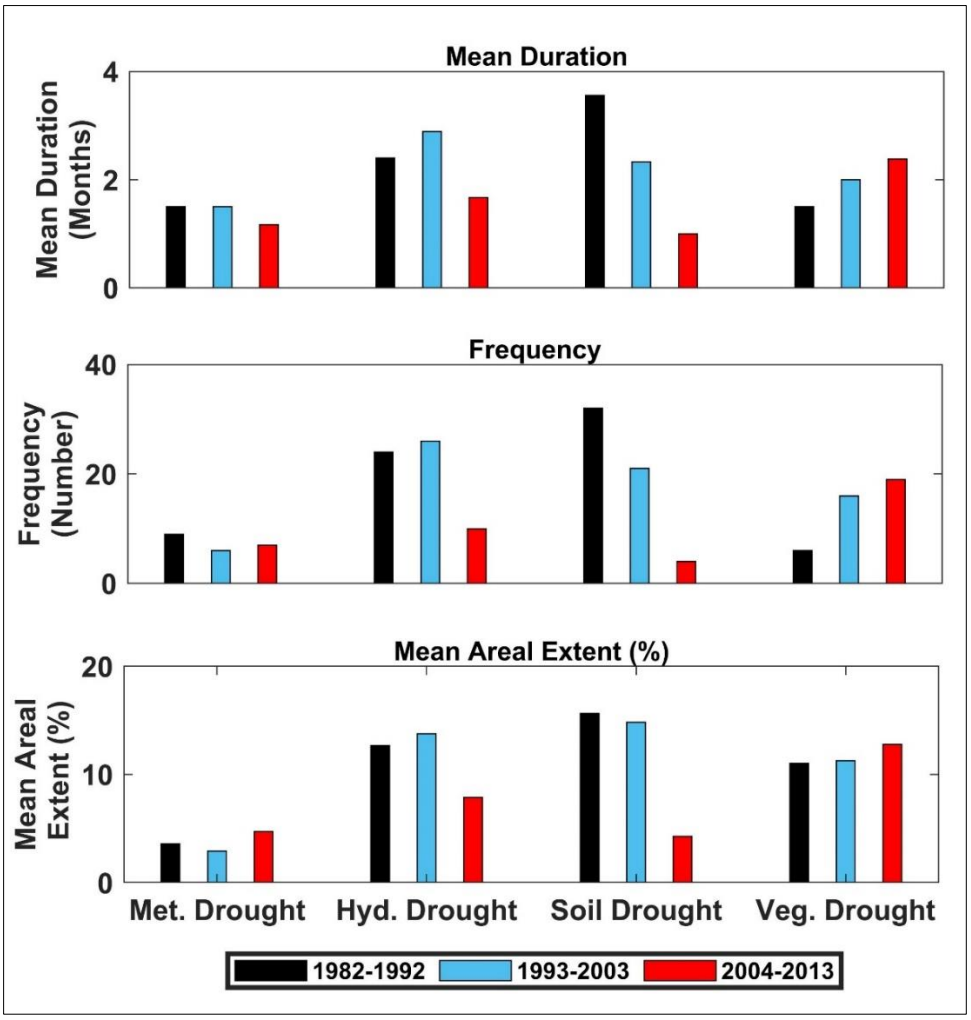



**Figure 3** Drought trends based on drought mean duration, frequency, and areal extent.

Similarly, frequency trend indicates that vegetation drought indicates the increasing trend from 1982-1992 to 2004-2013. However, all other three drought types show a decreasing trend from 1982-1992 to 2004-2013. All these three droughts exhibit a reduction from 9 drought events to 7 drought events for meteorological droughts, 24 drought events to 10 drought events months for hydrological

droughts, and 32 drought events to 4 drought events for soil moisture droughts from 1982-1992 to 2004-2013 respectively. While the frequency of vegetation drought increases from 6 drought events to 19 drought events from 1982-1992 to 2004-2013.

The lowermost part of Figure 3 illustrates the trend in terms of mean areal extent, where vegetation and meteorological drought illustrates an increasing trend from 11% to 12.78% (mean areal extent) and 3.58% to 4.74% respectively. In case of soil moisture and hydrological droughts, a decreasing trend was observed i.e., 15.65% to 4.28% and 12.67% to 7.88% from 1982-1992 to 2004-2013 respectively. From this thorough investigation, it was found that more frequent, prolonged, and larger area of vegetation drought is estimated. Whereas all other three drought types were estimated as drought with lower frequency, less duration, and smaller areal extent.

### *3.4. Concurrent droughts*

As discussed in materials and methods section that concurrent drought can be computed by considering two or more than two drought indices values together for the same month. Table 3 indicates that regional droughts over Madhya Pradesh for each month during 1982-2013. From the investigation, 40concurrent droughts were observed during 1982-2013 over Madhya Pradesh. Further examination suggests that nearly 90% of concurrent droughts consists of hydrological droughts. Additionally, it is interesting to know that more than 82% of concurrent droughts were two-drought based conjunctions. These results indicate frequent hydrological drought as well as suggest the remarkable role of runoff over rainfall in Madhya Pradesh.

**Table 3** Concurrent droughts estimated using domain-averaged drought indices for every month in 1982-2013. The symbol of "+" represents the concurrent situation. Years, when at least three types of droughts occurred, are marked in bold.

| **Concurrent Droughts** | | | | | | | | | | | | |
|---|---|---|---|---|---|---|---|---|---|---|---|---|
| **Year** | **Jan** | **Feb** | **March** | **April** | **May** | **June** | **July** | **August** | **Sept** | **Oct** | **Nov** | **Dec** |
| 1983 | | | H+S | H+S | | | | | | | | |
| **1984** | | | | H+S | | | M+H | H+S | | | | |
| 1985 | | | | | | | | H+S | | | | |
| **1986** | | | | | | | | H+S | M+H+S | | | |
| **1987** | | | | | | M+V | M+S | H+S | | | | |
| 1989 | H+S | | | | | | | | | | | |
| 1990 | | | H+S | | | | | | | | | |
| **1991** | | H+S | H+S | H+S+V | | | | | M+H+S | | | |
| **1992** | H+S | H+S | | | | M+H+V | | | | | | |
| **1996** | | | | | H+S | M+V | | | | | | |
| 1997 | | | | | H+S | H+S | H+S | | | | | |
| **1998** | | | | H+S | H+S+V | H+S+V | | | | | | |
| 1999 | | | H+S | | | | | | | | | |
| **2000** | | | | | | | | M+H | M+H+S | H+S | | |

| | | | | | | | | | | | | |
|---|---|---|---|---|---|---|---|---|---|---|---|---|
| **2001** | M+H | | | | | H+V | | M+S | | | | |
| 2002 | | | | | | H+V | | | | | | |
| **2003** | | | | H+S+V | | | | | | | | |
| 2006 | M+H | | | | | | | | | | | |
| 2009 | H+S | | | | | | | | | | | |
| 2012 | | H+S | | | | | | | | | | |

**Note:** M, H, S, and V indicate meteorological, hydrological, soil moisture, and vegetation drought respectively.

### *3.5. Blockchain technology-based disaster risk management framework*

This study proposed a disaster risk management framework based on decentralized blockchain technology. This framework will provide safer and faster disaster response system and help in providing money, aid and fund to the needy people. This framework also reduces corruption during disaster management (Figure 4). The blockchain technology enables trustworthy information exchange and decision making between help requestors, help providers, and sources of information. The proposed framework is complete decentralized without any controlling authority.

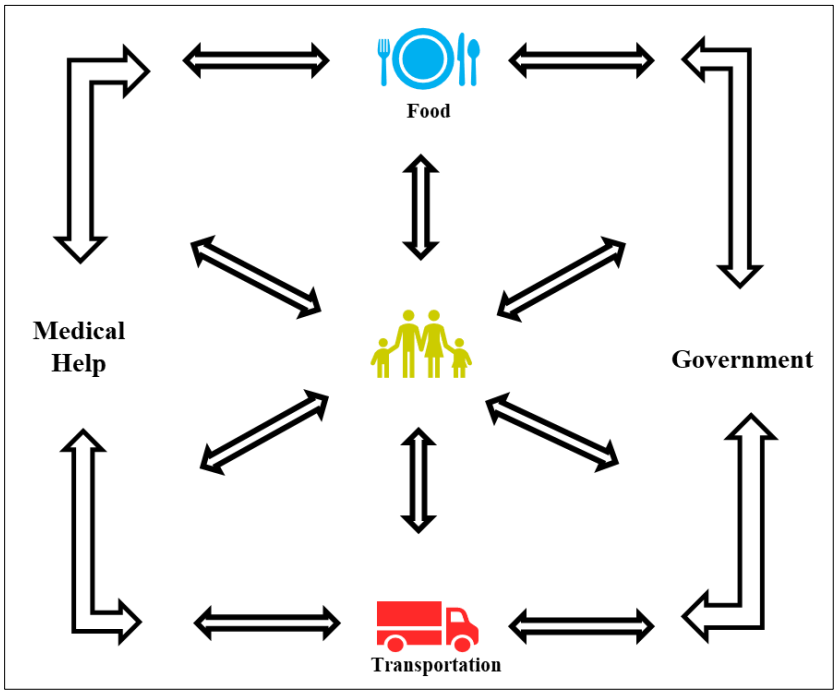



**Figure 4** Proposed blockchain-based disaster risk management framework.

## 4. Conclusions

In this study, we estimate the meteorological, hydrological, soil moisture, and vegetation droughts over Madhya Pradesh using the standardized precipitation index (SPI), standardized runoff index (SRI), standardized soil moisture index (SSI) and vegetation drought index (VCI) during the period 1982-2013 respectively. The study investigates the spatio-temporal distribution of droughts, individually and concurrently. Further, drought trend analysis is carried out in terms of their extent, duration, and frequency. Examinations indicate that soil moisture and hydrological droughts are more

extreme related to other drought types over Madhya Pradesh. Moreover, 90% of concurrent droughts include soil moisture drought as a major part. The proposed blockchain-based disaster management provides safer and effective system and provide help and funds to the needy people as fast as possible without any corruption in transparent environment. This study facilitates a comprehensive approach to better understand the dynamic characteristics of all major droughts and their complex interaction from various perspectives over Madhya Pradesh, and thus provides useful insights for policy makers to develop effective strategies for drought mitigation and sustainable ecosystem management in the state.

## References


Dracup, J. A., Lee, K. S., Paulson, E. G., & Jr. (1980). On the definition of droughts. *Water Resources Research*, *16(2)*.

Heim, R. R. (2000). Drought indices: a review. *A Global Assessment, Routledge Hazards and Disasters Series (UK)*, *1*, 159–167.

Hisdal, H., & Tallaksen, L. M. (2000). Assessment of the Regional Impact of Droughts in Europe. *Assessment of the Regional Impact of Droughts in Eurrope*, *6*, 41.

Jha, S., Das, J., Sharma, A., Hazra, B., & Goyal, M. K. (2019). Probabilistic evaluation of vegetation drought likelihood and its implications to resilience across India. *Global and Planetary Change*, *176*, 23–35. https://doi.org/10.1016/j.gloplacha.2019.01.014

Keyantash, J., & Dracup, J. A. (2002). The quantification of drought: An evaluation of drought indices. *Bulletin of the American Meteorological Society*, *83*(8), 1167–1180. https://doi.org/10.1175/1520-0477(2002)083<1191:TQODAE>2.3.CO;2

Kogan, F. N. (1995). Application of vegetation index and brightness temperature for drought detection. *Advances in Space Research*, *15*(11), 91–100. https://doi.org/10.1016/0273-1177(95)00079-T

Kogan, Felix N. (1997). Global Drought Watch from Space. *Bulletin of the American Meteorological Society*, *78*(4), 621–636. https://doi.org/10.1175/1520-0477(1997)078<0621:GDWFS>2.0.CO;2

Mallya, G., Mishra, V., Niyogi, D., Tripathi, S., & Govindaraju, R. S. (2015). Trends and variability of droughts over the Indian monsoon region. *Weather and Climate Extremes*, *12*, 43–68. https://doi.org/10.1016/j.wace.2016.01.002

McKee, T. B., Doesken, N. J., & Kleist, J. (1993). The relationship of drought frequency and duration to time scales. *Proceedings of the 8th Conference on Applied Climatology,Vol. 17. American Meteorological Society, Boston, MA, USA*, 179–184.

Mishra, A., & Singh, V. (2010). A Review of Drought Concepts. *Journal of Hydrology*, *391*, 202–216. https://doi.org/10.1016/j.jhydrol.2010.07.012

Nagarajan, R. (2003). Drought: Assessment, Monitoring, Management and Resources Conservation. *Capital Publishing Company, New Delhi*.

Ojha, R., Nagesh Kumar, D., Sharma, A., & Mehrotra, R. (2013). Assessing severe drought and wet events over india in a future climate using a nested bias-correction approach. *Journal of Hydrologic Engineering*, *18*(7), 760–772. https://doi.org/10.1061/(ASCE)HE.1943-5584.0000585

S., N. (2008). New drought indices. In L.-F. A. (Ed.), *Drought management: scientific and technological innovations* (Vol. 80, pp. 267–274). Zaragoza : CIHEAM. http://om.ciheam.org/om/pdf/a80/00800451.pdf

Svoboda, M., LeComte, D., Hayes, M., Heim, R., Gleason, K., Angel, J., Rippey, B., Tinker, R., Palecki, M., Stooksbury, D., Miskus, D., & Stephens, S. (2002). The drought monitor. *Bulletin of the American Meteorological Society*, *83*(8), 1181–1190. https://doi.org/10.1175/1520-0477(2002)083<1181:TDM>2.3.CO;2

Wilhite, D. A. (2000). Chapter1 Drought as a Natural Hazard. *Drought: A Global Assessment*, 147–162.

Wilhite, D. A. (2005). *The Role of Disaster Preparedness in National Planning with Specific Reference to Droughts* (Springer,).

World_Bank. (2003). India Financing Rapid Onset Natural Disaster Losses in India : *Report No. 26 844-IN*, *26844*, 126.

Zargar, A., Sadiq, R., Naser, B., & Khan, F. I. (2011). A review of drought indices. *Environmental Reviews*, *19*(1), 333–349. https://doi.org/10.1139/a11-013

# Theme XII

# Hydraulic Structures and Hydropower Engineering

*IN PROCEEDINGS OF 25th HYDRO 2020, INTERNATIONAL CONFERENCE,*
*NATIONAL INSTITUTE OF TECHNOLOGY ROURKELA, ODISHA, INDIA*
*26-28, March 2021, ISBN 978-93-90631-56-8*

Paper ID - 005

# FLOW PATTERN AROUND MULTIPLE VANE ARRANGEMENT

Karan Solanki[a], *Postgraduate Student*

Himanshu Sharma[a*], *Assistant Professor*

[a]*Department of Civil Engineering, Institute of Infrastructure Technology Research and Management, Ahmedabad, Gujarat, India-380026.*

*E-mail:* himfce@gmail.com ([*] Corresponding author)

## ABSTRACT

Submerged vanes are the foils placed skewed to the flow direction and are utilized to manage the sediment by altering the shear stress on the bed by generating the secondary currents on account of pressure difference between the two sides of vane. The range of angle of attack at which submerged vanes can be placed in the flow with respect to flow direction varies in between 10° to 40°. Since, there are few studies which consider non-rectangular submerged vanes but mostly with single tapered vane. Thus, present study studies the optimization of tapered vanes arranged as a vane pair and multiple vanes per rows. Numerical modelling of present study was done in ANSYS-CFX software using K-ω turbulence closure model to simulate the vortical flow. In present study it was observed that due to high vortical interaction for $\delta_n$ = H &2H, the vane are not able to work independently with one vane vortex suppressing another one's while for $\delta_n$ = 4H, the vanes induced the vortices individually and made a more efficient system.

## 1. INTRODUCTION

Fluvial system carries a large suspension of fine sediments along with the flow. These suspended sediments are responsible for the turbidity which in turn prohibit the entrance of light in the river. Restriction of the light entrance then affects the aquatic food-chain (Van Nieuwenhuyse and LaPerriere, 1986; Davies-Colley et al., 1992). The presence of suspended sediments results in smothering of the channel bed and changes the river morphology, which may have deleterious effects on aquatic fauna and flora (Nuttall, 1972; Wright and Berrie, 1987; Doeg and Koehn, 1994). Hence, it is important to alter the bed condition in such a way that the erosion may be restricted so that they may be barred to come in the core flow region as suspended sediments.

Submerged vanes are the foils placed skewed to the flow direction and are utilized to manage the sediment by altering the shear stress on the bed by generating the secondary currents on account of pressure difference between the two sides of vane (Odgaard and Spoljaric, 1986; Odgaard and Mosconi, 1987; Odgaard and Wang, 1991 a & b; Wang and Odgaard, 1993). The range of angle of attack at which submerged vanes can be placed in the flow with respect to flow direction varies in between 10° to 40° (Odgaard & Kennedy, 1983; Odgaard and Wang, 1991 a; Wang and Odgaard, 1993; Marelius and Sinha, 1998; Tan et al., 2005; etc.).

Submerged vanes outperforms the traditional methods of sediment management such as dikes, groins, etc. Traditional sediment management structures when placed normally to the flow redistribute eroded sediment flowing in the flow by utilizing the drag force and are less efficient in managing the sediment (Odgaard and Wang, 1991 a & b). While, submerged vanes minimize the skin drag acting over it and alter the flow structure by generating secondary currents (Wang and Odgaard, 1993). Several analytical and experimental studies have been reported in which the submerged vanes have been used to mitigate the problems related to sediment transport like river bank/bed erosion, intake shoaling etc. by efficiently inducing the secondary currents (Odgaard and Wang, 1991a; Wang and Odgaard, 1993; Marelius and Sinha, 1998; Neary et al., 1999; Tan et al,. 2005; and Ouyang et al., 2008). It has been observed that all the studies enlisted above consider the rectangular vane. However, there are few studies which consider

non-rectangular submerged vanes (Gupta et al. 2006, Gupta et al. 2007, Ouyang 2009, Ouyang and Lin 2016) as shown in Fig. 1.

## 2. METHODOLOGY

### 2.1. Model setup

In the beginning, to prepare the model of a submerged vane, a volume is created of the dimensions, 10 m long, 0.910 m wide and 0.152 m deep, which will acts as a channel section in which vane will be put. At 2m from the inlet of the prepared channel volume, a cuboidal volume is made having the dimensions as of 0.152 m long, 0.001 m thick and where the height of this volume was kept as 0.076 m. The smaller cuboidal volume, was thus, trimmed for different sweep angles which ranged from $10^o$ while the angle of attack of this volume was kept as $17^o$. After making the vane volume, the vane volume was duplicated and lateral spacing between the duplicated and original volume was varied from y = H to 4H (Here, H = height of vane). After developing a row, the row was copied and distance at which the copied row will be placed was varied from 3H to 8H. A total of 4 vane rows were placed.

After finishing the geometry, process of blocking was initialized. Blocking is the process to create a block or partition around the area of interest to capture the flow features in this volume at microscopic level. Therefore, a block or a partition like structure was prepared around the tapered vane and was made to coincide with the vane geometry. While developing the block around the vane, the edges of vane were split by using 'Split edges' option as shown in Fig. 4. After splitting the edges, development of the extra vertices over the surface was observed. Since the developed extra vertices are at presently unassociated, hence extra points were made over the surfaces where these vertices are to be connected over the points and hence completing the formation of blocking around the tapered vane. After having done with blocking, the block formed in the tapered vane was assigned to be 'SOLID' so that block becomes impermeable to the flow occurring in the flow domain.

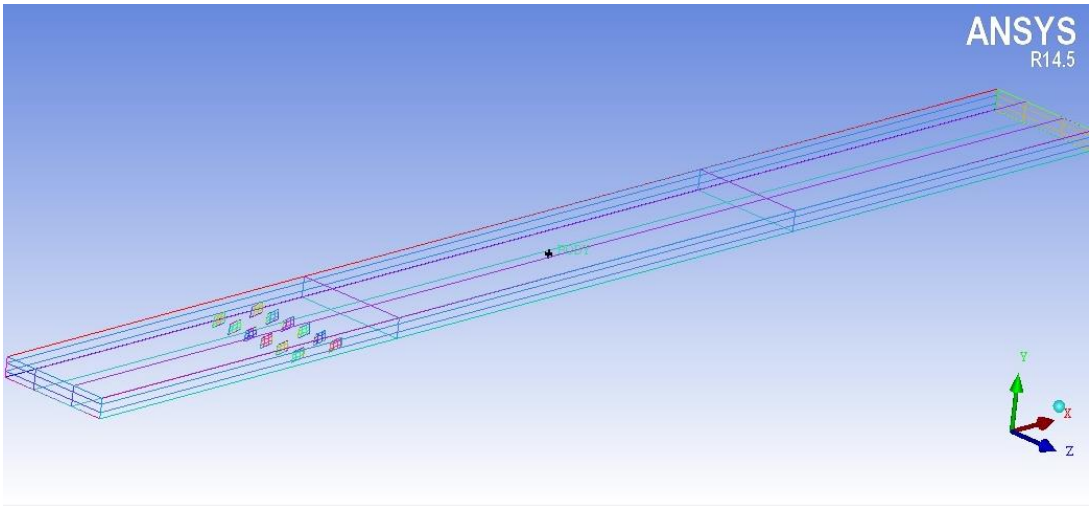



**Fig. 2** Model of submerged vanes generated by ICEM-CFD.

The global mesh size assigned was 10 mm and in the block area this mesh size logarithmically reduces to finer mesh in order to capture fine flow features. Mesh workability was also calculated through mesh quality parameter. In present study, it was observed to be within the range of 0.875 to 0.963 and according to Ansys CFX (2011) for a mesh to be workable, minimum value of mesh quality should be 0.3. After completion of all of the discussed, geometry is saved. Fig. 5, shows the meshed geometry of channel sections along with vanes. After saving the geometry, mesh file of geometry is imported to ANSYS CFX. After completion of geometry import, various surfaces of geometry were assigned the boundary in accordance with the role which they will serve, as shown in table 1.

**Table 1** Boundary conditions assigned to the model surfaces

| S. No. | Boundary conditions | Specifications | Remarks |
|---|---|---|---|
| 1 | Inlet | 0.24 m/s, inlet velocity | Assumed that there is no lateral and perpendicular component to the longitudinal velocity |
| 2 | Outlet | 0.24 m/s, inlet velocity | Assumed that there is no streamwise diffusion of velocity |
| 3 | Solid Boundaries | Wall boundary conditions | Represents that the flow cannot pass through these surfaces |
| 4 | Water Surface | Symmetry boundary condition | Modelled by assuming it to be a rigid lid which has no possibility of across flow |

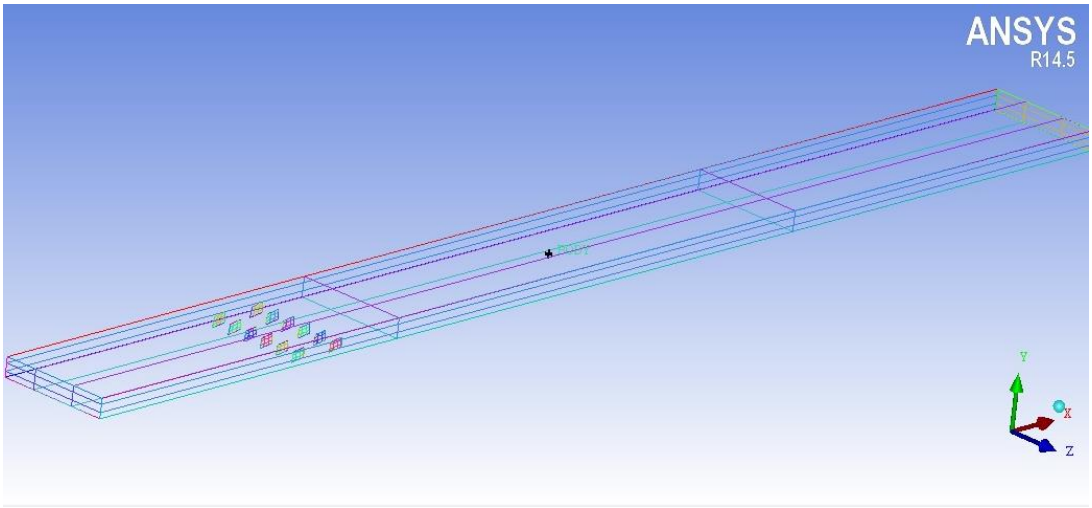



**Fig. 3** Blocking of submerged vanes.

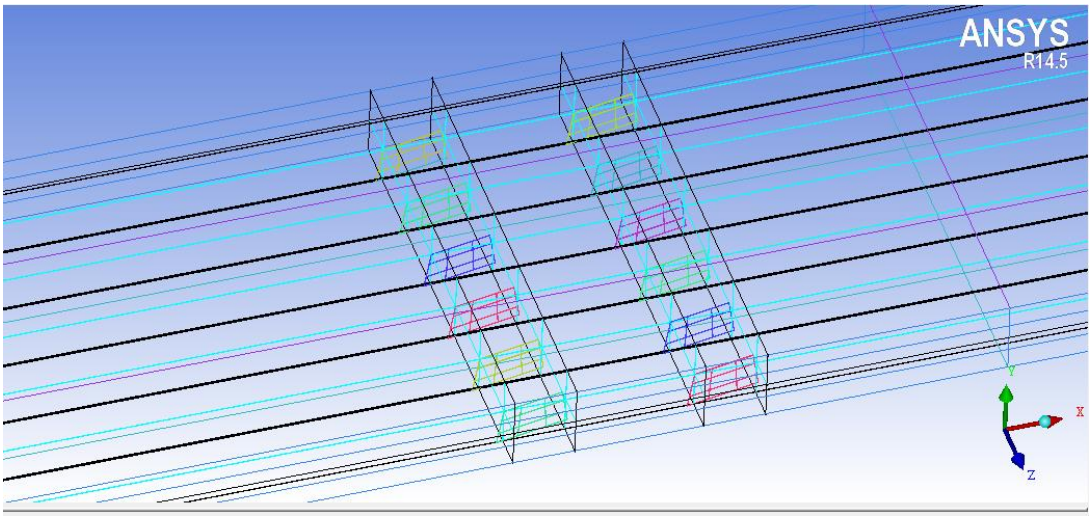



**Fig. 4.** Meshing of submerged vanes generated by ICEM-CFD.

The Table 2 provides the parameters used in simulating the various models of tapered vanes.

**Table 2** Summary of different model parameters used in the present study.

| S. No. | Models parameters | Range |
|---|---|---|
| 1 | Length of the channel | 10 m |
| 2 | Width of the channel | 0.910 m |
| 3 | Depth of flow | 0.152 m |
| 4 | Slope of the channel | 0.000174 |
| 5 | Upstream distance of first vane from inlet | 2 m |
| 6 | Height of Vane | 0.076 m |
| 7 | Length of Vane | 0.152 m |
| 8 | Thickness of Vane | 0.001 m |
| 9 | Angle of attack of vane | 17° |
| 10 | Tapered angle of vane | 10° (from vertical axis) |
| 11 | Lateral spacing between two vanes in a row | 0.076, 0.152 and 0.304 m |
| 12 | Longitudinal spacing between vane rows | 3H, 5H and 8H |
| 13 | Number of vanes per row | 2-6 |
| 14 | Velocity of fluid | 0.240 m/s |
| 15 | Froude number | 0.1967 |
| 16 | Turbulence modeling use | k-ω model |
| 17 | Average mesh qualities of models | Minimum 0.902 from 1 |

## 3. VALIDATION OF CFD MODEL

In the present study, model of channel flume was developed and meshed in the ICEM-CFD platform and simulation was done with the help of ANSYS-CFX for an experimental study conducted by Wang and Odgaard (1993). In order to check the efficacy of the developed model, the transverse velocity computed by model is compared with transverse velocities obtained experimentally in the study conducted by Wang and Odgaard (1993). It can be seen from Fig. 5 that modelled transverse velocities matched well with the experimental transverse velocities of Wang and Odgaard (1993). Therefore, it may be concluded that present model can be utilized to model the flow features in case of multiple tapered vanes.

Sensitivity analysis of the model was conducted to examine the effect of mesh size on the value of the transverse velocity calculated at transect. Three mesh sizes, 8 mm, 10 mm and 12 mm were utilized to mesh the domain and value of transverse velocity profile was calculated for three longitudinal distances, x = 2H, 8H and 20H at mid-width of channel. Fig. 6 shows the measured profile for all three mesh sizes at all aforesaid longitudinal distances.

It can be seen that transverse velocity profiles superimpose satisfactorily over each other for all mesh sizes. It suggests that present result for the given model is independent of mesh size and hence, either of the mesh size can be used to compute the results for present study.

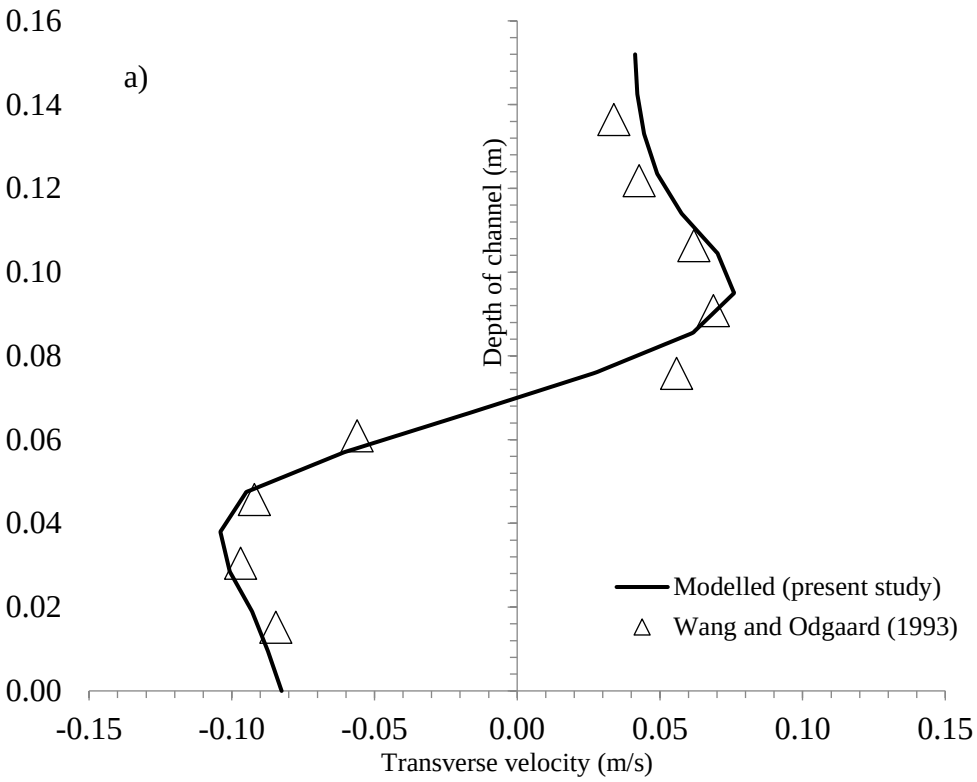
## 4. FLOW PATTERN AND PARAMETER OPTIMIZATION OF VANE PAIR

*a) Lateral spacing between two vanes*

Wang and Odgaard (1993) observed that described that when vane are put in proximity, vane generated secondary currents will interact with each other to reduce vane circulation value. They observed that as the distance between the vanes was increased, each vane tend to generate circulations, individually, thus, reducing their effectiveness. Thus, they provided 2 to 3 times vane height as optimum range of lateral spacing which will generate the maximum strength of secondary currents. Study conducted by Ouyang et al. (2008) confirmed the findings of Wang and Odgaard (1993) and put forth that lateral spacing must range in between 2 to 3 times vane height for generation of the secondary currents of maximum strength. Sharma et al. (2016) observed that for lateral spacing of 2.5 times height of vane, vanes generated secondary currents of maximum strength. In present study, vane were designed in

accordance with the recommendations provided by Solanki et al. (2020). A single row of two vanes was developed in the flow domain and three lateral spacing was kept in between the vanes, which are H, 2H and 4H. In Fig. 7, one can see the contours as well as vector plot along a plane for three different vane spacings *viz.* $\delta_n$ = H, 2H and 4H. It can be seen that for $\delta_n$ = H, in Fig. 7 a), the circulations generated by two vanes, started to merge with each other to make a single circulation, post separation and during mutual merger, circulation formed a single circulation of lower vorticity, which was in accordance with the Wang and Odgaard (1993). It was observed that the vortex formed by vortex then got consumed by the viscosity of fluid.

In Fig. 7 b), it was observed that for $\delta_n$ = 2H, the vanes generated individual vortices and these vortices were observed to exist in the flow by x = 20H, too. From the observation it can be inferred that for $\delta_n$ = 2H, vanes have able to generate the circulations to the further downstream than $\delta_n$ = H and the circulations were able to interact with each other and merge with each other after a distance of x = 20H. For lateral spacing of $\delta_n$ = 4H in Fig. 7 c), it was observed that vortices were now fully separated and efficacy of the vane rows were decreased as the viscosity now can counter the vortices individually and can suffice them.



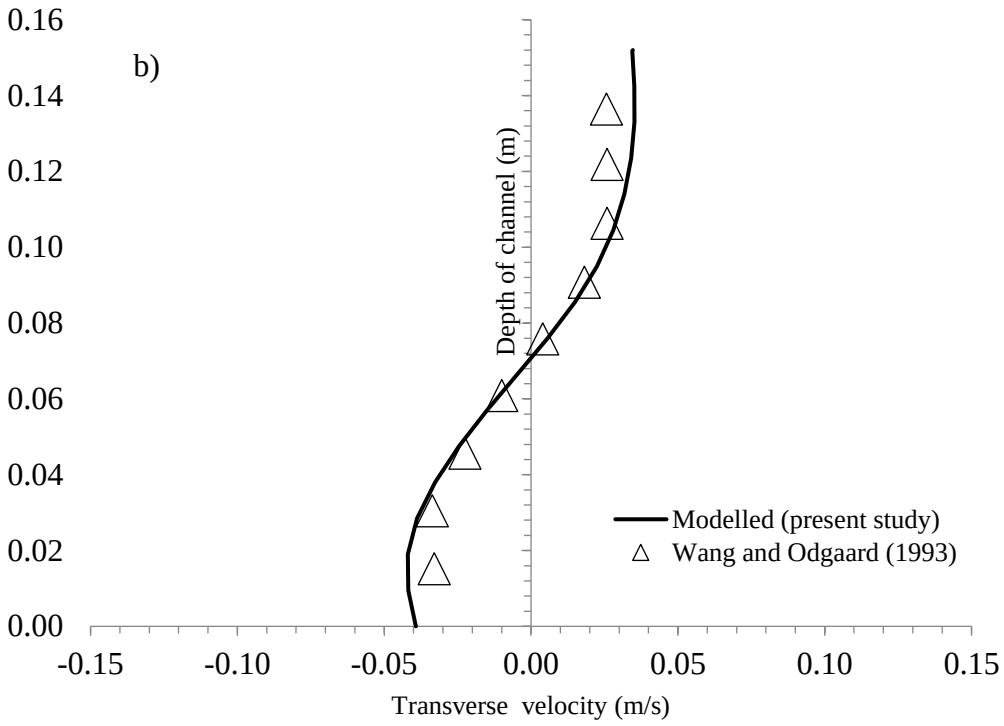
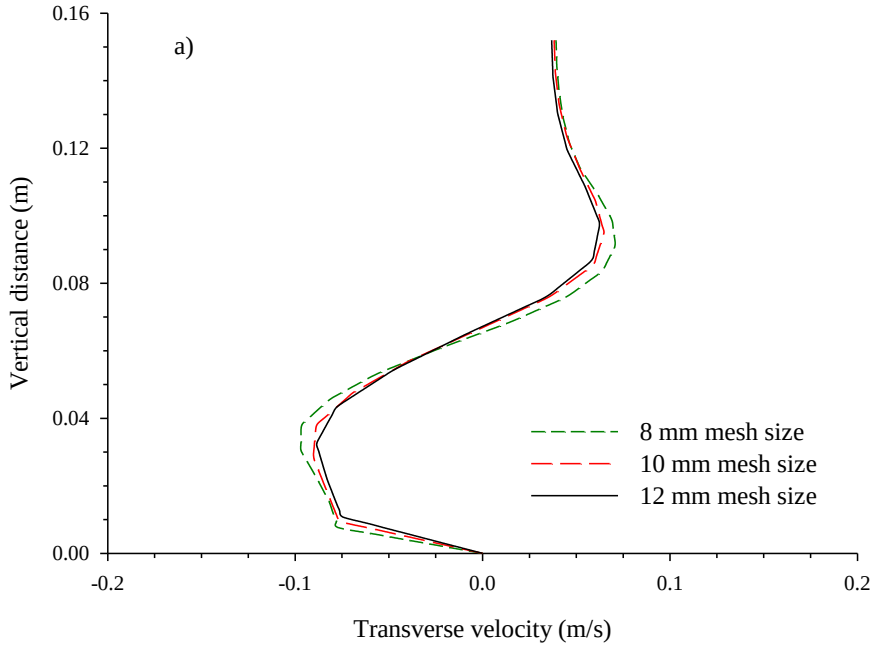



**Fig. 5** Validation of model for a) x = 2H; b) x = 20H (Here, H = height of vane).



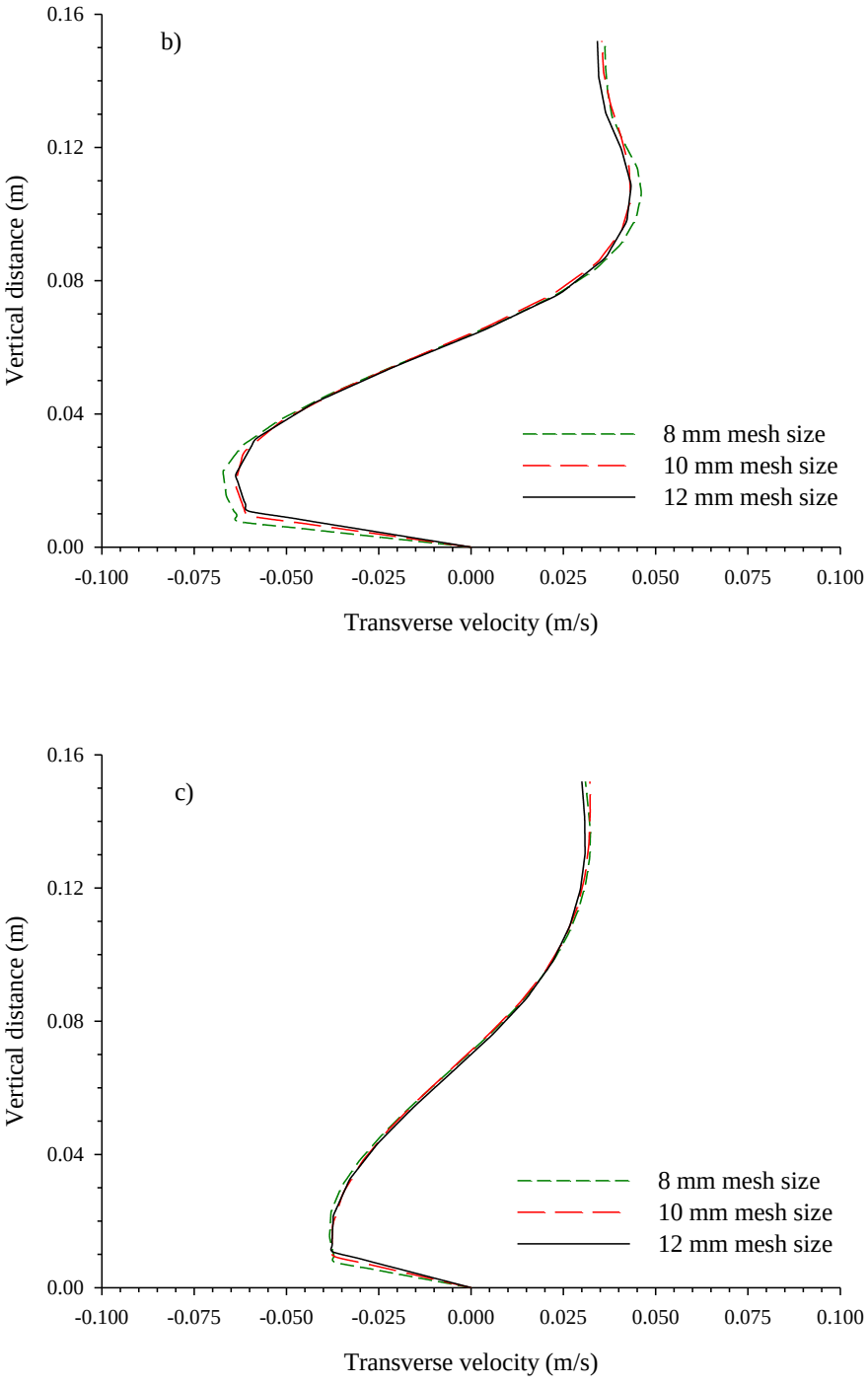



**Fig. 6** Sensitivity analysis of model for a) x = 2H; b) x = 8H; c) x = 20H.

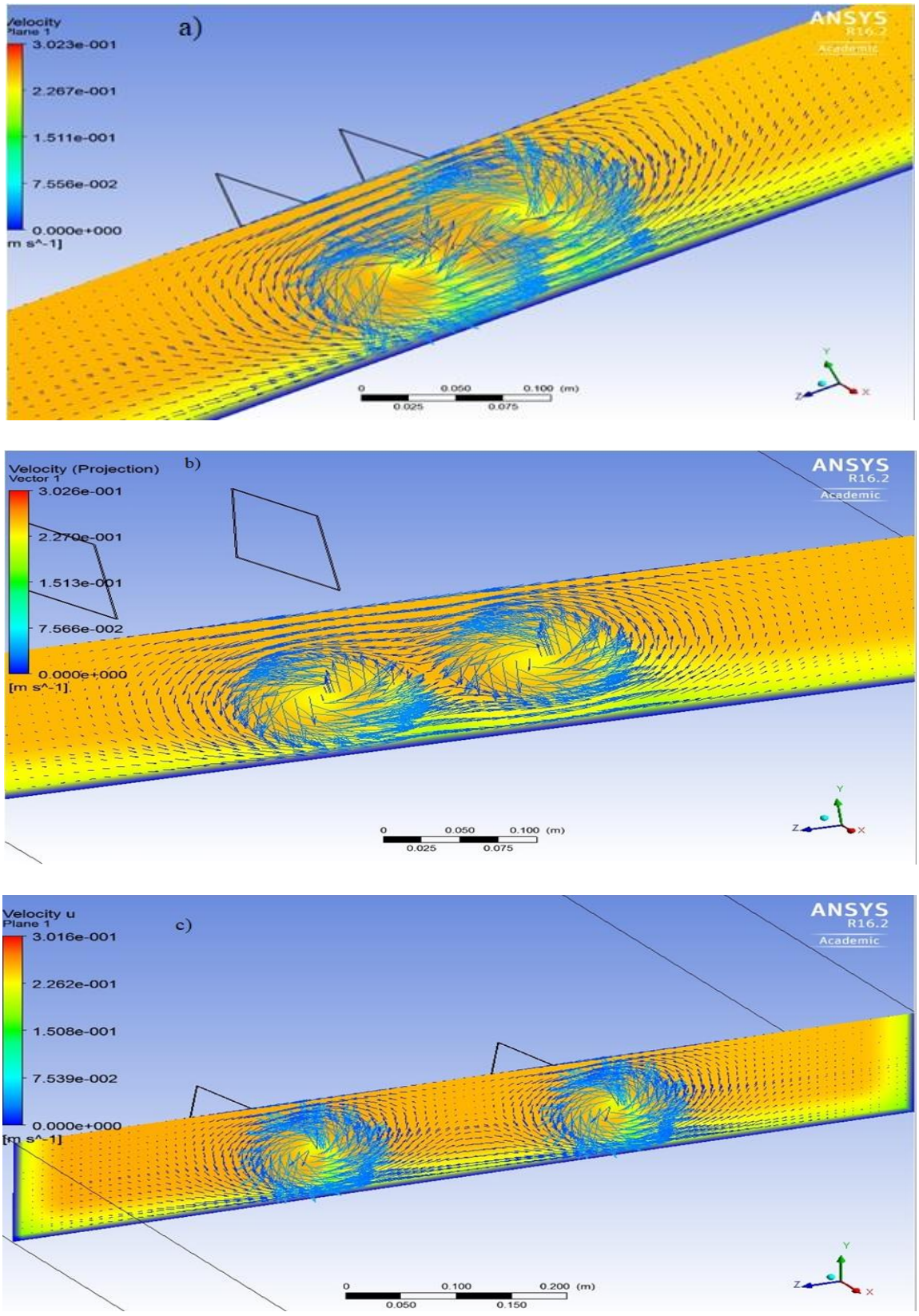



**Fig. 7** Flow pattern at downstream of tapered vane at x = 2H for a) $\delta_n$ = H; b) $\delta_n$ = 2H and c) $\delta_n$ = 4H (Here, $\delta_n$ = lateral spacing between the vanes).

## 5. CONCLUSIONS

Thus, from the present study, following conclusions can be drawn:

a) For lateral spacing of 4H the vane were involved equally to generate the secondary currents in the flow for lateral spacing of H and 2H, it was observed that the vortices start coalescing with each other to form a single vortex.
b) It was observed that for lateral spacing = H, the two individual vortices were generated at x = 2H and were merged by the transect x = 8H and that single vortex travelled further downstream. For lateral distance = 2H, similar to lateral spacing = H, initially two individual vortices were formed and at x = 8H, again two vortices coexisted in the flow with one vortex having more vorticity than another due to interaction of vanes. At x = 20H, the vortices were merged for the lateral spacing = 2H. For lateral spacing = 4H, vane formed the individual vortices and they coexisted even after the x = 20H.
c) When rectangular and tapered vane pair were compared, it was observed that tapered vane interacted more with each other as compared to rectangular vane due to higher down-wash generated by tapered vane which also signify the generation of higher vorticity.
d) It was observed that vorticity induced in flow were independent of the longitudinal distance between vane rows.

## 7. REFERENCES

Ansys CFX (2011). *Ansys ICEM CFD User's Manual.* Ansys Inc., USA.

Davies-Colley, R.J., Hickey, C.W., Quinn, J.M., & Ryan, P.A. (1992). Effects of clay discharges on streams: 1. Optical properties and epilithon. *Hydrobiologia, 248*, 215–234.

Doeg, T.J., & Koehn, J.D. (1994). Effects of draining and desilting a small weir on downstream fish and macroinvertebrates. *Regulated Rivers: Research and Management, 9*, 263–278.

Gupta, U.P., Sharma, N., & Ojha, C.S.P. (2006). Vorticity with different shapes of submerged vanes, *ISH Journal of Hydraulic Engineering, 12(1)*, 13-26.

Gupta, U.P., Sharma, N., & Ojha, C.S.P. (2007). Performance evaluation of tapered vane, *Journal of Hydraulic Research, 45(4)*, 472-477.

Marelius, F., & Sinha, S.K. (1998). Experimental analysis of flow past submerged vanes, *Journal of Hydraulic Engineering, 124(5)*, 542-545.

Neary, V.S., Sotiropoulos, F., & Odgaard, A.J. (1999). Three-dimensional numerical model of lateral-intake inflows, *Journal of Hydraulic Engineering, 125(2)*, 126-140.

Nezu, I., and Nakagawa, N. (1993). *Turbulence in open channel flows.* AA Balkema, Delft, The Netherlands.

Nuttall, P.M. (1972). The effects of sand deposition upon the macroinvertebrate fauna of the River Camel, Cornwall. *Freshwater Biology, 2*, 181–186.

Odgaard, A.J., & Kennedy, J.F. (1983). River bend bank protection by submerged vanes, *Journal of Hydraulic Engineering, 109(8)*, 1161-1173.

Odgaard, A.J., & Spoljaric, A. (1986). Sediment control by submerged vanes, *Journal of Hydraulic Engineering, 112(12)*, 1164-1181.

Odgaard, A.J., & Mosconi, C.E. (1987). Streambank protection by submerged vanes, *Journal of Hydraulic Engineering, 113(4),* 520-536.

Odgaard, A.J., & Wang, Y. (1991a). Sediment management with submerged vanes. Theory: I, *Journal of Hydraulic Engineering, 117(3),* 267-283.

Odgaard, A.J., & Wang, Y. (1991b). Sediment management with submerged vanes. Applications: II, *Journal of Hydraulic Engineering, 117(3),* 284-302.

Ouyang, H.T. (2009). Investigation on the dimensions and shape of a submerged vane for sediment management in alluvial channels, *Journal of Hydraulic Engineering*, *135*(3), 209-217.

Ouyang, H.T., Lai, J.S., Yu, H., & Lu, C.H. (2008). Interaction between submerged vanes for sediment management, *Journal of Hydraulic Research*, *46*(5), 620-627.

Ouyang, H.T., & Lin, C.P. (2016). Characteristics of interactions among a row of submerged vanes in various shapes, *Journal of Hydro-environment Research, 13,* 14-25.

Sharma, H., Jain, B., & Ahmad, Z. (2016). Optimization of submerged vane parameters, *Sadhana, 41(3),* 327-336.

Solanki, K., Sharma, H., & Joshi, N. (2020) Flow and parameter optimization of tapered vane, *Journal of Ecohydraulics*, Taylor and Francis (Accepted).

Tan, S.K., Guoliang, Y., Lim, S.Y., & Ong, M.C. (2005). Flow structure and sediment motion around submerged vanes in open channel, *Journal of Waterway, Port, Coastal and Ocean Engineering, 131(3),* 132-136.

Tennekes, H., and Lumley, J.L. (1972). *A first course in turbulence*. MIT Press, USA.

Van Nieuwenhuyse, E.E., & LaPerriere, J.D. (1986). Effects of placer gold mining on primary production in subarctic streams of Alaska. *Water Resources Bulletin*, *22*, 91–99.

Versteeg H.K., and Malalasekera W. (1995). *An introduction to computational fluid dynamics: The finite volume method.* Longman, New Delhi, India.

Wang, Y., & Odgaard, A.J. (1993). Flow control with vorticity. *Journal of Hydraulic Research, 31(4),* 549-562.

Wilcox, D.C. (1988). Reassessment of scale determining equation for turbulence models. *AIAA Journal, 26(11),* 1299-1310.

Wright, J.F., & Berrie, A.D. (1987). Ecological effects of groundwater pumping and a natural drought on the upper reaches of a chalk stream. *Regulated Rivers: Research and Management, 1,* 145–160.

IN PROCEEDINGS OF 25th HYDRO 2020, INTERNATIONAL CONFERENCE,
NATIONAL INSTITUTE OF TECHNOLOGY ROURKELA, ODISHA, INDIA
26-28, March 2021, ISBN 978-93-90631-56-8

Paper ID - 024

# Study of Energy Dissipator with Different Blocks to Reduce Basin Width and Trajectory: A Review

Shilpi Sippi Bhuinyan[1] Prof. Dr. Anand Kr. Sinha[2]

[1]*Research Scholar, Birla Institute of Technology, Mesra, Ranchi (Jharkhand), INDIA*
[2]*Professor, Birla Institute of Technology, Mesra, Ranchi (Jharkhand), INDIA*
*Email: ssbhuinyan@aissmscoe.com*
*Email: aksinha@bitmesra.ac.in*

## Abstract

One of the most powerful and cost-effective strategies for dissipating hydraulic energy from flood waters is to project the flows into a free trajectory jet shape to a position where the impact produces a downstream river bed dip pool. If takeoff speeds are increasing, ski jumps are standard features of dam spillways for efficient energy dissipation. A significant result of the Froud No. range approach flow, the relative height of the bucket and therefore the angle of the device is found. Using a physical hydraulic model, energy dissipation by a ski-jump can be assessed by evaluating several identified contributing parameters. Important parameters include;1) Geometric water jet trajectory profile such as distance of trajectory, trajectory height, horizontal and transverse impact width;2)Distribution of dynamic impact pressure; 3) average dynamic head of impact; 4) head of impact velocity; and 5) air entrainment. Deflectors are the element that is provided at the outlet to deflect the trajectory into a plunge pool area where sound rock is present so that less erosion occurs.

***Keywords:*** *Energy dissipation, Kinetic turbulence, Ski jump, stilling basin.*

## 1. Introduction

The hydraulic mechanisms are used in natural and built environments to regulate and maintain water flow. Which include structures for flow calculation such as weirs, conveyance structures such as culverts and structures for flood control such as dams. According to Hager & Boes (2014), hydraulic structures can be defined as engineering components, enabling improvement and/or modification of flow characteristics in water engineering, resulting in better desired flow conditions compared to natural flow of water. These structures require flexibility in design as well as high strength due to imposed forces generated by high velocities, large discharges as well as high hydrostatic pressures, so they are mainly made of concrete. In addition to the advances in dam engineering technology, Spillways is equipped with energy dissipation devices (e.g. – Stilling Basin, Chute Blocks, Buckets, Friction Blocks, End Sill) for energy dissipation resulting from the upstream and downstream energy level change of the structure. Energy dissipator must be sufficiently efficient to maintain the highest downstream flux speed.

Dam systems have undergone resurgence during recent years. This revival of interest came about because of numerous factors including advances in hydraulic instrumentation, the worldwide quest for clean renewable energy, and the need for experimental data modelling for computational fluid dynamics (CFD) and the growing demand for water access.

### 1.1 *Introduction of Spillway and Energy Dissipater:*

Spillways, in a dam, are safety devices. Many dam failures have been reported due to inadequate capacity or unsuitable spillway design, particularly for earthen and rock fill type dams that are likely to be destroyed, if overturned, unlike concrete dams that may not fail with slight overtopping for a short time.

Spillways are provided with energy dissipation devices (e.g. – Stilling Basin, Chute Blocks, Buckets, Friction Blocks, End Sill) for the dissipation of energy resulting from the upstream and downstream energy level changes of the structure. Energy dissipator shall be sufficiently efficient to maintain the highest flow speed on the downstream side of the dam.

### *1.1.1 Necessity of Spillway*

Among a dam's most significant structures is the spillway. It offers the opportunity to regulated or uncontrolled release of excess water. It ensures dam protection, and prevents dam overthrow. It is of vital importance that the spillway facilities be built with sufficient capacity to avoid overtopping the dam, particularly if the project selects an earth fill or rock fill type of dam. Spillway is used periodically to release water for water supply, production of hydroelectricity etc.

### *1.1.1 Necessity of Energy Dissipation Devices*

Energy dissipation systems dissipate excess flood kinetic energy by supplying equipment downstream of the dam to dissipate full water flow energy. It helps to obtain consistent downstream flow of water. It minimises the downstream harm from the erosion.

## 2. Literature Review

Energy dissipation devices dissipate excess flood kinetic energy by providing equipment on the downstream of the dam to dissipate maximum water flow energy. It helps in obtaining uniform water flow at downstream flow. It minimises downstream damage from the erosion. The following research work describes the dissipation methodology for the amount of energy in the spillway. The several experiments performed with hydraulic energy dissipator and results showed that the energy dissipation rate of 40 %-70 % was achieved.

Qian et al. (2016) attempted to increase energy dissipation and unit discharge on stepped chute. They introduced a new type of energy dissipator called a ski-jump-step energy dissipator; the new type of energy dissipator consists of two stages; each stage includes a ski-jump, a prestep, an aeration basin, and a stepped chute. Results showed that the unit discharge limit on stepped chute increases to 118 m2 / s and also increases the energy dissipation up to 75.8%.

Pfister et al. (2014) perform experiments on physical models. The results derived herein support the design process of ski jumps. Particularly the jet impact location onto the plunge pool surface may be derived, besides of its air features at this point. The latter support the assessment of the plunge pool stability in terms of scour. The design of ski jump includes additional criteria, as the maximum dynamic bottom pressures and bucket choking.

Jian-hua et al. (2016) gave the theoretical method of estimating the trajectory of ski-jumps, which was taken into account and modified. The present method is based in the sensitivity analysis of parameters on the effects of the take-off speed and the angle. The results showed that the velocity of take-off has a far greater effect on the point of impact than the angle of take-off.

Mujumdar et al.( 2001) tested a 1:100-scale ski jump energy dissipator model to determine the applicability of the design guidelines set out in IS 7365(1985), showing that energy dissipation was found to vary from 26% to 54.4% due to air intake and impact.

Utkarsh Nigam et al. ( 2015) analysed hydrodynamic uplift force on the apron of the stilling basin can be performed on a hydraulic model by measuring hydrodynamic forces using transducers acting on the stilling basin.

Jill Lucas et al. (2013), Performed simple-shaped deflectors allowing jet deflection in the tailwater, characterising the parameters of the trajectory under different conditions of approach flow.

Experimental results based on typical jet deflections for design conditions of the proposed elements are 20–25°. Higher deflections result only for approach flow Froude order numbers below 3, which are nonetheless irrelevant for design, and also cause conditions close to the flow shock. The relative height of the deflector increases the deflection to the jet.

Roman Juon et al. (2000) and Jill Lucas et al. (2013) focused on the use of ski-jump bucket deflector. Tests were conducted to find simple-shaped deflector, bottom pressure distribution, and lower and upper trajectory characteristics. The results showed that deflector geometry affects the shape of the jet and the dissipation of energy.

Azamathula et al. (2009) predicted the depth of the scour around hydraulic structures (trajectory spillways) accurately. The results were based on the experimental studies, and the developed equations are mainly of an empirical nature. In prediction of scouring below a flip bucket spillway, this paper evaluates the performance of the soft computing (intelligence) techniques, the Adaptive Neuron-Fuzzy System and the Genetic expression Programing approach.

## 3. Study Area

The Maithon Dam Project is located on the River Barakar, a tributary to the River Damodar in District Dhanbad of the state of Jharkhand. The River Damodar is a tributary to the River Ganga. Following BIS 11223-1985, the dam has been categorized as a large dam due to its storage and height. The Maithon Dam is located at latitude 23°47′13.06″ north and longitude 86°49′01.44″ east on the River Barakar. The Maithon town is situated just downstream of the dam. The catchment area has been estimated as 6391.74 km². It extends between latitude 23°46′34.12″ north and longitude 85°09′16.26″ east, to latitude 24°32′09.80″ north and longitude 86°53′19.20″ east. The dam has a height of 56.08 m above the lowest river bed level and a total length of 4426.76 m comprising 4064.35 m long earthen embankment and 362.41 m long concrete overflow section. The reservoir has a gross storage capacity of 1,093.54 Mm³ and a live storage capacity of 441.64 Mm³. The project was constructed between 1951 and 1957. The spillway, comprising 12 bays with gates 12.19 m wide and 12.50 m high gates over Ogee profile, was originally designed to pass a maximum discharge 13,592 m³/sec.




**Figure 1** Index Map of Maithon Dam
(Source: Flood Estimation report by Central water Commission, 2017)

### *3.1 Geographical Features*

The Ganga Basin mostly has level plains or slopes which are very gentle in general. But some parts of Uttarakhand, in the Lesser Himalayas and the Shiwalik ranges, has steep slopes. Steep slopes are also found in some parts of Madhya Pradesh. The lower parts of the basin viz., Jharkhand, Chhattisgarh and West Bengal, as also parts of Rajasthan have a gentle slope. Most part of the catchment is relatively flat, having a slope of 3% to 10%. High slopes are present only near the hills bordering the southern edge of the catchment The Ganga basin is home to a wide variety of soils. Alluvial soil, endowed with rich soil nutrients, covers more than 52 percent of the basin. While most parts of the Ganga Basin is covered with soil of fine texture, there are some parts of Uttarakhand and Bihar, which

have soils of very course texture, sometimes rocks. Soils with course texture are also noticed in parts of Haryana and Rajasthan. The major part of the Ganga basin (65.57 %) is under agriculture. Other major land cover types are deciduous forest (16 %), wasteland (8.89 %), built up land (4.28 %), water bodies (3.47 %), snow / glaciers (0.94 %) and grassland (0.85 %). The Ganga Basin supports nearly 600 million people, which includes some of the most densely populated regions of the world. It has 1949 cities and towns, with an estimated population of 125 million.

### *3.2 Salient Features of Maithon Dam*

The Maithon Dam is located at Maithon, 48 km from Dhanbad, in the state of Jharkhand. It is situated about 12.9 km above the confluence of the Barakar River with the Damodar River and has a catchment area of 6388.69 km². Maithon Dam is a composite earth and concrete structure. Its maximum height above the foundation is 56.08 m. Maithon hydropower station, on the left bank of the river, is an underground Power House. The present installed capacity of the generating units is 63.5 MW.

### *3.3 Technical Details of the Dam*

**Table 1** Technical Details of the Maithon Dam
(Source: Flood Estimation report by Central water Commission, 2017)

| SR. No. | Description | Value |
|---|---|---|
| **1.** | Gross storage capacity | 1093.54 Mm³ |
| **2.** | Live Storage capacity | 441.64 Mm³ |
| **3.** | Full reservoir level | 152.40 m |
| **4.** | Maximum Water Level | 150.88 m |
| **5.** | Minimum Draw Down Level | 132.59 m |
| **6.** | Dead Storage Level | 132.59 m |
| **7.** | Dam Top Level | 156.06 |
| **8.** | Lowest foundation level | 99.96 m |
| **9.** | Lowest river bed level | 103.63 m |
| **10.** | Crest level | 140.21 m |
| **11.** | Height above deepest foundation level | 56.08 m |
| **12.** | Length of dam at top | 4426.76 m |
| **13.** | Width of Dam at Top | 6.71m |
| **14.** | Maximum area of water spread | 99.55 Km² |
| **15.** | Spillway Type | Ogee |

| | | |
|---|---|---|
| **16.** | Type of Gates | Radial |
| **17.** | Size | 12.5 m (Ht) × 12.19 m (W) |
| **18.** | No. of Bays | 12 nos. |
| **19.** | Total Spillway Capacity | 13592 m³/s |

## 4. Hydraulic Modelling

Functional models address a lack of understanding of physical processes or dynamic boundary conditions in many problems of fluid mechanics / hydraulics that are not amenable to computational or analytical techniques. Studies of the physical model are invaluable methods for optimising different reservoir components and appurtenant structures. The hydraulic construction of different components of a project in the river valley includes two types of problems viz. Site unique problems and dynamic hydraulic flow dynamics related problems. The site-specific problems are due to place topography, foundation availability, soil and rock strata composition, etc. The problems of complex flow phenomena are many viz. Non-uniform flow in the approach section producing vortices, rapidly changing flow due to complex dynamics, high speed due to high head damage caused by cavitations, high turbulence causing hydrodynamic forces on the river bed structure and downstream banks, flow-induced vibration for wide range of operating conditions. These issues cannot actually be dealt with analytically, and so they must be solved by undertaking studies of these structures' physical models. The art of hydraulic modelling was an important tool in solving complex hydraulic problems for many decades.

A hydraulic model's advantage is its theoretical capacity to mimic many of the characteristics of a complicated flow situation. There are also conditions for which there is no recourse to design or operational decisions involving costly and complex hydraulic works other than hydraulic modelling. Such situations occur especially when complicated flow patterns or intricate transportation processes are involved for a variety of reasons, and accurate answers cannot be obtained through analytical solution or computer simulation.

### *4.1 Data Requirements for Model Studies*

Providing accurate information from the prototype is important for performing model experiments. The whole operation of the model depends on the prototype data being identical. The data would help to develop the model conformity pattern for the prototype and to improve the model's predictability. For the planning, design of spillway models and performing model studies, the following prototype data will generally be appropriate.

1. Maximum design outflow discharge for spillway and energy dissipater.
2. Gauge-discharge (Tail Water Rating) curve at downstream of the spillway up to the maximum outflow discharge.
3. Index plan showing location of dam and course of river for about 1 km upstream and 1 km downstream, water spread, tributaries upstream and downstream of the site, important structures etc.
4. Cross sections of the river at upstream and downstream of the dam axis.
5. A plan showing river course, dam complex, power intake, position of river cross sections and base line
6. Layout plan: Dam layout plan showing the chainages along the dam axis for the important structures such as left and right end of the spillway with reference to a baseline connected to the dam axis and location and orientation of the power intake.

7. Spillway section with details such as upstream and downstream crest profiles giving equations and radii of curves, tangent points, slopes and dimensioned details of energy dissipator. cross sections of the non-overflow section of the dam
8. Details of spillway gates and piers in plan and sections including distance of trunnion axis of radial gate with reference to dam axis/crest axis, gate seat elevation, geometric profile of breast wall and details of stoplog groove.
9. Details of power intake including plan and sections of bellmouth entrance, transition, trash rack piers and rib beams, dimensions of gate grooves.

### *4.2 Operation of Model*

Once the model is ready for experimentation, the model's operating programme should be carefully planned in order to assess the performance of the design proposed. One can divide the operating programme into two phases: The adjustment phase includes preliminary studies to identify model deficiencies and insufficiencies. These trial runs also show the need for partial redesign, overhaul or change of measuring instruments. The experimental phase contains standard model experiments after all the defects found during the adjustment process have been eliminated.

### *4.3 Numerical Modelling of Spillway Flows*

The spillway flows are usually studied using physical models. The drawbacks associated with spillway physical model studies are: construction expense, time delay in manufacturing and constructing model parts and performing experiments, and the difficulty in modifying structural details of various spillway components when carrying out parametric studies. Acquiring the required knowledge and understanding through physical models of the complete hydrodynamics of flow features over spillway requires sophisticated instrumentation to collect data that is costly, bulky and time consuming. The physical models for the simulation of air water flows are correlated with certain scale effects. Due to the complex nature of the flow, numerical modelling has been sparsely used in this area. The rapid growth in computer technology allowed numerical modelling of spillway flows as a viable complementary tool for physical modelling of spillway flows in terms of computer memory and processing speeds. With advanced CFD software, the simulation of flow over the spillway is possible as two phase air-water flows can be modelled.

## 5 Scope of the Work

**a.** Assess the scouring effect of different discharges on the plunge pool area due to impact of the trajectory.
**b.** Modeling the area of the impacted trajectory with scouring results.
**c.** Assess container dynamic pressure and speed distribution on vessel.
**d.** For high dam spills where full energy is required to dissipate bucket deflector.
**e.** Energy dissipation can be measured by air resistance, and total energy dissipation efficiency can be calculated.

## Conclusions

- Deflectors are an alternative to flip buckets with constructional ease yet of similar hydraulic features.
- Deflector angle is an important parameter for proper spray formation and maximum jet contraction.
- In skimming flows, the dissipation of energy in nappe flows is greater than that. The loss of energy resulting from end sills with smaller thicknesses is greater than that of end sills with larger thicknesses.

- Importance of the approach flow Froude number (3-6) and relative deflector height (50 mm) on the jet trajectory. The relevant jet parameters, including deflection angle (200), maximum jet elevation, and jet impact on the tailwater channel. The energy dissipation ranges from 40% to 70%,
- Stilling energy dissipators of form Jump with only one end sill is necessary to dissipate the energy in the Himalayan and plain region because the speed of the rivers in those areas is very high. Other energy dissipators such as Trajectory bucket, roller buckets with baffle blocks should be used to increase the speed in a low-velocity river that flows in any area.

## References

1. Bureau of Indian standards. "Criteria for hydraulic design of bucket type of energy dissipators." IS: 7365: 2010 (Second revision).
2. Flood Estimation report by Central water Commission, 2017.
3. Jian-hua, WU. Zhun XU., and Li, YAO. "Ski-jump trajectory based on take-off velocity." J. Hydrodynamics., 2016, 28(1): pp 166-169.
4. Jill Lucas, Willi H. Hager, Robert M. Boes "Deflector Effect on Chute Flow" J. Hydraul. Eng., 2013, 139(4): pp 444-449
5. Juon, R., and Hager, W. H. "Flip bucket without and with deflectors." J. Hydraul. Eng., 2000, 126(11): pp 837-845.
6. H. M. Azamathulla, A. A. Ghani and N. Azazi Zakaria "ANFIS-based approach to predicting scour location of spillway" Proceedings of the Institution of Civil Engineers Water Management 162 December 2009 Issue WM6 Pages 399–407.
7. M. Pfister, J. Lucas and W.H. Hager "Effect of pre-aerated approach flow on deflector-generated jets" 34th IAHR World Congress , 2011, pp 2554-2561.
8. Shangtuo, Qian. Jian hua, Wu. And Fei, Ma. "Hydraulic Performance of Ski-Jump-Step Energy Dissipater." J. Hydraulic. Eng., 2016, 05016004: pp 1-7.
9. Utkarsh Nigam,S Das,M R Choudhury "Overview Of Energy Dissipators And Stilling Basins With Design Aspects Of Hydraulic Jump Type Energy Dissipators'NCIT 2015, pp 1-9.
10. S K Mujumdar ,P L Patel "Model study of a ski jump type of Energy Dissipator" Hydro 2001,pp 425-432.

*IN PROCEEDINGS OF 25th HYDRO 2020, INTERNATIONAL CONFERENCE, NATIONAL INSTITUTE OF TECHNOLOGY ROURKELA, ODISHA, INDIA 26-28, March 2021, ISBN 978-93-90631-56-8*

Paper ID - 039

# Hydraulic modelling of headpond with lateral spillway weir structure for the Tamakoshi-V hydroelectric project, Nepal

Pradyumna Machhkhand[1]

[1]*CEO, Gomati Hydroinformatics Analytics & Engineering Pvt. Ltd., H.No.348, Chhote Atarmuda, Adarsh Nagar, Raigarh (Chhattisgarh) 496001, India*
*Email: pradyumna.machhkhand@ghyiae.com*
*Telephone/Mobile No.: +91 9999 326876*

## Abstract

The proposed operation of Tamakoshi-V hydroelectric project (TKVHEP), Nepal is completely determined by the discharge released from the power plant of Upper Tamakoshi hydroelectric project (UTKHEP), which led to the diversion of discharge from the already existing tailrace race tunnel (TRT) of UTKHEP to the interconnecting tunnel (ICT) that connects the said TRT and the headpond of TKVHEP; the flow in the TRT, the ICT, and the headpond being open-channel flow. Initially, the size of the headpond and the adjoined lateral spillway weir of TKVHEP were tentatively adjusted meeting the submergence criteria of the intake. However, in order to optimize the headpond size, the other criteria have been fixed by modelling the headpond reach (from the outlet point of the UTKHEP to the end of the headpond) using a physically-based and one-dimensional numerical model. The maximum discharge from the UTKHEP plant is Qmax = 68$m^3$/s. The normal depth of flow from the established hydraulic model corresponding to this discharge at headpond end has been observed at El.1155m, which is also the lowest regulated water level (LRWL) in the headpond, thereby meeting the intake's submergence criteria. Furthermore, the backwater development at the headpond due to sudden closure of TKVHEP plant and the propagation of wave towards the power tunnel have been modelled by considering the upstream boundary condition as constant discharge Qmax and the downstream boundary condition as transient flow at the headpond location in the model, which is based on the results of surge analysis (separately conducted) of the pressurized water conductor system of the TKVHEP. With the applied boundary conditions, the modelled headpond reach has been iteratively simulated, thereby changing the headpond dimensions and the crest length of the lateral spillway weir for each run. The crest level is fixed at El.1158.1m (0.1m above the recommended highest regulated water level, HRWL = El. 1158m) in the headpond. From the optimized model results, the maximum stage at headpond is observed at El.1159.1m and the design discharge through the lateral spillway weir has been deduced as the sum of inflow Qmax and the maximum transient flow opposite to the direction of inflow.

***Keywords:*** *TKVHEP; UTKHEP; TRT; ICT; headpond; open-channel flow; lateral spillway weir; transient flow; pressurized water conductor system; surge analysis*

## 1. Introduction

The Tamakoshi-V hydroelectric project (TKVHEP) is a dependent project that has been proposed to depend solely upon the operation of the power plant of Upper Tamakoshi hydroelectric project (UTKHEP). The key salient features of the UTKHEP are the Upper Tamakoshi Dam on the upstream of Tamakoshi River (Location 27°55'28.44"N 86°12'48.59"E; source: Google Earth), the intake at Upper Tamakoshi Reservoir, the headrace tunnel, the desander, the surge shaft, the pressure shaft, the power plant, and the tailrace tunnel (TRT). The power plant of UTKHEP receives inflow from the Upper Tamakoshi Reservoir via the headrace tunnel (HRT) and the pressure shaft. The turbines in the power house are high head Pelton turbines. With all units running in the power plant, the design maximum discharge that can be released from the UTKHEP plant is Qmax = 68$m^3$/s. As the power house of the UTKHEP is underground, the rock caverns have been excavated to construct tail pit to convey the released water from the turbines to the TRT, which further carries the released tail water as open-channel, thereby finally discharging into the Tamakoshi River. The TRT takes the shortest possible length between the UTKHEP tailrace exit location and the outfall location on the right bank of the Tamakoshi River.

The schematic view of the cascade arrangements of the UTKHEP and TKVHEP has been displayed below.

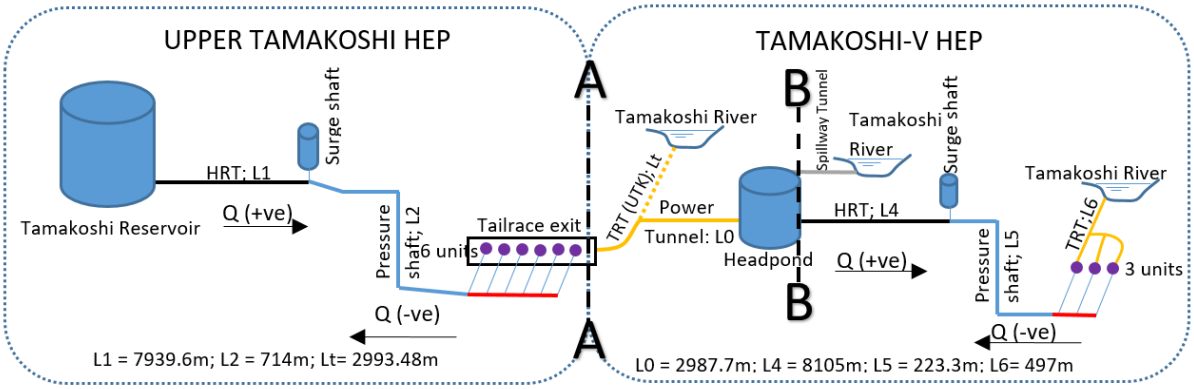



**Figure 1** Schematic view of the cascade arrangements of the UTKHEP and TKVHEP projects

### 1.1 *Planning and development of Tamakoshi-V hydroelectric project*

In the above Figure 1, the frame left to the section A-A represents the scheme of UTKHEP, whereas the frame right to section A-A includes the TRT that takes off from the tailrace exit of the UTKHEP and the frame also represents the TVKHEP. Initially, the TRT of UTKHEP was constructed to discharge into the Tamakoshi River; the alignment of the TRT being displayed in Figure 1 as dotted line.

Subsequent to the development of UTKHEP, the developer, Nepal Electricity Authority (NEA) planned to tap the release from the UTKHEP power plant so that a new hydroelectric project known as Tamakoshi-V hydroelectric project could be developed. In this context, as soon as the feasibility study was completed, the NEA awarded the detailed engineering design works to Lahmeyer International GmbH, where the author carried out the related design works as a hydraulic design and modelling expert. The present paper describes the hydraulic design of the headpond, where multi-objective optimization of the headpond is essential and it also illustrates how the objectives are achieved.

As indicated in Figure 1, the diversion of TRT was proposed for the development of TKVHEP. The frame right to the section A-A represents the scheme of TKVHEP (hereafter, both the TRT from UTKHEP and the diverted interconnecting tunnel (ICT) as a link to the headpond are clubbed together and called the power tunnel) as displayed above. The salient features of key elements of both the projects have also been displayed above. The section A-A to section B-B represents the reach of the open-channel flow that is conveying through the power tunnel and the headpond. In fact, the zone for hydraulic modelling of the headpond is between section A-A and section B-B. The focus of this paper is the hydraulic modelling of the proposed headpond, which also includes the hydraulic design and model study of the appurtenant structures related to the headpond of TKVHEP.

The proposed headpond is underground and is mounted with escape/lateral/side weir spillway to discharge the overflow from the headpond to the spillway outlet tunnel (open-channel) whose outfall is located at the right bank of the Tamakoshi River. It is important to understand the source of inflow to the TKVHEP in order to describe the proposed physical general layout of the TKVHEP itself. The source of the inflow to the TKVHEP project is the tail water release from the UTKHEP power plant. The following key factors have been considered while planning the TKVHEP as tabulated below.

**Table 1** Key factors for planning and development of Tamakoshi-V hydroelectric project

| Serial No. | Key Factors |
|---|---|
| 1 | The re-alignment of already constructed TRT of UTKHEP by taking maximum advantage of the existing alignment. |
| 2 | The point of diversion to be at an optimum distance to the proposed intake site of TKVHEP. |
| 3 | The lowest regulated water level (LRWL) shall be such that it meets the submergence criteria of the intake of the TKVHEP and is not less than the water level corresponding to the normal depth at the headpond during maximum inflow from the UTKHEP. |

| Serial No. | Key Factors |
|---|---|
| 4 | While UTKHEP is in operation and in case the handpond encounters backpropagation of flow through the intake due to shutting down of TKVHEP plant, an escape structure (lateral/side weir) is to be integrated with the headpond so that the flow could be discharged through the weir. |
| 3 | The underground headpond structure is to be optimally designed and located such that at any instance due to any backpropagation of water from the system must not affect the maximum tail water level (EL 1162.35m) at the tail pit of UTKHEP below the turbines. |

The proposed schematic layout plan of the TKVHEP featuring the start of the TRT of UTKHEP till the headpond has been refurbished below:

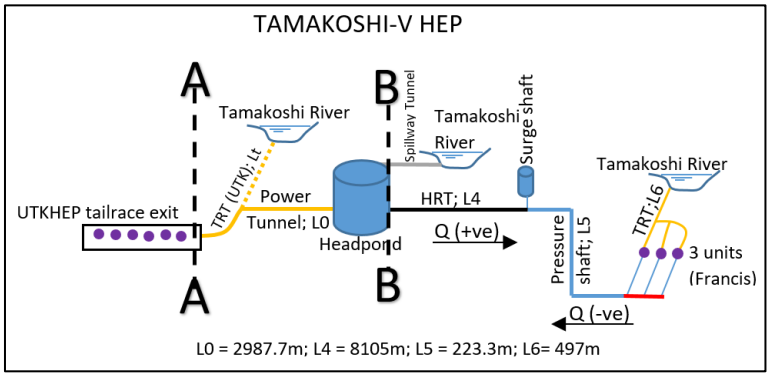



**Figure 2** Schematic view of TKVHEP project

The headpond structure is one of the salient features of the project Tamakoshi-V hydroelectric project (TKVHEP), Nepal. The headpond has been planned to receive the discharge (open-channel flow) via the power tunnel and to create head for the TKVHEP; the intake being at the end of the headpond, which connects the head race tunnel (HRT) of TKVHEP. Therefore, the inflow to the headpond entirely depends upon the operational release from the UTKHEP plant. The sketch of the general layout plan of the headpond, the power tunnel, the side weir spillway, and the spillway tunnel have been displayed below.

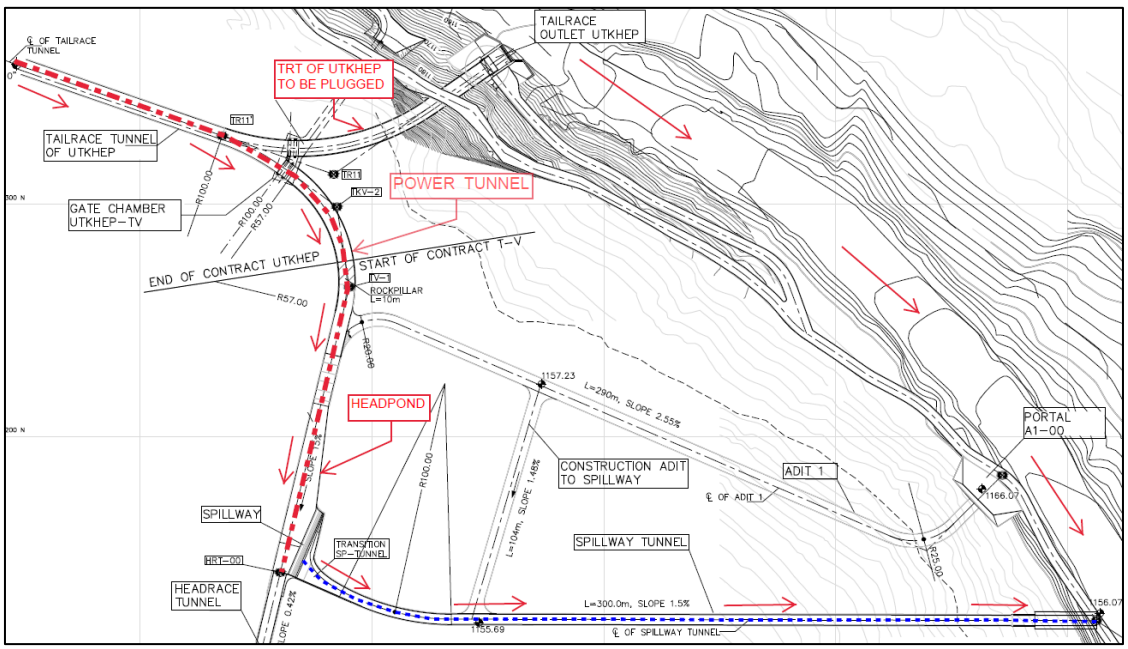



**Figure 3** Sketch of the general layout plan of the headpond, the power tunnel, the side weir spillway, and the spillway tunnel of Tamakoshi-V HEP (not to scale)

Initially, the headpond was designed based on the concept given by NEA during the feasibility stage, thereby keeping the highest regulating water level (HRWL) at EL. 1158m and the lowest regulating water level (LRWL) at EL.1155m. In fact, these data were the bases for the surge analysis conducted during detailed engineering stage. However, as the impact of surge development in the headpond on the UTKHEP power plant must be a part of the present study, the other design criteria have also been set and examined to optimize the size of the headpond. It is noted that the headpond design must be synchronous with the UTKHEP as well as with the TKVHEP without having any impact on the targeted energy of both the projects. This leads to the development of multiple criteria to optimize the headpond as described in the subsequent section.

## 2. Hydraulic design criteria of headpond

As the headpond and the power tunnel are proposed as open-channels and are to be constructed underground, the optimal design of headpond must conserve the principles of open-channel flow by maintaining sufficient freeboard in the power tunnel and the headpond. The hydraulic sections of these structures are rectangular with vertical lined walls on either side and with lined surfaces, whereas the freeboard sections are partly rectangular with finished arch cover. The sketch of the sections of the power tunnel and the headpond have been displayed below.

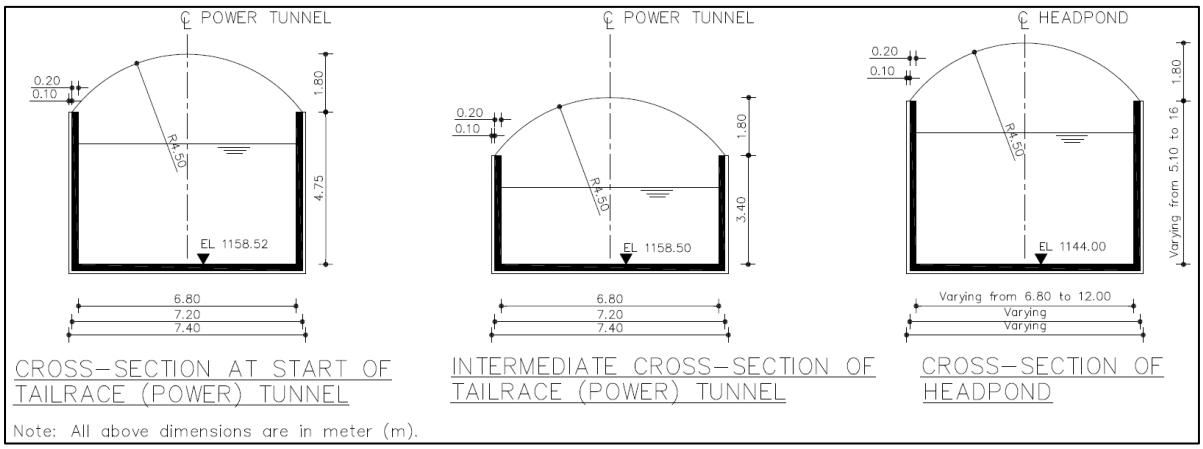



**Figure 4** Sketch of the sections of the power tunnel and the headpond

The hydraulic design criteria have been described in the subsequent sections below.

### 2.1 *Area-Capacity curve*

The area-capacity curve shall be based on the optimum size of the headpond as a result of hydraulic modelling of the headpond considering all the modelling criteria.

### 2.2 *Submergence for intake*

As the intake will receive controlled flow from UTKHEP, it is necessary to check the normal depth of flow at the intake when it receives the maximum release of Q = 68$m^3$/s from UTKHEP. The submergence shall be such that it suffices the required submergence depth criteria at Q = 68$m^3$/s and the LRWL at the intake remains unaffected.

### 2.3 *Spillway weir crest*

The spillway weir crest level shall be based on the model study of the headpond integrated with the spillway weir. It is to be ensured that the crest elevation is high enough as compared to the water levels in the river where the spillway outlet is discharging.

### 2.4 *Effect of backwater*

The effect of backwater shall be based on the critical condition, that is, when the headpond receives the maximum discharge from the UTKHEP, at the same instant the maximum transient flow in the reverse direction towards the headpond is witnessed due to sudden load rejection at TKVHEP considering the case of maximum magnitude of transient flow resulting from the surge analysis. The impact of this on the water level at the tail pit of UTKHEP shall not exceed the designed maximum tail water level (EL.1162.35m).

### 2.5 *Freeboard*

The freeboard in the power tunnel and the headpond must be greater than 1m from the maximum water levels in the system.

## 3. Hydraulic modelling of the headpond

In order to meet the above multiple criteria for hydraulic design of the headpond, the hydraulic modelling (physically-based numerical model) of the headpond and related structures become inevitable. The reaches of the headpond hydraulic model constitute the power tunnel reach (start point is where the TRT of UTKHEP begins) and the headpond reach (end point is where the intake/headrace tunnel of TKVHEP starts).

### 3.1 *Model setup*

The documents, Final Design Tailrace Tunnel *(Longitudinal Section, Cross-Section and Detail), 2011* and Tamakoshi V HEP Field Investigation and Data Collection: Detail Design Headworks Headpond Longitudinal Section Plan and Section *(Longitudinal Section, Cross-Section and Detail*), 2017, have been the bases for setting up the model:

#### 3.1.1 *Applied convention*

Following conventions have been applied:

a) depending upon the sectional change in the power tunnel and the headpond at varying intervals, both the reaches have been divided into 8 numbers of cross-sections for model study, which have been further divided/interpolated for model requirements;
b) as the power tunnel and the headpond are open channels, the one-dimensional (unsteady state) numerical modelling software, HEC-RAS by USACE has been used to model the system;
c) the critical condition in the headpond shall be the scenario where the Tamakoshi V plant shuts down suddenly when the UTKHEP is still discharging the maximum flow of 68$m^3$/s; and
d) the simulation date and time 05 September 0000 hours to 05 September 0025 hours are merely indicative of start time 0 sec to end time 1500 sec.

#### 3.1.2 *Brief description of the applied software, HEC-RAS*

The software, HEC-RAS developed by USACE is designed to perform one-dimensional (1D) and two-dimensional (2D) hydraulic computations numerically for a full network of natural and constructed channels. The HEC-RAS model comprises two major components; steady flow and unsteady flow. In the present study, both the components have been used. The steady component has been used to calibrate the model, whereas the 1D unsteady component has been used to model the power tunnel and

the headpond reaches. The physical laws which govern the flow of water in a stream or channel are expressed mathematically in the form of partial differential equations:

Conservation of mass (continuity) equation:

$$\frac{\partial Q}{\partial x} + \frac{\partial A}{\partial t} + q_1 = 0 \quad (1)$$

Conservation of momentum equation:

$$\frac{\partial Q}{\partial t} + \frac{\partial QV}{\partial x} + gA\left(\frac{\partial h}{\partial x} + S_f - S_o\right) = 0 \quad (2)$$

where:

$Q$ = discharge,
$A$ = total flow area,
$q_1$ = lateral inflow per unit length,
$x$ = distance along waterway,
$t$ = time,
$V$ = velocity,
$g$ = acceleration due to gravity,
$h$ = depth of flow,
$S_f$ = frictional slope, and
$S_o$ = bed slope.

### 3.1.3 *Cross-sections of the modelled reach*

The modelled reach has been divided into two parts, viz., the power tunnel reach and the headpond reach. The assignment of cross-sections in the reaches have been listed below.

**Table 2** Cross-sections of the power tunnel and the headpond

| Cross-sections (XS) | Distance from the immediate downstream XS (m) | Remarks |
|---|---|---|
| XS 8 | 10.00 | Power tunnel reach |
| XS 7 | 7.80 | Power tunnel reach |
| XS 6 | 2853.71 | Power tunnel reach |
| XS 5 | 22.06 | Headpond reach |
| XS 4 | 44.66 | Headpond reach |
| XS 3 | 17.00 | Headpond reach |
| XS 2 | 32.54 | Headpond reach |
| XS 1 | 0.00 | Headpond reach |

### 3.1.4 *Model calibration*

Using the above geometry and the available data of water levels at the TRT exit, a steady state model in HEC-RAS has been developed and calibrated. The Manning's roughness (n = 0.014) has been applied and the results concur with the previous study (NEA, 2016). For the hydraulic modelling of headpond, the Manning's roughness shall be n = 0.014.
It has been observed from the results that at Q = 68m$^3$/s, the water surface elevation at the headpond reaches EL 1155.08m. Later, the unsteady component of the HEC-RAS has been utilized to simulate the transient behavior of flow in the headpond as described in the subsequent sub-sections.

### 3.1.5 *Initial and boundary conditions*

The initial conditions and the upstream and the downstream boundary conditions have been tabulated below.

**Table 3** Initial and boundary conditions

| Station ID | Station name | Initial condition | Upstream boundary condition | Downstream boundary condition |
|---|---|---|---|---|
| XS ID - 8 | Power tunnel | Q = 6.8 $m^3/s$ | Inflow hydrograph | - |
| XS ID - 1 | Headpond | - | - | Transient flow hydrograph |

The upstream boundary condition is the inflow hydrograph with constant flow of 68 $m^3/s$ for the duration of time equal to 1500 sec at an interval of 1 sec.

The downstream boundary condition is the transient flow time series (duration 1500 sec) at the headpond due to load rejection scenario for minimum roughness case, which has been explained in the same report (Detail Engineering Design and Tender Document Preparation of Tamakoshi V Hydroelectric Project, Chapter 4, Lahmeyer International GmbH, Germany, 2018). The upstream and the downstream boundary conditions have been displayed in the figure below.

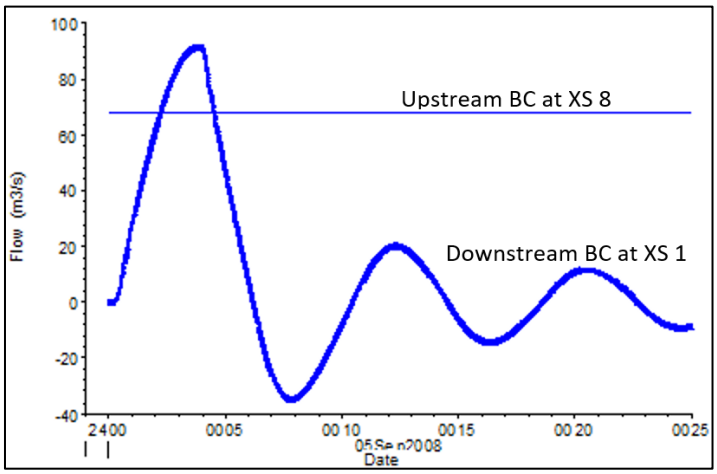



**Figure 5** Upstream and downstream boundary conditions

### 3.1.6 *Lateral/side spillway weir at the headpond*

The considered lateral/side spillway weir in the headpond shall be iteratively modelled, thereby changing the crest level and the crest length of the weir for each run till the optima crest level and length are achieved. The schematic plan and sections of the weir in the HEC-RAS model have been displayed in the figures below.

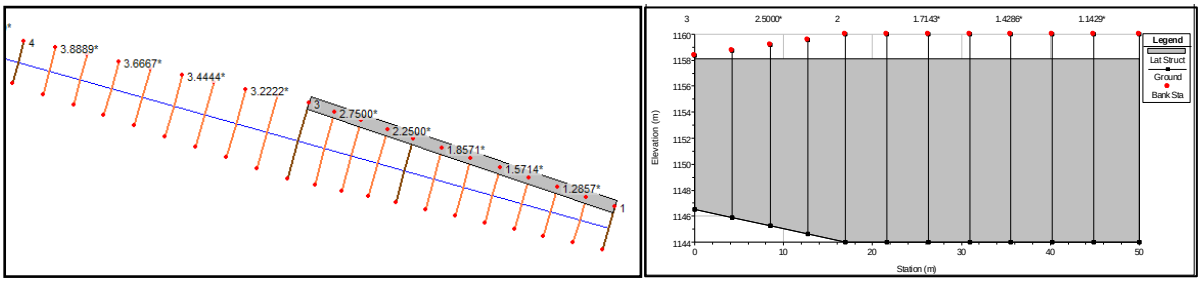



**Figure 6** Schematic plan (left frame) and section (right frame) of the weir in the HEC-RAS model

## 4. Results and discussions

The unsteady model discussed above has been simulated for 1500 sec. The longitudinal profile with maximum water surface elevations along the power tunnel and the headpond has been displayed in the figure below.

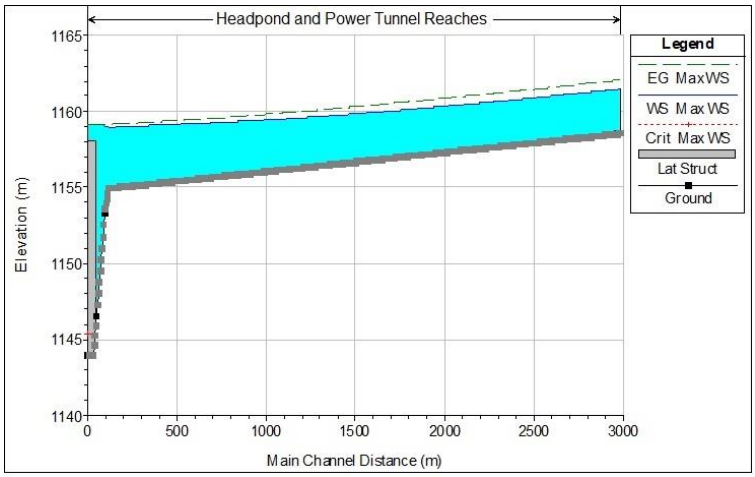



**Figure 7** Maximum water surface profile in the power tunnel and headpond reach

The above water surface profile has been further elaborated in the figure below.

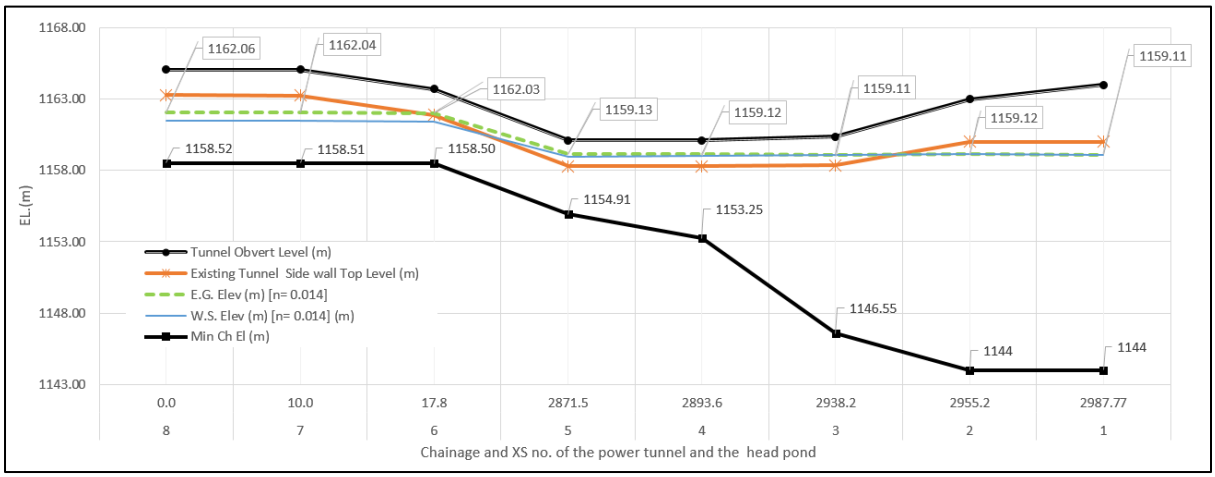



**Figure 8** Maximum water surface profile with details of the power tunnel and the headpond

The above figure displays the invert and obvert levels of the power tunnel and the headpond. It may be noted that minimum cover from the top of the side walls to the obvert levels of the tunnel is 1.8m. As the model has been developed considering the scenario of the transient condition that is critical for the headpond, the resulting maximum water surface profile does not exceed the maximum tailwater level EL 1162.35m of UTKHEP. Secondly, the available freeboard in the tunnel with reference to the maximum water surface levels ranges from 1.1m to 4.89m, which is acceptable and the modelled size of the headpond meets the critical condition scenario.

The results of simulated time series of flow and stage at XS-8 and XS-1 have been displayed in the figures below.

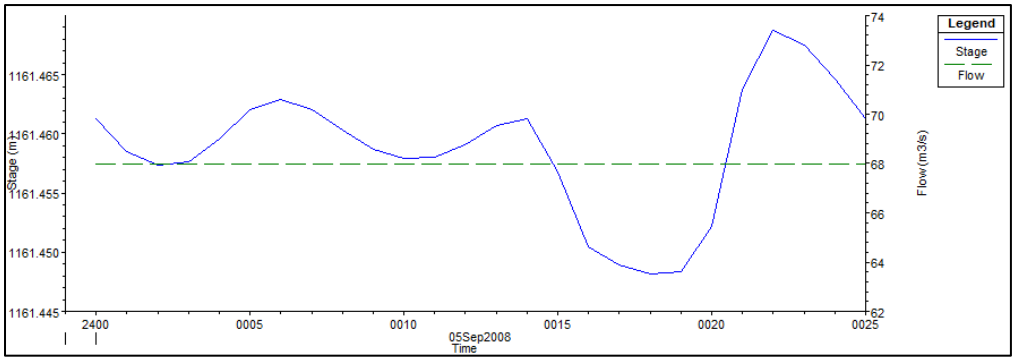



**Figure 9** Results of simulated stage-flow time series (time shown in minutes) at XS-8 (the start of the power tunnel)

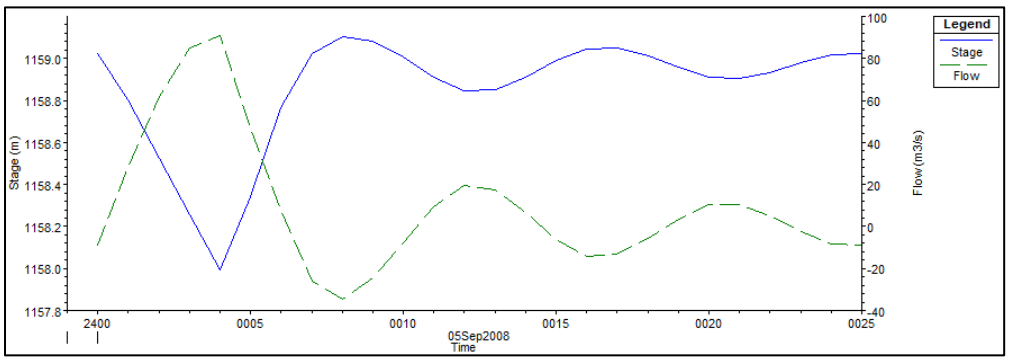



**Figure 10** Results of simulated stage-flow time series (time shown in minutes) at XS-1 (the end of the headpond)

Although the maximum stage that has resulted at headpond is 1159.1m, for the purpose of design of spillway chute and the appurtenances, the maximum inflow (Q =68$m^3$/s) from the tail outlet of UTKHEP and the maximum transient flow (Q =34.8 $m^3$/s) towards the headpond from Tamakoshi V intake have been summed up to result a design discharge through weir, Qd = 102.8 $m^3$/s. The same is advisable for the headpond design works.

The water levels of the Tamakoshi River at the spillway outlet of TKVHEP has been referred from the rating curve derived from the river model study considering the reach of the river near the spillway outlet (Lahmeyer International GmbH, Germany, 2018; Detail Engineering Design and Tender Document Preparation of Tamakoshi V Hydroelectric Project). The critical observatory discharges in the Tamakoshi River near the spillway outlet and their corresponding levels have been tabulated below.

**Table 4** Discharge and water levels of Tamakoshi River near spillway outlet of TKVHEP

| River Discharge (Q $m^3$/s) | Water surface elevation (m) | Lateral weir crest level (m) | Remarks |
|---|---|---|---|
| 68 | 1147.61 | 1158.10 | No impact on weir crest level |
| 300 | 1149.30 | 1158.10 | No impact on weir crest level |
| 2200 | 1155.28 | 1158.10 | No impact on weir crest level |
| 2800 | 1156.24 | 1158.10 | No impact on weir crest level |

In the above table, the discharge, Q =68$m^3$/s is hypothetically considered for the river because it is the maximum outflow from the UTKHEP plant that may spill out to the river due to closure of TKVHEP. The inflow at Upper Tamkoshi dam site when the UTKHEP shuts down is 300$m^3$/s (Nepal Electricity Authority, 2011; Feasibility Study of Tamakoshi-V Hydroelectric Project. Project Development Department, Engineering Services)). The river discharges, Q =2200$m^3$/s and Q =2800$m^3$/s represent the $Q_{1000yr}$ flow and the anticipated extreme flow, respectively. In all the above cases, the water levels in the Tamakoshi River are much below the lateral weir crest level, thereby causing no impact on the headpond structure.

## 5. Conclusions

Unlike the other forms of cascade hydroelectric projects, where the reservoirs exist on the surface of the rivers, the headpond of TKVHEP is to be constructed underground. As TKVHEP is a cascade development of UTKHEP, the TRT of the UTKHEP, which was initially constructed for discharging into the Tamakoshi River by taking the optimal route shall be diverted to form the headworks for the TKVHEP. The headworks include the said TRT, which is known as the power tunnel in this paper, and the headpond. It is anticipated that during the operation of TKVHEP, for any reason if the THVHEP plant shuts down and the UTKHEP is still in operation, the released water must find an escape. Therefore, the lateral weir at the headpond is found appropriate to serve this purpose. However, as the headpond must be synchronous with operations of both the plants upstream and downstream, the multi-objective optimization of the headpond is essential. The identified objectives are achieved by the one-dimensional hydraulic modelling of the headpond coupled with the transient flow results of surge analysis of TKVHEP as the downstream boundary condition; whereas the upstream boundary condition in the model being the constant maximum flow released from UTKHEP, Q = 68 $m^3/s$. A number of iterations have been attempted, thereby changing the dimensions of headpond and running the models. The paper presents the final successful model, where all objectives are achieved. The checklist showing the multiple hydraulic design criteria of headpond and the inferences drawn from the hydraulic modelling results have been tabulated below.

**Table 5** Checklist of the multiple criteria and the inferences from model study of headpond

| Sl. No | Hydraulic design criteria | Inferences from hydraulic modelling | Remarks |
|---|---|---|---|
| 1 | Area-capacity curve | The HRWL and the LRWL remain unchanged. | Recommended for further inclusion in the project works. |
| 2 | Submergence | At maximum inflow from UTKHEP, the required submergence depth merges with the normal depth at the headpond. | Recommended for further inclusion in the project works. |
| 3 | Lateral/Side weir | Design discharge = 102.8 $m^3/s$; weir length = 50m; weir crest level = EL.1158.1m; max. water level above the crest = EL.1159.1m, which is much higher than the water level of Tamakoshi River at the spillway outlet section. | Recommended for further inclusion in the project works. |
| 4 | Backwater | Critical transient condition has no negative impact on the UTKHEP power plant or on the headpond. | Recommended for further inclusion in the project works. |
| 5 | Freeboard | Sufficient freeboard is available at the power tunnel and the headpond structures. | Recommended for further inclusion in the project works. |

As the optimization of headpond size requires multiple criteria and constraints to be met, the inferences drawn from the hydraulic modelling of the headpond, the lateral weir structure, and the power tunnels dictate the same. As a corollary, the recommended length of the headpond length is 116.2m, whereas the recommended invert level in the headpond near the intake is EL.1144m; the same have been included in the model study.

## References

Nepal Electricity Authority (2011). *Feasibility Study of Tamakoshi-V Hydroelectric Project.* Project Development Department, Engineering Services, Nepal Electricity Authority, Kathmandu, Nepal.

Lahmeyer International GmbH, Germany (2018). *Detail Engineering Design and Tender Document Preparation of Tamakoshi V Hydroelectric Project*, Nepal Electricity Authority, Kathmandu, Nepal.

JV of Norconsult, Norway and Lahmeyer International GmbH, Germany (2016). *Final Report of Upper Tamakoshi Hydroelectric Project, Consultancy Services for Construction Supervision of Upper Tamakoshi Hydroelectric Project,* Nepal Electricity Authority, Kathmandu, Nepal.

Abbott, M. B, Pitman Publishing Ltd., London, (1979). *Computational hydraulics: Elements of the theory of free surface flows.*

*U.S. Army Corps of Engineers HEC-RAS (2008). River analysis system hydraulic reference manual. Institute for water resources, Hydrologic engineering center.*

*IN PROCEEDINGS OF 25th HYDRO 2020, INTERNATIONAL CONFERENCE, NATIONAL INSTITUTE OF TECHNOLOGY ROURKELA, ODISHA, INDIA 26-28, March 2021, ISBN 978-93-90631-56-8*

Paper ID - 076

# STAGE DISCHARGE RELATIONSHIP BY WEIR THEORY FOR CHANNEL FLOW MEASUREMENTS USING THE CONICAL CENTRAL BAFFLES

**Ankur Kapoor[1], Aniruddha D. Ghare[2], Avinash M. Badar[3]**

[1]*Research Scholar, Department of Civil Engineering, Visvesvaraya National Institute of Technology, Nagpur 440010, India.*

[2]*Professor, Department of Civil Engineering, Visvesvaraya National Institute of Technology, Nagpur 440010, India.*

[3]*Vice-Principal, KDK College of Engineering, Nagpur 440009, India*

***E-mail:*** *ankurkapoor06@yahoo.com*

## Abstract

The paper presents the use of weir theory to develop mathematical form of stage – discharge equation for measurement of flow in small rectangular open channels using conical central baffle flume. The flume is formed by placing a conical baffle axially in open channels which is mobile in nature and hence can be used for temporary flow measurements. The channel cross-section reduces around the central baffle and reaches its minimum at its central section. For this section, the discharge equation for the trapezoidal weir with crest height equal to zero can be used for flow measurement. The coefficient of discharge ($C_d$) in the weir discharge equation is expressed in non – linear form as function of apex angle of cone, contracted channel width and the upstream flow depth, to correct the nonrealistic assumptions. The empirical coefficients in the non – linear form of $C_d$ is determined by minimizing the summation of the absolute relative errors of the flow discharges, using the experimental data collected on laboratory flumes. The presented approach for discharge predication is compared with an analytical approach available in literature in which the stage – discharge relationship for the conical central baffle flume is derived using the energy concept. The average absolute error is found to be 3.55 % using the weir theory as against 4.24 % using the analytical approach for the same experimental data. This suggests that the weir theory can also be applied to predict discharge for the conical central baffle flume provided the coefficient of discharge should be determined by the developed non- linear form.

***Keywords***: *Conical flume, Flow measurement, Rectangular channel, Central baffle, Weir theory.*

## 1. Introduction

Water conservation is of utmost importance owing to the increased demand of agricultural, municipal, industrial, and recreational use of water. Open channels are often used for conveying water for several different purposes. Measurement of water in open channels will ensure equitable distribution of water and help in generating fair revenue share from the users. The revenue generated will help in upgrading the water management programs preventing excessive use of water. Globally, approximately 70 % of freshwater withdrawals are used for agriculture. This appeals for the water management programs to be primarily directed towards agriculture. Proper and accurate water measurement methods also help in the evaluation of seepage losses in unlined canals. Thus, measurement of flow rate in agricultural canals is essential to ascertain the volume of water reaching the field. Measurements of continuous flows, in case of an open channel, are performed using a hydraulic structure that establishes a unique depth-flow relationship. Installing canal flow measuring structures reduces the need for time-consuming current metering. Weirs have commonly been used for measurement of small to moderate flows in open channels but if the channel section upstream of the weir crest accumulates sediment then its accuracy reduces. For large flows, rating flumes have been commonly used which are calibrated using current meter measurements. A deposit on the floor of the rating flume changes the downstream flow conditions affecting the gage readings in such a way that the actual discharge values cannot be obtained making it not reliable for flow measurements. An improved Venturi flume proposed by Parshall (1926) for flow measurement obviated many of the disadvantages of weirs, rating flumes, etc. The Parshall flume had a throat section between the converging and diverging section and work on similar principle as that of the Venturi meter. The development of cutthroat flume (Robinson and Chamberlain, 1960; Skogerboe

and Hyatt, 1967) and RBC flume (Replogle, 1975) further improved the construction and accuracy of flow measuring devices in open channels. Hager (1985) first introduced the concept of using a portable flume instead of traditional flumes which were then in general use. The throat section was achieved by placing a cylindrical column vertically in a prismatic channel. The equations proposed by Hager (1985) measured the discharge with a precision of ± 5 %. Many modifications to Hager's proposed equation were made by Samani and Magallanez (1993, 2000), Badar and Ghare (2012) and Ghare et al. (2020). Hager (1988) also proposed a graphical approach for circular channels. Samani et al. (1991) replaced the graphical approach with a computer model which predicted discharge with a maximum error of 6 %. The use of Buckingham's π method of dimensional analysis along with physical modeling in a laboratory allowed Samani (2017) to develop a single calibration equation for discharge prediction in trapezoidal, rectangular, and circular channel cross-sections using a cylindrical column to achieve the required constriction. Ferro (2016) used the experimental data of Peruginelli and Bonacci (1997) and developed a stage – discharge equation for a flume formed using a mobile pier-shaped object termed as a central baffle. Kolavani et al. (2019) experimentally investigated the effect of various geometrical parameters for the central baffle flume (CBF) using dimensional analysis and energy conservation approaches. The use of cone by Kapoor et al. (2019) to achieve the constriction also illustrate the concept of using a mobile flume for temporary flow measurements in open channels.

## 2. Conical central baffle flume

Flow measurement in open channels is based on energy concept. Flow in open channels is governed by two types of energies namely, global or total and specific energy. According to the principle of specific energy, minimum energy produces a specific flow called critical flow for which the Froude number equals 1.

$$Fr^2 = \frac{Q^2 T}{g A^3} \tag{1}$$

It is evident from Eq. (1) that when critical flow occurs, the flow rate ($Q$) can be calculated using the area and top width of the flow which are function of the flow depth at that section. Therefore, it is necessary to create critical flow conditions to accurately measure flow in open channels by observing the flow depth at that section.

Kapoor et al. (2019) created the critical flow conditions by inserting a conical obstruction at the center of the channel (Fig. 1) and termed it as conical central baffle flume (CCBF). The proposed stage – discharge relationship (Eq. 2) was developed using the energy concept allowing the flow prediction by measurement of flow depth ($y_u$) at the cone face.

$$Q = C_d \sqrt{g \frac{\left(B_c\, y_c + c\, {y_c}^2\right)^3}{B_c + 2\, c\, y_c}} \tag{2}$$

$B_c$ : Contracted channel width; $B_c = B - d$
$B$ = Channel bed width
$d$ = Cone diameter

$c$ : $\tan(\theta/2)$
$\theta$ = Apex angle of cone

$y_c$ : Flow depth at critical section; $y_c = \frac{\left\{(3\,B_c - 4\,c\,y_u)^2 + 40\,c\,B_c\,y_u\right\}^{1/2} - (3B_c - 4\,c\,y_u)}{10\,c}$

$y_u$ : Observed flow depth at cone's face

$C_d$ : Discharge correction factor; $C_d = 1.1 \left(\frac{y_u}{B_c}\right)^{0.135}$

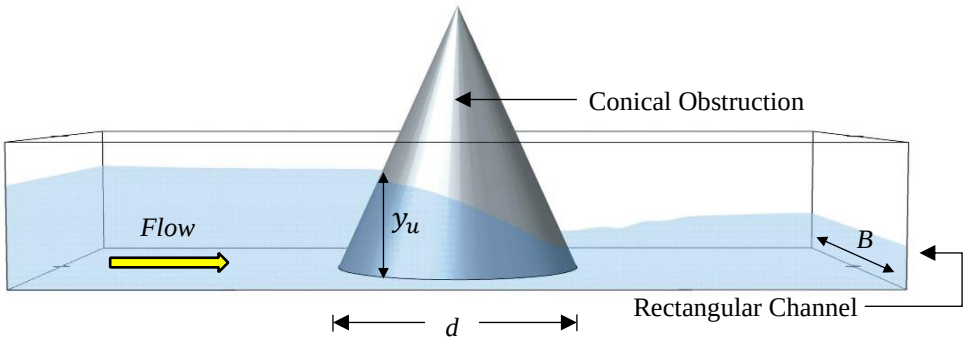



**Figure 1.** Conical central baffle flume

Kapoor et al. (2019) experimentally tested the proposed equations for flumes with different bed width and cone diameters. Cone of diameter 36 cm was inserted to achieve 60 % contraction in a 60 cm wide rectangular flume. Similarly, cones of diameter 20 cm and 27.5 cm were placed in a 30 cm wide rectangular flume to create 67 and 91.7 percent contraction respectively. Also, 80 % and 75 % contractions were achieved in a rectangular flume of 10 cm bed width using cones of diameters 8 cm and 7.5 cm respectively. The flow rate was varied between 0.001 $m^3/s$ to 0.052 $m^3/s$. Flow depths were recorded on the cone face for different discharge values. The maximum absolute relative error of the flow discharges was found to be less than 10 % with an average error of 4.24 % by implementing Eq. (2). In the present study, weir discharge equation for trapezoidal weir has been proposed to measure flow for the CCBF as the cross section of flume at the central section resembles a trapezoidal weir of zero crest height.

## 3. Weir theory for the CCBF

Weir theory can be used to work out the form of discharge equation for the CCBF (Vatankhah, 2020). The channel cross-section around the obstruction reaches its minimum at the central section. At this section, flow can be measured using the discharge equation (Eq. 3) for a trapezoidal weir with zero crest height.

$$Q = \frac{2}{3} C_d \sqrt{2g} \left( B_c {y_u}^{3/2} + 0.8\, c\, {y_u}^{5/2} \right) \tag{3}$$

where, $y_u$ is considered as the head for the trapezoidal weir of width $B_c$ and side slope $c$ (1 V: c H). $C_d$ is the discharge correction factor introduced to correct the assumption of streamline curvature due to contraction of the cross-section and the assumption related to approach velocity (Vatankhah and Khalili 2017). The correction factor $C_d$ is defined by the non – linear form (Eq. 4) which is a function of $c$, $y_u$ and $B_c$.

$$C_d = k_1 \left( \frac{y_u}{B_c} \right)^{k_2} c^{k_3} \tag{4}$$

The empirical coefficients $k_1$, $k_2$, and $k_3$ should be determined using the laboratory or field observations on the CCBF.

In the present study, the experimental observations on the CCBF reported by Kapoor et al. (2019) are used to determine the empirical coefficients of Eq. (4) by minimizing the summation of absolute relative errors of the flow discharges. Absolute relative errors between the calculated and observed discharges, after minimization, yields the following empirical coefficients of Eq. (4):

$$C_d = 0.705\left(\frac{y_u}{B_c}\right)^{0.177} c^{0.100} \quad (5)$$

Discharge is calculated using the weir discharge equation (Eq. 3) incorporating $C_d$ from Eq. (5). The distribution of absolute relative errors of Eq. (3) for all data reported by Kapoor et al. (2019) is plotted as shown in Fig. 2. The maximum absolute relative error was found to be 8.96 % with an average value of 3.55 %. The distribution of relative errors of Eq. (2) is also plotted in Fig. 2 which shows the maximum absolute relative error of flow discharges using Eq. (2) is 8.19 % having average error of 4.24 %.

The present study identifies the dimensionless parameters $y_u/B_c$ and $c$ as most influential parameters defining the correction factor $C_d$ of the weir discharge equation. The maximum and average values of errors using the weir theory show that the weir discharge Eq. (2) is as effective as the analytical approach (Eq. 3) in predicting discharge for the CCBF.

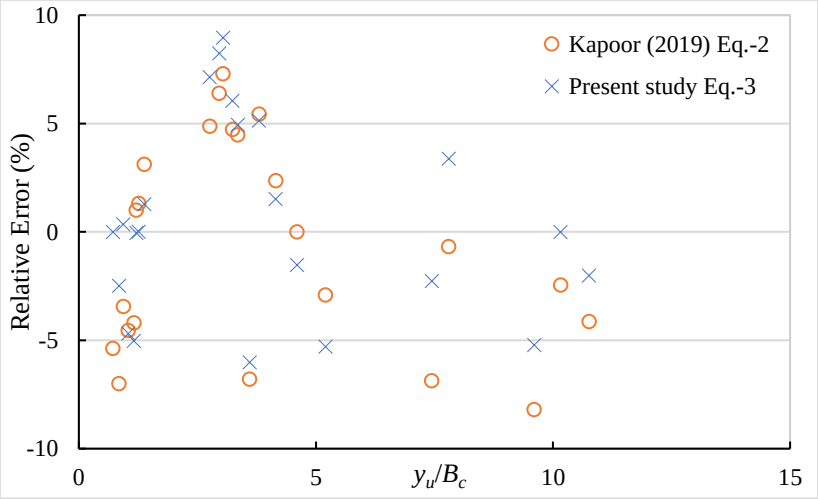



**Figure 2.** Relative error distribution of Eq. (2) – Eq. (3)

## 4. Conclusions

The theoretical weir discharge equation and non – linear form of discharge correction factor was used to define a simple stage – discharge relationship for use in conical central baffle flume. The proposed equation was calibrated using experimental data reported in literature for a similar flume. The present approach is simpler as it involves the use of a very general form of weir discharge equation against the analytical approach which requires $y_c$ to be calculated using a complex equation, yet the accuracy of the presented approach is similar to that of analytical one for the same flume. The present study also identifies two dimensionless parameters ($y_u/B_c$ and $c$) influencing the discharge correction as against only one ($y_u/B_c$) in the analytical approach. The maximum error within 10 % validated the proposed equation for use in CCBF. The approach presented in this study is general and can be applied to other similar flumes.

## Notations

The following symbols are used in this paper:

| | | |
|---|---|---|
| $A$ | : | Area of flow; |
| $B$ | : | Channel bed width; |
| $B_c$ | : | Contracted channel width; |

| | | |
|---|---|---|
| $C_d$ | : | Discharge correction factor; |
| $c$ | : | *tan (θ/2)*; |
| $d$ | : | Cone diameter; |
| $E$ | : | Upstream energy of flow; |
| $Fr$ | : | Froude number; |
| $g$ | : | Acceleration due to gravity; |
| $h$ | : | Height of cone; |
| $k_1$, $k_2$, $k_3$ | : | Empirical coefficients; |
| $Q$ | : | Discharge; |
| $Q_m$ | : | Measured discharge; |
| $T$ | : | Top width of flow; |
| $y_c$ | : | Flow depth at critical section; |
| $y_u$ | : | Observed flow depth at cone's face; |
| $\theta$ | : | Apex angle of cone. |

## References


1. Badar, A. M., and Ghare, A. D. (2012). "Development of discharge prediction model for trapezoidal canals using simple portable flume." *Int. J. Hydraul. Eng.* 1 (5): 37–42. https://doi.org/10.5923/j.ijhe.20120105.02.
2. Bijankhan, M., and Ferro, V. (2019). "Experimental study on triangular central baffle flume." *Flow Meas. Instrum.* 70. https://doi.org/10.1016/j.flowmeasinst.2019.101641.
3. Ferro, V. (2016). "Simple flume with a central baffle." *Flow Meas. Instrum.* 52: 53–56. https://doi.org/10.1016/j.flowmeasinst.2016.09.006.
4. Ghare, A. D., Kapoor, A., and Badar, A. M. (2020). "Cylindrical central baffle flume for flow measurements in open channels." *J. Irrig. Drain. Eng.* 146 (9): 06020007. https://doi.org/10.1061/(ASCE)IR.1943-4774.0001499.
5. Hager, W. H. (1985). "Modified venturi channel." *J. Irrig. Drain. Eng.* 111 (1): 19–35. https://doi.org/10.1061/(ASCE)0733-9437(1985) 111:1(19).
6. Hager, W. H. (1988). "Mobile flume for circular channel." *J. Irrig. Drain. Eng*. 114 (3): 520–534. https://doi.org/10.1061/(ASCE)0733-9437 (1988)114:3(520).
7. Kapoor, A., Ghare, A. D., Vasudeo, A. D., and Badar, A. M. (2019). "Channel flow measurement using portable conical central baffle." *J. Irrig. Drain. Eng*. 145(11): 06019010. https://doi.org/10.1061/(ASCE)IR.1943-4774.0001427.
8. Kolavani, F. L., Bijankhan, M., Stefano, C. Di., Ferro, V., and Mazdeh, A. M. (2019). "Experimental study of central baffle flume." *J. Irrig. Drain. Eng*. 145 (3): 62. https://doi.org/10.1061/(ASCE)IR.1943-4774.0001370.
9. Parshall, R. L. (1926). "The improved venturi flume." *Trans. ASCE* 89 (Mar): 841–880.
10. Peruginelli, A., and Bonacci, F. (1997). "Mobile prisms for flow measurement in rectangular channels." *J. Irrig. Drain. Eng*. 123 (3): 170–174. https://doi.org/10.1061/(ASCE)0733-9437(1997)123:3(170).
11. Robinson, A. R., and Chamberlain, A. R. (1960). "Trapezoidal flumes for open channel flow measurement." *Trans. Am. Soc. Agric. Eng*. 3 (2): 120–128. https://doi.org/10.13031/2013.41138.
12. Samani, Z., Jorat, S., and Yousaf, M. (1991). "Hydraulic characteristics of a circular flume." *J. Irrig. Drain. Eng.* 117 (4): 558–566. https://doi.org/10.1061/(ASCE)0733-9437(1991)117:4(558).
13. Samani, Z., and H. Magallanez. (1993). "Measuring water in trapezoidal canals." *J. Irrig. Drain. Eng.* 119

(1): 181–186. https://doi.org/10.1061/(ASCE)0733-9437(1993)119:1(181).
14. Samani, Z., and Magallanez, H. (2000). "Simple flume for flow measurement in open channel." *J. Irrig. Drain. Eng.* 126 (2): 127–129. https://doi.org/10.1061/(ASCE)0733-9437(2000)126:2(127).
15. Samani, Z. (2017). "Three simple flumes for flow measurement in open channels." *J. Irrig. Drain. Eng.* 143 (6): 04017010. https://doi.org/10.1061/(ASCE)IR.1943-4774.0001168.
16. Skogerboe, G. V., and Hyatt, M. L. (1967). "Rectangular cut throat flumes." *J. Irrig. Drain. Eng. Div*. 98 (4): 569–583.
17. Vatankhah, A. R. (2020). "Discussion of 'Channel flow measurement using portable conical central baffle' by Ankur Kapoor, Aniruddha D. Ghare, Avinash D. Vasudeo, and Avinash M. Badar" *J. Irrig. Drain. Eng.* 146(10): 07020009. https://doi.org/10.1061/(ASCE)IR.1943-4774.0001503.

*IN PROCEEDINGS OF 25th HYDRO 2020, INTERNATIONAL CONFERENCE, NATIONAL INSTITUTE OF TECHNOLOGY ROURKELA, ODISHA, INDIA 26-28, March 2021, ISBN 978-93-90631-56-8*

Paper ID - 082

# Study on Aeration Performance of P.K. weir with its Alternatives: A Review

Deepak Singh[1] and Munendra Kumar[2]

1. *Research Scholar, Department of Civil Engineering, Delhi Technological University, New Delhi-110042*

*Email: kumaindeepaksingh@gmail.com*

*2. Professor, Department of Civil Engineering, Delhi Technological University, New Delhi-110042 Email:*

*mkumar66@gmail.com*

## Abstract

Aeration is the phenomenon by which air is mixed with or dissolved in a liquid. Proper aeration over the hydraulic structures mitigates the risk of cavitation as well as used in maintaining the required Dissolved Oxygen (D.O.) concentration in the flowing water. In case of the open channel, the upper surface of the nappe exposes to the atmosphere, whereas the lower surface of nappe sometimes fully or partially submerged. Therefore, the lower surface of the nappe must be sufficient to ensure the proper aeration. The loss of the D.O. concentration in a stream or open channel flow due to the increment of salt concentration, the increment of the temperature of flowing water as well as the increment of cavitation effect can be remedied by enhancing the aeration performance of the weir structures. There are many ways to improve D.O. concentration in water by using self-aeration, mechanical aeration, and chemicals aeration or by hydraulic structures. However, the hydraulic structures used for aeration are weirs, notches, water jets, spillways, hydraulic jump, falls and close conduit flow arrangements etc. In the last decade, several studies have explored the aeration performances of the different types of free-flow structures such as rectangular, triangular, trapezoidal, semi-circular, labyrinth and Piano key weirs. This study reviews the past studies on the aeration performance of the different types of weirs such as rectangular, triangular, labyrinth weir and P.K. weirs. A closer look at the review shows that the P.K. weir has an excellent aeration performance to mitigate the risk of cavitation as well as used in maintaining the required Dissolved Oxygen (D.O.) concentration in the flowing water over the hydraulic structures.

***Keywords:*** *D.O. Concentration, Aeration, P.K. weirs, Aeration efficiency over different weirs.*

## 1. Introduction

The current scenario it is essential to maintain the water quality parameters at their desirable limits because day by day life the climatic conditions as well as pollution level is enhancing, which is directly or indirectly creating the problem in globally. Dissolved Oxygen is one of the essential parameters among them, which plays an indispensable role for the survivable of aquatic life in river, stream, lake, ponds and reservoir. According to environmental experts, the D.O. concentration varies from creature to creature. The amount of dissolved oxygen for worm's aquatic animals such as bottom feeders, crabs and oysters must contain 4 mg/L, while higher amount 4-15 mg/L oxygen level needs for shallow water fish,. The deficiency in D.O. concentration in any stream and rivers may create a hazard to the natural aquatic cycle. There are many ways to improve or enhance the D.O. concentration in river, stream, lake, ponds and reservoir. Still, aeration is one of the best economical and effective processes among them. In the aeration process the air is assorted within a liquid or water by constructing hydraulic structures, self-aeration, by mechanically, and by chemically. Hydraulic structures are the multipurpose structures; therefore, it can be efficiently used for aeration as well as many other purposes.

The aeration process over the hydraulic structures mitigates the risk of cavity formation as well as used in maintaining the required D.O. concentration in the flowing water. Hydraulic heads are naturally accessible in the river consequently no additional working expense is required for the maintaining the head, achieving aeration in the river/stream water, which makes the weir aeration

economically usable as compared to other artificial oxygen accelerators including mechanical aerators. Hydraulic structures help in boosting up the concentration of D.O. up to a large extent, even though being in contact with water for a concise period.

## 2. Historical Review on Nappe Aeration over Hydraulic Structures

The nappe alludes to the jet of water that passes over a weir structure. The behaviour of the nappe must be examined during the design/planning of weirs and spillways to guarantee optimum hydraulic performance, as well as to account for flow- actuated vibrations, pressure fluctuations, noise and flow surging (Falvey, 1980). The nappe aeration issues for different types of linear weirs have been thoroughly studied and well documented (Kandaswamy and Rouse 1957, Chow 1959).

Gameson (1957) was the first researcher to present the air circulation capability of the weir in rivers. Since then, various experimental studies have been performed at the level of laboratory-scale and investigated the aeration potential of different types of weirs, especially by Van der Kroon (1969a, b), Apted and Novak (1973), Avery and Novak (1978), and Nakasone (1987). Wilhelms *et al.*, (1992) presented a critical review of the aeration performance of the exiting hydraulic structures. Gulliver and Rindels (1993), specifically, examine issues related to field estimations of oxygen transfer and the level of vulnerability included. Wormleaton and Soufiani (1998) examined that the labyrinth weir has better aeration efficiency than the equivalent length linear weir. Emiroglu and Bayler (2003) contemplated air entrainment pace of sharp, broad crested and labyrinth weirs. Further Bagatur and Sekerdag (2003), Baylar and Bagatur (2006), Baylar *et al.*, (2008), Baylar and Ozkan (2006) and (Baylar *et al.*, 2010, 2011), have performed several investigation to find out the air/water flow ratio ($Q_a/Q_w$) and aeration efficiency ($E_{20}$) over different hydraulic structures, Some physical models of P.K. weirs have shown that the flow over weir naturally aerated, but this is, however, only true for relatively low head flows (Hein *et al.*, 2006 and Laugier *et al.*, 2013). Baylar and Bagatur (2000) conducted an experimental study over the different shapes of weirs to measure the aeration performance over a discharge range from 1 and 4 L/s with various drop heights ranges from 0.15-0.90 m. They found that the aeration performance or can say oxygen transfer efficiency is lowest in case of rectangular weir and highest for triangular weir. Baylar *et al.*, (2001) tested the different angled, triangular notch weir and found that the $90^0$ triangular notch weirs have shown better aeration efficiency than others. Further, linear regression and adaptive Neuro-Fuzzy Interference system in predicting the aeration efficiency of P.K. weir was investigated by Komal *et al.*, (2017). Jaiswal and Goal (2019) impersonated a systematic review of the aeration efficiency through the weirs.

Further, Jaiswal and Goal (2020) evaluated the aeration efficiency of the triangular weir by using Gaussian process and M5P approaches and concluded that, this technique has a good agreement between predicted and measured values. Crookston and Tullis (2012a) examined that the labyrinth weir has better efficiency at low heads, as the head increases, hydraulic efficiency declines, and consequently energy dissipation increases. They further expressed that the streaming release over the labyrinth weir relies upon different parameters such as crest length (Lc), cycle configuration and geometry (arced or straight), approach stream conditions (in-channel or reservoir application), and hydraulic circumstances. Crookston and Tullis, (2012d) introduced an intermediate step toward deciding the impact of nappe impedance on labyrinth weir hydrodynamics, for example, neighbourhood submergence. Crookston *et al.*, (2012) analysed four distinctive labyrinth weir nappe air circulation conditions which were seen during the laboratory analysis: clinging, aerated, partially aerated, and drowned. This analysis gives new hydrodynamics and bits of knowledge with respect to nappe conduct, nappe vibrations, nappe instability, and nappe ventilation (e.g., nappe breakers, aeration vents) to be utilized in amalgamation with the labyrinth weir design technique introduced in (Crookston and Tullis 2012a).

One of the main concerns identified by the previous studies is the presence of oscillating negative pressures behind the overflow nappe, the potential of these oscillations causing structural vibrations and the effect of artificially aerating the overflow nappe (Leite Ribeiro *et al.*, 2007) (Erpicum *et al.*, 2013a). The hydraulic performance of the weir depends on the geometry and aeration condition of the

nappe (Crookston & Tullis, 2013). In case of a PKW, the flow over the lateral and downstream inlet key crest forms a continuous curtain with an enclosed air pocket, i.e. a nappe (Denys *et al.*, 2017). The nappe thickness is dictated by the overflow location along the crest and hence the fall height. At higher flows or for narrow outlet keys, the flows from opposite lateral ridges may collide, but do not have a significant effect on the discharge efficiency if free flow conditions are adhered to (Machiels, 2012). Three typical nappe behaviours are observed for PKWs (unsubmerged conditions) and can all occur simultaneously at different locations along the lateral crests for a specific flow (Machiels *et al.*, 2011) (Machiels *et al.*, 2009).

These behaviours are summarised by (Johnson, 2000) in Figure: 1,. A clinging nappe occurs at low heads or velocities when there is no air beneath the nappe, and it clings to the crest and the downstream wall of the structure. · At higher heads, a depressed or leaping nappe occurs when the nappe starts to pull away from the wall but remains in contact with the downstream end of the crest. Generally, the pressure below the nappe is negative and is only partially ventilated or aerated. A free or springing nappe occurs at even higher heads when the nappe detaches from the upstream edge of the crest. The nappe is characterised by atmospheric pressure underneath the nappe, generally obtained by ventilating a weir.

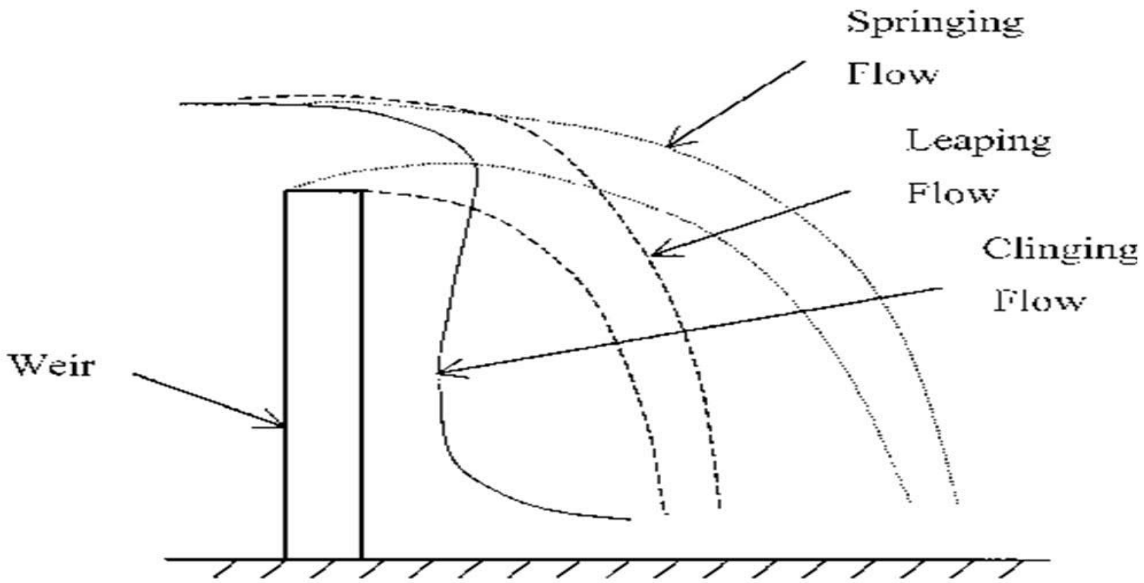



**Figure: 1 Nappe behaviour classification (Johnson, 2000)**

Nappe oscillations primarily occur during partially aerated nappe conditions rather than aerated and drowned nappe conditions. Although artificial aeration may have a reducing effect on the nappe instability (Crookston & Tullis, 2013), it does not necessarily prevent vibrations from occurring (Crookston & Tullis, 2011).

## 3. Basic Equations of Weir Aeration

Self-air circulation is a characteristic cycle of move of oxygen from the air towards the water over a free surface. The efficiency of aeration depends on the quality of air intake at the form state of water. D.O. is a highly inconsistent accumulates with a gas-water transfer rate that is controlled altogether by the liquid phase. Thus Gameson (1957) and Gulliver *et al.* (1990) stated that the concentration rate of oxygen changes over time in air-water phase system as water passes over hydraulic structures and can be expressed as,

$$\frac{dC}{dt} = K_L \frac{A}{V}(C_S - C) \quad (1)$$

Where C = D.O concentration; $K_L$= Coefficient of liquid- mass transfer; A = Surface area associated with the volume of water (V) over which the transfer occurs; $C_S$ = Saturation concentration at the equilibrium with the air phase is achieved; and t is the time. By integrating the Eqn. (1) we get the aeration efficiency.

$$E = \frac{C_d - C_u}{C_s - C_u} \quad (2)$$

Where, E= aeration efficiency, $C_d$ = D.O. concentration d/s of hydraulic structure, $C_u$ = D.O. concentration u/s of hydraulic structure, $C_s$ = D.O. at saturated level for a given ambient condition.

Gulliver *et al.*, (1990) developed the relationship based on mass exchange comparability to adjust aeration efficiency to $20^0$C and signified as $E_{20}$

$$E_{20} = 1 - (1 - E)^{1/f} \quad (3)$$

Where exponent f is expressed as follows:

$$f = 1 + 0.02103(T - 20) + 8.261 \times 10^{-5}(T - 20)^2 \quad (4)$$

Where T = Temperature in $^0$C

Holler (1971) assessed the aeration proficiency based on the hydraulic jump pre and post velocities as follows:

$$E_{20} = 1 - \frac{1}{1 + 0.0463\Delta V^2} \quad (5)$$

Where $\Delta V = V_1 - V_2$

Kucukali & Cokger (2009) presented a relation between aeration efficiency and energy dissipation rate as follows:

$$E_{20} = 0.0015w + 0.01 \quad (6)$$

Where, $w = (q \times \Delta H \times \gamma)$ rate of energy dissipation/width, q = flow rate/width and $\gamma$ = specific weight of water.

Lodomez *et al.*, (2017) addressed the two prevailing approaches (an images approaches and a sound approaches) to address aeration issues or nappe oscillation over the P.K. weir. In order to find the aeration performance of the P.K. weir, they conducted an experimental study along with various crest length and chute width configuration. The investigation shows that nappe motions are probably not going to happen on PKW, while they ought to happen on a labyrinth weir having a similar crest. PKW

has a preferred position contrasted with conventional vertical labyrinth whereby the establishment of air circulation lines may be perplexing. The peril of vibration, regardless, has all the earmarks of being less basic for the hydraulic structure that is a PK weir.

Vermeulen *et al.*, (2017) presented an air demand evaluation method reliant on made by (Ervine and Elsawy, 1975) on air driven by a rectangular channel stream falling into a volume of free water surface (Falvey 1980). This new appraisal procedure has been as of late endorsed by extents of air interest on Malarce dam PKW while flooding. The empirical formula was developed by the author, which predicts the measure of air flow in a stream $Q_{air}$ ($m^3/s$) as:

$$Q_{air} = (q_w \times L_n) \times 0.26 \times \left(\frac{L_n}{P_n}\right) \times \left(\frac{d_j}{h_n}\right)^{0.446} \times \left(1 - \frac{V_m}{V_i}\right) \quad (7)$$

Where,
$q_w$ = overflowing discharge through inlets or sidewalls ($m^3/s$), $L_n$ = width of nappe (m), $h_n$ = thickness of nappe (m), $P_n$ = perimeter of nappe which is equal to $P_n = 2*( L_n + h_n)$ (m), $d_n$ = height of falling jet (m), $V_i$ = speed of jet impact (m/s), and $V_m$ = Critical velocity required to entrain air. Nappe instabilities have been observed for fully aerated nappes (Crookston *et al.*, 2014) (Falvey, 1980) (Lodomez *et al.*, 2018a). Experimental studies by Lodomez *et al.*, (2018a) have shown that the air pocket behind the nappe only serves as an amplification and stabiliser factor and does not affect the occurrence of nappe vibrations.

According to Lombaard (2020) the nappe over the PK weir formed a continuous water curtain over the lateral and downstream inlet key crests. The flow surface was generally smooth and stable for lower discharge rates, which showed the nappe trajectory and characteristics, and however, for higher head the flow became more turbulent, making surface profile intricate or more difficult to nappe trajectory. The nappe profiles over the downstream crest and sidewalls of the inlet key, especially for low discharges, are noticeably affected by artificially aerating the nappe air cavity. It is best illustrated in the nappe surface profile measurements of the no aeration and completely aerated conditions (breaking the nappe) as shown in Figure: 2

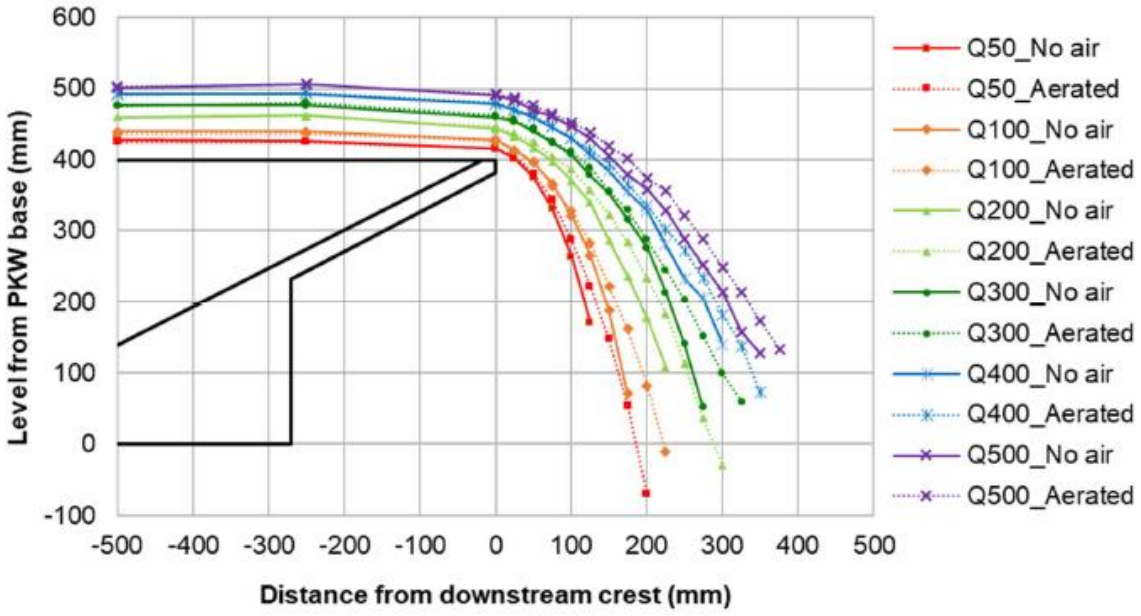



**Figure: 2 Measured of Nappe Profile (Adopted from Lombaard (2020))**

The purpose of this study is to present the review all the recent past work systematically investigate the aeration performance of the different types of the weir in terms of their discharge carrying efficiency.

## 4. Conclusion

The following recommendations can be made based on the findings of this hydraulic model study:

1. The aeration process over the hydraulic structures mitigates the risk of cavity formation as well as used in maintaining the required D.O. concentration in the flowing water.
2. The triangular weir shows the better aeration performance out of rectangular, triangular, trapezoidal and semi-circular geometries of weirs.
3. In comparison between weirs, Labyrinth weirs and PK weirs, PK weirs give better aeration potential at low head.
4. Artificial aeration testing under a great variety of conditions would be beneficial under low flow with $H/P \leq 0.10$ and therefore recommended when the expected discharge over a PKW high its lifecycle will mostly be within this range.
5. If nappe oscillations are expected for low flow conditions, artificial aeration can be considered as a mitigation measure to reduce the intensity of the fluctuations.
6. Considering that water mass has a damping effect on the natural frequency of the structure, the influence of increased downstream water levels on the vibrations can be evaluated.

**References**

1. Apted, R. W., and Novak, P., "Some Studies of Oxygen Uptake at Weirs", Proceedings of the XV Congress, IAHR paper B23, 1973.
2. Avery, S., and Novak, P., "Oxygen Transfer at Hydraulic Structures", Journal of Hydraulic Engineering, ASCE, Vol. 104, HY11, pp. 1521-1540, 1978.
3. Baylar A, and Bagatur, T. (2000). "Study of aeration efficiency at weirs." Turk J. Eng Environ Sci 24(4):255–264
4. Baylar, A, Bagatur, T and Tuna, A. (2001). "Aeration performance of triangular-notch weirs." Water Environmental J. 15(3), 203–206
5. Bagatur, T. and Sekerdag, N. (2003). Air-entrainment characteristics in a plunging water jet system using rectangular nozzles with rounded ends. Water SA, 29(1), pp.35-38
6. Baylar A, and Bagatur, T. (2006). "Experimental studies on air entrainment and oxygen content downstream of sharp crested weirs." Water Environmental J. 20(4), 210–216
7. Baylar, A. and Ozkan, F., 2006. Applications of venturi principle to water aeration systems. Environmental Fluid Mechanics, 6(4), pp.341-357.
8. Baylar, A., Hanbay, D. and Ozpolat, E. (2008). "An expert system for predicting aeration performance of weirs by using ANFIS". Expert Systems with Applications, 35(3), pp.1214-1222.
9. Baylar, A., Unsal, M. and Ozkan, F. (2010). "Hydraulic structures in water aeration processes". Water, Air, & Soil Pollution, 210(1-4), pp.87-100.
10. Baylar, A., Unsal, M. and Ozkan, F. (2011). "GEP modeling of oxygen transfer efficiency prediction in aeration cascades". KSCE, Journal of Civil Engineering, 15(5), pp.799-804.
11. Chow, V.T. (1959). Open-channel Hydraulics. McGraw-Hill, New York, NY.
12. Crookston, B. M., & Tullis, B. P. (2011). Hydraulic characteristics of labyrinth weirs. Labyrinth and Piano Key Weirs – PKW 2011 (pp. 25-32). CRC, Taylor & Francis Group.
13. Crookston, B.M. and Tullis, B.P. (2012a). "Hydraulic design and analysis of labyrinth weirs. Part 1: Discharge relationships. J. Irrig. Drain. Engr., ASCE, #(#). Posted ahead of print (date).
14. Crookston, B.M. and Tullis, B.P. (2012d). "Labyrinth weirs: Nappe interference and local submergence." J. Irrig. Drain. Engr., ASCE, 138(8), 757-765.

15. Crookston, B.M. ASCE, A.M. and Tullis, B.P. (2012). "Hydraulic design and analysis of Labyrinth weirs: Part-II: Nappe Aeration, Instability and Vibration". *J. Irrig. Drain. Engr., ASCE, 138(8), 757-765*.
16. Crookston, B. M., & Tullis, B. P. (2013). Hydraulic Design and Analysis of Labyrinth Weirs. II: Nappe Aeration, Instability, and Vibration. Journal of Irrigation and Drainage Engineering, 139, 371 - 377.
17. Crookston, B. M., Anderson, A., Shearin-Feimster, L., & Tullis, B. P. (2014). Mitigation Investigation of Flow-induced Vibrations at a Rehabilitated Spillway. 5th International Symposium on Hydraulic Structures 25 - 27 June. Brisbane: Hydraulic Structures and Society: Engineering Challenges and Extremes.
18. Denys, F. M., Basson, G., & Strasheim, J. (2017). Fluid Structure Interaction of Piano Key Weirs. Proceedings of the 3rd International Workshop on Labyrinth and Piano Key Weirs III - PKW 2017, (pp. 119-126).
19. Emiroglu, M. E. and Baylar, A.(2003). "The effect of broad crested weir shape on air entrainment. J. Hydraulic Res. 41(6): 649-655.
20. Erpicum, S., Laugier, F., Pfister, M., Pirotton, M., Cicero, G. M., & Schleiss, A. J. (2013a). Labyrinth and Piano Key Weirs II - PKW 2013. Proceedings of the 2nd International Workshop on Labyrinth and Piano Key Weirs II - PKW 2013 (p. 291). CRC Press, Taylor & Francis Group.
21. Ervine, D. A., & Elsawy, E. M. (1975). Effect of a Falling Nappe on River Aeration. 16th Congress of the International Associations for Hydraulic Research, (pp. 390-397) Brazil.
22. Falvey, H. (1980). "Practical experiences with flow-induced vibrations," edited by Naudascher, E., and Rockwell, D., Springer-Verlag, 386-398. Berlin/Heidelberg/New York.
23. Gameson, A. L. H., "Weirs and Aeration of Rivers", Journal of the Institution of Water Engineers, Vol. 11, 1957.
24. Gulliver J. S., Thene J .R. and Rindels, A. J. (1990) Indexing gas transfer in self-aerated flows. J. Environ. Eng., ASCE 116 (3) 503-523.
25. Gulliver, J. S., and Rindels, A. J. (1993) "Measurement of air-water oxygen transfer at hydraulic structures". *J. Hydraulic Engg. , ASCE, Vol. 119(3), pp. 327-349*.
26. Hien, T.C., Son, H.T., & Khanh, M.H.T. (2006). "Results of some piano keys weir hydraulic model tests in Vietnam". Proc. of the 22nd Congress of ICOLD, Barcelona, Spain.
27. Holler, A.G.(1971). "The mechanism describing oxygen transfer from the atmosphere to discharge through hydraulic structures". Proceeding of 14th International Association for Hydraulic Research World Congress, August 29-September 3, Paris, France pp: 372-382.
28. Jaiswal, A. and Goal, A. (2019). "Aeration through Weirs- A Critical Review". Sustainable Engineering, Lecture Notes in Civil Engineering 30, https://doi.org/10.1007/978-981-13-6717-5_19
29. Jaiswal, A. and Goal, A. (2020). "Evaluation of Aeration Efficiency of Triangular weirs by using Gaussian Process and M5P Approaches". Advanced Engineering Optimization Through Intelligent Techniques, Advanced in intelligent System and Computing 949, https://doi.org/10.1007/978-981-13-8196-6_66
30. Lombaard J. (2020). "Evaluation of the Influence of Aeration on the Discharge Capacity and Flow Induced Vibrations of Piano Key Weir Spillways" Masters of Engineering thesis. Copyright © 2020 Stellenbosch University.
31. Johnson, M. C. (2000). Discharge coefficient analysis for flattopped and sharp-crested weirs. Irrigation Science, 19(3), 133-137.
32. Kandaswamy, P. and Rouse, H. (1957). "Characteristics of flow over terminal weirs and sills." J. Hydr. Div., ASCE, no HY4, 1345 (83).
33. Komal, Kumar, M., Tiwari, N.K. and Ranjan, S.(2017). "Aeration performance Evaluation of Piano Key Weir using Linear regression and Adaptive Neuro Fuzzy Inference Sysem". ICET: EITM-2017, NIT Hamirpur, India, December16-18, 2017.
34. Kucukali, S. and Cokgor, S.(2009). " Energy concept for predicting hydraulic jump aeration efficiency". *J. Environ. Engg. 135: 105-107*.
35. Laugier F, Vermeulen J & Lefebvre V (2013). "Overview of Piano Key Weirs experience developed at EDF during the past few years." Proceedings of the 2nd International Workshop

on Labyrinth and Piano Key Weirs (PKW 2013), pp. 213-226. CRC Press, Taylor & Francis Group.

36. Leite Ribeiro, M., Boillat, J. L., Schleiss, A., Laugier, F., & Albalat, C. (2007). Rehabilitation of St-Marc Dam - Experimental Optimization of a Piano Key Weir. Proceedings of the 32nd Congress of IAHR.
37. Lodomez, M., Pirotton, M., Dewals, B., Archambeau, P., and Erpicum, S. (2017). "Could piano key weirs be subject to nappe oscillations?" Labyrinth and Piano Key Weirs III: Proceedings of the 3rd International Workshop on Labyrinth and Piano Key Weirs (PKW 2017), Feb 22–24, 2017, CRC Press, Qui Nhon, Vietnam
38. Lodomez, M., Pirotton, M., Dewals, B., Archambeau, P., & Erpicum, S. (2018a). Nappe oscillations on free-overfall structures: Experimental analysis. Journal of Hydraulic Engineering, 144(3).
39. Machiels, O., Erpicum, S., Archambeau, P., Dewals, B. J., & Pirotton, M. (2009). Large scale experimental study of piano key weirs. Proceedings of the 33rd Congress of IAHR. International Symposium on Hydraulic Structures.
40. Machiels, O., Erpicum, S., Dewals, B. J., Archambeau, P., & Pirotton, M. (2011). Experimental observations of flow characteristics over a Piano Key Weir. Journal of Hydraulic Research, 49(3), 359-366.
41. Machiels, O. (2012). Experimental study of the hydraulic behaviour of Piano Key Weirs. PhD thesis. HECE Research Unit, University of Liège, Belgium.
42. Nakasone, H. (1987). "Study of aeration at weirs and cascades". J. Environ. Eng., ASCE 113 (1) 64-81.
43. Van der Kroon, G. T. N., and Schram, A. H., "Weir Aeration - Part I", H2O, No.22, pp.528-537, 1969a.
44. Van der Kroon, G. T. N., and Schram, A. H., "Weir Aeration - Part II", H2O, No.22, pp.538-545, 1969b.
45. Vermeulen, J., Lassus, C., & Pinchard, T. (2017). Design of a Piano Key Weir Aeration Network. Proceedings of the 3rd International Workshop on Labyrinth and Piano Key Weirs III - PKW 2017, Qui Nhon, Vietnam, 22-24 February 2017 (pp. 127-134). London: Taylor & Francis Group.
46. Wilhelms, S. C., Gulliver, J. S., and Parkhill, K., "Reaeration at Low-Head Hydraulic Structures", Tech. Rep. HL-91, U. S. Army Engineer Waterways Experiment Station, Vicksburg, Miss, 1992.
47. Wormleaton, P. R., & Soufiani, E. (1998). Aeration performance of triangular platform labyrinth weirs. Journal of Environmental Engineering, 124(8), 709-719.

*IN PROCEEDINGS OF 25th HYDRO 2020, INTERNATIONAL CONFERENCE, NATIONAL INSTITUTE OF TECHNOLOGY ROURKELA, ODISHA, INDIA 26-28, March 2021, ISBN 978-93-90631-56-8*

Paper ID - 103

# STUDY OF FLOW CHARACTERISTIC OF RECTANGULAR LABYRINTH WEIR

Saurabh Sah [1*], Munendra Kumar[2]

[1,]Research Scholar Department of Civil Engineering

Delhi Technological University, New Delhi-110042, India

[2] Professor Department of Civil Engineering

Delhi Technological University, New Delhi-110042, India

## ABSTRACT

A rectangular labyrinth weir is characterized by a broken axis in plan as is seen in so that the effective length of crest is increased. This accounts for the spatial flow behaviour and defines the water surface profile along with the centre line of the labyrinth weir upstream channel. A physical model for the experimental studies design and analysis of rectangular labyrinth weirs. Hydraulic model tests of the weir showed that the behaviour of the labyrinth weir was convenient and that the discharge capacity presented a good agreement with theoretical calculations. It is the purpose of this paper to present a satisfactory developed physical model of labyrinth weir flow and provide engineers with a model capable of dealing with a variety of labyrinth weir configurations and flow conditions. This studies of rectangular labyrinth weir are performed between head to crest ratio, apex width, vertical aspect ratio, approach and conveyance channel conditions that increased the discharge capacity of rectangular labyrinth weir and design of rectangular labyrinth weir.

***Keywords:*** *Rectangular Labyrinth Weir, Hydraulic model, Physical model, Discharge Coefficient.*

## 1. Introduction

A rectangular labyrinth weir is built across a stream in order to raise of water level on the upstream side of river and allow the excess of water to flow over its entire length to the downstream side. Labyrinth weirs increase the spillway discharge capacity of dams and are often considered for renovation projects required due to an increase in expected flood inflow to the reservoir of dam. An effective way of increasing the spillway capacity is to use a rectangular labyrinth weir. The labyrinth weir is used to vary the plan shape of the crest in order to increase the effective crest length. Labyrinth weir (Q) under free flow condition in a channel is in terms of the following mathematical expression.

$$Q = \frac{2}{3} C_d \sqrt{2g}\, L h^{\frac{3}{2}} \qquad (1)$$

Where $C_d$ = coefficient of discharge, L = crest length of the weir, g = acceleration due to gravity, h = head over the crest. Cd depends on flow characteristics and geometry of the channel and the weir. In this paper are the results of the experimental study carried out to investigate the discharging capacity of a rectangular labyrinth weir plan form under free flow condition in a rectangular channel. The following equation for Cd was proposed by conducting experiments of broad crested curved weir.

$$C_d = \left(0.5 + 0.33\frac{h}{w} + \frac{h}{L}\right)^{0.06} \qquad (2)$$

Hay and Taylor followed up on Taylor's work and developed design criteria for labyrinth weirs. They suggested equation (3) for the discharge coefficient of labyrinth weirs.

$$C_d = 3.22 + 0.40\frac{h}{P} \tag{3}$$

Where Cd is the discharge coefficient; h is the depth of flow over the weir crest and P is the weir height. Lux has investigated model studies of the labyrinth weir and equation (4) is his suggested equation for calculation of the discharge of rectangular labyrinth weir.

$$Q = C_d\left(\frac{\frac{W_C}{P}}{\frac{W_C}{P+K}}\right)W_C H_t\sqrt{gH_t} \tag{4}$$

Where Q is the discharge over labyrinth weir $Cd$ is the discharge coefficient; $Ht$ is the total upstream head measured relative to the weir crest; $Wc$ is the channel width and P is the weir height. Magalhaes and Lorena calculated discharge coefficient ($C_d$) of labyrinth weir as function of L/w and $Ht/P$ parameters.

$$Q = C_d W_T 2gH_t{}^{1.5} \tag{5}$$

## 2. Experimental Set-up and Experiments

Experiments on the discharge capacity and flow characteristics of the rectangular labyrinth weirs were carried out using a physical model located in the hydraulic laboratory civil engineering department of Delhi Technological University, Delhi India. The experimental set-up includes sump, pumping system, collecting tank, rectangular flume, digital flow meter and rectangular labyrinth weir. Water is recirculated through 150 mm diameter of supply line using one 30 HP pumps. Water for experimental setup is taken from the supply line by means of a pipe with 100 mm diameter. The discharge was measured by means of an electromagnetic flow-meter installed in the supply line. For damping the water surface waves and reducing turbulence, baffle wall and wood surface dampener is provided. In the experiments, the upstream elevation was built higher than the downstream elevation so that free flow conditions occur downstream of the weir. Sheet metal materials which have 5 mm thickness ($t$) were used for labyrinth weirs. The upstream apex angle of the nappe breakers was taken as 90˚ and downstream apex shape was manufactured as rounded. Rectangular labyrinth weirs designed as two, three, fourth and five cycles. Schematic view of rectangular labyrinth and linear weirs is given in (Figure 2.1 to 2.5). Each labyrinth weir models with a sharp crested shape was tested in the experiments.

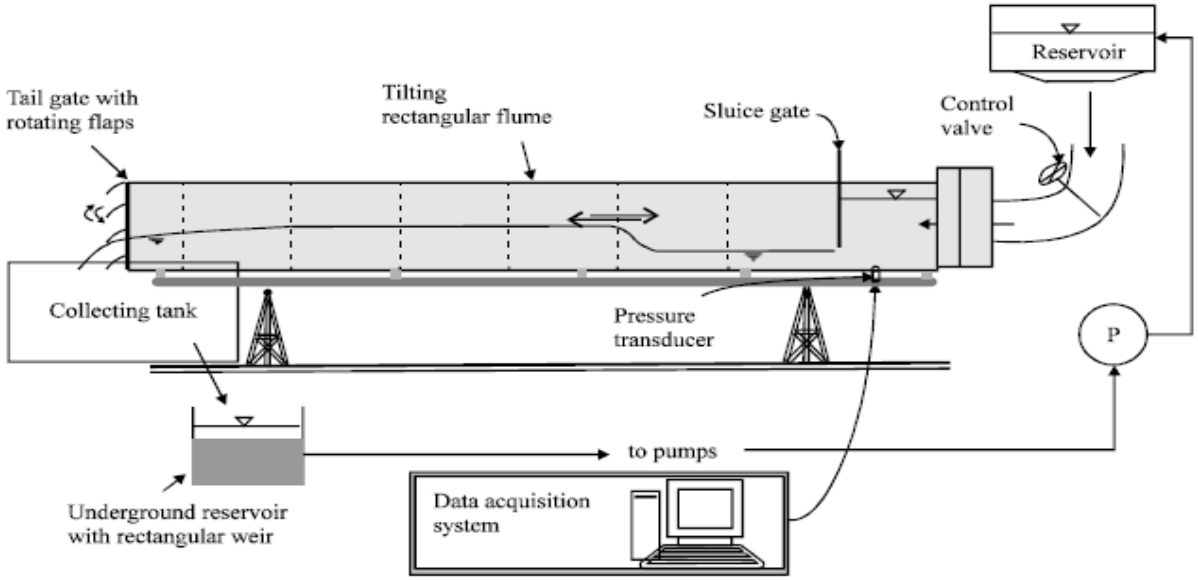



**Figure 2.1: Definition Sketch for Tilting Flume (10 m) Length**

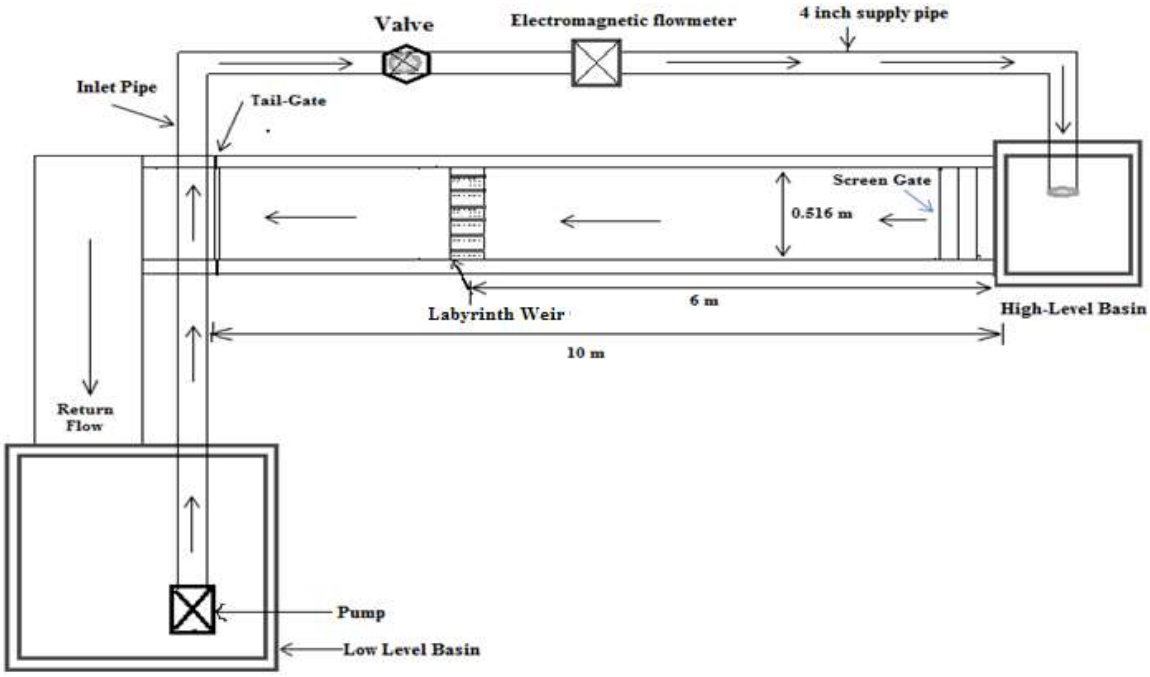



**Figure: 2.2. Schematic plan view of experimental setup.**

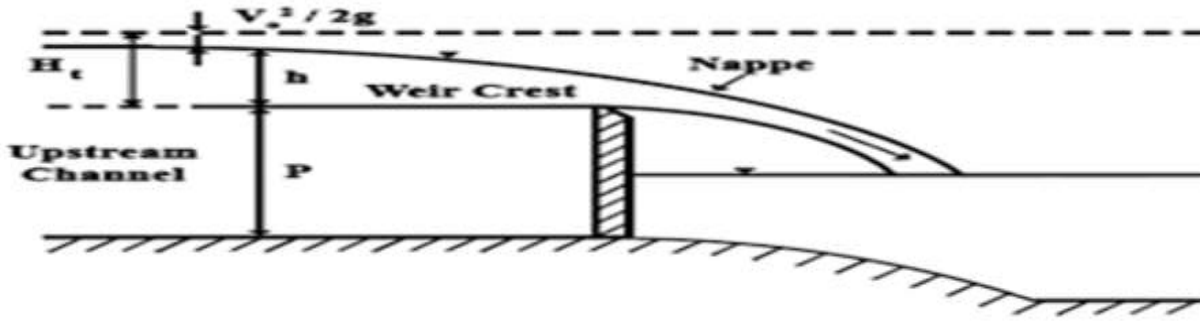



**Figure 2.3: Definition Sketch for Flow over a Sharp Crested Weir**



**Figure 2.4: Definition Sketch for Flow over a Rectangular Labyrinth Weir with Electromagnetic Flow Meter and Pointer Gauge.**

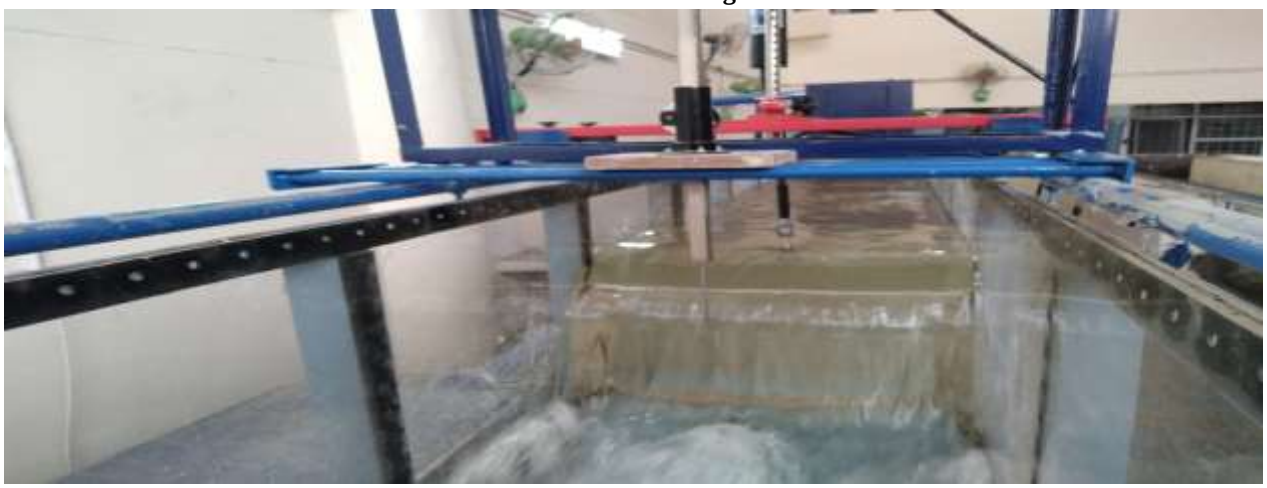


**Figure 2.5: Definition Sketch for Flow over a Rectangular Labyrinth Weir with ADV.**

## 3. Experimental Results and Analysis

Experiment study are carried out on twenty rectangular labyrinth weir models and their side wall angle of 0°,90°and linear weir models having sharp crested shape similar to labyrinth weir models. The head discharge measurement are taken for weir height of P= 15, 20, 25 and 30 cm. Total 20 different configurations were examined in this experiments shown in Table 1. The discharge coefficient was computed by labyrinth weir equation no (4). In this study the crest was spaced at a regular interval. From the experiments results the variation of Cd for rectangular labyrinth weir with Ht/P is plotted in (Figure 3.1 to 3.2).

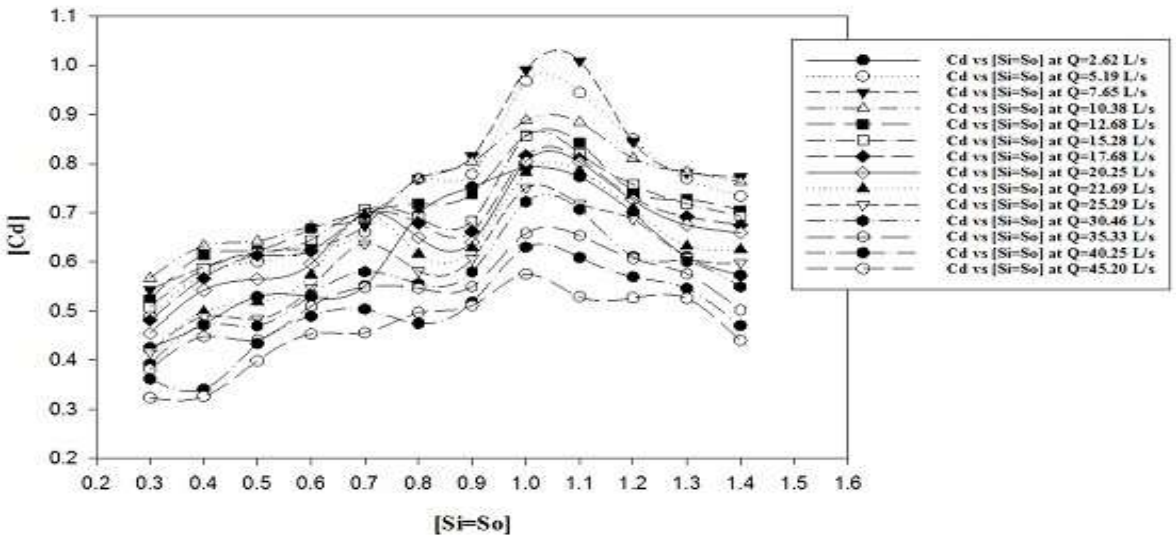



**Figure: 3.1: Variation of discharge coefficient [Cd] with different slopping floor [Si=So]**

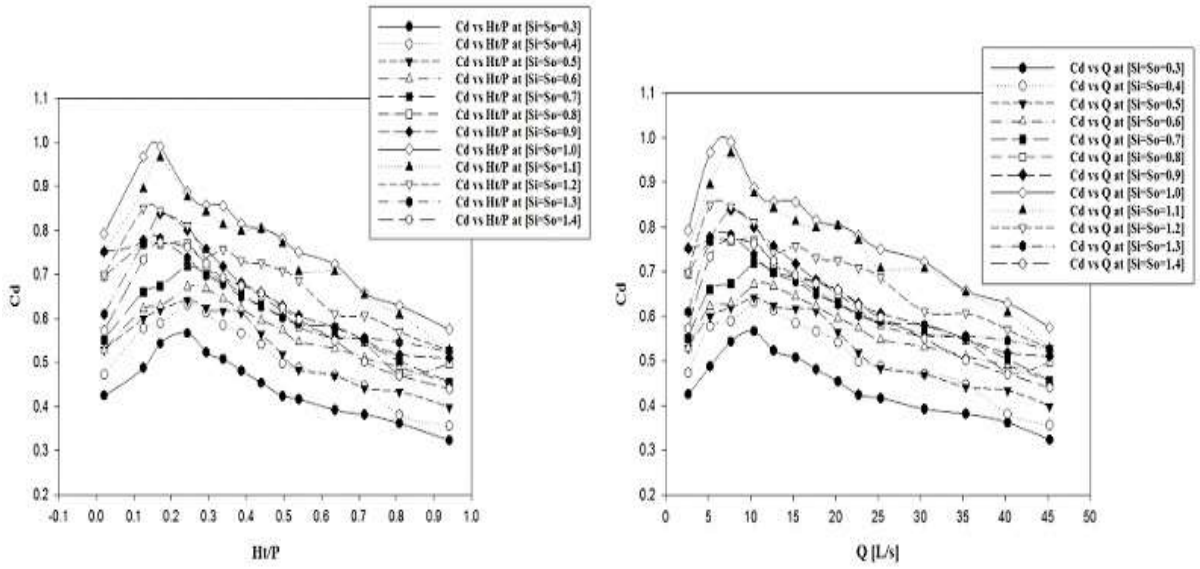



**Figure: 3.2. (a) Variation of Cd with Ht/P left and (b) variation of Cd with Q [L/s] right.**

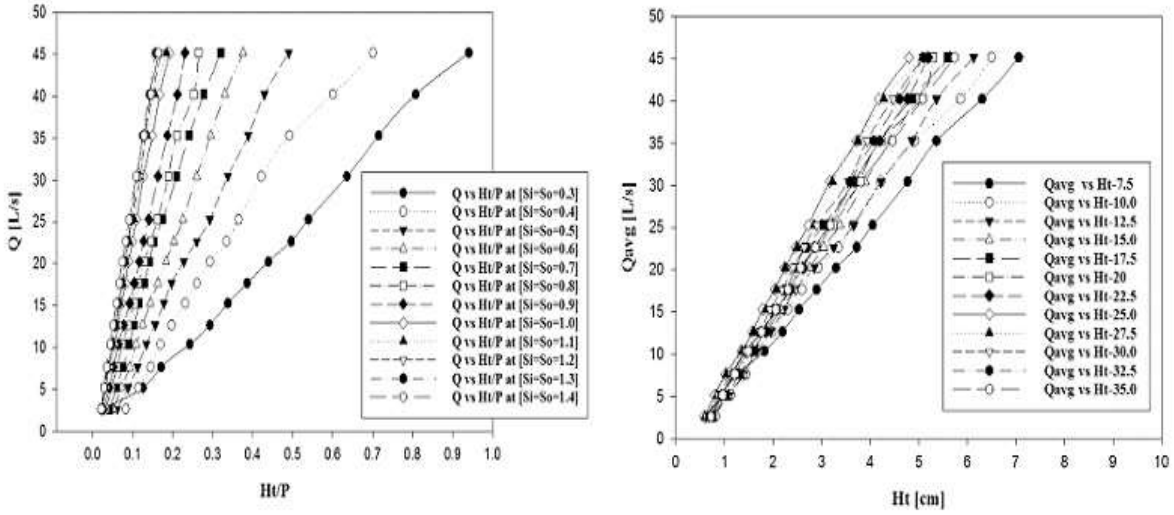



**Figure: 3.3: Variation of discharge Q with Ht/P and Ht.**

## 4. Conclusions

Rectangular labyrinth weir can pass large water flow at minimum head. The labyrinth weir can also be used easily to measures discharge metering device in open channel flow. The equation of Cd for weir has been obtained, which can be employed to find the value of Cd and θ in the corresponding range of the discharge of rectangular labyrinth weir**.** This study has found that rectangular labyrinth weir are more efficient than the linear weir and form the ease of construction and the increase discharge capacity. A problem for rectangular labyrinth weir is matching the outflow to downstream flow limitation. It is recommended that a study of the rectangular labyrinth weir design of physical model be undertaken to study the performances of different shapes and operations. In the study that recommended a rectangular labyrinth weir analysis and design to verified by a physical model study to same parameter with numerical modeling study for future work.

**Acknowledgments**

The author gratefully acknowledges the supports provided by the department of civil engineering, Delhi Technological University Delhi.

**Nomenclature**

$A =$ Inside apex width;
$B =$ Flume width;
$a, b$ = Coefficients;
$Cd$ = Coefficients of discharge for labyrinth weir;
$Fr =$ Froude Number;
$g$ = Acceleration due to gravity;
$Ht$ =Total upstream head on weir;
$Ht/P$ = Headwater ratio;
$l =$ Length of one cycle $(2L1 + A + D)$;

$L$ = Effective length of labyrinth = $N$ $(2L2 + 2A)$;
$N$ = Number of cycle;
$P$ = Weir height;
$Qo$ = Observed discharge;
$Qc$ = Computed discharge;
$R2$ = Determination coefficient;
$t$ = Weir wall thickness;
$Va$ = Velocity of approach;
$W$ = Total width of labyrinth weir;
$w$ = Width of one cycle of labyrinth;
$\theta$ = Vertex angle;
$\alpha$ = Angle of side edge or labyrinth angle;
ADV= Acoustic Doppler Velocimeter;

## References

1. Anderson, R. M. and Tullis, B. P., (2012) Comparison of Piano Key and Rectangular Labyrinth Weir Hydraulics. J. Hydraulic. Eng. 138:358-361.
2. Anderson, R.M. and Tullis, B.P. (2013) Piano Key Hydraulics and Labyrinth Weir Comparisons. *Journal of Irrigation and Drainage Engineering* (*ASCE*), **139**, 246-253.
3. Bilhan, O., Emiroglu, M.E. and Kisi, O. (2011) Use of Artificial Neural Networks for Prediction of Discharge Coefficient of Triangular Labyrinth Side Weir in Curved Channels. *Journal of Advances in Engineering Software*, **42**, 208-214.
4. Crookston, B.M. and Tullis, B.P. (2012) Arced Labyrinth Weirs. *Journal of Hydraulic Engineering* (*ASCE*), 138,555-562.
5. Crookston, B.M. and Tullis, B.P. (2012b) Discharge Efficiency of Reservoir-Application Specific Labyrinth Weirs. *Journal of Irrigation and Drainage Engineering* (*ASCE*), 138, 564-568.
6. Crookston, B.M. and Tullis, B.P. (2013) Hydraulic Design and Analysis of Labyrinth Weirs. II: Nappe Aeration, Instability, and Vibration. *Journal of Irrigation and Drainage Engineering* (*ASCE*), 139, 371-377.
7. Emiroglu, M.E., Kaya, N. and Agaccioglu, H. (2010) Discharge Capacity of Labyrinth Side Weir Located On a Straight Channel. *Journal of Irrigation and Drainage Engineering* (*ASCE*), **136**, 37-46.
8. Garde, R.J. and Ranga Raju, K.G. (2000). Mechanics of sediment transportation and alluvial stream problems. Wiley Eastern Limited, New Delhi.
9. Hassan I. Mohamed, "Flow over gabion weirs", J. Irrig. Drain Eng., 2010, 136(8): 573-577, Journal of Irrigation and Drainage Engineering © ASCE (2010).
10. Hay, N. and Taylor, G. (1970) Performance and Design of Labyrinth Weir. *Journal of Hydraulic Engineering* (*ASCE*), 96, 2337-2357.
11. J. Martı´nez, J. Reca, M.T. Morillas, J.G. Lo´ pez, Design and calibration of a compound sharp-crested weir, J. Hydraulic Eng. ASCE 131 (2) (2005) 112–116.
12. Kandaswamy, P. and Rouse, H. (1957) Characteristics of Flow over Terminal Weirs and Sills. *Journal of Hydraulics Division*, 83, 1-13.

13. Khode B.V., Tembhurkar A.R., Porey P.D., & Ingle R.N., (2010)." Determination of Crest Coefficient for Flow over Trapezoidal Labyrinth Weir". World Applied Sciences Journal, Vol.12, No.3, pp.324-329, 2011, (ISSN 1818- 4952), © IDOSI Publications, 2011
14. Khode, B. V., Tembhurkar, A. R. P. D. Porey and R. N. Ingle, (2012) Experimental Studies on Flow over Labyrinth Weir. Journal of Irrig. Drain Eng. ASCE, 138:548-552.
15. Lux, F. (1989) Design and Application of Labyrinth Weirs. Design of Hydraulic Structures 89, Balkema, Rotterdam.
16. Magalhaes, A. and Lorena, M. (1989) Hydraulic Design of Labyrinth Weirs. Report No. 736, National Laboratory of Civil Engineering, Lisbon, Portugal.
17. M.G. Bos (Ed.), Discharge measurement structures. International Institute for Land Reclamation and Improvement (ILRI) Publication 20, Wageningen, The Netherlands, 1989.
18. M.F. Sobeih, E.Y. Helal, T.H. Nassralla, A.A. Abdelaziz, Scour depth downstream weir with openings, Int. J. Civil Struct. Eng. 1 (3) (2012) 259–270.
19. Righetti M, Lanzoni S. Experimental study of the flow field over bottom intake racks. ASCE Journal of Hydraulic Engineering 2008; 134(1):15-22.
20. Tullis, B.P. and Waldron, D. (2005). Design of labyrinth spillways. *Journal of Hydraulic Engineering*, Vol 121, No 3.
21. Tullis BP, Amanian N, Waldron D. Design of labyrinth spillways. ASCE J Hyd Eng 1995; 121(3):247–55.
22. Tullis BP, Young JC,Chandler MA. Head-discharge relationships for submerged Labyrinth weirs. ASCE J Hyd Eng 2007; 133(3):248–53.
23. Venkataraman P. Discharge characteristics of an idealized bottom intake. Journal of the Institution of Engineers 1977; 58(2-3):99.
24. Yıldız, D. and Uzucek, E. (1996) Modeling the Performance of Labyrinth Spillways. *The International Journal on Hydropower and Dams*, **3**, 71-76.

*IN PROCEEDINGS OF 25th HYDRO 2020, INTERNATIONAL CONFERENCE, NATIONAL INSTITUTE OF TECHNOLOGY ROURKELA, ODISHA, INDIA 26-28, March 2021, ISBN 978-93-90631-56-8*

Paper ID - 110

# Hydrodynamic Cavitation: A Treatment to Secondary Effluent of STP to Reuse

Neha S. Baghele[1†], Anjali K. Khambete[2], Robin A. Christian[2]

[1]*Research Scholar, Civil Engineering Department, S. V. National Institute of Technology, Surat, India*
[2]*Faculty of Civil Engineering Department, S. V. National Institute of Technology, Surat, India*
*Email: neha.baghele19@gmail.com*
*Telephone/Mobile No.: +91 9579467759*

## Abstract

The degradation of secondary sedimentation tank effluent from the Sewage Treatment Plant (STP) using Hydrodynamic Cavitation (HC) for reuse has been investigated for the first time. The HC experiments has been designed for the study of HC process performance in Secondary Sedimentation Tank Effluent of Anjana STP, Surat, sampled for precised understanding of effect on inlet pressure (0.4 to 1.0 kg/cm2), the geometry of the cavitating device on reuse which was measured by COD parameter, has studied to maximize the rate of reduction of COD. The maximum reduction in COD as 64.12% for 2 mm hole is obtained under 0.8 kg/cm$^2$ optimized inlet pres sure. The pseudo-first-order kinetics has been used to described degradation. The hydrodynamic cavitation is zero sludge production, Physico-chemical treatment for SST effluent. The degradation COD has in the permissible limit for reuse the treated wastewater for various purposes like irrigation, plantation which helps to keep clean the environment.

***Keywords:*** *Chemical Oxygen Demand, Orifice Plate, Reuse, Secondary Sedimentation Tank Effluent.*

## 1. Introduction

Nowadays, the wastewater reuse is turned upward as potential substitute to deal with the expanding shortage hassle of water. Recycled water has been appropriate for a few applications like cleaning, toilet flushing, industrial reuse, irrigation, and ecological upgradation. On account of its steady quality, recycled wastewater of Sewage Treatment Plants from domestic source may be the dependable substitute asset of water (Gogate and Patil 2015; Jamwal and Mittal 2010; M. Amasha 2007). The reuse of wastewater produced from the domestic source could be acquired by the sewage treatment plant (STP) which is being practiced out of numerous years. Currently, it is perceived that conventional sewage treatment methods, includes rotational biological contractor, activated sludge processes (ASP), extended aeration process, trickling filters, up-flow anaerobic sludge blanket reactors are effective for degradation of carbonaceous contamination, however incapable to degrade nutrient successfully, especially nitrogen and phosphorus alongside microorganism/pathogen. (Kumar and Asolekar 2016). There is the presence of disease-causing pathogens in the wastewater treated by sewage treatment plants, if such effluent is disposed of then it can influence the microbiological life causing significant intimidation to individual health (Kumar, Tyagi, and Gupta 2011). The design of STPs are being made in consideration for effective degradation of organic matter, yet rarely have been arranged explicitly to kill pathogens from wastewater as a result of the economy. Consequently, after the treatment, there has been safe reuse of effluent from STPs. Thus, cautious analysis is needed by such STPs. The efficiency to remove pathogenic along with indicator microorganism STPs change as per the characteristic of sewage at the inlet, kind of treatment process, pH, temperature, Hydraulic Retention Time (HRT), Solid Retention Time, organic vegetation present in treatment plants, as well as the removal of suspended solids (Jamwal and Mittal 2010). Disinfection is a tertiary treatment of effluent coming from the secondary sedimentation tank (SST) of STP. The disinfection process or operation is a significantly slaughtered or controlled percentage of pathogenic microorganisms. Chlorination is most being practice by conventional STPs as a disinfection process which surplus the

chlorine in the form of residue for further contamination (Metcalf & Eddy 1991). Most widely, the Chlorination process of disinfection has been used for its effectiveness in killing pathogens. Further, the surplus amount of residual chlorine is toxic to aquatic life thus the effluent of the disinfection process should also be dechlorinated chemically. (Kumar, Tyagi, and Gupta 2011). Consequently, it becomes necessary to ascertain suitable technology, to improve the water quality and to meet up the permissible standards for reuse of treated effluent.

During last decade, several advance treatment methods are developed for the removal of an organic and inorganic pollutant from domestic and industrial wastewater like aeration, coagulation, and flocculation, membrane separation, ion exchange, wet air oxidation, ozonation, Fenton oxidation, photocatalytic degradation, along with general advanced oxidation processes (AOPs) (Metcalf & Eddy 1991). As compared to conventional treatment, the AOPs are an alluring option for the entire removal of contaminants with the production of zero sludge. AOPs includes the utilization of ozone, UV, $H_2O_2$, $TiO_2$, Fenton, persulfate, and photocatalysis, individually or in combination can be utilized for the generation and attack of the oxidizing hydroxyl radicals (•OH) which ultimately removal of impurities and mineralization of molecules (Boczkaj and Fernandes 2017). In the emergent technology, in the domain of AOPs, cavitation is a point of attraction for the degradation of ungovernable compounds. In collaboration with AOPs, The Hydrodynamic or Ultrasonic cavitation is being stated to be effectively worked in the degradation of several organic and inorganic pollutant from wastewater (Gogate and Patil 2015; Gore et al. 2014; Joshi and Gogate 2012; V. V. Patil et al. 2020; Zupanc et al. 2013). The study have been stated the effective degradation of wastewaters also provided extensive analysis on the hydrodynamic cavitation as good AOP. Cavitation consist of the production and resulting collapse of vapor-filled cavities by the utilization of hydrodynamic design of constrictions, generating local point that lead the chemical degradation. During the cavitation, the production of oxidizing radicals is the supplements of hydroxyl radical formation and attack in AOPs, typically leading to higher degradation. (Innocenzi et al. 2018; V. V. Patil et al. 2020).

In the present study, effluent from Secondary Sedimentation Tank from Anjana STP of Surat has been studied. Different physical, chemical, and biological treatment processes are designed and employed at STP. The characteristic of effluent is being correlated to the type of treatment process employed. The reclaim option has been analyzed by applying hydrodynamic cavitation to the effluent from SST nevertheless of chlorination to overcome. The study give an alternative for the treatment of SST effluent without producing toxic substance of sludge as by product to the STP.

## 2. Methodology

In this study, Anjana STP which is located in the Surat city of Gujarat were being sampled. The Anjana STP is applyning the activated sludge process as biological treatment and after that Chlorination as tertiary treatment. The total capacity of STP is 82.50 MLD to treat domestic wastewater. After treatment the effluent is being disposed into the Mithi Khadi lake. The wastewater characteristic has been analyzed of effluent, after the secondary sedimentation tank.

### *2.1. Sampling*

The effluent has been sampled in the month of February 2020. Effluent sample was collected at the end of secondary treatment process i.e. from the open channel constructed from SST to tertiary treatment. During the analysis period, STP has been sampled once in a day. The table 1 shows the minimum, maximum and average value of diffirent parameter analysied during year.

**Table 1:** Characteristic of SST effluent by Anajan STP

| | Temp. | TDS (mg/l) | SS (mg/l) | BOD (mg/l) | COD (mg/l) | O&G (mg/l) | Cl (mg/l) | pH |
|---|---|---|---|---|---|---|---|---|
| **Min** | 22.00 | 569.00 | 224.00 | 223.00 | 582.00 | 0.20 | 225.00 | 7.04 |
| **Max** | 30.50 | 798.00 | 1132.00 | 1012.00 | 2232.00 | 9.20 | 386.00 | 7.81 |
| **Average** | 25.97 | 659.62 | 629.15 | 585.94 | 1201.68 | 7.42 | 279.02 | 7.27 |

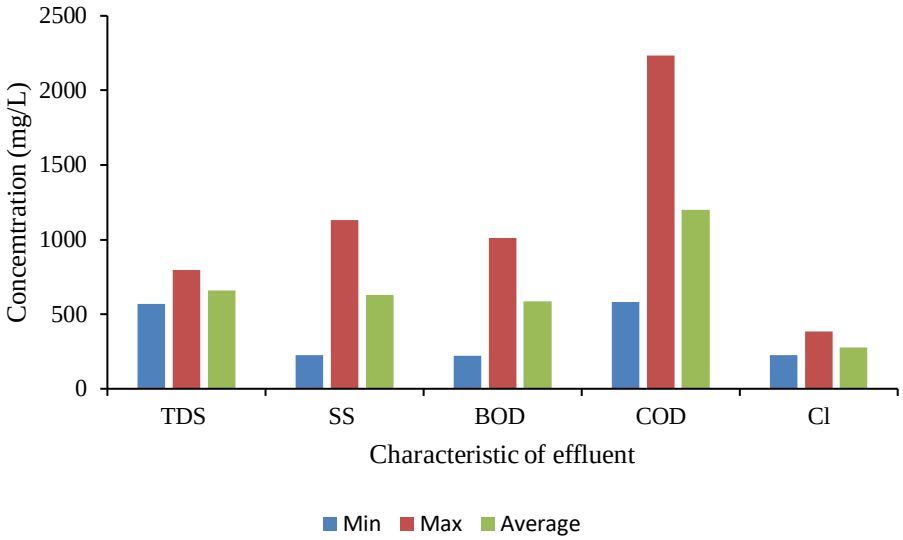



**Figure 1:** Major Characteristic of SST effluent

### *2.2. Experimental setup*

The lay out of the Hydrodynamic Cavitation experimental processes have been schematically represented in the figure 2. The hydrodynamic cavitation reactor comprises a storage tank whose capacity is approximately 20 L. The recirculation of the sample has been carried out through the mainline and bypass line by using a reciprocating pump of 0.5 kW power rating. To control the pressure at the required point, in this two-line pressure control valves are being provided. The measurement of the inlet pressure and recovers pressure are being noted by pressure gauges, installed in the mainline. In between the mainline, the orifice plate has been used as a cavitating device has been fitted having dimension as thickness 1.5 mm and the outer diameter of 55 mm. The concentric orifice hole having a 2 mm diameter for Anjana STP being used.

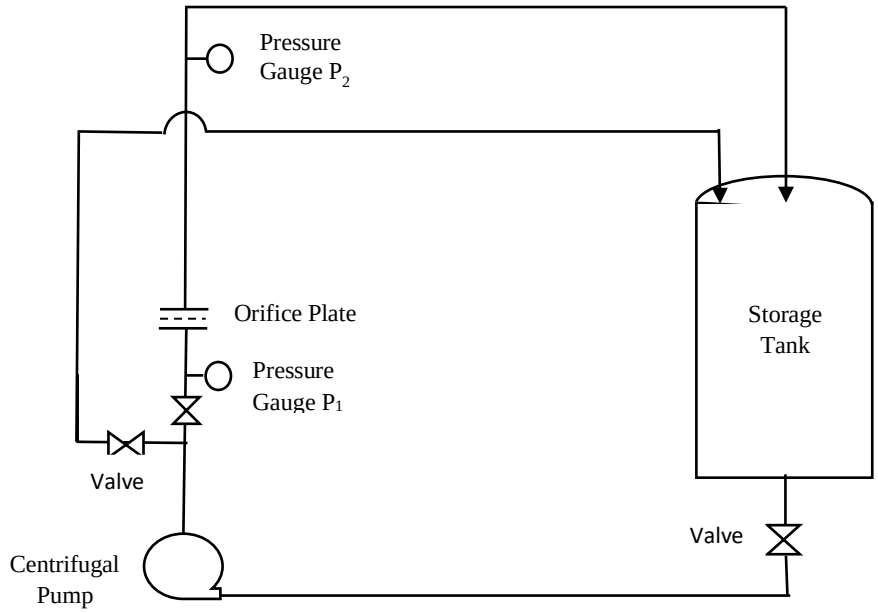



**Figure 2:** Experimental Setup of Hydrodynamic Cavitation Process

### *2.3. Analysis*

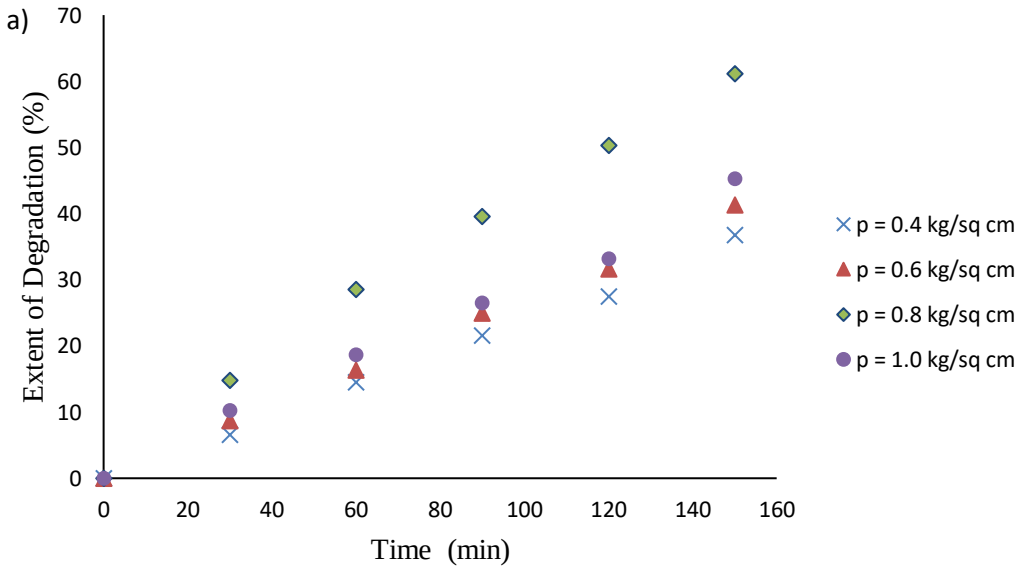
After collecting, samples were preserved at $4^0$ C for the transfer from STP to the laboratory. Instantaneously, in the laboratory of SVNIT, Surat, the samples were analyzed for pH, TDS, Electrical Conductivity, turbidity, and COD. All the parameter has analysed as per the procedure of the Standard Methods from APHA, 1998. The setup was run at an optimum inlet pressure of 0.8kg/cm$^2$. After every 30 min, the treated sample was collected and analyzed up to 150 min of recirculation of effluent from SST.

## 3. Result and Discussion

There are two major parameter i.e. geometrical parameters (geometry of the caviting device and cavitation number) and operating parameter (like characteristic of the liquid and inlet pressure) which gives the optimum efficiency of hydrodynamic cavitation (Innocenzi et al. 2018). For evaluation of process efficiency in the degradation rate of COD, at different operating conditions, several experiments were performed. The effect of the different operating parameters has been understood by analyzing the experiments and show up at a set of parameters which can give maximum COD reduction from the sampled wastewater.

### *3.1. Effect of inlet pressure*

The two significant parameters i.e. inlet pressure and cavitation number, in the process of hydrodynamic cavitation, give an impact on the cavity formed at interior of the cavitating device as well as impact on effectiveness of the HC process (Rajoriya et al. 2018). Degradation of Chemical Oxygen Demand has been examined at altering inlet pressures over the range of 0.4 to 1.0 kg/cm$^2$ for respective wastewater. The patterns for degradation, from figure 3(a) revealed that with increament in inlet pressure from 0.4 kg/cm$^2$ up to the optimum pressure of 0.8 kg/cm$^2$, the degree of degradation increased, beyond that, the rate of degradation. To examine the kinetic of order of reaction, the requisite analysis had been performed it was entrenched that the degradation rate sticks to first order kinetics, shown in figure 3(b). In table 2, the derived value of kinetic rate constants has been shown. Maximum degradation has been acquired at the optimum pressure was 64.11% and the first order reaction rate constant (K) of 6 x $10^{-3}$ min$^{-1}$ for 1.3 mm hole.



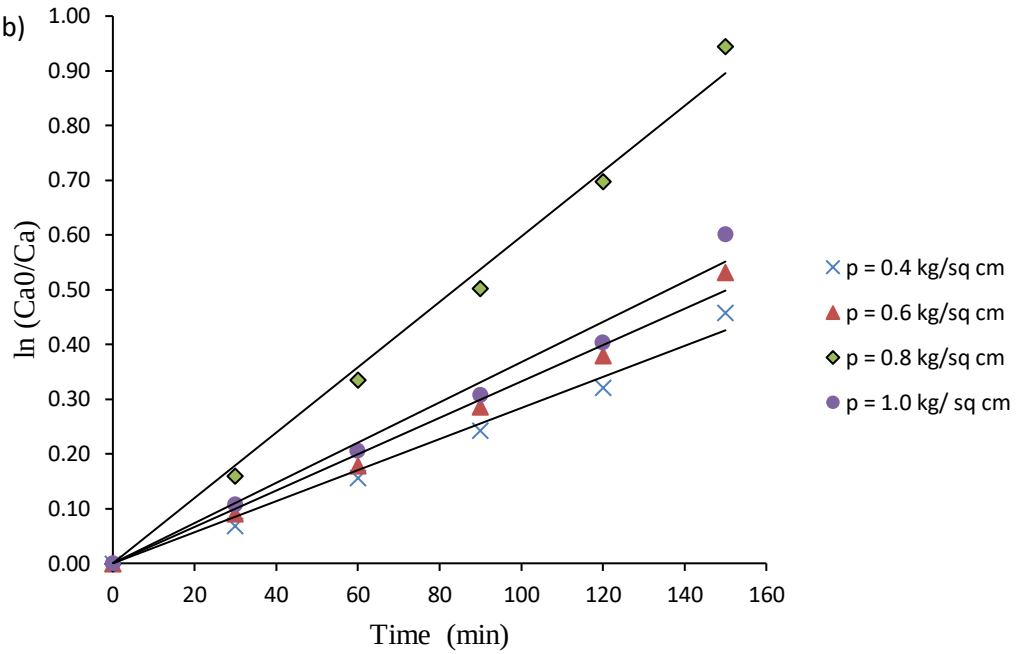



**Figure 3:** a) Effect of various inlet pressure on the degradation rate of COD. b) Kinetic data fitting for degradation rate of COD concerning various inlet pressure.

From inception, the number of cavities can be increased by increasing inlet pressure which results in enhancement of cavitational effects as of enhanced extent of degradation. The degree of the cavitational intensity within hydrodynamic cavitation process could estimated by using the cavitation number ($C_V$) that is formulated as follows,

$$C_V = \frac{P_2 - P_v}{(1/2)\rho v_0^2} \quad (1)$$

where $P_2$ and $P_V$ are completely recovered downstream pressure and vapor pressure of the liquid respectively and $v_0$ is the velocity in the throat of an orifice that could be estimated by determining the area of the constriction at an orifice plate and flow rate of the mainline. The higher will be the formation of cavities accompanied by collapse intensity if lower the cavitation number, which ultimately giving an increase for the rate of reduction. At extremely high pressures,4 extent of degradation is reduced beyond the optimum could be attributed to a cushioning effect results reduces the intensity of collapse from cavity i. e. cloud formation (numerous bubbles produced at increased pressures) (Barik and Gogate 2016; Gogate and Patil 2015; V. V. Patil et al. 2020; Rajoriya et al. 2018). Table 2 shows calculated value of cavitation number for different operating pressure.

**Table 2.** Cavitation number and kinetic rate constant at different inlet pressure for degradation of COD using Hydrodynamic Cavitation

| Pressure (kg/cm$^2$) | Cavitation Number ($C_v$) | The first order reaction rate constant (min$^{-1}$) | $R^2$ |
|---|---|---|---|
| 0.4 | 0.045 | 2.8 x 10$^{-3}$ | 0.986 |
| 0.6 | 0.037 | 3.3 x 10$^{-3}$ | 0.989 |
| 0.8 | 0.023 | 6.0 x 10$^{-3}$ | 0.992 |
| 1.0 | 0.016 | 3.7 x 10$^{-3}$ | 0.979 |

Patil and Gogate have also been described the same observation that at optimum pressure, 4 kg/cm$^2$, maximum reduction in methyl parathion found as 22.4% was secured thus minimizing the extent of methyl parathion reduction by increasing optimum pressures(P. N. Patil and Gogate 2012). A similar pattern had been reported by Prajapat and Gogate, by using an orifice as a cavitational device in the process of HC, with a rise of inceptional pressure to the optimum pressure accompanied the drop beside an additional increament of pressure resulting in increasing guar gum polymer degradation(Prajapat and Gogate 2015). Wu et al. had degraded phenol over assortment of initial pressure and obtained 17.6% and 46% reduction at pressure 0.1 MPa and 0.35MPa respectively also they found that over the complete range of operating pressure of experimental set up entrenched a constant increased(Wu et al. 2015). Likewise, Wang and Zhang by utilizing the swirling jet cavitational reactor obtained the reduction in alachlor was increased constantly beyond increasing inlet pressure in the range of 0.2 to 0.6 MPa(Wang and Zhang 2009). Additionally, Chakinala et al. used the HC reactor for to treat the industrial wastewater caused by the reactor containing liquid whistle operated at the scale of 700–1500 psi as the inlet pressure, obtained a similar pattern of a consistant increase in degradation of parameter of wastewater beyond increament in operating initial pressure and maximum efficiency of degradation had been found at 1500 psi (Chakinala et al. 2008). Due to the several designs of the hydrodynamic cavitation reactor, it is being observed that variations in the pattern of impact of pressure and also the optimum, that concludes the pressure for the coming of cloud generation.

### *3.2 Reuse potential of SST effluent*

In the present scenario, the total treated effluent of all STPs is being disposed into the natural pond knows as khadi. In Surat, out of total effluent, only 2% of Tertiary effluent is being utilized for industrial purposes which from Bamroli STP (Reverse osmosis as tertiary treatment) and rest of effluent is disposed into khadi. The total reclaimed treated effluent produced by STP find their path toward the open drains provide for storm water, thus complete treatment efforts are pointless. Figure 4 presents the potential of presented hydrodynamic cavitation set up under optimum operating conditions for Anjana STP of Surat city. The Anjana STP gave maximum degradation rate i. e. 64.12% at 0.8 kg/cm$^2$ inlet pressure and 2 mm concentric orifice plate. The COD of treated effluent from STP will be utilized for reuse in irrigation or agriculture if it is less than 100 mg/L (Donald R. Rowe 1995; Minisrey of Environment and forest 1986; US Environmental Protection Agency 2012) and obtained degradation of COD has range of 30 - 50 mg/L of the SST effluent treated by hydrodynamic cavitation process.

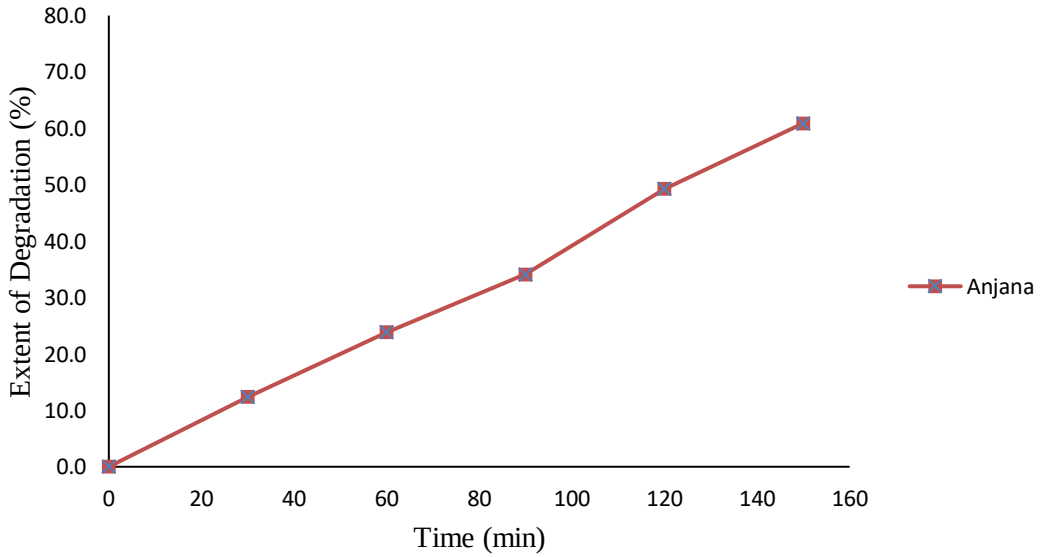



**Figure 4**. Effect of optimum operating condition on SST effluent of different STP for degradation of COD by using Hydrodynamic cavitation.

## 4. Conclusion

The present work states that COD in the effluent that is generated from SST of Sewage Treatment Plant could be degraded with the hydrodynamic cavitation approach as the better AOP. The HC decreases organic contamination more than 53.4% in the configuration of COD showed its potential application when being used in field conditions. By comparing the cavitating constriction, it was found that the orifice constriction having smaller diameter gives maximum efficiency in comparison to another plate in all of the parameters contemplated. It is because of amplified cavitational activity formed in the attribute for higher shear force observed by liquid forming a greater number of small cavities and subsequently, its collapse. For both cavitational constriction, with increasing inlet pressure, the optimum pressure was achieved at 0.8 kg/cm$^2$ that enhanced the extent of degradation. A study must establish the optimum cavitational number by concerning the impact of cavitation number based upon the design of constriction in an orifice. The examen discovered that at the inlet pressures of 0.8 kg/cm$^2$, obtained cavitation numbers as 0.01 for orifice plate with concentric 2 mm. The impact of reaction time concluded that liquid shows repetitive cavitation activity with increased time, and therefore contributes to the degradation of pollutants. For future study, the orifice plates can blended with the combination of hole in their shapes, number and diameter. This type in the construction of orifice could be beneficial in attaining various cavitational intensities that can be utilized in various applications. The HC reactors represent examen, have tremendous flexibility as far as for the operating inlet pressure, geometric conditions i. e. design of orifice plates, and flow rate. Contingent upon type of requirements along with the application, geometry, and operating conditions could be selected in the design of the HC reactor to optimize the cavitational impact at least possible energy consumption. In STP, as a replacement of conventional tertiary treatment i.e. chlorination which leftover chemicals in disposed effluent, HC is more effective in degrading organic and inorganic compounds with maximum energy efficiency.

## References

Barik, Arati J., and Parag R. Gogate. 2016. “Degradation of 4-Chloro 2-Aminophenol Using a Novel Combined Process Based on Hydrodynamic Cavitation, UV Photolysis and Ozone.” *Ultrasonics Sonochemistry* 30: 70–78.

Boczkaj, Grzegorz, and André Fernandes. 2017. “Wastewater Treatment by Means of Advanced Oxidation Processes at Basic PH Conditions: A Review.” *Chemical Engineering Journal* 320: 608–33.

Chakinala, Anand G., Parag R. Gogate, Arthur E. Burgess, and David H. Bremner. 2008. “Treatment of Industrial Wastewater Effluents Using Hydrodynamic Cavitation and the Advanced Fenton Process.” *Ultrasonics Sonochemistry* 15(1): 49–54.

Donald R. Rowe, Isam Mohammed Abdel-Magid. 1995. *Handbook of Wastewater Reclamation and Reuse*. Ist. CRC Press.

Gogate, Parag R., and Pankaj N. Patil. 2015. “Combined Treatment Technology Based on Synergism between Hydrodynamic Cavitation and Advanced Oxidation Processes.” *Ultrasonics Sonochemistry* 25(1): 60–69.

Gore, Mohan M et al. 2014. “Ultrasonics Sonochemistry Degradation of Reactive Orange 4 Dye Using Hydrodynamic Cavitation Based Hybrid Techniques.” *Ultrasonics - Sonochemistry* 21(3): 1075–82.

Innocenzi, V., M. Prisciandaro, F. Tortora, and F. Vegliò. 2018. “Optimization of Hydrodynamic Cavitation Process of Azo Dye Reduction in the Presence of Metal Ions.” *Journal of Environmental Chemical Engineering* 6(6): 6787–96.

Jamwal, Priyanka, and Atul K. Mittal. 2010. “Reuse of Treated Sewage in Delhi City: Microbial Evaluation of STPs and Reuse Options.” *Resources, Conservation and Recycling* 54(4): 211–21.

Joshi, Ravi K, and Parag R Gogate. 2012. “Ultrasonics Sonochemistry Degradation of Dichlorvos Using Hydrodynamic Cavitation Based Treatment Strategies.” *Ultrasonics - Sonochemistry* 19(3): 532–39.

Kumar, Dinesh, and Shyam R. Asolekar. 2016. “Significance of Natural Treatment Systems to Enhance Reuse of Treated Effluent: A Critical Assessment.” *Ecological Engineering* 94: 225–37.

Kumar, Dinesh, Neha Tyagi, and A B Gupta. 2011. “Selective Action of Chlorine Disinfection on Different Coliforms and Pathogens Present in Secondary Treated Effluent of STP .” 4(April 2011): 179–84.

M. Amasha, T. Elmaaty. 2007. “Wastewater Risk Assessment of Polyester Cabins in Egypt, Wastewater Reuse -

Risk Assessment, NATO Science for Peace and Security Series." (May).

Metcalf & Eddy, George Tchobanoglous. 1991. *Wastewater Engineering: Treatment and Reuse*. 3rd ed. ed. Franklin Louis Burton George Tchobanoglous. the University of Wisconsin - Madisonx: McGraw-Hill.

Minisrey of Environment and forest, India. 1986. "Standards Laid by Ministry of Environment and Forests , Government of India for Common Effluent Treatment Plants as per Environment Protection Rules , 1986." : 2–3.

Patil, Pankaj N., and Parag R. Gogate. 2012. "Degradation of Methyl Parathion Using Hydrodynamic Cavitation: Effect of Operating Parameters and Intensification Using Additives." *Separation and Purification Technology* 95: 172–79.

Patil, Vishal V., Parag R. Gogate, Akash P. Bhat, and Pushpito K. Ghosh. 2020. "Treatment of Laundry Wastewater Containing Residual Surfactants Using Combined Approaches Based on Ozone, Catalyst and Cavitation." *Separation and Purification Technology* 239: 116594.

Prajapat, Amrutlal L., and Parag R. Gogate. 2015. "Intensification of Depolymerization of Aqueous Guar Gum Using Hydrodynamic Cavitation." *Chemical Engineering and Processing: Process Intensification* 93: 1–9.

Rajoriya, Sunil, Swapnil Bargole, Suja George, and Virendra Kumar Saharan. 2018. "Treatment of Textile Dyeing Industry Effluent Using Hydrodynamic Cavitation in Combination with Advanced Oxidation Reagents." *Journal of Hazardous Materials* 344: 1109–15.

US Environmental Protection Agency. 2012. "Guidelines for Water Reuse." *Development* 26(September): 252.

Wang, Xikui, and Yong Zhang. 2009. "Degradation of Alachlor in Aqueous Solution by Using Hydrodynamic Cavitation." *Journal of Hazardous Materials* 161(1): 202–7.

Wu, C. D. et al. 2015. "Effects of Operating Parameters and Additives on Degradation of Phenol in Water by the Combination of H2O2 and Hydrodynamic Cavitation." *Desalination and Water Treatment* 53(2): 462–68.

Zupanc, Mojca et al. 2013. "Removal of Pharmaceuticals from Wastewater by Biological Processes, Hydrodynamic Cavitation and UV Treatment." *Ultrasonics Sonochemistry* 20(4): 1104–12.

IN PROCEEDINGS OF 25th HYDRO 2020, INTERNATIONAL CONFERENCE,
NATIONAL INSTITUTE OF TECHNOLOGY ROURKELA, ODISHA, INDIA
26-28, March 2021, ISBN 978-93-90631-56-8

Paper ID - 148

# New Methodology of Optimisation of Water Conductor System in Hydropower

Satyajeet Sinha

*Engineering Design and Research Centre, L&T Construction, Faridabad, 121003, India*
*Email: satyajeet.authentic@gmail.com*

## Abstract

Water conductor system in a hydro power projects conducts water required for generation of power from reservoir to the power house. The purpose of this study is to elaborate new methodology of optimisation of water conductor system in hydropower developed by a Practicing Engineer based on design experience and detail research carried out for verifying research output for a practical range applicable for major hydro power projects. The new optimisation methods of all the major components of water conductor system including intake, desilting basins, surge shafts and pressurised conduits are elaborated in this study. The optimisation of the desiting basins will be developed based on further studies carried out on the most read articles on the desiting basins on Google search engine published by the author. The optimisation of the tail race surge shaft published by the author and topped the list of Google Search Engine is taken as base to develop methodology for optimisation of surge shaft. The methodology of the optimisation of intake and tunnel are based on design experience of author. The optimisation methods suggested in this study will be useful in water conductor system optimisation and, hence, the cost of the hydropower projects can be minimized.

***Keywords:*** *Hydropower; optimisation; methodology; water conductor system.*

## 1. Introduction

A dam or diversion structure like a barrage obstructs the flow of a river and creates a potential head which is utilized by allowing the water to flow through the water conducting system up to the turbines driving the generators and then allowing it to discharge into the river downstream. Right from the intake of the water conducting system, where water enters from the main river, up to the outlet where water discharges off back into the river again, different structural arrangements are provided to fulfill certain objectives, the water inflowing into the conveyance system should be free from undesirable material, as far as possible, that may likely damage the turbines or the water conducting system itself. The energy of the inflowing water may be preserved, as far as possible, throughout the water course so that the turbine-generator system may extract the maximum possible energy out of the flowing water (NPTEL-Hydropower, 2020). The main components of water conductor systems are power intake, desilting basins, surge shafts and pressurised conduits. In this study new methodology of optimisation of these components is discussed based on design experiences of author and detail research carried out for verifying research output for a practical range applicable for major hydro power projects.

In this study power intake methodology of optimisation has been suggested by which the significant concrete, excavation and support quantities can be saved without any impact on overall performance of power intakes and power generation. Desilting basin optimization study discussed considering latest sediment management strategy adopted as per IHA (2020) guidelines. The recommendation proposed by the author for modern day desilting basins has been discussed along with monograph on desilting basins sizes estimation for a practical range of depth of desilting basins. Using all these studies output desilting basin sizing can be optimised efficiently. Surge shaft optimsation for tail race surge shaft is elaborated based on author contribution on the subject. Head race surge shaft optmisation steps are also discussed in this study. The general optimisation strategy of all pressure conduits in water conductor system including head race tunnel, pressure shaft and tail race tunnel are discussed in this study.

## 2. Power intakes

Intakes for power generation serve to provide hydraulically efficient water inlets to the water passages leading to the powerhouse. The passages may consist of conduits embedded in dams, excavated as tunnels, constructed as free-standing penstocks, or as short concrete passages between intakes constructed integrally with the powerhouses (ASCE:Hydroelectric-Waterways, 1989). The great majority of hydroelectric projects intakes are horizontal (ASCE, 1995).

Power intakes usually have gates and/or stop logs in series and parallel. The gates and/or stop logs are normally located in a rectangular flow section followed by a transition to the conduit cross-sectional shape (Miller, 1994).Intakes of rectangular shape with the largest dimension placed vertically are preferred for structural and mechanical reasons (Varshney, 2014). As per IS-9761 (1995), IS-11625 (1986), CEA (2004), and Varshney (2014), the bell mouth shape of power intake opening is generally an ellipse given by the following equations (1) and (2).

The Profile of roof and floor

$$\frac{x^2}{(1.1D_e)^2}+\frac{y^2}{(0.291D_e)^2}=1$$

The Profile of sides

$$\frac{x^2}{(0.55b_e)^2}+\frac{y^2}{(0.2143b_e)^2}=1 \quad (2)$$

As per ASCE (1995), some insight into the design of power intakes may be gained from intake shapes for high head outlet works. These equations are generally of the form:

$$\frac{x^2}{(3K_xD)^2}+\frac{y^2}{(K_yD)^2}=1 \quad (3)$$

Values of K for a rectangular flow section entrance are as follows:

Square or rectangular entrance $K_x = K_y = 0.33$

Suppressed one side only (rectangular entrance), for unsuppressed side $K_x = 0.33$, $K_y = 0.67$.

Substituting the above discussed $K_x$ and $K_y$ constant in equation (3) gives following equations (4) and (5).

The profile of Square or rectangular entrance

$$\frac{x^2}{D^2}+\frac{y^2}{(0.33D)^2}=1 \quad (4)$$

The profile of Suppressed one side only (rectangular entrance), for unsuppressed side

$$\frac{x^2}{D^2}+\frac{y^2}{(0.67D)^2}=1 \quad (5)$$

The above discussed equations (4) & (5) are also shown in IS-4880:(Part-III) (1976), CBIP-178 (1984), and USBR:Small-Dams (1987).

As per author`s experience of more than 20 hydropower projects at different stages (some projects at pre-feasibility stage, others at Feasibility stage, DPR stage and detail design stage), the equations (1) and (2) are preferred by those design Engineers who preferred IS code and CEA guidelines relevant to power intake guidelines and equations (4) and (5) are preferred by those design Engineers who observed equations (1) and (2) gives larger dimension of power intake and accordingly prefer equation (4) and (5). The general observation of author is that often where the intakes are

incorporated in concrete gravity dams or arch dams (ASCE:Hydroelectric-Waterways, 1989), equations (1) and (2) are preferred as it does not require a special structure except, perhaps, for the inlet portion, which is built integrally with the dam (mostly arch dams). For separate intake structures built at the power conduit portals, equation (5) is preferred, as the entrance with the bottom placed even with the upstream floor and with curved guide piers at each side of the entrance openings, both the bottom and side contractions will be suppressed and a sharper contraction will take place at the top of the opening. The curve from this equation will reduce the cost of intake structure by reducing intake quantity. Comparison between entrance profile of equation (5) in red and equation (1) in green for different diameter of intake tunnels is shown in Figure 1. From Figure 1, it is observed that there is significant concrete, excavation and support quantities are saved if equation (5) is used in comparison to equation (1).

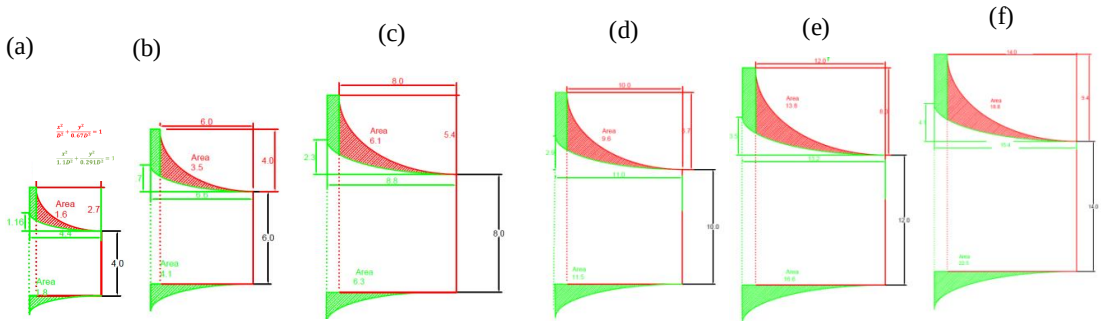



**Figure 1** Comparison between entrance profile of equation (5) in red and equation (1) in green for different diameter of intake tunnels: (a) D-4 m; (b) D-6 m; (c) D-8 m; (d) D-10 m; (e) D- 12 m; (f) D-14 m. (NTS).

Further in ASCE (1995), equation (3) curve may be too conservative for relatively low velocity hydropower intakes. As per USBR:Gravity-Dams (1976), and USBR:Arch-Dams (1977) the velocities in penstocks are considerably lower, the bell mouth does not have to be as streamlined as those designed for high-velocity river outlets. Experience on hydraulic models has shown that relatively simple rounding of corners eliminates most of the entrance losses when velocities are low. With the low velocities, pressure gradients in the bell mouth area are less critical.

As per ASCE (1995), for most hydropower intakes the value of C is in the range of 0.9 to 0.95 or in terms of K is in the range 0.24 to 0.10. Head loss coefficient for well-rounded intake is 0.10 and for slightly rounded intake is 0.25. As per IS-4880:(Part-III) (1976), CBIP-178 (1984), and USBR:Small-Dams (1987) average loss coefficient for slightly rounded entrances is 0.25, fully rounded entrances $\frac{r}{D} \geq 0.15$ are 0.10. For square bell mouth entrances, the minimum loss coefficient is 0.07, average loss coefficient is 0.16, and maximum loss coefficient is 0.20.

As per IS-4880:(Part-III) (1976), average permissible velocity in a concrete lined tunnel may be about 6 m/s. To further analyze the effect of head loss due to power intake entrance profile, study has been carried out to depict head loss in % w.r.t to gross head vs gross head of hydropower projects for minimum loss coefficient 0.1 and maximum loss coefficient of 0.25. All the practical range of velocity through intake conduit 3 m/s – 6 m/s were considered in the study. The output is shown in Figure 2.

It is suggested that the power intake structure can be optimized by adopting different entrance profile for different gross head of hydropower projects. For high head hydropower projects simple rounding of corners will be enough as % of head loss will not be enough as depicted in Figure 2. Similarly, for medium head hydropower project shorter bell mouth profile/simple rounding of corners can be adopted. The degree of intake shaping can be evaluated for head and energy losses and construction cost.

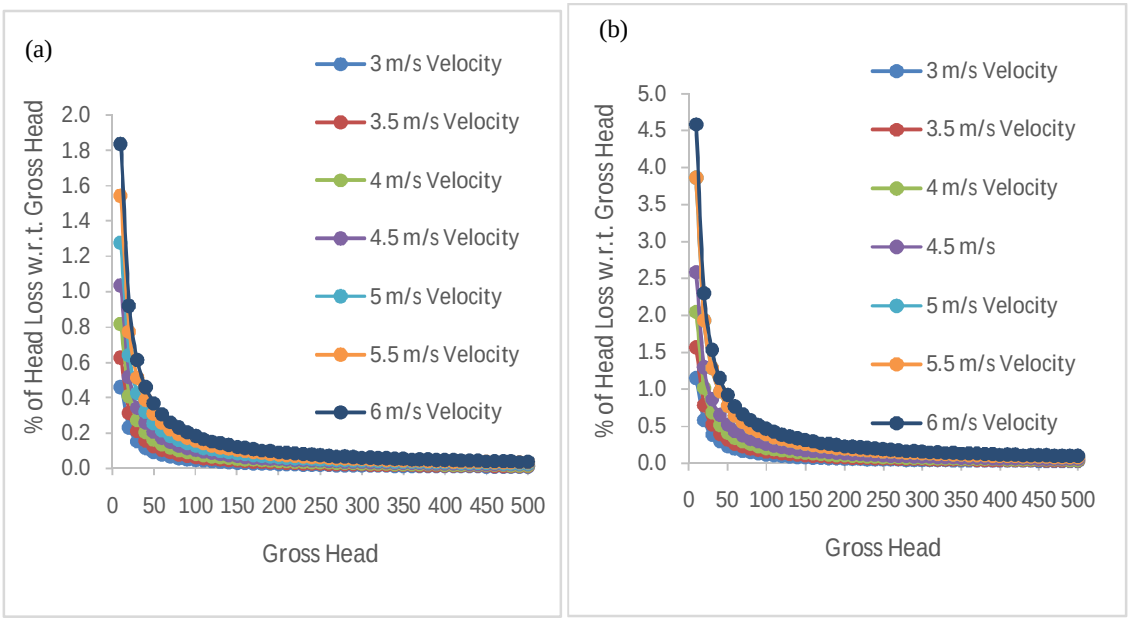



**Figure 2** % of Head loss w.r.t. Gross Head vs. Gross Head: (a) considering K as 0.1; (b) considering K as 0.25.

## 3. Desilting Basins

Hydropower projects constructed on erosive mountain faces severe issues due to sediment. The sharp-edged quartz sands transported by rivers in hilly terrain causes rapid wear of turbine runner blades/buckets due to abrasion (Sangal, Singhal, & Saini, 2018). Sediment entrained in water can severely abrade hydraulic machinery of all types, causing efficiency declines in turbines and pumps and also affecting valve and gate seals (Morris & Fan, Reservoir Sedimentation Handbook, 1998). Hardness of quartz on Mohs scale of hardness is 7 out of a maximum 10. Therefore, the river sediment containing a large percentage of quartz has abrasive action on hydro-mechanical equipment (Asthana, 2007).

### 3.1 *Latest sediment management strategy*

Sustainable sediment management seeks to achieve a balance between sediment inflow and outflow, restoring sediment delivery to the downstream channel, maximizing long-term storage, hydropower and other benefits, while minimizing environmental harm. As per Morris (2020), IHA (2020) management activities to address reservoir sedimentation may be classified into four broad categories as shown in Figure 3.Three categories focus on improving the sediment balance across reservoirs by: (a) reducing sediment yield from the watershed, (b) routing sediment-laden flows around or through the storage pool, and (c) removing sediment following deposition. The fourth category consists of adaptive strategies which respond to capacity loss, without addressing the sediment balance.

Strategies relevant to each reservoir will vary depending on technical, hydrologic, environmental, financial, legal and other conditions, and an optimal approach will frequently encompass a combination of both proactive and adaptive strategies. A combination of strategies will usually be used, and the techniques most suitable for implementation will change over time as sediment conditions change. The case studies of various projects worldwide are listed on IHA (2020) website.

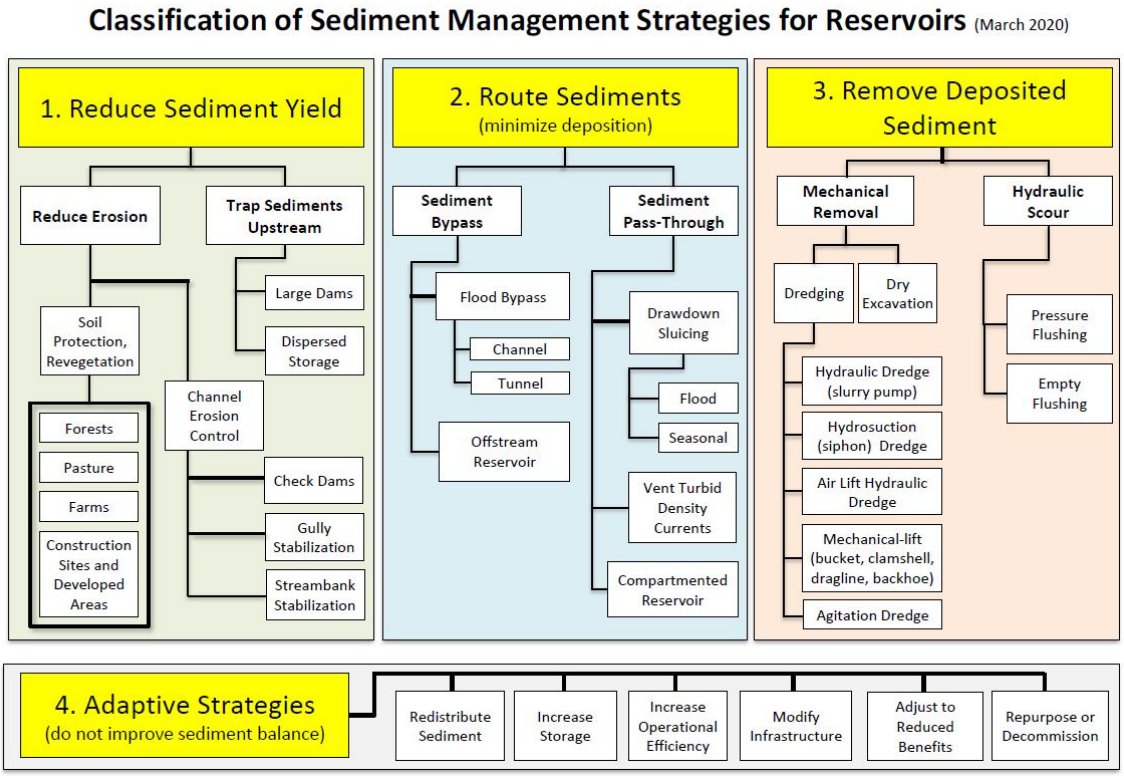



**Figure 3** Classification of strategies for managing reservoir sedimentation and its consequences, using flow lines to show categories and subcategories.

### 3.2 *Desilting Basin Concept*

In run-of-river hydel projects, when sediment load (particularly sharp-edged quartz sands) is high, sediment removal may be done by desilting basin (Singh & Kumar, 2016). The basic principle for sedimentation is to reduce the velocity of flow by increasing cross-sectional area of conduit so that suspended particle denser than water will settle into the bottom, in flowing water due to force of gravity(Nøvik , Dudhraj , Olsen , Bishwakarma , & Lia, 2014). These are removed through flushing arrangement. Once the minimum size of sediment to be excluded has been decided, the design of desilting basin involves the determination of the dimension of the desilting basin and the choice of method for removal of the deposited sediment, i.e., flushing arrangement.

Plants are often designed to remove most of the coarse sediment particles, while allowing fines (silt and clay) to flow through the turbines. However, even silt can cause significant abrasion if the quartz content of the silt and the pressure head are high enough. For example, the 1,500 megawatt Nathpa Jhakri hydropower plant in India contains four desilting chambers that are 525 meters long, 16.3 meters wide, and 27.5 meters high. The intent of these chambers is to remove coarse sediment before the water flows into the turbines (Figure 4(a)). In spite of the removal of the coarse sediment, the fines remaining in the water discharging through the turbines at Nathpa Jhakri caused significant abrasion. Not only is the quartz content of the silt very high, but the pressure head at the turbines is also high at 428 meters. The abrasion at Nathpa Jhakri after commissioning(Figure 4 (b)) was so severe that wet parts of the turbines had to be replaced within one year(Annandale, Morris, & Karki, 2016).



**Figure 4**(a) Dewatered Desilting Chambers at Nathpa Jhakri Hydropower Plant, 2010; (b) turbine damage at Nathpa Jhakri.

As per IHA:Nathpa-Jhakri (2017), the sediment management stratergy adopted afterwards are, all units were refurbished with HVOF-typeTungsten carbide coating, the upper limit of 5,000 ppm at the intake was decreased to 3,500 ppm, the upper limit of 5,000 ppm at the intake was decreased to 3,500ppm.

### 3.3 *Sinha and Singh recommendation for modern day desilting basins*

Most of the present day desilting basins are designed as wide rectangular basins; however, in general, width/depth ratio is not too high nor is the desilting basins completely rectangular in shape. Sinha & Singh(2018) proposed modifications in the existing empirical and analytical approaches that hold good for rectangular desilting basins by considering hydraulic radius parameter, cross-sectional and plan area so that the shape of desilting basin is addressed. Existing approaches that hold good for unlined desilting basins modified by incorporating friction factor parameter so that it can be used for both lined and unlined desilting basins. The generalized Camp-Dobbins graph represented in function of shear velocity incorporating hydraulic radius parameter and generalized overflow rate as per Sinha & Singh(2018) is shown in Figure 5.

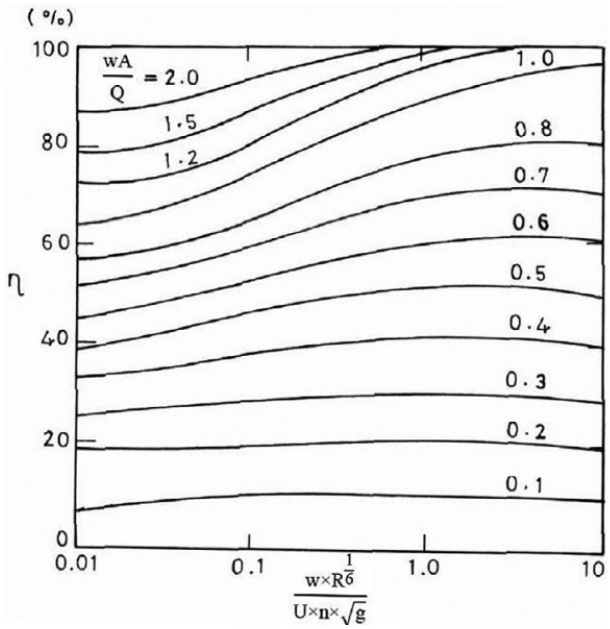



**Figure 5** Camp and Dobbins graph represented in function of shear velocity generalized using hydraulic radius parameter.

### 3.4 *Sinha`s monograph on desilting basins sizes estimation*

In Sinha, Monograph on desilting basins sizes estimation for hydropower projects (2019), a monograph was developed based on Teaching–Learning-Based Optimization and Gravitational Search algorithm for a practical range of depth of desilting basins. The parameters commonly used in hydropower projects for estimation of desilting basins sizing and its efficiency are used in this study. The outcome is further verified using a list of mega hydropower projects. This study will be useful in fixing the best optimized dimension of desilting basins. In this study A monograph has been developed comparing the result obtained by different analytical and empirical approaches for the practical range of depth of desilting basins and the data that are commonly considered in hydropower projects forestimation of desilting basins sizing. The length required for 90% efficiency with respect to the depth of desilting basin has been figured out. The designer can refer this study to find out the best optimized dimension of desilting basin for the given discharge. This study output data shall be used as a reference to suggest the length of the desilting basin and fine tuning shall be carried out considering actual parameters considered. The results obtained by different analytical and empirical approaches is elaborated in this study. The output obtained for 30 m depth is shown in Figure 6. For the relationship obtain for other depth kindly refer this study.

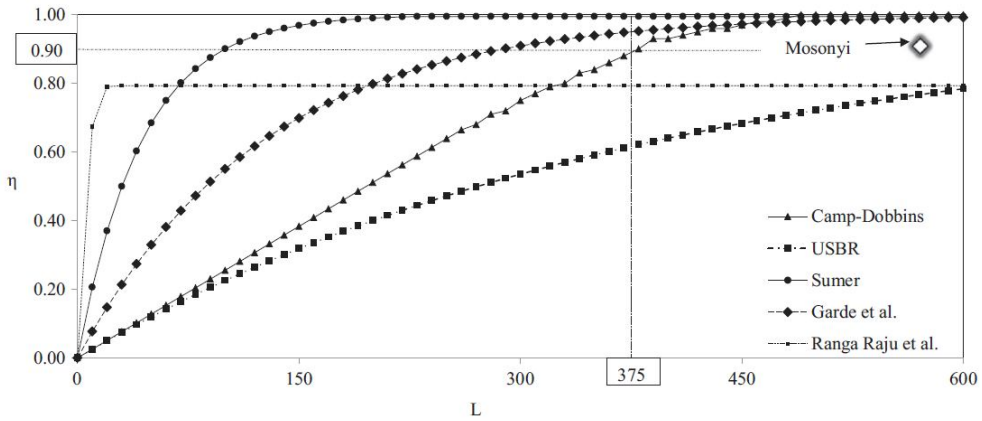



**Figure 6** Analytical and empirical approach comparison: efficiency versus length: depth 30 m.

## 4. Surge Shafts

In hydropower projects, turbine startup and shutdown time is a matter of a few seconds (Robinson & Zhao, 2011). The sudden startup and shutdown causes hydraulic transients in the water conductor system (Riasi, Raisee, & Nourbakhsh, 2010 ; Vereide, Lia, & Nielsen, 2015). Surge shaft is provided in water conductor systems to radically reduce the pressure surges due to water hammer and to prevent excessive internal loads on the pressure tunnel (Mosonyi, 1991; IS:7396-Part-1, 1985; Hanif, 2014). The surge shaft shall be designed to accommodate the maximum and minimum water levels anticipated under worst conditions. Mainly three types of surge shafts are commonly used in hydropower project (IS:7396-Part-1, 1985). The first is simple surge shaft/tank where a simple surge shaft/tank is connected to pressure tunnel directly or by a short connection of cross-sectional area not less than the area of the head race tunnel. The second type is restricted orifice surge shaft/tank where a simple surge shaft/tank in which the inlet is throttled to improve damping of oscillations by offering greater resistance and connected to the headrace tunnel with or without a connecting/communicating shaft. The third type is differential surge shaft/tank where differential surge shaft/tank is a throttled surge tank with an addition of riser pipe may be inside the main shaft, connected to main shaft by orifice or ports.

### 4.1 *Surge Analysis*

The commonly used software for surge analysis is WHAMO and HAMMER. WHAMO software was developed by the US Army Corps of Engineers and is widely used for transient analysis. WHAMO was developed to assist engineers in reducing water hammer by simulating water hammer and mass oscillation in networks that convey fluids, such as water and fuel. It provides dynamic simulation of fluid distribution systems in hydropower plants (WHAMO-Manual, 1998). It calculates time-varying flow and head in networks with pipes, valves, pumps, surge shaft, and turbines. WHAMO software uses an implicit finite difference method for calculating time-varying flows and pressures throughout the network being modelled. HAMMER software, developed by Bentley, uses the equations from the Method of Characteristics to calculate the changes in hydraulic grade and flow at each time step and pipe section point (incrementally along the pipeline length) (Bentley:HAMMER-Guide, 2009).

### 4.2 *Tailrace surge shaft optimization procedure by Sinha*

Tailrace surge shaft optimization procedure is proposed in Sinha, Tailrace surge shaft optimization procedure for minimum downsurge (2018). Tailrace surge shafts need to be applied after the turbines, if the spent water is conveyed under pressure through a long tailrace tunnel into the recipient (IS:7396-Part-2, 1985). For the tailrace system having a tailrace surge shaft, the conduit length affected by the water hammer decreases from the long tailrace tunnel to a short draft tube tunnel (conduit between draft tube and surge shaft) as the water hammer waves produced in the draft tube tunnel by load changes on the turbine are reflected back to the tailrace surge shaft. Owing to the reduction in the conduit length affected by water hammer, the change in pressure (pressure rise or pressure drop) will be less than that of the tailrace system without surge shaft. In addition, if the tailrace surge shaft is not connected at the junction of a draft tube tunnel and a tailrace tunnel, then the tailrace system needs to be designed to withstand the water hammer pressure (Kim, 2010). The water hammer pressure becomes enormous for the long tailrace tunnel system and the lining of the tailrace tunnel may not sustain such high surge pressure. Thus, to dampen the high surge pressure in the long pressurized tailrace system, the tailrace surge shaft is required. The other option is to ensure free flow conditions in the tunnel; however, this may prove extremely expensive, especially in the case of a long tailrace system (Varshney, 2014).

Based on numerous transient analyses carried out, it was observed that the cross-sectional area of the tailrace surge shaft can be optimized using the relationship between the tailwater level and the minimum downsurge level with respect to different cross sectional areas of the tailrace surge shaft and different available ranges of tailrace tunnel lengths. The output of the study considering 150 $m^3/s$ design discharge, with draft tube tunnel and tailrace tunnel diameter of 7.0 m is shown in Figure 7 ,to have a glimpse of the output.

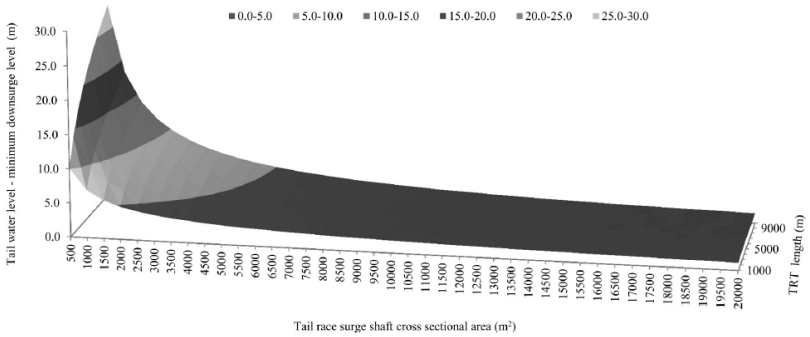



**Figure 7** Tailwater level – minimum downsurge level w.r.t. different tailrace surge shaft cross-sectional area and different tailrace tunnel length: 150 $m^3/s$ discharge.

The result of study demonstrated that a better solution is to increase the difference between the tailwater level and the minimum downsurge level. Raising the tailwater level must be avoided as it reduces the head for power generation. The best way is to lower the minimum downsurge level by lowering the bottom level of the tailrace surge shaft as much as possible. The tailrace surge shaft bottom level can be lowered to maximum extent depending upon the optimum turbine centerline level and other relevant factors. The optimization procedure that can be adopted is discussed below. For a given project, based on the topography, geology, and other constraints, the range of tailrace tunnel lengths can be determined to utilize the maximum permissible head for power generation. Transient analysis models need to be formulated based on the set lengths of tailrace tunnels and given tailwater levels apart from other design parameters, such as design discharge, diameter of tailrace system, etc. For the initial transient analysis, the top and bottom level of the tailrace surge shaft can be set at arbitrary higher and lower values, respectively, as the segment length of the surge shaft used in the transient analysis computation is calculated from the water surface elevation at the previous time step. The transient analysis simulations need to be carried out to determine the possible range of cross-sectional areas of the tailrace surge shaft. From transient analysis results, the relationship between the differences in the tailwater level and the minimum downsurge level at tailrace surge shaft obtained with respect to the different length of the tailrace tunnel and different cross-sectional area of the tailrace surge shaft need to be determined for the set tailrace tunnel length. The range of optimum cross-sectional areas of the tailrace surge shaft can be selected based on the trend of these graphs. With some cushion (say 2.0 m as perIS:7396-Part-1, (1985) from the minimum downsurge level for the selected cross-sectional areas, the bottom level of the tailrace surge shaft can be determined and the turbine centerlinecan be figured out accordingly. Fine tuning can be done after optimization.

The set of layouts with different cross-sectional areas of the tailrace surge shaft considered need to be checked for the additional cost owing to the increase in the length of the pressure shafts, the tailrace system, the access tunnel to the power house, etc. Also, the minimum Thoma criterion should be taken into account while selecting the minimum cross-sectional area of the tailrace surge shaft. A required minimum submergence of turbine installation as a function of rotational speed of runner derived by Pejovic, Karney, & Zhang, (2004) , needs to be established to control the water hammer pressure drop under a negligible level which does not lead to an excessive pressure rise to cause damage to the unit and waterways. By considering all these factors, the optimum cross sectional area of the tailrace surge shaft can be determined and the tailrace surge shaft can be optimized.

### 4.3 *Headrace surge shaft optimization procedure suggestions*

Headrace surge shafts need to be applied before the turbines, if the spent water is conveyed under pressure through a long headrace tunnel from the reservoir till the turbines. The maximum upsurge level and minimum downsurge level criteria for transient analysis study is just opposite of what in Tailrace surge shaft criteria. Turbine startup will produce maximum upsurge level in tailrace surge shaft and minimum downsurge level in headrace surge shaft. Similarly turbine shutdown will produce minimum downsurge level in tailrace surge shaft and maximum upsurge level in headrace surge shaft. The basic design criteria for surge analysis study discussed for tailrace surge shaft hold good for headrace surge shaft too such as minimum Thoma area check. For the initial transient analysis, the top and bottom level of the headrace surge shaft can be set at arbitrary higher and lower values, respectively, as the segment length of the surge shaft used in the transient analysis computation is calculated from the water surface elevation at the previous time step. Based on the transient analysis results the top and bottom level of headrace surge shaft can be determined afterwards. The top of headrace surge shaft may be taken as 1.5 m above the highest water level while the bottom of the surge shaft may be kept 2.0 m below the lowest surge level.

## 5. Pressure Conduits

The water conductor system from power intake till power house is pressurised conduits consisting of HRT, and/or Pressure shaft and/or Penstock. In case of reaction turbine and if power house is located far from outfall/river is also connected through pressure conduit called as Tailrace Tunnel.

### 5.1 *Headrace Tunnel*

Headrace tunnel is usually concrete lined tunnel. As per USBR:Design-Standard-3, (2014), concrete-lined water conveyance tunnels are designed with a usual flow velocity of about 10 feet per second (ft/s) (3.0 meters per second [m/s)] and a maximum velocity of 20 ft/s (6.1 m/s). As per IFC:Hydroelectric-Power, (2015), tunnel flow velocity is lower than 3-4 m/s to reduce head losses.

Economical diameter of HRT is calculated based on study of cost vs benefit of increasing HRT diameter. With increase of HRT diameter, the cost of constructing tunnel increases which includes additional cost of excavation and support but with increase in diameter head loss reduces which impact on over all unit cost of project. Thus the optimal HRT diameter shall be calculated considering this cost vs benefit study.

### 5.2 *Pressure shaft/Penstock*

The pressure shaft/penstock conveys pressurized water from the forebay or surge tank to the turbine. In addition to the pressure caused by static head, the pressure shaft/penstock must be able to withstand the pressure rise caused by the so-called water hammer, i.e., the pressure rise that occurs due to rapid turbine shutdown in emergencies. Pipe thickness is based on the internal pressure the pipe material must withstand; higher internal pressure requires greater pipe thickness(IFC:Hydroelectric-Power, 2015).

The pressure shaft/Penstock diameter and velocity are designed within an optimization analysis in which head losses are considered against penstock costs, which are determined by material, length, and thickness. The economic diameter of pressure shaft/penstock is calculating using the formula for calculating the economic diameter of penstocks given in IS-11625, (1986).

### 5.3 *Tailrace Tunnel*

Tailrace tunnel discharges turbine water into a receiver, a river,lake or ocean located far away from powerhouse location. Usually tailrace tunnel is connected from underground powerhouse consisting of reaction tubine to receiver.

Economical diameter of TRT is calculated based on study of cost vs benefit of increasing TRT diameter. With increase of TRT diameter, the cost of constructing tunnel increases which includes additional cost of excvation and support but with increase in diameter head loss reduces which impact on overall unit cost of project. Thus the optimal TRT diameter shall be calculated considering this cost vs benefit study.

## 6. Conclusion

In this study, power intake optımısation methodology been suggested by which the significant concrete, excavation and support quantities can be saved without any impact on overall performance of power intakes and power generation. It is suggested that the power intake structure can be

optimized by adopting different entrance profile for different gross head of hydropower projects. For high head hydropower projects simple rounding of corners will be enough as % of head loss will not be enough. Similarly, for medium head hydropower project shorter bell mouth profile/simple rounding of corners can be adopted. The degree of intake shaping can be evaluated for head and energy losses and construction cost.

Desilting basin optimization study discussed considering latest sediment management strategy adopted as per IHA (2020) guidelines. Reservoir sedimentation may be classified into four broad categories. Three categories focus on improving the sediment balance across reservoirs by: (a) reducing sediment yield from the watershed, (b) routing sediment-laden flows around or through the storage pool, and (c) removing sediment following deposition. The fourth category consists of adaptive strategies which respond to capacity loss, without addressing the sediment balance. The recommendation proposed by the author for modern day desilting basins has been discussed. Sinha & Singh (2018) proposed modifications in the existing empirical and analytical approaches that hold good for rectangular desilting basins by considering hydraulic radius parameter, cross-sectional and plan area so that the shape of desilting basin is addressed. Sinha, Monograph on desilting basins sizes estimation for hydropower projects (2019) is discussed in this study to utilize the monograph developed in this paper for optimized sizing of desilting basin. Using all these studies output desilting basin sizing can be optimized efficiently.

Tailrace surge shaft can be optimized using the optimization procedure is proposed in Sinha, Tailrace surge shaft optimization procedure for minimum downsurge (2018). Based on numerous transient analyses carried out, it was observed that the cross-sectional area of the tailrace surge shaft can be optimized using the relationship between the tailwater level and the minimum downsurge level with respect to different crosssectional areas of the tailrace surge shaft and different available ranges of tailrace tunnel lengths. The basic design criteria for surge analysis study discussed for tailrace surge shaft hold good for headrace surge shaft too such as minimum Thoma area check. For the initial transient analysis, the top and bottom level of the headrace surge shaft can be set at arbitrary higher and lower values, respectively, as the segment length of the surge shaft used in the transient analysis computation is calculated from the water surface elevation at the previous time step.

The economical diameter of HRT/ TRT are calculated based on study of cost vs benefit of increasing HRT/TRT diameter. With increase of HRT/TRT diameter, the cost of constructing tunnel increases which includes additional cost of excvation and support but with increase in diameter head loss reduces which impact on overall unit cost of project. Thus the optimal HRT/TRT diameter shall be calculated considering this cost vs benefit study. The pressure shaft/Penstock diameter and velocity are designed within an optimization analysis in which head losses are considered against penstock costs, which are determined by material, length, and thickness.

## Notation

| | |
|---|---|
| A | desilting basin plan area ($m^2$) |
| ASCE | American Society of Civil Engineers |
| | width of rectangular flow section in power intake structure after bell mouth (m) |
| C | coefficient of discharge (-) |
| | Central Broard of Irrigation and Power |
| CEA | Central Electricity Authority |
| | depth of rectangular flow section in power intake structure after bell mouth (m) |
| D | depth/diameter of the conduit (m) |

| | |
|---|---|
| DPR | Detail Project Report |
| etc | and so forth |
| ı.e. | For example/ in other words |
| g | acceleration due to gravity (m $s^{-2}$) |
| HRT | Head Race Tunnel |
| IS | Indian Standard Codes |
| K | loss coefficient (-) |
| | constant in x direction with respect to bell mouth entrance shape (-) |
| | constant in y direction with respect to bell mouth entrance shape (-) |
| L | length (m) |
| n | Manning's rugosity coefficient (s $m^{-1/3}$) |
| η | efficiency of removal of sediments (-) |
| NTS | Not to Scale |
| PEN | Penstock |
| PS | Pressure Shaft |
| Q | design discharge ($m^3s^{-1}$) |
| r | Radius of curve (m) |
| R | hydraulic radius (m) |
| TRT | Tail Race Tunnel |
| U | forward velocity (m $s^{-1}$) |
| USBR | United States Bureau of Reclamation |
| vs | versus |
| w | settling velocity (m $s^{-1}$) |
| WHAMO | Water Hammer and Mass Oscillation |
| w.r.t | with respect to |
| x | Coordinate in horizontal direction |
| y | Coordinate in vertical direction |

## ORCID

Satyajeet Sinha http://orcid.org/0000-0003-4518-3851

## References

Annandale, G. W., Morris, G. L., & Karki, P. (2016). *Extending the Life of Reservoirs Sustainable Sediment Management for Dams and Run-of-River Hydropower.* Washington : International Bank for Reconstruction and Development / The World Bank.

ASCE. (1995). *Guidelines for Design of Intakes for Hydroelectric Plants.* Reston,: American Society of Civil Engineers.

ASCE:Hydroelectric-Waterways. (1989). *Civil Engineering guidelines for planning and designing hydroelectric developments, Volume 2, Waterways.* New York: American Society of Civil Engineers.

Asthana, D. N. (2007). *Sediment management in water resources projects.* New Delhi: Central Board of Irrigation & Power.

Bentley:HAMMER-Guide. (2009). *Bentley HAMMER V8i Edition User's Guide.* Bentley, V8i, CONNECT Edition.

CBIP-178. (1984). *Manual on the planning and design of hydraulic tunnels.* New Delhi: Central Board of Irrigation and Power.

CEA. (2004). *Best practices in planning, designs & construction of civil.* Delhi: CEA Hydro Best Practices.

Hanif, C. M. (2014). *Applied hydraulic transients.* Springer.

IFC:Hydroelectric-Power. (2015). *Hydroelectric Power: A Guide for Developers and Investors.* Stuttgart Germany: IFC performance standards or World Bank safeguards.

IHA. (2020). Sediment management strategies. *International Hydropower Association (IHA)* .

IHA:Nathpa-Jhakri. (2017). *Case Study - Nathpa Jhakri.* London: International Hydropower Association (IHA).

IS:7396-Part-1. (1985). *Criteria for hydraulic design of surge tanks, simple restricted orifice and differential surge tanks.* New Delhi, India: Bureau of Indian Standards.

IS:7396-Part-2. (1985). *Criteria for hydraulic design of surge tanks, tail race surge tanks.* New Delhi, India.: Bureau of Indian Standards.

IS-11625. (1986). *Criteria for Hydraulic Design of Penstocks.* New Delhi: Indian Standards Institution.

IS-4880:(Part-III). (1976). *Code of practice for design of tunnels conveying water, part III Hydraulic Design.* New Delhi: Bureau of Indian standards.

IS-9761. (1995). *Hydropower Intakes - Criteria for Hydraulic Design.* New Delhi: Bureau of Indian Standards.

Kim, S. H. (2010). Design of surge tank for water supply systems using the impulse response method with the GA algorithm. *Journal of Mechanical Science and Technology , 24* (2), 629-636.

Miller, D. S. (1994). *Discharge Characteristics: IAHR Hydraulic Structures Design Manuals 8 (IAHR Design Manual)* . New York: Taylor & Francis.

Morris, G. L. (2020). Classification of Management Alternatives to Combat Reservoir Sedimentation. *MDPI-Water* , 861.

Morris, G. L., & Fan, J. (1998). *Reservoir Sedimentation Handbook.* New York: McGraw-Hill Book Co.

Mosonyi, E. (1991). *Water power development. Volume two/A. High-head power plants.* Akademiaikiado, Budapest.

Nøvik , H., Dudhraj , A., Olsen , N. R., Bishwakarma , M. B., & Lia, L. (2014). Numerical Modeling of Nonuniform Flow in Settling Basins. *Hydro Nepal: Journal of Water, Energy and Environment* , 27-35.

NPTEL-Hydropower. (2020). *Module 5, Hydropower Engineering, Lesson 2, Hydropower Water Conveyance System.* Kharagpur: IIT.

Pejovic, S., Karney, B., & Zhang, Q. (2004). Water column separation in long tailrace tunnel. *In Proceedings of Hydroturbo 2004, on Hydro-Power Engineering,Hydroturbo, Brno* , 1-10.

Riasi, A., Raisee, M., & Nourbakhsh, A. (2010). Simulation of transient flow in hydroelectric power plants using unsteady friction. *Journal of Mechanical Engineering , 56* (6), 377–384.

Robinson, A. C., & Zhao, Z. (2011). Intelligent flow control after load rejection at the juniper ridge hydroelectric power generation projectbend, Oregon. 21st Century dam design—advances and adaptations. *U.S. Society on Dams, San Diego, Calif.* , 477–492.

Sangal, S., Singhal, M. K., & Saini, R. P. (2018). Hydro-abrasive erosion in hydro turbines: a review. *International Journal of Green Energy* , 232-253.

Singh, G., & Kumar, A. (2016). Performance evaluation of desilting basins of small hydropower projects. *ISH Journal of Hydraulic Engineering* , 135-141.

Sinha, S. (2019). Monograph on desilting basins sizes estimation for hydropower projects. *International Journal of Green Energy* , 317-332, *https://doi.org/10.1080/15435075.2019.1566136* .

Sinha, S. (2018). Tailrace surge shaft optimization procedure for minimum downsurge. *Canadian Journal of Civil Engineering* , 446-457, *https://doi.org/10.1139/cjce-2017-0515* .

Sinha, S., & Singh, A. P. (2018). Sediment removal efficiency estimation criteria for modern day desilting basins. *ISH Journal of Hydraulic Engineering.* , 104-117, *https://doi.org/10.1080/09715010.2018.1426057* .

USBR:Arch-Dams. (1977). *Design of Arch Dams.* Colorado: United States department of the interior Bureau of Reclamation.

USBR:Design-Standard-3. (2014). *Water Conveyance Facilities, Fish Facilities, and Roads and Bridges, Chapter 4: Tunnels, Shafts, and Caverns Phase 4 (Final).* U.S. Department of the Interior Bureau of Reclamation.

USBR:Gravity-Dams. (1976). *Design of Gravity Dams.* Colorado: United States department of the interior Bureau of Reclamation.

USBR:Small-Dams. (1987). *Design of small Dams.* Washington, DC: United States department of the interior Bureau of Reclamation.

Varshney, R. S. (2014). *Hydro Power Structures.* ROORKEE: NEM CHAND & BROS.

Vereide, K., Lia, L., & Nielsen, T. K. (2015). Hydraulic scale modelling and thermodynamics of mass oscillations in closed surge tanks. *Journal of Hydraulic Research , 53* (4), 519–524.

WHAMO-Manual. (1998). *Water hammer and mass oscillation (WHAMO) 3.0 user manual.* US army corps of engineer's construction engineering research laboratories.

IN PROCEEDINGS OF 25th HYDRO 2020, INTERNATIONAL CONFERENCE,
NATIONAL INSTITUTE OF TECHNOLOGY ROURKELA, ODISHA, INDIA
26-28, March 2021, ISBN 978-93-90631-56-8

Paper ID - 165

# Numerical Simulation to Study Cavitation Characteristics of Centrifugal Pump

Ruchi Khare[1], Vishnu Prasad[2] Chinky Yadav[3]

*1Associate Professor, Civil, MANIT, Bhopal, India 462007*
*2 Professor, Civil, MANIT, Bhopal, India 462007*
*3MTech (Hydropower), MANIT, Bhopal India 462007*
*Email: ruchif4@rediffmail.com*
*Telephone/Mobile No.: +91 9425607454*

**Abstract**

Pumps are roto-dynamic devices used to enhance the energy of fluids. Centrifugal pumps are commonly used in water supply, irrigation and industries also. They are a common part of our day to day life. Their efficiency and performance is always an area of research. The performance of centrifugal pump depends on the operating conditions and cavitation characteristics of the pumps. In most of the cases the pumps capacity is determined by system head curve of the area where the pump is required to be installed. But in reality the pump hardly performs at best efficiency point. The performance of pump deteriorates at off design conditions which is mainly because of cavitation. Cavitation performance at off design conditions are required to be predicted before installation and commissioning of the centrifugal pumps. In present work numerical simulation of a radial flow centrifugal pump is carried out to study its performance in terms of efficiency and cavitation characteristics at constant rotational speed of 2900 rpm and 5 different discharge values which includes duty point and off design conditions. It is observed that as the pressure decreases in the suction side of the pump, losses at various parts of the pump increases, the increase in loss is more prominent in impeller and it increases with cavitation at suction side of the impeller.

***Keywords:*** *centrifugal pump, cavitation, NPSH, cavitation coefficient, pump characteristics*

## 1. Introduction

Centrifugal pump is one of the key device for fluid conveyance through long pipelines and has wide applications due to its centrifugal structure with wide range of flow rate, stable running operation, good suction performance and low maintenance. The energy consumed by the pump to transport the fluid has dominant role in pumping system and hence efficiency of pump is of great concern to both manufacturer and the customer. The suction performance improvement allows the user to reduce civil cost due to reduction in submergence and hence saving during the installation of pumps[Muttalli et al, 2014)]. The small improvement in the efficiency performance of pump can save huge amount of energy and money during operation of pumps.

In centrifugal pump, the curved flow passage and presence of solid rotating blades of impeller make the flow very complex. The geometry of the pump consists of suction pipe, impeller and delivery casing [Dazhuan et al, 2014]. The interpretation of flow physics within the pump is very important for designer. The flow through pump is complicated turbulent flow owing to the complex flow domain having stationary and rotating components. The designer has to make some assumptions to carry out the design and hence it becomes necessary to predict the pump performance. The physical model test of pump in laboratory is the conventional approach for

assessment of pump performance in terms of global design parameters and rarely in terms of local parameters like pressure and velocity (Rajendra et al. 2012, Mathew et al, 2014, Jafarzadeh et al 2011). The detailed knowledge of flow behavior inside the different components of pump is imperative for cost-effective design of pumps. It gives an insight to a designer and provides a direction to achieve the desired results.

The cavitation phenomenon which is due to the formation of the bubbles at low pressure zone (below the vapour pressure of the fluid) of the flow passage and its collapsing at high pressure zone effects the performance of centrifugal pumps considerably (Myung et al, 2012). The cavitation performance depends on the suction capacity or the net positive suction head required and net positive suction head available for the pump (Babayigit et al,2015).

The objective of present work is to study the cavitation (NPSHR) performance of a radial flow centrifugal pump by changing the boundary conditions of inlet and outlet. The Computational fluid dynamics is used to analyze the flow behavior in terms of head loss and velocity distribution at suction, impeller and delivery casing.

## 2. Formulae Used

The flow inside the centrifugal pump is a multiphase flow (Myung et al, 2012) . Hence partial differential governing equations which are based mainly continuity, momentum and energy equations are solved through CFD.

The numerical simulation gives values of pressure and velocity distribution in flow domain of pump. The following local and global flow and loss parameters are computed in non-dimensional form as:

| | | |
|---|---|---|
| Head developed | $H = \frac{TP_O - TP_I}{\rho g}$ | (1) |
| Relative loss in suction | $\xi_S = \frac{H_S}{H} x100$ | (2) |
| Relative loss in impeller | $\xi_I = \frac{H_I}{H} x100$ | (3) |
| Relative loss in casing | $\xi_C = \frac{H_C}{H} x100$ | (4) |
| Total head loss | $H_{HL} = H_S + H_I + H_C$ | (5) |
| Net Positive Suction Head | $\mathrm{NPSH} = \frac{\mathrm{Tp_I - Tp_{vap}}}{\rho g}$ | (6) |
| Power output | $P_{in} = \rho\, g\, QH/1000$ | (7) |
| Power input | $P_{out} = 2\pi NT/60000$ | (8) |
| Efficiency | $\eta_h$ =Power output/Power input | (9) |

Thomas cavitation factor $\sigma = NPSH/H_{net}$ (10)

## 2. Geometry and Meshing

The solid modeling of a centrifugal pump space in a single domain is very difficult because of large and complicated shape. Moreover, pump impeller is having some rotational speed and the inlet pipe and volute casing are fixed. So, the whole pump space is divided into three domains for geometric modelling. The 3D modelling is done in Ansys ICEM CFD and Ansys Blade Gen. The dimensions of the modelled pumps are given in table 1 & 2

**Table 1:** Dimensions of Centrifugal Pump Impeller

| | |
|---|---|
| Impeller hub diameter | 42.7 mm |
| Impeller inlet diameter | 120.2 mm |
| Impeller width at inlet | 27.3 mm |
| Impeller outlet diameter | 272.1 mm |
| Impeller width at outlet | 13.4 mm |
| Number of blades | 7 |

**Table 2:** Dimensions of Spiral Casing

| | |
|---|---|
| Inlet diameter of casing | 272.1 mm |
| Width at inlet | 13.4 mm |
| Casing rotation angle | $14^0$ |
| Outlet Diameter | 78.43 mm |

The complete flow path of the centrifugal pump is discretized through unstructured mesh in to 272880 nodes and 1521387 elements, keeping Y+ value less than 200.
The 3D turbulent flow analysis in a centrifugal pump domain is carried out using the Ansys CFX-14 software. The numerical flow simulation is first carried out for fixed rotational speed of 2900 rpm and discharge of water varying from 60%,80%,100% and 120% of 52.2 kg/s and with constant discharge with varying inlet pressure.
In the present flow simulation, SST k-ω turbulence model is used for the analysis and Rayleigh-Plesset Equation (RPE) model is used to estimate the rate of vapour production in case of cavitation (Philip et al, 2016, Maxime et al,2016).

## 3. Results & Discussions

The pump has been designed for the basic design parameters of 52.2 kg/s discharge, 89.95 m head and rotational speed of 2900 rpm. The numerical simulation has been carried out for the cavitation analysis. The boundary conditions are applied at the inlet of pipe and outlet of spiral

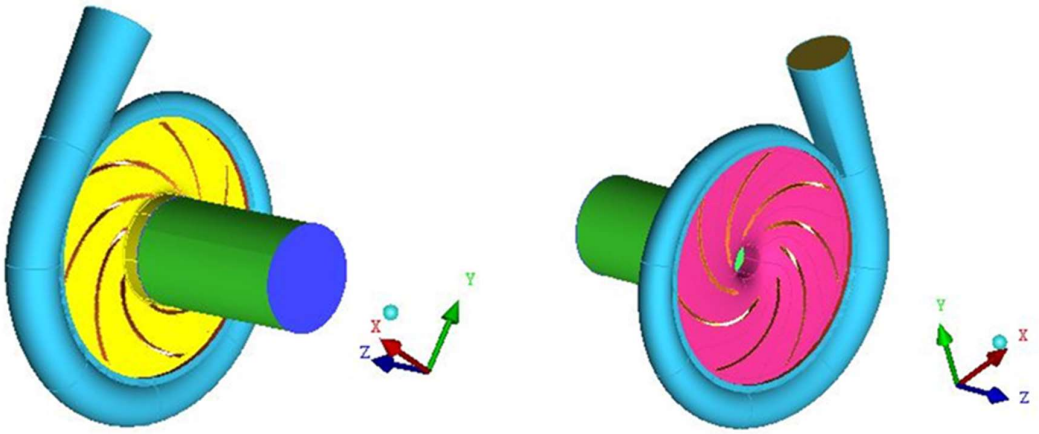



**Figure.1** : The geometry of complete assembly of centrifugal pump casing.

Grid dependency test is done by the varying the tetrahedral elements of the pump between 756825 to 1840889.It is found that the efficiency of pump improves by refining the meshing of the geometry. Efficiency is observed to be exactly same for the tetrahedral elements of 1521387 and 1840889. Therefore, all further numerical simulations for various speed and discharge has been carried out for 1521387 number of tetrahedral elements.

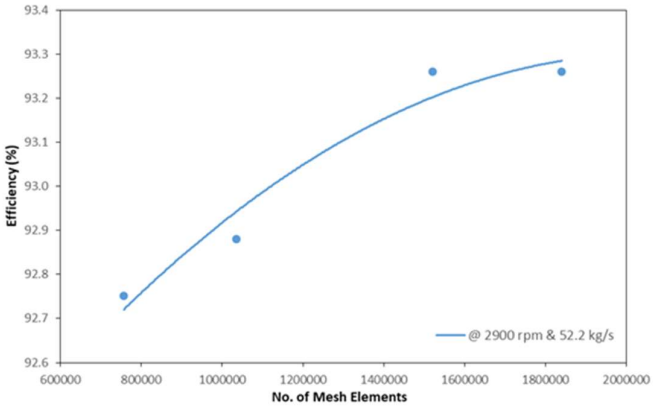



**Figure 2:** Grid Dependency test at Q=52.2 kg/s and N=2900 rpm

In this study of a centrifugal pump, numerical simulation is performed at the constant speed of 2900 rpm with discharge varying from 60%,80%,100%,120% of constant discharge of 52.2 kg/s with impeller rotational speed at 2900 rpm. Performance of a centrifugal pump for efficiency and NPSH with head is represented graphically. Pressure contours, velocity streamlines, are also shown for various loading conditions.

### 3.1 *Variation of Efficiency with NPSH*

The flow has been simulated for a value of discharge varies from 60%,80%,100% and 120% of 52.2kg/s at a constant speed of 2900 rpm with varying inlet pressure of 0.4 atm,0.6 atm,0.8 atm and 1 atm. Variation of hydraulic efficiency with NPSH is shown under different loading conditions. Figure 3 (a-d) shows the variation of efficiency with NPSH at all loading conditions. It is observed that efficiency decreases with reduction in NPSH value, it is because of bubble formation and cavitation at low NPSH values. The similar pattern of decrease in the net head with NPSH produced by the pump is also be observed in figure 4

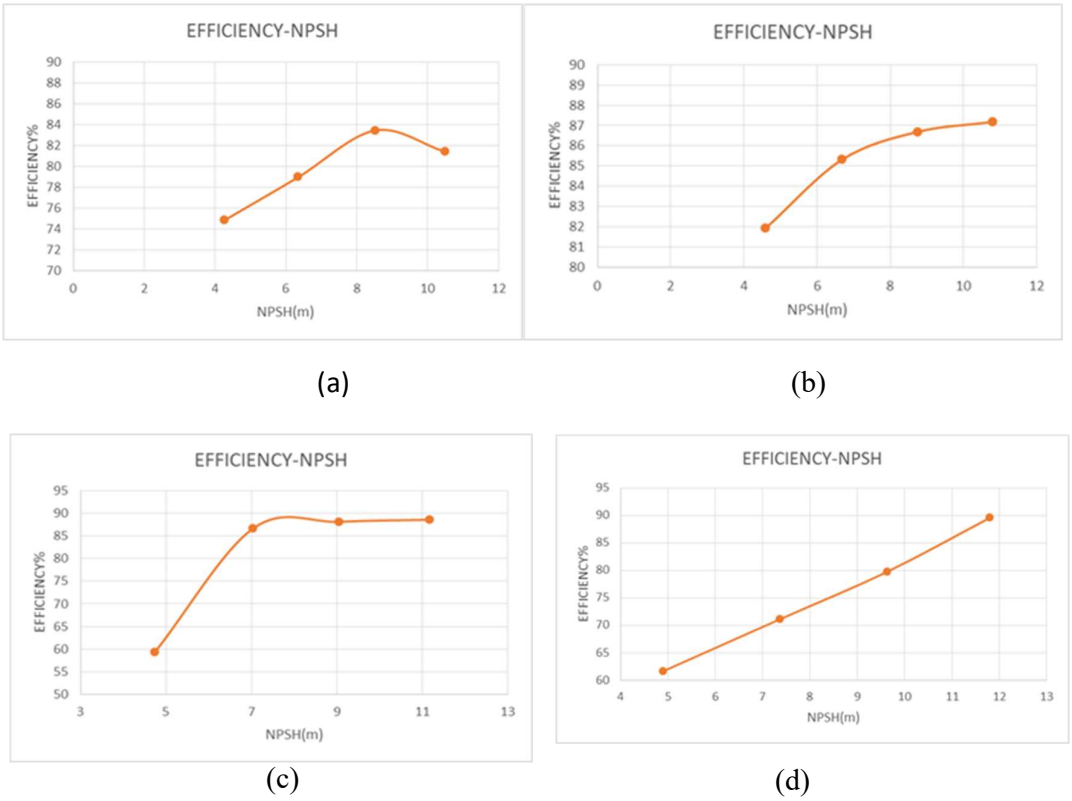



Figure 3: Variation of Efficiency with NPSH at (a) 60% (b) 80% (c) 100% and (d)120% loading

### 3.2 *Variation of Head*

The value of Required Net Positive Suction Head (NPSHr) for each loading is calculated corresponding to the 2% head drop (Ramadevi et al 2015). Variation of Head with NPSH is shown for different loading conditions and NPSHr is calculated.

**Table 3**: Net Positive Suction Head required($NPSH_r$) for different loading conditions

| Loading(%) | $NPSH_r$(m) |
|---|---|
| 60 | 5.5 |
| 80 | 5.9 |
| 100 | 6.8 |
| 120 | 11.6 |

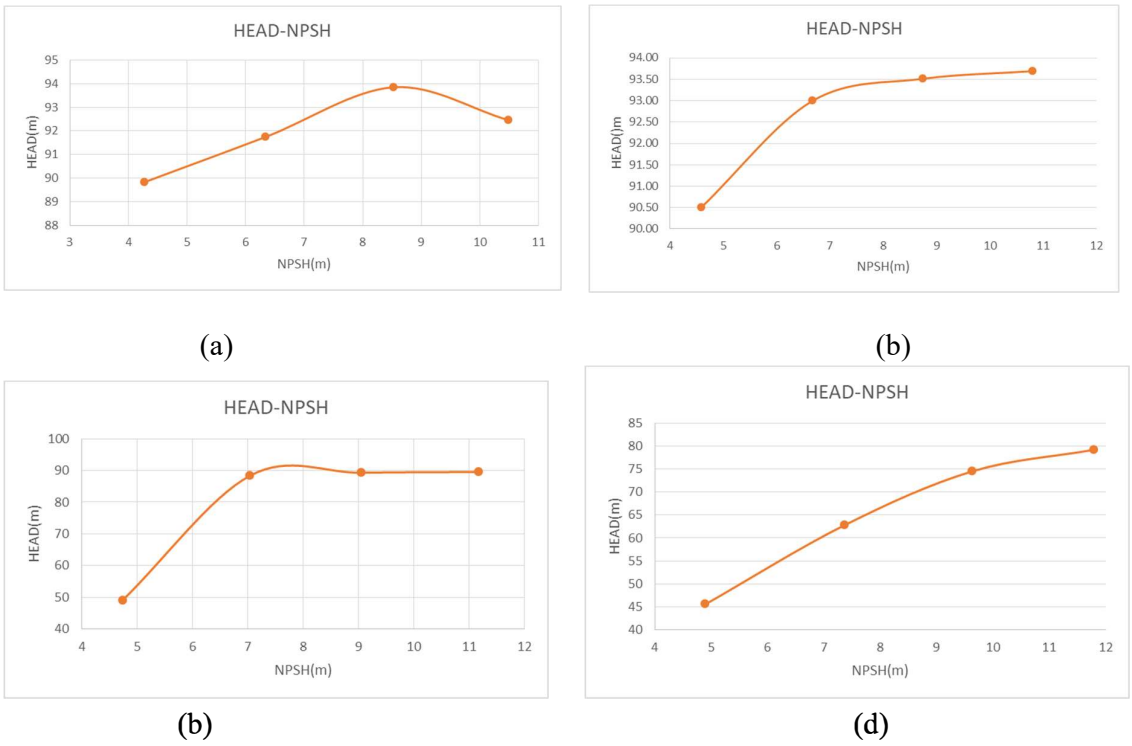
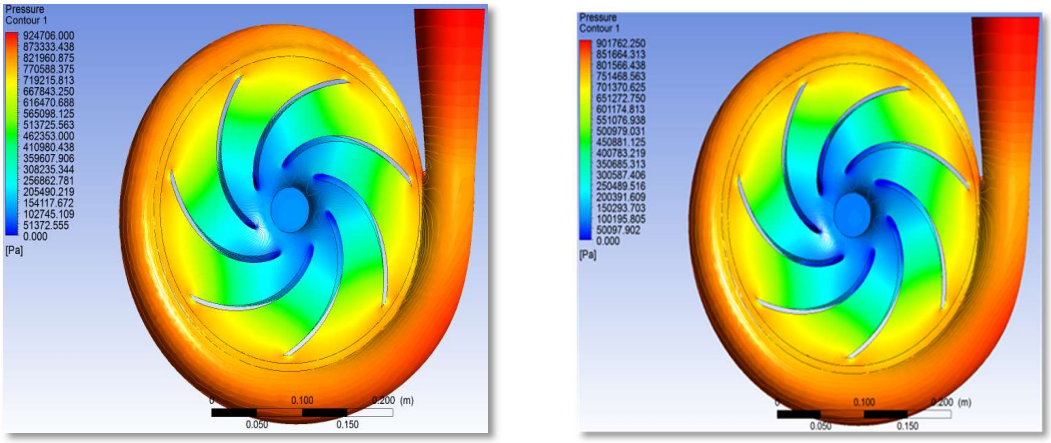
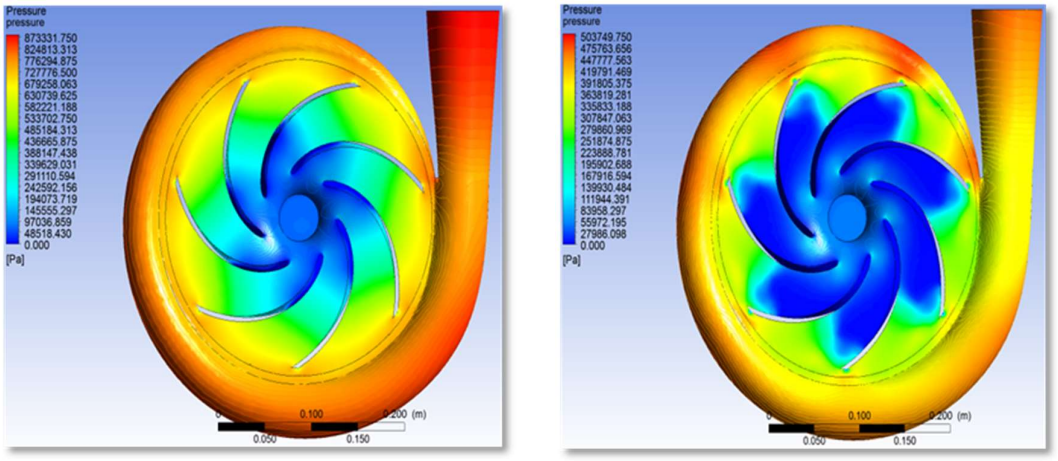



**Figure 4:** Variation of Net Head with NPSH at (a) 60% (b) 80% (c) 100% and (d)120% loading

### 3.3 *Pressure Contour at 100% Loading*

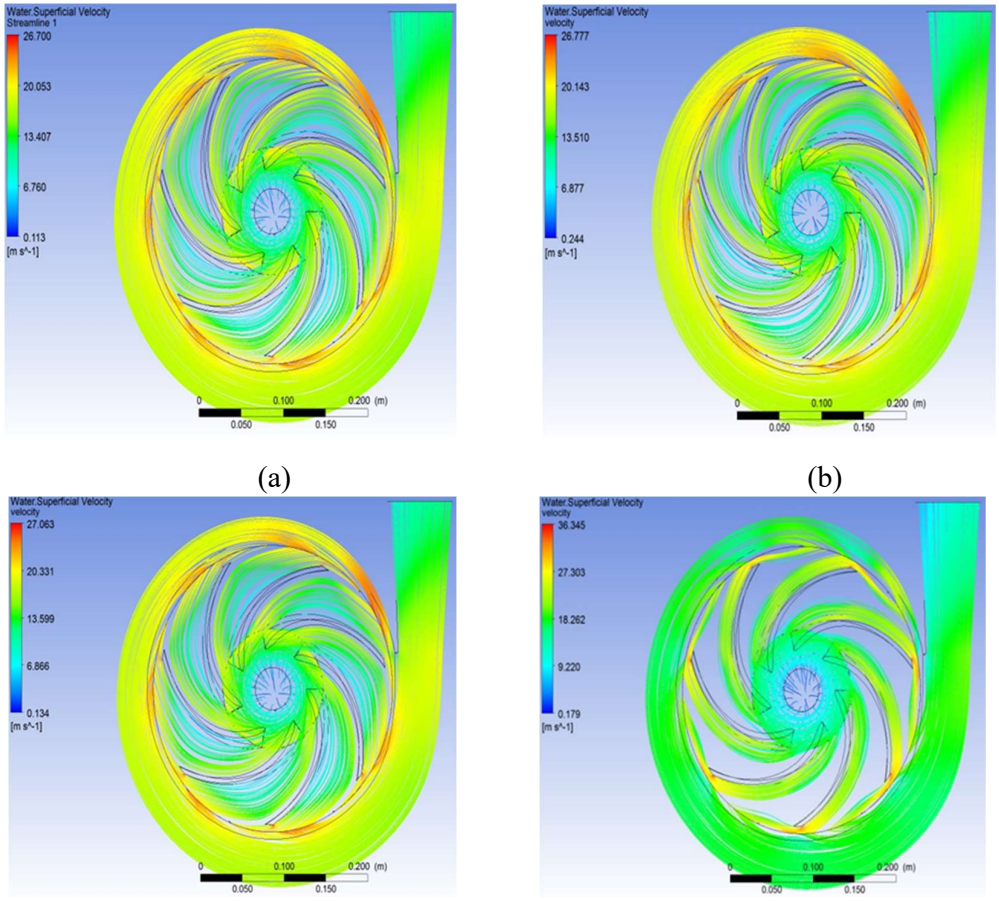
It is shown from the pressure contours that as the inlet pressure decreases maximum pressure inside the centrifugal pump also decreases. The development of cavitation i.e, the low pressure zone can be observed from figure 5. It can be seen that as long as pressure at suction side reduces the area of low pressure zone increases in impeller.






(c) (d)

**Figure 5** Pressure Contours for 100% loading & inlet pressure of (a)1atm (b) 0.8atm (c) 0.6atm (d) 4 atm




(a) (b)

(c) (d)

**Figure 6**:Velocity stream lines for 100% loading and inlet pressure of (a)1atm (b) 0.8atm (c) 0.6atm (d) 0.4atm

The same can also be observed in velocity stream lines for 100% loading as shown in figure 6., Which shows the increase in velocity by decreasing static pressure at inlet of the pump.

### 3.4 *Hydraulic losses in centrifugal pump*

Hydraulic losses of various parts of centrifugal pump such as inlet pipe, impeller and casing at constant rotational speed of 2900 rpm with discharge varying from 60%, 80%,100%,120% of designed discharge of 52.2 kg/sunder inlet pressure 0.4 atm,0.6 atm ,0.8 atm and 1atm is shown. Percentage loss is calculated with respect to net head. It has been observed that Inlet pipe has minimum loss as compared to other parts and maximum loss is found in impeller due to occurrence of cavitation at off design conditions..

**Table 4: Losses in percentage at different loading condition**

| %Loading | Q(kg/s) | P given(atm | Inlet Pipe Loss(% | Impeller Loss(%) | Casing Loss(%) | Total Loss(%) |
|---|---|---|---|---|---|---|
| 60% | 31.32 | 0.4 | 0.0345 | 17.967 | 8.304 | 26.3055 |
| 60% | 31.32 | 0.6 | 0.594 | 12.582 | 7.181 | 20.357 |
| 60% | 31.32 | 0.8 | 0.769 | 10.198 | 7.39 | 18.358 |
| 60% | 31.32 | 1 | 0.901 | 9.439 | 6.956 | 17.296 |
| 80% | 41.76 | 0.4 | 0.368 | 12.456 | 5.2 | 18.025 |
| 80% | 41.76 | 0.6 | 0.059 | 7.424 | 5.079 | 12.563 |
| 80% | 41.76 | 0.8 | 0.033 | 6.036 | 4.948 | 11.017 |
| 80% | 41.76 | 1 | 0.033 | 5.617 | 4.895 | 10.545 |
| 100% | 52.2 | 0.4 | 0.05 | 20.136 | 15.705 | 35.891 |
| 100% | 52.2 | 0.6 | 0.04 | 7.025 | 5.309 | 12.374 |
| 100% | 52.2 | 0.8 | 0.036 | 5.625 | 5.163 | 10.824 |
| 100% | 52.2 | 1 | 0.041 | 5.201 | 5.141 | 10.383 |
| 120% | 62.64 | 0.4 | 0.078 | 20.3 | 17.5 | 37.878 |
| 120% | 62.64 | 0.6 | 0.06 | 15.114 | 12.316 | 23.76 |
| 120% | 62.64 | 0.8 | 0.042 | 12.877 | 8.586 | 21.505 |
| 120% | 62.64 | 1 | 0.024 | 10.437 | 7.773 | 18.234 |

Table 4 shows that the total losses in the pump are increasing with loading on the pump. As long as the pressure decreases in the suction side of the pump, losses at various parts of the pump increases, the increase in loss is more prominent in impeller and it increases with cavitation at suction side of the impeller (Rambabu et al, 2015).

## 4. Conclusions

The numerical simulations of centrifugal pump at four different loading conditions and four different inlet pressure, It has been observed that the discharge and inlet pressure of centrifugal impeller significantly affects the local and global performance parameters of centrifugal pump.

Efficiency decreases with decrease in pressure at inlet o pump . Best efficiency is observed at 100% loading and its value is found to be 93.26 % without cavitation. The net head decreases with the increase in discharge and increases with inlet pressure for given loading condition. NPSHr value is calculated from the variation of head-NPSH curve. This value corresponds to the NPSH at 3% drop of head. The required NPSHr at 100% loading is calculated as 6.8 m.

**Nomenclature**

| | |
|---|---|
| | Hydraulic efficiency of turbine |
| | Contraction coefficient |
| ρ | Density of water(kg/m3) |
| g | Acceleration due to gravity(m/s2) |
| H | Net head (m) |
| Himp, Hs ,Hc | Head loss in impeller, suction and casing respectively (m) |
| Hl | Hydraulic loss (m) |
| N | Rotational speed of impeller (rpm) |
| NPSH | Net Positive Suction Head (m) |
| NPSHr | critical Net Positive Suction Head (m) |
| Q | Discharge (kg/s) |
| T | Torque on impeller blade (Nm) |
| Tpi | Total pressure at inlet of pump (pa) |
| Tpo | Total pressure at outlet of pump (pa) |
| Tvap | Vapour pressure of water at 20 degree Centigrade (pa) |

## References

Jafarzadeh B.,Hajari A., AlishahiM. M., and AkbariM. H. (2011). The flow simulation of a low-specific-speed high-speed centrifugal pump. *Applied Mathematical Modelling*, 35(1), 242-249.

Myung Jin Kim, Hyun Bae Jin, and Wui Jun Chung(2012) A Study on Prediction of Cavitation for Centrifugal Pump" World Academy of Science, Engineering and Technology *International Journal of Mechanical, Aerospace, Industrial, Mechatronic and Manufacturing Engineering* Vol.6, 345-354

Rajendran S., and Dr.PurushothamanK.(2012). Analysis of a centrifugal pump impeller using ANSYS-CFX., *International Journal of Engineering Research and Technology*, 1(3).1-6

LiuH. L., LiuD. X., WangY., WuX. F, and WangJ. (2013). Application of modified κ-ω model to predicting cavitating flow in centrifugal pump, *Water Science and Engineering*, 6(3), 331-339.

Dazhuan Wu,Shuai Yang,Binjie Xu,Qiaoling Liu,Peng Wu,Leqin Wang(2014), Investigation of CFD calculation method of a centrifugal pump with unshrouded impeller, *Chinese Journal of Mechanical Engineering* ,Volume 27(2),.376-384

MathewArun(2014)."Cavitation Modelling and Characteristic Study of a Centrifugal Pump Impeller" *International Journal of Innovative Research in Advanced Engineering (IJIRAE)* , 1(10) ,59-63

MuttalliRaghavendra S , AgrawalShweta ,WarudkarHarshla(2014),CFD Simulation of Centrifugal Pump Impeller Using ANSYS-CFX, International *Journal of Innovative Research in Science , Engineering and Technology*, Vol. 3(8), 15553-15561.

Babayigit O., Kocaaslan O., AksoyM. H., GulerenK. M., and OzgorenM. (2015). Numerical identification of blade exit angle effect on the performance for a multistage centrifugal pump impeller. *EPJ Web of Conferences, EDP Sciences, Vol. 92, 02003-02009*

Rambabu G, Sampath S, Karthik G., S. Siva Teja(2015). Flow analysis of centrifugal pump using CFX solver and remedies for cavitation mitigation."Int. Journal of Engineering Research and Applications, Vol. 5(7) ,52-58

Ramadevi (2015),Net Positive Suction Head Analysis for Testing the Condition of a Centrifugal Pump. Indian *Journal of Science and Technology*, 8(10), 300-304.

MaximeBinama , MuhirwaAlex, BisengimanacEmmanuel(2016), Cavitation Effects in Centrifugal Pumps-A Review, *Int. Journal of Engineering Research and Applications*, Vol. 6, Issue 5,173-185

Phillip Limbach, Tim Müller, Martin Blume, Romuald Skoda(2016),Numerical and experimental investigation of the cavitating flow in a low specific speed centrifugal pump and assessment of the influence of surface roughness on head prediction,*International Symposium on Transport Phenomena and Dynamics of Rotating Machinery at Hawaii*, Honolulu, 10-15 April.

IN PROCEEDINGS OF 25th HYDRO 2020, INTERNATIONAL CONFERENCE,
NATIONAL INSTITUTE OF TECHNOLOGY ROURKELA, ODISHA, INDIA
26-28, March 2021, ISBN 978-93-90631-56-8

Paper ID - 321

# 'Estimation of reservoir capacity of Singda dam, Manipur using modern Integrated Bathymetry System (IBS) - A case study'

**Ajit Singh[1] M.S. Bist[2] Ajay Sonawane[3] K Subbarao Murthy[4] M. Selva Balan[5]**

[1] *Research Assistant, Central Water & Power Research Station (CWPRS), Pune-411024, India*
[2] *Scientist-C, Central Water & Power Research Station (CWPRS), Pune-411024, India*
[3] *Assistant Research Officer, - Central Water & Power Research Station (CWPRS), Pune-411024, India*
[4] *Junior Engineer, Central Water & Power Research Station (CWPRS), Pune-411024, India*
[5] *Scientist- D, Central Water & Power Research Station (CWPRS), Pune-411024, India*
*Email: msbist1974@gmail.com*

## ABSTRACT

The Singda Dam is multipurpose project which is constructed across the Singda river and is one of the highest earthen dam in India. It has been catering the needs of drinking water and water for irrigation to most part of Imphal city and its nearby villages. The dam was built by National Projects Construction Corporation Limited (NPCCL) and completed in the year 1995. Since then more than 25 year of operation, the project authority decided to conduct the bathymetry survey for evaluating the existing storage capacity of the reservoir and estimate the silt deposited. By evaluating the present storage capacity of the reservoir, the project authority can be planned the distribution of water supply for irrigation and drinking purpose. The study also includes finding the possible methods to enhance the dam water storage capacity by means of removal of silt from the reservoir.

The CWPRS, Pune Instrumentation division team, carried out bathymetry survey of Singda dam during the month of Jan. 2020. The team deploying the modern Integrated Bathymetry System (IBS) at site consisting of echo-sounder sensor, DGPS with antenna mounted on a motorized boat with necessary fixtures and other auxiliary equipments and Laptop for data collection. This IBS system has depth accuracy in cms sub meters and position accuracy in sub meters. The bathymetric survey was done at an El 904.50 m. The data collection planning and analysis was carried out using software such as Hypack, Surfer. The Google earth and Global mapper software, was used for extracting survey area boundary of the reservoir.

After the analysis was done the gross storage capacity of the reservoir is calculated and it was found that there was a substantial reduction in storage capacity of the reservoir during span of 25 years after its operation.

***Key Words***: *Bathymetry, IBS DGPS, Echo-sounder, HYPACK, Surfer.*

## 1. INTRODUCTION

The Singda dam construction started in year 1975 and completed in 1995 by NPCCL. Since after completion, the dam has been catering the need of providing the drinking water to greater Imphal and water for irrigation its nearby villages. The Singda dam boundary on Google earth is shown in Photo1. After operation of more than 25 years of dam, the Executive Engineer, Water Resources Department, Govt. of Manipur has requested National Project Monitoring Unit (NPMU), for conducting bathymetry survey of Singda, dam, Manipur. Subsequently after accepting the proposal by CWPRS, the CWPRS team carried out hydrographic survey of Singda reservoir from 16th to 18th January, 2020.

The CWPRS team conducted the bathymetric survey by deployed Integrated Bathymetry system (IBS) consisting of dual frequency echo-sounder (210 Khz and 33 Khz) for measuring the water depth and a Global Positioning System (GPS) for finding the accurate location of boat moving on the

predefined grid lines loaded on the software in laptop. The data (depth and position) collected at site was logged in real time mode in laptop with survey software. Processing and calculations are done later by processing software such as Hypack and surfer. The Fig. 1 shows the Singda dam boundary with logged data in Google image.

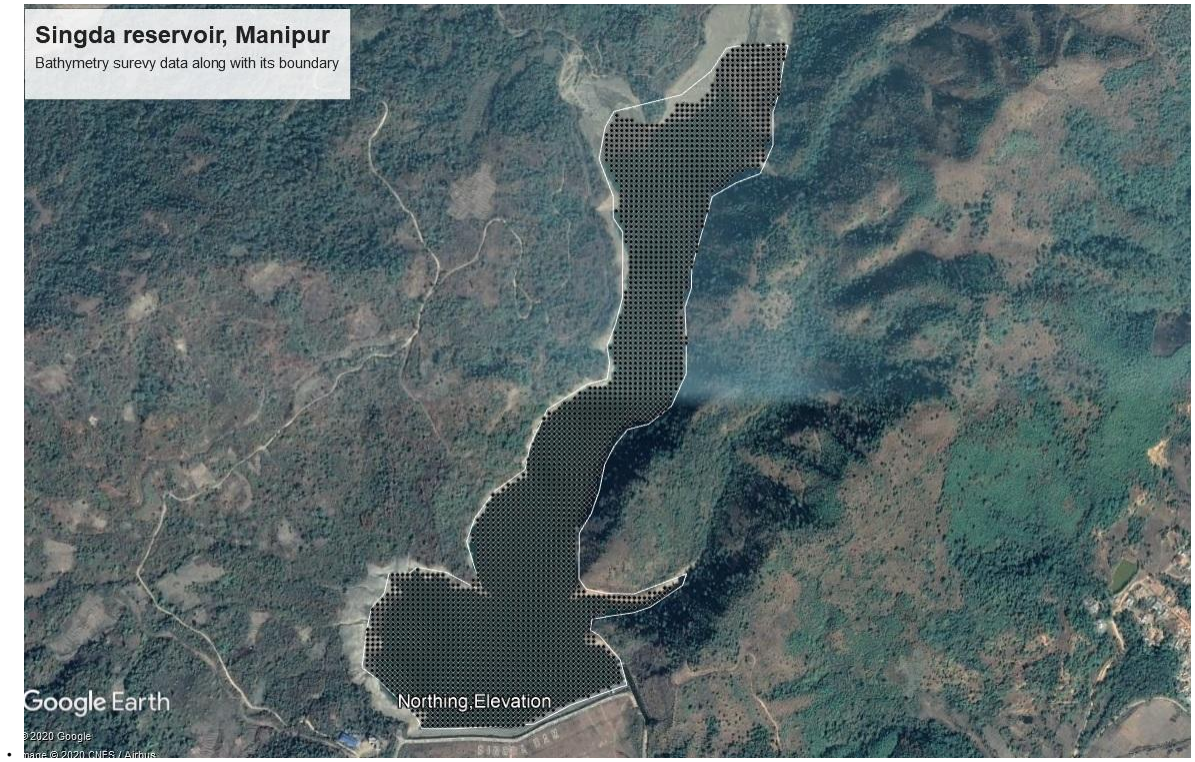



**Figure 1** Singda dam boundary in Google image.

## 2. COMPONENTS AND METHODOLOGY

The bathymetry survey was carried out with a boat equipped with the ultrasonic single beam dual frequency echo sounder (Single beam echo sounder Manual) Mobile GPS system with beacon correction and a lap-top for logging the real time data. The IBS system used during survey consists of the following components:

i) Single beam dual-frequency eco-sounder (210 Khz, 33 Khz) Knudsen make
ii) GPS make Trimble using beacon correction (GPS manual, Trimble make).
iii) Data collection laptop with Hypack software (Hypack manual) used for real time data acquisition.

A motorized boat was used for deploying the survey equipment during survey. The eco-sounder sensor with special fixture was fitted on one side of the boat and the GPS antenna was mounted on boat for receiving the satellite signal. The Hypack survey software was used for fixing of grid lines and interfacing of eco sounder and GPS equipment. The software logged the boat position longitude, latitude (x, y) data, and water depth (z) values at required interval/grid. The depth and position data is logged in real time mode in laptop with survey software. The Fig.2 shows GPS equipment with antenna fixed in boat and Fig.3 & Fig. 4 shows eco sounder and laptop screen showing data logging respectively. The echo sounder was calibrated for its accuracy before using it. The GPS correction for

boat location in accuracy of sub meter was achieved with beacon correction from near sea shore reference station.




**Figure 2** GPS with antenna




**Figure 3** Eco sounder

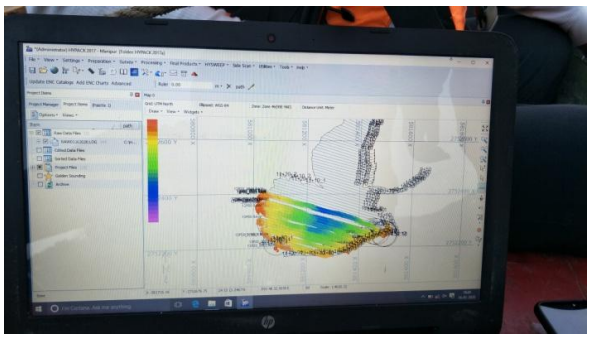


**Figure 4** Laptop screen showing data logging

The Fig.5 shows boat set up with survey equipment consisting of eco-sounder, GPS, attenna

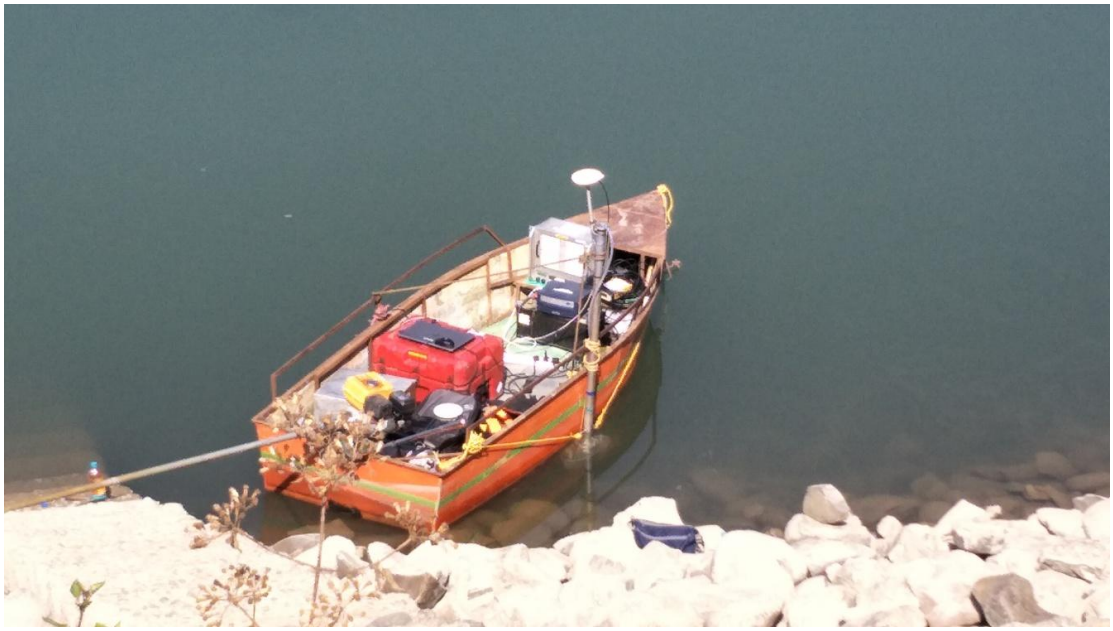


**Figure 5** Equipment set up in Boat

The survey is carried out by running the boat on the predefined straight grid line based on the pre survey process. This includes loading the survey boundary, assigning the proper coordinate system for the Global positioning system, setting the data logging protocol, zone, coordinate system etc. Similarly the echo sounder needs to be calibrated for the sound velocity before actual depth data logging. Boat navigation is also controlled by the software, so that boat tracks the grid line accurately while logging the data. The bathymetric survey was carried out during the month of June 2020 at the EL of 904.50 m.

The boundary profile was extracted from Google earth at CWPRS prior to the site visit. The same has been verified by running the boat on the actual cross section at site. After confirmation, the actual survey lines were carried out on the required cross-section. The bathymetry data collection was completed.

## 3. ANALYSIS AND RESULTS

After completing the survey, the data were filtered and noised were removed using software such as Surfer (Surfer Manual) /Hypack. During analyzing the data, the bathymetry raw data were converted in excel format. The grids were made using Krigging method and volume and corresponding area was calculated at survey EL of 904.50 m using Simpson 1/3 method and Simpson 1/6 method. The different volume value was calculated below survey level with an interval of 1m up to reservoir bottom. The elevation -volume-capacity, elevation- area curve, Digital Elevation Model (DEM) was plotted. The volumes at survey level and at dead storage level were calculated and compared. The Fig.6 shows surface map of Singda reservoir. The Fig. 7 and 8 shows elevation-capacity curve and Elevation- Area -Capacity curve of Singda reservoir respectively (CWPRS, Pune Technical Report No. 5835, July 2020)

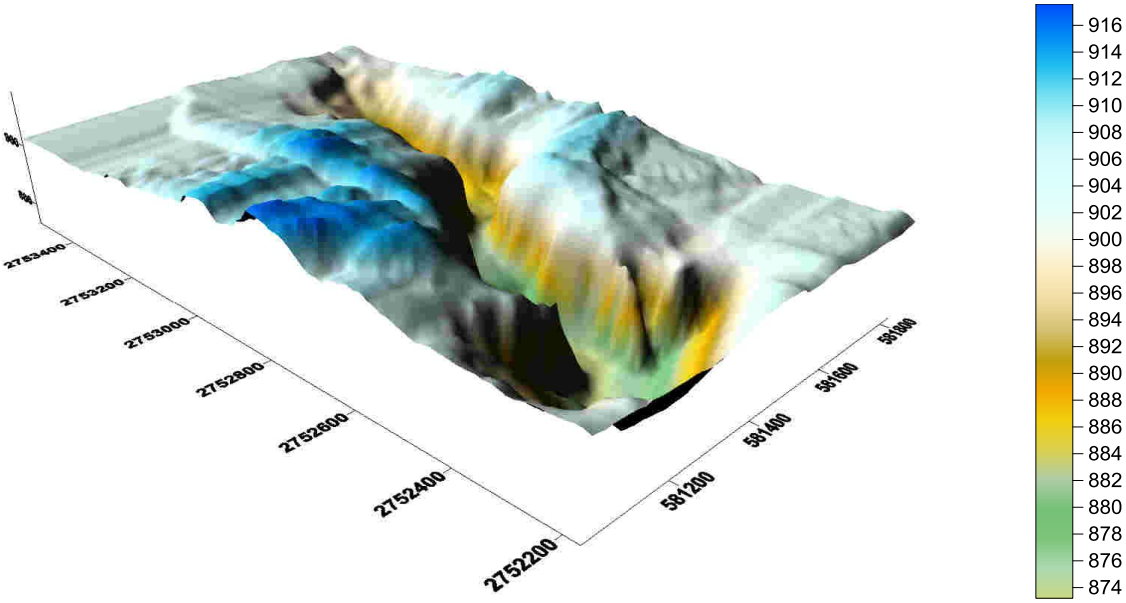



**Figure 6** Surface map of Singda reservoir

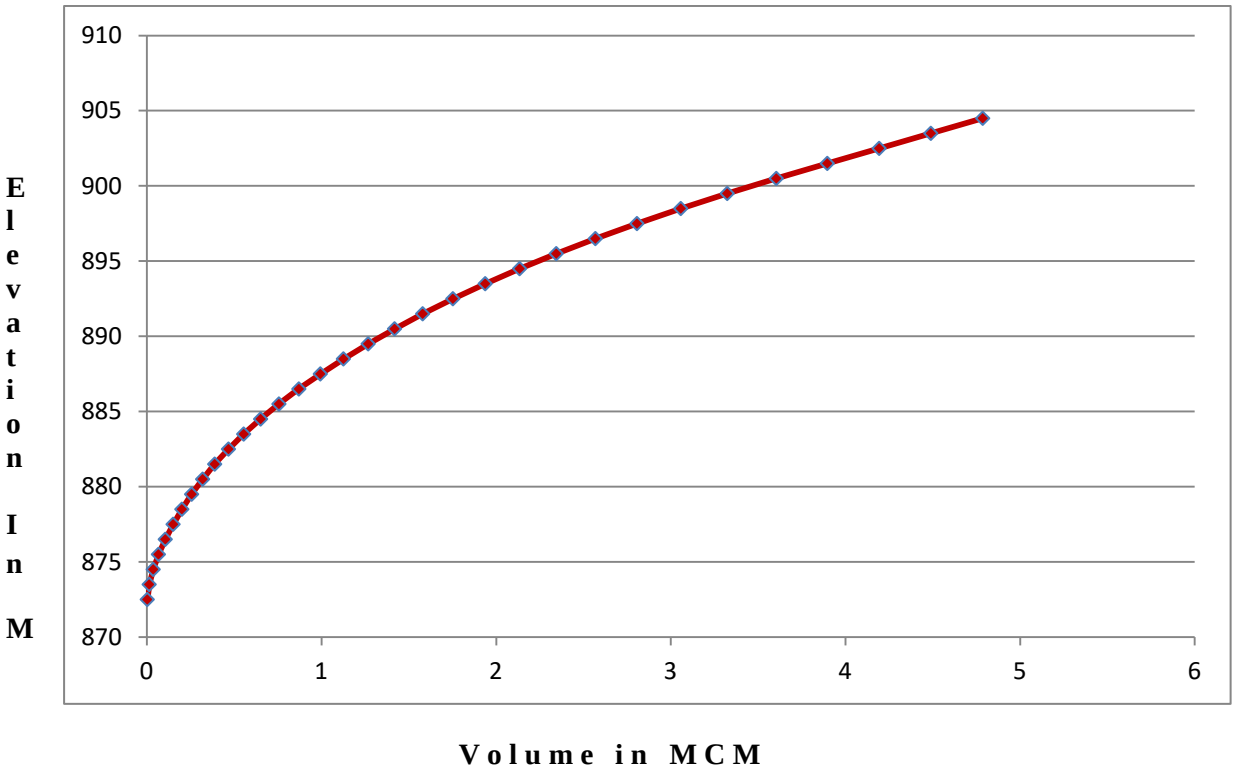



**Figure 7** Elevation- Capacity curve of Singda reservoir

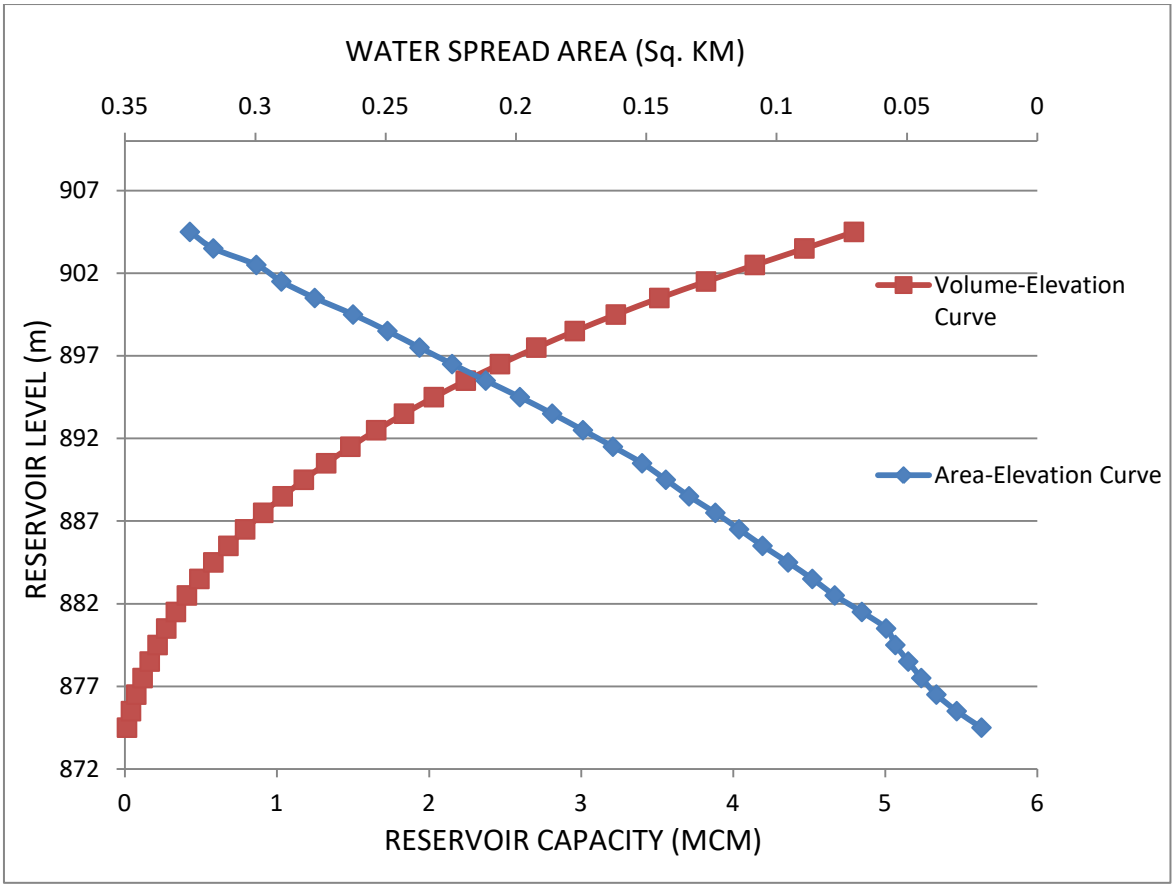



**Figure 8** Elevation- Area -Capacity curve of Singda reservoir

## 4. CONCLUSIONS

The collected data was edited and filtered and analyzed using HYPACK, Surfer. The volume-capacity curves, DEM, surface map, depth profile were drawn. The reservoir gross storage capacity calculated was 4.796 M.CM for water spread area of 0.325 sq. km at survey level 904.50 m RL. There is a reduction in volume of 2.45 MCM at survey RL i.e. 34 % when compared with the original gross storage capacity. Whereas there is a reduction of 25% in the live storage capacity of the reservoir.

## 5. ACKNOWLEDGEMENT

The authors wish to thank to Shri A. K. Agrawal, Director, CW&PRS for guiding them and giving his consent for publishing this paper. Our sincere gratitude to Dr. Prabhat Chandra, Scientist-E, who encouraged us during the preparation of this paper. Our sincere thanks to Shri Rohit Ahanthem, Superintending Engineer, Irrigation Circle-II, WRD, Govt. Manipur and his team of officials, Shri Irom Royal, Ex. Engineer, Shri Petlad K Haokip , E.E. and others in Irrigation division of Singda Dam project, Manipur who has extended their support in providing all necessary arrangements required for carrying out the hydrographic survey. The service of M/s. Geo Services Maritime Pvt. Ltd, Mumbai is duly acknowledged for their support in data collection activities.

## REFERENCES

AutoCAD Manual, Source: www.autodesk.com
CWPRS, Pune Technical Report No. 5835, (July, 2020).Bathymetry Survey of Singda Reservoir in Manipur State under National Hydrology Project (NHP).
GPS manual, Trimble make, Source: http:// www.trimble.com
Hypack Manual, Source: https://www.hypack.com
Surfer Manual Source: https://www.goldensoftware.com
Single beam echo sounder Manual, Knudsen makes. Source: https://www. knudseneng.co

# Theme XIII

# Groundwater Modelling and Management

*IN PROCEEDINGS OF 25th HYDRO 2020, INTERNATIONAL CONFERENCE, NATIONAL INSTITUTE OF TECHNOLOGY ROURKELA, ODISHA, INDIA 26-28, March 2021, ISBN 978-93-90631-56-8*

Paper ID - 027

# Study on subsurface hydraulic conductivity and soil moisture using Ground Magnetic Resonance (GMR)

Uttam Singh[1]; and Pramod K. Sharma[2]
Research Scholar[1]; Associate Professor[2]

[1,2]*Department of Civil Engineering, Indian Institute of Technology Roorkee-247667, Haridwar, India*
*Email: uttamsingh426@gmail.com; pramod.sharma@ce.iitr.ac.in*
*Mobile No.: +91 9455565229, +91 9456100806*

## Abstract

The ground magnetic resonance (GMR) equipment is working on the principle of magnetic resonance sounding (MRS). GMR equipment measures the magnetic signal from the subsurface water molecules via surface loop. It is a non-invasive method for estimation of relative hydraulic conductivity, which represents the ratio of unsaturated to the saturated hydraulic conductivity. The hydraulic conductivity in the capillary fringe zone can be considered as saturated because water content in this zone is considered equivalent to the water retention curve in equilibrium state. Hydraulic conductivity is the function of water content in the unsaturated zone of the aquifer. In this study, an attempt is made to perform field experiment using GMR and simultaneous inversion can be carrying out for obtaining the results of relative hydraulic conductivity, water content and decay time. Also, laboratory experiments shall be performed for finding saturated hydraulic conductivity and particle size distribution analysis. Finally, a relationship between unsaturated and saturated hydraulic conductivity shall be developed at different depths of subsurface.

***Keywords:*** *Hydraulic conductivity; ground magnetic resonance; water content; decay time*

## 1. Introduction

The Ground Magnetic Resonance equipment works on principle of the Nuclear Magnetic Resonance (NMR). It is a geophysical and ground water exploration technique was developed in recent decade. Nuclear magnetic resonance (NMR) phenomenon detects the sub surface water molecules (Hydrogen proton). Now a day's several methods are used for aquifer characterization. Most of them have correlation between electrical conductivity and water (Habberjam and Watkins 1967).

Schirov et al. (1991) studied the advantages of non-invasively detection of NMR signals at different depths by surface NMR equipment after that significant modifications and improvements are carried out in the hardware in past decades (Walsh, 2008 and Walsh et al., 2011). Mobile water content (seepage water) can be estimated by MRS in the vadose zone of the aquifer (Roy and Lubczynski, 2005). Roy et al. (2008) suggested that mobile and immobile water content cannot be detected in magnetic environment by standard FID. Bernard (2007) and Muller-petke et al. (2010) studied that Numis and hydroscope surface NMR equipment have effective dead time in the range of 30-40ms. New commercially available equipment GMR introduced in 2008 whose fixed dead time is 8ms and post processing effective dead time is 10ms plus 1/BW, BW is a user defined bandwidth (Hz). Further modifications were done in GMR equipment and the dead time was reduced up to 4ms and post processing dead time also 4ms plus 1/BW. Keating and knight (2007) and Grunewald and Knight (2011) found in their study that the characterization of water content fluxes due to mineral weathering is challenging because due to in-homogeneity in magnetic field minerals causes rapid changes in the phase of surfaces NMR FID signal. Permeability/hydraulic conductivity has been traditionally estimated for groundwater application using hydrological techniques. These techniques are expensive, time consuming and sometimes results may be erroneous. These problems were leading interest in the use

of surface NMR and well logging NMR measurements. Alternatively, hydraulic conductivity of the aquifer can be estimated by using Schlumberger-Doll research (SDR) equation (Dulbac et al., 2003)

Recently previous decade Vista Clara Inc. developed a multi-channel system, geomagnetic resonance (Vista clara, 2009). It is fully digitized and 50kHz strength of signal recording without any resonance circuit at receiving end (Walsh, 2008). The dead time of the system is about 5ms for capturing of time series data. The measurement loop placed at earth surface of required diameter and the loop can also be placed square shape or eight shape depending on the site condition and requirement. The depth of investigation depends upon excitation current and loop size and it is a depth dependent subsurface investigation. Dulgosch et al. (2011) studied that surface NMR method is not efficient as compared to laboratory NMR method because low signal to noise ratio (S/N) and very short relaxation time due to dead time of the equipment and long duration of excitation pulse. Under acceptable noise condition SNMR allows to estimate relative hydraulic conductivity and water content along the depth using NMR relaxation times $T_1$ and $T_2^*$. Type of NMR experiment will decide the relaxation time. Generally, free induction decay (FID) with single pulse excitation are considered for NMR applications because it saves time and energy both are key factors for field experimentation work (Grunewald and Knight, 2011).

In this study, our main objective is to estimate hydraulic conductivity and ground water content and also find the ground water by using GMR equipment.

### *1.1 Study Area*

The study area is located in south-western part of the Uttarakhand state in Haridwar district of Roorkee subdivision. The field experimentation was conducted at Roorkee site as shown in Figure 1. The latitude and longitude of the site was $29^\circ 54' 9.2''$ N and $77^\circ 57' 4.6''$ E, respectively and local magnitude of earth's magnetic field was $492161nT$. The magnetic inclination and magnetic declination was ($47.2160^\circ$) and ($1.3875^\circ$) respectively. This study site is situated under foot hill of Indo-Gangetic region of India. GMR equipment was setup at this location with three turns of 30m diameter of main loop (transmission/receiver loops) and two set of noise cancellation loops in different direction with 30m diameter size.

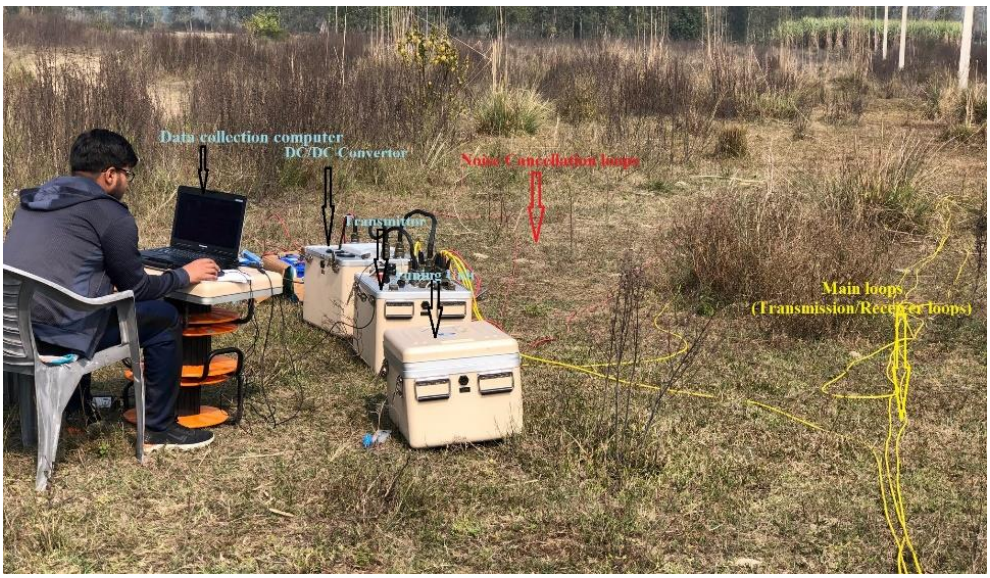



**Figure 1** GMR field experimentation setup.

## 2. Methodology

Hydrogen proton is present in the water molecules and its tendency to spin and surface NMR can be used for subsurface investigation. It is an intrinsic property of the hydrogen proton with the angular moment. Proton spin is not associated with physical rotation, Larmor frequency ( $f_L$ ) of hydrogen protons under static magnetic field ( $B_0$ ) is expressed as (Coates et al. 1999):

$$f_L = \frac{\omega_L}{2\pi} = \frac{-\gamma \times B_0}{2\pi} \quad (1)$$

Where; Proton gyro-magnetic, $\gamma = 0.2675 \times 10^9 \, s^{-1} T^{-1}$ and $\omega_L$ = Larmor angular frequency.

Larmor frequency depends on the strength of static magnetic field and it also depends on the type of NMR investigation. The static Earth's magnetic field ( $B_E$ ) for surface NMR lies between $25nT - 65nT$ . The net magnetic moment due to measure volume of water under thermal equilibrium in static magnetic field. This is summation of each proton moment in the same direction in static magnetic field. At the thermal equilibrium, net magnetization vector ( $M_0$ ) is given by Curie's law (Behroozmand et al. 2015).

$$M_0 = \frac{n\gamma^2 h^2}{4K_B T} B_0 \quad (2)$$

Where, $T$ is temperature; $K_B$ is Boltzmann's constant; $h$ is Plank's constant and $n$ is the number of protons.

The signal of surface NMR depends on the strength of magnetic field as well as inclination of magnetic field. So, effective energized magnetic field (transverse component) to Earth's magnetic field scaled with magnetic inclination. Generally, Earth's magnetic field is considered homogeneous within the experimentation site provided without strong magnetic material. Local resonance condition may be affected by temporal variation in Earth's magnetic field. Schirov and Legchenko (1991) conducted experiments in several aquifers at various depths in USSR region. The experimental curves (Figure 2) represents that curve shape depends on water content and depth of aquifer.

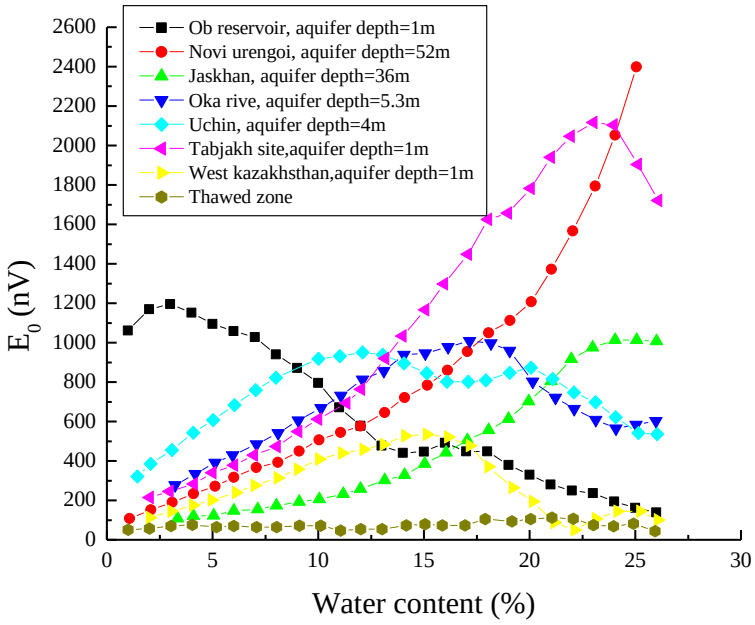



**Figure 2** Experimental curves represent variation in responses at different hydrological conditions in the USSR.

The wires can be spread on the surface in circular or square or figure 8 shape loop depending on the requirement and site condition, known as transmitting loop after that current passed under tuned Larmor frequency. The excitation pulse is generated and subsurface protons gets excited. The current pulse $(q)$ is the product of current amplitude $(I_0)$ and pulse duration $(\tau_p)$ and it develops energizing magnetic field $(\mathbf{B_T(r)})$. The direction and intensity of energizing magnetic field depends on subsurface material structure (electrical resistivity) and measuring configuration. Hertrich (2008) studied that long pulse duration (30-40ms) are used because of weak energizing magnetic field can penetrate up to 100m depth of subsurface. Energizing magnetic field becomes elliptically polarized when it reaches at its limiting depth of subsurface (100m).

$\mathbf{B_T(r)}$ is considered as homogeneous in the elementary volumes of each segment of subsurface for forward modeling of surface NMR. $\mathbf{B_T^{\perp}(r)}$ is a component of $\mathbf{B_T(r)}$ perpendicular to the Earth's magnetic field $(\mathbf{B_E})$. $\mathbf{B_T^{\perp}(r)}$ can also be decomposed in two co-rotating component $(\mathbf{B_T^{+}(r)})$ and counter-rotating component $(\mathbf{B_T^{-}(r)})$ in the form of following equation (Hertrich 2008).

$$\mathbf{B_T^{\perp}(r)} = \mathbf{B_T^{+}(r)} + \mathbf{B_T^{-}(r)} \tag{4}$$

Co-rotating component is the part of transmitting field component and it is in alignment with Earth's magnetic field $(\mathbf{B_E})$ from spin to tip. Tip angle in the surface NMR can be defined in the form of following equation.

$$\theta_T(\mathbf{r},\tau_p) = \omega_T(\mathbf{r})\tau_p = \gamma\left|\mathbf{B_T^{+}(r)}\right|\tau_p \tag{5}$$

Where $\omega_T(\mathbf{r})$ is an angular frequency of transmitting pulse and theoretically it is equal to the Larmor angular frequency.

Weak oscillating magnetic field is produced by free induction decay (FID) when energizing pulse is tuned off. The propagating signal travels inside the subsurface and it can be recorded by GMR equipment through surface receiver loop. Overlapping of energizing signals of each processing nuclear spins within Earth's volume at excited state is called as nuclear measured signal. Signal data was recorded in multiple stacks of pulses with phase and decay time (Figure 3). Subsurface depth information can be recorded by measuring signals in different exciting Earth's volume. Hertrich (2008) and Muller-Petke and Yaramanci (2010) proposed an expression for induced surface NMR voltage which is applicable for receiver loop.

$$V(q,t) = \int G(\mathbf{r},q)\int W\left(T_2^*,\mathbf{r}\right)e^{\frac{-t}{T_2^*}}dT_2^*d^3\mathbf{r} \tag{6}$$

The above equation is known as QT surface NMR inversion model. Where, $V(q,t)$ is measured surface NMR signal, $T_2^*$ is transverse relaxation time, $\mathbf{r}$ is a position vector, $W(T_2^*,\mathbf{r})$ is position of water content distribution at different transverse relaxation time and it is also known as partial/relative water content and $G(\mathbf{r},q)$ is a smoothing function known as Kernel function. Hertrich (2008) and Weichman et al. (2000) defined kernel function under on-resonance condition as follows.

$$G(r,q) = \omega_L M_0 \sin(-r\frac{q}{I_0}\left|\mathbf{B_T^+(r)}\right| \times \frac{2}{I_0}\left|\mathbf{B_R^-(r)}\right|.e^{[i(\xi_T(\mathbf{r},\omega_L)+\xi_R(\mathbf{r},\omega_L)]}$$
$$\times\left[\hat{\mathbf{b}}_{\mathbf{R}}^{\perp}(\mathbf{r},\omega_L).\hat{\mathbf{b}}_{\mathbf{T}}^{\perp}(\mathbf{r},\omega_L)+\mathbf{i}\hat{\mathbf{b}}_{\mathbf{0}}.\hat{\mathbf{b}}_{\mathbf{R}}^{\perp}(\mathbf{r},\omega_L)\times\hat{\mathbf{b}}_{\mathbf{T}}^{\perp}(\mathbf{r},\omega_L)\right] \tag{7}$$

Where, $\omega_L$ is angular Larmor frequency, $\mathbf{B_R^-(r)}$ is a counter-rotating component of virtual magnetic field and its projection lies in the plane perpendicular to Earth's magnetic field $(\mathbf{B_E})$, $\hat{\mathbf{b}}_{\mathbf{R}}^{\perp}$,$\hat{\mathbf{b}}_{\mathbf{T}}^{\perp}$ and $\hat{\mathbf{b}}_{\mathbf{0}}$ are the unit vectors, $\xi_T$ is transmitter to observation point phase lag, $\xi_R$ is observation point to receiver phase lag and other notations are as usual used in this study.

Generally, coincident transmission and receiver loop type configuration is used in the surface NMR study. So, same loop can be used for both energizing pulse and receiving NMR signal. For one dimensional (1 D) subsurface survey above 6 and 7 can be written as:

$$V(q,t) = \int G(q,z)\int W\left(z,T_2^*\right)e^{-\frac{t}{T_2^*}}dT_2^*dz \tag{8}$$

$$G(\mathbf{r},q) = \omega_L M_0 \sin\left(-\gamma\frac{q}{I_0}\left|\mathbf{B_T^+(r)}\right|\right)\times\frac{2}{I_0}\left|\mathbf{B_T^-(r)}\right|.e^{2i\xi_T(\mathbf{r},\omega_L)} \tag{9}$$

### *2.1 FID measurement of Surface NMR*

FID can be measured by single pulse acquisition scheme and transverse relaxation time $(T_2^*)$ is responsible for exponential decay of measured signal. Measured signal ideally having equal frequency to the energizing pulse which is equal to Larmor frequency. For detection of FID transverse relaxation time $(T_2^*)$ and static magnetic field $(B_0)$ are required because dead time ($t_{dead}$) and short duration ($\tau_p$) are approximately 10-40ms long with measured relaxation time. A significant duration of

relaxation can occur during pulse is known as relaxation during pulse (RDP). $T_2^*$ and $E_0$ can be accurately estimated by extrapolating signal from end of energizing pulse i.e., originating point of relaxation.

**Table 1** Values of $T_2^*$ and aquifer materials for Larmor frequency from Earth's magnetic field for 100MHz (Behroozmand et al. 2014).

| S.No. | Aquifer material | $T_2^*$ (ms) |
|---|---|---|
| 1. | Fine sand (0.03-0.2mm) | 140-300 |
| 2. | Medium sand (0.2-0.63mm) | 90-429 |
| 3. | Coarse sand(0.63-2mm) | 140-280 |

**Root mean square error (RMSE)**

Root mean square error is known as square root of mean of the square of all errors. It is commonly considered a very good indicator to evaluate the performance of numerical predictions.

$$RMSE = \sqrt{\frac{1}{N}\sum_{i=1}^{N}(X_i - Y_i)^2} \tag{15}$$

Where, $X_i$ is a observed by SNMR hydraulic conductivity, $Y_i$ is estimated by Kozeny's hydraulic conductivity and $N$ is number of infiltration data points.

**3. Results and Discussion**

Aquifer soil can also be classified based on the FID transverse relaxation time signals ($T_2^*$) along the depth of aquifer. In this study, aquifer consists the mixture of fine sand, medium sand and coarse sand (Table. 1). Hence, sand is the major material present in the aquifer. Top within one meter some FID transverse relaxation values exceeds the range of sand (Figure 3). It means this layer may have organic material impurity or presence of other soil such as gravel and silt etc.

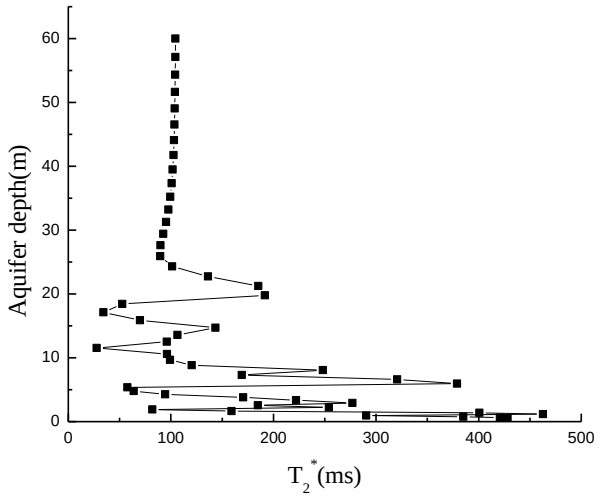



**Figure 3** FID transverse relaxation time ($T_2^*$) along the depth of aquifer.

Surface NMR cannot estimate water content and hydraulic conductivity in the unsaturated zone of the aquifer and fractured rock. Surface NMR has a hydraulic consideration that water content above the water table can be considered as zero and water content for fractured rock can be considered as 0.2%. The water content of the aquifer was indicated by surface NMR. Although, the sharp boundary of water table cannot be well determined by surface NMR inversion.

Mean water content (8%) of vadose zone (unsaturated) and saturation level of aquifer was reached at the depth of 4m. Saturated water content was more than 18% and it was estimated in lab (Figure 6) and also observed in the surface NMR inversion (Figure 4). Water content and hydraulic conductivity of the aquifer can be directly determined by surface NMR

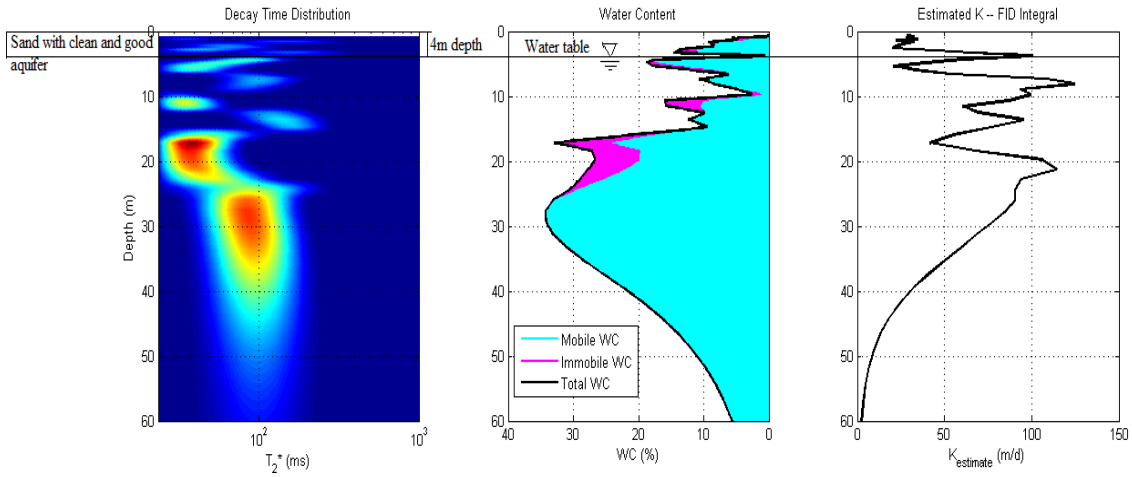



**Figure 4** Vertical distribution of mobile, immobile water content and unsaturated and saturated hydraulic conductivity of aquifer.

## 4. Conclusions

The study of this research indicated that surface NMR can play major role in subsurface characterization. Low amplitude and fast relaxation time NMR signals was a problem for vadose zone study. This problem has been overcome by incorporating short dead time, transmitting higher power for excitation pulse and minimization of relaxation pulse and maintain low signal to noise ratio.

**Based on above study following conclusion remarks are given below:**

1. Field experiment at site using SNMR shows water content and hydraulic conductivity variation below the ground surface. It is found that water table occurs at depth of 4 m below the ground surface.
2. Classification of aquifer material is based on FID transverse relaxation time ( $T_2^*$ ) (Bahroozmand et al. 2015). In this Surface NMR field study also, $T_2^*$ values indicates in the range of sand material.
3. RMSE of Surface NMR hydraulic conductivity and Kozeny's hydraulic conductivity was 4.68.

**References**

Behroozmand, A. A., Keating, K., and Auken, E. (2015). A review of the principles and applications of the NMR technique for near-surface characterization. *Surveys in geophysics*, *36*(1), 27-85.

https://link.springer.com/article/10.1007/s10712-014-9304-0

Bernard, J. (2007). Instruments and field work to measure a magnetic resonance sounding. *Boletín Geológico y Minero*, *118*(3), 459-472.

http://aguas.igme.es/Boletin/2007/118_3_2007/ART.%203.pdf

Coates, G. R., Xiao, L., and Prammer, M. G. (1999). *NMR logging: principles and applications* (Vol. 234). Houston: Haliburton Energy Services.

http://www.paper.edu.cn/scholar/showpdf/OUD2kN1IMTj0AxeQh

Dlugosch, R., Mueller- Petke, M., Günther, T., Costabel, S., and Yaramanci, U. (2011). Assessment of the potential of a new generation of surface nuclear magnetic resonance instruments. *Near Surface Geophysics*, *9*(2), 89-102.

https://doi.org/10.3997/1873-0604.2010063

Grunewald, E., and Knight, R. (2011). The effect of pore size and magnetic susceptibility on the surface NMR relaxation parameter. *Near Surface Geophysics*, *9*(2), 169-178.

https://doi.org/10.3997/1873-0604.2010062

Habberjam, G. M., and Watkins, G. E. (1967). The use of a square configuration in resistivity prospecting. *Geophysical prospecting*, *15*(3), 445-467.

https://doi.org/10.1111/j.1365-2478.1967.tb01798.x

Hertrich, M. (2008). Imaging of groundwater with nuclear magnetic resonance. *Progress in Nuclear Magnetic Resonance Spectroscopy*, *53*(4), 227. http://www.alphageofisica.com.br/vistaclara/PAPERS/Hertrich2008review_www.alphageofisica.com.br.pdf

Keating, K., and Knight, R. (2007). A laboratory study to determine the effect of iron oxides on proton NMR measurements. *Geophysics*, *72*(1), E27-E32.

https://doi.org/10.1190/1.2399445

Mueller-Petke, M., and Yaramanci, U. (2010). QT inversion—Comprehensive use of the complete surface NMR data set. *Geophysics*, *75*(4), WA199-WA209.

https://doi.org/10.1190/1.3471523

Roy, J., and Lubczynski, M. W. (2005). MRS multi- exponential decay analysis: aquifer pore- size distribution and vadose zone characterization. *Near Surface Geophysics*, *3*(4), 287-298.

https://doi.org/10.3997/1873-0604.2005024

Schirov, M., Legchenko, A., and Creer, G. (1991). A new direct non-invasive groundwater detection technology for Australia. *Exploration geophysics*, *22*(2), 333-338.

https://sci-hub.tw/10.1071/EG991333

Vista Clara I. (2009). *GMR Manual and Documentation* (User's Manual)

Walsh, D. O. (2008). Multi-channel surface NMR instrumentation and software for 1D/2D groundwater investigations. *Journal of Applied Geophysics*, *66*(3-4), 140-150.

https://doi.org/10.1016/j.jappgeo.2008.03.006

Walsh, D. O., Grunewald, E., Turner, P., Hinnell, A., and Ferre, P. (2011). Practical limitations and applications of short dead time surface NMR. *Near Surface Geophysics*, *9*(2), 103-113.

https://doi.org/10.3997/1873-0604.2010073

Weichman, P. B., Lavely, E. M., and Ritzwoller, M. H. (2000). Theory of surface nuclear magnetic resonance with applications to geophysical imaging problems. *Physical Review E*, *62*(1), 1290.
https://sci-hub.tw/10.1103/PhysRevE.62.1290

*IN PROCEEDINGS OF 25th HYDRO 2020, INTERNATIONAL CONFERENCE, NATIONAL INSTITUTE OF TECHNOLOGY ROURKELA, ODISHA, INDIA 26-28, March 2021, ISBN 978-93-90631-56-8*

Paper ID - 054

# MODFLOW, MODPATH and MT3DMS based simulation of groundwater flow and leachate transport from landfill

Shikha Kataki[1], Dr. Triptimoni Borah[2]

*[1]Dept of Civil Engineering, Assam Engineering College, Jalukbari, Assam, Guwahati-781013, India*
*[2]Associate Professor, Dept of Civil Engineering, Assam Engineering College, Jalukbari, Assam, Guwahati-781013, India*
*Email: shikhakataki@gmail.com*

## Abstract

This study presents an approach for simulation of three-dimensional groundwater flow in two-layer aquifer system developed using MODFLOW, MODPATH and MT3DMS models within the framework of GMS conceptual model. The model was developed to integrate the groundwater flow system, to identify a suitable site for landfill and to analyse the long-term effects of contamination from a landfill site. The study was applied to a hypothetical region. The model was first simulated for the distribution of head by MODFLOW in steady state condition. The zones of influence of all extraction wells in the study area were determined by MODPATH reverse particle tracking simulation for 20 years. The area was modelled for two different cases. In the first case, a suitable landfill site was proposed for that area without overlapping the zones of influences of extraction wells designated as W1, W2, W3, W4, W5 and W6. The transport of leachate concentration which is generated from the landfill was observed using MT3DMS simulation. The second case involved selecting the landfill site in a region having more probable interference with the zones of influence of an extraction well for 20 years. The minimum time required by array of particles to move from the landfill area to the nearest affected well was found out using MODPATH forward particle tracking simulation. The distribution of leachate concentration was also found out using MT3DMS simulation for 20 years at an interval of 2 years. The well W1 was observed to most contaminated for a pumping rate of 100 $m^3$/day. The leachate transport model was again simulated for different increase in pumping rates of wells and the contaminant concentrations were computed after 20 years. The results revealed that with increase in pumping rates, concentration increases and obtain its peak in the well W1 which is most affected by contamination and nearer to the landfill region. After attaining peak, there is a gradual decrease in concentration with further increase in pumping rates. But in the other wells W2, W3, W4, W5 and W6 which are located gradually far from the landfill site, the concentration increases with increase in pumping rates.

***Keywords:*** *MODFLOW; MODPATH; MT3DMS; landfill; leachate.*

## 1. Introduction

Groundwater is considered one of the most reliable sources of fresh water available on Earth that can be extracted easily using shallow or deep tube-wells. The quality of groundwater may be affected by a wide variety of naturally occurring situation and human activities. Good groundwater management of aquifers requires the ability to predict the groundwater system movement as well as predict the changes which are implemented on the groundwater system by the nature and human activities. In support of the planning and decision-making processes involved in groundwater management, groundwater modelling has become an important methodology. So many scientists and researchers have adopted different methodologies in ground water management model and various application of softwares to prepare a groundwater management strategy and to improve the efficiency of the model. Pramada, S. K. et al. (2020) developed a surface water and groundwater interaction model and applied to a case study. A finite-difference code was developed for the modeling of river water quality. A program is written in MATLAB using the explicit finite difference method. MODFLOW was used to model the groundwater flow and MT3DMS was used to model the contaminant transport flow in groundwater. Finally, the interaction between the surface water and groundwater was studied from the surface and groundwater quality models. Zhang, H. et al. (2020) adopted HYDRUS-1D model to explore water content and $NO_3^-$ distribution in the unsaturated zone above groundwater table in an agricultural area. The resulting estimates of water flux and $NO_3^-$ leaching through the unsaturated zone were used as input data in the application of the groundwater flow model Visual MODFLOW and mass transport model MT3DMS via a concentration recharge boundary. Horriche, J. et al (2020) carried out a study to

examine the impact of an artificial recharge site on groundwater level and salinity using treated domestic wastewater for the Korba aquifer (north eastern Tunisia) using MODFLOW and MT3DMS softwares. Restrepo, J. I. et al. (2005) carried out a study for understanding the changes that occur in wetlands by simulating the surface water movement and its interaction with ground water and wetland slough channels. They developed a computer package for the widely used MOD-FLOW code that would simulate three-dimensional wetland flow hydroperiods and wetland interactions with aquifers and slough channels. Lasserre, F. et al. (1999) developed a simple GIS-linked model for groundwater nitrate transport in the IDRISI GIS environment.

This study aims to achieve the following main objectives:

- Development of a ground water flow model for an illustrative study area using MODFLOW simulation;
- Proposing a suitable site for landfill for the study area without overlapping the zones of influence of extraction wells using MODPATH simulation;
- Finding the region of potential contamination from a landfill in an illustrative area for a specified time using MODPATH model;
- Development of a model for studying effect of contamination transport from the landfill in the extraction wells;
- Variation in the effect of contamination generated from the landfill for the increase in pumping rates of extraction wells.

## 2. Study area

The illustrative study area utilized for making various comparative analyses, is shown in Figure 1.

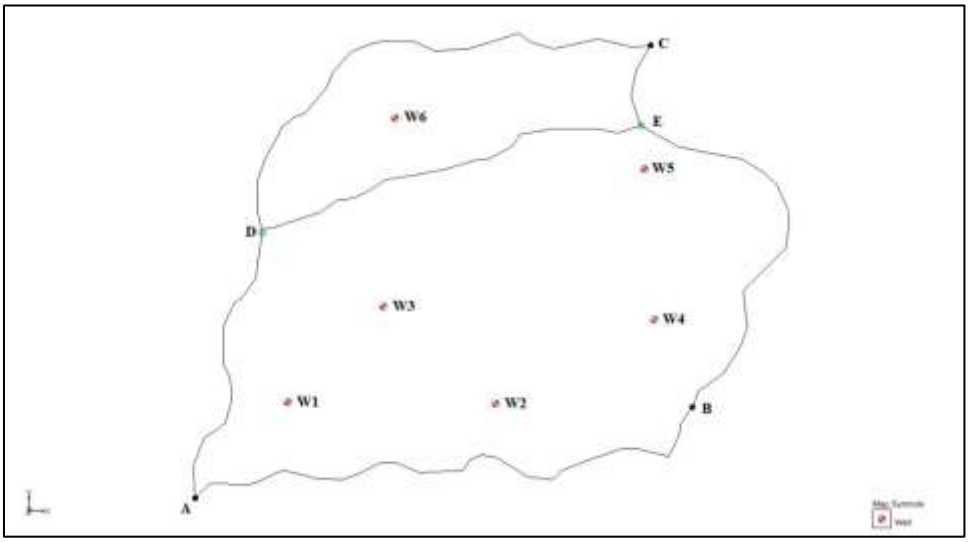



**Figure 1** Plan view of illustrative study area

The area covers 2578710.37 $m^2$ and is assumed to be homogeneous, isotropic with three-dimensional flow and transport processes having two layers of aquifers. Two rivers AB and AC on the southern and north-western boundaries of the area respectively, converges into the point A. The eastern boundary BC of the region is assumed to have no flow. A drain DE passes through the region meeting the river AC at point D. There are six extraction wells - W1, W2, W3, W4, W5, W6 located as shown in the figure 1 maintaining the uniformity in the whole area. These wells are fully penetrating to the two layers of aquifers.

### 2.1 *Hydro-geological data*

The detailed hydro-geological data for creating the model of the study area are given below.

### *2.1.1 River*

**Table 1** River Parameters

| Rivers | Length (m) | Nodes | Head stage (m) | Conductance ($m^2$/day/m) |
|---|---|---|---|---|
| AB | 2062.14 | A | 180 | 1 |
| | | B | 205 | |
| AC | 2988.91 | A | 180 | 1 |
| | | C | 195 | |

### *2.1.2 Drain*

**Table 2** Drain parameters

| Drain | Length (m) | Depth at point D (m) | Depth at point E (m) | Conductance ($m^2$/day/m) |
|---|---|---|---|---|
| DE | 1485.77 | 30 | 15 | 200 |

### *2.1.3 Aquifer Parameters*

**Table 3** Aquifer Parameters

| Aquifer Layer | Depth (m) | Horizontal Hydraulic Conductivity (m/day) | Vertical Anisotropy | Porosity | Longitudinal Dispertivity | TRPT | TRVT | DMCOEF |
|---|---|---|---|---|---|---|---|---|
| Top layer | 70 | 5 | 3 | 0.3 | 20 | 0.2 | 0.1 | 0 |
| Bottom layer | 75 | 10 | 3 | 0.4 | 20 | 0.2 | 0.1 | 0 |

### *2.1.4 Rainfall Recharge*

The influx into the system is primarily through recharge due to rainfall. The annual rainfall throughout the region assigned is 150 cm. Assuming 5% of the total rainfall meet the groundwater through infiltration, the recharge rate is 0.0002 m/day.

## 3. Modelling Approach

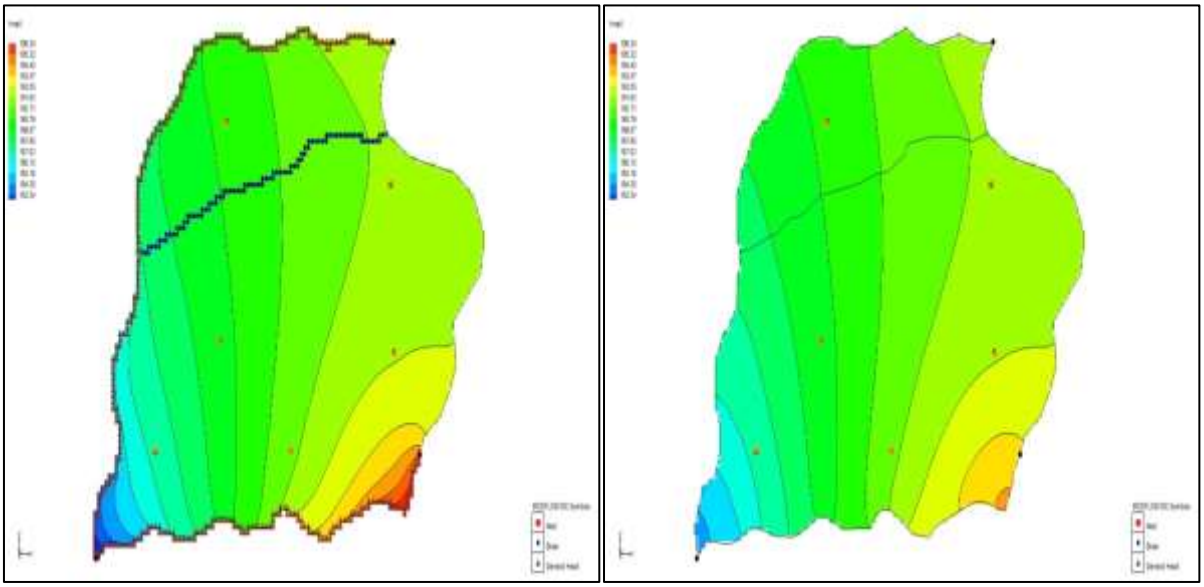
This study is carried out with an overall objective of developing a simulation model for flow and transport process of the contaminants in groundwater aquifers by coupling of MODFLOW, MODPATH and MT3DMS modelling tool in the platform of most advanced Groundwater Modelling System (GMS). In this study, a conceptual model of a hypothetical study area has been developed in GMS for knowing the dynamics of groundwater flow system. The concept model is based on a two-layer aquifer system, characterised with two rivers and a drain with steady state flow regime. The influx into the system is primarily through recharge due to rainfall. The groundwater is extracted from the system by the six pumping wells which are fully penetrating to the two layers of aquifers. Using MODFLOW, the steady state groundwater heads are first determined. This information is then input to MODPATH. MODPATH calculates the three-dimensional pathlines and travel time information of water. The path of imaginary particles of water in each cell which consist of those extraction wells in the study area are tracked back using MODPATH reverse particle tracking for 20 years of simulation. From this, we get the origin points of the water particles in each cell of extraction wells before 20 years and the software gives the diagrammatic view of three-dimensional influence zone of each extraction well. With this model solution, we can easily find a suitable place for landfill without contaminating the water of extraction wells. In this study, the characterisation of water particle pathlines is again scrutinised assuming two different cases. In the first case, a landfill site generating leachate of 22000 ppm at constant rate has been proposed without overlapping the influence zones of extraction wells. Then the

pathlines of particles starting from the landfill site is again tracked for 20 years using MODPATH forward particle tracking simulation. From this we get the ending position of the particles which travel from the landfill site. In the second case, a landfill site which also generate leachate of 22000 ppm has been chosen which can probably more contaminate the water of extraction wells. This model set-up is simulated using MODPATH forward particle tracking approach for 20 years of duration. To know the quantitative distribution of leachate for this worst case, the model is simulated using MT3DMS software at interval of 2 years for 20 years of stress period. The effect of contaminants transport in each well are found out. Another separate simulation approach has also been taken to know the effect of leachate transport with increase in pumping rates of extraction wells.

## 4. Results and analysis

### 4.2.1 *Water Head distribution in the aquifer system using MODFLOW*

The model of the illustrative study area as discussed above is simulated for knowing the water head distribution using MODFLOW under steady state condition. The pumping rates of the extraction wells are taken as 100 $m^3$/day. Initial head during simulation is assumed to be at the top elevation of the upper aquifer layer. A network of grids covering the study area of cell size 20 m x 20 m in both the aquifer layers created to simulate the model. The distribution of head in both the aquifer layers when there is steady pumping of 100 $m^3$/day, taking bottom elevation of lower aquifer layer as datum are shown in figure 2(a) and figure 2(b) below.

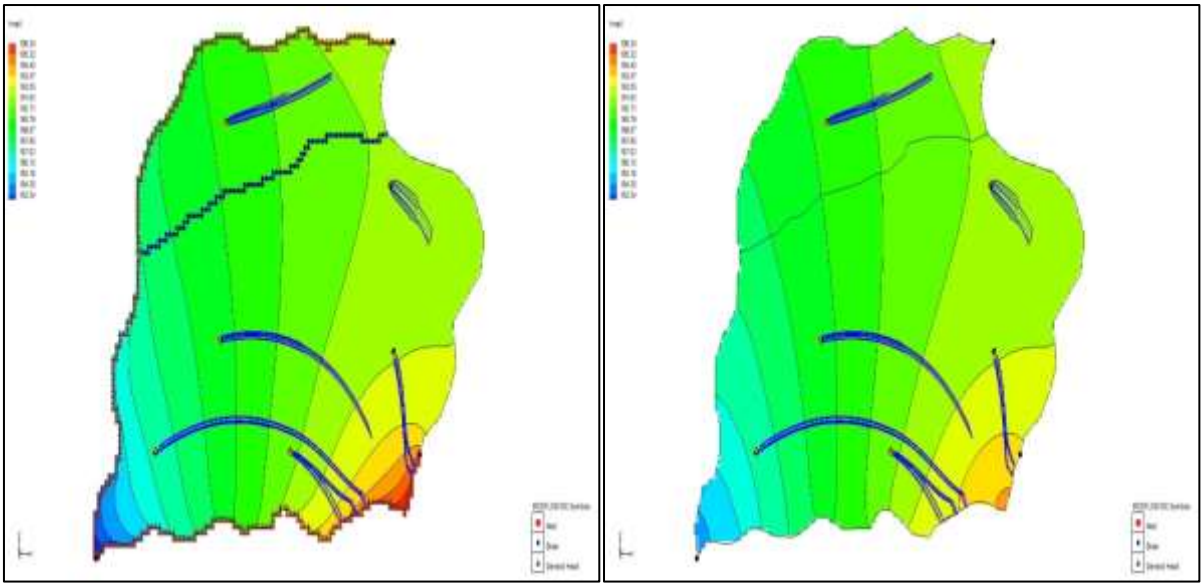


(a) Top aquifer (b) Bottom aquifer

**Figure 2** Head distribution in aquifer layers

### *4.2.2 Particle tracking simulation using MODPATH*

The MODFLOW solution is again simulated for knowing the zones of influence of all the extraction wells for 20 years by using MODPATH software. Imaginary set of particles starting locations at every cell that contains extraction wells are generated. Each set of particle consists of six particles. Reverse particle tracking simulation for 20 years are performed and the set of pathlines from wells in the direction of particle flow in both the aquifer layers are shown in figure 3(a) and figure 3(b) below.



(a) Top aquifer (b) Bottom aquifer

**Figure 3** 20 years tracking of particles generated at wells

### *4.2.3 Selection of Landfill sites*

From the outcomes of MODPATH reverse particle tracking simulation, we can see the zones of groundwater which have no or little influence to the water extracted by wells. The study area is modelled for two different cases. In the first case, a suitable landfill site of area 62658.28 $m^2$ generating leachate of 22000 ppm is proposed for the study area without overlapping the zones of influences of extraction wells. The second case involved selecting the landfill site of same area generating leachate of 22000 ppm in a region having more probable interference with the zones of influence of an extraction well in 20 years. In both cases, the leachate rate in the landfill region assigned is 0.00006 $m^3$/day and it generates leachate of 22000 ppm at steady rate. The two cases are discussed below.

#### *4.2.3.1 Case study 1*

The location of the Landfill designated as L1 is as shown in figure 4 below. The leachate rate from the landfill is assumed to be 0.00006 $m^3$/day This recharge rate is small relative to the rate assigned to the other region. This is because that landfill will be capped and lined and thus will have a small recharge value.

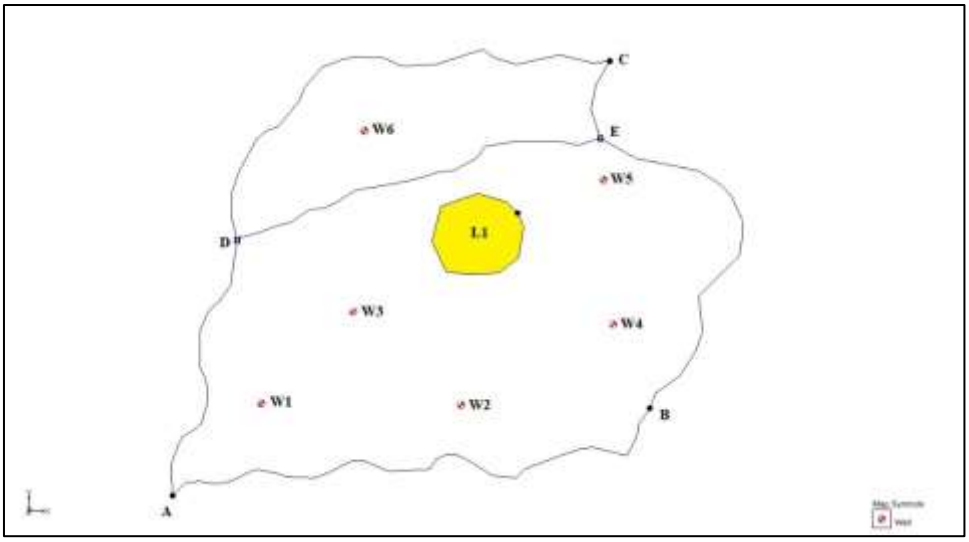
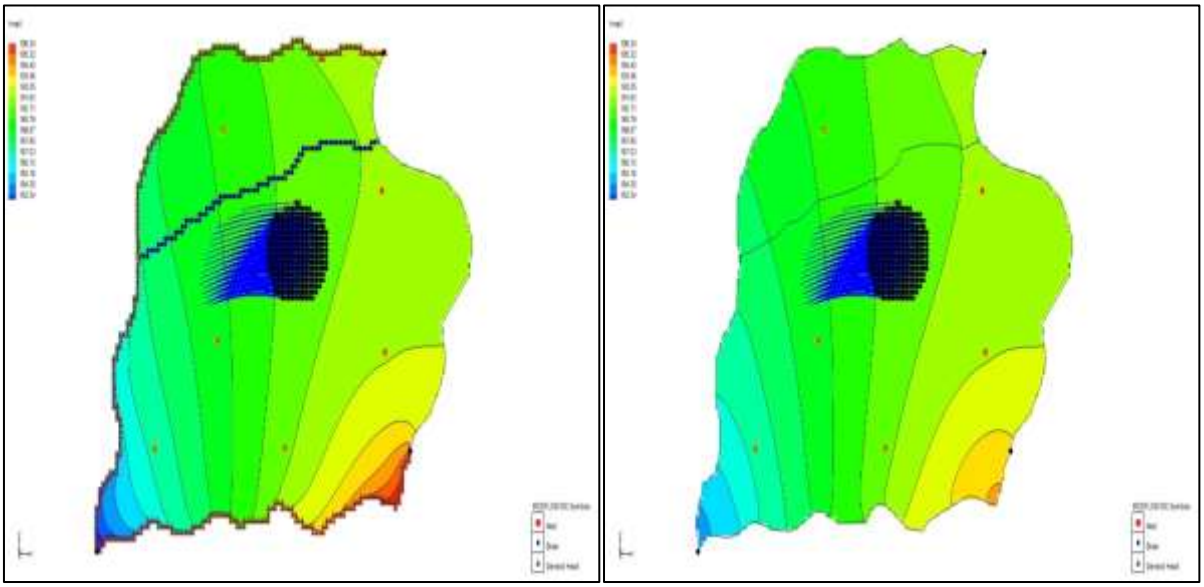



**Figure 4** Plan view of illustrative study area containing landfill L1

The area is simulated using MODPATH forward particle tracking to again verify the non-interference or little interference of the contaminants to the water extracted by wells. The pathlines of particles from the landfill site in 20 years where the sets of particles are generated in the cells covering the landfill L1 are shown in the figure 5(a) and figure 5(b) below.



(a) Top aquifer (b) Bottom aquifer

**Figure 5** MODPATH Forward particle tracking in 20 years for particles generated at Landfill L1

From the figures above, it is clear that no particles from the landfill are captured by the wells in 20 years of duration. This means the landfill site is suitable for minimising the effects of contamination in wells.

### *4.2.3.2 Case Study 2*

Here, the location of landfill is chosen as shown in figure 6 such that the contamination from the landfill affects the wells more.

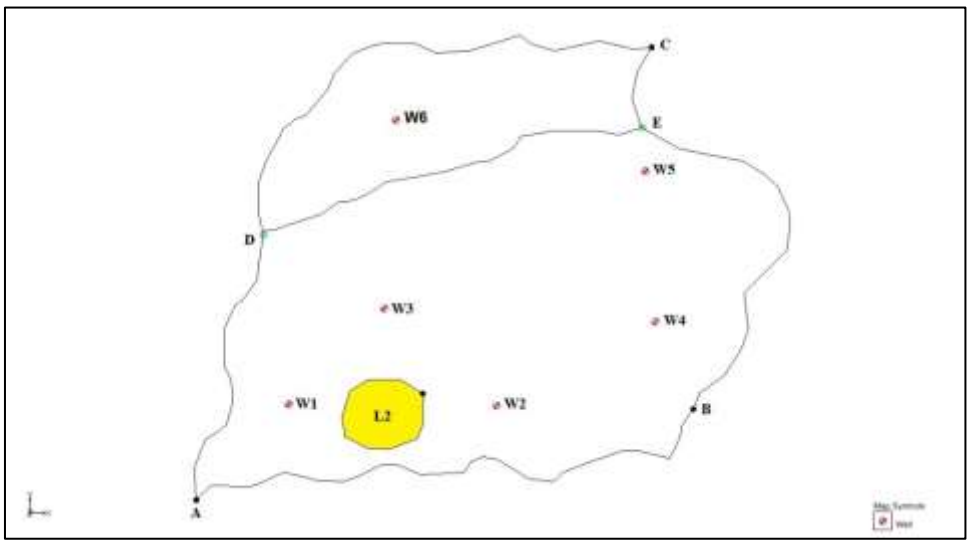
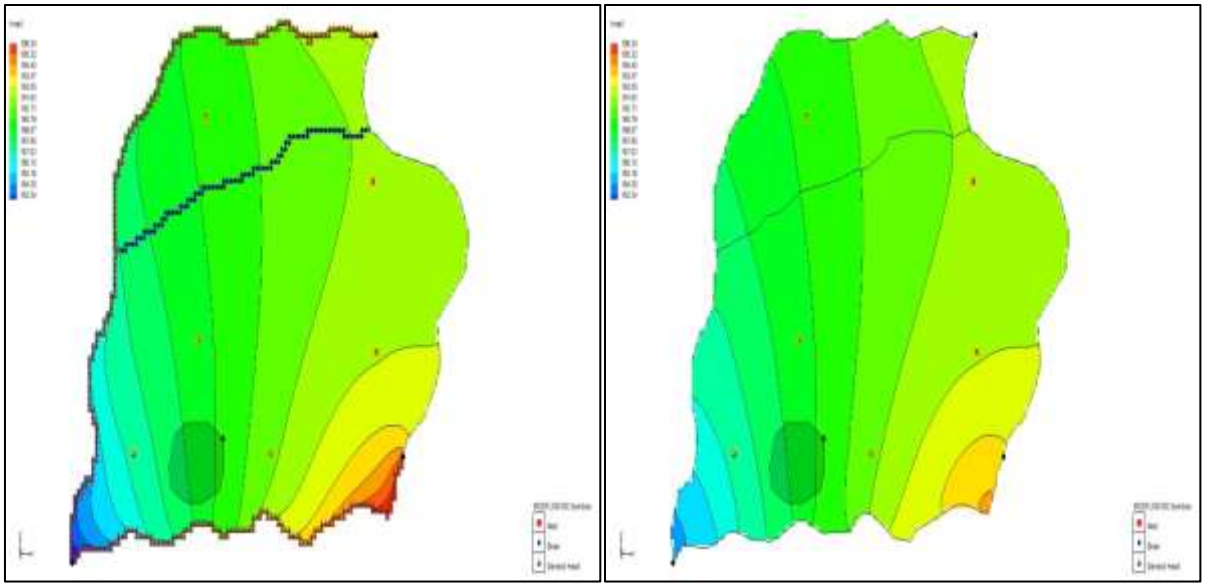



**Figure 6** Plan view of illustrative study area containing landfill L2

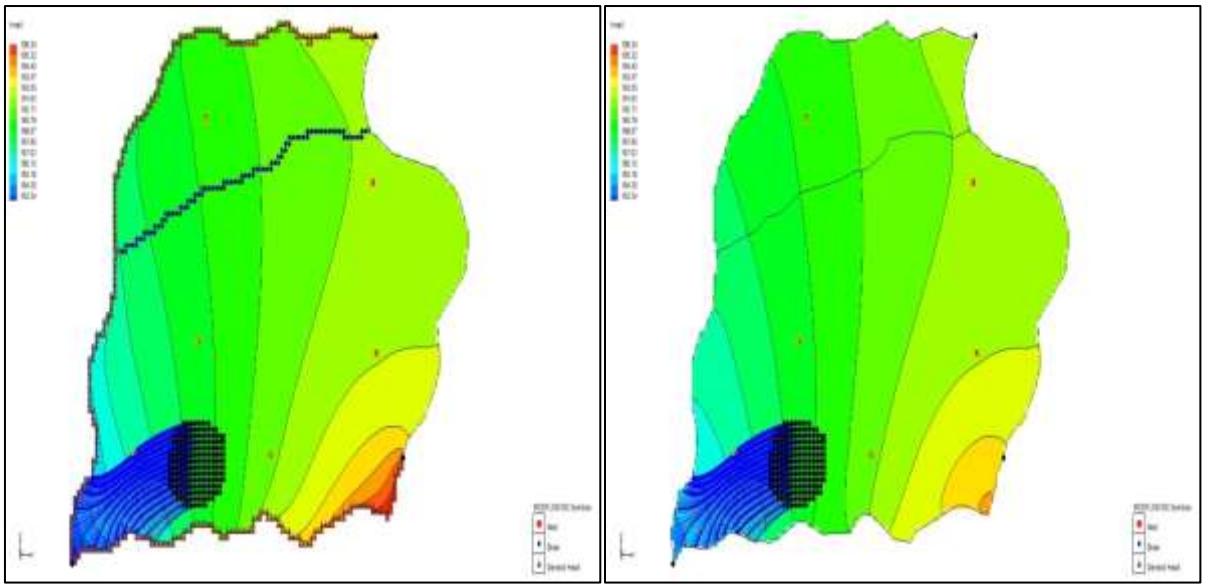
The distribution of water head of the study area containing landfill L2 using MODFLOW is shown in figure 7(a) and figure 7(b) below. The simulation is done considering steady pumping rate 100 $m^3$/day through extraction wells.



(a) Top aquifer (b) Bottom aquifer

**Figure 7** Water Head distribution of the study area containing landfill L2

The result of this MODFLOW simulation is used as input for the MODPATH forward particle tracking simulation.The pathlines of particles from the landfill site in 20 years where the sets of particles are generated in the cells covering the landfill L2 are shown in the figure 8(a) and figure 8(b) below.

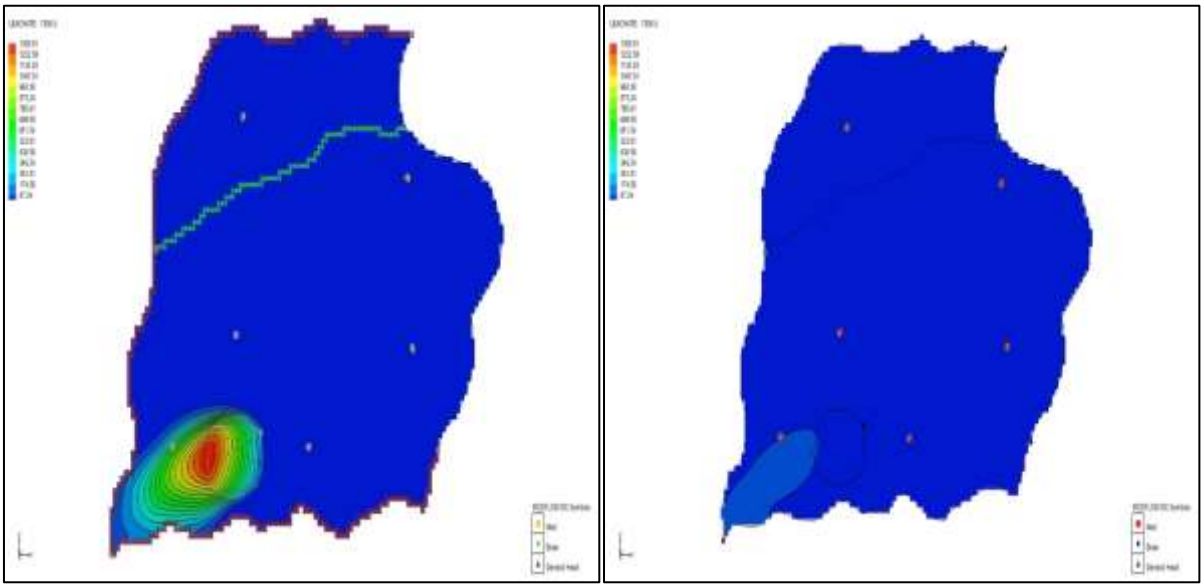


(a) Top aquifer (b) Bottom aquifer

**Figure 8** MODPATH Forward particle tracking in 20 years for particles generated at Landfill L2

It is seen that some of the particles from the landfill terminate at the well W1. Other wells are not affected by it. The minimum time required by array of particles to move from landfill site to the well W1 found out using the MODPATH simulation is 3735.49 days i.e. it takes minimum 3735.49 days for contaminant to travel from landfill site to the well W1.

The area consisting landfill L2 is again simulated using MT3DMS software to know the concentration distribution of leachate generated from the landfill. The simulation is done at an interval of 2 years for 20 years duration. The below figure 9(a) and 9(b) show the leachate distribution after 20 years.



(a) Top aquifer (b) Bottom aquifer

**Figure 9** 20 years concentration contours of leachate generated from the landfill

It can be seen that; the leachate is spreading more in the south-west direction contamination W1. In the top aquifer, the pollution starts affecting the downstream water of river AB and AC. Bottom aquifer water is less contaminated in comparison to that of top aquifer.

The amount of concentrations observed at each cell containing the extraction wells are shown in table 4 and table 5 below.

**Table 4** Leachate concentration (ppm) observed at each cell containing wells in top aquifer layer

| Well | Leachate concentration (ppm) in | | | | | | | | | |
|---|---|---|---|---|---|---|---|---|---|---|
| | 2 Years | 4 Years | 6 Years | 8 Years | 10 Years | 12 Years | 14 Years | 16 Years | 18 Years | 20 Years |
| W1 | 0.097485 | 14.98794 | 83.74281 | 194.6304 | 311.9679 | 410.3335 | 480.5386 | 524.88 | 550.4569 | 564.178 |
| W2 | 2.48E-12 | 2.65E-09 | 1.04E-07 | 1.01E-06 | 4.56E-06 | 0.000013 | 0.000027 | 0.000045 | 0.000066 | 0.000085 |
| W3 | 5.06E-07 | 0.000018 | 0.000075 | 0.000146 | 0.000202 | 0.000236 | 0.000255 | 0.000264 | 0.000269 | 0.000271 |
| W4 | 0 | 4.51E-38 | 1.15E-34 | -1.71E-31 | -4.21E-30 | -6.28E-28 | -2.66E-26 | 2.29E-25 | 1.18E-23 | 1.28E-22 |
| W5 | 0 | 0 | 0 | 0 | 0 | 0 | 0 | -1.94E-42 | 2.73E-41 | 3.13E-39 |
| W6 | 0 | 0 | 0 | 0 | 0 | 0 | 2.54E-39 | 6.08E-37 | 4.81E-35 | 1.86E-33 |

**Table 5** Leachate concentration (ppm) observed at each cell containing wells in top aquifer layer

| Well | Leachate concentration (ppm) in | | | | | | | | | |
|---|---|---|---|---|---|---|---|---|---|---|
| | 2 Years | 4 Years | 6 Years | 8 Years | 10 Years | 12 Years | 14 Years | 16 Years | 18 Years | 20 Years |

| | | | | | | | | | | |
|---|---|---|---|---|---|---|---|---|---|---|
| W1 | 0.021114 | 2.02627 | 11.80175 | 29.28592 | 48.87284 | 65.43981 | 77.04957 | 84.20435 | 88.23473 | 90.32801 |
| W2 | 1.36E-12 | 1.74E-09 | 6.70E-08 | 5.89E-07 | 2.37E-06 | 6.02E-06 | 0.000011 | 0.000017 | 0.000023 | 0.000028 |
| W3 | 1.17E-07 | 3.85E-06 | 0.000015 | 0.000028 | 0.000037 | 0.000044 | 0.000047 | 0.000049 | 0.000049 | 0.00005 |
| W4 | 0 | 1.29E-36 | 5.20E-33 | -2.81E-30 | -4.40E-29 | -1.99E-27 | -2.28E-26 | 4.24E-24 | 8.76E-23 | 7.15E-22 |
| W5 | 0 | 0 | 0 | 0 | 0 | 0 | 0 | -1.40E-40 | 9.26E-40 | 6.93E-38 |
| W6 | 0 | 0 | 0 | 0 | 0 | -6.96E-41 | 3.81E-38 | 9.43E-36 | 7.16E-34 | 2.60E-32 |

### *4.2.4 Analysis of the effect of change in pumping rate of wells in contaminant transport*

In the case study 2, if we gradually increase the pumping rate of extraction wells, the change in leachate concentrations transported to the wells are observed after 20 years of simulation using MT3DMS software. Table 6 and table 7 below shows the concentrations of contaminant observed at each cell containing the wells with gradual increase in pumping rates of extraction wells, for steady state generation of leachate 22000 ppm from landfill L2.

**Table 6** Concentrations of contaminant observed at each well in top aquifer layer with increase in pumping rates of wells

| Pumping rate ($m^3$/day) | Leachate concentration (ppm) in | | | | | |
|---|---|---|---|---|---|---|
| | W1 | W2 | W3 | W4 | W5 | W6 |
| 100 | 564.178 | 0.000085 | 0.000271 | 1.28E-22 | 3.13E-39 | 1.86E-33 |
| 200 | 596.4594 | 0.000082 | 0.000137 | 2.13E-22 | 1.84E-39 | 3.05E-33 |
| 400 | 606.9373 | 0.000122 | 0.000128 | 6.11E-22 | -2.24E-37 | 8.45E-33 |
| 1600 | 615.4534 | 0.000212 | 0.000129 | 3.25E-21 | 3.48E-36 | -2.71E-32 |
| 3200 | 509.5258 | 0.03798 | 0.00015 | 3.74E-20 | 9.45E-31 | 1.81E-25 |
| 6400 | 207.9907 | 37.92716 | 0.000751 | 3.50E-17 | 1.47E-22 | 2.84E-17 |

**Table 7** Concentrations of contaminant observed at each well in bottom aquifer layer with increase in pumping rates of wells

| Pumping rate ($m^3$/day) | Leachate concentration (ppm) in | | | | | |
|---|---|---|---|---|---|---|
| | W1 | W2 | W3 | W4 | W5 | W6 |
| 100 | 90.32801 | 0.000028 | 0.00005 | 7.15E-22 | 6.93E-38 | 2.60E-32 |
| 200 | 95.85317 | 0.00003 | 0.000034 | 1.02E-21 | 2.83E-38 | 2.63E-32 |
| 400 | 107.7176 | 0.000032 | 0.000018 | 2.01E-21 | -1.61E-36 | 3.47E-32 |
| 1600 | 127.3417 | 0.000061 | 0.000017 | 6.80E-21 | 1.63E-35 | -5.75E-32 |
| 3200 | 145.9925 | 0.00549 | 0.000016 | 4.92E-20 | 3.92E-30 | 2.77E-25 |
| 6400 | 76.84093 | 9.356566 | 0.000115 | 5.24E-17 | 3.57E-22 | 3.30E-17 |

From the above tables, it is found that the well W1 is more exposed to the leachate from the landfill. Transport of contamination in other wells are very less or almost nil. The top aquifer layer is more affected than the bottom aquifer. The variation pattern in concentration of leachate with the increase in pumping rates of wells are observed at each well are shown graphically below from figure 10 to figure 15.

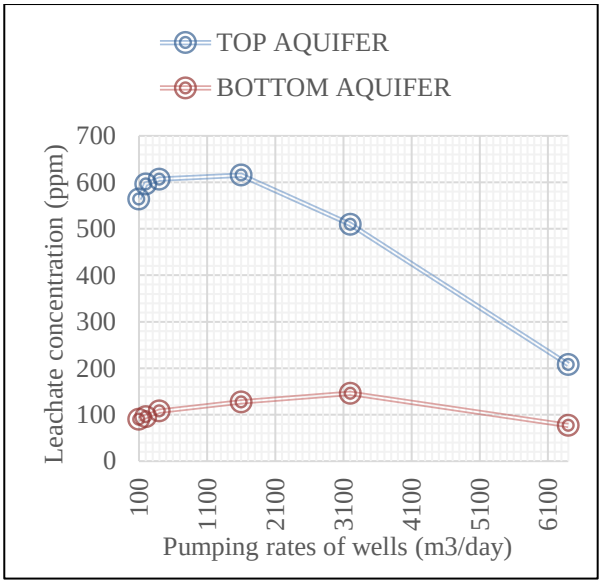



**Figure 10** Variation in leachate concentration at W1 with the increase in pumping rates of wells

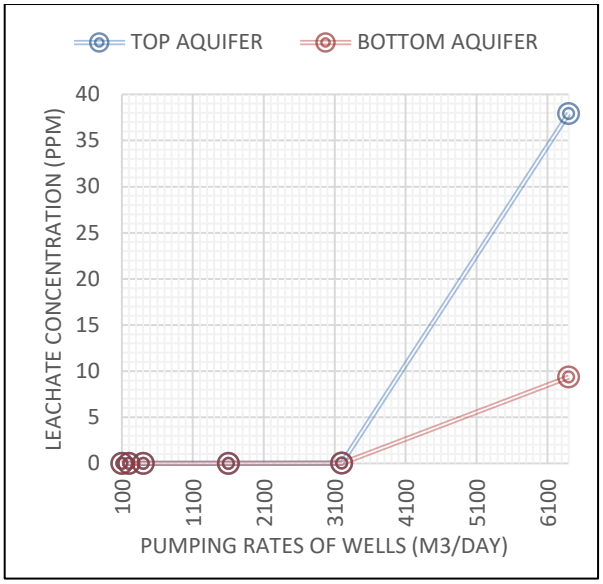



**Figure 11** Variation in leachate concentration at W2 with the increase in pumping rates of wells

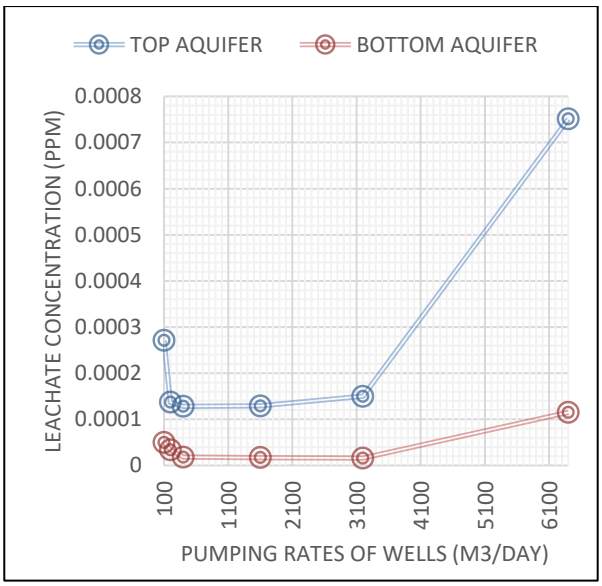



**Figure 12** Variation in leachate concentration at W3 with the increase in pumping rates of wells

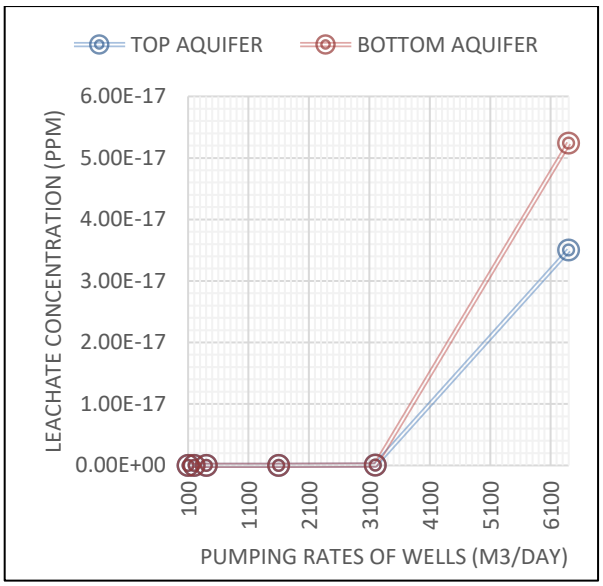



**Figure 13** Variation in leachate concentration at W4 with the increase in pumping rates of wells

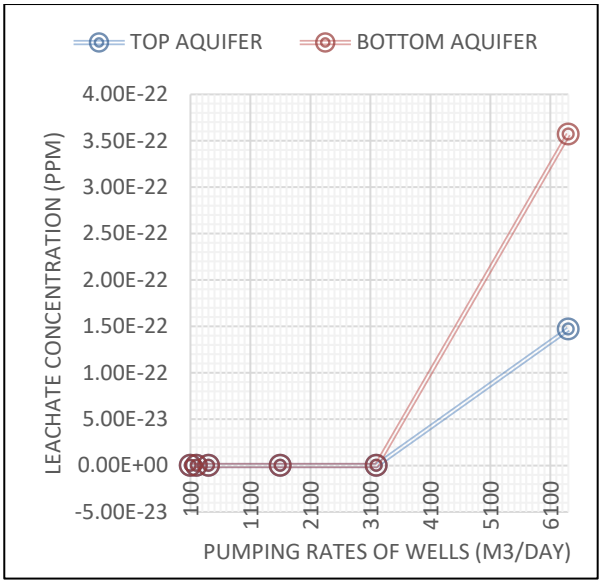



**Figure 14** Variation in leachate concentration at W5 with the increase in pumping rates of wells

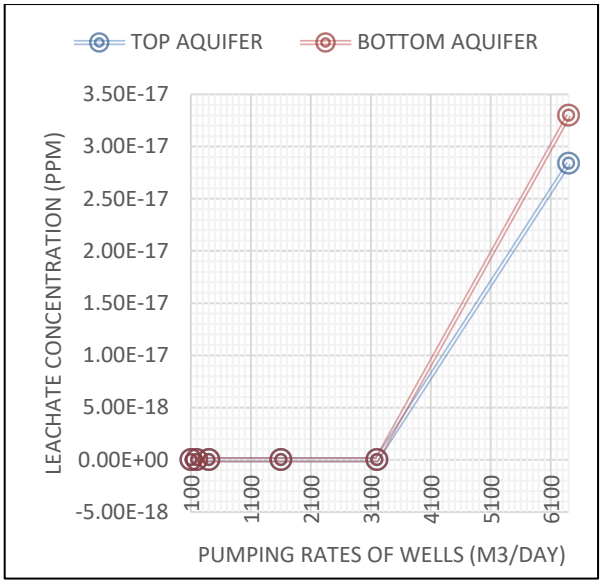



**Figure 15** Variation in leachate concentration at W6 with the increase in pumping rates of wells

The figure 10 shows the variation in leachate concentration at W1 with the increase in pumping rates of wells. In top aquifer, the curve rises from 564.178 ppm to 615.4534 ppm for increase in pumping rates of wells from 100 $m^3$/day to 1600 $m^3$/day. The curve again declines to 207.9907 ppm with further increase in pumping rate upto 6400 $m^3$/day. In bottom aquifer, the curve also follows the same pattern of increase or decrease. The maximum concentration attained is 145.9925 ppm for pumping rate of 3200 $m^3$/day.

The figure 11 shows the variation in leachate concentration at W2 with the increase in pumping rates of wells. It shows that, in both the aquifer, the concentration of leachate is almost nil for increase in pumping rate upto 3200 m3/day. With further increase in pumping rates of wells up to 6400 $m^3$/day, the maximum concentration attained in top and bottom aquifers are 37.92716 ppm and 9.356566 ppm respectively.

The figure 12 shows the variation in leachate concentration at W3 with the increase in pumping rates of wells. It shows that, in both the aquifers, the concentration in well W3 is very less or almost nil. But an increasing or decreasing pattern of concentration in well W3 can be observed in both the aquifers with increase in pumping rates. For 100 $m^3$/day of pumping rates, the concentrations at W3 are 0.000271ppm and 0.00005 ppm in top and bottom aquifers respectively. Then the concentration falls to 0.000128 ppm in top aquifer at 400 $m^3$/day of pumping rates and 0.000016 ppm in bottom aquifer at 1600 $m^3$/day of pumping rates. After that, it again increases with further increase in pumping rates and attained maximum concentration of 0.000751pmm and 0.000115 ppm in top and bottom aquifer respectively at 6400 $m^3$/day of pumping rates.

The figure 13, figure 14 and figure 15 show the variation in leachate concentration at W4, W5 and W6 respectively with the increase in pumping rates of wells. The contamination is very less or negligible in these three wells. The curves show an increasing pattern of concentration and maximum concentration attained for maximum pumping rate of 6400 $m^3$/day.

From the above all graphs, it is seen that the well W1 which is located just at the downward gradient to the landfill L2, is more contaminated. With the increase in pumping rates of wells, the contamination concentration increases and obtain its peak. After attaining peak, there is a gradual decrease in concentration with further increase in pumping rates. This means the polluted water are consumed by us more due to over-extraction of water.

Due to excessive pumping, even the other wells W2, W3, W4, W5 and W6 which are located gradually far from the landfill site and at upward slope to it, start to be contaminated. With increase in pumping rates, the pollutants start moving also against the groundwater head flow.

## 5. Conclusion

The results of these simulation in this study, give an idea of flow and contaminant transport pattern of groundwater. In the first case, when we selected the landfill site L1 based on the result of MODPATH reverse particle tracking simulation, it is seen from the diagrammatic view that the water particles from the landfill site have not reached the extraction wells in 20 years of duration. That is, the water extracted from the wells are yet free from any contamination that may occur due to leakage of leachate from landfill. But while choosing the landfill site L2, we can clearly observe the contamination effect in the pumping well W1 due to leakage from the landfill.

From this model, we can also see the causes of over-extraction of water in groundwater pollution. It is seen that in the well W1, the concentration increases with increase in pumping rates and reach saturation points. After that further increase in pumping, the concentration decreases. But in the other wells, this pattern is not seen. There, with increases in pumping, the concentration also increases. With more over-extraction, the extent of contaminated area is more. A stage wise designed pollution monitoring network is found to be useful in improving the efficiency of groundwater management strategy. A possible extension of this study would be the practical applicability of the proposed methodology to know the behaviour of groundwater flow in large aquifer system. Some remediation strategy can be applied to the area influenced by contaminant transport in groundwater. Performance of this measures can be evaluated by applying the GMS programming tool. Placing some artificial recharge methods like construction of recharge pit around the area, we can observe its effect on reducing the contamination in groundwater. Finally, a study of the economic aspects of this design in the context of real-life problems can be very useful and interesting.

## References

Abd-Elaty. Ismail et al. (2019) “Integrated Modelling for Groundwater Contamination from Polluted Streams Using New Protection Process Techniques”, MDPI Water 2019, 11, 2321, pages 1-23.

Bora, G. (2016) “Solution of aquifer simulation process problem by using GMS and potential sources of groundwater contamination and its remediation”, Department of Civil Engineering, Assam Engineering College, Guwahati.

Chakrabarty, D. (2001) “Identification of unknown groundwater pollution sources and simultaneous parameter estimation using linked optimization- Simulation Approach”, Department of Civil Engineering, Indian Institute of Technology Kanpur.

Chunmiao Zheng, P. (1999) “MT3DMS: A Modular Three-Dimensional Multispecies Transport Model for Simulation of Advection, Dispersion, and Chemical Reactions of Contaminants in Groundwater Systems; Documentation and User's Guide”, Department of Geological Sciences University of Alabama, Tuscaloosa, AL 35487.

Harbaugh, A. W. et al. (2000) “MODFLOW-2000—User Guide to Modularization Concepts and the Ground-Water Flow Process”, U.S. Geological Survey.

Horriche, Faten Jarraya and Benabdallah, Sihem (2020), “Assessing Aquifer Water Level and Salinity for a Managed Artificial Recharge Site Using Reclaimed Water”, Water (20734441), Feb2020, Vol. 12 Issue 2, p341. 1p.

https://aquaveo.com

https://britannica.com

https://water.usgs.gov

https://wikipedia.org

http://www.hwe.org.ps/

Langevin, C. D. et al. (2006) “MODFLOW/MT3DMS–Based Simulation of Variable-Density Ground Water Flow and Transport” Ground Water, Volume 44, No. 3, pages 339-351.

Lasserre, F. et al. (1999) “A GIS-linked model for the assessment of nitrate contamination in groundwater”, Journal of Hydrology, Volume 224 (1999), pages 81–90.

Lautz, L. K. et al. (2006) “Modeling surface and ground water mixing in the hyporheic zone using MODFLOW and MT3D”, Advances in Water Resources 29 (2006), pages 1618–1633.

Melki, S. (2020) "Actual and Predictive Transport Modeling of Fluoride Contamination of the Sfax-Agareb Coastal Aquifer in the Mediterranean Basin", Hindawi-Journal of Chemistry, Volume 2020, Article ID 4745057, pages 1-14.

Murcia, F. (2020) "Modeling of the dispersion of pollutants in porous media: Case of the Jacarezinho landfill", Journal of Chemical Information and Modeling, Volume 53, Issue 9, pages 1689-1699

Pramada, S. K. and Venugopal, Sowmya (2020) "Interaction Between Groundwater and Surface Water and Its Effect on Groundwater Quality", Environmental Processes and Management, Pages 381-395.

Prommer, H. et al. (2003) "A MODFLOW/MT3DMS based reactive multi-component transport modelling", Ground Water, Volume 42, Issue 2, pages 247-257.

Restrepo, J. I. et al. (1998) "A Wetland Simulation Module for the MODFLOW Groundwater Model", Ground Water, Volume 36, No. 5, pages 764-770.

Sahu, S. K. et al. (2019) "Application of groundwater transport modelling in groundwater development and management: a review", International Journal of Advanced Geosciences, Volume 7, Issue 1, pages 47-51.

W. Harbaugh, A. W. et al. (2001) "MODFLOW-2000, The U.S. Geological Survey Modular Ground-Water Model—User Guide to Modularization Concepts and the Ground-Water Flow Process", U.S. Geological Survey.

X. X. Guanhua Huang et al. (2011) "Using MODFLOW and GIS to Assess Changes in Groundwater Dynamics in Response to Water Saving Measures in Irrigation Districts of the Upper Yellow River Basin", Water Resources Management, volume 25, Issue 8, pages 2035-2059.

Yan, S. (2019) "Non-negative numerical solutions of the two-dimensional full- tensor diffusion/dispersion problems using flux-corrected transport, and implementation for the groundwater transport simulator MT3DMS", University of Illinois at Urbana-Champaign.

Zhang, H. et al. (2020) "Modeling fertilization impacts on nitrate leaching and groundwater contamination with HYDRUS-1D and MT3DMS", Paddy and Water Environment, Volume 18, Issue 3, pages 481-498.

Zheng, C. and Wang, P. P. (1999) "MT3DMS: A Modular Three-Dimensional Multispecies Transport Model for Simulation of Advection, Dispersion, and Chemical Reactions of Contaminants in Groundwater Systems; Documentation and User's Guide", University of Alabama, Strategic Environmental Research and Development Program, Contract Report SERDP-99-1.

*IN PROCEEDINGS OF 25th HYDRO 2020, INTERNATIONAL CONFERENCE, NATIONAL INSTITUTE OF TECHNOLOGY ROURKELA, ODISHA, INDIA 26-28, March 2021, ISBN 978-93-90631-56-8*

Paper ID - 061

# Hydro-Chemical Characterization and Quality Appraisal of Groundwater using Water Quality Index in District Jaipur, Rajasthan

Santosh Ojha[1], Gunwant Sharma[2], Deepesh Machiwal[3]

[1,2]*Malaviya National Institute of Technology, Jaipur , India*
[3]*Central Arid Zone research Institute (CAZRI), Jodhpur , India*
*Email: santosh16mar@gmail.com*

## Abstract

The study aims to assess the hydrochemistry of groundwater and its suitability for drinking purpose for district Jaipur. Groundwater quality parameters data of 196 locations in the study area were collected and analyzed using Gibb's plot and Piper Trillinear diagram. According to Gibbs diagram, based on TDS and the concentration of cations and anions; the predominant samples fall in the rock-water interaction dominance and evaporation dominance. Higher Cation ratio suggests that dissolution of silicate minerals are the dominant controlling factor of the groundwater chemistry of the study area. Piper's diagram classification shows that majority of the samples belong to Na-$HCO_3$ and Na-Cl-$SO_4$ hydrochemical facies, GIS based Inverse Distance Weighing (IDW) interpolation technique was used to signify spatial variation of water quality index (WQI) in the study area. Analysis of WQI reveals that Majority of samples belong to excellent to good water type (13.78 % and 45.41 %, respectively). The water samples within poor quality, and very poor quality contributed 33.16 and 6.13% of groundwater samples and can be used for drinking with some treatment and conventional disinfection, whereas Water "unsuitable for drinking purposes" covers only 1.53 % of groundwater samples could only be used for aquaculture, irrigation, and industrial purposes. The Spatial distribution map of water quality index shows that excellent quality found in the North Western and few patches in central part of the study area, due to high elevation area having less dissolution and infiltration, god water type identified in north, north-east and central part., poor and very poor water qualities were found in the south and south-west and few patches in central part of the study area and water unsuitable for drinking purpose observed in block Dudu and Phagi, located in southern part of the study area are unsuitable for drinking purpose.

*Keywords: hydrochemistry, chemical classification, Gibbs diagram, piper diagram, WQI*

## 1. Introduction

The quality of water resources is a subject of ongoing concern. The health and happiness of the human race are closely tied up with the quality of the water used for consumption where the per capita consumption of water is an index of quality of life of the people as well as their economic and social condition. In previous few decades, there has been unprecedented amplify in the requirement for fresh water supply is owing to a tremendous increase in population, industrialization, urbanization, and intense agricultural activities (Dhanasekarapandian, Chandran, Devi, & Kumar, 2016; Raju, Shukla, & Ram, 2011). Due to insufficient availability of surface water which is further aggravated by pollution, urbanization, and industrialization, and also due to the notion that groundwater is pollution free, the majority of the populace in India depends on groundwater assets for drinking and household, industrial, and agricultural uses (Raju et al., 2011). Groundwater is highly valued because of certain properties not possessed by surface water. Groundwater systems are dynamic and water is continuously in slow motion down gradient from areas of recharge to areas of discharge. The chemistry of subsurface water is controlled by many natural as well as anthropogenic factors. Natural factors which have control over water chemistry include precipitation pattern and amount, geological features of watershed and aquifer, meteorological factors, and various

rock–water interaction processes in the aquifer (Arnade, 1999; Raju, Patel, Reddy, Suresh, & Reddy, 2016; Singh, Raju, & Ramakrishna, 2015). Human activities which influence the water chemistry include dumping of solid waste, domestic and industrial waste, and mining and agricultural activities (Hem, 1991; Raju, 2007; Singh, Raju, Gossel, & Wycisk, 2016; Todd, 1980). Residential, municipal, commercial, industrial, and agricultural activities can all affect groundwater quality. Human health is threatened by most of the agricultural development activities particularly in relation to excessive application of fertilizers and unsanitary conditions. Rapid urbanization, especially in developing countries like India, has affected the availability and quality of groundwater due to it's overexploitation and improper waste disposal,

Water quality is also a major determinant for the health of ecosystems. Proper monitoring and assessment of the quality is essential for efficient groundwater management, which in turn can ensure human welfare and environmental sustainability. Groundwater quality acts a crucial role in groundwater security and excellence preservation. Hence, evaluation of the groundwater quality is essential not only for use by present generation but also for future consumption. The chemistry of groundwater is an important factor determining its use for domestic, irrigation and industrial purposes. The knowledge of hydrochemistry is important to assess the ground water quality in any area in which the groundwater is used for both irrigation and drinking needs (Srinivas et al. 2013). The water quality assessment may give clear information about the subsurface geologic environments in which the water presents (Raju et al. 2011). The present study was carried out for qualitative analysis based on physico-chemical parameters of groundwater. In the current study, an effort has been made to calculate the groundwater quality indices for the aptness of groundwater resource for drinking and agricultural purpose and identify the influences of natural and anthropogenic actions on groundwater chemistry.

## *1.1 Description of Study Area*

The Jaipur district is situated under semi-arid climatic zone with geographical area of 11061.44 $km^2$, extending between north latitudes $26^o25'$ and $27^o51'$ and east longitudes $74^o55'$ and $76^o18'$ and administrated by 13 blocks. The normal annual rainfall in the district is 565 mm. The area under irrigation is about 35.27% of the total area of the district. Jaipur records the lowest humidity in the month of April. May onward humidity picks up and increases gradually to reach its highest in the month of August. Due to indiscriminate disposal of industrial waste, groundwater has become susceptible to pollution and it is perceived that pollutant/contaminant level would further rise due to population growth, rapid urbanization and industrialization etc.

### *1.1.1 Geology and Hydrogeology*

The district is characterized by broad continuum of landscapes including hillocks, pediments, undulating fluvial plains, aeolian dune fields, ravines, palaeo-channels etc. Structural hills (mainly in north and NE parts) moving towards NNE-SSW are generally composed of Delhi quartzite. The district area is dominated by undulating plains of fluvial/ fluvial-aeolian origin forming landforms of river terraces, floodplains and buried channels of various drainage systems.

In the area, gneisses and schists of Bhilwara Super Group are the oldest rock types overlain by quartzite, schists, conglomerates, dolomitic limestone etc. belonging to Alwar and Ajabgarh groups of Delhi super group along with granite, pegmatite and amphibolite intrusive of post-Delhi age. Groundwater in the district occurs both in unconsolidated

quaternary formations and consolidated formations of Bhilwara and Delhi super groups, and also post-Delhi granites.

Groundwater in the district occurs both in unconsolidated quaternary formations and consolidated formations of Bhilwara and Delhi super groups, and also post-Delhi granites. In a large portion of the district, alluvial deposits mainly fine sand and silt serve as potential aquifers in addition to gravel zones. Ground water in the district is contained in several different lithologic units ranging in age from Younger alluvium to old Gneisses. Important aquifers are formed in Younger alluvium (which occupies about 39% area of all the aquifers in the district) followed by Older alluvium, Gneiss, Schist, Quartzite and partly in Granite. Some parts of these aquifers are saline also.

Depth of wells in the district generally varies from 50 to 100 m in alluvium and 50 to 200 m in combination/consolidated formation areas. Specific capacity of wells varies from 58 to 500 liters per minute per meters. Transmissivity value and storage coefficient varies from 10 to 850 $m^2$/day and $4.70\times10^{-5}$ to $1.05\times10^{-3}$ respectively.

### *1.1.2 Soil, Land Use and Irrigation*

Soils in the study area can be classified as loamy sand to sandy loam, sandy clay loam and sandy clay. About 20% of the total area is not suitable for cultivation because of forest, hills, pasture land, barren lands, and ponds. In addition, about 21% area is found suitable for cultivation but is presently not under cultivation due to non-availability of irrigation water sources and other reasons. About 85% of the total district area is under cultivation, and irrigation is applied only in 26% of the total district area.

### *1.1.3 Topography*

The general slope of Jaipur city and its surroundings is from north to south and then to south-east. Nearly all ephemeral streams flow in this direction. Higher elevations in the north exist in the form of low, flat-topped hills of Nahargarh (587 meters). Jaigarh, Amber and Amargarh hills are deeply dissected and eroded. An isolated hillock called ‘Moti Dungri’ upon which an old royal castle exists is near the Rajasthan University. Further in the south, topographical levels of the plain areas varies between 280 meters along Bandi and Dhund rivers to some 530 meters in the north-east of Chomu near Samod hills. The overall trend is a decline of slope from the areas bordering the hills in the north to low lying gentle plains in the south.

## 2. Experimental Program

A total of thirteen groundwater quality parameters (i.e., Ca, Mg, Na, K, $SO_4$, Cl, $NO_3$, $CO_3$, $HCO_3$, F, TDS, EC and pH ) of 196 sampling sites in the area for pre- monsoon season of eighteen year period (2001-2018) were collected from Rajasthan State Ground Water Board, Jaipur (Fig. 1). However, the groundwater quality data of 2015 and 2016 could not be available.

### *2.1 Hydrochemical Processes*

Identifiying and understanding the hydrochemical processes are essential to evalaute the causes for changes in groundwater quality for planning groundwater protection. Gibbs (1970) plot is widely used to establish the relationship of water composition and aquifer lithological characteristics, showing major processes controlling groundwater chemistry. Gibbs diagrams were constructed by the equivalence ratios of

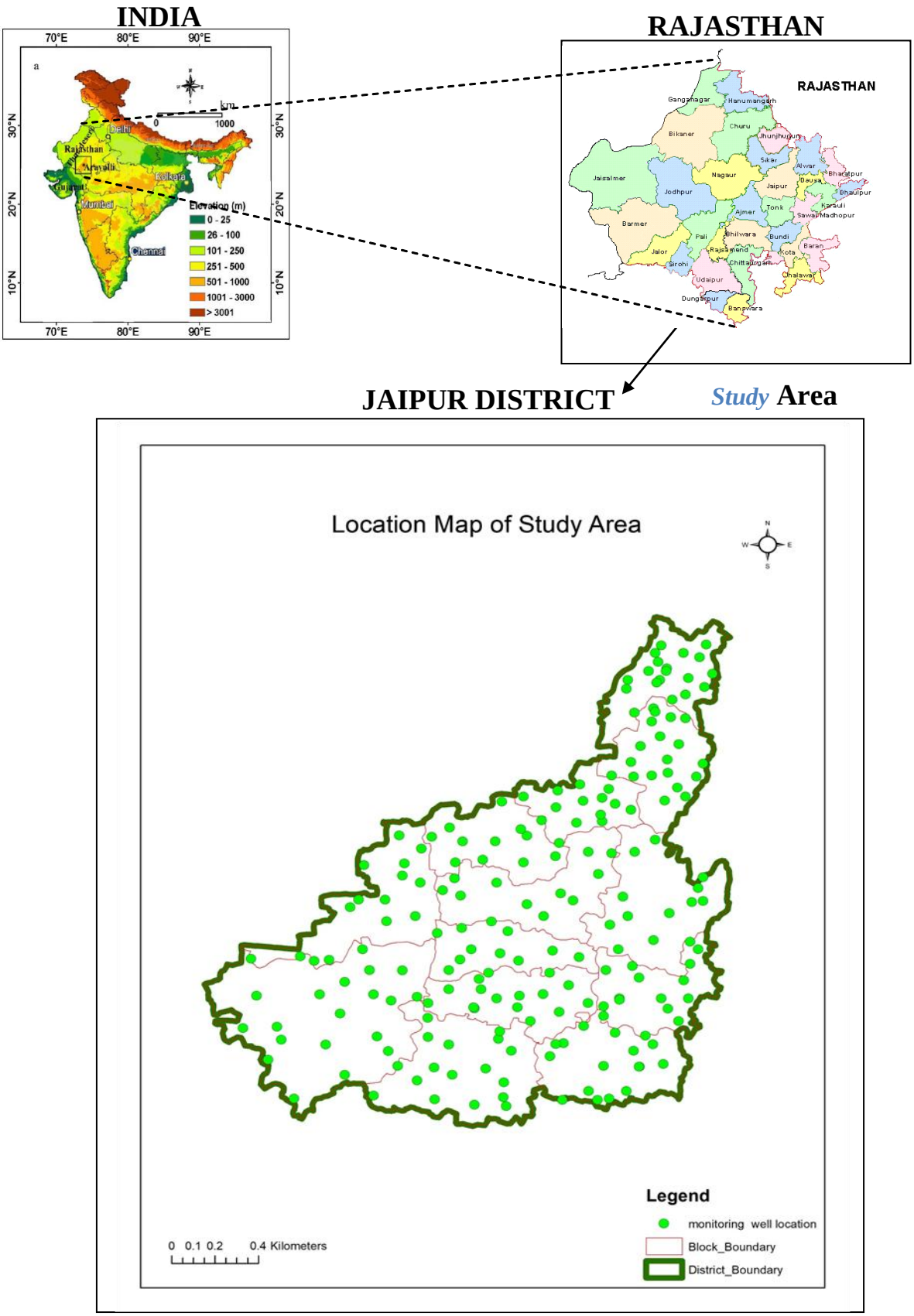



**Fig. 1. Location map of study area**

$(Na^{+}+K^{+)}/(Na^{+}+K^{+}+ Ca^{2+)}$ and $Cl^{-}/(Cl^{-} + HCO_3^{-})$ versus TDS. This method has been widely used to identify hydro geochemical evolution, which involves precipitation, rock weathering, and evaporation–crystallization processes. The positioning of groundwater either on the left or right side of diagram depends on soil and aquifer properties. The rock-water interaction dominance field indicates the interaction between rock chemistry and the chemistry of the percolated waters under the subsurface.

Evaporation crystallization is the dominant factor leading to increased salinity and therefore poor quality of groundwater (Srinivasamooorthy et al, 2008).

## *2.2 Chemical Classification of Groundwater*

The term hydrochemical facies is a function of solution kinetics, rock water interactions, geology and contamination sources used to describe the quantities of water that differ in their chemical composition. Piper trilinear diagram is used to categorize the water facies on the basis of dominant ions (Piper, 1944). The cations expressed as percentage of total cations in meq/l as a single point on the left triangle while anions plot in the right triangle. Each point is then projected into the upper field along a line parallel to the upper margin of the field and the point where the extension intersects indicates the character of the water as represented by the relationship among $Na^{+}+K^{+}$, $Ca^{2+} + Mg^{2+}$, $CO_3^{2-} + HCO_3^{-}$ and $Cl^{-}$, $SO_4^{2-}$ . This classification system shows the anion and cation facies in terms of major-ion percentages. The water types are designated according to the area in which they occur on the diagram segments.

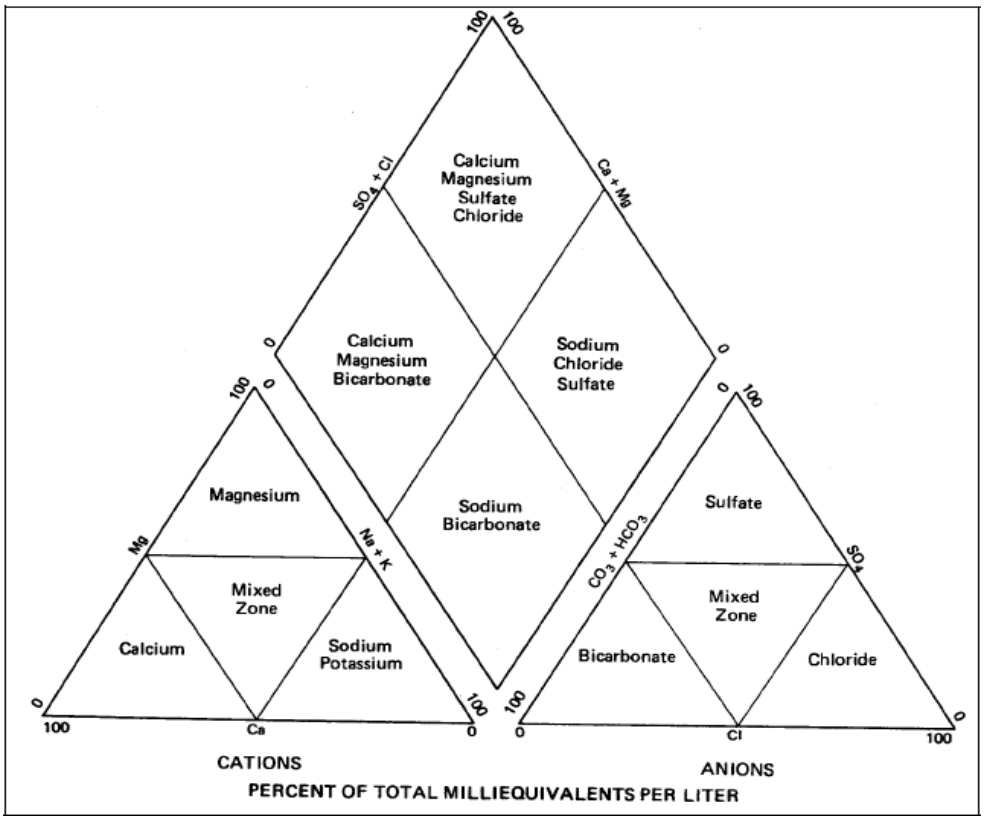



**Fig. 2: Trillinear Piper Diagram showing Water Type Categories**

### *2.3 Water Quality Index Calculation*

Water quality index is defined as a rating reflecting the composite influence of different water quality parameters based on several key parameters of groundwater chemistry. Water quality is assessed on the basis of calculated water quality indices. WQI describes as a method of ranking that gives the combined control of major water quality parameters on the whole excellence of water for human utilization (Singh et al., 2016). The data obtained through quantitative analysis and WHO water quality standards were used for calculating water quality indices. Firstly, special weights (wi) in a scale of 1 (slightest consequence on water quality) to 5 (highest outcome on water quality) was allocated to every elemental parameter, on the basis of their supposed impact on primary health and their relative magnitude in the quality of drinking water (Sener & Davraz, 2013).

The parameters having serious health impact and whose occurrence above the critical concentration amount could result in confined usage of the resource for household and drinking purposes were given the highest weight five. The highest weight of 5 has been allocated to the parameters like nitrate, TDS and fluoride because of their foremost significance in water excellence evaluation (Table1).

**Table 1: Relative Weight of Major Physico-chemical Parameters for Drinking Purpose**

| Chemical Parameters | WHO Standards | Weight ($w_i$) | Relative Weight ($W_i$) |
|---|---|---|---|
| TDS (mg/l) | 500 | 5 | 0.135 |
| $Na^+$ (Mg/l) | 200 | 4 | 0.108 |
| $K^+$ (Mg/l) | 250 | 3 | 0.081 |
| $Ca^{2+}$ (Mg/l) | 75 | 3 | 0.081 |
| $Mg^{2+}$ (Mg/l) | 50 | 2 | 0.054 |
| $Cl^-$ (Mg/l) | 250 | 3 | 0.081 |
| $SO_4^{2-}$ (Mg/l) | 250 | 4 | 0.108 |
| $CO_3^{2-}$ (Mg/l) | 100 | 2 | 0.054 |
| $HCO_3^-$ (Mg/l) | 500 | 1 | 0.027 |
| $NO_3^{2-}$ (Mg/l) | 45 | 5 | 0.135 |
| $F^-$ (Mg/l) | 1.5 | 5 | 0.135 |

The relative weight was computed from the following equation:

$$Wi = wi/\sum_{i=1}^{n} wi \quad (1)$$

Where,
Wi is the relative weight,
wi is the weight of each parameter
n is the number of parameters

The quality rating scale for each parameter is calculated by dividing its concentration in each water sample by its respective standards (World Health Organization 2011) and multiplied the results by 100.

$$Q_i = (C_i/Si) \times 100 \quad (2)$$

Where,
Qi is the quality rating
Ci is the concentration of each chemical parameter in each sample in milligrams per liter
Si is the World Health Organization standard for each chemical parameter in milligrams per liter according to the guidelines of the (WHO 2011)

The final step to compute the value of WQI, the P is first determined for each parameter i.e. the multiplication of the relative weight and quality rating. The sum of P values gives the water quality index for each sample.

$$Pi = Wi \times Qi \quad (3)$$

$$WQI = \sum_{i=1}^{n} Pi \quad (4)$$

Where,
Pi is the sub index of ith parameter

### *2.31 Spatial Distribution Analysis of Groundwater Quality Index using ArcGIS*

GIS based Inverse Distance Weighing (IDW) interpolation technique was used to signify spatial variation of water quality index (WQI) in the study area. The groundwater quality of district Jaipur for drinking purpose was evaluated through water quality index method. The map was categorized based on the classification shown in Table 2.

**Table 2: Water Quality Classification based on Water Quality Index (WQI)**

| Range | Type of Water |
|---|---|
| < 50 | Excellent |
| 50– 100 | Good |
| 100- 200 | Poor |
| 200– 300 | Very Poor |
| >300 | Unsuitable for drinking purpose |

## Conclusions

The conventional hydro-geochemical techniques and quality indices are used to find out the status of groundwater quality for its utilization to drinking purpose. The study of groundwater controlling mechanism using According to Gibbs diagram, the predominant samples fall in the rock–water interaction dominance and evaporation dominance field. Higher cation ratio suggests that dissolution of silicate minerals are the dominant controlling factor of the groundwater chemistry of the study area. Further, surface contamination sources such as irrigation return flow and anthropogenic impacts probably affect the quality of groundwater through increasing of Na and Cl contents. Evaporation greatly increases the concentrations of ions formed by chemical weathering of rock, leading to higher salinity.

Hydro-geochemical analysis of groundwater samples reveals that the study region is dominated by Na-$HCO_3$ and Na-Cl-$SO_4$ type facies. Na and $CO_3^{2-}$ +$HCO_3^-$ are dominant ions among the studied cations and anions. This process indicates that alkalis ($Na^+$+ $K^+$) dominated over the alkaline earth ($Ca^{2+}$+$Mg^{2+}$).

Water quality has been classified under 5 categories based on the WQI values. The groundwater samples exhibits large variation of water quality for the study region (33.147 to 713.37). The spatial distribution of Water Quality Indices exhibits that 13.78 % of groundwater samples in in the North Western and few patches in central part and 45.41 % groundwater samples in north, north-east and central part of the study area falls under excellent and good water type, respectively. This part of the study area is less affected by surface contamination such as irrigation return flow and anthropogenic impacts due to high elevation area having less dissolution and infiltration. The water samples within poor quality, very poor quality, and unsuitable for drinking purposes contributed 33.16, 6.13 and 1.53% of groundwater samples. Poor and very poor water qualities were found in the south and south-west and few patches in central part of the study area and cannot be used for drinking without any treatment and conventional disinfection, whereas water “unsuitable for drinking purposes” could only be used for aquaculture, irrigation, and industrial purposes and observed in 1.53 % of groundwater samples in block Dudu and Phagi, located in southern part of the study area are unsuitable for drinking purpose.

## References

Ackah, M., Agyemang, O., Anim, A.K., Osei, J., Bentil, N.O., Klatch, L Hanson, J.E.K. (2011). Assessment of groundwater quality for drinking and irrigation: The study of Teiman-Oyarifa Community, Ga East Municipality, Ghana. Proceedings of the International Academy of Ecology and Environmental Sciences, 1(3–4), 186–194.

Abbasi, T., Abbasi, S. A., 2012. Water quality indices, Great Britain, Elsevier, 384 p.

Arkoc, O., 2011. Assessment of water quality of east part of the Ergene basin, Turkey. Journal of Environmental Protection and Ecology, 11 (4), 1644-1655.

Arnade, l.j (1999). Seaonal correlation of well contamination and septic tank distance groundwater. 37(60, 920-923l.

Avvannavar, S.M., & Shrihari, S. (2008). Evaluation of water quality index for drinking purposes for river Netravathi, Mangalore, South India. Environmental Monitoring and Assessment, 143(1–3), 279–290.

Ballukraya PN, Ravi R (1999) Characterization of groundwater in the unconfinedaquiferofChennaicity,India.JGeolSocIndia54:1–11

Bairu, A., Tadesse, N., Amare, S., 2013. Use of geographic information system and water quality index to assess suitability of groundwater quality for drinking purposes in Hewane areas, Tigray, Northern Ethiopia. Ethiopian Journal of Environmental Studies and Management, 6 (2), 110-123.

BIS (1991) (Bureau of Indian Standards) 10500 Indian Standard drinking water specification, 1st rev, 1–8

Boyacioglu, H., 2010. Utilization of the water quality index method as a classification tool. Environmental Monitoring and Assessment, 167 (1-4), 115-124.

Dhanasekarapandian, M., Chandran, S., Devi, D.S., & Kumar, V. (2016). Spatial and temporal variation of groundwater quality and its suitability for irrigation and drinking purpose using GIS and WQI in an urban fringe. Journal of African Earth Sciences, 124, 270–288.

Gibbs, R.J. (1970). Mechanism controlling world's water chemistry. Science, 170, 1088–1090.

Gibrilla, A., Bam, E. K. P., Adomako, D. S., Ganyaglo, S., Osae, S., Akiti, T. T., Kebede, S., Achoribo, E., Ahialey, E., Ayanu, G., Agyeman, E. K., 2011. Application of water quality index (WQI) and multivariate analysis for groundwater quality assessment of the Birimian and Cape Coast Granitoid Complex: Densu River Basin of Ghana. Water Quality Exposure Health, 3 (2), 63-78.

Gorai, A. K., Kumar, S., 2013. Spatial distribution analysis of groundwater quality index using GIS: A case study of Ranchi Municipal Corporation (RMC) area. Geoinformatics & Geostatistics: An Overview. doi:10.4172/2327-4581.1000105.

Gowd, S.S. (2005). Assessment of groundwater quality for drinking and irrigation purposes: A case study of Peddavanka watershed, Anantapur District, Andhra Pradesh, India. Environmental Geology, 48(6), 702–712.

Haritash, A.K., Kaushik, C.P., Kaushik, A., Kansal, A., & Yadav, A.K. (2008). Suitability assessment of groundwater for drinking, irrigation and industrial use in some North Indian villages. Environmental Monitoring and Assessment, 145(1–3), 397–406.

Hem, J.D. (1991). *Study and interpretation of the chemical characteristics of natural water*. (3rd ed., p. 263). Jodhpur, India: Scientific publication 2254

Jerry AN (1986) Basic environmental technology (water supply, waste disposal and pollution control). Wiley, New York

Magesh NS, Krishnakumar S, Chandrasekar N, Soundranayagam JP (2013) Groundwater quality assessment using WQI and GIS techniques, Dindigul district, Tamil Nadu, India. Arab J Geosci 6(11):4179–4189

Mishra, P.C., & Patel, R.K. (2001). Quality of drinking water in Rourkela, Outside the steel township. Journal of Environment and Pollution, 8(2), 165–169.

Mitra, B.K., Sasaki, C., Enari, K., Matsuyama, N., & Fujita, M. (2007). Suitability assessment of shallow groundwater for agriculture in sand dune area of northwest Honshu Island Japan. Applied Ecology and Environmental Research, 5(1), 177–188.

M. N. Tijani, "Hydrochemical assessment of groundwater in Moro area, Kwara State, Nigeria," Environmental Geology, vol. 24, no. 3, pp. 194–202, 1994.

Piper, A.M. (1944). A graphic procedure in the geochemical interpretation of water-analyses. *Transactions, American Geophysical Union, 25*, 914–923.

Raju, N.J. (2007). Hydrogeochemical parameters for assessment of groundwater quality in the upper Gunjanaeru River basin, Cuddapah District, Andhra Pradesh, South India. *Environmental Geology*, 52(6), 1067–1074.

Raju, N.J., Shukla, U.K., & Ram, P. (2011). Hydrogeochemistry for the assessment of groundwater quality in Varanasi: a fast-urbanizing center in Uttar Pradesh, India. Environmental Monitoring and Assessment, 173, 279–300. doi:10.1007/s10661-010-1387-6

Raju, N.J., Ram, P., & Gossel, W. (2014). Evaluation of groundwater vulnerability in the lower Varuna catchment area, Uttar Pradesh, India using AVI concept. *Journal of the Geological Society of India, 83*(3), 273–278.

Sadat-Noori, S. M., Ebrahimi, K., Liaghat, A. M., 2014. Groundwater quality assessment using the Water Quality Index and GIS in Saveh-Nobaran aquifer, Iran. Environmental Earth Sciences, 71 (9), 3827-3843.

Selvakumar, S., Ramkumar, K., Chandrasekar, N., Magesh, N.S., & Kaliraj, S. (2017). Groundwater quality and its suitability for drinking and irrigational use in the Southern Tiruchirappalli district, Tamil Nadu, India. Applied Water Science, 7(1), 411–420.

Sener, E., & Davraz, A. (2013). Assessment of groundwater vulnerability based on a modified DRASTIC model, GIS and an analytic hierarchy process (AHP) method: The case of Egirdir Lake basin (Isparta, Turkey). *Hydrogeology Journal, 21*(3), 701–714.

Singh, S., Raju, N.J., & Ramakrishna, C. (2015). Evaluation of groundwater quality and its suitability for domestic and irrigation use in parts of the Chandauli-Varanasi region, Uttar Pradesh, India. Journal of Water Resource and Protection, 7(7), 572.

Srinivasamoorthy, K., Chidambaram, S., Prasanna, M.V., Vasanthavihar, M., Peter, J., & Anandhan, P. (2008). Identification of major sources controlling groundwater chemistry from a hard rock terrain – A case stu88dy from Mettur taluk, Salem district, Tamil Nadu, India. Journal of Earth System Science, 117(1), 49–58.

Sreedevi, P.D. (2004). Groundwater quality of Pageru river basin, Cudapah district, Andhra Pradesh. Journal of the Geological Society of India, 64, 619–636.

Subba Rao N (2006) Seasonal variation of groundwater quality in a part of Guntur district, Andhra Pradesh, India. Environ Geol 49:413–429

Todd DK (1980) Groundwater hydrology. Wiley, New York.

Vasanthavigar M, Srinivasamoorthy K, Vijayaragavan K, Rajiv Ganthi R, Chidambaram S, Anandhan P, Manivannan R, Vasudevan S (2010) Application of water quality for groundwater quality assessment: Thirumanimuttar Sub basin, Tamil Nadu, India. Environ Monit Assess 171(1–4):595–609

Wang, S. (2013). Groundwater quality and its suitability for drinking and agricultural use in the Yanqi Basin of Xinjiang Province, Northwest China. Environmental Monitoring and Assessment, 185(9), 7469–7484.

WHO (2011) WHO Guidelines for Drinking-water Quality, fourth ed. World Health Organization

*IN PROCEEDINGS OF 25th HYDRO 2020, INTERNATIONAL CONFERENCE, NATIONAL INSTITUTE OF TECHNOLOGY ROURKELA, ODISHA, INDIA 26-28, March 2021, ISBN 978-93-90631-56-8*

Paper ID - 221

# Assessment of Groundwater Potential Zones using AHP Technique in Darbhanga District of Bihar

Sumit Kumar[1], Vivekanand Singh[2]

[1]*PG student, Dept. of Civil Engineering, National Institute of Technology Patna, Patna and 800005, India.*
[2] *Professor, Dept. of Civil Engineering, National Institute of Technology Patna, Patna and 800005, India.*
*Email: sumitjaynagar@gmail.com, vsingh@nitp.ac.in*
*Telephone/Mobile No.: +91 8149943305, +91 7544006310*

## Abstract

Darbhanga district is situated in North Bihar. In this region, 80 % of the irrigation demand is met by groundwater though it has annual rainfall of about 1200 mm. The increasing population and industrialization are likely to overexploit the groundwater and day by day groundwater level is declining. Thus it is important to delineate the groundwater potential zones in the study area, so that better planning and management of groundwater resources can be done. In this study, groundwater potential zone of Darbhanga district in Bihar has been delineated using GIS based Analytical Hierarchical Process (AHP). The parameters, which contribute the groundwater are geology, soil, slope, drainage density, lineament density, geomorphology, land use and rainfall. The thematic map of these parameters have been prepared by using remote sensing, meteorological and geological data of the study area. Different weights have been assigned to these parameters depending upon the influence of that parameter on groundwater potential. Geometric mean of weightage of these parameters have been computed using AHP technique. All the thematic map have been integrated in ArcGIS. Groundwater potential zones have been classified into five categories, such as very poor, poor, moderate, good and very good. Based on the above data, the groundwater potential zones have been delineated and computed using AHP technique for these classifications. The groundwater potential zones are: Very Poor - 9.90 %, Poor - 25.73 %, Moderate - 36.95 %, Good - 25.41 %, and Very Good - 2 %.

***Keywords:*** *Groundwater potential zone; Darbhanga; Remote sensing; GIS; Analytic Hierarchy Process.*

## 1. Introduction

Groundwater is very important natural resource and it is about 30 % of the world's freshwater resources. It provides critical input for the sustenance of life being in arid and semi-arid zones. It is natural fresh resources which is 34% of the total annual water supply (Shekhar and Pandey, 2014). In hard rocky terrain, availability of groundwater is limited due to groundwater confined with the fracture and weathered zone. In fact, there is a requirement of groundwater for agriculture, domestic and industrial needs for developed as well as for developing countries. Due to rapid increase in population and industrialization, fresh water requirement has been increased tremendously, which over exploits the groundwater. The availability of groundwater is decreasing gradually due to misuse and in absence of proper planning, maintenance and management. To overcome with this problem, it is necessary to understand the use of water and to replenish the groundwater through recharge, so that the availability of groundwater can be improved regionally as well as on locally for the sustainability. Groundwater is replenished through recharge by surface water sources such as lakes, rivers, ponds, and runoff. Effective way of groundwater recharge is through artificial recharge of aquifer for the management of groundwater resource. Thus, it is paramount important to demarcate the high groundwater potential zones. Earth having the various features such as geology, geomorphology, soil type, lineament, land use and land cover drainage etc. are influencing the recharge of the groundwater.

Many researchers have identified the groundwater potential zone in different region using Remote Sensing (RS) and Geographic Information System (GIS) based Analytic Hierarchy Process (AHP) technique and suggested that these methods are useful tool to delineate groundwater potential in any region (Preeja et al., 2011; Agarwal et al., 2013; Kaliraj et al., 2013; Mohammadi et al, 2018; Kumar et al., 2020; Saranya and Saravanan, 2020). Remote Sensing and GIS based AHP technique is the new method to study the groundwater resources (Jasrotia et al., 2013) other methods are also developed using RS and GIS to further study of groundwater resource (Adji and Sejati, 2014; Agarwal and Garg,

2016). Some researchers have also worked on groundwater potential zone using geomatics approach integrated by remote sensing and GIS (Elewa and Qaddah, 2011; Nag and Ghosh, 2012; Pandian and Kumanan, 2013; Aluko and Igwe, 2017). In India, several researchers have carried out the studies on groundwater recharge, groundwater potential and other studies related to groundwater for different catchments (Magesh et al., 2012; Shekhar and Pandey, 2014; Aneesh and Deka, 2015; Siva et al., 2017). Performing study on groundwater mapping and groundwater recharge in hard rock region is very difficult. To overcome these difficulties of mapping and recharge of groundwater in hard rock terrain the integration of modern technique with remote sensing and GIS is very useful. Delineation of groundwater potential zones in hard rock terrain using integrated RS, GIS and AHP method by researchers have been reported (Muralitharan and Palanivel, 2015). In recent years, various methods have been developed to improve groundwater studies using RS and GIS.

This study has been conducted to delineate the groundwater potential zones in Darbhanga district using multi-criteria decision analysis technique, Analytic Hierarchy Process (AHP). AHP technique was originally developed by Saaty (1990) for analyzing and organizing the complex decision. The AHP technique simplify the complex multi-criteria decision problem in the hierarchy based pair-wise comparison matrix of the different criteria and sub-criteria. The AHP has been approached for decision making by judgments, organizing perception into a hierarchy structure that shows the forces that control a decision. It was used for multi-criteria decision. Data have been collected from the satellite image, central groundwater board (CGWB) and SWAT climate data website of rainfall to approach the target of groundwater potential. This study delineates groundwater potential zones using 8 thematic layer like drainage density, soil, slope, lineament density, geology, geomorphology, land use and rainfall of region.

## 2. Study area

Darbhanga district is one of the district of Bihar with Darbhanga town as its administrative headquarter. It is located between longitude 85º45' and 86º25' E and latitude 25º53' and 26º27' N as shown in Figure 1. The study area touches the north by Madhubani district, on the south by Samastipur district, on the east by Saharsa district and on the west by Sitamarhi and Muzaffarpur district. Elevation of the Darbhanga is 52 m above mean sea level and total geographical area of the district is 2288.15 $km^2$. The average annual rainfall in the district is 1200 mm, 80 % of this rainfall occurs during monsoon seasons. The soil of this area is very fertile with terai, sandy and loamy soils (Sinha et al., 2018; CGWB). Darbhanga district belongs to the Bagmati sub-basin of the Ganga basin. There are 3 major drainage systems in the district namely, Bagmati, Kamla and Tiljuga. The district has three sub-division, namely Darbhanga sadar, Benipur and Birul. Darbhanga district has, 1269 villages, 329 Panchayats, 23 police station and 19 development block. Darbhanga district forms a vast monotonously flat plain along with low relief to the south of Tarai/Bhabhar and high relief belt in Himalayas region in Nepal. About 82 % area is Culturable with kharif crop has highest about 96 % and in ravi crop wheat is the highest. 70 % area is irrigated by groundwater through dugwells and tube wells. Depth to groundwater level was varying from 1.77 to 6.09 m bgl in pre-monsoon and from 1.7 to 2.7 m bgl in the monsoon season (CGWB).

## 3. Methodology and Data used

Thematic layers have been prepared by using the digital image processing of remote sensing, meteorological and geological data. To demarcate the groundwater potential zone in the study area, thematic layers of drainage density, geology, geomorphology, lineament density, land use, soil, slope and rainfall are required. Shuttle Radar Topography Mission (SRTM) Digital Elevation Model (DEM) data for drainage density and slope map and, Landsat data for land use and land cover have been downloaded from the earth explorer USGS (http://earthexplorer.usgs.gov) in the raster format. For rainfall map required rainfall data which was downloaded from the SWAT climate website (http://www.globalweather.tamu.edu) and geology, soil, geomorphology and lineament density map were downloaded from Bhukosh (http://www.bhukosh.gsi.gov.in). It was the geo-scientific database of survey of India. Flow chart for the methodology has been presented in Figure 2.

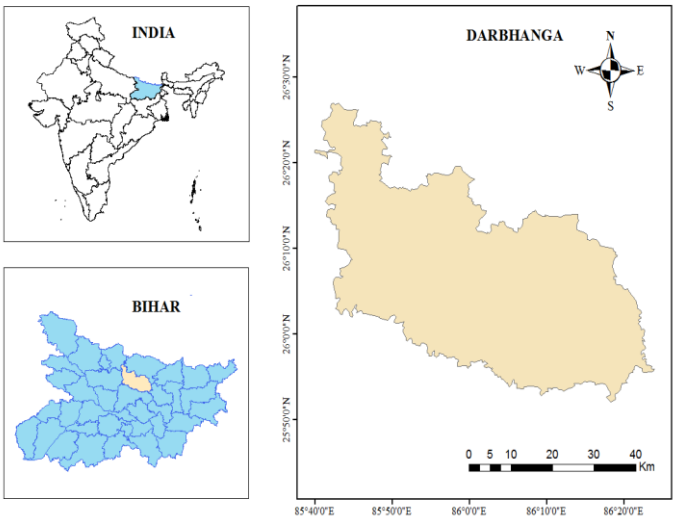



**Figure 1** Location map of study area

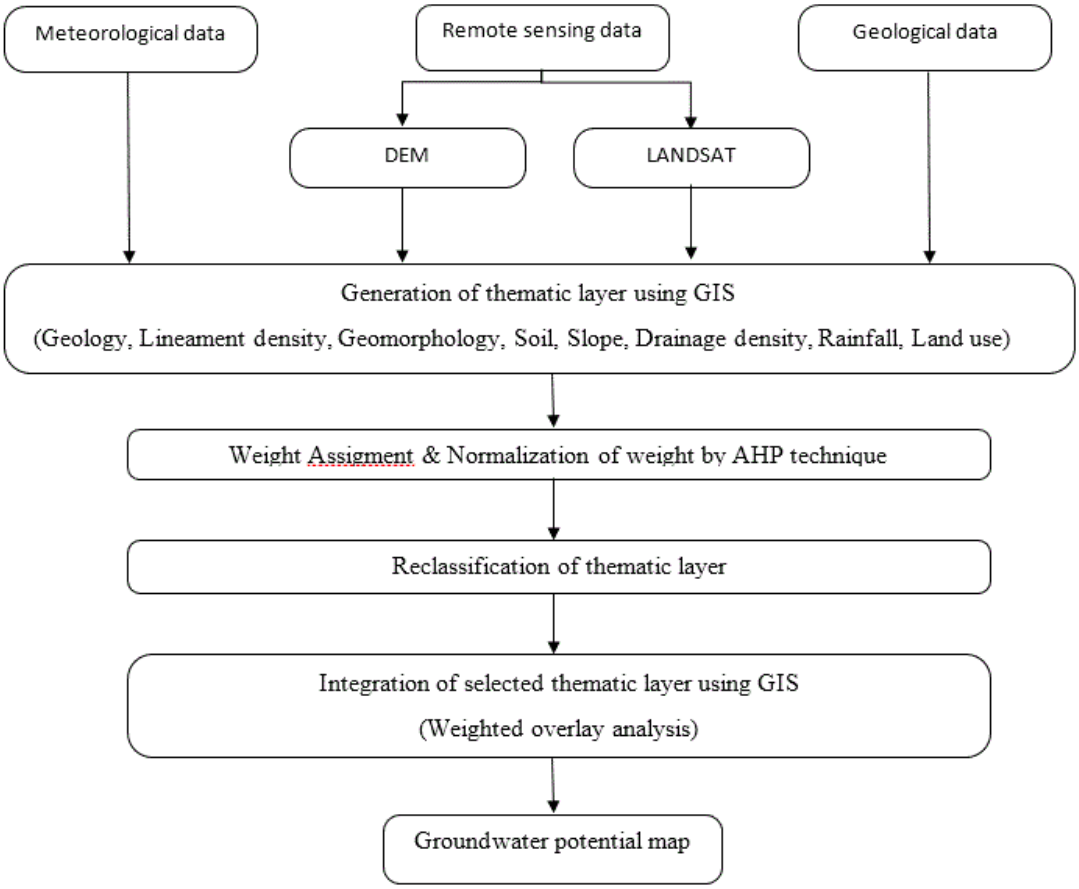



**Figure 2** Flow chart of the methodology of this study

### 3.1 *Analytic Hierarchy Process (AHP)*

AHP technique applied for break down the complex multi-criteria decision problem into the hierarchy based pair-wise comparison of the important of direct parameters and indirect parameters. First a pair-wise comparison matrix was constructed for the different parameters based on their influence toward the groundwater potential. AHP was used to demarcate the groundwater potential zones which was

proposed by Saaty (1990). AHP method is based on the geometric mean. In AHP, pair wise matrix was developed by the scale weight parameters, based on direct and indirect relationship between the parameters toward the groundwater potential.

### 3.2 *Scale weight*

The scale weight is assigned as 1 for the parameters, which have direct influence towards the groundwater and it is assigned as 0.5 for the parameters, which have indirect influence towards the groundwater. The scale weight have been presented in Table 1.

**Table 1** Scale weight calculation of selected thematic layer by assigning score value

| Factor | Geology | Lineament density | Geomorphology | Soil | Slope | Drainage density | Rainfall | Land-use | Scale Weight |
|---|---|---|---|---|---|---|---|---|---|
| Geology | 1.0 | 1.0 | 1.0 | 1.0 | 0.5 | 0.5 | 0.5 | 1.0 | 6.5 |
| Lineament density | 0.5 | 1.0 | 0.5 | 0.5 | 0.5 | 1.0 | 0.5 | 1.0 | 5.5 |
| Geomorphology | 0.5 | 1.0 | 1.0 | 0.5 | 1.0 | 1.0 | 0.5 | 1.0 | 6.5 |
| Soil | 0.5 | 0.5 | 0.5 | 1.0 | 0.5 | 0.5 | 0.5 | 1.0 | 5.0 |
| Slope | 0.5 | 0.5 | 1.0 | 0.5 | 1.0 | 1.0 | 1.0 | 0.5 | 6.0 |
| Drainage density | 0.5 | 0.5 | 0.5 | 0.5 | 0.5 | 1.0 | 1.0 | 0.5 | 5.0 |
| Rainfall | 0.5 | 1.0 | 0.5 | 0.5 | 0.5 | 1.0 | 1.0 | 0.5 | 5.5 |
| Land-use | 0.5 | 0.5 | 0.5 | 0.5 | 0.5 | 0.5 | 0.5 | 1.0 | 4.5 |

### 3.3 *Geometric mean*

Geometric mean is define as the ratio of sum of scale weight of all parameters to the total number of the parameter. Geometric mean of the parameter have been shown in the Table 2.

**Table 2** Normalized pairwise matric analysis for geometric mean calculation of selected parameter

| Factor | Geology | Lineament density | Geomorphology | Soil | Slope | Drainage density | Rainfall | Land-use | Geometric mean |
|---|---|---|---|---|---|---|---|---|---|
| Geology | 1 | 1.18 | 1 | 1.3 | 1.08 | 1.3 | 1.18 | 1.44 | 1.18 |
| Lineament density | 0.84 | 1 | 0.84 | 1.1 | 0.91 | 1.1 | 1 | 1.2 | 0.99 |
| Geomorphology | 1 | 1.18 | 1 | 1.3 | 1.08 | 1.3 | 1.18 | 1.44 | 1.18 |
| Soil | 0.77 | 0.9 | 0.76 | 1 | 0.83 | 1 | 0.9 | 1.11 | 0.91 |
| Slope | 0.92 | 1.09 | 0.92 | 1.2 | 1 | 1.2 | 1.09 | 1.33 | 1.09 |
| Drainage density | 0.77 | 0.9 | 0.76 | 1 | 0.83 | 1 | 0.9 | 1.11 | 0.91 |
| Rainfall | 0.84 | 1 | 0.84 | 1.1 | 0.91 | 1.1 | 1 | 1.2 | 0.99 |
| Land-use | 0.69 | 0.81 | 0.69 | 0.9 | 0.75 | 0.9 | 0.81 | 1 | 0.81 |

### 3.4 *Factor influencing of the groundwater potentiality of the study area*

Factors considered for the delineation of groundwater potential of the study area are geology, lineament density, geomorphology, soil, slope, drainage density, rainfall and land use. The details for these factors have been given in Table 3.

**Table 3** Assigned weight and normalized weight of feature classes of selected parameter

| Parameters | Feature Class | Assigned Weight (AW) | Geometric Mean (G) | Normalized weight (N=AW/G) |
|---|---|---|---|---|
| Geology | Fluvial(slit, clay, alluvium) | 9 | 1.18 | 7.63 |
| Lineament density | 0-0.00235 | 9 | 0.99 | 9.09 |
| | 0.00235-0.0047 | 7 | | 7.07 |
| | 0.0047-0.00705 | 5 | | 5.05 |
| | 0.00705-0.0094 | 3 | | 3.03 |
| Geomorphology | Older flood plain | 1 | 1.18 | 0.85 |
| | Younger Alluvial plain | 3 | | 2.54 |
| | Pond | 5 | | 4.24 |
| | River | 7 | | 5.93 |
| | Water bodies-unclassified | 9 | | 7.63 |
| Soil | Clay loam | 1 | 0.91 | 1.99 |
| | Loam | 3 | | 3.3 |
| Slope | 0-1.52 | 1 | 1.09 | 0.92 |
| | 1.52-2.66 | 3 | | 2.75 |
| | 2.66-4.06 | 5 | | 4.59 |
| | 4.06-6.10 | 7 | | 6.42 |
| | 6.10-32.41 | 9 | | 8.26 |
| Drainage density | 0-0.07 | 7 | 0.91 | 7.69 |
| | 0.07-0.14 | 5 | | 5.49 |
| | 0.14-0.21 | 3 | | 3.3 |
| | 0.21-0.27 | 2 | | 1.1 |
| Rainfall | 1556-1512 | 5 | 0.99 | 5.05 |
| | 1512-1480 | 7 | | 7.07 |
| | 1480-1449 | 9 | | 9.09 |
| | 1449-1418 | 11 | | 11.11 |
| | 1418-1367 | 13 | | 13.13 |
| Land-use | Build-up land | 1 | 0.81 | 1.23 |
| | Plantations | 3 | | 3.7 |
| | Shrub land | 5 | | 6.17 |
| | Crop land | 7 | | 8.64 |
| | Fallow land | 9 | | 11.11 |
| | Wasteland | 11 | | 13.58 |
| | Permanent Wetland | 13 | | 16.05 |
| | Water bodies | 15 | | 18.52 |

### *3.4.1 Geology*

The geological setting of the study area depend on the underlain by sedimentary Rock. Geology map download from the bhukosh (http://www.bhukosh.gsi.gov.in) which is the geo-scientific database of survey of India. Preparation of thematic layer of geology of Darbhanga district by extraction from the downloaded data by clip tool. Figure 3 presents the geology of study area. One type of formation i.e. Fluvial has been found in the study area.

### *3.4.2 Lineament density*

Lineaments is the linear geological formation due to the tectonic origin. It is identified as narrow, long and straight alignment visible in the satellite images. Lineament may be fault, fracture and master joint. It is a geological formation in the form of long and linear. Lineament is responsible for the infiltration of water into the sub-surface. Lineament density is also called secondary permeability. This feature express underlying structure in surface topography. Lineament is hydro-geologically very important for the pathway of groundwater movement. Lineament map was downloaded from the bhukosh (http://www.bhukosh.gsi.gov.in) which is the geo-scientific database of survey of India. It is defined as total length of lineament that is fault, fracture and joints divided by the catchment area. Lineament density value lies between 0 and 0.0094 (km/km$^2$). The lineament density have been classified into four category: low (0-0.00235), moderate (0.00235-0.0047), high (0.0047-0.00705) and very high (0.00705-0.0094). Most of the area have no lineament density. Low lineament density have been found in eastern part and high lineament density have been found in the south-west portion in the Darbhanga district (Figure 4).

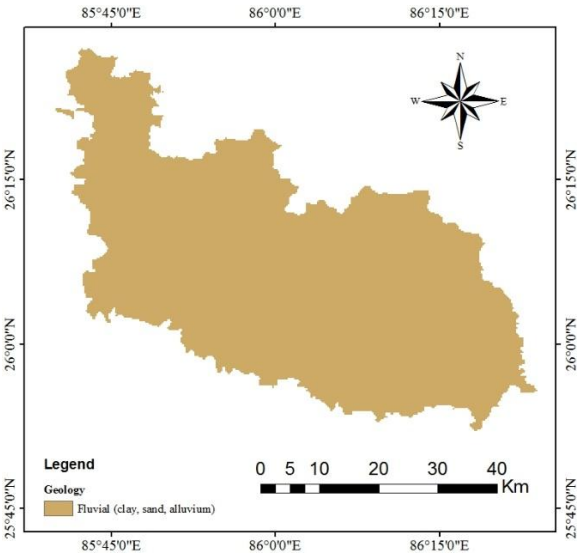



**Figure 3** Geology of study area

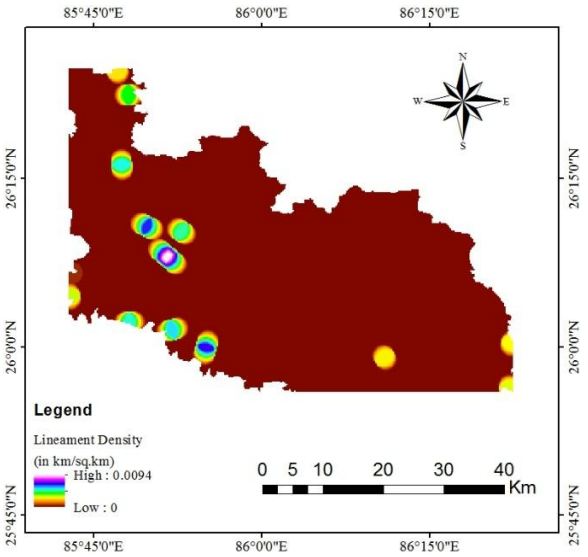



**Figure 4** Lineament density map of Study area

### *3.4.3 Geomorphology*

Geomorphology of the study area was highly influenced by the rock and formation of underlying structure. It was one of the most important feature for delineating the groundwater potential zones, because it is the study of the hydrogeology and structure (Bahuguna et al. 2003; Rao and Jugram 2003; Kumar et al. 2008). Land material associate with the water bodies and flood plain have high groundwater potential. Landform plays very important role for the distribution of groundwater and occurrence of the rain. Geomorphology of the study area have been mostly overlaid by the land such as younger alluvial plain, older flood plain, River, Pond and Water bodies (Figure 5).

### *3.4.4 Soil*

Porosity of soil helps the water movement (Subba et al., 2001). Soil map is download from the FAO digital soil map of the world (DSMW) (http://www.fao.org.in) in the ESRI shape file format. Soil map of study area extract from the DSMW by clip tool in ArcGIS and found that two type of soils in study area - loam and clay loam. Clay loam soil has less influenced in the groundwater potential whereas loam soil has high influenced in the groundwater potential (Figure 6).

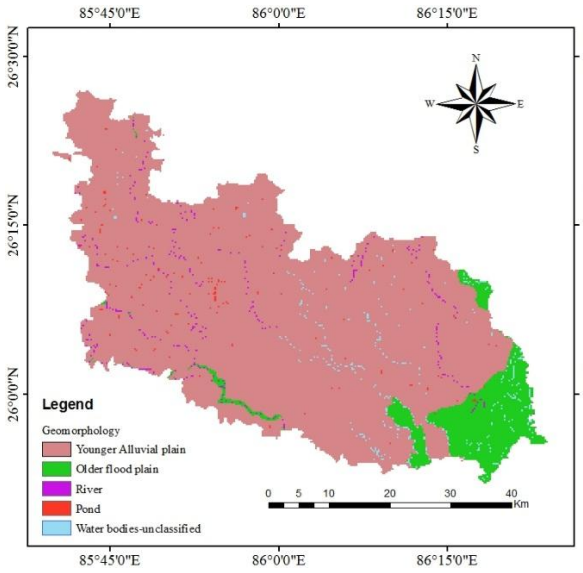



**Figure 5** Geomorphology of the study area

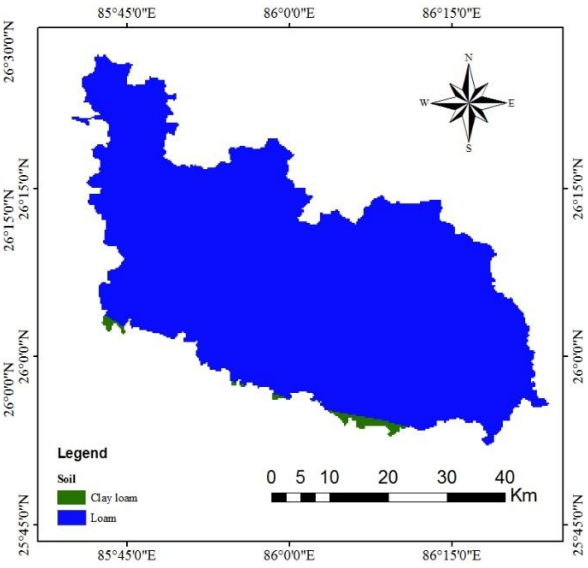



**Figure 6** Soil map of the study area

### *3.4.5 Slope*

Drainage pattern develop on the basis of slope. Slope plays significant character in determination of infiltration and is inversely proportional to infiltration. Slope value of the study area varies 0º to 6º (Figure 7). Slope have been classified into 5 classes: 0º-1.53º, 1.54º-2.67º, 2.68º-4.07º, 4.08º-6.10º and 6.11º-32.41º which have represented very low, low, moderate, high and very high slope, respectively. Low value slope have very high influenced in groundwater potential and vice versa. Most of the region belongs low to very low slope and central region belongs to moderate slope.

### *3.4.6 Drainage density*

Drainage density is express as the closeness of spacing of all stream channel. Drainage density is define as the total length of all order stream to the catchment area. High drainage density means high run-off and results low groundwater potential and vice versa. Drainage density map prepared by the DEM of the study area through Arc hydro tool. Drainage density value lies between 0-0.27 km/km$^2$ (Figure 8). It have been classified into four classes: 0-0.07 km/km$^2$ (low), 0.07-0.14 km/km$^2$ (moderate), 0.14-0.21 km/km$^2$ (High) and 0.21-0.27 km/km$^2$ (Very High). South East region has very high drainage density and North West region has low drainage density.

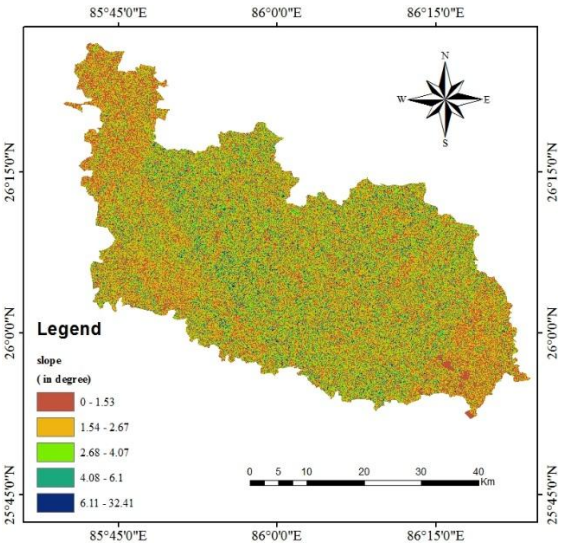



**Figure 7** Slope map of the study area

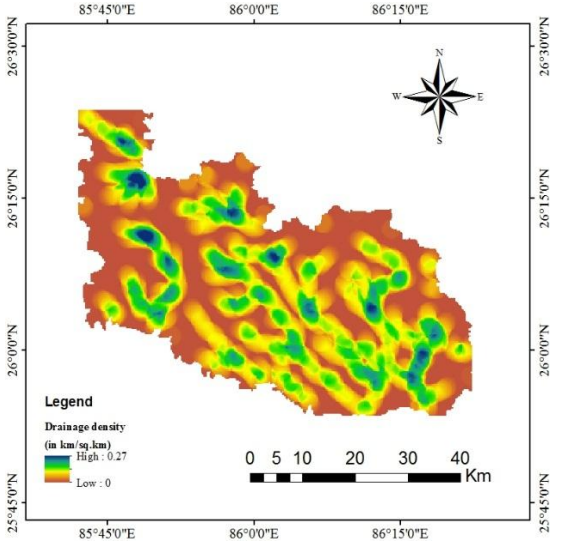



**Figure 8** Drainage density map of the study area

### *3.4.7 Rainfall*

Rainfall is the important resource for the groundwater recharge (Magesh et al. 2012; Shekhar and Pandey. 2014). It measures the amount of water percolated into the groundwater zones. Therefore, rainfall is major hydrological factor for the groundwater potential (Adiat et al. 2012). Daily data of rainfall at 16 gauging sites have been taken from the SWAT climate data website (http://www.globalweather.tamu.edu). Rainfall map have been shown in the Figure 9. Daily rainfall data have been converted into annual average rainfall. Rainfall map has been prepared by Interpolation using by the inverse distance weighted (IDW) technique under the spatial analyst tool. The rainfall have been divided into five subdivisions: 1367-1418 mm, 1418-1449 mm, 1449-1480 mm, 1480-1512 mm and 1512-1556 mm. South west region has low rainfall as compare to north east region. Central portion area has the moderate rainfall. High rainfall value has high influenced in groundwater potential and vice-versa.

### *3.4.8 Land use*

Land use map of the study area have been classified into eight categories i.e Crop land, Build-up land, Shrub land, Fallow land, Wasteland, Water bodies, Plantation and permanent wetland. The Fallow land and Water bodies has high influenced in groundwater potential and build-up land and shrub land has less influenced in groundwater potential (Figure 10).

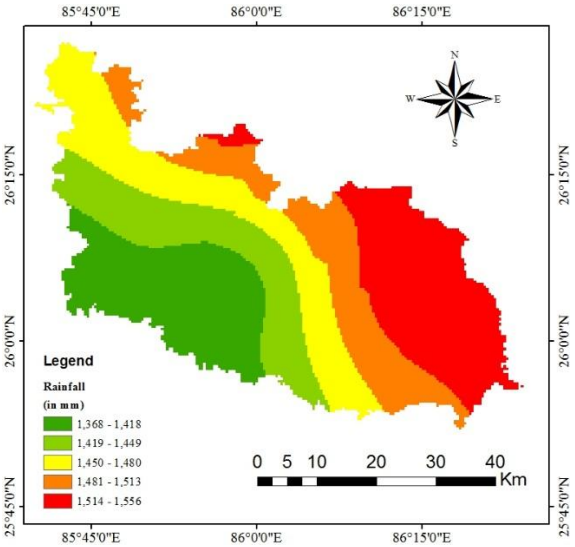



**Figure 9** Rainfall map of the study area

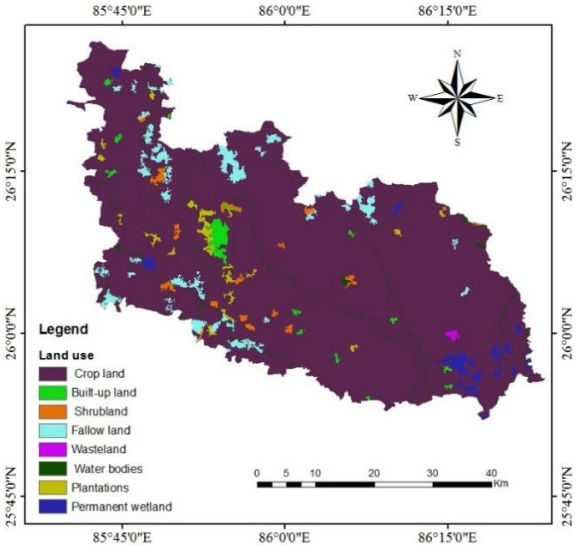



**Figure 10** Land use map of the study area

## 4. Results and Discussion

The groundwater potential zone was delineated on the basis of normalized weight determined for all the feature classes of thematic layers. All the eight thematic layers were overlaid step by step on one another in ArcGIS. Eight parameters (geology, geomorphology, soil, slope, drainage density, lineament density, rainfall and land use) were selected and these feature classes were assigned weight based on their influence on the groundwater potential. For delineating groundwater potential zones all vector layer have been converted into raster format and integrated step by step one-another using overlay analysis in ArcGIS (Mohammadi et al., 2018).

$$GWPI = (G_wG_r) + (L_wL_r) + (M_wM_r) + (S_wS_r) + (T_wT_r) + (D_wD_r) + (U_wU_r) + (R_wR_r) \quad (1)$$

Where, GWPI is groundwater potential index, which was computed by multiplying the assigned weight (w) with its corresponding feature class rate of contributing parameter and G refer for the geology, L refer for the lineament density, M refer for the geomorphology, S refer for the soil type, T refer for the topography of slope, D refer for the drainage density, U refer for the land use and R refer for the average annual rainfall.

The groundwater potential zones have been classified into 5 categories: very poor, poor, moderate, good and very good. Total 226.65 km$^2$ area has been found as very poor groundwater potential zones, which was 9.90 % of total area, 588.71 km$^2$ area has been found as poor groundwater potential zones which was 25.73 % of total area, 845.57 km$^2$ area has been found as moderate groundwater potential zone, which was 36.95 % of the area, 581.50 km$^2$ area has in good groundwater potential zones, which was 25.41 % of the area, and 45.71 km$^2$ area has in very good groundwater potential zones, which was about 2 % of the area. The groundwater potential zones statistics have been presented in the Table 4. Figure 11 presents the groundwater potential zones in the study area.

**Table 4** Groundwater potential zones in terms of area as well as in percentage

| Sr. no. | Class | Area (in km$^2$) | Area (in %) |
|---|---|---|---|
| 1. | Very good | 45.71 | 1.99 |
| 2. | Good | 581.50 | 25.41 |
| 3. | Moderate | 845.57 | 36.95 |
| 4. | Poor | 588.71 | 25.73 |
| 5. | Very poor | 226.65 | 9.90 |

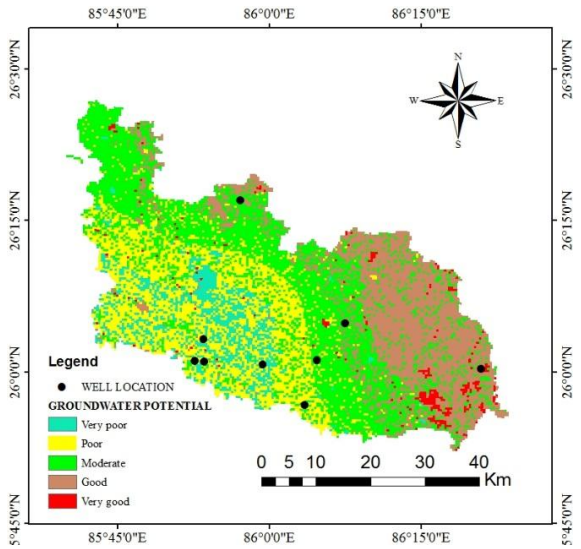



**Figure 11** Groundwater potential map of the study area

## 5. Conclusions

Remote sensing and GIS based Analytical Hierarchy Process (AHP) techniques has been used for the delineation of Groundwater potential zones in the Darbhanga district considering remote sensing, meteorological and geological data. The groundwater potential has been classified into 5 categories: Very poor, poor, moderate, good and very good. Darbhanga district has 9.9 % of very poor, 25.73 % poor, 36.95 % moderate, 25.41 % good and 1.99 % very good groundwater potential. It can be concluded that Darbhanga district has poor to good groundwater potential with percentage of moderate is the highest. The application of remote sensing, geographical information system based analytical hierarchy process will be helpful for planning, design and management of groundwater for the sustainable development of the study area.

## References

Adiat, K., Nawawi, M., and Abdullah, K. (2012). Assessing the accuracy of GIS-based elementary multi criteria decision analysis as a spatial prediction tool-A case of predicting potential zones of sustainable groundwater resources. J Hydrology, 440, 75–89.

Adji, T.N., and Sejati, S.P. (2014). Identification of groundwater potential zones within an area with various geomorphological units by using several field parameters and a GIS approach in Kulon Progo Regency, Java, Indonesia. Arab. J. Geosci. 7, 161–172.

Agarwal, E., Agarwal, R., Garg, R.D., and Garg, P.K. (2013). Delineation of groundwater potential zone: an AHP/ANP approach. Journal of Earth System Science 122, 887–898.

Agarwal, R., and Garg, P. K. (2016). Remote sensing and GIS based groundwater potential & recharge zones mapping using multi-criteria decision making technique. Water Resources Management, 30(1), 243-260.

Aluko, O. E., and Igwe, O. (2017). An integrated geomatics approach to groundwater potential delineation in the Akoko-Edo Area, Nigeria. Environmental Earth Sciences, 76(6), 240.

Aneesh, R., and Deka, P.C. (2015). Groundwater potential recharge zonation of Bengaluru urban district - a GIS based analytic hierarchy process (AHP) technique approach. International Advanced Research Journal in Science, Engineering and Technology 2, 129–136.

Bahuguna, I. M., Nayak, S., Tamilarasan, V., and Moses J. (2003). Groundwater prospective zones in basaltic terrain using remote sensing. J Indian Soc Remote Sens 31(2):107–118.

CGWB, (2013). Groundwater Information Booklet, Darbhanga district, Bihar.

Elewa, H.H., and Qaddah, A.A., (2011). Groundwater potentiality mapping in the Sinai Peninsula, Egypt, using remote sensing and GIS-watershed-based modeling. Hydrogeol. J. 19, 613–628.

Jasrotia, A.S., Bhagath, B.D., Ajay, K., and Rajesh, K. (2013). Remote sensing and GIS approach for delineation of groundwater potential and groundwater quality zones of Western Doon Valley, Uttarakhand, India. Jour. Indian Soc. Remote Sensing. 41, 365–377.

Kaliraj, S., Chandrasekar, N., and Magesh, N.S. (2013). Identification of potential groundwater recharge zones in Vaigai upper basin, Tamil Nadu, using GIS based analytical hierarchy process (AHP) technique. Arab. J. Geisci. 7:1385-1410

Kumar, T., Gautam, K., and Kumar, T. (2014). Appraising the accuracy of GIS based multicriteria decision making technique for delineation of groundwater potential zones. Water Resour. Manag. 28, 4449–4466.

Kumar, V A, Mondal, N C and Ahmad, S. (2020). Identification of Groundwater Potential Zones Using RS, GIS and AHP Techniques: A Case Study in a Part of Deccan Volcanic Province (DVP), Maharashtra, India, Journal of the Indian Society of Remote Sensing. https://doi.org/10.1007/s12524-019-01086-3.

Magesh, N.S., Chandrasekar, N., and Soundranayagam, J.P. (2012). Delineation of groundwater potential zones in Theni district,Tamil Nadu, using remote sensing, GIS and MIF techniques. Geosci. Front. 3, 189–196.

Mohammadi-Behzad, H.R., Charchi, A., Kalantari, N., Mehrabi Nejad, A., and Karimi Vardanjani, H. (2018). Delineation of groundwater potential zones using remote sensing (RS), geographical information system (GIS) and analytic hierarchy process (AHP) techniques: a case study in the Leylia–Keynow watershed, southwest of Iran. Carbonates Evaporites. https://doi.org/10.1007/s13146-018-0420-7.

Muralitharan, J., and Palanivel, K. (2015). Groundwater targeting using remote sensing, geographical information system and analytical hierarchy process method in hard rock aquifer system, Karur district, Tamil Nadu, India. Earth Sci. India 8 (4), 827–842. http://doi.org/10.1007/s12145-015-0213-7.

Nag, S.K. and Ghosh, P. (2012). Delineation of groundwater potential zone in Chhatna Block, Bankura District, West Bengal, India using remote sensing and GIS techniques. Environ Earth Sci: 1–13. doi:10.1007/s12665-012-1713-0.

Pandian, M., and Kumanan, C.J. (2013). Geomatics approach to demarcate groundwater potential zones using remote sensing and GIS techniques in part of Trichy and Karur district, Tamilnadu, India. Arch Appl Sci Res 2013 5(2):234–240.

Preeja, K.R., Sabu, J., Jobin, T., and Vijith, H. (2011). Identification of groundwater potential zones of a tropical river basin (Kerala, India) using remote sensing and GIS techniques. J Indian Soc Remote Sens 39(1):83–94. doi:10.1007/s12524-011-0075-5.

Rao, Y.S., Jugran, D.K. (2003). Delineation of groundwater potential zones and zones of groundwater quality suitable for domestic purposes using remote sensing and GIS. Hydrological Sciences-Journal-des Sciences Hydrologiques 48, 821–833.

Saaty, T. L. (1990). How to make a decision: The analytic hierarchy process? European Journal of Operational Research, 48, 9–26.

Saranya, T. and Saravanan, S, (2020). Groundwater potential zone mapping using analytical hierarchy process (AHP) and GIS for Kancheepuram District, Tamilnadu, India, Modeling Earth Systems and Environment, https://doi.org/10.1007/s40808-020-00744-7.

Shekhar, S., and Pandey, A.C. (2014). Delineation of groundwater potential zone in hard rock terrain of India using remote sensing, geographical information system (GIS) and analytic hierarchy process (AHP) techniques. Geocarto Int 30(4):402–442.

Sinha, R, Gupta, Surya and Nepal, Santosh, (2018). Groundwater dynamics in North Bihar plains, Current science, 114(12), 2482-2493.

Siva, G., Nasir, N., and Selvakumar, R. (2017). Delineation of groundwater potential zone in sengipatti for thanjavur district using analytical hierarchy process. IOP Conf. Ser. Earth Environ. Sci. 80, 012063.

Subba, R. N., Chakradhar, G.K.J., and Srinivas, V. (2001). Identification of groundwater potential zones using remote sensing techniques in and around Gunur town, Andhra Pradesh, India. J Indian Soc Remote Sens 29:69–78.

*IN PROCEEDINGS OF 25th HYDRO 2020, INTERNATIONAL CONFERENCE, NATIONAL INSTITUTE OF TECHNOLOGY ROURKELA, ODISHA, INDIA 26-28, March 2021, ISBN 978-93-90631-56-8*

Paper ID - 241

# Investigation on submarine groundwater discharge (SGD) and Saltwater intrusion (SWI) zones along Mangaluru to Udupi coast

Dr. Ramesh H [1], Sunilkumar P S [2*], Vijay Suryawanshi [3]

[1]*Associate Professor, Dept. of Water Resources and Ocean Engineering, National Institute of Technology Karnataka (NITK), Surathkal, Mangalore-575025, India.*

[2* & 3]*Ph.D. Research Scholar & Junior Research Fellow, Dept. of Water Resources and Ocean Engineering, National Institute of Technology Karnataka (NITK), Surathkal, Mangalore-575025, India.*

*Corresponding author, Email: sunilkumarpscivil36@gmail.com*

*Mobile No.: +918660577407*

## Abstract

Submarine groundwater discharge (SGD) is a complex hydrogeological phenomenon it describes the exchange of fresh and recirculated saline groundwater from coastal aquifers into the ocean. The increase of population and rapid changes in urbanization, industries in coastal areas, and The increase of population and rapid changes in urbanization, industries in coastal areas, and its release of sewage recharged into coastal groundwater. This outflow of the Contaminated submarine groundwater pathway for transport of various chemical substances such as nutrients, metals, organic compounds to the marine environment. Hence, the identification and flux quantification of SGD in coastal regions is important. The main focus of this study is the identification and potential mapping of SGD zones using archival research and field-based in-situ sampling along with Mangalore to Udupi coast. The field-based water sampling measurement of well water, pore water, and seawater have been done using Hanna multi water quality parameter sensor instrument. The measured water quality parameters are pH. EC, Salinity, TDS, Temperature, and DO. these parameters have been processed, interpreted, and mapped by using IDW and Topo raster interpolation tool using ArcGIS platform. From the results, it reveals that the SGD zones 1 to 7 have observed freshwater with lower groundwater table concerning Mean sea level (MSL) and higher GWL more than 7.5m concerning MSL and also less than 32PPT of salinity in pore water samples are susceptible to SGD. Similarly, Saltwater intrusion zones (SWI) 1 to 16 have observed higher water quality parameter values like EC (> 1000 uS/cm), Salinity (> 3 PPT), pH (> 7.6), TDS (> 800), and temperature (> 29) along with the lower value of DO (< 3 mg/lit) indicate the traces of seawater intrusion. The complete assessment of salinity and electrical conductivity is cited in the result.

***Keywords:*** *SGD zones, SWI zones, Insitu measurements, GWL, IDW and Toporaster, Porewater, EC, Salinity.*

## 1. Introduction

The importance of submarine groundwater discharge (SGD) as a source of dissolved solids and nutrients to the ocean has become increasingly recognized. Recent studies suggest that SGD derived chemical loading may rival other major sources such as rivers in many coastal areas (Moore, 1996; Bugna et al., 1996; Palash Debnath et al., 2015). Submarine groundwater discharge is a pathway for groundwater flowing into the ocean through pores of rocks medium (terrestrial) and also across sea sand bed at the coast. The effect of discharged groundwater as SGD influence on coastal environment and its chemistry. For example, nutrients, metals, and nitrogen loading into ocean environments can result in eutrophication, which can lead to an effect on available oxygen content, lead to an algal bloom, kills fish, and also affects flora (Valiela et al., 1992; Slomp and Van Cappellen, 2004). Another major problem over a coastal area is seawater intrusion. Nowadays seawater intrusion (SWI) rapidly increasing in coastal areas due to the over-extraction of freshwater from coastal aquifers (Lathashri and Mahesha 2015, 2016; Mahesha and Lakshmikant 2014) which is due to the demand for water (drinking, agriculture, and industries) from the increased population of coastal communities. Seawater intrusion is the movement of seawater towards the landmass and mixing with the freshwater aquifers and makes aquifers unfit for drinking and other urge demands (Mahesha et al. 2012; Sathish and Elango 2015; Manivannan and Elango 2019).

Generally, SGD and SWI occur whenever the coastal aquifers are hydraulically connected with the sea and groundwater table above or below the sea level (Burnett et al. 2006; W. Al-Muqdadi and J. Merkel 2012). Further, some of the terrestrial and marine forces drive the SGD and SWI at the coast (Zektser and Dzhamalov 1981; Moore 2010). The forces are topographical elevation, the hydraulic head

difference across coastal barriers, excessive pumping (freshwater extraction), tidal fluctuation, wave setup, and land-use changes ( Corbett et al. 1999; Charette et al. 2007; Taniguchi et al. 2007; Moore 2010; Szymczycha and Pempkowiak 2016). Tidal fluctuation at the coast one of the most important marine factor which influences on SGD and SWI. During low tide, the ocean tends to charm the terrestrial coastal groundwater towards the sea as SGD, and during high tide, the ocean pushed backs saline water towards the landmass as seawater intrusion ( Li et al. 1999; Burnett et al. 2003, 2006; Post 2005; Ding et al. 2014; Tait et al. 2013; Gopalan and Chikkamadaiah 2015; Lecher et al. 2016; Suresh Babu et al. 2018). Studies confirm that 90% of the total SGD is constituted by recirculated seawater and terrestrial freshwater constitutes only 10% on a global scale (Burnett and Dulaiova 2003). But this percentage varies with seasons, the freshwater component is dominant in the monsoon season due to precipitation and recharger of groundwater (higher groundwater levels), while the recirculated SGD and SWI component increases in the summer season due to lower groundwater levels and marine forces (Moore 2010).

The submarine groundwater discharge (SGD) and Saltwater intrusion are spatially and temporarily variable components and difficult to identify its zones and flux quantification. Generally, SGD and SWI occur all over the world where the landmass is connected with the ocean. The many studies on SGD has been conducted worldwide, including Biscayne Bay, Florida (Langevin 2003), Newyork coast in america (Joseph J. Tamborski et., al, 2015), Kinvara Bay in Ireland (Margaret McCaul. et al., 2016), French Mediterranean coast (Simon Bejannin et al., 2017), coastal Gulf of Mexico (Burnett and Dulaiova 2003), Sea embayment in Tianjin (Liu et al. 2015), Western Mediterranean coast of Spain (Mejías et al. 2012), coastal karst aquifers in southern Spain (Montiel et al. 2018), A French Aquitanian coast in Western Europe (Anschutz et al. 2016), Dead sea (Akawwi et al, 2008), American east coast (Gonneea et al, 2013), Japan (Taniguchi et al. 2002; Burnett et al. 2006; Zhu et al. 2018), China (Zing et al, 2014, Yi et al, 2019 ) and Antarctica (Uemura et al, 2011) respectively using different methods such as hydraulic head variation, groundwater modelling (Numerical technique), thermal infrared remote sensing (TIRS), hydrograph separation technique, water balance equation, resistivity survey and geochemical tracers such as radon, radium and strontium, groundwater and porewater salinity and pore water temperature. Several researchers identified the seawater intrusion ( Paniconi et al. 2001; Karahanoglu and Doyuran 2003; Kim et al. 2005; Sherif et al. 2012; Mahesha and Lakshmikant 2014; Zhao et al. 2016; Najib et al. 2017).

Very few studies have been conducted on SGD on the Indian coastline. It includes the western coast of India at Kerala and Gujarat, the eastern coast at Tamilnadu and Orissa, and the northern coast of India at West Bengal. In Kerala at Kozhikode coast ( Jacob et al. 2009; Suresh Babu et al. 2009, George et al. 2018) was identified submarine groundwater discharge (SGD) zones using IR satellite imageries (for SST to identify groundwater anomalies over sea surface), in-situ groundwater, and porewater analysis (hydrochemical analysis), hydraulic head variation and electrical resistivity survey at selected points. In Tamilnadu, the presence of SGD has been conformed at Manapad, Tuticorin coast (Antony Ravindran and Ramanujam 2014) using a 2D electrical resistivity survey and also he concludes that the resistivity ranges from 31 to 174 Ohm act as a permeable pathway for freshwater discharge into the sea. The SWI and SGD zones were identified in the south part of Chennai in Tamilnad using Numerical groundwater modeling and electrical conductivity (EC) of in situ groundwater and porewater samples (Sathish and Elango 2015; Manivannan and Elango 2019). In West Bengal, the presence of SGD has been confirmed at South Pargana and East Medinipur district coast using radon ($^{222}Rn$) and porewater electrical conductivity (EC) method (Krishan et al. 2015).

Towards the west coast of India at Karnataka, most of the studies have been conducted on seawater intrusion, groundwater quality modeling for shoreline aquifers and as wells as aquifers in riverbanks of Gurupura and Nethravati, and groundwater numerical modeling, and its assessment (Mahesha et al. 2012; Mahesha and Lakshmikant 2014; Sylus and Ramesh 2015; Lathashri and Mahesha 2015a; b). very little information available on SGD in the coastline of Karnataka (Malavika and Ramesh H 2019). Hence, The present study was carried out to recognize potential zones of submarine groundwater discharge (SGD) and saltwater intrusion (SWI) between Mangaluru to Udupi coast using archival data (groundwater level and water quality) and in-situ hydrochemical analysis of groundwater and porewater samples.

## 2. Study area

Study area situated within the coast and near the shoreline of the western coast of India between Mangaluru to Udupi of Karnataka state. length of the study area on the coastline is about 65 km and lies between 12° 40' to 13° 30' North latitude and 74° 20' to 75° 50' East latitude. the study area receives an annual rainfall of around 4000 mm (CWC) and experiences the max. temperature 35 °C in summer and a minimum of 28 °C In winter . the coastline is bounded between in east western ghat with dense biodiversity and also the origin for many west-flowing rivers namely, Nethravati, Gurupur, Pavanje, Udyavara, Sita river and the unpolluted Arabian Sea in the west. The shoreline has a sandy and rocky type of nature and a downward gradient from east to west. The coastline of the study area is comprised of alluvial soil, red soil, laterite soil, and forest loamy soil that often with a medium grain, sand, clay, and gravels. some parts of the coastline of the study area are quite dynamic with dense geomorphology and high landforms. The commonly seen landforms like a pit, bar, tidal flat, dune flood plain, ridges, and these landforms are destroyed or created within a few years by different geomorphic processes.

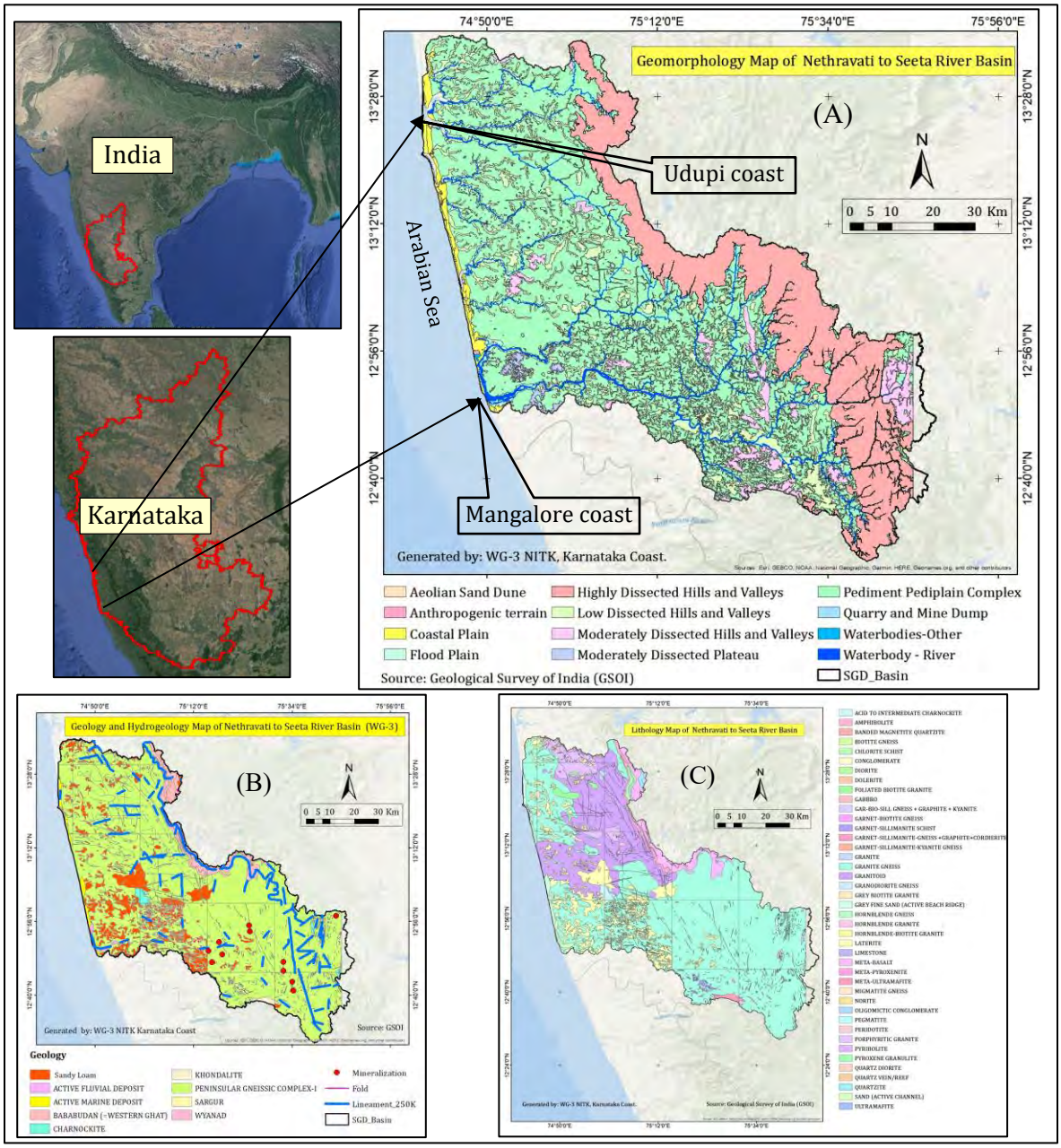



**Figure 1** (A) Location of study area between Mangaluru to Udupi coast and geomorphology of the basin, (B) geology and hydrogeology map of the study area, and (C) lithology map.

## 3. Materials and methods

For the successful completion of this study, archival research is one of the important techniques. Archival research is a method of collecting data from different sources (primary, secondary, and tertiary) that already exist. Here, in this study Archival data's such as Groundwater level, Rainfall, Water quality, Satellite imageries, Toposheet, Geology & Hydrogeology, Taluk & coastal Village boundaries were collected from various organizations like Central Ground Water Board (CGGB), State Ground Water Board (SGWB), Water Resources information Systems (WRIS), Indian Meteorological Department (IMD), Geological Survey of India (GSOI), Survey of India Nakshe portal, (SOI), Earth Explorer (USGS), Earth data and Bhuvan platform. For the analysis, A total of 19 years (2000-2019) Groundwater level (GWL) data of Udupi and Dakshina Kannada district has been used for both summer (Jan-March) and post-monsoon (Oct-Dec) season. Data were used to delineate groundwater level contour thought out the study area. 0.5-degree rainfall gridded data was collected from the National Datacenter, IMD, Pune from 1971 to 2005. And also district-wise precipitation data (Dakshina Kannada & Udupi) was collected from WRIS and IMD from 1998 to 2018. The year 2000 to 2016 averaged water quality parameter data was collected from WRIS and CGWB and It is been included average water quality parameters such as pH, EC (µmhos/cm), SAR, RSC, CHLORIDE, CA, MG, BICARBONATE, SULPHATE, FLUORIDE, TOTAL ALKALINITY, NITRATE, K, NA, CARBONATE, FE, TH. Aster DEM 30 m resolution and Landsat 8 satellite images were collected from the earth explorer and Bhuvan platform for different periods from 2014 to 2019. Here, Dem has been used to extract the elevation of the well location to the conversion of groundwater level meter below ground level to Above Mean Sea Level (AMSL) and Satellite imageries have been used to preparation of sea surface temperature to identify the groundwater anomalies over the sea surface.

The methods adopted to investigate submarine discharge and Saltwater intrusion zones in the study area are (i) water table elevation identification (groundwater gradient) and water quality analysis using collected groundwater level from Central Ground Water Board (CGWB) and (ii) *in situ* hydrochemical analyses of water samples and electrical conductivity measurements in coastal wells and as well of pore water samples.

For identification of water table elevation, 2014 and 2018 (Summer and Post monsoon) groundwater level data were considered. Water table elevation w.r.t. mean sea level has been calculated using extracted elevation from Digital Elevation Model (DEM) for a respective well location for 2018 groundwater level (Summer and Post monsoon). Groundwater contours for both summer and post-monsoon were plotted by interpolating the groundwater level (2018) values through Inverse Distance Weighted (IDW) interpolation using the Geostatistics module in ArcGIS to identify the hydraulic gradient of the region. Water quality data (CGWB) were used for the analysis of various physicochemical parameters (e.g., pH, EC, Chloride, Temperature, and D.O) to understand the seasonal changes in water quality for beach face wells. These seasonal changes in physicochemical parameters can help us to suspect the location of SGD or saltwater intrusion.

Consequent to the archival data analysis, detailed hydrological and hydro-chemical surveys are necessary to characterize the coastal aquifers. The common approach for local to regional scale estimation of groundwater discharge into the sea is based on naturally-occurring geochemical tracers (Burnett et al., 2006). An advantage of groundwater tracers is that they present an integrated signal as they enter the marine water via, various pathways in the aquifer (Burnett et al., 2006). A Hydrochemical study exposes the water quality by measuring the concentration of parameters and comparing them with the different water samples and water quality standards.

Here in this study to assess SGD and SWI, the detailed water sampling investigations were carried at 1km intervals along with Nethravati mouth (Mangalore coast) to the Udyavara River (Udupi coast). Different Water samples like Well water, Porewater, and Seawater have been collected from coastal wells, Porewater samples (below beach sand), and ocean (Spring, etc.,) during pre-summer (Jan-2020). The collected water samples (well water, Porewater, and seawater ) and its physio-chemical parameters such as temperature, pH, salinity, EC, dissolved oxygen, TDS, ORP, and Seawater sigma have been tested instantly using a portable multi-parameter water quality analyzer. Measurement Porewater samplings have been done during low tide that is less than 1.0 m wave height. Similarly, the well water

collected and its been measured morning time during high tide and also recorded basic details namely Latitude, Longitude, Locations, type of well, and depth of water table. the salinity of well-water, Porewater, and seawater has been measured instantly in the field using Salinity Refractometer. Groundwater samples have collected carefully using a polyethylene bottle at every 5 km interval along the study area. Collected water Bottles were stored at minimum temperature to be testing.




**Figure 2** (A) showing well water, Porewater, and seawater locations, (B) measurement of groundwater table for coastal well, (C) water quality parameters measurement using Hanna water quality parameters sensor instrument, (C) measurement of groundwater salinity using a refractometer, (D) collection of porewater samples using push point sampler with syringe tube.

### *3.1 Identification of SWI and SGD zones*

The analysis of the in-situ Hydrochemical parameters and archival data has been used to identify the saltwater intrusion (SWI) and submarine groundwater discharge (SGD) zones in Coastal wells. It is found that SGD and SWI are specially and temporally variable during both the seasons i.e. summer and monsoon. Study results point out that the seawater intrusion and Submarine groundwater discharge takes place at coastal wells during summer and winters due to topographical elevation, changes in the hydraulic head, density difference (Water), and other marine forces (tides). The following criteria are used to identify the SGD and SWI zones in the study area (Table 1 & Table 2).

**Table 1** Criteria for identification of Submarine Groundwater Discharge (SGD) zones.

| Water Samples | pH | EC uS/cm | TDS Mg/lit | Salinity | Temperature | Groundwater Table (AMSL) |
|---|---|---|---|---|---|---|
| Porewater | 6.5 to 7.8 | < 1000 | < 800 | < 32 PPT | < 29 | |
| Seawater | 7 to 8.1 | < 35000 | < 15000 | < 32 PPT | < 30 | |
| Groundwater (Wells) | 6 to 8.5 | 0 to 1000 | 200 to 600 | 0 to 0.5 | < 29 | > 7.5 m |

**Table 2** Criteria for identification of Saltwater intrusion (SWI) zones.

| Water Samples | pH | EC uS/cm | TDS Mg/lit | Salinity PPT | Temeprtaure | Groundwater Table (AMSL) |
|---|---|---|---|---|---|---|
| Groundwater (Wells) | 7.2 – 8.5 | >1000 | > 800 | > 2 | > 29 | < 2.5 m |
| Porewater | 7 to 8.1 | < 35000 | < 15000 | >32 PPT | < 30 | |

The wells having higher water quality parameters value of EC (> 1000 uS/cm), Salinity (> 3 PPT), pH (> 7.6), TDS (> 800), and temperature (29) along with the lower value of DO (< 3 mg/lit) indicate the traces of seawater intrusion. And also considering the water table, the wells having a < 2.5m groundwater level gradient with reference to above Mean sea level can be suspected to be SWI zones. Here contrary to this, in this study, some wells have recorded higher EC, TDS, Salinity, Temperature, and most prominently have the groundwater level up to 7.8 m concerning the mean sea level. This condition is aroused because prolonged SWI has led to the recharge of the coastal wells.

Similarly, the SGD condition is vice versa to the SWI. Generally, SGD occurs based on the GWL difference and marine forces along the coastline. The wells having 1) freshwater with lower groundwater table concerning Mean sea level and higher GWL more than 7.5m with reference to MSL, 2) and also less than 32PPT of salinity in pore water are susceptible to SGD.

Considering all the above factors and Hydrochemical chemical analysis, both the SWI & SGD zones have been characterized. This can be summarized in table 3.

## 4. Results and Discussion

### *4.1 Aquifers 3D Visualization*

3D volume model can enhance the visual interpretation and understanding of the complex subsurface settings of different geological units as well as the hydraulic strata. This type of representation also helps the non-professionals to get ideas about the subsurface complexity. From the volume model, each of the layers is individualized using their spatial properties and therefore volumes can be calculated to estimate the water availability in each layer. One of the important requirements in groundwater management is to know how much water is available in the subsurface of an area. Usually, to calculate this, the volume of water-bearing strata is generalized from thickness and area. But the model provides the layer volume considering the geological settings and variable thickness of the layers and visually allows visualization of the relationship with the other units.

The boundary of the study area was taken as the Arabian Sea in the west, and western ghat in the east, Ullal in the south, and Udupi in the north. The Electrical Resistivity Tomography (ERT) and borehole data (Geological Survey of India (GSOI) - 2018) show that the depth of bedrock from the surface falls between 20-35m. ERTs prepared from the resistivity survey across Mangalore city represent that the Sand layer has recorded the higher resistivity values 1295 ohm-m, clay 55 ohm-m, the highly weathered rock 55 ohm-m, and weather rock 194 ohm-m. further, The borehole data confirmed the presence of sand (0-6 m), clay sand (6-12), laterite (12-18), lateritic clay (18-25m), weathered rock, fractured rock, and the massive hard bedrock (>25m).

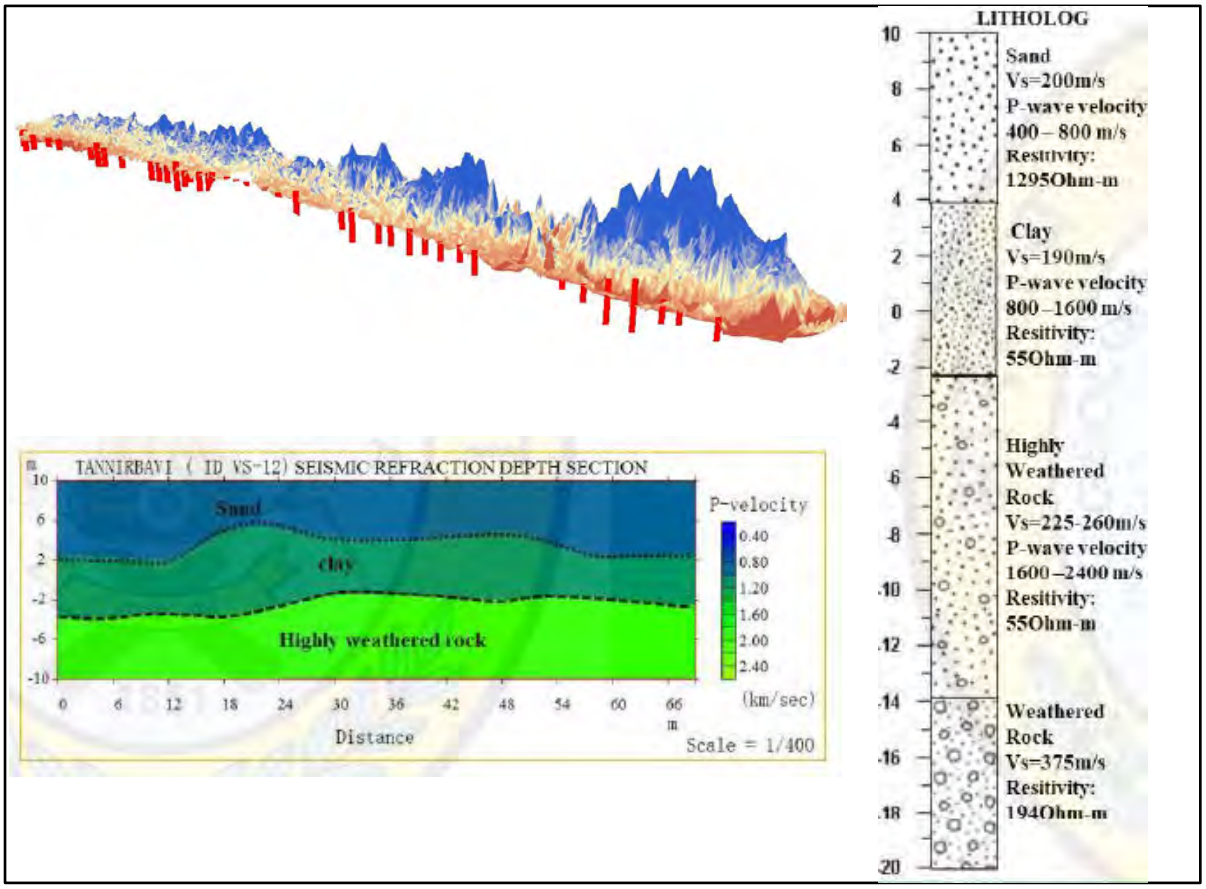



**Figure 3** Borehole lithology of the study area. (Geological Survey of India (GSOI) - 2018)

### *4.2 Monthly Rainfall*

Rainfall is spatially and temporally distributed over the study area for a period of 35 years (1971 to 2005). From the rainfall trend analysis, it reveals that during summer (Jan to April ) western ghat receives normal rainfall of about 125 mm to 2203.29 mm as compared to the coastline and mid part of the study area receives least rainfall 10 mm to 1250 mm. Similarly in monsoon, coastline and mid part of the study area except western ghat receives maximum rainfall was about 6000 mm to 54518.75 mm (sum of monthly rainfall for 35 years). western ghat receives only 2500 mm to 17000 mm rainfall for the entire 35 years. Further, the north part of the study area (Udupi. Karkala, and Moodbidre) receives maximum rainfall was about 475 mm to 16634 during post-monsoon (October to December). In post-monsoon, western ghat and coastlines receives less rainfall.

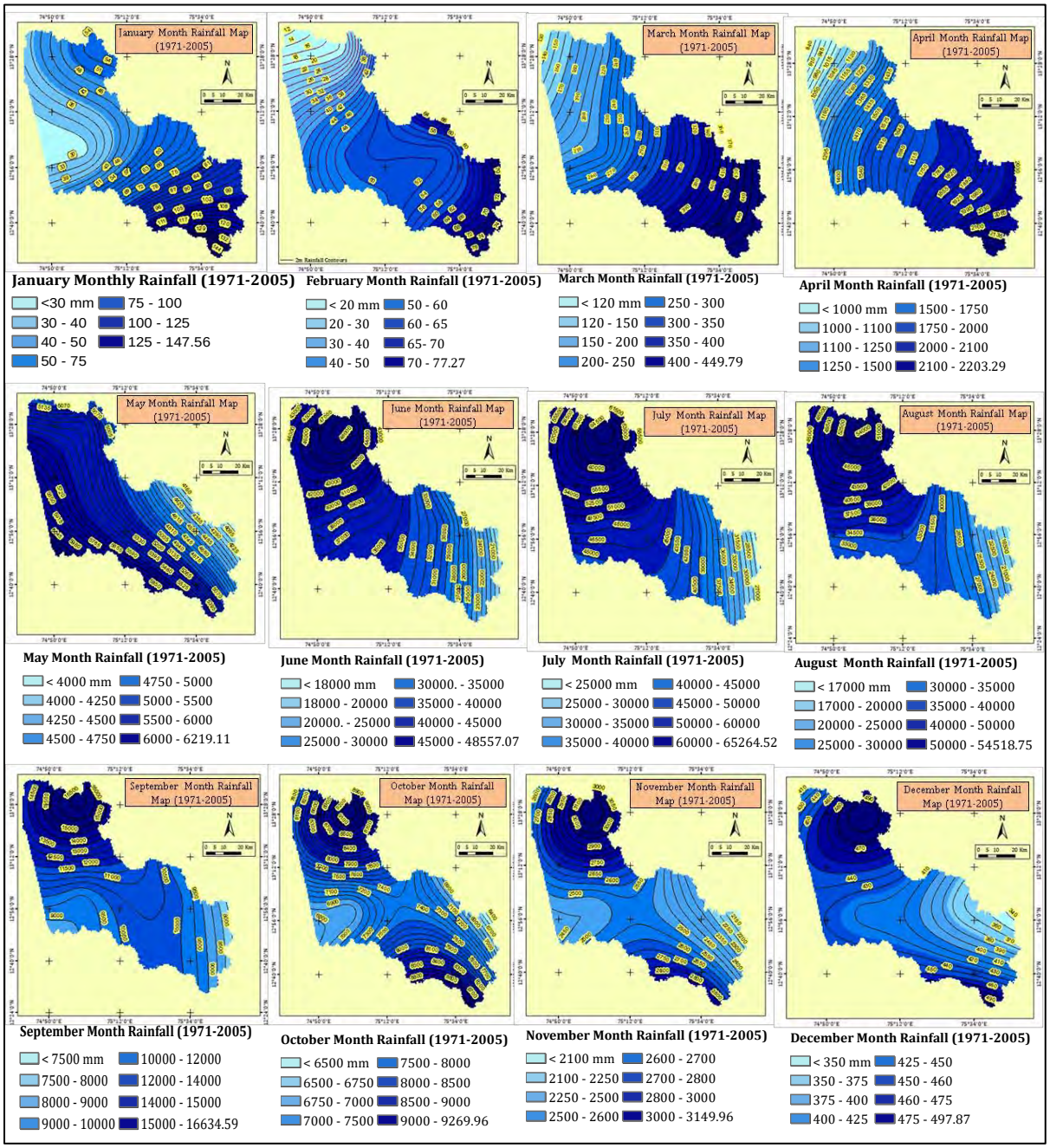



**Figure 4** Sum of monthly rainfall variation across the study area for the period of 35 years (1971 to 2005)

### *4.3 Groundwater Table*

Detection of the hydraulic head at different sampling points using GPS and collected groundwater level data from CGWB helped in delineating the hydraulic gradient for Mangalore to Udupi coast (Fig.4) in a catchment scale and also coastal micro watershed scale. A higher gradient was noticed in the region Tannir bhavi, Surathkal Hejamadi, Padubidri, Tenka, Mattu, and maple beach from collected CGWB GWL data (2018). Similarly, the lower hydraulic head was noticed in the region of Bengre circle, Menna kalli, Shashihitlu, Nadsala, Utpadi, and Shanti Nagar. The hydraulic gradient varied between -1.2 m to 17m concerning Mean Sea Level (MSL). Tannir bhavi, Hosabettu, Surathkal, Hejamadi, Tenka, and Bada showing a downward trend towards the sea which marks the potential zone of groundwater discharge. The flow of coastal groundwater from coast to the sea occurring from a higher gradient to lower gradient has been identified as potential zones of Submarine groundwater discharge (SGD) at six locations namely Tannir bhavi, Hosabettu, Surathkal, Hejamadi, Tenka, and Bada. Fig. 5 shows the suspected location of saltwater intrusion and submarine groundwater discharge zones of the study area.

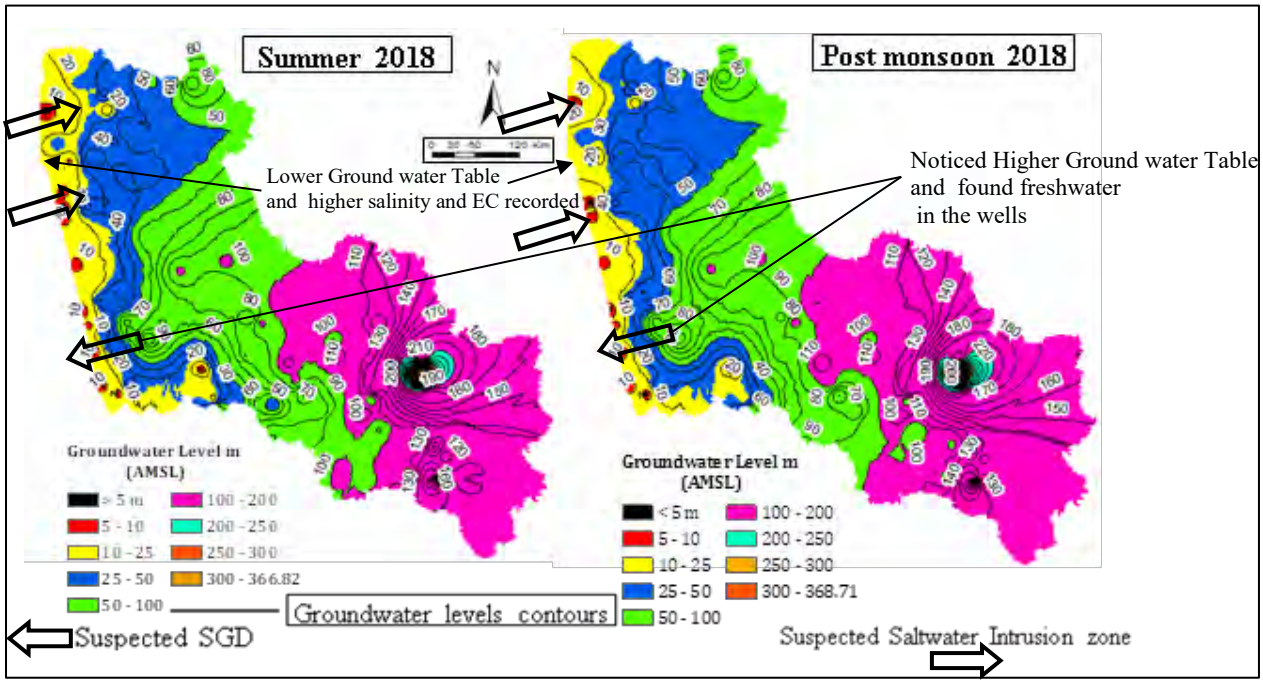



**Figure 5** shows the suspected location of saltwater intrusion (SWI) and submarine groundwater discharge (SGD) zones.

### *4.4 Groundwater (Salinity, and EC) Assessment*

From the in-situ water quality measurements of groundwater 53 wells were carried out during Summer 2020. 28 wells were identified with salinity higher than 2 PPT, 18 were identified with EC higher than 700 uS/cm, and similarly, 10 wells were identified with TDS higher than 400 mg/lit. all these wells are located to the shoreline and beach face wells. Among the 28 saline wells, 2 wells are located on the Panambur coast, another 10 wells are located between Shashitlu to Padubidri coast, and the remaining saline wells are found between Padu to Shanti Nagar (maple beach) showing the locations of ingression in summer. The presence of tidal inlets and Udyavaer River (Running parallel to the coast and gets saline during summer) at Padu to Shantinagar coast is responsible for the higher salinity in the wells. But the region Tannirbhavi, Hosabettu, Surathkal, Hejamadi, Tenka, and Bada coast wells recorded salinities below 2 PPT, <800 EC, and <400TDS suggesting the presence of freshwater discharging to the coast. Further, it is cross-examined with images obtained through interpolation of water table

elevation from CGWB groundwater level data and obtained through GPS and they matched the potential locations of SGD and SWI zones.

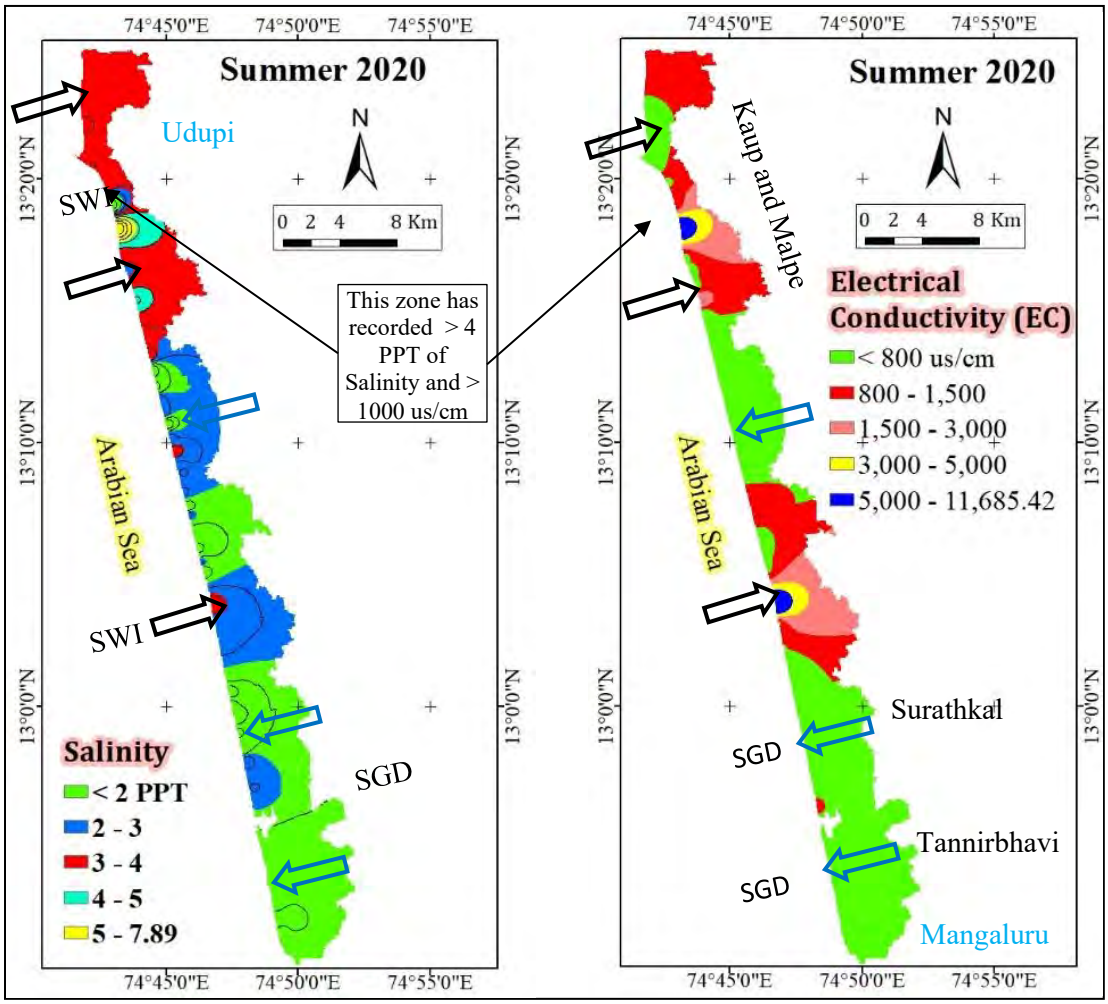



**Figure 6** In situ groundwater (a) Salinity, and (b) Electrical Conductivity variations from Mangalore to Udupi coast.

### *4.5 Groundwater and Porewater temperature assessment*

From the in-situ Temperature measurements of groundwater and porewater samples, the survey was carried out in 53 locations during Summer 2020. Most of the porewater location temperature were identified higher than 28 °C, and the same temperature observed in the groundwater samples for the place Malpe Shantinagar, Kaup, Shashihitlu, Padubidri, Tenka, and Bada at the same time these locations have recorded higher EC and Salinity it indicates the presences of saltwater intrusion. Similarly, Surathkal, Tannirbhavi, Hejmadi, and Padu location has observed lesser groundwater temperature than porewater temperature and the hydraulic gradients (Water table) of these locations is higher concerning mean sea level and there is a chances groundwater discharging to seas due to higher groundwater level gradient.

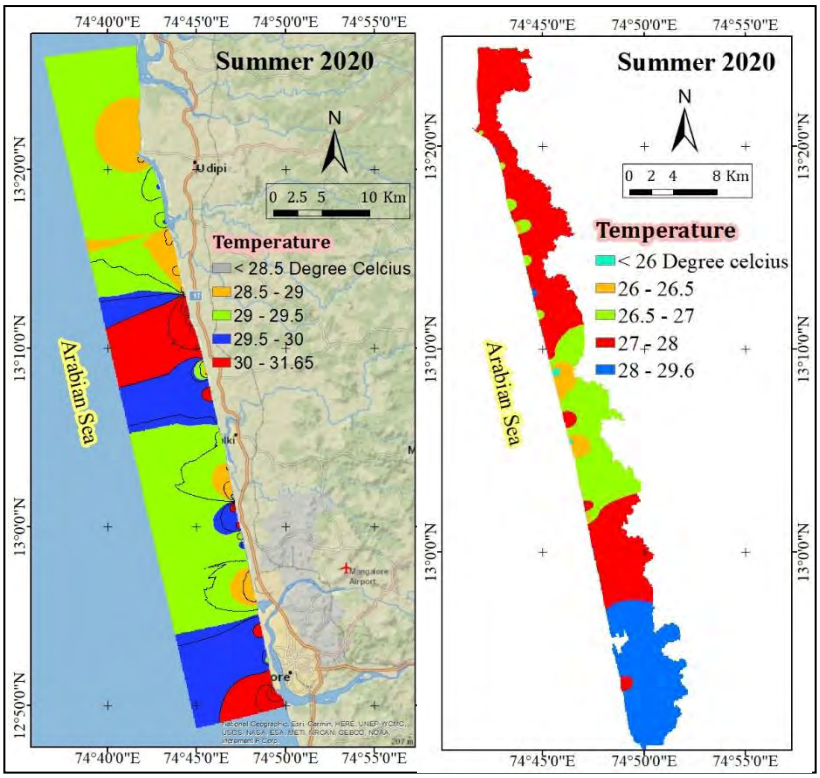



**Figure 7** In-situ groundwater and Porewater temperature variation from Mangalore to Udupi coast

### *4.6 Suspected SGD and SWI zones*

Considering the assessment of the groundwater table, salinity, electrical conductivity, and temperature of porewater and groundwater samples following zones have been identified. Figure 8 and Table 3 shows the details about zones.

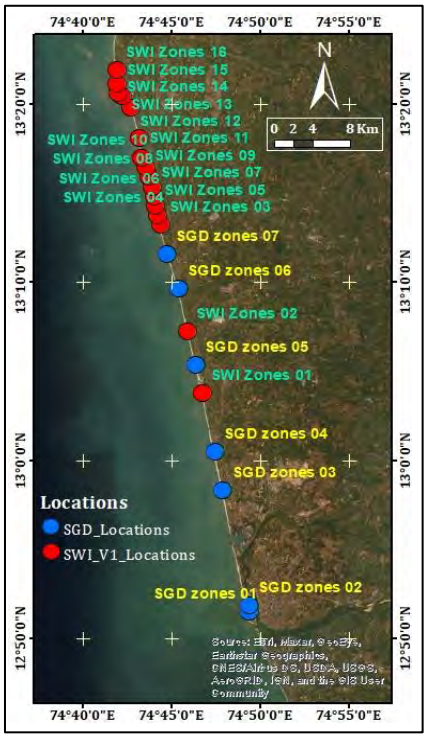



**Figure 8** SGD and SWI zones along the study area

**Table 3** Details of suspected SGD and SWI zones

| Sl. No. | Location | Well Nos. | Latitude | Longitude | Zones | Justifications |
|---|---|---|---|---|---|---|
| 01 | Shashihitlu 4 | WW-22 | 13.0637194 | 74.77885833 | SWI 1 | These wells have been recorded higher water quality parameter values like EC (> 1000 uS/cm), Salinity (> 3 PPT), pH (> 7.6), TDS (> 800), and temperature (29) along with the lower value of DO (< 3 mg/lit) indicate the traces of seawater intrusion. |
| 02 | Padubidri 1 | WW-27 | 13.1217056 | 74.76497778 | SWI 2 | |
| 03 | Padu 1 | WW-39 | 13.2211278 | 74.73930278 | SWI 3 | |
| 04 | padu 2 | WW-40 | 13.2297528 | 74.73662778 | SWI 4 | |
| | polipu 1 | WW-41 | 13.2387389 | 74.7346 | SWI 5 | |
| 05 | polipu 2 | WW-42 | 13.2472972 | 74.73372222 | SWI 6 | |
| 06 | kaiparjal | WW-43 | 13.2564583 | 74.73123611 | SWI 7 | |
| 07 | mattu 1 | WW-44 | 13.2653639 | 74.72861111 | SWI 8 | |
| 08 | mattu 2 | WW-45 | 13.2749694 | 74.72520833 | SWI 9 | |
| 09 | Udyavara 1 | WW-46 | 13.2834528 | 74.72185 | SWI 10 | |
| 10 | Udyavara 2 | WW-47 | 13.3019778 | 74.7194 | SWI 11 | |
| 11 | Utpadi 2 | WW-49 | 13.3306556 | 74.71148889 | SWI 12 | |
| 12 | Paduke | WW-50 | 13.3413083 | 74.70311389 | SWI 13 | |
| 13 | Shantinagar | WW-51 | 13.3438694 | 74.69988056 | SWI 14 | |
| 14 | Malpe Beach 1 | WW-52 | 13.3526083 | 74.698925 | SWI 15 | |
| 15 | Beach 2 (Udupi) | WW-53 | 13.3648972 | 74.698575 | SWI 16 | |
| 16 | Bengre circle | WW-02 | 12.8593889 | 74.82339167 | SGD 1 | Porewater salinity of these two locations was found less than 32 PPT. |
| 17 | Bengre kasaba | WW-03 | 12.8653222 | 74.82260278 | SGD 2 | |
| 18 | Hosabettu | WW-12 | 12.9732 | 74.79825 | SGD 3 | These wells are found higher water table elevations concerning MSL and freshwater well also. There is a chance of SGD. A detailed investigation has to be carried out. |
| 19 | Surathkal | WW-16 | 13.00895 | 74.79071667 | SGD 4 | |
| 20 | Hejamadi 2 | WW-24 | 13.0902917 | 74.77258333 | SGD 5 | |
| 21 | Tenka 2 | WW-32 | 13.1611417 | 74.75634722 | SGD 6 | |
| 20 | Bada 4 | WW-36 | 13.19365 | 74.74528611 | SGD 7 | |
| | **SWI:** Saltwater Intrusion | | **SGD:** Submarine Groundwater Discharge | | | |

## 4.7 Conclusions

Identification and potential mapping of SGD zones was an attempt from Mangalore to Udupi coast using archival research and field-based in-situ analysis. the primary and secondary data sets like GWL, water quality parameters, Rainfall, DEM, and all Hydrogeological layers have been collected from CGWB, WRIS. The field measurement of well water, pore water, seawater has been done using Hanna multi water quality parameter sensor instrument. The measured water quality parameters such as pH, EC, Salinity, TDS, Temperature, and DO have been processed, interpreted, and mapped by using IDW and Topo raster interpolation tools in the ArcGIS platform.

The wells having the higher water quality parameters values of EC (> 1000 uS/cm), Salinity (> 3 PPT), pH (> 7.6), TDS (> 800), and temperature (29) along with the lower value of DO (< 3 mg/lit) indicate the traces of seawater intrusion. And also considering the water table, the wells having a < 2.5m groundwater level gradient regarding above Mean sea level can be suspected to be SWI zones. Here contrary to this, in this study, some wells have recorded higher EC, TDS, Salinity, Temperature, and

most prominently have the groundwater level up to 7.8 m concerning the mean sea level. This condition has aroused because prolonged SWI has led to the recharge of the coastal wells. Similarly, the SGD condition is vice versa to the SWI. Generally, SGD occurs based on the GWL difference and marine forces along the coastline. The wells having 1) freshwater with lower groundwater table concerning Mean sea level and higher GWL more than 7.5m concerning MSL,2) and also less than 32PPT of salinity in pore water are susceptible to SGD.

From the results, it reveals that The pH of the groundwater and porewater is slightly acidic to neutral. the pH of the groundwater is higher than the porewater. the Well Water (WW) 22, WW27, WW 39, WW 40, WW 41, WW 42, WW 43, WW 45, WW 46, WW 47, WW 48,WW 49, WW 50, WW 51, WW 52 and WW 53 has recorded higher Electrical Coducitivy (EC) (> 1000 uS/cm), Salinity (> 3 PPT), pH (> 7.6), TDS (> 800), and temperature (29) along with the lower value of DO (< 3 mg/lit) indicate the traces of seawater intrusion. Similarly, WW 02, WW 03, WW12, WW 16, WW 24, WW 32, and WW-36 found freshwater with lower groundwater table concerning Mean sea level and higher GWL more than 7.5m concerning MSL and also less than 32PPT of salinity in pore water are susceptible to SGD. In the northern part of the study area (Udupi), the electrical conductivity and salinity of the groundwater is higher and indicates the presence of seawater intrusion. Initially, Archival research and in-situ analysis was the better method for identification of SGD and SWI zones along the coastline. A further detailed investigation has to be done in the above-identified location to quantify SGD flux and the nutrients discharging to the coastal ecosystem.

## Acknowledgments

We thank the National Centre for Earth Science Studies (NCESS ) - Ministry of Earth Science (MoES) and National Institute of Technology Karnataka (NITK) for providing research facilities and funds. Thanks, are also due to the Dept. of Water Resources and Ocean engineering staff members (JRF and supporting staff), of NITK for their assistance and support all through the work and especially in the field.

## References

Anschutz, P., Charbonnier, C., Deborde, J., Deirmendjian, L., Poirier, D., Mouret, A., Buquet, D., and Lecroart, P. (2016). “Terrestrial groundwater and nutrient discharge along the 240-km-long Aquitanian coast.” *Mar. Chem.*, 185, 38–47.

Antony Ravindran, A., and Ramanujam, N. (2014). “Detection of submarine groundwater discharge to coastal zone study using 2d electrical resistivity imaging study at Manapad, Tuticorin, India.” *Indian J. Mar. Sci.*, 43(2), 224–228.

Burnett, W. C., Aggarwal, P. K., Aureli, A., Bokuniewicz, H., Cable, J. E., Charette, M. A., Kontar, E., Krupa, S., Kulkarni, K. M., Loveless, A., Moore, W. S., Oberdorfer, J. A., Oliveira, J., Ozyurt, N., Povinec, P., Privitera, A. M. G., Rajar, R., Ramessur, R. T., Scholten, J., Stieglitz, T., Taniguchi, M., and Turner, J. V. (2006). “Quantifying submarine groundwater discharge in the coastal zone via multiple methods.” *Sci. Total Environ.*, 367(2–3), 498–543.

Burnett, W. C., Bokuniewicz, H., Moore, W. S., and Taniguchi, M. (2003). “Burnett_2003_Biogeochemistry.pdf.” *Biogeochemistry*, 66, 3–33.

Burnett, W. C., and Dulaiova, H. (2003). “Estimating the dynamics of groundwater input into the coastal zone via continuous radon-222 measurements.” *J. Environ. Radioact.*, 69(1–2), 21–35.

Charette, M. A., Moore, W. S., and Burnett, W. C. (2007). “CHAPTER-5 Uranium-and Thorium- Series Nuclides as Tracers of Submarine Groundwater Discharge CHAPTER-5 Uranium-and Thorium-Series Nuclides as Tracers of Submarine Groundwater Discharge.” 234–289.

Corbett, D. R., Chanton, J., Burnett, W., Dillon, K., Rutkowski, C., and Fourqurean, J. W. (1999). “Patterns of groundwater discharge into Florida Bay.” *Limnol. Oceanogr.*, 44(4), 1045–1055.

Ding, F., Yamashita, T., Lee, H. S., and Pan, J. (2014). “A modelling study of seawater intrusion in the liao dong bay coastal plain, china.” *J. Mar. Sci. Technol.*, 22(2), 103–115.

George, M. E., Babu, D. S. S., Akhil, T., and Rafeeque, M. K. (2018). “Investigation on Submarine Groundwater Discharge at Kozhikkode Coastal Aquifer, SW Western Ghats.” *J. Geol. Soc. India*, 92(5), 626–633.

Gopalan, C. V., and Chikkamadaiah, K. (2015). “Salt Water Intrusion Impacts and Quality of Ground Water along Coastal Area from Thalapady to Kumbala, Kasaragod District, Kerala, India.”

Jacob, N., Suresh Babu, D. S., and Shivanna, K. (2009). "Radon as an indicator of submarine groundwater discharge in coastal regions." *Curr. Sci.*, 97(9), 1313–1320.
Krishan, G., Rao, M. S., Kumar, C. P., Kumar, S., and Rao, M. R. A. (2015). "A Study on Identification of Submarine Groundwater Discharge in Northern East Coast of India." *Aquat. Procedia*, 4(Icwrcoe), 3–10.
Langevin, C. D. (2003). "Simulation of Submarine Ground Water Discharge to a Marine Estuary: Biscayne Bay, Florida." *Ground Water*, 41(6), 758–771.
Lathashri, U. A., and Mahesha, A. (2015). "Simulation of Saltwater Intrusion in a Coastal Aquifer in Karnataka, India." *Aquat. Procedia*, 4(Icwrcoe), 700–705.
Lathashri, U. A., and Mahesha, A. (2016). "Groundwater sustainability assessment in coastal aquifers." *J. Earth Syst. Sci.*, 125(6), 1103–1118.
Lecher, A. L., Fisher, A. T., and Paytan, A. (2016). "Submarine groundwater discharge in Northern Monterey Bay, California: Evaluation by mixing and mass balance models." *Mar. Chem.*, 179, 44–55.
Li, L., Barry, D. A., Stagnitti, F., and Parlange, J. Y. (1999). "Submarine groundwater discharge and associated chemical input to a coastal sea." *Water Resour. Res.*, 35(11), 3253–3259.
Liu, L., Yi, L., Cheng, X., and Tang, G. (2015). "Distribution of 223Ra and 224Ra in the Bo Sea embayment in Tianjin and its implication of submarine groundwater discharge." *J. Environ. Radioact.*, 150, 111–120.
Mahesha, A., and Lakshmikant, P. (2014). "Saltwater intrusion in coastal aquifers subjected to freshwater pumping." *J. Hydrol. Eng.*, 19(2), 448–456.
Mahesha, A., Vyshali, Lathashri, U. A., and Ramesh, H. (2012). "Parameter Estimation and Vulnerability Assessment of Coastal Unconfined Aquifer to Saltwater Intrusion." *J. Hydrol. Eng.*, 17(8), 933–943.
Manivannan, V., and Elango, L. (2019). "Seawater intrusion and submarine groundwater discharge along the Indian coast." *Environ. Sci. Pollut. Res.*, 26(31), 31592–31608.
Mejías, M., Ballesteros, B. J., Antón-Pacheco, C., Domínguez, J. A., Garcia-Orellana, J., Garcia-Solsona, E., and Masqué, P. (2012). "Methodological study of submarine groundwater discharge from a karstic aquifer in the Western Mediterranean Sea." *J. Hydrol.*, 464–465, 27–40.
Montiel, D., Dimova, N., Andreo, B., Prieto, J., García-Orellana, J., and Rodellas, V. (2018). "Assessing submarine groundwater discharge (SGD) and nitrate fluxes in highly heterogeneous coastal karst aquifers: Challenges and solutions." *J. Hydrol.*, 557, 222–242.
Moore, W. S. (2010). "The effect of submarine groundwater discharge on the ocean." *Ann. Rev. Mar. Sci.*, 2(1), 59–88.
Post, V. E. A. (2005). "Fresh and saline groundwater interaction in coastal aquifers: Is our technology ready for the problems ahead?" *Hydrogeol. J.*, 13(1), 120–123.
Sathish, S., and Elango, L. (2015). "Numerical Simulation and Prediction of Groundwater Flow in a Coastal Aquifer of Southern India." *J. Water Resour. Prot.*, 07(17), 1483–1494.
Suresh Babu, D. S., Anish, M., Vivekanandan, K. L., Ramanujam, N., Nathakiri Murugan, K., and Antony Ravindran, A. (2009). "An account of submarine groundwater discharge from the SW Indian coastal zone." *J. Coast. Res.*, 25(1), 91–104.
Suresh Babu, D. S., Padmalal, D., and Purnachandra Rao, N. (2018). "Submarine groundwater discharge in the Indian context." *Curr. Sci.*, 115(12), 2197–2198.
Sylus, K. J., and Ramesh, H. (2015). "The Study of Sea Water Intrusion in Coastal Aquifer by Electrical Conductivity and Total Dissolved Solid Method in Gurpur and Netravathi River Basin." *Aquat. Procedia*, 4(Icwrcoe), 57–64.
Szymczycha, B., and Pempkowiak, J. (2016). *The Role of Submarine Groundwater Discharge as Material Source to the Baltic Sea. Role Submar. Groundw. Disch. as Mater. Source to Balt. Sea*.
Tait, D. R., Santos, I. R., Erler, D. V., Befus, K. M., Cardenas, M. B., and Eyre, B. D. (2013). "Estimating submarine groundwater discharge in a South Pacific coral reef lagoon using different radioisotope and geophysical approaches." *Mar. Chem.*, 156, 49–60.
Taniguchi, M., Burnett, W. C., Cable, J. E., and Turner, J. V. (2002). "Investigation of submarine groundwater discharge." *Hydrol. Process.*, 16(11), 2115–2129.
Taniguchi, M., Ishitobi, T., Burnett, W. C., and Wattayakorn, G. (2007). "Evaluating ground water-sea water interactions via resistivity and seepage meters." *Ground Water*, 45(6), 729–735.
W. Al-Muqdadi, S., and J. Merkel, B. (2012). "Interpretation of Groundwater Flow into Fractured Aquifer." *Int. J. Geosci.*, 03(02), 357–364.
Zektser, I. S., and Dzhamalov, R. G. (1981). "Groundwater discharge to the pacific ocean." *Hydrol. Sci. Bull.*, 26(3), 271–279.

*IN PROCEEDINGS OF 25th HYDRO 2020, INTERNATIONAL CONFERENCE, NATIONAL INSTITUTE OF TECHNOLOGY ROURKELA, ODISHA, INDIA 26-28, March 2021, ISBN 978-93-90631-56-8*

Paper ID - 242

# Surface Water Groundwater Interactions in Estimating Groundwater Recharge using Genetic Programming

Ajay[1], Chidara Nagamanikanta Sai[1] & Om Prakash[1]

*1 Department of Civil and Environmental Engineering, IIT Patna, Bihta-801103, Bihar, India*
*Email: ajayrs1013@gmail.com*

## Abstract

Groundwater constitutes a significant part of the water resources required to meet the global water demand. Unweighted usage with added uncertain climatic conditions have depleted many groundwater resources making it unsustainable for future exploitation. Groundwater depletion is one of the biggest threat to humanity's sustenance and require proper management strategy. For long groundwater has been considered as separate resource. It is well established, that groundwater continuously interacts with surface water, water mass being exchanged between the two under different hydrogeological and hydrological stress conditions. These interactions happen on small scale to over regional scale. Even the time scale of these interactions can vary from a few hours to several decades. Therefore, effective water management must consider surface water and groundwater as "connected" single resource.

Proper groundwater management of an aquifer requires accurate estimation of groundwater recharge. There are many direct and indirect methods and sophisticated models for estimating recharge. However, most of them require many field data or model parameters, which limit their actual field application. In this study groundwater interaction in estimating recharge is presented for a semiarid climatic region which gets recharged from high storm events using Genetic Programming.

Genetic Programming (GP) as an Artificial Intelligence tool for predicting groundwater level fluctuations helps us to predict future groundwater recharge for various storm events. Only when the antecedent conditions are ripe a rainfall event results in groundwater recharge. A large portion of the precipitation infiltrates into the ground and gets consumed in raising the moisture content of the soil column above the water table until saturation. Storm events that result in groundwater recharge are looked at for both diffused recharge (directly falling on the ground surface) and focused recharge (indirectly as runoff to lakes, streams and rivers) for varying antecedent conditions. Precipitation in the upstream region results in diffuse recharge and also contributes to focused recharge in the downstream region through runoff in stream. The GP models are trained using large number of realizations of rainfall and stream flow fluctuations for differing input variable scenarios. Rainfall data from both upstream and downstream regions, groundwater level data from various boreholes, stream stages and antecedent soil moisture index is used for training the GP model. These evaluated results show efficiency in predicting groundwater recharge for storm events at different hydrogeological time scales.

***Keywords:*** *Groundwater management; Groundwater Recharge; Genetic Programming; Focused Recharge; Diffused Recharge; Antecedent Conditions*

## 1. Introduction

Groundwater use is of fundamental importance to meet the rapidly expanding urban, industrial, and agricultural water requirements, particularly in (semi-)arid zones. To quantify the current rate of groundwater recharge is thus a prerequisite for efficient and sustainable groundwater resource management in these dry areas, where such resources are often the key to economic development.

Most of the sustainable management strategy (Giambastiani et al., 2012, Iverach et al., 2017) are based on zero deficit of groundwater over different time horizon i.e. the amount of water abstracted is replenished by the recharge pathways during the time period. Diffuse (areal) recharge and recharge through stream channels (or focused recharge) are the major source of groundwater replenishment (Lerner et al., 1990, Scanlon et al., 2006, Iverach et al., 2017). However, there is no well-established method to quantify individual contributions of these recharge components to the groundwater. It is also found that under varying hydrological and hydrogeological stresses groundwater may discharge into

the stream channel. Figure 1 shows the qualitative linking of groundwater with other hydrological process.

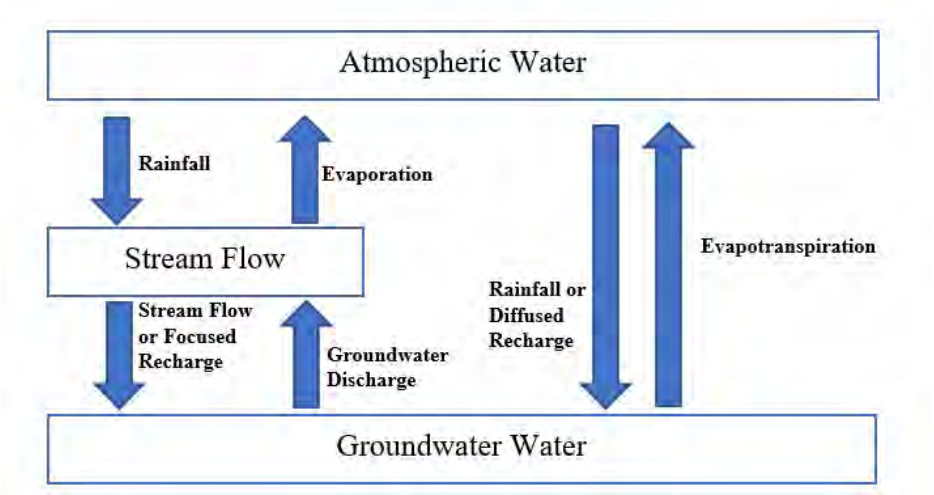



**Figure 1** Groundwater surface water interaction

Not all rainfall results in groundwater recharge. There are various hydrological (rainfall intensity, rainfall duration and rainfall frequency) and hydrogeological factors (aquifer thickness, soil type, infiltration rate, vegetative cover etc.) that have a direct bearing on groundwater recharge. Small intensity rainfall or infrequent high intensity rainfall may not push the zero-flux plane to reach the groundwater table (Freeze and Cherry, 1979, Lerner et al., 1990, Healy and Scanlon, 2010). Long dry spell could create enough moisture deficit in the unsaturated soil moisture zone that most of the rainfall is consumed in replenishing the soil moisture deficit. Hence, a lot depends on the antecedent conditions that can trigger a groundwater recharge with same intensity of rainfall. Only when the conditions are right a given rainfall incident would contribute to groundwater recharge.

River or stream flow also originates as a result of rainfall and the discharge quantum is governed by similar antecedent conditions. A river may gain from groundwater system (perennial rivers during low rainfall season) or loose to groundwater in form of focused recharge (Barlow et al., 2000, Chen and Chen, 2003, Ha et al., 2008, Maharjan and Donovan, 2016). However, under what conditions does a recharging river become a discharging river is a matter of scientific investigation and interpretation. What is even more important is the quantification of recharge/discharge as it is vital in designing a wholistic water management strategy. This study aims to understand these interactions with groundwater and determine the necessary condition in quantifiable terms that trigger groundwater recharge. The study also aims to find the quantitative contribution of focused recharge and diffused recharge especially in the context of climate change.

At present, the utilization of machine learning techniques is gaining momentum to predict accurate estimates in the field of water resources engineering. The major principle of machine learning is to learn effectively from the training set of data (either from records or experimental) provided by the user. Based on the existing literature, it was noticed that the multi gene Genetic Programming (GP) is efficient and capable to predict the behavior of different water resources problems. There is a lack of simplified solution for predicting groundwater recharge. Hence, in the present study, an attempt has been made to develop a model for predicting groundwater recharge using GP techniques.

## 2. Study Area

This study is based on field sites in the Maules Creek Catchment in northwestern New South Wales. Located on the western slopes of the Great Dividing Range, the 1,475 km$^2$ catchment is bound to the north and the east by the New England Fold Belt and the Nandewar Range (Andersen and Acworth, 2009). The Namoi River enters the study area from the south at Gins Leap Gap, which is a narrow constriction (< 2 km) of the alluvium between the low ridge of hills of Pilliga Forest and the Leard State Forest. It is believed to be controlling groundwater flow entering the catchment from the south

(Crawford et al., 2009, Giambastiani et al., 2012, McCallum et al., 2013). To the north the extent of this study ends where the Bibbla Creek enters the Namoi River. The upstream and downstream boundaries are chosen to include the government operated stream gauges at Boggabri (BOG) and Turrawan (TUR) (Figure 2).

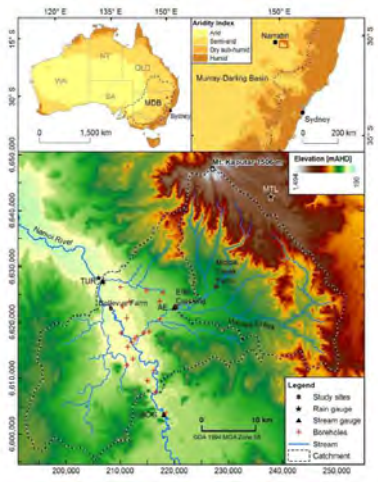



**Figure 2** Plan view of the study area (Li, 2018)

The point of highest elevation is Mt. Kaputar (1506 m) in the Nandewar Range. Away from the ridgelines, the topography is gently undulating with ground slope generally less than 10%. The topography of the alluvial plains is gently sloped from approximately 340 m AHD in the mountain front area to 230 m AHD near the Namoi River over a distance of about 20 km.

## *2.1. Rainfall in the catchment*

Daily average rainfall data from NCRIS rain gauge station at Middle Creek are analyzed to understand the rainfall pattern in the catchment. Figure 3 shows the daily cumulative rainfall at Middle Creek. Rainfall record at Middle creek starts from 6 July 2012 only.

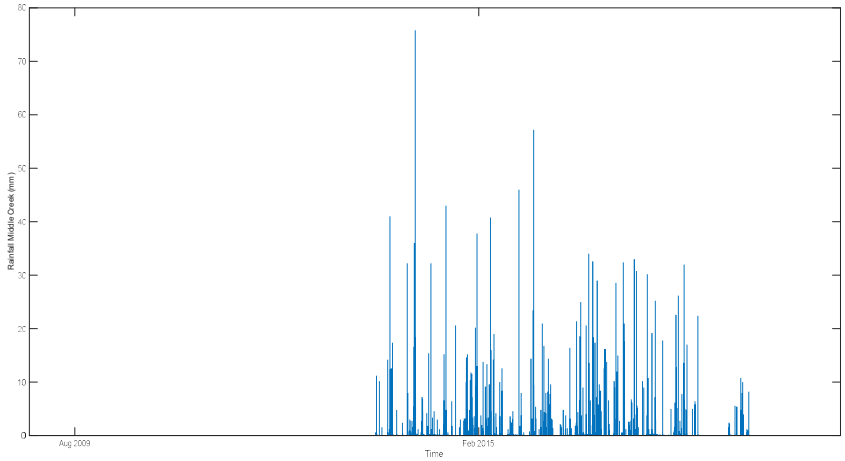



**Figure 3** Daily cumulative rainfall at Middle Creek

## *2.2. Stream Flow*

Stage in the stream in the study area is measured at Middle Creek using stilling well. The daily average stage in the stream at Middle Creek is shown in figure 4. Middle Creek which is up stream of Elfin crossing shows an ephemeral behavior. There are phases when there is no water flowing in the Middle Creek Section.

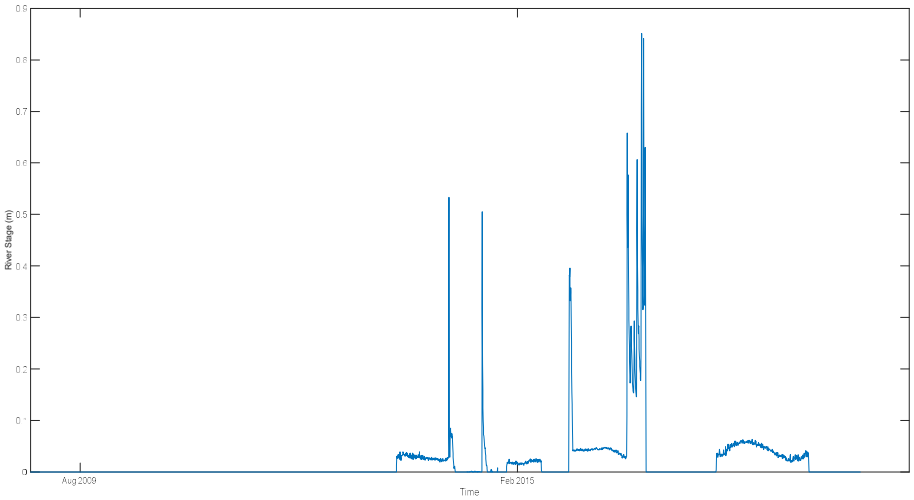



**Figure 4** River stage at Middle Creek

## 3. Groundwater Recharge Processes

It is already established that the major drivers of groundwater recharge are focused recharge from the stream, diffused recharge from rainfall and lateral groundwater movement. However, the recharge mechanism from each of these drivers differ in process and in magnitude. It is important to understand the major aspects of each of these recharge mechanism and what role each of the factors play in contributing to groundwater recharge.

### *3.1. Streamflow recharge or focused recharge*

Based on the flow in the stream it is generally categorized as ephemeral (flow for short durations) and perennial (continuous flow throughout the year). When there is no flow in the stream no groundwater recharge happens and any fluctuations in groundwater level is only caused due to lateral groundwater flow in the direction of declining hydraulic gradient. A storm event of certain proportion may cause some temporal flow in river. Some of the flowing water seeps through the river bed and percolates down to recharge the groundwater. This creates a mound due to rise in water table under the river bed which spreads laterally if there is sustained flow in the river. If a piezometer is installed near the bank of the river (Figure 5) change in the groundwater level can be noted as result of focused recharge. However, it is to be noted that the stage in the river (depth of flow) fluctuates with time and so does the amount of recharge from the stream. The most challenging aspect is to estimate groundwater recharge in such unsteady flow scenarios.

To understand focused recharge mechanism from an ephemeral stream let us consider a scenario of groundwater recharge from a stream as shown in figure 5. If we assume the aquifer system to be isolated and flow in the river to be steady and uniform, then the groundwater level in the piezometer will rise till groundwater level and flow level in the river are same, when measured from a fixed datum. Recharge is governed by hydraulic head difference between the river flow level and the groundwater level in the adjacent surrounding. Essentially, flow happens till a hydraulic gradient exists (Darcy's law).

In a real-world scenario the aquifer is neither isolated nor the flow in the stream is steady and uniform. Flow depth in the stream may change from $H_{SW}^{T_1}$ at time $T_1$ to $H_{SW}^{T_2}$ at later time $T_2$ (figure 5). At any time $T_1$ if the flow depth in the stream (measured from a fixed datum) is $H_{SW}^{T_1}$ and the groundwater level measured in a piezometer close to the stream is $H_{GW}^{T_1}$, then focused recharge gradient ($FRG$) is a function of the difference of the two heads (equation 1a).

$$FRG^{T_1} \propto f\,(H_{SW}^{T_1} - H_{GW}^{T_1}) \qquad (1a)$$

Similarly, focused recharge gradient at time $T_2 = T_1 + \Delta T$ is given by equation (1b).

$$FRG^{T_2} \propto f\,(H_{SW}^{T_2} - H_{GW}^{T_2}) \quad (1b)$$

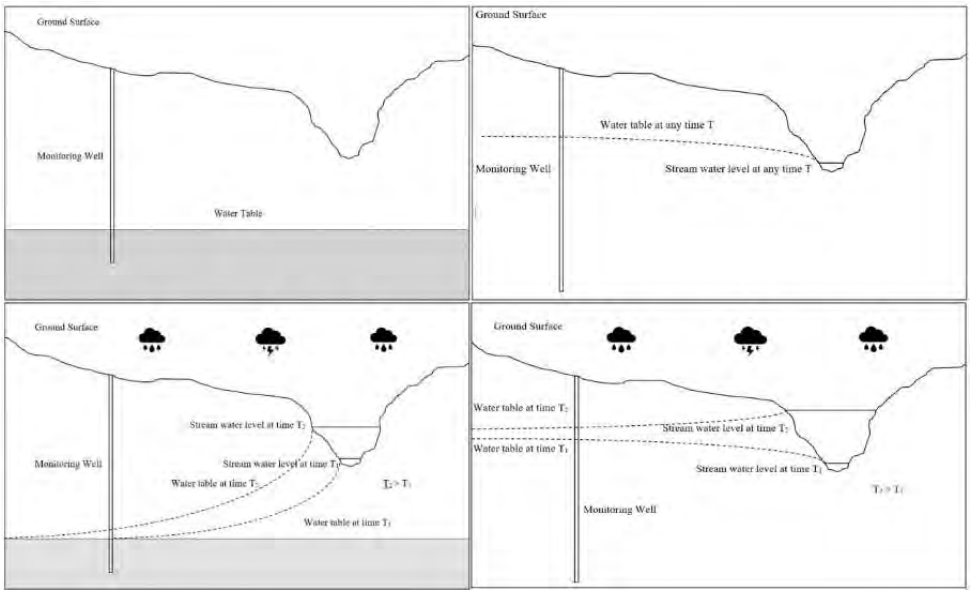



**Figure 5** Cross-section of the ephemeral and perennial river stream during recharge

Groundwater level surrounding a perennial stream section is higher than the stream flow level, thus having a flow gradient towards the stream (figure 5). In perennial river systems, flow in the stream is maintained during dry season as a result of contribution from groundwater flow. However, in extreme drought conditions the groundwater level may fall below the stream bed level and create conditions of no flow (figure 5) or the stream may behave as an ephemeral stream during intermediate intensity rainfall events.

During ordinary conditions the stream flow level in a perennial section is lower than the adjoining groundwater table. However, during rainfall event stage in the river rises quickly compared to groundwater level in the adjoining area as contribution from over land flow is faster than percolation into the ground. This creates a temporary scenario where the stage in the river is higher than the surrounding groundwater level which reversers the natural flow gradient from the stream towards the surrounding area by creating a focused recharge gradient. Thus, we see that both in ephemeral as well as perennial streams the main driver causing focused recharge is focused recharge gradient. Therefore, any change in the groundwater level in the surrounding area should be a function of the focused recharge gradient.

In real life world it is difficult to get absolute continuous field measurement of hydrogeological parameters (river stage, water table etc.). To handle such situation, we can assume that the measured hydrogeological parameters are in a state of temporal quasi-equilibrium at discrete times. Any focused recharge that happens can be attributed to the temporal quasi-equilibrium $FRG$ at that time. Since $FRG$ is a function of the head difference hence the change in the groundwater level is proportional to the hydraulic head difference $(H_{SW}^{T_1} - H_{GW}^{T_1})$ at that temporal quasi-equilibrium state.

The head difference may change due to fluctuation in the flow depth in the stream which changes the focused recharge gradient and in turn affects the groundwater level in the surrounding area. Thus, groundwater level changes from one temporal quasi-equilibrium state to another in reaction to the change in $FRG$ until $FRG$ becomes 0. In actual this is a continuous process and rarely would groundwater level equal stream flow level except in case of a big and long duration flood events.

### *3.2. Rainfall recharge or diffused recharge*

Rainfall recharge or diffused recharge is conceptually well understood and hence not overemphasized in this section. Not all rainfall infiltrate through the ground surface but some is lost in form of

evaporation, transpiration, overland flow and temporary surface storages. Only those rainfall events that causes enough infiltration to push the zero-flux plane to meet the groundwater table result in diffused recharge. Whether infiltration from a rainfall event will contribute to groundwater recharge depends if the rainfall is intense and durable enough to push the zero-flux plane to meet the existing groundwater table. Infiltration from rest of the rainfall events only result in increasing soil moisture content but do not raise the groundwater level through diffused recharge.

A large portion of the infiltrated rain is consumed in raising the moisture content of the soil column above the water table until saturation. The amount of infiltrated rain consumed depends on the antecedent moisture content of the soil matrix above the water table. Even the existing groundwater table may fluctuate resulting in more/less soil matrix getting saturated. A rainfall event may not contribute to the groundwater recharge but will alter the antecedent conditions for the next rainfall event. This is a continuous process where the immediate pre-existing antecedent condition determine groundwater recharge from a rainfall event. Thus, a time series of antecedent condition can be analyzed using rainfall and evapotranspiration as the input parameters. The antecedent condition is represented as Antecedent Index ($AI$). The antecedent index is an indicator of conditions suitable for diffused recharge.

Assuming a known time $T_0$ when the soil column above the water table is saturated, and all the excess infiltrated rain contributes to diffused groundwater recharge, then at such a time the $AI_{T_0} = 0$. Starting from such a point the $AI_T$ at any time becomes a function of the loss of soil moisture due to evapotranspiration ($EVT$) and rainfall ($I$) during the time period ($\mathrm{T} - T_0 = \Delta\mathrm{T}$) and rainfall. Evapotranspiration during time interval is measured using a pan evaporation (EVA) such that the loss of soil moisture from the subsurface is a fraction of the pan evaporation ($EVT = \lambda \times \mathrm{EVA}$). Only fraction of the total rainfall infiltrates the ground surface where the rest becomes overland flow. A rainfall event causes diffused recharge only when the antecedent index at a previous time step is zero. A time series of antecedent condition can be created for monitoring station using the formulations given in equations 2a & 2b.

$$AI_T = AI_{T-\Delta\mathrm{T}} + \lambda \times EVA_T - \gamma(I_T \times \Delta T) \quad \text{if } AI_{T-\Delta\mathrm{T}} \geq 0 \tag{2a}$$

$$AI_T = 0 + \lambda \times EVA_T - \gamma(I_T \times \Delta T) \quad \text{if } AI_{T-\Delta\mathrm{T}} < 0 \tag{2b}$$

where

$AI_T$ is the Antecedent Index at any time $T$

$AI_{T-\Delta\mathrm{T}}$ is the Antecedent Index at any time $T - \Delta T$

$T$ is time in days from a known day $T_0$ when the soil moisture is zero ($AI_{T_0} = 0$)

$\lambda$ is a fraction indicating amount of evapotranspiration

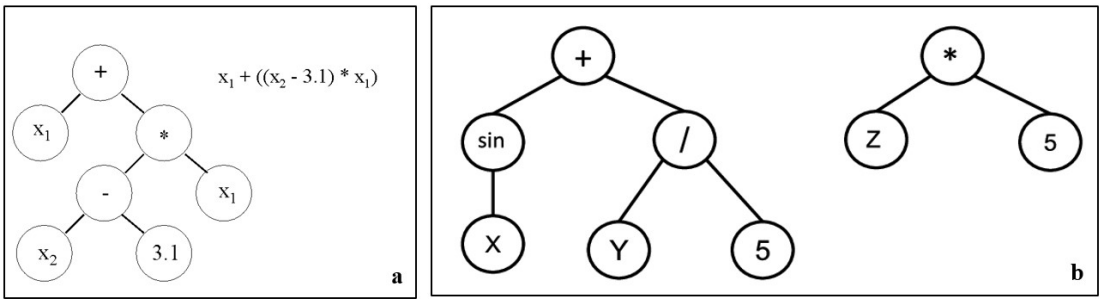
$\gamma$ is a fraction indicating amount of rainfall infiltration

## 4. Development of GP based groundwater recharge model

Genetic programming (GP) is an extension of genetic algorithms (GA) and biologically supervised machine learning method. It attempts to discover the most fit computer programs through an evolutionary search, based on the principles of genetics and natural selection (Koza, 1994). The genetic operators of GA and GP are almost similar. However, the representation of the final solution may differentiate both the methods. GA is used to optimize the model parameter and generate the result in terms of a string number. Whereas, GP generate the result in the form of a computer program and represented as a tree structure. The GP can provide the structure of the model through evolution together with the value of its parameters. In the case of GA, the user should define the structure of the model.

Primarily, the symbolic expression of a computer model is randomly generated. It consists of nodes which are represented as tree structures, subject to user-defined gene number or tree depth. Nodes are the elements, defined by the user to solve a certain problem prior to its modeling. It comprises a set of functions and terminals. The functional set includes basic mathematical operators, trigonometric functions, logical operators, Boolean operators or any other user-defined functions. Whereas, the terminal set composed of numerical constants or variables or logical constraints as shown in figure 6a. A typical GP tree starts with a root node and extends up to the randomly selected functional or terminal sets. After the generation of a population of expressions using a random selection process, the fitness function was used to assess the ability of individual expression for solving the problem. The major aim

of this process is to reduce the error (deviation between the model output and actual output), which is generated from the model. During the process, a part of the initial population is selected based on their fitness value. It was copied to a new population through various evolutionary mechanisms, namely, reproduction, crossover, and mutation. Various mechanisms available for the selection of population in GP include roulette-wheel selection, tournament, and ranking. This process is continued until the termination criterion is satisfied. The criteria can be either to reach an admissible error or the maximum number of generations defined by the user.




Multi-Gene Genetic Programming is a new variant of GP (Searson et al. 2010; Searson 2015). This method is designed to formulate the empirical relationship between the inputs and outputs in a mathematical expression which is just a weighted linear combination of the outputs. The expression developed from a number of evolved genes may consider as an individual GP tree. Figure 6b shows the schematic representation of multi-gene model used to predict the output. The input and functional parameters of the model are $x, y, z$ and $sin$, $+$, $\times$, $/$, $5$, respectively.

### *4.1. Study duration and input data*

The developed methodology is used to estimate time series of groundwater head at monitoring location. Middle Creek section of the study area has been chosen as the site for estimating the time series. A total of 6 bore wells are present Middle Creek section, though all of them show similar groundwater recharge characteristics (figure 7). Modelling groundwater level change in one borewell (BH 18-4) would also be representative of the other bore wells in this section as there is very small variation in the groundwater

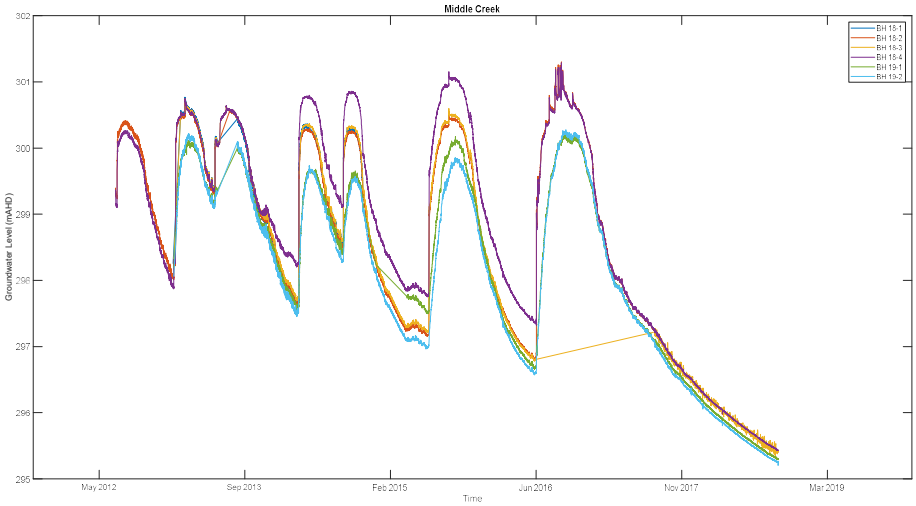



**Figure 7** Groundwater Level at Middle Creek bores

level data in the 6 borewells. Borewell BH 18-4 is chosen as the groundwater level data from this borehole has least gaps or missing data when compared to the other boreholes in Middle Creek section. Middle Creek section has a weather station that records rainfall (figure 3) and a stream gauge to measure the flow depth in the stream (figure 4) at this section. Given the completeness of the measurement data of all the necessary parameters required to fit the model, BH 18-4 is chosen as the candidate site.
The data selected for developing the model to predict groundwater recharge consists of input and output parameters. The major parameters, which influence the groundwater recharge were considered as input parameters. These parameters include precipitation, River stage level, and antecedent index. Whereas, the ground water level is considered as the output index. The antecedent index for different values of λ and γ is shown in the plot below (figure 8).

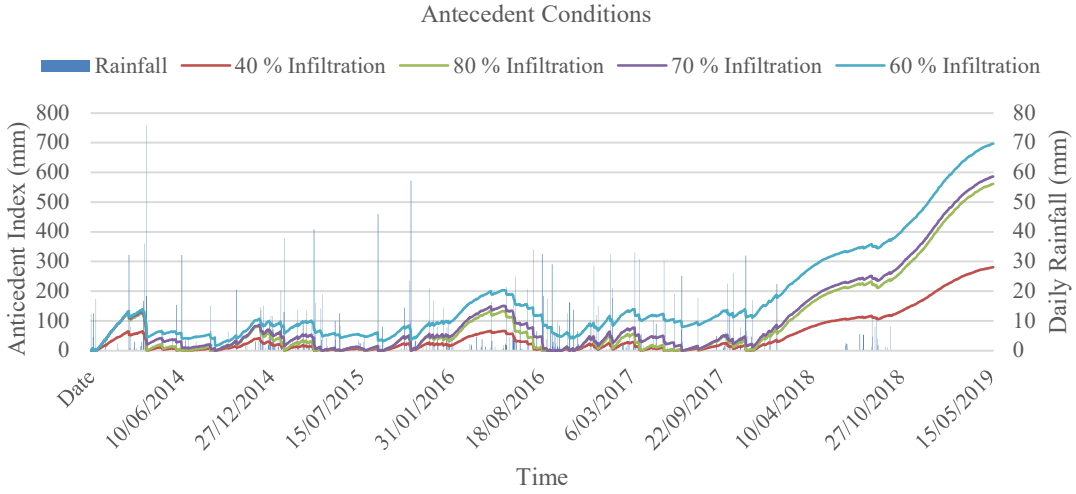



**Figure 8** Antecedent Index time series

The entire groundwater level data at BH 18-4 is split into training data set and the testing data set (figure 9). The river stage data, rainfall data and the antecedent index data are given as input and groundwater level change data as output is utilized for training and testing the GP model.

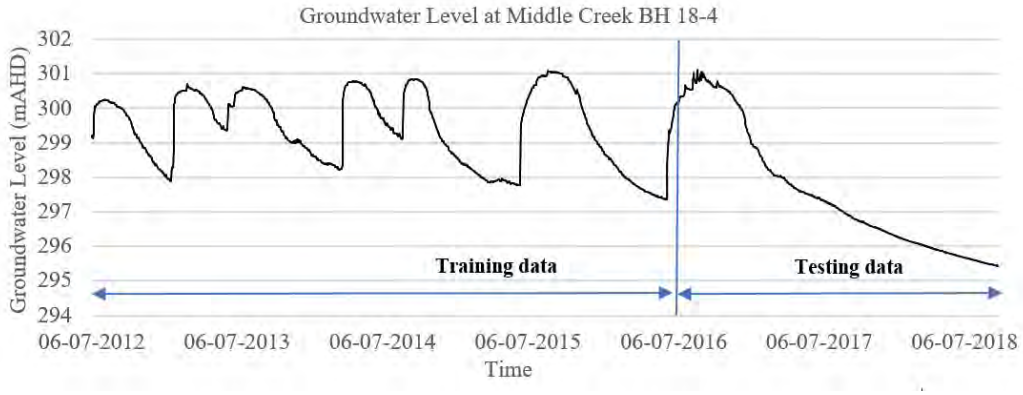



**Figure 9** Groundwater level data for training and testing

## 5. Performance evaluation results of the developed GP model

The performance evaluation result of the developed GP model is discussed in this section. The empirical relationship representing the input and the output is given by equation (3).

$$y = x_2 - 3.58\text{x}10^{-11}\, x_1 - x_3 - 3.3\text{x}10^{-10} \sin(x_1^3 + x_2) + 7.48\text{x}10^{-7} \quad (3)$$

where,
y = groundwater level change (AHDm)
$x_1$ = Intensity of rainfall (in mm)
$x_2$ = River stage level from datum (in mm)
$x_3$ = Antecedent index (in mm)

Groundwater level predicted using the empirical relationship obtained from the developed GP model both for training and testing is shown in figure 10 and figure 11, respectively. The efficacy of developed

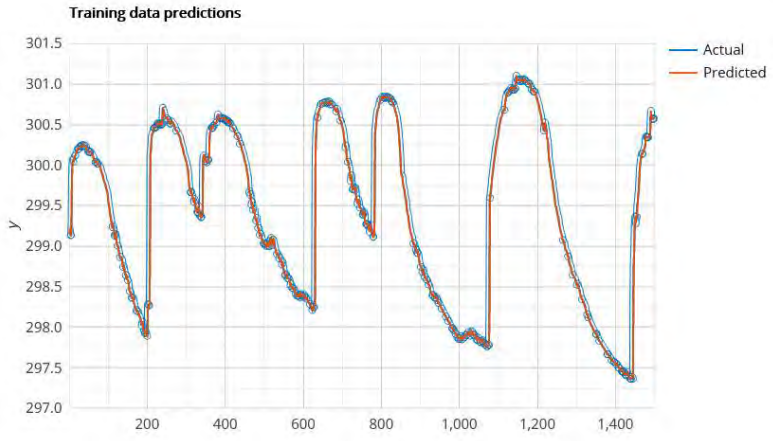



**Figure 10** Predicted and actual groundwater level during training phase

models was evaluated through different performance indices. It includes Mean square error (MSE), Root mean square error (RMSE), Coefficient of correlation (R), Coefficient of determination ($R^2$). The model with lower RMSE, MSE, and higher R, $R^2$ were considered as an optimum model.

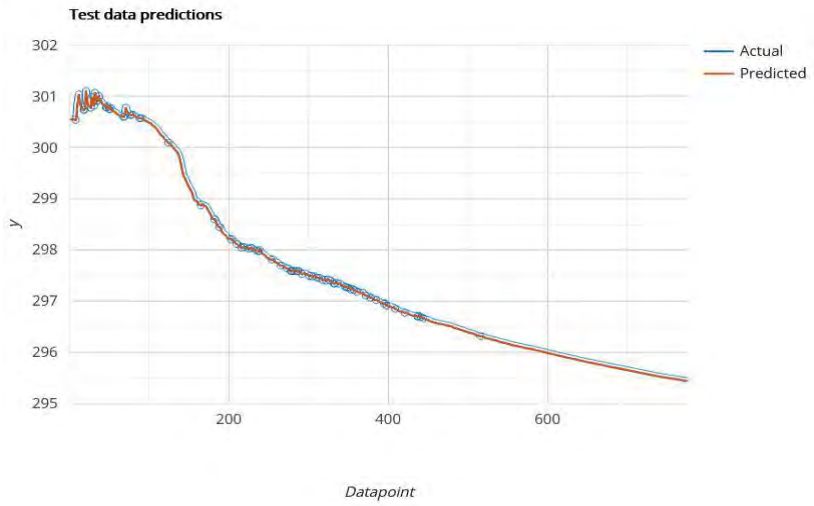



**Figure 11** Predicted and actual groundwater level during testing phase

Figure 12a shows the correlation between predicted and actual values for the training dataset obtained from the model. The accuracy of the models with the actual results was studied in terms of coefficient of determination ($R^2$). From the figure, a good match was observed between predicted and observed values of the training set. Similarly, the correlation between predicted and actual values for the testing

dataset is shown in Fig. 12b. The predicted groundwater recharge using the testing data set has shown good agreement with the actual results.

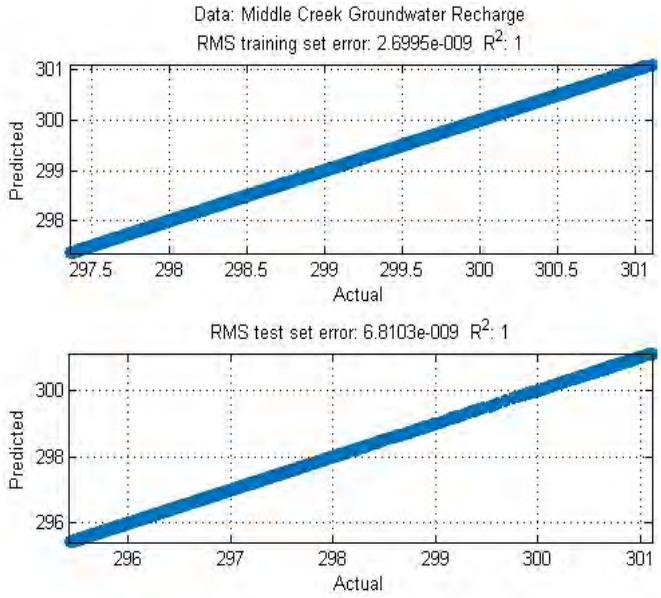



**Figure 12 (a) and (b)** Correlation between predicted and actual results for training and testing

To obtain this accuracy in the model set for training and testing data we used pareto tournaments to bias the model discovery process to low complexity models. Here 4 genes were used with a biased term limited to depth of 4 so as to obtain the model form as:

$$Y_{predicted} = C_0 + C_1 \times Tree_1 + C_2 \times Tree_2 + C_3 \times Tree_3 + C_4 \times Tree_4 \quad (4)$$

Where

$Y_{predicted}$ = output predicted

$C_0$ = bias term

$C_1, C_2, C_3, C_4$ = gene cofficients

Different set of performance matrices obtained in developing this model both during training and testing is are provided in following table 1.

**Table 1** Performance metrics during training and testing of the developed GP model

| Performance Metric | Training | Testing |
|---|---|---|
| Goodness of fit (coefficient of determination), [$R^2$] | 1 | 1 |
| Root mean squared error, [RMSE] | $2.6995 \times 10^{-9}$ | $6.8103 \times 10^{-9}$ |
| Mean absolute error, [MAE] | $2.349 \times 10^{-9}$ | $6.1659 \times 10^{-9}$ |
| Sum of squared errors, [SSE] | $1.0931 \times 10^{-14}$ | $3.5991 \times 10^{-14}$ |
| Mean squared error, [MSE] | $7.2873 \times 10^{-18}$ | $4.638 \times 10^{-17}$ |
| Max. abs. error | $5.5875 \times 10^{-9}$ | $1.04 \times 10^{-8}$ |

## 6. Discussion and Conclusion

In this study 10 years of groundwater level data along with rainfall and stream flow data for Maules Creek catchment in northwestern New South Wales, Australia is analyzed. GP is utilized for developing a machine learning based groundwater level prediction model. The GP model was found to be near accurate in predicting the groundwater level in this area. Based on the analysis, it was found that the river stage level was the most influencing parameter for groundwater region in this area. It was also

seen that the precipitation barely impacts the groundwater level in this area thus hardly have any contribution from diffused recharge.

Here, the GP model also found very efficient in predicting the groundwater level. The performance evaluated through different performance indices was found to be satisfactory. The resonance parameters predicted from by GP model have shown good agreement with the field data. Overall, genetic programming is viable option to develop accurate groundwater level prediction models and the generated empirical equation representing the output as a function of input can be utilized for future predictions of groundwater recharge.

## References

BARLOW, P. M., DESIMONE, L. A. & MOENCH, A. F. 2000. Aquifer response to stream-stage and recharge variations. II. Convolution method and applications. *Journal of Hydrology,* 230**,** 211-229.

CHEN, X. & CHEN, X. 2003. Stream water infiltration, bank storage, and storage zone changes due to stream stage fluctuations. *Journal of Hydrology,* 280**,** 246-264.

FREEZE, R. A. & CHERRY, J. A. 1979. *Groundwater*, Prentice-Hall.

GIAMBASTIANI, B., MCCALLUM, A., ANDERSEN, M., KELLY, B. & ACWORTH, R. 2012. Understanding groundwater processes by representing aquifer heterogeneity in the Maules Creek Catchment, Namoi Valley (New South Wales, Australia). *Hydrogeology Journal,* 20**,** 1027-1044.

HA, K., KOH, D.-C., YUM, B.-W. & LEE, K.-K. 2008. Estimation of river stage effect on groundwater level, discharge, and bank storage and its field application. *Geosciences Journal,* 12**,** 191-204.

HEALY, R. W. & SCANLON, B. R. 2010. *Estimating Groundwater Recharge*, Cambridge University Press.

IVERACH, C. P., CENDÓN, D. I., MEREDITH, K. T., WILCKEN, K. M., HANKIN, S. I., ANDERSEN, M. S. & KELLY, B. F. J. 2017. A multi-tracer approach to constraining artesian groundwater discharge into an alluvial aquifer. *Hydrol. Earth Syst. Sci.,* 21**,** 5953-5969.

Koza JR (1994) Genetic programming as a means for programming computers by natural selection. Stat Comput 4(2):87–112

LERNER, D. N., ISSAR, A., SIMMERS, I. & HYDROGEOLOGISTS, I. A. O. 1990. *Groundwater Recharge: A Guide to Understanding and Estimating Natural Recharge*, Heise.

Li Calvin. 2018. Surface Water Groundwater Interaction in Semi-arid Catchments and Implications for Groundwater Management and Reach Classification. *The University of New South Wales*.

MAHARJAN, M. & DONOVAN, J. 2016. Groundwater response to serial stream stage fluctuations in shallow unconfined alluvial aquifers along a regulated stream (West Virginia, USA). *Respuesta del agua subterránea a una serie de escenarios de fluctuaciones de una corriente en acuíferos aluviales someros no confinados a lo largo de una corriente regulada (West Virginia, EEUU).* 24**,** 2003-2015.

SCANLON, B. R., KEESE, K. E., FLINT, A. L., FLINT, L. E., GAYE, C. B., EDMUNDS, W. M. & SIMMERS, I. 2006. Global synthesis of groundwater recharge in semiarid and arid regions. *Hydrological Processes,* 20**,** 3335-3370.

Searson DP (2015) GPTIPS 2: an open-source software platform for symbolic data mining. In: Handbook of genetic programming applications, pp 551–573

Searson DP, Leahy DE, Willis MJ (2010) GPTIPS: an open source genetic programming toolbox for multigene symbolic regression. Int Multiconf Eng Comput Sci 1:77–80 Semblat JF, Lenti L, Jacqueline D, Leblond JJ, Grasso E (2011)

*IN PROCEEDINGS OF 25th HYDRO 2020, INTERNATIONAL CONFERENCE, NATIONAL INSTITUTE OF TECHNOLOGY ROURKELA, ODISHA, INDIA 26-28, March 2021, ISBN 978-93-90631-56-8*

Paper ID - 315

# A review of evolutionary algorithms in inverse modelling for groundwater flow and transport parameter estimation

Alice Thomas[1] and T. I. Eldho[2]

[1] *Research Associate, Hydrological processes group, National Centre for earth science studies, Thiruvananthapuram, India*
[2] *Professor, Department, Civil Engineering, Indian Institute of Technology Bombay, Mumbai, India*
*Email: alicearackalpadickal@gmail.com*
*Telephone/Mobile No.: +91 9930443475*

## ABSTRACT

The groundwater flow and transport model prediction accuracy highly relies on the ability to accurately and reliably quantify parameters such as transmissivity, hydraulic conductivity, longitudinal and transverse dispersivities, storativity and areal recharge. Consequently, an important component of groundwater flow and contaminant transport model is the solution of the inverse problem, i.e. the estimation (identification) of groundwater flow and contaminant transport model parameters. When compared to the trial and error method, the time required for inverse solutions are substantially less. Simulation-optimization (S-O) models are extensively used in previous studies to assess aquifer parameters by inverse modeling (IM) approach where the groundwater flow and transport processes are simulated by Mesh Free (MFree) method, Finite Element (FEM), Finite Difference (FDM), Boundary Element and Analytical Element Methods. In the solution of the inverse problem, the forward problem is solved many times till the unknown parameters are optimally calculated. Many heuristic optimization algorithms, such as Genetic algorithm -GA, Differential Evolution-DE, Particle Swarm Optimization-PSO, Ant Colony Optimization-ACO, Cat swarm optimization- CSO have been used for aquifer parameter estimation by inverse modeling. The heuristic optimization methods do not require derivative calculations or a well thought out initial point to start the search process unlike traditional gradient based methods. Lesser chance of getting trapped in a local optimum and having a higher probability to find a near-optimal solution as compared to conventional optimisation methods are other advantages reported of these evolutionary methods. In this paper, an attempt is made to review the applications of recent heuristic optimization techniques like GA, DE, ACO, PSO and CSO in parameter estimation problem considering the advantages and challenges while applying them in inverse modeling. Here, an application of DE for a hypothetical case study is also demonstrated for the parameter estimation of transmissivity in a confined aquifer.

***Keywords:*** *Groundwater parameter estimation, Inverse modeling, Heuristic optimization algorithms*

## 1. Introduction

According to Franssen et al. (2009), inverse modeling is the process of gathering information on the model and/or its parameters from measurements of what is being modelled. To compute hydraulic head or concentration distribution in groundwater systems, hydrogeological characteristics, dimensions of aquifer and boundary conditions, transmissivity (T), longitudinal and transverse dispersivity ($\alpha_L$,$\alpha_T$), aquifer recharge (Q), storativity (S) are primarily required as input parameters of the model. These input variables are used to determine groundwater head and concentration values in a forward problem where the governing partial differential equations are solved for the applicable boundary conditions. Alternatively, in situations where parameters like T, $\alpha_L$, $\alpha_T$ or Q are unknown but the observed head distribution in the aquifer is available, the unknown parameters can be computed by solving the forward problem for an assumed set of parameters. Assumed set keeps improving with every simulation call until the simulated head or concentration distribution comes in good agreement with the actual observed groundwater head or concentration values. This process is often referred as solution by inverse modeling. Inverse parameter estimation problem is thus the optimal determination of parameters by agreement between the dependent variable collected in the spatial and time domains and simulated results (Sun, 2004). The state of art of inverse modeling is summarized in the Table 1. Finite Element (FEM), Finite Difference (FDM), Boundary

Element (BEM), Analytical Element (AEM) and more recently Meshfree Methods and Software based on these methods like GMS (FDM), COMSOL (FEM) etc. have been found adequate by researchers for simulation modeling. For optimization, there is a trend to use evolutionary algorithms (EA) replacing the conventional numerical techniques for nearly last two decades. As these methods do not depend upon the initial set of chosen decision variables and as they do not require the first or second order gradient of the objective function with respect to the decision variables, numerical instability is avoided and a near global optimal solution is guaranteed. In particular, EA can handle implicit and higher order objective function and can handle combinatorial optimization problems which are involved in groundwater inverse modeling. Evolutionary algorithms like Genetic Algorithm (GA), Particle Swarm Optimization (PSO), Ant Colony Optimization (ACO), Cat Swarm Optimization (CSO) and Differential Evolution (DE) are used in a wide spectrum of problems in engineering and sciences. This study aims at reviewing the application of recent heuristic optimization techniques like GA, DE, ACO, PSO and CSO specific to parameter estimation problem in groundwater hydrology.

## 2. Groundwater Parameter Estimation Using Evolutionary Algorithms

### *2.1 Ant colony Optimization*

Ant colony optimization (ACO) initially proposed by Dorigo (1992) is an evolutionary algorithm inspired by ant colonies. Various applications of ACO in groundwater related problems can be found in Thomas and Rastogi (2011). Abbaspour et al. (2001) used ACO algorithm to estimate hydraulic parameters of unsaturated soil. A hybrid ant colony-simulated annealing method for groundwater parameter estimation was developed by Li et al. (2006) to determine storage coefficients and transmissivity for a two-dimensional unsteady state groundwater flow model. From the literature, it was observed that the disadvantage with ACO is it's large amount of computer run time consumption since there are several pre-defined parameters in this technique which influence the algorithm's search behavior. Literature also lacks in giving clear guidelines about picking up these ant colony parameters and therefore this method is not pursued seriously by researchers in inverse modeling. However, authors feel that there is a possibility to explore and experiment with this method to make it more user friendly in aquifer parameter estimation.

### *2.2 Particle swarm optimization*

PSO developed by Eberhart (1995) is a very popular population-based search algorithm inspired by flock of birds. Here a population of random solutions, called particles are initialized and each of it is associated with a velocity which corresponds to advancement in the solution which improves the initially assumed solution as it gradually moves towards the optimum solution. Particles move in the search domain with dynamically adjusted velocities based on their historical behaviours to a more focused search area. It was particularly observed in this technique that the improvement in solution is derived from two main considerations which firstly, looks to betterment in the individual solution in a particular iteration and secondly it also engages the best of all the previous solutions. Such behaviour takes it to a faster convergent growth and the near optimal solutions are delivered faster. Additionally this method is easier from programing convenience and enough guidance is available in the literature to pick up some user defined parameter for this method.

Swathi and Eldho (2014) in their study developed an improved method where Meshless Local Petrov Galerkin (MLPG) was used for ground water flow simulation which was coupled with Particle Swarm Optimization (PSO) for inverse modeling of groundwater parameters. Guneshwar et al. (2018) in their study developed a simulation optimization model by coupling Radial point collocation method (RPCM) with PSO for source identification to identify the unknown groundwater contaminant sources from the simulated

contaminant concentration data in the aquifer. Swathi and Eldho (2018) in their study developed a model based on Meshless Local Petrov Galerkin (MLPG) flow simulation model which is coupled with Particle Swarm Optimization (PSO) for inverse modeling of parameter structure identification. The model is applied to a hypothetical confined aquifer to compute transmissivity in different zones of the aquifer. It could be understood from these studies that PSO is an effective tool and can be further applied for determining parameters in the regional groundwater systems. PSO algorithm is simple, easy to implement, not affected by the nature of the objective function it optimizes but only by the magnitude of the objective function. Complexity in objective functions can hence be easily implemented. PSO parameters are problem specific. Extensive sensitivity analysis is necessary.

### *2.3 Cat swarm optimization*

A relatively new heuristic optimization algorithm viz., Cat Swarm Optimization (CSO) was presented by Chu and Tsai (2006). It is based on two major traits of cats. These traits are termed as "Seeking mode" and "tracking mode", which model upon the behaviours of cats. These two modes individually represent different procedure in the algorithm to imitate the behaviours of cats, and they are dictated to join with each other by a mixture ratio MR. The cat mostly spends time in seeking prey and little time in chasing prey. Thus, the MR is assigned in such a way that a higher number of cats belongs to seeking mode and a lower number of cats belongs in tracking mode.

Thomas et al. (2018) applied the CSO algorithm to a field case study to determine the flow parameters using inverse modeling. The decision and state variables were zonewise transmissivity values and hydraulic heads at the predefined locations, respectively. Their study showed the effectiveness of RPCM-CSO model for aquifer parameter estimation. Thomas et al. (2019) also presented a comparative assessment of simulation-optimization (S-O) models to estimate aquifer parameters such as transmissivity, longitudinal dispersivity, and transverse dispersivity. Premature convergence and stagnation point error in PSO is found tackled in seeking and tracking modes of CSO.

### *2.4 Genetic algorithm*

Genetic Algorithm (GA) is a search algorithm for optimization based on the mechanics of natural selection and natural genetics (Goldberg, 1989). Survival of the fittest among individuals, along with a structured yet randomized information exchange, and also few of the advanced skills of human search forms GA. Prasad and Rastogi (2001) coupled GA with Galerkin's finite element to estimate optimal aquifer parameters of net recharge and hydraulic conductivity for a real case aquifer. Huggi and Rastogi (2003) added the concept of solute transport parameter estimation by this method. They coupled their FEM based solute transport model with GA and ascertained the success of the method to obtain optimal estimate of aquifer parameters. Morshed and Kaluarachchi (1998) and Bhattacharjya and Datta (2009) linked GA based simulation-optimization model with artificial neural networks ANN for deriving certain objective management strategies for coastal aquifers. As GA performs too many fitness evaluations, it may generate slower solutions in real time. Hence ANN-GA was used to develop faster solutions in real time. Yao and Guo (2014) recommended a hybrid algorithm, combination of an improved genetic algorithm (GA) and Gauss-Newton method (GNM) for estimating parameters in groundwater problems. In this hybrid algorithm, the advantages of both GA and GNM were utilized. GA is effective in searching the whole finite space whereas GNM is good for a local search if its initial value is assigned appropriately. GA is efficient for estimating the hydrogeological parameters, but its limitation of generating solutions slowly gives rise to opt for a hybrid algorithm. Good convergence to the global solution with high probability, precision and efficiency makes GA efficient for inverse modeling. According to Deb (2001), GA ensures global optimal solution

and is efficient in handling problems having discrete variables. Instead of the actual parameters, GA uses the coded version. GA in general has a broad applicability and ease of use. GA instead of derivatives makes use of objective function information. Also instead of deterministic rules GA uses probabilistic search rules. Akbarpour et al.(2020) used GA and PSO to evaluate optimal pumping policy in an hypothetical aquifer and the results indicated that the GA has better performance than the PSO in optimizing groundwater pumping well locations.

### *2.5 Differential Evolutionary Algorithm*

Storn and Price (1997) considered a heuristic approach called differential evolution (DE) for global optimization. Differential evolution developed by Storn and Price in 1995 is a meta-heuristic method where a population set is maintained and new individual solutions are created by performing difference operation on the already existing population set. The new individuals will replace the old population only if the fitness function value of new solution is greater than the old solution.

Rastogi et al. (2014) discussed how DE is used for parameter estimation like transmissivity, aquifer recharge and boundary flows and also compared DE with GA. They concluded that DE performs better when compared to GA in terms of solution accuracy and computational time. DE is simple, powerful and easier to implement. DE has over ten variants and therefore it offers a wider choice from its variant selection for a particular problem of inverse modeling. Most of these variants pick three to five random solutions and improve upon their difference to make it more compatible for optimal solution. There are convenient rules to accept or reject the new solutions and which is a definite strength of this method. Anand (2016) also coupled DE to MFree based simulation model to estimate transmissivity in a real field aquifer. From the literature, it is found that there is scope of application of DE in inverse groundwater modeling to estimate system parameter which is an essential step towards groundwater planning and management. In the present study, DE is used to demonstrate the use of EA for inverse modelling.

Patel et al. (2020) proposed a hybrid-metaheuristic Differential Evolution- Particle Swarm Optimization (DE-PSO) to obtain aquifer parameters and to avoid getting stuck in the sub optimial solution. The results of this study show that the hybrid-metaheuristic based DE-PSO optimization algorithm is an efficient and robust tool for inverse groundwater problem of estimating the aquifer parameters. These new evolving global optimization techniques have largely replaced conventional numerical optimization methods particular for its application in inverse modeling. Despite all the literature available, knowledge gap does exist in parameter estimation process in highly heterogeneous and dynamic settings.

**Table 1:** State of Art of Inverse modeling

| References | Year | Methodology | Estimated Parameters |
|---|---|---|---|
| **Strecker and Chu** | 1986 | USGS's method of characteristics combined with parameter identification procedure | Transmissivity and Dispersivity |
| **Rooy et al. Rooy et al.** | 1989 | Stochastic approach and optimization using Levenberg-Marquardt algorithm | Transmissivity, dispersivity concentration source |
| **Keidser and Rosbjerg** | 1991 | Stochastic approach and optimization using Levenberg-Marquardt algorithm and Feed-back method | Transmissivity field, dispersivity values and concentration |
| **Wagner** | 1992 | Non-linear maximum likelihood estimator and SUTRA | Hydraulic conductivities, effective porosity, boundary flux and contaminant flux at the source, longitudinal and transverse dispersivity |
| **Medina and Carrera,** | 1996 | Maximum likelihood method along with parameters prior information and optimization using Marquardt algorithm | Transmissivity, recharge, leakage, dispersivity, molecular diffusion, porosity, retardation linear decay |
| **Sonnenborg et al.** | 1996 | Method of characteristic combined with nonlinear least square multiple regression and optimization using Levenberg-Marquardt strength | Transmissivity, porosity and longitudinal dispersivity, leakage factor and source |
| **Iribar et al.** | 1997 | TRANSIN II code with maximum likelihood estimation approach and optimization using Marquardt algorithm. | Transmissivity pattern |
| **Franssen and Hernandez** | 2003 | Sequential self-calibrated method | Transmissivity |
| **Sanz and Voss** | 2006 | Coupled SUTRA with UCODE (Universal inverse CODE) | Permeability, solute molecular diffusivity, freshwater inflow and porosity |
| **Franssen et al.** | 2009 | Regularized Pilot Points Method | Transmissivity and hydraulic head fields and the well catchment |
| **Franssen and Kinzelbach** | 2009 | Ensemble Kalman Filtering (EnKF) | Transmissivity |
| **Hosseini et al.** | 2011 | Sequential self-calibrated (SSC) approach | Transmissivity |
| **Ebrahimi et al** | 2016 | Modflow and remote sensing | groundwater recharge |
| **Wang et al.** | 2017 | Stochastic Newton approach and geostatical approaches | Transmissivity |
| **Singh et al.** | 2018 | Mesh free RPCM and PSO | Contaminant Source |
| **Swathi et al.** | 2018 | Mesh free -MLPG and PSO | Structure Pattern |
| **Thomas et al.** | 2019 | Mesh Free RPCM and CSO, PSO, DE and GA | Transmissivity, longtitudinal and transverse dispersivity |
| **Patel et al.** | 2020 | FEM and hybrid-metaheuristic based DE-PSO | Transmissivity |
| **Akbarpour et al.** | 2020 | FEM and GA, PSO and Firefly algorithm | Optimal pumping well locations |



*IN PROCEEDINGS OF 25th HYDRO 2020, INTERNATIONAL CONFERENCE, NATIONAL INSTITUTE OF TECHNOLOGY ROURKELA, ODISHA, INDIA 26-28, March 2021, ISBN 978-93-90631-56-8*

## 3. Model Development

The simulation model used here is radial point collocation based Mesh Free (MFree method). In MFree method a system of algebraic equations are established for the entire problem domain without any predefined mesh or grid. Here a set of nodes which are scattered within the problem domain and on the boundaries represent the problem domain along with its boundaries. Details of governing equations for the groundwater flow model and the MFree formulation can be found in Thomas et al. (2014). For the present study, PSO is used as an optimization tool. The coupled simulation optimization model is developed for the transient conditions in MATLAB. In optimization model, the input data are obtained from the developed flow model and the objective function considered is the sum of the weighted squared difference of the simulated and observed head values as given in model formulation. The objective function in the form of Eq. (1) is used for inverse modeling. Using this objective function, the parameters are estimated by the stochastic population based meta-heuristics PSO.

Mathematically a groundwater inverse model for aquifer parameter estimation can be expressed as, (Sun, 1994).

$$Min\ (F) = \sum_{n=1}^{L} \sum_{t=t_o}^{t^f} w\,(\mathrm{h_{sim}(P)} - \mathrm{h_{obs}})^2 \qquad (1)$$

Subject to lower bound and upper bound on parameters

$$T_{i,min} \le T_i \le T_{i,max} \qquad (2a)$$

$$h_{l,t}^{c} = f(T_i) \qquad (2b)$$

Where, $\mathrm{h_{obs}}$ is the observed hydraulic head value; $\mathrm{h_{sim}(P)}$represents the simulated and observed head values; $F$ is objective function which is implicitly connected to system parameter P; $T_i$ is the transmissivity at node $i$; $L$ is the total number of monitoring wells; $t_o$ and $t_f$ are beginning and ending time of observations. w is a weighting coefficient. The present study assumed the weight $(w)$ coefficient as unity since it's a synthetic problem. However in field problems weightage can be based upon the quality of observed data. If the observed head values are obtained from real aquifer, there can be instrumentation and personal errors in which case weights can be assumed according to the reliability of the observed data from the field.

## 4. Case Study

To validate the Meshfree RPCM-DE model for inverse modeling, a hypothetical confined aquifer of 36 sq. km area (Tamer Avyaz, 2007) is considered. The flow domain as shown in Figure 1(a), has on south a constant head boundary of 100 m, on the west there is a flux boundary of inflow 0.25 $m^2$/day. Both the northern and eastern boundaries are characterised by no-flow boundaries. A recharge zone exists at the north with recharge a rate of 0.00015 m/day. Three pumping wells are also present in the aquifer with pumping rates of $Q_1$ = 3000 $m^3$/day, $Q_2$ = 6000 $m^3$/day, and $Q_3$ = 800$m^3$/day. Assumed storage coefficient for the aquifer domain is 0.001 and the aquifer is parameterized into four zones with transmissivity values varying from 50 to 300 $m^2$/day with assumed $T_1$ = 50$m^2$/day, $T_2$ = 300$m^2$/day, $T_3$ = 100 $m^2$/day and $T_4$ = 200$m^2$/day. The considered flow problem is solved using RPCM model with 625 nodes as shown in Figure. 1(b) with Δx = Δy = 250m and with a circular support domain with a radius equal to three times the nodal distance. Time step considered for simulation of groundwater head is 1 day and the value of $\alpha_c$ is taken as 3 after initial tuning of the parameter. The hydraulic heads obtained by the RPCM model for the known transmissivity values for the flow problem are taken as observed heads in the inverse modeling. The upper bound and lower bound of the transmissivity are assumed as 300 $m^2$/day and 0 $m^2$/day respectively. Figure.

1(b) shows the nodal distribution and also location of the thirty seven observation wells where groundwater head is measured. The objective function is evaluated by finding the difference in observed and simulated head values at these observation wells. Observed head data are generated at these thirty seven observation points after 100 days of pumping.

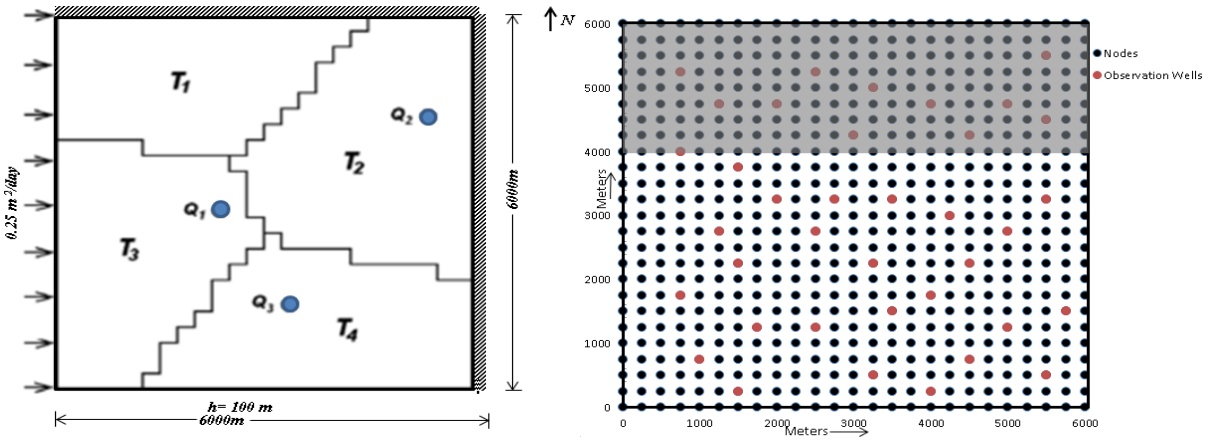



**Figure 1**: **a)**: Aquifer domain and zonation pattern **b)** Nodal distribution

The estimated transmissivity parameters corresponding to minimum objective function value are listed in Table 2. It could be inferred from the results that the error in predicted transmissivity values when compared to the actual values are negligible proving the effectiveness of the developed MFree RPCM-DE model for parameter estimation in groundwater system. Among the various variants of DE, DE/rand/1/bin is used in the present study. Also the DE model characteristics considered are: Population size (N) 40, Mutation factor (F) 0.8 and Crossover (CR) 0.9 Final objective function values for the optimal solution 0.0031.

**Table 2:** Estimated transmissivity values

| Zone | True values ($m^2/d$) | Estimated values using PSO ($m^2/d$) | % Difference with true values |
|---|---|---|---|
| 1 | 50 | 49.58 | 0.84 |
| 2 | 300 | 298.89 | 0.37 |
| 3 | 100 | 99.51 | 0.49 |
| 4 | 200 | 198.82 | 0.59 |

The final optimal transmissivity values obtained are satisfactory as it can be seen from Table 2 as the maximum error of estimated values when compared to true values is rather small (0.84%). This study found that MFree-DE is an effective tool for inverse modeling and can further be applied to real case studies involving estimation of solute transport parameters.

## 5. Conclusions

Determining the various input parameters for groundwater simulation models like transmissivity or hydraulic conductivity, storativity/ specific yield, aquifer recharge, longitudinal and transverse dispersivity is one of the major challenges found in groundwater modeling. Therefore developing a computationally efficient and adequate inverse model capable of determining the input field parameters is an essential

requirement. The parameter estimation for the coupled flow and solute transport groundwater problems are not attempted widely. In inverse modeling, the above-mentioned aquifer parameters are estimated from the state variables (hydraulic head, solute concentration) using a simulation-optimization approach. In the simulation optimization problem, the simulation model is called many times over to deliver the optimal parameters by the optimization model. Hence a fine tuning of the optimizers in terms of population size, objective function value and number of iteration is required. The MFree-DE is found to be an effective tool for inverse modeling and can be further applied to real case studies such as transport parameter estimation. It is understood that these heuristic optimization methods has a major advantage that they neither require derivative calculations nor initial point to start search processes and also convergence to an optimal solution does not depend on the initially chosen estimates. User defined parameters affect the algorithm's search behaviour which is found to be a common concern for the evolutionary algorithms discussed here. Since these are problem specific, therefore adequate sensitivity analysis is essential for determining the same. The study explores the effectiveness of evolutionary algorithms GA, DE, ACO, PSO and CSO in inverse modeling and suggests it's future scope in application to the real field confined and unconfined aquifers.

## References

Abbaspour KC, Schulin R, Van Genuchten MT. (2001) Estimating unsaturated soil hydraulic parameters using ant colony optimization. *Advances in Water Resources. Aug 31;24(8)*:827-41.

Akbarpour, A., Zeynali, M.J. & Nazeri Tahroudi, M. (2020) Locating Optimal Position of Pumping Wells in Aquifer Using Meta-Heuristic Algorithms and Finite Element Method. *Water Resources Management 34*, 21–34.

Anand Kumar (2016) Groundwater inverse modelling using meshfree based simulation and differential evolution based optimization methods. *M. Tech dissertation report*, IIT Bombay

Carrera J, Alcolea A, Medina A, Hidalgo J, Slooten LJ. (2005). Inverse problem in hydrogeology. *Hydrogeology Journal*. Mar 1;13(1):206-22.

Carrera J, Neuman SP. Estimation of aquifer parameters under transient and steady state conditions: 1. Maximum likelihood method incorporating prior information. *Water Resources Research. 1986 Feb 1;22(2):*199-210. 10.1029/WR022i002p00199

Chu, S. C., & Tsai, P. W. (2007). Computational intelligence based on the behavior of cats. *International Journal of Innovative Computing, Information and Control, 3(1)*, 163-173.

Deb, K. (2001) Multi-Objective Optimization Using Evolutionary Algorithms, *John Wiley & sons Ltd, London*.

Dorigo, M.( 1992).Optimization, learning and natural algorithms, *Ph.D. thesis, DEI*, Politecnico di Milano, Italy.

Eberhart, R. C., & Kennedy, J.( 1995) A new optimizer using particle swarm theory, *Proceedings of the Sixth International Symposium on Micro Machine and Human Science: Oct*.

Ebrahimi, H., Ghazavi, R., & Karimi, H.(2016). Estimation of Groundwater Recharge from the Rainfall and Irrigation in an Arid Environment Using Inverse Modeling Approach and RS. *Water Resources Management, 30(6)*, 1939-1951.

El Harrouni K, Ouazar D, Walters GA, Cheng AD. (1996) Groundwater optimization and parameter estimation by genetic algorithm and dual reciprocity boundary element method. *Engineering Analysis with Boundary Elements. Dec 1;18(4):*287-96.

El Harrouni K, Ouazar D, Wrobel LC, Cheng AD.(1997) Groundwater parameter estimation by optimization and DRBEM. *Engineering Analysis with Boundary Elements. Mar 1;19(2):*97-103.

Franssen HH, Alcolea A, Riva M, Bakr M, Van der Wiel N, Stauffer F, Guadagnini A.(2009) A comparison of seven methods for the inverse modelling of groundwater flow. Application to the characterisation of well catchments. Advances in Water Resources. Jun 30;32(6):851-72.

Franssen, H. H., & Gómez-Hernández, J. J . (2003) Impact of measurement errors in stochastic inverse conditional modelling by the self-calibrating approach. *Advances in water resources, 26(5)*, 501-511.

Franssen, H. J. H., Gómez-Hernández, J., & Sahuquillo (2003) A Coupled inverse modelling of groundwater flow and mass transport and the worth of concentration data. *Journal of Hydrology, 281(4)*, 281-295. .

Franssen, Hendricks H.J. and Kinzelbach, W. (2009), Ensemble Kalman filtering versus sequential self-calibration for inverse modelling of dynamic groundwater flow systems. *Journal of Hydrology 365*, 261–274

Goldberg, D.E. (1989). Genetic Algorithm in Search, Optimization, and Machine Learning, *Addison-Wesley Publishing Company, Inc.*

Guneshwor, L., Eldho, T. I., & Kumar, A. V. (2018). Identification of Groundwater Contamination Sources Using Meshfree RPCM Simulation and Particle Swarm Optimization. *Water Resources Management, 32(4),* 1517-1538.

Hendricks Franssen, H. J., Alcolea, A., Riva, M., Bakr, M., van der Wiel, N., Stauffer, F., & Guadagnini, A.(2009) A comparison of seven methods for the inverse modelling of groundwater flow. Application to the characterisation of well catchments. *Advances in Water Resources, 32(6),* 851–872

Hosseini, A. H., Deutsch, C. V., Mendoza, C. A., & Biggar, K. W.(2011). Inverse modeling for characterization of uncertainty in transport parameters under uncertainty of source geometry in heterogeneous aquifers.*Journal of Hydrology,* 405(3), 402-416.

Huggi VP, Rastogi A. K.(2003) Estimation of solute transport parameters of groundwater systems using genetic algorithm. *Water and Energy International.60(4):*38-45.

Iribar, V., Carrera, J., Custodio, E. and Medina, A.(1997) Inverse modeling of seawater intrusion in the Llobregat delta deep aquifer. *Journal.Hydrology.,v.198,* pp.226-244.

Keidser,A. and Rosbjerg, D.(1991) A comparison of four inverse approaches to groundwater flow and transport parameter identification. *Water Resources Research., v.27(9),* pp.2219-2232.

Li S, Liu Y, Yu H.(2006) Parameter estimation approach in groundwater hydrology using hybrid ant colony system. *Lecture Notes in Computer Science*. Aug 16;4115:182.

Mayer, A.S. and Huang, C.(1996). Development and application of a coupledprocess parameter inversion model based on the maximum likelihood estimation method. *Advances in Water Resources, v.22(8),* pp.841-853.

Medina, A. and Carrera, J. (1996) Coupled estimation of flow and solute transport parameters. *Water Resources Res., v.32(10),* 3063-3076.

Morshed Jahangir and Kaluarachchi, Jagath J.(1998) Parameter estimation using artificial neural network and genetic algorithm for free-product migration and recovery. *Water resources research vol. 34, no. 5,* 1101-1113

Poeter EP, Hill M.C.(1997) Inverse models: A necessary next step in ground-water modeling. *Groundwater. 1;35(2):*250-60.

Prasad KL, Rastogi A.K.(2001) Estimating net aquifer recharge and zonal hydraulic conductivity values for Mahi Right Bank Canal project area, India by genetic algorithm. *Journal of Hydrology. 15;243(3):*149-61.

Rastogi AK, Rosemary Cyriac and Vidya Munuswami (2014). PSO and DE application in Groundwater Hydrology: Pumping cost optimization and inverse solutions of aquifers. *Lambert academic publishing.*

Rastogi A.K.(2007) Numerical groundwater hydrology. *Penram International Publication,* New Delhi; India.

Rooy, D.V., Keidser, A. and Rosbjerg, D.(1989) Inverse modelling of flow and transport. *Groundwater Contamination. I,AHS Publ. no.185,* pp.11-23.

Sanz, E. and Voss, C.I.(2006) Inverse modeling for seawater intrusion in coastal aquifers: Insights about parameter sensitivities, variances, correlations and estimation procedures derived from the Henry problem. *Advances in Water Resources, v.29(3),* pp.439-457.

Sharad Patel & T.I. Eldho & A.K. Rastogi, (2020). Hybrid-Metaheuristics Based Inverse Groundwater Modelling to Estimate Hydraulic Conductivity in a Nonlinear Real-Field Large Aquifer System. *Water Resources Management: An International Journal, Published for the European Water Resources Association (EWRA), Springer;European Water Resources Association (EWRA), vol. 34(6),* 2011-2028.

Sonnenborg, T.O., Engesgaard, P. and Rosbjerg, D.(1996) Contaminant transport at a waste residual deposit Inverse flow and nonreactive transport modeling. *Water Resources Res., v.32(4),* pp.925–938.

Strecker, E.W. and Chu, W-S. (1986) Parameter identification of a groundwater contaminant transport model. *Ground Water, v.24(1),* pp.56-62.

Storn, R., & Price, K. (1997). Differential evolution–a simple and efficient heuristic for global optimization over continuous spaces. *Journal of global optimization, 11(4),* 341-359.

Swathi, B., & Eldho T.I. (2014). Inverse Modeling of Groundwater System Using Coupled PSO-MLPG Techniques.*Internationl conference on hydroinformatics.*

Swathi, B., & Eldho, T. I. (2018). Aquifer parameter and zonation structure estimation using meshless local Petrov–Galerkin method and particle swarm optimization. *Journal of* Hydroinformatics, 20(2), 457-467.

Thomas A, Eldho TI, Rastogi AK. (2014). A comparative study of point collocation based meshfree and finite element methods for groundwater flow simulation. *ISH Journal of Hydraulic Engineering* ;20(1):65-74.

Thomas, A., & Rastogi, A. K.(2011) A review of ant colony in water resources optimization, *Proceedings of National conferences of advances in Civil Engineering*, 52-59.

Thomas, A., Eldho, T. I., Rastogi, A. K., & Majumdar, P. (2019). A comparative study in aquifer parameter estimation using MFree point collocation method with evolutionary algorithms. *Journal of Hydroinformatics*, https://doi.org/10.2166/hydro.2019.105.

Wagner B.J.(1992) Simultaneous parameter estimation and contaminant source characterization for coupled groundwater flow and contaminant transport modelling. *Journal of Hydrology*. 1992 Jul 1;135(1-4):275-303.

Wang X, Jardani A, Jourde H.(2017) A hybrid inverse method for hydraulic tomography in fractured and karstic media. *Journal of Hydrology*.

Yao Leihua and Guo Yufei.(2014). Hybrid Algorithm for Parameter Estimation of the Groundwater Flow Model with an Improved Genetic Algorithm and Gauss-Newton Method. *Journal of Hydrology*. *2014 Eng.19:*482-494

Zimmerman D.A, Marsily G.D, Gotway C.A, Marietta M.G, Axness C.L, Beauheim R.L, Bras R.L, Carrera J, Dagan G, Davies PB, Gallegos DP.(1998). A comparison of seven geostatistically based inverse approaches to estimate transmissivities for modeling advective transport by groundwater flow. *Water Resources Research*.*34(6):*1373-413.

*IN PROCEEDINGS OF 25th HYDRO 2020, INTERNATIONAL CONFERENCE,*
*NATIONAL INSTITUTE OF TECHNOLOGY ROURKELA, ODISHA, INDIA*
*26-28, March 2021, ISBN 978-93-90631-56-8*

Paper ID - 417

# IMPACT OF CLIMATE CHANGE ON GROUNDWATER RECHARGE

Puja Tripathy[1], K.C. Patra[2], Uma Maheswar Rao[3]

*1, MTech. Scholar, Department of Civil Engineering, NIT Rourkela, Odisha 769008, India*
*Email: pujatripathy99@gmail.com*
*2, Professor, Department of Civil Engineering, NIT Rourkela, Odisha 769008, India*
*Email: kcpatra@nitrkl.ac.in*
*3, PhD Scholar, Department of Civil Engineering, NIT Rourkela, Odisha 769008, India*
*Email: mahesh93.happy@gmail.com*

## Abstract

Groundwater is an important natural resource for its use in domestic, agricultural, industrial and various purposes. Due to increase in population its demand is also increasing by each passing day. Though in India, surface water availability is more than ground water but as the later can be accessed more easily and widely, it is extracted more leading to decrease in ground water table by each passing day. Climate change also has a severe effect on groundwater. Increase in atmospheric concentrations of greenhouse gasses leads to change in hydrologic cycle through evaporation, soil moisture, precipitation with increasing temperature. So, along with growing population, climate change leads to inadequate recharge of groundwater thus resulting in declined groundwater levels. Thus, it is very important to predict the impact of climate change on future groundwater recharge. General Circulation Models (GCMs) are the main tools that gives fairly precised climate data on global or regional scale and have the ability to simulate present climate and predict changes in climate in future caused due to increased greenhouse gas concentrations. Therefore, this study aims to evaluate long term average annual groundwater recharge (2000-2019) based on the given scenarios of 2000-2019 and predict future groundwater recharge (2050-2059). A hydrological model, WetSpass is used for estimation of groundwater recharge and its spatial variation and future atmospheric conditions are predicted by downscaling climate data (precipitation, temperature and windspeed) from two CMIP5 GCMs (MIROC-ESM-CHEM and GFDL-CM3) under four RCP scenarios (2.6,4.5,6.0,8.5) using SD-GCM V2.0. The results of this study are expected to help in future planning and management of groundwater resources and to take suitable and necessary measures due to climate change impact.

***Keywords**: Climate change, groundwater recharge, GCMs, WetSpass, SD-GCM V2.0*

## 1. INTRODUCTION

Overutilization of groundwater is defined as a condition in which, over the course of time, recharge process is inadequate in comparison of the rate of extraction. The over exploitation of groundwater for domestic, agricultural irrigation and industrial use has led to the falling of groundwater level in many parts of the world and more so in India. Due to its easy availability, low capital cost and less prone to pollution groundwater is the most preferred source of water.

The Dynamic Ground water resources assessment of 2017 shows that the total annual ground water recharge of India is 432 billion cubic meters (bcm), out of which the total natural discharges is 39 bcm. Thus, Annual extractable Ground Water Resources is 393 bcm. Contribution of rainfall to the total annual groundwater recharge of India is 67%, the major source being monsoon rainfall which is 58% i.e., 252 bcm. Recharge from water conservation structures, ponds, tanks, irrigation return flow, canal seepage contributes 33% of the total annual groundwater recharge. The overall stage of development of groundwater in India is 63%. The total groundwater extraction of India for the year 2017 has been evaluated as 248.69 bcm, agriculture sector being the primary consumer. About 89% of total annual groundwater extraction is for irrigation purpose i.e., 221.46 bcm and only 11% is for Domestic and Industrial use i.e., 27.23 bcm. Clearly the major component of extracted groundwater is used for irrigation. Wells provide 61.6% of water for irrigation and 24.5% is provided by canals. Over the years, surface water use is decreased and groundwater use is increased for irrigation purpose and the use of

tube wells has increased sharply thus increasing the consumption of groundwater for irrigation. Due to its increasing demand in various sectors and with increasing population in India, available groundwater resources fail to meet the demand targets.

Contribution of human activities to climate change is significant due to inclusion of $CO_2$ and other heat-trapping gases to the atmosphere, thus increasing greenhouse gas emissions resulting in the rise of Earth's surface temperature. In 2014 India's total GHG emissions were 3,202 million metric tons of carbon dioxide (MtCO2e) equivalent to 6.55% of world's GHG emissions. With changing temperature, climate changes that can have severe consequences on all components of water cycle through precipitation, evapotranspiration, infiltration and others. Groundwater recharge mainly depends on precipitation and changing of climate has a direct impact on precipitation and surface water bodies. Due to variation in rainfall distribution floods and droughts takes place. Due to increasing sea levels saline intrusion has increased in coastal and island aquifers thus affecting groundwater quality and quantity. Thus, climate change plays a drastic role in reducing the quantity and quality of water resources.

The relationship between groundwater and changing climatological variables is more complex and is not clearly understood as compared to surface water. Thus, it is very important to understand climate variability over the long term and accordingly plan and manage groundwater resources well into the future keeping in mind that with increasing population industrial, agricultural, and domestic needs also increases thus stresses on groundwater resources also increases. General Circulation Models (GCMs) are the main tools that gives fairly precised climate data on global or regional scale and have the ability to simulate present climate and predict changes in climate in future caused due to increased greenhouse gas concentrations. To predict the climate change impact on groundwater recharge, it is very important to predict reasonably accurate climatic variables and also precisely evaluate the groundwater recharge. So GCMs are downscaled in basin scale and then coupled with hydrological model for estimating the effect of climate change on groundwater recharge. Groundwater recharge depends not only on climatic factors but also on a variety of other factors such as local geological composition, land use and topography in the considered area and elements of hydrologic cycle.

In this study, the hydrological model used is WetSpass (Water and Energy transfer between soil, plants and atmosphere under quasi steady state) constructed on the basis of spatially distributed water balance model depending on time (Batelaan and De Smedt, 2001, 2007). Kahsay, Pingale and Hatiye **(**2017) in their paper evaluated the impacts of climate change on groundwater recharge and base flow in Tekeze sub-catchment in Ethiopia using WetSpa. The future climatic parameters (precipitation and temperature) were procured from CORDEX under RCP 2.6 and 4.5. The results showed annual rainfall is declining and average temperature and evapotranspiration is increasing for RCP 2.6 and 4.5. Shrestha, Bach and Pandey 2016 in their study used WetSpass model to estimate climate change impact on groundwater recharge and used MODFLOW to evaluate the groundwater level and storage in Mekong Delta. The future climatic variables were obtained from five GCMs (CNRM-CM5, HadCM3, CanESM2, MIROC4H, CMCC-CM) under two different RCP (4.5, 8.5). Results indicated decrease in future groundwater recharge thus decreasing groundwater levels and storage in future. Meresa, Girmay and Gebremedhin 2019 in their research estimated components of seasonal water balance and long term annual average using WetSpass for Bikri Watershed. The study concluded that WetSpass is a good indicator for assessing of water balance components. Shrestha, Hoang and Bhatta 2018 studied impact of climate change on groundwater recharge in four cities of Asia i.e. Lahore, Bandung, Bangkok and Ho Chi Minh City and classify alternate options. Future climatic variables were obtained from 4 RCMs (CCAM, CCAM, REMO 2009, RCA4) under RCP scenarios 4.5 and 8.5. Two hydrological models were used. SWAT was used for Lahore, HCMC, and Bandung cities and WetSpass was applied to Bangkok. Pandian.M 2014 in his paper studied the effect of land use changes on groundwater recharge using WetSpass for the parts of Coimbatore and Tiruppur districts.

The primary objective of this study is assessment of groundwater recharge and downscaling of future climatic variables i.e., rainfall, temperature, windspeed from selected GCM under four different RCPS (2.6, 4.5, 6.0, 8.5) using SD-GCM V2.0 and study their effect on future groundwater recharge using WetSpass.

## 2. MATERIALS AND METHODOLOGY

### 2.1 *Study Area*

This study has been done for Bardhhaman district of West Bengal (Figure 1). The study area lies within the geographical limits of 22.930771°N to 23.879951 °N latitude and 86.790939°E to 88.416061°E longitude surrounded by three major rivers i.e., Bhagirathi-Hooghly river in east, Ajay river in the north and Damodar river in the southwest. It comprises 32 community development blocks with a total area of 7024 km$^2$. According to Block wise Ground Water Resources Assessment -2017, 11 blocks of the study area is in semi-critical zone i.e., MANGOLKOTE, BHATAR, KETUGRAM – II, KETUGRAM – I, KATWA-I, KATWA-II, RAINA – II, RAINA – I, MEMARI- II, KALNA – II, MANTESWAR. A total of 34.375% of the district is in semi-critical zone. The mean annual rainfall of the study area ranges from 1200mm-1400mm, 74% percent of which is contributed during the months of June, July, August and September.

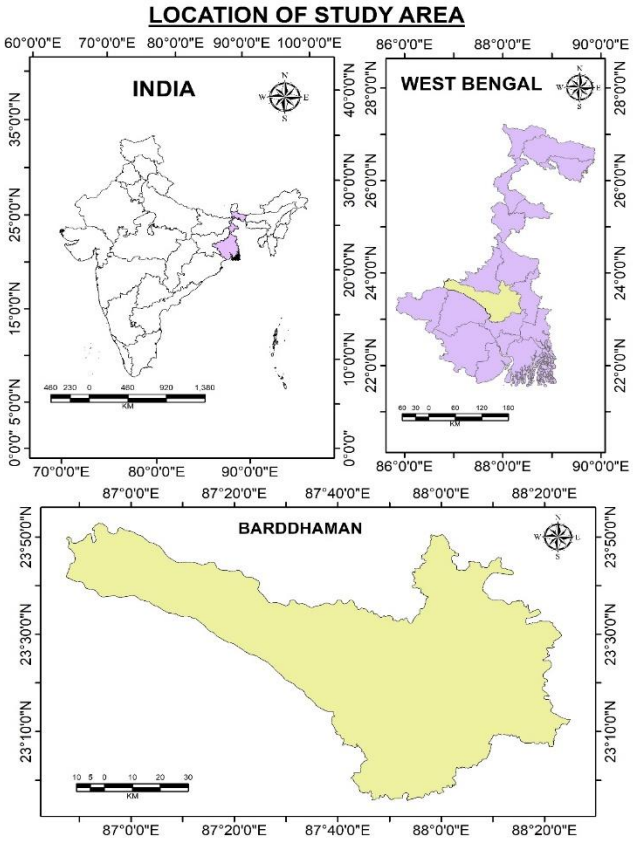



**Figure 1** Location map of study area

### 2.2 *Methodology*

Methodology is shown in Figure 2a. Various data and software used are given in Table 1 and Table 2 respectively. Two CMIP5(5th Coupled Model Intercomparison Project) GCMs were selected i.e., MIROC-ESM-CHEM and GFDL-CM3 because of data availability for all four RCP (2.6,4.5,6.0,8.5) scenarios. Observed station data was compared with GCMs' historical data (1990-2006) to find which GCM is more suitable for the study region. Overall, MIROC-ESM-CHEM showed better correlation (temperature-.93, windspeed-0.6 and precipitation-0.3) than GFDL-CM3(temperature- 0.95 windspeed-0.4 and precipitation- 0.24). So, the study has been proceeded using MIROC-ESM-CHEM. This GCM showed better correlation with temperature (.93) and windspeed (0.6) than precipitation (0.3). Initially the GCM outputs are gridded to the resolution of observed data i.e., 0.5°×0.5°.SD-GCM V2.0 software is used then to downscale precipitation, temperature, windspeed data from MIROC-ESM-CHEM. The downscaled outputs can have systematic biases. To remove the biases, bias correction is used. In this

study, Quantile Mapping is used as it showed better correlation (temperature- 1 windspeed- 0.998 and precipitation- .696) than Delta Method (temperature- 1 windspeed- .998 and precipitation- .695) and Empirical Quantile Mapping (temperature- 1 windspeed- .998 and precipitation- .687).
Arcinfo grid files of input data i.e., soil, slope, topography, land use, rainfall, wind speed, potential evapotranspiration, groundwater depth and temperature are prepared and also parameter tables i.e. land use summer, land use winter, runoff coefficient, soil in dbf format are prepared to be used as input in WetSpass. All grid files should have same number of columns and rows, cell size, number of bands, spatial reference and extent. The input files to the model were resampled to 5555*3527 raster cells with a cell size of (30*30) m. The model requires seasonal input parameters, so, four months i.e. June, July, August, and September (JJAS) are considered summer (main rainy season) and the remaining eight months i.e. January, February, March, April, May, October, November, December (JFMAMOND) are winter (dry season). The input maps (2000-2019) are shown in Figure 4. Potential Evaporation (PET) calculated using Thornthwaite formula given as

$$PET=16\times Lo\times(10\times T/I)^{a} \ldots\ldots\ldots\ldots\ldots (1)$$

where, T is the average monthly temperature. Lo = adjustment factor depending on the latitude of that place, a is an empirical constant given as

$$a= 6.75\times10^{-7}\times I^{3}-7.71\times10^{-5}\times I^{2}+1.792\times10^{-2}\times I+.49239\ldots\ldots\ldots\ldots\ldots (2)$$

$I=\sum i$ from January to December

$i=(T/5)^{1.514}$

Firstly, the meteorological data and other inputs are used as inputs to WetSpass to estimate the current recharge of groundwater, then the bias corrected future climate variables and other inputs are used as inputs to WetSpass for the prediction of future groundwater recharge. The difference between recent and future groundwater recharge is the impact of climate change.

**Table 1** Input Data and Sources

| SL.NO. | INPUT PARAMETERS | SOURCES |
|---|---|---|
| 1. | Soil | FAO |
| 2. | DEM(Topography & Slope) | USGS Earth Explorer |
| 3. | Land use Land cover | LANDSAT 8, USGS |
| 4. | Groundwater depth | India-WRIS, WebGIS |
| 5. | Precipitation (Summer & Winter) | power.larc.nasa.gov |
| 6. | Temperature (Summer & Winter) | power.larc.nasa.gov |
| 7. | Wind speed (Summer & winter) | power.larc.nasa.gov |
| 8. | Look up tables | Wetspass & Literature Review |
| 9. | GCMs | climate4impact.eu |

**Table 2** Software used in this study

| SL.NO. | SOFTWARE | FUNCTIONS |
|---|---|---|
| 1. | ERDAS Imagine | Layer stacking, LULC classification & Accuracy Assessment. |
| 2. | ArcMap 10.3 | Grid data preparation, Spatial data analysis, interpretation of data. |
| 3. | ArcView 3.3 & WetSpass Extention | Running Wetspass Model. |
| 4. | SD-GCM V2.0 | Downscaling of GCMs & Bias Correction. |

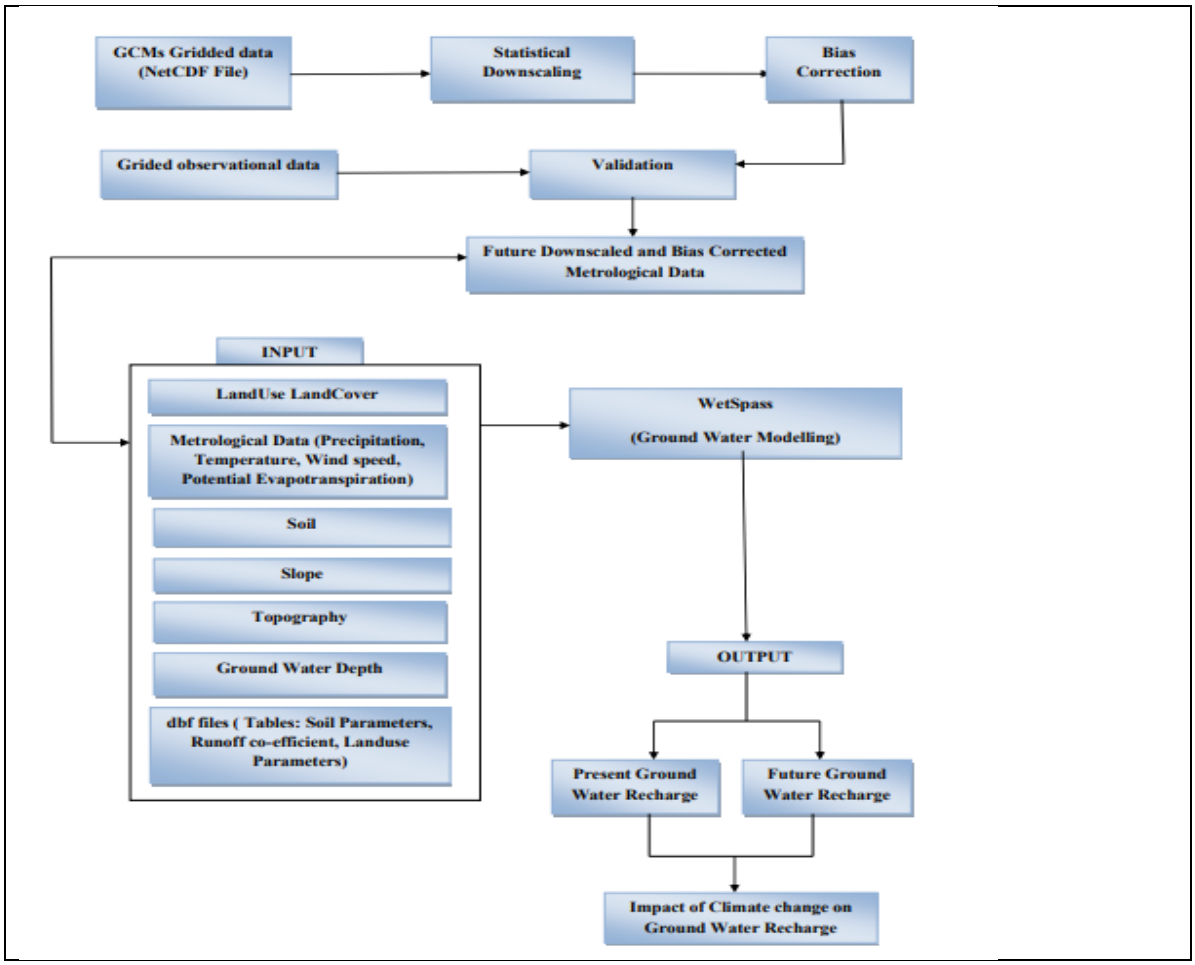



**Figure 2** Methodology

## 2.3 *WetSpass Model*

WetSpass (Water and Energy Transfer between Soil, Plants and Atmosphere under quasi–Steady State) is a distributed seasonal-water balance model, that requires ArcInfo grid files (soil, slope, topography, land use, rainfall, wind speed, groundwater depth, temperature and potential evapotranspiration) and as well as parameter tables in the form of dbf files (land use summer, land use winter, soil, runoff coefficient) as input for estimating annual and seasonal groundwater recharge values. WetSpass is a raster model integrated in GIS ArcView coded in Avenue. The spatially distributed recharge results obtained from WetSpass model can improve groundwater level forecasting, and the locations of discharge and recharge areas for a steady-state groundwater model. The model considers the area as a regular pattern of raster cells divided into four parts i.e., bare soil(s), impervious surface (i) vegetated(v) and open water(o) fractions. The independent water balances of these four fractions of a raster cell are shown in the Figure 3.

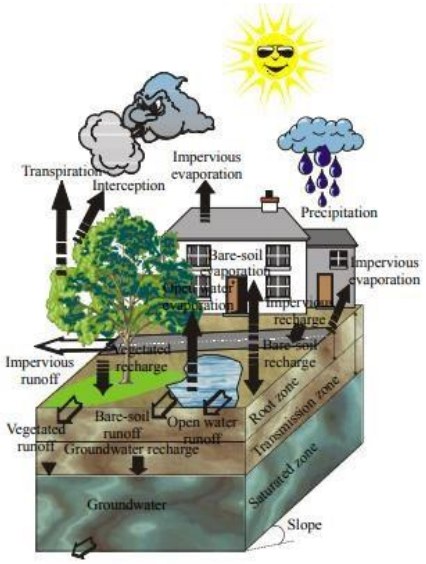
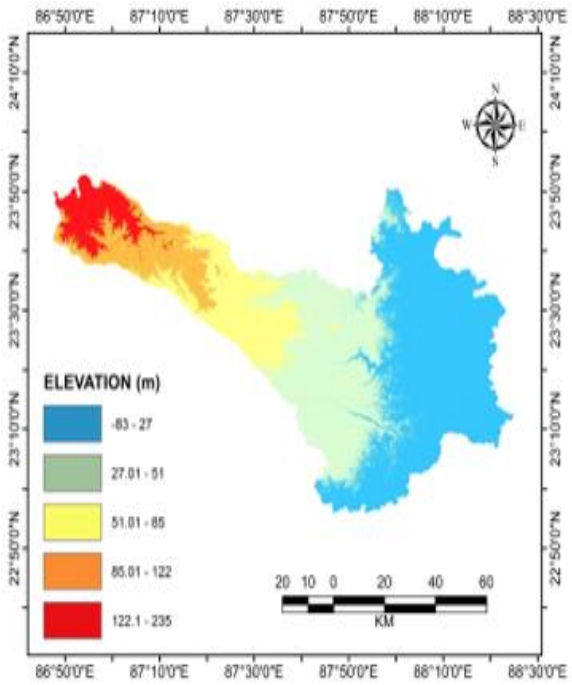


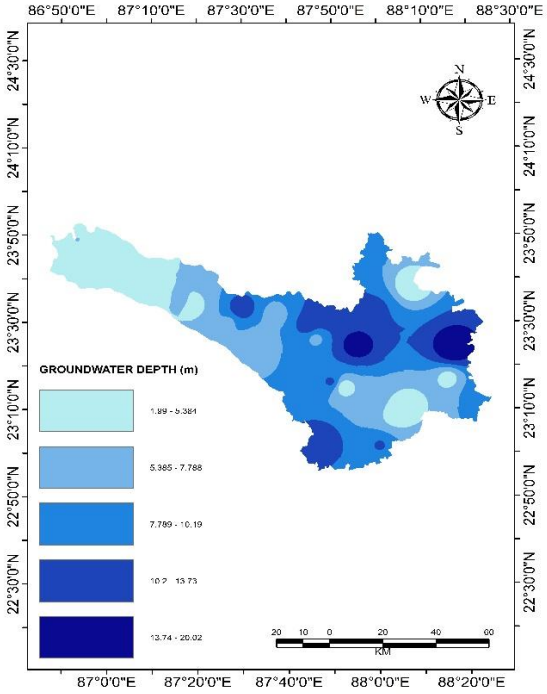

**Figure 3**. Schematic representation of water balance of a hypothetical raster cell (Batelaan and De Smedt 2001)

The recharge of groundwater is obtained from the following equation
$R=P-S-ET-E_S-I$…….. (3)

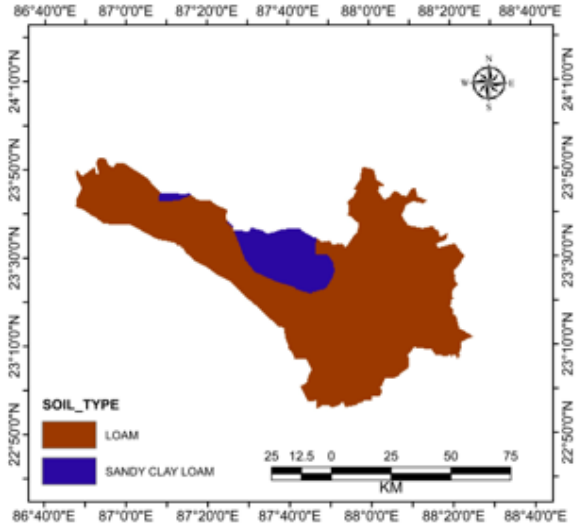
where, P= Precipitation [$LT^{-1}$]
R=Groundwater Recharge [$LT^{-1}$]
ET= Actual Evapotranspiration [$LT^{-1}$]
S=Surface Runoff [$LT^{-1}$]
$E_S$=Evaporation from bare soil [$LT^{-1}$]
I=Interception [$LT^{-1}$]
The total water balance of a raster cell as shown below:
Total Evapotranspiration, $ET_{raster} = a_sE_s + a_iE_i + a_vET_v + a_oE_o$ …….... (4)
Surface Runoff, $S_{raster} = a_sS_s + a_iS_i + a_vS_v + a_oS_o$ …….... (5)
Groundwater Recharge, $R_{raster} = a_sR_s + a_iR_i + a_vR_v + a_oR_o$ …….... (6)
$a_s$, $a_i$, $a_v$ and $a_o$ are the bare soil, impervious area, vegetated and open water fractions of a raster soil respectively.
The calibration and validation of WetSpass model is quite complex as compared to other hydrological models. However, the best way to calibrate and validate the groundwater recharge is by using Groundwater Modelling System (GMS) like MODFLOW. The groundwater recharge from WetSpass is used as input to MODFLOW to get groundwater depth as output. The output is then compared with the groundwater depth which was used as input to WetSpass. Due to unavailability of data, MODFLOW cannot be used so the model is assumed to be correct at first iteration.



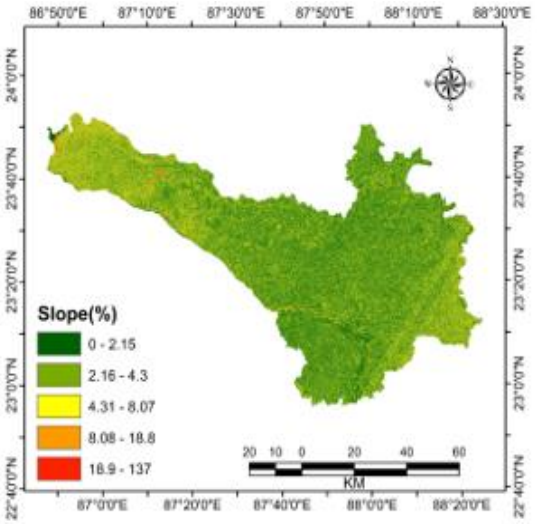

a. DEM of study area



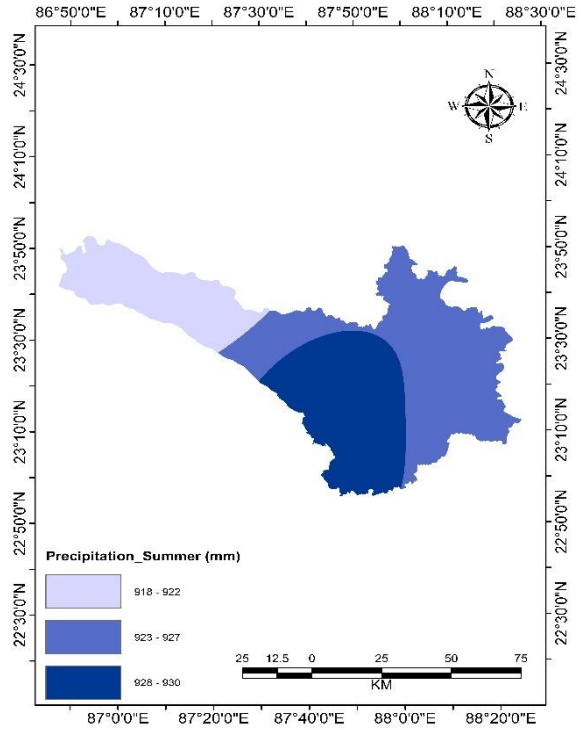

b. Groundwater Depth



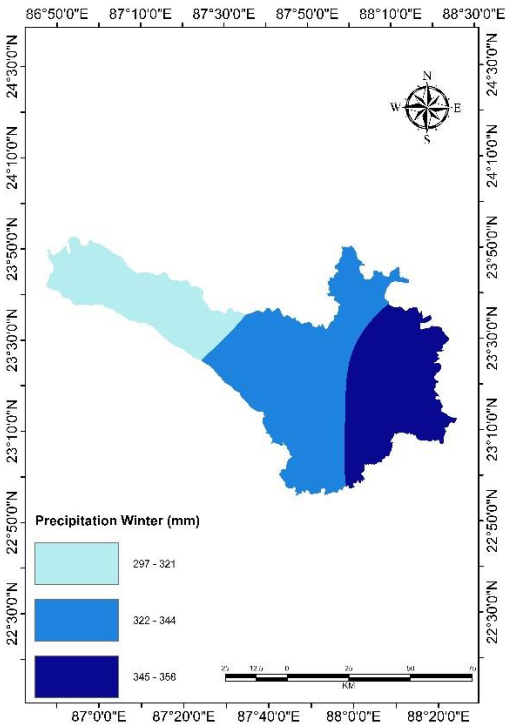

c. Soil Map of study area



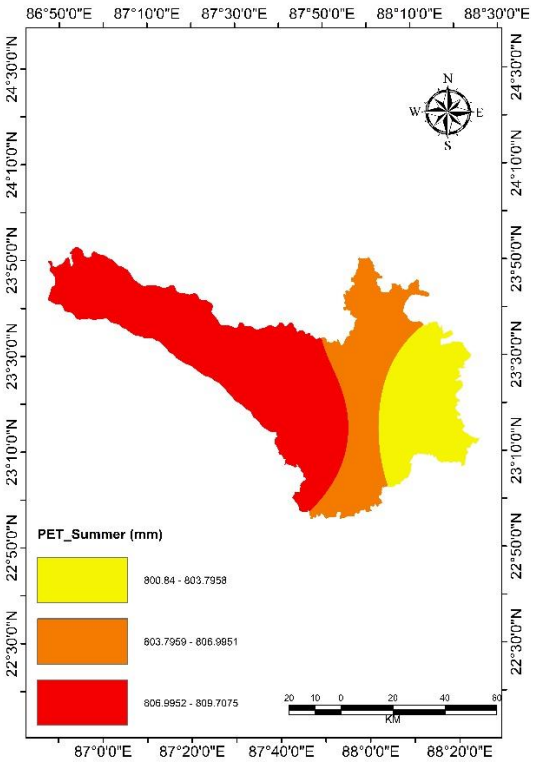

d. Slope Map of study area



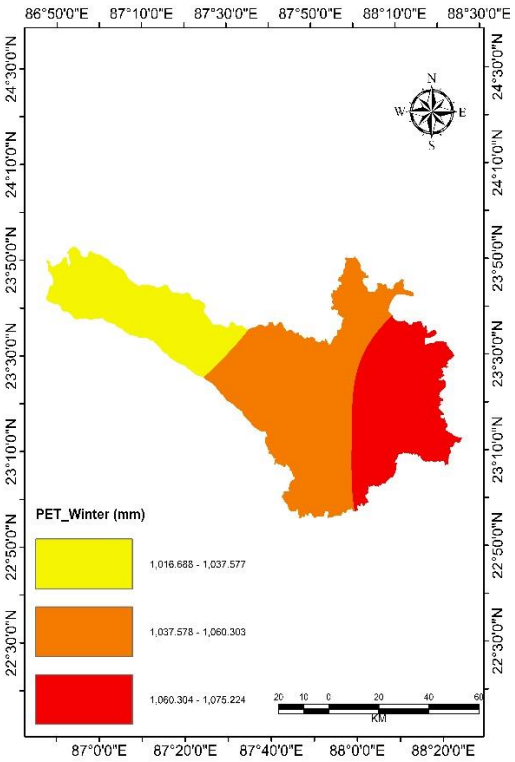

e. Average Precipitation (Summer)



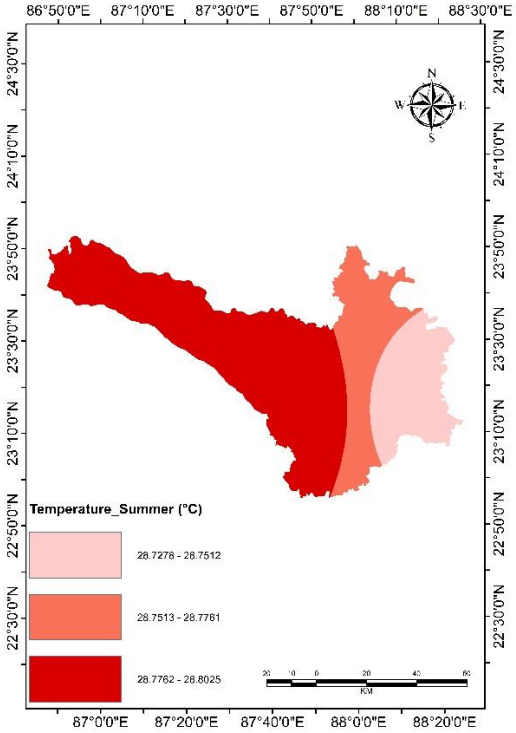

f. Average Precipitation (Winter)



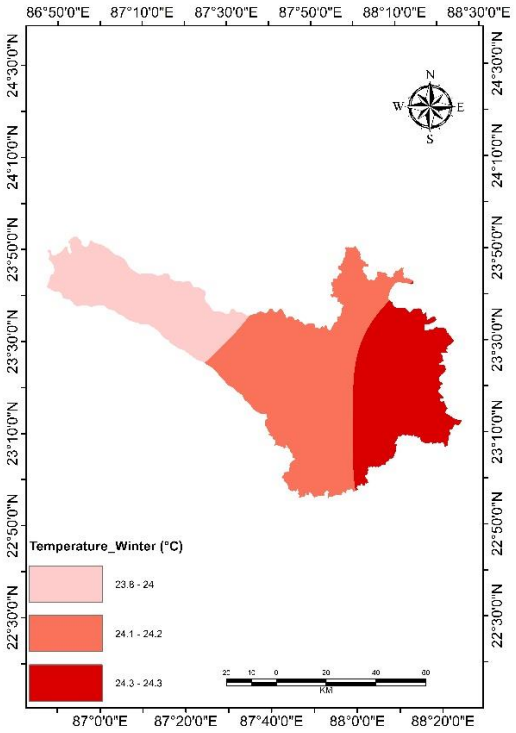

g. Average PET (Summer)



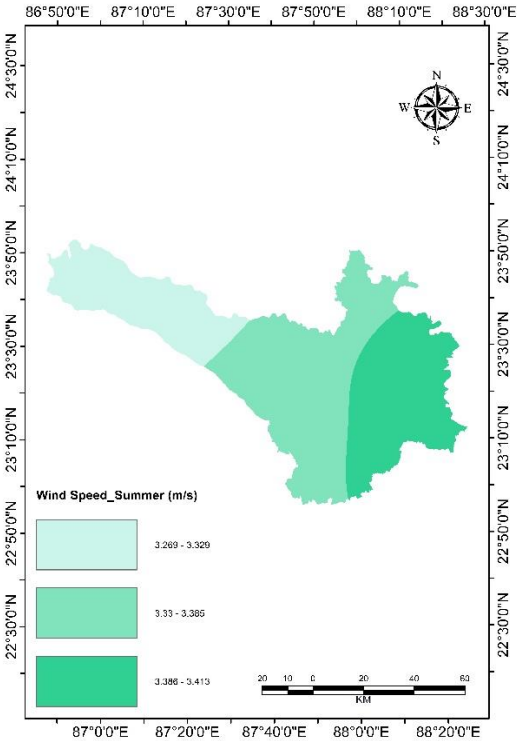

h. Average PET(Winter)



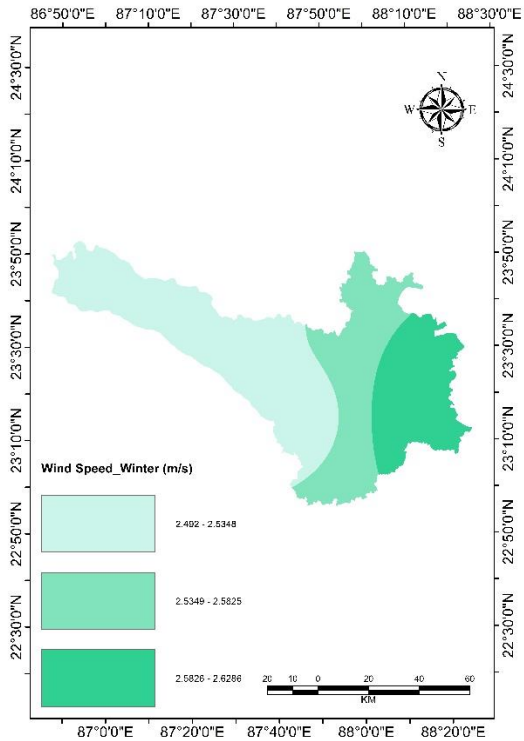

i. Average Temperature (Summer)



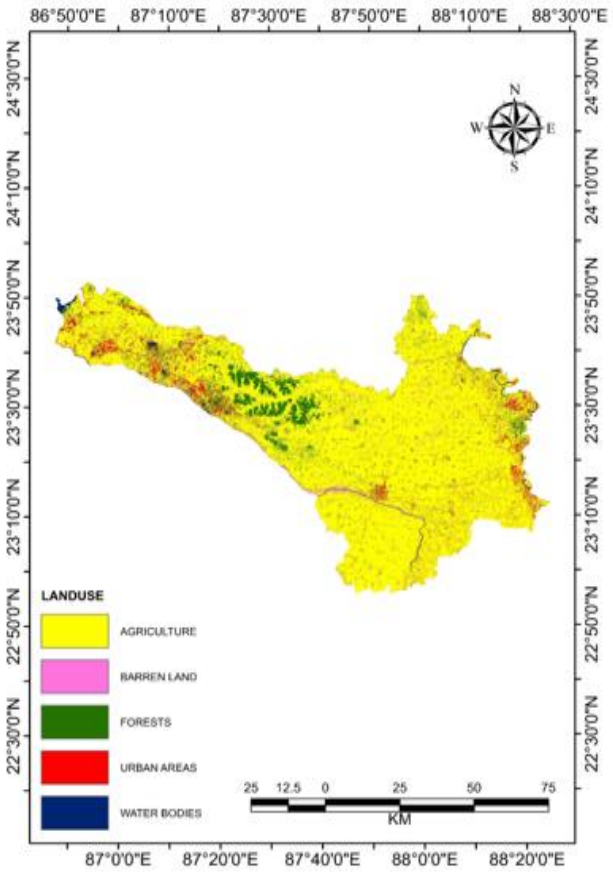

j. Average Temperature (Winter)




k. Average Windspeed (Summer)




l. Average Windspeed (Winter)




m. Landuse of Study Area

**Figure 4** Input Data for WetSpass Model (a to m)

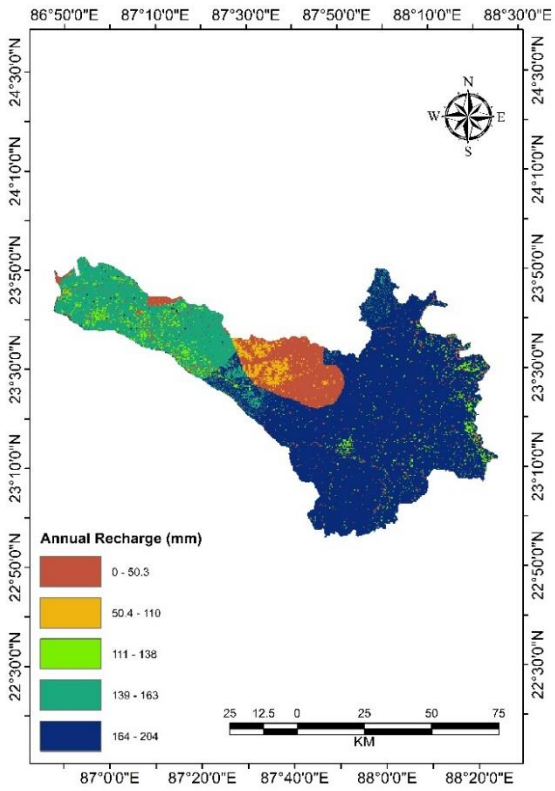
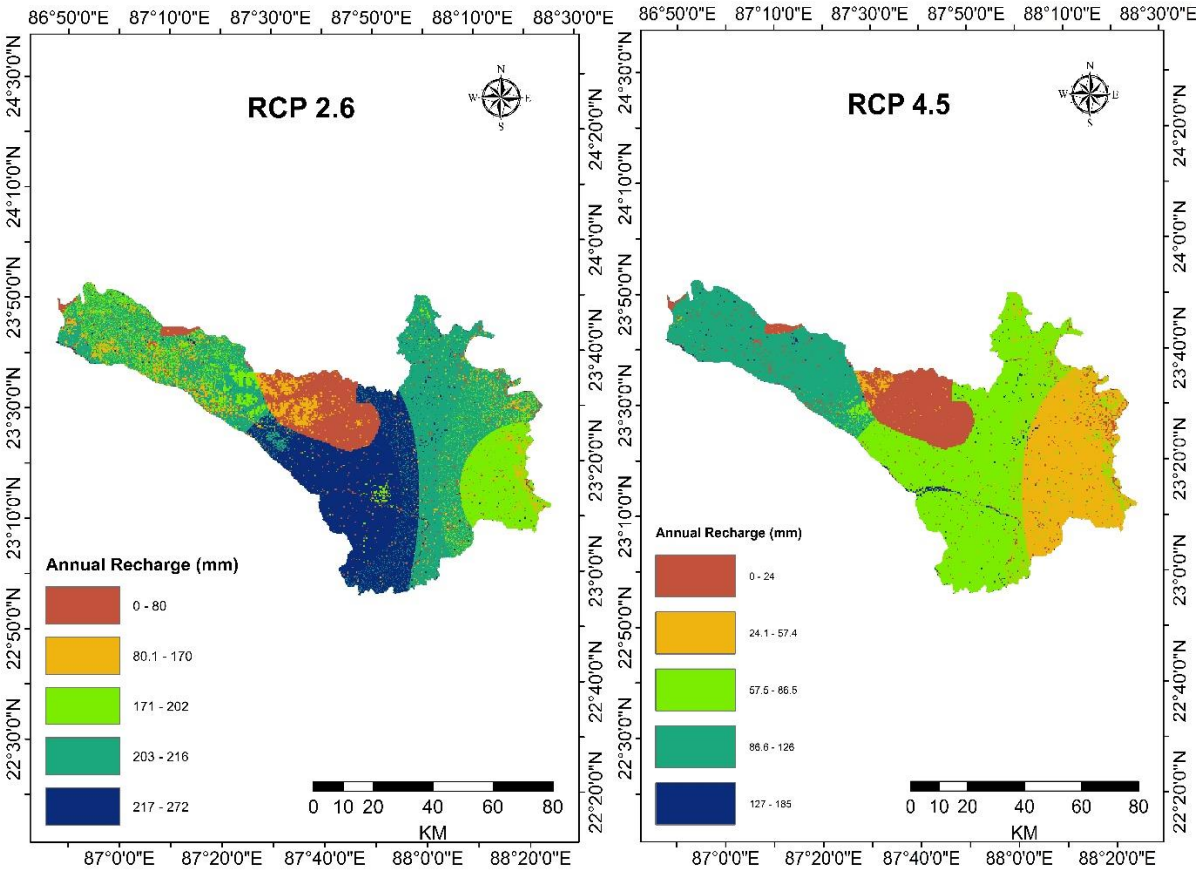



**Figure 5** Groundwater Recharge (2000-2019)

## 3.RESULTS

The average annual groundwater recharge of baseline period (2000-2019) is shown in Figure 5 ranging between 0-204 mm/year (the mean value being 102 mm/year) which accounts for 16.25% of precipitation. As per the climate change scenarios (2.6,4.5,6.0,8.5) , the average annual groundwater recharge for the future(2050-2059) is shown in Figure 6. In RCP 2.6 the average annual groundwater recharge varies from 0 to 272 mm/year( 21.725% of precipitation) with a mean of 136mm/year. Similarly for RCP 4.5 , RCP 6.0 and RCP 8.5 the average annual groundwater recharge varies between 0 to 185 mm/year(15.937% of precipitation) , 0 to 279 mm/year (21.6% of precipitation), 0 to 315 mm/year (22.24% of precipitation) with a mean of 92.5 mm/year, 139.5mm/year and 157.5mm/year respectively.All scenarios except RCP 4.5 has shown increase in groundwater recharge. The decrease in groundwater recharge in RCP 4.5 could be due decrease in precipitation though there is little decrease in temperature and windspeed. This indicates that an increase or decrease in precipitation has more effect than other climatic parameters in the region.



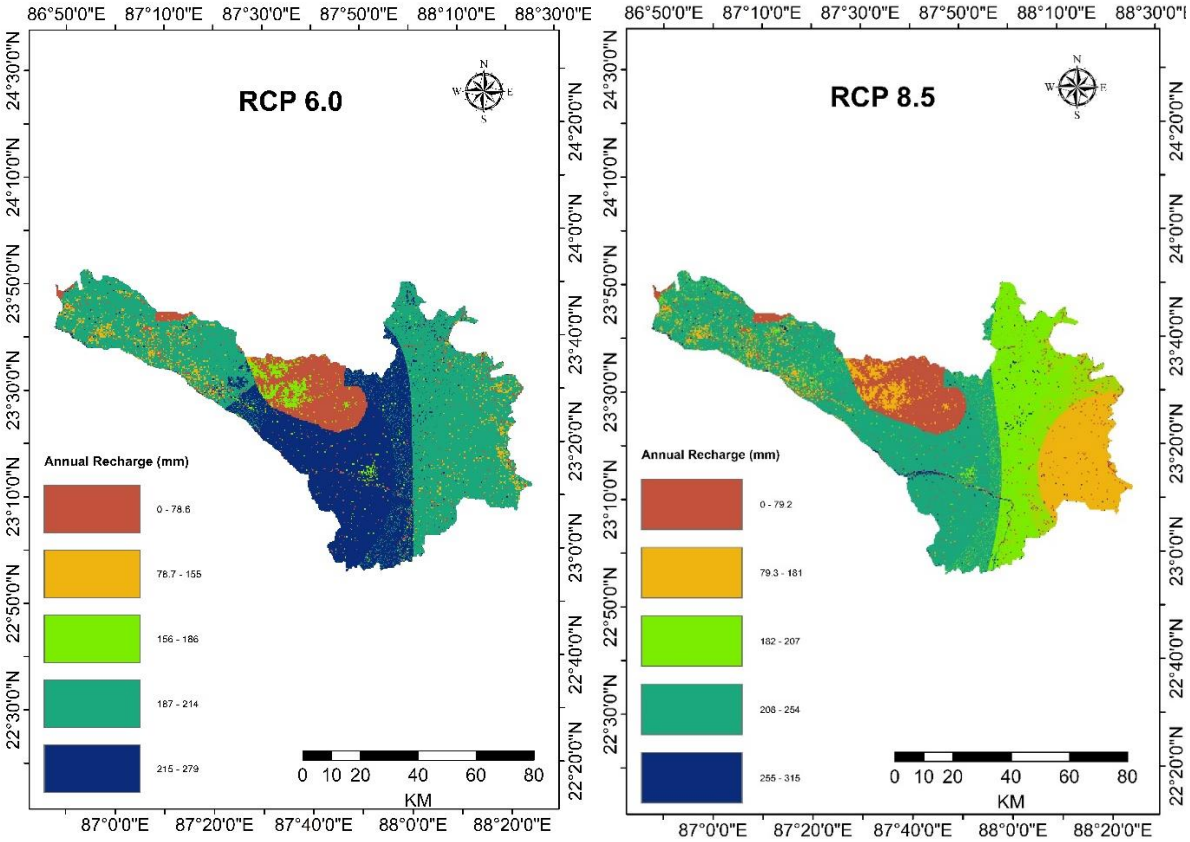



**Figure 6** Average Groundwater Recharge (2050-2059)

## 4.CONCLUSIONS

- Groundwater is a very important resource and is required to be preserved and protected from over-exploitation, climate change and pollution. In a developing country like India whose economy is mostly reliant on agriculture, the increasing population demands more and therefore effects of climate change on groundwater may be felt more severely.
- Research on climate change impact on groundwater are limited as long-time historical data are required that may not be always available.
- The main focus of this study was to present the effect of climate change on rainfall and other climatic parameters and study their impact on groundwater recharge. Rainfall has more impact on groundwater recharge in study area than other climatic parameters.
- The accuracy of MIROC-ESM-CHEM in predicting rainfall for this region is low.
- Even though uncertainties are there, response strategies based on the model may be valuable and accordingly proper strategies must be adopted to reduce or prevent the consequences of climate variability on groundwater resources.

## 5.LIMITATIONS

- In this study certain assumptions are taken such as land use of the study area is assumed to be unchanged in the future period.
- Uncertainties are less in the predicted data if ensemble of multi-model GCMs are used.

## REFERENCES


- Armanuos Asaad ,M. Negm Abdelazim ,Yoshimura C. Valeriano Oliver C.Saavedra, "Application ofWetSpass model to estimate groundwater recharge variability in the Nile Delta aquifer". Arabian Journal of Geosciences · July 2016 DOI: 10.1007/s12517-016-2580-x
- Batelaan, o. En f. De Smedt, WetSpass a flexible, "GIS based, distributed recharge methodology for regional groundwater modeling". 2001
- Central Ground Water Board Department of Water Resources, RD & GR Ministry of Jal Shakti Government of India, "Dynamic Ground Water Resources of India, 2017"
- Ghouili Nesrine, Horriche Faten Jarraya, Zammouri Mounira, Benabdallah Sihem.Farhat Boutheina , "Coupling WetSpass and MODFLOW for groundwater recharge assessment: case study of the Takelsa multilayer aquifer, northeastern Tunisia". Geosciences Journal GJ
- Hassan Waqed Hammed. (2020). "Climate change impact on groundwater recharge of Umm er Radhuma unconfined aquifer Western Desert, Iraq". International Journal of Hydrology Science and Technology. 10. 392. 10.1504/IJHST.2020.108268
- Kahsay Kiflom Degef, Pingale Santosh M "Impact of Climate Change on Groundwater Recharge and Base Flow in the Sub-Catchment of Tekeze Basin, Ethiopia, Groundwater for Sustainable Development", https://doi.org/10.1016/j.gsd.2017.12.002
- Meresa, Esayas ,Girmay Abbadi, Gebremedhin Amare A. (2019). "Water Balance Estimation Using Integrated GIS-Based WetSpass Model in the Birki Watershed, Eastern Tigray, Northern Ethiopia". Physical Science International Journal, 22(3)
- M Pandian, UAB Rajasimman., & J Saravanavel, "Identification of Groundwater Potential Recharge Zones using WETSPASS Model in parts of Coimbatore & Tiruppur Districts in Tamil Nadu", India. International Journal of Water Research
- Singh R. D. & Kumar C. P, "IMPACT OF CLIMATE CHANGE ON GROUNDWATER RESOURCES."
- Shrestha Sangam, Anh Ngoc,Hoang Thi, Shrestha Pallav Kumar, Bhatta Binod "Climate change impact on groundwater recharge and suggested adaptation strategies for selected Asian cities"
- Shrestha Sangam, Bach Tran Viet, Pandey Vishnu Prasad, "Climate change impacts on groundwater resources in Mekong Delta under representative concentration pathways (RCPs) scenarios". Environmental Science and Policy.
- Taylor Richard, "Ground water and climate change"

*IN PROCEEDINGS OF 25th HYDRO 2020, INTERNATIONAL CONFERENCE, NATIONAL INSTITUTE OF TECHNOLOGY ROURKELA, ODISHA, INDIA 26-28, March 2021, ISBN 978-93-90631-56-8*

Paper ID - 425

# Appraising Prolific Zones of Groundwater in hard rock phreatic aquifers from sub-watersheds of Upper Bhima Basin, Western India using Geospatial and MIF techniques

**Himanshu Gaikwad[1] Bhavana Umrikar*[1] Mandira Majumdar[2] C Krishnaiah[2]**

[1]*Department of Geology, Savitribai Phule Pune University, Pune 411007, Maharashtra, India*

[2]*CWPRS, Khadakwasla, Pune 411024, Maharashtra, India*

*Email: bnumrikar@gmail.com (Dr. Bhavana Umrikar- corresponding author)*
*himanshugaikwad23@gmail.com (Mr. Himanshu Gaikwad) mandira5ism@gmail.com (Dr. Mandira Majumdar)*
*krishnac26@gmail.com (Dr. Krishnaiah Chevva)*

## Abstract

A study on sub-watersheds of upper Bhima river basin namely BM-7,8,9,12,17,18,26,27,34 and 35 covering an area of 2360 sq.km was performed to decipher the potential groundwater zones. In remote and hilly areas, groundwater is considered as the primary source of water for drinking along with agricultural practises. The need for sustainable management of this resource is on rise due to the increase in demands. In the field of hydrogeology there has been a sudden breakthrough in exploring the subsurface water resources with the help of potentiality map. Keeping this in view, a prolific groundwater zonation map is prepared by applying the geospatial and Multi-Influencing-Factor (MIF) techniques. Various themes such as geology, geomorphology, slope, land utilization pattern, drainage and lineament densities, soil type and rainfall were considered as influencing factors and raster layers of the same were generated using satellite imageries and topographic sheets. MIF helps in assigning appropriate weightages and ranks to thematic layers and their feature classes that make some impact on groundwater occurrence. The map obtained by overlay analysis has been grouped in 5 classes from poor to excellent groundwater potential. This potential zonation map helps in planning and steady state development of this precious subsurface resource for efficiently meeting the future needs.

***Keywords**: Groundwater, basaltic aquifers, GIS, MIF, western India*

## 1. Introduction

A global population of around 2 billion is primarily dependant on groundwater as a source of fresh drinkable water (Alley et al. 2002). More than 50% of this fresh water resource, has been used for irrigation in many parts of the world (Famiglietti, 2014). Globally it is seen that groundwater accounts for nearly 30% of whole fresh water reserves and is significant in food security vis-a-vis human resource development (Aeschbach-Hertig & Gleeson, 2012). With increase in demands from growing population, rapid industrialization and modern agricultural practices there has been an evident water scarcity over the past few decades. According to Lewis (2011) one of the biggest challenges in 21st century would be securing water in order to meet the growing demands. In most parts of Asia, groundwater recharge is largely dependent on the rainfall where water precipitates on the ground and infiltrates through the soils reaching the aquifers and replenishing the groundwater reserves. But with increasing variability in the precipitation rates and more extreme weather events observed in light of climate change would lead to increase in duration of draughts or flooding, thus having direct impacts on the availability and dependency on groundwater. Thus, in order to combat drought, achieve water resource management and sustainable development, identifying groundwater prolific areas is highly essential (Umrikar, 2015; Mundalik et al. 2018; Raskar et al. 2019; Datta et al. 2020; Rajasekhar et al. 2020).

With a population of over a billion, India is considered to be one of the largest consumers of groundwater, wherein approximately 230 cubic km/year is the average rate of consumption (Fienen & Arshad,2016). Groundwater catastrophe in this country is mainly associated with the meagreness of government's management plans, unscientific development, unjudicial utilization, industrial and agricultural interventions. According to reports published by CGWB (2013) an estimate consumption

of groundwater for irrigation, agriculture and urban water supply is 62%, 85% and 45% respectively. Evaluation of CGWB (2017), the primary origin of replenishable groundwater resources is recharge through rainfall, which accounts for 67% groundwater reserves. India being a country where the main source of income for the rural population is agriculture and farming and the consumption rate of groundwater in these regions is more than 90%, hence it is very essential to identify the potential zones of groundwater.

The Deccan Traps having an aerial extent of 500,000km$^2$ are one of the extensive formations in which groundwater is generally found in phreatic state in weathered zones just above the hard rocks and in confined/semi-confined state in cracks, joints, fissures, secondary porosities of vesicular amygdaloidal basalts in between successive lava flow (Limaye, 2010). Groundwater recharge in Deccan basalts is not easy as it seems to be. Recharging Groundwater in these terrains is not simply pushing the surface water into the subsurface and increasing volumes. Hence in order to determine the groundwater potential sites a lot of researchers have adopted various techniques. Both direct and indirect techniques have been used in an approach to quantify natural groundwater regime (Scanlon et al. 2006; Mondal et al. 2012). The direct method such as tracer techniques, in which a recharge pulse is said to directly move through the pores in subsurface estimating the groundwater potential zones. This technique has been used been used almost all over the world by many scientists (Wright 1964; Reznek 1979; Krishnan 2015; Sebastian et al. 2018; Hoffmann et al. 2019). Stable isotope techniques are also one of the vastly used methods to determine the source and also the age of groundwater (Gonfiantini et al. 1998; barbeta et al. 2018, Yoon et al. 2018). Water table Fluctuation method (Yang et al. 2018; Bourgault 2016; Blarasin et al. 2016; Mondal and Singh 2004) is one of the Hydrogeological approaches along with base flow separation method (Gonzales 2009; Kouanda et al. 2018; Risser 2009) been used to estimate the groundwater potential. In addition to these various Geophysical techniques (Shailaja et al. 2018; Singh et al. 2016; Maliva 2009) especially electrical resistivity surveys are beneficial in characterization of aquifer. Geospatial and Geostatistical approach (Mallick et al. 2015) and Entropy based methods (Mondal and Singh 2010) have also been used. However, all these methods are time consuming, expensive and cannot be carried out everywhere in relation to highly undulating topography. Hence a simple and cost-effective method is used in this study.

Integrated Remote Sensing and GIS (RS-GIS) techniques have been deployed by many researchers for understanding the groundwater potential (Sohail et al.2019; Raju et al. 2019; Bhattacharya et al. 2020; Senapati et al. 2020; Zghibi et al. 2020; Paul et al.2020). Moreover, multi-criteria decision making (MCDM), probabilistic models (PM), bivariate statistics (BS), multivariate statistics (MS), and data-mining/machine learning (DM/ML) are some of the methods adopted for more accurate groundwater potential zone mapping in various regions worldwide. In this study an attempt has been made to decipher the groundwater potential zones (GWPZs) of upper Bhima River catchment area using Multi Influencing Factor (MIF) techniques. Thematic layers such as LU/LC, Lineament density, Rainfall, drainage density, Geomorphology, Soil and slope are used for deciphering the GWPZs. MIF is an effective technique that assigns scores to different parameters based on their major and minor influence on determining the GWPZs. This technique has been widely accepted by many researchers (Magesh et al. 2012; Das et al. 2017; Thapa et al. 2017; Fagbohun, 2018; Nasir et al. 2018; Anbarasu et al. 2019; Etikala et al. 2019; Kanagaraj et al. 2019) as it helps in identifying the most sensitive areas of GWPZ and assessing the error that leads to greater certainty.

## 2. Study Area

The study area is included in the Junnar, Ambegaon, Khed and Shirur Taluka of Pune District

(Fig:1). Detailed pre and post monsoon hydrogeological investigations were carried out in parts of Shirur, Manchar, Loni, Pabal, Kasari and Ganegaon villages. The area constitutes of major reservoirs namely Yedgaon, Dimbe, Chinchani dams. Kukadi, Meena, Kar and Ghod are the rivers draining the study area. The study region has an aerial extent of 2360 km.sq and lies between $18^0$ 30' 00" and $19^0$ 15' 00" North
latitudes and between $73^0$ 30' 00" and $74^0$ 30' 00" East longitudes.. The area is well accessible from Pune City (India) on 70km by road (Pune-Ahmednagar highway). The sub-watersheds show monsoon in month of June to September with uncertain and erratic rainfall with average annual of 497mm. It experiences hot tropical climate having 39°C-40°C temperature in summer months of April and May. The average yearly maximum temperature is about 33°C and minimum 22°C. Agriculture is the dominant occupation in the sub-watersheds and with rise in population the demand of groundwater is growing. The area is having availability of groundwater with canal water supply, sugarcane and elsewhere onion, legumes, vegetable are grown.

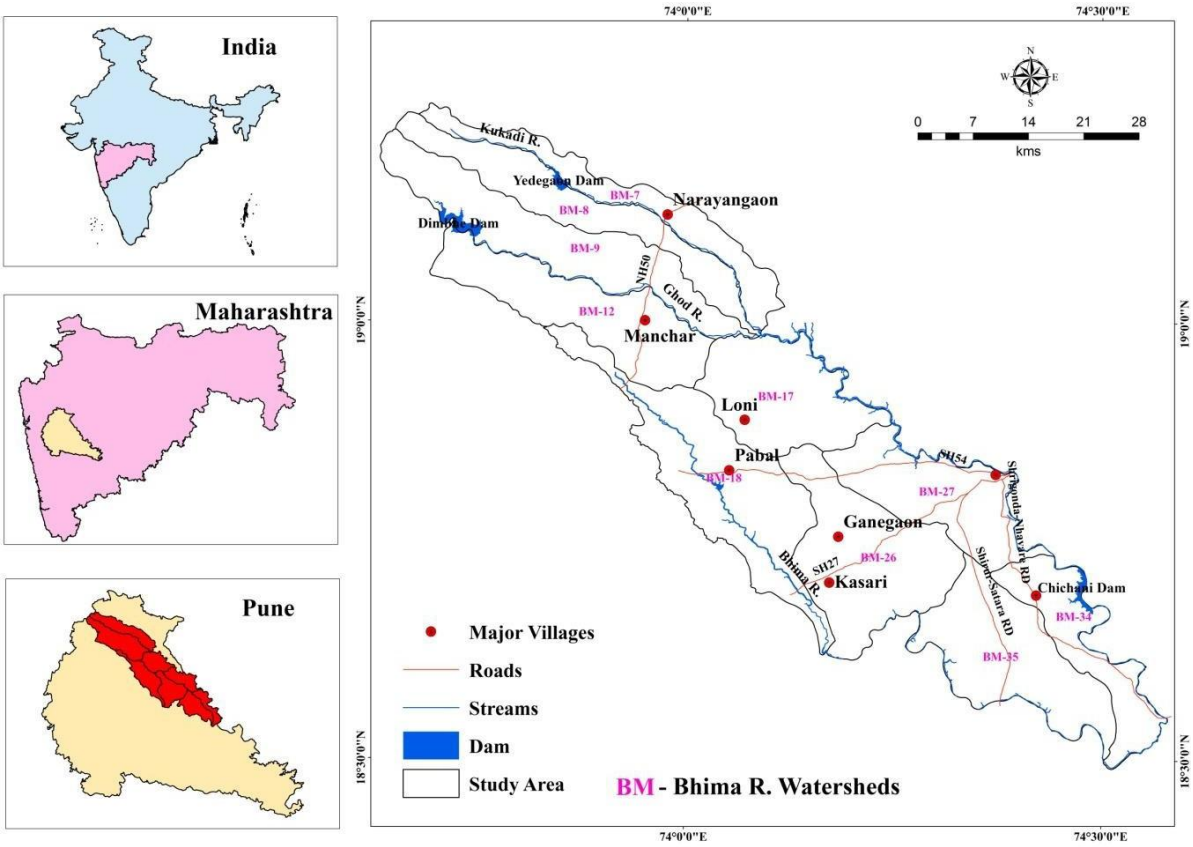



Fig 1: Location map of study area

## 3. Geology

The sub-watersheds of Upper Bhima basin area are covered by basalt flows of Cretaceous - Paleocene age with Quaternary alluvial and colluvio-alluvial deposits along the river banks. Geological mapping of the area has been done by Geological Survey of India (Sabale and Thorat, 1991) and the generalized geological map is created from the district map of GSI that gives the distribution of the various geological units (Fig. 2). The lava pile exposed in the area is made up of both compound pahoehoe flows and a`a flows; which have been grouped into Ratangarh and Indrayani Formations of the Sahyadri group of Deccan Trap Super Group. Also dissected patches of Karla Formation are seen in the north. The low-lying areas drained by Ghod and Kukadi rivers expose compound pahoehoe flows and megacrysts, with average elevation of 580m above msl. The compound pahoehoe flows which dominate the lower part of the pile form part of the Upper Ratangarh Formation.

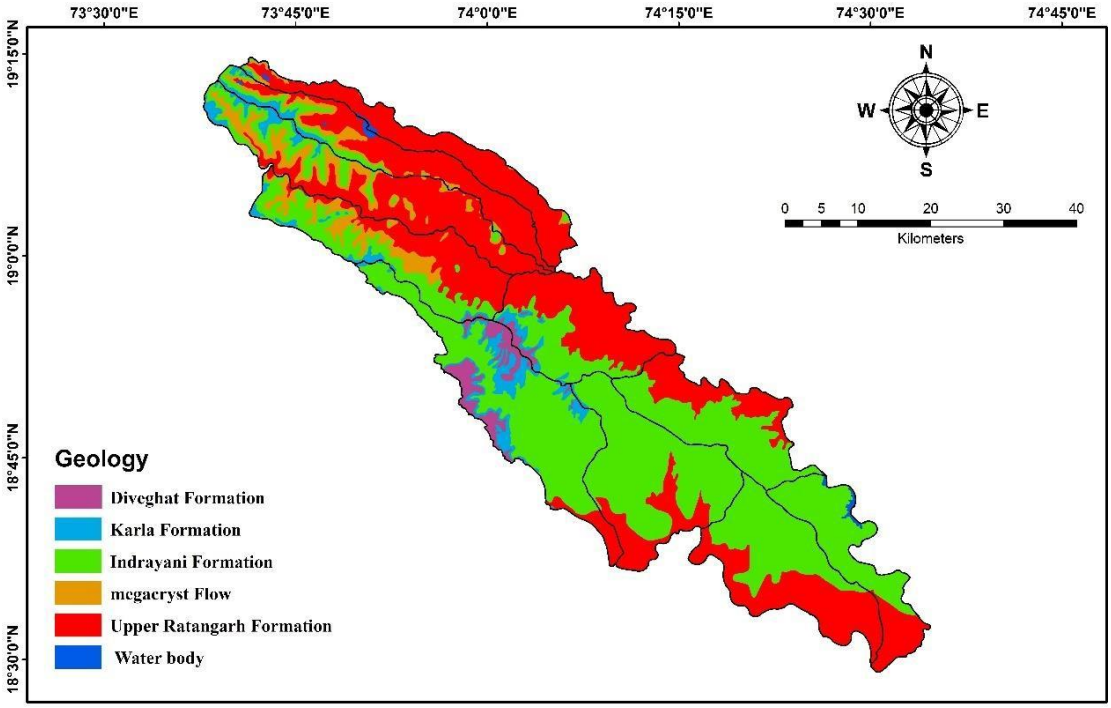



Fig 2: Geology of the area

The pahoehoe flows are compound in nature, with numerous small flow lobes/ units. The individual lobes show characteristic features like squeeze ups and in crack fillings. Plateau forming areas, mostly expose aà flows. Some of the isolated hills are constituted of alternating aà and pahoehoe flows. These flows belong to the Indrayani Formation and vary in thickness from 15 to 40m and exhibit crude columnar jointing and overall boulder appearance. The typical aa flows have a lower basal clinker, massive core and upper flow top breccia. Some flows of Indrayani Formation do not exhibit typical characters of a`a flow or pahoehoe flow. Basal clinker is rarely seen with intermittent exposures of brecciated flow top and at places only vesicular top. These flows show mixed characters, could be of transitional type. Red interflow horizons, commonly referred to as Red boles, are observed separating most of the flows. At places, where, distinct interflow horizons could not be delineated, the flow contacts were established based on the change in texture, jointing pattern and geomorphic expression. Mega phenocryst flows or giant plagioclase flows are delineated in the area, separates the dominantly pahoehoe pile below from the a`a pile above, i.e. the Upper Ratangarh Formation and Indrayani Formation and has been referred to as M3 megacryst. These flows that have giant plagioclase phenocrysts, with 2-3cm long plagioclase phenocrysts serve as marker horizons and aid in correlation. This M3 flow shows typical compound pahoehoe characters in area around Shirur. A well section near Shirur, exposes M3 marker horizon, where plagioclase laths measuring up to 3 -4cm are seen. It was observed that the frequency and size of laths vary, and some units are made up of only medium size phenocrysts. Megascopically, the flows are light to dark grey, fine to coarse grained, non- porphyritic to porphyritic. The porphyritic ones are mostly plagioclase phyric, with fine to coarse size phenocrysts exhibiting sparsely to moderately porphyritic nature. The pahoehoe flows exhibit fewer regular joints as compared to a`a flows. They exhibit sheet joints towards to top, parallel to the flow unit tops. The a`a flow in the area highly jointed, forming colonnade and entablature zones and more than one tiers. Fractures in the area trend NNW-SSE, NE-SW. The Deccan basalts are unconformably overlain by Quaternary alluvial and alluvio-colluvial sediments. The Quaternary deposits are thin and occur as discontinuous patches within the rivers Kukadi and Ghod. The alluvium is medium to coarse grained and calcareous in nature.

## 4. Material and Methodology

The processing of remotely sensed, field investigations and ancillary data was undertaken to decipher the areas having groundwater potential wherein the integration of all the themes has been carried out in GIS environment (Fig. 3).

To delineate the watershed boundary, ASTER-Global Digital Elevation Map (GDEM, 30m spatial resolution) was downloaded in Geo-TIFF format. The drainage lines were procured by applying hydro tool available in GIS software. The drainage divide line was digitized to generate the study area boundary and sub-watersheds were defined with the help of drainage network. Apart from this the DEM was also used to obtain the land slope. Lineament map and LULC map were generated from Landsat 8 image. Soil map is generated by referring the NBSS data.

The ranks were assigned to various parameters and weights were allocated to every sub-feature class under the specific factor using MIF techniques. Further, the rasterization of all themes for weighted overlay analysis was carried out assigning 30m*30m pixel resolution in ArcGIS 10 software. The integrated resultant map was divided into five classes depending on the potential variability. The verification of groundwater favourable zones was conducted using the data from 57 dug wells collected for static water depths by preparing and superimposing point vector data.

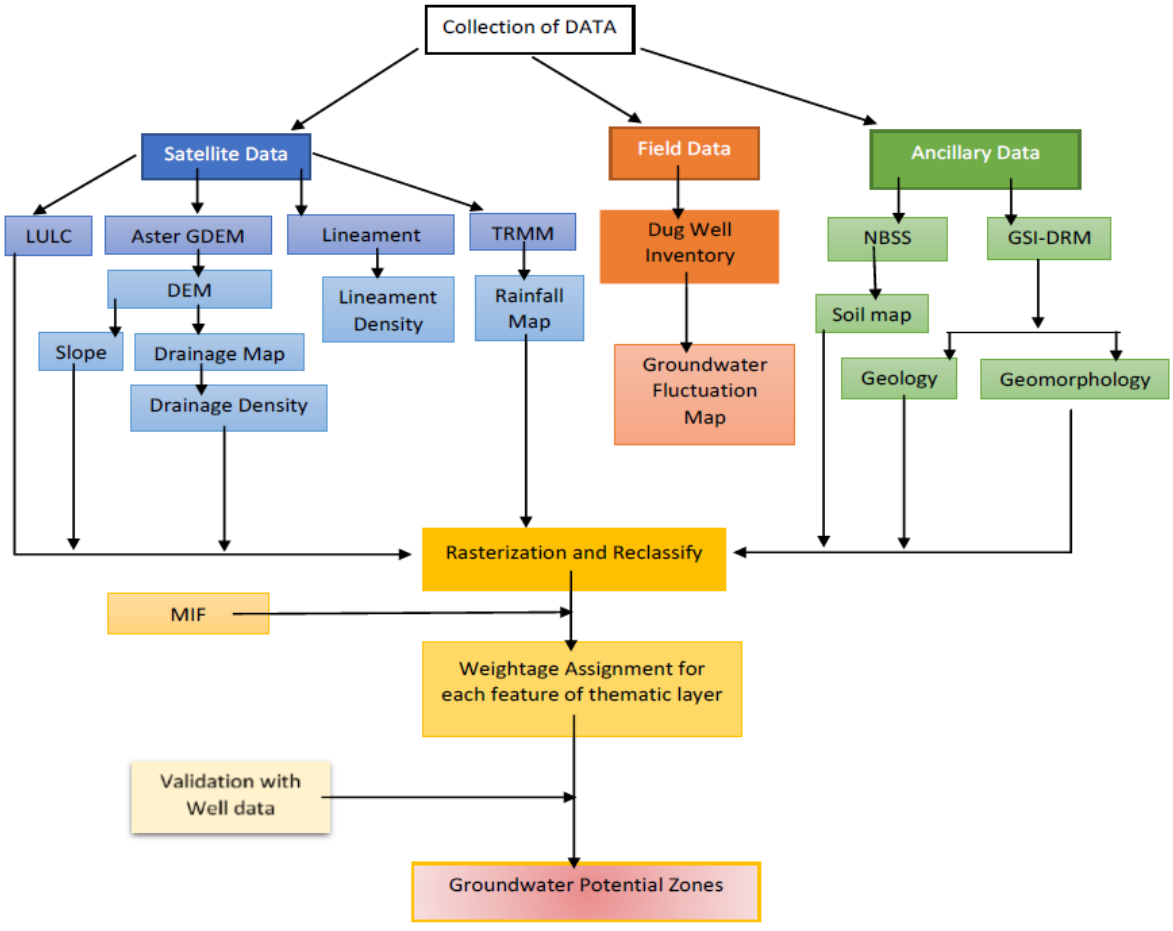



Fig 3: Flow chart of methodology.

### 4.1 Multi-influential Factors in zonation of groundwater potentiality

There are several direct and indirect indicators that have been generally considered for understanding the groundwater potential in a region. However, the degree of influence on groundwater potential

varies and hence there is a necessity to build an inter-relationship between them. Thus, the seven themes namely geomorphology, soil, land-use patterns, slope, rainfall, drainage and lineaments were submitted to establish a MI Factors network and weights were computed statistically to assign to each influencing factor for the delineation of potential sites (Fig. 4).

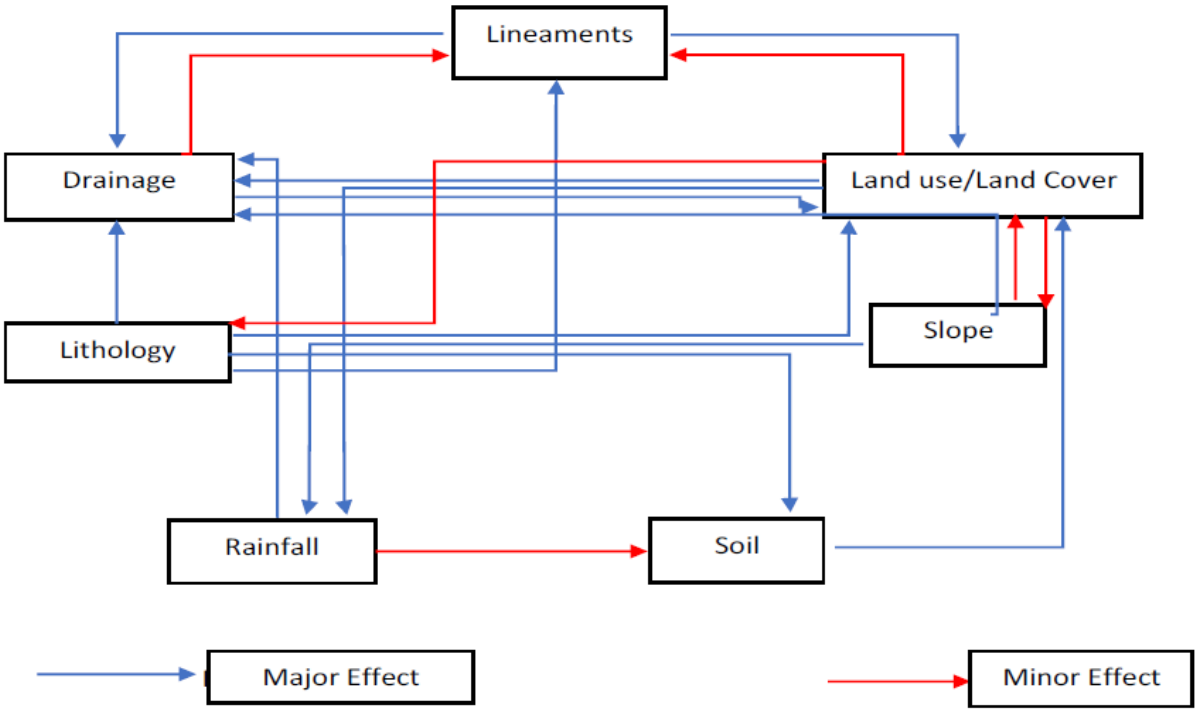



Fig 4: Interrelationship between the multi influencing factors concerning the GWPZ

Depending on the degree of influence on groundwater potential, various parameters were assigned with the higher and lower weights and ranks. The reclassified thematic raster maps were combined using weighted overlay tool to understand the cumulative impact of influence for delineating groundwater potential zones.

## 4.2 Assigning Weightage to Individual Parameters

The groundwater potential in a region is governed by various physiographical, climatic, hydrological and hydrogeological components. Each component is related to each other strongly or weakly. Thus, the strongly influential factors were allocated with a weightage of 1 and the effect of minor factor was assigned a value of 0.5. The totality of assigned weights has submitted as input data to compute the relative rates that facilitated the computation of final score (Eq. 1) of individual parameter.

$$\left[\frac{(A+B)}{\sum(A+B)} \times 100\right] \qquad \text{…….. Eq. 1}$$

Where, A: major interrelationship and B: minor interrelationship between two influential factors.

Table 1: Effect of influencing factor, relative rates and score for each potential factor

| Influential factors | Major Effect (A) | Minor Effect (B) | Proposed Relative Rates (A+B) | Proposed Score |
|---|---|---|---|---|
| Lineament Density | 1+1 | 0 | 2 | 13 |
| LULC | 1+1 | 0.5+0.5+0.5 | 3.5 | 22 |
| Geomorphology | 1+1+1+1 | 0 | 4 | 25 |
| Drainage Density | 1 | 0.5 | 1.5 | 9 |
| %Slope | 1+1 | 0.5 | 2.5 | 16 |
| Precipitation | 1 | 0.5 | 1.5 | 9 |
| Soil | 1 | 0 | 1 | 6 |
| | | | Σ16 | Σ100 |

Table 2: Rank assignment of subclasses as per the influence.

| **Sr. No** | **Classes** | **Subclasses** | **Rank** |
|---|---|---|---|
| 1 | Rainfall(mm) | Very high (1047-1466) | 9 |
| | | High (794-1047) | 7 |
| | | Moderate (597- 794) | 5 |
| | | Low (415 - 597) | 3 |
| | | very Low (178-415) | 1 |
| 2 | Slope(%) | Flat(0-5.6) | 16 |
| | | Gentle (5.7-16.9) | 12 |
| | | Moderate (17-35.2) | 8 |
| | | Moderately Steep (35.3-56.3) | 4 |
| | | Steep (>56.4) | 2 |
| **3** | Geomorphology | HDP-A, Denudational Hills. | 5 |
| | | MDP-B, Denudational Slopes. | 10 |
| | | MDP-C, Plateau. | 15 |
| | | Point Bar. | 20 |
| | | Shallow Alluvium Plain | 25 |
| **4** | Drainage Density | Very high | 9 |
| | | High | 7 |
| | | Moderate | 5 |
| | | Low | 3 |
| | | Very low | 1 |
| **5** | LULC | Hills | 1 |
| | | Settlement | 2 |
| | | Barren land | 5 |
| | | Fallow land | 8 |
| | | Agriculture | 15 |
| | | Vegetation | 22 |
| | | Waterbody | 0 |
| **6** | Lineament density ($m/km^2$) | Very high (4319.37-6883.97) | 13 |
| | | High (2645.62-4319.36) | 9 |
| | | Moderate (1457.79-2645.61) | 5 |
| | | Low (593.92-1457.78) | 3 |
| | | Very Low (0 – 593.91) | 1 |
| **7** | soil | Clayey Soil | 1 |
| | | Fine Soil | 3 |
| | | Loamy Soil | 6 |

## 5. Results and Discussion

### *5.1 Rainfall*

Rainfall is generally the most dominant factor of the hydrological cycle and thus has very important part to play in determining the potentiality of groundwater in any region irrespective of the type of geological set-up (Kadam et al. 2020). Most of the rainfall in the study region is received from the South- Westerly Monsoons. It ranges as high as 1466 mm mostly towards the NW part and lowest range observed it 178mm mostly towards the southern region(fig:5). Based on the influence it is categorised as Very High, high, moderate, low and very low classes. Keeping in mind that higher rainfall would result in higher potential of groundwater. However, in the NW parts of the study area is subjected to orographic type of monsoon due to presence of Hills and higher drainage density resulting in water being washed out in the form of runoff and extremely low infiltration rates. Hence proving the importance of other factors such as Drainage Density, Land use patterns and slopes giving a better picture to decipher the potentiality of the study regions. The highest rainfall is occurring in source region gets washed to below basin part due the high rainfall-runoff relationship results into low potential area in upstream part of study area.

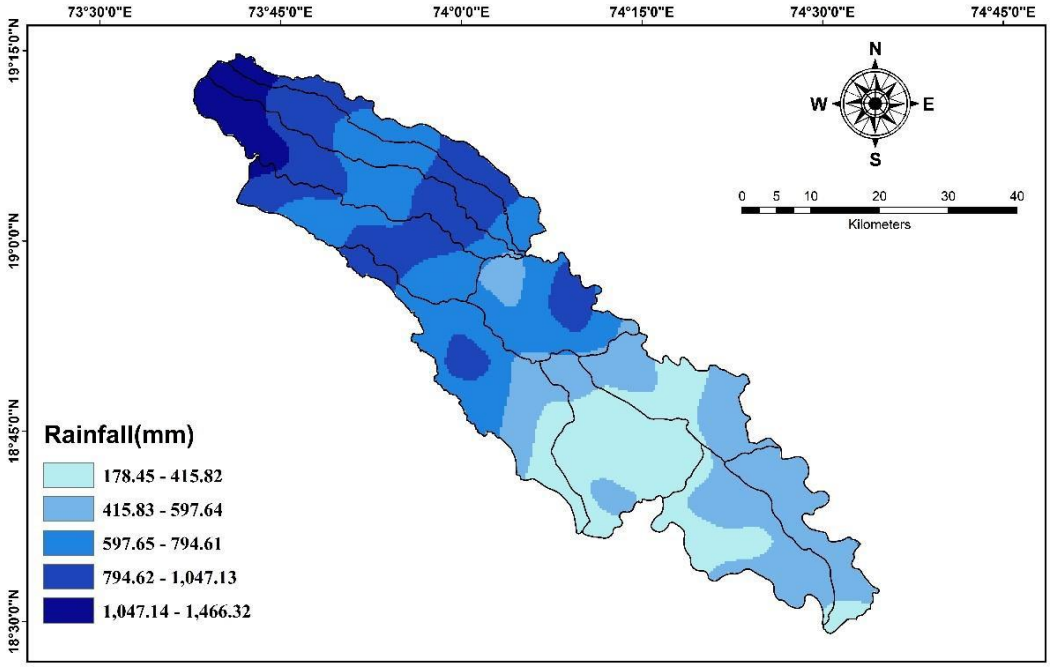



Fig 5: Rainfall of the study area

### *5.2 Slope*

The toporaphy of a region has a large role to play in the surface runoff generation and rate of infiltration and thus the slope of a region is important factor to determine the recharge and development of groundwater(Detty & Mcguire, 2010). The land capability and land utilization patterns are influenced by the presence of topographic slopes. Rainfall-runoff and rainfall-recharge ratios are aslo influenced by the types of slopes. The slopes in upper Bhima Basin is categorised as flat, gentle, moderate, moderately steep and steep(Fig:6). Most of the study area is having flat to gentle slopes, however with the presence of Hills (Western Ghats) in the peripheral parts of north western region steep slopes are observed. As the study area comprises of the Deccan Traps, presence of moderate to steep slopes is common. Flat to gentle slopes results in less runoff thus increasing time for infilration and hence are considered as higher ranks for determining the potentiality of groundwater followed by lower ranked steep slopes genreating high surface runoff.

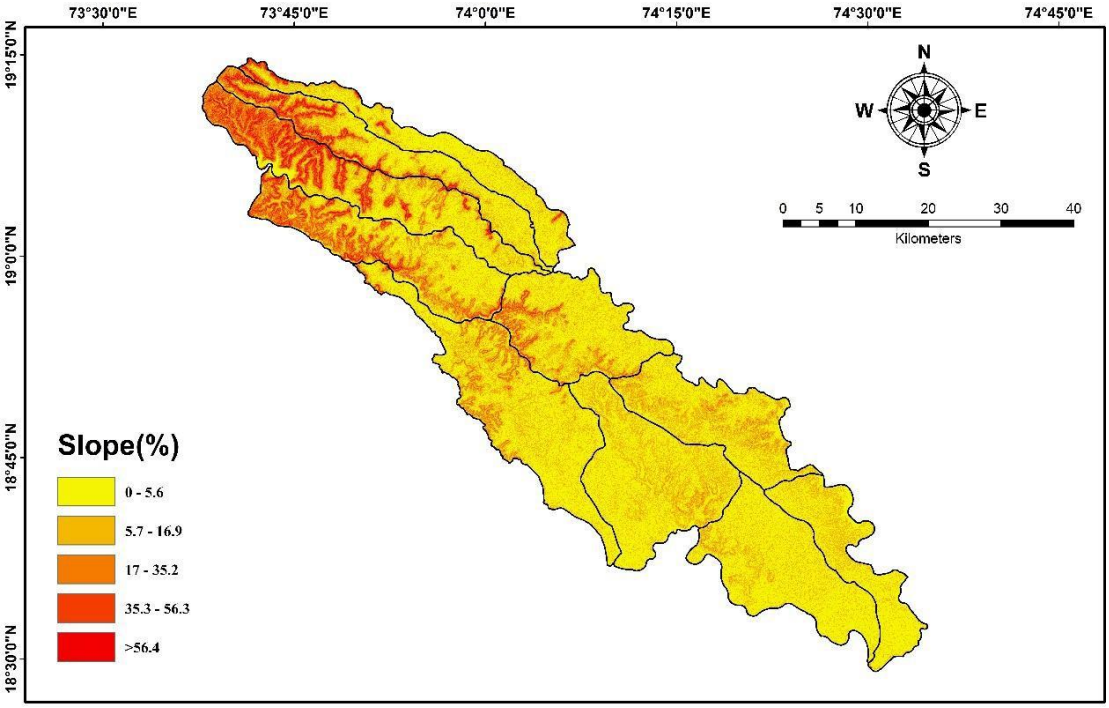



Fig 6: Slope of the study area

### *5.3 Geomorphology*

Geomorphological studies are mainly based on the mapping and delineation of various landforms. It also includes the investigation of drainage characteristics of the given area (Datta et al. 2020). These geomorphological investigations significantly help in correlating groundwater occurrence, flow and identifying the prolific areas in the region. Geomorphological set up is basically dependent on the factors such as climate, lithology and structure. There are different geomorphic elements observed in study area(Fig:7) especially the landforms that are categorized into dome type denudational hills(1.2%), highly dissected plateau with exposed rock and negligible soil cover(17.2%), moderately dissected plateau with exposed rock and thin soil cover(12.6%), moderately dissected plateau with moderate soil cover(34.4%), moderately dissected plateau with thick soil cover and thick weathered zone(24%), massive type denudational hills(0.1%), massive type residual hills(0.2%), Plateau top(2.3%), point bar (0.1%), shallow alluvial plain (2%), water body(2.3%), denudational slopes(3.3%). Highly dissected plateau along with moderately dissected plateau make up to more than 50% of the study area and act as good groundwater potential zones.

### *5.4 Drainage Density*

Drainage Denisty of any region is mainly dependant by the presence of geological, geomorphological setup and topographic relief (Horton, 1945). Dendrrtic drainainge pattern which is characteristic of deccan volcanic province is observed with parallel to sub parrallel arrangements in the first order streams(Fig:8). In the central parts of the area the streams are sparsely placed generating lowering density values. Especially in the NW of the area due to the presence of hills, there are higher concentrations of streams. Density values have been formulated as Very high, high, moderate, low and very low. Lower drainage density provides more time for infiltration and higher desnities gnerally show high surface runoff. Hence high ranks have been given to class having lower drainage density and vice versa(Fig:9).

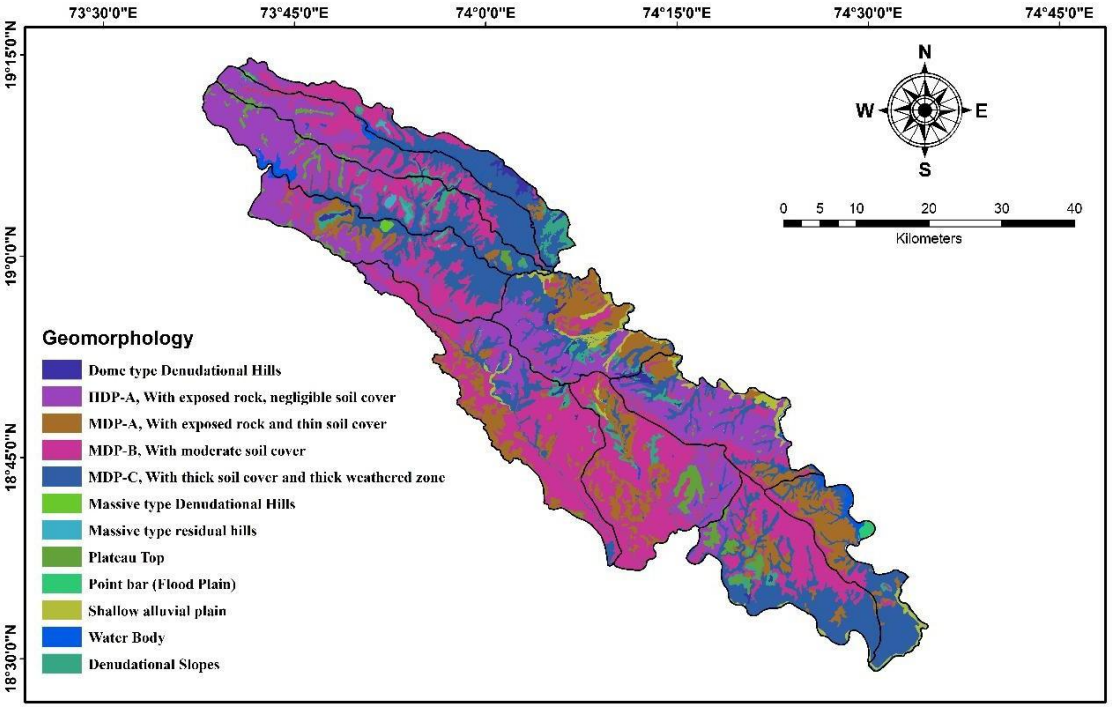



Fig 7: Geomorphology of the study area

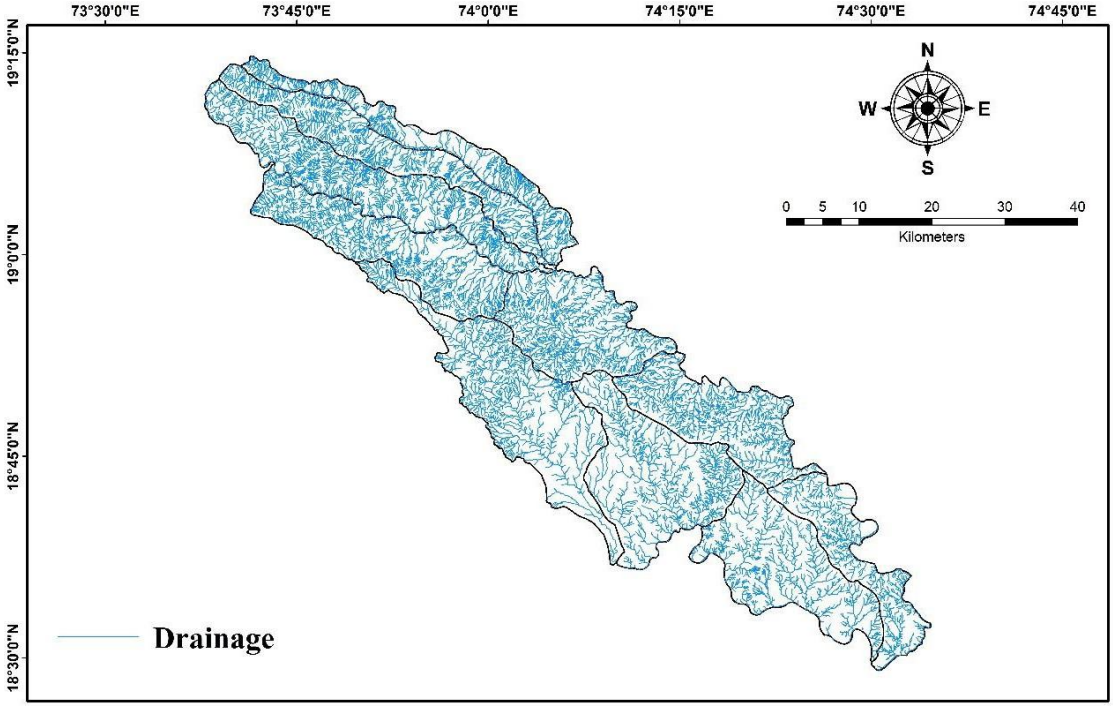



Fig 8: Drainage of the study area

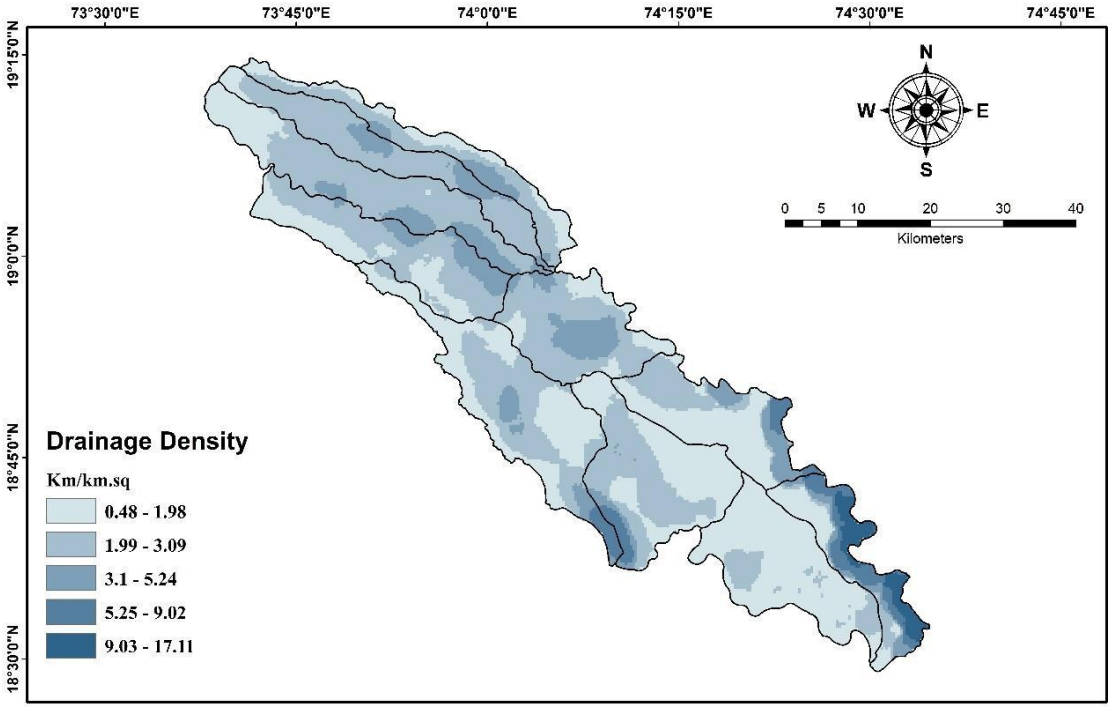



Fig 9: Drainage Density of the study area

### *5.5 Land Use Patterns*

Among the many decisive factors responsible for the governing of groundwater recharge, land utilization patterns are imperative. The changes in land patterns is a major concern for researchers globally, keeping into mind the rapid urbanisation. In order to estimate the groundwater recharge of a region, the knowledge of land use-land cover is must. The land use patterns observed in the study region(Fig:10) are Agriculture (38.6%), Barren land (18.4%), Fallow land (5.5%), Hills (33.5%), Settlement (1.2%), Vegetation (0.5%) and Water Body (2.3%). The agricultural land is major land use type present on plain land is having ample scope for recharge of surface water in subsurface strata result into high groundwater availability (Kadam et al. 2020). The second highest land cover in the region is Hills which is given low ranks as it does not facilitate the recharge of groundwater.

### *5.6 Lineament Density*

The storage and movement of groundwater in Deccan Volcanic Provinces are largely dependent on the presence of lineaments (Henriksen & Braathen, 2006). In the Upper Bhima Basin various major and minor lineaments whose lengths may vary from few centimeters to kilometers are present (Fig:11). These lineaments have potential to establish the hydraulic connectivity between shallow unconfined and deeper confined aquifers in the area. Thus, five classes namely poor, moderate, good, very good and excellent of lineament density have been formulated and maximum weight is given to higher the lineament density being more is it suitable for groundwater potential zones (Fig:12).

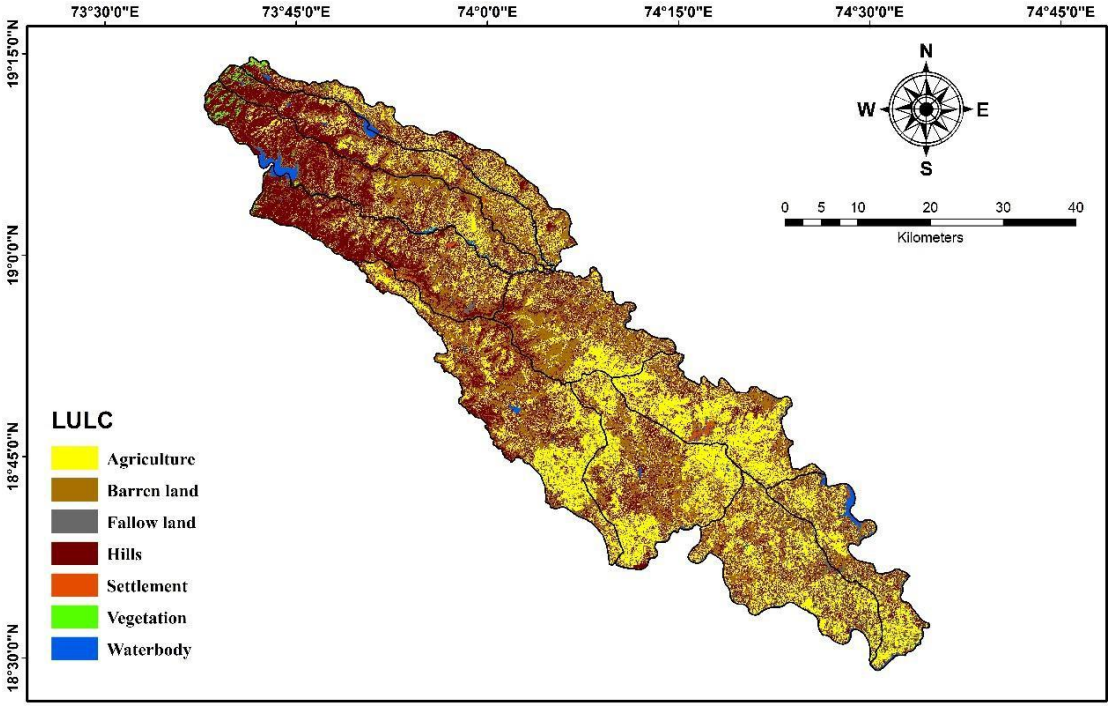



Fig 10: LULC of the study area

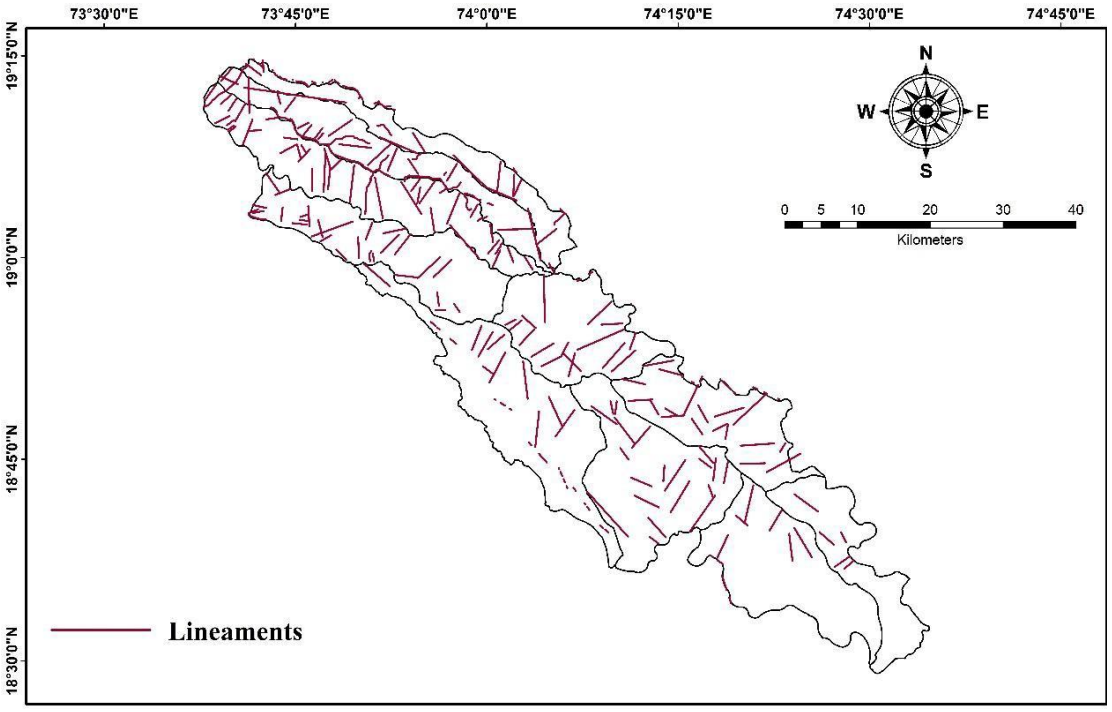



Fig 11: Lineaments of the study area

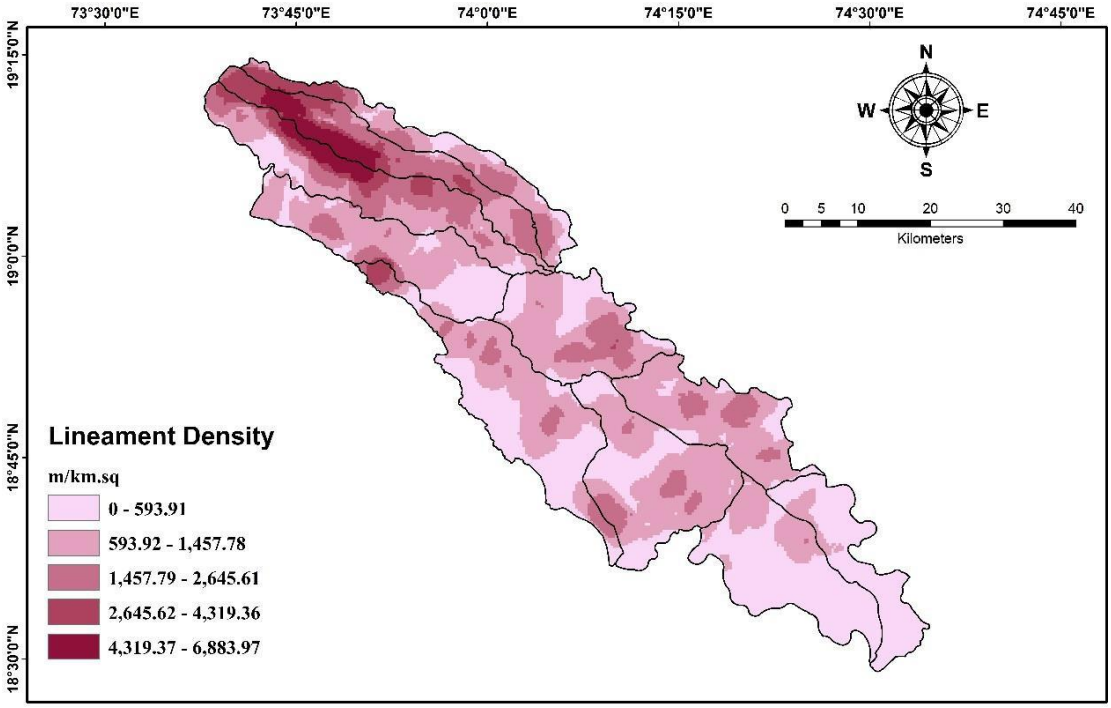



Fig 12: Lineament Density of the study area

### *5.7 Soil*

The type of soil is determined by the texture, strength and pore size distribution, etc. which further controls its porosity, permeability and infiltration capacity (Singhai et al. 2019). The soils of the area are mainly derived from Deccan basalts(Fig:13). The soil types observed in the area are mostly calcareous, clayey (36%), loamy(39%) and fine soil(25%). If the clay contain is increasing in the soil then it slows down the infiltration rate. The soil derived from basalt contains montmorillonite and kaolinite clay minerals. Based on the properties clayey, fine and loamy soils are categorized as poor, moderate and good respectively. The upstream part of study area is having clayey soil showing less groundwater potential due to less porosity, loamy soil is having porosity having capacity to infiltrate water showing high groundwater potential.

## 6. Potential areas for groundwater

The integration of rainfall, slope, soil, drainage density, lineament density, geomorphology, Land Use/Land Cover thematic layers using WOA has formulated the resultant map showing areas with variable degree of groundwater potential. The weightage derived from MIF techniques are used to conduct the analysis. From the technique, maximum weightage was given to geomorphological landforms whereas minimum weightage was assigned to soil types. The weights of different feature classes of each geo- environmental factor also show considerable variability based on their significance on the occurrence of groundwater. However, the weightage assigned to each factor may vary from region to region and is not constant.

The resultant map was further categorized as Excellent (Rank-5), Very Good (Rank-4), Good (Rank-3), Moderate (Rank-2), and Poor potential zones (Rank-1). About 7.6% of the area falls in excellent category(Fig:14). In this particular region there is a presence of weathered geomorphology of deposited plains and farming parcel with 0-6% of slope. It indicates that, geomorphology and gradient performed an important part in groundwater escalation. About 18.6% of the entire area present in the

'very good' zone, 29.6% present in 'good' zone due to the presence of dissected geomorphology, 34.7% falls in 'moderate' GWPZ, and 9.5% of the area is covered in 'poor' area. From this study it is observed that geomorphology, LULC, topographic relief and lineaments play a significant role in deciphering the potential zones. Excellent potential zones are dominantly observed in the catchment area of Chinchani Dams in and around Shirur village. Low to moderate groundwater potential zones are observed in the regions which have steep slopes in hard rock terrains.

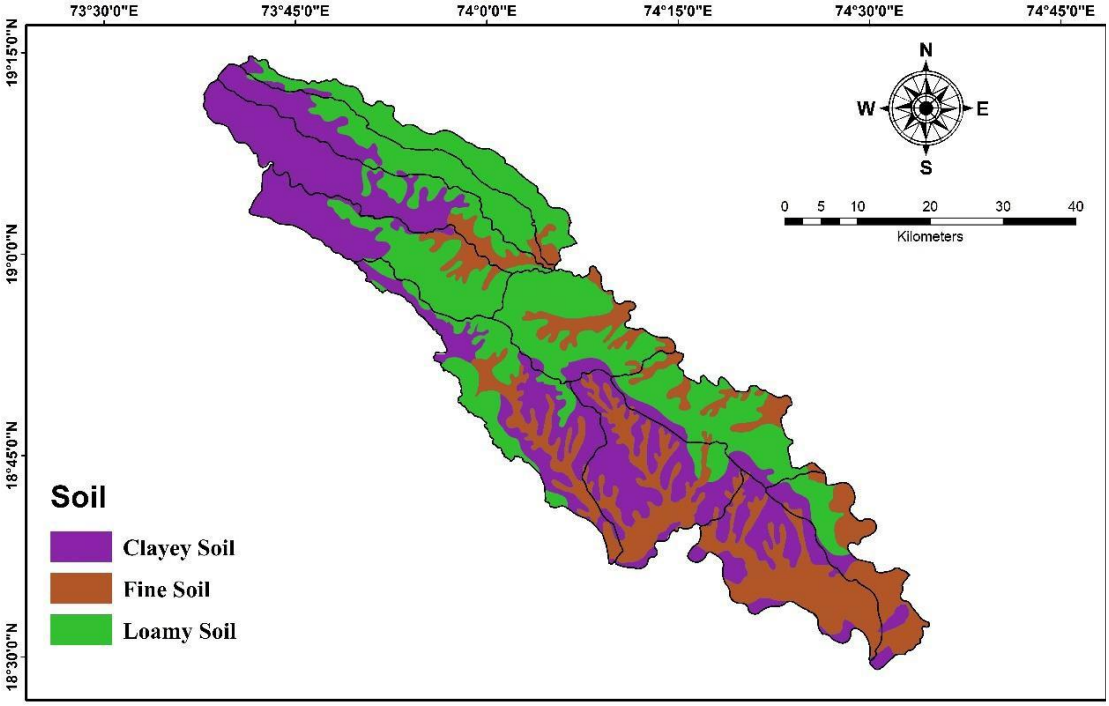



Fig 13: Soil of the study area

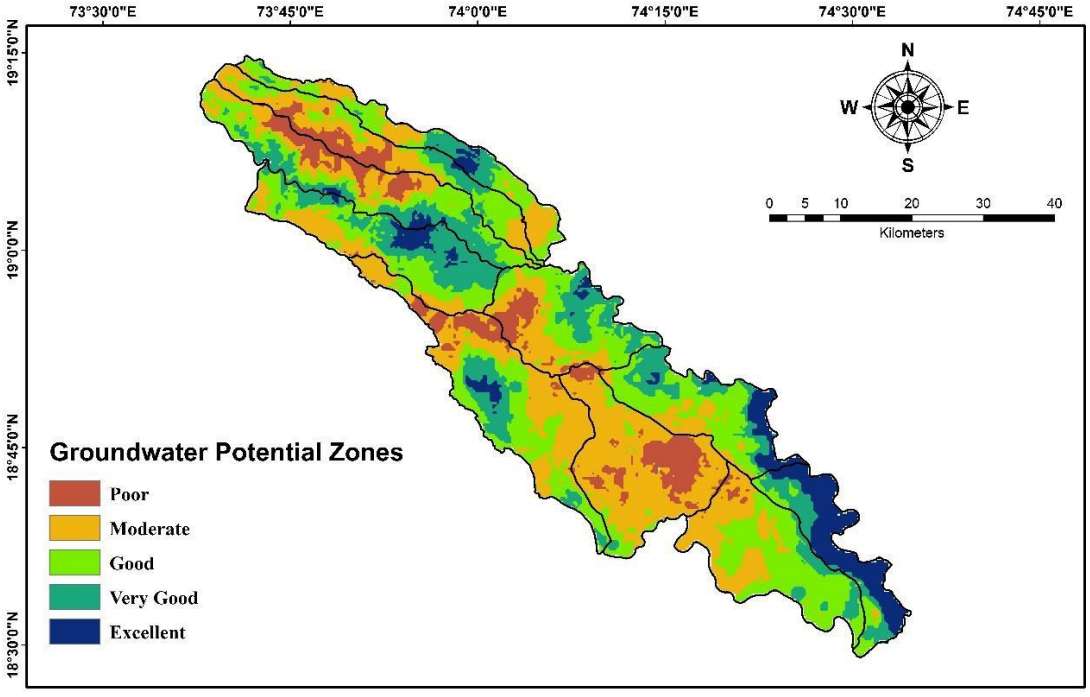



Fig 14: Groundwater Potential Zones of the study area

### 6.1 Groundwater Fluctuation

Well inventory was conducted and groundwater levels for both winter and summer seasons were recorded, from which a fluctuation map has been prepared. Lower groundwater level fluctuation is depicting higher groundwater storage, whereas higher groundwater fluctuation is depicting lower groundwater storage(Fig:15).

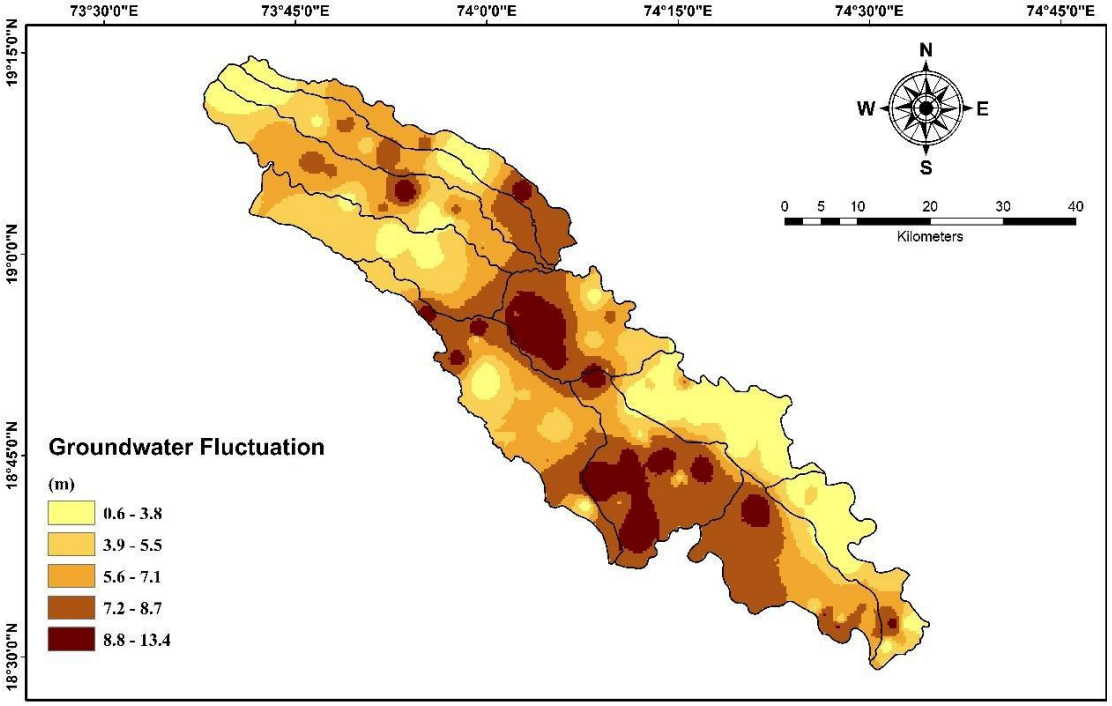



Fig 15: Groundwater Fluctuation of the study area

## 7. Conclusion

The groundwater potential zones of the upper Bhima Basin was generated using the RS-GIS and MIF techniques. Geospatial tools have proven to be beneficial in anticipating, surveying and appraising the groundwater resources, keeping in mind its ability of consumption in time. This research is focussed on the application and outcome of these advanced techniques to bring about sustainable development and management. Each thematic layer such as rainfall, relief, drainage density, lineament density, LULC and geomorphology provides certain clues that can be interpreted to understand the storage and movement of groundwater. Hence all these factors are integrated in one single layer by providing a suitable factor based on their degree of influence on replenishment of groundwater. The resultant map obtained was divided into five classes namely, 'poor' accounting nearly 118 $km^2$ (5%), 'moderate' 818.9 $km^2$ (34.7%), good 698.5$km^2$ (29.6%), very good 438.9$km^2$ (18.6%) and excellent nearly 179.3 $km^2$ (7.6%). The resultant data proves that MIF techniques is effective tool in groundwater management studies.

## 8. References

Aeschbach-Hertig, W., & Gleeson, T. (2012). Regional strategies for the accelerating global problem of groundwater depletion. Nature Geoscience, 5(12), 853-861.

Alley, W. M., Healy, R. W., LaBaugh, J. W., & Reilly, T. E. (2002). Flow and storage in groundwater systems. science, 296(5575), 1985-1990.
Anbarasu, S., Brindha, K., & Elango, L. (2019). Multi-influencing factor method for delineation of groundwater potential zones using remote sensing and GIS techniques in the western part of Perambalur district, southern India. Earth Science Informatics, 1-16.
Barbeta, A., Ogée, J., & Peñuelas, J. (2018). Stable-Isotope techniques to investigate sources of plant water. In Advances in Plant Ecophysiology Techniques (pp. 439-456). Springer, Cham.
Bhattacharya, S., Das, S., Das, S., Kalashetty, M., & Warghat, S. R. (2020). An integrated approach for mapping groundwater potential applying geospatial and MIF techniques in the semiarid region. Environment, Development and Sustainability, 1-16.
Blarasin, M. & Bécher Quinodoz, Fátima & Cabrera, Adriana & Matteoda, Edel & Alincastro, Nahuel & Giuliano Albo, María. (2016). Weekly and Monthly Groundwater Recharge Estimation in A Rural Piedmont Environment

using the Water Table Fluctuation Method. International Journal of Environmental & Agriculture Research (IJOEAR). 2. 104-113.
Bourgault, M., Larocque, M., & Garneau, M. (2016). Quantification of peatland water storage capacity using the water table fluctuation method. Hydrological Processes. 31. 10.1002/hyp.11116.
CGWB 2013 "Ground water pollution by industrial clusters. Bhu-Jal news, 28 (1–4), Ministry of Water Resources, river development and ganga rejuvenation, government of India". (Accessed 28 October 2019).
CGWB, 2017. Dynamic Groundwater Resources of India (As on 31st March 2013). Central Ground Water Board, New Delhi.
Das, S., Gupta, A., & Ghosh, S. (2017). Exploring groundwater potential zones using MIF technique in semi-arid region: a case study of Hingoli district, Maharashtra. Spatial Information Research, 25(6), 749-756.
Datta, A., Gaikwad, H., Kadam, A., & Umrikar, B. N. (2020). Evaluation of groundwater prolific zones in the unconfined basaltic aquifers of Western India using geospatial modeling and MIF.
Detty, J. M., & McGuire, K. J. (2010). Topographic controls on shallow groundwater dynamics: implications of hydrologic connectivity between hillslopes and riparian zones in a till mantled catchment. Hydrological Processes, 24(16), 2222-2236.
Etikala, B., Golla, V., Li, P., & Renati, S. (2019). Deciphering groundwater potential zones using MIF technique and GIS: A study from Tirupati area, Chittoor District, Andhra Pradesh, India. HydroResearch, 1, 1-7.
Fagbohun, B. J. (2018). Integrating GIS and multi-influencing factor technique for delineation of potential groundwater recharge zones in parts of Ilesha schist belt, southwestern Nigeria. Environmental earth sciences, 77(3), 69.
Famiglietti, J. S. (2014). The global groundwater crisis. Nature Climate Change, 4(11), 945-948.
Fienen, M. N., & Arshad, M. (2016). The international scale of the groundwater issue. In Integrated Groundwater Management (pp. 21-48). Springer, Cham.
Gonfiantini, R., Fröhlich, K., Araguás-Araguás, L., & Rozanski, K. (1998). Isotopes in Groundwater Hydrology. 10.1016/B978-0-444-81546-0.50014-8.
Gonzales, A.L. & Nonner, J. & Heijkers, J. & Uhlenbrook, Stefan. (2009). Comparison of Different Base Flow Separation Methods in a Lowland Catchment. Hydrol. Earth Syst. Sci., 13, 2055-2068, 2009. 13. 10.5194/hess-13- 2055-2009.
Henriksen, H., & Braathen, A. (2006). Effects of fracture lineaments and in-situ rock stresses on groundwater flow in hard rocks: a case study from Sunnfjord, western Norway. Hydrogeology journal, 14(4), 444-461.
Hoffmann, R., Wajid, U., Goderniaux, P., Dassargues, A., Maréchal, J. C., Chandra, S., ... & Selles, A. (2019). Cold water injections as innovative smart tracer technique in hot fractured aquifers.
Horton, R. E. (1945) Erosional development of streams and their drainage basins; hydrophysical approach to quantitative morphology. Geological society of America bulletin, 56(3), 275-370.
Kadam, A. K., Umrikar, B. N., & Sankhua, R. N. (2020). Assessment of recharge potential zones for groundwater development and management using geospatial and MCDA technologies in semiarid region of Western India. SN Applied Sciences, 2(2), 312.

Kanagaraj, G., Suganthi, S., Elango, L., & Magesh, N. S. (2019). Assessment of groundwater potential zones in Vellore district, Tamil Nadu, India using geospatial techniques. Earth Science Informatics, 12(2), 211-223.
Kouanda, B., Coulibaly, P., Niang, Dial., Fowe, T., Karambiri, H., Paturel, J. (2018). Analysis of the Performance of Base Flow Separation Methods Using Chemistry and Statistics in Sudano-Sahelian Watershed, Burkina Faso. Hydrology: Current Research. 09. 10.4172/2157-7587.1000300.
Krishan, G. (2015). Environmental tracer techniques in groundwater investigations. Water and Energy International. 58. 57-63.
Lewis, L. (2011). Water in Crisis: Spotlight Rural and Urban Issues in Africa. The Water Project, www. thewaterproject. org/water-in-crisis-rural-urban-africa. ph p (accessed on January 8, 2013).
Limaye, S.D. Hydrogeol J (2010) 18: 543. https://doi.org/10.1007/s10040-009-0566-4
Magesh, N. S., Chandrasekar, N., & Soundranayagam, J. P. (2012). Delineation of groundwater potential zones in Theni district, Tamil Nadu, using remote sensing, GIS and MIF techniques. Geoscience frontiers, 3(2), 189-196. Maliva, R.G., Clayton,E.A., Missimer, T.M. (2009) Application of advanced borehole geophysical logging to managed aquifer recharge investigations. Hydrogeol J 17(6):1547–1556
Mallick, J., Singh, C., Al-Wadi, H., & Mohd, m., & Rahman, A. (2015). Geospatial and geostatistical approach for groundwater potential zone delineation. Hydrological Processes. 29. 10.1002/hyp.10153.
Mondal, N.C., & Singh, V.P. (2010) Entropy-based approach for estimation of natural recharge in Kodaganar River basin, Tamil Nadu, India. Curr Sci 99(11):1560–1569
Mondal, N.C., & Singh, V.S. (2004) A new approach to delineate the groundwater recharge zone in hard rock terrain. Curr Sci 87(5):658–662
Mondal, N. C., Singh, V. P., & Ahmed, S. (2012). Entropy-based approach for assessing natural recharge in unconfined aquifers from Southern India. Water resources management, 26(9), 2715-2732.
Mundalik, V., Fernandes, C., Kadam, A. K., & Umrikar, B. N. (2018). Integrated geomorphological, geospatial and AHP technique for groundwater prospects mapping in basaltic terrain. Article history 2, 16.
Nasir, M. J., Khan, S., Zahid, H., & Khan, A. (2018). Delineation of groundwater potential zones using GIS and multi influence factor (MIF) techniques: a study of district Swat, Khyber Pakhtunkhwa, Pakistan. Environmental Earth Sciences, 77(10), 367.
Paul, R. S., Rawat, U., SenGupta, D., Biswas, A., Tripathi, S., & Ghosh, P. (2020). Assessment of groundwater potential zones using multi-criteria evaluation technique of Paisuni River Basin from the combined state of Uttar

Pradesh and Madhya Pradesh, India. Environmental Earth Sciences, 79(13), 1-24.
Rajasekhar, M., Gadhiraju, S. R., Kadam, A., & Bhagat, V. (2020). Identification of groundwater recharge-based potential rainwater harvesting sites for sustainable development of a semiarid region of southern India using geospatial, AHP, and SCS-CN approach. Arabian Journal of Geosciences, 13(2), 24.
Raju, R. S., Raju, G. S., & Rajasekhar, M. (2019). Identification of groundwater potential zones in Mandavi River basin, Andhra Pradesh, India using remote sensing, GIS and MIF techniques. HydroResearch, 2, 1-11.
Raskar, T., Gaikwad, H., Kadekar, O., & Umrikar, B. N. (2019). Impact Assessment of Water Harvesting Structures in Micro-Watersheds of Nira River Basin, Maharashtra, India.
Reznek, S., Hayden, W., & Lee, M. (1979). Analytical Note—Fluorescein Tracer Technique for Detection of Groundwater Contamination. Journal-American Water Works Association, 71(10), 586-587.
Risser DW, Gburek WJ, Folmar GJ (2009) Comparison of recharge estimates at a small watershed in east-central Pennsylvania, USA. Hydrogeol J 17(2):287–298
Sabale. A. B. and Thorat. P. K. (1991) Geology of parts of Pune and Ahmednagar districts, Maharashtra. Unpublished Progress Report for FS 1989-90
Scanlon, B. R., Keese, K. E., Flint, A. L., Flint, L. E., Gaye, C. B., Edmunds, W. M., & Simmers, I. (2006). Global synthesis of groundwater recharge in semiarid and arid regions. Hydrological Processes: An International Journal, 20(15), 3335-3370.

Sebastián, C. & Maguiña, J. & Maghella, G.. (2018). Determination of Flow Velocities in Groundwaters by the Aid of Tracer Techniques. Journal of Chemistry and Chemical Engineering. 12. 10.17265/1934-7375/2018.02.001 Senapati, U., & Das, T. K. (2020). Assessment of Potential Land Degradation in Akarsa Watershed, West Bengal, Using GIS and Multi-influencing Factor Technique. In Gully Erosion Studies from India and Surrounding Regions (pp. 187-205). Springer, Cham.

Shailaja, G., Kadam, A., Gupta, G., Umrikar, B., & Pawar, N.J. (2018). Integrated geophysical, geospatial and multiple-criteria decision analysis techniques for delineation of groundwater potential zones in a semi-arid hard-rock aquifer in Maharashtra, India. Hydrogeology Journal. 10.1007/s10040-018-1883-2.

Singh, A., Erram, V., Arora, S., & Gupta, G. (2016). Resistivity Survey: A Case Study of the Konkan Coastal Belt, Maharashtra.

Singhai, A., Das, S., Kadam, A. K., Shukla, J. P., Bundela, D. S., & Kalashetty, M. (2019). GIS-based multi-criteria approach for identification of rainwater harvesting zones in upper Betwa sub-basin of Madhya Pradesh, India. Environment, Development and Sustainability, 21(2), 777-797.

Sohail, A. T., Singh, S. K., & Kanga, S. A (2014) Geospatial Approach for Groundwater Potential Assessment Using Multi Influence Factor (MIF) Technique. water resources, 15(12), 21.

Thapa, R., Gupta, S., Guin, S., & Kaur, H. (2017). Assessment of groundwater potential zones using multi- influencing factor (MIF) and GIS: a case study from Birbhum district, West Bengal. Applied Water Science, 7(7), 4117-4131.

Umrikar, B. N. (2015). GIS Technique in Management of Watershed Developed along the Konkan Coast, Maharashtra, India. Journal of Geographic Information System, 7(03), 280.

WRIGHT, E. (1964). Tracer Techniques in Hydrology. Nature. 202. 1254-1255. 10.1038/2021254a0.

Yang, L., Qi, Y., Zheng, C., Andrews, C., Yue, S., Lin, Si., Li, Y., Wang, C., Xu, Y., & Li, H. (2018). A Modified Water-Table Fluctuation Method to Characterize Regional Groundwater Discharge. Water. 10. 503. 10.3390/w10040503.

Yoon, Y. Y., Kim, Y. C., & Lee, K. Y. (2018). Study for artificial recharge process of groundwater using natural isotope tracers. Journal of Radioanalytical and Nuclear Chemistry, 318(3), 2213-2218.

Zghibi, A., Mirchi, A., Msaddek, M. H., Merzougui, A., Zouhri, L., Taupin, J. D., ... & Tarhouni, J. (2020). Using Analytical Hierarchy Process and Multi-Influencing Factors to Map Groundwater Recharge Zones in a Semi-Arid Mediterranean Coastal Aquifer. Water, 12(9), 2525.

*IN PROCEEDINGS OF 25th HYDRO 2020, INTERNATIONAL CONFERENCE,*
*NATIONAL INSTITUTE OF TECHNOLOGY ROURKELA, ODISHA, INDIA*
*26-28, March 2021, ISBN 978-93-90631-56-8*

Paper ID - 430

# Estimating confined aquifer parameters using Particle Swarm Optimization technique

R. A. Panchal[1], Dr. H. M. Patel[2]

*[1]Assistant Professor, G H Patel College of Engineering & Technology, Vallabh Vidyanagar-388120, India*
*[2]Professor, Faculty of Technology & Engineering, The M. S. University of Baroda, Vadodara-390001, India*
*Email: [1]ratanpanchal@gcet.ac.in, [2]hmpatel-ced@msubaroda.ac.in*

## Abstract

Groundwater management is an important part of the water resources planning and management. The transmissivity (T) and storage coefficient (S) of the aquifers control the movement and extraction of groundwater in the geological formations. These hydraulic parameters of the aquifers, which are key inputs for groundwater modeling and management, widely estimated using pumping tests. After obtaining the time-drawdown data from pumping test results, the parameters of the aquifer system are traditionally determined by means of manual curve matching approaches. Although these approaches are simple to employ, some errors might be introduced since the accuracy of these approaches is mostly dependent to the modeler's ability. Therefore, use of the simulation-optimization models becomes popular tools to determine the aquifer parameters. The purpose of this study is to develop algorithm using Particle Swarm Optimization (PSO) technique to estimate the aquifer parameters T and S and its fitness is checked by Sum Squared Error (SSE) of observed and simulated drawdown. The drawdown is simulated using Theis function. The model is tested with results of curve matching technique (Todd and Larry, 1980). The SSE obtained by PSO optimized parameters is found less than that obtained using Curve matching. In this study, the PSO algorithm is selected due to its strong searchability, fast convergence speed, and high efficiency.

***Keywords:*** *Confined aquifer, Aquifer parameters, Theis function, Particle Swarm Optimization (PSO)*

## 1. Introduction

Hydrological parameters of the aquifers control the movement and abstraction of groundwater in the geological formations. To determine the hydrological parameters such as storativity, transmissivity and leakage coefficients aquifer tests are used. The hydrogeological parameters are hidden in the field test data and their identification is possible using the available of physically plausible models suitable for the prevailing field circumstances. Estimation of aquifer parameters, namely, transmissivity T, and storage coefficient S, from aquifer test data has been a continual area of research (Birpinar 2003). These hydraulic parameters of the aquifers, which are key inputs for groundwater modeling and management, widely estimated using pumping tests (Srivastava and Guzman 1994). For this purpose, many efforts have been made for the development of the most simple and rapid methods. The first study on this topic was made for the confined aquifers with isotropy, homogeneity, and uniform geometry by Theis in 1935. Later, a large number of analytical and graphical methods were applied to analyze aquifer pumping test data in nonleaky confined aquifers by many researchers (Cooper and Jacob; Chow; Papadopulos and Cooper; Şen; Wikramaratna). These all methods make use of curve matching procedures to analyze the drawdown measurement. In the slope-matching technique, which is one of the numerical methods, various finite difference approaches are used to determine the aquifer parameters (Cimen 2009). An equation developed by Theis in 1935 is used to determine the transmissivity and storage coefficient in a homogenous, isotropic, infinite areal extent confined aquifer using the measured drawdowns in an observation well located at a specific distance from a fully-penetrated tube well which is pumped at a constant rate. He proposed a curve-matching approach to determine the aquifer parameters, but this approach is tedious, requiring to know argument u and well function (W(u)); which involves errors due to individual judgment in determination of the best match between the observed and theoretical curves, especially when only early drawdowns are measured (Naderi 2019). Although these approaches are simple to employ, some errors perhaps occur as the accuracy of these approaches is mostly dependent on the individual's skill. Therefore, simulation–optimization models have become popular tools to determine aquifer parameters. The current literature includes various solution approaches integrating different simulation and optimization models for

determining aquifer parameters. These models work in a similar manner, but they have some differences in terms of the utilized optimization approaches such as simulated annealing (SA), genetic algorithm (GA), particle swarm optimization (PSO) etc. (Ayvaz and Gurarslan 2019)

The present study includes developed algorithm using Particle Swarm Optimization (PSO) technique and where aquifer parameters S and T is estimated to compare it with the results of curve matching technique using Theis function.

## 2. Methodology

### *2.1 Theis Method*

The influence of discharge always extents outward with time for a fully penetrated well in an extensive confined aquifer when pumped at a constant rate. The discharge will be equal the rate of decline of head times the storage coefficient when summed over the of influence. With the reduction of storage within the aquifer, the head will continue to decline as long as the aquifer is effectively infinite and therefore, unsteady or transient flow exists. However, the rate of decline decreases continuously with expansion of the area of influence. Theis in 1935 obtained a solution for the applicable differential equation in plane polar coordinates based on the analogy between groundwater and heat conduction (Todd and Larry 1980).

The written form of Theis solution in terms of the aquifer drawdown, s, which describes unsteady radial flow in confined aquifer is,

$$s = \frac{Q}{4\,\pi\,T}\,W(u) \tag{1}$$

Where in the above equation Q is the well discharge (Constant), T is the aquifer transmissivity, W(u) is known as well function. Well function W(u) represents an exponential integral which can be written as convergent series as

$$W(u) = \int_u^{\infty} \frac{e^{-u}}{u}\,du = -0.577 - \ln u - \sum_{k=1}^{\infty}(-1)^k\,\frac{u^k}{K.K!} \tag{2}$$

Also, u in the equation is given by

$$u = \frac{r^2\,S}{4\,T\,t} \tag{3}$$

where in the above equation r represents the distance between the pumped well and observation well, S represents the storage coefficient and t is the pumping time. Also, u and W(u) both are the dimensionless terms (Yeh 1987).

Equation (3) is known as the nonequilibrium or *Theis* equation. From the pumping tests of wells, constants S and T can be determined by this nonequilibrium equation. Because a value of S can be determined, only one observation well is required, shorter period of pumping is necessary and no assumption of steady – state flow condition is required, this equation is widely accepted.

Following are the essential assumptions to be considered in equation (2) while applying non-equilibrium equation so that it won't lead to erroneous results. They are:

1. The aquifer is homogeneous, isotropic, of uniform thickness and of infinite areal extent.
2. The piezometric surface is horizontal before pumping and the well is pumped at a constant discharge rate.
3. The pumped well penetrates fully in the aquifer and flow is everywhere horizontal within the aquifer to the well.

4. The pump diameter is tiny so that storage within the well can be neglected and for decline of head water removed from the storage is instantly discharged.

These assumptions seldom satisfied in real field conditions. However, the recognition of them can create an awareness of approximations involved for employing the non-equilibrium equation. Under the influence of a constant pumping rate and by observing the change in drawdown within one or more observation wells in the vicinity of pumped well, average values of S and T can be obtained.

Now, rewriting equation (3) as

$$\frac{r^2}{t} = \left(\frac{4\,T}{S}\right) u \tag{4}$$

from equation (1) and (4) it can be clearly seen that the relation between W(u) and u must be similar to that between s and $r^2/t$ because the terms in parentheses in the two equations are constants. Giving this similarity, Theis suggested an approximate solution for S and T based on a graphic method of superposition. As per this method, a *type curve*, a plot of W(u) versus u on logarithmic paper is prepared. The values of W(u) for a wide range of u is given in one of the tables in Groundwater Hydrology by D. K. Todd. Then on logarithmic paper of the same size and scale as for the type curve, values of drawdowns are plotted against the values of $r^2/t$. The observed time-drawdown data then are superimposed on the type curve, and keeping the coordinate axes of the two curves parallel and adjusting until a position is found by trial whereby most of the plotted points of the observed data all on a segment of the type curve. After selecting any convenient point, the coordinates of this match point are recorded. With values of W(u), u, s and $r^2/t$ thus determined, finally S and T can be obtained from equation (1) and (4). (Todd and Larry 1980)

The above method given by Theis (1935) and those suggested by Cooper-Jacob (1946) and Chow (1952) are commonly used to calculate values of S and T by pumping tests in the field. However, these methods require data plotting work and during curve-fitting procedure require personal judgment which makes them burdensome and tedious. Although these approaches are effortless to make use of it, they may anticipate errors during the procedures as the precision of these approaches is mainly depending on individual's ability. Therefore, on the other hand simulation-optimization models have become well liked tools to discover aquifer parameters (Ayvaz and Gurarslan 2019).

This study includes the use of Theis approach to simulate the drawdown and Particle Swarm Optimization (PSO) algorithm to prepare the simulation-optimization model. PSO algorithm is selected due to its quick convergence speed, powerful search ability and high-level efficiency. PSO got many advantages such as quick search speed, remembrance, less parameters and simple structure.

*2.2 Particle Swarm Optimization (PSO)*

Kennedy and Eberhart in the year 1995 introduced PSO for the very first time to simulate the social behaviour which was conventionalized by the bird flocking or fish shoaling. The process of PSO follows comparison of movement of bird flocks or fish shoals for social reasons which makes use of the familiarisation of the individual member of the swarm along with mutual experience of all members (Eberhart and Kennedy 1995).

As discussed by (Meenal and Eldho 2012) out of two alternatives of PSO viz. consideration of global neighbourhood and consideration of local neighbourhood, the first alternative is selected in this study where each particle progresses towards its previous best position and towards the best particle in the swarm to develop the model. The position of individual particles updated is given by

$$x_{N+1}^{i} = x_{N}^{i} + v_{N+1}^{i} \tag{5}$$

where, velocity is calculated as

$$v_{N+1}^{i} = wv_{N}^{i} + c_1 r_1 \left(P_N^i - x_N^i\right) + c_2 r_2 \left(P_N^g - x_N^i\right) \quad (6)$$

where in the above equations $x_N^i$ is representing particle position, $v_N^i$ is representing particle velocity, $x_{N+1}^i$ is the updated position of the particle. $P_N^i$ is representing best 'remembered' individual particle position, $P_N^g$ is representing best 'remembered' swarm position and $v_{N+1}^i$ is the updated velocity of the particle. Also, $c_1$ & $c_2$ are the cognitive and social parameters, $r_1$ & $r_2$ are the random numbers between 0 and 1 and $w$ is the inertia.

*2.3 Model Development in MATLAB*

For development of simulation-optimization model, PSO algorithm is selected and programming is carried out in MATLAB. The drawdown is simulated using Theis function and the fitness of the model is checked by summed squared of residual which is usually labelled as SSE. Following is the prepared objective function for main PSO program:

SSE = ObjFunc (Q, r, nt, t, so, S, T)

where Q is discharge in cumecs, r is the distance of observation well in meter, nt is no. of observations, t is the time for which drawdown is measured in seconds in the data of pumping test, so is the observed valued of drawdown in the data of pumping test, S is the storage coefficient and T is transmissivity in $m^2$/sec.

For objective function taking SSE = 0 initially and for i = 1: nt,

u = (r^2) * S / (4*pi*T) (7)

Taking w as a well function, the equation for w from equation (2) is given as,

w = Well_func(u)
w = -0.577216 – log (u) + u (8)

Also, the equation for simulated drawdown from equation (1) is given as,

sc(i) = (Q*w) / (4*pi*T) (9)

The fitness of the model is checked by SSE taking in consideration of observed and simulated drawdown, which is given as,

SSE = SSE + (so(i) - sc(i)) ^2 (10)

The SSE measures the total deviation of the response values from the fit to the response values. A value closer to 0 indicates that the model has a smaller random error component, and that the fit will be more useful for prediction.

Main PSO program for analysis of pumping test data is prepared. Taking objective function and defining other parameters as stated above the PSO parameters were first initialized. The PSO program is prepared for population size of 40 with maximum iteration as 30. Values for $c_1$ an $c_2$ were considered as unity and inertia value was considered as linear variation between wmax and wmin. The values for wmax equals to 1 and wmin equals to 3 were considered and kept to same value for constant w value. Giving problem and velocity bounds in the program, random positions and velocities were then initialized. After that objective for all the particles were evaluated and gbest and pbest values were found out. For maximum value of iteration, the velocities and positions were updated and objectives were evaluated

again to get new gbest and pbest values. Finally, the global best values, gbest were determined for the best fitness value.

## 3. Results

In this study to validate the pertinency and accuracy of the prepared model, three pumping test data set are used. They are as follows:

### *3.1 Data Set – 1:*

A well penetrating homogeneous and isotropic confined aquifer pumped at a uniform rate of 0.038 cumec ($m^3$/sec). During the pumping period drawdowns were measured in an observation well situated 60 m away and observations of *s and t* are listed in the Table 1. The values for storage coefficient (S) and Transmissivity (T) were determined using Theis method and found to be 2.35 x $10^{-4}$ and 0.017 $m^2$/sec respectively. These values were kept as expected values in the model for PSO algorithm in MATLAB. The results obtained by PSO for gbest as storage coefficient (S) and Transmissivity (T) were 2.36 x $10^{-4}$ and 0.0169 respectively. Also, the fitness value was found to be equals to 0.000003.

**Table 1** Pumping test data set - 1

| t, sec | s, m | t, sec | s, m |
|---|---|---|---|
| 300 | 0.471 | 6000 | 0.997 |
| 600 | 0.590 | 7200 | 1.029 |
| 900 | 0.661 | 8400 | 1.056 |
| 1200 | 0.712 | 9600 | 1.080 |
| 1500 | 0.751 | 10800 | 1.101 |
| 1800 | 0.783 | 12600 | 1.129 |
| 2100 | 0.811 | 14400 | 1.152 |
| 2400 | 0.834 | 16200 | 1.173 |
| 2700 | 0.855 | 18600 | 1.198 |
| 3000 | 0.874 | 21000 | 1.219 |
| 3600 | 0.906 | 23400 | 1.239 |
| 4200 | 0.933 | 25800 | 1.256 |
| 4800 | 0.957 | 29400 | 1.279 |
| 5400 | 0.978 | 33000 | 1.300 |

### *3.2 Data Set – 2:*

This data set includes the published pumping test data on page no. 166 of Todd and Larry. A well penetrating homogeneous and isotropic confined aquifer pumped at a uniform rate of 0.0289 cumec (2500 $m^3$/day). During the pumping period drawdowns were measured in an observation well situated 60 m away and observations of *s and t* are listed in the Table 2. The values for storage coefficient (S) and Transmissivity (T) were determined using Theis method and found to be 2.06 x $10^{-4}$ and 0.00128 $m^2$/sec (1110 $m^2$/day) respectively. These values were kept as expected values in the model for PSO algorithm in MATLAB. The results obtained by PSO for gbest as storage coefficient (S) and Transmissivity (T) were 2.17 x $10^{-4}$ and 0.01333 respectively. Also, the fitness value was found to be equals to 0.00820.

**Table 2** Pumping test data set – 2 from Todd and Larry 1980

| t, sec | s, m | t, sec | s, m |
|---|---|---|---|
| 60 | 0.20 | 1440 | 0.67 |
| 90 | 0.27 | 1800 | 0.72 |
| 120 | 0.30 | 2400 | 0.76 |
| 150 | 0.34 | 3000 | 0.81 |
| 180 | 0.37 | 3600 | 0.85 |
| 240 | 0.37 | 4800 | 0.90 |
| 300 | 0.41 | 6000 | 0.93 |
| 360 | 0.42 | 7200 | 0.96 |
| 480 | 0.48 | 9000 | 1.00 |
| 600 | 0.53 | 10800 | 1.04 |
| 720 | 0.57 | 12600 | 1.10 |
| 840 | 0.60 | 14400 | 1.12 |
| 1080 | 0.63 | - | - |

*3.3 Data Set – 3:*

A well penetrating homogeneous and isotropic confined aquifer pumped at a uniform rate of 0.0138 cumec ($m^3$/sec). During the pumping period drawdowns were measured in an observation well situated 251.15 m away and observations of *s and t* are listed in the Table 3. The values for storage coefficient (S) and Transmissivity (T) were determined using Theis method and found to be 2.09 x $10^{-5}$ and 0.00141 $m^2$/sec respectively. These values were kept as expected values in the model for PSO algorithm in MATLAB. The results obtained by PSO for gbest as storage coefficient (S) and Transmissivity (T) were 2.1 x $10^{-5}$ and 0.001416 respectively. Also, the fitness value was found to be equals to 0.01688.

**Table 1** Pumping test data set - 3

| t, sec | s, m | t, sec | s, m |
|---|---|---|---|
| 180 | 0.091 | 4200 | 1.859 |
| 300 | 0.213 | 4800 | 1.920 |
| 480 | 0.396 | 5400 | 2.042 |
| 720 | 0.640 | 6000 | 2.133 |
| 1200 | 0.975 | 7800 | 2.286 |
| 1440 | 1.097 | 9600 | 2.529 |
| 1800 | 1.249 | 12000 | 2.590 |
| 2280 | 1.432 | 15600 | 2.804 |
| 2820 | 1.554 | 19200 | 2.956 |
| 3000 | 1.615 | 22800 | 3.108 |
| 3600 | 1.737 | 30000 | 3.322 |

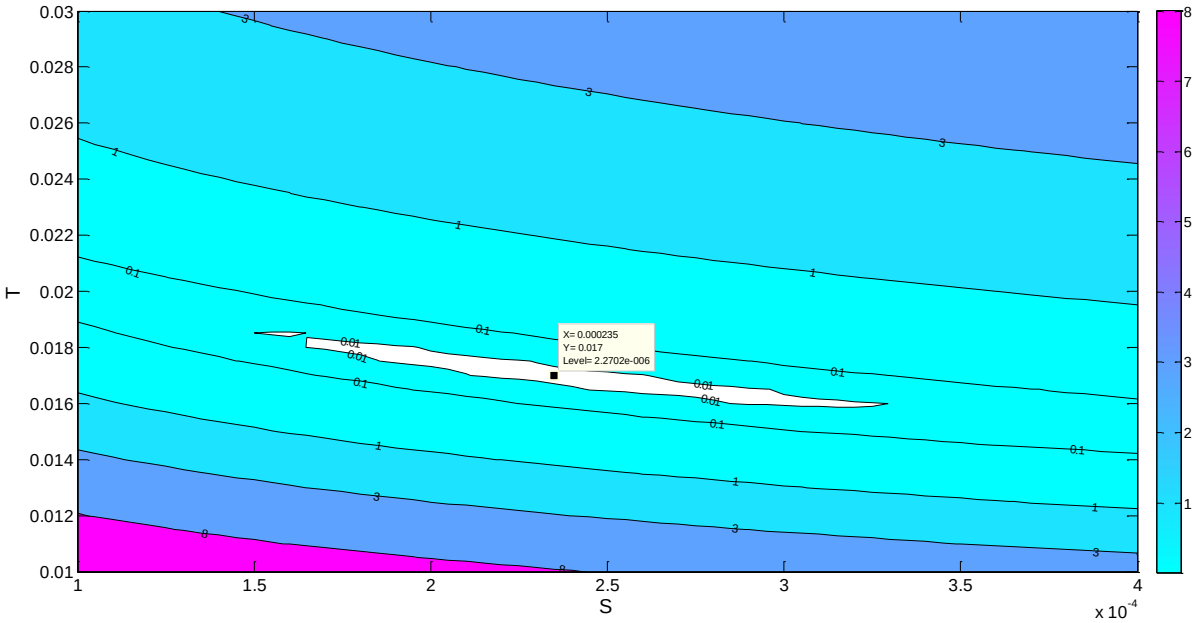



**Figure 1** Counters of SSE near optimum solution

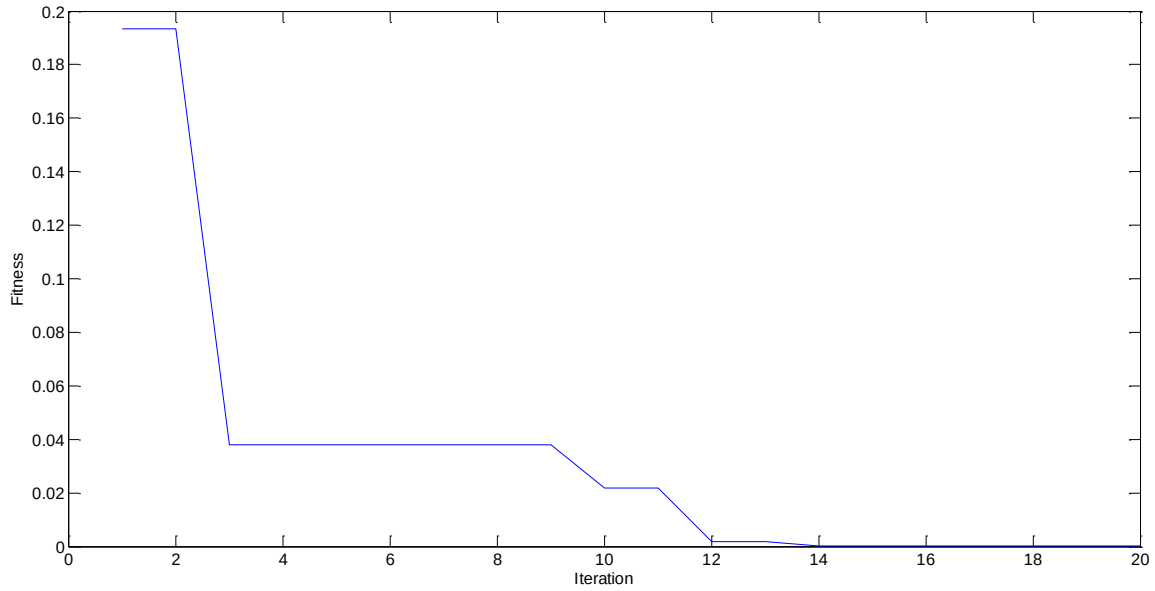



**Figure 2** Fitness value vs. Iteration

Fig.1 shows how function SSE varies on solution space near the optimum solution for selected problem. Fig 2 indicates how the solution is converged with reduction in fitness function after each iteration.

## 4. Discussion

The study indicates that pumping tests are often used to determine the aquifer parameters, storage coefficient and transmissivity. And to estimate the aquifer parameter using pumping tests, several methods have been developed. However, all those methods suffer from various shortcomings. Theis method utilized in this study to simulate the drawdown also make use of non-truncated well function W(u) that can be apply to all drawdown data for estimation of aquifer parameters but it still suffers from personal judgment in curve matching which is tedious procedure and also require values for Theis well function W(u) and u (Naderi 2019). On the other hand, simulation-optimization model prepared using PSO shows relatively quick and accurately estimated values in comparison with Theis method. For all

three data sets, result shows that estimated aquifer parameter S and T are identical and matches with expected values of Theis method. Also, the fitness value, SSE for all three data sets are almost 0. However, there is quite variation in the SSE values for all three data sets and that may be due to heterogeneity of the aquifer.

## 5. Conclusion

Storage coefficient (S) and Transmissivity (T) which are the key parameters for aquifer modelling are often estimated using pumping tests. In this study, simulation-optimization model is prepared to estimate aquifer parameters using PSO algorithm in MATLAB and drawdown is simulated using Theis function and its fitness is checked by SSE function. The results indicate that use of simulation-optimization model beat the insufficiency of the manual curve matching approach. It does not require curve matching, construction of a graph and values of the W(u) and u. Also, the fitness value, SSE function value for all three data sets is acceptable and the model is validated.

## References

Ayvaz, M., and Gurarslan, G. (2019). A hybrid optimization approach for parameter estimation of confined and leaky confined aquifers. *Water Supply, 19.8,* 2359-2366.

Birpinar, M. (2003). Aquifer parameter identification and interpretation with different analytical methods. *Water SA, 29*(3), 251-256.

Cimen, M. (2009). Effective Procedure for Determination of Aquifer Parameters from Late Time-Drawdown Data. *Journal of Hydrologic Engineering, 14*(5), 446-452.

Eberhart, R., and Kennedy, J. (1995). A New Optimizer Using Particle Swarm Theory. *Sixth International Symposium on Micro Machine and Human Science, IEEE,* 39-43.

Meenal, M., and Eldho,T. (2012). Simulation-optimization model for groundwater contamination remediation using meshfree point collection method and particle swarm optimization. *Sadhana, 37*(3), 351-369.

Naderi, M. (2019). Estimating confined aquifer parameters using a simple derivative-based method. *Heliyon, 5,* e02657.

Srivastava, R., and Guzman, A. (1994). Analysis of Slope-Matching Methods for Aquifer Parameter Determination. *Ground Water, 32*(4), 570-575.

Todd, D., and Mays, L. (1980). Groundwater Hydrology. *Third Edition.*

Yeh, H. (1987). Theis' Solution by Nonlinear Least-Squares and Finite-Difference Newton's Method. *Ground Water, 25*(6), 710-715.

# Theme XIV

# Computational Fluid Dynamics / Numerical Modelling

*IN PROCEEDINGS OF 25th HYDRO 2020, INTERNATIONAL CONFERENCE, NATIONAL INSTITUTE OF TECHNOLOGY ROURKELA, ODISHA, INDIA 26-28, March 2021, ISBN 978-93-90631-56-8*

Paper ID - 034

# CFD Analysis of Flow through Concentric, Eccentric and Segmental Orifice Meters

Dr. I. Siva Parvathi[1], Miss. G. Prema Swathi[2]

[1]*Associate Professor, Department of Civil Engineering, Andhra University College of Engineering, Viskhapatnam-530003, India*

[2]*Assistant Professor, Department of Civil Engineering, GIET Engineering College, Rajahmundry, India.*

*Email: isparvathi@gmail.com*

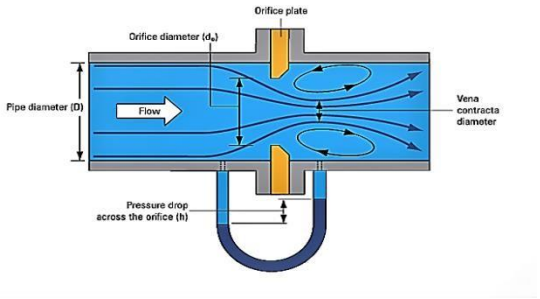
## Abstract

Accurate measurement of fluid flow is an essential task for many industries. An orifice meter is widely used in process industry, chemical industry, oil, and gas industry for flow rate measurement of steam, oil, gas, etc. The common types of orifices used in industries are concentric, eccentric, and segmental orifices. The concentric orifice is the most used design because of its proven reliability in a variety of industrial applications. Eccentric orifice plates are generally used when the process material contains foreign matter that may block the orifice in the case of concentric configuration. Segmental orifice plates are used to measure the flow of light slurries and fluids with a high concentration of solids. The present study aims to determine the coefficients of discharge, pressure contours, and velocity streamline patterns for selected concentric, eccentric, and segmental orifices by using ANSYS CFD software. From the results, it is observed that the sharp edge with $45^0$ back cut concentric orifice meter has the maximum discharge coefficient value, velocity streamlines, and minimum pressure drop value when compare with square-edged and square-edged with 45° back-cut concentric orifice meters. The discharge coefficient and velocity streamlines are gradually increased and pressure drop decreases with the increasing of the eccentricity of the orifice. In the case of segmental orifice, with increasing the opening of orifice the discharge coefficient value is increases, and the pressure drop value is decreased. The results can be used to select the most suitable geometry of the orifice plate in practical applications.

***Keywords:*** *Computational Fluid Dynamics, Orifice Meter, Concentric, Eccentric, Segmental Orifice and ANSYS-Fluent*

## 1. Introduction

An orifice meter is a type of flow meter used to measure the rate of flow of liquid or gas, especially steam, using the differential pressure measurement principle. The sectional view of the orifice meter is shown in Figure 1. To create a pressure drop and thereby assess the flow, an orifice plate is inserted in between the inlet and outlet sections. As illustrated in Figure 2, to accommodate multiple flows measuring work, the orifice plate bore can be made in several configurations. To see which of the setups is sufficient for each calculation work; the running conditions should be tested. Orifice meters are designed in various ways depending on the particular requirements of the application, the type, scale, and placement of holes on the orifice plate. Orifices are commonly used in flow metering due to their robustness, simple mechanical construction and other established advantages (Shah et al. 2012). Due to its demonstrated reliability in a variety of industrial applications and the significant amount of study carried out on this system, the concentric orifice is the most prevalent configuration.



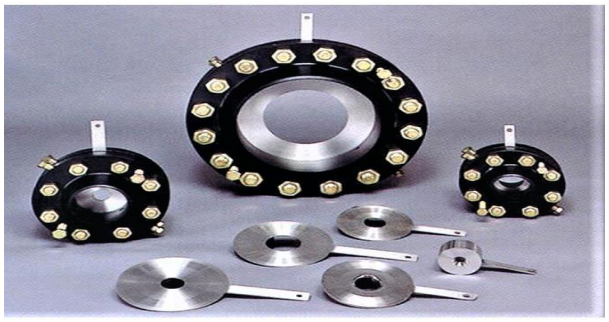



**Figure 1** Sectional view of orifice meter

**Figure 2** Orifice plates

A circular opening (bore) tangent to the inside wall of the pipe is present in the eccentric plate. These plates are used to measure the velocity of solid-carrying fluids and are often used for measuring liquid-carrying gases. The opening is equivalent to a partially opened gate valve in a segmental orifice plate. The placement of these orifice plates depends on the type of fluid used in the device of the pipe. These plates can either be positioned on top or at the bottom of a horizontal shaft, depending on the form of fluid. This plate is usually used to weigh liquids or gases that bear impurities that are non-abrasive, such as light slurries or extremely dirty gases. Concentric, eccentric, and segmental orifice plates are as shown in Figure 3.

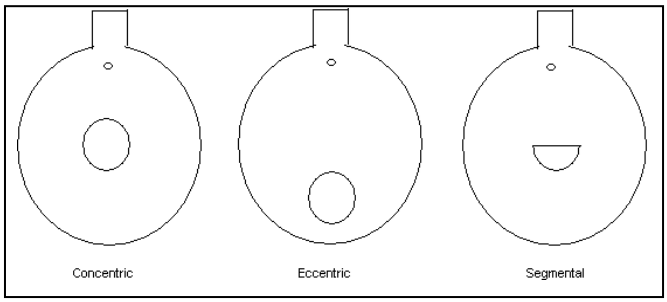



**Figure 3** Concentric, eccentric and segmental orifice plate

Lucien(1961) carried out an experimental analysis to determine the discharge coefficients for a segmental orifice with various openings. From his observation, he concluded that when compared to concentric and eccentric orifices, the discharge coefficient values for the segmental orifices are very small. Four distinct diameter orifices put experimentally in a pipe by James (1965), the consequence of increasing eccentricity is assessed. He indicated that the discharge coefficient of the orifice from the concentration position to the maximum eccentric position is also increased with increasing eccentricity. In comparison with the classical concentric orifice plate, Zahariea (2016) tested for an eccentric orifice plate is qualitative from the point of view of the sedimentation potential of solid particles in the fluid whose flow rate is measured. The numerical pattern of streamlines for both orifice plates has been evaluated for this reason. Using ANSYS Fluent program, the numerical work was carried out to solve the Reynolds-averaged Navier-Stoke's equations with the k-$\omega$ SST turbulence model. By using the ANSYS CFD methodology, Sanghani et al. (2016) conducted a comparative study of various orifice geometries for pressure reduction. The simulation results showed that the square-edged with 45° back-cut orifice plate has the maximum pressure loss under the same diameter ratio and thickness condition, and the streamline

approach orifice plate has minimum pressure loss. Comparison of the experimental, theoretical and simulation findings for pressure drop in sharp-edged orifice meters was also performed by Sanghani et al. (2016). Using the Navier-Stokes (N-S) equations by Mohamed et al. (2015), a theoretical analysis of turbulent flow in an orifice plate inside a pipe is conducted. By taking into account (k-ε) turbulence models, the analysis is carried out by varying Reynolds numbers and aspect ratio. Within the pipe and around the orifice, the observations reveal the velocity pattern, differential pressure, and vorticity of the moving fluid. Orifice meter flow attributes have been simulated in the CFD by Manish et al. (2012). A method has been suggested for placing the pressure tap in the vena contract to measure the flow with greater precision and consistency in the orifice meter. Tukiman et al. (2017) also done a CFD simulation of flow into an orifice meter. The findings were stated in terms of flow pattern, velocity, and pressure profiles. From CFD simulations, the vena-contract location was determined. Two-phase flow pressure drops through thin and thick orifices have been studied numerically with air–water flow in horizontal pipes. Calculations of the two-phase computational fluid dynamics (CFD) by using Eulerian–Eulerian model were used to measure the pressure drop through the orifices (Manmatha and Sukanta 2012).

The shape, size of the opening, eccentricity, and location of the orifice influence the discharge coefficient in the orifice meter. In the present case, concentric, eccentric, and segmental orifices are considered by numerical simulation using computational fluid dynamics analysis to calculate discharge coefficients, pressure contours, and velocity streamlines.

The objectives of the present study are:

(i) To determine the discharge coefficient for selected concentric orifices of a square-edged orifice, square-edged with $45^0$ back cut and sharp-edged with $45^0$ back cut orifices.
(ii) To determine the discharge coefficient in eccentric orifice meter with increasing the eccentricity from center of the axis to 0.238 cm, 0.476 cm, 0.572 cm, and 0.715 cm from concentric position placed in 5.08 cm diameter pipe.
(iii) To determine the discharge coefficient for chosen segmental orifices in three cases (one- quarter open, semi-circle open, and three-quarters open).

## 2. CFD Analysis

Computational Fluid Dynamics (CFD) is a computer-oriented numerical simulation technique. It isn't always possible to experimentally test the orifice meter. Since, when studying them experimentally, there are issues such as time-intensive, costly, and scaling issues, etc. Therefore, as compared to experimental work, researching them numerically is a successful method. In CFD, the underlying theory is to add boundary conditions and evaluate fluid flow by solving equations. In the present study, flow characteristics were analyzed in three-dimensional (3D) models using an orifice meter CFD analysis. The governing equations for fluid are given by applying the fundamental laws of mechanics to a fluid. A series of coupled, nonlinear, partial differential equations are generated by these equations, along with the conservation of energy equations. For other engineering problems, these equations cannot be analytically solved. However, it is possible to find approximate computer-based solutions to the related equations for several engineering problems. It is necessary to solve the governing equations (continuity and momentum) with the related Reynolds stress closure. The standard k-epsilon turbulence model by Launder and Spalding (1974) was used in the present analysis. The k-epsilon turbulence model is easy to use, simple, most commonly validated and has excellent performance for many industrial flows (Versteeg and Malalasekera 1995).The basic equations governing the flow inside and outside the orifice are the equation of continuity and the equation of force-momentum and the energy equation:

***Continuity Equation:***

$$\frac{D\rho}{Dt} + \rho\frac{\partial U_i}{\partial x_i} = 0 \tag{1}$$

***Momentum Equation:***

$$\rho\frac{\partial U_j}{\partial t} + \rho U_i\frac{\partial U_j}{\partial x_i} = -\frac{\partial P}{\partial x_j} - \frac{\partial \tau_{ij}}{\partial x_i} + \rho g_j \tag{2}$$

$$\text{where } \tau_{ij} = -\mu\left(\frac{\partial U_j}{\partial x_i} + \frac{\partial U_i}{\partial x_j}\right) + \frac{2}{3}\delta_{ij}\mu\frac{\partial U_k}{\partial x_k} \tag{3}$$

$\rho\frac{\partial U_j}{\partial t}$ =Local change with time; $\rho U_i\frac{\partial U_j}{\partial x_i}$ =Momentum convection ; $\frac{\partial P}{\partial x_j}$ = Surface Force

$\frac{\partial \tau_{ij}}{\partial x_i}$ = Molecular- dependent momentum exchange (diffusion); $\rho g_j$ =Mass Force

***Energy Equation:***

$$\rho c_\mu\frac{\partial T}{\partial t} + \rho c_\mu U_i\frac{\partial T}{\partial x_i} = -P\frac{\partial U_i}{\partial x_i} + \lambda\frac{\partial^2 T}{\partial x_i^2} - \tau_{ij}\frac{\partial U_j}{\partial x_i} \tag{4}$$

$\rho c_\mu\frac{\partial T}{\partial t}$ =Local energy change with time; $\rho c_\mu U_i\frac{\partial T}{\partial x_i}$ =Convection term; $P\frac{\partial U_i}{\partial x_i}$ = Pressure work

$\lambda\frac{\partial^2 T}{\partial x_i^2}$ =Heat flux (diffusion); $\tau_{ij}\frac{\partial U_j}{\partial x_i}$ =Irreversible transfer of mechanical energy into heat

## 3. Details of the present study

The present study evaluated discharge coefficients, pressure contours, velocity streamline patterns for flow regions of concentric, eccentric, and segmental 3D model orifice meters using the ANSYS CFD device. A set of 10 different orifice meter models have been operated for a single discharge to analyze the impact on flow characteristics due to a shift in shape and the location of the orifice plate includes:

(i) Three models of square-edged, square-edged with 45° back-cut, and sharp-edged with 45° back-cut concentric orifice meters.
(ii) Four models of concentric orifice meter with increasing the eccentricity from the center of the axis to 0.238 cm, 0.476 cm, 0.572 cm and 0.715 cm from concentric position placed in 5.08 cm diameter pipe.
(iii) Three models of 1/4 opening, 1/2 opening, and 3/4 opening of the segmental orifice meters.

### *3.1 Numerical analysis data*

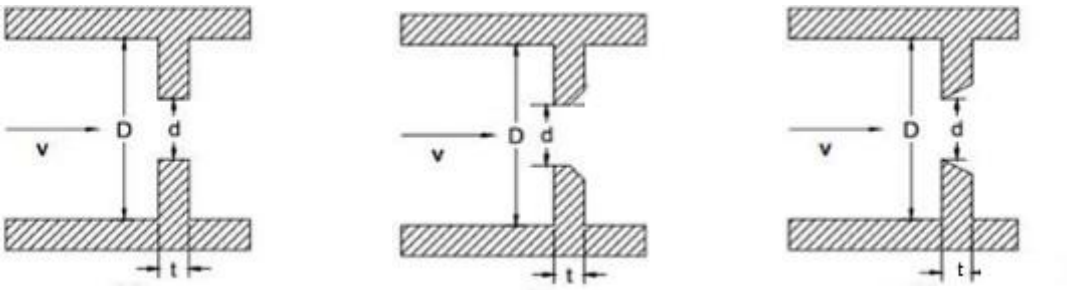
Diameter of the pipe = 5.08cm; Diameter of the orifice plate = 3.65cm; Length of the pipe = 200cm; Thickness of the orifice plate = 0.6cm; Velocity at inlet = 8 m/s; Density of water = 998.2 kg/m$^3$; Viscosity of water = 1.003× 10$^{-3}$ kg/(m-s); Gravitational acceleration = 9.81 m/s$^2$. The flow path was taken in the path of the Z-axis and the Y-axis is the vertical component of the orifice meter. Velocity input for the condition of the inlet boundary and pressure outlet for the condition of the outlet boundary is considered. The stationary motion of the wall and the "no-slip" state of

the pipe walls and the orifice plate were also considered. Gravity is tested and the value for the Y-axis is given as -9.81 m/s$^2$ since gravity operates in a downward direction, which is opposite to the Y-directional vector. The turbulence model was selected as the model of k- ε and the pressure-based solver is used. SIMPLE is chosen as one of the solution types. These are pressure-based separated algorithms and are recommended for steady flow environments. The second-order upwind scheme is used in spatial control for momentum, kinetic energy, and dissipation equations. Normal initialization is chosen for greater consistency in the configuration of the system. After the initial values of pressure and velocity are given, the measurement is performed from the inlet. The number of iterations for stronger iteration convergence is known to be 1000.

## 4. Results and Discussions

### *4.1 Analysis of flow through concentric orifice meter*

The flow is evaluated by observing the pressure contours, streamlines, and discharge coefficients. In CFD analysis, the discharge coefficient of the orifice meter is derived from the mass flow rate and pressure drop. The sectional view of square-edged, square edge with 45$^0$ back cut, and sharp edge with 45$^0$ back cut concentric orifices are as shown in Figure 4. The flow model of sharp-edged orifice with 45$^0$ back cut concentric orifice is represented in Figure 5.




(i) Square edged (ii) Square edged with 45$^0$ back cut (iii) Sharp edged with 45$^0$ back cut

**Figure 4** Sectional view of concentric orifices

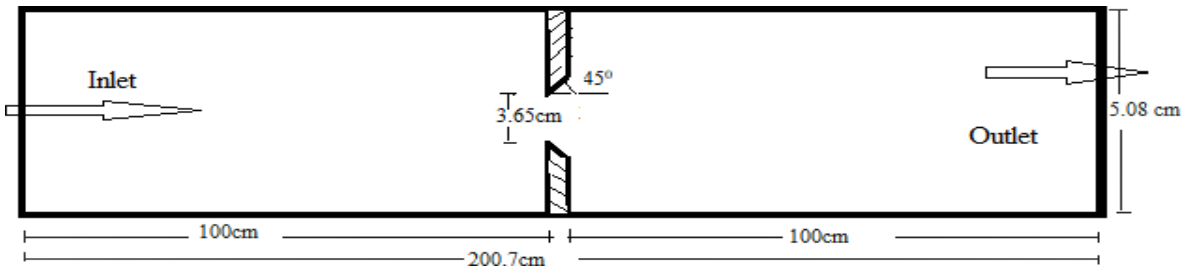



**Figure 5** Sharp edged orifice with 45$^0$ back cut concentric orifice

The obtained velocity streamlines of the three types of concentric orifice meters are shown in Figure 6. The maximum velocity values of square-edged, square-edged with 45° back-cut, and sharp-edged with 45° back-cut orifices attained are 19.39 m/s, 19.71 m/s, and 19.90 m/s for concentric orifices.

### *4.2 Discharge coefficients of various concentric orifice meters*

In CFD analysis, Coefficient of discharge [ISO 5167] is computed from mass flow rate by using the following formula:

$$C_d = \frac{4Q_m\sqrt{1-\beta^4}}{\varepsilon\pi d^2\sqrt{2\rho\Delta P}} \quad (5)$$

Where, $C_d$ = Coefficient of discharge, $Q_m$= mass flow rate of fluid (kg/s), $\rho$=Density of fluid (kg/m$^3$), $\Delta P$= pressure drop (pascal's), d = Orifice diameter (m), $\varepsilon = 1$ is the expansion factor, where $\beta$ = d/D is the diameter ratio, D is the pipe diameter.

The effect of the orifice shape on the discharge potential of the orifice meter is calculated by the analysis of the discharge coefficients of various orifice forms (square-edged, square-edged with 45°back-cut, and sharp-edged with 45° back-cut orifices), and the values obtained are presented in Table 1. The square-edged with 45° back-cut orifice has the maximum pressure drop and sharp-edged with 45° back-cut orifice has minimum pressure drop, due to the effect of orifice shape. The sharp-edged with 45° back- cut orifice has the maximum discharge coefficient and the square-edged with 45° back-cut has the minimum discharge coefficient. With the increasing sharpness of the orifice plate, the discharge coefficient increases.

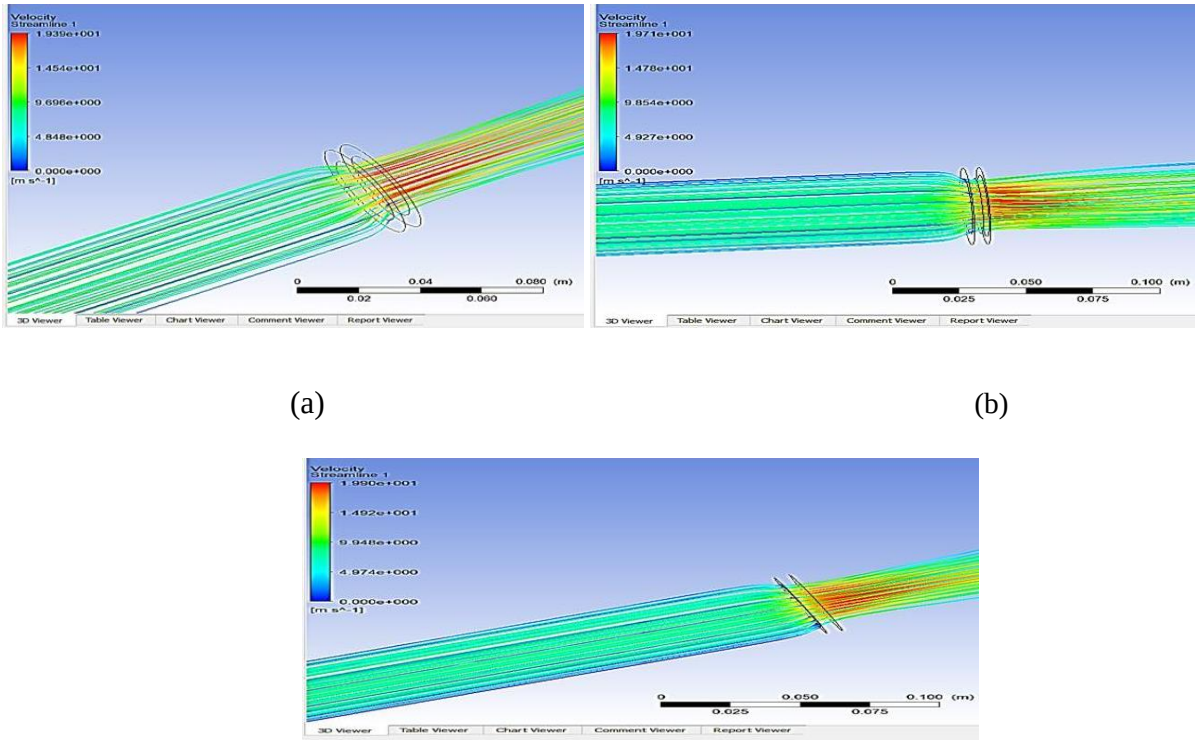


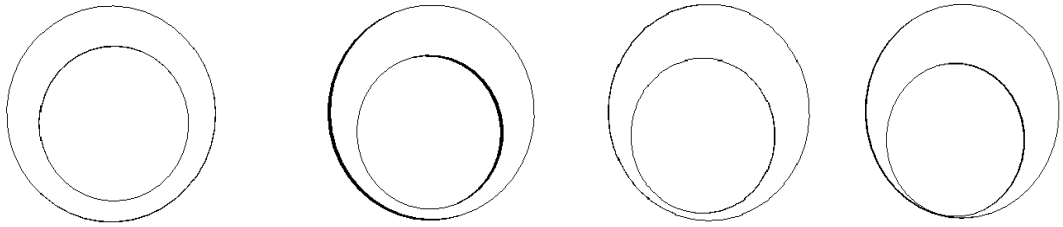

**Figure 6** Velocity streamlines of the (a) square-edged (b) square-edged with 45° back-cut (c) sharp-edged with 45° back-cut concentric orifice meter

**Table 1** Discharge coefficients for concentric orifice meters

| S.No | Type of the concentric orifice meter | Pressure drop (MPa) | Mass flow rate (kg/s) | Max. velocity streamlines (m/s) | Discharge coefficient, $C_d$ |
|---|---|---|---|---|---|
| 1 | Square-edged | 0.2669 | 16.028 | 19.71 | 0.573 |
| 2 | Square-edged with 45° back-cut | 0.2688 | 16.028 | 19.39 | 0.571 |
| 3 | Sharp-edged with 45° back-cut | 0.2033 | 16.028 | 19.90 | 0.650 |

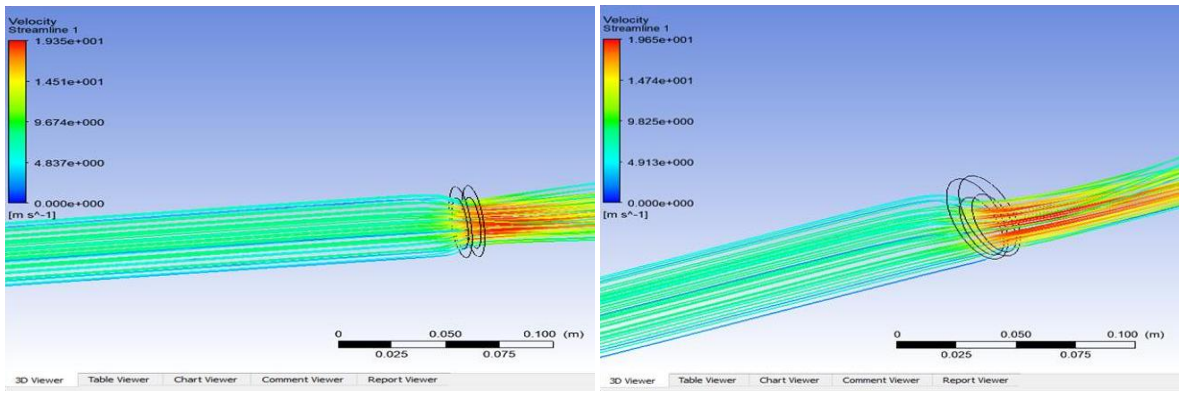
### *4.3 Analysis of flow through eccentric orifice meter*

The sectional view of eccentric orifices is as shown in Figure 7. The velocity streamlines of the four types of eccentric orifice meters are presented in Figure 8. The maximum velocity streamlines are then increased by increasing the eccentricity of the orifice from the concentric location.

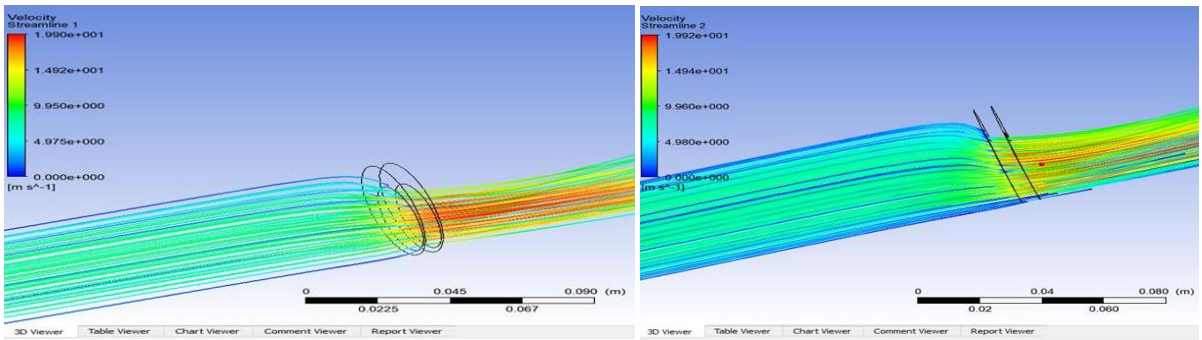


(i) (ii) (iii) (iv)

**Figure 7** Sectional view of eccentric orifices at (i) 0.238cm (ii) 0.476 cm (iii) 0.572 cm and (iv) 0.715 cm from the center of the axis




(a) (b)




(c) (d)

**Figure 8** Velocity streamlines of eccentric orifice at (a) 0.238cm (b) 0.476cm (c) 0.572cm from the center of axis and (d) full eccentric orifice meter

The effect of the location of the orifice plate on the discharge potential of the orifice meter is calculated by the analysis of the discharge coefficients of the various eccentric orifice meters (increased eccentricity as 0.238 cm, 0.476 cm, 0.572 cm, and 0.715 cm (full eccentric) from the

concentration location set in the 5.08 cm diameter pipe) and the values obtained are presnted in Table 2. Increasing the orifice's eccentricity from the concentric location, then a decrease in the magnitude of the pressure drop is observed. The discharge coefficient also increases with the rise in the eccentricity of the orifice from the concentric location.

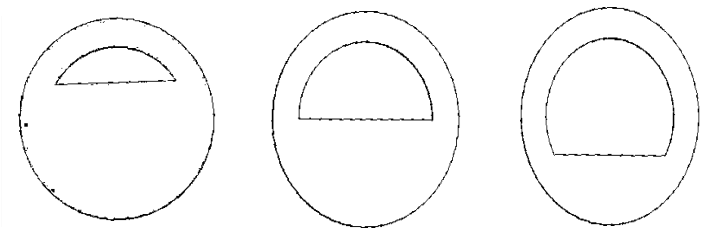
**Table 2** Discharge coefficients for eccentric orifice meter

| S.no | Eccentricity from concentric position | Pressure drop(MPa) | Mass flow rate (kg/s) | Max. velocity streamlines (m/s) | Discharge coefficient $C_d$ |
|---|---|---|---|---|---|
| 1 | 0.238 cm | 0.2634 | 16.049 | 19.35 | 0.593 |
| 2 | 0.476cm | 0.2609 | 16.049 | 19.65 | 0.596 |
| 3 | 0.572cm | 0.2546 | 16.049 | 19.90 | 0.603 |
| 4 | 0.715cm (full eccentric) | 0.2543 | 16.039 | 19.92 | 0.604 |

### *4.4Analysis of flow through segmental orifice meter*

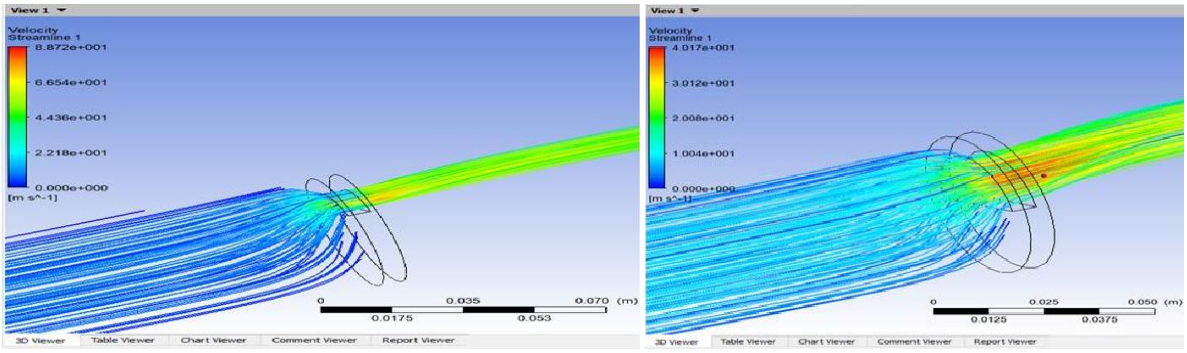
The effect of the location of the orifice plate on the discharge potential of the orifice meter is calculated by the analysis of the discharge coefficients of the various eccentric orifice meters (increased eccentricity as 0.238 cm, 0.476 cm, 0.572 cm, and 0.715 cm (full eccentric) from the concentration location set in the 5.08 cm diameter pipe) and the values obtained are presnted in Table 2. Increasing the orifice's eccentricity from the concentric location, then a decrease in the magnitude of the pressure drop is observed. The discharge coefficient also increases with the rise in the eccentricity of the orifice from the concentric location

The sectional view of the segmented orifice meter is shown in Figure 9.Velocity streamlines in segmental orifice meters of the three types of openings as shown in Figure 10. The 1/4 opening, 1/2 opening, and 3/4 opening orifices maximal velocity streamlines obtained are 88.72 m/s, 40.17 m/s, and 24.90 m/s respectively. The effect of orifice plate openings on the discharge capacity of the orifice meter is determined by studying the discharge coefficients of different orifice openings, such as 1/4 opening, 1/2 opening and 3/4 opening, and Table 3 presents the values obtained. The pressure drop of the segmental orifice decreases as the opening of the orifice increases. The discharge coefficient of the segmental orifice is increased with the increasing the opening of the orifice.

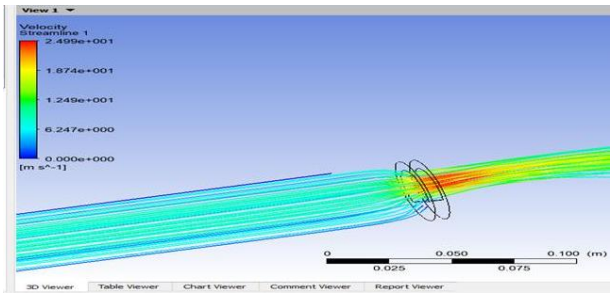


(i)1/4 opening (ii) 1/2 opening (iii) 3/4 opening

**Figure 9** Sectional view of segmental orifices




(a) (b)




(c)

**Figure 10** Velocity streamlines of (a) ¼ opening (b) ½ opening (c) ¾ opening segmental orifice meter

**Table 3** Discharge coefficients for segmental orifice meter

| S. No | Type of the segmental orifice meter | Pressure drop(MPa) | Mass flow rate (kg/s) | Max. velocity streamlines (m/s) | Discharge coefficient $C_d$ |
|---|---|---|---|---|---|
| 1 | 1/4opening | 6.77 | 16.028 | 88.72 | 0.116 |
| 2 | 1/2 opening | 1.23 | 16.028 | 40.17 | 0.274 |
| 3 | 3/4 opening | 0.44 | 16.028 | 24.90 | 0.450 |

## 5. Conclusions

**In concentric orifices:**

Sharp edge with 45° back-cut concentric orifice meter has the maximum discharge coefficient value ($C_d$ = 0.650) and square-edged with 45° back-cut concentric orifice has minimum discharge coefficient value ($C_d$ = 0.573). Square-edged with 45° back-cut concentric orifice has maximum pressure drop and minimum velocity value and sharp edge with 45° back-cut concentric orifice meter has minimum pressure drop and maximum velocity value.

***In eccentric orifices:***

The Cd value is found to be increased with the increasing eccentricity of the orifice from the concentric location. With an increasing eccentricity of the orifice from concentric position pressure drop value is observed to be decrease and velocity streamlines value increases.

***In segmental orifices:***

The $C_d$ value is reported to be increased by increasing the opening of the segmental orifice. With increasing the opening of segmental orifice pressure drop value is observed to decrease. The segmental orifice has a slightly less discharge coefficient compared to the concentric and eccentric orifice.

## References

1. ANSYS User's Manual V 16, 2016.
2. ISO 5167 (2003). Measurement of fluid flow by means of pressure differential devices inserted in circular cross-section conduits running full.
3. James E. Casale (1965). The eccentric orifice as a flow measuring device in small diameter pipes. MS Thesis, Mechanical Engineering, University of Missouri At Rolla.
4. Launder and Spalding D (1974). The numerical computation of turbulent flows. *Comput. Methods Appl. Mech. Eng.* 3,pp. 269-289.
5. Lucien E. Rising (1961).Efflux from eccentric and segmental orifices. MS Thesis, Mechanical Engineering, the University of Arizona.
6. Manish S.Shah, Jyeshtharaj B.Joshi, ،Avtar S.Kalsi ,C.S.R.Prasad, (2012). Analysis of flow through an orifice meter: CFD simulation. *Journal of Chemical Engineering Science*, Volume 71, 26 March, pp 300-309.
7. Manmatha K. Roul and Sukanta K. Dash (2012). Single-phase and two-phase flow through thin and thick orifices in horizontal pipes. *Journal of Fluid Engineering*, ASME, Vol: 134, pp 1-14.
8. Mohamed A. Siba, Wan MohdFaizal Wan Mahmood, MohdZ. Nuawi, RasidiRasani, and Mohamed H. Nassir (2015). Modeling and applications of 3d flow in orifice plate at low turbulent Reynolds numbers. *International Journal of Mechanical & Mechatronics Engineering*, IJMME-IJENS Vol:15(4).
9. Sanghani C. R, Jayani D. C, C. R. Dobariya, G. K. Sabhadiya, J. R. Gohil (2016). Comparative Analysis of Different Orifice Geometries for Pressure Drop. IJSTE - *International Journal of Science Technology & Engineering*, Volume 2, Issue 10, April.
10. Sanghani C. R, Jayani D. C, Hingu, A. H, Jadav M. Y, .Jiyavia D. V (2016). Comparison of experimental, theoretical and simulation result for pressure drop in sharp edged orifice meter. IJSTE - *International Journal of Science Engineering & Technology*, Volume 5, Issue 3, March.
11. Shah M. S, JoshiJ. B, Kalsi A.S, PrasadC.S.R, and Shukla D.S(2012). Analysis of flow through an orifice meter: CFD simulation. *Chemical Engineering Science*, Vol. 71, pp. 300–309.
12. Tukiman M M , M N M Ghazali , A Sadikin , N F Nasir , N Nordin , A Sapit , M A Razali (2017). CFD simulation of flow through an orifice plate., *IOP Conf. Series: Materials Science and Engineering* 243, 012036 doi:10.1088/1757-899X/243/1/012036.
13. Versteeg H K and Malalasekera W (1995). An introduction to computational fluid dynamics: The finite volume method (England: Pearson Ed)
14. Zahariea D (2016). Numerical analysis of eccentric orifice plate using ANSYS Fluent software. 20th *Innovative Manufacturing Engineering and Energy Conference* (IMEE 2016), doi:10.1088/1757-899X/161/1/012041.

*IN PROCEEDINGS OF 25th HYDRO 2020, INTERNATIONAL CONFERENCE, NATIONAL INSTITUTE OF TECHNOLOGY ROURKELA, ODISHA, INDIA 26-28, March 2021, ISBN 978-93-90631-56-8*

Paper ID - 096

# HYDRAULIC STRUCTURE DESIGN WITH 3D CFD MODEL

Prashant Prakash Huddar[1], Vishwanath Govind Bhave[2]

[1]*Director HPD, Flat no.16, Saord 1B, Nadbramha Society, Waraje Naka, Pune, India 411058*
[2]*Consultant HPD, S24 Indranagari, Survey No 31/2 Kothrud, Dahanukar Colony Lane no15, Pune 411038*
*Email: prashant@hpdglobal.com / vgbhave@yahoo.com*

## Abstract

Design of hydraulic structures requires various inputs for dealing with Structural and Hydraulic aspects. Hydraulic structures like pump intake, Fish ladder and barrage need input in the form of water level, velocity as well as real picture of flow taking place at and around the structure. Design of intake structure must ensure that prevailing norms are adhered, flow is as axial as possible, and vortices are not formed during operation. This aspect needs to produce 3D picture of flow in the pump-sump area. Such a view can be obtained through 3D simulations using either hydraulic scale model or mathematical models. Each of this technique has its own advantage and limitations. At times it is necessary to know the behavior of the structure from sediment movement perspective. Authors have been using CFD modelling technique of structures like intake, barrage, and fish ladder over one decade and have carried out designs of above structure on river and estuaries. CFD modelling is becoming popular tool due to inherent advantages like less time required, flexibility to simulate different scenario and relatively less cost than hydraulic scale model. It is proposed to present design aspects of above structures and case study of an intake channel and pump station on river Narmada in the state of Madhya Pradesh using FLOW3D software.

***Keywords:*** *CFD Modelling, Flow3D, Hydraulic Structures*

## 1. Introduction

Narmada-Jhabua-Petlawad-Thandla-Sardarpur Micro Lift Irrigation Scheme (MLIS) of M/s Narmada Valley Development Agency (NVDA) is proposed to irrigate an area of 57422 ha of actual cultural command area in 202 villages of Dhar and Jhabua district in Madhya Pradesh. Details are presented in Table 1 below:

**Table 1 :** Details of Area & Beneficiary Villages in MLIS

| District | Tehsil | No. of villages | Command (ha) |
|---|---|---|---|
| Dhar | Sardarpur | 59 | 25422 |
| Jhabua | Jhabua, Petlawad, Meghnagar and Thandla | 143 | 32000 |
| Total | | 202 | 57422 |

The project envisages lifting water upto 18 $m^3/s$ (and likely to increase to 20 $m^3/s$) in rabi season from river Narmada. It is proposed to supply water through MS pipeline extending up to 55 km with static head of 459.36 m. Adequate pressure would be maintained for water supply through drip / sprinkler irrigation system. Minimum pressure head of 20 m upto 2.5 ha chak is proposed. Total cost of the project is expected to be more than 2050 cr.

Out of the work components related to structural and hydraulic design of the proposed lift irrigation scheme awarded to M/s HPD Consultants by M/s JMC Projects (India), hydraulic design of intake structure was carried out by the authors. Details are discussed in this paper.

### 1.1 *Scope of work*

Out of the total works related to structural and hydraulic design of the proposed lift irrigation scheme carried out by M/s HPD Consultants, scope of work related to hydraulic design of intake channel included the following:

a) Hydraulic design of intake channel connecting river Narmada to forebay and forebay to sump based on bathymetric survey
b) Confirmation and finalization of alignment and intake channel size for discharge of 18 $m^3/s$
c) Confirm the shape and size of approach channel and fore bay
d) Study the sedimentation and propose silt collection and removal mechanism

### 1.2 *Data used*

Majority of the data were supplied by M/s JMC Projects (India). Additional data available in public domain were also used. Data used in the present studies include:

a) Geometry of river Narmada for stretch of 300 m on upstream and almost same length on the downstream of proposed intake location
b) Daily water levels, corresponding discharge and sediment load in river Narmada for a period of 31 years from 1985 - 2016
c) Details of fore bay and sump area of intake structure near Kukshi village

### 1.3 *Methodology*

It is proposed to complete the task through the following work components:

a) Inspection of site with client
b) Design of intake channel from river Narmada upto fore bay for a discharge of 18 $m^3/s$ (with extension upto 20 $m^3/s$)
c) Analysis of gauge, discharge and sediment load data at Mandaleshwar site
d) Derivation of sediment rating curve in the form of sediment load versus discharge
e) Derivation of gauge discharge relation at the downstream end of Narmada river reach
f) Setting up 1D hydrodynamic model covering reach of river Narmada described above and intake channel from river Narmada upto pump location using appropriate boundary data
g) Simulation runs under steady and unsteady scenario, with and without sediment, load for periods extending to 1 year, 2 years and five years at a stretch
h) Analysis of results and derivation of inputs for setting up 3D hydrodynamic model
i) Setting up 3D hydrodynamic model and analysis of 3D model results
j) Suggest possible remedial measures keeping in mind the sedimentation aspect.
k) Arrive at conclusions and suggest recommendations for smooth operation in the rabi season

## 2. Results and discussions

Inspection of site was carried out and discussions were held with the client for appraisal of the likely situation that would prevail in rabi season. It was apprehended that sediment would be deposited both in approach channel and sump area. In order to minimise the sediment entry into the sump, different combinations of bed slope for intake channel and fore bay (up to sump) were considered and discussed with client. Finally, continuous bed slope of 1/100 is adopted.

Design of Intake channel was carried out for expected higher discharge of 20 $m^3/s$. It was noticed that a trapezoidal section with bed width of 18 meters and side slope of 1 v : 1 h would be required.

### 2.1 *1D hydrodynamic model*

HEC RAS, hydrodynamic model developed by US Army corps of Engineers (2016), was selected for the present study because it has capability to simulate a junction of open channel and the boundary data available was adequate to simulate different scenarios contemplated in the design. HEC-RAS was set up to include intake structure and river Narmada for stretch of 300 m upstream as well as downstream of the intake structure. The structure included intake channel, fore bay and sump area.

Geometry of intake channel was specified using design cross section and supplemented with sump and fore bay.

Daily discharge data series at Mandleshwar gauging site was analysed to derive the following

1 ) Top five annual maximum peak flows
2 ) Three time series of 1 year, 2 year and 5 year duration. Each of the series contained water year data (from 1st June to 31st May of the succeeding year) for the year in which peak flow was observed. Five year time series were derived corresponding to peak flows and placed back to back in descending order of peak flows.
3 ) Three time series of sediment load corresponding to the periods of five peak flows.
4 ) Sediment rating curve (**Figure 1**)

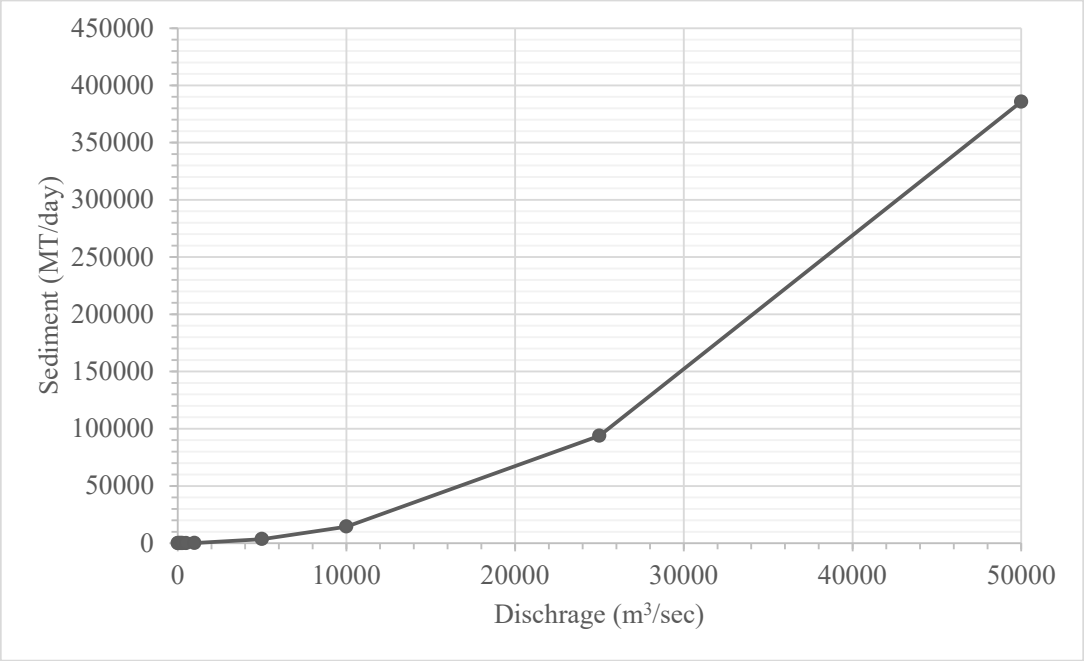



**FIGURE 1:** Sediment Rating Curve

Time series of discharges was considered as upstream boundary, gauge discharge curve derived at the last cross section was used to specify for the downstream boundary condition of main river Narmada and constant discharge required under full development scenario was specified as downstream boundary at the end of intake channel at sump.

Review of sediment data indicated that major part of sediment is in fine range and accordingly Acker's White sediment transport equation was adapted. Distribution of sediment load was specified as per the gradation curve derived by Harish Gupta and G. J. Chakrapani (2005).

The main objective of the study is to determine sediment deposition in the intake area near pump, accordingly, results related to intake channel are only presented and discussed JMC Report (2020).

Change in bed level of intake channel at the end of three simulation runs namely R1, R2 and R5 corresponding to period of 1 year, 2 year and 5 year were obtained through unsteady simulation with HEC-RAS model. These are presented in **Figure 2** alongwith initial bed level**.** The maximum rise in bed level at the end of intake channel was 0.794 m, 0.392 m and 0.943 m for runs R1, R2 and R5 respectively. Changes in cross section at pump location and at the entry of intake channel from river

Narmada were also derived and saved. The results are summarised in **Table 2** and typical sections after sedimentation at the pump location superimposed on initial section are presented in F**igure 3**.

**Table 2: Summary of Sediment Accumulation**

| Location | Average depth (m) at the end of | | |
|---|---|---|---|
| | 1st year | 2nd year | 5th year |
| Intake channel at Pump | 0.458 | 0.608 | 0.718 |
| End of Intake channel | 0.794 | 0.392 | 0.943 |

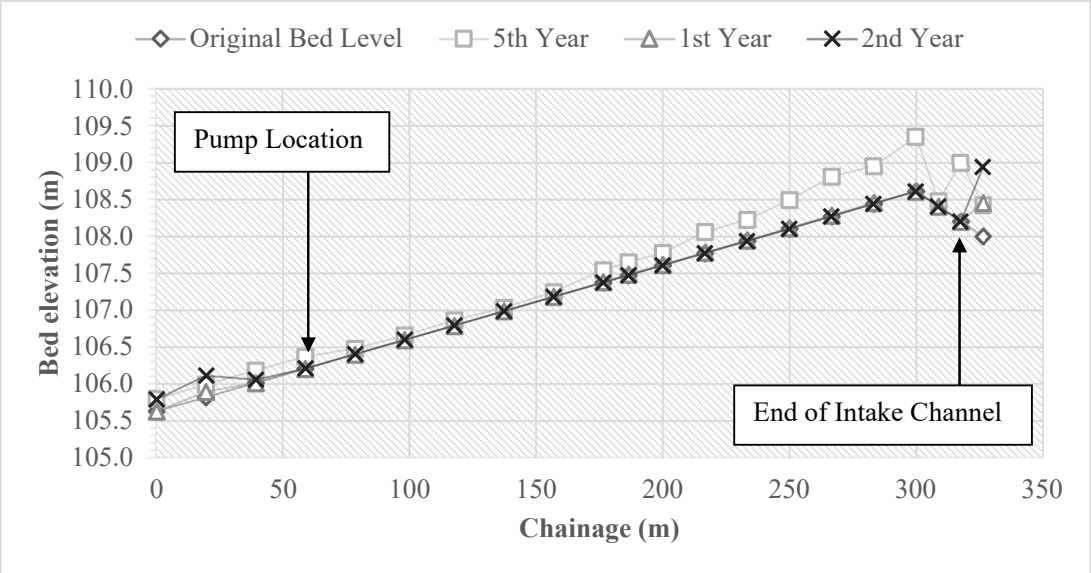



**FIGURE 2:** Sediment Deposition Profiles

It can be observed from **Figure 3** that the deposition of sediment, entering the intake channel, takes place along the left bank. This aspect needs to be seen in detail during 3D model studies.

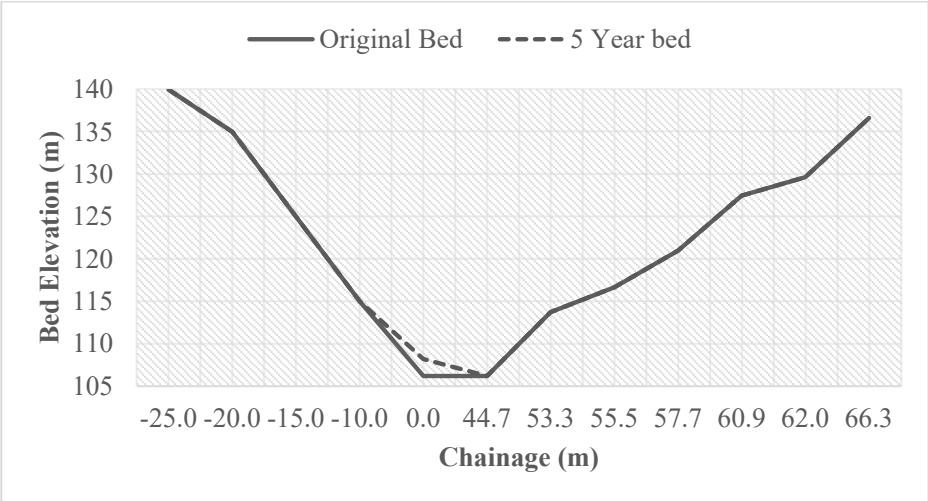



**FIGURE 3:** Sediment Deposition at Pump Location

The change in bed levels of intake channel at the end of 1, 2 and 5 year period of simulation presented in **Figure 2** indicates that there is rise in bed level at pump location. The results summarized in **Table 2** show that rise in bed level at pump location indicates rising trend; as deposition of 0.458 m at the end of first year is increasing to 0.608 m and 0.718 m at the end of 2 and 5 year period respectively.

### 2.2 *Flow-3D model study*

Flow of water in intake channel shows variation in water level and velocity in all the three directions. Accordingly, simulation of these conditions has to be done using 3D hydrodynamic model. Flow-3d model, developed by Flow Science, USA (2017), was selected for the present studies because of the capability to simulate sediment particle motion in a junction of channels. The model is based on the computational fluid dynamics (CFD) principle and has 3D hydrodynamic equation solver based on finite volume approach.

Model inputs starts with definition of the geometry of the water body. The task is completed by defining the elevations of different locations using meshing technique. Meshing proposed in the present study is presented in **Figure 4.**

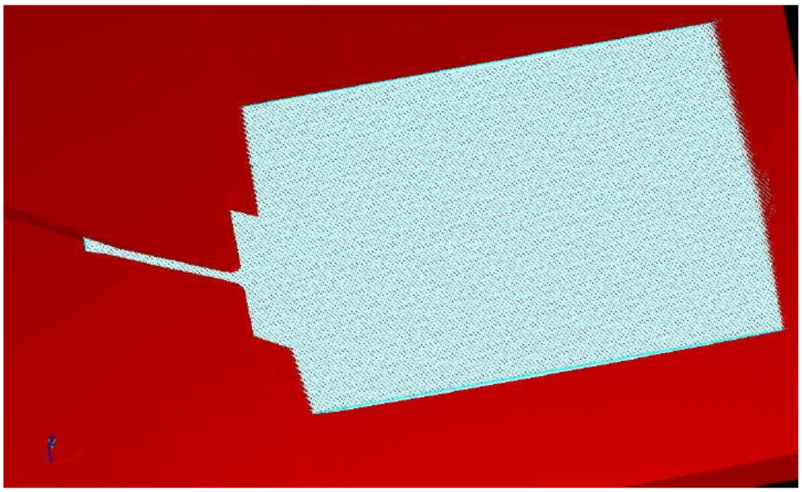


**FIGURE 4:** Meshing in Flow 3D Model

Similar to 1D model, upstream boundary in river Narmada was set as discharge of 934 $m^3/s$, which is likely to prevail in post monsoon season. Water level of 110.64 m was maintained as downstream boundary at the end of river reach and withdrawal at nearly 1.9 times full scheme discharge of 18 $m^3/s$ was set as downstream boundary at the pump location in model set up. Results of 1D model were reviewed and block of 1000 particles of sediment with typical diameter of 0.020m were released at the upstream end of the model. Simulation Run for a period of 1200 seconds was taken to ensure that steady state is reached. Typical velocity distribution pattern at pump location and entry of intake channel particle tracking at the end of simulation period is presented in **Figure 5**.

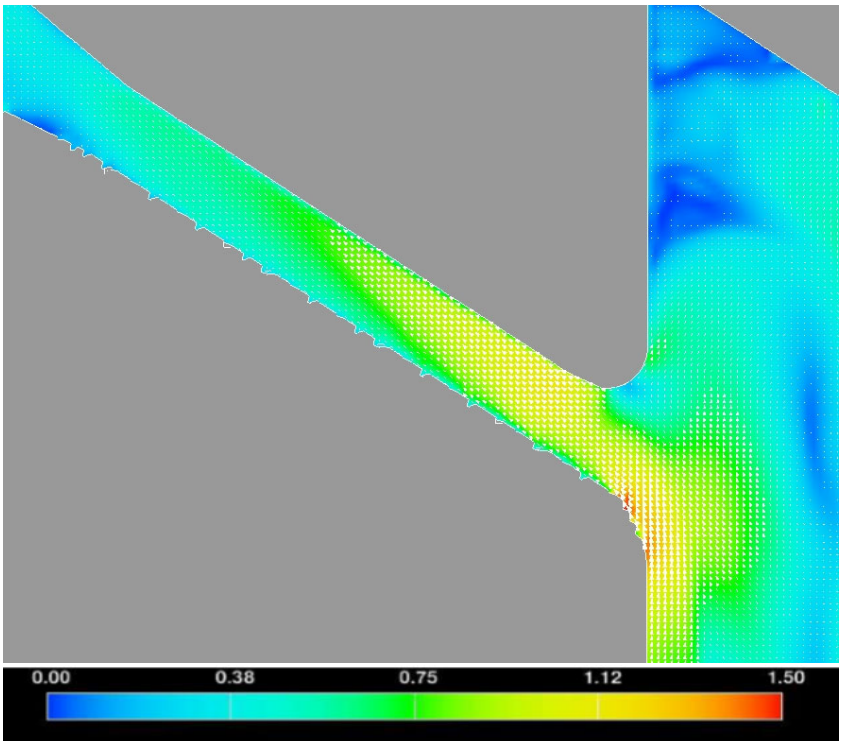



**Figure 5:** Velocity Contour for 3D Hydrodynamic Model

Blue areas in **Figure 5** indicate low velocity zones near pump location as well as entry of intake channel. These are indicators of the likely areas of sediment deposition. Accumulation of sediment near left bank of intake channel noticed in 1D model results thus corroborates with the low velocity zone clearly seen in **Figure 5**.

Sediment entry in intake channel is due to rotational or return flow at the junction with Narmada river channel. This situation can be minimized by providing fluming or smoothening sharp corners at the junction of intake channel and Narmada river-banks.

A qualitative review of sediment particles movement was taken using particle tracking utility of the model. It is indicated above that number of particles entering the model were constant, particles entering the intake channel and leaving the model reach need to be tracked for reviewing the situation. Results are presented (**Figure 6**) as bar chart showing number of particles entering the intake channel and leaving the model reach.

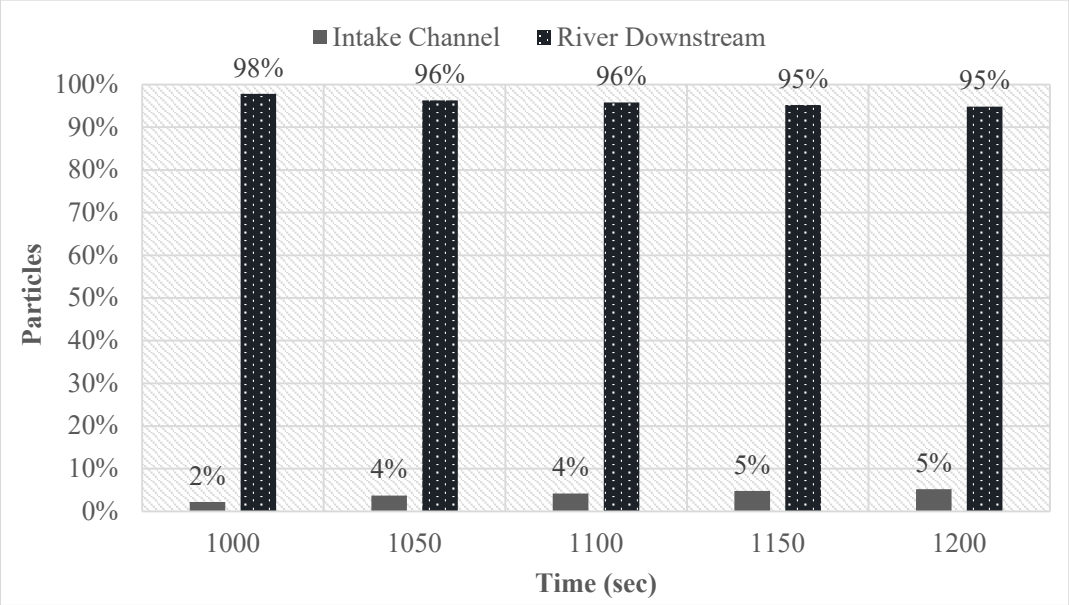



**Figure 6:** Sediment Particle Distribution - Intake Channel & River

It can be seen that upto 5 % of the sediment particles enter the channel at the end of simulation and majority of the sediment moves towards downstream end, ie back into river. However, it is indicated here that the results are qualitative in nature.

## 3. Conclusions

A combined 1D and 3D modelling approach has been used in the design of intake structure for Narmada Jhabua Petlawad Thandla Sardarpur Micro Lift Irrigation Scheme located in the state of Madhya Pradesh. A-y junction of channels formed by 600 m length of river Narmada and about 300 m long intake channel was included in the simulation reach.

1D hydrodynamic HEC-RAS model was used for simulation of water and sediment flows for a period of 1 year, 2 year and 5 years in succession. Discharge hydrograph was used as upstream boundary. Gauge discharge curve was specified as downstream boundary for river Narmada and full capacity discharge of lift irrigation scheme was used for defining downstream boundary of intake channel. Sediment load - discharge relation was derived using concurrent daily data at Mandaleshwar site on river Narmada and was used to define sediment load entering the river at upstream end. Acres White relation was selected for deriving sediment transport rate in the modelled stretch of river Narmada and intake channel junction.

It was noticed that deposition of sediment takes place along bed of intake channel; deposition being high near pump location. The trend of deposition was rising with time. The trend is in order considering that maintenance to remove accumulated sediment is not carried out.

Results of 1D model indicated the areas to be seen in detail with 3D model. Results of 3D model indicated low velocity zone near the locations of deposition noticed in 1D model, thus corroborating the results of 1D model.

Entry of sediment in intake channel can be due to rotational or return flow at the junction of river and intake channel.

### 3.1 *Recommendations*

In order to minimize the sedimentation that is likely to occur near pump location and along the low velocity zone in intake channel, it is recommended that

1) Silt traps be provided at the location of low velocity zones for collection of incoming sediment with slurry pumps for removing the sediment and transporting to properly identified location.

2) Periodic maintenance of the entire intake structure i.e. off-take from river Narmada upto the location of pump be carried out to ensure removal of the accumulated sediment before starting operation of lift irrigation scheme.

3) Necessary stop log structures are to be provided at the entry for segregating the area of intake structure.

4) Smoothening of sharp corners at the junction is to be carried out by provision of fluming structure.

### 3.2 *Acknowledgement*

Design of intake structure for Jhabua Micro lift irrigation scheme was carried out as requested by M/s JMC Projects (India). The work was sponsored by them and authors express deep gratitude to M/s JMC Projects authorities for granting permission to present the work done in HYDRO 2020 conference.

## References

"Flow3D user manual you can write – FLOW3D V12.0 user manual" (2017), Flow Science, Inc. 683 Harkle Road, Santa Fe, NM 87505, 2017 edition

Harish Gupta and G. J. Chakrapani (2005) "Temporal and Spatial Variations in Water Flow and Sediment Load in Narmada River Basin, India: Natural and Man-made Factors", Int Joul of Environ Geol 48: 579–589

"HEC-RAS River Analysis System, User's Manual," Feb (2016), U S Army Corps of Engineers, Institute of Water Resources, Hydrologic Engineering Centre, 609 Second Street, Davis, CA - 95616,

"Simulation of Sediment Transport for Hydraulic Design of Jhabua LIS Inatke PS1_R1" (2020), Oct 2020, Report submitted to JMC

*IN PROCEEDINGS OF 25th HYDRO 2020, INTERNATIONAL CONFERENCE, NATIONAL INSTITUTE OF TECHNOLOGY ROURKELA, ODISHA, INDIA 26-28, March 2021, ISBN 978-93-90631-56-8*

Paper ID - 130

# Performance of Mac-Cormack finite difference scheme with TVD and Artificial Viscosity

Jyotiprakash Tarei[1], Bandita Barman[2]

[1]*MTech student, Sardar Vallabhbhai National Institute of Technology Surat, Surat and Gujarat 395007, India*
[2]*Assistant professor, Sardar Vallabhbhai National Institute of Technology Surat, Surat and Gujarat 395007, India*
*Email: bandita@ced.svnit.ac.in*
*Telephone/Mobile No.: +91 9085778672*

## Abstract

Numerical experiments for instantaneous dam break flow are presented in this paper. The governing equations for one-dimensional shallow water hydrodynamic are solved using Mac-Cormack finite difference scheme. Numerical scheme to simulate dam break flow requires shock capturing capabilities. Here, we applied two different methodologies to dampen the numerical oscillation. Firstly, artificial viscosity is added to the Mac-Cormack Scheme. Numerical performance of the scheme is presented at various pre-break upstream to downstream flow depth ratio. Secondly, a Total Variation Diminishing (TVD) scheme is added to the Mac-Cormack Scheme to verify the same. We have observed better shock capturing capacity while using TVD Mac-Cormack scheme. A flood hydrograph is also simulated using original Mac-Cormac scheme, artificial viscosity and Total Variation Diminishing (TVD) scheme. Similar results are observed from all three approaches in case of flood hydrograph simulation however, it is observed from dam break analysis that TVD scheme has better shock capturing capability.

***Keywords:*** *Mac-Cormack scheme; artificial viscosity; Total Variation Diminishing*

## 1. Introduction

A dam is a barrier to the control and usage of water for human purposes or is an obstacle built over a waterway. The purposes are like to overcome on floods/surges, stored water can fulfil various requirement like water supply towards downstream for drinking and irrigation purposes, generation of hydroelectricity etc. After considering all the safety criteria in designing, construction and operation, dam breach may be occurring due to unpredictable events. Dam failure floods often cause a great deal of property destruction and loss of lives. In recent years, therefore, enormous attempts have been made to achieve satisfactory solutions (Rahaman and Andallah 2018). If we can estimate or approximate the water area elevations, the time travel resulting from a dam break, an area to be flooded, the time of arrival, then we can plan to avoid all the failures and losses due to a dam break (Naik and Khatua 1987). Mathematical or computational models may calculate this because calculation of field in real time is prohibitively difficult to do in the case of a dam break.

Shallow water dam break flow models are used for all types of applications, for example in flood warning systems, water level changes and weather forecasts. In this study, we used shallow water equation to analyze the dam break flow. The dam break flow analysis is critical for the spatial and temporal production of flood event and safety analysis (Rahaman and Andallah 2018). The shallow water equations can be obtained by numerically integrating the depth into the Navier-stock equations and taking hydrostatic pressure distribution into account (Kalita 2016). These equations are derived from the preservation of mass and momentum method and are commonly used for simulations of hydrodynamic flows in water bodies such as rivers, lakes and estuary areas (Kalita 2016). Such equations are, mathematically, first order partial hyperbolic differential equations, without considering several approximations and without a closed form analytical solution.

This results in the use of various numerical techniques, including FDM, FEM, FVM ((Tseng and Chu 2000); (Brufau et al. 2002); (Sreeja and Gupta 2007); (Liang et al. 2007); (Kouassi et al. 2013); (Sanyal et al. 2014); (Bellos and Tsakiris 2015) for solution of these equations (Kalita 2016).

There are different types of numerical techniques for simulating hydrodynamic flows. (Garcia and Kahawita 1986) and (Garcia et al., 1993) used the explicit shock tracking Mac-Cormack scheme (Mac-Cormack 1971). (Robert and Chaudhry 1991) reviewed and compared Mac-Cormack, Gaubutti, and Preissmann schemes (Wang 2000).

Mac-Cormack is one of the excellent schemes for resolving the above-mentioned governing equations for the class of Finite Difference Schemes (Mac-Cormack 1971). The explicit numerical method of Mac-Cormack has become very common in recent years when it comes to dealing with 1D and 2D unsteady open channel flows. This scheme is especially ideal for dam-break problems because accurate results and fairly simple' weak solutions' can be obtained. However, implementing of the equation scheme for finite differences includes carefully handling the usual dissipation and dispersion errors of the first-order and second-order schemes (Anderson et al. 1984). This error leads to spurious oscillation which results unstable solution. To prevent this type of oscillations (Robert and Chaudhry 1991) bring out a new technique named as artificial viscosity which gives smoothness to the large spurious oscillation area. (Tsakiris and Bellos 2014) have recently developed a new technique to handle such numerical oscillations by introducing an additional term to the corrector step in the conventional Mac-Cormack Predictor corrector scheme. After they implement this new artificial viscosity to the model in different cases the result obtained was good but the methodology has same problem of trial and error approach (Kalita 2016).

To overcome this trial and error approach, a theory called TVD (Total Variation Diminishing) techniques which removes sharp discontinuity and gives smooth results this was proposed by (Tsakiris and Bellos 2014), this was added as an extra term to the Mac-Cormack predictor-corrector scheme. Originally the methodology was given by (Harten 1984) to solve hyperbolic equations, the benefit of that is that the necessary dissipation can be taken automatically at different locations in the computational domain; it also has no terminology of adjustable parameters (Tseng and Chu 2000). Later, several researchers (Tseng and Chu 2000a); (Vincent et al. 2001); (Campisano et al. 2014)) Using this method, the governing shallow water flow equations were resolved to simulate various hydrodynamic problems and obtained very good results. (Louaked and Hanich 1998) this technique was first used for shallow water calculations using another system known as the Lax-Wendroff scheme, which is precisely the second order, This approach has the advantage that the Eigen values and Eigen vectors of the equations do not have to be solved, and thus, the calculation costs here are small (Kalita 2016). (Liang et al. 2007) was first used this TVD technique in Mac-Cormack predictor corrector scheme for simulating unsteady shallow water flow.

Later a large number of researcher ((Liang et al. 2007); (Ouyang et al. 2013); (Ouyang et al. 2015)) investigate or research based on this TVD scheme techniques, they implement this techniques to their hydrodynamic model to simulate the model. Based on (Kalita 2016), Strang 1968 during their research in his model he convert the 2D problem into two 1D problems, later the 1D problem was solved by using traditional predictor corrector method with extra addition of the TVD term to it (Kalita 2016).

The main objectives of the present study are to perform the numerical experiments on dam break flood using total variation diminishing (TVD) and artificial viscosity (AV) in Mac-Cormack scheme and compare their results and to perform the numerical experiments on flood hydrograph using Mac-Cormack scheme and then compare these results with TVD, Artificial Viscosity and with Mac-Cormack Predictor-Corrector scheme.

## 2. Research methodology

### *2.1 Governing equation*

As per Anderson (2010) the incompressible 3-dimensional Navier equations and some easier theories originate from this Shallow water system and that of the Saint Venant. The partial differential equation that represents the 1-D incompressible flow of an open channel used in this model is the Saint Venant's continuity and moment (1) and (2).

The continuity equation in 1D form

$$\frac{\partial h}{\partial t} + \frac{\partial}{\partial x}(hu) = S \tag{1}$$

The momentum equation in 1D form

$$\frac{\partial}{\partial t}(hu) + \frac{\partial}{\partial x}\left(hu + \frac{gh^2}{2}\right) = gh(S_0 - S_f) \quad (2)$$

Where, $S_0$ is the slope of the bed with height z of the ground surface. z. $S_f$ represents the energy slope.

$$S_0 = \frac{dz}{dx}\ , S_f = \frac{n^2 * u^2}{h^{\frac{4}{3}}} \quad (3)$$

For a 1-dimensional system, the shallow water equation can be expressed as follows.

$$\frac{\partial U}{\partial t} + \frac{\partial F}{\partial x} = S \quad (4)$$

$$U = \begin{pmatrix} h \\ hu \end{pmatrix}\ F = \begin{pmatrix} uh \\ u^2h + gh^2/2 \end{pmatrix}\ S = \begin{pmatrix} 0 \\ gh(S_{0x} - S_{fx}) \end{pmatrix} \quad (5)$$

### *2.2 Mac-Cormack discretized method*

The implementation of Mac-Cormack predictor-corrector method to the hyperbolic equation i.e. on shallow water equation proceeds by two methods; a predictor step followed by a corrector step. The predictor step consists of forward finite difference scheme while corrector step consists of backward finite difference scheme. finally, the final time step at (n+1) is calculated by averaging both the predictor and corrector results.
The shallow water equation is written as;

$$\frac{\partial U}{\partial t} + \frac{\partial F}{\partial x} = S \quad (6)$$

Then

$$\frac{\partial U}{\partial t} = S - \frac{\partial F}{\partial x} \quad (7)$$

Here U represents vectors with discrete variables h, u; F are flux vectors and are functions of U; S is source term. The SWE problem is solved here with the process Mac-Cormack. Now the above equation is discretized in its conservative form using the predictor-corrector scheme, proposed by Chaudhary (2008),
After that, Mac-Cormack method is called on shallow water equation by using predictor-corrector approach.
Predictor step:
Now find the value of U at time step t+1 from known time step t and using forward difference scheme

$$[U_i^{n+1}]_P = [U_i^n] - \left[\{(F_i^n) - (F_{i-1}^n)\} * \frac{\Delta t}{}\right] - (S_i^n) * \Delta \quad (8)$$

Corrector step:

$$[U_i^{n+1}]_C = [U_i^n] - \left[\{(F_i^P) - (F_{i-1}^P)\} * \frac{\Delta t}{}\right] - (S_i^P) * \Delta \quad (9)$$

Then, at step n + 1, we have the solution with a average between the predictor and the corrector

$$U_i^{n+1} = \frac{[U_i^{n+1}]_P + [U_i^{n+1}]_C}{2} \quad (10)$$

where Δx is the grid spacing in x-direction designated by the subscript i, Δt is the grid spacing in the time axis (time step) designated by the superscript n, where, superscripts p and c stands for predicted and corrected values respectively.

## 2.3 Numerical techniques

### 2.3.1 Numerical techniques for TVD

The proposed shallow water equations are solved with a TVD Mac-Cormack Predictor system. The following finite differences are obtained from this new TVD technique which is proposed by Kalita (2016).

$$U_i^{n+1} = \frac{[U_i^{n+1}]_P + [U_i^{n+1}]_C}{2} + \{[G(r_i^+) + G(r_{i+1}^-)] * [\Delta U_{i+1}^n - U_i^n]\} - \{[G(r_{i+1}^+) + G(r_i^-)] * [\Delta U_i^n - U_{i-1}^n]\} \quad (11)$$

$$r_i^+ = \frac{(h_i^n - h_{i-1}^n)*(h_{i+1}^n - h_i^n) + (hu_i^n - hu_{i-1}^n)*(hu_{i+1}^n - hu_i^n)}{(h_{i+1}^n - h_i^n)*(h_{i+1}^n - h_i^n) + (hu_{i+1}^n - hu_i^n)*(hu_{i+1}^n - hu_i^n)} \quad (12)$$

$$r_i^- = \frac{(h_i^n - h_{i-1}^n)*(h_{i+1}^n - h_i^n) + (hu_i^n - hu_{i-1}^n)*(hu_{i+1}^n - hu_i^n)}{(h_{i+1}^n - h_i^n)*(h_{i+1}^n - h_i^n) + (hu_{i+1}^n - hu_i^n)*(hu_{i+1}^n - hu_i^n)} \quad (13)$$

The expression for the function G ()is given as

$$G(x) = 0.5 * C_i^n * [1 - \emptyset(x)] \quad (14)$$

$$\emptyset(x) = \max(0, \min(2x, 1)) \quad (15)$$

$$C_i^n = Cr_i^n(1 - Cr_i^n) \quad \text{for } Cr_i^n <= 0.5$$
$$= 0.25 \quad \text{for } Cr_i^n > 0.5 \quad (16)$$

$$Cr_i^n = \frac{mod((U_i^n) + \sqrt{g * h_i^n})}{\Delta x} \Delta t \quad (17)$$

$$U_i^n = \frac{Q_i}{A_i} \quad (18)$$

From the expression above, it seems that the present technique requires no calculation of individual values or own vectors. The additional TVD term added after the predictor-corrector is made up of some variables that can be determined easily based on the flux variables in a known time step.

### 2.3.2 Numerical techniques for Artificial Viscosity

In order to apply this approach on the basis of normalized form of the calculated water-surface gradients, we calculate the following parameter:

$$V_i^{n+1} = \frac{|y_{i+1}^n - 2*y_i^n + y_{i-1}^n|}{|y_{i+1}^n| + 2*|y_i^n| + |y_{i-1}^n|} \quad (19)$$

$$V_{i+\frac{1}{2}}^{n+1} = k * \max(V_{i+1}^{n+1}, V_i^{n+1}) \quad (20)$$

Where k is a constant, We use the following expressions in place of Eq(33) when $y_{i+1}$ and $y_{i-1}$ do not exist.

$$V_i^{n+1} = \frac{|y_i^n - y_{i-1}^n|}{|y_i^n| + |y_{i-1}^n|} \quad (21)$$

$$V_i^{n+1} = \frac{|y_{i+1}^n - y_i^n|}{|y_{i+1}^n| + |y_i^n|} \quad (22)$$

The measured vector F will then be updated as

$$F_i^{n+1} = F_i^{n+1} + V_{i+\frac{1}{2}}^{n+1} * \left(F_{i+1}^{n+1} - F_i^{n+1}\right) - V_{i-\frac{1}{2}}^{n+1} * \left(F_i^{n+1} - F_{i-1}^{n+1}\right) \quad (23)$$

F refers to both h as well as to u.

*2.3.3 Stability condition*

For an explicit finite difference scheme, it must satisfy the courant condition. The expression for courant number is given in the equation i.e.

Courant no = Cn = u*($\Delta t/\Delta x$) (24)

Where 0≤Cn≤ 1 and

u = flow velocity

Δx = space interval

Δt = time interval

## 3. Model validation and comparison

In this current paper, Mac-Cormack finite difference scheme is applied to perform the numerical experiments. A TVD and artificial viscosity is incorporated with the original Mac-Cormack scheme to analyze the dam break flow. Both approaches are applied on a same numerical problem to check the performance of the schemes, similarly another numerical experiment done on hydrograph simulation using TVD, Artificial Viscosity and Mac-Cormack Predictor-corrector scheme to compare the performance of these schemes.

### *3.1 Model validation for TVD*

In the first example which is referred from Kalita(2016), a classical dam-break flow is repeated with the proposed model. It demonstrates the shock capability of the numerical system with particular attention to the motion of the front wave. The canal is considered a rectangular channel with a length of 1000 m without friction or horizontal. The dam is in the middle of the lake. The original water levels are 10 m and 2 m upstream and downstream of the dam. The dam is breached immediately at the beginning (t = 0). Because of this separation, downstream a positive wave travels, and upstream a negative wave. The present model used for numerical simulation of the channel with delx = 0.8 m. The banks are simulated as free slip limits because the solution has no effect. The value of the time step is delt = 0.01s. Conduct a value of average $Cn \leq 1$.

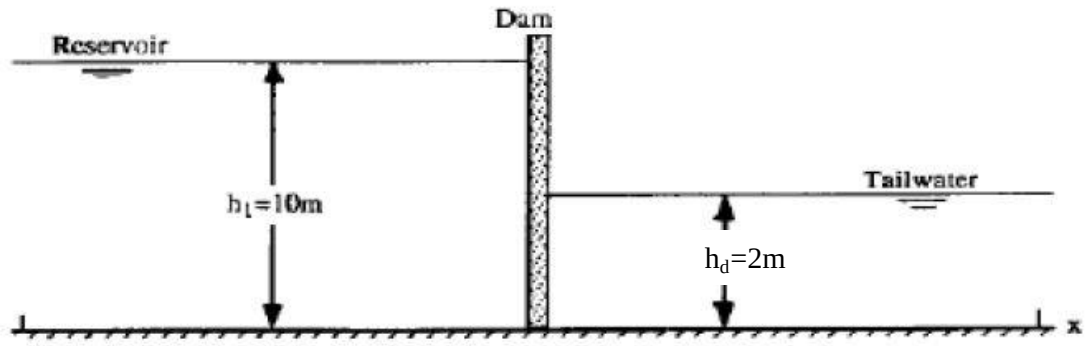



**Figure 1** Schematic representation of model

Initial boundary condition

At time t = 0, the initial boundary conditions are given below

$h(x) \mid_{t=0} = h_0(x)$

$q_x(x) \mid_{t=0} = q_{x0}(x)$

For initial condition and boundary condition, no slip condition assumed, then $h_L$ (0) (upstream) water level taken 10m where, the velocity at upstream $U_L$ (0) =0 m/s, at downstream $h_d$ (1000) water level is taken as 2m, velocity at downstream $U_d$ (1000) =0 m/s.

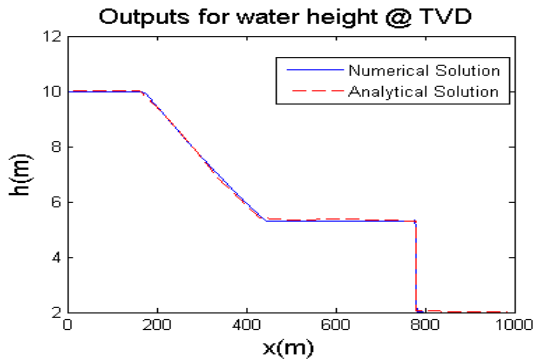



**Figure 1a Model validation for Artificial Viscosit**

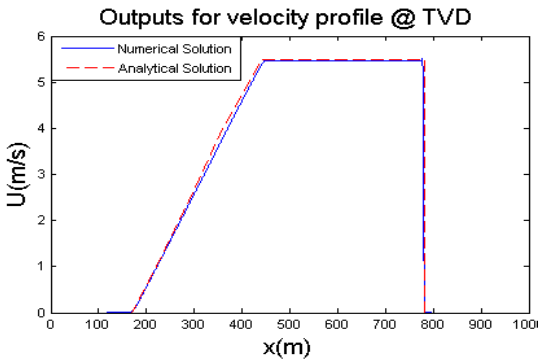



**Figure 1b** Outputs for velocity profile @TVD

The same numerical experiment explained in the previous section is simulated applying artificial viscosity. Fig 2 shows the results with artificial viscosity. Here, we observed some numerical oscillation on the water surface simulation. However, this oscillation is not present in the TVD simulation.

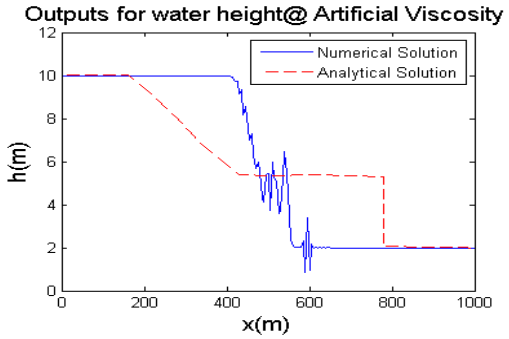



**Figure 2a** Outputs for water height @ Artificial Viscosity

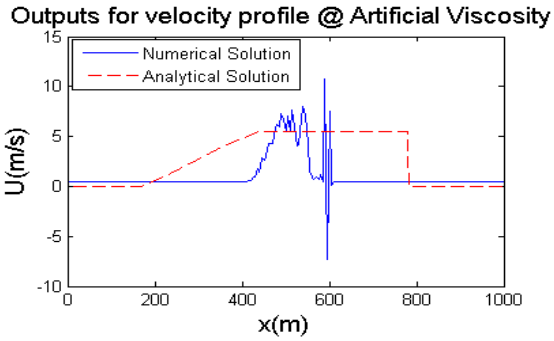



**Figure 2b** Outputs for water height @ Artificial Viscosity

### *3.3 Model validation for hydrograph*

A benchmark problem is considered from Naik and Khatua (2015), from which data collected from a hydrograph and compare it with performing different numerical experiments. It's a length of 25000 ft long and 13500 ft wide and del x=1000 ft and del t= 200seconds that is scaled in this realistic case. The rest of the surface base is dry. At time t = 0, the dam is drained completely and rapidly; the water flows down the valley. No slip limiting conditions on the foundation geography are authorized. All the initial data required are given, i.e., the initial depth of the water in the reservoir, and the numerical formulae for each grid point, as per the explicit Mac-Cormack Scheme, are written for every grid point to resolve the next grid value. The downstream output is determined, such as the hydrographic flow and phase hydrographs. After the calculation process, the outputs and the comparison and conclusion are given in the following sections.

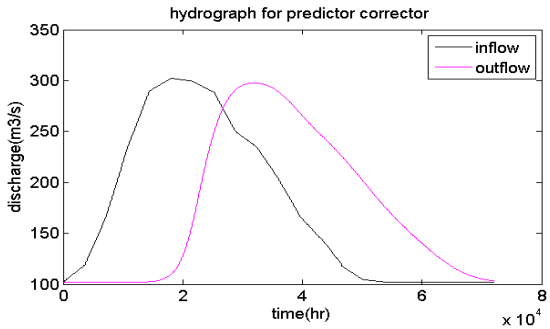



**Figure 3** Outputs of hydrograph in predictor-corrector method

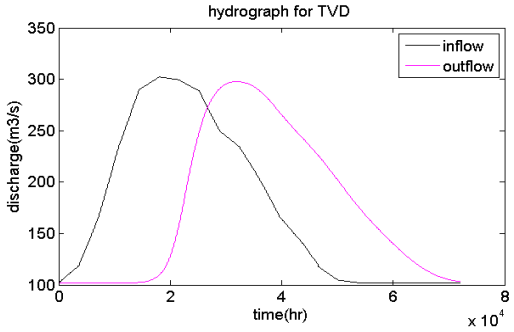



**Figure 4** Outputs of hydrograph in TVD method

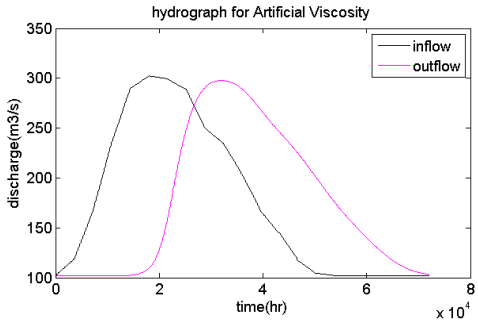



**Figure 5** Outputs of hydrograph in Artificial Viscosity method

### *3.4 Discussion of the result*

From the output, we have observed that the performance of TVD and AV using the Mac-Cormack predictor and corrector method was tested for a dam break analysis at both the experiments. The result shows that TVD is more shock capturing and more accurate than AV in the case of dam break analysis. The results are found to be quite accurate with analytical solutions and with Kalita (2016). Similarly, we performed an artificial viscosity experiment based on this same benchmark problem and it found that artificial viscosity becomes more unstable at the time of dam break, it gives results for the period of 7.2 sec, afterward, it becomes unstable and gives high oscillation inflow. For this, we take delx=5 and delt=0.01. But the result in plotting hydrograph in all three cases i.e. predictor-corrector method, TVD, AV they all gives a similar output.

## 4. Conclusions

This study focuses on the performance test for the TVD and Artificial viscosity Mac-Cormack predictor-corrector scheme for the solution of flow governing equations. As a predictor-corrector method based on the present model, it is simpler, easier to implement and more precise. Then adding TVD and AV makes oscillations more robust and unwanted. In this present model, we check the performance of both TVD and AV in terms of comparing a benchmark problem. The result is quite distinct which shows that for analytical dam break over horizontal friction bed, TVD is more accurate and more shock capturing while Artificial Viscosity becomes unstable and gives more oscillation to model. This study concluded that TVD is a more accurate method than AV and to verify its efficacy in real-life applications, a detailed model experiment is required. There is also a necessity of validating the model for two dimensional dam break flow and also for curvilinear coordinate system.

## References

Anderson, J. . (2010). *Computational fluid dynamics, second edition*. McGraw-Hill INc., New York.

Bellos, V., and Tsakiris, G. (2015). "Comparing Various Methods of Building Representation for 2D Flood Modelling In Built-Up Areas." *Water Resources Management*, 29(2), 379–397.

Brufau, P., Vzquez-Cendon, M. E., and Garca-Navarro, P. (2002). "A numerical model for the flooding and drying of irregular domains." *International Journal for Numerical Methods in Fluids*, 39(3), 247–275.

Campisano, A., Cutore, P., and Modica, C. (2014). "Improving the evaluation of slit-check dam trapping efficiency by using a 1D unsteady flow numerical model." *Journal of Hydraulic Engineering*, 140(7), 1–11.

Cao, Z., Pender, G., and Wallis, S. (2004). "Computational Dam-Break Hydraulics over Erodible Sediment Bed." *Journal of hydraulic engineering*, 130(October), 1013–1024.

Chaudhry, H. (2008). *open channel flow*. Springer Science+Business Media, Columbia.

Das and Bagheri (2015). "Modelling of shallow-water equations by using compact Mac-Cormack-Type schemes with application to dam-break problem," *International Journal of Advances in Applied Mathematics and Mechanics*,

Fagherazzi, S., Furbish, J., and Hussaini, M. (2004). "Numerical Solution of the Dam-Break Problem with a Discontinuous Galerkin Method." *Journal of hydraulic engineering*, 130(december), 1013–1024.

G-Navarro. et al (1993). "1-d open-channel f l o w simulation using t v d - m c c o r m a c k scheme." 118(10), 1359–1372.

Garcia-Navarro, P., Fras, A., and Villanueva, I. (1999). "Dam-break flow simulation: Some results for one-dimensional models of real cases." *Journal of Hydrology*, 216(3–4), 227–247.

Garcia, R., and Kahawita, R. A. (1986). "Numerical solution of the St. Venant equations with the MacCormack finite-difference scheme." *International Journal for Numerical Methods in Fluids*, 6(5), 259–274.

Harten. (1984). "On a Class of High Resolution Total-Variation-Stable Finite-Difference Schemes." 21(1), 1–23.

Harten, Yee (1985), " On the Implementation of a Class of Upwind Schemes for System of Hyperbolic Conservation Laws ", *NASA Ames Research Center*.

Hicks, F. ., and Steffler, P. . (1997). "One-dimensional dam-break solutions for variable width channels." *Journal of Hydraulic EngineeringofHydraulic Engineering*, 123(10), 464–468.

Hu, C., and Sueyoshi, M. (2010). "Numerical simulation and experiment on dam break problem." *Journal of Marine Science and Application*, 9(2), 109–114.

Jovanović, M., and Djordjević, D. (1995). "Experimental verification of the MacCormack numerical scheme." *Advances in Engineering Software*, 23(1), 61–67.

Kalita, H. M. (2016). "A New Total Variation Diminishing Predictor Corrector Approach for Two-Dimensional Shallow Water Flow." *Water Resources Management*, 30(4), 1481–1497.

Kouassi, K. L., Kouame, K. I., Konan, K. S., Sanchez Angulo, M., Deme, M., and Meledje, N. H. E. (2013). "Two-Dimensional Numerical Simulation of the Hydro-Sedimentary Phenomena in Lake Taabo, Côte d'Ivoire." *Water Resources Management*, 27(12), 4379–4394.

Liang, D., Lin, B., and Falconer, R. (2011). "Simulation of rapidly varying flow using an efficient TVD–MacCormack scheme." *International Journal for Numerical Methods in Fluids*,

65(October 2010), 236–253.

Liang, D., Lin, B., and Falconer, R. A. (2007). "A boundary-fitted numerical model for flood routing with shock-capturing capability." *Journal of Hydrology*, 332(3–4), 477–486.

Liska, R., and Wendroff, B. (1999). "Two-dimensional shallow water equations by composite schemes." *International Journal for Numerical Methods in Fluids*, 30(4), 461–479.

MacCormack. (1971). "The effect of viscosity in hypervelocity impact cratering."

Naik, S., and Khatua, K. K. (2015). "Numerical Simulation of a Dam Break Flow Using Finite Difference Method." 37–41.

Ouyang, C., He, S., and Xu, Q. (2015). "MacCormack-TVD finite difference solution for dam break hydraulics over erodible sediment beds." *Journal of Hydraulic Engineering*, 141(5), 1–9.

Ouyang, C., He, S., Xu, Q., Luo, Y., and Zhang, W. (2013). "A MacCormack-TVD finite difference method to simulate the mass flow in mountainous terrain with variable computational domain." *Computers and Geosciences*, Elsevier, 52, 1–10.

Peng, S. H. (2012). "1D and 2D numerical modeling for solving dam-break flow problems using finite volume method." *Journal of Applied Mathematics*, 2012.

Rahaman, M., and Andallah, L. (2018). "Numerical simulation of shallow water dam break flow problem." *International Journal of Scientific & Engineering Research*, 9(11), 13–22.

Robert, B., and Chaudhry, H. (1991). "E x p l i c i t m e t h o d s for 2-d transient free-surface flows." 116(8), 1013–1034.

Sanyal, J., Densmore, A. L., and Carbonneau, P. (2014). "2D Finite Element Inundation Modelling in Anabranching Channels with Sparse Data: Examination of Uncertainties." *Water Resources Management*, 28(8), 2351–2366.

Sreeja, P., and Gupta, K. (2007). "An alternate approach for transient flow modeling in urban drainage systems." *Water Resources Management*, 21(7), 1225–1244.

Sun, G., Wei, W., and Liu, Y. L. (2010). "Numerical scheme for simulation of 2D flood waves." *Proceedings - 2010 International Conference on Computational and Information Sciences, ICCIS 2010*, IEEE, 846–849.

Tsakiris, G., and Bellos, V. (2014). "A Numerical Model for Two-Dimensional Flood Routing in Complex Terrains." *Water Resources Management*, 28(5), 1277–1291.

Tseng, M. H., and Chu, C. R. (2000a). "Two-dimensional shallow water flows simulation using TVD-MacCormack scheme." *Journal of Hydraulic Research*, 38(2), 123–131.

Tseng, M. H., and Chu, C. R. (2000b). "The simulation of dam-break flows by an improved predictor-corrector TVD scheme." *Advances in Water Resources*, 23(6), 637–643

Van Leer, B. (1979), Towards the Ultimate Conservative Difference Scheme, V. A Second Order Sequel to Godunov's Method, *J. Com. Phys..*, *32*, 101–136

Vincent, S., Caltagirone, J. P., and Bonneton, P. (2001). "Numerical modelling of bore propagation and run-up on sloping beaches using a MacCormack TVD scheme." *Journal of Hydraulic Research*, 39(1), 41–49.

Vosoughifar, H. R., Dolatshah, A., and Sadat Shokouhi, S. K. (2013). "Discretization of multidimensional mathematical equations of dam break phenomena using a novel approach of

finite volume method." *Journal of Applied Mathematics*, 2013.

Wang. (2000). "Finite-difference TVD scheme for computation of Dam-breakk problems." 126(April), 253–262.

Wang, Z., and Shen, H. (1999). "LAGRANGIAN SIMULATION OF ONE-DIMENSIONAL DAM-BREAK FLOW." *Journal of Hydraulic Engineering*, 125(November), 1217–1220.

Zoppou, C., and Roberts, S. (2000). "Numerical solution of the two-dimensional unsteady dam break." *Applied Mathematical Modelling*, 24(7), 457–475.

Zoppou, C., and Roberts, S. (2003). "Explicit schemes for dam-break simulations." *Journal of Hydraulic Engineering*, 129(1), 11–34.

*IN PROCEEDINGS OF 25th HYDRO 2020, INTERNATIONAL CONFERENCE,*
*NATIONAL INSTITUTE OF TECHNOLOGY ROURKELA, ODISHA, INDIA*
*26-28, March 2021, ISBN 978-93-90631-56-8*

Paper ID - 217

# Development of two dimensional 9-noded Lagrangian quadratic isoparametric element mesh generation tool for Finite Element Models

Lokesh Mangal[1], C. Gowri Shankar[2], Manasa Ranjan Behera[3*]

[1]*Junior Research Fellow, Department of Civil Engineering, IIT Bombay, Mumbai-400076, India*
[2]*Research Associate, Department of Civil Engineering, IIT Bombay, Mumbai-400076, India*
[3*]*Associate Professor, Department of Civil Engineering, IIT Bombay, Mumbai-400076, India*
*Email: manasa.rb@iitb.ac.in*
*Telephone/Mobile No.: +91 22 2576 7313*

## Abstract

With the advent of high performance computing facilities, PDEs representing most complex physical processes are solved using numerical methods, such as Finite Difference Method (FDM), Finite Volume Method (FVM) and Finite Element Method (FEM). FEM is widely adopted and requires inversion of property matrix to obtain the behavior matrix that is a time consuming step. However, the Explicit FEM (EFEM) suggested by Gray and Lynch (1979) uses the 9-noded Lagrangian quadratic isoparametric elements with Simpson's 9-point integration rule resulting in a diagonal property matrix. The solution of the diagonal property matrix is straightforward and substantially reduces the computational effort. The 9-noded element can capture the field variables more accurately within the element, which further enhances the accuracy of numerical results, which may not be possible through other type of elements. Because of these properties of 9-noded Lagrangian quadratic isoparametric element, it is used to discretize large domains such as Bay of Bengal, Arabian Sea, Indian Ocean, etc. for the solution of Ocean dynamics and processes; such as, tidal flow and tsunami propagation. The importance of 9-noded Lagrangian quadratic isoparametric element mesh and unavailability of open source software/modules for mesh generation motivated to develop an in house 9-noded mesh generation tool. Initially, a tool (programmed using MATLAB) has been developed to generate quadrilateral elements mesh for rectangular and circular domains. The tool could generate uniform mesh using quadrilateral elements for the mentioned standard domain shapes. The tool also has the option to extract the nodal coordinates and nodal connectivity of the elements required for Finite Element Analysis models. The program was further extended to generate 9-noded mesh for two-dimensional rectangular region, and obtain nodal coordinate and element connectivity matrices, which are very useful in solving standard two-dimensional problems using Finite Element Method. The tool can be extended for various domain shapes inclusive of obstructions for versatile applications.

***Keywords:*** *9-Noded Lagrangian Quadratic Isoparametric Element; Simpson's 9-point Integration; Mesh Generation; Finite Element Method*

## 1. Introduction

Mesh generation is defined as the process of discretizing a physical domain into smaller sub domains (elements), in order to generate a numerical solution for a partial differential or integral equation. Mesh generation is used for a wide range of engineering applications and physical simulations such as finite element analysis and computational fluid dynamics. Surface (2D) domains may be subdivided into triangular or quadrilateral shapes and other 2D elements, while volumes (3D) may be subdivided primarily into tetrahedral or hexahedral shapes. Meshing algorithms ideally define the shape and distribution of the elements. The finite element method has become a mainstay for engineering design and analysis, in recent decades and is being used in simulation of complex designs.

Initially, finite element method was capable of simulating designs utilizing only tens or hundreds of elements. Very careful and thorough preprocessing was required to subdivide domains into usable elements, but at present the users expect to mesh complex domains with thousands or millions of elements. The mesh generation problem aims to define a set of nodes and elements in order to best describe a geometric domain, subject to various element sizes and shape criteria, where the geometry is most often composed of vertices, curves, surfaces and solids.

In order to solve the differential equations numerically, the continuous physical domain needs to be identified with a large set of discrete locations called nodes. The number of these discrete data points

(spatial resolution) should be so large such that the differential equation solution is close to the exact or bench-mark solution (Lo 2015).

MATLAB has been used by researches for finite element analysis of different problems since it has vast predefined mathematical library, which enables user to write code for implementing numerical methods, and are user friendly. Implementation of algorithm is the main task as the vector and linear tools are already defined. The advantage of using MATLAB as a tool to generate mesh for a 2D FEM problem is that it requires only a few hundred lines of code, while the same problem needs few thousands of lines of codes in C++ or FORTRAN to be able to solve it (Chessa 2002). Since MATLAB is an interpretive language; each line of code is interpreted by the MATLAB command line interpreter and executed sequentially at run time. Bartels et al. (2006) developed a MATLAB tool for the solution of elliptical problems such as stationary flow problem in 2D with triangular and quadrilateral quadratic isoparametric elements. A finite element analysis through MATLAB was presented by Behzad and Berardo (2013) for the computation of stress and strain of elasticity plane using 9-noded Lagrangian quadratic isoparametric elements. Predefined mathematical library "distmesh" was used by Koko (2015) for unstructured triangular mesh generation of 2D domain. The finite element solutions for point, line or surface loads were presented by Sun and Lueth (2018) by extending the concept of MATLAB PDE toolbox. The use of MATLAB for finite element analysis is not limited to these studies; it is widely adopted and used extensively because of its efficient capability of setting up, solving and post processing 2D problems.

Gray and Lynch (1979) suggested Explicit FEM (EFEM) and used the 9-noded Lagrangian quadratic isoparametric elements with Simpson's 9-point integration rule which results in a diagonal property matrix for tidal flow computation. The solution of the diagonal property matrix is straightforward and substantially reduces the computational effort. Mahadevan and Latha (2001) estimated the influence of coastal flooding on surge along the east coast of India by using EFEM and the domain was discretized using 9-noded Lagrangain quadratic isoparametric elements. Behera et al. (2008) adopted unstructured EFEM and simulated Indian Ocean tsunami propagation for Bay of Bengal and Northern part of Indian Ocean using shallow water equation for irregular coastline and used 9-noded Lagrangain quadratic isoparametric elements with Simpson's 9-point integration rule to reduce computation time. The advantage of using unstructured grids is to resolve the complicated and multiscale geometry of coastal environments and helps in obtaining proper resolution of the important topographic variability (Walters 2006).

### *1.1 Finite Element Method (FEM)*

An approximation to real solution of the PDEs is constructed using different types of discretization methods in the form of algebraic equations. The solutions to these algebraic equations are generally found out using different numerical methods such as FDM (Finite Difference Method), FEM (Finite Element Method), and FVM (Finite Volume Method) etc. In FEM the algebraic equations are solved at nodal points and interpolated between nodes by using shape functions. The low order polynomial functions are typically used as shape function. If the shape functions of the elements are written by using Lagrangian polynomial and the equations of shape function are of order 2 in both the direction then the element is called Lagrangian bi-quadratic element. The term isoparametric is derived from the use of the same shape functions to define the element's geometric shape as are used to define the primary unknowns within the element (Behzad and Berardo 2013). In 9-noded element, 4 nodes are defined at corners, 4 nodes at the edge center and 1node at the center of element as shown in Figure 1. The 9-noded Lagrangian quadratic isoparametric element has the application for the finite element solution of coastal dynamics defined for large physical domains such as Bay of Bengal, Arabian Sea and Indian Ocean, etc.

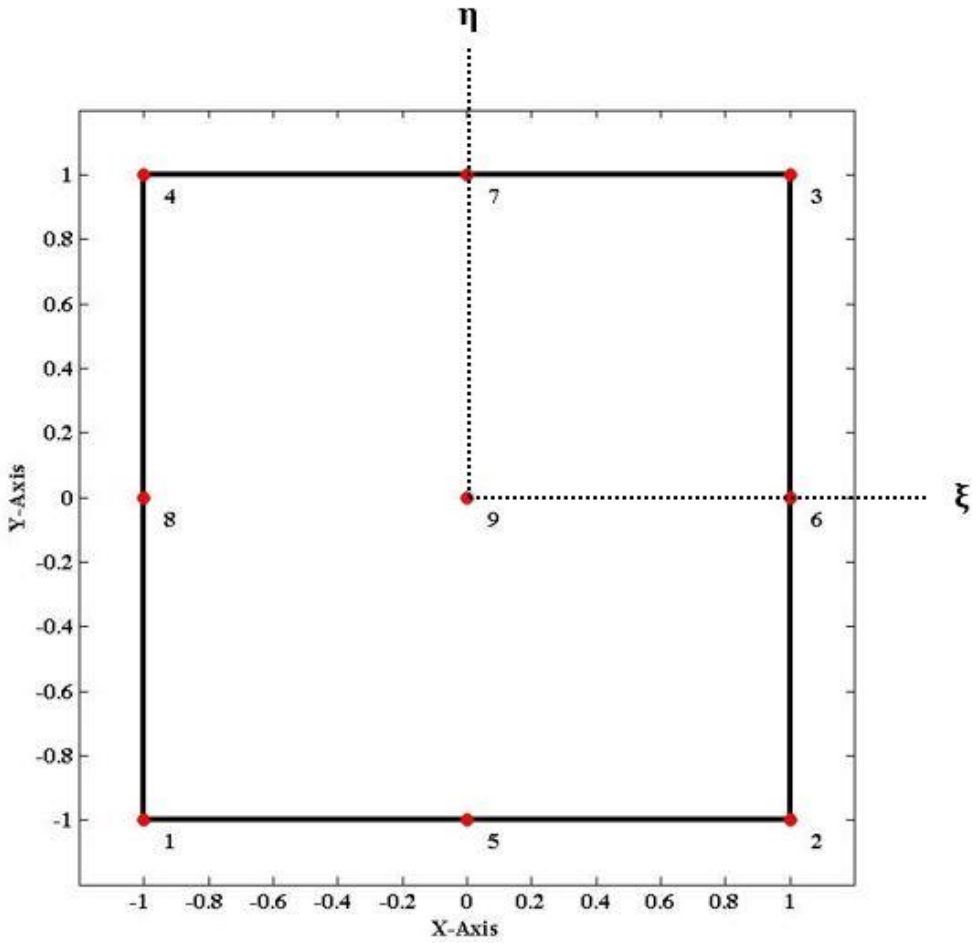



**Figure 1** Schematic representation of a 9-node isoparametric element

The shape functions of 9-noded Lagrangian quadratic isoparametric element expressed as shown in eq.'s. (1-9). $N_i(\xi,\eta)$ represents the shape function at node 'i'.

$$N_1(\xi,\eta) = \left(\frac{\xi}{2}\right)(1-\xi)\left(\frac{\eta}{2}\right)(1-\eta) \quad (1)$$

$$N_2(\xi,\eta) = \left(\frac{\xi}{2}\right)(1+\xi)\left(-\frac{\eta}{2}\right)(1-\eta) \quad (2)$$

$$N_3(\xi,\eta) = \left(\frac{\xi}{2}\right)(1+\xi)\left(\frac{\eta}{2}\right)(1+\eta) \quad (3)$$

$$N_4(\xi,\eta) = \left(-\frac{\xi}{2}\right)(1-\xi)\left(\frac{\eta}{2}\right)(1+\eta) \quad (4)$$

$$N_5(\xi,\eta) = (1-\xi^2)\left(-\frac{\eta}{2}\right)(1-\eta) \quad (5)$$

$$N_6(\xi,\eta) = \left(\frac{\xi}{2}\right)(1+\xi)(1-\eta^2) \quad (6)$$

$$N_7(\xi,\eta) = (1-\xi^2)\left(\frac{\eta}{2}\right)(1+\eta) \quad (7)$$

$$N_8(\xi,\eta) = \left(-\frac{\xi}{2}\right)(1-\xi)(1-\eta^2) \quad (8)$$

$$N_9(\xi,\eta) = (1-\xi^2)(1-\eta^2) \quad (9)$$

## 2. General Methodology for finite element analysis

Typical steps of finite element analysis are pre-processing, processing and post-processing. The pre-processing step involves in setting up of the mathematical model to define the physical problem in terms of algebraic equations. The solution to these governing algebraic equations are obtained with help of finite element modelling for which the model parameters such as element type, mesh density, solution parameters (loading, forcing conditions) and boundary conditions are prescribed during the pre-processing step. Once the pre-processing step is completed the processing section takes place where the defined problem is solved with the help of mathematical model and finite element parameters specified in pre-processing. Post-processing section is the analyzer in which the output is analyzed and errors are estimated. Error assessment of the finite element solution of mathematical model and validation of result obtained provides the information about the discrepancies made in previous steps of the modelling process. If the estimated error exceeds the limit values then the solution is not acceptable and therefore the improvement should be initiated either in meshing definition or mathematical model or both. Validated results obtained after acceptable error can be interpreted for further analytical assessment and other secondary parameters required for the study can also be calculated.

## 3. MATLAB Programming and mesh generation

The first step after defining the problem is to discretize the domain using different types of elements known as meshing. A problem domain can be defined by specifying the dimensions for regular domains (rectangular or circular) or by providing the coordinates of boundary points of the domain of irregular shapes. The defined domain is discretized for finite element analysis for which meshing element parameters such as no. of nodes per element, total no. of elements, total no. of nodes in the domain etc. need to be defined. For rectangular domain the parameters are defined along length and breadth directions whereas for circular domain parameters are defined along angular and radial directions.

After defining the domain extent and meshing parameters, the domain is discretized using the “linspace” MATLAB function for rectangular domain and using “meshgrid” function for circular domain. To represent the discretization of the domain, we define a set of nodes and nodal coordinates that are stored in the nodal coordinate matrix. For circular domain the radial coordinates are converted to Cartesian coordinates before the generation of nodal coordinate’s matrix. The elements are connected at the nodes in counter-clockwise order (to ensures the Jacobian’s are positive) and are stored in a matrix named as element connectivity matrix.

## 4. Development of mesh generation tool

The information needed for finite element analyses are the nodal coordinates and nodal connectivity of the elements when a structure is discretized that are used for further analysis. The Mesh generation algorithm explained in previous section was used for the development of MATLAB tool for different cases which are explained in the following sections.

### *4.1 Four noded element mesh generation*

#### *4.1.1 Rectangular domain*

A tool was programmed and developed using MATLAB to generate the 4-noded element mesh for a rectangular domain. The dimension of the rectangular domain was set to 1×1 (Length × Width) and the spatial resolution was discretized to 10 elements in -x and y- axes direction. After defining the domain dimensions and required no. of elements, the total length and width of the domain was finally discretized using “linspace” function in MATLAB to generate the nodal coordinate matrix. The generated nodal coordinates were stored in nodal coordinate matrix and was connected in counter-

clockwise direction to generate the four noded element mesh and also the connectivity matrix. The discretized 4-node element mesh is represented through Figure 2.

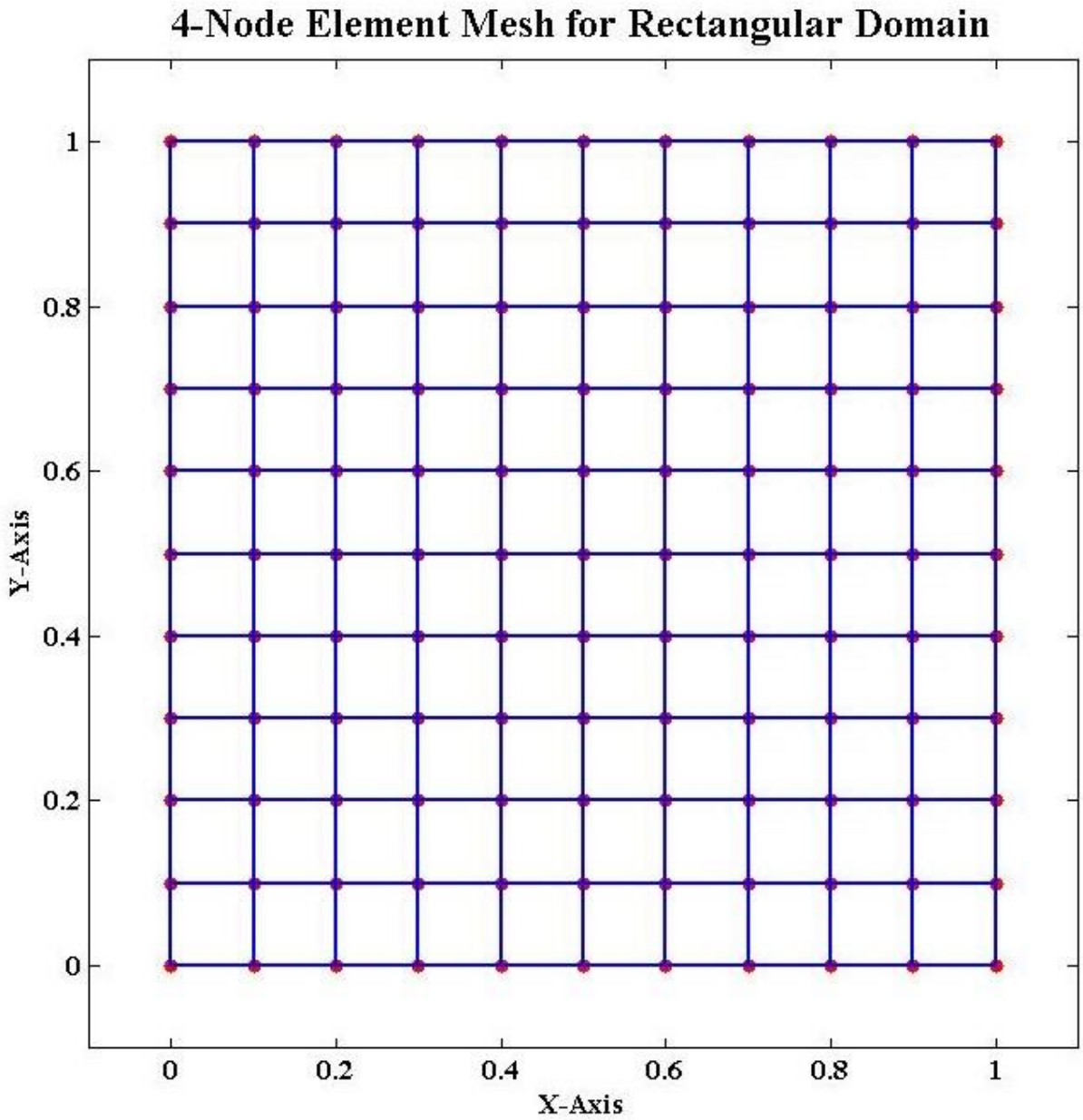



**Figure 2** Generated 4-Noded Element Mesh for Rectangular domain

### *4.1.2 Circular domain*

The tool developed for rectangular domain was extended for circular domain of radius 1 unit and of 360º angle. The no. of angular sectors and elements along radial direction of each angular sector was considered as 20 and 10, respectively and discretized using "meshgrid" function of MATLAB. Further the radial coordinate parameters were converted to Cartesian coordinate and the nodal coordinate matrix was obtained. Finally four noded element mesh was generated by connecting the corresponding nodes. The elements at the center location where node coordinates are repeating a 3-node element was formed. The element connectivity matrix was also formed and generated mesh was plotted as shown in Figure 3 for visualization of the discretized circular domain.

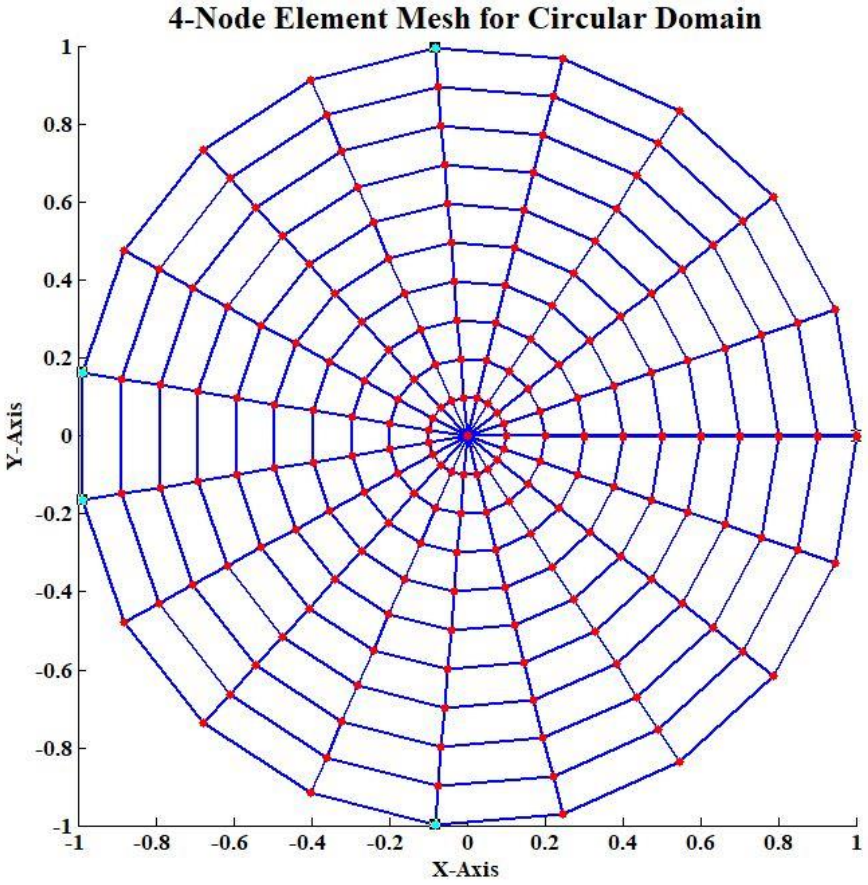



**Figure 3** Generated 4-Noded Element Mesh for Circular domain

### *4.2 Use of PDE library of MATLAB to generate triangular mesh for domain defined*

The triangular mesh for a domain defined as a rectangle of 2×2 dimension and a circle of 0.25 radius centered at (1,1) was generated using "PDE" function of MATLAB library. The circle was removed from the rectangular domain (which may be thought of as the circular feature such as island or pile present in the domain) and geometry of the model was plotted using "decsg" MATLAB function as shown in Figure 4.

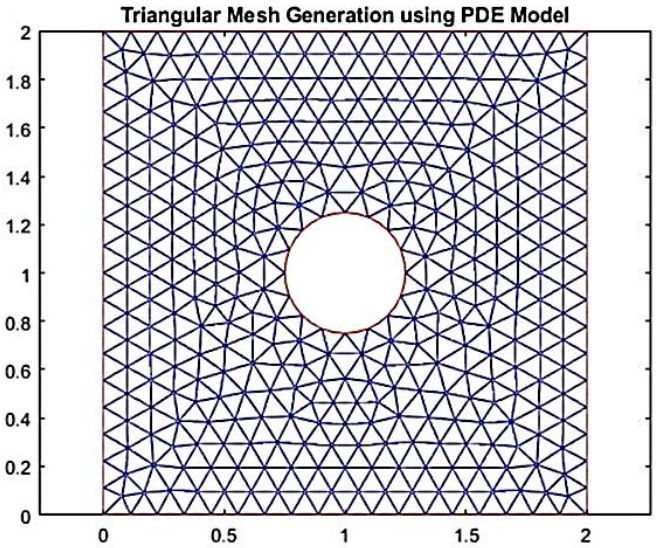



**Figure 4** Generated triangular mesh for rectangular domain with inset circular domain

### *4.3 9-Node element mesh generation for rectangular domain*

A rectangular domain of dimension 1×1 (Length × Width) was considered with spatial resolution of 4 elements along each direction. The discretization of defined domain was done using "linspace" MATLAB function and a nodal coordinate matrix was formed. The generated nodal coordinates were connected in counter-clockwise direction and element connectivity matrix was formed. Finally, the generated 9-noded element mesh was plotted as shown in Figure 5.

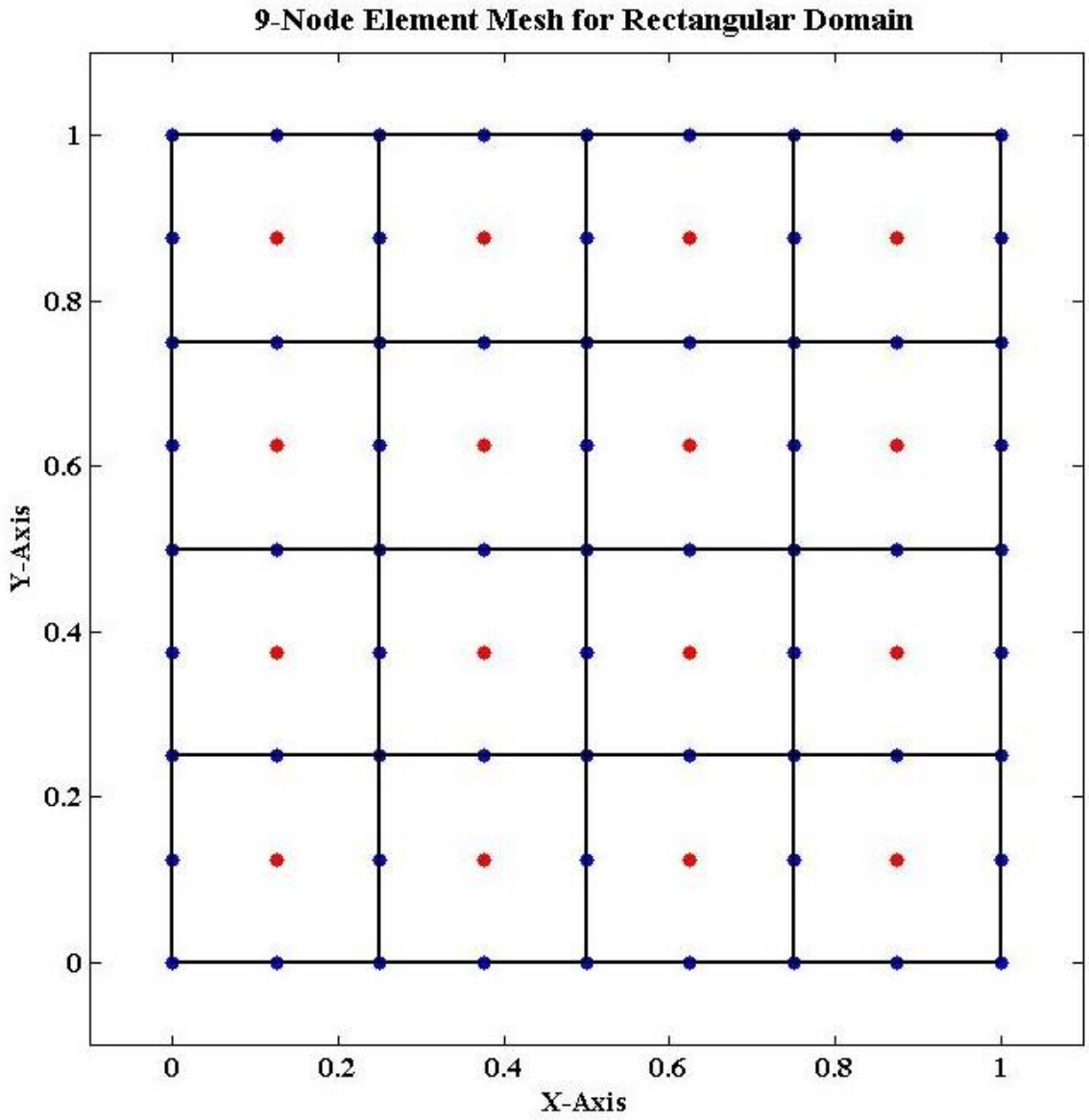



**Figure 5** Generated 9-noded element mesh for rectangular domain

### *4.4 MATLAB Programme for 9-Noded Lagrangian Quadratic Isoparametric Element*

A code to generate shape functions properties for a 9-node Lagrangian quadratic isoparametric element was developed using MATLAB. The isoparametric coordinates were written for the 9-noded element and converted to Lagrangian quadratic form. Finally shape function properties were plotted using "surf" plotting function depicted in Figure 6.

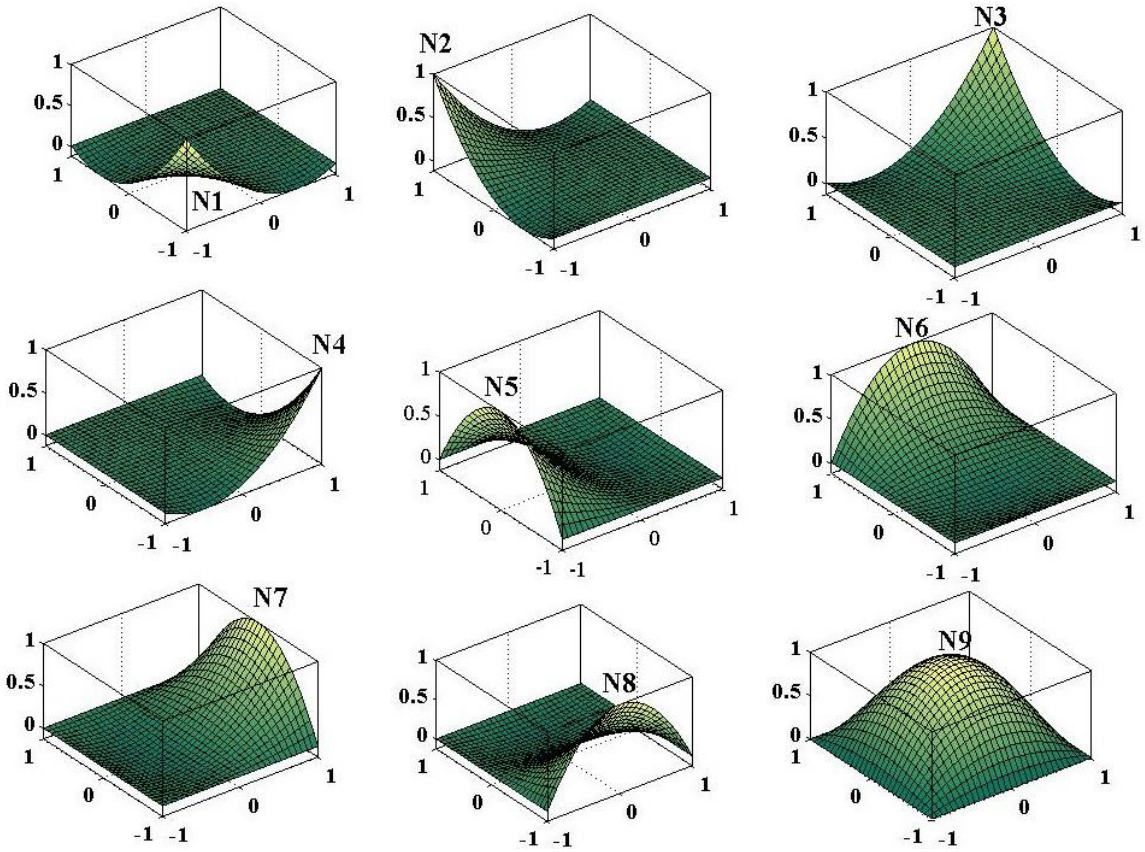



**Figure 6** 9-noded Element Shape Function Properties generated using MATLAB Programme

## 5. Conclusions

The use of 9-noded Lagrangian quadratic isoparametric element is important for discretization of large domain areas such as Bay of Bengal, Arabian Sea, Indian Ocean, etc. for the solution of coastal dynamics and environment such as tidal flow computation and tsunami computations. A MATLAB tool was developed to generate quadrilateral elements mesh for rectangular and circular domains. The developed tool was used to generate uniform mesh using quadrilateral elements for the pre-defined standard domain shapes. The nodal coordinates and nodal connectivity of the elements required for Finite Element Models were extracted using the developed tool. The program was further extended to generate 9-noded mesh for a two-dimensional rectangular region. The developed tool can also be further modified and extended for various domain shapes inclusive of obstructions for versatile applications.

## References

Bartels, S., Carstensen, C., and Hecht, A., (2006). P2Q2Iso2D= 2D isoparametric FEM in Matlab. *Journal of computational and applied mathematics*, 192(2), 219-250.

Behera, M.R., Murali, K., Sannasiraj, S.A., and Sundar, V., (2008). Explicit FE modeling of Indian Ocean Tsunami using unstructured mesh. *International Journal of Ecology & Development*, 10, 115-129.

Behzad, V. Farahani., and Berardo, José. (2013). *Technical report on, An Analysis of a Quadrangular Lagrangian Element with 9 Nodes for the Elasticity Plane So as to Compute Stress and Strain through Programming in Matlab.* Portugal: University of Porto.

Gray, W.G., and Lynch, D.R., (1979). On the control of noise in finite element tidal computations: a semi-implicit approach. *Computers & Fluids*, 7(1), 47-67.

J. Chessa., (2002). Programming the Finite Element Method with Matlab. Evanston, Illinois: Northwestern University.

Koko, J., (2015). A Matlab mesh generator for the two-dimensional finite element method. *Applied Mathematics and Computation*, 250, 650-664.

Lo, D.S.H., (2015). Finite Element Mesh Generation. Boca Raton, Florida: CRC Press.

Mahadevan, R., and Latha, G., (2001). Influence of coastal flooding on surge estimates along the east coast of India. *Indian Journal of Marine Sciences*, 30, 115-122.

Sun, Y., and Lueth, T.C., (2018). Extension of the FEM Analysis Using the PDE-Toolbox of Matlab with Regard to Point Loads, Line Loads, and Freeform Surface Loads: Feature Surface Concept. *In 2018 IEEE International Conference on Robotics and Biomimetics (ROBIO)*, pp. 1151-1158.

Walters, R.A., (2006). Design considerations for a finite element coastal ocean model. *Ocean Modelling*, 15(1-2), 90-100.

*IN PROCEEDINGS OF 25th HYDRO 2020, INTERNATIONAL CONFERENCE, NATIONAL INSTITUTE OF TECHNOLOGY ROURKELA, ODISHA, INDIA 26-28, March 2021, ISBN 978-93-90631-56-8*

Paper ID - 254

# Application of computational fluid dynamics in investigating orifice spillway flow

M. S. Bhadange[1],R. R. Bhate[2], Dr. S. D. Khandekar[3]

[1]*PG Student, Sinhgad College of Engineering, Pune-411041, India.*
[2]*Scientist B, Central Water and Power Research Station. Pune-411024, India.*
[3]*Professor, Sinhgad College of Engineering, Pune-411041, India.*
*Email: mayur.bhadange@gmail.com*

## Abstract

Orifice spillways are provided in Run-of-the river diversion dams in Himalayan region where the management of sediment along with flood is the main issue. Analysis of hydraulic behavior of flow over orifice spillway is very significant considering the safety and efficiency of the dam. Orifice spillways are exposed to two-phase flow, high velocity, cavitation, scouring and downstream erosion. Conventionally, physical modelling is a proven technique for simulating such complex hydraulics problems, but it is time-consuming and uneconomical. However, computational fluid dynamics modelling is advantageous because of recent developments in high-performance computing. The performance and reliability of numerical modeling depend upon grid convergence studies and the selection of the turbulence model. This paper aims at the selection of the grid and turbulence model for analyzing the flow over orifice spillway with ski-jump dissipator. The spillway considered in this study is one of the run-of-river hydropower schemes in the Himalayan region. It is designed to pass a flood discharge (PMF) along with GLOF. Physical model studies were carried out to analyze the flow through the breastwall spillway incorporating one full span and two half spans in a 1:40 scale sectional model at the CWPRS laboratory. CFD software, FLOW-3D based on VOF was used for numerical model studies. For verification studies, the technique of Grid Convergence Index as suggested by the ASME was utilized to determine appropriate grid dimensions and minimize discretization errors. The RNG turbulence model was used for numerical simulation. The data in terms ofdischarging capacity, pressure distribution along with the spillway profile and water surface profile were computed in the numerical model. Validation of numerical model results with physical model results was done. It was found from the present study that the RNG turbulence model is slightly better than K- ε and K-w turbulence model and FLOW-3D could able to simulate the various hydraulic parameters of spillway flows accurately as there was close agreement between the simulated values and experimental results.

***Keywords:****Orifice spillway, CFD, Grid Convergence, FLOW- 3D, Turbulence model, Discharging Capacity, Pressure Distribution, Water Surface Profile.*

## 1. Introduction

Spillway is one of the most significant components of a dam and identification of hydraulic characteristics for a spillway flow is a difficult issue because of the rapid changes in the state of flow. Orifice spillways are provided in run-of-the-river diversion to serve the dual purpose of flushing of sediments accumulated and flood disposal. These spillways are constructed mostly in the mountainous terrains such as Himalaya, where the large amount of sediments areencountered and has high heads for power generation.About 75% of the hydro potential of India will come from the Himalayan river systems i.e. the Indus - Ganga- Brahmaputra river system and rest 25% from other river systems (2008) CWPRS Technical Memorandum.Hydraulic models are used to visualize, to understand and to explain hydraulic phenomena in and around the hydraulic structures. Physical modeling and Numerical modeling techniques are the toolsused for the purpose. It is a well-established and widely accepted fact among the hydraulic engineering professionals that the physical hydraulic scale model test is not only a choice but an essential tool for testing hydraulic structures,due to its ability to solve complex hydraulic problems. However, due to advances in computational power and numerical techniques, it is now possible to obtain the required insightthrough numerical modeling. CFD modelling is time efficient, economical and has less uncertainties and difficulties associated with the scaling effects. CFD modelling is thereliable toolto encounter complex hydraulics in orifice spillway. Although the CFD modelling has a lot of advantages with respect to the physical modelling, it should

be verified and validated with the physical modelling.Verification and Validation studies are essential aspects of a successful numerical modelling study. Methodologies and definitions regarding these studies are well outlined by Stern et al. (2001). The correctness of a CFD solution is influenced by the number of cells contained by the mesh i.e. the finer is the meshing, the better is the solution accuracy. However, it is true upto certain extend, beyond which only computation time is increased. CFD solutions are highly dependent on the grid size and flow physics. Systematic grid-convergence studies are the most common; most straightforward and arguably constitute the most reliable technique for the quantification of numerical uncertainty (Roache, 1997). American Society of Mechanical Engineer`s (ASME) Journal of Fluid Engineering Editorial Policy Statement for reporting numerical modelling studies (Celik, I. B.,2008) is followed for grid convergence study. Similarly, Percent of relative error and R-square method (Junagade et al. 2018) was used for turbulence model comparisons.

## 1.1 *Physical model*

Thespillway considered for this study is an orifice spillway on one of the Himalayan hydropower projects.Seven numbers of rectangular orifice openings with of dimensions 6.5m (W)×12.6m (H) is provided to pass the design dischargeof 11,811$m^3$/s(PMF). The design head is of 50m above the crest. Radial gates of 15.75 m radius are providedto control the flow. Cross section of spillway is as show in the figure 1.The studies were conducted on 1:40 scale G.S. model at CWPRS, Pune laboratory.

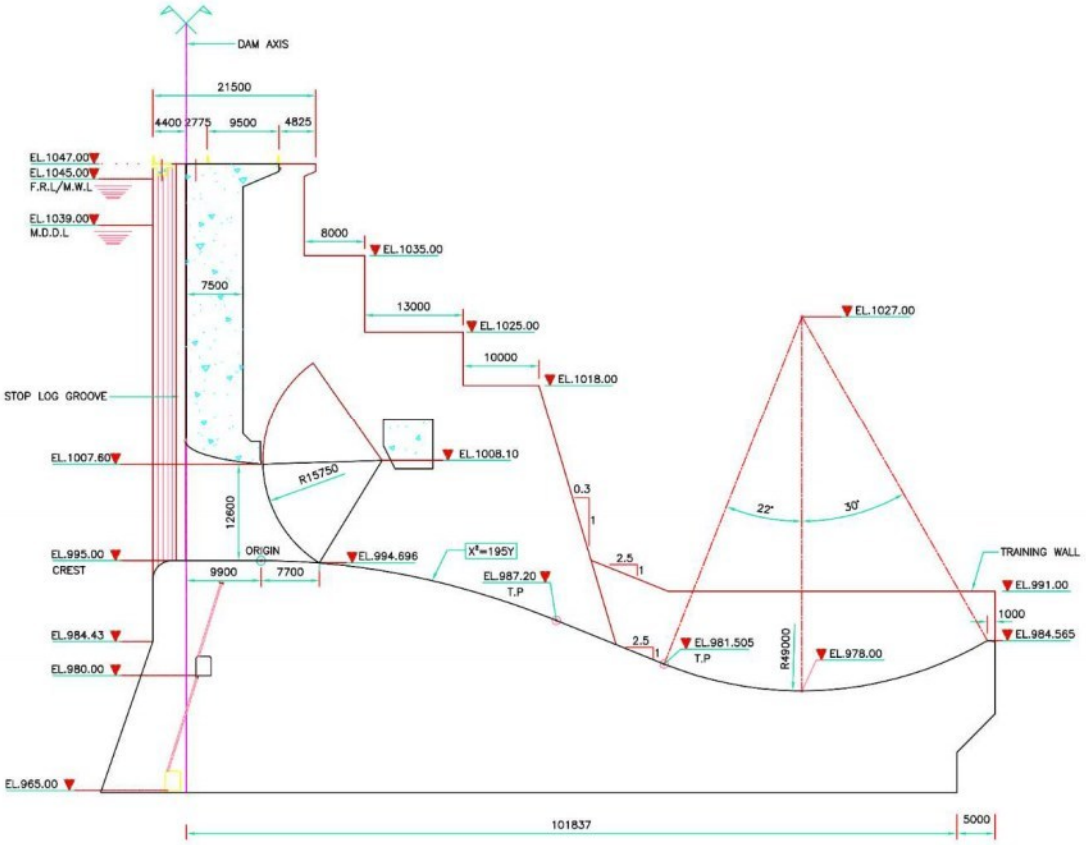



**Figure 1**Cross section of orifice spillway

### 1.1.1 *Numerical model*

For CFD modeling, commercially available software FLOW 3D was used. The geometry was created in AutoCAD and imported in FLOW 3D. The domain was extended 100 m upstream and 300mdownstreamof the dam axis making the total domain 400m long.History probes along the

spillway profile resemble the piezometers. Cases of ungated and gated conditi for various discharges were considered for the study. Physics like air entrainment, gravity, surface tension, viscosity and turbulence were specified.

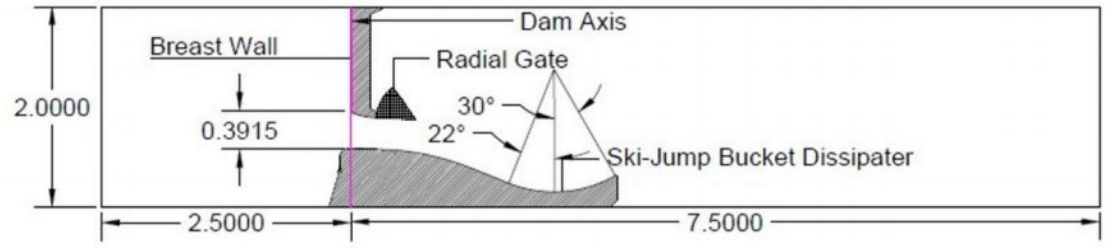



**Figure 2**Cross section of numerical model in scale 1:40

## 2.Grid conversion study

In CFD, various errors are introduced due to the use of iterative methods and various input parameters that are spatially and temporally dependent. Thus, Convergence of a numerical model consists of two elements-iterative convergence and grid convergence. The GCI method is an acceptable and recommended method that has been evaluated over several hundred CFD cases for convergence. Roache suggested the Grid Convergence Index method based on generalized Richardson Extrapolation. Accordingly, GCI is defined as a scale to evaluate how far the solution is from the asymptotic value and he highlighted that a small value of GCI is indicative of negligible numerical uncertainty due to the discretization error. Three meshes with successive refinement for the case of 75% discharge with ungated operation were generated for grid convergence study. The details of the meshes are as given in Table 1.

**Table 1**GCI mesh details

| Sr. No. | Mesh Type | $h$-Mesh Cell size (m) | Fluid Element Count (N) | Refinement Factor(r) | $f$-Discharge kg/s |
|---|---|---|---|---|---|
| 1 | Fine | 0.02 | 17,13,156 | 1.5 | 254.5326 |
| 2 | Medium | 0.03 | 5,47,607 | 1.5 | 257.7947 |
| 3 | Coarse | 0.045 | 1,76,199 | | 257.9983 |

Due to computational limitations, grid sizes used were roughly uniform for smooth transitions and the refinement factor considered was 1.5,which was larger than 1.3 i.e. the suggested minimum refinement factor. Discharge was considered as a GCI parameter. Steady state discharge values through inlet were observed at 80 seconds. Based on the GCI results mentioned in Table 2, the finest mesh was selected.

**Table 2**GCIresults

| Steps | Terms | Values |
|---|---|---|
| 1 | N1, N2, N3 | 1713156, 547607, 176199 |
| 2 | $r_{21} = \frac{h2}{h1}$ | 1.5 |
| 3 | $r_{32} = \frac{h3}{h2}$ | 1.5 |
| 4 | $f_1$ | 254.5326 |
| 5 | $f_2$ | 257.7947 |
| 6 | $f_3$ | 247.2463 |
| 7 | $\phi_{21} = f_2 - f_1$ | 3.2621 |

| | | |
|---|---|---|
| 8 | $\phi_{32} = f_3 - f_2$ | -10.5484 |
| 9 | $e_{21} = \left\lvert \frac{f_2 - f_1}{f_1} \right\rvert$ | 0.012816041 |
| 10 | $e_{32} = \left\lvert \frac{f_3 - f_2}{f_2} \right\rvert$ | 0.040917757 |
| 11 | $GCI_1 = \frac{1.25 e_{21}}{r^p - 1}$ | 0.00731 |
| 12 | $GCI_2 = \frac{1.25 e_{32}}{r^p - 1}$ | 0.0233 |

where,

$$p = \frac{\ln\left(\frac{e_{32}}{e_{21}}\right)}{\ln(r_{21})} + \frac{1}{\ln(r_{21})}[\ln(r_{32} - 1) - \ln(r_{21} - 1)] = 2.86 \quad (1)$$

$r_{21}$ and $r_{32}$refinement factor respectively.
$e_{21}$ and $e_{32}$are relative approximate error respectively.
$p$ is order of accuracy.

For validation purpose, finest mesh Pressure Profile of 23 piezometers along the spillway were compared with physical model results and found ingood agreement. Similarly, Water surface elevation profile with respect to chainage from dam axis was compared with physical model results and found in good agreement.

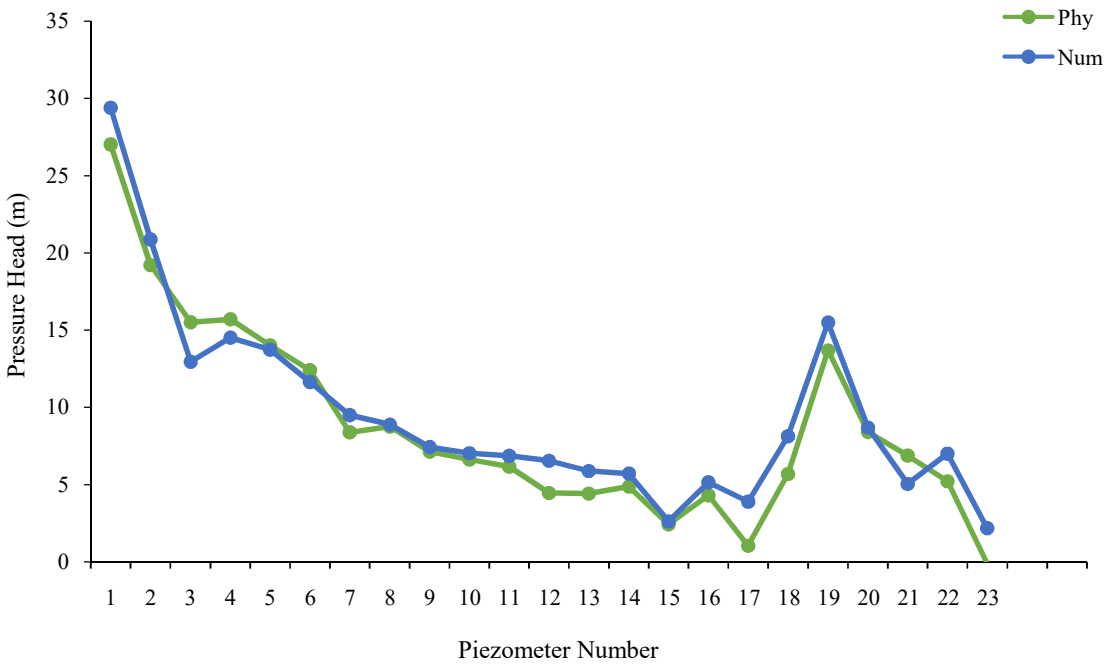



**Figure 4** Pressure profile comparison for mesh cell size 0.02

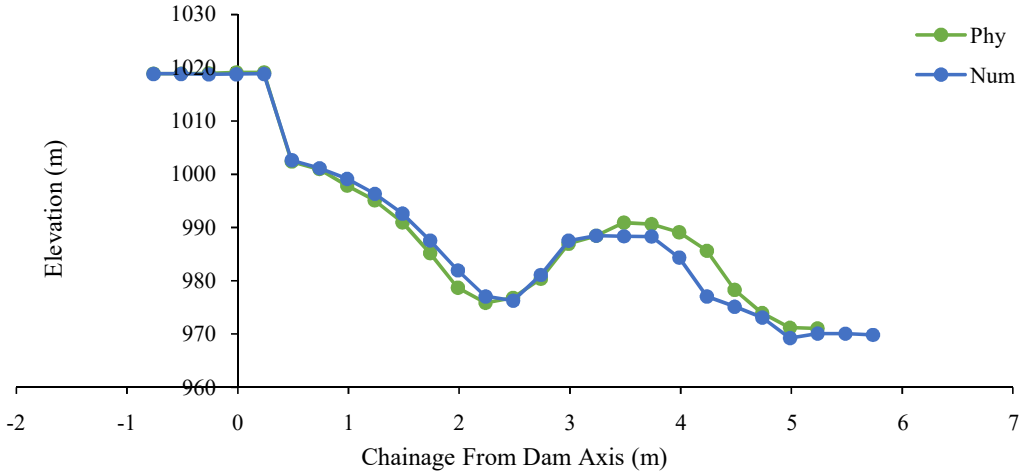



**Figure 5** Water surface elevations profile comparison for mesh cell size 0.02

Figure 4 and 5 implies a good comparison however at some points the small difference can be seen. Further comparison of other parameters such as tail water level and reservoir level and discharge for different mesh type is shown in Table3.

**Table3**Comparison of other parameters in GCI studies

| Sr. No. | Mesh Type | Tail Water Level (m) | Reservoir Level (m) | Discharge (kg/s) | Computational Time (HR:MM: SS) |
|---|---|---|---|---|---|
| 1 | Fine | 24.375 | 25.425 | 254.5326 | 16:04:06 |
| 2 | Medium | 24.39 | 25.4475 | 257.7947 | 13:21:04 |
| 3 | Coarse | 24.39 | 25.451 | 257.9983 | 08:54:26 |
| 4 | Physical Model | 24.46 | 25.4725 | 250.1023 | |

Along with this, Residual RMS error values have reduced to an acceptable value typically $10^{-4}$ or $10^{-5}$. FLOW-3D (2012) user manual recommends having an aspect ratio near to 1, which was maintained. The numerical results were also found to be in agreement with the physical modeling results which denote the efficiency numerical modelling. The error in discharge is found to be 1.14% for the selected fine mesh. It indicates that the 2D section model yields excellent results for water level studies.

## 3. Turbulence model Selection

In computation of turbulent flows, various turbulence model options such as Renormalized group model (RNG), Two-equation (K-ε) and Two-equation (k-w) model are available in Flow 3D. Case of 100% (11811 $m^3$/**s**) discharge with the ungated condition was considered for turbulence model comparison. Discharge is given as an input from upstream boundary condition (Daneshkhah et al. ,2012) with fine mesh. Discharge in cubic meter and respective computational time of turbulence models after simulation are as shown in Table 4.

**Table 4**Turbulence model comparison

| Turbulence Models | Discharge of Numerical Modelling ($m^3$/**s**) | Discharge of Physical Modelling ($m^3$/**s**) | Percentage of Relative Error | $R^2$ | Computational Time (HR:MM: SS) |
|---|---|---|---|---|---|
| RNG | 11866.670 | 11811.000 | 0.469129 | 0.9556 | 13:16:11 |
| K- ε | 11857.635 | 11811.000 | 0.393291 | 0.9557 | 14:14:27 |
| K-w | 11900.946 | 11811.000 | 0.755789 | 0.9572 | 23:07:06 |

$$\text{Percentage of Relative Error} = \frac{\text{Numerical Model} - \text{Physica}}{\text{model}} * 100 \quad (2)$$

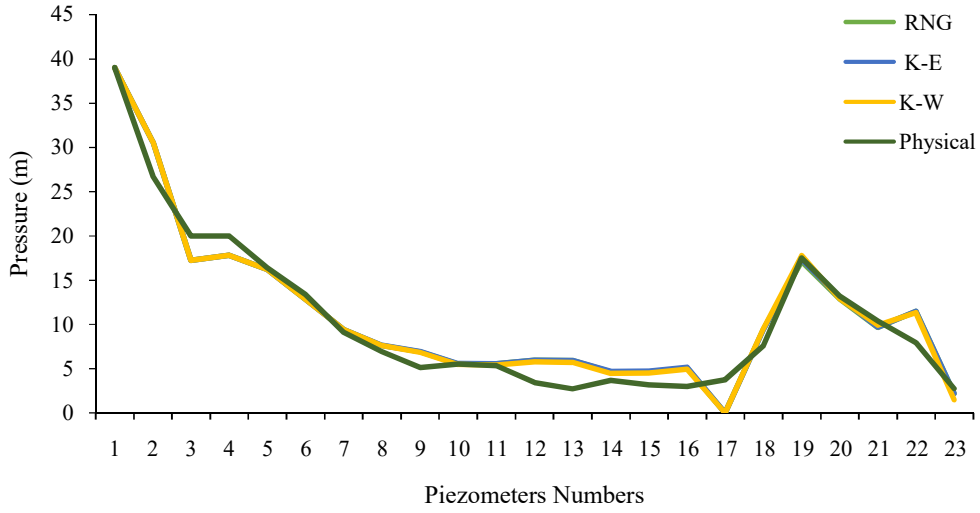



**Figure 6**Pressure profile comparison between different turbulence models and physical model

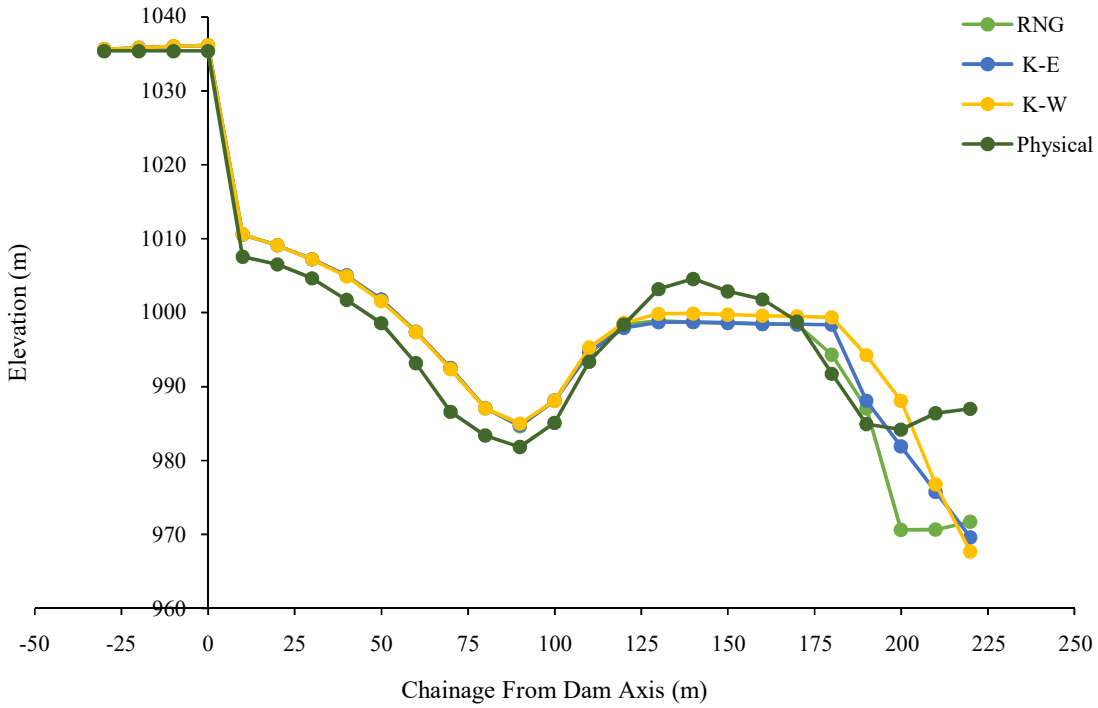



**Figure 7**Water surface elevation profile comparison between different turbulence models and physical model

Despite of the good estimation on discharge for all turbulence models, there are some problems in the pressure head estimations in the simulations. Because of curvature there is high turbulence occur and insufficient number of grid points along the flow depth. Scatter plots of pressure profile between different turbulence models and physical model were plot and it is observed that RNG turbulence

model is in good fit with physical model. Hence this turbulent model was adopted for further simulations.

## 4. Results and discussions

Table 5 shows list of cases which were considered for comparison between numerical and physical model results for discharges, RWL and TWL.It was observed that there were slightly higher discharges in the numerical model than physical model and this range increases with an increase in the head, but it was an acceptable difference. Overall discharge capacity comparison is satisfactory.

**Table 5**List of cases considered for numerical modelling

| Case No | Type and Condition | Physical Model | | | Numerical Model | | |
|---|---|---|---|---|---|---|---|
| | | Discharge ($m^3/s$) | RWL (m) | TWL (m) | Discharge ($m^3/s$) | RWL (m) | TWL (m) |
| 1 | 75%-Ungated | 8858 | 25.47 | 25.47 | 8997 | 25.45 | 25.45 |
| 2 | 75%-Gated | 8858 | 26.12 | 26.12 | 8857 | 26.12 | 26.12 |
| 3 | (PMF)100%-Ungated | 11,811 | 25.83 | 25.83 | 11,876 | 25.82 | 25.82 |
| 4 | (PMF)100%-Gated | 11,811 | 26.12 | 26.12 | 11,825 | 26.11 | 26.11 |
| 5 | (PMF+GLOF)-Ungated | 12,981 | 25.98 | 25.98 | 12,954 | 25.96 | 25.96 |

Performance of numerical and physical models were carried out by calculating statistical parameters such as $R^2$ and RMSE to indicate the absolute and relative fit of the numerical model to physical model data. Table 6 shows the error estimation for all the cases.

**Table 6** Error estimation for various cases

| Case No. | Water Surface Profile | | Pressure Profile | |
|---|---|---|---|---|
| | RMSE(m) | $R^2$ | RMSE(m) | $R^2$ |
| 1 | 5.3372 | 0.9559 | 2.4656 | 0.9605 |
| 2 | 7.212 | 0.9327 | 2.5055 | 0.9913 |
| 3 | 4.5886 | 0.9546 | 1.7721 | 0.9695 |
| 4 | 5.6698 | 0.9714 | 3.6814 | 0.9677 |
| 5 | 1.435 | 0.9960 | 0.8781 | 0.9947 |

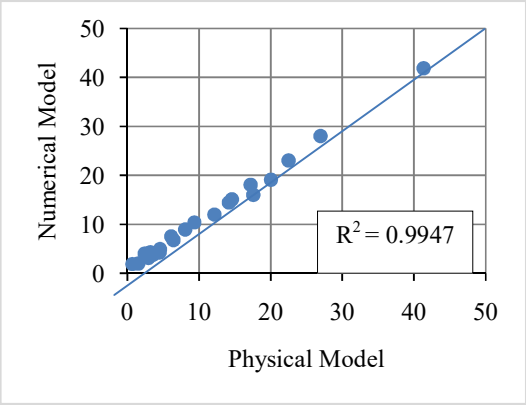



**Figure 9** Scatter plot of pressure for physical modelling and numerical modelling for case no. 5

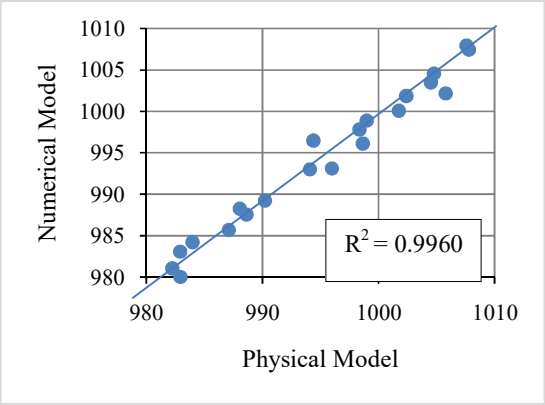



**Figure 11** Scatter plot of water surface elevation for physical modelling and numerical modelling for case no. 5

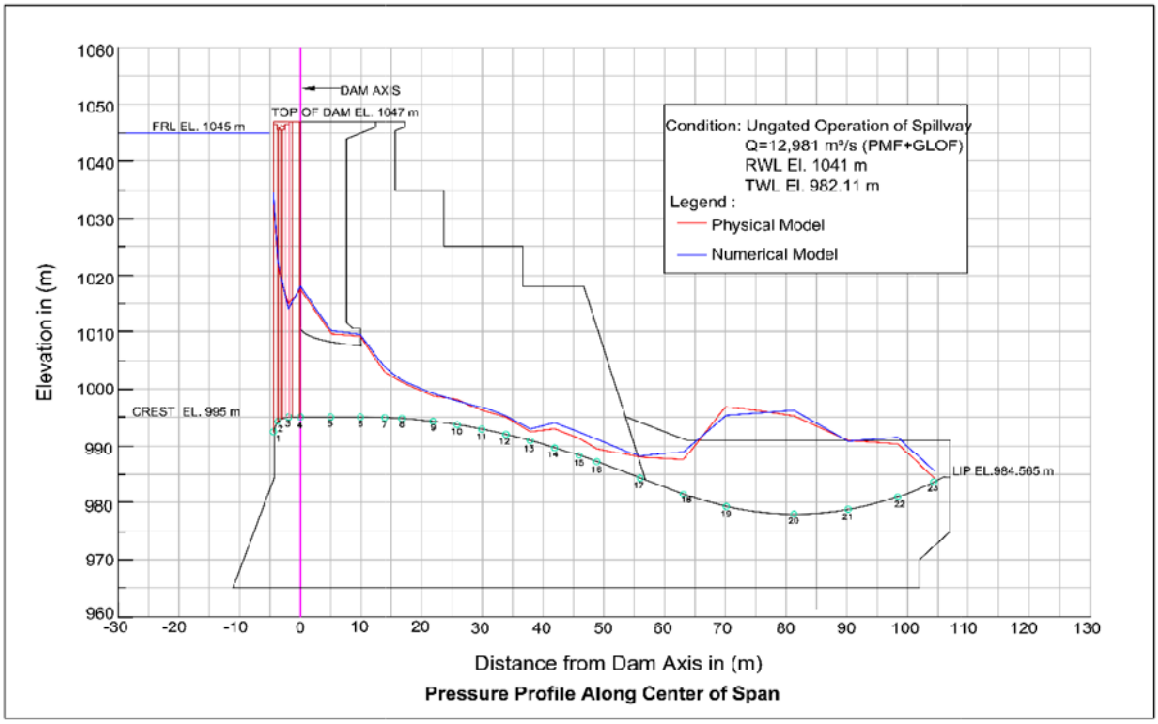



**Figure 8** Pressure profile comparison for case no.5

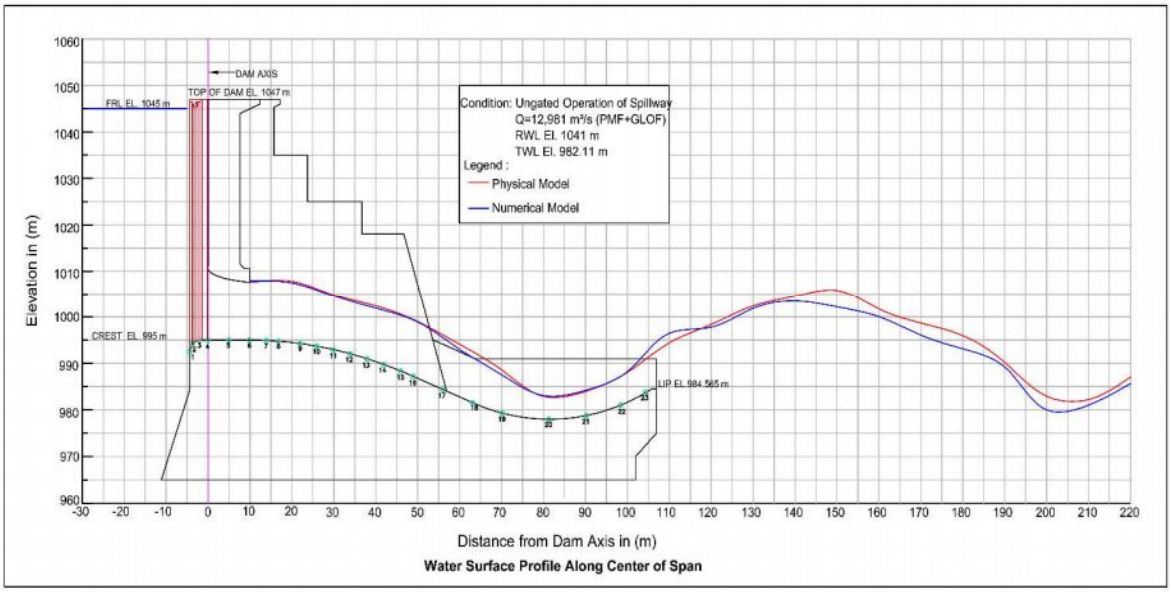



**Figure 10** Water surface profile comparison for case no. 5

Figure 10 and 11 shows the scatter plot of pressure and water surface elevation for Case No.5. It wasobserved that there were deviations compared to the experimental results in the flip bucket part of the spillway. This is because of the high curvature within this region which could not be captured very efficiently. Despite of the good estimation of discharge, there were problems in the pressure head estimations in the simulations. This was because of the insufficient number of grid points along the flow depth. Therefore, the large variations were seen after the pier ends. Also, error may be

cumulative effect of variations in terms of material properties, input parameters and human error in physical modelling measurements. The studies were carried out on model scale and hence may not reflect the prototype behavior exactly. However, this can be justifiable since physical model studies were used for validation studies, hence the use of scaled model was indispensable.

Although CFD tools still have some limitations such as long run times and numerical instabilities, they are more economical and can provide more details about hydraulic characteristics than a scaled physical model. Furthermore, many more scenarios could be easily tested with easy modifications to the numerical model. Thus, the numerical models have the flexibility in studying in different flow phenomena. However, it is important to select an appropriate mesh, with correct initial and boundary conditions for an accurate numerical solution.

## 5. Conclusion

The ability of the CFD software Flow3D to model orifice spillway flow behavior proved to be quite useful. The following conclusions can be drawn from this study:

- Investigation of the hydraulics characteristics of the flow over orifice spillway for 75%, 100% discharge and PMF+ GLOF cases were successfully done. Simulated and the numerical model discharges were observed to be in good agreement with the physical model discharges. Thus, it can be concluded that Flow3D is generally capable of providing spillway discharges that are within considerably accuracy range of physical model experimental data.
- The GCI method is most reliable for grid convergence based on that 0.02 fine mesh was adopted. In turbulence models comparison, the RNG turbulence model was slightly better than the K- ε and K-w turbulence model.
- The water surface profiles and pressure profile over the spillway were found to be almost the same as that of those obtained in physical model up to the pier end. The RMSE and $R^2$ values were found to be in the range of 1.435 to 7.212 and 0.9327 to 0.9960 for water surface profile. While for pressure profile the range is 0.8781 to 3.6814 and 0.9605 to 0.9947, respectively. Thus, it was seen that Flow3D could successfully model orifice spillway's water surface profile and pressure profile for a variety of discharge conditions to physical model testing.

Overall, it can be concluded that this numerical study yielded good results for head- discharge relations, tail water levels, pressures and water surface profiles up to the pier end. Thus, this study, even though not a total replacement to physical model study, was seen to be an efficient and cost-effective preliminary study.

## 6. Acknowledgements

The authors are grateful to Dr. Mrs. V. V. Bhosekar, Ex. Director- Central Water and Power Research Station allowing to use the resources for the study. We also thank Dr. M. R. Bhajantri, Scientist 'E', Spillways and Energy Dissipators Division, CWPRS for his valuable guidance during the study.

## References

[1] Celik, I. B., (2008) "Procedure for estimation and reporting of discretization error in CFD applications".In Statement on the Control of Numerical Accuracy of the Journal of Fluids Engineering (Editorial Policy), ASME Fluids Engineering Division.

[2] Daneshkhah, A., Vosoughifar, H., (2012), "Solution of Flow Field Equations to Investigate the Best Turbulent Model of Flow Over A Standard Ogee Spillway in Finite Volume Method." The first international conference on dams and hydropower

[3] Fred Stern, Robert V. Wilson, Hugh W. Coleman and Eric G. Paterson, (2001), "Comprehensive approach to verification and validation of CFD simulations- Part 1: methodology and procedures." ASME Journal of Fluids Engineering, Vol. 123-793

[4] FLOW-3D, v10.1 User Manual, (2012).

[5] Hydraulic Design of Orifice Spillway, (2008) CWPRS Technical Memorandum.

[6] Johnson, M.C., Savage, B.M., (2006) "Physical and Numerical Comparison of Flow Over Ogee Spillway in The Presence of Tailwater", Journal of Hydraulic Engineering, ASCE, Vol. 132, No. 12.

[7] MrunmayJunagade, K. C., S. K. and R. R. Bhate (2018) "Analysis of Performance of Orifice Spillway using Computational Fluid Dynamics" Hydro (2018).

[8] Roache, P. J. (1997), "Quantification of the uncertainty in computational fluid"

*IN PROCEEDINGS OF 25th HYDRO 2020, INTERNATIONAL CONFERENCE, NATIONAL INSTITUTE OF TECHNOLOGY ROURKELA, ODISHA, INDIA 26-28, March 2021, ISBN 978-93-90631-56-8*

Paper ID - 257

# Study on influence of vegetation in open channel using CFD model

Anitha Gopinath A[1], Miji Cherian R.[2]

[1] *PG Student, Department of Civil Engineering, Government Engineering College, Thrissur and 680009, India*
[2] *Assistant Professor, Department of Civil Engineering, Government Engineering College, Thrissur and 680009, India*
*anithagopinath17@gmail.com*

## Abstract

Vegetation in open channel flow will cause some roughness and generate drag on flowing water. The drag force generated by this will reduce the water discharge and also influences the sediment load transportation. The prediction is very difficult because the flow in open channels is usually turbulent; the geometry is irregular and can vary with time. In the present study, influence of the vegetation on the flow characteristics was determined numerically using computational fluid dynamics (CFD). For the numerical study of the vegetated channel, two CFD approaches viz., the stem scale approach and the porous zone approach were used. The obtained results were then compared with the available experimental results. The various hydraulic parameters which describe the flow characteristics of the vegetated channel were also determined using two CFD approaches and compared. The CFD model with the porous zone approach, which better predicted the hydraulic parameters, was found to be superior to the stem scale approach. The average value of the Manning's roughness coefficient for each vegetation cover was determined and it was found that the roughness coefficient increases with increase in the vegetation cover.

***Keywords:*** *CFD, Stem scale approach, Porous zone approach*

## 1. Introduction

Vegetation can be defined as a collection of plants acting as a covering to the ground or the surface. Vegetation that grows inside the channel can be categorized into submerged, emergent, floating leaf and free floating. This presence of vegetation can be beneficial and harmful. Vegetation in open channel flow will cause some roughness and generate drag on flowing water. Drag force generated by this will reduce water discharge and also influences the sediment load transportation. Thus, it becomes important to estimate the flow resistance in river directly leaving an impact on the channel flow parameters. The calculation of flow characteristics is one of the most important tasks in river engineering and related areas. The prediction is very difficult because the flow in open channels is usually turbulent, the geometry is irregular and can vary with time.. In the present study, influence of vegetation on flow characteristics was determined numerically using computational fluid dynamics (CFD). From previous studies it was found that in most of the cases, influence of vegetation on open channel flow was determined experimentally. Sometimes it may be impractical to conduct studies on natural channels or laboratory flumes and in such situations numerical modelling can be adopted. Numerical modelling is accurate, cost effective, and less time-consuming approach. It was noticed from the previous results that very less work has been done using CFD models to validate the flow through vegetated channel. Porous zone approach was also less used. For modeling vegetated channel two CFD approaches available in the literature are stem scale and porous zone approaches ( Tsavdaris et al., 2013) and hence, adopted in this study. In stem scale approach channel was modeled considering the dimensions of vegetation. In porous zone approach vegetated area was considered as porous bed and then modeled.

### 1.1 *Numerical procedure in ANSYS Fluent using experimental data - flow characteristics*

Mulahasan et al. (2017) conducted an experimental study for determining the flow resistance of inline vegetation in open channel flow. Their setup consists of a rectangular main channel of 0.3 m wide, 0.3 m deep and 10 m long with rigid cylindrical rods spaced at 0.125 m. In this experiment three different vegetation cover were used (31.8%, 15.9% and 7.95%). Velocity values are measured at three different points ( at X = 4.76, 7.76, 8.15) and average value were taken.

### 1.1.1 *Stem scale approach - Geometry creation and mesh generation*

In stem scale approach, channel was modeled considering the dimensions of vegetation used in the experimental setup. The geometry of the experimental setup for three vegetation cover, proposed in the journal is created in the design modeler module in ANSYS Workbench 16.0. Names of the boundaries were given using the option 'named selection'and it includes these six parts: Inlet, Outlet, Cylinders, Sidewalls, Bottom and Top. The meshing was carried out in ANSYS ICEM CFD module in ANSYS Workbench 16.0. Figure 1 and 2 shows geometry and generated mesh for three different percentages of vegetation cover.

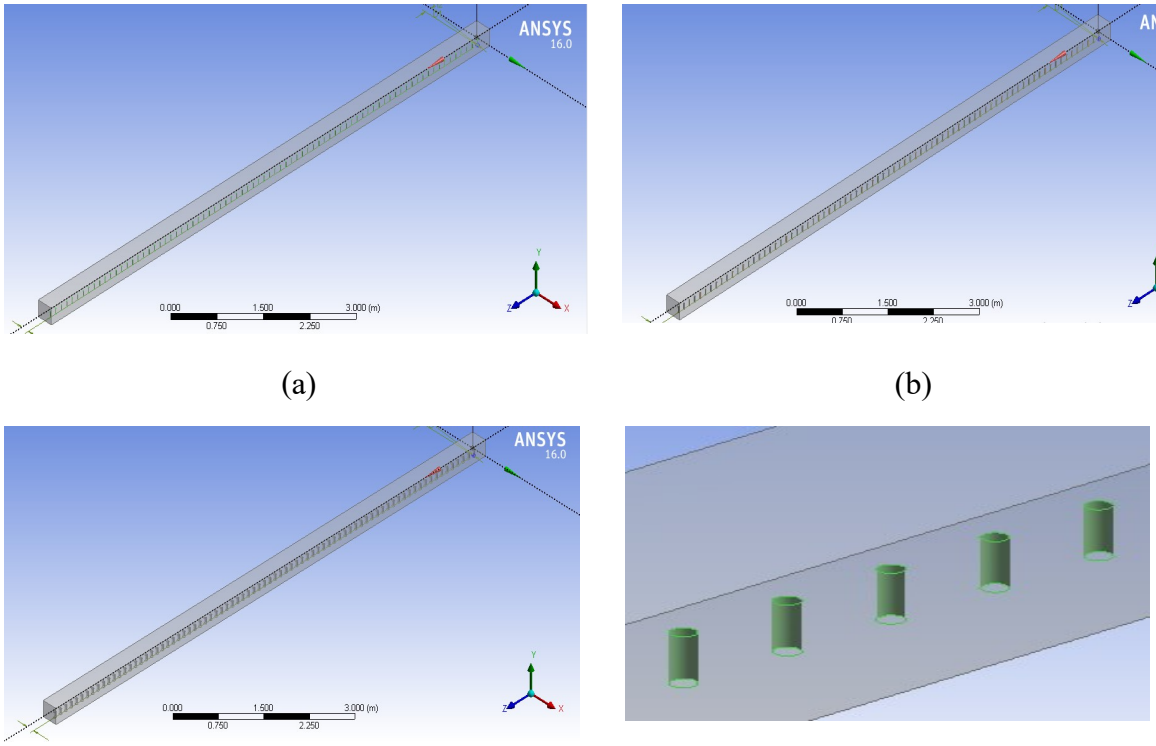
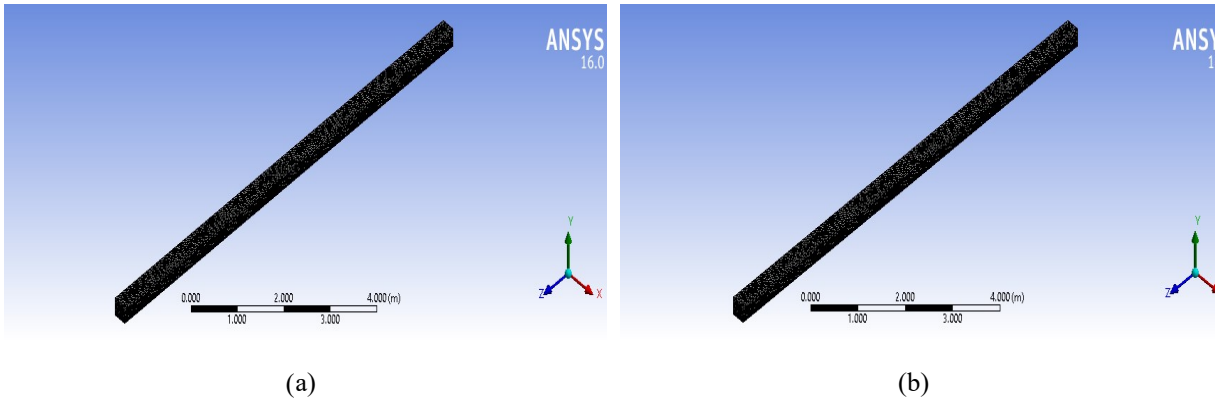
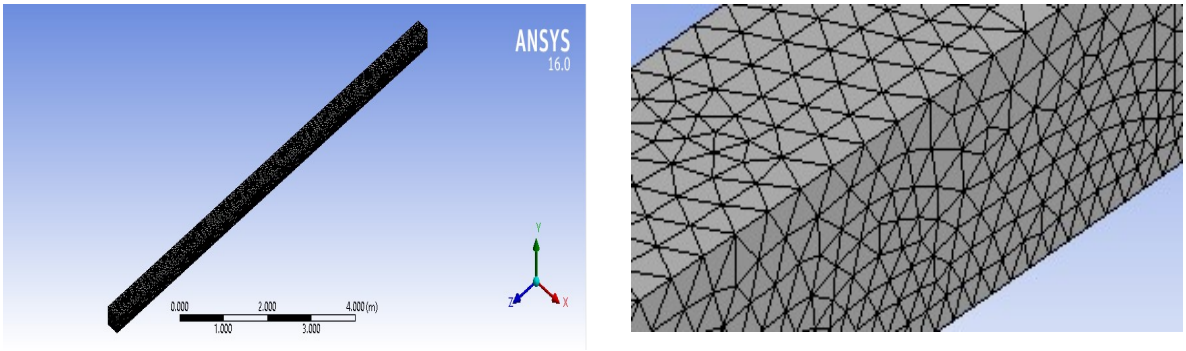



**Figure 1** Geometry of channel with a) Vegetation cover-7.95% b) Vegetation cover-15.9% c) Vegetation cover-31.8% d) Enlarged view






(c) (d)

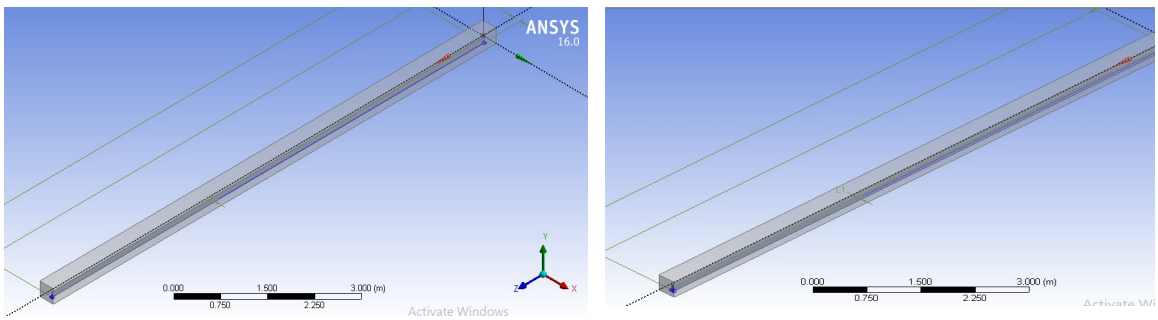
**Figure 2** Mesh generated a) Vegetation cover-7.95% b) Vegetation cover-15.9% c)Vegetation cover - 31.8% d) Enlarged view

The CFD solver ANSYS Fluent is used for simulation. From the Fluent Launcher window, double precision option, serial processing option and 3D options were selected. The pressure-based solver was selected for simulation since incompressible flow was modeled. Velocity formulation was selected as absolute. The velocity formulation will result in most of the flow domain having the smallest velocities in that frame, thereby reducing the numerical diffusion in the solution and leading to a more accurate solution. Time was specified as steady since time variation does not affect the flow change and the gravity was provided in the negative Y-direction.Volume of fluid (VOF) model was selected with air as primary phase and water as secondary phase. From VOF model open channel flow was selected as sub-model.

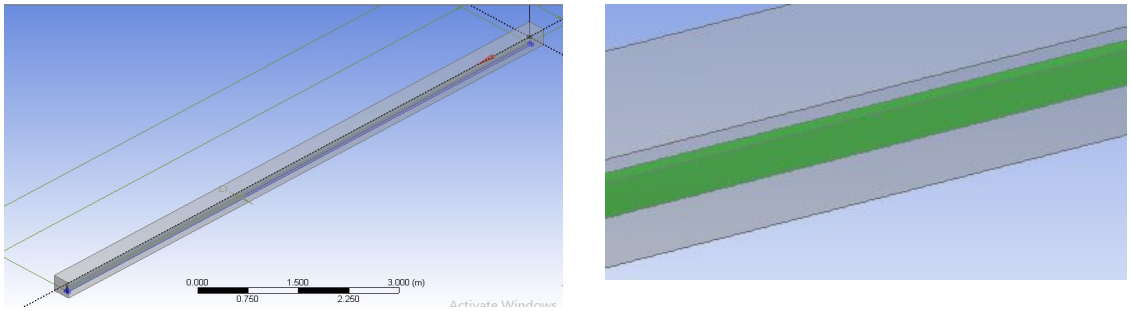
The turbulence was modelled using standard k-ε model with standard wall function. Boundary conditions were set for Inlet (velocity inlet), cylinder (wall), Sidewall, Top (Symmetry), Bottom wall, Outlet (pressure outlet).The pressures at the outlet boundaries were considered as zero gauge pressure. In multiphase, open channel option is selected and flow depth is entered. No slip condition of shear is given for all wall surfaces. For the pressure-velocity coupling SIMPLE algorithm was selected. Least square cell-based method was selected for spatial discretization. For momentum, second order upwind discretization was selected and first order discretization was selected for turbulent kinetic energy and turbulent dissipation rate. For volume fraction compressive discretization was selected . For all the solution control parameters, default values are set. These values are to be reduced if the iterations are showing divergence. The next step is to initialize the solution using standard initialization. After setting all the parameters for the calculation, the calculation activity was started .

### 1.1.2 *Porous zone approach - Geometry creation and mesh generation*

In porous zone approach vegetated area was considered as porous bed and then modeled. Porous bed was created in ANSYS Fluent with width as diameter of vegetation and height as 0.1m. After creating geometry, meshing was carried out in ANSYS ICEM CFD module in ANSYS Workbench 16.0. Figure 3 and 4 shows geometry and generated mesh for three vegetation cover.

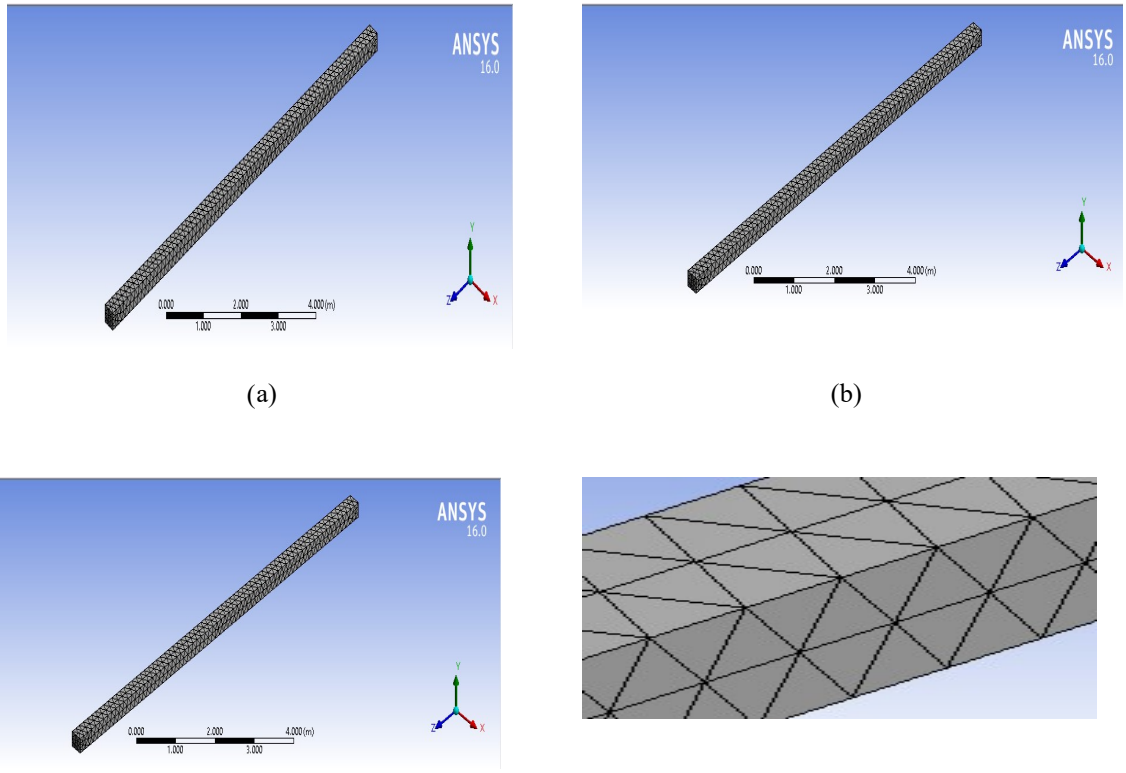



(a) (b)




(c) (d)

**Figure 3** Geometry of channel with a) Vegetation cover-7.95% b) Vegetation cover-15.9% c) Vegetation cover-31.8% d) Enlarged view




(a) (b)

(c) (d)

**Figure 4** Mesh generated a) Vegetation cover-7.95% b) Vegetation cover-15.9%

c) Vegetation cover - 31.8% d) Enlarged view

Boundary conditions were set for inlet (velocity inlet), porous zone, sidewall, top (symmetry), bottom wall and outlet (pressure outlet). Porous media constants α (permeability) and C2 (inertial resistance factor) are calculated for providing in cell zone conditions. Equation used for the calculation of porous media constants (Tsavdris et al. 2013) are given below.

$$\alpha = \frac{D_p^2 \varepsilon^2}{150(1-\varepsilon^2)} \tag{1}$$

$$C_2 = \frac{3.5(1-\varepsilon)}{D_p^2 \varepsilon^3} \tag{2}$$

$$\varepsilon = 1 - (N \times A_v) \tag{3}$$

Where, $D_p$ = Stem diameter, N = No. of cylinders, $A_v$ = Area of stem, α = Permeability, γ = Specific weight of water, A = Cross-sectional area of flow, b = Width of channel, y = Depth of flow, and ε = Porosity.

Table 1 shows porous media constant calculated for three vegetation cover. Solution setup was provided similar to stem scale approach.

**Table 1** Porous media constants

| Vegetation cover (%) | 1/α | $C_2$ |
|---|---|---|
| 7.95 | 92.1045 | 2.769 |
| 15.9 | 391.05 | 5.879 |
| 31.8 | 2025.008 | 15.222 |

## 1. Hydraulic parameters

Various hydraulic parameters such as Reynolds number (Re), Frouds number (Fr), Manning's roughness coefficient (n) were calculated for both CFD approaches to describe the hydraulic characters of open channel flow due to the influence of vegetation. The obtained values are then compared with experimental results. Following equations are used for the calculation of hydraulic parameters.

$$\text{Reynolds Number,} \quad \text{Re} = \frac{VD}{\upsilon} \tag{4}$$

$$\text{Frouds Number,} \quad \text{Fr} = \frac{V}{\sqrt{gy}} \tag{5}$$

$$\text{Manning's formula,} \quad \text{V} = \frac{1}{n} R^{\frac{2}{3}} S^{\frac{1}{2}} \tag{6}$$

Where, $V$ = velocity, $D$ = diameter of stem, $\upsilon$ = kinematic viscosity, $y$ = water depth, $g$ = acceleration due to gravity, $R$ = hydraulic depth, $S$ = slope of channel, $n$ = Manning's roughness constant.

## 3.Results and Discussion

For open channel flow with vegetation, a series of simulation were carried out to study the flow characteristics using two CFD approaches i.e, stem scale and porous zone approach. Grid independence study was conducted, and the number of elements were selected based on the grid quality. The obtained numerical results after simulation were validated with the experimental results. Various hydraulic parameters were also calculated for different vegetation cover and compared with experimental results.

### 3.1 *Model validation for flow characteristics*

Validation of the model for both stem scale and porous zone approach can be carried out by comparing the average value of velocity at three different location (at X = 4.76, 7.76, 8.15) at corresponding depth provided in the reference journal (Mulahasan et al., 2017). Percentage error was also calculated for each simulation. Table 2 and 3 shows the validation of stem scale and porous zone approaches with experimental results.

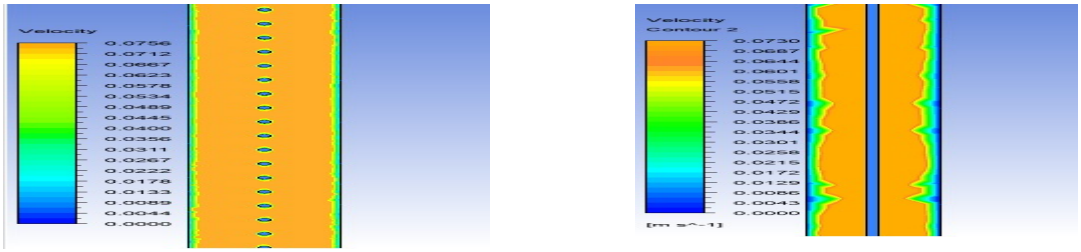
**Table 2** Validation of stem scale approach

| Vegetation cover (%) | y (m) | Vexperiment (m/s) | Vstem (m/s) | Percentage error |
|---|---|---|---|---|
| 31.8 | 0.0687 | 0.0727 | 0.0756 | 3.99 |
| | 0.076 | 0.0767 | 0.0794 | 3.52 |
| | 0.0832 | 0.0801 | 0.0828 | 3.37 |
| | 0.0902 | 0.0831 | 0.0853 | 2.65 |
| 15.9 | 0.0557 | 0.1047 | 0.1056 | 0.86 |
| | 0.0622 | 0.1071 | 0.1084 | 1.21 |
| | 0.0754 | 0.1105 | 0.1118 | 1.18 |
| | 0.0895 | 0.1117 | 0.1127 | 0.90 |
| 7.95 | 0.0487 | 0.1368 | 0.1442 | 5.41 |
| | 0.0605 | 0.1377 | 0.1452 | 5.45 |
| | 0.0694 | 0.144 | 0.151 | 4.86 |
| | 0.0759 | 0.1537 | 0.1577 | 2.60 |

**Table 3** Validation of Porous zone approach

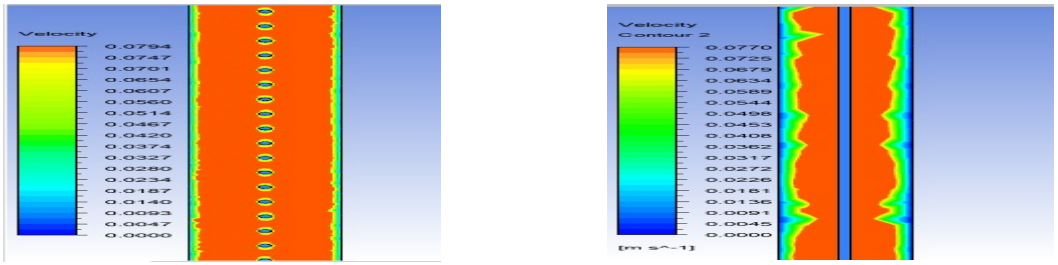
| Vegetation cover (%) | y (m) | Vexperiment (m/s) | Vporous (m/s) | Percentage error |
|---|---|---|---|---|
| 31.8 | 0.0687 | 0.0727 | 0.0731 | 0.55 |
| | 0.076 | 0.0767 | 0.077 | 0.39 |
| | 0.0832 | 0.0801 | 0.0806 | 0.62 |
| | 0.0902 | 0.0831 | 0.0834 | 0.36 |
| 15.9 | 0.0557 | 0.1047 | 0.1048 | 0.10 |
| | 0.0622 | 0.1071 | 0.1073 | 0.19 |
| | 0.0754 | 0.1105 | 0.1108 | 0.27 |
| | 0.0895 | 0.1117 | 0.1118 | 0.09 |
| 7.95 | 0.0487 | 0.1368 | 0.1371 | 0.22 |
| | 0.0605 | 0.1377 | 0.1379 | 0.15 |
| | 0.0694 | 0.144 | 0.1444 | 0.28 |
| | 0.0759 | 0.1537 | 0.1540 | 0.20 |

Numerical study shows that the values of velocity obtained from numerical simulation over estimate that of experimental values with error less than 6% for stem scale and less than 1% for porous zone approaches. Figure 5, 6, 7 and 8 shows velocity contours obtained for stem scale and porous zone approaches at different water discharge.



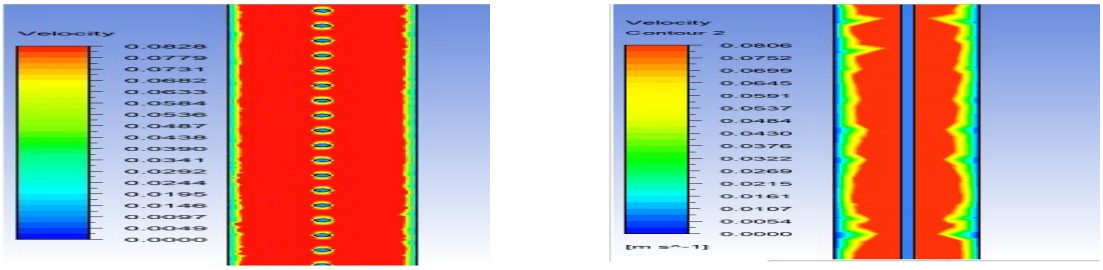
(a) (b)

**Figure 5** Velocity contour at discharge 1.58 *l/s* & water depth 0.0687 m a) Stem scale b) Porous zone



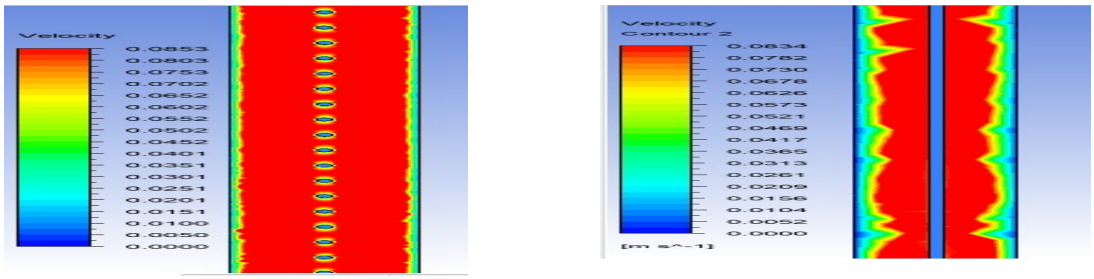
(a) (b)

**Figure 6** Velocity contour at discharge 1.78 *l/s* & water depth 0.076 m a) Stem scale b) Porous zone



(a) (b)

**Figure 7** Velocity contour at discharge 2 *l/s* & water depth 0.0832 m a) Stem scale b) Porous zone



(a) (b)

**Figure 8** Velocity contour at discharge 2.24 *l/s* & water depth 0.0902 m a) Stem scale b) Porous zone

For both stem scale and porous zone approaches, maximum velocity was obtained near the vegetation and it reduces near the boundary. In stem scale approach, at most of the part the velocity was same for all cases. In porous zone approach, for the same discharge there is a variation in velocity vector compared to stem scale and it can be due to continues modeling of porous zone along the channel.

## 3.2 Hydraulic parameters

Hydraulic parameters such as the Reynolds number, the Manning's roughness coefficient, and the Frouds number were calculated for both the CFD approaches and compared with the experimental results. Table 4, 5, and 6 shows the comparison of hydraulic parameters obtained for stem scale and porous zone approaches with experimental results.

**Table 4** Hydraulic parameters - Reynolds Number

| Vegetation cover (%) | y (m) | Q(*l*/*S*) | Experiment | Stem scale | Porous |
|---|---|---|---|---|---|
| 31.8 | 0.0687 | 1.58 | 3613.320 | 3757.455 | 3633.201 |
| | 0.076 | 1.78 | 3812.127 | 3946.322 | 3827.038 |
| | 0.0832 | 2 | 3981.113 | 4115.308 | 4005.964 |
| | 0.0902 | 2.24 | 4130.219 | 4239.563 | 4145.129 |
| 15.9 | 0.0557 | 1.75 | 2601.889 | 2624.254 | 2604.374 |
| | 0.0622 | 2 | 2661.531 | 2693.837 | 2666.501 |
| | 0.0754 | 2.46 | 2746.024 | 2778.330 | 2753.479 |
| | 0.0895 | 3.06 | 2775.845 | 2800.696 | 2778.330 |
| 7.95 | 0.0487 | 2.02 | 1699.801 | 1791.750 | 1703.529 |
| | 0.0605 | 2.5 | 1710.984 | 1422.962 | 1713.469 |
| | 0.0694 | 3.06 | 1789.264 | 2016.650 | 1794.235 |
| | 0.0759 | 3.5 | 1909.791 | 2138.419 | 1913.519 |

**Table 5** Hydraulic parameters - Frouds Number

| Vegetation cover (%) | y (m) | Q(*l*/*S*) | Experiment | Stem scale | Porous |
|---|---|---|---|---|---|
| 31.8 | 0.0687 | 1.58 | 0.089 | 0.092 | 0.089 |
| | 0.076 | 1.78 | 0.089 | 0.092 | 0.089 |
| | 0.0832 | 2 | 0.089 | 0.092 | 0.089 |
| | 0.0902 | 2.24 | 0.088 | 0.091 | 0.089 |
| 15.9 | 0.0557 | 1.75 | 0.142 | 0.143 | 0.142 |
| | 0.0622 | 2 | 0.137 | 0.139 | 0.137 |
| | 0.0754 | 2.46 | 0.128 | 0.130 | 0.129 |
| | 0.0895 | 3.06 | 0.119 | 0.120 | 0.119 |
| 7.95 | 0.0487 | 2.02 | 0.198 | 0.209 | 0.198 |
| | 0.0605 | 2.5 | 0.179 | 0.149 | 0.179 |
| | 0.0694 | 3.06 | 0.175 | 0.197 | 0.175 |
| | 0.0759 | 3.5 | 0.178 | 0.199 | 0.178 |

**Table 6** Hydraulic parameters - Mannings Roughness

| Vegetation cover (%) | y (m) | Q(*l/s*) | Experiment | Stem scale | Porous |
|---|---|---|---|---|---|
| 31.8 | 0.0687 | 1.58 | 0.040 | 0.039 | 0.040 |
| | 0.076 | 1.78 | 0.040 | 0.038 | 0.040 |
| | 0.0832 | 2 | 0.040 | 0.038 | 0.039 |
| | 0.0902 | 2.24 | 0.040 | 0.039 | 0.039 |
| 15.9 | 0.0557 | 1.75 | 0.025 | 0.025 | 0.025 |
| | 0.0622 | 2 | 0.026 | 0.026 | 0.026 |
| | 0.0754 | 2.46 | 0.028 | 0.027 | 0.027 |
| | 0.0895 | 3.06 | 0.029 | 0.029 | 0.029 |
| 7.95 | 0.0487 | 2.02 | 0.018 | 0.017 | 0.018 |
| | 0.0605 | 2.5 | 0.020 | 0.024 | 0.020 |
| | 0.0694 | 3.06 | 0.020 | 0.018 | 0.020 |
| | 0.0759 | 3.5 | 0.020 | 0.018 | 0.020 |

Average value of the Reynolds number for both the approaches were greater than 2000, and it shows that flow is turbulent due to the impact of vegetation. Average value of the Froud's number for both the stem scale and the porous zone approaches were greater than 1, it shows that flow is subcritical. In both cases, the Manning's roughness increases with vegetation cover. It was found that porous zone approach predicted the experimental values of hydraulic parameters better than stem scale approach. The computational time was also less for porous zone approach compared to stem scale approach .

## 2. Conclusion

Flow characteristics of a vegetated channel was studied using two CFD approaches (i.e. stem scale and porous zone approaches) available in the ANSYS Fluent software. For the validation of the model numerical results are then compared with the experimental results from the reference journal. To study the flow characteristics of the vegetated channel, various hydraulic parameters were calculated for both the CFD approaches and compared with the experimental results. For studying the influence of vegetation three different type of vegetation cover i.e, 31.81%, 15.91% and 7.95% were modeled. The average value of the Manning's rougness coefficient for each vegetation cover were determined and it was found that the roughness coefficient increases with the increase in the vegetation cover. Numerical study of vegetated channel shows that the values of velocity obtained from the CFD simulation over estimate that of experimental values with error less than 6% for the stem scale approach and 1% for the porous zone approach.The CFD model with the porous zone approach predicted the hydraulic parameters and found to be better than stem scale approach. The computational time is also less for the porous zone approach compared to stem scale approach.

This model can be used to predict the hydraulic characteristics for different vegetation cover under different hydraulic condition in natural channels, thus it can be an alternative to experimental setup and reduce the time and effort. The Manning's *n* value for different type of vegetation are important for the design of vegetated channels like stormwater pond. The porous zone approach was found to be more accurate than stem scale approach, thus can be applied for modeling the natural channels.

## References

1. Cheng,N.S. and Nguyen,H.T (2011). Hydraulic radius for evaluating resistance induced by simulated emergent vegetation in open-channel flows. *Journal Hydraulic Engineering*, 137(9), 995–1004.

2. Ebrahimi,N., Gharibreza,M., and Ashraf,M.A (2017). Experimental study on the impact of vegetation coverage on flow roughness coefficient and trapping of sediment *Geology, Ecology, and Landscapes,* 1(3), 167–172.

3. Gao,G., Falconer,R.A., and Len,B. (2011). Modelling open channel flows with vegetation using a three dimensional model *Journal of water resource protection*, 3, 114-119

4. Jordanova,A.A., and James,C.S (2003). Experimental study of bed load transport through emergent vegetation *Journal of Hydraulic Engineering ASCE*, 129, 474-478.

5. Kumar,M. and Aggrwal,S. (2017). Flow analysis of rigid and flexible vegetation using ANSYS Fluent *ASCE India Conference, New Delhi* , 12-14 December.

6. Mulahasan,S. and Stoesser,T. (2017). Flow resistance of inline vegetation in open channel flow *International Journal of River Basin Management*, 329-334.

7. Panigrahi,K. and Khatua,K.K. (2015). Prediction of velocity distribution in straight channel with rigid vegetation *International conference on water resources,coastel and ocean engineering 2015, Surathkal,* 12-14 March 819-825.

8. Stoesser,T., Kim,S.J. and Diplas,P. (2010). Turbulent Flow through Idealized Emergent Vegetation *Journal of Hydraulic Engineering*, 136(12),1003-1017.

9. Tsavdaris,A., Steve Mitchell,S. and Williams,J.B. (2013). Use of CFD to model emergent vegetation in detention ponds *ARPN journal of Engineering and Applied science*, 8(7).

10. Yiping, Li., Wei,D., Zhongbo,Y., Tang C., Wang,Y., Janet,L., and Acharya, K.,(2014). Impact of flexible emergent vegetation on flow turbulence and Kinetic energy characteristics in flume experiment *Journal of Hydro-Environment research* , 1-14

*IN PROCEEDINGS OF 25th HYDRO 2020, INTERNATIONAL CONFERENCE, NATIONAL INSTITUTE OF TECHNOLOGY ROURKELA, ODISHA, INDIA*
*26-28, March 2021, ISBN 978-93-90631-56-8*

Paper ID - 277

# Computation of gradually varied flow depths in a channel system using numerical methods

Rohini Rani[1,*], Pravas Ranjan Pradhan[2], Kishanjit Kumar Khatua[3]

[1]*M.Tech Scholar, Department of Civil Engineering, National Institute of Technology Rourkela, Rourkela 769008, Odisha, India.*
[2]*M.Tech Scholar, Department of Civil Engineering, National Institute of Technology Rourkela, Rourkela 769008, Odisha, India.*
[3]*Professor, National Institute of Technology Rourkela, Rourkela 769008, Odisha, India.*
*Email: rohinirani002@gmail.com, jubu.pp@gmail.com, kkkhatua@nitrkl.ac.in.*

## Abstract

A channel helps in transportation of water from a main source to the field where the crops are located thus making possible to feed our nation. It is very important to predict the water level at different section of channel because this will help to determine if the water level, at a specific point, and will provide the necessary discharge of water. It has been established that flow through channels are basically gradually varied flow. Due to differences in the hydraulic and geometric properties of channels, we have to look for the numerical methods that provide accurate results. In this paper, computation of gradually varied flow has been done by using different software like MATLAB and HEC-RAS. In MATLAB, algorithm has been encoded to determine water level at different sections by using Direct step method and Fourth-order Runge-Kutta method. The result obtained from software has been compared well and percentage error has been calculated to find out the better method. Merit and demerits of the methods are discussed.

***Keywords:*** *channel; water level; gradually varied flow; numerical methods; MATLAB; algorithm*

## 1. Introduction

For engineering applications, it is necessary to compute the water surface elevation along the channel length for a specific discharge. The knowledge water-surface elevation is required for many hydraulic engineering purposes like planning, design and operation of open channels to assess the effects of various engineering works and channel modifications. The addition of a dam, for example, raises water levels upstream of the dam and therefore it become necessary to determine the flow depths in the upstream region to determine the extent of flooding.

There are many methods to compute gradually varied flow. Two traditional methods are Direct step method and Standard step method. Computations in these methods progress step by step from one section. There are also numerical methods to integrate the governing differential equation. We may classify these methods into the following two categories (McCracken and Dorn, 1964; Chapra and Canale, 1988):

1. Single-step methods, and
2. Predictor-corrector methods

There are several single-step methods (McCracken and Dorn, 1964). However, some of the frequently used methods are:

1. Euler method
2. Modified Euler method
3. Improved Euler method
4. Fourth-order Runge-Kutta method

Some of these methods have been used in various general purpose computer programs for computing water-surface profiles [Soil Conservation Service; 1976; U.S. Army Corps of Engineers, 1982; and Geological Survey, 1976]. Of these programs, HEC-RAS developed by the Army Corps of Engineers is most widely used.

## 1.1 *Methodology*

In this paper calculation of water-surface elevation has been done by Direct step method, Fourth-order Runge-Kutta method and HEC-RAS program. The first and second model has been developed using the program MATLAB, where an algorithm was produced. To test and compare the results, a particular channel dimension was specified, and different parameters were measured such as top width, Froude's number, energy gradient, water surface elevation keeping the length of reach constant.

### 1.1.1 *Direct Step Method*

The direct step method can be expressed in two forms, depending on the variable that you want to determine. If we know the flow depth at a point 1 and the distance between the section 1 and 2 is known for a specific discharge, the flow depth at point 2 can be determined, refer to figure 1.

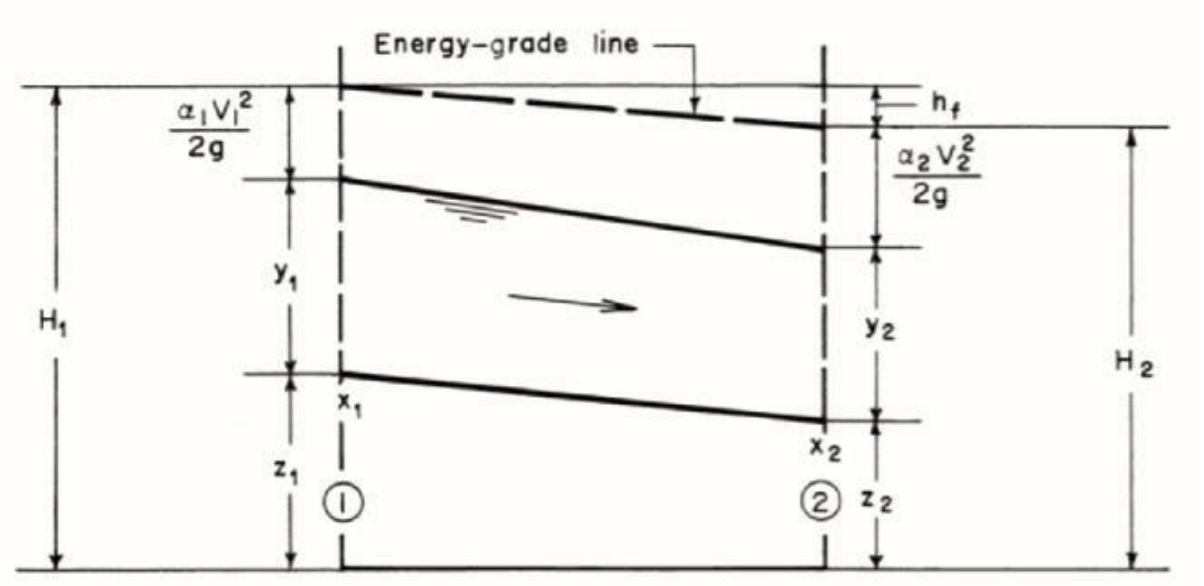



**Figure 1** Definition sketch for Direct Step Method (Chaudhry, 2008)

Equations used in the estimation of water surface elevation in gradually varied flow are following (Chaudhry, 2008):

$$T_b = B + (2 * m * y_u) \quad (1)$$

$$A = 0.5 * (Tb + B) * y_u \quad (2)$$

$$P = B + (2 * y_u * (m^2 + 1)^{0.5}) \quad (3)$$

$$R = A / P \quad (4)$$

$$V = Q / A \quad (5)$$

$$S_f = (n^2 * V^2) / (R^{1.33}) \quad (6)$$

$$dy/dx = (S_o - S_f) / (1 - (a * T_b * Q^2) / (g * A^3)) \quad (7)$$

Where $T_b$= top width; B= bottom width; m= side slope; A= area of flow; $y_u$= initial depth; P= wetted perimeter; R= hydraulic radius; V= velocity of flow; $S_o$= bottom slope; $S_f$= friction slope; n= manning's coefficient;

The following approximations have been used (U.S. Army Corps of Engineers, 1982) to select a representative value of $\bar{s}_f$ (average friction slope) for the channel length between sections 1 and 2:

Average friction slope

$$\bar{s}_f = (S_{f1} + S_{f2}) / 2 \quad (8)$$

Geometric mean friction slope

$$\bar{s}_f = (S_{f1} * S_{f2})^{0.5} \quad (9)$$

Harmonic mean friction slope

$$\bar{s}_f = (2 * S_{f1} * S_{f2}) / (S_{f1} + S_{f2}) \quad (10)$$

Based on some formulations, it has been recommended to use equation 8 for the computation of average friction slope.

In direct step method, water surface elevation at the end of each reach is computed directly by using the initial depth by using the following equation:

$$y_d = y_u + (dy/dx * L_R) \quad (11)$$

Where, $y_d$= water surface elevation at the end of each reach; $L_R$= length of each reach.

To calculate $y_d$, MATLAB program has been used. Figure 2 represent flow-chart of the algorithm used in MATLAB to determine the flow depth at a section 2 knowing the values of flow depth and elevation at section 1, using the direct step method.

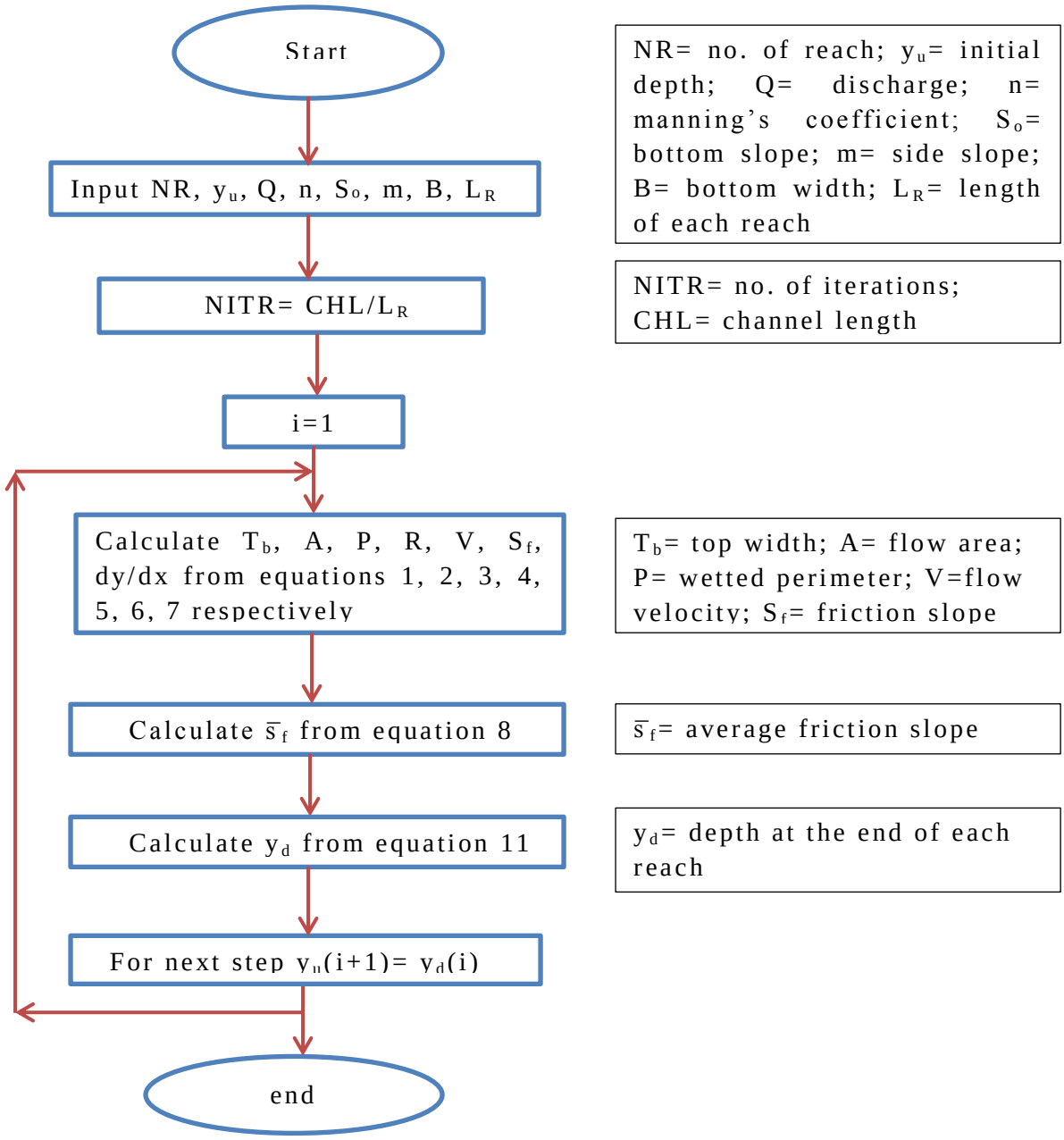



**Figure 2** Flow chart of algorithm used in MATLAB for Direct step method

1.1.2 *Fourth-order Runge-Kutta method*

Direct step method is only first order accurate. Hence the error in the calculation of water surface elevation is more. To improve the accuracy, Fourth-order Runge-Kutta method is used. This method is fourth order accurate. Therefore, this method gives better results than direct step method.

Let denote dy/dx from equation 7 as $f(y_u)$ because as we can see in the equation that dy/dx is a function of yu and $L_R$ as Δx.

Denoting constant k1, k2, k3 k4 as

$$k1= f(y_u(i)) \quad (12)$$

$$k2 = f(y_u(i) + (0.5 * k1 * \Delta x)) \quad (13)$$

$$k3 = f(y_u(i) + (0.5 * k2 * \Delta x)) \quad (14)$$

$$k4 = f(y_u(i) + (k3 * \Delta x)) \quad (15)$$

Then the equation used for the calculation of water surface elevation after each interval of reach is following

$$y_u(i+1) = y_u(i) + [(1/6) * (k1 + 2k2 + 2k3 + k4) * \Delta x] \quad (16)$$

Figure 3 represent flow-chart of the computations to determine the flow depth after each interval of reach using Fourth-order Runge-Kutta method.

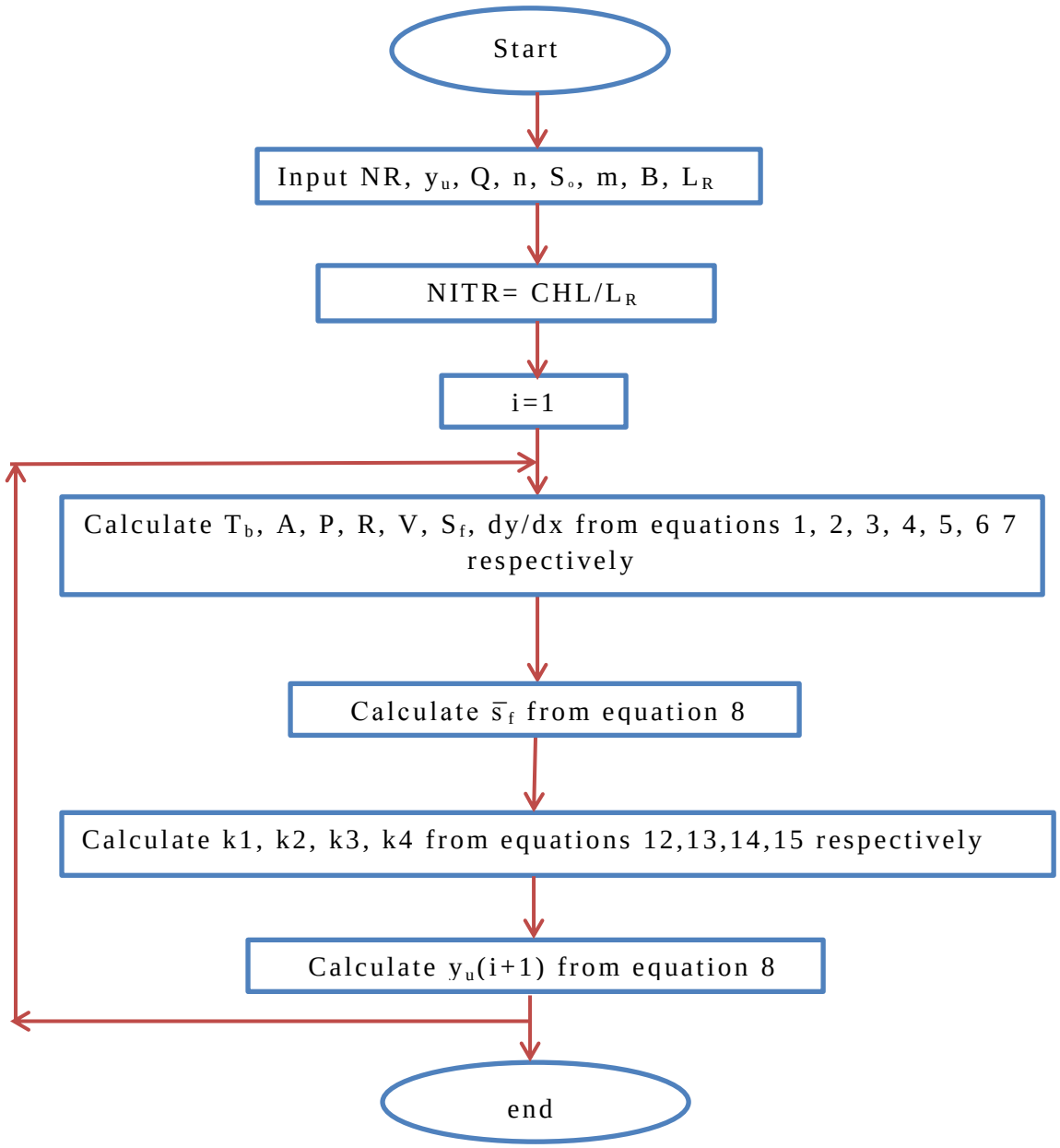



**Figure 3** Flow chart of algorithm used in MATLAB for Runge-kutta method

## 2. Experimental program

The case of study proposed for this paper was a series of channel. The channel has a length of 1200 meters and has a trapezoidal cross-section; which was prepared by the program HEC-RAS, is illustrated in figure 4. Geometric properties of the channel are listed on the table 1. This information was used to create the model with the program HEC-RAS and MATLAB. A definition sketch was prepared by the program HEC-RAS to illustrate this series of channel, figure 6.

For channel the initial discharge will be 399.5$m^3$/s and it is assume that there will not be any lateral inflow or outflow along the distance of channel. Also the upstream water depth at the first section of the channel and the initial depth estimate will be 8.0 meters.

**Table 1:** Channel properties

| Channel Property | Value |
|---|---|
| Bottom slope, $S_o$ | 0.0001 |
| Length | 1200 m |
| Manning's Roughness Coefficient, n | 0.02 |
| Bottom width, B | 10 m |
| Lateral Slope, m (m Horizontal : 1 Vertical) | 1.5 |
| Number of reaches | 12 |
| Length of each reach | 100 |
| Kinetic energy coefficient, α | 1 |

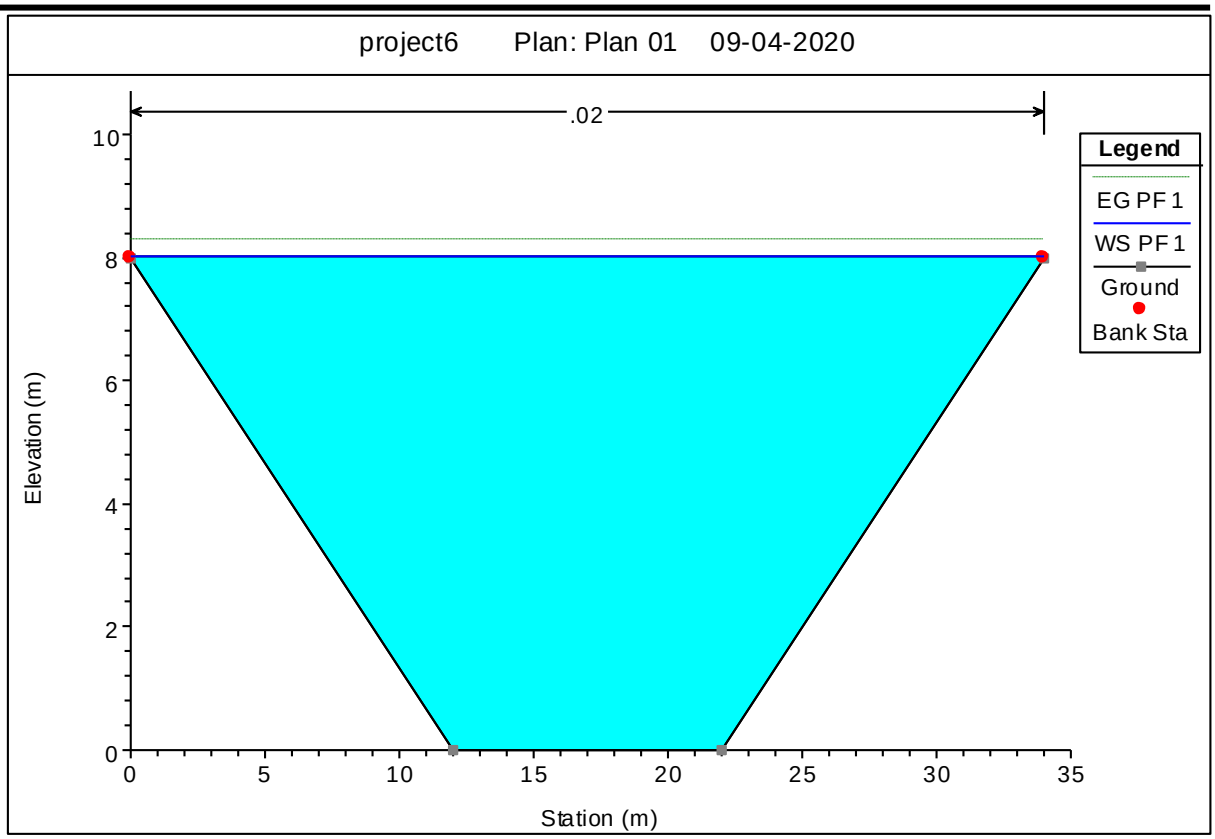



**Figure 4** Upstream Cross section

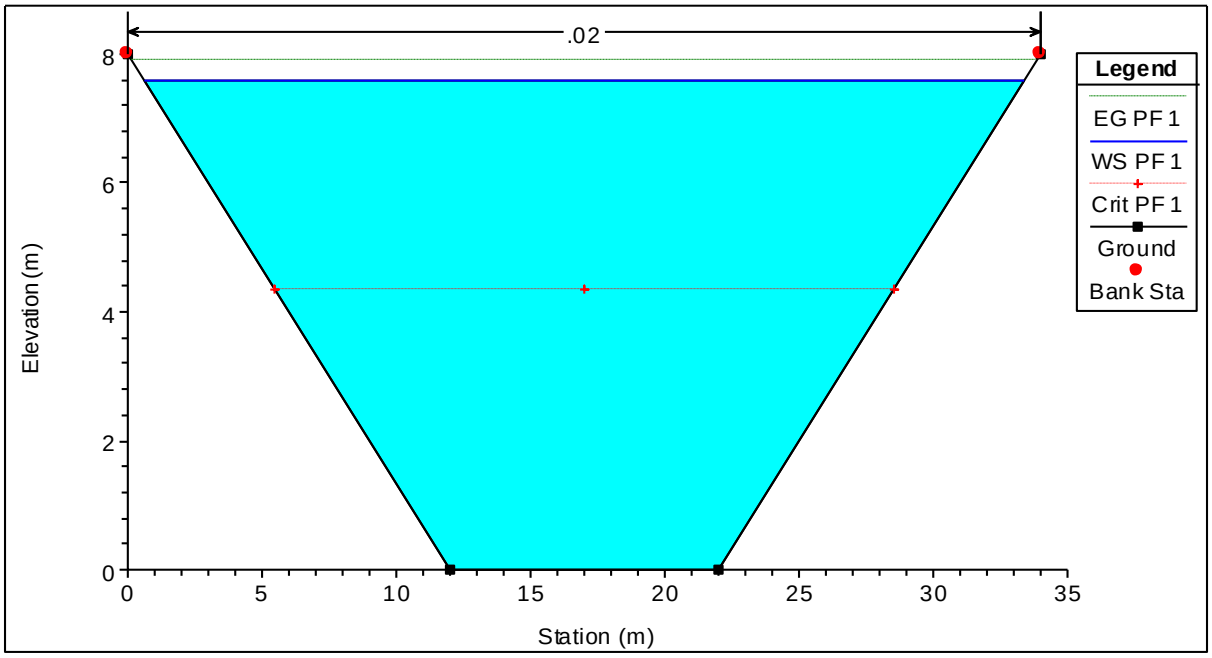



**Figure 5** Downstream cross section

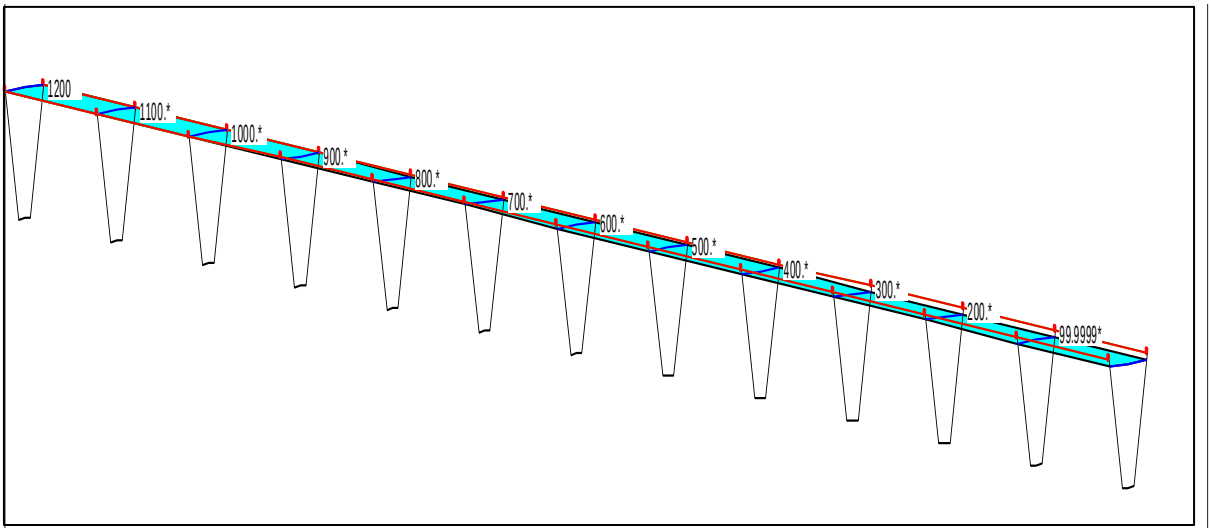



**Figure 6** Sketch of the channel in series (HEC-RAS)

## 2.1 Results and analysis

The results of direct step method and Runge-Kutta method obtained from MATLAB program is shown in table 2 and table 3 respectively and for Hec-RAS program is shown in table 4. Then the value of water surface elevation obtained from all the three methods has been compared in table 4. Also in this table, the percentage of error of water surface elevation had been calculated between each reach, where the theoretical water surface elevation is 8m. Figure 6 shows the water surface profile obtained from the Direct step method, Runge- Kutta method and HEC-RAS program.

**Table 2** Results of Direct step method from MATLAB program

| Reach | Flow depth | Flow area | Top width | Velocity | E.G. Slope |
|---|---|---|---|---|---|
| 0 | 8.000 | 176.000 | 34.000 | 2.270 | 0.0000276 |
| 100 | 7.980 | 175.334 | 33.941 | 2.279 | 0.0000279 |
| 200 | 7.960 | 174.657 | 33.881 | 2.287 | 0.0000282 |
| 300 | 7.940 | 173.970 | 33.820 | 2.296 | 0.0000285 |
| 400 | 7.920 | 173.271 | 33.758 | 2.306 | 0.0000288 |
| 500 | 7.898 | 172.562 | 33.695 | 2.315 | 0.0000291 |
| 600 | 7.877 | 171.841 | 33.631 | 2.325 | 0.0000295 |
| 700 | 7.855 | 171.108 | 33.566 | 2.335 | 0.0000298 |
| 800 | 7.833 | 170.363 | 33.499 | 2.345 | 0.0000302 |
| 900 | 7.810 | 169.604 | 33.431 | 2.356 | 0.0000305 |
| 1000 | 7.787 | 168.833 | 33.362 | 2.366 | 0.0000309 |
| 1100 | 7.768 | 168.048 | 33.291 | 2.377 | 0.0000313 |
| 1200 | 7.740 | 167.249 | 33.219 | 2.389 | 0.0000317 |

**Table 3** Results of Runge- Kutta method from MATLAB program

| Reach | Flow depth | Flow area | Top width | Velocity | E.G. Slope |
|---|---|---|---|---|---|
| 0 | 8.0000 | 176.0000 | 34.0000 | 2.2699 | 0.00002763 |
| 100 | 7.9883 | 175.8013 | 33.9825 | 2.2725 | 0.00002771 |
| 200 | 7.9765 | 175.402 | 33.9472 | 2.2776 | 0.00002788 |
| 300 | 7.9526 | 174.5961 | 33.8759 | 2.2881 | 0.00002823 |
| 400 | 7.9284 | 173.7802 | 33.8036 | 2.2989 | 0.00002859 |
| 500 | 7.8915 | 172.5366 | 33.693 | 2.3155 | 0.00002915 |
| 600 | 7.8663 | 171.6939 | 33.6179 | 2.3268 | 0.00002953 |
| 700 | 7.8408 | 170.8396 | 33.5416 | 2.3385 | 0.00002993 |
| 800 | 7.8213 | 170.191 | 33.4835 | 2.3474 | 0.00003024 |
| 900 | 7.8017 | 169.7548 | 33.4444 | 2.3534 | 0.00003045 |
| 1000 | 7.7884 | 169.0944 | 33.3851 | 2.3626 | 0.00003077 |
| 1100 | 7.7683 | 168.4268 | 33.3251 | 2.372 | 0.0000311 |
| 1200 | 7.7479 | 167.7515 | 33.2642 | 2.3815 | 0.00003144 |

**Table 4** Results from HEC-RAS program

| Reach | Flow depth | Flow area | Top width | Velocity | E.G. Slope |
|---|---|---|---|---|---|
| 0 | 8.00 | 176.00 | 34.00 | 2.27 | 0.000273 |
| 100 | 7.98 | 175.39 | 33.95 | 2.28 | 0.000277 |
| 200 | 7.95 | 174.33 | 33.85 | 2.29 | 0.000282 |
| 300 | 7.92 | 173.26 | 33.76 | 2.31 | 0.000287 |
| 400 | 7.89 | 172.17 | 33.66 | 2.32 | 0.000292 |
| 500 | 7.85 | 171.05 | 33.56 | 2.34 | 0.000297 |
| 600 | 7.82 | 169.91 | 33.46 | 2.35 | 0.000302 |
| 700 | 7.78 | 168.76 | 33.35 | 2.37 | 0.000308 |
| 800 | 7.75 | 167.58 | 33.25 | 2.38 | 0.000314 |

| | | | | | |
|---|---|---|---|---|---|
| 900 | 7.71 | 166.38 | 33.14 | 2.4 | 0.000320 |
| 1000 | 7.68 | 165.16 | 33.03 | 2.42 | 0.000326 |
| 1100 | 7.64 | 163.91 | 32.92 | 2.44 | 0.000333 |
| 1200 | 7.62 | 162.64 | 32.8 | 2.46 | 0.000340 |

**Table 4** Comparison of percentage error of water elevation

| Reach | % error (Direct step method) | % error (Runge- Kutta method) | % error (HEC- RAS program) |
|---|---|---|---|
| 100 | 0.245 | 0.14625 | 0.25 |
| 200 | 0.495 | 0.29375 | 0.625 |
| 300 | 0.74875 | 0.5925 | 1 |
| 400 | 1.00625 | 0.895 | 1.375 |
| 500 | 1.27 | 1.35625 | 1.875 |
| 600 | 1.5375 | 1.67125 | 2.25 |
| 700 | 1.81 | 1.99 | 2.75 |
| 800 | 2.0875 | 2.23375 | 3.125 |
| 900 | 2.37125 | 2.47875 | 3.625 |
| 1000 | 2.66 | 2.645 | 4 |
| 1100 | 2.9 | 2.89625 | 4.5 |
| 1200 | 3.25 | 3.15125 | 4.75 |

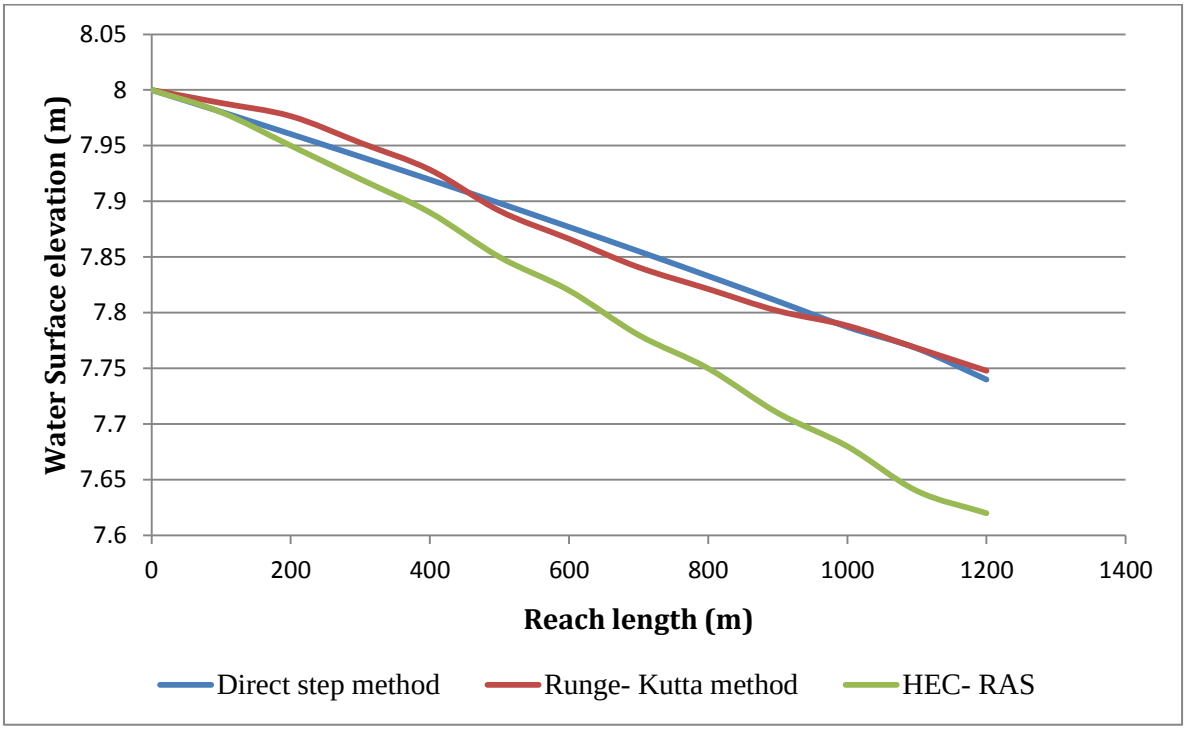



**Figure 7** Plot of water surface elevation vs reach length

## 3. Conclusions

Given the results for the direct step method, Runge- Kutta method and HEC-RAS method, it can be said that Runge- Kutta method estimates the flow depth very accurate, since the percentage of error is small in comparison to other methods. HEC-RAS program use 1-D Saint-Venant equation for water surface profile calculation. Direct step method and HEC-RAS program give second order accurate results while Runge- Kutta method gives fourth accurate results. It was demonstrated that the water surface profile graphs (figure 7), for all the three cases of study, follow the theoretical paths and assumptions established on the literature.

This study shows that if we want more accurate results to do more precise experiments, we have to adopt Runge- Kutta method. But it has complex algorithm and it does not give pictorial representation of the work. But HEC-RAS program is very efficient in giving fast results for less accuracy with pictorial representation of all the work that we have done. Pictorial representation helps in getting a wider picture of the events that are happening as we see figure 4, figure 5, figure 6, figure 7 which was obtained from HEC-RAS. In the figures we can clearly see how the water surface profile is changing from upstream to downstream.

In conclusion to all, we can say that we need to develop software that work on complex methods like Runge- Kutta methods which should give results up to fourth order accurate for getting more accurate results along with pictorial representation of each step so that the prediction of water surface profiles will become more precise and the construction of hydraulic structures will be more easier and less time consuming.

## References

Chaudry, H. M. (2008). *Open-Channel Flow* (Second Edition ed.). New York, NY: Springer Science+Business Media, LLC.

Collazo, F. L. S., and Araya, W.S.(2014). *Computation of Gradually Varied Flow in a Channel System*. Puerto Rico, https://www.researchgate.net/publication/270566726.

Henderson, F. M. (1966). *Open Channel Flow*. New York, NY: Macmillan Publishing Company., Inc.

U.S. Army Corps of Engineers (USACE). (2010). HEC-RAS, River Analysis System. User Manual.

*IN PROCEEDINGS OF 25th HYDRO 2020, INTERNATIONAL CONFERENCE, NATIONAL INSTITUTE OF TECHNOLOGY ROURKELA, ODISHA, INDIA 26-28, March 2021, ISBN 978-93-90631-56-8*

Paper ID - 283

# Numerical solution of 1D Saint-Venant equation by MacCormack Method and Comparison of result with Preissmann Implicit Method

Pravas Ranjan Pradhan[1], Rohini Rani[2], Kishanjit Kumar Khatua[3]

[1]*M.Tech Scholar, Department of Civil Engineering, National Institute of Technology Rourkela, Rourkela 769008, Odisha, India.*
[2]*M.Tech Scholar, Department of Civil Engineering, National Institute of Technology Rourkela, Rourkela 769008, Odisha, India.*
[3]*Professor, National Institute of Technology Rourkela, Rourkela 769008, Odisha, India.*
*Email: jubu.pp@gmail.com, rohinirani002@gmail.com, kkkhatua@nitrkl.ac.in.*

## ABSTRACT

In water resources management river flow prediction is highly essential. For the river flow prediction unsteady flow analysis plays an important and vital role than the steady state analysis because in practical scenarios there is no existence of steady flow. For the study of unsteady flow in open channels Saint-Venant introduced two equations (Continuity and Momentum equation) in the form of Non-linear partial differential equation. As these equations are highly nonlinear so they don't have analytical solutions. To solve these equations numeric methods can be utilized effectively. This Paper presents the numerical solution to the Saint-Venant equation that governs the propagation of flood wave by using a finite difference method. To solve these nonlinear partial differential equations a mathematical model with the initial and boundary conditions is established. The Model is then discretised by using a MacCormack finite difference method and implemented on MATLAB. The output parameters like depth of water (y), the fluid velocity (u) and the volumetric flow rate (Q) are simulated numerically and values are obtained for the different time at different cross sections to plot outflow hydrograph for the downstream sections. To solve these highly nonlinear equations through the MATLAB programming proper discretization with proper selection of grid size and time step is highly essential. Conversion of these equations into ordinary partial differential equation forms and the simple discretization of these equations by MacCormack explicit scheme using CFD techniques and the comparison of the result with other implicit and explicit models are presented in this paper.

***Keywords:*** *Saint-Venant equations, MATLAB, MacCormack scheme, CFD, Explicit, Implicit*

## 1. Introduction

Many environmental problems are now associated with the sudden climate change which affect also to the rainfall. More heavy rain is one of the important signs of climate change. As the atmosphere warms, more water evaporates from soils, plants, lakes, and oceans. For every additional 1°F of warming, the atmosphere is capable of holding an additional 4 percent of water vapor. So, when this additional water vapor condenses into precipitation, it leads to heavier rain. These sudden heavy rains produce Flash Flood in the downstream sections of natural streams and rivers. Flash floods are very dangerous floods that can happen with little or no warning. So, the computation of unsteady free-surface flows is required to estimate the arrival time, discharge and height of a flood waves at any downstream location in a river flow.

To estimate the arrival time and height of a flood waves at any downstream location in a river flow, there is a need to do the computation of unsteady free-surface flows. St. Venant's equations also sometime referred to as shallow water equations, describe one-dimensional unsteady free-surface flows, which are derived assuming hydrostatic pressure distribution. These equations are nonlinear first-order, hyperbolic partial differential equations. The closed-form solutions of these equations are not available. Therefore, these equations are solved numerically. In this paper detailed study has been done for for simulation of the unsteady flow in a channel by comparison of explicit and implicit schemes and the results obtained are presented.

Many researchers have done a lot of experiment and numerical modelling to find the solution of Saint Venant equation by applying several explicit and implicit models such as lax diffusive scheme and Preissman implicit scheme. These two techniques are most commonly used for the hydraulic flood routing. In Lax diffusive method both the time complexity of the programming is less and the finite differentiation of the Saint Venant equation are simpler and easy to handle. But the main disadvantage of Lax diffusive method is the accuracy of the result is less and it requires stability condition to get solution. Similarly, in Preissmann implicit scheme the time complexity of the programming is higher than the explicit model and the finite differentiation of the Saint Venant equation are complex and very difficult to handle. In this research paper the main objective is to use MacCormack finite difference method which can be used as a efficient hydraulic flood routing model with less time complexity and also can give more accurate result than the Lax diffusive model.

## 1.1 *Governing Equations*

The dynamic routing model is based on the Saint-Venant equation's dynamic wave theory. For prismatic channels having no lateral inflow or outflow the continuity and momentum equations defined as

Continuity equation

$$\frac{\partial \mathrm{A}}{\partial \mathrm{t}} + \frac{\partial \mathrm{Q}}{\partial \mathrm{x}} = 0 \tag{1}$$

Momentum equation

$$\frac{\partial Q}{\partial t} + \frac{\partial}{\partial x}\left(\frac{Q^2}{A}\right) + \frac{1}{2} g \frac{\partial}{\partial x}\left(\frac{A^2}{B}\right) - g\, A\,(S_o - S_f) = 0 \tag{2}$$

Another governing equation is the equation of the discharge hydrograph that can be represented as a function of time. So The U/S discharge hydrograph (Qt) is generally sinusoidal in nature and is a function of time (*t*), base flow (Qb) and peak flow (Q) is given by:

$$Q(t) = \frac{Q_p}{2} \sin\left(\frac{\pi t}{t_p} - \frac{\pi}{2}\right) + \frac{Q_p}{2} + Q_b \qquad \text{for} \quad t < t_b$$

$$Q(t) = \frac{Q_p}{2} \cos\left(\pi \frac{t - t_p}{t_b - t_p}\right) + \frac{Q_p}{2} + Q_b \quad \text{for} \quad t_p < t \leq t_b$$

$$Q(t) = Q_b \quad \text{for} \quad t > t_p \tag{3}$$

The above equation (3) can be used only at upstream boundary means only at the upper exterior grid points and cannot be used for the interior grid points. Similarly, for the downstream boundary condition the positive characteristic equation as well as the manning's equation is used. Both the positive and negative characteristics equations are derived from the Saint-Venant equation of continuity and momentum and given by:

$$\frac{\partial Q}{\partial t} - \left(\frac{Q}{A} + \sqrt{\frac{gA}{B}}\right)\frac{\partial A}{\partial t} = gA(S_0 - S_f) \tag{4}$$

$$\frac{\partial Q}{\partial t} - \left(\frac{Q}{A} - \sqrt{\frac{gA}{B}}\right)\frac{\partial A}{\partial t} = gA(S_0 - S_f) \tag{5}$$

Here equation (4) represents the positive characteristic equation and equation (5) represents the negative characteristic equation.

### 1.1.1 *Finite Difference Method*

The continuity and momentum equations set of nonlinear first-order, hyperbolic partial differential equations. So analytical solutions or closed-form solutions cannot be obtained for these equations. Therefore, these equations are solved numerically. Finite difference method is one of the common numerical methods applied for the solution of these types of equations. The finite difference techniques are completely based upon the Taylor series expansion of any partial derivative term with some error approximations that permit replacing differential equations by finite difference equations. The solutions of these finite difference approximations which are in algebraic form, are related to grid points. After that the equations are solved at each grid point with appropriate initial and boundary conditions to obtain the values of unknown variables.

### 1.1.2 *Mac-Cormack Explicit Scheme*

The MacCormack method is a widely used discretization scheme in computational fluid dynamics for the numerical solution of hyperbolic partial differential equations. This method was introduced by Robert W. MacCormack in 1969 [1] The MacCormack method is easy to understand and program. This procedure provides the best results for nonlinear equations. MacCormack scheme is equivalent to the Lax–Wendroff method for linear equations.

Both the continuity and momentum equations can be written in the following simplified differential form:

$$\frac{\partial \boldsymbol{U}}{\partial t} + \frac{\partial \boldsymbol{F}}{\partial x} + S = 0 \tag{6}$$

where the vectors $\boldsymbol{U}$, $\boldsymbol{F}$ and $\boldsymbol{S}$ are defined as:

$$\boldsymbol{U} = \begin{pmatrix} A \\ Q \end{pmatrix},\ \boldsymbol{F} = \begin{pmatrix} Q \\ \frac{Q^2}{A} + 0.5g\frac{A^2}{B} \end{pmatrix},\ S = \begin{pmatrix} 0 \\ -g\,A\,(S_o - S_f) \end{pmatrix}$$

In this study, the original and improved McCormack scheme both are investigated. One of the basic advantages of the original scheme is that it can calculate gradually and rapidly varied flow, when needed to simulate water flow during flush floods. For implementation in the explicit time-marching algorithm the inclusion of the source terms is relatively simple and suitable. The standard algorithm which is based on McCormack original scheme (McCormack 1971) involves a two-stage procedure also known as the predictor–corrector method and it can be written as:

$$\boldsymbol{U}_i^p = \boldsymbol{U}_i^n - \frac{\Delta t}{\Delta x}(\boldsymbol{F}_{i+1}^n - \boldsymbol{F}_i^n) + \Delta t \boldsymbol{S}_i^n \tag{7}$$

$$\boldsymbol{U}_i^c = \boldsymbol{U}_i^n - \frac{\Delta t}{\Delta x}(\boldsymbol{F}_i^p - \boldsymbol{F}_{i-1}^p) + \Delta t \boldsymbol{S}_i^p \tag{8}$$

where the superscripts $p$ and $c$ refer to the predictor and corrector step and $n$ is the time level. The final updating formula, representing the solution at the next time level ($n$ + 1) has a form:

$$\boldsymbol{U}_i^{n+1} = \frac{1}{2}(\boldsymbol{U}_i^p + \boldsymbol{U}_i^c) \tag{9}$$

### 1.2 *Initial and Boundary Conditions*

Values of discharge (Q), depth (y), area of cross section (A) and at the beginning of the time step are to be specified at all the grid points along the assumed rectangular channel as the initial condition. The two boundary conditions that are required by the model are the inflow discharge hydrograph at the upstream boundary, and the zero-depth at the downstream boundary. To find the discharge value at the downstream boundary the positive characteristics equation (4) along with the Manning's equation is used In the MacCormack scheme, the equations 7, 8 and 9 are used at the interior grid points to compute the unsteady flow discharge and the Area of cross section. These equations cannot be used at the boundaries, since there is no grid point outside the flow domain. Therefore, in this procedure, we solve the positive characteristic equation simultaneously for explicit schemes with the condition imposed by the boundary for the downstream-end condition. Unlike the explicit schemes, here we can directly include the equations describing the end conditions in the system of equations. Or we can say that we do not have to use the characteristic equations or the reflection procedures. This is one of the main advantages of the implicit schemes.

### 1.3 *Stability of the Method*

For the stability of this explicit schemes, the courant number must be less than or equal to 1. And the courant number is defined as:

$$C_n = \frac{|V| \pm \sqrt{gy}}{\Delta x / \Delta t}$$

Here, the courant number depends upon the flow velocity, spatial grid spacing and the flow depth, which are basically the functions of space and time. Sometime it is required to reduce the value of Δt and Δx for stability because the flow depth and the flow velocity change significantly during the computations. So, for every computational interval Courant condition must be satisfied at each grid point.

## 2. Method of solution

To find the solution of the equation at all the grid point by MacCormack scheme, first the grid points are generated as the requirement of the channel to be routed. Then the initial condition is applied at all the nodes at zero-time level. Then from the known initial conditions and using the discretized equations 7,8 and 9 and by solving the positive characteristic equation simultaneously with the downstream end boundary condition (Manning's Equation) and the negative characteristic equation with the upstream-end boundary condition equation 3, the values of Q and A, are obtained at all the nodes.

### 2.1 *Results and discussions*

To find the solution of the equations and to find the values of discharge and depth at every node Δt = 15 sec for more accuracy. Bed slope is taken So = 0.00061 and Manning's n value = 0.023 for this channel Total duration of the hydrograph is taken 20 hours. A 30 km length of the rectangular channel is considered for the flood routing. The time axis is divided into 4800 grids. Similarly, the value of Δx = 1 km = 1000 m. So, the length of the channel (Space axis) is divided into 30 grids. So, a mesh of 30×4800 is prepared and by using MacCormack method along with initial and boundary condition the value of depth (y) and discharge (Q) are found at all the nodes by using MATLAB Programming.

The inflow hydrograph having a peak discharge of 300 $m^3/s$, which is routed using Saint Venant equation is shown in the figure below:

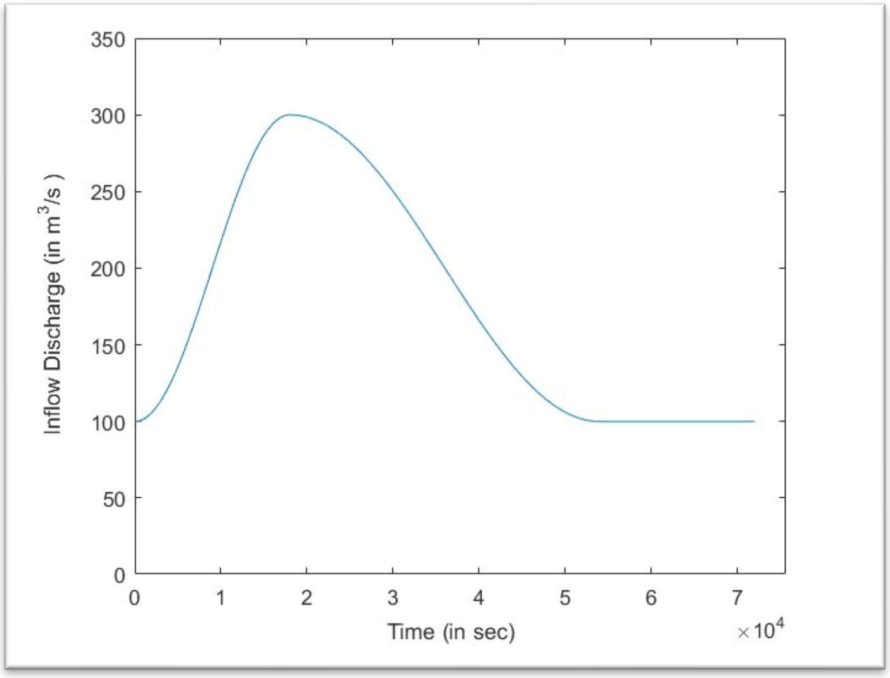



**Figure 1** Inflow hydrograph at upstream section

The values of discharges are obtained by the MacCormack method at the downstream end and the flood hydrograph is obtained for the required downstream ends:

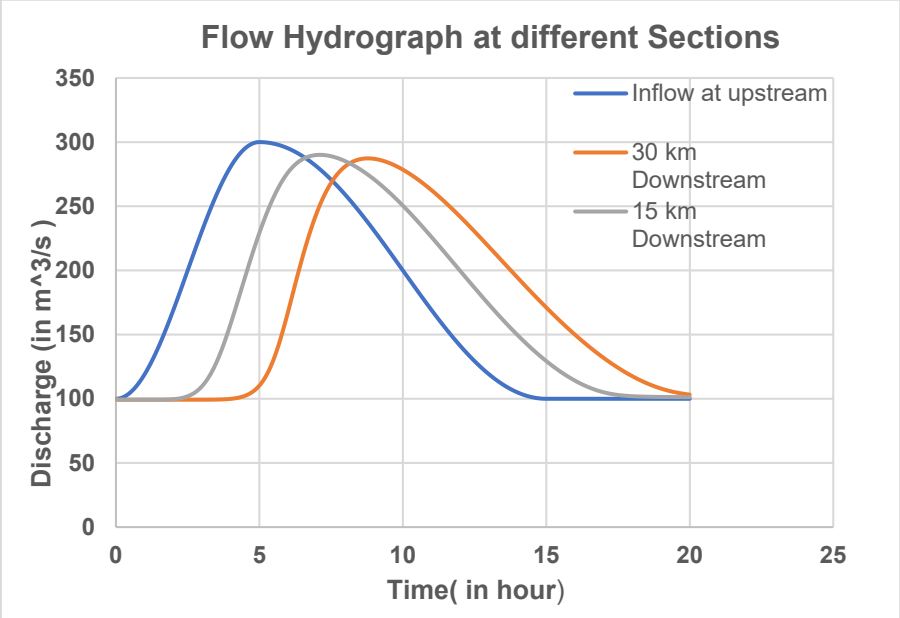



**Figure 2** Inflow vs Outflow hydrograph obtained by MacCormack Method at 15 km and 30 km from the upstream section

## 2.2 *Comparison of Result with Other models*

With the same channel dimension ,Same flow condition and also by using the same initial and boundary conditions the value of depth and discharge are calculated by other researcher's (Akbari G.,

Firoozi B., 2010 "*Implicit And Explicit Numerical Solution of Saint-Venant Equations For Stimulating Flood Wave In Natural Rivers*",5th National Congress On Civil Engineering, Ferdowsi University Of Mashhad, Mashhad, Iran.). They have used the Lax-Diffusive explicit model and Preissmann Implicit model to find the outflow hydrograph at different downstream section. So, a comparison of the result at same cross section is made with their model and the MacCormack model which is used in this paper.

**Table 1** Comparison of discharge hydrograph value calculated by different methods at 15 km from the upstream:

| Time (hour) | At upstream section | At 15 km from the Upstream section | | |
|---|---|---|---|---|
| | | Lax-Diffusive Method | Preissmann Implicit Method | Mac Cormack Method |
| | Q (in $m^3/s$) | Q (in $m^3/s$) | Q (in $m^3/s$) | Q (in $m^3/s$) |
| 0 | 100.00 | 100.00 | 100.00 | 100.00 |
| 1 | 111.19 | 100.00 | 100.00 | 99.27 |
| 2 | 169.11 | 105.60 | 100.00 | 99.69 |
| 3 | 230.92 | 129.60 | 110.40 | 109.80 |
| 4 | 280.91 | 175.20 | 163.20 | 158.59 |
| 5 | **300.00** | 230.40 | 235.20 | 229.32 |
| 6 | 295.10 | 271.20 | 284.40 | 276.45 |
| 7 | 280.89 | **285.60** | **296.40** | **289.96** |
| 8 | 258.77 | 283.20 | 290.40 | 285.05 |
| 9 | 230.89 | 270.00 | 274.80 | 270.90 |
| 10 | 199.99 | 248.40 | 253.20 | 250.48 |
| 11 | 169.09 | 223.20 | 226.80 | 225.96 |
| 12 | 141.21 | 196.80 | 199.20 | 199.58 |
| 13 | 119.09 | 170.40 | 172.80 | 173.47 |
| 14 | 104.89 | 146.40 | 148.80 | 149.54 |
| 15 | 100.00 | 128.40 | 127.20 | 129.32 |
| 16 | 100.00 | 115.20 | 112.80 | 114.08 |
| 17 | 100.00 | 109.20 | 103.20 | 105.05 |
| 18 | 100.00 | 104.40 | 100.80 | 102.00 |
| 19 | 100.00 | 103.20 | 100.80 | 101.44 |
| 20 | 100.00 | 102.00 | 100.80 | 101.44 |

**Table 2** Comparison of discharge hydrograph value calculated by different methods at the downstream end (at 30 km distance):

| Time (hour) | At upstream section | At downstream end (30 km from the upstream) | | |
|---|---|---|---|---|
| | | Lax-Diffusive Method | Preissmann Implicit Method | Mac Cormack Method |
| | Q (in $m^3/s$) | Q (in $m^3/s$) | Q (in $m^3/s$) | Q (in $m^3/s$) |
| 0 | 100.00 | 100.00 | 100.00 | 100.00 |
| 1 | 111.19 | 100.00 | 100.00 | 99.27 |
| 2 | 169.11 | 100.00 | 100.00 | 99.27 |
| 3 | 230.92 | 102.00 | 100.00 | 99.28 |
| 4 | 280.91 | 111.60 | 100.00 | 99.94 |
| 5 | **300.00** | 138.00 | 108.00 | 110.31 |
| 6 | 295.10 | 183.60 | 168.00 | 167.99 |
| 7 | 280.89 | 232.80 | 248.40 | 244.95 |
| 8 | 258.77 | 265.20 | 286.80 | 281.26 |
| 9 | 230.89 | **277.20** | **292.80** | **286.96** |
| 10 | 199.99 | 273.60 | 284.40 | 278.51 |
| 11 | 169.09 | 259.20 | 267.60 | 262.51 |
| 12 | 141.21 | 238.80 | 246.00 | 241.76 |
| 13 | 119.09 | 214.80 | 220.80 | 218.40 |
| 14 | 104.89 | 190.80 | 195.60 | 194.29 |
| 15 | 100.00 | 169.20 | 171.60 | 171.04 |
| 16 | 100.00 | 148.80 | 150.00 | 149.89 |
| 17 | 100.00 | 133.20 | 132.00 | 131.79 |
| 18 | 100.00 | 121.20 | 116.40 | 117.53 |
| 19 | 100.00 | 114.00 | 106.80 | 107.93 |
| 20 | 100.00 | 109.20 | 102.00 | 107.93 |

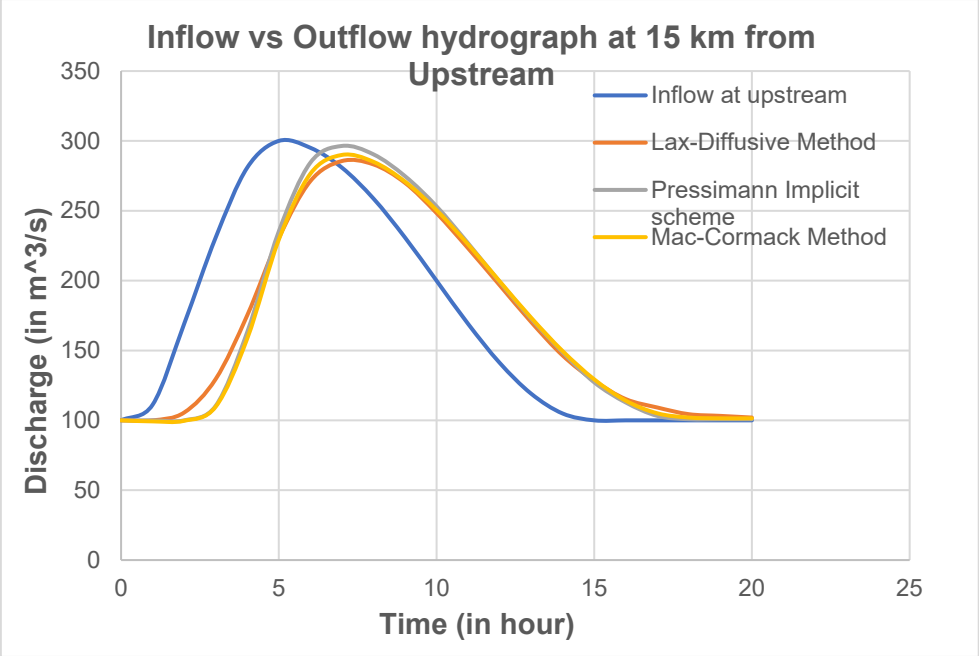



**Figure 3** Inflow vs outflow hydrograph obtained by different models at 15 km from upstream

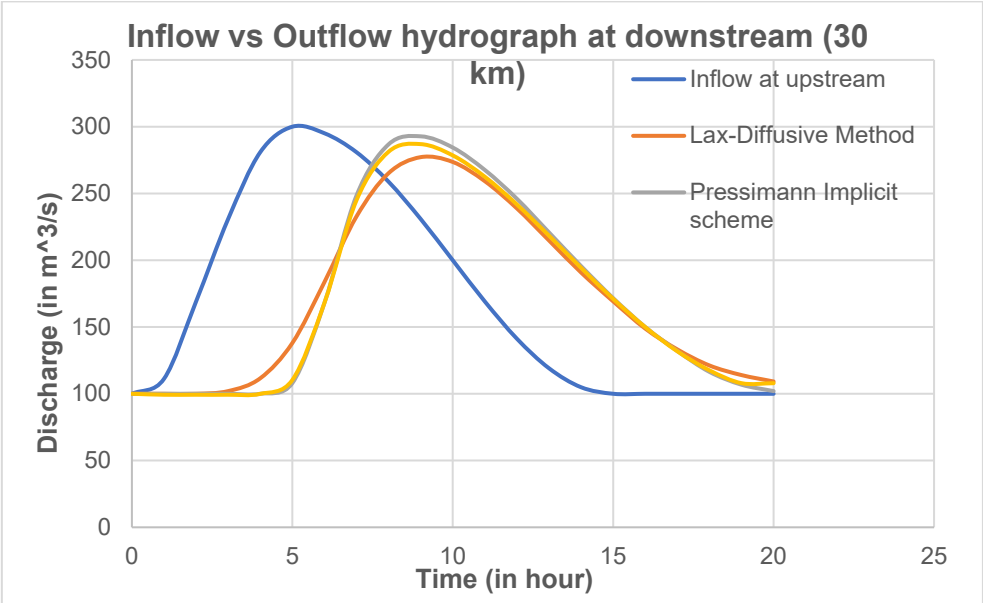



**Figure 4** Inflow vs outflow hydrograph obtained by different models at 15 km from upstream

From the above tables and graphs, it is observed that at 15 km d/s section the peak flood obtained by Lax-Diffusive explicit model and Preissmann Implicit model are 285.6m$^3$/sec and 296.4 m$^3$/sec respectively and the value obtained in this paper by MacCormack model is 289.96 m$^3$/sec. Similarly, at 30 km d/s section the peak flood obtained by Lax-Diffusive explicit model and Preissmann Implicit model are 277.2 m$^3$/sec and 292.8 m$^3$/sec respectively and the value obtained in this paper by MacCormack model is 286.96 m$^3$/sec. So, it is clearly distinguished that MacCormack explicit model gives more accurate result than Lax-Diffusive explicit model because the result MacCormack method is closer to the result of implicit method.

## 3. Conclusion

In this research paper the solution of the 1D Saint Venant equation is found by MacCormack numerical method and it is used for hydraulic flood routing problems in a wide rectangular river with the help of MATLAB and the result is compared with other implicit and explicit model. To design a hydraulic structure at any point in a river the flood hydrograph and the value of peak flood is the most important parameter to be considered. For the flood management and dam break situation hydraulic flood routing plays an important role. So, the obtained d/s hydrograph should be accurate and should be calculated quickly through the computer simulation. This model is an explicit model so the complexity of solving the equation is less here as well as the time of simulation is less. In terms of accuracy this model gives more accurate result than other model by taking small time interval ($\Delta t$) for the calculation as discussed in the above section. This model can also be used for the flash flood simulation as it gives more accurate time lag than the other explicit model. Further this model can also be used to solve the 2D Saint Venant equation and also it can be used in practical field.

## References

Akbari G., Firoozi B., 2010 "*Implicit and Explicit Numerical Solution of Saint-Venant Equations For Stimulating Flood Wave In Natural Rivers"*,5th National Congress On Civil Engineering, Ferdowsi University Of Mashhad, Mashhad, Iran.

Sharp, Zachary B., "*Applications of Computational Fluid Dynamics in Flow Measurement and Meter Design*" (2016). All Graduate Theses and Dissertations Utah State University. 4887.

Kalita H. M, Sarma A. K , "*Efficiency and performances of finite difference schemes in the solution of saint Venant's equation"* Department of Civil Engineering, Indian Institute of Technology, Guwahati, India.

Elisa Aldrighetti, Prof. Vincenzo Casulli and Dott. Paola Zanolli, "*Computational hydraulic techniques for the Saint Venant Equations in arbitrarily shaped geometry*" Universit`a degli Studi di Trento.

Hossam Elhanafy, Graham J.M. Copeland, *"Flash floods simulation using saint venant equations"*Civil Engineering Department, Strathclyde University, Scotland, U.K.

*IN PROCEEDINGS OF 25th HYDRO 2020, INTERNATIONAL CONFERENCE, NATIONAL INSTITUTE OF TECHNOLOGY ROURKELA, ODISHA, INDIA 26-28, March 2021, ISBN 978-93-90631-56-8*

Paper ID - 342

# Numerical Simulation Of Undular Hydraulic Jump on Smooth Bed

G.Rahul Indivar[1], Kishanit Kumar Khatua[2]

[1]*MTech Scholar, Department of Civil Engineering, NIT Rourkela, Odisha 769008, India*
[2]*Professor, Department of Civil Engineering, NIT Rourkela, Odisha 769008, India*
*Email:* rahulindivar7@gmail.com

## Abstract

In Open Channel Flow, the transition from supercritical to subcritical flow is called hydraulic jump. For low upstream Froude numbers free surface on the downstream side of jump develops undulations, these hydraulic jump is known as undular hydraulic jump. In this study, flow model is presented to predict the undular hydraulic jump in rectangular channel with smooth bed. The model is based on the general two-dimensional Reynolds-Averaged Navier–Stokes flow equations. The resulting set of partial differential equations is solved using the Ansys Fluent program.

***Keywords:*** *Undular hydraulic jump; Navier-Stokes Equation; Numerical simulation; Ansys Fluent;*

## 1. Introduction

The transition from supercritical flow to subcritical flow is known as Hydraulic jump. According to Chow (1959), a strong jump occurs when inflow Froude number is greater than 9, a steady jump occurs when inflow Froude number is between 4.5 and 9, an oscillating jump occurs when inflow Froude number is between 2.5 and 4.5, a weak jump occurs when inflow Froude number is between 1.7 and 2.5, and an undular jump occurs when inflow Froude number is between 1 and 1.7 .Generally for hydraulic jumps there will be significant roller length so there will be considerable amount of energy dissipation in the jump. For undular hydraulic jump as there is no roller, there will be significantly less amount of energy dissipation in the hydraulic jump.

When an undular jump takes place in a channel, waves of large amplitudes develop and propagate downstream of the jump. These undulations may overtop and damage extensively the channel banks. The propagation of free-surface waves downstream of undular jumps must be taken into account for the design of canals and for the maintenance of natural channels. . In addition, information regarding the formation of undular jumps can be useful when planning water-sport facilities such as rafting chutes. Undular-jump formations can also be an attractive feature of flowing water in a landscape.

Several studies were carried out on undular hydraulic jump. Chanson and JS Montes performed experiments on characteristics of undular hydraulic jump in a rectangular channel with fully developed upstream shear flow conditions. They reported the disappearance of undular jump occurs for Froude numbers ranging from 1.5 to 2.9 and that the wave length and amplitude of the free-surface undulations are functions of the upstream Froude number and the aspect ratio yc/W. Castro-Orgaz and Chanson examined the characteristics of the undular flows based on the Boussinesq-type energy equation, which allowed for friction effects and streamline curvature.

Fatemeh Rostami simulated undular hydraulic jump on a rough bed and smooth bed in rectangular channel using the VOF technique to predict the wavy shape of the surface profile. The RNG turbulence model was used to determine the effects of turbulence on the mean flow. The resulting set of equations were solved using Flow-3D solver. Three types of undular jumps were simulated in rectangular channel for different upstream Froude numbers.

Due to the Numerical difficulties in predicting flow characteristics of undular hydraulic jump Wilhelm Schneider proposed iteration procedure, which is based on an asymptotic analysis, appears suitable to lend essential support to the numerical solution of near-critical free-surface flows. He observed the choice of the turbulence model has little effect on the results for the elevation of the free surface, while the results for the wall shear stress show a more substantial dependence on the turbulence model.

In the present work undular hydraulic jump is simulated in Ansys Fluent 3D which solves Reynolds Averaged Navier-Stokes equations. Numerical equations are discretized using finite volume method. . For displacement of the free surface, the volume of fluid method is adopted.

### 1.1 Governing Equations

The governing equations are developed from the basic laws of the system i.e. conservation of mass and conservation of momentum. The turbulence model is solved with these equations for the Reynolds Stress. As the flow pattern is assumed to be two-dimensional, two momentum equations in the x and z directions are solved. The differential equation of mass conservation equation is as follows:

$$\frac{\partial(\alpha\rho)}{\partial t}+\frac{\partial(\alpha\rho u)}{\partial x}+\frac{\partial(\alpha\rho w)}{\partial z}=0 \tag{1}$$

Where u and w are the velocity components in the length, x and z are height directions,α is fraction of fluid, ρ is the density of fluid. The momentum equation for the fluid velocity components in the two directions are the Navier–Stokes equations, which are as follows:

$$\alpha\rho g_x-\frac{\partial P}{\partial x}+\frac{\partial\tau_{xx}}{\partial x}+\frac{\partial\tau_{zx}}{\partial z}=\alpha\rho\left(\frac{\partial u}{\partial t}+u\frac{\partial u}{\partial x}+w\frac{\partial u}{\partial z}\right)$$

$$\alpha\rho g_z-\frac{\partial P}{\partial z}+\frac{\partial\tau_{xz}}{\partial x}+\frac{\partial\tau_{zz}}{\partial z}=\alpha\rho\left(\frac{\partial w}{\partial t}+u\frac{\partial w}{\partial x}+w\frac{\partial w}{\partial z}\right) \tag{2}$$

Where $g_x$ and $g_z$ are the components of acceleration due to gravity in lengths x and z respectively is the pressure, α is the fraction of fluid, $\rho$ is the fluid density, u and w are the velocity components in the length. Meanwhile,$\tau_{xx}$, $\tau_{zz}$ and $\tau_{xz}$ are viscous stresses, which are proportional to the element strain rates and coefficient of viscosity as follows :

$$\tau_{xx}=2\mu\frac{\partial u}{\partial x}$$

$$\tau_{zz}=2\mu\frac{\partial w}{\partial z} \tag{3}$$

$$\tau_{xz}=\tau_{zx}=\mu\left(\frac{\partial w}{\partial x}+\frac{\partial u}{\partial z}\right)$$

The free surface profile is calculated using the Volume of Fluid Model. The VOF formulation relies on the fact that two or more fluids are not interpenetrating. The fluid volume fraction is denoted by function α(x,y,t). The computational cells can be classified as empty, full, or partially filled with fluid. The fluid fraction for each cell in the computational domain varies from zero to one, depending on the quantity of fluid in the cells. Thus, when α = 1, show a cell filled by fluid and α = 0 correspond void region, and for 0<α<1 the cell contains interface between the fluid and other fluid. The tracking of free surface is accomplished by solution of continuity equation for volume fraction function, the equation has the following form:

$$\frac{\partial\alpha}{\partial t}+\frac{\partial(\alpha u)}{\partial x}+\frac{\partial(\alpha w)}{\partial z}=0 \tag{4}$$

To consider the turbulence effects on the flow field, the renormalization group (RNG) model is utilized. The RNG based turbulence model is derived from the instantaneous Navier-Stokes equations, using a mathematical technique called "renormalization group" (RNG) methods. The analytical derivation results in a model with constants different from those in the standard model, and additional terms and functions in the transport equations for turbulent kinetic energy (k) and rate of dissipation of kinetic energy (ϵ).The RNG model improves the accuracy by adding additional term in ϵ-equation and RNG model provides an analytically derived differential formula for effective viscosity that accounts for low Reynolds number effects. The following are the transport equations for calculating turbulent kinetic energy (k) and rate of dissipation of kinetic energy (ϵ):

$$\frac{\partial k}{\partial t} + \frac{1}{V_F}\left(uA_x\frac{\partial k}{\partial x} + wA_z\frac{\partial k}{\partial z}\right) = P_T + Diffr - \epsilon$$

Where k is turbulent kinetic energy and $P_T$ is the turbulent kinetic energy production. The diffusion term is as follows
:

$$P_T = \frac{\mu}{\rho V_F}\left\{2A_x\left(\frac{\partial u}{\partial x}\right)^2 + 2A_z\left(\frac{\partial w}{\partial z}\right)^2 + \left(\frac{\partial u}{\partial z} + \frac{\partial w}{\partial x}\right)\left(A_z\frac{\partial u}{\partial z} + A_x\frac{\partial w}{\partial x}\right)\right\}$$

The diffusion term is:

$$Diffr = \frac{1}{V_F}\left\{\frac{\partial\left(v_k A_x\frac{\partial k}{\partial x}\right)}{\partial x} + \frac{\partial\left(v_k A_z\frac{\partial k}{\partial z}\right)}{\partial z}\right\}$$

Where $v_k$ is the diffusion coefficient computed based on the local value of the turbulent viscosity. The transport equation for rate of dissipation of kinetic energy is as follows:

$$\frac{\partial k}{\partial t} + \frac{1}{V_F}\left(uA_x\frac{\partial \epsilon}{\partial x} + wA_z\frac{\partial \epsilon}{\partial z}\right) = \frac{C_1\epsilon}{k}(P_T + C_3.G) + Diff_\epsilon - C_2.\frac{\epsilon^2}{k}$$

The diffusion term of rate of dissipation, $Diff_\epsilon$ is as follows:

$$Diff_\epsilon = \frac{1}{V_F}\left\{\frac{\partial\left(v_\epsilon A_x\frac{\partial \epsilon}{\partial x}\right)}{\partial x} + \frac{\partial\left(v_\epsilon A_z\frac{\partial \epsilon}{\partial z}\right)}{\partial z}\right\}$$

Here $C_1$, $C_2$, $C_3$ are all dimensionless parameters that are equal to 1.42, 1.68 and 0.2, respectively, for RNG model.

### 1.2 Numerical Simulation

A flow with incompressible and unsteady state condition and viscose effects was considered in this study. The two dimensional Reynolds Averaged Navier-Stokes equation in incompressible form of mass and momentum equations was applied to determine the flow parameters.
The level of detail generated by the program depends on the shape of the geometry, the type of mesh grid used and quality of mesh grid. The mesh grid is adjusted to achieve skewness factor less than 0.9,element quality near to 1,and aspect ratio near to 1 in order to get good quality mesh.

Generally, the steps taken to develop the model in Ansys Fluent were:
1. Create the geometry of the flume,
2. Generate the geometry grid,and
3. Define the boundary conditions,

After this step in development, the geometry, mesh and boundary conditions could be applied to the model according to the boundary conditions taken.

**Table 1**
**Boundary conditions on geometrical boundaries for the flume**

| Boundary Condition | Type |
|---|---|
| **Inlet** | Pressure Inlet |
| **Bed** | Wall |
| **Sidewalls** | Wall |
| **Outlet** | Pressure Outlet |
| **Interior Material** | Fluid |

The VOF method was used to determine the water surface profile by calculating the water level in each control volume . The VOF of water, when $\alpha = 1$, show a cell filled by fluid and $\alpha = 0$ correspond void region, and for $0<\alpha<1$ the cell contains interface between the fluid and other fluid. The grid geometry used in the VOF method, where the domain extends from 0 to 1, is shown in Fig. 2.

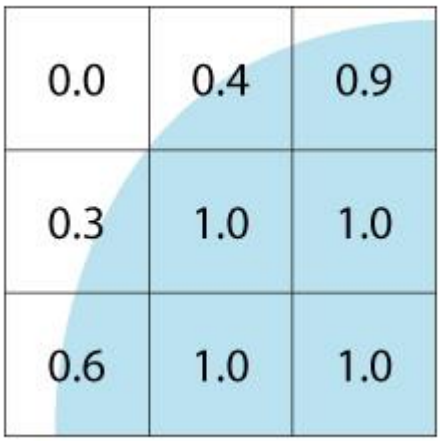



**Fig.1 Volume of Fraction Mesh**

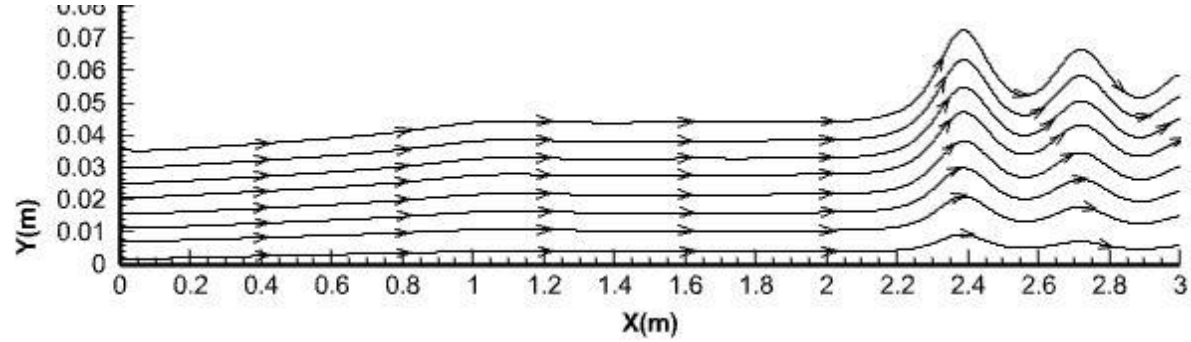
Specific parameters of the numerical model must be changed to suit the boundary conditions before it can be solved: the state of the flow must be set to transient, components of acceleration due to gravity should be given, the RNG k-$\epsilon$ turbulence model was selected to calculate effects of turbulence , pressure discretization was applied as the flow is gravity driven, first-order discretization was employed for the momentum, dissipation and turbulence kinetic energy equations, and PISO pressure–velocity coupling was used for simulation. Required number of time step and number of iterations per time step is given for the calculation.

## 2. Results

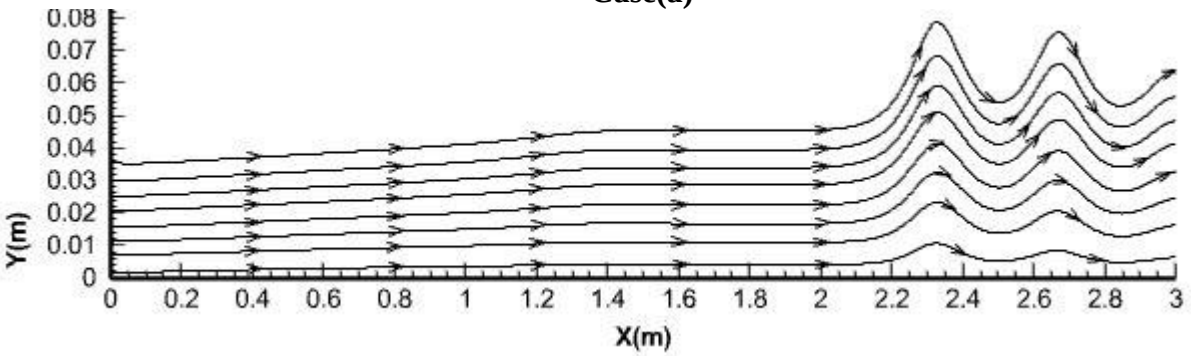
Different types of undular hydraulic jump with different values of Froude number are simulated. Characteristics of the simulation are listed in the table below-

| Case | Discharge($m^3/s$) | Upstream Froude Number | Time Step Taken(s) |
|---|---|---|---|
| (a) | 0.031 | 1.411 | 0.01 |
| (b) | 0.033 | 1.495 | 0.01 |
| (c) | 0.035 | 1.577 | 0.01 |

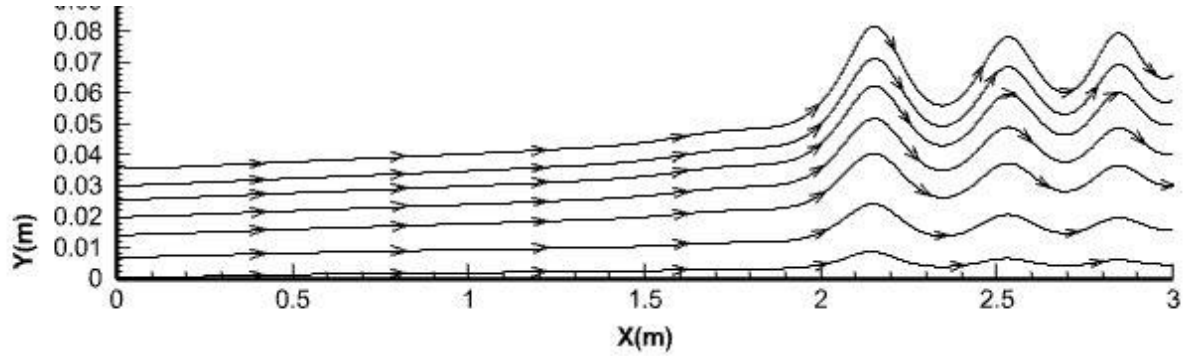
The boundary conditions of the simulations are show in table 1.The upstream flow rate for different undular hydraulic jumps are $0.031m^3/s$, $0.033m^3/s$ and $0.035m^3/s$. The pressure discretization was used as the flow was gravity driven and the PISO pressure-velocity coupling was used to simulate. The RNG k-ϵ turbulence model was used to simulate the turbulence effects.




**Case(a)**




**Case(b)**




**Case(c)**

**Fig.2 Streamlines for various cases**

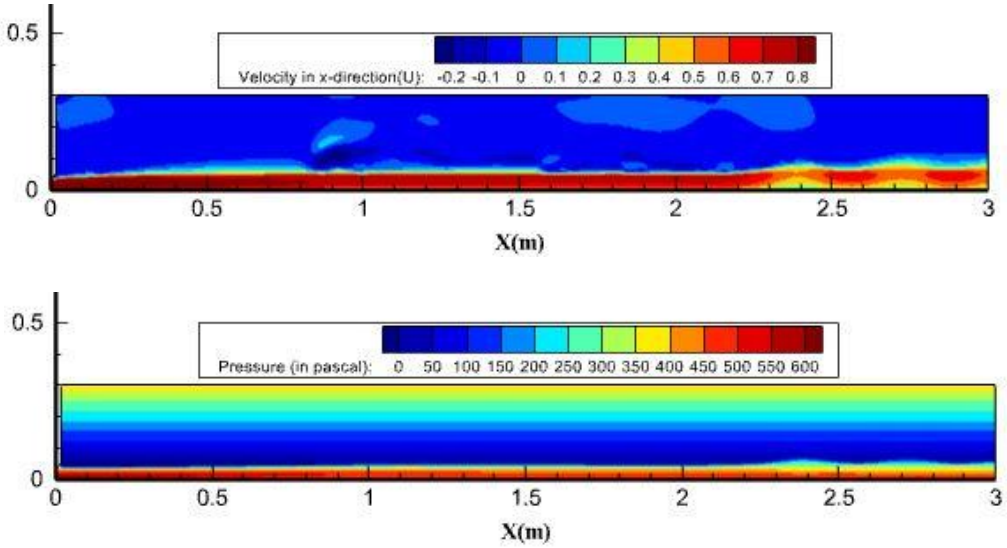



**Fig.3 Velocity and Pressure Contour For Case (a)**

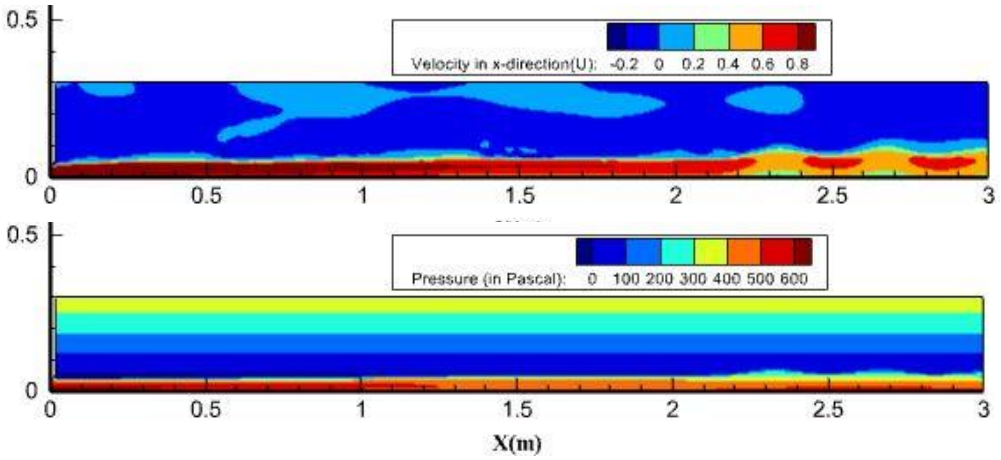



**Fig.4 Velocity and Pressure Contour For Case (b)**

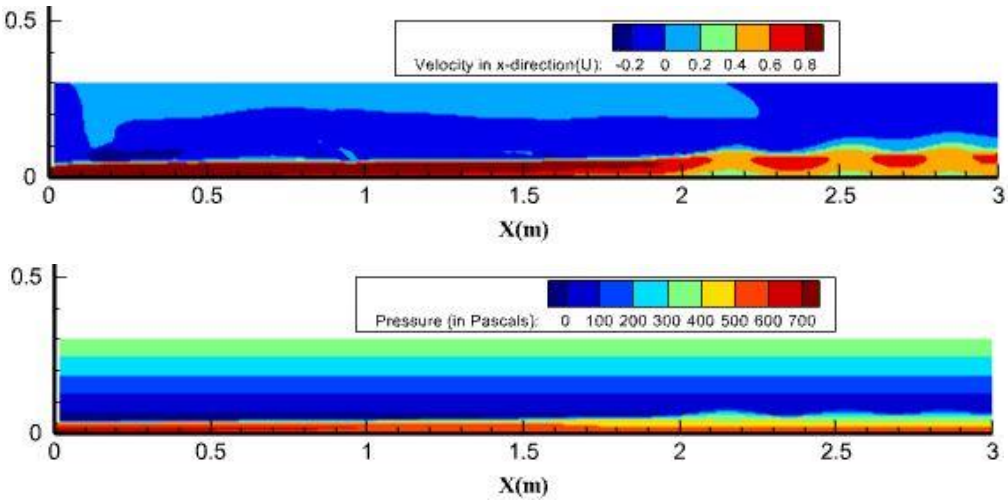



**Fig.5 Velocity and Pressure Contour For Case (c)**

The streamlines show the curvature and flow path of the flow. Streamlines for various cases are shown in figure 2.From the figure we can observe that the undular jumps distance from the inlet is decreasing with increase in rate of flow. The height of the waves generated, increase with increase in rate of flow. In all of the above cases we can observe highest velocity occur at the trough of the wave and in flow

before the undular jump. The variation of the pressure is not hydrostatic in the jump due to curvature of the streamlines. The variation of the pressure is different for concave and convex curves of the streamline.

.

## 3. Conclusion

Hydraulic jump occur when flow transition takes place from supercritical flow to subcritical flow. When the supercritical upstream flow, Froude number is near unity undular hydraulic jump occurs during transition from supercritical flow to subcritical flow. In this study an attempt is made to simulate undular hydraulic jump on smooth bed in Ansys Fluent using Volume of fraction method, pressure discretization and PISO velocity-pressure coupling. The undular hydraulic jump was simulated for three different discharges, it was found that the velocity was highest at trough of the wave and the pressure variation was not hydrostatic in wave.

## References

1. Fatemeh Roatami,Mahdi Shahrokhi, Md Azlin Md Saod, Saeed Reza Sabbagh Yazdi, Numerical simulation of undular hydraulic jump on smooth bed using volume of fluid method
2. Fatemeh Rostami, Saeed Reza Sabbagh Yazdi, Md Azlin Md Said and Mahdi Shahrokhi, Numerical simulation of undular hydraulic jumps on graveled bed using volume of fluid method.
3. H.Chanson,Characterstics of Undular Hydraulic Jumps,Comparison with near critical flows,University of Queensland,Australia,Dept. of Civil Engineering,1995.
4. H.Chanson,J.S.Montes,Characterstics of Undular Hydraulic Jumps, Experimental Apparatus and Flow Pattern,J.Hydraul. Eng-ASCE 121 (1995)
5..Hans G. Hornung, Christian Willert, Stewart Turner, The flow field downstream of a hydraulic jump.
6. I. Ohtsu, Y. Yasuda, H. Gotoh, Flow conditions of undular hydraulic jumps in horizontal rectangular channels.
7. J.S.Montes,A study of the undular jump profile.
8. J.S.Montes,Undular hydraulic jump-discussion,J.Hydraul. Division,ASCE 105 (1979) 1208-1211.
9. M.B. Abbott, G.S. Rodenhuis, A numerical simulation of the undular hydraulic jump
10. Shaymaa Abdul Muttaleb Al-Hashumi, Khitam Abdulhussein Saeed, Thameen N. Nahi, Experimental and CFD modeling of Hydraulic jumps forming at submerged Weir.
11. Wilhelm Schneider , Richard Jurisits , Yee Seok Bae, An asymptotic iteration method for the numerical analysis of near-critical free-surface flows.
12. Ven Te Chow, Open-Channel Hydraulics.
13. Frank M.White, Fluid Mechanics.

*IN PROCEEDINGS OF 25th HYDRO 2020, INTERNATIONAL CONFERENCE, NATIONAL INSTITUTE OF TECHNOLOGY ROURKELA, ODISHA, INDIA 26-28, March 2021, ISBN 978-93-90631-56-8*

Paper ID - 471

# Numerical modelling in shoreline evolution prediction: case study of inlet channel at Kasargod, Kerala

Jiweshwar Sinha[1], S.N. Jha[2], Vaibhawi Roy[3], Prabhat Chandra[4]

*[1]Scientist D, [2]Assistant Research Officer , [3]Research Assistant and [4]Scientist E*
*Central Water and Power Research Station, Pune – 411 024, India Email: jsinha_cwprs@yahoo.com*

## Abstract

Longshore sediment transport comprising complex phenomena is an important factor in shoreline change in response to marine structures. Longshore sediment is mainly driven by waves rather than tides and ocean currents. Prediction of beach morphological changes is of paramount importance for various coastal engineering projects and proper management of coastal zone. In the present study, mathematical modelling is applied for prediction of shoreline evolution for the proposed 700 m curve shaped extension of North breakwater in the inlet channel at Kasargod, Kerala located at confluence of the northern creek and the downstream of the river Chandragiri. The study includes evaluating historic shoreline performance and changes in its behavior. The paper demonstrates that LITPACK package developed by DHI could be successfully applied to reproduce the natural conditions and altered conditions due to manmade implementation in the shoreline environment. The LITDRIFT module showed annual longshore sediment transport. The LITLINE module predicted the shoreline morphological evolution. Shoreline evolution of the proposed scenario after 2 years, 4 years, 6 years and 10 years are gradually enhancing. As per model simulation, after 10 years cross-shore movement in northern side is about 355 m and in southern side about 72 m.

***Keywords:*** *Fishing harbour; wave; creek inlet; shoreline; longshore transport*

## 1. Introduction

Coastal zones are the most dynamic regions due to the continuous wave action and the direction of wave attack resulting into the complex phenomena of littoral transport. When marine structures such as groins, breakwaters are built in the nearshore regions, they block the natural longshore transport of sand creating scarcity of sand in the down-drift direction and sand deposition in the up-drift direction and causing imbalance in the nature at those regions.

There are many methods and tools to study littoral drift distribution and shoreline change in coastal engineering. A number of different models have been developed to simulate littoral drift distribution and shoreline change since the first model was proposed by Pelnard-Considère in 1956 (Dean 2002). There are several commercially available models for the short /medium term prediction such as (Delft, 1993; Vriend, 1987 and Broker et. al., 1991). Among them GENESIS, UNIBEST, LITPACK are the popular 1-D models being widely used by the majority of researchers. Several literatures are available reporting the Longshore sediment transport rates for different coastal regions of the Kerala coast. The annual net transport of 0.3 million $m^3$ (southward) and the gross transport of 0.7 million $m^3$ was estimated for Manjeshwar coastal regions located at about 30 km north of the present study area of Kasargod as per the previous study at CWPRS. Based on studies carried out at CWPRS the annual net and the gross transports of 0.413 million $m^3$ and 0.649 million $m^3$, respectively was estimated for Ajanur coastal regions which is about 20 km south of Kasargod. Other literatures (Sajeev et al., 1997; Sanilkumar et al., 2006) are available wherein longshore sediment transport rate of nearby locations is mentioned. They estimated annual the net and the gross transport of 0.736 million $m^3$ and 0.958 million $m^3$ (southward), respectively at Kozikode coastline.

Kasargod Fishing Harbour is situated at the northern bank of the river Chandragiri at the confluence of the northern creek and the downstream of the river Chandragiri at Kasargod, Kerala. Location map of the study area is shown in Figure 1. At present two breakwaters having length 530 m (northern) and

570 m (southern) are existing across the inlet channel of width 100 m to facilitate navigation of fishing vehicles such as trawlers, boats etc. Another fishing harbour is located at about 450 m north of the northern breakwater in the western side of the creek. Figure 2 shows the present status and position of the inlet channel at Kasargod.




**Figure 1** Location map of the study area




**Figure 2** Present status of the inlet channel

Past history of the inlet channel shows that due to the littoral transport prevailing at the site, the inlet was getting shifted along the shore towards north upto about 700 m from its present position. It further shows that the width of the northern and the southern shorelines varies in the range of 100-300 m and 75-450 m, respectively in cross-shore direction. Figure 3 presents the past behaviour of the inlet channel. Post construction of both the breakwaters and the closure of the natural northern channel, it is observed that the maneuvering of fishing vehicles through the inlet channel is getting difficult due to the wave and current actions near the entrance of the inlet causing sedimentation in the channel and around both the breakwaters as observed in Figure 2.




(a) Before the year 2009 (b) During the year 2016

**Figure 3** Past status and position of the inlet channel

A curved breakwater of 700 m (Figure 4) was evolved at CWPRS through wave tranquility studies for providing necessary tranquility at the entrance and in the harbour area. This paper demonstrates the suitability of this breakwater layout to restrict entering of littoral sediment into the channel and on the shore line changes.

## 2. Site conditions and input data

For simulation of littoral drift distribution and shoreline changes, nearshore wave data is essential. In the present study, wave data observed by ships plying in offshore region of Kasargod fisheries harbour reported by India Meteorological Department (IMD) during the past 30 years were used to arrive at nearshore wave data. Analysis of wave climate data for the entire year indicated that predominant wave directions in deep water were from SSW to NNW with the maximum wave height of the order of 4.5 m.

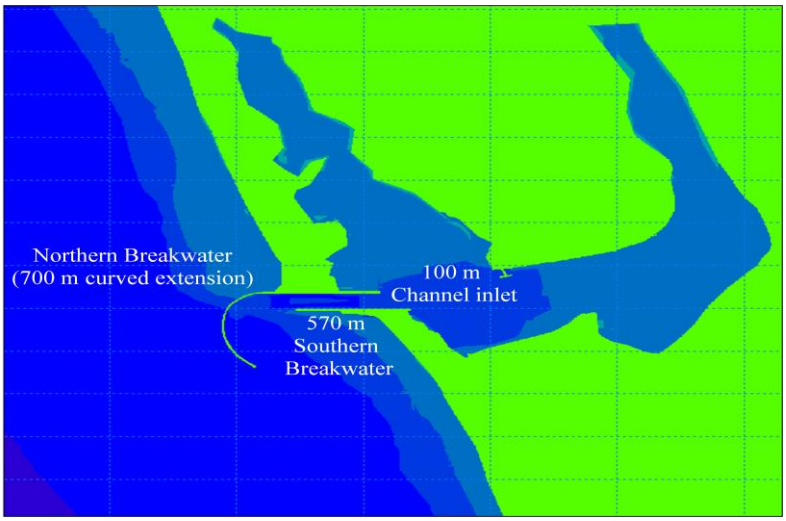



**Figure 4** Proposal with Extension of northern breakwater

Predicted tide at Kasargod reveals that spring and neap tidal range is of the order of 1.6 m and 1.0 m respectively. Bathymetric data of offshore region were taken from CMAP database which shows that bed slope is mild (1:500) and contours are parallel to the shoreline. Bed sediment of the upstream

river area is mostly of fine sand type with mean diameter ($D_{50}$) falling in the range of 0.4 mm to 0.75 mm whereas, it is silt-clayey in the sea portion.

## 3. Modelling techniques

For wave transformation from deep water to nearshore region, the MIKE 21 Spectral Wave (SW) model was used. The model is capable of simulating the growth, decay and transformation of wind generated waves and swells in both offshore and coastal areas, which takes into account coastal phenomena like wave growth by influence of wind, non-linear wave-wave interaction, diffraction effects, dissipations due to white-capping, bottom friction and depth-induced breaking.

In order to simulate littoral drift distribution and shoreline changes, LITDRIFT and LITLINE modules of LITPACK software is used. In LITDRIFT module, the cross-shore distribution of longshore current, wave height and setup for an arbitrary beach profile are computed by solving the longshore and cross-shore momentum balance equations. The annual sediment budget is calculated based on the contribution of transport from each of the wave incidents occurring during the year. LITLINE calculates coastline evolution by solving continuity equation for sediment in the littoral zone. The basic input data for running the model are the longshore relative coastline alignment, cross-shore profile description and bathymetry, active depth of transport and depth contour angles at each grid point, environmental data with wave properties, tidal currents and water levels position and size of structures etc.

## 4. Model setup

An area of 200 km alongshore and 50 km cross-shore upto -10 m depth contour with an unstructured mesh was considered for simulation of MIKE 21 SW model. The model was run for incident wave of wave height 4.5 m for all the predominant wave directions in deep sea.
Using LITDRIFT module, littoral drift was simulated for beach profile of 3.5 km extending upto about -10.0 m depth contour. Profile was discretized into 350 grid points with uniform grid size of 10 m.

For shoreline evolution (LITLINE) model, shoreline of 10.0 km length was considered. The length was divided into 1000 grid points with uniform grid size of 10 m. Projection of the proposed extension of northern breakwater was taken for evolution of the shoreline. The model was run with the schematic layout for a period of 10 years.

## 5. Results and discussions

The nearshore wave climate during the entire year (shown in Figure 5) obtained from MIKE 21 SW model indicates that predominant wave directions are SSW to WNW with the maximum wave height of the order of 3.5 m from West direction with percentage of occurrence 23%.

The general orientation of coastline at Kasargod is NNW-SSE making an angle of about $337^0$ N. The model was simulated for the cross-shore profile for the annual wave climate. The transport rate is reported in the Table 1 and its distribution is shown in Figure 6.

**Table 1** Annual transport rate (million $m^3$)

| Period | Net | Gross | North | South |
|---|---|---|---|---|
| Annual | 0.188 | 0.359 | 0.086 | 0.274 |

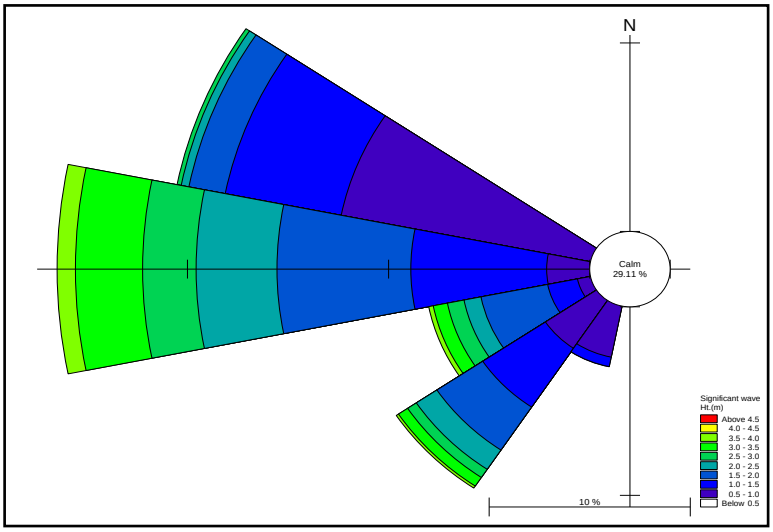



**Figure 5** Wave Rose at Kasargod for Annual Period (Jan-Dec)

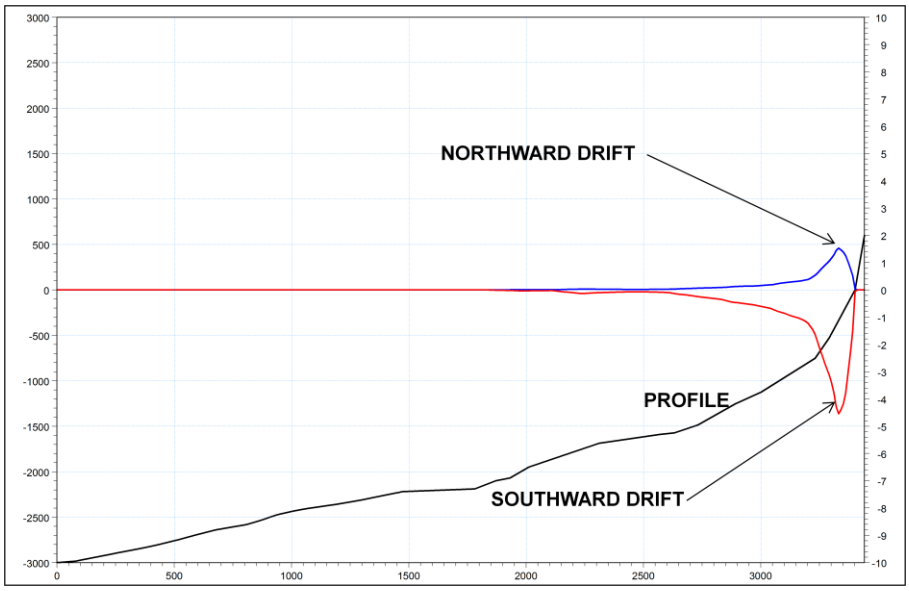



**Figure 6** Profile and Cross-shore distribution of littoral transport for annual period

It could be seen from the table and from the figure that the annual northward and southward drift are 0.086 million $m^3$and 0.274 million $m^3$, respectively while the net and the gross transports are 0.188 million $m^3$ and 0.359 million $m^3$, respectively. The net transport is towards south. The distribution of littoral transport rates indicates that the sediment drift moves within a range of 750 m from the shoreline as the cross-shore profile has mild slope. Further, it could also be seen that the peak transport occurs at about 150 m from the shoreline and about 75% transport occurs between 0 m to 350 m from shoreline i.e. between +0.0 to –3.0 m depth contours.

The predicted shoreline change obtained from the model simulation is shown in Figure 7. Being net transport towards south, the deposition on north side of the northern breakwater is noticed. Model was simulated subsequently for a period of 2, 4, 6, 8 and 10 years and maximum cross-shore advancement for each period was obtained as 128 m ,208 m, 268 m, 316 m and 355 m respectively from the prevailing coastline position on northern side of the extended north breakwater (see Figure 7).

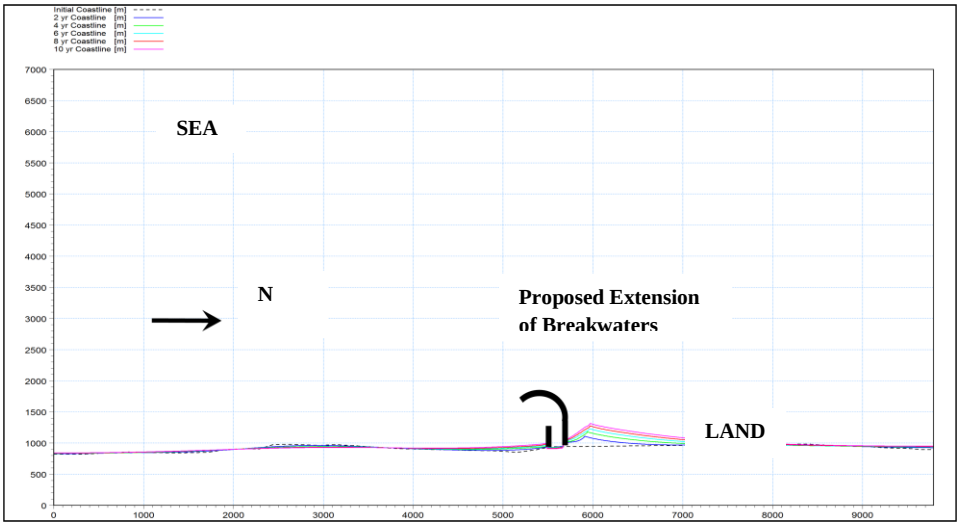



**Figure 7** Shoreline evolution at 2nd, 4th, 6th, 8th, 10th year

Also, the maximum cross-shore advancement for a period of 2, 4, 6, 8 and 10 years was obtained as 12 m, 25 m, 42 m, 57 m and 72 m respectively on the south of the southern breakwater. Further, the corresponding longshore effect of deposition in northern and southern sides was felt for a length of about 2.53 km and 1.8 km, respectively.

## 5 Conclusions

Mathematical model studies have been carried out to estimate littoral drift distribution at the inlet channel at Kasargod of Kerala state. Following are the main conclusions obtained from the present studies:

1) Annual southward and northward transports are computed to be 0.274 million cum and 0.086 million cum, respectively with the net and the gross transports being 0.188 million cum and 0.359 million cum, respectively. Net longshore transport is towards south.

2) Based on the distribution of annual longshore transport, the transport is confined within a range of 1000 m from shoreline and southward transport is more than northward transport. The peak transport occurs at about 150 m from the shoreline and about 75% transport occurs between 20 m to 500 m from shoreline i.e. between +0.0 to –3.0 m depth contours..

3) Significant quantity of sediment movement due to littoral drift occurs within a reach of 500 m from the shoreline, the extension of the existing breakwater by about 700 m in a semi-circular shape (i.e. upto about -5.8 m depth contour) at Kasargod inlet is found to be suitable.

4) As the net transport is directed towards south, deposition is expected on north side of the northern breakwater. After a period of for a period of 2, 4, 6, 8 and 10 years and maximum cross-shore advancement for each period would be obtained as 128 m ,208 m, 268 m, 316 m and 355 m respectively from the prevailing coastline position. The corresponding longshore effect on northern side of the breakwater would be felt upto 2.83 km. Further, due to extension of northern breakwater in semi-circular shape, a mild deposition is also expected on the south of the southern breakwater. For a period of 2, 4, 6, 8 and 10 years maximum cross-shore advancement in the southern side for each period would be obtained as would be obtained as 12 m, 25 m, 42 m, 57 m and 72 m respectively from the prevailing coastline position.

## Acknowledgement

The authors are grateful to Shri A.K. Agrawal, Director, CWPRS for his guidance. The authors express their deep gratitude for according permission to publish this paper. The authors are thankful to the Project Authority for providing data during the course of the study.

## References

LITPACK (2005), An Integrated Modelling System for Littoral Processes and Coastal Kinetics, Danish Hydraulic Institute.
MIKE 21 SW (2013), User manual, Danish Hydraulic Institute (DHI), Denmark.
Sajeev R., P. Chandramohan, V. Josanto, and V. N. Sankaranarayanan. (1997), 'Studies on sediment transport along Kerala coast, south west coast of India' Indian Journal of Geo-Marine Sciences 26:11–15.
SanilKumar, V., Pathak, Pednekar, P., K. C., Raju, N. S. N and Gowthaman, R., (2006), 'Coastal Processes along the Indian Coastline', Current Science, Vol. 91, pp 530 - 536.
Dean, R. G. 2002. Beach nourishment theory and practice, advanced series on ocean engineering – Volume 18. River Edge, NJ: World Scientific Publishing.
Delft (1993). "UNIBEST user's manual". Version 4.0. Delft Hydraulics Laboratory, The Netherlands.
Vriend, H.J. (1987). "2DH mathematical modelling of morphological evolutions in shallow water". Coast. Engg., 11, pp. 1–27.
Broker, H.I., Deigaar, R. and Fredsoe, J. (1991). "Onshore/offshore sediment transport and morphological modelling of coastal profiles". Coastal Sediment, ASCE.

# Theme XV

# Sediment Transport

*IN PROCEEDINGS OF 25th HYDRO 2020, INTERNATIONAL CONFERENCE, NATIONAL INSTITUTE OF TECHNOLOGY ROURKELA, ODISHA, INDIA 26-28, March 2021, ISBN 978-93-90631-56-8*

Paper ID - 059

# Breakwater construction effects on hydrodynamics and sedimentation pattern in open coast

A K Singh1 Naval S Jagatap2 L.R.Ranganath3 J.D.Agrawal4

*1Scientist B, Central Water and Power Research Station, Pune- 411 024, India.*
*2Research Assistant, Central Water and Power Research Station, Pune- 411 024, India.*
*3 Scientist D, Central Water and Power Research Station, Pune- 411 024, India.*
*4 Scientist E, Central Water and Power Research Station, Pune- 411 024, India.*
*Email: dak_singh@rediffmail.com*

## Abstract

A coast is a geological system that is subject to constant movement and change. Shorelines, beaches, and coastal areas in effect affect human lives, and vice versa Sediment transport driven by current, wind and wave plays an important role in influencing the evolution of offshore and onshore bed morphologies by deposition and erosion. Government of Karnataka is keen to expand the fishing harbours and fish landing centres to give a new dimension to the livelihood of the fishing community. Hangarkatte Port lies at latitude 13°26'40.04"N and 74°42'8.09"E, at the mouth of Sitanadi and Swarra River at Hangarkatte in Udupi District. At present the navigation of this port is through sand bar. By construction of suitable breakwater and river training walls it is possible to develop this port into a regular all-weather port which will also serve as a fishing harbor.

Hydrodynamics and sedimentation studies were conducted using MIKE 21 HD FM and MIKE 21 MT sediment transport models to study the tidal hydrodynamic behavior of flow and probable siltation pattern in the area of the proposed development of fish landing center at Hangarkatte and Kodibengre. The sea mouth entrance region opposite to Hangarkatte jetty acts as an approach for the two locations Hangarkatte and Kodibengre from the open sea. This inlet region has shallow patches and boats have difficulty to enter the estuary. To improve the navigation condition, it is proposed to a construct breakwater so as to give protection to Hangarkatte jetty. A proposed layout with two parallel breakwaters at the River mouth was studied and was found to be helpful to facilitate safe navigation of fishing boats and to keep the mouth, free from sand deposition. Sedimentation studies with Proposed layout indicated that the zone of deposition is mainly in the northern and southern side of the proposed breakwater as the two parallel breakwaters 950m (northern break water) and 680m (southern breakwater) are extended beyond the littoral zone (-3m contour) and also a slight tendency of erosion inside the inlet entrance is seen towards the offshore region which ranges from 5 to 10cm.

From the hydrodynamic studies it was observed that with the proposed layout, consisting of parallel breakwaters with 200 m opening and dredging the channel and basin to -3m the current magnitude in the channel increased facilitating natural flushing of the channel to some extent. Sedimentation studies reveal that the maintenance dredging tends to increase in the basin area due to dredging upto -3m depth. The annual deposition of siltation is expected, as the velocities are weak compared to the existing condition at the fish landing area. This tendency of sediment deposition in the harbor basin needs to be tackled by maintenance dredging. Hence, based on the model studies the proposed layout is recommended for the development of fish landing centers at Hangarkatte, Udupi, Karnataka.

***Keywords:*** *hydrodynamics, sedimentation, harbor, dredging, breakwater*

## 1. Introduction

About more than 90% of India's trade by volume is conducted via the country's maritime route, there is a continuous need to develop India's ports and trade related infrastructure to accelerate growth in the manufacturing industry and to assist the 'Make in India' initiative. India has 13 major ports and approximately 200 non-major ports administered by Central and State Governments respectively. The demand for its ports and trade infrastructure will continue to mount as trade diversifies and grows, making a compelling case for the rapid and efficient expansion of India's port sector.

Karnataka's coastline called Karavali stretches 300 km between Mangalore in Dakshina Kannada district and Karwar in Uttara Kannada district. Udupi is a coastal District towards the south-west of the state of Karnataka. The major fishing places in Udupi are Malpe, Hejamadi, Hangarkatte and Gangolli. Hangarkatte is a minor sea-port mainly used for fishing purpose. Government of Karnataka is keen to expand the fishing harbours and fish landing centers to give a new dimension to the livelihood of the fishing community. Hangarkatte is a minor sea-port mainly used for fishing

purpose. Hangarkatte Port lies at latitude 13°26'40.04"N and 74°42'8.09"E, at the mouth of Sitanadi and Swarra River at Hangarkatte in Udupi District as shown in Figure 1.

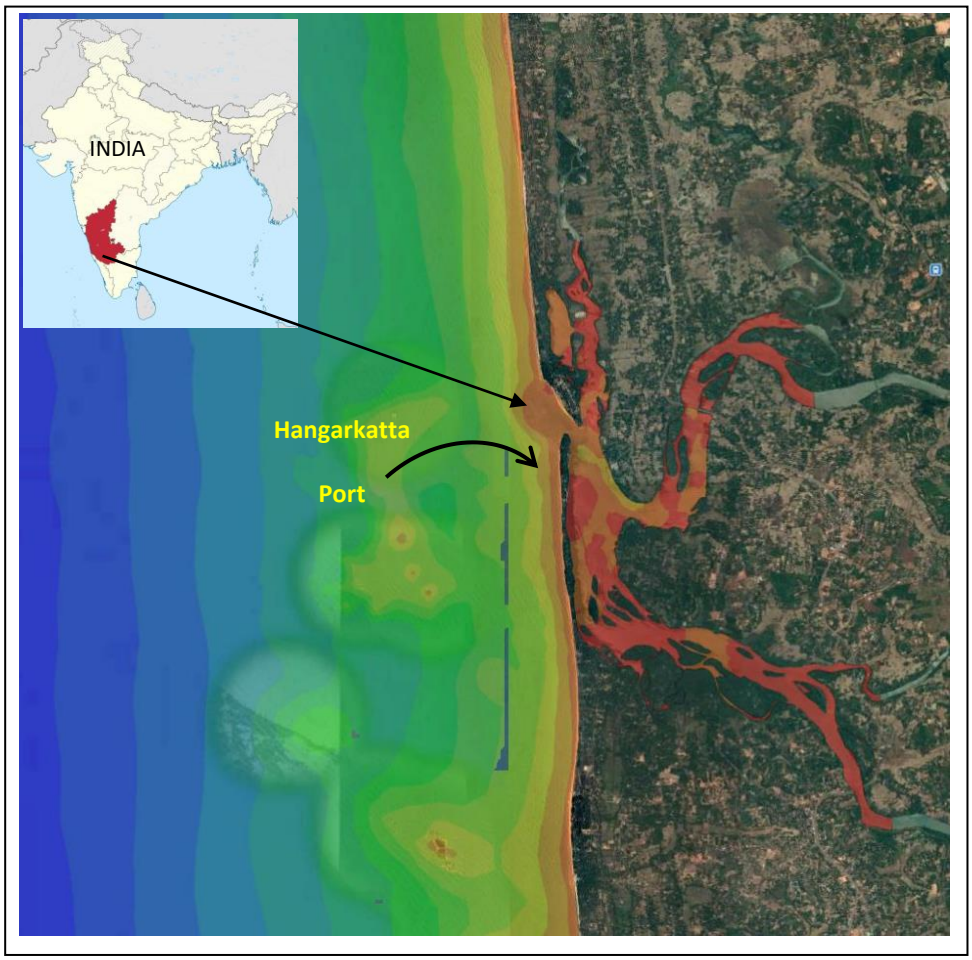



**Figure 1** Location map

In order to extend the port capacity and to develop a fishing harbour the navigation of the vessels entering and leaving should be efficient. The current existing conditions hampers the navigation due to the sedimentation at the mouth. By constructing a suitable breakwater at the mouth of the sea it is possible to develop this port into a regular all-weather port which will also serve as a fishing harbor.

## 2. Methodology

The sea mouth entrance region opposite to Hangarkatte jetty acts as an approach for the two locations Hangarkatte and Kodibengre from the open sea. This inlet region has shallow patches and boats have difficulty to enter the estuary. To improve the navigation condition, it is proposed to a construct breakwater so as to give protection to Hangarkatte jetty and approaches. Parallel alignments of breakwaters to assess the flow conditions and sedimentation pattern in and around the Hangarkatte port was studies. This paper describes the mathematical model studies carried out to understand the tidal hydrodynamic behavior of flow and probable siltation pattern in the area of the proposed development of fish landing center at Hangarkatte and Kodibengre.

A 2-D mathematical model was developed incorporating the features of the project site. MIKE-21 HD model was used to simulate tidal flow pattern in the region. The sedimentation aspect was simulated using MIKE21-MT model using sediment characteristics at the site. The model was calibrated both for hydrodynamic aspect for the existing condition using the filed observed data. The hydrodynamic model studies include simulation of flow field for the existing conditions as well as with the proposed layout of breakwaters. These model studies help us in evaluating the probable

changes in the hydrodynamic conditions and formation of tidal circulations, if any, due to the proposed developments. The results of the tidal hydrodynamic simulation form the basic input to the integrated sediment transport model.

The mud transport model is used to simulate siltation pattern in and around the Hangarkatte Port, considering both tide induced currents. These studies predict the probable zone of siltation and erosion in and around the proposed breakwater layout.

## 3. Data analysis

### *3.1 Bathymetry*

The bathymetry data was taken from MIKE CMAP. The Bathymetry so obtained from MIKE CMAP was used in the study. Figure 2. Shows the detailed bathymetry of existing condition used for the model study.

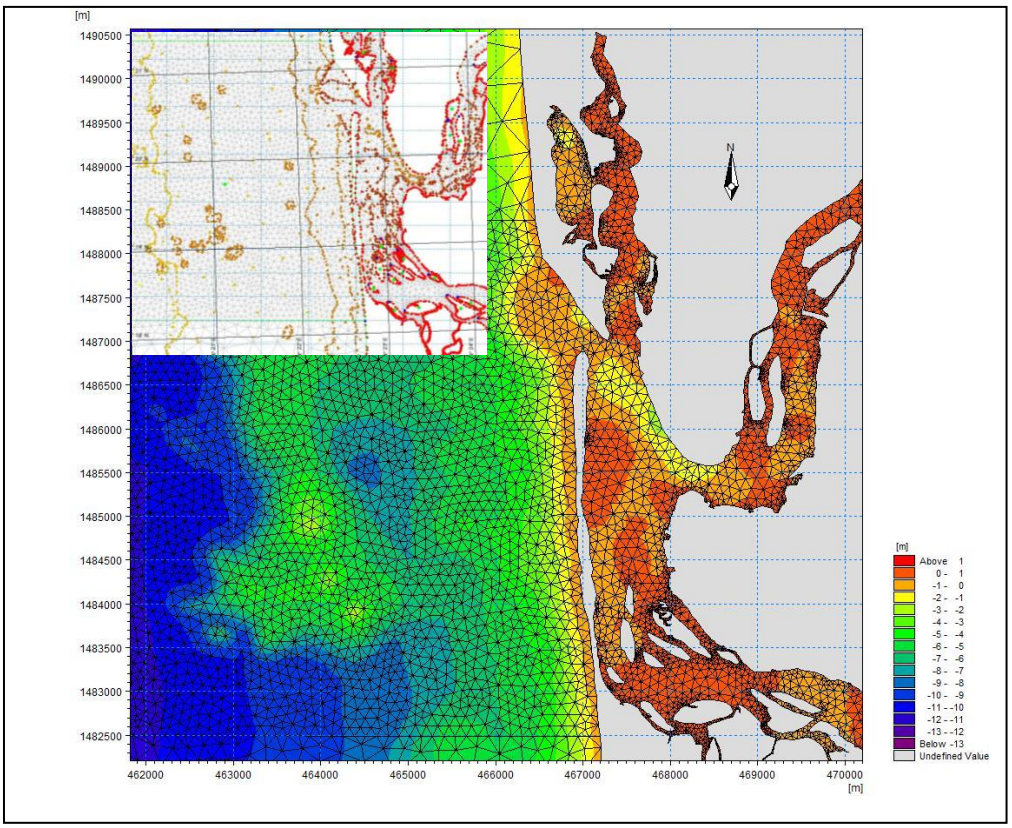



**Figure 2** Bathymetry

### *3.2 Tide Data*

Field observed tidal data was available for the period of 21 days at (74.6630°E & 13.4540°N). The data analysis indicated that the observed tidal range was 2.0m during high tide and about 0.91m during low tide and the same was considered for the model studies. Tides experienced in and around Kodibengre are of mixed semi-diurnal type having two highs and two lows with unequal amplitudes. The tide used for model studies is shown in Figure 3.

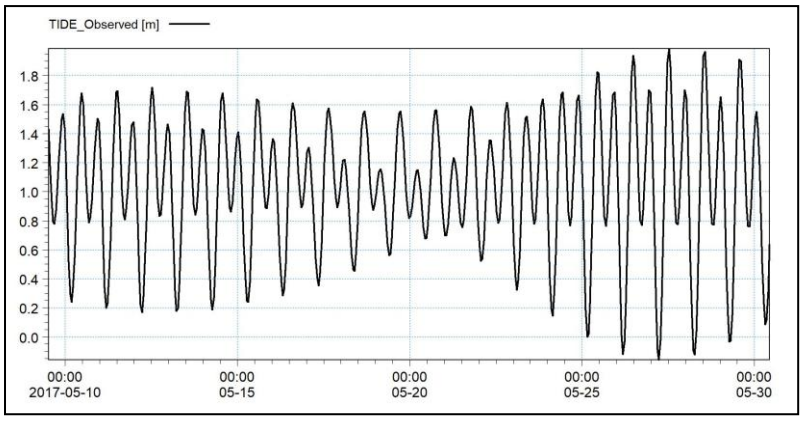



**Figure 3** Boundary tide

### *3.3 Current Data*

Currents observed at the location as shown in Figure 4, near shore currents (Longitude 74.6630°E & Latitude 13.4540°N) at a depth of 10m was measured with 10m interval.

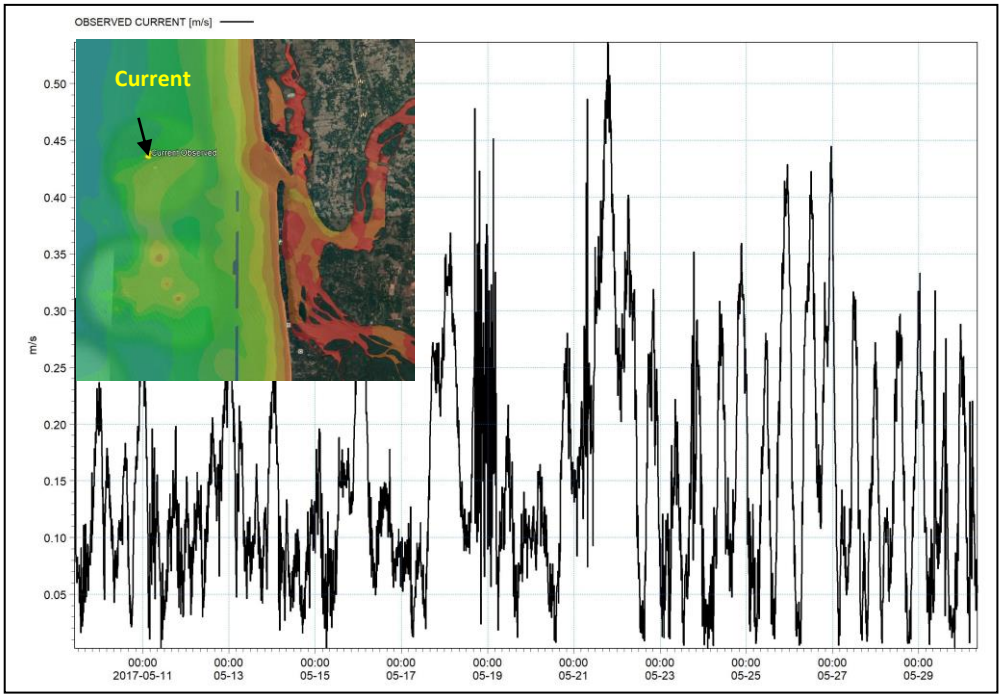



**Figure 4** Observed current speed and direction

### *3.4 Sediment Data*

Water samples were collected at three depths surface, mid and bottom twice in neap and twice in spring at low tide & high tide. The samples were analyzed during different phases of tide and water depth. The average value of 0.01kg/m3 was considered in the model studies. The average D50 value of the sediments was observed to be around 0.10mm at site, which was considered for simulation.

**Table No. 1** Suspended sediment concentration

| Spring Phase 11 May 2017 | | Neap Phase 18 May 2017 | |
|---|---|---|---|
| STATIONS | SPM(mg/l) | STATIONS | SPM(mg/l) |
| 1S | 5.2 | 1S | 11.1 |
| 1M | 8.5 | 1M | 8.2 |
| 1B | 16.5 | 1B | 5.4 |
| 2S | 7.8 | 2S | 2.4 |
| 2M | 5.6 | 2M | 2.1 |
| 2B | 16.7 | 2B | 2 |
| 3S | 3.2 | 3S | 5.2 |
| 3M | 3.2 | 3M | 3.8 |
| 3B | 9.7 | 3B | 2.2 |
| 4S | 3.1 | 4S | 10.6 |
| 4M | 4.5 | 4M | 8.1 |
| 4B | 7.6 | 4B | 6.4 |
| 5S | 4.1 | 5S | 3.6 |
| 5M | 4.4 | 5M | 2.8 |
| 5B | 20.6 | 5B | 2.1 |
| 6S | 9.4 | 6S | 4.1 |
| 6M | 3.3 | 6M | 4 |
| 6B | 12.9 | 6B | 3.8 |
| 7S | 5.0 | 7S | 9.1 |
| 7M | 4.8 | 7M | 7.8 |
| 7B | 9.4 | 7B | 6.9 |
| 8S | 4.0 | 8S | 3.5 |
| 8M | 4.2 | 8M | 3.1 |
| 8B | 14.3 | 8B | 2.8 |
| 9S | 3.2 | 9S | 6.7 |
| 9M | 3.2 | 9M | 4.1 |
| 9B | 12.2 | 9B | 3.2 |
| 10S | 4.2 | 10S | 10.8 |
| 10M | 4.2 | 10M | 9.9 |
| 10B | 17.9 | 10B | 8.2 |
| 11S | 6.8 | 11S | 9.1 |
| 11M | 4.1 | 11M | 5.1 |
| 11B | 21.5 | 11B | 4.3 |
| 12S | 3.2 | 12S | 8.9 |
| 12M | 3.2 | 12M | 8.6 |
| 12B | 12.2 | 12B | 7.4 |

## 4. Setting up of mathematical model

### 2-Dimensional Hydrodynamic Model

For any major developments in coastal areas it is necessary to know dynamics of the water body in terms of velocity and water level fluctuations beforehand. The appropriate governing equations for studying water movement in coastal areas are Shallow water equations based on 3D Governing Equations in Catresian Co-ordinates. The model is based on the situation of the three-dimensional incompressible Reynold's averaged Navier-Stokes equations, subject to the assumptions of Boussinesq and hydrostatic pressure.

The local continuity equation is written as

$$\frac{\partial u}{\partial x}+\frac{\partial v}{\partial y}+\frac{\partial w}{\partial z}= S \qquad (2.1)$$

And the two horizontal momentum equations for the x-and y- component, respectively

$$\frac{\partial u}{\partial t}+\frac{\partial u^2}{\partial x}+\frac{\partial vu}{\partial y}+\frac{\partial wu}{\partial z}=fv-g\frac{\partial \eta}{\partial x}-\frac{1}{\rho_0}\frac{\partial p_a}{\partial x}-\frac{g}{\rho_0}\int_z^n \frac{\partial p}{\partial x}dz-\frac{1}{\rho_0 h}\left[\frac{\partial s_{xx}}{\partial x}+\frac{\partial s_{xy}}{\partial y}\right]+$$

$$F_u+\frac{\partial}{\partial z}\left[v_t\frac{\partial u}{\partial z}\right]+u_s s \qquad (2.2)$$

$$\frac{\partial v}{\partial t}+\frac{\partial v^2}{\partial y}+\frac{\partial uv}{\partial x}+\frac{\partial wv}{\partial z}=-fu-g\frac{\partial \eta}{\partial y}-\frac{1}{\rho_0}\frac{\partial p_a}{\partial y}-\frac{g}{\rho_0}\int_z^n \frac{\partial p}{\partial y}dz-\frac{1}{\rho_0 h}\left[\frac{\partial s_{yx}}{\partial x}+\frac{\partial s_{yy}}{\partial y}\right]+$$

$$Fv+\frac{\partial}{\partial z}\left[v_t\frac{\partial v}{\partial z}\right]+v_s s \qquad (2.3)$$

Where,
t = time
x,y and z = Cartesian co-ordinates
η = surface elevation
d = still water depth
h = η+d total water depth
u,v and w = velocity components in the x,y and z direction.

$f = 2\Omega sin\Phi$, Coriolis parameter (Ω is the angular rate of revolution and φ the geographic Latitude)

Also, g is the gravitational acceleration; ρ is the density of water ; $s_{xx}, s_{xy}, s_{yx}$ and $s_{yy}$ are components of the radiation stress tensor; $v_t$ is the vertical turbulent (or eddy) viscosity; $p_a$ is the atmospheric pressure; $\rho_0$ is the reference density of water . S is the magnitude of the discharge due to point source and $(u_s, v_s)$ is the velocity by which the water is discharged into the ambient water. The horizontal stress terms are described using a gradient- stress relation, which is simplified to

$$F_u=\frac{\partial}{\partial x}\left(2A\frac{\partial U}{\partial X}\right)+\frac{\partial}{\partial y}\left[A\left(\frac{\partial u}{\partial y}+\frac{\partial v}{\partial x}\right)\right] \qquad (2.4)$$

$$F_v=\frac{\partial}{\partial x}\left[A\left(\frac{\partial u}{\partial y}+\frac{\partial v}{\partial x}\right)\right]+\frac{\partial}{\partial y}\left(2A\frac{\partial v}{\partial y}\right) \qquad (2.5)$$

Where 'A' is the horizontal eddy viscosity.

The surface and bottom boundary condition for $u, v \; and \; w$ are

At z=η:

$$\frac{\partial n}{\partial t}+u\frac{\partial \eta}{\partial x}+v\frac{\partial \eta}{\partial y}-w=0, \quad \left[\frac{\partial u}{\partial z},\frac{\partial v}{\partial z}\right]=\frac{1}{\rho_0 v_t}\left(\tau_{sx},\tau_{sy}\right) \qquad (2.6)$$

At z=-d:

$$u\frac{\partial d}{\partial x}+v\frac{\partial d}{\partial y}+w=0, \quad \left[\frac{\partial u}{\partial z},\frac{\partial v}{\partial z}\right]=\frac{1}{\rho_0 v_t}\left(\tau_{bx},\tau_{by}\right) \qquad (2.7)$$

Where $\left(\tau_{sx},\tau_{sy}\right)$ and $\left(\tau_{bx},\tau_{by}\right)$ are the x and y components of the surface wind and bottom stresses.

The total water depth h can be obtained from the kinematic boundary condition at the surface, once the velocity field is known from the momentum and continuity equations. However, a more robust equation is obtained by vertical integration of the local continuity equation

$$\frac{\partial h}{\partial t} + \frac{\partial h\bar{u}}{\partial x} + \frac{\partial h\bar{v}}{\partial y} = hS + \hat{P} - \hat{E} \quad (2.8)$$

Where $\hat{P}$ and $\hat{E}$ are precipitation and evaporation rates, respectively, $\bar{u}$ and $\bar{v}$ are the depth-averaged velocities.

### *4.1 Sediment Transport Module*

The two-dimensional depth averaged sediment transport module (MIKE-21-MT) takes into account conservation of mass of sediment, depth averaged velocities, longitudinal dispersion coefficient, lateral diffusivity, settling velocity, critical deposition stress, and critical erosion stress for the given sediment. A simple explicit, upstream finite volume technique is used to solve this advection diffusion equation. The model takes into account the currents generated due to waves along the littoral zone. The rates of deposition and erosion are computed based on the critical shear stress condition. In case of significant bed load movement, the model takes into account the additional sediment source in the transport equation. Thus, the model considers the total load while predicting the morphological changes.

The calibration of sediment transport model is difficult because morphological changes are too slow and temporal bed changes are too variable to measure anything significant for comparison. The sediment fluxes at various locations may differ and the following factors contribute to these variations:

- unsteadiness of flow,
- mixtures of sediment in suspension,
- variability of supply of mobile sediment on the bed,
- presence of sandy (non cohesive) sediment,
- omission of depth variation,
- effect of wave stirring.

### *4.2 Computational Model for Hydrodynamic Studies*

A 2-D mathematical model was developed using bathymetry taken from MIKE CMAP as shown in Figure 2. The mathematical model domain consists of open sea portion up to -21 m contour and a portion of Sitanadi and Swarra River at Hangarkatte and Kodibengre influenced with tidal fluctuation. A model area of 20 km x 20 km to cover the entire proposed breakwater and surrounding area was considered. The bathymetry data extracted from the MIKE CMAP was reproduced in mathematical model for the existing conditions and is shown in Figure 6.

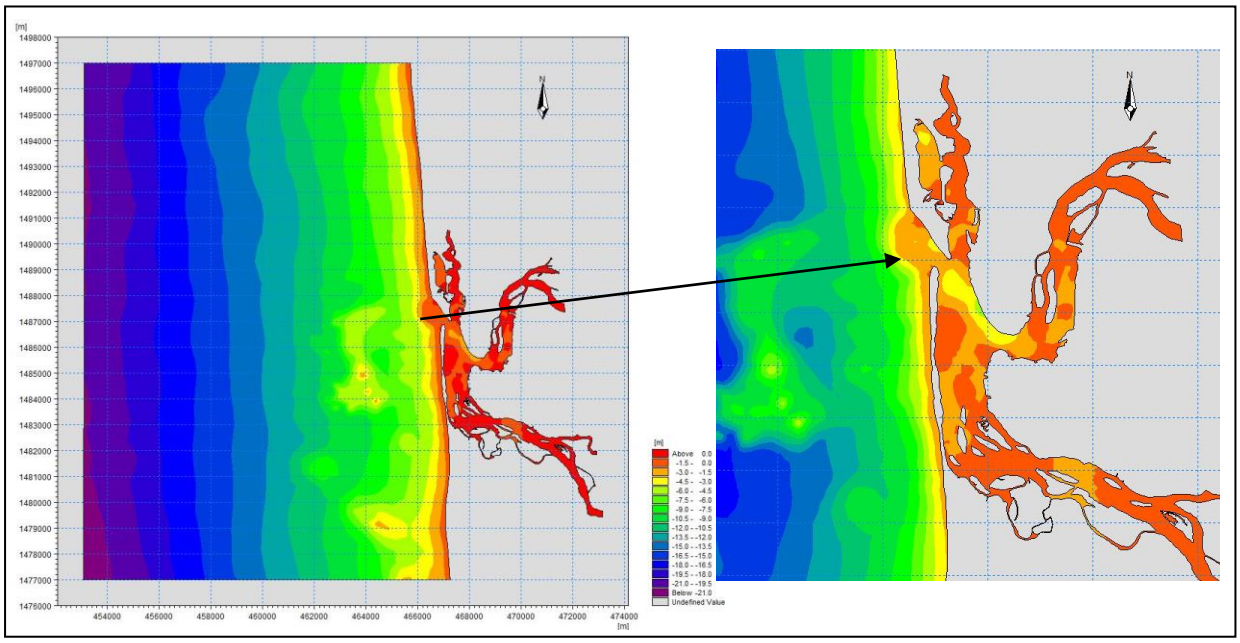
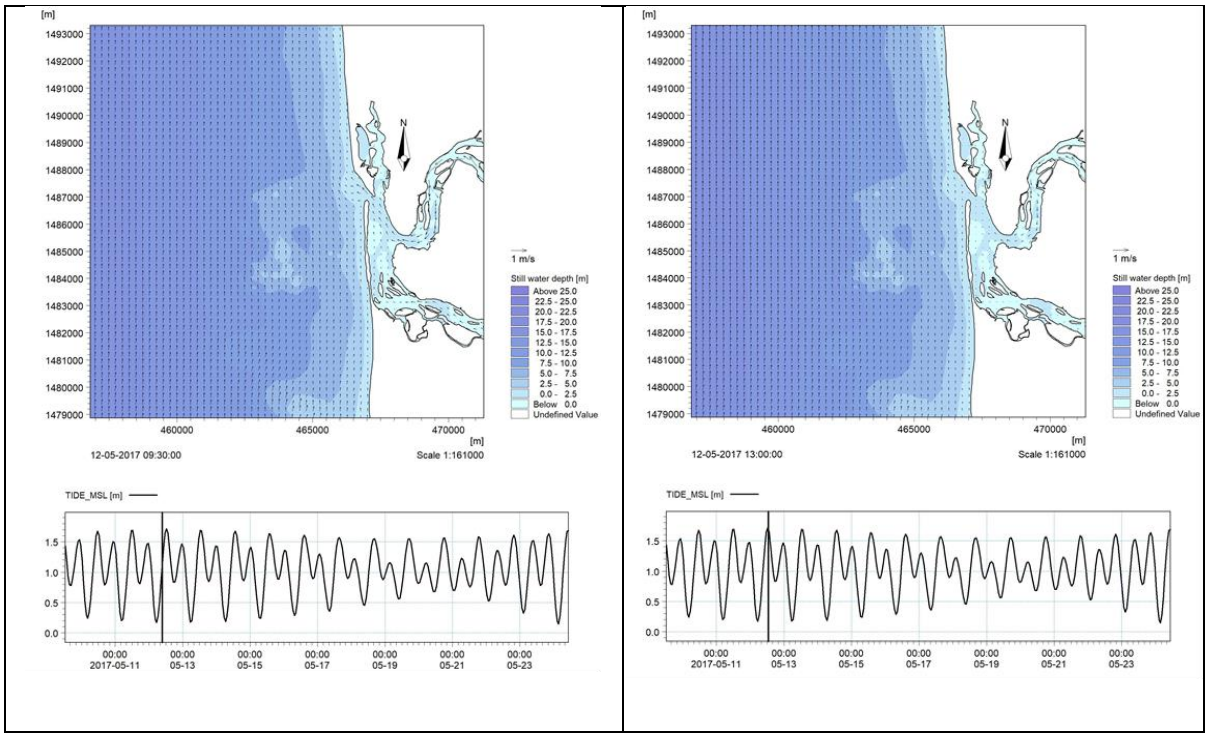


**Figure 5** 2-D View of computational model

### *4.3 Simulation of Flow Field with Existing Condition*

Initially, model was simulated for the existing conditions with typical field observed tide for 15 days duration considering non-monsoon season. The tidal input was provided along the northern and southern open boundaries with appropriate phase lag. The discharge from the Sitanadi and Swarra River was also considered during setting up of the model. The flow simulations were carried out with different model parameters until computed value nearly matches with the field observed values and thus the model was calibrated. The flow fields at every 30 minutes were recorded for the existing condition and typical flow fields during different phases of tide are shown in Figure 7 (A) to Figure 7 (D).



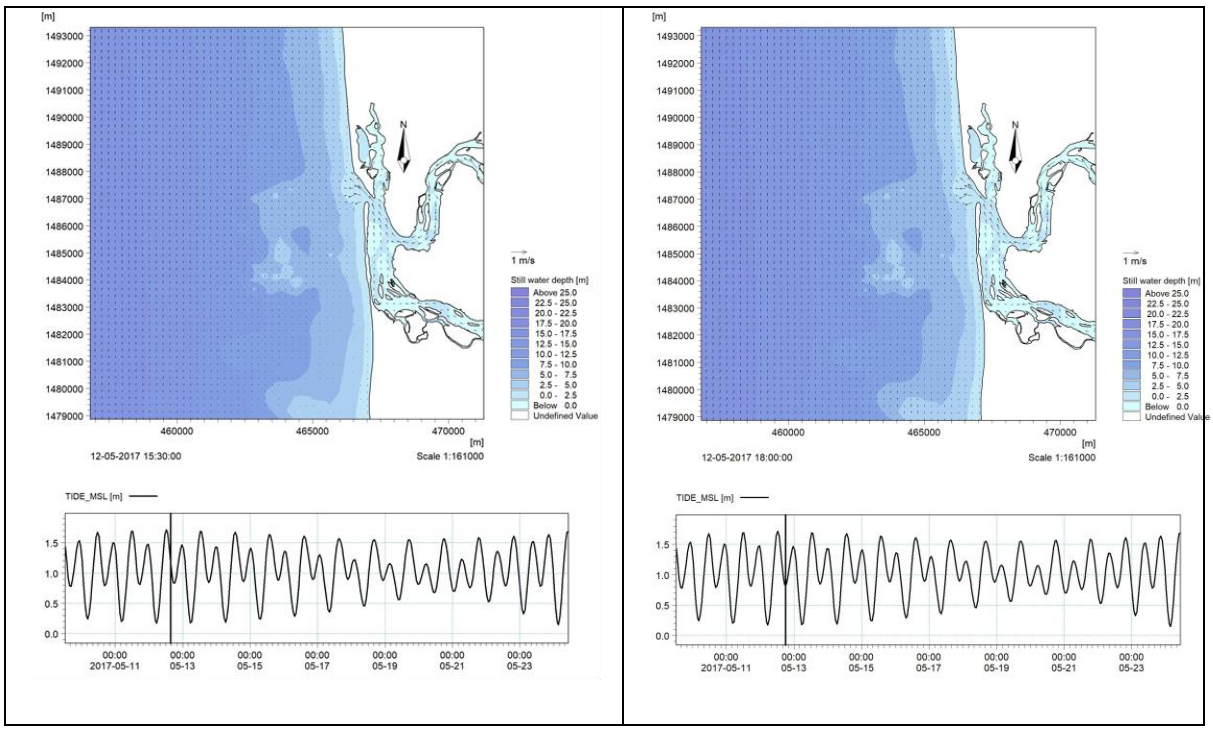



**Figure 6(A-D)** Typical flow field during different phases of tide in existing condition

From the above simulations it is observed that magnitude of currents varied in the range of 0 to 0.35m/sec indicating that the currents are moderate in offshore and near the proposed harbour region during entire tidal cycle except at the inlet where the magnitude of currents are of the order of 0.7m/s which may be attributed to the jetting action due to constriction at inlet mouth. Comparison of observed and computed currents is shown in Figure 7.

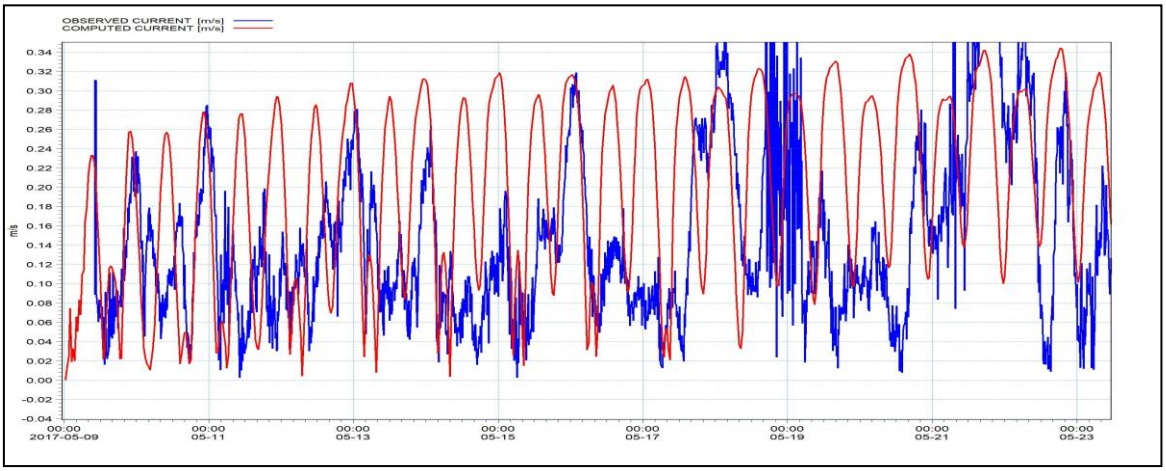



**Figure 7** Comparison of currents (observed Vs computed)

## 5. Simulation of Flow Field with Proposed layout

Initially two parallel breakwaters were proposed with a spacing of 200m to facilitate fishing boats to enter the fish landing facility inside the estuary. The computational model was modified by

incorporating the proposed developments. The channel between the breakwaters was dredged up to -3.0m depth uniformly all along, and natural depths were maintained inside the inlet i.e. the Sitanadi and Swarra River side up to existing jetty location at Hangarkatte and Kodibengre. A Northern breakwater of 950m length and southern breakwater of 680m length having a clear gap of 200m in between them was incorporated in the model as shown in Figure 8 (A). A 2-D view of the computational model with proposed port development is shown in Figure 9 (B).

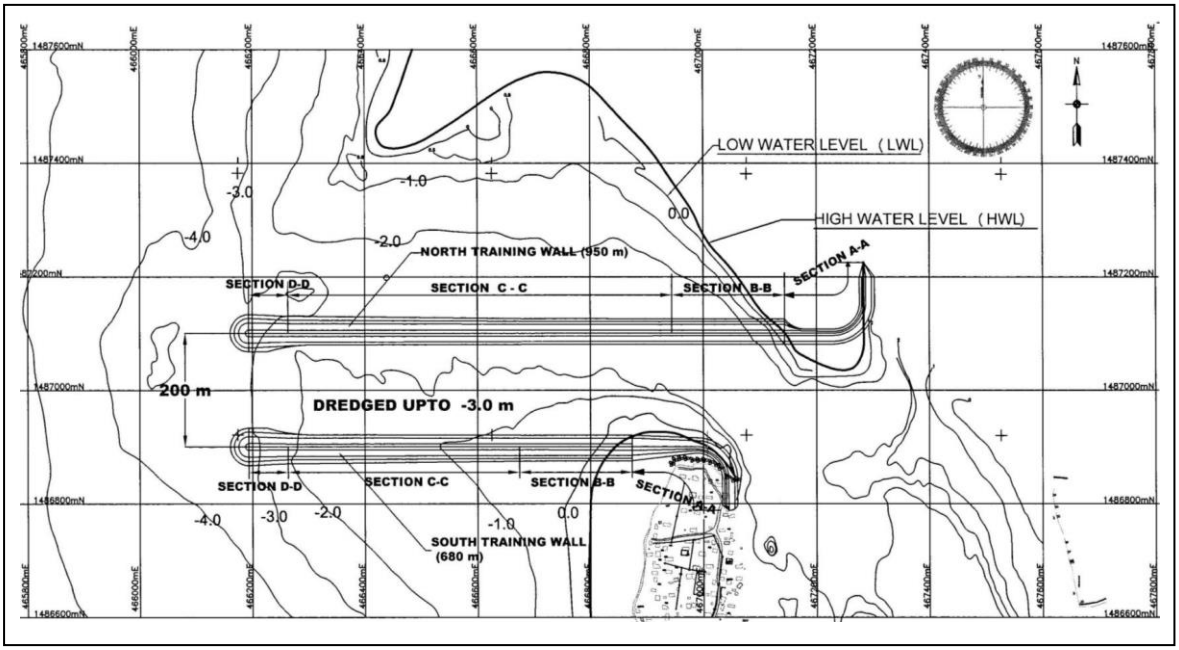



**Figure 8 (A)** Proposed breakwater layout

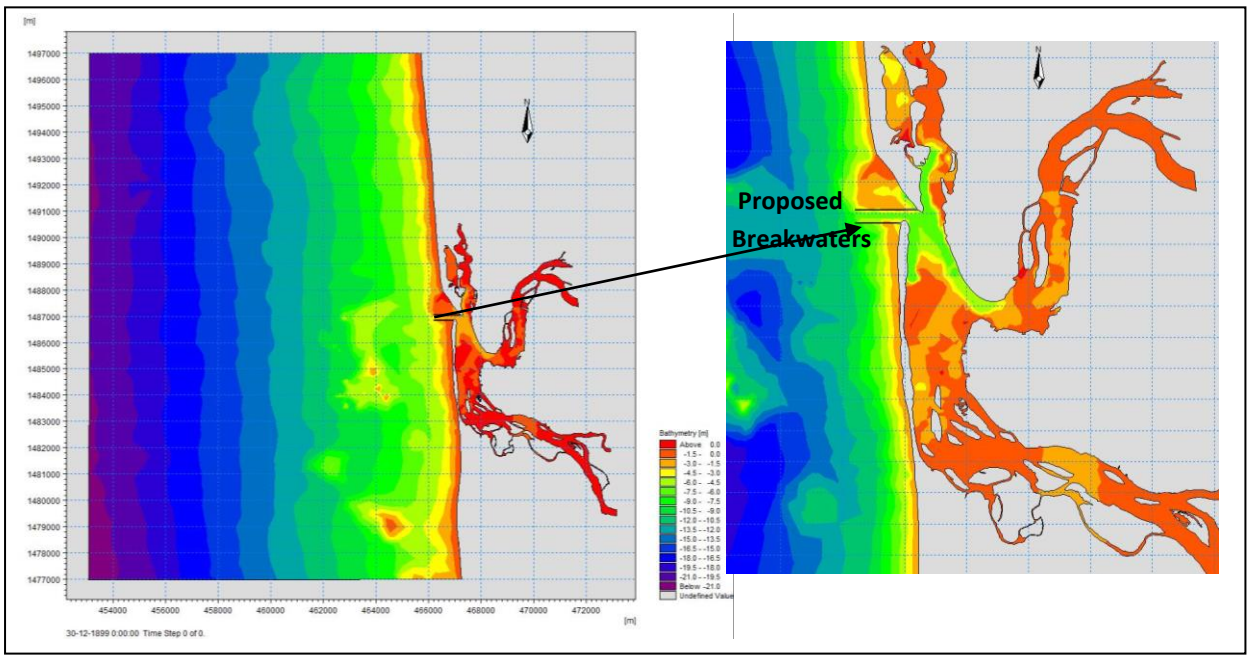



**Figure 8 (B)** Computational model in proposed condition

The flow fields at every half an hour were recorded for the proposed development and a typical flow during different phases of tide are shown in Figure 9 (A) to Figure 9 (D).

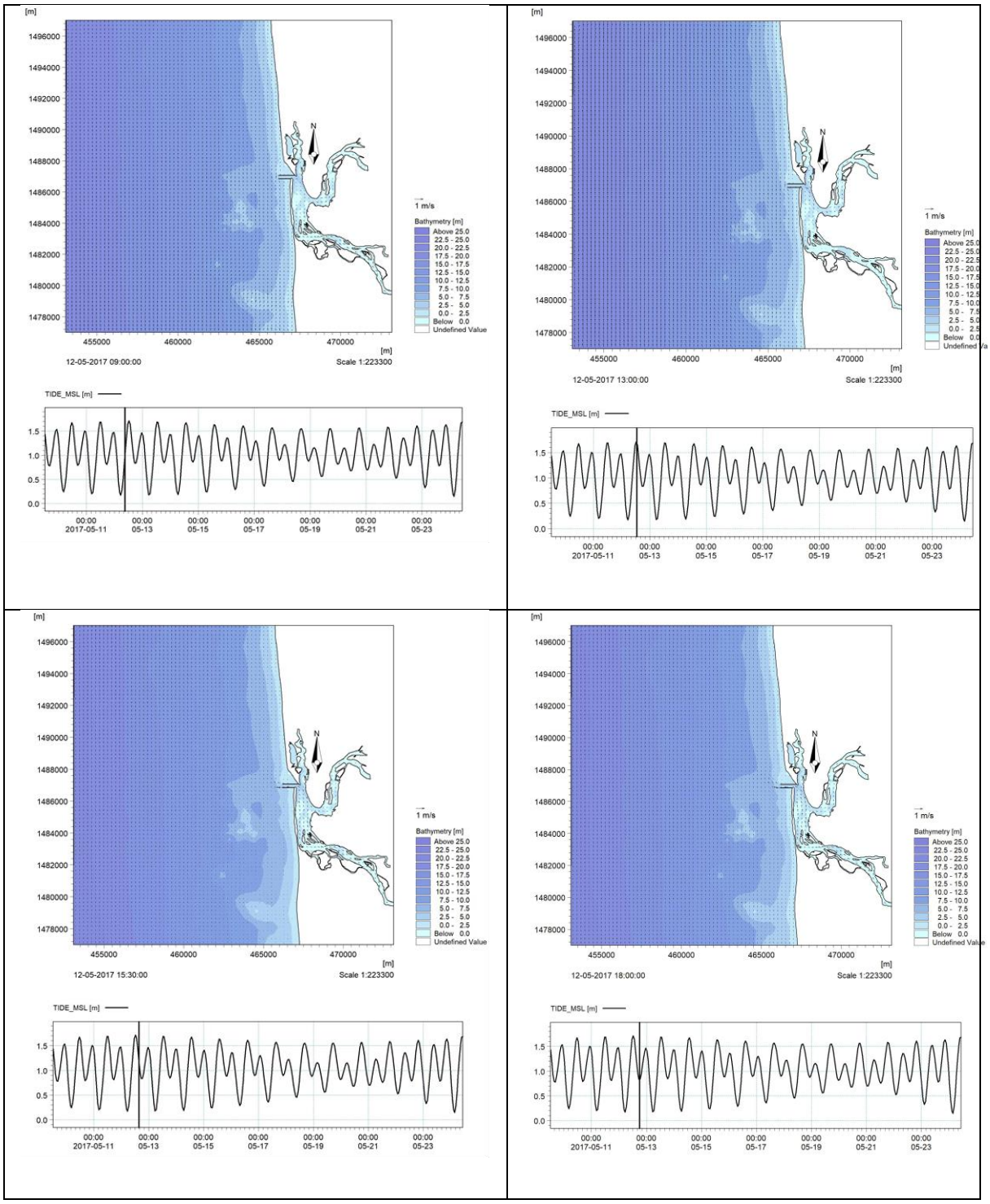



**Figure 9 (A-D)** Typical flow field during different phases of tide with proposed layout

The magnitude and direction of flow along with flow pattern were observed. The magnitude of currents monitored along the entrance channel at four points varied in the range of 0.01 to 1.1m/s that the currents are higher in entrance channel as compared to that of the existing condition. But, in the inlet channel the flow is streamlined. It is also observed that there is no tidal circulation or eddy formation inside the fishing harbour.

## 6. Sedimentation studies

Hangaraktte Port lies at the mouth of Sitanadi and Swarra River. At present the navigation of this port is through sand bar. The sea mouth entrance region opposite to Hangarkatte jetty acts as an approach for the two locations Hangarkatte and Kodi Bengre from the open sea. This inlet region has shallow patches and boats have difficulty to enter the estuary. Siltation in the approach channel and the harbour basin is a serious problem in west coast, which is being experienced by New Mangalore Port and other major ports on the west coast of India. By construction of suitable break-water and river training walls, it is possible to develop this port into a regular all-weather port which will also serve as a fishing harbor. In this regard sedimentation studies are an important element in any port development especially in this region during the design and implementation stage.

### *6.1 Sedimentation Studies with Existing Condition*

The sediment transport studies were carried out with the existing conditions i.e., without any development by considering spring and neap tidal conditions. The sedimentation during different phases of the tide was observed. A typical siltation pattern over a period for existing condition is shown in the Figure 10. From the bed thickness change plot, it is observed that there is negligible sediment accumulation in front of jetty area in Sitanadi and Swarra River and at the river mouth. The average depth of sediment deposition varies from 10 to 20cm in a period of 30 days.

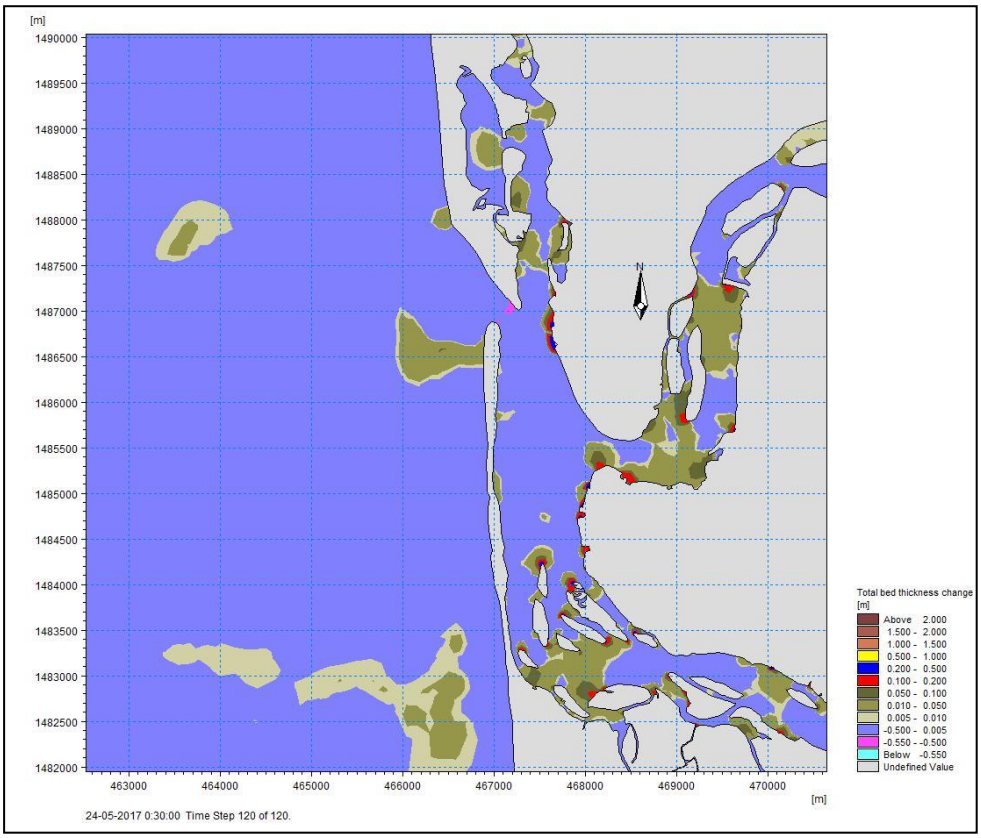



**Figure 10** Siltation Pattern during existing condition

### *6.2 Sedimentation studies with Proposed Layout*

The model was then operated for predicting the siltation pattern with the proposed developments i.e. initially two parallel breakwaters were proposed with a spacing of 200m to facilitate fishing boats to enter the fish landing facility inside the Hangarkatte harbor. A typical siltation pattern over a period of two weeks during non-monsoon with the proposed parallel breakwater layout is shown in Figure 12(A-B). It could be seen that the zone of deposition is mainly in the northern and southern side of

the proposed breakwater as the two parallel breakwaters are extended beyond the littoral zone (-3m contour) and also a slight tendency of erosion inside the inlet entrance is seen towards the offshore region which ranges from 5 to 10cm, this may be attributed to the strong currents (Flushing capacity) as the width of the opening is 200m. Inside the Harbor there is a slight tendency of sediment deposition over the shadow region of the basin which is very marginal. But inside the river i.e., just behind the inlet there is a trend of deposition and may be of the order of 10 to 20cm.

## 7. Conclusions

- From hydrodynamic studies it is noticed that two parallel breakwaters at the River mouth would be helpful to facilitate safe navigation of fishing boats and to keep the mouth, free from sand deposition.

- Hydrodynamic studies with proposed condition consisting of parallel breakwaters with 200m opening shows that the magnitude of currents varied in the range of 0.01 to 1.1m/s indicates that the currents are higher in entrance channel as compared to that of the existing condition. But in the inlet channel the flow is streamlined. It is also observed that there is no tidal circulation or eddy formation inside the fishing harbor.

- Sedimentation studies with Proposed condition indicated that the zone of deposition is mainly in the northern and southern side of the proposed breakwater as the two parallel breakwaters 950m (northern break water) and 680m (southern breakwater) are extended beyond the littoral zone (-3m contour) and also a slight tendency of erosion inside the inlet entrance is seen towards the offshore region which ranges from 5 to 10cm, this may be attributed to the strong currents (Flushing capacity).

- From the study it is finally concluded that the parallel arrangement of the breakwater will facilitate safe navigation and prove efficient in the port expansion in the future.

## Acknowledgements

The authors wish to thank Shri. A.K. Agrawal, Director, CWPRS for his consistent support, encouragement and kind consent for publishing this paper.

## Reference

Technical Report No 5796, March 2020 “Mathematical Model Studies for the Development of Fish Landing Centre at Hangarkatta, Udupi, Karnataka”.

*IN PROCEEDINGS OF 25th HYDRO 2020, INTERNATIONAL CONFERENCE, NATIONAL INSTITUTE OF TECHNOLOGY ROURKELA, ODISHA, INDIA 26-28, March 2021, ISBN 978-93-90631-56-8*

Paper ID - 063

# INTERLINKING PROSPECT OF GODAVARI RIVER WITH KRISHNA RIVER

Kamalini Devi[1], Bhabani Shankar Das[2], Jnana Ranjan Khuntia[3], Gutha Ruthwikesh Reddy[4], Annepu Laxmi Prasad[5]

[1]*Associate Professor, Vidyajyothi Institute of Technology, Hyderabad*
[2] *Assistant Professor, NIT Patna, Bihar*
[3]*Assistant Professor, Civil Engineering Department, St. Martin's Engineering college, Secunderabad, 500100, Telangana, India*
[4,5]*B. Tech student, Vidyajyothi Institute of Technology, Hyderabad*
*Email: kamalinidevi@vjit.ac.in*
*Telephone/Mobile No.: +91 9437729134*

## Abstract

India is highly vulnerable to flood, so a major portion of its population is greatly facing problems every year due to the irregular distribution of rainfall in space and time. In 1980, Central Water Commission formulated a National Perspective Plan (NPP) in which an innovative plan called "Interlinking of Rivers in India" was approached for effective management of floods. The essential feature of this National Perspective Plan is to provide proper distribution of water by transferring water from surplus basin to deficit basin. Under NPP plan, about 30 interlinking of rivers are proposed to be done on 37 Indian rivers. The rivers in India are basic means of human beings as well as for wild-life. It also helps in irrigation, generation of electricity as well as a source of livelihood for the ever-increasing population. Hence most of the major cities of India are found to be at the banks of holy rivers. Due to uncertainty of Monsoon, proper management of river water is needed in India as the country invariably depends upon the agriculture. Moreover, the improper distribution of rainfall leads to severe problem in lack of irrigation in one region and water logging in others. So depleting status of water resources in India may be one of the most critical resource issues of the 21st century. So, the Present study investigates the purpose of river linking which is planned by Government of India for benefit and welfare of the society. It focusses on linking two or more rivers by creating a canal network manually and provide a land area that otherwise does not have river water access. Present study investigates the designing of canals which connects the river Godavari and river Krishna to control floods and to use surplus water for irrigation and other purpose. Manning's method is used for design of canals. Flood frequency analysis has been conducted for both the rivers. These analyses have been proven to be great asset to our planning. The magnitude of Krishna river floods has greatly been declined over the years and the chances of floods in Krishna are very slim. Whereas there are chances of floods in Godavari. It is planned that the flood water can be diverted to river Krishna. These promising results have increased the possibility of success of our planning. The principal objective is to draw water from Godavari river to Krishna river which can be done by connecting the Polavaram right canal to Krishna river at Ibrahimpatnam and thereafter to Srisailam Dam.

***Keywords:****Interlinking, River basin; Tributaries; Diversions; Reservoirs; canals; Flood frequency analysis; Design.*

## 1. Introduction

Water is the most essential natural resource next to air, required for sustaining life on the earth. It is required for drinking and industrial uses, for irrigation to meet the growing food and fibre needs, for power generation, navigation and recreation. The development, use and conservation of water, therefore, play a vital role in the country's development planning. The water resources scarce in the country, however, limited considering the future demands. The rainfall in the country is mostly confined to the monsoon season and is unevenly distributed with respect to both space and time. As a result, some parts of the country are affected by frequent droughts whereas floods affect other parts. Nearly, one-third of the country is drought prone. In the very near future, water will become a scarce resource due to increasing thrust of population and increasing demand for various uses. Some researchers have estimated that by 2025 more than half of the world population facing water-based crisis and suggested that by 2030, in some developing regions of the world, water demand will exceed supply by 50%. Therefore, it need not be emphasized that water should be harnessed in the most scientific and efficient

manner. This is where the idea of interlinking of rivers rises. By interlinking the rivers, the water that is going waste into the ocean can be harnessed. For example, every year about 1500 to 2000 TMC of Godavari water is going waste in the ocean. This can be harnessed by linking River Godavari to River Krishna. So, in this project an attempt has been made to prepare a plan and design of canals to link River Godavari to River Krishna.

The Godavari to Krishna canal link aim is to draw the surplus water in the Godavari river to the Krishna river. This plan is intended to benefit the districts of twin states which depend on the Krishna river. The link will divert the major portion of water from the Godavari river at Polaravam by the Polavaram project right canal to the Krishna river at Vijayavada which is lifted to the Pullichintalu then to Nagarjuna Sagar and at last to srisailam. The water is stored in portions in the reservoirs along the way and then can be supplied for various purposes. The plan is divided into different components as the plan is not only to link the two rivers, but also to use the water by storing them in different reservoirs till srisailam.

## 2.Literature Review

*Verma and Kumar (2015), "Interlinking of rivers in India: Proposed Sharda-Yamuna Link".*The main concern of the paper is to study the proposed inter-basin water transfer Sharda – Yamuna Link including its size, area and location of the project. The enrouted and command area of the link canal in the States of Uttarakhand and location of the project. The purpose of S-Y link canal is to transfer the water from surplus Sharada River to deficient Yamuna River for use of water in drought prone western areas like Uttar Pradesh, Haryana, Rajasthan and Gujarat of the country. It could be one of the effective plans of flood and drought management and other water-based activities for future.

*Kale et al.,(2016), "Interlinking of Rivers and its Advantage".* The interlinking of rivers involving inter basin water transfer has canals, tunnels or water lifts, for water to flow from one river basin tot another and making use of excess water. In India rainfall is dependent on the south-west and north-west monsoons or on the shallow cyclonic depression and disturbance and on violent local storms which form regions where cool humid winds of the sea meet the dry winds from the land and occasionally reach cyclonic dimension. Hence some areas are affected by the droughts while other areas are affected by seasonal floods. There is a general perception that with growing human population and rising standards of living, the available supplies of fresh water on the planet are becoming insufficient to meet demand. It will be scarce, expensive to develop and maintain and valuable in use.

*Pasi and Asardon, (2012) "Inter-Linking of Rivers: A Solution for Water Crisis in India or a Decision in Doubt?".*This paper looks into the history of adoption of the ILR project, its current status, and future implementation and presents a critique of the existing debts the support or question its feasibility. A brief discussion on the global trends of water resources management in context to the development of big water projects, especially for the rise and fall in big water projects is also presented. Finally, a set of policy alternative have been recommended that meet the goals of the ILR project while minimizing the social and environmental impacts in this paper.

*Rane and Chaudhari (2017), "Interlinking of River".* The core objectives of this paper are to study issues and challenges in interlinking of rivers in Indian and to study environmental impact of Indian-River Linking Projects (IRL). At the backdrop of this, the present paper is an attempt to study issues and challenges in interlinking of rivers in India from the point of view of society at large.

*Ameer et al., (2016), "Interlinking of Rivers: Concerns and Benefits".* The main objective of this paper is topromote sustainable development and management of the water resources and also to understand the challenges and prospects in 'Interlinking of Rivers' with reference to the 'Indian Rivers Inter-link Project'.

## 3. Flood Frequency Analysis and Project plan

### 3.1 *Flood Frequency Plan*

Flood frequency analysis is a technique used by hydrologists to predict flow values corresponding to specific return periods (also known as recurrence interval or repeat interval, is an average time or an estimated average time between floods) or the probabilities along a river. The flood frequency analysis is needed to know the occurrence of the floods in Godavari and Krishna rivers. The linking of these two rivers is to divert the surplus water to Krishna river. By these analyses a canal of required capacity can be designed.

Godavari river is the second longest river in the India after Ganga. It has an overall length of 1,465km from its origin (near Trimbak in Nashik District) to the end (flows into Bay of Bengal at Narasapuram in West Godavari District). In Telangana, four stations are present where the flow rate of Godavari river can be measured. Dummagudem, Bhadrachalam, Kaleshwaram and Eturunagaram are the four station points where the flow data are measured. Fig. 1 to 4 shows the flood data at those stations. The blue line shows the max. water level at the period. As per the records the highest flood in Godavari river was recorded in 1986 with a magnitude of 3.6 million cusecs which caused devastating effects. But the floods after that where failed to have that magnitude till now. Even though chances of occurring flood is high and there is a good flow.

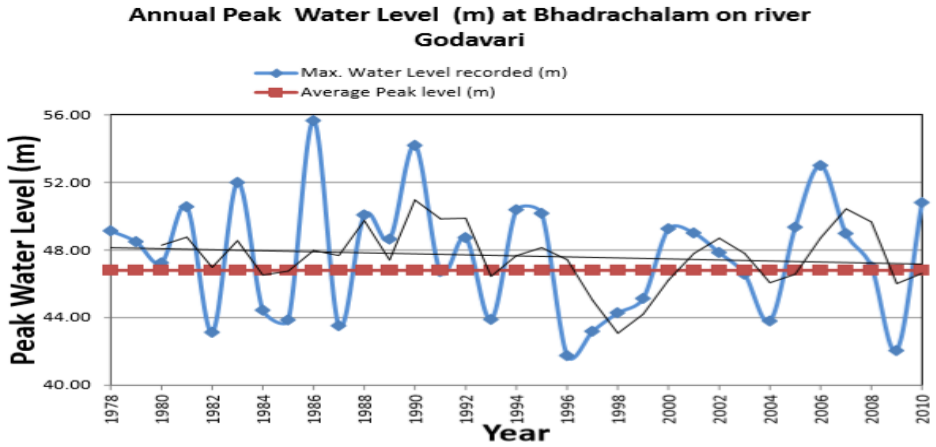



**Figure 1**Annual peak Level (m) at Dummugudem

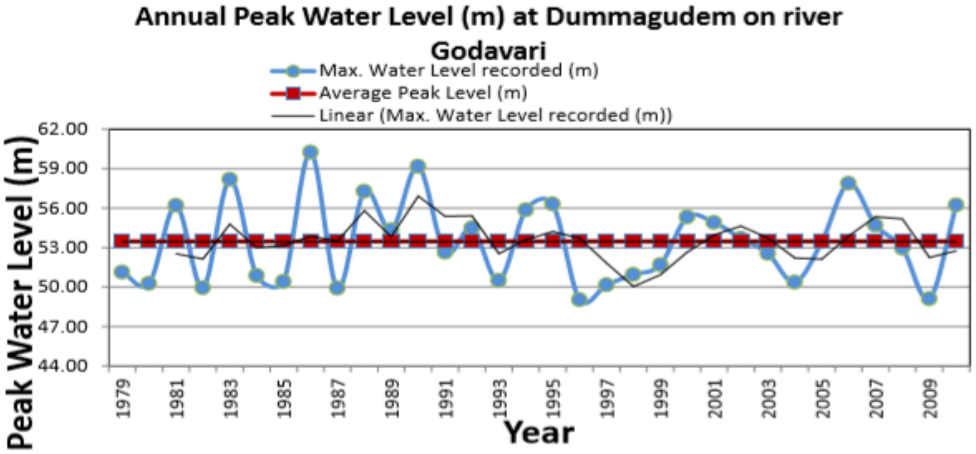



**Figure 2**Annual Peak Level (m) at Bhadrachalam

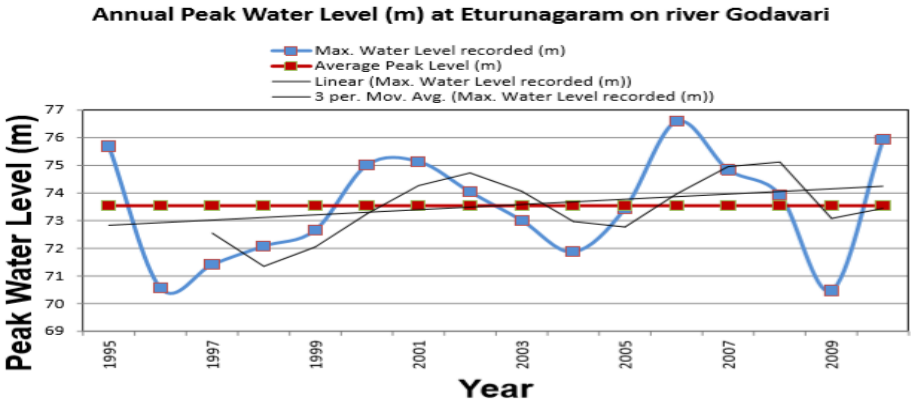



**Figure 3** Annual Peak Water Level (m) at Kaleshwaram

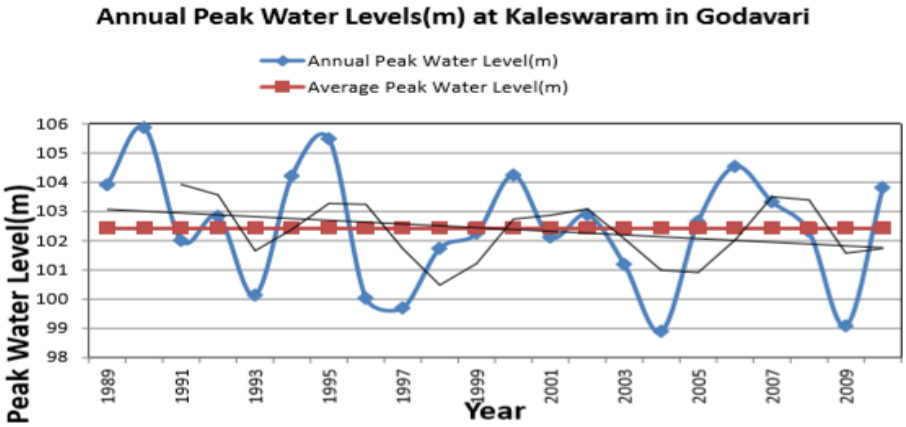



**Figure 4**Annual Peak Water Level (m) at Eturunagaram

Krishna river is the fourth longest river in the India. It has a total length of 1400km from its origin (at Mahabaleshwar near Jor village in Satara district, Maharashtra) to its end (falls into Bay of Bengal at Hamasaladeevi near Koduru in A.P. In Twin-Telugu states Krishna river has larger flow length compared to T.S. When the flood data are analyzed, it is found that the highest flood in Krishna occurred in 2009 with a magnitude of 10.94 Lakh Cusecs. After 2009 the magnitude of the floods has heavily declined as shown in table I

**Table 1**Krishna river flood data

| Occurrence (Year) | Quantity (Lakh Cusecs) |
|---|---|
| Oct 7, 1903 | 10.60 |
| Aug 11, 1914 | 9.48 |
| Nov 2, 1917 | 9.55 |
| Sep 24, 1949 | 9.24 |
| Oct 2, 1964 | 9.87 |
| Oct 17, 1998 | 9.32 |
| Sep 21, 2005 | 7.40 |
| Oct 5, 2009 | 10.94 |
| Oct 26, 2013 | 4.67 |
| Oct 24, 2016 | 1.39 |
| Aug 17, 2019 | 8.21 |

Now even the usual flow in Krishna is also very low. Most of the water in Krishna river is being used

by the dams on upstream before entering into the A.P. The Almatti Dam which is located at Karnataka state in Bijapur district had FRL at 519 m MSL with a grosss capacity of 123.08 TMC. Now the dam FRL is being to be raised at 524 m FRL which is going to increase the gross capacity of the dam to total of 200 TMC. This will even decrease the flow in Krishna river. So, there no harm in diverting the Godavari river water to Krishna river.

### 3.2 *Project Plan*

To connect the both the rivers , a canal route plan is required. There are five possibilities to link these two rivers. These five possibilities are listed below.

1. Sriram Sagar to Srisailam
2. Echampally to Srisailam
3. Kanathallapally to Srisailam
4. Dummugudem to Srisailam
5. Polavaram to Srisailam

**Sriram Sagar to Srisailam:** Sriram ram sagar dam is located in, Nizamabad district of Telangana. It is the first dam that will be encountered in Telangana on Godavari river along its route as shown in Fig. 5. It has a capacity of 90 TMC. The plan is to link Srisam Sagar to Srisailam dam, which has a capacity of 196 TMC located at Srisailam. This link has a high possibility of success. But, at present Sriram Sagar doesn't have good amount of water to its capacity and no hope in the future too. This is because of the huge number of the dams on the Godavari river in Maharashtra. So, this possibility can be rolled out.

**Icchampally to Srisailam:** The second one is from Icchampally to Srisailam. Icchampally dam is after Indravathi river as shown in Fig. 5. Due to the Kaleshwaram project there is no much flow for Echampally. So, diverting to Krishna river is out of the question.

**Kanathallapally to Srisailam:** The third option is from kanathallapally to Srisaialm. It has got two problem. One is as same as the second option there is no enough flow to divert. The second one is that if link is made from Kanathallapally to Srisailam the canal has to pass through the Telangana. As at present the political issues stands between two Telugu states this idea will face difficulties for the approval.

**Dummugudem to Srisailam:** The fourth option is from Dummugudem to Srisailam. Dummugudem after Devadula Project where a new dam, Sitarama project is being constructed. But this project lake the capacity to divert required amount of water to Krishna river.

**Polavaram to Srisailam:** The last option and most suitable for the link, from Polavaram to Srisailam. Polavaram Project, which is in A.P. as shown in Fig. 5 is being constructed and hoped to be finished in the near future. The flow increases after the Sabari river which is prior to Polavaram. This makes it the most suitable choice for the link.

The Polavaram project is located at Polavaram, West Godavari district, A.P. It is a Concrete spillway, Non over flow masonry dam and Earth dam. Polavaram is going to be the largest project in terms of discharge pushing back Three Gorges Dam to second place. Polavaram has a gross capacity of 194 TMC at an FRL of 150 ft from MSL and can discharge about 84 TMC for 110 days from its right canal. The Polavaram to Srisailam link is divided into 7 links. Through these 7 links Godavari waters can be successfully diverted to Krishna river all the way to Srisailam. The 7 links are as following.

1. Link 1, Polavaram to Ibrahimpatnam
2. Link 2, Ibrahimpatnam to Pulichintala Dam
3. Link 3, Pulichintala Dam to Nagarjuna Sagar Tail Pond
4. Link 4, Nagarjuna Sagar Tail Pond to Nagarjuna Sagar

5. Link 5, Nagarjuna Sagar to Bugga Dam
6. Link 6, Bugga Dam to Marrivemula Reservoir
7. Link 7, Marrivemula Reservoir to Srisailam

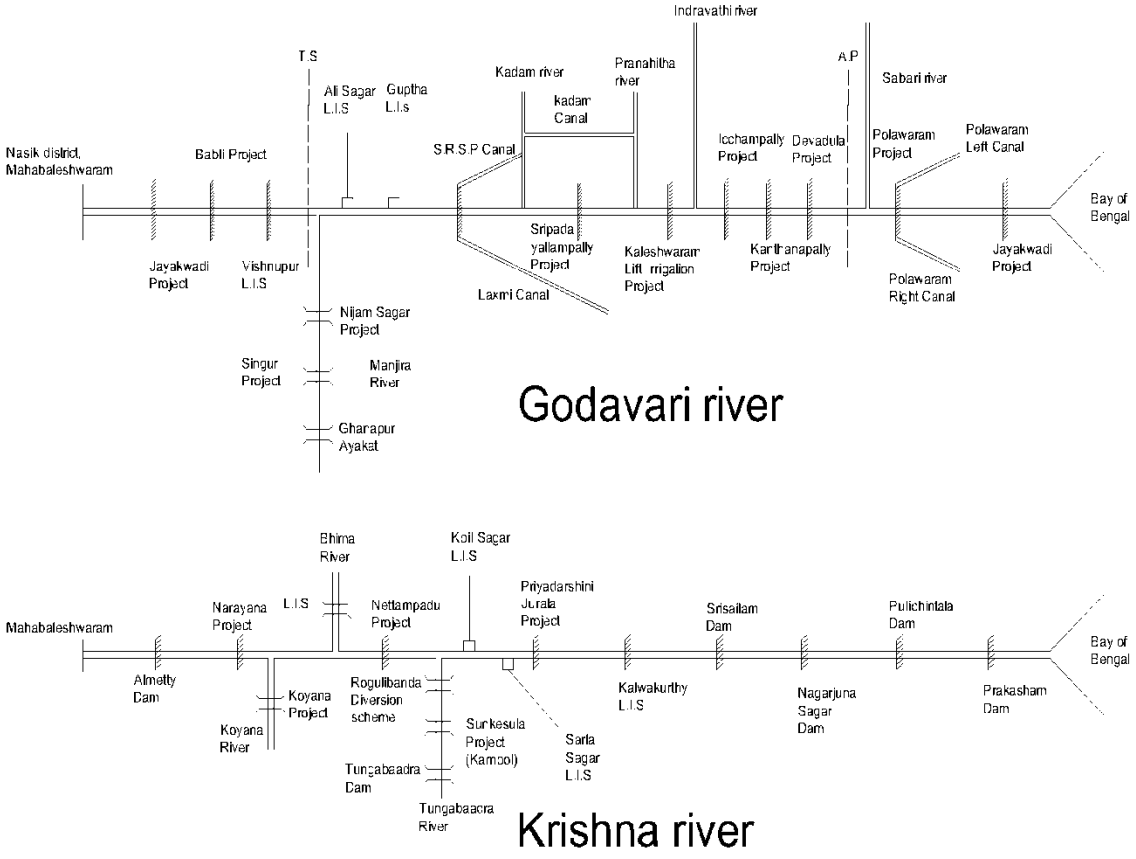



**Figure 5** Projects on Godavari and Krishna Rivers

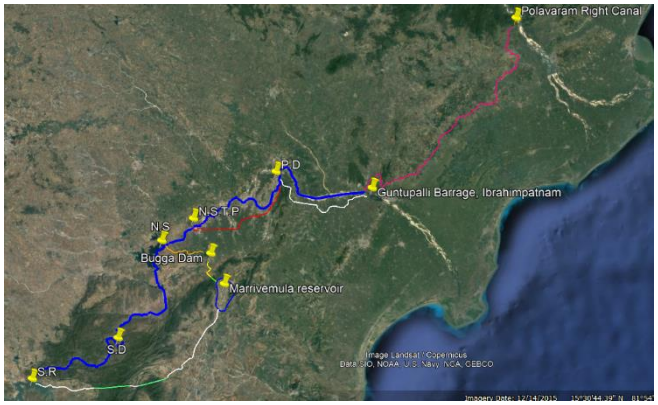



**Figure 6** Polavaram to Srisailam canal route

**Link 1 – Polavaram to Ibrahimpatnam:** The link from Polavaram right canal to Ibrahimpatnam comes under link 1. It starts from Polavaram right canal to Pavitra Sangamam at Ibrahimpatnam as shown in Fig. 6. At present the temporary project at Pattiseema can lift water from Godavari. So, this canal is needed to be linked from Pattiseema. But once the right canal construction is finished, the water can directly be drawn from it, though gravity flow to Ibrashimpatnam. The link has a canal of length of 174 km from Polavaram and joins the cooling canal of length about 16 km. This cooling canal is used

for drawing water from the Krishna river about 11,000 cusecs by pumping, as the part of the alternate cooling system for thermal station at Ibrahimpatnam.

**Link 2 – Ibrahimpatnam to Pulichintala Dam:** The second link is from Ibrahimpatnam to Pulichintala Dam as shown in Fig. 6. The water from Ibrahimpatnam should be lifted up to Pulichintala at it is at upstream. Normally this lifting should be done from Prakasham barrage. But Vijayawada which is one of the major cities of A.P. is situated on the left abutment of the barrage. If water is drained to the barrage, there is a high chance of the Vijayawada city submerge. So, a new barrage 7.81 km has been proposed prior to Prakasham barrage with a capacity of 6 TMC, Guntupalli barrage as shown in Fig. 7. This link needs a canal of length 73.9 km, a tunnel of length 789 m and pump house at Guntupalli barrage.




**Figure 7**Guntupalli Barrage

**Link 3 – Pulichintala Dam to Nagarjuna Sagar Tail Pond:**Pulichintala dam is located at Pulichinta village, Bellamkonda mandal, Guntur district, A.P. Pulichintala dam has a gross capacity of 45.77 TMC at FRL, which is a multipurpose project serving irrigation needs, hydro power generation and flood control. Water is lifted from Pulichintala dam to Nagarjuna Sagar Tail Pond. This link has a canal of length 73.9 km and a pump house to lift water to N.S.T.P. The link is clearly shown in the Fig. 6.

**Link 4 – Nagarjuna Sagar Tail Pond to Nagarjuna Sagar:** Nagarjuna Sagar Tail Pond is a multipurpose reservoir located 21 km downstream from the Nagarjuna Sagar Dam across the Krishna river with a gross storage of 6 TMC. It has a pump house that pumps water back to Nagarjuna Sagar and the power generation. So, this pump house can be used to lift the water that it has received from Pulichintala dam to Nagarjuna Sagar.

**Link 5 – Nagarjuna Sagar to Bugga Reservoir:** The link 5 connects Nagarjuna Sagar to Bugga reservoir as shown in Fig.6. Nagarjuna Sagar Dam is a masonry dam across the Krishna river at Nagarjuna Sagar which straddles the border between Guntur district, A.P and Nalgonda district, T.S. Already the Nagarjuna Sagar main canal is linked to Bugga reservoir which will act as the link 5 with a length of 28.8 km as shown in the Fig. 8. However, the capacity of the Bugga reservoir should be increased from 3 TMC to 10TMC.

**Link 6 – Bugga Reservoir to Marrivemula Reservoir:** As the part of this link, it has been proposed for a construction of new balancing reservoir at Marrivemula of 120 TMC as shown in the Fig. 8. Normally it would have been to connect the Nagarjuna Sagar directly to Srisailam by skipping both link 5 and link 6. A canal cannot be dug through Nallamala forest as it is a restricted area for any type of construction. So, it has to take a detour by link 5 and link 6. This link needs a canal of length 19.6 km,

a tunnel of length 5 km (as shown in Fig. 8 with green line) and a pump house at Marrivemula.




**Figure 8**MarrivemulaReservoire

**Link 7 – Marrivemula Reservoir to Srisailam:** This link connects the Marrivemula reservoir to Saisailam reservoir which is at a distance of 85.7 km Srisailam dam across the Krishna river. The right main canal of the Srisailam project takes-off from this reservoir. The canal of length 145.36 km takes-off from Marrivemula reservoir and connects the both reservoirs. It goes through two long tunnels. These tunnels are clearly shown in the Fig. 8 as green lines.

The total number of new canals, new tunnels, new pump houses, new barrages and new reservoirs are given in the below Table 2.

**Table 2** Requirements

| S. no. | Requirement name | Requirement number |
|---|---|---|
| 1 | New canals | 5 |
| 2 | New tunnels | 4 |
| 3 | New pump houses | 4 |
| 4 | New barrages | 1 |
| 5 | New reservoir | 1 |

## 4. Design of canals

The design of canals is done by using Manning's equation recommended by IS 10430-2000. The Fig. 9 shows the design sketch of the canal.
The Manning's equation is given below,

$$V = \frac{1}{n} R^{2/3} S^{1/2} \quad (1)$$

where,V = velocity of water, *n* = rugosity Co-efficient, S = bed slope, A = area of deep cut portion, P = wetted perimeter of the section, b = bed width, d = depth of water, θ = angle of side slope

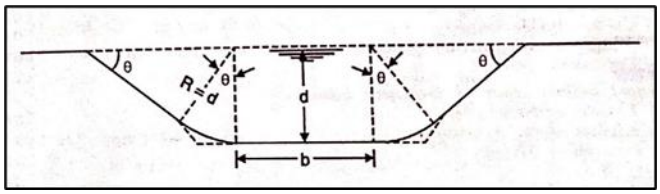



Figure 9 Design Sketch of canal

"*n*" the rugosity coefficient is suggested in the IS 10430-2000 for different kind of lining and side slope

are also referred basing on the type of soil considered.

The design parameters of the canal are discharge, bed width, water depth in the canal, side slope, bed slope, free board and berm. These parameters are needed to be calculated for designing the canals. If discharge is known, water will be sent through each canal depending upon the requirement. Next the water depth is assumed for each canal relating to soil parameter through which it passes. Bed slop is also assumed based on the topography. The berm, side slope and free bored are fixed as recommended in IS 10430-2000. Then by using the Manning's equation bed width is calculated.

## 5. Results

For linking Godavari to Krishna which is from Polavaram to Srisailam-5 new canals, 4 new tunnels, 4 new pump houses, 1 new barrage, 1 new reservoir are required to be constructed. The five new canals design results are given in the Table 3. In design results the design parameters of the 5 canals are specified.

**Table 3**Canal Design Results

| | |
|---|---|
| Link 1 - Canal | Polavaram to Ibrahinpatnam |
| Discharge | 327.73 cusecs (i.e., 11574 cumecs) |
| Bed width | 52.74 m |
| Water depth | 5 m |
| Side slope | 1.5:1 |
| Bed slope | 1 in 20000 |
| Free board | 0.75 m |
| Berm | 5 m |
| | |
| Link 2 - Canal | Ibrahinpatnam to Pulichintala |
| Discharge | 655.45 cusecs (i.e., 23148 cumecs) |
| Bed width | 92.61 m |
| Water depth | 4.5 m |
| Side slope | 15:1 |
| Bed slope | 1 in 10000 |
| Free board | 0.75 |
| Berm | 5 m |
| | |
| Link 3 - Canal | Pulichintala to N.S.T.P |
| Discharge | 655.45 cusecs (i.e., 23148cumecs) |
| Bed width | 92.61 m |
| Water depth | 4.5 m |
| Side slope | 15:1 |
| Bed slope | 1 in 10000 |
| Free board | 0.75 |
| Berm | 5 m |
| | |
| Link 6 - Canal | Bugga Reservoir to MarrivemulaResevoir |
| Discharge | 655.45 cusecs (i.e., 23148cumecs) |
| Bed width | 101.58 m |
| Water depth | 4 m |
| Side slope | 1.5:1 |
| Bed slope | 1 in 8000 |
| Free board | 0.75 m |
| Berm | 5 m |

| | |
|---|---|
| Link 7 - Canal | Marrivemula Reservoir to Srisailam Reservoir |
| Discharge | 655.45 cusecs (i.e., 23148cumecs) |
| Bed width | 26.45 m |
| Water depth | 9.5 m |
| Side slope | 0.5:1 |
| Bed slope | 1 in 15000 |
| Free board | 0.75 m |
| Berm | 5 m |

The A.P Government has taken up the Polavaram project in hoping to at least use 1100 TMC of water that is going waste. But, while it is under the construction, its potential is limited. So, only 252 TMC of water can be released from right canal (i.e., Patiseema). From which 96 TMC will be used along the way to Ibrahimpatnam. The remaining water will used by the projects on Krishna river. Basing on these facts water has to be distributed for all the projects, which is given in Table 4.

**Table 4**Water Distribution

| S. no. | Projects | Quantity in TMC |
|---|---|---|
| 1 | Guntupalli Barrage | 3 |
| 2 | Pulichintala Dam | 20 |
| 3 | Nagarjuna Sagar Dam | 40 |
| 4 | BuggaRecervoir | 6 |
| 5 | Marrivemula Reservoir | 37 |
| 6 | Srisailam Reservoir | 50 |
| Total | | 156 |

Due to this project the benefited districts are given are following

1. Krishna
2. Vijayawada
3. Guntur
4. Nalagonda
5. Kurnool
6. Kadapa
7. Anantapur
8. Prakasham
9. Nellore
10. Mahbubnagar

## 6. Conclusions

The link from Polavaram to Srisailam is designed which connects River Godavari to River Krishna. This link has the potential to draw the surplus water from Godavari to Krishna even at the time of high floods. Thus, the main objective of this linking is to take a full advantage of the floods in Godavari river. This link divides itself into many sub-links to connect various major projects on Krishna river along the way to Srisailam, which forming a long chain that connects several major projects on Krishna river to Godavari river. The Polavaram project, which is the diversion point on Godavari river can release about 159 TMC of water to Krishna river, in beneficial all the districts in A.P and Telangana which come under the command area of these projects.

The authors conclude in hoping for many new river interlinking projects like this to come in future, so

that a long network of river inter-linking in the country will be established that have the potential to carry water to the various parts of the country where the droughts are ruling.

## References

1. Ameer, S., Rafi, A., and Ahmad, A. (2016). Interlinking of rivers: Concerns and benefits. *Journal of Civil Engineering and Environmental Technology*, *3*(6), 544-548.
2. Garg, S. K. (1991). Irrigation engineering and hydraulic structure.
3. http://www.irrigation.telangana.gov.in/img/projectspdf/kaleshwaram.pdf
4. IS 10430 2000.: Criteria for Design of Lined Canals and Guidance for Selection of Type of Lining. Bureau of Indian Standards, New Delhi, India
5. Kale A, Gothankar P.,Kadam N and Mehetre D. (2016), Interlinking of rivers and its advantages. *International journal of engineering sciences & management* Shirke, TECHNOPHILIA: February 2016, ISSN:2277-5528.
6. Pasi N, Smardon R. (2012). Inter-linking of rivers: A solution for water crisis in India or a decision in doubt?. *Journal of Science Policy and Governance*, Volume 2, Issue 1, pp1-42.
7. Punmia, B. C., Lal, P. B. B., Jain, A. K., and Jain, A. K. (2009). Irrigation and water power engineering. Laxmi Publications, Ltd.
8. Rane, P. J. ; Chaudhari, S. C. (2017). Interlinking of river. *International Conference on Modern Trends in Engineering, Science and Technology (ICMTEST) 2017*, Maharashtra, India, pp.410-416 ref.14
9. Report on "Kaleswaram Project" by Irrigation Department, Government of Telengana.
10. Report on "Nagarjuna Dam" by Water Resources Department, Government of Andhra Pradesh.https://irrigationap.cgg.gov.in/wrd/static/approjects/Nagarjuna.html
11. Reporton "Srisailam Right Main Canal"by Water Resources Department, Government of Andhra Pradesh.https://irrigationap.cgg.gov.in/wrd/static/approjects/Srisailam_right_bank_canal.html
12. Report on Trend of Flood Peaks in Godavari Basin by P. Devender Rao, Director, CWC, New Delhi.
13. Subramanya, K. (2013). Engineering hydrology. Tata McGraw-Hill Education.
14. Verma A and Kumar N. (2015), Interlinking of rivers in India: Proposed Sharda-Yamuna Link. *IOSR Journal of Environmental Science, Toxicology and Food Technology*. Volume 9, Issue 2,pp-28-35.

*IN PROCEEDINGS OF 25th HYDRO 2020, INTERNATIONAL CONFERENCE, NATIONAL INSTITUTE OF TECHNOLOGY ROURKELA, ODISHA, INDIA 26-28, March 2021, ISBN 978-93-90631-56-8*

Paper ID - 149

# Estimation of Sediment Production Rate using Josh and Dash model- A case study of Rel River, Banaskantha District

Himadri Shah1 , Sudhanshu S. Dixit2 , V. M. Patel3 , Nimrabanu Memon 4Dhruvesh P. Patel5

1M.E. Student, CED, L. D. College of Engineering, Ahmedabad (380015), Gujarat, India
2Assistant Professor, CED, L. D. College of Engineering, Ahmedabad (380015), Gujarat, India
3Associate Professor, CED, L. D. College of Engineering, Ahmedabad (380015), Gujarat, India
4Research Scholar, CED, SOT, PDPU University, Gandhinagar (382007), Gujarat, India
5Associate Professor, CED, SOT, PDPU University, Gandhinagar (382007), Gujarat, India
Email: himadrishah98@gmail.com

## Abstract:

Spatial changes in rainfall are observed in India since past few years due to climate change and associated changes in the Indian summer monsoon circulation and the general atmospheric circulation. This indicates increase in rainfall parameter in western zone. Effect of this phenomenon is started to reflect in the semi-arid region of Gujarat and Rajasthan; a drought prone region which experienced severe flash floods in the years 2017 and 2015. This flood water carried unprecedented amount of sediments in the downstream. This research paper is aimed at estimation of sediment production rate of rel river sub watershed located between 24˚29'15" to 24˚46'18" North latitude and 72˚0'28" to 72˚27'5" East longitude covering 441.58 sq. km area in Gujarat Rajasthan boundary region. Sediment flow from the sub watershed during the floods in July 2017 posed a greater disaster in the localities near the outlet of sub watershed. Dhanera, a tehsil located in Banaskantha district located near the outlet of the sub watershed was sunk under 1 to 2 feet thick layers of muck disrupting many lives and properties. It took almost 2 months for Dhanera to stand up again. Estimation of sediment production rate will be helpful in selecting techniques for soil conservation. Moreover, we have classified the sub watershed into 52 micro watersheds and ranked them is the ascending order of sediment production rate. This guides to prioritize the sub watershed for urgency of soil conservation measures to be adopted. For this analysis geospatial technology such as Geographic Information System and Remote Sensing technology are used.

***Keywords***: *Summer monsoon rainfall western shift, sediment production rate, soil conservation, Geographic Information System*

## 1.Introduction:

### 1.1 *Description of study area:*

Rel river sub watershed covers total geographic area of approx. 441.58 sq.km. including some part of Gujarat Rajasthan region. Geographically it is located between $24^0$29'15" to $24^0$46'18" North latitude and $72^0$0'28" to $72^0$27'5" East longitude.

Maximum length of the watershed in North –South direction is 29.34 km while in East – West direction it covers 46.34 km. The area is classified as semi-arid-region. Sub watershed has elongated shape in East-West direction. The terrain is generally levelled to gentle slope. The soil of study area is dominantly coarse loamy, which is basic in nature and excessively drained. The parent rock is identified as calcareous rocks, and the soil layer is classified as Aeoline (transported by wind). The sub watershed is bisected by a non-perennial 2nd order stream known as 'Sukal Nadi' which originates in the Aravalli hills near Pindwara of Sirohi district (Rajasthan) at elevation of 372.5m above M.S.L. and drains into the Banas river from left bank. The length of the river is 38 km in monsoon during full flow condition. Sukal Nadi is named as 'Rel River' locally in Gujarat. The mean temperature of study area is $35^0$C in winters [1].ɪ $19^0$C during

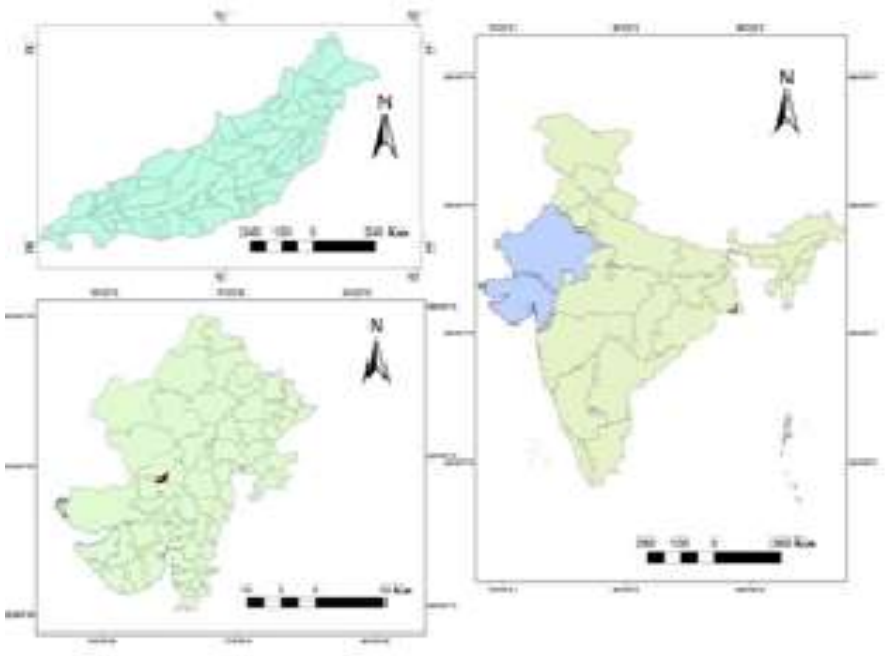


**Figure 1** geographic location of study region

### 1.2 *Rainfall variability and Dhanera flash flood, 2017:*

Impact of climate change gain worldwide attention in early 1990s when the global sea level observed rise of 15cm. Many scientists and researchers studied the variations in climatic parameters and predicting future trends of precipitation, wind direction, temperature. In India prof Nityananda Singh of Indian Institute of Tropical Meteorology, Pune studied the climatic fluctuations of Indo-Gangetic plains and predicted westward shift of Indian summer monsoon precipitation. He estimated the increase rate of summer monsoon precipitation in western zone of India as 170mm/100 years since 1900s [3]. Moreover, he analyzed and suggested westward shift in the occurrence of severe rainstorms. The early symptoms of this shift were visible in July 2015, when rainfall of 532mm which was 105% higher than average rainfall struck the region. After 2 years glimpse of the soil-water disaster was evident when 267% higher rainfall occurred in the region. The Jetpura dam in Jhalore distict of Rajasthan was washed away which caused the flood water to enter North Gujarat flooding the 10 districts Banaskantha, Mehsana, Patan, Morabi, Sabarkantha, Ahmedabad, Anand, Aravalli, Mahisagar and Surendranagar. The worst affected areas were extreme north Gujarat regions. These regions are considered as drought prone regions. So the flood awareness and soil conservation practices are totally absent in these region. Dhanera, a tehsil located near the outlet of sub watershed was sunk under 1 to 2 feet thick layers of muck disrupting many lives and properties. The sediment washed away from watershed created havoc in Dhanera as the people and cattle were stuck in the mud and deluged the tehsil beyond comprehension.[5]
The soil of sub watershed is non cohesive in nature. Moreover, as the region is semi-arid, there is minimal amount of vegetation or parameters which can obstruct soil erosion. Hence, the flood waters caused heavy flow of sediments disrupting lives in the nearby habitats and districts. In this paper, we are trying to draw attention towards urgency of soil-water conservation measures to be adopted. For this pilot sediment production rate of the sub watershed is estimated.

## 2. Material and methods

DEM of Cartosat-1with 30m resolution of the study area at scale 1:50000was obtained from National Remote Sensing Centre. The watershed boundary was generated with help of surface tool of ArcGIS. After generating the watershed boundary, using contours, the sub watershed was further divided in 52 sub parts and was given IDs in ascending order of area enclosed. These sub parts are various drainage pockets of sub watershed. The sediment production rate was estimated according to catchment characteristics using 'Josh and Dash Model'.
For estimation of sediment production rate of any catchment, various shape factors are essential and needed to be considered. As our study region is between10, 000 -50,000 ha (44158 ha) it is classified as sub watershed. Following are some of the shape parameters of sub watershed which are essential to estimate the sediment production rate.

### 2.1 *Form Factor*

It is obtained by calculating the ratio between area of the watershed to the square of the length of the watershed [6]. Higher the value of form factor indicates more circular watershed, whereas long narrow watershed has low form factor value, which is nearer to zero. The watersheds with high form factor have high peak flows for shorter duration, while the elongated watersheds with low form factor have low peak flows for longer duration [7].

$$R_f = A/L^2 \quad (1)$$

### 2.2 *Circularity Ratio*

According to Miller (1953) [10], circularity ratio (Rc) can be defined as the ratio of the watershed area (A) to the area of enclosed by circle corresponding to watershed in such a manner that perimeter of circle is equal to perimeter of the watershed. Mathematically it is stated as below

$$C_r = 12.57 * A/P^2 \quad (2)$$

Watersheds with low value of circularity ratio refer the elongated shape of watershed with high relief, steep slopes and its higher value represents more circularity in shape, moderate relief with gentle slopes [2].

### 2.3 *Compactness Coefficient*

According to Gravelius [8], compactness coefficient (Cc) was the ratio of the perimeter of watershed to the circumference of circular area, which equals the area (A) of the watershed and mathematically, it can be expressed by

$$C_c = 0.2821\ P/\ A^{0.5} \quad (3)$$

The value of Cc indicates the rate of erosion and nature of watershed shape. When watershed shape is a perfect circle, Cc is equal to unity.

### 2.4 *Elipticity Index*

Elipticity index is ratio of square of the watershed length (Lb) and the total area (A) of watershed [10] and calculated by the formula:

$$Ei = 0.79 * Lb2/A \quad (4)$$

The value of elipticity index varies from unity to infinity and its higher value indicates more elongated shape of the watershed.

### 2.5 *Estimation of Sediment Production Rate*

Sediment production rate is the volume of sediment produced per unit watershed area per unit time. The sediment production rate of the sub watershed has been estimated based on the model suggested by Jose and Das (1982) [3] and is expressed by the following equation:

$$\text{Log (SPR)} = 4919.80 + 48.64 \log (100 + Rf) - 1337.77 \log (100 + Cr) - 1165.64 \log (100 + Cc) \quad (5)$$

Where, SPR is sediment production rate, Rf is form factor, Cr is circulatory ratio and Cc is compactness coefficient.

### 2.6 *Estimation of Run-off Rate*

Runoff is the excess water that flows on the surface of earth after the infilteration. It depended on the amounts of rainfall, evapotranspiration losses and percolation losses which in turn are affected by climatic conditions, topography, soil characteristics, structure, relief and other surface properties [9]. Generally, run-off rate is relatively low in the plain areas because of low relief, gentle slope which results high permeability of the terrain. Run-off rate of the watershed was estimated using Jose and Das (1982) model, which expressed by the formula:

$$\text{Log Q} = 2238.43 + 22.12 \log (100 + Rf) - 608.28 \log (100 + Cr) - 530.02 \log (100 + Cc) \quad (6)$$

where, Q is run-off of the watershed, Rf is form factor, Cr is circulatory ratio and Cc is compactness coefficient.

## 3. Result and Discussion:

### 3.1 *Form Factor*:

The form factor value of the Rel river sub watershed is 0.2056 which indicates more elongated in nature with flatter peak flow for longer duration.

### 3.2 *Circulatory ratio:*

The circulatory ratio of the sub watershed is 2.23 which indicates elongated watershed.

### 3.3 *Compactness coefficient:*

Compactness coefficient of watershed is 0.22 which indicates that watershed is prone to erosion and is not circular.

### 3.4 *Elipcity Index:*

The value obtained for the study area is 4.86, indicating elongated shape of the watershed.

### 3.5 *Sediment Production Rate:*

The SPR was found to be 10.3024901 cubic meter/sq.km/yr which indicates that the sub watershed produces higher amount of sediments annually due to non-cohesive nature of soil. Also, the sub watershed is divided into 52 sub parts and sediment production of individual sub part is calculated and ranked as per ascending order as shown in fig.1 This will guide to decide which region of sub watershed should be considered first for soil conservation measures. Table 1 depicts the erosion class of the sub parts of sub watershed. Geographic orientation of same is depicted in fig.2.

### 3.6 *Runoff rate:*

The total runoff value obtained for the Rel river sub watershed is 0.7405 cm/sq.km suggesting that the area is characterized by low discharge of runoff for standard rainfall and high permeability due to rugged topography and leveled terrain. But effect of higher amount of rainfall is not studied as the adequate data for rainfall run-off analysis are not available. Only one rain gauging station 'Bapla, Rajasthan' is available in sub watershed. The immediate nearby stations are 'Panthwada, Gujarat' located at 15.34 km from Bapla and 'Badgaon, Rajasthan' located at 7.58 km from Bapla. There is urgent requirement of establishing more rain gauging station in this sub watershed as well as entire West zone of India to estimate the flood and soil erosion impacts in this zone due to climate change and hence, mitigate the painful effects of climate change.

## 4. Conclusion:

Rel river sub watershed is elongated watershed with high sediment production rate. This rate is expected to increase more due to increasing trend of rainfall in the region. Hence, more rain gauging stations should be installed in the area and soil conservation measures should be taken as per the ranking given for sub parts of our sub watershed.

## 5. Acknowledgement

We are thankful to PDPU, for felicitating for this Project. Moreover, we are thankful to State Water data center, Gandhinagar and National Remote Sensing Center for providing us with the required data.

**Table 1.** Erosion category of sub parts of Rel river sub watershed

| Erosion category | Ws ID | % Area |
|---|---|---|
| high | 1,2,3,4,5,6,8,13,14,15,20,26,27,30,32,34,35,36,42,45,50 | 33.91% |
| moderate | 7,9,11,12,18,19,21,22,23,24,25,29,31,33,37,38,39,40,41,44,46,47,48,49,51 | 52.41% |
| low | 10,16,17,28,52 | 10.57% |
| very low | 43 | 3.11% |

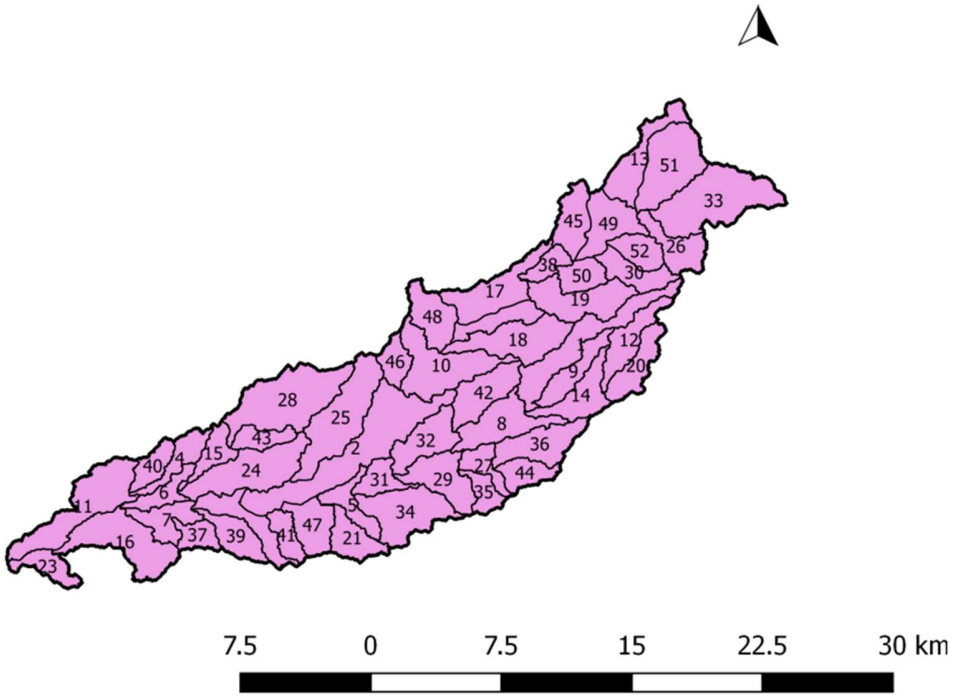



**Figure 2** Ranking Map

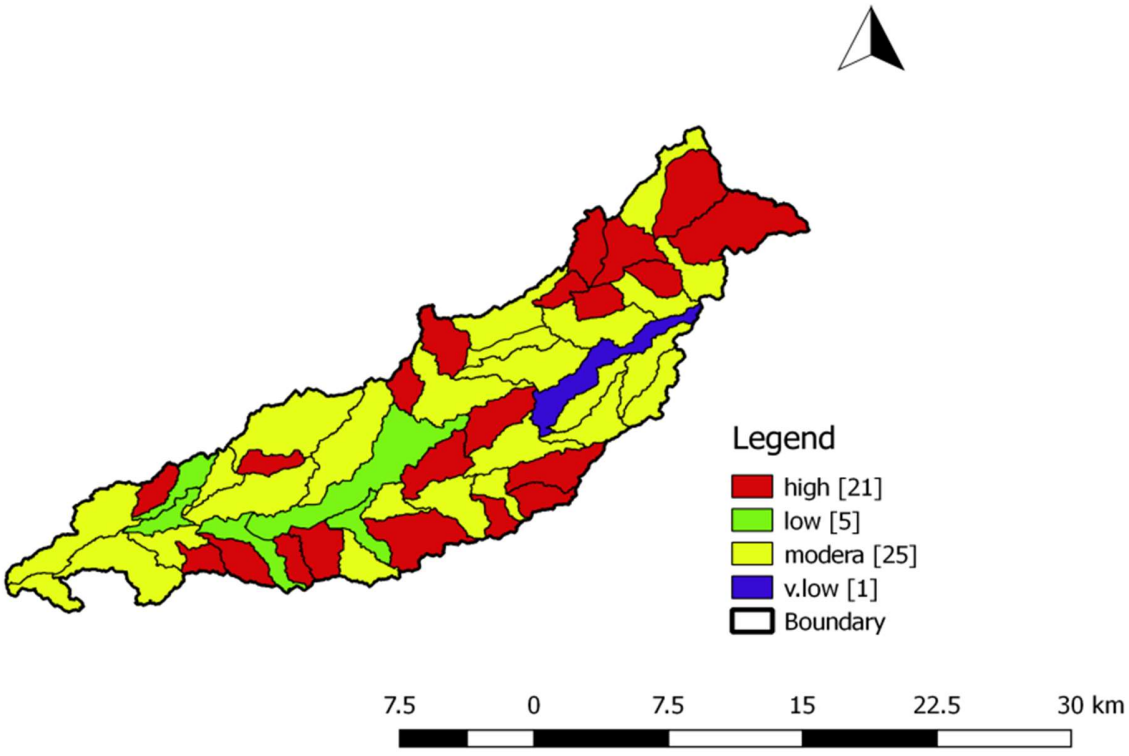



**Figure 3** Prioritization Map based on Erosion Class

## References

1. http://www.indiawris.nrsc.gov.in/wrpinfo/index.php?title=Banas

*2.* P. N. Rymbai* and L. K. Jha, (2012) *Estimation of sediment production rate of the Umbaniun Micro Meghalaya, India Department of Environmental Studies, North Eastern Hill University, Shillong, Journal of Geography and Regional Planning Vol. 5(11), pp. 293-297, 13 June, 2012.*

*3.* P. Thirumalai, D. Sudha, K. Chitra, R. Surulivel, P. Priya and R. Senthil Kumar, (2014) *watershed based on sediment production rate around Arasalar-Palavar division of Nagapattinam using GIS, Dept. of Geography, Govt. Arts College(A), Kumbakonam, Tamil Nadu, India, Arch, . Appl. Sci. Res., 2014, 6 (5):156-162*

4. NityanandSingh,N. A. Sontakke,(2002) *Fluctuations and Environmental Changes of the Gangetic Plains, India , Climatic Change 52: 287 2002. © 2002 Kluwer Academic Publishers. Printed in the Netherlands*.

5. https://timesofindia.indiatimes.com/city/rajkot/dhanera sinks-in-muck-stench-rot/articleshow/59814321.cms /

*6.* Horton, R.E. (1945)*: Erosional development of streams and their drainage basins: hydrophysical approach to quantitative morphology. Geological America Bulletin, 56 (3), pp.275*

*7.* Miller, V.C. (1953)*: A quantitative geomorphic study of drainage basin characteristics on the Clinch Mountain area, Virgina and Tennessee. Project NR 389 Tech. Rep. 3, Columbia University, Department of Geology, ONR, New York.*

*8.* Gravelius, H. (1914)*: Flusskunde. Goschen Verlagshan dlung Berlin. In: Zavoianu I, editor. Morphometry of drainage basins. Amster dam: Elsevier*

*9.* Sinha, N.K.P. (1966): *northern Rupununi, British, Guiana. Ph. (Unpublished), Department of Geography, McGill University, Montreal, Canada.*

*10.* Stoddart, D.R. (1965): *Review and reassessment. Progress in Physical Geography, 1, pp.159 –222.*

*IN PROCEEDINGS OF 25th HYDRO 2020, INTERNATIONAL CONFERENCE, NATIONAL INSTITUTE OF TECHNOLOGY ROURKELA, ODISHA, INDIA 26-28, March 2021, ISBN 978-93-90631-56-8*

Paper ID - 182

# Evaluation of hydrodynamics and sedimentation due to construction of jetty

A K Singh1 Naval S Jagatap2 L.R. Ranganath3 J.D. Agrawal4

*1Scientist B, Central Water and Power Research Station, Pune- 411 024, India.*
*2Research Assistant, Central Water and Power Research Station, Pune- 411 024, India.*
*3 Scientist D, Central Water and Power Research Station, Pune- 411 024, India.*
*4Scientist E, Central Water and Power Research Station, Pune- 411 024, India.*
*Email: dak_singh@rediffmail.com*

## Abstract

Gujarat with its favorable location and availability of a long coastline is a prime destination for executing maritime economic activities. The increasing importance attached to maritime economic activities has further led to the development of many port related activities. Okha port is an all-weather, non-major intermediate port handling dry-bulk cargo, owned and managed by the Gujarat Maritime Board (GMB). It is located in the North-West coast of Saurashtra Peninsula, at the mouth of Gulf of Kutch, Devbhumi Dwarka District, Gujarat.Hydrodynamics and sedimentation studies were conducted using MIKE 21 HD FM and MIKE 21 ST sediment transport models to evaluate the tidal hydrodynamic behavior of flow and probable siltation pattern in the port area with a 200 m x 20 m proposed Jetty. The computational model considered for tidal flow and sediment simulation covered an area of 22 km x 18 km. The model area covers the jetty region including the Beyt Dwarka jetty.From the hydrodynamic studies it was observed that with construction of proposed Jetty and approach channel there is no cross flow which is conducive for the proposed development. The siltation observed in the Jetty area and approach channel is very less this may be attributed due to the hard strata/ rocky bed in the vicinity, which indicates that the proposed jetty construction is feasible from siltation point of view.

***Keywords:*** *hydrodynamics, sedimentation, harbor, dredging, breakwater*

## 1.0 Introduction

Gujarat is the nearest maritime outlet to Middle East, Africa and Europe for India. 32% of total national cargo is handled only by Non – Major Ports in Gujarat (2015-16). With 49 ports which includes 1 major port and 48 non-major ports Gujarat state has the highest number of operational ports and commercial cargo ports. To meet the ever-increasing demand for port development and to sustain, facilitate and excel in developing multipurpose port and logistic facilities and shipping related industry via its competent services and timely infrastructure development Gujarat is leading its way in port development.

Okha port is an all-weather; non-major intermediate port handling dry-bulk cargo, owned and managed by the Gujarat Maritime Board (GMB). It is located in the North-West coast of Saurashtra Peninsula, at the mouth of Gulf of Kutch, Devbhumi Dwarka District, Gujarat. Latitude: 22o 27’ 59” N Longitude: 60o 04’ 10” E. The port primarily imports coal, coke, wheat, sulphur, fertilizers, lime stone and exports calcium bauxite, onion, clinker, raw bauxite, chemicals, soda ash. A 200 x 20 m jetty is proposed in front of back up area between DCB pier and the passenger jetty at Okha Port to enhance the port operations. A mathematical model study to evaluate the conditions due to proposed Jetty was done and is presented in this paper. Figure 1 (A-B) show the location of the proposed area. Figure 1(A). Location Map of Proposed Site at Okha.

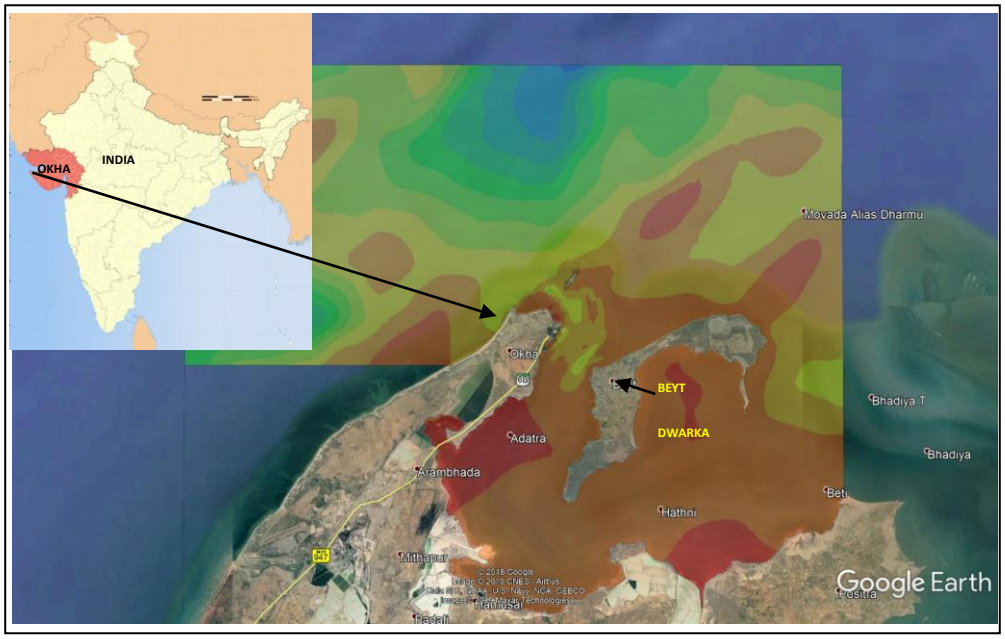



**Figure 1(A)** Location map of proposed site at Okha

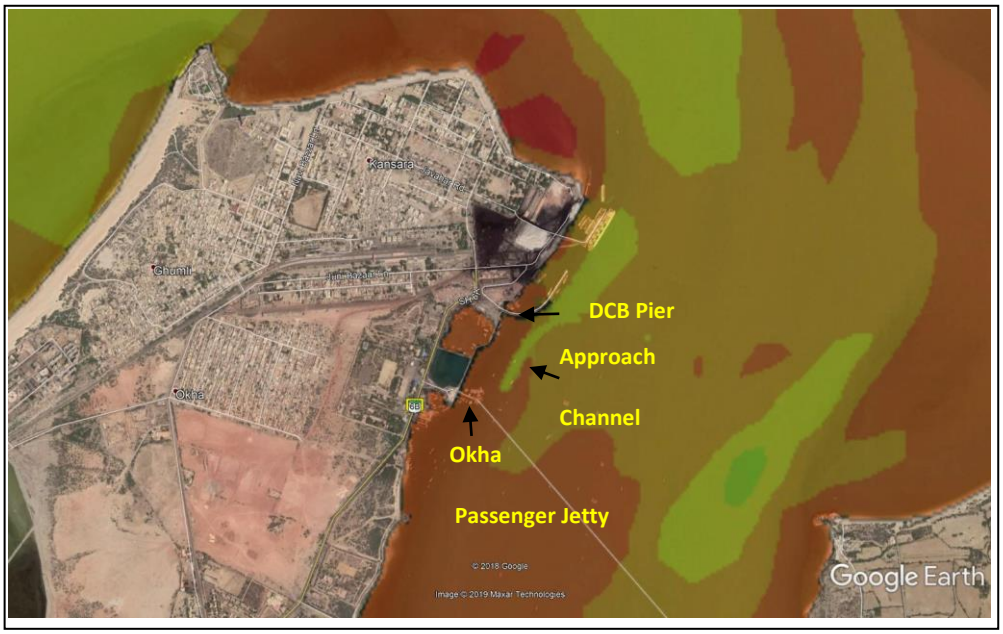



**Figure 1(B)** Proposed site at Okha

## 2.0 Methodology

MIKE-21 HD model was used to simulate tidal flow pattern in the region using the information about the bathymetry and other hydraulic parameters like tide, current, waves etc. The model was calibrated for hydrodynamics aspects by comparing the currents in existing condition with the field observed data available. The hydrodynamic model studies include simulation of flow field for the existing conditions as well as with the proposed construction of jetty and approach. These model studies help us in evaluating the probable changes in the hydrodynamic conditions and formation of tidal circulations, if any, due to the proposed developments. Sediments are being carried by tidal currents and the strength of this current at

any instant in space and time is responsible for siltation/erosion. The sedimentation aspect was simulated using MIKE21-ST/MT model using sediment characteristics at the site. The sediment transport model is used to simulate siltation pattern in and around the Okha Port, considering both tide and wave induced currents. These studies predict the probable zone of siltation and erosion around the proposed jetty at Okha Port.

## 3.0 Data analysis

The data required for the model studies are mainly bathymetry, tide, waves, wind, currents and sediment data. The details of the field data collected along with the locations are shown in the Figure 2.

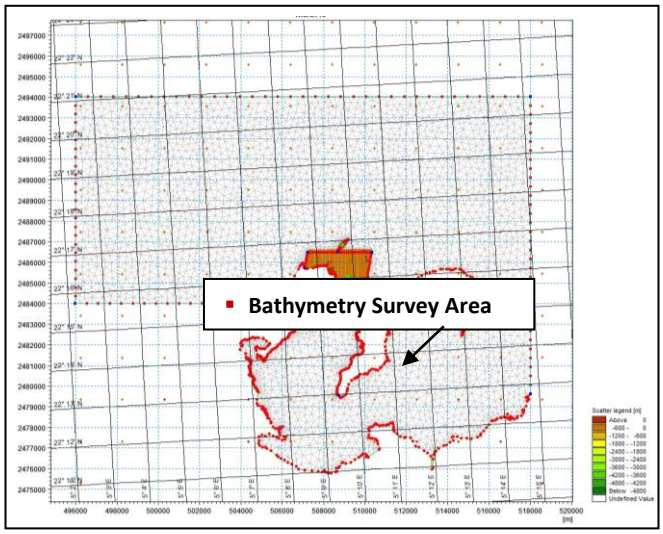



**Figure 2** Bathymetry survey area

### *3.1 Bathymetry*

The bathymetric data for the offshore region was obtained by bathymetry survey as shown in Figure 2. at Okha Port covering an area of 9 km2 into the sea at 50 m line spacing. The bathymetry data is used for development of computational model.

### *3.2 Tide Data*

The tide data was obtained from MIKE CMAP during the period of April 2019. Time series plot of water level variation during the period tide data from CMAP is shown in Figure 3.

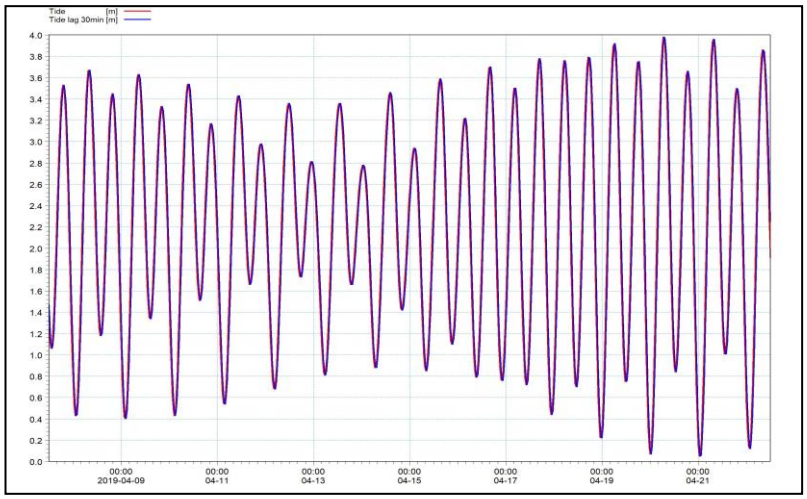



**Figure 3. Boundary tide**

### *3.3 Current Data*

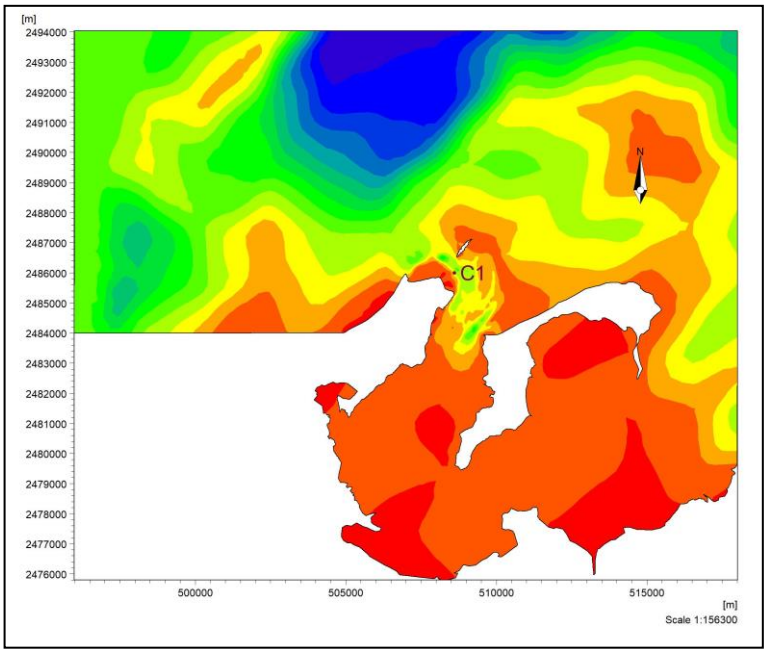



**Figure 4. Current observation locations (C1)**

The current measurements were available at C1 location (22°28’34.80” N, 69°5’08.46” E) as shown in Figure 4. The maximum current observed at the surface, mid-depth at this station were 1.4 m/s whereas the peak current at the bottom was 1.2 m/s. The minimum currents were 0.03 m/s and 0.02 m/s at surface and bottom respectively whereas the minimum current at the mid-depth was 0.5 m/s. The current directions at all levels were dominantly 180° during the flood tide and 30° during the ebb tide. This data was used for model calibration the current plot is shown in Figure 5.

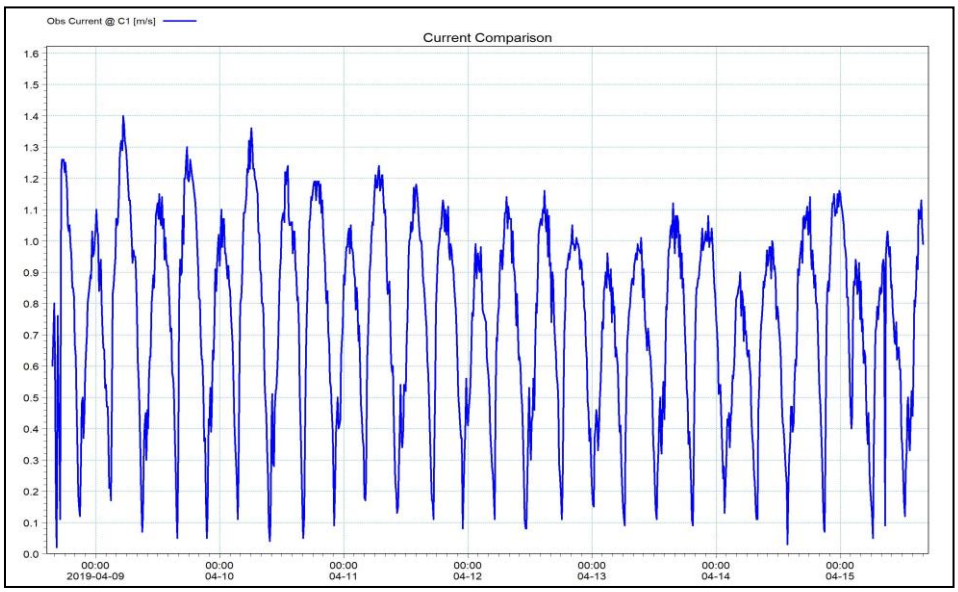



**Figure 5. Observed current**

## *3.4 Sediment Data*

### *3.4.1 Suspended sediment concentration*

The suspended sediment in the seawater sampling was available at two sites Stn. SW1 (22°28'00.16" N, 69°4'46.13" E) and Stn. SW2 (22°28'55.00" N, 69°4'46.58" E). The SSC measurements were ranging from a minimum of 20 mg/l to maximum 68 mg/l during the survey period.

### *3.4.2 Bed material*

The seabed sediment samples data was available for two locations SS1(22°28'00.16" N, 69°4'46.13" E) and SS2 (22°28'55.00" N, 69°4'46.58" E). The $d_{50}$ for the sample determined as fine sand was 0.23 mm.

**Table No. 1** Bed sample

| | Classification of Soil | Coarse Sand % | Medium Sand % | Fine Sand % | Silt & Clay % |
|---|---|---|---|---|---|
| SS1 | Fine Sand | 9.6 | 11.7 | 63.9 | 14.8 |
| SS2 | Medium Coarse Sand | 45.1 | 47 | 7 | 0.9 |

## 4.0 Computational model for hydrodynamic studies

The computational model considered for tidal flow and sediment simulation covered an area of 22 km x 18 km. The model area covers the jetty region including the Beyt Dwarka jetty. The complete model area has been discretized into computational coarse and fine mesh near proposed development. Figure 6. shows the 2-D view of the computational model in existing condition.

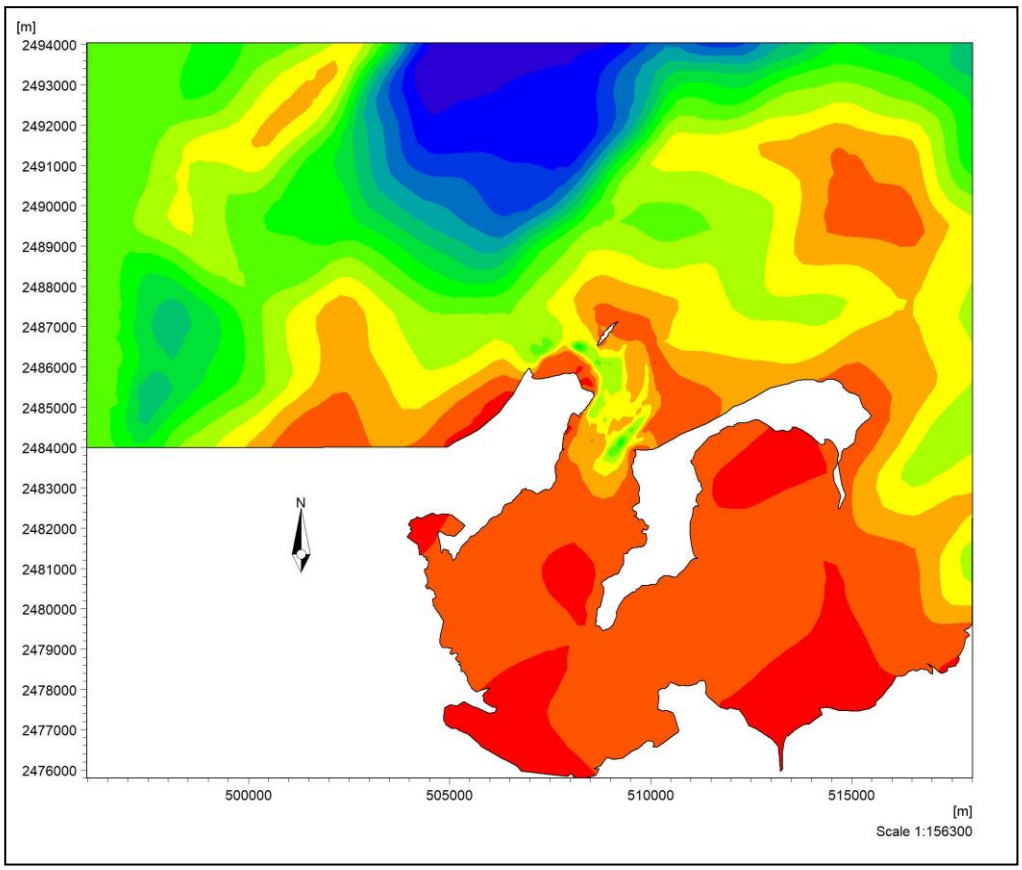



**Figure 6** 2-D View of computational model (existing)

### *4.1 Simulation of flow field with existing condition*

The studies were conducted with the existing conditions in the jetty area and Beyt Dwarka area. Initially the flow simulations were carried out by providing tide with a tidal range of 4 m, as the current observations at C1 location was also available for the same time near proposed location. The tidal boundaries were provided along the Western and Eastern boundaries with appropriate phase lag. As the flow is almost parallel to the contours along the southern boundary, no cross flow near boundary was considered. The model was calibrated with the observed current near proposed location. The typical velocity vector plots during different phases of the spring tide are shown in the Figure 7 (A-B).

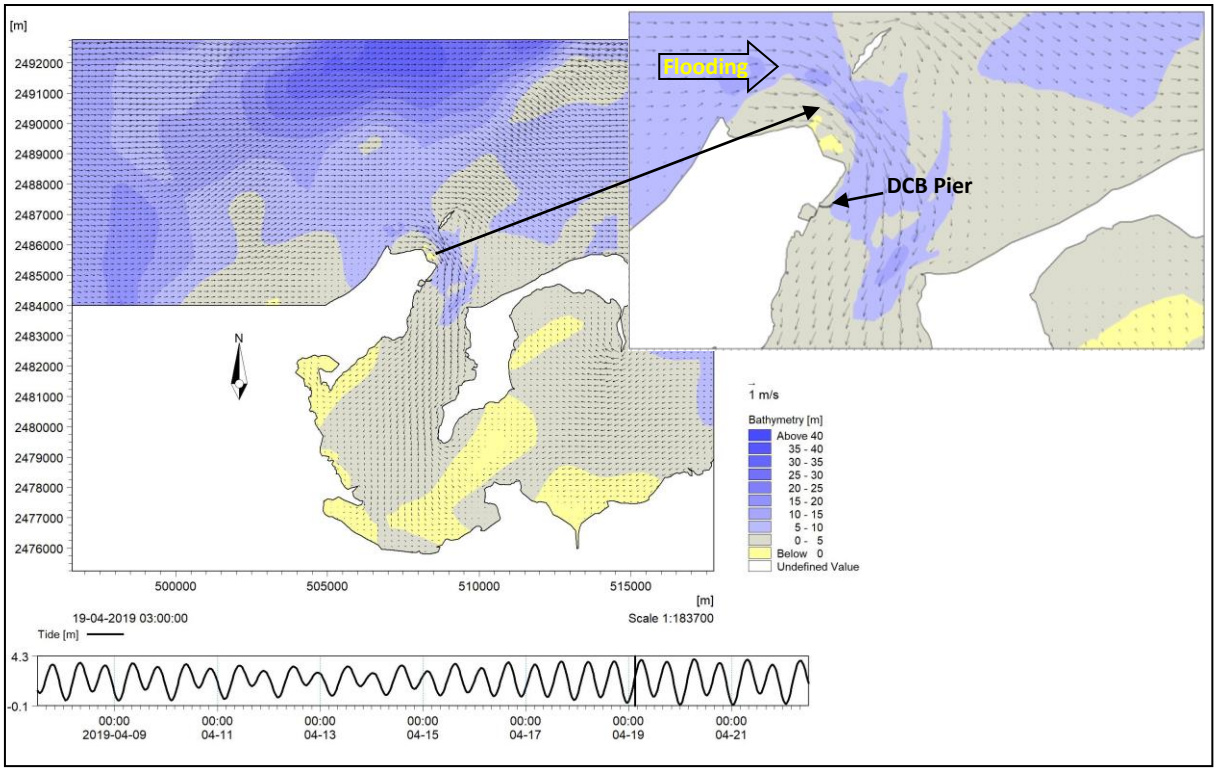



**Figure 7(A)** Typical flow field during peak flood (existing)

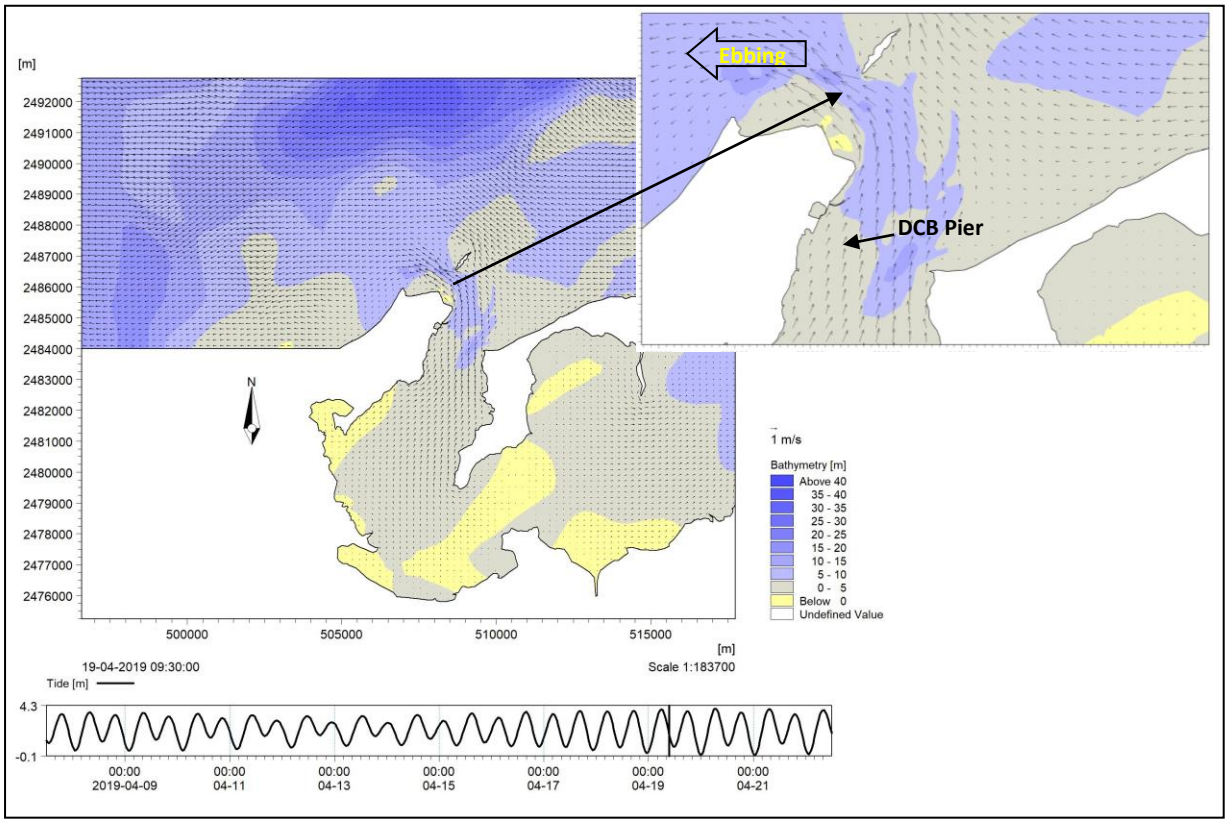



**Figure 7(B)** Typical flow field during peak ebb (existing)

From the simulations it was observed that there was no cross circulation near the jetty area and the current at C1 location was observed to be 0.02 to 1.4 m/s during spring tide and it varies from 0.08 m/s to 1.0 m/s during neap tide. The comparison of currents with the field observed and a model result is shown in Figure 8. It was observed that the computed current matches well with the observed current at C1 location. Thus, the model was calibrated and same model setup was then considered for prediction of flow conditions for the different proposals.

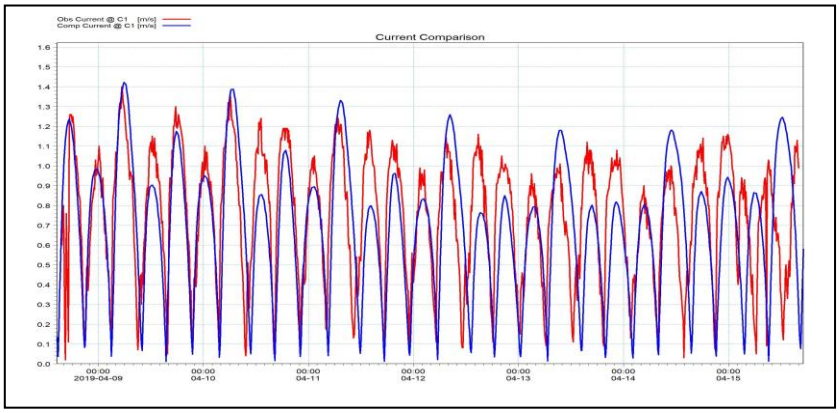



**Figure 8** Comparison of currents (observed Vs computed)

## *4.2 Simulation of Flow Field with Proposed Jetty*

The same model set up of existing condition was used to simulate hydrodynamics for the proposed layout. 2-D view of the computational model is shown in Figure 9. It is proposed to construct a 200 x 20 m jetty in front of back up area between DCB pier and the passenger jetty at Okha Port with approach channel and same has been interpreted in to the model to simulate flow conditions for the proposed layout.

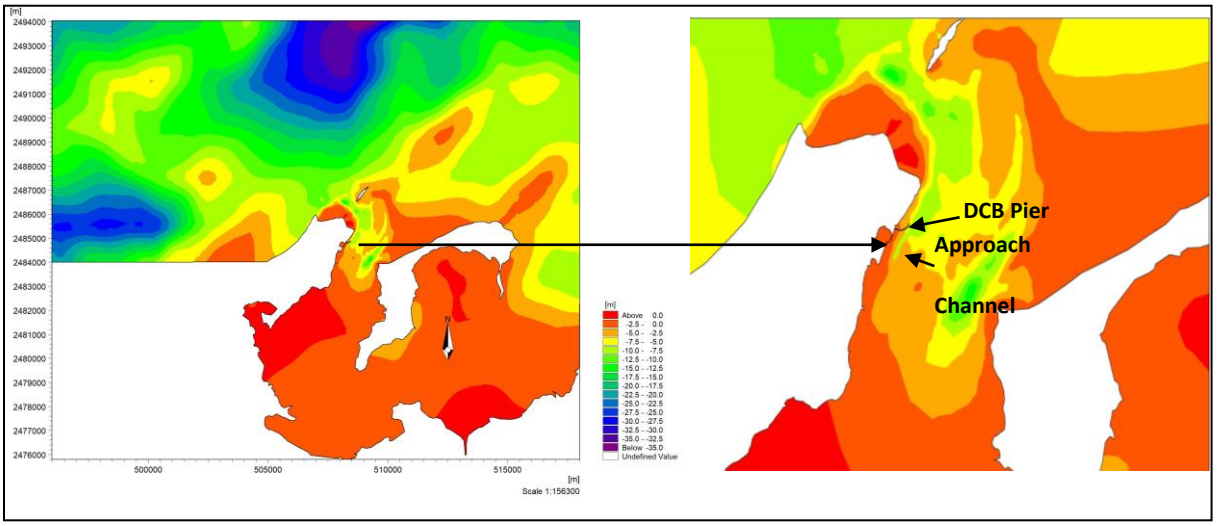



**Figure 9** 2-D view of computational model proposed

The boundary conditions for the model would remain same as that of existing condition. The typical velocity vector plots during different phases of the spring tide are shown in the Figure 10 (A-B). It was observed that there is no cross circulation and no significant change in current velocity near the jetty area and the current varies from 0.03 to 1.4 m/s during spring tide and it varies from 0.01 m/s to 0.95 m/s during neap tide.

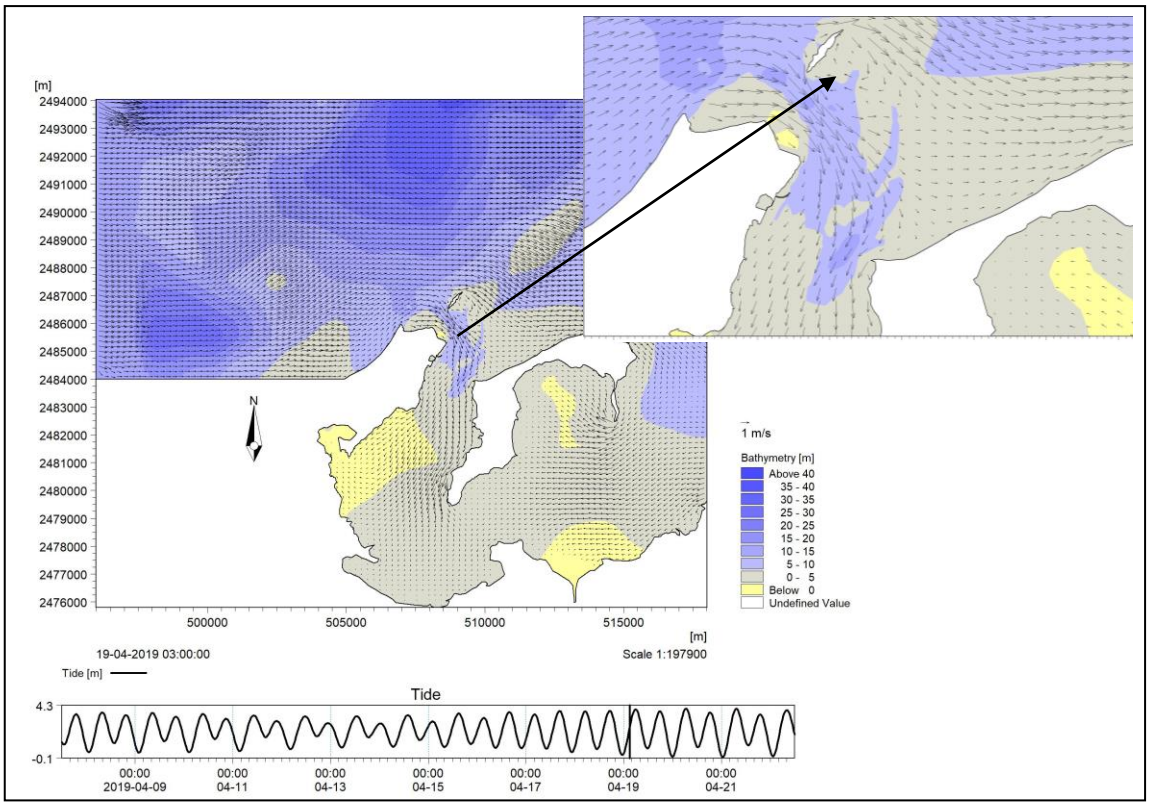



**Figure 10(A)** Typical flow field during peak flood (proposed)

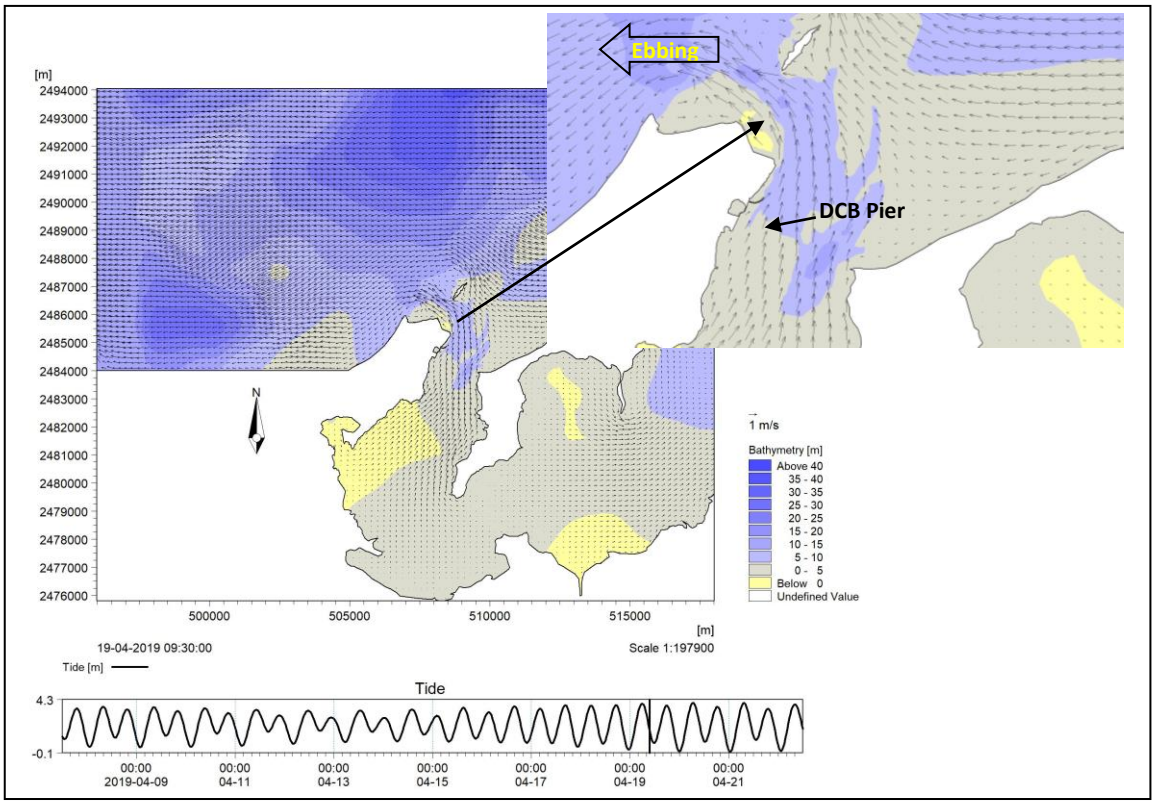



**Figure 10(B)** Typical flow field during peak ebb (proposed)

## 5.0 Sedimentation studies

### *5.1 Sedimentation Studies with Existing Condition*

Initially the sediment transport studies were carried out with the existing conditions in the jetty area and Beyt dwarka area. The sedimentation during different phases of the tide was observed. The siltation pattern for existing condition is shown in the Figure11.

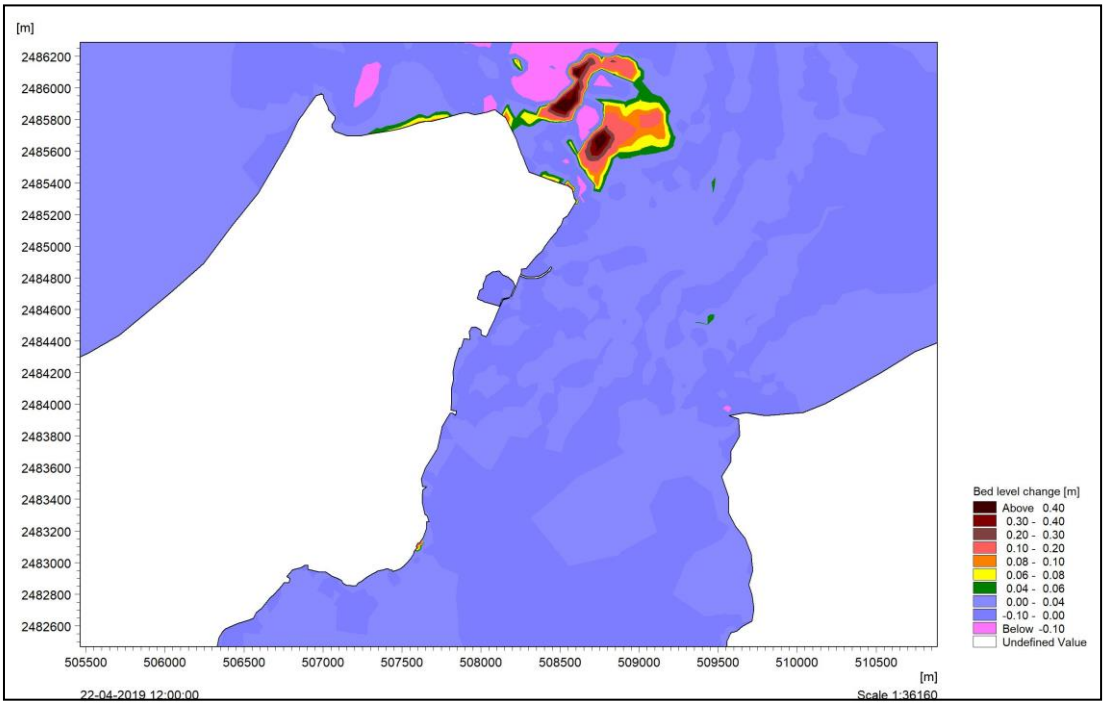



**Figure 11** Siltation pattern (existing)

It is found that minimum siltation is observed around the jetty area. Further studies were conducted with the proposed construction of Jetty to study the changes in sedimentation pattern in order to study its impact on the proposed construction.

### *5.2 Sedimentation studies with the proposed jetty construction*

The sediment transport studies were carried out with the same model set up of that of existing condition after incorporating the proposal of Jetty construction. The 200 m x 20 m jetty is proposed to be constructed in front of back up area between DCB pier and the passenger jetty at Okha Port. 22°27'58.57"N, 69°4'44.73"E location was incorporated. The model was simulated for a simulation period of 30 days. The sedimentation during different phases of the tide was observed. The siltation studies indicated that the siltation in the Jetty area and approach channel is very less and this may be attributed due to the hard strata/ rocky bed in the vicinity. The siltation pattern with proposed layout is shown in the Figure 12 (A-B). It also shows the siltation pattern after one month near the proposed jetty and approach channel is of the order of 0.08 m.

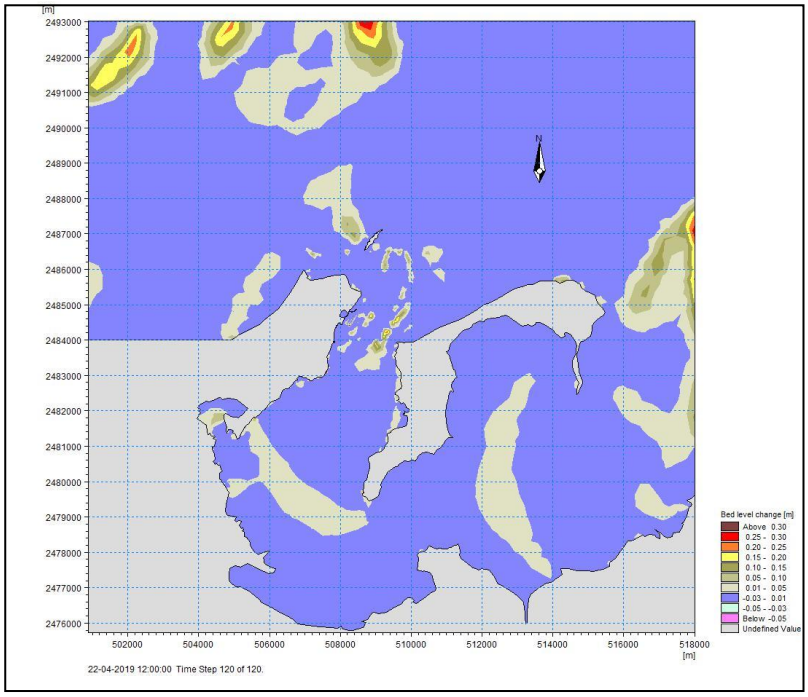



**Figure 12 (A)** Siltation pattern (proposed)

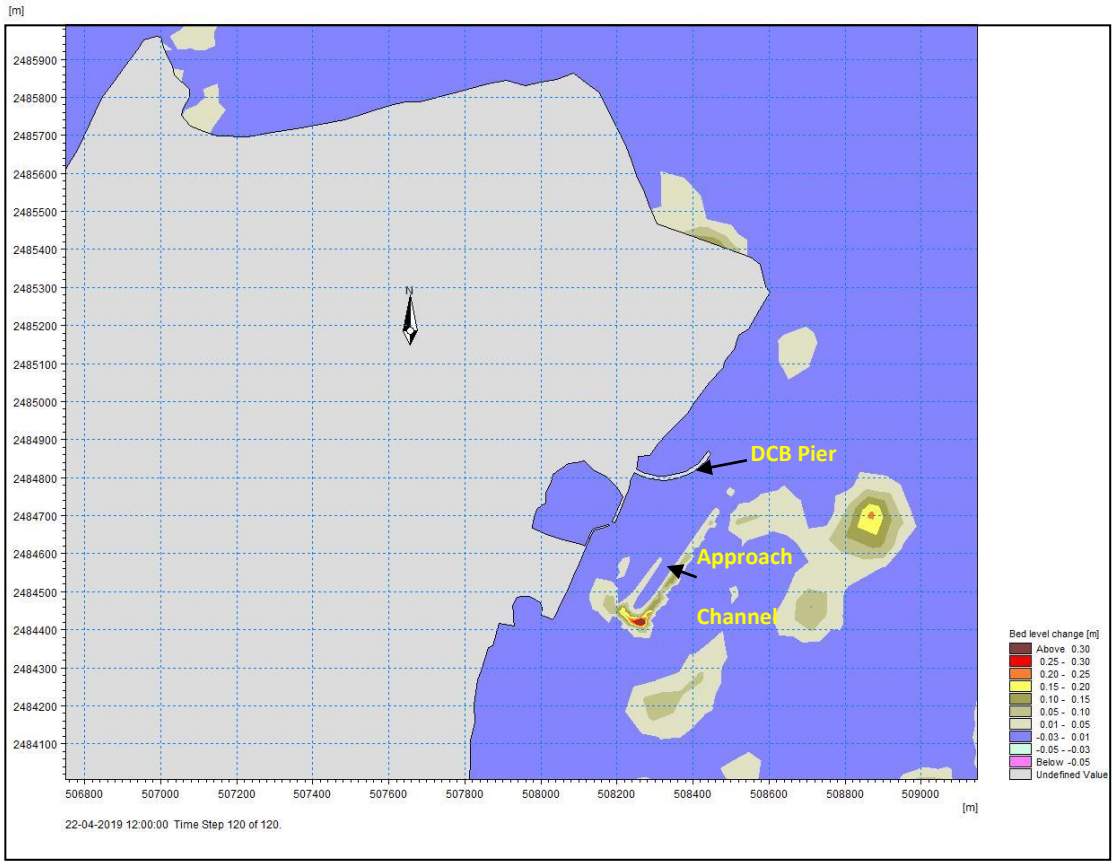



**Figure 12 (B)** Siltation pattern in approach channel (proposed)

## 7.0 Conclusions

The mathematical model studies for hydrodynamics and sedimentation were carried to evaluate flow condition and sedimentation pattern near proposed location of jetty. The mathematical models MIKE21-HD and MIKE21-ST were used for simulation of hydrodynamics and sedimentation respectively. The flow conditions and siltation in the vicinity of the proposed jetty location were studied.

- From hydrodynamic studies with proposed layout it is noticed that flow direction is almost parallel to the contours along the northern and southern boundary and it was observed that there is no cross flow which is conducive for the proposed development.
- The siltation observed in the Jetty area and approach channel is very less. This may be attributed due to the hard strata/ rocky bed in the vicinity, which indicates that the proposal of jetty is feasible from siltation point of view as well.
- The estimated capital dredging in approach channel would be in the order of 0.153 M-cum and annual maintenance dredging in approach channel would be of the order of 50000 cum.

It is suggested that periodical maintenance dredging is required to maintain proper draft for smooth navigation of vessels and the dredging data is to be monitored regularly and reported for analysis. The analysis of such data can be used to identify the annual maintenance dredging in the approach channel.

## Acknowledgements

The authors wish to thank Shri. A.K. Agrawal, Director, CWPRS for his consistent support, encouragement and kind consent for publishing this paper.

## Reference

Technical Report No 5799, March 2020 “Mathematical Model Studies to Evaluate Hydrodynamics and Sedimentation Due to Proposed Construction of Jetty and Approach at Okha Port, Gujarat”.

*IN PROCEEDINGS OF 25th HYDRO 2020, INTERNATIONAL CONFERENCE, NATIONAL INSTITUTE OF TECHNOLOGY ROURKELA, ODISHA, INDIA 26-28, March 2021, ISBN 978-93-90631-56-8*

Paper ID - 188

# COMPARISON OF SEDIMENTATION IN DREDGED OPEN BASIN AND ENCLOSED BASIN– A CASE STUDY

*[1]V.B. Sharma[2]M D Sawant[3]Dr. Prabhat Chandra*

*[1]Scientist "B" [2]Assist. Research Officer[3]Scientist "E",*
*Central Water and Power Research Station, Khadakawasla, Pune-411024;*
***Email:**vipin_bihari@yahoo.com*

## ABSTRACT

Technical feasibility and maintenance cost of any harbour play an important role in deciding its layout. Cost of Maintenance dredging is a major factor in maintenance cost of a harbour. In general, it is observed that obstruction of flow causes sedimentation in the area but this is not always true. The other phenomena which is important in sedimentation is the amount of sediment flux moving over the dredged area as part of sediment flux gets trapped in the dredged area and the tidal exchange. This phenomenon was observed while carrying out studies for Mormugao Port Trust to develop POL berth, fisheries harbour, Passenger, Port craft jetties and Mooring dolphins in Vasco bay, Goa. Maximum spring tidal range in at Mormugao is 2.4 m while the maximum currents in the area are 0.30 m/s. The bed material in the Vasco bay area is of soft - silty - clayey type.

The proposed developments in Vasco bay included construction of; a POL berth (length 294 m) dredged to (-) 13.1 m below chart datum, Passenger jetty and Port craft jetty and a fisheries harbour dredged to (-) 3.1 m and Mooring dolphins. The studies indicated that the Scenario – II with solid bund structures has been found to be more suitable from the considerations of maintenance dredging compared to Scenario – I with piled structure and maintenance dredging would reduce to 0.22 Mcum from 0.34 Mcum. In the present study, 2-Dimensional hydrodynamic model MIKE 21 HD, spectral wave model MIKE 21 SW and mud transport Model, MIKE 21 MT have been used to simulate the flow field and sediment transport in the existing and the proposed scenarios under prevailing tidal and wave conditions.

***Keywords:**Tide, current, sedimentation, maintenance dredging*

## 1. INTRODUCTION

Coastal areas play an important role in the socio-economic development of a country because seaborne trade remains the cheapest method of transporting large quantities of goods over long distances. Globalization requires movement of large quantities of raw materials and finished goods, and consequently there is strong emphasis on expansion of existing ports and harbours.Accordingly Mormugao Port Trust (MPT) proposes to develop POL berth, fisheries harbour, Passenger, Port craft jetties and Mooring dolphins in Vasco bay, Goa. The Vasco bay is located at about 3.0 km upstream from the existing breakwater at Mormugao port. The size of the Vasco bay is about 800m x 1000m and the existing depths lies between(-)2 m to (-)4m below chart datum. The layout consists of POL jetty with dredged of (-) 15.1 m while in the fishing harbour the dredged levels are (-) 3.1 m (Figure -1).The capital dredging for this development is estimated to be about 2.25 Mcum. It is proposed to determine the impact of construction on hydrodynamics and sedimentation considering the structures to be on piles (Scenario-I) and on solidrubble bund (Scenario-II).Accordingly, 2-Dimensional hydrodynamic model MIKE 21 HD, spectral wave model MIKE 21 SW and mud transport Model, MIKE 21 MThave been used to simulate the flow field and sediment transport in the

existing and the proposed scenarios under prevailing tidal and wave conditions and a suitable option has been evolved.

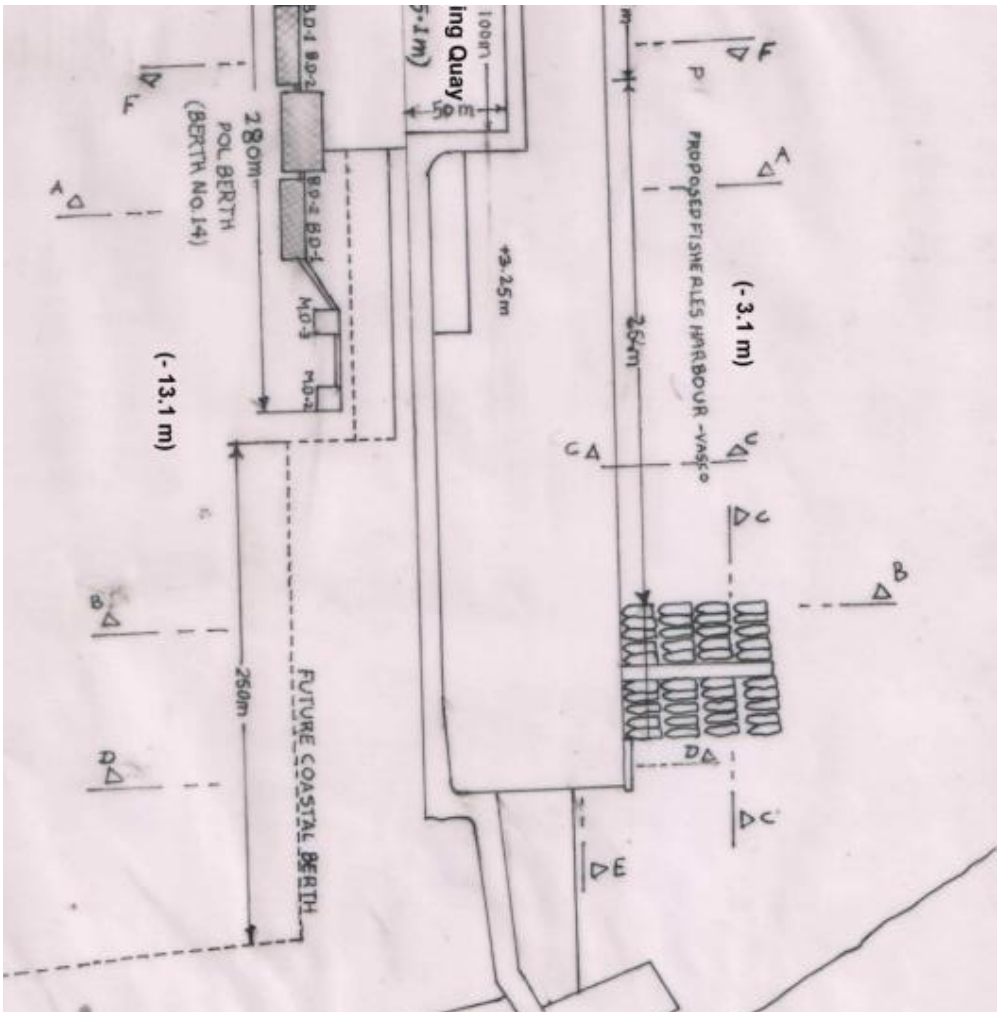



**Figure1: Layout of development in Vasco bay**

## 2. ANALYSIS OF PROTOTYPE DATA

The basic inputs for hydrodynamic and sedimentation studies are bathymetry, tidal data, current data, wave data, sediment characteristics, suspended sediment concentration etc. Bathymetry was obtained from available hydrographic charts as supplied by the MPT and from MIKE-21 C map dataupto (-) 56 depth contour as shown in Figure 2. Tides in the estuary are semidiurnal with pronounced diurnal inequality having considerable difference in the tidal ranges and the elevation of low waters and high waters in the successive tidal cycles. The spring tidal range in the Zuari estuary is about 2.4 m. A typical observed tide at Mormugao is shown in Figure 3.

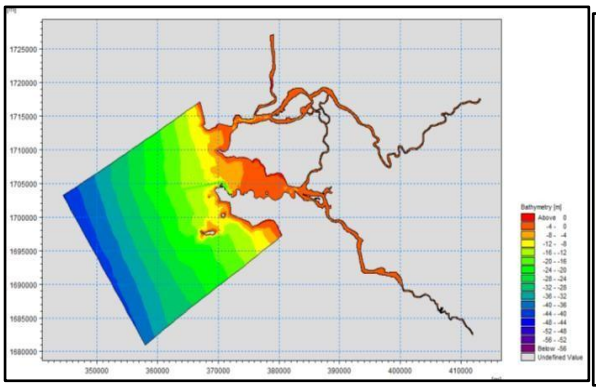


**Figure 2: Bathymetry of model area**

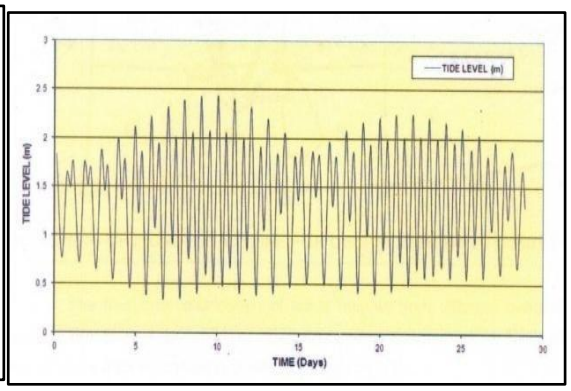



**Figure 3: Observed Tide at Mormugoa Port**

On the basis of the analysis of water sample data, the average sediment concentration has been considered as 0.04ppt during the monsoon season and 0.012 ppt during the non-monsoon season in the port and channel areas. $D_{50}$ of suspended sediment is about 0.002 mm under dispersed state and the bed material may be classified as soft – silty and clayey type.During monsoon period, flood discharge in Mandovi river is about 4 to 5 times higher as compared to the Zuari river. The maximum river discharges in Mandovi and Zuari rivers have been observed to be 4000 $m^3/s$ and 970 $m^3/s$ respectively. The average discharges in Mandovi and Zuari river are about 1000 $m^3/s$ and 250 $m^3/s$ respectively.

## 3. MODELING APPROACH

Two Dimensional hydrodynamic model, MIKE 21 HD and mud transport Model, MIKE 21 MT are used to simulate flow field and transport of sediment in existing as well as proposed conditions of fishery harbour for predetermined boundary conditions.The Hydrodynamic Module is based on the numerical solution of the two- dimensional shallow water equations integrated over the depth and assumed to be incompressible ReynoldsaveragedNavier-Stokesequations. The governing equations behind the MT module are essentially based on Mehta et al. (1989). In MIKE-21 HD model, turbulence modelling is included in the momentum equations in the terms containing laminar stresses and Reynolds stresses. It can be either used as a constant in the horizontal stress terms or by using the Smagorinsky's formulation (1963) to express sub-grid scale transports by using an effective eddy viscosity related to characteristic length scale (Lily, 1989).

The wave induced radiation stresses are the depth integrated and wave averaged excess momentum fluxes due to waves as defined by Longuet-Higgins and Stewart (1964). Radiation stresses are responsible for set-up, set-down and longshore current in the near shore zone. This approach is used in MIKE-21 SW model to simulate radiation stresses.

The cohesive sediment transport module or mud transport (MT) module deals with the movement of mud in a fluid and the interaction between the mud and thebed.The transport of the mud is described by equation given by Teisson, 1991.
The two dimensional depth averaged sediment transport model (MIKE- 21MT/AD) takes into account conservation of mass of sediment, depth averaged velocities, longitudinal dispersion coefficient, lateral diffusivity, settling velocity, critical deposition stress, and critical erosion stress for the given sediment. Flocculation of mud particles is described as function of

suspended sediment concentration as given by Burnt 1986. The numerical values of these parameters were modified within their ranges such that the prevailing sedimentation in the existing approach channel is achieved.

## 4. MODEL CALIBRATION

The computational model considered for tidal flow simulation covered an area of 70 km x 40 km. The model area covers the entire proposed port area upto (-) 56m depth contour. In order to take into account the impact of waves on hydrodynamics, MIKE-21 SW model was used. MIKE-21 NSW model was simulated for average significant wave height of 3.0 m for the waves coming from west direction corresponding to the Southwest monsoon.

The model area consists of 5 open boundaries: two river boundaries and three sea boundaries. As the flow is almost parallel to the contours along western boundary, no cross flow condition was provided at this boundary. The model parameter like bottom roughness coefficient, surface elevation etc. were adjusted to get the required prototype conditions in the model. The model was simulated for a period of one month. The vector velocity plots in peak flood and ebb phase of tide are shown in Figures 4.

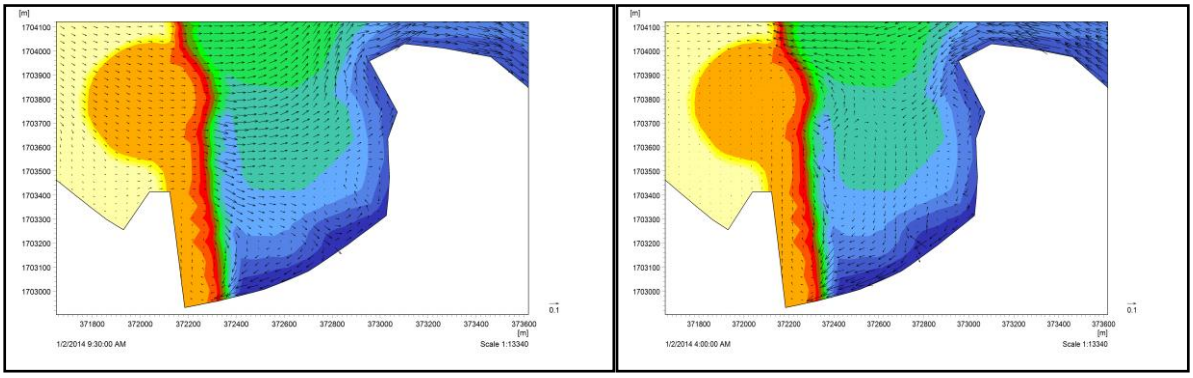



**Figure 4: Vector Velocity Plot in Vasco Bay during Flooding and Ebbing**

## 5. MODEL EXPERIMENTS

- **In Scenario-I (All structures on Piles)**

In this scenario, the change in magnitude of currents and movement of sediment flux prevailing in the region would be insignificant. The existing bathymetry was modified to incorporate proposed dredging of -15.1 m in front of POL jetty and -3.1 m in fishing harbour area. The model was simulated for a period of 15 days to cover both spring and neap tide without changing the hydraulic parameters of the model for which model was calibrated. . The flow conditions obtained in the Vasco bay during flood and ebb tides after simulating the proposed dredged levels are shown in Figure 5.

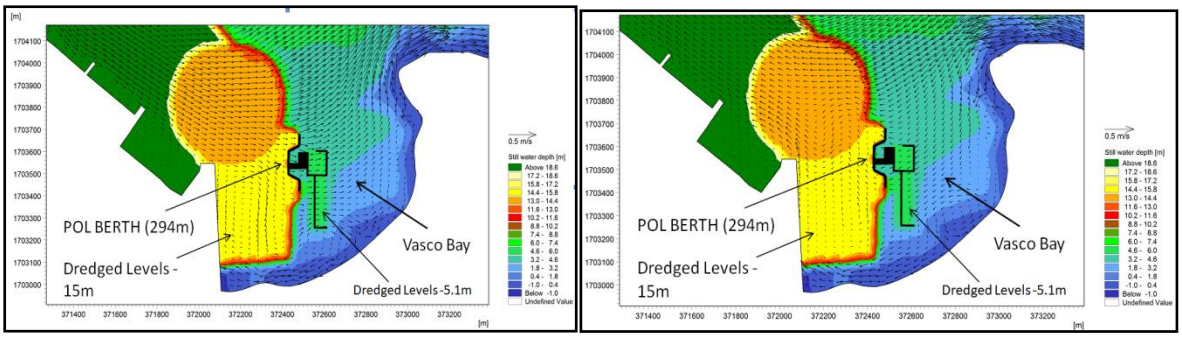



**Figure 5: Hydrodynamic condition in Vasco bay at the strength of flood tide and Ebb tide**

It can be observed from these figures that the currents are very weak in the bay area and the maximum current is about 0.10 m/s both during flood and ebb tides and some weak circulation patterns are also observed in the Vasco bay with their strengths less than 0.10 m/s. Hence, there would be no navigation and berthing problems in the Vasco bay on account of prevailing currents.

Mud transport model was simulated for 15 days to estimate sedimentation in the proposed condition using MIKE-21MT model integrated with MIKE-21HD. The siltation pattern after 15 days during the monsoon season are shown in Figure -6. The model studies indicated that the annual depth of siltation in the dredged portions in the Vasco bay for the proposed development would be about 1.5 m. The annual maintenance dredging requirement would be about 0.34 Mcum which is about 15% of the total capital dredging. The sedimentation in the dredged areas occur due to the flow crossing the Vasco bay during flood and ebb tides and subsequent deposition of the suspended sediments while crossing the deepened areas near POL berth, passenger and port craft jetties and in the fisheries harbour. Most of the siltation, say more than 90%, occurs during the four months of the southwest Monsoon season.

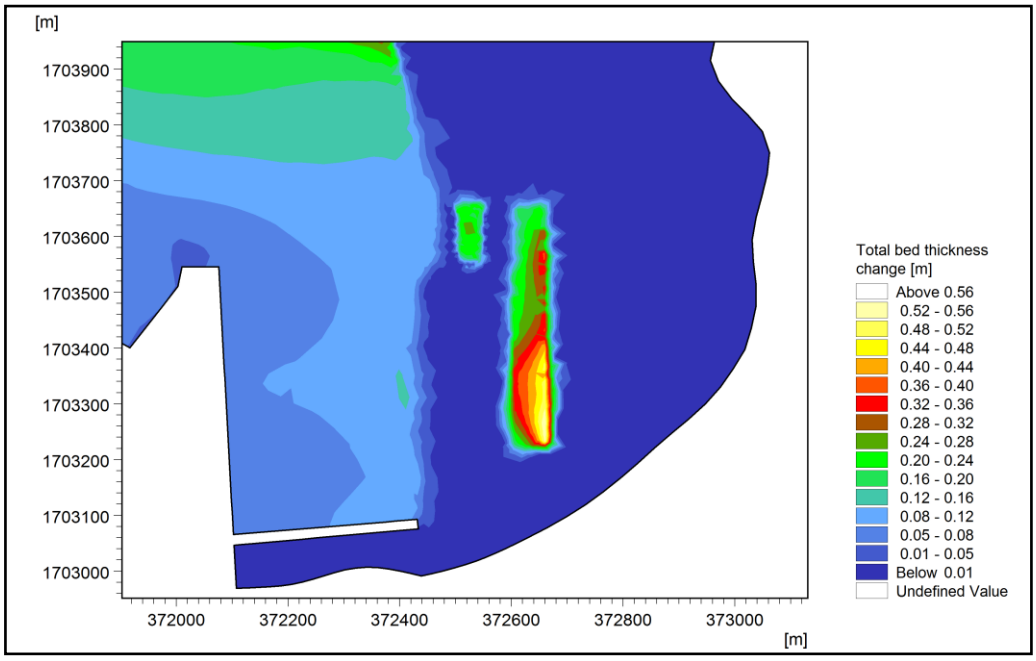



**Figure 6: Siltation patterns in Vasco bay for the proposed Scenario-I**

- **In Scenario-II (Solid bund Structures)**

The hydrodynamics model was simulated for scenario-II without changing the hydraulic parameters for which model was calibrated. The Figure7 shows the flow conditions in the Vasco bay area at the strength of flood and ebb tides respectively.

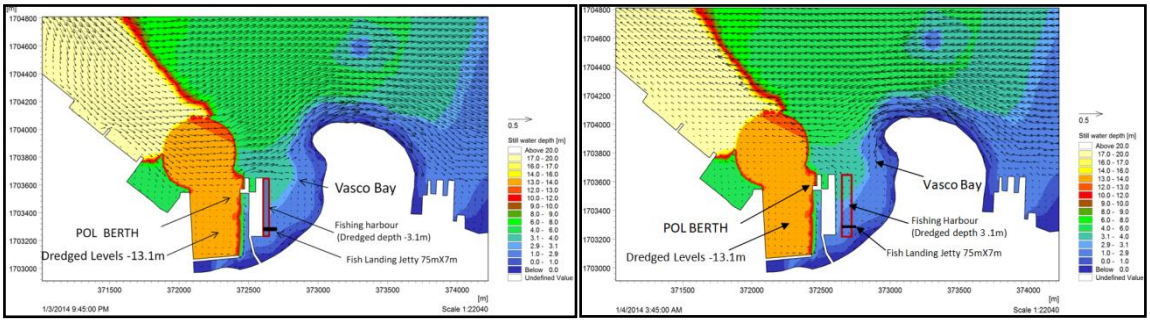



**Figure7: Hydrodynamic condition in Vasco bay at the strength of flood tide**

It can also be observed from these figures that the currents are very weak in the Vasco bay area and the maximum current is about 0.10 m/s both during flood and ebb tides and some weak circulation patterns are also observed in the Vasco bay with their strengths less than 0.10 m/s. These currents further reduce to 0.02 m/s after dredging in area of POL jetty and after construction of proposed layout. This indicates that the exchange of flow would reduce in the basin. There would be an overall reduction in the magnitude of currents in the bay due to construction of proposed layout by solid bund.

Mud transport model was simulated for 15 days for this scenario. The siltation pattern after 15 days during the monsoon season is shown in Figure 8. It is observed that due to the less exchange of flow, the maintenance dredging for the proposed solid bund layout would be less. The model studies indicated that the annual depth of siltation in the dredged portions in the Vasco bay for the proposed development would be about 1.0m. The annual maintenance dredging requirement would be about 0.22 Mcum which is about 10% of the total capital dredging.

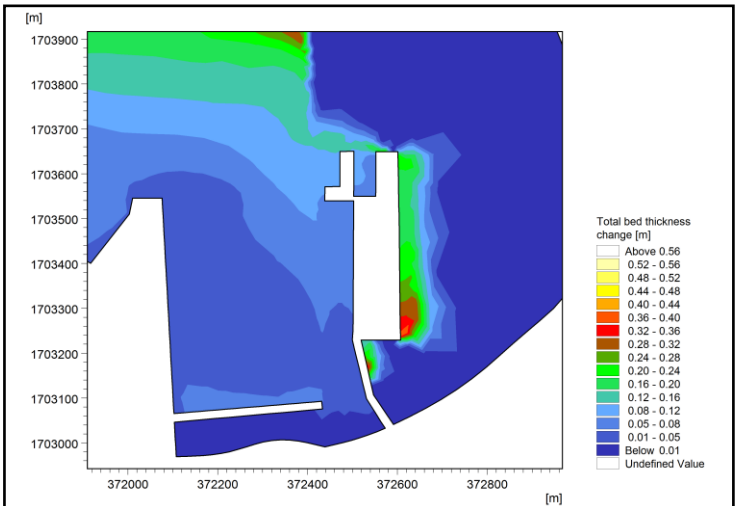



**Figure 8: Siltation patterns in Vasco bay for the proposed development**

## 6. RESULTS AND DISCUSSION

From the considerations of hydrodynamics, free flow of water is always desirable to reduce siltationin dredged portions in case of strong exchange of flow. The dredged portions act like a trap and more sediment get silted up in these areas. The locations of two scenarios at monitoring points P1, P2 and P3 as shown in Figure9 and the comparison of currents are shown in Figures 10. It could be seen from these figures that there is a fall in the magnitude of current in the enclosed portion of POL jetty in Vasco bay for scenario –II which indicates that due to the very less the exchange of flow in the basin with incorporation of solid bunds, it would not act like a trap for sediments.

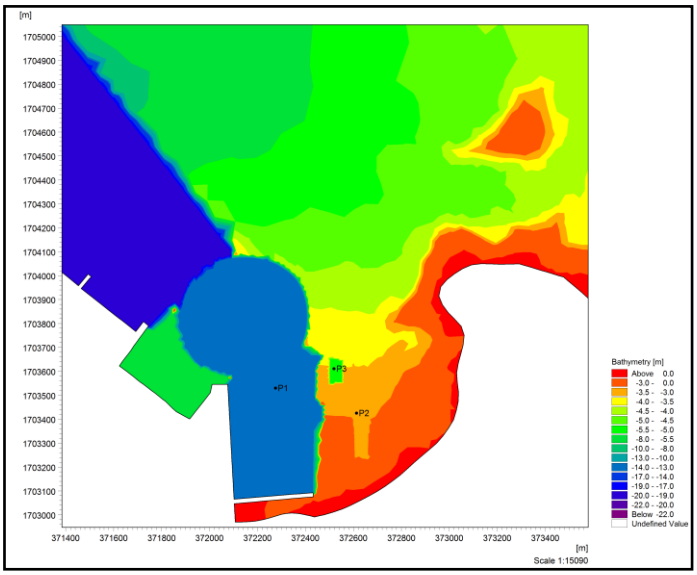



**Figure 9: Locations of monitoring points**

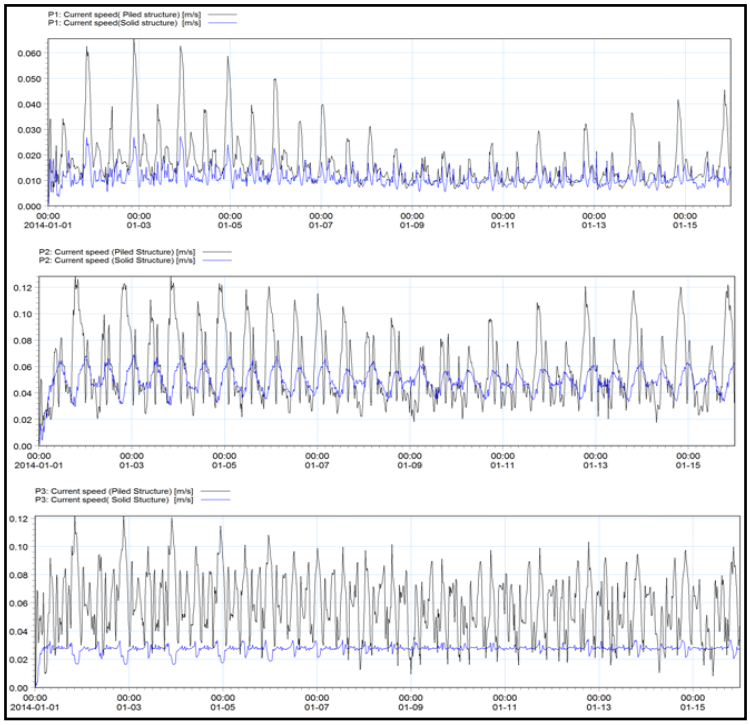



**Figure 10: Comparison of currents at 3 locations**

In general, the currents are quite weak in the Vasco bay area for scenario – I both during flood and ebb tides. Due to the embayment in Vasco bay, the circulation patterns are also noticed in Scenario-I which is too weak to cause any navigational problem in the development area. Siltation in the dredged areas in the Vasco bay occurs as a result of deposition of the suspended sediments. The suspended sediment concentration is much more during the monsoon season as compared to the non-Monsoon season. Most of the siltation is expected to occur during the Monsoon season and the annual depth of siltation in the dredged portions for the proposed development in the Vasco bay is estimated to be about 1.5m. The annual maintenance dredging requirement would be about 0.34 Mcum which is about 15% of the total capital dredging.

For Scenario – II, the POL jetty area is enclosed from three sides. This results in reduction in velocity in the basin. It could be seen from the figure that the currents drop drastically in Scenario –II which reduces the exchange of flow which in turn reduces the sedimentation in the basin marginally as compared to earlier layout (Scenario-I). The annual maintenance dredging requirement would be about 0.22 Mcum which is about 10% of the total capital dredging. In the fishing harbour area, the annual siltation is estimated to be about 1.0 m and the depths would be reduced to about 2.0 m. It would be worthwhile to provide for cushion dredging of about 1.0m to (-) 4.0 m so that during the year, the navigable depths may not be below (-) 3.0 m.

## 7. CONCLUSIONS

- The Scenario – II with solid bund structures has been found to be more suitable from the considerations of maintenance dredging compared to Scenario – I with piled structure and maintenance dredging would reduce to 0.22Mcum from 0.34Mcum.
- The annual depth of siltation in the dredged areas for the proposed development in the Vasco bay and in the fisheries harbour for Scenario – II, is estimated to be about 1.0 m.
- It would be worthwhile to provide for cushion of about 1.0 m by dredging to (-) 4.0 m below CD in the fishing harbour area so that during the year, the navigable depths may not fall below (-) 3.1m.

## ACKNOWLEGDMENT

The authors are grateful to Shri A.K. Agrawal, Director, CWPRS for his guidance and constant encouragement during the course of study. The authors express their deep gratitude for according permission to publish this paper.

## REFERENCES

Burnt, N., 1986 Field settling velocities of estuary muds. In: Estuarine cohesive sediment Dynamics, Edited by Mehta, A J Spring – Veriag, Berlin, Heidelberg, New York, Tokyo, 126-150

Longuet-Higgins, M. S., & Stewart, R. W., 1964, August. Radiation stresses in water waves; a physical discussion, with applications. In Deep Sea Research and Oceanographic Abstracts (Vol. 11, No. 4, pp. 529-562). Elsevier.

Lilly, D. K., 1989, February. The length scale for sub-grid-scale parameterization with anisotropic resolution. In Annual Research Briefs, 1988 (Vol. 1, pp. 3-9)

MIKE 21 (2014). Scientific background, DHI, Denmark.

Mehta, A.J., Hayter, E.J., Parker, W.R., Krone, R.B. and Teeter, A.M., 1989. Cohesive sediment transport. I: Process description. Journal of Hydraulic Engineering – ASCE 115 (8), 1076–1093.

Smagorinsky, J., 1963. General circulation experiments with the primitive equations: The basic experiment. Monthly weather review, 91(3), 99-164.

Teisson, C., 1991. Cohesive suspended sediment transport: feasibility and limitations of numerical modelling. Journal of Hydraulic Research 29 (6), 755–769.

TR No. 5557 (2018). Mathematical model studies to assess the impact of deepening at NMPT, New Mangalore.

*IN PROCEEDINGS OF 25th HYDRO 2020, INTERNATIONAL CONFERENCE, NATIONAL INSTITUTE OF TECHNOLOGY ROURKELA, ODISHA, INDIA 26-28, March 2021, ISBN 978-93-90631-56-8*

Paper ID - 197

# Erosion of river Ganga upstream and downstream of Farakka Barrage- A review

Mayuraksha Bardhan

*River Research Institute, P.O- Mohanpur, District-Nadia, West Bengal, Pin-741246, India*
*Email: mayur.bardhan@gmail.com*
*Mobile No.: +91 9432100700*

## Abstract

The Himalayan Rivers continuously change courses in their lower reaches and the Ganga and its tributaries are no exception. The river Ganga has continuously changed its geometry of meandering in West Bengal during the last three decades. Migration of river Ganga towards the left bank upstream and right bank downstream of the barrage has resulted in unprecedented erosion of the left bank towards Malda district upstream of the barrage and its right bank towards Murshidabad district downstream of the barrage. In an uncontrolled regime, the changing course of the river is governed by skewed hydrography, bank-stratigraphy, influent and effluent seepage, sediment load. After construction of Farakka barrage, the dynamics of bend migration changed appreciably. The sequential maps help to understand how the river Ganga has changed its course. During the period 1968 to 1990, the upstream meander has migrated towards left bank by about 3 km eastward with an average migration rate of about 136 m per year. Between 1990 and 2005, it has further migrated about 4 km eastward which corresponds to an average migration rate of about 266 m per year. On the downstream side, the right bank of the river also has similar erosion problem. Continued erosion of the river upstream and downstream of the barrage has resulted in colossal loss of agricultural and household properties and subjected the poor people living on the banks to unimaginable sufferings. Two Experts Committees (P. Singh Committee in 1980 and G. Keskar Committee in 1996) constituted to explore the possible remedial measures to combat erosion, submitted their reports. Both committees recommended revetments with boulders to protect the banks from impinging currents and construction of spurs to deflect the flow towards the opposite bank. The Government of India has recently constituted the Ganga Control Authority with the objectives of pollution abatement and restoration of minimum ecological flow. It is equally important is to design a scientific land use plan for the flood plain of the river Ganga which shifts its course like a pendulum in the lower reach.

***Keywords:*** *River Bank Erosion; Sediment Load; Skewed Hydrography*

## 1.0 Introduction

River is a general term applied to a natural stream of water flowing regularly or intermittently over a bed in a definite channel following the slope of the land. River changes its own course and shapes the surrounding landscapes in different stages by continuous changing its hydrodynamic and morpho-dynamic processes following the slope, terrain characteristics, rock and soil characteristics, vegetation cover in the region. The old stage of a river is characterized by the low elevation with very gentle slope of land. The river Ganga, the most important river of India, emerges from a glacier at Gangotri , about 7010 m above mean sea level in the Himalayas and flows down to the Bay of Bengal covering a a distance of about 2525 km. Ganga starts its old stage while entering West Bengal (Parua 2010) and swings the Rajmahal hill range and then flows towards south. The Ganga has continuously changed its geometry of meandering in West Bengal during the last three decades. There are instances when the Ganga has gone back to its former courses after reaching the limit of its meander belts, but there is no specific time for these reversals. The bed and suspended load carried by the rivers were trapped in barrage-ponds. The bed of the Ganga experienced uninterrupted sedimentation in the reach upstream of Farakka Barrage (Mandal 2015). After the construction of Farakka barrage, the dynamics of bend migration changed appreciably. What apparently seems to be bank failure is largely the response by

the river system to the massive engineering intervention which impedes the flow of water and sediment load.

## 2.0 Review of Literature

Some literature or Articles are studied by me for preparation of this paper.There are many articles, Case study or documentary available in different Internet sources .Many governmental and non-governmental organisationsare work on Impact of Farakka Barrage and water diversion through Feeder Canal on its upstream and downstream areas. They indicate the different impacts-like-hydrological, geomorphological, social and economical. A report by Banerjee M, on "the impact of Farakka Barrage on the human fabric" emphasis the problem of the rural impeverisation and marginalization and response to the situation faced by the human beings (Banerjee 1999). According to the official report by Irrigation and Waterways Department, Govt. of West Bengal, there could be number of reason for the culmination of left swing and initiation of the right swing of main channel. One of the possible reasons could be the progressive diversion of flow from the main channel. A particular channel might have dominated over the other in course of time due to its more favourable orientation and ultimately became the carrier of main flow (Ray 2004). The official records regarding land erosion are available in Malda since 1931, which also took note of the fact that the river *Ganga* is slowly shifting its course in Malda district (Rudra 2006). Laha Chalantika and Bandyapadhya Sunando indicate-How Ganga Channel is shifted with the time in upstream and downstream of Farakka Barrage (Laha Chalantika 2013). Parua P.K says how the river bank is eroding for construction of Farakka Barrage in Malda and Murshidabad districts. He described the causes of bank erosion and role of Farakka Barrage (Parua 1999, 2002). Chakrabarti and Nag (2015) reported on the mechanism of bank failure in upstream and downstream of Farakka Barrage that retreat of water after the initial high discharge, removal of fine materials (sand/silt) by the water force accelerates the process of bank failure. Rudra (2000) discussed on the bank failure issue of Malda district that un-working of almost 54 sluice gates of Farakka barrage by the side of Malda has been obstructing the flow of Ganges during rainy season and leads to emerge a long strip of land in upstream of the barrage which is also responsible for severe erosion in Malda district. Dhulian and its surrounding areas in the downstream section of Farakka Barrage have been facing the problem of bank erosion by river Ganga and total municipality area lies in highly risky zone caused by severe bank erosion problem of river Ganga. Ghosh (2018) reported on the problem of erosion in Dhulian. According to Flood Preparedness and Management Plan (2014), Government of West Bengal, Dhulian town has been shifted four times due to devastating bank erosion problem. The present paper deals with the problem of bank erosion of river Ganga upstream and downstream of Farakka Barrage in the state of West Bengal.

## 3.0 The Ganga in West Bengal

The entire 174 km stretch along the Ganga, from Bhutni in Malda to Jalangi in Murshidabad has been facing erosion . The mighty river, after its long eastward journey of more than 2000 km, enters the plains of Bengal and begins to throw off distributaries. The Ganga divides into two major distributaries, Padma and Bhagirathi-Hugli, in a village called Mithipur (in Murshidabad district) which is located about 40 km downstream of Farakka. The Padma carries the bulk of the discharge, flows about 65 km along the Indo-Bangladesh border and finally leaves Indian territory at Jalangi. The Bhagirathi-Hugli branch flows southward from Mithipur for about 500 km and ultimately discharges into the Bay of Bengal. Fig 1 shows river Ganga and its tributaries near Farakka. Fig 2 shows average longitudinal slope of river Ganga.

Farakka barrage-about 2.6 km long- was constructed in the year 1967 across river Ganga with the objective of forcibly diverting flow from the parent river Ganga to its tributary river Hoogly. The river Hoogly (initial stretch of which is known as Bhagirathi) was drying up due to silting of it's off take point at a place called Jangipur resulting in gradual reduction of fresh upland flow from Ganga. Hoogly River flows through West Bengal for a length of about 500 km from its off take to its outfall

in Bay of Bengal. It is the lifeline of West Bengal as it is the principal source of water for drinking and industrial uses for Kolkata and Howrah cities and many other important towns located on either bank of Hoogly which is a navigable and a tidal river. Kolkata port located on river Hoogly was drying up due to siltation, as the fresh water upland discharge was reducing. The Farakka barrage was constructed with the objectives of flushing the sediment load into the sea, making the Bhagirathi-Hooghly channel free from navigational hazard.

In post Farakka period, the intensity of erosion by the Ganga in Maldah and Murshidabad districts increased rendering thousands of people homeless (Rudra 2009). In the reach between Rajmahal and Farakka, the Ganga flows between outliers of the Rajmahal Hills along the right bank and the old alluvium of Barind tract along the left bank. Three moribund distributaries, Kalindri, Chota Bhagirathi and Pagla, mark the old course of the Ganga. Three other channels flow through newly emerged riverine islands, locally known as char. At the time of construction of the Farakka barrage, from the early 1960s the Ganga formed a mighty bend encroaching eastward. However, since the monsoon season of 2007, the river has started to swing westward. In the section downstream of the Farakka Barrage, where the river followed the Indo-Bangladesh border in 1947, the encroachment was southward (i.e. towards India) in most of the reaches.

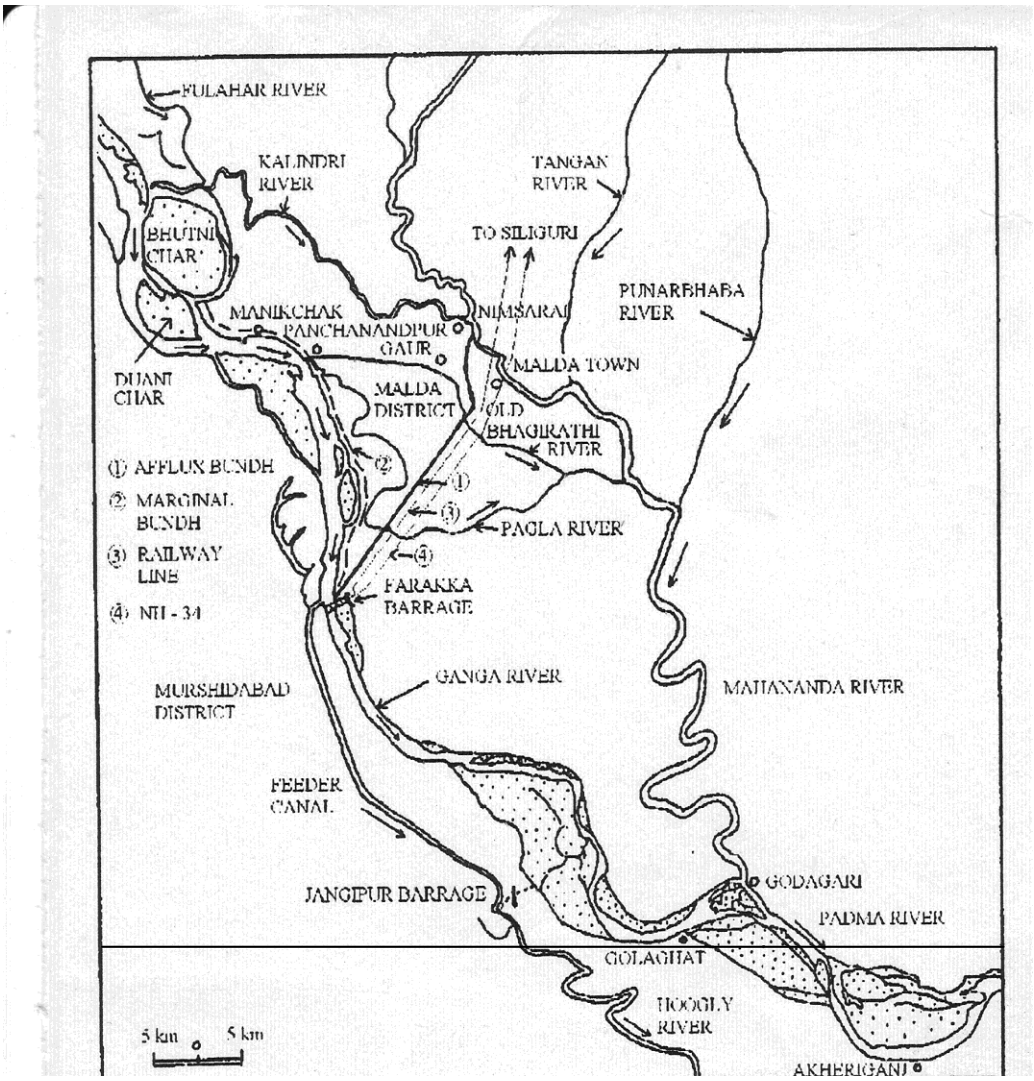



**Fig 1** : River Ganga and its Tributories near Farakka

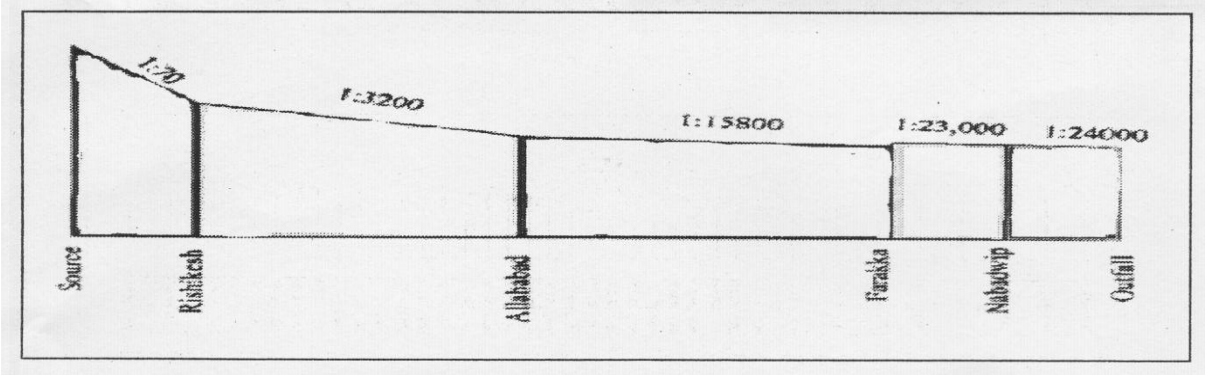



**Fig 2** : Average longitudinal Slope of Ganga (after Parua 2010)

## 4.0 Migration of river Ganga and resultant erosion

Fig 3 depicts shifting of course of river Ganga from the year 1920 to 2010.

### *4.1 Between Rajmahal and Farakka upstream of the barrage*

In the second half of the 18th Century, the Ganga was bifurcated near Rajmahal with a riverine island called Bhutni. The situation remained unchanged until the mid-19th century. The Ganga then flowed flanking the northeastern side of Bhutni. Today, the river flows along the southwestern side of the island. Furthermore, the shape of the island has changed appreciably. In the stretch between Rajmahal and Farakka, the changing course can be understood with reference to the site of Gaur, which was the mediaeval capital of Bengal. Its archaeological ruins, along with Kalindri and Bhagirathi, two moribund distributaries of the Ganga, are still recognizable. Mukherjee (1938) reported ‘‘Leaving the hills of Rajmahal the Ganges seemed to have passed north-wards through modern Kalindri, and then southwards into the lower course of the Mahananda, east of the ruins of ancient Gaur’’. Rennell (1793) wrote in his Memoir of a Map of Hindustan, ‘‘No part of the site of ancient Gour is nearer to the present bank of Ganges, than four miles and a half; and some parts of it, which were originally washed by the river, are now 12 miles from it”. The abandoned channels found in the western part of Ganga have depicted the fact that before the year 1973, Ganga shifted up to this extent in west, then again moved on towards east and occupied the position of 1973. In the year 2010, the left bank has engulfed some abandoned channels located in the eastern part of the course of 1973. The distance between the right bank and the western side abandoned channels has also become less, which means that Ganga has shifted eastward and widened its course from 1973 to 2010.

Fig 4 and Fig 5 show the course of river Ganga between Rajmahal and Farakka for the years 1982 and 2006-2007. The massive structural intervention across the Ganga at Farakka started in 1962–1963, and the barrage was completed in 1971. Since then, 87 $Mm^3$ of water was impounded above the barrage and the water level was raised by about 6.71 m. The river adjusted by widening, and backflow reached beyond Bhagalpur (Parua 1999, 2002). The river formed an eastward meander bend. The eastward encroachment of the Ganga continued until the rainy season of 2006, when the river reached the limit of its meander belt. In the process of easterly flight, during the period 1969-1999, 4.5 lakh people were affected by left bank erosion of the Ganges in Malda district, upstream of the Farakka Barrage. River Ganga engulfed 22 mouzas in Manickchak, Kaliachak I and Kaliachak II Blocks. Other affected areas were in Kaliachak III, Ratua I and Ratua II locks. The worst-hit areas lie in the left bank of the river stretch between Bhutnidiara and Panchanandapore in the Kaliachak II block. The Ganga Bhangan Pratirodh Action Nagarik Committee’s survey revealed a loss of 750 square km area in Kaliachak and Manikchak. 60 primary schools, 14 high schools, coveted mango orchards were engulfed by the river Ganga leaving 40,000 affected families. During the period 1990-2001 Hiranandapur, Manikchak, Gopalpur of Manikchak Block and Kakribondha Jhaubona of Kaliachak II Block were badly affected by river bank erosion. In 2004-05 large scale erosion took place in

Kakribondha Jhaubona and Panchanandapur-I gram panchayats of Kaliachak II and Dakshin Chandipur, Manikchak, and Dharampur gram panchayets of Manikchak Block. Kakribondha Jhaubona, a gram panchayat, was totally lost by river bank erosion.

Since 2007, the main flow of the Ganga has followed the middle channel, impinging the land along the left bank just upstream of the Farakka Barrage. The older maps further show that the sites of Rajmahal and Farakka are two nodal points where the river has not changed its course. This was presumably one of the reasons for selecting Farakka as the site of the barrage. It is clearly understood from the recent satellite images that the Ganga water has been flowing through four channels below Rajmahal and the middle channel is most active now. Fig 6 shows erosion of river Ganga at Chakbahadurpur in Kaliachak Block 3 in Malda District during pre-monsoon period as observed on 2.7.2020. Fig 7 shows sedimentation on river bed upstream of Farakka Barrage.

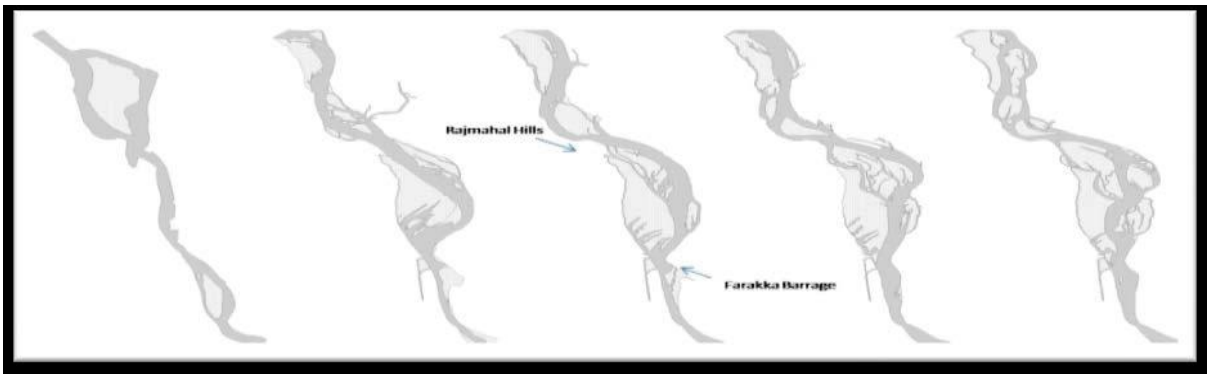



**Fig 3** : Migration of river Ganga time.( Source :Laha Chalantica & Bandyapadhyay Sunanda 2013)

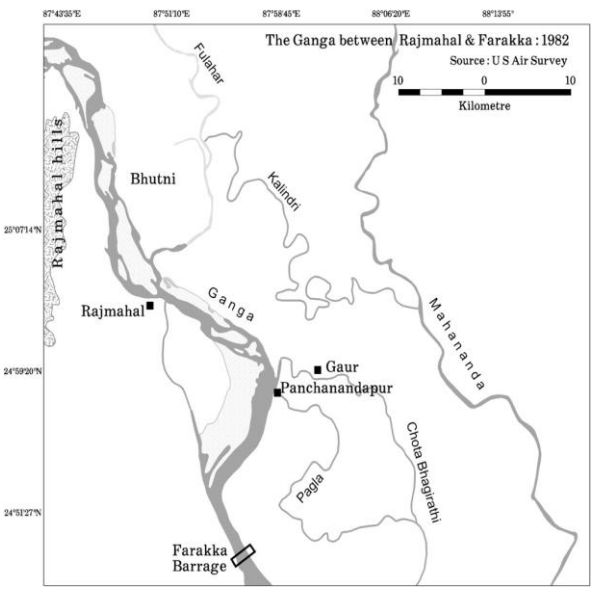



**Fig 4** : The course of the Ganga between Rajmahal and Farakka 1982 (after Rudra 2009)

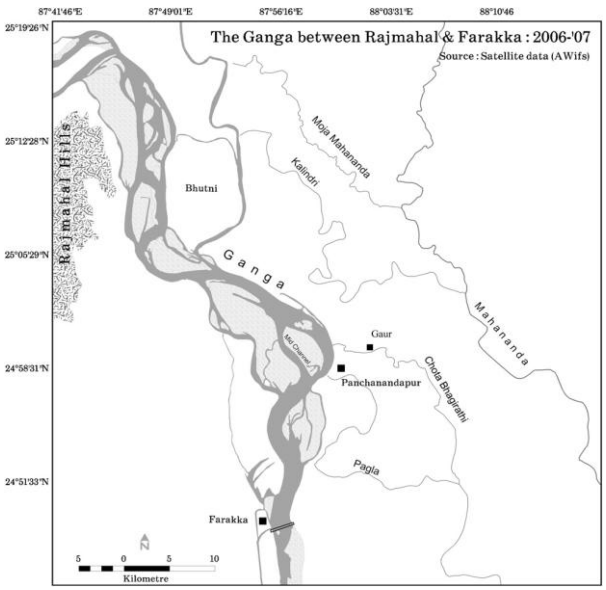



**Fig 5** : The course of the Ganga between Rajmahal and Farakka 2006-2007 (after Rudra 2009)



**Fig 6** : Erosion of river Ganga at Chakbahadurpur in Kaliachak Block 3 in Malda District during pre-monsoon period as observed on 2.7.2020. (Source Anandabazar Patrika dated 3.7.2020)



**Fig 7** : Sedimentation on river bed upstream of Farakka Barrage (after Mandal 2015)

### *4.2 In and around Murshidabad downstream of the barrage*

Fig 8 depicts the change in the course of river Ganga between Farakka and Lalgola from the year 1972 to 2018. Fig 9 and Fig 10 depict the course of river Ganga between Akheriganj and Jalangi for the years 1982 and 2006-2007. The river Gange has a bank-line of 94 km along its right bank from downstream of Farakka Barrage to Jalangi. Severe erosion occurs all along this bank. Since the inception of the Farakka barrage, the hydraulic gradient of the river has been changed, relatively silt-free water released from the under sluices incised the valley deeply in the downstream section and the river has became progressively deep and narrow. The water released from the barrage eroded the right bank and the channel gradually shifted further west. This is clearly visible by comparison of the US Air Survey Map of 1982 and the satellite images of 2006–2007. The Farakka Barrage Authority has dumped huge boulders to protect the structure from imminent danger of erosion.

During the late 1960s and 1970s, the towns located downstream of the Farakka such as Dhulian, Nimtita, Sankopara, and Suti, and adjoining areas, suffered from severe erosion (Ghosh 2018) and the railway connecting North and South Bengal and the national highway was realigned further west. The present Dhulian town is a relocated site after the original site was engulfed by the river. In the late 1980s and early 1990s, severe erosion was observed in Akherigang. The local market area, high school, bank and many villages were plunged in the river. The road connecting the site with Berhampur, the district headquarters, was damaged. The engineering measures to protect the bank proved futile. The present Akherigang is a relocated cluster of settlement. The original site which now lies on the other side of the river is at least 3 km north of present site. A large number of erosion victims have settled on the newly emerged land, locally known as Nirmal Char, along the northern bank of river. The impinging river eroded 207 square km of land in Murshidabad during the period 1988–1994 and more than 79,000 people were displaced (Rudra, 1996). Since erosion at Akherigang ceased, the point of severe erosion has shifted further east to Jalangi. Jalangi situated 50 km east of Baharampur district headquarter has suffered tremendously in 1994-95. At Jalangi Bazaar severe erosion started in September 1995 engulfing nearly 400 metre width of land within a week and then

high built up homestead land thereby destroying Jalangi High School, Gram Panchayat Office, Thana and innumerable buildings rendering nearly 12000 people homeless. Even the road leading to Karimpur collapsed into the river. Fig 11 shows severe bank slip on right bank of river Ganga upstream side of Sankopara under Maheshpur GP Block –Farakka District Murshidabad as observed on 6.9.2014. Fig. 12 shows erosion of river Ganga in Mondalpara area in Samserganj Block in Jangipur Sub-division in Murshidabad District as observed on 5.9.2020.

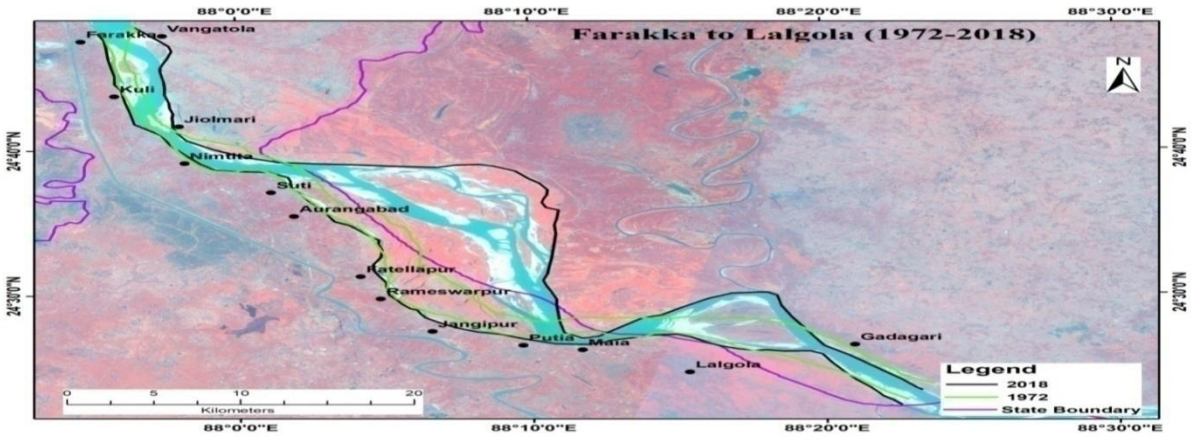



**Fig 8** : Changes in the course of River Ganga between Farakka and Lalgola (after Sen 2019)

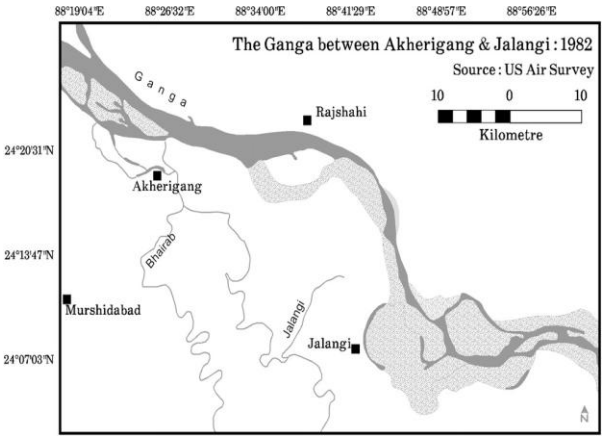



**Fig 9** : The course of the Ganga between Akherigang and Jalangi 1982 (after Rudra 2009)

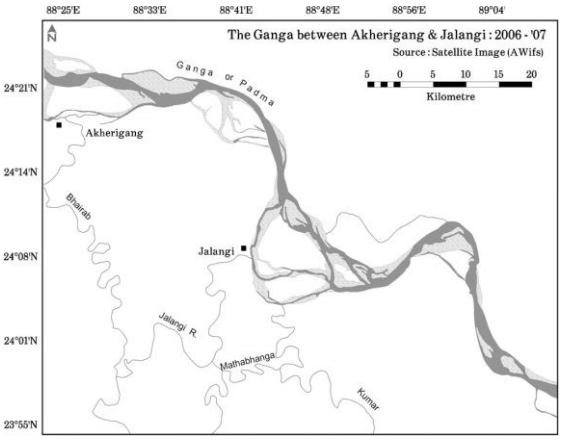



**Fig 10** : The course of the Ganga between Akherigang and Jalangi 2006-2007



**Fig 11** : Photograph shows severe bank slip on right bank of river Ganga upstream side of Sankopara under Maheshpur GP Block –Farakka District Murshidabad as observed on 6.9.2014.



**Fig 12** :Photograph shows erosion of river Ganga in Mondalpara area in Samserganj Block in Jangipur Sub-division in Murshidabad district as observed on 5.9.2020. Villages namely Dhanghara, Kuldiar and Purono Shibpur disappeared completely.
(Source Anandabazar Patrika dated 7.9.2020)

## 5.0 Mechanism of river bank erosion

River bank erosion is a natural and inevitable phenomenon of river and can be defined as a dynamic natural process which involves the removal of materials from the banks of a river. The bank erosion will be occurred when the magnitude of flowing water exceeds the strength or shearing resistance of materials or sediments on the basal part of a river bank. The sediments at basal part of the bank are washed out by the running water (rising stage of discharge or effluent flow of ground water into the river) leads to form vacuum at the base and form a steep wall or cliff above which ultimately collapses by hydraulic pressure, geotechnical events or combined effect of both. Bank erosion mainly occurs in meandering river. In meandering river, river shifting takes place through bank erosion and deposition on the point bar.

The rivers continuously transfer water and sediment load in the downstream direction. Tropical rivers such as the Ganga have some unique fluvio-geomorphological characteristics. The hydrograph of the Ganga as recorded and plotted is extremely skewed because more than 80% of annual discharge passes during the monsoon months of June–September. The suspended sediment load carried annually by river Ganga has been estimated by many experts. It is stated to be 800 million tons by Abbas and Subramaniam (1984). Each year in Malda, the riverbed is rising at the rate of 50 cm resulting in declining slope in the opposite direction between Farakka and Rajmahal (Mandal 2015). Human intervention into the fluvial regime impairs dynamic equilibrium and the processes of changing course is often delayed or accelerated. In an uncontrolled regime, the changing course of the river is governed by skewed hydrography, bank-stratigraphy, influent and effluent seepage, sediment load and the ratio between peak and lowest discharge. The width of the meander belt is related to the discharge flowing in the river: the greater the discharge, the wider the meander belt. The shelving bank of Ganga exposed during lean months shows a layer of loose and unconsolidated basal layer of sand with a comparatively thin layer of silt-clay on top. The impinging current of the monsoon erodes the basal sand-layer during the rising stage and leads to collapse of the bank. When the river is in spate, the influent seepage recharges the ground water pool. The effluent seepage towards the river creates voids in the basal layer during the falling stage, resulting in extensive bank failure (Ghosh 2018). Fig 13 and Fig 14 show photographs (pre-monsoon and post-monsoon) of bank protection works carried out at Moya, Lalgola in Murshidabad district during the year 2017 and the said protection work was effective in reducing bank erosion at that location.



**Fig 13** :Bank Protection Works (before monsoon) in 2017 at Moya, Lalgola in Murshidabad (after Sen 2019)

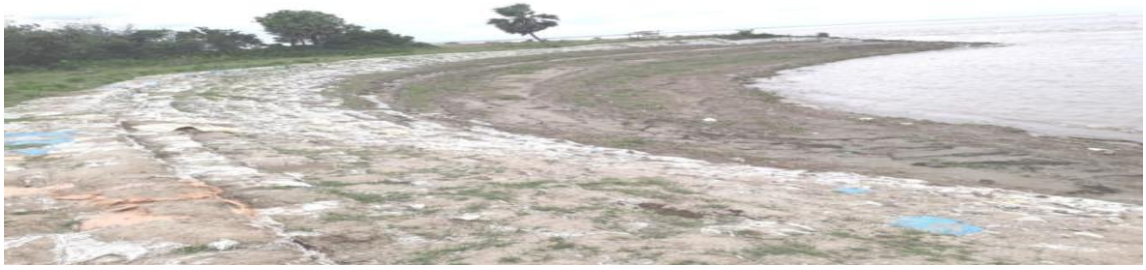


**Fig 14** :Bank Protection Works (after monsoon) in 2017 at Moya, Lalgola in Murshidabad (after Sen 2019)

## 6.0 Formation of Expert Committee

Two Experts' Committees (P. Singh Committee in 1980 and G. Keskar Committee in 1996) constituted to explore the possible remedial measures to combat erosion, submitted their reports. Both committees recommended revetments with boulders to protect the banks from impinging currents and also construction of spurs to deflect the flow towards the opposite bank (Singh 1980). Total cost of the short term and long term measures suggested by the committee was about Rs.10,000 million based on 1996 price index (Mazumder 2000). A master plan of riverbank protection, both upstream and downstream of the barrage, was drawn to control erosion of river banks and prevent further migration of the river at a cost of about Rs. 927 crores as per the recommendations of Pritam Singh and Keskar Committee. Unfortunately, the recommended conventional protective measures, consisting of impermeable earth-core type spurs protected with stone pitching and crated stone bed spurs over stone mattress, have miserably failed to perform. Most of the impervious spurs are destroyed due to heavy erosion at their heads and toes. They settle (due to scouring/winnowing of foundation soil) ,crack and the high velocity current flows through the cracks eventually washing out the spurs. The river banks made of very fine non-cohesive alluvial soil are subjected to the fury of the river causing erosion of the bank. The sand and silt layers underneath the bank get eroded first and the top clayey bank caves in the scoured area due to lack of any support from bottom (Mazumder 2004). The Government of India has recently constituted the Ganga Control Authority with the objectives of pollution abatement and restoration of minimum ecological flow.

## 7.0 Conclusions

In spite of elaborate and very costly river training measures adopted so far, river Ganga is creating unforeseen problems due to uncontrolled erosion of its left bank upstream and right bank downstream of Farakka barrage. Uncontrolled erosion and deposition process in the vicinity of Farakka barrage has resulted in development of meanders and its migration towards Malda district in West Bengal ( on left bank) upstream of the barrage and Mushidabad district in West Bengal (on right bank)

downstream of the barrage resulting in flooding, loss of life, agricultural lands and other properties on both the banks. The river course of Ganga has shifted gradually towards east from 1973 to 2010. During the period from 1973 to 1977, the rate of migration was higher about 147 m / year. After that from 1977 to 2010, the rate was less about 60 m / year. In the period of four years from 1973 to 1977, just after construction of Farakka Barrage, the rate of channel widening process was tremendously high. It can be concluded that such abnormal rate of channel widening process may be as a result of immediate impact of human intervention over the natural flow. It is necessary to understand the basic mechanisms of aggradations / degradation, flow instability and meandering processes in a river like Ganga near Farakka for proper planning and design of river training works. Conventional measures consisting of embankments, stone mattresses and groynes are found to be ineffective due to deep scour near the river banks. An in-depth analysis of erosion mechanism and failure of the protective works are necessary. In addition to that, it is also equally important is to design a scientific land use plan for the flood plain of the river Ganga which shifts its course like a pendulum in the lower reach.

## References

Abbas, N., Subramaniam, V.,( 1984). Erosion and sediment transport in the Ganga River Basin (India). Journal of Hydrology 69, 173–182.

Banerjee Manisha(1999), South Asia Network on Dams, Rivers and People. A report on the impact of Farakka Barrage on the human fabric -A study of the upstream and downstream areas of Farakka Barrage. Submission to World Commission on Dams New, Delhi: 110 088-India, November 1999

Chakrabarti, P., Nag, S. (2015). "River of West Bengal changing scenario. Geoinformatic and Remote Sensing Cell West Bengal State Council of Science and Technology, Govt. of West Bengal", pp. 62-66.

Flood preparedness & Management Plan (2014). Office of the District Magistrate,, Murshidabad, West Bengal-2014.

Ghosh,D. & Sahu, A.S. (2018)- Regional Science Enquiry Vol X (2), 2018, pp 205-214.

Laha Chalantika & Bandyapadhyay Dr. Sunando. Research Scholar (2013), Dept. Of Geography, University Of Calcutta. Analysis of the Changing Morphometry of River Ganga, shift monitoring and Vulnerability Analysis using Space-Borne Techniques: A Statistical Approach. International Journal of Scientific and Research Publications, Volume 3, Issue 7, July 2013.

Mandal, I. (2015)- "Impact of Farakka Barrage at Farakka and its surrounding area"- Journal of Engineering Computers and Applied Sciences" (JECAS), Vol 4, no. 6, June 2015, ISSN No. 239-5606.

Mazumder, S.K. (2000) "Role of Farakka Barrage on the Disastrous Flood at Malda (West Bengal) in 1998" Proc. 8th ICID Intl. Drainage Workshop 'Role of Drainage and Challenges of 21st Century Vol. III, sponsored by ICID –CIID & Min. of Water Resources and org. by ICD & WAPCOS, New Delhi Jan 31 - Feb 4, NewDelhi

Mazumder, S.K. (2004)" Aggradation/Degradation of Ganga near Farakka Barrage", Proc. Seminar on "Silting of Rivers- Problems and Solutions" org. by Min of Water Resources, Govt. of India, New Delhi Feb. 12-13.

Mukherjee, R.K., 1938. The Changing Face of Bengal/A Study in Riverine Economy. University of Calcutta.

Parua P.K, (1999)Superintending Engineer, Farakka- Barrage Project. Erosion problems of the river Ganga in the districts of Malda and Murshidabad in West Bengal; Bi-monthly Technical Journal of American Society of Civil Engineers - Indian Section; vol. XIII, no. 2, March-April 1999.

Parua, P.K., 2002. Fluvial geomorphology of the River Ganga around Farakka. Journal of Institution of Engineers 82, 193–196.

Parua,P.K. (2010) –The Ganga : Water use in the Indian subcontinent", Water Science & technology Library, Springer, e-ISBN 978-90-481-3103-7, Springer Dordrecht Heidelberg, London, New York.

Ray. S.C. (2004), A study Report on Control of left Bank Erosion of River Ganga between Rajmahal and Farakka by Irrigation and Waterways Department,. Govt. of West Bengal.

Rennell, J.,(1793).Memoir of aMap of Hindustan. (Reprinted in India in 1976) pp.147, 385.

Rudra, Kalyan, (1996) Problems of bank erosion in Murshidabad District of West Bengal. Journal of Geography and Environment 1, 25–32. Vidyasagar University, West Bengal.

Rudra, Kalyan, (2000). Living on the edge: the experience along the bank of the Ganga in Malda district, West Bengal. Indian Journal of Geography and Environment 5, 57–67. Vidyasagar University, West Bengal.

Rudra, Kalyan, (2006). Shifting of the Ganga and Land Erosion in West Bengal/A Socio-ecological Viewpoint. CDEP Occasional Paper-8. Indian Institute of Management Calcutta, pp. 1–43.

Rudra, K. (2009). "Dynamics of the Ganga in West Bengal (1764–2007): implications for science–policy interaction". Quatern Int 227(2):161–169

Sen, D.J. (2019), Lecture on "Morphological study of Rivers Hooghly, Mahananda and Mahanadi using Remote Sensing Technique", River Research Institute, West Bengal, Mohanpur, Nadia, June 2019.

*IN PROCEEDINGS OF 25th HYDRO 2020, INTERNATIONAL CONFERENCE, NATIONAL INSTITUTE OF TECHNOLOGY ROURKELA, ODISHA, INDIA 26-28, March 2021, ISBN 978-93-90631-56-8*

Paper ID - 214

# A Study of Flow and Sediment Transport Analysis using HEC-RAS

Harapriya Panda [1*], Ratnakar Swain [2], Bibhuti Bhusan Mukharjee[3]

[1]*Department of Civil Engineering, CAPGS, BPUT Rourkela, Berhampur and 760010, India*
*Email: harapriyapanda2414@gmail.com (*Corresponding Author)*

[2]*Assistant Professor, Department of Civil Engineering, National Institute of Technology, Rourkela, Odisha, India, E-mail: swainrk@nitrkl.ac.in*

[3]*Associate Professor, Department of Civil Engineering, CAPGS, BPUT Rourkela, Rourkela and 769015, India*
*E-mail:bibhuti.2222@gmail.com*

## Abstract

River engineering is defined as controlling and predicting river behaviors and evaluate the sediment transport, which are utmost important for the hydraulic engineers now-a-days. The design of a model to determine the water conveyed with minimal erosion and sedimentation. The HEC-RAS model can perform the mobile bed sedimentation with computed an unsteady (hydrograph) flow series data. The conceptual and physical parameters required the HEC-RAS model were determined through calibration and direct measurement, and different parameters used in sediment transport analysis. The saint-venant (continuity and momentum) equation is then solved in the variation of discharge with time along the length of the water body, using the real-time sedimentation. Manning's roughness coefficient value is calibrated and simulated using the HEC-RAS model using the discharge of unsteady flow measurement, sediment discharge, and deposition rates at different levels of flow in the river. Herein, the main objective of the work is to analyze the flow and sediment transport simultaneously for Jaraikela-Panposh reach of the Brahmani River of length 37 km. The calibration and validation was carried out for the Mannings's roughness coefffcient (n) and optimal sediment transport function (STF), using daily sediment-discharge time series data from 01-January, 2001 to 31-December, 2001 and from 01-January, 1996 to 31-December, 2000. From performance evaluation measures, the optimum 'n' value was found to be 0.05 and optimum STF is found to be Mayer Peter Muller method. During the calibration of 'n' value, the performance evaluation measures such as Nash and Sutcliffe Efficiency (NSE), Root Mean Square Error (RMSE) and Coefficient of determination ($r^2$) were found to be 97.13%, 130.95 $m^3/s$, and 0.97 respectively. Similarly, during calibration of optimum STF, the performance evaluation measures such as NSE, RMSE and $r^2$ were found to be 95.97%, 155.14 $m^3/s$ and 0.97 respectively. In this study it is concluded that the HEC-RAS can be used for simultaneous analysis of both flow and sediment transport very efficiently.

***Keywords:*** *HEC-RAS; Sediment Transport; Unsteady Flow; Flow Routing; Brahmani River*.

## Introduction

The sediment transport was a mobile base channel and is a numerical model. The flow of water in a channel (natural or artificial), it tries to scour its surface. The silt, gravel, and even larger boulders are detached from the bed or side of a channel, and particles are spread downstream by the moving water known as sediment transport and The objective of this method was pressure distribution, the velocity distribution of water. The sediment transport causes large scale scouring and siltation of the irrigation canal, it's increasing their maintenance and huge economic loss to the public exchequer of Sediment transport was erosion, deposition, and change in the platform, area of study. It refers to the loose, non-cohesive material transported by suspended in or deposited by water. These sediment properties are two categories- non-cohesive and cohesive aggregate of particles. The distinctive feature of sediment transport was grain size distribution, fall velocity, the shape of the particle, particle specific gravity, angle of repose underwater, bulk specific weight of the sediment. The physical and conceptual parameters used in the HEC-RAS model, to determine calibrated and validated measures.

Flow forecasting enquired by the morphological of a river that illustrates the geometry of river, bed shape and longitudinal profile, cross-section, and change of river shape (Haghiabi and Zaredehdasht, 2012). The saint-venant equation involved in the diffusive wave and dynamic model and evaluated the amount of ground load and convey the chance of land and water resource project was carried by a river

bend of a narrowing river, flood control, navigation. The purpose of reservoir is to store the necessary demand of water.

Hameed and Ali, (2013) studied the manning's coefficient give the results for computed hydrograph in the investigated area. The HEC-RAS model is calculated by steady flow, unsteady flow, and movable boundary flow. The steady flow element used standard step method which is used for the gradually varied flow.

Parhi et al., (2012) analyzed the hydraulic model for flood forecasting and found that the flood plain mapping was a sensitive parameters of the HEC-RAS model. The numerical models used in different streams improve the flood forecasting and inundation mapping and hydrodynamic model performance. Routing the movable boundary element used the subordinate of sediment, and one of the various sediment transport equations to calculate river bed alluviation and/or abjection. The volume of erosion or deposition studied by the armoring and sorting algorithms of the alignment using the continuity equation in both algorithms by Brunner and Gibson, 2005.

Van Rijn, (1993) and Graf, (1984) studied the forecasting of sedimentation transport in the river. The study found the benefit of the mathematical design of the geomorphological study and show the complication of the sediment transport. Haghiabi and Zaredehadasht, (2012) studied the assumption of sediment load using HEC-RAS model and observed input data.

Gibson et al., (2006) studied the one-dimensional approach for various cross-section geometry cross-section in the sediment erosion and deposition. The US Army Corps of Engineers (USACES), (2015); Gibson et al., (2006) studied the technical feasibility in dealing with decreased the sediment trapping efficiency to altering the reservoir operation by (Shelley et al., 2009). Ochiere et al., (2015) studied the flow transport with minimum erosion and deposition and calibration the model using the recent operating condition and determined the flow and sediment discharge. The HEC-RAS model used Acker's White equation for sediment routing using large range of the sediment size in the area of study (Mohammad et al., 2016).

## Methodology

### 2.1 *The HEC RAS Model Accounting the Unsteady Flow Condition of Sedimentation*

The one-dimensional unsteady flow was gradually varied by this HEC-RAS model; the model was developed in a saint venant equation. The continuity and momentum equation (1) and (2), have been used in the inundation measured of the Brahmani river.

$$\frac{\partial A}{\partial t} + \frac{\partial Q}{\partial x} = q_l \tag{1}$$

$$\frac{\partial A}{\partial t} + \frac{\partial \left(\frac{Q^2}{A}\right)}{\partial x} + gA \cdot \frac{\partial H}{\partial x} + gA(s_F - s_0) = 0 \tag{2}$$

Where Q = Discharge of unsteady flow; flow depth y and water profile gradient, $\frac{\partial y}{\partial x}$; A= cross-sectional area of water flow; $q_l$= lateral flow per unit channel length; g = acceleration due to gravity; H = water surface elevation above a specified datum, also called stage; $s_o$= bed slope; $s_f$ = energy slope; x= longitudinal distance along the river channel from the upstream, and t = time variable. This numerical scheme has been used corresponds to the weighting factor (θ) of 0.6 for the unsteady flow simulation. The detail procedure of the study is illustrated in **Figure 1**.

### 2.2 *Performance Evaluation Measures*

To assess the performance of HEC-RAS model, three of performance evaluation measures are used herein such as;

1. Nash and Sutcliffe coefficient for routing discharge (NSEq) and estimating the corresponding flow depth (NSEy).

$$e = 1 - \frac{\sum_i^n (o_i - s_i)^2}{\sum_i^n (o_i - \bar{o})^2} \quad (3)$$

2. Coefficient of determination for discharge (r2q) and stage (r2y).

$$r^2 = \frac{\sum_i (s_i - \bar{o})^2}{\sum_i (o_i - \bar{o})^2} \quad (4)$$

3. Root mean square error for discharge (RMSEq) and stage (RMSEy).

$$RMSE = \sqrt{\frac{\sum_i^n (W_O - W_S)^2}{n}} \quad (5)$$

Where, *Wo* = Observed water level in meter (above mean sea level); *Ws* = Simulated water level in meter; *n* = Total no. of reference data points; $O_i$ = Sum of the observed value; $\overline{O}$ = Average value of the observed value and $S_i$ = Sum of the simulated value.

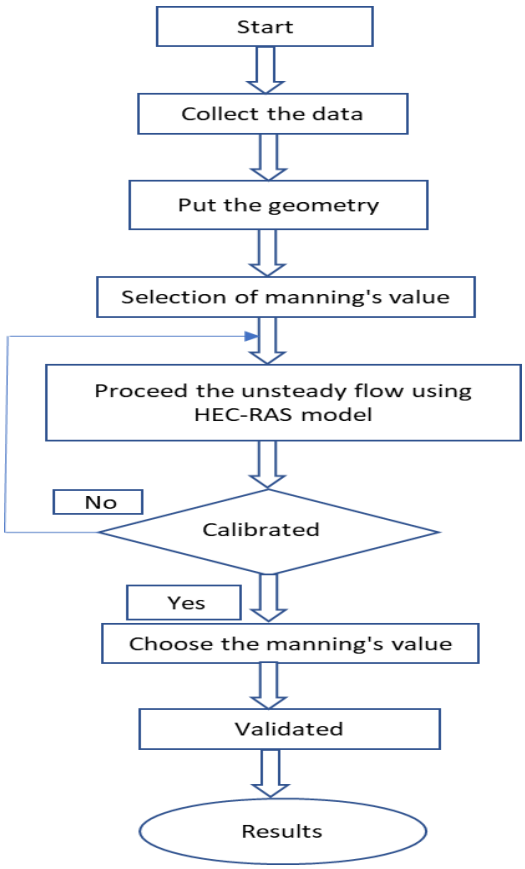



**Figure 1**: Steps of one-dimensional HEC-RAS model

## Study Area and Data Collection

### *3.1 Study Area and Data Collection*

The study is caried out using the Hydro-meteorological data of the Brahmani river, the second largest river of the northern part of Odisha state, India. The Brahmani river is created by both trbutaries the sankh river and the koel river. Jaraikela-Panposh (**Figure 2**) reach of length 37km is considered herein.

The watershed area of Jaraikela station and Panposh station are 15265880 km$^2$ and 202763.416 km$^2$ respectively.

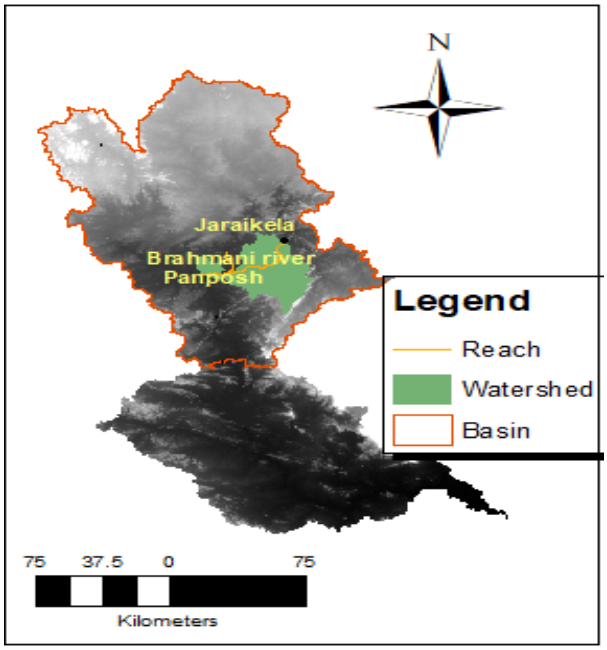



**Figure 2**: The index map of the Brahmani River Basin showing the Jaraikela-Panposh water shed.

Herein, the daily stage-discharge data for the year 1996-2001 and cross-section data of Jaraikela and Panposh gauging stations were collected form central Water Commission (CWC). To assess the soil type, the soil classification is carried out using Food and Agriculture organization (FAO) soil map as shown in **Table-1**. The calibration and validation of Manning's roughness coefficient is carried out for the period from 01 January 2001-31 December 2001 and 01 January 1996-31 December 2000.

**Tabel 1:** Soil property and texture

| | | | | | | Weighted mean | | | |
|---|---|---|---|---|---|---|---|---|---|
| Soil Mapping Unit Symbol | DOM Soil Unit | Sand % top soil | Silt % top soil | Clay % top soil | percentage | Sand % top soil | Silt % top soil | Clay % top soil | Soil texture |
| Lf92-1a | Lf | 74.6 | 9.6 | 15.9 | 60 | 44.76 | 5.76 | 9.54 | Sandy loam |
| I-Ne | I | 58.9 | 16.2 | 24.9 | 50 | 29.45 | 8.1 | 12.45 | Sandy clay loam |
| | | | | | | 74.21 | 13.86 | 21.99 | Sandy clay loam |

## Results and Discussions

### 4.1 *Calibration and validation of Manning's Roughness Coefficient*

The calibration of Manning's roughness coefficient is carried out using observed flow data for year 2001 for the optimum value of NSE. Different values of Manning's roughness coefficient (n) in the rage of 0.015-0.055 were considered in the calibration. The performance evaluation measures for different 'n' values during calibration is mentioned in **Table-2** and show in **Figure 3- 4**. The optimum 'n' value is found to be n=0.05 corresponding to best performance evaluation measures. During

calibration the performance evaluation measures NSE, RMSE, $r^2$ at n=0.05 were found to be 98.63, 120.74 and 0.986 respectively.

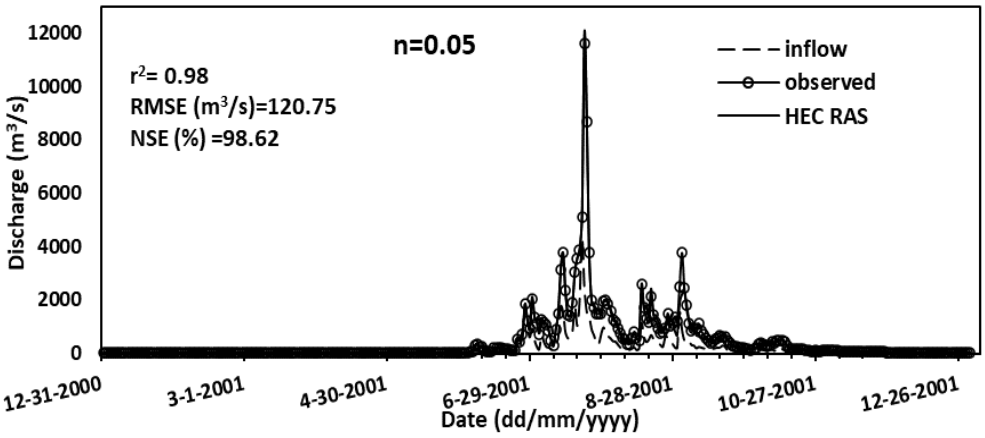



**Figure 3**: Discharge hydrograph at optimum n=0.05 during calibration

**Table 2**: Performance evaluation measures during calibration of the manning's roughness coefficient.

| Year | n | NSE (%) | $r^2$ | RMSE ($m^3/s$) |
|---|---|---|---|---|
| 01 January 2001 - 31 December 2001 | 0.015 | 98.14 | 0.982 | 140.55 |
| | 0.020 | 98.092 | 0.981 | 142.39 |
| | 0.025 | 98.161 | 0.982 | 139.83 |
| | 0.030 | 98.07 | 0.980 | 143.30 |
| | 0.035 | 97.90 | 0.982 | 149.43 |
| | 0.040 | 98.09 | 0.981 | 142.39 |
| | 0.045 | 98.17 | 0.982 | 139.26 |
| | 0.050 | 98.63 | 0.986 | 120.74 |
| | 0.055 | 97.92 | 0.981 | 148.76 |

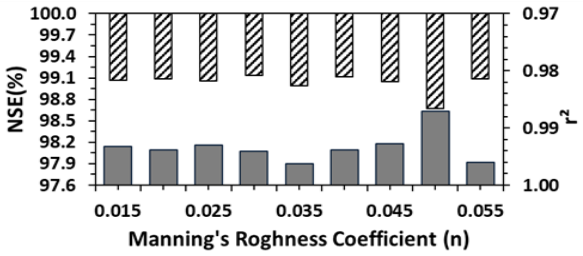



**Figure 4**: Illustration of NSE, $r^2$ values obtained during calibration of 'n'

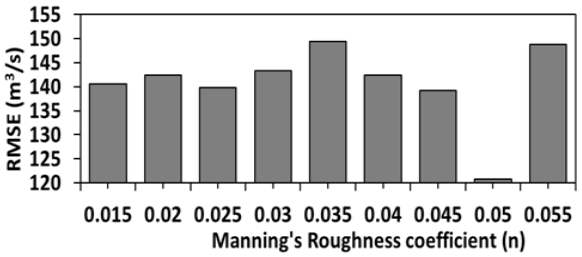



**Figure 5**: Illustration of RMSE values obtained during calibration of 'n'

The validation of 'n' value is carried out annually and continuously from the year 1996-2000. The performance evaluation measures such as NSE, RMSE and $r^2$ found during validation is given in **Table 3**. The reproduction of discharge hydrographs annually and whole period from year 1996-2000 are presented in **Figure 6-7.**

**Table 3**: Performance evaluation measures during validation of the manning's roughness coefficient.

| Year | n | NSE (%) | $r^2$ | RMSE ($m^3/s$) |
|---|---|---|---|---|
| 1996 | 0.05 | 98.15 | 0.98 | 131.07 |
| 1997 | | 96.83 | 0.98 | 141.35 |
| 1998 | | 97.76 | 0.98 | 118.90 |
| 1999 | | 95.28 | 0.96 | 159.40 |
| 2000 | | 95.98 | 0.96 | 95.98 |
| 196-2000 | | 97.13 | 0.97 | 130.95 |

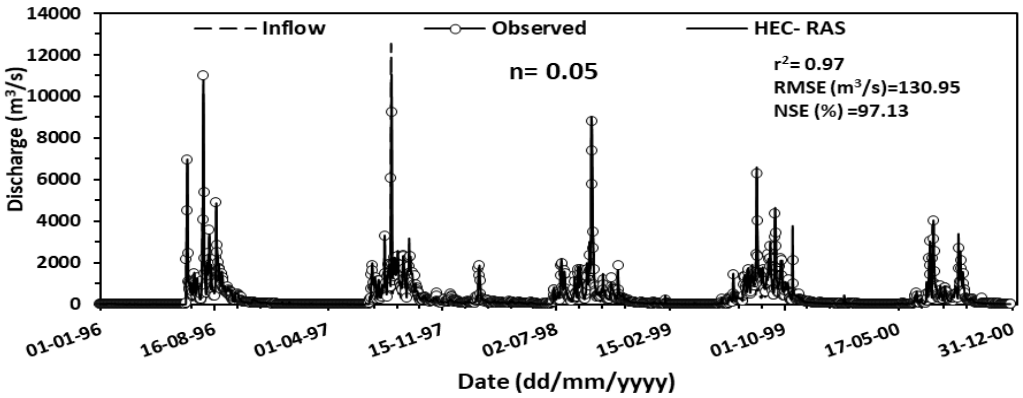



**Figure 6**: Reproduction of observed and simulated discharge time-series hydrograph from 1996-2000.

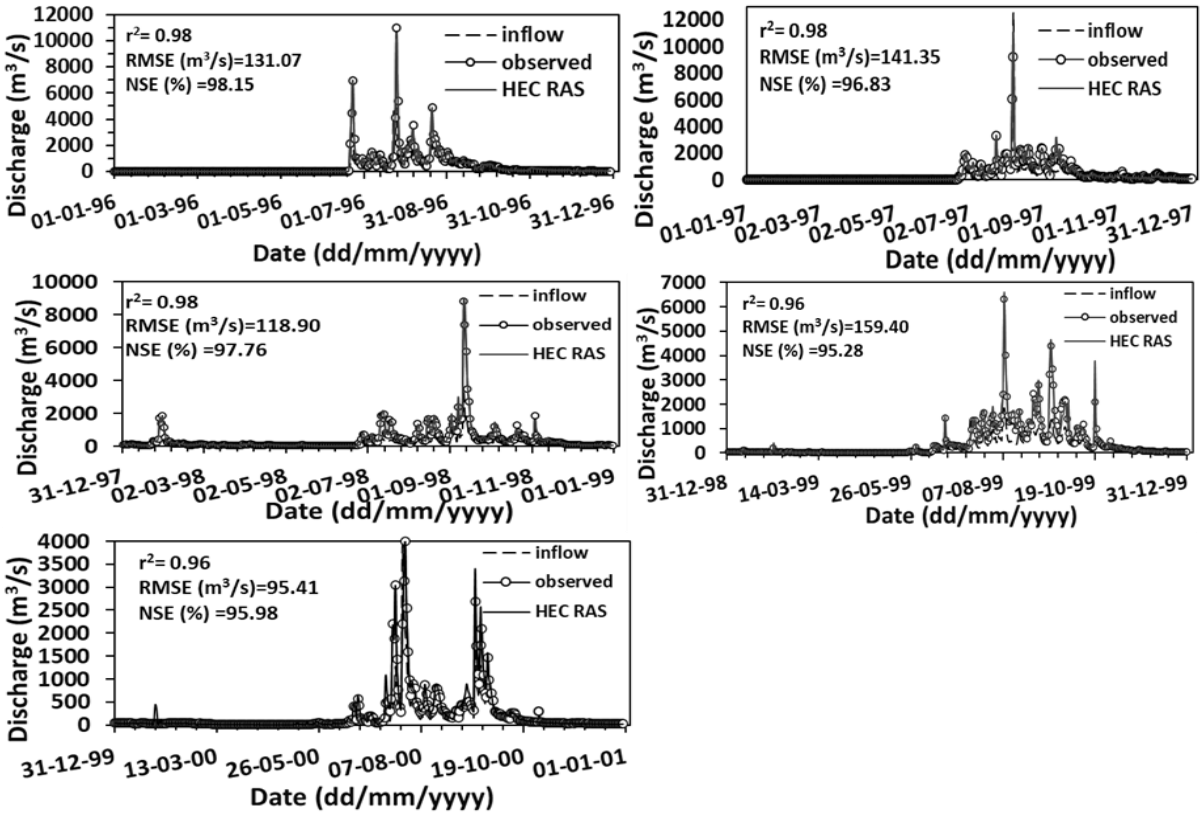



**Figure 7**: Reproduction of annual observed and simulated discharge hydrographs from 1996-2000.

### 4.3 *Calibration and validation of Sediment Transport Function*

The calibration and validation of type of sediment transport function is carried out for different sorting methods and fall velocity methods. The performance evaluation for different combinations of sediment transport function, sorting methods and fall velocity methods are evaluated (**Table-4-5**) using HEC-RAS. The performance evaluation measured found during calibration and validation is mentioned in Table-5.3 and Table-5.4 respectively. The values of performance evaluation measures during calibration are also illustrated in **Figure 9-10**. During calibration and validation of sediment transport function the validated 'n'=0.05 is used. During calibration the optimum sediment transport function is found to be Mayer Peter Muller, optimum sorting method is found to be Copeland (EX7) and optimum Fall Velocity method found to be Van Rijn. The simulated and observed sediments load distribution plot of the calibration results is shown in **Figure 8-9.** Similarly, the sediment Transport function is validated annually and continuously from year 1996-2000 and performance evaluation measures were estimated as shown in **Figure 5**. The simulated and observed sediments load distribution plot of the validation results is shown in **Figure 11.**

**Table 4**: Performance evaluation measures during calibration of the sediment transport function.

| Sediment Transport Function | Sorting Method | Fall Velocity Method | NSE (%) | $r^2$ | RMSE ($m^3/s$) |
|---|---|---|---|---|---|
| Laursen (Copeland) | Copeland (EX7) | Ruby | 97.92 | 0.987 | 148.55 |
| Ackers White | Active Layer | Van Rijn | 97.96 | 0.986 | 147.08 |
| Mayer Peter Muller | Copeland (EX7) | Van Rijn | 98.11 | 0.988 | 141.39 |

| | | | | | |
|---|---|---|---|---|---|
| Engelund Hansen | Copeland (EX7) | Van Rijn | 97.95 | 0.987 | 147.35 |
| Engelund Hansen | Active Layer | Van Rijn | 97.94 | 0.982 | 147.91 |
| Engelund Hansen | Active Layer | Ruby | 97.92 | 0.986 | 148.63 |
| Mayer Peter Muller | Active Layer | Ruby | 97.93 | 0.987 | 148.24 |
| Laursen (Copeland) | Active Layer | Ruby | 97.93 | 0.987 | 148.10 |
| Mayer Peter Muller | Copeland (EX7) | Ruby | 97.92 | 0.986 | 148.65 |
| Laursen (Copeland) | Active Layer | Van Rijn | 97.95 | 0.987 | 147.43 |
| Mayer Peter Muller | Active Layer | Van Rijn | 97.95 | 0.986 | 147.90 |
| Laursen (Copeland) | Copeland (EX7) | Van Rijn | 97.96 | 0.986 | 147.23 |
| Ackers White | Active Layer | Ruby | 97.9378 | 0.986 | 148.07 |

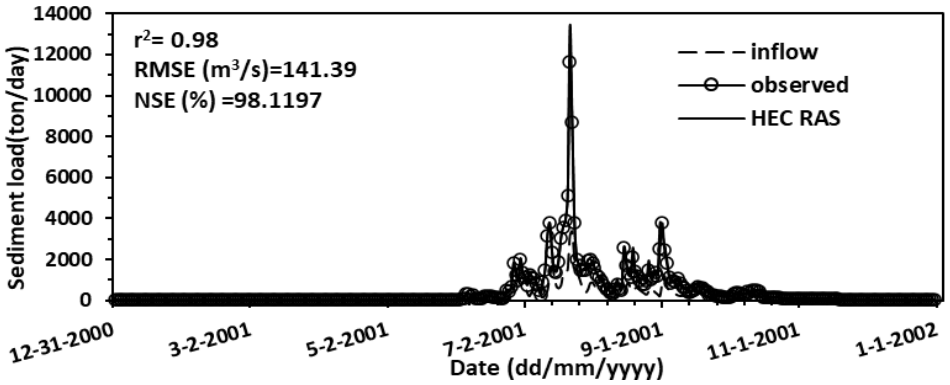



**Figure. 8**: Reproduction of simulated and observed sediment load rate distribution during calibration.

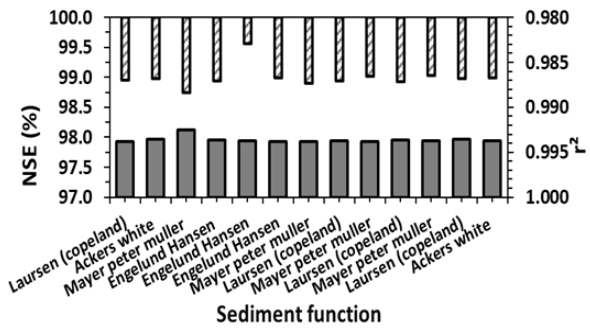



**Figure 9**: Compared the NSE (%) and $r^2$ using sediment transport function

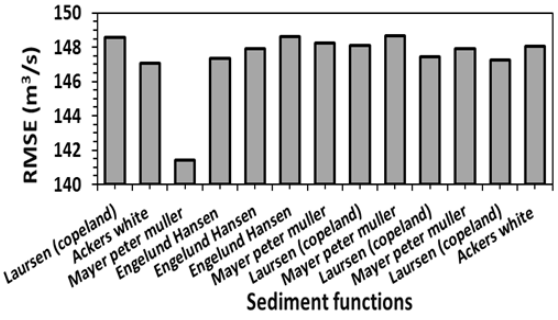



**Figure 10**: Compared the RMSE ($m^3/s$) using sediment transport Function

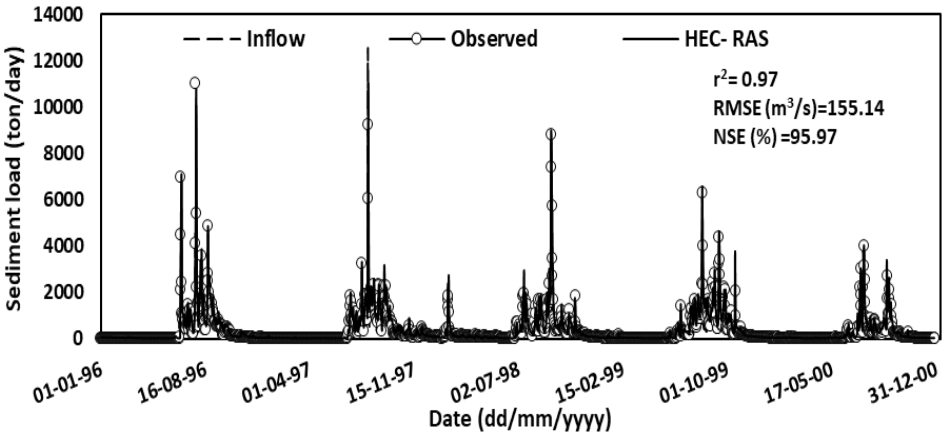



**Figure 11**: Reproduction of observed sediment load hydrographs of the total year by the model.

**Table 5**: Performance evaluation measures during validation of the sediment transport function.

| Year | n | Sediment Transport Function | Sorting Method | Fall Velocity Method | NSE (%) | $r^2$ | RMSE ($m^3/s$) |
|---|---|---|---|---|---|---|---|
| 1996 | 0.05 | Mayer Peter Muller | Copeland (EX7) | Vanrijn | 96.44 | 0.97 | 181.97 |
| 1997 | | | | | 96.25 | 0.98 | 153.70 |
| 1998 | | | | | 95.73 | 0.97 | 164.32 |
| 1999 | | | | | 95.00 | 0.95 | 164.08 |
| 2000 | | | | | 95.75 | 0.97 | 98.71 |
| 1996-2000 | | | | | 95.97 | 0.97 | 155.14 |

## Conclusions

The Jaraikela-Panposh reach of the Brahmani River was used for simultaneous simulation of flood and sediments transport using HEC-RAS model. The calibration and validation of 'n' value and sediment transport function was carried out using observed flow and sediment data.

i. The one-year calibration result shows a close agreement between observes and simulated flow data (NSE=98.63%, RMSE=120.74$m^3$/s, r2=0.986) at optimum n value 0.05.
ii. The validation result 'n' gives NSE=97.13%, RMSE=130.95 $m^3$/s, $r^2$=0.97 at n=0.05.
iii. The calibration result of the sediment function also gives close proximity between observed and simulated sediment load distribution (NSE (98.12%, RMSE=141.39$m^3$/s, $r^2$=0.988) the optimum combinations is found to be sediment transport function: Mayer peter muller, shorting method: Copeland (ex7) and fall velocity method: Van Rijn.
iv. The validation result of optimum sediment transport function gives NSE=95.97%, RMSE=155.14$m^3$/s, and $r^2$=0.97.
v. The result also that the total outflow sediment load is less than the total inflow sediment load. Considering conservation of mass principle, it can concluded that the channel may undergoing erosion during flood propagation from u/s to d/s.

## References

Brunner, G. W., & Gibson, S. (2005). Sediment transport modeling in HEC RAS. *In Impacts of Global Climate Change (pp. 1-12).*

Gibson, S., Brunner, G., Piper, S., & Jensen, M. (2006, April). Sediment transport computations in HEC-RAS. *In Eighth Federal Interagency Sedimentation Conference (8thFISC), Reno, NV (pp. 57-64).*

Graf, W. H. (1984). Hydraulics of sediment transport. *Water Resources Publication*.

Haghiabi, A. H., & Zaredehdasht, E. (2012). Evaluation of HEC-RAS ability in erosion and sediment transport forecasting. *World Applied Sciences Journal, 17(11)*, 1490-1497.

Hameed, L. K., & Ali, S. T. (2013). Estimating of Manning's roughness coefficient for Hilla River through calibration using the HEC-RAS model. *Jordan Journal of Civil Engineering*, 159(701), 1-10.

Mohammad, M. E., Al-Ansari, N., Issa, I. E., & Knutsson, S. (2016). Sediment in Mosul Dam reservoir using the HEC-RAS model. *Lakes & Reservoirs: Research & Management, 21(3), 235-244*

Ochiere, H. O., Onyando, J. O., & Kamau, D. N. (2015). Simulation of sediment transport in the canal using the Hec-Ras (Hydrologic Engineering Centre–River Analysis System) in an underground canal in the Southwest Kano Irrigation Scheme–Kenya. *International Journal of Engineering Science Invention, 4(9)*, 15-31.

Parhi, P. K., Sankhua, R. N., & Roy, G. P. (2012). Calibration of channel roughness for Mahanadi River,(India) using the HEC-RAS model. *Journal of Water Resource and Protection*, 4(10)

Shelley, J., Gibson, S., & Williams, A. (2009). Unsteady flow and sediment modeling in a large reservoir using HEC-RAS 5.0. *In Federal Interagency Sediment Conference*.

USACE (2015). HEC-RAS River Analysis System, Version 5.0, *Hydrologic Engineering Center User Manual.*

Van Rijn, L. C. (1993). Principles of sediment transport in rivers, estuaries, and coastal seas (Vol. 1006, pp. 11-3). *Amsterdam: Aqua publications.*

*IN PROCEEDINGS OF 25th HYDRO 2020, INTERNATIONAL CONFERENCE, NATIONAL INSTITUTE OF TECHNOLOGY ROURKELA, ODISHA, INDIA 26-28, March 2021, ISBN 978-93-90631-56-8*

Paper ID - 237

# FLOOD PROTECTION MEASURES AND ANTI EROSION WORKS ALONG PALHORI KHAD TRIBUTARY OF RIVER YAMUNA.

B. Raghuram Singh[1], Jotsana G. Ambekar[2], Dr. R. G. Patil[3]

[1]*Scientist 'C', Central Water and Power Research Station, Pune - 411024, India*

[2]*Research Assistant, Central Water and Power Research Station, Pune - 411024, India*

[3]*Scientist 'E', Central Water and Power Research Station, Pune - 411024, India*

*Email:banothuraghu@yahoo.com, jotsana.ambekar@rediffmail.com, patil.rg@cwprs.gov.in*

## Abstract

Palhori Khad is a tributary of River Yamuna. Palhori Khad and its various Nallahs are flashy torrents which pose threat to valuable cultivated lands of this region during rainy season. The flood rises very fast due to reducing longitudinal slope and conveyance of the river downstream. For the past several years, flooding of banks and bank erosion is affecting the development of villages and agriculture lands on both the banks of Palhori Khad. Heavy floods occurred during the year 2013-14 that washed away the crops in 400 acres of land and farmers had suffered huge revenue loss. The construction of the embankments (levees) would help in passing the floods easily as the flood wave would not get attenuated and conveyance of the river would be higher. In view of this, Govt. of Himachal Pradesh has planned to take up flood protection measures along the affected reaches of Palhori Khad. The study reach of Palhori Khad for a length of 7.1 km from upstream of Palhori village to boundary of Haryana and Himachal Pradesh was simulated in mathematical model HEC-RAS using 25 river cross sections. The discharge given by project authorities 173.88 $m^3/s$ is used for proving studies and the discharges obtained as per CWC flood estimation method for western Himalayas (Zone 7) are used for designing the flood embankments along Palhori Khad. The analysis of the results indicated that the heights of the protection works proposed by project authorities are overtopping at some locations with the discharge of 1 in 50 years and 1 in 100 years return flood. In view of this, CWPRS has recommended to increase the height of embankments for safe passage of flood. In this paper the probable causes, mechanisms and methods of predictions of bank erosion and sustainable strategies of different bank protection measures are briefly discussed.

***Keywords:*** *Water levels, velocity, afflux, free board, slope protection, launching apron.*

## 1. Introduction

The Village Palhori is situated on both the banks of Palhori Khad at the border of Himachal Pradesh and Haryana as shown in Figure 1. The Palhori Khad and its tributaries are flashy torrents which pose threat to valuable cultivated land of this region during rainy season [CWPRS Technical Report No. 5714]. For the past several years, flooding of banks and bank erosion is affecting the development of villages & agriculture land on both the banks of Palhori Khad. Heavy flood during the year 2013-14 washed away the crops in 400 acres of land and farmers had to suffer huge revenue loss. To safeguard these areas Govt. of Himachal Pradesh has planned to take up flood protection measures along the affected reaches of Palhori Khad.

Joint inspection of the site was conducted and the problems were discussed. Based on the data, mathematical model studies were carried out for deciding the protection works. This technical paper describes the studies conducted for evaluation of the proposed protection works along Palhori Khad.

## 2. Proposal of project authorities

The project engineers had proposed a tentative alignment and locations of flood protection based on the necessity of protecting areas on the country side of the Palhori Khad. The same are presented in Table 1(a).

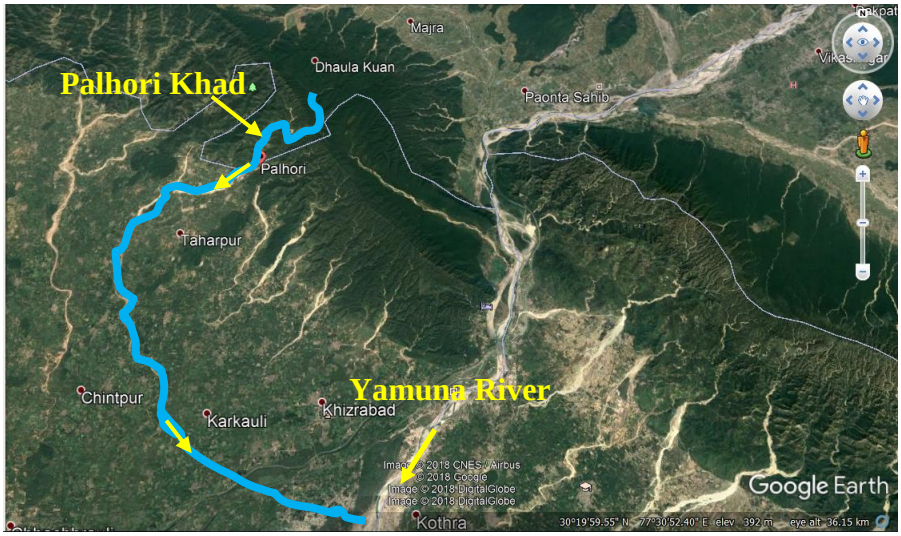



**Figure 1** Google map of Palhori Khad

These proposals were decided based on the previous flood experience and necessity of protecting the country side area depending on the importance of the property on the country side [CWPRS Technical Report no. 5714]. The same were submitted to CWPRS for model studies. The project authorities also submitted the proposed height of the gabion walls derived from previous flood levels as shown in Table 1(b). I&PH department, Poanta Sahib had earlier calculated the 1 in 25 year return period flood discharge of Palhori Khad using ryves formula as 173.88 $m^3$ /s and corresponding water levels at various RD's were also submitted. Based on the catchment area and rainfall data of Palhori Khad and its tributaries, flood frequency analysis was conducted using CWC flood estimation method for western Himalayas (Zone 7) and estimated peak flood discharges corresponding to 1 in 25 years, 1 in 50 years and 1 in 100 years return period for catchments is presented in Table 2. The rainfall data from the Daula Kuan site of Sirmour district is used for flood frequency analysis. This gauge site is 7 km from the study area. Therefore, the rain fall pattern of this location is appropriate for flood frequency analysis.

**Table 1(a)** Alignment and locations of the proposed embankments on left and right bank of Palhori Khad for flood protection (Project authority)

| Sr. No | RD (m) | Left embankment location along cross section from Zero line, (m) | Right embankment location along cross section from Zero line, (m) | Sr. No | RD (m) | Left embankment location along cross section from Zero line, (m) | Right embankment location along cross section from Zero line, (m) |
|---|---|---|---|---|---|---|---|
| 1 | 0 | Not proposed (NP) | 45 | 34 | 3800 | 0 | 50 |
| 2 | 100 | NP | 60 | 35 | 3900 | 0 | 50 |
| 3 | 200 | NP | 60 | 36 | 4000 | 0 | 50 |
| 4 | 300 | NP | 60 | 37 | 4100 | 0 | 50 |
| 5 | 400 | NP | 60 | 38 | 4200 | 0 | NP |
| 6 | 500 | NP | 45 | 39 | 4300 | 0 | 40 |
| 7 | 600 | NP | 45 | 40 | 4400 | 0 | NP |
| 8 | 700 | NP | 60 | 41 | 4500 | 0 | NP |
| 9 | 800 | NP | 60 | 42 | 4600 | NP | 50 |
| 10 | 900 | NP | 60 | 43 | 4700 | NP | 50 |
| 11 | 1000 | NP | 90 | 44 | 4800 | NP | 50 |
| 12 | 1100 | NP | 90 | 45 | 4900 | NP | 40 |
| 13 | 1200 | 0 | 90 | 46 | 5000 | NP | 40 |
| 14 | 1300 | 0 | 75 | 47 | 5200 | NP | 40 |
| 15 | 1400 | 0 | NP | 48 | 5300 | NP | 45 |

| | | | | | | | |
|---|---|---|---|---|---|---|---|
| 16 | 1500 | 0 | NP | 49 | 5400 | NP | 50 |
| 17 | 1800 | 0 | NP | 50 | 5500 | NP | 50 |
| 18 | 1900 | 0 | 50 | 51 | 5600 | 0 | NP |
| 19 | 2000 | 0 | 50 | 52 | 5700 | 0 | 50 |
| 20 | 2100 | NP | 50 | 53 | 5800 | 0 | 50 |
| 21 | 2200 | 0 | 75 | 54 | 5900 | 0 | 50 |
| 22 | 2300 | 0 | 45 | 55 | 6000 | 0 | 50 |
| 23 | 2400 | 0 | 45 | 56 | 6100 | 0 | 50 |
| 24 | 2500 | 0 | 45 | 57 | 6200 | 0 | 50 |
| 25 | 2800 | NP | 45 | 58 | 6300 | 0 | 50 |
| 26 | 2900 | NP | 45 | 59 | 6400 | 0 | 60 |
| 27 | 3000 | 0 | 45 | 60 | 6500 | 0 | 90 |
| 28 | 3100 | 0 | 45 | 61 | 6600 | 0 | 90 |
| 29 | 3300 | 0 | NP | 62 | 6700 | 0 | NP |
| 30 | 3400 | 0 | NP | 63 | 6800 | 0 | NP |
| 31 | 3500 | 0 | NP | 64 | 6900 | 0 | NP |
| 32 | 3600 | 0 | NP | 65 | 7000 | 0 | NP |
| 33 | 3700 | 0 | NP | 66 | 7100 | 0 | NP |

**Table 1(b)** Height of the proposed embankments on left and right bank of Palhori Khad for flood protection (project authority)

| Palhori Khad left bank from RD 1200 m to 7100 m | | | | |
|---|---|---|---|---|
| Sr. No. | RD in 'm' | | Length in 'm'. | Av. Height of crate wall in 'm' |
| | From | To | | |
| 1 | 1200 | 1500 | 300 | 2.20 |
| 2 | 1800 | 2000 | 200 | 2.20 |
| 3 | 2200 | 2500 | 300 | 2.20 |
| 4 | 3000 | 3100 | 100 | 2.30 |
| 5 | 3300 | 3400 | 100 | 2.30 |
| 6 | 3500 | 3920 | 420 | 2.30 |
| 7 | 4000 | 4500 | 500 | 2.30 |
| 8 | 5600 | 5900 | 300 | 2.40 |
| 9 | 6000 | 7100 | 1100 | 2.50 |
| | | Total length | 3320 | |
| Palhori Khad Right bank from RD 0 m to 6900 m | | | | |
| Sr. No. | RD in 'm' | | Length in 'm' | Av. Height of crate wall in 'm' |
| | From | To | | |
| 1 | 0 | 1300 | 1300 | 2.20 |
| 2 | 1850 | 2550 | 700 | 2.20 |
| 3 | 2800 | 3100 | 300 | 2.20 |
| 4 | 3800 | 4100 | 300 | 2.30 |
| 5 | 4300 | 4350 | 50 | 2.30 |
| 6 | 4600 | 5000 | 400 | 2.30 |
| 7 | 5200 | 5500 | 300 | 2.40 |
| 8 | 5700 | 6600 | 900 | 2.50 |
| | Total length | | 4250 | |
| | Total Length (L.B. +R.B.) | | 7570.00 m | |

**Table 2** Peak flood discharges for different return periods of Palhori Khad

| S. No | Return period in Years | Peak flood discharge in $m^3/s$ |
|---|---|---|
| 1. | 25 | 400.2 |
| 2. | 50 | 428.7 |
| 3. | 100 | 485.9 |

## 3. Mathematical model studies and proving studies

The existing cross sections (without embankment) of Palhori Khad were reproduced on mathematical model as per the data supplied by the project authorities. Studies were conducted for the above mentioned discharges.

### *3.1 HEC-RAS Model*

HEC-RAS is an integrated package of hydraulic analysis programs, in which the user interacts with the system through the use of a Graphical User Interface (GUI). The system is capable of performing steady and unsteady flow water surface profile calculations, and will include sediment transport and several hydraulic design computations.

### *3.2 Reach simulated in mathematical model*

The study reach of Palhori Khad for a length of 7.1 km i.e., from upstream of Palhori village to boundary between the states of Haryana and Himachal Pradesh was simulated in mathematical model HEC-RAS using 25 river cross sections. The discharge given by project authorities i.e., 173.88 $m^3/s$ is used for proving studies and the discharges obtained as per CWC flood estimation method for western Himalayas (Zone 7) are used for designing the flood embankments along Palhori Khad.

### *3.3 Boundary conditions*

Model studies were initially carried out with the given discharge of 173.88 $m^3/s$. The downstream boundary was taken as normal depth with a bed slope of 0.0126.

**Table 3** Comparison of water levels at various locations along Palhori Khad for the discharge of 173.88 $m^3/s$.

| S. No. | Chainage in 'm' | Water level given by Project authority in 'm' | Water level computed in 'm' (HECRAS) |
|---|---|---|---|
| 1. | 0 | 445.52 | 445.49 |
| 2. | 3500 | 403.09 | 403.35 |
| 3. | 7000 | 364.47 | 364.45 |

The proving studies were conducted by comparing the results of the mathematical model studies with the known water level at various locations along Palhori Khad for the discharge of 173.88 $m^3/s$ as shown in Table 3. The mathematical model was run by varying the manning's 'n' and the value of 'n' for which the water level matched well with the known water level data was selected for further studies. For Palhori Khad, the water level obtained by the mathematical model is in close agreement with data supplied by the project authorities for manning's 'n' value of 0.03 as shown in Table 3. In view of this, the model was considered as proved with the manning's 'n' value of 0.03.

Studies were conducted for existing condition (without embankments) with discharges obtained as per CWC flood estimation method for Western Himalayas (Zone 7) are used for designing the flood embankments along Palhori Khad as shown in Table 2. The simulations were carried out and the velocity of flow and water levels were computed at various locations with manning's 'n' value equal to 0.03. The computed water levels along Palhori Khad for the above mentioned discharges are shown in Figs. 2, 3&4.

## 4.0 Studies with embankments proposed by project authority

The proposals of project authorities as shown in Table 1(a) & 1(b) were reproduced as per the drawings provided by the project authorities in the mathematical model. Simulations were carried out for the above mentioned discharges and the velocity of flow and water levels were

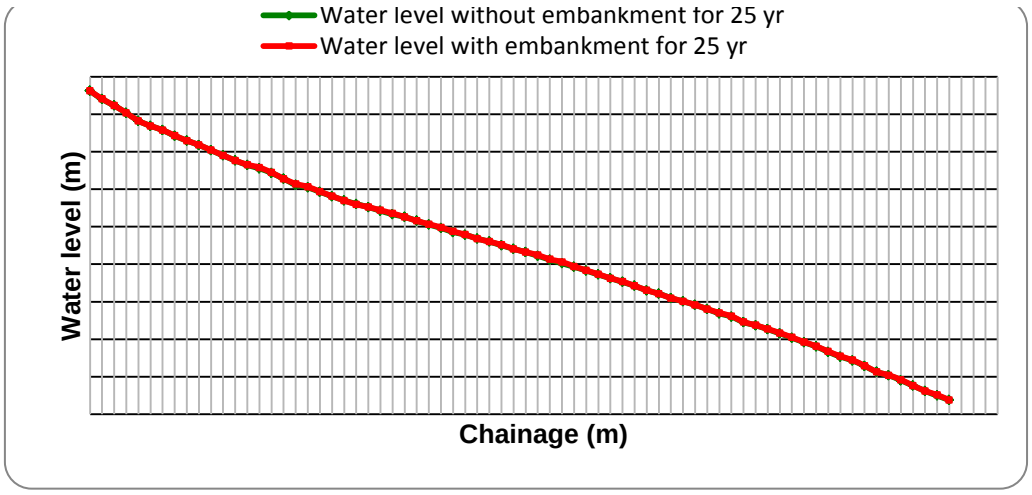



**Figure 2** Water level profile of Palhori Khad with and without embankments by the project authority for the 25 year return period discharges of 400.2 $m^3/s$

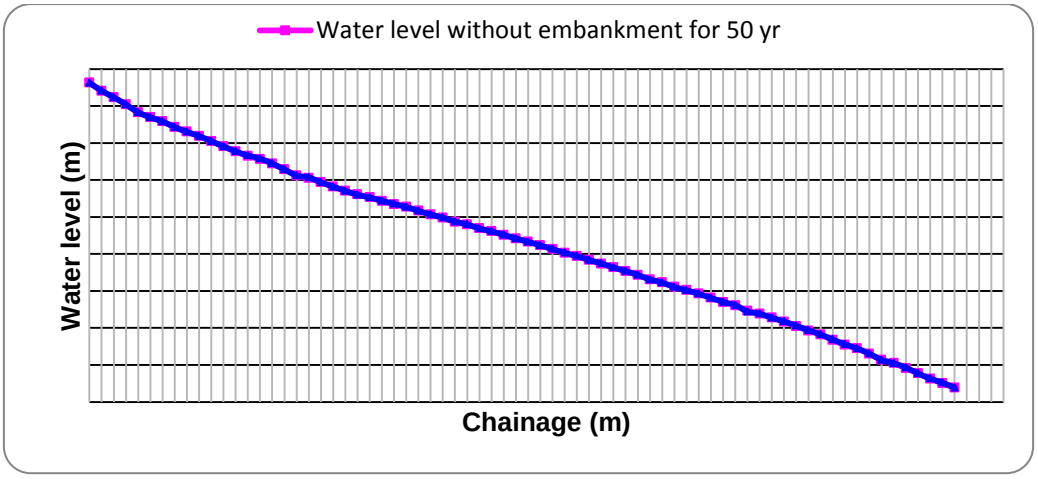



**Figure 3** Water level profile of Palhori Khad with and without embankments by the project authority for the 50 year return period discharges 428.7 $m^3/s$.

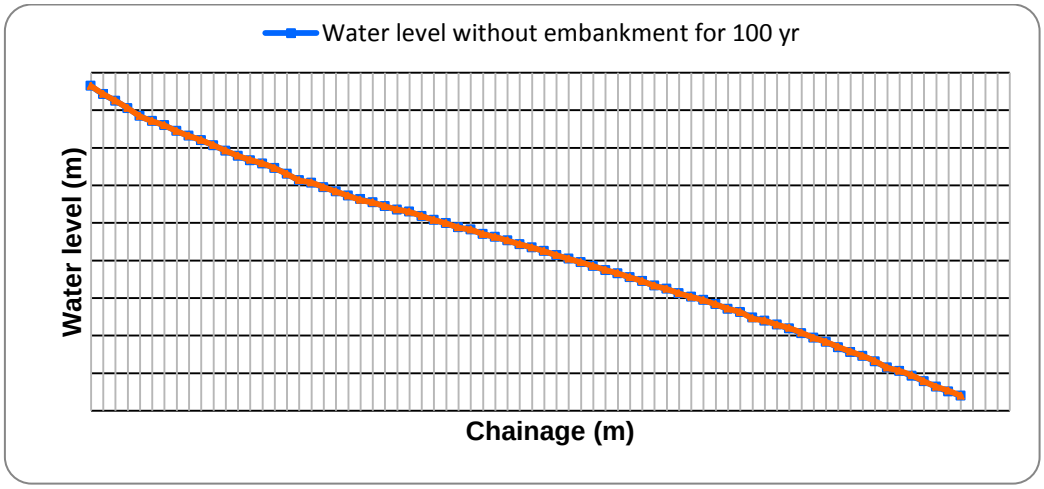



**Figure 4** Water level profile of Palhori Khad with and without embankments by the project authority for the 100 year return period discharges of 485.9 $m^3/s$

computed at various locations with manning's 'n' value equal to 0.03. The computed water levels values along Palhori Khad with embankments as proposed by project authorities are shown in Figs 2, 3&4. It was observed that, at RD's 2200 m and 4200 m the computed afflux values were more than 40 cm for 25 year, 50 year and 100 year return period discharges; at RD's 1300 m, 5200 m and 5300 m the afflux values are more than 40 cm for 50 year and 100

year return period discharges. In view of this, studies were conducted with modified alignments and heights of embankments (Table 4 & 5) that will reduce the effective afflux.

## 5.0 Studies with modified embankments

The heights of the protection works proposed by project authorities are overtopping at some locations with the discharge of 1 in 50 years and 1 in 100 years return flood. In view of this, the height of embankments was increased for safe passage of flood as shown in Table 4. Model studies were carried out with modified embankments for various return period discharges given in Table 2. It was observed that at some locations the waterway designed for safe passage of flood is not sufficient and it is showing higher values of afflux (more than 40 cm) at some locations. To minimize the afflux values, the waterway was increased by changing the

**Table 4** Modified height of embankments on left and right bank of Palhori Khad

| Palhori Khad left bank from RD 1200 m to 7100 m | | | | |
|---|---|---|---|---|
| Sr. No. | RD in 'm' | | Length in 'm'. | Av. Height of crate wall in 'm' |
| | From | To | | |
| 1 | 1200 | 1500 | 300 | 2.80 |
| 2 | 1800 | 2000 | 200 | 2.60 |
| 3 | 2200 | 2500 | 300 | 2.80 |
| 4 | 3000 | 3100 | 100 | 2.80 |
| 5 | 3300 | 4500 | 1200 | 3.40 |
| 6 | 5600 | 7100 | 1500 | 2.70 |
| | | Total length | 3600 | |
| Palhori Khad Right bank from RD 0 m to 6600 m | | | | |
| Sr. No. | RD in 'm' | | Length in 'm' | Av. Height of crate wall in 'm' |
| | From | To | | |
| 1 | 0 | 1300 | 1300 | 3.00 |
| 2 | 1900 | 2500 | 600 | 2.80 |
| 3 | 2800 | 3100 | 300 | 2.80 |
| 4 | 3800 | 4300 | 500 | 3.40 |
| 5 | 4600 | 5000 | 400 | 2.60 |
| 6 | 5200 | 5500 | 300 | 3.50 |
| 7 | 5700 | 6600 | 900 | 2.60 |
| | Total length | | 4300 | |
| | Total Length (L.B. +R.B.) | | 7900.00 m | |

**Table 5** Modified location of proposed embankments on left and right bank of Palhori Khad

| Sr. No. | RD | Left station | Right station |
|---|---|---|---|
| 1 | 1300 | 0 | 60 |
| 2 | 2000 | -15 | 60 |
| 3 | 2100 | Not proposed | 60 |
| 4 | 2200 | 0 | 65 |
| 5 | 2300 | -15 | 60 |
| 6 | 2400 | -15 | 60 |
| 7 | 2500 | -15 | 60 |
| 8 | 4300 | -15 | 50 |
| 9 | 5200 | Not proposed | 50 |
| 10 | 5300 | Not proposed | 60 |

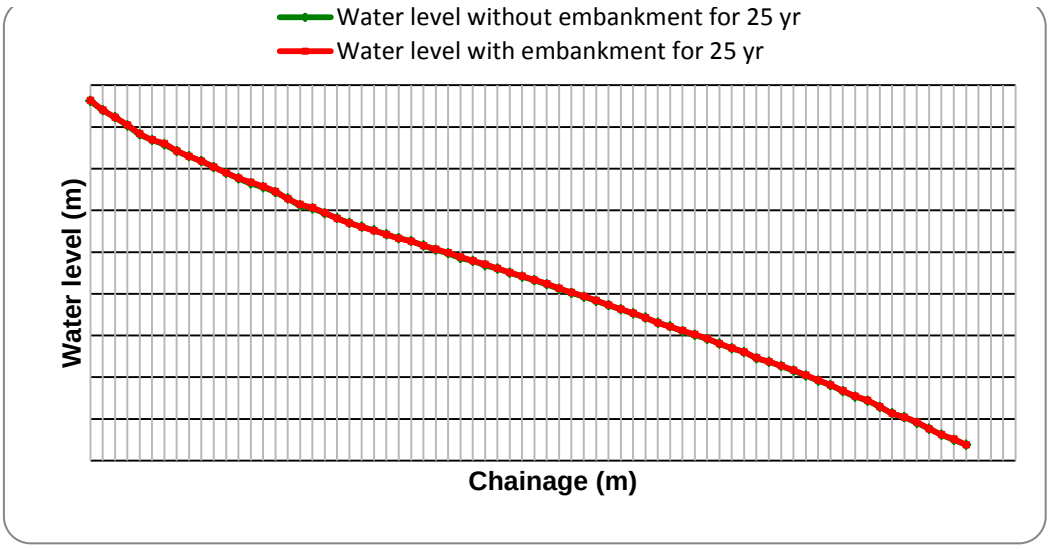



**Figure 5** Water level profile of Palhori Khad with and without embankments as modified by the CWPRS for the 25 year return period discharges of 400.2 $m^3/s$

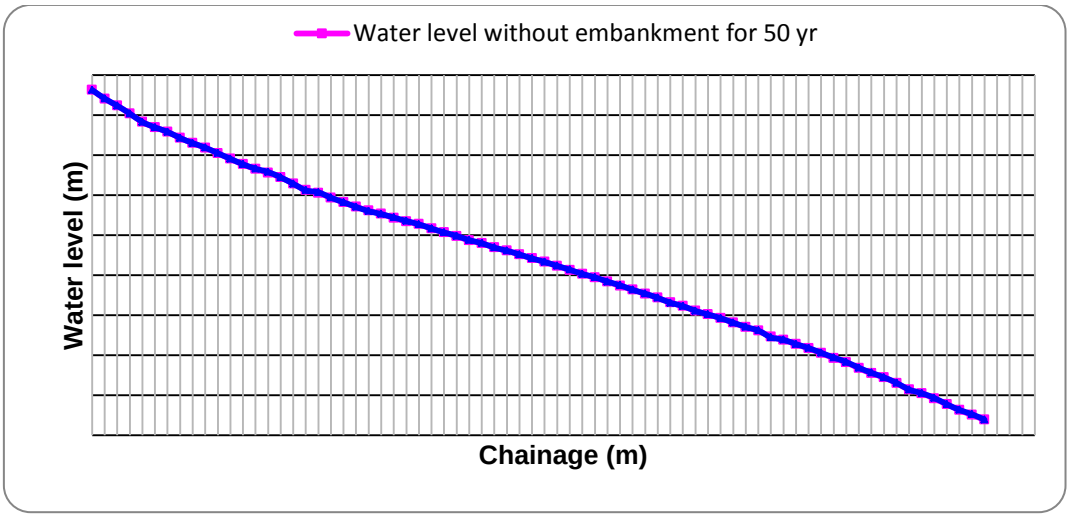



**Figure 6** Water level profile of Palhori Khad with and without embankments as modified by the CWPRS for the 50 year return period discharges 428.7 $m^3/s$.

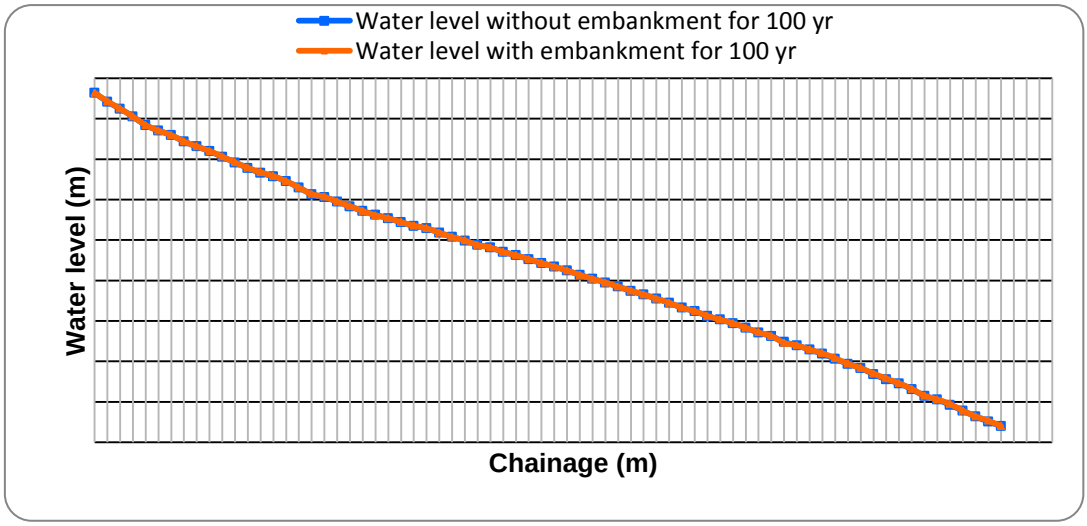



**Figure 7** Water level profile of Palhori Khad with and without embankments as modified by the CWPRS for the 100 year return period discharges of 485.9 $m^3/s$

alignment locations of levees towards the bank as shown in Table 5. The proposals as shown in Tables 4&5 were reproduced in the mathematical model. Simulations were carried out for the above mentioned discharges and the velocity of flow and water levels were computed at various locations with manning's 'n' value equal to 0.03. The computed water levels along Palhori Khad with proposed modified embankments are shown in Figs 5, 6 &7. The computed afflux values along the Palhori Khad were of the order of less than 10% of normal flow depth i.e., below 40 cm for modified embankments. Figures 5, 6 & 7 show the water level profile with and without embankments along Palhori Khad for the discharges of 400.7 $m^3/s$, 428.7 $m^3/s$ and 485.9 $m^3/s$ respectively.

## 6.0 Flood protection measures

The site inspection and subsequent mathematical model studies indicated that the longitudinal slopes vary in the range of 1 in 204.08 to 1 in 27.70 for Palhori Khad. The steep sloped reaches experience a maximum velocity of flow of the order of 4.0 m/s to 4.73 m/s. Under these hydraulic conditions, the regular bank protection works in the form of embankments or slope protection works may not sustain during the floods. Therefore,it is felt that the gabion walls with launching apron and toe protection to the walls is desirable type of protection works for the study reach under consideration. The height of gabion walls are computed from the maximum water levels obtained from model studies with embankments by adding sufficient free board. The vertical gabion wall with launching apron of sufficient length is designed to protect the toe of the gabion wall as shown in Figure 8. Typical drawings of gabion stone filled crate walls of height 2.74 m and 3.65 m with launching aprons are shown in Figures 8 & 9. These protection works may be decided and adapted based on the general bed level and computed HFL (1 in 25 year, 1 in 50 year and 1 in 100 year) with sufficient free board as per IS 10635.

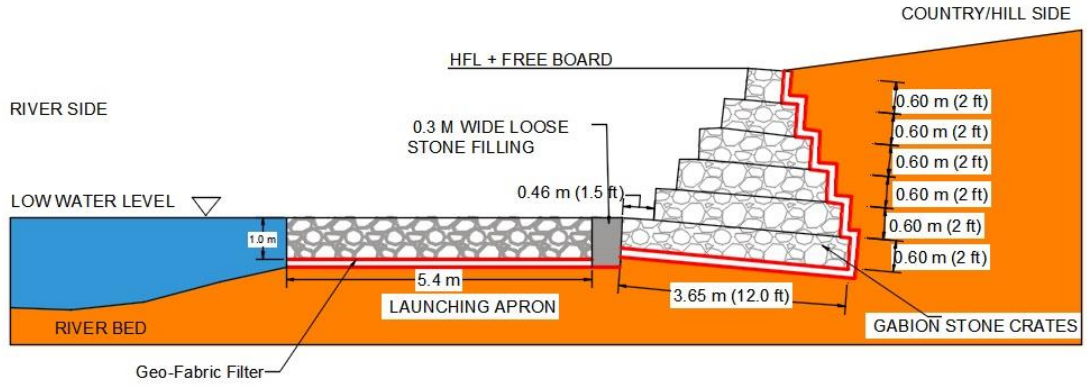



**Figure 8** Typical section of Gabion wall up to the height of 12 ft (3.65 m)

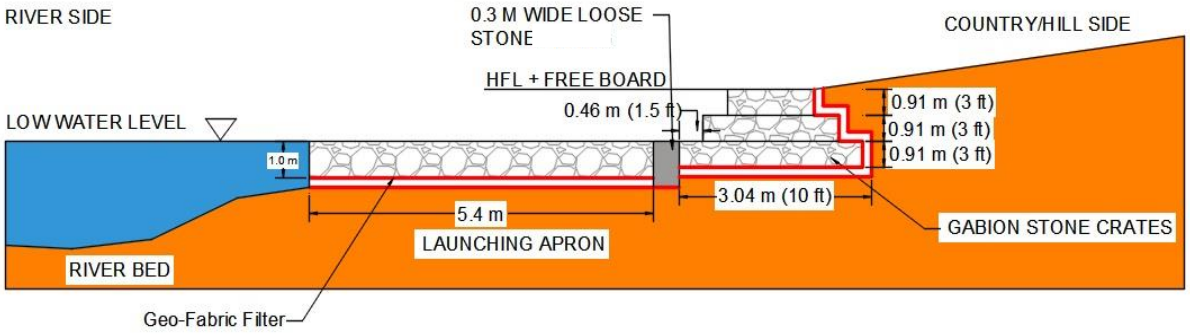



**Figure 9** Typical section of Gabion wall up to the height of 9.0 ft (2.74) m

## 7.0 Conclusion and recommendations

Based on the mathematical model studies for flood protection works of Palhori Khad, following recommendations are made:

- Flood protection works in the form of slope protection works or vertical gabion wall with launching apron as toe protection may be provided along Palhori Khad. The slope protection work may be adopted for velocities till 4.5 m/s and beyond vertical gabion walls may be adopted.

- The protection work shall be streamlined in plan in the vicinity of confluence of tributaries with the main river. where ever there is tributary joining the main river and the protection work is not taken up for the tributary, in such cases the protection works shall be extended in to the tributary for at least 50 m or for a length of 1.5 time the width of the tributary mouth whichever is maximum.

- The ends of the protection works (either u/s or d/s) shall be properly embedding into the country side (about 5 m) so that the flow does not outflank the protection works.

- Bank protection works (excluding launching apron) shall not encroach the original river width more than 15%. This is necessary to pass the given flood through the cross section without causing any much obstruction to the flow.

- Height of the gabion wall may be raised above the computed maximum water levels by providing sufficient free board as per IS-10635. In extreme flood exceeding the design flood, the free board plays an important role. Higher the free board, higher will be flood retention period on country side. Considering this apprehension, it is advised to keep the free board not more than 0.5 m for various protection works suggested here. However, it can be as per standard for a reach where important structures such as industries, densely populated areas are to be protected.

- The alignment of the modified gabion walls (Table 4 & 5) shall be same as in proposal, otherwise the flow parameters are bound to change.

- The alignment of the embankments shall be such that the meanders of the river are within the embankments and the width covers the thalweg of the river.

- Geo-fabric filter as per the specification is necessary and hence recommended. while placing geo-fabric filter below the protection works, care may be taken to place 15 cm thick layer of sand below the filter and also 15 cm thick sand layer above the filter (sandwiching the geo-fabric filter between sand layers) to avoid rupture of filter material.

- The stone crates may be filled up with graded stones so that maximum density is achieved and crates are efficient in arresting the high velocity flow approaching the embankment.

- If the width of river is narrow and the launching aprons of both the banks overlap, the project authorities may provide a single layer of launching apron connected through the bed of the river, the top of such launching apron being at the average bed level of the cross section.

- The bank protection works for the tributaries near the confluence should be integral part of the protection works of Palhori Khad. The protection works near the confluence in plan shall be streamlined to induce smooth merging flow of both the rivers/khads

- To drain the storm water collected in the country side, proper storm water drainage facility such as culverts/pipes along with non-return flap gates on the river side should be provided. The dimensions of such vent/pipes and numbers may be designed based on the hydrological features of the catchment area.

## 8. References

Technical Report No. 5714 of CWPRS, "Mathematical model studies for evolving flood protection measures and anti erosion works along Palhori Khad tributary of river Yamuna, Paonta Sahib, Himachal Pradesh". June 2019.

*IN PROCEEDINGS OF 25th HYDRO 2020, INTERNATIONAL CONFERENCE, NATIONAL INSTITUTE OF TECHNOLOGY ROURKELA, ODISHA, INDIA 26-28, March 2021, ISBN 978-93-90631-56-8*

Paper ID - 250

# Estimation of sediment yield in Chalakudy River

Maneesha K Sankar[1], Dr. Suman K.S[2]

*Mdneesha K Sankar, MTech Student in Water Resources and Hydroinformatics, Government Engineering college Trichur, Thrissur and 680009, India*

[2] *Dr. Sumam K.S, Professor in Civil Engineering, Government Engineering college Trichur, Thrissur and 680009, India*

*Email: manujune20@gmail.com , sumam@gectcr.ac.in*

*Telephone/Mobile No.: +91 9746861008 , +91 9496167977*

## Abstract

Neural networks are a user-friendly alternative to physically complex models for the prediction of soil erosion. The purpose of the study is to find out the best Artificial Neural network model for predicting the sediment yield by considering different input parameters like discharge, rainfall and flow velocity. The input data's for a period of 28 years (1990 to 2018) were considered for this study. Models were developed for two periods 1990-1997 and 2010-2017. Five years of data were used for training the model and the remaining two years of input data were used for validating the model. The training was conducted using the Levengerg – Marquardt algorithm. For selecting the best performing model, minimum value of RMSE and NSE were taken as criteria for the evaluation of model. From the analysis of result, it was found that the Discharge – Rainfall model gave the best results in predicting the sediment yield.

***Keywords:*** *Artificial neural network; Sediment yield; Chalakudy River.*

## 1. Introduction

Sedimentation is one of the serious environmental issues that are widely recognized all across the world. It has an impact on water quality, a reduction in reservoir capacity and low agricultural productivity due to the removal of top nutrient soils. Sediment outflow from the watershed depends upon the process through which the soil materials are removed, transported and deposited by runoff and precipitation. Estimation of suspended sediment is necessary, to deal with issues like the design of reservoirs or dams and the transport of pollutants and sediments through streams and rivers. The increasing effect of sediment loads causes an enormous burden on water infrastructures due to the increasing operation cost, particularly in the case of water extraction and treatment for community water supply. The interaction between soil texture, geology, land use, topography and climate change seems to be increasing the number of sediment loads produced and transported from the watershed. The production and transportation of sediment in the watershed are deeply connected to the synergistic influences of land use and climate. As a result of temperature and climatic change, indirectly affects the rainfall which will influence the frequency and magnitude of sediment flow. The changes in land use and soil management activities have a greater effect on sediment flow compared to climate variability. However, the extent to which the intensity and magnitude of sediment flows are affected by climate change and land use remains a topic for discussion.

Sedimentation is a mechanism in which soil particles are separated and transported by running water and deposited as a layer of solid particles in water bodies. It is the phenomenon that soil particle attains a certain velocity under the action of the gravitational field. This translation velocity is known as the sedimentation of the settling velocity. Sedimentation is a complicated phenomenon that varies with sediment yield of the watershed, transport rate and mode of deposition. The accumulation of sediments reduces the storage capacity and lifespan of reservoir.

Sedimentation remains one of the most serious issues to river ecosystems across the world. A research was performed on the 145 rivers on the world with long-term sediment records and results demonstrate that about 50 percent of rivers have a statistically significant downward trend due to

sedimentation (Walling and Fang, 2003). Sumi and Hirose (2009) reported that the global gross storage capacity of the reservoir is approximately 600 $km^3$ and the annual sedimentation rate of the reservoir is approximately 31 $km^3$ (0.52 per cent). This means that by the year 2100, the global storage capacity of the reservoir would be reduced to 50% at this sedimentation rate.

The direct calculation is the most accurate sediment load estimation process, but the sampling of sediment concentration is costly and it can't be carried out regularly. For the estimation of sediment loads, data-driven models such as numerical models have proven their effectiveness. Many techniques have been made use of forecasting sediment yield models with high accuracy and the research in this field is continuing. Statistical models based on the time series have been used for hydrological forecasting and some of the statistical models are a simple regression model, multiple regression models, and autoregressive moving average models. The statistical approach uses classical methods to analyze historical data to develop forecasting models for estimating sediment concentrations. Nonetheless, these models are not meant to represent the non-linear processes involved in the transformation of rainfall into sediment yield. Artificial intelligence (AI) methods meet this need. Major AI methods that have wide range of applications in water resources engineering are Genetic Algorithm, Artificial Neural Network, and Fuzzy Logic.

For any watershed, estimation of sediment becomes one of the important criteria for water quality analysis. The outflow of sediment from the watershed depends upon the detachment, transport and deposition of soil particles by discharge and rainfall. The estimation of sediment yield is expected to resolve issues like the construction of reservoirs and dams, sediment - pollutant transport in lakes and streams. Hence it is necessary to have an appropriate method to analyze the amount of sediment deposited in the river so that proper measures have to be taken to reduce the reservoir sedimentation and protect water resources.

The objective of the study is to develop the best combination among rainfall, discharge and flow velocity in ANN by predicting sediment yield for the watershed and comparing its prediction performance with observed data.

## 1.1 *Artificial Neural Network*

An artificial neural network (ANN) is an information processing paradigm inspired by biological nervous systems, like the processing of information by the brain. The novel structure of the information processing system is the key aspect of this model. It consists of many highly interconnected processing elements (neurons) which work together to solve specific problems. An artificial neural network learns by examples, just the way human learns. An ANN is designed through a learning algorithm for a particular task, such as pattern recognition or data classification. Learning in a biological system involves the adaptation of the synaptic connections between the neurons.

Artificial neural networks are regression estimators which can estimate any measurable function with a high degree of accuracy, is selected for this study. The development of artificial intelligence in the field of hydrology and water resources simulation has generated several promising results. In the past few years, numerical models can be used for modelling rainfall-runoff forecasting, prediction of surge water levels and flash flood forecasting and the result shows convincing.The artificial intelligence computational methods provide a great benefit over traditional modelling, by handling a large number of noisy data from complex and nonlinear systems whose relations are not fully understood. These techniques can be effectively exploited for the construction of powerful intelligent systems.

### *1.1.1 Architecture of Neural networks*

Feedforward ANNs allow signals to travel from input to output only. The feedback loops do not have any effect on the output of the same layer. Feedforward is usually simple networks associating

input with outputs. They are commonly used to recognize patterns. This type of organization is called the bottom-up or top-down organization.

The feedback network can have signals going in both directions through the network loops. It is a very strong and complicated networking system. The feedback network is a highly complex system which continually changes until it finds a balance. It stays in the balance until their information updates or a new equilibrium is found.

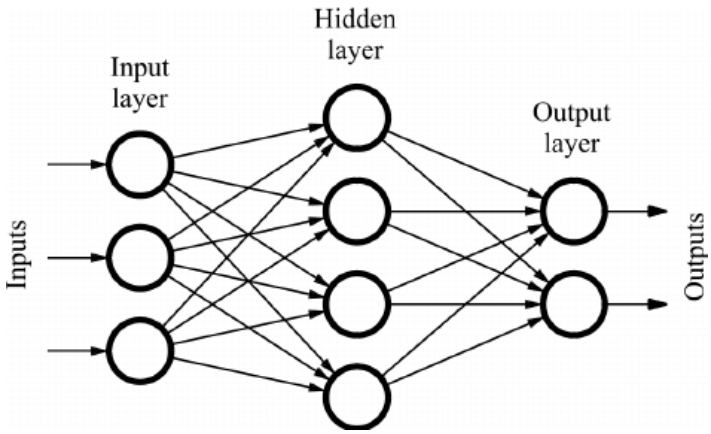



**Figure 1** An example of a simple feed-forward network

### *1.1.2 Network layers*

The most common form of the artificial neural network consists of three unit layers. An "input" unit layer is connected to hide a unit layer which is then connected to an "output" unit layer (figure 1). The input unit activity represents the raw information that is transmitted to the network. The hidden unit's activity is determined by the activities of the inputs and the weight of the connection between the input and the hidden units. The performance of the output unit depends on the operation of the weights and hidden node. This simple form of network contains the hidden units in it, which helps to construct their inputs layout freely. The weights between the input and the hidden units are calculated by the activation function of the input unit and the hidden unit.

### *1.1.3 Back Propagation Algorithm*

To minimize the error between the desired output and the actual output, the neural network must be trained to adjust the weight of each variable. Through this process, the neural network architecture calculates the weight error derivative (EW). EW computes the error changes for a slight difference in the weights. For determining EW, back propagation algorithm is the most widely used method.

In the back propagation algorithm, the entire unit in the network is linear. The algorithm computes each EW by first computing the EA, the rate at which the error changes at the activity level of a unit is changed. For output units, the EA is simply the difference between the actual and the desired output. To compute the EA for a hidden unit in the layer just before the output layer, identify all the weight between the hidden units and the output units to which it is connected. Then multiply those weights by the EA of those output units and add the products. This sum equals the EA for the chosen hidden unit. After calculating all the EAs in the hidden layer just before the output layer, compute the EAs for the other layers, moving from layer to layer in opposite direction in the way activities propagate through the network. This is called backpropagation. Once the EA has been computed for a unit, it is straightforward to compute EW for each coming connection of the unit. The EW is the product of EA and the activity through the incoming connection.

### *1.1.4 Neural Networks Training Algorithm*

The Levenberg - Marquardt algorithm is designed to approach the second-order training speed without computing the Hessian Matrix. In most of the cases, the best results for ANN models are given by the LM algorithm. So for the study, the LM algorithm is selected. Minimisation of the global error E is the objective of the training algorithm. Error E can be calculated by the following equation:

$$E = \frac{1}{M}\sum_{m=1}^{M} E_m \quad (1)$$

where M is the total no. of training patterns and $E_m$ is the error of the training pattern. $E_m$ is derived as:

$$E_m = \frac{1}{2}\sum_{k=1}^{n}(O_k - t_k)^2 \quad (2)$$

Where the total number of output nodes denoted by n, $O_k$ is the network output at the $k^{th}$ output node and $t_k$ target output at the $k^{th}$ output node.

## 2. Models developed using different input combinations

In this study, different combinations of four input variables such as Discharge, Rainfall and Flow velocity will be considered for training the ANN model to forecast sediment yield. Models will be developed for two different periods 1990-1997 and 2010-2017. From these 10 models, the best model will be used for forecasting the sediment yield.

**Table 1** Input combination

| Model Name | Model Period | Model Parameters | Input Layer | Output layer |
|---|---|---|---|---|
| M1 | 1990 -1997 | $Q_t$, $S_t$ | $Q_t$ | $S_t$ |
| M2 | 2010 – 2017 | | | |
| M3 | 1990 -1997 | $P_t$, $S_t$ | $P_t$ | $S_t$ |
| M4 | 2010 – 2017 | | | |
| M5 | 1990 -1997 | $V_t$, $S_t$ | $V_t$ | $S_t$ |
| M6 | 2010 – 2017 | | | |
| M7 | 1990 -1997 | $P_t$, $Q_t$ and $S_t$ | $P_t$, $Q_t$ | $S_t$ |
| M8 | 2010 – 2017 | | | |
| M9 | 1990 -1997 | $P_t$, $V_t$ and $S_t$ | $P_t$, $V_t$ | $S_t$ |
| M10 | 2010 – 2017 | | | |

Where $Q_t$ = Discharge in $m^3$/sec, $P_t$ = Precipitation in mm, $F_t$ = Flow velocity in $m^2$/sec and $S_t$ = Sediment Yield in g/litre.

## 3. Model Evaluation criteria

World Meteorological Organisation (WMO) and other researchers (Nash and Sutcliffe) proposed different methods of verification criteria for the evaluation and the comparison of the numerical models. For the present study, the root means square error (RMSE) and the Nash Sutcliffe coefficient (NSE which is also called the coefficient of simulation efficiency COE) is used as the numerical indicators. The equation for calculating RMSE and COE value are given below,

$$RMSE = \sqrt{\frac{\sum_{i=1}^{n}(X_i - X_i')^2}{n}} \quad (3)$$

$$COE = \frac{\sum_{i=1}^{n}(X_i - X_i')^2}{\sum_{i=1}^{n}(X_i - \bar{X})^2} \quad (4)$$

where, $X_i$ is the observed value of sediment; $X_i'$ is the predicted values sediment; $\bar{X}$ is the average value of observed sediment; and $n$ is the number of observations.

Model errors can be indicated by the value of the RMSE in terms of the dimensioned quantity. A perfect match between the observed and predicted values indicates that RMSE and COE values are close to zero and 1 respectively.

## 4. Description of study area and data

The Chalakudy River is one of the longest rivers of Kerala. The five streams Parambikulam, Kuriarkutty, Sholayar, Karappara and Anakkayam originating from the Anamalai Hills of Western Ghats, are confluence to form Chalakudy River. The rivers Parambikulam and Sholayar originate in the Tamilnadu whereas the rivers Karappara and Kuriarkuthti originate from the Palakkad district of Kerala. At 470m above the Mean sea level, the Parambikulam joins with the Kuriarkutty River and the river Sholayar is joined by 9 km down. The Karappara and Anakkayam meet the main river about 455 m and 8 km further down at 365 meters above the MSL respectively. The river reaches the plains of Athirapally by passing through the dense forests.

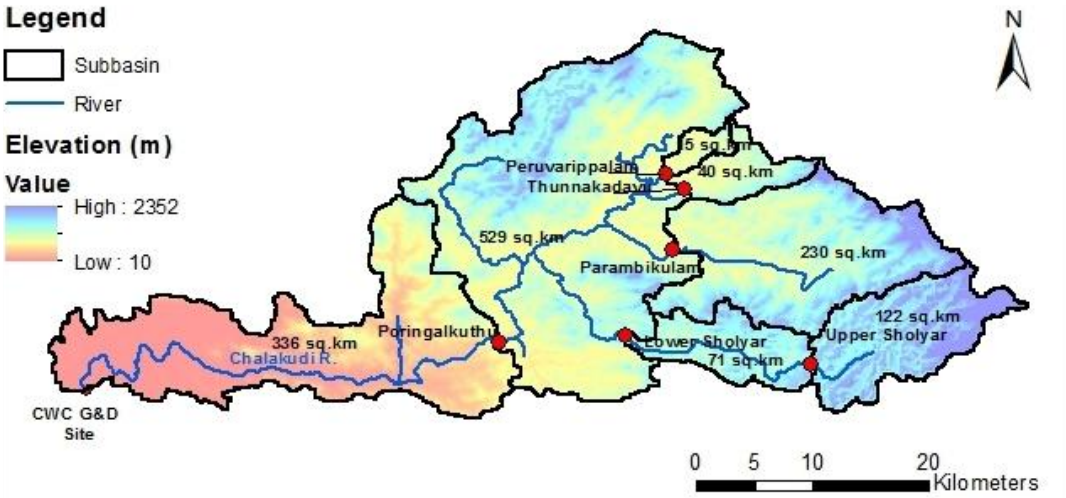



**Figure 2** Map of Chalakudy River Up To Arangali G&D Site of CWC

Data used for the present study are collected from Arangali Hydrological observation station, situated in Trichur district Kerala, under the Central Water Commission. Central Water Commission has built a series of sediment observation stations and stream gauging stations for observing hydrological parameters. Periyar River is the main tributary in the hydrological observation station and its sub tributary is Chalakudy River. The catchment area is 1342 $Km^2$ and lies in the Longitude of 76°18'55" and Latitude of 10°16'53".

The data required for this study are Discharge, Rainfall, Flow velocity and Sediment Yield. The data for the present study is described in the table given below:

**Table 2** Date description

| Data Required | Data Description |
|---|---|
| Discharge | The daily discharge in $m^3/s$ from the year 1990 Jan to 2018 Dec from Arangaly station. |
| Rainfall | The daily precipitation data from the year 1990 Jan to 2018 Dec from Arangaly station |
| Flow velocity | The daily flow velocity data from the year 1990 Jan to 2018 Dec from Arangaly station |
| Sediment Yield | The daily sediment data from the year 1990 Jan to 2018 Dec obtained from Arangaly station |

## 5. Results and discussion

Throughout this analysis, the various combinations of discharge, precipitation and flow velocity were used as input variables to develop monthly sediment models. The description of different models to be developed is given in table 1. For developing the models, seven years (1990-1997 and 2010-2017) of monthly data of discharge, rainfall and flow velocity were used. For training the model five years of data will be used and the remaining two years of data will be used for testing the model. The trial and error method will be used for determining the number of neurons in the hidden layers. The best ANN model will be selected based on COE, $R^2$ and RMSE values.

In Model 1, discharge is taken as the input parameter for the period of 1990 – 1997 and sediment yield is taken as a target for developing an ANN model. Five-year data will be used for training the model and the remaining two-year data will be used for testing the model. Results obtained from model 1 are shown below.

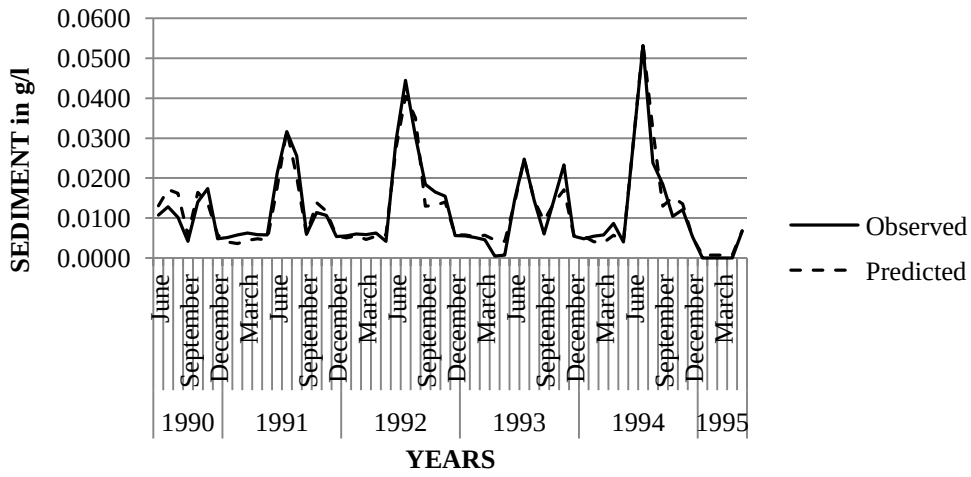



**Figure 3** Graph obtained for the sediment for a training period of 1990-1997

The RMSE value and COE obtained for training the model is 0.0027 and 0.934427 respectively and it shows a perfect match with the standard values.

This trained model will be used for simulating the sediment yield for a period of 1996 -1997. The graph of observed vs predicted sediment is plotted again as in figure 4. RMSE and COE value will be

calculated for testing the model, to check its compatibility with the trained model values. RMSE and COE values obtained for testing the model is 0.002859 and 0.853889. RMSE value and COE value calculated for the testing period shows a slight difference for the training period. Still, results hold well, because RMSE value and COE value are close to the standard result.

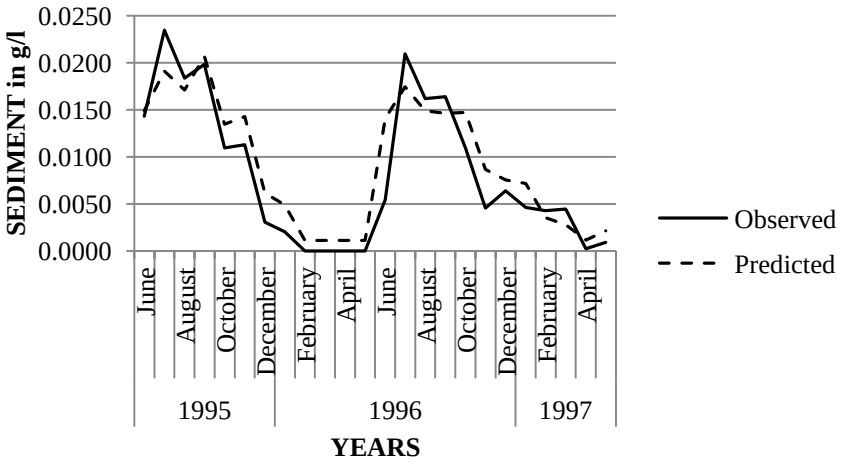



**Figure 4** Graph obtained for the observed and predicted sediment for a training period of 1996-1997

Similarly all 10 models were developed, out of which model 7 gives the best performance for predicting the sediment yield. In Model 7, discharge and rainfall are taken as the input parameter for the period of 1990 – 1997 and sediment yield is taken as a target for developing an ANN model. Here two input parameters were considered for predicting the sediment yield. Five-year data, which is seventy percentages of data, is used for training the model and the remaining two-year data is used for testing the model. Results obtained from model 7 are shown below.

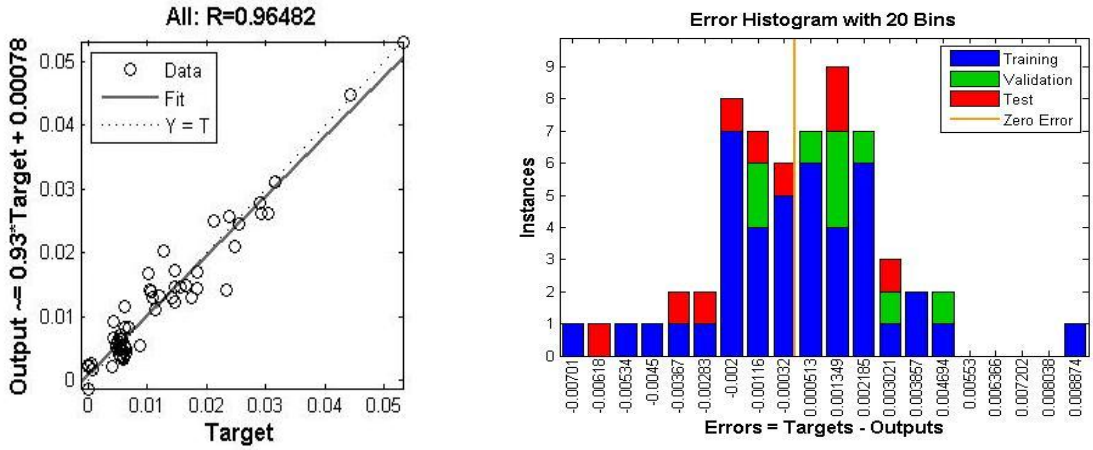



**Figure 5** Regression plot of model 7 and Error histogram of the model 7

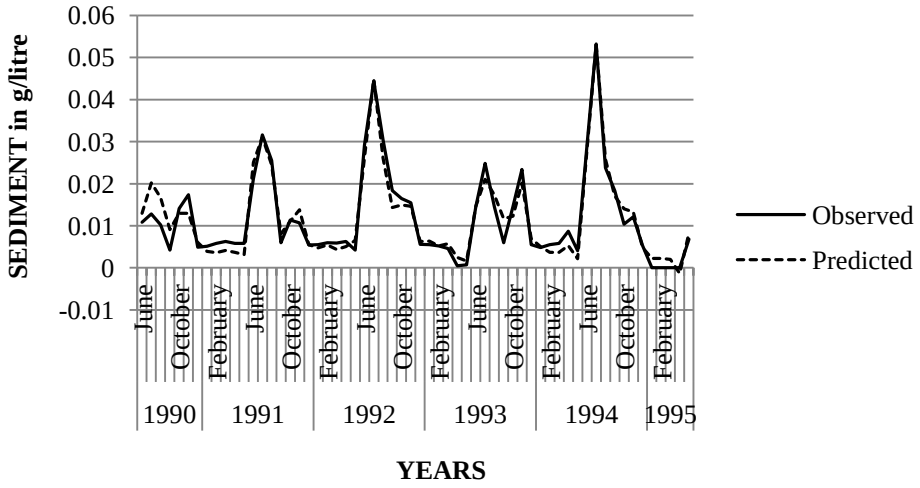



**Figure 6** Graph obtained for the observed and predicted sediment for a training period of 1990-1995

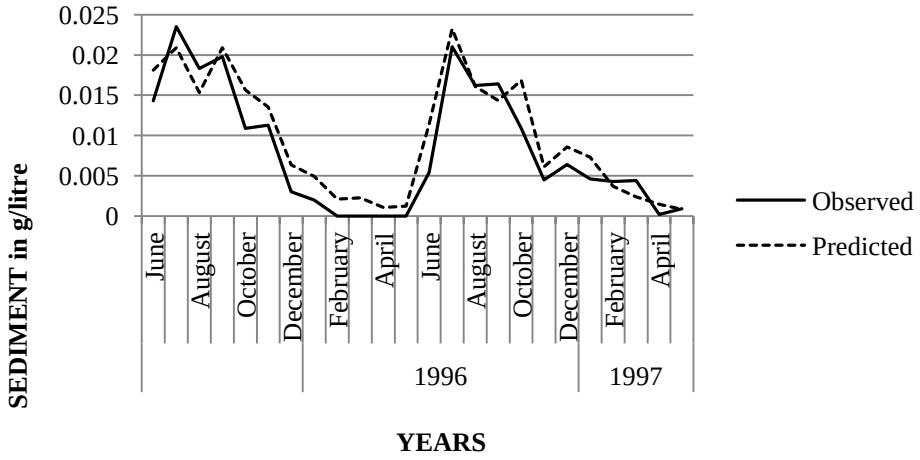



**Figure 7** Graph obtained for the observed and predicted sediment for a testing period of 1996-1997

The RMSE and COE values obtained for training the model is **0.0025708** and **0.9425** respectively and for testing the model it is obtained as **0.0026537** and **0.8744**. There is a slight difference in the values of training and testing. Since the RMSE and COE values are close to the standard values, one can say that model holds a good result. This model gives a better RMSE and COE values than discharge and rainfall, by considering the inputs individually. Two input parameters give a better result than the single input parameter models. So it's evident that by increasing the input parameters can improve the efficiency of sediment prediction of the model. The overall output obtained for these 10 models are given in Table 3.

By analyzing all these 10 models, it can be concluded that ANN models can be used for the prediction of sediment yield. Discharge, rainfall and flow velocity can be used as input for developing sediment yield. From the models, it is evident that models with discharge as input gives values more close to observed values of sediment yield as compared to those predicted using the rainfall and flow velocity as input.

**Table 3** Results obtained for all models developed for predicting sediment yield

| Model | Period | Input | RMSE | | COE | |
|---|---|---|---|---|---|---|
| | | | Training | Testing | Training | Testing |
| Model 1 | 1990-1997 | Discharge | 0.003 | 0.003 | 0.934 | 0.854 |
| Model 2 | 2010-2017 | | 0.005 | 0.003 | 0.771 | 0.703 |
| Model 3 | 1990-1997 | Rainfall | 0.004 | 0.003 | 0.847 | 0.809 |
| Model 4 | 2010-2017 | | 0.005 | 0.003 | 0.726 | 0.672 |
| Model 5 | 1990-1997 | Flow Velocity | 0.004 | 0.003 | 0.888 | 0.791 |
| Model 6 | 2010-2017 | | 0.006 | 0.004 | 0.620 | 0.577 |
| Model 7 | 1990-1997 | Discharge & Rainfall | 0.003 | 0.003 | **0.943** | **0.874** |
| Model 8 | 2010-2017 | | 0.004 | 0.003 | 0.827 | 0.759 |
| Model 9 | 1990-1997 | Flow Velocity & Rainfall | 0.003 | 0.003 | 0.921 | 0.836 |
| Model 10 | 2010-2017 | | 0.005 | 0.003 | 0.767 | 0.694 |

Models developed for 1990-1997 performs better than 2010-2017 models. The models with two input parameters performed better than the model with the single input parameter. Out of 10 models, Model 7 gives the best result to predict sediment yield and this model's input is a combination of discharge and rainfall.

## 6. Conclusions

Artificial neural network models were developed to predict monthly sediment yield from easily available information on discharge, rainfall and flow velocity. Different neural network architectures were developed by considering the input variables and hidden neurons. For developing the models seven years of data of discharge, rainfall, flow velocity and sediment yield from the year 1990-2018 were used. Models are developed for two periods 1990-1997 and 2010-2017. For training, the models five years of data were used and remaining two-year data were used to test the models. The conclusions arrived from the study are as follows.

1. ANN models can be used for the prediction of sediment yield.
2. Rainfall, Discharge and flow velocity can be used as input parameters for the prediction
3. Increase of the number of the input parameters can increase the efficiency of the model..
4. Combination of Discharge and Rainfall model gives the best result compared to other models
5. To forecast the sediment yield for any year, ANN models can be used if rainfall and discharge are known.

## References

Agarwal, A., Rai, R. K., and Upadhyay, A. (2009) Forecasting of runoff and sediment yield using artificial neural networks, *Journal of Water Resources and Protection*, 1(05), 368–375.

Ajai Singh, Mohd. Imtiyaz, R. K. Isaac, and Denis, D. M. (2013) Comparison of Artificial Neural Network Models for Sediment Yield Prediction at Single Gauging Station of Watershed in Eastern India, *Journal of Hydrologic Engineering*, 18(1): 115-120.

ASCE Task Committee on Application of Artificial Neural Networks in Hydrology. 2000a. Artificial neural networks in hydrology. I: Preliminary concepts, *J. Hydrologic Eng., 52, 115–123*

ASCE Task Committee on Application of Artificial Neural Networks in Hydrology. 2000b. Artificial neural networks in hydrology. II: Hydrologic applications, *J. Hydrologic Eng., 52, 124–137*

Behera, S., and Panda, R. K. (2006) Evaluation of management alternatives for an agricultural watershed in a sub-humid subtropical region using a physical process based model, *Agric. Ecosyst. Environ*., 113(1–4), 62–72

Bhattacharya, Sarangi, A., and A. K. (2005) Comparison of artificial neural network and regression models for sediment loss prediction from Banha watershed in India, *Agric. Water Manage.*, 78(3), 195–208.

Cigizoglu, H. K. and Kisi, O. (2006) Methods to improve the neural network performance in suspended sediment estimation, *Journal of Hydrology*, 317(3–4), 221–238.

Cigizoglu, H. K. and Alp, M., (2007) Suspended Sediment load simulation by two artificial neural network methods using hydro meteorological data, *Environmental Modelling & Software*, January 2007, 2-13, 22(1), 2–13.

Cigizoglu, H. K. and Partal, T., (2008) Estimation and forecasting of daily suspended sediment data using wavelet-neural networks, *Journal of Hydrology*, 358(3–4), 317–331

De Farias, Alves, F. M., Santos, C. A. G., and Koichi, S. (2010) An ANN-based approach to modelling sediment yield: a case study in a semi-arid area of Brazil, Proc., ICCE Symp.: Sediment Dynamics for a Changing Future, *International Commission on Continental Erosion, Rennes, France*, 337, 316–321.

Mutlu, E., Chaubey, I., Hexmoor, H., and Bajwa, S. G. (2008) Comparison of artificial neural network models for hydrologic predictions at multiple gauging stations in an agricultural watershed, *Hydrol. Processes*, 22(26), 50–97.

Nagy, H.M., Watanabe, K., Hirano, M., (2002) Prediction of sediment load concentration in rivers using Artificial Neural Network Model, *Journal of Hydraulic Engineering* (ASCE) 128 (6), 588-595

Raghuwanshi N. S., Singh, R. and Reddy, L. S. (2006) Runoff and Sediment Yield Modeling Using Artificial Neural Networks: Upper Siwane River, India, *Journal of Hydrologic Engineering*, Vol. 11, No. 1, January 1, 2006, 10.1061/(ASCE)1084- 0699(2006)11:1(71).

Rajaee, T., Mirbagheri, S. A., Zounemat-Kermani, M., and Nourani, V. (2009) Daily suspended sediment concentration simulation using ANN and neuro-fuzzy models, *Science of the Total Environment*, 407(17), 4916–4927.

Sumi, T. And Hirose, T. (2009) Accumulation of sediment in reservoir, in water storage, Transport and Distribution, *Encyclopaedia of Life Support systems*, Vol. 1, pg 489. ISBN 978-1-84826-176-1

Walling and Fang (2003) Recent trends in the suspended sediment loads of the world's rivers, *Global and Planetary Change*, 39 (2003) 111 – 126

Wang, Y. M., Kerh, T., and Traore, S. (2009) Neural networks approaches for modelling river suspended sediment concentration due to tropical storms, *Global NEST J.*, 11(4), 457–466

Zhu, Lu X. X, and Zhou Y. (2007) Suspended sediment flux modeling with artificial neural network: An example of the Longchuanjiang River in the Upper Yangtze Catchment, China, *Geomorphology* 84 (2007) 111–125

*IN PROCEEDINGS OF 25th HYDRO 2020, INTERNATIONAL CONFERENCE, NATIONAL INSTITUTE OF TECHNOLOGY ROURKELA, ODISHA, INDIA 26-28, March 2021, ISBN 978-93-90631-56-8*

Paper ID - 300

# 1-D hydrodynamic modelling in HEC-RAS for prediction of water levels and sediment transport in Narmada River

V. K. Bind [1, 2], and B. K. Samtani [3]

[1]*Post Graduate, Water Resource Engineering, Department of Civil Engineering, Sardar Vallabhbhai National Institute of Technology, Surat 395007, India*

[2] *PhD Scholar, Discipline of Earth System Science, Indian Institute of Technology, Gandhinagr, 382355, India*

[3] *Professor, Department of Civil Engineering, Sardar Vallabhbhai National Institute of Technology, Surat 395007, India*

*Email: vivekbindce@gmail.com*

*Telephone/Mobile No.: +91 8447791811*

## Abstract

Sediment transport modeling is intricate because there are so many parameters responsible for the movement of particles like fluid characteristics, soil type, shape and size of the particles, turbulence in the fluid, and so on. Prediction of water levels and sediment transport across the river could help design the hydraulic structure. The 1-D hydrodynamic model was developed using HEC-RAS from Barmanghat to Handia to predict the water levels and sediment transport. The daily discharge and water levels and bed material size was collected from CWC, Bhopal and geometric data collected from India-WRIS for four stations, namely Barmanghat, Sandia, Hoshangabad, and Handia of Narmada River for 2011 and 2013 monsoon period. The calibration and validation of the model were done for Manning's n by comparing water levels at Sandia and Hoshangabad. The calibrated Manning's value for the 2011 monsoon period was found to be 0.037 for Sandia and 0.035 for Hoshangabad with minimum RMSEs 0.5052 m and 0.5158 m, respectively. That Manning's n value validated for the 2013 monsoon period at Sandia and Hoshangabad, the RMSEs were obtained as 0.7921 m and 0.9425 m, respectively. The calculated total load for these four stations using Yang's equation is close to the total simulated load with $R^2$= 0.86 for the 2013 monsoon. This study could help in the designing of water resources structures across the channels and flood management.

***Keywords:*** Hydrodynamic Model, Simulation, Sediment transport, Calibration, HECRAS.

## 1. Introduction

The term load represents the amount of sediment transport in the river. It is the rate at which the sediment transport occurs in the river. If average bed shear stress generated by flow is $\tau_0$ is more than the critical shear stress $\tau_{0c}$ for the initiation of sediment particles motion (Shield, 1936). First bed load equation given by (Du Boys, 1879) assumed that movement of bed material took place in the form of layer parallel to the bed of the channel. Velocity fluctuations i.e., Turbulence interact with the particles and play important role for the transport of the sediment in the mode of bed load as well as suspended load (Dey, 1999). Transport of bed material occur due to successive contact of the particle with the bed being limited by effect of gravity defined by Bagnold (1956). Stream velocity and fall velocity of the particles are sensitive parameter for sediment transport (Yang, 1973). Bed load transport rate is the function of number, particle size and average speed of the particle in motion, fluid force and fluctuations due to turbulence (Kalinske, 1947). Relative roughness $\frac{d_{50}}{D}$ is considered to know about sediment discharge using regression analysis (Rottner, 1959), fall velocity concept was used for bed load calculation (Einstein, 1950), a mathematical model was established using effective shear stress to calculate bed load (Yadav and Samtani, 2009), bed load formula was developed using water discharge (Schoklitsch, 1934). HEC-RAS is used for the estimation of sediment transport modelling (Haghiabi and Zaredehdasht, 2012), hydrodynamic model was developed in HEC-RAS for prediction of water level in lower Tapi river (Timbadiya et al., 2011). So, there are many parameters which plays important role for sediment transport. River conveys sediment along with water from the catchment and from the channel itself. Construction of reservoir and dams across the river decrease the sediment transport and reduces the capacity of reservoir due to aggradation of sediment (Zhang et al., 2012). The phenomenon of sediment transport is a major issue as far as the multi-purpose projects on the river. The study of such

kind of issue can help in proper project management. Study related to transport is necessary for the various major problem related to river and multi-purpose project like change in reservoir operation policy due to reservoir sedimentation, reduction in the discharge carrying capacity of the river and channels, reduction of the storage capacity of the reservoir, reducing the life span of the reservoir, impact of change in watershed characteristics on the sediment yield, design and maintenance of stable irrigation channels, River training and bed formations. Objective of this study is to Development of 1-D hydrodynamic model between Barmanghat to Handia station using The Hydrologic Engineering Center River Analysis System (HEC-RAS) with the help of flood year data 2011 (for calibration) and 2013 (for validation) for prediction of water level and sediment transport.

## 2. Study area and data collection

The Narmada is the 5th largest river flowing in India previously it was also known as Nerbudda. It is a central Indian river mostly flows in Gujarat and Madhya Pradesh. It originates from Amarkantak plateau and terminates to the Arabian Sea covering 1312 km length flowing from east to west. It is flowing 1077 km in Madhya Pradesh, 74 km in Maharashtra and 161 km in Gujarat state nearly.
Narmada basin covering approximately 92672.42 square km area between longitudes $72^0 38'$ to $81^0 43'$ in the east and between latitudes $21^0 27'$ to $23^0 37'$ in the north covering 3% area of the total geographical area of India. Geographical location of study area can be seen from the figure 1 of index map. Narmada River is geographically bounded by Maikala rages in east, the Arabian Sea in the west, Vindhyas in the North and Satpuras in the south. The basin covers a large area in M.P. and Gujarat states as compare to other two state that is Maharashtra and Chhattisgarh.

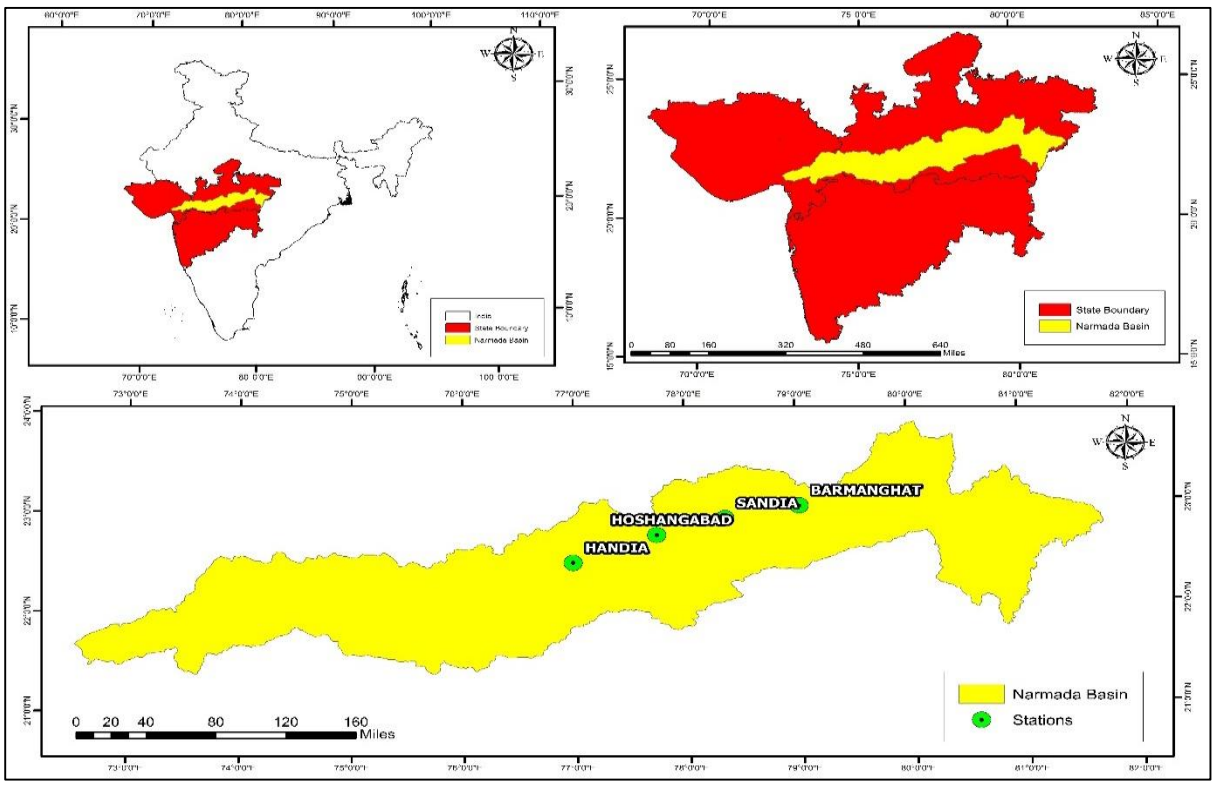



**Figure 1** Index map of study area

### *2.1 Data collection*

Daily discharge, water level data and grain-size distribution of bed material data (for 2013 year) for monsoon season was collected from CWC, Bhopal for all four stations Barmanghat, Sandia, Hoshangabad and Handia. Flood hydrograph was used upstream boundary condition at Barmanghat and stage hydrograph was used as downstream boundary condition at Handia. Area of cross-section data of

2012 was available on Water Resources Information System (India-WRIS) site it was collected from there, rest of the cross-section data in between the stations obtained by interpolation using HEC-RAS geometry tool. Particles mean size was collected from Narmada Valley Development Authority (NVDA).

## 3. Theoretical Background

### *3.1 Hydrodynamic Modelling*

Hydrologic routing is governed by the Continuity equation and flow/storage relationship, while hydraulic routing is governed by both Continuity and Momentum equations. HEC-RAS uses distributed flood routing. The alternative of hydraulic flood routing is used for calculation of the flow rate at the chosen location, and then calculate the corresponding water level by using the established rating curve at the same location. The advantage of a hydraulic flood routing over the hydrologic routing is that hydraulic routing calculates and updates the water level and flow rate simultaneously in the time domain and hence, more closely approaches the actual unsteady non-uniform nature of flow propagation in a channel.

The hydrodynamic models describing the flood routing in the river are, invariably, based on the solution of unsteady gradually varied flow equation, i.e., Saint-Venant equation. The analytical solution of the Saint-Venant equation for distributed routing is not feasible but it can be solved by numerical schemes. An implicit scheme is used in HEC-RAS for solving the Saint-Venat equation. A system of an algebraic equation is generated by applying a Saint-Venant equation simultaneously to all the unknown values on a timeline. The adopted numerical scheme for HEC-RAS is a four-point implicit finite difference scheme, some well-known numerical schemes used are Preissmann four-point scheme (Chow, 1988) developed by Preissmann.

### *3.2 Sediment theory in HEC-RAS*

Sediment transport analysis was done by the Quasi-unsteady Sediment hydrodynamic modelling to know about the quantity of sediment transport with the help of available equations in the model. Sediment transport modelling is very difficult because of uncertain sediment data and empirical equations. A brief discussion about Quasi- unsteady flow is given here.

#### *3.2.1 Quasi-unsteady flow*

It represents a discrete steady flow profile series of continuous hydrographs. Each step is divided into three steps, Flow duration, computational increment, and bed mixing. HEC-RAS updates the cross-sections and hydraulics at every computational increment and further divides these time steps into bed mixing time steps and updates the gradation of the bed.
The largest time step is Flow Duration; HEC-RAS assumes temperature and stage flow constant over the duration. The computational increment is the sediment time step, usually subdivide the duration. It may be equal to the duration but cannot be more than the duration. Flow duration is constant, but it may vary. The computational time step is further subdivided into the bed mixing time step (called the SPI parameter). HEC-RAS updates the gradation of the bed considering armoring and sorting many times in a single computation increment.

## 4. Methodology

1-D Hydrodynamic model was developed using the cross-section area, and River-network (created from Arc-GIS) exported in HEC-RAS shown in figure 2. The cross-sectional data were collected for four stations, and the rest of the cross-sections were generated at 500 m intervals by interpolation using HEC-RAS. The model performance was checked by changing the roughness parameter and comparing the observed and simulated water levels. The upstream boundary condition was taken as a flow

hydrograph at Barmanghat, and the downstream boundary condition was taken as a stage hydrograph at Handia. Afterward, the model was used to predict water levels and sediment transport. Total sediment transport calculated with the help of equation (i) or (ii) using $d_{50}$ data while for simulation grain size distribution was used for the 2013 monsoon period.

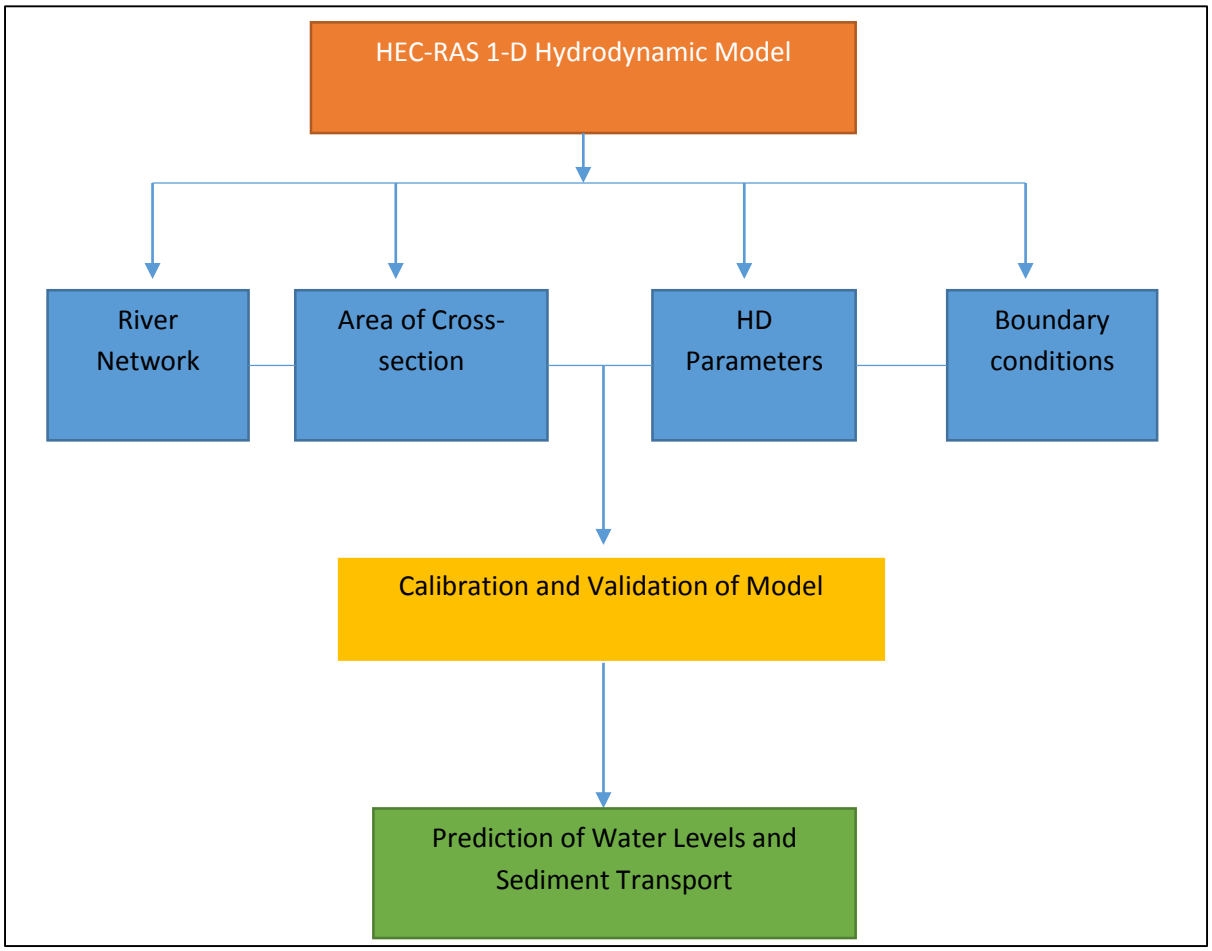



**Figure 2** Flow chart of methodology

(Yang, 1984) gave the sediment transport equation was given for gravel and sand for single grain size represented by:

$$logC_t = 5.435 - 0.28log\frac{wd_m}{\upsilon} - 0.457log\frac{u_*}{w} + \left(1.799 - 0.409log\frac{wd_m}{\upsilon} - 0.314log\frac{u_*}{w}\right)log\left(\frac{VS}{w} - \frac{V_{cr}S}{w}\right) \quad (1)$$

For sand $d_m < 2mm$

$$logC_t = 6.681 - 0.633log\frac{wd_m}{\upsilon} - 0.481log\frac{u_*}{w} + \left(2.784 - 0.305log\frac{wd_m}{\upsilon} - 0.282log\frac{u_*}{w}\right)log\left(\frac{VS}{w} - \frac{V_{cr}S}{w}\right) \quad (2)$$

For sand $d_m \geq 2mm$

Where, $C_t$ = Total sediment concentration, $w$ = Particle fall velocity, $d_m$ = Median particle diameter, $\upsilon$ = Kinematic viscosity, $u_*$ = Shear velocity, V= Average channel velocity.

### *4.1 Boundary Conditions*

The flow hydrograph was taken as an upstream boundary condition at the Barmanghat gauging station, and the stage hydrograph was taken as a downstream boundary condition at the Handia gauging station. The daily data of flow and stage were collected from CWC for the 2011 and 2013 floods in the monsoon period (from June to September).

### *4.2 Calibration and Validation of the Model*

Calibration and validation of the model are necessary for the reliability of the result coming from the model itself. The calibration of the model was done by varying the Manning's roughness n. The upstream and downstream boundary conditions taken were taken as flow hydrograph at Barmanghat and stage hydrograph at Handia, respectively. By changing the Manning's n value, the observed and simulated water level is compared between Sandia and Hoshangabad.

### *4.3 Performance Indices*

For the performance evaluation of the result obtained various performance indices have been used.

#### *4.3.1 Root mean square error (RMSE)*

The RMSE is the most commonly used error index statistic and used by most of the modeler to evaluate their model. The expected value should come close to zero.

$$\text{RMSE} = \sqrt{\sum_{i=1}^{N} \frac{(O_i - P_i)^2}{N}} \quad (3)$$

Where, $O_i$= represent the observed value, $P_i$ = represent the simulated value and $N$ = Total observations.

#### *4.3.2 Coefficient of Determination ($R^2$)*

It indicates the collinearity degree between the observed and simulated data. The coefficient of determination defines the proportion of the variance in the measured data. Its values lies between 0 and 1, the higher values indicates good result.

## 5. Result Discussion

The calibrated manning value was found to be 0.037 for Sandia and 0.035 for Hoshangabad with minimum RMSEs of 0.5052 m and 0.5158 m, respectively. The obtained Manning's n value validated for the 2013 monsoon period at Sandia and Hoshangabad, and the RMSEs are obtained as 0.7921 m and 0.9425 m, respectively, as shown in table 1.

**Table 1** Root mean square error (m) in the Calibration and Validation of the model

| | Year | Manning's n | Sandia | Hoshangabad |
|---|---|---|---|---|
| **Calibration** | | 0.020 | 1.0024 | 1.1021 |
| | | 0.025 | 0.7199 | 0.8796 |
| | | 0.030 | 0.8713 | 0.684 |
| | | 0.035 | 0.5384 | **0.5158** |
| | | 0.037 | **0.5052** | 0.5224 |
| | | 0.040 | 0.5075 | 0.5383 |
| **Validation** | **2013** | | 0.7921 | 0.9425 |

The model is used for the prediction of sediment transport using the equation given in the model. Yang's equation gave better than other equations results with the calculated value of sediment transport at all four stations. The Observed and predicted water levels for Sandia and Hoshangabad were found to be close, as shown in figure 3 and figure 4, respectively. The obtained $R^2$ between observed and predicted

water levels for Sandia and Hoshangabad were found to be 0.94 (shown in figure 5) and 0.96 (shown in figure 6), respectively.

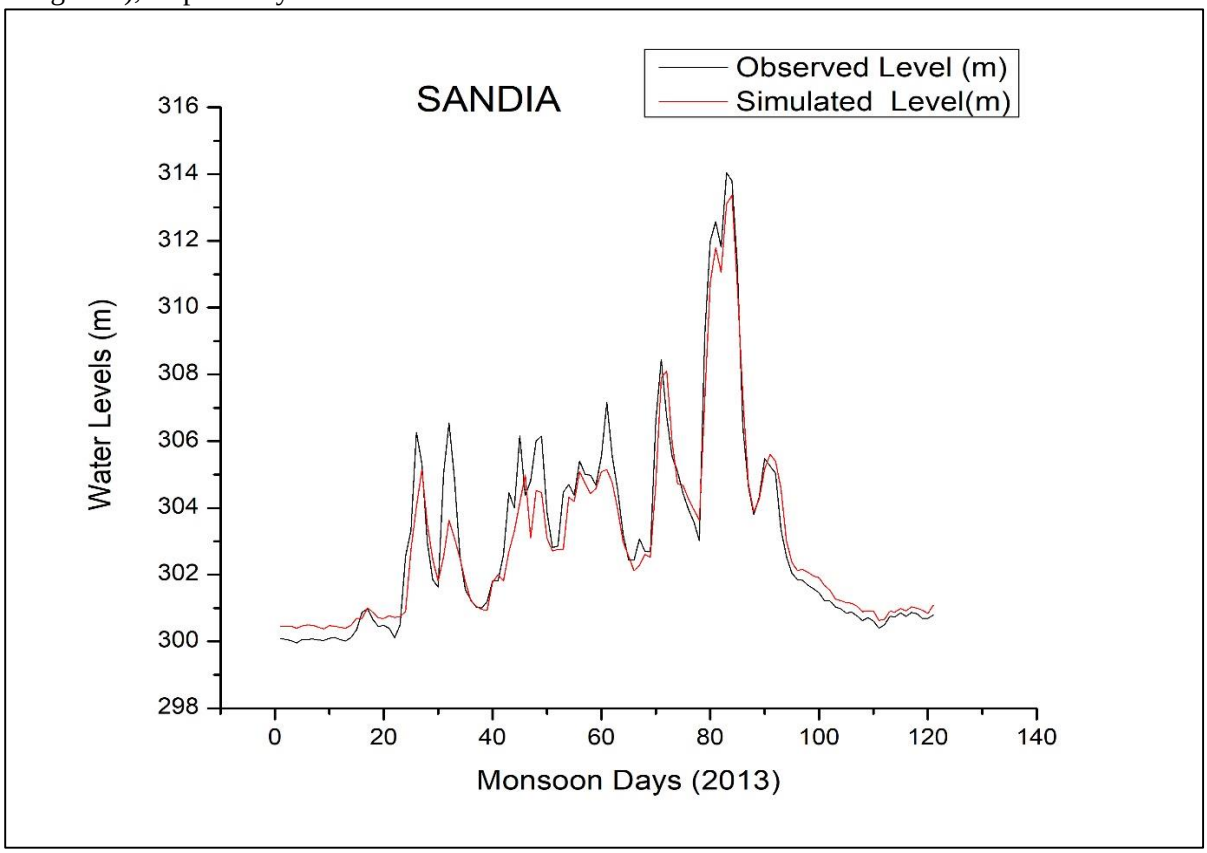



**Figure 3** Observed and simulated water level at Sandia

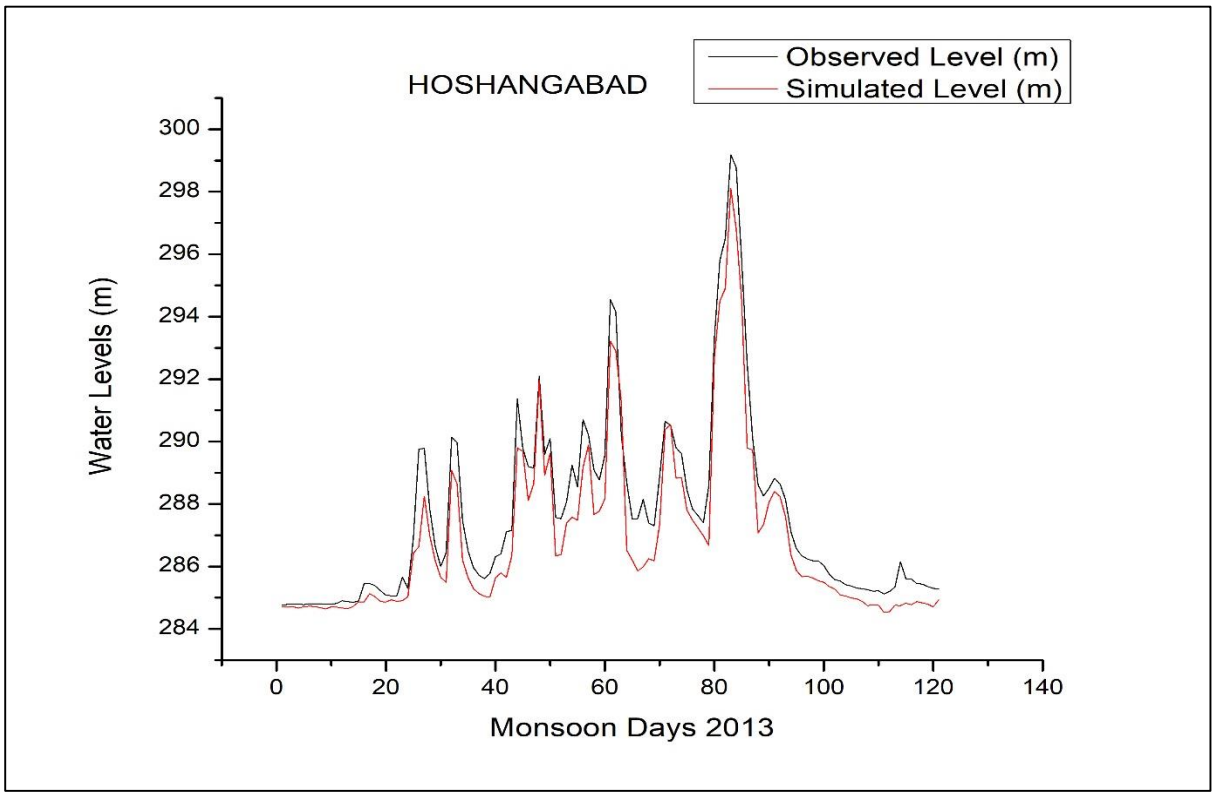



**Figure 4** Observed and simulated water level at Hoshangabad

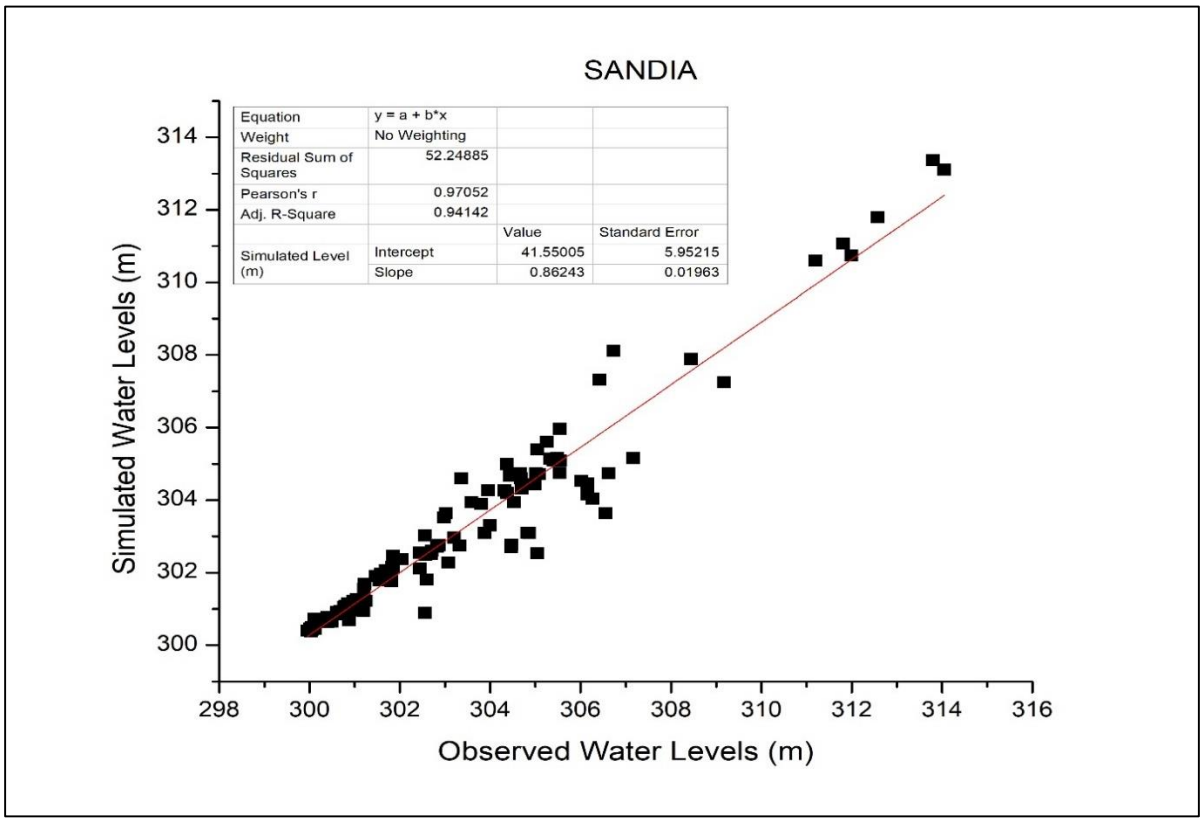



**Figure 5** Collinearity degree between observed and predicted Water Level at Sandia for the year 2013 HEC RAS

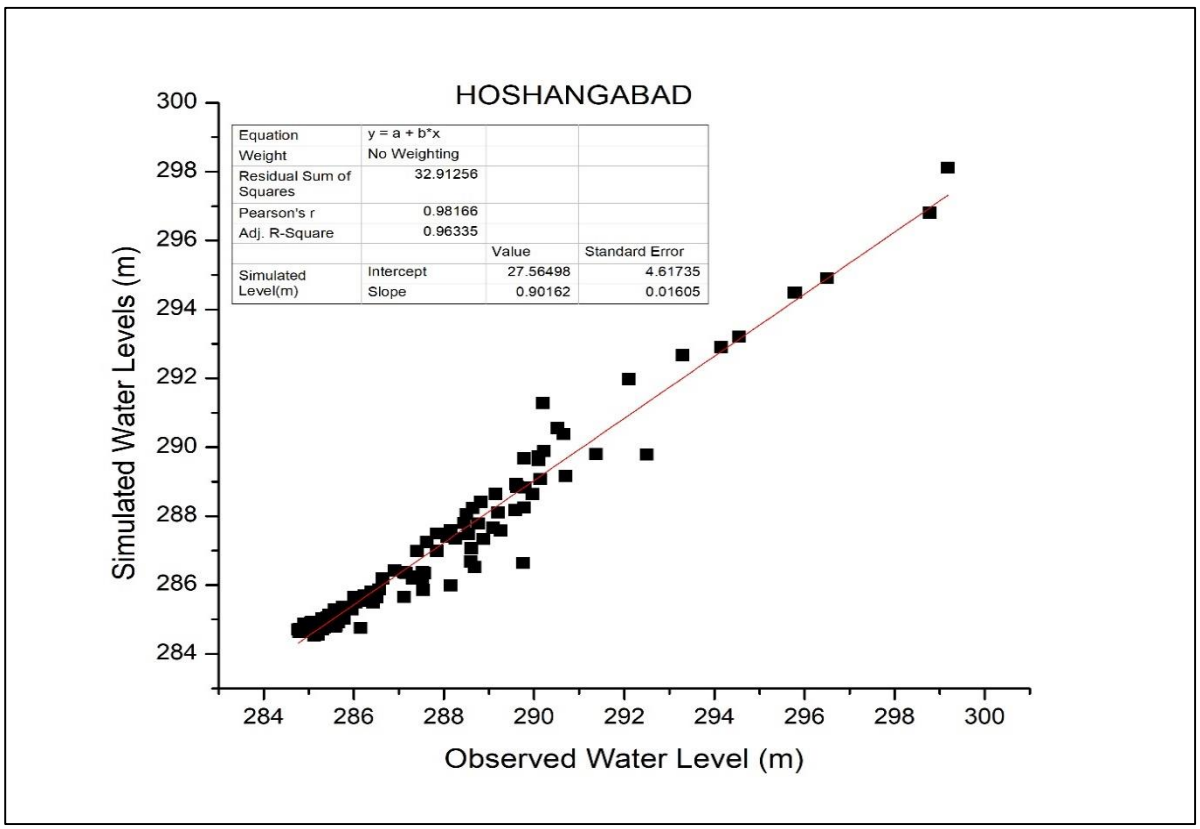



**Figure 6** Collinearity degree between observed and predicted Water Level at Hoshangabad for the year 2013 HEC-RAS

The total simulated sediment for the four stations is shown in Figures 7, 8, 9, and 10. Some important points of result discussion is given below.

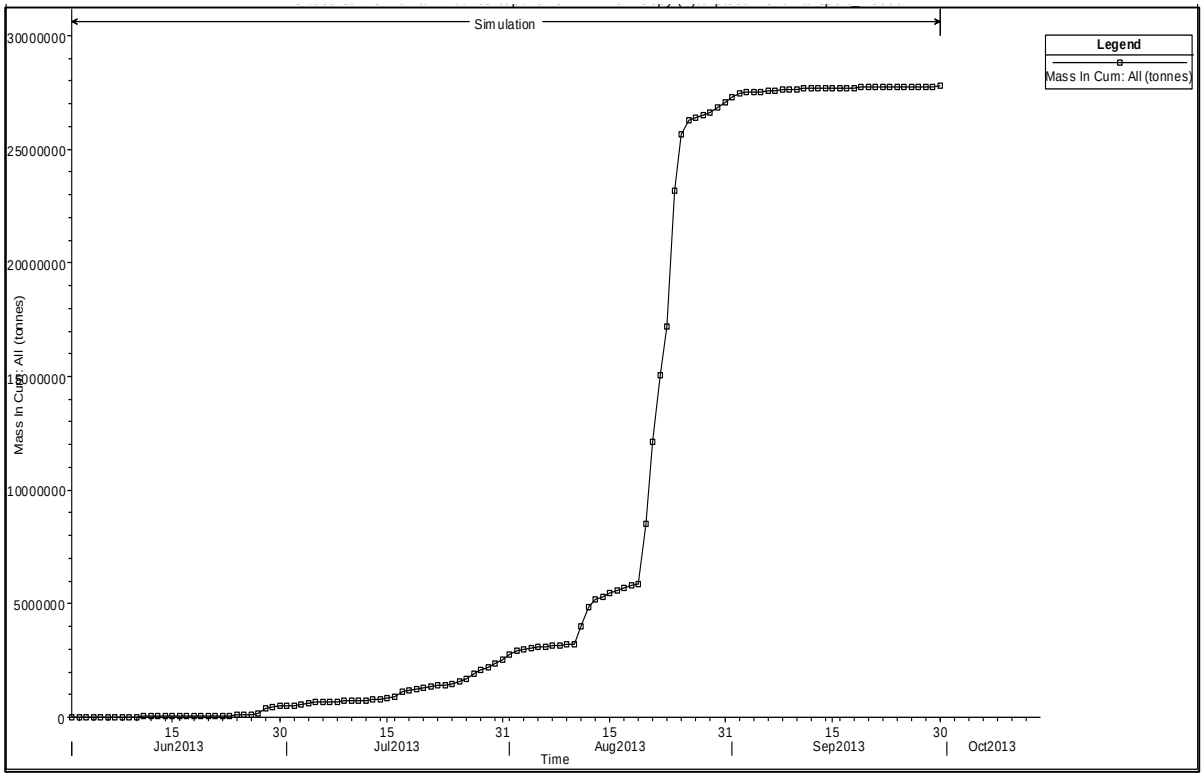



**Figure 7** Simulated Cum. Total load (Tonne) at Barmanghat for 2013 monsoon

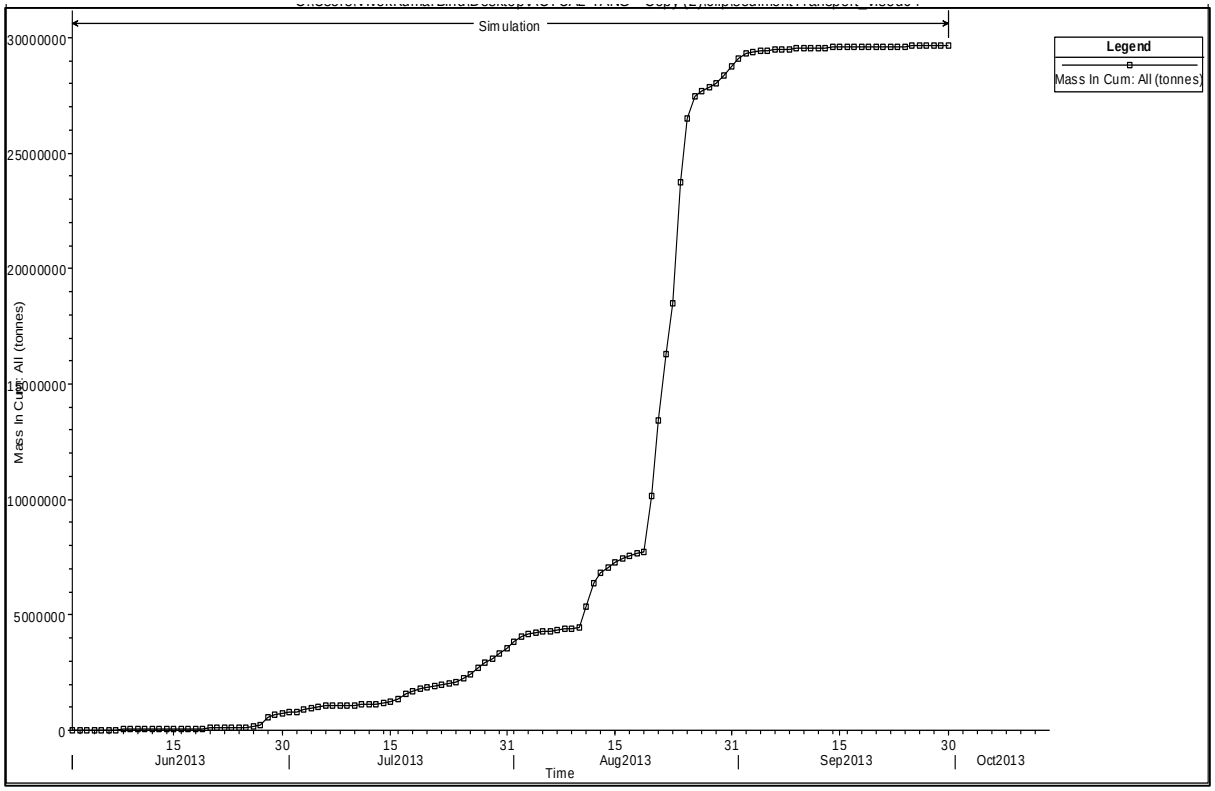



**Figure 8** Simulated Cum. Total load (Tonne) at Sandia for 2013 monsoon

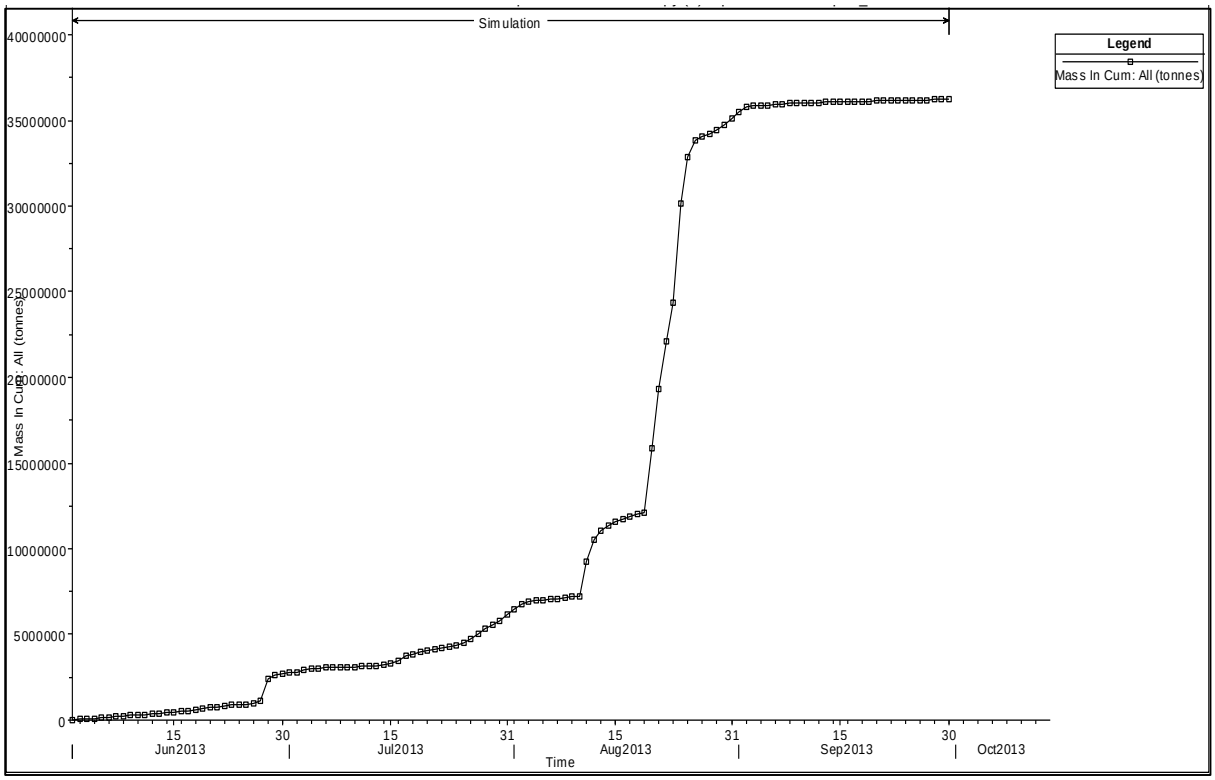



**Figure 9** Simulated Cum. Total load (Tonne) at Hoshangabad for 2013 monsoon

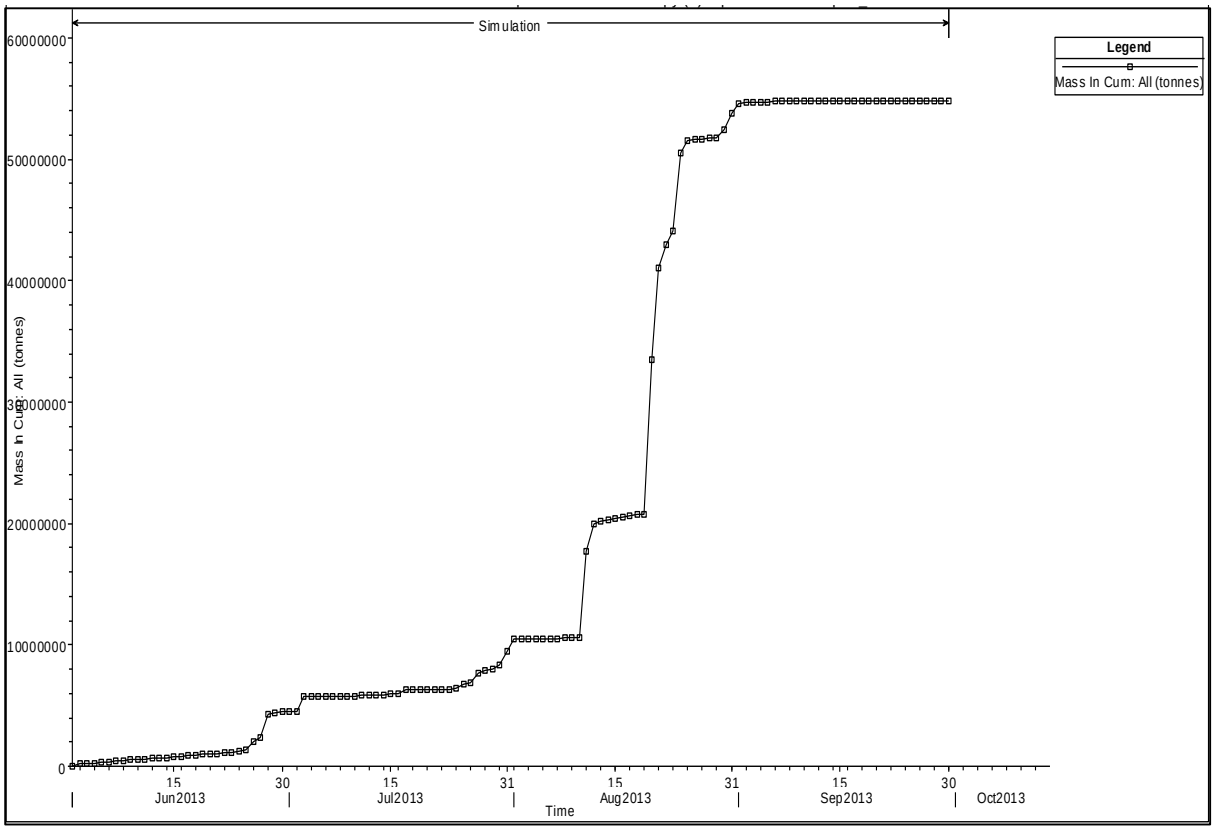



**Figure 10** Simulated Cum. Total load (Tonne) at Handia for 2013 monsoon

The calibrated Manning's value was found to be 0.037 for Sandia and 0.035 for Hoshangabad with minimum RMSEs 0.5052 m and 0.5158 m, respectively. The obtained Manning's n value was validated for the 2013 monsoon period at Sandia and Hoshangabad with RMSEs values 0.721 m and 0.9425 m, respectively. The observed and simulated water levels at Sandia and Hoshangabad were very close during validation with R2 =0.94 and R2 = 0.96, respectively. It shows good agreement between simulated and observed water levels. The maximum observed and simulated water levels at Sandia are 299.18 m and 298.11 m, respectively. Whereas, the maximum observed and simulated water levels at Hoshangabad are 314.05 m and 313.37 m, respectively, for the 2013 flood. Yang's method in HEC-RAS gives better results than another method because it is fall velocity and unit stream power (velocity×shear stress) factor gives good result when applied in the field and flume. The average total load calculates using Yang's equation with the help of the mean size of the particle obtained as 3.40×107 tonne, 2.01 ×107 tonne 3.88×107 tonne, and 7.69×107 tonne at Barmanghat, Sandia, Hoshangabad and, Handia, respectively for monsoon 2013. The total simulated load was obtained 2.77×107 tonne, 2.96×107 tonne, 3.62×107 tonne, and 5.47×107 tonne at Barmanghat, Sandia, Hoshangabad, and Handia, respectively for monsoon 2013. The total calculated cum. sediment load is in close agreement with total simulated cum. load with R2 = 0.86. Comparison between calculated and simulated total cum. The load is shown in table 2. The calculated and simulated total cum. Loads are found very close with R2 = 0.86, as shown in figure 11.

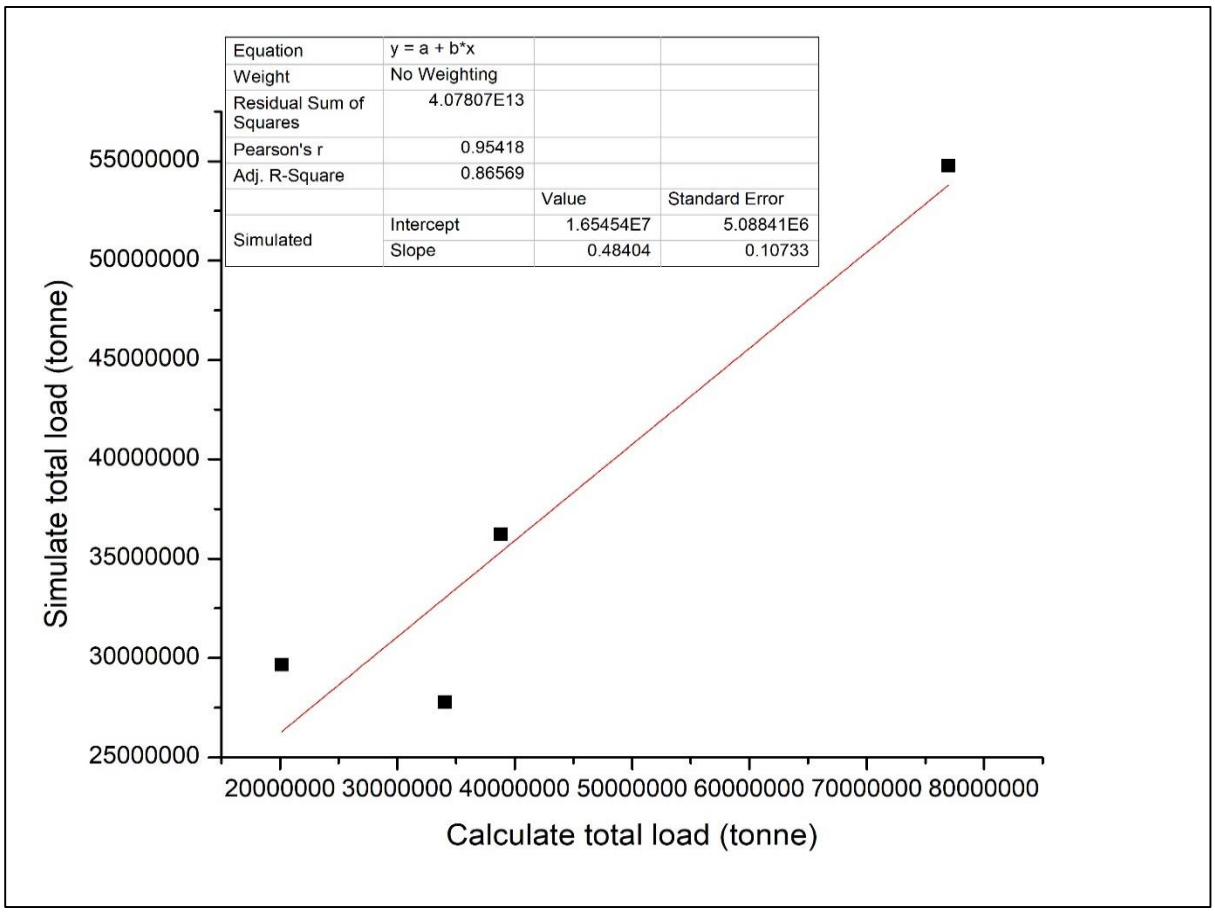



**Figure 11** Comparison between calculated load and simulated load

**Table 2** Comparison of Total Load in monsoon for 2013 for different stations

| Stations | Calculated ($\times 10^7$Tonne) | Simulated ($\times 10^7$Tonne) |
|---|---|---|
| Barmanghat | 3.40 | 2.77 |
| Sandia | 2.01 | 2.96 |
| Hoshangabad | 3.88 | 3.62 |
| Handia | 7.69 | 5.47 |

Empirical equations are based on some assumptions. This is also one of the major reasons for deviation in the result.

## 6. Conclusions

The 1-D hydrodynamic model was developed using HEC-RAS for the prediction of water levels and sediment transport. The data collected from CWC, India-WRIS, and NVDA. The quasi-unsteady model setup is done using HEC-RAS for computing sediment load. The model calibration is done for Manning's n. The calibrated Manning's value was 0.037 for Sandia and 0.035 for Hoshangabad obtained during calibration with the minimum RMSEs 0.5052 m and 0.5158 m respectively for the 2011 flood. That Manning's n value validated for the 2013 monsoon period at Sandia and Hoshangabad. The RMSE obtained was 0.72 m with R2 =0.94 at Sandia, whereas the RMSE obtained was 0.94 m with R2 = 0.96 at Hoshangabad. The predicted water levels are very close to the observed water levels for both stations. The calculated total load using Yang's equation is close to the total simulated load with R2 = 0.86. The model can be used for the prediction of total load for the Narmada river at Barmanghat, Sandia, Hoshangabad, and Handia. The study could help in making water resources structure in any section in the reach.

### Acknowledgements

The authors are thankful to CWC, Bhopal, NVDA and India-WRIS for providing required data.

## References

Bagnold, R. A. (1966). "An approach to the sediment transport problem from general physics". *Geological Survey Professional Paper* 422-I, U.S.A.
Chow, V. T., Maidment, D. R., and Mays, L. W. (1988). "Applied hydrology". *McGraw-Hill, New York.* pp. 272-330.
Dey, S. (1999). "Sediment threshold". *Applied Mathematical Modelling*, 23(5), 399-417.
Du Boys (1879). "The Rhone and streams with movable beds". *Annals des Pontes et Chaussees*, sec. 5, vol. 18, pp. 141-195.
Einstein, H. A. (1950). ''The bed-load function for sediment transportation in open channel flows.'' Technical Bull. No. 1026, U.S.D.A, *Soil Conservation Service*, Washington, D.C.
Fread, D. L. (1973). "Technique for implicit dynamic routing in rivers with tributaries". *Water Resources Research*, 9(4), 918-926.
Haghiabi, A. H., & Zaredehdasht, E. (2012). "Evaluation of HEC-RAS ability in erosion and sediment transport forecasting". *World Applied Sciences Journal*, *17*(11), 1490-1497.
HEC-RAS reference manual version 5.0.6 (2016). "HEC-RAS river analysis system" *U.S. Army corps of engineer.* (530)756-1104.
Kalinske, A. A. (1947). "Movement of sediment as bed load in rivers". *Eos, Transactions American Geophysical Union*, 28(4), 615-620.
Rottner, J. (1959). "A Formula for bed-Load Transport," *La Houille Blanche*, vol. 14, no. 3, pp.285-307.
Schoklitsch, A. (1934). "Der Geschiebetrieb und die Geschiebefracht," *Wasserkraft und Wasserwirtchaft'* vol. 29, n 4, pp. 37-43.
Sheilds, A. (1936). "Anwendung der Aechnlichkeitsmechanik und der Turbulenzforchung auf die Geschiebebewegung". *Mitteilungen d. Preuss. Versuchansta f. Wasserbau u. Schiffbau*. Berlin, Nr. 26.
Timbadiya, P. V., Patel, P. L., & Porey, P. D. (2011). "HEC-RAS based hydrodynamic model in prediction of stages of lower Tapi River". *ISH Journal of Hydraulic Engineering*, 17(2), 110-117.
Yang, C.T. (1973). "Incipient Motion and Sediment Transport". *JHD, Proc. ASCE*, Vol. 99, no. HY-10.
Yang, C. T. (1984). "Sediment transport and unit stream power function". *Journal of the Hydraulics Division*, 108(6), 774-793.
Zhang, W., Wei, X., Jinhai, Z., Yuliang, Z., & Zhang, Y. (2012). "Estimating suspended sediment loads in the Pearl River Delta region using sediment rating curves". *Continental Shelf Research*, 38, 35-46.



# With Best Compliments from Our Sponsors



DHI

# TEQIP - III

TECHNICAL EDUCATION QUALITY IMPROVEMENT PROGRAMME - III

**NIT ROURKELA**

## ABOUT THE INSTITUTE

National Institute of Technology (NIT), Rourkela was founded as Regional Engineering College, Rourkela in 1961. It is a prestigious Institute with a reputation for excellence at both undergraduate and postgraduate levels, fostering the spirit of national integration among the students, close interaction with industry, and a strong emphasis on research, both basic and applied. Its been consistently ranked within TOP 20 engineering institutes for 5 consecutive years as per MHRD's NIRF, Govt. of India and has retained a good world ranking among its peer institutes. The city of Rourkela is a bustling industrial town, cosmopolitan by nature, and is well connected to all parts of the country by road and rail. It is en-route Howrah-Mumbai main line of South-Eastern Railway. Nesting amidst greenery on all sides, the NIT campus is approximately 7km from Rourkela railway station. The nearest airports are Jharsuguda, Ranchi, Kolkata, and Bhubaneswar.

## ABOUT DEPARTMENT OF CIVIL ENGINEERING

Civil Engineering is concerned with the improvement in the quality of basic needs of human civilization and taking care of the natural and humanly built environments with their planning, designing, construction, operation, and maintenance. The Civil Engineering Department at NIT Rourkela is earnestly working to develop solutions to major sustainability challenges of the country and committed to producing leaders impacting the society at large.

The Department is actively involved in basic and applied research in the field of Structural Engineering, Geotechnical Engineering, Transportation Engineering, Water Resources Engineering, and Environmental Engineering along with high-quality technical advisory support to various organizations through R&D projects and consultancy. A broad area of the current research focus of the Department includes liquefaction and landslide remediation, ground improvement, vibration control, composite structures, seismic evaluation and retrofitting, river hydraulics, remote sensing and GIS, pavement design, transportation planning, wastewater management, air pollution, and solid waste management.

## ABOUT INDIAN SOCIETY FOR HYDRAULICS

The Indian Society for hydraulics (ISH) has established in the year 1992 as a technical, educational, and non-profit voluntary National organization to encourage and foster understanding amongst engineers, scientists, and other technical personnel engaged in various activities related to Hydraulics and Resources Engineering. Its main objectives include:

- To disseminate information through the conduct of Seminars/Conferences/workshops & Symposia.
- To encourage its member to update their knowledge, skills in and outside the country.
- To publish a paper to research/review/design and investigation in the Journal of Hydraulic Engineering for a wider audience.
- To accord recognition to the outstanding Researchers/Engineers who are striving hard in Hydraulics and Water Resources Engineering field.

Paramount Publishing House

A-531, H.No. 4-32-521, Phase-1, Allwyn Colony,
Kukatpally, Hyderabad - 500 072.
Ph. : 7799000082

ISBN 978-93-90631-56-8
9 789390 631568 >